37th EPS
European Peptide Symposium

14th IPS
International Peptide Symposium

25 - 29 August 2024

PROCEEDINGS



http://doi.org/10.17952/37EPS

Proceedings of the 37th European and the 14th International Peptide Symposium

Florence, Italy, 25-31 August 2024

Edited by:

Michal Lebl

Spyder Institute Prague, Czech Republic

Copyright ©2024 European Peptide Society
All rights reserved. No part of the material protected by this copyright notice may be reproduced or utilized in any form or by any means, electronic or mechanical, including photocopying, recording or by any information storage and retrieval system, without written permission from the copyright owner.

Introduction

The 37th European Peptide Symposium / 14th International Peptide Symposium was held in Florence, Italy, 25-31 August 2024, and its success was made possible by the contributions of 1,022 registered participants from 45 countries, alongside the generous support of over 30 sponsors and exhibitors. With a rich program featuring 95 oral presentations, 38 young scientist communications, and 632 posters, the symposium stood out as a significant milestone in advancing the dynamic field of peptide science.

The International Scientific Advisory Board played a key role in shaping the program, ensuring a comprehensive blend of traditional and innovative topics. These included advancements in peptide chemistry, cutting-edge industry technologies, emerging peptide-based applications, bioactive and therapeutic peptides, antimicrobial and antiviral peptides, peptide structural studies, computational approaches to peptide discovery, delivery systems, peptide materials, and the intersection of peptides with chemical biology. This diversity provided opportunities for both seasoned researchers and early-career investigators, with special emphasis on young scientists.

The 2024 symposium introduced several exciting new features to enhance engagement and accessibility. For the first time, Young Investigators' flash communications and parallel sessions were incorporated, significantly increasing the number of oral presentation slots. Additionally, recordings of the parallel sessions were made available to participants on the symposium website. Following the main program, three workshops provided an in-depth exploration of key topics: applying computational AI/ML in peptide research and its implications for peptide drug and material development, fostering innovation and sustainability in peptide synthesis, and navigating entrepreneurship and technology transfer in peptide discovery and development.

The impact and breadth of the symposium are reflected in this Proceedings book. Thanks to the dedicated efforts of Dr. Michal Lebl and the adoption of a new format, which incorporates PDF contributions of lectures and posters, this collection showcases 422 poster contributions and 8 lectures, capturing the wide range of topics addressed during the symposium.

We extend our heartfelt gratitude to all participants, invited speakers, the International Scientific Advisory Board, the Local Organizing Committee, the organizing secretariat OIC Group, and our sponsors and exhibitors. Your invaluable contributions have made this symposium a truly memorable and impactful event.

Anna Maria Papini & Paolo Rovero

Editor's Comments

This proceedings is quite different. Since many Symposium participants were experiencing this type of meeting for the first time, many of them had no idea that the production of symposium proceedings has a long tradition, starting with the first peptide symposium in Prague in 1958, organized by Professors Rudinger and Šorm. Every word presented at that meeting, including the discussion after each lecture was transcribed and published in the special issue of Collection of Czechoslovak Chemical Communication, which became the first book of proceedings. Today, understandably, not everything presented at the symposium makes it into the book since it is up to the authors whether they would submit their work or not. In the book of proceedings from 36thEPS only 96 (<20%) out of more than 500 presentations were submitted to the collection. And it did not fulfill the original idea of Rudinger and Šorm that the peptide symposium should bring together scientists working in this area to share their ideas and "cross-pollinate" their thinking.

I remember the times when it was a thing of high prestige to have the presentation accepted for a plenary lecture and therefore automatically for the book of proceedings. There were no poster presentations, and when the posters were introduced, not every poster was accepted for publication. Yes, there were not as many participants as today, but the idea of sharing the knowledge beyond the weeklong meeting should be revisited again.

And Meldal's Nobel prize in chemistry best illustrated the importance of publishing your work in the Proceedings. The priority of Meldal's work was unambiguously established by his article in the proceedings of the American peptide symposium (Tornoe W.T. and Meldal M., in "Peptides, The Wave of the Future; Proceedings of the Second International and the Seventeenth American Peptide Symposium" (Lebl M. and Houghten R.A., Eds.), American Peptide Society, 2001, p. 263).

So, we decided to change the format of the proceedings book based on the following principles:

- Every lecture or poster is available electronic form – usually the Powerpoint presentation or pdf file.
- Once the lecture or poster is presented at the symposium, everything in it is legally public knowledge.
- Presentation at the meeting is considered preliminary publication and should not prevent publication of the full version of the particular paper in Science or Nature.
- Every presentation receives the doi identifier once it is included in The Proceedings.
- Authors do not have to do anything else in addition to preparing their lecture or poster. Just submit their pdf through The Proceedings web site.
- If the author decides to write a classical proceedings mnuscript like in the past, it will be included into the collection as well. But there is no way to submit both versions of the same work.

In this way the original idea of the founders utilizing the technologies which were not available at their time is revitalized. (Personally, I believe that Prof. Rudinger would approve this without hesitation.)

Some observation from this year's book production. We still did not achieve the goal of including everything what was presented in this symposium, especially the lectures. However, the lectures are still available at the symposium web page. Poster's situation is much better – 422 posters are included in the proceedings – 67% of all posters were captured and provided with DOI numbers. Out of all submitted pdfs only 28 (7%) were created as the classical proceedings papers.

Let us hope that the next European Peptide Symposium will have even higher sucess in capturing all new ideas presented there!

Michal Lebl

Organization

Co-Chairs



Anna Maria Papini



Paolo Rovero

Scientific Advisory Board

Fernando Albericio, University of KwaZulu-Natal, South Africa
Steven Ballet, Vrije Universiteit Brussel, Belgium
Annette G. Beck-Sickinger, Leipzig University, Germany
Christian F.W. Becker, University of Wien, Austria
Elisabetta Bianchi, IRBM, Italy
Florence Brunel, Novo Nordisk, USA
Miguel A.R.B. Castanho, University of Lisbona, Portugal
Florine Cavelier, CNRS, Montpellier, France
Gong Chen, Nankai University, China
Philip Dawson, Scripps Research, USA
Marc Devocelle, Royal College of Surgeons, Ireland
Assaf Friedler, University of Jerusalem, Israel
Shiroh Futaki, Kyoto University, Japan
Rosario González Muñiz, Instituto de Química Médica, Spain
Thimmaiah Govindaraju, JNCASR, India
Tom N. Grossmann, VU University Amsterdam, The Netherlands
Wendy Hartsock, AralezBio, USA
Knud J. Jensen, University of Copenhagen, Denmark
Yangmee Kim, Konkuk University, Seoul, Korea
Rafal Latajka, Wroclaw University of Science and Technology, Poland
Michael Lebl, Czech Academy of Sciences, Czech Republic
Xuechen Li, University of Hong Kong, Hong Kong
William D. Lubell, University of Montreal, Canada
Lara Malins, Australian National University, Australia
Istvan Mandity, Semmelweis University, Hungary
Giancarlo Morelli, Università di Napoli "Federico II", Italy
Ines Neundorf, University of Cologne, Germany
Tamara Pajpanova, Bulgarian Academy of Sciences, Bulgaria
Joel Schneider, Center for Cancer Research, NIH, USA

Oliver Seitz, Humboldt University, Germany
Ved Srivastava, Perpetual Medicine, USA
Claudiu T. Supuran, University of Florence, Italy
Meritxell Teixidó, Gate2Brain, Spain
Andreas Tzakos, University of Ioannina, Greece
Helma Wennemers, ETH, Switzerland
Dek N. Woolfson, University of Bristol, United Kingdom

Local organizing committee
Sara Aquilia
Carla Bazzicalupi
Chiara Bellini
Claudia Bello
Silvia Bracci
Francesco Brenzini Biagioni
Michele Casoria
Mario Chelli
Andrea Di Santo
Fosca Errante
Carmen Gallo
Marina Macchiagodena
Margherita Marino
Francesca Nuti
Lorenzo Pacini
Marco Pagliai
Michael Quagliata
Feliciana Real-Fernandez
Luca Rosi
Matilde Rossi
Lucrezia Sforzi
Angela Sofia Tino

EPS Council

EPS National Representatives

Christian Becker, Austria
Steven Ballet, Belgium
Dancho Danalev, Bulgaria
Ruža Frkanek, Croatia
Michal Lebl, Czech Republic
Tomas Eiland Nielsen, Denmark
David Fewer, Finland
Oleg Melnyk, France
Roderich Süßmuth, Germany
Andreas Tzakos, Greece
Gábor Tóth, Hungary
Mark Devocelle, Ireland
Norman Metanis, Israel
Maria Luisa Mangoni, Italy
Ingrid Dijkgraaf, The Netherlands
Markus Baumann, Norway
Aleksandra Kesik-Misicka, Poland
Nuno Correia Santos, Portugal
Ekaterina Kolesanova, Russia
Jan Bakos, Slovakia
Tomaž Bratkovič, Slovenia
Rosario Gonzalez-Muñiz, Spain
Alesia A. Tietze, Sweden
Jeffrey W. Bode, Switzerland
Steven Cobb, United Kingdom

Awards

Josef Rudinger Memorial Award
Sponsored by PolyPeptide Group
The Josef Rudinger Memorial Lecture Award is presented "in commemoration of Josef Rudinger's role in the foundation of the European Peptide Symposia and of diverse contributions he made to peptide chemistry".

Awardee: **David Andreu**, Pompeu Fabra University, Spain and **Fernando Albericio**, University of KwaZulu-Natal, South Africa and University of Barcelona, Spain.

Leonidas Zervas Award
The Leonidas Zervas Award is presented in commemoration of his outstanding contributions to peptide science. The award is given to the scientist who has made the most outstanding contributions to the chemistry, biochemistry and/or biology of peptides in the five years preceding the date of selection and is sponsored by the donation of **Dr. Rao Makineni**.

Awardee: **Ashraf Brik**, Technion-Israel Institute of Technology, Haifa, Israel.

Miklós Bodanszky Award
Sponsored by BCN Peptides
The Miklos Bodanszky Award is presented in commemoration of Miklos Bodanszky's contributions to peptide research, to a young scientist who has in the opinion of the General Assembly of the Society made the most outstanding contribution to peptide research in the period of maximum ten years after obtaining the PhD degree.

Awardee: **Cesar De La Fuente**, University of Pennsylvania, USA

Invited speakers

Morten Meldal (University of Copenhagen – Denmark)
Fernando Albericio (University of Kwa-Zulu, South Africa)
Emel Adaligil (Genentech – USA)
David Andreu (Pompeu Fabra University, Spain)
Baptiste Aussedat (Chemitope Glycopeptide – USA)
Annette Beck-Sickinger (Leipzig University – Germany)
Christian Becker (University of Vienna – Austria)
Ashraf Brik (Technion Haifa – Israel)
Florence Brunel (Novo-Nordisk, USA)
Miguel Castanho (Universidade de Lisboa – Portugal)
David Craik (University of Queensland – Australia)
Phil Dawson (Scripps Research – USA)
Cesar de la Fuente (University of Pennsylvania, USA)
Richard Di Marchi (Indiana University – USA)
Ikuo Fujii (Osaka Metropolitan University – Japan)
Shiroh Futaki (Kyoto University – Japan)
Thimmaiah Govindaraju (Jawaharlal Nehru Centre for Advanced Scientific Research – India)
Christian Gruber (Medical University of Vienna – Germany)
Christian Hackenberger (Leibniz-Forschungsinstitut für Molekulare Pharmakologie – Germany)
Wendy Hartsock (Aralez Bio – USA)
Gosuke Hayashi (Nagoya University – Japan)
Hironobu Hojo (Osaka University, Japan)
Akhter Hossain (The Florey, University of Melbourne – Australia)
Mattan Hurevich (Hebrew University of Jerusalem – Israel)
Diana Imhof (Pharmaceutical Institute – Germany)
Knud Jensen (University of Copenhagen – Denmark)
Daniela Kalafatovic (University of Rijeka – Croatia)
Rui Kamada (Hokkaido University – Japan)
Aphrodite Kapurniotu (Technical University of Munich – Germany)
Stephen Kent (University of Chicago – USA)
Beate Koksch (Freie Universitaet Berlin – Germany)
Xuechen Li (University of Hong Kong – Hong Kong)
Yu-Shan Lin (Tufts University – USA)
Ewa Lis (KoliberBio – USA)
William Lubell (Université de Montréal – Canada)
Shi-Zhong Luo (Beijing University, China)
Lara Malins (Australian National University – Australia)
Istvan Mandity (Semmelweis University – Hungary)
Hiroshi Matsui (Cornell Medical College – USA)
Katsumi Matsuzaki (Kyoto University – Japan)
Kevin McDonnel (Bicycle Therapeutics – USA)
Norman Metanis (Hebrew University of Jerusalem – Israel)
Hiroshi Murakami (Nagoya University – Japan)
Ikuhiko Nakase (Osaka Metropolitan University – Japan)
Ines Neundorf (University of Cologne – Germany)
Atsushi Ohta (Chugai Pharmaceutical – Japan)
Nir Qvit (Bar-Ilan University – Israel)
Ronald Raines (Massachusetts Institute of Technology – USA)
Kazuyasu Sakaguchi (Hokkaido University – Japan)
Viji Sarojini (University of Auckland – New Zealand)

Joel Schneider (National Institutes of Health – USA)
Oliver Seitz (Humboldt University Berlin – Germany)
Pernille T. Shelton (Gubra – Denmark)
Roderich Suessmuth (Technische Universität Berlin – Germany)
Hiroaki Suga (University of Tokyo – Japan)
Meritxell Teixido (Gate2Brain – Spain)
Helma Wennemers (ETH – Switzerland)
Derek Woolfson (University of Bristol – United Kingdom)
Shlomo Yitzchaik (Hebrew University of Jerusalem – Israel)

Sponsors and Supporters











































MOTIF BIOTECH

CHRISTOF SENN LABORATORIES AG

TELEDYNE | Teledyne LABS

vapourtec
fast-flow for peptides

PEPTISYSTEMS
Scalability. Flowthrough. Automation.

ANASPEC

RAPP POLYMERE

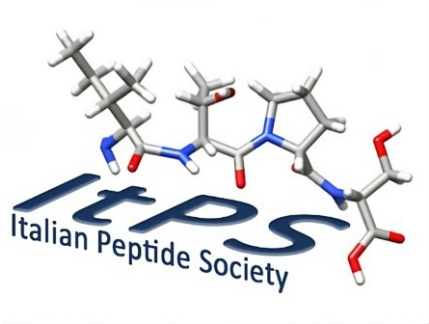

SENN

List of Lectures

L003 Synthesis of β-turn mimics without stereogenic carbons: expanding the modular approach for diversity-oriented synthesis of tetrasubstituted benzotriazepinones
Xiaozheng Wei, Sarah-Maude Harvey, Debora Iaculli, Steven Ballet, William D. Lubell
L005 Fundamental aspects of SPPS and the Green future
Stephen Kent
L020 tCAP conjugate: an affinity peptide-based antibody conjugation system to generate highly functional antibody
Yuji Ito
YIF02 Bimodal use of chiral α-Trifluoromethylalanine in Aib Foldamers: study of the position impact towards the helical screw-sense preference
Nathan Picois, Lizeth Bodero, Pierre Milbeo, Thierry Brigaud, Grégory Chaume
YIF09 Designed cyclic peptides as inhibitors of amyloid self-assembly and cross-seeding of amyloid-beta peptide and islet amyloid polypeptide
Beatrice Dalla Volta, Melanie Roth, Yuan Tian, Alessia Calzi, Jürgen Bernhagen, Aphrodite Kapurniotu
YIF13 Targeting West Nile virus replicases: NS3 and heterodimers inhibitors
Daniele Volpin, Cristina Peggion, Riccardo Rigo, Matia Sturlese
YIF20 Short Catalytic Peptides for Carbon Dioxide Sequestration
Kalpana Kumari, Vibin Ramakrishnan
YIF21 Bioactive Self-assembled Peptide Hydrogels for 3D Cancer Model Applications
Burcu Sırma Tarım, Sedef Tamburacı, Ayben Top

List of Posters

P1002 Convergent synthesis of peptidomimetic based on a chloroalkene dipeptide isostere and its application to inhibition against amyloid β aggregation
Takuya Kobayakawa, Chika Azuma, Kenichi Yamamoto, Kohei Tsuji, Hirokazu Tamamura
P1003 Optimization of IEDDA reaction parameters
Rasheda Aktar Samiha, Samir Das, Arundhati Nag
P1004 Identification of reactivity hotspots at the interfaces of protein–protein interactions
Nathalie M. Grob, Clint Remarcik, Simon L. Rössler, Jeffrey Y. K. Wong, John C. K. Wang, Jason Tao, Corey L. Smith, Andrei Loas, Stephen Buchwald, Dan Eaton, Magdalena Preciado López, Bradley Pentelute
P1005 Using N-acylation as a disulfide lock simplifies chemical protein synthesis
Vincent Diemer, Vangelis Agouridas, Benoît Snella, Rémi Desmet, Oleg Melnyk
P1007 Synthesis of Peptide Hydrazides: Hydrazone Resin vs. Hydrazine 2CT Resin
Maria Leko, Polina Filippova, Karin Rustler, Thomas Bruckdorfer, Sergey Burov
P1009 Facilitating the access to repeat proteins by a novel water-compatible oligomerization process
Eliott Roy, Oleg Melnyk, Vincent Diemer
P1012 Technetium-99m tricarbonyl complexes containing amino acid derivatives for cancer imaging
João D.G. Correia, Rúben D.M. Silva, Cristina P. Matos, Catarina I.G. Pinto, Joana F. Guerreiro, Lurdes Gano, Filipa Mendes
P1013 Development of methodology for late-stage acylation of threonine residue enabled by chemoselective acyl transfer followed by desulfurization
Daiki Sato, Chiho Shinozaki, Masaya Denda, Akira Otaka
P1014 Towards the total synthesis of the bacteriocin Nisin A on solid support
Ilia Perov, Bethan Donnelly, Tyler Mallett, John Vederas
P1015 Protein semi-synthetic approach to probe C-terminal hyperphosphorylation of the Alzheimer-relevant protein Tau
Bingjia Yan, Léa EI Hajjar, Wenyi Lia, Caroline Smet-Nocca, Christian P. R. Hackenberger
P1016 Structural Optimization Study Leading to Orally Bioavailable Cyclic Peptides Inhibiting an Intracellular Tough Target
Mikimasa Tanada, Ryuji Hayashi, Mirai Kage, Atsushi Ohta, Hitoshi Iikura,Takuya Shiraishi
P1017 Chemical Engineering of Artificial Transcription Factors
Omer Harel, Xiaoxi Lin, Muhammad Jbara
P1018 Peptides Targeting DNA Four-Way Junctions
Eleanor Ivens, Andrew Beekman, Mark Searcey

P1019 C-Glycosylation of Aromatic Amino Acids by Pd-Catalyzed Cross-Coupling
Calvin Matula, Norbert Sewald
P1020 Efficient Peptide Thioester Synthesis from Hydrazides Using Near-Stoichiometric Thiol Quantities
Julie Di Adamo, Nathalie Ollivier, Vincent Diemer, Oleg Melnyk
P1021 Electrostatic Assistance of NCL Catalysis by 4-Mercaptophenylacetic Acid
Nathalie Ollivier, Eliott Roy, Remi Desmet, Vangelis Agouridas, Vincent Diemer, Oleg Melnyk
P1022 An efficient strategy to bioconjugate disulfide-rich peptides via thiol-maleimide chemistry while preserving their bridging pattern
Lylia Azzoug, Hervé Meudal, Karine Loth, Séverine Morisset-Lopez, Carlo Pifferi,Vincent Aucagne
P1023 Auxiliaries in Native Chemical Ligation: Exploring the Reactivity Landscape with new Scaffolds
Sebastian Trunschke, Antonia Feida, Oliver Seitz
P1025 Superfast Desulfurization for Protein Chemical Synthesis and Modification
Zhenquan Sun, Yihui Cao, Xuechen Li
P1026 An iron-catalyzed protein desulfurization method reminiscent of aquatic chemistry
Rémi Desmet, Céline Wichlacz, Aurélie Tasiemski, Vangelis Agouridas, Oleg Melnyk
P1027 Chemoselective P-S coupling of aminophospholes to peptides under mild conditions
Emmanuelle Rémond, Laure Liénart, Miyanou Rosales-Hurtado, Sébastien Clément, Jean-Alain Fehrentz, Jean-Louis Banères, Florine Cavelier
P1029 Flow – SPPS towards greener and more efficient peptide manufacturing
Oliver Kracker, Eike-Fabian Sachs
P1030 Design of Experiments as Powerful Tool for Peptide Cleavage Development
Teresa Friedrichs, Alexander P. Galow
P1031 Synthetic combinatorial OPA-cyclic peptide library
Kin Nam Adrian Chu, Carina Hey Pui Cheung, Xuechen Li
P1032 Direct synthesis of peptidomimetics containing non-coded amino acids via photocatalytic carbamoylation reaction
T. Gandini, M. L. Gelmi, R. Bucci
P1034 Thiol-yne Mediated Macrocyclisation and Derivatisation Strategies
Conor Williams, Dearbhla Tully, Susannah H. Calvert, Joanna F. McGouran, Eoin M. Scanlan
P1036 Synthesis and biological activity of ultra-short antimicrobial peptides bearing a novel noncoded amino acid
Barbara Biondi, Fernando Formaggio, Cristina Peggion, Andrea Schivo, Teodora Calin, Simona Oancea, Emma Khachatryan, Liana Hayriyan, Ashot Saghyan, Anna Mkrtchyan
P1037 Evaluation of the stability of oxytocin and vasopressin under oxidative stress conditions
Stefano Tartaggia, Claudia Honisch, Martina Rotondo, Paolo Ruzza
P1038 Biocatalytic Synthesis of Dihalogenated Tryptophan Derivatives
Bjarne Scharkowski, Nicolai Montua, Norbert Sewald
P1039 Silicon-containing amino acids for 18F labeling of neurotensin analogues targeting NTS1 receptor
Miyanou Rosales Hurtado, Emmanuelle Rémond, Delphine Vimont, Alexis Reinbold, Elif Hindié, Clément Morgat, Florine Cavelier
P1042 Preclinical Development of Myrcludex B Derivatives: Physicochemical Properties
Tyra Christian, Sabrina Wohlfart, Christian Kleist, Philipp Uhl, Stephan Urban, Walter Mier
P1044 Exploring the structure-function relationship of heme binding to blood coagulation factor VIII based on peptide models
Lorena Kröner, Diana Imhof, Marie-T. Hopp
P1046 Site-specific post-translational modifications of Tau4
Miriam M. K. Preissler, Dominik Vogl, Christian F. W. Becker
P1047 Synthesis of the natural peptide product Fusahexin
Carmen Bäuerlein, Armin Geyer
P1049 Organocatalytic Surfactants for Direct Asymmetric Aldol Reactions in Aqueous Media
Susanta Kumar Behera, Ramesh Ramapanicker
P1050 O-to-O Acyl Transfer for Epimerization-free Peptide C-terminal Salicylaldehyde Ester Synthesis
Zhixiang Zhong, Wang Xia, Bing-Wen Li, Han Liu, Zhi-Xiang Yu, Xuechen Li
P1051 New electrochemical method for Arylation of Cysteine containing peptides
Shen Linhua, Olivier Monasson, Elisa Peroni, Franck Le Bideau, Samir Messaoudi
P1052 N-Aminoimidazol-2-one Peptide Mimic Tools for Deciphering Active Conformations
Yousra Hamdane, Pradeep Chauhan, Suresh Vutla, Darince Truong, William D. Lubell

P1054 Ring Pucker Control in β-Prolines
Nassim Maarouf Mesli, William D. Lubell
P1055 Nature-Inspired Gallinamides Are Potent Antischistosomal Agents: Inhibition of the cathepsin B1 Protease Target and Binding Mode Analysis
P. Spiwokova, M. Horn, L. Maresova, J. Fanfrlik, A. Jilkova, P. Fajtova, A. Leontovyc, R. Houstecka, L. Bielikova, J. Brynda, M. Chanova, H. Mertlikova-Kaiserova, E. Caro-Diaz, J. Almaliti, N. El-Sakkary, W.H. Gerwick, C.R. Caffrey, M. Mares
P1056 Study on interactions of LL-37 human cathelicidin peptide fragment with Cu(II) ion
Jakub Brzeski, Dariusz Wyrzykowski, Bogusław Pilarski, Joanna Makowska
P1058 Peptide stapling - application in antibacterial therapies
Monika Wojciechowska, Julia Macyszyn, Michal Burmistrz, Joanna Miszkiewicz, Malgorzata Lobka, Joana Trylska
P1059 Translocation-Enhancing Peptides: FacilitateTransport of Molecules and Lipid Scrambling
Ladislav Bartoš, Robert Vácha
P1062 Antimicrobial activity of Histatin 5 based metallopeptides
Gabriela Vieira Silva Zolin, Renan Lira de Farias, Saulo Santesso Garrido
P1063 De novo design of miniproteins binding to PD-L1
Juan Lizandra Pérez, Natalia Miodowska, Łukasz Berlicki
P1064 Metal complexes of ATCUN-like peptides for sequence-specific DNA cleavage
Ivan N. Unksov, Lena K. Müller, Hanna Zdhannova, Alexander Gräwe, Joshua Stahl, Viktor Stein, Daniel Tietze, Alesia A. Tietze
P1067 Development of peptide-based inhibitors against β-catenin using in silico approach
Minami Fujita, Amika Kikuchi, Kyohei Arita, Takashi Misawa, Yosuke Demizu
P1068 An Intracellular Cyclisation Screen Generates Short Helical Peptide Inhibitor of Alpha Synuclein Aggregation
Scott G. Allen, Richard M. Meade, Robert J. Williams, Jody M. Mason
P1070 Synthesis and study of modified Temporin analogs with unnatural amino acids Citrulline and Ornithine as potential antibacterial agents
Nelly Georgieva, Dilyana Dimitrova, Tsvetelina Foteva, Veronika Nemska, Dancho Danalev
P1071 New unique analogs of anorexigenic cocaine- and amphetamine-regulated transcript peptide
Andrea Pačesová, Vilém Charvát, Miroslava Blechová, Blanka Železná, Jaroslav Kuneš, Lenka Maletínská
P1072 Antibacterial and anti-biofilm activity of branched peptides derived from antimicrobial peptides
Eva Tollapi, Alessandro Rencinai, Giada Meogrossi, Silvia Scali, Chiara Falciani
P1073 AMP32: a short cyclic peptide as an environmentally friendly alternative to counteract late blight symptoms in crops
Elena Marone Fassolo, Demetrio Marcianò, Stefano Rosa, Lucia Feni, Vaibhav Srivastava, Andrea Tagliani, Silvia Laura Toffolatti, Sara Pellegrino, Vincent Bulone, Simona Masiero, Paolo Pesaresi
P1075 Water-soluble longibramide E analogs: synthesis and antibacterial activity
Renato B. Pereira, Ana Gomes, Mariana Ferreira, Paula Gameiro, Paula Gomes
P1076 Generation of a Peptide Library from human Bone Marrow for the discovery and identification of novel bio active bone-marrow derived peptides
Nico Preising, Armando A. Rodriguez, Merve Karacan, Sebastian Wiese, Dennis Freisem, Fabian Zech, Dietmar Thal, Konstantin Sparrer, Jan Münch, Frank Kirchhoff, Ludger Ständker
P1079 Synthesis and antibacterial activity of new analogues of Aurein 1.2
Nora Angelova, Tsvetelina Foteva, Veronica Nemska, Nelly Georgieva, Dancho Danalev, Emilia Naydenova
P1080 Tackling antibiotic resistance by blocking signalling pathways
Rachel A. Johnson, Susanne Gebhard, Jody M. Mason
P1081 Synthesis and evaluation of β-secretase inhibitory activity of new Galantamine derivatives comprising peptide moiety
Emilia Naydenova, Lyubomir T. Vezenkov ,Valentin Lozanov, Daniela S. Tsekova
P1082 Searching for biologically active peptide fragments of hACE2 interacting with the S1 protein of the SARS-CoV-2 virus
Aleksandra Czerchawy, Manoj Kumar Muthyala, Beata Kolesińska
P1084 Synthesis of Aza-Amanitins to Enhance Cytotoxicity for Targeted Cancer Therapeutics
Kayla C. Newell, F. Cruz Custodinho, Juliette Froelich, Katherine Bessai, Cassandra M. Sgarbi, David M. Perrin
P1085 In situ mechanistic insight to antibacterial action of membrane-incising β-peptide lamellae
Kamal el Battioui, Imola Cs. Szigyártó, Sohini Chakraborty, Judit Tóth, Dániel Molnár, Tünde Juhász, Loránd

Románszki, Andrea Bodor, Kata Horváti, István Mándity, Zoltán Varga, Judith Mihály, Csenge Lilla Szabó, Szilvia Bősze, Gergő Gyulai, Mayra Quemé-Peña, András Wacha, Bálint Jezsó, Tamás Beke-Somfai

P1087 Novel peptide inhibito of SARS-CoV-2 infection

Nina Raasch, Lucas Weißenborn, Elie Richel, Olena Denysenko, Simon Schäfer, Heinrich Sticht, Klaus Überla, Jutta Eichler

P1088 Investigating protein prenylation using cell-permeable peptides

Martin Matijass, Merlin Klußmann, Annika Klimpel Ines Neundorf

P1090 Cytotoxicity and phototoxicity effects of modified temporin analogs with unnatural aminoacids

Tsvetelina Foteva, Ivan Iliev, Rositsa Hristova, Dilyana Dimitrova, Veronica Nemska, Nelly Georgieva, Dancho Danalev

P1092 Triazole-bridged peptides with enhanced antimicrobial activity and potency against pathogenic bacteria

Joshua Grabeck, Jacob Mayer, Axel Mayer, Michele Casoria, Michael Quagliata, Denise Meinberger, Andreas R. Klatt, Isabelle Wielert, Berenike Maier, Anna Maria Papini, Ines Neundorf

P1094 Rational design of a miniprotein to inhibit the oncogenic transcription factor MYC

B. Ellenbroek, J. Kahler, D. Arella, C. Lin, W. Jespers, S. Pomplun

P1095 Novel, non-covalent peptide furin inhibitors suppressing Zika virus replication

Aleksandra Helbik-Maciejewska, Gabriela Brzuska, Dawid Dębowski, Agata Gitlin-Domagalska, Andrea Lipińska, Ewelina Król, Krzysztof Rolka

P1096 Molecular investigation on peptide regulated Mfn 1 and Sirt 1 protein interactions in mitochondrial dynamics

Mahesh Kumar Cinthakunta Sridhar, Nir Qvit

P1098 The role of β-hairpins in aggregation of β-amyloid derived peptides

Elisabetta Galluppo, Claudia Honisch, Stefano Tartaggia, Mauro Carraro, Paolo Ruzza

P1099 Biological Evaluation of New Fell Analogues as Potential PDE4 Inhibitors

Veronica Nemska, Boryana Borisova, Marie Cochard, Stéphane Gérard, Dancho Danalev

P1100 Investigation of the role of Mfn2 and Drp1 protein-protein interactions in mitochondrial dynamics and its biological implications in cardiovascular diseases

Berhe Hayelom, Qvit Nir

P1101 Peptide and Probe: A two-pronged approach to investigating menaquinone binding peptides

Eilidh J. Matheson, Roy A. M. van Beekveld, Sarah Gothard, Paolo Innocenti, Nathaniel I. Martin, Markus Weingarth, Stephen A. Cochrane

P1104 A series of novel, selective matriptase inhibitors

Dębowski Dawid, Aleksandra Helbik -Maciejewska, Agata Gitlin-Domagalska, Malihe Hassanzadeh, Antoine Désilets, Pierre-Luc Boudreault, Richard Leduc, Anna Łęgowska, Krzysztof Rolka

P1105 Total synthesis and semi-synthesis of fluorinated analogues of the antifungal cyclic lipopeptide iturin A

Periklis Karamanis, Matthew Kiernan, Jimmy Muldoon, Paul Evans, Cormac D. Murphy, Marina Rubini

P1106 Design and antimicrobial activity of short and novel peptides

Ilaria Di Stefano, Silvia Rizzo, Dario Corbisiero, Francesca Bonvicini, Giovanna Angela Gentilomi, Walter Cabri, Tainah Dorina Marforio, Lucia Ferrazzano, Alessandra Tolomelli

P1109 Short Analogues Of Cathelicidins Pmap-36 And Bmap-27: Structure-Activity Relationship And Stability To Proteolysis

C. Peggion, A. Schivo, F. Albini, A. Di Stasi, B. Biondi, M. Mardirossian

P1110 HBP-5: A Leading Heparin-Binding Peptide with Remarkable Activity against Gram-negative Bacteria

Roberto Bello Madruga, Daniel Sandín, Javier Valle, David Andreu, Marc Torrent

P1112 Inhibitory activity and proteolytic stability in human serum of peptide inhibitors of the Vascular Endothelial Growth Factor A165/Neuropilin-1 complex

Dagmara Tymecka, Patrycja Redkiewicz, Piotr F.J. Lipinski, Aleksandra Misicka

P1113 Unlocking the Potential of Conotoxins: Chemical Synthesis Strategies and Biological Activity

Yazid Souf, Nicolas Inguimbert, Sebastien Dutertre

P1114 Mucroporin-M1 analogues: synthesis, conformation and structure-activity correlation

Claudia Storti, C. Peggion

P1115 Ferrocene-peptide conjugates with potential antitumor activity

Barbara Biondi, Beatrice Calderaro, Annalisa Bisello, Roberta Cardena, Renato Schiesari, Saverio Santi

P1116 Fragments of fibroblast growth factors useful in regenerative medicine components

Katarzyna Czerczak-Kwiatkowska, Adrianna Wierzbicka, Dorota Bociaga, Justyna Fraczyk, Beata Kolesinska

P1117 CR22DK-S18G Breakthrough: Revealing a novel antimicrobial peptide with rifampicin and isoniazid-like potency against Mycobacterium tuberculosis - a comprehensive exploration from synthesis to immune modulation

and selective action
Cesar Augusto Roque-Borda, Laura Maria Duran Gleriani Primo, Rafaela Melo Pogianeli, Lucas Henrique Domingos da Silva, Isabela Caroline dos Santos, Flávia Aparecida Resende, Henrik Franzyk, Paul Robert Hansen, Fernando Rogério Pavan
P1119 In silico identification and chemical remodelling of tick protein epitopes for vaccine antigen development
Stepan S. Denisov, M. Amine Jmel, Wouter Peeters, Maya Idema, Michalis Kotsyfakis, Johannes H. Ippel, Tilman M. Hackeng, Ingrid Dijkgraaf
P1121 Harnessing GPCRs Biased Signaling: Novel Macrocyclic Analogs for Enhanced Cardiovascular Treatment with Reduced Side Effects
Kien Tran, Xavier Sainsily, Jérôme Côté, David Coquerel, Pierre Couvineau, Sabrina Saibi, Lounès Haroune, Élie Besserer-Offroy, Alexandre Murza, Jean-Michel Longpré, Mannix Auger-Messier, Michel Bouvier, Philippe Sarret, Pierre-Luc Boudreault
P1122 A Novel Regulation Method of mRNA by Recruiting Regnase-1 Using Binding Motif-Antisense Oligonucleotide Conjugates
Masayuki Fujii
P1124 Deoxythymidine-based antimicrobial peptidomimetics to combat drug-resistance
Eun Young Kim, Dinesh Kumar, Sung Tae Yang, Song Yub Shin
P1125 Fine-Tuning the Immune-Stimulatory and Cancer Cell Binding Properties of Immune System Engagers (ISErs)
Hannah Back, Manuel Felkl, Susanne Kremer, Claudia Altdorf, Ute Steinbusch, Christian FW Becker
P1126 Targeted Acidosis Mediated Delivery of Antigenic MHC-Binding Peptides
Joey J. Kelly, Emily T. Ankrom, Sarah E. Newkirk, Damien Thévenin, Marcos M. Pires
P1128 Hybrid synthetic approach and biological characterization of a branched heterodimer for overcoming prostate cancer heterogeneity
Santo Previti, Sacha Bodin, Emmanuelle Rémond, Clément Morgat, Florine Cavelier
P1129 Epitope-directed peptide screening and machine learning for HER2-targeted antibody-mimetic peptides
Tetsuya Kadonosono, Yutaka Saito
P1130 Enhancing the Gastrointestinal Stability of Salmon Calcitonin thought Peptide Stapling
Hiba Ghareeb, Norman Metanis
P1131 Development and Antifungal Efficacy of Hydrocarbon-Stapled Peptide Analogs Based on Human Antimicrobial Peptides for Candidiasis Therapy
Hyosuk Yun, Ganbaatar Byambasuren, Chul Won Lee
P1132 Prevention of the Spread of Virus Infection in Global Societies: Anti-SARS-CoV-2 Agents Learned from HIV Researches
Hirokazu Tamamura, Nobuyo Higashi-Kuwata, Hiroaki Mitsuya, Kohei Tsuji, Takahiro Ishii, Takuya Kobayakawa
P1133 Bicycle Radionuclide Conjugates (BRCs) as agents for tumour targeting
Anusha Regupathy, Ben Blakeman, Luca Mascheroni, Simone Pellegrino, Johanna Lahdenranta, Lisa-Charlotte Domogalla, Malgorzata Sulewska, Matthias Eder, Ann-Christin Eder, Gemma Mudd
P1134 Development of gut-restricted antibiofilm peptides to target gastrointestinal biofilms
B. Jandl, M. Lang, A. Makristathis, C. Gasche, M. Muttenthaler
P1135 Development of peptide modulators targeting proteinprotein interactions of the Sodium Leak Channel Complex
Emma Beyer, Stephan Pless
P1136 Application of membrane-active peptide-based therapeutics in the management of stromal melts associated with microbial keratitis
Jyoti Sood, Sujithra Shankar, Sushmita G. Shah, Shikha Yadav, Archana Chugh
P1137 One-bead-one-compound combinatorial libraries for the discovery of ligands towards SIRPα and checkpoint CD47 proteins
P. Quesada-Martínez, M. Sánchez-Navarro
P1138 Impaired metabolic phenotyping in mice with deletions of GPR10 and NPFFR2 receptors: Implications for lipidized PrRP analog therapy in obesity
Veronika Strnadová, Magdalena Škrlová, Jaroslav Kuneš, Lenka Maletínská
P1139 Latarcins as membrane active peptides for therapeutic applications
Sivalingam Ayyanar, Prasanjeet Kaur, Deepthi Poornima Budagavi, Nisha Ponnappan, Archana Chugh

P1140 Intranasal effects of an analogue of the gliopeptide ODN on energy homeostasis
Omayma Dlimi, Karthi Duraisamy, Arnaud Arabo, Léa Killman, Marie Jean-Claude Do Rego, Marie Jean-Luc Do Rego, Benjamin Lefranc, Amine Bourzam, Nicolas Chartrel, Jérôme Leprince
P1142 Enhancing biomedical metal implants with synthetic peptides: improved bioactivity and in vitro safety
Adrien Mourgot, Farzin Arjmand, Olivier Monasson, Michel Boissiere, Madjid Djemai, Souad Ammar-Merah, Guy Dirras, Elisa Peroni
P1143 StreaMLine - Machine learning guided development of novel GLP-1 receptor agonists
Claudia Hjørringgaard, Jens Christian Nielsen, Mads Mørup Nygaard, Anita Wester, Lisbeth Elster, Trine Porsgaard, Randi Bonke Mikkelsen, Silas Rasmussen, Andreas Nygaard Madsen, Morten Schlein, Niels Vrang, K. Rigbolt, Louise S. Dalbøge
P1144 Development of a HPMC-patch containing RGD and KTTKS peptide sequences for application in tissue healing
Naiara Maia Pereira, Reinaldo Marchetto
P1146 Optimisation of a TREM2 receptor inhibitor peptide
Claudia Honisch, M. Rotondo, E. Galluppo, S. Tartaggia, C. Gallo, M. Dell'Isola, D. Carbone, E. Manzo, A. Fontana, P. Ruzza
P1149 Synthesis and Characterization of Tumor Targeted Peptide (TTP) Conjugated with Magnetic Nanoparticles for Thermo-ablation
Sima Alvani Alamdari, Justyna Fraczyk, Joanna Waśko, Anita Plazinska, Beata Kolesinska
P1150 Synthesis and characterization of phenethyl isothiocyanate conjugated with magnetic nanoparticles modified by tumor targeting peptide (TTP) using in cancer treatment
Sima Alvani Alamdari, Łukasz Janczewski, Justyna Fraczyk
P1151 Analysis of Mannan (polymannose) Conjugated with 35-55 Immunodominant Epitope of Myelin Oligodendrocyte Glycoprotein for the Treatment of Multiple Sclerosis
Carmen Simal, Areti Gkika, Maria-Eleni Androutsou, Georgia Biniari, Alexios Aletras, Theodore Tselios
P1152 A Nanomolar Potency Macrocyclic Peptide Inhibitor of SARS-CoV-2 Spike through Deep Mutational Scanning
Antonius J.P. Hopstaken, Oliver J. Debski-Antoniak, Preeti Hooda, Daniel L. Hurdiss, Seino A.K. Jongkees
P1153 Intelligent wound dressing with antimicrobial properties
Sebastian Kersting, Sophia Ohnesorg, Markus von Nickisch-Rosenegk
P1154 High Throughput Phage Display Screening Identified Peptide Inhibitors Targeting the α-Synuclein for Parkinson's Disease Treatment
Haiyan Zhou, Zhaohui Liang, Chenyin Wang, Wai Lok Ngai, Michael K. Chan, Chaogu Zheng, Xuechen Li
P1155 Linear peptides as IgG-epitope mimetic for allergic immunotherapy against birch pollen
Alessandro Streuli, Lara Šošić, Marta Paolucci, Agathe Duda, Klaus Eyer, Pål Johansen, Christian Steuer
P1160 Discovery of a novel α-helical peptide targeting GTP-bound K-Ras(G12D)
Hannah Comfort, Sarah Ross, Jefferson Revell, Thomas Murray, Carole Urbach, Bethan Archer, Darerca Owen, Helen Mott
P1161 Peptide Inhibitors of Protein-Protein Interactions Targeted to Src Homology 2 Domains: A Combined Computational and Spectroscopic Design Approach
Paolo Calligari, Claudia Storti, Chiara Innamorati, Chiara Fulci, Alessia Damiani, Cristiano DI Stefano, Chiara Cocca, Cristina Peggion, Barbara Biondi, Gianfranco Bocchinfuso, Lorenzo Stella
P1162 Peptide-based vesicle isolation method for P. aeruginosa
Tania Henriquez, Ismael Castañón, Silvia Scali, Chiara Falciani
P1164 Antibacterial, Anti-inflammatory and Anti-biofilm Activities of Novel Short Antimicrobial Peptides Designed from the Cecropin A-Melittin Hybrid Antimicrobial Peptide, BP100
Eun Young Kim, Dinesh Kumar, Sang Hyun Park, Song Yub Shin
P1165 Study on the stability of new promising antimicrobial peptides against protease activities present in infection sites
Clelia Cortese, Giovanni Cappello, Laura Cresti, Virginia Niccolini, Marco Scocchi, Marialuisa Mangoni, Alessandro Pini
P1170 Revolutionizing Peptide Production: Introducing An Engineered TEV Protease
R. Guerrette, C. Schwarz, B. Wetzel
P1172 Spatio-temporal control of cellular differentiation for cartilage tissue engineering
Jules Simonin Garcia, Cécile Echalier, Emmanuel Belamie, Marie Morille, Gilles Subra

P1173 Development of a novel alternative method for liraglutide production
Gabriela R. Barredo-Vacchelli, Jésica A. Rodríguez, Joaquín A. Eloy, Silvia A. Camperi
P1174 Comparison of in vitro immunogenicity between δ-ctenitoxin-Pn2a and epitope-based immunogens
Jésica A. Rodríguez, Gabriela R. Barredo-Vacchelli, Ariadna M. Birocco, Agustín Blachman, Gerardo Acosta, Fernando Albericio, Graciela C. Calabrese, Silvia A. Camperi
P1176 Extracellular-Vesicle Catch-and-Release isolation System using a Net-charge Invertible Curvature-sensing peptide
Kenichi Kawano, Yuki Kuzuma, Koichi Yoshio, Kenta Hosokawa, Yuuto Oosugi, Takahiro Fujiwara, Fumiaki Yokoyama, Katsumi Matsuzaki
P1178 Multifunctional peptides for the synthesis of photothermally active gold nanoparticles
Alžbeta Runová, Helma Wennemers
P1179 Intracellular Peptide Library Screening for Covalent Transcription Factor Inhibitors
Andrew Brennan, Keith Vance, Scott Lovell, Jody Mason
P1182 Innovative microfluidic preparation of monodisperse peptidic nanoparticlesfor ultrasound guided gene delivery
Guy Gouarin, Vicentiu Moraru, Samir Cherkaoui
P1186 Environment Responsive Peptide Dimers Bind and Stabilize dsRNA
Niall M. McLoughlin, Marvin A. Albers, Estel Collado Camps, Jannik Paulus, Youri A. Ran, Saskia Neubacher, Sven Henning, Roland Brock, Tom N. Grossmann
P1187 Engineered oxalyl thioester-containing protein domains as a building block for synthetic biopolymers
Francesco Terzani, Simindokht Rostami, Chen Wang, Benoît Snella, Birgit Wiltschi, Oleg Melnyk, Vangelis Agouridas
P1188 Improved Sortase A-Catalyzed Transpeptidation by Selective Electrostatic-Assisted Aminolysis Trapping
Chen Wang, Benoît Snella, Rémi Desmet, Oleg Melnyk, Vangelis Agouridas
P1189 Photocontrollable probes for the investigation of neuropeptide signalling
Konstantin Raabe, Predrag Kalaba, Hilary Yong, Erik Keimpema, Victor Anggono, Markus Muttenthaler
P1191 Bind&Bite: Covalently stabilized heterodimeric coiled-coil peptides for the site-selective chemical modification of proteins
Jannis Beutel, Riccardo di Vincenzo, Klaus Überla, Jutta Eichler
P1194 Protein Interface Catalysed Capture (PICC) to Resolve the Structure of the Tau-PSD95 Protein Complex
Reuben Blades, Kanishka Pushpitha, Gene Hart-Smith, Muhammad Bin Zenaidee, Daryl Ariawan, Lars Ittner, Ole Tietz
P1195 In vitro selection of highly N-alkylated cyclic peptides for targeting intracellular protein-protein interactions
Takeo Iida, Atsushi Ohta, Yusuke Yamagishi, Tetsuo Kojima, Hitoshi Iikura
P1200 Study on the Role of Helix-Stabilized Peptides in Transporting Antisense Morpholino Oligomers into Cells: Relationships among Helicity, Cellular Uptake, and Antisense Activity
Hiroyuki Takada, Keisuke Tsuchiya, Yosuke Demizu
P1203 Synthesis of Bacteria-Derived Lipopeptides and Applications in Antibiotic Discovery
Glenna Swinand, Katherine Bowen, Samir Olatunji, Martin Caffrey, Eoin M. Scanlan
P1204 Controlled Intracellular Trafficking and Gene Silencing by Oligonucleotide-Signal Peptide Conjugates
Masayuki Fujii
P1205 Polysaccharides modified with attenuated cationic lytic peptides: Formation of microparticles and their use in cytosolic antibody delivery
Junya Michibata, Yoshihiro Sasaki, Kazunari Akiyoshi, Shiroh Futaki
P1206 Probing the interplay between Ubiquitination and Adenosine-Di-Phosphate ribosylation
Max S. Kloet, Jim Voorneveld, Qiang Liu, Robbert Q. Kim, Ivan Đikić, Huib Ovaa, Dmitri V. Filippov, Gerbrand J. van der Heden van Noort
P1207 Virucidal Peptide-Based Drugs to Target Influenza
Shadi Kordbacheh, Francesca Olgiati, Francesco Stellacci
P1210 Linkerology of Cryptophycin Drug Conjugates
Jan-Niklas Bollnow, Cedric Dessin, Norbert Sewald
P1211 The series of a new fluconazole-based conjugates with cell penetrating and antimicrobial peptides
Natalia Ptaszyńska, Daria Łada, Wioletta Brankiewicz, Katarzyna Serbakowska, Jan Lica, Marek Drab, Natalia Maciejewska, Anna Łęgowska, Piotr Szweda, Krzysztof Rolka
P1212 Click-to-Release-based Cryptophycin Drug Conjugates
Jona Voss, Peter Bitsch, Cedric Dessin, Harald Kolmar, Norbert Sewald

P1213 Strategies for designing hepatocyte-selective carriers using helical peptides as stable scaffolds
Takahito Ito, Takashi Misawa, Nobumichi Ohoka, Michihiko Aoyama, Takao Inoue, Akiko Ishii-Watabe, Yosuke Demizu
P1214 Synthesis and characterization of bioconjugates containing peptide moiety with potential anticancer activity
Dancho Danalev, Polya Miladinova, Yordan Todorov, Ivan Iliev
P1216 Rational design, synthesis and evaluation of mitoxantrone conjugated with mutated Gonadotropin Releasing Hormone (GnRH) for the treatment of hormone-dependent cancer
Georgia Biniari, Agathi Nteli, Christos Markatos, Vlasios Karageorgos, Alexios Vlamis-Gardikas, George Liapakis, Maria Venihaki, Theodore Tselios, Carmen Simal
P1217 New peptide-porphyrin conjugates targeting brain-residing viruses
Toni Todorovski, Giuseppina Guida, Patrizia Janković, Diogo Mendonça, Christine Cruz-Oliveira, Marco Cavaco, Daniela Kalafatović, Sira Defaus, Andrea Da Poian, Miguel Castanho, David Andreu
P1218 Development of Daunomycin-Peptide Antitumor Conjugates Containing Neurotensin-Based Homing Moiety
Levente E. Dókus, Eszter Lajkó, Orsolya Láng, László Kőhidai, Gábor Mező
P1220 Peptide fibrils as nanocarrier for targeted therapy
Justyna Sawicka, Milena Czeszejko, Ewa Wieczerzak, Paweł Niedziałkowski, Tomasz Kulesza, Kamila Kitkowska, Rafał Sądej, Sylwia Rodziewicz-Motowidło
P1221 De novo Semi-synthetic Platform for Monitoring Protein degradation in Live Cells
Mahdi Hasan, Deepanjan Panda, Guy Mann, Ashraf Brik
P1223 Design of aptamer conjugates as monoclonal antibody mimics
Jordan Cossu, Océane Ricloux, Corinne Ravelet, Véronique Frachet, Eric Peyrin, Didier Boturyn
P1224 Conjugates containing homing peptide, cell penetrating peptide and a cytostatic or marker potentially useful in the diagnosis or treatment of lung cancer diseases
Piotr Jedrzejczak, Anna Gajda, Justyna Fraczyk, Beata Kolesinska
P1225 Development of novel amphipathic stapled peptides as DDS carriers for intracellular delivery of nucleic acids
Motoharu Hirano, Hidetomo Yokoo, Makoto Oba, Takashi Misawa, Yosuke Demizu
P1227 Development of selective peptide-based radiopharmaceuticals for targeted therapy and diagnosis of high malignant cancers
Anna Giorgio, Nicola Salvarese, Annarita Del Gatto, Michele Saviano, Cristina Bolzati, Laura Zaccaro
P1228 Control of biological processes using metallopeptides
Jessica Rodriguez Villar
P1229 pH-Dependent Cellular Uptake of CPPs – Guanidinium versus OxyguanidiniumProline
Rahel Heeb, Laura Massaad, Helma Wennemers
P1230 Lipophilic Prodrug Charge Masking- insights into new method of peptide prodrugs synthesis conception
Agata Gitlin-Domagalska, Anna Olejnik, Natalia Ptaszyńska, Jaroslaw Ruczyński, Mladena Glavaš, Mikolaj Marszałek, Dawid Dębowski, Aleksandra Helbik-Maciejewska, Anna Łęgowska, Chaim Gilon, Krzysztof Rolka
P1231 Amphipathic Proline-Rich Cell Penetrating Peptides for Mitochondria Targeting
Adeline M. Schmitt, Helma Wennemers
P1233 Optimization of Anti-Vasoconstricting UT-II-Derived Biogels
Thibault Cauwenbergh, Juliana Dallagnol, David Chatenet, Charlotte Martin, Steven Ballet
P1234 Development of cell penetrating peptide-based ubiquitin ligase ligand for the development of PROTAC
Hidetomo Yokoo, Zhou Dongrui, Yosuke Demizu
P1236 Design and characterization of CD20 antigen surfaces for the selection of rituximab peptide mimics
Océane Ricloux, Chanantida Jongwohan, Jordan Cossu, Liliane Guerente, Didier Boturyn
P1240 Development of Novel Angiopep-2 Conjugates for Cancer Treatment
Gábor Mező, Levente Dókus, Diána Vári-Mező, Krisztina Kiss, Lilla Pethő, Ivan Ranđelović, József Tóvári, Szilvia Bősze
P1241 Systematic Determination of the Effects of Macrocyclization on Peptide Permeability into Mycobacteria
Rachita Dash, Irene Lepori, Han Zhang, Wonpil Im, M. Sloan Siegrist, Marcos M. Pires
P1242 Lipophilic Prodrug Charge masking strategy for novel oxytocin prodrugs production
Agata Gitlin-Domagalska, Natalia Ptaszyńska, Anna Olejnik, Jaroslaw Ruczyński, Mladena Glavaš, Dawid Dębowski, Aleksandra Helbik-Maciejewska, Anna Łęgowska, Chaim Gilon, Krzysztof Rolka
P1243 Drug-likeness of cyclic peptides beyond Rule of 5
Shojiro Shinohara, Mikimasa Tanada, Yuya Morita, Kazuhiko Nakano, Takuya Shiraishi, Hitoshi Iikura
P1244 POM-peptide hybrid against Alzheimer's Desease
Marta Giacomini, Claudia Honisch, Elisabetta Galluppo, Genny Orso, Haihong Yu, Mauro Carraro, Paolo Ruzza

P1245 The potential use of peptides in pancreatic cancer
Martina Rotondo, Giovanna Bossio, Sofia Parassia, Andrea Mattarei, Claudia Honisch, Ildikò Szabò, Lucia Biasutto, Paolo Ruzza
P1246 Evaluation of different spin labels for the study of protein-peptide interaction in cellular extract using Electron Paramagnetic Resonance spectroscopy techniques
Claudia Toso, Giovanni Loprete, Elisabetta Bergantino, Simone Fabbian, Massimo Bellanda, Sylvain Marque, Gerard Audran, Marina Gobbo, Marta De Zotti, Donatella Carbonera, Marco Bortolus, Marilena DI Valentin
P1247 Development of a cell penetrating peptide carrying a biological active HPV16 E6 inhibitory molecule for delivery into cervical cancer cells
Anna Lucia Tornesello, Luisa Dassi, Vincenza De Gregorio, Giorgia Imparato, Marilisa Leone, Lu Wuyuan, Noemy Starita, Andrea Cerasuolo, Luigi Buonaguro, FrancoMaria Buonaguro, Maria Lina Tornesello
P1249 The Antimicrobial Peptide SET-M33: In Vivo Efficacy and Toxicity in Different Animal Species and Encapsulation in Inhalable Polymeric Nanoparticles for Pulmonary Delivery
Laura Cresti, Giovanni Cappello, Clelia Cortese, Virginia Niccolini, Alessandro Pini
P1250 Affibody-mediated peptide nucleic acid pretargeting for delivery of cytotoxic payloads to HER2 positive carcinoma
Jacob Clinton, Kristina Westerlund, Amelie Eriksson Karlström
P1251 Structure-activity relationship study on the P4 structure of macrocyclic BACE1 inhibitors
Kazuya Kobayashi, Momoka Kawakita, Takuya Otani, Yasaunao Hattori, Shinya Oishi
P1253 Non-Enzymatic Protein Catalyses Amide Bond Formation
Nicolas Brauckhoff, Laura Fang, Anissa Haim, Tom N. Grossmann
P1254 β-Sheet mimetics that Target the Transcriptional Coactivator β-Catenin
M. Wendt, A. Yeste-Vázquez, T. van Ramshorst, R. J. Hana, N. M. Pearce, S. Hennig, T. N. Grossmann
P1255 Solid-phase synthesis of peptoids with structure-inducing tert-butyl side chains: A unique challenge finally met
Zacharie Bordas, Sophie Faure, Olivier Roy, Claude Taillefumier
P1256 Combinatorial solid phase peptide synthesis of peptides on glass slides and thermographic investigation on CO2 -binding affinity
Jessica Jung-Fittkau, Katharina Moro, Josef Diebold, Andrea Kruse, Hans-Peter Deigner, Magnus Schmidt
P1257 Stabilization of a miniprotein fold by an unpuckered proline surrogate
Madison M. Wright, Benjamin H. Rajewski, Taylor A. Gerrein, Lorna J. Smith, W. Seth Horne, Juan R. Del Valle
P1259 Exploring the potential of CXCR4 mimetic peptides to target cancer cells
Showmika Srirangan, Chafia Chiheb, Sebastian Stäbler, Anja Bosserhoff, Jutta Eichler
P1260 The ornithine-based siderophore as a potential carrier of peptide nucleic acid into Escherichia coli
Uladzislava Tsylents, Michał Burmistrz, Piotr Maj, Monika Wojciechowska, Joanna Trylska
P1261 Stepwise chemical control in the formation of beta-peptide assemblies
Imola Cs. Szigyártó, Kristóf Ferentzi, Kamal el Battioui, Olivér Pavela, András Wacha, Viktor Farkas, Tamás Beke-Somfai
P1262 Low-Molecular α-Amino Acid-Based Derivatives as Nanocarriers of Plant Growth Regulators
Vasilena Kondova, Borislav Anchev, Konstantin Dochev, Daniela S. Tsekova, Mariana Sichanova, Maria Geneva
P1264 From Peptides to Bioactive Lactam-constrained Foldamers
Maxime Fillaudeau, Alexandre Messerschmitt, Arie Van der Lee, Lubomir Vezenkov, Luc Brunel, Young Kee Kang, Jean Martinez, Baptiste Legrand, Muriel Amblard
P1265 Development of Neurotensin(8-13) Analogs as Potent NTS1/NTS2 Receptor Ligands with Enhanced Effects on a Mouse Model of Parkinson's Disease
Nikolay T. Tzvetkov, Toni Kühl, Maya G. Georgieva, Harald Hübner, Maria Lazarova, Polina Petkova-Kirova, Tamara I. Pajpanova, Reni Kalfin, Lyubka Tancheva, Aneliya A. Balacheva, Peter Gmeiner, Diana Imhof
P1266 Synthesis and biological application of a short peptidomimetics based on bacterial cell wall peptidoglycan monomer
Marcela Šišić, Leo Frkanec, Ruža Frkanec
P1267 Antimicrobial peptidomimetics against methycillin-resistant Staphylococcus aureus (MRSA)
Katarzyna Łada, Maria Dzierżyńska, Agnieszka Gajewicz-Skrętna, Łukasz Grabowski, Alicja Węgrzyn, Franciszek Kasprzykowski, Sylwia Rodziewicz-Motowidło
P1268 Synthesis of 5-member heteroaromatics containing peptide backbone: pro and cons of structural constrains induced by amide bond surrogates
Francesco Brenzini Biagioni, Corentin Layec, Karine Porte, Pierre-Yves Renard, Anna Maria Papini

P1270 PepFuNN: Novo Nordisk open-source toolkit to enable peptide in silico analysis
Rodrigo Ochoa, Kristine Deibler
P1271 A peptide database from human feces to foster the discovery of novel bioactive peptides
Armando A. Rodriguez, Nico Preising, Merve Karacan, Thomas Seufferlein, Martin Wagner, Frank Kirchhoff, Jan Münch,Ludger Ständker, Sebastian Wiese
P1272 Application of the MALDI-MS and MALDI-IMS in the identification of the GPR146 receptor in tissue preparations
Joanna Waśko, Aleksandra Ryk, Wojciech Fendler, Beata Kolesińska
P1273 Searching for biomarkers characteristic for severe stage of COVID-19
Aleksandra Czerchawy, Joanna Waśko, Beata Kolesińska
P1274 Identification of Delftia lacustris Proteins in Response to Cadmium Stress.
Ximena Carolina Pulido Villamil, Jefferson Beltrán, Maryeimy Varón-López, Cesar Augusto Jaramillo
P1275 Proteins Involved in the Plant Growth Promotion of Pseudomonas orientalis in the Presence of Cadmium
Ximena Carolina Pulido Villamil, Jefferson Beltrán, Maryeimy Varón López, Cesar Augusto Jaramillo
P1276 Identification of protease inhibitors from the human peptidome to develop novel antivirals
Armando A. Rodríguez, Jan Lawrenz, Nico Preising, Merve Karacan, Bernd Schröppel, Rene van Erp, Eberhard Barth, Marion Schneider, Ludger Ständker, Frank Kirchhoff, Jan Münch, Sebastian Wiese
P1277 An Advanced Database for GlycoPeptide Structure Exploration to build GlycoPeptideStructure Hub: GPS Hub
Michele Casoria, Marina Macchiagodena, Carla Bazzicalupi, Claudia Andreini, Gianni Cardini, Anna Maria Papini, Marco Pagliai
P1278 Machine Learning Reveals Structural Properties of Monosaccharides and their Peptide Conjugates
Michele Casoria, Marina Macchiagodena, Carla Bazzicalupi, Claudia Andreini, Gianni Cardini, Anna Maria Papini, Marco Pagliai
P1279 Mechanistic basis for the role of acidic tail of Rad6 (ubiquitin-conjugating enzyme) in Bre1 (E3 ligase) mediated recognition of histones in Saccharomyces cerevisiae
Pawan Yadav, Manish Gupta, Mohan Kamthan, Pankaj Kumar
P1280 Arginine-rich peptides vs. lysine-rich peptides: interaction with differently charged lipid bilayers
Andreja Jakas, Lea Pašalić, Danijela Bakarić
P1283 Prediction and simulation of the S100A1ct peptide with a membrane environment
Tommaso Bartoloni, Manuel Glaser, Julia Ritterhof, Patrick Most, Rebecca Wade
P1285 Engineering Stable Miniproteins: The Journey from Computational Design to Tertiary Structure Stability
Natalia Miodowska, Ewa Rudzińska-Szostak, Vitaly Kovalenko, Łukasz Berlicki
P1286 Enhancing computational peptide therapeutic design with quantum chemistry and quantum computing
Vikram K. Mulligan, Tristan Zaborniak, P. Douglas Renfrew, Benjamin Brown
P1287 Formation of native disulfide bond patterns in small antifungal proteins and their gamma-core optimized analogs
Györgyi Váradi, László Galgóczy, András Czajlik, Attila Borics, Gábor Bende, Csaba Papp, Zoltán Kele, Gyula Batta, Gábor K. Tóth
P1290 Alanine scanning analysis of the antimicrobial peptide lyp1987 using a template-based approach
Jomari Fernando, Jeremiah Batucan, Jacquelyn Peran, Lilibeth Salvador-Reyes, Aaron Joseph Villaraza
P1292 Synthesis and assessment of amyloidogenic activity of the C-peptide fragments
Joanna Waśko, Beata Kolesińska
P1293 High-Throughput Synchrotron Radiation Circular Dichroism (HT-SRCD) for the screening of G-quadruplex ligands
Martina Rotondo, Claudia Honisch, Barbara Biondi, Pietro Spanu, Fausta Ulgheri, Giovanni Loriga, Andrea Beccu, Rohanah Hussain, Giuliano Siligardi, Paolo Ruzza
P1295 Design and Synthesis of a Diamino Diacid-based Short Cyclic Peptide with Tunable Self-Assembly
Devki Nandan, Ramesh Ramapanicker
P1296 Effect of lipid peroxidation on protein conformational stability
Claudia Honisch, M. Rotondo, S. Tartaggia, R. Hussain, G. Siligardi, P. Ruzza
P1297 Three-dimensional structure and membrane permeability relationship of cyclopropane-restricted cyclic peptides
Yuki Yamazaki, Hiroyuki Kumeta, Satoshi Shuto, Mizuki Watanabe
P1298 Methyl-based NMR methods for characterization of large peptide self-assemblies
Dörte Brandis, Fanny Kozak, Christian W. F. Becker, Dennis Kurzbach

P1299 Silaffin 1A1: Insights to the Processes of Tailored Silica Precipitation
Fanny Kozak, Fabian Daus, Dörte Brandis, Armin Geyer, ChristianW. F. Becker, Dennis Kurzbach
P1302 Rational design of polyfluorinated peptide-based materials: Self-assembly of an amphiphilic motif
Maurizio Iannuzzi, Suvrat Chowdhary, Holly Fiedler, Kilian Haoues, Boris Schade, Andreas F. Thünemann, Elisa Quaas, Beate Koksch
P1303 Let's do the Twist - Chiral Information Transfer in Supramolecular Peptide Complexes
Danielle Aria Liebnitz, Pernille Vosbein-Christensen, Andrew Thomson
P1306 Tailoring the self-assembly of cyclic peptide scaffolds for prostate cancer imaging
Fátima Santillán, Carlie Charron, Betty C. Galarreta, Leonard G. Luyt
P1307 Computational/Experimental Symbiosis in the Design of Supramolecular Peptide Architectures
Ivan R. Sasselli, Laura Perez-Chirinos, Aitziber L. Cortajarena, Zaida Alvarez
P1310 Ultrasound-assisted formation of therapeutic peptide microcapsules
Gabriele Rossi, Erica Belforte, Francesca Cavalieri, Ana Aguilera, Mariano Venanzi
P1311 Tailoring Peptide Self-Assembly with Electron Donor Functionalization Towards Formation of Vesicles, Helical Ribbons, and Fibers
Laura Brüchle, Thomas Heim, Milan Kivala, Franziska Thomas
P1312 Crosslink reaction of α-/ω-substituted diacrylate polyethylene-glycol in Fmoc-FF hydrogel matrices
Carlo Diaferia, Paolo Pellegrino, Giancarlo Morelli, Rosaria Rinaldi, Antonella Accardo
P1313 Innovative Strategies for Sustainable Materials: Developing Protein-Based Bioplastics from Rapeseed By-Products for a Circular Economy
Sara Aquilia, Michele Pinna, Anna Maria Papini, Francesco Ciardelli, Luca Rosi, Claudia Bello.
P1314 Self-assembled Peptides for Biomimetic Mineralization and Enamel Repair
Yue Li, Rong Chang, Yang-Jia Liu, Feng Chen, Yong-Xiang Chen
P1315 Cationic amphiphilic peptide-based delivery platforms for negatively charged active pharmaceutical ingredients including short interfering RNA
M. Rosa, C. Diaferia, A. Accardo, G. Morelli
P1316 Synthesis of peptidomimetics using Diaryl-β2,3 amino acids for the preparation of smart materials
Dulce A. Quintana-Romero, Raffaella Bucci, Merve Gul, Maria M. Pérez-Madrigal, Carlos Alemán, M. Luisa Gelmi
P1317 Conformational and self-assembly studies of a protein-mimetic peptide from Pseudomonas aeruginosa's YeaZ protein
Elettra Fasola, Giulia Alboreggia, Stefano Pieraccini, Francesco Oliva, Fatima Ezzahra Agharbaoui, Michela Bollati, Giovanni Bertoni, Sandro Recchia, Marcello Marelli, Umberto Piarulli, Sara Pellegrino, Silvia Gazzola
P1318 A comparative study between phenylglycine- and phenylalanine-derived peptide hydrogels
Jolien Bertouille, Ulrich Hennecke, Charlotte Martin, Ana V. Cunha, Steven Ballet
P1319 Peptides stapling as a tool for improving molecular recognition of C-reactive protein
K. Szot-Karpińska, M. Lubos, N. Cwalina, J. Pícha, J. Kaminský, J. Jiráček, M. Majewska, M. Narajczyk, J. Niedziółka-Jönsson
P1320 A structural sight on peptides forming stable LLPS: a combined experimental and computational investigation
Gianfranco Bocchinfuso, Francesca Cavalieri, Daniel O. Cicero, Annachiara Ferrara, Hilda Garay-Perez, Greta Petrella, Marco Savioli, Mariano Venanzi
P1321 From Synthesis To Application: Peptide-Functionalized Nanoformulations For Biomedical Applications
Shubhi Joshi, Gaurav Verma, Avneet Saini
P1322 Sustainable Development of Cross-Linked Films from Rapeseed Meal
Sara Aquilia, Michele Pinna, Anna Maria Papini, Francesco Ciardelli, Luca Rosi, Claudia Bello
P2002 Suspension Bead Loading (SBL): An Economical Protein Delivery Platform to Study URM1's Behavior in Live Cells
Reem Mousa, Abhishek Saha, Yam Alalouf, Pradeep Sadhu, Mahdi Hasan, Shaswati Mandal, Guy Mann, Ashraf Brik
P2003 Synthesis and Conformational Analysis of β,β-Diaryl-α-Amino Acids: on the Way to Molecular Gearing
Timo Zimmer, Armin Geyer
P2004 A green peptide synthesis protocol for improving peptide production: a new approach
Luana Lastella, Barbara Biondi, Ivan Guryanov, Fernando Formaggio, Marco Macis, Antonio Ricci
P2005 A Rapid and Efficient Photochemical Modification Strategy for Late-Stage Peptide and Protein Functionalization
Meng-Qian Zhang, Yan-Mei Li

P2008 Novel Selectively Cleavable Dmb-Based Protecting Groups for Side Chain Amino Groups of Amino Acids
Raimund Maier, Karin Rustler, Thomas Bruckdorfer, Udo Kalejs, Vilnis Liepins, Kai Holland-Nell, Jacqueline Dalski, Stephan Pritz
P2009 Conformational editing and intracellular delivery of intrinsically disordered protein domain
Alexis Jouin, Alastair McEwen, Pierre Poussin-Courmontagne, Bruno Kieffer, Vladimir Torbeev
P2010 Palladium-mediated S-arylation and S-allylation for late stage peptide functionalization and protein conjugation
Ross D. Ballantine, Mingxiang Zhu, Ameni Hadj Mohamed, Aromal Asokan, Linhuan Shen, Mélanie Chenon, Ana Novak, Vincent Robert, Séverine Morisset-Lopez, Massimiliano Beltramo, Carlo Pifferi, Vincent Aucagne, Samir Messaoudi
P2011 Total Chemical Synthesis of Nanobodies for Targeted Cancer Therapy
Keziah Poggenpoel, Kevin Beijerling, William Kelton, Jiwon Hong, Margaret A. Brimble, Iman Kavianinia
P2012 Green Synthesis of a Novel Primary Amine Protecting Group for Solid-phase Peptide Synthesis
Clouie Justin Aguilar, Makhdoom Sarwar, Margaret A. Brimble, Iman Kavianinia
P2013 New Opportunities for Side-Chain Functionalization of Halogenated Amino Acids
Laura Cerveson, Norbert Sewald
P2014 Sculpting cavities in alpha-helical bundles to accommodate ligands of different size and shapes
Katarzyna Ozga, Rokas Petrenas, Joel J. Chubb, Derek N. Woolfson
P2015 Efficient and glycoeconomic synthesis of densely clustered mucin glycopeptides
Arseniy Galashov, Ekaterina Kazakova, Oliver Seitz
P2017 Targeting LAT1 with technetium(I)-99m-labeled tryptophan derivatives for SPECT imaging
Rúben D.M. Silva, Cristina P. Matos, Catarina I.G. Pinto, Joana F. Guerreiro, Lurdes Gano, Filipa Mendes, João D.G. Correia
P2018 Applications of Thiol-ene and Thiol-yne Chemistry for Peptide Stapling and Bioconjugation
Inés Rabadán González, Joshua Mclean, Nikitas Ostrovitsa, Sheila Fitzgerald, Andrea Mezzeta, Lorenzo Guazzelli, Donal O'shea, Eoin M. Scanlan
P2019 Greening Peptide Purification Through Use of Elevated Temperatures
Colin Simpson, Drew Cesta, Sandeep Singh, Jonathan Collins
P2020 Enzymatic Peptide and Protein Bromination: The BromoTrp Tag
Nicolai Montua, Norbert Sewald
P2021 Combining quaternary ammonium compounds and peptides- its application to antimicrobials and beyond
Rolland Lin, Margaret A. Brimble, Brian H. Northrop, Alan J. Cameron
P2022 Fluorescent Amino Acids with large Stokes Shift
Nicolas Schnatmann, Norbert Sewald
P2023 Propargylamine Amino Acids as Constrained Nε-Substituted Lysine Mimetics
Kevin Van holsbeeck, Mathias Elsocht, Steven Ballet
P2024 Synthesis and Structural Characterization of Trifluoromethylated Tetrahydroisoquinolines as New Constrained Aromatic Amino Acid Surrogates
Lilian Loisons, Steven Ballet, Thierry Brigaud, Simon Gonzalez
P2025 Cysteine Thioaldehydes : Photolytic Generation and Reactivity
Ardra Karthika, Matthew Murray, Guillermo Palop, Lee-Ann Keane, Patrick McArdle, Luke Crehan, Nicholas Yates, Alison Parkin, Martin Fascione, Eddie L. Myers
P2026 Application of a new green protocol in Solid-Phase Peptide Synthesis: identification of a new green solvent mixture compatible with ETT/TBEC
G. Vivenzio, M. Scala, P. Campiglia, M. Sala
P2029 Modular Access to Structurally Defined Ubiquitin Chains
Moritz Urschbach, Susanne Huhmann, Luca Ferrari, Dominik Vogl, Dominik Appel, Sascha Martens, Christian F. W. Becker
P2034 Tetrahydropyranyl and Tetrahydrofuranyl as New Backbone Protecting Groups For Enhanced Fmoc SPPS
Samuel J. Paravizzini, Craig A. Hutton, John A. Karas
P2035 Exploring Innovative Liquid-Phase Peptide Synthesis Strategies with Silane-Containing Molecules
Naoki Nishizawa, Akihiro Nagaya, Shota Murase, Yuji Mimori, Michiharu Handa, Ayumu Matsuda, Yutaka Kobayashi, Haruaki Kurasaki, Douglas R. Cary, Keiichi Masuya
P2037 Influence of tryptophan insertion on the fibrillation capacity and antimicrobial efficacy of β-Hairpin Antimicrobial Peptides
Dhanya Mahalakshmi Murali, Jian Xu, Dai Thien Nhan Tram, Pui Lai Rachel Ee

P2040 Cyclic Antimicrobial Peptides Guanidino-based Analogues of Temporin L
I. Boccino, R. Bellavita, M.R. Loffredo, F. Cappiello, B. Casciaro, M.L. Mangoni, P. Grieco, F. Merlino
P2041 From clotting to calcification: Gla-domains as guardians of vascular remodeling
S.M. Agten, A. Gentier, D.P.L. Suylen, S. Peijenborgh, M. Hochstenbach, L.J. Schurgers, T.M. Hackeng
P2042 Design and Synthesis of Peptide Modulators of Gαi/s Proteins
Anna Pepanian, Sabriye Aydoğdu, F. Ayberk Binbay, Pradipta Ghosh, Dehua Pei, Diana Imhof
P2045 Synthesis of Macrocyclic Thiolactone Peptides via Radical Acyl Thiol-Ene
Alby Benny, Eoin M. Scanlan
P2046 Divalent metal ions-directed release of C-terminally modified peptides at 60 °C under mild conditions
Rebeca G. Moura, Thiago de Souza Freire, M. Terêsa Machini
P2047 Exploring the Three-Dimensional Structures and Activity Relationships of N-Methyl and N-Desmethyl Analogues of Cyclodepsipeptide Destruxin E
Takayuki Doi, Hiroshi Sato, Hiroshi Nakagawa, Masahito Yoshida
P2048 Green solvents and Safe Reagents in SPPS taking advantage of induction heating and automation: synthesis and HPLC-free purification of difficult sequences
L. Pacini, M. Muthyala, O. Marder, L. Aguiar, R. Zitterbart, P. Rovero, A. Papini
P2049 Simple one-pot peptide cleavage and spontaneous macrocyclization through Paal- Knorr-like reactions using 2,5-dialkylfuran derivatives
Alex Manicardi, Atiruj Theppawong, Marleen Van Troys, Annemieke Madder
P2050 Sustainable Scale-Up of GLP-1 Agonist Peptides through Green Solid Phase Peptide Synthesis
L. Pacini, M. Muthyala, R. Zitterbart, P. Rovero, A. Papini
P2051 Searching for peptide inhibitors of TNFR2/TNFαcomplex formation using a virtual
Paulina Stencel, Artur Giełdoń, Beata Gromadzka, Sylwia Rodziewicz-Motowidło, Marta Spodzieja
P2054 Core-shell type resins for SPPS
Kwanwoo Kim, Seok-In Kim, Yoon-Sik Lee
P2055 Nature-inspired unique antimicrobial peptides from Chilean marine sediments
L. I. Beyer, A.-B. Schäfer, A. Undabarrena, I. Mattsby-Baltzer, D. Tietze, E. Svensson, A. Stubelius, M. Wenzel, B. Camara, A. A. Tietze
P2056 The role of the quorum sensing peptide PlnA in the microbiome-sarcopenia axis
Amélie Descamps, Anton De Spiegeleer, Liesbeth Crombez, Morten Kjos, Evelien Wynendaele
P2058 Unlocking Mango's Peptide Potential: Exploring Bioactive Peptides in Pulp, Peel and Seed
Mahya Bahmani, Michelle L. Colgrave, Cassandra L. Pegg, Angéla Juhász
P2059 Alca1, a cyclotide extracted and isolated from Allexis cauliflora (Violaceae): Synthesis and biological activities
Olivier Ndogo Eteme, Letícia Oliveira Catarin Nunes, Marcela Nunes Argentin, Norival Alves Santos-Filho, Ilana Lopes Baratella Da Cunha Camargo, Eduardo Festozo Vicente
P2060 Microporous Scaffold-Mediated Myeloid Cell Activation in Situ for Robust Peptide-Based Cancer Vaccine
Shao-Hua Zhuo, Wen-Hao Li, Jing-Yun Su, Yan-Mei Li
P2062 The “Sand in a gearbox” effect of antimicrobial peptides: beyond pore formation on model membranes and real bacteria cells
Daniela Roversi, Z. Vaezi, A. Bortolotti, C. Di Stefano, S. Bonacorsi, V. Santucci, C. Aisenbrey, M. M. Konai, Y. Acharya, R. Khosravi-Far, B. Bechinger, J. Haldar, L. Stella
P2064 Design and Structural Analysis of Fluorinated Polyproline-Type Foldamers and their Ability to Interact with Membrane Models
Chloe Cayrou, Simon Gonzalez, Astrid Walrant, Delphine Ravault, Karine Guitot, Sylvie Noinville, Françoise Illien, Sandrine Sagan, Thierry Brigaud, Olivier Lequin, Sandrine Ongeri, Gregory Chaume
P2065 Cyclic peptides as Connexin43 and Pannexin1 inhibitors for the treatment of inflammatory disorders
Debora Iaculli, Arthur Lamouroux, Malaury Tournier, Jade Montgomery, Anne Caufriez, Mathieu Vinken, Filippo Molica, Brenda R. Kwak, Steven Ballet
P2066 Antimicrobial peptidomimetics: design, synthesis, and surface binding
Marc Mathieu
P2067 New Insights Into Antibacterial And Antitumor Effects Of Structurally Versatile Amino Acid- Based And Non-Proteinogenic Compounds
Martina I. Peeva, Maya G. Georgieva, Aneliya A. Balacheva, Svetoslav Dimov, Nikolay T. Tzvetkov
P2068 Chemical Synthesis and Intracellular Delivery of P53 Transactivation Domain (TAD) Constructs
Mo’ath Yousef, Vladimir Torbeev

P2071 Development of a retro-inverso tetrapeptide collagen modulator as anti-aging active principle
Fosca Errante, Marco Pallecchi, Gianluca Bartolucci, Elena Frediani, Francesca Margheri, Lisa Giovannelli, Anna Maria Papini, Paolo Rovero
P2076 A BMP-2-derived peptide conjugated to chitosan improves osteoblast proliferation and antibacterial properties of membranes for oral surgery
Cristian Balducci, Annj Zamuner, Martina Todesco, Andrea Bagno, Antonella Pasquato, Giovanna lucci, Federica Bertela, Chiara Battocchio, Luca Tortora, Luca Sacchetto, Paola Brun, Erilberto Bressan, Monica Dettin
P2077 Transmembrane peptide-loaded ionic liquid nanocarriers targeting ErbB2-positive cancer
Helal Abujubara, Pankaj Bharmoria, Samantha W. Alvarez, Enoch Appiah, Kasper Moth- Poulsen, Volkan I. Sayin, Alesia A. Tietze
P2078 Characterization of Aurora-A Activation and Allosteric Regulation by TACC-3 Peptidomimetics
Diana Gimenez, Martin Walko, Jennifer A. Miles, Richard Bayliss, Megan H. Wright, Andrew J. Wilson
P2080 Synthesis, conformational analysis and biological activity evaluation of novel antiviral peptides blocking the SARS-CoV-2 cell-entry
M. Quagliata, M.A. Stincarelli, A. Di Santo, L. Pacini, F. Real-Fernandez, R. Arvia, S. Rinaldi, S. Giannecchini, A.M. Papini, P. Rovero
P2083 Synthesis, characterization and biological activity evaluation of a dual-drug based on the antibacterial peptide lugdunin functionalized with the Carbonic Anhydrase sulfonamide inhibitor acetazolamide
M. Quagliata, F. Brenzini Biagioni, S. Giovannuzzi, V. De Luca, C. Capasso, A. Nocentini, C. T. Supuran, P. Rovero, A.M Papini
P2085 Phosphorylation and GlcNAcylation of the RNA polymerase II C-Terminal domain and their effect on recognition by Pin1 and Protein Phosphatase 1
Alina Herfort, Emanuele Piemontese, Corina Maller, Maja Köhn, Oliver Seitz
P2086 How a single non-conventional amino acid can modify the effectiveness of amphibian antimicrobial peptides
Maria Rosa Loffredo, Bruno Casciaro, Giacomo Cappella, Rosa Bellavita, Diego Brancaccio, Floriana Cappiello, Francesco Merlino, Paolo Grieco, Lorenzo Stella, Alfonso Carotenuto, Maria Luisa Mangoni
P2087 Development of bioactive peptides of cosmetic interest through environmentally sustainable processes
L. Sforzi, F. Errante, J. Makowska, P. Rovero, A. Papini
P2088 Thermodynamic and kinetic effects on the activity and selectivity of antimicrobial peptides
F. Carneri, E. Franci, C. Troiano, G. Giaquinto, A. Leoci, D. Roversi, M. R. Loffredo, Y. Park, A. Toto, S. Gianni, M. L. Mangoni, H. Franzyk, L. Stella
P2091 Different approaches in optimisation of miniprotein structure for improvement of affinity towards target and inhibitory activity
Paweł Noceń, Łukasz Berlicki
P2092 Developing autoinducing peptides for regulating the quorum sensing system in S. lugdunensis
Iben Jensen, Benjamin S. Bejder, Martin S. Bojer, Hanne Ingmer, Christian A. Olsen
P2093 Design of fluorinated Aib foldamers: synthesis, structural study and capacity to interact with amyloid proteins
Marine Pietri, Olivier Monasson, Julia Kaffy, Elisa Peroni, Sandrine Ongeri, Grégory Chaume, Nathalie Lensen
P2094 Antimicrobial peptides with varied chemical compositions trigger hyperpolarization of the bacterial membrane
Anasztázia Hetényi, Kaushik Nath Bhaumik, Réka Spohn, Anett Dunai, Lejla Daruka, Csaba Pál, Tamás A. Martinek
P2095 Synthetic glucosylated peptide antigens of the bacterial protein adhesin of nontypeable Haemophilus influenzae to detect antibodies in Multiple Sclerosis
F. Nuti, F. Real-Fernandez, H. Berhane Tesfaya, P. Strauss, R. Aharoni, M. Hurevich, P. Rovero, A.M. Papini
P2098 Design, synthesis, and biological activity of tumor necrosis factor-alpha peptides for adalimumab recognition
Feliciana Real Fernandez, Andrea Di Santo, Kalina Kirilova Kirilova, Silvia Rinaldi, Gabriele Simonini, Paolo Rovero
P2099 Computational design of ultrashort peptide inhibitors for the RBD of the SARS-CoV-2 S-protein
Pengfei Pei, Shi-Zhong Luo
P2100 In vitro effect of the acidic pH on the susceptibility of the antimicrobial peptide Esc(1-21) against respiratory pathogens in cystic fibrosis lung environment
Giacomo Cappella, Maria Rosa Loffredo, Bruno Casciaro, Floriana Cappiello, Arianna Turchini, Maria Luisa Mangoni
P2103 Bismaleimidohexane-Stapled Anoplin Analogs
Magdalena Bobier, Aaron Joseph Villaraza, Portia Mahal Sabido

P2104 Glycine- and histidine-rich peptides derived from Shepherin I: study of candidacidal activity, metal-chelation properties and mode of action
Gustavo Nunes, Lohanna Lopes, Ernani Lacerda, Ana M. C. Ferreira, Carlos Marques, Breno P. Esposito, M. Terêsa Machini
P2107 ReCHEMbinant protein engineering – synthetically enhanced protein therapeutics for Myc targeting
Jan Pascal Kahler, Brecht D. Ellenbroek, Sebastian Pomplun
P2108 Cecropin A-Melittin B Hybrid CA(1-7)M(2-9) Analogs with Improved Antibacterial Activity, Low Toxicity, and Good Protease Stability
Talia Chetty, Jessica T. Mhlongo, Ayman Y. Waddad, Fernando Albericio, Beatriz G. de la Torre
P2109 Optimizing Ham Curing Process: Impact of overripening and the use of nitrifying salts on Peptide Bioactivity.
Noelia Hernández Correas, Cindy Bande-De León, Adela Abellán Guillén, Teresa Muela Clemente, Eva Salazar Serna, Jose María Cayuela García, Luis Tejada Portero
P2110 Functional and structural understanding of the angiotensin II receptor type 1 (AT1R) biased signaling
Margot Hadjadj, Alexandre Murza, Brian Holleran, Yoon Namkung, Stéphane Laporte, Richard Leduc, Mannix Auger-Messier, Pierre-Luc Boudreault
P2111 Molecular determinants of the anti-amyloid function of the cross-interaction of the human cathelicidin LL-37 with islet amyloid polypeptide
Valentina Armiento, Hendrik Wunderlich, Aphrodite Kapurniotu
P2114 Use of alternative curing salts in the cured ham production process. Effect on the generation of bioactive peptides
Cindy Bande-De León, Noelia Hernández Correas, Manuel Hernández Lorca, Pablo Gómez San Miguel, Gregorio Molina Valero, Estefanía Bueno Gavilá, María Dolores Gil Martínez, Adela Abellán Guillén
P2116 Development of a potent and specific peptide inhibitor for the E. coli MazF toxin
Luiz R. Pizzolato-Cezar, Phelipe Vitale, Carolina D. Lacerda, Mario A. R. Pineda, Roberto K. Salinas, M. Terêsa Machini
P2120 Buforin-Derived Synthetic Peptides with Potential Application in Medicine
Dana Maria Copolovici, Cristian Moisa, Andreea Ioana Lupitu, Oana Gavriliuc, Florina Bojin, Mihaela Dochia, Dorina Chambre, Lucian Copolovici
P2121 Exploring antimicrobial peptides: a new frontier in cancer treatment innovation
Lucian Copolovici, Cristian Moisa, Andreea Ioana Lupitu, Dorina Chambre, Dana Maria Copolovici
P2122 High level soluble expression of human Glucagon-Like Peptide-1 (GLP-1) analogue as a recombinant peptide in E. coli
S. Sushmita, Esha Shukla, Gaurav Pandey
P2124 Combining peptide fragments for the high-throughput generation and screening of large libraries
Anne Zarda, Xingwang Deng, Edward Will, Maylin Romero, Christian Heinis
P2126 Designed Peptide based on Plant Original Cyclic Scaffold facilitate Rheumatoid Arthritis Diagnosis
Mingshu Zhang, Sunithi Gunasekera, Liyan Mei, Erik Jakobsson, Camilla Eriksson, Helena Idborg, Per-Johan Jakobsson, Ulf Göransson
P2127 Highway to Cell: Internalization of CFTR-Stabilizing Peptides as Potent Cystic Fibrosis Treatment
Clementine Teko-Agbo, Emilie Josse, Quentin Seisel, Dean R. Madden, Magali Taulan Cadars, Prisca Boisguerin
P2128 Effects of peptide labeling on fluorescence binding assays to Src homology 2 domains: the case of protein-protein interactions inhibitors of the oncogenic phosphatase SHP2
Sara Bobone, Chiara Fulci, Chiara Innamorati, Alessia Damiani, Claudia Storti, Paolo Calligari, Daniela Roversi, Luca Pannone, Simone Martinelli, Gianfranco Bocchinfuso, Fernando Formaggio, Cristina Peggion, Barbara Biondi, Lorenzo Stella
P2129 Bicyclic peptidomimetics enable efficient transport of proteins across brain endothelium
Maria C. Lucana, Roberta Lucchi, Fabien Gosselet, Cristina Díaz-Perlas, Benjamí Oller-Salvia
P2132 Synthesis of Halogenated Cyclic RGD-Peptides as Potent SMDC-ligands
Beate Nachtigall, Norbert Sewald
P2133 Supramolecular anticoagulants with on-demand reversibility
Millicent Dockerill, Daniel J. Ford, Simona Angerani, Imala Alwis, Luke J. Dowman, Jorge Ripoll-Rozada, Rhyll E. Smythe, Joanna S. T. Liu, Pedro José Barbosa Pereira, Shaun P. Jacksond, Richard J. Payneb, Nicolas Winssinger
P2134 Adalimumab and anti-adalimumab antibodies a novel method of detection and quantification in human sera based on surface plasmon resonance technique

Andrea Di Santo, Fosca Errante, Manuela Capone, Alessandra Vultaggio, Matteo Accinno, Lorenzo Cosmi, Francesco Annunziato, Anna Maria Papini, Paolo Rovero, Feliciana Real-Fernandez

P2136 Innovative liquid chromatographic-mass spectometric technologies to purify and identify biologically active antibody-drug conjugates

Margherita Marino, Paolo Rovero, Walter Mier, Hendrik Rusche, Anna Maria Papini

P2140 High-Throughput Permeability Assay for the Discovery of Cell Penetrating Cyclic Peptides

Hanna Stokes, Noora Azadvari, Parisa Hosseinzadeh

P2143 UL144-derived peptides as modulators of the BTLA/HVEM signaling pathway

Magdalena Lipińska, Piotr Ciura, Sylwia Rodziewicz-Motowidło, Anna Wardowska, Marta Spodzieja

P2144 β-Hairpin peptide fibrillation and bacteria trapping in hydrogel

Peiyan Yu, Mrunmayee Deshpande, Nhan Dai Thien Tram, Pui Lai Rachel Ee

P2145 Peptide Nanonets as Antimicrobial and Anti-inflammatory Agents

Pui Lai Rachel Ee, Nhan Dai Thien Tram, Jian Xu, Dhanya Mahalakshmi Murali, Peiyan Yu, Wai Shiu Fred Wong, Lakshminarayanan Rajamani

P2146 Protein-Protein Interactions: Unraveling the link between HTLV-1 Tax-1 oncoprotein and human Drosophila discs large tumor suppressor

Wael El Yazidi Mouloud, Sibusiso B. Maseko, Yasmine Brammerloo, Inge Van Molle, Adria Sogues Castrejon, Charlotte Martin, Remaut Han, Steven Ballet, Oleksandr Volkov, Jean-Claude Twizere

P2148 Esc peptides for novel therapeutics against Pseudomonas aeruginosa pulmonary infections: beyond antimicrobial activity

Maria Rosa Loffredo, Loretta Ferrera, Floriana Cappiello, Bruno Casciaro, Giacomo Cappella, Ivana D'Angelo, Y. Peter Di, Maria Luisa Mangoni

P2150 Synthesis and antimicrobial activity of hybrid peptides as dual inhibitor of intracellular targets in ESKAPE pathogens

Aman Kumar Mahto, Rikeshwer Prasad Dewangan

P2152 Disrupting the RANK-TRAF6 Interface: A Novel Approach for Bone Metastases Treatment

Sofia A. Martins, Cátia Rosa, Marco Cavaco, Rita Melo, David Andreu, Javier Valle, Vera Neves, Miguel A. R. B. Castanho, João D.G. Correia

P2154 Targeting MRGPRX2 with venom peptide P17: A therapeutic avenue for DSS-Induced colitis

Karthi Duraisamy, Mukesh Kumar, Abdullah Nawabjan, Emily Kwun Kwan Lo, Benjamin Lefranc, Elsa Bonnafé, Michel Treilhou, Hani El-Nezami, Billy K.C. Chow, Jérôme Leprince

P2158 Fight-TB: Design of Novel Vaccine Antigens to Fight Tuberculosis

Marina Sala, Giovanni Barra, Maria Carmina Scala, Pietro Campiglia, Rita Berisio, Alessia Ruggiero

P2161 Advances on the green synthesis of Etelcalcetide

Koula Achilleos, Andreas Sergides, Styliana Mirallai, Charalambos Ioannou, Vicky Nicolaidou, Christos Petrou, Christakis Sergides, Yiannis Sarigiannis

P2163 Determination of the Oligomerization States of the Transmembrane Domains from SARS-CoV-2 Membrane Proteins

Tyler G. Hobart, Andrew M. Rehak, Timothy M. Reichart

P2164 Exploiting the features of short peptides to recognize specific cell surface markers

Michela Buonocore, Angelo Santoro, Enza Napolitano, Elena Ciaglia, Francesco Montella, Francesca Boccafoschi, Valeria Perugini, Matteo Santin, Anna Maria D'Ursi

P2167 Obtaining, Optimizing, and Evaluating the Activity of Anticancer LfcinB-Derived Peptides on in vitro Models against Melanoma

Karla Rodriguez, Jose Mendoza, Javier García, Zuly Rivera, Joel Lopez, Ricardo Fierro

P2169 Design and characterization of a multistage peptide-based vaccine platform to target Mycobacterium tuberculosis infection

Chiara Bellini, Emil Vergara, Fruzsina Bencs, Szilvia Bősze, Denis Krivić, Bernadett Bacsa, Sára Eszter Surguta, József Tóvári, Rajko Reljic, Kata Horvati

P2171 Engineering mRNA display for GPCR drug discovery – de novo discovery of cyclic peptide GLP1R binders

Esther Meron, Jens C. Nielsen, Mads M. Nygaard, Dennis Worm, Ulrike Leurs, Morten Lundh, Joseph M. Rogers

P2172 Novel functionalized acylation reagents for Glyand Lys-His tag acylation on proteins

Delphine N. Møller, Christian Kofoed, Mikkel B. Thygesen, Kasper K. Sørensen, Tuule Treiberg, Knud J. Jensen

P2173 KLVFF peptide functionalization of graphene oxide as suitable Aβ biomarker detection platform

Rita Turnaturi, Giuseppina Sabatino, Giuseppe Di Natale, Giuseppe Nocito, Angela Scala, Viviana Scuderi, Simona Filice, Antonino Mazzaglia, Silvia Scalese, Giuseppe Pappalardo

P2174 On-Resin Synthesis and Modification of Novel Peptide Heterocycles
Ciaran McGrory, Eddie Myers
P2175 Use of Green Solid Phase Peptide Synthesis to Obtain Tripeptide-85
M. C. O. A. Brasil, C. R. Princival, V. Kuchenbecker, E. Katekawa, W.V. Magalhães, E.M. Cilli
P2176 Affinity Peptide Extraction Using Small-Molecule, Thermoresponsive Zwitterionic Liquid Materials
Yen-Ho Chu, Yu-Hsin Chung
P2178 Optimization of pDNA delivery by WRAP cell-penetrating-peptide
K. Konate, S. Deshayes, P. Boisguérin, E. Vivès, S. Faure, P. De Santa Barbara
P2180 Application of coumarin-type chemiluminophore toward in vivo detection
Yukie Nohara, Keiko Taniguchi, Hiromi Ii, Shun Masuda, Hiroko Kawakami, Masakatsu Matsumoto, Susumu Nakata, Toshiyuki Sakai, Taku Yoshiya
P2181 Development of novel automated solid phase peptide synthesizers ensuring economic, effective, scalable and green synthesis
Krisztina Kiss, Soma Ránky, László Molnár
P2183 Discovery and Characterization of a Short Peptide Possessing a Latent Warhead Undergoing Intramolecular Cyclization in the Aqueous Environment
Riku Katsuki, Masumi Taki
P2186 A fishing technology of glycated peptides
F. Nuti, M. Marino, P. Ledwon, R. Latajka, A. Lapolla, M. Chorev, P. Rovero, A.M. Papini
P2188 Programmable Chemical Synthesis & in-situ Modifications of Peptides
Jacopo Zero, Tristan Tyler, Leroy Cronin
P2191 Peptide-based Coacervates as Evolutionary Roads of Catalytic Function
David Reis, Sara Pereira, Ana P. Ramos, Pedro M. Pereira, Leonor Morgado, Ana S. Pina
P2194 An all-in-one automated peptide purification and synthesis solution
Luísa Aguiar, M. Muthyala, S. Lüdtke, Dominik Sarma, Robert Zitterbart
P2195 Riding new Tides: Synthesis of oligonucleotides on PurePep® Chorus
Luisa Aguiar, Dominik Sarma, Robert Zitterbart
P2196 The first endocrine-disrupting chemical inhibiting a coactivator peptide's binding
Masaki Iwamoto, Takahiro Masuya, Mari Hosose, Tomaka Ishibashi, Ayami Matsushima
P2197 PYY peptides and Fc-PYY conjugates selectively agonise Y2R
Elise Bernard, Siobhan O'Brien, Nicole Burmeister, Jacqueline Naylor, Stephanie Oldham, Arthur Suckow, Hamid Salari, Maria A. Bednarek
P2200 Pipeline for development of acylated peptide-based CGRP receptor antagonist with extended half-life for migraine treatment
Jens Bjelke Kristensen, Lisbeth Elster, Morten Lundh, Borja Ballarín-González, Flora Alexopoulou, Martin Kræmer, Ditte Marie Jensen, Ulrike Leurs, Jens Christian Nielsen, Henrik H. Hansen, Matilda Degn, Kristian A. Haanes
P2201 Peptide-conjugates derived from bacterial ParE toxin: synthesis and biological studies
Jose Gregorio Martín Bedoya, Naiara Maia Pereira, Reinaldo Marchetto
P2202 Identification and Characterization of Small Molecule Nucleotide Binding and Oligomerization Domain 2 (NOD2) Receptor Agonists
Liora E. Wittle, Karl L. Ocius, Marcos M. Pires
P2203 Influence of Hydrophobic Moieties on the Formation and Stability of Collagen Heterotrimers
Maša Stopinšek, Valdrin Islami, Giuseppe Antoniazzi, Philipp Bittner, Renato Zenobi, Helma Wennemers
P2207 Exploring Novel Peptide-Based Natural Products as a Payload for the Generation of Antibody and Peptide-Assisted Targeted Cancer Therapy
Suzie M. Chan, Makhdoom Sarwar, Jeanine Giarolla Vargas, J. da Silva, Margaret A. Brimble, Iman Kavianinia
P2208 Bispecific DNA-Peptide Conjugates for Targeting Cancer Cells
Pritam Ghosh, Huyen Dinh, Oliver Seitz
P2209 Memantine and Adamantine KLVFF Conjugates: Synthesis, Ab interaction and Effects on Recognition Memory in Mice.
Giuseppe Pappalardo, Eleonora Bocchieri, Stefania Zimbone, Maria Laura Giuffrida, Giuseppe Di Natale, Giuseppina Sabatino, Graziella Vecchio, Santina Chiechio
P2210 Chemoselective arylation of amino acids, peptides and proteins
Ahmed M. Embaby, Sanne Schoffelen, Christian Kofoed, Morten Meldal, Frederik Diness

P2211 Glycopeptides as synthetic antigenic probes for MOG Antibody-Associated Disease
Silvia Braccia, Feliciana Real-Fernandez, Christine Patte-Mensah, Christian Klein, Nicolas Collongues, Jérôme de Sèzed, Paolo Rovero, Anna Maria Papini
P2212 Designing self-assembling lipopeptide for tissue regeneration
Dhriti Shenoy, Lauren Roberts, Michela Pesenti, Kaliroi Peqini, Stefania Crespi, Cécile Echalier, Gilles Subra, Sara Pellegrino
P2213 Optimizing biological activity of Lactoferricin derived peptides: Conjugation with non peptidic motifs as a strategy
Daniel Castellar, Javier García, Zuly Rivera, Ricardo Fierro
P2215 Introducing Novel Titanium Binding Peptides; Effect of the Sequence of Amino Acids on Their Adsorption Energy to TiO2
Roja Rahmani, Alexander P. Lyubartsev
P2216 Peptides Conjugated to Sugars as Therapeutics for Ebola & Cancer disease
Fayna García-Martín, Óscar Suárez, Gonzalo Millán, Filipa Marcelo, Ana Gimeno, Elena Lalinde, Jesús R. Berenguer, Juan Anguita, Héctor Busto, Jesús Manuel Peregrina, Asuka Nanbo, Jesús Jiménez-Barbero, Francisco Corzana
P2217 Synthetic strategies to prepare novel bioactive lysine and peptide conjugates with triazolium derivatives
Claudia Bello, Michał Jewginski, Patrycja Ledwon, Francesca Nuti, Paolo Rovero, Rafal Latajka, Anna Maria Papini
P2222 Effect Of Azaglycine On The Internalization Of Penetratin Derivatives
Karima Tarchoun, Dóra Soltész, Ildikó Szabó, Zoltán Bánóczi
P2223 Molecular Design for Cytosolic Delivery of Antibodies Using an Intracellular Delivery Peptide
Yoshimasa Kawaguchi, Shiroh Futaki
P2224 Synthesis and characterization of nucleolin receptor recognizing F3 peptide fragment-drug conjugates
Bettina Basa, Diána Vári-Mező, Kata Nóra Enyedi, József Tóvári, Szilvia Bősze, Krisztina Kiss, Gábor Mező
P2225 Leuprorelin Peptide Drug Complexes with Permeability Enhancers to Increase Bioavailability
Adel Penhasi, Zeina Zaatari, Moustafa Ghanyem, Deborah E. Shalev
P2226 Designing selective peptide binders for Methicillin resistance Staphylococcus aureus
Yaara Zandany, Zvi Hayouka
P2228 Phosphopeptides as a replacement of bisphosphonates for bone targeting
Mazen Jamous, Barbara Roether, Uwe Haberkorn, Walter Mier
P2231 Site-specific Conjugation of Cell-penetrating Peptides: A Strategy to Ameliorate Antibody Therapy
Niklas van den Bergh, Verena Merke, Sabrina Wohlfart, Philipp Uhl, Walter Mier
P2234 Synthesis of cell-penetrating peptides with peroxisomal targeting signal 1
Christine Krofta, Anne Sophie Hammann, Sven Thoms, Norbert Sewald
P2235 Surface peptide-modified black phosphorus nanosheets: a novel multifunctional nanoadjuvant
Tian-Yang Wang, Wen-Hao Li, Xue-Feng Yu, Yan-Mei Li
P2236 Non-ionic surfactants for the solubilisation of lipopeptides and enhancement of their biological activity
Ágnes Ábrahám, Gergő Gyulai, Judith Mihály, Andrea Horváth, Orsolya Dobay, Éva Kiss, Kata Horváti
P2238 Nanobody CDR3 loop peptidomimetic improves binding on living Acinetobacter baumannii
Kevin Van holsbeeck, Anke Breine, Charlotte Martin, Morgane Mannes, Els Pardon, Jan Steyaert, Han Remaut, Charles Van der Henst, Steven Ballet
P2239 High-Throughput Analysis of Peptide Accumulation in Mammalian Cells
Sobika Bhandari, George Ongwae, Marcos M. Pires
P2240 Electrostatically modulated peptide-based drug delivery against resistant cancer
Yvonne Christian, Amay Sanjay Redkar, Naveen Kumar, Shine Varghese Jancy, Aneesh Chandrasekharan, T.R. Santhoshkumar, Vibin Ramakrishnan
P2241 Novel viral peptide-based tandemized carriers: Structure prediction and in vitro evaluation
Katalin Uray, Martin Krátký, Jiří Horčic, Levente Lakatos, Előd Méhes, Bálint Jezsó, Jarmila Vinšová, Szilvia Bősze
P2242 Small Additive Molecules to Enhance the Effective Accessibility of Delivered Nucleic Acid by Cell-Penetrating Peptide
Geeta Arya, Ly Porosk, Chigozie Nkwocha, Margus Pooga
P2244 Fluorogenic cell surface labelling using fluorescent molecular rotor-labelled peptide boronic acid conjugates
Alen Koçak, Pritam Ghosh, Oliver Seitz

P2247 Synthesis and application of β-amino γ-lactam (Bgl) residues
Charity D. Yongo-Luwawa, William D. Lubell
P2250 Development of Cyclopropane-Based Foldamers Mimicking Protein Secondary Structures
Makoto Nagata, Nanase Ochiai, Akiko Yoshida, Satoshi Shuto, Mizuki Watanabe
P2253 Gq protein peptidomimetics as allosteric modulators of the ghrelin receptor
Morgane Mannes, Esaü Vangeloven, Charlotte Martin, Marjorie Damian, Sonia Cantel, Jean-Alain Fehrentz, Julie Kniazeff, Jean-Louis Banères, Steven Ballet
P2255 A reductive amination approach for the synthesis of catalytic peptide foldamers
M. Pollastrini, A. Moretto
P2257 DARPin-based Pretargeting: Zeroing in on Cancer
K. Westerlund, M. Oroujeni, A. Van Deventer, Z. Wang, J. Clinton, I. Zelepukin, E. Papalanis, Y. Liu, A. Orlova, V. Tolmachev, A. Eriksson Karlström
P2258 Rational design of novel peptidomimetics against influenza a virus: biological and computational studies
M.C. Scala, M. Agamennone, M. Marchetti, F. Superti, P. Campiglia, M. Sala
P2259 Development of peptide nucleic acids-based molecules targeting non-canonical nucleic acids structures
Matilde Rossia, Paola Gratteri, Anna Maria Papini, Carla Bazzicalupi
P2260 Macrocyclic mimetics of the Suppressor of Cytokine Signaling 1 and 3 proteins (SOCS1-SOCS3)
A. Cugudda, S. La Manna, D. Florio, D. Marasco
P2262 Modulation of the antagonistic properties of an insulin mimetic peptide by disulfide bridge modifications
Marta Lubos, Jan Pícha, Irena Selicharová, Jiří Žák, Miloš Buděšínský, Katarína Mitrová, Lenka Žáková, Jiří Jiráček
P2263 Combinatorial libraries of bipodal insulin receptor binders
Irena Selicharová, Benjamin Fabre, María Soledad Garre Hernández, Marta Lubos, Jan Pícha, Zdeněk Voburka, Katarína Mitrová, Jiří Jiráček
P2266 AI-driven design of β-secretase 1 inhibitors
Marko Njirjak, Daniela Kalafatovic, Goran Mauša
P2267 Application of Deep learning Imputation to Peptide Bioactivity and Property Prediction
Samar Mahmoud, Himani Tandon, Matthew Segall, Ruibo Zhang, Robert E Thompson, Jeffrey W Schubert, Dipannita Kalyani, Dan Sindhikara
P2268 PICKAPEP: Visualization and Calculation of Cyclized and Modified Peptidomimetics Made Easy
Vanessa Erckes, Mattis Hilleke, Clemens Isert, Christian Steuer
P2274 Metalloproteins Investigation for the Development of new Inhibitors
Matteo Orlandi, Piero Procacci, Marina Macchiagodena, Fabrizio Carta, Claudiu T. Supuran, Marco Pagliai
P2275 Deep learning for Peptide Classification: From Data to Effective Models
Marko Njirjak, Marko Babić, Patrizia Jankovic, Erik Otović, Daniela Kalafatovic, Goran Mauša
P2276 Scoring the Synthesizability of Any Novel Non-natural Amino Acid
Gökçe Geylan, Mikhail Kabeshov, Samuel Genheden, Thierry Kogej, Ola Engkvist, Leonardo De Maria
P2277 Chemoenzymatic synthesis of protein pseudo-[2]rotaxane
Elodie Soehnlen, Shalene Ofner, Judit Osz, Natacha Rochel, Vladimir Torbeev
P2279 Structural and Mechanistic Insights Into the Advances of FXIIIa Inhibitors
Ivan P. Bogdanov, Arijit Biswas, Diana Imhof, Nikolay T. Tzvetkov
P2280 Can large scale structural modeling be applied to peptide screening and deorphanization?
Shaima Hashem, Jérôme Leprince, Pierre Tuffery
P2281 Impact of backbone N-amination on the stability of parallel beta-sheets
Syrah Starnes, Seth Horne, Juan Del Valle
P2283 How do Disulfide, Thioacetal and Lanthionine Bridges Influence the Conformations of Macrocyclic Peptides?
William T. P. Darling, Lianne H. E. Wieske, Declan T. Cook, Abil E. Aliev, Laurent Caron, Emily J. Humphrys, Angelo Miguel Figueiredo, D. Flemming Hansen, Máté Erdélyi, Alethea B. Tabor
P2284 Characterizing bradykinin-derived membrane-sensing peptides through Molecular Dynamics
Carlo Guardiani, A. Giacomello
P2285 Effect of antifreeze activity and lipid interaction of tryptophan scanning of 11-residue lysine homopeptide
R. Rojas, M. Aróstica, C. Cardenas, L. Aguilar, F. Albericio, F. Guzmán
P2286 Structural Ensemble of Peptide-induced Membrane Poration by Heterogeneous Magainin Peptides
Bing Zan, Charles Chen, Martin Ulmschneider, Jakob Ulmschneider-Mayer

P2288 Helical peptides bearing dual triplet-spin/fluorescent labels enable the first parallel distance measurements by electron spin resonance and Förster resonance energy transfer
Marta De Zotti, Arnau Bertran, Chiara Dalla Torre, Jack Sawyer, Derren Heyes, Sam Hay, Christiane Timmel, Marilena DI Valentin, Alice Bowen
P2289 Antiparallel β-Double Helices from α,γ-Hybrid Peptides
DRGKoppalu R. Puneeth Kumar, Gijo George, Uddipan Bhattacharya, Arnab Mukherjee, Hosahudya N. Gopi
P2290 Aromatic-aromatic interactions as an intrinsic modulator of amyloid formation
Artem Pavlov, Beate Koksch
P2291 Structure-Activity Relationship Study of β-Hairpin Peptides with Antibiotic Activity
Aparna Palakkurussi Rathessan, Suvrat Chowdhary, Johannes Kupke, Marcus Fulde, Beate Koksch
P2293 Molecular insights into the lipid bilayer interaction of the cyclic lipodepsipeptide tolaasin
Benjámin Kovács, Tünde Juhász, Niels Geudens, José C. Martins, Tamás Beke-Somfai
P2294 A comprehensive structural study on AT1 Receptor Variants: Towards the Design of Potent Biased Agonists
Malihe Hassanzadeh, Audrey Collette, Brian Holleran, Stéphane Laporte, Richard Leduc, Pierre-Luc Boudreault
P2295 Structural analysis of a peptide-based simplified model reproducing SARS-CoV-2 S RBD/ACE2 binding site
Michela Buonocore, Rosanna Lucignano, Angelo Santoro, Anna Maria D'Ursi, Delia Picone
P2296 Planar aggregation of the influenza viral fusion peptide alters membrane structure and promotes poration
Richard W. Pastor, Amy Rice, Paul S. Blank, Joshua Zimmerberg
P2298 Unlocking HIV's Secrets: Synthesis of Histone H3K36Me3 to Investigate LEDGF Protein Binding to Modified Nucleosomes using Cryo-Electron Microscopy
Ramesh M. Chingle, Samanthreddy Kedika, Tao Jing, Dmitry Lyumkis, Terrence R. Burke
P2300 Elucidating the role of phosphoserines in Tau protein by combined computational and synthetic methods
Martina Tuberti, Fintan Kelleher, Gemma K. Kinsella
P2300 Elucidating the role of phosphoserines in Tau protein by combined computational and synthetic methods
Martina Tuberti, Fintan Kelleher, Gemma K. Kinsella
P2301 Theoretical and biological studies of oxytocin containing conformationally fixed analogue of Tyrosine Tic(OH) (1,2,3,4-Tetrahydro-7-hydroxyisoquinoline-3-carboxylic acid)
Michal Lebl, Jiří Jiráček, Marta Lubos, Jakub Kaminský
P2305 Can we improve Coarse-Grained simulations of peptide selfassembly and aggregation by cluster analysis inputs?
Marko Babić, Daniela Kalafatović
P2306 Design and Exploration of Tubular Assemblies of Hybrid Cyclic Peptides
Souvik Panda Mahapatra, Hosahudya N. Gopi
P2307 Antimicrobial and cell-adhesive peptide-based hydrogels for biomedical applications
Nabila Mehwish, Patricia López-Gómez, Maria Pau-Ginebra, Carles Mas-Moruno
P2309 De novo design of collagen-like peptides for cell-based technologies
Maryana Baran, Eileen Gentleman, Maxim Ryadnov
P2310 Self-assembling dipeptides as vehicles for the delivery of peptide therapeutics
Peter Divanach, Eirini Fanouraki, Vagelis Harmandaris, Anastassia N. Rissanou, Anna Mitraki
P2314 Self-assembly of histidine-containing peptides and applications
C.P Apostolidou, Chrysoula Kokotidou, Varvara Platania, Vasilis Nikolaou, Georgios Landrou, Emmanouil Nikoloudakis, Georgios Charalambidis, Maria Chatzinikolaidou, Athanassios G. Coutsolelos, A. Mitraki
P2315 Tuning the Assembly of Proteins and Peptides in Lipid Bilayers
Sebastián Jiménez Millán, Ivan Sasselli, Armando Maestro
P2318 Design of fluorinated peptide-based hydrogels for sustained drug release application
Aurélie Honfroy, Jolien Bertouille, Ana-Maria Turea, Thibault Cauwenbergh, Jessica Bridoux, Nathalie Lensen, Jessica Mangialetto, Niko Van den Brande, Jacinta F. White, James Gardiner, Thierry Brigaud, Steven Ballet, Sophie Hernot, Grégory Chaume, Ch
P2319 Single glycans shape viscoelastic properties of a mucin-inspired peptide hydrogel
Jonas Proksch, Marlene Dal Colle, Frederick Heinz, Jacqueline Gottwald, Robert Schmidt, Martina Delbianco, Bettina Keller, Ulrike Alexiev, Michael Gradzielski, Beate Koksch
P2330 Cardiolipin-specific peptides, designed to possess cell penetrating ability, rescue mitochondrial dysfunction
Gwangsu Shin, Dongwoo Kim, Yoonhwa Choi, Hyeong woon Choe, Seung Hee Yang, Jaehoon Yu
P2331 Efficient synthesis of three-helix bundle proteins using ligase-mediated trimerization of HIV-1 fusion inhibitor T20 on a dendrimer scaffold
Xiaohong Zhang, Yiyin Xia, Chuan-Fa Liu, James P. Tam

P3332 Broaden the Applications of Peptidyl Asparaginyl Ligases

Yiyin Xia, Hongxia Li, Jiayong Liu, James P.Tam, Chuan Fa Liu

LECTURES

Proceedings of the 37th European Peptide Symposium
Michal Lebl, Editor
European Peptide Society, 2024
http://doi.org/10.17952/37EPS.2024.L003

Synthesis of β-turn mimics without stereogenic carbons: expanding the modular approach for diversity-oriented synthesis of tetrasubstituted benzotriazepinones

Xiaozheng Wei,[1] Sarah-Maude Harvey, [1] Debora Iaculli,[1,2] Steven Ballet,[2] and William D. Lubell[1]

[1]Département de Chimie, Université de Montréal, 1375 Ave. Thérèse-Lavoie-Roux, Montréal, Québec, H2V 0B3, Canada; [2]Research Group of Organic Chemistry, Departments of Chemistry and Bioengineering Sciences, Vrije Universiteit Brussel, 1050 Brussels, Belgium

Introduction

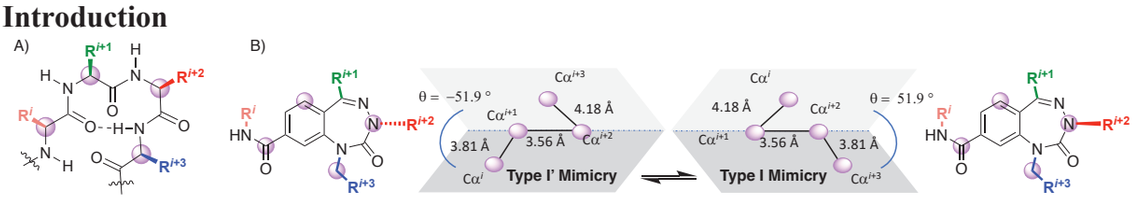

Figure 1. A) β-turn indicating α-carbons, B) dynamic turn mimicry by benzotriazepinone

Benzotriazepinones are "privileged structures" exhibiting promising biological and medicinal properties [1]. Benzotriazepinone crystal structures have shown that the N3 nitrogen is pyramidalized and exists in dynamic equilibrium between two configurations [2,3]. In the context of peptide science, X-ray analysis indicated tetrasubstituted benzotriazepinones replicate the topology of β-turn secondary structures [2]. Superimposing key atoms of the tetrasubstituted benzotriazepinone with the four α carbon atoms ($C\alpha^{i}$–$C\alpha^{i+1}$–$C\alpha^{i+2}$–$C\alpha^{i+3}$) within a tetrapeptide has demonstrated capacity to mimic both type I and I' β-turns which are topologically defined by the dihedral angle θ (Figure 1) [2,4].

A modular synthesis route to tetrasubstituted benzotriazepinones was developed starting from *tert*-butyl 4-acetyl-3-aminobenzoate (Figure 2) [2]. Aldol condensation provides the *i*+1 residue substituent. Annulation with an aza-glycine residue adds the *i*+2 substituent. The *i*+3 and *i* residue substituents are introduced by amide coupling and alkylation.

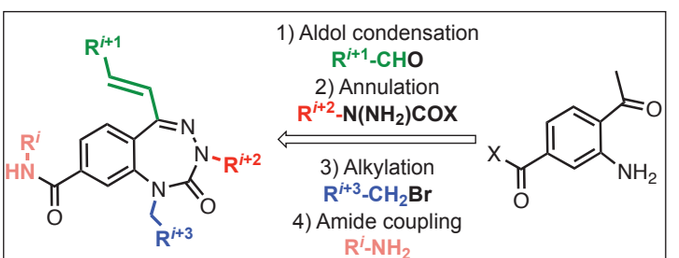

Figure 2. Modular benzotriazepinone turn mimic synthesis

A tetrasubstituted benzotriazepine library was rationally designed, synthesized, and shown to contain urotensin receptor (UT) allosteric modulators [2,5]. A G protein-coupled receptor, UT has two endogenous ligands, *h*UII and URP [5]. Differentiation of pathophysiological roles of *h*UII and URP has been pursued for medical applications, such as cardiovascular disease therapy. Tetrasubstituted benzotriazepinones exhibited respectively selective modulator ability on the activity of *h*UII and URP as positive and negative allosteric modulators with neutral activity on the ligand counterpart [5].

Results and Discussion

Diversity-oriented methods were studied to expand the modular route to β-turn *i*+1 and *i*+3 substituents by the synthesis of amino acid **1** and benzophenone analog **2** (Scheme).

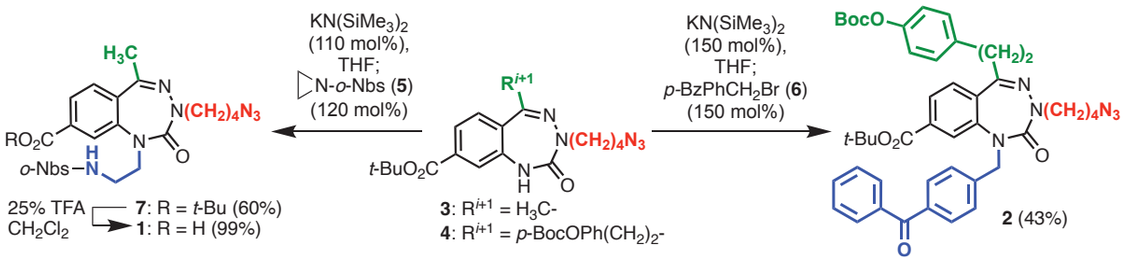

Scheme. Synthesis of tetrasubstituted benzotriazepines **1** and **2**

Benzotriazepines **3** and **4** were respectively prepared from 4-keto-3-aminobenzoates using the reported annulation protocol [2]. The aza-glycinate derived from *p*-nitrophenyl chloroformate and benzophenone hydrazone reacted with 3-aminobenzoates, *i*-Pr_2EtN in CH_2Cl_2 to give glycinamides. Benzotriazepines **3** and **4** were obtained by glycinamide alkylation with $Br(CH_2)_4Cl$ and Et_4NOH in THF, annulation with 1N HCl, and chloride displacement with NaN_3 in 4:1 NMP:H_2O [2].

Respective alkylations of benzotriazepinones **3** and **4** using $KN(SiMe_3)_2$ in THF with *N*-*o*-nitrosulfonyl (*o*-Nbs)aziridine (**5**) [6] and *p*-benzoyl benzyl bromide (**6**) afforded *o*-Nbs-amino ethyl and benzophenone benzotriazepinones **7** (m/z = 601.2) and **2** (m/z = 771.5). Subsequent treatment of *o*-Nbs-amino ester **7** with F_3CCO_2H in CH_2Cl_2 gave acid **1**, which exhibited diastereotopic methylene proton signals at 3.41 and 4.30 ppm indicative of a chiral nitrogen center.

Modular synthesis of β-turn benzotriazepinone mimics has been expanded through diversification of the *i*+3 position substituent by novel alkylation chemistry which has respectively provided amino acid **1** and benzophenone **2** for applications in peptide synthesis and photoaffinity labeling.

Acknowledgments

We are grateful for funding from the Natural Sciences and Engineering Research Council of Canada (NSERC, Discovery Research Project RGPIN-2019-04079), the Canadian Institutes of Health Research (CIHR, Project PJT-168839), and the Fonds de Recherche du Québec - Nature et Technologie (FRQNT, CGCC, FRQNT-2020-RS4-265155-CCVC). Assistance is acknowledged from members of the Université de Montréal facilities: Dr. P. Aguiar (NMR spectroscopy) and Dr. A. Fürtös (mass spectrometry). D.I. and S.B. thank the Research Foundation Flanders (FWO Vlaanderen) and the Research Council of the VUB for support of Strategic Research Programmes SRP50 and SRP95. S.M.H. thanks NSERC and FRQNT for Summer undergraduate research fellowship support.

References

1. Harvey, S.-M.; Wei, X.; Darince, D. and Lubell, W. D. Benzotriazepine synthesis, conformational analysis, and biological properties. *Can. J. Chem.* **2024**, *102*, 469-498. https://doi.org/10.1139/cjc-2023-0146
2. Wei, X.; Douchez, A.; Lubell, W. D. 1,3,5,8-Tetrasubstituted 1,3,4-benzotriazepin-2-one scaffolds for β-turn mimicry without Stereogenic Carbon Centers: synthesis and conformational analysis. *J. Org. Chem*. **2023**, *88*, 4633–4648. https://doi.org/10.1021/acs.joc.3c00113
3. Douchez, A. and Lubell, W. D. Chemoselective Alkylation for Diversity-Oriented Synthesis of 1,3,4-Benzotriazepin-2-ones and Pyrrolo[1,2][1,3,4]benzotriazepin-6-ones, Potential Turn Surrogates *Org. Lett.*, **2015**, *17*, 6046-6049. https://doi.org/10.1021/acs.orglett.5b03046
4. Hata, M. and Marshall, G. R. Do benzodiazepines mimic reverse-turn structures? *J. Comput. Aided Mol. Des*. **2006,** *20*, 321-31. https://doi.org/10.1007/s10822-006-9059-x
5. Wei, X.; Diarra, S.; Douchez, A.; Dallagnol, J. C. C.; Hébert, T. E.; Chatenet, D. and Lubell. W. D. Urotensin II Receptor Modulation with 1,3,4-Benzotriazepin-2-one Tetrapeptide Mimics. *J. Med. Chem.* **2023**, *66*, 14241-14262. https://doi.org/10.1021/acs.jmedchem.3c01307
6. Sanz-Rodríguez, C.E., Hoffman, B., Guyett, P.J., Purmal, A., Singh, B., Pollastri, M.P. and Mensa-Wilmot, K. Physiologic targets and modes of action for CBL0137, a lead for human african trypanosomiasis drug development. *Mol. Pharmacol*. **2022**, *102*, 1-16. https://doi.org/10.1124/molpharm.121.000430

https://doi.org/10.17952/37EPS.2024.L005

Fundamental aspects of SPPS and the Green future

Stephen Kent

Department of Chemistry

THE UNIVERSITY OF CHICAGO



European Peptide Symposium
Florence, Italy
August 2024

In 1963, Merrifield introduced solid phase peptide synthesis.

After initial fierce skepticism, SPPS has become almost universally used for the chemical synthesis of peptides, in both academic research and in industry.

In this brief talk, I will describe the fundamental physicochemical properties of peptide-resins that make SPPS so useful.

I will suggest ways to retain that utility in a 'Green' SPPS.

Then I will explain how to combine Green SPPS with chemical ligation for more efficient production of peptide molecules.

Solid Phase Peptide Synthesis (Merrifield 1963)

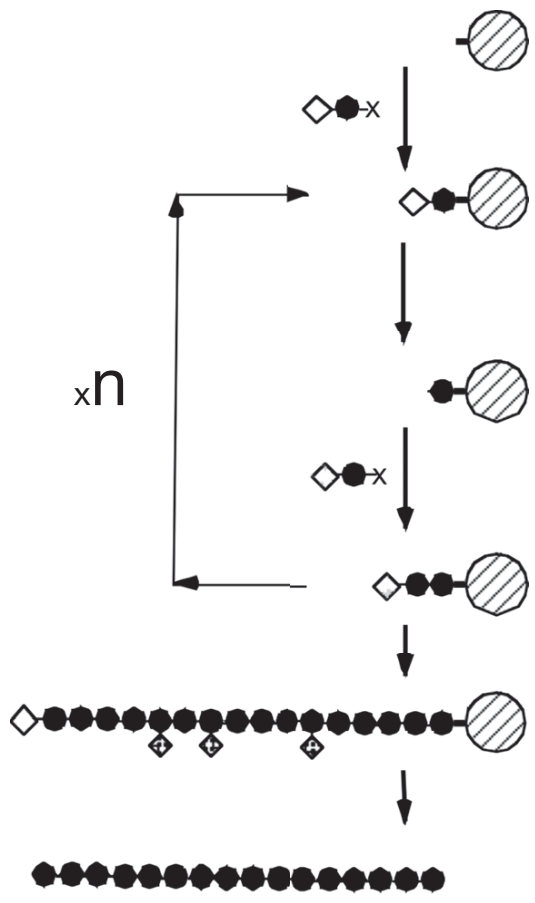

- C-terminal Xaa attached to resin beads
- stepwise chain elongation
- maximal protection of side chains
- global deprotection/release from resin

Is SPPS ‘Green’?

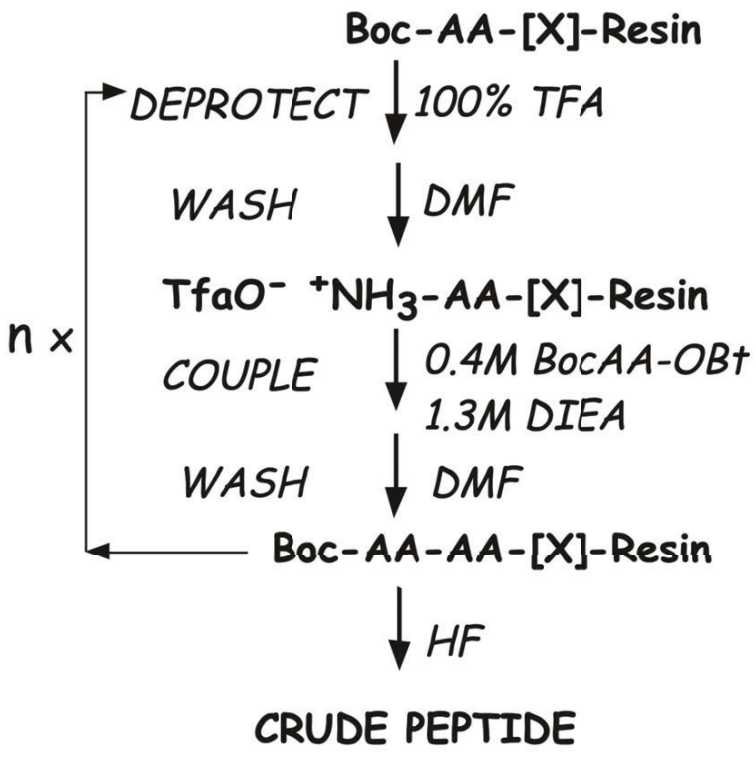

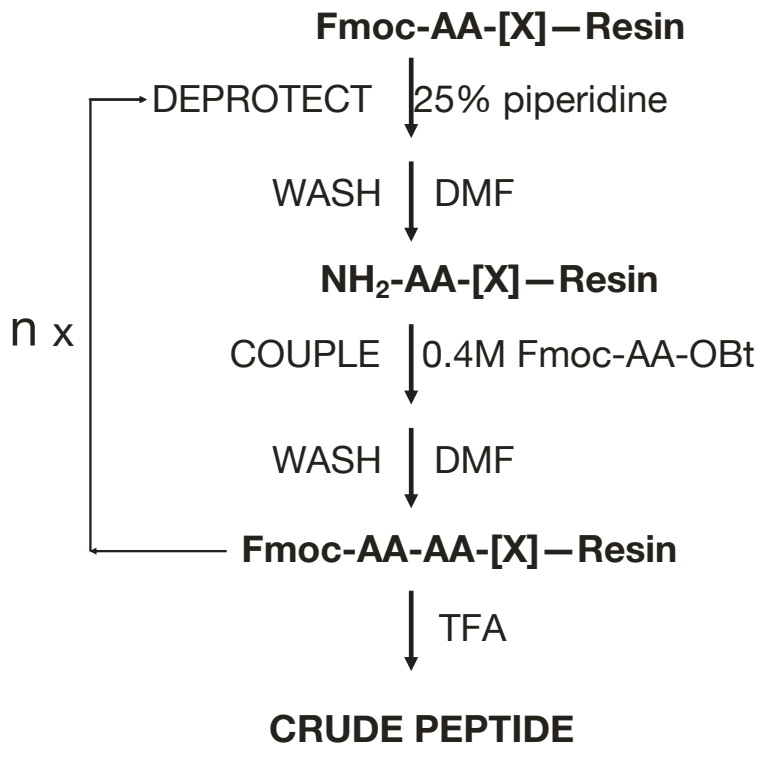

Is SPPS ‘Green’?

NO!

Boc-AA-[X]-Resin

Fmoc-AA-[X]—Resin

Poor atom economy:

* maximal use of protecting groups
* large excesses of reactants

Process mass intensive (PMI):

* corrosive/toxic chemicals
* inefficient purification
* high volume waste streams

Can we preserve the inherent advantages of SPPS

for ‘Green’ peptide synthesis?

Advantages of SPPS

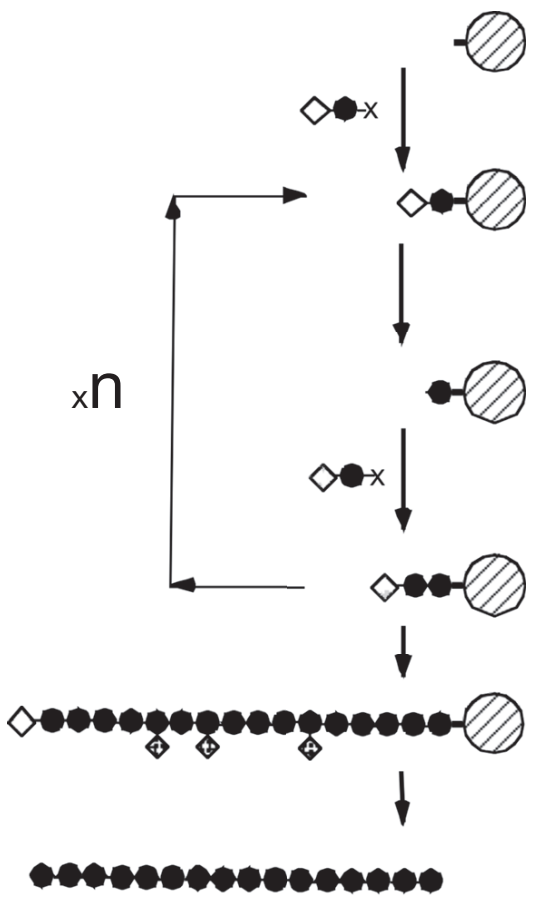

- ***enhanced solvation***
- stepwise synthesis
- purification by filtration
- quantitative recoveries
- general protocols
- automation

SPPS

Principles of Polymer Chemistry

(Paul Flory)

resin beads:

- randomly crosslinked
- IPN

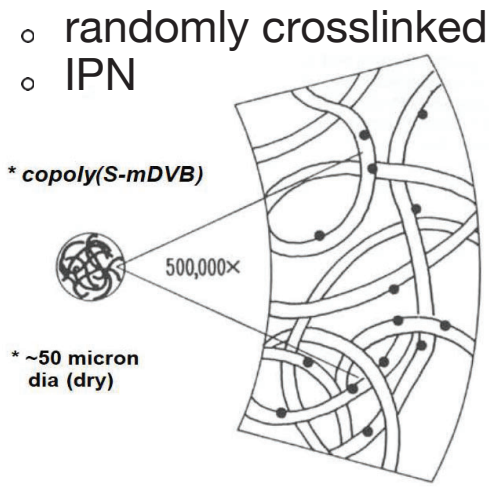

synthesis occurs ***within*** solvent-swollen beads:

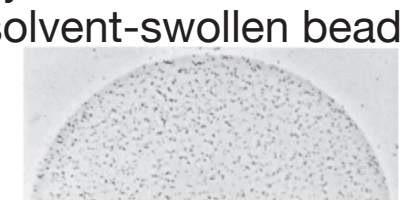

~10^{14} peptides per bead

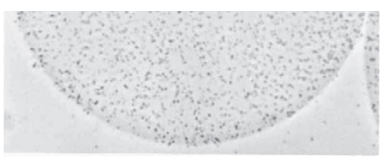

resin-bound peptides are effectively in solution - τ_c <10^{-8} sec

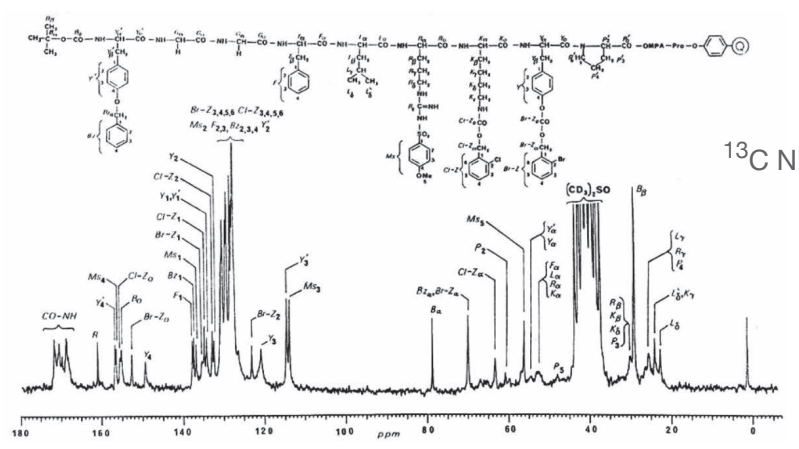

^{13}C NMR peptide-resin

peptide-resin super swelling

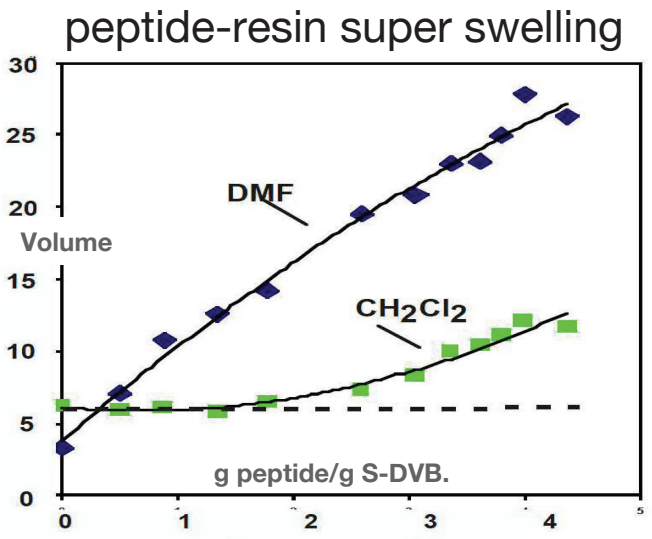

Solvation of resin-bound peptides

Enhanced solvation of peptides within solvent-swollen resin beads is the *fundamental reason* for the *efficacy* and *versatility* of SPPS

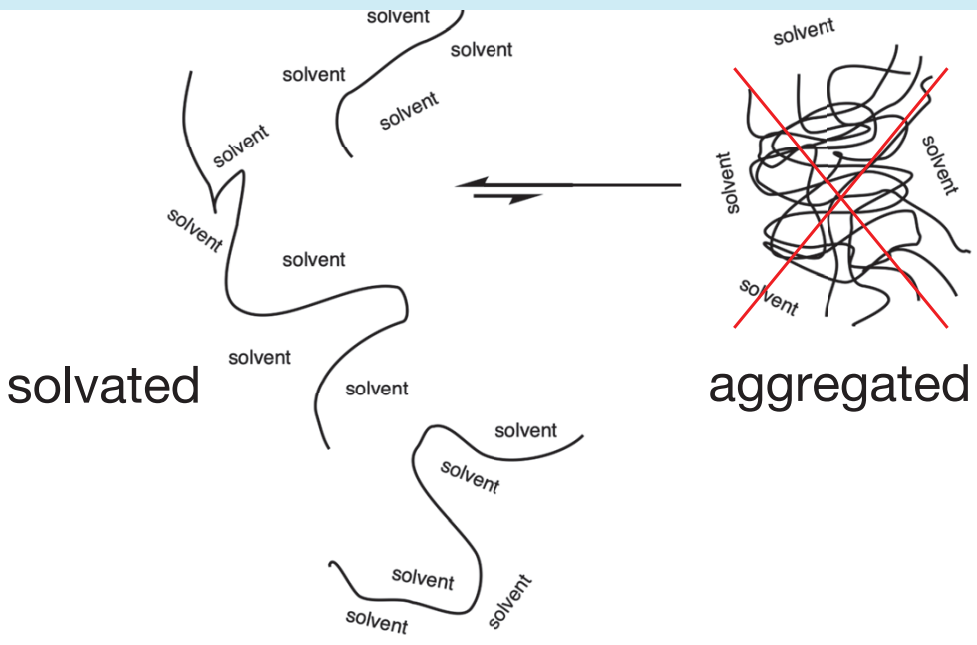

disfavored in peptide-resin

- *cross-links* prevent phase separation
- *dissimilar* properties of resin & peptide

the extent of solvation depends on the *relative free energies* of these two states

Dang, Dhayalan, & Kent
Org. Lett. 2015, **17**, 3521–3523

Features of a Green SPPS

- **atom economy**
  - minimal protecting groups
  - minimal excess reactants
- **benign reactants & reagents**
- **benign solvent**
- **efficient purification (PMI)**

“Controlled Synthesis of Peptides in Aqueous Solution.

1. The Use of α-Amino Acid N-Carboxyanhydrides.” (NCAs)

- **atom economy** ✓
  - minimal protecting groups
  - minimal excess reactants
- **benign reagents** ✓
- **benign solvent** ✓

Denkewalter, et al.
J.Am.Chem.Soc.
88, 3163-3164 (1966)

SPPS using α-Amino Acid N-Carboxyanhydrides on ChemMatrix resin

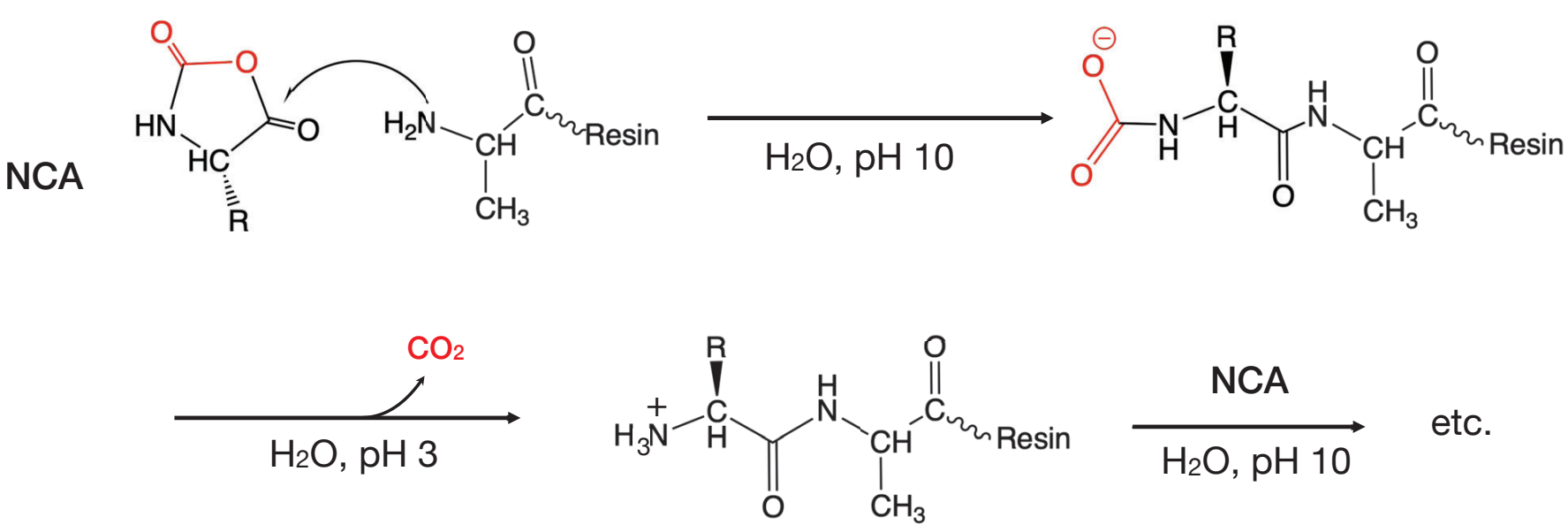

De Marco, Gentilucci, et al., *ACS Sustainable Chem. Eng.* **1,** 566–569 (2013)

Green Solid Phase Peptide Synthesis

Atom economy

- N-carboxyanhydrides
  - minimal side-chain protection
    - Lys
    - Ser/Thr(?)
- high resin loading
  - >1 millimol/g resin
- maximum ***concentration*** of NCA
- minimal ***excess*** of NCA

Solvent

- water

Resin

- aqueous solvent-compatible

Preparation of chemically defined resins for SPPS

BioBeads Sx1 (Biorad)

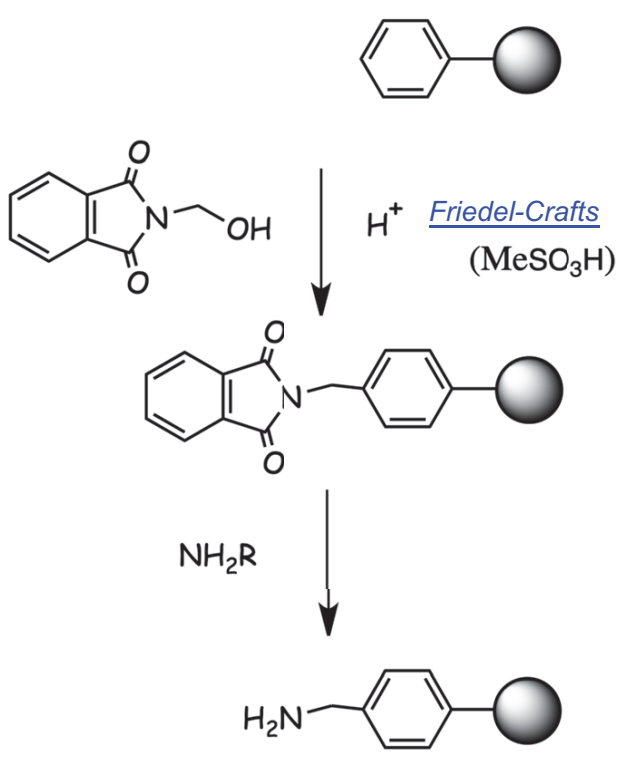

Paul W. R. Harris et al. ,
Tetrahedron Letters
52 (2011) 6024–6026

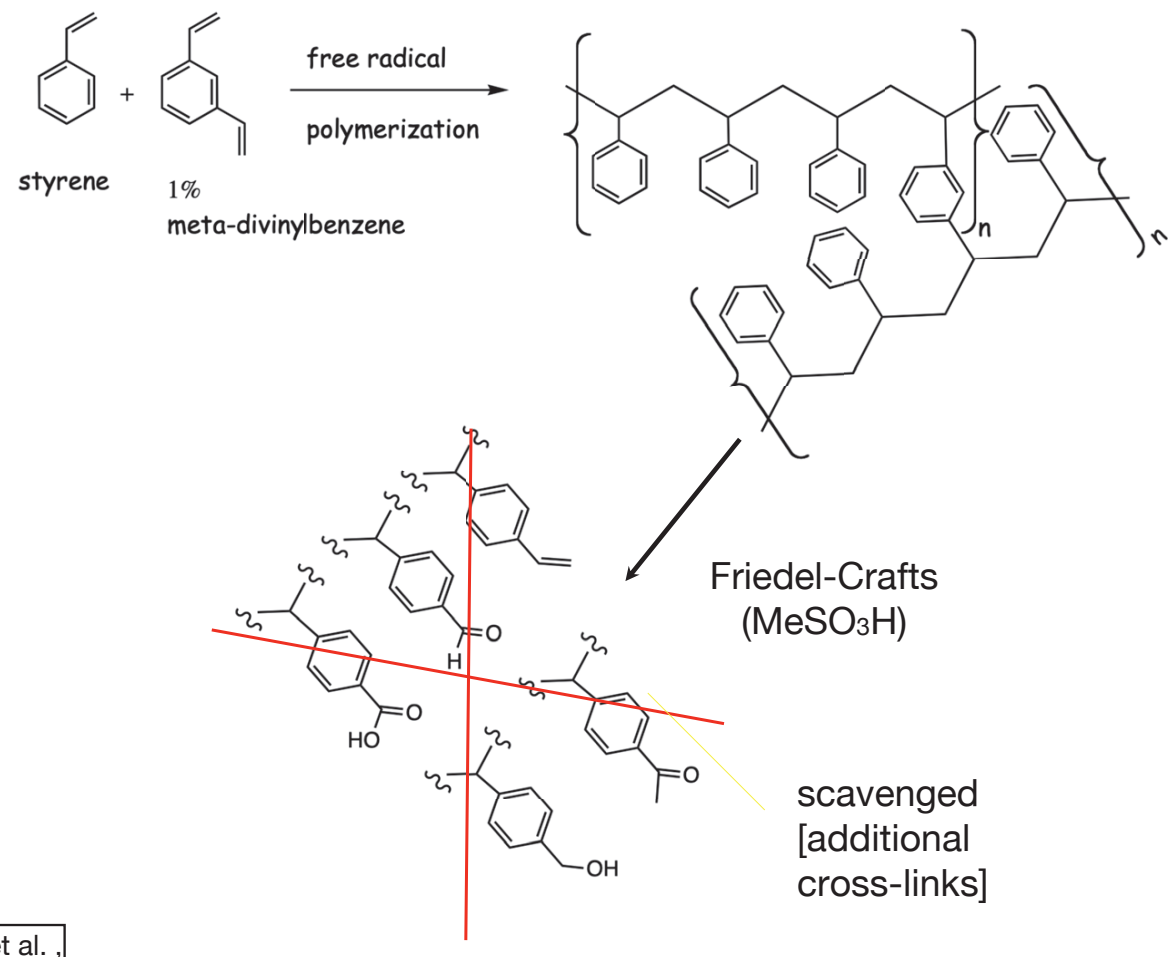

Mitchell A.R., Kent S.B.H., Engelhard M., Merrifield R.B.
J. Organic Chem **43**, 2845-2852 (1978).

Aqueous solvent-compatible resin for SPPS

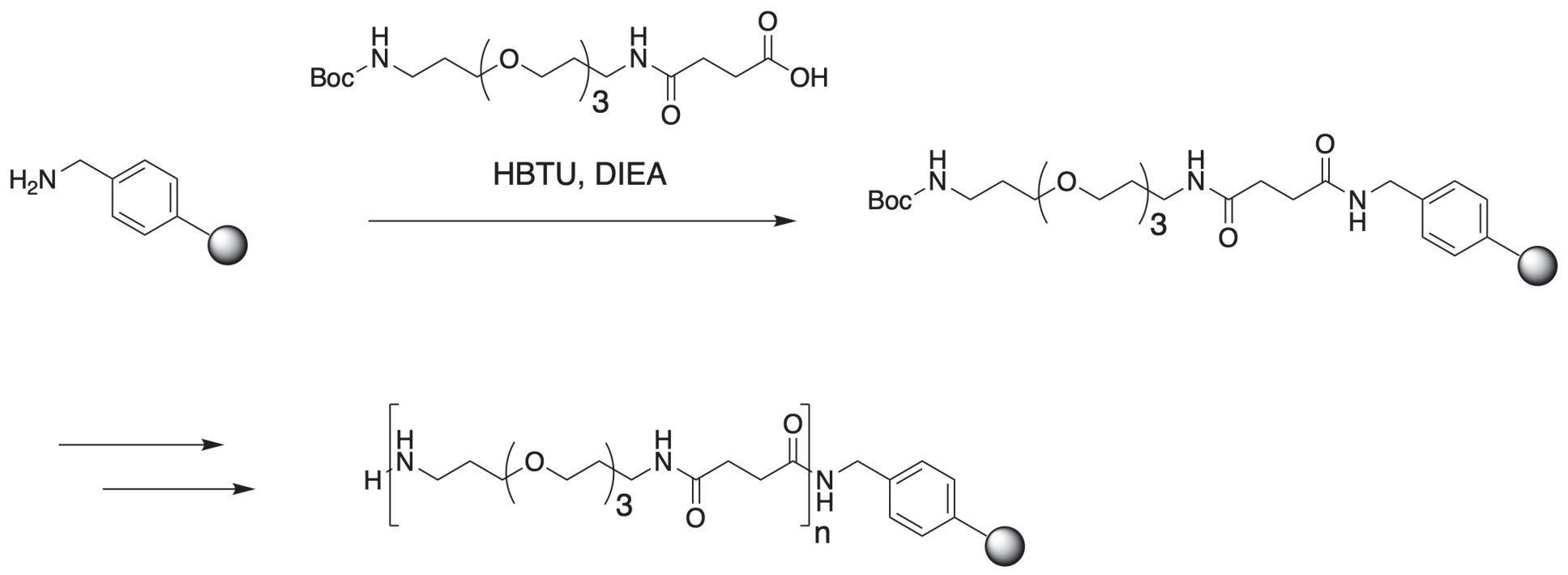

NH_2–(TTD-Succ)$_n$–Resin

Zachary P. Gates, Balamurugan Dhayalan, Stephen B. H. Kent, *Chem.Communications,* 2016,**52**,13979—13982.

Green Solid Phase Peptide Synthesis

Atom economy

- N-carboxyanhydrides
  - minimal side-chain protection
    - Lys(Boc)
    - Ser/Thr?
- high resin loading
  - ~1 millimol/g resin
- maximum ***concentration*** of NCA
- minimum ***excess*** of NCA

Solvent

- water

Resin

- aqueous solvent-compatible

Deprotection/cleavage/purification

- *without* TFA
- efficient purification (PMI)
  - tag-assisted
  - displacement mode prep HPLC

Convergent chemical synthesis

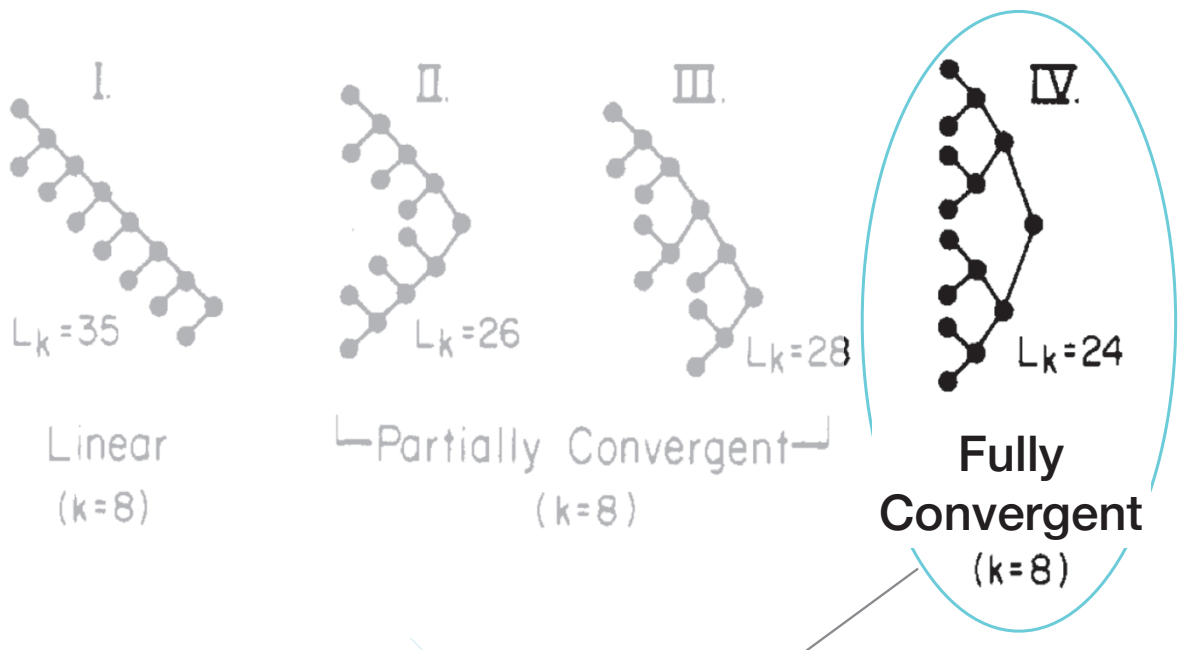

Systematic Synthesis Design. 6.
Yield Analysis and Convergency

James B. Hendrickson

Journal of the American Chemical Society / 99: 5439 (1977)

- most efficient use of starting materials
- minimum exposure to reaction conditions
- versatile analogue synthesis
- ***isolation of intermediate products***
- ***enhanced yields & purity***

Convergent segment ligation *vs.* stepwise synthesis

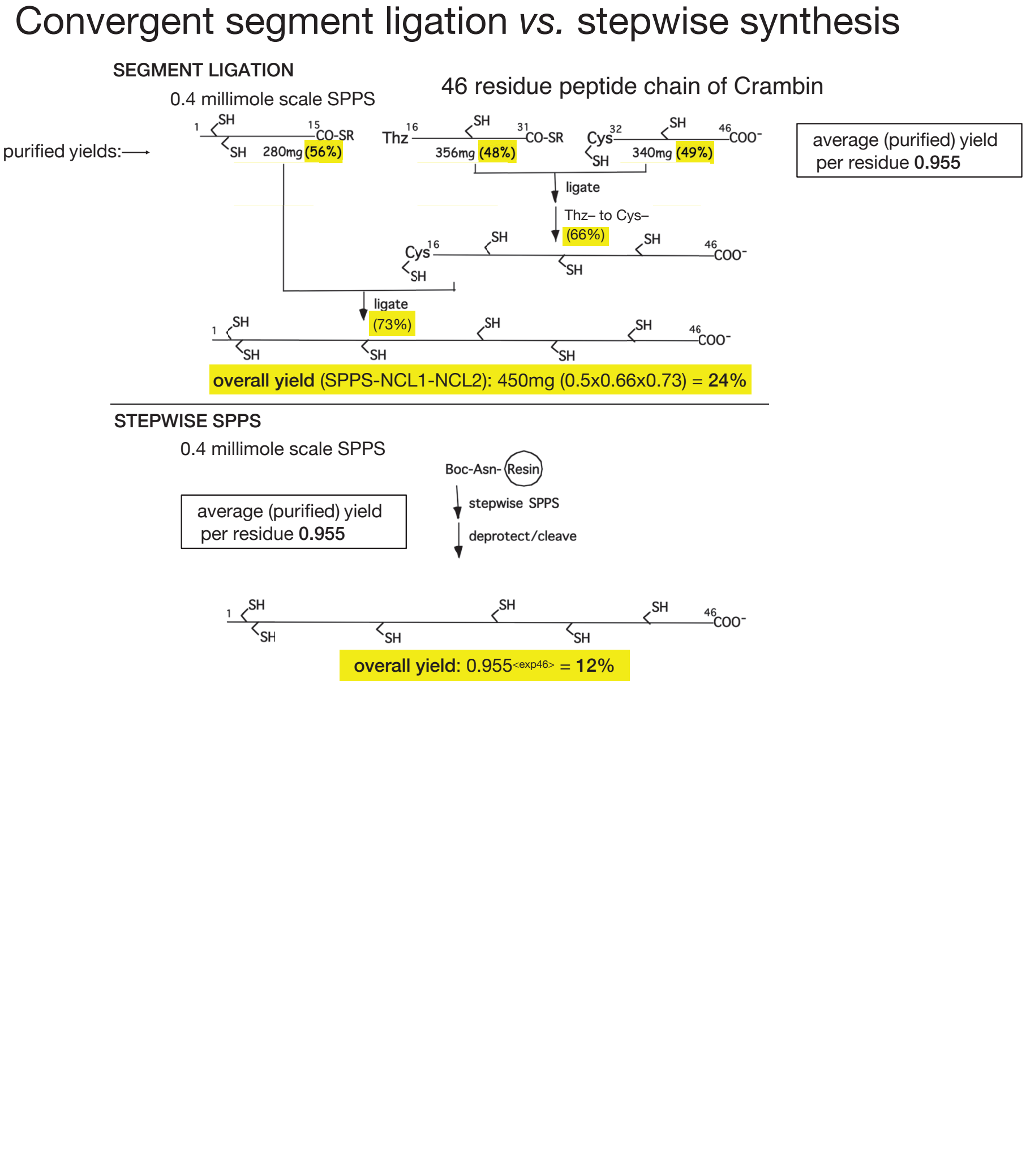

Chemical ligation condensation of unprotected peptides is inherently ’Green’*!*

* Protecting groups - minimal/none
* Reaction conditions - benign
* Solvent - water (w or w/o ‘solubility modifiers’)
* Energy - reactions at/near room temperature
* Efficiency - minimal excesses of reactants
* Atom economy - complete/very good
* Products - degradable

commercial availability* of β-SH Xaa’s*

– please! –

Green peptide synthesis

stepwise SPPS using N-carboxyanhydrides

convergent segment condensation by NCL

- enhanced yields
- enhanced purity

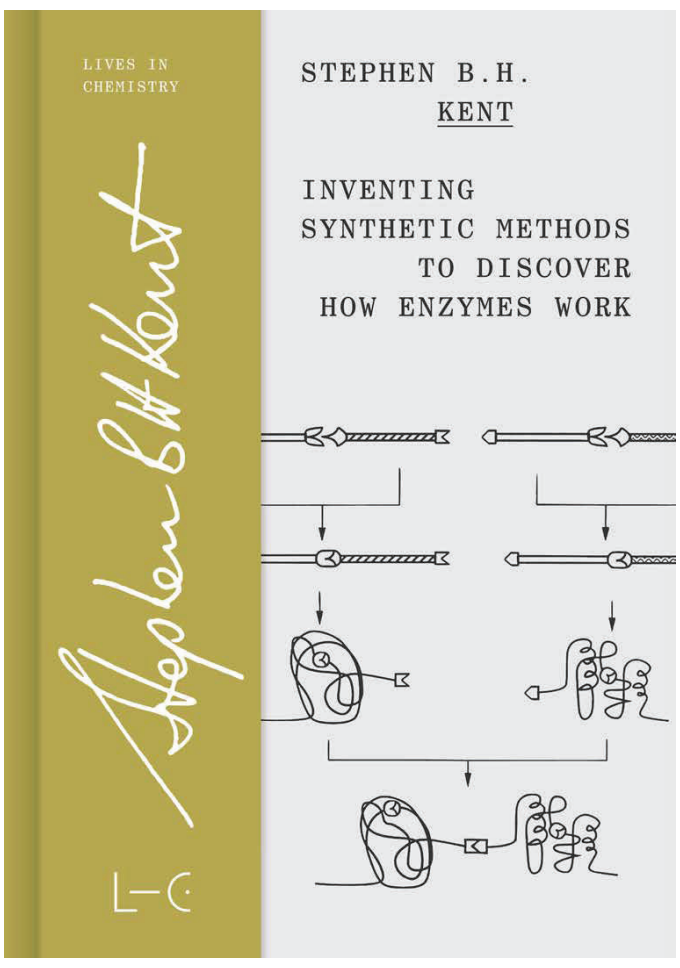

LIVES IN CHEMISTRY

GDCh HISTORY OF CHEMISTRY DIVISION

Outstanding chemists unveil

- how they started they career
- how their ideas evolved
- how they balanced work & life
- how they built a team
- how they overcame hurdles
- how they survived harsh conditions

GDCh

GERMAN CHEMICAL SOCIETY

https://doi.org/10.17952/37EPS.2024.L020

EPS-IPS 2024
Florence, Italy, Aug 26th, 2024

tCAP conjugate: an affinity peptide-based antibody conjugation system to generate highly functional antibody

Yuji Ito[1], Rafique Abdur[1], Shun Masuda[2], Yukie Nohara[2], Shugo Tsuda[2], Taku Yoshiya[2]

[1]Kagoshima University, Kagoshima, Japan, [2]Peptide Institute, Inc., Osaka, Japan

High functional drug with DDS by tissue-specific targeting antibody AccumBody®

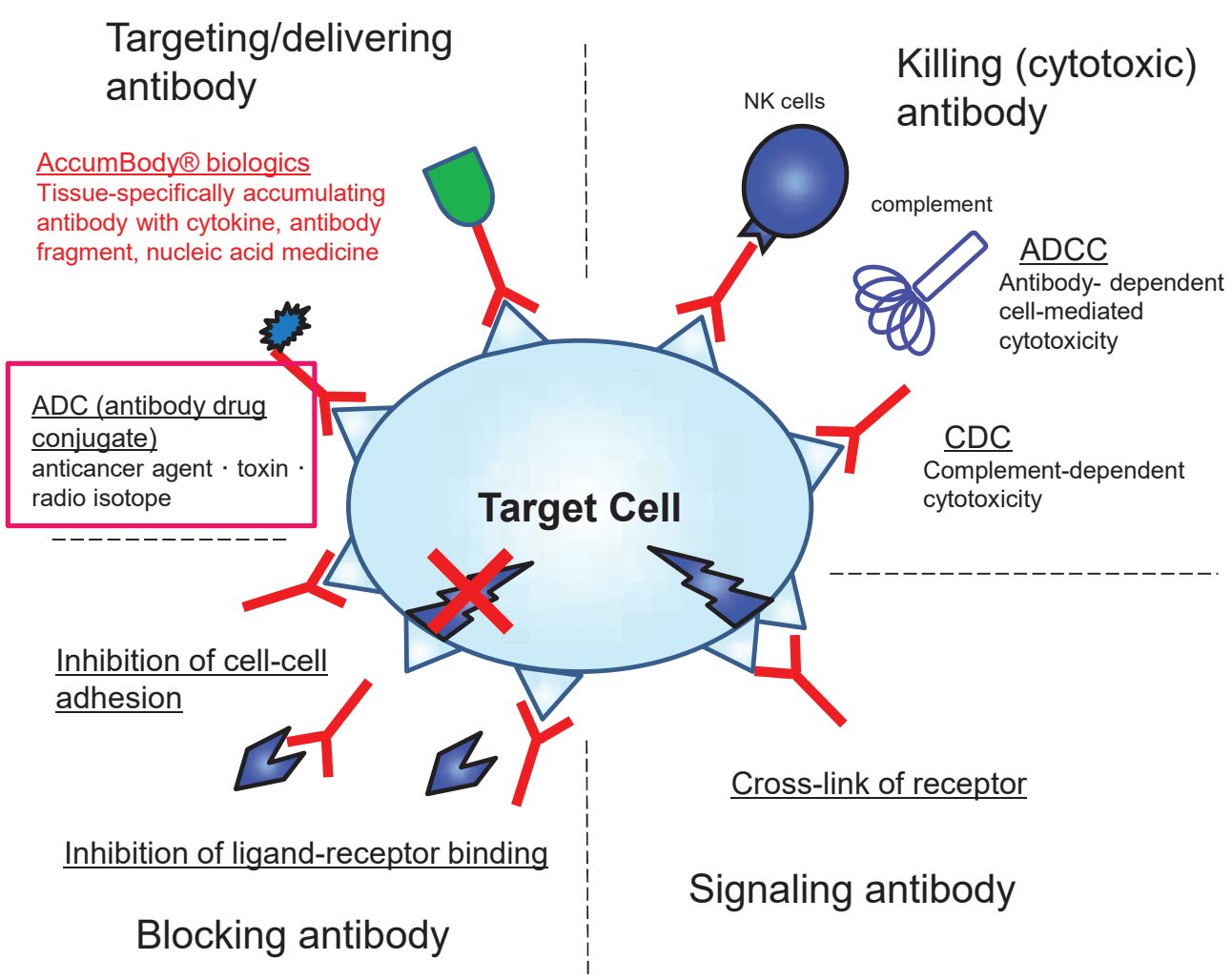

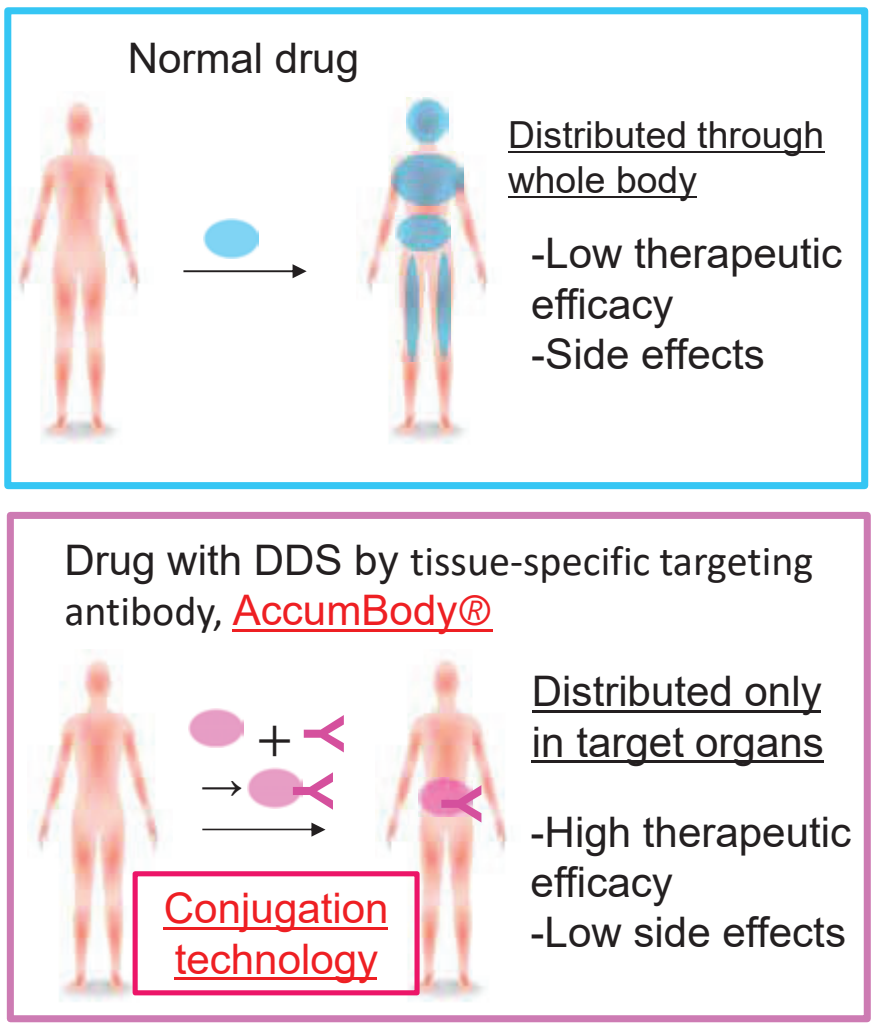

CCAP （Chemical conjugation by affinity peptide）

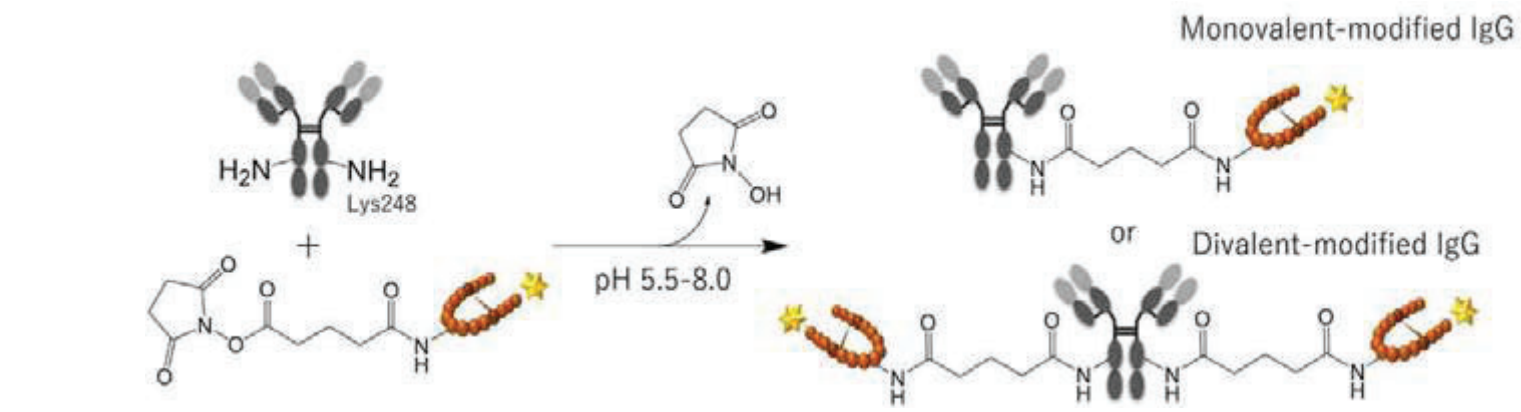

Kishimoto, S. et al. Bioconjug. Chem. 30, 698–702 (2019).

Patent-filed as WO2016186206.

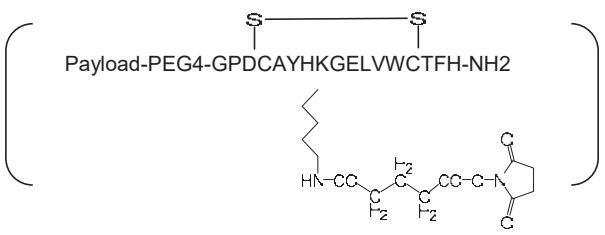

Hunan IgG-Fc and IgG-BP complex

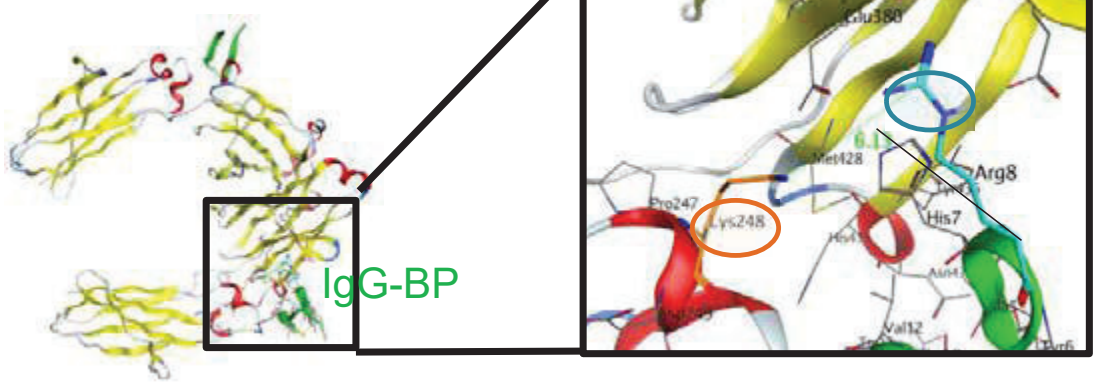

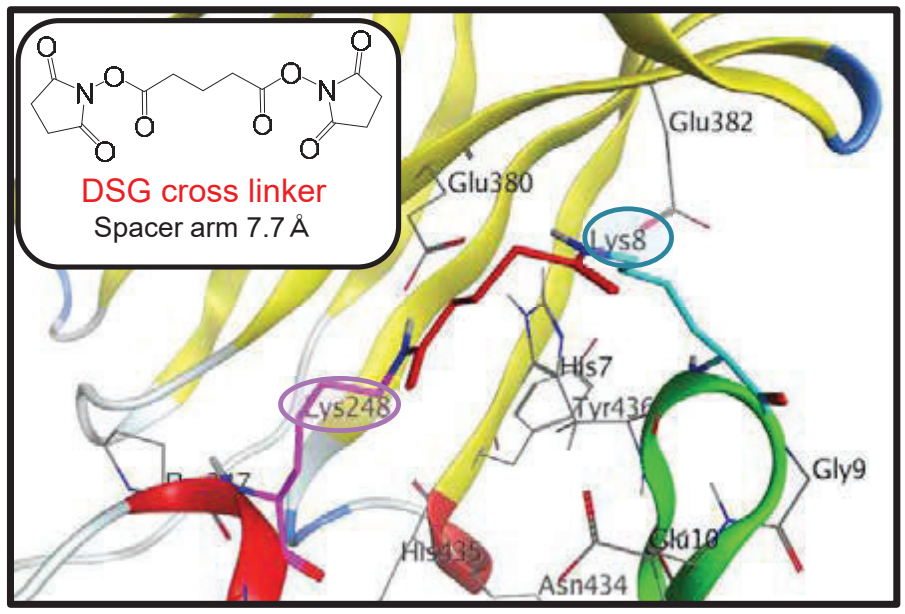

Various ADC prepared by CCAP

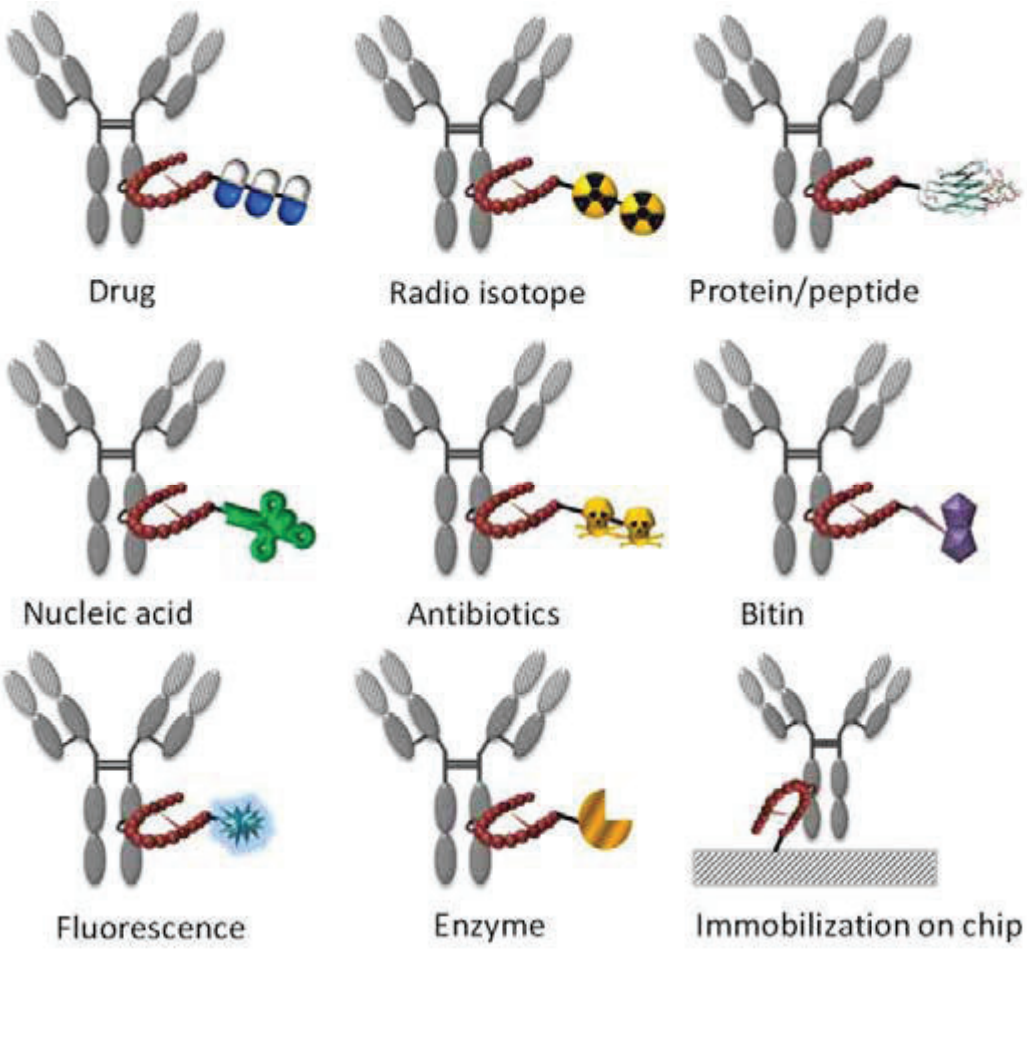

Serum half-life and Fc receptor binding ability of CCAP conjugates



[Dose] 5 mg/kg, I.V.
[Animal] Slc: ICR male, 5 weeks old
[Sampling] 1, 4, 24 h, 2, 3 and 7 d

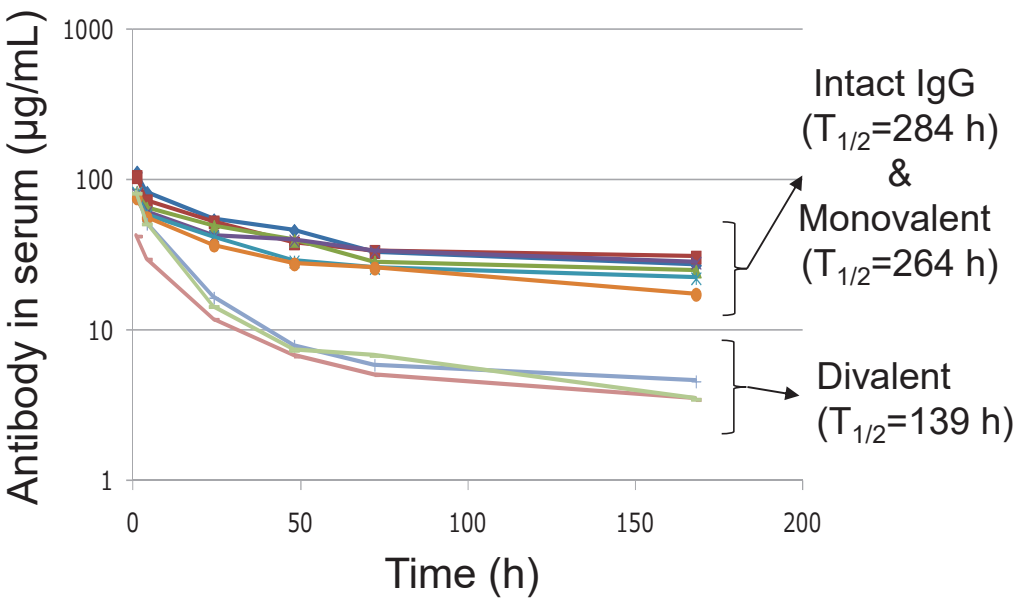

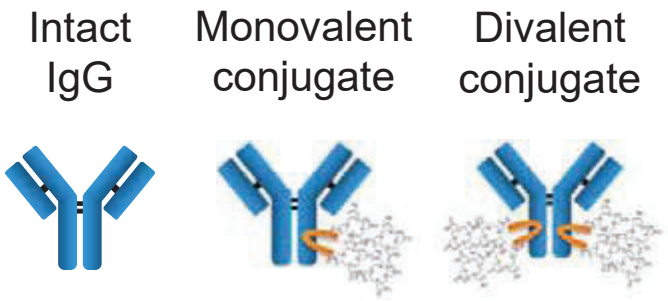

	Trastuzumab (Intact IgG)	Monovalent	Divalent
FcRn	ka=1.2 × 10^6 (/Ms) kd=4.0 × 10^{-2} (/s) K_D=36 nM	ka=5.6 × 10^5 (/Ms) kd=3.3 × 10^{-2} (/s) K_D=59 nM	No binding
FcγR Ⅰ	ka=2.3 × 10^5 (/Ms) kd=5.7 × 10^{-3} (/s) K_D=24 nM	ka=3.1 × 10^5 (/Ms) kd=5.4 × 10^{-3} (/s) K_D=17 nM	ka=2.9 × 10^5 (/Ms) kd=4.8 × 10^{-3} (/s) K_D=16 nM
FcγR Ⅲ A	ka=9.4 × 10^4 (/Ms) kd=1.5 × 10^{-2} (/s) K_D=160 nM	ka=8.2 × 10^4 (/Ms) kd=8.4 × 10^{-3} (/s) K_D=100 nM	ka=1.1 × 10^5 (/Ms) kd=5.0 × 10^{-3} (/s) K_D=45 nM

Next-generation CCAP technology: tCAP

Z34C : CH3CO-FNMQCQRRFYEALHDPNLNEEQRNAKIKSIRDDC-NH2

CCAP→ αZ34C : DSG-FNMQCQRRFYEALHDPNLNEEQRNARIRSIRDDC-NH2

tCAP→ αZ34C : Cargo-MeNbz-Gaba-NMQCQRRFYEALHDPNLNEEQRNARIRSIRDDC-NH2

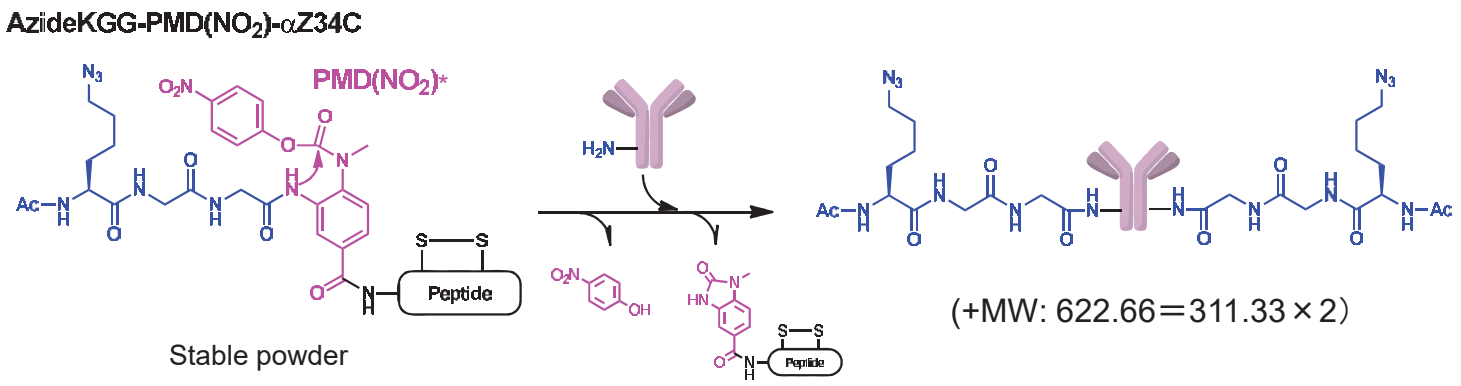

* Phenoxycarbonylated *N*-methyl-diaminobenzene (PMD):

1) Pala-Pujadas, J. et al., *Angew.Chem.Int.Ed.*, **57**,16120 (2018);
2) Tsuda, S. et al., *Chem.Commun.*, **54**, 8861 (2018).

Next-generation CCAP technology: tCAP

	Z34C :	CH3CO-FNMQCQRRFYEALHDPNLNEEQRNAKIKSIRDDC-NH2
CCAP→	αZ34C :	DSG-FNMQCQRRFYEALHDPNLNEEQRNARIRSIRDDC-NH2
tCAP→	αZ34C :	Cargo-MeNbz-Gaba-NMQCQRRFYEALHDPNLNEEQRNARIRSIRDDC-NH2

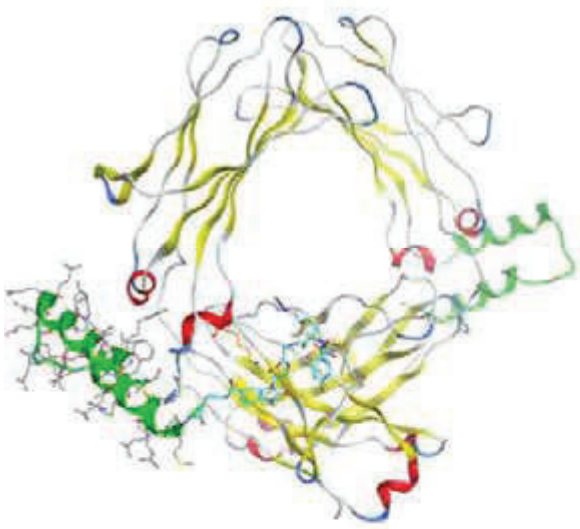

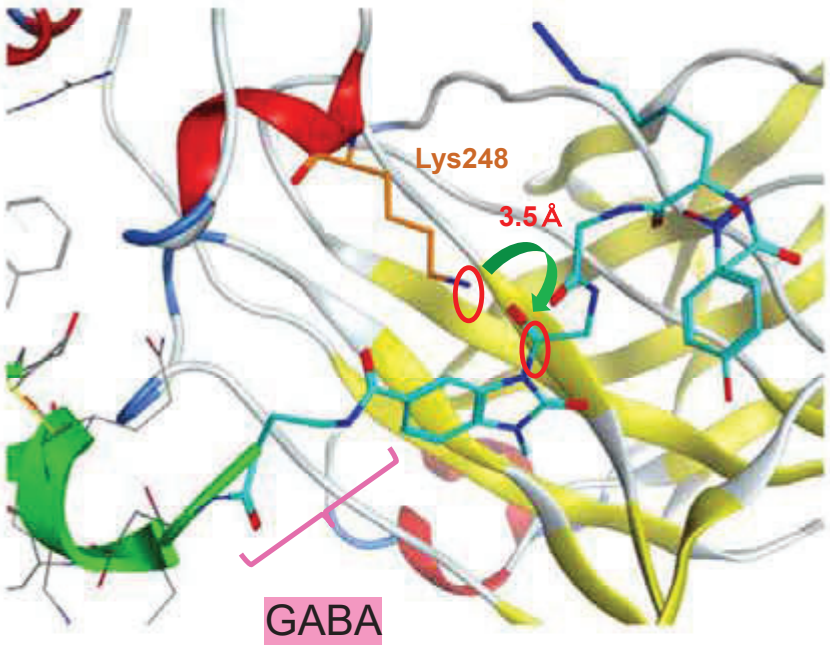

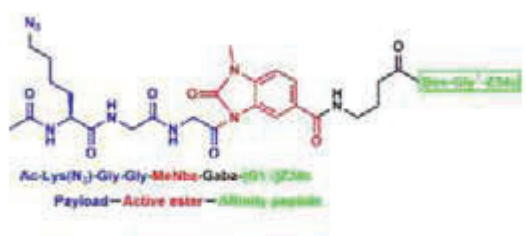

pH dependent reaction of tCAP reagent with human IgG1

Analytical method:

Antibody (15.6 μM) + 5 folds excess reagent
→At different pH and R.T. for 2 h →LC-MS

LC (RP-HPLC):

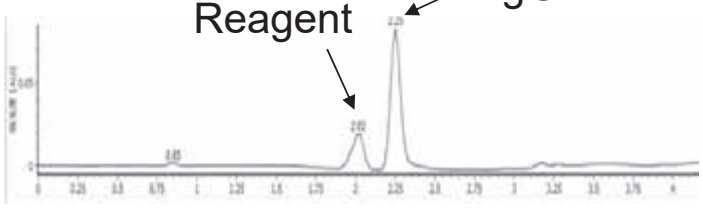

Intact IgG

Monovalent

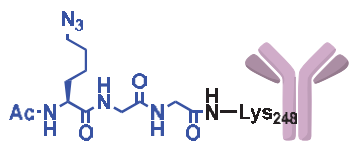

Divalent

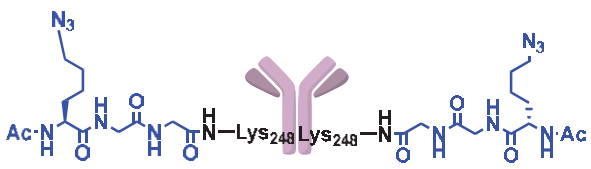

MS of IgG:

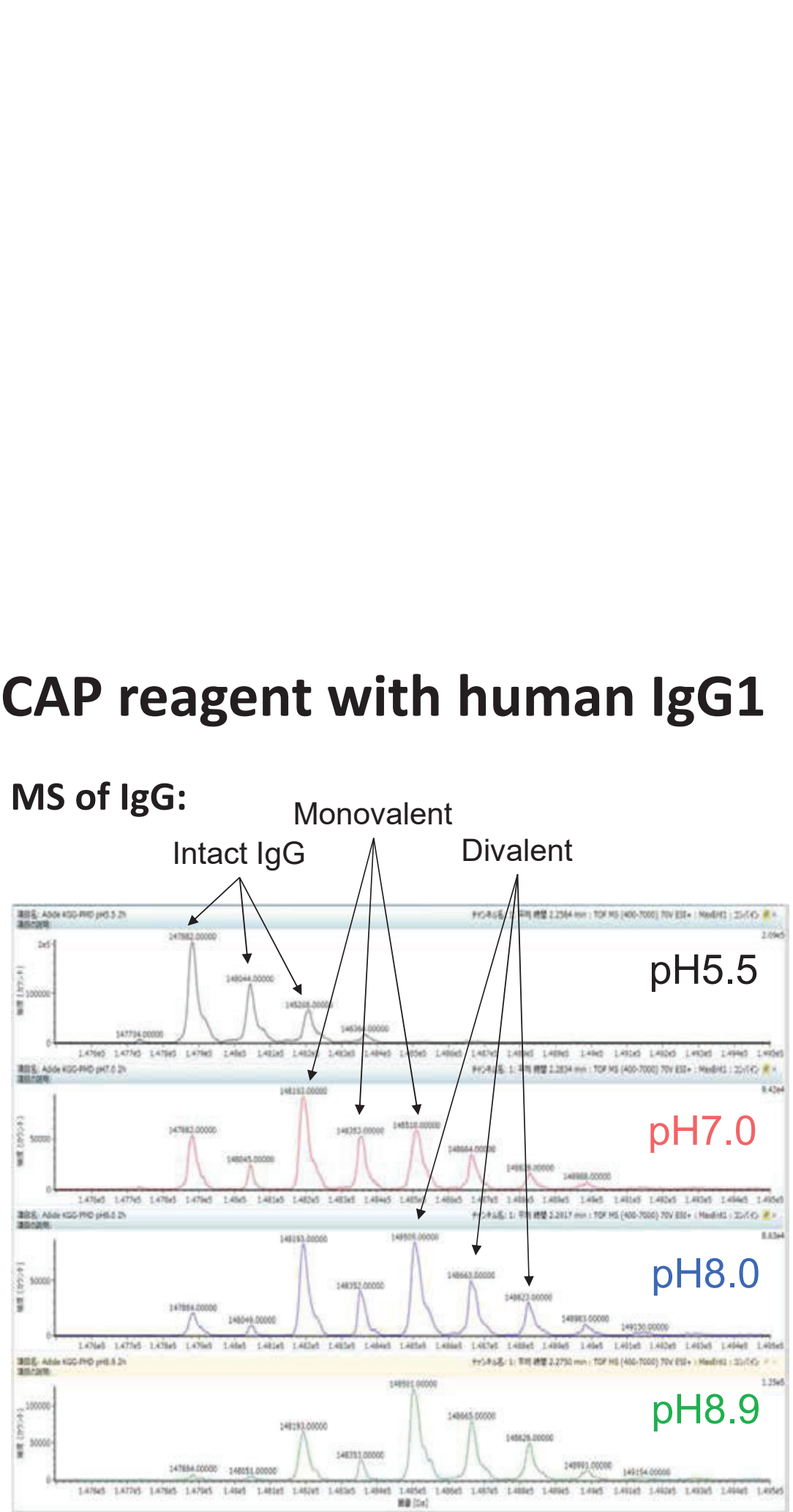

Kinetic binding of tCAP-modified IgG (Trastuzumab) for FcγR and FcRn on BIAcore

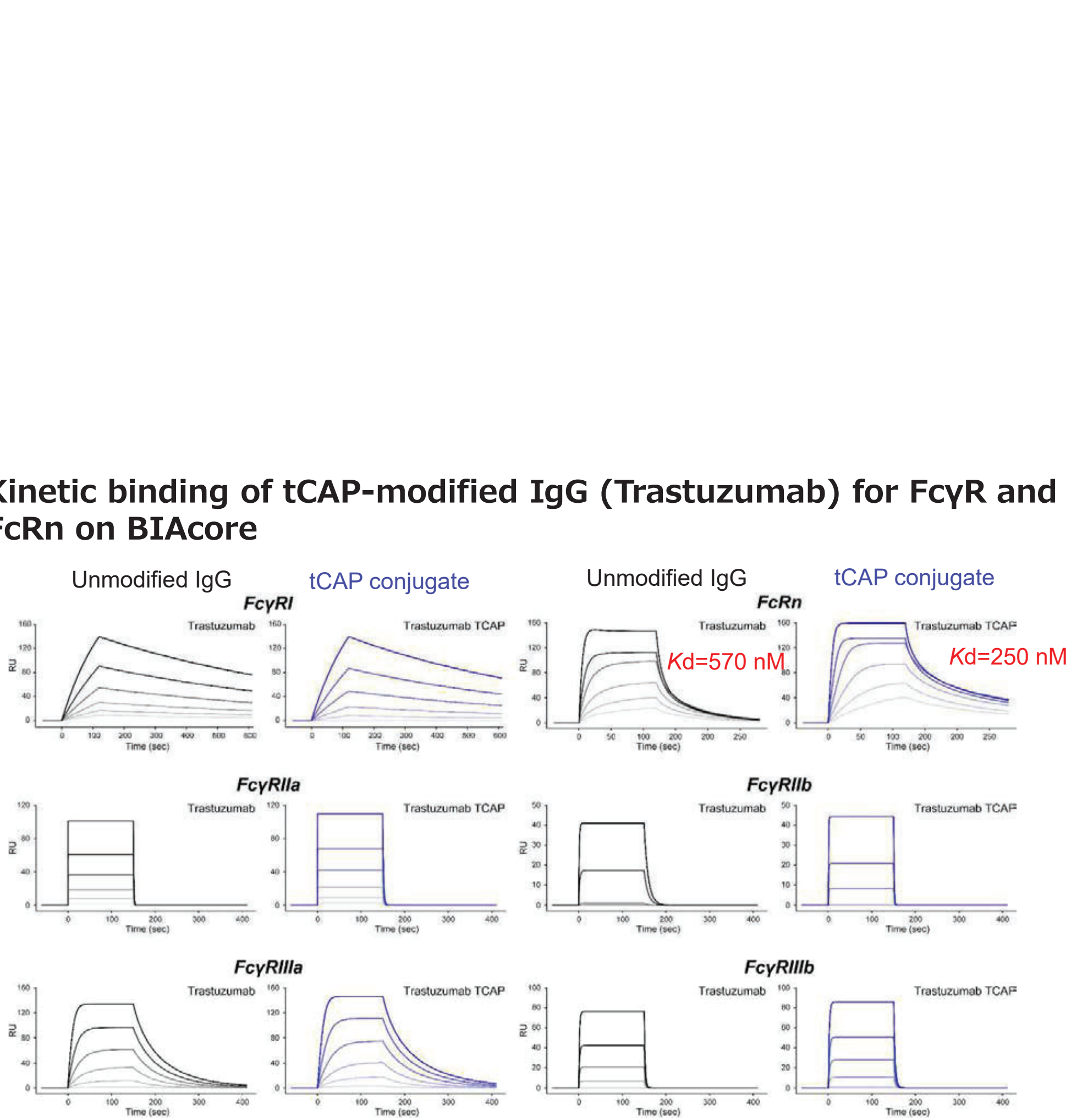

Preparation of Bispecific antibody and AOC by t-CAP

(A) Preparation of conjugate by t-CAP

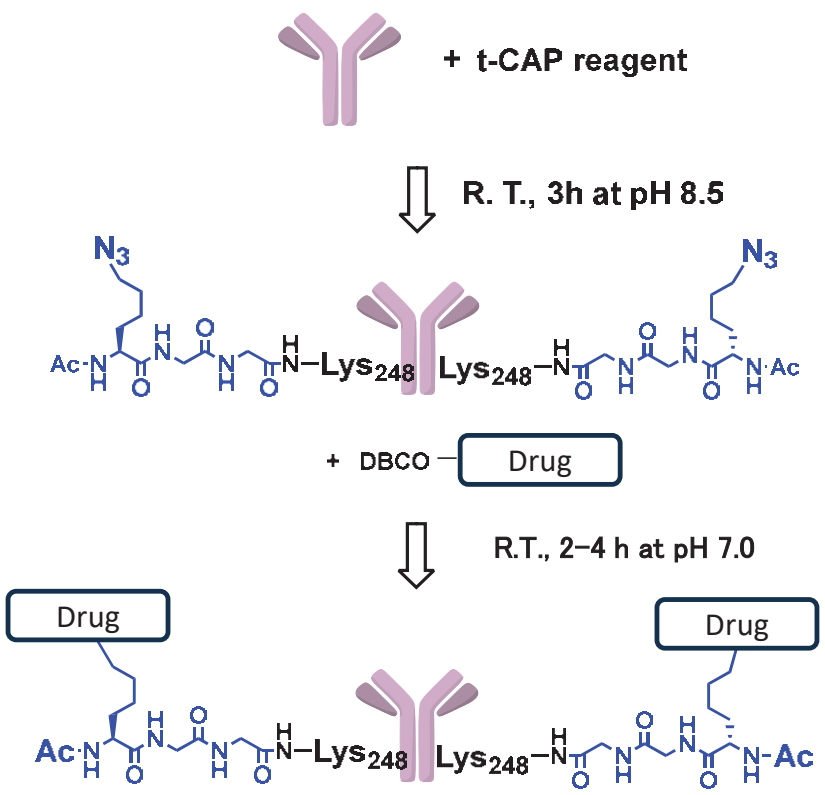

(B) Bispecific antibody (IgG + VHH)

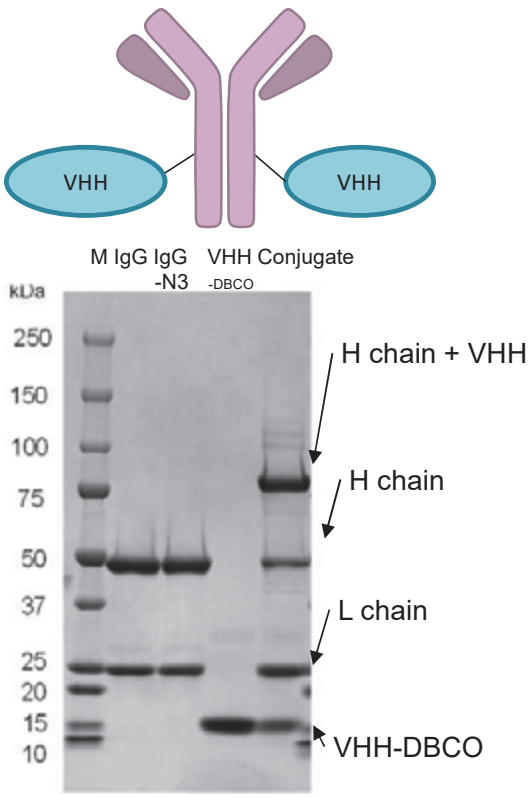

(C) Antibody oligonucleotide conjugate (AOC) (VHH-Fc + oligonucleotide)

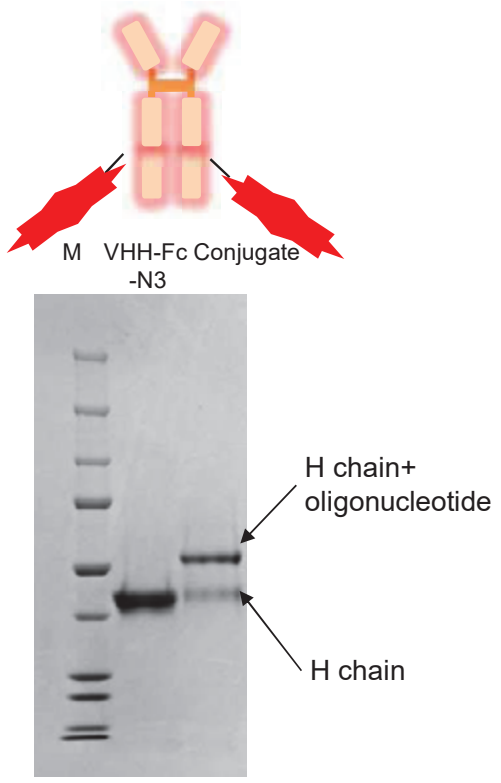

LC-MS analysis of ASO antibody conjugates by tCAP

Attachment of an azide group to 4D5 scFv-Fc by tCAP

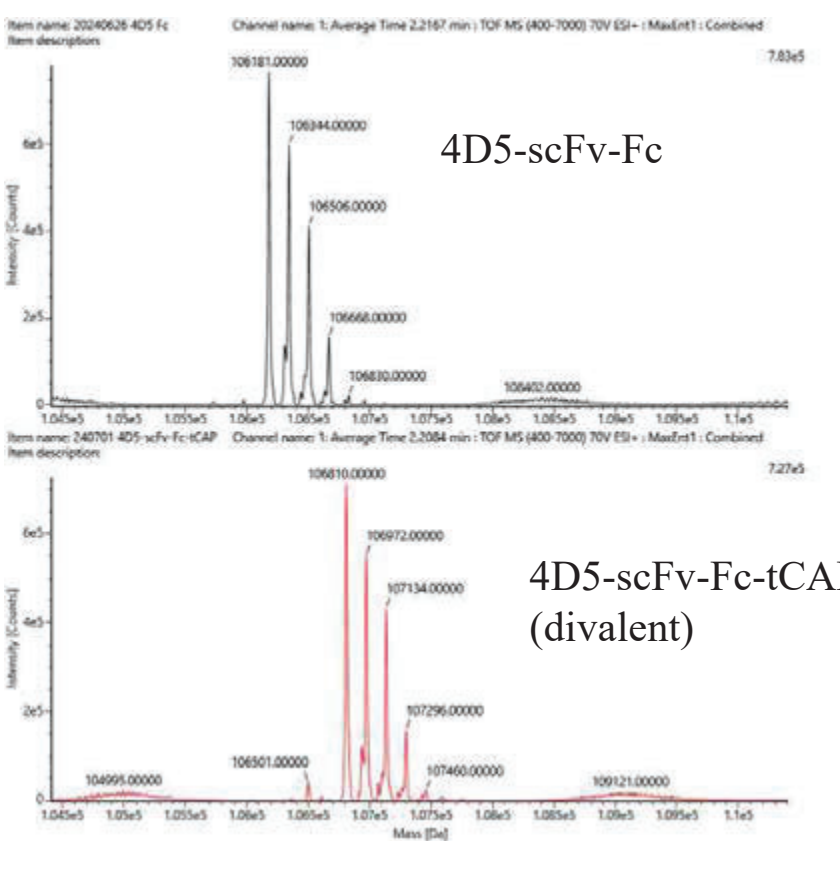

Introduction of oligonucleotide into scFv-Fc antibody by click reaction

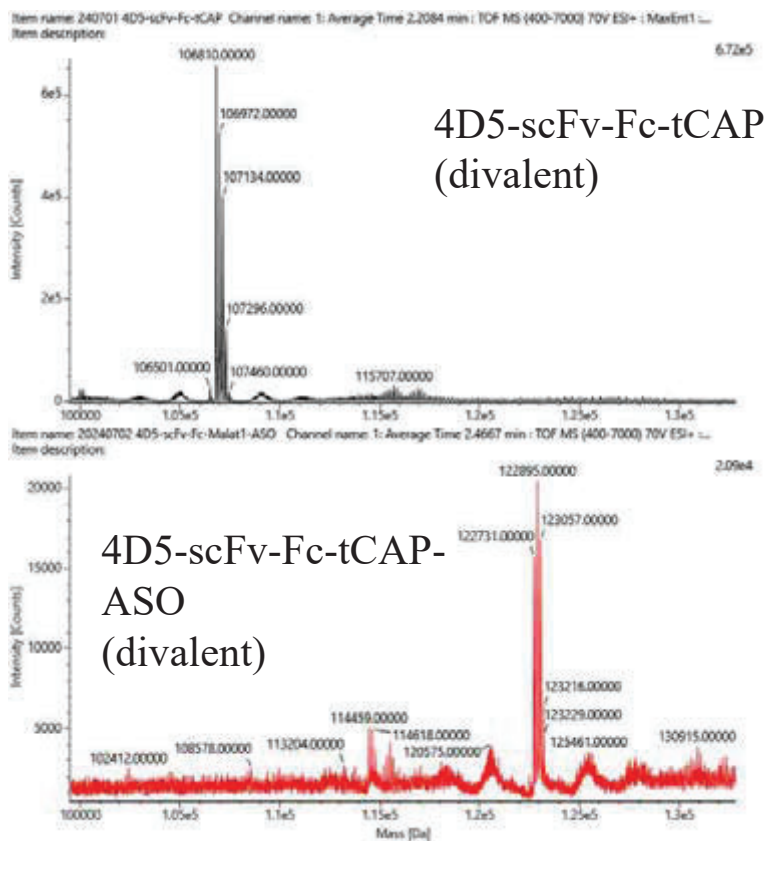

FcRn binding of tCAP conjugates with payloads

FnRn binding evaluation by FnRn- immobilized column*

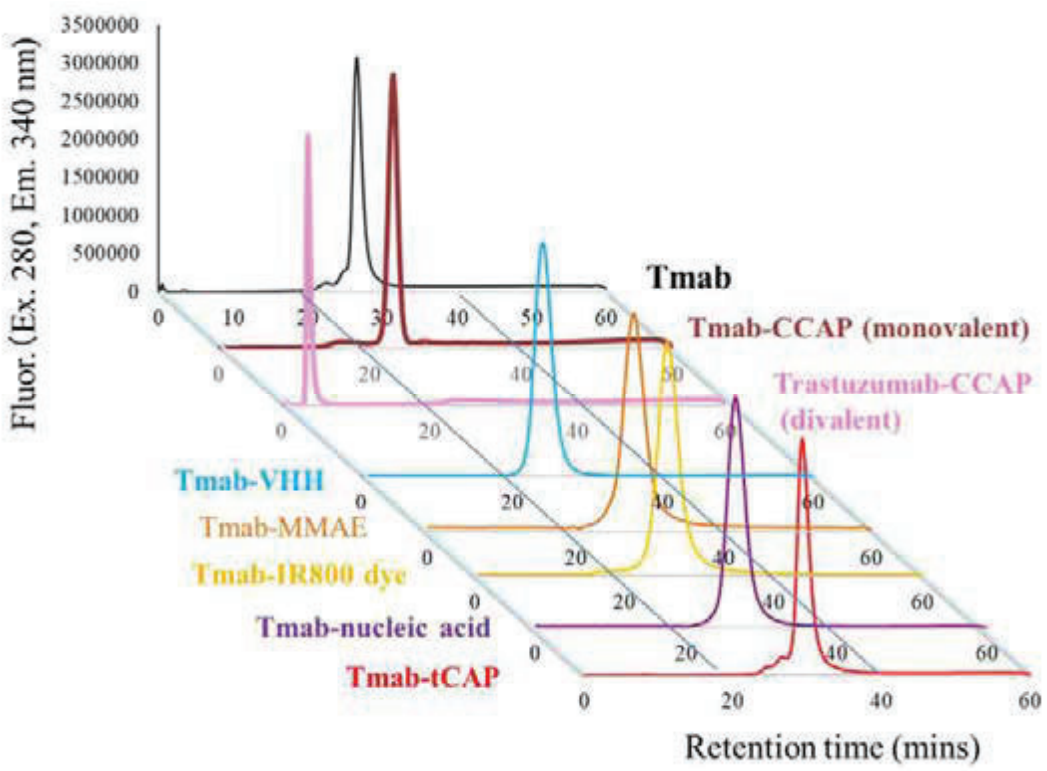

*Bindings with FnRn was evaluated using an FnRn-immobilized column (β version) from Tosoh Corp.

Development of Tissue-Specific Migrating Antibody, AccumBody and Its Application to Next-Generation antibody drug

Drug

Tissue-Specific Migrating Antibody 『AccumBody』

Next-Generation antibody drug

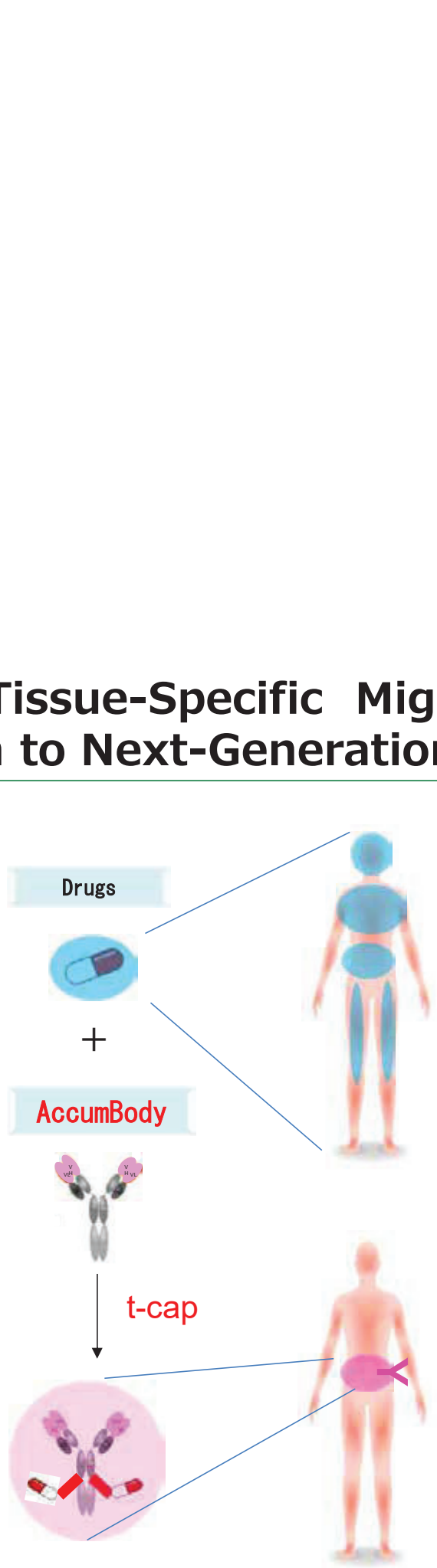

Distributed in whole body

Novel drug candidates for unmet medical needs

C.N. : multiple sclerosis
Muscle : muscular dystrophy
Bowel : IBD

Distributed in target tissue only

- High therapeutic efficacy with small side effects

Collaborators
Professor Y. Kazuki (Tottori Univ.)
Professor K. Tomizuka (Tokyo Phar. Univ.)

Isolation of AcuumBody® by antibody phage library

Immunization with tissue, or protein antigens

In vitro and/or *in vivo* panning

Identification of antibodies by NGS analysis

Fully human antibody-producing TC animals

Alpaca

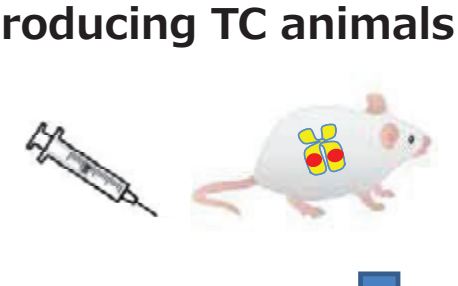

Construction of antibody phage library

Cells

Mice

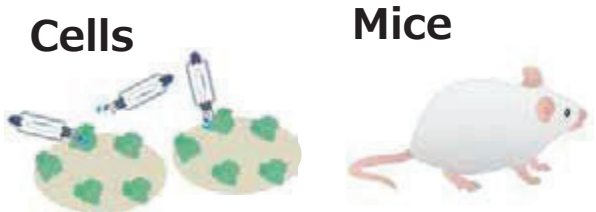

Panning

Recovery

Proliferation of phages

The enriched phages

NGS analysis of H chain

(Illumina Miseq)



Phylogenetic tree analysis on SOPRA program



Identification of specific antibody sequences

Tissue specific targeting AccumBody®

AcuumBody®-Bowel (Anti GPA33 antibody)

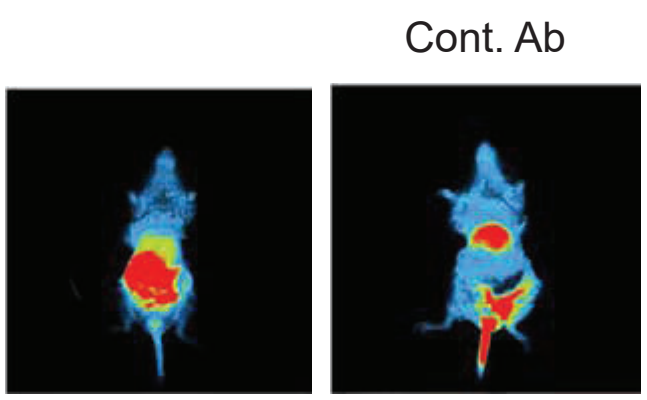

After tail vein administration to Balb/c mice at 5 mg/kg, the mice were perfused and opened at 24 hours for fluorescence imaging.

AccumBody®-Muscle

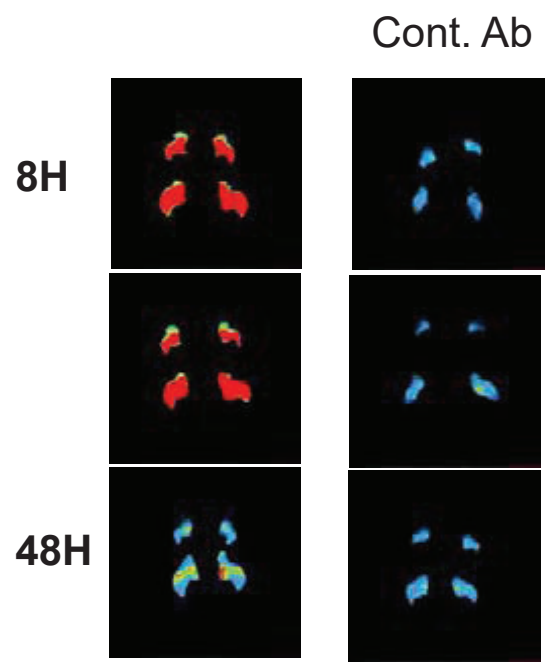

Balb/c mice were perfused at each time after i. v. injection at 5 mg/kg and the muscles of the upper and lower limbs were subjected to fluorescence imaging.

Summary

1. tCAP, a site-specific modification method using antibody Fc-affinity peptides was developed. This method is a useful modification method for the preparation of ADCs, because it does not affect the antigen binding and Fc function including Fc receptor bindings.

2. AccumBodies that target antigens specifically expressed in the brain, bowel and muscle were developed. AccumBodies can deliver the drug to diseased tissues and are useful as DDS tools for highly effective therapeutics.

3. For AccumBody-bowel and -muscle, the technology to promote cellular uptake are necessary to develop. A common issue for the future is the development of cleavable linkers for ADCs.

https://doi.org/10.17952/37EPS.2024.YIF02

Nathan PICOIS

Supervisors : Pr T. Brigaud, Pr G. Chaume et Dr P. Milbeo

***BioCIS** laboratory (UMR CNRS 8076) - Pr T. Brigaud*

Bimodal Use of Chiral α-Trifluoromethylalanine in Aib Foldamers: Study of the Position Impact Towards the Helical Screw-Sense Preference

Young Investigators Mini Symposium flash communications – *29th August 2024*

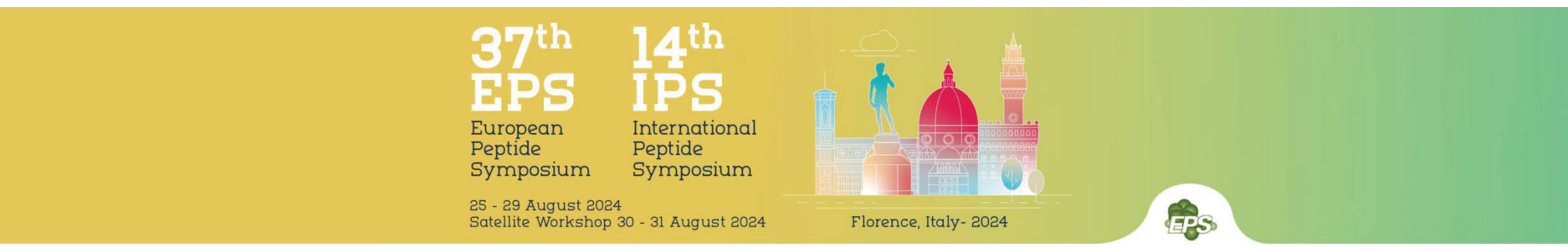

Context and results of the first study

α-Aminoisobutyric acid (Aib) oligomers

- Formation of stable right- (***P***) or left-handed (***M***) $\mathbf{3_{10}}$ helices

Nature **2022**, *607*, 387-392.

J. Org. Chem. **2014**, *79*, 10, 4659–4675.

The chiral inducer promotes a screw-sense preference

X These systems need independently a **chiral inducer** along with an NMR **reporter**

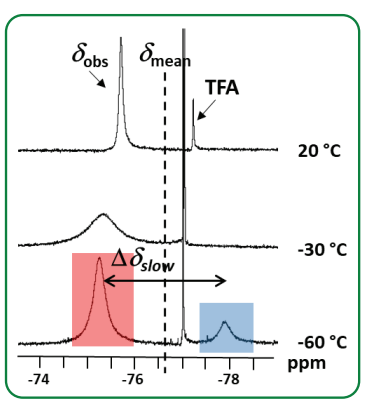

h.e. by **^{19}F NMR** fits with results obtained through **^{1}H** NMR **reporter**

✓ **α-TfmAla** as a **chiral inducer** and **^{19}F** NMR **reporter**

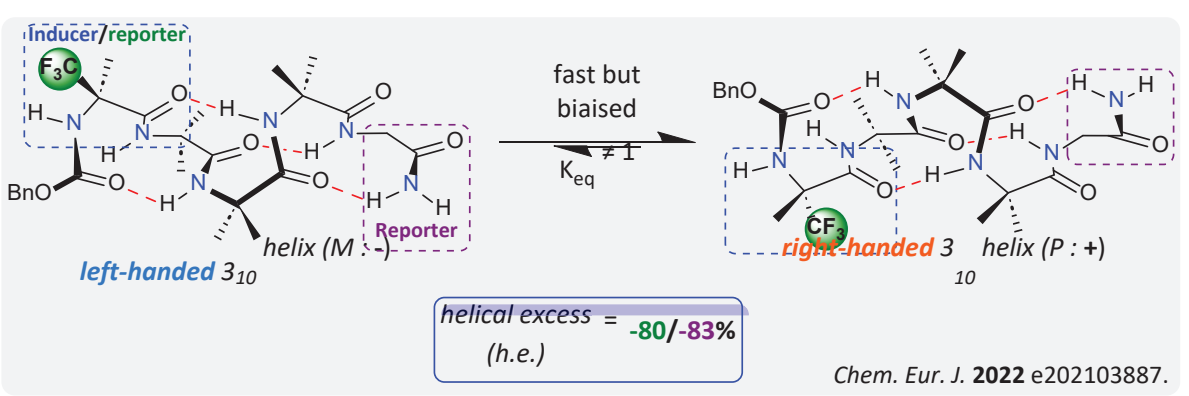

Chem. Eur. J. **2022** e202103887.

Bimodal use of α-TfmAla : study of the position impact

R -CF3 or Me

AA = Aib or α-TfmAla

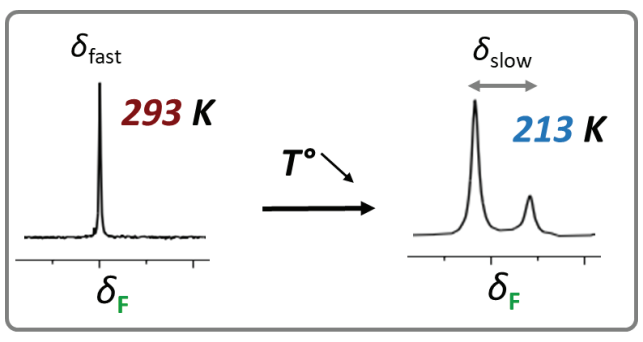

^{19}F NMR allows **helical excess determination at low T°**

CD allows **screw-sense preference determination**

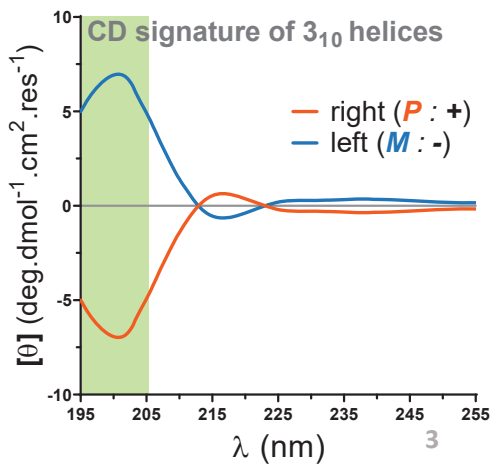

Chem. Eur. J. **2024**, *30*, e202400540.

Helical screw-sense inversion : dipole alignment of the $-CF_3$ group

Chem. Commun. **2014**, *50*, 7949-7952

- Stereo-electronic effect of **-CF_3** group seems to be the principal contribution
- Dipole alignment observed in the solid state
- ✓ Versatility of **α-TfmAla** residue to induce and determine helical excess in Aib oligomers

Want to learn more ?

Proceedings of the 37th European Peptide Symposium
Michal Lebl, Editor
European Peptide Society, 2024 http://doi.org/10.17952/37EPS.2024.YIF09

Designed cyclic peptides as inhibitors of amyloid self-assembly and cross-seeding of amyloid-beta peptide and islet amyloid polypeptide

Beatrice Dalla Volta[1], Melanie Roth[1], Yuan Tian[2], Alessia Calzi[1], Jürgen Bernhagen[2], and Aphrodite Kapurniotu[1]

[1]Division of Peptide Biochemistry, TUM School of Life Sciences, Technical University of Munich (TUM), Freising, D-85354, Germany; [2]Division of Vascular Biology, Institute for Stroke and Dementia Research (ISD), Klinikum der Universität München, Ludwig-Maximilian-University (LMU), D-81377, Munich, Germany

Introduction

Increasing evidence suggests a link between the pathogenesis of Alzheimer's disease (AD) and type 2 diabetes (T2D). In this context, the key amyloid polypeptides of AD and T2D amyloid-β peptide (Aβ (Aβ40(or 42)) and islet amyloid polypeptide (IAPP) have been reported to co-localise in brain or pancreas of AD and T2D patients [1,2]. In addition, IAPP or Aβ fibrils were found to act as cross-seeds of the amyloid self-assembly of the two polypeptides [3,4]. Therefore, molecules that inhibit amyloid self-assembly and cross-seeding of IAPP and Aβ may offer promising leads for anti-amyloid drugs in both diseases.

Our earlier studies revealed high affinity interactions between Aβ and IAPP and were consistent with cross-interactions and amyloid self-assembly being mediated by the same "hot segments" [5,6]. We used the identified IAPP "hot segments" to design peptides as inhibitors of amyloid self-assembly of IAPP, Aβ, or both polypeptides [7,8]. Our more recently developed IAPP-derived amyloid inhibitors were the 17-residue long macrocyclic peptides termed "macrocyclic inhibitory peptides" or MCIPs [8]. The lead MCIP **2e** turned out to be a nanomolar inhibitor of Aβ amyloid self-assembly and in addition it exhibited a good proteolytic stability in human plasma *in vitro* and blood-brain barrier (BBB) crossing in a cell model. However, **2e** was unable to inhibit IAPP amyloid self-assembly. The aim of the work presented here was to design novel cyclic peptides with optimized properties and functions.

Results and Discussion

Systematic MCIP shortening and optimisation yielded a new class of cyclic peptides. Peptides were synthesized by Fmoc-based solid phase peptide synthesis (SPPS) methodology. We used the amyloid specific thioflavin T (ThT) binding assay in combination with transmission electron microscopy (TEM) to study their effects on fibril formation of IAPP or Aβ42. To determine their effects on formation of cytotoxic assemblies, we used the MTT reduction assay in cultured RIN5fm for IAPP-related studies or cultured PC12 cells for Aβ42-related studies. According to the ThT binding assay and TEM, in the presence of the cyclic peptides IAPP fibril formation was fully suppressed. In addition, the cell viability assay showed that formation of cytotoxic IAPP aggregates was fully suppressed as well. Furthermore, the cyclic peptides suppressed Aβ42 amyloid self-assembly while the lead cyclic peptide suppressed IAPP/Aβ42 cross-seeding as well. Thus, the cyclic peptides of our study might be promising candidates for drugs targeting pathogenic amyloid self-assembly in both AD and T2D and studies toward their further development are in progress.

Acknowledgements

This work was supported by Deutsche Forschungsgemeinschaft (DFG) grant SFB1035 B06 to AK (part of SFB1035, project number 201302640) and by DFG under Germany's Excellence Strategy within the framework of the Munich Cluster for Systems Neurology EXC 2145 SyNergy-ID 390857198 to JB. We thank K. Hille and J. Jekel for help with peptide synthesis and purification.

References

1. Jackson, K., et al. *Ann. Neurol.* **74**, 517-26 (2013), https://doi.org/10.1002/ana.23956
2. Martinez-Valbuena, I., et al. *Ann. Neurol.* **86**, 539-551 (2019), https://doi.org/10.1002/ana.25570
3. O'Nuallain, B., et al. *J Biol Chem* **279**, 17490-17499 (2004), https://doi.org/10.1074/jbc.M311300200
4. Moreno-Gonzalez, I., et al. *Mol Psychiatry* **22**, 1327-1334 (2017), https://doi.org/10.1038/mp.2016.230
5. Yan, L.M., et al. *Angew Chem Int Ed Engl* **46**, 1246-1252 (2007), https://doi:10.1002/anie.200604056
6. Andreetto, E., et al. *Angew Chem Int Ed Engl* **49**, 3081-3085 (2010), https://doi.org/10.1002/anie.200904902
7. Andreetto, E., et al. *Angew Chem Int Ed Engl* **54**, 13095-1310 (2015), https://doi.org/10.1002/anie.201504973
8. Spanopoulou, A., et al. *Angew Chem Int Ed Engl* **57**, 14503-14508 (2018), https://doi.org/10.1002/anie.201802979

https://doi.org/10.17952/37EPS.2024.YIF13

Targeting West Nile virus replicases: NS3 and heterodimers inhibitors

PhD student: **Daniele Volpin** [a]

Cristina Peggion [a] (supervisor), Riccardo Rigo [b] (co-supervisor), Mattia Sturlese [b]

[a] Department of Chemical Sciences, University of Padova, 35131, Padova, Italy
[b] Department of Pharmaceutical and Pharmacological Sciences, University of Padova, 35131, Padova, Italy

INTRODUCTION and AIM OF THE PROJECT

The **West Nile virus** (**WNV**) is a flavivirus of the Flaviviridae family. It circulates through a mosquito–bird–mosquito cycle and it is transmitted to humans through Culex mosquitoes. ⟶ Urgency for the **development of new WNV antiviral compounds**.

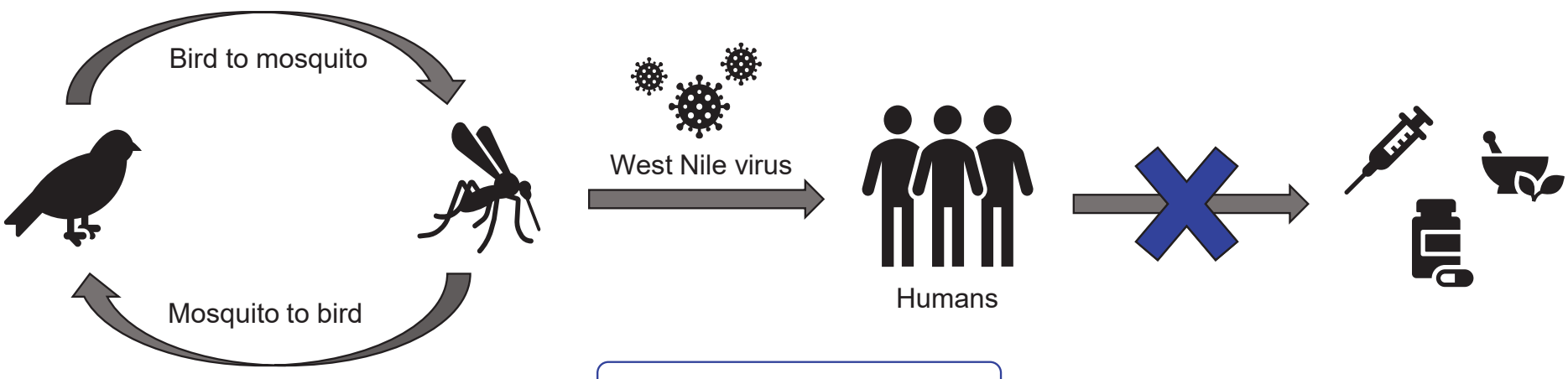

AIM OF THE PROJECT

A **direct approach** targeting the **active site of NS2B-NS3 protease.**

↓

Peptides/peptidomimetics as potential inhibitors.

An **indirect approach** targeting protein-protein interactions essential for NS3 activity.

↓

Peptides to disfavour NS2B-NS3 heterodimer.

Tri and tetra-peptide inhibitors

Several peptides and peptidomimetics were synthesized as possible NS2B-NS3 inhibitors of WNV, tested and their IC_{50} value was evaluated.

Peptide name	Interaction	MW (g/mol)	Purity	IC_{50} (μM)
Nona-D-Arginine	NON – COVALENT	1422.73	87%	20.70 ± 3.60
PhAc-Lys-Lys-Arg-NH_2		547.71	97%	130.4 ± 8.3
Aun-Lys-Lys-Arg-NH_2		612.86	96%	34.43 ± 3.65
Palm-Lys-Lys-Arg-NH_2		667.99	95%	29.43 ± 3.81
PhAc-Lys-Lys-Arg-(cyclic-dehydro)		514.67	96%	**8.33** ± 0.33
Aun-Lys-Lys-Arg-(cyclic-dehydro)		579.83	98%	**8.34** ± 0.78
Palm-Lys-Lys-Arg-(cyclic-dehydro)		634.95	97%	**10.34** ± 1.71
PhAc-Lys-Lys-Arg-H	COVALENT	532.69	95%	**3.14** ± 0.19
Aun-Lys-Lys-Arg-H		597.85	97%	**7.05** ± 0.97

NS2B-NS3 ACTIVE SITE INHIBITORS

Tri and tetra-peptide inhibitors

Several peptides and peptidomimetics were synthesized as possible NS2B-NS3 inhibitors of WNV, tested and their IC_{50} value was evaluated.

Peptide name	Interaction	MW (g/mol)	Purity	IC_{50} (μM)
Nona-D-Arginine	NON – COVALENT	1422.73	87%	20.70 ± 3.60
PhAc-Lys-Lys-Arg-NH_2		547.71	97%	130.4 ± 8.3
Aun-Lys-Lys-Arg-NH_2		612.86	96%	34.43 ± 3.65
Palm-Lys-Lys-Arg-NH_2		667.99	95%	29.43 ± 3.81
PhAc-Lys-Lys-Arg-(cyclic-dehydro)		514.67	96%	**8.33** ± 0.33
Aun-Lys-Lys-Arg-(cyclic-dehydro)		579.83	98%	**8.34** ± 0.78
Palm-Lys-Lys-Arg-(cyclic-dehydro)		634.95	97%	**10.34** ± 1.71
PhAc-Lys-Lys-Arg-H	COVALENT	532.69	95%	**3.14** ± 0.19
Aun-Lys-Lys-Arg-H		597.85	97%	**7.05** ± 0.97

Cyclic peptide inhibitor

Cyclization of the tripeptides to increase the inhibitory efficacy and to disfavor their degradation.

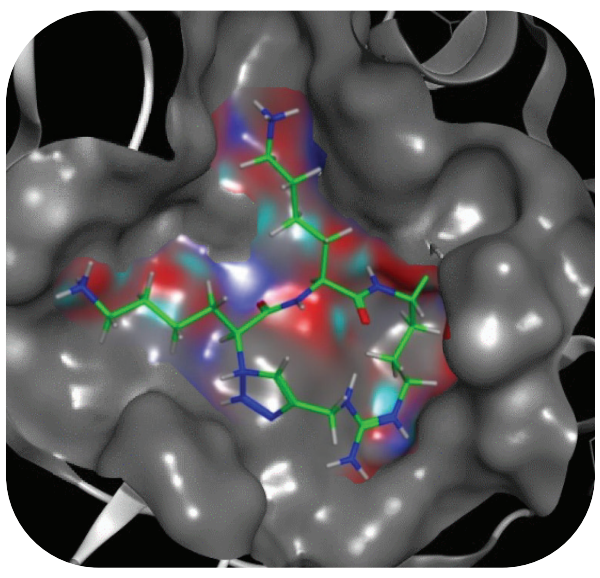

Superimposition of cyclic tripeptide on the active site pocket of NS2B-NS3 protease of WNV.

NS2B-NS3 ACTIVE SITE INHIBITORS

Tri and tetra-peptide inhibitors

Several peptides and peptidomimetics were synthesized as possible NS2B-NS3 inhibitors of WNV, tested and their IC_{50} value was evaluated.

Peptide name	Interaction	MW (g/mol)	Purity	IC_{50} (μM)
Nona-D-Arginine	NON – COVALENT	1422.73	87%	20.70 ± 3.60
PhAc-Lys-Lys-Arg-NH_2		547.71	97%	130.4 ± 8.3
Aun-Lys-Lys-Arg-NH_2		612.86	96%	34.43 ± 3.65
Palm-Lys-Lys-Arg-NH_2		667.99	95%	29.43 ± 3.81
PhAc-Lys-Lys-Arg-(cyclic-dehydro)		514.67	96%	**8.33** ± 0.33
Aun-Lys-Lys-Arg-(cyclic-dehydro)		579.83	98%	**8.34** ± 0.78
Palm-Lys-Lys-Arg-(cyclic-dehydro)		634.95	97%	**10.34** ± 1.71
PhAc-Lys-Lys-Arg-H	COVALENT	532.69	95%	**3.14** ± 0.19
Aun-Lys-Lys-Arg-H		597.85	97%	**7.05** ± 0.97

Cyclic peptide inhibitor

Cyclization of the tripeptide to increase the inhibitory efficacy and to disfavor its degradation.

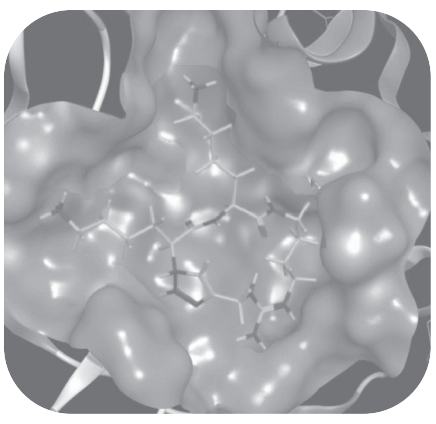

Retro-inverse peptide inhibitors

To increase the inhibitory efficacy and to disfavor its degradation.

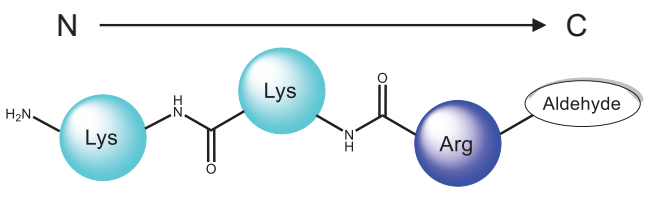

Reference peptide

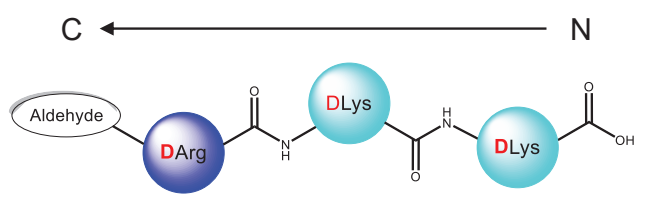

Retro-inverso peptide

NS2B-NS3 ALLOSTERIC SITE INHIBITORS

We designed **different tripeptides** that mimic the structure of an already known reversible allosteric inhibitor (SID:852843) of the formation of the functional conformation of the NS3 protease of WNV and we studied these **possible allosteric inhibitors by docking**.

- **Active tripeptide allosteric inhibitor**

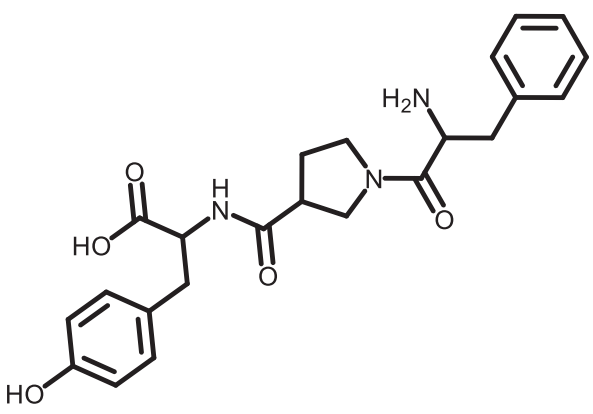

Phe-βPro-Tyr-OH

IC_{50} = **48.30** ± 11.07 μM

NS2B-NS3 ALLOSTERIC SITE INHIBITORS

We designed **different tripeptides** that mimic the structure of an already known reversible allosteric inhibitor (SID:852843) of the formation of the functional conformation of the NS3 protease of WNV and we studied these **possible allosteric inhibitors by docking**.

Active tripeptide allosteric inhibitor

Phe-βPro-Tyr-OH

IC_{50} = **48.30** ± 11.07 μM

Protein-peptides interactions by NMR studies

2D NMR BEST-TROSY spectrum of the Trp-βPro-Trp peptide, which interacts with the NS2B-NS3 protease, as evidenced by Chemical Shift Perturbations.

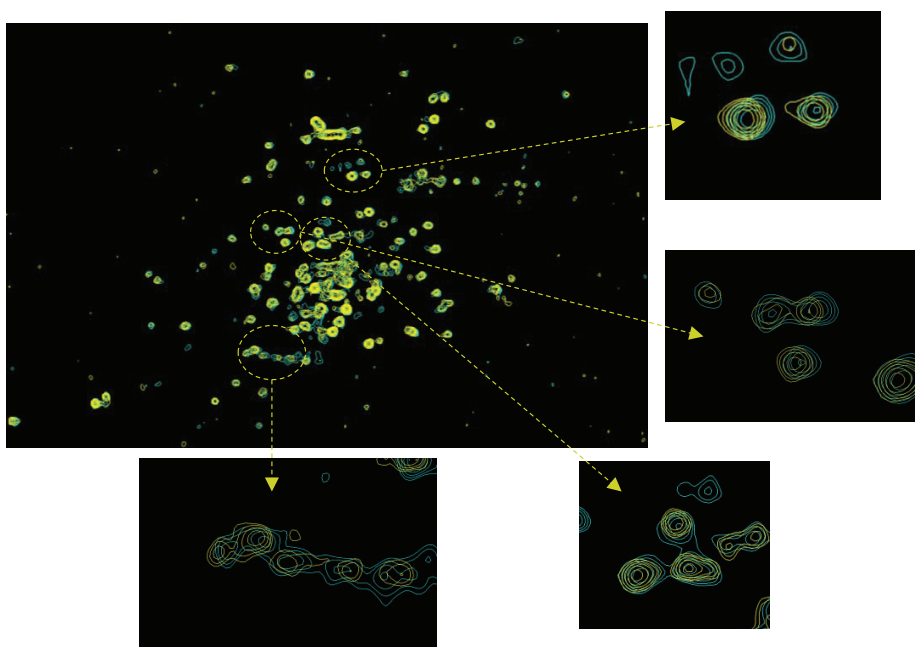

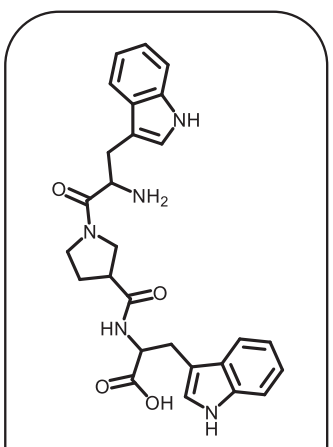

Trp-βPro-Trp-OH

AKNOWLEDGMENTS

Prof. **Cristina Peggion**: supervisor

University of Padova - Department of Pharmaceutical and Pharmacological Sciences

Dr. **Riccardo Rigo**: co-supervisor

Prof. **Mattia Sturlese**

Caterina Zulian
Thomas Stella

University of Padova - Department of Pharmaceutical and Pharmacological Sciences

Prof. Arianna Loregian
Prof. Beatrice Mercorelli

University of Cagliari - Department of life and environmental sciences

Prof. Angela Corona
Prof. Enzo Tramontano

Fondazione INF-ACT

Funded by the European Union
NextGenerationEU

https://doi.org/10.17952/37EPS.2024.YIF20

IIT GUWAHATI

Short Catalytic Peptides for Carbon Dioxide Sequestration



Young Investigators Mini Symposium Flash Communications

37th European Peptide Symposium
14th International Peptide Symposium
25th - 29th August 2024
Florence, Italy

Kalpana Kumari
Doctor of Philosophy

Molecular Informatics & Design Laboratory
Biosciences & Bioengineering
IIT Guwahati, Assam, India

Supervisor: Vibin Ramakrishnan

Motivation and Problem Statement

IIT GUWAHATI



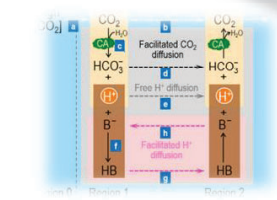

Fluid secretion

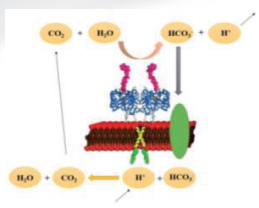

pH control



Respiration

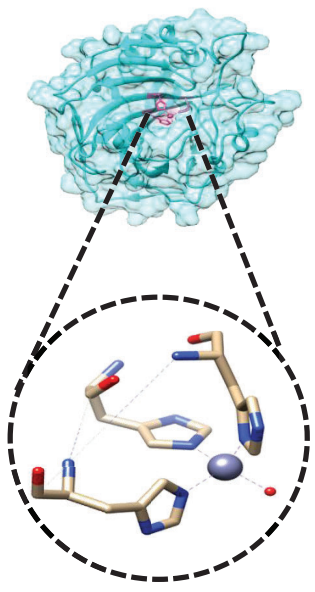

Active site of human carbonic anhydrase II (PDB ID:2CBA)

Why peptide catalyst?

1. Self-assembly
2. Inherent biological origin
3. Biocompatible & Biodegradable
4. Low immunogenicity

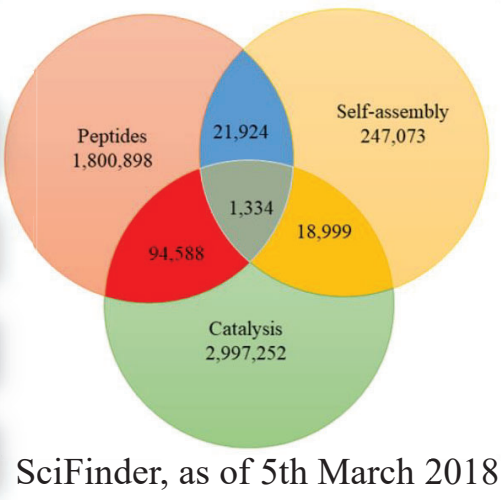

SciFinder, as of 5th March 2018

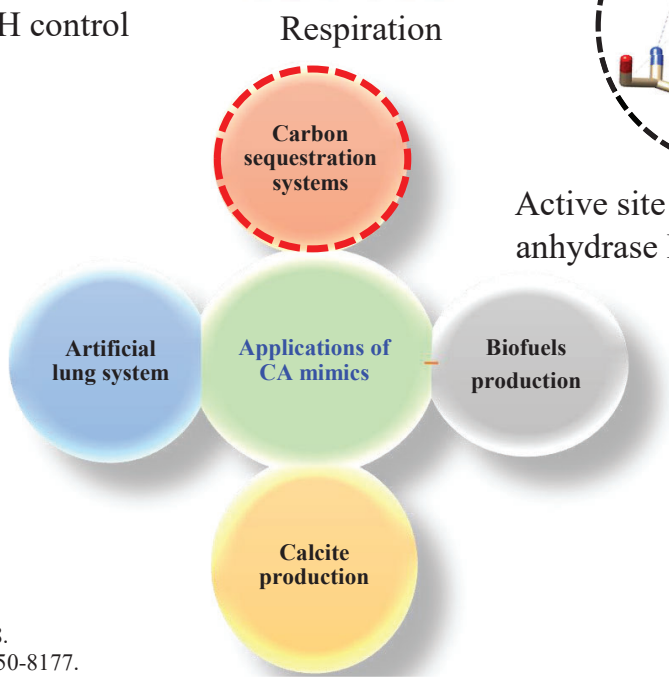

O. Zozulia, M. A. Dolan, and I. V. Korendovych, "Catalytic peptide assemblies," *Chem. Soc. Rev.*, vol. 47, no. 10, pp. 3621–3639, 2018.
Fleming, S., and Ulijn, R. V. (2014) Design of nanostructures based on aromatic peptide amphiphiles, *Chemical Society Reviews 43*, 8150-8177.

Work done on Problem

IIT GUWAHATI

Morphological Characterization of Designed Peptides by Field-Emission Scanning Electron Microscope

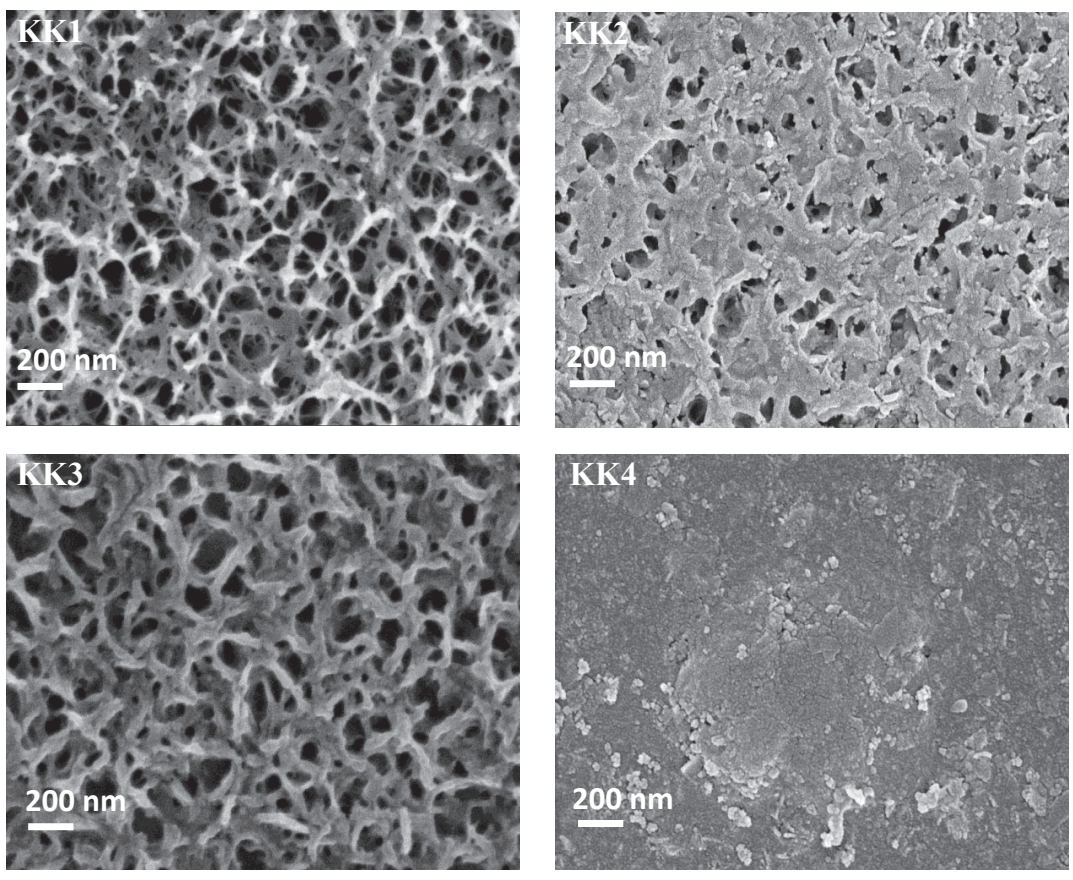

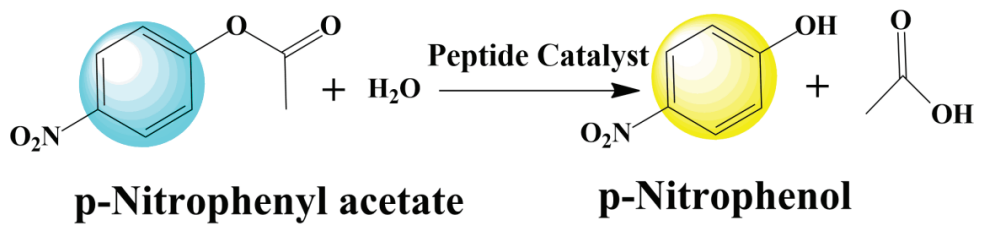

Kinetic parameters of Peptide Catalysts

Kinetic parameters	KK1	KK2	KK3	KK4
v_{max} (mM/s)	9.39×10^{-4}	0.41×10^{-4}	6.18×10^{-4}	(No activity)
K_M (mM)	0.131	0.329	0.212	-
$K_{cat} = v_{max}$/ Peptide concentration (s^{-1})	93.9×10^{-4}	4.1×10^{-4}	61.8×10^{-4}	-
Catalytic efficiency = K_{cat}/K_M ($M^{-1}s^{-1}$)	71.67	1.246	29.15	-

Patent Filed: R20243014268

Catalytic efficiency: KK1> KK3> KK2> KK4

Work done on Problem

IIT GUWAHATI

Catalytic Activity of Peptide at varying pH and Temperature

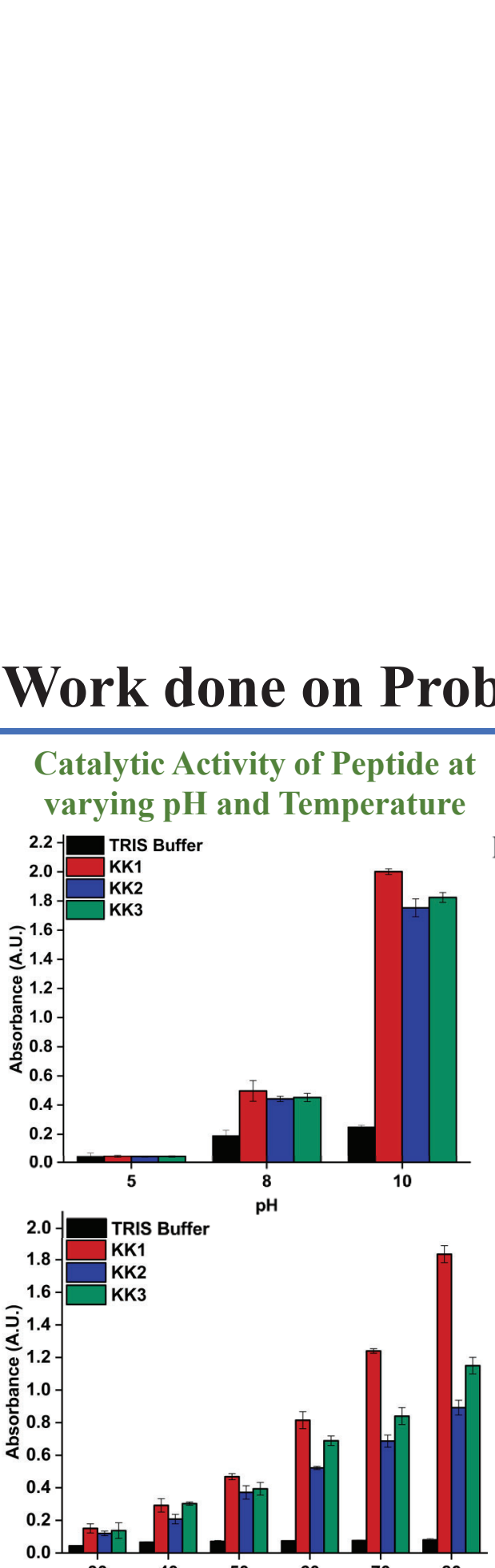

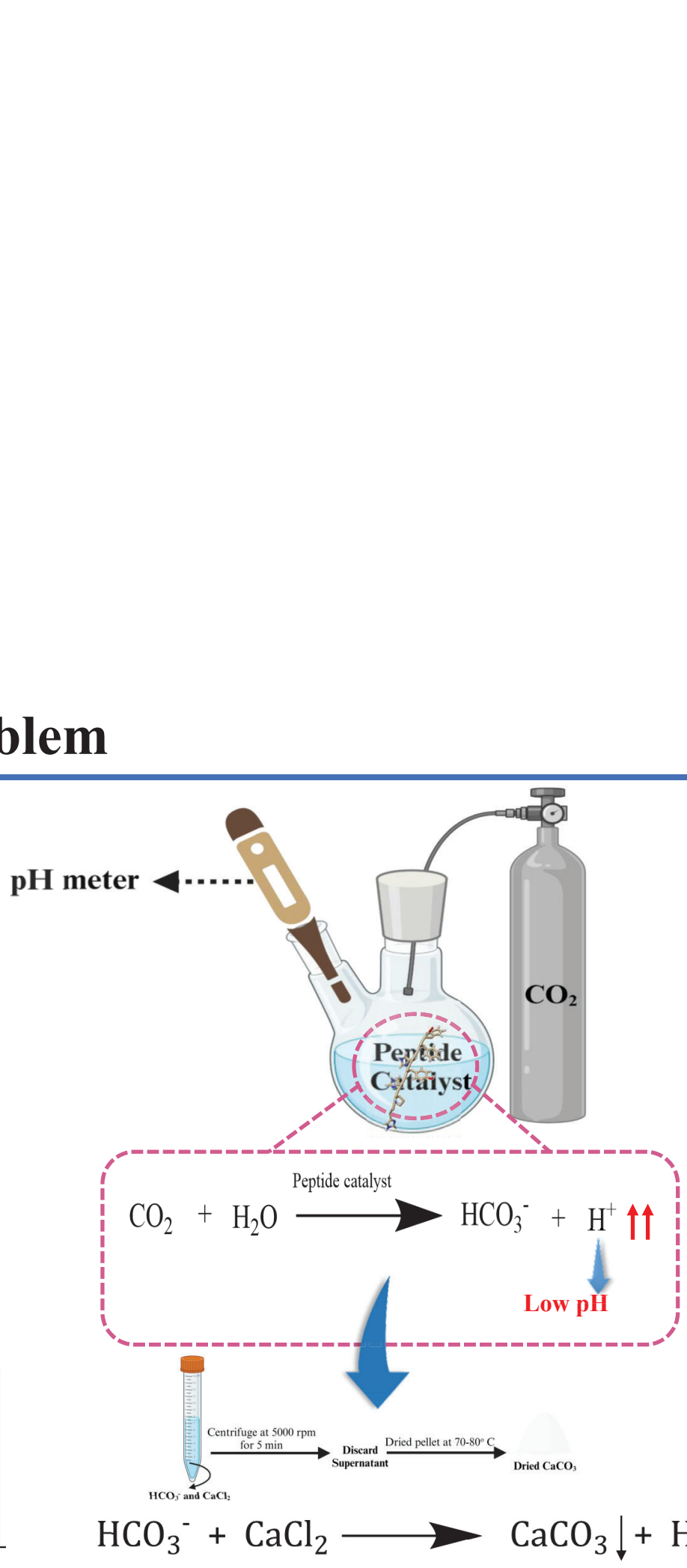

pH changes during the hydration of CO_2 Followed by Formation of $CaCO_3$ during Sequestration in the Presence of Different Catalysts

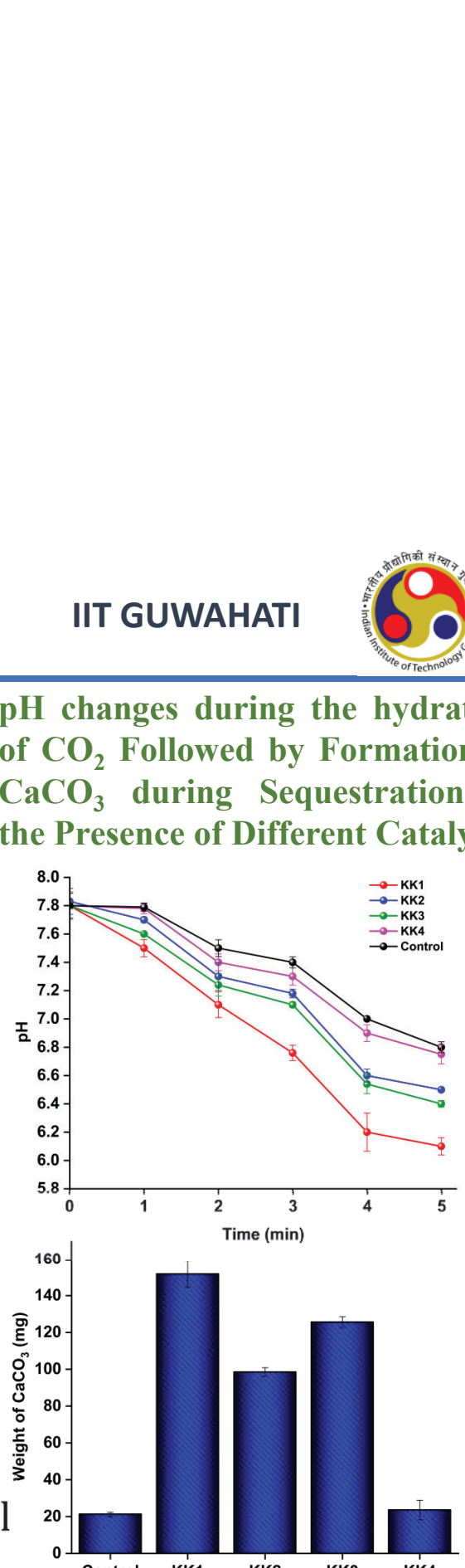

Patent Filed: R20243014268

Proceedings of the 37th European Peptide Symposium
Michal Lebl, Editor
European Peptide Society, 2024 *http://doi.org/10.17952/37EPS.2024.YIF21*

Bioactive Self-assembled Peptide Hydrogels for 3D Cancer Model Applications

Burcu Sırma Tarım, Sedef Tamburacı, Ayben Top
Izmir Institute of Technology, Department of Chemical Engineering, Izmir, Turkey

Purpose:
Investigation of the proliferation, invasion, and drug-resistance behavior of cancer cells requires the application of cancer models that mimic the tumor environment. Hydrogels, structurally similar to extracellular matrix (ECM), have been widely used in 3D cancer models [1]. Peptides with regularly alternating hydrophobic and hydrophilic amino acids and specific charge distributions can form nanoarchitectures resembling the ECM through non-covalent interactions. Furthermore, bioactive motifs such as cell adhesion units can be incorporated into the peptide sequences during the synthesis [1,2]. In this study, we designed peptide hydrogelators containing a fibronectin-binding motif, leucine-aspartic acid-valine (LDV) for 3D cancer model applications. Self-assembly properties and in vitro cell interactions of these peptide hydrogels were studied.

Methods:
Peptides were synthesized using the solid phase peptide synthesis method based on Fmoc chemistry. Matrix-assisted laser desorption/ionization-time of flight mass spectroscopy (MALDI-TOF-MS) and reverse phase high-pressure liquid chromatography (RP-HPLC) were used to assess peptide purity. Secondary structures of the peptides were determined using Attenuated Total Reflection-Fourier Transform Infrared (ATR-FTIR) spectroscopy. The morphological and viscoelastic properties of the hydrogels were evaluated using atomic force microscopy (AFM) and oscillatory rheometer measurements, respectively. A549 cells were encapsulated in the peptide hydrogel matrices. In vitro cell proliferation, cell viability, and spreading tests were performed using Alamar blue assay, live-dead assay, and DAPI and phalloidin staining, respectively.

Results:
Molar mass and purity of the peptides were confirmed by MALDI-TOF-MS and RP-HPLC. ATR-FTIR results indicated the formation of β-sheet structures. Nanofibrous network structures were observed in the AFM images of the hydrogels. The storage moduli determined via the frequency sweep measurements are comparable to those of the other peptide hydrogels. The hydrogels supported the proliferation of the cells, and the cells encapsulated in the hydrogels started to colonize in 3D morphology after 7 days.

Conclusions:
The designed peptide hydrogels containing LDV sequences have potential in 3D cancer model applications. Testing of the anticancer drugs in these 3D matrices is underway.

Acknowledgments:
This project was financially supported by The Scientific and Technological Research Councilof Turkey (TÜBİTAK) (grant number: 122M821).

References:
[1] Xu, J., Qi, G., Wang, W., & Sun, X. S. (2021). Advances in 3D peptide hydrogel models in cancer research. *npj Science of Food*, 5(1), 14.
[2] Seow, W. Y., & Hauser, C. A. (2014). Short to ultrashort peptide hydrogels for biomedical uses. *Materials Today*, 17(8), 381-388

POSTERS

Convergent synthesis of peptidomimetic based on a chloroalkene dipeptide isostere and its application to inhibition against amyloid β aggregation

Takuya Kobayakawa, Chika Azuma, Kenichi Yamamoto, Kohei Tsuji, Hirokazu Tamamura
Institute of Biomaterials and Bioengineering, Tokyo Medical and Dental University

https://doi.org/10.17952/37EPS.2024.P1002

Introduction

~Background~

Alkene type dipeptide isosteres (ADIs), which have been designed based on a native peptide bond in a ground state conformation, are expected as "peptide bond isosteres" because of high structural homology with natural dipeptides. Practically, many groups have investigated to replace amide bonds in peptides with ADIs, and their positive effects have been demonstrated in biological molecules.[1] However, there are several problems in diversity, synthetic efficiency toward ADIs, etc.

~This Study~

In this situation, we have developed an efficient synthetic method for chloroalkene dipeptide isosteres (CADIs) as peptide bond equivalents.[2-6]

In a convergent synthetic method, Fmoc-protected carboxylic acids can be synthesized via Evans *syn* aldol reaction followed by [3.3] sigmatropic rearrangement from *N*- and *C*-terminal analogs corresponding to each amino acid as starting materials. By the synthetic strategy, an Fmoc-protected CADI can be applied for solid-phase peptide synthesis.

Design of chloroalkene dipeptide isostere (CADI)

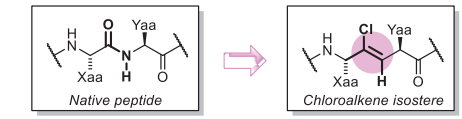

X	VDR[c] (pm)	Electronegativity
O	152	3.4[a] (3.5)[b]
H	120	2.2[a] (2.3)[b]
F	147	4.0[a] (4.1)[b]
Cl	175	3.2[a] (2.8)[b]

[a] Pauling value, [b] Allred-Rochow value
[c] VDR is Van der Waals Radius.

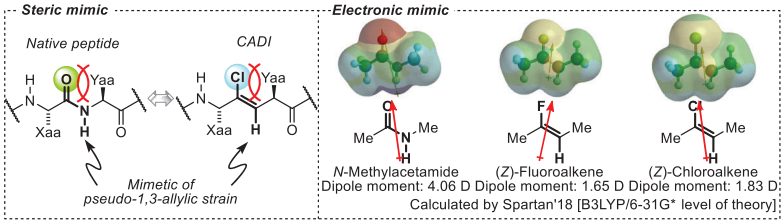

Results and discussion

[1] Retrosynthetic analysis for chloroalkene dipeptide isostere (CADI)

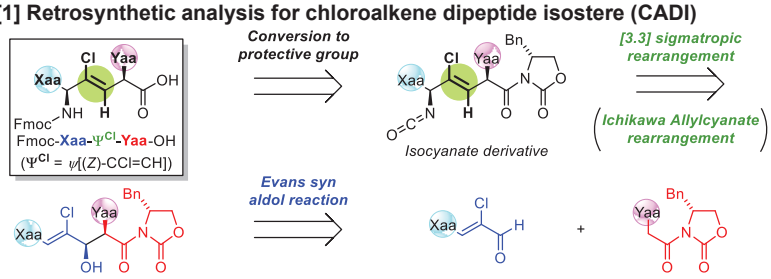

[2] Convergent synthesis for Fmoc-Val-ψ[(*Z*)-CCl=CH]-Phe-OH[6]

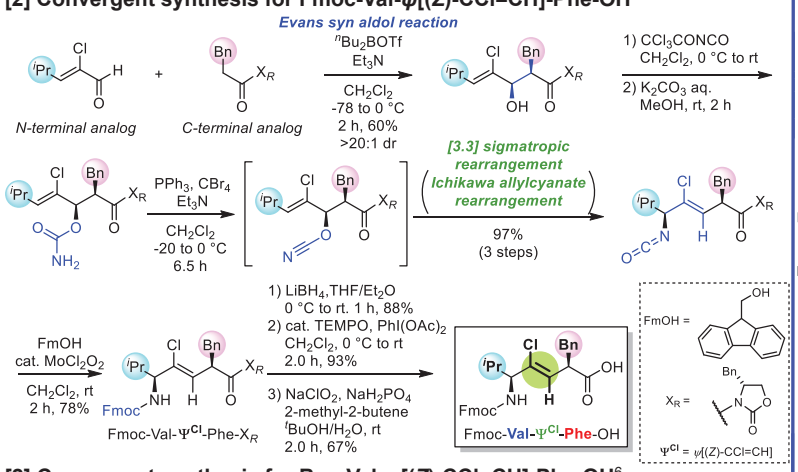

[2] Convergent synthesis for Boc-Val-ψ[(*Z*)-CCl=CH]-Phe-OH[6]

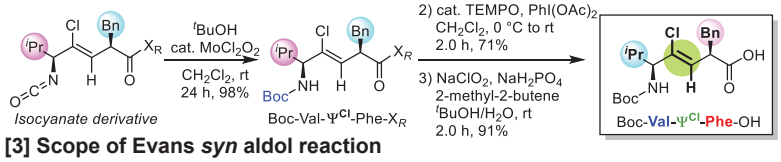

[3] Scope of Evans *syn* aldol reaction

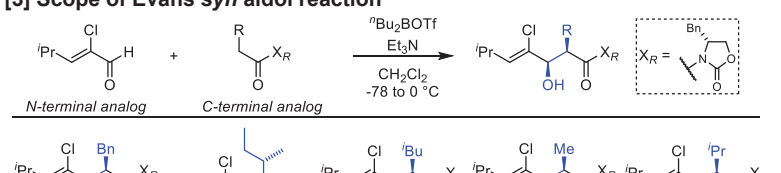

[4] Scope of a [3.3] sigmatropic rearrangement

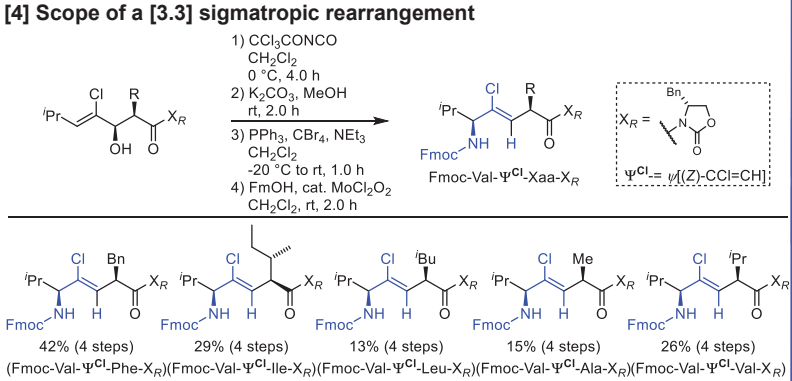

[5] Application of CADI for cyclic KLVFF peptide as Aβ aggregation inhibitor[6]

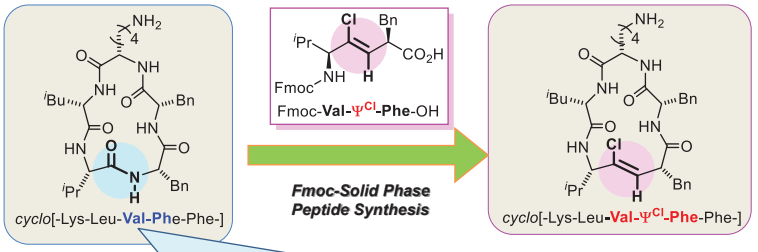

Aβ$^{1-42}$:DAEFRHDSGYEVHHQ**KLVFF**AEDVGSNKGAIIGLMVGGVVIA
(16 20)

➢ **Hydrophobic central region important for Aβ aggregation**

Incorporation into *cyclo*[KLVFF][7], an *anti*-aggregation peptide of amyloid-β (Aβ) peptide hypothesized to cause Alzheimer's disease
Synthesis of CADI based on the developed synthesis method
Introduction into Aβ aggregation Inhibitory peptide *cyclo*[KLVFF] by Fmoc-solid phase peptide synthesis

[6] Synthesis of cyclic KLVFF peptide including CADI structure[6]

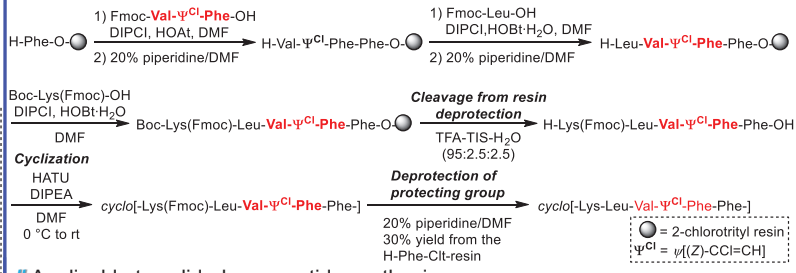

Applicable to solid-phase peptide synthesis

[7] Evaluation of Aβ aggregation inhibition by Thioflavin-T dye assay[6]

entry	Compound (Ψ[Cl] = ψ[(Z)-CCl=CH])	ThT fluorescence intensity [%][a] inhibitor 20 μM (10 μM)
1	H-Lys-Leu-Val-Phe-Phe-OH	90.2 ± 8.3
2	H-Lys-Leu-Val-Ψ[Cl]-Phe-Phe-OH	79.6 ± 15.6
3	*cyclo*[-Lys-Leu-Val-Phe-Phe-]	20.3 ± 1.9 (77.9 ± 2.5)
4	*cyclo*[-Lys-Leu-Val-Ψ[Cl]-Phe-Phe-]	24.6 ± 0.9 (**30.1 ± 3.3**)
5	Morin	36.0 ± 8.9

[a]Relative fluorescence intensity of Aβ1–42 (20 μM) + inhibitor (20 or 10 μM) vs. Aβ1–42 (20 μM) alone incubated for 6.0 h. All data shown are mean values of at least three independent experiments.

✔ Higher inhibitory activity of the CADI containing KLVFF peptide than that of the parent KLVFF peptide
✔ Increase of interaction with Aβ by the stabilized whole structure compared to the parent KLVFF peptide

Summary

[1] Development of an efficient synthetic method for (L,L)-type CADIs

We have also succeeded to establish of the convergent synthesis for CADIs, which was used by *N*- and *C*-terminal analogs corresponding amino acids as starting materials, via Evans syn aldol reaction followed by [3.3] sigmatropic rearrangement of the allyl cyanate.

[2] Application to peptide synthesis and introduction to a bioactive peptide

Utilizing the above methodology, a CADI was incorporated into a cyclic KLVFF peptide by solid-phase peptide synthesis. As a result, the cyclic KLVFF peptidomimic has shown higher activity than the parent cyclic peptide.

Acknowledgement

We acknowledge Prof. Yoshio Hayashi and Assoc. Prof. Atsuhiko Taniguchi (School of Pharmacy, Tokyo University of Pharmacy and Life Sciences) for evaluation of inhibitory activity for Aβ aggregation.

References

[1] Tamamura H.; Kobayakawa T.; Ohashi N. Mid-size drugs based on peptides and peptidomimetics: a new drug category. In: *Springer Briefs in Pharmaceutical Science & Drug Development*, *Singapore*, **2018**, 1-100. [2] Kobayakawa, T.; Tamamura, H. *J. Synth. Org. Chem. Jpn.* **2019**, *77*, 904-911. [3] Kobayakawa, T.; Narumi, T.; Tamamura, H. *Org. Lett.* **2015**, *17*, 2302-2305. [4] Kobayakawa, T.; Tamamura, H. *Tetrahedron* **2017**, *73*, 4464-4471. [5] Kobayakawa, T.; Matsuzaki, Y.; Hozumi, K.; Nomura, W.; Nomizu, M.; Tamamura, H. *ACS Med. Chem. Lett.* **2018**, *9*, 6-10.[5] Kobayakawa, T.; Azuma, C.; Watanabe, Y.; Sawamura, S.; Taniguchi, A.; Hayashi, Y.; Tsuji, K.; Tamamura, H. *J. Org. Chem.* **2021**, *86*, 5091-5101. [6] Arai, T.; Araya, T.; Sasaki, D.; Taniguchi, A.; Sato, T.; Sohma, Y.; Kanai, M. *Angew. Chem., Int. Ed.* **2014**, *53*, 8236-8239.

Optimization of IEDDA reaction parameters

https://doi.org/10.17952/37EPS.2024.P1003

37th European Peptide Symposium, Florence, Italy

Rasheda Aktar Samiha, Samir Das, Arundhati Nag

Carlson School of Chemistry and Biochemistry, Clark University, Worcester, MA 01610, USA

Introduction

Inverse Electron Demands Diels-Alder (IEDDA) reaction is a biorthogonal reaction that potentially can be used for various applications such as bioconjugation, imaging, screening etc. The reaction kinetics of the IEDDA reaction varies based on the nature of the substitutions on the tetrazine and diene. Incorporation of S, S-disubstituted tetrazine in peptides is synthetically much less challenging than the incorporation of an aromatic N,N-tetrazines, using the thiol functionality of Cys.

We have synthesized S, S-tetrazine cyclic peptides, and we want to study the reactivities of these peptides with different dienes, as there is very limited information about IEDDA reactions with S, S-tetrazine. We synthesized norbornene-containing or cyclopropene-containing dienes and incorporated them in peptides to increase the mass of the resultant products. The reactions of these peptides with S, S-dimethyl tetrazine are being studied under various conditions, to identify a diene with suitable reactivity that can be used for IEDDA reaction of S, S-tetrazine cyclized peptides with biomolecules like proteins.

Materials and methods

(1) IEDDA reaction with norbornene acid and tetrazine

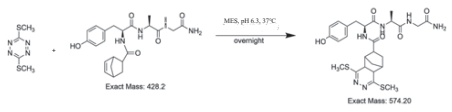

(2) IEDDA reaction with norbornene methyl and tetrazine

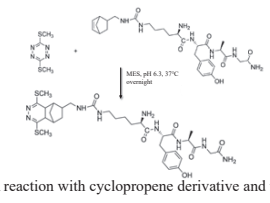

(3) IEDDA reaction with cyclopropene derivative and tetrazine

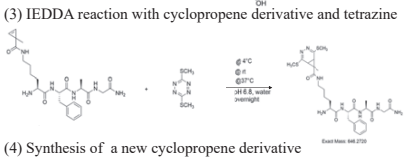

(4) Synthesis of a new cyclopropene derivative

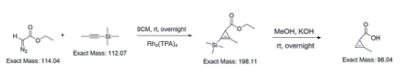

Results

(1) LC-MS result of IEDDA product. Dienophile: Norbornene-Lys-Tyr-Ala-Gly (1 eq), Diene: 3,6-Bis (methylthio)-1,2,4,5 tetrazine (5 eq).

(2) Dienophile: Norbornene methyl-Lys-Tyr-Ala-Gly (1 eq), Diene: 3,6-Bis (methylthio)-1,2,4,5 tetrazine (5 eq).

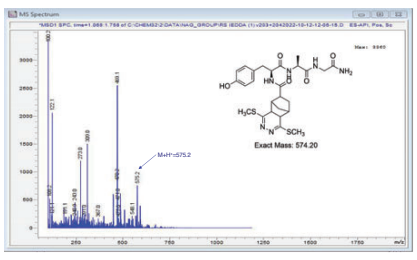

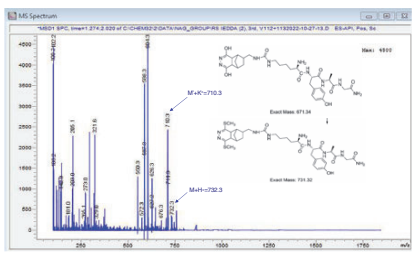

(3) LC-MS result of IEDDA product at 4ºC (left), and 37ºC (right). Dienophile: Cycp-Lys-Phe-Ala-Gly (1 eq), Diene: 3,6-Bis (methylthio)-1,2,4,5 tetrazine (1 eq).

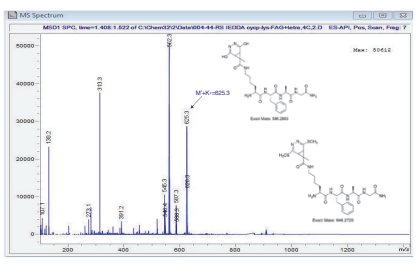

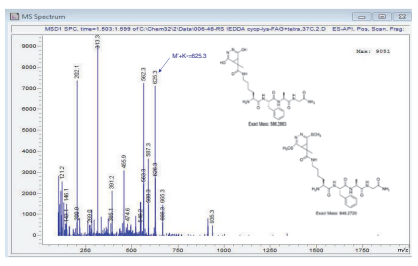

(4) ^{13}C NMR result of 2-methylcycloprop-2-enecarboxylic acid and LC-MS result of Cycp-Lys-Phe-Ala-Gly

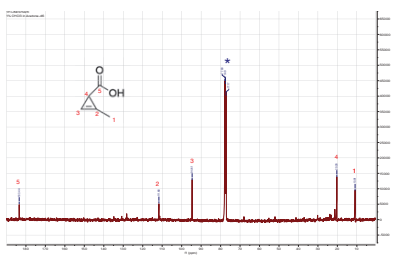

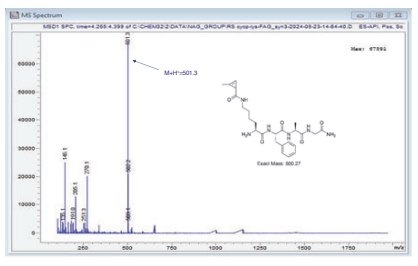

Conclusions

- Various dienophiles like norbornene-containing and cyclopropene-containing molecules have been synthesized successfully.
- IEDDA reactions with different dienophiles have been carried out.
- Color change was observed for IEDDA reaction of S, S-tetrazine with alkenes in solution but the correct product was not detected in LCMS analysis.
- IEDDA reaction with cyclopropene ring has shown more reactivity than norbornene
- Acidic pH may be leading to hydrolysis of the tetrazine.
- More reactive dienophile is going to be synthesized to occur the IEDDA reaction at room temperature to avoid hydrolyzation.
- More experiments in basic condition will be conducted to optimize IEDDA reaction conditions using cyclopropene derivative as a dienophile.

Literature cited

1. Oliveira, B., Guo, Z. & Bernardes, G. Inverse electron demand Diels–Alder reactions in chemical biology. *Chemical Society Reviews* **46**, 4895-4950 (2017).
2. Wu, H. & Devaraj, N.K. Advances in tetrazine bioorthogonal chemistry driven by the synthesis of novel tetrazines and dienophiles. *Accounts of chemical research* **51**, 1249-1259 (2018).
3. Yu, Z., Pan, Y., Wang, Z., Wang, J. & Lin, Q. Genetically encoded cyclopropene directs rapid, photoclick-chemistry-mediated protein labeling in mammalian cells. *Angewandte Chemie* **124**, 10752-10756 (2012).
4. Lang, K. et al. Genetically encoded norbornene directs site-specific cellular protein labelling via a rapid bioorthogonal reaction. *Nature chemistry* **4**, 298-304 (2012).

Acknowledgments

Research reported in this poster was supported by NIGMS of the National Institute of Health. I would also like to thank Dr. Nag and Dr. Das for their support and guidance.

https://doi.org/10.17952/37EPS.2024.P1004

Identification of reactivity hotspots at the interfaces of protein–protein interactions

Nathalie M. Grob[1‡], Clint Remarcik[2], Simon L. Rössler[1], Jeffrey Y. K. Wong[1], John C. K. Wang[2], Jason Tao[1], Corey L. Smith[3], Andrei Loas[1], Stephen Buchwald[1], Dan Eaton[2], Magdalena Preciado López[2], Bradley Pentelute[1]

[1] MIT, Department of Chemistry, Cambridge MA, USA; [2] Calico Life Sciences, San Francisco CA, USA; [3] AbbVie Bioresearch Center, Worcester MA, USA

[‡] Current Affiliation: ETH Zürich, Department of Chemistry and Applied Biosciences, Institute of Pharmaceutical Sciences, Zürich, Switzerland

Swiss National Science Foundation

RATIONALE

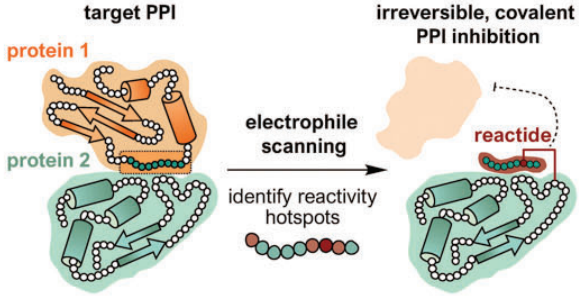

Covalent binding can enhance the activity of drugs by prolonged target engagement and increased selectivity. Peptides, which are prone to rapid degradation and elimination, may benefit from this approach. However, selecting a residue for covalent binding is challenging due to the effects of the local microenvironment. We propose *electrophile scanning* to identify reactivity hotspots in peptide ligands to covalently bind and disrupt disease-related protein–protein interactions (PPIs).

TARGET

VL9, a 9-mer peptide antigen presented by HLA-E on healthy cells was subjected to an electrophile scan. The complex is recognized CD94–NKG2A on natural killer (NK) cells to prevent their cytotoxic activation. Many cancer cells overexpress HLA-E on their cell surface to evade attacks by NK cells.[1]

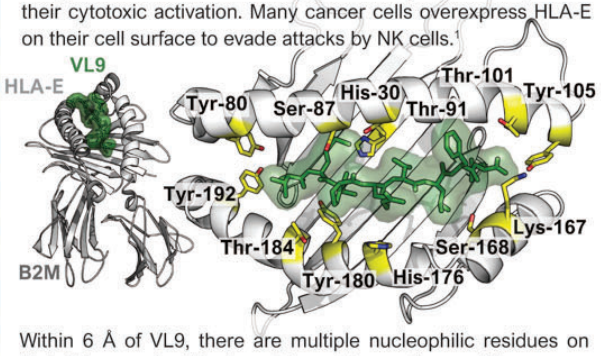

Within 6 Å of VL9, there are multiple nucleophilic residues on HLA-E for covalent binding with protein-reactive modifier.

1) Borst et al. *Clinical Cancer Research* **2020**, *26* (21), 5549-5555

REACTIDE SYNTHESIS

Unprotected, crude analogs of VL9 were equipped with versatile meta-sulfonyl fluoride (mSF) in one step. A palladium oxidative addition complex (Pd-OAC) introduced the electrophilic group on Cys-modified analogs of VL9.[2] mSF was used for initial studies due to broad reactivity by Sulfur(VI) Fluoride Exchange.[3]

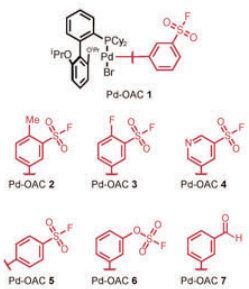

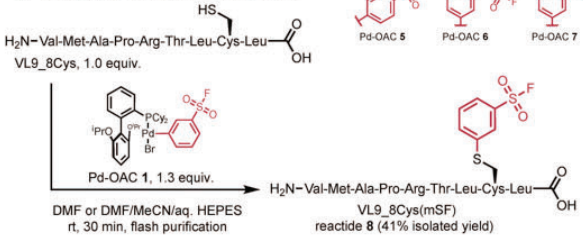

2) Narayanan et al. *Chemical Science* **2015**, *6* (5), 2650-2659
3) Vinogradova et al. *Nature* **2015**, *526* (7575), 687-691

CROSSLINKING RESULTS

Several reactides showed potent covalent binding in a crosslinking reaction with HLA-E.

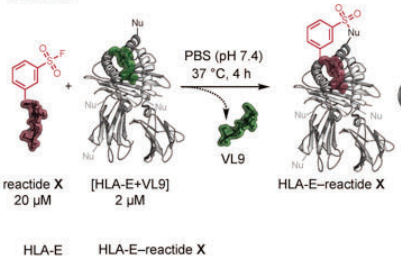

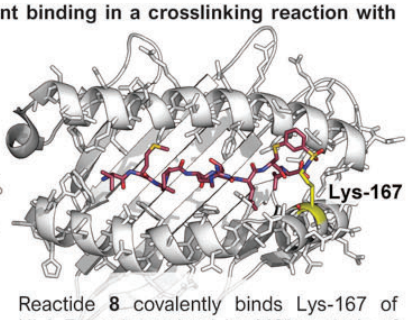

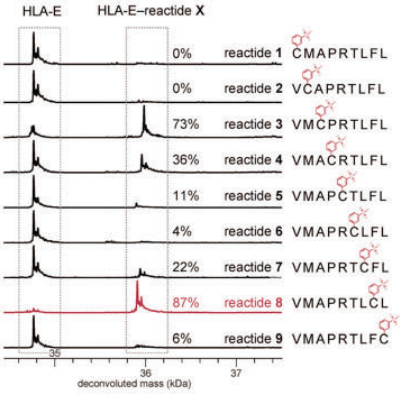

Reactide **8** covalently binds Lys-167 of HLA-E as determined by MS² analysis of the conjugate. No binding was found with off-target proteins, and reactide controls.

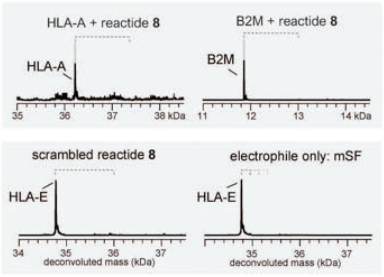

Pd-OACs **2–7** were used to explore the crosslinking potential of diverse electrophilic groups on VL9_8Cys. The readily available, shelf-stable Pd-OACs allow for further optimization of reactivity and stability profiles at reactivity hotspots.

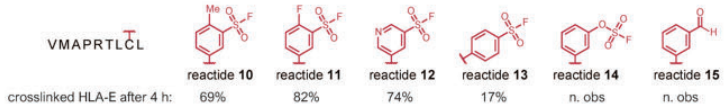

PPI INHIBITION

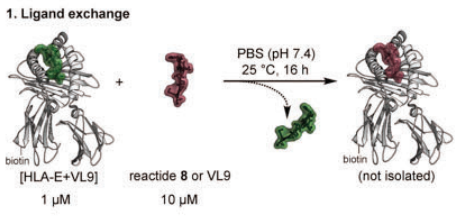

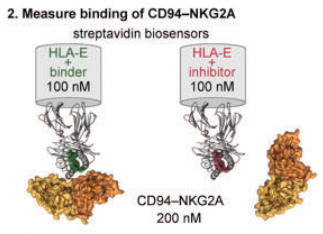

Reactide 8 inhibits the PPI of HLA-E and CD94–NKG2A. After ligand exchange in the antigen-binding groove of HLA-E and covalent binding by reactide **8**, the receptor heterodimer of NK cells showed reduced binding to HLA-E. Inhibiting the molecular recognition of cancer cells by NK cells could be a useful intervention in cancer immunotherapy.

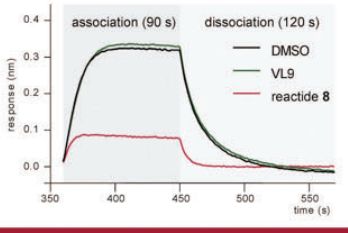

CONCLUSION

Peptides with covalent modes of action are a promising modality for the modulation of therapeutically relevant PPIs. Electrophile scanning identifies reactivity hotspots at early stages of ligand discovery and development and provides targeting options to guide further maturation efforts.

Full paper:
Grob NM, et al. *ACS Chem Bio* **2024**, *19* (1), 101-109

Current activities:
Grob Group for Peptide-based Drug Discovery at ETH zürich

Acknowledgments: Financial support was received from Calico Life Sciences (to BLP). NMG and SLR are grateful for the Postdoc Mobility fellowship of the SNSF (PN 195351 and 195700). The Massachusetts Life Sciences Center is acknowledged for financial support for the Orbitrap Eclipse mass spectrometer. We thank Millipore-Sigma for the generous gift of RuPhos.

Using *N*-acylation as a disulfide lock simplifies chemical protein synthesis

Vincent Diemer,[1] Vangelis Agouridas,[1,2] Benoît Snella,[1] Rémi Desmet,[1] Oleg Melnyk[1]

[1] *Univ. Lille, CNRS, Inserm, CHU Lille, Institut Pasteur de Lille, U1019 - UMR 9017 - CIIL – Center for Infection and Immunity of Lille, F-59000 Lille, France;*
[2] *Centrale Lille, F-59000 Lille, France.*

https://doi.org/10.17952/37EPS.2024.P1005

Introduction

There is an increasing evidence that cells utilize some post-translational modifications to remotely control the physico-chemical properties of thiols, and hence their capacity to engage in biochemical processes. For example, recent investigations show that lysine acylation is a post-translational modification that enables to modulate the catalytic activity of the protein disulfide isomerase, a cysteine enzyme that accelerates the folding of proteins.[1] Mimicking nature and tuning thiol reactivity by a chemical event occurring remotely is an appealing strategy to create controllable chemical systems. This concept is illustrated here in the context of chemical protein synthesis.

We discovered that the stability of the cyclic disulfide called SutCys towards reduction increases dramatically upon *N*-acylation, locking its opening and hence its reactivity in the presence of a mild reductant. Only the addition of a significantly stronger reductant in the reaction mixture can restore the SutCys reactivity. In this communication, we show how locking transiently SutCys ring-opening enables us to synthesize cyclic polypeptides through the concatenation of peptide segments on a water compatible solid support using native chemical ligation (NCL).

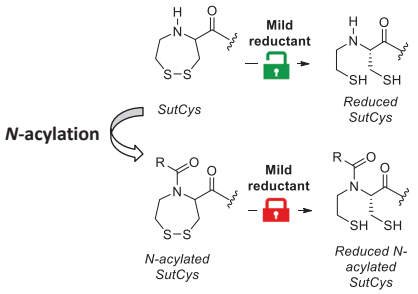

N-Acylation locks SutCys ring-opening

To compare the redox properties of SuCys peptides with their *N*-acylated derivatives, a 1:1 mixture of two model compounds was partially reduced using *tris*(2-carboxyethyl)phosphine (TCEP). To monitor the equilibration between the reduced and oxidised SutCys species present in solution, the reduced forms of SutCys were trapped by thiol alkylation with an excess of iodoacetamide prior to HPLC analysis.

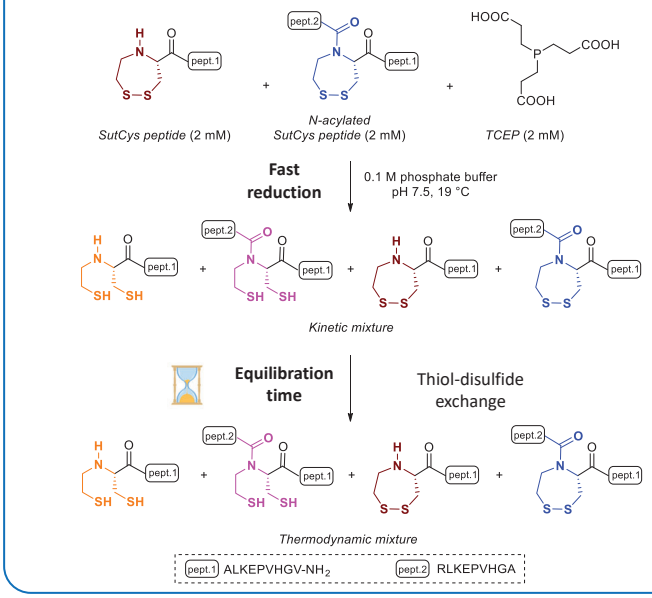

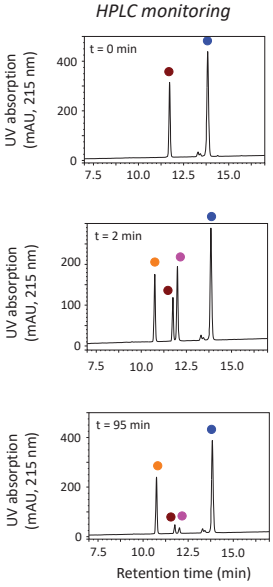

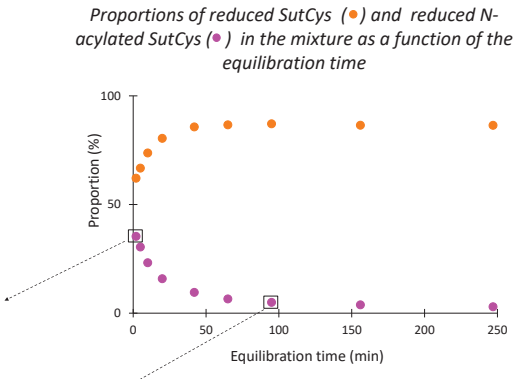

Equilibration through thiol-disulfide exchange favours the formation of reduced SutCys.

Stabilization of SutCys disulfide bond by *N*-acylation

SutCys as a novel linker for the assembly of cyclic polypeptides on solid support

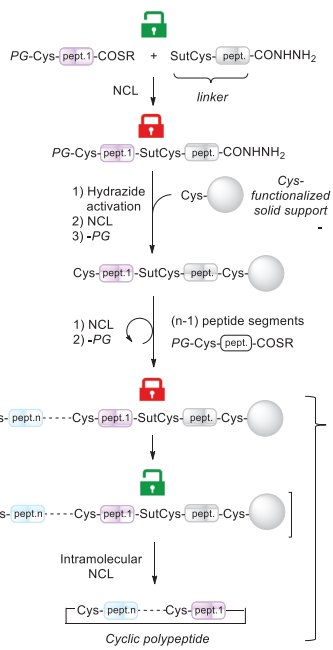

① **Linker pre-assembly by *N*-acylation** locks SutCys in the presence of MPAA

NCL: MPAA, pH 7.2

② **Connection to the solid support** of the linker and first peptide segment

NCL: MPAA, pH 7.2

③ **Elongation**

NCL: MPAA, pH 7.2

④ **SutCys activation, cyclisation and detachment** from the solid support

Activation and cyclative NCL: TCEP, MPAA, pH 5.5

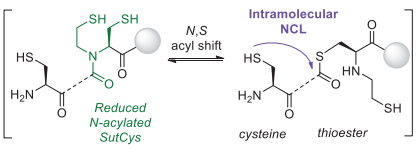

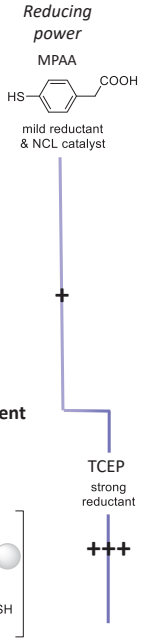

The synthesis of the target cyclic polypeptides on the solid support relies on MPAA-catalyzed NCL reactions[2-5] and uses *N*-peptidyl SutCys as a linker.

In this process:

- SutCys is acylated in solution by NCL leading to the pre-assembly of a linker that is stable under the reductive conditions imposed by the MPAA catalyst.
- *N*-peptidyl SutCys is silent during the solid phase attachment and elongation of the peptide sequence by a series of NCL reactions.
- *N*-peptidyl SutCys is activated by reduction of the S-S bond with TCEP and acts as a an acyl donor[6] during the final NCL leading to the cyclization and the detachment of the polypeptide.

LC-MS analysis of the purified cyclic polypeptide assembled from 2 peptide segments (n = 2)

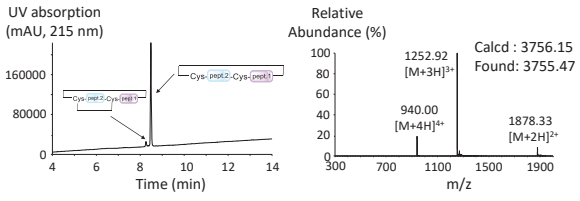

16%, 5 steps (69% per step) from the solid support

PG = -PG = NH_2OH, pH 4.0

pept.1 PDTRPAPGSTAPPAHGVTA
pept.2 PDTRPAPGSTGPPAHGVTA
pept. ALKEPVHGA

Conclusion

N-Acylation of SutCys by NCL stabilizes the disulfide bond of this cysteine derivative and leads to the formation of a thioester surrogate that is latent under mild reducing conditions classically used to concatenate peptide segments by NCL. Illustrated with the synthesis of cyclic peptide sequences on solid support, this concept opens the way towards the design of novel synthetic strategies in chemical protein synthesis.[7-8]

References

1) Caba, C.; Ali Khan, H.; Auld, J.; Ushioda, R.; Araki, K.; Nagata, K.; Mutus, B. *Front. Mol. Biosci.* **2018**, *5*, 18. 2) Agouridas, V.; Diemer, V.; Melnyk, O. *Curr. Opin. Chem. Biol.* **2020**, *58*, 1. 3) Dawson, P. E.; Muir, T. W.; Clark-Lewis, I.; Kent, S. B. H. *Science* **1994**, *266*, 776. 4) Agouridas, V.; El Mahdi, O.; Diemer, V.; Cargoët, M.; Monbaliu, J.-C. M.; Melnyk, O. *Chem. Rev.* **2019**, *119*, 12, 7328. 5) Diemer, V.; Firstova, O.; Agouridas, V.; Melnyk, O. *Chem. Eur. J.* **2022**, *28*, 16, e202104229. 6) Ruff, Y.; Garavini, V.; Giuseppone, N. *J. Am. Chem. Soc.* **2014**, *136*, 6333. 7) A manuscript is in preparation. 8) The ANR is acknowledged for financial support (Projet-ANR-21-CE06-0006).

https://doi.org/10.17952/37EPS.2024.P1007

Synthesis of Peptide Hydrazides: Hydrazone Resin *vs.* Hydrazine 2CT Resin

Maria Leko[a], Polina Filippova[a], Karin Rustler[b], Thomas Bruckdorfer[b] and Sergey Burov[a]
[a] Medico-Biological Research-Industrial Complex "Cytomed", St-Petersburg, Russia
[b] Iris Biotech GmbH, Adalbert-Zoellner-Str. 1, 95615 Marktredwitz, Germany, www.iris-biotech.de

Introduction

Peptide hydrazides are widely applied as precursors of peptide thioesters, valuable building blocks for the synthesis of proteins by native chemical ligation. Conversion of hydrazides into azides or isocyanates makes them useful intermediates for the conjugation with different nucleophiles. Finally, they can be applied for the selective modification of cargo or carrier molecules using hydrazone ligation technique (Fig. 1).

Solid-phase synthesis of peptide hydrazides commonly can be achieved by hydrazinolysis of peptidyl-Wang resin or using standard cleavage/deprotection protocols and hydrazine 2CT resin[1,2,3]. Both methods possess their own limitations depending on peptide sequence and protecting group combination. Previously, we described the synthesis of a new pyruvoyl hydrazone resin (Fig. 2) and examples of its practical application[4]. Herein, we report a comparative investigation of different synthetic protocols in parallel synthesis of peptide hydrazides using hydrazine 2CT and hydrazone resin.

Results and Discussions

In this study, we demonstrated that in the case of the hydrazone resin, all synthetic procedures from the attachment of the linker group to the cleavage of the final product can be performed by using only "recommended" and "usable" organic solvents (Fig. 3; Table 1). Moreover, the resin permits to fulfil selective Mtt group removal and possesses complete stability to acidic additives such as 6-Cl-HOBt and OxymaPure during peptide chain elongation (Fig. 4; Table 2).

In contrast, synthesis of the Fmoc-hydrazine 2CT resin in "usable" and green solvents proceeds with moderate efficiency (Fig. 5). Attempts of Mtt group removal with 4% TFA solution in DCM or toluene resulted in complete peptide release from the solid support (Table 2).

At the same time, HPLC analysis of different peptide hydrazides synthesized using hydrazine 2CT and hydrazone resin demonstrated comparable purity of the crude products (Fig. 6).

Investigation of the cleavage conditions revealed that apart from TFA, the peptide can be efficiently released from the polymeric support with simultaneous removal of ^{t}Bu based protecting groups using 5% HCl (aq) in acetone. While this protocol demands subsequent peptide deprotection in the case of other protecting groups, it benefits of significantly reduced TFA consumption.

It should be mentioned that cleavage and deprotection of peptide hydrazides using TFA can be accompanied with the side reaction of hydrazide trifluoroacetylation. In accordance with the literature data, extent of trifluoroacetylation can be reduced by the additional amount of water (8%) in the cleavage cocktail[5]. However, in the case of peptide with C-terminal glycine we still observed about 10% of the corresponding side product. Subsequent experiments demonstrated that its formation can be minimized by the addition of 10% of HCl (aq) to the cleavage cocktail (Fig. 7; Table 3).

To prove the practical utility of the suggested resin, we synthesized a set of model compounds including, but not limited to SV40 T antigen nuclear localization signal, *cyclo*-RGDfK(TPP), and an analog of Szeto-Schiller peptides (Table 4). Parallel synthesis of several peptides using hydrazine 2CT and hydrazone resin demonstrated comparable weight gain, cleavage yield, and crude peptide purity in both cases. Taking into account the improved stability in acidic conditions, the possibility of selective Mtt group removal and peptide cleavage using green solvent, hydrazone resin can be considered as a useful alternative for peptide hydrazides synthesis.

Conclusions

- Synthesis of peptide hydrazides on hydrazine 2CT and hydrazone resin resulted in comparable weight gain, cleavage yield, and crude peptide purity.
- Hydrazone resin permits to fulfil selective Mtt group removal and possesses complete stability to acidic additives during peptide chain elongation.
- Side reaction of hydrazide trifluoroacetylation can be minimized by the addition of 10% HCl (aq) to the cleavage cocktail.

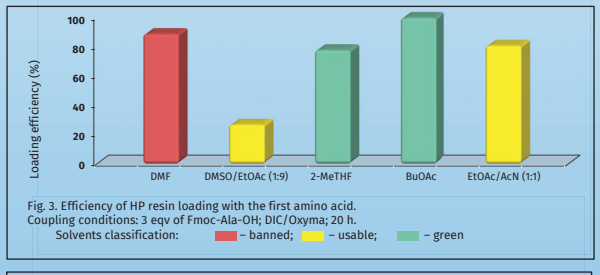

Fig. 3. Efficiency of HP resin loading with the first amino acid.
Coupling conditions: 3 eqv of Fmoc-Ala-OH; DIC/Oxyma; 20 h.
Solvents classification: – banned; – usable; – green

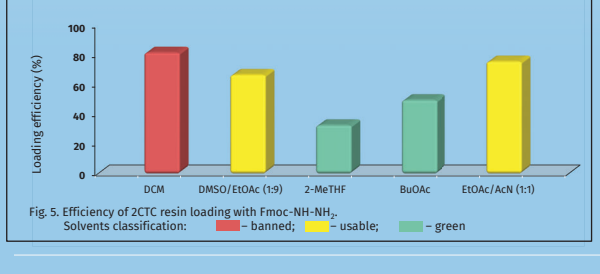

Fig. 5. Efficiency of 2CTC resin loading with Fmoc-NH-NH_2.
Solvents classification: – banned; – usable; – green

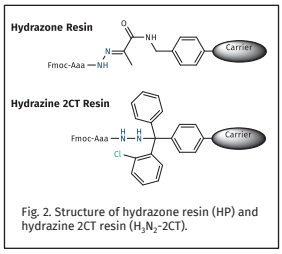

Fig. 2. Structure of hydrazone resin (HP) and hydrazine 2CT resin (H_3N_2-2CT).

Fig. 1. Applications of peptide hydrazides

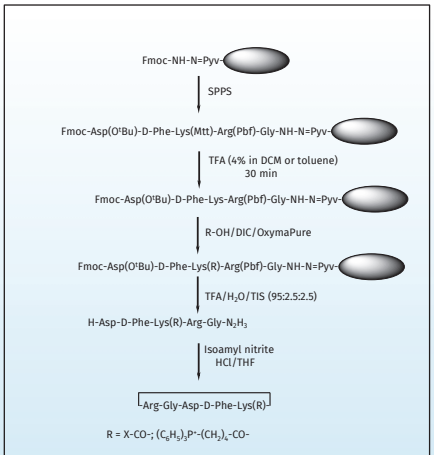

Fig. 4. Synthesis of cyclic RGD analogs using hydrazone pyruvoyl resin.

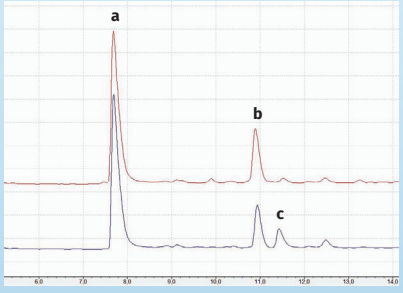

Fig. 6. HPLC analysis of crude product. Synthesis on H_3N_2-2CT resin (red) and HP resin (blue). Cleavage conditions: TFA/H_2O/TIS (95:2.5:2.5).
a - PKKKRKVG hydrazide;
b - Trifluoroacetyl hydrazide;
c - Peptide with free carboxyl group.

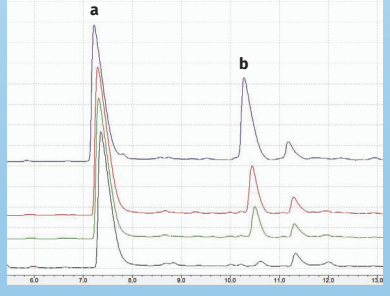

Fig. 7. Suppression of hydrazide trifluoroacetylation using different cleavage cocktails. TFA/DODT/TIS 95:2.5:2.5 (blue); TFA/H_2O/TIS 95:2.5:2.5 (red); TFA/H_2O/TIS 89.5:8:2.5 (green); TFA/HCl(aq)/TIS 87.5:10:2.5 (black)
a - PKKKRKVG hydrazide;
b - Trifluoroacetyl hydrazide.

Table 1. Synthesis of peptide hydrazides in "greener" solvent mixtures.

Entry	Hydrazone resin	H_3N_2-2CT resin
Attachment of the linker group	DMSO/EtOAc	EtOAc/AcN
Resin loading with the first amino acid residue	BuOAc	DMSO/EtOAc
Coupling and Fmoc removal	DMSO/EtOAc	DMSO/EtOAc
Cleavage/deprotection	HCl(aq)/Acetone; TFA/H_2O	HCl(aq)/Acetone; TFA/H_2O

Table 2. On-resin removal of Mtt group from DfKRG precursor.

Solvent	Polymer capacity (mmol/g)			
	HP resin		H_3N_2-2CT resin	
	A	B	A	B
DCM	0.28	0.35*	0.46	0.00
Toluene	0.28	0.35*	0.46	0.03

A – Before the treatment with 4% TFA for 30 min.
B – After the treatment.
*The loading value was recalculated due to Mtt group removal.

Table 3. Trifluoroacetylation of PKKKRKVG hydrazide in the course of peptide deprotection.

Cleavage cocktail	Desired product (%)	Trifluoroacetylation (%)
TFA/DODT/TIS 95:2.5:2.5	53.6	27.6
TFA/H_2O/TIS 95:2.5:2.5	70.4	14.8
TFA/H_2O/TIS 89.5:8:2.5*	75.4	10.6
TFA/HCl(aq)/TIS 92.5:5:2.5	76.1	9.3
TFA/HCl(aq)/TIS 87.5:10:2.5	80.8	2.3

*Recommended in the literature for the suppression of trifluoroacetylation[5].

Table 4. Synthesis of peptide hydrazides on hydrazone resin.

Entry	$[M+H]^+$		Yield* (%)
	Calc.	Found	
PKKKRKVG	953.66	953.67	55
TKPR	514.33	514.33	42
FrFK	610.37	610.36	47
RADA	445.24	–**	35
RADARADA	858.44	858.44**	41
cyclo-RGDfK(TPP)	948.45	948.48	28

* Yield of purified hydrazides and peptide obtained by azide cyclization.
TPP – triphenylphosphonium moiety.
** Peptides were prepared from the common precursor.

References:
1. Preparation of polymer-bound trityl-hydrazines and their application in the solid phase synthesis of partially protected peptide hydrazides; G. Stavropoulos, D. Gatos, V. Magafa, K. Barlos; *Letters in Peptide Science* 1996; **2**: 315-318. https://doi.org/10.1007/bf00162245
2. Facile synthesis of C-terminal peptide hydrazide and thioester of NY-ESO-1 (A39-A68) from an Fmoc-hydrazine 2-chlorotrityl chloride resin; Y.-C. Huang, C.-C. Chen, S.-J. Li, S. Gao, J. Shi, Y.-M. Li; *Tetrahedron* 2014; **70**: 2951-2955. https://doi.org/10.1016/j.tet.2014.03.022
3. A Shelf Stable Fmoc Hydrazine Resin for the Synthesis of Peptide Hydrazides; M. J. Bird, P. E. Dawson; *Pept Sci (Hoboken)* 2022; **114**: e24268. https://doi.org/10.1002/pep2.24268
4. Convenient method of peptide hydrazide synthesis using a new hydrazone resin; P. S. Chelushkin, K. V. Polyanichko, M. V. Leko, M. Y. Dorosh, T. Bruckdorfer, S. V. Burov; *Tetrahedron Letters* 2015; **56**: 619-622. https://doi.org/10.1016/j.tetlet.2014.12.056
5. Total chemical synthesis of proteins without HPLC purification; S. F. Loibl, Z. Harpaz, R. Zitterbart, O. Seitz; *Chemical science (Royal Society of Chemistry : 2010)* 2016; **7**: 6753-6759. https://doi.org/10.1039/c6sc01883a

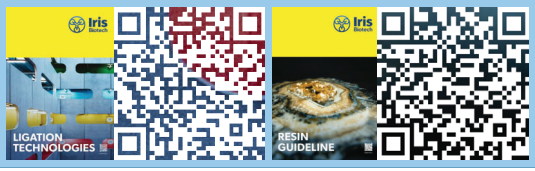

https://doi.org/10.17952/37EPS.2024.P1009

Facilitating the access to repeat proteins by a novel water-compatible oligomerization process

Eliott Roy, Oleg Melnyk, Vincent Diemer

Univ. Lille, CNRS, Inserm, CHU Lille, Institut Pasteur de Lille, U1019 - UMR 9017 - CIIL - Center for Infection and Immunity of Lille, F-59000, Lille, France

Introduction

In nature, **repetitive motifs** are frequently **contained in proteins**[1] and are known to be associated with important physical or biological functions. Logically, producing such domains is an appealing strategy for engineering minimal protein mimics endowed with desired properties.

In this context, we aim to develop a method enabling the total synthesis of proteins made of repetitive motifs by **spontaneous and chemoselective oligomerization of peptide segments**. Using NCL as an oligomerization method, this strategy is classically complicated by the **intramolecular cyclization of the bifunctional monomer used for polymerization**. To solve this, we exploited the non classical reactivity of the *N*-selenoethyl cysteine (**SetCys**), a chemical device recently discovered by the team,[2] through native chemical ligations (NCL)[3,4] for peptide segments oligomerization.

Principle of oligomerization process

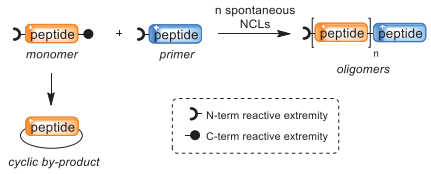

1) SetCys properties

The three important SetCys properties for this work:

- *Property 1.* ***N*-acylation of the SetCys leads to a reversible amide bond** under NCL conditions
- *Property 2. N*-selenoethyl **arm self-immolation after selenosulfide bond reduction**
- *Property 3. N*-selenoethyl **arm is stable when SetCys α-amino group is acylated**

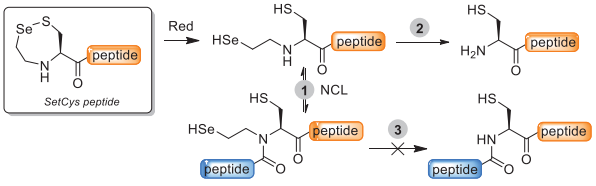

2) SetCys enables peptide oligomerization using NCL

➢ Preliminary results

As a proof of concept, we compared the NCL-mediated oligomerization of peptide segments using monomers equipped with either a Cys or SetCys residue. The reaction is initiated by a cysteinyl peptide (called primer).

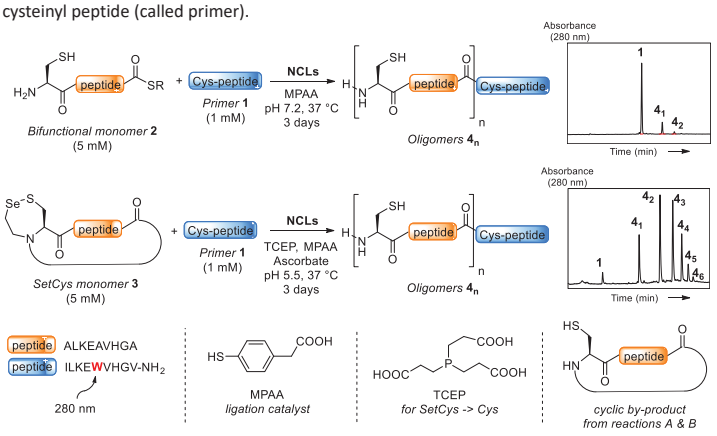

In the case of SetCys monomer, TCEP is added to reduce the selenosulfide bond and hence induce the loss of *N*-selenoethyl arm. The latter process displays the fastest rate at pH 5.5. Sodium ascorbate is used as radical inhibitor to avoid deselenization of SetCys by TCEP. MPAA is used as a catalyst for NCL reactions.[5]

This experiment shows that **using cyclic SetCys monomers enabled peptide oligomerization by spontaneous NCL** reactions whereas Cys bifunctional monomers mainly led to the intramolecular cyclized by-product.

➢ Optimization of the process

The optimization aims to **increase the degree of polymerization (DP)** of the process, i.e. the number of successive ligations.

After screening of pH, temperatures, monomer nature and various additives, the optimal reaction conditions resulted in a **DP of 2.4 and 55% conversion of monomer into oligomers** using 5 equivalents of monomer.

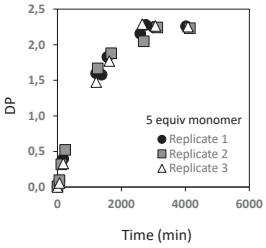

3) Repetitive additions of monomer

Then, the impact of monomer excess on the length of oligomers was then explored:

- Surprisingly, increasing the **monomer equivalents from 5 to 10** resulted in a small **increase in DP, from 2.4 to 3.0**
- In contrast, **repetitive additions** of 2 x 5 equiv of the monomer led to a further **increase in DP, reaching 4.0**

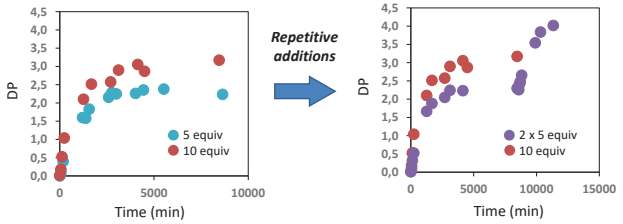

The slow continuous addition of monomer was also performed but the experiments displayed the same results than the one batch addition.

4) Impact of the size of the monomer on DP

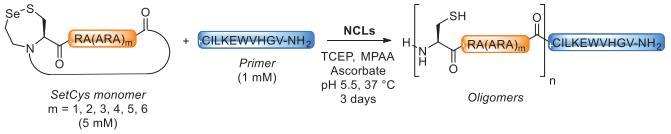

Number of AAs	6	9	12	15	18	21
DP	1.46	2.42	2.33	2.35	2.26	1.86
Isolated yield (%)	23	36	30	36	38	38

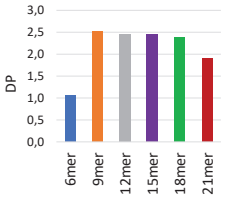

The process achieves **optimal DPs** using a monomer containing **between 9 and 18 AAs**.

5) Post-oligomerization modification

Due to the high frequency of Ala in proteins, the **combination of NCL with a Cys desulfurization** step is a **powerful synthesis tool** for biological applications.[6,7,8]

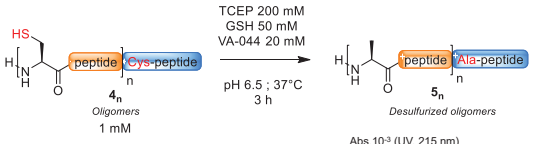

To initiate the chemical synthesis of the target proteins, the **compatibility between the oligomerization process and Cys desulfurization** was assessed.

HPLC purified oligomers were engaged in a desulfurization reaction, which was **completed after 3 h** even for the largest oligomers which contain more cysteines.

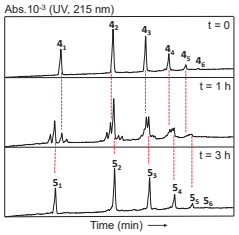

Conclusion

In literature, the only described strategy to avoid intramolecular cyclization of monomers in oligomerization processes is the conformational rigidification of monomers.[9] However, this strategy does not enable the oligomerization of most of the small peptides due to their conformational flexibility.

We **achieved and optimized an innovative oligomerization process** using **SetCys residue.** The fact that the process favours the formation of oligomers over of intramolecular cyclization is ascribed to the **reversibility of the Xaa-SetCys peptide bond under NCL conditions.**

Moreover, the compatibility of the process with post-oligomerization modifications has been established. This **enlarges the scope of the study** and will **enable the synthesis of bio-inspired and functional repeat protein mimics**.

Acknowledgements to the Agence Nationale de la Recherche (ANR 2021, REPEAT).

References

[1] Di Domenico, T. et al. *Nucleic Acids Res.* **2014**, *42*, 1-6. DOI.
[2] Diemer, V. et al. *Nat. Comm.* **2020**, *11*, 1-14. DOI.
[3] Dawson, P.E. et al. *Science*. **1994**, *266*, 776-779. DOI.
[4] Agouridas, V. et al. *J. Med. Chem.* **2020**, *63*, 15140-15152. DOI.
[5] Diemer, V. et al. *Chem. Eur. J.* **2022**, *28*, e202104229. DOI.
[6] Yan, L. Z. et al. *J. Am. Chem. Soc.* **2001**, *123*, 526-533. DOI.
[7] Wan, Q. et al. *Angew. Chem. Int. Ed.* **2007**, *46*, 9248-9252. DOI.
[8] Diemer, V. et al. *Chem. Soc. Rev.* **2024.** DOI.
[9] Van der Heden van Noort, G. et al. *Org. Lett.* **2017**, *19*, 6490-6493. DOI.

P1.012

Technetium-99m tricarbonyl complexes containing amino acid derivatives for cancer imaging

https://doi.org/10.17952/37EPS.2024.P1012

João D.G. Correia[1,2*], Rúben D.M. Silva[1], Cristina P. Matos[1], Catarina I.G. Pinto[1], Joana F. Guerreiro[1], Lurdes Gano[1,2], Filipa Mendes[1,2]

[1] C²TN – Centro de Ciências e Tecnologias Nucleares, Instituto Superior Técnico, Universidade de Lisboa, Portugal

[2] DECN – Departamento de Engenharia e Ciências Nucleares, Instituto Superior Técnico, Universidade de Lisboa, Portugal

*jgalamba@ctn.tecnico.ulisboa.pt

Positron Emission Tomography (PET) Radiopharmaceuticals in clinical use for assessing enhanced cancer metabolism[1]

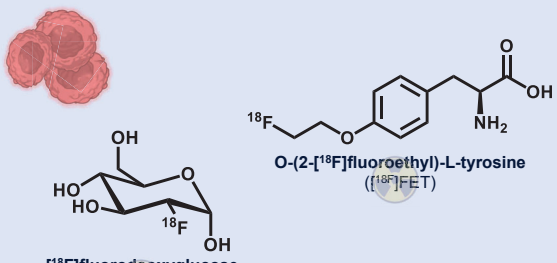

99mTc-(I)-complexes bearing cationic amino acids as potential cancer imaging tools

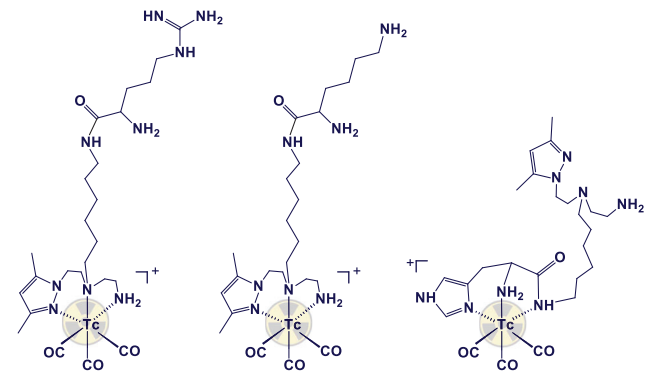

Design and biological evaluation of cationic amino acid **(Aa)-bearing radiometal (technetium-99m, 99mTc) complexes** to assess **upregulation of amino acid transporters** (*e.g.* Cationic Amino Acid Transporter 1, CAT 1, or Amino Acid Transporter $B^{0,+}$, $ATB^{0,+}$) *in vivo* by Single Photon Emission Computed Tomography (**SPECT**) for *Cancer Imaging*[2,3].

Cellular Uptake

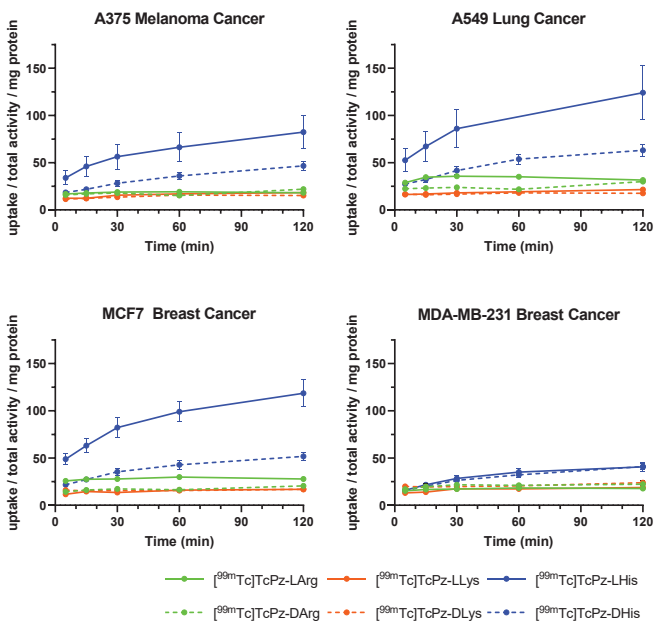

Cellular Internalization

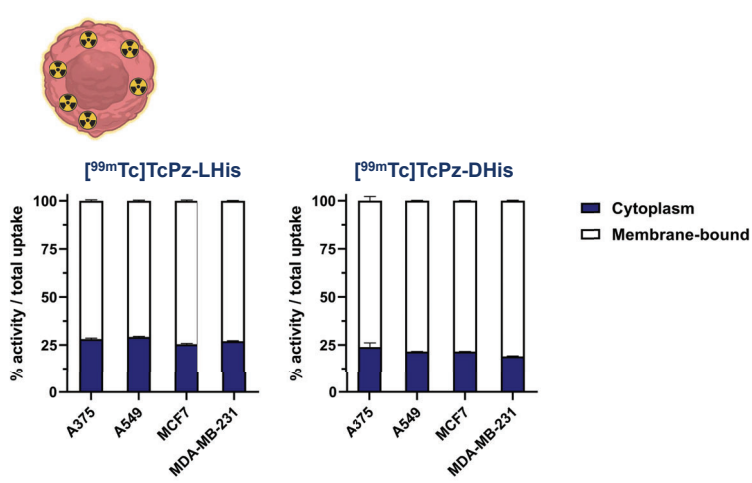

Results (N = 4) were normalized by protein content

Biodistribution studies of [99mTc]TcPz-LHis in Balb/c-Nude mice bearing A549 Lung Cancer xenografts (*N = 3*)



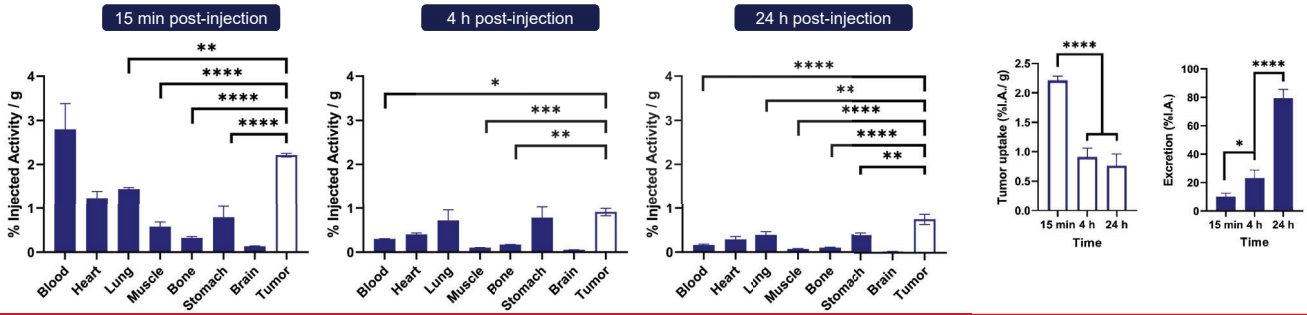

Conclusions

- Cellular uptake of the radiocomplexes depends on the amino acid moiety. The histidine-bearing complexes present the highest uptake in all cancer cell lines, with ~25% of the total cell-related activity found intracellularly.
- A549 cancer cell line shows the highest overall uptake, with the breast cancer cell line MDA-MB-231 showing the lowest uptake.
- **[99mTc]TcPz-LHis** shows high and fast tumor uptake in tumor-bearing mice, with good retention in the tumor 24 h after injection (~30% compared with 15 min post-injection).

References:

[1] Katsanos et al., *Clin. Nucl. Med.* **2019**, *44*, 864

[2] Jain et al., *Front. Oncol.* **2023**, *13*, 983023

[3] Morais et al., *Dalton Trans.* **2017**, *46*, 14537

Centro de Ciências e Tecnologias Nucleares thanks Fundação para a Ciência e Tecnologia (FCT) for funding through project UID/Multi/04349/2020. The work was also funded by FCT project PTDC/QUI-OUT/3854/2021 and PhD fellowships to RDMS (DFA/BD/4978/2020) and CIGP ((DFA/BD/07119/2020).

https://doi.org/10.17952/37EPS.2024.P1013

Development of methodology for late-stage acylation of threonine residue enabled by chemoselective acyl transfer followed by desulfurization

○Daiki Sato, Chiho Shinozaki, Masaya Denda, Akira Otaka
(Institute of Biomedical Sciences and Graduate School of Pharmaceutical Sciences, Tokushima University)

1. Background

Construction of ester linkage between threonine (Thr) hydroxyl side chain and carboxylic acid has been a synthetic challenge and would be useful for syntheses of both druggable peptides and function-unknown proteins. However, the low nucleophilicity of Thr hydroxy group has prevented a development of efficient acylation protocol.

2. Conventional acylation method[2]

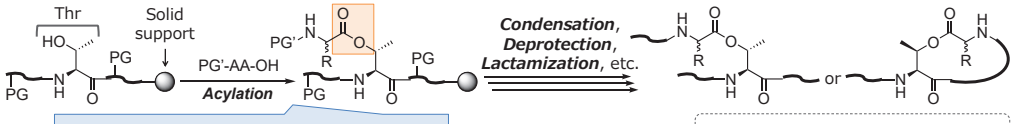

3. "Intramolecular" acylation of Thr using thiol-incorporated threonine derivative (Thr(SH))[3]

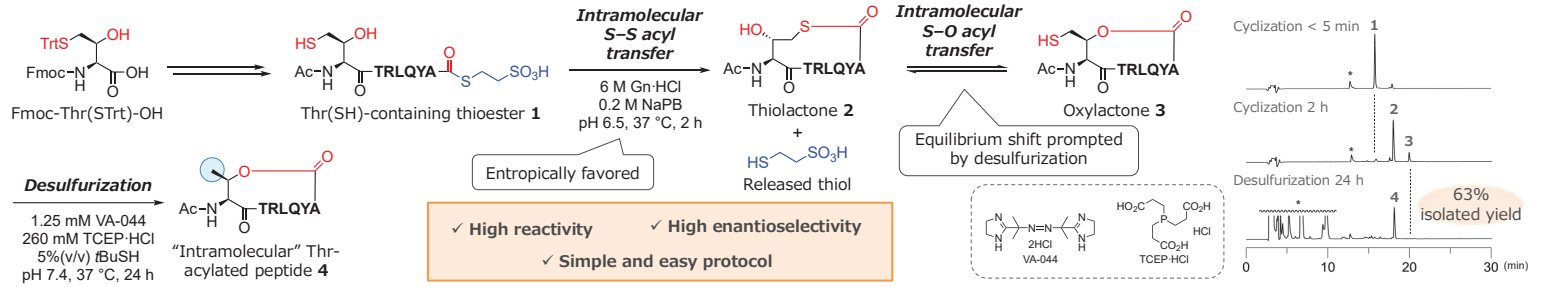

HPLC conditions: Linear gradient of 0.1%(v/v) TFA–MeCN in 0.1%(v/v) TFA aq. (5:95–45:55 over 30 min); *: non-peptidyl compounds.; **T**: Threonine, **R**: Arginine, **L**: Leucine, **Q**: Glutamine, **Y**: Tyrosine, **A**: Alanine

4. Scope of the developed intramolecular acylation

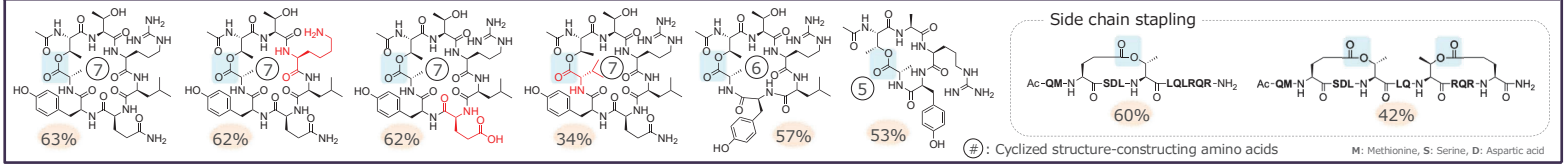

5. Strategy for accelerating entropically unfavored intermolecular S–S acyl transfer

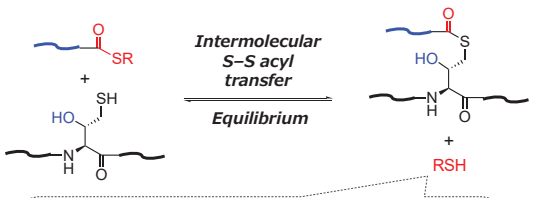

6. Optimization of reaction conditions (acylation steps)

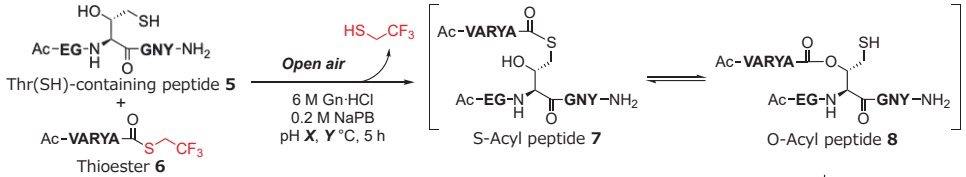

Entry	5:6	X	Y	Products
1	1:1	6.5	37	**7, 8, 9**
2	2:1	6.5	37	**7, 8, 9**
3	1:1	5.0	37	**7, 8, 9**
4	1:1	6.5	4	**7, 8, 9**
5	1:2	6.5–7	37	**9**

Entry 5: optimized condition in acylation steps

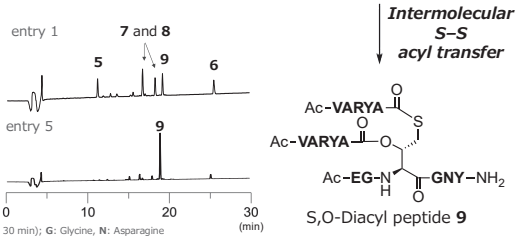

HPLC conditions: Linear gradient of 0.1%(v/v) TFA–MeCN in 0.1%(v/v) TFA aq. (5:95–45:55 over 30 min); **G**: Glycine, **N**: Asparagine

7. Optimization of reaction conditions (deacylation–desulfurization steps)

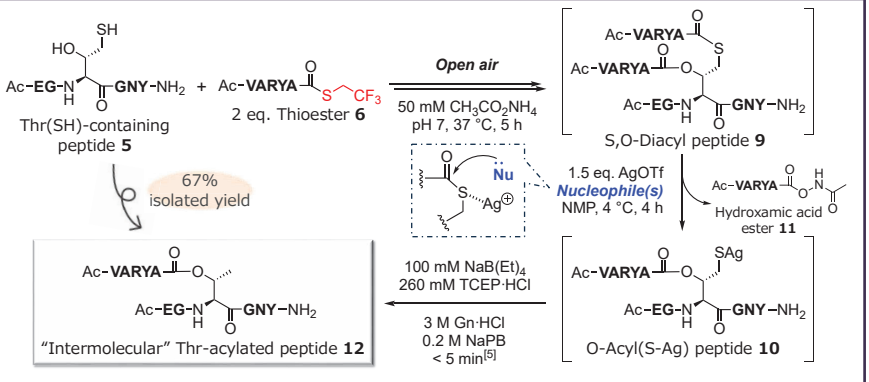

Entry	Nucleophile(s)	Ac-VARYA-Nu
1		Fair conversion
2		
3		Great conversion (64% yield)

Entry 3, Desulfurization 5 min

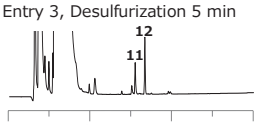

One-pot manner

HPLC conditions: Linear gradient of 0.1%(v/v) TFA–MeCN in 0.1%(v/v) TFA aq. (5:95–45:55 over 30 min)

8. Recover of the substrate

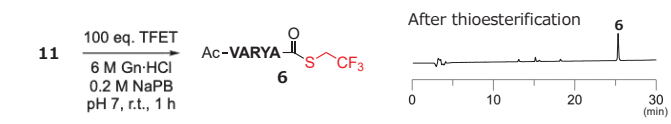

HPLC conditions: Linear gradient of 0.1%(v/v) TFA–MeCN in 0.1%(v/v) TFA aq. (5:95–45:55 over 30 min)

9. Scope of the intermolecular Thr acylation

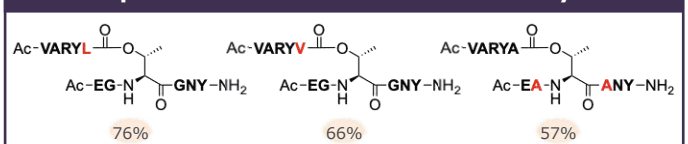

10. Conclusion

We developed an unprecedented late-stage Thr O-acylation protocol using sequential acyl transfers–desulfurization. The thiol unit on the Thr derivative allows for the facile deriver of an acyl moiety on the low nucleophilic neighboring hydroxy group. Developed protocol features high acylation efficiency and enantioselectivity. We next plan to synthesize ubiquitinated protein using developed protocol.

Acknowledgement: JST SPRING Grant Number JPMJSP2113, Japan

1. Kuan-Chuan Pao, Nicola T. Wood, Axel Knebel, Karim Rafie, Mathew Stanley, Peter D. Mabbitt, Ramasubramanian Sundaramoorthy, Kay Hofmann, Daan M. F. van Aalten, and Satpal Virdee *Nature* **2018**, *556*, 381–385. 2. Hao Sun, Roman Meledin, Sachitanand M. Mali, and Ashraf Brik *Chem. Sci.* **2018**, *9*, 1661–1665. 3. Daiki Sato, Masaya Denda, and Akira Otaka *Chem. Commun.* **2022**, *58*, 2918–2921. 4. Robert E. Thompson, Xuyu Liu, Noelia Alonso-Garcia, Pedro Jose Barbosa Pereira, Katrina A. Jolliffe, and Richard J. Payne *J. Am. Chem. Soc.* **2014**, *136*, 8161–8164. 5. Zhenquan Sun, Wenjie Ma, Yihui Cao, Tongyao Wei, Xiaoyong Mo, Hoi Yee Chow, Yi Tan, Carina H. P. Cheung, Jiamei Liu, Hung Kay Lee, Edmund C. M. Tse, Han Liu, and Xuechen Li *Chem.* **2022**, *8*, 2542–2557.

Towards the total synthesis of the bacteriocin Nisin A on solid support

Ilia Perov[1], Bethan Donnelly[1], Tyler Mallett[1], John Vederas[1]
[1] University of Alberta, Edmonton, Canada

perov@ualberta.ca
LinkedIn



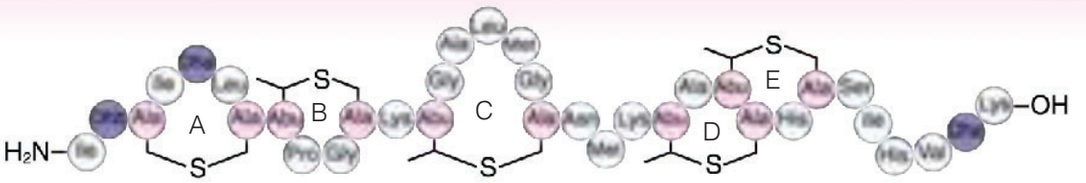

Background

What is nisin?

Nisin A is an antimicrobial peptide produced by *Lactococcus lactis*. It is active against a broad spectrum of Gram-positive bacteria at nanomolar concentrations. Nisin has been widely used as a food preservative (E234) in the past 50 years.

Why bother to synthesize it chemically if bacteria can produce it?

Despite its antimicrobial activity, nisin A is not used as a drug (yet)! It is unstable *in vivo* and is degraded very fast by proteases. The total synthesis of nisin A on solid support would allow us to conduct structure-activity relationship studies and potentially find analogues more suitable as antibiotic drugs.

Why hasn't anyone synthesized nisin A on the solid phase yet?

Nisin A's chemical structure contains dehydrated amino acids and (methyl)lanthionine rings, which are challenging to synthesize and incorporate in solid phase peptide synthesis. Take a look at our approach!

Our approach

Solid phase peptide synthesis (SPPS)

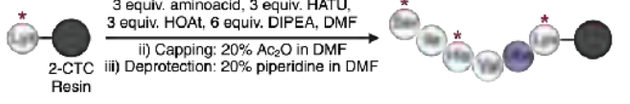

*Acid labile side chain protection

Dehydrated residues

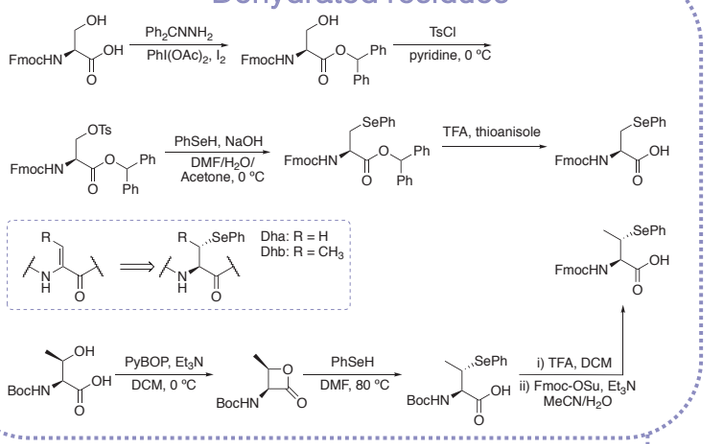

(Methyl)lanthionine rings

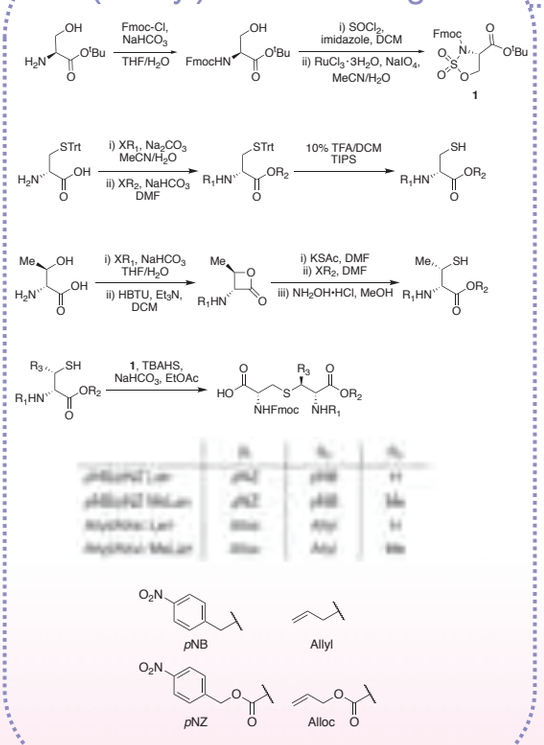

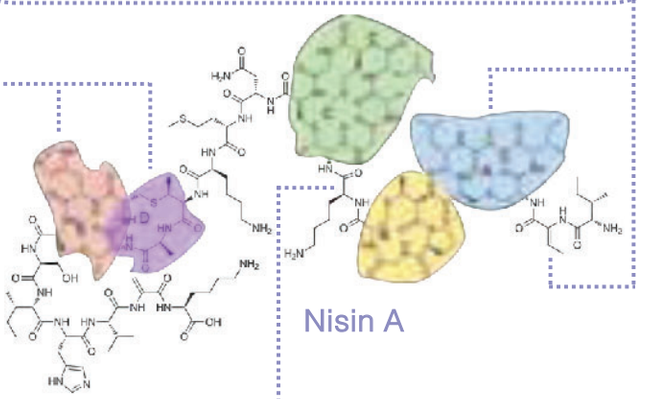

Ligation of two fragments and desulfurization

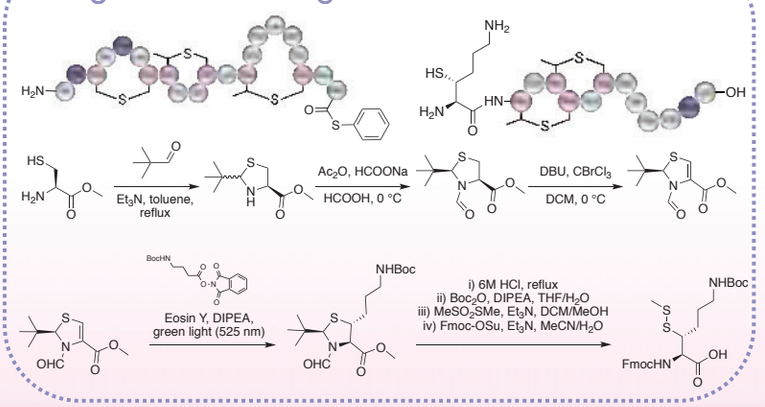

[1] D. Field *et al., FEMS Microbiology Reviews* **2023**, 47 (3), fuad023
[2] M. Gieselman *et al., Org. Lett.* **2001**, *3, 9, 1331–1334*
[3] D. Engelhardt *et al., Org. Biomol. Chem.* **2022**, *45, 8988-8999*
[4] Yin *et al., J. Am. Chem. Soc.* **2020**, *142, 33, 14201–14209*

https://doi.org/10.17952/37EPS.2024.P1014

NSERC CRSNG

Protein semi-synthetic approach to probe C-terminal hyper-phosphorylation of the Alzheimer-relevant protein Tau

Bingjia Yan[a], Léa El Hajjar[b,c], Wenyi Li[a], Caroline Smet-Nocca[b,c], Christian P. R. Hackenberger[a,d]

[a] Leibniz-Forschungsinstitut für Molekulare Pharmakologie, Robert Roessle-Str. 10, 13125 Berlin, Germany. [b] University Lille, Inserm, CHU Lille, Institut Pasteur de Lille, U1167-RID-AGE-Risk Factors and Molecular Determinants of Aging-Related Diseases, Lille, France. [c] CNRS EMR9002 Integrative Structural Biology, Lille, France. [d] Humboldt-Universität zu Berlin, Brook-Taylor-Str. 2, 12489 Berlin, Germany

https://doi.org/10.17952/37EPS.2024.P1015

Background

- Microtubule-associated Tau plays an important role in Alzheimer's disease (AD)[1].
- PTMs play a major role in the regulation of tubulin polymerization and/or stabilization of microtubule assembly[2-4].
- The PHF-1 epitope (Ser396, Ser400, and Ser404) of Tau comprising three phosphorylation sites is believed to be essential in the progression of AD[5].

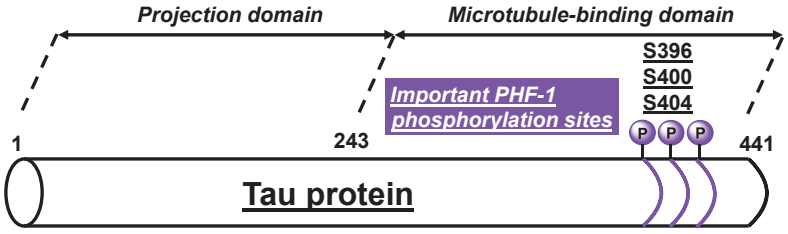

Aim: To obtain homogeneous PTM-patterns in C-terminus of Tau by Expressed Protein Ligation ➡ EPL strategy[6-8]

Semi-synthetic strategy to prepare homogeneous site-specific 2N4R PHF1-3P Tau protein

Concerns: 1. Impossible to synthesize multiple-phosphorylated C-terminal Tau peptides (390-441) *via* a single SPPS run.
2. Low ligation efficiency of NCL in preparation of C-terminal Tau peptides (390-441).

C-terminal Tau: A^{390}EIVYKSPVVS G^{401}DTSPRHLSN VSSTGSIDMV DSPQLATLAD EVSASLAKQGL^{441}-OH

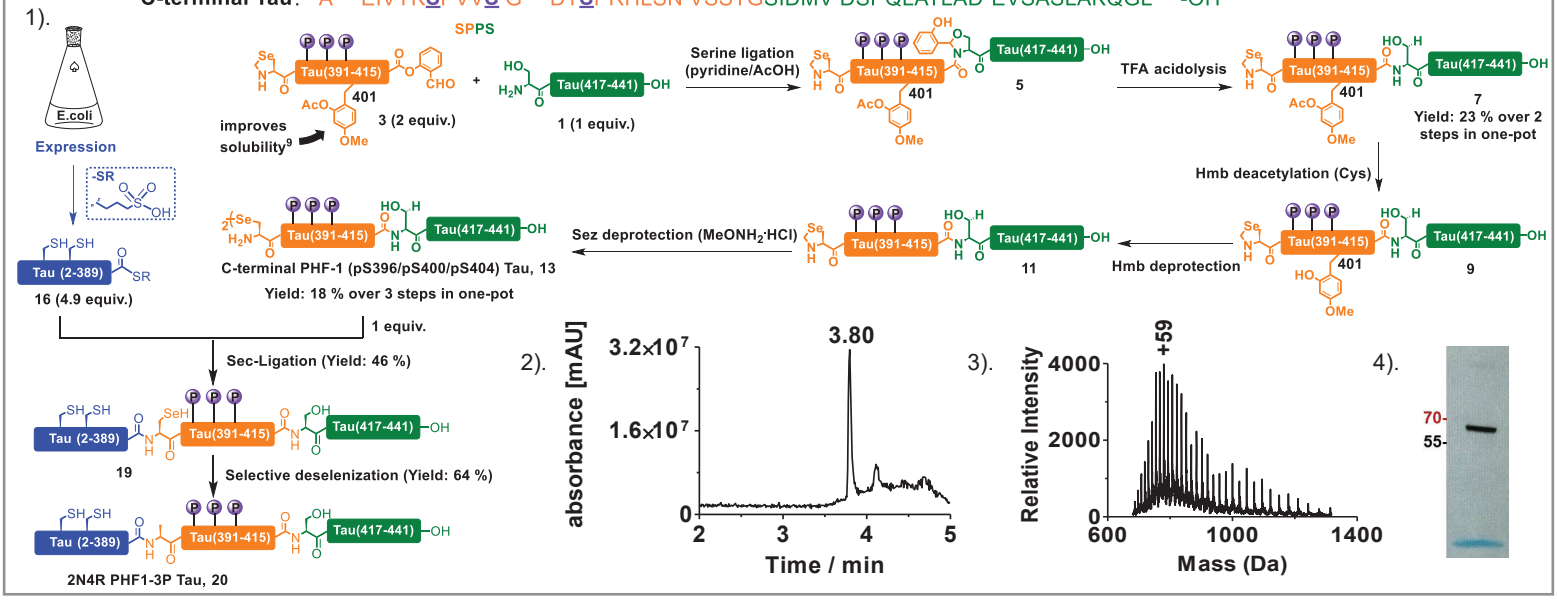

2).

3).

4).

Heparin-induced *in vitro* Tau aggregation assay

1).

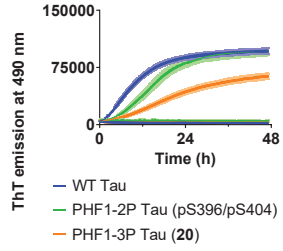

2).

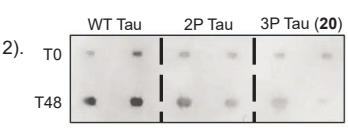

3).

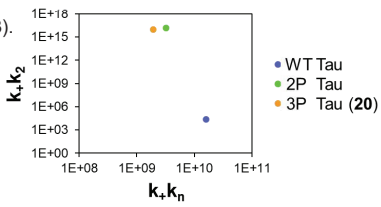

4).

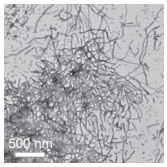

WT Tau

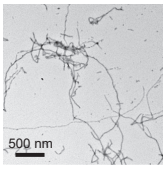

2P Tau

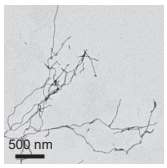

3P Tau (**20**)

- 10 μM Tau: 2.5 μM Heparin.
- PHF1-3P Tau (**20**, orange) exhibits a **slowest** onset of aggregation.
- PHF1-3P Tau (**20**) involves both **primary** (k_n) and **secondary** nucleation pathways (k_2).

Tau seed-induced *in vitro* Tau cross-seeding aggregation assay

1).

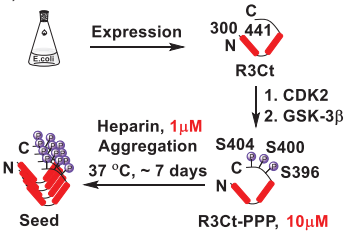

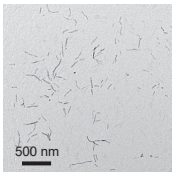

- **Flexible short** fibrils.

2).

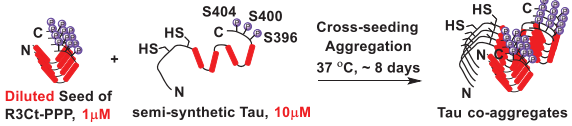

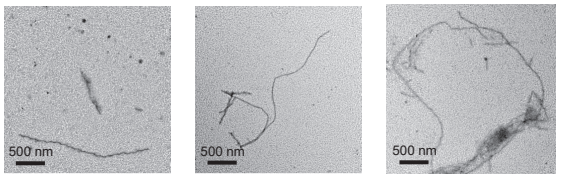

R3Ct-PPP with WT Tau | R3Ct-PPP with 2P Tau | R3Ct-PPP with 3P Tau (**20**)

- **Clusters** of Tau co-aggregates in R3Ct-PPP with 3P Tau (**20**).

Conclusion and future work

- **Combination of Sec- and Ser-Ligation** in preparation of homogeneous site-specific 2N4R PHF1-3P Tau.
- PHF1-3P Tau **inhibits** heparin induced aggregation.
- PHF1-3P Tau **facilitates** the development of elongated PHF-like fibrillar aggregates in cross-seeding aggregation.
- ❑ **cryo-EM** analysis of the generated Tau filaments.
- ❑ **Liquid-liquid phase separation (LLPS)** of semi-synthetic Tau proteins.
- ❑ *ex-vivo* Tau filaments **delivery** assay on neuronal cell line.
- ❑ **Seeding** of Tau aggregation in biosensor cells (HEK293T).

@PhosphorusFive
@BingjiaYan

References

1. M-Y Lee *et. al., Annu Rev Neurosci,* **2001,** *24,* 1121-1159.
2. Grundke-Iqbal *et. al., Proc. Natl. Acad. Sci. U. S. A.,* **1986,** *83,* 4913-4917.
3. Braak *et. al., Neurobiol. Aging,* **1995,** *16,* 271-278.
4. Hanger *et. al., Trends Mol. Med.,* **2009,** *15,* 112-119.
5. Drewes *et. al., EMBO J.,* **1992,** *11,* 2131-2138.
6. Smet-Nocca *et. al., Mol Biosyst,* **2011,** *7,* 1420-1429.
7. Haj-Yahya *et. al., J. Am. Chem. Soc.,* **2018,** *140,* 6611-6621.
8. Ellmer *et. al., Angew. Chem. Int. Ed.,* **2019,** *58,* 1616–1620.
9. Li *et. al., Org. Lett.,* **2016,** *18,* 5944-5947.

Structural Optimization Study Leading to Orally Bioavailable Cyclic Peptides Inhibiting an Intracellular Tough Target

Mikimasa Tanada, Ryuji Hayashi, Mirai Kage, Atsushi Ohta, Hitoshi Iikura, Takuya Shiraishi.
(Chugai Pharmaceutical Co. Ltd., Research Division)
https://doi.org/10.17952/37EPS.2024.P1016

CHUGAI
Roche Group

AP8784 (mRNA display Hit)
- 7 *N*-alkyl amino acids, cLogP = 12.7
- PPI KRAS^{G12D}-SOS1 IC_{50} = 54 nM
- Cellular IC_{50} > 20,000 nM (AsPC-1)

LUNA18 (Clinical compound)
- 8 *N*-alkyl amino acids, cLogP = 14.5
- PPI KRAS^{G12D}-SOS1 IC_{50} < 2 nM
- Cellular IC_{50} = 1.4 nM (AsPC-1)
- Oral BA = 21%(Mouse), 22%(Rat), 26%(Monkey), 47%(Dog)

(1) *J. Am. Chem. Soc.* 2023, *145*, 16610, (2) *Bioorg. Med. Chem.* Accepted (10.1016/j.bmc.2024.117830)

LUNA18-bound KRAS^{G12D} (X-ray, 7YV1)

No scaffold hopping

Orange: AP8784 (7YV1)
Blue: LUNA18 (7YUZ)

AP8784 / LUNA18 — SOS — RAS GDP (Inactive) — RAS GTP (Active) — GAP — Pi

LUNA18 mouse xenograft study (NCI-H441, oral QD)

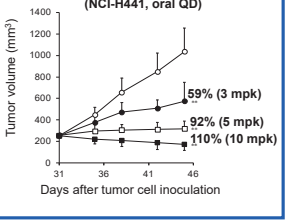

RAS protein structure was dramatically changed through induced-fit to our peptide side chain.

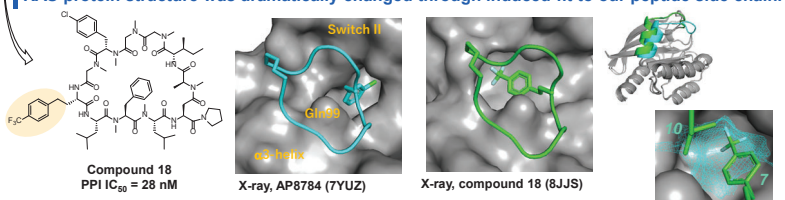

Compound 18
PPI IC_{50} = 28 nM

X-ray, AP8784 (7YUZ)

X-ray, compound 18 (8JJS)

Glid analysis

SBDD of side-chains located in the pocket was effective to improve bioactivity.

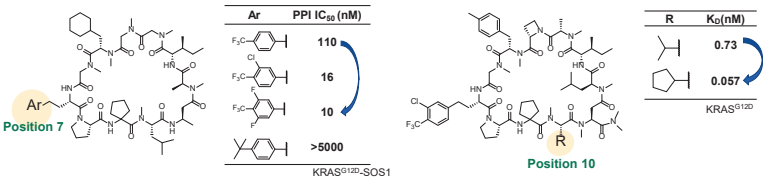

Semi-quantitative understanding of peptide structure by φ/ψ plot enabled rational restriction of cyclic peptide conformation resulting in improved membrane permeability.

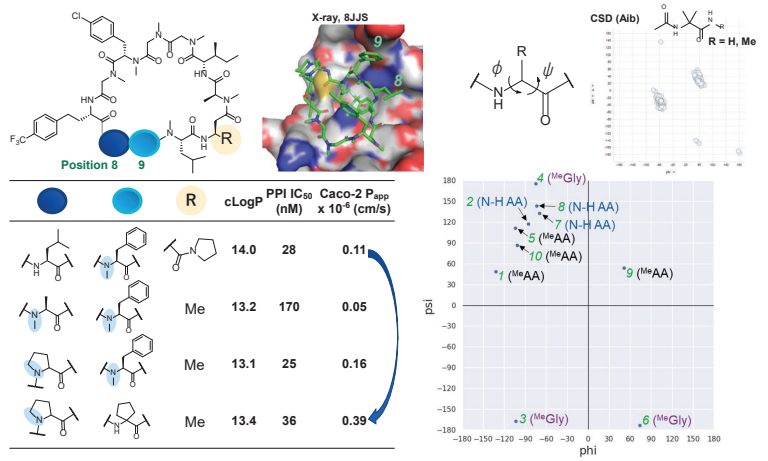

		R	cLogP	PPI IC_{50} (nM)	Caco-2 P_{app} x 10^{-6} (cm/s)
			14.0	28	0.11
		Me	13.2	170	0.05
		Me	13.1	25	0.16
		Me	13.4	36	0.39

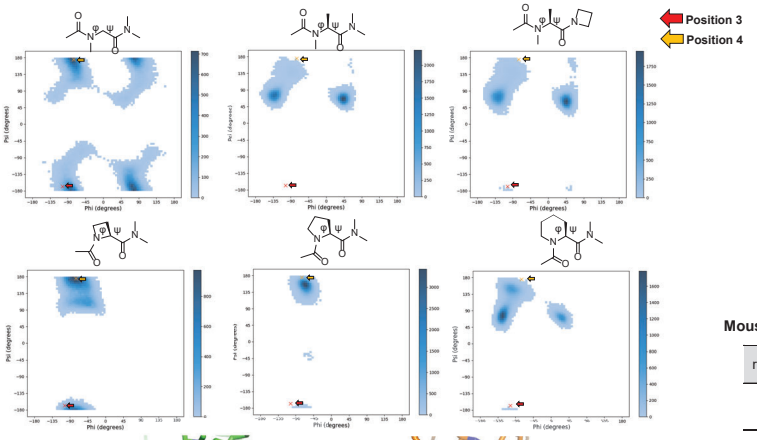

MeAla-Aze(2) model structure (based on 8JJS)

X-ray structure of LUNA18 (7YV1)

After identification of the membrane-permeable backbone, we were able to obtain LUNA18 by the combination of SAR.

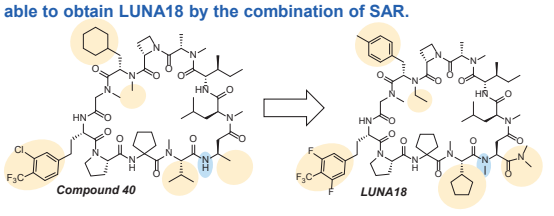

A single atom modification is enough to change the PK profile

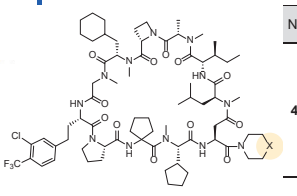

No.	species	route	dose (mg/kg)	$T_{1/2}$ (h)	AUC_{inf} (ng h/mL)	CL (mL/min/kg)	V_{ss} (L/kg)	F (%)
41	Mouse	iv	1	5.98	1350	12.4	3.0	-
		po	20	4.16	3880	-	-	14
	Rat	iv	1	5.57	2140	7.81	0.85	-
		po	10	3.96	3520	-	-	16
	Monkey	iv	0.167	8.14	673	4.30	0.82	-
		po	15	7.71	12500	-	-	21
42	Mouse	iv	1	8.62	2860	5.90	2.6	-
		po	20	6.46	3270	-	-	5.7
	Rat	iv	1	6.23	7970	2.13	0.37	-
		po	10	3.95	5770	-	-	7.2
	Monkey	iv	0.168	7.30	1590	1.81	0.49	-
		po	10	8.65	10700	-	-	11

Through the overall structural optimization from Hit to LUNA18…

- Strong Affinity (K_D=35 pM) was achieved without using polar side chains such as amino groups and carboxylic acids.
- Main exploration range of cLogP was as narrow as 13–15, which was sufficient to acquire membrane permeability.

Our Approach

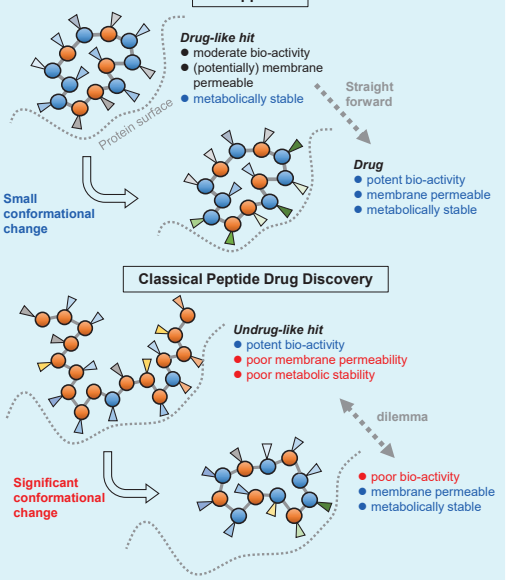

Desired values to acquire membrane permeable and metabolically stable cyclic peptide

Number of residues	Number of N-alkyl amino acids	cLogP	Amino acids
9 to 11	≧6	≧12.9	No polar amino acids such as Lys, Asp, Glu etc.

J. Am. Chem. Soc. 2023, 145, 24035

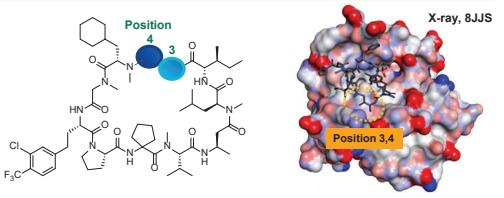

MeGly — MeAla — Aze(2) — Pro — Pic(2)

No.			cLogP	KRAS^{G12D}-SOS PPI IC_{50} (nM)	AsPC-1 IC_{50} (nM)	Caco-2 P_{app} x 10^{-6} (cm/s)
28	MeGly	MeGly	13.9	11	230	0.73
32	MeAla	MeGly	14.4	4900	>3000	N.T.
33	Aze(2)	MeGly	13.7	51	1100	1.38
34	Pro	MeGly	14.2	170	1200	1.75
35	Pic(2)	MeGly	14.8	3800	>3000	N.T.
36	MeGly	MeAla	14.4	2500	>3000	N.T.
37	MeGly	Aze(2)	13.7	22	230	0.99
38	MeGly	Pro	14.2	61	720	1.57
39	MeGly	Pic(2)	14.8	990	>3000	N.T.
40	MeAla	Aze(2)	14.2	24	110	1.62

Mouse SDPK (*compound 40*)

route	dose (mg/kg)	$T_{1/2}$ (h)	AUC_{inf} (ng h/mL)	CL (mL min^{-1} kg^{-1})	V_{ss} (L/kg)	F (%)
iv	5	3.16	65200	1.29	0.2	-
po	50	3.27	49700	-	-	7.6

https://doi.org/10.17952/37EPS.2024.P1017

Chemical Engineering of Artificial Transcription Factors

Omer Harel, Xiaoxi Lin, and Muhammad Jbara*
School of Chemistry, Raymond and Beverly Sackler Faculty of Exact Sciences, Tel Aviv University, Tel Aviv, 69978 Israel
E-mail: Jbaram@tauex.tau.ac.il

Abstract

The demand for site-selective functionalization strategies is crucial for generating precisely defined proteins and for advancing basic research and biomedical applications.[1,2] Cysteine-based reactions facilitate diverse transformations for modified proteins[3], yet achieving site selectivity or multiple transformations remains challenging. This study presents a site-selectivity methodology by manipulating C-S bond properties using palladium(II) complexes, enabling selective cysteine site editing in complex proteins.[4] Our orthogonal palladium(II) strategy allows rapid diversification of multiple cysteine sites, producing six covalently bound dimeric transcription factors (TFs) and six stapled linear analogs, on a milligram scale, with enhanced stability and potent DNA binding activity. This methodology facilitates protein editing and holds promise for engineering novel biomolecules, advancing biological understanding, and developing innovative therapeutics.

Selective Cys Modification via an Orthogonal Palladium(II) Strategy

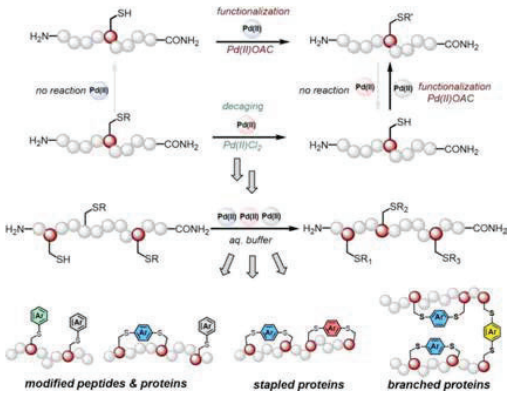

Late-Stage Dimerization and Editing of Minimized Transcription Factors Using Palladium(II) Strategy

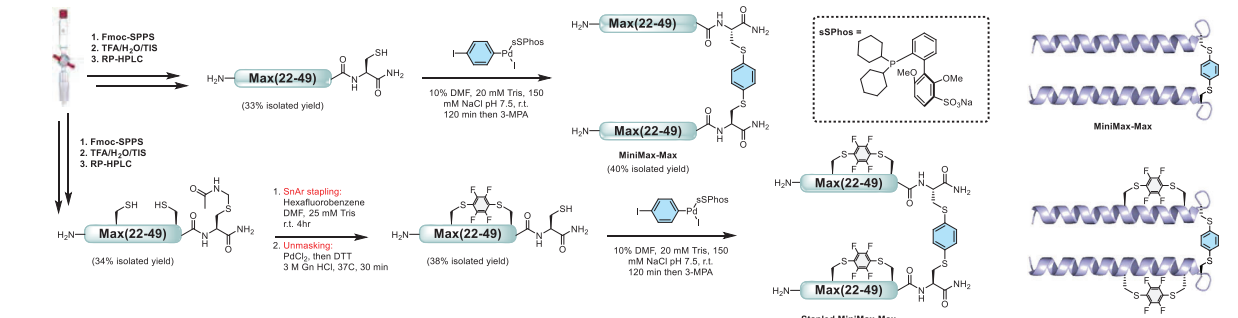

Chemical Synthesis of Stabilized Transcription Factors via Orthogonal Palladium(II) Strategy

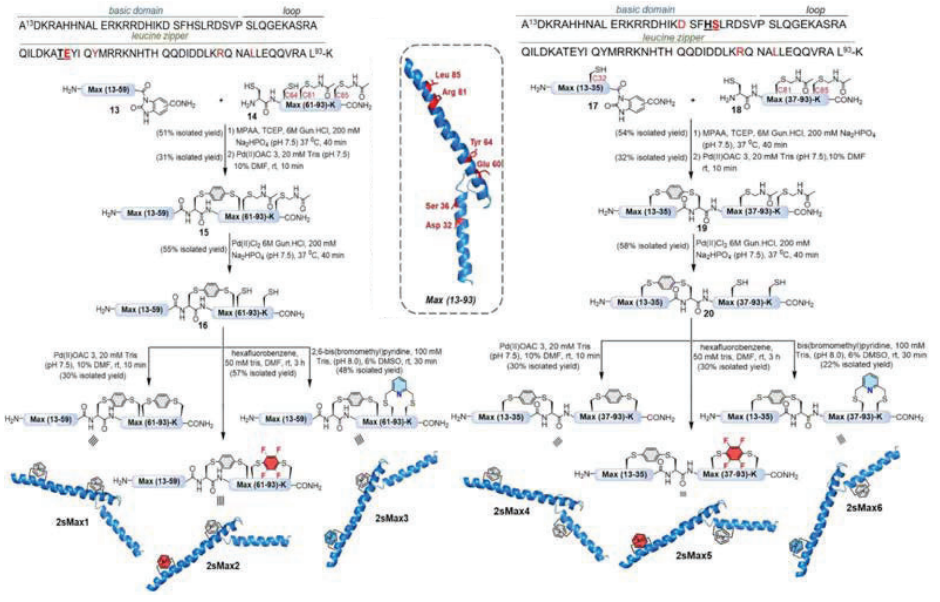

DNA Binding Activity of Stabilized Synthetic Max

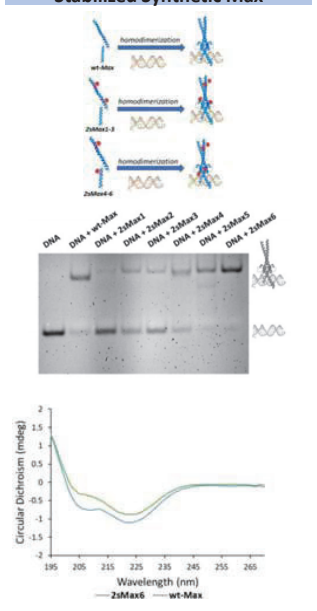

- *Chemical synthesis of a focused library of dimeric and stabilized TFs by using orthogonal palladium(II) chemistry and native chemical ligation.*
- *The stapled monomeric TFs exhibit enhanced stability and retain potent DNA binding activity with the canonical E-box sequence.*

Check out my CV | *Find me on LinkedIn*

References:

1. Harel, O. & Jbara, M. *Angew. Chem. Int. Ed. 62, e202217716* ***(2023)***
2. Harel, O. & Jbara, M. *Molecules 27(14), 4389* ***(2022)***
3. Lin, X., Nithun, R. V., Samanta, R., Harel, O., and Jbara, M. *Org. Lett. 25, 4715* ***(2023)***
4. Lin, X., Harel, O. & Jbara, M. *Angew. Chem. Int. Ed. 63, e202317511* ***(2024)***

Peptides Targeting DNA Four-Way Junctions

Eleanor Ivens, Andrew Beekman and Mark Searcey
School of Pharmacy, University of East Anglia, Norwich, NR4 7TJ, UK. E.Ivens@uea.ac.uk
https://doi.org/10.17952/37EPS.2024.P1018

University of East Anglia

Introduction

- Higher-order DNA structures are formed by the assembly of DNA into various 3D shapes.
- Four-Way Junctions (4WJs) are formed by the crossing over of DNA strands belonging to two separate double-stranded DNA segments.
- 4WJs are common intermediates in DNA repair and can be targeted in cancer and bacterial cells.[1]

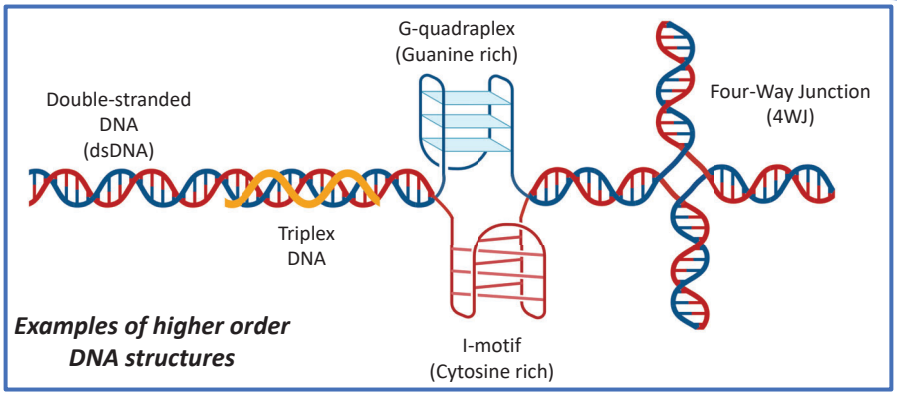

Examples of higher order DNA structures

Aims and approach

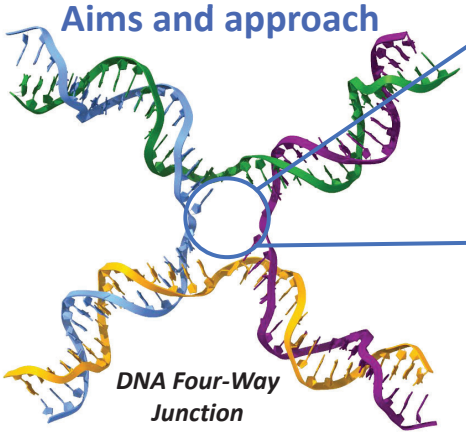
DNA Four-Way Junction

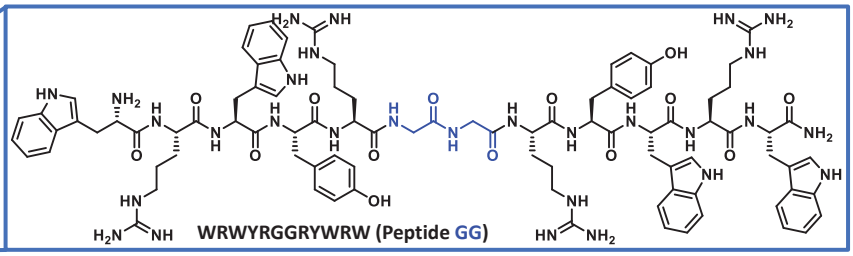
WRWYRGGRYWRW (Peptide GG)

- Peptide GG binds to the DNA 4WJ and has anti-bacterial effects.[2]
- During this project, peptides analogues were synthesised, based on the structure of Peptide GG.
- A series of biological assays were developed to test the ability of the peptide analogues to bind to the DNA 4WJ.

Results - synthesis

- Peptides synthesised using Solid-Phase Peptide Synthesis (SPPS).
- GG replacement groups (linkers) were added as unnatural amino acids.
- Cyclic peptides were produced, by combining the N^D-N^L linker with another linker.

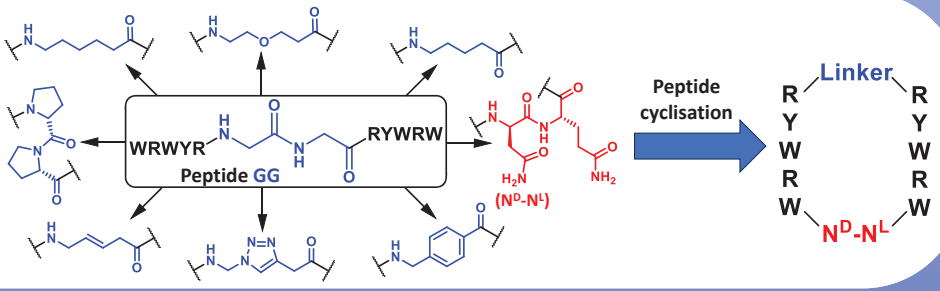

Results – Biological

Gel electrophoresis[3]

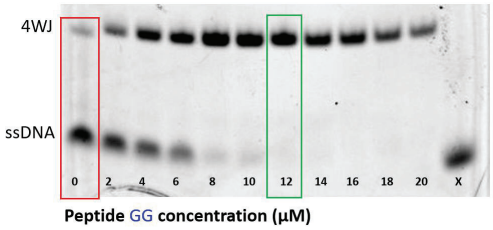

When four ssDNA strands were annealed in the absence of peptide, mostly ssDNA was formed. In the presence of peptide GG, the DNA was fully trapped as 4WJ.

Fluorescence Polarisation[4,5]

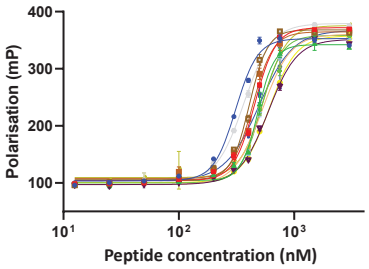

An increase in polarisation was observed when peptide was titrated into Fam-labelled 4WJ DNA.

Förster Resonance Energy Transfer (FRET)[6]

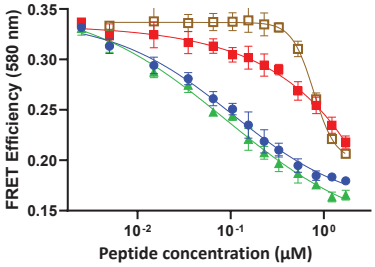

In solution the 4WJ was X-stacked, allowing FRET to occur. As peptide was added the 4WJ opened and FRET decreases.

Similar results were obtained for the linear/cyclic peptide analogues.

Different rates of 4WJ opening were observed. This indicates that although the peptides may have similar binding affinity, they may have different binding modes.

Future work

- Test the peptide analogues for selectivity against other DNA structures.
- Screen the peptide analogues for antibacterial activity, comparing to Peptide GG.
- Obtain crystal structures of the peptide:4WJ complex for further SAR studies.

References: 1) Ivens et al, *Bioorg. Med. Chem.* **2022**, 69, 116897. 2) Rideout et al, *Peptides.* **2013**, 40, 112. 3) Howell et al, ChemMedChem. 2012, 7, 792. 4) Fogg et al, J Mol Biol. 2001, 313(4), 751. 5) Lin et al, Int. J. Mol. Sci. 2023, 24(1), 580. 6) Clegg et al. Biochemistry, 1992, 31(20), 4846.

https://doi.org/10.17952/37EPS.2024.P1019

Faculty of Chemistry - Organic and Bioorganic Chemistry - OCIII

UNIVERSITÄT BIELEFELD

C-Glycosylation of Aromatic Amino Acids by Pd-Catalyzed Cross-Coupling

***Calvin Matula* and Norbert Sewald**

Organic and Bioorganic Chemistry, Faculty of Chemistry, Bielefeld University, Germany.

calvin.matula@uni-bielefeld.de

Glycopeptides and their features

- Glycoproteins play important roles in many biological processes, among them cell adhesion, cell differentiation or regulation of cell growth[1,2]
- Glycosylation in proteins modifies conformation, hydrophilicity and stability of peptides[3]
- Especially in peptide based drugs the introduction of glycosyl residues may lead to a higher membrane permeability (e.g. BBB)[4]
- *C*-Glycosides bear a higher stability towards hydrolysis in comparison to *N*- and *O*-Glycosides[5]
- Pd-catalyzed cross-coupling reactions offer a high potential to generate *C*-Glycosides[6, 7]
- Orthogonal protecting groups are used to imply their use as building blocks in peptide-based chemistry as SPPS

Generation of Boronates

- Generation of glycal boronic acids takes place through deprotonation by ^{t}BuLi followed by transmetallation with $B(OMe)_3$ and hydrolysation
- Boronic acids should be used short after its synthesis

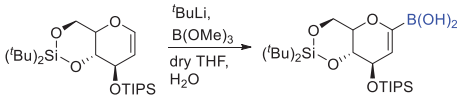

- Boronic acid esters can also be implemented in Suzuki cross coupling reactions
- Advantage of them being less prone to hydrolysis while storage

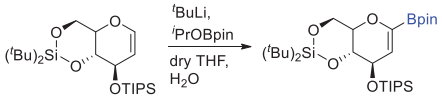

Suzuki cross coupling

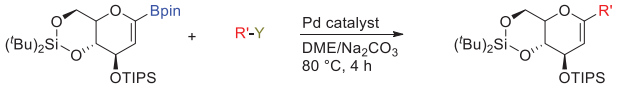

- Suzuki cross-coupling has been established for D-Glucal
- Generally Pd-catalyzed cross couplings are challenging for electronrich compounds like indole and tryptophane
  - Oxidative addition to the Pd-catalyst requires electronpoor aryl halides
- Enhancement of reaction conditions to obtain good yields and to ensure reproducibility

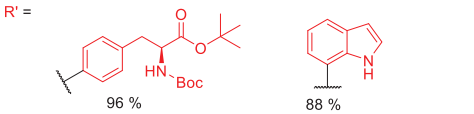

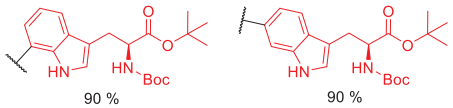

Heteroaromatic glucal library

Library of **16** new heteroaromatic glucals in very good yields

(Un)substituted and aminofunctionalised pyridines and pyrimidines were employed

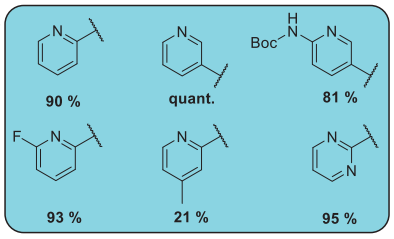

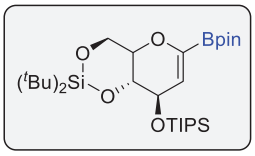

\+ HetAr-**Br**

Chinolines, benzofuranes, benzothiazoles and thiophenes were cross coupled

4-, 5-, 6- and 7-bromoindoles and 3-carbaldehyde-5-bromoindole have been implemented

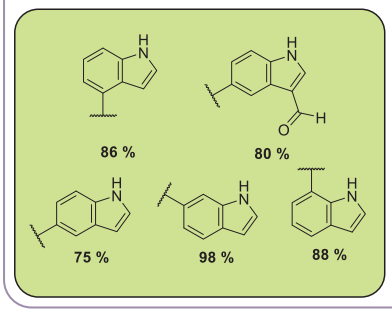

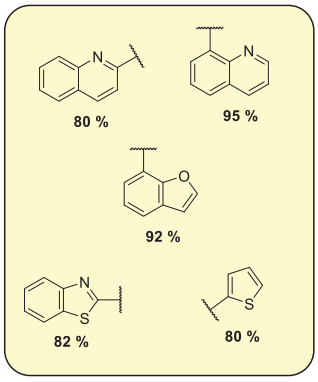

Glucal oxidation

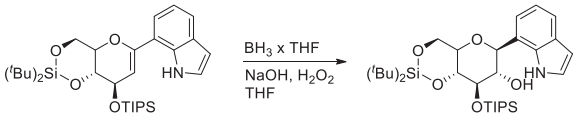

Hydroboration-Oxidation

- Anti-Markownikow addition of borane to alkene → **syn-addition**
- Stereoselective reaction to yield **β-anomer**

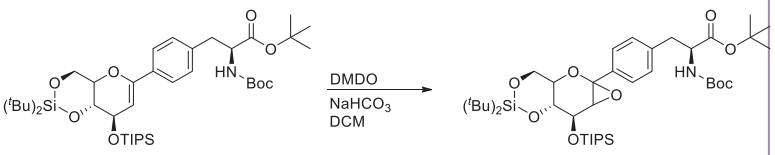

Epoxidation

- Epoxidation followed by reduction of oxirane
- Stereoselective reaction is supposed to yield **α-anomer**
- not suitable for indoles

References

[1] C. R. Apostol, M. Hay, R. Polt, *Peptides* **2020**, *131*, 170369.
[2] R. A. Dwek, *Chem. Rev.* **1996**, *96*, 683.
[3] N. Sewald, H. D. Jakubke, *Peptides: Chemistry and Biology*, Wiley-VCH, Weinheim, DE, **2002**.
[4] R. Polt, M. Dhanasekaran, C. M. Keyari, *Med. Res. Rev.* **2005**, *25*, 557.
[5] M. H. D. Postema, *Tetrahedron* **1992**, 8545.
[6] M. Ousmer, V. Boucard, N. Lubin-Germain, J. Uziel, J. Augé, *Eur. J. Org. Chem.* **2006**, *2006*, 1216.
[7] K. Parkan, R. Pohl, M. Kotora, *Chem. Eur. J.* **2014**, *20*, 4414.

37th EPS European Peptide Symposium
14th IPS International Peptide Symposium
25 - 29 August 2024
Satellite Workshop 30 - 31 August 2024
Florence, Italy- 2024

www.sewaldlab.de

SCAN ME

https://doi.org/10.17952/37EPS.2024.P1020

Efficient Peptide Thioester Synthesis from Hydrazides Using Near-Stoichiometric Thiol Quantities [1]

Julie Di Adamo[1], Nathalie Ollivier[1], Vincent Diemer[1], Oleg Melnyk[1]

[1]Univ. Lille, CNRS, Inserm, CHU Lille, Institut Pasteur de Lille, U1019 - UMR 9017 - CIIL - Center for Infection and Immunity of Lille, Lille, France

Introduction

Peptide alkyl thioesters serve as versatile peptide reagents across various synthetic applications. Consequently, significant efforts have been directed over the past two decades towards accessing peptide thioesters through both solution and solid-phase methods. Notably, the generation of peptide thioesters from **peptide hydrazides** is particularly prevalent in the field, owing to the ease of access to the latter via Fmoc-SPPS.

However, a notable limitation of many of these synthetic approaches, including the hydrazide technique, is the requirement for **a substantial excess of thiol reagent**.[2] This limitation confines these synthetic strategies to the production of thioesters from relatively **simple and cheap alkyl thiol nucleophiles**.

We present here a novel method to access various types of alkyl thioesters using nearly **stoichiometric quantities** of the alkyl thiol nucleophile.

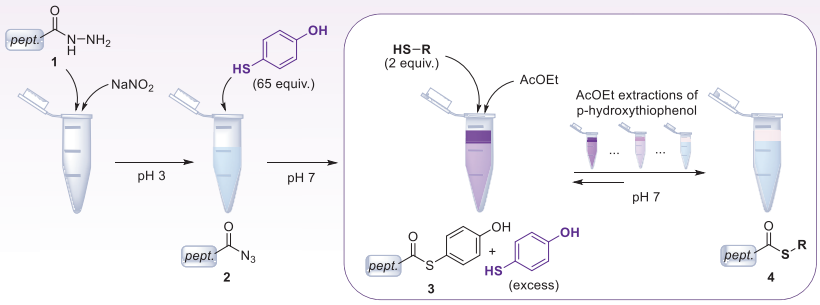

Fig. 1: One pot synthesis of peptide alkyl thioesters from peptide hydrazides is favoured by shifting thiol-thioester equilibrium through aryl thiol extraction.

Method

Initially, the hydrazide undergoes **activation** with sodium nitrite to yield a peptide azide (1→2, Fig.1). Subsequently, an excess of aryl thiol is added to the peptide azide solution under neutral pH conditions, resulting in the formation of an **intermediate aryl thioester** (2→3, Fig.1)**,** following a procedure reported by Liu and colleagues.[3]

In our method, an additional step involves a **thiol-thioester exchange** between the in situ formed aryl thioester and an alkyl thiol added in **quasi-stoichiometric amounts** to the reaction, under conditions enabling to concomitantly remove the excess of aryl thiol (3→4, Fig.1).

The excess of aryl thiol is essential to displace the azide and neutralize any remaining nitrous acid, but logically inhibits the formation of the alkyl thioester which proceeds through an **equilibrated thiol-thioester exchange** process.

In contrast, the removal of the aryl thiol during the thiol-thioester exchange reaction accelerates and promotes the formation of the alkyl thioester. This was conveniently achieved by using ***p*-hydroxythiophenol**, a thiol extractable under neutral pH conditions. (*Fig. 1*)

Results and discussion

As the aim of our method is to **shift the equilibrium** of the thiol thioester exchange by means of **extractions** to favor the formation of the desired thioester, we initially focused on this exchange to form **three thioesters** (thioester of MPA*, MPA-R_6L-NH_2 and coenzyme A) using two different methods.

The first method starts from the **p-hydroxy thiophenyl ester without extractions** (Method A) and the other from the **peptide hydrazide under extractive condition** (Method B). (*Fig. 2*)

Then, we compared these exchanges thanks to the **kinetics data** we obtained during the synthesis of our thioesters using both methods. (*Fig. 3*)

* MPA = 3-Mercaptopropionic acid

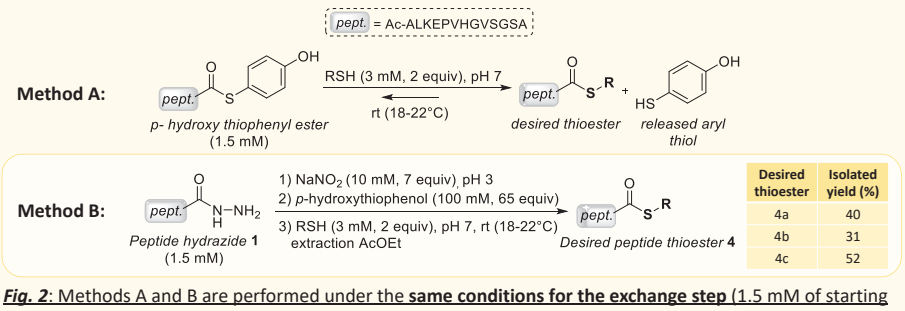

Desired thioester	Isolated yield (%)
4a	40
4b	31
4c	52

Fig. 2: Methods A and B are performed under the **same conditions for the exchange step** (1.5 mM of starting material, 2 equiv of alkyl thiol, pH 7) but Method B allows the extractions of *p*-hydroxythiophenol.

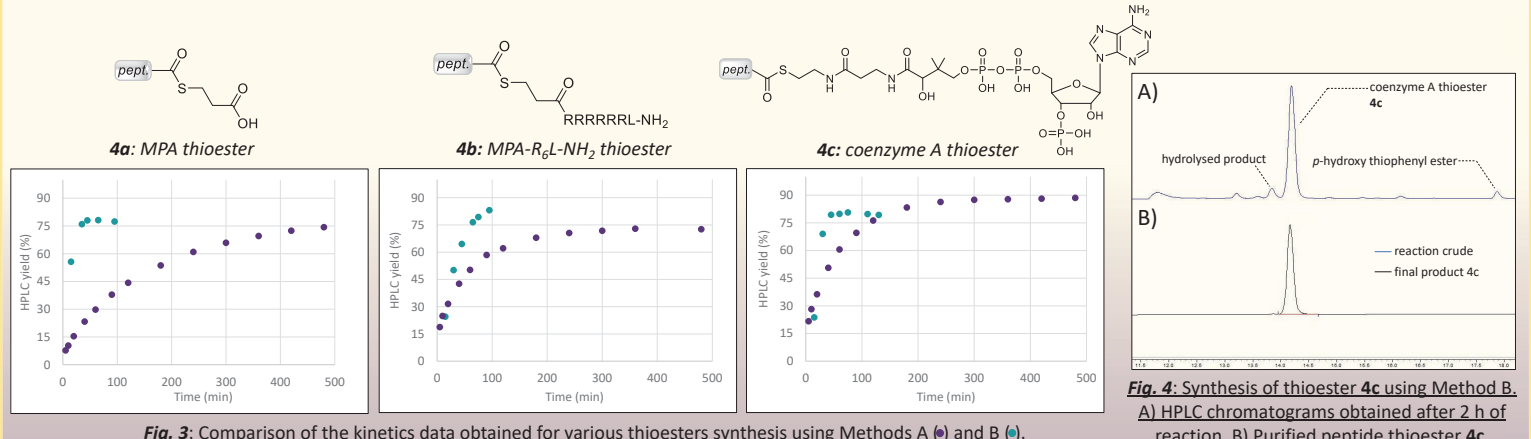

Fig. 3: Comparison of the kinetics data obtained for various thioesters synthesis using Methods A (●) and B (●).

Fig. 4: Synthesis of thioester **4c** using Method B. A) HPLC chromatograms obtained after 2 h of reaction. B) Purified peptide thioester **4c**.

Figure 3 highlights that by shifting the equilibrium of the thiol-thioester exchange using Method B, the desired maximum thioester yield can be achieved **more quickly**. In addition, for some thioester the **HPLC yield** using method B are higher.

The improvement in alkyl thioester synthesis obtained using Method B is due to the fact that both the initial excess of aryl thiol and the released aryl thiol are removed by extraction, while in Method A the released *p*-hydroxythiophenol remains in solution and favours the backward reaction.

Conclusion

Our method has proven **highly effective** in accessing peptide thioesters from a variety of alkyl thiols. Indeed, the extraction of the initial aryl thiol and aryl thiol released during the exchange **shifts the equilibrium** of the reaction, favouring the formation of the desired alkyl thioester using **near-stoichiometric conditions**.

The method is thus applicable to the use of **complex or expensive thiols** such as coenzyme A.

References:

[1] Di Adamo, J.; Ollivier, N.; Cantel, S.; Diemer, V.; Melnyk, O. *J. Org. Chem.* **2024**. https://doi.org/10.1021/acs.joc.4c01251

[2] Agouridas, V.; El Mahdi, O.; Diemer, V.; Cargoët, M.; Monbaliu, J.-C. M.; Melnyk, O. *Chem. Rev.* **2019**, *119* (12), 7328–7443.

[3] Fang, G.-M.; Li, Y.-M.; Shen, F.; Huang, Y.-C.; Li, J.-B.; Lin, Y.; Cui, H.-K.; Liu, L. *Angew. Chem. Int. Ed.* **2011**, *50* (33), 7645–7649.

Electrostatic assistance of NCL catalysis by 4-mercaptophenylacetic acid[1]

Nathalie Ollivier[a], Eliott Roy[a], Remi Desmet[a], Vangelis Agouridas[a,b], Vincent Diemer[a] and Oleg Melnyk[a]

[a] Univ. Lille, CNRS, Inserm, CHU Lille, Institut Pasteur de Lille, U1019 - UMR 9017 - CIIL - Center for Infection and Immunity of Lille, F-59000 Lille, France
[b] Centrale Lille, F-59000 Lille, France

https://doi.org/10.17952/37EPS.2024.P1021

Introduction.

The native chemical ligation (NCL)[2] reaction is a powerful tool enabling the semi or total chemical synthesis of proteins[3]. The water-soluble aryl thiol 4-mercaptophenylacetic acid (MPAA)[4] is the gold standard catalyst for this reaction. In classical conditions and using peptide alkyl thioesters as acyl donors, it has to be used in large excess for achieving practically useful rates (up to 50-100 equivalents).

We report here that the rate of NCL using MPAA as catalyst is dramatically enhanced when the alkyl thioester features several arginines in the departing thiol from the thioester, due to the electrostatic assistance of the catalysis step (Figure →). By doing so, the electrostatically assisted NCL reaction ([e]NCL) proceeds very rapidly by using sub-stoichiometric concentrations of MPAA.

Principle of the electrostatic assistance of NCL catalysis step by MPAA

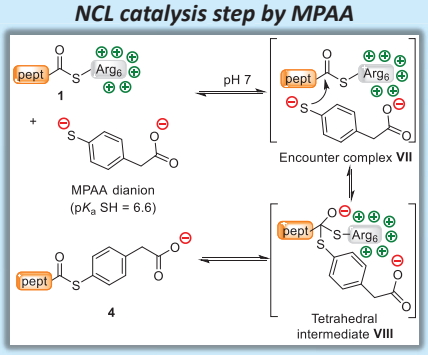

Electrostatic assistance of MPAA catalysis

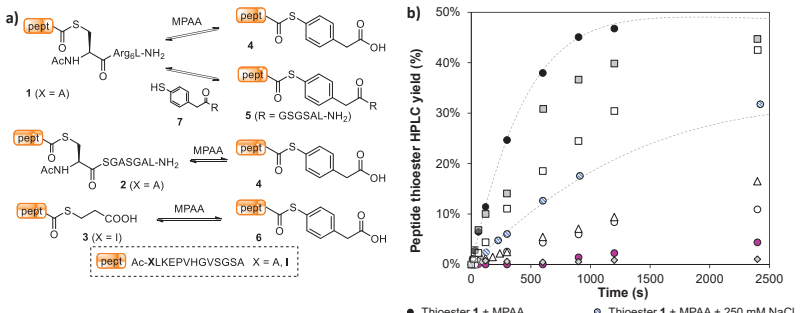

a) Reactions studied. b) Time course of peptide arylthioester formation (HPLC, 215 nm). Reaction conditions: [peptide thioester] = 50 µM, [arylthiol] = 250 µM, 10 mM sodium phosphate buffer, pH 7, 19 °C. The dots correspond to the experimental data, the dashed lines to the fitting curves.

Guanidinium chloride denaturant inhibits the assistance, while urea is tolerated.

Electrostatic assistance of NCL

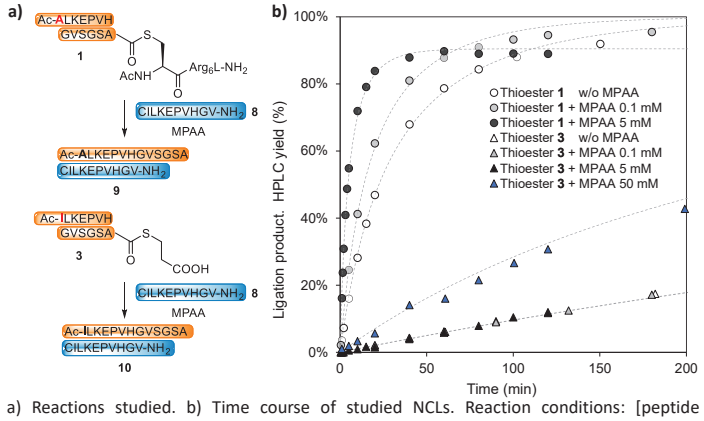

a) Reactions studied. b) Time course of studied NCLs. Reaction conditions: [peptide thioester] = 1 mM, [**8**] = 1,5 mM, 10 mM sodium phosphate buffer, pH 7, 19 °C. The dots correspond to the experimental data, the dashed lines to the fitting curves.

Due to the electrostatic assistance of the NCL catalysis step, NCL proceeds much faster than under classical conditions, while using only sub-millimolar concentrations of MPAA.

Applications.

[e]NCL enabled useful synthetic applications. Combining [e]NCL and classical NCL enabled performing one-pot kinetically controlled ligations. In another application, a one-pot [e]NCL/desulfurization process could be performed in one-pot because the sub-millimolar concentration of MPAA used for [e]NCL did not impair the desulfurization step.

One-pot kinetically controlled [e]NCL/NCL sequential ligation process

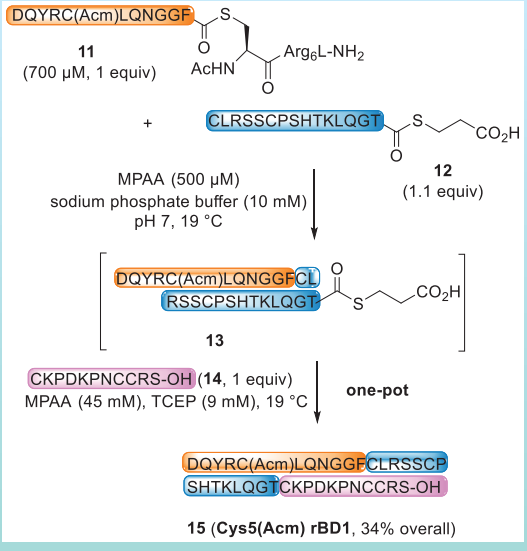

One-pot [e]NCL/desulfurization

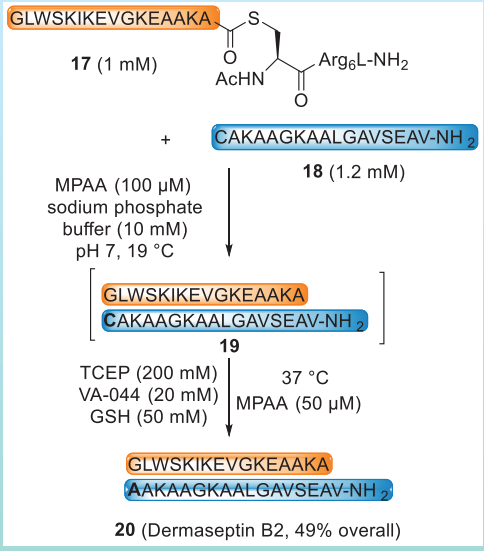

Conclusion.

The catalysis of NCL by MPAA can be boosted by using the negatively charges present in the catalyst at neutral pH for enabling attractive electrostatic interactions with the positively charged thioester reactant. Introducing the positive charges in the departing thiol in the form of arginines makes the assistance traceless while bringing solubility to the peptide thioester reactant. [e]NCL proceeds very fast using only sub-stoichiometric concentrations of MPAA.

References.

(1) Ollivier, N.; Roy, E.; Desmet, R.; Agouridas, V.; Diemer, V.; Melnyk, O. Electrostatic assistance of 4-mercaptophenylacetic acid catalyzed Native Chemical Ligation. Org. Lett. 2023, 25, 2696-2700.
(2) Dawson, P.E.; Muir, T.W.; Clark-Lewis, I.; Kent, S.B.H. Science 1994, 266, 776-779.
(3)a) Agouridas, V.; El Mahdi, O.; Melnyk, O. J. Med. Chem. 2020, 63, 15140-15152. b) Agouridas, V.; El Mahdi, O.; Diemer, V.; Cargoet, M.; Monbaliu, J.C.M.; Melnyk, O. Chem. Rev. 2019, 12, 7328-7443. c) Agouridas, V.; El Mahdi, O.; Cargoet, M.; Melnyk, O. Bioorg. Med. Chem. 2017, 25, 4938-4945.
(4) Johnson, E.C.; Kent, S.B.H. J. Am. Chem. Soc. 2006, 128, 6640-6646.

An efficient strategy to bioconjugate disulfide-rich peptides *via* thiol-maleimide chemistry while preserving their bridging pattern

Lylia Azzoug, Hervé Meudal, Karine Loth, Séverine Morisset-Lopez, Carlo Pifferi and Vincent Aucagne

Centre de Biophysique Moléculaire – UPR CNRS 4301 – Rue Charles Sadron 45071 Orléans Cedex 2, France

https://doi.org/10.17952/37EPS.2024.P1022

Background and project's aim

The generation of specific antibodies against weakly-immunogenic peptides requires their covalent conjugation to large protein carriers, such as keyhole limpet hemocyanin (KLH). Through such a general strategy, known as "hapten-carrier" approach, the carrier protein component has a dual function: (i) upon being processed by antigen-presenting cells (APCs), it provides a source of $CD4^+$ peptide epitopes that will be essential for the activation of helper T-cells; (ii) it also works as a scaffold for the display of several copies of hapten at once, which promotes B-cell receptor -mediated uptake and antibody production.

Most hapten-carrier approaches exploit the highly-efficient thiol-maleimide ligation, which enables for the attachment of multiple copies of peptides displaying a single cysteine thiol group onto a variety of commercial maleimide-functionalized carriers. Indeed, in addition to its fast kinetics and easy set-up, this benchmark reaction can be carried out under mild conditions (aqueous buffers, nearly-neutral pH, room temperature), compatible with a wide array of biomolecules (**Scheme 1**).

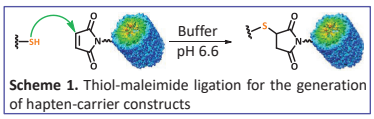

Scheme 1. Thiol-maleimide ligation for the generation of hapten-carrier constructs

While this methodology has been extensively applied for simple linear peptides by introducing a spare thiol residue in their sequence (for example an extra cysteine) the conjugation of disulfide-containing haptens by thiol-maleimide ligation has an inherent limitation (**Scheme 2**): the reducing ability of the free thiol group can disrupt the disulfide bridging pattern of the hapten leading to a mixture of incorrectly folded structures.

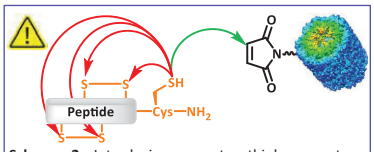

Scheme 2. Introducing an extra thiol group to a disulfide-containing hapten for ligation purposes can disrupt the disulfide bridging pattern.

To circumvent this limitation, Katayama *et al.* [1,2] introduced a PEG-based spacer (31 atoms) between the thiol function and the disulfide-containing hapten prior to thiol-maleimide conjugation. However, the extent of disulfide scrambling under the conjugation conditions has not been investigated.

With this project, we aim to develop a general strategy for the synthesis of disulfide-containing peptide conjugates that maintains the disulfide pattern unaltered under thiol-maleimide coupling conditions. As model peptide, we focused our attention on the well-structured N-terminal region of the Lingo-1 protein, a 20-mer peptide containing two disulfide bridges, that we coupled to a small battery of thiol-containing spacers (34 to 139 atoms), either flexible or rigid.

Model peptide

Lingo-1[1-20]

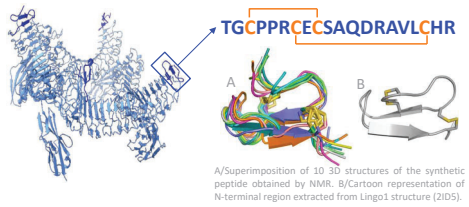

A/Superimposition of 10 3D structures of the synthetic peptide obtained by NMR. B/Cartoon representation of N-terminal region extracted from Lingo1 structure (2ID5).

Small disulfide-constrained peptide mimicking the 3D structure of the extracellular N-terminal part of LINGO-1, a membrane protein involved in neurodegenerative diseases.

Spacers to reduce disulfide scrambling

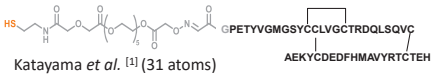

Katayama *et al.* [1] (31 atoms)

- $(GGGGS)_2GGC(SH)$ ≡ 52 atoms
- $(GGGGS)_4GGGGC(SH)$ ≡ 88 atoms
- $(GGGGS)_8GC(SH)$≡ 139 atoms

Flexible spacers

- $P_6C(SH)$ ≡ 34 atoms
- $P_{12}C(SH)$ ≡ 52 atoms

Rigid spacers

Polyproline as rigid "molecular rulers"
Wilhelm *et al.*[3]

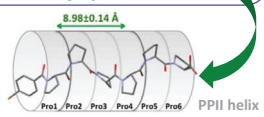

1. Synthesis of Lingo-1[1-20]

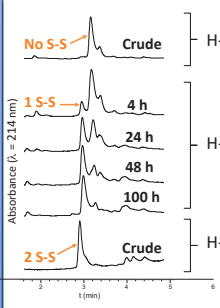

Lingo-1[1-20]

H-TGC(Acm)PPRCEC(Acm)SAQDRAVLCHRGK(N_3)-NH_2

380 µM peptide
10% aq. DMSO,
RT, 100 h [*then lyophilization*]

H-TGC(Acm)PPRCEC(Acm)SAQDRAVLCHRGK(N_3)-NH_2

1 mM peptide, 10 mM I_2
6.25% aq. HCl (160 mM) in AcOH, RT, 2 h
[*then ppt with Et_2O*]

H-TGCPPRCECSAQDRAVLCHRGK(N_3)-NH_2

Overall yield after 1 HPLC purification = 20%

2. Synthesis of thiol-(SH) spacers

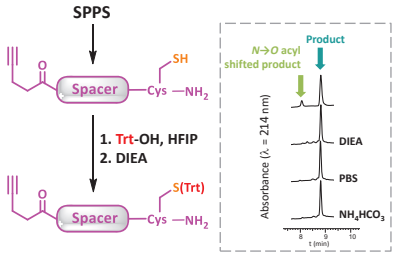

- **Trityl** protection prevents disulfide scrambling during CuAAC at pH 7
- **DIEA** treatment to reverse the Ser *N→O* shift

3. Copper-catalyzed Azide Alkyne Cycloaddition (CuAAC)

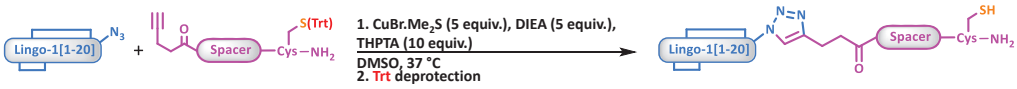

Spacer	Yield (%)
$(GGGGS)_2GGC(Trt)-NH_2$	43
$(GGGGS)_4GGGGC(Trt)-NH_2$	35
$(GGGGS)_8GC(Trt)-NH_2$	43
$P_6C(Trt)-NH_2$	78
$P_{12}C(Trt)-NH_2$	42

- **Trityl** deprotection with TFA/H_2O/Phenol/DODT/iPr_3SiH : 83/5/5/5/2 followed by precipitation in cold Et_2O.
- HPLC purification after step 1. Lingo-1[1-20]-SPACER-SH **crudes** are used for the scrambling monitoring.

Scrambling evaluation

Incubation of the Lingo-1[1-20]-SPACER-SH constructs under standard thiol-maleimide conjugation conditions: 20 mM phosphate buffer pH 6.6, 30 mM EDTA and 150 mM NaCl.

- HPLC and LC-MS monitoring at t=0 and up to t=2 h at RT and at t=24 h at 4 °C (recommended conditions for conjugation to maleimide activated proteins).
- ✓ *All solutions were thoroughly degassed and flushed with Ar to avoid dimer formation (confirmed by MS).*

HPLC monitoring of scrambling at λ = 214 nm

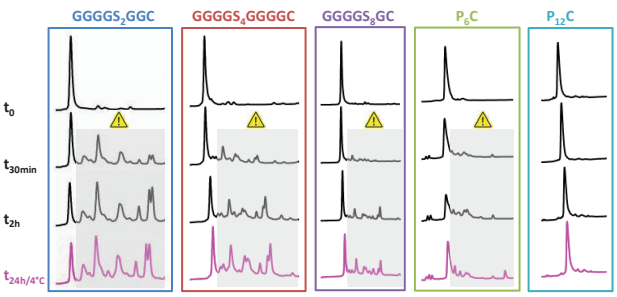

% of intact construct after incubation at 4 °C for 24 h

Spacer	%
$(GGGGS)_2$-GGC	11
$(GGGGS)_4$-GGGGC	18
$(GGGGS)_8$-GC	30
P_6C	45
$P_{12}C$	97

⚠ **Disulfide scrambling**

Chromolith, 3 mL/min flow rate. Gradient: 10-30% CH_3CN/H_20 (+0.1% TFA) over 5 min for **GGGGS** spacers, and, 10-45% CH_3CN/H_20 (+0.1% TFA) over 7.5 min for **polyproline** spacers, 25 °C.

Immunization studies

Immunization of one rabbit with the Lingo-1[1-20]-P_{12}-KLH conjugate

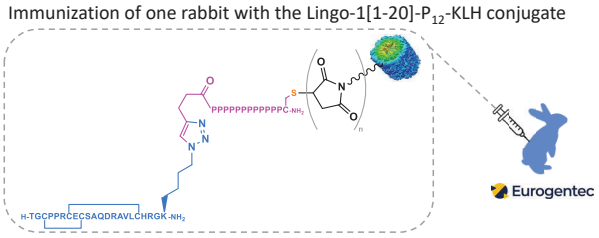

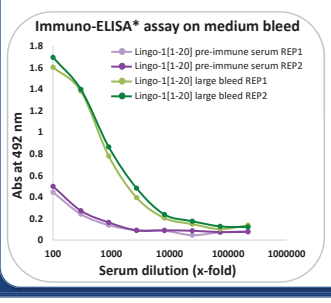

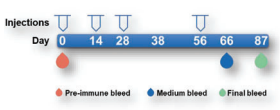

* Coating: Lingo-1[1-20]-GK(N_3)

- ✓ ELISA assay on post-immunization serum confirmed the presence of Lingo-1[1-20]-specific IgG antibodies
- ➢ Final bleed ELISA assay is undergoing.

Conclusions and prospectives

In this study, using the Lingo-1[1-20] model peptide, we systematically evaluated the contribution of different spacer moieties in limiting the extent of disulfide scrambling upon incubation of the "hapten-spacer-thiol" system alone, under standard reaction conditions used for thiol-maleimide coupling (*e.g.* buffered aqueous solution pH 6.6, for 2 hours at room temperature, or 24 hours at 4 °C). Strikingly, our results demonstrated that a **flexible** 52-atom spacer [$(GGGGS)_2GG$C] performed very poorly in maintaining unaltered the hapten disulfide pattern, with ≈20% of the native hapten being present after 2 hours at room temperature, and ≈10% after 24 hours at 4 °C. In sharp contrast, a **rigid**, proline-based 52-atom spacer [P_{12}C], allowed to maintain ≈100% of the native disulfide pattern, in both conditions, and it was therefore chosen as optimal spacer to carry out a hapten-carrier conjugation approach.

To further validate the importance of having a rigid linker, we will next perform circular dichroism (CD) on our proline-based compounds to confirm the presence of a PPII helix. At an early stage of the project we validated by NMR that the Lingo-1[1-20] synthetic peptide structure is superimposable with the corresponding N-terminal region from the native Lingo-1 protein. Then, immunization studies involving the corresponding KLH-based conjugate were performed, and immuno-ELISA assays with post-immunization serum confirmed the generation of hapten-specific antibodies. The next important step will be to assess whether the generated anti-Lingo-1[1-20] antibodies are capable to bind the native receptor; this could open interesting avenues to utilize these antibodies for follow-up projects involving the Lingo-1 protein.

References: [1] Katayama, H. and Mita, M. Bioorg. Med. Chem., **2016**, *24*, 3596. [2] Katayama, H.; Mizuno, R. and Mita, M. *Biosci. Biotechnol. Biochem.*, **2019**, *83*, 1791. [3] Wilhelm, P.; Lewandowski, B.; Trapp, N.; Wennemers, H. *J. Am. Chem. Soc.*, **2014**, *136*, 15829.

Auxiliaries in Native Chemical Ligation: Exploring the Reactivity Landscape with new Scaffolds

Sebastian Trunschke, Antonia Feida, Oliver Seitz*

Institut für Chemie, Humboldt-Universität zu Berlin, 12489 Berlin, Germany

https://doi.org/10.17952/37EPS.2024.P1023

The auxiliary-mediated native chemical ligation (NCL) serves as an essential tool in expanding the scope of NCL beyond cysteine, allowing for the selection of any amide bond for retrosynthetic scission of proteins. While long conceived as limited to "easy junctions" like Gly-Gly, our newest generation of auxiliaries are capable of tackling reactions of two β-branched amino acids and are feasible for ligation with phosphorylated or glycosylated amino acids at pH 7 or in acidic medium.

Base Catalysis in Auxiliary-mediated NCL

❑ auxiliary-mediated NCL can be enhanced via intramolecular base catalysis[1, 2, 3]

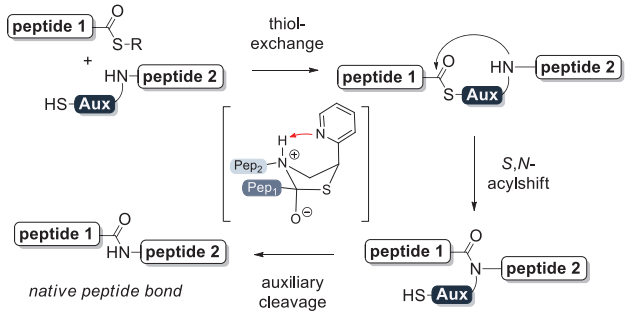

❑ A small history of ligation auxiliaries:

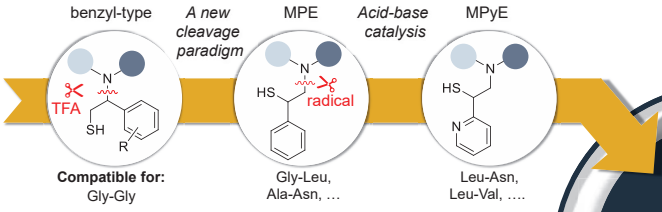

The Holy Grail of Ligations

❑ exceptional ligation rate with new conditions enables Leu-Val ligation in 4 h

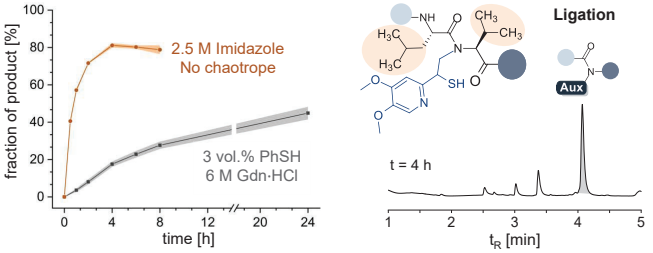

❑ Ligation with two β-branched amino acids become possible (Ile-Ile)

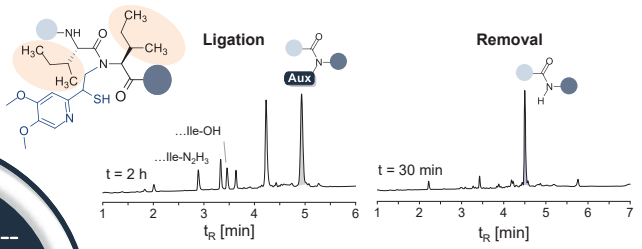

Connecting Basicity with Reactivity

❑ ligation rate correlates with basicity of the auxiliary

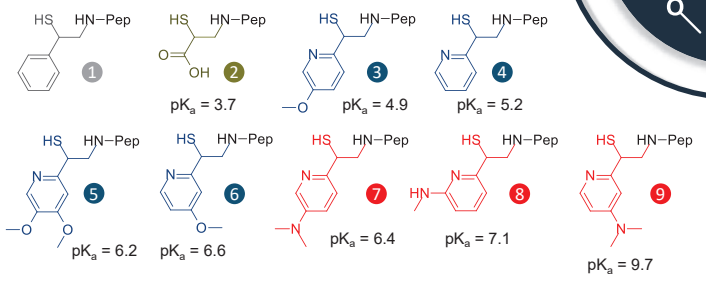

Ala-Asn Ligation

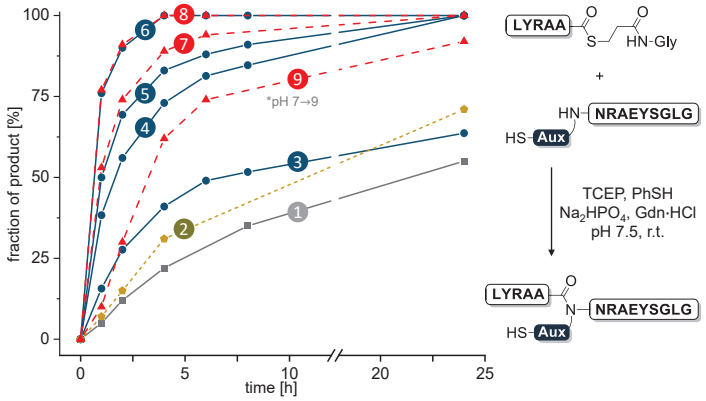

Protein Synthesis in Acidic Medium

❑ auxiliaries enable protein synthesis directly from peptide hydrazides

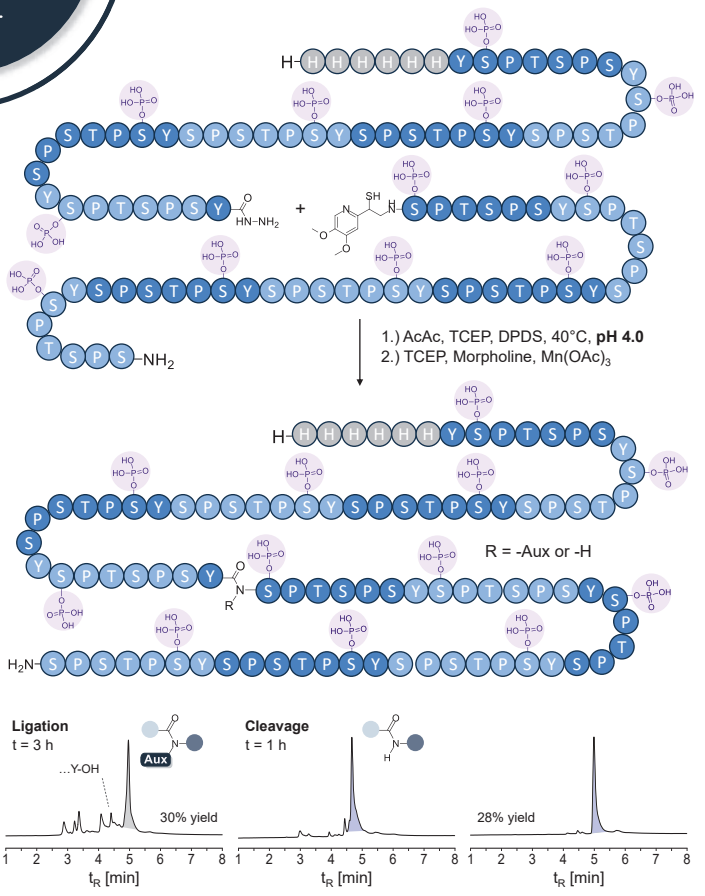

What Makes a Perfect Auxiliary?

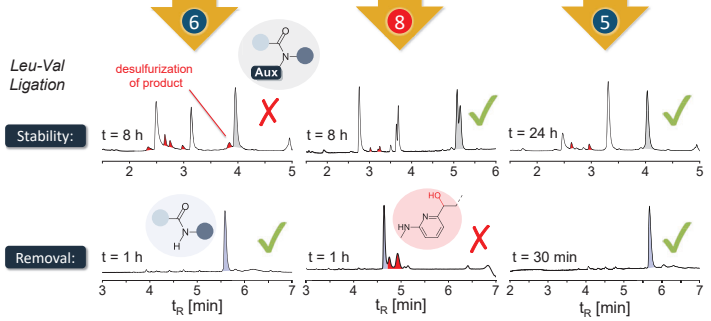

Conclusions

- ❑ crucial correlation between ligation rate and auxiliary basicity uncovered, confirming the postulated mechanism of intermediate proton abstraction
- ❑ a novel auxiliary for ligation of two amino acids with β-branching points
- ❑ with auxiliaries, ligation with phosphorylated and glycosylated amino acids are possible
- ❑ ligation at acidic pH feasible

[1] a) S.F. Loibl, Z. Harpaz, O. Seitz, Angew. Chem. Int. Ed., 2015, 54, 15055-15059; b) S.F. Loibl, A. Dallmann, K. Hennig, C. Juds, Chem. Eur. J., 2018, 24, 2623-3633.

[2] O. Fuchs, S. Trunschke, H, Hanebrink, M. Reimann, O. Seitz, Angew. Chem. Int. Ed., 2021, 60, 19483-19490.

[3] S. Trunschke, E. Piemontese, O. Fuchs, S. Abboud, O. Seitz, Chem. Eur. J., 2022, 28, e202202065

37th European Peptide Symposium
14th International Peptide Symposium
IPS 2024

https://doi.org/10.17952/37EPS.2024.P1025

Superfast Desulfurization for Protein Chemical Synthesis and Modification

Zhenquan Sun[1], Yihui Cao[1], Xuechen Li[1,*]

[1]*Department of Chemistry, State Key Laboratory of Synthetic Chemistry, University of Hong Kong, Hong Kong SAR, P. R. China (xuechenl@hku.hk)*

1. Introduction

A Chemical Protein Synthesis and Challenges of Desulfurization

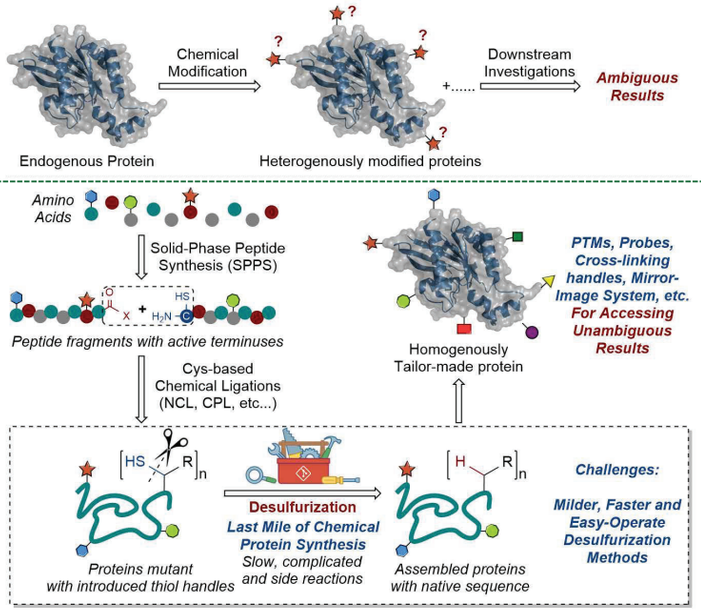

B This study

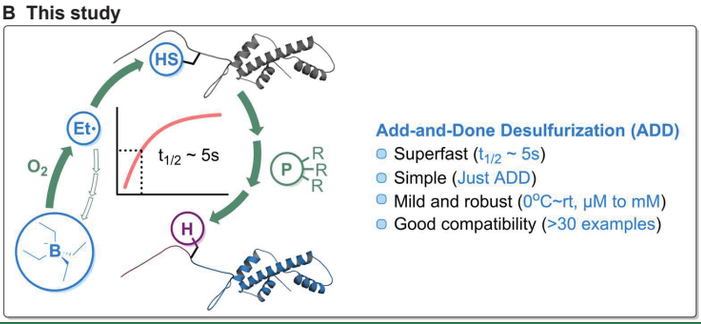

2. Kinetic Study and Substrate Scope Examination

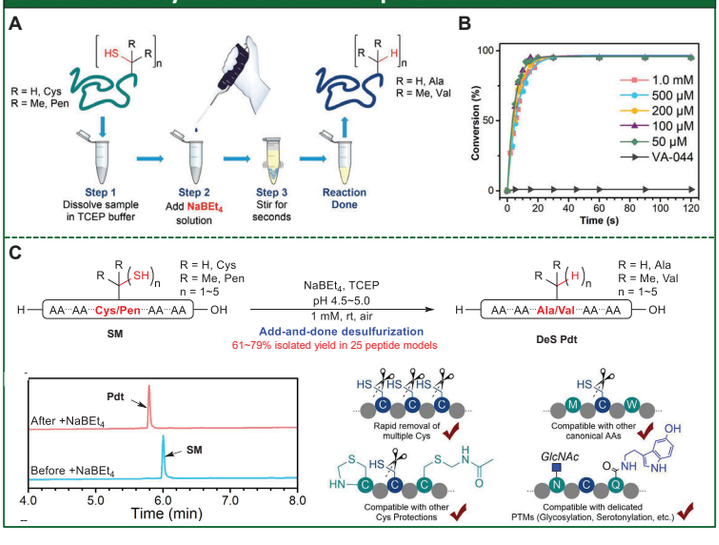

3. Application in Protein Modification and Protein Synthesis

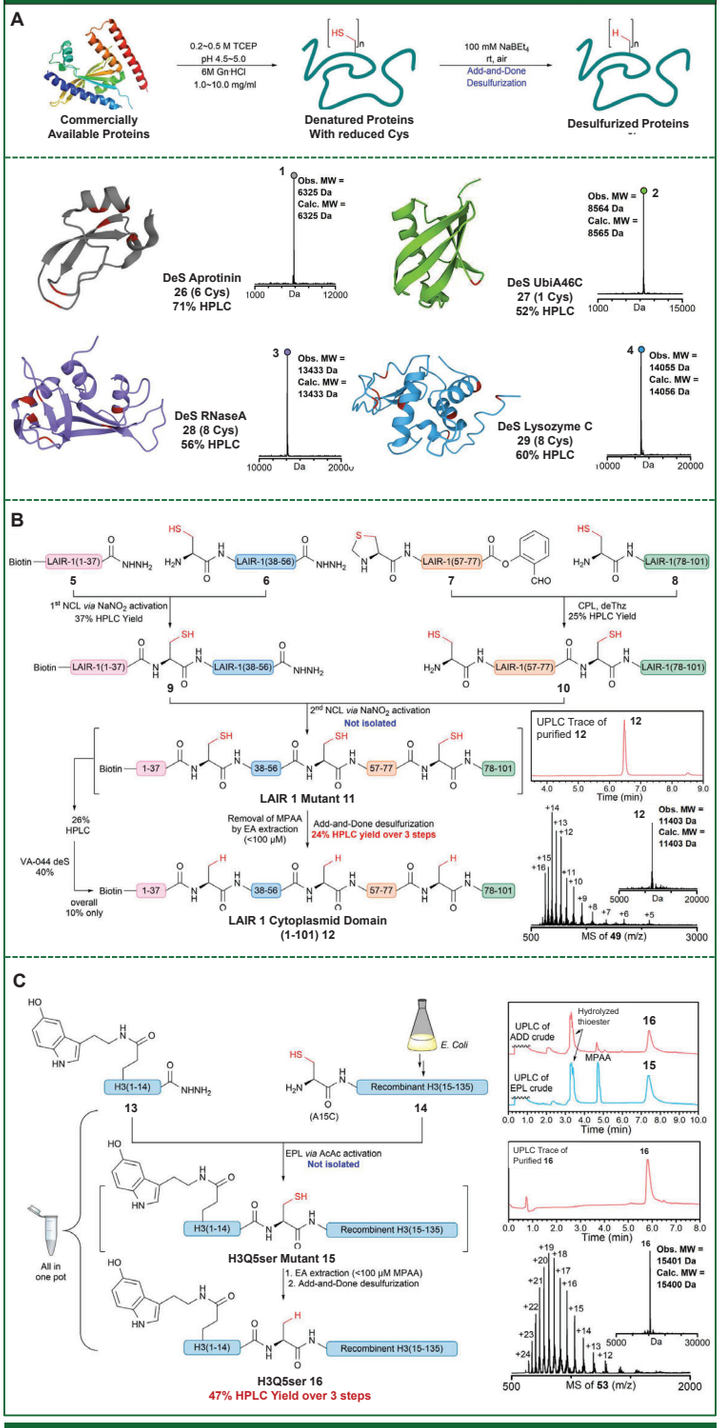

4. Reference

1. Sun, Z., Li, X.*, et al. *Chem* **2022**, 8, 2543-2557.
2. Sun, Z., Wei, T., Cao, Y., Li, X.* *STAR Proctoc.* **2023**, 4, 102042.

Scan QR code to access the superfast desulfurization paper

Acknowledgement: This work was supported by the Research Grants Council of University Grants Committee of the Hong Kong SAR, China (C7147-20G, 17303920, 17302621, and AoE/P-706/16).

https://doi.org/10.17952/37EPS.2024.P1026

An Iron-Catalyzed Protein Desulfurization Method Reminiscent of Aquatic Chemistry[1]

Rémi Desmet,[1] Céline Boidin-Wichlacz,[1] Reda Mhidia,[3] Aurélie Tasiemski,[1] Vangelis Agouridas,[1,2] Oleg Melnyk[1]

[1] CIIL - Center for Infection and Immunity of Lille, Univ. Lille, CNRS, Inserm, CHU Lille, Institut Pasteur de Lille, U1019 - UMR 9017, F-59000 Lille, France ; [2] Centrale Lille, F-59000 Lille, France ; [3] XProChem, 70 Rue du Dr. Yersin, F-59120 Loos, France.

1. Introduction.

One pillar of protein chemical synthesis based on the application of ligation chemistries to cysteine is the group of reactions enabling the selective desulfurization of cysteine residues into alanines.[2] Modern desulfurization reactions use a phosphine as a sink for sulfur under activation conditions involving the generation of sulfur-centered radicals. Here we show that cysteine desulfurization by a phosphine such as *tris*(2-carboxyethyl)phosphine TCEP can be effected efficiently by micromolar concentrations of iron under aerobic conditions in hydrogen carbonate buffer, that is using conditions that are reminiscent of iron-catalyzed oxidation phenomena occurring in natural waters.

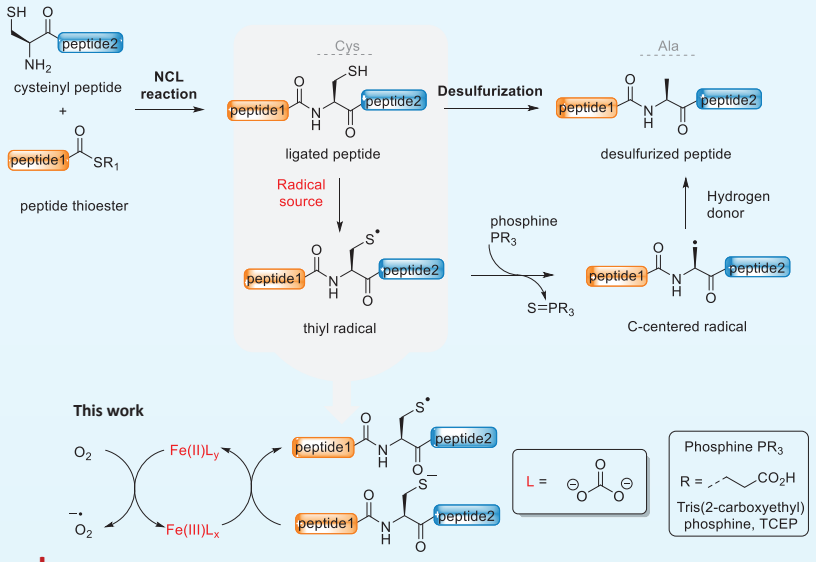

2. Influence of thiol type, thiol concentration and hydrogen carbonate concentration

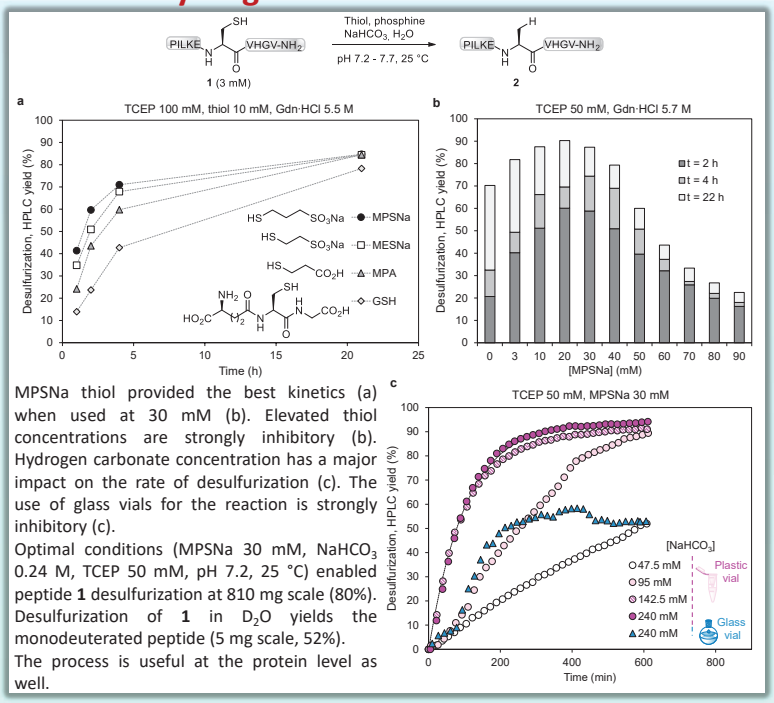

MPSNa thiol provided the best kinetics (a) when used at 30 mM (b). Elevated thiol concentrations are strongly inhibitory (b). Hydrogen carbonate concentration has a major impact on the rate of desulfurization (c). The use of glass vials for the reaction is strongly inhibitory (c).

Optimal conditions (MPSNa 30 mM, $NaHCO_3$ 0.24 M, TCEP 50 mM, pH 7.2, 25 °C) enabled peptide **1** desulfurization at 810 mg scale (80%). Desulfurization of **1** in D_2O yields the monodeuterated peptide (5 mg scale, 52%).

The process is useful at the protein level as well.

3. Implication of molecular oxygen

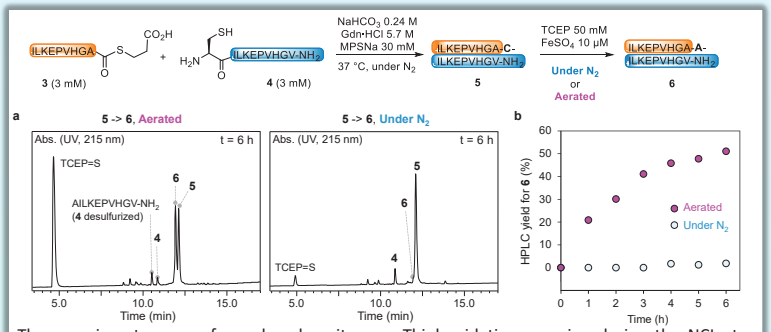

The experiment was performed under nitrogen. Thiol oxidation occuring during the NCL step enabled to consume the dissolved molecular oxygen remaining in the buffer solutions. The desulfurization carried out subsequently proceeded only with the aerated sample.

4. Implication of iron

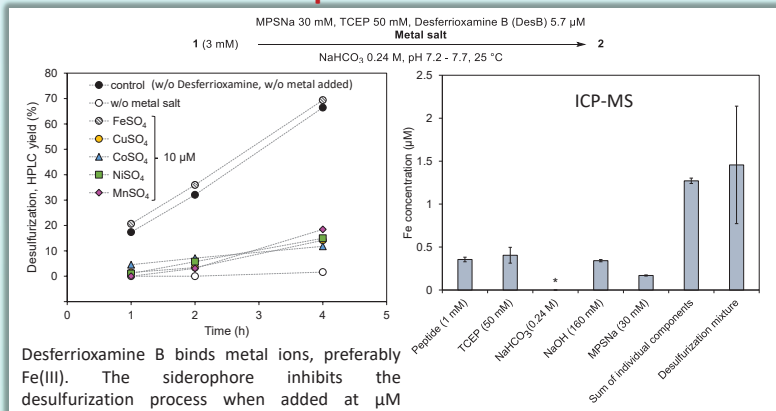

Desferrioxamine B binds metal ions, preferably Fe(III). The siderophore inhibits the desulfurization process when added at µM concentrations. The desulfurization process can be restored to the level of the control by adding $FeSO_4$, but not other metal salts.

The natural Fe content of a desulfurization mixture is ~1.5 µM. * Below quantification limit (0.01 µM).

5. Discussion & conclusion

In our experiments, the concentration of iron species is three orders of magnitude less (µM) than the peptide concentration (mM). In such conditions, Fe(II) species must be recycled into Fe(III) to achieve useful desulfurization yields.

Several studies established that the rate of oxidation of Fe(II) into Fe(III) by molecular oxygen is critically dependent on iron speciation. In particular, King and coworkers showed that in natural waters containing more than 1 mM of carbonate ions, the ferrous carbonate complex $Fe(CO_3)_2^{2-}$ is the most kinetically active species at neutral pH for reacting with molecular oxygen, and hence plays a major role in the degradation of organic matter in many aquatic systems.[3]

Our calculations of iron speciation support the presence of $Fe(CO_3)_2^{2-}$ in the desulfurization mixture.[1] Therefore, we think that part of the iron(II)-catalyzed peptide desulfurization process reported here is likely reminiscent of the iron-catalyzed oxidation phenomena occurring naturally in aquatic systems.

References

1. Desmet, R.; Boidin-Wichlacz, C.; Mhidia, R.; Tasiemski, A.; Agouridas, V.; Melnyk, O. An iron-catalyzed protein desulfurization method reminiscent of aquatic chemistry. Angew. Chem. Int. Ed. 2023, 62 (18), e202302648, DOI.
2. a) Diemer, V.; Melnyk, O. Protein desulfurization: Sodium tetraethylborate makes it fast. Chem 2022, 8, 2571-2573, DOI. b) Diemer, V.; Roy, E.; Agouridas, V.; Melnyk, O. Chem. Soc. Rev., DOI.
3. King, D. W. Role of carbonate speciation on the oxidation rate of Fe(II) in aquatic systems. Environmental Science & Technology 1998, 32, 2997-3003.

Chemoselective P-S coupling of aminophospholes to peptides under mild conditions

Miyanou Rosales-Hurtado,[1] Laure Liénart,[1] Sébastien Clément,[2] Jean-Alain Fehrentz,[1] Jean-Louis Banères,[1] Florine Cavelier,[1] Emmanuelle Rémond.[1]

[1]Pôle Chimie Balard, IBMM - UMR 5247, 1919, route de Mende, 34293 MONTPELLIER cedex 5 ; [2]Pôle Chimie Balard, ICGM - UMR 5253, 1919, route de Mende, 34293 MONTPELLIER cedex 5

emmanuelle.remond@umontpellier.fr ; florine.cavelier@umontpellier.fr

https://doi.org/10.17952/37EPS.2024.P1027

INTRODUCTION

Phospholes are dienes bridged with a tetrahedral phosphorus atom, which offer excellent resistance to photobleaching, and the phosphorus center can be easily transformed into derivatives with adjustable spectroscopic properties.[1] However, despite their low molecular weight, their absence of toxicity, and high photochemical stability compared to other fluorophores, the use of fluorescent phospholes in bioimaging is rare.[2] Strategies required for the chemistry and functionalization of phospholes are often associated with harsh conditions that cannot be used for biolabeling. To tackle this problem, we explored the attachment of phosphole-based fluorophores to peptides through the phosphorus atom under mild conditions, by P-heteroatom bond formation.[3]

COUPLING P-HYDROXYPHOSPHOLES OXIDE OR SULFIDE

We have recently reported the synthesis of P-hydroxyphosphole-oxide or sulfide by trapping the dibromobinaphthyl dianion with a dichlorophosphine reagent (Cl_2POMe or Cl_2PNEt_2), followed by oxidation or sulfuration of the P-center. Finals compounds **1a,b** were obtained by saponification or acid hydrolysis.[4]

Labeling amino acids and peptides in solution or on solid support

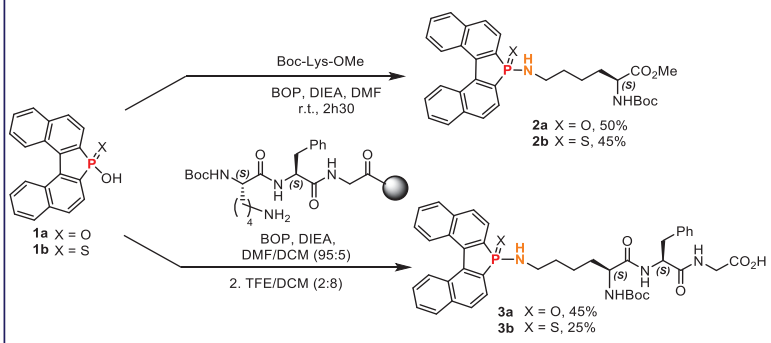

Labeling JMV2959 and FRET assays

This strategy was used to label JMV2959,[5] an antagonist of the Growth Hormone Secretagogue Receptor type 1a (GHSR1a), to the glycyl group or through spacers (Figure 1).

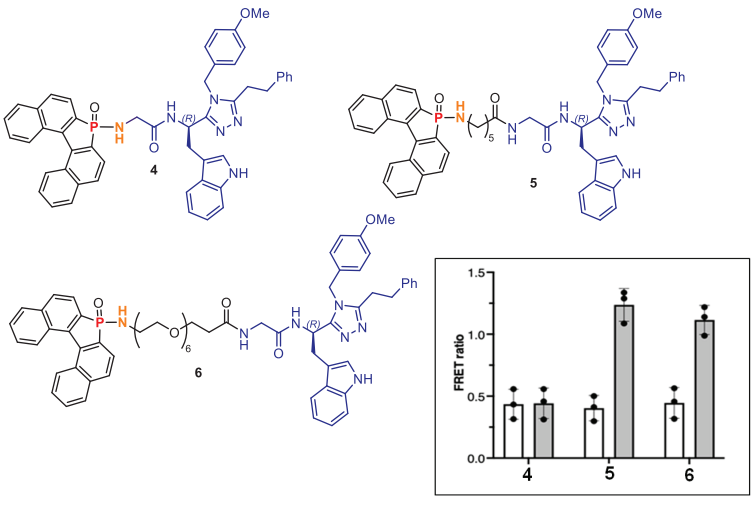

- Binaphtylphosphole oxide: fluorophore donor (λ_{abs} 380 nm; λ_{em} 464 nm)
- Recombinant GHSR labeled with AF488 dye: fluorophore acceptor (λ_{em} 525 nm)

Figure 1. Structure of conjugates **4-6** and FRET ratio with the labeled receptor GHSR1a

FRET-based binding assays demonstrate that the presence of a spacer is required to maintain high binding affinity (Figure 1).

CHEMOSELECTIVE COUPLING OF P-AMINOPHOSPHOLES

Alternatively, we have successfully developed a new method for coupling aminophospholes to biomolecules under neutral and reagent-free conditions.

Competitive experiments between amino acids

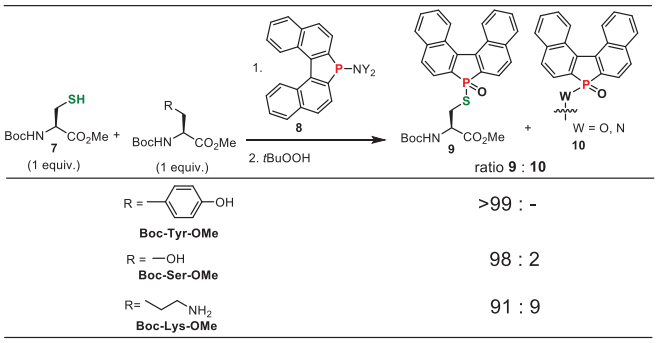

High selectivity of coupling to cysteine P-S >> P-N > P-O

Chemoselective labeling of cysteinylpeptides

Grafting aminophospholes onto cysteinyl pentapeptides which contain tyrosine, serine, or lysine residues, exhibit high chemoselectivity at the cysteine position. Only one product was observed in UPLC analysis.

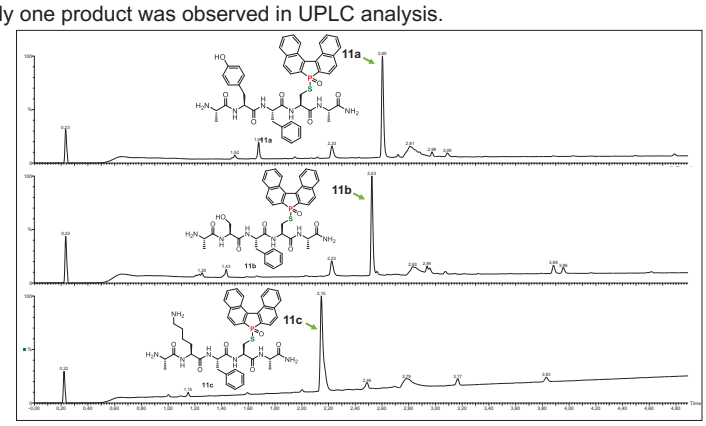

Figure 2: UPLC analysis of crude product **11a-c**

This innovative methodology has been applied for labeling peptide of interest such as Ghrelin [1-8]-Cys9, the natural ligand of GHSR1a.[6]

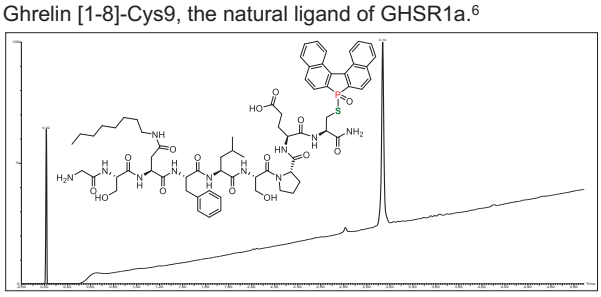

Figure 3: UPLC chromatogram of pure binaphtylphosphole Ghrelin[1-8]Cys9 conjugate

CONCLUSION

We have developed new classes of fluorophores derived of phospholes, the P-hydroxyphosphole-oxide or -sulfide and P-aminophospholes, for coupling to amino acids or peptides by formation of P-N or P-S bond, respectively, under mild conditions with high chemoselectivity. This latter strategy is currently explored for labeling proteins as well as other biomolecules.

References: (1) Y. Asok, *et al. Acc. Chem. Res.* **2023**, 56, 536−547; (2) M. Schenk, *et al. ChemBioChem* **2024**, e202300857; (3) J. Vantourout *et al. J.Am. Chem. Soc.* **2020**, 17236−17242; (4) E. Rémond, *et al.*, *Chem. Eur. J.* **2022**, 28, e202201526; (5) A. Moulin, *et al.*, *Amino Acids* **2013**, *44*, 301-314; (6) T.D. Müller, *et al. Mol. Metab.* **2015**, 4, 437–460.

Acknowledgments: We thank Dr. Ludovic MAILLARD for HPLC preparative apparatus and Pierre SANCHEZ for UPLC/MS analysis.

Flow – SPPS towards greener and more efficient peptide manufacturing

Oliver Kracker[1], Eike-Fabian Sachs[1]

[1] Corden Pharma International GmbH, Frankfurt am Main, Germany
PeptiSystems, Uppsala, Sweden

https://doi.org/10.17952/37EPS.2024.P1029

Collaboration with PeptiSystems



PeptiPilot: 0.1–12 mmol for development

Process development

- Reactions by flow through column (**re-circulation mode**)
- No calibration due to use of HPLC pumps
- Fully automated process
- Online monitoring implemented (**UV-Vis**)
- No visual inspection of resin due to steel column

Ready for production

- Process transferable from mmols to several mols
- Additional detection modes installable (**RI**)
- Custom made based on individual requirements



PeptiPro – up to 5 mol for production



UV-Detector
- Live in-line monitoring of coupling and washing steps



Heater
- Optional
- Efficient heat transfer

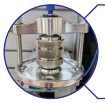

Column
- Interchangeable columns
- Up to 5 columns parallel



Preactivation vessel
- Volume adjustment
- Mixing of components

Case study – GLP-1 agonist Exenatide

- 39 amino acid linear peptide found in venom of „Gila lizard“

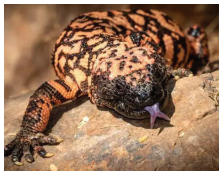

HGEGTFTSDLSKQMEEEAVRLFIEWLKNGGPSSGAPPPS-NH$_2$

Generic protocol (non-optimized)

- **Amino acid** / Oxyma / DIC (**1.5** / 1.5 / 3.0 eq)
- Rink amide resin (**0.65 mmol/g**), (0.085 g resin / mL column)
- Synthesized on 25 mL columm (1.38 mmol scale)
- **80 min coupling** duration for each cycle (**50 °C**)
- **6 CV washes** – 4 CV after DeFmoc, 2 CV after capping (4+2) (*can be reduced to 2 CV and 1 CV with 100 mL column (**2+1**)*)

Results

- **89% crude yield** over all steps
- High crude **purity 59%**
- **25% less AA**/Oxyma used
- **35–61% less solvent** consumption

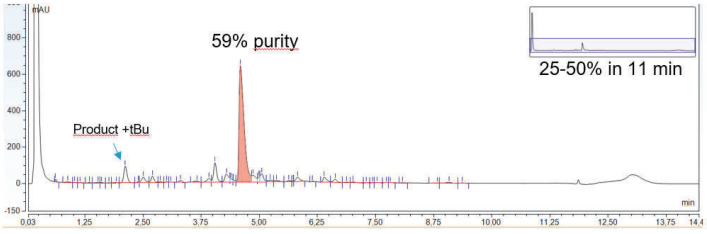

Fmoc deprotection

20% piperidine in DMF flow:

- Dibenzofulvene wash-out monitored by UV (full conversion ensured)
- **~50% less piperidine** utilized compared to batchwise SPPS

DMF washing step

- complete washing out of piperidine monitored via **RI**
- **2 CV are sufficient**, might be further reduced

PAT (RI) monitoring (100 mL column)

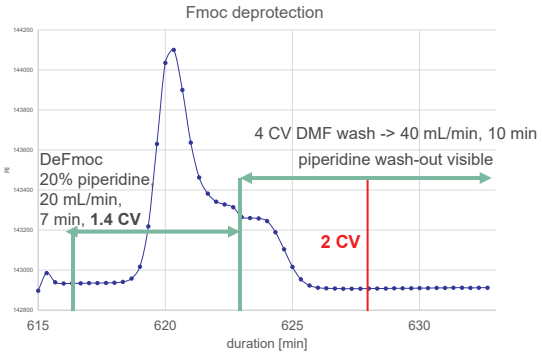

References

- Lukas TJ, Prystowsky MB, Erickson BW (**1981**). *PNAS*, *78*(5), 2791–2795.
- Sletten ET, Nuño M, Guthrieb D, Seeberger PH (**2019**). *Chem. Commun.*, *55*, 14598-14601
- de la Torre BG, Ramkisson S, Albericio F, Lopez J. (**2021**). *Org. Process Res. Dev.* 25(4), 1047-1053

Contact details

Oliver.Kracker@cordenpharma.com

Eike.Sachs@cordenpharma.com




https://doi.org/10.17952/37EPS.2024.P1030

Design of Experiments as Powerful Tool for Peptide Cleavage Development

Teresa Friedrichs[1], Alexander P. Galow[1]

[1] Corden Pharma International GmbH, Frankfurt am Main, Germany

Corden Pharma

OFAT vs. DoE

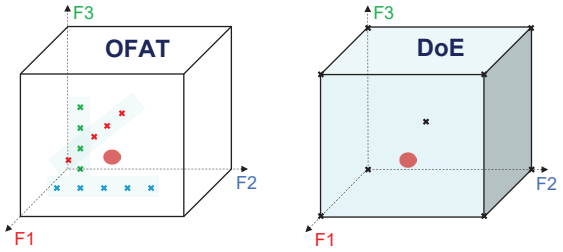

Exemplary Standard Approaches

OFAT: 3 factors, 5 levels
3 × 5 settings - 2 replicates = 13 experiments

DoE: 3 factors, 2 levels
2^3 + 3 replicates = 11 experiments

Which factors to screen?

- Ishikawa or brainstorming
- Identify most critical factors
- Focus on quantitative factors

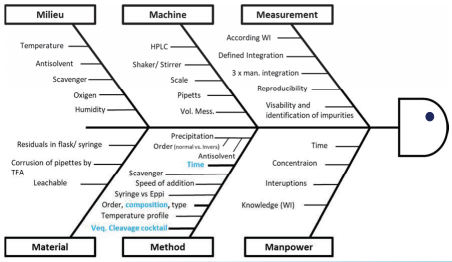

OFAT	- Small designed space
One Factor at a Time	- Iterative experiments - No information about factor interactions
DoE	- Large designed space covered
Design of Experiments	- Parallelization of experiments - Information about factor impact and interactions

Case study of peptide with ~20 AA, linear, Cysteine contained

Factor	Generic	OFAT	OFAT^{TBMTP}	Exp. SP^{TBMTP}	Exp. SP^{TBMTP}	Rob. SP
Cocktail Veq.	20.0 Veq.	15.0 Veq.	15.0 Veq.	13.0 Veq.	13.0 Veq.	12.8 Veq.
Time	120 min	90 min	90 min	90 min	90 min	90 min
Water	2.5%	2.0%	2.0%	5.5%	5.5%	5.6%
TIPS	2.5%	8.0%	8.0%	7.0%	7.0%	7.0%
Thioscavenger	2.5%	6.0% (DTT)	6.0% (TBMTP)	7.5% (TBMTP)	7.5% (TBMTP)	7.5% (TBMTP)
TFA	92.5%	84.0%	84.0%	80.0%	80.0%	79.9%
Yield	30.4 mAU·min	53.7 mAU·min	51.3 mAU·min	51.8 mAU·min	51.8 mAU·min	
Purity	64.0%AN	71.2%AN	69.8%AN	71.5%AN	71.5%AN	
Theo. Yield			45.3 mAU·min			47.6 mAU·min
Theo. Purity			73.0%AN			75.9%AN

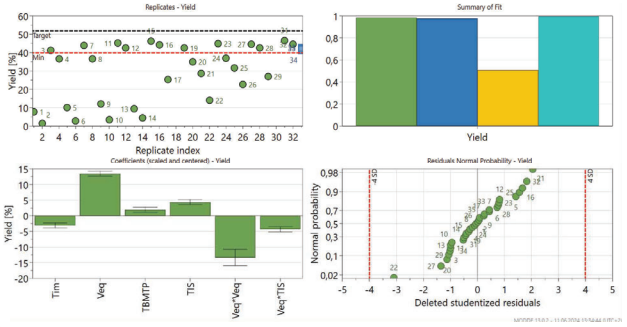

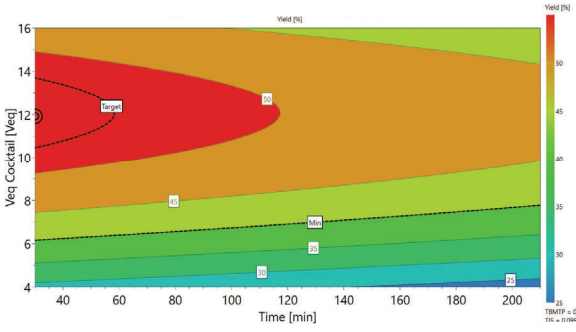

OFAT Optimization

- Approx. 1 week of time

DoE Optimization

- 1 day lab, 1 day office
- Trends clearly visible

PMI* / Cost

- Reaction time of 10 min is too short for upscale
- $\frac{1}{3}$ PMI for $\frac{4}{5}$ yield compared to optimum

Red: High yield
Orange / yellow: Good to moderate yield
Green to blue: Low yield

*PMI: Process Mass Intensity

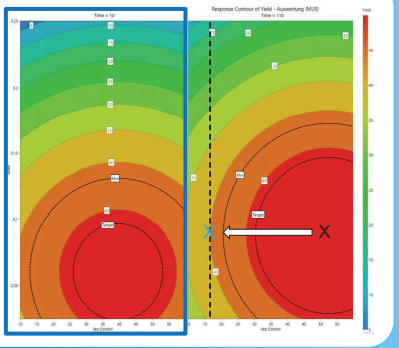

Conclusion

- DoE for in-depth evaluation results
- Qualitative factors preferable with OFAT in addition to DoE
- Similar number to less experiments than with OFAT
- Not as intuitive as OFAT
- Less time consuming
- Very positive customer feedback

- Main **DoE expertise** in peptidyl resin cleavage in **early-stage development** (50 mg scale)
- **Upscale successfully performed** with adaptions according to 'RGT' rule
- Other **process** steps in peptide synthesis were also **successfully optimized**
  E.g. (on-resin) cyclization, deprotections, reduction

Contact Details

Teresa.Friedrichs@cordenpharma.com
Alexander.Galow@cordenpharma.com

香 港 大 學
THE UNIVERSITY OF HONG KONG

https://doi.org/10.17952/37EPS.2024.P1031

Synthetic combinatorial OPA-cyclic peptide library

Kin Nam Adrian Chu[1], Carina Hey Pui Cheung[1], Xuechen Li[1]*
[1]Department of Chemistry, State Key Laboratory of Synthetic Chemistry, The University of Hong Kong, Hong Kong, P. R. China, SAR

Abstract

Cyclic peptides have a rising popularity as novel drug due to its improved stability and lower entropic cost for binding. In order to look for potential cyclic peptide drug, a high-throughput screening on various drug target can be done using a cyclic peptide library. Among various types of peptide library, we have chosen to synthesize a cyclic peptide library using the One-Bead-One-Compound (OBOC) strategy. In the design of our cyclic peptide library, we utilized ortho-phthalaldehyde (OPA) to do an on-resin peptide cyclization[1]. After the cyclic peptide library has been synthesized, we conducted a bead-based biological screening on various drug targets, for example, BamA and Walk-EPAS. We have successfully screened a few potential binders through this technique.

OPA chemistry:

Ortho-phthalaldehyde (OPA) can react with an amine group to form a phthalimidines [Two-Component product]. (Figure 1b)[1]
When there is a thiol group, OPA will react with both amine and thiol to form an isoindole ring [Three-Component product]. (Figure 1a)[1]

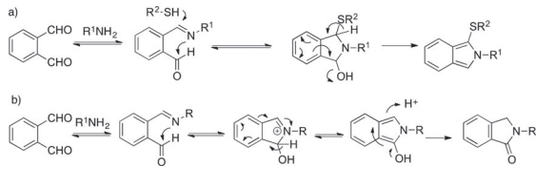

Figure 1: (a) Proposed Three-Component Reaction Mechanism; (b) Proposed Two-Component Reaction Mechanism

Library design:

- Synthesize a One-Bead-One-Compound (OBOC) OPA-cyclic peptide library. (Figure 2)
- Two layers in our library: outer layer is the cyclic peptide; inner layer is the linear peptide, which is the coding tag.

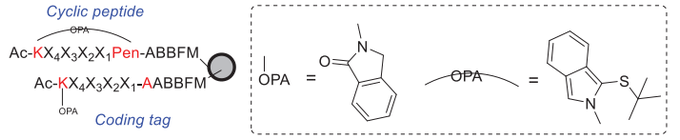

Figure 2: OBOC OPA-cyclic peptide library , B = β-Alanine, Pen = Penicillamine, X_n = canonical amino acids

- 16 canonical amino acids (Lys, Cys, Met, Ile not included) were used to form a random tetrapeptide region.
- Theoretical diversity of the library = 16^4 = 65536 peptides

Library construction:

- 3 key steps for library construction:
  - Spatial segregation: split the beads into 2 layers[2]
  - Split-and-pool synthesis: generate the random region[2]
  - On-resin OPA cyclization: cyclize the outer layer

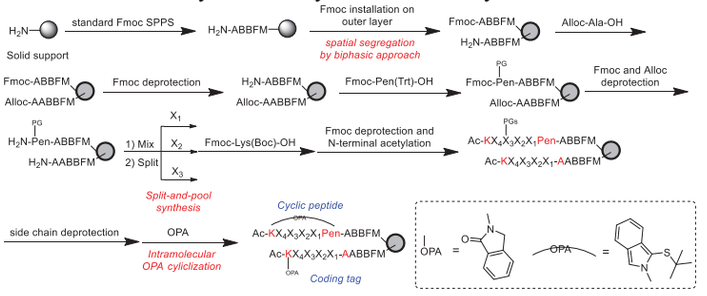

Figure 3: Synthetic scheme of the OBOC OPA-cyclic peptide library, B = β-Alanine, Pen = Penicillamine

Library screening & isolation of +ve hits:

- The OPA-cyclic peptide library will incubate into labelled target protein of interest (POI). (Figure 4)

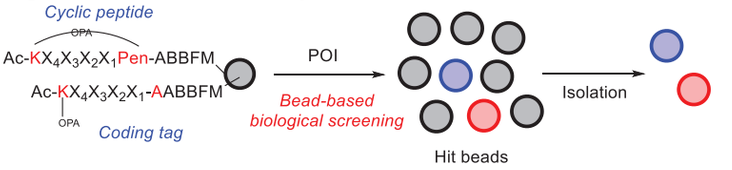

Figure 4: General scheme for library screening & isolation of positive hits

- Do magnetic screening & fluorescent screening to isolate positive hits
  - Magnetic screening: use biotin-labelled POI, isolated by streptavidin magnetic beads and a strong magnet.
  - Fluorescent screening: use fluorescent dye-labelled POI, isolated by picking the beads under confocal microscope (Figure 5)

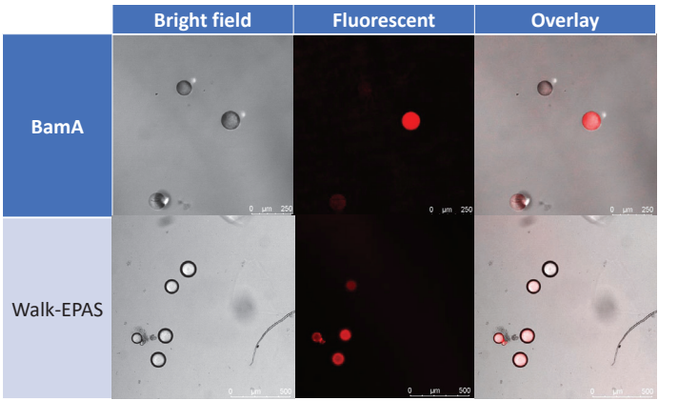

Figure 5: Visualization of positive beads under confocal microscope

Structural determination:

- Positive hits are cleaved from the beads by CNBr and send to Tandem MS/MS to obtain the sequence of positive hits. (Figure 6)
  - CNBr cleaves the C-terminal of Met to a homoserine lactone

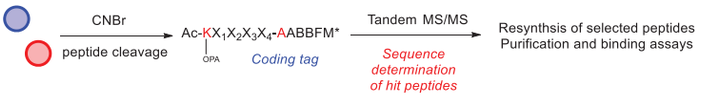

Figure 6: General scheme for structural determination, M* = homoserine lactone

- Results of BamA and Walk-EPAS screening (Table 1)

Proteins	Number of peptide sequences
Walk-EPAS	19
BamA	18

Table 1: Number of peptide sequences obtained from bead-based screening

References

[1] Zhang, Y., et al., Journal of the American Chemical Society, **2019**, 141(31), p. 12274-12279.
[2] Liu, Ruiwu et al., QSAR & combinatorial science, **2005,** 24(10), p. 1127–1140.

Direct synthesis of peptidomimetics containing non-coded amino acids via Photocatalytic carbamoylation reaction

T. Gandini, M. L. Gelmi, R. Bucci

DiSFarm, Sezione di Chimica Generale e Organica «A. Marchesini», Università degli Studi di Milano, Via Venezian 21, 20133 Milano, Italy
e-mail: raffaella.bucci@unimi.it

@BucciRaff

https://doi.org/10.17952/37EPS.2024.P1032

INTRODUCTION AND AIM OF THE WORK

Nowadays, peptidomimetics are widely studied, being useful tools in drug discovery and medicinal chemistry. They are indeed able to mimic the conformation of natural peptides and, thanks to small structural modifications, as the insertion of non-natural amino acids, could present improvements respect to natural peptides, such as higher affinity and selectivity toward a target receptor and an enhanced conformational and metabolic stability.
Here, we present an **innovative photocatalytic approach** for the synthesis of peptidomimetics by using dihydropyridines (DHPs)[1], functionalized with natural amino acids (AAs) or peptides, and imines.[2]

Formation of non-conventional peptidomimetics:

- R^1 could be of biological interest (i.e. sulfonyl group) or a protecting group;
- R (aromatic heterocycle/aryl) is the side chain of the *in situ* generated non-coded amino acid
- the DHP is functionalized with amino acids or peptides

Peptidomimetics Synthesis
this work

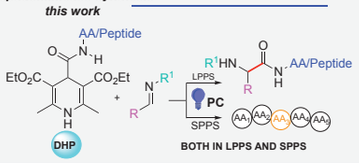

AA_3 = Non-coded amino acid
R = aryl groups
R^1 = sulfonamides or cleavable protecting group

- Green reaction conditions (metal-free approach);
- **Protocol validated also in SPPS**

SCOPE OF THE REACTION -LPPS-

N-benzylidenemethanesulfonimide (1) and DHP-Phe (2) were used to optimize the reaction, testing: **PCs (photocatalyst)**, **additives**, **solvents**, **concentrations**, **PC loading** and **LED lamps**.

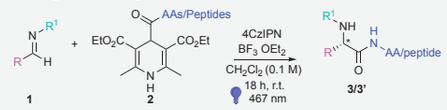

Imine scope

R- substituent on aldimine

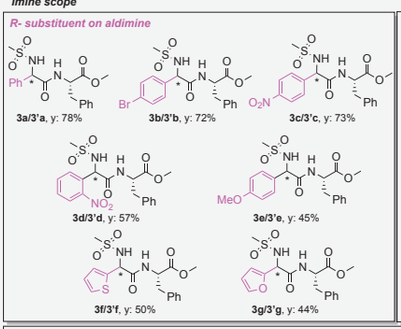

R^1- substituent on aldimine

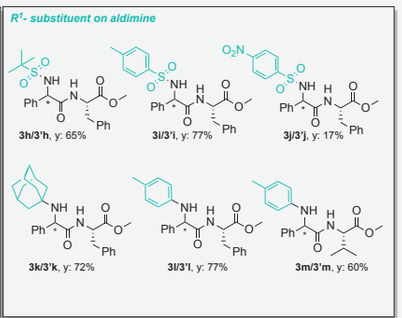

AA/Peptide Scope on DHP

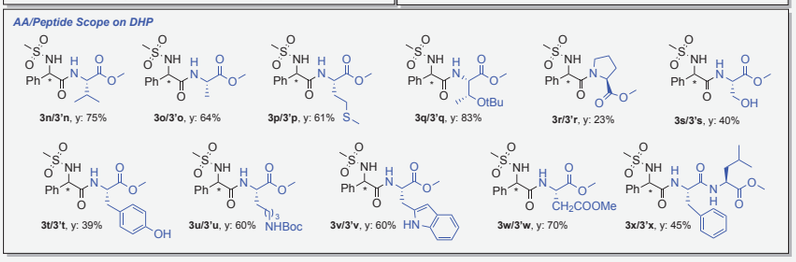

Scope of our carbamoylation reaction. y = yield. Reaction conditions: Imine **1** (1.0 equiv.), DHP-AA/Peptide **2** (1.3 equiv.), 4CzIPN (0.025 equiv.), BF_3OEt_2 (1.0 equiv.) in dry CH_2Cl_2 (3.0 mL, 0.1 M)

SYNTHESIS OF 4a-c/4'a-c and 6/6' -SPPS-

To further demonstrate the versatility of our method, we explored the deprotection of the sulfonamide moieties. Envisaging the possibility of using our protocol for longer peptide sequences with orthogonal protecting groups on AA side chains, we investigated on both acid and basic condition for the *N*-terminus sulfonamide deprotection.

Thus, starting from **3h/3'h** using acid conditions and from **3j/3'j** with basic ones, we succeeded in obtaining compound **5/5'** with high yield.

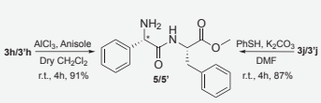

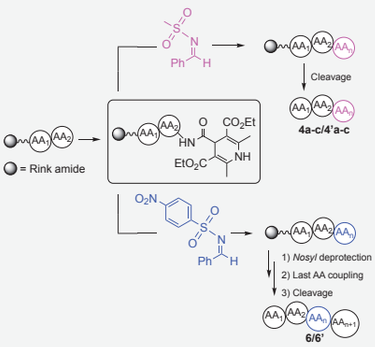



Experimental setup in solid phase.

The reaction on peptides with different lenght and conformations was studied to demonstrate its feasibility regardless from the **steric hindrance** and **peptide secondary structure**

SPPS approach

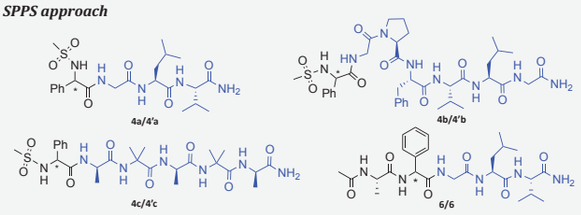

PROPOSED MECHANISM

Stern-Volmer analyses suggest two reductive quenching mechanisms both starting with the formation of radical intermediate **I**, formed thanks to the reduction of the photocatalyst from its excited state to its radical-anion form ($4CzIPN^{\bullet-}$)[3,4].

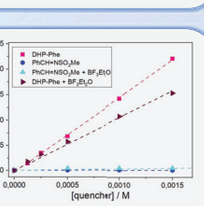

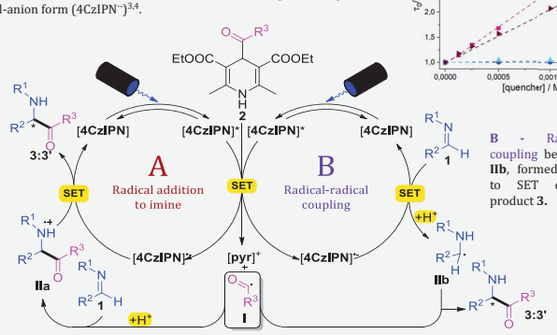

A - Radical addition of **I** to imine **1** facilitated by the presence of a Lewis acid additive to form **IIa**, leads to the product **3** upon SET event with $4CzIPN^{\bullet-}$.

B - Radical-radical coupling between **I** and **IIb**, formed subsequent to SET event gives product **3**.

ELECTROCHEMICAL CHARACTERIZATION

When separated, the diastereomers were fully characterized by NMR and similar behaviour in terms of chemical shift and protons patterns were observed for **3** and **3'** series.

X-Ray analysis

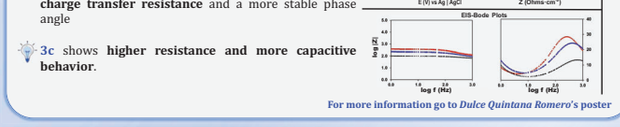

Electrochemical Characterization

3'c, with a more favourable spatial disposition, **exhibits better electron transfer efficiency, resulting in lower charge transfer resistance** and a more stable phase angle

3c shows **higher resistance and more capacitive behavior**.

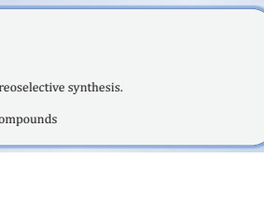

For more information go to *Dulce Quintana Romero's* poster

FUTURE PERSPECTIVES

- To improve the atom economy of the reaction;
- To develop a methodology for peptidomimetics diastereoselective synthesis.
- To investigate the electrochemical behaviour of **3/3'** compounds

REFERENCES

[1] N. Alandini, L. Buzzetti, G. Favi, T. Schulte, L. Candish, K. D. Collins, P. Melchiorre, *Angew. Chem. Int. Ed.* **2020**, *59*, 5248-5253.
[2] T. Gandini, F. Vaghi, Z. Laface, G. Macetti, A. Bossi, M. Penconi, M. L. Gelmi, R. Bucci, *under revision.*
[3] M. A. Bryden, E. Zysman-Colman, *Chem. Soc. Rev.* **2021**, *50*, 7587-7680.
[4] H.-H Zhang, S. Yu, *J. Org. Chem.* **2017**, *82*, 9995-10006.

Thiol-yne Mediated Macrocyclisation and Derivatisation Strategies

Conor Williams, Dearbhla Tully, Susannah H. Calvert, Joanna F. McGouran and Eoin M. Scanlan

Trinity Biomedical Sciences Institute, Trinity College Dublin, 152-160 Pearse St., Dublin, Ireland

Contact: cowillia@tcd.ie, scanlae@tcd.ie

IRISH RESEARCH COUNCIL
An Chomhairle um Thaighde in Éirinn

https://doi.org/10.17952/37EPS.2024.P1034

Introduction

- Peptides offer significant potential as therapeutics. However, poor membrane permeability and susceptibility to peptidases are of concern [1]
- Replacement of disulfide bonds offers a solution to increase stability [2]
- Thiol-yne 'click' cyclisation has been poorly explored [3]
  - Mild, metal free, selective and light mediated solution
  - Provides a new functional handle for further functionalisation

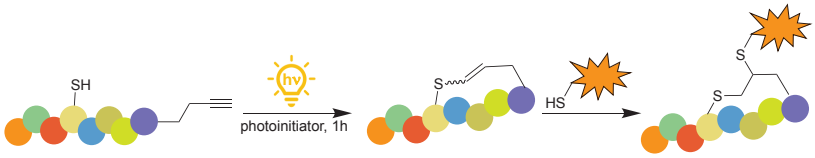

Thiol-yne Optimisation

- Alkyne containing peptides synthesised through incorporation of an alkyne amino acid or carboxylic acid

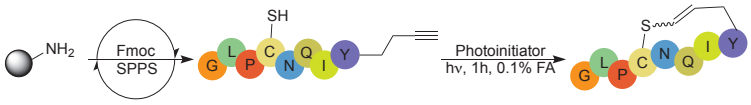

- Optimisation carried out exploring photoinitiator, pH, concentration and solvent effects

Photoinitiator	Photoinitiator eq.	Concentration (mM)	Solvent	Additive(s)	Conversion (%)
DPAP	1	1.7	H_2O : AcN	0.1% TFA, MAP	N.R.
DPAP	0.5	0.5	DMF	–	26%
Irgacure 2959	0.5	0.5	DMF	–	31%
Irgacure 2959	0.5	0.5	DMF	0.1% TFA	16%
Irgacure 2959	0.5	0.5	DMF	0.1% FA	60%
Irgacure 2959	0.5	1	DMF	0.1% FA	81%
Irgacure 2959	**0.5**	**1.5**	**DMF**	**0.1% FA**	**>95%**
Irgacure 2959	0.5	2	DMF	0.1% FA	89%

- Reaction can be modified for use in aqueous conditions or with Blue LED initiation, for compatibility with biological applications

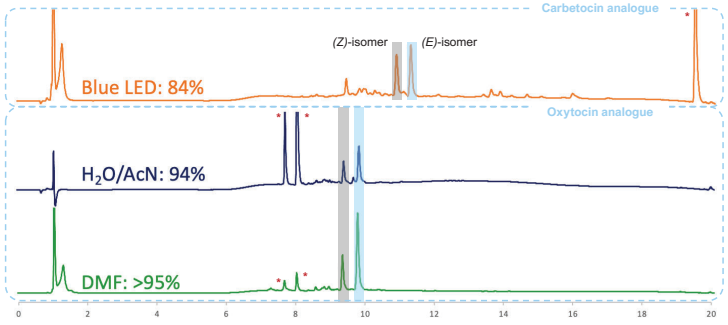

* Photoinitiator by-products

Propargylated Amino Acids

- Variety of SPPS compatible alkyne handles available

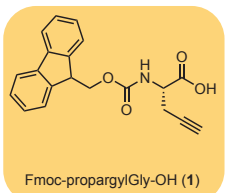

Fmoc-propargylGly-OH (**1**)

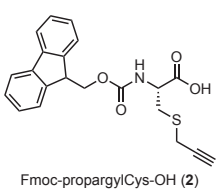

Fmoc-propargylCys-OH (**2**)

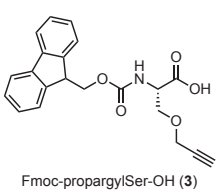

Fmoc-propargylSer-OH (**3**)

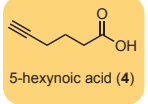

5-hexynoic acid (**4**)

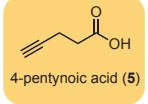

4-pentynoic acid (**5**)

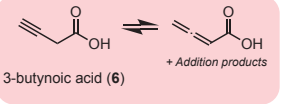

3-butynoic acid (**6**)

\+ Addition products

: Commercially Available

: SPPS incompatible [4]

- Propargylated Fmoc AAs readily synthesised with minimal purification [5]

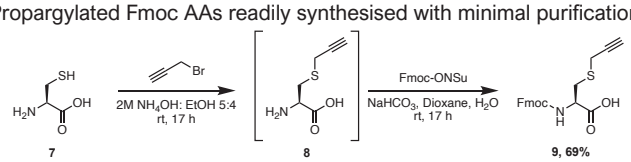

7 **8** **9, 69%**

Cyclic Neuropeptide Analogues

- Variety of Oxytocin, Carbetocin and Somatostatin analogues synthesised by SPPS and solution phase thiol-yne cyclisation
- *(E)* and *(Z)* isomers separable by HPLC

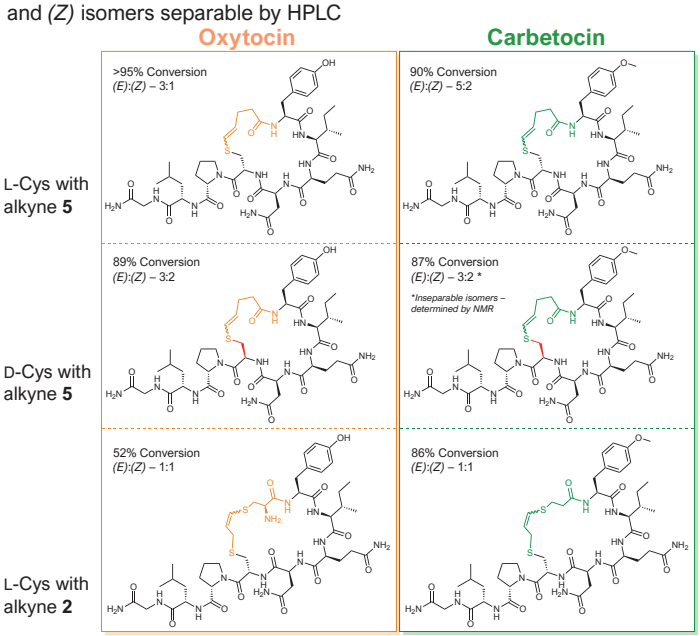

- Additional Somatostatin and small ring peptides currently in preparation
- Biological activity assays of neuropeptide analogues are being carried out in collaboration with the Muttenthaler group, University of Vienna [6]

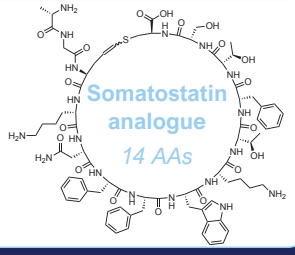

On-resin Cyclisation & Modification

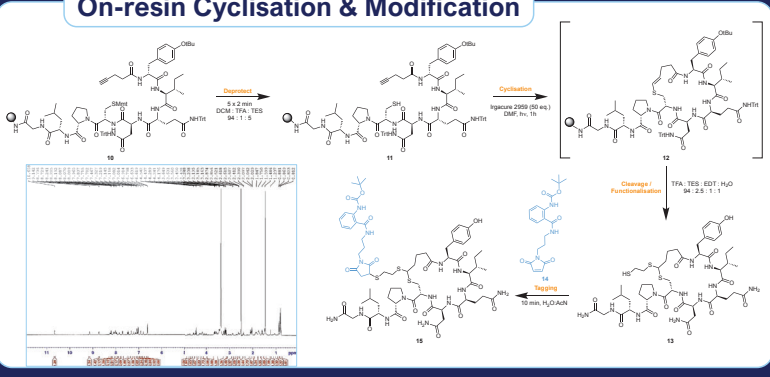

Conclusions and Future Work

- ✓ SPPS Compatible
- ✓ "Click" type reaction
- ✓ Compatible with biological systems
- ✓ Mild, photo-radical conditions
- ✓ Rapid 1h reaction
- ✓ Utilises Cys handle
- Exploration into thiol-ene functionalisation of alkyne handle currently underway

References

1. L. Wang, N. Wang, W. Zhang, X. Cheng, Z. Yan, G. Shao, X. Wang, R. Wang and C. Fu, *Sig. Transduct. Target Ther.*, 2022, **7**, 48.
2. S. Tomassi, A. M. Trotta, C. Ieranò, F. Merlino, A. Messere, G. Rea, F. Santoro, D. Brancaccio, A. Carotenuto, V. M. D'Amore, F. S. Di Leva, E. Novellino, S. Cosconati, L. Marinelli, S. Scala and S. Di Maro, *Chem. Eur. J.*, 2020, **26**, 10113–10125.
3. Y. Tian, J. Li, H. Zhao, X. Zeng, D. Wang, Q. Liu, X. Niu, X. Huang, N. Xu and Z. Li, *Chem. Sci.*, 2016, **7**, 3325–3330.
4. A. J. Cameron, P. W. R. Harris and M. A. Brimble, *Angew. Chem. Int. Ed.*, 2020, **59**, 18054–18061.
5. G. Fumagalli, R. J. Carbajo, J. W. M. Nissink, J. Tart, R. Dou, A. P. Thomas and D. R. Spring, *J. Med. Chem.*, 2021, **64**, 17287–17303.
6. A. D. De Araujo, M. Mobli, J. Castro, A. M. Harrington, I. Vetter, Z. Dekan, M. Muttenthaler, J. Wan, R. J. Lewis, G. F. King, S. M. Brierley and P. F. Alewood, *Nat. Commun.*, 2014, **5**, 3165.

Synthesis and biological activity of ultra-short antimicrobial peptides bearing a novel non-coded amino acid

Barbara Biondi,[1] Fernando Formaggio,[1,2] Cristina Peggion,[1,2] Andrea Schivo,[2] Teodora Calin,[3] Simona Oancea,[4] Emma Khachatryan,[5] Liana Hayriyan,[6] Ashot Saghyan,[5,6] Anna Mkrtchyan[5,6]

[1]Institute of Biomolecular Chemistry (Padova Unit), CNR, 35131 Padova, Italy
[2]Department of Chemistry, University of Padova, 35131 Padova, Italy
[3]Laboratory of Diagnostic and Investigation, Directorate of Public Health, 550178 Sibiu, Romania
[4]Lucian Blaga University of Sibiu, 550024 Sibiu, Romania
[5]SPC "Armbiotechnology" NAS RA, 0056 Yerevan, Armenia
[6]Institute of Pharmacy, Yerevan State University, 0056 Yerevan, Armenia

https://doi.org/10.17952/37EPS.2024.P1036

Aim

Antimicriobial resistance is a major concern for human health worldwide. Antimicrobial peptides and lipopeptides represent a promising alternative to conventional drugs in the fight against bacterial infections because of their ability to destroy cell membranes, causing damage difficult to fix, with a mechanism different from that of conventional antibiotics that act on specific targets. The major drawback in using peptides as drugs is their easy degradability by the enzymatic system of the human organism. The introduction of non-coded amino acids (NCAAs) should impart resistance to proteolysis.
We focused on 2-amino-3-(1H-imidazol-1-yl)propanoic acid as the NCAA for our investigation, synthesizing both enantiomers in high yield and optical purity. Starting from known ultrashort antimicrobial peptides bearing a lipid moiety at the N-terminus (1), we designed and synthesized different analogs in which we inserted a new NCAA at different positions. We also investigated whether the insertion of the lipid chain at the C-terminus impacts the biologic activity of these compounds.

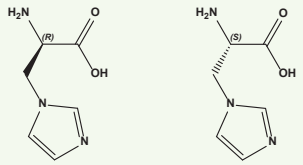

(R)- and (S)-2-amino-3-(1H-imidazol-1-yl)propanoic acid
(**D-** and **L-His°**)

Peptide Sequences	
P10	Palm-His-Ala-D-Ala-His-NH_2
P11	Palm-L-His°-Ala-D-Ala-L-His°-NH_2
P12	Palm-D-His°-Ala-D-Ala-D-His°-NH_2
P13	Ac-His-Ala-D-Ala-His-Aun-NH_2
P14	Ac-L-His°-Ala-D-Ala-L-His°-Aun-NH_2
P15	Ac-L-His°-Ala-D-Ala-L-His°-Aun-NH_2
P16	Laur-His-Ala-D-Ala-His-NH_2
P17	Laur-L-His°-Ala-D-Ala-L-His°-NH_2
P18	Laur-D-His°-Ala-D-Ala-D-His°-NH_2

Palm=$C_{15}H_{31}$-CO- ; **Laur**= $C_{11}H_{23}$-CO-

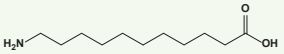

11-aminoundecanoic acid (**Aun**)

Amino Acid Synthesis

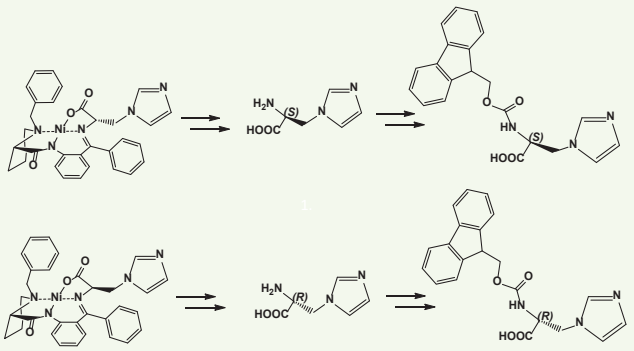

Belokon', Y. N., Sagyan, A. S., Djamgaryan, S. M., Bakhmutov, V. I., & Belikov, V. M. (1988). Asymmetric synthesis of β-substituted α-amino acids via a chiral Ni(II) complex of dehydroalanine. Tetrahedron, 44(17), 5507–5514.

SPPS & Peptides Characterization

SPPS
- Fmoc/tBu
- Activation: DIC/Oxyme
- Cleavage: TFA/TIS/H_2O (95:2.5:2.5)

Sample	R_t(min)*	Purity (%)	MW_{calc}	MW_{exp}
P10	20,0	97	671,9	671,4
P11	19,9	95	671,9	671,4
P12	19,8	95	671,9	671,4
P13	10,6	99	658,8	658,4
P14	10,6	99	658,8	658,3
P15	10,9	99	658,8	658,4
P16	16,0	96	615,8	615,3
P17	16,2	96	615,8	615,3
P18	16,3	95	615,8	615,3

*column Phenomenex Kinetex, 0.46x10cm, 100Å, 3.5µ; 5-95%B over 30 min

NMR characterization of P17

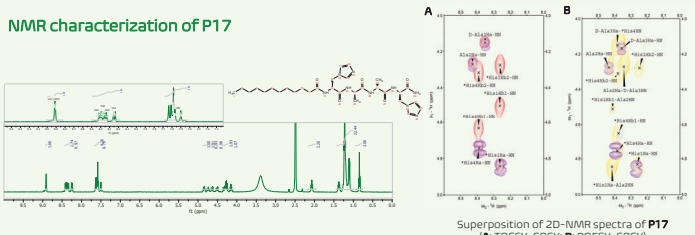

Superposition of 2D-NMR spectra of **P17**
(**A**: TOCSY-COSY; **B**: ROESY-COSY)

In serum stability

The stability of the peptides in the presence of human serum was monitored by HPLC–MS. The rate of peptide degradation was calculated as the **percentage of intact peptide** detected at defined time points.

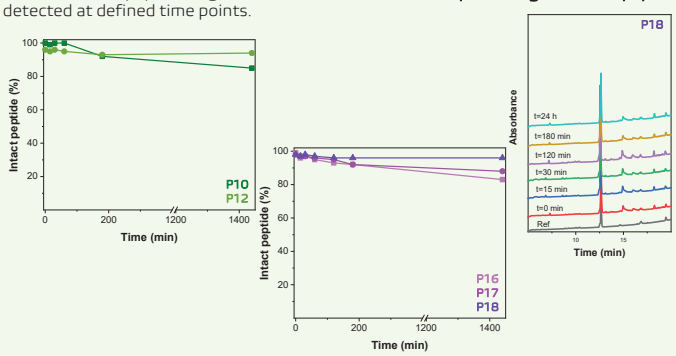

The introduction of the NCAA 2-amino-3-(1H-imidazol-1-yl)propanoic acid does not affect significantly the resistance to degradation *in serum* of the ultrashort peptides under investigation, regardless of the acyl chain at N-terminus.

Antimicrobial activity

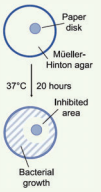

The antibacterial activity was tested on different Gram-positive and Gram-negative bacterial strains, according to the standardized disk diffusion Kirby–Bauer method. (2) Peptide activity was determined by measuring the diameters (in mm) of bacteria growth inhibition around the paper disks.

	Gram-negative bacteria				
Sample	Klebsiella aerogenes ATCC 13048	Salmonella enterica ATCC 13076	Escherichia coli ATCC 25922	Pseudomonas aeruginosa ATCC 27853	Acinetobacter baumannii ATCC 19606
P10	-	10	-	-	-
P11	-	-	-	-	-
P12	-	8	-	-	-
P13	-	-	-	-	-
P14	-	-	-	-	-
P15	-	-	-	-	-
P16	-	9	-	-	-
P17	10	8	9	8	-
P18	9	-	7	8	-

	Gram-positive bacteria									Fungi (yeast)
Sample	Bacillus Subtilis ATCC 6633	Staphylococcus aureus ATCC 25923	Enterococcus faecalis ATCC 29212	Streptococcus pyogenes ATCC 19615	Streptococcus mitis (clinical isolate)	Streptococcus oralis (clinical isolate)	Streptococcus pyogenes Group A (clinical isolate)	Streptococcus Group G (clinical isolate)	Enterococcus faecalis ATCC 51299	Saccharomyces cerevisiae ATCC 9763
P10	-	-	-	-	-	-	-	-	-	-
P11	-	-	-	-	-	-	-	-	-	-
P12	-	-	-	10	8	8	8	-	-	-
P13	-	-	-	-	-	-	-	-	-	-
P14	-	-	-	-	-	-	-	-	-	-
P15	-	-	-	-	-	-	-	-	-	-
P16	-	-	-	-	-	-	-	-	-	-
P17	11	9	12	-	-	-	-	-	-	12
P18	12	12	9	17	10	-	12	-	-	14

P17 and P18, containing the NCAA and the lauryl moiety at the N-terminus, resulted as the most promising candidates with a broad spectrum of activity against both Gram-positive and Gram-negative bacteria and yeast. Cytotoxicity tests are in progress.

References

1. Makovitzki A, Avrahami D, Shai Y. Ultrashort antibacterial and antifungal lipopeptides. *Proc Natl Acad Sci USA* **2006** , *103*, 15997-6002.
2. Bauer AW, Kirby WM, Sherris JC, Turck M. Antibiotic susceptibility testing by a standardized single disk method. *Am. J. Clin. Pathol.* **1966,** *45*, 493-496

barbara.biondi@cnr.it

This work was carried out with the support of a Joint Bilateral Agreement CNR/MESRA (2022-2024): "Synthesis of non-coded amino acids to improve the properties of two specific classes of antibacterial and anticancer peptides".

https://doi.org/10.17952/37EPS.2024.P1037

Evaluation of the stability of oxytocin and vasopressin under oxidative stress conditions

Stefano Tartaggia[1], Claudia Honisch[1], Martina Rotondo[2], Paolo Ruzza[1]
1 Institute of Biomolecular Chemistry of CNR, Padova Unit, via F. Marzolo, 135131 Padova, Italy,
2 University of Naples Federico II, Dept. of Biology, Napoli, Italy
stefano.tartaggia@cnr.it

Introduction

Oxytocin and vasopressin are neuropeptides produced in the hypothalamus that play a well-known role in social and emotional behavior, as well as in the regulation of body fluids tonicity. In recent studies, oxytocin was suggested to act as a neuroprotective factor by inhibiting neuro inflammation, oxidative stress, free radical formation and neuronal apoptosis, preventing mitochondrial dysfunction, activating free radical scavengers and several antioxidant enzymes. [1] Herein, we investigated the stability of oxytocin and vasopressin under oxidative stress conditions, such as UV irradiation, treatment with ROS and lipoxidation byproducts, similarly to our previous study on other neuropeptides.[2]

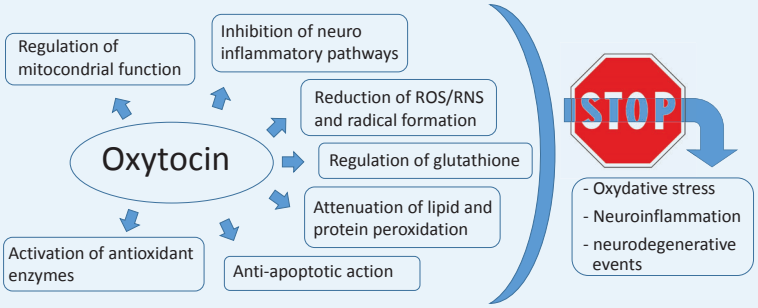

Synthesis

Oxytocin and vasopressin are cyclic nonapeptides with similar sequence of CYIQNCPLG and CYFQNCPRG respectively. The cysteine residues cyclize the structure through a disulfide bond and the C-terminus is found as a primary amide. Both peptides were prepared by solid phase peptide synthesis from rink amide resin and Fmoc-protected aminoacids. Activation of each residues was achieved with HBTU/HOBt and Fmoc deprotection was performed with piperidine. After cleavage and deprotection, the disulfide bridge is spontaneously obtained through oxidative folding.

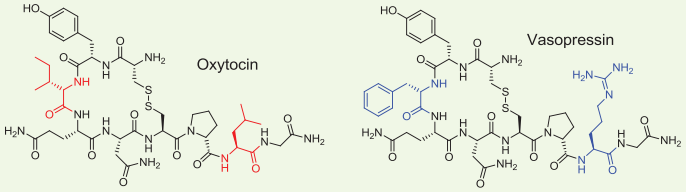

Reactivity under irradiation

Both peptides present a positive CD band at 226 - 228 nm and a negative band at 195 nm. Vasopressin display another negative band at 203 nm in TFE. The most evident spectral change after UV irradiation (254 nm) is the disappearance of the positive band in both aqueous (phosphate buffer) and organic (trifluoroethanol) environments, which is related to the opening of the disulfide bridge.

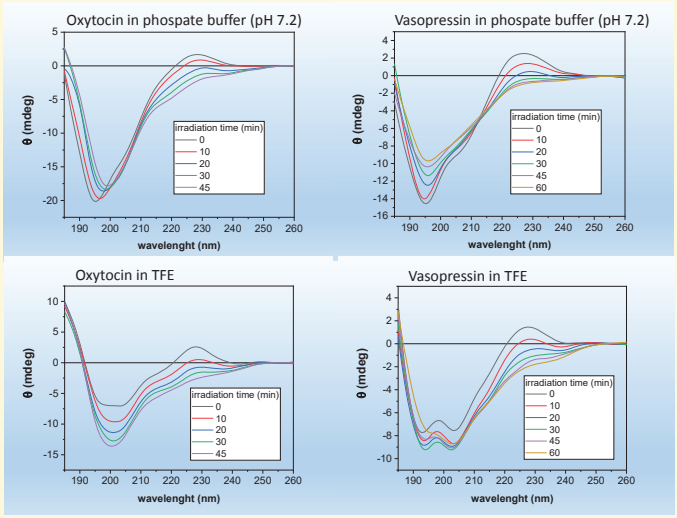

HPLC-MS analysis evidenced the formation of ΔAla -oxytocin and -vasopressin as the main irradiation products, together with a complex mixture of degradation and oligomerization by-products. We are determining wherever the desulfurization is a radical process caused by the ROS generated upon UV irradiation, or a photochemical reaction.
We are also optimizing the desulfurization process in order to clearly define in which Cys residue is occurring the β-elimination process *via* NMR investigations. It is worth noting that ΔAla oxytocin was previously suggested to act as an intermediate in the thermal degradation of oxytocin formulations but it was not directly detected. [3]

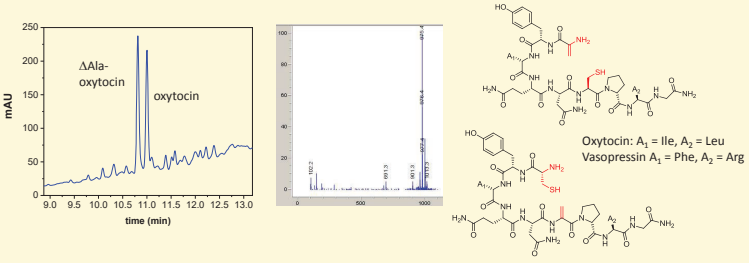

Reactivity with aldehydes

We tested the reactivity of our peptides with glyoxal and pyruvic aldehyde, which can be found in cells and tissues as lipid oxidation by-products. Although a significant change of CD spectra can be observed in organic media (TFE), HPLC-MS analysis evidenced the formation of imine condensation products also in aqueous media. Glyoxal exhibited the highest reactivity towards condensation reactions with respect to pyruvic aldehyde. Indeed, the condensation on arginine side chain resulted the major adduct with vasopressin, while oxytocin provided a condensation product currently under investigation.

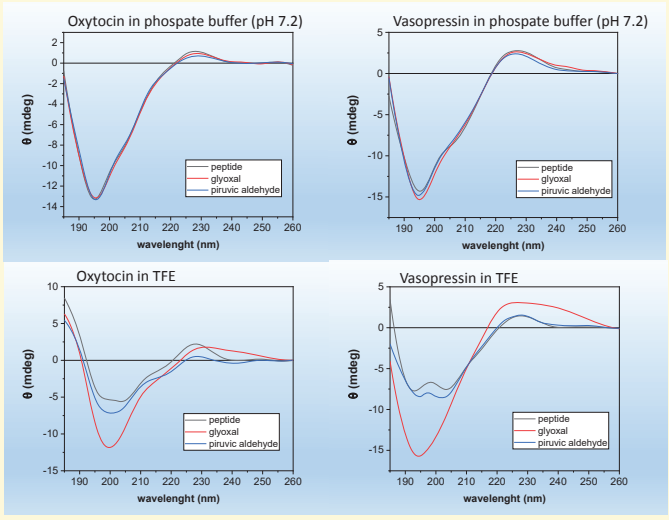

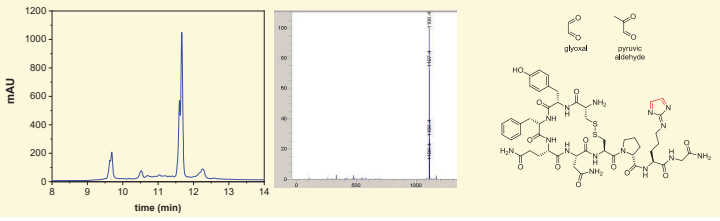

References

[1] R. Kamrani-Sharif, A. W. Hayes, M. Gholami, M. Salehirad, M. Allahverdikhani, M. Motaghinejad, E. Emanuele, Neuropeptides, 2023, 101, 102352.
[2] M. Rotondo, C. Honisch, S. Tartaggia, P. Ruzza, Molecules, 2023, 28, 484.
[3] K. Wisniewski, J. Finnman, M. Flipo, R. Galyean, C. D. Schteingart, Pept. Sci. 2013, 100, 408-421.

https://doi.org/10.17952/37EPS.2024.P1038

Faculty of Chemistry - Organic and Bioorganic Chemistry - OCIII

UNIVERSITÄT BIELEFELD

Biocatalytic Synthesis of Dihalogenated Tryptophan Derivatives

Bjarne Scharkowski[1], *Nicolai Montua*[1], *and Norbert Sewald*[1]

[1] Organic and Bioorganic Chemistry, Faculty of Chemistry, Bielefeld University, Germany.

Contact: bjarne.scharkowski@uni-bielefeld.de

Flavin-Dependent Halogenases

- **Flavin-dependent halogenases** (FDHs) offer an attractive strategy for the chlorination, bromination, and iodination of electron-rich arenes.
- They exhibit **remarkable regioselectivity** and simultaneously **obviate harsh conditions** typically found in conventional halogenation reactions.[1,2,3]
- Trp-FDHs can address even **electronically disfavored positions** on the indole moiety of tryptophan (**1**), otherwise not accessible by conventional halogenation.[1,2]
- **Cross-linking** of Trp-FDHs in tandem with an **enzymatic regeneration system** (→ combiCLEAs) allows for preparative synthesis of halotryptophans.[4]

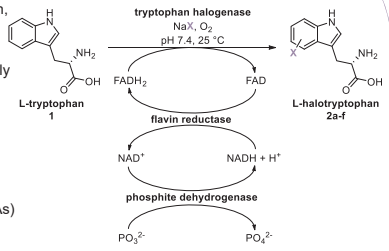

- **Bromo substituent** can be functionalized via e.g. transition metal catalyzed cross-coupling reactions, giving access to a plethora of fine chemicals.[5,6]

Dihalogenation by Combining Trp-FDHs

- Cross-coupling of halotryptophans **removes the halogen substituent**, which could otherwise be useful in modulating the bioactivity or stability of target molecules.

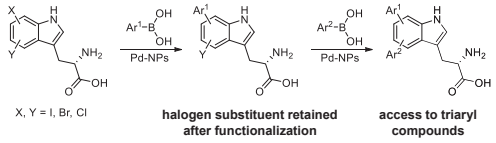

- Four representative Trp-FDHs were tested to identify viable combinations. The selection included Trp-5-halogenase **PyrH**, Trp-6-halogenase **Thal**, Trp-7-halogenase **RebH**, and Trp-5,7-dihalogenase **AetF** (**WT** and **S523A**).[7]
- Semi-preparative assays were conducted using the products of the respective other Trp-FDHs. **Specific activities** and **regioselectivities** were determined using HPLC(-MS) and NMR spectroscopy.

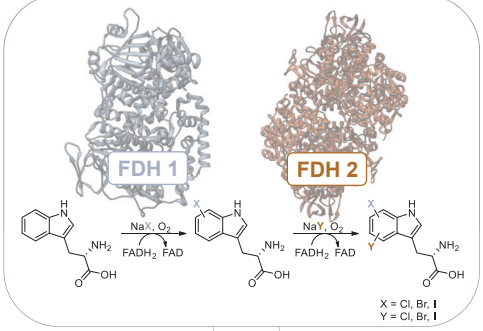

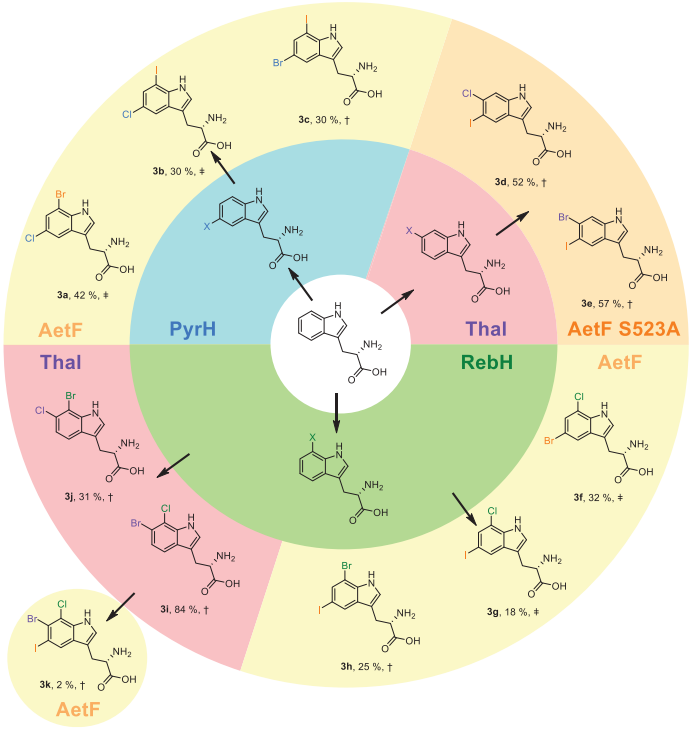

Figure 1: Obtained di- and trihalogenated tryptophan derivatives **3a-k**. Every colored section is marked with the halogenase used for the last halogenation step. † purification (RP-H/MPLC) was performed prior to the last halogenation step; ‡ no purification was performed between the last two halogenation steps. X = Cl, Br.

Orthogonal Cross-Coupling using SMC

- **Orthogonal addressability** of the halides in the dihalotryptophan derivatives **3a**, **3b**, **3f**, **3g** and **3i** was tested using **Suzuki-Miyaura cross-coupling** (SMC).
- **Pd-nanoparticles** (Pd-NPs) were employed as a catalyst using a procedure established by Dachwitz *et al.*[6]

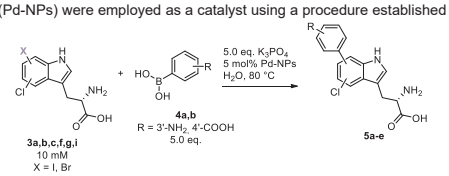

- To address the less reactive bromine substituent, **3-aminophenylboronic acid** (**4a**) was chosen, as good reactivity was previously reported when coupled to halotryptophans.[6]

X = Br, R = 3'-NH$_2$
→ Bromo-substituent addressable, orthogonality not always ideal

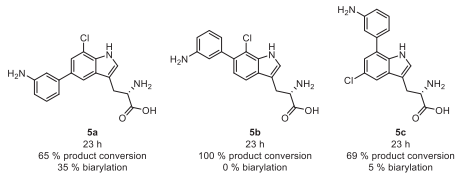

- The more reactive **iodine substituent** promised better orthogonal addressability.
- **4-Carboxyphenylboronic acid** (**4b**) with more sluggish reactivity was chosen to further avoid side product formation.[6]

X = I, R = 4'-COOH
→ Iodo-substituent addressable, orthogonality given

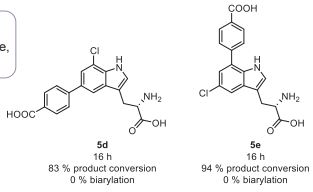

- Based on the **biarylation** observed when coupling bromo-chloro-tryptophans (**3a,b,c**), **7-Cl-substituent** might be **addressable** using Pd-NPs and a highly reactive boronic acid.
- Good orthogonality of iodo- and chloro-substituents indicated, that **orthogonal coupling of both substituents** is possible.

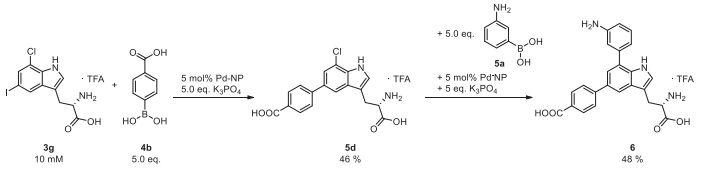

both halogen substituents orthogonally addressable in SMC

Conclusion

- A selection of Trp-FDHs was successfully combined to iteratively introduce **orthogonal halogenation patterns** in L-tryptophan (**1**).
- Most halogenases retained their native regioselectivity. Due to the *ortho*-directing effect of the halogen substituents, **PyrH**-catalyzed halogenation of 7-halo-Trp (**2e,f**) and **RebH**-catalyzed halogenation of 5-Br-Trp (**2b**) proceeded with **C6-regioselectivity**.
- **5,6-**, **5,7-** and **6,7-dihalotryptophans** bearing **two different halogen substituents** were well accessible with the chosen panel of Trp-FDHs and could be isolated on a preparative scale.
- **AetF** proved to be especially valuable for this application, even allowing for the synthesis of a **trihalogenated** bromo-chloro-iodo-tryptophan **3k**.
- **Orthogonal addressability** of several dihalotryptophans was tested in SMC using Pd-NPs. While in Br-Cl-Trp only a preference for the bromo-substituents was found for some patterns, the respective Cl-I-Trp could be **selectively functionalized**.
- In 7-chloro-5-iodo-tryptophan (**3c**) **both halogen substituents** could be **orthogonally addressed** in two consecutive SMCs.

References

[1] H. Minges, N. Sewald, *ChemCatChem* **2020**, *12* (18), 4450–4470.

[2] M. C. Andorfer, J. C. Lewis, *Annu. Rev. Biochem.* **2018**, *87*, 159–185.

[3] Y. Jiang *et al.*, *Angew. Chem., Int. Ed.* **2022**, *61* (51), e202214610.

[4] M. Frese, N. Sewald, *Angew. Chem., Int. Ed.* **2015**, *54* (1), 298–301.

[5] A. D. Roy *et al.*, *Chem. Commun.* **2008** (39), 4831–4833.

[6] S. Dachwitz *et al.*, *Chemistry* **2020**, *26* (69), 16357–16364.

[7] L. Dai et al.,. *Int. J. Biol. Macromol.* ***2024***, 260, 129312.

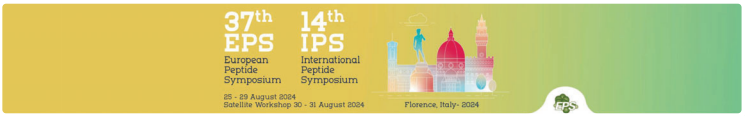

https://www.sewaldlab.de/

Silicon-containing amino acids for ^{18}F labeling of neurotensin analogues targeting NTS$_1$ receptor

Miyanou Rosales-Hurtado,[a] Emmanuelle Rémond,[a] Lina Ali,[b] Delphine Vimont,[b] Alexis Reinbold,[a] Elif Hindié,[b,c] Clément Morgat,[b,c] Florine Cavelier.[a]

[a] Pôle Chimie Balard, IBMM - UMR 5247, 1919, route de Mende, 34293 MONTPELLIER cedex 5 ; [b] INCIA, UMR CNRS 5287 - Bordeaux F-33000, France
[c] Département de médecine nucléaire, Groupe Hospitalier Pellegrin - CHU de Bordeaux
✉ emmanuelle.remond@umontpellier.fr; florine.cavelier@umontpellier.fr
https://doi.org/10.17952/37EPS.2024.P1039

INTRODUCTION

Targeting the neurotensin receptor-1 (NTS$_1$) is of great interest for the treatment of several cancers with aggressive phenotypes, including pancreatic adenocarcinoma, triple-negative breast cancer and colorectal cancer.[1] In this field, we have reported ^{68}Ga-radiolabeled NT[8-13] analogue conjugates, stabilized by the non-natural silylated amino acid (L)-trimethylsilylalanine (TMSAla) and sequence modifications, for PET imaging of tumors over-expressing NTS$_1$[2] or NTS$_2$[3] receptors. Herein, we present new NT[8-13] analogues designed for ^{18}F labeling, with a half-life of 110 min enabling later imaging than ^{68}Ga (half-life = 68 min) to potentially visualize more lesions with a better signal-to-noise ratio.

Silicon-containing amino acid pre-marker

Alkylation of the bis-lactim ether with diisopropylsilane led to diastereoisomers (*cis*/*trans* 25 :75) in 75% yield. After separation, hydrolysis of the *trans* diastereoisomer, saponification and protection, the N-Fmoc protected amino acid was isolated in 52% yield (Scheme 1). SPPS was then performed on a 2-chlorotrityl resin pre-loaded with this silanol amino acid pre-marker, which is adapted for radiolabeling by the formation of an Si-^{18}F bond.

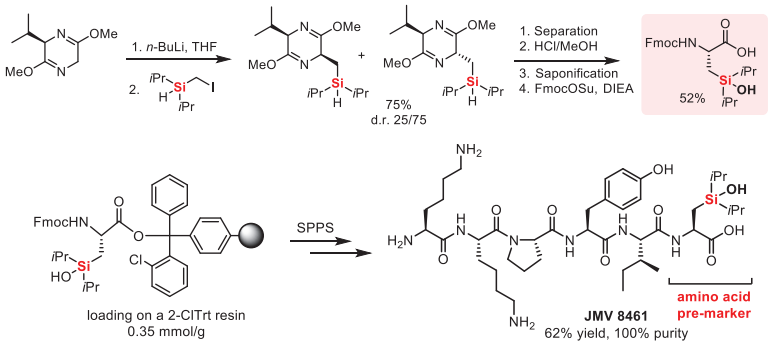

Scheme 1. Diastereoselective synthesis of silanol amino acid and SPPS

NT[8-13] analogue conjugates with an arylsilane

We have also developed conjugates by coupling di-*t*-butyl or diisopropyl arylsilane to NT[8-13] analogues containing TMSAla in the C-terminal position, via an APAc or (β-Ala)$_2$ linker in yield of 10-59% and purity of over 96% (Figure 1). To increase resistance to enzymatic degradation, analogues containing a reduced bond between the two lysines [Lys^{8}CH$_2$NHLys^9] were also synthesized.

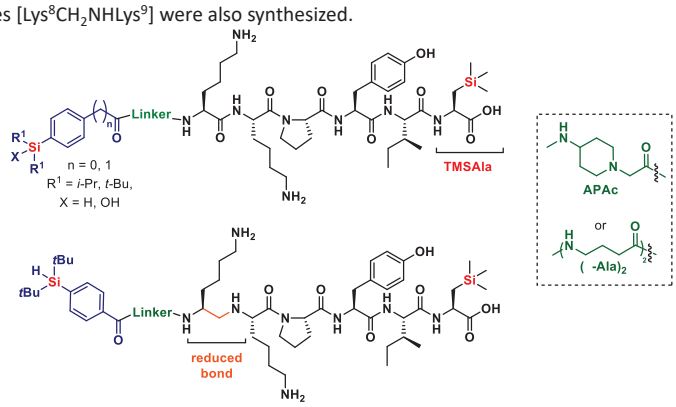

Figure 1. Structure of conjugates with an arylsilane attached at the N-terminal position

NT[8-13] analogues designed for ^{18}F-radiolabeling with a macrocycle

Conjugates JMV 8362 and JMV 8530 were radiolabeled with ^{18}F by the aluminium fluoride method, as well as with ^{68}Ga and ^{64}Cu for direct comparison. ^{64}Cu is another PET radionuclide with longer half-life (12.7h, available from ARRONAX, Nantes, France). *In vitro* characterization (internalization assay) of **^{68}Ga/^{18}F/^{64}Cu-JMV 8362** and **^{68}Ga/^{18}F/^{64}Cu-JMV 8530** was carried out on HT-29 human colorectal cancer cells over-expressing NTS$_1$. The DOTA reference compounds ^{68}Ga-JMV 6659 and ^{68}Ga-JMV 7490 were used as internal comparators (Figure 2, left). ^{68}Ga-JMV 8530 showed better NTS$_1$-internalization than the DOTA reference compound ^{68}Ga-JMV 7490. ^{68}Ga-JMV 8362 showed similar NTS$_1$-internalization to the reference compound ^{68}Ga-JMV 6659. Both ^{18}F-labeled conjugates showed very high internalization overpassing ^{68}Ga-JMV 6659 and ^{68}Ga-JMV7490. Surprisingly, ^{64}Cu-JMV 8530 showed weaker internalization than ^{64}Cu-JMV 8362 which exhibited long internalization in HT-29 cells (still 25% internalization 24h after incubation).

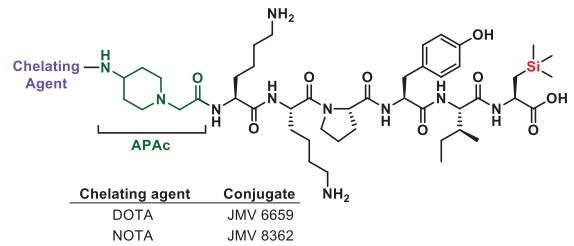

Chelating agent	Conjugate
DOTA	JMV 6659
NOTA	JMV 8362

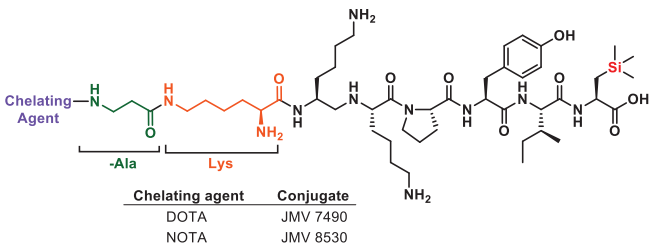

Chelating agent	Conjugate
DOTA	JMV 7490
NOTA	JMV 8530

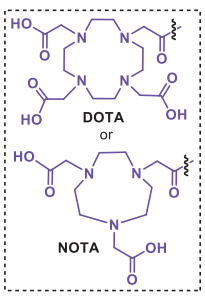

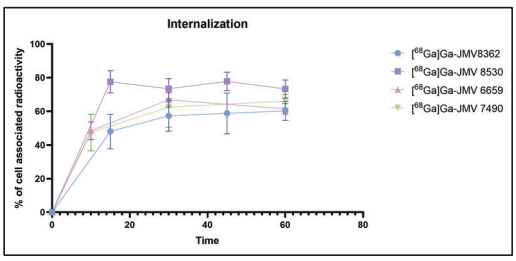

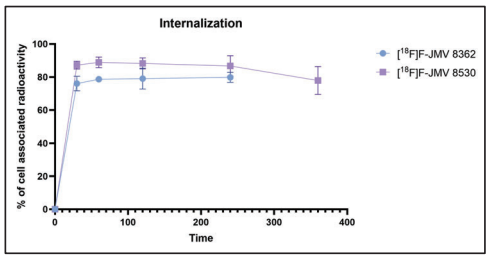

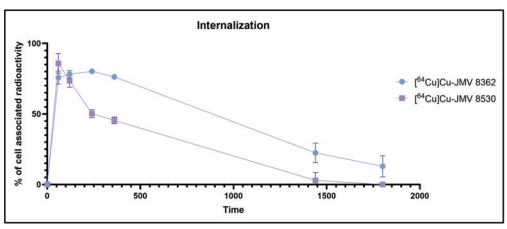

Figure 2. Structure of conjugates and internalization assay of **^{68}Ga/^{18}F/^{64}Cu-JMV 8362** and **^{68}Ga/^{18}F/^{64}Cu-JMV 8530** performed on HT-cells. *Left*: internalization of ^{68}Ga-NOTA-conjugates compared to ^{68}Ga-DOTA-conjugates. *Middle*: internalization of ^{18}F-NOTA-conjugates. *Right:* internalization of ^{64}Cu-NOTA-conjugates

CONCLUSION

We explored an innovative strategy for ^{18}F-radiolabeling of NT[8-13] analogues by introducing of a new class of silylated amino acid as pre-marker for fluorination, through the formation of a Si-^{18}F bond which should be further investigated for direct late labeling, either internally (C-terminal position) or prosthetically at the N-terminal position. As preliminary results to compare radionuclides, we have successfully developed new conjugates by coupling NT[8-13] analogues to chelating agents for radiolabeling with ^{68}Ga/^{18}F/^{64}Cu. These results show the the superiority of the NOTA over the DOTA and underline the value of developing fluorine labeling.

References: [1] a) Kim, J. T. et al. *Int. J. Oncol.* **2017**, *50*, 2200-2206. b) Dupouy, S. et al. *Biochimie* **2011**, *93*, 1369-1378. c) Norris, E. J. et al. *J. Pathol.* **2019**, *248*, 352-362. d) Morgat C et al. *Breast Cancer Res Treat.* **2021**, *190*, 403-413. [2] Fanelli, R. et al. *Bioconjugate Chem.* **2020**, *31*, 2339-2349. [3] Bodin, S. et al *ACS Omega* **2023**, *8*, 6994−7004.

https://doi.org/10.17952/37EPS.2024.P1042

Preclinical Development of Myrcludex B Derivatives: Physicochemical Properties

HEIDELBERG FACULTY OF MEDICINE

Tyra Christian[1,2], Sabrina Wohlfart[1], Christian Kleist[1], Philipp Uhl[2], Stephan Urban[3] & Walter Mier[1]

[1]Department of Nuclear Medicine, Heidelberg University Hospital, Heidelberg, Germany
[2]Department of Pharmaceutical Technology, Institute of Pharmacy and Molecular Biotechnology, Heidelberg University, Germany
[3]Department of Infectious Diseases, Molecular Virology, University Hospital Heidelberg, Germany

INTRODUCTION

When developing novel drugs, preclinical characterization is required to narrow down the number of lead candidates. For this purpose, several physicochemical properties have to be evaluated and compared.

About 5% of the 296 million people chronically infected with Hepatitis B (HBV) are estimated to be coinfected with the satellite virus Hepatitis D (HDV). HDV is a defective virus that is dependent on the envelope proteins of HBV to infect liver cells[1] (Fig. 1). Eventually, chronic HDV coinfection will cause more severe courses of disease, leading to hepatocellular carcinoma or liver cirrhosis.

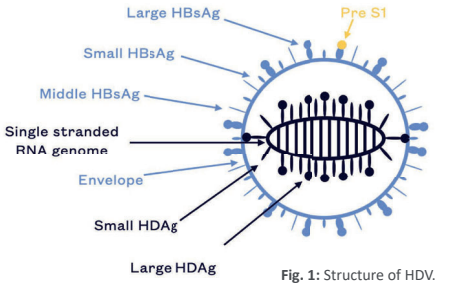

Fig. 1: Structure of HDV.

Until recently, the therapy was restricted to nucleosides and cytokines that induce antiviral response. In 2020, the first in class entry inhibitor Myrcludex B, sold under the name HepcludexTM, was approved by the FDA and the EMA. It is derived from the myristoylated pre S1 protein of the large HBsAg and consists of the first 47 amino acids. In order to further improve the treatment, derivatives of the original drug were designed and tested for their physicochemical properties as compared to the original drug.

RESULTS

LogD Determination

LogD determination revealed a wide range of logD values at varying pH values (Fig. 3). For some pH values, no logD values could be determined because the compounds did not dissolve at sufficient concentrations. In general, logD values decreased with increasing pH values. Extending over 1 log step, Myrcludex B showed the widest range of logD values.

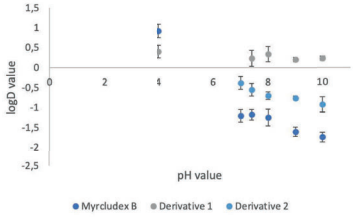

Fig. 3: Results of logD determination.

At pH 7.4, Myrcludex B was found to be the most hydrophilic compound with a logD value of -1.18 ± 0.13, Derivative 1 the most hydrophobic with logD7.4 0.23 ± 0.20. Derivative 2 was in between those two but closer to Myrcludex B with -0.55 ± 0.16. Because all compounds indicate to be in general more hydrophilic in behavior at pH 7.4, it is suggested that they will probably show poor permeation across biological membranes when administered orally.

Isoelectric Focusing

For the determination of the pIs, a calibration curve was generated from marker components with known pIs. This resulted in a linear equation used to calculate the pIs of Myrcludex B and the two derivatives. Additionally, the buffer used to dissolve the samples was applied in order to exclude interference (Fig. 4). Because Myrcludex B resulted in several pI values, three pIs were calculated representing the highest and lowest measurable pIs and middle pI. The calculated pIs distribute between 5.99 ± 0.09 and 4.35 ± 0.03 with a calculated mean of 5.17 ± 0.04. The pIs were calculated to be 5.95 ± 0.16 for Derivative 1 and 5.27 ± 0.07 for Derivative 2. Concluding, all three examined compounds are slightly acidic but the pIs of Myrcludex B and Derivative 2 are more alike to each other than the pI of Derivative 1.

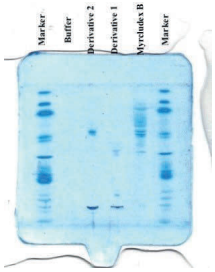

Fig. 4: Isoelectric focusing.

Serum Stability

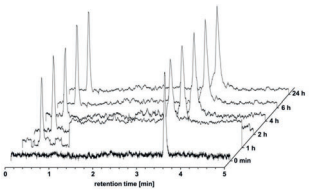

Fig. 5: Myrcludex B serum stability results.

Serum stability was determined using 125I-labeled compounds. All three compounds show high stability for 24 h without emerging side peaks (Fig. 5). The measurements for Myrcludex B are shown representatively. The first peak represents free 125I, which the samples were not purified from before the measurements, and the second peak represents Myrcludex B itself.

Protein Binding

Determination of protein binding of Myrcludex B or its derivatives proved to be quite difficult. In methods that include membrane separations, Myrcludex B notoriously clogs the membranes, prohibiting the compound from passing and distributing according to its albumin affinity. Precipitation of the serum proteins with acetonitrile delivered unstable results when measuring the remaining proportions of compound in the supernatant via HPLC. The magnetic beads and ultracentrifugation provided the most recent approaches, with the latter being the most promising one. However, these methods are still in their validation steps and so far, no conclusive experiments with either Myrcludex B or the derivatives could be done. The correct ratios of serum and compound have still to be determined and especially Myrcludex B showed to precipitate, when centrifuged with albumin, in several pre-trails.

METHODS

LogD Determination

Buffers with different pH values were produced and saturated with octanol. Myrcludex B and the two derivatives chosen were dissolved in the different buffers at a concentration of 0.5 mg/ml. Afterwards, the water-saturated octanol was added in a 1:1 ratio. The experiments were performed according to the OECD prescription[2] with some improvements:

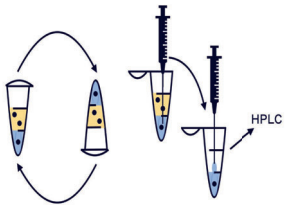

Fig. 2: LogD determination workflow.

1. No different solvent ratios were used
2. The microcentrifuge tubes were inverted for 45 ± 15 min, briefly centrifuged and allowed to stand for about 30 min (Fig. 2).
3. The octanol phase was discarded, and a small amount of the buffer phase taken using a syringe in order to avoid contamination of the sample with octanol.
4. The buffer phase was measured via HPLC because the signal-to-noise ratio was better than the one of the octanol phase.

Isoelectric Focusing

A separation and control unit was used to determine the isoelectric points (pI) of Myrcludex B and its two derivatives, together with pH gradient gels that separate samples according to their pI between 3 and 9.
The samples were dissolved in phosphate buffer pH 7.4 with a concentration of 0.5 mg/ml and 100 µL of the dissolved samples were loaded onto the gel together with a 1:5 diluted marker that consists of different substances with a known pI.
The experimental set up was cooled to 15 °C and after the electrical parameters reached the desired magnitude, the applicator, that was placed closest to the cathode, was automatically applied to the gel. One run lasted about 1.5 h and was completed, when 500 Vh were reached. Afterwards, the gels were stained with a Coomassie brilliant blue solution.

Serum Stability

Myrcludex B and the two derivatives were dissolved in phosphate buffer at pH 8.5 and labeled with 125I. Subsequently, they were incubated with human AB serum and measurements were made at incubation times of 1, 2, 4, 6 and 24 h. For this purpose, the serum proteins in the samples were precipitated with acetonitrile and the supernatant was measured by HPLC.

Protein Binding

To determine protein binding, several different approaches were pursued:

1. The first method tried was ultrafiltration. Filters sizes of 30 kDa and 100 kDa were used. As a pre-trail, 1 mg/ml Myrcludex B was centrifuged without serum, but this method had to be discontinued because Myrcludex B clogged the membranes.
2. The second approach contained dialysis. For this purpose, a chamber was manufactured that consisted of two halves between which a membrane could be placed. Into one half, the serum was pipetted, while the other half contained buffer with Myrcludex B or one of its derivatives. After a certain incubation time, a sample was supposed to be taken from the chamber containing the buffer and measured by HPLC and afterwards, the integrated area under the curve was intended to be compared to a stock solution measurement.
3. For the third approach, it was tried to precipitate the serum proteins with acetonitrile and measure the amount of Myrcludex B or the derivatives in the supernatant, compared to a stock solution.
4. The fourth approach included the use of magnetic beads which were coated with anti-HSA antibodies. The beads were first treated with 1% casein solution in order to block unspecific binding sites for Myrcludex B or its derivatives. Then, a saturating concentration of HSA was added and incubated, before Myrcludex B was added gradually. After each addition, a sample was taken and measured by HPLC. When the integrated areas under the curve were added to a graph, the slope should be greater after the saturation point was reached. Using this saturation point, the protein binding should have been calculated.
5. The last approach employed ultracentrifugation. HSA was diluted with phosphate buffer pH 7.4 and Myrcludex B and its derivatives were dissolved at 1 mg/ml. Centrifugation lasted 17 to 18 hours and a sample was taken from the top 1 ml after centrifugation, measured by HPLC and compared to the measurement of the stock solution.

SUMMARY

Several physicochemical properties of the first in class entry inhibitor Myrcludex B and two derivatives were determined. LogD determination showed mostly a decreasing behavior with increasing pH value. At pH 7.4, Myrcludex B and Derivative 2 were hydrophilic, while Derivative 1 was hydrophobic. Calculating the pIs revealed them to be slightly acidic, with Myrcludex B and Derivative 2 being very close to each other. Serum stability results proved all three compounds to be stable for at least 24 h. The results of protein binding are still subject of investigation because of the high complexity of the required workflow. Further investigations must be done, and improvements must be done to achieve oral availability of Myrcludex B and its derivatives.

References

[1]Lemp, F. and Urban, S. (2017). Hepatitis Delta Virus: Replication Strategy and Upcoming Therapeutic Options for a Neglected Human Pathogen. Viruses *9*, 172
[2] OECD (1995). Test No. 107: Partition Coefficient (n-octanol/water): Shake Flask Method. OECD Publishing *Section 1.*

MFHD

https://doi.org/10.17952/37EPS.2024.P1044

university of koblenz
Mathematics / Natural Sciences

Exploring the structure-function relationship of heme binding to blood coagulation factor VIII based on peptide models

Lorena Kröner[1], Diana Imhof[2], Marie-T. Hopp[1]

[1]Bioorganic Chemistry, Institute for Integrated Natural Sciences, University of Koblenz, Koblenz, Germany
[2]Pharmaceutical Biochemistry and Bioanalytics, Pharmaceutical Institute, University of Bonn, Bonn, Germany

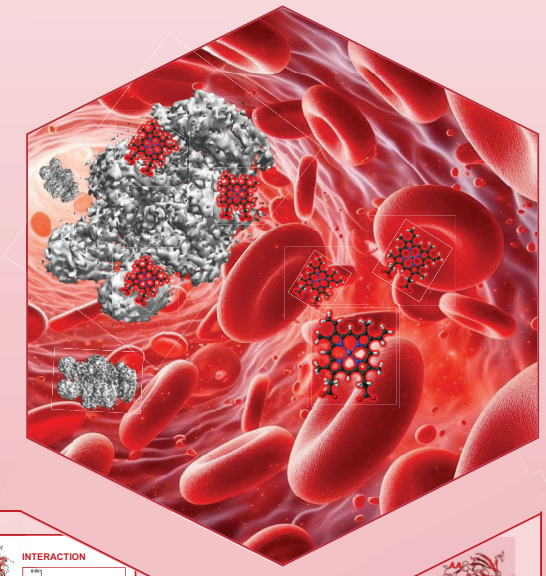

Background

Patients with hemophilia A often suffer from hemorrhage leading to massive accumulation of heme in, for example, the bleeding joint. To target the underlying deficiency of coagulation factor VIII (FVIII) and the associated complications, the protein is usually substituted. In this regard, it has been reported that direct FVIII injection into the bleeding site, meaning into the heme-rich environment, shows significantly fewer side reactions.[1] However, basic information about an interaction between FVIII and heme as well as the functional consequences thereof are still missing.[2,3] In the past, peptides arose as suitable models for the prediction of heme-binding proteins, mimicking potential surface-exposed Cys-, His- and/or Tyr-based heme-binding stretches, so-called "heme-binding motifs" (HBMs).[4] Spectroscopic characterization of the heme-binding capacity of protein-derived peptides allowed for the transfer onto protein level, as demonstrated by several proteins.[4,5] These results led to the establishment of a webserver, called "HeMoQuest", for the sequence-based prediction of HBMs in proteins.[4,6] Herein, we thus transferred the usage of protein-derived peptides as HBM models for the first time onto a procoagulant blood coagulation factor, namely FVIII, which is highly relevant in the therapy of hemophilia A patients.[7]

Results

Identification of heme-binding sites in FVIII by peptide models

The sequence of FVIII was screened for potential heme-binding motifs (HBMs) by using HeMoQuest (*http://131.220.139.55/SeqDHBM/*).[6] Manual refinement (= exclusion of non-exposed motifs and combination of overlapping motifs) led to a selection of 17 potential HBMs in FVIII.[7] These motifs were synthesized as peptides following standard Fmoc/*t*Bu solid phase peptide synthesis. Heme binding to these FVIII-derived peptides (5-10 µM) was investigated by UV/Vis spectroscopy upon incubation with heme (increasing concentrations from 0.4 to 40 µM), which revealed four high affinity HBMs (**9**, **15**, **13**, and **17**) and one HBM (**16**) with moderate heme-binding affinity in the FVIII light chain as well as four HBMs (**1**, **3**, **4**, and **8**) with moderate affinity in the heavy chain. The heme-binding mode of select peptides was characterized by rRaman spectroscopy showing e.g., the presence of penta-coordinated complexes in case of peptides **9**, **15**, and **17** (**Fig. 1**).[7]

Analysis of heme binding to FVIII (Transfer onto protein level)

UV/Vis spectroscopic titrations of heme (18 µM) to full-length-FVIII (FL-FVIII; Octocog alpha; 900 nM) and B-domain-deleted-FVIII (BDD-FVIII; Simoctocog alfa; 900 nM) were performed to specify the heme-binding capacity of FVIII. This analysis revealed that both forms of FVIII, FL- and BDD-FVIII, are able to transiently bind up to seven heme molecules on their surface (**Fig. 2**).[7] Furthermore, heme binding occurred immediately upon mixture of FVIII with heme and stably over a time period of 60 min.[7]

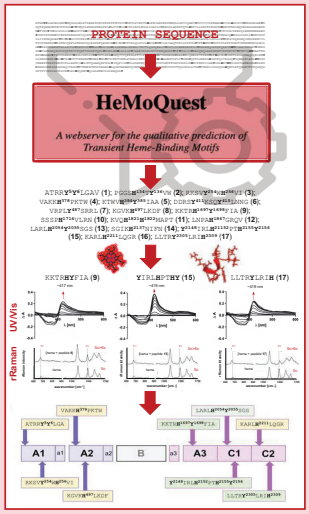

Figure 1. Prediction of HBMs by HeMoQuest and analysis of heme binding with FVIII-derived peptides as HBM models.[6,7]

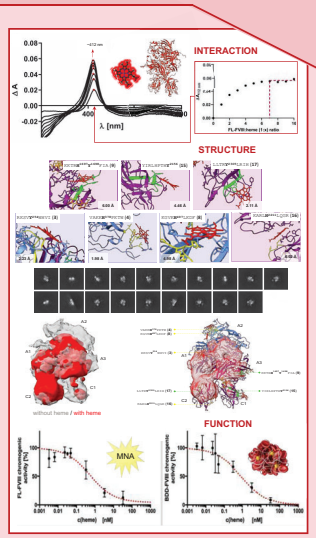

Figure 2. Heme binding affects the structural flexibility and functional activities of coagulation factor VIII.[7]

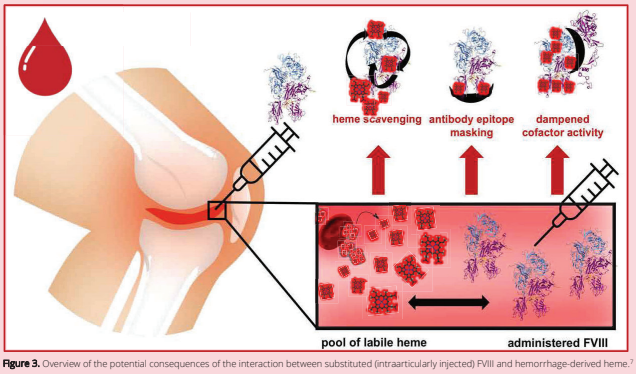

Figure 3. Overview of the potential consequences of the interaction between substituted (intraarticularly injected) FVIII and hemorrhage-derived heme.[7]

Cryo-EM and *in silico* characterization of the FVIII-heme complex

Heme was docked to FVIII (PDB: 2r7e) to each of the seven identified HBMs and remained there over a 50 ns molecular dynamics simulation, which confirmed stable binding of seven heme molecules to FVIII.[7] RMSF values suggested increased flexibility of distinct regions upon heme binding, which was further supported by single-particle cryo-EM-based studies (**Fig. 2**).[7] While FVIII (without heme) was able to form dimers, upon incubation with heme no dimers could be observed anymore. In contrast, only a core structure around the high affinity HBMs remained in structural map analysis, which (together with MALDI-TOF-MS and *in silico* analysis) suggests increased flexibility with a potential of functional consequences for the protein due to the importance of the affected regions for function-related essential protein-protein interactions.[7]

Impact of heme on the function of FVIII

In the presence of heme, the procoagulant cofactor activity of FVIII is inhibited in a chromogenic and a clotting assay with IC_{50} values of ~0.53 nM (FL-FVIII) and ~0.89 nM (BDD-FVIII) as well as ~3.44 nM (FL-FVIII) and ~1.54 nM (BDD-FVIII), respectively (**Fig. 2**).[7] These results show that heme tends to anticoagulant effects with respect to its interaction with FVIII.[7] More importantly, a potential immunomodulating effect of heme on FVIII will be tested in future.

Conclusions

Heme binding to 19 FVIII-derived peptides was analyzed, revealing 7 HBMs. ● FVIII binds heme rapidly and stably. ● Heme binding induces structural flexibility in FVIII with functional consequences. ● Heme diminishes FVIII's procoagulant cofactor activity. ● Further studies are necessary to gain insights into the immunomodulating role of the FVIII-heme complex formation in FVIII substitution therapy of hemophilia A patients (**Fig. 3**). ● Model peptides will allow for the characterization of all blood coagulation proteins in future.

References

1. Zhang et al. (**2020**) *Hum. Gene Ther.* 31: 448. DOI: 10.1089/hum.2019.355
2. Repessé et al. (**2012**) *J. Thromb. Haemost.* 10: 1062. DOI: 10.1111/j.1538-7836.2012.04724.x
3. Hopp & Imhof (**2021**) *J. Clin. Med.* 10: 427. DOI: 10.3390/jcm10030427
4. Wißbrock et al. (**2019**) *Biosci. Rep.* 39: BSR20181940. DOI: 10.1042/BSR20181940
5. Hopp et al. (**2021**) *Antioxid. Redox. Signal.* 34: 32. DOI: 10.1089/ars.2019.7992
6. Paul George et al. (**2020**) *BMC Bioinformatics* 21: 124. DOI: 10.1186/s12859-020-3420-2
7. Hopp et al. (**2024**) *Thromb. Res.* 237: 184. DOI: 10.1016/j.thromres.2024.04.006

Acknowledgement

This work is funded by the Society of Thrombosis & Haemostasis Research e.V. (GTH Early Career Research Grant to M.T.H.), the Deutsche Forschungsgemeinschaft (DFG) under the project number 507218303 (to M.T.H.), and the Günther Landbeck Excellence Award (by Takeda). Conference grants (to L.K.) are gratefully acknowledged by the German Chemical Society (GDCh), Max Buchner Research Foundation (DECHEMA e. V.), and the University of Koblenz.

Contact

Jun.-Prof. Dr. Marie T.-Hopp, Department of Chemistry, Institute for Integrated Natural Sciences, University of Koblenz, Universitätsstraße 1, D-56070 Koblenz, +49 261 287 2259, mhopp@uni-koblenz.de

Site-specific post-translational modifications of Tau4

Miriam. M. K. Preissler[1a, b], Dominik Vogl[1a, b] & Christian F. W. Becker[1a]

[1]a) University of Vienna, Faculty of Chemistry, Institute of Biological Chemistry, Währinger Str. 38, 1090 Vienna, Austria
[1]b) University of Vienna, Vienna Doctoral School in Chemistry (DoSChem), Währinger Str. 42, 1090 Vienna, Austria

https://doi.org/10.17952/37EPS.2024.P1046

BACKGROUND

- **Molecular basis of Alzheimer's disease (AD):** proteinaceous materials of amyloid β, microtubule-associated protein tau
- **Tau fibrils are hyperphosphorylated** in AD patient's brains [1]
- ***In vitro* liquid-liquid phase separation (LLPS):** aberrant process may advance fibril formation *in vivo* [2]

OBJECTIVES

- **Investigation of site-specific modifications** and their effects on aggregation and LLPS
- **Achieved by combination of recombinant expression and solid phase peptide synthesis (SPPS)** [3]
- **Native chemical ligation** yields full length tau

SEMISYNTHETIC STRATEGY

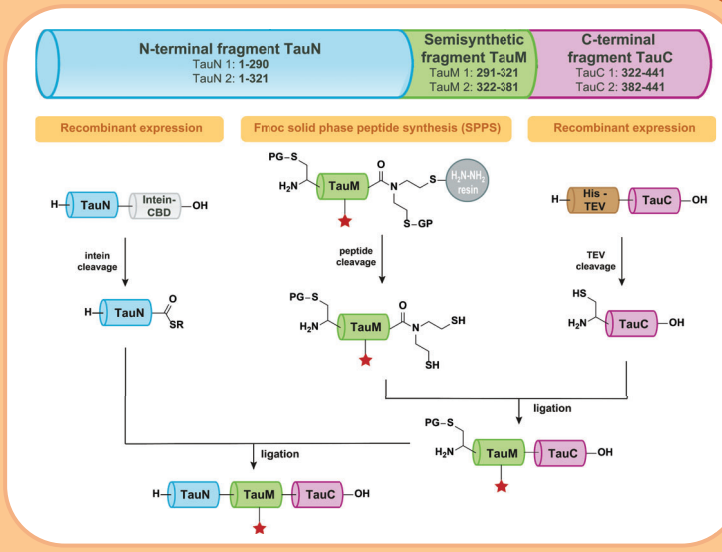

- **Semisynthesis of Tau 1** previously established [3]
- **TauM 2 purified**
- **TauN 2 yet to be purified**
- Next: TauC 2, C2 + M2 ligation

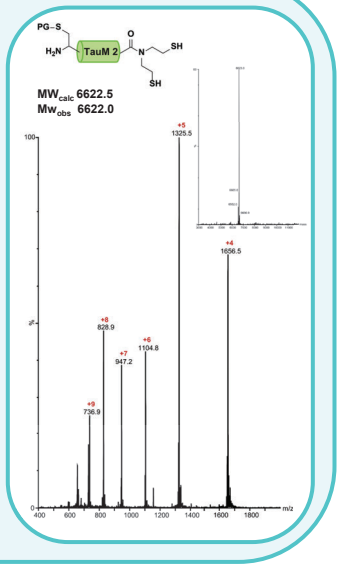

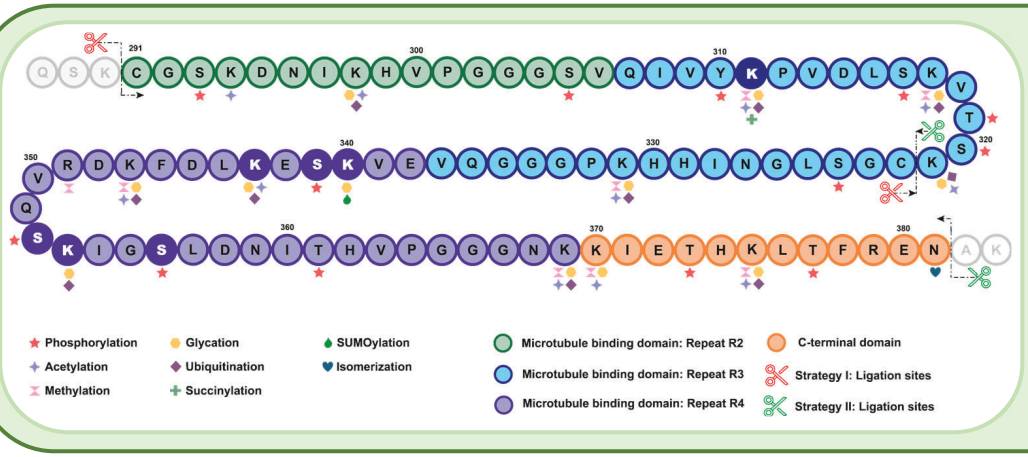

- **Longest isoform 4R2N** [1]
- **1st Semisynthetic variant**
  - Carbamylation K311
  - Succinylation K311
- **2nd Semisynthetic variant**
  - Phosphorylation S341, S352, S356
  - Acetylation K340, K343, K353

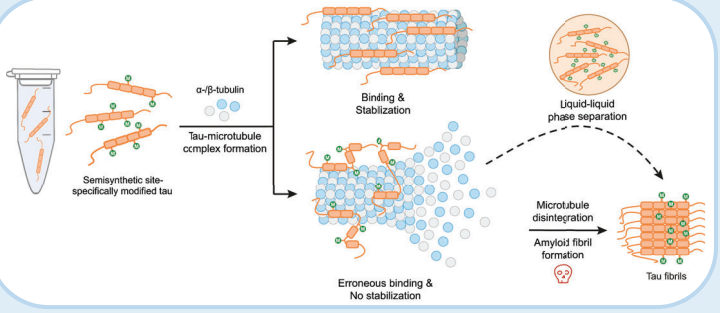

Microtubule binding & fibrillation

- **Potentially protective effect** of Ac294
- **Potentially toxic effect** of Ac311, Ac294/Ac311
- **Next:** Effects of new modified variants

LLPS

- **Modified variants to be tested:** pS341, pS341/pS352, Ac340/Ac343/Ac353, pS341/pS352/Ac340/Ac343/Sc353, CarbK311, SucK311

References:

[1] C. Tapia-Rojas, F. Cabezas-Opazo, C. A. Deaton, E. H. Vergara, G. V. W. Johnson, R. A. Quintanilla, *Progress in Neurobiology* 2019, *175*, 54-76.
[2] H. Zhang, X. Ji, P. Li, C. Liu, J. Lou, Z. Wang, W. Wen, Y. Xiao, M. Zhang, X. Zhu, *Science China Life Sciences* 2020, *63*, 953-985.
[3] D. Ellmer, M. Brehs, M. Haj-Yahya, H. A. Lashuel, C. F. W. Becker, *Angewandte Chemie International Edition* 2019, *58*, 1616-1620.

Contact:
Prof. Dr. Christian F. W. Becker
Mail: christian.becker@univie.ac.at
Tel.: +43-1-4277-70510
Miriam Preissler
Mail: miriam.preissler@univie.ac.at
Tel.: +43-1-42777-0518

Synthesis of the natural peptide product Fusahexin

Carmen Bäuerlein and Armin Geyer
Department of Chemistry
Philipps-University Marburg, Germany

https://doi.org/10.17952/37EPS.2024.P1047

Introduction

The cyclic hexapeptide Fusahexin was isolated and characterized by WESTPHAL *et al.*[1] It contains a 6,5-bicyclic dipeptide which is similar to β-turn mimics proposed by BALDWIN and CLARIDGE[2] but in a different configuration because the D-*allo*-Thr (**ehr**) was not investigated as a β-turn mimic before. Substituents on the 6-membered ring can restrict the valerolactam puckering and identify efficient β-turn mimics.[3] The aim of this project is the synthesis of Fusahexin and the characterization of the conformational restriction exerted by ehr=Pro.

Expansion of the literature known spectra of the isolated Fusahexin from WESTPHAL, 600 MHz, 308 K, DMSO-d_6

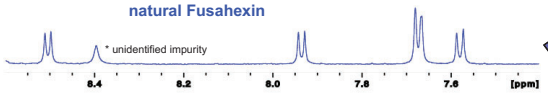

All possible strategies to the natural peptide product Fusahexin

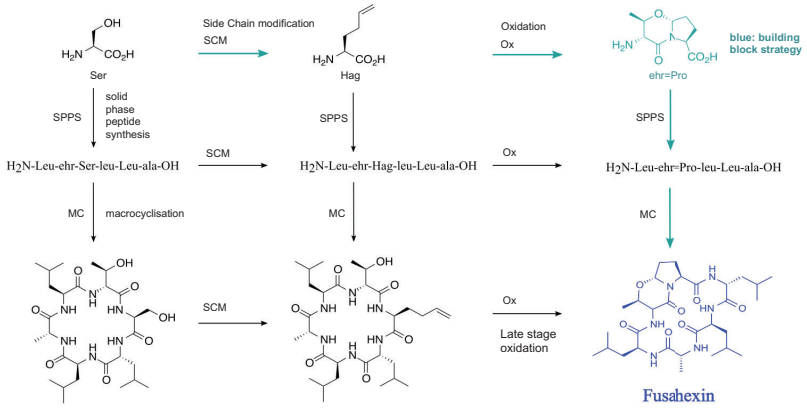

Homoallylglycine (**Hag**) was synthesized according to the literature[5] and after cleavage of the Boc protecting group,was used in a dipeptide coupling with Fmoc-ehr-OH. The resulting dipeptide was used in a LEMIEUX-JOHNSON oxidation to yield the storable building block Fmoc-ehr=Pro-OH which was used in SPPS for the linear precursor peptide of Fusahexin.The tricyclic peptide natural product can be isolated and characterized after head to tail macrocyclisation. The synthetic Fusahexin was characterized with NMR spectroscopy and compared with the literature known data of the isolated one. Both spectra show nearly the same chemical shifts and coupling constants.

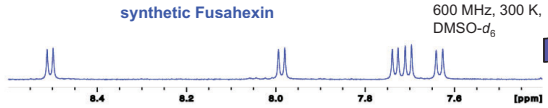

Modeling

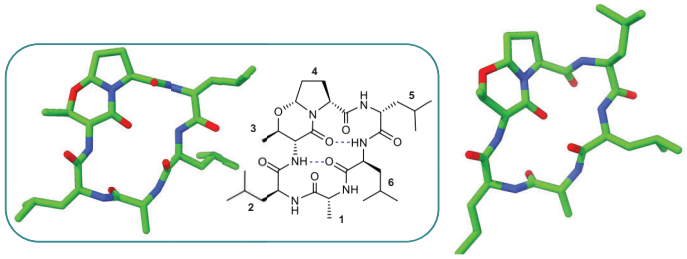

Left: 3D model of Fusahexin *cyclo*[-Leu-ehr=Pro-leu-Leu-ala]
Middle: Hydrogen bonding pattern of Fusahexin
Right: 3D model of *cyclo*[-Leu-ehr=Pro-Leu-Leu-ala]

The alternating sequence of D- and L- configurated amino acids and the bicyclic ring system ehr=Pro determine the conformation of Fusahexin. NOEs, ^3J coupling constants and temperature coefficients identify the 3D structure in a computer model (left). The leu^{5}NH→Leu^{6}NH NOE is characteristic for a βII´-turn with ehr=Pro in the i to i+1 position (middle).

We inverted the configuration of amino acid 5 and characterized the cyclic hexapeptide *cyclo*[-Leu-ehr=Pro-Leu-Leu-ala] by NMR and modeling (above right). ehr=Pro remains in the long side although the β-turn flips to βI-conformation. Further peptides confirm the β-turn-inducing properties of ehr=Pro.

Building block synthesis

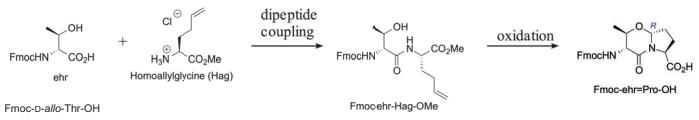

The building block Fmoc-ehr=Pro-OH was synthesized in 9 steps, starting from the natural amino acid L-serine. During the whole synthesis the N-terminus was protected with the Fmoc protection group which is necessary for the SPPS. The bridge head forms stereoselectively in *R* configuration independently of the peptide sequence. The stereoselective ring closure was proven by 2D-NMR like ROESY, where the bridge head proton shows a contact to the α-proton and to the γ-protons of ehr.

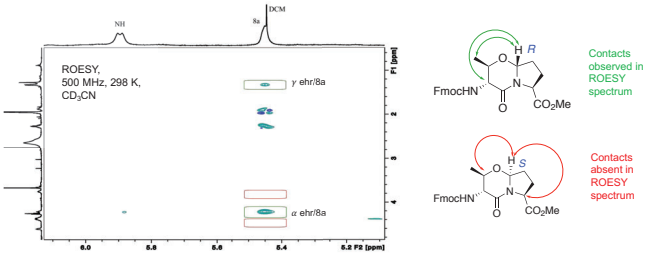

The independence of the bridge head configuration from the peptide sequence was further proven by the synthesis of *cyclo*[ehr-Hag-Phe-Gly-Gly-Gly] and the late-stage oxidation to *cyclo*[ehr=Pro-Phe-Gly-Gly-Gly], where the bridge head was again *R* configurated.[6]

Conclusion and Outlook

The building block Fmoc-ehr=Pro-OH can be synthesized in a 9 step synthesis with the LEMIEUX-JOHNSON oxidation as the key step. With this dipeptide the synthesis of the peptide natural product fusahexin was possible and 10 mg were isolated as a white solid. Because of the similiarity to the dipeptide which BALDWIN & CLARIDGE proposed as a β-turn mimic the Fmoc-ehr=Pro-OH building block is a possible β-turn mimic. In further studies the building bock is going to be used in more different peptide sequences to see if it is introducing a β-turn. Bioactivity studies are in progress.

References

[1] Westphal, K.R. et al., *J. Nat. Prod.*, **2021**, *84*, 2070-2080.
[2] Baldwin, J.E., Hulme C., Schofield C.J., Edwards A.J., *J. Chem. Soc., Chem. Commun.*, **1993**, 935-936. Claridge, T.D.W., Hulme C., Kelly R.J., Lee V., Nash I.A., Schofield C.J., *Bioorg. Med. Chem. Lett.*, **1996**, *6*, 485-490.
[3] Eckhardt, B., Grosse W., Essen L.O., Geyer A., *PNAS*, **2010**, *107*, 18336-18341.
[4] H. Kessler, *Angew. Chem.*, **1982**, *94*, 509-520.
[5] F. Daus, X. Xie, A. Geyer, *Org. Biomol.Chem.* **2022**, *20*, 3387-3396.
[6] Thesis A. Wuttke, Synthetische Oligomere von amyloidogenen Peptiden durch reversible Chemie, **2016**, Philipps-University Marburg, Germany.

Organocatalytic Surfactants for Direct Asymmetric Aldol Reactions in Aqueous Media

Susanta Kumar Behera and Ramesh Ramapanicker*
Department of Chemistry, Indian Institute of Technology Kanpur, Uttar Pradesh, India
skbehera@iitk.ac.in

https://doi.org/10.17952/37EPS.2024.P1049

Abstract

We have developed a peptide surfactant (Pepfactant) based organocatalyst that bears a proline unit as an efficient organocatalyst for the reaction between aromatic aldehydes and cyclohexanone in aqueous media and at room temperature. Using a catalytic loading of 20 mol%, the aldol products were obtained in high yields (99%) and with excellent enantioselectivity (93%) and good diastereoselectivity (95:5). The aqueous solution containing the surfactant could be reused for reactions between four different sets of substrates one after the other without the loss of selectivity. This method provides a greener strategy for carrying out organocatalytic reactions in aqueous media.

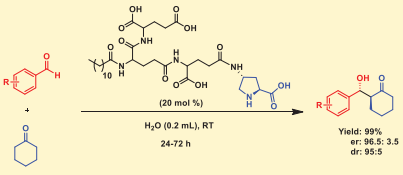

Design and Synthesis

Synthesis of Precursors I - IV

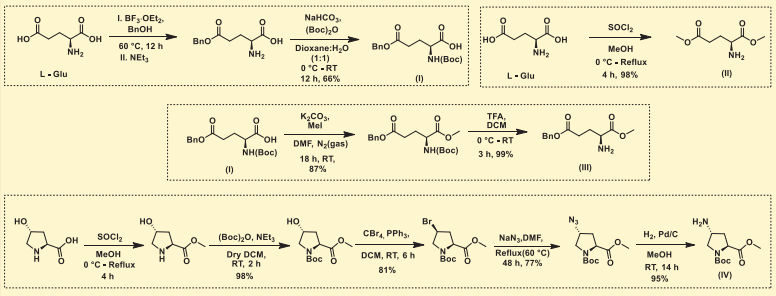

All precursors are synthesized from commercially available L-glutamic acid and *trans*-4-hydroxy-L-proline.

Synthesis of the Catalyst

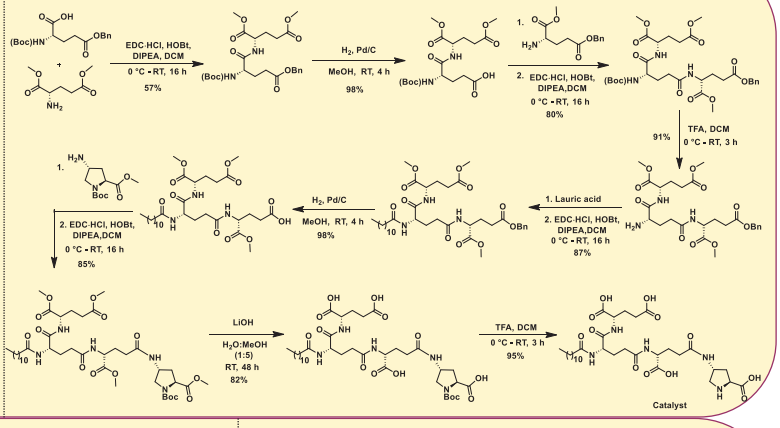

Optimization

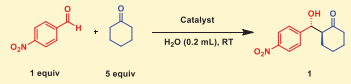

S. No.	Catalyst (mol%)	Time (h)	Yield[a] (%)	ee[b] (%)
1	1	58	80	88
2	5	58	99	92
3	10	30	98	91
4	20	24	99	93

(a) Isolated yield after column chromatography. (b) ee as determined by HPLC analysis using a Chiral AD-H Column.

Substrate Scope

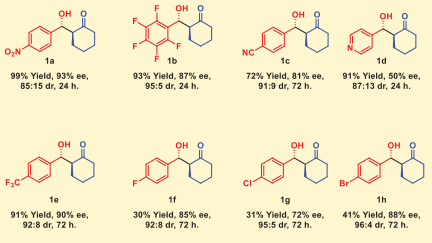

Reactions were performed with catalyst (0.08 mmol), aromatic aldehyde (0.4 mmol) and cyclohexanone (2 mmol) in water (0.2 mL) at room temperature. Isolated yield after column chromatography. Diastereomeric ratio was determined by ^{1}H NMR on a crude sample. ee as determined by HPLC analysis using different Chiral AD-H, OD-H and AS-H Columns.

Recyclability Test

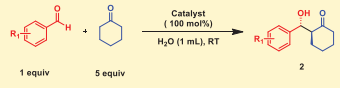

S. No.	R_1	Time (h)	Yield[a] (%)	ee[b] (%)
1	NO_2	15	88	90
2	CN	34	89	83
3	C_6F_5	12	91	89
4	CF_3	24	84	91

(a) Isolated yield after column chromatography. (b) ee as determined by HPLC analysis using different Chiral AD-H, OD-H and AS-H Columns.

Representation of Recyclability

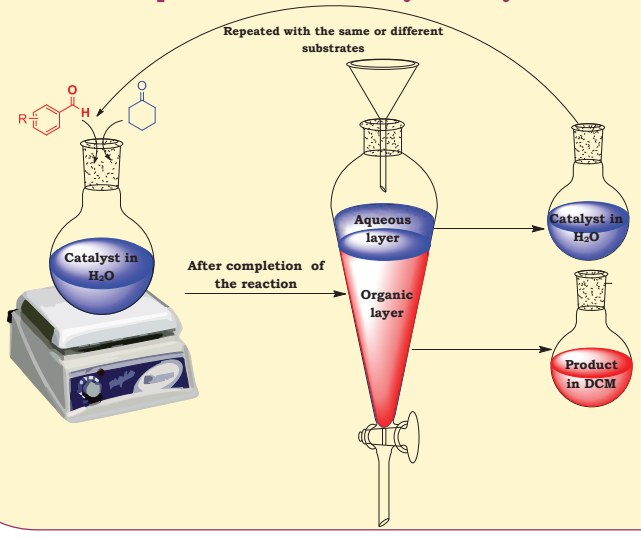

Conclusion

- We have designed and synthesized a new water-soluble peptide surfactant (Pepfactant) that contains a proline unit as an organocatalyst.
- These reactions are performed exclusively in water without the use of any additive and at room temperature.

References

- Hayashi, Y.; Sumiya, T.; Takahashi, J.; Gotoh, H.; Urushima, T.; Shoji, M. Angew. Chemie - Int. Ed. 2006, 45 (6), 958–961
- Mase, N.; Nakai, Y.; Ohara, N.; Yoda, H.; Takabe, K.; Tanaka, F.; Barbas, C. F. J. Am. Chem. Soc. 2006, 128 (3), 734–735.
- Al-Momani, L.; Lataifeh, A. Ind. Eng. Chem. Res. 2022, 61 (6), 2417–2424.

O-to-*O* Acyl Transfer for Epimerization-free Peptide C-terminal Salicylaldehyde Ester Synthesis

Zhixiang Zhong[1], Wang Xia[1], Bing-Wen Li[2], Han Liu[1], Zhi-Xiang Yu[2], and Xuechen Li[1]

[1]*Department of Chemistry, The University of Hong Kong, Hong Kong, China.*

[2]*College of Chemistry, Peking University, Beijing, China.*

https://doi.org/10.17952/37EPS.2024.P1050

THE UNIVERSITY OF HONG KONG

Abstract

Peptide salicylaldehyde esters are the requisite coupling partner in Ser/Thr ligation reactions towards chemical protein synthesis. In general, it would be cost-effective and efficient to use side chain protected peptide acids, after Fmoc-solid phase peptide synthesis, for direct C-terminal derivatization, however this has yet to be achieved, due to an intrinsic epimerization pathway. Here, we report the development of 2-(dichloromethyl)phenol (**DCP**) as a reagent which can directly form peptide salicylaldehyde esters in an epimerization-free manner. The peptide salicylaldehyde ester reaction products have been applied in the convergent total chemical synthesis of linker histone H1.2 using sequential Ser/Thr ligation reactions.

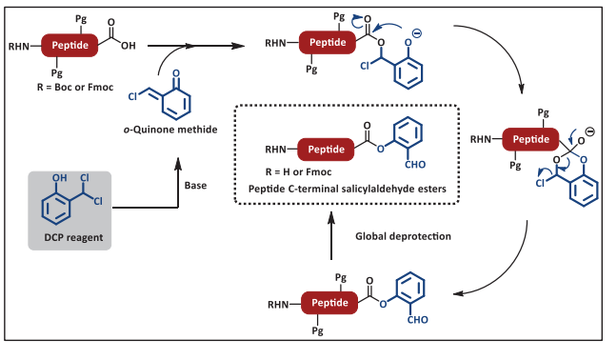

Results and Discussion

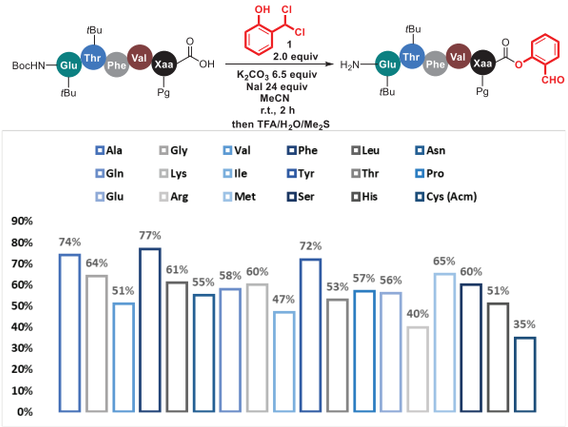

Figure 1. *Peptide SAL ester formation of different C-terminal residues using DCP reagent.*

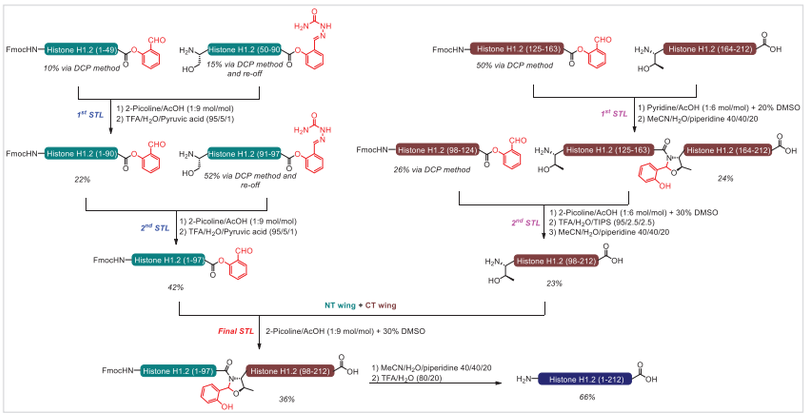

Figure 3. *Convergent synthesis of Histone H1.2 via serine/threonine ligations.*

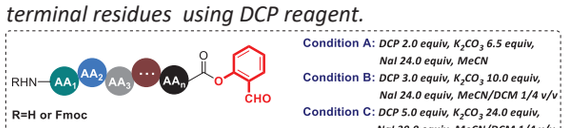

Sequence	Number of AA	Method applied	Isolated yield
NH_2-TNNDTGEYF-COSAL	9	B	68%
NH_2-SAKGVRYQNA-COSAL	10	C	55%
NH_2-TARKLGDQITHAPDEVNRSG-COSAL	20	C	31%
NH_2-TMSAKEKGKFEDMAKADKARYEREM-COSAL	25	C	30%
NH_2-SELLSGMGVSALEKEEPDSENIPCELL-COSAL	27	C	32%
NH_2-PRNGTVHLYLTKPLYTSAPSLQHLC$_{31Bn}$RL-COSAL	27	C	20%
NH_2-TYIPPKGETKKKFKDPNAPKRPPSAFFLF-COSAL	29	C	37%
NH_2-AFYRDPGVHAGLIYSAGVRKVILCQTNKGA-COSAL	30	C	28%
NH_2-PGLIGPKGDIGETGVPGAEGPRGFPGIQGRKGEPGEG-COSAL	37	C	27%

Figure 2. *Substrate scope of the peptide SAL ester formation using DCP reagent.*

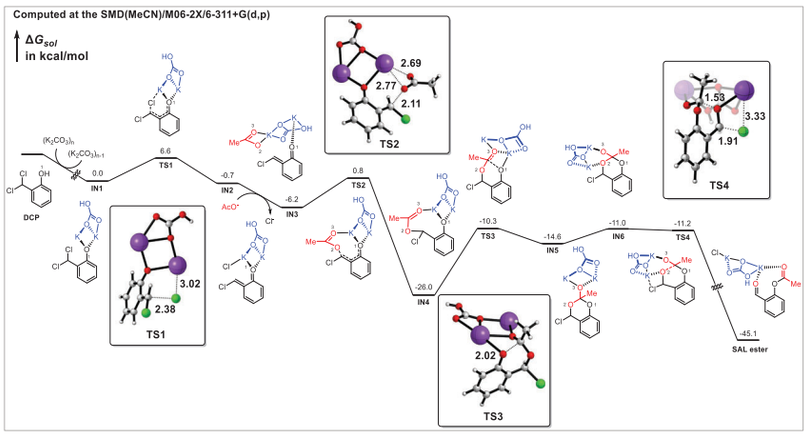

Figure 4. *Computational study of the mechanism*

Conclusion

The epimerization-free synthesis of peptide C-terminal salicylaldehyde (SAL) esters is achieved directly from solid phase synthesized side chain protected peptides using 2-(dichloromethyl)phenyl (DCP) reagent via a nontypical *O*-to-*O* acyl transfer. The scope of this method was demonstrated with syntheses of peptide SAL esters of various lengths ranging from 5 to 49 amino acids. The resulting peptide SAL esters were successfully applied for the convergent total chemical synthesis of 212-residue linker histone H1.2 protein using serine/threonine ligations.

References

[1] Xia, W., Li B-W., Zhong Z., Liu, J., Liu, H., Yu, Z*. & Li, X*. *O*-to-*O* acyl transfer for epimerization-free peptide C-terminal salicylaldehyde ester synthesis. *Nat. Synth.* **2024**, https://doi.org/10.1038/s44160-024-00570-0

[2] Zhang, Y., Xu, C., Lam, H. Y., Lee, C. L. & Li, X*. Protein chemical synthesis by serine and threonine ligation. *Proc. Natl. Acad. Sci. U. S. A.* **2013**, *110*, 6657-6662.

[3] Liu, H. & Li, X*. Serine/threonine ligation: origin, mechanistic aspects, and applications. *Acc. Chem. Res.* **2018**, *51*, 1643-1655.

Acknowledgement

The work was supported by the Grants Research Council of University Grants Committee of Hong Kong (C7017-18G, 17302621, 17306521, AoE/P-706/16), and National Natural Science Foundation of China (22177097).

New electrochemical method for Arylation of Cysteine containing peptides

Shen Linhua[1], Olivier Monasson[2], Elisa Peroni[2], Franck Le Bideau[1], Samir Messaoudi[1]
CNRS, BioCIS Université Paris-Saclay, 92290 Orsay, France, Orsay, France, 2CNRS, BioCIS CY Cergy Paris Université, 95000-Cergy-Pontoise, France, Cergy-Pontoise, France

https://doi.org/10.17952/37EPS.2024.P1051

INTRODUCTION

Functionalized peptides have emerged as a privileged class of bioconjugates with a diverse range of potential therapeutic applications, including cancer therapy, inflammation, and infection[1].

Thus, the development of peptide bioconjugates is a growing area of research and holds great potential for the treatment of various diseases. As a consequence, the need for new site-selective bioconjugation methods under biocompatible conditions is highly desirable.

Here we report a simple electrochemical route towards the synthesis of S-arylated peptides by a site selective coupling of Cysteine containing peptides with aryl halides under base free conditions. This approach demonstrates the power of electrochemistry to access both highly complex peptide conjugates and cyclic peptides [3].

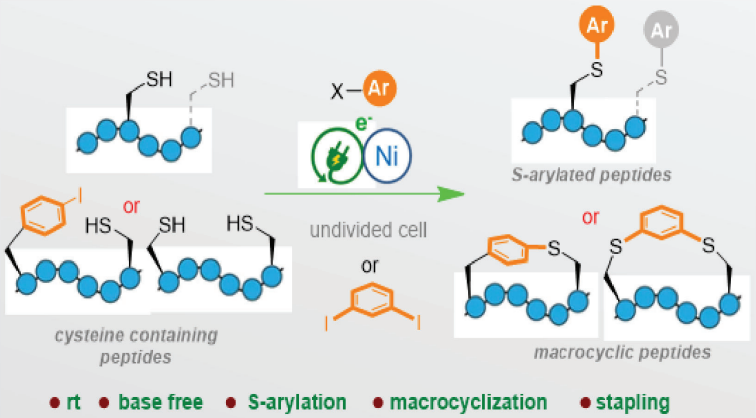

Electrochemical S-arylylation of native Peptides

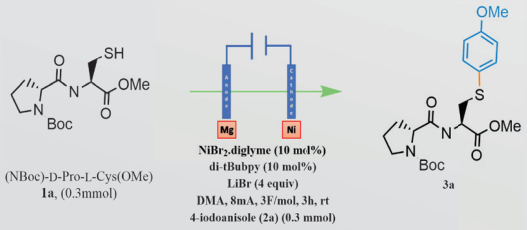

Entry	Deviation from the standard conditions	Yield %
1	None	89
2	(4mA, 6h), instead of (8mA, 3h)	84
3	4-Br-Anisole instead of 4-I Anisole	57

Reaction Optimization

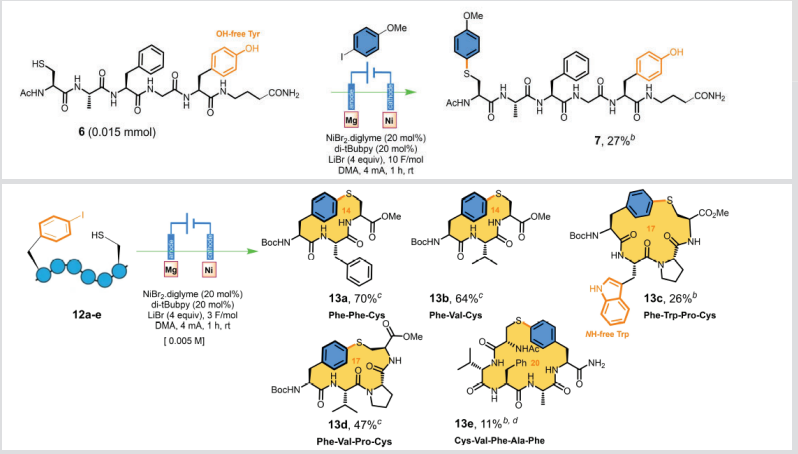

Access to linear and cyclic peptides

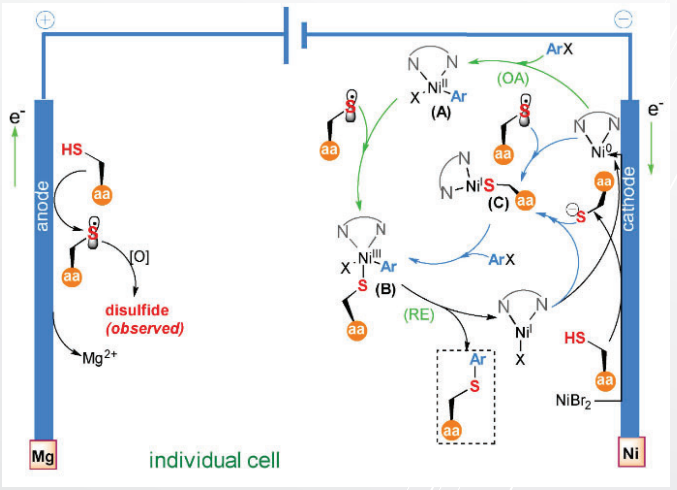

Proposed Mechanism

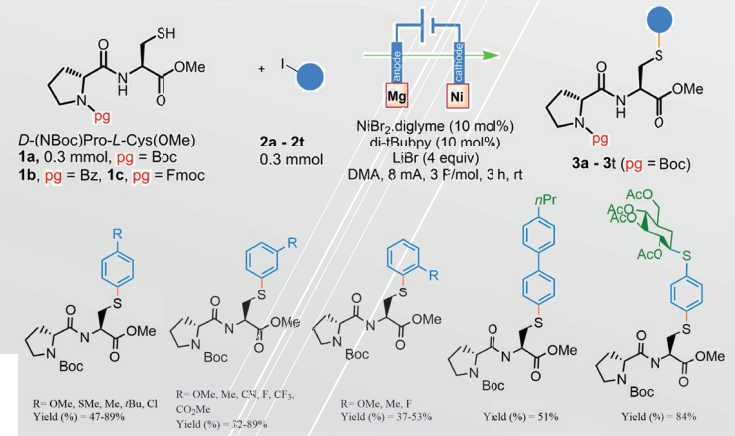

Aryl/Alkenyl/alkynyl halides Scope

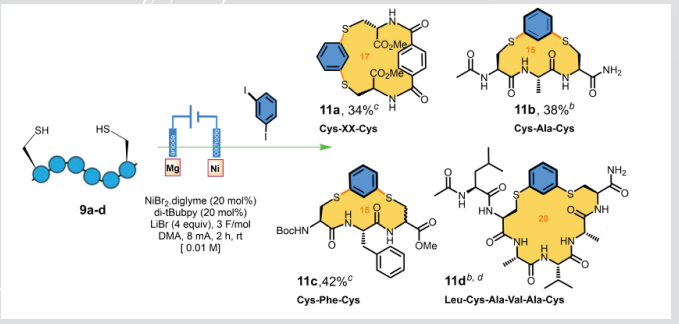

Access to stapled peptides

CONCLUSION ET PERSPECTIVES

We developped the first electrochemical method for the coupling of cystein containing peptides with halides under mild reaction conditions, without precious metals or halide excess. We obtained linear, cyclic and stapled peptide, with or without protecting groups. Further studies on the applications of this method to obtain macrocyclic peptides are ongoing

[1] M. H. Baig, K. Ahmad, M. Saeed, A. M. Alharbi, G. E. Barreto, G. Md Ashraf, I. Choi, *Biomed. Pharmacother.* 2018, 103, 574–581. [2] Y. Weng, C. Song, C. W. Chiang, A. Lei, *Commun. Chem.* 2020, 3, 171.
[3] L. Shen, O. Monasson, E. Peroni, F. Le Bideau, S. Messaoudi, Angew. Chem.Int. Ed.2023, 62, e2023157.

Proceedings of the 37th European Peptide Symposium
Michal Lebl, Editor
European Peptide Society, 2024
http://doi.org/10.17952/37EPS.2024.P1052

N-Aminoimidazol-2-one Peptide Mimic Tools for Deciphering Active Conformations

Yousra Hamdane[1], Pradeep Chauhan[1], Suresh Vutla[1], Darince Truong[1] and William D. Lubell[1]

[1]*Département de Chimie, Université de Montréal, Montréal, Québec H3C3J7, Canada*

Introduction

Peptide mimics serve as tools for studying structure-activity relationships in biomedical applications to improve selectivity and pharmacokinetic properties.[1-3] Among peptide mimics (Figure 1), *N*-aminoimidazolidin-2-one (Aid, **3**)[4] and *N*-aminoimidazol-2-one (Nai, **4**)[5] residues combine properties of the covalent constraint found in α-amino-γ-lactam (Agl, **1**)[6] residues and the stereoelectronic effects of azapeptides (**2**).[7] The Nai residues enable potential for adding ring substituents to mimic amino acid side chains in constrained χ-dihedral angle orientations to improve activity and selectivity.[5]

Results and Discussion

The synthesis of 4-substituted Nai residues was first investigated by a *5-endo-dig* cyclisation of aza-propargylglycine analogs (e.g., **5**, Figure 2).[8] 4,5-Disubstituted Nai analogs were next prepared by diversification of the 5-position using palladium catalysis and Vilsmeier chemistry to install respectively aryl and formyl groups (e.g., **7** and **8**).[9,10] Organic catalysis using azoglycine residues gave later 5-substituted Nai residues which were used to study peptide ligands of the cluster of differentiation-36 receptor (CD36).[11] For example, oxidation of Fmoc-azaGly-Phe-O*t*-Bu (**9**) using *N*-bromosuccinimide gave azopeptide **10**. Subsequent reaction of the azopeptide with aryl acetaldehydes and proline as organocatalyst, followed by acid-mediated dehydration gave 5-aryl Nai dipeptides **11a** and **11b** (Figure 3), which after ester deprotection, were installed into peptides **14a** and **14b** by conventional solid-phase synthesis.[11]

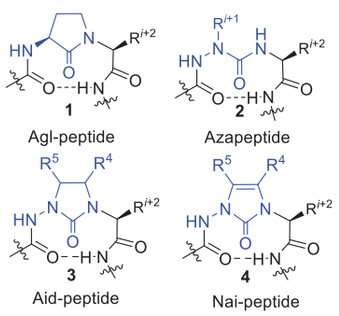

Fig. 1 Agl, aza-, Aid and Nai peptide mimics.

X-ray and computational analyses of model Nai peptides have demonstrated preferences for the *i* + 1 residue of type II' β- and γ-turns as well as potential to mimic side chain function and χ-space orientation contingent upon ring substituent position.[5]

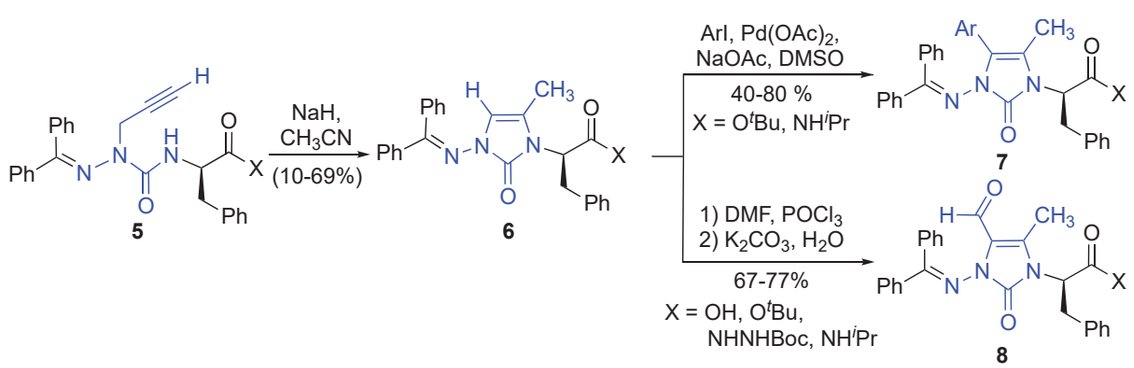

Fig. 2. Synthesis of Nai analogs by way of 5-endo-dig cyclisation of aza-propargylglycines.

Previously, [(5-Ar)Nai[4]]-GHRP-6 analogs **14a** and **14b** exhibited relatively high CD36 binding affinity and reduced NO production by macrophages exposed to a toll-like receptor-2 agonist. The *N*-amino cyclic urea of **14a** and **14b** adopted likely the $i + 1$ residue of a type II' β-turn with aryl substituent in *gauche* χ-space.[11]

With interest to further explore the active conformer, 4,5-disubstituted Nai peptides (e.g., **15**) are under investigation. For example, treatment of azopeptide **10** with 1-phenylpropan-2-one and proline, followed by acid catalyzed dehydration gave (4-Ph,5-Me)Nai **12** in 74% yield from azaGly **9**. Insertion of disubstituted Nai **12** into GHRP-6 analog **15** is now being pursued to detail the active conformation for CD36 modulation towards prototypes for mitigating macrophage-driven inflammation.

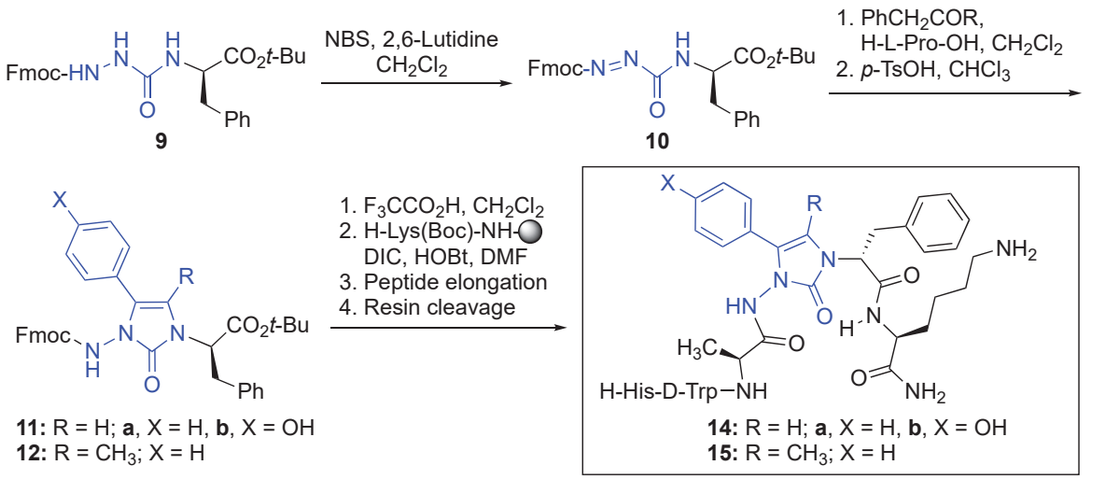

Fig. 3. Organocatalytic approach for Nai peptide synthesis for applications as CD36 modulators.

Acknowledgments

We are grateful for funding from the Natural Sciences and Engineering Research Council of Canada (NSERC, Discovery Research Project RGPIN-2019-04079), the Canadian Institutes of Health Research (CIHR, Project PJT-186296), and the Fonds de Recherche du Québec - Nature et Technologie (FRQNT, CGCC, FRQNT-2020-RS4-265155-CCVC). Assistance is acknowledged from members of the Université de Montréal facilities: Dr. P. Aguiar (NMR spectroscopy) and Dr. A. Fürtös (mass spectrometry).

References

1. Lubell, W. D. *Preface*, In *Peptidomimetics I*; Lubell, W. D., Ed.; Springer International Publishing: Cham, **2017**, v–xiv.
2. Robertson, N. S.; Spring, D. R. *Molecules* **2018**, *23*, 959, https://doi.org/10.3390/molecules23040959
3. Qvit, N.; Rubin, S. J. S.; Urban, T. J.; Mochly-Rosen, D.; Gross, E. R. *Drug Discovery Today* **2017**, *22*, 454, https://doi.org/10.1016/j.drudis.2016.11.003
4. Doan, N.-D.; Hopewell, R.; Lubell, W.D. *Org. Lett.* **2014**, *16*, 2232-5, https://doi.org/10.1021/ol500739k
5. Hamdane, Y.; Poupart, J.; Lubell, D. W. *Synthesis* **2022**, *54*, 1518–1526, DOI: 10.1055/s-0040-1719862
6. Freidinger, R. M. *J. Med. Chem.* **2003**, *46*, 5553-5566, https://doi.org/10.1021/jm030484k
7. Proulx, C.; Sabatino, D.; Hopewell, R.; Spiegel, J.; García Ramos, Y.; Lubell, W. D. *Future Med. Chem.* **2011**, *3*, 1139-1164, https://doi.org/10.4155/fmc.11.74
8. Proulx, C.; Lubell, W. D. *Org. Lett.* **2012**, *14*, 4552-4555, https://doi.org/10.1021/ol302021n
9. Poupart, J.; Doan, N.-D.; Berube, D.; Hamdane, Y.; Medena, C.; Lubell, W. D. *Heterocycles* **2019**, *99*, 279-293, DOI: 10.3987/COM-18-S(F)22
10. Poupart, J.; Hamdane, Y.; Lubell, W. D. *Can. J. Chem.* **2020**, *98*, 278-284, https://doi.org/10.1139/cjc-2019-0479
11. Hamdane, Y.; Chauhan, P. S.; Vutla, S.; Mulumba, M.; Ong, H.; Lubell, W. D. *Org. Lett.* **2021**, *23*, 3491-3495, https://doi.org/10.1021/acs.orglett.1c00936

Proceedings of the 37th European Peptide Symposium
Michal Lebl, Editor
European Peptide Society, 2024 *http://doi.org/10.17952/37EPS.2024.P1054*

Ring Pucker Control in β-Prolines

Nassim Maarouf Mesli and William D. Lubell
Département de Chimie, Université de Montréal, 1375 Ave. Thérèse-Lavoie-Roux, Montréal, Québec, H2V 0B3, Canada

Introduction

Pyrrolidine ring puckering influences proline localization in peptide conformations.[1, 2] The dihedral angles χ^1 and χ^2 define respectively the C^γ *endo* ($\chi^1 > 0$, $\chi^2 < 0$) and *exo* ($\chi^1 < 0$, $\chi^2 > 0$) puckers.3-6 In peptides, proline (e.g., **1**) prefers usually the C^γ *endo* ring pucker with the C^α carbonyl in the pseudoaxial orientation (**Figure 1**). Pyrrolidine ring substituents can significantly influence proline puckering and consequently peptide folding.[3-6] For example, (4*R*)-*trans*-hydroxy- and fluoro-prolines favour the *exo* over the *endo* ring pucker in peptides due to stereoelectronic effects.[5] Moreover, *N*-acyl (4*R*)-*trans*- and (4*S*)-*cis*-*tert*-butyl prolines adopt respectively *endo* and *exo* ring puckers.[6]

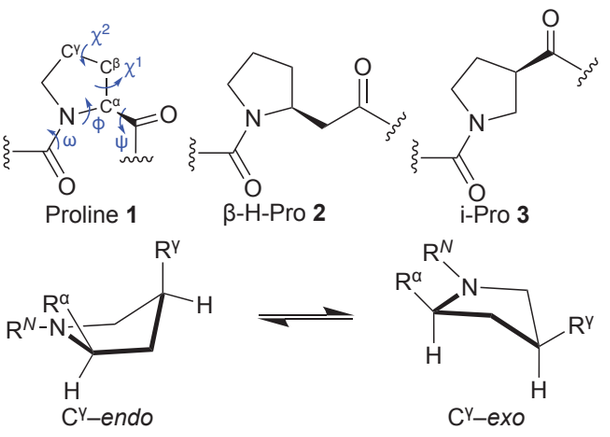

Figure 1. Prolyl and β-prolyl residues and related pyrrolidine ring puckerings.

The *N*-acetyl analogs of the β-prolines, β-homoproline and isoproline (e.g., **2** and **3**) are predicted to adopt preferred *exo* puckering with pseudoequatorial orientations of the respective C^α and C^β substituents.[7, 8] Exploring the synthesis and conformational preferences of homo-isoproline (Hip) chimeras, we have characterized influences of nitrogen hybridization on ring puckering and peptide topology.

Results and Discussion

The effects of nitrogen hybridization on ring puckering and conformation were examined using di-*N'*-methyl amides of *N*-toluensulfonyl (Ts) and *N*-*p*-nitrophenyl (*p*Np) *cis*-homo-isoprolines *cis*-Ts-Hip(NHMe)-NHMe (**4**) and *cis*-*p*Np-Hip(NHMe)-NHMe (**5**), which were respectively synthesized and characterized by ^{1}H NMR spectroscopy and X-ray crystallography.[9] In sulfonamide **4** the nitrogen is sp^3 hybridized and the *exo* ring pucker is favoured due in part to pseudoequatorial orintations of the C^α and C^γ substituents which minimize steric repulsion (**Figure 2**). Sulfonamide **4** exhibited spectral and crystallographic data for χ^1 and χ^2 dihedral angles in agreement with an *exo* ring pucker as previously reported for 4-substituted prolines.[6] *p*-Nitrophenyl analog **5** is expected to adopt the sp^2 nitrogen hybridization and induce $A^{1,3}$ strain with the C^α substituent which takes a pseudo-axial orientation eclipsing the C^β proton in a flattened C^γ *exo* ring pucker as characterized by X-Ray crystallography (**Figure 2**). The application of the ring puckering effects of homo-isoproline are under further study in peptide mimics.[9]

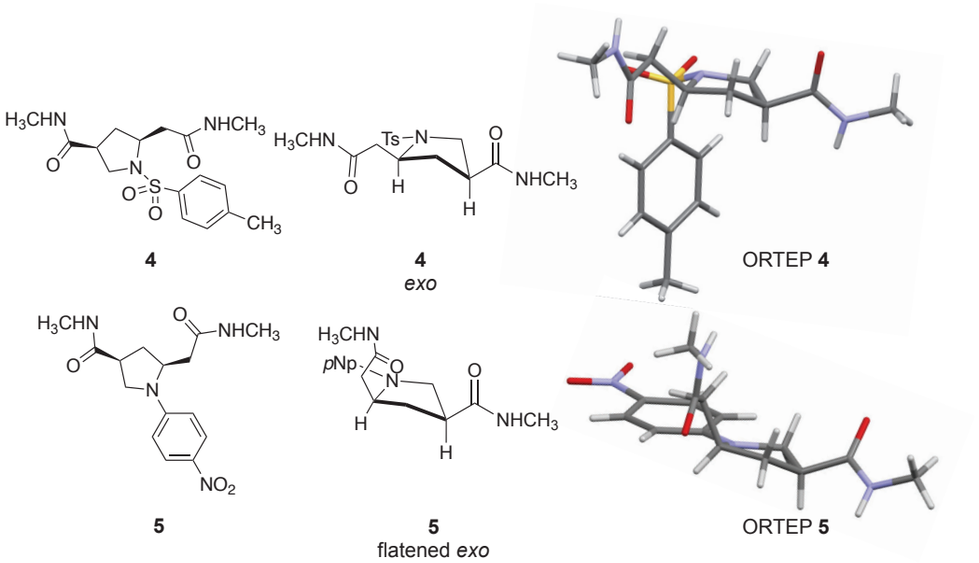

Figure 2. *N*-Substituted homo-isoproline diamides **4** and **5** and favored ring puckerings.

Acknowledgments

We thank the Canadian Institutes of Health Research (CIHR) for project PJT-190158, the Natural Sciences and Engineering Research Council of Canada (NSERC) for funding Discovery Research Project RGPIN-2019-04079, and the Fonds de Recherche du Québec - Nature et Technologie (FRQNT) for support of the Centre in Green Chemistry and Catalysis (CGCC, FRQNT-2020-RS4-265155-CCVC). The authors acknowledge the assistance of members of the Université de Montréal facilities: Dr. P. Aguiar and Dr. C. Malveau (NMR spectroscopy) and Dr. A. Fürtös, Ms. K. Gilbert and Dr. M.-A. Vaudreuil (mass spectrometry), Dr. T. Maris and Dr. D. Chartrand (X-ray). NMM thanks NSERC for an Alexander Graham Bell Fellowship and the EPS for a registration fee waiver.

References

1. Milner-White, E. J.; Bell, L. H.; Maccallum, P. H., Pyrrolidine ring puckering in cis and trans-proline residues in proteins and polypeptides: Different puckers are favoured in certain situations. *J. Mol. Biol.* **1992**, 228 (3), 725-734.
2. DeTar, D. F.; Luthra, N. P., Conformations of proline. *J. Am. Chem. Soc.* **1977**, 99 (4), 1232-1244.
3. Berger, G.; Vilchis-Reyes, M.; Hanessian, S., Structural Properties and Stereochemically Distinct Folding Preferences of 4, 5-cis and trans-Methano-l-Proline Oligomers: The Shortest Crystalline PPII-Type Helical Proline-Derived Tetramer. *Angew. Chem. Int. Ed.* **2015**, 54 (45), 13268-13272.
4. Beausoleil, E.; Lubell, W. D., Steric effects on the amide isomer equilibrium of prolyl peptides. Synthesis and conformational analysis of N-acetyl-5-tert-butylproline N ‘-methylamides. *J. Am. Chem. Soc.* **1996**, 118 (51), 12902-12908.
5. DeRider, M. L.; Wilkens, S. J.; Waddell, M. J.; Bretscher, L. E.; Weinhold, F.; Raines, R. T.; Markley, J. L., Collagen stability: insights from NMR spectroscopic and hybrid density functional computational investigations of the effect of electronegative substituents on prolyl ring conformations. *J. Am. Chem. Soc.* **2002**, 124 (11), 2497-2505.
6. Koskinen, A. M.; Helaja, J.; Kumpulainen, E. T.; Koivisto, J.; Mansikkamäki, H.; Rissanen, K., Locked conformations for proline pyrrolidine ring: synthesis and conformational analysis of cis-and trans-4-tert-butylprolines. *J. Org. Chem.* **2005**, 70 (16), 6447-6453.
7. Góbi, S.; Knapp, K.; Vass, E.; Majer, Z.; Magyarfalvi, G.; Hollósi, M.; Tarczay, G., Is β-homo-proline a pseudo-γ-turn forming element of β-peptides? An IR and VCD spectroscopic study on Ac-β-HPro-NHMe in cryogenic matrices and solutions. *PCCP* **2010**, 12 (41), 13603-13615.
8. Sandvoss, L. M.; Carlson, H. A., Conformational behavior of β-proline oligomers. *J. Am. Chem. Soc.* **2003**, 125 (51), 15855-15862.
9. Mesli Maarouf, N.; Lubell W.D. Unpublished results.

https://doi.org/10.17952/37EPS.2024.P1055

Nature-Inspired Gallinamides Are Potent Antischistosomal Agents: Inhibition of the Cathepsin B1 Protease Target and Binding Mode Analysis

Spiwokova P.[1], Horn M.[1], Maresova L.[1], Fanfrlik J.[1], Jilkova A.[1], Fajtova P.[1], Leontovyc A.[1], Houstecka R.[1], Bielikova L.[1], Brynda J.[1], Chanova M.[2], Mertlikova-Kaiserova H.[1], Caro-Diaz E.[3], Almaliti J.[3,4], El-Sakkary N.[4], Gerwick W.H.[3,4], Caffrey C.R.[4], and Mares M.[1]

[1] Institute of Organic Chemistry and Biochemistry, Czech Academy of Sciences, Prague, Czech Republic, [2] Charles University and General University Hospital, Prague, Czech Republic, [3]Scripps Institution of Oceanography, University of California, San Diego, United States, [4]University of California, Skaggs School of Pharmacy and Pharmaceutical Sciences, San Diego, United States

Introduction

Gallinamide A is a natural product of marine cyanobacteria. This compound and its derivatives can bind cysteine proteases in a covalent-irreversible manner. Here we analyze the interaction of gallinamides with *Schistosoma mansoni* cathepsin B1 (SmCB1), a central digestive protease, which has recently been validated as molecular target against schistosomiasis. This parasitic disease is caused by blood flukes of the genus *Schistosoma* and is a global health problem with over 240 million people infected. Treatment relies on just one drug and new therapies are needed. Adult schistosomes live in the blood vessels and host blood proteins are the main source of nutrients.



- *Schistosoma mansoni* cathepsin B1 (SmCB1) is a validated drug target against schistosomiasis
- We screened a library of synthetic analogues of gallinamide A for inhibition of SmCB1 and identified inhibitors with low nanomolar potency.
- Gallinamides exhibit a strong suppression effect on live schistosomes in culture.
- We solved the first high-resolution crystal structures of gallinamides in complex with SmCB1 and determined their binding mode in the active site.

Electron density maps and B-factors

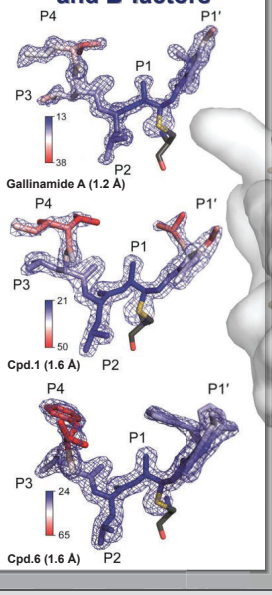

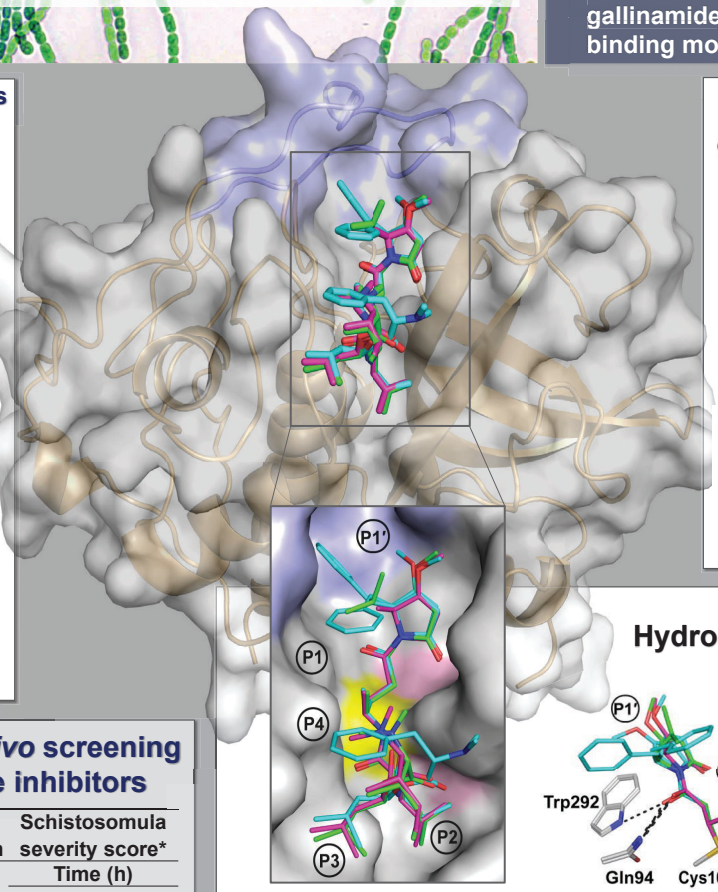

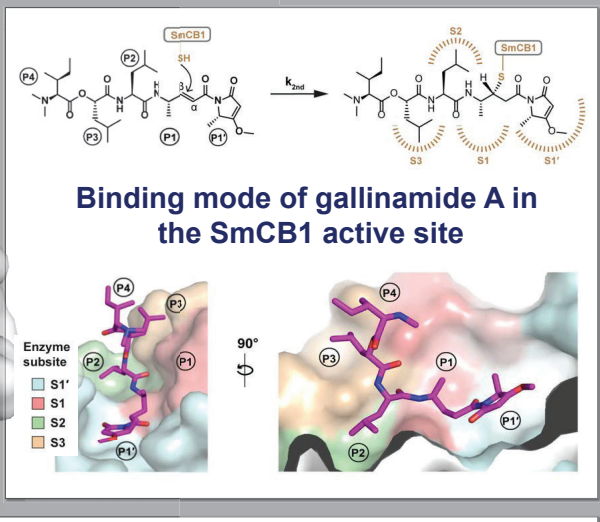

Hydrogen bonds

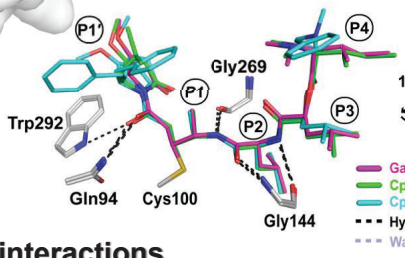

Water bridges

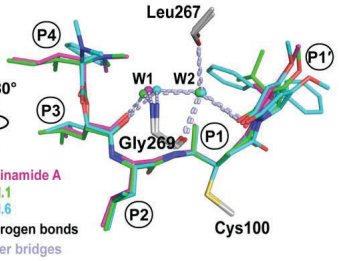

Hydrophobic interactions

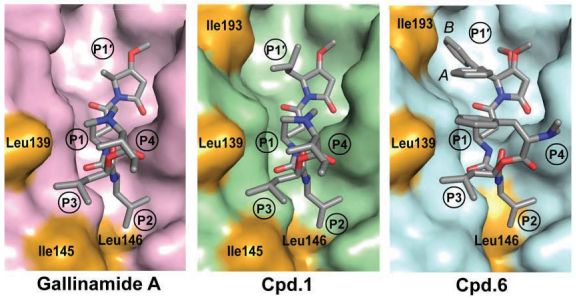

In-vitro and *ex-vivo* screening of gallinamide inhibitors

Compound name	SmCB1 Inhibition k_{2nd} ($M^{-1} \cdot s^{-1}$)	Schistosomula severity score* Time (h) 24	48	72
Gallinamide A	6644	0	2	4
1	3394	2	4	4
2	3334	0	2	4
3	2902	0	0	2
4	2894	0	0	4
5	2792	0	4	4
6	1930	3	4	4
7	942	0	3	4
8	886	1	4	4
9	793	0	1	4
10	537	0	2	4
11	295	0	3	4
12	212	1	4	4
13	109	0	3	4
14	55	0	4	4
15	41	0	3	4
16**	36	0	0	0
17	18	0	2	4
18	16	0	0	3

*Induction of phenotypic alterations by the inhibitors was determined with newly transformed schistosomula of *S. mansoni*. The inhibitors were tested at 1 μM concentrations for 3 days and the resulting phenotypes were graded by severity score from 0 to 4 being the most severe.

**Gallinamide A without warhead

Parasite phenotypic screening

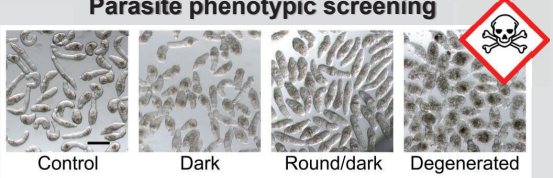

Quantum chemical calculation of interaction energy

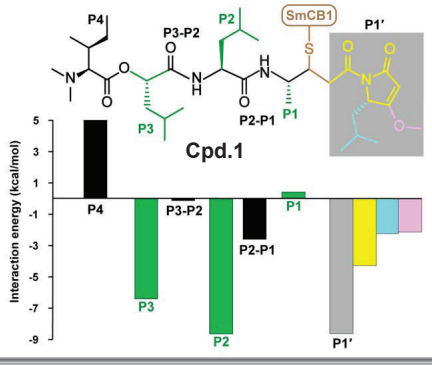

This work was supported by grants LTAUSA19109 and LUAUS23050 from the Ministry of Education, Youth, and Sports of the Czech Republic and institutional project RVO 61388963.

ÚOCHB IOCB PRAGUE

EUROPEAN UNION
European Structural and Investment Funds
Operational Programme Research, Development and Education

MINISTRY OF EDUCATION, YOUTH AND SPORTS

Study on interactions of LL-37 human cathelicidin peptide fragment with Cu(II) ion

Jakub Brzeski[1], Dariusz Wyrzykowski [1], Bogusław Pilarski[2], Joanna Makowska [1]

[1]Faculty of Chemistry, University of Gdańsk, Wita Stwosza 63, 80-308 Gdańsk, Poland

[2]Cerko Sp. z o.o. Sp.k, Al. Zwycięstwa 96/98, 81-451 Gdynia, Poland

https://doi.org/10.17952/37EPS.2024.P1056

NMR structure of LL-37 in sodium dodecyl sulfate (SDS) micelles and its selected variants.
G. Wang, W. D. Treleaven, R. J. Cushley, *Biochim. Biophys. Acta.*, 1996, 1301, 174–184.

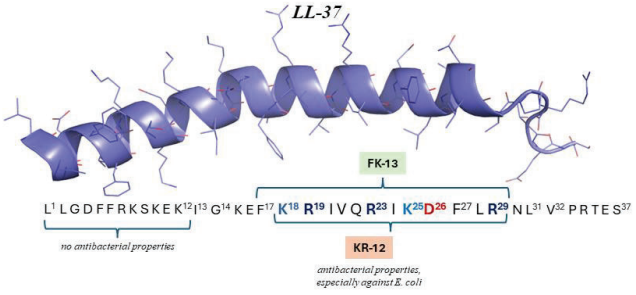

KR-12

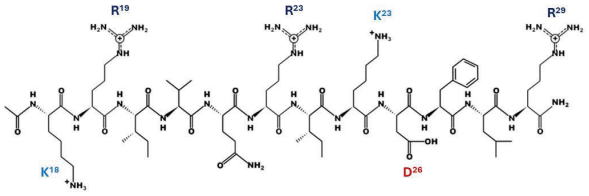

Biologically essential metal Cu(II) ions could have a two-fold effect on the activity of antimicrobial peptides (AMPs): (a) AMPs bind them, so that microbes do not get enough metals essential for their survival and virulenceor , (b) AMPs require a given metal ion to enhance their antimicrobial activity.

The human Cationic Antimicrobial Protein (hCAP) corresponding to overlapping sequences of hCAP (151-162) named KR-12 peptide is the smallest portion of the only type of human *Cathelicidin*, which has been shown that could be modified into more effective antimicrobials. The Isothermal Titration Calorimetry technique and *in silico* analysis were used to determine potential metal Cu(II) binding sites of KR-12. Based on density functional theory (DFT) calculations, we propose the most likely coordination modes of Cu(II) to peptide as well as to discuss the chemical nature of the interactions. The specific behavior of basic residues presented in the investigated peptide in a solution can govern the process of binding ions to the system. The presented results provide important structural and thermodynamic information to understand the influence of Cu(II) ions on the activity of KR-12 peptide.

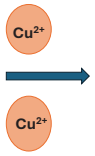

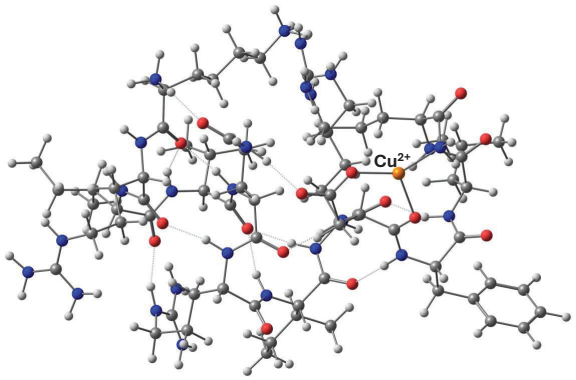

Isothermal titration calorimetry (ITC)

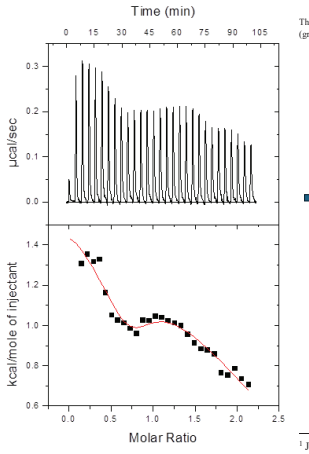

The conditional thermodynamic parameters of Cu^{2+} binding to KR-12 and previously established data for LL-37[1] (grey column) in the 10 mM CACO buffer of pH 6, at 298.15 K.

Parameter	LL-37//Cu^{2+}	KR-12//Cu^{2+}
$\log K_{ITC(1)}$	**4.23** (±0.02)	**5.73** (±0.08)
$\Delta_{ITC}H_{(1)}$ [kcal/mol]	4.08 (±0.03)	1.46 (±0.05)
$T\Delta_{ITC}S_{(1)}$ [kcal/mol]	10.8	9.28
$\Delta_{ITC}G_{(1)}$ [kcal/mol]	-6.72 (±0.03)	-7.82 (±0.11)
$\log K_{ITC(2)}$		**4.20** (±0.18)
$\Delta_{ITC}H_{(2)}$ [kcal/mol]		-5.78 (±2.39)
$T\Delta_{ITC}S_{(2)}$ [kcal/mol]		-0.05
$\Delta_{ITC}G_{(2)}$ [kcal/mol]		-5.73 (±0.25)
$\log K_{ITC(3)}$		**5.16** (±0.19)
$\Delta_{ITC}H_{(3)}$ [kcal/mol]		15.40 (±4.58)
$T\Delta_{ITC}S_{(3)}$ [kcal/mol]		22.44
$\Delta_{ITC}G_{(3)}$ [kcal/mol]		-7.04 (±0.26)
$\log K_{ITC(4)}$		**5.01** (±0.20)
$\Delta_{ITC}H_{(4)}$ [kcalmol]		-10.85 (±2.71)
$T\Delta_{ITC}S_{(4)}$ [kcal/mol]		-4.01
$\Delta_{ITC}G_{(4)}$ [kcal/mol]		-6.84 (±0.28)

[1] J. Makowska, D. Wyrzykowski, E. Kamysz, A. Tesmar, W. Kamysz, L. Chmurzyński, *Journal of Thermal Analysis and Calorimetry*, 2019, **138** (6), 4523-4529

The analysis of the presented data at the given theoretical level (GFN2-xTB/ALPB)

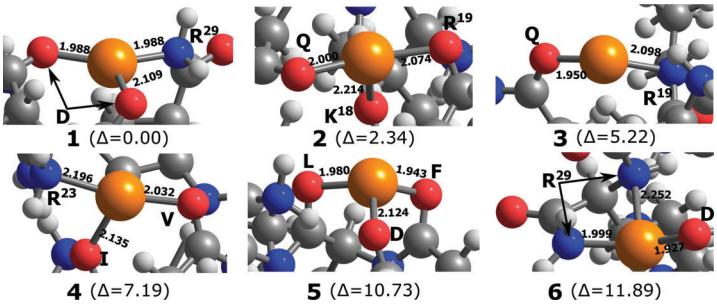

The KR-12 interacts with metal ions mostly via the main chain's oxygen atoms, however, the two types of amino acids that are expected to be vital for the interaction of Cu(II) are D and R29. Former due to the overall negative charge arising from the deprotonated carboxylic group within its side chain. Later via O atoms of the main chain, also characterized by significantly nucleophilic character arising from polarization due to the substantial positive character of the guanidine moiety. Additionally, the obtained results indicate that the oxygen atoms of the main peptide chain in KR-12, especially those with positively charged side chains may be crucial when it comes to interaction with electrophiles, such as Cu(II) ions. The most probable and stable dominant structures of the investigated complexes have been selected based on calculations. The presented results provide important structural and thermodynamic information for further study to understand the influence of Cu(II) ions on the activity of the KR-12 peptide.

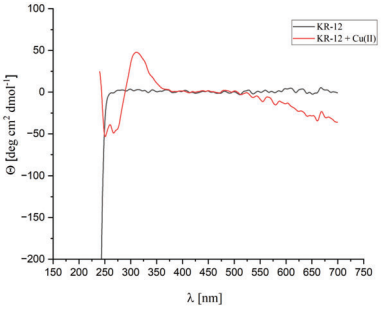

The CD spectra recorded for the KR-12 peptide (black line) at 298K as well as their copper(II) complex (red line) in CACO buffer (pH 6)

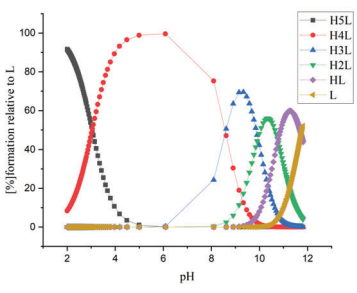

Species distribution diagram of the KR-12 peptide (H_5L) as a function of pH calculated based on the acid dissociation constants obtained from potentiometric titration data.

Peptide stapling - application in antibacterial therapies

Monika Wojciechowska, Julia Macyszyn, Michał Burmistrz, Joanna Miszkiewicz, Małgorzata Lobka, Joanna Trylska

Centre of New Technologies, University of Warsaw, Banacha 2c, 02-097, Warsaw, Poland

m.wojciechowska@cent.uw.edu.pl

https://doi.org/10.17952/37EPS.2024.P1058

Introduction

Membrane-active peptides (MAPs) are short chains of amino acids that interact with cell membranes, primarily targeting lipid bilayers and inducing changes in their structure. MAPs have wide-ranging applications in medicine and biotechnology, particularly in antimicrobial therapies (**antimicrobial peptides**, AMPs), anticancer therapies, and drug delivery (**cell-penetrating peptides**, CPPs). Their ability to disrupt cell membranes makes them particularly promising against pathogens that are resistant to traditional antibiotics. We have proposed to stabilize the biologically active structures of selected MAPs with a peptide stapling technique, enhancing their proteolytic stability and antibacterial activity without increasing their hemolytic activity or toxicity to other human cells. Additionally, to enhance the effectiveness of some stapled peptides, we conjugated them with **aminoglycosides**.

Goal of our reaserch

We employed a **hydrocarbon stapling technique**, a specific method of peptide stapling that involves creating hydrophobic bridges composed of hydrocarbons between amino acid residues within the peptide. This process introduces synthetic amino acids containing alkene groups (unsaturated hydrocarbons) into precise positions (*X* and *X + 4*) in the peptide chain.

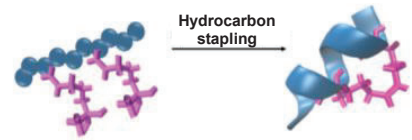

As aminoglycosides, we chose **amikacin** (AMK) and **neomycin** (NEO). We proposed two methods for conjugating peptides with AMK and NEO: a non-cleavable triazole ring formed through a 'click chemistry' reaction, and a disulfide bond, which is cleavable in the bacterial cytosol.



Results

Hydrocarbon staples were introduced into the sequences of several peptides: **anoplin**, an AMP with low antibacterial activity; **(KFF)$_3$K**, a CPP which facilitates the transport of molecules into the bacterial interior; and three desi9gned peptides rich in lysine and leucine residues (**KAL**, **KAL2** and **KAL3**). All selected peptides exhibited an amphipathic nature, a positive net charge, and a propensity to form a helical structure in a lipid environment.

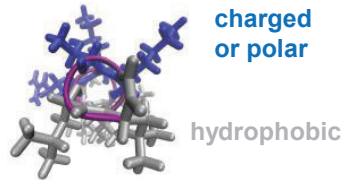

Amphipathic helical structure of a peptide

The staples were inserted into the peptides in a manner that preserved their amphipathicity, hydrophobicity, and net charge.

Secondary structure

The secondary structures of the peptides were determined by **circular dichroism (CD)** spectroscopy in phosphate buffer and in the presence of various lipid membrane environments, including micelles and liposomes. Unlike the unmodified peptides, the stapled analogs exhibited a stable **α-helical structure** in phosphate buffer, as indicated by minima at 208 nm and 222 nm in the CD spectrum. Furthermore, all peptides adopted a helical structure in each lipid environment.

Proteolytic stability

The proteolytic stability of the tested peptides was investigated in **trypsin** (for anoplin analogs), **chymotrypsin** (for (KFF)$_3$K analogs), or **human blood serum** (for peptides rich in lysines and leucines). All modified peptides exhibited increased proteolytic stability.

Antibacterial activity and hemolysis

Antibacterial activity was examined against gram-positive (*Staphylococcus aureus*) and gram-negative (*Escherichia coli*) bacterial strains. Peptides containing the hydrocarbon staple demonstrated greater antibacterial activity than the unmodified linear ones, with only a slight increase in hemolytic activity.

Peptide	Sequence	MIC [μM] *E. coli* K12 MG1655	MIC [μM] *S. aureus* ATCC 29213	Hemolysis [%] at 16 μM
anoplin	GLLKRIKTLL	32	>64	0.7
anoplin [2-6]	GS$_5$LKRS$_5$KTLL	4	16	2.8
anoplin[5-9]	GLLKS$_5$IKTS$_5$L	16	4	29.8
(KFF)$_3$K	KFFKFFKFFK	32	>32	0.35
(KFF)$_3$K[2-6]	KS$_5$FKFS$_5$KFFK	2	16	2.3
(KFF)$_3$K[5-9]	KFFKS$_5$FKFS$_5$K	2	8.6	2.0
KAL	KALKKLLAKWL	16	64	0.4
KAL[2-6]	KS$_5$LKKS$_5$LAKWL	4	8	4.6
KAL[3-7]	KAS$_5$KKLS$_5$AKWL	4	8	0.8
KAL2	KALAKLLKKWL	32	>64	0.8
KAL2[2-6]	KS$_5$LAKS$_5$LKKWL	2	4	10.8
KAL2[3-7]	KAS$_5$AKLS$_5$KKWL	2	4	2.5
KAL2[6-10]	KALAKS$_5$LKKS$_5$L	2	4	0.2
KAL3	KALKKLLKAWL	8	>64	0.4
KAL3[2-6]	KS$_5$LKKS$_5$LKAWL	2	4	15.0
KAL3[3-7]	KAS$_5$KKLS$_5$KAWL	2	4	4.4
KAL3[6-10]	KALKKS$_5$LKAS$_5$L	2	4	2.1
NEO-anoplin	NEO-GLLKRIKTLL	8	16	3.4
NEO-anoplin[2-6]	NEO-GS$_5$LKRS$_5$KTLL	8	8	3.9
AMK-anoplin	AMK-GLLKRIKTLL	16	32	4.3
AMK-anoplin[2-6]	AMK-GS$_5$LKRS$_5$KTLL	4	16	3.2
NEO-SS-anoplin[2-6]	NEO-SS-GS$_5$LKRS$_5$KTLL	8	4	2.7
NEO-SS-anoplin[2-6]	NEO-SS-GS$_5$LKRS$_5$KTLL	8	4	21.4

S$_5$ - (S)-2-(4'-pentene)alanine

Conclusions

- The hydrocarbon stapling technique **stabilized the active α-helical structures** of modified peptides, which was crucial for enhancing their antibacterial activity
- Stapled peptides, compared to unmodified ones, **exhibited up to 8-fold enhanced antibacterial activity** against *E. coli* and *S. aureus* strains, along with **improved proteolytic stability**, while **showing no hemolytic or cytotoxic effects**.
- AMG-peptide conjugates demonstrated only slightly enhanced antimicrobial activity compared to their unconjugated counterparts, particularly against resistant strains. No synergistic effects were observed between the unconjugated segments.
- **Overall, the hydrocarbon stapling technique proved to be the most effective modification tested for enhancing the antibacterial activity of MAPs.**

References

Stapled anoplin as an antibacterial agent, *Frontiers in Microbiology* DOI: doi.org/10.3389/fmicb.2021.772038

Conjugates of aminoglycosides with stapled peptides as a way to target antibiotic-resistant bacteria, *ACS Omega* DOI:doi.org/10.1021/acsomega.3c02071

Structural dynamics influences the antibacterial activity of a cell-penetrating peptide (KFF)$_3$K, *Scientific Reports* DOI:doi.org/10.1021/acsomega.3c02071

Acknowledgements: This work was supported by National Science Centre (2019/35/D/NZ1/01957)

https://doi.org/10.17952/37EPS.2024.P1059

Translocation-Enhancing Peptides: Facilitate Transport of Molecules and Lipid Scrambling



Ladislav Bartoš[a], and Robert Vácha[a,b]*

a) CEITEC – Central European Institute of Technology, Masaryk University, Brno, Czech Republic b) Faculty of Science, Masaryk University, Brno, Czech Republic * robert.vacha@muni.cz

Motivation

- Despite textbook knowledge that only small molecules can spontaneously cross cell membrane, amphiphilic molecules such as cell penetrating peptides were observed to do the same. Their translocation mechanism remains elusive[1-3]
- Scramblases are proteins facilitating bidirectional & energy-independent transport of phospholipids between membrane leaflets[4]
- Insertases facilitate membrane insertion of proteins by local membrane defect, which also facilitates lipids scrambling[5]

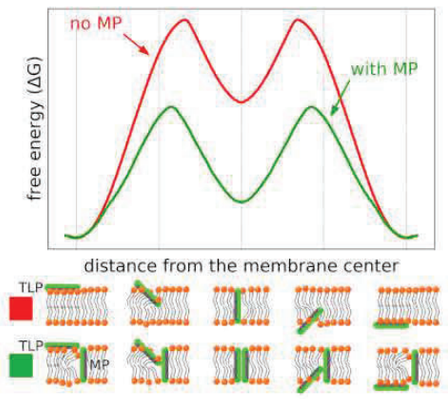

Methods

Molecular dynamics simulations:

- NPT molecular dynamics using Gromacs package versions 5.1.4 and 2021.4 [6]
- MARTINI 2.2 [7] with downscaled LJ interactions between protein beads[8]
- Lipid scrambling also all-atom with Slipids[9] and Amber 99SB-ILDN[10]
- Membrane composed of POPE:POPG 3:1
- Free energy calculations using umbrella sampling technique with collective variable including distance between peptide end and local membrane center of mass[11] for scrambling the lipid was pulled by phosphorus atom

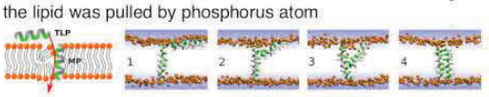

- water defect is average number of water beads in a cylinder around the transmembrane peptide

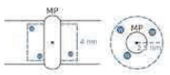

Funding

101001470

European Research Council

MINISTRY OF EDUCATION YOUTH AND SPORTS

LX22NPO5103

CZECH RECOVERY PLAN

NIVB

Funded by the European Union NextGenerationEU

Results

Properties of transmembrane peptide affect the translocation barrier

Size of hydrophilic patch[12]

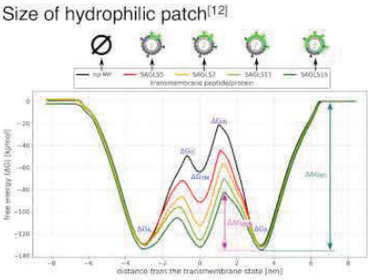

Patch depth, compactness and residue composition

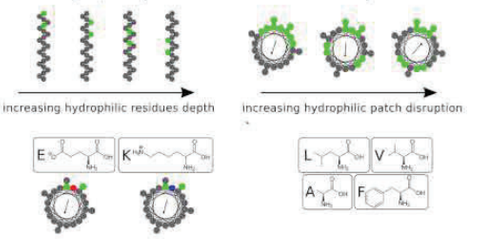

Membrane disruption – water and tails

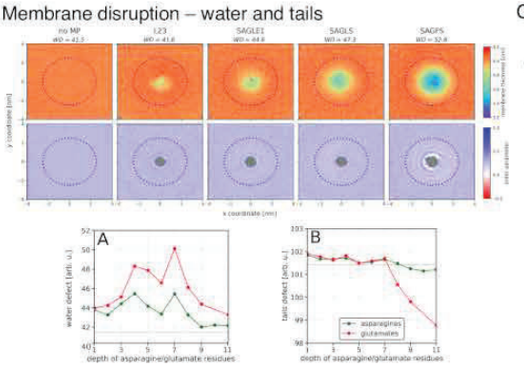

Optimized sequences

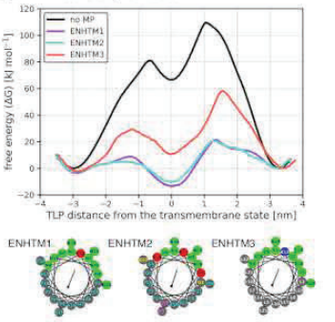

Lipid flip-flop / scrambling along transmembrane peptides

Simulations

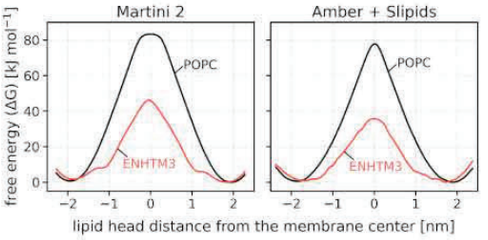

Coarse-grained
All-atom

Experiments

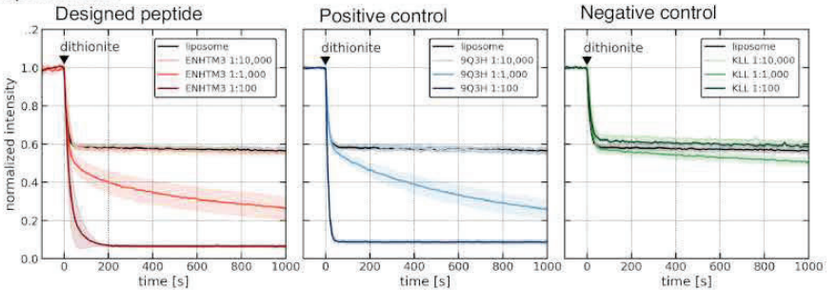

Conclusions

- transmembrane proteins/peptides with a hydrophilic patch enhance the translocation of amphiphilic molecules (e.g. peptides and lipids) by stabilizing them in the membrane[13]
- local membrane disruption is mainly responsible for the translocation enhancement
- transport of amphiphilic molecules in cells could be enhanced by native scramblases and insertases or artificial translocation-enhancing peptide

References:

1) Wang J. et al. Med Res Rev 39, 831–859, 2019.
2) Guidotti G. et al. Trends Pharmacol Sci 38, 406–424, 2017.
3) Allolio C. et al. PNAS 2018, 115, 11923.
4) Sakuragi T. et al. Nat Rev Mol Cell Biol 2023, 24, 576–596.
5) Bartoš L. et al. Structure 2024, 32, 4, 505-510.
6) Abraham, M. et al. SoftwareX 2015, 1–2:19–25.
7) Marrink S.J. et al. J Phys Chem B 108, 750–760, 2004.
8) Javanainen M. et al. PLOS ONE 12, e0187936, 2017.
9) Jambeck J. P. M. et al. J Chem Theor Comput 2012, 8, 2938–2948.
10) Lindorff-Larsen K. et al. Proteins 2010, 78, 1950–1958.
11) Kabelka I. et al. J Chem Inf Model 2021, 61 (2), 819–830.
12) Bartoš L. et al. Biophys J 2021, 120 (11), 2296-2305.
13) Bartoš L. et al. Biophys J 2024, 123, 1–13.

https://doi.org/10.17952/37EPS.2024.P1062

37th European Peptide Symposium and
14th International Peptide Symposium

Antimicrobial activity of Histatin 5 based metallopeptides

Gabriela Vieira Silva Zolin[1], Renan Lira de Farias[2], Saulo Santesso Garrido[1]

[1]Department of Biochemistry and Organic Chemistry, Institute of Chemistry, São Paulo State University, Araraquara, Brazil; [2]Department of Chemistry, Pontifical Catholic University of Rio de Janeiro, Rio de Janeiro, Brazil.

PURPOSE

With the aim of developing new antifungal agents to combat *Candida albicans* infections, whose resistance is increasing worldwide[1], proteolytic fragments of Histatin 5[2], a salivary peptide, were complexed with silver ions. Studies have reported that Hst5 activity is enhanced when arginine residues replace some lysine residues[3]. Therefore, this amino acid exchange was applied to the developed fragments, which were also complexed with silver ions.

METHODOLOGY

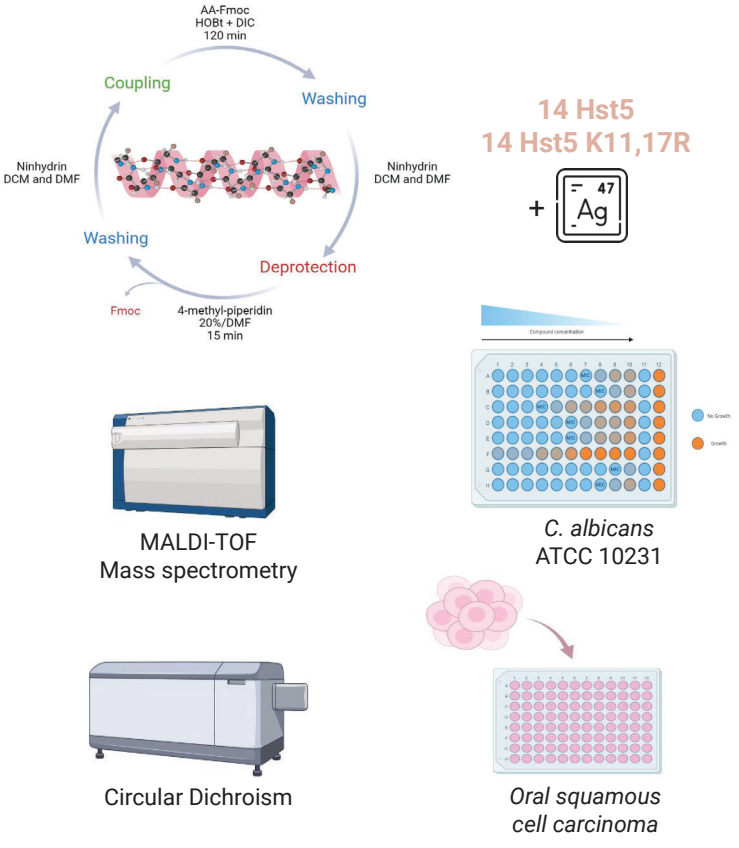

RESULTS

Metallopeptide	Theoretical molecular mass (g mol $^{-1}$)	Experimental molecular mass (g mol^{-1})
14 Hst5 – Ag	2141,13	2129,92
14 Hst5 K11,17R – Ag	2197,16	2195,98

MALDI-TOF mass spectrometry comparing the experimental molecular mass obtained for the two metallopeptides and the predicted theoretical molecular mass. The coordination compounds were prepared in a 1:1 (v/v) ratio with a 10 mg/mL 2,5-dihydroxybenzoic acid (DHB) matrix, analyzed by a Bruker Daltonics Ultraflextreme MALDI spectrometer, with TOF/TOF analyzer, and MS and MS/MS data acquisition (reflector mode).

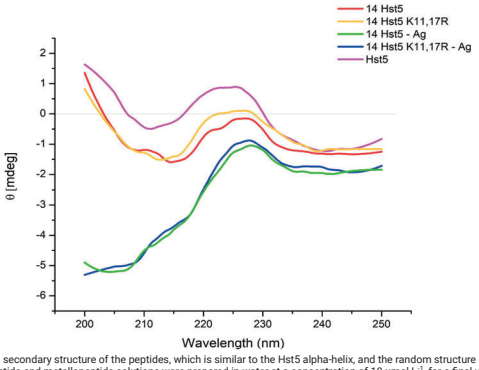

Circular dichroism showing the secondary structure of the peptides, which is similar to the Hst5 alpha-helix, and the random structure adopted by the peptides when coordinated with Ag(I). The peptide and metallopeptide solutions were prepared in water at a concentration of 10 μmol L^{-1}, for a final volume of 500 μL. The spectra were obtained with an accumulation of 12 scans, from 200 to 250 nm, with measurements every 0.1 nm, at a speed of 100 nm min^{-1}.

Concentration (μmol L^{-1})	Compound	% Inhibition (planktonic cells)[1]	% Inhbition (biofilm)[2]	% Cell viability (OSCC)
160	*14 Hst5*	96,82	97,61	47,08
	14 Hst5 – Ag	93,47	95,97	0
	14 Hst5 K11,17R	98,44	71,15	44,94
	14 Hst5 K11,17R - Ag	93,58	96,89	0
80	*14 Hst5*	96,91	81,75	55,25
	14 Hst5 – Ag	97,06	94,68	0
	14 Hst5 K11,17R	96,94	0,0	50,33
	14 Hst5 K11,17R - Ag	97,35	96,39	20,46
40	*14 Hst5*	6,51	0,55	51,35
	14 Hst5 – Ag	97,54	87,52	25,12
	14 Hst5 K11,17R	94,27	0,41	49,43
	14 Hst5 K11,17R - Ag	97,19	95,22	45,32
20	*14 Hst5*	6,03	0,76	61,86
	14 Hst5 – Ag	97,19	1,41	73,90
	14 Hst5 K11,17R	6,31	0,16	51,51
	14 Hst5 K11,17R - Ag	97,33	15,30	76,46

Inhibition of *Candida albicans* growth in planktonic and biofilm conformation by peptides and metallopeptides and cell viability of OSCC. The concentrations of peptides and metallopeptides in the inhibition assays were 160 to 5 μmol L^{-1} for planktonic cells and 320 to 10 μmol L^{-1} for biofilm. The peptides and metallopeptides were incubated with the sponsored cells for 48 h before reading the OD at 595 nm. The peptides and metallopeptides were incubated with OSCC cells at the same concentration as in the planktonic cell assay for 48 h, and the resazurin method was used to evaluate cell viability by reading the OD at 570 and 600 nm.

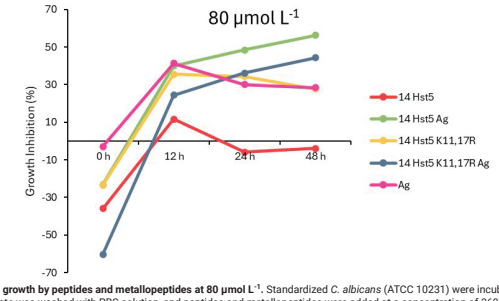

Inhibition of mature biofilm growth by peptides and metallopeptides at 80 μmol L^{-1}. Standardized *C. albicans* (ATCC 10231) were incubated for 48 h in a 96-well cell plate for maturation. The plate was washed with PBS solution, and peptides and metallopeptides were added at a concentration of 360 to 10 μmol L^{-1}. OD reading at 595 nm was taken 0, 12, 24, and 48 h after peptides and metallopeptides were added. The percentage of growth inhibition was calculated according to the positive and negative growth controls.

CONCLUSION

The coordination between the proposed peptides and Ag(I) occurred effectively, in the molar ratio 1:1. The antifungal activity against biofilms was optimized in both peptides when compared with Hst5, and the coordination with Ag(I) further improved the inhibition of growth of resistant *C. albicans*. The metal without the presence of the peptide did not show the same inhibition profile against the same strains, reinforcing the synergism. The cytotoxicity presented by the compounds were below 50% in most of the cases.

FUNDING AND ACKNOWLEDGMENTS

CAPES FAPESP Instituto de Química

REFERENCES

[1] PERLIN, D. S. et al. The global problem of antifungal resistance: Prevalence, mechanisms, and management. **The Lancet Infectious Diseases**, v. 17, n. 12, p. e383–e392, 2017.
[2] HELMERHORST, E. J. et al. Oral fluid proteolytic effects on histatin 5 structure and function. **Archives of Oral Biology**, v. 51, n. 12, p. 1061–1070, 2006.
[3] IKONOMOVA, S. P. et al. Effects of histatin 5 modifications on antifungal activity and kinetics of proteolysis. **Protein Science**, v. 29, n. 2, p. 480-493, 2020.

https://doi.org/10.17952/37EPS.2024.P1063

De novo design of miniproteins binding to PD-L1

Juan Lizandra Pérez, Natalia Miodowska, Łukasz Berlicki.

Department of Bioorganic Chemistry, Wrocław University of Science and Technology, Wybrzeże Wyspiańskiego 27, 50-370 Wrocław

juan.lizandra-perez@pwr.edu.pl

Wrocław University of Science and Technology

Objectives

De novo design of miniproteins, ideal drug candidates that cover the space between small molecule drugs and antibodies, has emerged in the past 40 years as an excellent tool for the development, with atomic accuracy, of bioactive molecules. However, a significant challenge remains due to the absence of tools capable of efficiently design sequences incorporating non-canonical amino acids. In the present work, we intend to *de novo* design a miniprotein with a EHEE topology (E – extended; H – Helix) targeting programmed cell death ligand 1 protein (PD-L1). The design approach allows the incorporation of three β-amino acids in an αβααβααβ pattern, ensuring that the structural integrity and binding capabilities of the design remain unaffected.

Materials and methods

Miniprotein design was performed combining Rosetta blue-print design with fast design protocol. Designs were filtered using the Rosetta scores, AlphaFold2, Rosetta *ab initio* calculations and molecular dynamics (MD). Designs were synthesized by Solid Phase Peptide Synthesis, purified by High Performance Liquid Chromatography (HPLC), and characterized with mass spectrometry, analytical HPLC and Circular Dichroism (CD). The affinity studies towards PD-L1 are done with BioLayer Interferometry (BLI).

Conclusions

Here, we successfully designed a novel PD-L1 miniprotein binder with a EHEE topology. Moreover, the design approach allowed to incorporate three β-amino acids in the helical region while preserving the structural integrity and improving the binding capacity for the target by 5-fold.

Design

Sequence of inhibitors **BABB_1** and **BABB_T1**.

Entry	Sequence
BABB_1	VKITIKQIPTEE**L**AKK**L**AK**L**LLRDPGVHVWIHNGVLIVIKL
BABB_T1	VKITIKQIPTEE⬟AKK⬟AK⬟LLRDPGVHVWIHNGVLIVIKL

⬟ =  (1*S*,2*S*) Aminocyclopentanecarboxylic acid (*trans*-ACPC)

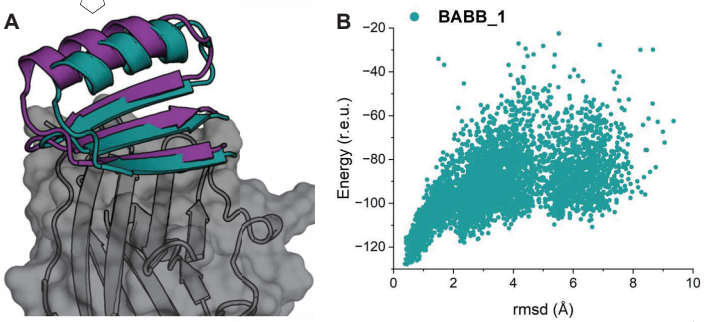

A) Pymol alignment of AlphaFold2 prediction (Violet) over the designed model (Cyan) in complex with PD-L1 with RMSD = 1.563 Å. B) Folding energy landscape of **BABB_1** from Rosetta *ab initio* structure prediction

Designs were filtered based on Alphafold2 prediction confidence, of the inhibitor as a monomer and in complex with PD-L1. Subsequentially, we performed Rosetta *ab initio* structure prediction simulations, leading to a total of 7 designs from which **BABB_1** was selected for its positively charged character, known to enhance binding capacity for PD-L1.

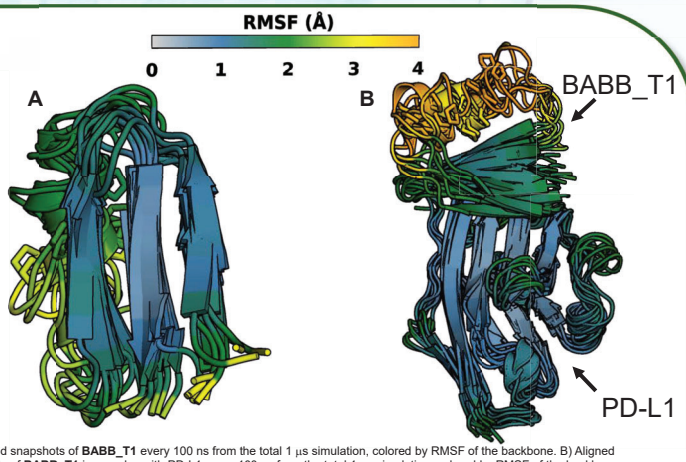

A) Aligned snapshots of **BABB_T1** every 100 ns from the total 1 μs simulation, colored by RMSF of the backbone. B) Aligned snapshots of **BABB_T1** in complex with PD-L1 every 100 ns from the total 1 μs simulation, colored by RMSF of the backbone

Amber/20 was used for MD simulations of **BABB_T1**, both as a monomer and in complex with PD-L1, due to the lack of structure prediction tools for β-amino acid-containing miniproteins. With a total simulation time of 1μs, it is visible that the structure remains stable after the introduction of the *trans*-ACPC as well as the complex predicted from the design. However, the helical region showed increased flexibility, likely due to *trans*-ACPC constrained nature limiting its ability to accommodate electronic density compared to leucine.

Characterization

T_m and K_D, of inhibitors **BABB_1** and **BABB_T1**, *precipitation during measurement.

Entry	T_m (°C)	K_D (nM)
BABB_1	73.7 ± 1.1*	961 ± 11.6
BABB_T1	64.7 ± 0.4*	192 ± 2.2

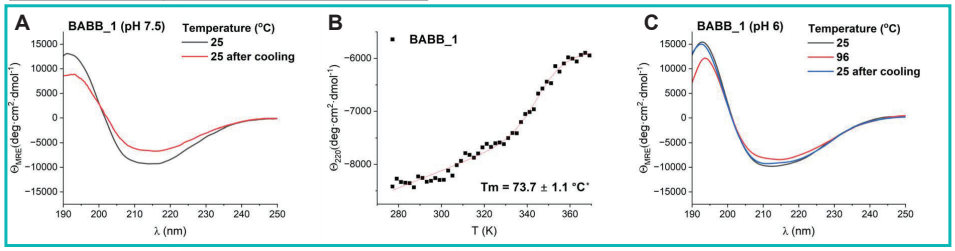

A) CD spectra pH 7.5 at 25 °C before and after thermal denaturation. B) Thermal denaturation plot recorded at 220 nm and pH 7.5. C) CD spectra pH 6 at 25, 96 and 25 °C of the same sample. Top figures correspond to **BABB_1**, lower figures correspond to **BABB_T1** at 25 μM in phosphate buffer.

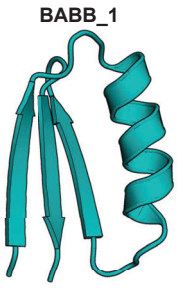

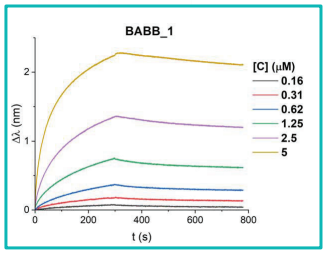

BLI sensograms at pH 6.9 in HEPES buffer of **BABB_1** (top) and **BABB_T1** (below).

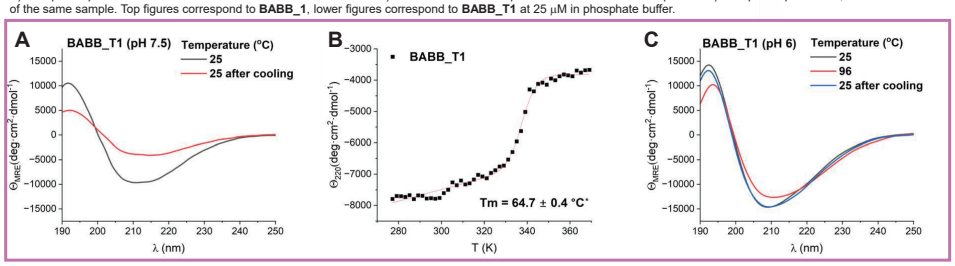

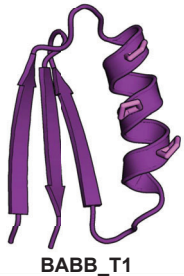

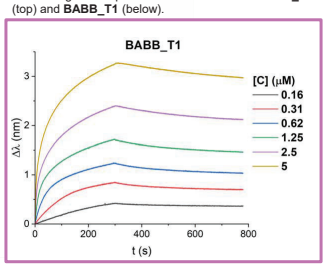

CD structural determination indicated the presence of folded structures in solution. However, at pH 7.5, precipitation was observed during thermal denaturation, precluding accurate T_m determination. Modification of pH to 6 showed high thermal stability of both inhibitors (>96 °C) and no apparent precipitation. Affinity studies by BLI at pH 6.9 reflected nanomolar affinities for PD-L1 with a 5-fold higher binding affinity of the β-amino acid-containing miniprotein than the designed partner.

Acknowledgments and references

Project financed by National Science Center "De novo designed, structurally extended peptide foldamers and their use for construction of PD-1/PD-L1 interaction inhibitors"; NCN, OPUS 2018/31/B/ST5/02631.

Ciesiołkiewicz A., Lizandra-Perez J., Skalniak Ł., Nocen P., Berlicki Ł., Miniprotein engineering for inhibition of PD-1/PD-L1 interaction, *Protein Science,* **2024**, 33, 8.
Roy, L. Shi, A. Chang, et al., "De novo design of highly selective miniprotein inhibitors of integrins αvβ6 and αvβ8". *Nat Commun*, **2023**, 14, 5660.
Ciesiołkiewicz A., Lizandra-Perez J., Berlicki Ł., Miniproteins in medicinal chemistry, *BMCL*, **2022**, 71, 128806.

WALLENBERG CENTRE FOR MOLECULAR AND TRANSLATIONAL MEDICINE

Metal complexes of ATCUN-like peptides for sequence-specific DNA cleavage

UNIVERSITY OF GOTHENBURG

https://doi.org/10.17952/37EPS.2024.P1064

Ivan N. Unksov,[1] Lena K. Müller,[2] Hanna Zdhannova,[1] Alexander Gräwe,[3] Joshua Stahl,[2] Viktor Stein,[3] Daniel Tietze,[1] and Alesia A. Tietze*[1]

1 Department of Chemistry and Molecular Biology, Wallenberg Centre for Molecular and Translational Medicine, University of Gothenburg, Kemigården 4, 412 96 Göteborg, Sweden
2 Clemens Schöpf Institute for Organic Chemistry and Biochemistry, Darmstadt University of Technology, Alarich-Weiss-Str. 4, 64287 Darmstadt, Germany
3 Darmstadt University of Technology, Department of Biology, Schnittsphanstr. 12, 64287 Darmstadt, Germany

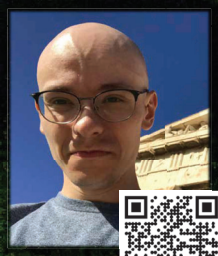

Join me on LinkedIn!

Peptides with Amino-Terminal Cu(II) and Ni(II) binding motif (ATCUN) motif are known to bind to the DNA minor groove and cleave the DNA, being promising for antimicrobial and antitumor activities. A typical ATCUN motif is Gly-Gly-His. We synthetized another His-containing peptide and two mutants where the His is substituted by Ala and Asp, and study whether these form complexes with Cu(II), bind to a DNA and exhibit cleavage activity.

ATCUN–like peptides can coordinate metals

Ac-Dap-β-Ala-His/Asp/Ala-PEG_4

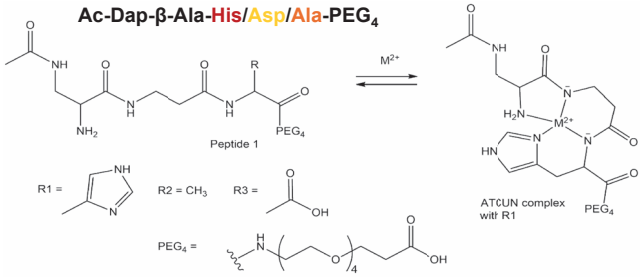

The peptides are simulated to bind to the DNA minor groove

Molecular docking shows binding for all three peptide complexes with Cu(II).

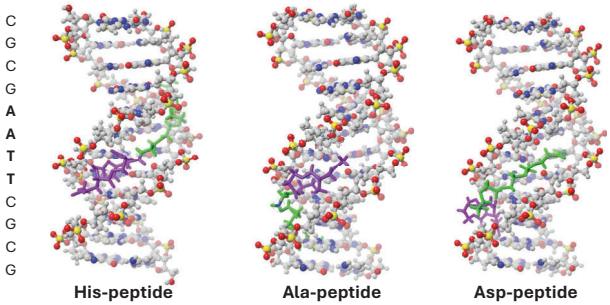

His-peptide 7.6 kcal/mol

Ala-peptide 7.1 kcal/mol

Asp-peptide 7.7 kcal/mol

The peptides displace a dye from DNA minor groove

The **Hoechst 33258** fluorescent dye binds to the minor groove with AT-specificity. Metallopeptides displace Hoechst and redistribute the dye from AT rich sites in the minor groove more prominently than a peptide with the classic Gly-Gly-His ATCUN motif.

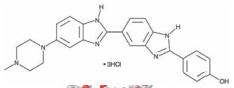

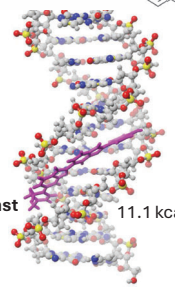

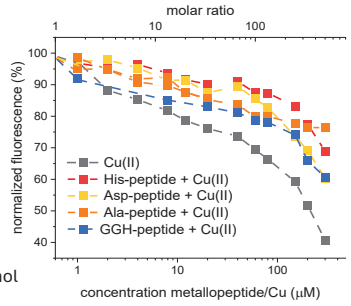

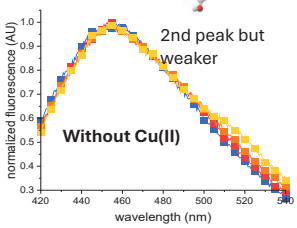

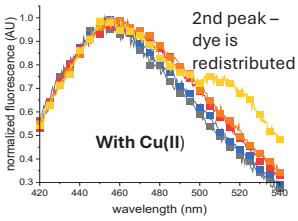

Antibiotic resistance plasmids are cleaved region-specifically

a, b – ampicillin-resistant plasmids

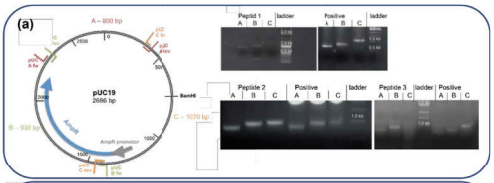

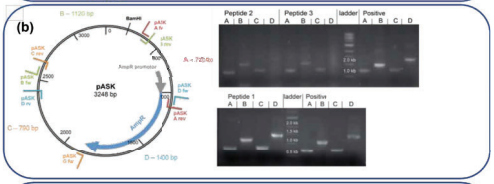



c – chloramphenicol-resistant plasmids

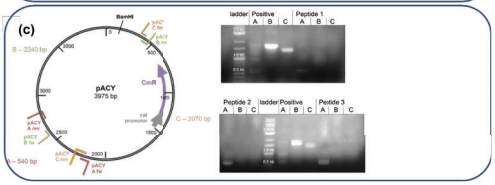

The peptides do not intercalate between DNA base pairs

Ethidium bromide is an intercalator dye but its fluorescence is not displaced or redistributed as compared to Cu(II) alone.

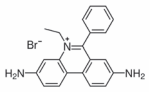

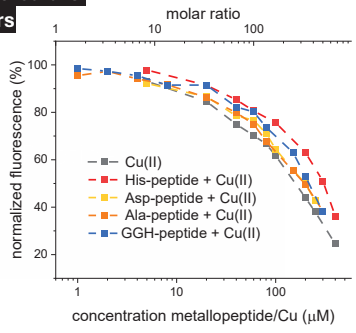

CONCLUSION

- All three peptides, even without His, bind to Cu(II).
- All our peptides, and especially the Asp-containing one, redistribute the fluorescent dye from the AT rich sites in the minor groove.
- All peptides linearize three studied plasmids.
- The Asp- and His-containing peptides cleave the DNA with specificity to AT-rich sites.
- These small metallopeptides are promising for drug design from anticancer to antimicrobial treatment.

Interested in more? Follow this QR code to see our lab's work.

CANCERFONDEN
Vetenskapsrådet
Knut och Alice Wallenbergs Stiftelse

The Knut and Alice Wallenberg Foundation via the Wallenberg Centre for Molecular and Translational Medicine (AT), Swedish Research Council (2020-04299) (AT) and Cancerfonden (AT) are gratefully acknowledged.

For additional information, please contact:
Ivan Unksov ivan.unksov@gu.se
Alesia Tietze alesia.a.tietze@gu.se

Development of peptide-based inhibitors against β-catenin using *in silico* approach

Minami Fujita[1,2], Amika Kikuchi[1], Kyohei Arita[1], Takashi Misawa[2], Yosuke Demizu[1,2]
1. Graduate School of Medical Life Science, Yokohama City University
2. National Institute of Health Sciences

https://doi.org/10.17952/37EPS.2024.P1067

01 Background

Wnt/β-catenin signaling pathway

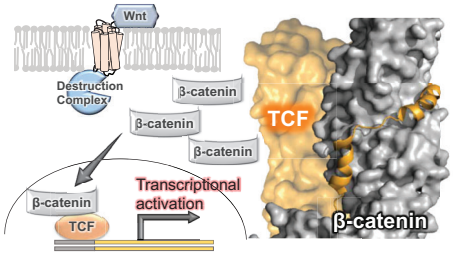

✧ The Wnt/β-catenin signaling pathway is transcriptionally activated through the interaction between β-catenin and T-cell factor (TCF).

✧ Excessive transcriptional activation of Wnt/β-catenin pathway is associated with the pathogenesis of various cancers.

Development of a peptide-based PPI inhibitor

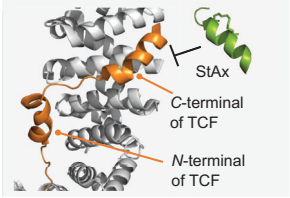

✧ The formation of TCF is induced when TCF interacts with β-catenin. In particular, the *N*-terminal region of TCF is important for interaction with β-catenin.

✧ Axin-derived stapled peptide (StAx) that inhibits *C*-terminal helix of TCF and β-catenin showed anticancer activity.[1)]

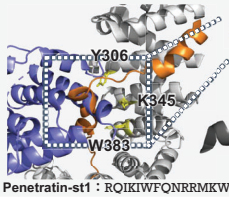

Penetratin-st1 : RQIKIWFQNRRMKWKK-βAla-AA-S_5*-LDY-S_5*-Nle-CNY

Stapling
✔ Stabilize secondary structure
✔ Improve protease resistance

Cell-penetrating peptides (CPP)
✔ Improve cell-membrane permeability
Ex.) Penetratin, Oligoarginine

✧ The binding surfaces of the *N*-terminal region of TCF and LRH-1 on β-catenin partially overlap. Furthermore, the crystal structure analysis revealed that Y306, K345, and W383 of β-catenin are important for interaction with LRH-1.[2)]

✧ We designed peptide-based inhibitors using a partial sequence of LRH-1.[3)]
✧ The inhibitory activity of the **Penetratin-st1** was not sufficient (20 μM).
➢ Improving the peptide structure is required to enhance the inhibitory activity of **Penetratin-st1**.
➢ To reduce effort and costs, efficient peptide design using *in silico* methods was implemented.

1) G. L. Verdine, *et al.*, *Proc. Natl. Acad. Sci. U.S.A.* **2012**, *109*, 17942.
2) F. Yumoto, *et al.*, *Proc. Natl. Acad. Sci. U.S.A.* **2012**, *109*, 143.
3) K. Tsuchiya, *et al.*, *Bioorg. Med. Chem.* **2022**, *73*, 117021.

02 *In silico* design of peptides

► An integrated scientific computing software, Molecular Operating Environment (MOE) was used to optimize the peptide sequence targeting β-catenin based on affinity scores.

1. Residue Scan

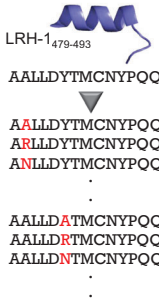

■ Each amino acid residue in the sequence was replaced by the other 19 natural amino acids.

2. Scoring

■ The affinity of the peptide mutants for β-catenin was evaluated by dAffinity which was measured as a difference between the binding energies of the wild-type and mutants.

Negative dAffinity
⇨Peptide-protein complex was stabilized.

Positive dAffinity
⇨Peptide-protein complex was destabilized.

Mutation	dAffinity
C487R	-5.38
D483R	-4.08
C487M	-3.41
.	.

dAffinity	Number of mutants
0<	114
≧0	146
total	260

Ex.) C487R
β-Catenin/peptide mutant complex was stabilized.
▷ Predicted to interact with higher affinity

■ Mutations with dAffinity value of -1 or less were extracted.

dAffinity	Number of mutants
0<	600
≧0	60
total	660

3. Residue Scan

■ Mutations were only introduced to amino acid residues that side chains are located at the interaction interface with β-catenin.



Amino acid residue	Mutation
A480	Y, F, Q, R
D483	M, L, H, R
C487	Y, F, L, Q, N, V, W, M, I, R
N488	K

4. Scoring

■ Peptides **2** and **3** which have dAffinity value of -10 or less were selected as candidates.

Peptide	Sequence	dAffinity
2	ARLLLYTMRNY	-10.76
3	AFLLLYTMRNY	-10.16

deficit : mutations

03 Synthesis of peptides

► Nle (norleucine)-derivative peptides **2** and **3** were designed. In addition, a stapled peptide **st3** and its penetratin conjugated peptide **Penetratin-st3** were also designed.

Peptide	Sequence
1	βAla-AALLDYT-Nle-CNY
2	βAla-ARLLLYT-Nle-RNY
3	βAla-AFLLLYT-Nle-RNY
st3	βAla-AF-S_5*-LLY-S_5*-Nle-RNY
Penetratin-st3	RQIKIWFQNRRMKWKK-βAla-AF-S_5*-LLY-S_5*-Nle-RNY
Penetratin-st1	RQIKIWFQNRRMKWKK-βAla-AA-S_5*-LDY-S_5*-Nle-CNY

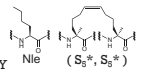

C terminal = NH_2
Nle = norleucine
deficit : mutations

04 MD simulations

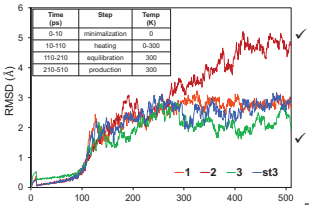

✓ Peptides **1**, **3**, and **st3** showed similar RMSD values, and were predicted to form stable complex with β-catenin.

✓ RMSD value of **2** was larger than the others.

RMSD : Root Mean Square Deviation

05 Binding activity

► The binding activity of 5(6)-carboxyfluorescein-labeled (F-) peptides to β-catenin was evaluated by the fluorescence polarization assay.

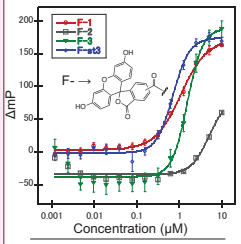

Peptide	K_d value (μM)
F-1	1.10
F-2	4.99
F-3	1.56
F-st3	0.71

✓ Peptide **F-3**, designed using MOE, showed similar binding activity as the lead peptide **F-1**.

✓ The stapled peptide **F-st3** further enhanced binding activity.

✗ Peptide **F-2**, which was expected to improve, showed reduced affinity.

MD simulation results showed that peptide **2** was more flexible than the other peptides, suggesting that peptide conformational flexibility may correlate with the binding affinity.

06 Interaction analysis

1. Mutational analysis

► The interaction surface of peptides for β-catenin was analyzed by binding assay using mutant of β-catenin (Y306A, K345A, W383A).

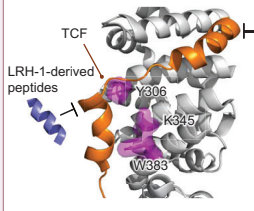

Peptide	K_d value (μM) WT	K_d value (μM) MT
F-35	0.072	0.054
F-1	0.35	2.1
F-3	0.77	4.2
F-st3	0.38	1.4

✓ The binding activity of **F-35** (StAx), which binds to β-catenin at a different region, was maintained.

✓ Peptides **F-1**, **F-3**, and **F-st3** showed reduced affinity.

2. Cryo Electron Microscopy

► Cryo-EM analysis of the structure of β-catenin/peptide was attempted.

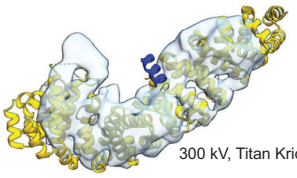

✓ In this experiment, a map with a resolution of 4.07 Å was obtained. Conditions are being optimized to obtain higher resolution maps to allow analysis of peptide binding sites. In addition, preparations for crystal structure analysis are underway.

07 Cell based assays

1. Evaluation of cell growth inhibitory activity

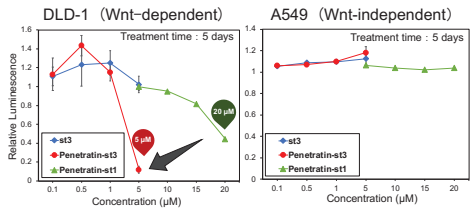

✓ **Penetratin-st3** inhibited the growth of only DLD-1 cells at 5 μM.
▷ The peptide has a specific growth inhibitory effect on the Wnt-signaling pathway.

✓ **Penetratin-st3** has higher inhibitory activity than the reported peptide **Penetratin-st1**.

2. Evaluation of Wnt signaling-mediated inhibitory activity

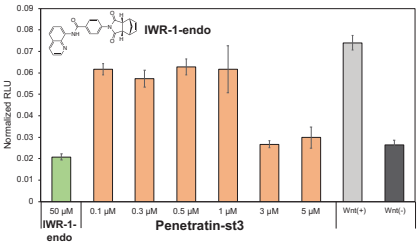

✓ A concentration-dependent decrease in luminescence intensity was observed for cells treated with **Penetratin-st3**.
▷ **Penetratin-st3** intracellularly binds to β-catenin to inhibit its transcriptional activity by preventing the formation of the TCF/β-catenin complex.

08 Conclusion

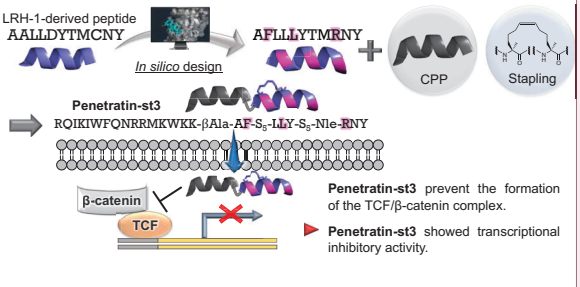

Penetratin-st3 prevent the formation of the TCF/β-catenin complex.

Penetratin-st3 showed transcriptional inhibitory activity.

✓ In this study, the peptide sequence was designed using MOE.[4)]

✓ **Penetratin-st3** was found to have four-fold stronger inhibitory activity than previously reported peptides.[4)]

4) M. Fujita, *et al.*, *Bioorg. Med. Chem.* **2023**, *84*, 117264.

An Intracellular Cyclisation Screen Generates Short Helical Peptide Inhibitor of Alpha Synuclein Aggregation

Scott G .Allen, Richard M. Meade, Robert J. Williams, Jody M. Mason

Department of Life Sciences, University of Bath, Bath, UK. Sga46@Bath.ac.uk J.Mason@Bath.ac.uk

https://doi.org/10.17952/37EPS.2024.P1068

1. Introduction and Previous Work

- Alpha-Synuclein (αS) is heavily associated with Parkinson's Disease (PD) pathology [1]. αS aggregates into toxic oligomers and fibrils within neuronal cells, ultimately resulting in cell death [1], and PD symptoms (Fig 1A).
- αS adopts an α-helical conformation in the presence of lipids, which is required for its proposed role in synaptic transmission[2]. Key residues involved in lipid binding are found in the N-terminal region (Fig 1B, Purple Region).
- Short peptides have been shown to reduce αS aggregation and associated toxicity [3,4].
- We have previously shown that helical, N-terminal based peptides can effectively inhibit αS aggregation, resulting in the formation of the potent inhibitor, $\alpha S_{2\text{-}12}$ (Fig 1C and D).
- Here, we utilised a novel intracellular cyclisation screening method, to further improve $\alpha S_{2\text{-}12}$.

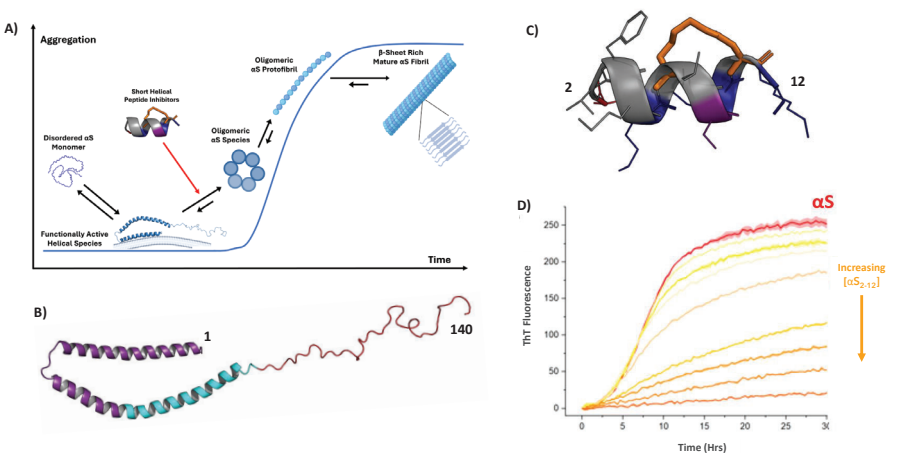

Figure 1. A) Schematic of αS aggregation. B) αS contains three domains: The N-terminal (Purple), The NAC region (Blue) and the C-terminal (Red) (PDB=1XQ8). C) Solution NMR structure of $\alpha S_{2\text{-}12}$ peptide (PDB 80L8). D) ThT assay showing dose dependent inhibition of αS aggregation by $\alpha S_{2\text{-}12}$.

2. Protein Fragment Complementation Assay

- We screened a peptide library using the Protein-fragment Complementation Assay (PCA).
- PCA selects interactions between a peptide and a target protein by recovering bacterial survival in the presence of trimethoprim (TMP). TMP selectively inhibits bacterial Dihydrofolate Reductase (DHFR). Bacterial survival is recovered by supplementing the bacterial cells with a split, exogenous murine DHFR (mDHFR).
- Peptides that bind αS recombine mDHFR resulting in cell survival. A winning peptide hit is selected as the fasting growing colony in liquid passaging.

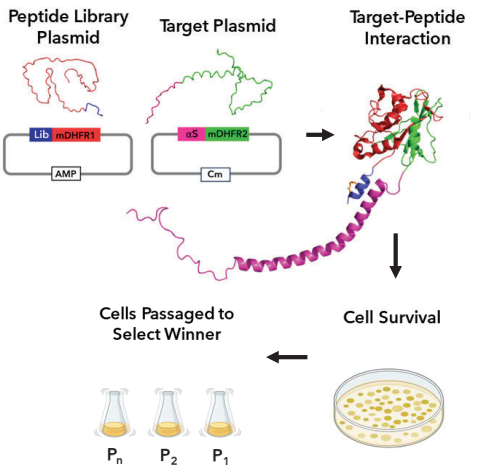

Figure 2. Protein-Fragment Complementation Assay used to screen peptide library.

3. Library Design and Selection of $\alpha S_{2\text{-}12}W$

- A 20-million-member library was designed to generate a charged, polar, and hydrophobic residue options at each position (Fig 3A).
- The library design permits intracellular i→i+4 cyclisation, locking the peptide into an α-helical arrangement by the addition of a peptide stapling agent.

A)

Residues 6 and 10 stapled

$\alpha S_{2\text{-}12}$ Sequence	1 D	2 V	3 F	4 M	5 K	6	7 L	8 S	9 K	10	11 K
Peptide Library Options	D	V	F	M	K		L	S	K		K
	V	I	L	V	I		V	I	I		I
	I	G	V	G	G		M	L	G		G
	N	E	Y	E	V		Q	V	V		V
	E	K	D	R	E		E	G	E		E
	K	R	H	K	R		K	N	R		R
								D			
								R			
								H			
								K			
20,155,392 Library Members								E			
								Q			

- A winning peptide ($\alpha S_{2\text{-}12}W$) was selected after 4 liquid passages, corresponding to the clean pool sequence readout (Fig 3B).

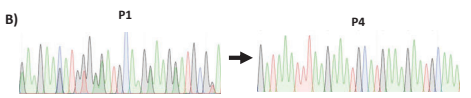

Figure 3. A) Peptide library generated based on the $\alpha S_{2\text{-}12}$ peptide. B) Sequencing shows a clean readout in the fourth passage, indicating a single peptide sequence in the screen.

4. Biophysical Analysis Confirms Intracellular Stapling Induces Helicity

- Addition of an N-terminal SUMO tag facilitated purification of $\alpha S_{2\text{-}12}W$ following bacterial expression in the presence or absence of a constraining agent.
- A mass increase corresponding to the constraint was observed, thus confirming the intracellular cyclisation of $\alpha S_{2\text{-}12}W$ (Fig 4A).

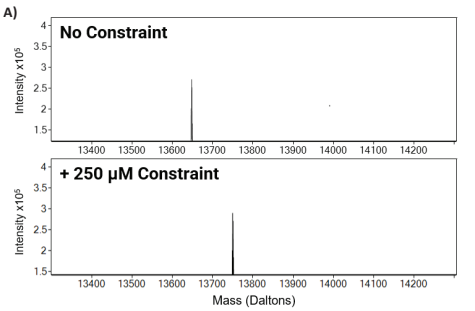

- CD was next used to confirm that the addition of the stapling agent induced helicity in the $\alpha S_{2\text{-}12}W$ peptide (Fig 4B).

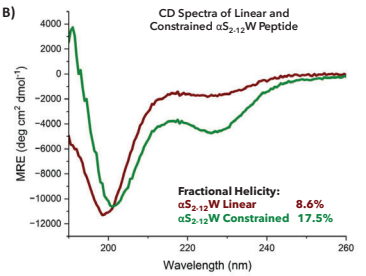

Figure 4. A) Intact mass spectrum shows a mass increase equivalent to the addition of the constraint, indicating successful *in vivo* cyclisation of the peptide sequence. B) CD Spectrum confirming induction of helicity in $\alpha S_{2\text{-}12}W$ by the stapling agent.

5. $\alpha S_{2\text{-}12}W$ Inhibits αS aggregation

- ThT fluorescence studies were used to analyse the inhibition of αS aggregation by $\alpha S_{2\text{-}12}W$.
- $\alpha S_{2\text{-}12}W$ is more potent than $\alpha S_{2\text{-}12}$ at substoichiometric concentrations (Fig 5A).
- TEM shows addition of the $\alpha S_{2\text{-}12}W$ peptide significantly reduces the formation of αS fibrils (Fig 5B).

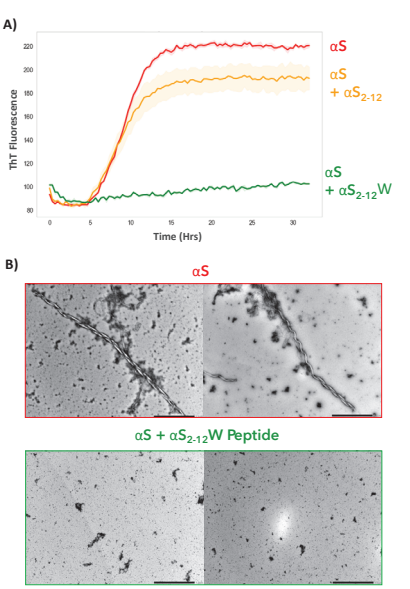

Figure 5. A) ThT assay shows the $\alpha S_{2\text{-}12}W$ peptide hit further improves inhibition from the initial $\alpha S_{2\text{-}12}$ peptide. B) TEM shows reduction in αS fibril formation in the presence of $\alpha S_{2\text{-}12}W$.

6. Conclusions and Next Steps

- We have developed a novel intracellular cyclisation method, utilising the PCA peptide screening platform, to generate a potent inhibitor of αS aggregation.
- The peptide, $\alpha S_{2\text{-}12}W$, inhibits αS aggregation at substoichiometric concentrations.
- Further characterisation for the specific mode of action of $\alpha S_{2\text{-}12}W$ inhibition is currently ongoing using several biophysical techniques.
- We next plan to study the impact of different constraints on the activity of $\alpha S_{2\text{-}12}W$ and collect cytotoxicity data.
- We aim to publish this work in the coming months.

LinkedIn, Contact Details, and Digital Poster:

Thank you to the SWBio DTP and ARUK for funding

7. References

1. Meade, R.M et al. (2019). Alpha-synuclein structure and Parkinson's disease - lessons and emerging principles. *Molecular Neurodegeneration* 14:29.

2. Bartels, T et al. (2011). α-synuclein occurs physiologically as a helically folded tetramer that resists aggregation. *Nature* 477, 107–110.

3. Meade, R.M., Allen SG., *et al.* (2023). An N-terminal alpha-synuclein fragment binds lipid vesicles to modulate lipid-induced aggregation. *Cell Reports Physical Science, 4(9),101563.*

4. Allen, S.G., Meade, R.M. *et al.* (2023) 'Peptide-based approaches to directly target alpha-synuclein in Parkinson's disease', *Molecular Neurodegeneration*, 18:80.

Background Work

SYNTHESIS AND STUDY OF MODIFIED TEMPORIN ANALOGS WITH UNNATURAL AMINO ACIDS CITRULLINE AND ORNITHINE AS POTENTIAL ANTIBACTERIAL AGENTS

Nelly Georgieva, Dilyana Dimitrova, Tsvetelina Foteva, Veronika Nemska, Dancho Danalev

Biotechnology Department, University of Chemical Technology and Metallurgy, 8 Kliment Ohridski blvd, Sofia 1797, Bulgaria

https://doi.org/10.17952/37EPS.2024.P1070

Introduction

Antimicrobial resistance (AMR) has reached almost critical levels and is listed by the WHO as one of top ten global health threats. In 2019 AMR was clearly accountable for 1.27 million deaths globally and contributed to 4.95 million deaths. The search for new alternatives in the treatment of bacterial infections has become a primary objective [1].

A promising new substitute are antimicrobial peptides (AMPs), which are biologically active compounds with low toxicity, high selectivity and can be administered alone or in combination with other antimicrobial agents for a synergistic effect [2]. They are highly hydrophobic and have a positive net charge, a wide range of activity against Gram-negative and Gram-positive bacteria, fungi, and yeast, as well as some additional anticancerogenic properties. In addition, they appear to be non-toxic against the human red blood cells [2, 3].

Temporin A (FLPLIGRVLSGIL-NH_2) is an AMP secreted from the European red frog *Rana temporaria*, with a length of 13 amino acids, hydrophobic, basic and amidated at the C-terminus. It is proven to be effective against gram-positive bacteria, including methicillin- and vancomycin-resistant strains [4, 5].

Results

The new analogs are fully characterized, and the results are summarized in **Table 1.** The HPLC profiles and MS data for the determination of the structure and purity are shown in **Fig. 2a** and **2b**.

Table 1 Structure and characteristics of the synthesized peptides

Entry	Chemical Formula	MM $_{exact}$ [g/mol]	$[M+H]^+_{observed}$ [g/mol]	$[M+Na]^+_{observed}$ [g/mol]	RT [min]	α_D^{20} [°]*	M.p. [°C]
DTA	$C_{68}H_{117}N_{17}O_{14}$	1395,90	1397,00	1418,95	4,513	-38	158 ± 2
DTCit	$C_{68}H_{116}N_{16}O_{15}$	1396.88	1397.75	1419.75	5.793	-34	182 ± 2
DTOrn	$C_{67}H_{115}N_{15}O_{14}$	1353.87	1354.70	1376.70	4.364	-42	123 ± 2

*methanol (c=1)

Fig. 2a HPLC profiles: Temporin TA, Temporin TThr and Temporin TTyr4 (from left to right)

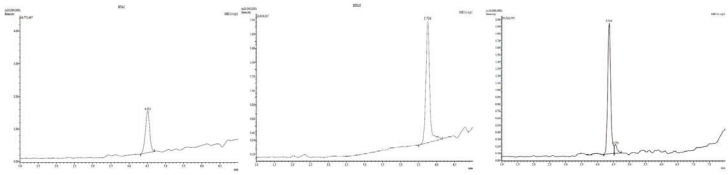

Fig. 2b MS data: Temporin TA, Temporin TThr and Temporin TTyr4 (from left to right)

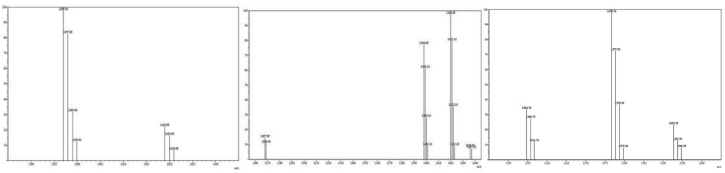

The novel analogs Temporin DTCit and DTOrn, as well as the parent peptide Temporin TA were studied for their antibacterial properties against *B. subtilis* strain 3562, *A. oxydans* 9333, *E. coli* 8785 *and P. aeruginosa* 3700. .The results are summarized in **Table 2.** The activity of the modified analogs were compared to that of the parent peptide in **Fig. 3**.

Table 2 Minimal inhibitory concentration (MIC) in μg/mL of DTA, DTCit and DTOrn

	Peptide	Sequence	*B. subtilis* 3562	*E. coli* 8785	*A. oxydans* 9333	*P. aeruginosa* 3700
1	DTA	Phe-Leu-Pro-Leu-Ile-Gly-**Arg**-Val-Leu-Ser-Gly-Ile-Leu-NH_2	80 μg/mL	320 μg/mL	80 μg/mL	320 μg/mL
2	DTCit	Phe-Leu-Pro-Leu-Ile-Gly-**Cit**-Val-Leu-Ser-Gly-Ile-Leu-NH_2	NI	NI	160 μg/mL	NI
3	DTOrn	Phe-Leu-Pro-Leu-Ile-Gly-**Orn**-Val-Leu-Ser-Gly-Ile-Leu-NH_2	160 μg/mL	NI	160 μg/mL	NI

*NI – no inhibition

Fig. 3 Comparison of the MIC values against tested strains

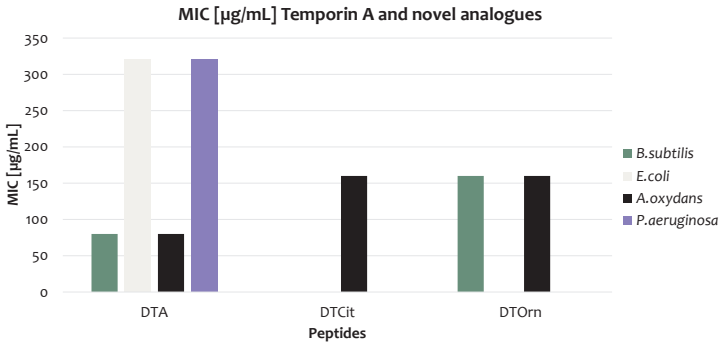

Materials & Methods

Here we report synthesis of new temporin A analogs with modification of Arg residue in position 7 with Citrulline (FLPLIG-**Cit**-VLSGIL-NH2) and Ornithine (FLPLIG-**Orn**-VLSGIL-NH2).

Synthesis of the novel Temporin A analogs

The peptides were synthesized by the Fmoc/OBu^t solid (9-fluorenylmethoxycarbonyl) phase peptide synthesis. Solid-phase peptide synthesis (SPPS) is a method for peptide synthesis, in which a peptide chain bonded to a polymer carrier is grown by presenting suitably protected amino acids (**Fig. 1**). The solid-phase carrier was Rink-amide MBHA resin, and the coupling agent was either N,N,N′,N′-Tetramethyl-O-(1H-benzotriazol-1-yl)uronium hexafluorophosphate (HBTU) or Diisopropylcarbodiimide (DIC). The monitoring of the reactions of deprotection and coupling was carried out using Kaiser test. The peptides were then cleaved from the resin using a mixture of trifluoracetic acid (TFA), triisopropyl silane (TIS) and water. They were then crystalized. The structure and purity were determined using HPLC-MS technique.

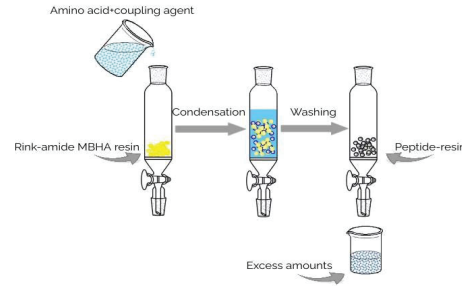

Fig. 1 General scheme for SPPS synthesis (Own drawing, modified based on [6])

Antibacterial activity of the novel Temporin A analogs

The minimal inhibitory concentration (MIC) of the peptides in concentration range from 0 to 320 μg/mL were determined using the broth dilution method. Stock solutions of the peptides with a concentration of 10 mg/mL in 10% EtOH/H_2O were prepared. Suspensions of the bacteria in the corresponding media were added to 96-well U-shaped bottom polystyrene plates and exposed to the peptide in concentration range from 0 to 320 μg/mL, as well as a 10% EtOH/H_2O control, diluted using the same scheme as the peptides. The plates were then incubated for 24h under aerobic conditions at the corresponding temperature. The MIC (μg/mL) was assumed as the lowest concentration of the antimicrobial, where there was visible inhibition of the strain. The absorbance was measured at 630 nm. To determine the minimal bactericidal concentration (MBC) 10 μl from concentrations greater than or equal to the MIC were placed on the corresponding solid nutrient medium. The Petri dishes were then incubated at 30 or 37° C for 24 h.

Discussion

The purity of the newly synthesized peptides is satisfactory as seen by the HPLC profiles. The desired sequences are also accomplished and proven by the MS data.

The peptides show lower MIC values against the Gram-positive bacteria *B. subtilis* 3562 and *A. oxydans* 9333. The parent peptide Temporin TA shows a MIC value of 80 μg/mL against the Gram(+) strains and 320 μg/mL against the Gram(-). The modification with Citrulline in position 7 proves to be redundant because the novel peptide shows no antibacterial activity in the chosen concentration range. An interesting observation can be made that DTCit shows inhibitory effect only against A. oxydans 9333. However, the substitution of the Arg residue with a Orn one, keeps the inhibitory effect, but at a higher concentration of the peptide. The analog DTOrn has a bactericidal effect at 320 μg/mL against *B. subtilis* 3562 and at 160 μg/mL against *A. oxydans* 9333. DTCit also has a MBC value of 160 μg/mL against *A. oxydans* 9333.

Conclusions

If looking over the obtained MIC values and taking into consideration the differences in the Arginine, Ornithine and Citrulline, a conclusion can de drawn that a bulkier, longer, and thus more basic side chain is needed at position 7 in order to have a lower MIC value. Additionally, the removal of positive charge in the lateral chain leads to a loss of the antibacterial properties evident with the analog DTCit.

Acknowledgement

This study is funded by the European Union-NextGenerationEU, through the National Recovery and Resilience Plan of the Republic of Bulgaria, project № BG-RRP-2.004-0002, "BiOrgaMCT".

References

[1] https://www.who.int/news-room/fact-sheets/detail/antimicrobial-resistance, visited on 06.02.2024

[2] Wei, Shuangshuang, et al. "A temporin derived peptide showing antibacterial and antibiofilm activities against Staphylococcus aureus." Protein & Peptide Letters, vol. 30, no. 2, Feb. 2023, pp. 183–192, https://doi.org/10.2174/0929866530666221202123011.

[3] Felício, Mário R., Osmar N. Silva, Sónia Gonçalves, Nuno C. Santos, Octávio L. Franco. "Peptides with Dual Antimicrobial and Anticancer Activities." Frontiers in Chemistry, vol. 5, 2017, https://doi.org/10.3389/fchem.2017.00005.

[4] David Wade, Jerzy Silberring, Rabah Soliymani, Sami Heikkinen, Ilkka Kilpeläinen, Hilkka Lankinen, Pentti Kuusela. "Antibacterial Activities of Temporin A Analogs." *FEBS Letters*, vol. 479, no. 1-2, 2000, pp. 6–9., https://doi.org/10.1016/s0014-5793(00)01754-3.

[5] Louise A. Rollins-Smith, Cynthia Carey, J. Michael Conlon, Laura K. Reinert, Jennifer K. Doersam, Tomas Bergman, Jerzy Silberring, Hilkka Lankinen, and David Wade. "Activities of Temporin Family Peptides against the CHYTRID Fungus (*Batrachochytrium Dendrobatidis*) Associated with Global Amphibian Declines." *Antimicrobial Agents and Chemotherapy*, vol. 47, no. 3, 2003, pp. 1157–1160., https://doi.org/10.1128/aac.47.3.1157-1160.2003.

[6] Hojo K, Shinozaki N, Nozawa Y, Fukumori Y, Ichikawa H. Aqueous Microwave-Assisted Solid-Phase Synthesis Using Boc-Amino Acid Nanoparticles. *Applied Sciences*. 2013; 3(3):614-623. https://doi.org/10.3390/app3030614

Website of the university

Proceedings of the 37th European Peptide Symposium
Michal Lebl, Editor
European Peptide Society, 2024 *http://doi.org/10.17952/37EPS.2024.P1071*

New unique analogs of anorexigenic cocaine- and amphetamine-regulated transcript peptide

Andrea Pačesová[1], Vilém Charvát[1], Miroslava Blechová[1], Blanka Železná[1], Jaroslav Kuneš[1,2], Lenka Maletínská[1]

1 Institute of Organic Chemistry and Biochemistry of the Czech Academy of Sciences, 160 00 Prague, Czech Republic

2 Institute of Physiology of the Czech Academy of Sciences, 142 00 Prague, Czech Republic

Scientific background: Cocaine- and amphetamine-regulated transcript peptide (CARTp) is an important anorexigenic neuropeptide expressed in the hypothalamus that contains three disulfide bridges important for the biological activity [1]. Its expression is stimulated by leptin, the main regulator of energy homeostasis, which highlights its importance in food intake regulation [2]. CARTp receptor is still unknown, however, Maletínská et al. described the specific binding of CARTp to pheochromocytoma PC12 cells [3]. Subsequent study of Blechová et al. defined the CARTp analog CART(61-102) with only two disulfide bridges, 2-SS-CART(61-102), as the shortest analog with preserved binding affinity and food intake-lowering properties after application to the 3rd brain ventricle [4]. However, natural CARTp is not capable of central action after peripheral administration. Therefore, we designed new lipidized analogs that were tested for their potential anorexigenic properties.

Methods: Lipidized analogs of 2-SS-CART(61-102) were designed and synthesized at the Institute of Organic Chemistry and Biochemistry of the Czech Academy of Sciences in Prague (IOCB CAS in Prague) using Fmoc strategy. The purity and identity of all lipidized analogs were determined by analytical HPLC and using a MALDI-TOF/TOF (Bruker Daltonics, Germany)/Q-TOF micro (Waters) MS technique. The structures are shown in Table 1.

Table 1 Structure of 2-SS-CART(61-102) and its lipidized analogs

Analogue	Sequence
2-SS-CART(61-102)	
acyl-2-SS-CART(61-102)	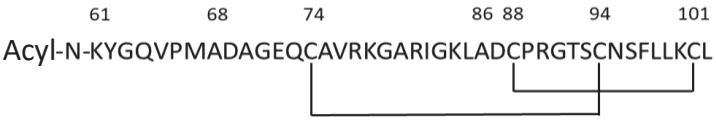

Acyl: octanoyl (oct), mirystoyl (myr), palmitoyl (palm)

Their binding affinity was tested in PC12 cells, either in naïve cells or those differentiated to neuronal phenotype by nerve growth factor (NGF). The effect on food intake regulation and body weight change was investigate after chronic subcutaneous (SC) application to mice with obesity induced by application of monosodium glutamate (MSG) to newborn mice, day 2-5 after birth, at a dose 4 mg/kg.

Results and discussion: All lipidized analogs showed binding affinity to PC12 cells, naïve or NGF-differentiated, comparable to 2-SS-CART(61-102), as shown in Table 2. palm-2-SS-CART(61-102) showed even higher binding affinity than the natural CART(61-102) with three disulfide bridges [3].

Table 2 Binding affinity of lipidized 2-SS-CART(61-102) analogs

Analog	Naïve PC12 cells	NGF-differentiated PC12 cells
	^{125}I-CART(61–102) K_i [nM]	^{125}I-CART(61–102) K_i [nM]
2-SS-CART(61–102)	261.3 ± 209,80	10.26 ± 9.04
oct-2-SS-CART(61–102)	76.09 ± 17.66	43.9 ± 10.41
myr-2-SS-CART(61–102)	12.1 ± 3.40	14.34 ± 0.33
palm-2-SS-CART(61–102)	1.43 ± 0.41	0.39 ± 0.14

The palm-2-SS-CART(61-102) was subsequently SC administered for 3 weeks to MSG obese mice. The treatment significantly reduced food intake and body weight of the MSG mice. Furthermore, palm-2-SS-CART(61-102) decreased the plasma level of leptin, which is produced by white adipose tissue, and insulin. It is possible that palm-2-SS-CART(61-102) regulates the activity of pancreatic β-cells [5]. In conclusion, we designed new unique CARTp analogs with central effect after peripheral application with strong anorexigenic and antiobesity potential.

Dedication:

This research was supported by the project National Institute for Research of Metabolic and Cardiovascular Diseases (Programme EXCELES, ID Project No. LX22NPO5104) - Funded by the European Union - Next Generation EU, and by RVO: 61388963 and RVO:67985823 of the CAS.

References:

1. Thim, L.*, et al.*, *Int J Biochem Cell Biol* **1998,** 30.
2. Kristensen, P.*, et al.*, *Nature* **1998,** 393.
3. Maletinska, L.*, et al.*, *Eur J Pharmacol* **2007,** 559.
4. Blechova, M.*, et al.*, *Peptides* **2013,** 39.
5. Wierup, N.*, et al.*, *Peptides* **2022,** 149.

37th European Peptide Symposium and 14th International Peptide Symposium

Antibacterial and anti-biofilm activity of branched peptides derived from antimicrobial peptides

Eva Tollapi[1*], Alessandro Rencinai[1], Giada Meogrossi[1], Silvia Scali[1], Chiara Falciani[1]

Department of Medical Biotechnologies, University of Siena

https://doi.org/10.17952/37EPS.2024.P1072

This work was realized thanks to EU funding within the NextGeneration EU-MUR PNRR Tuscany Health Ecosystem (Project no ECS00000017-THE)

Background

Antibiotic resistance is a global public health issue that reduces the effectiveness of conventional antibiotics. Overuse of antibiotics led to the development of multi-drug-resistant microorganisms. Developing new anti-infective agents is crucial to protect the efficacy of standard antibiotics and reduce the risk of antibiotic resistance. Antimicrobial peptides (AMPs) are short, cationic, and amphipathic molecules found in all living organisms, belonging to the innate immune system. AMPs can potentially replace antibiotics having a wide range of activity against Gram-positive and Gram-negative bacteria, fungi, protozoa, and viruses. Moreover, they show immunomodulatory and antibiofilm activity, and they are less likely to induce resistance mechanisms compared to antibiotics (*Uddin SJ et al. 2021*). The synthesis of AMPs in branched structure not only improves the resistance profile to protease degradation but also generates the possibility to form polyvalent interactions increasing the binding avidity *(Falciani et al. 2007).*

Tetra-branched antimicrobial peptides (BAMPs)

A small library of **tetra-branched peptides** was solid-phase synthesized starting from 9-10-residue linear sequences derived from natural AMPs.

The prediction of the linear analogues' tertiary structure with APPTEST protocol (*Brendan Timmons et al. 2021)* revealed that **BAMP2** displayed an extensive amphipathic alpha helix arrangement, **BAMP39** showed an alpha helix structure involving only three central residues whereas **BAMP49** exhibited a fully alpha helix arrangement. Differently, **BAMP37** and **BAMP45** presented a random linear form. Structural modelling studies confirmed that the predicted tertiary structure of the peptides was maintained in the tetra-branched forms.

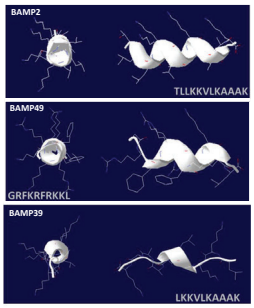

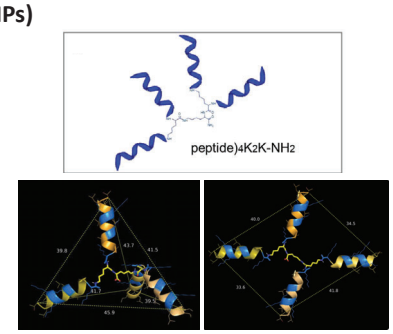

Antibacterial activity

Minimum Inhibitory Concentration (μM)

Name	BAMP2	BAMP37	BAMP39	BAMP45	BAMP49
Sequence	(TLLKKVLKAAAK)$_4$K$_2$K	(KKLLGKNWKLM)$_4$K$_2$K	(LKKVLKAAAK)$_4$K$_2$K	(INLKKLAKL)$_4$K$_2$K	(GRFKRFRKKL)$_4$K$_2$K
Origin	Dermaseptin	Mastoparan	Dermaseptin	Mastoparan	Cathelicidin
***E. coli* TG1**	1.5	3	1.5	0,7	6
***E. coli* LC711** (colR*)	3	>25	6	6	>25
***P. aeruginosa* ATCC 27853**	6	3	6	3	6
***P. aeruginosa* FI-25 (bla_{VIM-1}*)**	12	NT	NT	NT	NT
***P. aeruginosa* FI-29 (bla_{GES-5}*)**	12	NT	NT	NT	NT
***K. pneumoniae* ATCC 43816**	6	25	12,5	12	25
***K. pneumoniae* (colR*)**	6	>25	>25	6	>25
***E. faecalis* 51299**	25	>25	>25	>25	> 25
***E. faecium* FI-48 (van,*)**	6	NT	NT	NT	NT
***S. aureus* USA 300**	>25	>25	>25	>25	>25

** blaVIM-1, VIM-type -lactamase; bla GES-5, GES-5 type -lactamase; colR, colistin resistance; vanA, vancomycin resistance; NT: not tested.*

All the BAMPs were active against planktonic forms of Gram-negative strains of *E. coli*, *P. aeruginosa* and *K. pneumoniae*. Notably, BAMP2, BAM39 and BAMP45 were also active against strains carrying the gene for resistance to colistin, a peptide antibiotic used in clinical practice. The most promising peptide proved to be **BAMP2** also demonstrating activity against strains of *P. aeruginosa* resistant to β-lactamases.

Activity against *E. faecalis* and *S. aureus* Gram-positive strains was poor for all peptides.

Anti-biofilm activity

	E.coli TG1				*K. pneumoniae* ATCC 43816			
μM	BAMP2	BAMP37	BAMP39	BAMP49	BAMP2	BAMP37	BAMP39	BAMP49
MIC	1,5	3	1,5	6	6	25	12,5	>25
BPC	1,5	3	6	25	50	50	>50	50
MBIC	3	25	50	50	50	50	50	50

BPC: lowest concentration of peptide that results in 80% lower biofilm formation compared to untreated controls.

MBIC: lowest concentration of peptide that results in 80% reduction in preformed biofilm compared to untreated controls.

AMPs have amphipathic surfactant structure that facilitates penetration of the biofilm matrix down to the outer bacterial membrane favouring biofilm disruption and bacterial eradication *(Srinivasan, Ramanathan et al., 2021)*. Therefore, the antibiofilm activity of BAMPs was evaluated.

BAMP2 proved the best against *E. coli* biofilm, inhibiting its formation and disrupting existing layers at the MIC and double the MIC, respectively.

BAMP37, **BAMP39** and **BAMP49** were more efficient at inhibiting biofilm formation, and less at disrupting existing *E. coli* biofilm.

K. pneumoniae biofilm was 80% disrupted by higher concentrations, i.e. 50 μM, by all peptides.

Mechanism of action

The mechanism of action of **BAMPs** was evaluated in *E. coli* TG1 with electron microscopy experiments (TEM and SEM) revealing that the peptides had a **detergent-like effect**: they disrupted the bacterial membrane causing the wrinkling of the surface, the enlargement of the cells and an overall loss of surface smoothness leading to rapid permeabilization of the membrane and bacterial death.

The loss of membrane integrity was also confirmed by the internalization of non-permeable fluorophores within 10 minutes after adding the peptides, demonstrating rapid **dysregulation of homeostasis.**



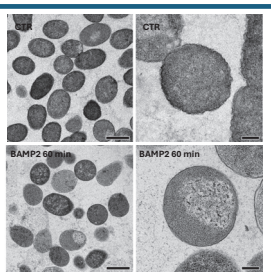

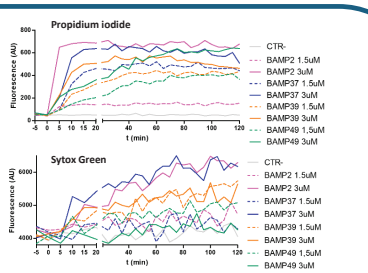

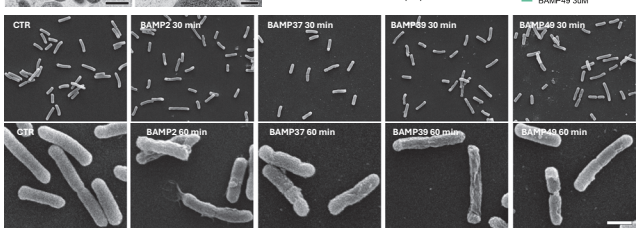

Conclusion

Among all the tested BAMPs, **BAMP2** showed to be the most effective antibacterial agent, probably thanks to its extensive amphipathic alpha helix conformation. The promising antibacterial and antibiofilm activity of these BAMPs could be exploited for the development of new therapeutic molecules to fight mild infections such as dental ones, often associated with the presence of multi-resistant biofilms. Thus, using AMPs instead of antibiotics in oral cavity infections may be beneficial in maintaining the effectiveness of standard antibiotics in more severe infections.

https://doi.org/10.17952/37EPS.2024.P1073

AMP32: a short cyclic peptide as an environmentally friendly alternative to counteract late blight symptoms in crops

Elena Marone Fassolo[1], Demetrio Marcianò[1], Stefano Rosa[1], Lucia Feni[2], Vaibhav Srivastava[3], Andrea Tagliani[1], Silvia Laura Toffolatti[4], Sara Pellegrino[2], Vincent Bulone[3,6,7,8], Simona Masiero[1] and Paolo Pesaresi[1]

[1]Department of Biosciences (DBS), University of Milan, 20133, Milan, Italy; [2] Department of Pharmaceutical Sciences (DISFARM), University of Milan, 20133, Milan, Italy ;[3]Division of Glycoscience, Department of Chemistry, School of Engineering Sciences in Chemistry, Biotechnology and Health, Royal Institute of Technology (KTH), AlbaNova University Centre, 10691, Stockholm, Sweden [4]Department of Agricultural and Environmental Sciences (DISAA), University of Milan, 20133, Milan, Italy; [5]School of Agriculture, Food and Wine, University of Adelaide, Waite Campus, Urrbrae, South Australia, 5064, Australia; [6]ARC Centre of Excellence in Plant Cell Walls, School of Agriculture, Food and Wine, University of Adelaide, Waite Campus, Urrbrae, South Australia, 5064, Australia; [7]Adelaide Glycomics, School of Agriculture, Food and Wine, University of Adelaide, Waite Campus, Urrbrae, South Australia, 5064, Australia



(I) Potato late blight (*P. infestans*) infection, (II) *P.infestans* sporangia, (III) and mycelium.

Abstract

Oomycetes, e.g. *Phytophthora infestans*, a widespread pathogen that causes late blight and affects most *Solanaceae* species, cause crop losses of several billion USD every year. Oomycetes life cycle consist in the production of sexual oospores and asexual zoospores, this event occurs numerous times during a single vegetative season. Defence against fungal plant pathogens is mainly based on the use of chemical fungicides[1] , which give rise to great concerns for risks associated with human health, environmental toxicity, or fast development ofresistance in target pathogens. Among those, several compounds have been banned or included in a list of candidates for substitution by the EU Commission, thus novel and sustainable molecules with low environmental impact are needed. Our group identified, through a Yeast Two-Hybrid-based combinatorial library of cyclic peptides (CYCLIC), an antimicrobial peptide (AMP32) able to bind a bait (i.e., target) of interest[2]. This approach aims to increase the specificity toward the targeted protein and, as consequence, toward the desired pathogen, thus reducing the risks of negative effects on other organisms. In this work, the glycosyltransferase domain of the *P. infestans* Cellulose synthase 2 (PiCesA2) was selected as bait because of its essential role in cellulose biosynthesis and cell wall integrity[3]. Chemically synthesized AMP32 was tested for its antimicrobial activity in in vitro and ex vivo assays and showed a strong *P. infestans* growth inhibition both *in vitro* and *ex vivo*. Noteworthy, the absence of toxicity in non-target organisms was also successfully addressed. Moreover, AMP32 showed similar antimicrobial effects when tested on other oomycete species with a high homology sequence for the PiCesA2, suggesting a broad-spectrum activity. A deeper investigation has confirmed that AMP32 compromises cell viability in *P. infestans*, showing a fungistatic activity and the ability to interfere with *P. infestans* cell membrane integrity. Other undergoing studies will deepen our understanding of the structural and biochemical insights of AMP32-PiCesA interaction and mode of action (MoA) and will provide useful information for peptide modification and chemical formulation suitable for field application.

1 W. Leesutthiphonchai, A. L. Vu, A. M. V. Ah-Fong, H. S. Judelson, How Does Phytophthora infestans Evade Control Efforts? Modern Insight into the Late Blight Disease, (2018) Phytopathology 108:8, 916-924
2 Rosa S, Tagliani A, Barbaro C, Tadini L, Visentin C, Gourlay LJ, Prod'S, Feni L, Pellegrino S, Pesaresi P and Masiero S (2023) The cyclic peptide GACP2 enables the modulation of galactose metabolism in yeast by interfering with GAL4 transcriptional activity. Front. Mol. Biosci. 10:1017757. doi: 10.3389/fmolb.2023.1017757
3 Erwig, L., Gow, N. "Interactions of fungal pathogens with phagocytes". Nat Rev Microbiol 14, 163–176(2016)

Distribution map of *Phytophthora infestans* and intensities of fungicide sprayings



Source: The CIP webpage (http://www.cipotato.org)

A

Targeting cell wall biosynthesis in Oomycetes

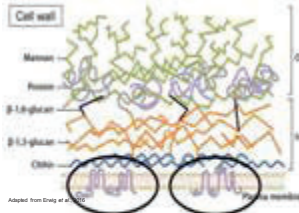

Adapted from Erwig et al., 2016

CAbohydrate enZymes (CAZymes):
- Cellulose synthases (CesAs)
- Chitin synthase (CHSs)
- Putative transglycosylases

WHY?

- Resistance to environmental stresses
- Mediates nutrient uptake
- Signaling interface

→ **Essential for development and infection process**

Yeast Two-Hybrid assay

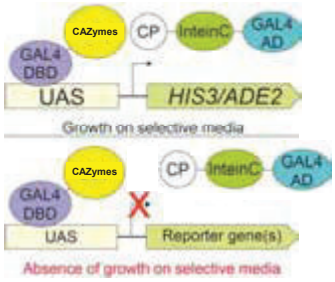

Combinatorial librarY of cyCLIC peptides (CYCLIC)

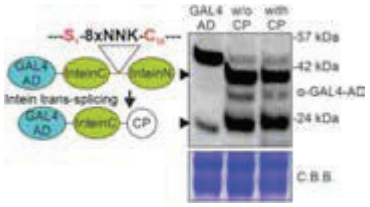

B

Bioactivity assay

Peptides identification → Peptides synthesis → Peptides testing

***In vitro* viability assay**

% metabolic activity inhibition of P. infestans sporangia

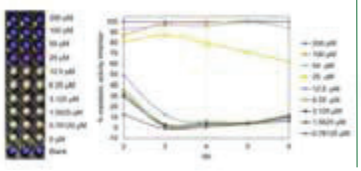

***Ex vivo* bioactivity assay on leaf disks**

% reduction on *P. infestans*-related symptoms

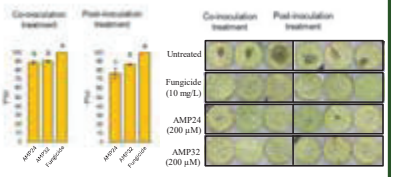

C

Toxicity test

Toxicity test on off-target organisms

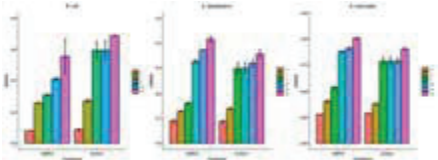

MTT assay on human cells

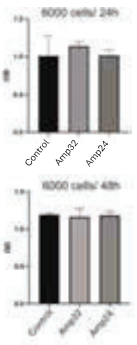

Photosynthetic performance measured using Imaging PAM on grapeine leaves

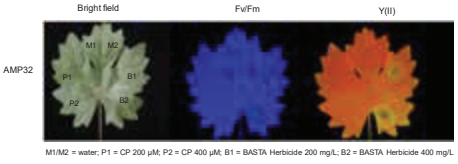

M1/M2 = water; P1 = CP 200 µM; P2 = CP 400 µM; B1 = BASTA Herbicide 200 mg/L; B2 = BASTA Herbicide 400 mg/L

D

Molecular characterization

AMP32 interfere with PiCesA2

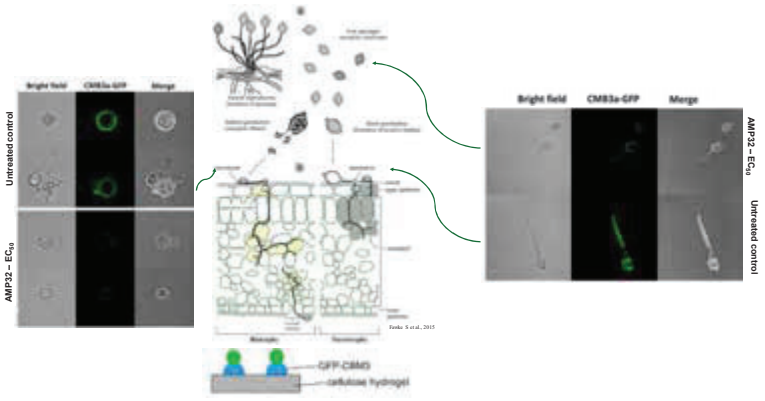

Cellulose quantification

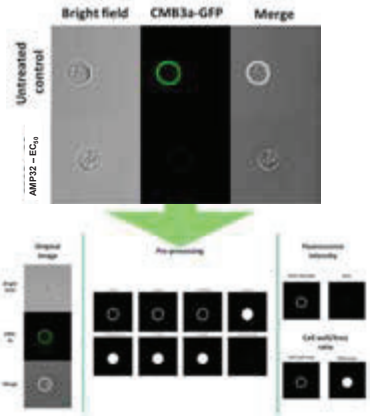

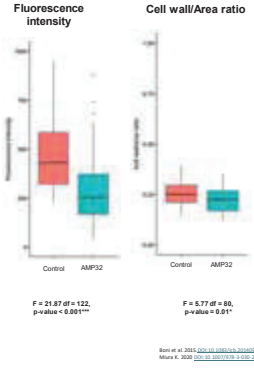

Boni et al. 2015 DOI: 10.1083/jcb.201409123
Miura K. 2020 DOI: 10.1007/978-3-030-22386-1_2

Outcome: identification of peptides with antimicrobial activity for a sustainable agriculture

Bibliography:

1. Erwig, L., Gow, N. "Interactions of fungal pathogens with phagocytes". Nat Rev Microbiol 14, 163–176 (2016).
2. Barreto, Kris, and C. Ronald Geyer. "Screening combinatorial libraries of cyclic peptides using the yeast two-hybrid assay." Yeast Protocols. Humana Press, New York, NY, 2014. 273-309.
3. Fawke S, Doumane M, Schornack S.2015.Oomycete Interactions with Plants: Infection Strategies and Resistance Principles. Microbiol Mol Biol Rev79:. https://doi.org/10.1128/mmbr.00010-15
4. Boni, Andrea, et al. "Live imaging and modeling of inner nuclear membrane targeting reveals its molecular requirements in mammalian cells." *Journal of Cell Biology* 209.5 (2015): 705-720.
5. Miura, Kota. "Measurements of Intensity Dynamics at the Periphery of the Nucleus." *Bioimage Data Analysis Workflows* (2020): 9-32.

37th EPS European Peptide Symposium
14th IPS International Peptide Symposium
25 - 29 August 2024
Satellite Workshop 30 - 31 August 2024
Florence, Italy- 2024
https://doi.org/10.17952/37EPS.2024.P1075

Water-soluble longibramide E analogs: synthesis and antibacterial activity

Renato B. Pereira,[1*] **Ana Gomes**,[1] **Mariana Ferreira**,[1] **Paula Gameiro**,[1] **Paula Gomes**[1]

[1]LAQV-REQUIMTE, Departamento de Química e Bioquímica, Faculdade de Ciências, Universidade do Porto, P-4169-007 Porto, Portugal

*Email: renato.pereira@fc.up.pt

Introduction/Aim

The overuse and misuse of antibiotics have significantly contributed to the emergence of antibiotic-resistant bacteria, making infections harder to treat, and increasing the risk of spread. To address this challenge, the development of new classes of antibacterial drugs is crucial. In this context, peptaibols are promising membrane-active peptides since their antibacterial action does not involve specific cellular targets, reducing the likelihood of bacterial resistance development. Recently, Zhang *et al.* 2022 [1] isolated a series of new 11-residue peptaibols, denominated longibramides, from *Trichoderma longibrachiatum*. Among them, longibramide E sparked us particular interest due to its activity against *S. aureus* MRSA T144 [1]. However, a major drawback to the exploitation and application of peptaibols is their poor water solubility and longibramide E offers no exception to this limitation. Our current study demonstrated that the removal of the acetylation in the *N*-terminus and the replacement of the relatively expensive *C*-terminal leucinol moiety by a leucine amide markedly improve peptide hydrophilicity. Aiming at the further improvement of peptide water solubility, other Lys-containing analogs have been synthesized. Furthermore, based on the growing body of evidence that acylation of the *N*-terminus with a fatty acid increases peptide antimicrobial properties [2], a longibramide E analog featuring a *n*-octanoyl in the *N*-terminus was synthesized. Both manual and automated solid phase synthesis were used to compare synthesis method efficiency for this class of metabolites, whose antibacterial activity was determined against susceptible strains and multidrug-resistant clinical isolates of Gram-positive and Gram-negative bacteria.

Methodology

Peptides **1**, **3**, **6-9** were synthesized using Symphony® X (Gyros Protein Technologies) at a 100 µmol scale, using a low loading rink amide AM resin (0.29 mmol/g), and following a Fmoc/tBu orthogonal protection scheme. Deprotection of the resins was carried out with a solution of 20% piperidine in DMF and coupling steps were conducted in the presence of HCTU and NMM. To optimize the outcome of these synthesis, different conditions were tested (**Table 1**). Coupling steps were followed by a capping step, with a solution of Ac_2O/Lut/DMF (5:6:89), for 5 min at room temperature. For longibramide E and peptides **3** and **4**, *N*-terminal acetylation was achieved using Ac_2O/DIEA/DMF (1.3:4.8:93.9). The rink amide (peptides **1-3** and **6-9**) and L-Leucinol-2-chlorotrityl (longibramide E and peptide **4** and **5**) resins were cleaved with a solution of TFA/TIS/H_2O (95:2.5:2.5) and TFA/DCM/TIS (50:47.5:2.5) for 2 hours at room temperature, respectively.

Table 1. Methods used to synthesize the target peptides.

Method	Coupling		Deprotection		Capping
	Time (min)	T (ºC)	Time (min)	T (ºC)	
A - Manual	60	RT	20	RT	☒
B – Automated RT	2 × 60	RT	2 x 2.5	RT	☑
C – Automated IR	2 × 10	75	2 x 2.5	RT	☑

Results

1. Comparing synthesis methodologies

Table 2. Sequences produced in this study.

Peptide	Sequence	Method	Purity (%)
Longibramide E	Ac-Aib-Asn-Ile-Ile-**Aib**-Hyp-Leu-Leu-Aib-Pro-Lol	A	99.9
1	Aib-Asn-Ile-Ile-**Aib**-Hyp-Leu-Leu-Aib-Pro-**Leu-NH_2**	A/B/C	91.3
2	Aib-Asn-Ile-Ile-Hyp-Leu-Leu-Aib-Pro-**Leu-NH_2**	A	95.7
3	Ac-Aib-Asn-Ile-Ile-Aib-Hyp-Leu-Leu-Aib-Pro-**Leu-NH_2**	B	98.3
4	Ac-Aib-Asn-Ile-Ile-Hyp-Leu-Leu-Aib-Pro-Lol	A	99.5
5	Aib-Asn-Ile-Ile-Aib-Hyp-Leu-Leu-Aib-Pro-Lol	C	90.5
6	Aib-Asn-Ile-Ile-Aib-Hyp-**Lys-Lys**-Aib-Pro-**Leu-NH_2**	B	90.6
7	**Lys-Lys-Lys-Ala**-Aib-Asn-Ile-Ile-Aib-Hyp-Leu-Leu-Aib-Pro-**Leu-NH_2**	C	97.3
8	Aib-Asn-Ile-Ile-Aib-Hyp-Leu-Leu-Aib-Pro-Leu-**Ala-Lys-Lys-Lys-NH_2**	B	98.9
9	***n*Oct-Lys-Lys-Lys-Ala**-Aib-Asn-Ile-Ile-Aib-Hyp-Leu-Leu-Aib-Pro-**Leu-NH_2**	C	91.3

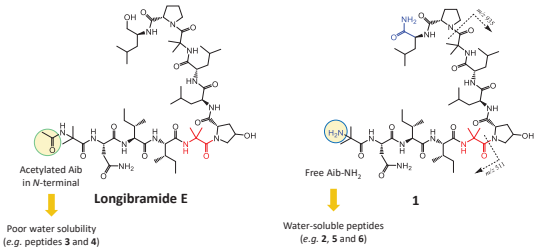

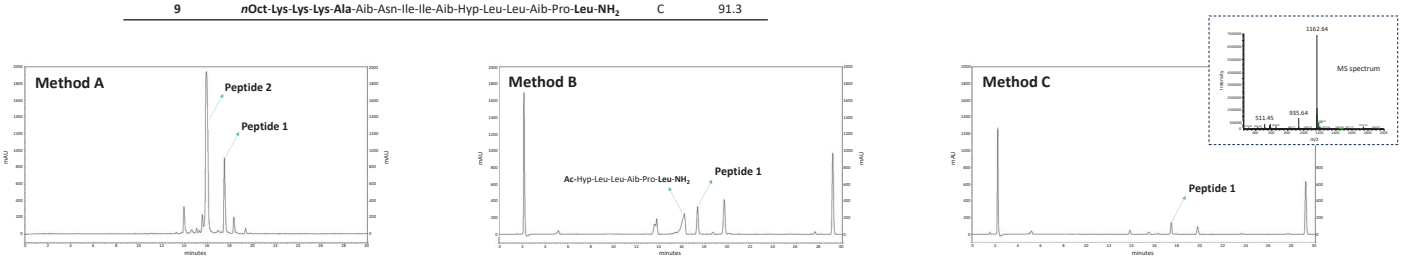

Figure 1: HPLC chromatogram of the crude peptide **1** synthesized manually without capping (Method A), automatically at room temperature (Method B), and automatically using infrared heating (Method C).

2. Assessment of antibacterial activity

Table 3: Activity of the peptides under study against Gram-positive and Gram-negative bacteria.

Bacterial strains	MIC in µg/mL (µM)									
	Longibramide E	1	2	3	4	5	6	7	8	9
S. aureus (ATCC 29213)	> 256 (215)	128 (110)[a]	1024 (950)[a]	> 256 (213)	> 256 (231)	256 (223)[a]	> 1024 (859)	64 (40)[a]	512 (316)[b]	4 (2)[b]
HJS-SA007 [1]	> 256 (215)	64 (55)[a]	1024 (950)[a]	> 256 (213)	> 256 (231)	256 (223)[a]	> 1024 (859)	32 (20)[c]	256 (158)[b]	4 (2)[b]
Sa3-SA3 [2]	> 256 (215)	128 (110)[b]	-	-	-	256 (223)[a]	-	32 (20)[b]	> 256 (158)	4 (2)[a]
E. coli (ATCC 25922)	> 256 (215)	512 (440)[b]	> 1024 (950)	> 256 (213)	> 256 (231)	512 (445)[a]	> 1024 (859)	8 (5)[a]	128 (79)[a]	8 (4)[a]
Ec1-SA1 [3]	> 256 (215)	> 256 (220)	> 1024 (950)	> 256 (213)	> 256 (231)	512 (445)[b]	> 1024 (859)	32 (20)[a]	> 256 (158)	8 (4)[a]
HSJ-EC004 [4]	> 256 (215)	> 256 (220)	-	-	-	> 256 (223)	-	16 (10)[a]	256 (158)[a]	4 (2)[a]

Antimicrobial resistance pattern: [1] CIP; CLI; ERY; GEN; OXA; LEV; MOX. [2] VAN; AMC; AMP; CXI; IMI; CIP; OXA. [3] AZT; CTZ; CTA; TET; AMP; TRS; CIP; GEN. [4] AMC; AMP; CXA; CXM; CIP; PIT; LEV. [a] MBC = MIC. [b] MBC = 2 × MIC. [c] MBC = 16 × MIC. AMC: amoxicillin/clavulanic acid; AMP: ampicillin; AZT: aztreonam; CTZ: ceftazidime; CIP: ciprofloxacin; CLI: clindamycin; CTA: cefotaxime; CXA: cefuroxime axetil; CXM: cefuroxime sodium; ERY: erythromycin; CXI: Cefoxitin; GEN: gentamicin; IMI: imipenem; LEV: levofloxacin; MOX: moxifloxacin; OXA: oxacillin; TRS: Trimethoprim/Sulfamethoxazole; TET: tetracycline; PIT: piperacillin/Tazobactam; VAN: vancomycin.

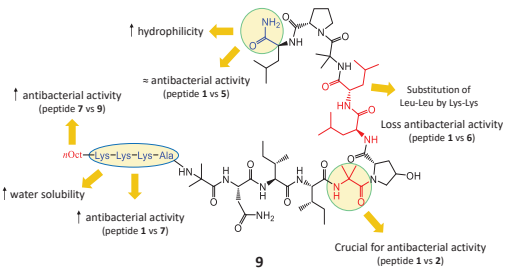

Conclusions

- The use of infrared (IR) heating markedly improved the synthesis of this class of metabolites, as the coupling of Aib to Hyp was significantly more efficient.
- The Aib coupled to Hyp is crucial for the antibacterial activity (peptide **1** vs **2**), contrarily to the substitution of the expensive *C*-terminal alcohol by a leucine amide (**1** vs **5**).
- The incorporation of **Lys-Lys-Lys-Ala-** in the *N*-terminus (**7**) markedly improved peptide water solubility and enhanced antibacterial activity.
- The addition of ***n*-octanoyl** (**9**) further potentiated the antibacterial activity.
- Peptide **9** may be a promising molecule to tackle infections caused by resistant Gram-positive and Gram-negative bacteria.

References

[1] Zhang, S.-H.; Zhao, X.; Xu, R.; Yang, Y.; Tang, J.; Yue, X.-L.; Wang, Y.-T.; Tan, H.-Y.; Zhang, G.-G.; Li, C.-W. Chem. Biodiversity 2022, 19, e202200627.
[2] Zhong, C.; Liu, T.; Gou, S.; He, Y.; Zhu, N.; Zhu, Y.; Wang, L.; Liu, H.; Zhang, Y.; Yao, J.; Ni, J. Eur. J. Med. Chem. 2019, 182, 111636.

Funding: This research was funded by Fundação para a Ciência e Tecnologia/Ministério da Ciência, Tecnologia e Ensino Superior (FCT/MCTES, Portugal), through project KIWIBOL (PTDC/ASP-PLA/2440/2021, DOI 10.54499/PTDC/ASP-PLA/2440/2021). **Acknowledgements**: This work received support and help from FCT/MCTES (LA/P/0008/2020 DOI 10.54499/LA/P/0008/2020, UIDP/50006/2020 DOI 10.54499/UIDP/50006/2020 and UIDB/50006/2020 DOI 10.54499/UIDB/50006/2020), through national funds. Renato B. Pereira and Mariana Ferreira thank FCT and LAQV/REQUIMTE for the contract (REQUIMTE 2023-05) and the post-doc fellowship (REQUIMTE 2019-34), respectively. Ana Gomes thanks FCT for funding through the Scientific Employment Stimulus - Individual Call (Ref. 2022.08044.CEECIND/CP1724/CT0004).

CRC 1279 ulm university · universität ulm

https://doi.org/10.17952/37EPS.2024.P1076

Generation of a Peptide Library from human Bone Marrow for the discovery and identification of novel bio active bone-marrow derived peptides

Nico Preising[1], Armando A. Rodriguez[1,2], Merve Karacan[1], Sebastian Wiese[2], Dennis Freisem[3], Fabian Zech[3], Dietmar Thal[4], Konstantin Sparrer[3], Jan Münch[3], Frank Kirchhoff[3] and Ludger Ständker[1]

[1] Core Facility Functional Peptidomics, Ulm University Medical Center, Ulm, Germany , [2] Core Unit Mass Spectrometry and Proteomics, Ulm University Medical Center, Ulm, Germany
[3] Institute of Molecular Virology, Ulm University Medical Center, Ulm, Germany, [4] Laboratory of Neuropathology, Department of Imaging and Pathology, Leuven Brain Institute, Leuven,Belgium

Human bone marrow contains an abundance of proteins and peptides that are essential for the formation of blood cells. Thus, bone marrow is expected to contain a wealth of factors that influence cell growth, differentiation, and function. Aiming to identify novel bioactive peptides in human bone marrow, we established a method to generate a peptide library from primary human material. To this end, 25 kilograms of human bone (femur) from donors were collected, and the bone marrow was extracted. The eluted peptides were separated into 285 fractions, and consecutively tested for bioactivity e.g. immune modulation, cell viability and growth, and anti-viral activity. After further iterative bioassay guided sub-fractionation, peptides responsible for the function can be identified. In summary, our data show that human bone marrow contains peptides that modulate autophagy and inhibit viral infections. This project provides the basis for establishing peptide extraction methods from complex human tissues to identify novel peptide modulators of cellular processes.

Generation of the Peptide Library

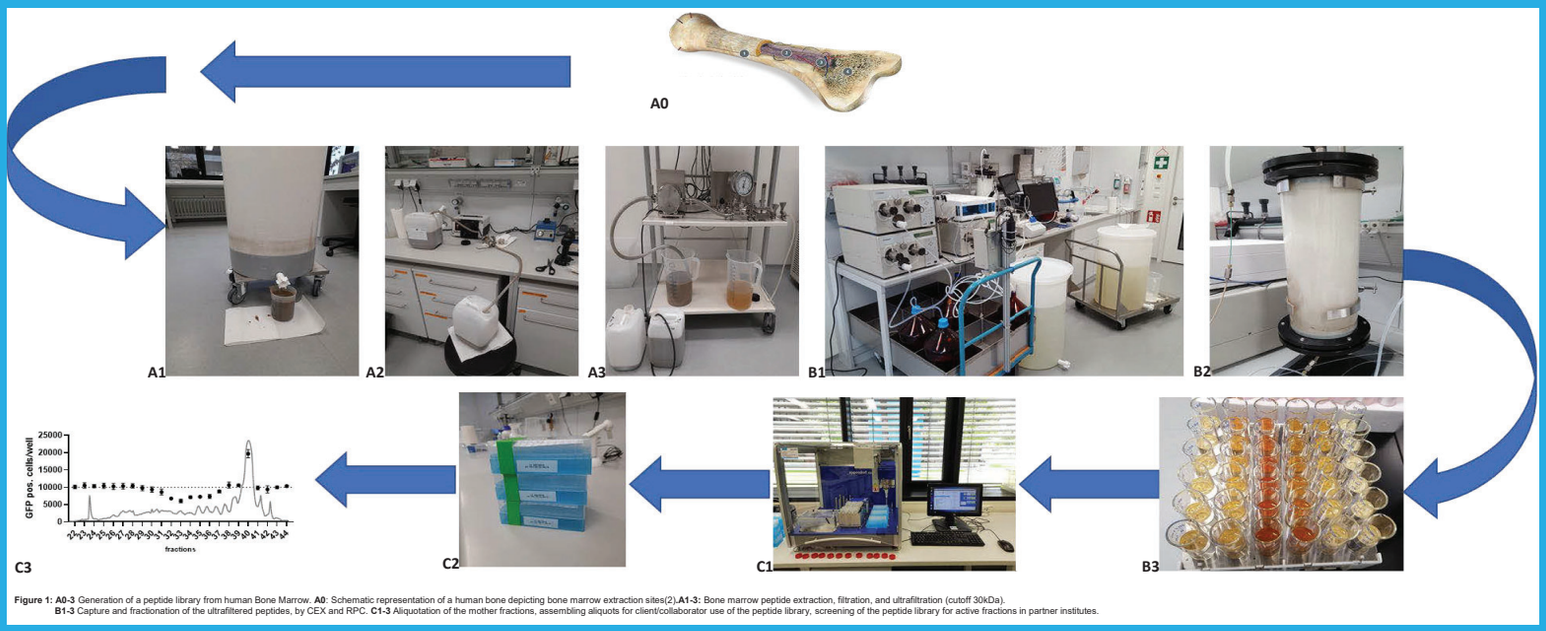

Figure 1: A0-3 Generation of a peptide library from human Bone Marrow. **A0**: Schematic representation of a human bone depicting bone marrow extraction sites(2).**A1-3:** Bone marrow peptide extraction, filtration, and ultrafiltration (cutoff 30kDa).
B1-3 Capture and fractionation of the ultrafiltered peptides, by CEX and RPC. **C1-3** Aliquotation of the mother fractions, assembling aliquots for client/collaborator use of the peptide library, screening of the peptide library for active fractions in partner institutes.

Screening for Bioactive Fractions

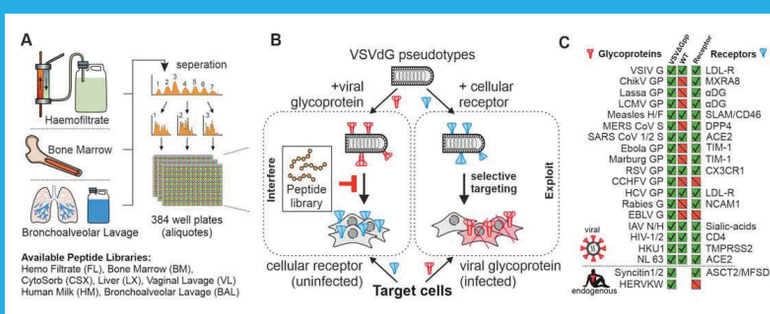

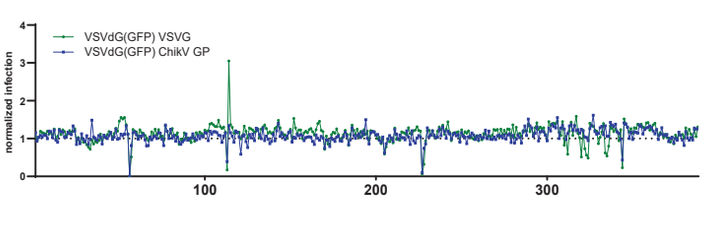

Figure 2: A Schematic depiction of the generation of human-derived peptide libraries. **B** Outline of the two major strategies of the project: Interfere (left) and Exploit (right).
C List of the already established Vesicular Stomatitis Indiana Virus ΔG pp, as well as corresponding wild type viruses and, if identified, their receptors.

Figure 3: Isolation of candidate peptides that selectively inhibit Chikungunya virus GP-mediated infection. A Full proof-of-concept dual-colour screen, of the bone marrow peptide library including over 350 wells.

References:

- Kaygisiz, K. et al. Data-mining unveils structure-property-activity correlation of viral infectivity enhancing self-assembling peptides. Nat. Commun. 14, 5121 (2023)
- Bone. https://www.mibe.de/gesundheit/knochenstoffwechsel/wunderwerk-knochen
- Logo 37th EPS https://eps2024.com/

Contact:

Nico Preising
Core Facility Functional Peptidomics
Ulm University Medical Center
Meyerhofstraße 4
89081 Ulm, Germany
Email: nico.preising@uni-ulm.de

Summary and Perspectives

- Human bone marrow-derived peptides were extracted and collected
- A human bone marrow peptide library was generated.
- The peptide library was screened for autophagy modulation and activity against different viral glycoproteins
  - → Chromatographic purification of the active peptides.
  - → Mass spectrometry and sequencing of the pure peptides.
  - → Identification of the active peptides and testing synthetic variants of them.

SYNTHESIS AND ANTIBACTERIAL ACTIVITY OF NEW ANALOGUES OF AUREIN 1.2

Nora Angelova, Tsvetelina Foteva, Veronica Nemska, Nelly Georgieva, Dancho Danalev, Emilia Naydenova
University of Chemical Technology and Metallurgy, Sofia, Bulgaria

https://doi.org/10.17952/37EPS.2024.P1079

INTRODUCTION

Antimicrobial peptides are identified as the most promising option to the conventional molecules used nowadays against infections because they mimic the natural metabolic effects within the body with low toxicity and better selectivity which proves they're one of the alternatives for therapeutic intervention. Aurein 1.2 is a short multi-functional antimicrobial peptide isolated from Litoria aurea and Litoria raniformis skin secretion. Aurein peptides can be classified into five distinct groups (Aureins -1 to -5), among which Aurein-1 peptides are considered to be one of the shortest α-helical peptides with antimicrobial and anticancer activity. Many antimicrobial peptides have the ability to cross cell membranes and destroy bacteria. Biological activity of Aurein has been widely investigated however, its lack of a potent action failed to provide Aurein 1.2 with a competitive edge for further development as a therapeutic agent for clinical use.

METHODS

The conventional solid-phase peptide synthesis based on Fmoc (9-fluorenylmethoxycarbonyl) chemistry was employed to synthesize a series of new analogs of Aurein 1.2. Rink-amide MBHA resin was used as a solid-phase carrier to obtain C-terminal amides. TBTU (2-(1Hbenzotriazole-1-yl)-1,1,3,3-tetramethyluronium tetrafluoroborate) or DIC (N,N′-Diisopropylcarbodiimide) were used as a coupling reagents. The peptide purity was monitored on a RP-HPLC. The LC/MC spectra were recorded on a LTQ XL OrbitrapDiscovery instrument. The optical rotation was also measured. The obtained new analogues were estimated for their antibacterial activity against Gram positive Bacillus subtilis strain 3562 and Gram-negative E. coli NBIMCC 8785 using broth microdilution method in concentrations from 0 to 320 μg/mL to determine the minimal inhibitory concentration (MIC).

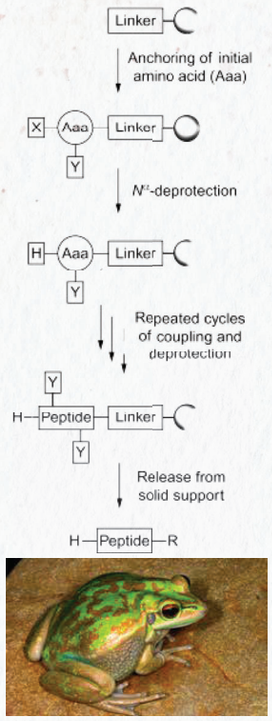

PURPOSE

Aurein 1.2 was chosen as a template for rational modification to achieve a higher bio-functionality. The modifications of the six new analogues were made in the primary structure by incorporating unnatural amino acids in order to improve the pharmacodynamics of the new peptides. Aurein 1.2 was modified at position 7 and 8.

The six new modified analogs followed the structure:

Gly-Leu-Phe-Asp-Ile-Ile-**Xxx**^{7}-**Xxx**^{8}-Ile-Ala-Glu-Ser-Phe-NH_2

where Xxx is Orn or Dab (diaminobutyric acid). Lysine residues were replaced sequentially and simultaneously with the unnatural amino acids.

Fig.1 Structure of Aurein 1.2

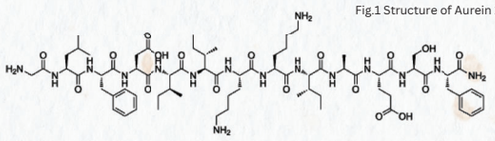

RESULTS

The MIC of the original peptide Aurein 1,2 is 160 μg/ml, and the MIC of the derivatives decreases to 80 μg/ml, which indicates better antibacterial activity of the newly synthesized peptides. Only in EH [Dab] 7,8 the value of MIC is the same as in the starting compound (Table 1).

The values of the minimum bactericidal concentration are higher than the MIC - 320 μg/ml for the newly obtained compounds, and for EH [Dab] 7,8 and the starting peptide are not reported, which means that the derived compounds have a bacteriostatic effect against B. subtilis 3562. The replacement of lysine with the unnatural amino acids Orn and Dab leads to a increase in the antibacterial activity of the obtained peptides compared to Aurein 1,2 against the B. subtilis 3562.

The test results with Gram negative strain E. coli K12, showed that the MIC of the newly synthesized peptides increased - 80 μg/ml, even for EH [Dab] 7,8 the MIC was 160 μg/ml, compared to the starting peptide Aurein 1,2, in which MIC is 40 μg/ml. This means that in the case of derivative compounds, the antibacterial effect is significantly reduced. A minimum bactericidal concentration was not reported against E. coli K12, which indicates a very weak bacteriostatic effect of the studied peptides against this strain.

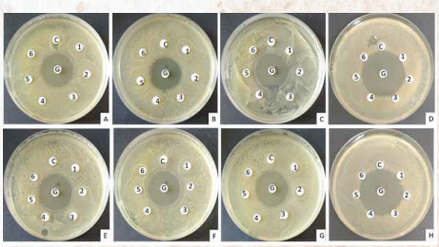

The disk diffusion assay - B. subtilis 3562

Legend: A – Aurein 1,2; B - EH [Orn]7; C - EH [Orn]7,8; D – EH[Dap]7,8; E - EH[Dab]8; F - EH[Dab]7; G - EH[Dab]7,8; H – EH[Orn]8
1 – 10 μg/ml peptide; 2 - 20 μg/ml peptide; 3 – 40 μg/ml peptide; 4 – 80 μg/ml peptide; 5 – 160 μg/ml peptide; 6 – 320 μg/ml peptide; G –10 μg/disc Gentamicin;

Name	*Bacillus subtilis* 3562		*Escherichia coli* K12	
	MIC μg/ml	MBC μg/ml	MIC μg/ml	MBC μg/ml
1. Aurein 1,2	160	NA	40	NA
2. EH [Orn]^{7}	80	320	80	NA
3. EH [Orn]^{8}	80	320	40	NA
4. EH [Orn]^{7,8}	80	320	80	NA
5. EH [Dab]^{7}	80	320	80	NA
6. EH [Dab]^{8}	80	320	80	NA
7. EH [Dab]^{7,8}	160	NA	160	NA

Table 1. Minimal inhibitory concentration and minimal bactericidal concentration of tested peptides against B. subtilis 3562 and E. coli K12

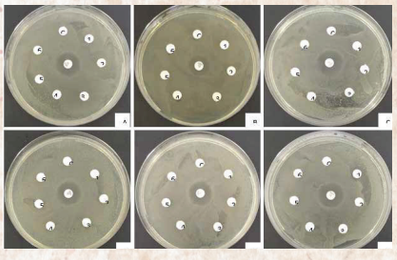

The disk diffusion assay - E. coli K12

CONCLUSIONS

The replacement of Lysine with the unnatural amino acids Orn and Dab in the primary structure of Aurein 1.2 leads to a significant increase in the antibacterial activity of the obtained peptides against the investigated microorganisms

[1] Roudi, R.; Syn, N.L.; Roudbary, M. Antimicrobial peptides as biologic and immunotherapeutic agents against cancer: A comprehensive overview. Front. Immunol. 2017, 8, 1320

Acknowledgement: This study is funded by the European Union-NextGenerationEU, through the National Recovery and Resilience Plan of the Republic of Bulgaria, project № BG-RRP-2.004-0002, "BiOrgaMCT"

Tackling antibiotic resistance by blocking signalling pathways

Rachel A. Johnson[1], Susanne Gebhard[2], Jody M. Mason[1]

[1] Department of Life Sciences, University of Bath, UK
[2] Institute of Molecular Physiology, Johannes Gutenberg-Universität Mainz, Germany

https://doi.org/10.17952/37EPS.2024.P1080

1. Context

- BceRS is a two-component system (TCS) in *Bacillus subtilis*.
- BceRS enables *B. subtilis* to respond in the presence of bacitracin, a cell wall acting antibiotic.
- BceS is a histidine kinase and forms a key part of this signalling pathway.

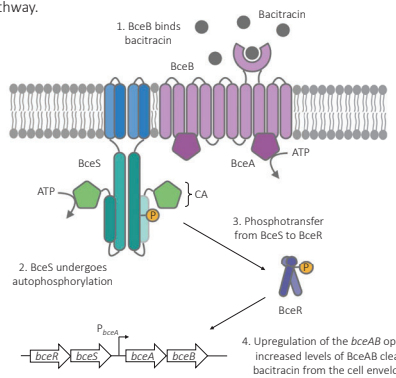

Figure 1: Schematic of the typical signalling pathway of the BceRS two-component system and its cognate transporter BceAB.[1]

2. Project Approach

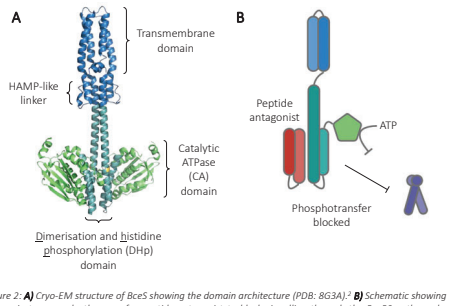

*Figure 2: **A)** Cryo-EM structure of BceS showing the domain architecture (PDB: 8G3A).*[2] *__B)__ Schematic showing the project approach: the use of a peptide antagonist to block signalling through the BceRS pathway by disrupting BceS dimerisation.*

AIM: To disrupt BceS dimerisation and block BceRS signalling using a peptide antagonist, rendering *B. subtilis* unable to respond to bacitracin.

WHY: This constitutes a novel means of tackling AMR with reduced evolutionary pressure to develop resistance and leverages the sequence specificity of histidine kinase dimerisation domains.

IMPACT: There is the potential to translate this approach to other two-component systems in clinically relevant pathogens.

3. Screening Methodology

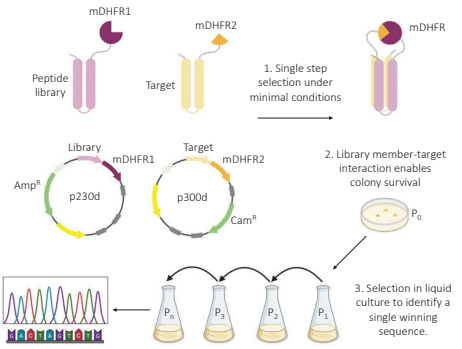

Figure 3: Schematic showing the protein-fragment complementation assay used to screen peptide libraries.

- Peptide libraries were screened using an **intracellular protein-fragment complementation assay** (PCA) based on murine dihydrofolate reductase (mDHFR).
- This methodology selects the strongest binder whilst also **profiling for biostability, solubility and selectivity**.[3,4]

4. Library Generation & Screening

- A DHp homodimerisation experiment showed colony survival under minimal conditions only in the presence of IPTG.
- This suggests the **BceS DHp** domain can **homodimerise** *in vivo* and is **amenable to PCA**.

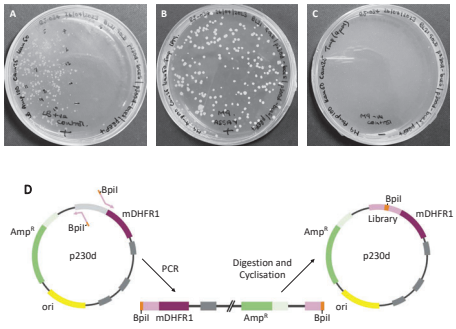

*Figure 4: Plate image from the PCA BceS DHp homodimerisation experiment. **A)** Positive control lacking trimethoprim. **B)** Assay conditions containing trimethoprim and IPTG. **C)** Negative control showing no growth in the absence of IPTG. **D)** Schematic describing library generation using whole plasmid PCR followed by restriction enzyme digest and intramolecular circularisation*

Initial ***adg*** Library

```
                1   2   3   4   5   6   7   8
Heptad:     bcdef gabcdef gabcdef gabc  ef gabcdef gabcdef gabcdef gab
adg Lib.: DELMA WIHEVKT PLTAMHL IIDRMEDKA LKSQLSY EWLRIHL LLDQQLH QKR
              I  LN  I   LI  L   LN          II  I   VL  L   IQ  L  L
              S  L   Q       K                   Q   L       Q
                                Q                   L       K
adg Hit:  DELMA WIHEVKT PLTALHL IIDRMEDKA IKSQLSY LWLRIHL LLDQLLH LKR
```

- An initial **14.1-million-member library** containing randomisation at the ***a***, ***d*** and ***g*** positions was generated using whole plasmid PCR.[5]
- A single winning sequence was identified but exhibited **poor solubility**.

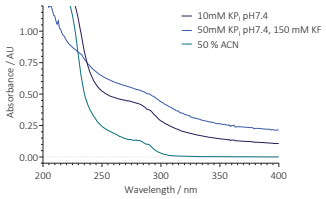

*Figure 5: Permutations included in the initial **adg** peptide library and the selected hit. This hit was synthesised with an additional C-terminal TAT sequence for cell permeability, but poor solubility was observed, as shown by the elevated baseline by UV-vis at 10 µM.*

Solubility Library

```
                1   2   3   4   5   6   7   8
Heptad:     bcdef gabcdef gabcdef gabc  ef gabcdef gabcdef gabcdef gab
Sol Lib.: DELMA WIHEVKT PLTALHL IIDRMEDKA IKSQLSY LWLRIHL LLDQLLH LKR
          E   E   R   K   K   R   E         R   H   R   R   E   R
          N   K   Q   N   R       N             N           N   Q
          K   T                   K                         K
Sol2:     KELMA WIQEVKK PLKALHL IIDRMEDKA IKSQLSY LWRRIHR LLDQLLR LKR
Sol3:     DELME WIREVKT PLTALHR IINRMEDKA IKRQLSY LWLRIHR LLEQLLR LKR
```

- Next, an additional ~1-million-member **solubility library** was incorporated into the initial hit sequence.
- Two sequences showed an **increase** in the **number of hydrophilic residues** and gave a **strong helical response** when analysed by CD.

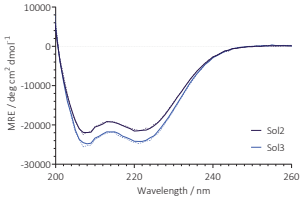

Figure 6: Permutations included in the solubility library and the selected hits. CD analysis of the two solubility library peptides at 50 µM in 10 mM HEPES pH 7.4, 50 mM NaCl prior to (solid lines), and following (dashed lines), a 1-95 °C melt.

5. Target Expression

A truncated **BceS construct** (Q97-V334) containing the **DHp and CA domains** was recombinantly expressed and purified for use in biophysical characterisation. It was shown to **exist as a homodimer**.

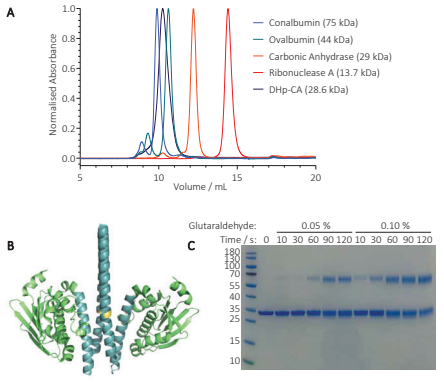

*Figure 7: **A)** Size exclusion chromatogram showing the DHp-CA target construct exists as a homodimer in solution. **B)** Predicted structure of the DHp-CA construct.*[2] *__C)__ SDS-PAGE gel shows time and concentration dependent crosslinking of BceS Q97-V334 with glutaraldehyde, consistent with dimer formation.*

6. Binding Characterisation

- An equimolar combination of the DHp-CA target with a solubility library hit resulted in precipitation.

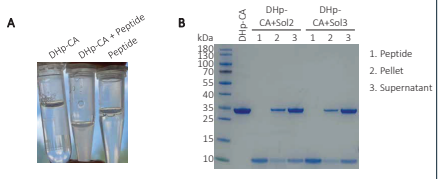

- Analysis of the supernatant showed the presence of a shoulder, potentially indicating disruption of homodimerisation.

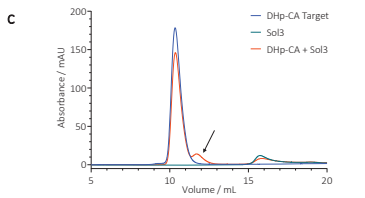

*Figure 8: **A)** Image showing the presence of precipitation having combined a PCA hit with the target. **B)** SDS-PAGE showing the composition of the pellet and supernatant following precipitation. **C)** Size exclusion chromatogram showing the presence of a shoulder, suggesting the formation of a complex of lower MW.*

7. Conclusions & Next Steps

- Two peptide libraries have been screened and hits identified.
- When combined with the target, precipitation was observed, but SEC analysis of the supernatant showed the presence of a shoulder.
- The composition of this shoulder should be confirmed.
- Further modification of the peptides, such as downsizing may facilitate easier handling.
- Investigate alternative buffer conditions to stabilise a potential antagonist-target complex.
- Expression of the DHp-CA BceS target construct is soluble, therefore the PCA hits could also be fused to the CA domain to assess binding, should peptide solubility continue to be an issue.

8. Selected References

1. Koh A. *et al. Mol. Micro.* **2021**, *115* (1), 157-174. DOI: 10.1111/mmi.14607
2. George N. L.; Orlando B. J. *Nat. Comms.* **2023**, *14* (1). DOI: 10.1038/s41467-023-39678-w
3. Pelletier J. N. *et al. PNAS USA* **1998**, *95* (21), 12141-12146. DOI: 10.1073/pnas.95.21.12141
4. Arndt K. M. *et al. Structure* **2002**, *10* (9), 1235-1248. DOI: 10.1016/s0969-2126(02)00838-9
5. Kong X. D. *et al. ACS Chem. Bio.* **2020**, *15* (11), 2907-2915. DOI: 10.1021/acschembio.0c00497

37th EPS European Peptide Symposium
14th IPS International Peptide Symposium
25 - 29 August 2024 Satellite Workshop 30 - 31 August 2024
Florence, Italy- 2024

TOPIC: Bioactive peptides

https://doi.org/10.17952/37EPS.2024.P1081

SYNTHESIS AND EVALUATION OF β-SECRETASE INHIBITORY ACTIVITY OF NEW GALANTAMINE DERIVATIVES COMPRISING PEPTIDE MOIETY

Emilia Naydenova[1], Lyubomir T. Vezenkov[1] ,Valentin Lozanov[2], Daniela S. Tsekova[1]

[1] Department of Organic chemistry, University of Chemical technology and metallurgy, Sofia[1]

[2] Department of Medical Chemistry and Biochemistry,Medical University of Sofia, Sofia 1000, Bulgaria

The Alzheimer's disease leads to neurodegenerative processes and affecting negatively million people worldwide. The treatment of the disease is still difficult and incomplete in practice. One of the most useful in a medicine practice cholinesterase inhibitors is Galanthamine (Gal). It inhibit the β-amiloid aggregation and decrease the toxicity of the β-amyloid peptide (Aβ) [1]. The enzyme β-secretase plays an important role in the process of proteolytic cleavage and progression of AD, therefore we directed our research in the search of new potent beta-secretase inhibitors.

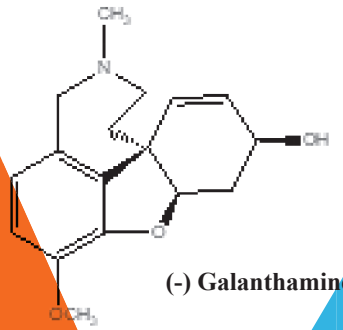

(-) Galanthamine structure

Purpose:

The purpose of this work is synthesis of new derivatives of galanthamine comprising peptide moiety as well as study of their β-secretase inhibitory activity.

Methods:

The solid-phase peptide synthesis (SPPS) by Fmoc (9-fluorenylmethoxycarbonyl) chemistry was used to synthesize target compounds.



The peptide purity was monitored on a RP-HPLC. The LC/MC spectra were recorded on a LTQ XL Orbitrap Discovery instrument. The optical rotation was also measured. Analysis of the inhibitory activity of the compounds against β-secretase was performed using the commercial kit (β-secretase activity assay kit (F).

Results:

In our previous studies, we found that incorporation of an anti-aggregating peptide motif at position 6 of Galantamine significantly increased β-secretase inhibitory activity [2].

Compound structure	Concentration [nM]	Inhibition %	IC_{50} [nM]
6-*O*-[Boc-Leu-Val-Phe-Phe-Gly]-Gal	2.1	19.98	5.26
6-*O*-[H-Leu-Nva-Phe-Phe-Gly]-Gal	2.17	51.19	1.95
6-*O*-[Boc-Leu-Nva-Phe-Phe-Gly]-Gal	2.15	27.24	3.95
6-*O*-[H-Leu-Tle-Phe-Phe-Gly]-Gal	2.04	46.03	1.96
6-*O*-[Fmoc-Nle-Val-Phe-Phe-Gly]-Gal	1.86	23.01	4.04

Here we report the synthesis of six novel peptide-galantamine derivatives in which the substitution is at the 11-position of Galantamine in order to establish the influence of the position on biological activity. Inhibitory activity was shown by two of the investigated compounds, which have the following structure:

Table 1 Inhibition of the studied compounds towards BACE-1

Compounds structure	MW	Tested concentration	% inhibition	IC50 calculated
11-N-demethyl-11-N,N-[H-Asp(Lys-Leu-Val-Phe-Phe)]-Gal	1023.35	1 mg/ml	5	5.6 uM
11-N-demethyl-11-N,N-[H-Asp(Tle-Asp-Leu-Ala)]-Gal	801.40	1 mg/ml	8	12.5 uM

Conclusion:

After the studies carried out, we found that the inclusion of peptide moiety at position 11 of galantamine did not result in a significant increase in beta inhibitory activity, unlike that at position 6.

References:

[1] Matharua B, Gibsona BG, Parsons R, Huckerby TN, Moore SA,Cooper LJ, et al.Galanthamine inhibits β-amyloid aggregation and cytotoxicity. J Neurol Sci 280(1-2):49-58(2009)

[2] Vezenkov, L. T., Danalev, D. L., Iwanov, I., Lozanov, V., Atanasov, A., Todorova, R.,Vassilev N., Karadjova, V. Synthesis and biological study of new galanthamine-peptide derivatives designed for prevention and treatment of Alzheimer's disease. Amino Acids, 54(6), 897-910, (2022).

Acknowledgement: This study is funded by the European Union-NextGenerationEU, through the National Recovery and Resilience Plan of the Republic of Bulgaria, project № BG-RRP-2.004-0002, "BiOrgaMCT"

Proceedings of the 37th European Peptide Symposium
Michal Lebl, Editor
European Peptide Society, 2024 *http://doi.org/10.17952/37EPS.2024.P1082*

Searching for biologically active peptide fragments of hACE2 interacting with the S1 protein of the SARS-CoV-2 virus

Aleksandra Czerchawy[1], Manoj Kumar Muthyala[2], Beata Kolesińska[1]

[1] Institute of Organic Chemistry, Faculty of Chemistry, Lodz University of Technology, Zeromskiego 116, Lodz, 90-543, Poland [2] Gyros Protein Technologies AB, Schillerstraße 20, Teltow, 14513, Germany

Introduction

Over four years after the COVID-19 pandemic outbreak, we still lack a perfect diagnostic tool for detecting the SARS-CoV-2 virus infection. While the rt-qPCR gained great popularity and became the analytical gold standard, it also has notable drawbacks such as high costs connected with long-term procedures, and the necessity to perform the analysis by well-trained personnel in biosafety level 3 (BSL-3) laboratories. Furthermore, the results are highly dependent on the type and method of sample collection and storage, symptom duration and severity, thus influencing the variable viral load and leading to an increasing number of false-positive results [1]. As an alternative, the rapid test indicating the presence of the virus's spike protein or specific antibodies in the form of LFI tests was used. Nevertheless, they are characterised by lower sensitivity and are typically suitable only for symptomatic individuals, limiting their effectiveness as a broad screening tool.

In response to these challenges, researchers have increasingly focused on developing new types of biomedical tests indicating COVID-19 disease. One promising option is the use of biosensors as small, reliable and portable devices providing real-time results. The receptor layer, typically composed of biological molecules, can ensure high selectivity and specificity with small sample volumes and without the need to isolate the target analyte from the mixture [2]. The covalent immobilization of the biological component offers additionally higher resistance to external factors and allows even for sensor regeneration.

However, the use of protein structures is associated with problematic and time-consuming biosensor development. Their synthesis, isolation and purification are expensive. Additionally, proteins are also prone to enzymatic degradation, thus affecting their stability. A different approach could involve using peptide fragments that maintain the biological activity instead of using the whole protein. Peptides are characterised by higher durability for pH and temperature changes and stability in sterilization and storage conditions. Their smaller size reduces the cost of the synthesis and provides an excellent opportunity for structure modification, enhancing desired properties. What's more, their self-assembling properties can result in forming monolayers with better orientation levels, ensuring also higher density surface, fast binding kinetics and lower risk of aggregation during the interaction, compared with proteins [3]. Fragments mimicking the activity of the receptor would recreate the outer sphere of the protein and be involved in protein-protein or protein-peptide interaction. One of the key receptors, responsible for binding spike protein of the SARS-CoV and SARS-CoV-2 viruses is human angiotensin-converting enzyme type 2 (hACE2).

Result and Discussion

Research conducted in the Institute of Organic Chemistry at the Lodz University of Technology focuses on the development of biosensors indicating the presence of the SARS-CoV-2 virus physiological fluids (e.g. blood, urine, saliva particles, exhaled air) or in the air using hACE2 peptide fragments. The procedure established in our Institute enables the selection of fragments with potential biological activity based on the Dot-blot methodology and involves multiple steps [4].

The initial phase considered the automated SPOT synthesis of overlapping peptide fragments covering the primary structure of the hACE2 on cellulose matrixes with the use of 1,3,5-triazine derivatives (DMT/NMM/$TosO^-$) [5]. Next, the incubation of the received 399-element library with HRP-labelled S1 protein subunit of the SARS-CoV-2 virus and further enzymatic oxidation of 4-chloro-1-naphtol into coloured 4-chloro-1-naphtone allowed the selection of fragments interacting with spike protein (Figure 1).

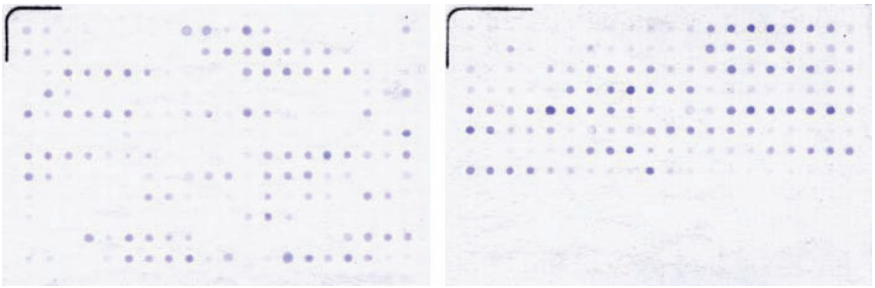

Fig. 1. *Scans of the cellulose matrix with immobilized decapeptides of hACE2 protein after the incubation with HRP-labelled S1 protein subunit of the SARS-CoV-2 virus. The intensity of each coloured complex represents the strength of the peptide-protein interaction.*

Based on the intensity of the received complexes, measured on a 256-grey scale, 32 structures with different lengths of peptide chains were chosen, including 16 fragments strongly interacting with the spike protein and 16 peptides with moderate affinity (Table 1).

Table 1. *Peptide fragments of hACE2 protein selected during the Dot-blot with the use of the HRP-labelled S1 protein subunit of the SARS-CoV-2 virus.*

No.	Locant	Peptide fragment	No.	Locant	Peptide fragment
1.	505-526	H-HVSNDYSFIRYYTRTLYQFQFQ-OH	9.	755-776	H-VGIVILIFTGIRDRKKKNKARS-OH
2.	667-692	H-EEDVRVANLKPRISFNFFVTAPKNVS-OH	10.	385-394	H-YAAQPFLLRN-OH
3.	779-788	H-NPYASIDISK-OH	11.	699-718	H-EVEKAIRMSRSRINDAFRLN-OH
4.	545-562	H-SNSTEAGQKLFNMLRLGK-OH	12.	265-282	H-HLLGDMWGRFWTNLYSLT-OH
5.	641-666	H-YLFRSSVAYAMRQYFLKVKNQMILFG-OH	13.	239-256	H-HLHAYVRAKLMNAYPSYI-OH
6.	611-632	H-SPYADQSIKVRISLKSALGDKA-OH	14.	103-122	H-NGSSVLSEDKSKRLNTILNT-OH
7.	733-746	H-PPNQPPVSIWLIVF-OH	15.	467-484	H-EIPKDQWMKKWWEMKREI-OH
8.	587-606	H-YFEPLFTWLKDQNKNSFVGW-OH	16.	123-132	H-MSTIYSTGKV-OH

The further step concerned the resynthesis of chosen fragments using the SPPS method and Fmoc/t-Bu strategy. For some of the fragments, characterized by poor solubility, high hydrophobicity or tendency of aggregation, the process involved automated synthesis with an induction-heating system and "catch-and-release" purification. For this purpose, the coupling of the oxime-based linker to the *N*-terminal amine group of the desired peptide structure was performed. The key benefit of using the linker developed by Zitterbart's team is the rapid, selective immobilization ("catch") of the product to an aldehyde-modified agarose resin. The oxime ligation for the catch step is very robust allowing a wide pH range, the use of organic solvents (ie. dimethylsulfoxide or hexafluoroisopropanol) and chaotropic reagents, thus facilitating the synthesis and purification of "problematic" fragments. After immobilization, any impurities, including by-products, salts and truncated peptides can be washed out. The later traceless cleavage ("release") of the product from solid support is possible through the reduction of an aryl azide to aniline and following acid-catalysed 1,6-elimination of the linker (Figure 2). Moreover, the linker is stable (in its azide form) to acidic environment necessary for peptide cleavage [6].

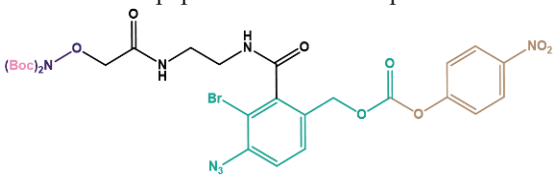

Fig. 2. *The Boc-protected structure of an oxime-based linker. Black colour represents a catch tag (Boc protected), green colours shows a cleavable unit with aryl azide and, brown – leaving group [6].*

The use of the above peptide purification method allowed for obtaining 6 peptide fragments of the hACE2 protein with purities above 90% (Table 2).

Table 2. *Peptides synthesized and purified using an induction-heating system and "catch-and-release" method.*

No.	Locant	Peptide fragment	PEC purity
1.	611-623	H-SPYADQSIKVRIS-OH	97,73 %
2.	755-767	H-VGIVILIFTGIRD-OH	95,21 %
3.	385-394	H-YAAQPFLLRN-OH	95,29 %
4.	699-718	H-EVEKAIRMSRSRINDAFRLN-OH	98,85 % *
5.	265-275	H-HLLGDMWGRFW-OH	94,92 % *
6.	111-122	H-DKSKRLNTILNT-OH	96,84 %

* *represents purities including the oxidation of Met residue.*

The last step of the research will include the confirmation of peptides' biological activity towards the SARS-CoV-2 virus particles in MST analysis.

Conclusions

The rapid advancement of natural and technical sciences has led to the development of innovative analytical tools that may find their application in medical diagnostics. Despite the limitations of current diagnostic methods for the SARS-CoV-2 virus identification, promising alternatives are being developed, including biodetecting devices utilizing hACE2 as the receptor structure. The procedure presented in this work shows an alternative approach

and may facilitate the process of searching for biologically active peptides, as well as their subsequent synthesis and purification for biomedical application. However, extensive testing would be required to validate the utility and accuracy of such prepared devices.

Acknowledgements

The research was founded by "Young Scientist Fund" no. W-3D/FMN/16G/2023.
I would like to acknowledge the support of Gyros Protein Technologies, in particular Dr. Manoj Muthyala, during the internship at the PECS laboratory in Teltow, Germany, for assisting with the synthesis and PurePep® EasyClean purification of several peptides mentioned in this work. PurePep® EasyClean technology described here can be purchased from Gyros Protein Technologies.

References

[1] Pan, Y., et al. *Clin. Chem.* **66(6)**, 794-801 (2020), https://doi.org/10.1093/clinchem/hvaa091
[2] Barbosa, A.J.M., Oliveira, A.R., Roque, A.C.A. *Trends Biotechnol.* **36 (12)**, 1244-1258 (2018), https://doi.org/10.1016/j.tibtech.2018.07.004
[3] Zhu, Q., Zhou, X. *J. Hazard. Mater.* **425**, 127923 (2022), https://doi.org/10.1016/j.jhazmat.2021.127923
[4] Kolesińska, B. et al. *Engineering of Biomaterials* **148**, 41 (2018).
[5] Frączyk, J., Walczak, M., Kamiński, Z.J. *J. Pept. Sci.* **24**, e3063 (2018), https://doi.org/10.1002/psc.3063
[6] Zitterbart, R. et al. *Chem. Sci.* **12 (7)**, 2389–2396 (2021), https://doi.org/10.1039/D0SC06285E

Synthesis of Aza-Amanitins to Enhance Cytotoxicity for Targeted Cancer Therapeutics

Kayla C. Newell, F. Cruz Custodinho, Juliette Froelich, Katherine Bessai, Cassandra M. Sgarbi, David M. Perrin*

Department of Chemistry, University of British Columbia, 2036 Main Mall, Vancouver, B.C., V6T 1Z1, Canada

https://doi.org/10.17952/37EPS.2024.P1084

Abstract

- The development of cancer therapies in which cancer-specific agents can be used to deliver a cytotoxic agent to cancer cells is at the forefront of drug research[1,2]
- There has been more research into antibody drug conjugates (ADCs) as a method of targeted cancer therapy[3]
- α-amanitin, a highly selective inhibitor of RNA polymerase II (Pol II), produced by the death-cap mushroom targets tumors in a cell-cycle independent manner[4]
- α-amanitin as a drug payload for ADCs enhances therapeutic potential and specificity

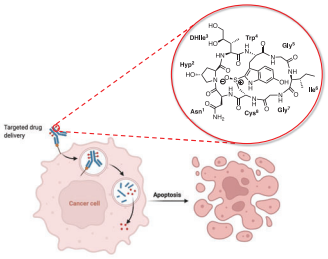

Introduction

- Rationally designed amanitin analogs have been shown to influence cytotoxicity on various cell lines[5]
- Replacing glycine at position 7 with an aza-glycine amino acid results in increased cytotoxicity on CHO, HEK293 and HeLa cells
- May enhance aza-peptide stability to enzymatic and chemical degradation
- Constraints on the φ and Ψ dihedral angles → favor turn geometry
- α-amanitin contains a β - turn at Ile[6]

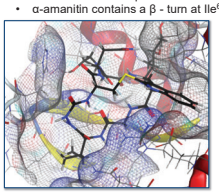

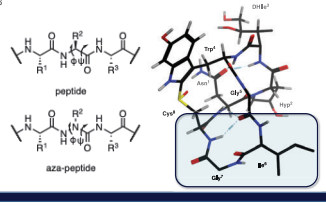

Objectives

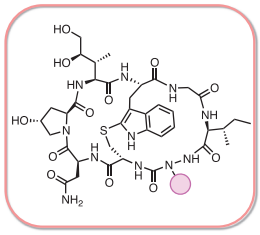

- Accessing aza-amino acids for amanitin analogs
- Probe the structure activity relationship
- Discover aza-amanitin analogs with enhanced cytotoxicity

Synthesis

Aza-Amino Acid Substrate Scope

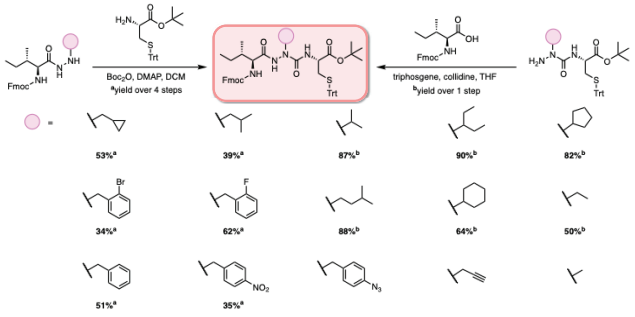

Synthesis of Aza-Amanitin Analogs

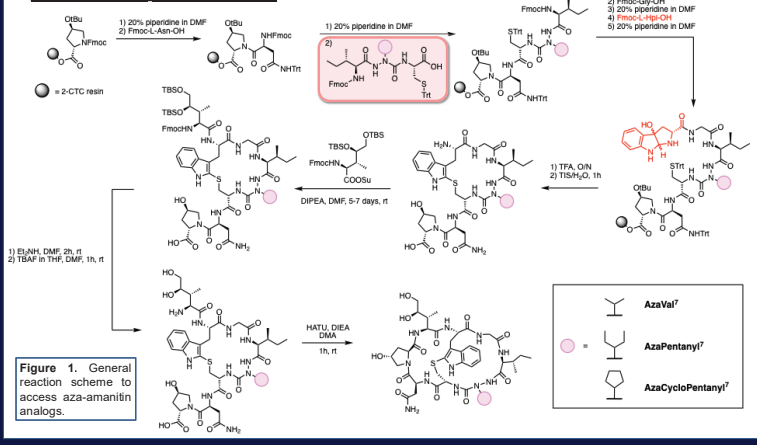

Figure 1. General reaction scheme to access aza-amanitin analogs.

Optimization

Optimization of Aza-Amino Acid Synthesis

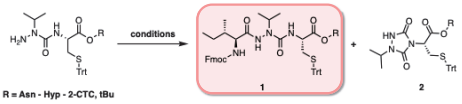

Entry	Phase	Amino Acid	Conditions (coupling agent, base, solvent)	Percent Conversion (%)[d,e] 1	2
1	SPPS	Fmoc-Ile-OH[a]	Triphosgene (2.5 eq), 2,4,6-collidine (15 eq), THF	30	56
2	SPPS	Fmoc-Ile-OH[a]	DIC (7.5 eq), HOBt (7.5 eq), DIPEA (15 eq), DMF	5	35
3	SPPS	Fmoc-Ile-OH[a]	PyBOP (7.5 eq), DIPEA (15 eq), DMF	9	32
4	SPPS	Fmoc-Ile-OH[a]	HATU (7.5 eq), DIPEA (15 eq), DMF	31	32
5	SPPS	Fmoc-Ile-OH[a]	COMU (7.5 eq), DIPEA (15 eq), DMF	37	45
6	Solution	Fmoc-Ile-OSu[b]	2,4,6-collidine (3 eq), DMF	0	0
7	Solution	Fmoc-Ile-OH[b]	DCC (3 eq), DMAP (3 eq), DCM	0	0
8	Solution	Fmoc-Ile-OH[c]	Triphosgene (3 eq), 2,4,6-collidine (15 eq), THF	87[f]	0

[a] 7.5 eq; [b] 3 eq; [c] 9 eq; [d] Conversion determined by HPLC; [e] Remaining material was determined to be unconverted starting material; [f] Isolated yield

Cytotoxicity Assays

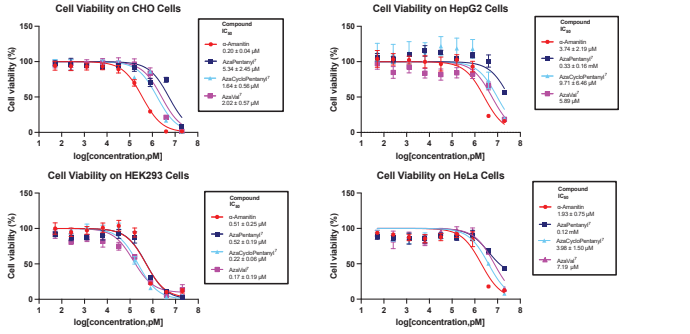

Figure 2. In vitro cytotoxicity of aza-amanitin analogs and α-amanitin. CHO, HepG2, HEK293, and HeLa cells were treated with various concentrations of toxins. Cell viability was determined by MTT assays.

Circular Dichroism

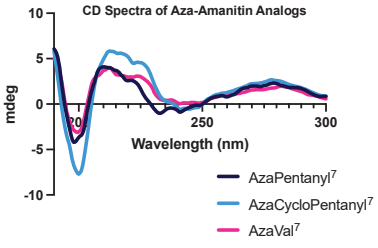

Conclusions & Future Directions

Conclusions

- Route to access aza-amino acids was determined
- New amanitin analogs were synthesized and cytotoxicity was evaluated
- AzaVal[7] and AzaCyclePentanyl[7] were more cytotoxic than natural α-amanitin in HEK293 cells
- AzaPentanyl[7] had comparable cytotoxicity in HEK293 cells

Future Directions

- Synthesis and biological assays of more aza-amanitin analogs to provide further insight into structure activity relationship

References

1. Teicher, B. A. *Curr. Opin. Oncol.* **26**, 476–483 (2014)
2. Ho, R. J. Y. & Chien, J. *J. Pharm. Sci.* **103**, 71–77 (2014).
3. Senter, P. D. *Curr. Opin. Chem. Biol.* **13**, 235–244 (2009).
4. Matinkhoo, K. *et al. J. Am. Chem. Soc.* **140**, 6513–6517 (2018).
5. Todorovic, M. *et al. J. Med. Chem.* **65**,*10357-10376 (2022).*

Acknowledgments

CHEMISTRY
Maria Ezhova, NMR

MOLECULAR AND CELL BIOLOGY
Bioservices, Department of Chemistry, UBC
Jessie Chen, Dr. Elena Polishchuck

THE UNIVERSITY OF BRITISH COLUMBIA

37th EPS European Peptide Symposium
14th IPS International Peptide Symposium
Florence, Italy

CIHR IRSC Canadian Institutes of Health Research / Instituts de recherche en santé du Canada

NSERC CRSNG

In situ mechanistic insight to antibacterial action of membrane-incising β-peptide lamellae

https://doi.org/10.17952/37EPS.2024.P1085

Kamal el Battioui [1], Imola Cs. Szigyártó[1], Sohini Chakraborty[1], Judit Tóth[2], Dániel Molnár [2], Tünde Juhász[1], Loránd Románszki[1], Andrea Bodor [3], Kata Horváti[1], István Mándity [1], Zoltán Varga[1], Judith Mihály[1], Csenge Lilla Szabó[3], Szilvia Bősze[3], Gergő Gyulai[3], Mayra Quemé-Peña[1], András Wacha[1], Bálint Jezsó[1], Tamás Beke-Somfai [1,*]

[1] Institute of Materials and Environmental Chemistry, HUN-REN Research Centre for Natural Sciences, Budapest, Hungary
[2] Institute of Molecular Life Sciences, HUN-REN Research Centre for Natural Sciences, Budapest, Hungary
[3] Institute of Chemistry, Eötvös Loránd University, Budapest, Hungary
E-mail: beke-somfai.tamas@ttk.hu

Introduction

β[3]-peptides exhibit:
- Resistance against protease degradation
- Unique folding architecture
- Therapeutic applications (delivery systems, bionanomaterials)

Our short cationic β[3]-peptides:
- Non-natural β[3]-amino acids
- Amino acids with alternating R and S chirality
- Rich in hydrophobic residues (Leu)
- Several positively charged residues (Lys)

Main goals

- Exploit the **self-assembly** capacity in various conditions
- Characterize **membrane activity**
- Study interactions with biologically relevant phosphate agents
- Test their antibacterial effect

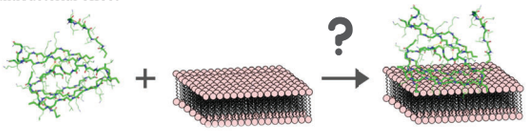

Results

Previous Results - Structure and assembly manipulated by environmental parameters

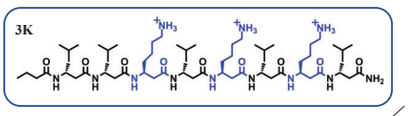

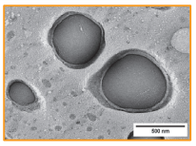

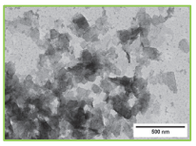

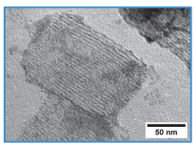

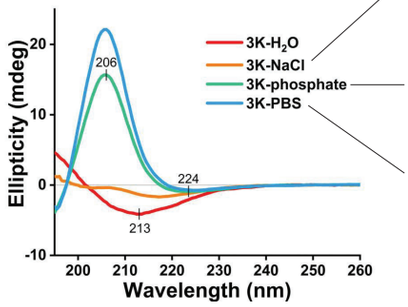

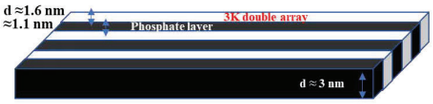

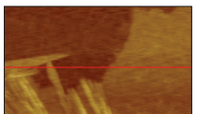

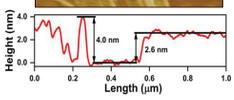

- Double arrays of 3K in parallel orientation, where intermolecular H-bonds stabilized the assembly while the two arrays formed a hydrophobic core composed of the leucine side chains.
- Several double arrays of 3K are connected by a narrow layer of phosphate ions that coordinate lysine side chains.
- The zig-zag 3K molecules span ~ 3.1 nm, whereas the width of the double 3K arrays and the hydrophilic lysine-phosphate region is approximated to be 1.8 nm and 1.1 nm, respectively.

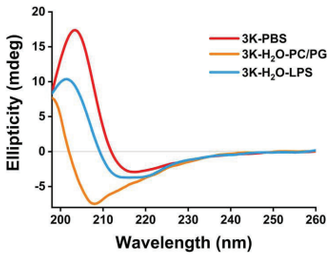

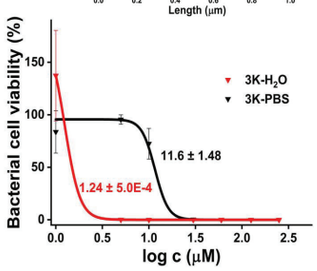

Interactions with biologically relevant phosphate agents

3K:AMP (1:4)

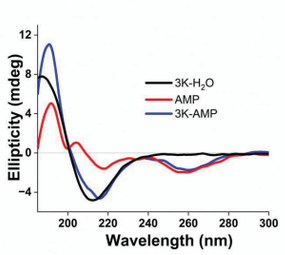

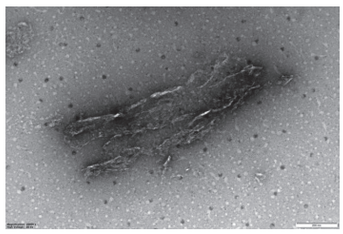

Less packed and more disperse objects

3K:ADP (1:4)

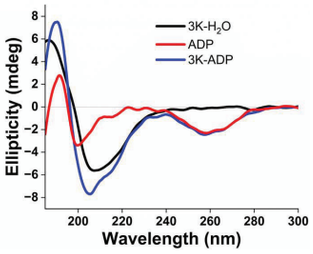

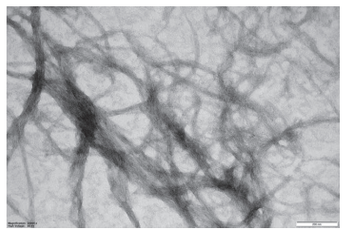

Similar sub-unit packing as 3K-PBS
→ long fibril-like thread morphologies

3K:ATP (1:4)

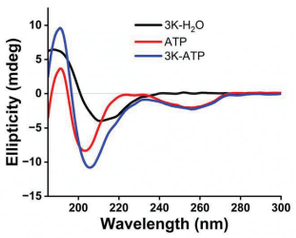

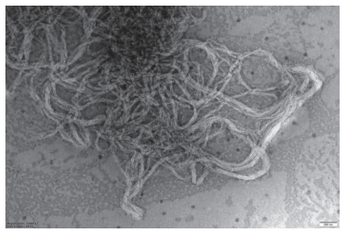

Similar sub-unit packing as 3K-PBS
→ infinite fibril-like thread morphologies

Conclusion

- Short cationic/hydrophobic β[3]-peptides can effectively self-assemble to associate with various morphologies depending on the conditions.
- Previously, we exploited the environmental sensitivity of 3K in various environments → 3K in PBS resulted in high antibacterial efficacy and low cytotoxicity.
- Triggered by these observations, we studied the interactions of various other phosphate moieties with 3K.
- Initial results from CD and TEM suggest that the different oligophosphates contribute effectively to the co-assembly formation resulting in unique morphologies.
- Similar to biological filaments, such as actin and amyloids, fibrillar morphologies are observed which appear to be continuous and infinite. The length of these fibrils are influenced by the number of phosphates.
- Owing to their unique morphologies, these fibrils could potentially act as peptide nanonets to inhibit the bacterial growth on specific sites in the human body.

References

- Hiutung Chu *et al.* Humana-Defensin 6 Promotes Mucosal Innate Immunity Through Self-Assembled Peptide Nanonets. *Science.* 337, 477-481 (2012).
- Szigyártó, I. Cs. *et al.* Membrane active Janus-oligomers of β[3]-peptides. *Chem. Sci.* 11, 6868–6881 (2020).
- El Battioui, Kamal *et al.* In Situ Captured Antibacterial Action of Membrane-Incising Peptide Lamellae. *Nat. Comm.*, 15, Paper: 3424 (2024)

Acknowledgements

This work was funded by the Ministry of Innovation and Technology of Hungary from the National Research, Development and Innovation Fund, financed under the TKP2021-EGA-31 and the 2020-1-1-2-PIACI-KFI_2020-00021, KKP_22 144180, funding schemes. Support from Eötvös Loránd Research Network, grant n.o. SA-87/2021, is also acknowledged.

Department Chemie und Pharmazie

GRK 2504

FAU Friedrich-Alexander-Universität Erlangen-Nürnberg

Novel peptide inhibitors of SARS-CoV-2 infection

Nina Raasch[1], Lucas Weißenborn[1], Elie Richel[2], Olena Denysenko[3], Simon Schäfer[3], Heinrich Sticht[3], Klaus Überla[2] and Jutta Eichler[1]

[1]Department of Chemistry and Pharmacy, Friedrich-Alexander-Universität Erlangen-Nürnberg, 91058 Erlangen, Germany
[2]Institute for Clinical and Molecular Virology, Universitätsklinikum Erlangen, Friedrich-Alexander-Universität Erlangen-Nürnberg, 91054 Erlangen, Germany
[3]Institute of Biochemistry, Friedrich-Alexander-Universität Erlangen-Nürnberg, 91054 Erlangen, Germany

https://doi.org/10.17952/37EPS.2024.P1087

nina.raasch@fau.de

Infection with SARS-CoV-2 is based on the interaction of the viral Spike (S) protein with the ACE2 receptor on the human host cell [1]. With the aim to increase virus neutralizing activity we have generated and characterized a truncated and cyclized peptide variant of the SARS-CoV-2 neutralizing miniprotein LCB1 [2]. The 10-fold stronger antiviral activity of this peptide (LW25.13), as compared to LCB1 to the wild-type Spike receptor-binding domain (RBD), as well as its substantially improved proteolytic stability, make it a better potential candidate for SARS-CoV-2 therapy [3].

Nevertheless, there is a need for optimization of the peptides in order to facilitate neutralization of newer virus variants, such as BA.1/ BA.2/ BA.5 (omicron variants). Therefore, we have combined reverse mutation strategies with structural and bioinformatic analysis to design peptide variants of LW25.13 capable of efficiently neutralizing omicron virus variants.

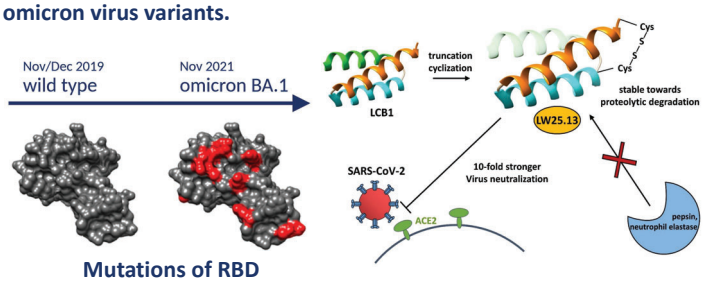

Results & Discussion

1) Peptide design and characterization

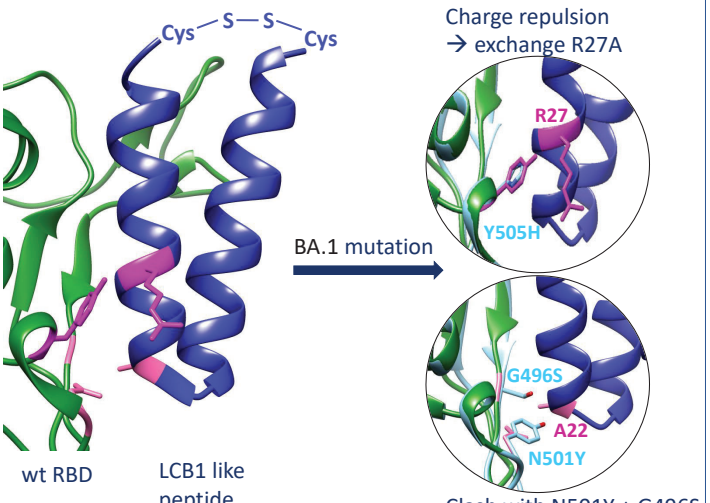

2) omicron BA.1 neutralization

- **Omicron RBD** has increased number of **positively** charged AA
- Reducing positive charge and insertion of negatively charged AA

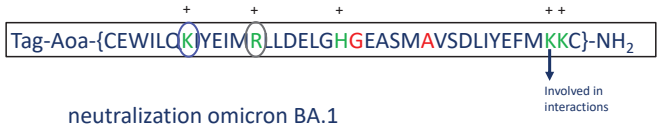

neutralization omicron BA.1

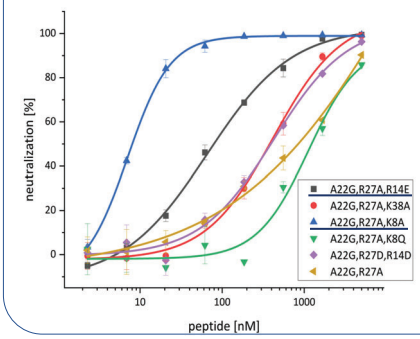

IC_{50} (A22G,R27A,K8A): 7.06 ± 0.35 nM
IC_{50} (A22G,R27A,R14E): 65.85 ± 0.45 nM
IC_{50} (A22G,R27A): > 1000 nM

3) Virus variant selectivity

neutralization A22G,R27A + **R14E** | neutralization A22G,R27A + **K8A**

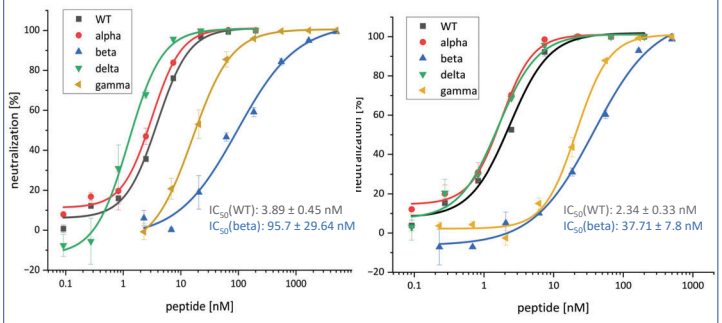

- Both charge exchange variants are **broadly neutralizing** peptides
- Peptide variants **gain neutralization activity**

4) Combined peptide variant

neutralization omicron BA.1

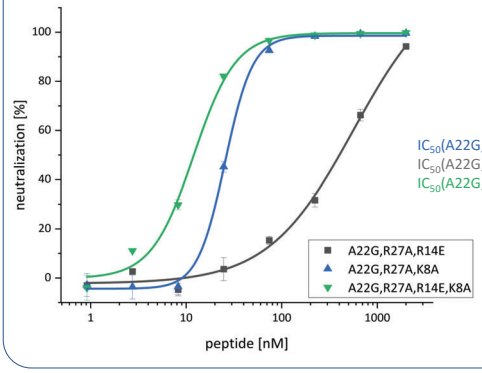

IC_{50}(A22G,R27A,K8A): 12.36 ± 0.06 nM
IC_{50}(A22G,R27A,R14E): > 500 nM
IC_{50}(A22G,R27A,R14E,K8A): 11.95 ± 1.16 nM

5) Discussion and Conclusion

- Targeting critical RBD mutations is the main goal in future peptide design → scaffold for "pandemic preparedness"
- Charge exchange variants of LW25.13 have a higher neutralization capacity against the BA.1 omicron variant
- **Broadly neutralizing peptides**

Outlook

- Further optimization of combined peptide variant
- H21 charge exchange variants
- Generation of bispecific antiviral peptides

References
[1] Jackson, C. B. et al. Nature Rev. Mol. Cell Biol. **2022**, 23(1), 3 - 20.
[2] Cao, L. et al. Science **2020**,370(6515), 426 - 431.
[3] Weißenborn, L. et al. Int. J. Mol. Sci. **2022**, 23(11), 6309.

LinkedIn



is funded by DFG

Investigating protein prenylation using cell-permeable peptides

Martin Matijass*, Merlin Klußmann*, Annika Klimpel Ines Neundorf*
*Institute of Biochemistry, University of Cologne, Germany

https://doi.org/10.17952/37EPS.2024.P1088

Abstract

Protein prenylation is an irreversible post-translational modification in which prenyltransferases attach an isoprenoid to a *C*-terminal CaaX-motif. This protein modification determines the localization and biological function of proteins. Targeting protein prenylation would be an exciting way to modulate their activity spectrum.

Recently, we developed cell-permeable CaaX-peptides that impaired Ras protein localization and their biological function as a molecular switch. The peptides combined a cell-penetrating peptide (CPP) with a *C*-terminal CaaX-motif of Ras proteins. They highly accumulated inside cells and exhibited pronounced toxicity to KRas mutated pancreatic cancer cells bearing a G12D mutation (PANC-1). Also, CaaX-peptides altered Ras localization causing a loss of membrane integrity and decreased KRas levels in PANC-1 cells. This likely affected other interactors as, for instance, the expression of the tumor suppressor and negative regulator of KRas, neurofibromin-1 (NF-1).

Based on these findings, my study aims to further investigate intracellular processing of CaaX-peptides and to study their influence on KRas expression and membrane localization, and how they affect distinct KRas interactors.

Design and Synthesis of cell-permeable CaaX-peptides

Design: H_2N — CPP (sC18*) — secondary signal — CaaX — OH

```
                1        10        11-160                170       180
Kras4B:  MTEKLVVVG.....................REIRKHKEKM SKDGKKKKKK SKTK CVIM
sC18*:                                    GL  RKRLRKFRNK
CaaX-1:                                   GL  RKRLRKFRNK SKTK CVIM
```

Name	Sequence	Mwcalc [Da]	Mwexp [Da]	Purity [%]
CaaX-1	GLRKRLRKFRNK-SKTK-CVIM-OH	2463.1	2463.645	>98
SaaX-1	GLRKRLRKFRNK-SKTK-SVIM-OH	2447	2447.568	>98
CF-CaaX-1	CF-GLRKRLRKFRNK-SKTK-CVIM-OH	2821.4	2821.992	>98
CF-SaaX-1	CF-GLRKRLRKFRNK-SKTK-SVIM-OH	2805.3	2806.022	90
Bio-CaaX-1	Bio-GLRKRLRKFRNK-SKTK-CVIM-OH	2689.4	2690.035	85
Bio-SaaX-1	Bio-GLRKRLRKFRNK-SKTK-SVIM-OH	2673.3	2673.735	80

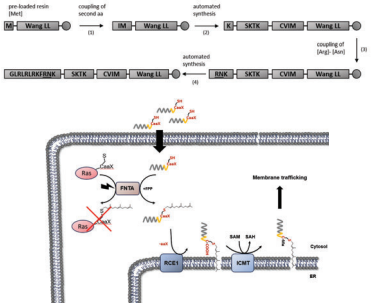

- Synthesis of CaaX-peptides derived from Ras proteins conjugated to the CPP sC18*

→ recognition of CaaX-peptides by the prenylation machinery

→ interference with Ras prenylation and subsequent signaling processes

In cellulo detection of Bio-CaaX-1

- 3 h peptide treatment (30 µM)

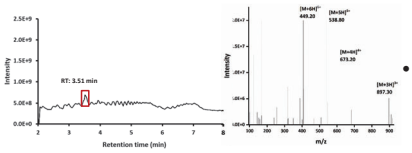

- Peptide isolation using magnetic streptavidin beads
- *In cellulo* detection of Bio-CaaX-1 by mass spectrometry

CaaX-1 interacts with FTase

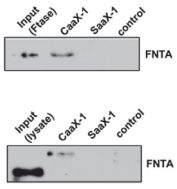

- 24 h peptide treatment (30 µM)
- Pulldown assay using magnetic streptavidin beads

→ CaaX-1 interacts with FTase

CaaX-1 is farnesylated *ex cellulo*

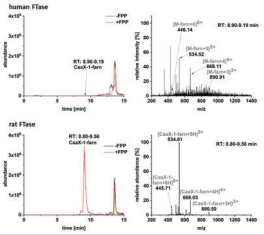

- 18 h reaction time
- 250 nM rat FTase + 50 µM CaaX-1 (+ 50 µM FPP)

→ CaaX-1 is farnesylated by FTase

CaaX-1 alters KRas abundance in PANC1

- 24 h peptide treatment (30 µM)

PANC-1: KRas G12D mutant pancreatic ductal adenocarcinoma
BxPC-3: KRas wildtype pancreatic ductal adenocarcinoma

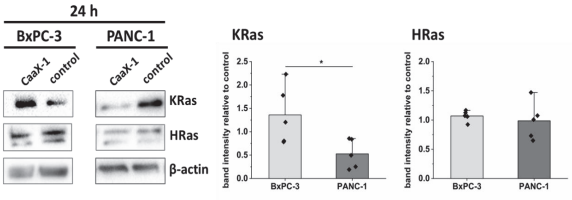

→ Influence of CaaX-1 on KRas expression levels depending on Ras genotype

Influence of CaaX-1 on KRas membrane localization

- 3 h peptide treatment (30 µM)

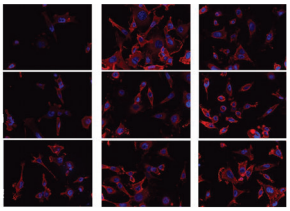

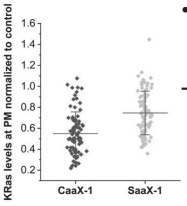

- Immunostaining using KRas antibody conjugate

→ Decrease of KRas membrane localization after CaaX-1 treatment

- 3 h peptide treatment (30 µM)

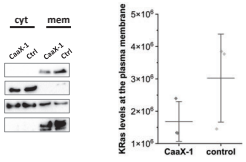

- Membrane fractionation using Digitonin (cytosol) and Triton X-100 (membrane)

→ KRas only detectable in membrane fraction

→ Decreased KRas levels in membrane fraction after CaaX-1 treatment

CaaX-1 alters Ras regulators and downstream effectors

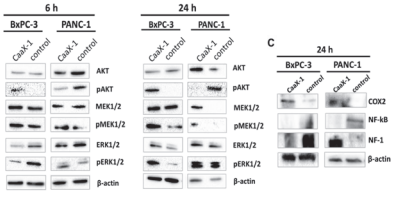

- 24 h peptide treatment (30 µM)

→ different expression levels of KRas and NF-1 potentially explain different activation of PI3K/AKT/mTOR signaling in PANC-1 and BxPC-3

Outlook

- Investigating alterations of Ras signaling using a phosphoproteomic approach
- How do CaaX peptides influence nanoclustering of KRas?
- Does CaaX-1 influence the interactome of KRas genotypes?

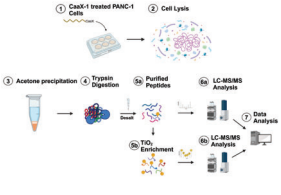

Created with BioRender.com

[1] Wang, M. & Casey, P. J. Protein prenylation: Unique fats make their mark on biology. *Nature Reviews Molecular Cell Biology* vol. 17 110–122 (2016).
[2] Palsuledesai, C. C. & Distefano, M. D. Protein prenylation: Enzymes, therapeutics, and biotechnology applications. *ACS Chemical Biology* vol. 10 51–62 (2015).
[3] Klimpel, A., Stillger, K., Wiederstein, J. L., Krüger, M. & Neundorf, I. Cell-permeable CaaX-peptides affect K-Ras downstream signaling and promote cell death in cancer cells. *FEBS J.* febs.15612 (2020) doi:10.1111/febs.15612.

https://doi.org/10.17952/37EPS.2024.P1090

Cytotoxicity and phototoxicity effects of modified temporin analogs with unnatural aminoacids

Tsvetelina Foteva[1], Ivan Iliev[2], Rositsa Hristova[2], Dilyana Dimitrova[1], Veronica Nemska[1], Nelly Georgieva[1], Dancho Danalev[1]

1 University of Chemical Technology and Metallurgy, Bulgaria, Sofia, 8 blvd. Kl. Ohridski;
2 Institute of Experimental Morphology, Pathology and Anthropology with Museum, Bulgarian Academy of Sciences, Bulgaria;
e- mail: tsvetelina.foteva@uctm.edu

Introduction

Antimicrobial peptides (AMPs) are promising candidates for a new generation of anti-infective agents. Temporins are known to be particularly active against Gram-positive bacteria and Gram-negative bacteria. In addition to antimicrobial activity, some kinds of AMPs exert rapid and selective cytotoxicity against malignant cells but show relatively lower cytotoxicity against untransformed proliferating cells. In this study the cytotoxicity and phototoxicity effects of novel Temporin A analogs with modification of Arg residue in position 7 with unnatural Cit (Phe-Leu-Pro-Leu-Ile-Gly-Cit-Val-Leu-Ser-Gly-Ile-Leu-NH2; DTCit) and Orn (Phe-Leu-Pro-Leu-Ile-Gly-Orn-Val-Leu-Ser-Gly-Ile-Leu-NH2; DTOrn) on BALB/3T3 cell lines were investigated.

Materials & Methods

The cell lines BALB 3T3 (mouse embryonic fibroblasts). Cell lines were obtained from the American Type Cultures Collection (ATCC, Manassas, VA, USA). Cells were cultured in Dulbecco modified Eagle's medium (DMEM) supplemented with 10% fetal bovine serum (FBS), 100 U/mL penicillin, and 0.1 mg/mL streptomycin (Sigma-Aldrich, Schnelldorf, Germany) in an incubator at 37 ◦C, 5% CO_2 and 95% humidity. Plastic flasks 75 cm2 (Biologix, Lenexa, KS, USA) were used to grow the cells.
The neutral red uptake (NRU) assay is a cell viability assay that allows in vitro quantification of modified peptide analogs-induced cytotoxicity. The assay relies on the ability of living cells to incorporate and bind neutral red, a weak cationic dye, in lysosomes. Cells were plated at a density of $1*10^4$ cells in a 100 µL culture medium in each well of 96-well microplates and allowed to adhere for 24 h. Peptides were dissolved in DMSO and diluted in culture medium to a concentration range 10 to 1000 µL were then added and the cell cultures were incubated for an additional 24 h. After treatment with Neutral Red medium, the absorption was measured on a microplate reader at wavelength 540 nm. The phototoxicity test was performed in parallel on the second 96-well plate, which was irradiated with a solar simulator (LED lamp) for 10 minutes.

Results

The cytotoxicity expressed in % relative to the negative control was determined. Dose–response dependence was observed for all peptide analogs (Fig. 1). At a concentration of 60 µg/mL, no cytotoxic effect was observed on the test peptides. CC50 values (50% cytotoxic concentration) were calculated through nonlinear regression analysis (Table 1). The peptide analogs tested had significantly lower toxicity ($p < 0.001$) than the natural peptide Temporin A. The exception was DTF, where increased toxicity (CC50 = 92.40 ± 2.82 µM) was observed. To evaluate the phototoxic potential of the investigated peptide analogs, we used the photo irritation factor (PIF), which was calculated using the following formula:
PIF = CC50 − Irr/CC50 + Irr.

Table 1 Cytotoxicity/phototoxicity in BALB 3T3, CC50 values and PIF factor

Compounds	Structure	Mean CC_{50} ± SD (µM)		PIF*
		- Irr	+ Irr	
DTA	Phe-Leu-Pro-Leu-Ile-Gly-**Arg**-Val-Leu-Ser-Gly-Ile-Leu-NH_2	106.32 ± 4.18	105.40 ± 4.88	1.01
DTF	Phe-Leu-Pro-Leu-Ile-Gly-**Lys**-Val-Leu-Ser-Gly-Ile-Leu-NH_2	92.40 ± 2.82	88.35 ± 1.48	1.05
DTCit	Phe-Leu-Pro-Leu-Ile-Gly-**Cit**-Val-Leu-Ser-Gly-Ile-Leu-NH_2	356.09 ± 7.64	331.78 ± 12.30	1.07
DTOrn	Phe-Leu-Pro-Leu-Ile-Gly-**Orn**-Val-Leu-Ser-Gly-Ile-Leu-NH_2	337.27 ± 7.09	345.1 ± 6.41	0.98

*Photo Irritation Factor: PIF < 2 not phototoxic, 2 < PIF < 5 probable phototoxicity, PIF > 5 phototoxic

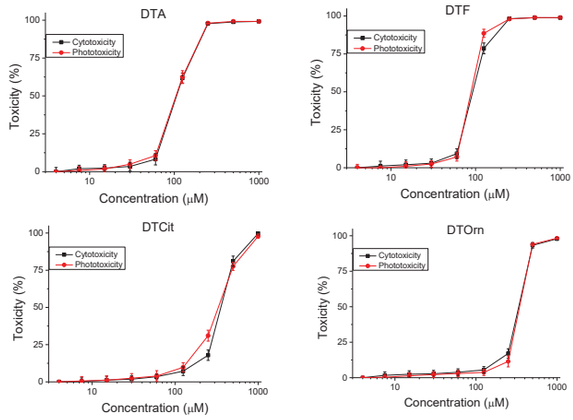

Fig. 1 Parent-peptide DTA and synthesized analogs DTF, DTDab and DTDap: Cytotoxicity/phototoxicity of peptide analogues determined in the cell line BALB/c 3T3 clone A31, n = 6

Conclusions

All modified temporin analogs do not show phototoxicity - no statistically significant difference in the CC_{50} values was observed for the irradiated peptides compared to the non-irradiated ones. The cytotoxic test shows that DTCit is the less toxic agent in comparison to Temporin A. materials proved efficient for use in both biosorption and tissue engineering applications.

ACKNOWLEDGEMENTS: This study is funded by the European Union-NextGenerationEU, through the National Recovery and Resilience Plan of the Republic of Bulgaria, project № BG-RRP-2.004-0002, "BiOrgaMCT".

https://doi.org/10.17952/37EPS.2024.P1092

Triazolyl-bridged peptides with enhanced antimicrobial activity and potency against pathogenic bacteria



Joshua Grabeck, Jacob Mayer, Axel Mayer, Michele Casoria, Michael Quagliata, Denise Meinberger, Andreas R. Klatt, Isabelle Wielert, Berenike Maier, Anna Maria Papini, Ines Neundorf

Department of Chemistry and Biochemistry, University of Cologne, Germany

Abstract

Still, there are no linear antimicrobial peptides (AMPs) available as treatment option against bacterial infections. This is caused by several drawbacks that come with AMPs as for instance their limited proteolytic stability and low selectivity against human cells. In this work, we screened a small library of rationally designed new peptides based on the cell-penetrating peptide sC18* towards their antimicrobial activity.[1] We identified several effective novel AMPs and chose one out of this group to further develop its potency. Therefore, we introduced a triazolyl-bridge at different positions to provide a preformed helical structure assuming that this modification would (i) improve proteolytic stability and (ii) membrane activity. Indeed, placing the triazolyl-bridge within the hydrophilic part of the linear version highly increased membrane-activity as well as stability against proteolytic degradation. The new peptides 8A and 8B demonstrated high activity against several bacterial species tested including pathogenic *N. gonorrhoeae* and methicillin-resistant *S. aureus*. Since they exhibited significantly lower activity against human cells, these novel peptides offer true alternatives for future clinical applications and are worth to study in more detail.[2]

1 Synthesis of triazolyl-bridged novel AMPs

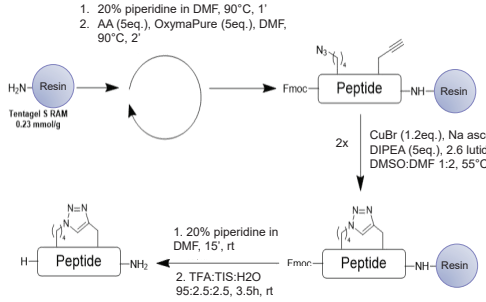

- Synthesis scheme of triazolyl-bridged peptides
- Cupper catalyzed alkyne azide click (CuAAC) reaction on solid support
- Bridge built between azidolysine and propargylglycine
- Reaction supported by using microwave
- Aim to improve stability and biological activity

Name	Sequence	$MW_{calc.}$ [Da]	$MW_{exp.}$ [Da]	Net charge
RL-8	GLRKLLRKFLNK	1485.9	1485.3	+6
8A	GLR-**Pra**-LLR-**Aza**-FLNK	1478.8	1478.2	+4
8B	GLR-**Aza**-LLR-**Pra**-FLNK	1478.8	1478.2	+4
8C	G-**Pra**-RKL-**Aza**-RKFLNK	1508.8	1508.2	+6
8D	G-**Aza**-RKL-**Pra**-RKLNK	1508.8	1508.2	+6

2 Secondary structure

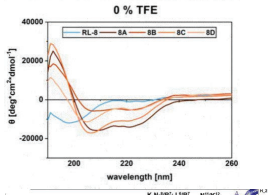

TFE content	0 %	25 %
RL-8	0.22	0.68
8A	0.88	0.77
8B	0.89	0.71
8C	0.63	0.75
8D	0.54	0.80

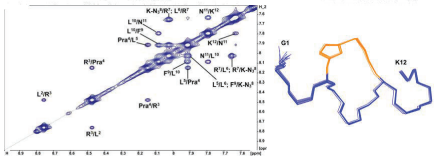

- CD spectroscopy confirmed an α-helical structure for peptides 8A-8D
- NMR data showed exemplary perfectly formed α-helix of 8A

→ **Triazolyl-bridged peptides stabilize secondary structure**

3 Analyzing antimicrobial activity

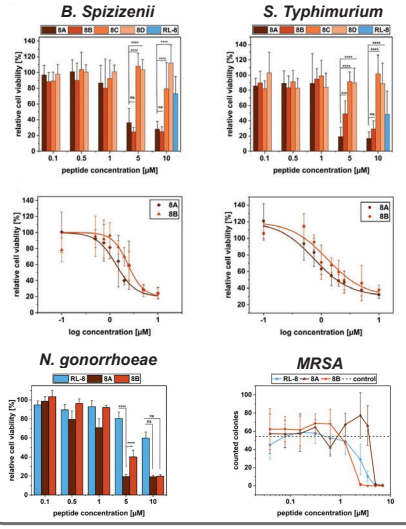

- Peptides 8A/8B exhibited higher antimicrobial activity compared to 8C/8D in gram-negative and -positive bacteria
- 8A and 8B were also potent against pathogenic species in the lower micromolar range
- High activity is related to the presence of the triazolyl-bridge

→ **Triazolyl-bridged peptides with enhanced antimicrobial activity**

4 Transmission electron microscopy to analyze peptide-membrane interaction

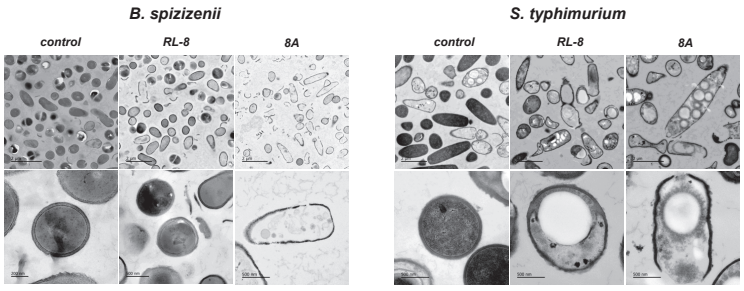

- Lytic activity detectable for both analyzed peptides
- Cyclopeptide 8A showed even stronger impact on membrane integrity

→ **Triazolyl-bridged peptides are highly membrane active**

5 Stability in serum and activity in human cells

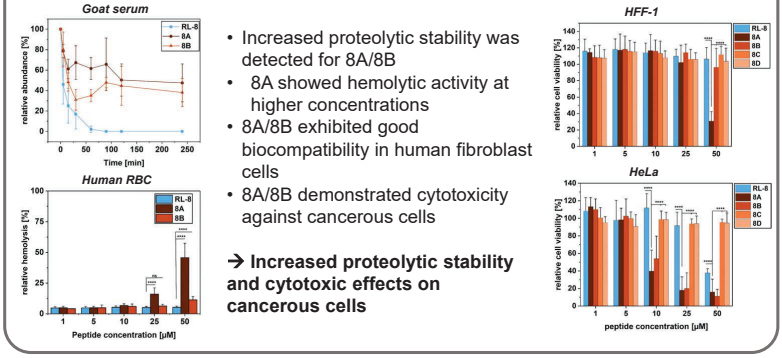

- Increased proteolytic stability was detected for 8A/8B
- 8A showed hemolytic activity at higher concentrations
- 8A/8B exhibited good biocompatibility in human fibroblast cells
- 8A/8B demonstrated cytotoxicity against cancerous cells

→ **Increased proteolytic stability and cytotoxic effects on cancerous cells**

Summary and Outlook

Antibiotic resistance is a growing threat, necessitating the development of new drugs to combat resistant bacterial strains. A novel antimicrobial peptide, 8A, demonstrated potent antibacterial activity, stability against proteolytic cleavage, selectivity for bacteria over human cells, and potential cytotoxic effects against cancer cells, making it a promising candidate for further research.

1. Drexelius, M., Reinhardt, A., Grabeck, J., Cronenberg, T., Nitsche, F., Huesgen, P. F., Maier, B., & Neundorf, I. (2021). Multistep optimization of a cell-penetrating peptide towards its antimicrobial activity. Biochemical Journal, 478(1), 63–78. https://doi.org/10.1042/BCJ20200698
2. Grabeck, J., Mayer, J., Miltz, A., Casoria, M., Quagliata, M., Meinberger, D., Klatt, A. R., Wielert, I., Maier, B., Papini, A. M., & Neundorf, I. (2024). Triazole-Bridged Peptides with Enhanced Antimicrobial Activity and Potency against Pathogenic Bacteria. ACS Infectious Diseases. https://doi.org/10.1021/acsinfecdis.4c00078

https://doi.org/10.17952/37EPS.2024.P1094

Rational design of a miniprotein to inhibit the oncogenic transcription factor MYC

Universiteit Leiden
The Netherlands

B. D. Ellenbroek[1], J. P. Kahler[1], D. Arella[1], C. Lin[1], W. Jespers[1], S. Pomplun[1]
[1]Department of Medicinal Chemistry, LACDR, Leiden University, the Netherlands

LACDR
Oncode Institute

The master regulator MYC is involved in >50% of human cancer

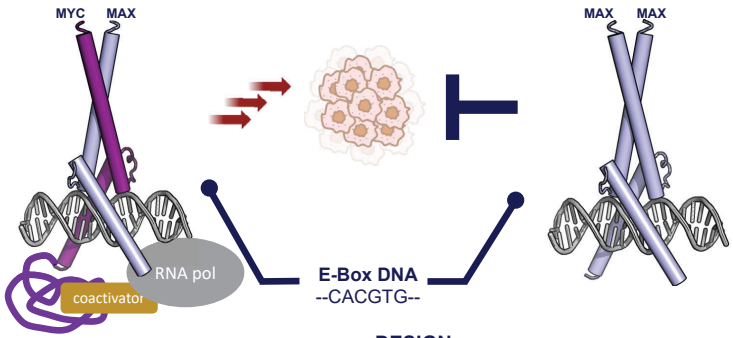

INTERACTION

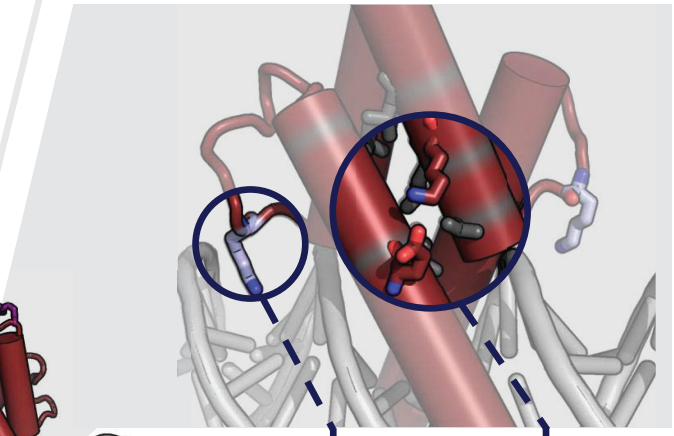

DESIGN

- **Omomyc** targets E-box DNA.[1]
- **Decreasing** protein size can **increase** cell permeability.[2]
- **DuoMYC** has been engineered to **inhibit** MYC activity.

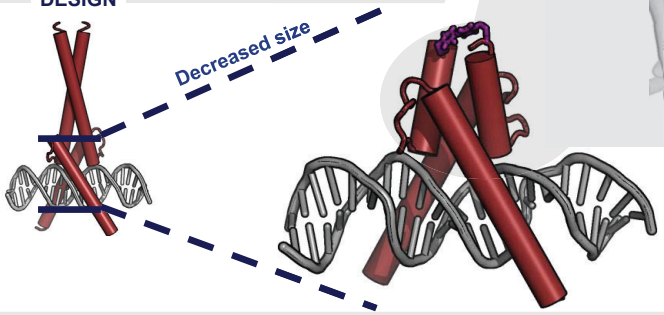

SYNTHESIS AND VALIDATION

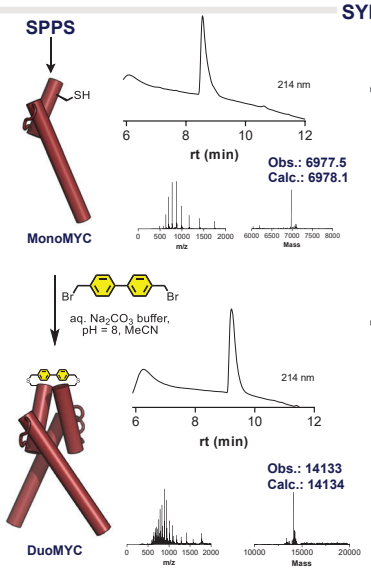

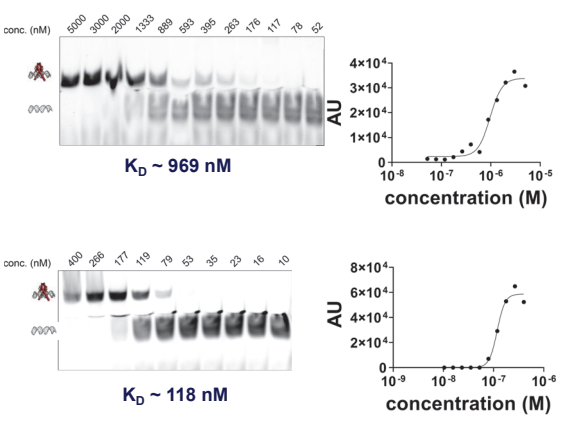

- DuoMYC shows **increased binding** compared to **MonoMYC** towards E-box DNA.

CHARACTERIZATION

Serum stability

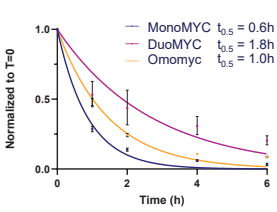

Circular Dichroism

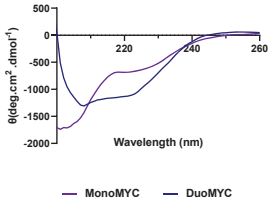

Biolayer interferometry (BLI)

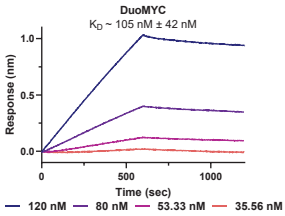

- **DuoMYC** shows serum stability.
- **DuoMYC** adopts a partial α-helix in solution.
- BLI **confirms** strong binding to E-box DNA.

CELL PENETRATION

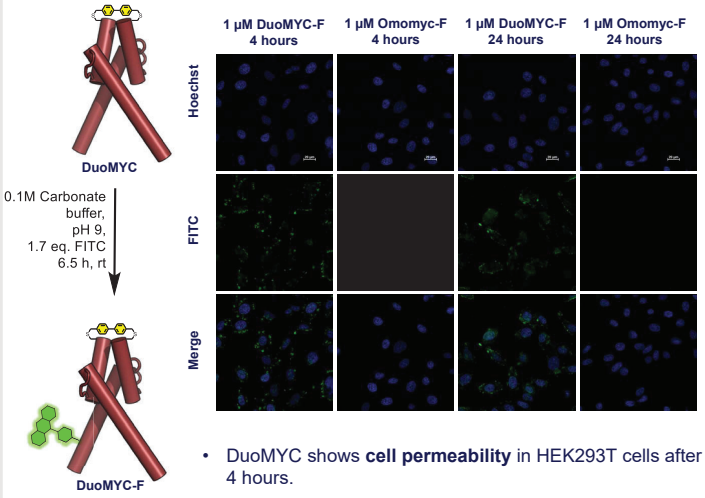

- DuoMYC shows **cell permeability** in HEK293T cells after 4 hours.

CELLULAR ACTIVITY

MYC reporter gene assay in HEK293T cells

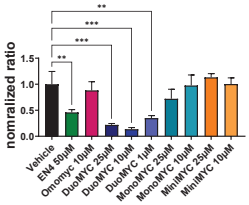

MYC reporter gene assay in Hela cells

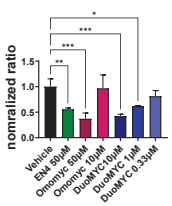

MYC reporter gene assay in HEK293T cells EC_{50} = 464 nM

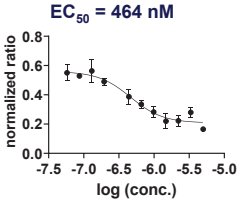

- DuoMYC shows **cellular activity** in multiple cell lines.

CONCLUSION

- We designed a small miniprotein called **DuoMYC** were we successfully replaced the leucine zipper domain with a chemical linker.
- DuoMYC shows **stability** in **human serum** and partial α-helix formation.
- DuoMYC shows **cell permeability.**
- DuoMYC successfully **inhibits** MYC from **binding** as shown in the reporter gene assays.

REFERENCES

[1] L. Soucek, M. Helmer-Citterich, A. Sacco, R. Jucker, G. Cesareni, S. Nasi, *Oncogene 1998 1719* **1998**, *17*, 2463–2472.
[2] N. J. Yang, M. J. Hinner, in Methods Mol. Biol., NIH Public Access, 2015, pp. 29–53.
PDB structures used: 5I50, 1NKP

Funding acknowledged by: erc

Contact information:
b.d.Ellenbroek@lacdr.leidenuniv.nl

Novel, non-covalent peptide furin inhibitors suppressing Zika virus replication

Aleksandra Helbik-Maciejewska,[1] Gabriela Brzuska,[2] Dawid Dębowski,[1] Agata Gitlin-Domagalska,[1] Andrea Lipińska,[3] Ewelina Król,[2] Krzysztof Rolka[1]

1. Department of Molecular Biochemistry, Faculty of Chemistry, University of Gdańsk, Gdańsk, Poland
2. Laboratory of Recombinant Vaccines, Intercollegiate Faculty of Biotechnology, University of Gdańsk and Medical University of Gdańsk, Gdańsk, Poland
3. Laboratory of Virus Molecular Biology, Intercollegiate Faculty of Biotechnology, University of Gdańsk and Medical University of Gdańsk, Gdańsk, Poland

https://doi.org/10.17952/37EPS.2024.P1095

Introduction

Furin is a subtilisin-like secretory **serine protease** widely distributed in various human tissues. It converts inactive precursor proteins into bioactive molecules (growth factors, neuropeptides or hormones).

Furin is also involved in the **development of various inflammatory diseases, cancers and pathogen infections (both viral and bacterial)**. Furin induces viral infections through processing of surface glycoproteins produced by numerous viruses (e.g. Zika, Dengue, SARS-CoV-2).

The **Zika virus (ZIKV)** infection results in relatively mild clinical symptoms, however it is associated with teratogenic effects on fetal development, so it is particularly dangerous for pregnant women. ZIKV is made up of 3 main structural proteins: capsid (C), membrane (M), which is created from its precursor premembrane (prM), and envelope (E). The host cell furin is involved in processing of prM and its transformation into mature M protein. This action is necessary to convert, immature, spiky, and noninfectious virus into a mature smooth, and infectious one. **Therefore, inhibition of furin seems to be a promising strategy to find new therapies against ZIKV infection.**

Fluorescein labeled inhibitors:

labeling peptides → biological tests

&[1]Lys-Arg-Arg-Cys(&[2])-Lys-Lys-Ser-Ile-Pro-Pro-Ile-Cys(&[2])-Phe&[1]
Fluo

&[1]Lys-Arg-Arg-Cys(&[2])-Lys-Lys-Ser-Ile-Pro-Pro-Ile-Cys(&[2])&[1]
Fluo

Fluo - 5(6)-Carboxyfluorescein

Concept and methods

&[1]Gly-Arg-Cys(&[2])-Thr-Lys-Ser-Ile-Pro-Pro-Ile-Cys(&[2])-Phe-Pro-Asp&[1]

Sunflower trypsin inhibitor, SFTI-1

X_i-X_k-Cys(&)-X_j-X_i-Ser-Ile-Pro-Pro-Ile-Cys(&)-Phe-NH_2

Peptide 1 was obtained by combinatorial chemistry followed by iterative deconvolution;

$X_i - X_j$ – variable amino acid residues

Our inhibitors

1. Arg-Arg-Cys(&)-Lys-Lys-Ser-Ile-Pro-Pro-Ile-Cys(&)-Phe-NH_2

Addition of basic residues (additional Arg or Lys residues - enhancement of the interaction of the inhibitor with furin) and additional cyclizations (increase proteolytic stability)

*Gitlin-Domagalska A., Dębowski D., Maciejewska A., Samsonov S., Maszota-Zieleniak M., Ptaszyńska N., Łęgowska A., Rolka K., ACS Med. Chem. Lett., **2023**, 14, 458−465*

2. Lys-Arg-Arg-Cys(&)-Lys-Lys-Ser-Ile-Pro-Pro-Ile-Cys(&)-Phe-NH_2
3. Arg-Arg-Arg-Cys(&)-Lys-Lys-Ser-Ile-Pro-Pro-Ile-Cys(&)-Phe-NH_2
4. &[1]Arg-Arg-Cys(&[2])-Lys-Lys-Ser-Ile-Pro-Pro-Ile-Cys(&[2])-Phe&[1]
5. &[1]Lys-Arg-Arg-Cys(&[2])-Lys-Lys-Ser-Ile-Pro-Pro-Ile-Cys(&[2])-Phe&[1]
6. &[1]Arg-Arg-Arg-Cys(&[2])-Lys-Lys-Ser-Ile-Pro-Pro-Ile-Cys(&[2])-Phe&[1]

Results

A) **Peptides 3, 5, 6 – potent furin inhibitors**

Inhibitor	K_i [nM]
3	0.27
5	0.21
6	0.25

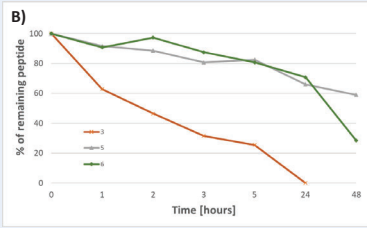

Fig. B) Stabilities of selected inhibitors in human serum

Results of biological tests of inhibitor 5

- Good membrane permeability
- Non-toxic at the concentration range 0.01-500 µM (Vero E6, A549 cells)
- Reduction of infectious virus progeny (Fig. A) as well as viral proteins level: E, pr and M (Fig. B)
- IC_{50} values were lower than those reported for commercial, covalent furin inhibitor decanoyl-Arg-Val-Lys-Arg-chloromethylketone (CMK) (Fig. E-G)

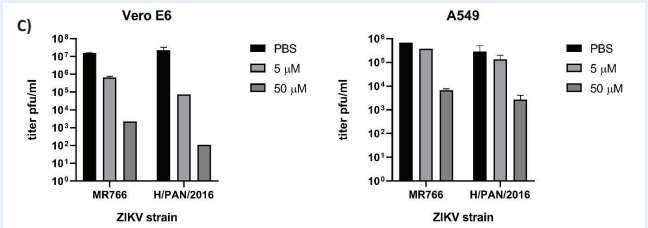

Fig. C) Antiviral assessment of inhibitor 5 against ZIKV. Vero E6 and A549 cells were infected with ZIKV (two strains: MR766 and H/PAN/2016) at 0.1 MOI and then incubated with inhibitor 5 (50 µM and 5 µM)/PBS for 48 hours. The virus was released into culture medium and then it was titrated on Vero E6 cells using the plaque method

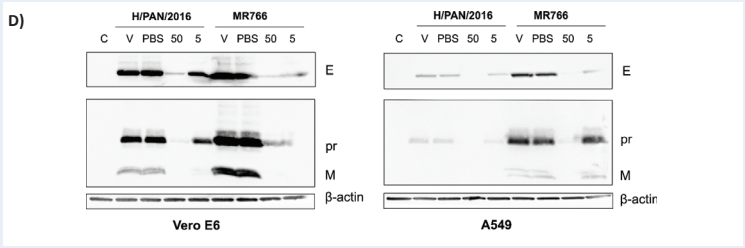

Fig. D) Western blot analysis of viral proteins (prM/M and E) in cell lysates after infection and after treatment with inhibitor 5 (50 µM and 5 µM)/PBS for 48 hours. C - uninfected cells; V - infected cells with ZIKV (MOI 0.1)

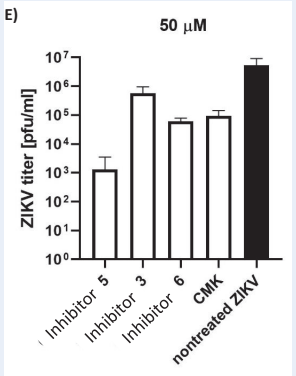

Fig. E) Comparsion inhibitory activity of inhibiotr 5 with other potent inhibitors (3 and 6) and comercial furin inhibitor (CMK). ZIKV titer in the culture medium after treatment with compounds (50 µM) of infected (MOI 0.1) Vero E6 cells for 48 hours

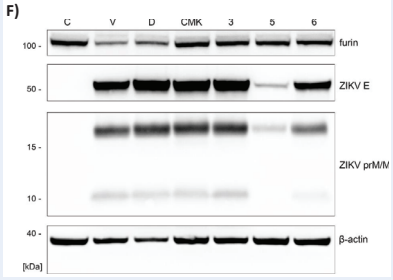

Fig. F) Expression of ZIKV proteins in cell lysates after 48 hours

G)

Inhibitor	IC_{50} [µM]	CC_{50} [µM]	SI
Dec-RVKR-CMK	9.06	615.2	**67.90**
3	22.25	707.3	**31.79**
5	3.69	1303	**353.12**
6	13.45	545.8	**40.58**

Fig. G) IC_{50} values of the tested inhibitors

Dec-RVKR-CMK – comercial furin inhibitor
IC_{50} – concentration of inhibitor necessary to reduce the number of infected cells by 50%
CC_{50} – cytotoxic concentration 50%
SI – selectivity index; SI = CC_{50} / IC_{50}

Conclusions

- We obtained 3 inhibitors more potent than the reference peptide (K_i = 0.49 nM; *Fittler, H. Depp, A. Avrutina, O. Dahms, S. O. Than, M. E., ChemBioChem 2015, 16 (17), 2441−2444*)
- Additional cyclization significantly improved the proteolytic stability of inhibitors
- Our inhibitors have extremely strong antiviral properties against ZIKV
- Inhibitor 5 is less cytotoxic than the comercial furin inhibitor (CMK) and its selectivity index (SI) is 5 times higher than SI value of CMK

Further plans

- Antiviral activity tests against other flaviviruses: tick-borne encephalitis virus (TBEV), West Nile Virus (WNV), Hepatitis C virus (HCV)
- Intestinal permeability *in vitro* tests: Parallel Artificial Membrane Permeability Assay (PAMPA test) and test based on the Caco-2 cell line
- Blood-brain barrier permeability test
- Synthesis of next generation inhibitors (improvement of their stability in proteolytic and reducing environment)

Acknowledgements

This work was supported by Ugrants-start-4 1220/158/2024

37th EPS European Peptide Symposium
14th IPS International Peptide Symposium
Florence, Italy

The Azrieli Faculty of Medicine
Bar-Ilan University

https://doi.org/10.17952/37EPS.2024.P1096

Molecular investigation on peptide regulated Mfn1 and Sirt1 protein interactions in mitochondrial dynamics

Mahesh Kumar Cinthakunta Sridhar [1], Nir Qvit [1]
The Azrieli Faculty of Medicine of Bar Ilan University, Israel

Aim and Abstract

Our study explores mitochondrial dynamics in cardiac cells with respect to myocardial infarction, focusing on the role of Mitofusin1 (**Mfn1**) and Sirtuin 1 (**Sirt1**) under hypoxia. We initially observed that Mfn1 interacts with Sirt1 to stabilize mitochondrial function during stress. We developed a peptide, **CVP-127**, designed to modulate this interaction. CVP-127 inhibited Mfn1-Sirt1 binding and promoted cell survival, enhanced mitochondrial potential, and protected against reactive oxygen species under hypoxic conditions. To understand this paradox, we are investigating how the inhibition of Mfn1/Sirt1 interaction by CVP-127 contributes to cell survival and identifying alternative mechanisms involved.

Our approach includes biochemical assays, gene expression analysis, and proteomics to uncover the underlying pathways that might compensate for the disrupted Mfn1/Sirt1 interaction and ensure cellular resilience under stress.

Graphical Representation

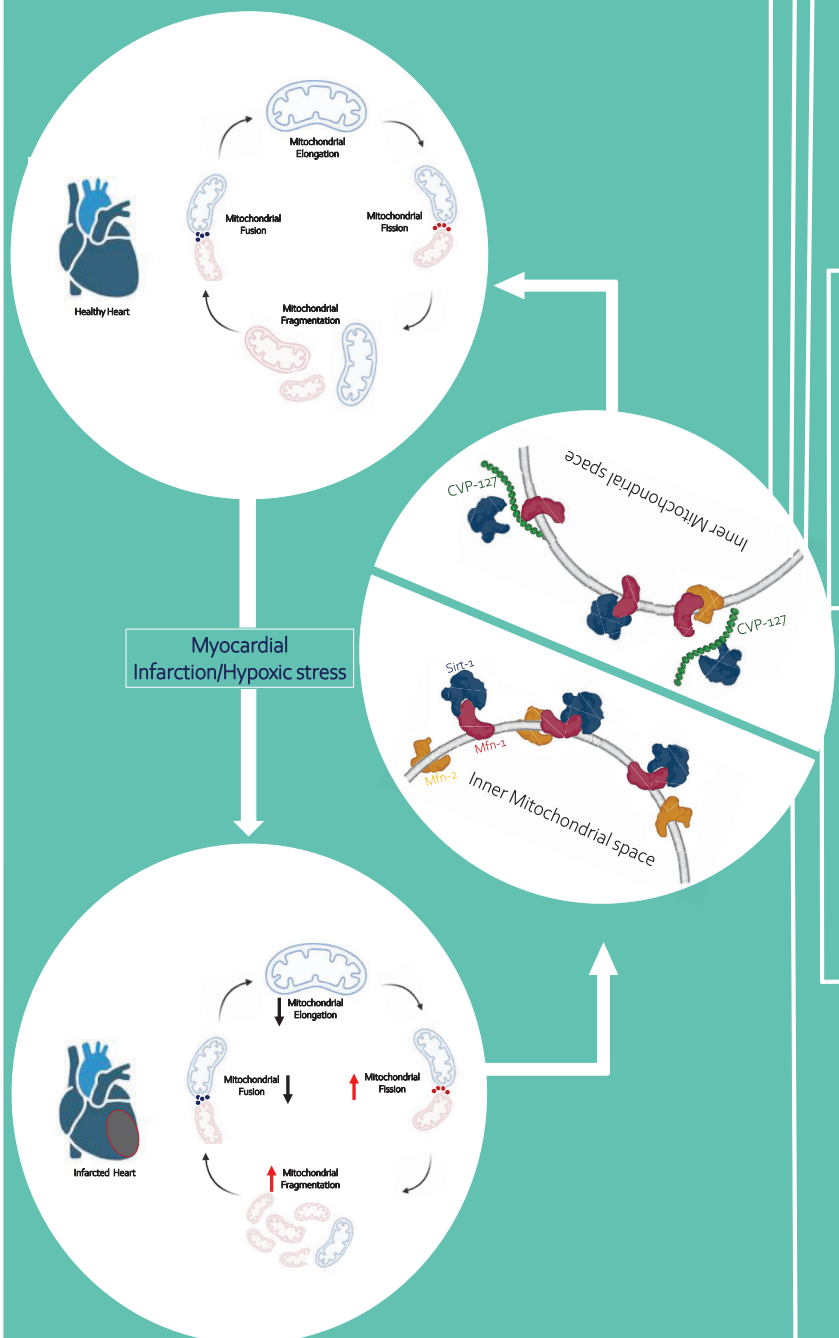

Results

1. Expression and purification of Sirt1 and Mfn1

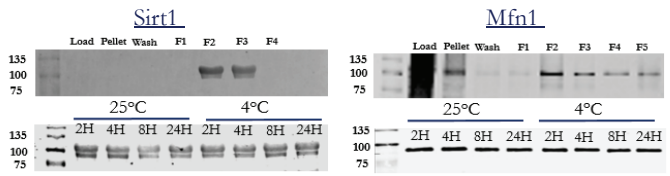

The proteins Sirt1 and Mfn1 were successfully expressed and purified. There was also found to be stable at 25° C and 4° C for about 24 hours

2. Protein-protein interaction between Sirt1 and Mfn1

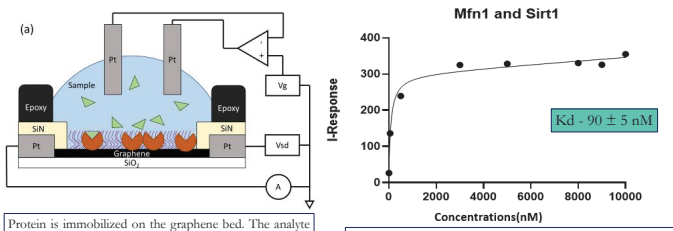

Protein is immobilized on the graphene bed. The analyte protein is made to react with the immobilized protein. Changes in the current during the interaction is measured.

We observed good interaction between Sirt1 and Mfn1 with K_D of 90 ± 5 nM using field emission Biosensing technique.

3. Protein-peptide interaction with Sirt1, Mfn1

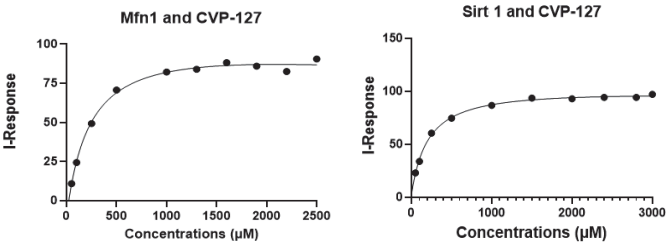

The peptide CVP-127 showed good interaction with the proteins Sirt1 and Mfn1 with K_D of 236.96 and 209.5 µM respectively

4. Protein-protein competitive interaction with peptide

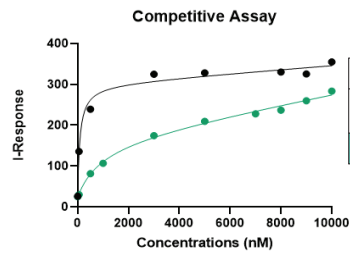

Experiment Name	Immobilized protein	Analyte	Peptide	K_D
Mfn1 and Sirt1 interaction (n=3)	Mfn1	Sirt1	-	90 ± 5 nM
Competitive interaction (n=3)	Mfn1	Sirt1	CVP-127 250 µM	938.07 ± 6 nM

The interaction between Sirt1 and Mfn1 was successfully inhibited by the peptide CVP-127 with K_D 938.07 (± 6 nM) higher than that of Sirt1 and Mfn1 interaction K_D 90 (± 5 nM)

5. Cell Viability assays

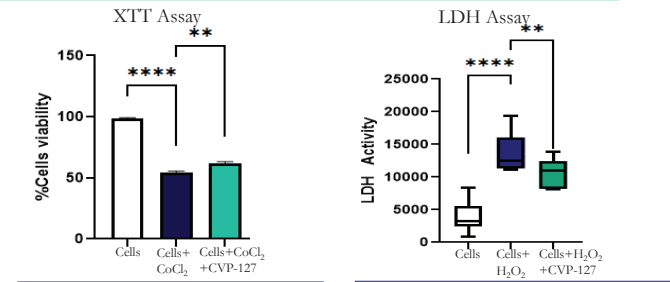

Under cobalt induced hypoxic stress the peptide was observed to significantly increase the H9c2 cell viability.

Under H_2O_2 induced hypoxic stress the peptide was observed to significantly decrease the release of LDH from H9c2 cells

6. Microscopic Assessment

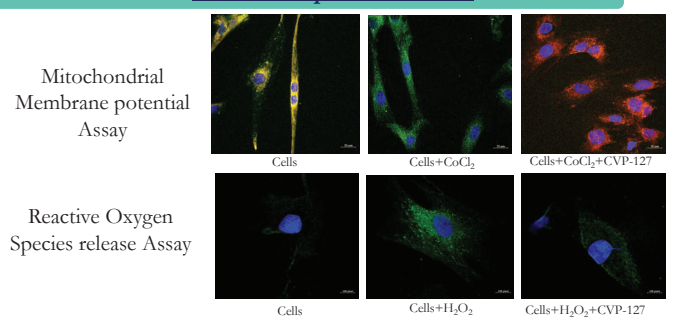

Conclusion We observed potential interactions between Sirt1 and Mfn1 using FEB technology. We developed a peptide that successfully inhibited the interaction between Sirt1 and Mfn1. The cells showed high viability and reduced release of LDH when treated with CVP-127 under hypoxic stress. Also, under stress when treated with peptide CVP-127 we observed high mitochondrial membrane potential and reduction in the release of Reactive Oxygen Species. These results prove that CVP-127 rescues H9c2 cells from hypoxic stress. Further we are evaluating the action of peptide on myocardial infarction in rats.

Contact details
Mahesh Kumar C S, PhD Student
The Azrieli Faculty of Medicine of Bar Ilan University, Israel
mahesh1996biu@gmail.com

The role of β-hairpins in aggregation of β-amyloid derived peptides

Elisabetta Galluppo[1], Claudia Honisch[1], Stefano Tartaggia[1], Mauro Carraro[2], Paolo Ruzza[1]

1. Institute of Biomolecular Chemistry of CNR, Padova Unit, Padova, Italy,
2. Dept. of Chemical Sciences, University of Padua, Padova, Italy

https://doi.org/10.17952/37EPS.2024.P1098

Alzheimer's disease (AD) is one of the most widely recognized and prevalent neurodegenerative conditions in today's society. However, despite its prevalence, effective pharmacological treatment is not currently available, leaving only palliative care options as the most helpful course of action. The pathogenesis of Alzheimer's disease (AD) involves the formation of proteinaceous plaques due to the aggregation of originally soluble oligomers of **amyloid-β peptides**[1]. These oligomers have been observed to adopt different conformations, including β-sheets, α-helices, and predominantly **β-hairpins**. β-hairpins are capable of assuming different configurations in space.

In order to investigate the mechanisms that govern β-hairpin orientation and develop an *in vitro* model of peptide aggregation for use in testing inhibitors of this process, two **Aβ17-36 derivatives** were synthesized; subsequently, their conformation was studied through circular dichroism spectroscopy (CD).

Synthesis

Fmoc-SPPS was conducted using a Wang resin preloaded with valine, employing HOBt/HBTU as the activator, while HATU was utilized exclusively for the couplings involving Ile[32] and D-Pro residues. To mitigate the propensity for β-sheet aggregation, an **N-Me-Gly (Sarcosine)** residue [2] was incorporated into both peptides, instead of a residue of glycine.

This residue modulates the hydrogen bonding pattern, promoting a *cis* conformation of the Ile-Sar peptide bond and disfavoring the aggregated form of the hairpin[3].

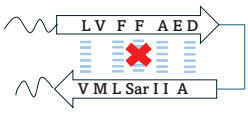

Purification

Purification of both peptides was carried out using reverse-phase HPLC on a C18 column with: (A) 0.05% TFA in H_2O and (B) 0.05% TFA in acetonitrile: H_2O 9:1 v/v. Linear binary gradient: 38-50 %B in 40 minutes. Due to the poor solubility of the peptides, to be eluted the samples are dissolved in a 9:1 v/v solution of acetonitrile: 10 mM ammonium acetate, pH 5.5.

*Sequence of **17-37pP** peptide:* $L^{17}VFFAED^{23}$-*pP*-$A^{30}IISarLMV^{36}$

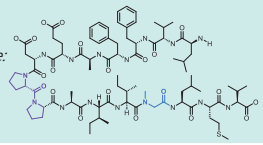

Compared to the original sequence Aβ17-36[2], we examined the conformation of two distinct loops: a sequential **homochiral (R)-(R-) dinipecotic acid (Nip)** segments[4] and the **D-Pro-L-Pro (pP)** loop[5] .

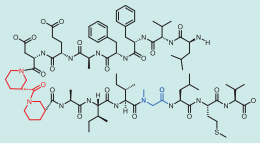

*Sequence of **17-37Nip** peptide:* $L^{17}VFFAED^{23}$-*Nip-Nip*-$A^{30}IISarLMV^{36}$

Circular Dichroism

Effect of pH

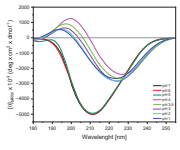

***(up) 17-36pP (down) 17-36Nip** peptide **titration** with H_2SO_4 0.05 M. Peptide was dissolved in PB buffer 10 mM (0.1 mg/ml), cell pathlength 1 mm.*

The far-UV CD spectra of both *17-36pP* and *17-36Nip* peptides are found to be influenced by the pH values. In a 10 mM phosphate buffer (PB) with a pH of 7.4, both spectra exhibit a negative band within the 195-210 nm range, which is indicative of an unordered conformation. A pH value lower than 4 units results in the CD spectrum of the ***17-36pP*** peptide developing a negative band near 225 nm, the growth of a positive band at approximately 200 nm, and a negative band near 180 nm. This is indicative of a class B spectrum, according to the Woody classification[7], which suggests the presence of a **β-turn**. The intensity of these bands is influenced by the pH values, from pH 7.4 to 1.5.

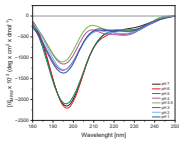

The CD spectrum of the peptide ***17-36Nip*** at lowering pH values demonstrated a reduction in the intensity of the negative band at 198 nm, accompanied by a blue-shift at a low wavelength (195 nm), and the emergence of a negative band at approximately 225 nm. For this peptide, as well, the intensity of the bands was affected by pH values. The shape of this spectrum could not be attributed to any β-turn described thus far.

Effect of time

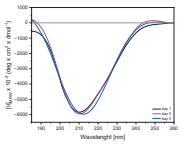

***(up) 17-36pP (down) 17-36Nip** peptide dissolved in PB buffer 10 mM (0.5 mg/ml) **pH 7.4**, cell pathlength 1 mm, over **5 day**.*

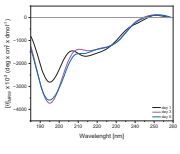

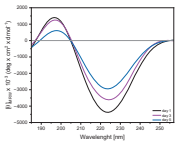

***(up) 17-36pP (down) 17-36Nip** peptide dissolved in PB buffer 10 mM (0.5 mg/ml) **pH 2.1**, cell pathlength 1 mm, over **5 day**.*

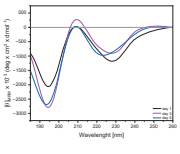

The ***17-36pP*** peptide exhibits no conformational change when incubated in PB buffer at pH 7.4 for five days at 25°C. However, at acidic pH conditions, the intensity of the CD bands of the peptide undergoes a change over time, indicating a tendency towards **aggregation**.

The pH 7.4 spectrum of the ***17-36Nip*** peptide is influenced by incubation at 25°C, resulting in an increase in the intensity of the negative band at approximately 190 nm from day 1 to day 3. The continuation of the incubation does **not induce any further change** in the dichroic spectrum, and from day 3 to day 5, there is no longer any difference. A similar behaviour can be observed at acidic pH.

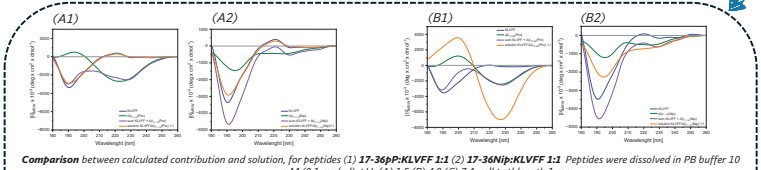

***Comparison** between calculated contribution and solution, for peptides (1) **17-36pP:KLVFF 1:1** (2) **17-36Nip:KLVFF 1:1** Peptides were dissolved in PB buffer 10 mM (0.1 mg/ml), pH: (A) 1.5 (B) 4.0 (C) 7.4, cell pathlength 1 mm.*

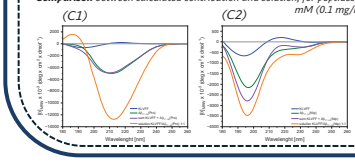

Further confirmation of the interaction of the KLVFF peptide with the two hairpins is obtained by comparing the measured spectrum for the hairpin/β-breaker mixture with the theoretical spectrum calculated by summing the contributions of the individual peptides at a given pH value.

Effect of concentration

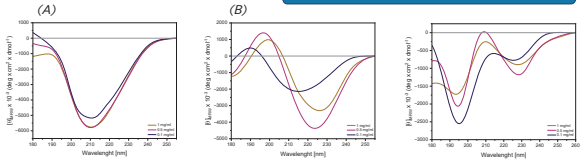

***17-36pP** peptide, dissolved in PB buffer 10 mM (1 mg/ml, 0.5 mg/ml, 0.1 mg/ml), pH (A) 7.4 (B) 2.1, cell pathlength 1 mm.*

***17-36Nip** peptide, dissolved in PB buffer 10 mM (1 mg/ml, 0.5 mg/ml, 0.1 mg/ml), pH 2.1, cell pathlength 1 mm.*

The CD spectrum of both peptides in PB is not influenced by peptide concentration (as evidenced by the spectra of *17-36pP*).

Conversely, in **acidic conditions**, the CD spectrum is **markedly influenced** by peptide concentration, indicating the potential for peptide interactions.

Hairpin and β breaker

The capability of the **β-breaker KLVFF** peptide to interact with both ***17-36pP*** and ***17-36Nip*** peptides has been evaluated by CD spectroscopy at the different pH values (the studies were carried out in presence of 5% of trifluoroethanol -TFE- as a cosolvent because of the poor solubility of KLVFF in aqueous solution).

The influence of pH on the CD spectrum of KLVFF peptide was evaluated[6]. At pH 7.4, the CD spectrum of peptide shows a negative band at about 193 nm and a positive band at 215 nm, suggesting the presence of an unordered conformation. It has been reported that this conformation is always in equilibrium with other structures like **β-turns and -strands, and PP_{II} helix**, due to the closely proximity of the respective dihedral angle values[8].

The decrease in pH values is mainly accompanied by a **hyperchromic behaviour** of the molar ellipticity of the band from -500 to -3500 deg•cm²•dmol⁻¹.

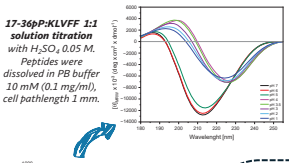

***17-36pP:KLVFF 1:1 solution titration** with H_2SO_4 0.05 M. Peptides were dissolved in PB buffer 10 mM (0.1 mg/ml), cell pathlength 1 mm.*

In the presence of the KLVFF peptide, the CD spectrum of the ***17-36pP*** peptide at neutral pH is characterized by the appearance of a positive band at about 195 nm and a red-shift displacement of the negative band from 210 to 213 nm, accompanied by an evident hyperchromic effect of the same. This effect persists throughout the range of pH values explored.

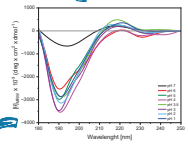

***KLVFF** peptide **titration** with H_2SO_4 0.05 M. Peptide was dissolved in PB buffer 10 mM (0.1 mg/ml), cell pathlength 1 mm.*

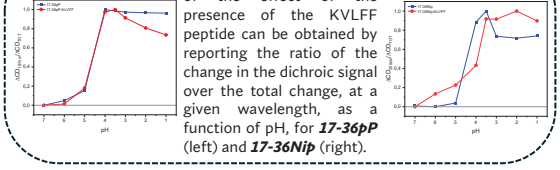

A qualitative representation of the effect of the presence of the KVLFF peptide can be obtained by reporting the ratio of the change in the dichroic signal over the total change, at a given wavelength, as a function of pH, for ***17-36pP*** (left) and ***17-36Nip*** (right).

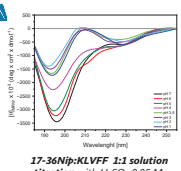

***17-36Nip:KLVFF 1:1 solution titration** with H_2SO_4 0.05 M. Peptides were dissolved in PB buffer 10 mM (0.1 mg/ml), cell pathlength 1 mm.*

Similarly, the presence of the peptide KLVFF also influences the CD spectrum of the peptide ***17-36Nip***, and in this case the effects can be observed as early as pH 6.2. For this peptide, too, the effect is essentially on the intensity of the dichroic bands, whereas at pH values below 4 units, the appearance of a weak positive band at 205 nm and an increase in the intensity of the negative band at around 230 nm are observed.

[1] Y. Yang, D. Arseni, W. Zhang, M. Huang; *SCIENCE*, **2022**, 375 (6577), 167-172
[2] S. Ruttenberg, A. Kreutzer, N. Truex, J. Nowick; *Biochemistry*, **2024**, 63, 212−218
[3] M. Teixidò, F. Albericio, E. Gitalt; J. *Peptide Res.*, **2005**, 65, 153−166
[4] Huck, J. Fisk, S. Gellman; *Org. Lett.*, **2000**, 17(2), 150-157
[5] B. Dasgupta et all.; *FEBS Letters*, **2007**, 581, 4529−4532
[6] L. Tjernberg, et all.; *J. of Biological Chemistry*, **1996**, *271* (15), 8545−8548
[7] . Woody, S. Venyaminov, N. Sreerama; *Protein Science*, **1999**, 8, 370-380

This work was supported by PRIN 2022 National Project (Grant N. 2022CAS9ZT, Development of HYbrid and Multifunctional Bio-conjugates against Alzheimer's Disease - HYMBAD)

37th European Peptide Symposium
Florence, Italy, 25-29th August 2024

BIOLOGICAL EVALUATION OF NEW FELL ANALOGUES AS POTENTIAL PDE4 INHIBITORS

https://doi.org/10.17952/37EPS.2024.P1099

Veronica Nemska[1], Boryana Borisova[1], Marie Cochard[2], Stéphane Gérard[2], Dancho Danalev[1]
*e-mail: vnemska@uctm.edu

[1]*University of Chemical Technology and Metallurgy, 8, Kliment Ohridski Blvd., 1797 Sofia, Bulgaria*

[2]*University of Reims Champagne-Ardenne, CNRS, ICMR, UFR Pharmacy, 51, Cognacq-Jay Str., 51096 Reims, France*

Introduction

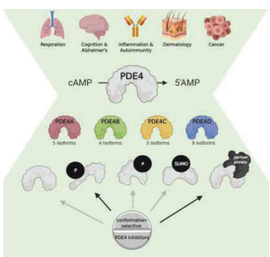

Fig. 1. PDE4 as a pharmacological target in a variety of disease areas [Paes et al., 2021].

In recent years, the inhibition of phosphodiesterase type-4 (PDE4) has been an attractive therapeutic strategy for treating a variety of diseases. PDE4 is a major enzyme class which is responsible for the hydrolysis of cyclic adenosine monophosphate (cAMP) – an intracellular second messenger, regulating a network of pro- and anti-inflammatory mediators.

As conventional first-generation selective PDE4 inhibitors show many side effects, the search for new therapeutics is a priority [1]. Bioactive peptides are a preferred alternative due to their small size, natural mechanism for elimination, low or lack of secondary effects, etc. FELL is a tetrapeptide, derived from human calcium-binding protein spermatid 1, showing promising anti-inflammatory properties [2].

Aim

The aim of this work was to determine the ability of 4 new FELL analogues, where Leu-residues in the 3rd and 4th positions were replaced by different hydrophobic amino acids (Leu, Val, Ile, Nle), to inhibit the enzyme PDE4.

Materials and methods

Synthesis of target peptides

The FELL analogues were synthesized by the conventional solid-phase peptide synthesis (SPPS) using the Fmoc (9-fluorenyl methoxycarbonyl)/OtBu strategy [2].

Phosphodiesterase assay

The PDE4 inhibition activity was determined by using a Cyclic nucleotide phosphodiesterase assay kit (Enzo Life Sciences, France) [1]. Tested compounds were previously dissolved in DMSO. A non-specific PDE inhibitor, 3-isobutyl-1-methylxanthine (IBMX) was used as a test control.

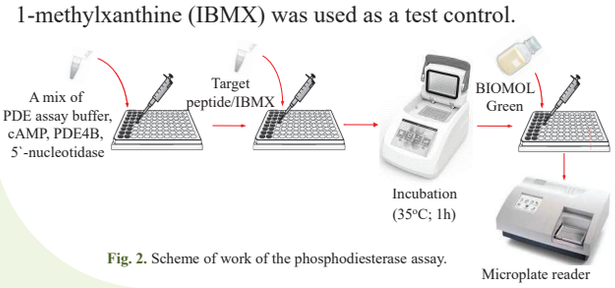

Fig. 2. Scheme of work of the phosphodiesterase assay.

Results and discussion

A series of analogues of the tetrapeptide FELL as N-terminus amide with general structure Phe-Glu-X-X-Z, where X = Leu (analogue BB1), Nle (analogue BB2), Ile (analogue BB4) or Val (analogue BB3), Z = C(=O)NH_2 (in the parent compound) was synthesized by SPPS using Fmoc/OtBu strategy [2]. Their PDE4 inhibition activity was evaluated by using a Cyclic nucleotide phosphodiesterase assay kit. All experiments were performed in triplicate. The obtained results are presented in **Fig. 2**:

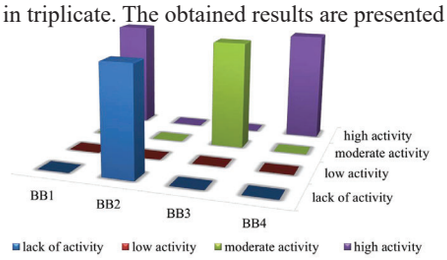

Fig. 2. Biochemical evaluation of FELL analogues as PDE4B inhibitors.

Legend: *0 – 10% -very low activity; 10.1 – 25% - low activity; 25.1 – 45% - moderate activity; > 45.1% - high activity*

Results showed that the newly synthesized FELL analogues possessed quite diverse PDE4 inhibition activity (**Fig. 2**). Except analogue BB2, which showed no activity, all other compounds had moderate to high PDE4 inhibition activity. The highest PDE4 inhibition activity was observed for analogue BB4 and the lowest – for analogue BB3.

Conclusion

Four new FELL analogues were successfully synthesized. Among the FELL analogues tested, the highest PDE4 inhibition activity was observed in analogues BB1 and BB4. At the same time, analogue BB2 was found to be practically inactive at the screening concentration whereas

Acknowledgements

This study is supported by the European Union-NextGenerationEU, through the National Recovery and Resilience Plan of the Republic of Bulgaria, Project № BG-RRP-2.004.0002, “BiOrgaMCT” and by University of Reims Champagne-Ardenne.

References

[1] Allart-Simon, I., Moniot, A., Bisi, N., Ponce-Vargas, M., Audonnet, S. Laronze-Cochard, M., Sapi, J., Henon, E., Velard, F., Gerard, S., RSC Med. Chem., 2021, 12, 584-592.

[2] Borisova, B., Nocheva, H., Gérard, S., Laronze-Cochard, M., Dobrev, S., Angelova, S., Petrin, S., Danalev, D., Pharmaceuticals, 2023, 16, 1183.

[3] Paes, D., Schepers, M., Rombaut, B., van den Hove, D., Vanmierlo, T., Prickaerts, J., Michel, M., Pharmacol Rev, 2021, 1016-1049.

https://doi.org/10.17952/37EPS.2024.P1100

Investigation of the role of Mfn2 and Drp1 protein-protein interactions in mitochondrial dynamics and its biological implications in cardiovascular diseases

Berhe Hayelom[1] and Qvit Nir[1*]

[1]The Azrieli Faculty of Medicine in the Galilee, Bar-Ilan University, Safed 1311502, Israel

Hayelom Berhe; hayelom.berhe8@gmail.com, Nir Qvit: nir.qvit@biu.ac.il

1. Introduction and Aim

Mitochondrial dynamics is a potential target for cardiovascular diseases (CVDs). Deregulation of dynamicity causes mitochondrial dysfunction, impacting on cellular functions and leading to disease.

Protein-protein interactions (PPIs) are promising therapeutic targets toward the embarrassment of medical conditions.

The interaction between **Drp1** and **Mfn2** suggests a regulatory mechanism where Mfn2 can influence the balance between fusion and fission. Specifically, Mfn2's interaction with Drp1 may promote mitochondrial elongation which can affect mitochondrial morphology. Thus, Drp1/Mfn2 PPI can lead to mitochondrial dysfunction and quality controls associated with various diseases.

Therefore, inhibiting Drp1/Mfn2 interactions may reduce excessive mitochondrial fusion, improving mitochondrial dynamics, morphology, and quality control.

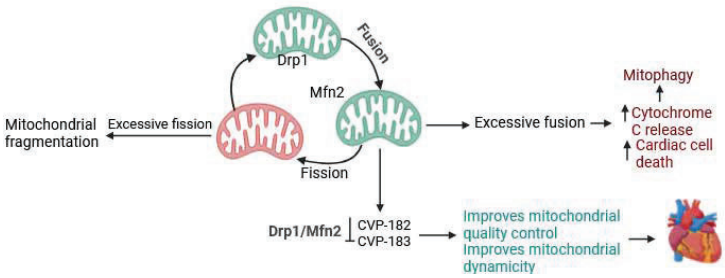

Figure 1. Schematic representation of excessive mitochondrial fusion affects mitochondrial dynamics and mitochondrial quality controls.

2. Materials and Methods

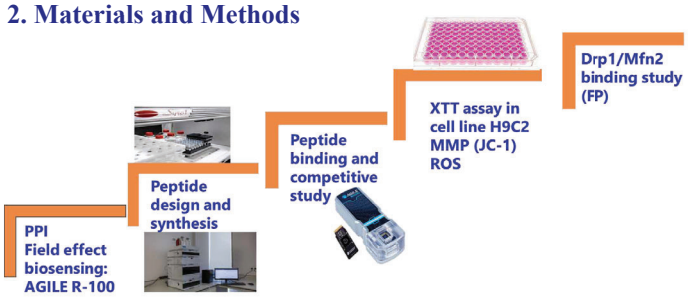

3. Result and Discussion

3.1. Protein-protein interactions

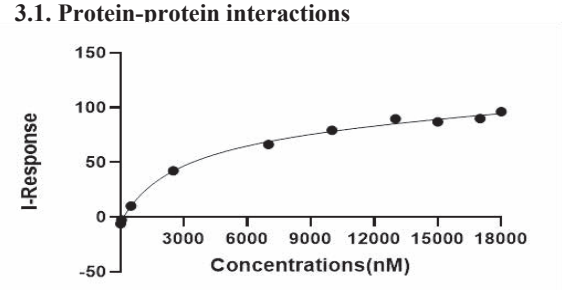

K_D: 2.646 ± 0.681 µM (n=3)

Figure 1. Drp1 and Mfn2 protein-protein interactions.

3.3. In vitro competitive study

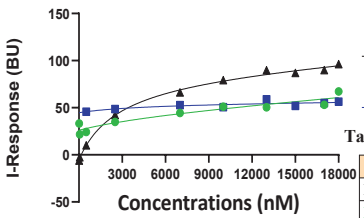

Table 1: K_D values of the competitive assay

Competitive assay	kD (µm)	R^2
Drp1/Mfn2	2.646 ± 0.681	0.99
Drp1/Mfn2-CVP-182	6.201 ± 0.945	0.99
Drp1/Mfn2-CVP-183	4.710 ± 0.902	0.99

Figure 3: Drp1/Mfn2 PPI inhibition curves of Drp1/CVP-182 and Mfn2/CVP-183, *in vitro* study.

3.4. Protein-peptide binding using FEB and fluorescence polarizations

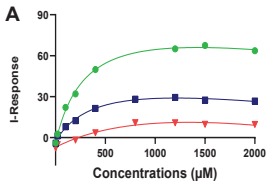

Peptide ID	K_D (µM)	R^2
Drp1/CVP-182	325.90 ± 28.13	0.99
Mfn2/CVP-183	454.50 ± 12.27	0.99

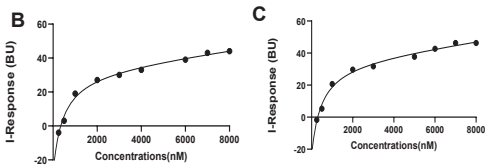

Peptide ID	Drp1/CVP-188 (B)	Mfn2/CVP-189 (C)
K_D (µM)	0.460 ± 0.684	0.439 ± 0.539
R^2	0.99	0.99

D. K_D values of the protein-peptides bindings

Figure 4: Protein-peptide binding curves. (**A**): protein-peptide binding curve using FEB. (**B & C**): Protein-peptide binding curves using fluorescence polarization. (**D**): Summary of K_D values of protein-peptide binding curves.

3.5. Cell viability study

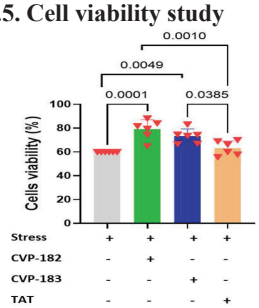

Figure 5: Cell viability study of CVP-182 and CVP-183 peptides using H9c2 cells.

3.6. Measurement of mitochondrial membrane potential (JC-1)

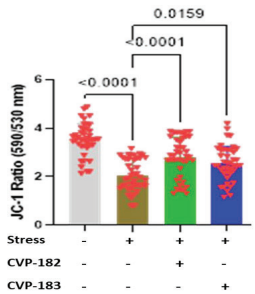

Figure 6: Measurement of mitochondrial membrane potential of H9c2 cells using CVP-182 and CVP-183 peptides.

3.7. Measurement of Reactive Oxygen Species (ROS) potential

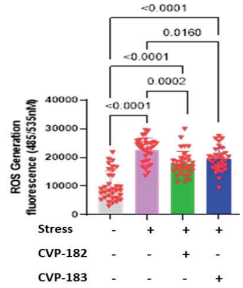

Figure 7. Measurement of Reactive Oxygen Species (ROS) for H9c2 cells using CVP-182 and CVP-183 peptides

Conclusion

Drp1 and Mfn2 proteins exhibit strong interactions. The peptides CVP-182 and CVP-183 have been synthesized with 100% purity. These peptides demonstrate high binding activities with Drp1 and Mfn2 proteins when assessed using field effect biosensor technology and fluorescence polarization (CVP-188 & CVP-189), respectively. Notably, CVP-182 and CVP-183 are biologically active in cultured cardiomyocyte (H9c2) cells, and they inhibit the interaction between Drp1 and Mfn2. These peptides enhance mitochondrial membrane potential and reduce reactive oxygen species (ROS) levels in H9c2 cells.

Future directions

- ✓ A study of CVP-182 and CVP-183 is necessary to advance therapeutic interventions in diseases characterized by mitochondrial dysfunction.
- ✓ The candidate peptides required studies of the optimal dosing and treatment intervals for cardio-protection in cardio-myocytes and other models.

Peptide and Probe: A two-pronged approach to investigating menaquinone binding peptides

Eilidh J. Matheson, Roy A. M. van Beekveld, Sarah Gothard, Paolo Innocenti, Nathaniel I. Martin, Markus Weingarth, Stephen A. Cochrane
School of Chemistry and Chemical Engineering, Queen's University, Belfast, UK, BT7 1NN, Biological Chemistry Group, Institute of Biology, Leiden University Sylviusweg 72, 2333 BE Leiden, NL, NMR Spectroscopy, Bijvoet Centre for Biomolecular Research, Department of Chemistry, Utrecht University, Utrecht, NL
ematheson01@qub.ac.uk, s.cochrane@qub.ac.uk

https://doi.org/10.17952/37EPS.2024.P1101

Background

In 2015, lysocin E was first reported. A broad spectrum depsipeptide with good activity against Gram positive bacteria.[1] Its novel mode of action involves binding to menaquinone (MK), an essential membrane bound enzyme cofactor involved in the electron transport chain. Since lysocin E, a number of other MK binding antimicrobial peptides (MBAMPs) have been reported, including WAP and MBA2.[2,3] It is thought that MK acts as an anchoring point for the MBAMPs into cell membrane, causing cell lysis. Beyond this, not much is known about this novel mode of action. Our lab has previously developed chemistry to selectively modify terminal isoprene units in simple polyprenols.[4] We sought to further apply this ω-modification chemistry to create a library of highly valuable MK-derived probes. These probes could then be utilised to better understand MBAMPs and their mode of action.

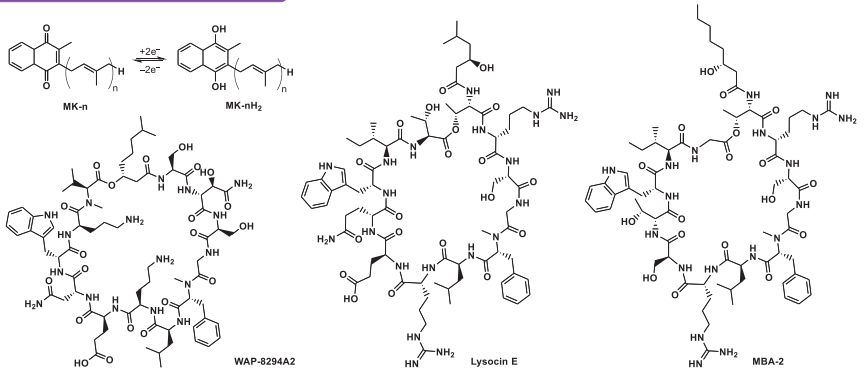

MK Probe Synthesis

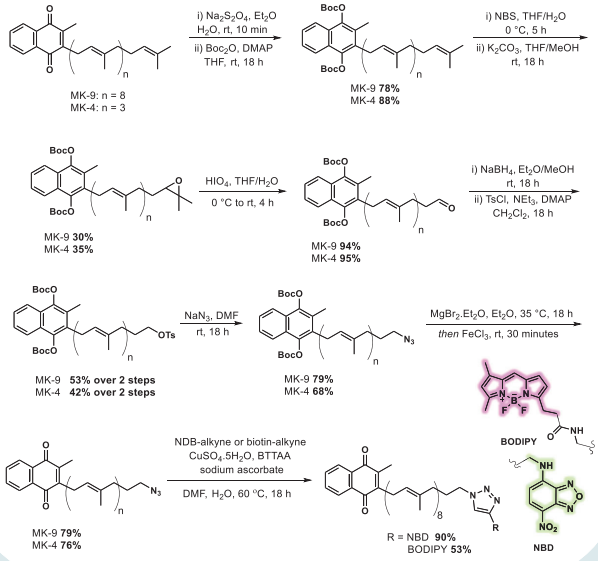

MBAMP Synthesis

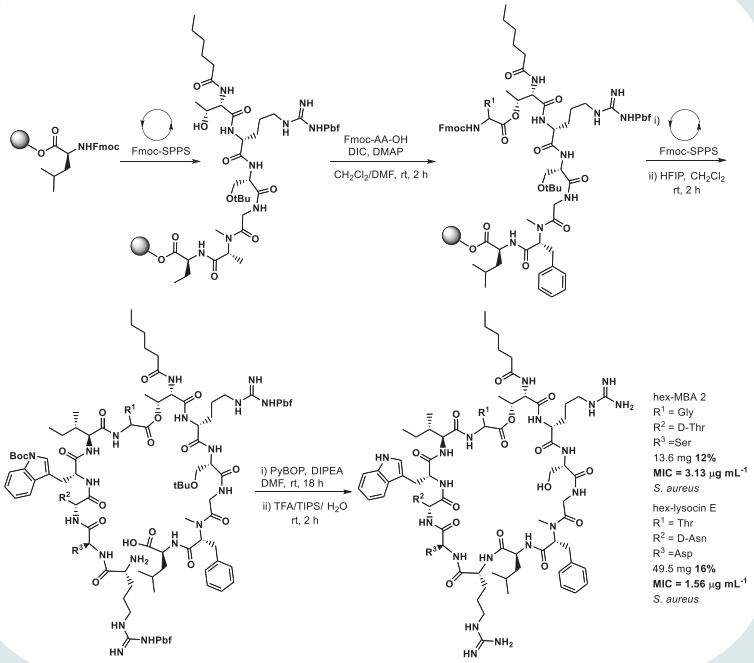

Do ω-modifications affect binding?

Antagonisation Studies

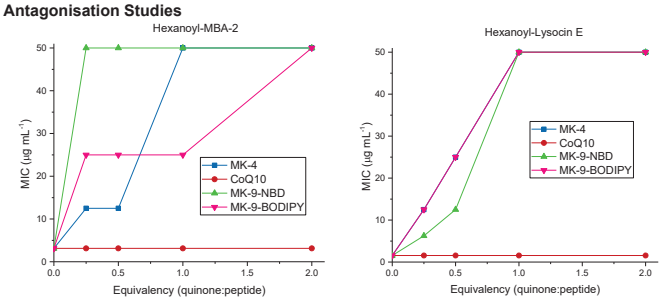

ITC Results

Quinone	Hexanoyl-Lysocin E		Hexanoyl-MBA-2	
	K_D (nM)	ΔH (kcal mol^{-1})	K_D (nM)	ΔH (kcal mol^{-1})
MK-4	59.2	– 8.49	56.9	– 5.63
MK-9	80.3	– 8.99	61.1	– 5.02
MK-9-NBD	101.4	– 5.02	84.3	– 8.37
MK-9-BODIPY			106.1	– 9.47
CoQ_{10}	0	0	0	0

Initial SAR MBA-2 Studies

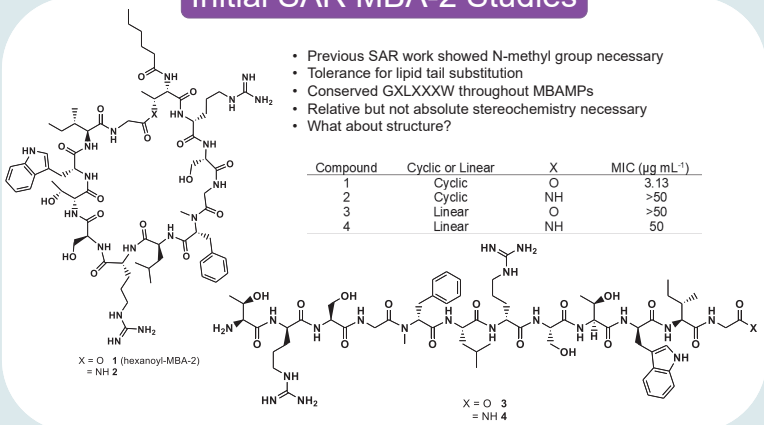

- Previous SAR work showed N-methyl group necessary
- Tolerance for lipid tail substitution
- Conserved GXLXXXW throughout MBAMPs
- Relative but not absolute stereochemistry necessary
- What about structure?

Compound	Cyclic or Linear	X	MIC (μg mL^{-1})
1	Cyclic	O	3.13
2	Cyclic	NH	>50
3	Linear	O	>50
4	Linear	NH	50

Model Membrane Studies

Giant unilamellar vesicles: 98% DOPC, 2% MK-9, 0.1% MK-9(ω-BODIPY)
(λ_{excit} = 488 nm, λ_{emis} = 496 – 669 nm)

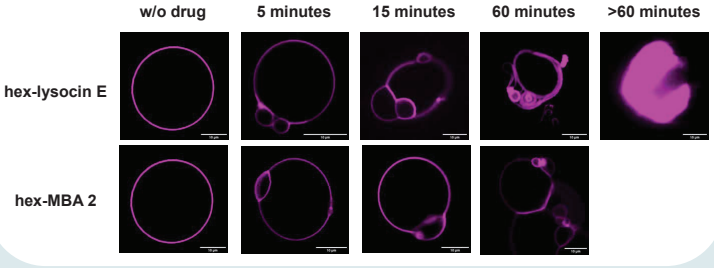

Cellular Uptake Studies

***Mycobacterium smegmatis* labelled with MK-9(ω-BODIPY)**

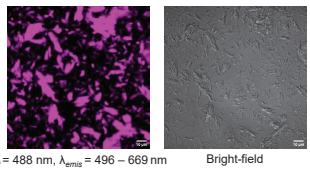

λ_{excit} = 488 nm, λ_{emis} = 496 – 669 nm Bright-field

Uptake conditions: 7H9 broth, 0.1% v/v TWEEN 80, 0.2% v/v glycerol solution (50% w/v Aq.) and 0.2% w/v glucose, 10 μM MK-9(ω-BODIPY), 20 h

Conclusions

- ω-modification chemistry to achieve MK probes
- ω-modification does not significantly affect binding
- MBAMPs cause MK localisation, causing membrane perturbation and vesiculation
- SAR work: cyclisation necessary and conformational flexibility important for activity
- *M. Smegmatis* will uptake MK-9(ω-BODIPY)

Ongoing:

- Continued whole cell uptake studies
- ssNMR to determine binding conformation

References

1. H. Hamamoto *et al.*, *Nat. Chem. Bio.*, 2015, **11**, 127 – 133.
2. H. Itoh *et al.*, *J. Org. Chem.*, 2018, **83** (13), 6924 – 6935.
3. L. Li, B. Koirala, Y. Hernandez *et al.*, *Nat. Microbiol.*, 2022, **7**, 120 – 131.
4. R. V. K. Cochrane, F. M. Alexander, C. Boland, S. K. Fetics, M. Caffrey and S. A. Cochrane, *Chem. Commun.*, 2020, **56**, 8603 –8 606.

Acknowledgements
Technical and safety staff at QUB, Leiden and Utrecht Universities. RSC CBBG and QUB Emily Sarah Montgomery scholarship for travel and conference funding.

https://doi.org/10.17952/37EPS.2024.P1104

A series of novel, selective matriptase inhibitors

Dawid Dębowski [1], Aleksandra Helbik-Maciejewska [1], Agata Gitlin-Domagalska [1], Malihe Hassanzadeh [2], Antoine Désilets [2], Pierre-Luc Boudreault [2], Richard Leduc [2], Anna Łęgowska [1], Krzysztof Rolka [1]

[1] Department of Molecular Biochemistry, Faculty of Chemistry, University of Gdansk, Gdansk, Poland;
[2] Faculty of Medicine and Health Sciences, and Institut de Pharmacologie de Sherbrooke Universitéde Sherbrooke,Sherbrooke, Québec (Canada)

Background

Even though both type II transmembrane serine proteases (TTSPs), matriptase-1 (MT1) and matriptase-2 (MT2) share significant structural similarity and substrate specificity, they differ in biological functions [1].

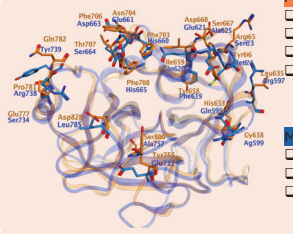

MT1-MT2 active site superimposition

MT1
- ❑ widely expressed in all types of epithelial tissues
- ❑ maintains integrity of epithelial tissues
- ❑ increased expression reported in epithelial cancers
- ❑ in breast and prostate cancers increased expression is considered as a predictive factor of poor disease prognosis

MT2
- ❑ mostly localized in the liver
- ❑ regulates iron homeostasis
- ❑ differently from MT1, a positive correlation between its increased level and prognosis in the breast cancer patients

We have shown recently, that the gradual shortening of the primary structure of Chinese frog-skin derived inhibitor (HV-BBI, *Huia versabilis* Bowman-Birk inhibitor, 18-amino acids) led to strong non-covalent, disulfide-bridged MT1 inhibitor (13-amino acids) with *C*-terminal amide group [2].

Gly[1]-Cys-Trp-Thr-Lys-Ser-Ile-Pro-Pro-Arg-Pro-Cys-Phe[13]-NH_2

strong MT1 inhibitor K_i = 8.5 nM
weak MT2 inhibitor K_i = 7900 nM

Moreover, this inhibitor has presented unprecedented specificity toward MT1 as compared to MT2. The K_i value was almost **1000-times lower for MT1 than for MT2**. To the best of our knowledge, such significant selectivity, combined with high inhibitory potency, have not been reported so far, for any known MT1 inhibitors.

Objectives

Molecular dynamic (MD) study was applied to explain significant difference in binding of the inhibitor with MT1 and MT2.



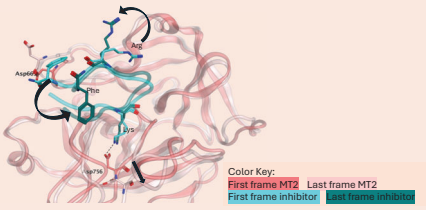

MT1
- ❑ the P1 inhibitor's Lys[5] forms a stable hydrogen bond with the MT1 Asp799 at the bottom of S1 pocket
- ❑ the inhibitor's Arg[10] forms a hydrogen bond interaction with the MT1 Arg662 (not present in MT2)
- ❑ initially, the inhibitor's *C*-terminal Phe[13] is in close distance to the MT1 Phe706 in S4 pocket (first frame), however, after reaching a stable conformation, the *C*-terminal tail bends towards the MT1 active site (last frame)

MT2
- ❑ the P1 inhibitor's Lys[5] don't form a hydrogen bond with the MT1 Asp756 in S1 pocket
- ❑ Asp756 relocates from its initial position, moving away from the inhibitor's P1 Lys[5]
- ❑ initially, the inhibitor's *C*-terminal Phe[13] is located in close distance to the MT2 Asp663 in S4 pocket and after reaching a stable conformation, the tail bends towards the MT1 active site

MD study has underscored dynamic behavior of the inhibitor's *C*-terminal tail. It was shown that the inhibitor's Phe[13] moves from the MT1 hydrophobic region towards the active site. As a result, an expected and potentially favorable interaction between Phe[13] and Phe706 benzene rings has been abolished.

Our goal was to verify experimentally these MD findings. Hence, the Phe[13] was substituted with various proteinogenic and non-proteinogenic amino acids including (Fig.1): (i) amino acids more hydrophobic than Phe which may provide stronger interactions with Phe706; (ii) more hydrophilic such as Lys; (iii) as well as Gly deprived of any side chain (considered as control).

Results

Table.1 List of synthesized peptides

Name	Inhibitor sequence
H	Gly-Cys(&)-Trp-Thr-Lys-Ser-Ile-Pro-Pro-Arg-Pro-Cys(&)-**Phe**-NH_2
H-1	Gly-Cys(&)-Trp-Thr-Lys-Ser-Ile-Pro-Pro-Arg-Pro-Cys(&)-**DPhe**-NH_2
H-2	Gly-Cys(&)-Trp-Thr-Lys-Ser-Ile-Pro-Pro-Arg-Pro-Cys(&)-**diPhe**-NH_2
H-3	Gly-Cys(&)-Trp-Thr-Lys-Ser-Ile-Pro-Pro-Arg-Pro-Cys(&)-**Bpa**-NH_2
H-4	Gly-Cys(&)-Trp-Thr-Lys-Ser-Ile-Pro-Pro-Arg-Pro-Cys(&)-**PheTrt**-NH_2
H-5	Gly-Cys(&)-Trp-Thr-Lys-Ser-Ile-Pro-Pro-Arg-Pro-Cys(&)-**PheF**-NH_2
H-6	Gly-Cys(&)-Trp-Thr-Lys-Ser-Ile-Pro-Pro-Arg-Pro-Cys(&)-**Bip**-NH_2
H-7	Gly-Cys(&)-Trp-Thr-Lys-Ser-Ile-Pro-Pro-Arg-Pro-Cys(&)-**NPhe**-NH_2
H-8	Gly-Cys(&)-Trp-Thr-Lys-Ser-Ile-Pro-Pro-Arg-Pro-Cys(&)-**PheNO$_2$**-NH_2
H-9	Gly-Cys(&)-Trp-Thr-Lys-Ser-Ile-Pro-Pro-Arg-Pro-Cys(&)-**Gly**-NH_2
H-10	Gly-Cys(&)-Trp-Thr-Lys-Ser-Ile-Pro-Pro-Arg-Pro-Cys(&)-**Trp**-NH_2
H-11	Gly-Cys(&)-Trp-Thr-Lys-Ser-Ile-Pro-Pro-Arg-Pro-Cys(&)-**Lys**-NH_2
H-12	Gly-Cys(&)-Trp-Thr-Lys-Ser-Ile-Pro-Pro-Arg-Pro-Cys(&)-**NMePhe**-NH_2
H-13	**Phe**-Cys(&)-Trp-Thr-Lys-Ser-Ile-Pro-Pro-Arg-Pro-Cys(&)-Phe-NH_2

& - cyclization, disulfide bridge

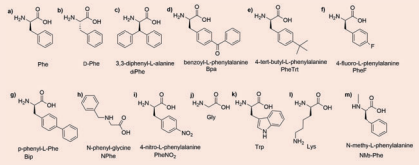

Fig.1 Amino acids introduced instead of Phe[13]

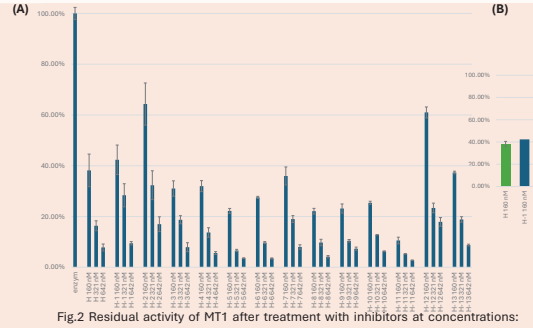

Fig.2 Residual activity of MT1 after treatment with inhibitors at concentrations: 160 nM, 321 nM, 642 nM; **(A)** all results together, **(B)** each concentration separately.

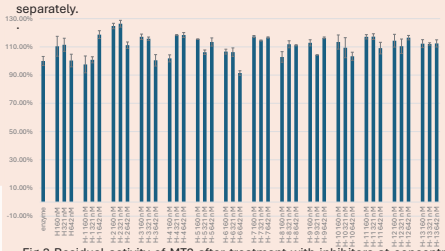

Fig.3 Residual activity of MT2 after treatment with inhibitors at concentrations: 160 nM, 321 nM, 642 nM.

Table 2. IC_{50} and K_i values measured for the selected most active inhibitors.

analog	AA in 13	nM	
		IC_{50}	K_i
H	Phe	31.60±4.6	26.15±3.81
H-5	PheF	16.80±1.20	**13.90**±0.99
H-6	Bip	17.60±1.30	**14.57**±1.08
H-9	Gly	33.10±2.70	27.39±2.23
H-11	Lys	19.30±1.10	**15.97**±0.91

Methods

Peptides were synthesized using Fmoc/tBu chemistry on Rink Amide resin. The peptide chain was elongated in the consecutive cycles of deprotection and coupling. Deprotection was performed with 20% piperidine in DMF, and peptide chains elongation was done using 3-fold molar excess of each Fmoc-protected amino acid, TBTU/HOBt/NMM (molar ratio 1:1:1:2). After completing the synthesis, peptides were cleaved from the resin and the protecting groups were removed in a one-step procedure using a mixture of TFA:phenol:triisopropylsilane:H_2O (88:5:2:5, v/v/v/v). The disulfide bridge was formed using a 0.1 M methanolic iodine solution.
Crude compunds were purified by reverse-phase high performance liquid chromatography (RP-HPLC) on PLC 2050 Gilson HPLC with Grace Vydac C18 HPLC column (22 × 250 mm, 10 µm, 300 Å). The solvent system was 0.1% TFA (A) and 80% acetonitrile in A (B). The purity of each peptide was checked by RP-HPLC on a Shimadzu Prominence-I LC-2050C 3D equipped with a Kinetex XB-C18 column (150 × 4.6 mm, 5 µm) and a UV-Vis detector. A linear gradient 10%-90%B for 20 min, flow rate 1 mL min^{-1}, and detection at 214 nm was used. The mass spectrometry analysis was carried out on MALDI MS (Autoflex maX MALDI-TOF spectrometer, Bruker Daltonics).
The activities of the purified, recombinant enzymes were assessed using fluorogenic substrate Boc-QAR-MCA by Fluostar Omega plate reader (BMG Labtech) with an excitation wavelength of 360 nm and emission wavelength 450 nm. The IC_{50} values (inhibitor concentrations giving 50% inhibition) were calculated using a four parameter fit model (GraFit Erithacus Software Ltd). The K_i values were calculated using the Cheng-Prusoff equation, assuming the competitive mode of inhibition, according to the following relationship: $IC_{50} = K_i(1+S/K_m)$ where K_m is Michaelis constant (48 µM), S is substrate concentration 10 µM. Enzyme concentration was 0.25 nM.
Molecular dynamic study: MT1 (PDB ID: 3P8F) and MT2 (Homology model). The homology model was constructed starting from the published crystal structure of MT1 [3]. GROMACS: MD simulation; 500 ns. MOE: Analysis and Visualization. The method was validated using SFTI-1 – MT1 complex (PDB:3P8F). "The first frame" and "The second frame" refer to the initial and last molecular dynamics poses of the inhibitors in the active sites of the MT1 and MT2 receptors.

Conclusions

- ❑ Despite various *C*-terminal modifications, all inhibitors retained inhibitory activity towards MT1 (Fig.2) and significant specificity – they did not block MT2 (Fig.3)
- ❑ Peptides H-5 (PheF[13]), H-6 (Bip[13]) and H-11 (Lys[13]) are stronger inhibitors of MT1 than the parent peptide H; their K_i values are almost 2 times lower than that of peptide H with Phe[13] (Table 2)
- ❑ High, almost the same activity of H-6 with hydrophobic and bulky 4-phenyl-phenylalanine (Bip[13]) and H-11 with hydrophilic Lys[13] may be regarded as an experimental confirmation of MD study that pointed out dynamic behavior of *C*-terminal tail.
- ❑ High activity of H-11 and weak activity of H-2 with hydrophobic, spatial diPhe[13] question the role of interaction between *C*-terminal inhibitor's tail and hydrophobic Mat1 S4 pocket surrounded by Phe703, Phe706, Phe708, and Trp826. This is consistent with MD study showing that the *C*-terminal tail appears to distance itself from this region and change its surroundings.
- ❑ It may be speculated that surprising difference in inhibitory activity between H-2 (low activity) and H-6 (high activity) is related to different space hindrances caused by diPhe[13] and Bip[13], rather than to, for example, entropic penalty.
- ❑ MD study underscores the importance of intramolecular hydrogen bonding, including interaction between the amide group of *C*-terminal Phe[12] and carbonyl oxygen of Trp[3], which stabilize specific inhibitor's conformation more conducive for binding to the enzyme. Low inhibitory activity of peptide H-12 with *N*-methylated Phe confirms this finding. *N*-methylated Phe is unable to form such interaction. However, the importance of intramolecular hydrogen bonding is challenged by peptide H-7 having NPhe (due to side chain C→N shift is unable to form hydrogen bond) which presents activity comparable to that of parent peptide H.
- ❑ Further MD study are necessary to explain the reported results.

References

1. Murza A., et. al (2020) Inhibitors of Type II transmembrane serine proteases in treatment of diseases of the respiratory tract. Expert Opinion on Therapeutic Patents. 30(11): 807-824.
2. Gitlin-Domagalska, A., Dębowski, D., et al. (2020) Truncation of Huia Versabilis Bowman-Birk Inhibitor Increases Its Selectivity, Matriptase-1 Inhibitory Activity and Proteolytic Stability. Biochimie, 171–172, 178–186.
3. St-Georges, C. et al. (2017) Modulating the Selectivity of Matriptase-2 Inhibitors with Unnatural Amino Acids. Eur. J. Med. Chem., 129, 110–123.

Total Synthesis and Semi-synthesis of Fluorinated Analogues of the Antifungal Cyclic Lipopeptide Iturin A

Periklis Karamanis[a,b*], Matthew Kiernan[a,b], Jimmy Muldoon[a], Paul Evans[a,b], Cormac D. Murphy[b,c], Marina Rubini[a,b]

[a] School of Chemistry, University College Dublin, Belfield, Dublin, Ireland, [b] BiOrbic Bioeconomy SFI Research Centre, University College Dublin, Belfield, Dublin, Ireland [c] School of Biomolecular and Biomedical Science, University College Dublin, Belfield, Dublin, Ireland

periklis.karamanis@ucdconnect.ie



https://doi.org/10.17952/37EPS.2024.P1105

Introduction

Iturin A

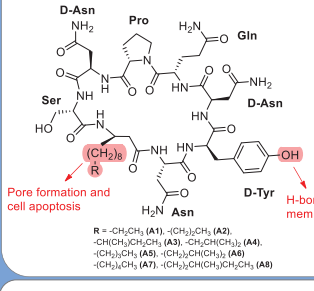

R = -CH_2CH_3 **(A1)**, -$(CH_2)_2CH_3$ **(A2)**, -$CH(CH_3)CH_2CH_3$ **(A3)**, -$CH_2CH(CH_3)_2$ **(A4)**, -$(CH_2)_3CH_3$ **(A5)**, -$(CH_2)_2CH(CH_3)_2$ **(A6)**, -$(CH_2)_4CH_3$ **(A7)**, -$(CH_2)_2CH(CH_3)CH_2CH_3$ **(A8)**



Cyclic lipopeptide produced by *Bacillus subtilis.*



Potent **antifungal agent** against several fungal pathogens, including *Fusarium graminearum and Candida albicans.*[1]



Its **structure** consists of seven α-amino acids and a β-amino acid with varying alkyl side chains (iturin A1-A8).[1]

Fluorine in Peptide Engineering



+ 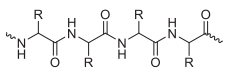 =

- Enhanced hydrogen bond formation capacity.
- Enhanced metabolic stability.
- Isostere of C-H and C-OH moieties.
- New characterization techniques available (such as ^{19}F NMR).[2,3]

Synthesis and characterization of iturin A analogues

1. Synthesis of the β-amino fatty acid

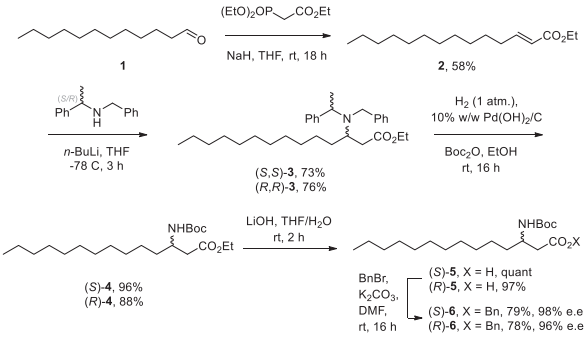

2. Solid phase peptide synthesis and cyclisation reactions

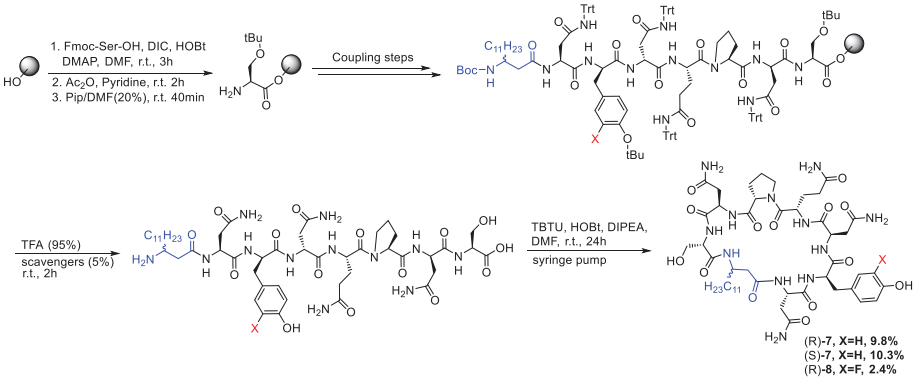

3. HPLC purification (blue) and ESI LC-MS characterisation (red) of the obtained cyclic lipopeptides

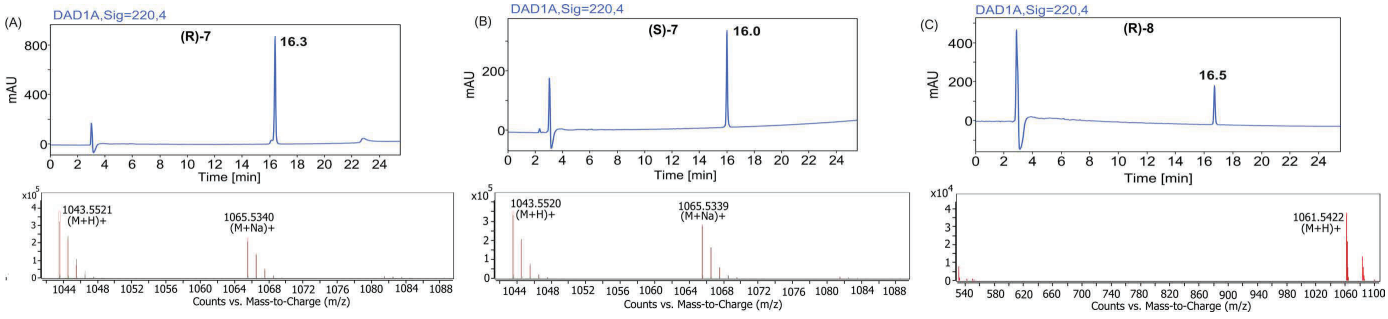

Late-stage trifluoromethylation of natural iturin A

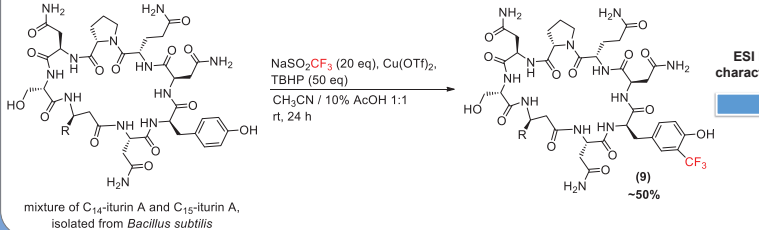

mixture of C_{14}-iturin A and C_{15}-iturin A, isolated from *Bacillus subtilis*

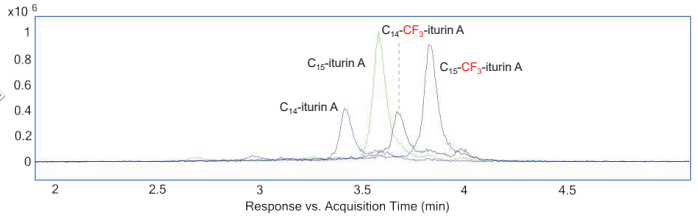

Antifungal assays

Compound	Minimum inhibitory concentration (μg/mL)	
	Fusarium graminearum	*Candida albicans*
Amphotericin B	<7.8	<7.8
Commercial iturin A	31.2	62.5
(R)-7	15.6	62.5
(S)-7	>1000	>1000
(R)-8	15.6	62.5

Concentration range tested: 7.8 – 1000 μg/mL

Conclusions and outlook

- A novel synthetic route to obtain iturin A analogues has been developed.[4]
- The importance of the stereochemistry of the β-amino fatty acid on the bioactivity of the natural lipopeptide has been elucidated, as the non natural epimer is significantly less bioactive.
- The obtained monofluorinated iturin A analogue displays identical bioactivity to the natural compound and can be a useful ^{19}F NMR probe.
- A high yielding semi-synthetic method to obtain trifluoromethylated iturin A analogues has been shown.

Future work:

- Antifungal assays to assess the bioactivity of the trifluoromethylated iturin A analogues, when compared to the natural lipopeptide.
- ^{19}F NMR studies to investigate the mode of binding of iturin A to the fungal membrane.

References

(1) D. A. Yaraguppi, Z. K. Bagewadi, N. R. Patil, N. Mantri, *Biomolecules* **2023**, *13*, 1515.
(2) C. Jäckel, B. Koksch, *Eur J Org Chem* **2005**, *2005*, 4483.
(3) D. Gimenez, A. Phelan, C. D. Murphy, S. L. Cobb, *Beilstein J. Org. Chem.* **2021**, *17*, 293.
(4) P. Karamanis, J. Muldoon, C. D. Murphy, M. Rubini, *Journal of Peptide Science* **2024**, *30*, e3569.

Acknowledgments

The authors would like to thank Dr Yannick Ortin for his aid in the NMR analyses, as well as Dr Mohd Faheem Khan and Dr Aniello Palma for the fruitful discussions regarding the antifungal assays and the peptide synthesis. Lastly, we would like to thank Finn Doyle for his contribution to the synthesis of the lipopeptides.

The A2P CDT is supported by the Science Foundation Ireland (SFI) and the Engineering and Physical Sciences Research Council (EPSRC) under Grant No. 18/EPSRC-CDT/3582.

BiOrbic, Bioeconomy SFI Research Centre, is an SFI Research Centre funded under the Science Foundation Ireland Research Centres Programme.

Design and antimicrobial activity of short and novel tripeptides

Ilaria Di Stefano[1], Silvia Rizzo[1], Dario Corbisiero[1] , Francesca Bonvicini[1] , Giovanna Angela Gentilomi[1], Walter Cabri[1], Tainah Dorina Marforio[1], Lucia Ferrazzano[1], Alessandra Tolomelli[1]
[1]Univesità di Bologna - Alma Mater, Bologna, Italy
Ilaria.distefano3@unibo.it

https://doi.org/10.17952/37EPS.2024.P1106

Introduction

Antimicrobial peptides (AMPs) are promising antibacterial agents that could avoid the problematic development of drug resistance. The main advantage of using AMPs is related to their peculiar mechanism of action involving the lytic disruption of the bacterial cellular membrane of both Gram-positive and Gram-negative bacteria. Among the AMPs, Lytixar (LTX-109) is an interesting short tripeptide containing a bulky hydrophobic moiety (Tbt) and cationic amino acids (Arg). In this work we explored structural amphiphilic alternatives to LTX-109 and investigated, through molecular modelling, their interaction with the bacterial membrane, disclosing the critical moieties involved in the lytic mechanism of action. Thus, structural changes were synthetically introduced to evaluate the effect on the antimicrobial activity and the metabolic stability of these new molecules. SAR studies were used to rationalize the combined effect of lipophilicity, steric hindrance and charges.

Synthesis

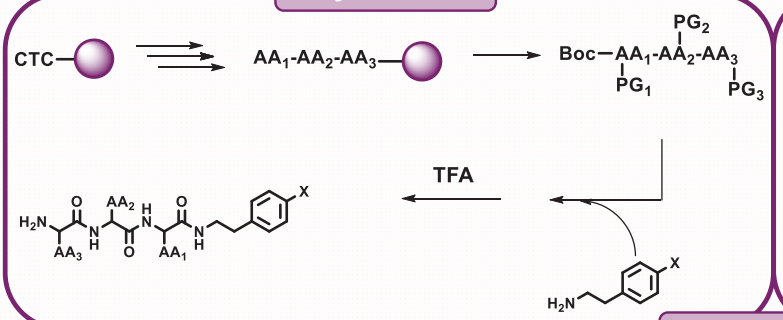

SAR studies

From SAR studies lipophilicity was evaluated, and eventually used to rationalize antibiotic activity. LogKow showed how *para* substitution influenced lipophilicity and, according to biological data, to higher values corresponded better activities. Introduction of 2,5,7-Tris-tert-butyl-tryptophan (tBt) lead to a significant increase of lipophilicity as it did for activity. Interestingly, hystidine substitution corresponded to an increase of LogKow values and, in some cases, to a better activity; especially in the sequences containing tBt instead of Trp.

	LogKow
RTR-H	5.50
RTR-I	6.67
RTR-F	5.70
RTR-CF_3	6.46
RTR-tBu	7.41
RWR-H	-0.23
RTH-H	6.28
HTR-H	6.28

Target Library

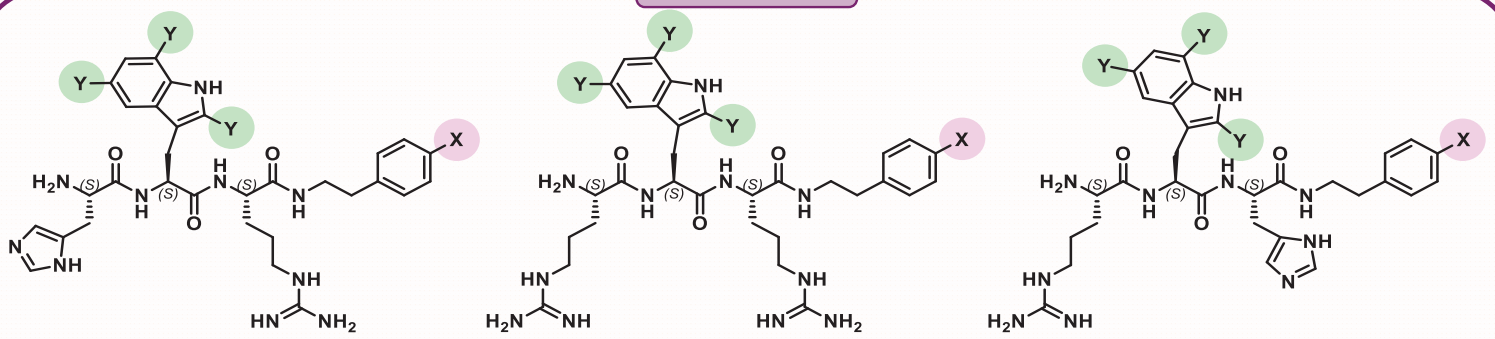

Biological results

According to IC50 values good results were obtained for peptides containing the bulky, unnatural tri-tert-butyl-triptophan residue (T) and little variation of activity was reported by the aromatic ring para-substituted compounds. The influence of these substitutions was tested on the W series tripeptides. Iodine derivatives demonstrated better activity than the -F and -CF_3 substituted, indicating that sterical effects might be more significant on biological activity than electronic ones. According to MHC and CC50 values none of the tested molecules demonstrated hemolytic activity (at MIC concentrations) nor relevant cytotoxicity. For what concerns selectivity (SI), all peptides of the T series showed good results compared to the original LTX.

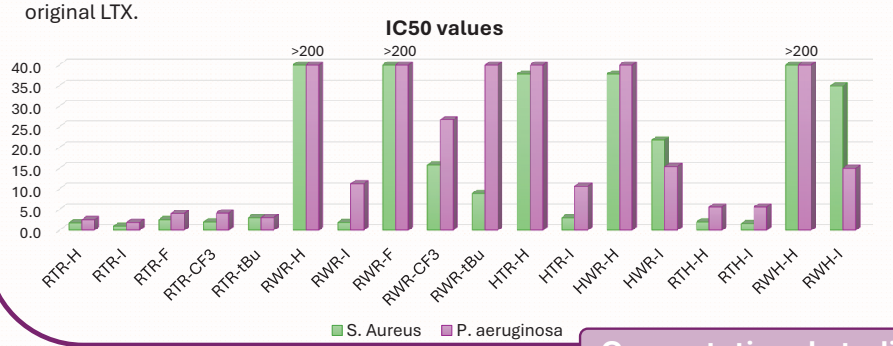

	CC50 (µg/mL)	Selectivity index (CC50/IC50)		MHC
	Hel299 cells	S. aureus	P. aeruginosa	
RTR-H	47.4	26.3	19.0	200.0
RTR-I	24.1	24.1	12.7	50.0
RTR-F	50.6	20.2	12.3	50
RTR-CF_3	28.9	14.4	6.9	25
RTR-tBu	19.39	6.4	6.4	6.25
RWR-H	200.0	n.d.	n.d.	>200
RWR-I	123.2	64.8	11.0	200.0
RWR-F	86.4	n.d.	n.d.	>200
RWR-CF_3	>200	>12.6	>7.5	200
RWR-tBu	200	n.d.	n.d.	200
HTR-H	54.0	18.0	5.1	100
HTR-I	179.6	6.8	1.9	>200
HWR-H	200.0	5.2	2.4	>200
HWR-I	>200	>9.2	>13.0	>200
RTH-H	29.5	14.8	5.3	50
RTH-I	23.7	14.8	4.2	25
RWH-H	200.0	n.d.	n.d.	>200
RWH-I	93.5	2.7	6.2	>200

Computational studies

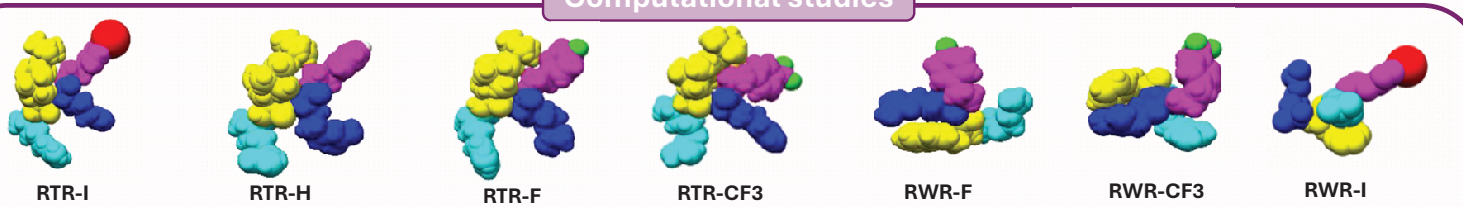

MD studies were performed to evaluate the most populated conformations in water. These results showed a characteristic "X" shape where the hydrophobic moieties of the tbt and Ph(X) are close in contact, pushing the arginines to the opposite side. Docking with Gram+ e Gram- bacterial membrane showed that X conformation is crucial for correct lytic mechanism of action influencing the orientation of interaction with the membrane as antibiotic activity. In fact, molecules containing Trp instead of tBt are not able to adopt this conformation and this behavior is reflected in their scarce antibiotic activity.

Wang J, Dou X, Song J, et al, Med Res Rev. **2019**; 39: 831–859, Koo HB, Seo J, Pept Sci. **2019**; 111:e24122; J. Isaksson, B.O. Brandsdal, M. Engqvist, G.E. Flaten, J.S.M. Svendsen, W. Stensen, J. Med. Chem. **2011**; A. Sivertsen, J. Isaksson, H.-K.S. Leiros, J. Svenson, J.-S. Svendsen, B.O. Brandsdal, BMC Structural Biology **2014**; Ferrazzano, F. Bonvicini, T.D. Marforio et al., manuscript under preparation.

https://doi.org/10.17952/37EPS.2024.P1109

SHORT ANALOGUES OF CATHELICIDINS PMAP-36 AND BMAP-27: STRUCTURE-ACTIVITY RELATIONSHIP AND STABILITY TO PROTEOLYSIS

C. Peggion,[1] A. Schivo,[1] F. Albini,[1]
A. Di Stasi,[3] B. Biondi,[2] M. Mardirossian[3]

[1] Department of Chemical Sciences, University of Padova, Padova, Italy
[2] Institute of Biomolecular Chemistry, CNR, Padova, Italy
[3] Department of Life Sciences, University of Trieste, Trieste, Italy

1 – Introduction

Due to the widespread use of antibiotics, bacterial antibiotic resistance has become a major global health problem in recent years. PMAP-36 and BMAP-27 are natural antimicrobial peptides that belong to the cathelicidin family and have broad-spectrum antibacterial activity. The mechanism of action of these peptides hampers the development of bacterial resistance, making them promising for the development of new drugs.

Poor stability in the cellular environment is a limitation for the use of these molecule, but it can be increased by inserting D-configured amino acids into the peptide sequences.

2 – Aim

We present the synthesis of peptide sequences derived from PMAP-36 and BMAP-27 containing all-L and all-D amino acids,

Aim:
- to understand whether the shortened analogues PMAP36(12-24) and BMAP27(1-18) retained the helical structure of the original peptides and thus their antimicrobial activity
- to investigate their stability in proteolytic medium and their cytotoxicity in cells.

List of the synthetized peptides and of their physico-chemical properties

	Name	Peptide Sequence
	PMAP-36	H-GRFRRLRKKTRKRLKKIGKVLKWIPPIVGSIPLGCG-NH_2
a	L-PMAP36(12-24)	Ac-KRLKKIGKVLKWI-NH_2
b	D-PMAP36(12-24)	Ac-krlkkigkvlkwi-NH_2
	BMAP-27	H-GRFKRFRKKFKKLFKKLSPVIPLLHLG-NH_2
c	L-BMAP27(1-18)	Ac-GRFKRFRKKFKKLFKKLS-NH_2
d	D-BMAP27(1-18)	Ac-grfkrfrkkfkklfkkls-NH_2

3 – Synthesis

SPPS
- Fmoc/tBu
- Activation: DIC/Oxyme
- Cleavage: TFA/TIS/H_2O (95:2.5:2.5)

PURIFICATION
- Authomatic flash chromatography (column: C18, 100 Å, 12g cartridge)

CHARACTERIZATION
- analytical HPLC
- ESI-MS

	Theoretical MW $[M+H]^+_{calcd}$	Experimental MW $[M+H]^+_{exp}$	Retention time* t_R(min)
a	1651.1	1651.1	13.5
b	1651.1	1651.1	12.4
c	2383.5	2383.1	11.4
d	2383.5	2383.1	14.7

*Retention time refers to 10-40%%B (CH_3CN/H_2O, 9:1) over 30 min gradient for **a** and **b** and 15-45%B over 30min gradient for **c** and **d**.

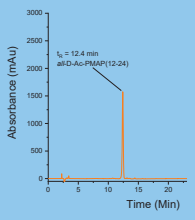

HPLC profile of peptide **b** (10-40%%B over 30 min

Biological Activity

- D-peptides are as active as L-peptides. In some cases, they are even more active
- D-peptides are not toxic at the concentrations required for bacterial activity

Proteolytic resistance

- The two L-peptides are rapidly degraded by both trypsin and human serum.
- In contrast, D-peptides are degraded at a much slower rate and remain intact for at least 24 hours.

Conformation

- Short PMAP and BMAP analogues retain the helical structure of the native peptide
- NMR confirms the helical propensity of the two shortened peptides: long range NOEs signals are observed

CONCLUSION

The designed short peptides, which contain D-amino acids, are
→ capable of maintaining both the conformation and the activity of the native peptides
→ stable in physiological proteolytic environments

4 – Conformation

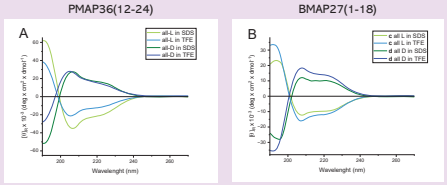

CD spectra of (**A**): L-PMAP36(12-24) (**a**) and D-PMAP36(12-24) (**b**). (**B**): L-BMAP27(1-18) (**c**) and D-BMAP27(1-18) (**d**). The spectra were taken in SDS (blue) and TFE (green), at 25°C.

Circular Dichroism (CD) measurements in 100mM sodium dodecyl sulphate (SDS) and 2,2,2-trifluoroethanol (TFE). SDS was selected as a membrane-like environment, while TFE was chosen as a helix inducer solvent. The secondary structure of the D-peptides is the mirror image of that of the L-peptides

NMR 2D spectra were registered for all the four peptides. Long range NOEs typical of helical conformation were observed.

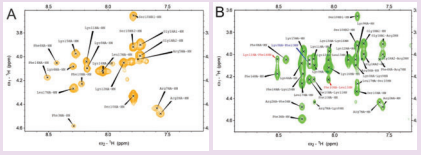

L BMAP(1-18): (**A**) Region of the TOCSY spectrum of peptide **c**. (**B**) Fingerprint region of the NOESY spectrum of peptide **c**. The αCH(i)→ NH(i+2) and αCH(i)→ NH(i+3) cross-peaks are highlighted in blue and red, respectively (600MHz, TFE d2, 308K).

5 – Biological activity

Peptide	MIC (μM) E.coli ATCC 25922	S.aureus ATCC 25923	A.baumanni ATCC 19606	K.pneumoniae ATCC 700603	P.aeruginosa ATCC 27853	S.epidermidis ATCC 12228
all-L-Ac-PMAP(12-24)	4	>64	2	4	8	4
all-D-Ac-PMAP(12-24)	2	16	2	4	4	4
all-L-Ac-BMAP(1-18)	8	16	8	16	16	2
all-D-Ac-BMAP(1-18)	4	8	8	8	8	1

Antibacterial activity against Gram-negative and Gram-positive bacteria. *MIC, minimum inhibitory concentration is the lowest peptide concentration causing no visible growth after 18 h incubation in Mueller–Hinton broth at 37°C.

High antimicrobial activity was observed for L-PMAP(12-24) and D-PMAP(12-24) toward *E. coli, A. baumannii, K. pneumoniae, P. aeruginosa, and S. epidermidis.* L-BMAP(1-18) and D-BMAP(1-18) are active against *S. epidermidis.*
All-D peptides are more toxic than L-peptides only at high concentrations.

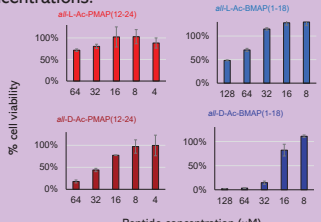

Cytotoxicity was measured by the MTT assay on human immortalized epidermal keratinocyte HaCaT cell line

6 – Proteolytic resistance

The stability of the peptides in presence of trypsin or serum was monitored by HPLC.

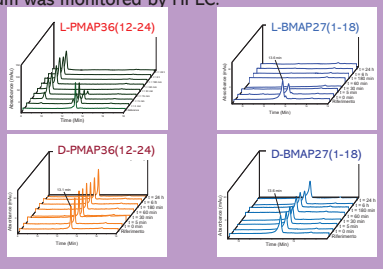

HPLC profiles of peptides in Trypsin. Left, peptides **a** and **b**; right, peptides **c** and **d**. Gradient 5-65%B in 30mins. UV-vis detector at 214nm.

Proteolytic resistance to trypsin: peptides with all L-amino acids were degraded in less than half an hour, whereas peptides with all D-amino acids were not degraded at all.

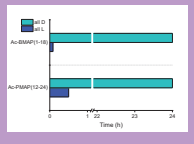

Results of the trypsin degradation tests on the four peptides in human serum at 37°C.

A similar result is obtained from the degradation in human serum, where D-peptides are not degratated in the firs 24 hours.

REF. Biondi, B.; De Pascale, L.; Mardirossian, M.; Di Stasi, A.; Favaro, M.; Scocchi, M.; Peggion, C., Sci. Rep., 2023, 13,15132

Finanziato dall'Unione europea NextGenerationEU

This work was supported by the NextGenerationEU-MUR PNRR Extended Partnership initiative on Emerging Infectious Diseases (Project no. PE00000007, INF-ACT)

HBP-5: A Leading Heparin-Binding Peptide with Remarkable Activity against Gram-negative Bacteria

Roberto Bello Madruga [1], Daniel Sandín [1], Javier Valle [2], David Andreu [2] and Marc Torrent [1]

roberto.bello@uab.cat

[1] Systems Biology of Infection Lab, Department of Biochemistry and Molecular Biology, UAB, Cerdanyola del Vallès 08193. Spain

[2] Universitat Pompeu Fabra, Department of Medicine and Life Sciences, Barcelona Biomedical Research Park, Barcelona 08003. Spain

https://doi.org/10.17952/37EPS.2024.P1110

BACKGROUND

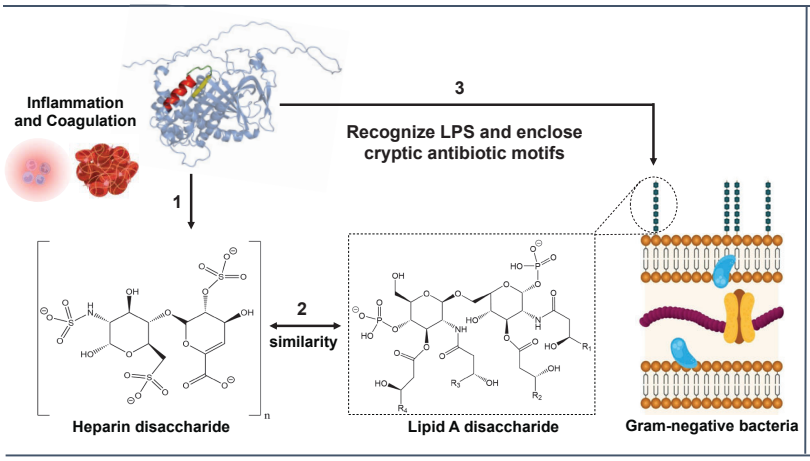

METHODOLOGY

- Use the AMPA predictor to identify antimicrobial regions in Heparin-Binding Proteins (HBPs).
- Identification of Heparin Binding sites (CPC` motif) in cryptic peptides and evaluation of their affinity by molecular docking.
- Synthesis and validation of the best candidates corresponding to the regions with the highest AMPA and Heparin-binding score.

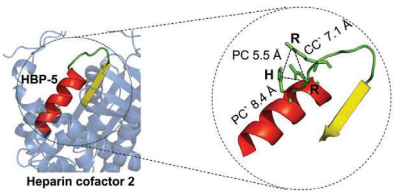

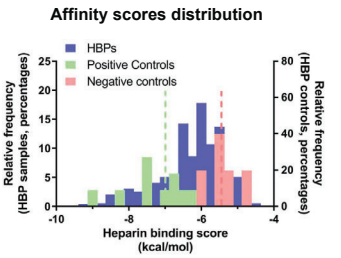

RESULTS

1 Antimicrobial Activity, Heparin-LPS Affinity and Toxicity of HBPs peptides

	Minimum Inhibitory Concentration (μM)						Heparin, LPS Affinity and Toxicity			
	E. coli	*A. baumannii*	*P. aeruginosa*	*S. aureus*	*E. faecium*	*L. monocytogenes*	Heparin Affinity (% Elution buffer)	LPS Affinity (EC50, μM)	Hemolysis % (125 μM of peptide)	MRC-5 cytotoxicity (IC50, μM)
HBP-1	1.6	1.6	3.1	50	100	6.3	60	42 ± 16	4.6 ± 0.6	>200
HBP-2	12.5	50	25	>100	>100	37.5	59	1500 ± 600	2 ± 1	>200
HBP-3	3.1	0.8	6.3	25	>100	6.3	68	7 ± 5	4 ± 1	>200
HBP-4	0.2	0.8	0.8	3.1	12.5	1.6	82	0.7 ± 0.6	15.5 ± 0.1	35 ± 1
HBP-5	0.4	0.2	0.8	6.3	25	1.6	98	0.9 ± 0.7	10.3 ± 0.2	69 ± 2
LL-37	1.6	6.3	0.8	25	0.8	0.8	50	0.9 ± 0.8	32.7 ± 0.7	26 ± 3

2 Mechanism of Action of HBP-derived Antimicrobial Peptides

Cell Membrane depolarization

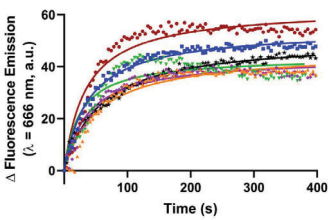

Outer Membrane permeabilization

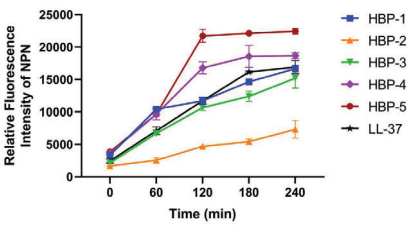

3 Structural Analysis by Circular Dichroism

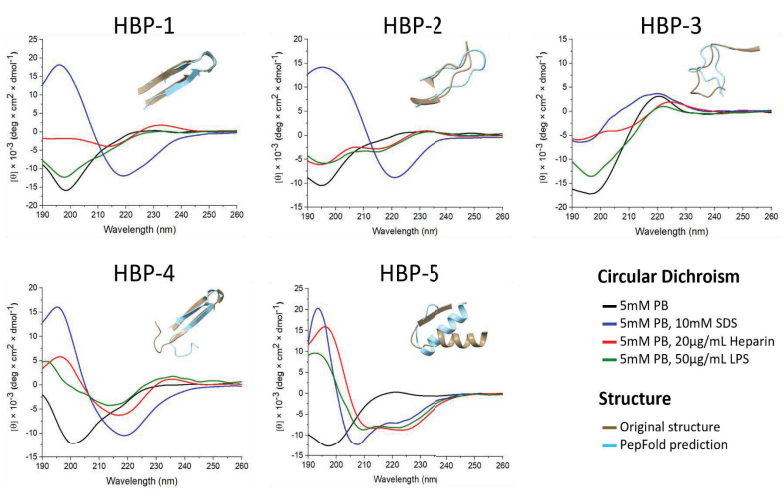

4 Characterization of HBP-5 peptide

Chemical shifts induced by Heparin

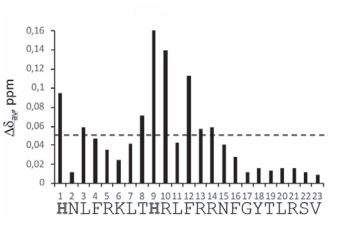

Distances between CPC' residues involved in Heparin binding

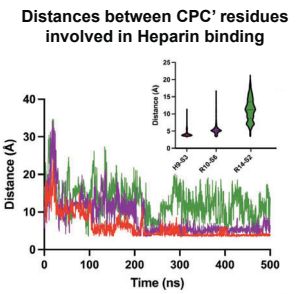

Why HBP-5 is a leading peptide ?

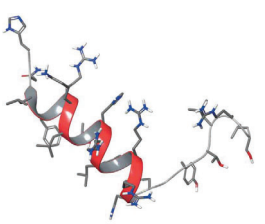

- Broad spectrum of antibacterial activity
- Non-cytotoxic and non-hemolytic
- Bacterial cell depolarization and permeabilization
- High affinity for LPS

Conclusions

- We have shown that **Glycosaminoglycans-binding proteins can be a source of new AMPs**, some with remarkable activity, **particularly against Gram-negative bacteria**.
- The fact that **these peptides can bind to both Heparin and LPS** is consistent with the **structural similarity hypothesis.**

What`s next

- Investigate the structural determinants of HBP-5 and their implication on the antibacterial mechanism.
- Optimize and evaluate HBP-5 peptide in an *in vivo* infection model.

https://doi.org/10.17952/37EPS.2024.P1112

INHIBITORY ACTIVITY AND PROTEOLYTIC STABILITY IN HUMAN SERUM OF PEPTIDE INHIBITORS OF THE VEGF-A_{165} / NRP-1 COMPLEX

Dagmara TYMECKA[1], Patrycja REDKIEWICZ[2], Piotr F.J. LIPIŃSKI[2], Aleksandra MISICKA[1]

[1] Faculty of Chemistry, University of Warsaw, Pasteura 1, 02-093 Warsaw, Poland,

[2] Department of Neuropeptides, Mossakowski Medical Research Institute Polish Academy of Sciences, Pawińskiego 5, 02–106 Warsaw, Poland

email addresses: dulok@chem.uw.edu.pl, (D. Tymecka) or misicka@chem.uw.edu.pl (A. Misicka)

INTRODUCTION

Neuropilin-1 (NRP-1) is a cell surface receptor involved in a wide variety of signaling pathways, including physiological and pathological processes of angiogenesis. Its overexpression is associated with tumor aggressiveness and metastasis, which is observed, inter alia, in breast, pancreatic, prostate, colon cancer or brain tumors (e.g. gliomas) [1].
One of the most important ligands of NRP-1 and the main mediators of angiogenesis is vascular endothelial growth factor A_{165} (VEGF-A_{165}), which acts as a pro-angiogenic factor by interacting with NRP-1.

Compounds that block this interaction are potential inhibitors of the VEGF-A_{165}/NRP-1 complex that may find application in the diagnosis and therapy of cancer.
One of a significant achievement in this field was the identification (by screening a mutant phage library) of the heptapeptide Ala-Thr-Trp-Leu-Pro-Pro-Arg (A7R), which selectively inhibits the binding of VEGF-A_{165} to NRP-1 and reduces angiogenesis and breast cancer growth *in vivo* [2, 3].

In our efforts along this track, based on the structure of the A7R C-terminal tetrapeptide, we designed stronger inhibitors, in particular: Lys(Har)-Dap-Pro-Arg (**1**) and Lys(Har)-Dab-Pro-Arg (**2**).
Detailed stability studies of these compounds in human plasma have shown that the first cleavage site is a detachment of the C-terminal arginine by carboxypeptidases, resulting in a loss of activity since arginine is a key element in the interaction between these inhibitors and NRP-1 [4].

PROJECT ASSUMPTIONS AND RESULTS

THE AIM OF OUR STUDY was to obtain more stable (and active) analogs of these branched peptidomimetics (**1** and **2**). To achieve this, we decided to substitute the C-terminal arginine with its mimetics (Table 1 and 2).

Table 1. Structure of the parent compounds and arginine mimetics used in our study.

PARENT COMPOUNDS

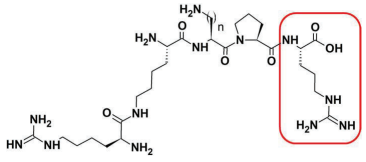

Dap[2] (n = 1) or Dab[2] (n=2)

ARGININE MIMETICS

Har	Agb	Agp	Cit	Phe(4-CH_2-NH_2)
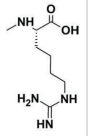	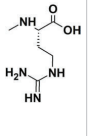	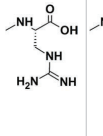	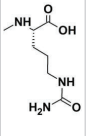	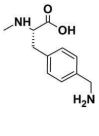

All compounds were synthesized using the standard SPPS-Fmoc/tBu protocol.

INTERACTION MODEL FOR COMPOUNDS 1 AND 2

In our previous work, based on molecular dynamics, we put forward an interaction model for compounds **1** and **2** [4]. According to this model:

- the branched peptidomimetics adopt more than one binding pose at the NRP-1 binding cleft, with two poses (BP1 and BP2) being dominant and in mutual equilibrium (Fig. 1);
- the peptidomimetics insert their C-terminal Arg residue in the shallow cleft at the protein surface and form several interactions, including H-bonds to Asp320, Ser346, Thr349;
- the middle and N-terminal parts of the peptidomimetic retain some residual mobility and switch between positioning BP1 and BP2, forming several interactions in each, including H-bonds to Gly318, Glu319, Glu324, Ser294, Tyr297, Glu348.

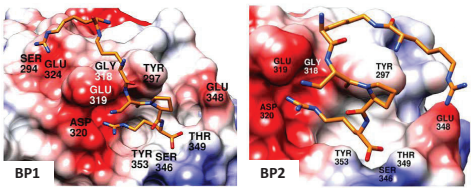

Figure 1. Two dominant binding poses found in molecular dynamics simulations for Lys(Har)-Dap-Pro-Arg as complexes with b1 domain of NRP-1. The NRP-1 receptor is depicted as an electrostatic color-coded surface (red: negative charges, white: neutral, blue: positive). Colors of ligands are orange, red and blue for carbon, oxygen and nitrogen, respectively. The peptidomimetics were modelled in the NRP-1 binding site (PDB: 2ORZ) using AutoDock4 (10.1002/jcc.21256).

DESIGN PRINCIPLES FOR PEPTIDES 3-12

With our desire to replace the C-terminal Arg, we took the described our previous model (Fig. 1) as a starting point for designing new peptides. We analyzed several possible modifications to the C-terminus:

- **Har**[4] - according to the crystal structure 5IJR [5], Har can be accommodated in the cleft although with some displacement of the binding mode compared to Arg is present in the cleft;
- **Agb**[4] or **Agp**[4] - we envisaged that some shortening in Xaa[4]-side chain should still be tolerated inside the binding cleft, given that the Lys(Har)[1] and Dap/Dab[2] side-chains are long and flexible and so that they should still be able to reach their interaction partners (Fig. 1);
- **Cit**[4] - for a kind of an acid-test to the importance of guanidine-Asp320 interactions: according to our modelling, Cit[4] side chain should enable forming one H-bond to Asp320 (but contrary to other analogues, without charge-assistance);
- **Phe(4-CH_2-NH_2)**[4] - to verify that the C-terminal residue with an aromatic ring could gain some affinity due to forming aromatic interactions with Tyr297.

INHIBITORY EFFECT OF OBTAINED PEPTIDOMIMETICS ON VEGF-A_{165} BINDING TO NRP-1

The inhibitory activity of the obtained compounds on VEGF-A_{165} binding to the NRP-1 was evaluated *in vitro* by modified competitive ELISA test following the previously described protocol [6].

Table 2. Inhibitory effect of obtained peptidomimetics on VEGF-A_{165} binding to NRP-1.

No	Structure	IC_{50} [μM] ± SD
A7R	Ala-Thr-Trp-Leu-Pro-Pro-Arg	11.3 ± 3.2
1	**Lys(Har)-Dap-Pro-Arg**	**8.4 ± 1.6**
2	**Lys(Har)-Dab-Pro-Arg**	**4.7 ± 0.6**
3	**Lys(Har)-Dap-Pro-Har**	**29.2 ± 1.8**
4	**Lys(Har)-Dab-Pro-Har**	**14.3 ± 2.3**
5	Lys(Har)-Dap-Pro-Agb	87.5 ± 10.3
6	Lys(Har)-Dab-Pro-Agb	105.7 ± 17.4
7	Lys(Har)-Dap-Pro-Agp	147.6 ± 45.9
8	Lys(Har)-Dab-Pro-Agp	164.7 ± 21.1
9	Lys(Har)-Dap-Pro-Cit	169.7 ± 55.6
10	Lys(Har)-Dab-Pro-Cit	193.3 ± 20.6
11	**Lys(Har)-Dap-Pro-Phe(4-CH_2-NH_2)**	**22.8 ± 5.9**
12	**Lys(Har)-Dab-Pro-Phe(4-CH_2-NH_2)**	**19.8 ± 1.8**

Odd numbers refer to compounds with Dap at position 2, where even numbers refer to compounds with Dab at position 2.
IC_{50} values were calculated from three independent experiments, each performed in duplicate.

Obtained results revealed that:

- extension of Arg^4 side chain (**1** and **2** vs. **3** and **4,** respectively) gives only a slight decrease in inhibitory activity;
- contrary to our speculation, shortening the Arg^4 side chain (**1** and **2**) to Agb (- 1 x CH_2, **5** and **6**) or further to Agp (- 2 x CH_2, **7** and **8**) leads to a significant reduction in the inhibition of VEGF-A_{165} binding to NRP-1;
- replacement of the guanidine group (Arg^4, in **1** and **2**) by the urea group (Cit^4, **9** and **10**) significantly reduces the inhibitory activity;
- interestingly, the replacement of the alkyl side chain of Arg^4 by the aromatic ring of Phe(4-CH_2-NH_2) coupled with the change of the guanidine to an amino group (**1** and **2** vs. **11** and **12**, respectively), resulted in a slight decrease in activity, comparable to that for Har.

METABOLIC STABILITY

The *in vitro* metabolic stability of the most potent peptidomimetics (**3**-**4** and **11**-**12** in comparison to **1**-**2**) has been determined in human serum.

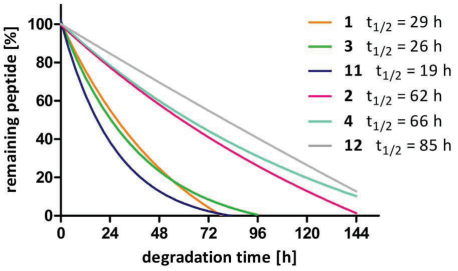

Figure 2. Comparison of the *in vitro* metabolic stability for **1**-**4** and **11**-**12**. For clarity of the figure, the markers on the curve and error bars have been removed.

Obtained results revealed that:

- all tested compounds degraded proteolytically at rates comparable to the parent compounds (**3**, **11** vs. **1** and **4**, **12** vs **2**), (Fig. 2);
- peptidomimetics containing Dab as the second residue are more stable as compared to those containing Dap, (Fig. 2);
- stability of compounds in the Dap^2 series changes as follows **1 > 3 > 11** while in the case of the Dab^2 series it changes in the opposite direction, i.e. **12 > 4 > 2**, (Fig. 2);
- all tested compounds were degraded in accordance with three independent and parallel metabolic pathways (Fig. 3).

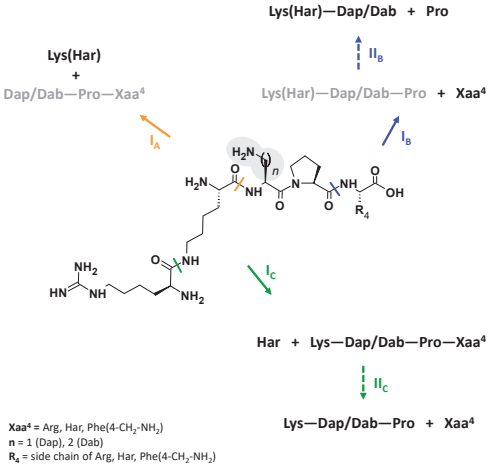

Figure 3. Probable degradation pathways and cleavage sites of **1**-**4** and of **11**-**12**. The general structure of these compounds is shown with marked locations of the first major enzymatic cleavage sites (for pathway I_A, I_B and I_C). Peptide sequences in grey have not been identified by mass spectrometry. II_B and II_C indicate further degradation pathways for Lys(Har)-Dap/Dab-Pro and Lys-Dap/Dab-Pro-Xaa peptides, respectively.

CONCLUSIONS

OUR STUDY SHOWED THAT:

- location of the guanidinium group (which strongly depends on the length of the methylene chain) in relation to Asp320 has a crucial effect on the inhibitory activity that changes as follows:

  Arg (3x CH_2) ≈ **Har** (4x CH_2) > **Agb** (2x CH_2) > **Agp** (1x CH_2)

- limited number of the interaction between the side chain of C-terminal residue and Asp320 strongly reduces inhibitory activity

  Arg (guanidine group) > > **Cit** (urea group)

- replacement of ionic interaction with aromatic interaction (inside the binding cleft) allows to maintain inhibitory activity at a similar level

  Arg (guanidine group) ≈ **Phe(4-CH_2-NH_2)** (aromatic ring)

- substitution of Arg^4 with its mimetics Har or Phe(4-CH_2-NH_2) does not significantly improve proteolytic stability compared to parent compounds. However, compounds with Dab^2 ($t_{1/2}$ = 62-85 h) are more stable than those with Dap^2 ($t_{1/2}$ = 19-29 h);
- proteolytic degradation occurs through the three independent and parallel pathways.

REFERENCES:

[1] Chaudhary B. *et. al.*, Cancer Immunol Immunother, 63 (2014), 81–99
[2] Starzec A. *et al.*, Life Sci, 79 (2006), 2370–2381
[3] Starzec A. *et al.*, Peptides, 28 (2007), 2397-2402
[4] Tymecka D. *et al.*, Eur. J. Med. Chem., 158 (2018) ,453-462
[5] Mota F. *et al.*, FEBS J., 285 (2018), 1290–1304
[6] Puszko A.K.. *et al.*, Med. Chem. Commun., 10 (2019), 332-340

ACKNOWLEDGEMENTS:

This work was supported by NCN grant no 2019/33/B/NZ7/02818.

Oxidative organic, aqueous or regioselective folding, what is the best strategy to unlock the potential of Conotoxins ?

Yazid Souf [1], Gonxhe Lokaj [2], Veeresh Kuruva [3],Tchikry Marena [1], Youssra Diani [1],Delphine Raviglione [1], Ashraf Brik [3], Annette Nicke [2], Sébastien Dutertre[4] and Nicolas Inguimbert [1]

[1] CRIOBE, Université de Perpignan, FRANCE; [2] Walther Straub Institute of Pharmacology and Toxicology, Faculty of Medicine, LMU Munich, Germany;

[3] Schulich Faculty of Chemistry, Technion-Israel Institute of Technology, Israel ;[4] IBMM, Université Montpellier, France

https://doi.org/10.17952/37EPS.2024.P1113

Introduction

Conotoxins, disulfide-rich peptides derived from cone snail venom, exhibit diverse biological activities and structural variations, leading to their classification into distinct subfamilies[1]. Each subfamily can target various pharmacological receptors. Due to their pharmacological significance, synthesizing these peptides is appealing but complicated by the presence of multiple disulfide bridges. Developing versatile chemical synthesis strategies for these compounds is essential to unlock their full potential[2]. In this work, we compare the results of three folding strategies applied to the unusual AdIIIB conotoxin, which features a single amino acid separating the fourth and fifth cysteine residues.

Conotoxin	Cone snail species	Sequence	Loop m/n/o	Disulfide linkage	Reference
AdIIIB	*Conus adamsonii*	KGCCSGVT−CPIYWKNVNICRCC−*	4/9/1	ND	This work
CnIIIF	*Conus consors*	−RCCGEGASCPRYFRNSQICSCC−*	5/9/1	ND	[3]
MIIIJ	*Conus magus*	ZKCCSGGS−CPLYFRDRLICPCC−*	4/9/1	ND	[4]
SIIID	*Conus striatus*	−−CCGEGSSCPKYFKNNFICGCC−*	5/9/1	C1–C4, C2–C5, C3–C6	[5]
MrIIIE	*Conus marmoreus*	−VCC−PFGGC−−−−−HELCYCCD*	4/3/1	C1–C5, C2–C4, C3–C6	[6]

Table 1 : M1-branch of M conotoxin superfamily , * amidated , ND: not determined , Z: Pyroglutamate

Methodology

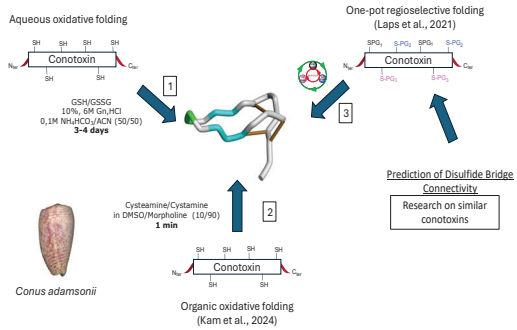

To synthesize these cyclic peptides, three methods have been compared:

1.Aqueous oxidative folding leads to the most stable isomer. In our case, we achieved optimal results using a 0.1M $NH4HCO_3$ buffer with acetonitrile as a co-solvent and reduced/oxidized glutathione[7].

2.Organic oxidative folding was performed in 90% morpholine as a solvent, with cysteamine/cystamine as disulfide bond mediators[8].

3.Regioselective oxidative folding combines several components. Disulfiram (DSF) acts as a disulfide bond oxidizing agent, ultraviolet light deprotects the nitrobenzyl (Nbzl) group, and palladium deprotects the acetamidomethyl (Acm) group. These elements enable chemoselective and regioselective cysteine activation, allowing for one-pot formation of multiple disulfide bonds in various peptides and proteins[9,10].

While oxidative folding methods generally lead to the most stable isomer without anticipating the specific arrangement of the disulfide bonds, directed folding allows for control over the formation of disulfide bonds, with the arrangement defined based on a literature survey.

Results

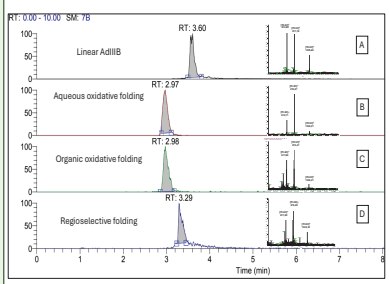

Figure 1: LC-MS analysis of the 3 different oxidative folding

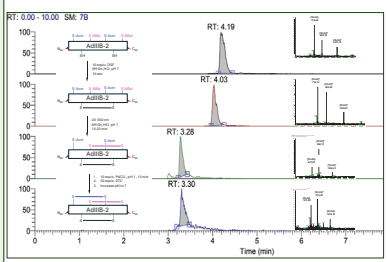

Figure 2: LC-MS analysis of the one-pot regioselective folding

1. Comparison of the three folding strategies.

Among the 15 different possible pairings starting from six cysteine residues, we obtained the following results:

•**Non-directed oxidative folding:** A single isomer, AdIIIB-1, containing three disulfide bonds, was obtained. This isomer elutes at 2.97 minutes, regardless of whether the folding occurred in aqueous or organic media (Figure 1: B, C).

•**Regioselective folding:** Starting from the linear precursor, we sequentially formed the disulfide bonds between C1–C4, C2–C5, and C3–C6, an arrangement based on the most active isomer of SIIID conotoxin, which has a sequence similar to AdIIIB. The elution time of this isomer, AdIIIB-2 (rt: 3.29 minutes, Figure 1: D), is different from that of the isomer obtained by non-directed oxidative folding.

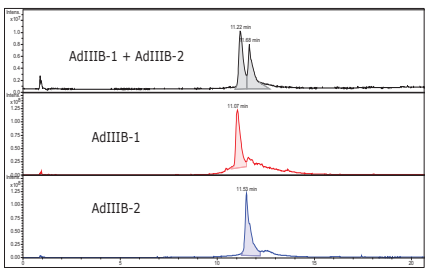

Figure 3: UHPLC analysis : Co-injection of the different isomer AdIIIB-1 & AdIIIB-2

	% Responce of current amplitude					
	10 µM AdIIIB-1			10 µM AdIIIB-2		
Rat receptors	Oocyte 1	Oocyte 2	Oocyte 3	Oocyte 1	Oocyte 2	Oocyte 3
αβγδ(muscle typ.)	28%	14%	20%	78%	76%	71%
α2β4	97%	96%	86%	100%	100%	90%
α2β2	88%	86%	-	97%	98%	-
α3β4	96%	90%	84%	99%	96%	99%
α3β2	72%	68%	-	91%	89%	91%
α4β4	93%	92%	88%	100%	99%	97%
α7	92%	91%	-	100%	100%	-

Table 2: inhibitory potency on different nAChRs subtypes

2. Co-Injection of the Isomers

Co-injection of the isomers AdIIIB-1 and AdIIIB-2, obtained respectively through oxidative and regioselective folding, confirms their structural differences (Figure 3). This observation underscores the limitations of relying solely on literature predictions for disulfide bridge configurations.

3. Inhibitory Test

The inhibitory potency of AdIIIB-1 and AdIIIB-2 was assessed using two-electrode voltage clamp analysis on rat nAChR subtypes. Results indicated that AdIIIB-1, derived from oxidative folding, exhibited significantly higher biological activity compared to AdIIIB-2. Furthermore, AdIIIB-1 demonstrated a selective affinity for the α1β1γδ nAChR subtype over other subtypes.

Conclusion & perspective

Comparing the three folding methods for conotoxin, the most prominent findings are:

•**Non-Directed Oxidation**: The isomer produced through non-directed oxidation exhibited the highest biological activity.

•**Organic Oxidative Folding**: This method was faster, but it requires improvements to simplify the purification of the cyclic peptide.

•**One-Pot Regioselective Oxidation**: This approach successfully yielded the desired isomer; however, the disulfide connectivity differed from that of the isomer obtained through non-directed methods.

•**Predictive Tools**: Utilizing tools like AlphaFold to predict disulfide bond formation could be beneficial in guiding the selection of folding strategies when applying the regioselective method.

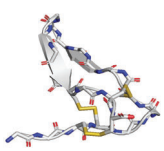

AlphaFold structure prediction of AdIIIB

References

1] K.B. Akondi, M. Muttenthaler, S. Dutertre, Q. Kaas, D.J. Craik, R.J. Lewis, P.F. Alewood, Chem Rev 114 (2014) 5815–5847.
[2] M. Góngora-Benítez, J. Tulla-Puche, F. Albericio, Chem. Rev. 114 (2014) 901–926.
[3] A. Violette, D. Biass, S. Dutertre, D. Koua, D. Piquemal, F. Pierrat, R. Stöcklin, P. Favreau, Journal of Proteomics 75 (2012) 5215–5225.
[4] M.J. Rybin, H. O'Brien, I.B.L. Ramiro, L. Azam, J.M. McIntosh, B.M. Olivera, H. Safavi-Hemami, D. Yoshikami, Toxins 12 (2020) 197.
[5] H. Wang, Y. Li, M. Yang, M. Zhou, Toxicon 210 (2022) 141–147.
[6] Y.-H. Han, Q. Wang, H. Jiang, L. Liu, C. Xiao, D.-D. Yuan, X.-X. Shao, Q.-Y. Dai, J.-S. Cheng, C.-W. Chi, FEBS Journal 273 (2006) 4972–4982.
[7] G. Bulaj, B.M. Olivera, Antioxidants & Redox Signaling 10 (2008) 141–156.
[8] A. Kam, S. Loo, Y. Qiu, C.-F. Liu, J.P. Tam, Angew Chem Int Ed Engl 63 (2024) e202317789.
[9] Y.M. Souf, G. Lokaj, V. Kuruva, Y. Saed, D. Raviglione, A. Brik, A. Nicke, N. Inguimbert, S. Dutertre, Marine Drugs 21 (2023) 356.
[10] S. Laps, F. Atamleh, G. Kamnesky, S. Uzi, M.M. Meijler, A. Brik, Angewandte Chemie Intl Edit 60 (2021) 24137–24143.

Mucroporin-M1 analogues: synthesis, conformation and structure-activity correlation

C. Storti [1,2], C. Peggion [2]

1. Department of Public Health, Experimental and Forensic Medicine, University of Pavia, Pavia, 27100, Italy
2. Department of Chemical Sciences, Università degli studi di Padova, 35131, Padova, Italy

https://doi.org/10.17952/37EPS.2024.P1114

INTRODUCTION and AIM

Mucroporin is a peptide of 17 amino acids deriving from the scorpion venom *Lychas mucronatus* with known antimicrobial properties (active against gram-positive bacteria). *Li et al.* [1] optimized the *Mucroporin* sequence by proposing ***Mucroporin-M1*** sequence with some amino acid substitutions (G3R, P6K, G10K and G11R). These modifications improved peptide activity at lower concentrations respect to the native peptide. Substitutions increase the net positive charge of the peptide, strengthening the amphipathic character of the peptide helix.

Previous studies have shown that Mucroporin-M1 also possesses antiviral activity: it interacts directly with viral particles and that, when the peptide attaches to the virus, its strong electrostatic affinity increases the interaction and destruction of the viral envelope [1-3].

The **aim** of this work was to further improve the **activity** of Mucroporin-M1 and develop its **analogues** by suitably modifying the amino acid sequence and studying the conformation of the synthesized compounds and the structure-activity relationship.

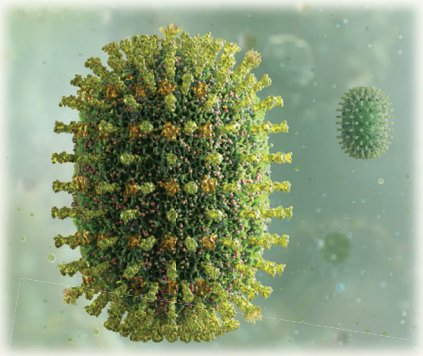

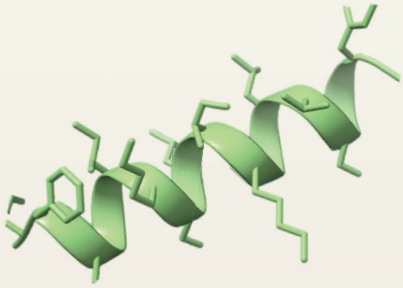

Mucroporin-M1

SEQUENCES

The summarized sequences are shown in the table. They were obtained by SPPS (Solid-Phase Peptide Synthesis), purified by preparative HPLC and characterized by HPLC-MS.

ABBREVIATION	COMPOUND	SEQUENCE
CS1	Mucroporin-M1 Long	LFRLIKSLIKRLVSAFK-NH_2
CS2	Mucroporin-M1 Short	LIKRLVSAFK-NH_2
CS3	Mucroporin-M2 Long	LFRLUKS LUKR LUSAFK-NH_2
CS4	Mucroporin-M2 Short	LUKR LUSAFK-NH_2
CS5	Palm-Mucroporin-M2 Short	Palm-LUKR LUSAFK-NH_2

RESULTS

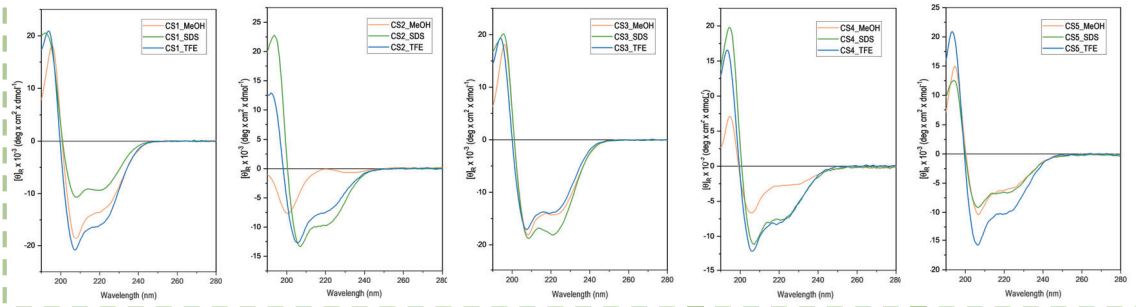

Conformational studies were conducted by **CD** in three different solvents: **MeOH** (organic solvent), **SDS 100 mM** (surfactant that forms micelles, which mimic cell membranes) and **TFE** (helix inducer solvent). Conformational studies by **NMR** are in progress.

In order to study resistance to enzymatic degradation, the synthesised peptides were tested with **Trypsin** (cut on the carboxyl of Lysine and Arginine), **Chymotrypsin** (cut on the carboxyl of apolar amino acids) and **Serum**. The enzymatic degradation reactions were followed by HPLC.

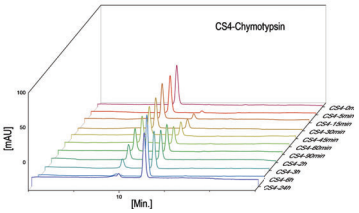

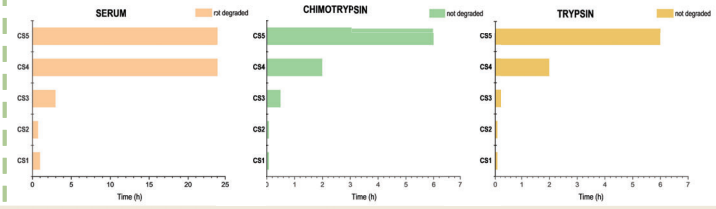

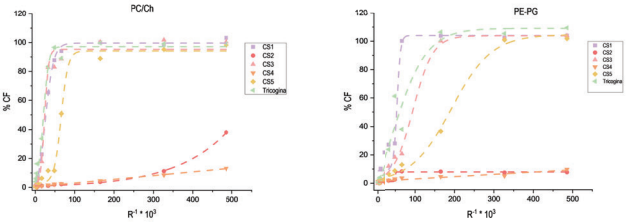

The **cytotoxicity** of the peptides was determined by MTT assay in 3 different cell lines (vero cell, vero E6 cell and MDCK cell). Preliminary **activity** studies were also conducted by leakage assays from liposomes to determine the ability to interact with membranes.

Peptide	Cytotoxicity , CC_{50} (μg/mL)		
	Vero cells (72h)	Vero E6 cells (72h)	MDCK cells (48h)
CS1	49	93	>100
CS2	>100	>100	>100
CS3	38	79	>100
CS4	>100	>100	>100
CS5	33	50	49

CONCLUSIONS

From the **structural studies**, we can observe that the helical structure is maintained in different solvents by the modified sequences, and that CS4 remains helical in MeOH, unlike CS2.

The **enzymatic degradation studies** show that the proposed modifications increase the products' resistance to enzymatic degradation, thereby enhancing their stability in serum.

Regarding **cytotoxicity**, it is noteworthy that the modified and shortened CS4 peptide is not cytotoxic in different cell lines. In-cell **activity studies** are currently underway. For now, a preliminary study has been conducted using leakage tests, which indicate a decrease in the ability to breach membranes as the peptide chain length decreases.

INF-ACT
Finanziato dall'Unione europea
NextGenerationEU

SCAN ME

https://doi.org/10.17952/37EPS.2024.P1115

FERROCENE-PEPTIDE CONJUGATES WITH POTENTIAL ANTITUMOR ACTIVITY

Barbara Biondi,[a] Beatrice Calderaro,[a] Annalisa Bisello,[b] Roberta Cardena,[b] Renato Schiesari,[b] Fernando Formaggio,[a,b] and Saverio Santi[b]

[a]Institute of Biomolecular Chemistry, Padova Unit, CNR, 35131 Padova, Italy; [b] Department of Chemistry, University of Padova, 35131 Padova, Italy

INTRODUCTION

New anticancer therapies are currently much needed. Our contribution aims at synthesizing and studying ferrocene(Fc)-peptide conjugates to be tested as anti-tumor agents. The peptide is intended to selectively address over-expressed integrins of cancer cells, whereas ferrocene is expected to display anti-proliferative activity through the production of reactive oxygen species (ROS) [1]. A concentration of ROS higher than normal favors carcinogenesis, but if this exceeds a certain value then a cytotoxic effect is observed. The exogenous production of ROS, consequently, represents a possible strategy to induce apoptosis in diseased cells.

SYNTHESIS

Inspired by previous contributions [2-7], we synthesized conjugates made up of four components (Figures 1 and 2):

i) an Fc unit as the electroactive element;
ii) an aromatic moiety to modulate the oxidation potential of Fc and thus to favor its oxidation under physiological conditions;
iii) an alkyl spacer to increase flexibility and, consequently, to improve integrins affinity, cellular uptake and antitumor activity [6];
iv) an oligopeptide, including the well-known RGD, able to interact with over-expressed receptors of the cancer cells.

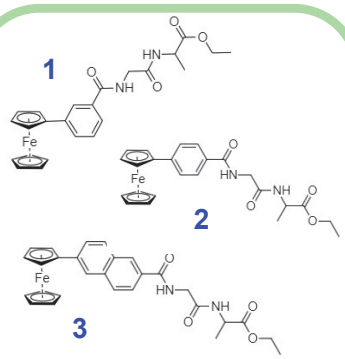

Figure 1. Known Fc-aromatic-peptide conjugates [3-6] synthesized as reference compounds.

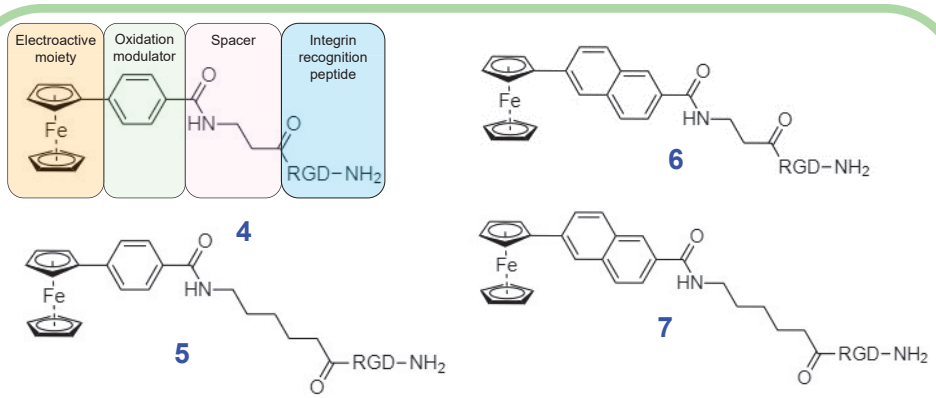

Figure 2. New Fc-aromatic-spacer-peptide conjugates synthesized in this work.

CONFORMATION in methanol

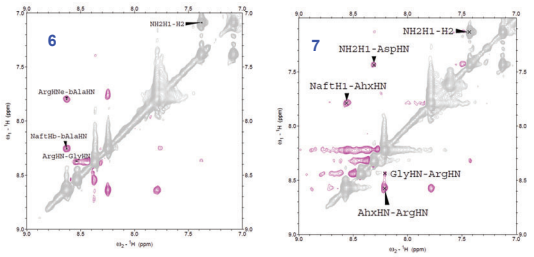

Figure 3. Amide region of the NOESY spectra of **6** and **7**. The sequential $NH_{i \rightarrow i+1}$ connectivities indicate a helical conformation.

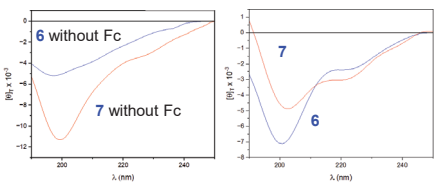

Figure 4. CD spectra in the amide absorption region of **6** and **7** (right panel) and of the same two conjugates missing the Fc-aromatic moieties (left panel).

ENZYMATIC STABILITY

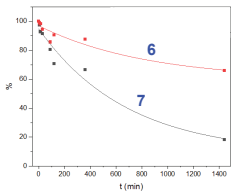

Figure 5. Conjugates **6** and **7** incubated for 24 hr in human serum.

CONCLUSIONS

- Conjugates 6 and 7 display a significant α-helical content, not observed when the Fc-aromatic moiety is removed.
- The Fc moiety prevents peptide degradation in human serum. After a 24 hours treatment, significant amounts of 6 and 7 are still detected. The shortest spacer gives the best results as Fc is closer to the peptide.
- Cyclic voltammetry measurements indicate a relevant influence of the aromatic groups on the Fc oxidation potentials.
- The anticancer activity of our conjugates is currently under scrutiny.

REFERENCES

[1] P. Kopf-Maier, H. Kopf, E. W. Neuse, *J. Cancer Res. Clin.*, **1984**, *108*, 336-340.
[2] A. Goel, D. Savage, S. R. Alley, P. N. Kelly, D. O'Sullivan, H. Mueller-Bunz, P. T. M. Kenny, *J. Organomet. Chem.*, **2007**, *692*, 1292-1299.
[3] A. J. Corry, N. O'Donovan, Á. Mooney, D. O'Sullivan, D. K. Rai, P. T. M. Kenny, *J. Organomet. Chem.*, **2009**, *694*, 880-885
[4] A. J. Corry, A. Mooney, D. O'Sullivan, P. T. M. Kenny, *Inorg. Chim. Acta*, **2009**, *362*, 2957-2961
[5] A. Mooney, A. J. Corry, D. O'Sullivan, D. K. Rai, P. T. M. Kenny, *J. Organomet. Chem.*, **2009**, *694*, 886–894
[6] B. Zhou, J. Li, B. Feng, Y. Ouyang, Y. Liu, F. Zhou, *J. Inorg. Biochem.*, **2012**, *116*, 19–25
[7] B. S. Ludwig, S. Tomassi, S. Di Maro, F. S. Di Leva, A. Benge, F. Reichart, M. Nieberler, F. E. Kühn, H. Kessler, L. Marinelli, U. Reuning, S. Kossatz, **Biomaterials**, **2021**, *271*, 120754.

THANKS TO

the Italian Ministry of Research (**PRIN Prot. 2020833Y75**). We also acknowledge contributions from a NextGenerationEU-MUR PNRR Extended Partnership initiative (Project no. PE00000007, INF-ACT) and a University of Padova Grant to S.S. (P-DiSC-2018).

Proceedings of the 37th European Peptide Symposium
Michal Lebl, Editor
European Peptide Society, 2024 *http://doi.org/10.17952/37EPS.2024.P1116*

Fragments of fibroblast growth factors useful in regenerative medicine components

Katarzyna Czerczak-Kwiatkowska[a], Adrianna Wierzbicka[b], Dorota Bociaga[b], Justyna Fraczyk[a], Beata Kolesinska[a]

[a]*Institute of Organic Chemistry, Łódź University of Technology, Żeromskiego 116, 90-924 Lodz, Poland*

[b]*Institute of Materials Science and Engineering, Lodz University of Technology, Stefanowskiego. 1/15, 90-924 Lodz, Poland*

Introduction

Tissue engineering and/or regenerative medicine is a field of life science using different methods to create a new tissues/organs and/or to promote the regeneration of damaged or diseased tissues/organs. Materials used as scaffolds must ensure appropriate micro-environment of the cells, adhesion, proliferation, differentiation and finally the reproduction of the parent tissue [1,2]. Concentrated Growth Factors (CGFs) are the newest and safest therapy in regenerative medicine. CGF is a new-generation autologous platelet concentrate containing equivalent or higher levels of TGF-B1, PDGF-BB, and VEGF than platelet-rich plasma (PRP) concentrates. CGFs has been shown to stimulate cell proliferation [3,4], allowing for use in regenerative medicine. [5]. CGF is easily obtained by centrifuging intravenous blood of the patient and does not require any synthetics or biomaterials to make a gel; hence, it is free from the risk of cross-contamination [6]. The fibroblast growth factor (FGF) family represents a broad group of signaling proteins with structural similarities and related actions. FGFs are involved in a number of processes taking place in the cells; they are involved in wound regeneration, angiogenesis or regulation of metabolism, among others. The FGF family consists of 22 proteins. Apart from FGF15 and FGF19, the remaining FGFs have analogous mouse and human structures (homology about 90%). FGFs have very similar biological effects and a similar mechanism of gene expression Fibroblast growth factor 1 (FGF1) is also known as acidic fibroblast growth factor (aFGF). It consists of 155 amino acid residues, the main chain includes residues 16-155. FGF1 occurs as a monomer or homodimer. FGF1 binds to all receptors FGFR (FGFR1-FGFR4). In addition to homodimers, FGF1 forms a complex with fibroblast growth factor binding protein 1 (FGFBP1) and FGF2. Fibroblast growth factor 2 is also known as basic fibroblast growth factor (bFGF). The FGF2 chain consists of 288 amino acid residues, residues 1-142 constitute the propeptide. The main chain includes amino acids 143-288. It occurs as a monomer or homodimer. It binds to FGFR1, FGFR2, FGFR3 and FGFR4 receptors. FGF2 levels are increased in acute wounds, supporting the formation of granulation tissue, re-epithelialization and reconstruction of the damaged site [7]. It also regulates the synthesis and function of ECM components and increases the migration of keratinocytes and fibroblasts [8]. In the case of chronic wounds, the level of FGF2 is reduced [9]. Recombinant FGF2 applied directly to the wound shows promising effects in the treatment of pressure ulcers [10]. Promising effects have also been shown in the treatment of diabetic foot [11]. Currently, derivatives of fibroblast growth factors are available for the treatment of ulcers and burns. FGF proteins are recommended by the American Wound Healing Society and the European Wound Management Association for the treatment of refractory ulcers. Studies on the

 http://doi.org/10.17952/37EPS.2024.P1116

family of these proteins show that FGF2, FGF7 and FGF10 are key in the regeneration of skin wounds.

The aim of the study was to find a set of short fragments of native FGFs involved in repairing damaged tissues. These sets should reproduce the outer sphere of proteins and have biological properties similar to native proteins due to their ability to interact with receptors. We focused our attention on the search for FGF1 and FGF2 fragments.

Results and discussion

Using the SPOT method, libraries of FGF 1 and FGF2 fragments immobilized on cellulose were obtained [12]. Based on the Dot-blot test, fragments of both proteins were selected forming an outer sphere of proteins capable of interacting with the corresponding receptor.

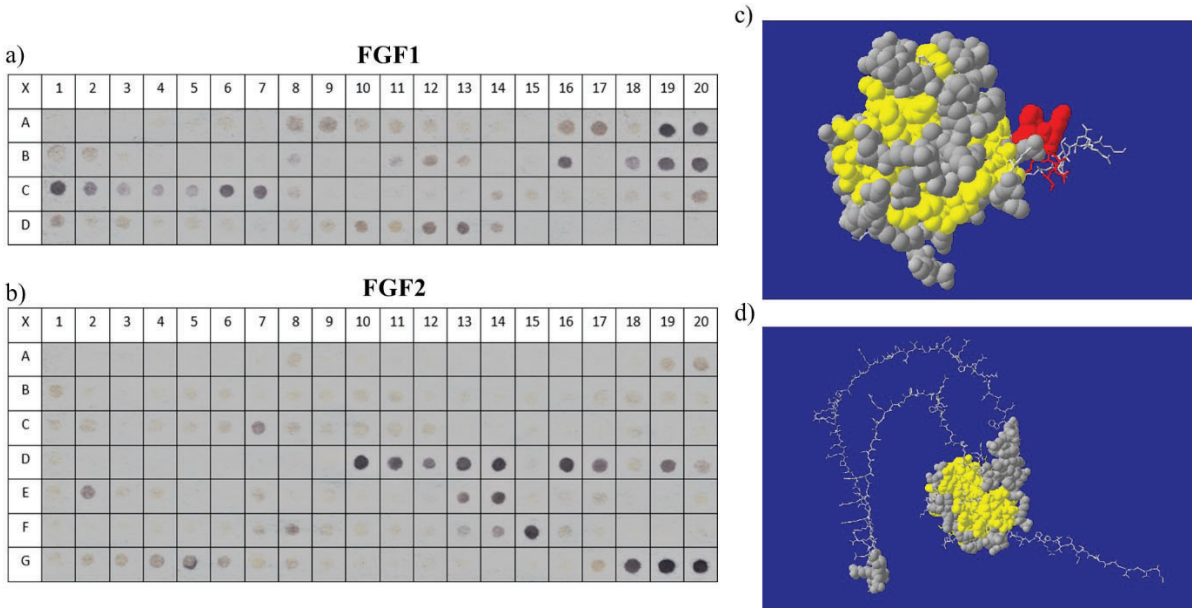

Fig. 1. a) Scan of a cellulose sheet containing the whole library of FGF1 fragments after reaction with antibodies. FGF1 map: 74 decapeptides, reading frame: 2 AA. b) Scan of a cellulose sheet containing the whole library of FGF2 fragments after reaction with antibodies. FGF2 map: 140 decapeptides, reading frame: 2 AA. c) FGF1 found fragments, AlphaFold model (Uniprot P05230). d) FGF2 found fragments, AlphaFold model (Uniprot P09038).

In the case of the FGF1 fragment library, 37 fragments able to interact with polyclonal antibodies were found based on the Dot-blot assay, including 17 fragments showing strong/very strong interaction. For the FGF2 fragment library, 20 fragments able to interact with polyclonal antibodies were found, of which 14 fragments showed strong/very strong interaction. The found fragments of FGF1 and FGF2 were synthesized on 2-chlorochlorotrityl resin using a triazine coupling reagent [13]. In the next step, FGF fragments were used in studies on NIH/3T3 cells to investigate their effect on the viability of cells incubated in a medium with the addition of FGF fragments.

 http://doi.org/10.17952/37EPS.2024.P1116

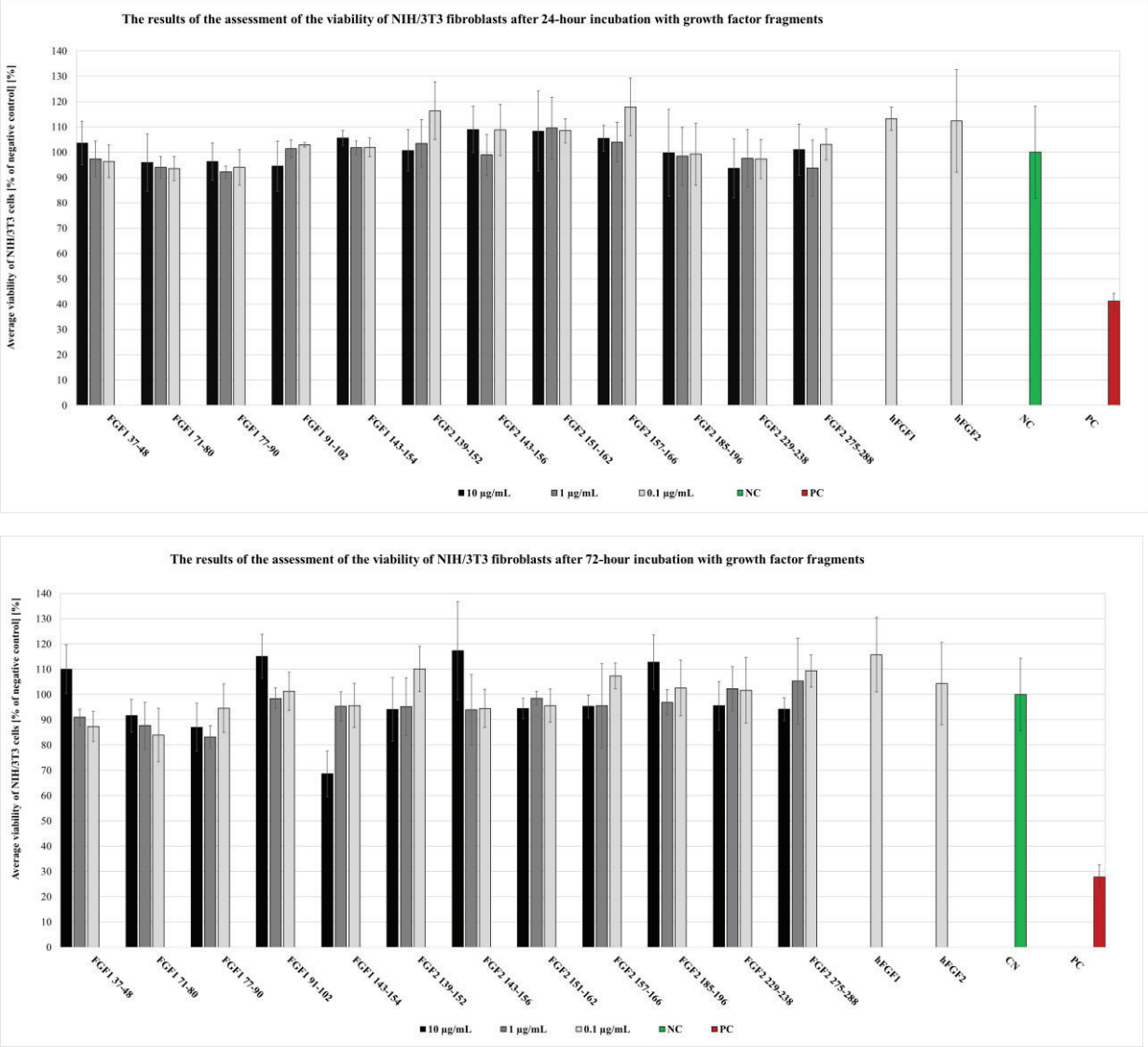

Fig. 2 Viability of NIH/3T3 cells grown in the presence of FGF1 and FGF2 fragments. Incubation for 24 h (top panel), incubation for 72 h (bottom panel).

Studies have shown that all FGF1 and FGF2 fragments have no negative effect on cell viability at concentrations of 1 and 0.1 µg/mL. However, at a concentration of 10 µg/mL, only one FGF1 fragment (cultured for 72 hours) showed a slight decrease in cell viability.

Conclusions

Selected FGFs fragments are useful in the regeneration of skin damage and treatment of difficult-to-heal wounds.

Literature

[1] Wobma, H., Vunjak-Novakovic, G. (2016) Tissue Engineering and Regenerative Medicine 2015: A Year in Review. *Tissue Eng. Part B Rev*. *22*, 101-113. doi: 10.1089/ten.TEB.2015.0535.
[2] Marx, V. (2015) Organs from the lab *Nature 522*, 373-377. doi.org/10.1038/522373a.
[3] Masuki, H., Okudera, T., Watanebe, T., Suzuki, M., Nishiyama, K., Okudera, H. (2016) Growth factor and pro-inflammatory cytokine contents in platelet-rich plasma (PRP), plasma rich in growth factors (PRGF), advanced platelet-rich fibrin (A-PRF), and concentrated growth factors (CGF). *Int. J. Implant Dent. 2*, 19. doi.org/10.1186/s40729-016-0052-4.
[4] Giannotti, L., Di Chiara Stanca, B., Spedicato, F., Nitti, P., Damiano, F., Demitri, C., Calabriso, N., Carluccio, M.A., Palermo, A., Siculella, L. (2023) Progress in Regenerative Medicine: Exploring Autologous Platelet Concentrates and Their Clinical Applications. *Genes 14*, 1669. doi.org/10.3390/genes14091669.

[5] Yahata, Y., Handa, K., Ohkura, N., Okamoto, M., Ohshima, J., Itoh, S., Kawashima, N., Tanaka, T., Sato, N., Noiri, Y., Hayashi, M., Okiji, T., Saito, M. (2023) Autologous concentrated growth factor mediated accelerated bone healing in root-end microsurgery: A multicenter randomized clinical trial. *Regen*. *Ther. 24*, 377-384. doi.org/10.1016/j.reth.2023.08.006.
[6] Rodella, L.F., Favero, G., Boninsegna, R., Buffoli, B., Labanca, M., Scarì, G., Sacco, L., Batani, T., Rezzani, R. (2011) Growth factors, CD34 positive cells, and fibrin network analysis in concentrated growth factors fraction. *Microsc. Res. Tech. 74*, 772-777. doi: 10.1002/jemt.20968.
[7] Powers, C.J., McLeskey, S.W., Wellstein. A. (2000) Fibroblast growth factors, their receptors and signaling. *Endocr. Relat. Cancer 7*, 165-197. doi:10.1677/erc.0.0070165.
[8] Sogabe, Y., Abe, M., Yokoyama, Y., Ishikawa, O. (2006)Basic fibroblast growth factor stimulates human keratinocyte motility by Rac activation. *Wound Repair Regen*. *14*, 457-462. doi:10.1111/j.1743-6109.2006.00143.x
[9] Robson, M.C. (1997)The role of growth factors in the healing of chronic wounds. *Wound Repair Regen*. *5*, 12-17. doi:10.1046/j.1524-475X.1997.50106.x
[10] Payne, W.G., Ochs, D.E., Meltzer, D.D., Hill, D.P., Mannari, R.J., Robson, L.E., Robson, M.C (2001) Long-term outcome study of growth factor-treated pressure ulcers. *Am J Surg*. *181*, 81-86. doi:10.1016/S0002-9610(00)00536-5.
[11] Uchi, H., Igarashi, A., Urabe, K., Koga, T., Nakayama, J., Kawamori, R., Tamaki, K., Hirakata, H., Ohura, T., Furue, M. (2009) Clinical efficacy of basic fibroblast growth factor (bFGF) for diabetic ulcer. *Eur. J. Dermatology*. *19*, 461-468. doi:10.1684/ejd.2009.0750.
[12] Fraczyk, J., Walczak, M., Kaminski, Z.J. (2018) New methodology for automated SPOT synthesis of peptides on cellulose using 1,3,5-triazine derivatives as linkers and as coupling reagents. *J. Pept. Sci.*, *24*, e3063. doi.org/10.1002/psc.3063.
[13] Kolesinska, B., Rozniakowski, K.K., Fraczyk, J., Relich, I., Papini, A.M., Kaminski, Z.J. (2015) The Effect of Counterion and Tertiary Amine on the Efficiency of N-Triazinylammonium Sulfonates in Solution and Solid-Phase Peptide Synthesis. *Eur. J. Org. Chem*., 401-408. doi: 10.1002/ejoc.201402862.

37th EPS European Peptide Symposium | 14th IPS International Peptide Symposium

CR22DK-S18G Breakthrough: Revealing a novel antimicrobial peptide with rifampicin and isoniazid-like potency against *Mycobacterium tuberculosis* - a comprehensive exploration from synthesis to immune modulation and selective action

Cesar Augusto Roque-Borda[1,2,3], Laura Maria Duran Gleriani Primo[1], Rafaela Melo Pogianeli[1], Lucas Henrique Domingos da Silva[4], Isabela Caroline dos Santos[4], Flávia Aparecida Resende[4], Henrik Franzyk[3], Paul Robert Hansen[3], João Perdigão[2], Fernando Rogério Pavan[1]

https://doi.org/10.17952/37EPS.2024.P1117

1) São Paulo State University (UNESP), School of Pharmaceutical Sciences, Araraquara, São Paulo – Brazil. 2) University of Lisbon. Faculty of Pharmacy, iMed.ULisboa–Institute for Medicines Research, Lisbon - Portugal. 3) University of Copenhagen, Faculty of Health and Medical Sciences, Department of Drug Design and Pharmacology, Denmark. 4) Research Center on Biotechnology – UNIARA, Araraquara, São Paulo – Brazil.

Introduction

According to WHO, 1.6 million people died from Tuberculosis (TB) in 2021, making TB the second-leading infectious killer after COVID-19.[1,2,3] In recent years, antimicrobial peptides (AMPs) with promising anti-TB activity have been identified. B1CTcu5 is a peptide amide, isolated in 2014 from the skin secretion of the Indian toad *Clinotarsus curtipes*, and showing initial MIC values of 12.5 µg/mL against *Mycobacterium tuberculosis* (MTB).[4] The objective of the present work was to generate a library of B1CTcu5 analogues by replacing Cys[15] and Cys[21] with Ala, Ser and/or Lys, and to evaluate their activity against MTB and cytotoxicity.

Materials and Methods

1. In silico prediction and molecular docking



6. Intracellular AMP transport

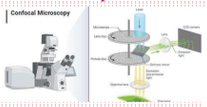

2. Solid Phase Peptide Synthesis (SPSS)

7. Efflux pumps inhibition

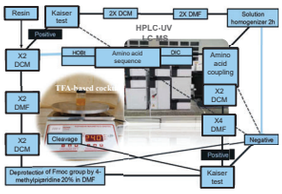

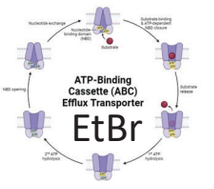

3. Antimicrobial activity and cytotoxicity

Mycobacterium tuberculosis

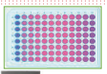

Fluorescence Microplate Reader



8. Galleria mellonella Infection model

Toxicity

Infection/Treatment

Histology

4. AMES test

Salmonella enterica subsp. *enterica* serovar Typhimurium

TA100
TA98
TA102
TA97a

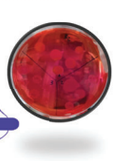



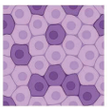

5. Morphological structure interaction

Scanning Electron Microscopy (SEM)

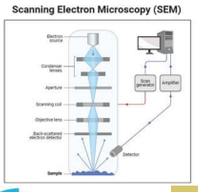

Conclusions

In conclusion, B1CTcu5 analogs show promise as a potential new peptide-based therapy against *Mycobacterium tuberculosis*, specially CRDK-s18G.

Results and Discussions

1

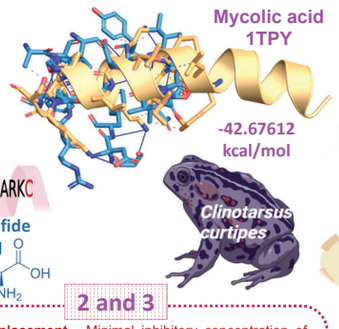

Multi-Drug Resistant MTB

3

AMP	MDR-MTB CF110 (ug/mL)	Fibroblast IC50 (ug/mL)
B1CTcu5	> 25	408.83
W-B1CTcu5	4.25	30.05
cB1CTcu5	8.63	203.72
cW-B1CTcu5	8.19	20.55
CR22D33	11.24	204.61
CR22D34	**3.74**	**233.17**
CR22D35	**1.17**	**662.94**
CR22DS20	> 25	875.30
CR22DS19	> 25	> 1000
CR22DS18(-G)	> 25	195.40
CR22DS18(G)	**1.20**	**593.74**
CR22DS17	22.72	> 1000
CR22DS16	21.48	466.08

2 and 3

Table 1. Cysteine replacement - Minimal inhibitory concentration of B1CTcu5 peptide analogs against *Mycobacterium tuberculosis* strains and cytotoxic activity on murine macrophages. Peptide analogs was evaluated at concentrations between 2 to 250 µg/mL.

AMP	Sequence	Molecular Weight	MTB H37Rv	Macrophage J774A.1	SI
B1CTcu5	**linear**	**2711.92**	**12.27**	**>250**	**20.38**
W-B1CTcu5	W-linear	2898.13	3.24	>250	77.18
cB1CTcu5	cyclic	2709.90	13.31	>250	18.79
cW-B1CTcu5	Trp cyclic	2896.11	4.68	125	26.70
CR2101	Lys	2305.89	14.02	124.34	8.87
CR2102	Ala	2197.70	31.87	178.31	5.60
CR2103	Lys and Ala	2248.80	13.31	>250	18.78
CR2104	**Trp, Ser, Ser**	**2409.91**	**7.42**	**>250**	**33.69**
CR2105	Trp, Ala	2396.49	10.73	21.36	1.99
CR2106	Trp, Ser	2296.76	22.31	>250	11.21
CR2107	**Trp, Lys, Ser**	**2451.01**	**7.21**	**>250**	**34.67**
CR2108	Trp, Ser, Lys	2451.01	17.73	>250	14.10
CR2109	Trp, Lys, Ser	2393.91	13.77	>250	18.15
CR2111	**Lys and Ala**	**2207.70**	**7.44**	>250	**46.59**
CR2111X	Cin-acid, Lys, Ala	2340.48	14.81	151.84	10.25
CR22D33	Ser and Ser	2679.78	10.64	>250	23.49
CR22D34	**Lys and Ser**	**2834.90**	**5.82**	**>250**	**42.93**
CR22D35	Ser and Ala	2663.78	>25	>250	2.50

* MIC and IC50 values was expressed in µg/mL.

Table 2. Screening of serine - Minimal inhibitory concentration of B1CTcu5 peptide analogs against *Mycobacterium tuberculosis* strains and cytotoxic activity on murine macrophages. Peptide analogs was evaluated at concentrations between 2 to 250 µg/mL.

AMP	Sequence	Molecular Weight	MTB H37Rv*	Macrophage J774A.1*	SI
CR22DK-S20	S...	2808.82	10.24	>250	24.42
CR22DK-S19	LS...	2808.82	>25	>250	2.50
CR22DK-S18(-G)	LIS...	2793.85	22.85	>250	10.94
CR22DS18(G)	**LISG...**	**2993.43**	**1.22**	**>250**	**204.42**
CR22DK-S17	LIAGS...	2808.82	10.35	>250	24.17
CR22DK-S16	**LIAGLS...**	**2850.09**	**1.45**	**>250**	**173.01**
CR22DK-S15	LIAGLAS...	2850.90	23.23	>250	10.76
CR22DK-S12	LIAGLAANFS...	2808.82	3.71	>250	67.48
CR22DK-S09	LIAGLAANFLPQS...	2808.82	25.00	>250	-
CR22DK-S08	LIAGLAANFLPQIS...	2808.82	25.00	>250	-
CR22DK-S05	LIAGLAANFLPQILKKS...	2808.82	25.00	>250	-

* MIC and IC50 values was expressed in µg/mL.

Selective Drug Discovery

3

AMP	E. coli MIC (µg/mL)	S. aureus MIC (µg/mL)
B1CTcu5	64	64
W-B1CTcu5	128	128
cB1CTcu5	128	64
cW-B1CTcu5	128	128
CR22D33	128	128
CR22D34	128	128
CR22D35	128	128
CR22DS20	128	128
CR22DS19	128	128
CR22DS18 (-G)	64	128
CR22DS18(G)	128	128
CR22DS17	128	128
CR22DS16	128	128
CR22DS15	128	128
CR22DS12	128	128
CR22DS09	128	128
CR22DS08	128	128
CR22DS05	128	128

7

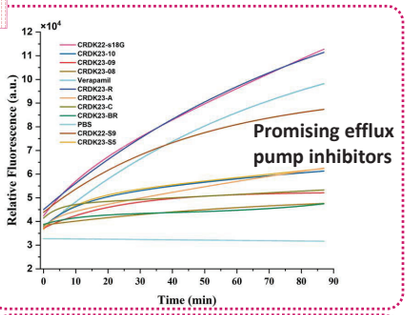

6

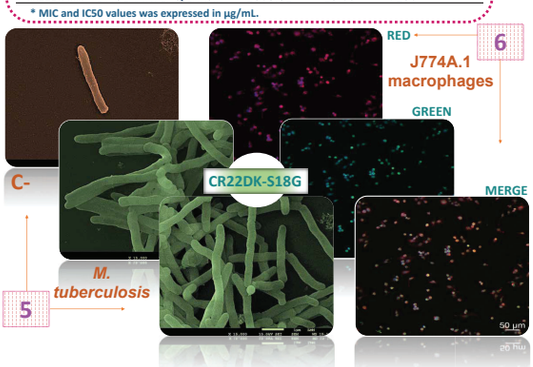

5

8

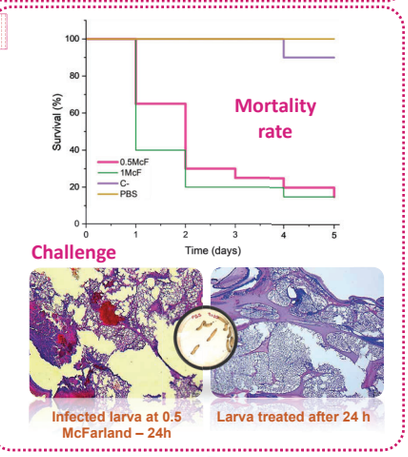

References

1. WHO Global tuberculosis report 2022; Geneva, 2022; ISBN 9789240061729.
2. Roque-Borda, C.A. et al. Biomaterials 2023, 293, 121978.
3. Roque-Borda, C.A. et al. Pharmaceutics 2021, 13.
4. Abraham, P. et al. Peptides 2020, 132, 170373.

Acknowledgments

This study was financed in part by the Coordenação de Aperfeiçoamento de Pessoal de Nível Superior - Brasil - Finance Code 001; and The São Paulo Research Foundation (FAPESP) from Brazil, Scholarship Process number 2021/14603-5 and 2020/16573-3.

The Company of Biologists | Disease Models & Mechanisms

In silico identification and chemical remodelling of tick protein epitopes for vaccine antigen development

https://doi.org/10.17952/37EPS.2024.P1119

Stepan S. Denisov[1,2], M. Amine Jmel[3], Wouter Peeters[1], Maya Idema[1], Michalis Kotsyfakis[3], Johannes H. Ippel[1], Tilman M. Hackeng[1], Ingrid Dijkgraaf[1*]

[1]*Department of Biochemistry, Maastricht University, Cardiovascular Research Institute Maastricht (CARIM), Maastricht, the Netherlands.*
[2]*Radcliffe Department of Cardiovascular Medicine, University of Oxford, the United Kingdom*
[3]*Institute of Parasitology, Biology Centre, Czech Academy of Sciences, České Budějovice, Czech Republic*

Introduction

Ticks and tick-borne diseases are severe burdens for healthcare systems and for animal husbandry amounting to billions of dollars in economic losses worldwide. Due to climate change, ticks' habitats are expanding, which makes the need for novel ways of tick control as pressing as never before. One of the desirable strategies is the development of anti-tick vaccines to elicit acquired tick resistance[1]. The challenge in the development of such vaccines often lies in the inherently low immunogenicity and proteolytical stability of tick proteins, which they acquired through millions of years of evolution. Here we present a pipeline for the development of anti-tick vaccine antigens (ATVA) which utilizes AlphaFold2 structure modelling of tick proteins, *in silico* identification of antigenic epitopes by the protrusion-based algorithm[2], chemical remodelling and multimerization using the tick salivary lectin pathway inhibitor (TSLPI) as a model protein.

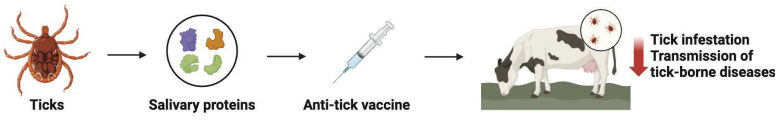

Bioinformatic pipeline allows mining of ATVA candidates

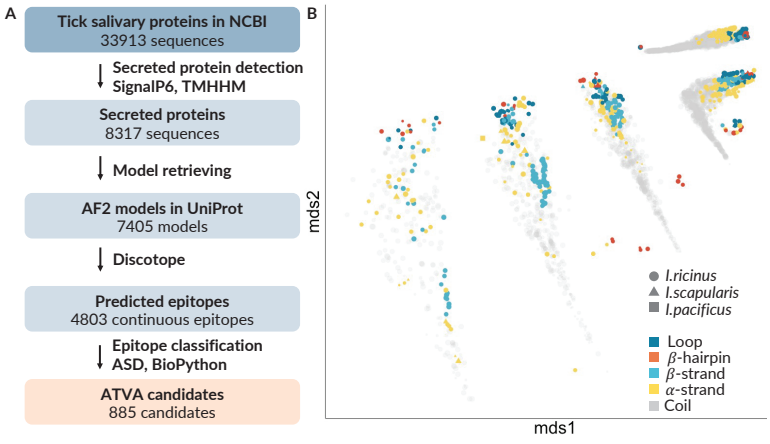

A. The pipeline for ATVA detection. **B.** The 2D representation of the epitope structural space based on amplitude spectrum distance (ASD)[3].

TSLPI contains a prospective epitope for ATVA

Tick salivary Lectin Pathway Inhibitor (TSLPI) from *Ixodes Scapularis* blocks the lectin pathway and facilitates transmission of *Borrelia burgdorferi*[4].



TSLPI AF2 model

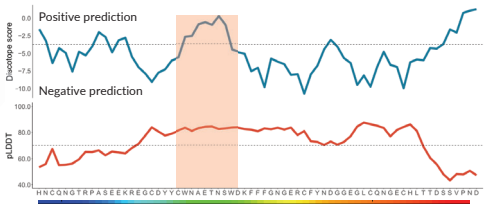

pLDDT and Discotope scores for TSLPI AF2 model. The selected for the synthesis epitope is highlighted in orange.

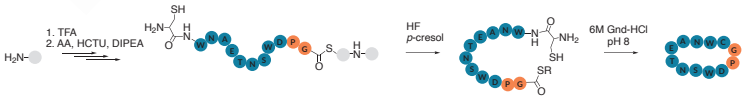

The synthesis scheme of the cyclic epitope using Boc-SPPS and intramolecular NCL. D-Pro-Gly turn is shown in orange.

Synthetic epitope mimics the parental TSLPI



Comparison of secondary chemical shifts for full-length TSLPI and the cyclic epitope.

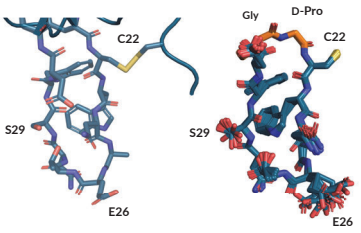

C22-D31 region in the TSLPI AF2 model (left) and overlay of 20 lowest-energy NMR structures of the cyclic epitope (right). D-Pro-Gly turn is shown in orange.

Epitope is multimerized for higher immunogenicity

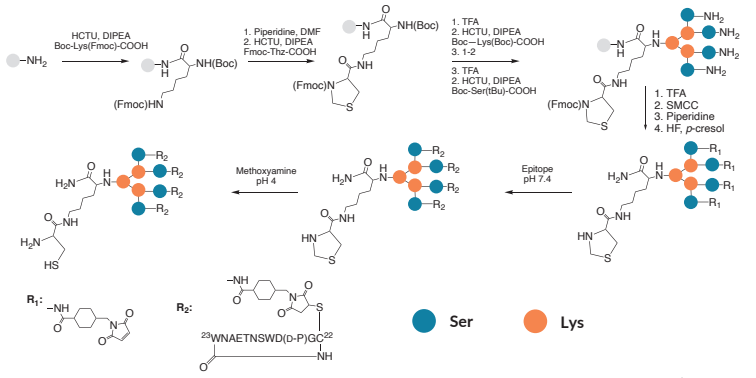

Synthesis of the tetrameric cyclic epitope coupled to a lysine wedge. SMCC, R_1: succinimidyl-4-(N-maleimidomethyl)cyclohexane-1-carboxylate

Synthetic epitopes elicit specific immune response

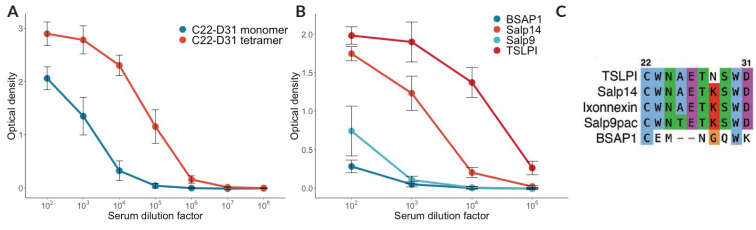

A. Level of TSLPI-specific antibodies in sera samples of mice vaccinated with KLH-peptide conjugates. **B.** Cross-reactivity of antibodies against tick proteins in sera samples of mice vaccinated with tetrameric cyclic epitope. **C.** Section of multiple sequence alignment of related to TSLPI proteins from *I.scapularis*.

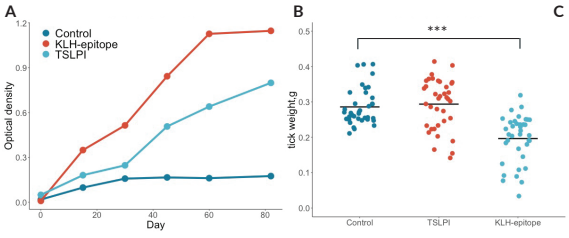

C

Egg hatching, %	
Control	79.4
TSLPI	67.2
KLH-epitope	41.9

Results experiments with naïve rabbits (control), immunized with the parent TSLPI and tetrameric-cyclic C22-D31 TSLPI epitope (KLH-epitope) challenged with *I.ricinus* ticks. The level of antibodies in rabbit sera (**A**), tick weight (**B**) and egg hatching percentage (**C**).

Conclusions

- AlphaFold and structure-based epitope prediction algorithms allows fast identification of ATVB
- The predicted epitope from *I.Scapularis* was chemically synthesised and modified to structurally mimic the parental protein
- Tertramerized TSLPI epitope elicits higher TSLPI-specific immune response in mice compared to the monomeric epitope
- Immunisation of rabbits with the tetrameric epitope might affect tick feeding and reproduction

References
1. J. de la Fuente, et al., Vaccine 2017, 35, 5089–5094
2. M. H. Høie, F. S. Gade, et al., Frontiers in Immunology 2024, 15.
3. C. Galiez and F. Coste, BMC Bioinformatics 2015, 16,256
4. Schuijt et al., Cell Host & Microbe 2011, 10, 2, 136-146

Funding:
The Netherlands Organization for Scientific Research (VIDI 723.013.009; Aspasia 015.010.005; ECHO 711.018.005 to I.D.; Rubicon to S.D.)
Maastricht University/ MUMC+: Kootstra Talent Fellowship to S.D.

Corresponding author:
Ingrid Dijkgraaf
i.dijkgraaf@maastrichtuniversity.nl

https://doi.org/10.17952/37EPS.2024.P1121

Harnessing GPCRs Biased Signaling: Novel Macrocyclic Analogs for Enhanced Cardiovascular Treatment with Reduced Side Effects

Kien Tran,[1,2] Xavier Sainsily,[1] Jérôme Côté,[1] David Coquerel,[1] Pierre Couvineau,[2] Sabrina Saibi,[1] Lounès Haroune,[1] Élie Besserer-Offroy,[1] Joël Flynn-Robitaille,[1] Martin Resua Rojas,[1] Alexandre Murza,[1] Jean-Michel Longpré,[1] Mannix Auger-Messier,[1] Michel Bouvier,[2] Éric Marsault, Philippe Sarret and Pierre-Luc Boudreault[1]

1. Institut de Pharmacologie de Sherbrooke, Faculté de Médecine et des Sciences de la Santé, Université de Sherbrooke
2. 2. Institut de Recherche en Immunologie et en Cancérologie, Université de Montréal

INTRODUCTION

The discovery of signaling bias and the development of biased ligands represents a recent and significant advancement in drug discovery, offering the potential for more selective and effective therapies with reduced side effects. Biased ligands can preferentially activate or inhibit specific signaling pathways downstream of a receptor, thus providing a novel approach to modulating biological functions with greater precision.1 The innovation of biased signaling is particularly relevant in the context of cardiovascular diseases, where the precise modulation of receptor pathways can have significant implications for heart function and blood pressure regulation. [Pyr1]-apelin-13, an isoform of the apelin peptide acting on the APJ receptor, exemplifies this potential. It plays a pivotal role in cardiovascular physiology, mediating effects such as vasodilation and cardiac contractility enhancement, which are beneficial in the treatment of heart failure and hypertension. However, the therapeutic application of [Pyr1]-apelin-13 and its analogs has been limited by factors such as rapid degradation in vivo and the activation of multiple signaling pathways, which could lead to side effects.

HYPOTHESIS

Stable and Biased ligands targeting the APJ receptor, designed to selectively modulate specific signaling pathways, will enhance therapeutic outcomes in cardiovascular diseases by improving efficacy and reducing side effects compared to non-biased ligands.

OBJECTIVES

Develop stable, biased, and potent macrocyclic analogs of Pyr-apelin-13 (Ape13).



N-terminal pharmacophores
- Affinity (essential)

C-terminal pharmacophores
- Affinity (important)
- Functional activation

SYNTHESIS

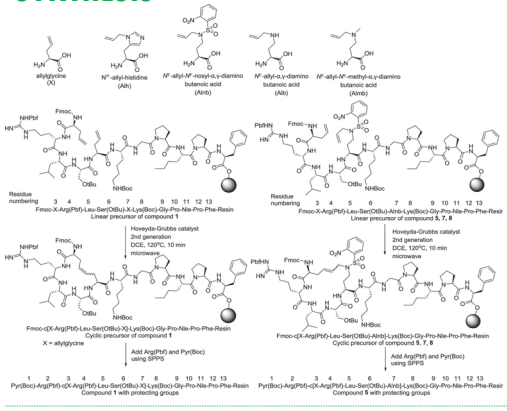

RESULTS

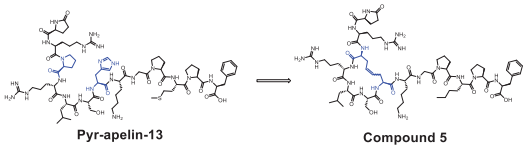

Macrocyclization of Ape13: Scan for macrocycle position

No	Macrocyclic analogues	Binding K_i (nM)	$G\alpha_i$ EC_{50} (nM)	β-arr2 EC_{50} (nM)	$T_{1/2}$ in vitro
Ape13	Pyr-R-P-R-L-S-H-K-G-P-M-P-F	0.7 ± 0.1	1.1 ± 0.2	60 ± 4	0.4 ± 0.1
2	c[X-R-P-R-X]c-S-H-K-G-P-Nle-P-F	5.7 ± 3.5	23 ± 6	857 ± 195	0.8 ± 0.2
3	Pyr-c[Rx-P-R-L-X]c-H-K-G-P-Nle-P-F	4.5 ± 1.4	6.0 ± 1.4	179 ± 21	2.2 ± 0.3
4	Pyr-c[X-P-R-L-X]c-H-K-G-P-Nle-P-F	509 ± 146	--	--	0.7 ± 0.1
5	Pyr-R-c[X-R-L-S-X]c-K-G-P-Nle-P-F	3.0 ± 0.1	3.7 ± 0.9	126 ± 26	3.9 ± 0.6
6	Pyr-R-P-c[Rx-L-S-H-X]c-G-P-Nle-P-F	9.1 ± 1.4	19 ± 5	512 ± 131	7.7 ± 0.3
7	Pyr-R-P-c[X-L-S-H-X]c-G-P-Nle-P-F	6074 ± 1168	--	--	9.9 ± 1.2
8	Pyr-R-P-R-c[X-S-H-K-X]c-P-Nle-P-F	41 ± 5	--	--	3.5 ± 0.8
9	Pyr-R-P-R-L-c[Sx-H-K-G-X]c-Nle-P-F	188 ± 84	--	--	> 24h
10	Pyr-R-P-R-L-c[X-H-K-G-X]c-Nle-P-F	268 ± 125	--	--	4.1 ± 0.8
11	Pyr-R-P-R-L-S-c[X-K-G-P-X]c-P-F	1.4 ± 0.4	20 ± 2	400 ± 35	6.6 ± 0.4
12	Pyr-R-P-R-L-S-H-c[X-G-P-Nle-X]c-F	14 ± 7	30 ± 7	825 ± 113	4.6 ± 0.7
13	Pyr-R-P-R-L-S-H-K-c[X-P-Nle-P-X]c	1.1 ± 0.1	19 ± 4	272 ± 7	8.6 ± 0.6
14	Pyr-R-P-R-L-S-H-K-G-c[X-Nle-P-F-X]c	310 ± 59	--	--	7.8 ± 1.1

N-terminus and C-terminus truncation

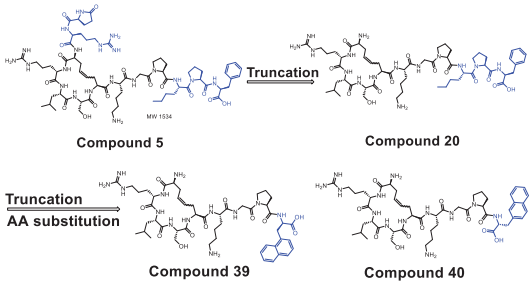

Functional activation

No	EC_{50} $G\alpha_{i1}$ (nM)	EC_{50} $G\alpha_{12}$ (nM)	EC_{50} β-arr2 (nM)
Ape13	0.8 ± 0.2 (100%)	49 ± 1 (100%)	37 ± 8 (100%)
5	3.7 ± 0.9 (101%)	22 ± 2 (98%)	126 ± 26 (98%)
20	6.7 ± 1.2 (100%)	45 ± 2 (98%)	143 ± 33 (98%)
39	0.8 ± 0.1 (103%)	> 10000 (3%)	31 ± 7 (70%)
40	5.0 ± 0.6 (105%)	2.4 ± 0.6 (40%)	232 ± 4 (55%)

Spider plots of Δlog(τ/KA) of analogs 39 and 40

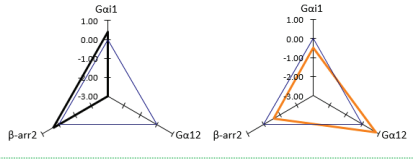

Long-lasting *in vivo* cardiac effect

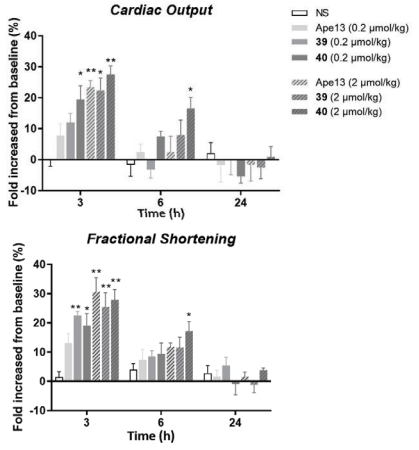

Pharmacokinetic *in vivo* in rat

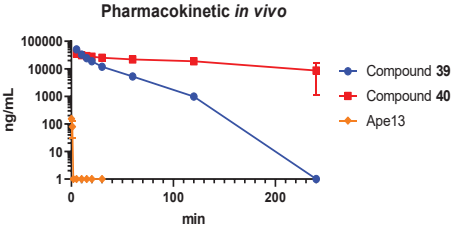

	Ape13	39	40
$T_{1/2}$ *in vivo*	< 1 min	24 min	220 min
AUC (mg/mL.min)	0.0002 ± 0.0001	1.33 ± 0.18	8.80 ± 0.41
Clearance (Cl) mL/(min.kg)	Very high	2.3	0.3

CONCLUSION

- The macrocyclization is a powerful method to improve the stability and affinity of the apelin peptide.
- Macrocyclic analogue **39** and **40** has significant lower MW (33%) than **apelin-13** but display similar potency.
- Compounds **39** is biased agonists of APJ receptor on the $G\alpha_{12}$ pathway.
- Analogue **39** and **40** display a longer half-life and long-lasting cardiac effect *in vivo* up to 6h after administration.

REFERENCES

1. Trân et al. *J. Med. Chem.* **2022**, *65* (1), 531–551.
2. Trân *et al. J. Med. Chem.* **2018**, *61* (6), 2266–2277.
3. Coquerel *et al. Critical Care Medicine* **2017**, *45* (11), e1139Yang *et al. Trends Pharmacol. Sci.* **2015**.

https://doi.org/10.17952/37EPS.2024.P1122

P1.122

A Novel Regulation Method of mRNA by Recruiting Regnase-1 Using Binding Motif-Antisense Oligonucleotide Conjugates

Masayuki Fujii

Department of Biological & Environmental Chemistry, Faculty of Humanity Oriented Science and Engineering, Kindai University, 11-5 Kayanomori, Iizuka, Fukuoka 820-8555, Japan

ABSTRACT

In the present study, a novel regulation method of mRNA using RNA stem-loop motif (SL) which is recognized by Regnase-1, an endoribonuclease responsible for suppression of inflammatory mRNAs, is described. Antisense oligonucleotides (ASO) linked to SL, ASO-SLs targeting *KRAS* mRNA codon 12 were prepared and suppression of *KRAS* mRNA by ASO-SLs was evaluated. ASO-3SL containing SL linked to 2'-OMeRNA ASO targeting *KRASwt* at its 3'-end suppressed $KRAS^{wt}$ mRNA 49.2% at 100nM and 66.8% at 1μM, respectively. On the other hand, ASO-5SL containing SL linked to 2'-OMeRNA ASO at its 5'-end did not affect $KRAS^{wt}$ expression at all at 1μM.

Introduction

Endoribonuclease involved in various biological functions such as cellular inflammatory response and immune homeostasis, glial differentiation of neuro-progenitor cells, cell death of cardiomyocytes, adipogenesis and angiogenesis. Functions as an endoribonuclease involved in mRNA decay (Interleukin-1-inducible MCPIP protein has structural and functional properties of RNase and participates in degradation of IL-1beta mRNA. (FEBS J. 2009, 276:7386-7399)

Regnase-1, MCPIP1 (Monocyte chemotactic protein-1-induced protein-1) ZC3H12A (AY920403)

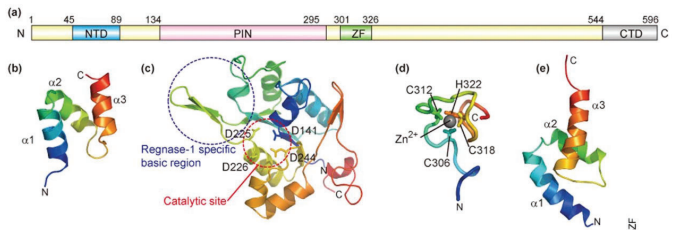

Figure 1: Structural and Function of Regnase-1.
From: Structural basis for the regulation of enzymatic activity of Regnase-1 by domain-domain interactions (F Inagaki et al, Scientific Reports 2016, 6: 22324)

Regnase-1 modulates the inflammatory response by promoting the degradation of a set of translationally active cytokine-induced inflammation-related mRNAs, such as IL6 and IL12B, during the early phase of inflammation (MCPIP1 endoribonuclease activity negatively regulates interleukin-17-mediated signaling and inflammation. Immunity 43:475-487 (2015). Regnase-1 prevents aberrant T-cell-mediated immune reaction by degradation of multiple mRNAs controlling T-cell activation, such as those encoding cytokines (IL6 and IL2), cell surface receptors (ICOS, TNFRSF4 and TNFR2) and transcription factor (REL) (Figure 2).



Figure 2. Degradation of Inflammatory mRNA by Regnase-1

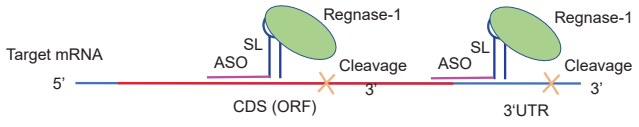

Figure 3. Recruitment of Regnase-1 and mRNA Cleavage by ASO-SL Conjugate

Results and Discussions

In the present study, we aimed to modulate Regnase-1 activity using Regnase-1 binding stem-loop motif (SL) linked to antisense oligonucleotide (ASO). We prepared two types of SL-ASO targeting *KRAS* codon 12 and 13, 2'-OMeRNA ASO linked to RNA SL at the 3'-end (ASO-3SL) and 2'-OMeRNA ASO linked to RNA SL at the 5'-end (ASO-5SL) as well as 2'-OMeRNA ASO and siRNA.

ASO: 5'-(CCUACGCCACCAGCUCCAACU)m-3'
siRNAwt: 3'-(AC)mCUCGACCACCGCAUCCGUU-5'
5'-GAGCUGGUGGCGUAGGCAA(GA)m-3'
siRNAG12D: 3'-(AC)mCUCGACUACCGCAUCCGUU-5'
5'-GAGCUGAUGGCGUAGGCAA(GA)m-3'
ASO-3SL: 5'-(CCUACGCCACCAGCUCCAACU)m-SL-3'
ASO-5SL: 5'-SL-(CCUACGCCACCAGCUCCAACU)m-3'

Suppression efficiencies of *KRASwt* mRNA in HeLa cells by ASO-3SL and ASO-5SL were evaluated by quantification of KRAS mRNA by RT-PCR and compared with those of ASO, siRNAwt and siRNAG12D (Figure 3).

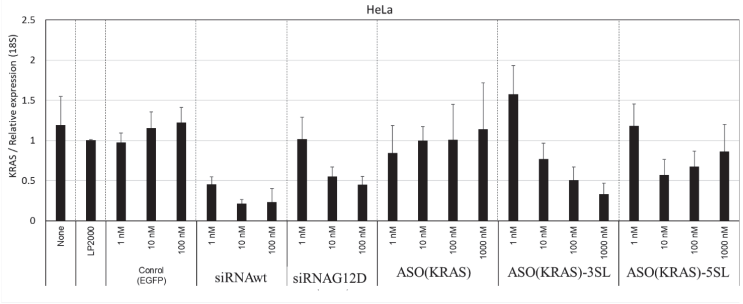

Figure 4. Suppression of *KRAS* mRNA by ASO-3SL and ASO-5SL

ASO-3SL suppressed $KRAS^{wt}$ mRNA in HeLa cells in 49.2% at 100nM. 66.8% at 1μM, while ASO-5SL did not affect *KRAS* mRNA level at all. The results indicate Regnase-1 recruited onto SL motif and cleaved mRNA at 3'-side of the SL. On the other hand, ASO-3SL suppressed $KRAS^{G12D}$ mRNA in PK-45H cells very slightly. ASO din not suppress $KRAS^{wt}$ mRNA at all at 1 μM and siRNAwt suppressed $KRAS^{wt}$ mRNA in 55.6% at 1 nM, 78.3% at 10 nM and 76.6% at 100 nM. Silencing efficiency of ASO-3SL was stronger than ASO but weaker than siRNA. The results indicate that ASO-3SL suppressed the target mRNA moderately but not too much because Regnase-1 can also regulate its own mRNA to keep the immune activity properly. This characteristic feature of ASO-3SL will be important to target immunity associated mRNAs.

Conclusion

Here we successfully report a novel regulation method of mRNA using RNA stem-loop motif. It is to be pointed out that ASO-SL could target ORF of cancer gene and that this regulation method is a universal method targeting any position of any types of mRNA. Moreover, ASO-SL is very selective and sensitive to single base mutation of cancer genes and will provide a great benefit in cancer immunotherapy such as CAR-T cell therapy and immune check point inhibitors.

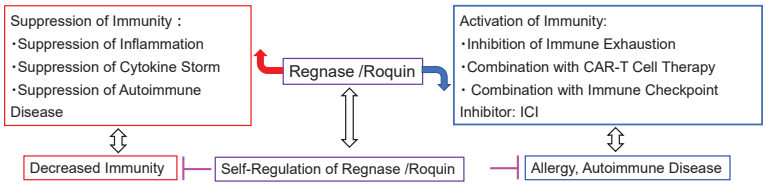

Figure 5. Immunity can be suppressed or activated by regulation of Regnase /Roquin.

COI: We have no conflict of interest to disclose for this presentation.

Deoxythymidine-based antimicrobial peptidomimetics to combat drug-resistance

https://doi.org/10.17952/37EPS.2024.P1124

Eun Young Kim[1], Dinesh Kumar[1], Sung Tae Yang[2] and Song Yub Shin[1,*]

[1]Department of Cellular & Molecular Medicine, School of Medicine, Chosun University, Gwangju, 61452, Republic of Korea
[2]Department of Department of Microbiology, School of Medicine, Chosun University, Gwangju, 61452, Republic of Korea

Abstract

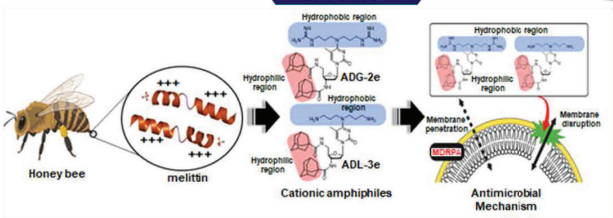

Deoxythymidine-based amphiphilic antimicrobial peptidomimetics, ADG-2e and ADL-3e, were assessed for their potential as novel classes of antimicrobial, antibiofilm, and anti-inflammatory agents. ADG-2e and ADL-3e demonstrated good resistance to physiological salts and human serum, with a low incidence of drug resistance. They also exhibit proteolytic resistance against pepsin, trypsin, α-chymotrypsin, and proteinase K. ADG-2e and ADL-3e were found to kill bacteria by an intracellular target mechanism and a bacterial cell membrane-disrupting mechanism, respectively. Furthermore, when combined with several conventional antibiotics against MRSA and MDRPA ADG-2e and ADL-3e showed effective synergistic effects. Importantly, ADG-2e and ADL-3e not only suppressed MDRPA biofilm formation but also effectively eradicated mature MDRPA biofilms. Additionally, ADG-2e and ADL-3e significantly reduced TNF-α and IL-6 gene expression and protein secretion in LPS-stimulated macrophages, indicating potent anti-inflammatory activity during LPS-induced inflammation. Our findings suggest that ADG-2e and ADL-3e have the potential to be further developed as novel antimicrobial, antibiofilm, and anti-inflammatory agents for combating bacterial infections.

Structure & Protease Stability

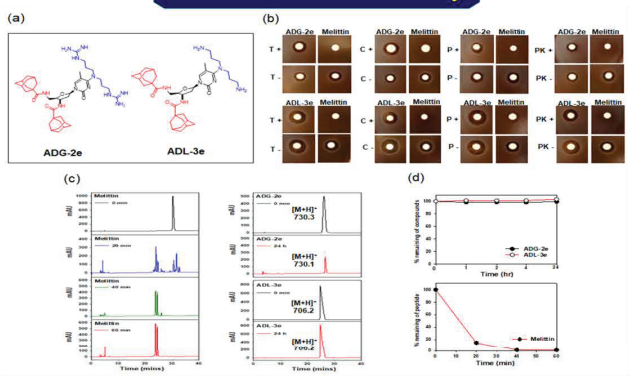

Fig. 1. (a) Chemical structures of deoxythymidine-based cationic amphiphiles, ADG-2e and ADL-3e. The blue and red colors indicated the cationic and hydrophobic moiety of amphiphiles, respectively. (b) Effect of protease on the bactericidal activity of ADG-2e and ADL-3e determined by radial diffusion assay. Compounds were incubated with pepsin, trypsin, α-chymotrypsin, or proteinase K for 4 h at 37°C. Subsequently, 20ul of the enzyme-treated compounds were added into wells in the *E. coli* (KCTC 1682) (10^5-10^6 CFU/ml) mixed MH-broth agar plate and incubated overnight at 37°C. T+: with trypsin, T-: without trypsin, C+: with α-chymotrypsin, C-: without α-chymotrypsin, P+: with pepsin, P-: without pepsin, PK+: with proteinase K, PK-: without proteinase K. (c) Reverse-phase high-performance liquid chromatography (RP-HPLC) profiles of tryptic digestion products of melittin, ADG-2e and ADL-3e obtained at varied intervals. The main eluents of trypsin-treated ADG-2e and ADL-3e for 24 h were collected, lyophilized and analyzed by electrospray ionization-mass spectroscopy (ESI-MS). (d) Stability of melittin, ADG-2e and ADL-3e to trypsin digestion.

Table 1. The MIC values of ADG-2e, ADL-3e and conventional antibiotics against MRSA, MDRPA and VREF

Bacterial strains	MIC (ug/ml)					
	ADG-2e	ADL-3e	CHL	TET	RIF	CIP
MRSA[a]						
CCARM 3001	32	16	512	64	32	128
CCARM 3089	16	16	1024	128	32	1024
CCARM 3090	16	16	1024	128	32	512
CCARM 3095	16	32	2048	256	8	1024
MDRPA[b]						
CCARM 2095	32	32	2048	256	16	1024
CCARM 2109	32	16	1024	128	32	512
VREF[c]						
ATCC 515675	32	32	128	256	64	128
ATCC 51559	16	16	1024	>2048	32	128

[a] MRSA: Methicillin-resistant *Staphylococcus aureus*
[b] MDRPA: Multidrug-resistant *Pseudomonas aeruginosa*
[c] VREF: Vancomycin-resistant *Enterococcus faecalis*
CHL: Chloramphenicol, TET: Tetracycline, RIF: Rifampicin, CIP: Ciprofloxacin

Table 2. The MIC values of ADG-2e, ADL-3e and antibiotics in the presence of physiological salts and human serum

Compounds	Control	NaCl 150 mM	KCl 4.5 mM	NH_4Cl 6 uM	$MgCl_2$ 1 mM	$CaCl_2$ 2.5 mM	$FeCl_3$ 4 uM	Human serum (25%)
MRSA (CCARM 3089)								
ADG-2e	16	16	16	16	16	16	32	32
ADL-3e	32	32	32	32	32	32	32	32
CHL	2048	2048	2048	2048	2048	2048	2048	2048
TET	256	256	256	512	512	256	512	512
RIF	8	16	16	8	8	8	8	16
CIP	1024	1024	1024	1024	1024	1024	1024	1024
MDRPA (CCARM 2095)								
ADG-2e	32	32	32	16	16	32	32	16
ADL-3e	32	32	32	32	32	32	32	32
CHL	2048	2048	2048	2048	2048	2048	2048	2048
TET	256	256	512	256	256	512	512	1024
RIF	16	32	16	16	16	32	32	32
CIP	1024	1024	1024	2048	2048	2048	2048	1024

Synergy Activity & Antibiofilm Activity

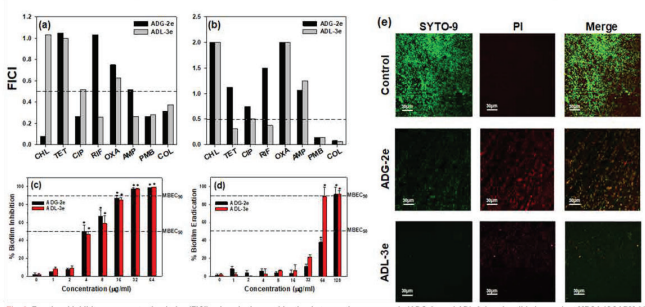

Fig. 2. Fractional inhibitory concentration index (FICI) values in the combination between the compounds (ADG-2e and ADL-3e) and antibiotics against MRSA (CCARM 3089) (a) and MDRPA (CCARM 2095) (b). The dotted line represents FICI=0.5. FICI ≤ 0.5 = synergy. In vitro antibiofilm activity of compounds. Biofilm inhibition (c) and eradication (d) activities of ADG-2e and ADL-3e against MDRPA (CCARM 2095). The values are expressed as the mean ± SEM of three independent experiments and are statistically significant at $^{*}p < 0.05$. (e) Confocal laser scanning microscopy (CLSM) images of compound-treated mature MDRPA biofilms. Biofilms were 24 h and then treated with PBS solution (control), ADG-2e ($MIEC_{90}$) and ADL-3e ($MIEC_{90}$) for 2h. Biofilms were stained with the live (green) and dead (red) stain kit, which uses SYTO-9 to stain live cells and propidium iodide (PI) to stain dead cells. The scale bar represents 30 um.

Drug Resistance & Time-Killing Kinetic

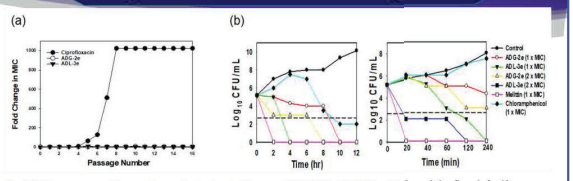

Fig. 3. (a) The emergence of drug resistance after treatment of *S. aureus* (KCTC 1621) with ADG-2e, ADL-3e, and ciprofloxacin for 16 passages at a sub-MIC concentration determined by the sequential passaging method. The fold change in MIC of the antimicrobials (compounds) was plotted against the number of passages. (b) Time-killing kinetic analysis of ADG-2e and ADL-3e against *E. coli* (KCTC 1682). The dotted line indicates a 50% reduction from the initial CFU.

Antimicrobial Mechanism

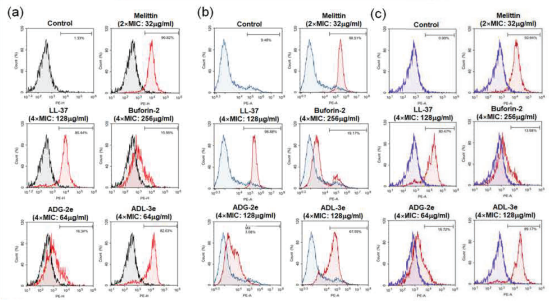

Fig. 4. Flow cytometric analysis of *E. coli* (KCTC 1682) (a), MRSA (CCARM 3089) (b) and MDRPA (CCARM 2095) (c) treated with 2xMIC or 4xMIC of ADG-2e, ADL-3e and control peptides (melittin, buforin-2 and LL-37) for 60 min and stained with PI.

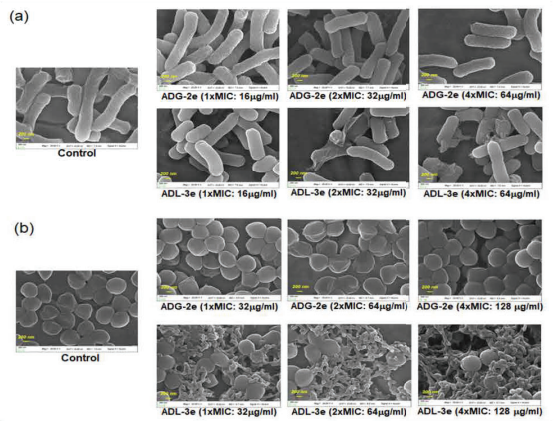

Fig. 5. Scanning electron microscopy (SEM) images of *E. coli* (KCTC 1682) (a) and MRSA (CCARM 3089) (b). Mid-logarithmic-phase bacteria cells were treated with compound at 1xMIC, 2xMIC and 4xMIC for 4 h. The control was done without compound. Scale bar: 200 nm.

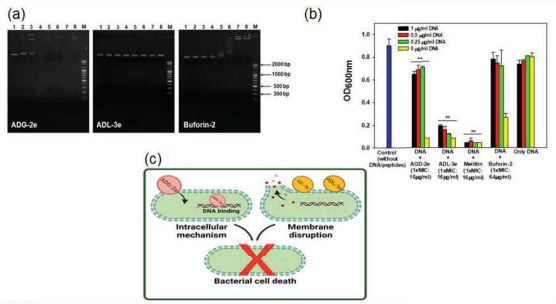

Fig. 6. (a) Interaction of compounds with *E. coli* (ATCC 25922) genomic DNA by a gel migration assay. Binding was assayed by measuring the degree of inhibition of migration by *E. coli* (ATCC 25922) genomic DNA (500 ng). DNA and compounds were co-incubated for 1 h at room temperature before electrophoresis on a 1.0% agarose gel. Line 1-8: The concentration of compounds was 0, 2, 4, 8, 16, 32, 64, and 128ug/ml, respectively. M: DNA marker (b) Inhibitory effect of *E. coli* (ATCC 25922) genomic DNA on antimicrobial activity of ADG-2e, ADL-3e, and control AMPs (melittin and buforin-2). The values are expressed as the mean ± SEM of three independent experiments and are statistically significant at $^{**}p < 0.01$. (c) Schematic diagram showing the potential antimicrobial mechanism of ADG-2e and ADL-3e

Anti-inflammatory Activity

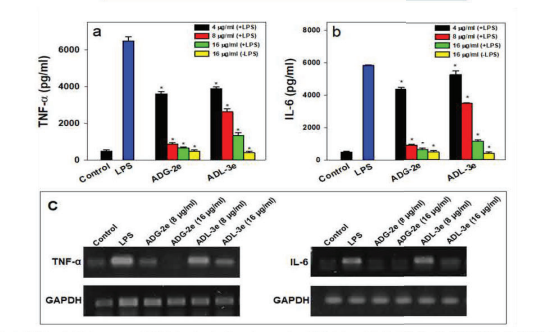

Fig. 7. ADG-2e and ADL-3e suppressed LPS-induced production and expression of TNF-alpha and IL-6 in LPS-stimulated RAW264.7 cells. (a) Effects of ADG-2e and ADL-3e on TNF-alpha production in LPS-stimulated RAW264.7 cells. (b) Effects of ADG-2e, ADL-3e, and LL-37 on IL-6 production in LPS-stimulated RAW264.7 cells. All bar graphs represent mean ± SEM from three independent experiments ($^{*}P < 0.05$, significantly different from the control group treated with LPS alone). (c) Effects of ADG-2e and ADL-3e on the mRNA levels of TNF-alpha and IL-6 in LPS-stimulated RAW264.7 cells. RAW264.7 cells ($5x10^5$ cells/well) were incubated with the compounds in the presence of LPS (20 ng/mL) for 3 h. Total RNA was isolated and analyzed to determine the TNF-alpha and IL-6 mRNAs levels by RT-PCR.

https://doi.org/10.17952/37EPS.2024.P1125

Fine-Tuning the Immune-Stimulatory and Cancer Cell Binding Properties of Immune System Engagers (ISErs)

Hannah Back[a,b], **Manuel Felkl**[a], **Susanne Kremer**[c], **Claudia Altdorf**[c], **Ute Steinbusch**[c], **Christian FW Becker**[a]

[a] Institute of Biological Chemistry, Faculty of Chemistry, University of Vienna, Währinger Str. 38, 1090 Vienna, Austria

[b] University of Vienna, Vienna Doctoral School in Chemistry (DoSChem), Währinger Str. 42, 1090 Vienna, Austria

[c] Syntab Therapeutics GmbH, ZBMT, Pauwelstrasse 17, 52074 Aachen, Germany

Email address: hannah.susanne.back@univie.ac.at

1. Introduction

- **Targeted therapies against cancer** have become a key therapeutic approach as distinct surface markers are addressed using specific compounds such as monoclonal antibodies (mAbs) or small molecule drugs.[1,2]
- **Immune system engagers (ISErs)**, a novel class of peptide-based therapeutics, offer potential advantages over mAbs with respect to issues such as poor tumor penetration, prolonged bioavailability, and high production costs. They consist of at least two binders recognizing cancer cell-specific targets and one or more effector moieties recruiting innate immune cells. The binders and effector are linked via a polyethylene glycol chain (PEG), mimicking the epitope length in antibodies.[3-5]

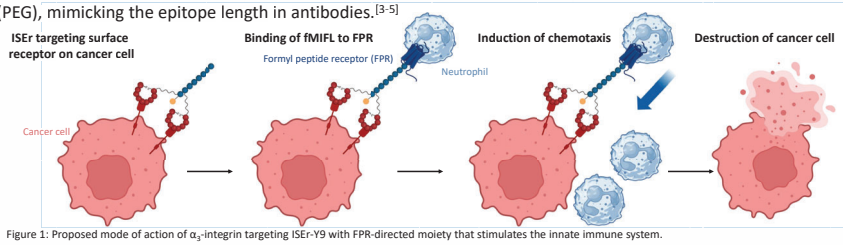

Figure 1: Proposed mode of action of α_5-integrin targeting ISEr-Y9 with FPR-directed moiety that stimulates the innate immune system.

- **Innate immune cell stimulation** is achieved with a chemoattractant, the short and very potent N-formylated peptide (fMIFL), which binds to formyl peptide receptors (FPRs), classified pattern recognition receptors (PRRs) expressed on innate immune cells.[6,7]

2. Motivation

- The goal of this work is the generation of ISEr variants with optimized binding affinities/avidity towards different cancer surface markers and with tailored immune stimulating properties.
- Establishing a **PEG linker library** and assessing the binding avidity via a competitive binding assays.

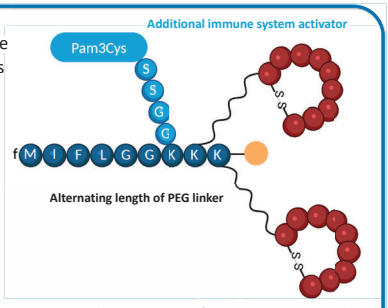

Figure 2: Schematic structure of an ISEr showing moieties that offer potential for possible modification sites.

- Toll-like receptor 2 (TLR2), an integral transmembrane glycoprotein and PRR, is targeted with the TLR2 agonist **Pam3Cys** (N-acyl-S-diacylglycerol cysteine). Binding leads to heterodimerization with TLR1 and stimulation of the MyD88-dependent signaling pathway, which triggers activation of the host defense mechanism via the innate immune system.[8]

3.A Results: ISEr-Y9 with varying PEG linkers

- PEG linkers increase the drug size and therefore circulation time and bioavailability.[9]
- Increased PEG linker lengths prevent the event of proteolysis, however, shorter linkers might improve ligand receptor interaction by limiting conformational freedom.[9]
- The ISEr-Y9 PEG series was successfully synthesized.
- In the competitive binding assay, the ISEr-Y9 PEG series was titrated against 50 nM Biotin-ISEr-Y9 PEG_{27}.
  ISEr-Y9 PEG_{27} showed lowest IC_{50} value in both human and murine breast cancer cell lines, indicating the best binding avidity in comparison to ISEr-Y9 with PEG_3 and PEG_{11} linker, respectively.

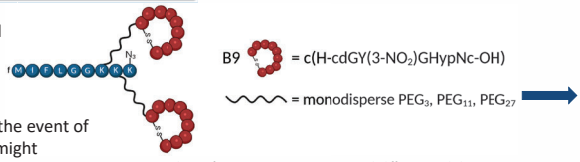

Figure 3: Library of integrin α_5-targeting ISEr-Y9 with different PEG linkers.

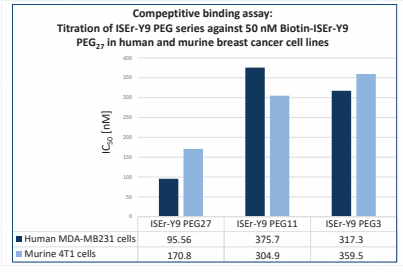

Figure 5: IC_{50} of ISEr-Y9 PEG series in human and murine breast cancer cell lines.

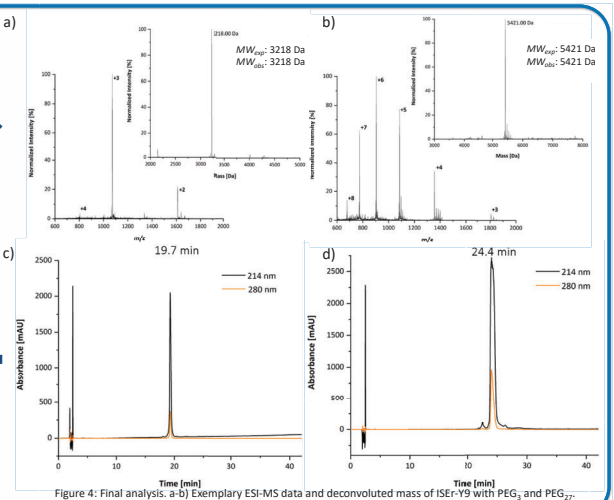

Figure 4: Final analysis. a-b) Exemplary ESI-MS data and deconvoluted mass of ISEr-Y9 with PEG_3 and PEG_{27}. c-d) Exemplary HPLC data (C4 column) of ISEr-Y9 with PEG_3 and PEG_{27} linker.

3.B Results: Palmitoylated ISEr

- Attachment of the amino acid Pam3Cys, which targets TLR2 on immune cells to induce an antimicrobial pathway that can be monitored by cytokine release.

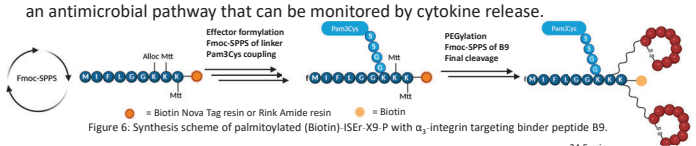

Figure 6: Synthesis scheme of palmitoylated (Biotin)-ISEr-X9-P with α_5-integrin targeting binder peptide B9.

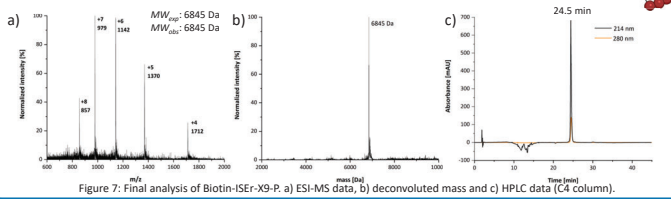

Figure 7: Final analysis of Biotin-ISEr-X9-P. a) ESI-MS data, b) deconvoluted mass and c) HPLC data (C4 column).

- ISEr-X9-P increases TNF-α, IL-6 and IL-8 levels in blood cells, indicating successful TLR2 stimulation.

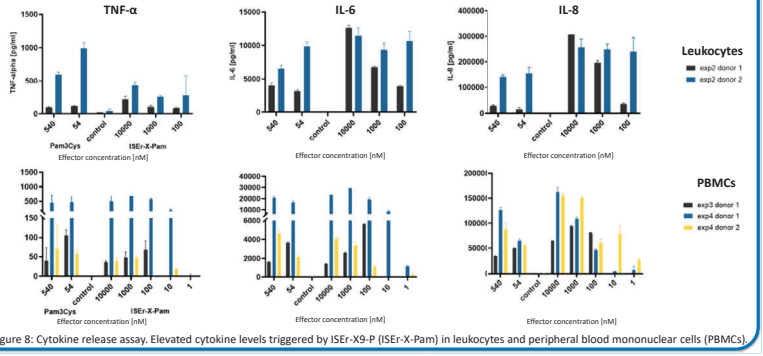

Figure 8: Cytokine release assay. Elevated cytokine levels triggered by ISEr-X9-P (ISEr-X-Pam) in leukocytes and peripheral blood mononuclear cells (PBMCs).

4. Summary & Outlook

- **Results I:** ISEr-Y9 with PEG_{27} linker showed the highest binding avidity on human and murine breast cancer cell lines. Next, the library will be extended with a PEG_{54} variant and evaluated for binding properties compared to previously synthesized PEG variants. Furthermore, this PEG library will be adapted to an ISEr series with an ephrin A2 targeting binder peptide (B59).
- **Results II:** Palmitoylated Biotin-ISEr-X9-P was successfully synthesized. The immunostimulatory effect of palmitoylated ISEr-X9-P on TLR2 was validated in a cytokine release assay and showed increased levels of TNF-α, IL-6 and IL-8. Next, the library will be extended to include a palmitoylated ISEr with an ephrin-A2 targeting binder peptide (B59) and will need to be evaluated for binding avidity and immunostimulatory potential.

5. References

[1] Scott, A. M. *et al. Nat Rev Cancer* **12**, 278-287 (2012).
[2] Padma, V. *et al. Biomedicine (Taipei)*, (2015).
[3] Conibear, A. C. *et al. Front Chem* **7**, 113 (2019).
[4] Mitra, S. *et al. J Genet Eng Biotechnol* **19**, 159 (2021).
[5] Potgens, A. J. G. *et al. Biochemistry* **58**, 2642-2652 (2019).
[6] Conibear, A. C. *et al. Chembiochem* **19**, 459-469 (2018).
[7] Dalpiaz, A. *et al. Eur J Pharmacol* **411**, 327-333 (2001).
[8] Nalla, N. *et al. Bioorg Med Chem* **23**, 5846-5855 (2015).
[9] Lim, C. *et al. Int J Nanomedicine* **18**,1615-1630 (2023).

Figures were created with BioRender.com

Targeted Acidosis Mediated Delivery of Antigenic MHC-Binding Peptides

Joey J. Kelly[1], Emily T. Ankrom[2], Sarah E. Newkirk[1] Damien Thévenin[2], Marcos M. Pires[1]
[1]Department of Chemistry, University of Virginia, Charlottesville, VA
[2]Department of Chemistry, Lehigh University, Bethlehem, PA
https://doi.org/10.17952/37EPS.2024.P1126

Abstract

Objective

One of the immune system's critical mechanisms for eliminating cancer is to target cancer-specific peptide antigens presented on the major histocompatibility complex (MHC).[1] However, cancers with low mutational burdens often manage to avoid immune clearance due to the limited presence of cancer-specific peptide antigens.[2] The lack of immunogenic peptides for display on MHC to immune cells greatly hinders the ability of the immune system to recognize and eliminate cancer.[3] To counteract this mechanism of immune evasion, we aimed to:

- Specifically deliver antigenic MHC binding peptides to cancer cells
- Demonstrate improved immune activation against targeted cancer cells

Background

Targeted Delivery of Antigenic Peptide

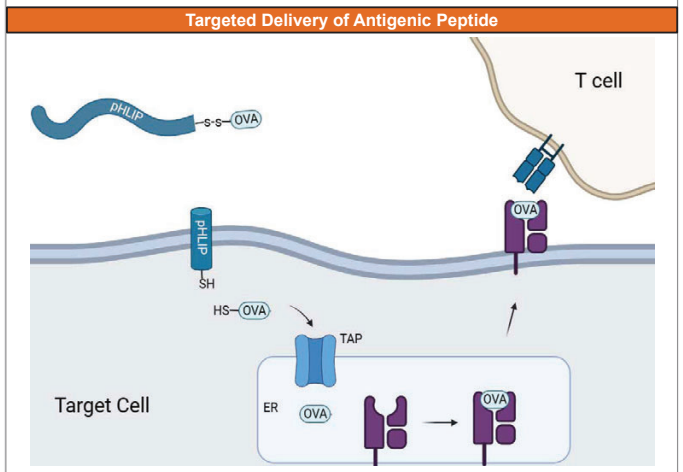

pH(low) insertion peptides (pHLIP) selectively insert into the membrane of cells in acidic microenvironments – a hallmark of cancer biology.

SIINFEKL (OVA) is a model peptide antigen from the protein ovalbumin that readily binds to MHC and activates the immune system.

Disulfide release enables OVA to enter the antigen presentation pathway.

Presentation of OVA on MHC alerts T cells to activate a cytotoxic response

References

1) Schappert, A. et al. *Life Sci*. **2018.** 209: 255-258
2) Jardim, D. et al. *Cancer Cell*. **2021.** 39: 154-173
3) Zou, X. et al. *Front. Immunol*. **2021**. 12: 689076

Pires research lab

Methods and Results

RMA-S Stabilization Assay is a Well-Established Method to Measure MHC Affinity

RMA-S cells display empty MHC molecules that can bind exogenous peptide.

Peptide-MHC affinity can be quantified by the amount of pMHC complexes stabilized on the surface of the cell.

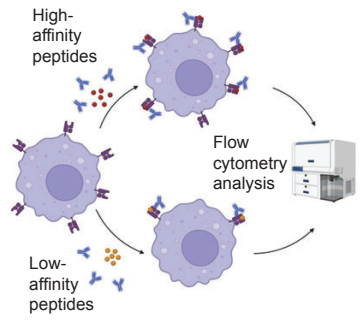

CSIINFEKL Retains Potent MHC Binding and T Cell Activation

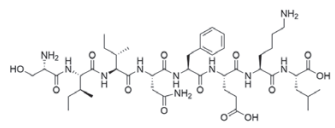

We synthesized a library of SIINFEKL derivatives to identify sites amendable to cysteine modifications.

Modifications near the N-terminus were well tolerated for MHC binding.

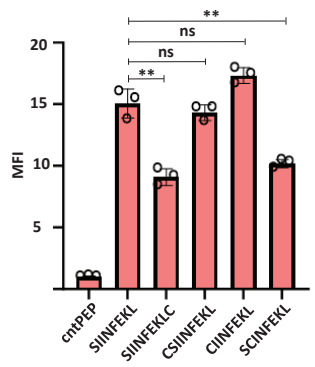

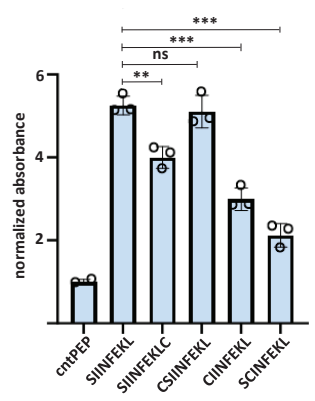

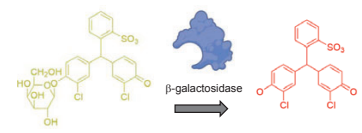

Reporter T cell line with OVA-specific T cell receptor measured T cell activation.

CSIINFEKL (CysOVA) proved to be least disruptive to T cell activation.

Results

pHLIP-CysOVA Selectively Inserts into Lipid Bilayers at Low pH

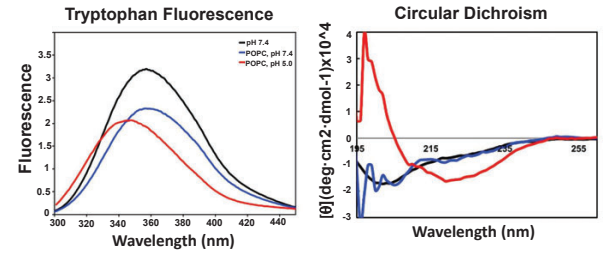

Synthesized pHLIP-CysOVA conjugate and confirmed pH dependent membrane anchoring using tryptophan fluorescence and CD spectrometry.

Disulfide Reduction is a Necessary Step for MHC Presentation

RMA-S cells display empty MHC molecules when incubated at 26ºC that can bind exogenous peptide.

Peptide-MHC affinity can be quantified by the amount of pMHC complexes stabilized on the surface of the cell.

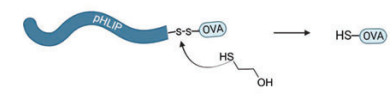

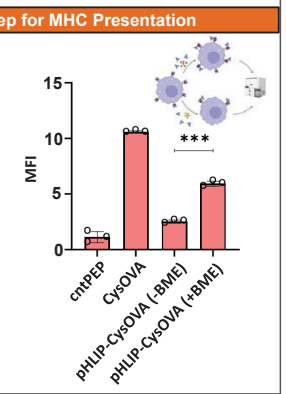

pHLIP-CysOVA Improves Activity of Antigen-Specific T cells

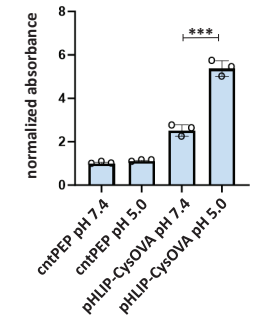

Treatment of pHLIP-CysOVA at low pH improves T cell activation.

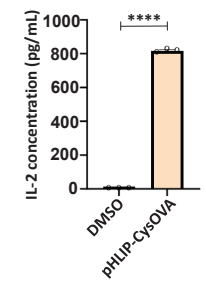

ELISA results also confirmed proinflammatory IL-2 secretion

https://doi.org/10.17952/37EPS.2024.P1128

Hybrid synthetic approach and biological characterization of a branched heterodimer for overcoming prostate cancer heterogeneity

Santo Previti,[a,b] Sacha Bodin,[c,d] Emmanuelle Rémond,[a] Clément Morgat,[c,d] and Florine Cavelier[a]

[a] Pôle Chime Balard, IBMM, UMR 5247, F-34293 Montpellier, France; [b] Department of Chemical, Biological, Pharmaceutical, and Environmental Sciences, University of Messina, Viale Stagno d'Alcontres 31, 98166 Messina, Italy; [c] University of Bordeaux, CNRS, EPHE, INCIA UMR 5287, F-33400 Talence, France; [d] CHU Bordeaux, Department of Nuclear Medicine, F-33000 Bordeaux, France.

BACKGROUND

Prostate cancer is the fifth cause of cancer-related death in men over the world (375 000 cases in 2020) ⟶ 5-year survival rate of 31% at the late stage.[1]

Radiolabelled Prostate-Specific Membrane Antigen (PSMA) inhibitors entry in clinical practice for imaging (**[^{68}Ga]Ga-PSMA-11**) and therapy (**[^{177}Lu]Lu-PSMA-617**).[2]

80% of prostate cancers show high heterogeneity ⟶ low expression of PSMA and presence of multiple distinct tumour foci.[3]

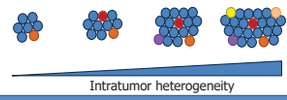

AIM OF THE RESEARCH

Development of heterodimers addressing two distinct targets expressed by tumoral prostate tissues.[4]

Neurotensin (NT) system was found to be involved in the growth of prostate cancer cells.

NTS1 ⟶ valid onco-target for imaging and therapy of PSMA-negative prostate cancer lesions.

pGlu-Leu- Tyr-Glu-Asn- Lys-Pro-**Arg^{8}-Arg^{9}-Pro^{10}-Tyr^{11}- Ile^{12}-Leu^{13}-OH**

⇩

H-Arg^{8}-Arg^{9}-Pro^{10}-Tyr^{11}- Ile^{12}-Leu^{13}-OH ⟹ **H-Lys^{8}-Lys^{9}-Pro^{10}-Tyr^{11}- Ile^{12}-Leu^{13}-OH**

NT8-13 -> NTS1, K_i = 1.5 nM — **JMV 438** -> NTS1, K_i = 4 nM [6]

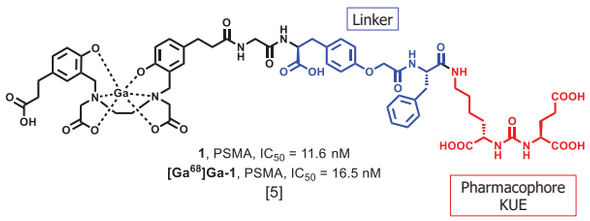

1, PSMA, IC_{50} = 11.6 nM

[Ga^{68}]Ga-1, PSMA, IC_{50} = 16.5 nM

[5]

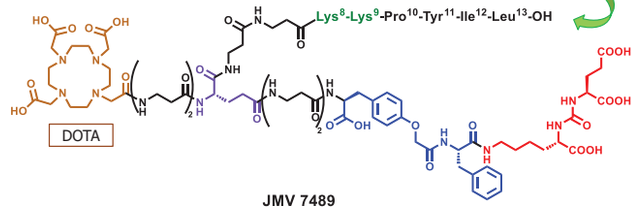

JMV 7489

SYNTHESIS

Synthesis of PMSA linker in solution

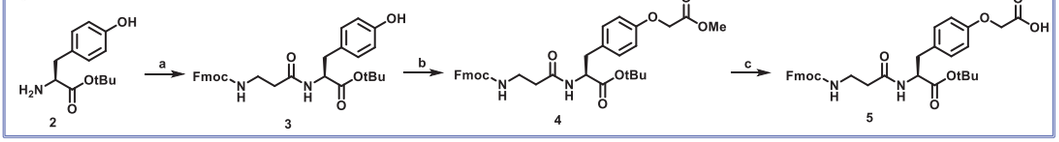

a = HATU, DIPEA, DMF, rt, on
b = Methyl bromoacetate, K_2CO_3, ACN, rt, on
c = NaOH, $CaCl_2$, ISA/H2O 7:3, rt, TLC mon.
d = 20% piperidine in DMF, rt, 1h
e = HATU, DIPEA, DMF, 45 min
f = 20% piperidine in DMF, 5 min (x 3)
g = TFE/DCM/AcOH (8:1:1), 4h
h = TFA/H_2O/TIS (95:2.5:2.5), 7h

Crucial steps report ★

Syntesis of NT arm

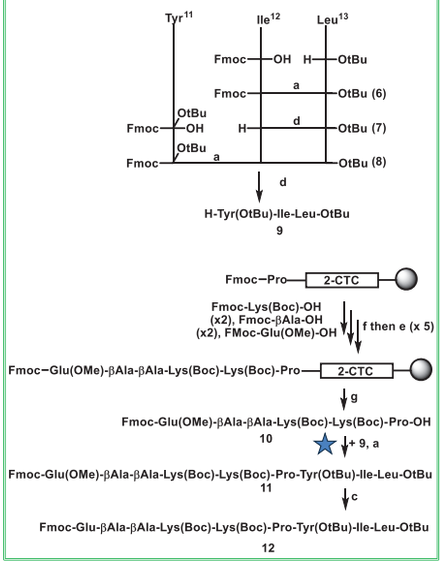

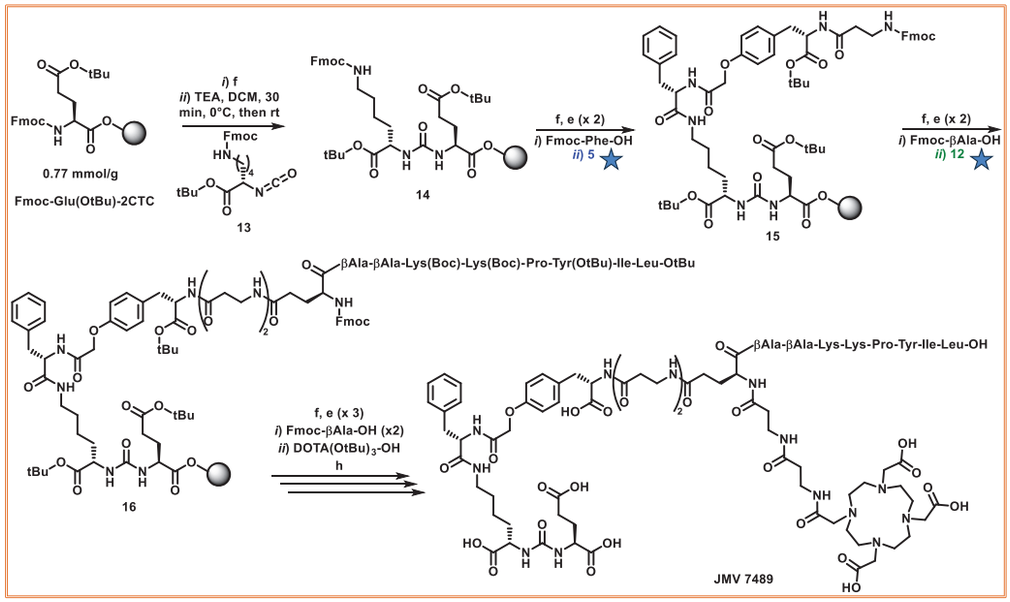

BIOLOGICAL INVESTIGATION

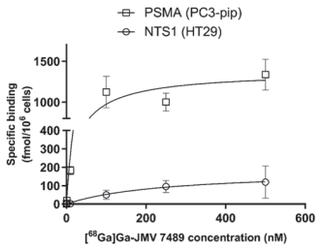

	Affinity towards NTS1 nM	Affinity towards PSMA nM
[^{68}Ga]Ga-**JMV 7489**	246 ± 1 (HT-29 cells, K_d)	53 ± 17 (PC-3 pip cells, K_d)
JMV 438	4.0 (CHO-K1 expressing hNTS1, K_i) [6]	-
[^{68}Ga]Ga-**1**	-	16.5 (LnCaP cells, IC_{50}) [5]
[^{68}Ga]Ga-**JMV 7089**	154.7 ± 13.2 (HT-29 cells, K_d)	-

⇩ DOTA-(βAla)$_2$-JMV438

- Loss of affinity with respect to the monomers was observed, more evident in NTS1 binding.
- The NT monomer **JMV 7089** was synthesized using SPPS.
- **JMV 7089** showed lower affinity towards NTS1 if compared with **JMV 438**.
- The linker and the DOTA macrocycle are the main responsible for the loss of affinity.
- The integration of the NT-pharmacophore into the DOTA-β-Ala-β-Ala-NTS1-PSMA heterodimer was quite well tolerated at the NTS1 (1.6-fold decrease in affinity **JMV 7489** *versus* **JMV 7089**).

CONCLUSION AND PERSPECTIVES

- A hybrid synthetic pathway, which includes both synthesis in batch and solid phase, was successfully employed.
- The linker and chelating macrocycle play a key role for binding affinity, in particular towards NTS1.
- These findings could be taken in consideration for future development of NTS1-PSMA radiopharmaceuticals.

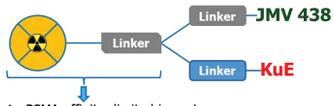

- PSMA affinity: limited impact
- NTS1 affinity: notable impact

FUNDINGS

REFERENCES

[1] Cancer.net., Prostate Cancer: Statistics, https://www.cancer.net/cancer-types/prostate-cancer/statistics; [2] Capasso G. et al., *Eur J Med Chem* **2024**, *263*, 115966; [3] Haffner M.C. et al., *Nat Rev Urol* **2021**, *18*, 79-92; [4] Schollhammer R. et al. *Cancers* **2023**, *15*, 2345; [5] Zha Z. et al., *Nucl Med Biol* **2018**, *59*, 36-47; [6] Previti S. et al., *Front Chem* **2020**, *8*, 406.

P1.129
The 37th EPS and 14th IPS Symposia

Epitope-directed peptide screening and machine learning for HER2-targeted antibody-mimetic peptides

○ Tetsuya Kadonosono[1] and Yutaka Saito[2] ([1]Tokyo Tech, JAPAN, [2]AIST, JAPAN)

東京工業大学 Tokyo Institute of Technology

tetsuyak@bio.titech.ac.jp

https://doi.org/10.17952/37EPS.2024.P1129

INTRODUCTION

Small antibody mimetics can serve as lower cost alternatives to current monoclonal antibody drugs. Recently, we developed an epitope-directed peptide screening system called Monoclonal Antibody-Guided Peptide Identification and Engineering (MAGPIE) screen [1]. In this system, candidate peptides are bound to antigens on the mammalian cell surface by displaying peptide library on antigen-expressing cells, followed by evaluation of their epitope by a fluorescently labelled guide antibody (gAb) that bind to the desired epitope.

The current study described the development of human epidermal growth factor receptor 2 (HER2)-targeted antibody-mimetic peptides using a combination of MAGPIE screen and machine learning.

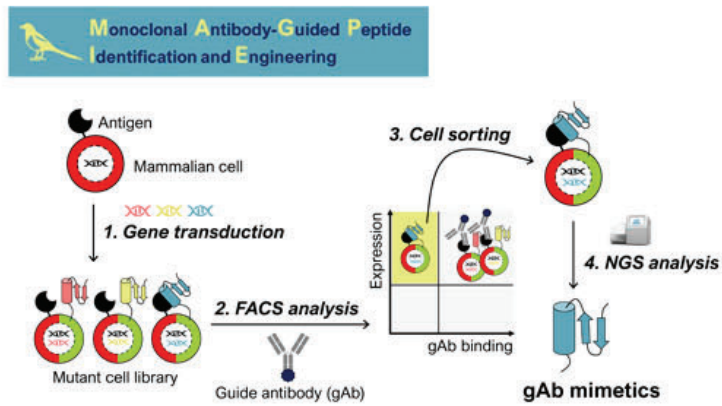

RESULT

1. Construction of mutant cell library

Cells coexpressing HER2 and peptide library were constructed by lentiviral gene transduction.

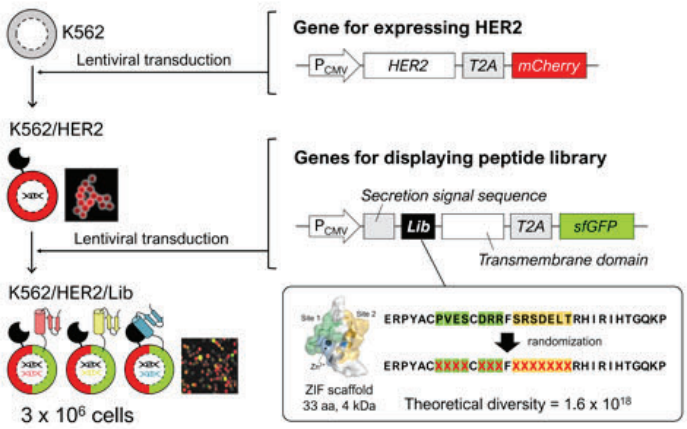

Mutant cell library was constructed.

2. MAGPIE screen of Pertuzumab-mimetic peptides

Cells expressing Pertuzumab-mimetic peptides were sorted with gAb and their sequences and affinity were analyzed.

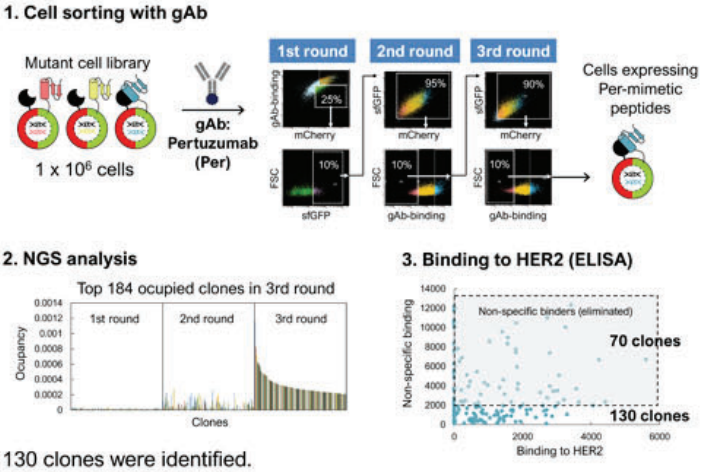

130 clones were identified.

3. Prediction of high-affinity peptides

Prediction model for Per-mimetic peptides was constructed by machine learning using HER2 affinity and sequences of 130 clones as training data.

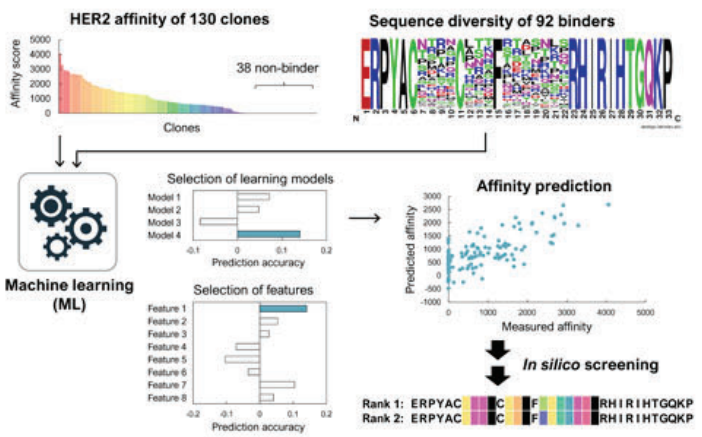

Two candidate peptides were predicted.

4. Characterization of predicted peptides

Affinity and drug efficacy of predicted peptides were evaluated by biolayer interferometry and cell proliferation assay, respectively.

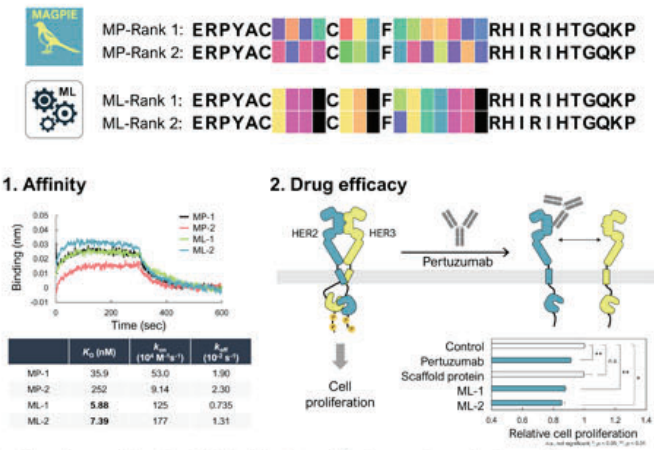

	K_D (nM)	k_{on} (10^4 $M^{-1}s^{-1}$)	k_{off} (10^{-2} s^{-1})
MP-1	35.9	53.0	1.90
MP-2	252	9.14	2.30
ML-1	5.88	125	0.735
ML-2	7.39	177	1.31

Predicted peptides had high binding affinity and good drug efficacy.

CONCLUSION and PROSPECTS

1. MAGPIE screen could identify many antigen-binding peptides with various affinities and sequences.
2. Predicted peptides had high binding affinity and good drug efficacy like Pertuzumab.
3. Smart design can be used with any available mAbs.

[Ethics] All recombinant DNA experiments were performed with approval of the recombinant DNA advisory committees of Tokyo Institute of Technology (No. I2016020, I2021017).
[COI] We have no financial relationship to disclose.

PUBLICATION

1. "Antibody-guided design and identification of CD25-binding small antibody mimetics using mammalian cell surface display", *Sci Rep*, **11 (1)**, 22098 (2021)
2. PCT/JP2022/39963

[Acknowledgement]
We thank the FACS Core Laboratory at the Institute of Medical Science, University of Tokyo for providing us with technical assistance in operating flow cytometer. This study was supported by AMED under Grant Numbers JP19am0401023h0001, JP20am0401023h0002, JP21am0401023h0003, and JP22am0401023h0004.

Enhancing the Gastrointestinal Stability of Salmon Calcitonin thought Peptide Stapling

Hiba Ghareeb[1] Norman Metanis[1]*
1 Institute of Chemistry, The Hebrew University of Jerusalem,
Safra Campus Givat Ram, Jerusalem 91904, Israel

https://doi.org/10.17952/37EPS.2024.P1130

Abstract

Salmon calcitonin (sCT) is a polypeptide hormone available in the clinic. sCT is degraded in the gastrointestinal tract in minutes. In this work, a stapled analogue of salmon calcitonin, KaY-1(R24Q), was developed using the cooperative stapling between Lys and Tyr, with R24Q substitution. The analogue exhibited an improved stability in simulated gastric and intestinal fluid and retain the ability to activate calcitonin receptor. This work will serve as a starting point for the development of an oral sCT drug.

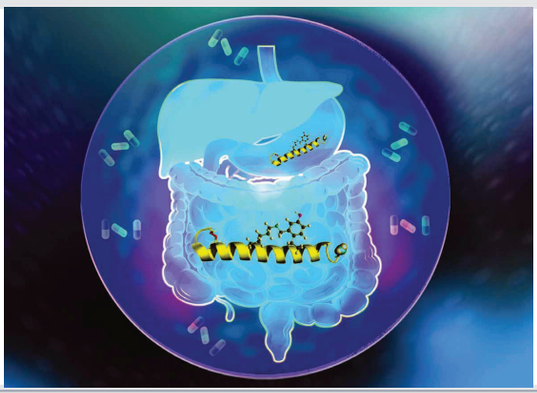

Method

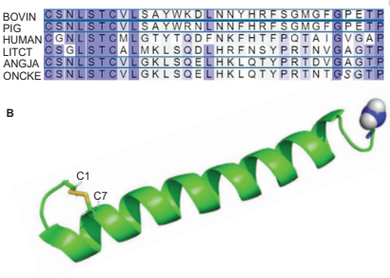

Designing of analogues using modification and helix stapling

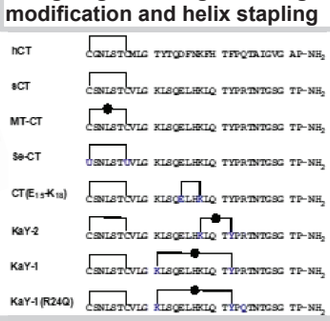

Chemical protein synthesis for macrocyclic peptide

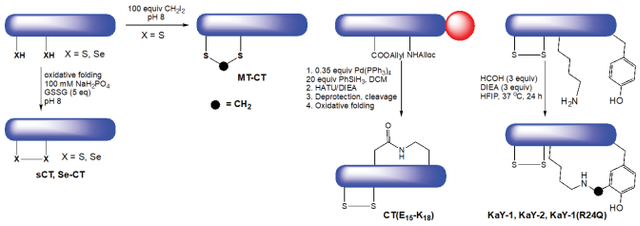

Results

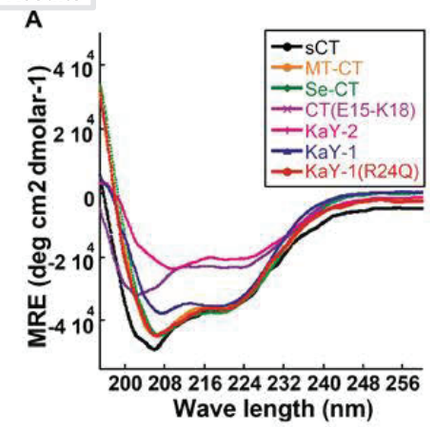

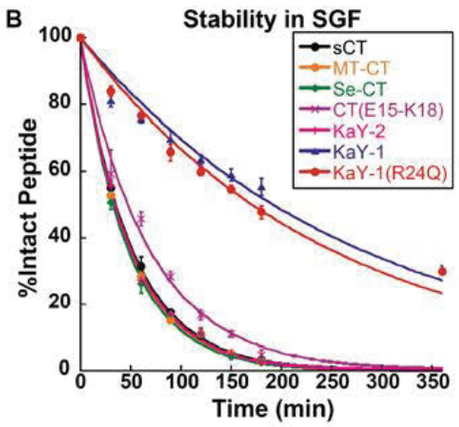

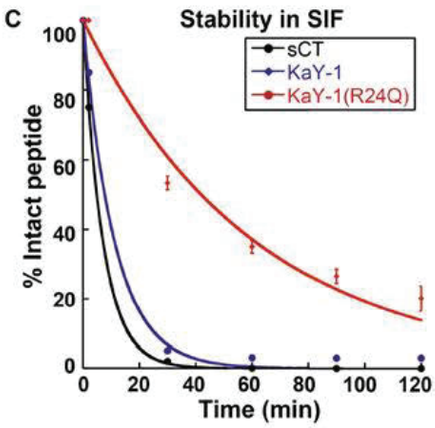

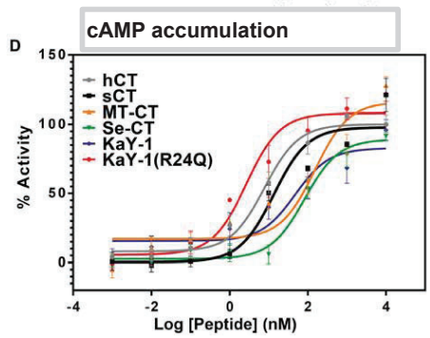

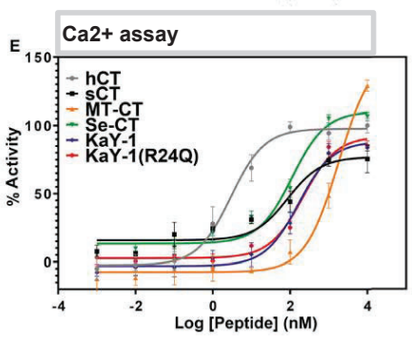

CT analogue	SGF $t_{1/2}$ (min)	SIF $t_{1/2}$ (min)	cAMP EC_{50} (nM)	Ca^{2+} EC_{50} (nM)
hCT	n.d.	n.d.	7.8±1.6	2.9±0.6
sCT	35.6±0.1	4.9±0.7	13.5±4.5	87.0±17.5
MT-CT	33.5 ±0.2	n.d.	1666±60	7304±700
Se-CT	32.6±0.5	n.d.	82.7±16.5	112.5±18.3
CT(E_{15}-K_{18})	47.3±1.9	n.d.	n.d.	n.d.
KaY-2	34.5±0.3	n.d.	n.d.	n.d.
KaY-1	191.2±66.1	7.1±0.7	47.6±24.1	165.5±34.8
KaY-1(R24Q)	170.6±32.2	41.9±6.1	2.7±0.8	215.8±43.8

(**A**) All analogues obtained α- helicity. (**B**) KaY-1 and KaY-1(R24Q) have 5 fold longer $t_{1/2}$ in SGF. (**C**) KaY-1(R24Q) has 6 fold longer $t_{1/2}$ in SIF (**D**) KaY-1(R24Q) enable cAMP accumulation with EC_{50} 2.7 nM. (**E**) KaY-1(R24Q) enable Ca2+ accumulation in cytosol with EC_{50} 216 nM

Conclusions

The present study demonstrated that KaY-1(R24Q) obtained by stapling reaction between Lys11 and Tyr22 retained helical structure, exhibited increased stability in both SGF and SIF, and retained activity. Our results provided a starting point for the development of oral sCT analogue for the treatment of postmenopausal osteoporosis, Paget`s disease and hypercalcemia.



Ghareeb, H., & Metanis, N. (2023). Enhancing the gastrointestinal stability of salmon calcitonin through peptide stapling. Chemical Communications, 59(44), 6682-6685.

https://doi.org/10.17952/37EPS.2024.P1131

Development and Antifungal Efficacy of Hydrocarbon-Stapled Peptide Analogs Based on Human Antimicrobial Peptides for Candidiasis Therapy

Hyosuk Yun, Ganbaatar Byambasuren, and Chul Won Lee*

Department of Chemistry, Chonnam National University, Gwangju 61186, South Korea
*Corresponding author : cwlee@jnu.ac.kr

Abstract

KR-12, derived from the human antimicrobial peptide LL-37, maintains the antimicrobial properties of LL-37 while minimizing human cell toxicity. The KR-12 analog, named KR-12-pa, is characterized by its amphipathic α-helical structure, contributing to its strong antimicrobial and anti-inflammatory effects. In this study, we designed hydrocarbon-stapled peptide analogs based on KR-12-pa incorporating chiral non-natural amino acids at positions i and i+4. All stapled peptides were synthesized by solid-phase peptide synthesis method, verified by LC-MS. The stapled peptides showed broad-spectrum antifungal activities, with minimum inhibitory concentrations (MIC) ranging from 2 to 32 μg/mL, against pathogenic *Candida* strains including the fluconazole-resistant *Candida krusei* strain. Notably, a subset of these analogs, specifically S3, S5, and S7, demonstrated low human cell toxicity comparable to the original KR-12 peptide. Among these, S3 stood out for its balance of potent antifungal activity and minimal toxicity, making it a promising candidate for further development.

Further structural analysis through circular dichroism indicated that S3 maintains an α-helical conformation in buffer solutions, differing from the wild-type peptide. Preliminary *in vivo* assessments using the *Galleria mellonella* model underscored S3's reduced toxicity and heightened antifungal efficacy. Altogether, these results position the S3 stapled analog of KR-12-pa as a viable and effective option for treating candidiasis, highlighting its potential as a therapeutic innovation.

Introduction

Antimicrobial peptides (AMPs) are an important component of the innate immune system and are produced by almost all living organisms, from plants and insects to mammals, including humans. The ability to physically destroy bacterial cell membranes and induce lysis allows AMPs to target bacteria, fungi, and enveloped viruses and renders them a potential alternative to conventional antibiotics LL-37 is a natural antimicrobial peptide expressed in the human body.

❖ KR-12-pa

LL-37	LLGDFFRKSKEKIGKEFKRIVQRIKDFLRNLVPRTES
KR-12	KRIVQRIKDFLR
KR-12-pa	KRIVKRIKKFLR

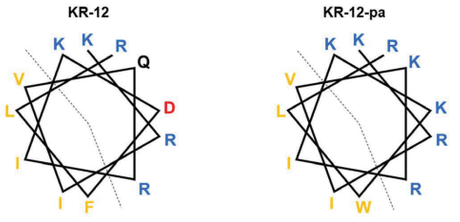

- Primary sequences and helical wheel diagrams of LL-37, KR-12, and KR-12-pa. Positively charged residues are in blue
- Negatively charged residues are in red. Hydrophobic residues are in yellow

❖ NMR structure of KR-12-pa

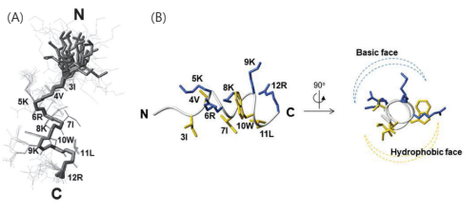

(A) Stereo view of twenty converged line structures of KR-12-pa for backbone heavy atoms
(B) The lowest target function structure of KR-12-pa

Results

Design and synthesis of stapled peptide analogs based on KR-12-pa

Design of stapled peptides

		Sequence	MW Linear	MW Stapled
No stapled	WT	KRIVKRIKKWLR-NH_2	1623.10	-
Single stapled (i, i+4)	S1	**X**RIV**X**RIKKWLR-NH_2	1645.14	1617.08
	S2	K**X**IVK**X**IKKWLR-NH_2	1589.11	1561.01
	S3	KR**X**VKR**X**KKWLR-NH_2	1675.17	1647.11
	S4	KRI**X**KRI**X**KWLR-NH_2	1674.18	1646.12
	S5	KRIV**X**RIK**X**WLR-NH_2	1645.14	1617.08
	S6	KRIVK**X**IKK**X**LR-NH_2	1559.08	1531.03
	S7	KRIVKR**X**KKW**X**R-NH_2	1675.17	1647.11
	S8	KRIVKRI**X**KWL**X**-NH_2	1617.12	1589.07

- X : (S)-2-(4-pentenyl)Ala-OH

Synthetic scheme of stapled peptides

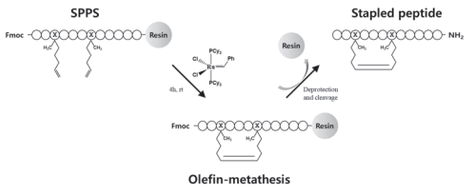

Preparation of KR-12-S3 stapled peptides

Instrumental conditions of peptide with LC-MS	
LC-MS system	Shimadzu-10AD/AB Sciex API2000
Column	Sunfire C18 (4.5 x 250 mm)
Buffer	A: 100% H_2O containing 0.05% TFA B: 100% ACN containing 0.05% TFA
Method	5-65% for 30 min
Detector	230 nm
Flow rate	1 mL/min

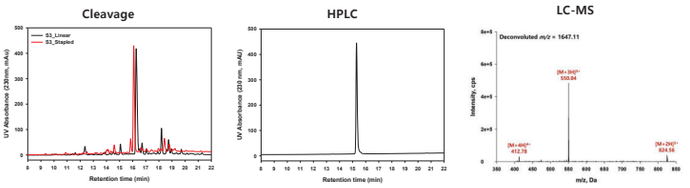

Helical wheel diagrams

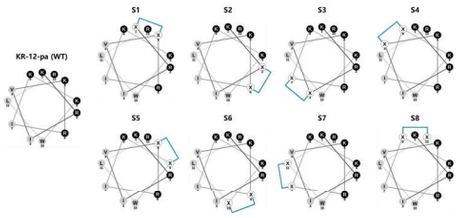

CD spectra of WT and S3

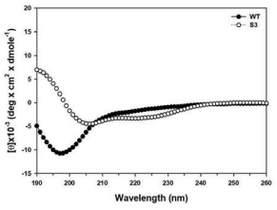

- Jasco, J-810
- 20 ℃
- 200 μM in 50 mM sodium phosphate

Antimicrobial activity

Strain		MIC (μg/mL) WT	S1	S2	S3	S4	S5	S6	S7	S8
C. parapsilosis	ATCC 22019	16	16	4	4	2	16	4	4	2
C. albicans	ATCC MYA-2876	64	16	4	8	4	32	16	16	4
C. glabrata	ATCC 90030	8	4	2	2	2	4	2	2	2
C. glabrata	ATCC 2001	>64	64	4	8	8	>64	8	16	8
C. krusei	ATCC 6258	64	16	4	4	4	16	8	16	4
C. tropicalis	ATCC 750	4	8	2	2	2	4	2	4	2

- Antifungal susceptibility strains : ATCC 22019, MYA-2876, 750
- Antifungal susceptible-dose dependent(SDD) strains : ATCC 90030, 2001
- Antifungal resistant strains : ATCC 6258

Hemolytic activity

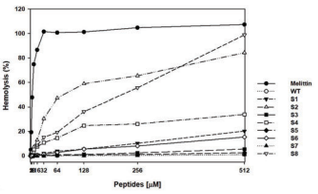

S5, S7 < WT < S3 < S6 < S1 < S4 < S2 < S8

Effect of S3 stapled peptide from *Galleria mellonella*



Galleria mellonella larvae

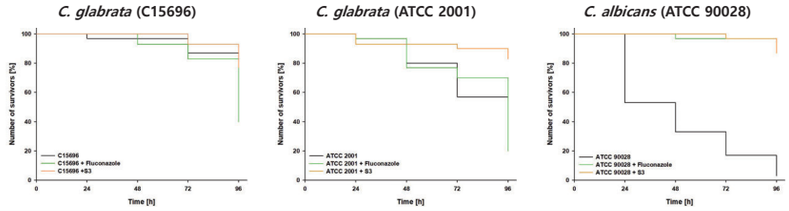

Conclusion

Eight stapled peptides based on KR-12-pa, derived from the human antimicrobial peptide LL-37, were synthesized using solid-phase synthesis and purified by RP-HPLC. Among the eight stapled peptides, S3 demonstrated high antifungal activity and low hemolytic activity. The CD spectrum showed that S3 maintains an α-helical conformation in buffer solutions. Preliminary *in vivo* assessments of the S3 peptide, confirmed using *Galleria mellonella* larvae, showed low toxicity and heightened antifungal efficacy.

1. Yun, H., Min, H. J. & Lee, C. W. (2020) NMR structure and bactericidal activity of KR-12 analog derived from human LL-37 as a potential cosmetic preservative, *J Anal Sci Technol.* **11**.
2. Walensky, L. D. & Bird, G. H. (2014) Hydrocarbon-Stapled Peptides: Principles, Practice, and Progress, *Journal of Medicinal Chemistry.* **57**, 6275-6288.
3. Li, X., Chen, S., Zhang, W.-D. & Hu, H.-G. (2020) Stapled Helical Peptides Bearing Different Anchoring Residues, *Chemical Reviews.* **120**, 10079-10144.

Prevention of the Spread of Virus Infection in Global Societies: Anti-SARS-CoV-2 Agents Learned from HIV Researches

○Hirokazu Tamamura,[1] Nobuyo Higashi-Kuwata,[2] Hiroaki Mitsuya,[2] Kohei Tsuji,[1] Takahiro Ishii,[1] Takuya Kobayakawa,[1]

[1]Tokyo Medical and Dental University, [2]National Center for Global Health and Medicine Research Institute

https://doi.org/10.17952/37EPS.2024.P1132

Introduction

More than three years have passed since the beginning of the pandemic of the novel emerging infection disease, COVID-19 which is produced by SARS-CoV-2. Since SARS-CoV-2 main protease (M^{pro}) is essential for viral replication and there is no human enzyme closely homologous with the M^{pro}, it is an important and attractive drug discovery target for treatment of COVID-19. Recently, inhibitors of the SARS-CoV-2 M^{pro}, Nirmatrelvir and Ensitrelvir, were developed. However recent studies warned of the possibility of the emergence of drug-resistant SARS-CoV-2 variants against the Nirmatrelvir therefore development of novel drugs and an increase in the repertory of the drugs are urgently needed. In order to meet this challenge, we previously reported highly potent M^{pro} inhibitors, **TKB198** and **TKB211**, based on YH-53/5h, which was developed by Hayashi et al. in 2013 as a SARS-CoV M^{pro} inhibitor. More recently, our further studies led to the development of more potent inhibitors, **TKB245** and **TKB248**. In this study, we report our structure-activity relationship studies and evaluation of the anti-SARS-CoV-2 activity of derivatives of these inhibitors.

✔ Replication cycle of SARS-CoV-2

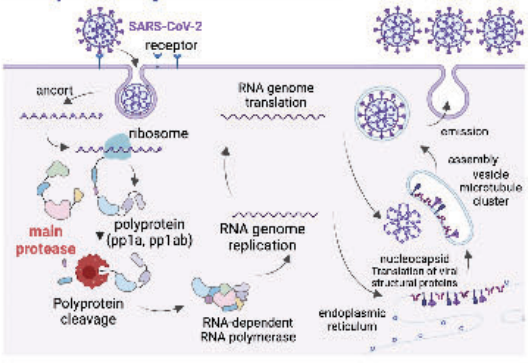

✔ Potential problems of Nirmatrelvir

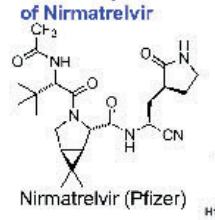

Nirmatrelvir (Pfizer)

Owen, D. R., et al. Science 2021, 374, 1586-1593.

Problems
- antiviral activity
- metabolic stability

→Solve these problems

✔ YH-53/5h

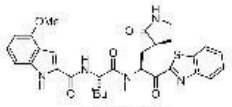

YH-53/5h
(SARS-CoV M^{pro} inhibitor)

Thanigaimalai, P., et al. Eur. J. Med. Chem. 2013, 65, 372-384.

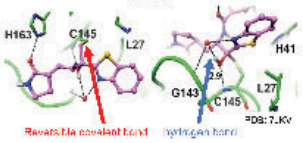

Hatton, S., et al. Wat. Commun. 2021, 12, 618.

✔ Fluorination and thioamidation of the lead compound

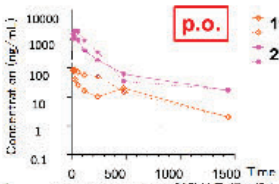

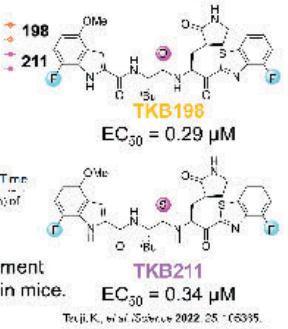

Thioamide bond replacement improved blood stability in mice.

Teji, K., et al. JScience 2022, 25, 105335.

TKB245 & TKB248

✔ Co-crystal structures of SARS-CoV-2 M^{pro} with TKB198(8DOY) or Nirmatrelvir (7RFW)

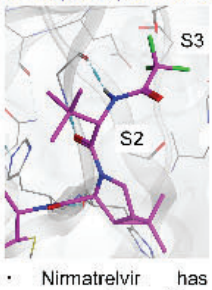

- Nirmatrelvir has numerous interactions in the S2-S3 region of SARS-CoV-2 M^{pro}.

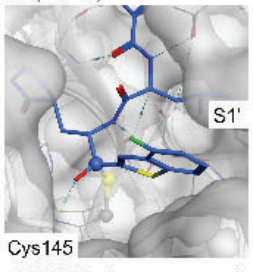

- **TKB198** forms a covalent bond with Cys145, the active center of SARS-CoV-2 M^{pro}. Also, it inactivates the enzymatic activity of M^{pro}.

✔ Hybridization of SARS-CoV-2 inhibitors with Nirmatrelvir and TKB198



Nirmatrelvir

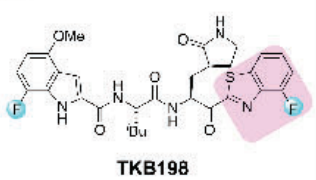

TKB198

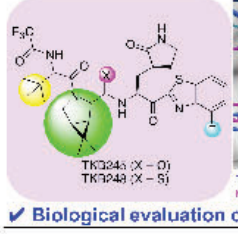

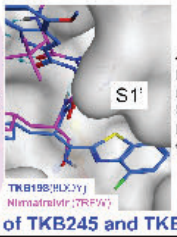

4-F benzothiazole moiety occupies SARS-CoV-2 M^{pro} pocket (S1') effectively.

✔ Biological evaluation of TKB245 and TKB248

Compound	EC_{90} (μM)	EC_{95} (μM)	IC_{90} (μM)	IC_{95} (μM)	$T_{1/2}$ (h)	Oral [a] (%)
YH-53	2.6	9.47	0.13	1.5	0.27	n.d.
TKB198	0.27	0.83	0.023	0.75	0.83	1.98
TKB245	0.03	0.53	0.007	0.14	3.82	48
TKB248	0.22	0.87	0.074	6	4.34	72
Nirmatrevir	0.94	7.81	0.013	0.77	1.03	56

[a]Oral = AUC per unit dose after oral administration / AUC per unit dose after intravenous administration. [b]PK test was performed using human liver stomach mice (TKB245, TKB248, and Nirmatrelvir) and ICR mice (YH-53 and TKB198).
[c]EC_{xx}: Drug concentration to inhibit half of the multiplication of SARS-CoV-2.

✔ Co-crystal structures of SARS-CoV-2 M^{pro} with TKB245 or TKB248

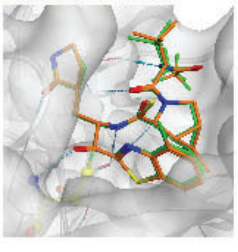

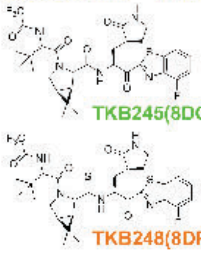

Results & Discussion

✔ Structure-activity relationship studies

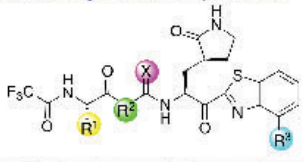

Compound	R^1	R^2	R^3	X	EC_{90} (μM)	CC_{50} (μM)
TKB245			F	O	0.012	> 100
TKB248			F	S	0.31	> 100
TKB269			F	O	0.36	> 100
TKB255			F	O	0.095	> 100
TKB263			F	O	2.4	> 100
TKB253			F	O	0.25	> 100
TKB267			F	O	2.8	> 100
TKB265			F	O	0.59	> 100
TKB286			Cl	O	0.019	> 100
TKB287			Br	O	0.063	> 100

✔ Short summary

R^1 : L-*tert*-Leu residue is suitable.

R^2 :  is the best amino acid among the tested derivatives.

R^3 : F and Cl is tolerable.

TKB245 and **TKB248** are still the most promising compounds. In addition, we found **TKB286**, which the activity is comparable to that of **TKB245**.

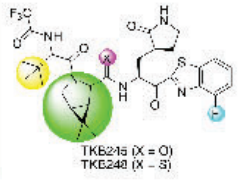

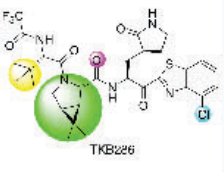

✔ Antiviral activity in various target cells

Cell line	TKB245	TKB248	Nirmatrelvir	Ensitrelvir hemisulfate
	EC_{50} (μM)			
VeroL6	0.03	0.22	1.02	0.11
VeroE6 + 2 μM CP100356	0.001	0.03	0.026	-
HeLa-ACE2-TMPRSS2	0.021	0.16	0.24	0.2
A549-ACE2-TMPRSS2	0.0027	0.199	0.017	-

- CP100356 is P-glycoprotein inhibitor

✔ Stability against acid treatment

Compound	EC_{50} (μM)		CC_{50} (μM)
	acid (-)	acid (+)	
TKB245	0.074	0.087	>100
TKB248	0.31	0.32	>100
Nirmatrelvir	1.4	2.5	>100

- The acid (-) means test compounds dissolved in PBS without acid treatment.
- The acid (+) means test compounds treated with 0.1 M HCl aq. in PBS, incubated for 1h at 37 °C, and then neutralized with 0.1 M NaOH aq. in the mixture.

✔ Antiviral activity against mutant strains

Compound	EC_{50} (μM)				
	WK-521	o/BA.1	o/BA.2	o/BA.5	o/BA.2.75
TKB245	0.03	0.014	0.052	0.016	0.049
TKB248	0.22	0.282	0.16	0.066	0.43
Nirmatrelvir	0.94	1.047	1.3	1.126	0.985

✔ Selectivity among cysteine proteases

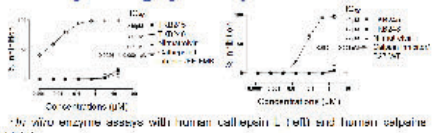

- In vitro enzyme assays with human cathepsin L (left) and human cathepsin (right).
- Human cathepsin L Inhibitor screening and human cathepsin activity assay kits are designed to measure human cysteine protease activity and identify inhibitors of these enzymes.

✔ Evaluation of potential immune response

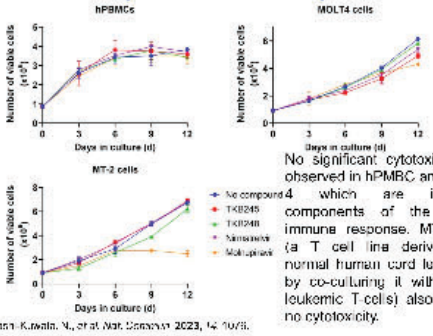

No significant cytotoxicity was observed in hPMBC and MOLT-4 which are important components of the human immune response. MT-2 cells (a T cell line derived from normal human cord leukocytes by co-culturing it with human leukemic T cells) also showed no cytotoxicity.

Higashi-Kuwata, N., et al. Wat. Commun. 2023, 14, 1075.

Teji, K., et al. J. Med. Chem. 2023, 66, 13516-13529.

Conclusion & Acknowledgement

As the results of the SAR studies of **TKB245**, a 4-fluoro or 4-chlorobenzothiazole ketone was suitable as the P1' unit. Biological evaluation demonstrated that **TKB245** and **TKB248** showed preferable acid stability in the test conditions and no significant cytotoxicity in hPMBCs, MOLT-4 cells and MT-2 cells.
These data supported that **TKB245** and **TKB248** can be orally administrable drug candidates for COVID-19 therapy as M^{pro} inhibitors.

We deeply thank to Prof. Yoshio Hayashi and Dr. Sho Konno from Tokyo University of Pharmacy and Life Sciences for the valuable discussions.

https://doi.org/10.17952/37EPS.2024.P1133

Bicycle Radionuclide Conjugates (BRCs) as agents for tumour targeting

Abstract #

#

Anusha Regupathy[1], Ben Blakeman[1], Luca Mascheroni[1], Simone Pellegrino[1], Johanna Lahdenranta[2], Lisa-Charlotte Domogalla[3,4], Malgorzata Sulewska[3,4], Matthias Eder[3,4], Ann-Christin Eder[3,4], Gemma Mudd[1]

[1]BicycleTx Ltd, Portway Building, Granta Park, Cambridge CB21 6GS, United Kingdom
[2]Bicycle Therapeutics, 35 Cambridgepark Drive, Cambridge, MA, 02140, United States.
[3]Department of Nuclear Medicine, University Medical Center Freiburg, Faculty of Medicine, University of Freiburg, Freiburg, Germany
[4]Division of Radiopharmaceutical Development, German Cancer Consortium (DKTK), partner site Freiburg, Freiburg, Germany and German Cancer Research Center, Heidelberg, Germany

ABSTRACT

USING THE BICYCLE PHAGE DISPLAY PLATFORM TO DESIGN NOVEL PEPTIDE BASED RADIOLIGANDS

- Targeted Radionuclide Therapy (TRT) is emerging as a promising therapeutic approach for cancer treatment. TRT is centered on delivering a cytotoxic radioactive payload to cancer cells via target receptors on the membrane.
- Membrane type 1 matrix metalloproteinase (MT1-MMP) is overexpressed in many solid tumours such as breast and non-small cell lung cancer making it a high value target for cancer therapy.[1,2]
- Using Bicycle's proprietary phage platform, bicyclic peptides with high affinity to MT1-MMP were identified, optimized and incorporated in Bicycle Radionuclide Conjugates (BRCs) for diagnostic imaging and TRT.

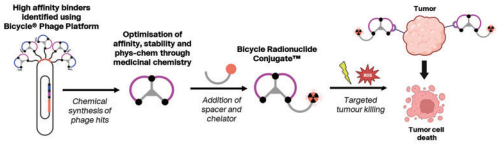

Figure 1: Overview of identification and design of Bicycle Radionuclide Conjugate for TRT using Bicycle's proprietary phage platform.

INTRODUCTION

- Bicycle® molecules are short linear peptides stabilized by a central chemical scaffold.
- The scaffold constrains the peptide in its bioactive form, resulting in high affinity whilst also imparting stability compared to their linear counterparts.
- The small size (1-3kDa) enables rapid penetration in tumours, allowing rapid delivery of payload.
- The relatively large binding footprint allows for exquisite selectively to close analogues of target protein.
- Bicycle® molecules have a short biological half-life, which allows fast clearance from circulation. This spares healthy tissue from prolonged radiation exposure, making Bicycle® molecules an ideal modality for targeted radionuclide delivery.
- Due to their fast clearance from circulation and rapid penetration in tumours at early timepoints, BRCs are well suited for both cancer diagnosis (through imaging) and therapy and can be applied in the new emerging field of thernaostics.

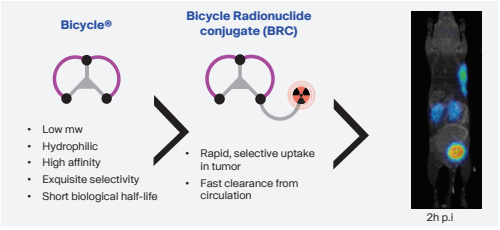

Figure 2: Left: Properties of Bicycle® molecules that render them most suitable for radioactive payload delivery. Right: PET image of a MT1-MMP targeting ^{68}Ga-BRC in a HT1080 tumour carrying mouse at 2h p.i.

MT1-MMP AS A TARGET FOR RADIOTHERANOSTIC APPROACH IN CANCER

- Membrane type 1 matrix metalloproteinase (MT1-MMP) plays a role in cancer metastasis and overexpression in solid tumours such as non-small cell lung cancer, esophageal and triple negative breast cancer.
- Early positron emission tomography (PET) imaging in preclinical models highlighted the promise for MT1-MMP as a target for cancer diagnosis and potential therapy.[3]
- In this study BRCs targeting MT1-MMP were optimised to selectively deliver high levels of radioactivity to tumours whilst minimising uptake in healthy tissue.

METHODS

STUDY APPROACH

- PET imaging to assess selectivity and biodistribution of MT1-MMP targeting BRCs in a mouse tumour xenograft model.
- Affinity improvement through structural activity relationship (SAR) exploration and co-crystal structure guided design.
- In-vitro profiling of BRCs in cellular uptake assays to measure internalisation.
- Iterative rounds of medicinal chemistry design to optimize the biodistribution profile to increase tumour uptake and tumour-to-tissue ratios.

RESULTS

PET IMAGING OF EARLY MT1-MMP TARGETING BRC SHOWS SELECTIVE UPTAKE INTO MT1-MMP EXPRESSING TUMOUR

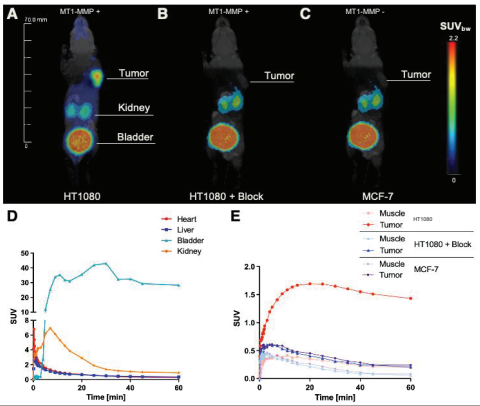

Figure 3:Whole-body maximum intensity projections of 150 pmol ^{68}Ga-labeled BCY1 in HT1080 (A, B) and MCF-7 (C) tumor-bearing BALB/c nu/nu mice (right flank) 60 min p.i. obtained from small animal PET/MR imaging. Blocking experiments (B) were performed with an excess of non-labeled peptide (30 nmol) 5 min prior to radiotracer administration. (D) Corresponding time activity curves (TAC) for organs of interest from 0 to 60 min p.i. of 150 pmol of [^{68}Ga]Ga-BCY1 in the HT1080 xenograft. (E) Detailed TACs of tumor and muscle tissue of all animals.

^{177}Lu LABELLED BRC IS RETAINED IN TUMOUR OUT TO LATER TIMEPOINTS

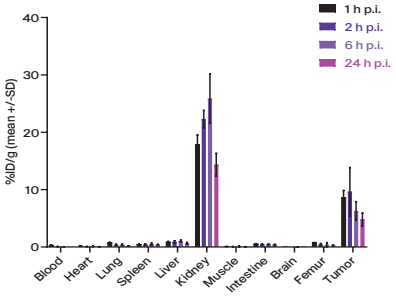

Figure 4:Organ distribution of 150 pmol ^{177}Lu-labeled BCY at 1, 2, 6 and 24 h p.i. in HT1080 mouse xenograft. Data are expressed as mean % ID/g tissue ± SD (n=3)

CO-CRYSTALLISATION WITH MT1-MMP PROTEIN

- A co-crystal structure of MT1-MMP protein and bicyclic peptide was obtained using co-crystallisation techniques and analysed using x-ray crystallography.
- This structural information was used to study molecular interactions and guide chemical optimisation.

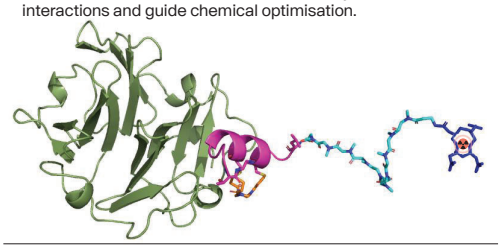

Figure 5: Illustration of Bicycle Radionuclide Conjugate binding to MT1-MMP protein in green (derived from Bicycle co-crystal structure)

IMPROVING BRC AFFINITY FOR MT1-MMP THROUGH SAR EXPLORATION

- Optimisation to improve binding kinetics with the aim of increasing tumour uptake and retention.
  - >100 compounds were designed and synthesised
  - Highly potent binders with affinity (K_D) of 20 pM and off-rate of 1.3E-4 s^{-1} were identified

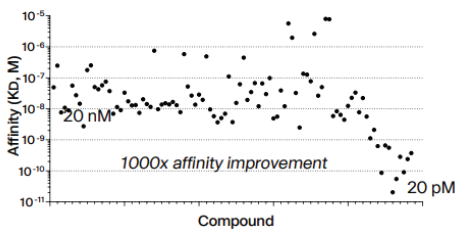

Figure 6: Graph showing affinity (K_D, M) of compounds for MT1-MMP over course of optimisation

BINDING KINETICS OF HIGH AFFINITY BINDERS WITH SLOW DISSOCIATION

- Bicycle® molecules can bind to target protein with high affinity (K_D) and slow dissociation (Kd) and have comparable binding kinetics to monoclonal antibodies.
- Slow dissociation rate (Kd) of BRCs in the range of 1.3E-4 s^{-1} could result in long residence time at the tumour receptor

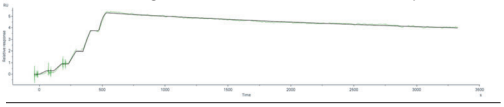

Figure 7: Bicycle® molcule binding to human MT1-MMP characterized using a 5-point 2-fold titration up to 10nM; fitted with a 1:1 binding model

MT1-MMP BRCS SHOW RAPID INTERNALISATION IN IN-VITRO CELLULAR ASSAYS

- Internalisation of Bicycle® molecules into MT1-MMP positive cells were assessed using both fluorescence imaging as well as gamma counting of radioactivity.
- MT1-MMP expressing cells after incubation with fluorophore conjugated bicycle molecules were imaged using confocal microscopy. Pink punctate signal indicates internalised bicycle fluorophore conjugate.
- ^{177}Lu-BRCs were incubated with HT1080 cells and internalised fractions were collected and radioactivity measured using a gamma counter.
- High levels of internalisation into both cell lines were observed.

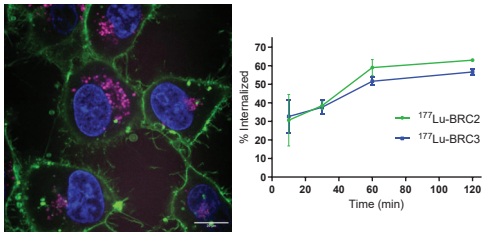

Figure 8: Left: MT1-MMP expressing cells incubated with Bicycle fluorophore conjugate (Alexa Fluor 647, red) at 100 nM concentration for 4 hours, washed, the nuclei counterstained with Hoechst (blue) and the cell membrane counterstained with CellMask (green). Images of live cells taken on an Olympus IX53 using a 100X objective. Right: % Internalisation of MT1-MMP targeting ^{177}Lu-BRCs in HT1080 cells over 120 minutes post incubation.

OPTIMISATION OF BIODISTRIBUTION PROFILE OF BRCS

- Chemical optimisation led to BRCs with increased tumour uptake and retention, along with reduced kidney uptake / retention.
- Medicinal chemistry can be used to optimise the in-vivo biodistribution profile of BRCs.

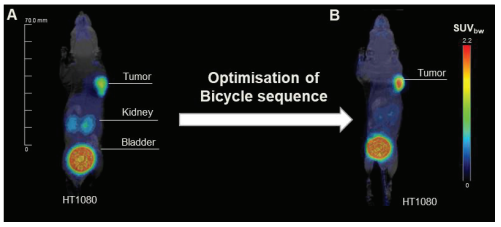

Figure 9:Whole-body maximum intensity projections of 150 pmol ^{68}Ga-labeled BRC1 (A) and optimized BRC4 (B) in HT1080 tumor-bearing BALB/c nu/nu mice (right flank) 60 min p.i. obtained from small animal PET/MR imaging.

CONCLUSIONS

HIGH TUMOUR UPTAKE, LOW HEALTHY TISSUE UPTAKE

- Bicycle® molecules are suitable vectors for delivering radionuclides to tumours due to their favourable pharmacokinetic properties (specific tumour uptake, rapid penetration and rapid renal clearance).
- Due to their rapid clearance from blood circulation and minimal non-specific uptake into healthy tissue (apart from kidneys), they can be used effectively as diagnostic PET agents.
- The biodistribution profile of the Bicycle Radionuclide Conjugates (BRCs) can be optimised to maintain high tumour uptake whilst significantly reducing kidney levels.
- BRCs emerge as promising agents for a theranostic approach.

UNIVERSITÄTS KLINIKUM FREIBURG
CCCF COMPREHENSIVE CANCER CENTER FREIBURG

dkfz.
German Cancer Consortium
Partner site Freiburg

REFERENCES

1. Kessenbrock K et al. Matrix metalloproteinases: regulators of the tumor microenvironment. Cell. 2010;141:52-67
2. Wang YZ et at. MMP-14 overexpression correlates with poor prognosis in non-small cell lung cancer. Tumour Biol. 2014;35:9815-9821.
3. Eder M et al. Bicyclic Peptides as a New Modality for Imaging and Targeting of Proteins Overexpressed by Tumors. Cancer Res. 2019;79:841-852.

Bicycle Therapeutics, Inc.
35 Cambridgepark Drive, Suite 350
Cambridge, MA 02140
USA
T. +1 617-945-8155

BicycleTx Limited
Portway Building
Granta Park, Cambridge
CB21 6GS, UK
T. +44 (0)1223 261503

Company number 11036101.
Registered in England.

bicycletherapeutics.com

Development of gut-restricted antibiofilm peptides to target gastrointestinal biofilms

https://doi.org/10.17952/37EPS.2024.P1134

Bernhard Jandl[1,2,3,4], Michaela Lang[4], Athanasios Makristathis[5], Christoph Gasche[4,6] and Markus Muttenthaler[1,3]

[1]Institute of Biological Chemistry, Faculty of Chemistry, University of Vienna, 1090 Vienna, Austria.
[2]University of Vienna, Vienna Doctoral School in Chemistry (DoSChem), Währinger Str. 42, 1090 Vienna, Austria.
[3]Institute for Molecular Bioscience, The University of Queensland, 4072 Brisbane, Queensland, Australia.
[4]Division of Gastroenterology and Hepatology, Department of Internal Medicine 3, Medical University of Vienna, 1090 Vienna, Austria.
[5]Division of Clinical Microbiology, Department of Laboratory Medicine, Medical University of Vienna, 1090 Vienna, Austria.
[6]Loha for Life, Center for Gastroenterology and Iron Deficiency, 1190 Vienna, Austria.

Email: bernhard.jandl@univie.ac.at

Introduction

Inflammatory bowel diseases (IBD) and **irritable bowel syndrome (IBS)** are gastrointestinal (GI) disorders that together **affect 10–15%** of the Western population. A recent study identified **mucosal biofilms** in **57% of IBS, 34% of ulcerative colitis (UC)** and **22% of Crohn's disease (CD) patients** compared with **6%** in the **control group**.[1] No drug is on the market that selectively targets biofilms and conventional antibiotics are mostly ineffective, leaving jet-washing during endoscopy the only way to remove gut biofilms.

This work explores the potential of antimicrobial peptides (AMP) as antibiofilm agents and investigates chemical strategies to improve potency and gut-stability. Gut-stable antibiofilm peptides are promising therapeutic candidates to target mucosal biofilms in patients with GI disorders, as their large size prevents systemic uptake and reduces side effects by keeping them gut-restricted when orally administered.

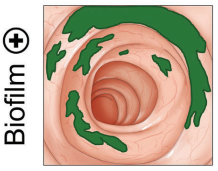

57% of IBS
34% of UC
22% of CD
6% of healthy patients

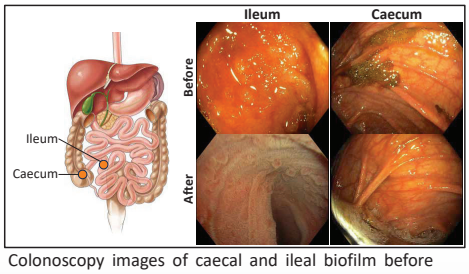

Colonoscopy images of caecal and ileal biofilm before and after jet-washing.

Therapeutic target

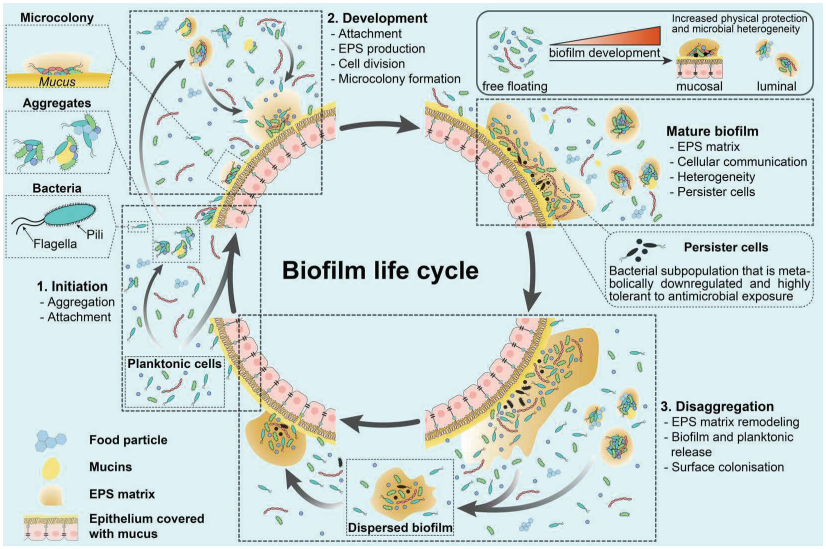

The biofilm life cycle. The four stages of the biofilm life cycle are: initial adhesion, early development, biofilm maturation and biofilm dispersal. **Therapeutic approaches** focus on these stages of the biofilm life cycle, aiming to **(i) inhibit bacterial surface adhesion**, **(ii) inhibit biofilm formation**, and **(iii) eradicate mature biofilms**.

Approach

We have chemically synthesized a medium-size AMP compound library (>40 peptides), including peptides produced by ants, bees, frogs, and wasps. By screening of our library we identified 16 hits with promising antibiofilm activity. Out of these hits, we selected **MMBJ040** to conduct a systematic **structure-activity relationship (SAR)** using diverse medicinal chemistry approaches.

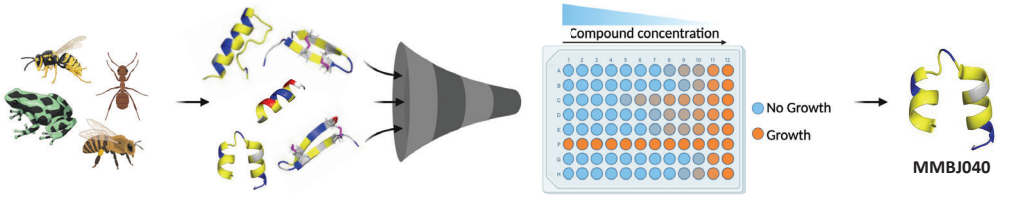

1) Synthesis of an AMP library **2) Antibiofilm screening using clinical isolates** **3) Hit to lead**

Study design

We applied Chemical strategies such as truncation, lipidation and the establishment of mirror images and evaluated the **minimum inhibition concentration (MIC)**, **minimum biofilm inhibition concentration (MBIC)**, and **minimum biofilm eradication concentration (MBEC)** using two clinical isolates from biofilm-positive patients (*Streptococcus parasanguinis* (Gram-positive (G^+)) and *Escherichia coli* (Gram-negative (G^-))) and two biofilm-forming type strains (*Staphylococcus aureus* (G^+) and *Pseudomonas aeruginosa* (G^-)). Further, we determined the gut stability of our best-performing candidates using **simulated gastric fluid (SGF)** and **simulated intestinal fluid (SIF)** assays.

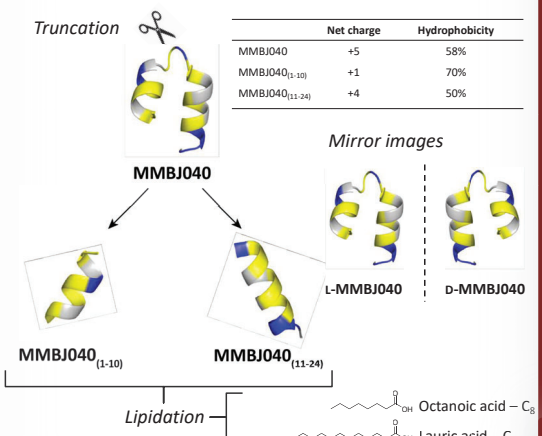

	Net charge	Hydrophobicity
MMBJ040	+5	58%
$MMBJ040_{(1-10)}$	+1	70%
$MMBJ040_{(11-24)}$	+4	50%

blue – positively charged residues, red – negatively charged residues and yellow – hydrophobic residues

Results

Antibiofilm activity

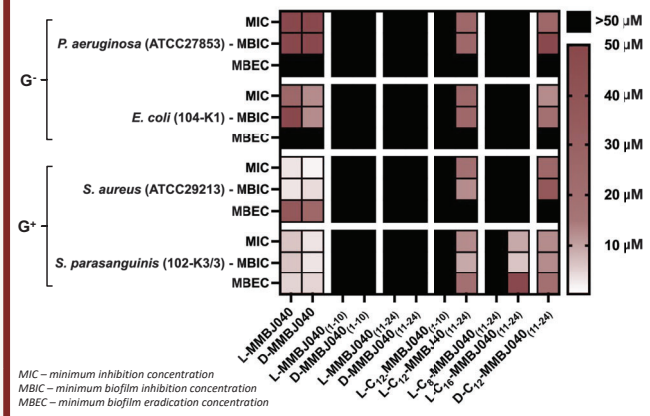

MIC – minimum inhibition concentration
MBIC – minimum biofilm inhibition concentration
MBEC – minimum biofilm eradication concentration

Gut stability

Half-life ($t_{1/2}$) of **L-MMBJ040 [<1 min] and mirror image D-MMBJ040 [>24 h]** in **simulated gastric fluid (SGF)** and **simulated intestinal fluid (SIF)**.

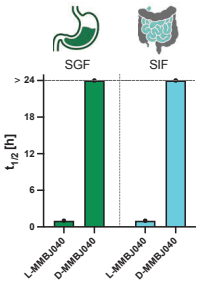

Truncation: Our MMBJ040 SAR exploration revealed that the two truncated α-helical domains $MMBJ040_{(1-10)}$ and $MMBJ040_{(11-24)}$ had no antimicrobial or antibiofilm activity. **Lipidation:** The lipidation of $MMBJ040_{(11-24)}$ reestablished antimicrobial activity but did not increase the antibiofilm activity, and C_{12} fatty acid conjugation led to the best result; lipidation of $MMBJ40_{(1-10)}$ did not display antimicrobial activity. **Mirror images:** All-D versions of active all-L parent peptides were also active. **D-MMBJ040** has the most potent antibiofilm activity.

In conclusion, we developed the gut-stable peptide **D-MMBJ040** with potent antibiofilm activity against G^+ biofilm-forming bacteria. Moreover, we identified that fatty acid substitution of hydrophobic domains in antimicrobial peptides could serve as an attractive approach to lower the production costs of antimicrobials.

Acknowledgement

We gratefully acknowledge financial support by the Vienna Science and Technology Fund (WWTF) – funding: LS18-053

Reference [1] Baumgartner, M. *et al*, Mucosal Biofilms Are an Endoscopic Feature of Irritable Bowel Syndrome and Ulcerative Colitis. *Gastroenterology* **2021**, *161* (4), 1245-1256.e20.

Development of peptide modulators targeting protein-protein interactions of the Sodium Leak Channel Complex

https://doi.org/10.17952/37EPS.2024.P1135

LUNDBECK FONDEN

Emma Beyer, Stephan Pless

University of Copenhagen, Denmark

1 The Sodium Leak Channel (NALCN) Complex

The Sodium leak channel, non-selective (NALCN) conducts a current of monovalent cations into neurons thereby adjusting the membrane potential and excitability. (PMID: 17448995)

NALCN consists of 4 domains connected by intracellular linkers. The DI-DII linker forms a loop which binds to a hydrophobic surface of uncoordinated protein-79 (UNC79). The DII-DIII linker forms alpha helical structures which interact with uncoordinated protein-80 (UNC80). (PMID: 32494638).

Mutations in NALCN, UNC79 and UNC80 are rare in humans but cause severe neurodevelopmental symptoms. (PMID: 30167850) Here, we aim to use the linker structures as a starting point to develop complex inhibiting peptides.

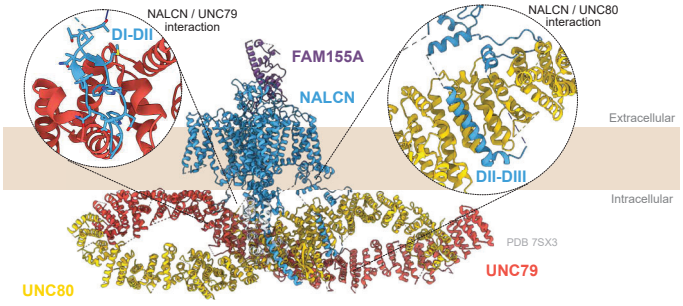

2 Two-electrode voltage clamp

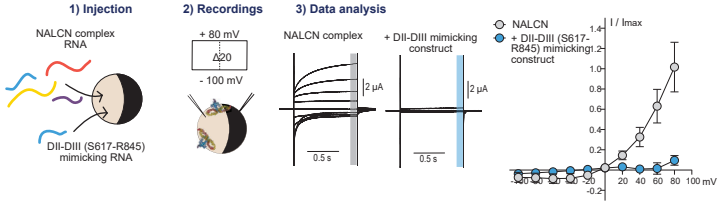

We express the NALCN complex in *Xenopus leavis* oocytes and use two-electrode voltage clamp (TEVC) to measure NALCN activity. From these experiments, we found that a construct mimicking the DII-DIII linker fully inhibits NALCN currents.

3 DI-DII linker mimicking constructs

We also evaluated the inhibitory effect of DI-DII mimicking constructs and peptides in NALCN-expressing oocytes. However, none of these inhibited NALCN activity.

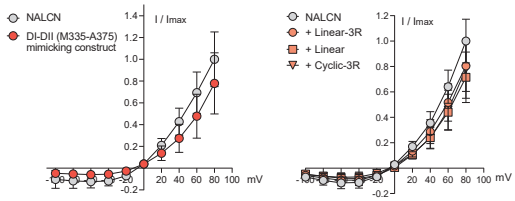

4 Membrane anchored DI-DII linker constructs

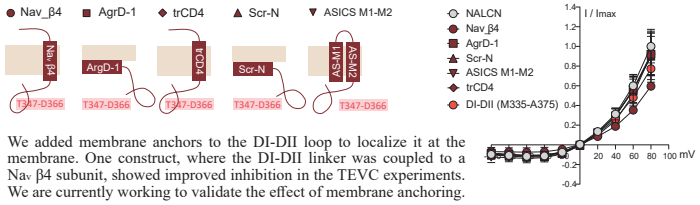

We added membrane anchors to the DI-DII loop to localize it at the membrane. One construct, where the DI-DII linker was coupled to a Na_V β4 subunit, showed improved inhibition in the TEVC experiments. We are currently working to validate the effect of membrane anchoring.

5 SICLOPPS (cyclic) DI-DII linker constructs

Split-intein circular ligation of peptides and proteins (SICLOPPS) is a method used to create circular proteins and peptides through the use of split inteins. (PMID: 28258013)

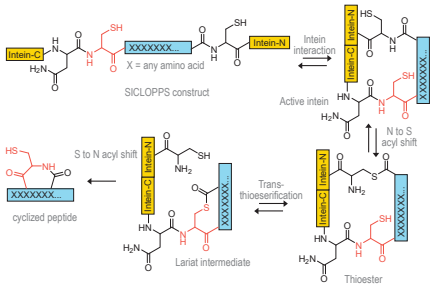

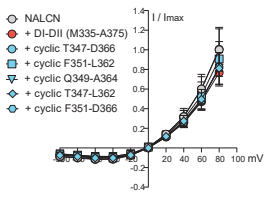

We designed and evaluated SICLOPPS constructs encoding cyclic peptides which mimic the DI-DII linker loop. However, none of the cyclic peptide inhibited NALCN activity.

6 DII-DIII linker mimicking constructs

To identify key interaction sites of the DII-DIII mimicking construct, we shortened it by dividing it into halves and quarters.

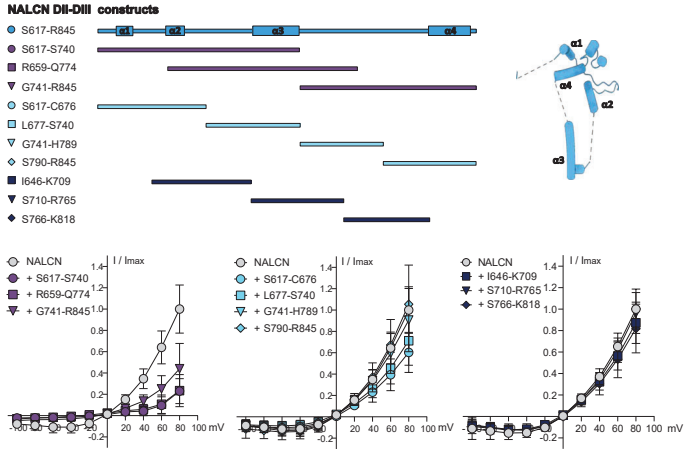

We found that the N-terminal and middle half (120 AA) of the DII-DIII linker also inhibited NALCN currents, while the C-terminal half was not as efficient. Shortening the construct further (60 AA) abolished the effect.

7 Alanine scan of the DII-DIII linker

To pinpoint important interaction sites in the N-terminal half of the DII-DIII linker (S617-S740), we introduced alanine mutations in stretches of 10-15 residues.

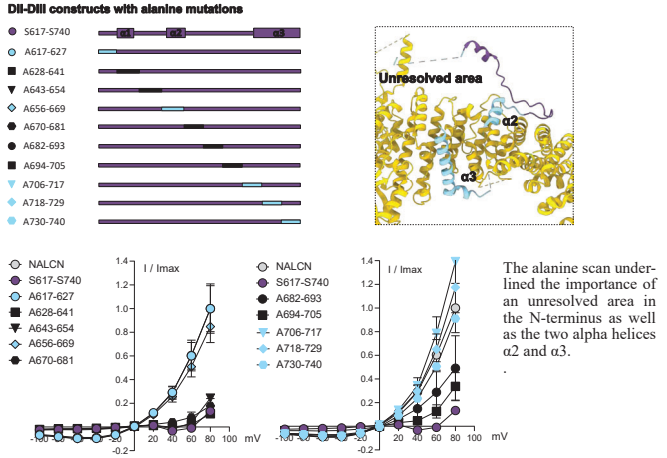

The alanine scan underlined the importance of an unresolved area in the N-terminus as well as the two alpha helices α2 and α3.

.

8 Stapled alpha helical peptides

We synthesized peptides with stapled alpha-helical folds to mimic the α2-helix of the DII-DIII linker. Two N-capped peptides inhibited outward currents at positive potentials. We are currently expanding our library of alpha-helical peptides which mimic structures of the α2- and α3-helices.

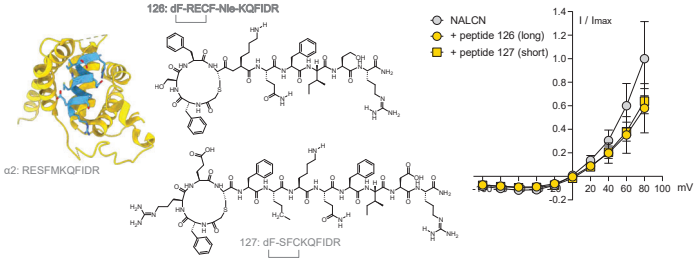

9 Future perspectives

The DI-DII / UNC79 interaction

Confirm the effect of membrane anchoring the DI-DII linker

Expand the library of membrane anchored DI-DII linker constructs

Other interaction partners

Identify and evaluate binding epitopes of other NALCN binding partners

The DII-DIII / UNC80 interaction

Narrow down binding epitopes by shortening alanine stretches

Expand library of stapled α2 and α3 mimicking peptides

Evaluate peptide stability in oocytes

Optimize conditions for injecting peptides

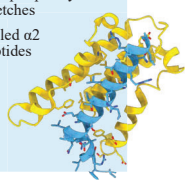

Application of membrane-active peptide-based therapeutics in the management of stromal melts associated with microbial keratitis

https://doi.org/10.17952/37EPS.2024.P1136

Jyoti Sood[1] , Sujithra Shankar[1, 2], Sushmita G. Shah[3] , Shikha Yadav[4] , Archana Chugh[1*]

***Corresponding author email: achugh@bioschool.iitd.ac.in**

[1]Indian Institute of Technology Delhi, New Delhi, India, [2]Duke-NUS Medical School, Singapore, Singapore,
[3]Eye Life Hospital, Mumbai, India, [4]National Institute of Biologicals, Noida, India

ABSTRACT

Advanced **microbial keratitis** causes corneal ulceration and stromal melts. An imbalance of matrix metalloproteinases (MMPs) and exogenous collagenases or other enzymes released by the infecting pathogen degrades corneal tissue. It causes **tissue damage resulting in blindness**. No targeted treatments exist to stop corneal melting. An **antimicrobial peptide targeting the cornea** of anterior eye was designed. With its **collagen interaction properties**, it is anticipated to be a promising agent for preventing microbial keratitis-induced stromal melts.

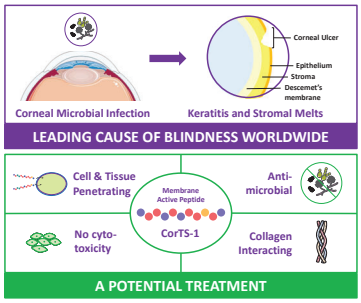

Fig. 1. Graphical abstract

METHODOLOGY

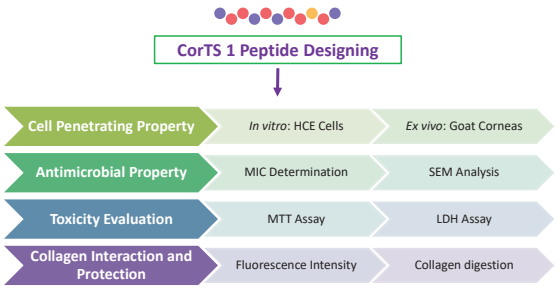

Fig. 2. Summarized methodology

RESULTS

1. Cell Penetrating Property

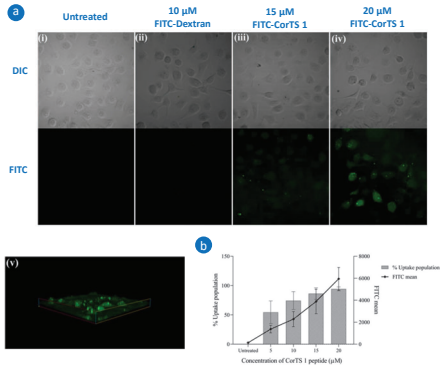

Fig. 3. (a) Confocal microscopy of (i-iv) CorTS 1 uptake on HCE cells (v) a z-section image of HCE cells treated with 20 µM FITC CorTS 1, (b) Percentage uptake population and FITC mean of HCE cells treated with CorTS 1 as measured by flow cytometry.

2. Peptide- Collagen Interaction

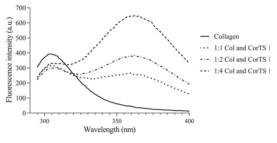

Fig. 4. Fluorescence emission spectra of 5 µM Collagen alone and in presence of CorTS 1 at different ratios.

3. Anti-microbial Property Investigation

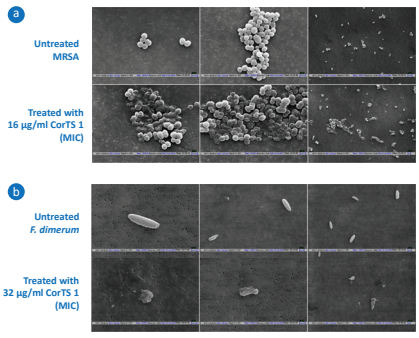

Fig. 5. Scanning electron microscopic analysis of (a) Methicillin-Resistant *Staphylococcus aureus* (MRSA) (b) *Fusarium dimerum* after CorTS 1 treatment.

4. Peptide Localization in Cornea

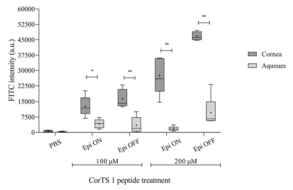

Fig. 6. Fluorometric results of tissue penetration of CorTS 1 after 30 min of topical application in goat eyes with intact epithelium (ON) and debrided epithelium (OFF).

5. Collagen Protective Property Investigation

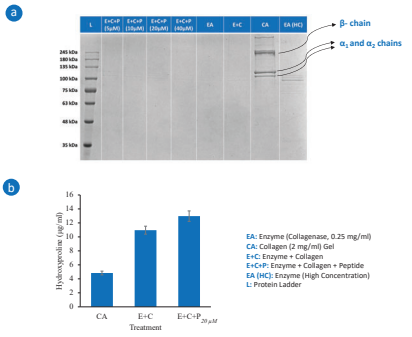

Fig. 7. Analysis of collagen gel digestion by collagenase in presence and absence of peptide by (a) SDS-PAGE profile and (b) Hydroxyproline assay (***Unpublished Results***)

6. Toxicity Evaluation

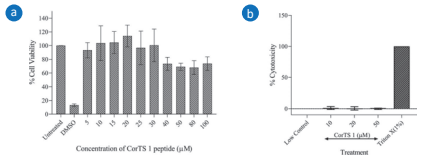

Fig. 8. (a) Percentage viability of HCE cells treated with CorTS 1 for 24 hr evaluated by MTT assay. (b) Percentage cytotoxicity in HCE cells treated with CorTS 1 evaluated by LDH assay.

DISCUSSION AND FUTURE

CorTS-1 is a **cornea targeting cell penetrating peptide** with its localization in cornea.

It has **antimicrobial** effect as well as **collagen interaction** properties with no cytotoxicity towards mammalian cell lines.

Although it is **not able to protect the collagen gel** from collagenase digestion ***in vitro***, it is hypothesized to show anti-collagenolytic effect in complex systems.

Other aspects such as its **matrix metalloproteinase inhibitory activity** needs to be checked before investigation in complex systems.

REFERENCES

1. Shankar, S., Shah, S. G., Yadav, S., & Chugh, A. (2021). Novel corneal targeting cell penetrating peptide as an efficient nanocarrier with an effective antimicrobial activity. *European Journal of Pharmaceutics and Biopharmaceutics*, 166, 216-226.
2. Chugh, A., Shankar, S. & Shah, S. Novel Corneal targeting CPP for ocular disease management. Indian Patent Application Number: 202111002997, Date of Filing: 21/01/2021
3. García-López, C., Rodríguez-Calvo-de-Mora, M., Borroni, D., Sánchez-González, J. M., Romano, V., & Rocha-de-Lossada, C. (2023). The role of matrix metalloproteinases in infectious corneal ulcers. *Survey of Ophthalmology*, 68(5), 929-939.

ACNOWLEDGEMENTS

Authors are thankful to CRF-IIT Delhi for providing research facilities. JS is thankful to IIT Delhi for proving Junior Research Fellowship and travel support. JS is also thankful to Department of Biotechnology- CTEP Programme and European Peptide Society for providing travel grant and registration waiver, respectively to attend this symposium. Fig. 1 and Fig. 2 were drawn in part using images from Servier Medical Art. Servier Medical Art is licensed under CC BY 4.0.

CONTACT DETAILS

Jyoti Sood
Ph. D. Student, IIT Delhi, India
jyoti.sood@bioschool.iitd.ac.in

Prof. Archana Chugh
Professor, IIT Delhi, India
achugh@bioschool.iitd.ac.in

One-bead-one-compound combinatorial libraries for the discovery of ligands towards SIRPα and checkpoint CD47 proteins

P. Quesada-Martínez,[a] M. Sánchez-Navarro [a]

[a] *Instituto de Parasitología y Biomedicina "López-Neyra"- CSIC, Avda. Conocimiento 17,18016, Granada, Spain*
e-mail: paula.quesada@ipb.csic.es

https://doi.org/10.17952/37EPS.2024.P1137

Abstract

Library screening is a powerful tool to find new peptide-based drug candidates, allowing rapid identification of ligands from a large number of diverse compounds. Among these methods, one-bead-one-compound (OBOC) peptide libraries, encoding for lineal, branched or cyclic peptides, including natural and unnatural amino acids, hold great potential.

CD47 is a glycoprotein expressed on the surface of cells. Its interaction with signal-regulating protein alpha (SIRPα) of dendritic cells induces an antiphagocytic signal, known as "don't-eat-me" signal. This mechanism is not only exploited by certain tumours to escape immune surveillance, but some pathogens, such as the *Plasmodium malariae*, induce CD47 overexpression. Since the activation of CD47 expression is not related to the pathogen-host specific interaction, CD47 appears as a therapeutic target to treat a wide range of infection agents. In these terms, peptides might be used to inhibit this interaction and enhance phagocytosis.

Our main objective is to discover new protease resistant peptides with affinity for the CD47/SIRPα axis, so as to inhibit their interaction. We decided to use and design linear and cyclic OBOC library comprised non-proteinogenic amino acids. After synthesis of these libraries, they are evaluated using affinity selection-mass spectrometry (AS-MS) to identify binders for the proteins of interest.

One-bead-one-compound (OBOC) library

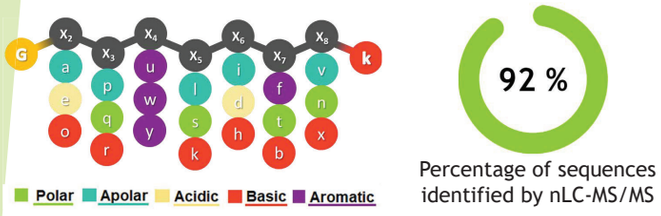

***Figure 1*. OBOC Library synthesized.** Three different D-amino acids have been introduced in seven positions of the sequence. 2187 possible peptides. After analysis via nLC-MS/MS, most of the peptide were detected.

His-Tagged SIRPα protein expression

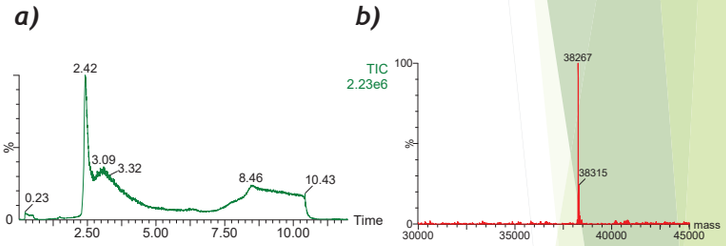

***Figure 2*. Characterization of His-Tagged SIRPα. a)** Chromatogram of SIRPα, showing a retention time of 2.42 minutes **b)** Mass spectra after deconvolution, the molecular weight obtained matches the theoretical one (3264.67 Da). The protein was successfully obtained.

Affinity Selection-Mass Espectrometry (AS-MS) assay

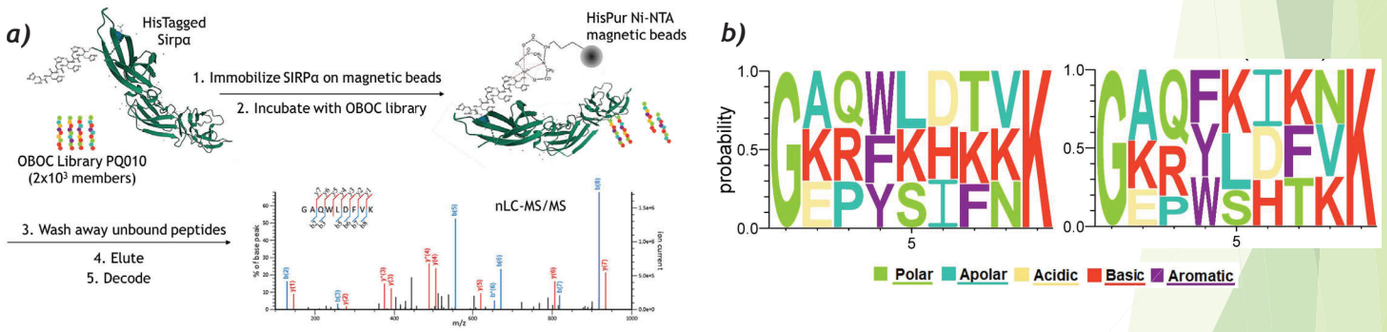

***Figure 3*. a) Workflow of AS-MS assay**. The OBOC library is incubated with immobilized His-SIRPα. After incubation and wash, hits are decode by MS analysis**. b) Positional frequency plot** showing theoretical possibilities of finding the selected amino acids in each position**.** Assay performed at different OBOC library concentrations (1 and 10 nM respectively). None of the positions are biased towards an specific type of amino acid.

Conclusions

·A OBOC protease-resistant peptide library has been designed, its synthesis has been performed by SPPS and its characterization was done by nLC/MS-MS, identifying 92% of the population.

·AS-MS assay was performed using SIRPα against OBOC library, but results show the need of using larger libraries to identify posible hits.

Future Perspectives

·Methods to optimize analysis of the elution from the AS-MS assays are being developed and other approaches are being taken into consideration as an alternative for the analysis of this library.

·Larger OBOC libraries have been synthesized and are ready to be tested.

References

[1] *Amino Acids, 2020, 52, 1207-1226.*
[2] *Antibodies 2020, 9(3), 44.*
[3] *Nat. Commun. 2020, 11, 3183.*

Proceedings of the 37th European Peptide Symposium
Michal Lebl, Editor
European Peptide Society, 2024 *http://doi.org/10.17952/37EPS.2024.P1138*

Impaired metabolic phenotyping in mice with deletions of GPR10 and NPFFR2 receptors: Implications for lipidized PrRP analog therapy in obesity

Veronika Strnadová[1], Magdalena Škrlová[1], Jaroslav Kuneš[1,2], Lenka Maletínská[1]

[1] *Institute of Organic Chemistry and Biochemistry of the Czech Academy of Sciences, 16600 Prague, Czech Republic*
[2] *Institute of Physiology of the Czech Academy of Sciences, 14200 Prague, Czech Republic*

Scientific background: Obesity is a growing global health concern with limited treatment options. Prolactin-releasing peptide (PrRP) is a neuropeptide that can reduce food intake when administered centrally but loses this effect when given peripherally. However, lipidization of peptides can enhance their stability and efficacy after peripheral administration. Our previous work showed that lipidized PrRP analogs effectively reduced food intake and body weight in mice[1]. PrRP binds to its GPR10 receptor and with high affinity to neuropeptide FF receptor type 2 (NPFFR2)[2], both of which are involved in regulating food intake and energy homeostasis.

Palmitoylated analog of PrRP31, palm^{11}-PrRP31 improved its binding and agonist activity for both receptors[3,6,7]. We have previously shown that deletion of GPR10 resulted in increased food intake, elevated insulin levels, impaired glucose tolerance, and altered lipid metabolism gene expression[4]. NPFFR2 knockout mice showed severe glucose intolerance, which worsened with a high-fat diet (HFD), and developed hypothalamic insulin resistance due to reduced insulin pathway signaling proteins[5]. Deletion of both GPR10 and NPFFR2 caused sex-specific and diet-dependent metabolic changes, including impaired glucose tolerance and hyperglycemia on a high-fat diet.

Methods: In this study, we examined the effect of palm^{11}-PrRP31 on mice with deletion of either GPR10 or NPFFR2 or both receptors (GPR10/NPFFR2 KO or dKO mice). Male mice were fed a HFD starting at 8 weeks of age for a duration of 5 months. During the final month, they received a 4-week subcutaneous treatment with either saline or palm^{11}-PrRP31 (5 mg/kg) administered twice daily. An oral glucose tolerance test (OGTT) was performed in the third week of the interventions, and fasting plasma was collected to measure insulin levels. Finally, the mice were euthanized by decapitation, and organs (brain, liver, adipose tissue) were collected for further analysis.

Results and discussion: The palmitoylated palm11-PrRP31 analog demonstrated strong appetite-suppressing and glucose-lowering effects in obese wild-type (WT) mice. Treatment with palm11-PrRP31 led to a significant reduction in body weight and food intake in GPR10 KO mice, whereas in NPFFR2 KO mice, the reduction in body weight was less pronounced and food intake was only slightly reduced. In dKO mice, which lack both GPR10 and NPFFR2 receptors, there was no reduction in body weight or food intake.

 http://doi.org/10.17952/37EPS.2024.P1138

Palm^{11}-PrRP31 significantly improved glucose tolerance in WT mice, but had no effect in any of the KO models, suggesting that the activation of both GPR10 and NPFFR2 receptors is essential for its anti-obesity and anti-diabetic effects.

Previous studies have shown that the GPR10 and NPFFR2 receptors are involved in regulating energy balance, food intake, and glucose homeostasis. The dual agonism of these receptors by palm^{11}-PrRP31 may enhance anorectic signaling pathways, reduce insulin resistance, and promote glucose uptake in peripheral tissues, which are critical mechanisms for weight loss and improved metabolic control. Moreover, lipidization of PrRP analogs, such as palm^{11}-PrRP31, increases their stability and prolongs their half-life, enhancing their therapeutic efficacy. Therefore, targeting both GPR10 and NPFFR2 receptors with lipidized PrRP analogs could offer a promising strategy for treating obesity and related metabolic disorders by addressing both appetite regulation and glucose metabolism, potentially overcoming the limitations of current therapies that target only a single pathway.

Dedication:
This research was supported by the project National Institute for Research of Metabolic and Cardiovascular Diseases (Programme EXCELES, ID Project No. LX22NPO5104) - Funded by the European Union - Next Generation EU, by grant 21-03691S Czech Science Foundation of the GACR and by RVO: 61388963 and RVO:67985823 of the CAS.

References:

1. Maletínská L. et al., Int J Obes (2015), 39, 986–993
2. Engström M. et al., J Pharmacol Exp Ther (2003), 305(3):825-32
3. Pražienková V., Holubová M. et al.,PLoS ONE 12(8): e0183449
4. PražienkováV. et al., Gene (2021), 774-145427
5. Karnošová A., Strnadová V. et al., Clin Sci (2023), 137 847–862
6. Strnadová V. et al., Neuropeptides 98 (2023), 102319
7. Karnošová A. et al., Int J Mol Sci (2021), 22, 8904

https://doi.org/10.17952/37EPS.2024.P1139

Latarcins as membrane active peptides for therapeutic applications

Sivalingam Ayyanar[1], Prasanjeet Kaur[1], Deepthi Poornima Budagavi[1,2], Nisha Ponnappan[1,3], Archana Chugh[1*]

* Corresponding Author e-mail : achugh@bioschool.iitd.ac.in

[1]Kusuma School of Biological Sciences Indian Institute of Technology Delhi, New Delhi, India
[2]Cold Spring Harbor Laboratory, New York, United States [3]Medicine Discovery Catapult, Macclesfield, United Kingdom

37th EPS European Peptide Symposium
14th IPS International Peptide Symposium
25 - 29 August 2024
Florence, Italy

ABSTRACT

Venoms, a rich source of bioactive peptides present promising avenues for drug discovery and development. Latarcins, a class of seven linear membrane active peptides (MAPs) isolated from the ant spider *L.tarabaevi*, exhibit notable biological activities including antimicrobial and anticancer effects. Studying the membrane-targeting ability of Latarcins is crucial for understanding their molecular mechanisms. Our ongoing research focuses assessment of antimicrobial efficacy of Latarcins, revealing a broad spectrum of activity. Propidium Iodide (PI) uptake assay confirms the membrane-disrupting activity of Latarcins on MRSA cells. Time kill kinetics assays demonstrated rapid microbial killing effect (Mentioned data is not published yet). Cellular translocation and cargo delivery efficiency of modified Latarcin peptide sequences fused with a nucleus- targeting sequence (LDP-NLS) was also investigated. Also, *in-vitro* anticancer activity is currently being investigated in different cancer cell lines. Collectively, this multidimensional exploration combined with *in-silico* Molecular Dynamics (MD) studies contribute to our understanding of molecular interaction of these MAPs with biological membranes and holds potential for the development of efficacious therapeutics.

APPROACHES

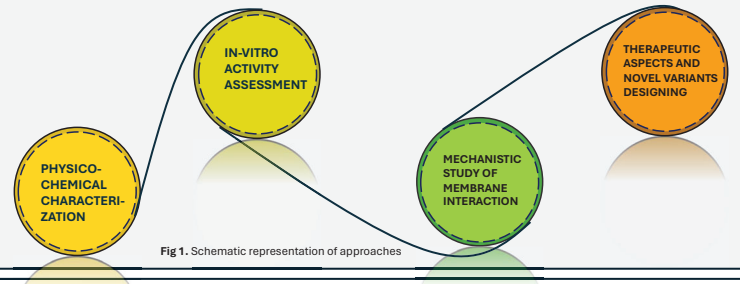

Fig 1. Schematic representation of approaches

RESULTS

MEMBRANE TARTGETING ANTIBACTERIAL ACTIVITIES (Data unpublished)

MIC AND MBC DETERMINATION

Strain	Ltc1	Ltc2a	Ltc3	Ltc4	Ltc5	Ltc6	Ltc7
Methicillin resistant *Staphylococcus aureus*	16, 32	4, 8	8, 16	4, 8	8, 16	>128	>128
Escherichia coli	128,128	8,128	128,128	128,128	128,128	>128	>128
Pseudomonas aeruginosa	16,16	8,8	128,128	>128	32,32	>128	>128
Vibrio cholerae	128,128	32,32	64,64	64,64	128,128	>128	>128
Rhizopus zygospores	>128	32,32	>128	>128	>128	>128	>128
Mucor indicus	>128	32,32	>128	>128	>128	>128	>128
Fusarium dimerum	16	4,8	32,64	32,64	32,64	>128	128, >128

Table 1. MIC and MBC values of Ltcs **Fig 2.** A) Bar graph representation of MIC values of Ltcs B) Bar graph representations of MBC values of Ltcs against different pathogens

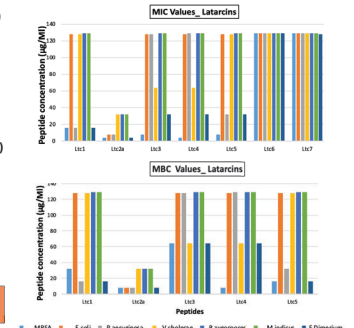

Ltc2a exhibited broad-spectrum antimicrobial activity at lower concentrations;
The close correspondence between the MIC and MBC values highlights their bactericidal nature

PROPIDIUM IODIDE (PI) UPTAKE ASSAY

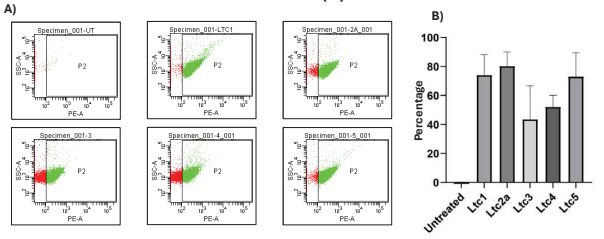

Fig 3. Flow cytometry analysis of PI uptake A) i) Untreated ii) Ltc1 iii) Ltc2a iv) Ltc3 v) Ltc4 vi) Ltc5 B) Population cell death percentage in treated and untreated cells.

After 1h treatment, ~50 or more percent of cells were stained with PI in Ltcs treated populations

TIME KILL KINETICS

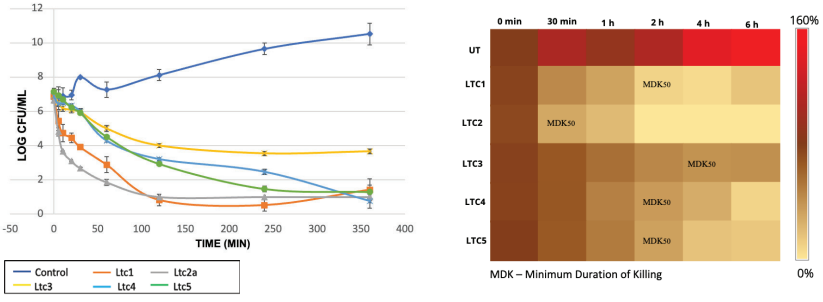

Fig 4. A) Time kill curve for Ltc treated cells. B) Heat map representation of population viability over time in ltc treated populations

At 6h post treatment the population size declined nearly to Log1 (~100 %) (Except Ltc3) ; Ltc2a treated cells showed ~log5 reduction after 2h treatment

MEMBRANE INTERACTION AND MEMBRANE DAMAGE EFFECTS

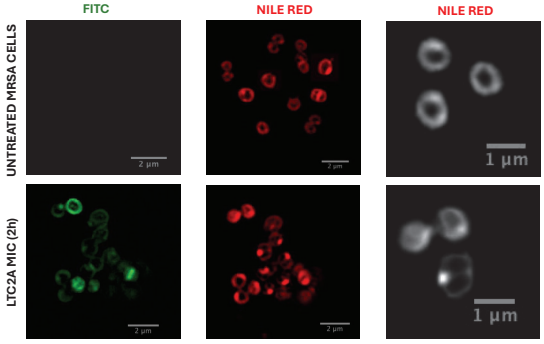

Fig 5. SIM images of FITC-Ltc2a treated cells stained with Nile Red.

Nile red dye accumulation and diffusion confirms the membrane damage in Ltc2a cells

CELL PENETRATING ACTION INSIDE FUNGAL SPORES AND ANTIFUNGAL EFFECTS (Budagavi et al., 2018)

CELL PENETRATION ACTION OF LTC VARIANTS

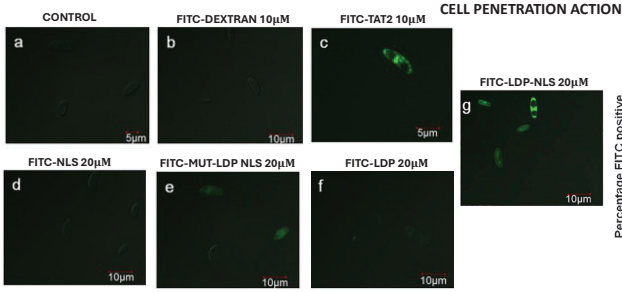

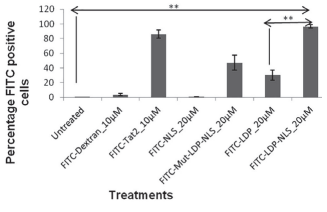

Fig 6. Epi fluorescence microscopy images of FITC-Latarcin variants treated cells.

Fig 7. Flow cytometry analysis of FITC-Latarcin variants treated cells.

Fluorescence microscopy and flow cytometry analyses confirm the penetration of FITC-LDP-NLS inside fungal spores

ANTIFUNGAL ACTIVITY OF VARIANTS AGAINST *Fusarium solani*

S.No.	Peptide name	Sequence[a]	MIC of peptides against *F. solani* (µM)	
			Spores	Hyphae
1.	LDP-NLS	KWRRKLKKLRPKKKRKV	2.5–5	20–30
2.	LDP	KWRRKLKKLR	5–10	30–40
3.	Mut-LDP-NLS	AWRRKLKALAPAKKARV	20–25	> 50
4.	NLS	PKKKRKV	No effect till 50 µM	No effect till 50 µM
5.	Tat2	RKKRRQRRRRKKRRQRRR	5–10	15–30

Table 2. MIC determination of Latarcin derived variants against *F.solani* spores and hyphae

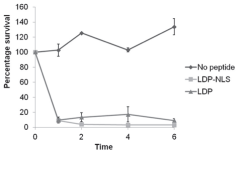

Fig 8. Killing kinetics of variants

LDP-NLS showed effective anti-fungal activity against *F.solani* spores and hyphae

DISCUSSION

Currently, mechanistic aspects of membrane damage induced bactericidal action of Ltcs are being investigated using microscopic and biophysical approaches. Beyond their antimicrobial and cell-penetrating capabilities, these MAPs also exhibit promising anticancer properties (data is not shown). Ongoing research is focused on the *in-vitro* validation of their anticancer efficacy and elucidating the mechanistic pathways involved in their cytotoxic effects. By offering a strong foundation for investigating the various biological functions of these MAPs, these integrated, multidisciplinary approaches demonstrate their potential as viable therapeutic candidates in the future.

REFERENCES

- Gostaviceanu, Andreea, et al. "Membrane-active peptides and their potential biomedical application." *Pharmaceutics* 15.8 (2023): 2091.
- Dubovskii, Peter V., et al. "Latarcins: versatile spider venom peptides." *Cellular and Molecular Life Sciences* 72 (2015): 4501-4522.
- Budagavi, Deepthi Poornima, Sheeba Zarin, and Archana Chugh. "Antifungal activity of Latarcin 1 derived cell-penetrating peptides against Fusarium solani." *Biochimica et Biophysica Acta (BBA)-Biomembranes* 1860.2 (2018): 250-256.
- Wadhwani, Parvesh, et al. "Membrane interactions of latarcins: antimicrobial peptides from spider venom." *International Journal of Molecular Sciences* 22.18 (2021): 10156.

ACKNOWLEDGEMENTS

The authors are thankful to the Indian Institute of Technology Delhi and GATE Fellowship for providing project funds, scholarship and travel grant. The authors are thankful to CRF IIT Delhi and SATHI facility for providing research facilities. The authors are thankful to the Department of Biotechnology (DBT) – CTEP program and EPS-IPS 2024 for providing travel support and registration fee waiver for the conference participation.

CONTACT

SIVALINGAM AYYANAR
Ph.D Student
School of Biological Sciences
IIT Delhi
asivalingam2000@gmail.com

To visit our lab

https://doi.org/10.17952/37EPS.2024.P1140

INTRANASAL EFFECTS OF AN ANALOGUE OF THE GLIOPEPTIDE ODN ON ENERGY HOMEOSTASIS

Omayma Dlimi[1], Karthi Duraisamy[1], Arnaud Arabo[2], Léa Killman[2], Marie Jean-Claude Do Rego[3], Marie Jean-Luc Do Rego[3], Benjamin Lefranc[1,2], Amine Bourzam[1,4], Nicolas Chartrel[1], Jérôme Leprince[1,2]

[1]INSERM U1239, LABORATORY OF NEUROENDOCRINE, ENDOCRINE AND GERMINAL DIFFERENTIATION AND COMMUNICATION - NORDIC, ROUEN NORMANDY UNIVERSITY, ROUEN, FRANCE
[2]INSERM US51, CNRS UAR 2026, HERACLES, ROUEN NORMANDY UNIVERSITY, ROUEN, FRANCE; [3] UNIV ROUEN NORMANDIE, ANIMAL BEHAVIOUR PLATFORM SCAC, ROUEN, FRANCE
[4]LABORATOIRE DE NEUROPHYSIOLOGIE ET PHYSIOPATHOLOGIE CELLULAIRE ET VALORISATION DES BIOMOLÉCULES, UNIVERSITÉ DE TUNIS EL MANAR, TUNIS, TUNISIE

CONTACT: omayma.dlimi1@univ-rouen.fr

OBESITY MAJOR PUBLIC HEALTH PROBLEM IN INDUSTRIALIZED COUNTRIES

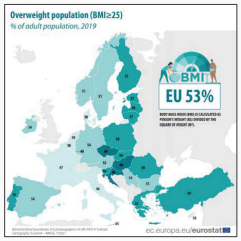

Overweight and obesity - BMI statistics

RISK FACTORS:

→ TYPE 2 DIABETES
→ CARDIOVASCULAR DISEASE
→ CANCERS

Levian et al.,2014

HYPOTHALAMIC REGULATION OF FOOD INTAKE
▪ NEURONAL COMPONENT

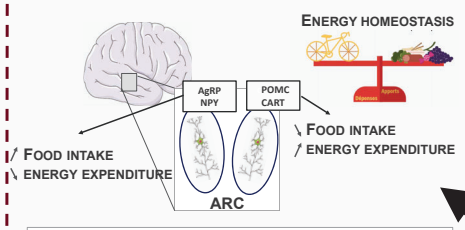

The hypothalamus strongly contributes to the homeostatic control of energy balance by integrating information linked to the nutritional status and arising from peripheral organs

HYPOTHALAMIC REGULATION OF FOOD INTAKE
▪ GLIAL COMPONENT

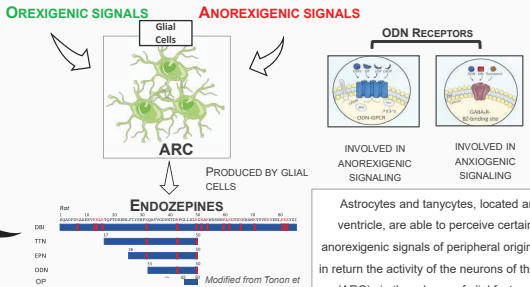

Astrocytes and tanycytes, located around the third ventricle, are able to perceive certain orexigenic or anorexigenic signals of peripheral origin and to modulate in return the activity of the neurons of the arcuate nucleus (ARC) via the release of glial factors. Among these different molecules, the endozepines and particularly ODN are a family of gliopeptides of interest.

Lebrun et al., 2021

THERAPEUTIC ROLE OF THE ODNERGIC SYSTEM IN THE TREATMENT OF OBESITY?

1 The i.n. administration of OP as an alternative to i.c.v. route



OP:

- C-terminal part of ODN
- Bioactive analog of ODN
- As potent as ODN *in vitro* $[Ca^{2+}]_i$ mobilization in astrocytes

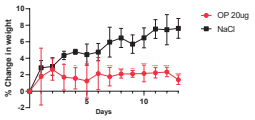

- Intranasal administration of OP (20 µg/day/mice), an ODN-derived analog, results in the cessation of body weight gain in adult normally fed mice starting from the 3rd day of treatment.

2 Cerebral biodistribution of dansyl-OP

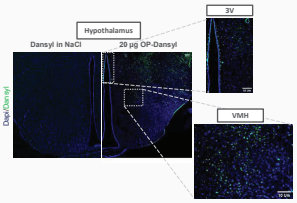

- To monitor the delivery of our peptide to the target brain regions through the intranasal route, we conjugated the OP sequence with dansyl. These preliminary results allow for the visualization of the peptide at the brain level, primarily in the cortex, hippocampus, around the third ventricle, and the VMH.

3 Hypothalamic areas activated by i.n. administration of OP

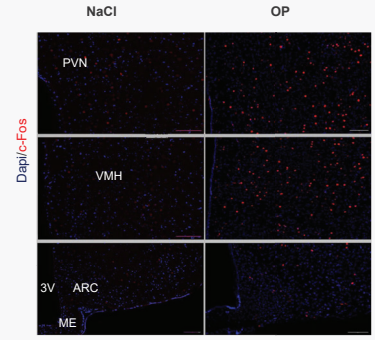

- Fluorescence microscopy allowed visualization of doubly labeled neuronal populations (c-Fos, Dapi) within the mice hypothalamus. The immunohistochemistry images obtained show specific c-Fos labeling limited to 3 main regions, namely the paraventricular (PVN), arcuate (ARC) and ventromedial nuclei (VMH) .

4 The intranasal administration of OP affects metabolic parameters

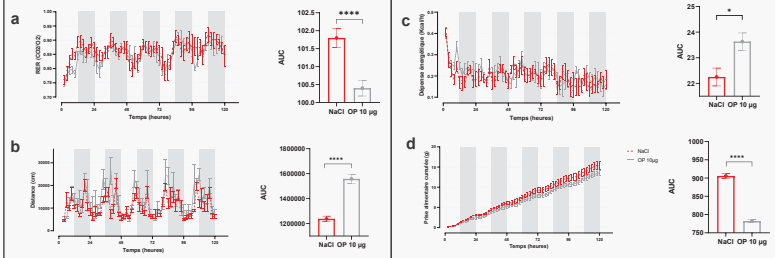

The results show that the intranasal administration of OP in obese mice has significant effects on energy metabolism and appetite regulation. A dose of 10 µg of OP leads to a notable decrease in the respiratory exchange ratio (RER) (a), indicating an increase in the use of lipids as an energy source from body reserves. OP also increases motor activity (b) and energy expenditure in the mice (c), while reducing their food intake (d).

5 The effect of i.n. administration of OP on mRNA expression in the hypothalamus

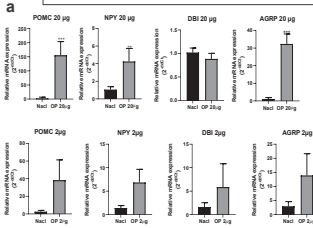

- The representative Western blot revealed a significant increase in POMC protein levels in hypothalamic extracts following i.n. administration of 20 µg OP, in contrast to treatment with NaCl (fig b). This finding was corroborated by real-time RT-PCR, which demonstrated elevated expression levels of the POMC, NPY, and AGRP genes in the hypothalamus following the same 20 µg OP administration, indicating a potential shift toward anorexigenic neuropeptide activity (POMC) from orexigenic neuropeptides (NPY and AGRP) (panel a).

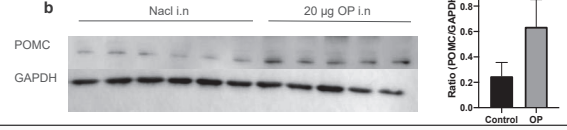

Conclusions and perspectives

In summary, our findings demonstrate the efficacy of the i.n. route for delivering OP to the brain, resulting in activation of identical hypothalamic regions as observed with i.c.v. injection. **These data affirm the therapeutic promise of the ODN/GPCR system in addressing human conditions linked to energy metabolism.**

➢ THE IMPACT OF I.N. ADMINISTRATION OF OP ON ENERGY METABOLISM IN WT MICE

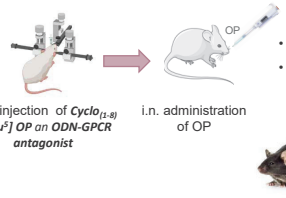

i.c.v. injection of ***Cyclo$_{(1-8)}$ [$_D$Leu^5] OP an ODN-GPCR antagonist***

i.n. administration of OP

Evaluation of:

- **Food intake**
- **Body weight**



➢ ANOREXIGENIC EFFECT OF OP IN F77I MICE

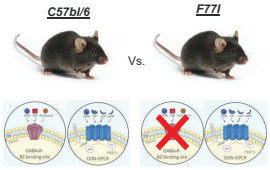

1. i.c.v. injection of **ODN**
   → **No** anxiogenic effect expected

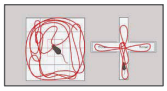

2. **c-Fos** immunohistochemistry
3. OP instilation in normally fed and diet-induced obesity mice

➢ NEUROANATOMICAL PATHWAYS AND HYPOTHALAMIC TARGETS OF THE OP

Monitor the mode of OP penetration in the nasal epithelium and then its central and peripheral biodistributions by β-imaging of a radioactive analogue of OP ([^{3}H]OP) in collaboration with the CEA.

References:

- Guillebaud F., Duquenne M., Djelloul M., Pierre C., Poirot K., Roussel G., Riad S., Lanfray D., Morin F., Jean A., Tonon MC., Galgé S., Lebrun B., Dallaporta M., Leprince J., Prevot V., Troadec JD. (2020) Glial endozepines reverse high-fat diet-induced obesity by enhancing hypothalamic response to peripheral leptin. Mol. Neurobiol. 57, 3307-3333
- Lebrun B., Barbot M., Tonon MC., Prévot V., Leprince J., Troadec JD. (2021) Glial endozepines and energy balance: Old peptides with new tricks. Glia. 69, 1079-1093/
- Levian C., Ruiz E., Yang X. (2014) The pathogenesis of obesity from a genomic and systems biology perspective. Yale J. Biol. Med. 87, 113-126.
- Overweight and obesity - BMI statistics. Eurostat statistics-explained.
- Tonon MC., Vaudry H., Chuquet J., Guillebaud F., Fan J., Masmoudi-Kouki O., Vaudry D., Lanfray D., Morin F., Prevot V., Papadopoulos V., Troadec JD., Leprince J. (2020) Endozepines and their receptors: Structure, functions and pathophysiological significance. Pharmacol. Ther. 208, 107386.

https://doi.org/10.17952/37EPS.2024.P1142

Enhancing biomedical metal implants with synthetic peptides: improved bioactivity and in vitro safety

A. Mourgout,[1] F. Arjmand,[2] E. Groult,[3,4] O. Monasson,[3] S. Ammar,[2] A. Hattal,[5] M. Djemai,[5] G. Dirras,[1] M. Boissiere,[4] E. Peroni[3]

[1]Université Sorbonne Paris Nord, LSPM, CNRS-UPR 3408, 93430 Villetaneuse, France; [2]Université Paris Cité, CNRS, ITODYS (UMR 7086), 75205 Paris; France; [3]CY Cergy Paris Université, CNRS, BioCIS, 95000, Cergy Pontoise, France; [4]CY Cergy Paris Université, ERRMECe, 95000, Cergy Pontoise, France.
[5]Z3DLAB, SAS, 2 Chemin de Coye, 95270-Chaumontel, France
Elisa.peroni@cyu.fr

Modern solutions in biomedical engineering imply innovative strategies at the frontier between chemistry, material science, and biology to develop biofunctionalized substitutes able to restore, maintain or improve tissue integrity. These substitutes are materials that are designed to positively interact with a living biological system for a therapeutic purpose while introducing mechanical, physical and/or chemical functions to the body. Commonly speaking, they are defined as biomaterials [1].

It is of paramount importance to enhance the bioactivity of materials scaffolds by combining biomaterials with biological cues to drive a particular tissue function [2]. In practice, biocompatibility can be achieved by first choosing bioinert solids and then coating them with bioactive molecules.

Interestingly, different biological effects may be targeted when implanting a biomaterial by combining peptides from diverse nature. In the field of bone regeneration, the use of BMP-2 derived peptides is of crucial importance to promote osteodifferentiation of mesenchymal stem cells (MSCs) and guide bone formation [3].

Peptides are easily modifiable for functionalization of surfaces, reaching, in some cases, similar biological activity to the total protein for a specific target [4].

A simple though useful approach to improve the performance of peptidic molecules is to combine peptide sequences with synergistic or complementary effects, enabling to address two or more biological effects. In this way, multifunctionality may be installed on biomaterials without using proteins.

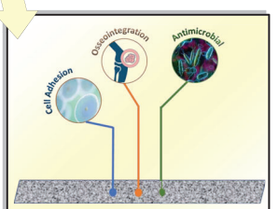

Our goal is to develop a new family of safe & bioactive HEAs

High Entropy Alloys (HEAs) are a novel class of materials known for their exceptional mechanical properties and corrosion resistance. These alloys generally are composed of multiple principal elements in equimolar or non/near-equimolar ratios, with elemental concentrations ranging from 5% to 35%. Among these HEAs have been specifically developed for biomedical applications. Notable examples include equiatomic and non-equiatomic alloys like TiZrNbTaMo, which have attracted significant attention as a new generation of biomaterials. However the integration of such materials as implants into bone is only adressed as a passive process. In such an approach, the fixation is mainly mechanical, with anchorage failure. Therefore, the increase of the biointegration of the implant and the bone tissue is becoming a research hotspot. Such an active integration is usually achieved by grafting bioactive molecules on the surface of the metal implant.

Proadhesion and osteogenic peptides synthesis for multifunctional alloy coating

Peptide selection

	Peptide sequences	Description
P1	**KIPKASSVPTELSAISTLYL**	These 2 peptides sequences are the BMP-2(73-92) fragment of the Bone morphogenetic proteins BMP-2, that is the most investigated and potent osteoinductive growth factors in bone regeneration[5].
P2	**KIPKASSVPTELSAISTLYLK(TAMRA)PEG$_9$-NH$_2$**	
P3	**TAMRA- GGCRGD**	RGD peptide has been demonstrated to be able to increase the expression of osteogenic markers and mineralization in hMSCs culture[6]

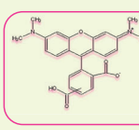

Fluorescent Probe

5(6)-Carboxytetramethylrhodamine (TAMRA).
λ_{ex} = 555 nm et λ_{em} = 580 nm

Synthetic conditions:

Peptides were synthesized in solid-phase using a microwave-assisted protocol (MW-SPPS) on a Liberty Blue™ automated peptide synthesizer (CEM Corporation, Matthews, NC, United States), following the Fmoc/tBu strategy.

The introduction of an additional lysine (Lys[93]) in the BPM-2(73-92) fragment allows the introduction of the fluorescent probe in C terminus by coupling of the carboxylic moiety of TAMRA to the amino function of the side chain through the formation of an amide bond. For this purpose, we chose 4-methyltrityl group (Mtt) which is removed in very weak acid conditions. In order to increase the peptide solubility and to facilitate the on resin TAMRA coupling, a PEG9 linker has been introduced in C terminus.

Peptide assembly was performed by repeating the standard MW-SPPS coupling cycle for each amino acid, using Fmoc-protected amino acids (5 equiv, 0.2 M in DMF), OxymaPure® (5 equiv, 1 M in DMF), and DIC (5 equiv, 0.5 M in DMF).

Polyethylene glycol-based spacer (PEG), containing 9-atoms chain (Fmoc-8-amino-3,6-dioxaoctanoic acid) (2.5 equiv) and TAMRA were coupled in C and N terminal position of peptide P2 and P3, respectively, as follows: Fmoc-8-amino-3,6-dioxaoctanoic acid (2.5 equiv) and TAMRA (2,5 equiv), TBTU (2,5 equiv) and DIPEA (3,5 equiv) were dissolved in DMF with a final dilution of 1 mL DMF for 100 mg of resin. Couplings were performed 45 min at room temperature

	HPLC Rt (min)	HPLC gradient (%)	ESI-MS found (calc)
P1	1min85	10 - 90	$[M+H]^+$=2118,31 (2118,53)
P2	2min12	30 - 50	$[M+H]^+$=2805,12 (2805,23)
P3	1min35	20-60	$[M+H]^+$=979,96 (976,06)

Mtt deprotection

After the Lys(Mtt) loading, the synthesis was carried out with MW-assisted SPPS strategy. The following peptidil-resin was then washed several times with DCM and dried under vacuum:

K(Boc)**IPK**(Boc)**AS**(tBu)**S**(tBu)**VPT**(tBu)**E**(tBu)**LS**(tBu)**AIS**(tBu)**T**(tBu)**LY**(tBu)**LK**(Mtt)-PEG$_9$-*—RinkResin*

A satisfactory deprotection of Lys(Mtt) was accomplished in just three cycles of 1% TFA in DCM. The reaction was monitored by RP-HPLC from collected solutions.

Cleavage from the resin and side-chain deprotection were achieved by treatment with a TFA/TIS/water solution (95 : 2.5 : 2.5 v/v/v, 1ml/100mg of resin-bound peptide).
Lyophilized crude peptides were purified by semi-preparative Waters RP-HPLC (Milford, MA, USA) on a Phenomenex Jupiter C18 (10 µm, 250mm× 10mm) column at 4 ml/min. The solvent systems used were 0.1% TFA in H_2O (A) and 0.1% TFA in CH_3CN (B), and the gradients used are presented in Table 1. All peptides were obtained with a purity >95%.
Characterization of the peptides was performed by analytical RP-UPLC ESI-MS (Waters Acquity UPLC coupled to a Waters 3100 ESI-SQD MS) supplied with an Aeris Widepore C1 200A (3.6 µm 250 × 4.6 mm) column at 25 °C at 0.6 mL/min with solvent systems A (0.1% TFA in H_2O) and B (0.1% TFA in CH_3CN). Data were acquired and processed using MassLynx software (Waters, Milford, MA, USA).

HEAs Surface functionalization & characterization

The final goal of the project is the development of safe, non-destructive and biocompatible strategies to modify the surface of HEAs for applications in the field of medical implants .The main aim of this research is to enhance the osseointegration of two types of HEAs (formulated and pre-alloyed) by immobilizing peptides providing a favorable medium to biological reactions on the alloy surface. This was accomplished by modification of the alloy surfaces by the aryl amine coating via diazonium salt (Ds) electrochemical grafting and then covalent bonding of the peptide.

2 types of HEAs:
$Ti_{35}Nb_{25}Zr_{25}Ta_{7.5}Mo_{7.5}$ Formulated
$Ti_{35}Nb_{25}Zr_{25}Ta_{7.5}Mo_{7.5}$ Pre-alloyed

Electrochemical grafting of Ds-NO_2 and its electrochemical reduction to Ds-NH_2

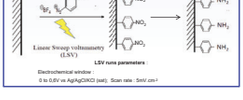

Peptide immobilization protocole

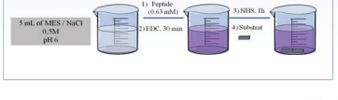

Epifluorescence Microscopy images of peptide grafted HEAs

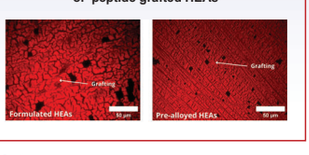

AFM 3D images of grafted grafted HEAs

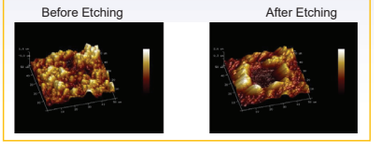

Biological data

BMP2 like peptide bioactivity → change in C2C12 morphology (21 days)

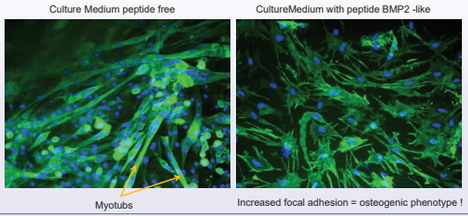

Assessment of the safety and biological activity of the BMP2 like peptide in cultured cell line models

In vitro cytotoxicity evaluation of bio-functionalized alloy surfaces and assessment of their biological performances toward osseointegration

Morphology of cell incubated with peptide grafted alloys

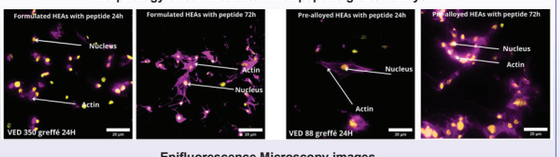

Epifluorescence Microscopy images

This work was funded by:
CY Initiative (grant "Investissements d'avenir" ANR-16-IDEX-0008)
ANR CoCoA-Bio (ANR-20-CE08-0032-01)
CY Fondation "Chaire RETIS"

References:
[1]. Will Williams, D.F. *Biomaterials* **2009**, 30, 5897–5909. [2] Förster Y, Rentsch C, Schneiders W, et al. *Biomatter.* **2012**; 2(3): 149- 157. [3] Mas-Moruno C. et al. *ACS Appl. Mater. Interfaces* **2014**, 6, 9, 6525–36. [4] Williams DF. *Biomaterials.* **2011**;32(18):4195-4197. [5]. A. Saito, et al, *J. Biomed. Mater. Res. A* **2005**, 72 77–82 [6] A.K. Jha, et al *PLoS One* **2014**, 9, e98640

https://doi.org/10.17952/37EPS.2024.P1143

StreaMLine - Machine learning guided development of novel GLP-1 receptor agonists

Authors: Claudia Hjørringgaard[1], Jens Christian Nielsen[1], Mads Mørup Nygaard[1], Anita Wester[1], Lisbeth Elster[1], Trine Porsgaard[1], Randi Bonke Mikkelsen[1], Silas Rasmussen[1], Andreas Nygaard Madsen[1], Morten Schlein[1], Niels Vrang[1], Kristoffer Rigbolt[1], Louise S. Dalbøge[1]*

[1]Gubra, Hørsholm Kongevej 11B, Hørsholm, Denmark. ***Corresponding author:** Louise S. Dalbøge, lsd@gubra.dk

1 Accelerated peptide screening and drug development with streaMLine

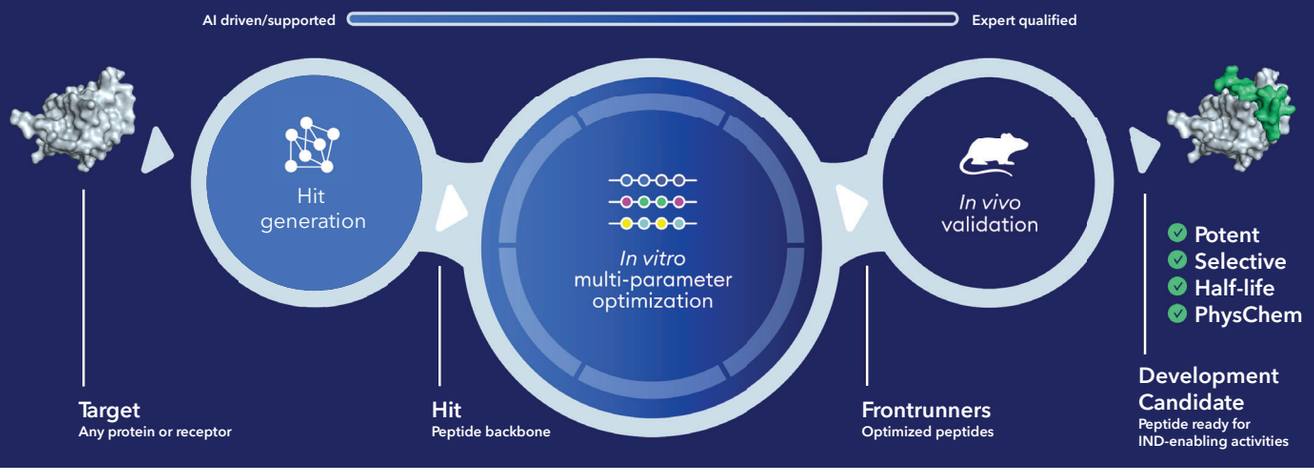

2 The **streaMLine** drug development process

Peptide library generation

+ Systematic design of peptide libraries
+ Rapid solid-phase peptide synthesis and characterization

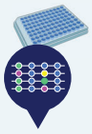

High through-put multi-parameter screening

Functional assays | Biophysical parameters | Metabolic stability

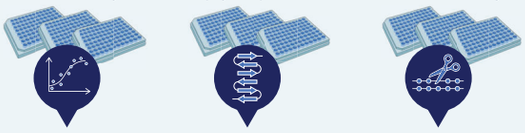

Building the ML model

Explaining the importance of AA substitutions



3 Using **streaMLine** to make novel GLP-1 receptor agonists

Engineering novel GLP-1 receptor agonist starting from the biophysically robust Secretin peptide

+ **StreaMLine platform** used to screen complete peptide sequence and identify key positions that accurately control GLP-1 receptor selectivity

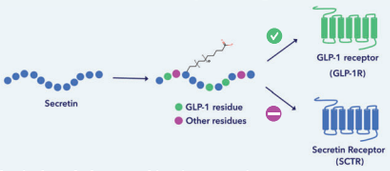

+ **Parallel optimization of potency, selectivity, biophysical- and pharmacokinetic properties**

Deep mutational scan

Positional understanding of the peptide backbone

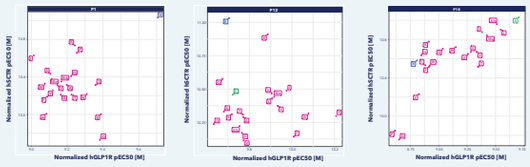

Lipidation (HLE) and glutamate scan

Extending half-life and improving solubility



4 Development candidate characterization

Compound	hGLP-1R EC_{50} (nM)	hSCTR EC_{50} (nM)	Solubility, pH 7 (mg/mL)	Chem. stab., pH 7 (% degradation)	Fibrillation, pH 7 (Yes/No)	$T_{1/2}$, mini pig IV (h)
Secretin	1500	0.0025	-	-	-	-
GLP-1	0.0022	800	-	-	-	-
GUB021794	0.019	190	≥10	-1.4	No	71

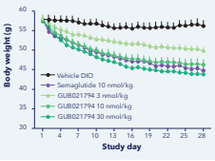



Claudia Hjørringgaard, PhD
Principal Scientist, Chemistry
chj@gubra.dk

Scan the QR code to read full story in *J. Med. Chem.* 2024

Scan the QR code and find out more about Drug Discovery at Gubra A/S

https://doi.org/10.17952/37EPS.2024.P1144

Development of a HPMC-patch containing RGD and KTTKS peptide sequences for application in tissue healing

Naiara Maia Pereira, Reinaldo Marchetto

UNESP – Institute of Chemistry – Department of Biochemistry and Organic Chemistry, Araraquara, São Paulo, Brazil

INTRODUCTION

The tissue healing is a complex process involving biological and molecular cascades events including hemostasis, inflammation, cell proliferation and remodeling phases. Studies indicates that RGD and KTTKS peptides are able to stimulate the Extracellular Matrix to increase an and sustains these events, due to the ability of the RGD sequence to stimulate cell adhesion in fibronectins [1] and KTTKS sequence to trigger cellular processes to induce Extracellular Matrix synthesis, collagen and fibronectin expression [2]. Therefore, peptide based on these sequences can be used in compounds meant for tissue recovery and healing, such as transdermal films. Thus, the peptide named NMC was designed, synthesized and loaded in patches prepared using different hydroxypropyl methylcellulose (HPMC) types and concentrations. The peptide was incorporated during the gel preparation process. The patches were cut as disks of 5 mm diameter and characterized by scanning electron microscopy (SEM), x-ray diffractometry (XRD) and Fourier transform infrared spectroscopy (FT-IR). The cytotoxic effect was investigated by MTT assay in HaCaT cells (BCRJ 0341). The antimicrobial activity was evaluated by the minimum inhibitory concentration (MIC) assay in Staphylococcus aureus (ATCC 14458).

METHODOLOGY AND RESULTS

Peptide

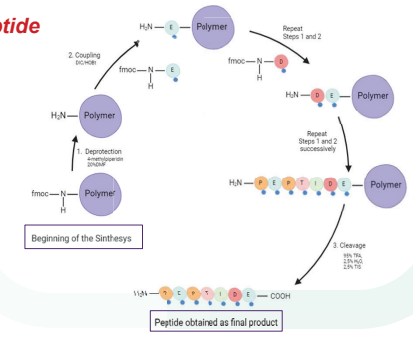

Film

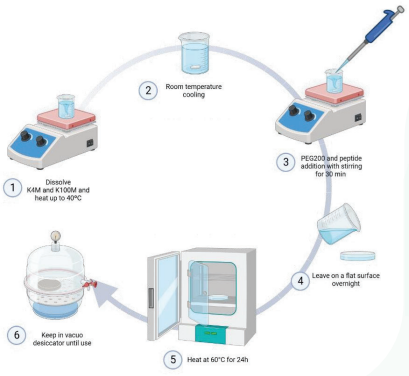

Films preparation

The solvent evaporation technique was used in the films preparation. Various formulations were tested using different types and concentrations of HPMC, combined with another polymers and solvents as previous described [3,4,5,6]. The best formulation (V30) was obtained by dissolving of HPMC K4M and K100M (3:1) at 40ºC, followed by cooling to RT. Then, PEG200 and the peptide (for V30P), when necessary, were added and stirred for more 30 minutes. The obtained gel was left on a flat surface overnight until air bubbles disappeared. Afterwards, the set was taken to an oven at 60ºC for 24 hours. The formed film was then left in a vacuo desiccator until use.

In vitro assays

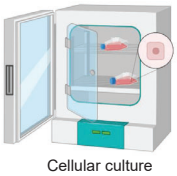

Cellular culture

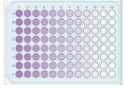

Citotoxicity and proliferation assays



Bacterial cultivation and preparation of inoculum



Antimicrobial assay

Synthesis, purification and characterization of peptide

The peptide NMC, WTGRGDSP-Ahx-KTTKS, was synthesized by solid-phase methodology, using Fmoc/tBu Chemistry with a RinK amide MBHA resin (0.55 mmol.g^{-1}) and DIC/HOBt activation. After deprotection and cleavage with TFA/water/EDT/TIS (94.5:2.5:2.5:0.5) for 2h at RT, the peptide was precipitated, solubilized and dried under vacuum. Analysis and purification was performed by RP-HPLC and the identity confirmed by ESI-MS.

Material Characterization

SEM images were obtained with a JSM-7500 scanning electron microscope. The samples were sputter coated with a 6 nm thick carbon layer. The morphology was observed at an accelerating voltage of 2 kV. XRD patterns were performed on a SmartLab SE Rigaku Diffractometer with a Kβ filter and Cu Kα radiation from 4° to 80°.
FTIR spectra were obtained with dried samples on a Bruker Hyperion 2000 Fourier transform infrared spectrophotometer, with ATR detector.

X Ray Difraction

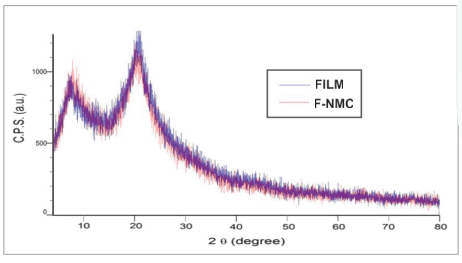

The pure HPMC film had broad diffraction peaks at around 7.72º and 20.48º attributable to the (101) and (002) crystalline planes and indicates its semi crystalline polymer nature (FILM). No significative variation was showed after peptide incorporation (F-NMC).

Cytotoxicity and proliferation assays

Cytotoxicity analysis was performed using the MTT colorimetric method for 72 h, using HaCaT cells, immortalized human keratinocytes (BCRJ 0341). To perform the MTT assay, the films were removed, the supernatants were discarded and 100 µl of sterile PBS buffer was added to the wells to remove dead cells and other metabolic residues present. Next, 180 µL of DMEM and PBS (1:4) solution were added, followed by the addition of 20 µL of MTT solution at 1.0 mg.mL^{-1}. The plates were kept in incubation for 4 hours at 37°C and 5% CO_2. Finally, the supernatants were discarded and 100 µL of a mixture 1:1 of isopropyl alcohol and dimethyl sulfoxide was added to each well to dissolve the formed crystals, keeping the set protected from light and under agitation for 1 hour. The absorbance was read using a microplate reader spectrophotometer at 540 nm.

Antimicrobial activity

Antimicrobial activity was performed using the plate microdilution method with modifications described by the Clinical and Laboratory Standards Institute (CLSI – M7-A10, 2015 and M27-A3, 2017). After initial growth, a cellular suspension was adjusted to McFarland scale 0.5 (10^8 CFU/mL) and diluted to 10^7 CFU/mL. For peptide analysis, 80 µL of media and 100 µL of peptide solution were added to each well, followed by 20 µL of microbial suspension, and incubated for 24 hours at 37°C. Similarly, 5mm discs were used in place of peptide solution under the same conditions. Positive controls were prepared similarly, using microorganisms and media as growth controls. Negative controls included media-only for peptide plates and media with a pure film disc for film analysis. After the incubation period, bacterial growth was assessed by measuring the optical density at 595 nm using a microplate reader spectrophotometer.

Peptide Structure and Characterization

WTG**RGD**SP-Ahx-**KTTKS**-NH_2

Calculated MW (g.mol^{-1})	ES+	ES m/z (g.mol^{-1})	Obtained MW (g.mol^{-1})
1.533,68	+1	1535,69	1534,67
	+2	767,90	
	+3	512,33	
	+4	384,80	

Scanning Electron Microscopy

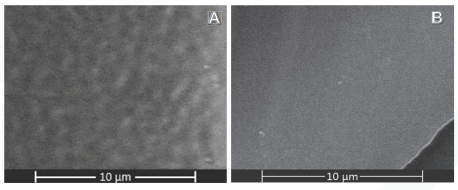

SEM images shows that the films exhibited smooth and homogeneous morphology with no sign of phase separation, which indicated the complete miscibility between HPMC and PEG200 (A). In addition, the film blended with peptide displayed smoother and more homogeneous topography (B).

FTIR spectra

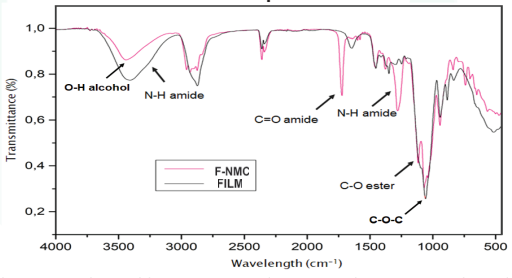

Characteristic vibrational frequencies assigned to HPMC and PEG200 were observed at 3500–3200 cm^{-1} (OH stretching), 2909 cm^{-1} (CH stretching of CH_2 and CH_3 groups), 1645 cm^{-1} (water OH bending), 1425 cm^{-1} (CH_2 symmetric bending), 1370 cm^{-1} (CH bending), 1160 cm^{-1} (antisymmetric bridge C–O–C stretching). Spectroscopy analysis showed bands assigned to amide I (3300-3180 cm^{-1}), C=O amide (1700 cm^{-1}) and amide II (~1300 cm^{-1}), which confirms the peptide incorporation on the films (indicated by arrows).

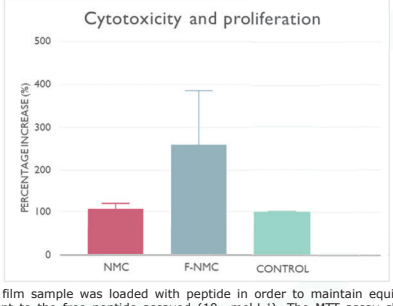

Each film sample was loaded with peptide in order to maintain equivalent amount to the free peptide assayed (10 µmol.L^{-1}). The MTT assay showed that peptide-loaded film (F-NMC) had low cytotoxicity and higher proliferation capacity of queratinocytes compared to the free peptide (NMC).

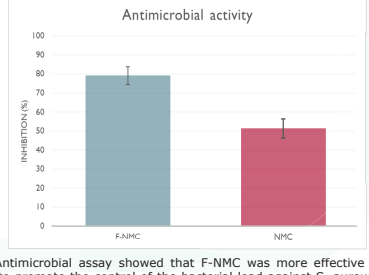

The Antimicrobial assay showed that F-NMC was more effective than the NMC to promote the control of the bacterial load against S. aureus with an inhibition rate of 79,18%±6,95 and 51,43%±5,33, respectively, for the same concentration.

CONCLUSIONS

The peptide-loaded film were successfully obtained using a modified peptide from natural human fibronectin containing the RGD and KTTKS sequences. The addition of the peptide to didn't show significantly changes on film chemical or physical properties but increased positively the cytotoxicity, proliferation and antimicrobial activity in comparison to the behavior of the free peptide. In general, the peptide-loaded film is very promising for use in biomedical applications, especially in cutaneous tissue healing as a transdermal patch.

Support

CAPES CNPq FAPESP

REFERENCES

[1] HERSEL, U.; DAHMEN, C.; KESSLER, H. *Biomaterials*, 24(24), p. 4385-4415, 2003
[2] ABU SAMAH, N.H.; HEARD, C.M. *Int. J. Cosmetic Sci.*, 33(6), p. 483-490, 2011.
[3] KHAN, S.; et al.; *AAPS PharmSciTech.*, 16(4), 800–810, 2015.
[4] KATHE, K.; HATHPALIA, H. *Asian J. Pharm. Sci.*, 12(6), 487–97, 2017.
[5] PATEL D.P.; et al.; *AAPS PharmSciTech.*, 10(2), 437–42, 2009.
[6] VIJAYA, R.; et al. *Int. J. Pharm. Chem. Biol. Sci.*, 5(3), 548–56, 2015.

Optimization of a TREM2 receptor inhibitor peptide

Honisch C.[1], Rotondo M.[2], Galluppo E.[1], Tartaggia S.[1], Gallo C.[3], Dell'Isola M.[3], Carbone D.[3], Manzo E.[3], Fontana A.[3], Ruzza P.[1]

[1]Institute of Biomolecular Chemistry of CNR, Padua Unit, Padova, Italy,
[2]University of Napoli Federico II, Dept. of Biology, Napoli, Italy
[3]Institute of Biomolecular Chemistry of CNR, Pozzuoli, Italy

https://doi.org/10.17952/37EPS.2024.P1146

Introduction

Triggering receptor expressed on myeloid cells 2 (TREM2) is an immune receptor regulating the inflammatory response and involved in neurodegenerative, chronic and autoimmune diseases. TREM2 is an orphan receptor, and the research of new ligands has recently become a hot topic. In this context, the peptide sequence 1A9 (H-IFLIKILAA-OH) has been rationally designed for inhibition of TREM2 [1]. In order to deeper analyze the mechanism of interaction with TREM2 and select molecules with specific binding, we synthetized a series of 1A9 peptide analogues where the **Lys** residues was replaced by either **Gly** or **Ala** to explore the effect of the residue side chain charge and polarity in this position that is believed to be fundamental for ligand interaction. Their conformation, their ability to interact with membranes, and their biological activity was investigated.

Synthesis and purification

Peptides were synthesized by Fmoc-SPPS starting from a 2-chlorotrytil resin. The lipophilic nature of the sequences required 5% piperazine + 2% DBU for Fmoc removal, in order to suppress aggregation during chain elongation, and HATU as coupling reagent.

RP-HPLC purification was challenged by the low solubility of peptides in conventional solvents and buffers but was overcome dissolving the peptides in either DMSO or HFIP (1,1,1,3,3,3-Hexafluoro-2-propanol).

In order to investigate the interaction of peptides with membranes as a function of counterion, the RP-HPLC purified peptides were repeatedly dissolved in diluted hydrochloric acid solution and freeze-dryed in order to exchange TFA with HCl.

Conformational characterization

Circular Dichroism in solution

The secondary structure of a peptide in a membrane environment can be characterized using conventional CD in aqueous dispersions of small unilamellar vesicles or exploiting TFE as membrane-mimetic solvent.

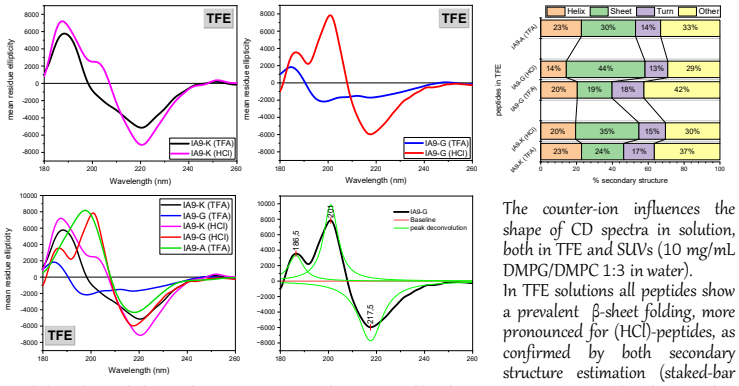

The counter-ion influences the shape of CD spectra in solution, both in TFE and SUVs (10 mg/mL DMPG/DMPC 1:3 in water).
In TFE solutions all peptides show a prevalent β-sheet folding, more pronounced for (HCl)-peptides, as confirmed by both secondary structure estimation (staked-bar plot) and signal deconvolution (as an example 1A9-G(HCl)), where an intense negative band centered at ~217 nm and a positive signal at 187 nm is detected. However, (HCl)-peptides show two positive signals, one centered around at 186 nm and one at 201 nm, the first more intense in 1A9-K, the second in 1A9-G.
1A9-G (TFA) shows a positive band at ~186 nm and two negative bands at 198 and 217 nm, suggesting an equilibrium between unordered and β-sheet folding due to the proximity of the respective dihedral angles. 1A9-A instead shows a single positive signal centered at 198 nm, and a negative one at 222 nm, suggesting a β-stranded structure, with the negative band red-shifted compared to the canonical value of 217 nm, suggesting a possible antiparallel conformation [2].

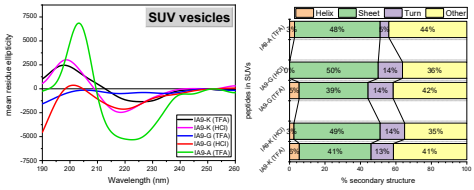

In SUVs 1A9 peptides shows a more prevalent β-sheet folding compared to TFE solutions, as confirmed by secondary structure estimation (staked bar plot). All spectra show a negative band, progressively red-shifted in the series 1A9-K(HCl) > 1A9-G(HCl) > 1A9-K(TFA)> 1A9-G(TFA) > 1A9-A(TFA), suggesting a prevalently antiparalel β-conformation [2].

Oriented Circular Dichroism (OCD)

OCD is used to evaluate the conformation and orientation of membrane-active peptides in oriented membrane systems.

The most studied peptides in this fiels are mainly folded in α-helical conformation, and show different OCD spectra when bound to the surface or when inserted perpendicularly or tilted in between the membrane phospholipids. The CD signal indeed depends on the angle between the helix axis and the electric field vector of the circularly polarized light beam, which is perpendicular to the direction of propagation [3]. Little data is reported for β-sheet folded peptides, only comparing the OCD signal to the CD spectral features observed in solution.

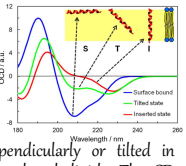



20μg of peptide were mixed with 500μg of DMPG/DMPC 1:3 dissolved in MeOH/$CHCl_3$ 1:1 v/v, deposited on quartz windows and dried for 24h under vacuum. The sample is humidified via the gas phase derived from saturated K_2SO_4 solution, which achieves a relative humidity of ~98%.
The same humidity is ensured by the presence of the K_2SO_4 solution in the cell's reservoir.

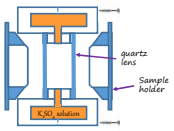



Custom-built cell

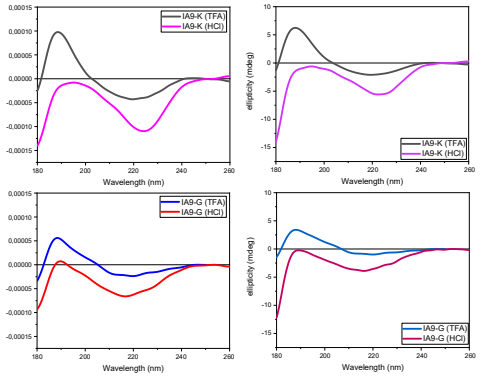

Spectra are reported in g-factor (ellipticity over absorbance) to account for the different thickness of each sample.
The different counterions seem to affect the interaction of the peptides with the membranes.
(TFA)-peptides show a positive band at ~190 nm and a broad negative one at ~220 nm, while in (HCl)-peptides the intensity of the positive band is diminished, and the negative one increases and is red-shifted.

Biological activity

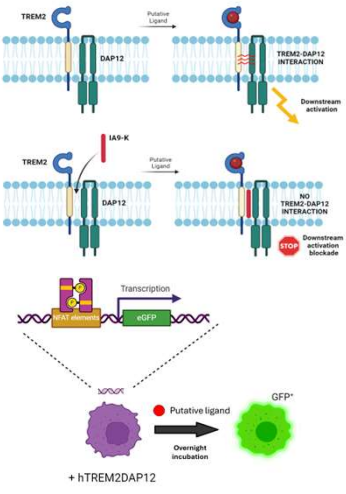

The signaling chain homooligomerization (SCHOOL) strategy aims to block multi-chain receptors in a ligand-independent manner using short peptides [4].
In the figure is reported the scheme of SCHOOL strategy for TREM2. Briefly, a competition for DAP12 binding occurs between the short peptide and the transmembrane portion of TREM2.
IA9-K with DAP12 interaction prevents message transduction in the presence of the putative ligand, causing blockade of downstream signaling. This mechanism appears to have a maximum effectiveness of 50% reduction.

2B4 reporter T cells stably transfected with enhanced green fluorescent protein (eGFP) under consensus sequences of NFAT (transcriptional factor of TREM2 pathway) and human TREM2/DAP12 cDNA has been employed to assay the inhibitory capacity of the synthetic peptides.

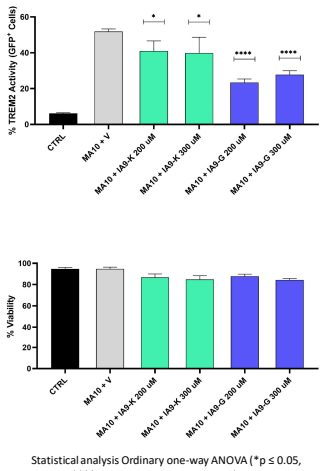

Statistical analysis Ordinary one-way ANOVA (*p ≤ 0.05, **** p ≤ 0.0001 versus MA10 + V), n=2

Different solvent conditions and concentrations have been tested to obtain the optimal result. 1A9-K (TFA) and 1A9-G (TFA) have been dissolved in DMSO/PBS (1:1 v/v) and tested at 200 μM and 300 μM.
Mycolic Acid, a known TREM2 putative ligand [5], has been used to induce receptor activation measured as eGFP+ positive cells by FACS at the concentration of 10 μg/mL (MA10) after overnight incubation.
In this model both 1A9-K and 1A9-G have been able to reduce TREM2 acivity significantly, in particular 1A9-G has shown greater inhibitory effectiveness by reducing the GFP+ population of the 50% compared to vehicle control (MA10 + V). These results are in line with data reported in the literature regarding the *in vivo* experiments.

The cell viability evaluation excluded potential toxic effect induced by peptides treatment. Propidium iodide dye has been used for flowcytometric analysis. No differences have been measured in presence of 1A9-K and 1A9-G compared to CTRL (vehicle).

Future perspectives

CD spectra of 1A9 peptides, adopting a prevalently β-sheet folding in different membrane-like environment, revealed the influence of the counter-ion on peptide conformation. Future investigation will focus on the effect of the different counter-ions on the ability of the peptides to interact with the receptor and their influence on the biological activity.

References

1. Sigalov, A.B. Inhibition of TREM-2 Markedly Suppresses Joint Inflammation and Damage in Experimental Arthritis Int. J. Mol.Sci. **2022**, 23, 8857.
2. Micsonai, A.; Wien, F.; Kernya, L.; Lee, Y.-H.; Goto, Y.; Réfrégiers, M.; Kardos, J., Accurate secondary structure prediction and fold recognition for circular dichroism spectroscopy. **2015**, 112, (24), E3095–E3103.
3. Bürck J, Wadhwani P, Fanghänel S, Ulrich AS. Oriented Circular Dichroism: A Method to Characterize Membrane-Active Peptides in Oriented Lipid Bilayers. Acc Chem Res. **2016** Feb 16;49(2):184–92.
4. Sigalov AB. SCHOOL of nature: ligand-independent immunomodulatory peptides. Drug Discov Today. 2020 Aug;25(8):1298–1306.
5. Iizasa E, Chuma Y, Uematsu T, Kubota M, Kawaguchi H, Umemura M, Toyonaga K, Kiyohara H, Yano I, Colonna M, Sugita M, Matsuzaki G, Yamasaki S, Yoshida H, Hara H. TREM2 is a receptor for non-glycosylated mycolic acids of mycobacteria that limits anti-mycobacterial macrophage activation. Nat Commun. **2021** Apr 16;12(1):2299.

Proceedings of the 37th European Peptide Symposium
Michal Lebl, Editor
European Peptide Society, 2024 *http://doi.org/10.17952/37EPS.2024.P1149*

Synthesis and Characterization of Tumor Targeted Peptide (TTP) Conjugated with Magnetic Nanoparticles for Thermo-ablation

Sima Alvani Alamdari[1], Justyna Fraczyk[1], Joanna Waśko[1], Anita Plazinska[2], Beata Kolesinska[1]

[1]Institute of Organic Chemistry, Faculty of Chemistry, Lodz University of Technology, Zeromskiego 116, 90-924 Lodz, Poland.
[2]Department of Biopharmacy, Faculty of Pharmacy, Medical University of Lublin, Chodźki 4a, 20-093 Lublin, Poland.
Email: sima.alvani-alamdari@dokt.p.lodz.pl

Introduction :

Nanotechnology is transforming various industries by enabling the manipulation of materials at the nanometer scale, leading to breakthroughs in drug delivery, water purification, data management, and the creation of advanced nanoscale materials for healthcare and industrial applications. By leveraging the unique properties of nanometric materials—such as their small size, large surface area, and customizable surfaces—scientists are developing innovative solutions with significant potential, particularly in targeted drug delivery [1-3].

Magnetic nanoparticles (MNPs), especially superparamagnetic iron oxide nanoparticles (SPIONs), have emerged as key players in biomedical research due to their promising applications in cancer treatment and other medical fields. These nanoparticles can be precisely engineered to enhance the delivery of therapeutic agents directly to cancer cells, reducing side effects and improving treatment efficacy.

Peptides are an attractive alternative to antibody-based targeted therapies. Unlike antibodies, peptides are easy to synthesize in large quantities, and their smaller size improves tissue penetration while preventing nonspecific uptake by the reticuloendothelial system. In addition, peptides can be chemically modified to alter affinity, charge, hydrophobicity, stability, and solubility, and can be optimized for in vivo use through modification. Importantly, peptides can exhibit receptor affinity similar to antibodies. Tumor-targeting peptides (TTPs) are an effective alternative for selectively targeting specific tumor receptors. Compared to antibodies, TTPs have better tumor/tissue penetration and are easy to synthesize and chemically modify to improve stability and pharmacokinetics. Peptides can be used for targeted drug delivery. They can be designed to have the ability to destroy cancer cells and inhibit tumor growth. Examples of TPPs are [4]: RGD-4C, iRGD, NGR, which act on: B16 melanoma, MDA-MB-435, HL-60, MMTV-PyMT, KRIB, C8161, K14-HPV16/E2 RIP1-Tag2, K14-HPV16.

This project focuses on synthesizing and characterizing novel hybrid nanomaterials (MNP-CPP-TM-drug) that combine MNPs with active anti-cancer compounds (EGF fragments connected with cytostatic). The goal is to develop a multifunctional nanostructure capable of not only delivering drugs with high specificity but also enabling targeted thermo-ablation for enhanced cancer.

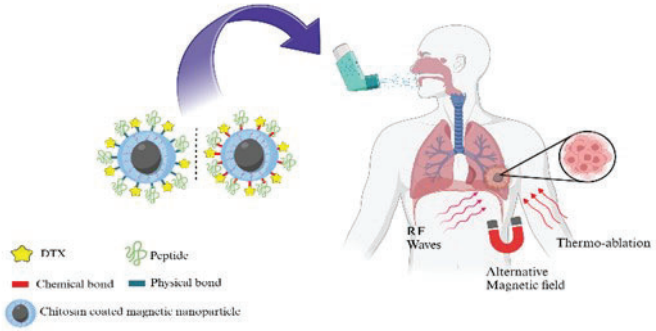

http://doi.org/10.17952/37EPS.2024.P1149

Methodology :

In the first stage of the research, magnetic nanoparticles (size: 14-29 nm, 99.5%) were coated with chitosan (low molecular weight) physically and chemically modified by different cross-linkers. Chitosan coating is biodegradable and helps attach other elements, such as anticancer drugs and targeting peptides by cross-linker. Targeting molecules were EGF fragments capable of interacting with the EGF receptor (EGFR). Docetaxel was used as an anticancer drug in this research.

EGF fragments in this research were prepared by solid-phase peptide synthesis (SPPS) with Fmoc/tBut strategy using triazine coupling reagent (4-(4,6-dimethoxy-1,3,5-triazin-2-yl) -4-methylmorpholinium toluene-4-sulfonate (DMT/NMM/TosO-))[5]. All EGF fragments were characterized by a high ability to interact with EGFR (microscale thermophoresis (MST)) [6].

Results and discussions :

Nanoparticles were characterized with SEM, DLS, FTIR, and TGA. Additionally, the peptides were characterized by LC-MS.

Table 1. LC-MS analysis of EGF fragments.

peptide	Sequence	Molecular wight	M/Z	HPLC Purity%
EGF fragment	^{10}HDGYCL^{15}	706.263	$[M+H]^{1+}$=707.2867 $[M+2H]^{2+}$=354.1477	96%
EGF fragment	^{43}QYRDL^{47}	693.334	$[M+H]^{1+}$=694.3590 $[M+2H]^{2+}$=347.6831	90%

Comparing coated magnetic nanoparticles with different cross-linkers: Dynamic light scattering (DLS) measurement was used to compare the sizes of MNPs (table 2), and simple Acid-base titration was used to evaluate the number of primary amine groups on the surface of MNPs (table 3).

Table 2. DLS measurement of MNPs (pH=7).

No.	MNPs	Size (nm)
1	Fe_3O_4@CS(300CPS)/TPP	70-71
2	Fe_3O_4@CS(30CPS)/TPP	55
3	Fe_3O_4@CS/Citric acid	90-130
4	Fe_3O_4@CS/Squaric acid	105
5	Fe_3O_4@CS/glutaraldehyde	253-263

Table 3. Result from Acid-base titration method.

sample	Cross-linker	$V_{ave./mL}$	NH_2 group (mol /mg)
1	TPP	1.73	0.293
2	Citric Acid	1.96	0.383
3	Squaric acid	1.85	0.272
4	Glutaraldehyde	1.63	0.065

Magnetic nanoparticles were also characterized by scanning electron microscopy (SEM), thermogravimetric analysis (TGA), and Fourier transform infrared spectroscopy (FT-IR) (Figure 1).

http://doi.org/10.17952/37EPS.2024.P1149

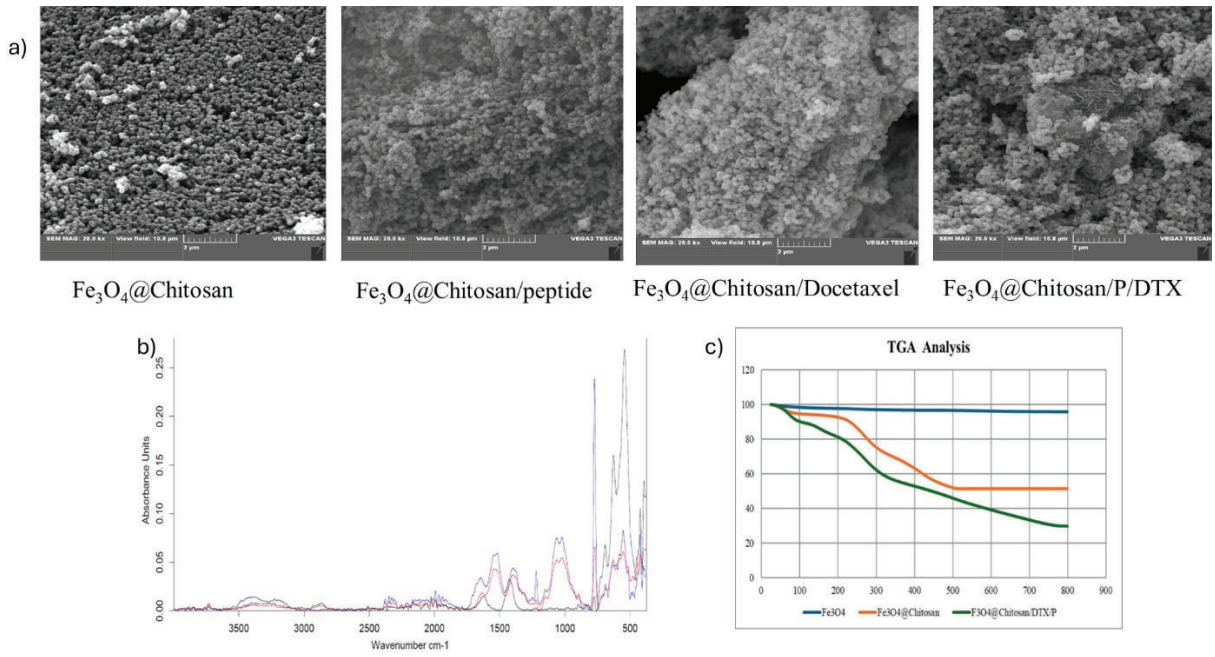

Figure 1. a) SEM images of chitosan-coated magnetic nanoparticles, b) FT-IR spectra of 1)Fe3O4, 2)Fe3O4@Chitosan, 3)Fe3O4@Chitosan/DTX/P, and c) TGA spectra of synthesized nanoparticles

Conclusion :

In this research, an effective method for coating magnetic nanoparticles with chitosan was developed. Tripolyphosphate (TPP) was chosen as the optimal cross-linker for synthesizing these coated MNPs. In the second step, an anticancer drug (DTX) and a peptide derived from EGF fragments were attached to the MNPs both physically and chemically. The thermo-ablation properties of these nanoparticles were also studied, and they are currently in their preliminary phase of research.

The nanoparticles were characterized using SEM, DLS, FTIR, and TGA. Additionally, peptides were characterized by LC-MS. The biological activity of the tumor-targeting peptide conjugated with magnetic nanoparticles and the cytostatic agent was confirmed.

Acknowledgments:

Research reported in this publication is supported by the "FU²N - Fund for Improving the Skills of Young Scientists" program, internal grants were awarded in the discipline of Chemical Sciences under grant No. 503-3-32-4-1 from the Lodz University of Technology.

References :

[1] Zhou, L. et al., J. Mater. Chem. 2011,21, 9, 2823-40.
[2] Ziegler-Borowska, M. et al., Catalysts. 2017, 7, 1, 26.
[3] Azarmi, S.et al., Adv. Drug Deliv. Rev. 2008, 60, 8, 863-75.
[4] Simón-Gracia, L. et al., Molecules, 2018, 23, 1190.
[4] Kamiński, Z.J. et al., J. Am. Chem. Soc. 2005, 127, 48, 16912-20.
[5] Czerczak-Kwiatkowska, K. et al. Int. J. Mol. Sci. 2024, 25, 3, 1470.

Proceedings of the 37th European Peptide Symposium
Michal Lebl, Editor
European Peptide Society, 2024 *http://doi.org/10.17952/37EPS.2024.P1150*

Synthesis and characterization of phenethyl isothiocyanate conjugated with magnetic nanoparticles modified by tumor targeting peptide (TTP) using in cancer treatment

Sima Alvani Alamdari[1], Łukasz Janczewski[1], Justyna Fraczyk[1]
[1]*Institute of Organic Chemistry, Faculty of Chemistry, Lodz University of Technology, Zeromskiego 116, 90-924 Lodz, Poland.*
Email: sima.alvani-alamdari@dokt.p.lodz.pl

Introduction:

Many isothiocyanates, both natural and synthetic, show anticarcinogenic activity because they decrease activation of carcinogens and increase their detoxification. They exhibit anti-tumor activity. [1].

One of the greatest challenges in cancer therapy is to selectively deliver chemotherapeutics to the cancer cells, thus achieving therapeutic efficacy while limiting damage to healthy tissues. The effective strategy of targeted drug delivery to tumor tissues is based on cellular heterogeneity which is characteristic of all organs and tissues including pathological tissues such as tumors. One of the biological properties of tumor cells is the expression or overexpression of a unique set of proteins or receptors on the cell surface. Activation of these receptors often results in deregulated signaling, increased cell proliferation and decreased cell apoptosis. Selective targeting of these tumor-specific receptors provides the opportunity for targeted drug delivery. Several types of tumor targeting ligands have been developed including antibodies, antibody fragments, polypeptides, small molecules, and others [2]. Tumor-targeting peptides (TTPs, targeting peptide (TM), homing peptide) are an efficient alternative for selective targeting of tumor specific receptors. Compared to antibodies, tumor-targeting peptides have better tumor/tissue penetration and are easy to synthesize and modify chemically to improve stability and pharmacokinetics. The first generation tumor homing peptides, RGD and NGR, have entered clinical trials. As a molecular targets of NSCLC, have been investigated: epidermal growth factor receptor (EGFR), Kirsten rat sarcoma viral oncogene homolog (KRAS), anaplastic lymphoma kinase (ALK), human epidermal growth factor receptor 2 (HER2) [3]. EGFR, one of these molecular targets with a high frequency of mutation, is a transmembrane receptor tyrosine kinase involved in the signaling pathways regulating cell proliferation, apoptosis, angiogenesis, and invasion [4].

In this study, we report the synthesis and characterization of phenethyl isothiocyanate (PEITC) conjugated onto the surface of magnetic nanoparticles (MNPs) modified by a tumor-targeting peptide (TTP) for enhanced cancer treatment and to facilitate targeted drug delivery [5]. PEITC, , which is one of the most studied ITCs, shows anti-cancer and chemopreventive properties and inhibits the growth of cancer cells by inducing apoptosis and inhibiting the cell cycle, making it an attractive candidate for cancer therapy. Additionally, TTP was incorporated to improve specificity towards cancer cells.

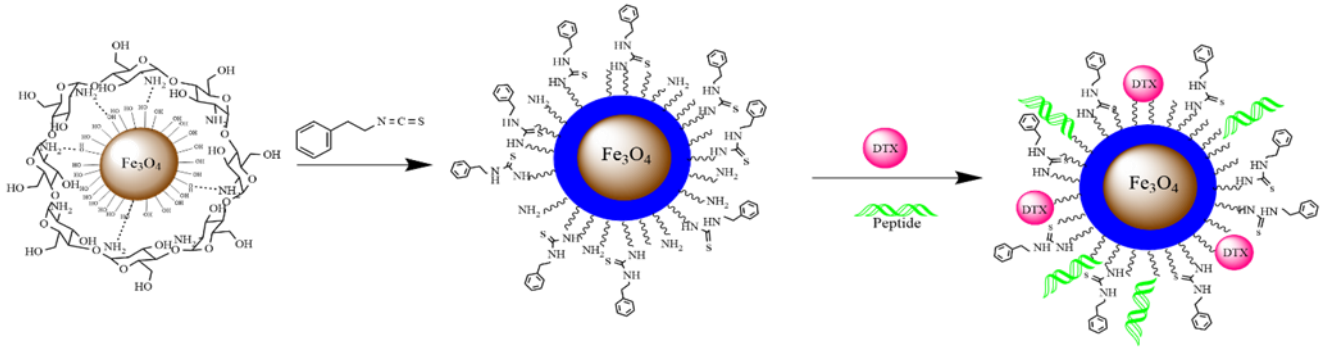

 http://doi.org/10.17952/37EPS.2024.P1150

Moreover, MNPs offer several advantages such as biocompatibility, ease of functionalization, and the ability to be guided to specific sites using an external magnetic field. By conjugating PEITC onto MNPs, we aimed to enhance its delivery to cancer cells while minimizing off-target effects.

Methodology:

In this synthesis method, phenethyl isothiocyanate (PEITC) is chemically attached to the chitosan (low molecular weight) using the method described by Bae et al.'s method [6]. Then magnetic nanoparticles (size: 14-29 nm, 99.5%) were coated by phenethyl isothiocyanate conjugated chitosan. Following PEITC conjugation, a tumor-targeting peptide (TTP) is incorporated onto the surface of the nanoparticles to impart specificity to cancer cells. TTP were EGF fragments capable of interacting with the EGF receptor (EGFR) [7]. Additionally, Docetaxel was used as an anti-cancer drug.

EGF fragments in this research were prepared by solid-phase peptide synthesis (SPPS) with Fmoc/t-Bu strategy using triazine coupling reagent (4-(4,6-dimethoxy-1,3,5-triazin-2-yl) -4-methylmorpholinium toluene-4-sulfonate (DMT/NMM/$TosO^-$)) [8].

Results and discussions :

Nanoparticles were characterized with TEM, DLS, FTIR, and TGA, and the structure of chitosan modified with PEITC was confirmed with NMR and FT-IR (Figures 1 and 2). Additionally, the peptides were characterized by LC-MS.

Characterization of modified chitosan :

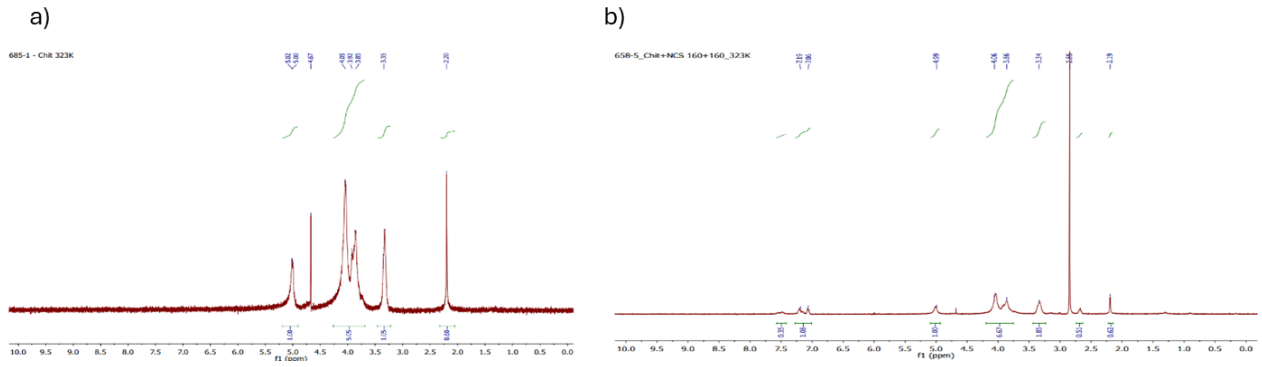

Fig. 1 ^{1} H NMR NMR (700 MHz, D_2O) spectra's of a) Free chitosan (CS) and b) Modified chitosan with PEITC.

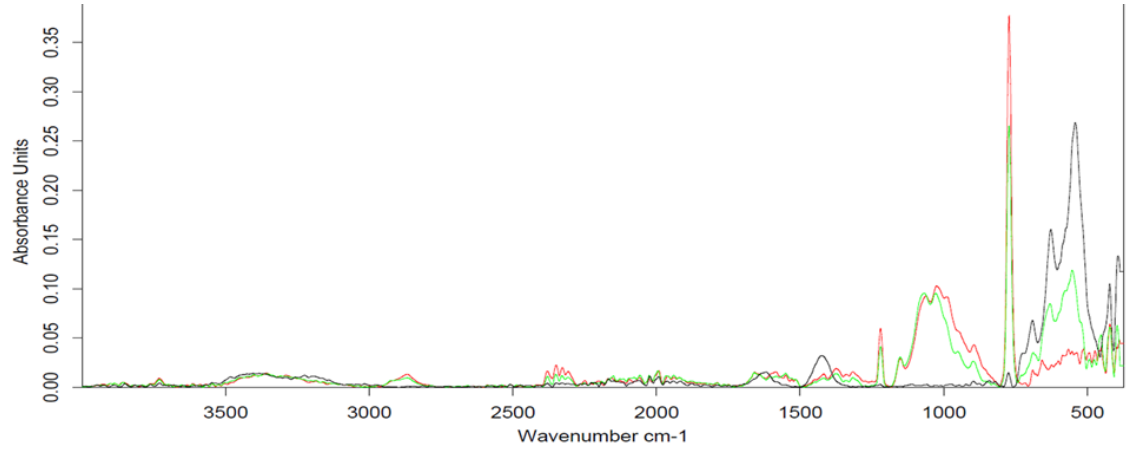

Fig. 2 FT-IR spectra's of a) Fe_3O_4, b) Chitosan(CS), and c) Fe_3O_4@CS/PEITC.

Proceedings of the 37th European Peptide Symposium
Michal Lebl, Editor
European Peptide Society, 2024
http://doi.org/10.17952/37EPS.2024.P1150

Characterization of peptides by LC-MS :

Table 1. LC-MS analysis of EGF fragments.

Peptide	Sequence	Molecular weight [g/mol]	m/z	HPLC Purity [%]
EGF fragment	^{10}HDGYCL^{15}	706.263	$[M+H]^{1+}$=707.2867 $[M+2H]^{2+}$=354.1477	96%
EGF fragment	^{43}QYRDL^{47}	693.334	$[M+H]^{1+}$=694.3590 $[M+2H]^{2+}$=347.6831	90%

Characterization of chitosan-coated MNPs modified with peptide and anti-cancer drug:

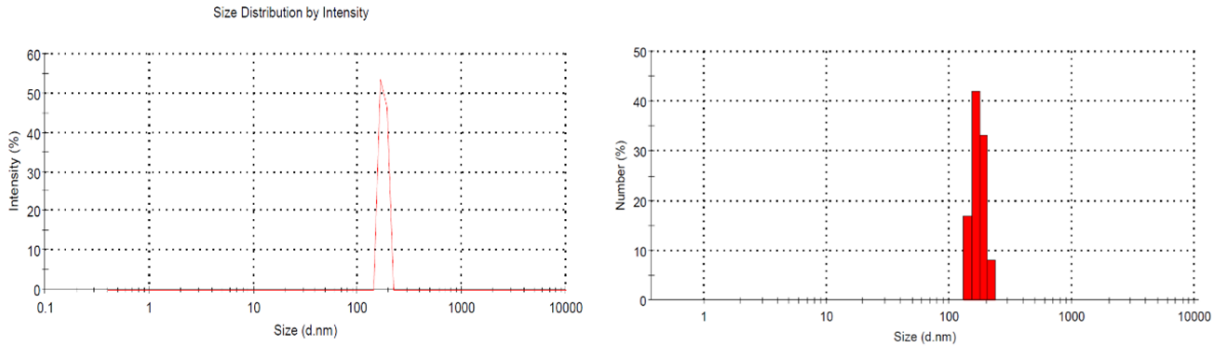

Fig. 3 DLS spectra of Fe_3O_4@chitosan/PEITC (Ave. size: 176 nm).

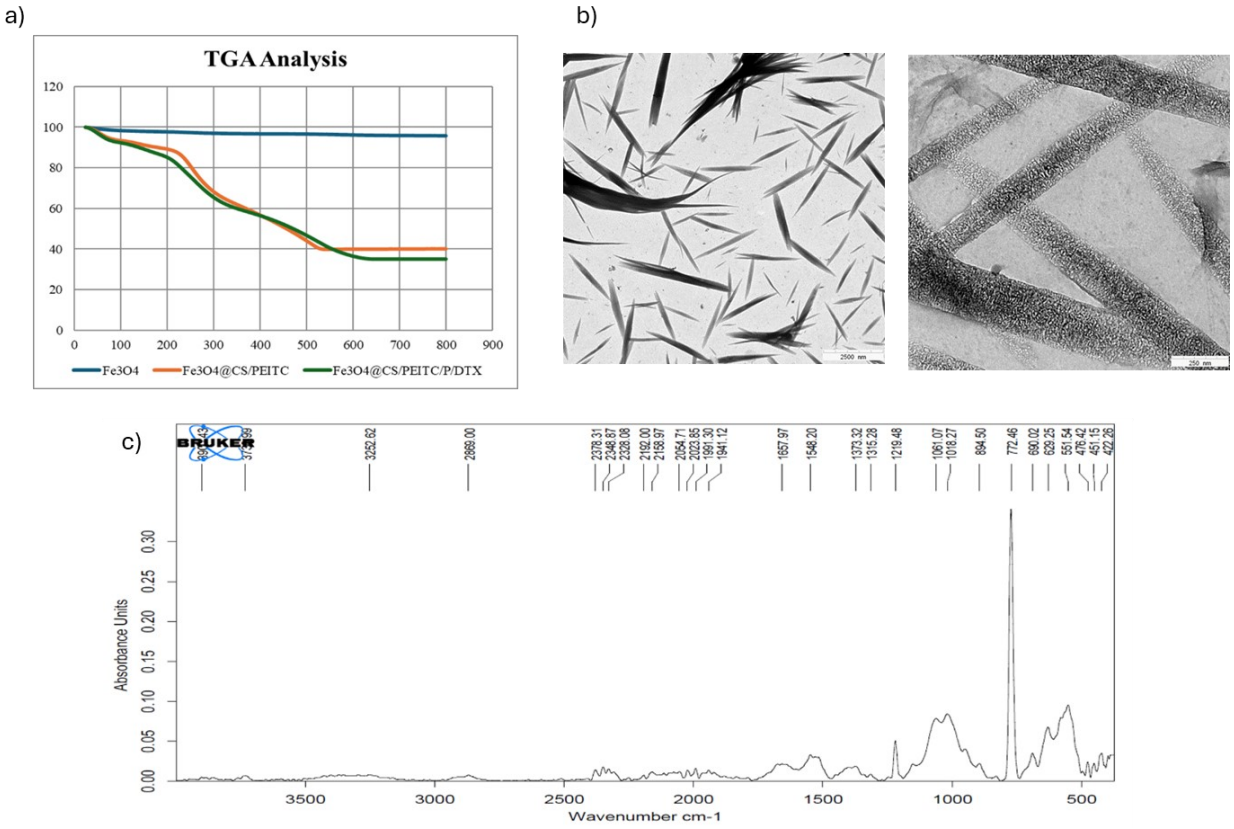

Fig. 4 a) TGA spectra of synthesized nanoparticles, b) TEM images of Fe_3O_4@chitosan/PEITC, and c) FT-IR spectra of Fe_3O_4@chitosan/PEITC/DTX/Peptide.

 http://doi.org/10.17952/37EPS.2024.P1150

Conclusion:

In this project, an effective method for synthesizing phenethyl isothiocyanate conjugated with magnetic nanoparticles was developed. In the second step, an anticancer drug (DTX) and a peptide derived from EGF fragments were attached to the MNPs both physically and chemically interaction. The nanoparticles were characterized using TEM, NMR, DLS, FTIR, and TGA. Additionally, peptides were characterized by LC-MS, and their structures were confirmed. The interaction between peptides and MNPs will be studied.

References:

[1] Wu, X. et al., *Acta Pharmacol. Sin*. 2009. *30*, 501–512.
[2] Raucher, D. *Curr. Opin. Pharmacol*. 2019, *47*, 14-19.
[3] Cheng, Z et al., *BMC Med. Imaging* 2017, *17*, 5.
[4] Nishino, M.et al., *Radiology*, 2014, *271*, 6-27.
[5] Laurent, S. et al., *Chem. Rev*. 2008, *108*, 2064-2110.
[6] Bae, I. et al., *Int. J. Mol. Sci.* 2022, *23*, 13802.
[7] Czerczak-Kwiatkowska, K. et al., *Int. J. Mol. Sci*. 2024, 25, 3, 1470.
[8] Kamiński, Z.J. et al., *J. Am. Chem. Soc*. 2005, 127, 48, 16912-20.

https://doi.org/10.17952/37EPS.2024.P1151

Analysis of Mannan (polymannose) Conjugated with 35-55 Immunodominant Epitope of Myelin Oligodendrocyte Glycoprotein for the Treatment of Multiple Sclerosis

Carmen Simal[1], Areti Gkika[1], Maria-Eleni Androutsou[2], Georgia Biniari[1], Alexios Aletras[1], Theodore Tselios[1]

[1]Department of Chemistry, University of Patras, 26504 Rion Patras, Greece.

[2]Vianex S.A., Varibobi 8, Nea Erythrea, 14671 Athens, Greece.

Scan me

Introduction

Multiple sclerosis (MS) is a prevalent autoimmune disease characterised by the destruction of myelin, leading to paralysis and severe health complications. The immunodominant epitope 35-55 of myelin oligodendrocyte glycoprotein (MOG_{35-55}) is a crucial autoantigen implicated in the progression of MS. Numerous studies have focused on the use of mannan polysaccharide (derived from Saccharomyces cerevisiae) conjugated with the MOG_{35-55} epitope to induce antigen-specific immune tolerance against the clinical symptoms of chronic experimental autoimmune encephalomyelitis (EAE), an animal model of MS [1,2]. In this context, we present a promising approach to MS immunotherapy where the MOG_{35-55} peptide is conjugated to mannan *via* Schiff base formation between the aldehydes of oxidised mannan and the amino groups of the $(LysGly)_5$ bridge located at the *N*-terminus of the peptide [3]. To confirm the integrity of the conjugation reaction and investigate any potential alterations in the peptide throughout the different stages of mannan-MOG_{35-55} conjugate production, a competitive enzyme-linked immunosorbent assay (ELISA) was developed. This assay was used in combination with sodium dodecyl sulfate-polyacrylamide gel electrophoresis (SDS-PAGE) and a colorimetric assay. **These mannan-MOG_{35-55} conjugates are currently undergoing a Phase I clinical trial conducted by a Greek pharmaceutical company.**

Experimental

Synthesis and conjugation of MOG_{35-55} to mannan

The $[(LysGly)_5MOG_{35-55}]$ was synthesised on CLTR-Cl resin using the Fmoc/tBu methodology. Purification and identification of the peptide were achieved by semi-preparative RP-HPLC and ESI-MS, respectively. Mannan (poly-mannose from Saccharomyces cerevisiae) was oxidised to poly-aldehyde using sodium periodate ($NaIO_4$) and purified by size exclusion chromatography using a Sephadex G-25 Medium column. The $[(LysGly)_5MOG_{35-55}]$ peptide was then mixed with oxidised mannan and incubated for 48 h at room temperature. Conjugation was achieved through the formation of a Schiff base between the aldehydes of the oxidised mannan and the amines of Lys residues in the $(LysGly)_5$ linker. The completeness of the reaction was confirmed by sodium dodecyl sulfate-polyacrylamide gel electrophoresis (SDS-PAGE).

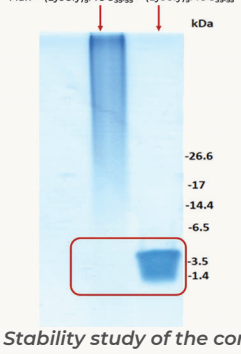

Fig.1: Confirmation of the conjugation of oxidised mannan with $(LysGly)_5MOG_{35-55}$ was achieved by SDS-PAGE in a 16.5% acrylamide gel and Coomassie Brilliant Blue staining. The conjugate of oxidised mannan with the peptide analogue $(LysGly)_5MOG_{35-55}$ appears as a diffuse band ranging from 20-200 kDa due to the variability in the number of mannose molecules in the main and side chains of the polysaccharide, leading to differentiation in peptide-mannan conjugation. The band with a molecular weight of 3.0-3.5 kDa corresponds to the peptide $(LysGly)_5MOG_{35-55}$. **In the lane containing the conjugate, no band corresponding to the free peptide (indicated by the red square) is observed, indicating that the conjugation is successful.**

Stability study of the conjugate stored at -20 °C ± 2 °C

A competitive ELISA was developed to detect the MOG_{35-55} peptide, even when conjugated with mannan polysaccharide. This method can identify alterations in the MOG_{35-55} epitope that may occur during storage at -20 °C ± 2 °C for at least three years.

Concentration of peptide in the conjugate (pmol/mL)	Log (C)	Average %Inhibition	Average %Inhibition
1600	3.20	54.96	72.14
800	2.90	49.61	57.04
400	2.60	44.84	36.11
200	2.30	33.68	24.60
100	2.00	30.69	17.91
50	1.70	24.64	0.07

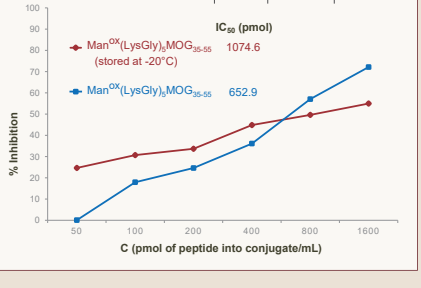

Fig.2: Inhibition curves for conjugate Man^{ox}-$(LysGly)_5MOG_{35-55}$ using polyclonal antibodies against MOG_{36-55} at six concentration levels of the peptide (50–1600 pmol/mL). Each data point represents the mean value of a triplicate measurement ± SD. The stored conjugate showed increased recognition at low concentrations (50–400 pmol/mL) or reduced recognition at high concentrations (800–1600 pmol/mL) by the antibody. The reduced range of inhibition percentage indicates decreased recognition of the epitope by the antibody. This is likely due to potential alterations of the peptide or conformational changes that hinder the antibody's ability to recognize the epitope.

Study of the oxidative conditions and parameters for mannan oxidation

The oxidation of mannan was studied to optimize the conditions, specifically reaction time and the amount of oxidizing agent, using the reagent 2,4-dinitrophenylhydrazine (DNPH). The absorbance of the resulting yellow-coloured product was measured at 349 nm.

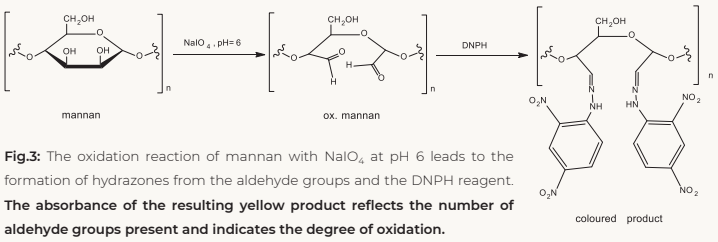

Fig.3: The oxidation reaction of mannan with $NaIO_4$ at pH 6 leads to the formation of hydrazones from the aldehyde groups and the DNPH reagent. **The absorbance of the resulting yellow product reflects the number of aldehyde groups present and indicates the degree of oxidation.**

Oxidizing Agent Monitoring

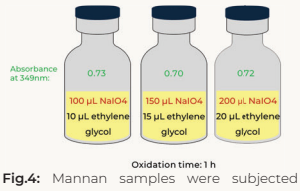

Fig.4: Mannan samples were subjected to an oxidative reaction for 1 h using three different amounts of $NaIO_4$. The **absorbances measured for these samples indicated that all three amounts of the oxidizing agent resulted in the same degree of oxidation.**

Reaction Time Monitoring

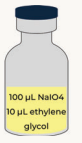

Oxidation time	Absorbance at 349nm
0 min	0.48
5 min	0.76
30 min	0.83
1 h	0.78
1.5 h	0.76
2 h	0.75

Fig.5: Oxidation reaction of mannan samples using a constant amount of $NaIO_4$ was conducted over 6 different reaction times. **The absorbances of these samples showed that the reaction was completed within 5 min.**

Conclusions

The Man^{ox}-$(LysGly)_5MOG_{35-55}$ conjugate is of significant interest in the fight against multiple sclerosis (MS) and is currently in phase I clinical trials. The developed methodology is both sensitive and reliable, making it suitable for monitoring peptide mutations of the conjugate during synthesis and storage. Furthermore, these methods could be applied not only to mannan conjugates but also to the analysis and identification of various bioactive glycoproteins.

References

[1] Dagkonaki, A. *et al. Front. Immunol.*, **2022**, 13: 972003. doi:10.3389/fimmu.2022.972003.

[2] Androutsou, M.E. *et al. Int. J. Mol. Sci.*, **2020**, 21(20):7566. doi: 10.3390/ijms21207566.

[3] Gkika, A. *et al. J Pept Sci.*, **2023**, 29(10): e3493. doi: 10.1002/psc.3493.

Acknowledgements

This research has been co-financed by the EU and Greek national funds through the Operational Program Competitiveness, Entrepreneurship and Innovation, under the call RESEARCH-CREATE-INNOVATE (project code: T1EDK-01859). We would like to thank Vianex S.A. pharmaceutical company for financial support of the study for MS treatment.

Contact details: Theodore Tselios
Department of Chemistry,
University of Patras, Rion, Greece.
ttselios@upatras.gr

Co-financed by Greece and the European Union

Chemists Don't Want You to Know This Simple Trick!

A Nanomolar Potency Macrocyclic Peptide Inhibitor of SARS-CoV-2 Spike through Deep Mutational Scanning

Antonius (Twan) J.P. Hopstaken[1], Oliver J. Debski-Antoniak[2], Preeti Hooda[2], Daniel L. Hurdiss[2], Seino A.K. Jongkees[1]
[1] Vrije Universiteit Amsterdam, Netherlands, [2] Utrecht University, Netherlands
https://doi.org/10.17952/37EPS.2024.P1152

Our previous mRNA display hit inhibits SARS-CoV-2 and related sarbecoviruses through binding of a conserved pocket deep within the spike protein [1]

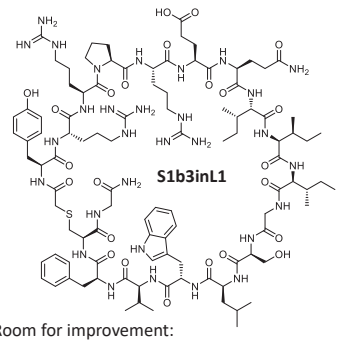

Room for improvement:
- **Potency** of virus infection inhibition
- **Solubility**
- Little information about tolerated mutations available from the sequencing data

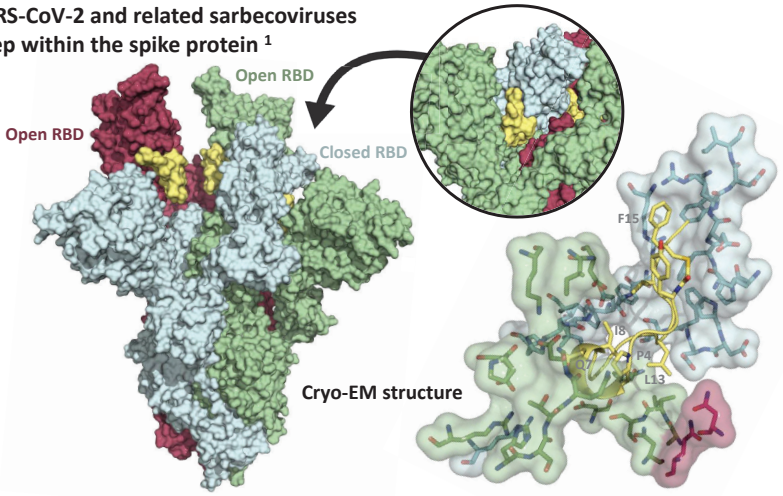

Variants of concern pseudovirus neutralization

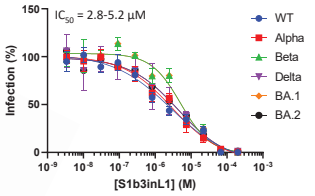

Sarbecovirus pseudovirus neutralization

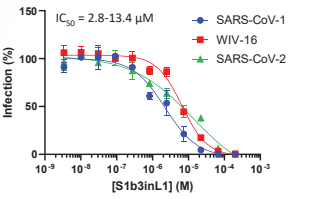

Deep mutational scan setup

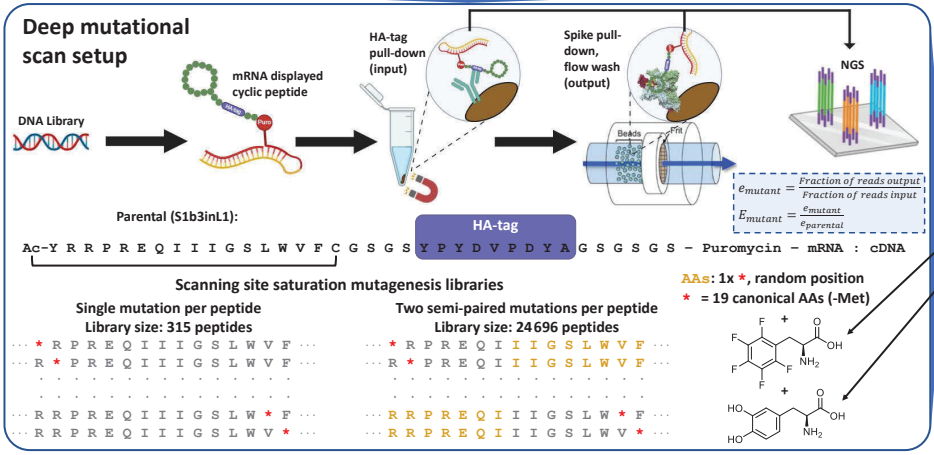

Scanning site saturation mutagenesis libraries

Single mutation per peptide
Library size: 315 peptides

Two semi-paired mutations per peptide
Library size: 24696 peptides

AAs: 1x *, random position
* = 19 canonical AAs (-Met)

Enrichment scores

Single mutation library

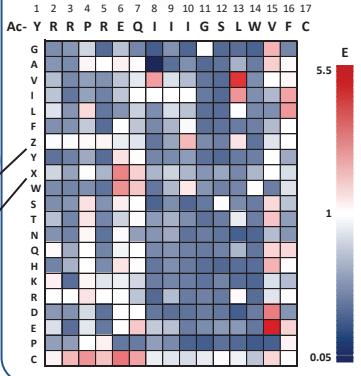

Semi-paired mutation library
Top 1000 E-scores

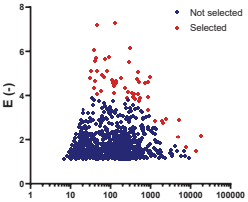

- **Positions 3, 9, 11, 12, 14** completely **conserved**
- High E-scores of cysteine mutations likely an artifact caused by dimerization, since cysteines were not enriched at similar positions in the larger library

Purified peptides all show improved potency and generally better solubility

SARS-CoV-2 pseudovirus neutralization

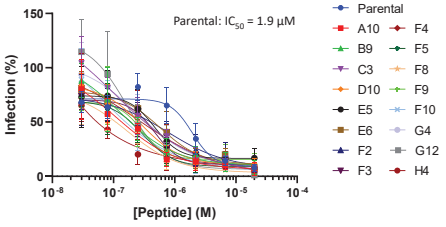

Nephelometry

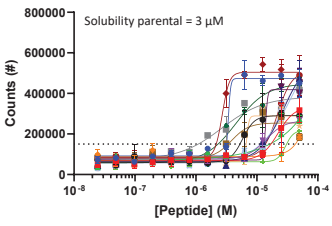

- **H04** is the **most potent hit**, combining 5 mutations that by themselves increase potency (Q7E, I8V, L13V, V15T, F16L) and 1 mutation that is detrimental as single mutation (P4S)
- SPPS of H4-P4S for further testing

- All peptides show **improved solubility** compared to parental **except** those with a mutation introducing another **tryptophan**
- Nephelometry is an extremely sensitive method for the detection of small particles, no turbidity could be observed by eye for any of the peptides even at 50 µM

Effects of single mutations on potency are additive when combined

- **96 peptides** were selected for **SPPS** based on favorable **E-scores** and predicted improved **solubility**
  - **25** from the single mutation libary + **6** shorter cycle peptides
  - **51** double or triple mutants from the larger library
  - **13** peptides with increasing amount of mutations
- **Crude peptides** tested for **potency**

SARS-CoV-2 pseudovirus neutralization

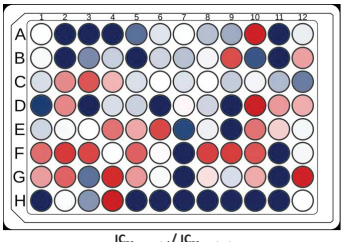

A01	R2K	C02	R2K, L13V	E03	E6X, V15A	G04	P4A, I8V, F16P
A02	P4L	C03	P4A, V15T	E04	E6X, V15T	G05	P4S, I8V, F16P
A03	P4S	C04	P4D, I8V	E05	E6N, I8V	G06	P4S, I8V, V15H
A04	R5Z	C05	P4D, V15T	E06	E6N, V15T	G07	E6X, I10Z, V15D
A05	E6X	C06	P4E, V15T	E07	E6S, V15S	G08	E6W, Q7X, V15E
A06	E6W	C07	P4K, V15T	E08	E6T, V15T	G09	I8V, L13V, V15G
A07	Q7E	C08	P4L, I8V	E09	E6W, I10Z	G10	L13V, V15E, F16L
A08	Q7X	C09	P4L, V15A	E10	E6W, L13V	G11	R5Z, I8V, L13V, V15E
A09	Q7W	C10	P4N, I8V	E11	E6W, V15A	G12	P4L, E6W, I8V, L13V, V15E
A10	I8V	C11	P4N, V15T	E12	E6Y, F16P	H01	P4S, E6X, I8V, I10Z, V15T
A11	I10Z	C12	P4R, V15T	F01	E6Y, V15T	H02	E6X, Q7E, I8V, V15E, F16Q
A12	L13I	D01	P4S, F16P	F02	Q7D, I8V	H03	P4S, Q7E, I8V, L13V, V15D, F16E
B01	L13V	D02	P4S, I8V	F03	Q7L, V15E		
B02	L13Z	D03	P4S, V15Q	F04	Q7W, L13V	H04	P4S, Q7E, I8V, L13V, V15T, F16L
B03	V15D	D04	P4T, V14A	F05	Q7W, V15E		
B04	V15E	D05	Parental	F06	Q7W, V15Q	H05	P4L, E6X, Q7W, I8V, I10Z, L13V, V15E, F16L
B05	V15Q	D06	P4T, V15Q	F07	I8V, I10Z		
B06	V15H	D07	P4T, V15T	F08	I8V, L13V	H06	R2K, P4L, R5P, E6X, Q7W, I8V, I10Z, L13V, V15E, F16L
B07	V15Q	D08	P4V, V15T	F09	I8V, V15E		
B08	V15S	D09	P4Z, V15T	F10	I8V, V15Q	H07	V15C, del16-17
B09	V15T	D10	R5P, V15T	F11	I10Z, F16L	H08	Q7C, C17A
B10	F16E	D11	R5V, V15T	F12	L13I, F16L	H09	E6C, C17A
B11	F16I	D12	E6H, V15T	G01	L13V, F16L	H10	R5C, C17A
B12	F16L	E01	E6X, F16P	G02	L13V, V15E	H11	P4C, C17A
C01	F16Q	E02	E6X, L13V	G03	V15T, F16E	H12	R3C, C17A

- **I8V**, **V15T** and **F16L** result in the **highest increase** in **potency** (with I8V > V15T > F16L)
- **No paired effects** observed for double or triple mutants, effect of single mutations additive when combined

Mutant peptides maintain activity across related sarbecoviruses

Pseudovirus neutralization

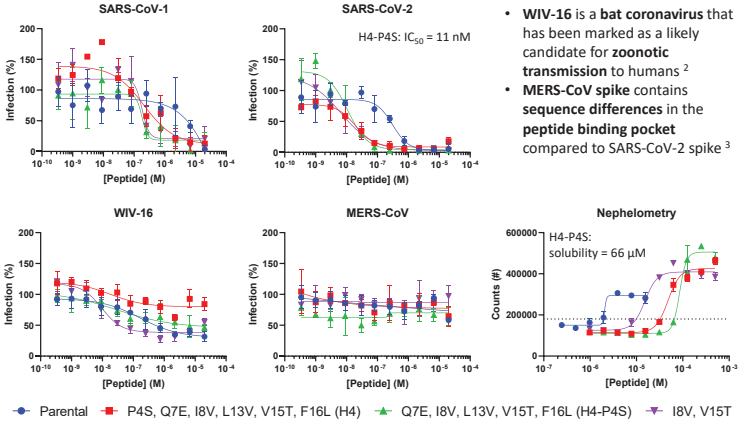

- **WIV-16** is a **bat coronavirus** that has been marked as a likely candidate for **zoonotic transmission** to humans [2]
- **MERS-CoV spike** contains **sequence differences** in the **peptide binding pocket** compared to SARS-CoV-2 spike [3]

Summary

- We found multiple **point mutations** that **improved** the **potency** with which our peptide **inhibits SARS-CoV-2** pseudovirus **infection**, most notably **I8V** and **V15T**
- When mutations were combined the **effect** on **potency** was **additive**
- Increase in potency went hand in hand with **increase** in **solubility**, likely because of the focus on mutations to soluble resiudes in the selection of the first set of 96 peptides
- A small set of our most promising hits showed **broad activity**, targeting **closely related coronaviruses** as well

Outlook

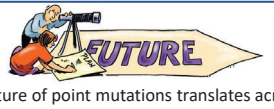

- **Potency** tests on **actual viruses**
- Further improve **solubility** of peptides
- For future deep mutational scans: see if additive nature of point mutations translates across all peptides / targets
- If so, a logical workflow would be: synthesize all peptides with point mutations that are tolereated in the deep mutational scan, then test for a metric and combine the best mutations

References

1. Thijssen, V. et al. A broad-spectrum macrocyclic peptide inhibitor of the SARS-CoV-2 spike protein. Proceedings of the National Academy of Sciences 120, e2303292120 (2023).
2. Yang, X.-L. et al. Isolation and Characterization of a Novel Bat Coronavirus Closely Related to the Direct Progenitor of Severe Acute Respiratory Syndrome Coronavirus. Journal of Virology 90, 3253–3256 (2016).
3. Hatmal, M. M. et al. Comprehensive Structural and Molecular Comparison of Spike Proteins of SARS-CoV-2, SARS-CoV and MERS-CoV, and Their Interactions with ACE2. Cells 9, 2638 (2020).

Intelligent wound dressing with antimicrobial properties

Sebastian Kersting[1], Sophia Ohnesorg[1], Markus von Nickisch-Rosenegk[1]

[1] Fraunhofer Institute for Cell Therapy and Immunology, Branch Bioanalytics and Bioprocesses IZI-BB, Am Muehlenberg 13, D-14476 Potsdam, Germany

https://doi.org/10.17952/37EPS.2024.P1153

Fraunhofer IZI-BB

Fraunhofer Institute for Cell Therapy and Immunology, Branch Bioanalytics and Bioprocesses IZI-BB

Poorly healing wounds such as the so-called "diabetic foot" are often treated inadequately and unspecifically. The KISMADI project aims to create an intelligent wound dressing with additional antimicrobial properties. In addition to the continuous sensor-based wound monitoring and AI-supported digital feedback, an antimicrobial function in the wound dressing is achieved using antimicrobial peptides (AMPs)

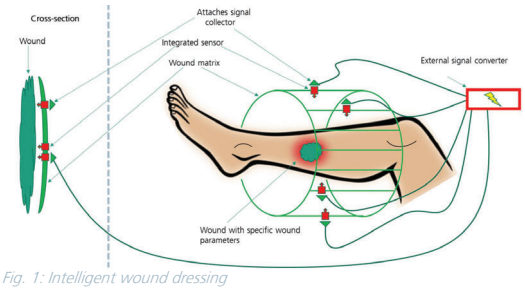

Fig. 1: Intelligent wound dressing

Selection of antimicrobial peptides

In the project, various natural or naturally derived peptides as well as sequence-optimized short peptides were selected and subsequently evaluated based on their effect on relevant resistant bacterial and fungal pathogens (e.g. MRSA, *Pseudomonas aeruginosa, Candida auris*).

Rational designed AMPs

Rational designed, artificial AMPs with biocompatible properties were developed. Important structural motifs were identified and optimized peptide sequences were generated. These peptides showed improved antimicrobial activity towards important bacterial pathogens in comparison with naturally occurring AMPs. At the same time, negative cytotoxic or cytostatic effects were evaded. The generation of a deletion and substitution library revealed the minimal sequence requirements and therefore reduced manufacturing costs. These optimized artificial antimicrobial peptides are suitable as therapeutic agents and may be used as templates for the development of new antimicrobial peptides with unique secondary structures.

Surface immobilization strategies

After activating the base material for the wound dressing (silica gel fiber fleece from Fraunhofer ISC), various covalent chemical coupling methods and linker systems were utilized. A selection was made based on the optimal density of peptide and mode of activity of the systems.

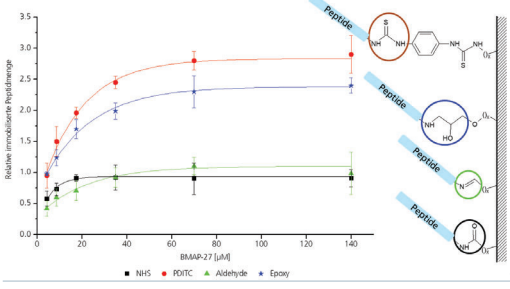

Fig. 2 Example for BMAP-27 based antimicrobial surface coating. Different immobilization strategies lead to differences in surface saturation and activity. Optimization of threshold concentration with lowest amount of peptide.

Characterization of surface couples AMPs

Rapid and efficient screening procedures have been established that allow for the identification and investigating of biologically active peptides for a specific application or to maintain the biocidal activity in an immobilized state. Suitable AMPs that exhibit high antimicrobial activity against disease-specific pathogens but low cytotoxicity are to be preferred for certain applications. Minimal inhibitory concentrations (MIC) against several gram-negative and gram-positive bacterial strains were examined. The membrane disruption properties of AMPs towards the outer and inner membrane were evaluated using a genetically modified bacterial strain.

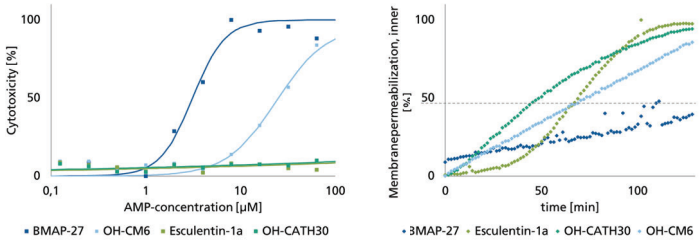

Fig. 3 Percentage cytotoxicity of three AMPs against HCEC-12 cells (left). Permeabilization of the inner bacterial membrane by addition of various peptides (right).

Biological testing of surface coupled AMPs

The activity of the immobilized peptides was tested with relevant bacterial and fungal strains. In the tests, up to a 5-log reduction in the bacterial load was achieved after 2 hours of incubation.

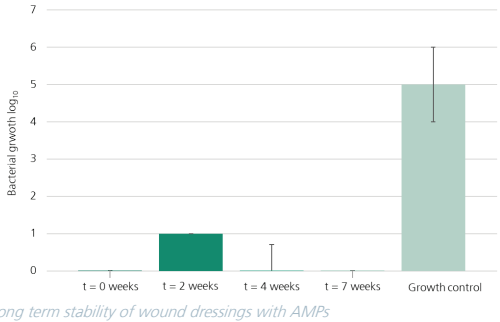

Fig. 4 Long term stability of wound dressings with AMPs

In addition, the wound dressing with AMPs was tested for long-term stability in different temperatures, pH values, and serum. In summary, it can be stated that the approach helps to maintain the sterility of the wound material and to reduce possible biofilm formation. The KISMADI wound dressing with decentralized sensor measurement of important parameters for wound healing, AI-supported digital feedback, and active antimicrobial coating could optimize wound management and extend wearing intervals.

Contact

Dr. Sebastian Kersting
Molecular Bio Engineering
Tel. +49 331 58187-214
sebastian.kersting@izi-bb.fraunhofer.de
Fraunhofer IZI-BB
Am Mühlenberg 13
D-14476 Potsdam
www.izi-bb.fraunhofer.de

Fraunhofer ZDD · Fraunhofer IZI-BB · Fraunhofer ISC · Fraunhofer IZM · Fraunhofer FIT

High Throughput Phage Display Screening Identified Peptide Inhibitors Targeting the α-Synuclein for Parkinson's Disease Treatment

香 港 大 學
THE UNIVERSITY OF HONG KONG

Haiyan Zhou[1], Zhaohui Liang[2], Chenyin Wang[3], Wai Lok Ngai[1], Michael K. Chan[2], Chaogu Zheng[3], Xuechen Li[1]

[1]*Department of Chemistry, The University of Hong Kong, Hong Kong SAR, P. R. China*
[2]*School of Life Sciences, The Chinese University of Hong Kong, Hong Kong SAR, P. R. China*
[3]*School of Biological Sciences, The University of Hong Kong, Hong Kong SAR, P. R. China*



https://doi.org/10.17952/37EPS.2024.P1154

Introduction

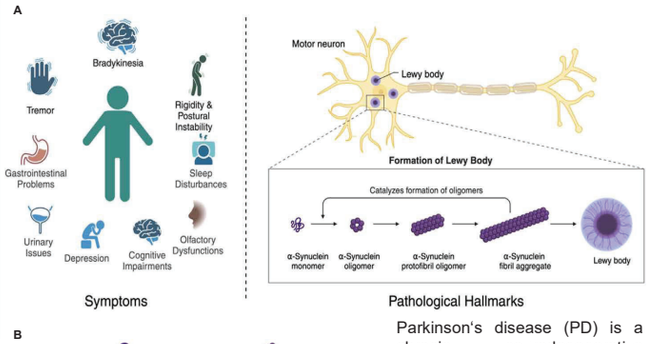

Fig. 1. Peptide inhibitor discovered for inhibition α-syn aggregation in PD. (A) α-Syn aggregation in Parkinson's disease. **(B)** Schematic illustration of SUMO1-derived peptide inhibitors suppresses early-stage α-syn aggregation.

Parkinson's disease (PD) is a chronic neurodegenerative disorder affecting 10 million worldwide. α-Syn aggregation is a key driver of PD pathogenesis and a therapeutic target. Previously we have discovered a SUMO-derived peptide inhibitor, which effectively suppresses α-syn aggregation. To enhance binding affinity, we aim to develop a SUMO-biased phage-displayed peptide library to identify peptides with enhanced binding affinity to α-syn, providing a promising avenue for developing novel therapeutics for PD.

Methods

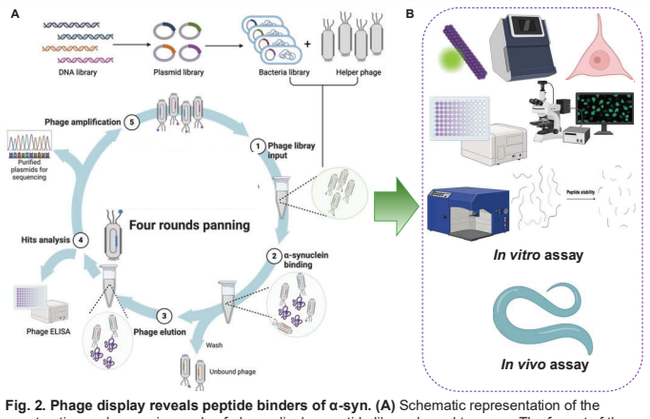

Fig. 2. Phage display reveals peptide binders of α-syn. (A) Schematic representation of the construction and screening cycle of phage display peptide library bound to α-syn. The format of the phage peptide library was marked in the cycle's center. **(B)** The biological activity evaluation of the selected peptide hits.

Conclusion & Future work

(1) We designed a phage display peptide library based on SUMO1 scaffold and identified PD-6 peptide targeting syn with a nanomolar affinity.

(2) PD-6 inhibits syn aggregation, penetrates neuronal cells, reduces toxic oligomer formation, and is resistant to protease degradation *in vitro*.

(3) PD-6 suppressed syn-induced toxicity in *C. elegans* PD models.

(4) We plan to evaluate the neuroprotective effect of PD-6 in a mouse model.

Acknowledgement:

We would like to thank the Hong Kong Research Grants Council, CUHK Center of Novel Biomaterials, and the National Natural Science Foundation of China for their kind support of this project.

Results

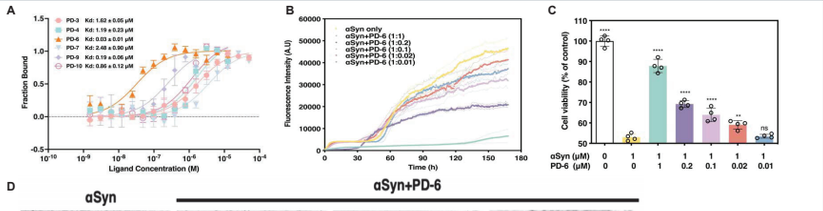

Fig. 3. PD-6 against α-syn aggregation *in vitro*. (A) MST assay. **(B)** Thioflavin-T (ThT) assay. **(C)** MTT assay. **(D)** TEM imaging.

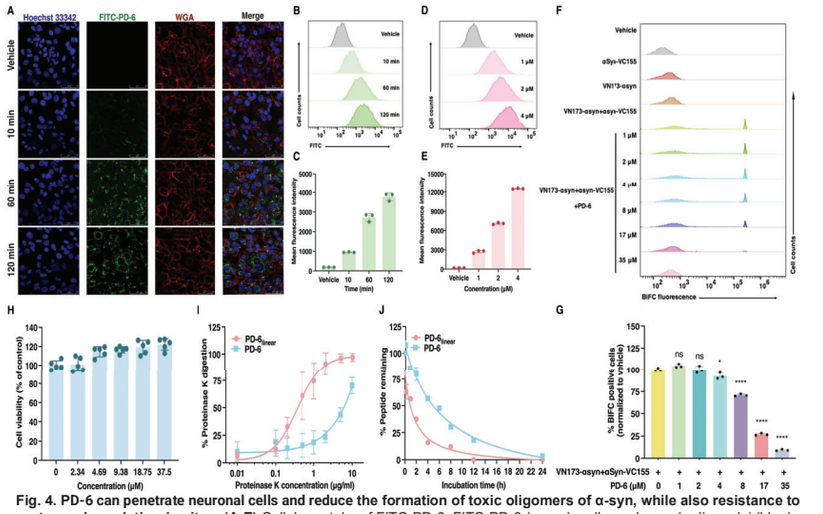

Fig. 4. PD-6 can penetrate neuronal cells and reduce the formation of toxic oligomers of α-syn, while also resistance to protease degradation *in vitro*. (A-E) Cellular uptake of FITC-PD-6. FITC-PD-6 (green), cell membrane (red), nuclei (blue). **(F-G)** BiFC assay. (**H**) CCK8 assay. **(I-J)** Representative degradation curves of peptides under Proteinase K and human serum stability assay.

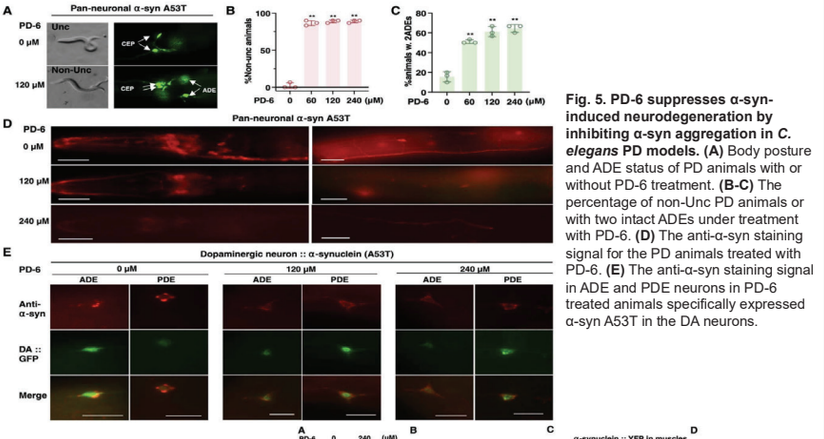

Fig. 5. PD-6 suppresses α-syn-induced neurodegeneration by inhibiting α-syn aggregation in *C. elegans* PD models. (A) Body posture and ADE status of PD animals with or without PD-6 treatment. **(B-C)** The percentage of non-Unc PD animals or with two intact ADEs under treatment with PD-6. **(D)** The anti-α-syn staining signal for the PD animals treated with PD-6. **(E)** The anti-α-syn staining signal in ADE and PDE neurons in PD-6 treated animals specifically expressed α-syn A53T in the DA neurons.

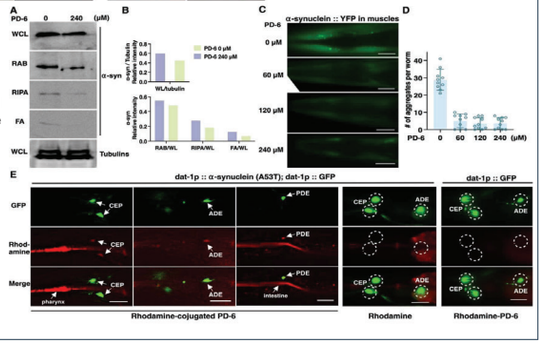

Fig. 6. PD-6 enters *C. elegans* neurons to inhibit α-syn aggregation. (A-B) WB analysis of the whole worm lysate (WCL) and the high-salt soluble (RAB), detergent soluble (RIPA), and insoluble (FA) fractions of the lysate for α-synuclein in the UM10 animals pan-neuronally expressing α-syn A53T and treated with or without PD-6. **(C-D)** Muscle aggregates of α-syn::YFP in the NL5901 strains under the treatment of various concentrations of PD-6. **(E)** Visualization of rhodamine-conjugated PD-6 in the DA neurons that express α-syn A53T.

Linear peptides as IgG-epitope mimetic for allergic immunotherapy against birch pollen

Alessandro Streuli[1], Lara Šošić[2], Marta Paolucci[2], Agathe Duda[2], Klaus Eyer[3], Pål Johansen[2], Christian Steuer[1]

[1]Institute of Pharmaceutical Sciences, ETH Zurich; [2]Department of Dermatology, University Hospital Zurich ; [3]Department of Biomedicine, Aarhus University

https://doi.org/10.17952/37EPS.2024.P1155

1 Introduction

Allergies present an increasing health burden affecting nearly one billion individuals with allergen immunotherapy (AIT) as the sole causative treatment via stimulation of allergen-specific IgG antibodies[1,2]. Although these antibodies are acknowledged for their protective potential, elevated levels in AIT-treated patients do not consistently represent the success of treatment, indicating further critical factors[3]. In this study, the antibody repertoire of treated and non-treated allergic patients was characterized serologically and on a single-cell level. IgG antibodies found in sera of patients were tested for their binding capacity and strength towards Bet v 1. Four main IgG binding epitopes were identified using linear epitope mapping. The insights were used to produce six hypoallergenic peptides tested *in vitro* and *in vivo*[4].

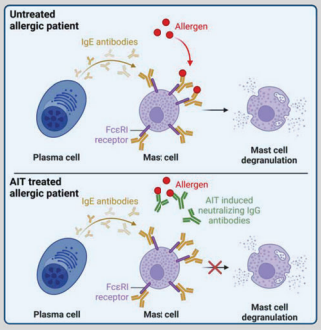

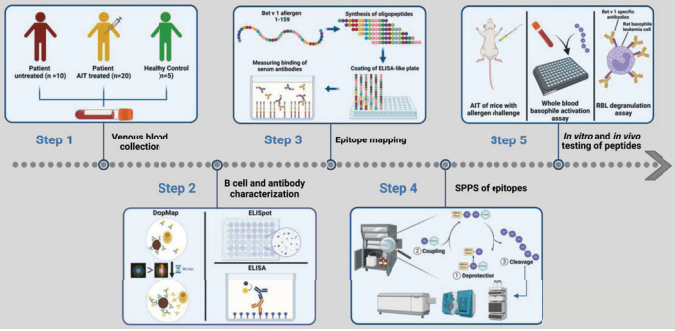

2 Antibody and B cell characterization

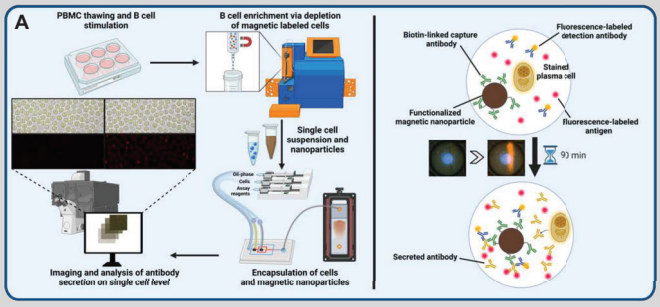

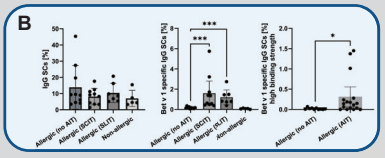

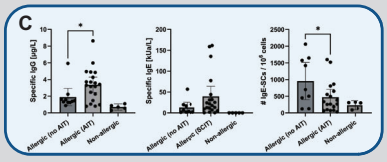

A: Workflow of used DropMap[5] assay to characterize memory B cells of patients.

B: DropMap results displayed more Bet v 1 specific IgG-secreting cells (SC) and particular SCs with high binding strength in both treatment groups while having constant SC over all groups.

C: ImmunoCAP measurements showed higher Bet v 1 specific IgG and IgE levels in allergic patients with and without treatment. ELISpot results showed a similar trend in the B cell memory.

3 Epitope mapping

A: Binding of IgG antibodies in patients either treated via subcutaneous AIT (SCIT) or sublingual AIT (SLIT) towards linear Bet v 1 epitope indicated four novel IgG binding sites (Lin 1-4).

B: Visualisation of identified binding regions (PDB = 1BV1). Lin 1 is indicated in blue, Lin 2 in green, Lin 3 in purple, and Lin 4 in orange.

C: Visualisation of 2 out of 6 defined linear epitope mimetics (PDB = 1BV1).

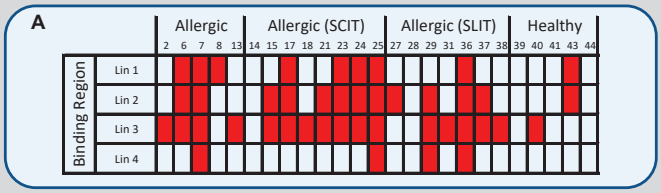

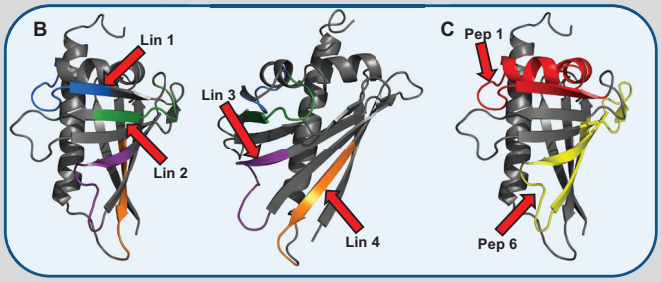

4 Synthesis of defined epitopes

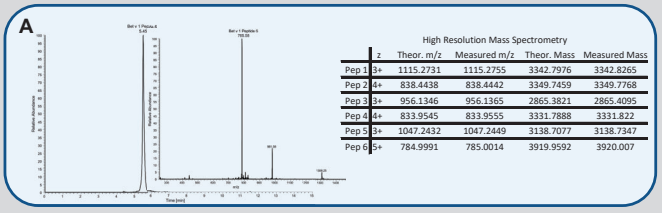

	z	Theor. m/z	Measured m/z	Theor. Mass	Measured Mass
Pep 1	3+	1115.2731	1115.2755	3342.7976	3342.8265
Pep 2	4+	838.4438	838.4442	3349.7459	3349.7768
Pep 3	3+	956.1346	956.1365	2865.3821	2865.4095
Pep 4	4+	833.9545	833.9555	3331.7888	3331.822
Pep 5	3+	1047.2432	1047.2449	3138.7077	3138.7347
Pep 6	5+	784.9991	785.0014	3919.9592	3920.007

A: Mass accuracy of successfully synthesised linear peptides was performed via LC-MS and high-resolution mass spectrometry. Representative LC-MS results for peptide 6 are shown. The table depicts the high resolution MS results for all peptides. Purity was determined to be >95% via LC-UV, and peptide sequence identity was validated via LC-MS/MS.

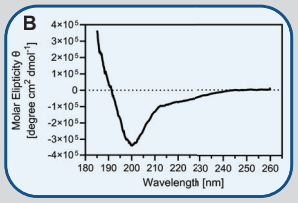

B: CD spectra of peptide 6, 50 µM in PBS (pH 7.4) with NaF, at 25 °C. Results were evaluated using the BeStSel web server and the structure was determined as predominantly uncoiled with smaller amounts of antiparallel and turn parts[6].

5 *In vitro* and *in vivo* testing

A: RBL degranulation assay showed that Bet v 1 protein, but none of the six peptides triggered β-hexosaminidase release.

B: Mice were immunised three times with each peptide and alum as adjuvant. Native Bet v 1 protein was used as positive control. Immune responses were detected for peptides 1 and 6.

C: Titer of mice immunised with peptide 1, peptide 6, or a mix of all peptides with either alum or MPLA as adjuvant. Peptide 1 showed no Bet v 1 specific IgG 1 titer. Immunisation using peptide 6 induced Bet v 1 specific IgG 1 in all mice.

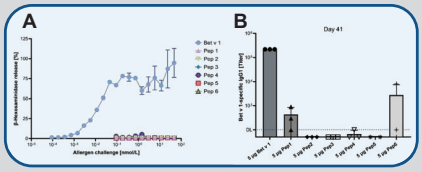

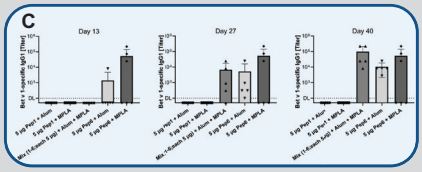

6 Conclusion and Outlook

We characterized the antibody and the memory B cell repertoire of 30 hay fever patients via ImmunoCAP, ELISpot, and on a single-cell level via DropMap. Further, the serum of patients was used to identify four novel IgG bindings regions on Bet v 1 via epitope mapping. Six corresponding linear peptides were synthesised as epitope mimetics via SPPS. Degranulation assays showed no allergenicity induced by the six peptides. Peptides 1 and 6 showed induction of Bet v 1 specific IgG 1 antibodies in the first round of *in vivo* testing which could be confirmed in the second round for peptide 6. The potency of desensitisation via AIT of peptide 6 still needs to be tested.

References

1 Roberts, G. *et al.* EAACI Guidelines on Allergen Immunotherapy: Allergic rhinoconjunctivitis. *Allergy* **73**, 765-798 (2018)
2 Shamji, M. H. *et al.* The role of allergen-specific IgE, IgG and IgA in allergic disease. *Allergy* **76**, 3627-3641 (2021)
3 James, L. K. *et al.* Long-term tolerance after allergen immunotherapy is accompanied by selective persistence of blocking antibodies. *J Allergy Clin Immunol* **127**, 509-516 e501-505 (2011)
4 Sosic, L. *et al.* Allergen immunotherapy: progress and future outlook. *Expert Rev Clin Immunol* **19**, 745-769 (2023)
5 Eyer, K. *et al.* Single-cell deep phenotyping of IgG-secreting cells for high-resolution immune monitoring. *Nat Biotechnol* **35**, 977-982 (2017)
6 Micsonai, A. *et al.* Accurate secondary structure prediction and fold recognition for circular dichroism spectroscopy. *Proc Natl Acad Sci U S A* **112**, E3095-3103 (2015).

Acknowledgement

We thank the European and International Peptide Symposium for covering the registration fee. Figures were partially created with BioRender.com.

Contacts

ETH Zurich, Pharmaceutical Analytics, Institute of Pharmaceutical Sciences
Vladimir-Prelog-Weg 1-5/10, CH-8093, Zürich
AS: alessandro.streuli@pharma.ethz.ch, Tel.: +41 44 633 73 28
CS: christian.steuer@pharma.ethz.ch, Tel: +41 44 633 74 19

https://doi.org/10.17952/37EPS.2024.P1160

Discovery of a novel α-helical peptide targeting GTP-bound K-Ras(G12D)

Hannah Comfort[1], Sarah Ross[2], Jefferson Revell[3], Thomas Murray[4], Carole Urbach[4], Bethan Archer[4], Darerca Owen[1] and Helen Mott[1]

[1]Department of Biochemistry, University of Cambridge, UK; [2]Oncology R&D, AstraZeneca, Cambridge, UK; [3]Discovery Sciences, AstraZeneca R&D, Cambridge, UK; [4]Biologics Engineering, AstraZeneca R&D, Cambridge, UK

1. Introduction

- K-Ras inhibition has been a major goal of cancer drug discovery for decades and there remain no clinically approved therapeutics directly targeting common K-Ras mutants such as G12D or G12V[1].
- Oncogenic K-Ras activates tumourigenic signalling pathways by binding to effector proteins, such as cRaf, in the GTP-bound form. Effector proteins bind predominately at the K-Ras switch regions, whose conformation is distinct in GTP- and GDP-bound K-Ras.
- Helical peptides can provide efficacious inhibitors of large protein-protein interfaces, such as that of K-Ras and its downstream effectors.
- A phage display screen of an α-helical peptide library identified a novel K-Ras(G12D) binder, which has been characterised biochemically and in a cellular context.

2. Biochemical characterisation of P39 binding

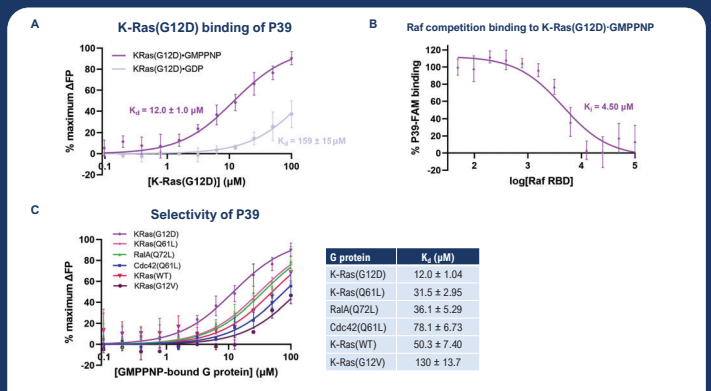

G protein	K_d (μM)
K-Ras(G12D)	12.0 ± 1.04
K-Ras(Q61L)	31.5 ± 2.95
RalA(Q72L)	36.1 ± 5.29
Cdc42(Q61L)	78.1 ± 6.73
K-Ras(WT)	50.3 ± 7.40
K-Ras(G12V)	130 ± 13.7

Figure 5. Characterisation of hit from naïve screen (P39)
(A) Fluorescence polarization (FP) of FAM-39 was measured with shown concentrations of GDP or GMPPNP-bound K-Ras(G12D). **(B)** FP was detected following addition of cRaf RBD to a complex of K-Ras(G12D)·GMPPNP and FAM-39. **(C)** FP of FAM-39 was measured with shown concentrations of various GMPPNP-bound G proteins.

A naïve screen of a helical peptide library against K-Ras(G12D) yielded numerous hits. Of these, P39 was selected for further characterisation and was found by FP to bind K-Ras(G12D) bound to the GTP analogue GMPPNP with >10-fold selectivity over the GDP-bound form (Figure 1A).

The K-Ras effector cRaf can also compete with P39 for K-Ras(G12D)·GMPPNP binding (Figure 1B), suggesting that the peptide may bind at the effector-binding interface.

Finally, P39 has some selectivity for K-Ras(G12D) binding over other G proteins as well as WT K-Ras and other common oncogenic mutants (Figure 1C).

3. NMR titration to map P39 binding site

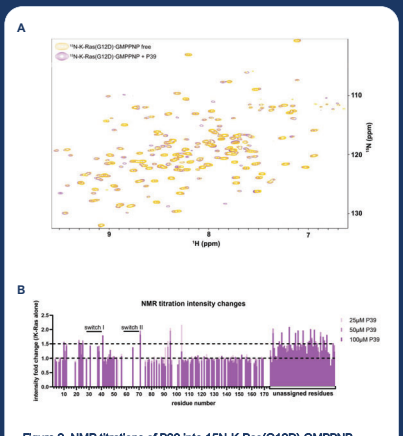

Figure 2. NMR titrations of P39 into 15N-K-Ras(G12D)·GMPPNP
(A) HSQC of ^{15}N-K-Ras(G12D)·GMPPNP was detected before (orange) and after (pink) addition of P39. **(B)** Intensity changes of peaks in ^{15}N-K-Ras(G12D)·GMPPNP HSQC upon addition of P39.

NMR was utilised to map the P39 binding site of K-Ras(G12D). Titration of P39 into ^{15}N-labelled K-Ras(G12D)·GMPPNP revealed an increase in intensity in numerous peaks in the HSQC spectrum (Figure 2A).

The residues for which peaks increased in intensity were found to be in or around the switch regions of K-Ras (Figure 2B). In addition, a number of new peaks appeared in the spectrum. These are likely to be within the switch regions, whose peaks are too weak to be assigned in free K-Ras.

This suggests that P39 likely binds to the switch I and switch II regions of K-Ras(G12D) and stabilises their conformation, increasing their HSQC peak intensity. K-Ras effector proteins also bind at the switch regions, consistent with the Raf-competitive binding of P39.

4. MD simulations of the P39-K-Ras(G12D) complex

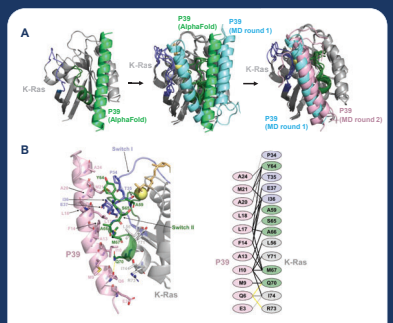

Figure 3. MD simulations of the P39-K-Ras(G12D) complex
(A) Starting from an AlphaFold model of the P39-K-Ras(G12D) complex a series of 300ns MD simulations revealed a stable binding site for P39. **(B)** Contacts between P39 and K-Ras(G12D)·GMPPNP over the simulation with the lowest P39 RMSD. Switch I is coloured blue, switch II is coloured dark green. Yellow line = polar contact.

Molecular dynamics (MD) simulations of an AlphaFold model of the P39-K-Ras(G12D) complex were used to predict the binding site of P39.

The initial three replicas differed, with one replica predicting a significant deviation from the AlphaFold model (Figure 3A center image). Performing three replica MD simulations from this starting point revealed a stable P39 binding pose between switch I and switch II (Figure 3A right image), supporting the NMR titration data.

Analysis of P39-K-Ras contacts reveals a largely hydrophobic interface (Figure 3B).

5. P39 interaction with K-Ras in HEK-293T cells

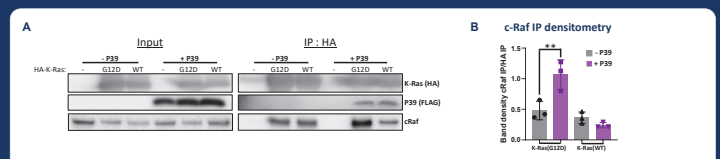

Figure 4. Co-immunoprecipitation of P39 with K-Ras when co-expressed in HEK-293T cells
(A) HA-K-Ras and P39-FLAG or empty vector were co-transfected into HEK-293T cells. HA-K-Ras was immunoprecipitated with anti-HA magnetic beads and associated proteins were identified by Western Blot. **(B)** Quantification of band intensity for cRaf from three independent co-immunoprecipitation experiments in HEK-293T cells co-transfected with K-Ras and P39 or empty vector. ** = 0.0021<p<0.033 by t-test.

To assess whether P39 interacts with K-Ras in a cellular context, HEK-293T cells were co-transfected with HA-tagged K-Ras(G12D) or K-Ras(WT) and FLAG-tagged P39 or an empty vector. K-Ras was immunoprecipitated and associated P39 was identified by Western Blot. P39 co-immunoprecipitated with both K-Ras(G12D) or K-Ras(WT) confirming the interaction (Figure 4A). The interaction between transfected HA-K-Ras and endogenous cRaf was also assessed, which surprisingly revealed an increase in the K-Ras(G12D)-cRaf interaction in the presence of P39 (Figure 4A/B).

6. Activity of P39 in KRAS(G12D)-mutant cells

To assess the effect of P39 on endogenous K-Ras(G12D) signalling, the KRAS(G12D)-mutant colon cancer cell line GP2D was utilised. P39 was appended with an octa-arginine sequence to enable cell penetration.

P39 treatment resulted in an increase in the K-Ras-Raf interaction in these cells (Figure 5A). This led to an increase in K-Ras signalling pathway markers in P39 treated cells, including MAPK pathway markers (pERK/pMEK) and PI3K pathway marker pAKT (Figure 5B). An increase in cleaved PARP was also seen indicating that Ras hyperactivity is driving apoptosis.

P39 did not increase Ras signalling or apoptosis in the K-Ras-independent BRAF(V600E)-mutant cell line HT29, indicating a specific response in the GP2Ds.

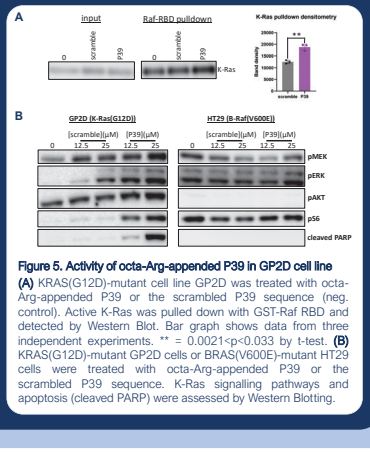

Figure 5. Activity of octa-Arg-appended P39 in GP2D cell line
(A) KRAS(G12D)-mutant cell line GP2D was treated with octa-Arg-appended P39 or the scrambled P39 sequence (neg. control). Active K-Ras was pulled down with GST-Raf RBD and detected by Western Blot. Bar graph shows data from three independent experiments. ** = 0.0021<p<0.033 by t-test. **(B)** KRAS(G12D)-mutant GP2D cells or BRAS(V600E)-mutant HT29 cells were treated with octa-Arg-appended P39 or the scrambled P39 sequence. K-Ras signalling pathways and apoptosis (cleaved PARP) were assessed by Western Blotting.

7. Conclusions

- A phage display screen of an α-helical peptide library against K-Ras(G12D) identified P39, which binds K-Ras(G12D) with **>10-fold selectivity for the active state**.
- P39 binding is somewhat selective for K-Ras over other G proteins (RalA and Cdc42) and for the G12D mutant over other K-Ras mutants (WT, Q61L and G12V).
- P39 is predicted to **bind between switch I and II** of K-Ras(G12D) through a largely hydrophobic interface.
- Octa-Arg-appended P39 **increases the K-Ras-Raf interaction in a KRAS(G12D)-mutant cancer cell line**, resulting in an increase in Ras signalling.
- Hyperactivation of Ras signalling by P39 **leads to apoptosis** in a KRAS(G12D)-mutant cancer cell line.

References

[1]Nussinov R and Jang H (2025) Direct K-Ras Inhibitors to Treat Cancers: Progress, New Insights, and Approaches to Treat Resistance. *Annu. Rev. Pharmacol.*

UNIVERSITY OF CAMBRIDGE

AstraZeneca

PEPTIDE INHIBITORS OF PROTEIN-PROTEIN INTERACTIONS TARGETED TO SRC HOMOLOGY 2 DOMAINS: A COMBINED COMPUTATIONAL AND SPECTROSCOPIC DESIGN APPROACH

Paolo Calligari[1], Claudia Storti[1, 2], Chiara Innamorati[1], Chiara Fulci[1], Alessia Damiani[1], Cristiano DI Stefano[1], Chiara Cocca[1], Cristina Peggion[3, 4], Barbara Biondi[4], Gianfranco Bocchinfuso[1], Lorenzo Stella[1]

[1]Dept. of Chemical Science and Technologies, Tor Vergata University of Rome, Rome, Italy,
[2]Department of Public Health, Experimental and Forensic Medicine, University of Pavia, Pavia, Italy,
[3]Department of Chemistry, University of Padua, Padua, Italy,
[4]Institute of Biomolecular Chemistry (Padova Unit), CNR, Padua, Italy

https://doi.org/10.17952/37EPS.2024.P1161

INTRODUCTION

SHP2 is an important molecular target for therapies against cancer and rare diseases, like RASopathies [1,2]. Mutations of the gene coding for SHP2, PTPN11, have been associated with cancer and developmental disorders. The structure of SHP2 includes two SH2 domains (N-SH2 and C-SH2) followed by the catalytic domain PTP. SH2 domains recognize and bind phosphopeptide [3]. They also have an important role in modulating the catalytic activity of the protein. Under basal conditions, the N-SH2 domain blocks the catalytic site and SHP2 is inactive. The association to binding partners favors a conformational transition from this autoinhibited conformation to an active state. Most of the SHP2 pathological amino acid substitutions perturb the autoinhibitory interaction in favor of open conformations, resulting in a hyperactivated protein [4]. SHP2 can be efficiently inhibited by targeting the binding of the N-SH2 domain to cognate proteins [5], furthermore the development of inhibitors of SHP2 protein-protein interactions can take advantage of the role of the C-SH2 domain for increasing both specificity and affinity.

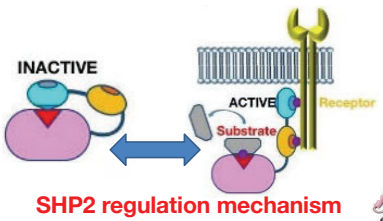

SHP2 regulation mechanism

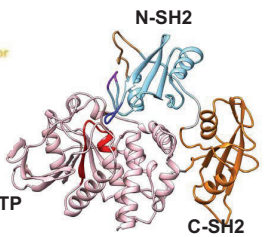

N-SH2

Current SHP2 inhibitors, which target either the catalytic site or an allosteric pocket, often lack specificity and are ineffective against disease-associated SHP2 mutants.
In response to the signaling hyperactivation caused by pathogenic lesions, we developed peptide-based molecules that exhibit nanomolar affinity for the N-SH2 domain of SHP2.
These peptides offer good selectivity, stability to degradation, and display 2–20 times higher affinity for pathogenic SHP2 variants compared to the wild-type protein.

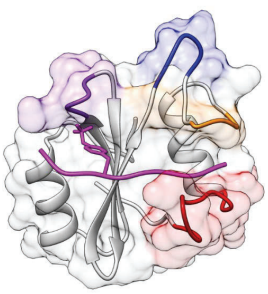

Binding affinity

Umbrella sampling simulations

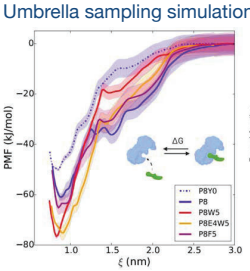

Fluorescence polarization assay

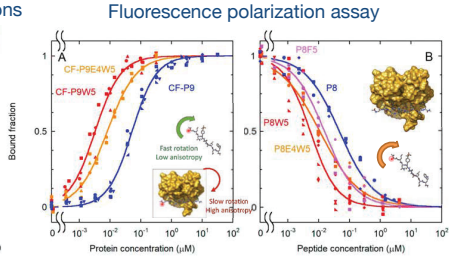

L N F2Pmp I D L D W

Selectivity for oncogenic variants

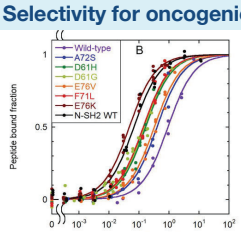

High specificity

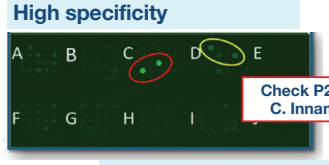

Check P2.128 !!!
C. Innamorati

Resistance to degradation

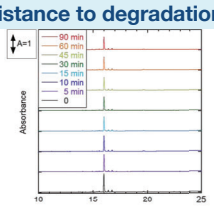

In vivo activity

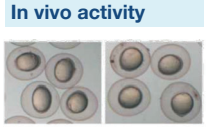

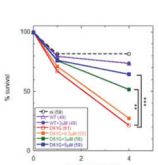

Further developments

US simulations

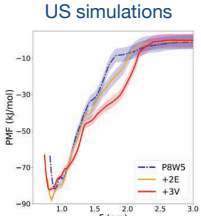

Fluorescence anisotropy assay

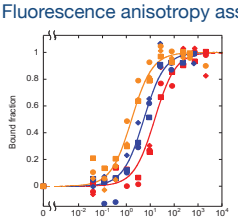

Affinity improvement

CF-GLN-pY-IDLDW K_d=(5.3±0.6) Nm

CF-GLN-pY-IDVDW K_d=(15.3±0.2) nM

CF-GLN-pY-HLDW K_d=(1.66±0.03) nM

L N pY I D L D W
+2 +3
E V

C-SH2

To evaluate the binding specificity of different peptide sequences for the C-SH2 domain, we conducted MD simulations of the domain complexed with high-affinity natural partners (PD1, GAB1, and IRS1) and their mutants, starting from the PD1 NMR structure (PDB ID: 6R5G). We also performed a similar analysis using crystallographic structures (PDB IDs: 5DF6, 5X7B, 5X94).

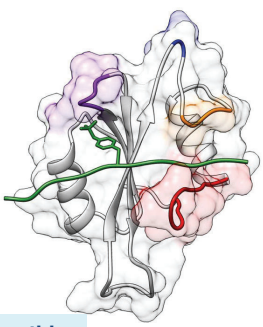

- GROMACS software package
- Force field AMBER99SB-ildn
- 1.2 μs

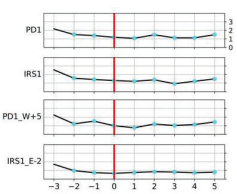

Structure and Dynamics of bound peptides

RMSF between peptide backbone and C-SH2 domain

Peptides stay within the binding cleft for the entire trajectory. The N-terminal portion exhibited higher mobility compared to the C-terminal side.

Ramachandran Plots of peptide backbone

Peptide maintain an extended conformation in the crystallographic structure. The central region (+1 to +3 residues) remains extended, occasionally extending to residue +4.

Residues +1 and +3 remained stably embedded in the hydrophobic groove.
Residues +2 and +4 point towards the solvent, so it is better to introduce polar residue in these positions.

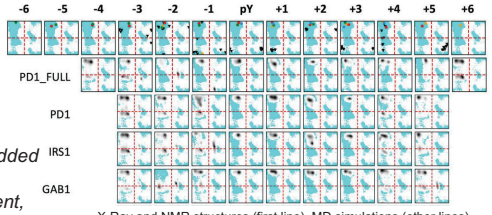

X-Ray and NMR structures (first line), MD simulations (other lines).

Hydrogen bond interactions

Backbone of the phosphopeptide residues +1, +2 and +4 forms HB respectively with the 169H^0, 205T^N and 203V^0 of C-SH2 domain.

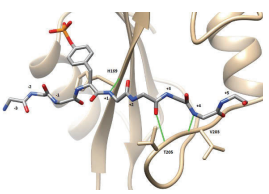

Inter-molecular ion-pair interactions

N-terminal and C-term portions of phosphopeptides can form different ion-pair interactions with the residue of the C-SH2 domain.

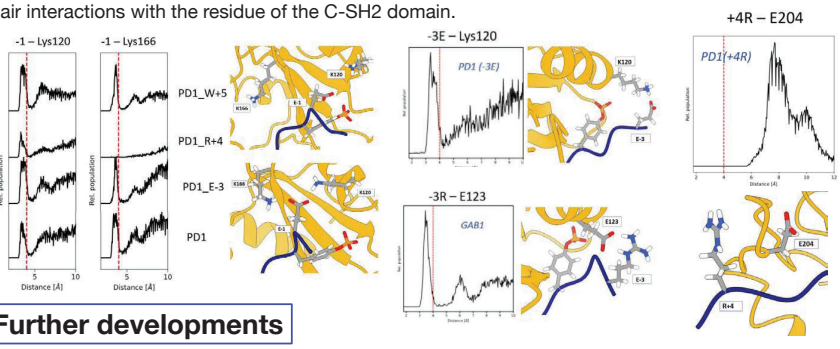

Further developments

Displacement assay

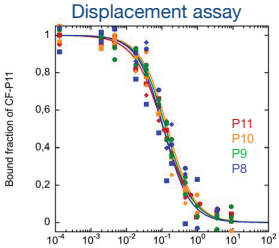

Minimal high affinity sequence length

	Sequence	Kd (nM)
P11	GETEpYATIVFP	77±4 (CF-P11, fluorescence anisotropy assay) 28±4 (displacement assay)
P10	ETEpYATIVFP	46±7 (displacement assay)
P9	TEpYATIVFP	38±4 (displacement assay)
P8	TEpYATIVF	29±5 (displacement assay)

All peptides showed comparable affinities toward C-SH2 domain.

REFERENCES

1. *Future Med. Chem.* 6 (2014) 1423–1437.
2. *Cancer Res.* 77 (2017) 5701–5705
3. *J Chem Inf Model* 60 (2020) 3157–71.
4. *Proteins* 66(2007) 963-974.
5. *J Med Chem* 64 (2021) 15973-15990.

Proceedings of the 37 th European Peptide Symposium
Michal Lebl (Editor)
European Peptide Society, 2024
https://doi.org/10.17952/37EPS.2024.P1162

Peptide-based vesicle isolation method for *P. aeruginosa*

Tania Henriquez, Ismael Castañón, Silvia Scali, Chiara Falciani.
Department of Medical Biotechnologies, University of Siena, Siena, Italy.

Introduction

Pseudomonas aeruginosa is an organism that can act as an opportunistic pathogen for humans and animals, where it can cause from mild diseases, such as otitis, to serious illnesses (life-threatening diseases) such as septicemia (1).

In the last decades, new elements have been associated with the pathogenicity of *Pseudomonas* strains (2). This is the case with outer membrane vesicles (OMVs), which are produced when part of the outer membrane (including periplasmic content) generates a bleb. Bacterial vesicles have diverse roles in physiology and virulence (3). However, the difficulties related to vesicle purification (i.e. long protocols or the need of specialized instruments) have become a major obstacle for their characterization. In this context, we decided to analyze the efficacy of a peptide designed in our lab to bind *P. aeruginosa* vesicles and use it to develop a new vesicle purification method.

Results and discussion

We first determine the best conditions to purify vesicles of *P. aeruginosa* PAO1 strain using a commercial kit (ExoBacteria OMV isolation kit) (Figure 1). To that end, we grew the strain in rich medium (KB) or M9 minimal medium. In parallel, we also used KB medium and M9 minimal medium without bacteria as negative control.

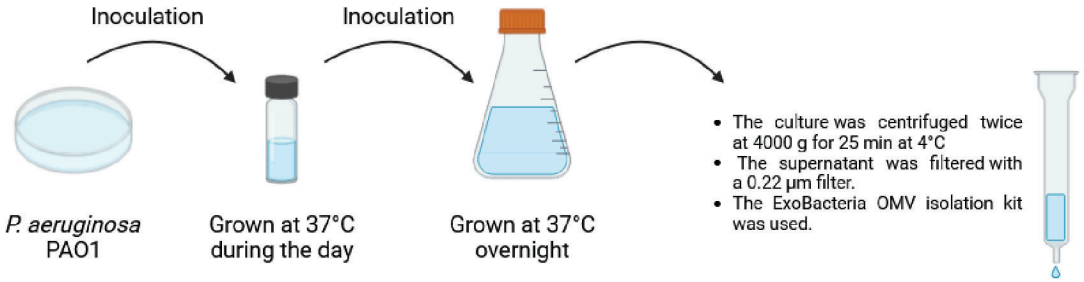

Figure 1. Diagram showing the main steps for vesicle purification. P. aeruginosa *PAO1 was grown in a cetrimide plate and then used to inoculate 2 ml of the corresponding medium. The strain was grown at 37°C during the day, and then used to inoculate 30 of fresh medium. After overnight incubation at 37°C and continuous shaking, the culture was centrifuged twice, filtered (0.25 µm) and processed with the ExoBacteria OMV Isolation according to the manufacturer instructions. Image created with BioRender.com*

We proceeded to characterize all samples—including those from *P. aeruginosa* cultures and negative controls in KB and M9 minimal media—using dynamic light scattering, electron microscopy, and protein quantification assays. Our findings demonstrated that the M9 minimal medium was the most effective for vesicle purification with the ExoBacteria OMV isolation kit. The negative control in M9 minimal medium exhibited a profile consistent with the absence of particle populations, whereas the negative control in KB medium (without bacteria) showed the presence of particle populations, likely due to protein aggregates (figure not shown). Furthermore, our analysis confirmed the presence of *P. aeruginosa* vesicles in the M9 minimal medium (Figure 2). Consequently, we selected these vesicles for subsequent experiments.

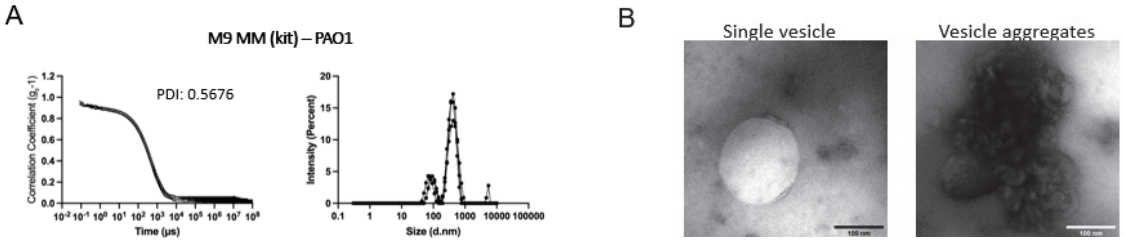

Figure 2. ExoBacteria OMV Isolation Kit was used to purify vesicles/particles from M9 minimal medium inoculated with P. aeruginosa *PAO1 strain. (A) Analysis of growth media for vesicle purification by Dynamic Light Scattering (DLS) using DLS (Zetasizer). The three curves in each graph represent the three readings of the instrument (triplicate). PDI: polydispersity index. (B) Electron microscopy images.*

We later synthesized an amphipathic and cationic 9-mer peptide that was previously described to bind LPS of *Escherichia coli* and *P. aeruginosa* (4) and used it to perform a modified Differential Radial Capillary Action of Ligand Assay (DraCaLa) assay (5). This DraCaLa assay relied on the colorimetric properties of our peptide conjugated to tetramethylrhodamine for visualization of migration on the nitrocellulose membrane (instead of the traditional radiolabeling). Our results suggested that the 9-mer peptide could bind the vesicles of *P. aeruginosa* PAO1. Interestingly, similar results were found for human exosomes (although with lower affinity).

Additional experiments are needed in order to determine the binding affinity between the peptide and the vesicles. In this context, ELISA experiments will be performed.
Altogether, these results contribute to broadening the knowledge on *Pseudomonas* vesicle purification and generate a new alternative for future applications.

Acknowledgments
We thank Eugenio Paccagnini, Mariangela Gentile and Pietro Lupetti for their help with Electron microscopy. Also, we thank Ilaria Clemente, Claudia Bonechi and Agnese Magnani for their help with the dynamic light scatter analysis.

References
(1) Iglewski BH. *Pseudomonas*. In: th, Baron S, editors. Medical Microbiology. Galveston TX: The University of Texas Medical Branch at Galveston.; 1996.
(2) Palleroni NJ. Pseudomonas. Bergey's Manual of Systematics of Archaea and Bacteria. 2015.
(3) Henriquez T, Falciani C. Extracellular Vesicles of *Pseudomonas:* Friends and Foes. Antibiotics 2023, 12, 703. https://doi.org/10.3390/antibiotics12040703.
(4) Falciani, Chiara & Lozzi, Luisa & Pollini, Simona & Luca, Vincenzo & Carnicelli, Veronica & Brunetti, Jlenia & Lelli, Barbara & Bindi, Stefano & Scali, Silvia & Di Giulio, Antonio & Rossolini, Gian & Mangoni, Maria & Bracci, Luisa & Pini, Alessandro. (2012). Isomerization of an Antimicrobial Peptide Broadens Antimicrobial Spectrum to Gram-Positive Bacterial Pathogens. PloS one. 7. e46259. 10.1371/journal.pone.0046259.
(5) Seminara AB, Turdiev A, Turdiev H, Lee VT. Differential Radial Capillary Action of Ligand Assay (DRaCALA). Curr Protoc Mol Biol. 2019 Apr;126(1):e84. doi: 10.1002/cpmb.84.

Antibacterial, Anti-inflammatory and Anti-biofilm Activities of Novel Short Antimicrobial Peptides Designed from the Cecropin A-Melittin Hybrid Antimicrobial Peptide, BP100

https://doi.org/10.17952/37EPS.2024.P1164

Eun Young Kim[1], Dinesh Kumar[1], Sang Hyun Park[2], and Song Yub Shin[1,*]

[1]Department of Cellular & Molecular Medicine, School of Medicine, Chosun University, Gwangju, 61452, Republic of Korea.
[2]Department of Animal Science, Institute of Agricultural Science and Technology, College of Agriculture & Life Science, Chonnam National University, Gwangju, 61186, Republic of Korea

Abstract

BP100 (KKLFKKILKYL-NH_2) is a short hybrid antimicrobial peptide (AMP) derived from cecropin A and melittin, two potent AMPs. We designed and synthesized several Trp-substituted BP100 analogs to enhance their antimicrobial activity therapeutic index. The therapeutic index represents the ratio of HC10 (the concentration causing 10% hemolysis of sheep red blood cells) to the geometric mean of MIC (minimal inhibitory concentration). Compared to BP100, the analogs BP5, BP6, BP7, BP8, BP11 and BP13 exhibited 1.4- to 5.8-fold higher therapeutic index. At a non-toxic concentration of 4 μM, both BP100 and some analogs (BP1, BP5, BP6, BP8, BP11, BP12 and BP13) suppressed the release of inflammatory cytokines, including tumor necrosis factor-α (TNF-α), interleukin-6 (IL-6) and monocyte chemoattractant protein-1 (MCP-1) in LPS-stimulated RAW 264.7 cells. This indicates that their potent LPS scavenging activity, similar to the control AMP LL-37. Furthermore, analogs BP5, BP6, BP7, BP8, BP11 and BP13 inhibited the biofilm formation of multidrug-resistant *Pseudomonas aeruginosa* (MDRPA) and eradicated preformed MDRPA by more than 90% at 8 μM. Thus, BP6, BP8, BP11 and BP13 exhibit higher potential than BP100 in terms of therapeutic index, anti-inflammatory and anti-biofilm activities. Additionally, we investigated the synergistic effects of BP100 and its analogs with conventional antibiotics against MDRPA, evaluating their potential as adjuvants in drug combination therapies.

Peptide Design

Table 1. Amino acid sequences and physicochemical properties of BP100 and its analogs

Peptides	Amino acid sequences [a]	Molecular mass (Da)		Net charge	R_t[b]	μH[c]
		Calculated	Observed			
BP100	KKLFKKILKYL-NH_2	1421.87	1420.74	+5	19.399	0.417
BP1	KKL**W**KKILKYL-NH_2	1460.91	1459.91	+5	20.091	0.469
BP2	KKLFK**W**LKYL-NH_2	1494.93	1493.80	+5	19.157	0.468
BP3	KKLFKKI**W**KYL-NH_2	1494.93	1493.77	+5	19.329	0.477
BP4	KKLFKKILK**W**L-NH_2	1444.91	1443.87	+5	20.714	0.545
BP5	KK**W**WKKILKYL-NH_2	1533.96	1532.86	+5	21.373	0.519
BP6	KK**W**FKKILK**W**L-NH_2	1517.96	1516.80	+5	21.424	0.595
BP7	KKL**W**KKI**W**KYL-NH_2	1533.96	1532.98	+5	19.185	0.519
BP8	KKL**W**KKILK**W**L-NH_2	1483.95	1482.94	+5	20.947	0.586
BP9	KKLFK**W**K**W**KYL-NH_2	1567.98	1566.80	+5	18.485	0.518
BP10	KKLFKK**W**LK**W**-NH_2	1567.98	1566.78	+5	18.859	0.518
BP11	KKLFKKI**W**K**W**L-NH_2	1517.96	1516.99	+5	19.807	0.595
BP12	KKLFKKILK**W**W-NH_2	1517.96	1516.96	+5	18.335	0.595
BP13	KK**W**FKK**W**LK**W**L-NH_2	1591.02	1589.89	+5	21.349	0.635
BP14	KKL**W**KK**W**LK**Y**W-NH_2	1607.02	1605.80	+5	19.263	0.560
BP15	KKL**W**KKI**W**K**Y**W-NH_2	1607.02	1605.82	+5	18.513	0.569
BP16	KKLFKK**W**K**W**L-NH_2	1591.02	1589.69	+5	20.229	0.635

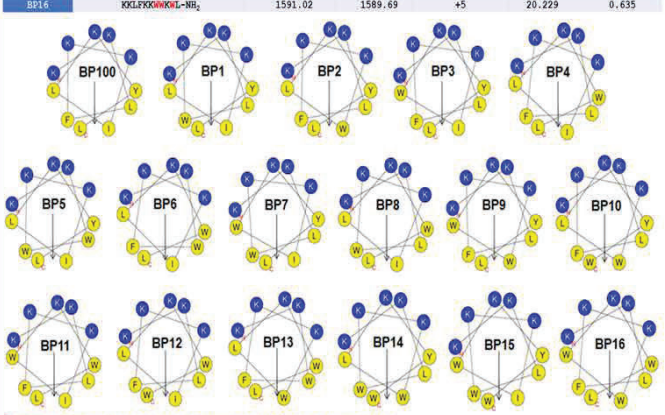

Figure 1. The α-helical wheel diagrams of BP100 and its analogs

Antimicrobial Activity & Cell Selectivity

Table 2. Antimicrobial Activities of BP100 and its analogs against bacterial strains

Bacterial strains	Minimal inhibitory concentration (MIC[a] (μM)																	
	BP100	BP1	BP2	BP3	BP4	BP5	BP6	BP7	BP8	BP9	BP10	BP11	BP12	BP13	BP14	BP15	BP16	Melittin
Gram-positive bacteria																		
S. aureus (KCTC 1621)	4	8	4	8	4	2	2	2	4	8	8	4	4	4	2	2	16	8
S. epidermidis (KCTC 1917)	4	8	2	8	8	1	2	2	2	4	8	4	4	8	2	4	16	32
B. subtilis (KCTC 3068)	8	8	8	16	4	2	4	4	8	16	16	8	8	8	4	4	16	16
Resistant Gram-positive bacteria																		
MRSA[b] (CCARM 3089)	32	32	16	64	64	4	8	8	16	64	64	8	64	32	16	16	16	32
MRSA (CCARM 3090)	64	64	16	64	64	8	16	32	16	64	64	32	64	32	32	64	128	8
VREF[c] (ATCC 51559)	64	64	128	64	16	8	8	32	16	64	128	16	128	16	64	64	64	64
Gram-negative bacteria																		
E. coli (KCTC 1682)	4	8	2	8	4	2	4	4	2	4	8	8	8	8	4	4	16	8
P. aeruginosa (KCTC 1637)	16	16	8	32	16	4	16	8	16	16	8	8	16	16	8	8	8	16
S. typhimurium (KCTC 1926)	4	8	8	4	2	2	4	2	4	4	8	2	4	8	8	4	16	16
Resistant Gram-negative bacteria																		
MDRPA[d] (CCARM 2095)	32	16	8	16	8	8	8	8	8	16	16	8	16	8	16	16	32	32
MDRPA (CCARM 2109)	16	16	4	16	16	4	16	4	16	16	16	16	16	16	8	8	32	32
GMᵉ	22.5	22.5	18.5	27.3	18.7	4.1	8.0	9.6	9.8	25.1	31.3	10.4	30.2	14.2	14.9	17.6	32.7	24.0
HC_{10}[f]	>256	>256	>256	>256	>256	>256	>256	>256	>256	>256	>256	>256	>256	>256	>256	>256	>256	2.0
TIᵍ	22.7	22.7	27.7	18.8	27.4	124.9	64.0	53.3	52.2	20.4	16.4	49.2	17.0	36.1	34.4	29.1	15.7	0.08

Resistance to Salts and Human serum

Peptides	Control	150 mM NaCl	4.5 mM KCl	6 μM NH_4Cl	1 mM $MgCl_2$	2.5 mM $CaCl_2$	4 μM $FeCl_3$	10% Human Serum
				E. coli (KCTC 1682)				
BP100	4	16	16	16	16	16	16	16
BP5	2	8	4	4	4	8	8	4
BP6	4	8	4	16	8	16	16	4
BP8	2	8	4	8	8	16	4	4
BP11	8	16	8	4	8	16	4	8
BP13	8	16	8	8	8	16	8	16
				S. aureus (KCTC 1621)				
BP100	4	16	16	16	16	16	16	32
BP5	2	4	4	4	4	4	4	4
BP6	2	4	4	4	4	4	8	4
BP8	4	4	4	4	4	4	4	4
BP11	4	8	4	4	4	16	4	8
BP13	4	8	8	8	8	8	8	8

Anti-biofilm Activity

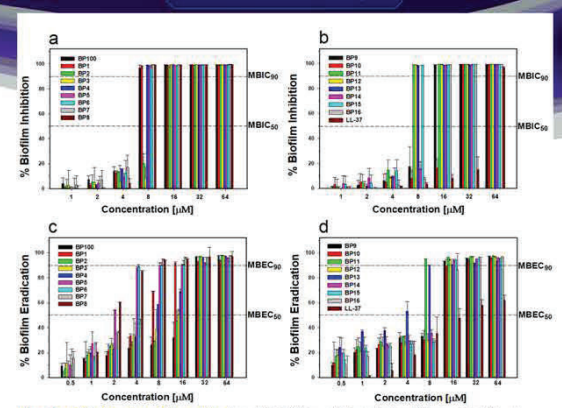

Figure 2. Antibiofilm activity of the peptides. (a and b) Inhibitory activity against multidrug-resistant *Pseudomonas aeruginosa* (MDRPA). (c and d) Eradication activity of preformed MDRPA biofilms. The dotted lines indicate 50% and 90% inhibition and eradication concentration.

Anti-inflammatory Activity

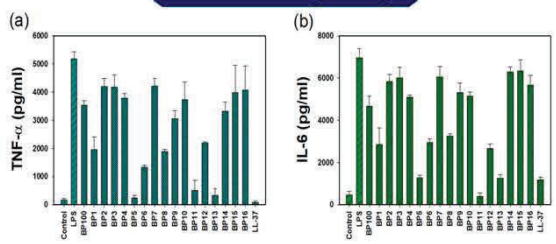

Figure 3. Effects of BP100 and its analogs on the release of TNF-α (a) and IL-6 (b) from LPS-stimulated RAW264.7 cells. The peptides were used at a concentration of 2μM for this experiment. All data represent at least three independent experiments and are expressed as means ± standard error of the mean (SEM). The data were analyzed using one-way analysis of variance (ANOVA) with Bonferroni's post-test. Asterisks indicate statistically significant differences (*P < 0.001 for each agonist).

Synergy Activity

Table 3. Synergistic antimicrobial activity of the peptide with ciprofloxacin (CIP) against MDRPA (CCARM 2095)

Peptides	MIC_A	[A]	FIC_A	MIC_B	[B]	FIC_B	FICI[a]	Interpretation
BP100	32	4	0.125	2048	512	0.25	0.375	synergy
BP5	8	0.5	0.0625	2048	512	0.25	0.3125	synergy
BP6	8	1	0.125	2048	512	0.25	0.375	synergy
BP8	8	0.5	0.0625	2048	512	0.25	0.375	synergy
BP11	8	0.5	0.0625	2048	512	0.25	0.3125	synergy
BP13	8	0.125	0.015625	2048	512	0.25	0.2656	synergy

Antimicrobial Mechanism

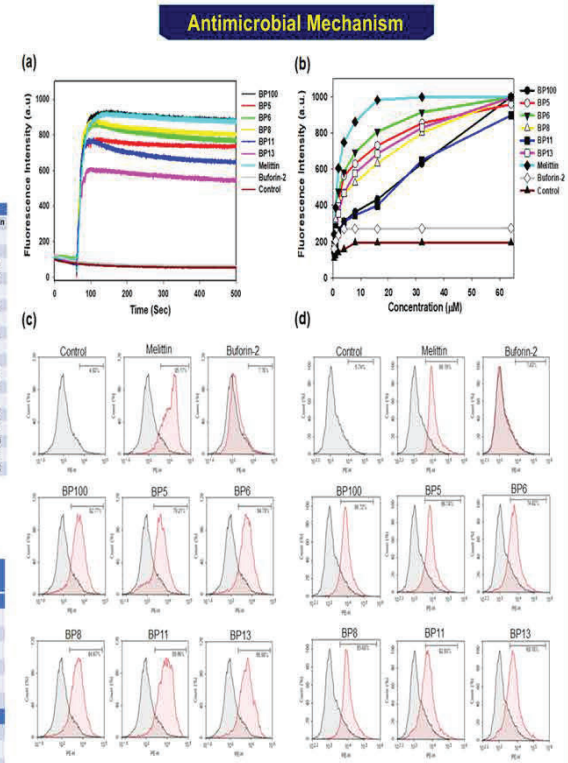

Figure 4. (a) Time-dependent cytoplasmic membrane depolarization of *S. aureus* (KCTC 1621) treated with the peptides (1×MIC), as assessed by the release of the membrane potential-sensitive dye $DiSC_3$-5. (b) Membrane uptake of 1-N-phenylnaphthylamine (NPN) by *E. coli* (KCTC 1682) in the presence of different concentrations of the peptides. (c) Membrane integrity of *E. coli* (KCTC 1682), as observed by flow cytometry. (d) Membrane integrity of *S. aureus* (KCTC 1621), as observed by flow cytometry.

https://doi.org/10.17952/37EPS.2024.P1165

Study on the stability of new promising antimicrobial peptides against protease activities present in infection sites

Clelia Cortese[1,4], Giovanni Cappello[1,4], Laura Cresti[1,4], Virginia Niccolini[1,4], Marco Scocchi[2], Marialuisa Mangoni[3], Alessandro Pini[1,4]

[1] *Department of Medical Biotechnologies - University of Siena, Italy*
[2] *Department of Life Sciences - University of Trieste, Italy*
[3] *Department of Biochemical Sciences - University of Rome "La Sapienza", Italy*
[4] *SetLance Srl - Siena, Italy*

Finanziato dall'Unione europea NextGenerationEU
Italiadomani PIANO NAZIONALE DI RIPRESA E RESILIENZA
Ministero dell'Università e della Ricerca

Bacterial respiratory infections are one of the leading causes of mortality worldwide, being associated with million deaths annually. Due to the increasing resistance of major respiratory bacteria to available antibiotics, coupled with the depletion of the traditional antibiotic pipeline, treatment options have become severely restricted. The emergence of **antimicrobial resistance** presents a significant threat to global health and highlights the urgent need for novel therapies.

Nature-inspired antimicrobial peptides (**AMPs**) are rapidly gaining attention for clinical translation, as they offer distinct advantages over conventional antibiotics by being molecules with multiple functions with rapid activity against a broad spectrum of microorganisms. AMPs of animal origin are molecules of the innate immunity of eukaryotes which act as a first-line defense against infections (many of them are evolutionarily conserved). They are less likely to elicit resistance than peptides of synthetic origin. Their structure differs from human AMPs, such as LL-37, minimizing the risk of inducing bacterial resistance to our endogenous AMPs or triggering autoimmune responses. Furthermore, AMPs are composed of amino acids: renewable and harmless compounds that do not persist in the environment and also provide harmless degradation products for human health. Therefore, AMPs demonstrate their intrinsic "green" nature through biodegradability and the absence of harmful degradation products. Several naturally occurring peptides with interesting properties were selected, such as (i) short helical AMPs active on the membrane of microorganisms (**MA-AMP**), (ii) or short, proline-rich AMPs that can act at an intracellular level by inhibiting protein synthesis (**PR-AMP**). The combined use of MA- and PR-AMP with different modes of action is expected to increase activity and significantly prevent or slow the incidence of resistance.

The objective of this study is to evaluate the properties of these AMPs for the development of a valid alternative to current therapies for the treatment of lung infections caused by "priority bacterial pathogens" such as *Staphylococcus aureus* and *Pseudomonas aeruginosa*. With this aim, **peptides stability** will be studied in environments where elastases of endogenous or bacterial origin are present. The peptide stability profile will be shown by HPLC and MALDI-TOF analyses. Trials for the development of a new peptide-based drug will continue for the most promising peptides.

STABILITY

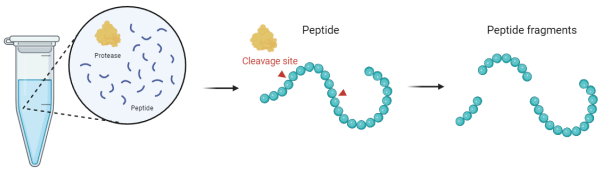

Figure 1. *Enzymatic action inside the test tubes and generation of fragments that will be analyzed by mass spectrometry (MALDI-TOF)*

PEPTIDEs

Peptide A – It is derived from larger peptides (21 residues). They are efficient in countering *P. aeruginosa* lung infection in mice, and they also inhibit *P. aeruginosa* biofilm formation under standard conditions.

Peptide B – It is an unusually short MA-AMPs (13 residues), mainly active against Gram-positive bacteria; can eradicate preformed *S. aureus* biofilms under standard conditions and are also active on intracellular *S. aureus*.

PROTOCOL

Peptide solution: 1 mg/mL
Peptide/enzyme ratio: 120 nmol / 1 unit
Reaction Volume: 130 µL

Incubation at 4 times: T_0, T_1, T_5 and T_{24}

HPLC analyses to verify the formation of fragments
MS analyses to identify the fragments from their weight.

TIME COURSE STABILITY

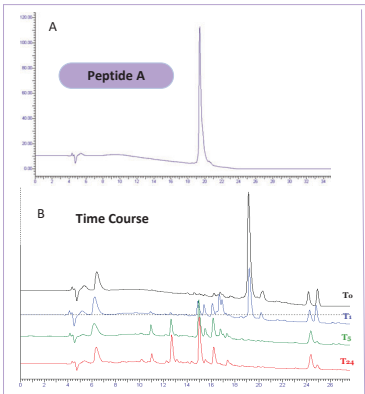

Figure 2. *A) HPLC analysis of Peptide A dissolved in TrisHCl 10 mM. B) HPLC analysis of Peptide A at 4 incubation times (0h, 1h, 5h, 24h) with human elastase in a ratio of 120nmol of peptide for 1unit of enzyme.*

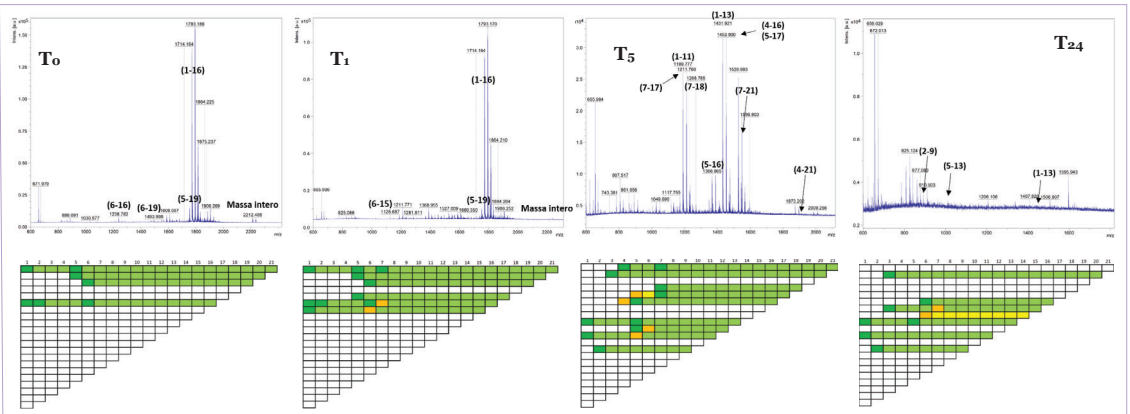

Figure 3. *Above, mass spectrometric analysis of Peptide A at 4 different incubation times. Below, graphic representation of the fragments found in the MS analyses.*

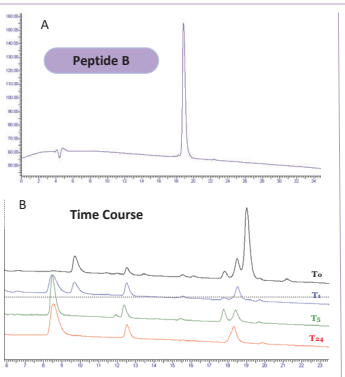

Figure 4. *A) HPLC analysis of Peptide B dissolved in TrisHCl 10 mM. B) HPLC analysis Peptide B at 4 incubation times (0h, 1h, 5h, 24h) with human elastase in a ratio of 120nmol of peptide for 1unit of enzyme.*

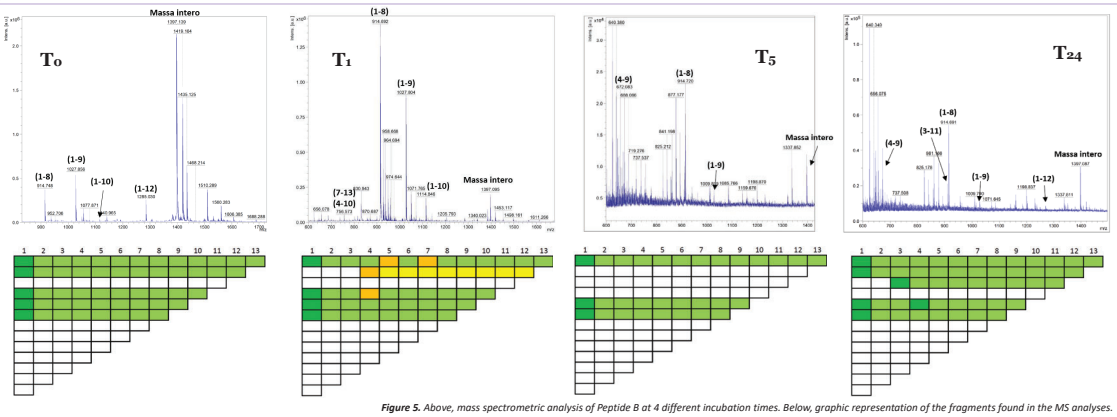

Figure 5. *Above, mass spectrometric analysis of Peptide B at 4 different incubation times. Below, graphic representation of the fragments found in the MS analyses.*

DISCUSSION

One of the main limits in using AMPs for treatment of lung infection is their susceptibility to enzymatic degradation. The lung environment of cystic fibrosis patients is rich in proteases and it is therefore important that any AMPs should not be susceptible to their enzymatic action. To determine whether these proteases affect the antimicrobial activity of peptides, their stability was analysed using purified human neutrophil elastase. AMP were incubated with the enzyme and the resulting solutions were analysed by HPLC and mass spectrometry at defined time points.

Peptide A undergoes complete degradation within 5 hours by human neutrophil elastase as confirmed by both HPLC and mass spectrometry analyses.

In contrast, **Peptide B** showed a faster degradation rate, according to the HPLC analyses, with minimal detectable quantities after 1 hour of incubation. However, mass spectrometry analyses, with a greater sensitivity, detect its presence even after 24 hours of incubation with the enzyme.

CONCLUSIONs

The purpose of this project is to identify the **best therapeutic peptides** for treatment of *P. aeruginosa* and *S. aureus* for lung infection starting from previously tested peptides that have shown promising results.

Among the peptides examined, **Peptide B** appears to have greater resistance to the enzymatic action of human elastase and, given the data previously observed, we expect that this stability will also persist against elastases of bacterial origin.

Other peptides will be tested for their stability. The most valid peptides will also be subjected to **efficacy**, **cytotoxicity**, **synergy** and **resistance** studies. For those peptide that will pass this first screening phase, further studies will be carried out in lung mimicking environments and then and will continue with the *in vivo* testing phase.

REFERENCEs

1 - Falciani *et al.* (2012). PloS ONE 7(10): e46259.
2 - Cappiello *et al.* (2016). Antimicrobal agents. , 60(12), 7252-7262.
3 - Cappiello *et al.* (2022). Pharmaceutics, 14(11), 2297.
4 - Mangoni *et al.* (2011). Journal of medicinal chem., 54(5), 1298-1307.
5 - Casciaro *et al.* (2019). Biomacromolecules, 20(5), 1876-1888.
6 - Scocchi *et al.* (2016). Cur. topics in medicinal chemistry, 16(1), 76-88.
7 - van der Weide *et al.* (2019). Int. Journ. of antimicrob., 54(2), 159-166.
8 - Degasperi *et al.* (2020). Microorganisms, 8(9), 1407.

NUMAFERM
The Peptein Company

Revolutionizing Peptide Production: Introducing An Engineered TEV Protease

R. Guerrette, C. Schwarz, B. Wetzel
https://doi.org/10.17952/37EPS.2024.P1170

What we do:

Numaferm specializes in **Pepteins** (without lenght limitation) **Peptide** and **Protein** production. Our Numaswitch platform is a **scalable** process that offers a **cost-effective** solution for **high-quality** biomolecule production for **R&D** up to **GMP grade** scale.

We bringing the **speed** of chemical synthesis for the first time to the world of peptide and protein while being **environmentally friendly** and **future proof**.

Numaswitch is a platform that offers State-of-the-art chemistry:

- fatty acids, fluorphores, PEGylation, toxins
- C-terminal amidation
- N-terminal acetylation
- Fermentative incorporation of **non-natural amino acids**
- Switchtags offer bioactive refolding of complex molecules up to 6 Cys bridges.
- **Endotoxin levels lower than < 1 EU/mg**.

Numaswitch® – The superiour Solution to conventional processes

Methodology	Chemical Synthesis	Biochemistry	Bioprocess
Platform	SPPS/hybrid approaches	NUMASWITCH™	Recombinant approaches
Developement Speed (for 100g Phase 1 trials)	~ 6–24 months	**6–9 months**	~ 12–24 months
Purity	> 90%	**> 98%**	> 95%

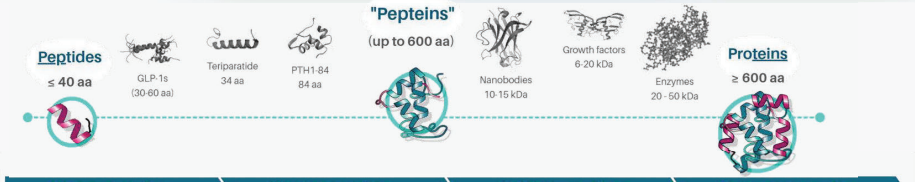

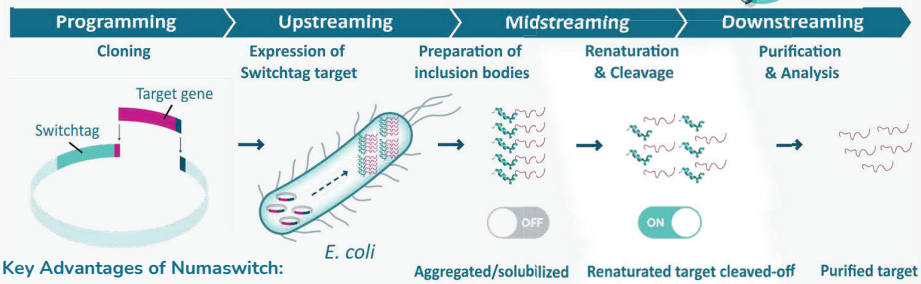

Our Roadmap to Commecial Production:

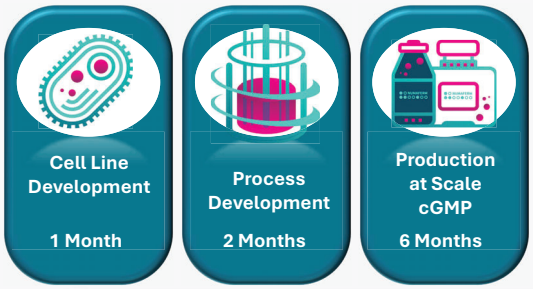

Key Advantages of Numaswitch:

- High product yields (g/L)
- Ultra-pure biomlecules (> 99%)
- Endotoxin-free products
- Scalable processes (mg to multi-ton scale)
- R&D and GMP-grade excellence
- Complex molecules

NumaCUT®

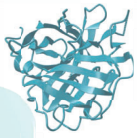

Meet the Family!

Tailored for you Experimental Needs

Evolved by directed evolution, the recognition site from wild type TEV protease (ENLYFQ↓S/G) was broadened to **ENLYFQ↓X** (X: any amino acid, except P). Fuse your target peptide or protein to the C-terminus of **any protein tag**, with an ENLYFQ sequence in between, which allows cleavage by the Numacut **regardless of the N-terminal amino acid.**

Experience Numacut's exceptional performance **tailored for your experimental needs**. It outperforms a competitor's wild type TEV protease from competitors, stays **highly active in high concentrations of chemicals, chaotropes, salts, and across a wide range of buffer systems and pH levels**. Trust Numacut for reliable and efficient cleavage, regardless of the condition.

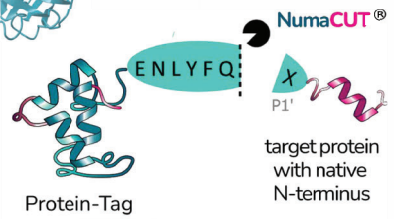

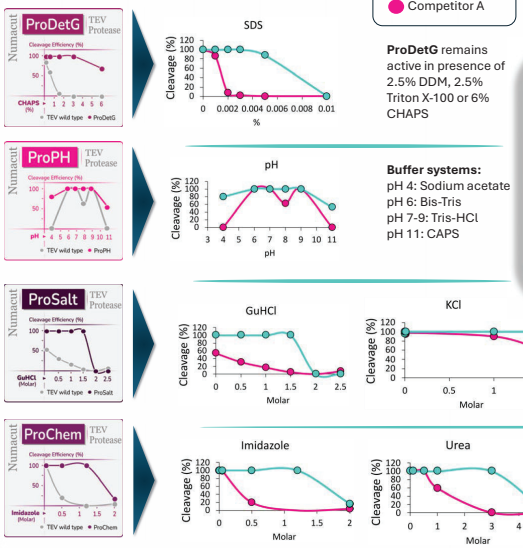

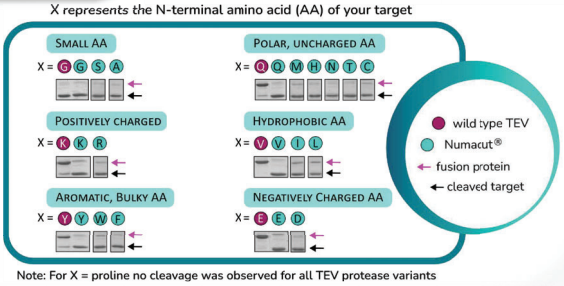

Note: For X = proline no cleavage was observed for all TEV protease variants

Contact us

Numaferm GmbH
Merowingerplatz 1a
40225 Düsseldorf
Phone: +49 (0) 211 97532900
E-Mail: info@numaferm.com

Small Scale or GMPc

Order Online Credit Card or a PO

Spatio-temporal control of cellular differentiation for cartilage tissue engineering

Jules SIMONIN GARCIA[1,2], Cécile ECHALIER[1], Emmanuel BELAMIE[2], Marie MORILLE[2], Gilles SUBRA[1]

[1]Institut des Biomolécules Max Mousseron, Univ. Montpellier, CNRS, ENSCM, Montpellier, France [2]Institut Charles Gerhardt de Montpellier, Univ. Montpellier, CNRS, ENSCM, Montpellier, France

https://doi.org/10.17952/37EPS.2024.P1172

Project context

Osteoarthritis (OA) : most prevalent joint disease (1/13 people worldwide). Defined by self-healing difficulties of cartilaginous lesions.

Our approach to treat OA : deliver cartilage producing cells (chondrocytes) to the chondral lesions.

The problem : chondrocytes undergo hypertrophy (RunX2 gene overexpression) and production of collagen II is limited.

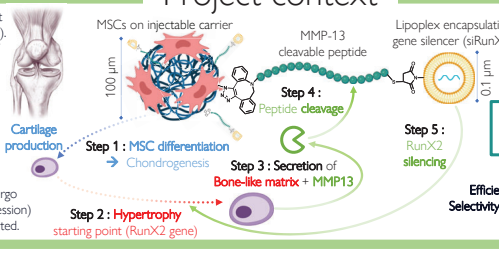

The new idea : use of the hypertrophy secretion of matrix-metalloproteinase 13 (MMP-13) to deliver a siRNA to down-regulate RunX2.

The project needs : a MMP-13 cleavable linker (peptide), very efficient and very selective against other synovial enzymes.

Efficiency : sequence cleavage rate for MMP-13.
Selectivity : sequence efficiency for MMP-13 / sequence efficiency for other proteases.

Poster summary

In this work, we present a new methodology for rapid screening of protease-cleavable peptide with high selectivity.

1. First, we designed a program capable of outputting protease-selective sequence libraries.
2. Then, we developed a fast and accurate method for the screening of efficiency and selectivity of peptide libraries.
3. Finally, we validated the program and the new screening method with established screening method (by UHPLC).

1 Computer Program and analysis optimizations

Programs available : **SELECTIVITY**
- SitePrediction and PeptideCutter (cleavage site)
- PepSite (binding sites)
- DeepPeptide (AI) and PoPS (substrate specificity)

Our program : **SELECTIVITY** **EFFICIENCY**

- based on the **score of amino acids**, per position and per enzyme (MEROPS), gives :
- **the most selective sequence** of the target protease
- **the sequence library** from the **most selective** to the **most efficient**
- **the most efficient protease** of the target sequence

n°	Sequences	n°	Sequences	n°	Sequences
1	GPKG(MNP)P	9	GPPG(MNP)P	17	GPLG(MNP)P
2	GPKG(MNG)P	10	GPPG(MNG)P	18	GPLG(MNG)P
3	GPKG(MRP)P	11	GPPG(MRP)P	19	GPLG(MRP)P
4	GPKG(MRG)P	12	GPPG(MRG)P	20	GPLG(MRG)P
5	GPKG(LNP)P	13	GPPG(LNP)P	21	GPLG(LNP)P
6	GPKG(LNG)P	14	GPPG(LNG)P	22	GPLG(LNG)P
7	GPKG(LRP)P	15	GPPG(LRP)P	23	GPLG(LRP)P
8	GPKG(LRG)P	16	GPPG(LRG)P	24	GPLG(LRG)P

24-peptide library
Target protease : MMP-13
Competing proteases : [MMP-1, MMP-2, MMP-3, MMP-9, ADAMTS-4, ADAMTS-5]
")(" : sequence cleavage bond

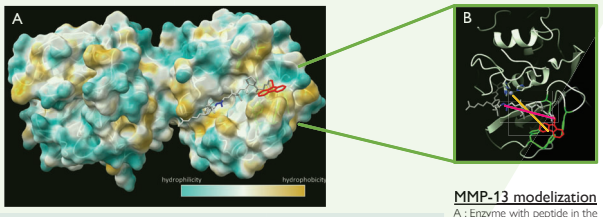

MMP-13 modelization
A : Enzyme with peptide in the catalytic pocket
B : Catalytic site zoom
: 15 A
: 14,5 A

An **aromatic area** was found near the cleavage site, **with matching distances** (N-ter--cleavage bond and Zn--aromatic area). All further studies were made with **Fmoc N-ter peptides (FIPs)** to allow peptides to **interact** with MMP-13.

2.a Indirect Fluorescence Competition (IFC) : Efficiency

Principle

FIP22 (interferent peptide, non fluorogenic)

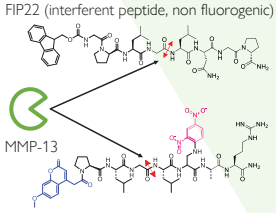

Mca-Dpa (MMP substrate, fluorogenic)

FIP22-induced slope decrease

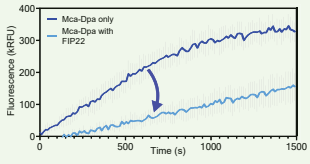

Mca-Dpa cleavage (MMP-13) : Fluorescence **increases**.
Mca-Dpa cleavage with interferent peptide : slope (hydrolysis rate) **decreases**.

Comparison of existing methods with IFC

	HPLC	Fluorescence	**IFC**
Precision	+ +	-	+
Analysis duration	- -	+ +	+ +
Costs	- -	- -	+ +
Suitable for large libraries	- -	-	+ +

Δ_S = % slope decrease with respect to substrate alone, ranked by sequence *in silico* scores
in silico scores calculated with the program (2nd option)

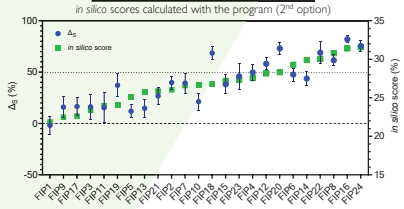

The IFC efficiency **increases** with the *in silico* score

2.b IFC : Selectivity

***in silico* score for chosen sequences and for every protease involved**
in silico scores calculated with the program (3rd option).

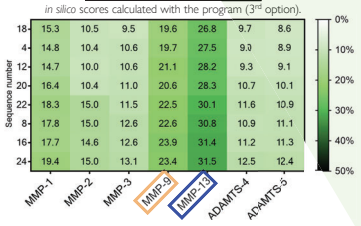

MMP-9 **most efficient protease** after MMP-13

Slope difference as a percentage of the Substrate slope
Comparison between MMP-13 and MMP-9

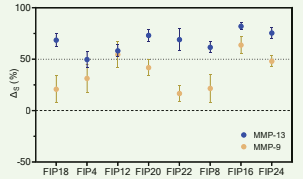

All peptides are **selective** towards MMP-13

Calculated selectivity of the 8 chosen peptides

FIP	$\Delta_{S,\ MMP-13}$ (%)	$\Delta_{S,\ MMP-9}$ (%)	Selectivity
18	68,5	20,8	3,29
4	49,7	31,3	1,59
12	58,1	54,5	1,07
20	73,0	41,7	1,75
22	69,0	16,6	4,16
8	61,5	21,5	2,86
16	81,9	63,7	1,29
24	75,4	47,9	1,57

FIP12 and FIP16 : **poor selectivity**
Probably due to **proline** at **P2** position
(higher MEROPS value for MMP-9 than MMP-13)

3 UHPLC Verification

Michaelis-Menten fit for FIP22

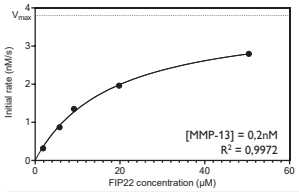

Kinetic reactions with **increasing** [FIPx] at a **fixed** [MMP-13]

K_M and k_{cat} of each MMP-13/peptide pairs

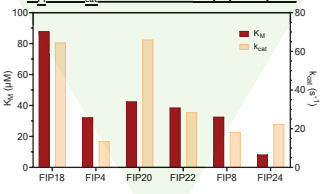

P1' position : **Leu** lowers more K_M than **Met**
P2' position : **Arg** lowers more K_M than **Asn**

k_{cap} (=k_{cat}/K_M) and Δ_S of each MMP-13/peptide pairs

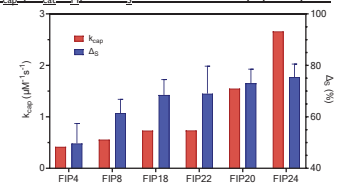

The IFC efficiency **increases** with the k_{cap} calculated with UPLC

Conclusion and perspectives

Selective and **efficient** methodology to screen **protease-sensitive peptides :**

Program predicting the **sequence library** to screen

New screening method that is **faster**, **cheaper** and **accurate** to rank peptides

Usable for **various projects**, depending on the specifications

Comparison of the specificity and selectivity of each MMP-13/peptide pairs

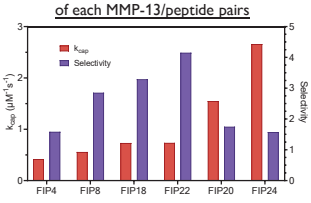

Use of **IP22** for the main project (the most selective one, with good efficiency) :
- **click chemistry** to the carrier;
- **thiol-Michael addition** to the siRNA lipoplexe.

Proof of method robustness on other enzymes complexes.
Research on the **theorical connection** between Δ_S and k_{cap}.

References

Global Burden of 369 Diseases and Injuries in 204 Countries and Territories, 1990–2019: A Systematic Analysis for the Global Burden of Disease Study 2019. *The Lancet* **2020**, 396 (10258), 1204–1222.

Scotti, C. *et al.*, Recapitulation of Endochondral Bone Formation Using Human Adult Mesenchymal Stem Cells as a Paradigm for Developmental Engineering. *Proceedings of the National Academy of Sciences* **2010**, 107 (16), 7251–7256.

Mathieu, M. *et al.*, Induction of Mesenchymal Stem Cell Differentiation and Cartilage Formation by Cross-Linker-Free Collagen Microspheres. *Eur Cell Mater* **2014**, *28*, 82–96; discussion 96-97.

Stay tuned for the publication

jules.simonin-garcia@umontpellier.fr
Tel : (+33)6 87 24 46 74

Pôle Chimie Balard Recherche
IBMM - UMR 5247 // ICGM - UMR 5253
1919, route de Mende
34293 MONTPELLIER cedex 5

37th European Peptide Symposium
14th International Peptide Symposium

Development of a novel alternative method for liraglutide production

Gabriela R. Barredo-Vacchelli[1,2], Jésica A. Rodríguez[1,2], Joaquín A. Eloy[1,2] and Silvia A. Camperi.[1,2]

[1]Universidad de Buenos Aires, Facultad de Farmacia y Bioquímica (FFyB), Cát. de Biotecnología, 1113 Ciudad Autónoma de Buenos Aires (CABA), Argentina
[2]UBA, Consejo Nacional de Investigaciones Científicas y Técnicas (CONICET), Instituto de Nanobiotecnología, 1113 CABA, Argentina

https://doi.org/10.17952/37EPS.2024.P1173

Introduction

Liraglutide (Fig.1) is applied in type-2 diabetes and obesity. Although, solid-phase peptide synthesis (SPPS) strategies have been designed, most of them are expensive and many of them are difficult to scale-up. Furthermore, this long peptide is prone to aggregate during its elongation, thereby hampering the yield and purity of the product.

Another disadvantage is the high cost of its purification by reverse phase high pressure liquid chromatography (RP-HPLC). In this work an alternative method for liraglutide production was developed to overcome the high cost and difficulties of current processes.

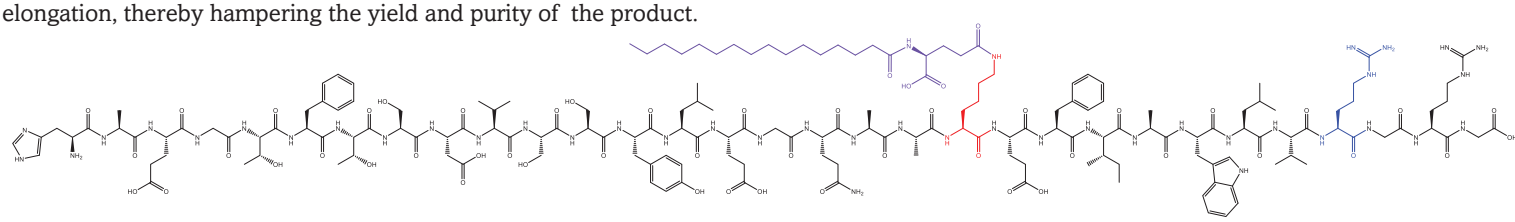

Fig. 1. Liraglutide sequence: His-Ala-Glu-Gly-Thr-Phe-Thr-Ser-Asp-Val-Ser-Ser-Tyr-Leu-Glu-Gly-Gln-Ala-Ala-Lys(γ-Glu-palmitoyl)-Glu-Phe-Ile-Ala-Trp-Leu-Val-Arg-Gly-Arg-Gly

Materials and Methods

The peptide was elongated by Fmoc/tBu solid-phase peptide synthesis on 4-(Hydroxymethyl)benzoyl-ChemMatrix resin (HMBA-CM). To prevent peptide aggregation the chaotropic agent LiCl was used as an additive in the coupling and deprotection mixtures. Side-chain protecting groups were removed with TFA, leaving the unprotected peptide attached to the solid support. The resin was thoroughly washed to eliminate the contaminants. Next, peptide was released with NaOH. Finally, liraglutide was purified by hydrophobic interaction low pressure liquid chromatography (HI-LPLC) using a TOYOPEARL Phenyl-650M column (Fig. 2).

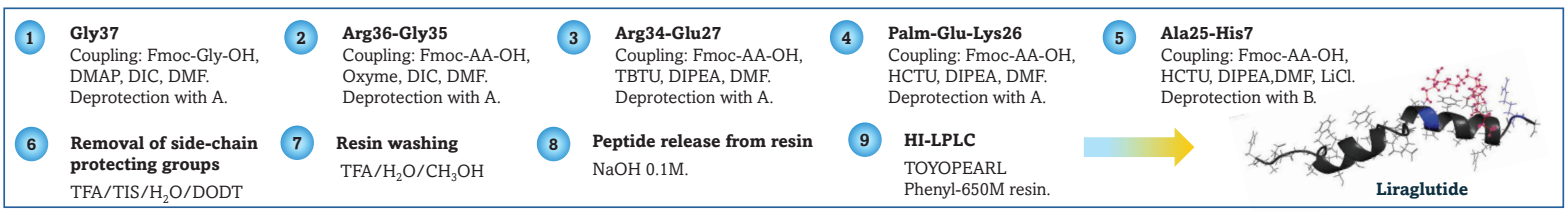

Fig 2. Liraglutide production protocol. A: piperidine/DMF (1:4); B: piperidine/LiCl 0.2 M in DMF (1:4).

Results and discussion

CM resin was suitable for the synthesis of this long peptide. LiCl was useful to prevent peptide aggregation. After side-chain protecting group removal, the resin was thoroughly washed and then the peptide was released from the resin. This two-stage procedure assures a high purity product. Afterwards, it was purified by HI-LPLC (Fig. 3) using an economic system with a peristaltic pump. The main peak was analyzed by RP-HPLC and showed a purity of 85% (Fig. 4). Its identity was analyzed by ESI-MS (Fig. 5). The main signals were $[M+4H]^{4+}$ (m/z=938.7) and $[M+3H]^{3+}$ (m/z=1251.3), which corresponded to the multiply protonated ions of liraglutide.

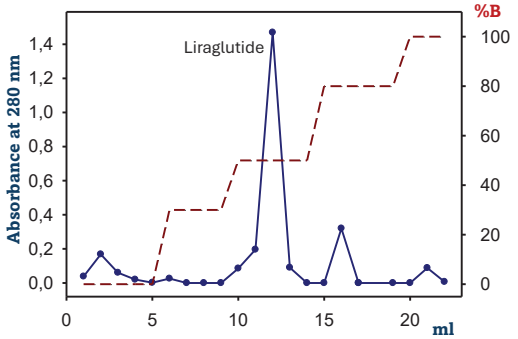

Fig. 3. Low-pressure hydrophobic interaction liquid chromatography. A: H_2O; B: Acetonitrile.

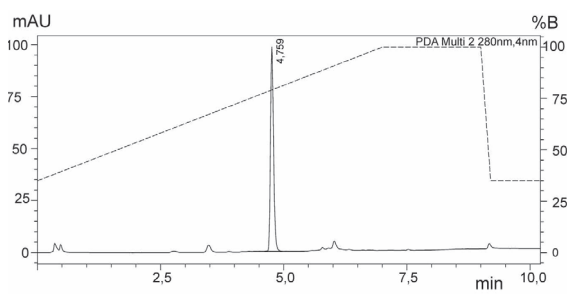

Fig. 4. Liraglutide RP-HPLC in C18 column. A: 0.045% TFA in H_2O. B: 0.036% TFA in acetonitrile.

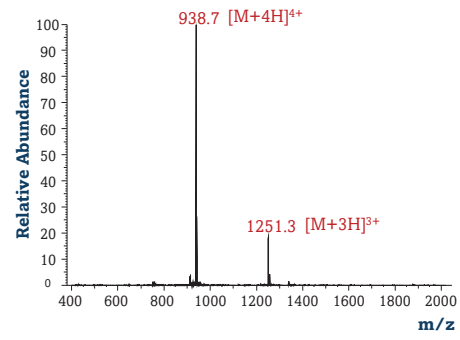

Fig. 5. Liraglutide ESI-MS.

Conclusions

This simple and economic method resulted in a product with high yield and purity as demonstrated by analytical RP-HPLC and ESI-MS while overcoming the high cost and difficulties of current processes. Although the SPPS has been performed manually with a domestic microwave, the method can be easily scaled-up by using an automated microwave peptide synthesizer. The present protocol can also be applied for the synthesis of similar incretin analogues.

scamperi@ffyb.uba.ar
https://nanobiotec.conicet.gov.ar/
nanobiotec.inst

https://doi.org/10.17952/37EPS.2024.P1174

37th European Peptide Symposium
14th International Peptide Symposium

Comparison of in vitro immunogenicity between δ-ctenitoxin-Pn2a and epitope-based immunogens

Jésica A. Rodríguez[1,2], Gabriela R. Barredo-Vacchelli[1,2], Ariadna M. Birocco[3], Agustín Blachman[3], Gerardo Acosta[5,6], Fernando Albericio[5,6,7], Graciela C. Calabrese[3,4] and Silvia A. Camperi.[1,2]

[1]Universidad de Buenos Aires, Facultad de Farmacia y Bioquímica (FFyB), Cát. de Biotecnología, 1113 Ciudad Autónoma de Buenos Aires (CABA), Argentina; [2]UBA, Consejo Nacional de Investigaciones Científicas y Técnicas (CONICET), Instituto de Nanobiotecnología, 1113 CABA, Argentina; [3]UBA, FFyB, Cát. de Biología Celular y Molecular, 1113 CABA, Argentina; [4]UBA-CONICET, IQUIFIB, 1113 CABA, Argentina; [5]CIBER-BBN, Networking Centre on Bioengineering, Biomaterials and Nanomedicine, and Department of Organic Chemistry, University of Barcelona, 08028 Barcelona, Spain; [6]Unidad de Péptidos, Universitat de Barcelona, Unidad Asociada al CSIC por el IQAC, Barcelona 08028, Spain; [7]School of Chemistry & Physics, University of KwaZulu-Natal, 4001 Durban, South Africa.

Introduction

Currently, the production of antivenom against the bite of *Phoneutria nigriventer* spider requires its capture and venom extraction by electrostimulation, a cumbersome, dangerous, and low-yielding method. Afterwards, the venom is injected into large mammalians to obtain immunoglobulins, which are then purified from plasma to make antiserum. Otherwise, those neurotoxins responsible for envenomation as well as epitope-based immunogens can be synthesized and used to optimize the



production of antivenoms for meeting their demands. The neurotoxin δ-ctenitoxin-Pn2a (UniPort: P29425) is the main responsible for the symptoms of *P. nigriventer* envenoming in humans. In previous studies we identified epitope G[34]YFWIAWYKLANCKK[48] from δ-ctenitoxin-Pn2a and used it to design immunogenic peptides. In this work δ-ctenitoxin-Pn2a was synthesized and its *in vitro* immunogenicity was compared with those immunogenic peptides.

Materials and Methods

δ-ctenitoxin-Pn2a was produced by automated microwave solid-phase peptide synthesis (SPPS) using Fmoc/tBu chemistry. Also, the epitope G[34]YFWIAWYKLANCKK[48] was synthesized manually by SPPS using Fmoc/tBu chemistry. The Cys was replaced by α-aminobutyric acid to avoid disulfide bonds formation resulting the peptide Ac-GYFWIAWYKLAN-Abu-KKG-NH_2 (a). The branched peptide (Ac-GYFWIAWYKLAN-Abu-KK)$_2$-KG-NH_2 (b) and the lipopeptide Palm-GYFWIAWYKLAN-Abu-KKG-NH_2 (c) were also manually synthesized to increase the immunogenicity. Cytotoxicity of δ-ctenitoxin-Pn2a and the epitope-based immunogens were evaluated on murine macrophage cell line RAW 264.7 using the 3-[4,5-dimethylthiazol-2-yl]-2,5-diphenyltetrazolium bromide (MTT) assay in the presence of increasing doses of each peptide (0.25–10.0 μM). The cellular distribution of the transcriptional factor NF-κB was examined by immunofluorescence after exposing macrophages to 0.5 μM of each peptide or δ-ctenitoxin-Pn2a.

Results and Discussion

δ-ctenitoxin-Pn2a did not show cytotoxicity between 0.25 and 10.0 μM (Fig. 1). On the other hand, Ac-GYFWIAWYKLAN-Abu-KKG-NH_2 (a) did not show cytotoxicity between the evaluated concentrations, while peptides Palm-GYFWIAWYKLAN-Abu-KKG-NH_2 (b) and (Ac-GYFWIAWYKLANAbuKK)$_2$-KG-NH_2 (c) did at concentrations equal or over 0.5 and 10.0 μM, respectively (Fig. 2).

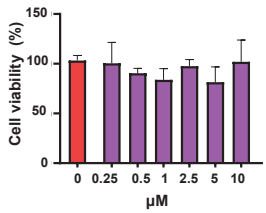

Fig. 1. Cell viability MTT assay histograms expressed as percentage of the control after their exposure to increasing concentrations of δ-ctenitoxin-Pn2a.

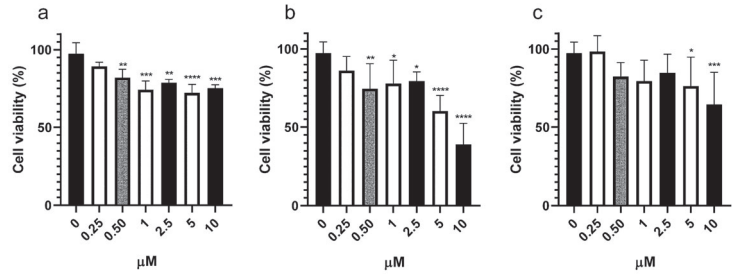

Fig. 2. Cell viability MTT assay histograms expressed as percentage of the control after their exposure to increasing concentrations of peptide.

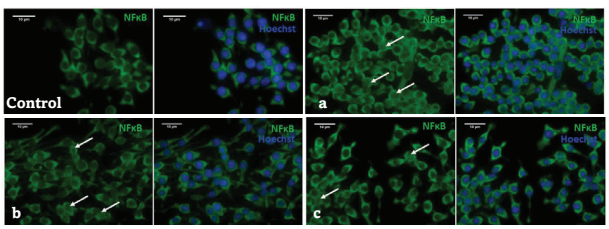

Fig. 3. NF-κB cellular distribution. Control cells, and cells treated with 0.5 μM of Ac-GYFWIAWYKLAN-Abu-KKG-NH_2 (a), Palm-GYFWIAWYKLAN-Abu-KKG-NH_2 (b) and (Ac-GYFWIAWYKLAN-Abu-KK)$_2$-KG-NH_2 (c).

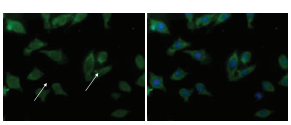

Fig. 4. NF-κB cellular distribution of cells treated with 10 μM δ-ctenitoxin-Pn2a.

NF-κB cellular distribution was detected by green immunofluorescence. Also, the nuclei were stained with Hoechst (blue). When immunogens activate cells, NF-κB migrates from the cytosol to the nucleus, where it upregulates cytokine gene expression. In resting macrophages (control), the transcription factor was restricted to the cytosol. In contrast, immunofluorescence was observed in the nucleus of the cells in the presence of 0.5 μM of each peptide thereby suggesting that they promote an immune response (Fig. 3). However, as shown in Fig. 4, δ-ctenitoxin-Pn2a only promote nuclear translocation at higher concentrations (10 μM). Probably, the cystine-knot motif of δ-ctenitoxin-Pn2a (Fig. 5) provides exceptional stability, thereby hampering immune response activation. Nevertheless, *in vivo* tests are still required to study the immunogenic capacity of the neurotoxin and the epitope-based immunogens for their use in the antivenom production.

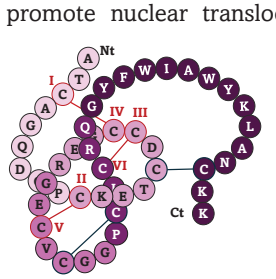

Fig. 5. Scheme of δ-ctenitoxin-Pn2a with the cystine-knot motif.

scamperi@ffyb.uba.ar
nanobiotec.inst
https://nanobiotec.conicet.gov.ar/

Extracellular-Vesicle Catch-and-Release isolation System using a Net-charge Invertible Curvature-sensing peptide

○Kenichi Kawano[1], Yuki Kuzuma[1], Koichi Yoshio[1], Kenta Hosokawa[1], Yuuto Oosugi[1], Takahiro Fujiwara[2], Fumiaki Yokoyama[3], Katsumi Matsuzaki[1]

1 Graduate School of Pharmaceutical Sciences, Kyoto University, Kyoto, Japan,
2 Institute for Integrated Cell-Material Sciences (WPI-iCeMS), Kyoto University, Kyoto, Japan,
3 Graduate School of Science, The University of Tokyo, Tokyo, Japan



https://doi.org/10.17952/37EPS.2024.P1176

Abstract

Extracellular vesicles (EVs) carry various informative components, including signaling proteins, transcriptional regulators, lipids, and nucleic acids. EVs have shown great promise as pharmaceutical-targeting vesicles and have attracted the attention of researchers in the fields of biological and medical science because of their importance as diagnostic and prognostic markers. However, the isolation and purification of EVs from cell-cultured media remain challenging. Ultracentrifugation is the most widely used method, whereas it requires specialized and expensive equipment. A simple method in a short time using general experimental equipment found in ordinary laboratories is required for researchers to reproducibly isolate EVs.

We proposed a novel methodology to isolate EVs using a simple and convenient method, *i.e.*, an EV catch-and-release isolation system (EV-CaRiS) using a newly designed biosensor, net-charge invertible curvature-sensing peptide (NIC). Curvature-sensing peptides recognize vesicles by binding to lipid-packing defects on highly curved membranes, regardless of the expression levels of biomarkers. NIC has a net positive charge at weakly acidic pH to bind to negatively charged EVs through electrostatic interactions, whereas it has a net negative charge at weakly basic pH to dissociate from EVs by electrostatic repulsion. NIC allowed us to achieve reproducible EV isolation from three human cell lines and single-particle imaging of EVs containing the ubiquitous exosome markers CD63 and CD81 by total internal reflection fluorescence microscopy. Moreover, the EVs isolated by EV-CaRiS exhibited immune-stimulation-activities and anticancer effects.

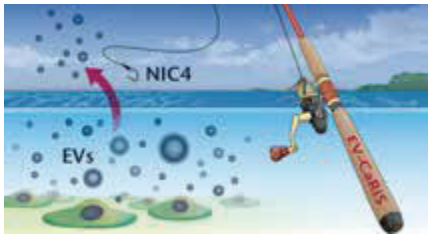

Published paper
Kawano et al., *Anal. Chem.* 96, 3754-3762 (2024)

Background

Curvature-sensing peptide

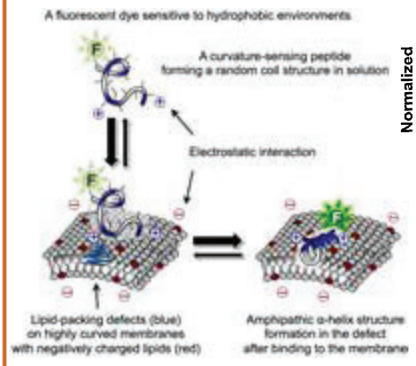

Size-dependent binding manner

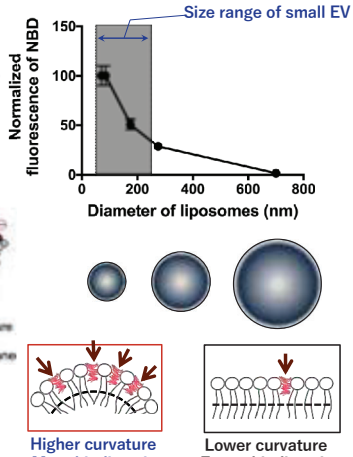

(1) Net-charge Invertible Curvature-sensing peptide (NIC)

Peptide	Amino acid sequence	pH 6	pH 9
NIC4	EZBLLZXLNZBTEBLSZX-GSGSC-NH_2	+0.7	−2.0

Net charge

Weakly acidic Weakly basic

Unusual amino acids

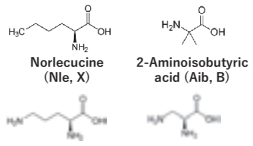

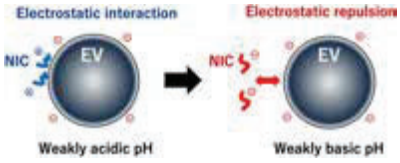

pH dependency of the net charge

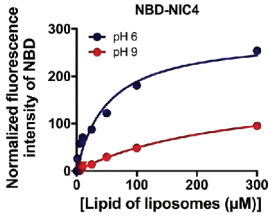

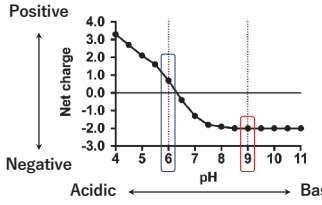

POPC : POPS : Cholesterol = 75 : 10 : 15 mol% (diamter : 80 nm)



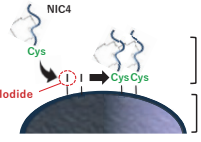

A schematic diagram of NIC4 coupling onto the SulfoLink™ resin

(2) EV Catch-and-Release isolation System (EV-CaRiS)

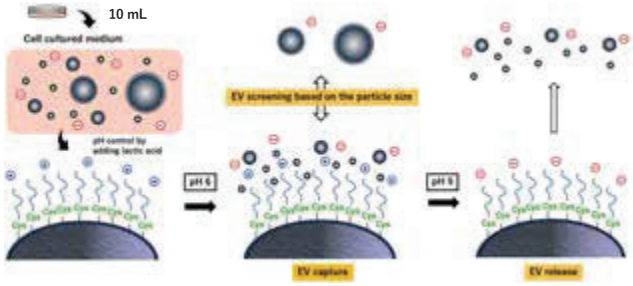

Nanoparticle tracking analysis (NTA)

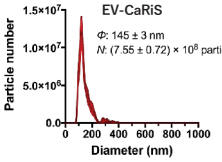

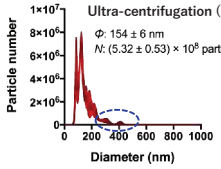

<Cell lines>
HeLa: human cervical cancer cell
PANC-1: human pancreatic carcinoma cell
MSC-R37: human bone marrow mesenchymal stem cell

The number of particles

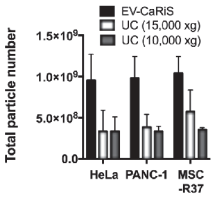

The size of particles

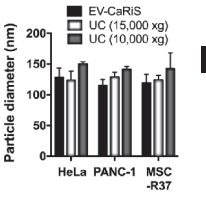

The time required

EV-CaRiS : 1.5 h

Conventional UC : 4–6 h

Immune activities

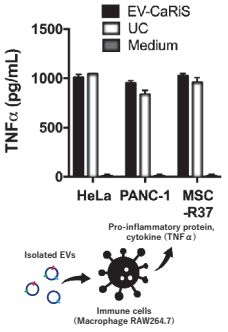

Anti-cancer activities

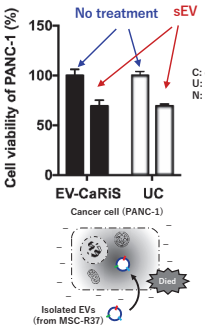

Western blotting

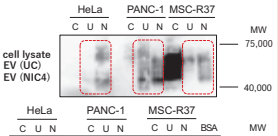

(3) Fluorescent Immunostaining (Single-particle Imaging)

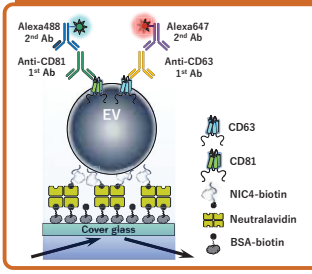

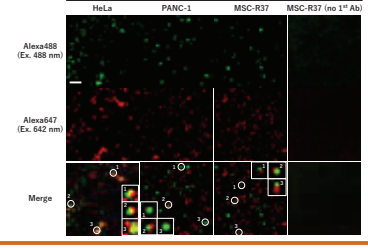

Conclusion

EV-CaRiS does not require any specialized experimental equipment and can isolate sEVs with high purity from a small amount of cell-cultured media (10 mL) in a relatively short time (~1.5 h). EV-CaRiS was clearly demonstrated as a simple and convenient methodology for sEV isolation.

Multifunctional peptides for the synthesis of photothermally active gold nanoparticles

Alžbeta Runová, Helma Wennemers*
Laboratory of Organic Chemistry, ETH Zürich, D-CHAB, 8093 Zürich, Switzerland

https://doi.org/10.17952/37EPS.2024.P1178

1 Introduction

Gold nanoparticles (AuNPs) have gained significant attention for therapy, imaging, and biosensing due to their unique properties that can be tailored by varying their size, shape, and coating.[1] Peptides offer multiple advantages for the formation and stabilization of AuNPs compared to traditional ligands.[2]
Here, we used a split-and-mix tripeptide library to identify peptides promoting AuNP formation without the need for external reducing agents. The lead peptide from our screening promoted the formation of stable anisotropic AuNPs with absorption in the near-infrared region. We envision that these peptide-coated AuNPs could become valuable tools for photothermal therapy.

2 Tripeptide library screening

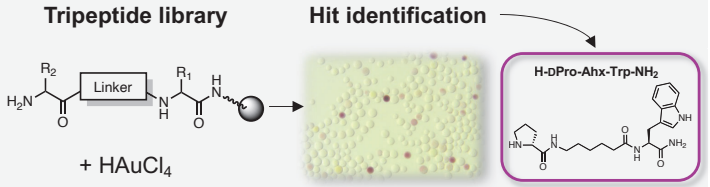

3 Sequence optimization

- **Alanine scan** revealed that the C-terminal tryptophan is crucial for NP formation, and the N-terminal proline is essential for anisotropy.
- **Stereochemistry studies** showed that peptides with an N-terminal L-amino acid form AuNPs without aggregation and with optimal dispersity, in contrast to those with a D-amino acid.
- **Linker optimization**

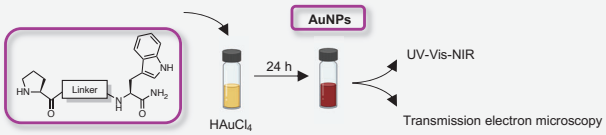

- Hydrophobic or positively charged linker → anisotropic NPs
- Aromatic, negatively charged or no linker → isotropic NPs
- Lead: **H-Pro-Gly-Trp-NH$_2$** → best dispersity, long-term stability

7 Conclusion

- **H-Pro-Gly-Trp-NH$_2$** is a reducing agent, stabilizer and a promoter of anisotropic AuNPs with NIR light absorption
- Potential photothermal agent
- Peptide modification for the formation of targeting AuNPs

4 NMR studies

NMR studies revealed a decrease of the Trp N-H proton signal after AuNP formation, indicating that Trp is involved in $HAuCl_4$ reduction and is oxidized in the process. A new signal at 8.13 ppm indicates the formation of an oxidation product.

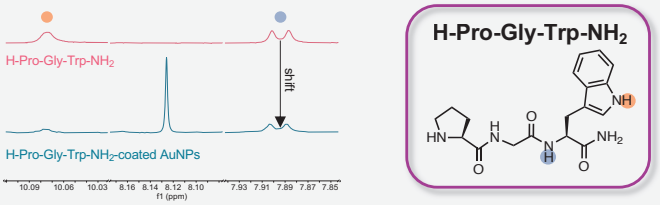

5 Thermal heating

H-Pro-Gly-Trp-NH$_2$-coated AuNPs

TEM image and absorption spectrum

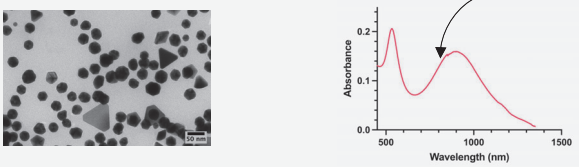

Photothermal effect

The AuNPs were irradiated by an 808 nm laser with a power density of 1.5 W/cm^2 for 5 min.

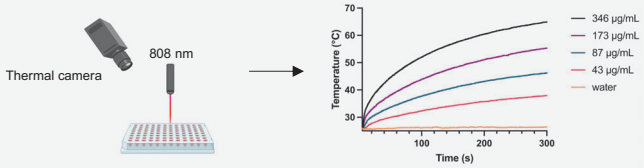

6 Functionalization of the lead peptide

Modification of the N-terminus resulted in AuNP aggregation, but C-terminal elongation is well tolerated.

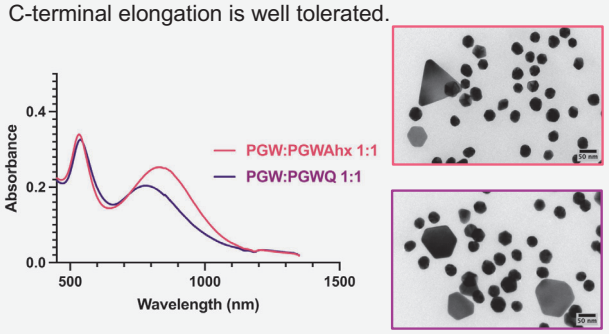

Absorption spectra and TEM images of peptide-coated AuNPs formed with 1:1 mixtures of H-Pro-Gly-Trp-NH$_2$ and H-Pro-Gly-Trp-Ahx-NH$_2$ or H-Pro-Gly-Trp-Gln-NH$_2$.

Derivatization opens up the possibility to equip the peptide at the C-terminus with a targeting moiety to form functionalized AuNPs tailored to specific applications.

References

[1] L. Wang, M. H. Kafshgari, M. Meunier, *Adv. Funct. Mater.*, **2020**, *30*, 2005400.
[2] K. Bhattacharjee, B. L. V. Bhagavatula, *Chem Soc Rev*, **2023**, *52*, 4121.

Figures created with BioRender.com

Partner/Sponsor:

Intracellular Peptide Library Screening for Covalent Transcription Factor Inhibitors

Andrew Brennan, Keith Vance, Scott Lovell and Jody Mason
Department of Life Sciences, University of Bath, UK

https://doi.org/10.17952/37EPS.2024.P1179

Biotechnology and Biological Sciences Research Council

1. Introduction

- The bZIP superfamily of transcription factors (TFs) bind DNA consensus sites as dimers, as shown for **cJun bound to TRE DNA**.[1]
- cJun is **upregulated in a range of diseases**, including cancer, making antagonism of its interaction with TRE DNA a promising therapeutic target.[2]
- The Transcription Block Survival (TBS) assay **screens peptide libraries to identify functional TF antagonists**.[3]
- **Cys269** in the cJun DNA-binding domain allows for the **possibility of selective covalent inhibition** of TF function.

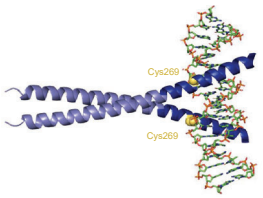

Crystal structure of a cJun homodimer bound to TRE DNA.[1]

2. TBS assay design

1. Inhibition of endogenous bacterial DHFR with TMP renders bacteria dependent on an exogenous TRE-mDHFR gene for cell survival.
2. cJun binds to TRE sites within TRE-mDHFR, sterically blocking RNA polymerase from transcribing the essential gene.
3. Only functional antagonism of the cJun/TRE interaction sequesters the bZIP to restore TRE-mDHFR transcription and therefore cell growth.

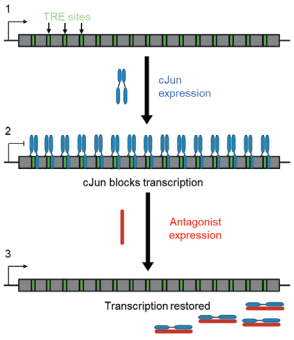

Assay benefits:

- Screen tens of millions of peptide library sequences, with growth rate as the assay readout which allows direct competition.
- Select for functional antagonism of protein-DNA interactions, not simply binding.
- Entirely tag-free system.
- *E. coli* system is robust and economical.
- Screening occurs *in vivo* which selects for favourable properties such as biostability, specificity, solubility and low toxicity.

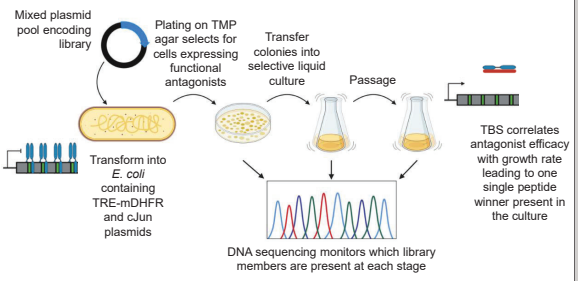

3. Previous antagonist development using TBS and subsequent rational optimisation

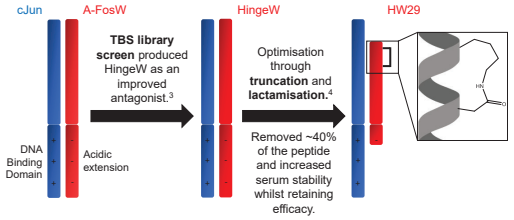

4. Cells with an oxidising cytoplasm can identify a covalent antagonist

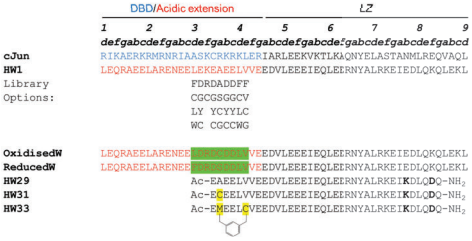

Screening a cysteine containing library in SHuffle Express cells facilitates disulphide formation between antagonist and target.

The position of the unique cysteine selected in SHuffle Express (OxidisedW) was incorporated into the optimised HW29 peptide to produce HW31 which we have shown to form an inhibitory disulphide with cJun.

5. Replacing selected cysteine with an electrophile irreversibly inhibits cJun

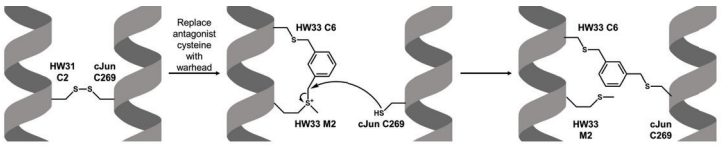

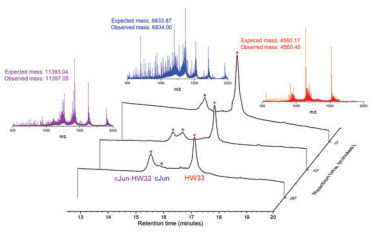

LC-MS analysis of the reaction of HW33 (40 μM) with cJun (20 μM) shows the formation of the conjugate over time.

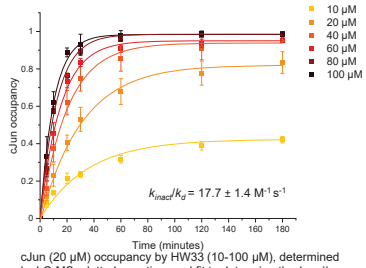

cJun (20 μM) occupancy by HW33 (10-100 μM), determined by LC-MS, plotted over time and fit to determine the k_{inact}/k_d.

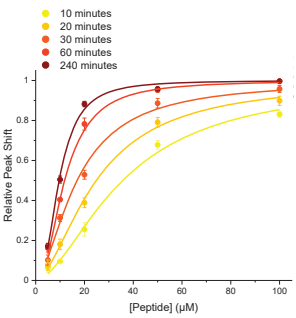

Circular dichroism cJun/TRE antagonism experiment shows an increase in IC_{50} over time as HW33 irreversibly reacts with cJun and prevents it binding to TRE DNA.

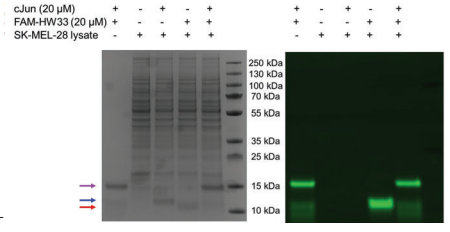

SDS-PAGE analysis of the reaction between cJun (20 μM) and FAM-HW33 (20 μM) after 24 hours incubation in SK-MEL-28 cell lysate which shows the selective reaction with the cJun bZIP.

6. HW33 shows efficacy in melanoma cells via cJun depletion

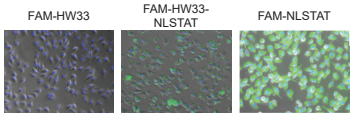

Imaging (overlay of brightfield, DAPI and FAM images) of SK-MEL-28 cells treated with 30 μM peptide for 6 hours at 37°C shows that NLSTAT is required to transport FAM-HW33-NLSTAT into cells, but the cargo reduces cell penetrance.

Western blot: 6 hours

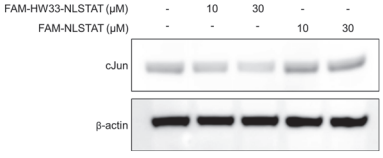

MTT: 24 hours

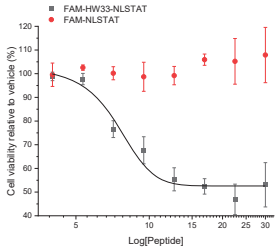

MTT assay on peptide-treated SK-MEL-28 cells (24 hours) shows a reduction in cell viability upon treatment with FAM-HW33-NLSTAT with an IC_{50} of 7.1 μM but the CPP alone produces minimal effect.

Western blot: 24 hours

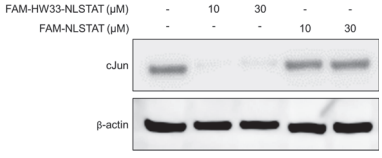

Western blot of peptide-treated cells (6 and 24 hours) shows time- and dope-dependent depletion of cJun upon treatment with FAM-HW33-NLSTAT.

7. Conclusions

- TBS correlates growth rate and protein-DNA antagonism, directly competing peptide library members to produce a single assay winner in the complex cellular environment.
- Screening cysteine containing libraries in SHuffle Express *E. coli* allows for the selection of cysteines capable of forming a disulphide with the target protein.
- The selected cysteine position was converted into an irreversible covalent antagonist capable of reducing melanoma cell viability via cJun depletion.

References

1. Glover, J.N., S.C. Harrison, *Nature*, 1995. **373**(6511).
2. Brennan, A., *et al.*, *J. Exp. Clin. Cancer Res.*, 2020. **39**(184).
3. Brennan, A., *et al.*, *JACS Au.*, 2022. **2**(996).
4. Brennan, A., *et al.*, *Cell Reports Physical Science*, 2022. **3**(101077).
5. Wang, D., *et al., Chem. Sci.*, 2019. **10**(4966).

https://doi.org/10.17952/37EPS.2024.P1182

Innovative microfluidic preparation of monodisperse peptidic nanoparticles for ultrasound guided gene delivery

Guy GOUARIN*, Vicentiu MORARU and Samir CHERKAOUI BRACCO SUISSE SA, Plan-les-Ouates, Switzerland guy.gouarin@bracco.com

BRACCO LIFE FROM INSIDE

INTRODUCTION

Context – Gas-filled microbubbles (MB), clinically approved as ultrasound (US) contrast agents, have demonstrated efficacy in drug and gene delivery by exploiting the sonoporation phenomenon.[1]

Problematic – Intravascular microbubbles (MB) have a relatively short lifespan and are unable to accumulate in tissues due to their large size (1 to 10 µm), thus limiting their efficacy.

Solution – Perfluorocarbon nanodroplets (ND) could overcome those challenges due to their submicrometric size. Moreover, an external ultrasound stimulus can convert them into gaseous microbubbles by a phenomenon called acoustic droplet vaporization (ADV).[2] Nanopeptisomes (NPP) represents a new class of nanodroplets taking advantages of peptide versatility.[3]

NANOPEPTISOME DESIGN

Hydrophilic cationic moiety using either Cell Penetrating Peptide (CPP) or Nuclear Localization Sequence (NLS) to bind anionic payload (PreS2, SV40, Pepfect14).

Cross-linking region is expected to enhance the NPP stability.

Hydrophobic fluorinated tail stabilize the PFC liquid core.

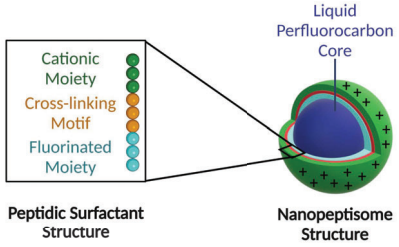

NANOPEPTISOME PREPARATION[4,5]

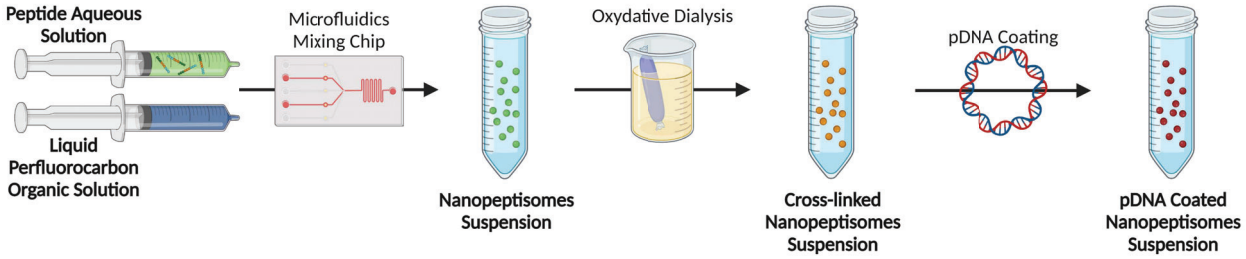

FORMULATION

- Shell: Peptidic Surfactants
- Core:
  - C_6F_{14}; Perfluorohexane PFH (b.p. 56°C)
  - C_5F_{12} Perfluoropentane PFP (b.p. 29°C)

MICROFLUIDICS PROCESS SETTINGS

- **Flow Rate Ratio (FRR):** Volumetric ratio of the aqueous & organic phases → 2:1 (aqueous : organic)
- **Total Flow Rate (TFR):** Total speed at which both fluid streams are injected → 10 mL/min

DIALYSIS

- **Solvent :**
  - Oxidation: Aqueous DMSO (2.5% v/v)
  - Purification: 5% Glucose
- **MWCO :** 10 kDa

pDNA Coating

- **Plasmid:** pCPG-hCMVSCEP-LucSH
- **Solvent:** 5% Glucose
- **Incubation:** 15 min, r.t.
- **NPP Concentration:** 10^9 p/mL
- **pDNA Concentration:** 10 µg/mL

CHARACTERIZATION

1 Particle characterization

- **Methods:** DLS, NTA and Fluorometry
- **Properties:**
  - Size (nm),
  - PolyDispersity Index (PDI),
  - ζ-Potential (mV),
  - Concentration (p/mL),
  - DNA Coating (µg/mL or µg/p).



Zetasizer Nano **DLS**



NanoSight NS300 **NTA**



Qubit 4 Fluorometer **Fluorometry**

2 Acoustical characterization

- Progressive increase of the acoustic pressure applied to the nanopeptisomes.
- **ADV threshold** defined as the minimum acoustic pressure required to convert liquid PFC non echogenic droplets into echogenic microbubbles.

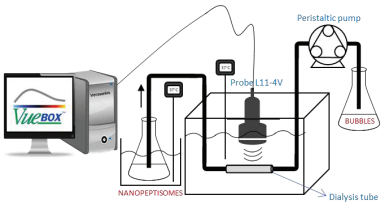

Home-made acoustic setup

RESULTS

Perfluorohexane Core NPP Characterization

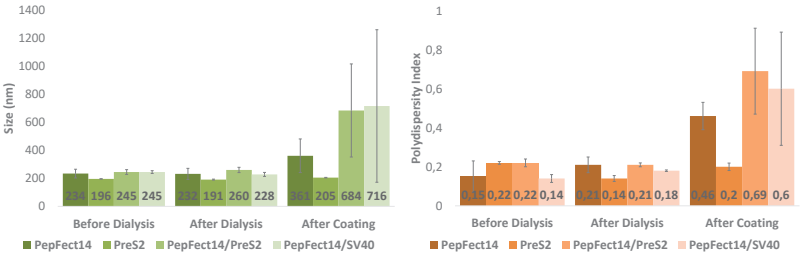

Peptide	Concentration (p/mL) Before Dialysis	After Dialysis	
PepFect14	$2,5x10^{10} \pm 0,2$	$7,6x10^{9} \pm 0,04$	↘
PreS2	*	*	
PepFect14/PreS2	$3,5x10^{10} \pm 0,3$	$1,0x10^{10} \pm 0,4$	↘
PepFect14/SV40	$2,6x10^{10} \pm 0,2$	$1,6x10^{10} \pm 0,03$	↘

* On going analysis.

Peptide	ζ-Potential (mV) Before Coating	After Coating
PepFect14	58,9 ± 9,1	-1,1 ± 3,3
PreS2	24,7 ± 0,7	-32 ± 1,1
PepFect14/PreS2	66,8 ± 3,5	-17,8 ± 4,6
PepFect14/SV40	60,8 ± 4,0	-18,6 ± 3,0

- Successful formulation of **monodispersed NPP** (PDI ≤ 0,2).
- **Oxidative dialysis** cause a **decrease** of NPP **concentration**.
- **Coating induce aggregation** (↗ Size, PDI and ↘ ζ-Potential) by **diminishing electrostatic repulsion** between NPP.

Perfluoropentane Core NPP Characterization

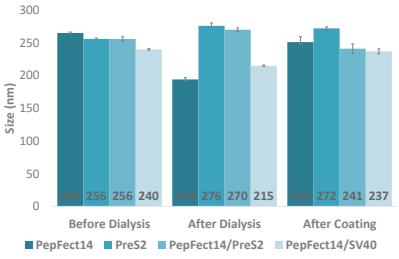

Peptide	ζ-Potential (mV) Before Coating	After Coating
PepFect14	31,5 ± 6,1	27,1 ± 1,0
PreS2	42,0 ± 0,4	33,1 ± 1,9
PepFect14/PreS2	53,6 ± 5,95	35,8 ± 3,5
PepFect14/SV40	33,1 ± 10,1	31,7 ± 2,6

- Similar trend to perfluorohexane NPP relative to the concentration evolution.
- **No aggregation observed** (= Size, PDI), ζ-Potential still highly positive, thus **maintaining electrostatic repulsion** between NPP.

Acoustic Response Study

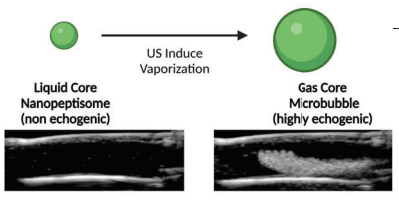

Gas	ADV Threshold (MPa)	Mechanical Index
C_6F_{14}	~ 10,20	~ 4,16
C_5F_{12}	~ 7,64	~ 3,13

- **Acoustic properties only driven** by the **perfluorocarbon liquid core**.
- **Mechanical Index** suitable **only** for **therapeutic applications**.

CONCLUSIONS

- **pDNA coated nanopeptisomes** offer an **innovative nanometric support** to **deliver genetic material** through sonoporation combined with echographic visualization.
- **Peptidic composition** of the shell display **little influence** on the **particle properties** (size, PDI, concentration and ζ-Potential) offering a **vast choice** of peptide sequence **depending on the target**.
- This **study underlines** the **importance** to **control** both **dialysis** and **coating steps** to ensure the best NPP properties.

REFERENCES

1. Fourrier et al., Microbubbles for human diagnosis and therapy, *Biotmaterials*, **2023**, 294
2. Melich et al., Microfluidic preparation of various perfluorocarbon nanodroplets: Characterization and determination of acoustic droplet vaporization (ADV) threshold - *Int. J. Pharm.*, **2020**, 587
3. Medina *et al.*, Fluorous Phase-Directed Peptide Assembly Affords Nano-Peptisomes Capable of Ultrasound-Triggered Cellular Delivery, *Angew. Chem. Int. Ed. Engl.*, **2017**, 56
4. Microfluidic preparation of fluorocarbon cross-linked vesicles – WO2023/08450048
5. Cationic Cross-Linked Vesicles - WO2024/133892

Environment Responsive Peptide Dimers Bind and Stabilize dsRNA

Niall M. McLoughlin,* Marvin A. Albers,* Estel Collado Camps, Jannik Paulus, Youri A. Ran, Saskia Neubacher, Sven Henning, Roland Brock, Tom N. Grossmann

Department of Chemistry and Pharmaceutical Sciences & AIMMS, VU Amsterdam, NL

https://doi.org/10.17952/37EPS.2024.P1186

Abstract: Double-stranded RNAs (dsRNA) possess immense potential for biomedical applications.[1] However, their therapeutic utility is limited by **low stability** and **poor cellular uptake**.[2] Different strategies have been explored to enhance the stability of dsRNA, including the incorporation of modified nucleotides, and the use of diverse carrier systems. Nevertheless, these have not resulted in a broadly applicable approach thereby preventing the wide-spread application of dsRNA for therapeutic purposes. Herein, we report the design of **dimeric stapled peptides** based on the RNA-binding protein TAV2b. These dimers are obtained via **disulfide** formation and mimic the natural TAV2b assembly. They **bind and stabilize dsRNA** in the presence of serum, protecting it from degradation. In addition, peptide binding also **promotes cellular uptake of dsRNA**. Importantly, peptide dimers **monomerize under reducing conditions** which results in a loss of RNA binding. These findings highlight the potential of **peptide-based RNA binders** for the stabilization and protection of dsRNA, representing an appealing strategy towards the **environment-triggered release of RNA**. This can broaden the applicability of dsRNA, such as short interfering RNAs (siRNA), for therapeutic applications.

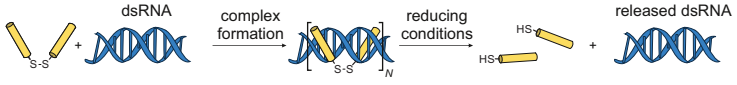

1. The Potential of RNA Therapeutics

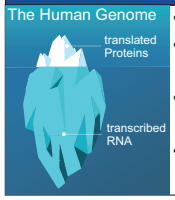

- Ribonucleic Acids are highly under-represented drug targets
- RNA interference (RNAi), activated by short RNAs, is an post-transcriptional mechanism that can degrade or block particular RNA sequences
- RNAi offers a specific and efficient therapeutic approach to silence any target gene[3]
- Despite considerable efforts the widespread application of siRNA-based therapeutics is hampered by lack of effective delivery systems

2. Design of TAV2b derived Dimers

TAV2b Structure

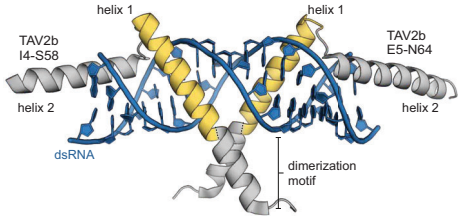

- TAV2b is a viral gene silencing supressor that binds dsRNA[4]
- We designed TAV2b inspired disulfide linked dimers
- High affinity binding in the oxidised dimeric vs. low affinity in the reduced monomeric form

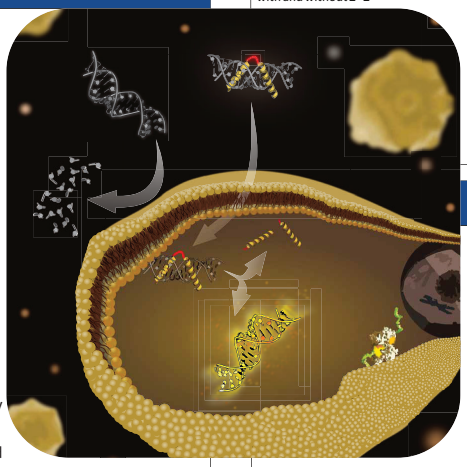

Designed Peptides

symbol	dimerization motif	RNA-binding helix
1L	PLHEIIRKLERMN	QKKQAQRKRHKLNRKER
1		MNQKKQAQRKRHKLNRKER
1'-1'		S-XβNQKKQAQRKRHKLNRKER S-XβNQKKQAQRKRHKLNRKER
2		MNQKKQAQRKRHKONRKOR
2'-2'		S-XβNQKKQAQRKRHKONRKOR S-XβNQKKQAQRKRHKONRKOR

- Synthesized by SPPS
- Peptides **2** and **2'-2'** are hydrocarbon stapled by RCM.
- **1L** includes the full dimerization motif

Figures: *top:* Crystal structure (pdb: 2zi0) of two TAV2b subunits (I4-S58 and E5-N64, yellow) bound to dsRNA (grey). Dimerization motif is indicated as well as helices 1 and 2. *bottom:* The sequence of TAV2b helix 1 and corresponding peptide derivatives (β = beta-alanine, X = 3-mercaptopropionic acid, O = (S)-2-(4-pentenyl)alanine).

3. Environment Responsive Binding

Electro-mobility shift assay (EMSA)

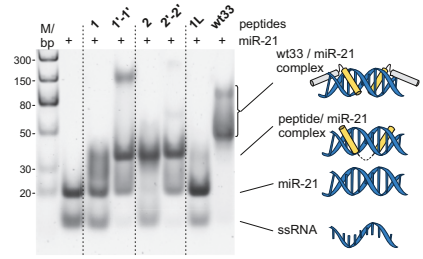

Isothermal titration calorimetry

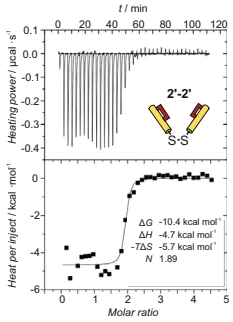

Reversible binding

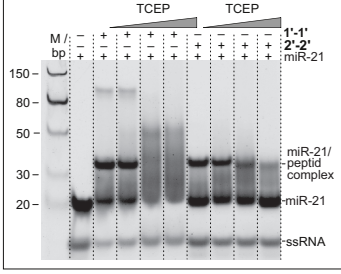

- **2'-2'** binds dsRNA (Kd = 31.7 nM)
- RNA binding is sequence independent (data not shown)
- Reducing conditions result in loss of binding
- Disulfide cleavage also at physiological glutathione concentrations (5mM) within 5 min(data not shown)

Figures: *top left:* EMSA of miR-21 (c = 3 µM) incubated with **1**, **1'-1'**, **2**, **2'-2'**, **1L** and **wt33** (c = 6 µM), native PAGE, TAE-buffer, SYBR gold stain. *top right:* ITC of **2'-2'** (c = 305 µM) with miR-21 (c = 15 µM) at 30 °C in 1xPBS. *bottom:* EMSA of miR-21 co-incubated with peptide dimers **1'-1'** or **2'-2'** and increasing concentrations of reducing agent TCEP (c = 6, 60 and 600 µM)

4. RNA Stabilization

- Increased miR-21 melting temperatures upon binding
- T_m increases in complex with **1'-1'** and **2'-2'**
- ΔT_m with **2'-2'** ~ 9 °C
- **2'-2'** extends miR-21 life-time in fetal-bovine serum (FBS) preventing its degradation by nucleases
- Up to 6h in 27.5 % FBS at rt

Figures: *top:* CD-derived thermal denaturation profiles (λ = 267 nm) of miR-21 in the presence and absence of **1, 1'-1'** (yellow) and **2, 2'-2'** (red). *bottom:* native PAGE of phenol/chloroform extracted miR-21 after incubation with increasing amounts of serum for 10 min at 37 °C with and without **2'-2'**

Thermal stability

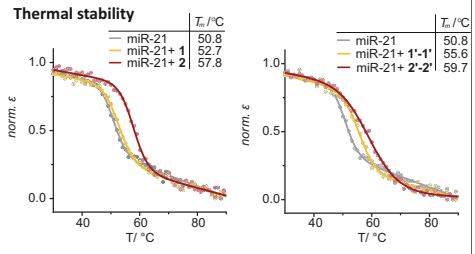

Serum stability

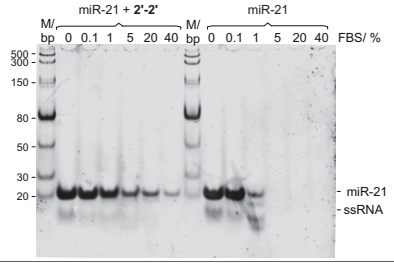

5. Promotion of Cellular Uptake

Confocal Microscopy

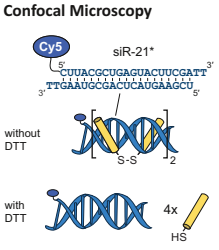

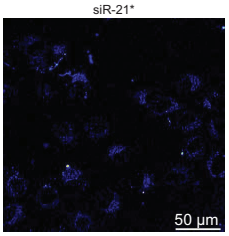

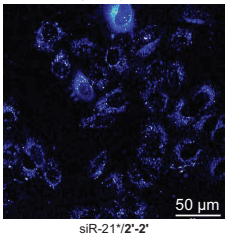

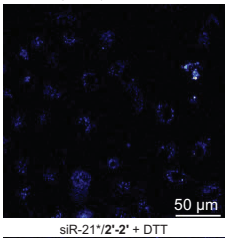

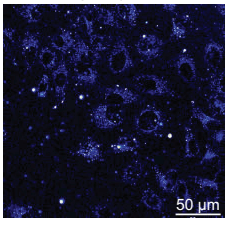

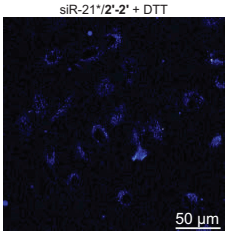

- HEK293 cells were incubated with Cy5-siRNA* with and without peptides **1'-1'** and **2'-2'**
- siR-21* alone showed low intracellular signal
- Increased cellular uptake with **1'-1'** and **2'-2'** (presumably endosomes).
- Again, low uptake with prior DTT treatment

Figures: *top left:* Cy5-labeled siRNA (siR-21*) and schematic representation of pre-treatment of **1'-1'** and **2'-2'** (c = 2 µM) with and without DTT before incubation with HEK293 cells. *Panels:* Confocal micrographs of HEK293 cells after incubation with siR-21* (c = 1 µM) for 1h with and without peptides **1'-1'** and **2'-2'**.

6. Conclusion

In this study, we designed and synthesized **novel dimeric peptides** derived from TAV2b, that **reversibly bind dsRNA**. Interestingly, dimer **2'-2'** increased the capability of RNA to **withstand degradation in serum** and **promoted the cellular uptake** of labeled siRNA. This study highlights how high affinity RNA ligands, can **stabilize dsRNA** and be equipped with **environment-responsive** binding properties, creating the basis for a significant advancement of dsRNA delivery strategies using peptides.

References

[1] K. Paunovska et al. , Nat. Rev. Genet. 2022, 23, 265
[2] J. N. Shukla et al. , RNA Biol. 2016, 13, 656
[3] D. Bumcrot et al. , Nat. Chem. Biol. 2006, 2, 711
[4] H.-Y. Chen et al. , EMBO Rep. 2008, 9, 754

Group

https://doi.org/10.17952/37EPS.2024.P1187

Engineered oxalyl thioester-containing protein domains as a building block for synthetic biopolymers

Francesco Terzani,[a] Simindokht Rostami,[b] Chen Wang,[a] Benoît Snella,[a] Birgit Wiltschi,[b] Oleg Melnyk,[a] Vangelis Agouridas[a]

[a] *Univ. Lille, CNRS, Inserm, CHU Lille, Institut Pasteur de Lille, U1019 - UMR 9017 - CIIL - Center for Infection and Immunity of Lille, F-59000 Lille, France*

[b] *Institute of Bioprocess Science and Engineering, University of Natural Resources and Life Sciences, Vienna*

Introduction and Aim

In recent years, the **production of genetically engineered protein biopolymers** has been the subject of intense research with promising applications in biomedical or materials science.[1] Despite significant advances, the access to tailored biopolymers and thus, the development of versatile and efficient approaches, remain major challenges. We recently documented the potential of **oxalyl thioester precursors (oxoSEA)** as reactive handles for the modification of peptides and proteins [2] (Scheme A). Upon **activation by a reductant**, they can react in an **NCL-fashion**[3] with an *N*-terminal cysteine residue to provide a ligated peptide. Notably, the reaction has been reported to be **highly chemoselective**, **triggered on-demand**, **fast (< 30 M^{-1} s^{-1})** and efficient in the high **nanomolar range**. The goal of this project is to build on the tremendous reactivity of oxalyl thioesters in order to access **high-molecular weight biopolymers by polycondensation of bifunctional protein-derived monomers** (Scheme B). This will be done by setting up a fully integrated approach from synthetic biology to chemistry, involving the **recombinant production** of monomeric units equipped with an *N*-terminal cysteine residue and a genetically encoded oxoSEA-amino acid derivative close to the *C*-terminus.

Scheme A: oxoSEA based ligation chemistry developed in our group

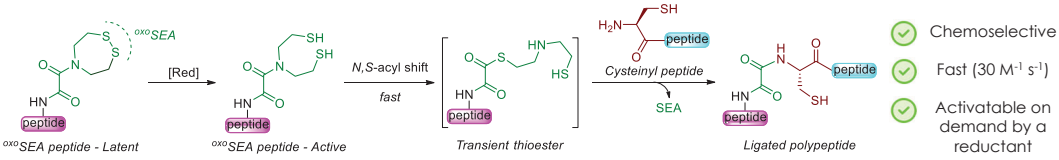

Scheme B: Reductant-triggered polycondensation from the recombinant production of *N*-cysteinyl oxoSEA monomers

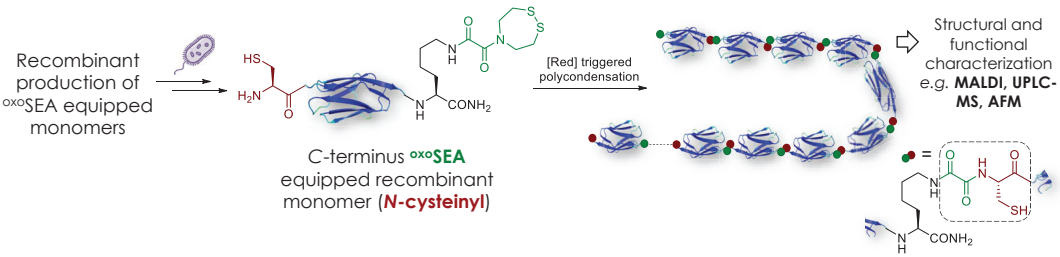

Genetic encoding of oxoSEA ncAAs: preliminary results

Up to now more than 150 non-canonical amino acids have been successfully incorporated ribosomally into proteins using the **amber stop codon approach**. The **pyrrolysyl-tRNA synthetase (PylRS)/$tRNA_{CUA}^{Pyl}$ pair** from the archaeon *Methanosarcina mazei* is known to be an efficient tool for the incorporation of lysine derived compounds presenting sterically hindered side chain similar to the oxoSEA fuctional group.[4]

Incorporation of **oxoSEA Lysine** as a first attempt

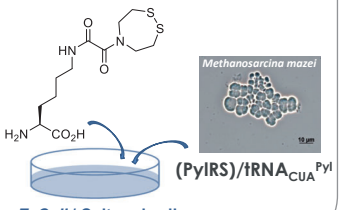

Despite structural similarities between previously incorporated lysine derived ncAAs and the oxoSEA lysine, initial results showed **no incorporation into the target protein sequence**

We identified **3 possible reasons** and we designed a **library of oxoSEA analogs** to help understand and to improve the incorporation of Lys(oxoSEA)

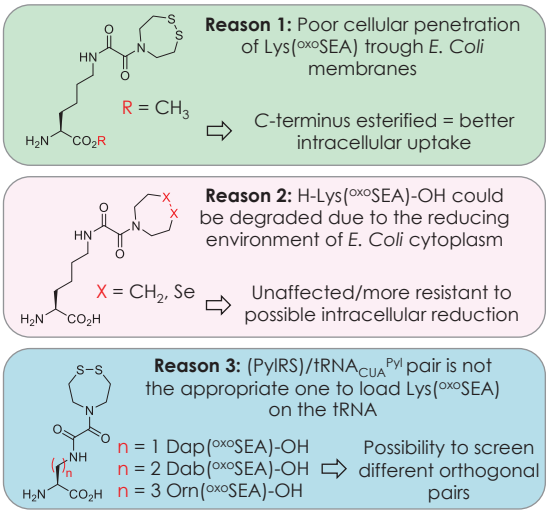

Synthesis of oxoSEA ncAAs

Synthesis of the oxoSEA building block 1 and the corresponding non-reactive version 2

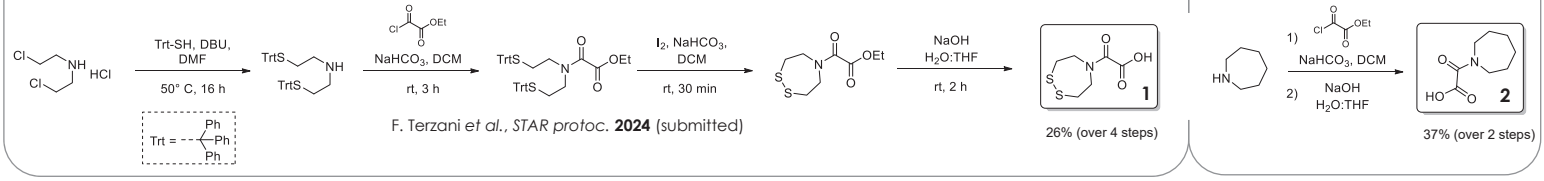

F. Terzani *et al.*, *STAR protoc.* **2024** (submitted)

Coupling of the oxoSEA building blocks with Lys,Orn, Dab and Dap

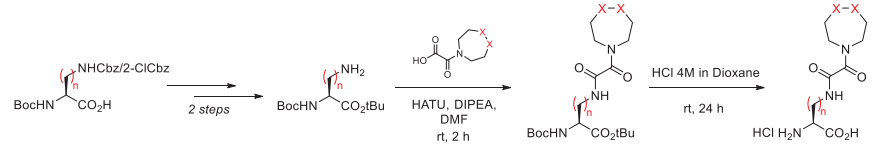

n	X	yield
4	S	20% (4 steps)
4	CH_2	18% (4 steps)
3	S	16% (4 steps)
2	S	38% (2 steps)
1	S	32% (2 steps)

Each compound has been purified *via* RP-HPLC semiprep. System e.g.

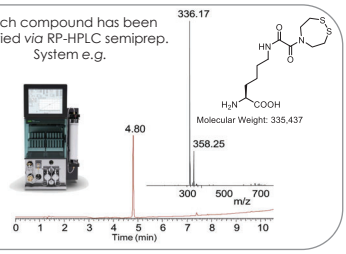

Conclusion

The library of oxoSEA ncAAs synthetized will help us understand the problems encountered during the first attempts of incorporation of the oxoSEA lysine and will hopefully allow us to achieve the ambitious challenge of genetically encode the latter in a target protein. Once this objective will be achieved we will be able to exploit the features of the oxoSEA based ligation chemistry for the development of a polycondensation method for the synthesis of tailored biopolymers.

(1) Werten, M. *et al*, *Biotechnology Advances*, **2019**, 642–666.
(2) a) Snella, B. *et al*, *Angew. Chem. Int. Ed.* **2022**, 61.
b) Grain, B. *et al*, *Org. Lett.* **2023**, 25, 5117-5122.
(3) a) Dawson, P. E. *et al*, *Science* **1994**, 266, 776.
b) Agouridas, V. *et al*, *Chem. Rev.* **2019**, 12, 7328.
(4) Dumas, A. *et al*, *Chem. Sci.* **2015**, 6, 50.

Acknowledgements to the Agence Nationale de la Recherche (**ANR-21-CE44-0031**) and the University of Lille (**R-PILOTE-19-0008-Molecular**).

https://doi.org/10.17952/37EPS.2024.P1188

Improved Sortase A-Catalyzed Transpeptidation by Selective Electrostatic-Assisted Aminolysis Trapping

Chen Wang,[a, b] Benoît Snella,[a] Rémi Desmet,[a] Oleg Melnyk,[a] Vangelis Agouridas[a,b]

[a] Univ. Lille, CNRS, Inserm, CHU Lille, Institut Pasteur de Lille, U1019 - UMR 9017 - CIIL
Center for Infection and Immunity of Lille, F-59000, Lille, France
[b] Centrale Lille, F-59000, Lille, France

Introduction

Sortase A (SrtA) and some variants thereof have been used in a wide range of applications including fluorescent labeling, protein cyclization and immobilization due to their mild reaction conditions and high specificity.[1] However, SrtA-catalyzed transpeptidation suffers the inherent limitation of being a reversible process which therefore requires an excessive amount of substrate to drive the reaction towards completion. Such an issue can prove prohibitive, especially in the case of high value-added substrate molecules.[2, 3]

In this context, we disclose a novel substrate engineering strategy that enables to achieve high levels of SrtA-mediated protein modification with nearly stoichiometric amounts of substrate. **Extension of the consensus sorting motif LPXTG with a positively charged peptidic module** allows to achieve sequence-specific removal of by-products by applying the concept of electrostatic-assisted aminolysis reaction recently described by our group.[4] The reaction equilibrium is driven to favor product formation, thereby greatly improving reaction yield.

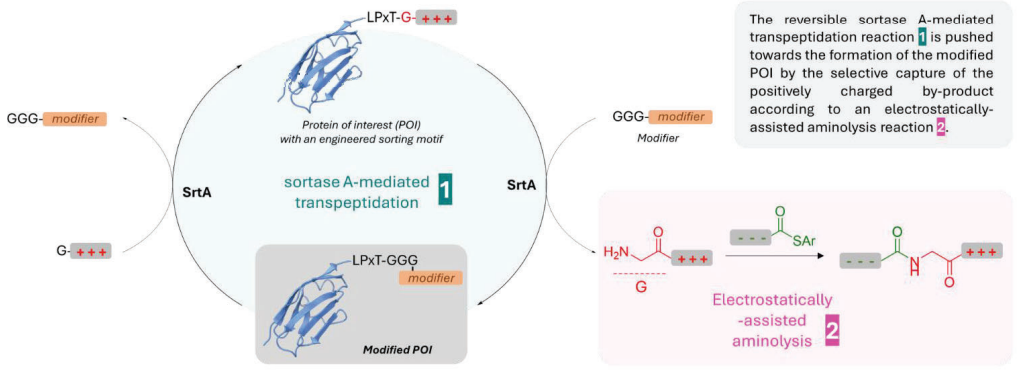

Proof-of concept

The model peptide **1** containing an Arg-rich positively charged module is incubated with the nucleophilic peptide **2** (1.2 equiv.) for 30 minutes. Thioester **3** equipped with a negatively charged module is added after 30 min (1.5 equiv.).

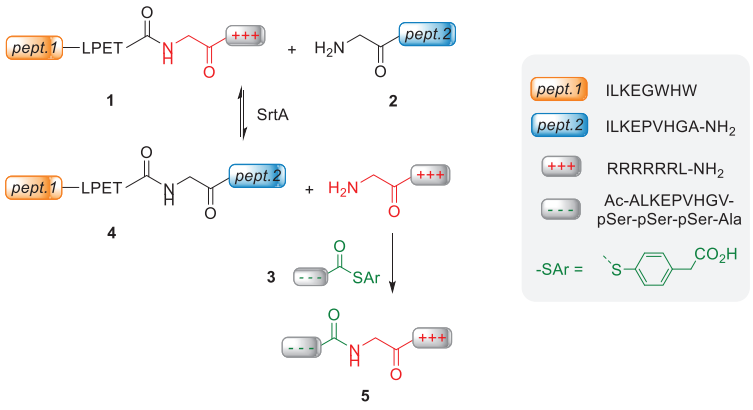

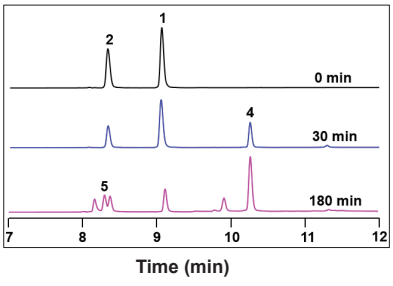

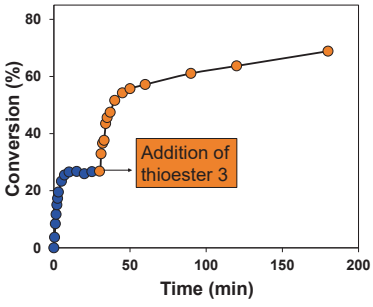

- ✓ In the first 30 minutes, the reaction plateaus at 26% conversion showing poor conversion to the transpeptidated product (yield calculation from Trp UV absorption at 280 nm).
- ✓ Addition of thioester **3** at 30 min immediately promotes peptide balance toward the product forming direction with a fast and instant conversion increase. The formation of the aminolysis product **5** can be observed by HPLC at 215 nm.
- ✓ After 3 additional hours, the conversion has almost tripled.

This experiment shows that the ligation byproducts are obviously removed and the yield is significantly increasing by the electrostatically assisted aminolysis reaction.

Optimization

1) Influence of the number of positive charges in the Arg-rich module

The number n of Arg residues was varied in the positively charged module with n = 2, 4, 6.

Result: $(Arg)_4$ and $(Arg)_6$ containing modules show similar results in the SrtA and electrostatically assisted reactions, both reaching 70% conversion after 180 minutes of reaction.
$(Arg)_2$ is less efficient in driving the SrtA transpeptidation equilibrium to high conversions despite reaching a higher plateau after 30 min. In this case, the electrostatically-assisted aminolysis is much less efficient.

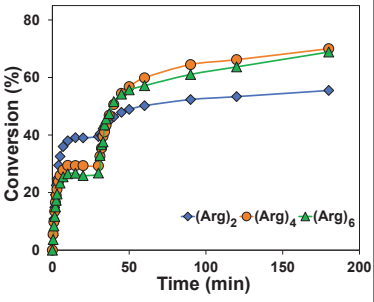

2) Repetitive additions of thioester 3.

The negatively charged thioester **3** is completely consumed one hour after the addition and cannot further promote the progress of the SrtA-catalyzed trans peptidation reaction. Therefore, repetitive additions of thioester **3** at 90 min and 180 min were tested.

Result: SrtA-mediated ligation is further displaced toward product formation after each thioester addition, resulting in 83% conversion after three additions.

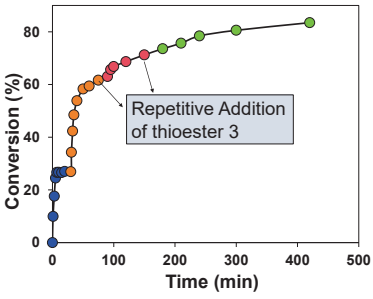

3) Addition of the thioester the beginning of the reaction

Peptide **1** (500 µM), peptide **2** (1 mM) and thioester **3** (750 µM) are added all together at the beginning of the reaction.

Result: the conversion reaches 74% after 3 hours. A second addition allows to increase the yield up to 85% after 2 additional hours of reaction.

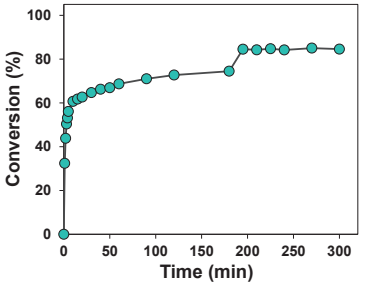

Conclusion

We have developed a straightforward method to significantly improve the efficiency of SrtA-mediated ligation by incorporating an electrostatically-assisted aminolysis to inactivate the reaction byproduct. Since positively charged sequences can be easily programmed into recombinant protein, this strategy enables efficient preparation of proteins with various modifications. The approach is currently being further developed and applied on protein models.

References

[1] Mao, H. et al. J. Am. Chem. Soc., **2004**, 126, 2670-2671.
[2] Morgan, H. E. et al. Chem. Soc. Rev., **2022**, 51, 4121-4145.
[3] Zou, Z. et al. Angew. Chem. Int. Ed. **2024**, 63, e202310910.
[4] Ollivier, N. et al. Nat. Commun. **2022**, 13, 6667.

Photocontrollable probes for the investigation of neuropeptide signaling

https://doi.org/10.17952/37EPS.2024.P1189

Konstantin Raabe,[A,B] Predrag Kalaba,[A] Hilary Yong,[C] Erik Keimpema,[D] Victor Anggono,[C] Markus Muttenthaler[A,E]*

a) University of Vienna, Institute of Biological Chemistry, Austria
b) University of Vienna, Vienna Doctoral School in Chemistry (DoSChem), Vienna, Austria
c) The University of Queensland, Clem Jones Centre for Ageing Dementia Research, Brisbane, Australia
d) Medical University of Vienna, Department of Molecular Neurosciences, Vienna, Austria
e) Institute for Molecular Bioscience, The University of Queensland, Brisbane, Australia

The Oxytocin/Vasopressin System and Photopharmacology

- Oxytocin/Vasopressin (OT/VP) are highly conserved neuropeptides playing a crucial role in physiological and neurological functions, including emotional responses and learning.[1-3]
- Dysfunctions in the OT/VP system have been linked to pathophysiological and psychological conditions, such as breast cancer, autism spectrum disorder, and major depressive disorder.
- Underpinning neuropeptide-mediated pathways have not been fully elucidated[1,3,4]
- Receptors widely expressed throughout the brain making it difficult to investigate specific effects of neuropeptides *via* intracerebroventricular or stereotaxic injections.[5]
- To address this complexity, we developed advanced photoprobes for OT and VP, enabling precise spatiotemporal control over neuropeptide activity *via* photopharmacology.
- Photolabile protecting groups (photocages) mask the peptides' bioactivity until exposed to light (1PE/2PE), allowing controlled release of OT and VP.
- The effectiveness of these probes was validated in cellular assays and *in vitro* experiments, offering a powerful tool for future studies on neuropeptide signaling in the brain
- Applications of our probes in prospective *ex vivo* and *in vivo* studies could potentially advance the understanding of neuropeptide related physiological and pathological conditions.

Rational: Potential for *in vivo* Applications

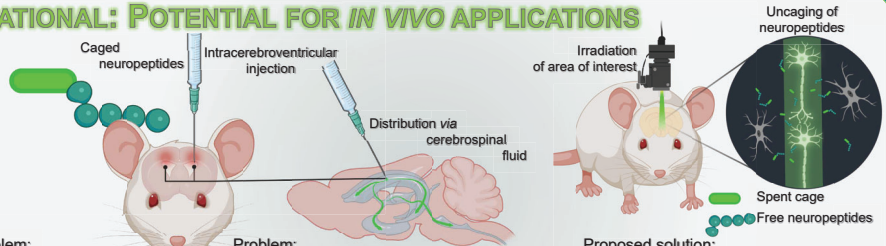

Problem:
- Injection stressful for the animal → Aberrant behaviour
- Usually anaesthesia required → Limited time window for behavioural experiments

Problem:
- Neuropeptide receptors widely expressed in various brain regions
- Diffusion away from original point of injection
- Interactions in non-targeted areas → Complicates evaluation of behavioural output in correlation to specific brain areas

Proposed solution:
- Combination with Photopharmacology → Photocaging → High spatiotemporal control → Uncaging during *in vivo* training → Simulation of endogenous release

Proposed *ex vivo* Experiments

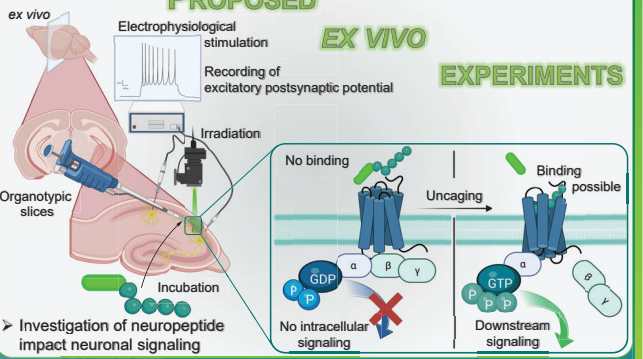

- Investigation of neuropeptide impact neuronal signaling

Synthesis

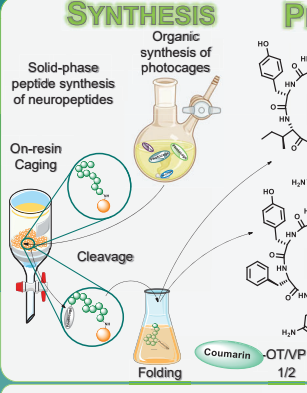

Probes

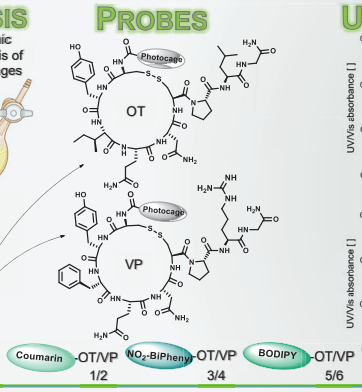

UV/Vis Absorbance

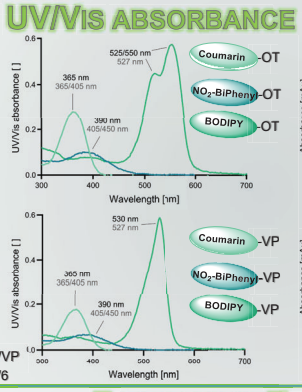

Uncaging with LEDs

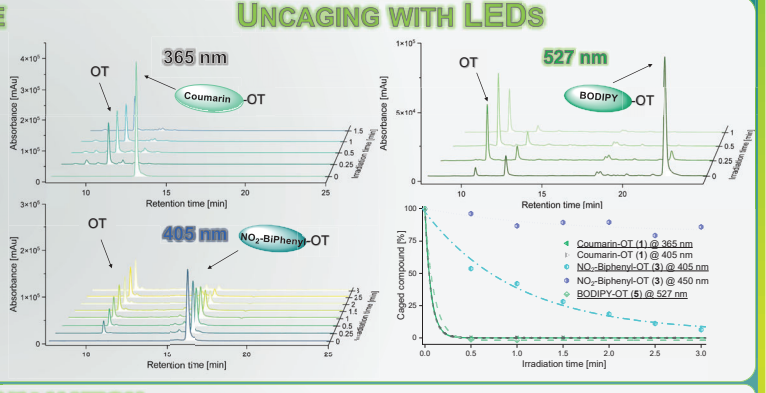

Biological Evaluation

Functional IP_1 Assays HEK-293

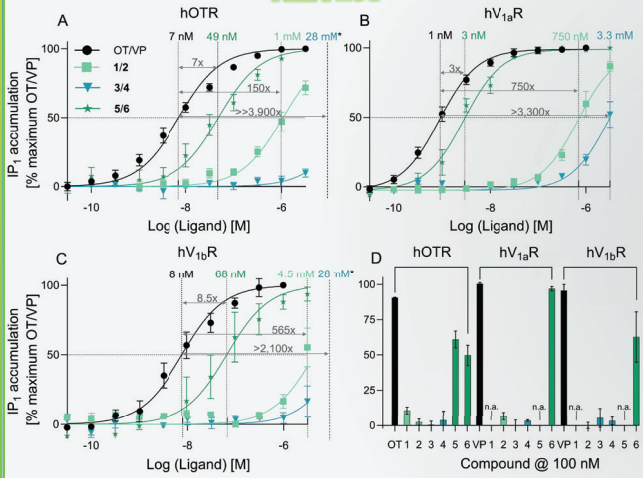

Confocal Scanning Microscopy Immunostaining & Quantification of pCREB

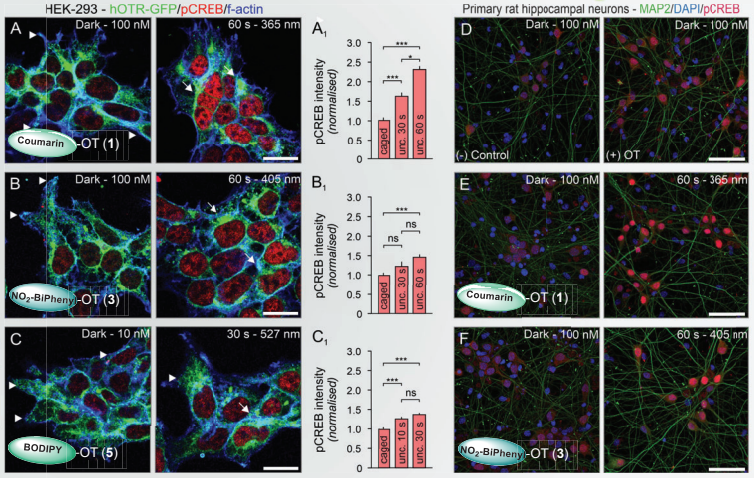

In vitro pharmacologically evaluation of photocaged neuropeptides. Cellular functional IP_1-assay performed on stable HEK-293 cells, overexpressing hOTR, hV1aR, or $hV_{1b}R$. Each point represents at least three independent measurements in technical triplicates. Results were normalised to OT/VP (100%) and negative control (buffer; 0%) activity. Error bars indicate the standard error of the mean. (A) hOTR, (B) $hV_{1a}R$, (C) $hV_{1b}R$, (D) 100 nM at each receptor. EC_{50} values shown above with same color coding for the corresponding compounds, asterisks indicate extrapolated values, grey numbers and lines indicate x-fold increase of EC_{50} values compared to parent peptide, n. a. no activity at 100 nM.

In vitro evaluation of the biological activity of OT photoprobes caged and uncaged. Left HEK-293 cells overexpressing hOTR-GFP. Phosphorylation of CREB (red) quantified after immunocytochemistry normalised to caged treatment. (A, A_1) Coumarin-OT (**1**), 100 nM, irradiation time 30 s and 60 s at 365 nm. (B, B_1) NO_2-Biphenyl-OT (**3**), 100 nM, irradiation time 30 s, 60 s at 405 nm. (C, C_1) BODIPY-OT (**5**), 10 nM, irradiation time 10 s, 30 s at 527 nm. Note transfer of hOTR-GFP signals (green) from membrane (blue, arrowheads) into cytosol (arrows), indicating receptor internalisation after uncaging. ns, non-significant; *P<0.05; ***P<0.001. Scale bars = 15 µm. Right primary rat hippocampal neurons. Phosphorylation of CREB (red) quantified after immunocytochemistry and normalised to negative control (aCSF). (D) Negative control (aCSF) and positive control (OT, 100 nM) dark, (E, E_1) Coumarin-OT (**1**), 100 nM, dark and irradiated at 365 nm for 60 s. (F, F_1) NO_2-Biphenyl-OT (**3**), 100 nM, dark and irradiated at 405 nm for 60 s. ns, non-significant; ***P<0.0005; ****P<0.0001. Scale bars = 50 µm.

Results

- Synthesis and comparison of three different photocages
- Reduced activities of caged compounds compared to parent peptides (up to >>3,900-fold)
- Fast and robust uncaging with easy-to-implement LED setup
- Uncaging *in vitro* possible and compatible with neuronal cells
- Irradiation induces cellular response comparable to endogenous peptides

Outlook

- Two-photon uncaging experiments
- Electrophysiology *ex vivo* experiments in organotypic tissue slices
- Selection of most promising compound for prospective *in vivo* experiments
- Extension to other important neuropeptides (Somatostatin, α-MSH, etc.)
- Manuscript in preparation

References
1. Pharmacol. Biochem. Behav. 2014, 119, 3-9.
2. J. Neuroendocrinol. 2021, 33 (1), e12911.
3. *Neuropeptides 2016, 55, 79-89.*
4. *Prog. Neurobiol. 2008, 84 (1), 1-24.*
5. *Eur. J. Pharmacol. 2010, 626 (1), 9-17.*

Figures created with smart.servier.com and BioRender.com

Legend
1PE: one-photon excitation; 2PE: two-photon excitation; aCSF: artificial cerebrospinal fluid
pCREB: phosphorylated cAMP response binding protein; GFP: Green fluorescent protein

Konstantin Raabe
konstantin.raabe@univie.ac.at
www.neuropeptidelab.com

universität wien
Vienna Doctoral School in Chemistry
The University of Queensland
AUSTRALIA
erc European Research Council
Institute of Biological Chemistry
Center for Brain Research Medizinische Universität Wien

https://doi.org/10.17952/37EPS.2024.P1191

Bind&Bite: Covalently stabilized heterodimeric coiled-coil peptides for the site-selective chemical modification of proteins

Jannis Beutel[1,3], Riccardo di Vincenzo[2], Klaus Überla[2] and Jutta Eichler[1]

[1]University of Erlangen-Nürnberg, Department of Chemistry and Pharmacy, Erlangen, Germany
[2]Institute for Clinical and Molecular Virology, Universitätsklinikum Erlangen, Friedrich-Alexander-Universität Erlangen-Nürnberg, 91054 Erlangen, Germany
[3]Institut Virion-Serion GmbH, Würzburg, Germany

Introduction

Ensuring site-selectivity in covalent chemical modification of proteins is one of the major challenges in chemical biology, medicinal chemistry and related disciplines [1]. We have modified a pair of heterodimeric coiled-coil peptides [2] to enable enzyme- and cysteine-free, covalent stabilization of the dimer. Fusion of one peptide to the protein of interest, in combination with linking the desired chemical modification to the complementary peptide, facilitates stable, site-selective protein labeling. Covalently crosslinking of the coiled-coil, also allowed for truncation of the peptides by one heptad [3]. This isopeptide/squaramide – based crosslinking strategy, was successfully used to selectively modify the HIV-1 envelope glycoprotein (Env).

Furthermore, mutually selective pairs of coiled-coil peptides were identified [3]. Ongoing research explores the Bind&Bite method in a biomedical context, as well its selectivity and versatility for the parallel, concurrent chemical modification of multiple proteins.

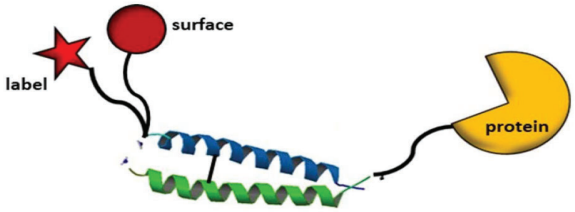

Bind&Bite principle

Activated glutamate residues in PepE can undergo proximity-enhanced isopeptide bond crosslink upon coiled-coil formation:

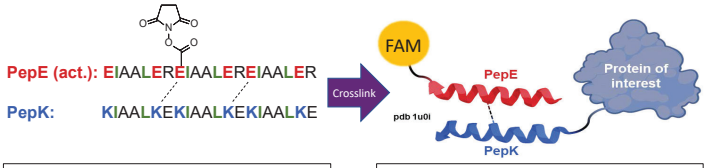

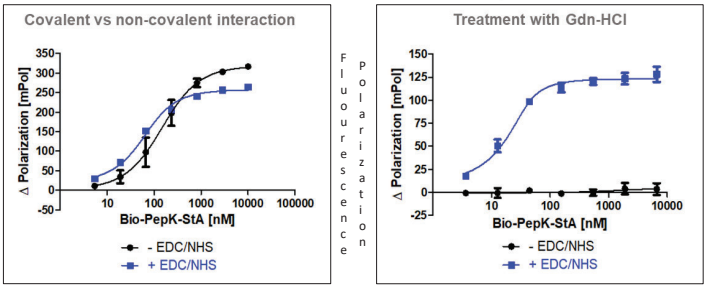

Labeling under challenging conditions

Robust and site-selective biotinylation achieved even in inhomogenous reaction conditions (Labeling of HIV-1 Env in DMEM/10 % FCS):

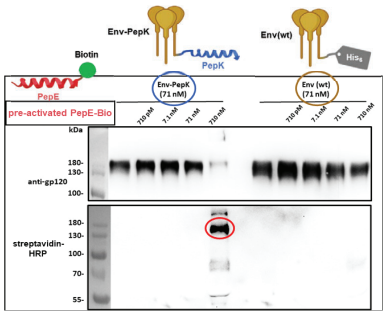

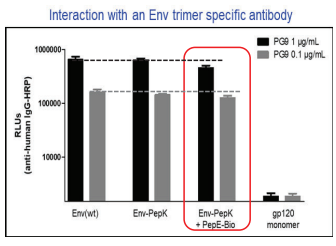

Antibody binding experiments (left):
Labeled protein is functional and retains its trimeric structure yielding responses similar to the his-tagged wildtype protein

Orthogonal Bind&Bite

Positional scanning of amine-reactive sites (PepE act.) vs. single lysine variants (PepK) yields mutually orthogonal pairs for covalent squaramide crosslinking:

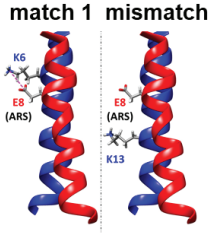

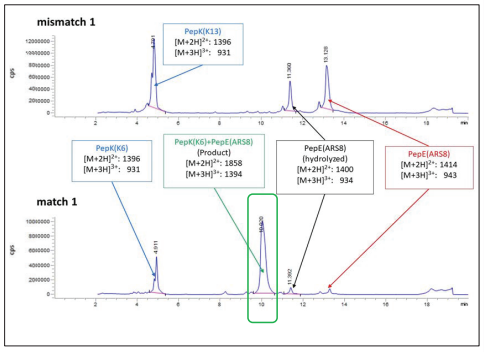

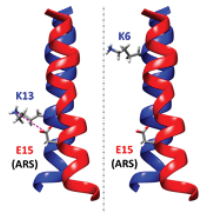

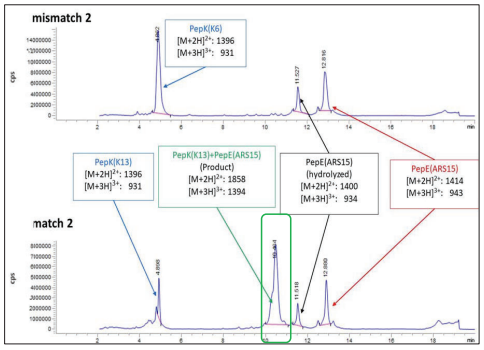

Covalent (squaramide) product formation is only observed for match 1 or match 2, no crossreactivity even after overnight incubation at high concentration (150 µM)
→ Orthogonal pairs

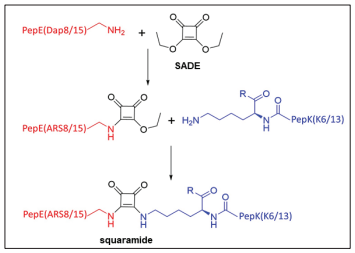

Multiple orthogonal Bind&Bite ligations

Applications of positionally encoded ligations:

Site-selective introduction of multiple tags in one protein:

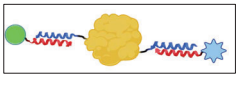

Controlled heterodimeric protein crosslinking:

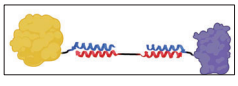

References

[1] O. Boutureira, G.J.L. Bernardes. Chem.Rev. 2015, 115, 2174–2195.

[2] A. Lindhout, J.R. Litowski, P. Mercier, R.S. Hodges, B.D. Sykes. Biopolymers, 2004, 75, 367–375.

[3] J. Beutel, P. Tannig, R. Di Vincenzo, T. Schumacher, K. Überla, J. Eichler. RSC Chem. Biol. 2023, 4, 794.

Protein Interface Catalysed Capture (PICC) to Resolve the Structure of the Tau-PSD95 Protein Complex

Reuben Blades, Kanishka Pushpitha, Gene Hart-Smith, Muhammad Bin Zenaidee, Daryl Ariawan, Lars Ittner, **Ole Tietz**

Dementia Research Centre, Macquarie Medical School, Macquarie University, Sydney, Australia
Australian Proteome Analysis Facility, Macquarie University, Sydney, Australia

Ole.Tietz@mq.edu.au
Reuben.Blades@hdr.mq.edu.au

https://doi.org/10.17952/37EPS.2024.P1194

TAU IN NEURODEGENERATIVE DISEASES

The microtubule associated protein tau (MAPT) has been implicated in multiple neurodegenerative conditions, such as Alzheimer's Disease (AD), Parkinson's Disease and a range of Frontotemporal Dementia's. The tau protein is intrinsically disordered in nature which severely limits our understanding of tau biology and hinders drug development efforts. Post-synaptic density protein (PSD95) is a key interaction partner of tau and is linked to disease progression through the mediation of post-synaptic excitotoxicity[1]. Misfolded tau aggregates have been shown to directly correlate to neuronal deficits in AD mouse models and that reducing the levels of post-synaptic tau mitigates excitotoxic effects[2]. Therefore, the resolution of tau's structure in complex is crucial for the development of effective therapies for AD and other neurodegenerative diseases.

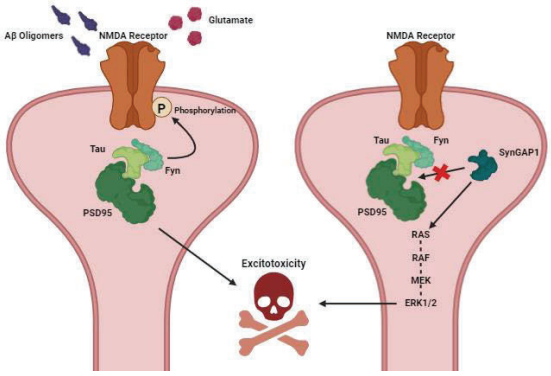

TAU – PSD95 BINDING REGIONS

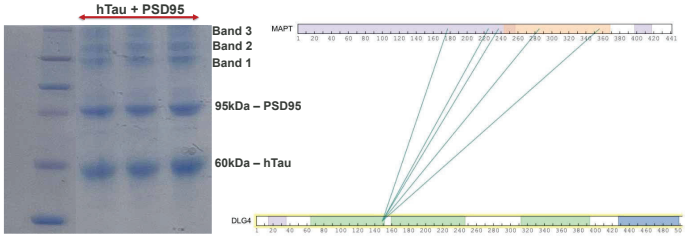

We performed an unbiased, low-resolution screen of hTau-PSD95 interaction sites, by applying crosslinking mass spectrometry (XL-MS) to the protein-protein complex. We utilized disuccinimidyl sulfoxide (DSSO), a MS cleavable crosslinker containing amine-reactive N-hydroxysuccinimide (NHS) ester groups. NHS esters react efficiently with primary amine groups and form stable amide bonds. Digestion and MS of bands 1-2 identified peptide sequences from the proline rich regions P1, P2, and the microtubule repeat region R2 of tau, which interact with PSD95's PDZ1 domain.

PROTEIN INTERFACE CATALYSED CAPTURE

Recent advances in protein chemistry allows for the installation of unnatural amino acid side chains into any position of a protein's backbone in a constitutionally 'scarless' manner[3]. The introduction of electrophilic haloalkyl side chains as native amino acid mimetics enables protein interface catalysed capture **(PICC)** of protein-protein complexes. In this process, the haloalkyl acts as a context-dependent 'protein alkylator' with cross linking reactivity for interacting nucleophiles at the protein-protein interface. This grants specificity for interacting residues as cross-linking reactions are restricted to genuine protein-protein interfaces.

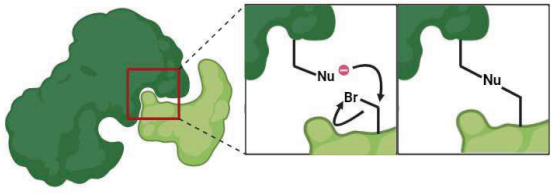

IN SILICO MODELING

We use a chymotrypsin digest followed by high resolution mass spectrometry analysis of the PICC complex. Initial experiments have identified a folded tau interface comprised of three anti-parallel regions of tau that interact with PSD95's PDZ1 domain. Experiments are ongoing to identify specific amino acid residues that are crucial to the tau-PSD95 interactome.

TAU PEPTIDE MODIFICATION

We designed biotinylated human tau peptides to represent the P1, P2 and R2 regions and installed PICC haloalkyl sidechains. We focused on five lysine residues **(K174, K180, K225, K234, K281)** and introduced single cysteine mutations in these positions. Reduction to Dha followed by light-driven radical chemistry using 4-bromobutyl boronic acid afforded five tau mutant peptides containing reactive lysine mimetics.

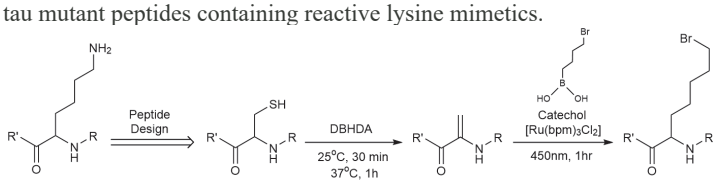

TAU - PSD95 BINDING RESIDUES

PICC tau peptides were incubated with full length PSD95 protein at low micromolar concentrations (2hr, 37ºC) and run on an SDS-gel under denaturing conditions, followed by western blot and Coomassie staining. Samples are treated with streptavidin to reveal biotinylated tau peptide signals crosslinked to PSD95.

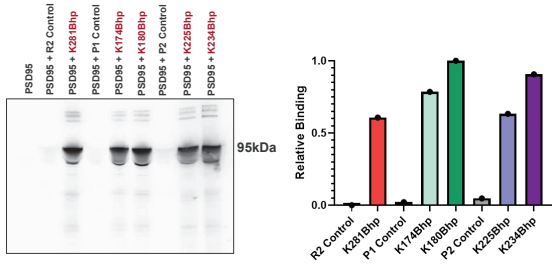

CONCLUSION

We demonstrate that PICC is a powerful tool that can be used to trap and study protein-protein interactions. Furthermore, we present the **first folded structure of tau protein fragments in complex** with an interacting protein. Future work seeks to resolve the structure of full-length tau and to develop specific PPI inhibitors for the treatment of Alzheimer's disease.

REFERENCES

1. Ittner, et al. *Biochem Cell Biol*, **2021**, Interaction between the guanylate kinase domain of PSD95 and the proline-rich region and microtubule binding repeats 2 and 3 of tau, 99(5), 606-616
2. Ittner, et al. *Cell*, **2010**, Dendritic functions of tau mediates Aβ toxicity in Alzheimer's disease mouse models, 142 (3), 387-397.
3. Davis, et al, Nature, **2020**, Light-driven post-translational installation of reactive protein side chains, 585 (7826), 530-537.

ACKNOWLEDGEMENTS

Dementia Research Centre
Australian Government
Australian Research Council
APAF
australian proteome analysis facility
Australian Government
National Health and Medical Research Council
NHMRC
Skipper Postgraduate/Early Career Researcher Travel Award
MACQUARIE University SYDNEY·AUSTRALIA

In vitro selection of highly N-alkylated cyclic peptides for targeting intracellular protein-protein interactions

○Takeo Iida, Atsushi Ohta, Yusuke Yamagishi, Tetsuo Kojima, Hitoshi Iikura
(*Research Division, Chugai Pharmaceutical Co. Ltd.*)
https://doi.org/10.17952/37EPS.2024.P1195

CHUGAI
Roche Roche Group

Abstract Peptides present a promising therapeutic approach to inhibiting protein-protein interactions (PPIs), a difficult goal often pursued by small molecule drugs. Techniques such as phage display and mRNA display have been employed to discover novel PPI inhibitor peptides. However, peptides derived from in vitro display selections, primarily composed of proteinogenic amino acids (AA), are not orally available, metabolically stable and lack cell membrane permeability. To achieve "drug-like" properties, including sufficient oral availability, metabolic stability and membrane permeability, significant chemical derivatization and optimization with substantial structural changes are necessary. Conversely, cyclosporine, a natural product derivative, shows the capability to inhibit intracellular proteins and oral availability. Two remarkable structural features of cyclosporine—backbone cyclization and N-alkylation of amide bonds—contribute to its "drug-like" properties.

In this study, we report "drug-like" cyclic peptides against KRAS using mRNA display. We employed amide cyclization and a genetic code rich in N-alkyl AA. The combination of Native Chemical Ligation (NCL) and radical-based desulfurization allows us to generate amide cyclic peptide library in an mRNA display. The genetic code was extensively engineered by using aminoacyl pCpA and mutant aminoacyl tRNA synthetases (mutARS), resulting in a codon table containing 10 N-alkyl AA and 4 other non-proteinogenic AA. We applied our "drug-like" library to the intracellular protein KRAS. The derived cyclic peptide, AP8784, contains 7 N-alkyl AA out of a total of 11 AA, similar to cyclosporine. AP8784 inhibited the KRAS-SOS1 interaction with an IC50 of 180 nM in an Alpha-Screen assay. X-ray structure analysis of the AP8784-KRAS complex revealed multiple interaction points between the cyclic backbone of AP8784 and the Gln99 residue of KRAS.
Ohta, et al. J. Am. Chem. Soc. 145, 24035−24051 (2023)

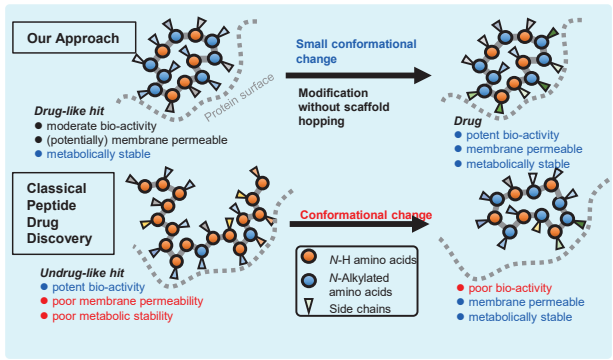

Binder enrichment cycle of cyclic peptides By mRNA display

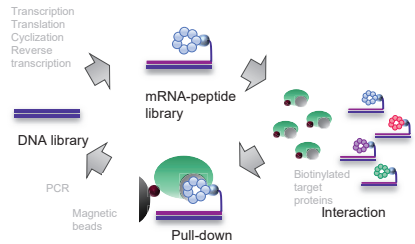

Amide cyclization method using native chemical ligation and desulfurization was established

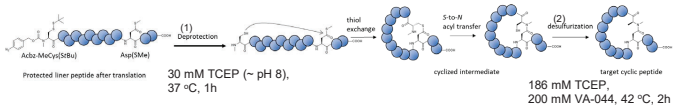

Ion chromatograms of peptides in each step

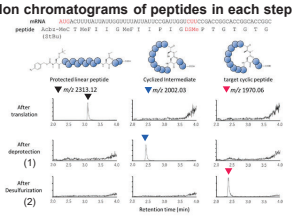

MALDI-TOF analysis of three different cyclic peptides

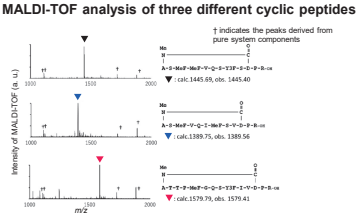

Peptide library oriented to our criteria was constructed

Amino acids and the codon table used in the panning

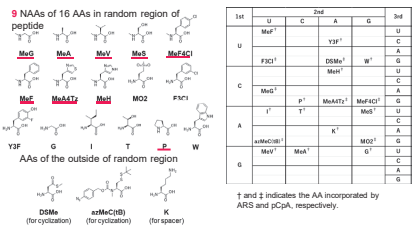

† and ‡ indicates the AA incorporated by ARS and pCpA, respectively.

Library design and properties of initial library

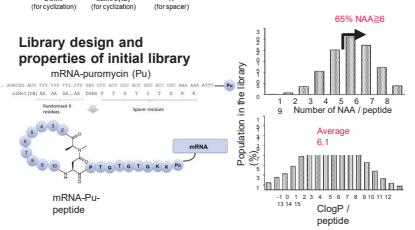

Consecutive NAA incorporations were improved by the pCpA and mutant ARS methods

The evaluation method of translation products

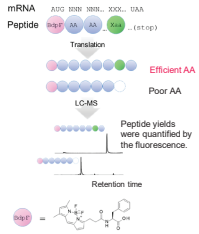

pCpA method

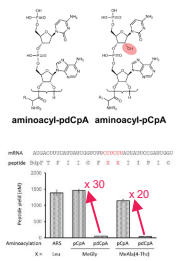

Mutant aminoacyl-tRNA synthetase (ARS) method

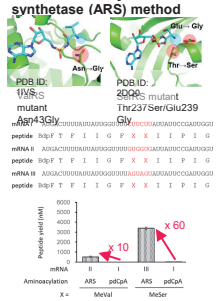

KRAS Inhibitors Were Acquired by mRNA Display

Top 10 enriched sequences in the panning and their properties

Compound No.	Frequency at round 5 (%)	Random region	No. of NAA	ClogP	K_D ‡ (μM)
1	36	W MeG Y3F MeF Y3F MeF4Cl I P T	5	10.5	2.1± 0.5
2	19	W MeG Y3F MeF Y3F MeF4Cl MeV P I	6	12.7	No binding response
3	7.8	MeG MeF MeG MeF T MeH T F3Cl F3Cl	6	7.8	5.2± 6
4	5.5	W MeG Y3F MeF Y3F MeF4Cl I P I	5	12.6	N.D.
5 (AP8784)	4.9	I MeG MeG MeF4Cl MeG F3Cl W MeF MeV	7	12.7	0.34± 0.04
6	4.9	W P Y3F F3Cl Y3F MeF4Cl T P MeV	5	11.1	No binding response
7	2.9	Y3F MeA4Tz MeA4Tz P Y3F MeV Y3F MeH Y3F	6	7.6	N.D.
8	1.8	W MeG I G MeF I F3Cl MeF MeA4Tz	5	11.5	2.9± 0.4
9	1.7	W MeF MeF4Cl P Y3F Y3F G MeH F3Cl	5	10.9	1.2± 0.3
10	1.5	Y3F MeA4Tz MeA4Tz P F3Cl MeV Y3F MeF4Cl F3Cl	6	12.8	No binding response

Pyt indicate pyrrolidine at C-term.
‡ indicate KD determination for GDP-KRAS-WT at 30 °C

Max. No. 7 12.8

KRAS as the tough target and identified PPI inhibitors

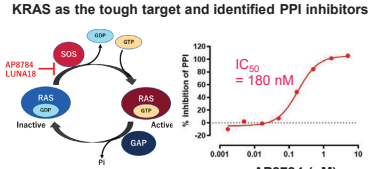

Structural analysis of KRAS-AP8784 complex

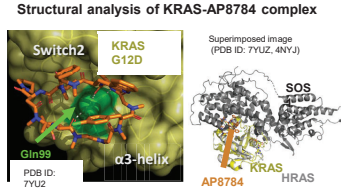

Lead optimization identified a clinical compound LUNA18

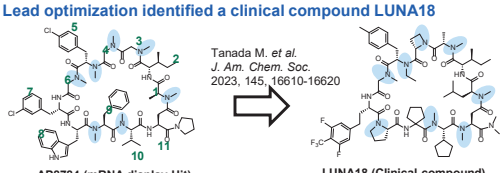

AP8784 (mRNA display Hit)
- 7 NAAs, ClogP = 12.7
- PPI $KRAS^{G12D}$-SOS1 IC_{50} = 54 nM
- Caco-2 Papp = 0.02 x 10^{-6} cm/s

LUNA18 (Clinical compound)
- 8 NAA, ClogP = 14.5
- PPI $KRAS^{G12D}$-SOS1 IC_{50} < 2 nM
- Caco-2 Papp = 2.3 x 10^{-6} cm/s

LUNA18 gave 21, 22, 47, and 26% bioavailability in mice (10 mg/kg), rats (10 mg/kg), dogs (0.3 mg/kg), and monkeys (3 mg/kg) after oral administration.

Cell growth inhibitory activity of LUNA18

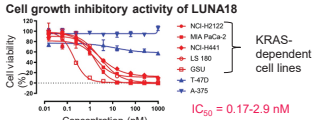

Mouse xenograft study of LUNA18 (NCI-H441, oral QD)

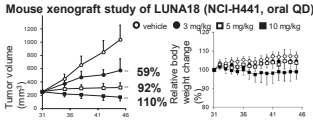

The main chains of AP8784 and LUNA18 in the KRAS binding form overlap well (no scaffold hopping)

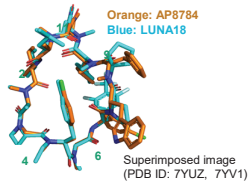

Conclusion

- Cyclic peptides were generated from our designated library contained 5–7 NAAs in 11-residue residues for KRAS.
- AP8784 from our library afforded orally available LUNA18 without scaffold hopping, which supports the validity of our concept.

https://doi.org/10.17952/37EPS.2024.P1200

Study on the Role of Helix-Stabilized Peptides in Transporting Antisense Morpholino Oligomers into Cells: Relationships among Helicity, Cellular Uptake, and Antisense Activity

Hiroyuki Takada[1,2], Keisuke Tsuchiya[1,3], ◯Yosuke Demizu[1,2,4]

[1]National Institute of Health Sciences, [2]Yokohama City University, [3]Sanyo-Onoda University, [4]Okayama University

1. Introduction

- Oligopeptides adopting well-defined secondary structures are called *peptide foldamers*. The secondary structures of cell-penetrating peptides (CPPs) influence their properties such as cell-membrane permeability, tolerability to proteases, and intracellular distribution. For example, **CPPs forming the stable α-helix structure are more cell-permeable compared with the conventional CPPs with random structures.**
- CPPs are a powerful tool for the intracellular delivery of impermeable macromolecules such as enzymes, antibodies, and oligonucleotides. In terms of the delivery of antisense oligonucleotides, several successful studies have been reported on the conjugates of cationic CPPs with phosphorodiamidate morpholino oligomers (PMOs) in cell-based assays and animal studies. However, **there are few studies where *peptide foldamers* are utilized for the delivery of PMOs.**

We designed and synthesized helix-stabilized CPPs by introducing α,α-disubstituted amino acids (dAAs) into the oligoarginine peptide and evaluated their effects on the cell permeability and antisense activity of the corresponding peptide-conjugated PMOs (PPMOs).

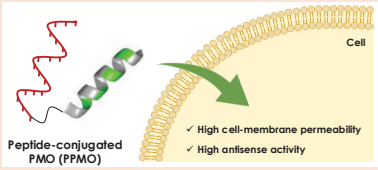

2. Design of helix-stabilized CPPs by introducing dAAs



Peptide	Sequence
2a	RRRRRRRRR
3a	RRX¹RRX¹RRX¹RRX¹RZ
4a	RRX²RRX²RRX²RRX²RZ
5a	RRX³RRX³RRX³RRX³RZ
6a	RRX⁴RRX⁴RRX⁴RRX⁴RZ

Z = 6-Azido-L-lysine

X¹ = Aib

X² = Ac_4c

X³ = Ac_5c

X⁴ = Ac_6c

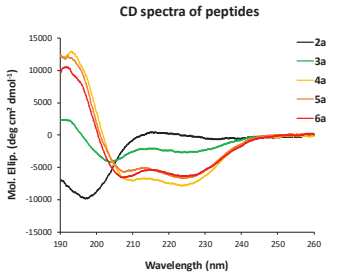

100 μM in 20 mM phosphate buffer (pH 7.4)

Peptides 3a–6a containing dAAs exhibited right-handed α-helix-like CD spectra, while the R9 peptide 2a showed a random-coil-like CD spectrum.

3. Antisense activity of helical CPP-PMO conjugates

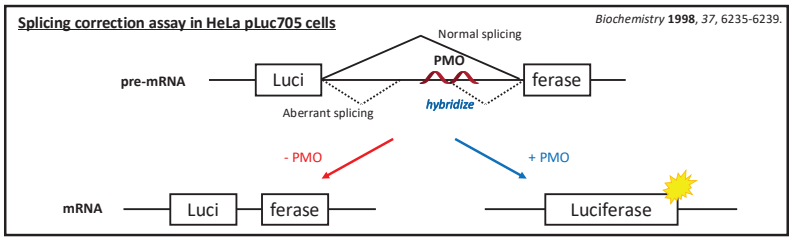

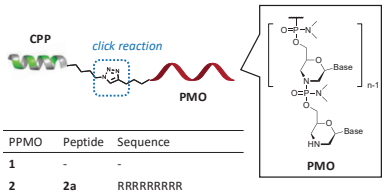

PPMO	Peptide	Sequence
1	-	-
2	**2a**	RRRRRRRRR
3	**3a**	RRX¹RRX¹RRX¹RRX¹RZ
4	**4a**	RRX²RRX²RRX²RRX²RZ
5	**5a**	RRX³RRX³RRX³RRX³RZ
6	**6a**	RRX⁴RRX⁴RRX⁴RRX⁴RZ

Z = 6-azido-L-lysine

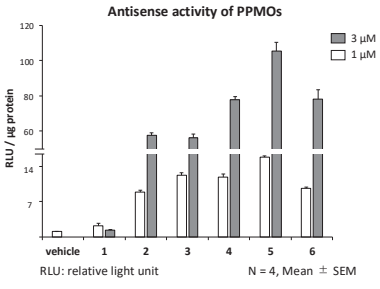

RLU: relative light unit

N = 4, Mean ± SEM

The helical CPP-PMO conjugates 3–6 exhibited higher antisense activities compared with the R9 peptide conjugate 2 in a dose-dependent manner. Among them, the conjugate 5 containing Ac_5c residues showed the best antisense activity.

4. Relationships among helicity, cellular uptake, and antisense activity

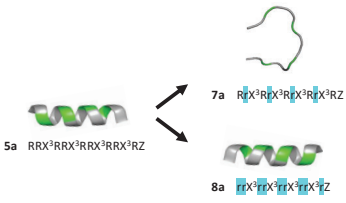

r = D-arginine, Z = 6-azido-L-lysine

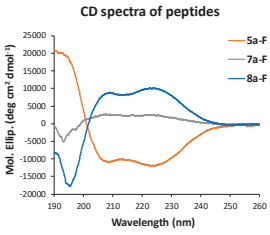

100 μM in 20 mM phosphate buffer (pH 7.4)

***5a-F, 7a-F, and 8a-F are modified with fluorescein at their N-terminus.**

The stereoisomers of 5a were synthesized, where the chirality of the Arg residues was altered. The peptide 7a showed a drastic decrease in helicity, while 8a exhibited a left-handed α-helical structure. These peptides have similar hydrophobicity, but different helicity.

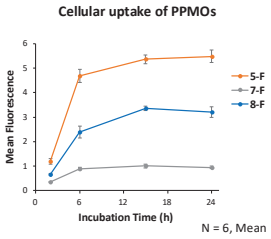

N = 6, Mean ± SEM

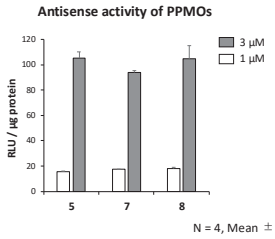

N = 4, Mean ± SEM

PPMO 5-F and 8-F containing helical CPPs exhibited higher cellular uptake compared with 7-F containing the non-helical CPP. By comparison, all PPMO 5, 7, and 8 showed comparable antisense activities regardless of the intracellular amounts of the PPMOs.

6. Confocal microscopy observation

Confocal microscopy images of HeLa pLuc705 cells treated with 5-F

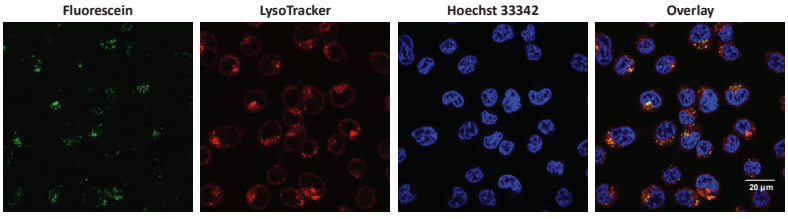

PPMOs containing arginine-rich CPPs are internalized into cells by endocytosis and they need to escape from the endosomes and move into the nuclei for the antisense activity. The confocal microscopy observation indicated that the green fluorescence of 5-F was distributed in a punctate pattern and colocalized with the endosome/lysosome marker, suggesting that most of the internalized helical CPP conjugates remained within endosomes or lysosomes and did not reach the nucleus.

7. Synergistic effects with endosomal escape enhancers

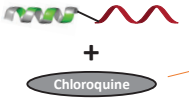



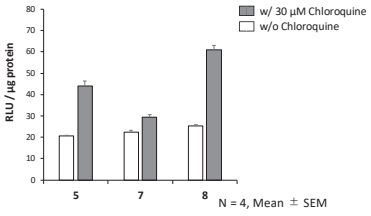

N = 4, Mean ± SEM

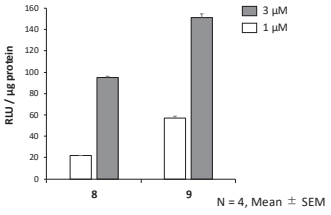

N = 4, Mean ± SEM

In the presence of chloroquine, an endosomolytic reagent, helical CPP-PMO conjugates 5 and 8 exhibited higher antisense activities than 7, suggesting synergistic effects of the efficient cellular uptake and cytosolic release of PPMOs. PPMO 9 with an endosomal escape domain peptide at its N-terminus exhibited high antisense activity compared with 8.

8. Summary

- ✓ We designed helix-stabilized arginine-rich peptides containing various dAAs to identify highly cell-permeable and potent PPMOs. Among them, the conjugate **5** containing Ac_5c residues exhibited a high antisense activity in the HeLa pLuc705 splicing correction assay.
- ✓ The relationships among the helicity of the peptides, cellular uptake, and antisense activity of PPMOs were investigated by using stereoisomers where the chirality of the Arg residues was altered. Consequently, it was demonstrated that helical CPPs can deliver the conjugated PMO into cells more efficiently than nonhelical CPPs, but the antisense activities were comparable regardless of the cellular uptake amounts due to endosomal entrapment.
- ✓ Co-administration of chloroquine, an endosomolytic reagent, synergistically improved the antisense activity of the helical CPP conjugates **5** and **8**, suggesting that stabilizing the helical structure of CPPs is effective to enhance the antisense activity of PPMOs when their endosomal escape is promoted.



Takada, H. *et al.*, *Bioconjugate Chemistry* **2022**, *33*, 1311-1318.

https://doi.org/10.17952/37EPS.2024.P1203

Synthesis of Bacteria-Derived Lipopeptides and Applications in Antibiotic Discovery

Glenna Swinand[1], Katherine Bowen[1], Samir Olatunji[2], Martin Caffrey[2], and Eoin M. Scanlan[1]

School of Chemistry[1] and School of Biochemistry and Immunology[2], Trinity Biomedical Sciences Institute, Trinity College Dublin, Ireland

swinandg@tcd.ie, eoin.scanlan@tcd.ie

Trinity College Dublin
The University of Dublin
IRISH RESEARCH COUNCIL
An Chomhairle um Thaighde in Éirinn

Introduction

Bacterial lipoprotein processing pathway (BLPP) in Gram-negative bacteria

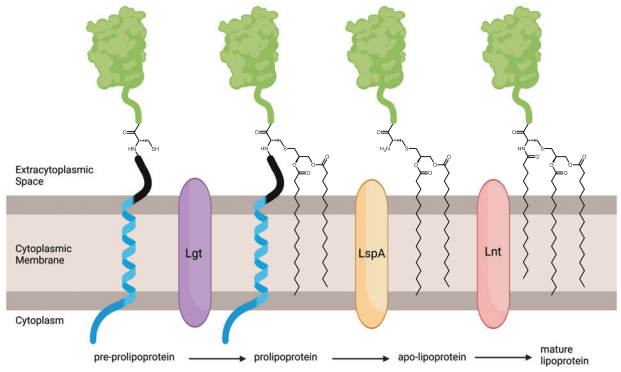

- The BLPP is a **post-translational modification** pathway of bacteria-specific enzymes.[1]
- Lipoproteins have **essential** functions in bacteria e.g. cell signalling, toxins, and for structural support.[2]
- Enzymes of the BLPP are potential **new antibiotic targets** therefore Inhibition of the BLPP offers novel opportunities for **antibiotic development**.
- Bacterial lipoproteins are **immunogenic** in humans and as potent TLR-2 agonists.[3]
- The first section of this work focuses on the **synthesis of fluorescent lipopeptide substrates** of LspA to probe the activity of this enzyme and to facilitate the discovery of **new inhibitors**.
- The second section focuses on a **convergent synthesis** methodology to access lipopeptides under mild **aqueous conditions**.

Lipopeptide Probe Synthesis

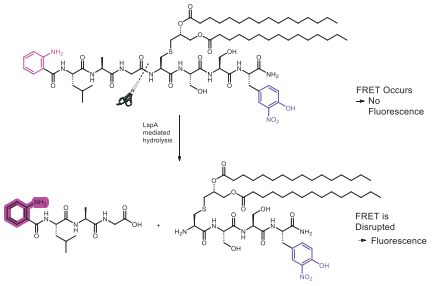

- Förster Resonance Energy Transfer (**FRET**) relies on the spectral overlap of a **donor** (pink) and an **acceptor** (purple) fluorescent moiety, and the **distance** between them.[4]
- Hydrolysis of the probe by LspA **disrupts FRET** resulting in an **increase in fluorescence** intensity corresponding to LspA activity.

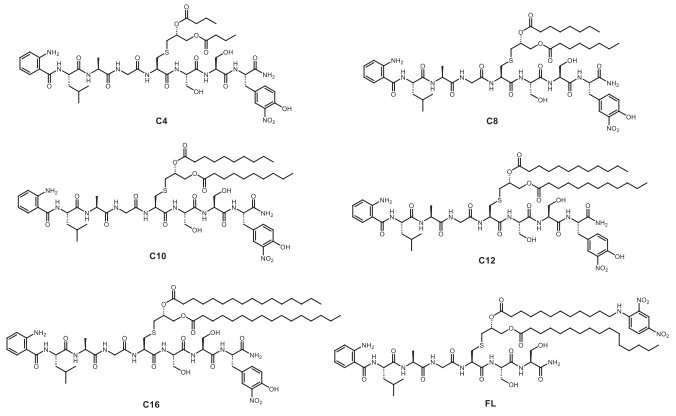

A range of lipopeptide probes for LspA with varying lipid lengths and structures were synthesised and tested as substrates for LspA.

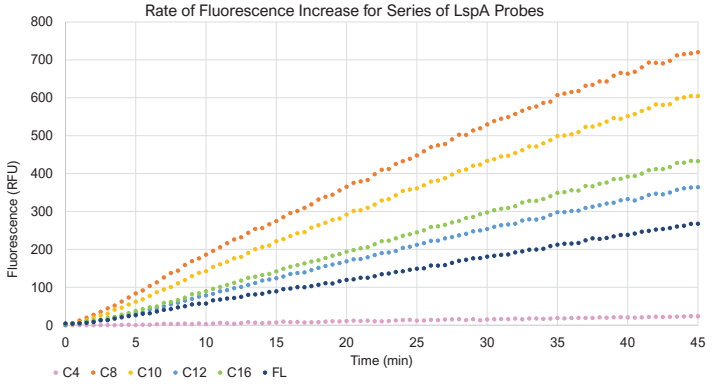

Peptide	C4	C8	C10	C12	C16	FL
Initial Rate (RFU/min)	0.606	19.4	16.0	9.4	10.7	6.41

Convergent Lipopeptide Synthesis

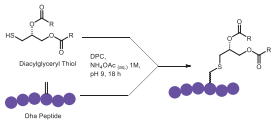

- ✓ Parallel assembly of starting materials
- ✓ Mild aqueous conditions
- ✓ Chemoselective late-stage addition

This methodology incorporates a thiol-Michael addition reaction between a Dha-containing peptide and a lipid-thiol that can be carried out under optimised aqueous conditions.

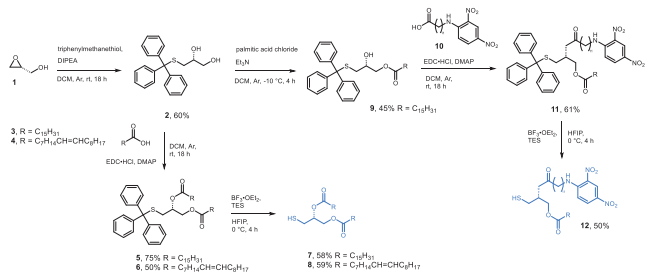

Three diacylglycerol lipid thiols were synthesised in good yield

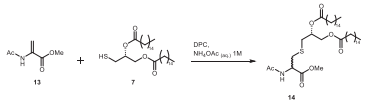

Conditions were optimised using a model reaction

Entry	Time (h)	pH	Consumption of Dha % (^{1}H NMR)
1	18	7	82%
2	18	4	69%
3	18	9	>99%
4	3	9	98%

- The conditions were then applied to a model peptide **15** with a series of lipids, showing the compatibility of this method with **saturated**, **unsaturated** and **complex lipids**.
- Lipid **16** was then reacted with a liraglutide-inspired peptide with excellent conversion.

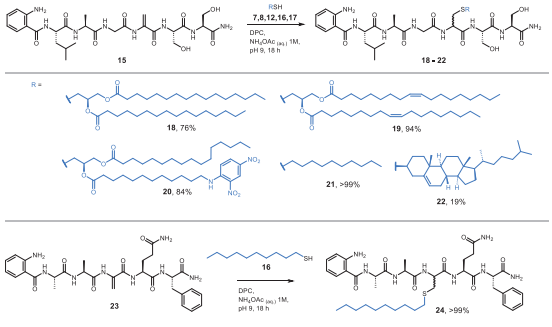

Lipopeptide **20** was found to be a substrate and an effective activity probe for LspA

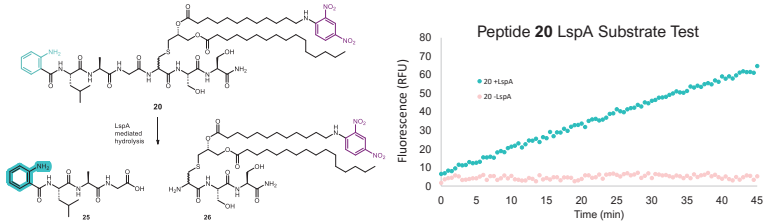

Conclusions and Future Work

A series of lipopeptide probes for LspA with varying lipid lengths were synthesised and the C8 analogue appeared to be the most sensitive followed by the C10 analogue. Future work includes enzyme kinetics experiments to characterise each probe.

A late-stage lipidation method was developed under mild aqueous conditions and demonstrated compatibility with a series of saturated, unsaturated, and complex lipids. The method was successfully used to make a novel probe for LspA.

References

1. L. Smithers, S. Olatunji and M. Caffrey, *Front. Microbiol.*, **2021**, 12, 788445.
2. S. Olatunji, X. Yu, J. Bailey, C.-Y. Huang, et. al. *Nat. Commun.*, **2020**, 11, 140.
3. S. Olatunji, K. Bowen, C.-Y. Huang, et. al. , *Nat. Commun.*, **2021**, 12, 4254.
4. H. Sahoo, *J. Photochem. Photobiol. C: Photochem. Rev.*, **2011**, 12, 20-30.

Acknowledgements: This work was supported by grants from the Irish Research Council and Science Foundation Ireland

P1.204

https://doi.org/10.17952/37EPS.2024.P1204

Controlled Intracellular Trafficking and Gene Silencing by Oligonucleotide-Signal Peptide Conjugates

Masayuki Fujii (mfujii@fuk.kindai.ac.jp)

1) Department of Biological and Environmental Chemistry, Kindai University, 11-6 Kayanomori, IIzuka, Fukuoka 820-8555, Japan

Abstract

In the present study, we investigated the intracellular delivery using some hybrid peptides as transfection reagents and the silencing effect of siRNA targeting human telomerase reverse transcriptase (hTERT) mRNA in 3 human cancer cell lines, Jurkat and HeLa [1,2,3]. The complex of siRNA and a specific amphiphilic peptide (Pfect?7) or its hybrid with an intracellular transport signal peptide could be effectively taken up into cells. The complex also showed a high silencing effect against hTERT mRNA

. Combination of siRNA-nuclear export signal (NES) peptide conjugates and the amphiphilic peptides suppressed the expression of BCR/ABL chimeric gene in chronic myelogenous leukemia (CML) cell line K562 up to 95.2 % [4]. The amphiphilic peptides and their hybrids showed almost no cyto-toxicity and protected siRNA against intracellular nuclease digestion in 10% FBS (half life time was over 48h).

Synthesis of Oligonucleotide-Peptide Conjugates by SPFC

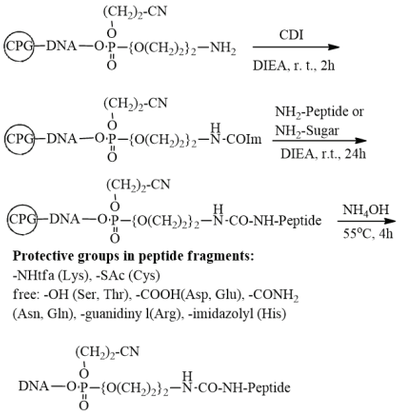

R-CONHCH$_2$CH$_2$OCH$_2$CH$_2$OPO$_3$-5'-CAGTTAGGGTTAG-3'

C1: R = Ac-GPKKKRKVGK- NH- (SV40 T antigen NLS)
C1f: R = FITC-GPKKKRKVGK- NH- (SV40 T antigen NLS)
C2: R = Ac-GRKKRRQRRRPPGGK- NH- (HIV-1 Tat NLS)
C2f: R = FITC-GRKKRRQRRRPPGGK- NH- (HIV-1 Tat NLS)
C3: R = - NH- ANSAAFEDLRVLS-OH (Influenza Virus nucleoprotein NLS)
C4: R = Ac-LPPLERLTLGK- NH- (HIV-1 Rev NES)
C4f: R = FITC-LPPLERLTLGK- NH- (HIV-1 Rev NES)
C5: R = - NH - ALRALLRALLRAL-OH (designed)
C5f: R = - NH - ALRALLRALLRAL-OH (designed)
C6: R = - NH - ARLRLRLRLRL-OH (designed)
C7: R = galactosamine

R-CONHCH$_2$CH$_2$OCH$_2$CH$_2$OPO$_3$-5'-s(CAGTTAGGGTTAG)-3'

C8: R = Ac-GPKKKRKVGK- NH- (SV40 T antigen NLS)
C8f: R = FITC-GPKKKRKVGK- NH- (SV40 T antigen NLS)

[1] Masayuki Fujii *et al., Org. Lett.*, **2003**, 5, 2623-2626.
Bioorg. & Med. Chem. Lett., **2005**, 15, 167-170.
Org. & Biomol.Chem., **2005**, 3, 3257 ? 3259.
Fronteers in Org. Chem., **2005**, 1, 229-241.
Bioorg. & Med. Chem. Lett., **2007**. 17, 6576-6578.
Curr. Org. Chem., **2009**, 13, 1366-1377.

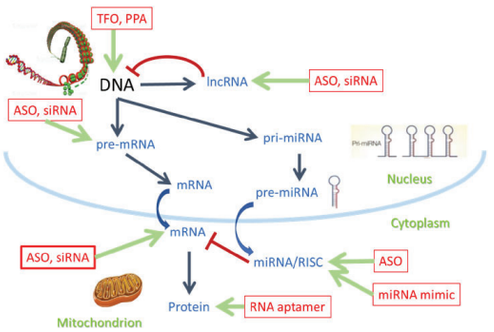

Nucleic Acid Therapeutics and Their Targets

Nucleic Acid Therapeutics should
(1) be stable enough chemically and biologically, inside and outside the cells,
(2) be delivered to the targeted tissue,
(3) be taken up into cells effectively,
(4) be localized in the specific intracellular organs,
(5) bind to the target molecule with enough affinity and specificity,
(6) not be toxic,
(7) not cause undesirable effect (off-target effect),
(8) not induce immunoresponse,
. . . .

Inhibition of hTERC by Antisense DNA-NLS Conjugate

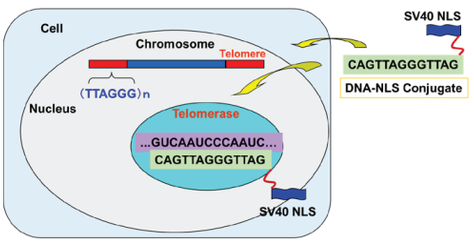

Ac-GPKKKRKVGK-εNH-CONHCH$_2$CH$_2$OCH$_2$CH$_2$OPO$_3$-5'-s(CAGTTAGGGTTAG)-3'
(SV40 T antigen NLS)

Inhibition of hTERC by Antisense DNA-NLS Conjugate

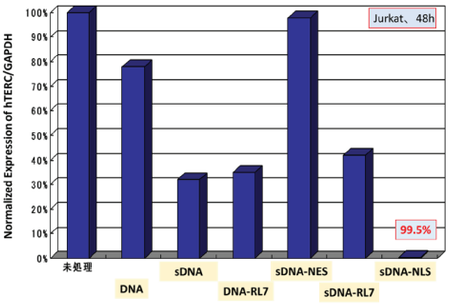

[2] M. Fujii, *et al.,* Org. & Biomol.Chem., 2005, 3, 3257-3259.
[3] Fujii M et al. (2020) Nucleosides, Nucleotides and Nucleic Acids 39(1-3):407-425.

Controlled Delivery of DNA-Signal Peptide Conjugates

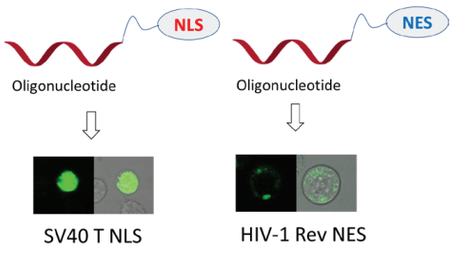

Chronic Myelogenous Leukemia (CML)

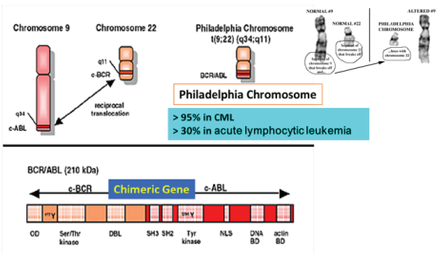

Target sequence of bcr/abl mRNA(355-390)
5'-ggauuuaagcagaguucaa/aagcccuucagcggcca-3'

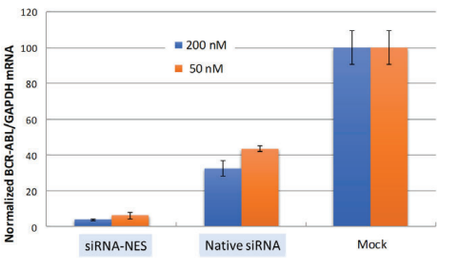

Silencing of bcr-abl mRNA by siRNA6 (HIV1 REV NES) in K562.

siRNA suppressed bcr-abl mRNA expression in K562 cells.
Normalized bcr-abl/GAPDH mRNA levels were measured in 24 h after transfection with Lipofectamine 2000™.

Delivery and Gene Silencing by Oligonucleotide-Peptide Conjugates

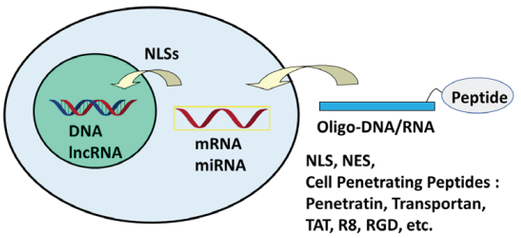

NLS, NES,
Cell Penetrating Peptides :
Penetratin, Transportan, TAT, R8, RGD, etc.

Specific Suppression of BCR-ABL mRNA by siRNA-NES Conjugates Targeting b3a2 Transcripts

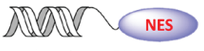

Target sequence of bcr/abl mRNA(355-390)
5'-ggauuuaagcagaguucaa/aagcccuucagcggcca-3'

siRNA
Sense; 5'-NES-GCAGAGUUCAAAAGCCCUUTT-3'
Antisense; 5'-AAGGGCTTTTGAACUCUGCTT-3'
NES Peptides:
C1; -NHCH$_2$CH$_2$CH$_2$CO-LPVLENLTL-OH (TFIIIA NES)
C2; AcNH-LPPLERLTL-K(εNH-)G-OH (HIV-1 REV NES)

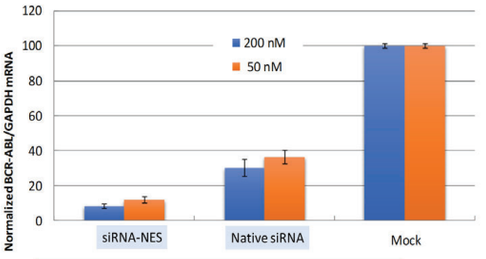

Silencing of bcr-abl mRNA by siRNA5 (TFIIIA NES) in K562.

siRNA suppressed bcr-abl mRNA expression in K562 cells.
Normalized bcr-abl/GAPDH mRNA levels were measured in 24 h after transfection with Lipofectamine 2000™.

[4] M. Fujii, *et al., Nucleic Acid Therapeutics*, 2017, 27(3), 168-175.

COI: We have no conflict of interest to disclose for this presentation.

Polysaccharides modified with attenuated cationic lytic peptides: Formation of microparticles and their use in cytosolic antibody delivery

Junya Michibata[1], Yoshihiro Sasaki[2], Kazunari Akiyoshi[2], Shiroh Futaki[1]
([1]Institute for Chemical Research, Kyoto University, [2]Graduate School of Engineering, Kyoto University)

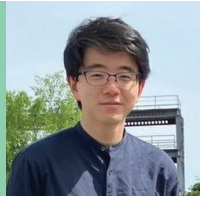

https://doi.org/10.17952/37EPS.2024.P1205

Summary

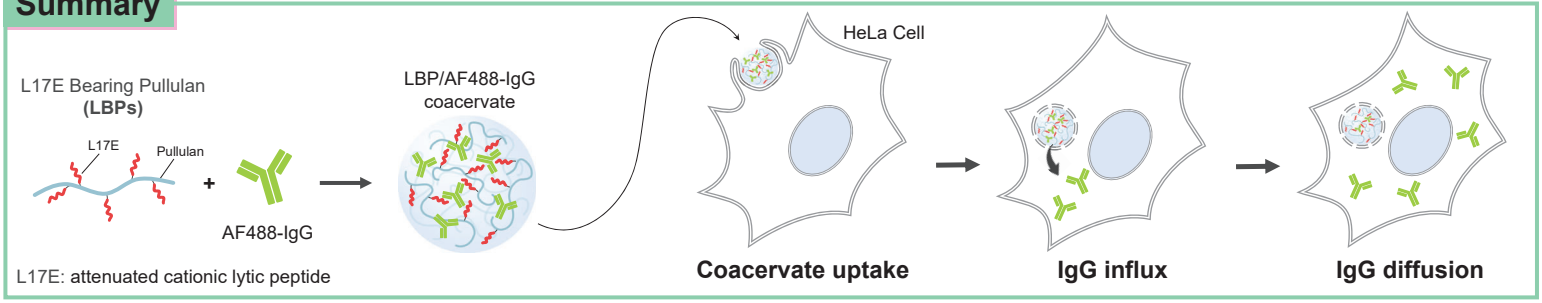

L17E: attenuated cationic lytic peptide

Background

- IgG does not penetrate cell membrane.
- With L17E, IgG can move into cytosol
  → but not efficient enough

L17E:IWLTALKFLGKHAAKHEAKQQLSKL-NH_2

Akishiba, M. *et al.* (2017) *Nat. Chem.* 9, 751-761.

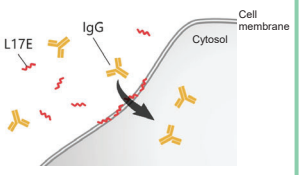

- $FcB(L17E)_3$, trimer of L17E, can deliver IgG into cytosol more efficiently by forming microdroplets with Alexa Fluor 488 labeled IgG (AF488-IgG).

Iwata, T. *et al.* (2021) *Angew. Chem. Int. Ed. Engl.* 60, 19804-19812.

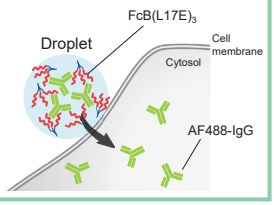

Develop more stable coacervate for future therapeutic application

Strategy

- Pullulan, a kind of polysaccharide, was used.
- Cholesterol bearing pullulan forms nanogel.

Akiyoshi, K. *et al.*, (1997) *Macromolecules.* 30, 857-861.

- Pullulan nanogel is hydrophilic and low toxic.

Kawasaki, R. *et al.*, (2021) *Adv. Healthc. Mater.* 10, e2001988.

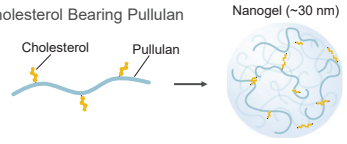

Pullulan modified with L17E instead of cholesterol

Coacervate formation?



Synthesis

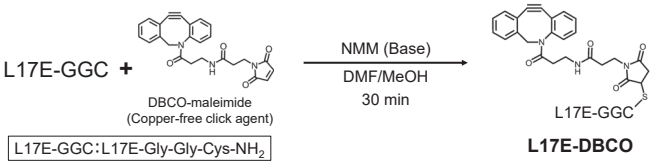

L17E-GGC:L17E-Gly-Gly-Cys-NH_2

L17E-DBCO

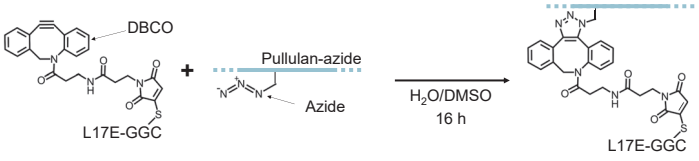

L17E Bearing Pullulan (LBP)

	Equivalence of added L17E-DBCO to 100 glucose units	Actual modification ratio to 100 glucose units
LBP-1	1	0.66
LBP-4	4	3.5
LBP-8	8	7.4
LBP-12	12	11.4
LBP-14	14	12.2

Actual modification ratio was measured by ^{1}H NMR.

Result

❑ LBPs can form 1-3 μm particles with AF488-IgG and multimerization of L17E is important for particle formation

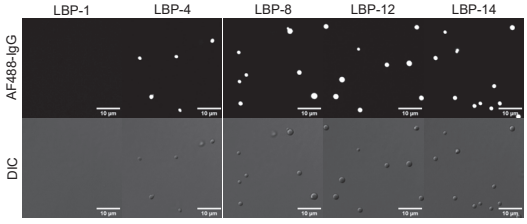

❑ LBPs efficiently delivered AF488-IgG into cells

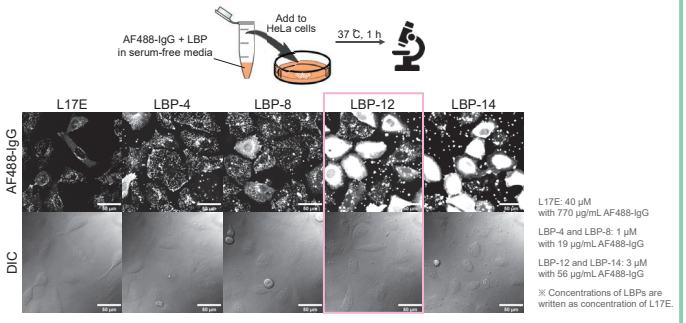

❑ AF488-IgG diffusion started from the particle and the particle induces the structural change of cell membrane

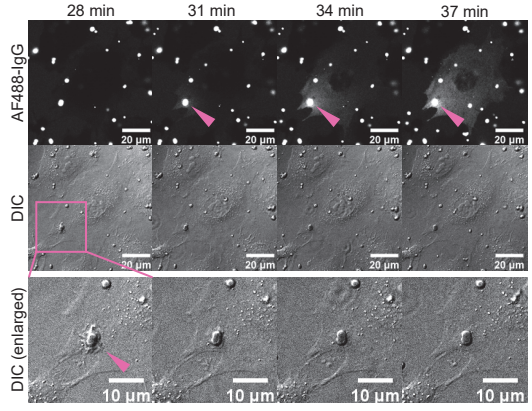

❑ The particle was inside the cell after delivery and it was wrapped by membrane

➢ Non-canonical or atypical mode of cellular uptake?

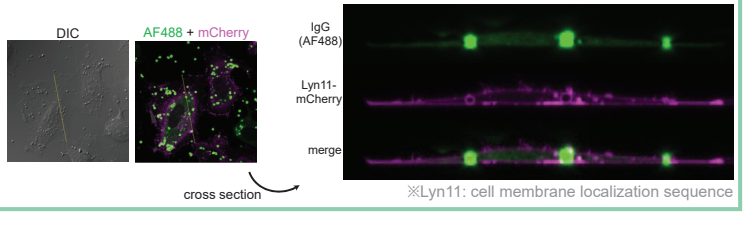

※Lyn11: cell membrane localization sequence

Leiden University Medical Center

Max S. Kloet[1], Jim Voorneveld[2], Qiang Liu[2], Robbert Q. Kim[1], Ivan Đikić[3], Huib Ovaa[1], Dmitri V. Filippov[2] and Gerbrand J. van der Heden van Noort[1*]

[1] Dept. of Cell and Chemical Biology, Leiden University Medical Centre, Leiden, NL
[2] Dept. of Bio-Organic Synthesis, Leiden Institute of Chemistry, Leiden, NL
[3] Inst. of Biochemistry II & Buchmann Inst. for Molecular Life Sciences, Goethe University, Frankfurt am Main, DE

https://doi.org/10.17952/37EPS.2024.P1206

Probing the interplay between Ubiquitination and Adenosine-Di-Phosphate ribosylation

ADP-ribosylation of Ub

The already difficult Ubiquitin code has recently been exposed to be even more complex as Ub can be post-translationally modified itself. Attachment of Adenosine-Di-Phosphate ribose (ADPr) on multiple distinct amino acids positions, such as Arg42, Thr66 or Gly76 in Ub leads to the formation of a variety of isotypes of Ub^{ADPr}. These modifications are tightly regulated by transferase and hydrolase enzymes that are involved in bacterial infections (by *Legionella pneumophila* and *Chromobacterium violaceum*) and mammalian DNA damage responses although the details of these processes are poorly understood. Unveiling this new layer of ubiquitin regulation and the molecular mechanisms and cell biological consequences of these distinct Ub^{ADPr}-isotypes will benefit from well-defined tools. We here report the chemical synthesis and application of Ub^{ADPr} substrates and activity-based probes.

Development of reagents and probes

Advantages of chemical synthesis:
- ADPr introduction possible on all amino acid positions
- Attachment of non-native amino acids, affinity-tags, fluorophores or warheads

Application potential:
- Biophysical studies on enzymes (kinetic parameters/ affinity/ selectivity preferences)
- Activity-based protein profiling (discovery of interactors, undisclosed enzymes)
- Structure determination (X-ray crystallography)



Ub^{ADPr} - toolbox

What can we do with new chemical methodologies?

native Arginine link[1]

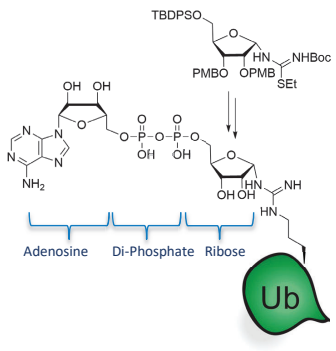

partially stabilised[2]

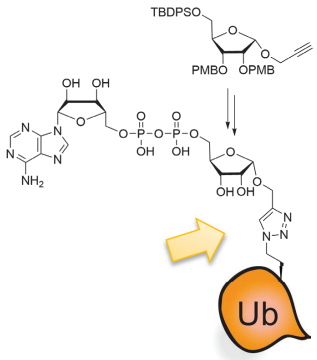

completely stabilised[3]

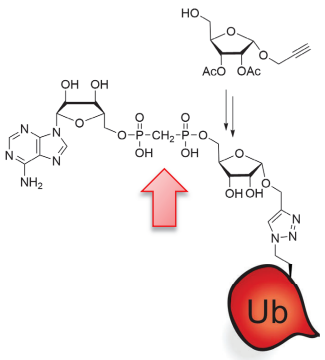

activity-based probes

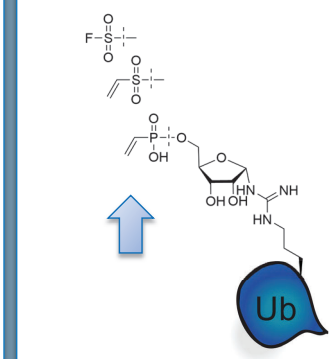

Profiling Legionella DupA activity

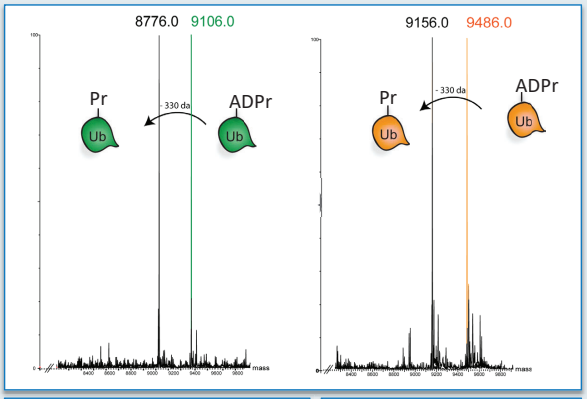

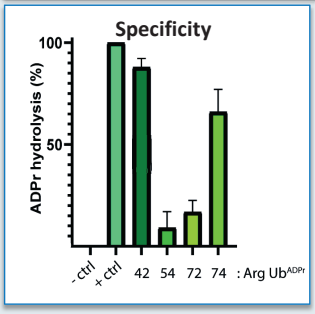

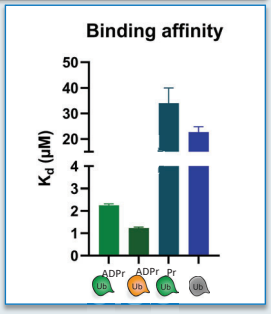

Pulldown & labelling of DupA

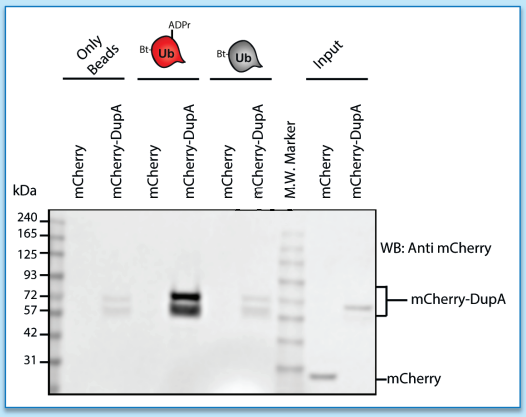

non-covalent interaction

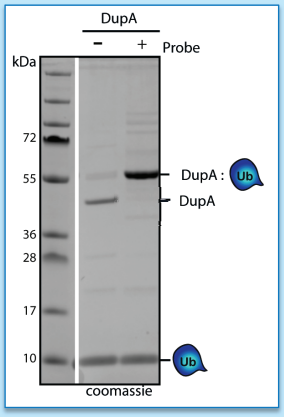

covalent adduct

Outlook

The newly developed chemical methodologies towards Ub^{ADPr}-substrates showcase the power of protein synthesis. This toolbox of Ub^{ADPr}-substrates and probes and proof-of-principle studies on Legionella effector enzyme DupA provides a platform to further interrogate the cell biology affected by all Ub^{ADPr} isotypes and opens the way to finding out if this modification is more prevalent then is known to date.

References: [1]] J. Voorneveld, M. S. Kloet, R. Q. Kim, A. Moutsiopoulou, M. Misra, I. Dikic, , D. V. Filippov, G. J. van der Heden van Noort, *submitted for publication* [2] Q. Liu, H. A. V. Kistemaker, S. Bhogaraju, I. Dikic, H. S. Overkleeft, G. A. van der Marel, H. Ovaa, G. J. van der Heden van Noort, D. V. Filippov, *Angewandte Chemie-International Edition* **2018**, *57*, 1659-1672 [3] R. Q. Kim, M. Misra, A. Gonzalez, I. Tomaskovic, D. Shin, H. Schindelin, D. V. Filippov, H. Ovaa, I. Dikic, G. J. van der Heden van Noort, *Chemistry*, **2021**, *27*, 2506-2512

* Correspondance to gvanderheden@lumc.nl

NWO Netherlands Organization for Scientific Research

École polytechnique fédérale de Lausanne

Institute of Materials - Institute of Bioengineering

sunmil.epfl.ch

Supramolecular NanoMaterials and Interfaces Laboratory

Virucidal Peptide-Based Drugs to Target Influenza

Shadi Kordbacheh, Francesca Olgiati, Francesco Stellacci

Institute of Materials Science & Engineering,
École polytechnique fédérale de Lausanne (EPFL), 1015-Lausanne, Switzerland

https://doi.org/10.17952/37EPS.2024.P1207

Aim of the Project

- Influenza viruses acquire point mutations in genes encoding the surface glycoproteins hemagglutinin (HA) and neuraminidase (NA).
- In case of HA, mutation mainly happens at the head region of the protein.
- Compounds targeting other regions of HA than receptor binding domain (RBD) are needed to decrease the chance of mutation.
- Antibodies are the best natural antiviral drugs. Inspired by portions of antibodies against influenza, peptide sequences were chosen as the targeting moiety.

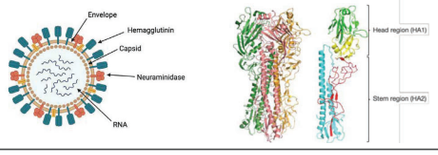

Peptide Extracts from Antibody

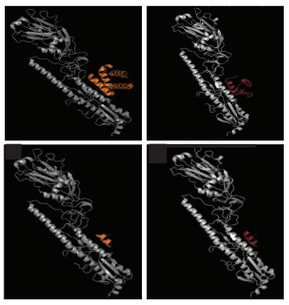

- Interaction of HB36.1 and HB80.4 Antibodies with HA
- Short Peptide Drives from Antibody:
  - ➢ Small portion of antibody is responsible for interaction with HA

Original protein	Peptide code	Peptide sequence
HB36.1	FW9	FDAAMRNMW
HB36.1	MF9	MRNMWAKVF
HB80.4	FA11	FSENIAKEIAA
HB80.4	EF11	ENIAKEIAASF

Peptide as the Targeting Moiety in the Virucidal Drug

- Synthesis of Peptide-Based Drugs

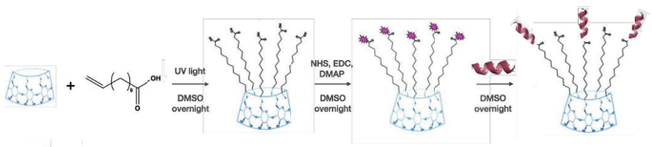

: Peptide

: Activated carboxylic acid

- Antiviral Activity of C11-Peptides Against A/Netherlands/602/2009

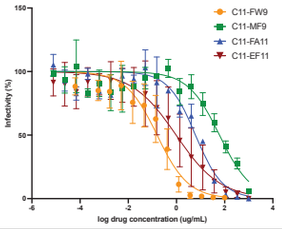

Molecule	Peptide sequence	EC50 (μg/mL)
C11-FW9	**FDAAMRNMW**	**0.16 (0.11-0.22)**
C11-MF9	MRNMWAKVF	60.9 (36.63-101.4)
C11-FA11	FSENIAKEIAA	6.19 (3.95-9.55)
C11-EF11	**ENIAKEIAASF**	**0.96 (0.60-1.55)**

- Virucidal Assay of C11-FW9 and C11-EF11

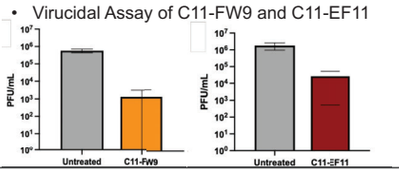

Mechanism of Action

- Individual Peptide

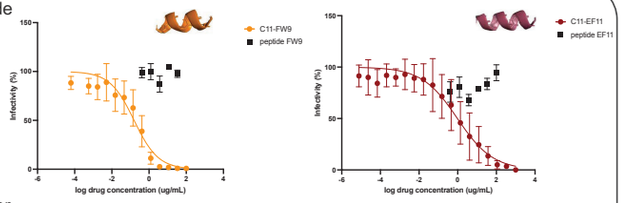

- PEGylated Linker

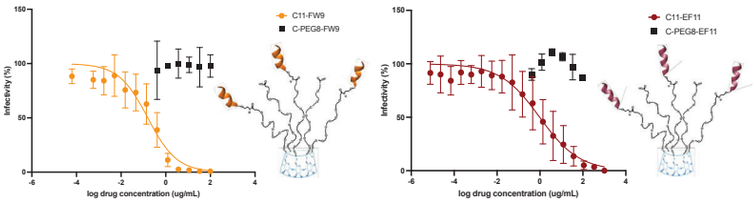

- Trypsin-Susceptibility Assay

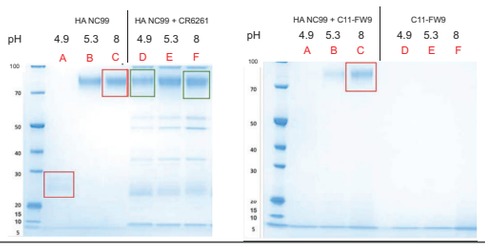

Key Amino Acids for Interaction

- The contact comes from the side chains of FM and W

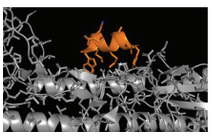

FDAAMRNMW

Peptide Code	Peptide sequence	Molecule	EC50 (μg/mL)
FW9	FDAAMRNMW	C11-FW9	0.16 (0.11-0.22)
EE9	EDAAARNAE	C11-EE9	34.31 (28.91-41.48)
SS9	SDAAARNAS	C11-SS9	>100
AA9	ADAAERNEA	C11-AA9	Not soluble

RBD is NOT the binding site

- Inhibition Assay with Mutants of the Original Virus

Mutation	EC50 (μg/mL)
No mutation (N09)	0.16 (0.11-0.22)
Cal09	2.09 (1.84-2.35)
G155E (N09 mutant)	1.72 (0.08-3.98)
N125D + D127E + A186D + S190R (N09 mutant)	0.43
K160E (N09 mutant)	2.58 (1.94-3.30)

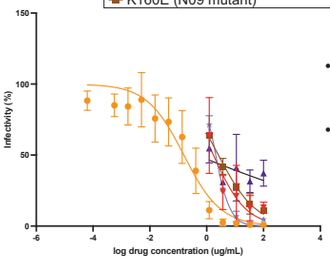

- C11-FW9 inhibited the viral replication of all the mutants
- **This results demonstrates that the binding site of the molecule is not the receptor binding domain**

Summary

- Virucidal drugs can be obtained exploiting interactions between peptide and HA of influenza virus
- The original virus mutants with a different receptor binding domain demonstrated the peptides bind to a different region of hemagglutinin than RBD

reference

- Ghafoori, S.M., Petersen, G.F., Conrady, D.G. *et al., Sci Rep* 13, 6940 (2023)
- Fleishman, S. J. et al. Computational Design of Proteins Targeting the Conserved Stem Region of Influenza Hemagglutinin. Science 332, 816–821 (2011)

https://doi.org/10.17952/37EPS.2024.P1210

Faculty of Chemistry - Organic and Bioorganic Chemistry - OCIII

UNIVERSITÄT BIELEFELD

Linkerology of Cryptophycin Drug Conjugates

***Jan-Niklas Bollnow*[1], *Cedric Dessin*[1], *and Norbert Sewald*[1]**

[1] Organic and Bioorganic Chemistry, Faculty of Chemistry, Bielefeld University, Germany.

Contact: jan-niklas.bollnow@uni-bielefeld.de

Introduction

- SMDCs consist of a cytotoxin connected to a small targeting ligand via a linker
- Payload is selectively delivered to the targeted cells through the homing device
- By utilizing cleavable linkers, the free payload is released at the target site
- Modified cryptophycin containing amino group was used as drug[1]
- Unit D is less exposed to the active site, making modifications in this unit promising[2]
- Cathepsin B cleavable linkers were attached using carbamate moiety
- Variation of peptide sequence in the linker for SAR study
- Folate receptor homing device was introduced via click reaction

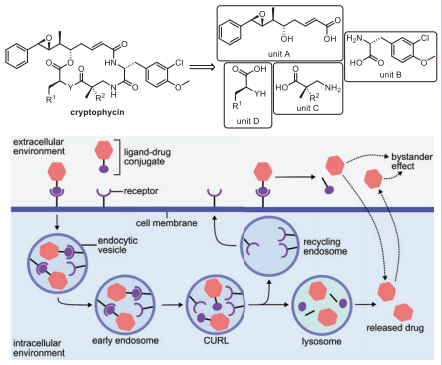

Figure 2: Pathways of drug conjugates that result in payload release, figure adapted from Low *et al.*[3] with modifications.

Homing Device

- Clickable folate ligand **8** adapted from vintafolide's homing device[4]
- Fluorophore conjugate **2** allows for FACS measurements
- >99% of KB-3-1 (FR+) cells were labelled, no labeling of HEK-293 (FR-) cells was detected
- Folic acid acts as inhibitor for labeling of KB-3-1 cells

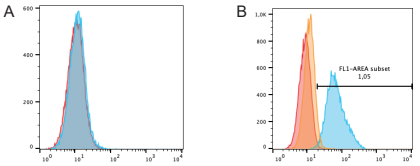

Figure 3: Flow cytometric analysis of conjugate **2** labeling FR- HEK297 (A) and FR+ KB-3-1 (B) cells. Unlabeled cells in red, cells incubated with **2** in blue, and cells incubated with **2** and 100 µm folic acid in orange.

Cytotoxicity Data

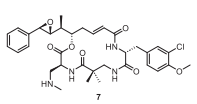

7

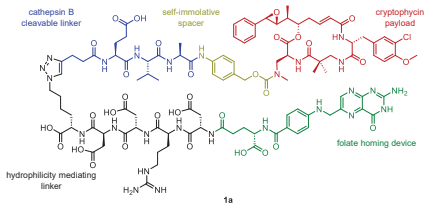

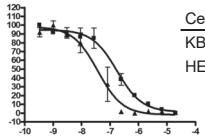

Cell Line	IC_{50} for **7**	IC_{50} for **1a**
KB-3-1 (FR+)	8.7 pM	155 nM
HEK 293 (FR-)	2.0 pM	32 nM

Targeting Index = 0.9

Figure 4: Dose-response curves of **1a** for cell viability of KB-3-1 (FR+) and HEK 293 (FR-) cells. Cell viability (%) plotted against logarithmic concentration (M^{-1}).

Synthesis of Conjugates

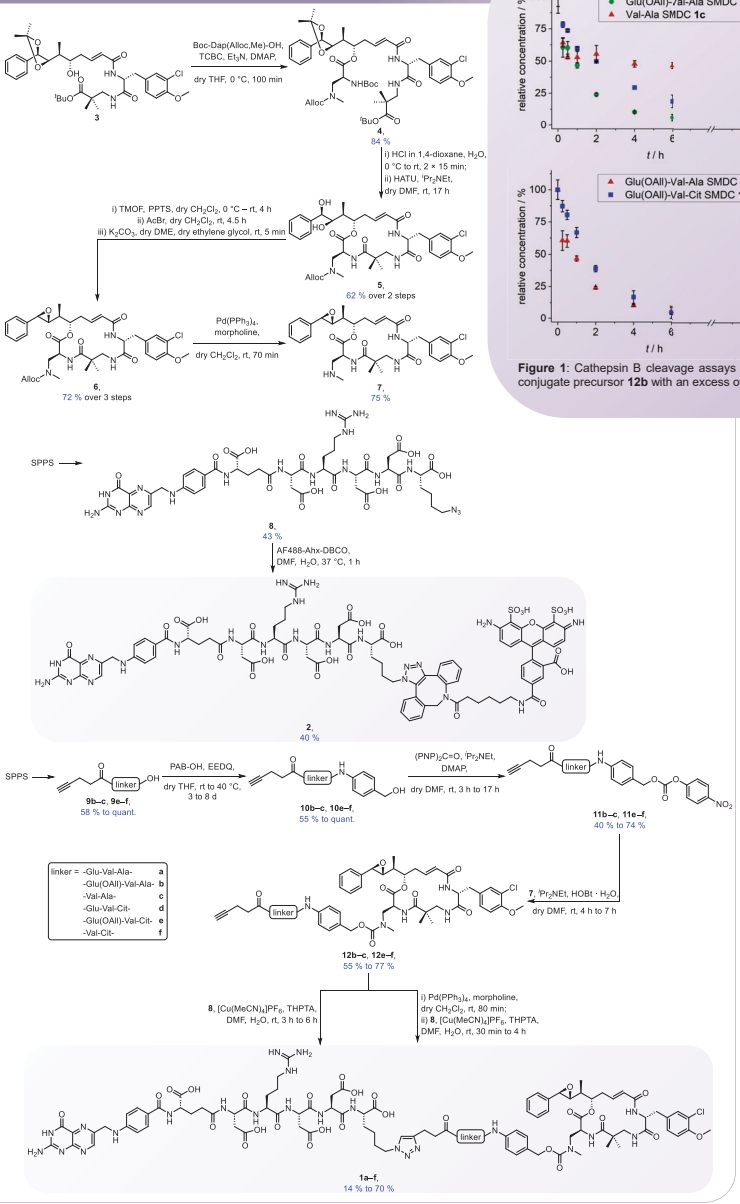

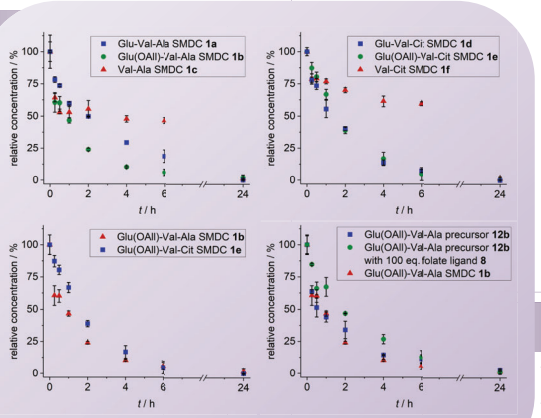

Figure 1: Cathepsin B cleavage assays of conjugates **1a–f**, conjugate precursor **12b**, and conjugate precursor **12b** with an excess of folate ligand **8**.

Cleavage Assays

- Substrate to enzyme ratio of 10:1, substrate concentration of 1 µM
- Glu(OAll)-Val-Ala SMDC **1b** is cleaved faster than Glu-Val-Ala SMDC **1a**
- Cit conjugates with glutamic acid (**1d**, **1e**) show similar cleavability
- Absence of glutamic acid (**1c**, **1f**) causes significant reduction in cleavability, in agreement with findings from TSUCHIKAMA *et al.*[5]
- Only minor influence of the recognition sequence (Val-Ala or Val-Cit)
- Cleavability of precursor **12b** comparable to the cleavability of allyl protected SMDC **1b**
- Only minor influence of excess folate ligand **8** on the cleavability of precursor **12b**

Conclusion

- Construction of library of enzymatically cleavable SMDCs **1a–f** and fluorophore conjugate **2**
- Folate ligand **8** acts as excellent homing device for targeting the folate receptor
- SMDC **1a** exhibits low targeting index and cytotoxicity is reduced by more than four orders of magnitude compared to cryptophycin **7**, both presumably caused by slow cleavage of the linker
- SAR study of the linker and its cleavability demonstrates that neither folate ligand **8** nor the glutamic acid in P^3 position are causes for the slow cleavage
- Glu-Val-Ala conjugate **1a** strikes optimal balance between cleavage kinetics of the linker and hydrophilicity of the conjugate
- Further SAR studies needed to optimize payload release

Further Info

For additional research regarding cryptophycins and corresponding conjugates, please visit Ninive Cati (P1-209), Dominic Seißenschmidt (P1-215), and Jona Voss (P1-212).

References

[1] C. Dessin, T. Schachtsiek, N. G. Blanchard, N. Sewald, N. Janson, International Patent WO2022/175222, **2022**.
[2] A.-C. Abel, T. Mühlethaler, C. Dessin, T. Schachtsiek, B. Sammet, T. Sharpe, M. O. Steinmetz, N. Sewald, *J. Biol. Chem.* **2024**, *300*, 107363.
[3] M. Srinivasarao, C. V. Galliford, P. S. Low, *Nat. Rev. Drug Discov.* **2015**, *14*, 203.
[4] M. Srinivasarao, P. S. Low, *Chem. Rev.* **2017**, *117*, 12133.
[5] Y. Anami, C. M. Yamazaki, W. Xiong, X. Gui, N. Zhang, Z. An, K. Tsuchikama, *Nat. Commun.* **2018**, *9*, 2512.

Let's get linked!

https://sewaldlab.de/

The series of a new fluconazole-based conjugates with cell penetrating and antimicrobial peptides

Natalia Ptaszyńska[1], Daria Łada[1], Wioletta Brankiewicz[2], Katarzyna Serbakowska[2], Jan Lica[3], Marek Drab[4], Natalia Maciejewska[2], Anna Łęgowska[1], Piotr Szweda[2], Krzysztof Rolka[1]

[1]Department of Molecular Biochemistry, Faculty of Chemistry, University of Gdańsk, Gdańsk, Poland,
[2]Department of Pharmaceutical Technology and Biochemistry, Faculty of Chemistry, University of Technology, Gdańsk, Poland,
[3]Department of Regenerative Medicine, Faculty of Medicine, Medical University of Warsaw, Warszawa, Poland,
[4]Unit of Nanostructural Bio-Interactions, Hirszfeld Institute of Immunology and Experimental Therapy, Polish Academy of Sciences, Wrocław, Poland

https://doi.org/10.17952/37EPS.2024.P1211

Drug

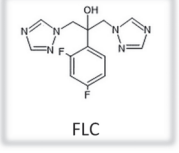

Fluconazole (**FLC**) is a **drug** used to treat a number of fungal infections (particularly *Candida* infections). It inhibits the lanosterol 14α-demethylase and decreases the level of ergosterol required for the integrity of fungal cell membranes. FLC causes the accumulation of the ergosterol precursors (lanosterol, 4,14-dimethylzymosterol, and 24-methylenedihydrolanosterol) inside the cell, resulting in the altered structure and functioning of the cell membranes [1]. Fluconazole was the first triazole antifungal drug introduced in the medicinal practice.

Linker

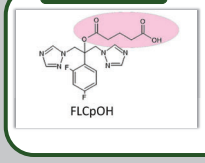

In all studied conjugates, **glutaric acid** served as a **linker,** forming covalent bonds between hydroxyl group of FLC and N-terminal amino group of the peptide (ester and amide moieties, respectively).

Peptide

Selected CPP and AMP peptides:

LFcinB(2-11)-NH_2: FKCRRWQWRM-NH_2
LFcinB[$Nle^{1,11}$]-NH_2: NleFKCRRWQWRNleKKLG-NH_2
HLopt2-NH_2 : CFQWKRAMRKVR-NH_2
TP10-NH_2 : AGYLLGKINLKALAALAKKIL-NH_2
TP10-7-NH_2 : AGYLLGKINLKPLAKL(AiB)KKIL-NH_2
P5-NH_2 : YIRKIRRFFKKLKKILKK-NH_2
P9-NH_2 : SYERKINRHFKTLKKNLKKK-NH_2

- CPPs serving as carrier peptides and are considered the fundamental part of an extensively developed concept of a drug delivery system; TP-10 is one of the most promising peptides in this family. These peptides effectively penetrate cell membrane.
- Modified fragments of bovine lactoferrin (LFcin) and human lactoferrin (HLopt2) are members of the AMP family, peptides that constitute an important segment of the body's natural immunity against microorganisms.
- P5 and P9 are AMPs, which are designed based on *Artisicluthys nobilia* interferon-I, inhibit Methicillin-resistant Staphylococcus aureus (MRSA) and show low cytotoxicity.

Peptide Fluconazole-Based Conjugates

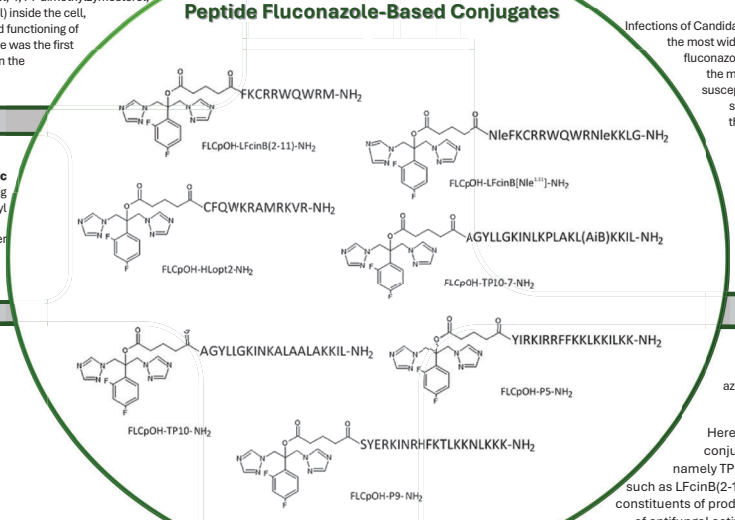

Introduction

Many pathogenic bacteria and fungi strains have become resistant to the most of commercially available antibiotics as the result of their common use in medical practice. The fungal infections have a major impact on quality of life and also exhibit high levels of mortality. That is why effective and safe therapeutic treatment of fungal infections is a major challenge for modern medicine.

Infections of Candida spp. etiology are frequently treated with azole drugs. Among azoles, the most widely used in the clinical practice remains fluconazole (FLC). However, fluconazole usage has developed some negative consequences, among which the most important are: (i) selection of fungal pathogens that exhibit lower susceptibility to fluconazole activity, including some non-albicans Candida spp. (e.g., *C. krusei*, *C.glabrata*); (ii) development of resistance against this agent among species that are naturally sensitive, e.g., *C. albicans*.

Promising results in treatment of dangerous, systemic *Candida* infections demonstrate the advantages of combined therapies carried out with combinations of at least two chemical molecules with different antimicrobial activity that in the end display a different mechanism of action than the parent compounds.

The aim of the work

In this study we proposed modification of fluconazole's (and other azoles') structure by covalently linking it to other substances-peptides with different structures and biological activities.

Herein we report the chemical synthesis and biological activity of conjugates of fluconazole with (i) cell-penetrating peptides (CPP), namely TP10-NH_2 and TP10-7-NH_2, or (ii) antimicrobial peptides (AMP), such as LFcinB(2-11)-NH_2, LFcinB[Nle1,11]-NH_2, HLopt2-NH_2, P5 and P9. Both constituents of produced conjugates (FLC and peptides) display different modes of antifungal activity and affect different molecular targets within fungal cells.

The major foreseen advantages of conjugates of FLC and selected CPPs or AMPs include improved antifungal (hopefully fungicidal) efficiency and increased drug delivery. Moreover, according to our previous research [2], we would like to check if synthesized fluconazole-based conjugates (especially those with P5 and P9) have also anti-cancer properties.

Table 1. MIC and MFC Values (in M) Determined for Compounds, As Well As for Two Control Antifungal Agents (AmB and FLC) against Various Yeast Strains [5].

Yeast Strains	MIC* and MFC ** (μM)	Compounds							
		FLCpOH	FLCpOH-TP10-NH_2	FLCpOH-TP10-7-NH_2	FLCpOH-LFcinB[$Nle^{1,11}$]-NH_2	FLCpOH-LFcinB(2-11)-NH_2	FLCpOH-HLopt2-NH_2	Fluconazole (FLC)	Amphotericin B (AmpB)
Candida albicans Cu4	MIC_{50}	>250	45	23	125	>250	>250	-	<0.1
	MIC_{90}	>250	62	31	250	>250	>250	31	<0.1
	MFC	-	62	31	-	-	-	-	<0.1
Candida albicans Cu5	MIC_{50}	>250	62	31	>250	>250	>250	-	<0.1
	MIC_{90}	>250	125	62	>250	>250	>250	>250	<0.1
	MFC	-	62	62	-	-	-	-	<0.1
Candida albicans 48	MIC_{50}	>250	45	15	250	250	250	-	<0.1
	MIC_{90}	>250	62	31	>250	>250	>250	>250	<0.1
	MFC	-	250	125	-	-	-	-	<0.1
Candida albicans 138	MIC_{50}	>250	45	23	23	190	>250	-	<0.1
	MIC_{90}	>250	62	31	31	250	>250	>250	<0.1
	MFC	-	250	125	-	-	-	-	<0.1
Candida albicans 190	MIC_{50}	>250	45	23	90	190	250	-	<0.1
	MIC_{90}	>250	62	31	125	250	>250	>250	<0.1
	MFC	-	250	125	-	-	-	-	<0.1
Candida albicans 247	MIC_{50}	>250	45	23	45	190	>250	-	<0.1
	MIC_{90}	>250	62	31	62	250	>250	>250	<0.1
	MFC	-	250	125	-	-	-	-	<0.1
Candida albicans 574	MIC_{50}	>250	45	23	45	190	250	-	<0.1
	MIC_{90}	>250	62	31	62	250	>250	>250	<0.1
	MFC	-	-	250	-	-	-	-	<0.1
Candida albicans 604	MIC_{50}	>250	45	23	45	190	>250	-	<0.1
	MIC_{90}	>250	62	31	90	250	>250	>250	<0.1
	MFC	-	250	250	-	-	-	-	<0.1

* MIC—minimum inhibitory concentration; ** MFC—minimum fungicidal concentration.

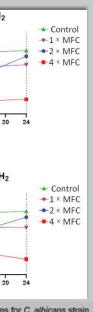

Figure 1. Time-kill determinations for *C. albicans* strain after treatment with FLCpOH-TP-NH_2 and FLCpOH-TP10-7-NH_2 alone at 1 x MFC, 2 x MFC and 4 x MFC. The x-axis represents the killing time, and the y-axis represents the logarithmic *C. albicans* SC5314 survival. [5].

- In reported conjugates, FLC was linked to the peptide by its hydroxyl group.
- Coupling of TP10-NH_2, analogues of LFcinB and HLopt2 to the FLC triazole ring yielding a practically inactive conjugates [3,4].
- Two of synthesized compounds, namely **FLCpOH-TP10-NH_2** and **FLCpOH-TP10-7-NH_2**, exhibit high activity against reference strains and fluconazole-resistant clinical isolates of *C. albicans*, including strains overproducing drug transporters.
- Moreover, both of them demonstrate higher fungicidal effects compared to fluconazole.
  - The MFC values against *C.albicans* reference strains were the same or only twice higher compared to MIC_{90}.
- The high fungicidal activity of both conjugates was also confirmed with the kill-time assay.
- Analysis performed with fluorescence and scanning electron microscopy as well as flow cytometry indicated the cell membrane as a molecular target of synthesized conjugates. In this respect, TP peptides behave like AMPs, disrupting cell membranes.
- Two compounds produced by us and reported herein appear to be potential candidates for novel antifungal agents. Some of the produced conjugates show promising activity and are good candidates for obtaining new effective antifungals.

Methods

Synthesis of analogue of FLC- FLCpOH

A solution of fluconazole (306 mg, 1 mmol), glutaric anhydride (1369 mg, 12 mmol) and DMAP (28,6 mg, 0,234 mmol) in 11 mL of DMF was heated at 85 °C for approximately 20 h under the reflux. After distillation of the solvent under reduced pressure, the resulting oil was dissolved in 40 ml of the solvent mixture water:acetonitril (4:1 v/v) and solid residue was filtered off. The crude product was purified on a preparative HPLC and the final product was confirmed by HPLC, MALDI-TOF and NMR.

Synthesis of Fluconazole-Based Conjugates

The mixture of purified FLCpOH, HOBt, and DIC (in molar ratio 1:1:1) was dissolved in 6 mL of DMF, added to SPPS vessel with peptidyl resins with free N-terminal amino groups. The coupling efficiency was monitored after 2 h using the chloranil test. In case of a positive test result, acylation was repeated using the mixture of purified FLCpOH, TBTU, HOBt and DIPEA (in molar ratio 1:1:1:2) dissolved in 6 mL of DMF. Usually, two repeats was required to complete the coupling. The conjugates were cleaved from the resin. The crude products were purified and analyzed the yields were 10–46%.

Time-Kill Assay

A starting inoculum was prepared by inoculating a tube of sterile water with growth from 24 h YPD agar plates (*C. albicans* SC5314), and OD660 was adjusted to about 0.1 (around 106 cells per 1 mL). The suspension was then diluted 10-fold with RPMI 1640 medium, and FLCpOH-TP10-NH_2 and FLCpOH-TP10-7-NH_2 were added at concentrations corresponding to 1 x MFC, 2 x MFC, and 4 x MFC. A negative control (growth medium without drug or organism) was also included at each time of testing. Tubes were incubated at 37 °C on an orbital shaker and vortexed before removing a sample for the determination of colony counts. After the appropriate time of incubation (0.5, 2, 4, 6, and 24 h), 1 mL of each suspension was centrifuged (2 min, 9170 g), and the pellet was re-suspended in 1 mL of PBS pH 7.4. Ten-fold serial dilutions with PBS were prepared, and 100 L of each was inoculated on YPD agar plates in duplicate. Plates were incubated for 24 h at 37 °C. Colony forming units in the range of 30–300 were counted (on the plates containing from 30 to 300 colonies) and the number of yeast cells in 1 mL (CFU/mL) was calculated.

Determination of Minimum Inhibitory Concentration (MIC) and Minimum Fungicidal Concentration (MFC)

Antifungal activity of the tested compounds against yeast cells was determined in 96- well plates as described in the CLSI document M27-A3, with minor modifications (CLSI, 2008). Suspensions of the microorganisms were prepared by taking one loop of pure culture into sterile water and adjusting optical density to 0.1 at 660 nm wavelength and further 50-fold dilution in RPMI 1640 medium, resulting in cell concentration of approximately 2 x 104 CFU/mL. Then, 100 L of cells were added to the wells of a 96-well microtiter plate that contained 16–500 M tested compounds and 16–500 M of FLC or 0.2–62 M AmB. The plates were incubated for 24 h at 37 °C. Each test was performed in triplicate. The final concentration of DMSO was ensured to be around 1% in all experiments. For determination of minimum fungicidal concentrations (MFC), small aliquots of suspensions (around 10 L) from each well were transferred using the pipette to YPD agar plates without inhibitors and incubated for 24 h at 37 °C.

Cytotoxicity Assay

Hs27 and HUVEC mammalian cell lines were cultured as mentioned above. Once cell lines were about 80% confluent, cells were counted by a hemacytometer (Hausser Scientific, Horsham, PA, USA) and plated in 96-well microtiter plates at concentrations of 4500 cells per well for Hs27 and 2000 cells per well for HUVEC. Cells were allowed to attach overnight. Drugs were serial dissolved (100–1.5 M) in cell culture medium and added to wells in 100 L, in triplicates. The final concentration of DMSO was ensured to be around 1% in all experiments. Cells were incubated with studied compounds for 72 h at 37 °C and 5% CO_2. After incubation, 20 L of MTT solution in PBS (4 mg/mL) was added to all wells and incubated further for 3 h at 37 °C. Formed formazan crystals were dissolved in 150 L DMSO, and absorbance was measured using an Asys UVM340 multi-well plate reader at λ = 540 nm. Cytotoxicity was determined compared to drug-free control. All experiments were performed in biological triplicates.

Membrane Permeabilization Assay Using Propidium Iodide Staining

Suspensions of *C. albicans* SC5314 were prepared by taking one loop of pure culture growth from 24 h YPD agar plates into RPMI 1640 medium and adjusting optical density to 0.1 at 660 nm wavelength. Then, FLCpOH-TP10-NH_2 and FLCpOH-TP10-7-NH_2 were added at concentrations corresponding to 8 x MIC and 4 x MIC. FLC (8 x MIC) was used as a negative control. The cell suspensions were then treated for 0.5, 2, 4, 6, and 24 h at 37 °C with continuous agitation (180 rpm). The cells were then centrifuged and resuspended in 200 L of PBS buffer (pH 7.4). Subsequently, cells were treated with propidium iodide (1 mg/mL, final concentration) and incubated for 30 min at room temperature in the dark. Cellular fluorescence was visualized using lens 20, using Olympus Fluorescence Microscope BX60 (Olympus, Tokyo, Japan). The images were also post-processed utilizing cell Sens program. The fluorescence intensity emitted by DNA-bound propidium iodide was measured using a flow cytometer (Merck Millipore guava easyCyte 8, Darmstadt, Germany). Data were obtained from at least two independent experiments.

Scanning Electron Microscopy (SEM)

Scanning electron microscopy of yeast was performed at a low accelerating voltage of the primary beam with or without the coating of the samples. *C. albicans* fungi suspension fixed with 2.5% glutaraldehyde was applied onto a silicon chip and allowed to adhere for 30 min. The samples were dehydrated in a series of methanol solutions (25–50–75–100–100%) in one-hour steps at 4 °C. Samples underwent critical point drying with methanol exchanged for liquid CO_2 in an automatized approach, (CPD300 AUTO, Leica Microsystems, Vienna, Austria) and were imaged with cross-beam scanning electron microscope equipped with Schottky field-emission cathode (Auriga 60, Carl Zeiss, Oberkochen, Germany) at 0.8 kV accelerating voltage; thus, the imaging was performed within a mode referred to as low-voltage, field-emission scanning electron microscopy (LV-FESEM) of non-labeled, critical point-dried sample. This process was implemented with the low-voltage field-emission scanning electron microscopy (LV-FESEM) mode and by applying the low-energy loss electron principle for generating the highly resolved chemical contrast. Images were acquired with the Everhart–Thornley electron detector (SE2 secondary electrons) and correlated with the energy-selective back-scattered electron detector (EsB), directly from the sample surfaces, with no coating or contrasting applied; thus, chemical cell-endogenous components were directly mapped. Polished silicon crystal used as a substrate for deposition of *C. albicans* allowed for chemical mapping of the sample's features and for identifying of the disintegrated pathogen cells in a correlative mode, with topography, contours and chemical aspects analyzed with pixel-to-pixel precision of correlation.

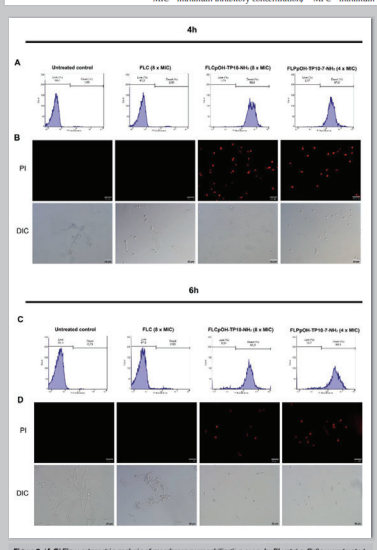

Figure 2. (**A**,**C**) Flow-cytometric analysis of membrane permeabilization assay by PI uptake. Cells were treated with FLC and FLC conjugates and stained with PI. After the completion of treatment and staining process, the cellular fluorescence was then analyzed via flow cytometry. (**B**,**D**) Fluorescence microscopy analysis of membrane permeabilization assay by PI uptake in treated as well as untreated yeast cells. The results of selected images are chosen as the best representatives of one of three different experiments with two replicates; similar results were observed each time. DIC—differentia interference contrast microscopy, PI—fluorescence microscopy. Scale bars correspond to 20 m [5].

Table 2. In vitro cytotoxicity (IC_{50} and IC_{90} SEM (M)) of the FLC conjugates and their constituents toward Hs27 and HUVEC cells [5].

Compound	Hs27		HUVEC	
	IC_{50}	IC_{90}	IC_{50}	IC_{90}
FLC	>100	>100	>100	>100
FLCpOH	>100	>100	>100	>100
FLCpOH-TP10-NH_2	12.00 ± 0.93	28.81 ± 0.87	14.45 ± 1.13	34.30 ± 1.00
FLCpOH-TP10-7-NH_2	13.07 ± 0.35	29.78 ± 0.29	15.16 ± 1.26	34.03 ± 1.90
FLCpOH-LFcinB[$Nle^{1,11}$]-NH_2	>100	>100	75.58 ± 1.73	>100
FLCpOH-LFcinB(2-11)-NH_2	>100	>100	>100	>100
FLCpOH-HLopt2-NH_2	>100	>100	>100	>100

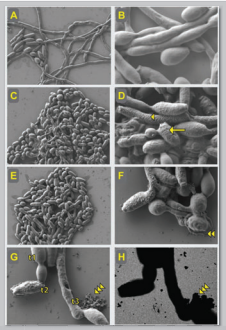

Figure 3. SEM analysis of the compounds' effects on the *C. albicans* cells. Control cells (**A**,**B**) demonstrating normal appearance of *C. albicans*, with long hyphae stage well-represented (**A**) and uniformly smooth surface (**B**). Compound FLC-TP10-7-NH_2 (**C**,**D**), in contrast, resulted in reduction of hyphae numbers (**C**), roughed cells surface (arrow) in large part of cell population, granularities (arrowhead), perforations and increased debris (**D**). Compound FLCpOH-TP10-NH_2, (**E**–**H**) demonstrated signs of stronger toxicity against *C. albicans*, lack of hyphae (**E**), with intense roughing of the cell surface and membrane disintegration or spreading (double arrowheads) (**F**), frequent perforations and granularities (**G**), membrane blebbing and more debris. (**G**,**H**) Different stages of deleterious effects of the compound, from mild (t1), through roughing (t2) to perforation and fragmentation of cells (t3). Chemical contrast imaging (**H**), correlated pixel-to-pixel with topography imaging. (**G**) Improved identification of blebbing and fragmentation of *C. albicans* cells (triple arrowheads). Gray appearance of the substrate in (**H**) stems from silicon polished crystal and facilitates detection of multiple organic fragments with dark appearance in (**H**), by chemical contrast mapping of no-coated samples. (**A**–**G**)—Everhart–Thornley detector, (**H**)—EsB detector imaging. (**A**,**C**,**E**)—magnification 5000 (field of view 60 m), (**B**,**D**,**G**,**H**)—magnification 20,000 (field of view 15 m).

Conclusions

References

[1] Kabir M.A., Ahmad Z., *ISRN Prev. Med.* 2013, 1–13, **2013**
[2] Lica J.J., et al. *Mol Pharmacol*, 105, 39–53, **2024**
[3] Ptaszyńska N., et al. *ACS Chem. Biol.*, 14, 2233–2242, **2019**
[4] Ptaszyńska N., et al. *Peptides*, 117, 170079, **2019**
[5] Brankiewicz W., et al. *Pharmaceutics*, *14*, 693, **2022**

Acknowledgments

This work was supported by the National Science Centre (NCN, Poland) under grant No. UMO-2016/21/B/ST5/00101

https://doi.org/10.17952/37EPS.2024.P1212

Faculty of Chemistry - Organic and Bioorganic Chemistry - OCIII

UNIVERSITÄT BIELEFELD

Click-to-Release-based Cryptophycin Drug Conjugates

***Jona Voss*[1], *Peter Bitsch*[2], *Cedric Dessin*[1], *Harald Kolmar*[2], *and Norbert Sewald*[1]**

[1] Organic and Bioorganic Chemistry, Faculty of Chemistry, Bielefeld University, Germany.
[2] Clemens-Schöpf Institute for Organic Chemistry and Biochemistry, Technical University of Darmstadt, Germany.

Contact: **jona.voss@uni-bielefeld.de**

Click-to-Release

- Traceless bioconjugation method for release of tetrazine-carbamate-bound payloads[1]
- Release by deliberate administration of an activator (strained alkene, e.g. *trans*-cyclooctene (TCO))
- Established by Robillard *et al.* in 2013 with a proof of concept in 2016 (Doxorubicin release)[2]

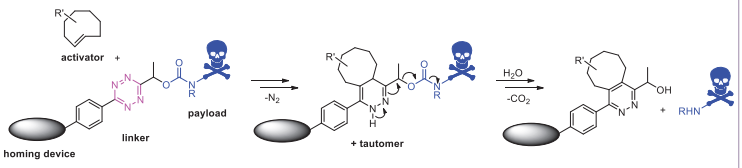

- Bioorthogonality through inverse electron-demand Diels-Alder reaction (iEDDA)
  - → High stability and selective formation of pyridazine-click-product
  - → Irreversibility through N_2 and concomitant CO_2 release
- Fast release kinetics (k_2 = 1 - 10^6 M^{-1})[3]
- Non-internalising antibodies as homing devices allow extracellular receptors as targets

in vitro Release

- In vitro study of release upon TCO addition (pH = 7.4, NH_4OAc buffer / MeCN, c_0 = 0.15 mM)
- Maximum "release yield" after 24 h (64%)

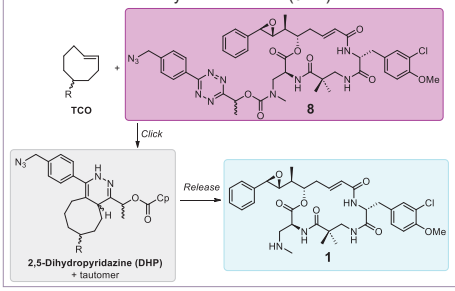

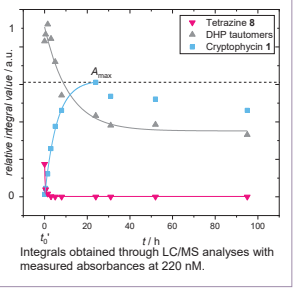

Integrals obtained through LC/MS analyses with measured absorbances at 220 nM.

Synthesis of Cryptophycin-Linkers

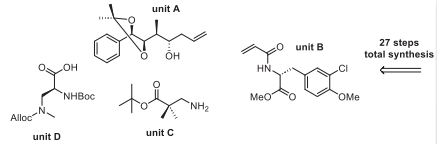

- Highly cytotoxic, usually in the pM range, even against multi-drug-resistant cell-lines[4]
- Modifications in unit D superior to retain high cytotoxicity[5]

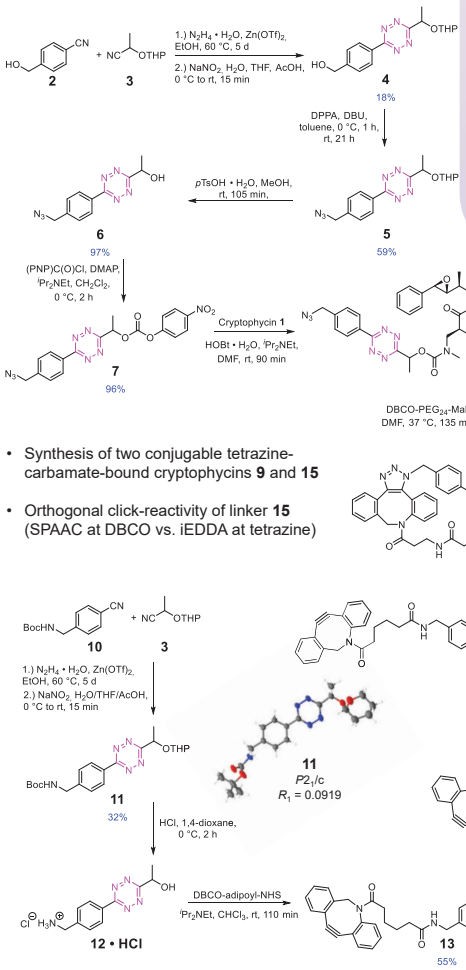

- Synthesis of two conjugable tetrazine-carbamate-bound cryptophycins **9** and **15**
- Orthogonal click-reactivity of linker **15** (SPAAC at DBCO vs. iEDDA at tetrazine)

Payload: Cryptophycin-unit D [Dap(Me)]

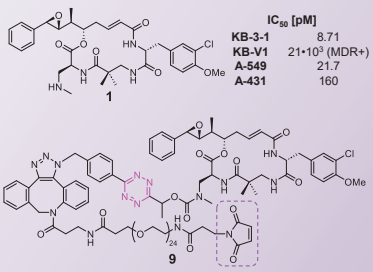

IC_{50} [pM]	
KB-3-1	8.71
KB-V1	21•10^3 (MDR+)
A-549	21.7
A-431	160

- Cysteine-addressable by Michael addition
- Azide-addressable by SPAAC

Antibody-Drug Conjugates

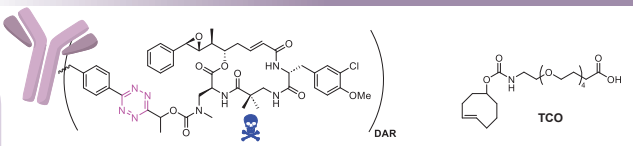

Trastuzumab-based ADCs

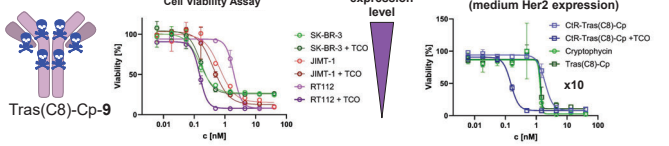

- Anti-Her2 mAb conjugated by Michael addition of Cryptophycin-Linker **9** to native cysteines
- Efficient cell-killing of medium and high Her2-expressing cell lines with **pM IC_{50}** values
- TCO activation only efficient for RT112 cells: proteolysis competing with internalization?

Sibrotuzumab-based ADCs

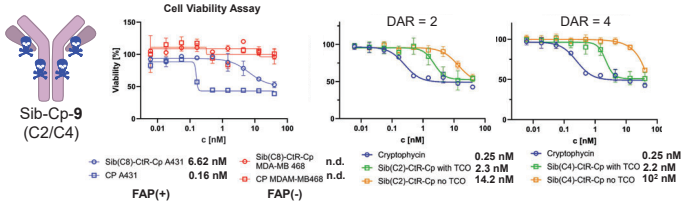

- Non-internalising mAb targeting cancer-associated fibroblasts (CAFs), conjugated to Cryptophycin-Linker **9** (with engineered cysteines)
- Efficient killing of FAP(+) cells with **pM efficacy** but no adverse effects against FAP(-) cells
- Increased toxicity (**x10**) after **washout** and activation with **TCO**

Dextramab [6]

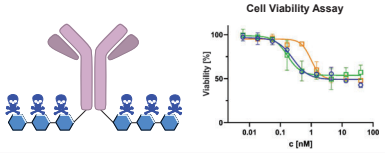

- Dextran-modified mAb (Sib) with azido groups for conjugation[6] with Linker **15**
- Increased potency as compared to sole Cryptophycin **1**

Further Info

For more Cryptophycin and Drug Conjugate research, please visit Jan-Niklas Bollnow (**P1.210**), Dominic Seißenschmidt (**P1.215**) and Ninive Cati (**P1.209**).

Reference

[1] R. M. Versteegen, R. Rossin, W. ten Hoeve, H. M. Janssen, M. S. Robillard, *Angew. Chem. Int. Ed.* **2013**, *52*, 14112.
[2] R. Rossin, S. M. J. van Duijnhoven, W. ten Hoeve, H. M. Janssen, L. H. J. Kleijn, F. J. M. Hoeben, R. M. Versteegen, M. S. Robillard, *Bioconjug. Chem.* **2016**, *27*, 1697.
[3] B. L. Oliveira, Z. Guo, G. J. L. Bernardes, *Chem. Soc. Rev.* **2017**, *46*, 4895.
[4] C. Weiss, E. Figueras, A. N. Borbély and N. Sewald, *J. Pept. Sci.* **2017**, *23*, 514.
[5] C. Dessin, T. Schachtsiek, G. Blanchard Nerin, N. Sewald, International Patent WO2022//175222, Bielefeld University, Bielefeld, **2022**.
[6] H. Schneider, L. Deweid, T. Pirzer, D. Yanakieva, S. Englert, B. Becker, O. Avrutina, H. Kolmar, *ChemistryOpen* **2019**, *8*, 354.

Let's get linked!

https://sewaldlab.de/

https://doi.org/10.17952/37EPS.2024.P1213

Strategies for designing hepatocyte-selective carriers using helical peptides as stable scaffolds

Takahito Ito,[1,2] Takashi Misawa,[2] Nobumichi Ohoka,[2] Michihiko Aoyama,[2] Takao Inoue,[2] Akiko Ishii-Watabe,[2] Yosuke Demizu[1,2,3]

1. Graduate School of Medical Life Science, Yokohama City University
2. National Institute of Health Sciences
3. Graduate School of Medicine, Dentistry and Pharmaceutical Sciences, Okayama University

1. Abstracts

Asialoglycoprotein receptor (ASGPR) is the representative targets for liver-selective DDS. ASGPR generally forms trimer, which trivalent GalNAc ligand is considered to be effective for hepatocyte-selective DDS. Representative triantennary GalNAc ligand (Tri-GalNAc) is already in medical use. Each GalNAc-binding site exists in the same orientation; however, due to GalNAc being mounted on flexible scaffolds, it faces disadvantages that prevent it from adopting a specific conformation. Helical structures can control the side-chain orientation due to their structural nature. Therefore, we thought to use helical peptide as a rigid scaffold to modulate the orientation of GalNAc and it could be more entropically favored structures. In this study, we designed helical peptides conjugated with GalNAc for hepatocyte selective carriers.

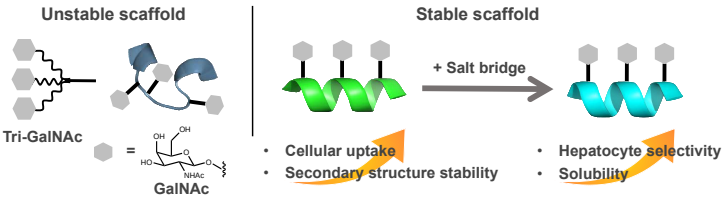

2. Design

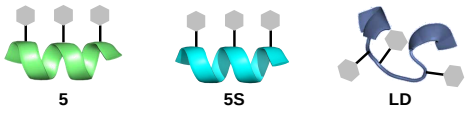

Peptide	Sequence
5	FITC-BL1SXSSLL2SXSSLL3SXSSL
5S	FITC-BS1EXSRLS2EXSRLS3EXSRL
LD	FITC-Bs1eXSrLs2eXSrLs3eXSrL

B = β-alanine

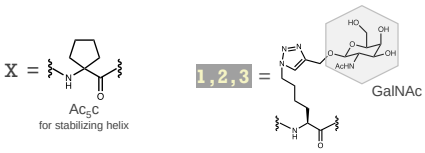

5S Based on **5**, introduced salt bridge to stabilize helix and improving solubility.
LD Based on **5S**, destabilize the secondary structure by introducing L and D-amino acids alternatively.

3. Secondary structure analysis

In silico conformational search (MD)

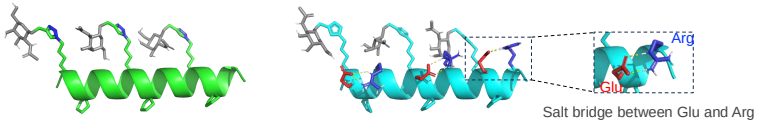

-297.5354 kcal/mol for **5**
-1020.4069 kcal/mol for **5S**
Salt bridge between Glu and Arg

CD spectra

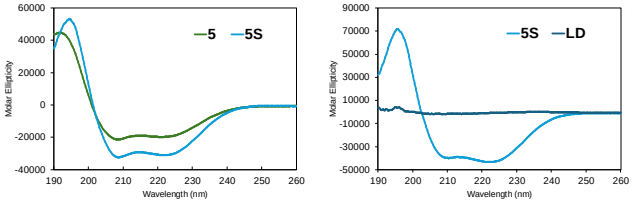

Left: 50% MeCN aqueous

	5	5S
Helicity	41%	93%

Right: 20 mM phosphate buffer (pH 7.2)

	5S	LD
Helicity	97%	0%

5S Secondary structure stability was confirmed by both MD and CD spectra by introducing salt bridge on peptide.
LD Did not showed specific secondary structure.

4. Cellular uptake studies

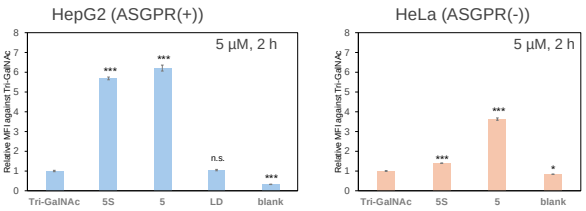

5 Better uptake than Tri-GalNAc but tissue-selectivity was low.
5S Equal activity to **5**, better tissue-selectivity.
LD Lower uptake than **5S** due to unstable secondary structure.

5. Cellular uptake of streptavidin

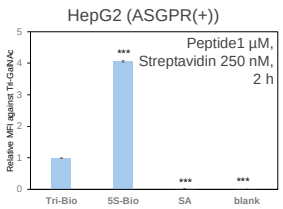

Peptide	Sequence
5S-Bio	Biotin-BS1EXSRLS2EXSRLS3EXSRL

Biotin =

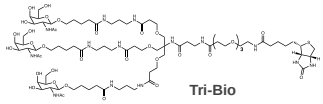

5S-Bio 4-folds better than **Tri-Bio**.
5S-Bio delivered protein into the hepatocytes.

SA: Alexafluor-647-labeled streptavidin without carriers.

6. Cell-based competitive binding study

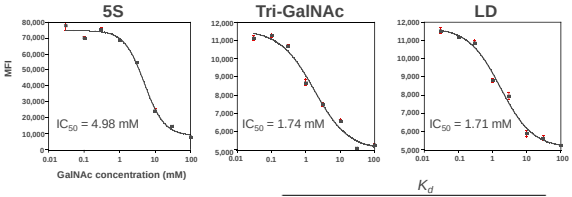

$$K_d = Ki \times \frac{Compound\ concentration}{IC_{50} - Ki}$$

K_i = 150 μM

	K_d
5S	155 nM
Tri-GalNAc	472 nM
LD	481 nM

Evaluation of the affinity against HepG2 by varying GalNAc concentration.
5S exhibited 3-folds better affinity than others.

7. Effects of number and position of GalNAc

Peptide	Sequence
5S-1-FITC	FITC-BS1EXSRLSAEXSRLSAEXSRL
5S-1'-FITC	FITC-BSAEXSRLS2EXSRLSAEXSRL
5S-1"-FITC	FITC-BSAEXSRLSAEXSRLS3EXSRL
5S-2-FITC	FITC-BS1EXSRLS2EXSRLSAEXSRL
5S-2'-FITC	FITC-BS1EXSRLSAEXSRLS3EXSRL
5S-2"-FITC	FITC-BSAEXSRLS2EXSRLS3EXSRL

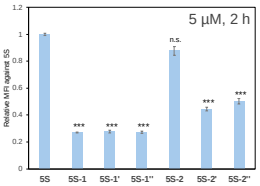

Peptides were designed to identify which GalNAc units contributes ASGPR bindings.

Single GalNAc Exhibits similar uptake trends.
Double GalNAc **5S-2** maintained the activity.

The pair of position 1 and 2 of GalNAc contributes to cellular uptake.

8. Application to protein degradation

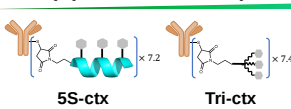

Evaluated the activity of membrane protein degradation (application as LYTACs).
Ctx: anti-epidermal frowth factor receptor (EGFR) antibody

Western blot

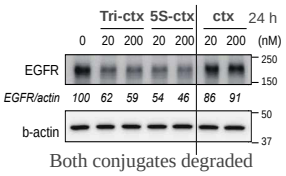

Both conjugates degraded EGFR in low concentration.

EGFR clearance from membranes

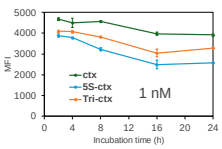

5S-ctx removed EGFR from membranes efficiently than Tri-GalNAc.

9. Conclusion

GalNAc conjugated helical peptides were more effectively taken up into hepatocytes than flexible ligands such as Tri-GalNAc and peptide LD. Peptide 5S exhibited high hepatocyte selectivity by introducing a salt bridge. Also, we clarified the effects of the number and position of GalNAc on cellular uptake. Furthermore, stronger binding to HepG2 cells was found to be associated with stronger uptake activity. Peptide 5S could be applicable to protein degradation and it facilitates endocytosis of EGFR efficiently than Tri-GalNAc. The results demonstrate a molecular design strategy using helical peptides as stable templates for ligands with specific orientations.

Acknowledgement

We appreciate a support from the Japan Science and Technology Agency (JST), the establishment of university fellowships towards the creation of science technology innovation and the Sasakawa Scientific Research Grant from The Japan Science Society.
We declare no conflict of interests.

Synthesis and characterization of bioconjugates containing peptide moiety with potential anticancer activity

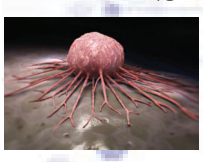

Dancho Danalev[1], Polya Miladinova[1], Yordan Todorov[1], Ivan Iliev[1,2]

[1]*University of Chemical Technology and Metallurgy, Department of Biotechnology, 8 Kliment Ohridski blvd., 1756 Sofia, Bulgaria*

[2]*Institute of Experimental Morphology, Pathology and Anthropology with Museum, Bulgarian Academy of Sciences, Acad. G. Bonchev str., bl. 25, 1113 Sofia, Bulgaria*

https://doi.org/10.17952/37EPS.2024.P1214

INTRODUCTION

According to the world database Globocan cases of cancer diseases worldwide in 2022 are close to 20 million. A quarter of this number is distributed in Europe. Cancers have long reached pandemic proportions, and their treatment has proven to depend both on their early diagnosis and the discovery of new selective chemotherapeutics. Somatostatin (SST) and the derivatives lanreotid, vapreotide, etc., are group of peptides successfully used for treatment of different type of cancers in the medicinal practice. BIM-23052 is a linear C-terminal amid analog of SST which show very good in vitro inhibitory activity against Growth hormone in nanomolar range of concentration, which make this molecule a possible candidate as a new anticancer drug. In addition, naphthalimide derivatives are attracting much attention due to their proven antitumor activity on various tumor models and excellent stability [1]. Taking into account our previous experience in the creation of bioconjugates in a searching of a synergic effect between both part of the molecule as well as a targeting of the newly synthesized molecules the purpose of this work is to create new bioconjugates between monofluorinated analog of BIM-23052 and naphthalimide derivatives with potential synergic effect for treatment of cancers.

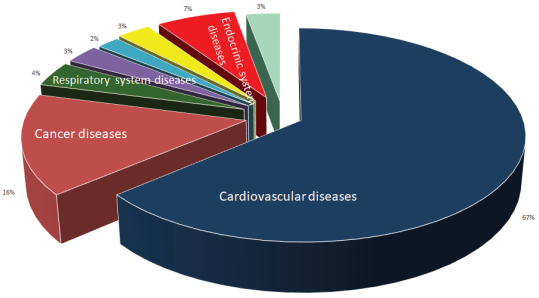

Data from the global database Globocan. estimated number of new cancer cases since 2020 until 2040
10 millions more, in total - close to 30 millions.

SYNTHESIS OF NEW BIOCONJUGATES

The 3 new bioconjugates of monofluorinated BIM-23052 with a general formula X-D-Phe-Phe(4-F)-Phe-D-Trp-Lys-Thr-Phe-Thr-NH_2, where X is A, B or C presented in Figure 1 were synthesized by using standard SPPS by means of Fmoc/O*t*Bu strategy (**Scheme 1**). Fmoc-Rink-Amide MBHA was used as a solid-phase carrier and DIC with additive of 1-hydroxysuccineimide (1-HOSu) served as coupling agent in a molar ratio Amino acid/DIC/1-HOSu/resin 3/3/3/1, respectively. The cleavage of the peptides from the resin was performed in acidic condition using a cocktail of . All deprotection and coupling reactions were monitored by standard Kaiser test.

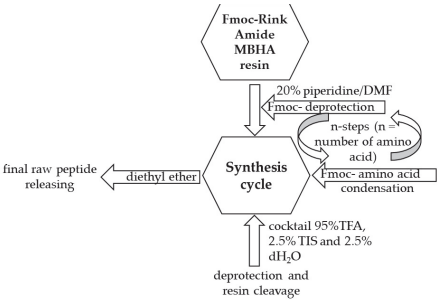

Scheme 1. SPPS synthesis of targeted bioconjugates

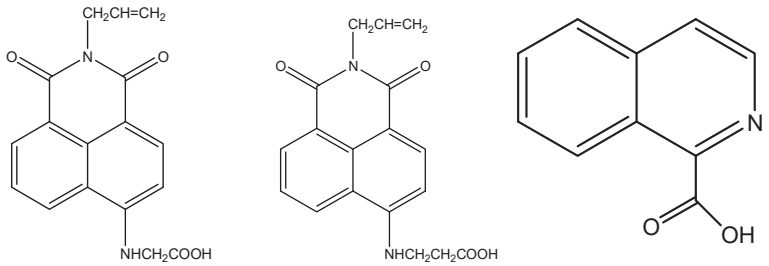

Figure. 1. A. N-allyl-4-(N-carboxymethyl)amino-1,8-naphtalimide (Nphtallyl-Gly); **B.** N-allyl-4-(N-carboxyethyl)amino-1,8-naphtalimide (Nphtallyl-β-Ala); **C.** Isoquinoline-1-carboxylic acid (IsoQui)

Code	Structure	Molecular formula	Mm exact, g/mol	$[M+nH]^+$ observed	t_R min	Chrom. purity, %
NIP1	Nphtallyl-Gly-D-Phe-Phe(4-F)-Phe-D-Trp-Lys-Thr-Phe-Thr-NH_2	$C_{78}H_{86}FN_{13}O_{13}$	1431.65	1432.75	6.680	99
NIP2	Nphtallyl-β-Ala-D-Phe-Phe(4-F)-Phe-D-Trp-Lys-Thr-Phe-Thr-NH_2	$C_{79}H_{88}FN_{13}O_{13}$	1445.66	1447.10	8.167	99
YT1	IsoQui-D-Phe-Phe(4-F)-Phe-D-Trp-Lys-Thr-Phe-Thr-NH_2	$C_{71}H_{79}FN_{12}O_{11}$	1294.60	1296.10	5.124	99

RESULTS AND DISCUSSION

Target structures with general formula X-D-Phe-Phe(4-F)-Phe-D-Trp-Lys-Thr-Phe-Thr-NH2, where X is a second pharmacophore A, B or C presented in Fig. 1 were synthesized. L-glycine or β-alanine in the fourth position of the naphthalimide ring are used as a linker between both parts of the molecule. The compounds were obtained by initially introduction of allylic group into the anhydride moiety and further the residue of the corresponding amino acid was introduced by nucleophilic substitution of a bromine atom. The second pharmacophore is also fluorescently active. Thus, the obtained bioconjugates could be also used as fluorescent markers in cancer diagnostics.

CHARACTERIZATION OF TARGETED BIOCONJUGATES

Purity of newly synthesized products was monitored by HPLC and their structures were proven by LC/MS/MS using Shimadzu Nexera X2, model 8045 apparatus with a linear binary gradient of phase A: H_2O (10 % AcCN; 0.1% HCOOH) and phase B: AcCN (5 % H_2O; 0,1 % HCOOH) and the following conditions:

time (min)	0.01	10.00	15.00	15.50	22.00
m.ph. A (%)	80	5	5	80	80
m.ph. B (%)	20	95	95	20	20

The other parameters of the chromatographic system are: Agilent Poroshell 120, 100 mm x 4.6 mm column; elution flow: 0.30 mL/min; temperature of column: 40ºC;
The structure of newly synthesized peptides is proven by ESI+ MS in SCAN mode in the following conditions:

Nebulizing gas flow	3 L/min
Heating gas flow	10 L/min
Interface temperature	350 ºC
DL temperature	200 ºC
Heat block temperature	400 ºC
Drying gas flow	10 L/min

CONCLUSIONS

Three new bioconjugates of monofluorinated BIM-23052 with a general formula X-D-Phe-Phe(4-F)-Phe-D-Trp-Lys-Thr-Phe-Thr-NH_2, where X is A, B or C presented in Fig. 1 were synthesized by using standard SPPS by means of Fmoc/O*t*Bu strategy and their structures and purity were proven with an HPLC/MS/MS. The anticancer activity is in a progress.

Acknowledgements:
This study is funded by the European Union-NextGenerationEU, through the National Recovery and Resilience Plan of the Republic of Bulgaria, project № BG-RRP-2.004-0002, "BiOrgaMCT"

References:

[1] Mateusz D. Tomczyk, Krzysztof Z. Walczak, 1,8-Naphthalimide based DNA intercalators and anticancer agents. A systematic review from 2007 to 2017, European Journal of Medicinal Chemistry, DOI: 10.1016/j.ejmech.2018.09.055

https://doi.org/10.17952/37EPS.2024.P1216

Rational design, synthesis and evaluation of mitoxantrone conjugated with mutated Gonadotropin Releasing Hormone (GnRH) for the treatment of hormone-dependent cancer

Georgia Biniari[1], Agathi Nteli[1], Christos Markatos[2], Vlasios Karageorgos[2], Alexios Vlamis-Gardikas[1], George Liapakis[2], Maria Venihaki[3], Theodore Tselios[1], Carmen Simal[1,*]

[1]Department of Chemistry, University of Patras, 26504 Rion, Greece
[2]Department of Pharmacology, School of Medicine, University of Crete, Heraklion, Greece
[3]Department of Clinical Chemistry, School of Medicine, University of Crete, 71003 Heraklion, Greece

Scan me

Introduction

Gonadotropin-releasing hormone (GnRH) or luteinizing hormone-releasing hormone (LHRH), has a significant role in fertility by initiating the regulation of gonadal axial, (1, 2). Several GnRH peptide analogues have been clinically used for the treatment not only to address fertility issues but also to treat hormone-dependent cancers, as GnRH receptors (GnRHR) are overexpressed in cancer cells. A promising strategy for selective immunosuppression of cancer cells, includes the development of delivery systems based on GnRH analogues conjugated with anti-cancer drugs to target the GnRHR on cancer cells (3). This targeted approach is advantageous due to the higher expression of GnRH receptors compared to healthy cells, allowing for more precise and effective treatment (2). In this study, we designed a modified mitoxantrone molecule (immunosuppressing agent) conjugated with an altered GnRH peptide *via* a disulfide bond (3). This conjugation aims to facilitate the *in situ* release of mitoxantrone through the reduction of the disulfide bond by the thioredoxin system.

Experimental

General synthetic route:

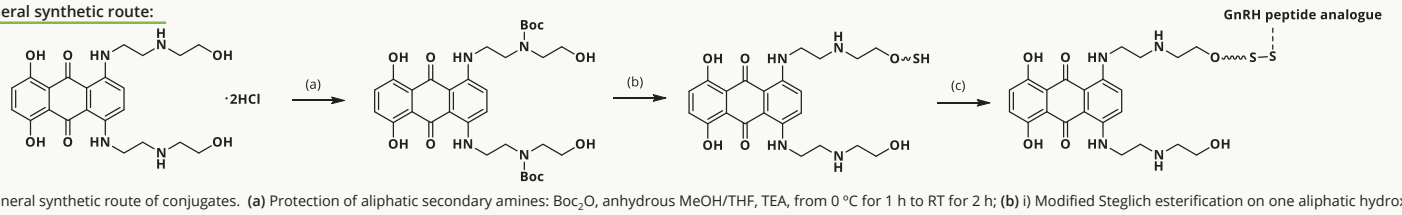

Fig.1: General synthetic route of conjugates. **(a)** Protection of aliphatic secondary amines: Boc_2O, anhydrous MeOH/THF, TEA, from 0 °C for 1 h to RT for 2 h; **(b)** i) Modified Steglich esterification on one aliphatic hydroxyl group: 3-(2-pyridyldithio)propanoic acid (con3) or $TrtSCH_2CO_2H$ (con7), DMAP, HOBt, DIC, CH_2Cl_2, 0 °C, 24 h; ii) Removal of protecting groups: TFA, TES, CH_2Cl_2, RT, 1.5 h; **(c)** Synthesis of conjugates: GnRH peptides analogues (synthesised in solid phase using CLTR-Cl or Ethyl Indole AM resin *via* Fmoc/ tBu methodology), MeOH, RT, 24 h (con3) or 6 h (con7) (3).

Structure of synthesised conjugates

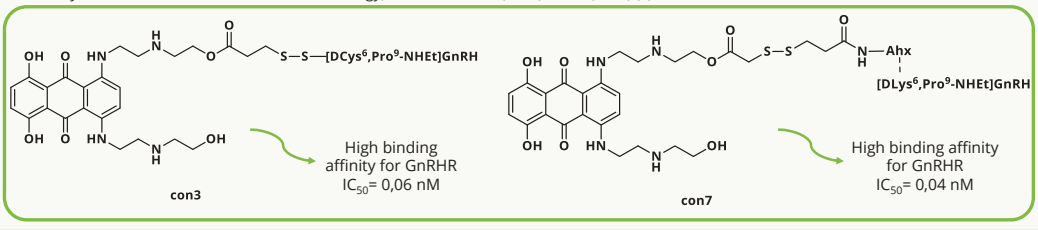

Identification of synthesised conjugates by ESI-MS and 1D/ 2D NMR studies.

Pharmacological evaluation

Cytotoxicity studies

Cytotoxicity studies achieved using **MTT assay**

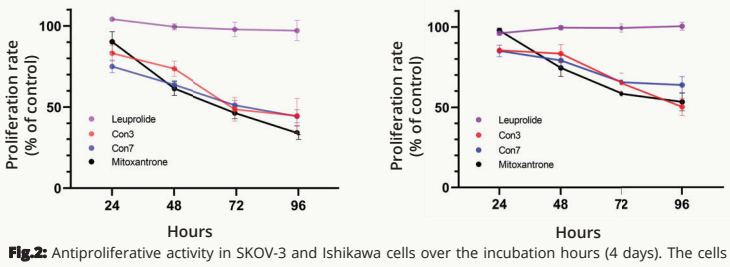

Fig.2: Antiproliferative activity in SKOV-3 and Ishikawa cells over the incubation hours (4 days). The cells were treated with 1μM of con3, con7, mitoxantrone analogue and the commercially available agonist Leuprolide. All analogs decreasing the proliferation rate in a time dependent manner.

- Cytotoxicity studies using MTT assay showed that the proliferation rate decreased in a **dose dependent manner** (data not shown)
- Leuprolide **did not affect** the viability of cells
- Conjugates con3 and con7 reduce the proliferation rate due to **the presence of mitoxantrone analogue**

Inhibition of Thioredoxin System

Cisplatin: Inhibitor of Thioredoxin Reductase ⟶ Thioredoxin system is not functional

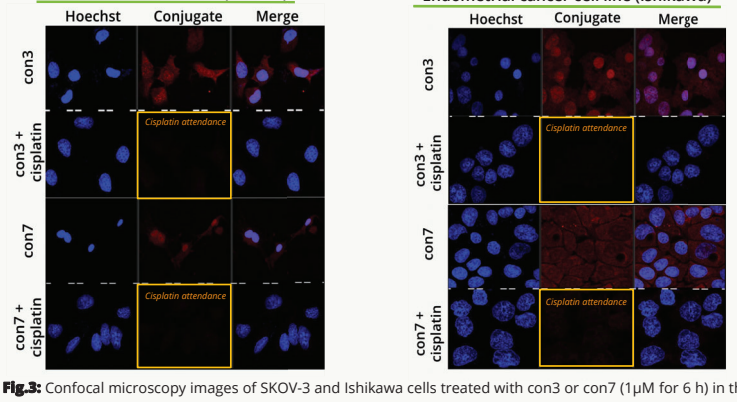

Fig.3: Confocal microscopy images of SKOV-3 and Ishikawa cells treated with con3 or con7 (1μM for 6 h) in the presence or absence of cisplatin. Cells' nuclei staining with Hoechst dye (blue) and the red ones depict the mitoxantrone fluorescence.

- Internalization of mitoxantrone analogue **only** when thioredoxin system is **functional** (active thioredoxin reductase).

Conclusions

The synthesised mitoxantrone-GnRH peptide conjugates were identified by 1D / 2D NMR studies and pharmacologically evaluated using several cancer cell lines. The conjugates con3 and con7 reduce cell proliferation in a time- and dose-dependent manner in SKOV-3 and Ishikawa cell lines. The cytotoxic effect of these conjugates is attributed to the release of the mitoxantrone analogue through the reduction of the disulfide bond by the cancer cells' thioredoxin system. This effect is confirmed by using cisplatin, an inhibitor of the thioredoxin system, which abolishes the intracellular accumulation of mitoxantrone.

References

1. A. V Schally et al., *Biochem. Biophys. Res. Commun*. 43, 393–399 (**1971**), doi:10.1016/0006- 291X(71)90766-2.

2. G. Emons et al., *Gynecol. Oncol.* 133, 427–432 (**2014**), doi:10.1016/j.ygyno.2014.03.576.

3. G. Biniari et al., *Int. J. Mol. Sci*. 24 (**2023**), doi:10.3390/ijms242015232.

Acknowledgements

This research has been co-financed by the European Union and Greek national funds through the Operational Program Competitiveness, Entrepreneurship and Innovation, under the call RESEARCH-CREATE-INNOVATE (acronym: **ORAMA**, project code: **T2EDK-02056**). Attendance at the conference has been funded by **MEDICUS** (ELKE, University of Patras).

Contact details: Carmen Simal, Department of Chemistry, University of Patras, Rion, Greece. **csimal@upatras.gr**

Co-financed by Greece and the European Union

New peptide-porphyrin conjugates targeting brain-residing viruses

Toni Todorovski[1,2], Giuseppina Guida[1], Patrizia Janković[2], Diogo Mendonça[3], Christine Cruz-Oliveira[3], Marco Cavaco[3], Daniela Kalafatović[2], Sira Defaus[1], Andrea Da Poian[4], Miguel Castanho[3], David Andreu[1]

[1] Department of Medicine and Life Sciences (MELIS), Universitat Pompeu Fabra, Barcelona, Spain; [2] University of Rijeka, Faculty of Biotechnology and Drug Development, Rijeka, Croatia; [3] Instituto de Medicina Molecular, Faculdade de Medicina, Universidade de Lisboa, Lisboa, Portugal; [4] Instituto de Bioquímica Médica Leopoldo de Meis, Universidade Federal do Rio de Janeiro, Rio de Janeiro, Brazil

Contact email: toni.todorovski@uniri.hr; toni.todorovski@upf.edu

https://doi.org/10.17952/37EPS.2024.P1217

Introduction

Flaviviruses (Zika, dengue, West Nile, yellow fever, tick-borne encephalitis) are enveloped viruses with positive-sense RNA, able to cross the blood-brain barrier (BBB) and thus infect adult brains. The infection can affect the central nervous system (CNS) causing severe neurological complications such as encephalopathy, encephalitis, Guillain-Barré syndrome and microcephaly. There is no current drug to target brain-infecting viruses, and any such development faces the challenge of delivering the drug across the BBB to reach virus at its most sensitive site of action, the brain. Herein we present a comparative study of various on-resin conjugation strategies to generate linear and multimerized (juxtaposed or branched) peptide-porphyrin conjugates (PPCs) able to cross BBB with good translocation rates and high antiviral activity [1, 2].

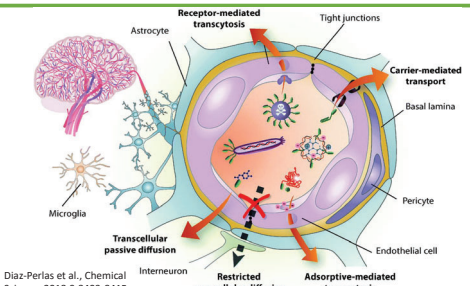

Diaz-Perlas et al., Chemical Science. 2018;9:8409-8415.

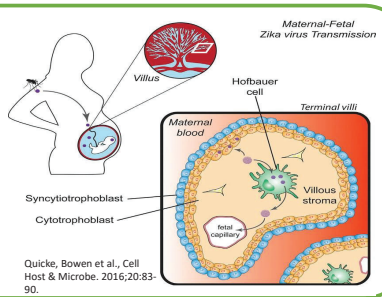

Quicke, Bowen et al., Cell Host & Microbe. 2016;20:83-90.

Conjugation chemistry

Entry number	Structure	M+H
P1	VQQLTKRFSL-amide	1218.7
P2*	VQQLTKRFSLK-amide	1346.8
P3	AGILKRW-amide	842.5
P4*	AGILKRWK-amide	970.6
P5	SGTQEEY-amide	812.3
P6*	SGTQEEYK-amide	940.4
Mesoporphyrin IX MPIX (MP)	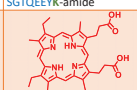	
Protoporphyrin IX PPIX (PP)	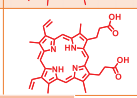	
8-amino-3,6-dioxooctanoic acid (O2Oc)	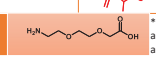	

*P2, P4, P6 are versions of P1, P3 and P5, respectively, elongated with an extra Lys residue (in bold green) to allow conjugation at the C-terminus

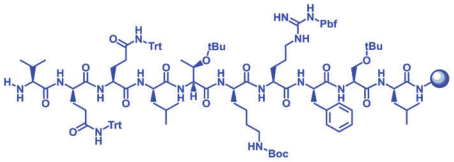

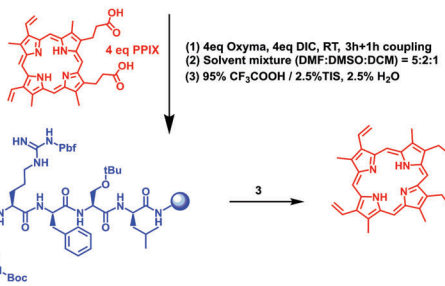

Porphyrin-peptide combinations	Activation method/Time (min)	Conversion (%)
PP-P1	PyBOP-DIPEA / 30	96.8
	HATU-DIPEA / 60	100
	TBTU-DIPEA / 30	97.6
	DIC-Oxyma / 180 + 60	**98.7**
MP-P3	PyBOP-DIPEA / 30	78.9
	HATU-DIPEA / 60	59.9
	TBTU-DIPEA / 30	98.6
	DIC-Oxyma-DIPEA / 180 + 60	**99.5**
PP-P3	TBTU-DIPEA / 30	90.1
	DIC-Oxyma / 180 + 60	**98.5**
MP-P1	TBTU-DIPEA / 30	67.3
	DIC-Oxyma-DIPEA / 180 + 60	**97.1**
P2-MP	**DIC-Oxyma-DIPEA / 180 + 60**	**99.6**
P2-PP	**DIC-Oxyma / 180 + 60**	**99.4**

The PPC production strategy involved six blood-brain barrier peptide shuttles (BBBpS), two porphyrins and one PEG-like linker (Table on the left side). Several on-resin conjugation chemistries and reaction times were tested (Table on the right side). The conjugation took place at *C*- (P2, P4 and P6) or *N*-terminal (P1, P3 and P5) part of the corresponding BBBpS. The scheme presented here show the synthesis of PP-P1 (conjugation at the peptide *N*-terminal part) using the optimized conditions. When conjugation was performed at the BBBpS *C*-terminal part, an additonal Lys with a orthogonally protected Mmt group was added at the peptide C-terminal end (Table on the left side, entries P2, P4 and P6). In these cases, first, the side-chain Mmt was selectively removed and afterwards the conjugation procedure is the same as showed in the scheme above. When the linker was used, coupling of the linker preceded the conjugation step.

BBB translocation rates and antiviral activity of some PPCs against Zika virus

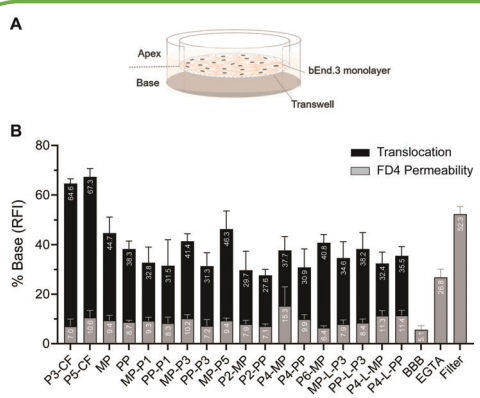

In vitro PPC translocation. (**A**) Schematic representation of the BBB model transwell system. (**B**) *in vitro* BBB translocation measurements. PPC translocation values are depicted in black, while FD4 permeability values post-translocation are in grey (BBB—only cells, EGTA—tight junctions disruption control, Filter—no cells).

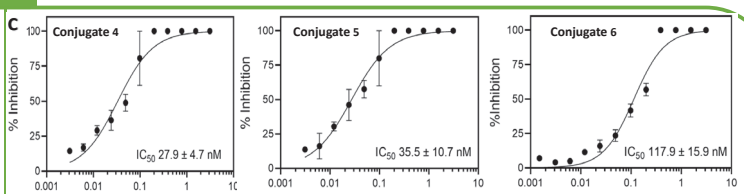

Conjugates 4, 5 and 6 were evaluated for Zika virus (ZIKV) inhibition *in vitro* using a plague assay **(C)**. The results showed that these PPCs are able to inhibit ZIKV *in vitro*, with IC_{50} values in the low nM range. These results are very promising, compared to IC_{50} values of the previously published PPCs [2] (Table on the right), and currently cytotoxicity and antiviral studies against other brain-residing viruses are undergoing.

	IC50 (μM)									
	MP	PP	MP-P1	MP-P5	PP-P1	PP-P5	P2-MP	P6-MP	P2-PP	P6-PP
ZIKV	> 50	> 50	> 50	25.07 ± 0.05	**1.08 ± 0.14**	> 50	> 50	> 50	> 50	> 50

Conclusions

- We have developed successful on-resin synthesis of new PPCs by DIC/oxyma activation strategy as most suitable and effective approach.
- All conjugates were well characterized with purity > 90 % and most of them were able to successfully pass the BBB.
- We have identified several PPCs with high antiviral activity (some of them reaching nanomolar range) against ZIKV.
- **In any event, one may propose peptide-porphyrin conjugation as a promising strategy to tackle brain-resident viruses.**

References

1. Mendonça, D.A. et al. *Bioconjugate Chemistry* **(2021),** 32 (6), 1067-1077.
2. Todorovski, T. et al. *Pharmaceutics* **(2022),** *14*, 738.

Acknowledgement

This project has received funding from La Caixa Foundation (HR17_00409) and from the European Union´s Horizon 2020 research and innovation programme under grant agreement No 828774.

Proceedings of the 37th European Peptide Symposium
Michal Lebl, Editor
European Peptide Society, 2024 *http://doi.org/10.17952/37EPS.2024.P1218*

Development of Daunomycin-Peptide Antitumor Conjugates Containing Neurotensin-Based Homing Moiety

Levente Endre Dókus[1], Eszter Lajkó[3], Orsolya Láng[3], László Kőhidai[3], Gábor Mező[1,2]

[1]HUN-REN-ELTE Research Group of Peptide Chemistry, Budapest, Hungary.
[2]Eötvös Loránd University, Faculty of Science, Institute of Chemistry, Budapest, Hungary
[3]Department of Genetics, Cell- and Immunobiology, Semmelweis University, Budapest, Hungary.

Introduction

Pancreatic ductal adenocarcinoma (PDAC) is one of the most dangerous cancerous diseases of the pancreas leading to high mortality [1]. Targeted tumor therapy could be a good tool to treat PDAC efficiently. From the literature it is known that PDAC cells overexpress the neurotensin-1 (NTSr1) receptor. This protein binds to neurotensin, a peptide hormone consisting 13 amino acids, as its ligand therefore, it can be a potential target for neurotensin-based homing peptide drug conjugates. The biological activity of neurotensin is attributed to its C-terminal part: ^{8}RRPYIL^{13} [2]. Our aim was to develop new peptide - drug conjugates containing daunomycin as an anticancer agent attached to the homing peptides *via* an oxime bond [3].

Results and Discussion

In the first round six different daunomycin - peptide conjugates were initially developed according to the literature background. In the case of three conjugates, enzyme labile spacer (GFLG) [4] was built into the sequences between the homing peptide and the aminooxy moiety used for oxime ligation. This spacer is cleavable by the lysosomal enzyme cathepsin B, making it suitable for enhancing the intracellular degradation and the release of the active metabolite.

The aminooxyacetyl-group containing homing peptide parts were synthetized by SPPS using Fmoc/^{t}Bu technique on Wang-resin. The payload (Dau) was coupled in solution phase (0.2 M NH_4OAc solution (pH=5)) to the cargo *via* oxime bond (Figure 1). The cytotoxic effect of the conjugates were characterized on PANC-1 (a PDAC type) cell line by an impedimetric technique, xCELLigence System.

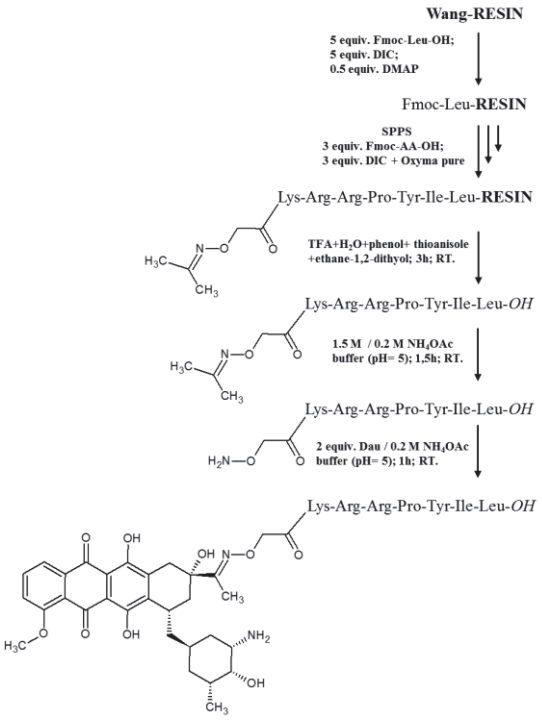

Fig. 1. Outline of the synthesis of conjugates

The results shown that from the first six constructions three conjugates (**2**,**5**,**6**) have a significant cytotoxic effect at 10^{-5} M concentration after 72 hours treatment, but the other three derivatives did not induce antitumor effect on PANC-1 cells (Table 1). The cellular uptake of these conjugates and their metabolism by lysosomal enzymes were also investigated (Figure 2 and 3).

These results were applied for design and prepare new non-natural amino acid (*e.g. tert*-leucine) containing derivatives to increase their enzyme stability [5]. Their antitumor effect (Table 1), internalization ability and lysosomal degradation were also investigated. (Figure 2 and 3)

In the next step the mentioned enzyme labile spacer was built in to the N-terminus of the two structures which resulted highest cellular uptake (**11** and **12**). Finally, these two structures with best internalization ability (**7**, **8**) were modified with additional non-natural amino acids and leaving of the *tert*-Leu. In the position[8] of this two structures Arg(Me), *h*-Lys, *h*-Arg, D-Lys, D-Arg or in one case L-Arg were built in resulted nine new conjugates. The antitumor activity were also characterized on PANC-1 cell line in 10^{-5} M and $3.3x10^{-5}$M concentrations using 72 or 96 hours incubation. Finally, the IC_{50} values of the three most efficient non-natural amino-acid containing derivatives were characterized (Table 1).

Table 1. Cytotoxic effect of the conjugates

	Sequence	Viability %		Sequence	Viability %
1	*Dau=Aoa*-RRPYIL-*OH*	**> 50**	10	*Dau=Aoa*-KRKPW^{t}LL-*OH*	102.6 ± 18.7
2	*Dau=Aoa*-KRRPYIL-*OH*	4.7 ± 1.8	11	*Dau=Aoa*-GFLGKRRPY^{t}LL-*OH*	116.4 ± 3.1
3	*Dau=Aoa*-KPRRPYIL-*OH*	**> 50**	12	*Dau=Aoa*-GFLGKRRPW^{t}LL-*OH*	116.6 ± 6.7
4	*Dau=Aoa*-GFLGRRPYIL-*OH*	**> 50**		Sequence	IC_{50} (μM)
5	*Dau=Aoa*-GFLGKRRPYIL-*OH*	13.0 ± 1.5			72 h / 96 h
6	*Dau=Aoa*-GFLGKPRRPYIL-*OH*	11.0 ± 1.7	13	*Dau=Aoa*-K-*h*Arg-RPYIL-*OH*	27.8 ± 5.9 / 23.1 ± 14.2
7	*Dau=Aoa*-KRRPY^{t}LL-*OH*	116.4 ± 3.1	14	*Dau=Aoa*-K-*h*Lys-RPWIL-*OH*	20.9 ± 2.3 / 13.1 ± 0.9
8	*Dau=Aoa*-KRRPW^{t}LL-*OH*	116.6 ± 6.2	15	*Dau=Aoa-K*-Arg(Me)-RPYIL-*OH*	22.9 ± 2.5 / 16.7 ± 2.4
9	*Dau=Aoa*-KRKPY^{t}LL-*OH*	110.0 ± 6.8	16	*Dau=Aoa*-K-D-Lys-RPWIL-*OH*	20.9 ± 2.2 / 20.3 ± 6.5

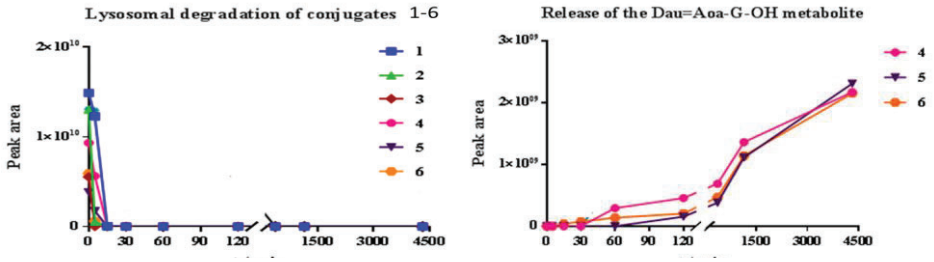

Fig. 2. Time dependent degradation of conjugates by lysosomal enzymes

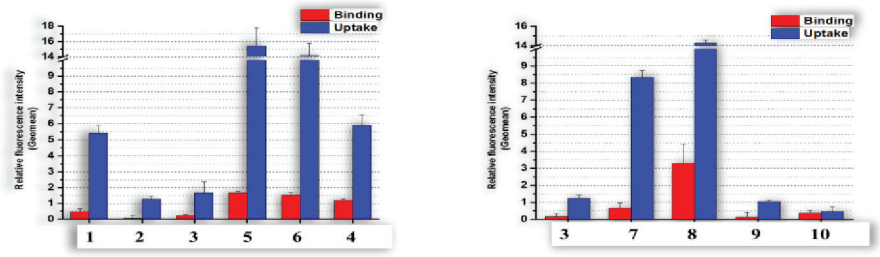

Fig. 3. Cellular binding and uptake of the conjugates

As discussion the results showed that three conjugates (**2, 5** and **6**) have significant cytotoxic effect at 10^{-5} M concentration (the cell (PANC-1) viability was lower than 15%). All of the investigated conjugates were fast degraded by lysosomal enzymes (within 30 minutes) but in case of GFLG containing constructions the presence of the smallest (active) metabolite in huge amount can be observed only after 60 minutes reaction time. (Figure 2) The presence of ^{t}Leu in the 12 position increases the cellular uptake (Figure 3), but these conjugates did not present any antitumor effect (Table 1). The presence of the enzyme labile spacer GFLG does not increase significantly the effectivity in case of different homing moieties.The incorporation of non-native amino acids into the position 8 of homing peptide results high cytotoxicity in case of **13**, **14**, **15**, and **16** conjugates, but only in higher (33 μM) concentration.

These conjugates might be good candidates for further development (other drugs and/or linker). In conclusion, the set of the developed neurotensin derivative – drug conjugates provide evidences to select appropriate molecules for further therapeutic experiments or as diagnostic tools.

Acknowledgments

The project was supported by the National Research, Development and Innovation Office (NKFIH K146039 and NVKP_16-1-2016-0036)

References

[1]: Jemal, A. et al. (2007) *CA Cancer J. Clin.* **57**, 43-66.
[2]: Gilbert, J.A. et al. (1989) *Biochem. Pharm.* **38**, 3377-3382.
[3]: Mező, G. et al (2024) *Int. J. Mol. Sci.* **2024**, *25*(3), 1864.
[4]: Peterson, J.J. et al. (1998) *Bioconj. Chem.* **9**, 618–626.
[5]: Hadden, M. K. et al. (2005) *Neuropharm.* **49**,1149-1159.

https://doi.org/10.17952/37EPS.2024.P1220

Peptide fibrils as nanocarrier for targeted therapy

Justyna Sawicka[1], Milena Czeszejko[1], Ewa Wieczerzak[1], Paweł Niedziałkowski[1], Tomasz Kulesza[2], Kamila Kitkowska [2], Rafał Sądej [2], Sylwia Rodziewicz-Motowidło[1]*

[1]Faculty of Chemistry, University of Gdańsk, Wita Stwosza 63, 80-308 Gdańsk

[2] Intercollegiate Faculty of Biotechnology of the University of Gdańsk and the Medical University of Gdańsk, Medical University of Gdańsk, Marii Skłodowskiej-Curie 3a, 80-210 Gdańsk

*e-mail: milena.czeszejko@phdstud.ug.edu.pl

INTRODUCTION

The use of drug delivery systems, particularly nanocarriers, has gained prominence as a result of their improved safety and efficacy compared to conventional therapies. Nanodrugs, consisting of nanocarriers conjugated with cytostatic molecules, have the ability to target cancer cells through active and/or passive targeting mechanisms. Antibody-drug conjugates (ADCs) offer a less burdensome, more selective, and potentially more effective therapeutic option. Despite its efficacy, the affordability of ADCs is a challenging issue, limiting access for a significant number of patients. Current approaches include a variety of biologically derived agents, including antibodies, peptides, and aptamers, to target nanotherapeutics to specific cancer cell receptors, such as HER2 [1]. Peptide fibrils, which self-organise from proteins and/or peptides, have a large surface-area-to-volume ratio, which allows for higher drug loading and attachment of targeting molecules. Their physicochemical and mechanical properties can also be regulated by altering the amino acid sequence of the peptides that form the fibrils. We studied the kinetics of fibril growth using an innovative method that combined electrochemical impedance spectroscopy (EIS) with cyclic voltammetry (CV). We also used a thioflavin (ThT) assay. The morphology of the fibrils was visualised using transmission electron microscopy (TEM) and atomic force microscopy (AFM). Additionally, we compared the molecular size of the peptide fibrils on day '7' of fibrillization using dynamic light scattering (DLS).

PEPTIDE DESIGN AND SYNTHESIS

One of the well-described fibril-forming peptides is the peptide with the sequence QAGIVV (FC). The amino acid sequence of the FC peptide is a fragment 55-60 of the human cystatin C (HCC) protein, whose sequence has been shuffled, the so-called shuffle peptide [2]. Our group conducted studies that confirm that its self-association ability does not disappear even after adding additional amino acid residues [3]. Two analogues were designed. The GFC peptide, which is the glycine analogue of the FC peptide, will serve as a carrier to which we will attach an antibody or affibody and a drug with known cytostatic activity. Additionally, we synthesized the CGFC peptide, which will enable drug attachment by forming a covalent bond.



Figure 1. *Amino acid sequence of the CGFC/GFC/FC peptide.*

All of the peptides were synthesised on a solid support using Fmoc chemistry, and then purified using reversed-phase high-performance liquid chromatography and mass spectrometry. Then, the obtained peptide was fibrillized. For this purpose, the peptide was dissolved in phosphate buffered saline (PBS) at pH 7.4, C = 1 mg/ml and incubated for 7 days at 37°C with constant orbital shaking.

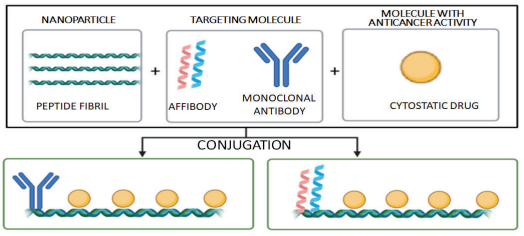

Figure 2. *Conceptual illustration of nanodrugs formation.*

METHODS AND RESULTS

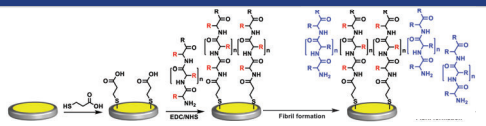

Figure 3. *Scheme of gold electrode functionalization with the correct peptide in order to obtain sensitive electrode fibrils growth.*

Each of the peptides was used for gold electrode functionalization purposes. The surface gold electrode was modified with mercaptocarboxylic acid to obtain carboxyl groups. This modification allows covalent attachment of the fibrilogenic peptide with the NH2 group in C-terminus (FC / GFC / CGFC) to the electrode surface (Figure 3). The preliminary of electrochemical impedance spectroscopy (EIS) spectra obtained show (Figure 4), that the electrode was functionalised successfully with the peptide. In the next step, the electrode was immersed in PBS buffer with the correct peptide (FC/GFC/CGFC) and incubated at 37°C using continuous shaking.

ELECTROCHEMICAL MEASUREMENTS

FC
NH_2-QAGIVV-NH_2

GFC
NH_2-**G**QAGIVV-NH_2

CGFC
NH_2-**CG**QAGIVV-NH_2

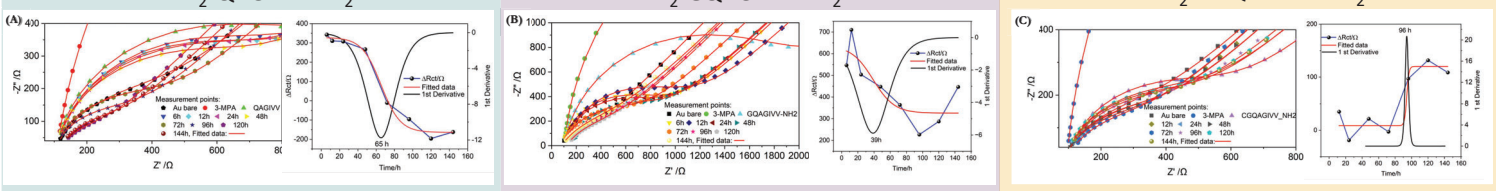

Figure 4. *Electrochemical impedance spectroscopy spectra obtained for modified electrodes and after incubation in fibril growth solution recorded at different time points for* ***(A)*** *FC;* ***(B)*** *GFC;* ***(C)*** *CGFC; peptide.*

Electrochemical impedance spectroscopy (EIS) spectra were obtained for modified electrodes before and after incubation in a fibril growth solution, recorded at different time points for the FC peptide. The electrode was immersed in a 1 mg/ml solution of the FC peptide in PBS buffer and incubated at 37°C with continuous shaking. The EIS spectra reveal that FC fibrils grew slowly during the first 20 hours, after which their growth rate increased rapidly, reaching a stable level after approximately 65 hours.

Electrochemical impedance spectroscopy (EIS) spectra were obtained for modified electrodes before and after incubation in a fibril growth solution, recorded at different time points for the FC peptide. The electrode was immersed in a 1 mg/ml solution of the FC peptide in PBS buffer and incubated at 37°C with continuous shaking. The EIS spectra reveal that GFC fibrils grew slow for the first 39 hours, after 80h, then their growth increased and after about 39 hours they reached a stable level.

Electrochemical impedance spectroscopy (EIS) spectra were obtained for modified electrodes before and after incubation in a fibril growth solution, recorded at different time points for the CGFC peptide. The electrode was immersed in a 1 mg/ml solution of the CGFC peptide in PBS buffer and incubated at 37°C with continuous shaking. The EIS spectra reveal that FC fibrils grew slowly during the first 75 hours, after which their growth rate increased rapidly, reaching a stable level after approximately 96 hours.

TIOFLAVIN T ASSAY

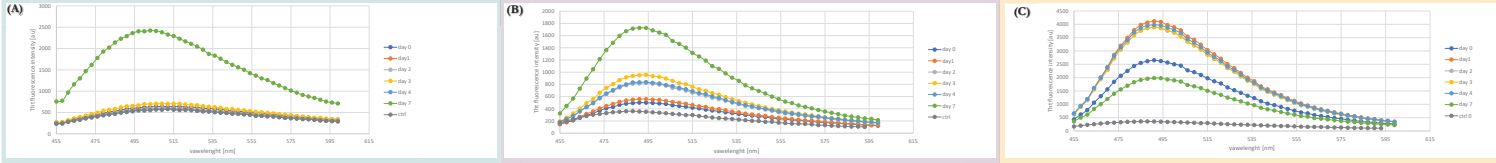

Figure 5. *Graph of the dependence of the fluorescence intensity of the peptide-thioflavin T complex on incubation time relative to the control consisting of PBS solution for* ***(A)*** *FC;* ***(B)*** *GFC;* ***(C)*** *CGFC; peptide.*

A 0.1 mg/ml FC peptide solution in PBS with thioflavin T (ThT), with a final peptide concentration of 10 μM, was used for the measurement. PBS with ThT served as the negative control. The sample was excited at 420 nm, and the emission spectrum was recorded in the range of 455 to 600 nm. The absorption maximum was observed at 482 nm. An increase in fluorescence intensity was observed over consecutive days. As shown in Figure 5 (A), the maximum fluorescence intensity was reached on day 7.

A 0.1 mg/ml FC peptide solution in PBS with thioflavin T (ThT), with a final peptide concentration of 10 μM, was used for the measurement. PBS with ThT served as the negative control. The sample was excited at 420 nm, and the emission spectrum was recorded in the range of 455 to 600 nm. The absorption maximum was observed at 482 nm In the following days the fluorescence intensity was observed at a similar level. As shown in Figure 5 (B), the maximum fluorescence intensity was reached on day 7.

A 0.1 mg/ml FC peptide solution in PBS with thioflavin T (ThT), with a final peptide concentration of 10 μM, was used for the measurement. PBS with ThT served as the negative control. The sample was excited at 420 nm, and the emission spectrum was recorded in the range of 455 to 600 nm. The absorption maximum was observed at 482 nm. An increase in fluorescence intensity was observed over consecutive days. As shown in Figure 5 (C), it can seen that the maximum of fluorescence intensity is at the first 3 days.

AFM / TEM

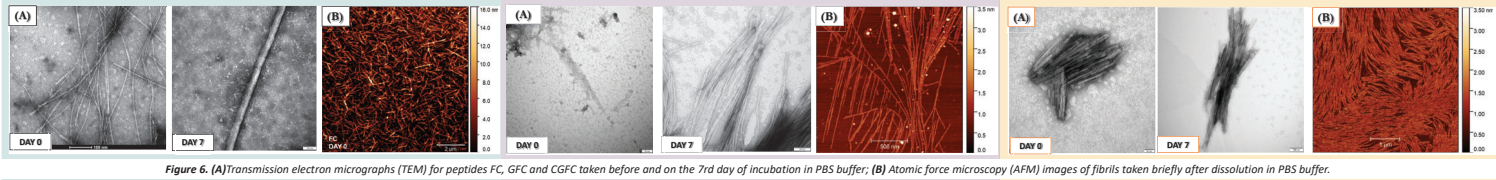

Figure 6. ***(A)****Transmission electron micrographs (TEM) for peptides FC, GFC and CGFC taken before and on the 7rd day of incubation in PBS buffer;* ***(B)*** *Atomic force microscopy (AFM) images of fibrils taken briefly after dissolution in PBS buffer.*

The FC peptide forms fibrils immediately after dissolving in PBS buffer. As observed in TEM images, the FC peptide forms very long fibers, exceeding 900 nm in length and approximately 10 nm in width. AFM images also reveal the formation of a dense, three-dimensional network of peptide fibrils.

The GFC peptide forms fibrils immediately after dissolving in PBS buffer. By the 7th day of incubation, the GFC peptide has developed a network of long, parallel fibrils. These fibrils are over 1 μm in length and approximately 5 nm in width, as seen in the images. The AFM image reveals a fibril arrangement resembling a horsetail pattern.

The CGFC peptide forms fibrils immediately after dissolving in PBS buffer. As seen in TEM images, the CGFC peptide forms fibers ranging from 100 to 500 nm in length and approximately 10 nm in width, which are tightly attached to one another. AFM images also show the formation of a dense, three-dimensional network of peptide fibrils.

DLS

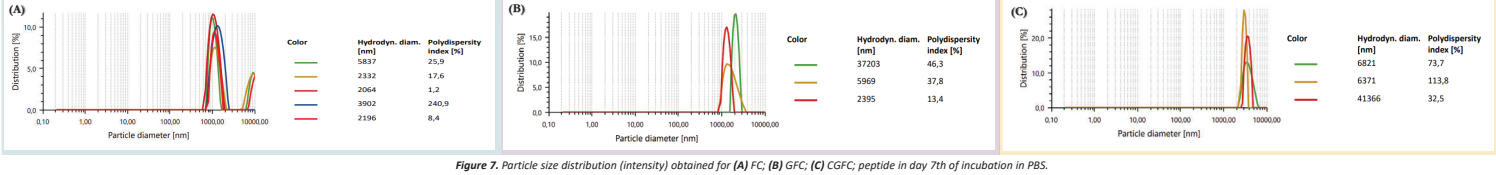

Figure 7. *Particle size distribution (intensity) obtained for* ***(A)*** *FC;* ***(B)*** *GFC;* ***(C)*** *CGFC; peptide in day 7th of incubation in PBS.*

The FC peptide has a mean hydrodynamic diameter of 3444 nm. A polydispersity index of 35.8% indicates moderate uniformity in particle size. Two dominant size peaks at 5665 nm and 4392 nm suggest the presence of two distinct particle populations.

The GFC peptide has an average hydrodynamic diameter of 15,189 nm, indicating the presence of large aggregates. The polydispersity index is 32.5%, reflecting moderate particle size variability. The primary size peak is observed at 1712.4 nm, with a higher light transmission of 75.1%.

The CGFC peptide is characterized by a large hydrodynamic diameter of 18,186 nm. The high polydispersity index of 73.3% indicates a broad distribution of particle sizes. The primary size peak is observed at 3480 nm.

CONCLUSION

Our study shows that minor changes in the peptide sequence (e.g., the addition of an additional amino acid residue) have a significant effect on their fibrilization properties, as illustrated by the differences between the FC, GFC, and CGFC peptides. The FC peptide shows slow initial fibril growth, as evidenced by ThT measurements that correlate with the EIS results. The FC formed very long fibrils, as observed by microscopy. The GFC peptide also reaches a peak in ThT fluorescence after 7 days, but are stabilized earlier (after 39 hours) and forms longer and narrower fibrils. The CGFC peptide, because of its ability to form dimers via disulphide bonds (owing to cysteine residues), resulted in significantly larger fibrils, as confirmed by DLS measurements showing a large hydrodynamic diameter. The ThT assay showed that the CGFC peptide stabilized its fibril growth after 96 hours, as also observed by EIS measurements. The combination of AFM/TEM, ThT assay, and EIS provided a comprehensive understanding of the fibril formation process, revealing differences in the kinetics, morphology, and structural properties of the peptides.

REFERENCES

[1] N. Zhang, J. Zhang, P. Wang, X. Liu, P. Huo, Y. Xu, W. Chen, H. Xu, Q. Tian, Investigation of an antitumor drug-delivery system based on anti-HER2 antibody-conjugated BSA nanoparticles. Anticancer Drugs. 2018 Apr;29(4):307-322.

[2] Sawicka J, Iłowska E, Deptuła M, Sosnowski P, Sass P, Czerwiec K, Chmielewska K, Szymańska A, Pietralik-Molińska Z, Kozak M, et al. Functionalized Peptide Fibrils as a Scaffold for Active Substances in Wound Healing. International Journal of Molecular Sciences. 2021; 22(8):3818.

[3] Iłowska, E. et al. Identification of a Steric Zipper Motif in the Amyloidogenic Core of Human Cystatin C and Its Use for the Design of Self-Assembling Peptides. Int J Mol Sci 23, (2022).

Thanks to the National Science Centre (grant nr 2022/45/B/NZ7/03889).

De novo Semi-synthetic Platform for Monitoring Protein degradation in Live Cells

Mahdi Hasan, Deepanjan Panda, Guy Mann and Ashraf Brik*

Schulich Faculty of Chemistry, Technion-Israel Institute of Technology, Haifa, 3200008, Israel. E-mail: mahdi.hasan@campus.technion.ac.il

https://doi.org/10.17952/37EPS.2024.P1221

Introduction

Depletion or inactivation of proteins is a powerful tool for evaluating their involvement in cellular pathways and in medicine. Proteolysis targeting chimera (PROTAC) is promising for both the development of therapeutics and studying protein turnover in biological pathways. The development of PROTAC depends on a known protein of interest (POI) binder and a suitable selection of an E3 recruiter. Although advanced progress has been made for the development of small molecule ligand for several proteins, developing a PROTAC requires significant efforts to optimize such a bifunctional molecule, containing a specific linker. Moreover, for many POIs there is a lack for a specific ligand to be used as part of the PROTAC, and the system requires extensive validation for the biological effect and its phenotype. Engineering degron technologies require a recombinant expression of a degron system, or genetically modifying the DNA to introduce the degrader to the POI. However, these methods are still restricted by the existence of a few ligands for E3 ligases. Inspired by these important approaches we thought to design a novel platform that is more flexible and systematically can be manipulated as well as can be activated on demand. Here we report our first steps towards building such a platform based on SpyTag/SpyCatcher system that allows tagging the POI with E3 ligand in test-tube, followed by cell delivery to monitor its degradation via the UPS.

1 SpyCatcher/SpyTag system

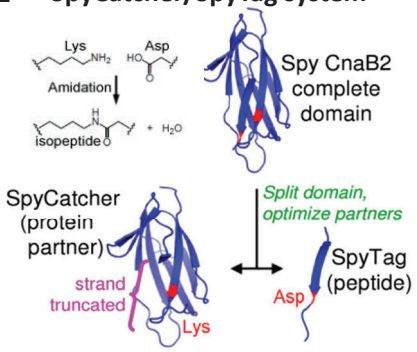

Zakeri, *et al*. 2012, *PNAS*.

Our strategy

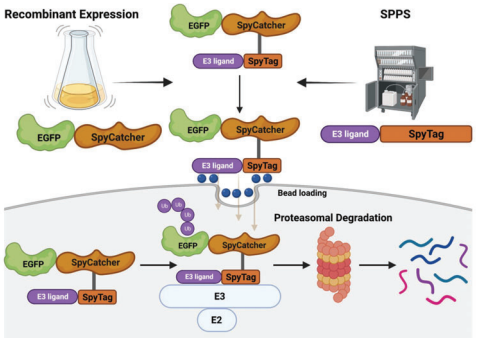

2 SpyTag-VHL synthesis

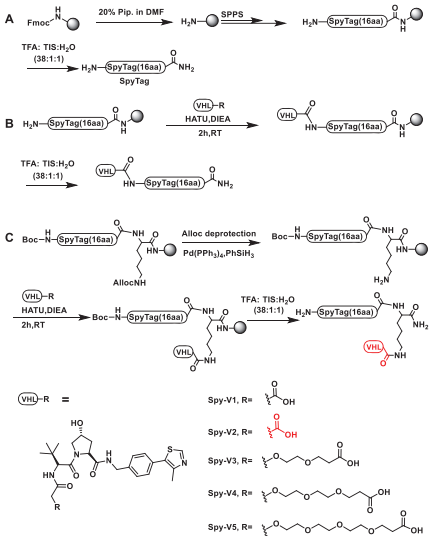

SpyCatcher/SpyTag reaction

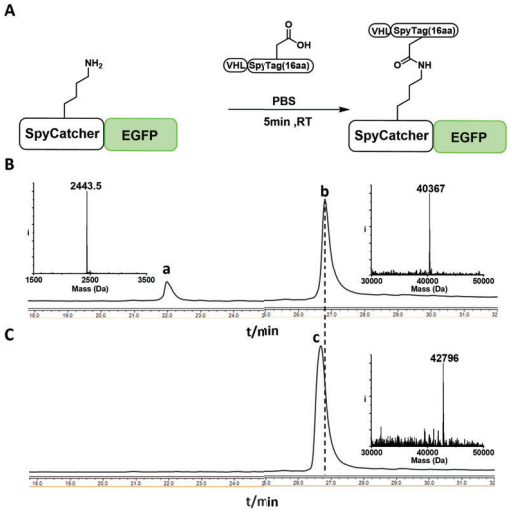

3 Results

SpyCatcher/SpyTag system promote ubiquitination and degradation of EGFP

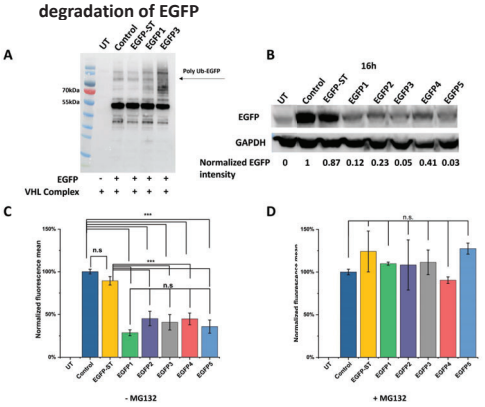

Figure 1.(A) In vitro ubiquitination assay using VHL complex. (B) WB analyses of the degradation of EGFP constructs in U2OS cells. (C) Flow cytometry analyses of the degradation of EGFP constructs, after 16h incubation in U2OS cells. (D) degradation rate of EGFP constructs in U2OS cells in the presence of proteasome inhibitor, MG132

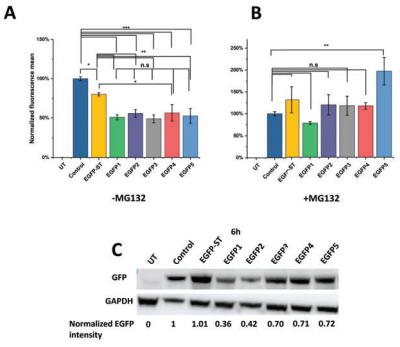

Figure 2.(A) Flow cytometry analysis of the degradation of EGFP constructs, after 6h incubation in U2OS cells. (B) Degradation rate of EGFP constructs in U2OS cells in the presence of proteasome inhibitor, MG132. (C) WB analyses of the degradation of EGFP constructs in U2OS cells

4 SpyTag VHL promote degradation of overexpressed EGFP-SpyCatcher U2OS cells after 4h

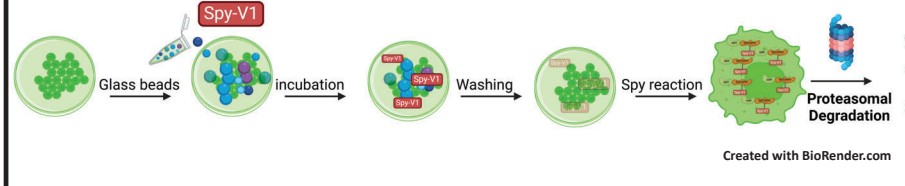

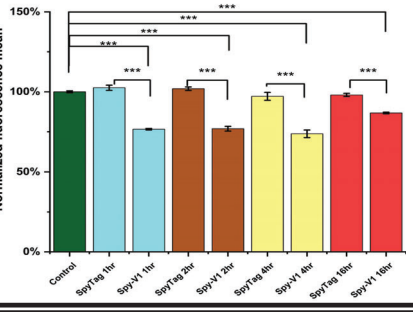

*Figure 3. Flow cytometry analysis of the degradation of overexpressed EGFP-SpyCatcher U2OS cells after 1,2,4 or 16 hours. SpyTag or Spy-V1 were delivered to U2OS via bead loading, the fluorescent intensity was normalized to DMSO treated cells (Control). Data are presented as normalized fluorescent mean ± SEM of two independent biological repeats with ≥10000 cells. The level of significance between the indicated treatments determined as: *p<=0.05, **p<0.01, ***p<0.001.*

Conclusion

- We have developed first generation of novel platform for monitoring the degradation of exogenous semi-synthetic proteins in live cells.
- We employed SpyCatcher/SpyTag system to modify EGFP with VHL ligand and used the bead loading approach to deliver it to live cells and monitor its proteasomal degradation.
- Our platform should allow rapid examination of different E3 ligands, as well as to introduce caged E3 such as the photocleavable VHL and bioorthogonal PROTAC that were recently developed.

Further reading

1- **Mahdi Hasan**, Deepanjan Panda, Guy Mann and Ashraf Brik. "De novo Semi-Synthetic Platform for Monitoring Protein degradation in Live Cells." *ChemBioChem* 25.3 (2024): e202300731.

2- Guy Mann, Pradeep Sadhu, and Ashraf Brik. "Multiplexed Delivery of Synthetic (Un) Conjugatable Ubiquitin and SUMO2 Enables Simultaneous Monitoring of Their Localization and Function in Live Cells." *ChemBioChem* 23.11 (2022): e202200122.

3- Bijan Zakeri, Jacob O Fierer, Emrah Celik, Emily C Chittock, Ulrich Schwarz-Linek, Vincent T Moy, Mark Howarth. "Peptide tag forming a rapid covalent bond to a protein, through engineering a bacterial adhesin." *PNAS* 109(12) (2012), E690-E697.

Design of aptamer conjugates as monoclonal antibody mimics

Jordan Cossu[1], Océane Ricloux[1], Corinne Ravelet[1], Véronique Frachet[1], Eric Peyrin[1] and Didier Boturyn[1]

[1] University Grenoble-Alpes, 38058 Grenoble Cedex 9, France
didier.boturyn@univ-grenoble-alpes.fr ; eric.peyrin@univ-grenoble-alpes.fr

https://doi.org/10.17952/37EPS.2024.P1223

Introduction

- In the late 90's, monoclonal antibodies (mAbs) became a major tool for therapeutic purposes. However, some restrictions provided strong arguments for the development of alternative agents like aptamers that integrate the benefits of mAbs while circumventing these limits.
- We propose to design **small synthetic mimics** of Rituximab, which is used to treat some lymphomas by targeting the CD20 antigen.
- **DNA aptamers** were chosen as recognition elements because of their **low immunogenicity**, their **high affinity** for their target, their chemical **stability** and the fact that their production is carried out by organic synthesis. Among methods used to produce aptamers, CE-SELEX (capillary electrophoresis-systematic evolution of ligands by exponential enrichment) technique was preferred due to its multiple benefits such as less consumption of samples, natural binding environments, and a higher screening efficiency.

CD20 synthesis

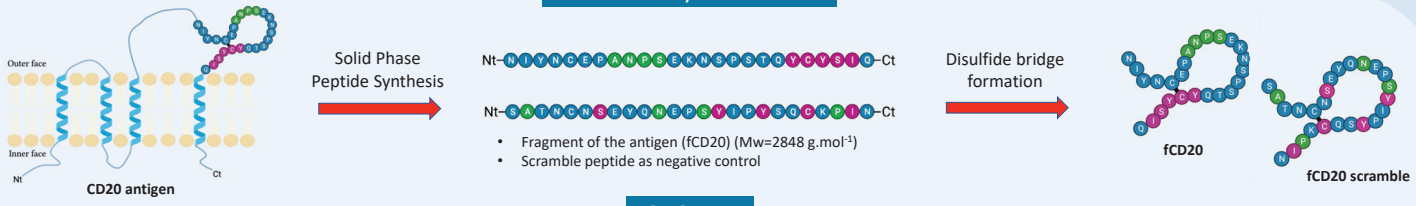

- Fragment of the antigen (fCD20) (Mw=2848 g.mol^{-1})
- Scramble peptide as negative control

CE-SELEX

Combination of a **separative method (CE)** and a **selection process (SELEX)**

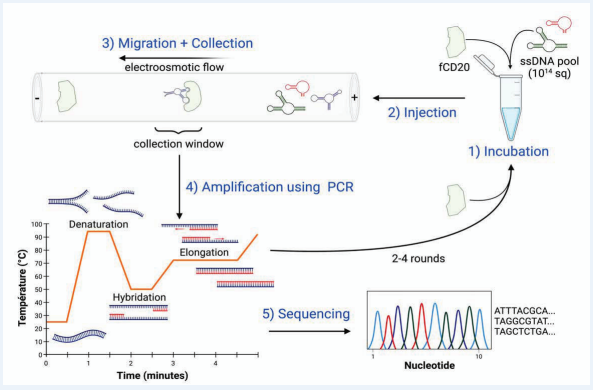

Schematic representation of the CE-SELEX process

Conditions for CE-SELEX process

Conditions	Round	[fCD20] (µM)	[ADN] (µM)	[fCD20]/[ADN]
TGK Buffer Tris 25 mM, Glycine 192 mM, KH_2PO_4 5 mM, **pH 8.3, 40 min**	1	1000	30	33.3
	2	0.5	0.17	3
	3	0.3	1	0.3
	4	0.03	1	0.03

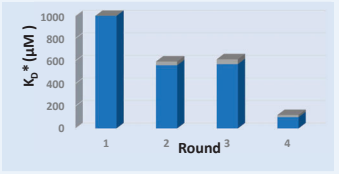

* Estimated dissociation constants (K_D) were calculated on one point from the decrease of the unbound DNA fractions

Dissociation constant (K_D) evaluated after each round of CE-SELEX

After sequencing, **two aptamers were selected** through CE-LIF analyses

Fragmentation from 2D structures

- **Secondary structures for Aptamer 1 and 2** simulated using mFold.
- **Three fragments** were designed.

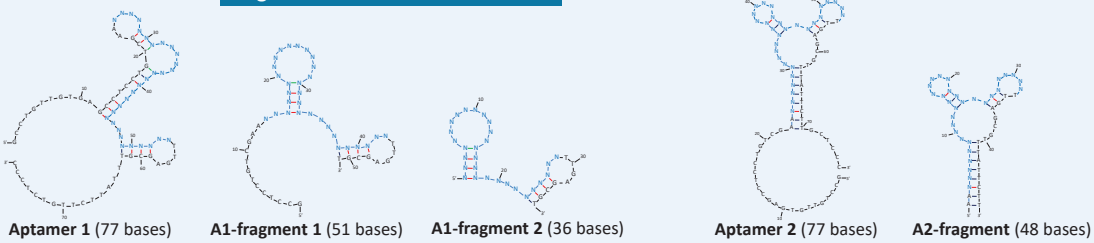

Aptamer 1 (77 bases) **A1-fragment 1** (51 bases) **A1-fragment 2** (36 bases) **Aptamer 2** (77 bases) **A2-fragment** (48 bases)

Isothermal Titration Calorimetry

	fCD20			fCD20 scramble		
Analyte	K_D (µM)	N (sites)	c	K_D (µM)	N (sites)	c
Apta 1	6.4 ± 0.9	0.86 ± 0.01	20.1	N/D	N/D	N/D
Apta 2	1.2 ± 0.2	1.49 ± 0.01	194	N/D	N/D	N/D
Apta 1-F1	9.0 ± 2.4	0.88 ± 0.02	14.7	> mM	N/D	N/D
Apta 1-F2	18.9 ± 3.3	1.07 ± 0.03	8.5	> mM	N/D	N/D
Apta 2-F	5.5 ± 1.3	1.46 ± 0.03	39.8	> mM	N/D	N/D

- The shrinking of the length led to a slight decrease of the affinity.
- The specificity remains high for the fCD20.

Flow cytometry

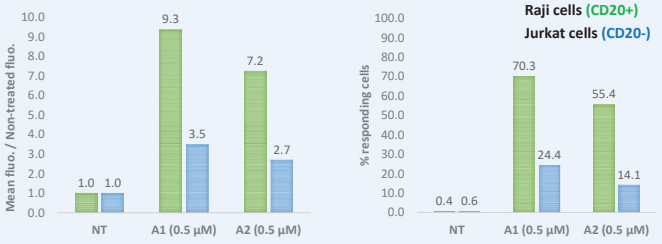

Mimic Design

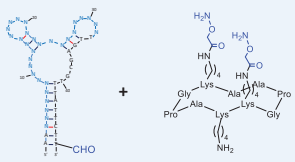

To improve the affinity of the selected compounds, multivalent systems will be designed using cyclopeptides as scaffolds. Up to 4 aptamers and a fluorophore or cytotoxic agent will be then grafted through chemical ligations.

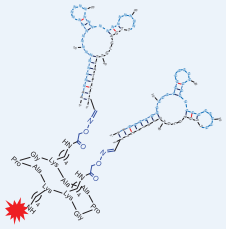

In vitro, in vivo tests



Summary and Outlook

- The first part of this project enabled us to select two aptamers with a suitable affinity (1-5 µM) and a high selectivity for the CD20 antigen.
- From their 2D structures, three fragments were designed and characterized. Similar affinities were found with high selectivity.
- *In cellulo* tests using flow cytometry were performed with the full aptamers showing promising results.
- In parallel, we started the synthesis of dimers using peptide scaffolds to assess multivalent effects.

Reference

J. Cossu, C. Ravelet, V. Martel-Frachet, E. Peyrin, D. Boturyn, Bioorganic & Medicinal Chemistry (**2024**)
DOI: https://doi.org/10.1016/j.bmc.2024.117831

Proceedings of the 37th European Peptide Symposium
Michal Lebl, Editor
European Peptide Society, 2024 *http://doi.org/10.17952/37EPS.2024.P1224*

Conjugates containing homing peptide, cell penetrating peptide and a cytostatic or marker potentially useful in the diagnosis or treatment of lung cancer diseases

Piotr Jedrzejczak[a], Anna Gajda[a], Justyna Fraczyk[a], Beata Kolesinska[a]

[a]*Institute of Organic Chemistry, Łódź University of Technology, Żeromskiego 116, 90-924 Lodz, Poland*

Introduction

Lung cancer causes 23% of total cancer deaths worldwide. It is the most deadly cancer, with minimal survival. There are two known forms: non-small cell lung cancer (NSCLC) (85% of cases) and small cell lung cancer (SCLC). NSCLC is sensitive to chemotherapy; however, response varies depending on the specific therapy [1]. Oral administration of anticancer chemotherapeutic agents is often limited by first-pass metabolism. Furthermore, due to their non-targeted nature, most chemotherapeutic agents act on normal tissues, leading to adverse effects. Despite this, classical chemotherapy is used in more than 70% of patients [2]. The chemotherapy drugs used are [3]: antimetabolites (capecitabine, floxuridine, methotrexate), alkylating agents (cisplatin, carboplatin), mechlorethamine, cyclophosphamide or mitomycin C), anitimicrotubule drugs (vinca alkaloids and taxanes), topoisomerase inhibitors (etoposide, doxorubicin, mitoxantrone, novobiocin). In recent years, two groups of drugs have been introduced to the treatment of lung cancer: molecularly targeted and immunotherapy drugs. Most clinically approved therapeutic mAbs are molecularly targeted therapies, they act passively by blocking the activity of receptors or activating the immune system [4]. mAbs have limitations such as nonspecific clearance of antibodies by the reticuloendothelial system which may lead to accumulation of antibody-conjugated drugs or toxins in undesirable sites [5]. Several types of tumor-targeting ligands have been developed, including antibodies, antibody fragments, polypeptides, small molecules, and others [6]. Peptides are an attractive alternative to antibody-based targeted therapies. Unlike antibodies, peptides are easy to synthesize in large quantities [7], and their smaller size improves tissue penetration while preventing nonspecific uptake by the reticuloendothelial system. In addition, peptides can be chemically modified to alter affinity, charge, hydrophobicity, stability, and solubility, and can be optimized for in vivo use through modification. Importantly, peptides can exhibit antibody-like affinity for receptors. The aim of the research is to develop methods for the synthesis of peptide conjugates that determine selective interaction with improve transport to the cell, as well as a compound with anticancer activity.

Results and discussion

Altretamine, a derivative of 1,3,5-triazine, is an anticancer drug. The structure of altreamine was modified by using other secondary amines and by adding a peptide that penetrates cell membranes. The syntheses began with obtaining penetrating peptides using the solid-phase synthesis strategy and obtaining monosubstituted dichlorotriazine derivatives. A quaternary N-triazinylammonium salt was used as the coupling reagent [8]. Then, monosubstituted

 http://doi.org/10.17952/37EPS.2024.P1224

dichlorotriazine derivatives (substituted with a methoxy group or an appropriate amino group) were attached to the obtained peptides on the solid phase.

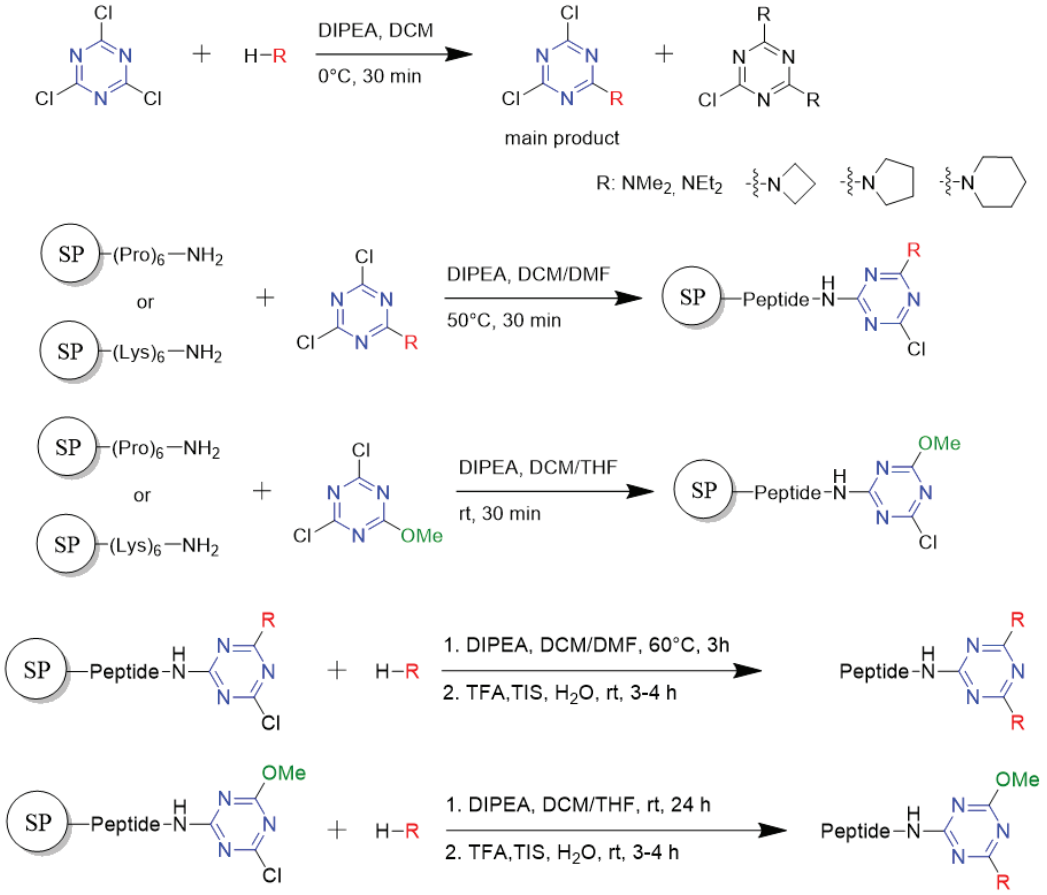

Fig. 1 Scheme for the synthesis of 1,3,5-triazine derivatives containing CPP attached to the triazine ring.

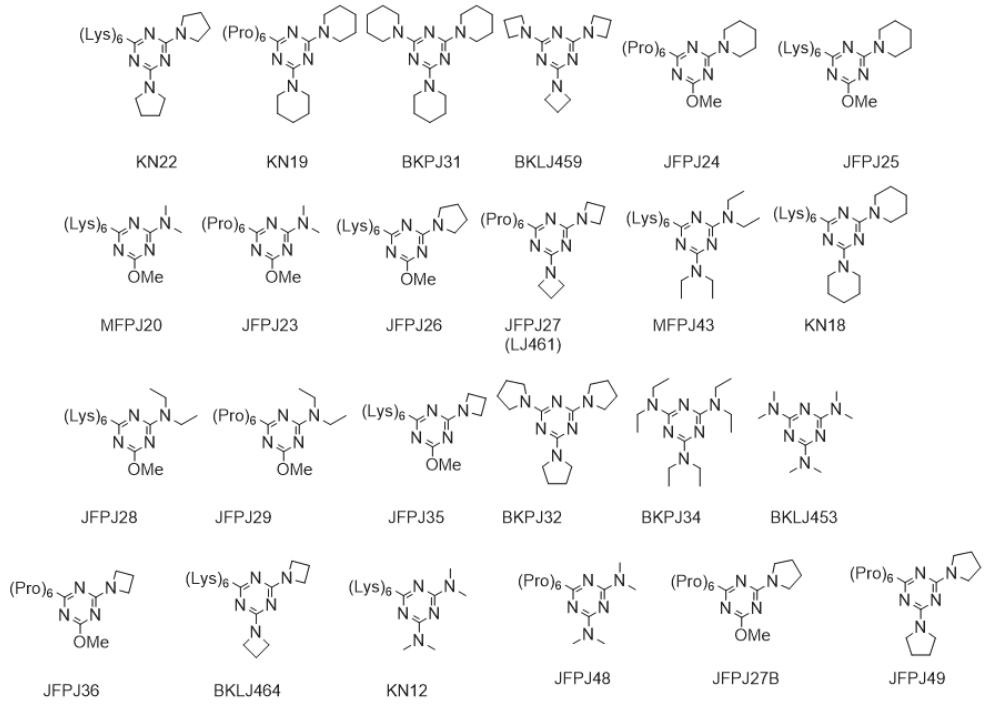

Fig. 2 Structures of the obtained 1,3,5-triazine derivatives (altretamine analogues) with CPP attached to the triazine ring.

 http://doi.org/10.17952/37EPS.2024.P1224

The final stage of the synthesis was the substitution of the last chlorine atom with an amino group and the cleavage of the compound from the solid phase. In total, 19 new compounds and aminoalkyl derivatives of 1,3,5-triazine were obtained, including altretamine as a standard.
In the final stage, the effect of the obtained compounds on A549 cells (non-small cell lung cancer, NSCLC) was assessed and the energy of interaction of the compounds with the EGF receptor was determined.

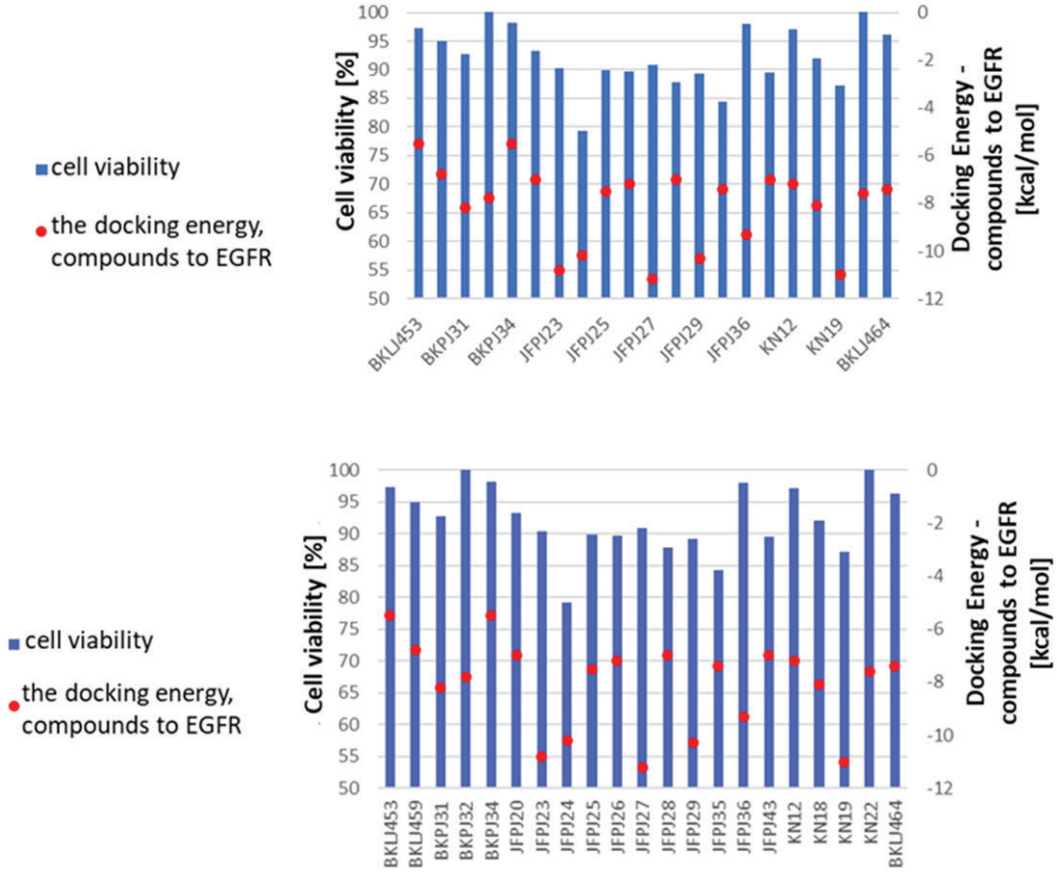

Fig. 3 The results of biological tests on the A549 cell line (NSCLC) and the calculated energy of interaction of compounds with the EGF receptor.

The biological studies carried out indicate the potential of the obtained compounds. However, due to the lack of specificity of CPP, it will be necessary to introduce an additional peptide fragment increasing the specificity towards cancer cells.

Conclusions

The results from first biological tests show increase in activity compared to control (altretamine). Further biological studies are carried out now to better characterize the obtained compounds.

Literature

[1] Jemal, A., Bray, F., Center, M.M., Ferlay, J., Ward, E., Forman, D.(2011) Global cancer statistics. *CA Cancer J. Clin.* 61, 69-90. doi: 10.3322/caac.20107.
[2] Gajarawala, S.N., Pelkowski, J.N. (2021) Telehealth Benefits and Barriers. *J. Nurse Pract*. 17, 218-221. doi.org/10.1016/j.nurpra.2020.09.013
[3] Zia, M.K., Siddiqui, T., Ali, S.S., Rehman, A.A., Ahsan, H., Khan, F.H. (2018) Chemotherapeutic Drugs and Plasma Proteins: Exploring New Dimensions. *Curr. Protein Pept. Sci*. 19, 937-947. doi.org/10.2174/1389203718666171002115547.
[4] Reichert. J.M. Valge-Archer, V.E. (2007) Development trends for monoclonal antibody cancer therapeutics. *Nat. Rev. Drug Discov*. 6, 349-56. doi: 10.1038/nrd2241.

 http://doi.org/10.17952/37EPS.2024.P1224

[5] Tabrizi, M.A., Tseng, C.-M.L., Roskos, L.K. (2006) Elimination mechanisms of therapeutic monoclonal antibodies. *Drug Discov. Today* 11, 81-88. doi: 10.1016/S1359-6446(05)03638-X.
[6] Raucher, D. (2019) Tumor targeting peptides: novel therapeutic strategies in glioblastoma. Curr. Opin. Pharmacol. 47, 14-19. doi: 10.1016/j.coph.2019.01.006.
[7] Bray, B.L. (2003) Large-scale manufacture of peptide therapeutics by chemical synthesis. *Nat. Rev. Drug Discov*. 2, 587-593. doi: 10.1038/nrd1133.
[8] Kolesinska, B., Rozniakowski, K.K., Fraczyk, J., Relich, I., Papini, A.M., Kaminski, Z.J. (2015) The Effect of Counterion and Tertiary Amine on the Efficiency of N-Triazinylammonium Sulfonates in Solution and Solid-Phase Peptide Synthesis. *Eur. J. Org. Chem*. 401-408. doi: 10.1002/ejoc.201402862.

https://doi.org/10.17952/37EPS.2024.P1225

Development of novel amphipathic stapled peptides as DDS carriers for intracellular delivery of nucleic acids

○Motoharu Hirano[1,2], Hidetomo Yokoo[2], Makoto Oba[3], Takashi Misawa[2], Yosuke Demizu[1,2]

1. Grad. Sch. Med. Life. Sci., Yokohama City Univ., 2. NIHS, 3. Kyoto Pref. Univ. Med.

01. Introduction

Messenger RNA (mRNA) has no risk of insertion into the host genome, and can express any encoded protein in the cell. Furthermore, small interfering RNA (siRNA) can target genes that cannot be targeted by conventional small molecule drugs and can suppress gene expression in a sequence-dependent manner through RNA interference. Therefore, nucleic acids such as mRNA and siRNA are expected to be next-generation modalities. However, nucleic acids are difficult to permeate cell membranes by themselves due to their high hydrophilicity and large molecular size. Therefore, it is important to develop drug delivery system (DDS) carriers that transport nucleic acids into cells, and cell-penetrating peptides (CPPs) have attracted attention as one of promising carriers.



	pDNA	mRNA	siRNA
Structure	Circular, Double-stranded DNA	Single-stranded RNA	Double-stranded RNA
Base pair	2~200K	~100	20~25
Function	-	Protein expression	mRNA degradation

02. Purpose

We have focused on magainin 2 (**Mag2**), a naturally occurring amphipathic antimicrobial peptide (AMP), and have developed helix-stabilized **Mag2** derivatives containing non-proteinogenic amino acids.[1,2] Because AMPs are capable of intracellular trafficking, they have potential applications as intracellular transport molecules for nucleic acids. In this study, we aimed to develop novel CPPs based on **Mag2** that efficiently transports several types of nucleic acids, such as pDNA, mRNA, and siRNA, into the cell.

1) M. Hirano *et al.*, *ChemPlusChem* **2020**, *85*, 2731-2736; 2) M. Hirano *et al.*, *Molecules* **2021**, *26*, 444.

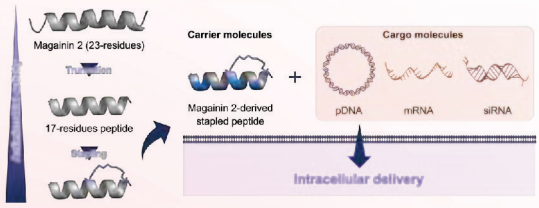

03. Design and Synthesis of Peptide

S5 = (*S*)-2-(4-Pentenyl)alanine, R8 = (*R*)-2-(7-Octenyl)alanine

Peptide	Sequence	Peptide	Sequence
Mag2	H-GIGKFLHSAKKFGKAFVGEIMNS-NH2	st7-1	H-R8*IKKFLKS5*AKKFVKAFK-NH2
Pep-1	H-GIKKFLKSAKKFVKAFK-NH2	st7-2	H-GR8*KKFLKSS5*KKFVKAFK-NH2
st4-1	H-S5*IKKS5*LKSAKKFVKAFK-NH2	st7-3	H-GIKKR8*LKSAKKS5*VKAFK-NH2
st4-2	H-GS5*KKFS5*KSAKKFVKAFK-NH2	st7-4	H-GIKKFR8*KSAKKFS5*KAFK-NH2
st4-3	H-GIKKS5*LKSS5*KKFVKAFK-NH2	st7-5	H-GIKKFLKR8*AKKFVKS5*FK-NH2
st4-4	H-GIKKFLKS5*AKKS5*VKAFK-NH2	st7-6	H-GIKKFLKSR8*KKFVKAS5*K-NH2
st4-5	H-GIKKFLKSS5*KKFS5*KAFK-NH2	Pep-1_R	H-GIRRFLRSARRFVRAFR-NH2
st4-6	H-GIKKFLKSAKKS5*VKAS5*K-NH2	st7-5_R	H-GIRRFLRR8*ARRFVRS5*FR-NH2

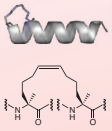



04. Intracellular Delivery of plasmid DNA (pDNA)

N/P ratio: Ratio of positive charge of peptide side chain to negative charge derived from nucleic acid.

(A) Transfection efficiency of pDNA

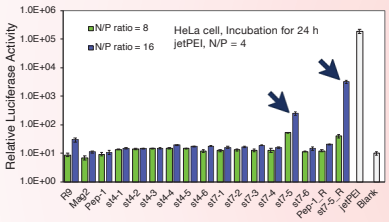

(B) The peptide/pDNA complex size and zeta-potential, gel shift

Peptide	N/P	Size (nm)	PDI (μ/Γ²)	Zeta-potential (mV)
R9	8	357.5 ± 0.3	0.21 ± 0.01	22.1 ± 0.3
	16	188.7 ± 0.7	0.19 ± 0.01	25.8 ± 0.2
st7-5	8	1522.0 ± 39.0	0.61 ± 0.02	23.4 ± 0.1
	16	234.0 ± 2.1	0.27 ± 0.02	25.6 ± 0.1
st7-5_R	8	352.2 ± 4.1	0.28 ± 0.00	22.3 ± 0.3
	16	125.1 ± 0.2	0.20 ± 0.01	27.0 ± 0.3

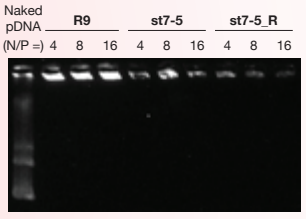

- ✓ The stapled peptide **st7-5_R** most efficiently introduced pDNA into the cell.
- ✓ **st7-5_R** formed the smallest complex with pDNA.

(C) Intracellular uptake of Cy5-labelled pDNA

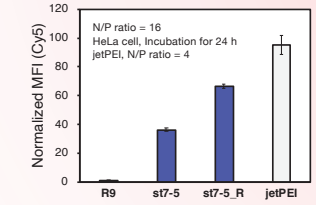

(D) Fluorescence microscopy images

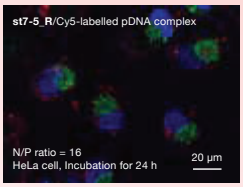

Red: Cy5-laballed pDNA, Blue: Nuclear, Green: Lysosome

(E) Intracellular uptake pathway of complex

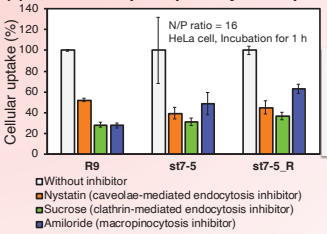

- ✓ The **st7-5_R**/pDNA complex was efficiently taken up into the cells.
- ✓ The **st7-5_R**/pDNA complex was suggested to enter the cell via multiple endocytosis pathways.

05. Intracellular Delivery of mRNA

(A) Transfection efficiency of mRNA

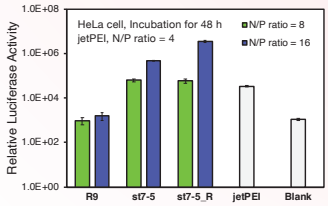

(B) The peptide/mRNA complex size and zeta-potential, gel shift

Peptide	N/P	Size (nm)	PDI (μ/Γ²)	Zeta-potential (mV)
R9	8	257.0 ± 2.5	0.28 ± 0.04	17.3 ± 2.2
	16	177.7 ± 28.8	0.48 ± 0.04	23.5 ± 3.4
st7-5	8	380.4 ± 16.2	0.35 ± 0.01	18.4 ± 0.6
	16	211.3 ± 3.2	0.39 ± 0.07	12.8 ± 1.8
st7-5_R	8	259.3 ± 13.1	0.39 ± 0.03	21.6 ± 1.3
	16	158.3 ± 47.4	0.50 ± 0.10	15.3 ± 1.6

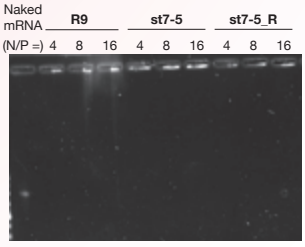

- ✓ **st7-5_R** transported mRNA into the cell more efficiently than other peptides.
- ✓ **st7-5_R** formed a small complex with mRNA.

06. Intracellular Delivery of siRNA

(A) Transfection efficiency of siRNA

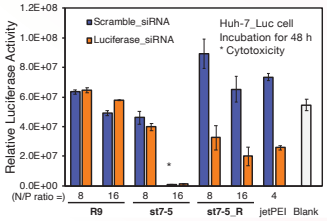

(B) The peptide/siRNA complex size and zeta-potential, gel shift

Peptide	N/P	Size (nm)	PDI (μ/Γ²)	Zeta-potential (mV)
R9	8	849.8 ± 6.5	0.35 ± 0.04	25.6 ± 0.3
	16	690.6 ± 8.7	0.20 ± 0.01	27.9 ± 0.7
st7-5	8	320.0 ± 4.7	0.34 ± 0.03	18.9 ± 0.5
	16	284.8 ± 21.1	0.43 ± 0.00	21.7 ± 1.1
st7-5_R	8	290.4 ± 6.7	0.33 ± 0.01	27.9 ± 1.1
	16	304.0 ± 5.7	0.42 ± 0.04	27.5 ± 2.1

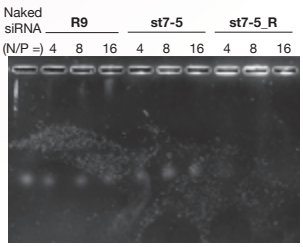

- ✓ **st7-5_R** delivered siRNA into the cell and suppressed luciferase expression.
- ✓ **st7-5_R** formed a small complex with siRNA.

07. Summary

- ◆ We designed and synthesized stapled peptides based on **Mag2** for the intracellular delivery of nucleic acids.
- ◆ The stapled peptide **st7-5_R** formed a small complex with pDNA and achieved efficient intracellular transport.
- ◆ The **st7-5_R**/pDNA complex was internalized into the cell by multiple endocytic pathways, independent of any specific pathway.
- ◆ **st7-5_R** also formed complexes with mRNA and siRNA to achieve their efficient intracellular transport.

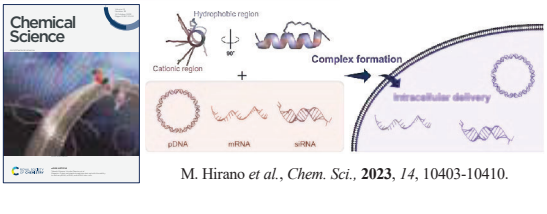

M. Hirano *et al.*, *Chem. Sci.*, **2023**, *14*, 10403-10410.

Development of selective peptide-based radiopharmaceuticals for targeted therapy and diagnosis of high malignant cancers

Anna Giorgio,[1,2] Nicola Salvarese,[3] Annarita Del Gatto,[2] Michele Saviano,[4] Cristina Bolzati,[3] and Laura Zaccaro[2]

[1]DiSC - University of Padua, Padova; [2]IBB-CNR, Napoli; [3]ICMATE-CNR, Padova; [4]IC-CNR, Bari.

anna.giorgio@phd.unipd.it.

https://doi.org/10.17952/37EPS.2024.P1227

RGDechi peptide derivatives can be considered interesting candidates as non-invasive diagnostic tracers in tumor imaging.

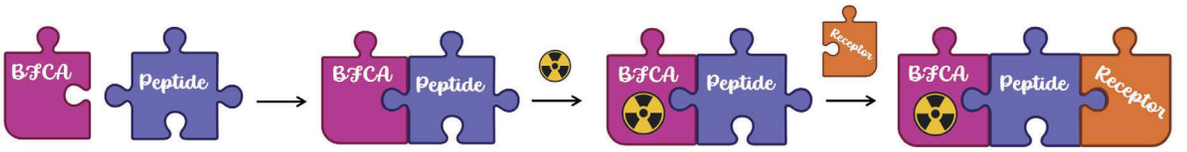

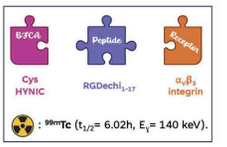

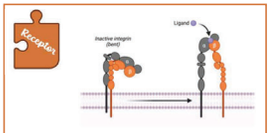

Integrins are heterodimeric trans-membrane glycoproteins composed of noncovalently associated α and β subunits.

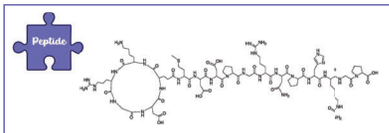

Properties[1,2,3,4]

- antiangiogenic activity;
- antiadhesive effect;
- antiproliferative effect;
- pro-apoptotic effect on human malignant melanoma cells.

$RGDechi_{1-17}$ is a bifunctional chimeric peptide composed of a cyclic RGD containing pentapeptide covalently linked by a spacer to an echistatin domain. This peptide can selectively modulate $\alpha_v\beta_3$ function, which is highly expressed in activated endothelial cells and in many solid tumors (e.g. melanomas).

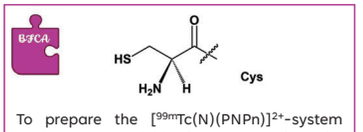

To prepare the $[^{99m}Tc(N)(PNPn)]^{2+}$-system conjugate to $RGDechi_{1-17}$ peptide, the labeling approach exploited involved the use of a Cys as a bifunctional chelating agent (BFCA), conjugated on Lys1 side chain.

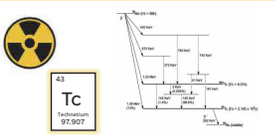

Technetium-99m ($t_{1/2}$=6.02 h, E_γ=140 keV) is the workhorse radionuclide in Nuclear Medicine for SPECT applications.

RADIOSYNTHESIS

$RGDechi_{1-17}$ peptide was prepared via solid-phase peptide synthesis. Exploiting the $[^{99m}Tc(N)(PNPn)]^{2+}$-technology,[5,6,7] a Cys residue was coupled on the side chain of Lys1, obtaining $RGDechi_{1-17}$-Cys, affording the final monocationic complex.[8]
Moreover, both the molecular weight and lipophilicity of the radiolabeled peptides were easily modified by varying substituents of the P atoms of PNP (Figure 1).

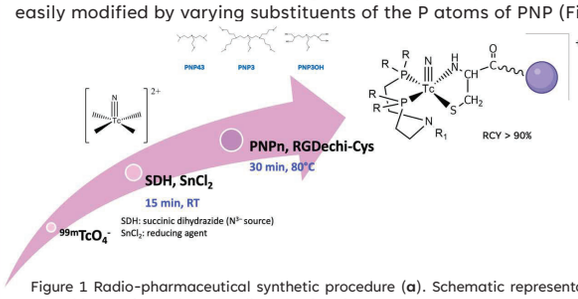

Complex	
$[^{99m}Tc(N)(RGDechi_{1-17}\text{-}Cys)PNP43]^+$	^{99m}**Tc1**
$[^{99m}Tc(N)(RGDechi_{1-17}\text{-}Cys)PNP3]^+$	^{99m}**Tc2**
$[^{99m}Tc(N)(RGDechi_{1-17}\text{-}Cys)PNP3OH]^+$	^{99m}**Tc3**

Table 1 – Radiolabeled peptides synthesized.

Figure 1 Radio-pharmaceutical synthetic procedure (**a**). Schematic representation of the PNP (PNP: bis-phosphino-amine) selected as ligands of Tc (**b**).

IN VITRO STUDIES

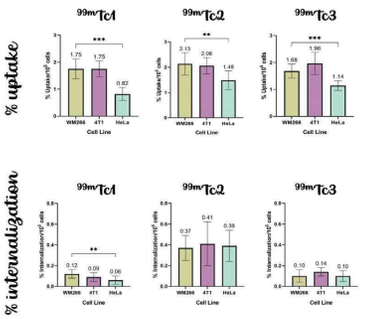

Preliminary studies were carried out incubating ^{99m}**Tc1-3** with $\alpha_v\beta_3$ overexpressing cell lines WM-266-4 (metastatic human melanoma) and 4T1 (breast cancer), and HeLa cells as control (Figure 5).
The radiolabeled peptides possess an almost similar accumulation profile showing a specific uptake in $\alpha_v\beta_3$-positive cells, which was dependent on the nature of $[^{99m}Tc(N)(PNPn)]$-synthon. ^{99m}**Tc1** seems to give the best results.

Figure 5 – Cells studies of ^{99m}**Tc1-3**. The cell uptakes were assessed in suspensions at 37 and 4°C. Data are expressed as percentage cell uptake of the total activity on 10^6 cells. Experiments were performed in triplicate.

STABILITY STUDIES AND METABOLITE IDENTIFICATION

Stability studies on radiolabeled peptides showed that they are stable in cell culture media, human and murine sera and after incubation in murine liver homogenate. Different behavior was detected after the exposure of ^{99m}**Tc1** to Mouse Kidney Homogenate (MKH): HPLC chromatogram collected after only 15 min incubation clearly shows a significant peak shifting.

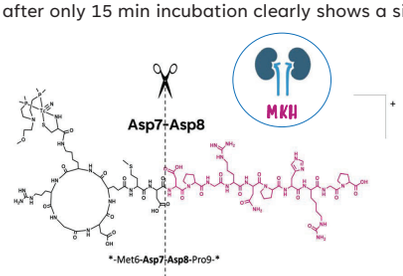

Figure 2 – Schematic representation of the enzymatic cleavage site observed after MKH exposure.

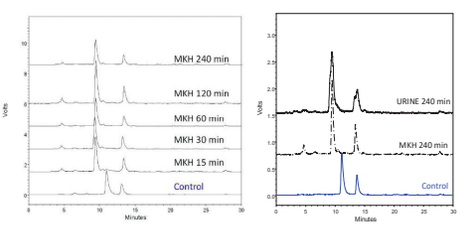

Figure 3 – Radio-HPLC of ^{99m}**Tc1** before and after incubation in MKH (left) and in murine urine sample (right).

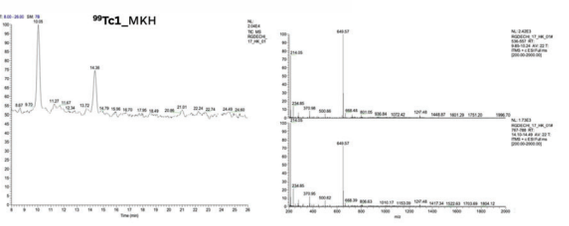

Figure 4 –LC-MS profiles of ^{99}**Tc1** after 1h of incubation, at 37°C, in MKH.

LC-ESI-MS analyses revealed for the two peaks (syn and anti isomers) a similar pattern consisting in a double-charged ion at m/z 649.96 (Figure 4), corresponding to a fragment that lacks the portion starting from Asp8 (Figure 2).

STABILIZATION OF RADIO-PEPTIDE

Given this result, Asp7 residue was replaced by α-methyl-L-Aspartic acid. $RGDechi_{1-17}$(αMeAsp7)-Cys peptide (^{99m}**Tc4**) was synthesized and characterized. Also, this peptide undergo biotransformation after incubation with MKH, but after 1h and not after only 15 minutes.

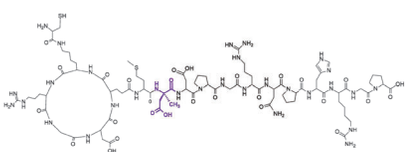

Figure 5 – Schematic representation of ^{99m}**Tc4**.

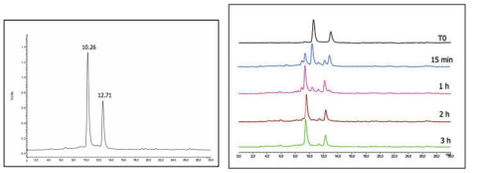

Figure 6 – Radio-HPLC of ^{99m}**Tc4** after purification (left) and before and after incubation in MKH (right).

IN CONCLUSION ...

^{99m}**Tc1–3** can selectively bind $\alpha_v\beta_3$ integrin and not to cross-react with $\alpha_v\beta_5$.
A cleavage site, common for different peptides, was identified between the Asp7 and Asp8 as a site of enzymes present in circulation and highly expressed in kidneys. The information collected from metabolism studies should be utilized to design, synthesized and characterized a more stable derivative, ^{99m}**Tc4,** in order to improve bioavailability and accumulation at tumor site.

The authors acknowledge AIRC for financial support (AIRC, IG2020 ID 24528)

References:

1. Del Gatto et al. 2006. *Journal of medicinal chemistry*, 49(11), 3416-3420. **2.** Santulli et al. 2011. *Journal of translational medicine*, 9(1), 1-10. **3.** Pisano et al. 2013. *Anticancer research*, 33(3), 871-879. **4.** Capasso et al. 2014. *PLoS One*, 9(9), e106441. **5.** Bolzati et al. 2002. *J. Am. Chem. Soc.*, 124, 11468-11479. **6.** Boschi et al. 2001. *Bioconj. Chem.*, 12, 1035-1042. **7.** Bolzati et al. 2018. *J Med Chem.*, 61, 9596-9611. **8.** Bolzati et al. 2018. Journal of medicinal chemistry, 61(21), 9596-9610.

https://doi.org/10.17952/37EPS.2024.P1228

Control of biological processes using metallopeptides

Jéssica Rodríguez

Universidade da Coruña, CICA–Centro Interdisciplinar de Química e Bioloxía, Rúa as Carballeiras, 15071, A Coruña, Spain

jessica.rodriguez.villar@udc.es

SUMMARY We have relied on transition metal chemistry to develop new tools for the controlled, specific recognition of DNA. We describe the potential of using nickel complexes as tethering coordination systems to promote DNA recognition and the use of a Pd-mediated cleavage to modulate the DNA-binding of a dimeric peptide.

Nickel-promoted DNA binding

1. Previous work

GCN4 TF binds to its consensus DNA as a homodimer of uninterrupted α-helices. Whereas an isolated basic region peptide fails to interact with its consensus DNA, we have shown that conjugation to an AT-hook anchor, allows the specific recognition of composite DNA sites featuring the binding sequences of the GCN4br and the AT-hook in tandem.

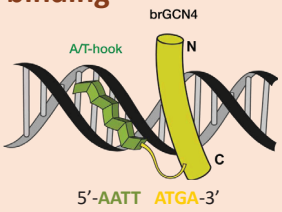

Chem. Sci., **2015**, 6, 4767.

2. Design of the metal-chelating peptide

We envisioned that incorporating a metal-chelating bipyridine moiety at the N-terminus of the fully peptidic GCN4br/AT-hook conjugate might allow, in the presence of an appropriate metal, the trapped of a designed GCN4br mutant featuring two coordinating histidines (**brHis$_2$**) and bind a cognate target DNA site with an extended palindromic TCAT-A$_2$T$_2$-ATGA sequence.

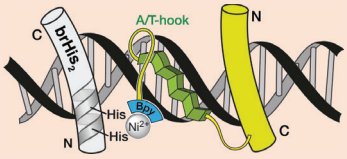

GCN4br: DPAAL KRARNTEAARRSRARKLQR
brHis$_2$: DPAA**H**KRA**H**NTEAARRSRARKLQR
brK: DPAAL KRARNTEAARRSRA**K**KLQR
AT-hook: KPRGRPKK

3. DNA binding properties

Incubation of **brk** with its consensus DNA, induces the formation of a retarded band corresponding to the expected DNA-peptide complex. Addition of Ni(ClO$_4$)$_2$ to this mixture does not generate new retarded bands, but subsequent addition of the metal-chelating **brHis$_2$** gives rise to a new, more retarded band that must correspond to the desired ternary complex.

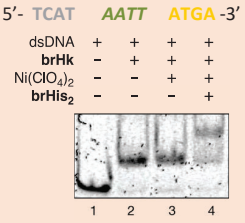

The key role of the Ni(II) ion prompted us to examine the possibility of disassembling the [(**brHis$_2$**)(**brK**)Ni]$^{2+}$/DNA complex by using an external chelator: addition of EDTA to the preformed metallosupramolecular complex with the consensus DNA promoted the disassembly of the complex. CD also showed a decrease in the degree of helicity.

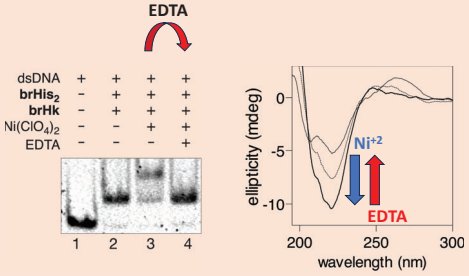

4. Conclusions

We have introduced a new approach for achieving a conditional and selective trivalent recognition of a long 12 base-pair DNA site. The strategy involves the nickel-promoted assembly of a supramolecular DNA binder

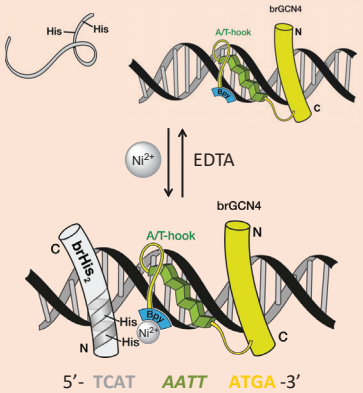

J. Rodríguez *et al., Chem. Eur. J.* **2016**, *22*, 13474.

Pd-mediated deactivation of DNA binding

1. Previous work

The leucine zipper in the GCN4 TF can be replaced by other dimerizing agents without significantly altering the DNA binding properties.

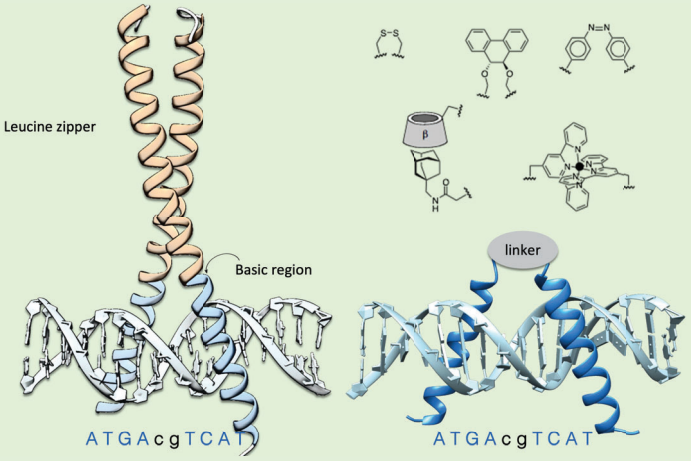

2. Synthesis of the dimer Pr(brC)$_2$

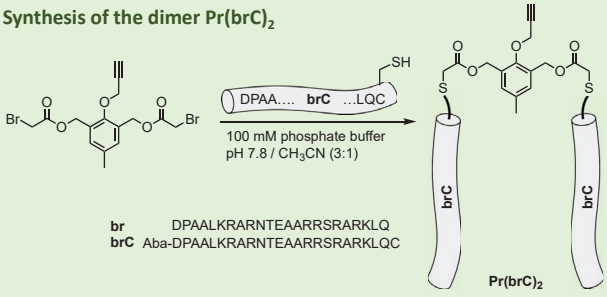

br DPAALKRARNTEAARRSRARKLQ
brC Aba-DPAALKRARNTEAARRSRARKLQC

3. DNA binding properties

When a ds-oligonucleotide containing the target ATF/CREB site was incubated with increasing concentrations of **Pr(brC)$_2$**, we observed the appearance of a new retarded band consistent with the formation of a specific DNA/**Pr(brC)$_2$** complex.

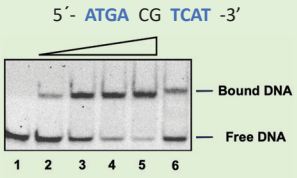

4. Palladium-promoted cleavage

When the **Pr(brC)$_2$**-DNA complex was treated with [Pd(allyl)Cl]$_2$ (**Pd1**) for 3 h, we observed the disappearance of most of the retarded band corresponding to the **Pr(brC)$_2$**-DNA complex (lanes 4-5). A control experiment with the disulfide dimer **(brGCC)$_2$** revealed that the DNA binding is retained after incubation with **Pd1** (lanes 2-3), which confirms that the cleavage/disassembly sequence only occurs with our responsive peptide dimer.

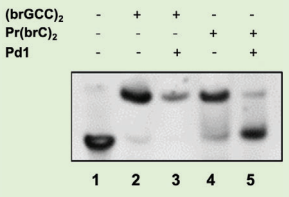

5. Conclusions

We describe the on-demand disassembly of dimeric peptides using a Pd-mediated cleavage of a designed self-immolative linker.

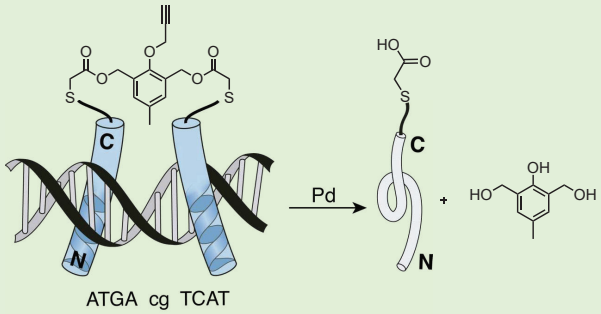

J. Rodríguez *et al., RSC Advances*, **2022**, *12*, 3500.

Acknowledgements. RYC2022-035154-I funded by MICIU/AEI/10.13039/501100011033 and by FSE+; PID2023-146174NA-I00 funded by MICIU/AEI/10.13039/501100011033 and by FEDER, UE.

https://doi.org/10.17952/37EPS.2024.P1229

pH-Dependent Cellular Uptake of CPPs – Guanidinium versus Oxyguanidinium Proline

Rahel Heeb, Laura Massaad, Helma Wennemers*
Laboratory of Organic Chemistry, ETH Zurich

Introduction

The delivery of bioactive molecules across cellular membranes represents a significant obstacle to developing protein and nucleic acid-based therapies. Cell penetrating peptides (CPPs) are attractive tools to transport such cargo across the cellular membrane.[1] Our group showed that rigid cationic oligo guanidinium proline (Gup_8) peptides exhibit higher cellular uptake in comparison to previously established flexible peptides (e.g., octa arginine).[2] Key to their high cellular uptake is their rigidity and charge arrangement in distances of ~9 Å along the PPII helical backbone, which enables tight ionic interactions between the cationic guanidinium prolines and anionic cell surface glycans. Building on this work, we developed a CPP analogue in which the guanidinium prolines were replaced with oxyguanidinium prolines (Gop).[3] We studied the conformational properties of Gop derivatives and the cellular uptake in normal versus acidic cancer cell microenvironments.[4]

Guanidinium versus Oxyguanidinium Proline

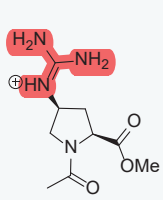

Ac-Gup-OMe
p*Ka* > 12

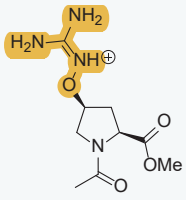

Ac-Gop-OMe
p*Ka* ~ 6.8

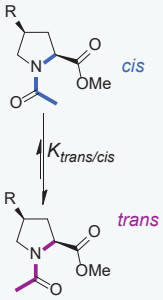

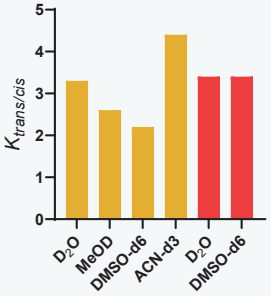

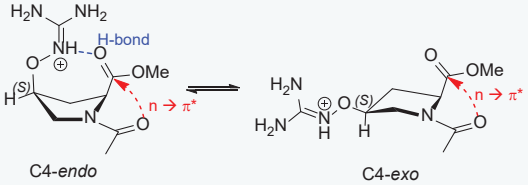

	acidic pH	basic pH
Ac-Gop-OMe	C4-*endo*	C4-*exo*
Ac-Gup-OMe	C4-*endo*	C4-*endo*

Structural Analysis of Octamers

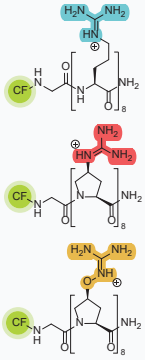

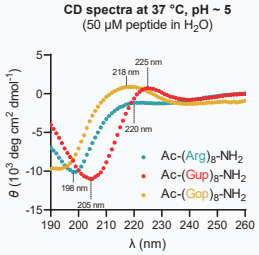

Ac-$(Arg)_8$-NH_2: "Random Coil"
Ac-$(Gup)_8$-NH_2: PPII helix
Ac-$(Gop)_8$-NH_2: PPI & shifted PPII helix

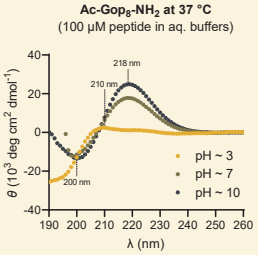

Acidic pH: Mixture of PPI and PPII helix
Basic pH: *Exo*-pucker and PPII helix with substituents pointing to the outside

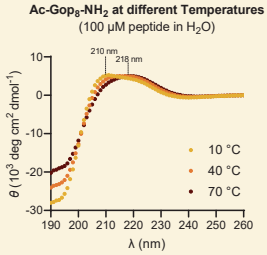

Higher temperature favours the PPII over the PPI helix

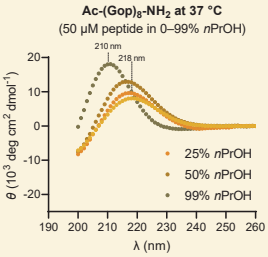

*n*PrOH favours the PPI helical conformation

Cellular Uptake Studies

Flow Cytometry

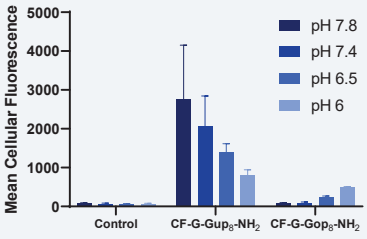

HeLa cells, 1 h, 37 °C, 5% CO_2, 10 µM

Ac-$(Gup)_8$-NH_2: lower uptake upon lowering the pH – cell surface charge change or inhibition of uptake mechanism

Ac-$(Gop)_8$-NH_2: higher uptake upon lowering the pH – protonation state of the peptide

Confocal Microscopy

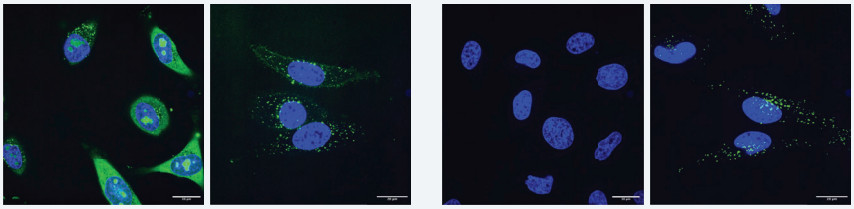

CF-G-Gup_8-NH_2 pH 7.5 | CF-G-Gup_8-NH_2 pH 6 | CF-G-Gop_8-NH_2 pH 7.5 | CF-G-Gop_8-NH_2 pH 6

HeLa cells, 1 h, 37 °C, 5% CO_2, live cells, 10 µM; green channel = CF-peptide, blue channel = Hoechst 33342 nucleus stain

Conclusion and Outlook

- Oxyguanidinium proline was introduced as an analogue of guanidinium proline
- The p*Ka* of Gop is 6.8, making it more than 10^5-fold more acidic than Gup
- The pucker of Gop depends on the pH
- The conformation of the Gop_8 depends on the pH, temperature and solvent
- Our findings render Gop-peptides promising as a tumour tissue specific delivery system

References

[1] P.A. Wender *et al.*; *Adv. Drug Deliv. Rev.* **2008**, *60*, 452-472
[2] Nagel, Y. A.; Raschle, P. S.; Wennemers, H.; *Angew. Chem. Int. Ed.* **2017**, *56*, 122–126
[3] For a study with canavanine, see: Calabretta, L. O., Thomas, V.M.; Raines R.T.; *Tetrahedron Lett.*, **2022**, *99*, 153848
[4] Riemann, A.; Reime, S.; Thews, O.; *Neoplasie*, **2017**, *19*, 1033-1042

Follow us:

Rahel Heeb | Wennemers group

D CHAB

https://doi.org/10.17952/37EPS.2024.P1230

Lipophilic Prodrug Charge Masking- insights into new method of peptide prodrugs synthesis conception

Agata Gitlin-Domagalska[1], Anna Olejnik[2], Natalia Ptaszyńska [1], Jaroslaw Ruczyński [1], Mladena Glavaš [1,3], Mikolaj Marszałek [1], Dawid Dębowski [1], Aleksandra Helbik-Maciejewska [1], Anna Łęgowska [1], Chaim Gilon[4], Krzysztof Rolka [1]

[1]Department of Molecular Biochemistry, Faculty of Chemistry, University of Gdansk, Gdansk, Poland;
[2]Department of Biotechnology and Food Microbiology, Faculty of Food Science and Nutrition, Poznan University of Life Sciences, Poznań, Poland;
[3]Laboratory for Synthetic Organic Chemistry, Division of Organic Chemistry and Biochemistry, Ruđer Bošković Institute , Zagreb, Croatia;
[4]Institute of Chemistry, The Hebrew University of Jerusalem, Jerusalem, Israel

Background

Lipophilic Prodrug Charge Masking (**LPCM**) strategy was first described in 2018 by Schumacher et al.[1] as an answer to a growing need of peptide drugs oral delivery. In short, LPCM assumes transitional masking of hydrophilic peptides' charge (especially those having positively charged residues such as Arg, Lys, and free amino terminus, as well as His or Trp in their sequence) by lipophilic moieties (alkoxycarbonyl) connected by a cleavable bond. The resultant prodrug displays improved intestinal permeability in compare to mother peptide. Once it gets into the systemic blood circulation the lipophilic moiety is cleaved by the serum esterases (mainly CES), and a free active peptide is released. Initial studies proved better permeability and, thus, enhanced oral bioavailability of cyclic model prodrug hexapeptides containing RGD motif.

This outcome encouraged us to look closer to LPCM as a method to transform peptides into bioavailable drugs. We intended to verify its application to commonly known and applied peptide drugs with proved biological activity, i.e. vasopressin and desmopressin

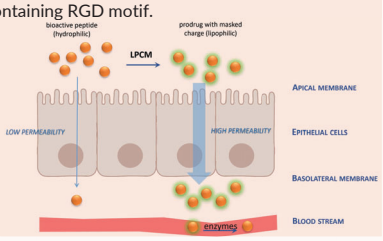

Objectives

We synthesized series of vasopressin (AVP) and desmopressin (DVP) prodrugs with masked charged in the *N*-terminus (in case of AVP) or on Arg/D-Arg side chain. Masking groups were various alkoxycarbonyl moieties differing in the alkyl chain length, bearing from 1 to 12 C atoms. The challenging modification of guanidinium group was described in our paper [2].

Obtained analogues permeability was examined using PAMPA test. We also incubated one of the DVP prudrugs (DVP(Hoc)) in rat serum to confirm its tranformation to unmodified peptide (DVP).

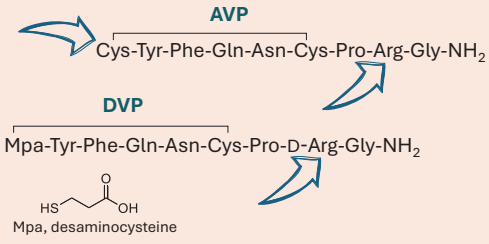

Masking group

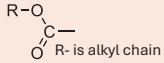

Following alkoxycarbonyl groups were introduced:

Et-etyloxycarbonyl,
Prop-propyloxycarbonyl,
MeOEt-2-methoxyethyloxycarbonyl,
But-butyloxycarbonyl,
Hoc-hexyloxycarbonyl,
Oct-octyloxycarbonyl,
Dec- decyloxycarbonyl,
Dod-dodecyloxycarbonyl

Results

PAMPA tests

compound	permeability P_e (10^{-6} cm/s)	Log Pe	Mass retention
caffeine	22	-5.01	26%
atenolol	1.24	-6.22	12%
AVP	5.15	-5.86	4%
Et-AVP	3.62	-5.67	58%
Prop-AVP	2.48	-5.84	41%
But-AVP	5.36	-5.63	57%
Hoc-AVP	4.26	-5.32	40%
Oct-AVP	0*	-	58%*
Dec-AVP	14.76	-4.88	80%
Dod-AVP	53.10	-4.32	81%
$AVP(Prop)_2$	1.27*	-5.99	37%*
$AVP(But)_2$	0.41*	-6.39	53%

*results unreliable; compound in the acceptor at the limit of qauntification, although its concentration decreased in the donnor side;

compound	permeability P_e (10^{-6} cm/s)	Log Pe	Mass retention
caffeine	33.80	-4.48	18.69%
atenolol	2.80	-5.66	0.10%
DVP	1.24	-5.95	2.73%
DVP(Et)	4.21	-3.48	9.77%
DVP(Prop)	4.77	-5.32	10.37%
DVP(But)	7.78	-5.11	9.32%
DVP(Hoc)	4.21	-4.97	23%
$DVP(Hoc)_2$	116*	-3.88	82.92%
DVP(Oct)	53.5*	-4.28	61.15%

caffeine- high permeability marker;
atenolol– low permeability marker;

High permeability > 4.0 × 10^{-6} cm/s; (in Caco-2 convention, according to Corning®)

DVP(Hoc) prodrug to drug DVP conversion in rat serum

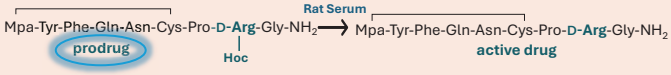

- Rapid, within 30min, conversion of DVP prodrug into mother peptide.
- DVP stable for at least 24 h

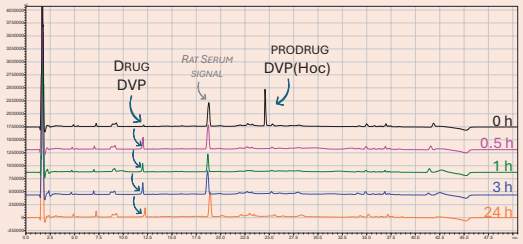

Methods

Synthesis

Peptides were synthesized using Fmoc chemistry on Prelude Peptide Synthesizer (Protein Technology, Inc., USA). Each peptide was synthesized on Rink Amide resin (loading 0.646 mmol/g, GL Biochem Shanghai). The protected derivatives of all Fmoc-amino acids were purchased from different commercial sources. The peptide chain was elongated in the consecutive cycles of deprotection and coupling. Deprotection was performed with 20% piperidine in DMF, and peptide chains elongation was performed using 3-fold molar excess of each Fmoc-protected amino acid, TBTU/HOBt/NMM (molar ratio 1:1:1:2). After completing the synthesis, peptides were cleaved from the resin and the protecting groups were removed in a one-step procedure using a mixture of TFA:phenol:triisopropylsilane:H_2O (88:5:2:5, v/v/v/v). Subsequently, the disulfide bridge was formed using a 0.1 M methanolic iodine solution.

Masking groups were introduced using corresponding alkyl chloroformates. In case of masking **N-terminal amine group** protection was intorduced on resin, using alkyl chloroformate and DIPEA (molar ratio 1:2) in DMF, reaction time 1-20h. Coupling was repeated until negativ chloranil test. **D-Arg side chain** was masked in solution. In short, eptide with formed disulphide bridge was dissolved in ACN/H_2O, 2.4 eq of DIPEA was added and cooled down to 0°C, later 1.2 eq of alkyl chloroformate in ACN was added dropwise. Reaction was monitored on HPLC and completed within 1h. Introduction of **two masking groups on Arg/D-Arg** side chain was more challanging and required preparation of Arg buidlduing blocks, as described in [2].

Obtained crude compunds were purified by reverse-phase high performance liquid chromatography (RP-HPLC) on PLC 2050 Gilson HPLC with Gilson Glider Prep. Software (Gilson, France), equipped with Grace Vydac C18 (218TP) HPLC column (22 × 250 mm, 10 µm, 300 Å, Resolution Systems). The solvent systems were 0.1% TFA (A) and 80% acetonitrile in A (B). The purity of each peptide was checked by RP-HPLC on a Shimadzu Prominence-I LC-2050C 3D equipped with a Kinetex XB-C18 column (150 × 4.6 mm, 5 µm) and a UV-Vis detector. A linear gradient from 10% to 90% B for 20 min, flow rate 1 mL min^{-1}, and detection at 214 nm was used. The mass spectrometry analysis of the synthesized compounds was carried out on MALDI MS (Autoflex maX MALDI-TOF spectrometer, Bruker Daltonics, Germany) using an α-cyano-4-hydroxycinnamic acid and/or 2,5-dihydroxybenzoic acid matrix.

PAMPA

PAMPA test was performed according to provider (**Corning®**) instructions.

Experiment conditions:
Caco-2 convention (top well is donor well)
Buffer: PBS pH 7.4
Incubation: 25 °C, 22h,
Sample concentration: 10 µM (AVP assay) and 50 µM (DVP assay)
Plates: **Corning® Gentest Pre-coated PAMPA Plate System**

- membrane construction: **lipid-oil-lipid trilayer**; hexane was used to disperse the contents of layers; The **oil layer** mimics the hydrophobic interior of the biological membrane and allows the amphiphilic lipids to anchor on it and is crucial for maintaining a robust and stable artificial membrane. **Lipid layer** is mixture of phospholipids.

PAMPA Caco-2 convention

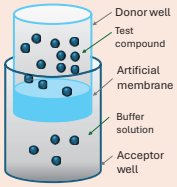

The concentrations of the tested compounds in each well of the acceptor and donor plates were determined by LC-MS technique. The analysis was conducted by UHPLC-MS system (Shimadzu Nexera X2 with LCMS-2020 detector) using a ReproSil Pure 120 ODS-3 column (Dr. Maisch GmbH, 100×2 mm, 2.4 µm particle size) with several gradients of ACN with 0.1% FA and 0.05% TFA at a flow rate of 0.3 mL/min. The eluted solution was monitored by ESI-MS detector operated in the positive ionization mode with the use of the select ion monitoring mode (SIM).

Conclusions and Future Perspectives

- ✓ Unmodified AVP shows good permeability P_e 5.15 x 10^{-6} cm/s
- ✓ But-AVP P_e was only slightly better than that of AVP, but mass retention was 14 times higher;
- ✓ P_e for AVP analogues with longest alikyl chains (**Dec- and Dod-AVP**) are very high (almost **3 and 10 times higher than for AVP**), but their concentration in the acceptor well was very low, on the detection limit;
- ✓ **Most compounds are characterized by high mass retention**, which suggests that they stay attached to the membrane, as their concentration in the donor well decreases;
- ✓ We improved DVP permeability (about 3-fold) when Et, Prop or Hoc groups were introduced on D-Arg side chain, while over **6 –fold** improvement was observed in case of **DVP(But)** prodrug;
- ✓ We proved that prodrug (DVP(Hoc)) is rapidly transformed in Rat Serum to active, unmodified peptide drug DVP within 30 min of incubation;
- ➢ DVP and its most promising prodrugs (DVP(Et)), (DVP(Prop)), (DVP(But)), (DVP(Hoc)), will be tested on Caco-2 cell model;
- ➢ Activity of DVP prodrug showing the highest P_{app} will be examined and compared to unmodified DVP in *in vivo* assay;

References

1. Schumacher-Klinger A., et al.., Enhancing Oral Bioavailability of Cyclic RGD Hexa-peptides by the Lipophilic Prodrug Charge Masking Approach: Redirection of Peptide Intestinal Permeability from a Paracellular to Transcellular Pathway, *Mol. Pharm.*, 2018, 15, 3468-3477.
2. Glavaš M., et al. Synthesis of Novel Arginine Building Blocks with Increased Lipophilicity Compatible with Solid-Phase Peptide Synthesis, Molecules, 2023, 28, 7780.

LPCM

Arg-buildiuing blocks

Acknowledgements

National Science Centre Poland

National Science Centre Poland Grant *Lipophilic Prodrug Charge Masking (LPCM) as a novel strategy to enhance oral bioavailability of charged active peptides. Optimization and generalization of the method*, **UMO-2019/35/D/NZ7/00174**

https://doi.org/10.17952/37EPS.2024.P1231

Amphipathic Proline-Rich Cell Penetrating Peptides for Mitochondria Targeting

Adeline M. Schmitt and Helma Wennemers*
Laboratory of Organic Chemistry, D-CHAB, ETH Zürich, Switzerland

Introduction

Cell penetrating peptides (CPPs) cross the cellular membrane and serve as delivery vectors to translocate cargo into cells.[1] They can also be useful for target-specific delivery, for example, of bioactive molecules to a specific cellular organelle. Here, targeting mitochondria constitutes an important goal since mitochondria dysfunction is associated with many diseases, including neurodegenerative and auto-immune diseases, diabetes, and cancer.[2] Selective delivery of bioactive compounds to mitochondria is challenging due to the dense and hydrophobic double layered-membrane.[3]

Background

Our group developed an oligoproline-based CPP (Z_8) that localizes in the cytoplasm and the nucleus. This CPP exhibits higher cellular uptake in comparison to more flexible peptides (e.g octaarginine) thanks to the preorganization of the cationic charges in defined positions along the rigid PPII helix. [4]

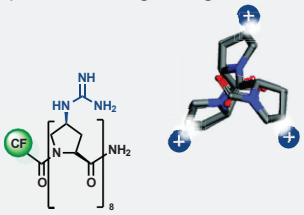

Z_8 peptide

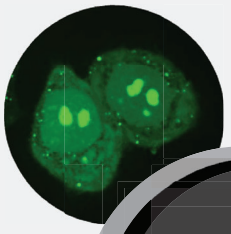

Concept

We envisioned that oligoproline peptides with hydrophobic amino acids installed at every third position allow for mitochondria targeting.[5] Selectivity would be achieved by the PPII helical conformation with two cationic faces and one hydrophobic face enabling the crossing of the mitochondria membrane.

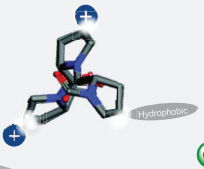

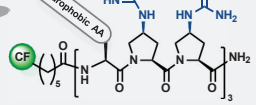

A cyclohexyl side chain enables the mitochondria targeting.

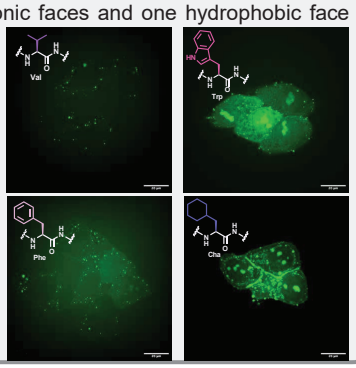

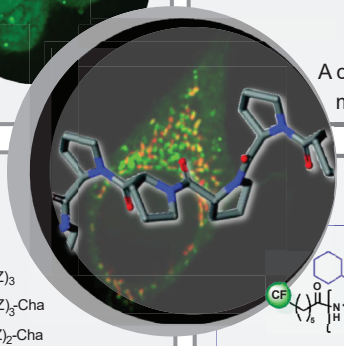

Circular Dichroism

All peptides are PPII helical

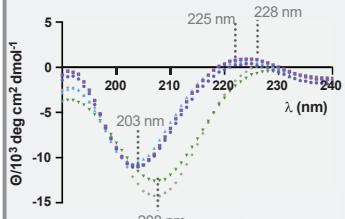

- $(ChaZZ)_3$
- $(ChaZZ)_3$-Cha
- $(ChaZZ)_2$-Cha
- $(ChProZZ)_2$-ChPro
- $(ChProZZ)_3$

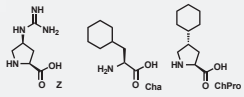

50 µM, H_2O

FACS Analysis

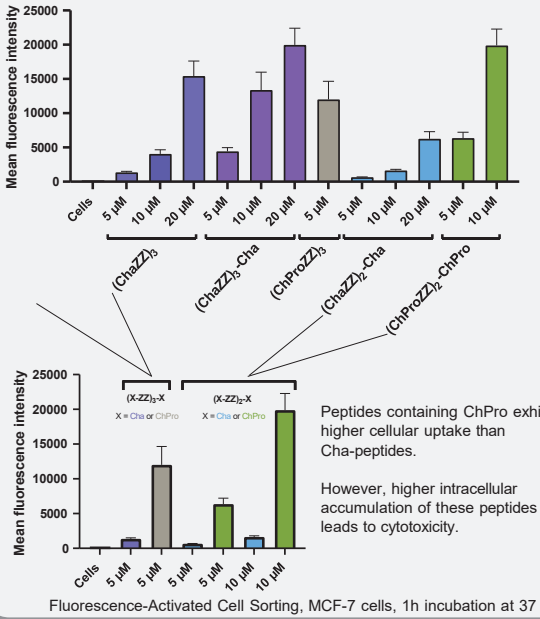

Peptides containing ChPro exhibit higher cellular uptake than Cha-peptides.

However, higher intracellular accumulation of these peptides leads to cytotoxicity.

Fluorescence-Activated Cell Sorting, MCF-7 cells, 1h incubation at 37 °C

Colocalization Studies in Live Cells

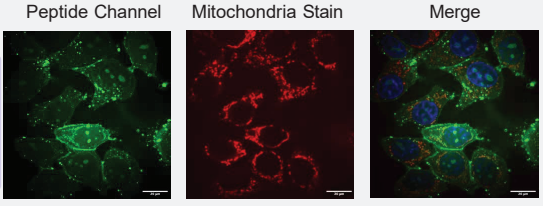

$(ChaZZ)_3$ peptide targets mitochondria but also the nucleus

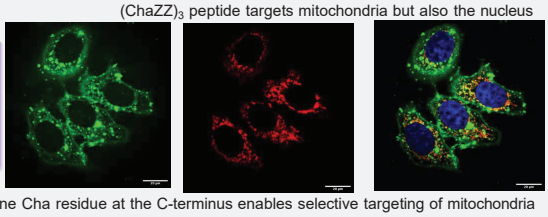

Adding one Cha residue at the C-terminus enables selective targeting of mitochondria



Also the shorter 7-mer is efficiently taken up and targets mitochondria but at higher concentration

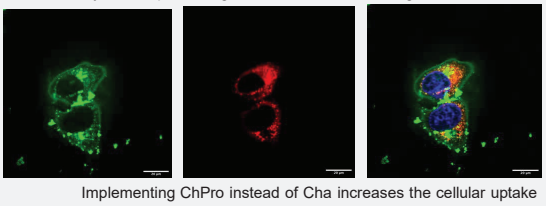

Implementing ChPro instead of Cha increases the cellular uptake

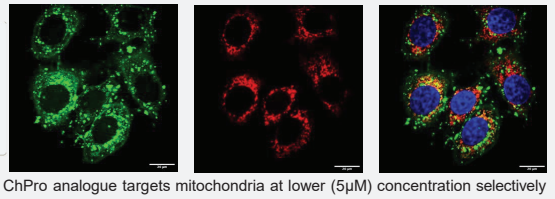

The 9-mer ChPro analogue targets mitochondria at lower (5µM) concentration selectively

Confocal microscopy, MCF-7 cells, 1h incubation at 37 °C



Let's keep in touch!

References

1 Langel, U., Cell-Penetrating Peptides, *Methods and Protocols*, **2011,** Humana, Totowa, NJ.
2 Heitz, F.; Morris, M. C.; Divita, G., *Br. J. Pharmacol.* **2009**, *157*, 195–206.
3 Bakovic, M.; Schenkel, L. C., *Int. J. Cell Biol.* **2014**, *2014*, 1–13.
4 Nagel, Y. A.; Raschle, P. S.; Wennemers, H.; *Angew. Chem. Int. Ed.* **2017**, *56*, 122–126.

For previous work on mitochondria targeting peptides, see
[5] [a] Jean, S. R.; Ahmed, M.; Lei, E. K.; Wisnovsky, S. P; Kelley, S. O.; *Acc. of Chem. Res.*, **2016,** *49*, 1893-1902
[b] Kalafut, D.; Anderson, T. N.; Chmielewski, J.; *Bioorg Med Chem Lett.* **2012,** *22*, 561-3.

https://doi.org/10.17952/37EPS.2024.P1233

Optimization of Anti-Vasoconstricting UT-II-Derived Biogels

Thibault Cauwenbergh[1], Juliana Dallagnol[2], David Chatenet[2], Charlotte Martin[1], Steven Ballet[1]

[1] Research Group of Organic Chemistry (ORGC) – Vrije Universiteit Brussel, Pleinlaan 2, Elsene (BE)
[2] INRS – Institut Armand-Frappier – Université du Québec, Québec (CA)
e-mail: thibault.cauwenbergh@vub.be

CO-FORMULATION VS. BIOGEL FORMULATION [1]

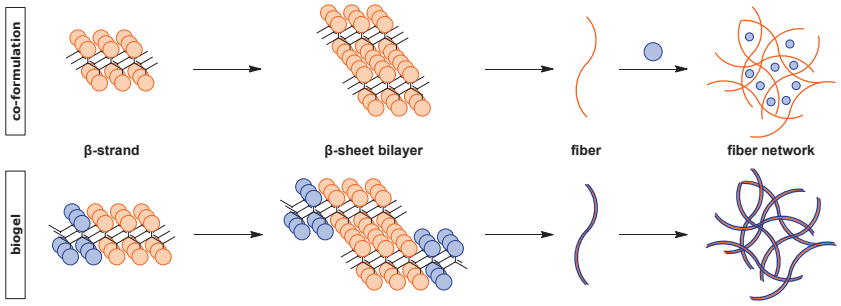

Templated on our in-house developed amphipathic hexapeptide hydrogel (H-Phe-Gln-Phe-Gln-Phe-Lys-NH_2), we designed a **self-assembling hydrogel-drug conjugate** platform, termed *biogel*, with a proof-of-concept for the sustained release of opioid peptides. This **prodrug** approach offers an elegant solution to the often difficult-to-control and fast release properties characteristic for traditional co-formulation-based hydrogel platforms. The work presented here focuses on the implementation of the developed biogel concept in **targeting the urotensin-II receptor** (UT-IIR).

UROTENSIN II RECEPTOR [2,3]

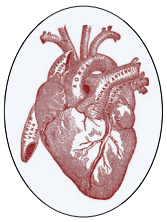

> G protein-coupled receptor
> somatostatin receptor homologue
> expressed in heart & pancreas
> intracellular Ca^{2+} mobilization
> strong vasoconstricting effect
> involved in renal failure & diabetes

hUT-II$_{(4-11)}$ & URP
Native agonists
Ultrapotent vasoconstrictors

Key ligand features
- ✓ -FWKY- (or closely related) core motif
- ✓ -SS- cyclic hexapeptide
- ✓ Type II' β-turn
- ✓ *N*- and *C*-terminal capping is tolerated

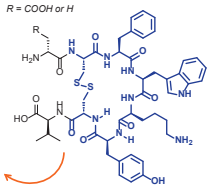

LEAD BIOGEL DESIGN [4]

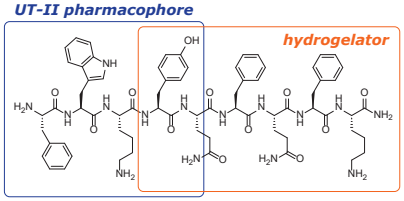

β-strand lead peptide
gel formation @ 2% w/v in PBS

β-STRAND ← ***GPCR activation*** (BRET biosensor assay on HEK293 cells) → ***β-HAIRPIN***

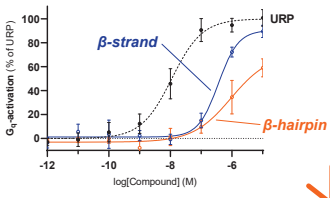

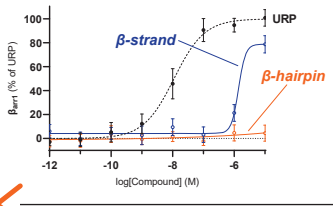

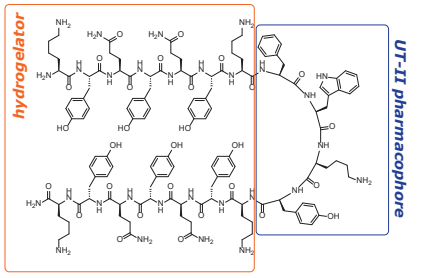

TYR SAR STUDY [5]

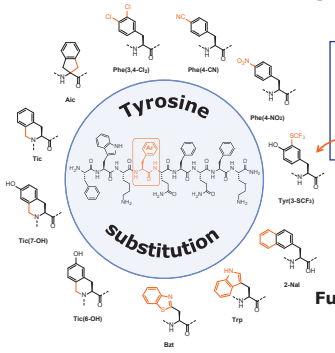

General considerations
- ❑ **Phe** most tolerant residue
- ❑ **Trp** tolerant to stereochemical inversion
- ❑ **Lys** 3/4 carbon (primary) aliphatic amine!
- ■ **Tyr** aromatic moiety!

Strong gel formation @ 2% w/v in PBS
except for constrained AAs (Tic(x-OH), Aic)

however

Full loss of G_q & β_{arr1} activation observed...
> under investigation

CYCLIZATION [6]

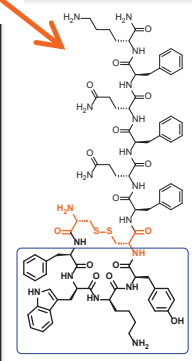

"Disulfide bridge is crucial for receptor recognition and activation"

Slightly reduced gel strength
but
Improved activity!

GPCR activation (BRET biosensor assay on HEK293 cells)

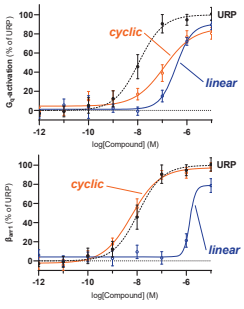

cyclization conditions
- on resin
- I_2 (10 equiv.)
- 2% v/v anisole in NMP
- MW
- 40 °C
- 15 min

PROTEOLYTIC RESISTANCE

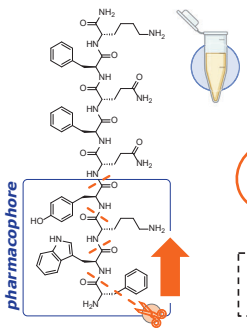

H-**FWKY**-QFQFK-NH_2
fast degradation
($t_{1/2}$ = 5.65 ± 0.26 min)

H-FQFQFK-**FWKY**-NH_2
($t_{1/2}$ < 2 min)

H-kfqfqf-**ykwf**-NH_2
($t_{1/2}$ = ?)

NEED FOR MORE PROFOUND MODIFICATIONS

N-capping

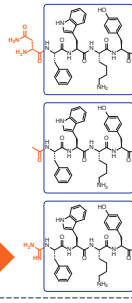

- **D-Asn-** $t_{1/2}$ = 93.59 ± 2.67 min
  C-ter cleavage H-nFW-OH metabolite
- **Ac-** $t_{1/2}$ = 70.64 ± 2.59 min
  C-ter cleavage Ac-FWK-OH metabolite
- **Gdn-** $t_{1/2}$ = 57.22 ± 3.80 min
  C-ter cleavage Gdn-FWK-OH metabolite

Trp modification

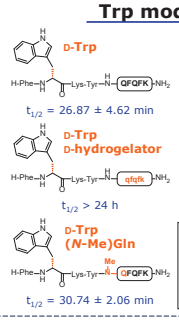

- D-Trp $t_{1/2}$ = 26.87 ± 4.62 min
- (*N*-Me)Trp $t_{1/2}$ = 45.16 ± 0.90 min
- D-Trp D-hydrogelator $t_{1/2}$ > 24 h
- Tcc $t_{1/2}$ = 47.56 ± 2.28 min
- D-Trp (*N*-Me)Gln $t_{1/2}$ = 30.74 ± 2.06 min

C-ter cleavage
Tcc preserves pharmacophore
substantial impact on gelation

Cyclization

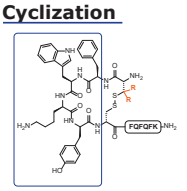

R = H (Cys) $t_{1/2}$ = 122.16 ± 2.63 min
R = Me (Pen) $t_{1/2}$ = 53.36 ± 1.51 min

pharmacophore preserved up to 24 h

CONCLUSIONS

> Search for highly active, long-acting UT-II-targeting conjugate hydrogel ('biogel')
> Cyclization of the pharmacophore enhances activity and proteolytic stability
> Unexpectedly, Tyr substitution yielded inactive linear peptide derivatives
> Proteolytic stabilization is needed to prolong peptide activity and preserve the pharmacophore

PERSPECTIVES

> Increase peptide activity, to compete with the parent peptide
> Test *in vitro* activity of the stabilized biogel analogues and their metabolites
> Further study & optimize the β-hairpin design
> Expand the biogel platform to other targets

ACKNOWLEDGEMENTS

We thank the Research Council of the VUB for financial support provided through the Strategic Research Program (SRP50 and SRP95) and the Research Foundation Flanders through FWO Hercules (OZR3584 and OZR3939).We thank Rode Kruis Vlaanderen for providing human blood plasma.

REFERENCES

[1] a) M. Bibian *et al.*, *J. Mater. Chem. B.* **2015**, *3*, 759–765; b) C. Martin *et al.*, *Med. Chem. Comm.* **2016**, *7*, 542–549; c) C. Martin *et al.*, *J. Med. Chem.* **2018**, *61*, 9784–9789.
[2] J. McDonald *et al.*, *J. Anesth.* **2007**, *21*, 378–389.
[3] a) R. Patacchini *et al.*, *Br. J. Pharmacol.* **2003**, *140*, 1155–1158; b) B. E. Maryanoff *et al.*, *J. Med. Chem.***2010**, *53*, 2695–2708.
[4] S. Bandholtz *et al.*, *J. Med. Chem.* **2016**, *59*, 10100–10112.
[5] a) D. Chatenet *et al.*, *J. Med. Chem.* **2006**, *49*, 7234–7238; b) b) A. Carotenuto *et al.*, *J. Med. Chem.* **2014**, *57*, 5965–5974; c) E. Billard *et al.*, *Biochem. Pharmacol.* **2017**, *144*, 100–107; d) J. Gregorc *et al.*, *J. Org. Chem.* **2023**, *88*, 13169–13177.
[6] a) A. Carotenuto *et al.*, *J. Med. Chem.* **2004**, *47*, 1652–1662; b) H. B. Zhang *et al.*, *Chin. Chem. Lett.* **2007**, *18*, 902–904.

Development of cell penetrating peptide-based ubiquitin ligase ligand for the development of PROTAC

https://doi.org/10.17952/37EPS.2024.P1234

OHidetomo Yokoo[1], Zhou Dongrui[1,2], Yosuke Demizu[1,2]
([1]National Institute of Health Sciences, Japan, [2]Yokohama City University, Japan)

P1.234

Abstract PROTAC (PROteolysis TArgeting Chimeric molecule) [1], which induces ubiquitination and degradation of protein of interest by recruiting ubiquitin ligase (E3) to target proteins, is expected to be a novel therapeutic modality. PROTAC is a chimeric molecule that combines the E3 ligand with the target protein ligand via an appropriate linker, and inhibits protein function through its degradation. We have developed peptide-based PROTAC by incorporating cell penetrating peptides and modifications like stapling structures to enhance cell membrane permeability [2, 3]. This molecule was expected to expand targets to include proteins considered undruggable by conventional small molecule-based drugs. However, low cell membrane permeability remains a problem for the development of PROTAC. Therefore, in this study, we enhanced the cell membrane permeability to the E3 ligand, a commonly used moiety in PROTACs. We designed a peptide-based E3 ligand moiety by conjugating it with cell penetrating peptides, including oligoarginine, endosomal escape domains (EEDs), and oligo-sarcosines, and attached a small molecule-based fluorophore as a model ligand for target proteins to the designated E3 ligand.

The designed peptides were synthesized through solid-phase synthesis, and their cell penetrating ability was evaluated by detecting the fluorescence from the fluorophore conjugated to the peptide. We found that controlling the introduction and sequence of oligoarginine, the EED and oligo-sarcosine could improve the efficiency of intracellular delivery of peptide-based E3 ligands. Therefore, the obtained E3 ligands were applied to PROTAC, in which peptide ligands called peptidomimetic estrogen receptor modulators (PERMs) for estrogen receptor α were introduced into the obtained E3 ligand peptides. Their degradation activities were evaluated by western blotting. As a result, the PROTAC with oligoarginine and the EED showed higher degradation activity than that of the parent peptide, suggesting that the developed E3 ligand peptide would be useful for the development of PROTAC.

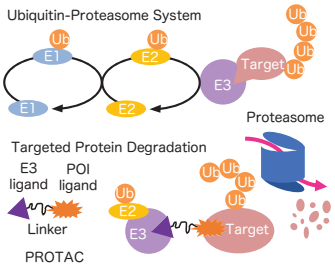

1) C. M. Crews, R. J. Deshaies et al. *Proc. Natl. Acad. Sci. USA* **2001**, *98*, 8554.
2) H. Yokoo, N. Ohoka, M. Demizu, Y. et al. *Int. J. Mol. Sci.*, **2021**, 22, 8772.
3) H. Yokoo, N. Ohoka, M. Naito, Y. Demizu, *Bioorg. Med. Chem.*, **2020**, *28*, 115595.

Design

The following peptides were designed by introducing VHL peptide ligand (ALAPYIP) as a model E3 ligase for VHL and fluorescent substance 5(6)-FAM as a model for small molecule target protein ligands.

R9 : 5(6)-FAM-GRRRRRRRRR-NH_2
VHL : 5(6)-FAM-βAla-ALAPYIP-NH_2
VHLR9 : 5(6)-FAM-βAla-ALAPYIP-R_9-NH_2
VHLSarnR9 : 5(6)-FAM-βAla-ALAPYIP-$(Sar)_n$-R_9-NH_2
R9VHLSarn : 5(6)-FAM-βAla-R_9-ALAPYIP-$(Sar)_n$-NH_2
R9VHLEEDSarn : 5(6)-FAM-βAla-R_9-ALAPYIP-Ahx-GFWFG-$(Sar)_n$-NH_2
EEDVHLSarnR9 : 5(6)-FAM-βAla-GFWFG-Ahx-ALAPYIP-$(Sar)_n$-R_9-NH_2
EEDVHLR9Sarn : 5(6)-FAM-βAla-GFWFG-Ahx-ALAPYIP-R_9-$(Sar)_n$-NH_2

Ahx; 6-aminohexanoic acid

Design of PROTAC

PROTAC1 : H-RILRCLLQ-G_3-ALAPYIP-NH_2

PROTAC1-R_9 : H-RILRCLLQ-G_n-ALAPYIP-R_9-NH_2 (n = 1 – 6)

H-RILRCLLQ-G_3-GFWFG-Ahx-ALAPYIP-$(Sar)_n$-R_9-NH_2 (n = 0, 5, 10, 20)

EED-PROTAC1-Sarn-R_9

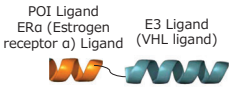

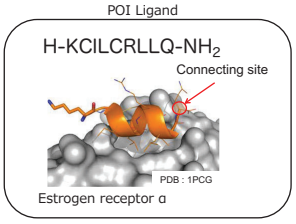

The E3 ligand was bound to sites facing outside that are unlikely to inhibit the binding to the target protein.

Cell-penetrating efficiency

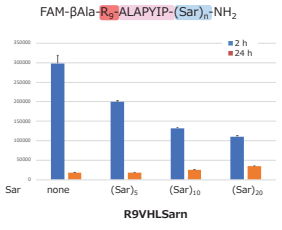

Uptake efficiency decreased as Sar elongated.

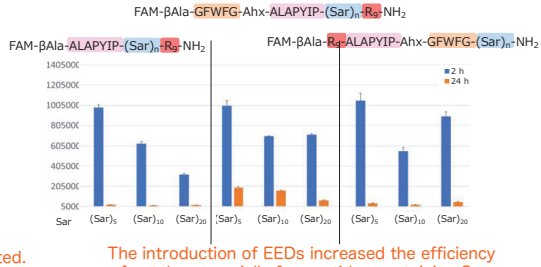

The introduction of EEDs increased the efficiency of uptake, especially for peptides containing Sar.

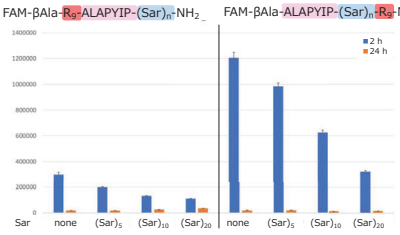

The uptake efficiency was greatly improved by introducing R_9 at the C-terminus and Sar as a linker.

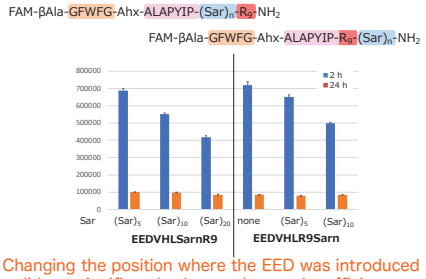

Changing the position where the EED was introduced did not significantly change the uptake efficiency.

Degradation activity

H-RILRCLLQ-G_3-ALAPYIP-NH_2
H-RILRCLLQ-G_3-ALAPYIP-R_9-NH_2
H-RILRCLLQ-G_3-GFWFG-Ahx-ALAPYIP-R_9-NH_2

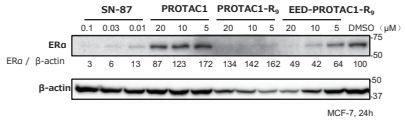

The introduction of cell penetrating peptides and EEDs resulted in higher degradation activity than simply peptide PROTAC.

H-RILRCLLQ-G_3-GFWFG-Hex-ALAPYIP-$(Sar)_n$-R_9-NH_2

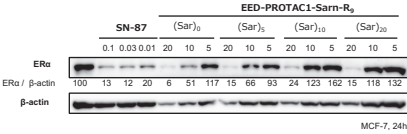

The peptide-based PROTAC with Sar also showed degradation activity.

H-RILRCLLQ-G_n-ALAPYIP-R_9-NH_2

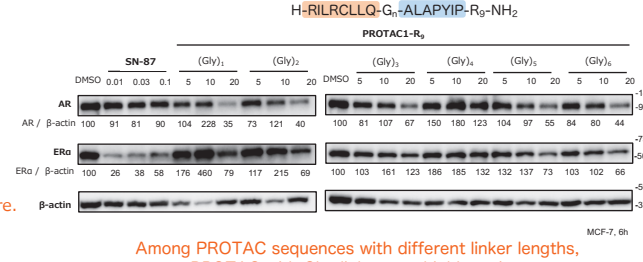

Among PROTAC sequences with different linker lengths, PROTAC with Gly_6 linker was highly active. Furthermore, the PROTAC degraded ERα and AR, The developed peptide will be useful as a model PROTAC.

Protease resistance

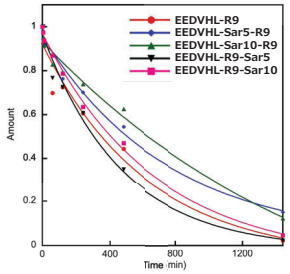

The introduction of Sar showed a slight increase in protease resistance.

CD sprectra

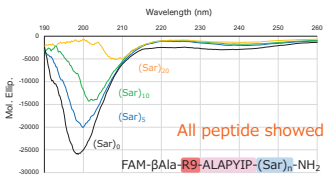

All peptide showed random structure.

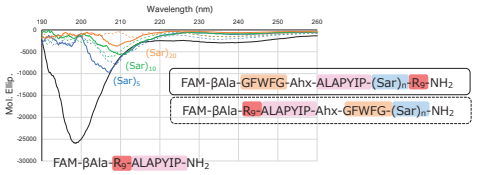

All peptide showed random structure.

Cell viability

H-RILRCLLQ-G_3-GFWFG-Ahx-ALAPYIP-$(Sar)_n$-R_9-NH_2

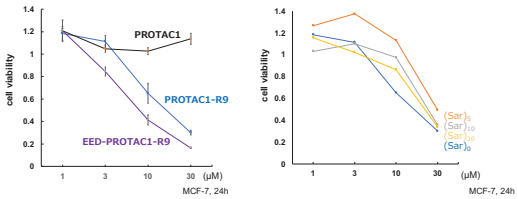

PROTAC with R_9 showed cell growth inhibitory effect on MCF-7 cells, and PROTAC with Sar showed similar activity.

Conclusion

- ✓ We designed and synthesized peptides with R_9, EED , and Sar.
- ✓ We found that the cellular uptake efficiency changed depending on the presence or absence of R_9, EED, and Sar and their order and that optimizing the sequences could improve the uptake.
- ✓ We designed and synthesized PROTAC using the obtained cell penetrating peptides.
- ✓ The peptide-based PROTAC with highly cell penetrability that is R_9 showed high activity.
- ✓ We developed a series of cell penetrating E3 ligand peptides that will be useful for optimizing degradation activity.

https://doi.org/10.17952/37EPS.2024.P1236

Design and characterization of CD20 antigen surfaces for the selection of rituximab peptide mimics

Océane Ricloux [1], Chanantida Jongwohan [1], Jordan Cossu [1], Liliane Guerente [1] and Didier Boturyn [1]

[1] *University Grenoble-Alpes, CNRS, DCM UMR 5250, 38058 Grenoble Cedex 9, France*

oceane.ricloux@univ-grenoble-alpes.fr ; didier.boturyn@univ-grenoble-alpes.fr

Introduction

Since the 90s, **monoclonal antibodies** (mAb) have emerged as a promising class of pharmaceuticals and were successfully used for cancer therapy. However, several **limitations** related to the nature of mAbs such as their cost, their low tissue penetration and immunogenicity limits their extensive clinical use. So, **new technological solutions**, as small organic mAb mimics, have to be explored. In this context, we are interested in the **development of mAb mimics** that recognize the CD20 antigen, which is expressed on B cells and is a key target for several cancer and autoimmune diseases. In this context, the **mAb Rituximab (RTX) that target CD20**, is routinely used to treat some Lymphoma. Herein, we propose to **design macromolecular compounds comprising cyclopeptides selected from the RTX Fab as recognition elements for CD20** in combination with a detection element and/or a cytotoxic unit for therapeutic applications. For this pupose, we **developed and characterized biomimetic surfaces** to mimic the surface of B cells in order **to screen and select the RTX mimics** before moving on to cell-based assays.

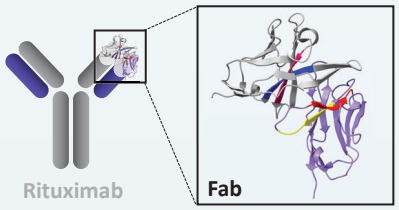

Development of antigenic surfaces for SPR

- The **biomimetic surfaces** were **characterize by Spectroscopic ellipsometry** (SE) coupled with **quartz microbalance** (QCM-D)

Grafting by **CuAAC** on a Self-Assembled Monolayer (SAM) of alcane thiols (N_3 or OH)
Antigen density is controlled by the N_3/OH ratio

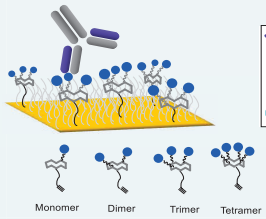

Compound	Surface density SE (pmol.cm^{-2})	Surface density QCM-D (pmol.cm^{-2})	Hydration (%)
Monomer *	37 ± 1	32 ± 6	66 ± 5
Dimer **	41 ± 4	32 ± 11	47 ± 13

Characterization of CD20 surfaces by SE coupled to QCM-D. SE areal densities were determined by *De Feijter* equation and QCM-D areal densities were extracted from *Sauerbrey* equation. * n = 2, ** n = 3

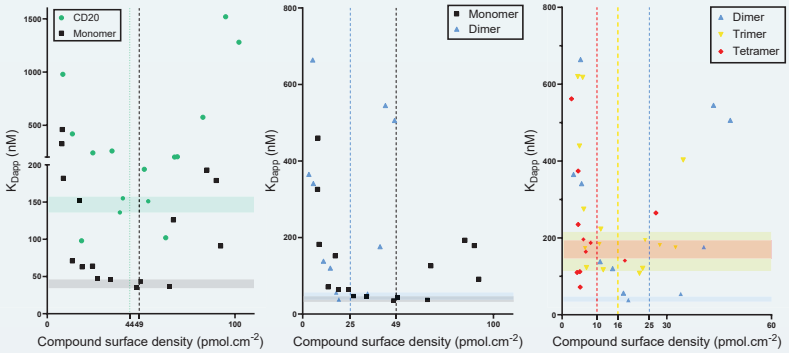

Impact of epitope surface density and clustering on RTX/CD20 affinity in SPR. K_{Dapp} were determined via the Heterogeneous Ligand (HL) model by the k_{off}/k_{on} ratio and areal densities by *Jung*'s formula.

Affinity of rituximab against CD20 at optimal surface density in SPR. K_{Dapp} were determined *via* the Heterogeneous Ligand (HL) model by the k_{off}/k_{on} ratio and areal densities by *Jung*'s formula. For the determination of inter-ligand distances, the projected surface of the compounds is considered circular. [a] n = 3, [b] n = 4

Compound	Surface density (pmol.cm^{-2})	K_{Dapp} * (nM)	Inter-ligand spacing (nm)
CD20 [a]	44 ± 8	147 ± 10	2.2 ± 0.2
Monomer [b]	49 ± 13	40 ± 5	2.1 ± 0.3
Dimer [a]	25 ± 11	49 ± 10	3.1 ± 0.6
Trimer [b]	16 ± 6	165 ± 50	3.8 ± 0.7
Tetramer [b]	10 ± 6	172 ± 25	5.0 ± 1.1

* K_D values ***in vitro*** : K_{Dapp} ≈ **5 - 19 nM**

Development of biosensors for BLI

Grafting by **Streptavidin/Biotin** interaction
Antigen density is controlled by the time of grafting

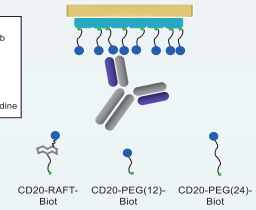

- **BioLayer Interferometry** (BLI) **biosensors** to **screen** RTX sequences to design the RTX mimics.

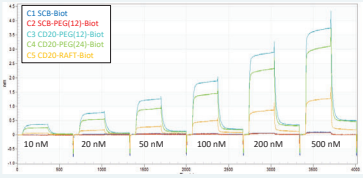

Compound	Loading response max (nm)	K_{Dapp} (nM)
SCB-Biot	0.8 ± 0.1	> mM
SCB-PEG(12)-Biot	1.3 ± 0.1	> mM
CD20-Biot	1.1 ± 0.1	> mM
CD20-PEG(12)-Biot	1.5 ± 0,1	250 ± 20
CD20-PEG(24)-Biot	1.5 ± 0.1	320 ± 10
CD20-RAFT-Biot	0.9 ± 0.1	560 ± 20

Impact of linker length on RTX/CD20 affinity in BLI. K_{Dapp} were determined *via* the Heterogeneous Ligand (HL) model by the k_{off}/k_{on} ratio.

Design and Evaluation of RTX mimics

❖ RTX peptide mimic design

Two types of RTX mimics :
- **multivalent mimics** displaying 2 to 4 times the same cyclopeptide from RTX consensus sequence
- **Bispecific mimics** displaying 2 different cyclopeptides, one from the heavy chain and one from the light chain sequences.

Multivalent RTX mimics

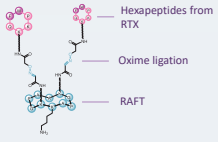

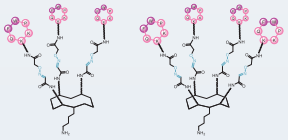

Bispecific RTX mimics

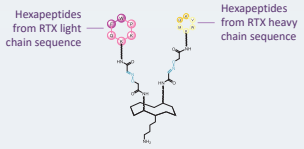

Hexapeptides from RTX containing a modified ketoaldehyde-lysine to carry out oxime ligation:



❖ Affinity of RTX peptide mimics for CD20

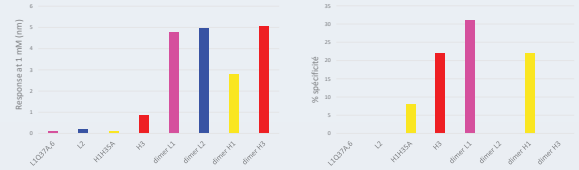

Impact of dimerization of RTX cyclopeptides on CD20 recognition by BLI model. The specificity percentage was determined by comparison with the "CD20-scramble" response at a concentration of 1 mM.

- **Dimerization** induces an **increase in response**
- **Dimerization** can **improve specificity** for the target

Study of RTX/CD20 interaction

❖ Amino acid significance of Rituximab-derived peptide sequences *via Ala-scan*

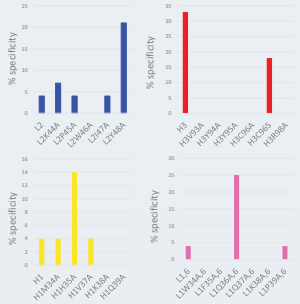

Ala-scan **peptide specificity results obtained on the BLI model.** The specificity percentage was determined by comparison with the "CD20-scramble" response at a concentration of 1 µM.

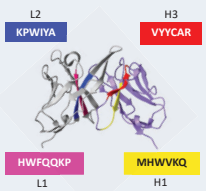



Representation of the Rituximab's binding pocket

- ***Ala-scan*** to determine the RTX amino acids involved in the RTX/CD20 interaction
- Presence of a **binding pocket** in RTX with two interaction areas

Conclusion & Outlooks

❖ Conclusion

- Design of antigenic surfaces with high specificity and affinity for its antibody
- Design of BLI biosensors for peptide screening
- Determination of the amino acids from RTX binding pocket involved in the interaction
- Design and synthesis of RTX mimics

❖ And now ?

- Evaluation of the affinity and the specificity of RTX mimics by BLI and SPR
- Biological assays with the hits

References

Bar, L.; Dejeu, J.; Lartia, R.; Bano, F.; Richter, R. P.; Coche-Guerente, L.; Boturyn, D. *Anal. Chem.* **2020**, *92*, 5396–5403.

Bar, L.; Nguyen, C.; Galibert, M.; Santos-Schneider, F.; Aldrian, G.; Dejeu, J.; Lartia, R.; Coche-Guerente, L.; Molina, F.; Boturyn, D. *Anal. Chem.* **2021**, *93*, 6865–6872.

Proceedings of the 37th European Peptide Symposium
Michal Lebl, Editor
European Peptide Society, 2024 *http://doi.org/10.17952/37EPS.2024.P1240*

Development of Novel Angiopep-2 Conjugates for Cancer Treatment

Gábor Mező[1,2], Levente Dókus[2], Diána Vári-Mező[2,3,4], Krisztina Kiss[2], Lilla Pethő[2], Ivan Ranđelović[4], József Tóvári[4], Szilvia Bősze[2,5]

[1]Eötvös Loránd University, Institute of Chemistry, Budapest, 1117 Hungary; [2]HUN-REN–ELTE, Research Group of Peptide Chemistry, Budapest, 1117 Hungary;[3]School of Ph.D. Studies, Doctoral School of Pathological Sciences, Semmelweis University, Budapest, 1085 Hungary; [4]Department of Experimental Pharmacology and the National Tumor Biology Laboratory, National Institute of Oncology, Budapest, 1122 Hungary; [5]Department of Genetics, Cell- and Immunobiology, Faculty of Medicine, Semmelweis University, Budapest, 1089 Hungary

Introduction

Transporting therapeutics through the blood-brain barrier (BBB) is a demanding/ambitious challenge in treating brain tumors. The BBB is semipermeable; therefore, most active substances are poorly transported through this barrier, decreasing therapeutic effects. Angiopep-2 (TFFYGGSRGKRNNFKTEEY) is a peptide containing 19 amino acids that was shown to be a ligand of the low-density lipoprotein receptor-related protein-1 (LRP1). This peptide can cross the blood-brain barrier *via* receptor-mediated transcytosis and simultaneously target glioblastoma. Thereby, dual targeting may be achieved [1]. Recently, we demonstrated that substituting the three conjugation sites (two lysine side chains and the N-terminus) with drug molecules is not the best choice for developing effective peptide-drug conjugates. The substitution of Lys in position 15 decreased the cellular uptake by U87 glioma cells, while the accessibility of Lys in position 10 was somewhat hindered; therefore, the drug release was inefficient (Figure 1). However, the side chain substitution of this Lys highly increased the cellular uptake [2].

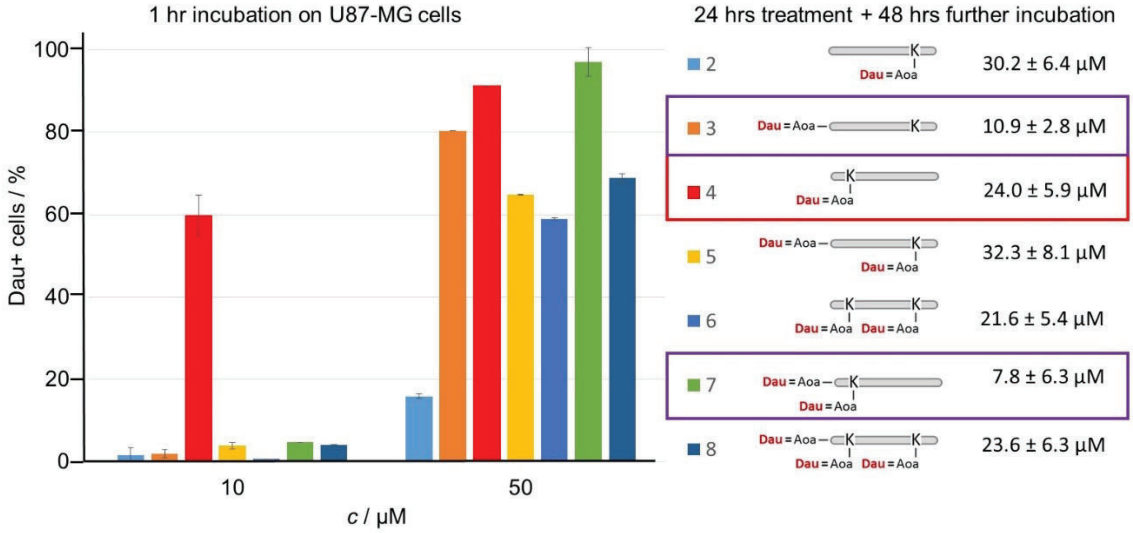

Figure 1. *In vitro* cellular uptake and cytostatic effect of Angiopep-2 – daunomycin conjugates

Thus, in this study, we developed daunomycin-Angiopep-2 conjugate in which the drug was attached to the N-terminus *via* oxime-linkage, and the side chain of Lys in position 10 was substituted with butyric acid (Dau=Aoa-TFFYGGSRGK(Bu)RNNFKTEEY-OH). The modification was used earlier efficiently in order to increase the cellular uptake and the antitumor effect of peptide-drug conjugates [3].

Results and Discussion

The Angiopep-2 peptide was built up on Wang resin by standard SPPS with Fmoc/tBu strategy. At the end of the sequence isopropylidene protected aminooxyacetic acid (Aoa) was attached similarly with Oxima Pure/HOBt coupling reagents. After the peptide cleavage from the resin the isopropylidene group was removed with 1M methoxyamine in 0.2M NH_4OAc buffer at pH 5 followed by purification and ligation with daunomycin (Dau) under the same condition. In the case of the butyrylated derivative the side chain of Lys in position 10 was protected with Mtt group that was removed prior the final cleavage with 2% TFA/DCM solution followed by butyrylation using butyric anhydride. The further reaction steps were the same as in the case of non-butyrylated derivative.

 http://doi.org/10.17952/37EPS.2024.P1240

The cellular uptake and the *in vitro* cytostatic effect of butyrylated conjugate was significantly higher (IC_{50} value was 0.678 ± 0.089 μM) than the non-butyrylated version (1.418 ± 0.153 μM), which confirmed our hypothesis (Figure 2).

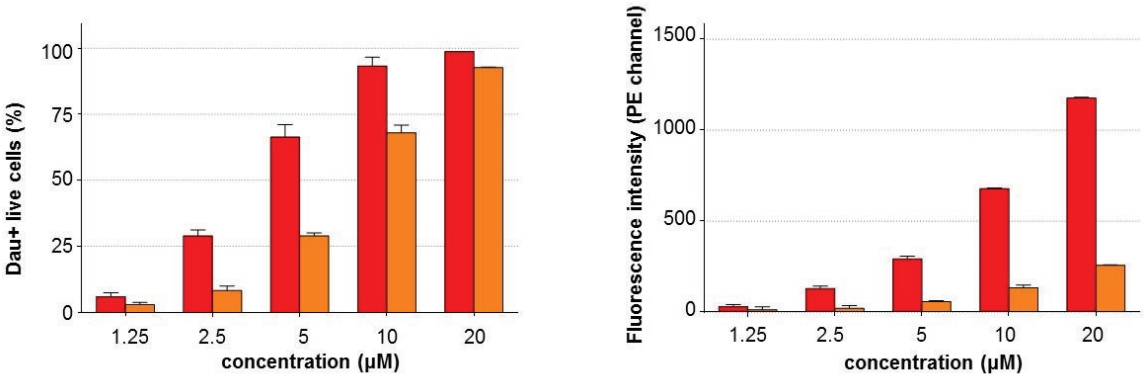

Fig. 2. Cellular uptake of Angiopep-2 – daunomycin conjugates (red: butyrylated; orange: non-butyrylated)

The short-chain acidic acid-containing conjugate showed a bit higher but insignificant (only 2%) passage through the BBB model [4] without LRP1. The conjugates were not cytotoxic on the endothelial cells.

According to these results, the conjugates were also investigated *in vivo* on U87MG *s.c.* tumor model. Dau had no tumor growth inhibition effect in the MTD concentration (1mg/kg) on this type of tumor model. However, the conjugates showed slight but not significant inhibition (10-15%) using a dose of 10 mg Dau content of conjugate/kg. The butyrylated conjugates elevated the tumor doubling time (11%) a bit and showed lower toxicity than the free Dau (Figure 3). Therefore, the butyrylated Angiopep-2 - drug conjugates might be good candidates for targeted tumor therapy, but more potent drug molecules should be used.

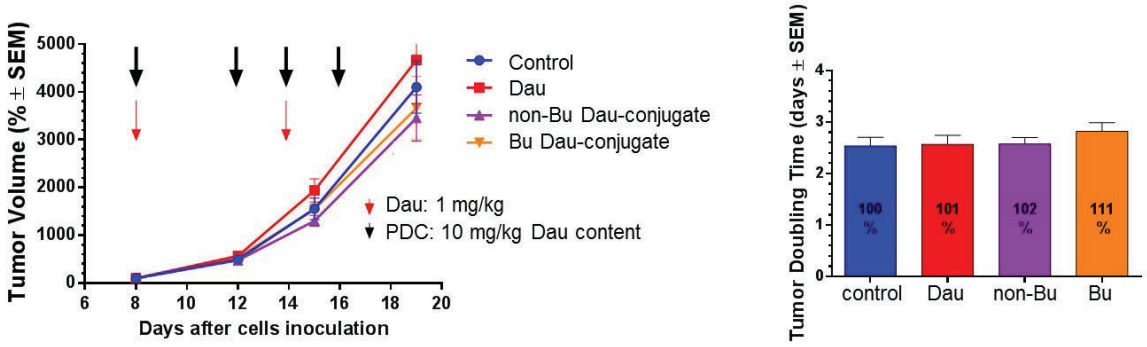

Fig 3. Tumor growth inhibition (black arrows: treatments with conjugates, red arrows: treatments with Dau) and tumor doubling time

Acknowledgments

The research was supported by the National Research, Development and Innovation Office under grants NKFIH K146039 and the National Laboratories Excellence program, as part of the National Tumor Biology Laboratory project (2022-2.1.1-NL-2022-00010).

References

1. Demeule, M., et al. *J. Pharmacol. Exp. Ther.* **324**, 1064-1072 (2008), doi: 10.1124/jpet.107.131318
2. Pethő, L., et al. *Int. J. Mol. Sci*. **24**, 3106 (2023), doi: 10.3390/ijms24043106.
3. Hegedüs, R., et al. *Eur. J. Med. Chem.* **56**, 155-165 (2012), doi: 10.1016/j.ejmech.2012.08.014
4. Baranyai, Zs., et al. *J. Med. Chem*. **64**, 2982-3005 (2021), doi: 10.1021/acs.jmedchem.0c01399

Systematic Determination of the Effects of Macrocyclization on Peptide Permeability into Mycobacteria

Rachita Dash[1], Irene Lepori[2], Han Zhang[3], Wonpil Im[3], M. Sloan Siegrist[2], Marcos M. Pires[1]

[1]Department of Chemistry, University of Virginia, Charlottesville, VA; [2]Department of Microbiology, University of Massachusetts, Amherst, MA; [3]Departments of Biological Sciences and Bioengineering, Lehigh University, Bethlehem, PA.

https://doi.org/10.17952/37EPS.2024.P1241

BACKGROUND

Tuberculosis (TB) is the World's Deadliest Infectious Disease!

Causative agent of TB is the bacterium *Mycobacterium tuberculosis (Mtb)*

10.6 million TB cases reported worldwide in 2022[1]

Current surge in U.S. incidence has reversed a decade-long decline[2]

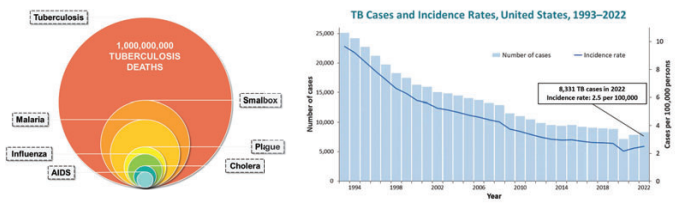

Figure: (Left) *Infectious-disease related deaths in the past 200 years.*[3] ***(Right)*** *TB cases in the U.S. per CDC.*[2]

A Major Bottleneck: The Mycobacterial Permeability Barrier[3]

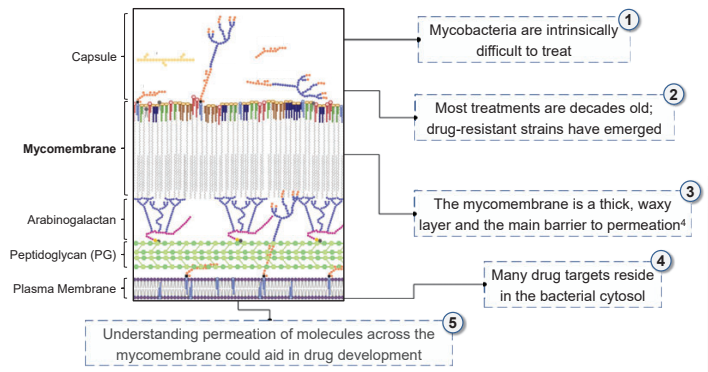

Assessing Permeability Across the Mycomembrane

Our group previously reported a robust, high-throughput assay to assess the permeability of molecules modified with an azide tag across the mycomembrane[5]

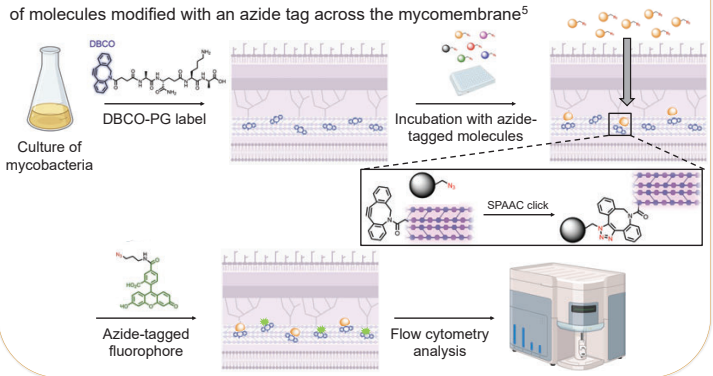

APPROACH AND DESIGN

Peptide drugs have recently gained more attention as therapeutics

- Like small molecules, they are synthetically accessible
- Like biologics, they possess structural pre-organization and selectivity

Peptide drugs are disadvantaged by their lack of permeability across membranes

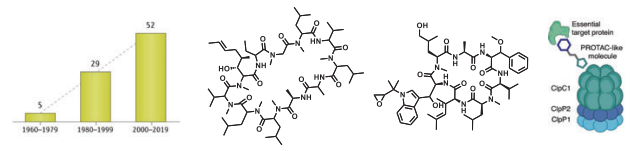

Figure: (Left) *Peptide drug approvals in the last six decades.*[6] ***(Center)*** Cyclosporin A *and* Cyclomarin A. ***(Right)*** *BacPROTAC.*[7]

Cyclization is extensively used to enhance passive membrane permeability in mammalian cells

- Can promote intramolecular hydrogen bonding
- Decreases solvent –accessible surface area

Cyclization as a permeability strategy has not yet been conclusively validated in mycobacteria

The unique composition of the mycobacterial cell envelope necessitates empirical testing of cyclization as a passive permeability strategy in mycobacteria

We set out to systematically isolate the impact of cyclization on peptide permeability across the mycomembrane in live cells

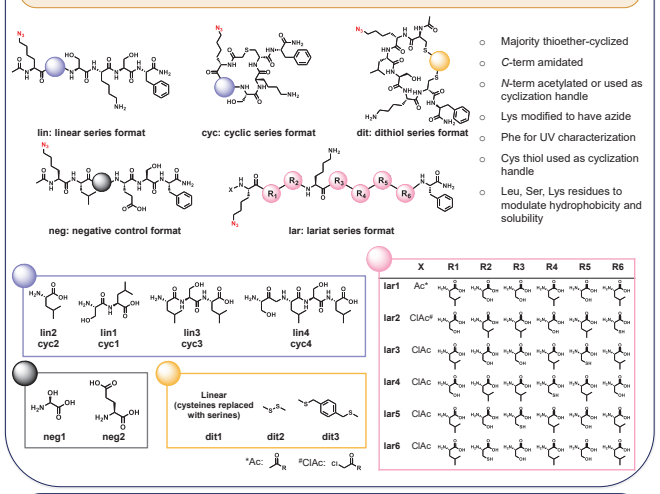

- Majority thioether-cyclized
- *C*-term amidated
- *N*-term acetylated or used as cyclization handle
- Lys modified to have azide
- Phe for UV characterization
- Cys thiol used as cyclization handle
- Leu, Ser, Lys residues to modulate hydrophobicity and solubility

RESULTS

Assay Development and Benchmarking in *M. smegmatis* (*Msm*)

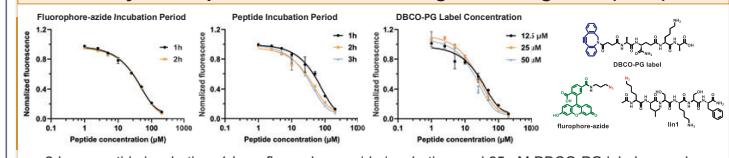

- 2-hour peptide incubation, 1-hour fluorophore-azide incubation, and 25 μM DBCO-PG label were chosen
- Permeability profile was largely unaffected by the number of DBCO moieties and fluorophore-azide incubation period

Effect of Cyclization on Peptide Permeability into Live *Mtb* and *Msm*

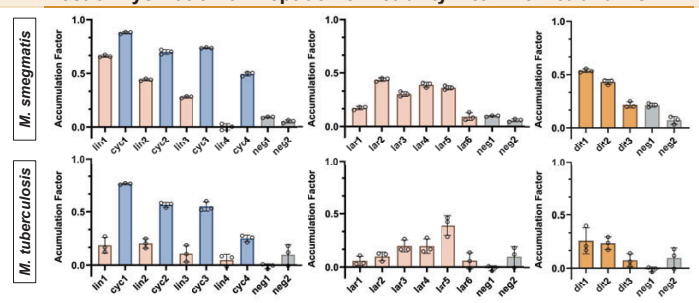

- Overall, peptides were less permeable across the *Mtb* mycomembrane when compared to *Msm*
- Thioether-cyclized peptides generally permeate the mycomembrane better than their linear counterparts

Peptide Reactivity and Membrane Integrity

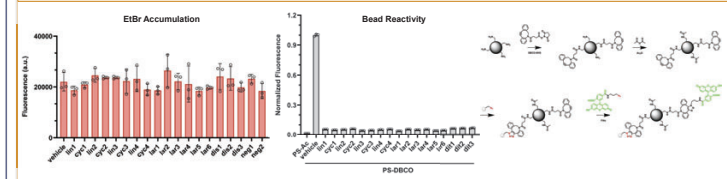

- EtBr accumulation unaffected by peptide incubation, confirming membrane integrity and cellular viability
- All peptides were found to readily react with beads displaying DBCO epitopes

Physicochemical Properties of the Peptide Library

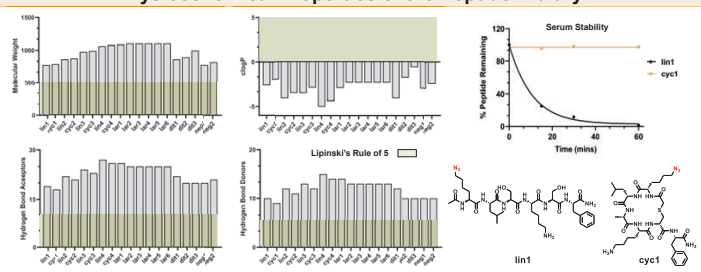

- The library breaks Lipinski's rule of 5
- cyc1 was found to be considerably more serum-stable than lin1

REFERENCES

1. Williams, Paula M. "Tuberculosis — United States, 2023." *MMWR* **2024**, Morbidity and Mortality Weekly Report 73.
2. CDCTB. "Reported TB in the U.S., 2021- National Data." **2023**, Centers for Disease Control and Prevention.
3. Paulson, T., *Nature* **2013,** 502(7470): S2–3
4. Dulberger, C. L. et al. *Nature Reviews Microbiology* **2020,** 18(1)
5. Liu, Z. et al. *Angewandte Chemie (International ed. in English)*, **2023**, 62(20): e202217777.
6. Muttenthaler, M. et al. *Nature Reviews Drug Discovery*, **2021** 20(4): 309–25.
7. Won, H. I. et al. *Nature Communications*, **2024** 15(1): 4065.

Pires research lab

NIH National Institutes of Health

https://doi.org/10.17952/37EPS.2024.P1242

Lipophilic Prodrug Charge Masking strategy for novel oxytocin prodrugs production

Agata Gitlin-Domagalska[1], Natalia Ptaszyńska[1], Anna Olejnik [2], Jaroslaw Ruczyński[1], Mladena Glavaš [1,3], Dawid Dębowski[1], Aleksandra Helbik-Maciejewska[1], Anna Łęgowska[1], Chaim Gilon[4], Krzysztof Rolka[1]

[1]Department of Molecular Biochemistry, Faculty of Chemistry, University of Gdansk, Gdansk, Poland;
[2]Department of Biotechnology and Food Microbiology, Faculty of Food Science and Nutrition, Poznan University of Life Sciences, Poznan, Poland;
[3]Laboratory for Synthetic Organic Chemistry, Division of Organic Chemistry and Biochemistry, Ruđer Bošković Institute , Zagreb, Croatia;
[4]Institute of Chemistry, The Hebrew University of Jerusalem, Jerusalem, Israel

Introduction

Lipophilic Prodrug Charge Masking strategy[1] is based on the introduction of transient charge masking group that would increse lipophilicity, and thus enhance peptide drug permeability. After permeation, enzymes (e.g. esterases) present throughout the body would bioconvert the prodrug to parent peptide with its original hydrophilic properties and activity. Masking groups used in this project are alkoxycarbonyl groups with general formula —R-O-C(=O)— . They vary in the alkyl chain lenghth, i.e. from 2 do 12 C atoms.

Oxytocin (OT) is a nonapeptide neurohormone produced in the hypothalamus, well characterized for its involvement in labor and lactation, but also social behavior, as well as affection. Its improper level was found in people suffering Autism Spectrum Disorders (ASD). ASD is a group of neurodevelopmental symptoms with specific pattern of abnormalities in social manners, manifested in problems with expressing emotions, which further leads to difficulties in communication and dealing with different social situations. Existing treatments focus mainly on behavioral therapy and there is no specific and effective drug treatment for the core dysfunctions of ASD reported. Those that are currently in use treat some symptoms like irritability, repetitive behavior but they cause many side effects and patients with autism may respond atypically[2].

Treatment with OT may improve social abilities and emotions recognition of autistic individuals [2,3]. Thus, the suggestion to deliver it directly to cerebrospinal fluid emerged. Intranasal route of drug administration, allowing to skip blood-brain barrier and deliver therapeutics directly to the central nervous system, seemed to be an answer for this need. Some studies show that daily administration of intranasal OT contributes to improvement ASD symptoms and increases social abilities while the other group showed no efficacy in administering OT intranasally to autistic adolescents [2,3]. These differences are not necessarily caused by therapeutic inefficiencies of OT, but the route of administration, imperfectness of used devices, resulting in dose and efficacy diversity. Additionally, ASD children, with communication problems and social dysfunctions, have significant difficulty to tolerate nasal sprays. Thus, the oral administration seems to be more convenient conserving good effectiveness of therapy.

Objectives

We synthesized series of OT prodrugs where charge on the *N*-terminus was masked with alkoxycarbonyl groups with various alkyl chain lengths from 2 to 12 carbon atoms (specified below).

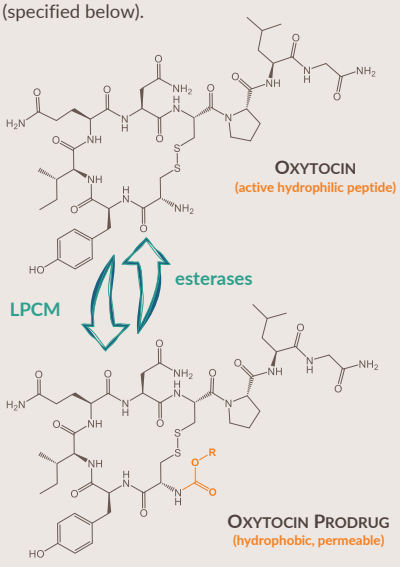

Following alkoxycarbonyl groups were introduced:

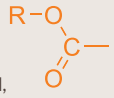

Et-etyloxycarbonyl,
Prop-propyloxycarbonyl,
MeOEt-2-methoxyethyloxycarbonyl,
But-butyloxycarbonyl,
Hoc-hexyloxycarbonyl,
Oct-octyloxycarbonyl,
Dec- decyloxycarbonyl,
Dod-dodecyloxycarbonyl;

Results

PAMPA test

Compound	Permeability P_e (10^{-6} cm/s)	Log P_e	Mass retention
caffeine	22	-5.01	26%
atenolol	1.24	-6.22	12%
OT	2.22	-5.65	19%
Et-OT	2.78	-5.56	16%
MeOEt-OT	2.37	-5.63	15%
Prop-OT	2.97	-5.53	33%
But-OT	2.2	-5.66	30%
Hoc-OT	4.67	-5.33	43%
Oct-OT	5.93	-5.23	33%
Dec-OT	9.28	-5.13	32%
Dod-OT	1.08	-5.79	67%

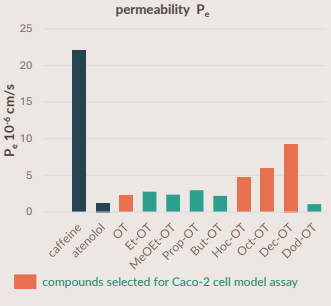

Caco-2 intestine epithelial model

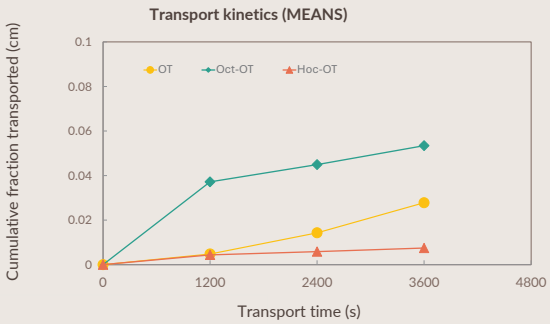

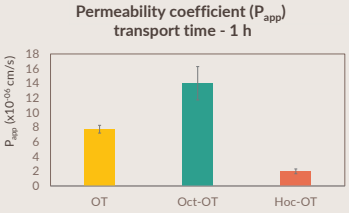

P_{app} ($\times10^{-6}$)	OT	Oct-OT	Hoc-OT
Mean	7.74	14	1.99
SD	0.53	2.27	0.33

**Dec-OT was excluded due to analytical dificulties*

Conclusions

- ✓ Most OT analogues showed higher permeability (P_e) in compare to unmodified OT in PAMPA test;
- ✓ Three OT analogues: **Hoc-OT, Oct-OT, Dec-OT showed high permeability in PAMPA test;**
- ✓ Dod-OT PAMPA permebaility was surprisingly low; however **mass retention was almost 70%;**
- ✓ OT and its derivatives were able to cross the Caco-2 monolayer in the absorptive direction, and significant differences in their permeability were observed
- ✓ **CFT** (cumulative fraction transported) **of Oct-OT was significantly higher than the CFT of OT**, Hoc-OT was characterized by a lower CFT than OT;
- ✓ **P_{app} value calculated for Oct-OT was approximately 1.8-fold higher than that obtained for OT,** suggesting relatively high Oct-OT oral availability;

Methods

Synthesis

OT was **synthesized** using Fmoc chemistry on Prelude Peptide Synthesizer (Protein Technology, Inc., USA). Each peptide was synthesized on Rink Amide resin (loading 0.646 mmol/g, GL Biochem Shanghai). The protected derivatives of all Fmoc-amino acids were purchased from various commercial sources. The peptide chain was elongated in the consecutive cycles of deprotection and coupling. Deprotection was performed with 20% piperidine in DMF and peptide chains elongation was performed using 3-fold molar excess of each Fmoc-protected amino acid and TBTU/HOBt/NMM (molar ratio 1:1:1:2). **Masking groups** vere introduced using corresponding alkyl chloroformates on resin after *N*-terminal cysteine Fmoc deprotection. In short, alkyl chloroformate and DIPEA (molar ratio 1:2) in DMF were added to the peptidyl resin, reaction time was 1-20h. Coupling was repeated until negativ chloranil test. After completing the synthesis, peptide was cleaved from the resin and the protecting groups were removed in a one-step procedure using a mixture of TFA/phenol/triisopropylsilane/H_2O (88:5:2:5, v/v/v/v). Subsequently, the **disulfide bridge** was formed using a 0.1 M methanolic iodine solution.
Obtained crude compunds were purified by reverse-phase high performance liquid chromatography (RP-HPLC) on PLC 2050 Gilson HPLC with Gilson Glider Prep. Software (Gilson, France), equipped with Grace Vydac C18 (218TP) HPLC column (22 × 250 mm, 10 µm, 300 Å, Resolution Systems). The solvent systems were 0.1% TFA (A) and 80% acetonitrile in A (B). The purity of each peptide was checked by RP-HPLC on a Shimadzu Prominence-I LC-2050C 3D equipped with a Kinetex XB-C18 column (150 × 4.6 mm, 5 µm) and a UV-Vis detector. A linear gradient from 10% to 90% B for 20 min, flow rate 1 mL min^{-1}, and detection at 214 nm was used. The mass spectrometry analysis of the synthesized compounds was carried out on MALDI MS (Autoflex maX MALDI-TOF spectrometer, Bruker Daltonics, Germany) using an α-cyano-4-hydroxycinnamic acid and/or 2,5-dihydroxybenzoic acid matrix.

PAMPA test

PAMPA test was performed according to provider (**Corning®**) instructions, following Caco-2 convention, where the top well is a donor well. **Experimental conditions:**
Buffer: PBS pH 7.4; Incubation: 25 °C, 22h; Sample concentration: 10 µM (AVP assay) and 50 µM (DVP assay); Plates: Corning® Gentest Pre-coated PAMPA Plate System; membrane construction: lipid-oil-lipid trilayer; hexane was used to disperse the contents of layers; The oil layer mimics the hydrophobic interior of the biological membrane and allows the amphiphilic lipids to anchor on it and is crucial for maintaining a robust and stable artificial membrane. Lipid layer is mixture of phospholipids.

Caco-2 intestine epithelial model

Caco-2 cells (ATCC HTB-37) were cultured at 37 °C under a 5% CO_2 atmosphere using Dulbecco's Modified Eagle's Medium (DMEM), supplemented with 20% (v/v) fetal bovine serum, non-essential amino acids 100× and gentamycin (50 mg/ml). For experiments, the Caco-2 cells were plated at a density of 4 × 10^5 cells per cm^2 on polyethylene terephthalate (PET) capillary pore membranes with a pore size of 0.4 µm (Greiner PET hanging, 1.13 cm^2). The growth medium of Caco-2 cultures was replaced every 2 days. All experiments were performed on differentiated Caco-2 cell monolayers 21 days post-seeding. To check the integrity of the Caco-2 monolayer, transepithelial electrical resistance (TEER) was measured by employing the Millicell Electrical Resistance System (Millipore, Merck). Moreover, fluorescein-5-(and-6)-sulfonic acid was used as a transport marker, added to the apical side of the Caco-2 cultures at 200 µg/mL concentration. Fluoresceinated sulfonic acid, with a molecular weight of 478 Da, is a hydrophilic, charged molecule at physiological pH and is considered to be cell impermeable.

Transepithelial transport experiment

The analyzed compounds at 100 µg/mL concentration were prepared in transport medium (Hank's balanced salt solution – HBSS). Before the experiments, the Caco-2 monolayers were washed twice with HBSS and pre-incubated at 37 °C for 30 min. Transport was initiated by adding HBSS to the acceptor (basolateral) side and the analyzed compounds to the donor (apical) side. The Caco-2 cell cultures were placed in the incubator (37 °C) and agitated using a plate shaker (120 rpm). At 20-minute intervals, a sample was taken from the acceptor compartment, and HPLC analyzed the concentration of the transported compound. Each sample volume was replaced with fresh pre-heated (37 °C) HBSS. To quantify the transport of compound across the Caco-2 cell monolayer, the apparent permeability coefficient (Papp) was determined according to the protocol previously described by Tavelin et al.

Tavelin S., Grdsjö J., Taipalensuu J., Ocklind G. and Artursson P., in Methods in Molecular Biology, Epithelial Cell Culture Protocols, ed. C. Wise, Humana Press Inc., Totowa, New Jersey, 2002, vol. 188, pp. 233–272

LC-MS

The concentrations of the tested compounds in each well of the acceptor and donor plates were determined by LC-MS technique. The analysis was conducted by UHPLC-MS system (Shimadzu Nexera X2 with LCMS-2020 detector) using a ReproSil Pure 120 ODS-3 column (Dr. Maisch GmbH, 100×2 mm, 2.4 µm particle size) with several gradients of ACN with 0.1% FA and 0.05% TFA at a flow rate of 0.3 ml/min. The eluted solution was monitored by ESI-MS detector operated in the positive ionization mode with the use of the select ion monitoring mode (SIM).

References

1. Schumacher-Klinger A., et al., Mol. Pharm., 2018, 15, 3468–3477
2. Anagnostou E., et al., Brain Res., 2014, 1580, 188–198.
3. Guastella A. J., et al., J. Child Psychol. Psychiatry, 2015, 56, 444–452.

LPCM

Acknowledgments

National Science Centre Poland

National Science Centre Poland Grant *Lipophilic Prodrug Charge Masking (LPCM) as a novel strategy to enhance oral bioavailability of charged active peptides. Optimization and generalization of the method,* **UMO-2019/35/D/NZ7/00174**

Drug-likeness of cyclic peptides beyond Rule of 5

○Shojiro Shinohara, Mikimasa Tanada, Yuya Morita, Kazuhiko Nakano, Takuya Shiraishi, Hitoshi Iikura
(*Research Division, Chugai Pharmaceutical Co. Ltd., Yokohama, Japan*)

https://doi.org/10.17952/37EPS.2024.P1243

Roche Group

Abstract

Drug discovery by small molecules accelerated after the emergence of the Rule of 5, a guideline defined by factors governing drug-likeness, such as membrane permeability and metabolic stability. To expand the drug discovery field to tough targets such as intracellular protein-protein interactions, it is critical to utilize compounds of molecular weight larger than 500 g/mol. One possible approach is to utilize cyclic peptides. However, outside the scope of the Rule of 5, general guidelines akin to the Rule of 5 have not been elucidated. In this study, we identified several governing factors needed for cyclic peptides to acquire drug-likeness—here defined as the compatibility of membrane permeability and metabolic stability—outside the scope of the Rule of 5.

To find a drug-likeness area and to determine the particular structural features that grant peptides drug-likeness, we evaluated the membrane permeability and metabolic stability of more than 700 cyclic peptides. The results suggest that a drug-likeness area can be defined by cyclic peptides, having about 11 residues, more than half of *N*-alkyl amino acids, and calculated logP (ClogP) of 12.9 or more. It is noteworthy that 11-residue peptides showed better possibility to be drug-like than peptides with fewer residues. This observation could be explained by the following hypothesis. Because 11-residue peptides like Cyclosporin A are structurally more flexible, a more lipophilic conformation could be feasible in the lipophilic membrane, while oxidative metabolism could be suppressed by a more hydrophilic conformation in water. Furthermore, an effect caused by differences in N-alkyl patterns on membrane permeability could be recognizable. The effect can be due to the ease of taking the lipophilic structure in the membrane. Moreover, we confirmed that it is preferable not to contain ionic functional groups. The number and types of acceptable polar functional groups would be more restricted compared to those of small molecules. Finally, the oral absorption of our drug-like cyclic peptides was validated by pharmacokinetic studies in several animal species.

The proposed criteria for drug-like cyclic peptides could be utilized both to design libraries for obtaining drug-like hits against intracellular targets and to facilitate optimization of them to a clinical compound.

[1] Ohta, A. *et al. J. Am. Chem. Soc.* 2023, 145, 24035-24051. [2] Tanada, M. *et al. J. Am. Chem. Soc.* 2023, 145, 16610-16620.

Proposed criteria for drug-like cyclic peptides

Cyclization	Number of residues	Number of N-alkyl amino acids	ClogP	Amino acids
Amide cyclization 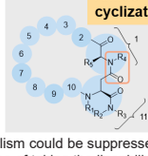	9 to 11	≥ 6	≥ 12.9	Membrane permeable/metabolically stable amino acids (No polar amino acids such as Lys, Asp, etc.)

Peptide Design for Drug-likeness Study as 1st campaign

Properties	553 peptides		Cyclosporin A
	min.	max.	
Number of amino acid residues	8	12	11
Number of *N*-alkyls	0	8	7
ClogP	4.4	15.2	14.4
Number of OH groups	0	1	1
MW (g/mol)	845	1,499	1,203

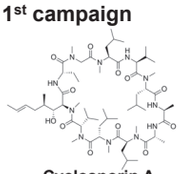

Cyclosporin A

hLM $CL_{int,mic}$ (+) = 72 μL/min/mg protein

Caco-2 P_{app} = 6.3 x 10^{-6} cm/s

53 incorporated amino acids

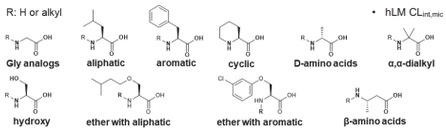

etc...

✓ Various types of amino acids

- ✓ Parameters of Cyclosporin A were referred
- ✓ Positions of *N*-alkyls and an OH group were randomly arranged to give a variety of structures

Part I. 11-residue peptides showed better possibility to be drug-like than peptides with fewer residues

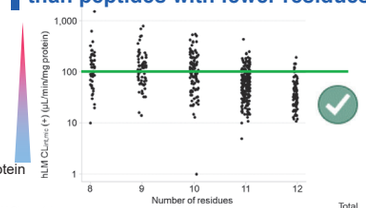

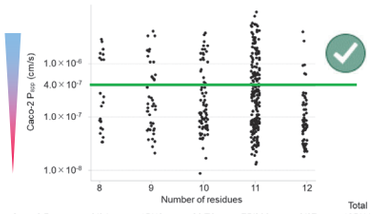

	8	9	10	11	12	Total
hLM $CL_{int,mic}$ (+) ≤100 (μL/min/mg protein)	25/51 49%	27/65 42%	56/106 53%	153/196 78%	75/82 91%	336/500 67%
Caco-2 P_{app} ≥4.0 × 10^{-7} (cm/s)	9/24 38%	15/43 35%	20/76 26%	75/200 38%	6/67 9%	125/410 30%
drug-like (hLM-Caco-2)	**1/24 4%**	**4/43 9%**	**8/74 11%**	**34/151 23%**	**4/65 6%**	**51/357 14%**

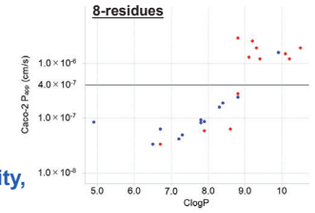

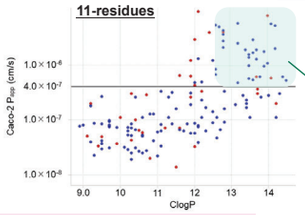

hLM $CL_{int,mic}$ (+) (μL/min/mg protein)
● ≤ 100
● > 100

Permeable Stable

Part II. Drug-likeness area can be defined by approximately 11-residue cyclic peptides with higher *N*-alkylation, higher lipophilicity, and fewer polar functional groups

11-residue peptides with 0~1 OH group from 1st and 2nd campaign

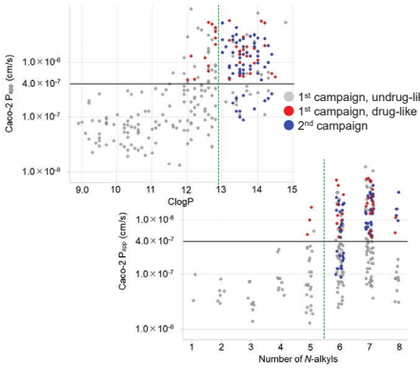

Drug-like

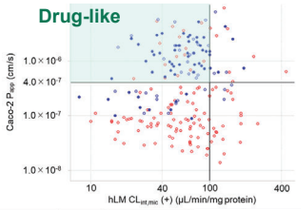

	1st campaign ClogP < 12.9 or *N*-alkyl < 6 ○	1st + 2nd campaign ClogP ≥ 12.9 & *N*-alkyl ≥ 6 ○+●
drug-like (hLM-Caco-2)	15/116 13%	63/95 66%

11-residue peptides from 1st, 2nd and 3rd campaign with ClogP ≥ 12.9 and the number of *N*-alkyls ≥ 6

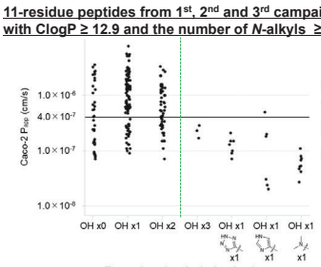

11-residue peptides from 1st, 2nd and 3rd campaign with 6 *N*-alkyls and 0~2 OH groups

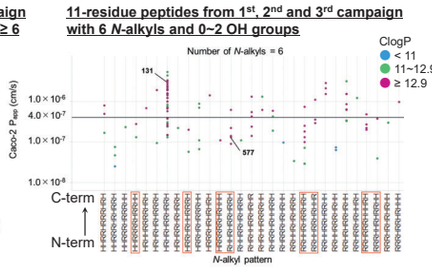

Caco-2 P_{app} ≥4.0 × 10^{-7} (cm/s)	0	1	2	3	4	5	6
	19/35 54%	81/105 77%	30/49 61%	0/3 0%	0/7 0%	1/6 17%	0/9 0%

peptide No.	Sequence	ClogP	*N*-alkyl pattern	Caco-2 P_{app} (x 10^{-6} cm/s)	hLM $CL_{int,mic}$ (+) (μL/min/mg protein)
131	D-Val MePhe Leu MeLeu Thr MeGly MeLeu Ser(tBu) MePhe MeVal Asp-pip	13.6	HRHRHRHRHRH	2.9	22
577	D-Phe_Phe(3-Cl) Ser(Pen) MeVal Thr MeGly MePhe Ser(Pen) MePhe MeVal Asp-pip	13.5	RHRHRHRHRHH	0.13	31

- 2nd campaign: 60 peptides with 11-residues, *N*-alkyl ≥ 6, ClogP ≥ 12.9, and 0~1 OH group
- 3rd campaign: 106 peptides with 11-residues, *N*-alkyl ≥ 6, ClogP ≥ 12.9, 0~3 OH groups, and 0~1 ionic functional group

- ✓ There is a clear difference in permeability of each *N*-alkyl pattern
- ✓ Permeability difference was observed between similar sequences with only one part difference in *N*-alkyl patterns
- ✓ hLM $CL_{int,mic}$ were acceptable for almost all *N*-alkyl patterns (*data not shown*)

Our hypothesis to explain the observation

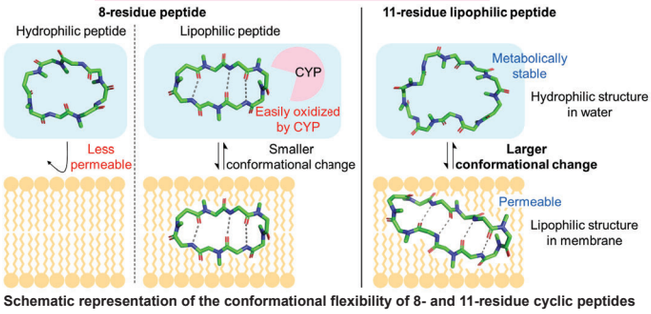

Schematic representation of the conformational flexibility of 8- and 11-residue cyclic peptides

Part III. Peptides satisfying our drug-like criteria showed acceptable oral bioavailability and *in vivo* exposure

***in vitro* properties of drug-like 11-residue peptides**

Peptide No.	ClogP	Number of *N*-alkyl	Caco-2 P_{app} (x 10^{-6} cm/s)	LM $CL_{int,mic}$ (+) (μL/min/mg protein) Human	Mouse
131	13.6	6	2.9	22	31
147	12.2	7	0.49	42	50
553	13.6	5	1.7	63	77
554	13.6	6	1.4	38	39
561	13.3	7	2.6	22	27
588	13.7	6	1.5	33	49
601	13.4	7	2.3	67	54
720	14.1	7	1.5	48	58
722	13.3	5	0.61	63	45

Pharmacokinetic parameters of these peptides in mice

Peptide No.	131	147	553	554	561
Dose (iv, mg/kg)	5	5	3	2	5
CL (mL/min/kg)	3.1 ± 0.3	5.3 ± 0.7	6.5 ± 0.8	1.3 ± 0.4	1.5 ± 0.1
V_{ss} (L/kg)	1.3 ± 0.2	0.20 ± 0.03	0.50 ± 0.04	0.35 ± 0.03	0.51 ± 0.06
Dose (po, mg/kg)	20	20	20	20	20
AUC_{inf} (po, ng·h/mL)	53,000 ± 1,600	4,400 ± 2,000	12,000 ± 1,700	46,000 ± 5,400	66,000 ± 20,000
F (%)	49 ± 1	6.8 ± 3.0	22 ± 3	18 ± 3	31 ± 10

Peptide No.	588	601	720	722
Dose (iv, mg/kg)	3	3	5	3
CL (mL/min/kg)	1.7 ± 0.2	3.9 ± 0.8	2.0 ± 0.2	1.3 ± 0.1
V_{ss} (L/kg)	0.67 ± 0.08	0.56 ± 0.09	0.34 ± 0.06	0.37 ± 0.07
Dose (po, mg/kg)	20	20	20	20
AUC_{inf} (po, ng·h/mL)	52,000 ± 17,000	11,000 ± 3,200	12,000 ± 5,900	34,000 ± 10,000
F (%)	27 ± 9	12 ± 4	7.1 ± 3.4	14 ± 4

✓ 5/9 peptides showed F of ≥15%

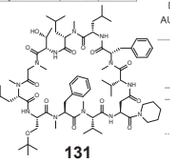

131

Pharmacokinetic parameters of 131 in various species

Species	Mouse	Rat	Dog	Monkey
Dose (iv, mg/kg)	5	1	0.25	0.5
CL (mL/min/kg)	3.1 ± 0.3	9.3 ± 1.5*	2.7 ± 0.6*	1.7 ± 0.3
V_{ss} (L/kg)	1.3 ± 0.2	3.0 ± 0.6*	1.9 ± 0.3*	0.70 ± 0.05
Dose (po, mg/kg)	20	20	3	1
AUC_{inf} (po, ng·h/mL)	53,000 ± 1,600	9,100 ± 3,800*	2,600 ± 960*	2,000 ± 940
F (%)	49 ± 1	25 ± 10*	13 ± 5*	20 ± 10

✓ 131 showed F of around 20% or more regardless of animal species

- Data of CL, V_{ss}, AUC_{inf}, and F are expressed as the mean ± SD of three animals
- * indicates that the data are expressed as the mean of four animals

iv, intravenous administration; po, oral administration; CL, *in vivo* plasma clearance; V_{ss}, volume of distribution at the steady state; AUC_{inf}, area under the curve from the time of dosing to the last measurable concentration and extrapolated to infinity; F, bioavailability

Conclusion

By comprehensively investigating the individual membrane permeability or metabolic stability of more than 700 cyclic peptides, this study revealed several key tendencies and proposed criteria for drug-like cyclic peptides

- ✓ around 11-residues, the number of *N*-alkyls ≥ 6, ClogP ≥ 12.9, and restricted polar functional groups
- ✓ The effect on the permeability by specific differences in *N*-alkyl patterns

https://doi.org/10.17952/37EPS.2024.P1244

POM-peptide hybrid against Alzheimer's Disease

Marta Giacomini[1], Claudia Honisch[2], Elisabetta Galluppo[2], Genny Orso[3], Haihong Yu[1], Mauro Carraro[1], Paolo Ruzza[2]

[1]Department of Chemical Sciences, University of Padova, Padova, Italy,
[2]Institute of Biomolecular Chemistry of CNR, Padova Unit, Padova, Italy,
[3]Department of Pharmaceutical and Pharmacology Sciences, University of Padova, Padova, Italy

Alzheimer's disease (AD) is the sixth leading cause of disability due to its high incidence and represents a huge health and social problem. AD, which culminates in cognitive decline, involves various pathological events, including accumulation in the brain **of beta-amyloid protein (Aβ) aggregates** responsible for triggering oxidative stress, synaptic degeneration, and neuronal death. Furthermore, increasing evidence posits that AD pathogenesis involves strong interactions with immunological mechanisms in the brain and microglia activation. Despite the current knowledge, the few drugs available can only mitigate symptoms without counteracting the multiple causes of AD. Within this scenario, a novel drug discovery paradigm, involving **multifunctional agents** able to interact with AD-relevant targets and compromised networks simultaneously will enable an effective therapeutic intervention.

POMs

Polyoxometalates (POMs) are nanosized metal oxides that exhibit promising biomedical applications properties. Due to their substantial polyanionic surface area, certain POMs are capable of interacting with the positively charged region of the Aβ peptide, thereby **preventing its aggregation** (1).

The purpose was to **develop hybrid POM-peptide** nanodrugs able to inhibit the formation of Aβ aggregates from the earliest stages.

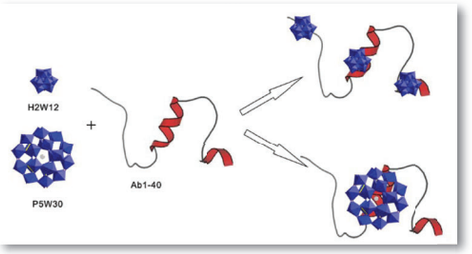

To this end, the KLVFF peptide, which has been shown to counteract the aggregation of the Aβ peptide, and its acetylated or fluorophore-labelled analogs were synthesized. The characterization of POM-peptide complexes was conducted through the use of circular dichroism (CD), dynamic light scattering (DLS), and transmission electron microscopy (TEM). Subsequently, these complexes were evaluated in a Drosophila model to assess their capacity to permeate the blood-brain barrier.

CIRCULAR DICHROISM

CD studies were carried out in the presence of trifluoroethanol (TFE) as a cosolvent due to the poor solubility of peptides in aqueous solutions. TFE facilitates intramolecular hydrogen bonding, thereby promoting folded conformations. As an illustration, the CD spectra of the Ac-KLVFF peptide at varying TFE concentrations are presented.
At a low TFE percentage (5%), the CD signature was indicative of an unordered structure. An increase in the TFE content (36%) resulted in a red shift of the negative band at approximately 210 nm, accompanied by the appearance of a positive band at 190 nm.

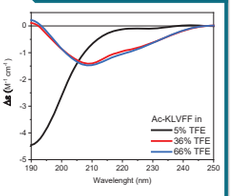

Far-UV CD spectra of the Ac-KLVFF peptide at different percentages of TFE at 25°C , cell 0.01 cm optical path.

Consequently, the conformational effects of POM on the secondary structure of peptides were investigated at two distinct TFE percentages (5 and 36%, respectively). The CD spectra of the Ac-KLVFF peptide in the presence of varying quantities of POM at different TFE percentages indicate that the **polyoxymetalate induces an ordered structure**.

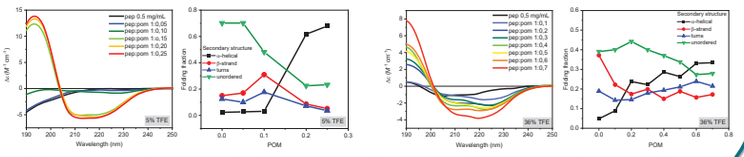

A *and* ***C****) Far-UV CD spectra of Ac-KLVFF peptide at different percentages of TFE in presence of increasing amount of POM at 25°C, cell 0.1 cm pathlength.* ***B*** *and* ***D****) Secondary structure estimation.*

DYNAMIC LIGHT SCATTERING

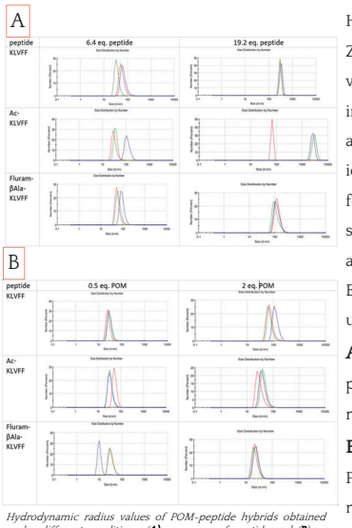

*Hydrodynamic radius values of POM-peptide hybrids obtained under different conditions: (**A**) an excess of peptide and (**B**) an excess of POM.*

Hydrodynamic diameter and Zeta potential measurements were used to investigate the interaction of the KLVFF peptide and its derivatives with POM and identify the optimal conditions for forming POM-peptide hybrid systems compatible with administration in Drosophila. Experiments were carried out under two distinct conditions:

A) in the presence of an excess of peptide, keeping the number of moles of POM constant (50 µm);

B) in the presence of an excess of POM, keeping the number of moles of peptide constant (60 µm).

The data obtained indicate that Fluram-βAla-KLVFF peptide-POM hybrid systems are **compatible** with the administration in Drosophila.

EX VIVO EXPERIMENTS IN DROSOPHILA

In order to evaluate the capacity of the peptide and POM-peptide systems to cross the blood-brain barrier (BBB) in Drosophila, *ex vivo* experiments were conducted. Third-instar larvae expressing an endoplasmic reticulum membrane marker (td-Tomato-Sec61β, red) in neurons were dissected and incubated for one hour with HL3 (untreated), Fluram-βAla-KLVFF (25 µM), and POM-fluram-βAla-KLVFF (100 µM).

The confocal microscopy images of the brain ganglia and muscle tissues indicate that **neither the peptide nor the POM-peptide hybrid is able to cross the BBB**, as no green signal is visible in the neuronal cells.

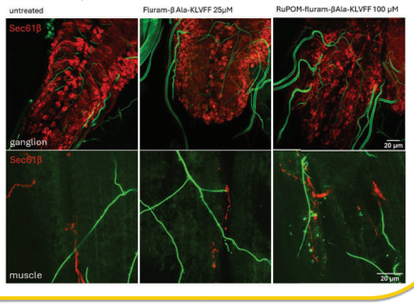

Representative images of dorsal ganglion and muscle tissue of untreated Drosophila tomato/elav III stage larvae treated with Fluram-βAla-KLVFF and POM/Fluram-βAla-KLVFF hybrid. Scale bar 20 µm.

Samples from the DLS analysis were lyophilised and subsequently subjected to TEM analysis. The sample comprising the hybrid POM KLVFF exhibited the presence of **extensive aggregates**, with dimensions spanning the micrometre range, and spherical nanoparticles, measuring approximately 100 nm. Hybrids comprising Ac-KLVFF and Fluram-βAla-KLVFF peptides also display large aggregates, albeit of a smaller size (approximately 500 nm) and in lower quantities.
The latter are predominantly characterised by **spherical particles** with a size of **100-200 nm**, exhibiting notable similarity.

TEM

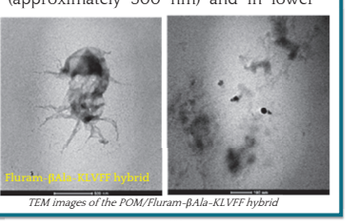

TEM images of the POM/Fluram-βAla-KLVFF hybrid

1. H. Chaudhary, I. A. Iashchishyn, N. V. Romanova, M. A. Rambaran, G. Musteikyte, V. Smirnovas, M. Holmboe, C. A. Ohlin*, Ž. M. Svedružić*, and L. A. Morozova-Roche ACS Appl. Mater. Interfaces 2021, 13, 26721−26734

This work was supported by PRIN 2022 National Project (Grant N. 2022CAS9ZT, Development of HYbrid and Multifunctional Bio-conjugates against Alzheimer's Disease - HYMBAD).

The potential use of peptides in pancreatic cancer

Martina Rotondo[1], Giovanna Bossio[2], Sofia Parassia[3], Andrea Mattarei[4], Claudia Honisch[2], Ildikò Szabò[3], Lucia Biasutto[5], Paolo Ruzza[2]

[1]Università Degli Studi di Napoli Federico II, Napoli, Italy
[2]Institute of Biomolecular Chemistry of CNR, Padua Unit, Padova, Italy
[3]University of Padova, Department of Biology, Padova, Italy
[4]University of Padova, Department of Pharmaceutical and Pharmacological Sciences, Padova, Italy
[5]Padua Unit, Neuroscience Institute of CNR, Padova, Italy
https://doi.org/10.17952/37EPS.2024.P1245

Pancreatic ductal adenocarcinoma (**PDAC**) is the most common type of pancreatic cancer and is among the most aggressive and still incurable cancers. Innovative and successful therapeutic strategies are extremely needed. Many approaches are under investigation to improve PDAC therapy. **The use of peptides is one of the possible delivery strategies to achieve tumor targeting.**

In recent decades, peptide-drug conjugates (**PDCs**) have been studied as new targeted therapies. PDCs combine a monoclonal peptide, a cytotoxic payload, and a linker, optimizing drug specificity and reducing adverse effects. These systems, composed of cyclic or linear peptides with low molecular weight, could allow for payload loading and better penetration into tumor tissues.

BACKGROUND

We found that several receptors capable of interacting with different peptides are overexpressed in pancreatic cancer cells, such as:

- The **CCK2R** receptor
- The **GRPR** receptor
- The **LDL-R** receptor
- The **Neuropilin-1**

Successively, the **Pan02** cell line, a murine pancreatic adenocarcinoma cell line, were selected to be tested.

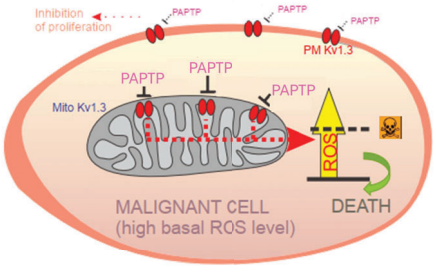

Among the various cargoes that could be tested for delivery to the cells, we opted for **PAPTP**, a mitochondria-targeted compound with promising anticancer effects. Mitochondria are emerging as a crucial target for cancer therapy and our derivative binds to and inhibits the **Kv1.3 channel** residing in the inner mitochondrial membrane, causing oxidative stress and selectively killing cancer cells while sparing normal ones.

SYNTHESIZED CONJUGATES

PEPTIDES

Elongated with a spacer containing an *alkyne group*

Linear Peptides

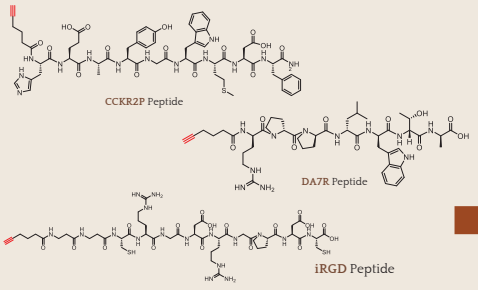

Cyclic Peptides

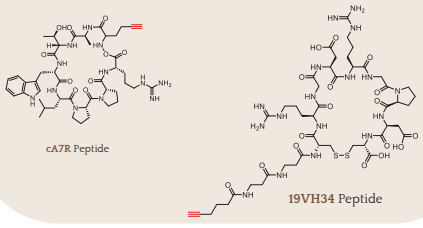

PAPTP

PAPTP is an antitumor drug derived from the psoralenic compound PAP-1. Its accumulation in the mitochondria is due to the presence of a permanent lipophilic cation, triphenylphosphonium (TPP+), attached to the molecule via a stable C-C bond.

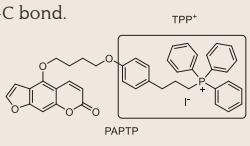

PAPTP was modified with the addition of a short linker containing an *azido moiety* to allow conjugation with the peptide in a position not interfering with binding to and inhibition of Kv1.3

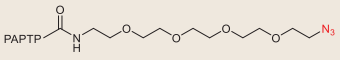

Other linkers have been used, such as the amino acid isoleucine (I), which allows peptide conjugation through an amide bond.

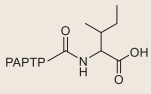

CLICK REACTION

- biologically compatible conditions (aqueous environment, room temperature, and physiological pH)
- limited or no production of by-products.

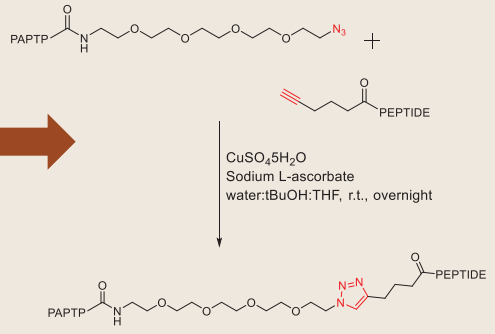

BIOLOGICAL TEST

Some of the peptides, when conjugated with PAPTPL, become haemolytic. This renders the PAPTPL-peptide construct unsuitable for *in vivo* applications, since the derivatives are expected to reach the bloodstream upon administration.

Haemolysis studies performed with red blood cells isolated from blood from mice. Data expressed as % haemolysis in comparison to that induced by Triton X -100.

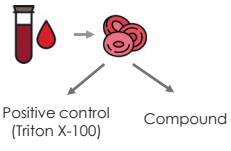

A7R variants:
(Parrasia S. et al, Pharmaceutics 2023)

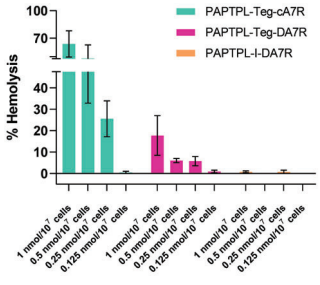

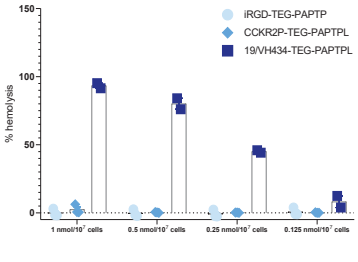

CONCLUSION

- The SPPS technique produced few by-products, avoiding the need for purification for most peptides.
- The CuAAC coupling reaction was effective under mild conditions for most peptides. The use of microwaves is suggested for future syntheses.
- Conjugation of peptides with PAPTP may cause unexpected properties of the resulting derivative, such as emolytic properties.
- *In vivo* experiments with a PDAC orthotopic mouse model are under way to test phramacokinetic and antitumoral properties of non-hemolytic derivatives.
- Non-hemolytic constructs are under study in mice, for their tissue distribution profiles, their ability to accumulate in the pancreas and PDAC, and their efficacy in reducing tumor mass in an orthotopic PDAC mouse model.

https://doi.org/10.17952/37EPS.2024.P1246

Evaluation of different spin labels for the study of protein-peptide interaction in cellular extract using Electron Paramagnetic Resonance spectroscopy techniques

Funded by the European Union NextGenerationEU

Claudia Toso[1], Giovanni Loprete[1], Elisabetta Bergantino[1], Simone Fabbian[1], Massimo Bellanda[1], Sylvain Marque[2], Gerard Audran[2], Marina Gobbo[1], Marta De Zotti[1], Donatella Carbonera[1], Marco Bortolus[1], Marilena DI Valentin[1]

[1]*University of Padova, Padova, Italy;* [2]*Aix Marseille Université, Marseille, France*

ABSTRACT

Calmodulin (CaM) is a protein involved in cellular signaling and undergoes specific conformational changes in the presence of Ca^{2+} ions and target peptides like M13.[1] In this study, some CaM mutants were labeled with two different nitroxide probes. Then, M13 was synthesized via SPPS and an aliquot was labeled with a porphyrin. Using EPR spectroscopy, CaM's conformational changes were observed both in buffer and in cell-mimetic environments, leading to evaluate the suitability of the selected probes, i.e., their resistance to reduction. Continuous Wave EPR reduction kinetics and pulsed EPR (DEER) experiments confirmed nitroxide probes' suitability and showed the major conformational changes of CaM in terms of interspin distances. Preliminary studies of nitroxide-labeled CaM's interaction with porphyrin-labeled M13 assessed triplet probe adequacy in perspective of distance measurements using dipolar EPR techniques coupled with photoexcitation. [2]

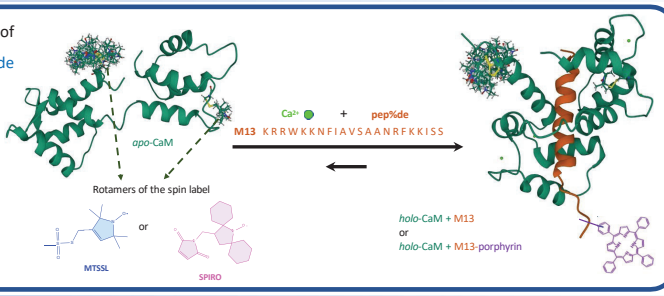

M13 pep'de synthesis

CaM's target peptide, M13, has a sequence rich in hydrophobic amino acids, allowing good interaction with CaM, which literally wraps the peptide creating a hydrophobic tunnel around it.[3,4] M13 (residues 1-19 of the peptide) was obtained through solid-phase peptide synthesis (SPPS), with a 63% final yield and a 92% purity. Porphyrin TPP was added to the N-terminal unprotected amine as TPP-COOH, by a standard coupling reaction.

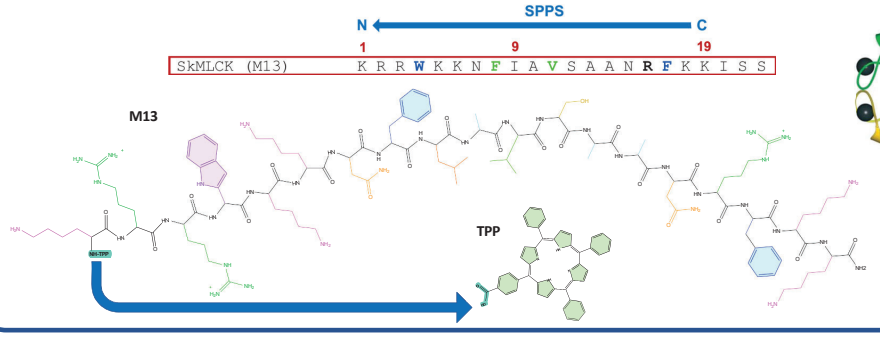

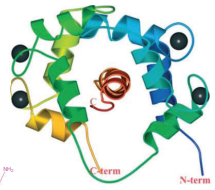

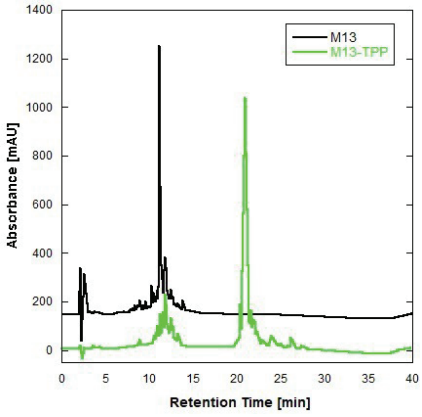

Con'nuous Wave EPR

Experimental setup. Block diagram of an EPR spectrometer.[5] The signal reflected from the resonant cavity is modulated at a specific frequency and then amplified by the lock-in amplifier. A derivative signal of the absorption spectrum, is obtained.

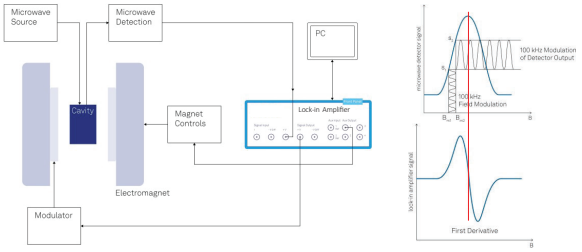

Experimental results. Kinetic measurements for the two different spin labels, MTSSL and SPIRO. In the figures below the results for the E114C mutant of CaM are reported, aquired in ascorbate and in cellular extract envoironments.

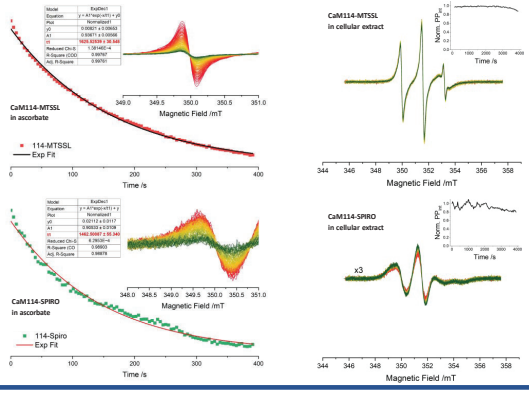

Double electron-Electron Resonance (DEER)

Experimental setup. DEER was used to obtain interspin distances in the protein complex. A four pulse sequence is employed, at two specific microwave frequencies, ω_A and ω_B.[6] The DEER signal is an oscillating and decaying function in time, whose modulations are given by the dipolar interaction between the interacting spins, i.e., depends on their mutual distance. The DEER traces in function of time are then converted into a distribution of distances.

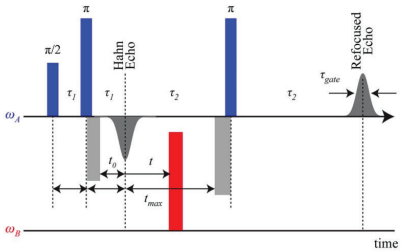

$$\omega_{AB}(\theta,r) = -\frac{\mu_0 g_A g_B \mu_B^2}{4\pi\hbar}\frac{1}{r_{AB}^3}(3cos^2\theta - 1)$$

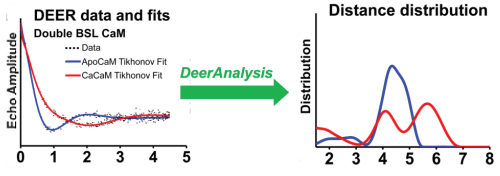

Experimental results. The DEER measurements provided structural distance costraints for the double mutants E6CI100C and E6CE114C of CaM, labeled with SPIRO. The results confirmed that CaM is at equilibrium between different conformations (closed/*apo*, open/*holo* in the presence of Ca^{2+}, compact in the presence of Ca^{2+} and M13). The results in cellular extract were comparable to the ones in buffer solution.

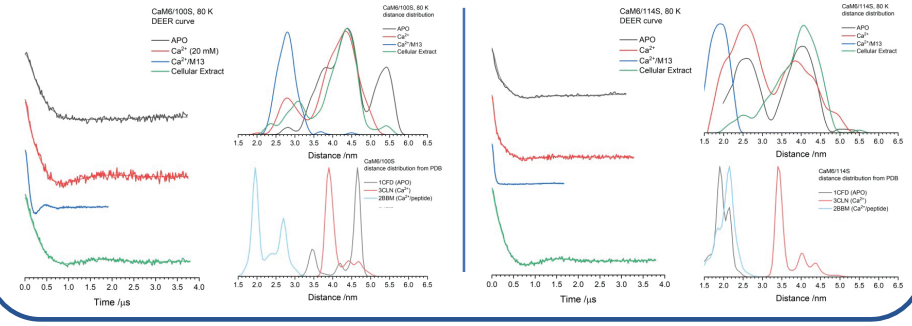

Future perspec'ves: light-induced pulsed EPR measurements in cell

The next steps include bringing EPR measurements directly into the cell, as well as the possibility of exploring the protein-ligand interaction by means of pulsed EPR measurements coupled to photoexcitation that could provide distance measurements between the protein and the porphyrin-labeled peptide.

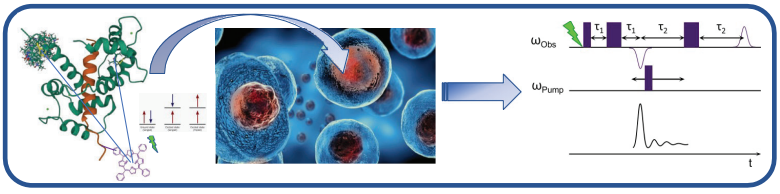

References:
1. Hultschig, C.; Hecht, H.-J.; Frank, R. *J Mol Biol* 2004, 343 (3), 559–568.
2. Di ValenHn, M. et al. *J. Am. Chem. Soc.* 2014, 136 (18), 6582–6585.
3. Ikura, M.; Clore, G. M.; Gronenborn, A. M.; Zhu, G.; Klee, C. B.; Bax, A. *Science* (1979) 1992, 256 (5057), 632–638
4. Hultschig, C.; Hecht, H.-J.; Frank, R. *J Mol Biol* 2004, 343 (3), 559–568.
5. hTps://www.zhinst.com/europe/it
6. Schiemann, O.; Jeschke, G. *et al, J Am Chem Soc* 2021, 143 (43), 17875–17890.

37th EPS European Peptide Symposium
14th IPS International Peptide Symposium
25 - 29 August 2024 Satellite Workshop 30 - 31 August 2024
Florence, Italy- 2024
ISTITUTO NAZIONALE TUMORI IRCCS - Fondazione Pascale

Development of a cell penetrating peptide carrying a biological active HPV16 E6 inhibitory molecule for delivery into cervical cancer cells

A.L. Tornesello [a], L. Dassi[b], V. De Gregorio[c], G. Imparato[d], M. Leone[e], L. Wuyuan[f], N. Starita[g], A. Cerasuolo[g], L. Buonaguro[a], F.M. Buonaguro[g], M.L. Tornesello[g],

https://doi.org/10.17952/37EPS.2024.P1247

[a]*Innovative Immunological Models Unit, Istituto Nazionale Tumori IRCCS Fondazione G. Pascale, Napoli, Italy;* [b]*Department of Precision medicine, Università della Campania, Luigi Vanvitelli, Napoli, Italy;* [c]*Interdisciplinary Research Centre on Biomaterials (CRIB), University of Naples Federico II, Naples, Italy; Center for Advanced Biomaterials for HealthCare@CRIB, Istituto Italiano di Tecnologia, Naples, Italy;* [d]*Center for Advanced Biomaterials for HealthCare@CRIB, Istituto Italiano di Tecnologia, Naples, Italy;* [e]*Institute of Biostructures and Bioimaging, Via Pietro Castellino 111, 80131 Naples, Italy;* [f]*Department of Biochemistry and Molecular Biology, University of Maryland School of Medicine, Baltimore, MD, United States of America;* [g]*Molecular Biology and Viral Oncology Unit, Istituto Nazionale Tumori IRCCS Fondazione G. Pascale, Napoli, Italy*

Introduction and Aim

The E6 oncoprotein encoded by high-risk human papillomaviruses (HPV) plays a crucial role in the development of cervical cancer mainly via degradation of the tumor suppressor protein p53. HPV E6 protein forms an heterodimer with the E3 ubiquitin ligase E6 associated protein (E6AP), which recruits p53 causing its ubiquitination and proteasomal degradation. Yeast two-hybrid screening of a randomized peptide expression library previously allowed the identification of the E6-binding 15-mer peptide, named pep11, which inhibited the formation of the E6/E6AP complex. The intracellular expression of pep11 caused the specific inhibition of colony formation of HPV16-positive cancer cells, abrogated p53 degradation and induced cell death selectively in HPV16-positive cancer cells[(1)]. Several attempts were made to chemically synthesize pep11, however, due to its aggregation tendency and high hydrophobicity, the yields were very poor and the peptide was insoluble in aqueous solution. Then, subsequent studies focused on the development of a modified pep11 sequence named pep11**[(2)].

We aimed to chemically synthesize a modified pep11 (CPP-pep11) containing a short cell penetrating peptide (CPP) moiety bound to the N-terminal end of the original pep11, in order to facilitate its solubility and delivery into HPV-positive cancer cells.

CPP - pep11
Biot-**RRRRRR**-**EFGSGCSCIVCIGLI**-NH_2

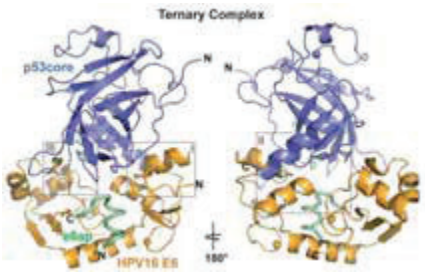

Figure 1: Structure of the HPV16 E6/e6ap/p53core ternary complex (green: E6AP peptide, gold: HPV16 E6, purple: p53 core[(3)]. Biotin was bound to the N-terminus.

Methods

Boc solid-phase peptide synthesis: The RRRRRR-EFGSGCSCIVCIGLI-NH2 (CPP-pep11) peptide was synthesized, at Laboratory of Biochemistry and Molecular Biology (Institute of Human Virology, Baltimore), on an automated peptide synthesizer, Applied Biosystems ABI 433, adopting the 0.250 mmol scale and using N,N-Diisopropylethylamine (DIPEA) in situ neutralization/HBTU activation protocol for Boc solid-phase peptide synthesis. Biotin at N-terminus was conjugated manually adding 1.2 equivalents of Biotin N-hydroxysuccinimide ester dissolved in DMF containing 2 equivalents of DIPEA. The coupling time was overnight at room temperature under stirring. The peptides derivatives were treated for the cleavage with anhydrous hydrofluoric acid (HF) in the presence of 5% p-cresol at 0 °C for 1h, followed by precipitation with cold diethyl ether. The precipitates were dried and solubilized in water (0.1% TFA) for the purification.

Analysis and purification: The crude compounds were purified by reverse-phase high-performance liquid chromatography RP-HPLC using a Waters C18 column eluted with H2O/0.1% TFA (A) and CH3CN/0.1% TFA (B) with linear gradient from 20 to 40% B over 2h at 40ml/min. Molecular weights were verified by electrospray ionization mass spectrometry (ESI-MS).

Cell culture and CPP-pep11 treatments: HPV16 positive cervical cancer-drived SiHa cell line (p53 wild type) were used for these studies. Cells were grown in Dulbecco's Modified Eagle's Medium (DMEM) high glucose supplemented with 10% fetal bovine serum (FBS), 2mM L-Glutammine and 100U/ml Penicillin - 100µg/mL Streptomycin at 37°C and 5% CO2. Cells were seeded in 6-well plate (3 x 10^5/well) and treated at decreasing concentrations of 20, 10, 5, 2, 1 µM for 5h, 24 and 48 h to monitor CPP stability at longer time and alteration in p53 levels.

Western blotting analysis: Cells treated with CPP-pep11 were washed three times with PBS1x and scraped into 300 µL RIPA buffer. Protein concentration was determined by Bradford method and 20 µg of proteins separated by electrophoresis either in 10% SDS-polyacrilammide gel, to detect cell proteins, or in 16% Tricine-SDS-page gel to detect CPP-pep11.

Confocal microscopy: SiHa cells were grown on glass coverslips in 6/well plate at a density of 3 x 10^5 and incubated for 24 hours in DMEM 10% FBS and then treated with CPP-pep11 and CPP-Scrpep11 20 µM, 2 µM and 0,5 µM for 5 h. Cells were fixed in 4% formaldehyde for 10 min at RT and permeabilized with 0.1% Triton ×100. The CPP-pep11 conjugates were incubated for 2 h. After incubation, the membrane-bound cargo was quenched with avidin. The intracellular cargo was then visualized with fluorescent streptavidin (streptavidin-Alexa488, in green). Nuclei were stained with DAPI (in blue), Phalloidin in red, CPP in green, DAPI in blue for nuclei.

Results

We have synthesized via Boc chemistry an optimized pep11 peptide containing a short cell penetrating peptide (CPP) at the N-terminus end (CPP-pep11). The CPP-pep11 was successfully synthesized and was further reacted with biotin. The CPP-pep11 yielded a 95-97% pure peptide, which was soluble in water at 20 µM concentration. The ability of CPP-pep11 to spontaneous penetrate cell membrane was evaluated on HPV-positive cervical cancer SiHa cells, which were incubated with serial dilutions (10, 5, 2, 1 µM) of biotin-labelled CPP-pep11 (bio-CPP-pep11) for 24, 48 and 72 hours. The cell uptake and intracellular distribution was evaluated by confocal microscopy (Figure 2. A-B). The CPP-pep11 at 2uM concentration showed an optimal internalization efficiency with homogenous distribution in the cytoplasm and in the nucleus. However, 20uM concentration of CPP-pep11 affected cell viability causing rupture of cell membranes. Western blot analysis of biotinylated CPP-pep11 in the cells showed levels of peptide concordant with the input, demonstrating stability over the time of CPP-pep11 in the cells.

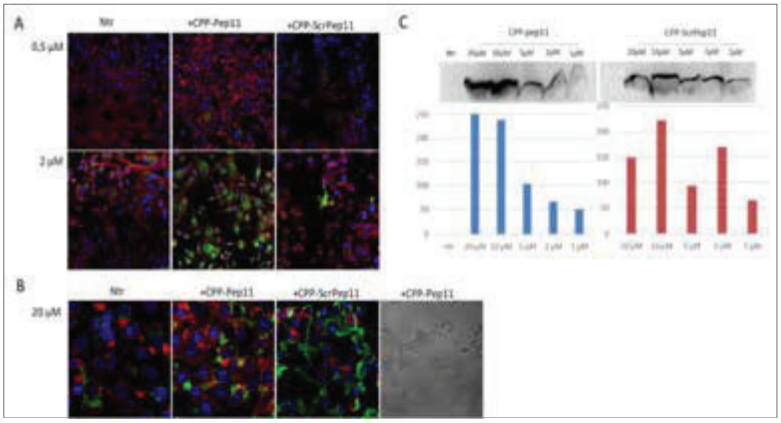

Figure 2: (A, B) Immunofluorescence of SiHa cells after treatment with CPP-pep11. The biotinylated internalized CPP-pep11 was visualized by confocal microscopy.
(C) immunoblotting of SiHa cellular exctracts afte 5 hours treatment with 20, 10, 5, 2 and 1 µM of CPPs. Lower, the graph indicates the CPP amount in the cells compared to the concentration used. The uptake of CPP-pep11 reduces on decreasing of micromolarity; for CPP-Scrpep11 is variable.

Conclusions

In conclusion, the addition of a CPP sequence to pep11 allowed to obtain a good yield of an extremely hydrophobic pepted, to enhance its solubility and to facilitate the uptake into the cells- The CPP-pep11 might be a promising anti-cancer moiety. Indeed, the CPP-pep11, by restoring the tumor suppressor function of p53, may hold promise as a potential therapeutic strategy for treating HPV-positive cervical carcinoma.

Correspondence should be addressed to: m.tornesello@istitutotumori.na.it; a.tornesello@istitutotumori.na.it;

References

1) Dymalla S, Scheffner M, Weber E, Sehr P, Lohrey C, Hoppe-Seyler F, Hoppe-Seyler K. A novel peptide motif binding to and blocking the intracellular activity of the human papillomavirus E6 oncoprotein. J Mol Med (Berl). 2009 Mar;87(3):321-31.

2) Zanier K, Stutz C, Kintscher S, Reinz E, Sehr P, Bulkescher J, Hoppe-Seyler K, Travé G, Hoppe-Seyler F. The E6AP binding pocket of the HPV16 E6 oncoprotein provides a docking site for a small inhibitory peptide unrelated to E6AP, indicating druggability of E6. PLoS One. 2014 Nov 10;9(11):e112514.

3) Martinez-Zapien D, Ruiz FX, Poirson J, Mitschler A, Ramirez J, Forster A, Cousido-Siah A, Masson M, Vande Pol S, Podjarny A, Travé G, Zanier K. Structure of the E6/E6AP/p53 complex required for HPV-mediated degradation of p53. Nature. 2016 Jan 28;529(7587):541-5.

37th EPS European Peptide Symposium
14th IPS International Peptide Symposium
Florence, Italy 25 - 29 August 2024

THE ANTIMICROBIAL PEPTIDE SET-M33: *IN VIVO* EFFICACY AND TOXICITY IN DIFFERENT ANIMAL SPECIES AND ENCAPSULATION IN INHALABLE POLYMERIC NANOPARTICLES FOR PULMONARY DELIVERY

Laura Cresti [1,2,3], Giovanni Cappello [1,2], Clelia Cortese[1], Virginia Niccolini[1], Alessandro Pini [1,2,3]

[1] Department of Medical Biotechnologies - University of Siena, Italy
[2] SetLance srl - Siena, Italy
[3] Azienda Ospedaliera Universitaria Senese, AOUS – Siena, Italy

https://doi.org/10.17952/37EPS.2024.P1249

BACKGROUND

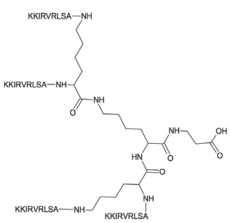

- Non-natural 9-aa cationic peptide synthetized in a tetrabranched form with four sequences linked by a lysine core
- Multiple Antigen Peptides (MAPs) acquire high resistance to protease and peptidase activity making these molecules good candidates for *in vivo* use.
- SET-M33 showed strong resistance to proteolytic degradation when synthetized in a tetrabranched form
- Strong antimicrobial activity against Gram-negative bacteria and MDR bacteria

AIM OF THE STUDIES

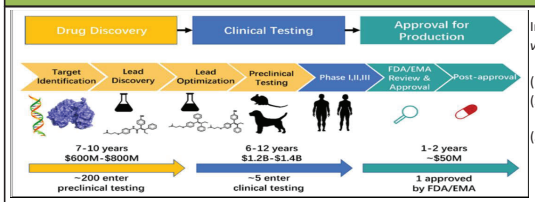

In recent years we focused on the pre-clinical development of the peptide in terms of *in vivo* efficacy and toxicity. In particular, we analysed:

(1) The local and systemic toxicity of SET-M33 in an inhalation study in mice;
(2) The efficacy of aerosolized SET-M33 in a mice model of endotoxin (LPS)-induced pulmonary inflammation;
(3) The toxicity study of SET-M33 by intravenous administration in rats and dogs, two animal species recommended as rodent and non-rodent test systems, respectively, by international guidelines.

Considering the certain degree of toxicity emerged by these studies, we concentrated our research on strategies to reduce the toxic effects at the local level, while maintaining its efficacy. With this purpose, the idea of peptide encapsulation in biocompatible nanoparticles (NPs) came up. A promising formulation approach is the encapsulation in a poly(lactide-co-glycolide) nanoparticles that mask the charges of SET-M33, preserve its bioactive structure, reduce side effects, facilitate transport to bacteria and achieve a prolonged therapeutic effect.

EFFICACY AND TOXICITY IN A MURINE MODEL OF PULMONARY INFLAMMATION

International Journal of Molecular Sciences
MDPI
Article

In Vivo Efficacy and Toxicity of an Antimicrobial Peptide in a Model of Endotoxin-Induced Pulmonary Inflammation

Laura Cresti [1,2], Giovanni Cappello [2,3], Silvia Vailati [4], Elsa Melloni [4], Jlenia Brunetti [2], Chiara Falciani [2], Luisa Bracci [1,2] and Alessandro Pini [1,2,*]

Int. J. Mol. Sci. **2023**, *24*, 7967. https://doi.org/10.3390/ijms24097967



Crl:CD-1(ICR) mice (for toxicity study)
Balb/c mice (for efficacy study)

1) Toxicity study of SET-M33 administered by snout inhalation exposure for 1 h/day for 7 days at doses of 5 and 20 mg/kg/day

2) Efficacy study of the peptide in an endotoxin (LPS)-induced pulmonary inflammation model. Intratracheal administration of SET-M33 at 0.5, 2 and 5 mg/kg

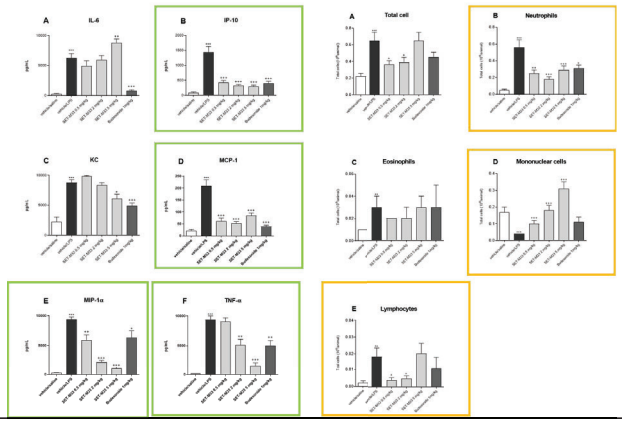

The no observable adverse effect level (**NOAEL**) for aerosol administration was considered to be **5 mg/kg/day in murine model**

The outcome of the *in vivo* toxicity and efficacy studies showed that a value ≤ NOAEL dose is compatible with anti-inflammatory efficacy

SAFETY EVALUATIONS IN RATS AND DOGS OF SET-M33 ADMINISTERED INTRAVENOUSLY



Sprague Dawley rats



Naive beagle dogs

scientific reports
OPEN

Safety evaluations of a synthetic antimicrobial peptide administered intravenously in rats and dogs

Laura Cresti[1,2], Chiara Falciani[2], Giovanni Cappello[1,2], Jlenia Brunetti[2], Silvia Vailati[4], Elsa Melloni[4], Luisa Bracci[1,2] & Alessandro Pini[1,2,*]

Scientific Reports | (2022) 12:19234 | https://doi.org/10.1038/s41598-022-23841-2

4-week daily administration by infusion for the evaluation of macroscopic and clinical signs of toxicity with a recovery period of 2 weeks for rats and 4 weeks for dogs.

Parameters evaluated: dose ranging finding (DRF), neurological toxicity, respiratory function, cardiac parameters, clinical laboratory investigations, bio-analytics and toxicokinetic, histopathology.

1) Daily administration of SET-M33 at the highest doses (15 mg/kg/day and 4mg/kg/day for rats and dogs, respectively) caused renal effects, such as tubule degeneration/regeneration, elevated blood concentrations of urea and creatinine, high glucose (only in rats), all of these identifying the **kidneys** as a target for toxic effects, thus suggesting a functional deficit. This confirms the bio-distribution and excretion data obtained previously with radio-iodinate SET-M33, which showed an evident uptake of the peptide by kidneys and bladder after intravenous administration of the peptide to mice (Brunetti J. *et al*, Sci Rep. 2016;6:26077. doi: 10.1038/srep26077).

2) The bioanalytical evaluation of blood parameters and the histological analysis did not suggest any possible toxic effects on other organs in rats and dogs. The lower doses did not provoke any detectable side effect for all organs evaluated.

3) The results obtained with SET-M33 administered intravenously indicate that the **NOAEL** resulted ≤1 mg/Kg/day.

INHALABLE POLYMERIC NANOPARTICLES FOR PULMONARY DELIVERY OF SET-M33: ANTIBACTERIAL ACTIVITY AND TOXICITY *IN VITRO* AND *IN VIVO*

SET-M33-loaded PLGA NPs

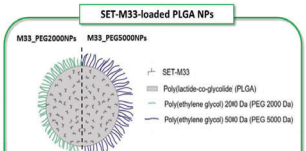

Production of nanoparticles

PLGA-based nanoparticles (NPs) containing SET-M33 peptide is prepared by a modified emulsion/solvent diffusion technique at 4% theoretical loading (4mg of M33 *per* 100 mg of NP). Formulation was prepared adding poly(lactic-co-glycolic acid) (PLGA) conjugated with polyethylene glycol (PEG) at two different molecular weight (2000 Da and 5000 Da) to the organic phase containing PLGA

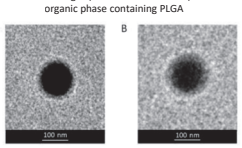

TEM images of M33-loaded NPs: M33_PEG2000 NPs (A) and M33_PEG5000 NPs (B).

In vitro release of SET-M33 peptide from nanoparticles

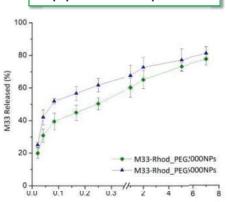

The two NPs formulations showed typical controlled release of the peptide lasting about 7 days.
The mechanism of release can be related to the diffusion process

In vitro diffusion studies across simulated lung barriers

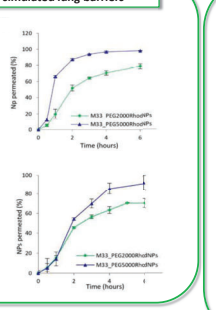

Anti-bacterial activity *in vitro*

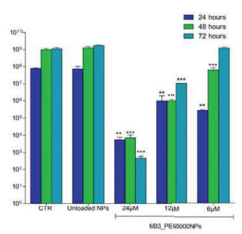

Antibacterial activity persisted up to 72 hours when M33_PEG5000 NPs were loaded at the higher concentrations and up to 48 hours with M33_PEG5000 NPs loaded with 6 μM SET-M33. Evident dose-dependent manner.

Anti-biofilm activity *in vitro*

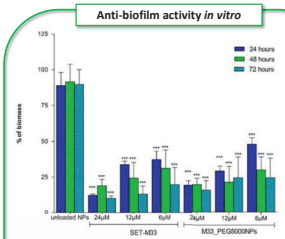

The profile of anti-biofilm activity of M33_PEG5000 NPs was very similar to that of the free peptide; it had a dose-dependent trend and the greatest reduction in biomass was at 24 μM. Like the free form of the peptide, M33_PEG5000 NP activity was strongest after 72 hours.

Cytotoxicity

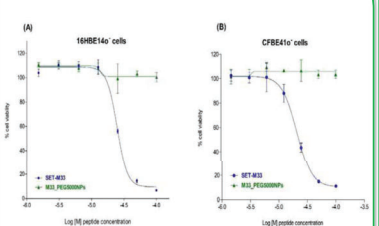

No toxicity was detected for M33_PEG5000 NPs, whereas the free peptide at the same concentrations as in the NPs showed an EC_{50} of ≈22μM on both cell lineage.

In vivo Acute Toxicity

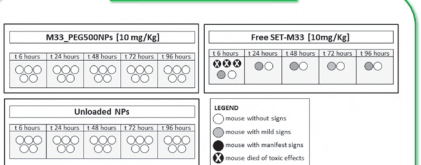

Mice were treated via i.t. administration of free SET-M33 and M33_PEG5000 NPs at the same peptide concentration (10 mg/Kg). Mice were checked for signs of toxicity for up to 96 h. No signs of toxicity were observed in mice treated via i.t. administration of M33_PEG5000 NPs and unloaded nanoparticles, confirming the absence of toxicity already seen in cytotoxicity tests, and the high biocompatibility of the material used.
i.t. administration of free SET-M33 caused three deaths within 6 h, mild signs in one mouse and no signs in another mouse.

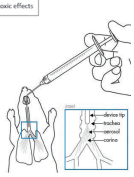

pharmaceutics
MDPI
Article

Inhalable Polymeric Nanoparticles for Pulmonary Delivery of Antimicrobial Peptide SET-M33: Antibacterial Activity and Toxicity In Vitro and In Vivo

Laura Cresti [1,2,3], Gemma Conte [4], Giovanni Cappello [2,3], Jlenia Brunetti [2], Chiara Falciani [2], Luisa Bracci [1,2], Fabiana Quaglia [5], Francesca Ungaro [5], Ivana d'Angelo [4,*] and Alessandro Pini [1,3,*]

Pharmaceutics **2023**, *15*, 3. https://doi.org/10.3390/pharmaceutics15010003

ACKNOWLEDGEMENT

SETLANCE
Azienda Ospedaliera Universitaria Senese
Zambon
labcorp Drug Development
PolyPeptide

CONTACTS

Dr. Laura Cresti, Ph.D.
Technologist
Department of Medical Biotechnologies
University of Siena
laura.cresti2@unisi.it

https://doi.org/10.17952/37EPS.2024.P1250

Affibody-mediated peptide nucleic acid pretargeting for delivery of cytotoxic payloads to HER2 positive carcinoma

Jacob Clinton[1], Kristina Westerlund[1] and Amelie Eriksson Karlström[1]

[1] Department of Protein Science, KTH - Royal Institute of Technology, Stockholm, Sweden

Key concepts

Pretargeted cytotoxic therapy is the concept of separating the tumor targeting agent from the cell-killing agent in order to reduce toxic exposure to healthy tissues.

1. First, a **tumor-targeting primary probe** is injected and allowed to bind the highly expressed tumor associated receptor

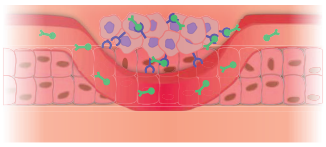

Tumor targeting with **primary probe**

2. A waiting time follows the first injection where any residual accumulated unbound primary probe is **cleared** from circulation and from healthy organs

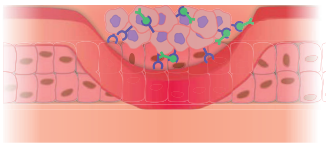

Clearance of unbound primary probe

3. After the waiting time, a fast clearing **cytotoxic secondary probe** is injected with high affinity and specificity to the primary probe, minimizing toxic exposure to healthy tissues

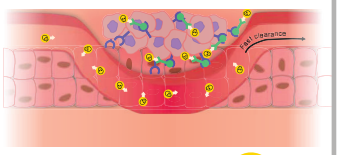

Injection of fast clearing **cytotoxic secondary probe**

The **primary probe** consists of the HER2-targeting **Affibody** ZHER2 conjugated to the single stranded peptide nucleic acid (**PNA**) sequence **HP9**

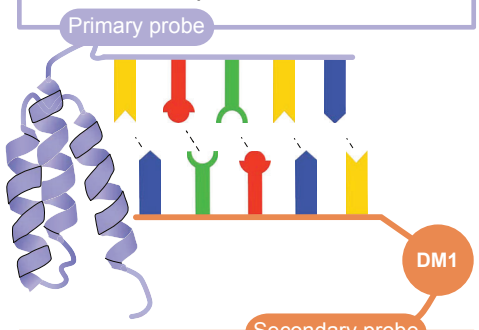

The cytotoxic **secondary probe** consists of the toxic molecule **DM1** coupled to the **complementary PNA** sequence to that of the HP9 probe

Aim and method

- Previously pretargeting has been successful in a system of targeted radiotherapy with a radioactive metal conjugated to the secondary probe.
- We explore the possibility of changing the radioactive metal on the secondary probe to the toxic molecule DM1.
- Six different 8-mer PNA base long secondary probes were produced. Their binding characteristics and cellular toxicity was analyzed with SPR and cytotoxicity assays.

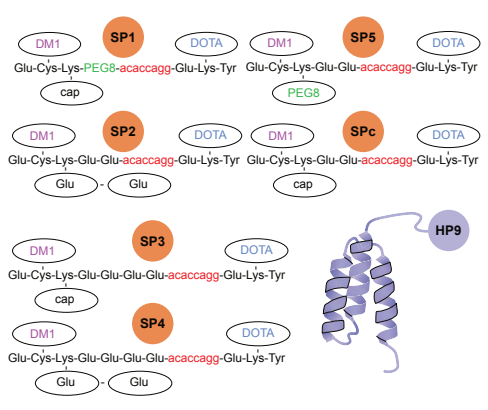

Figure 1: Sequences of the different secondary probes and schematic of the primary probe ZHER2-HP9 (purple).

Results

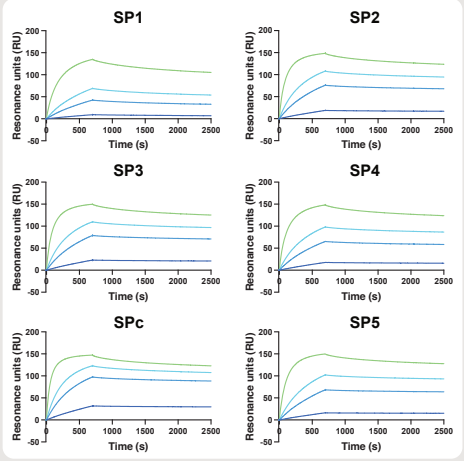

Figure 2: SPR sensorgrams of PNA hybridization between the immobilized ZHER2-HP9 and the six different secondary probes. Four concentrations ranging between 1.4 (dark blue)-70 (green) nM of each probe was used.

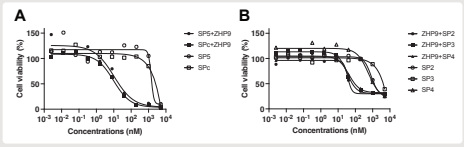

Figure 3: In vitro cellular cytotoxicity assay of secondary probes SP2-SP5 and SPc pre-incubated with and without the primary probe ZHER2-HP9 (ZHP9). Black dots, squares and triangles represent pre-incubated secondary and primary probe, whereas white ones are assays without the primary probe. A; AU565 cells and B; SKBR3 cells.

Conclusions

- Our aim is to utilize **pretargeting** in a new way where cytotoxic payloads are delivered to the tumor site while, at the same time, **minimizing toxic exposure to healthy tissues** and organs.
- We produced a panel of different mertansine (DM1) **cytotoxic secondary probes** with different hydrophilic properties to analyze binding characteristics to the **ZHER2-HP9 primary probe** together with their cell-killing potential.
- **SPR** results show that all six unique secondary probes have **strong picomolar hybridization** characteristics towards the complementary PNA sequence of ZHER2-HP9.
- Cellular **cytotoxicity assays** show **increased cell death** when cells are exposed to secondary probes combined with the ZHER2-HP9 primary probe, in contrast to secondary probes added alone.

CANCERFONDEN

Presenting author:
Jacob Clinton, Ph.D student
jclinton@kth.se

Structure-activity relationship study on the P4 structure of macrocyclic BACE1 inhibitors

○Kazuya Kobayashi[1], Momoka Kawakita[1], Takuya Otani[2], Yasunao Hattori[3], Shinya Oishi[1]

[1] *Laboratory of Medicinal Chemistry, Kyoto Pharmaceutical University, Kyoto, Japan*
[2] *Near InfraRed Photo-Immuno Therapy Research Institute, Kansai Medical University, Osaka, Japan*
[3] *Center of Instrumental Analysis. Kyoto Pharmaceutical University, Kyoto, Japan*

kkoba@mb.kyoto-phu.ac.jp

https://doi.org/10.17952/37EPS.2024.P1251

Introduction

β-Secretase (BACE1) is an aspartic protease involved in the production of amyloid β peptide (Aβ). Aβ accumulation in the brain is hypothesized to underlie the pathogenesis of Alzheimer's disease (AD), hence it is reasoned that inhibiting BACE1 will play a crucial role in the treatment of AD. Previously, we have synthesized and evaluated peptidic BACE1 inhibitors containing a hydroxyethylamine (HEA) type isostere[1,2] and discovered a macrocyclic inhibitor, inhibitor **3**, containing a hydrophobic bridge between the P1 and P3 side chains[3]. Despite displaying good activity, the membrane permeability of inhibitor **3** is constrained by high hydrophilicity, limiting its development as a drug. Therefore, we try to design macrocyclic derivatives of this inhibitor with lower hydrophilicity, to increase membrane permeability. In this study, the amino and carboxy groups of glutamic acid at the P4 position of inhibitor **3** significantly influence its hydrophilicity, hence some derivatives of inhibitor **3** with a less hydrophilic substituent at the P4 position were designed and synthesized, and their activities were evaluated.

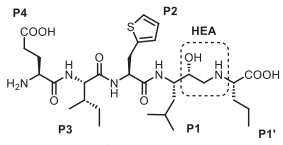

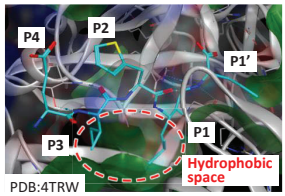

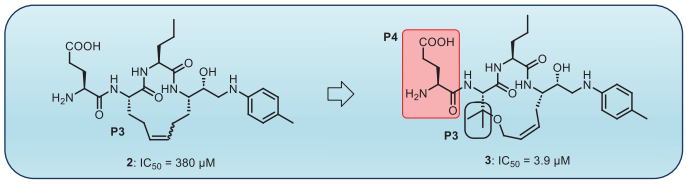

Results and Discussion

■ Synthesis of P1 fragment precursor 12

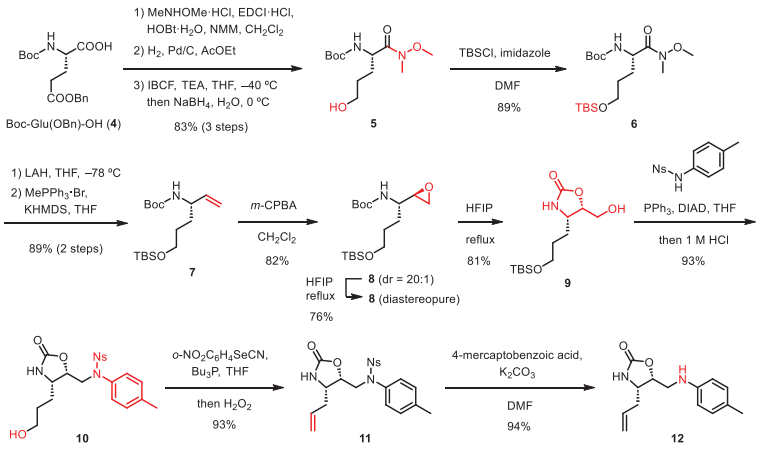

■ Synthesis of P3 fragment 19

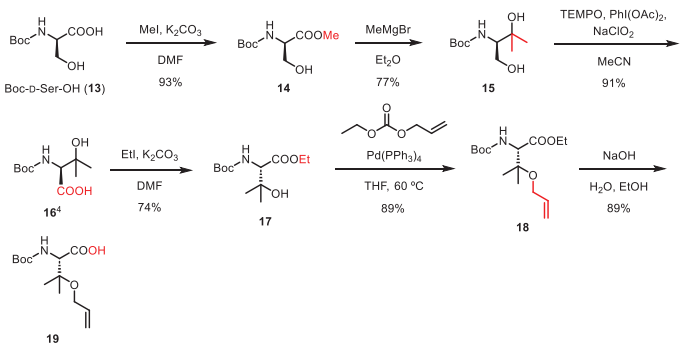

■ Synthesis of macrocyclic precursor 20

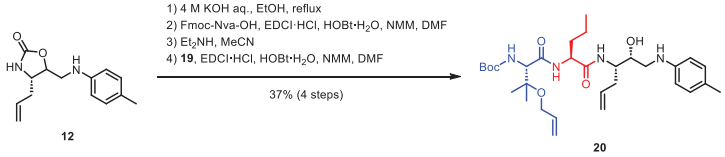

■ Synthesis of macrocyclic P4 derivatives

➢ Removal of the glutamic acid

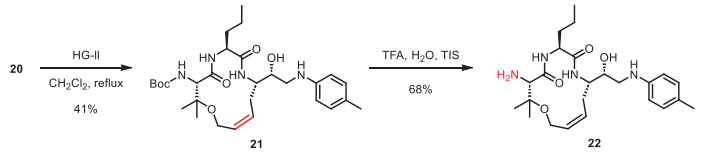

➢ Removal of the glutamic acid and reduction of the alkene

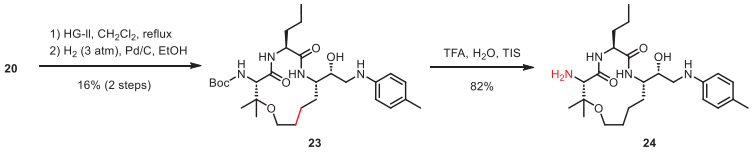

➢ Conversion of the glutamic acid to glutaric acid

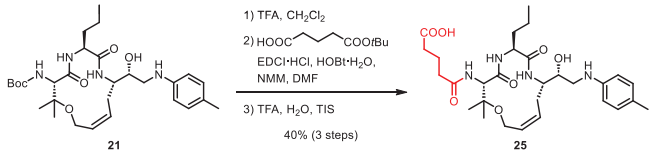

➢ Conversion of the glutamic acid to succinic acid

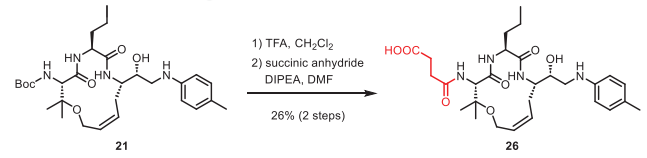

➢ Conversion of the glutamic acid to isophthalic acid (Not completed)

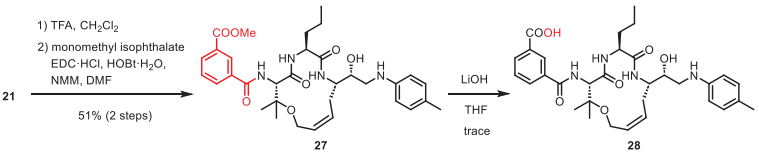

■ Evaluation of BACE1 inhibitory activity

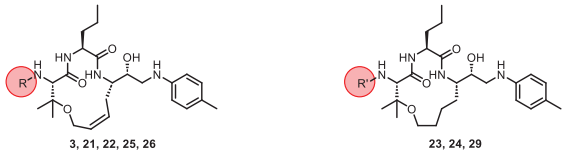

Comp.	R	IC_{50} (μM)	Comp.	R'	IC_{50} (μM)
3	H-Glu-	3.9	**29**[3]	H-Glu-	6.1
21	Boc-	124	**23**	Boc-	185
22	H-	177	**24**	H-	315
25	$HOOCCH_2CH_2CH_2CO$-	3.3			
26	$HOOCCH_2CH_2CO$-	14			

Summary

Synthesis and evaluation of macrocyclic P4 derivatives were conducted. Our study showed an alkene-containing macrocycle was a suitable ring structure for inhibitory activity compared to a reduced macrocycle (**21** and **22** vs. **23** and **24**, respectively), which was consistent with our previous work (**3** vs. **29**).

We also showed that the removal of the glutamic acid at the P4 position reduced inhibitory activity. However, the glutamate amino group has little effect on activity, while the positioning of the carboxy group is important. Optimization of the arrangement of the carboxy group is underway.

1. Hattori Y., Kobayashi K., Akaji K. *et al. Bioorg. Med. Chem.* **2015**, *23*, 5626-5640.
2. Kobayashi K., Akaji K. *et al. Bioorg. Med. Chem.* **2021**, *50*, 116459.
3. Otani T., Kobayashi K. *et al. Bioorg. Med. Chem.* **2021**, *52*, 116517.
4. Meng, Z.; Fürstner, A. *et al. J. Org. Chem.* **2018**, *83*, 6977-6994.

Non-Enzymatic Protein Catalyses Amide Bond Formation

Nicolas Brauckhoff,[a,b] Laura Fang,[a,b] Anissa Haim,[c] Tom N. Grossmann[a,b,c]

https://doi.org/10.17952/37EPS.2024.P1253

1 Principle Templated Amide Reaction

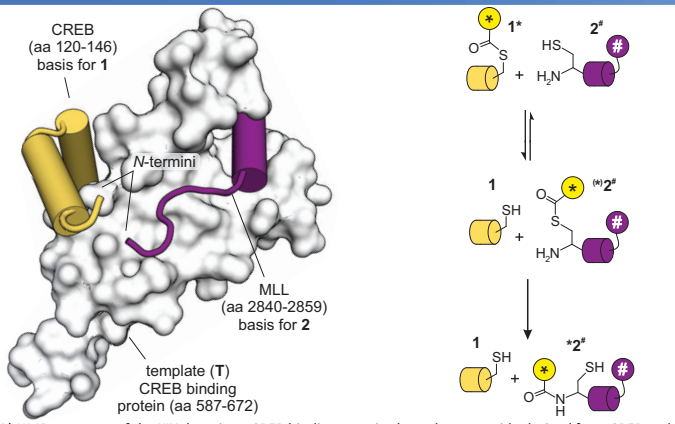

Figure 1: A) NMR-structure of the KIX domain or CREB binding proteins bound to a peptide derived from CREB and MLL (PDB ID 2lxt). N-termini of peptides are indicated. B) Principle of template-mediated transfer reaction based on native chemical ligation. * transferrable fluorescent group, # fluorescence quencher.

The spatial alignment of functional groups is a central aspect of most catalytic processes. Protein scaffolds with their exceptional molecular recognition properties have evolved into powerful biological catalysts. However, the rational design of artificial enzymes starting from noncatalytic protein domains proved challenging. Herein, we report the **use of a non-enzymatic protein as template for amide bond formation**. Starting from a protein adaptor domain capable of simultaneously binding to two peptide ligands, we designed **a catalytic transfer reaction based on the native chemical ligation**. This system was used for the **selective labelling of a target protein** validating its high chemoselectivity and potential as a novel tool for the **selective covalent modification of proteins**.

2 Peptide Design and Testing of Reaction

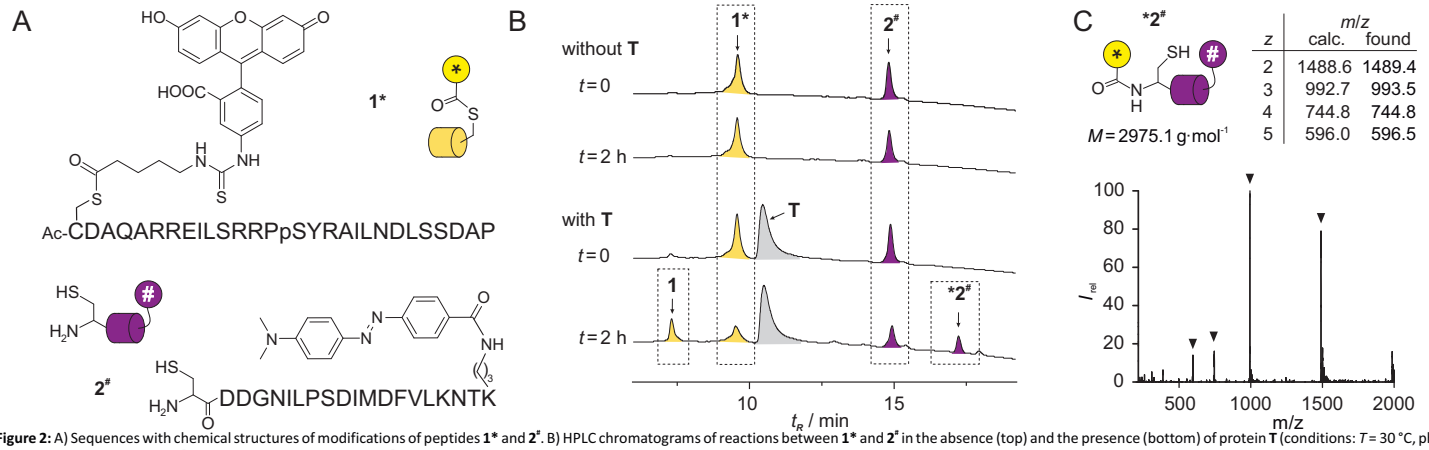

Figure 2: A) Sequences with chemical structures of modifications of peptides **1*** and **2#**. B) HPLC chromatograms of reactions between **1*** and **2#** in the absence (top) and the presence (bottom) of protein **T** (conditions: T = 30 °C, phosphate buffer, pH 7.4, c = 2.5 mM **1***, 5 mM **2#**, 2.5 mM **T**. C) MS spectrum of ***2#** including calculated and found m/z values.

3 Catalytic Cycle and Activity

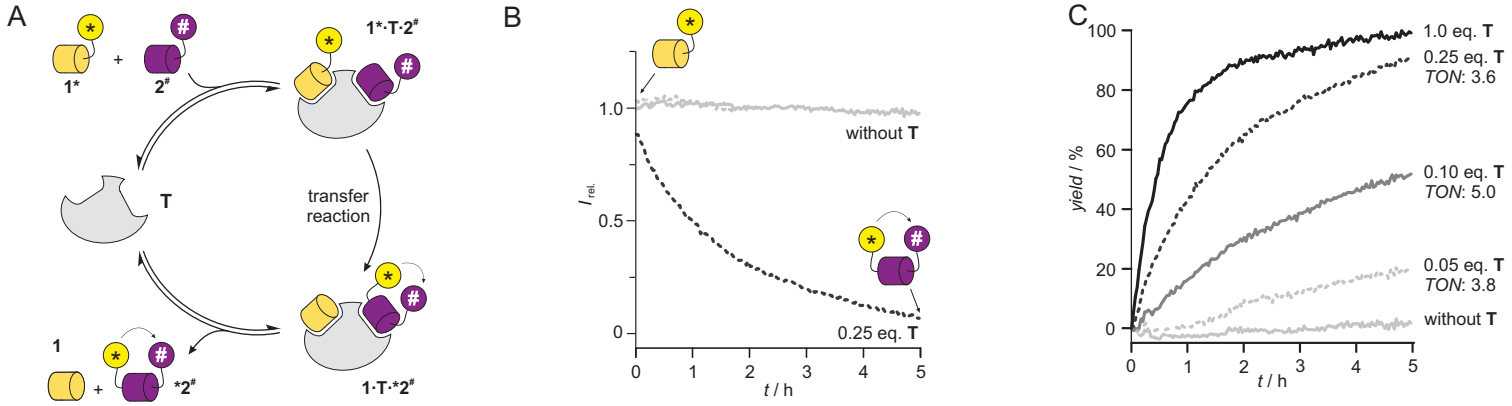

Figure 3: A) Scheme of catalytic cycle starting from **1*** and **2#** and providing reaction products **1** and ***2#**. B) Fluorescent readout of transfer reaction (conditions: T = 30 °C, phosphate buffer, pH 7.4, c = 5 mM **1***, 10 mM **2#**, 1.25 mM **T** (0.25 eq.). C) Reaction time course determined based on fluorescence intensity changes for different equivalents of **T** (conditions: T = 30 °C, phosphate buffer, pH 7.4, c = 5 mM **1***, 10 mM **2#**). Turnover numbers (TON) are provided.

4 Template-mediated Protein Labelling

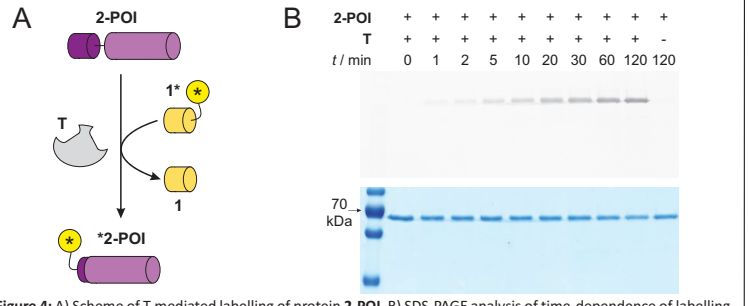

Figure 4: A) Scheme of T-mediated labelling of protein **2-POI**. B) SDS-PAGE analysis of time-dependence of labelling reaction with **1***, **2-POI** and **T** (each c = 1 mM, buffer: 20 mM sodium phosphate, pH 7.4, 500 mM TCEP, T = 30 °C). Top: Fluorescence imaging of gel indicating labelled protein ***2-POI**, Bottom: Coomassiestained gel indicative of total protein content **2-POI** and ***2-POI**.

Want to know more?

Support

Emmy Noether-Programm DFG · erc European Research Council · AstraZeneca · Bayer HealthCare · AIMMS · Merck · Boehringer Ingelheim · Bayer CropScience

[a]Chemical Genomics Centre of the Max Planck Society, Dortmund, 44227, Germany
[b]Department of Chemistry and Chemical Biology, Technical University Dortmund, Dortmund, 44227, Germany
[c]Department of Chemistry and Pharmaceutical Sciences & AIMMS, VU Amsterdam, NL

β-Sheet mimetics that Target the Transcriptional Coactivator β-Catenin

M. Wendt[1], A. Yeste-Vázquez[1], T. van Ramshorst[1], R. J. Hana[1], N. M. Pearce[1], S. Hennig[1] and T. N. Grossmann[1]

[1]Department of Chemistry & Pharmaceutical Sciences, VU University Amsterdam, NL

https://doi.org/10.17952/37EPS.2024.P1254

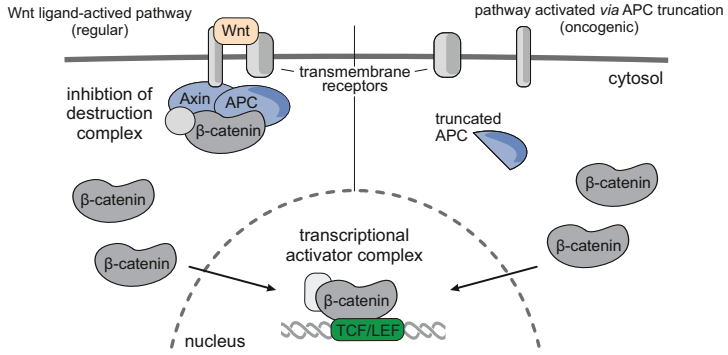

Protein complexes are defined by the three-dimensional structure of participating binding partners. Knowledge about these structures can facilitate the design of peptidomimetics which have been applied for example, as inhibitors of protein–protein interactions (PPIs). Even though β-sheets participate widely in PPIs, they have only rarely served as the basis for peptidomimetic PPI inhibitors,inparticular when addressing intracellular targets. Here,wepresent the structure-based design of β-sheet mimetics targeting the intracellular protein β-catenin, acentral component of the Wnt signaling pathway. Based on aprotein binding partner of β-catenin, a macrocyclic peptide was designed and its crystal structure in complex with β-catenin obtained. The presented design strategy can support the development of inhibitors for other β-sheet-mediated PPIs.

1 TCF Derived Tracer Peptide

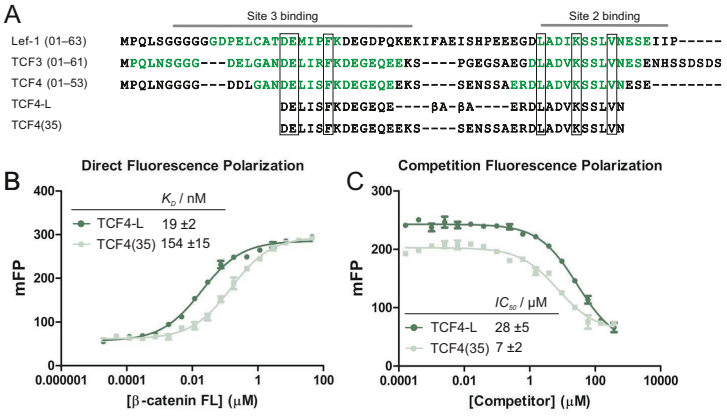

(A) Sequence alignment of the CBD's of Lef-1 (PDB ID 3ouw), TCF3 (PDB ID 1g3j), TCF4 (PDB ID 2gl7) and TCF4-L and TCF4(35). In green the resolved residues by X-ray. Framed the crucial residues for binding. (B) FP-binding assay of TCF4-L and TCF4(35) towards β-catenin. K_D-values were obtained from FP measurements (n=3, ± std. error). (C) FP competition assay with TCF4-derived tracer peptides c = 10 nM) and full-length β-catenin (c = 250 nM). Competitor concentration was varied (c = 1.6 x 10^{-1}–375 μM, n=2, ± std. error)

2 E-Cadherin-Derived Peptides

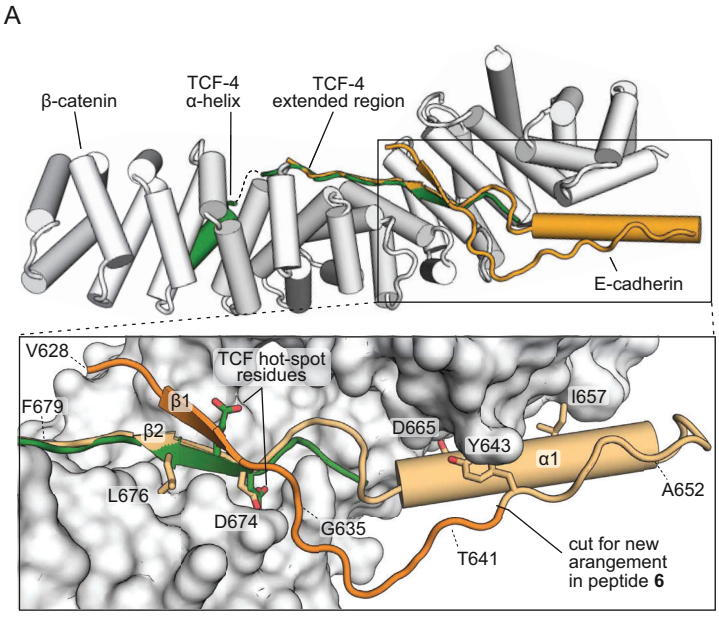

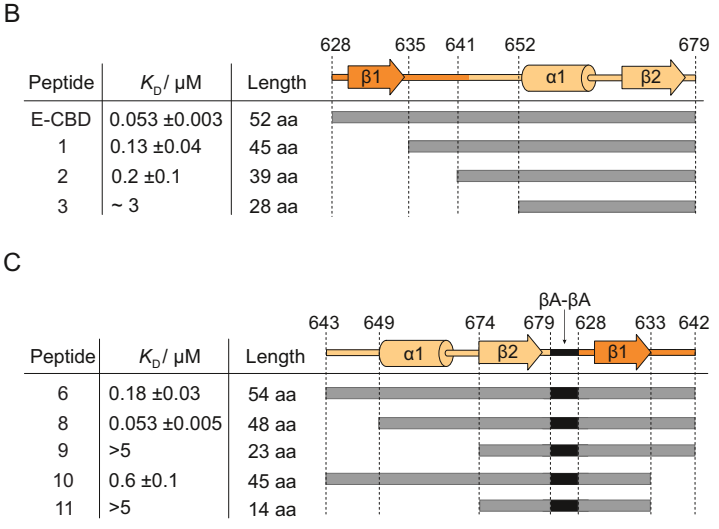

(A) Top: Crystal structure (PDB ID 2gl7) of β-catenin (grey) in complex with the CBD of TCF-4 (green) and superimposed with the CBD of E-cadherin (orange, PDB ID 1i7x, chain B). Bottom: Close-up of indicated region with b-catenin in surface representation (grey). Hot-spot amino acids of E-CBD (D665, I657, Y643, D674, L676) and TCF (D16, E17) are shown as stick. Terminal amino acids of peptides E-CBD, 1, 2 and 3 are indicated. Position where sequence of E-CBD was opened to generate peptide 6 is indicated. (B) Peptide affinities and lengths are shown including the visualization of involved peptide regions. K_D-values were obtained from FP measurements (n=3, ± std. error). (C) Table shows peptides derived from 6. The β-alanine loop (βA-βA) is highlighted in black. Measurements in analogy to Figure 1b..

3 A Cyclic Peptide Inhibits the β-Catenin/TCF4 Interaction

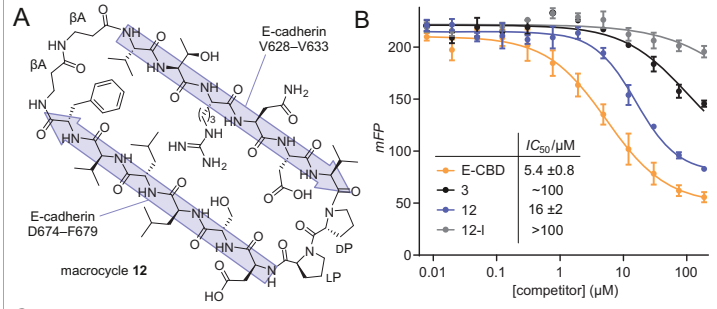

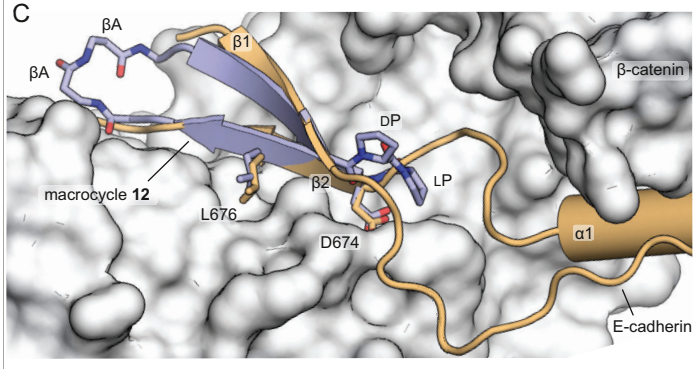

(A) Chemical structure of the macrocycle 12. Amino acids of β-strands β1 and β2 are highlighted in blue. (B) FP competition assay with TCF-4-derived tracer peptide c = 10 nM) and full-length β-catenin (c = 250 nM). Competitor concentration was varied (c = 7.9 x 10^{-3}–188 μM, n=3, ± std. error). (C) Crystal structure of β-catenin (grey, surface representation) in complex with peptide 12 (blue, cartoon representation, PDB ID 7ar4). The hot spot residues as well as βA-βAand the DP-LP turn are shown in stick representation (blue). 12 is superimposed with the CBD of E-cadherin (orange, cartoon representation, PDB ID 1i7x). Residues L676 and D674 are shown explicitly.

4 Conclusions

– This is the first crystal structure of a synthetic ligand bound to this site of β-catenin.

– A derivative peptide of **12** showed activity in Wnt reporter gene assay.

– Outlook is to improve cellular uptake further.

References

[1] M. Pelay-Gimeno, A. Glas, O. Koch, T. N. Grossmann, *Angew. Chem. Int. Ed.* **2015**, *54*, 8896–8927.

[2] H. Clevers, R. Nusse, *Cell* **2012**, *149*, 1192–1205.

[3] M. Wendt, R. Bellavita, A. Gerber, N-L. Efrem, T. van Ramshorst, N. M. Pearce, P. R. J. Davey, I. Everard, M. Vazquez-Chantada, E. Chiarparin, P. Grieco, Sven Hennig, T. N. Grossmann, *Angew. Chem. Int. Ed.* **2021**, 60, 13937–13944.

Financial Support

Solid-phase synthesis of peptoids with structure-inducing *tert*-butyl side chains: A unique challenge finally met

Zacharie Bordas, Sophie Faure, Olivier Roy, Claude Taillefumier

Université Clermont Auvergne, Clermont Auvergne INP, CNRS, ICCF, F-63000 Clermont–Ferrand, France

https://doi.org/10.17952/37EPS.2024.P1255

Institut de Chimie de Clermont-Ferrand

Peptoids as peptidomimetic foldamers

α-Peptide

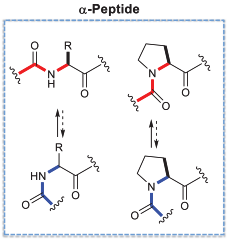

α-Peptoid (Zuckermann 1992)

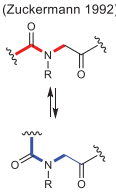

- No hydrogen bond donors
- Achiral backbone

Flexibility

- cis/trans isomerism

Oligomers of *N*-substituted glycines

- Efficient and scalable submonomer synthesis
- Great potential for diversity
- Higher proteolytic stability than peptides
- Better biodisponibility

Main side chains favoring *cis* peptoid amide bonds

Log (K*cis*/*trans*)

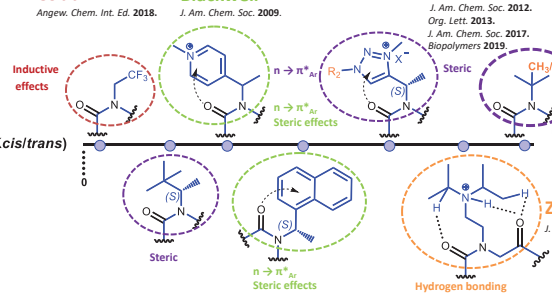

All-cis

PPI-like helix

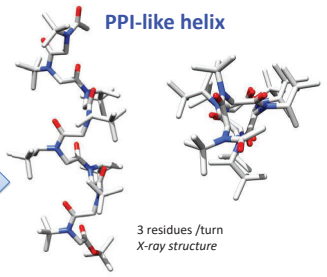

3 residues /turn
X-ray structure

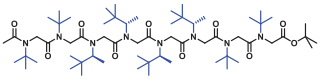

Homogeneous and robust helix comprising only aliphatic residues

- Right-handed PPI-type helix
- Remarkable conformational regularity
- Longest solid-state structure for linear peptoids

Roy, O.; Dumonteil, G.; Faure, S.; Jouffret, L.; Kriznik, A.; Taillefumier, C. *J. Am. Chem. Soc.* **2017**, *139* , 13533–13540.

Objectives

Rapid access to peptoid oligomers containing structure-inducing *tert*-butyl side chains

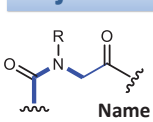

R =

Name of peptoid unit :

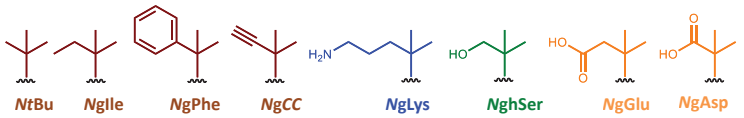

Incorporation of peptoid units bearing these side chains by solid-phase synthesis ?

Submonomer synthesis of α-Peptoids (Zuckermann)

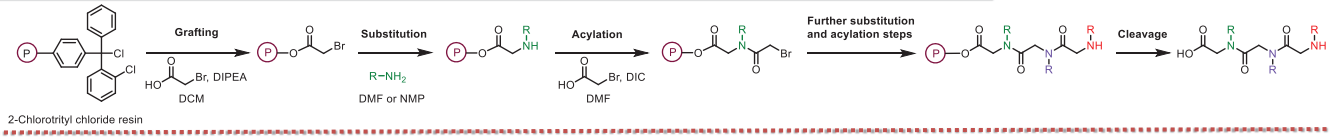

Solid-phase synthesis of the trimer model H-(*Nt*Bu)$_3$-OH

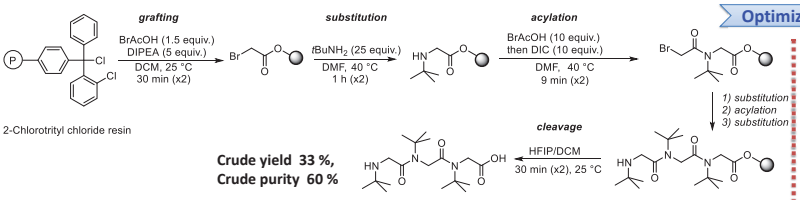

Crude yield 33 %,
Crude purity 60 %

Optimization

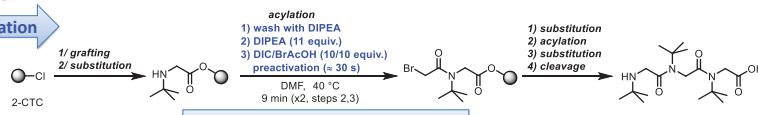

Acylation after incorporation of NtBu
- Wash with DIPEA before acylation
- Inclusion of DIPEA during acylation
- Pre-activation of BrAcOH with DIC

Crude yield 94 %,
Crude purity 83 %

Synthesis of the hexamer model H-(*Nt*Bu)$_6$-OH

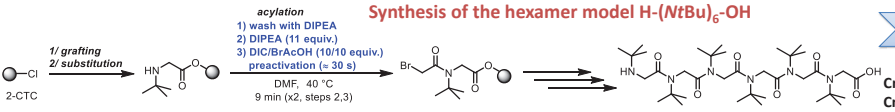

Crude yield = 55 %,
Crude purity = 67 %

Further optimizations

Other evaluated conditions for the acylation step :

- Coupling agents : DCC, HCTU, PyBOP, IBCF, MDPI, COMU, DIC + Oxyma, DIC + HOBt, and HBTU … ✗
- 60 °C or 25 °C or [BrAcOH] = 0.4 M or 2 × 20 min ✗
- ClAcOH instead of BrAcOH ✓

Solid-phase synthesis of *Nt*Bu peptoid homo-oligomers (up to 12-mer)

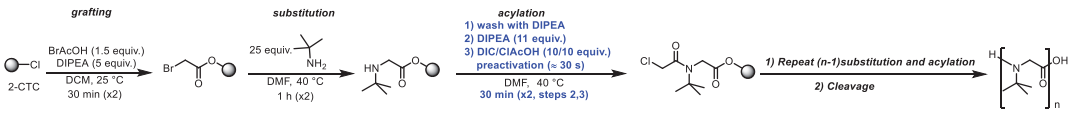

Peptoid	Sequence	Number of steps	Crude yield (%)	Crude purity (%)
4	H-(*Nt*Bu)$_2$-OH	5	100	81
5	H-(*Nt*Bu)$_3$-OH	7	93	91
6	H-(*Nt*Bu)$_4$-OH	9	81	87
7	H-(*Nt*Bu)$_5$-OH	11	68	85
3	H-(*Nt*Bu)$_6$-OH	13	94	94
8	H-(*Nt*Bu)$_7$-OH	15	51	77
9	H-(*Nt*Bu)$_8$-OH	17	55	71
10	H-(*Nt*Bu)$_9$-OH	19	47	63
11	H-(*Nt*Bu)$_{12}$-OH	25	36	71

Synthesis of trimers comprising *N*-Cα-*gem*-dimethyl side chains

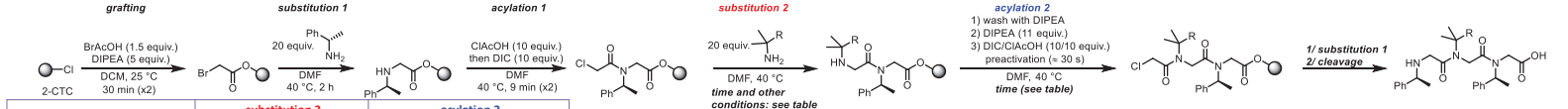

Monomer sequence	substitution 2 (time/other)	acylation 2 (time/other)
*Ns*1pe-*Nt*Bu-*Ns*1pe	2h	2x 30 min
*Ns*1pe-*Ng*Ile-*Ns*1pe	2h	2x 30 min
*Ns*1pe-*Ng*Phe-*Ns*1pe	2h 5 equiv. KI + 5 equiv. DIPEA	2x 30 min 22 equiv. DIPEA 20 equiv. DIC/ClAcOH
*Ns*1pe-*Ng*CC-*Ns*1pe	2x 2h 5 equiv. KI + 5 equiv. DIPEA	3x 30 min
*Ns*1pe-*Ngh*Ser(TBDMS)-*Ns*1pe	2h 5 equiv. KI + 5 equiv. DIPEA	3x 30 min
*Ns*1pe-*Ng*Lys(Cbz)-*Ns*1pe	24h 5 equiv. KI + 5 equiv. DIPEA	2x 30 min
*Ns*1pe-*Ng*Glu(All)-*Ns*1pe	24h 5 equiv. KI + 5 equiv. DIPEA	3x 30 min
*Ns*1pe-*Ng*Asp(Bn)-*Ns*1pe	16 h 5 equiv. KI + 5 equiv. DIPEA	3x 30 min

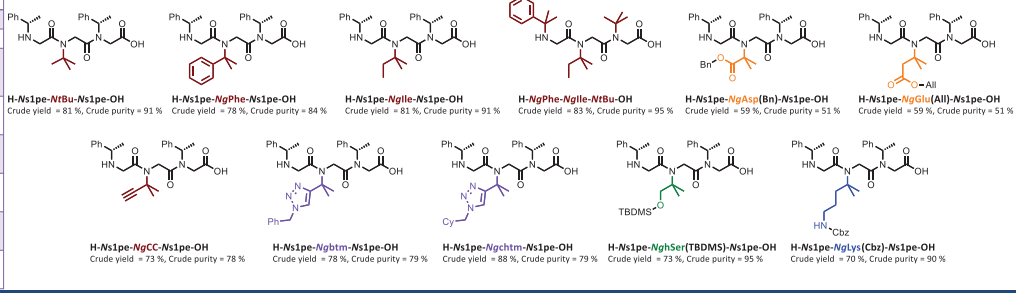

https://doi.org/10.17952/37EPS.2024.P1256

Combinatorial solid phase peptide synthesis of peptides on glass slides and thermographic investigation on CO_2-binding affinity

Jessica Jung-Fittkau[1,2], Katharina Moro[1], Josef Diebold[1], Andrea Kruse[2], Hans-Peter Deigner[1,3,4], Magnus Schmidt[1]

[1]Organic and Bioorganic Chemistry Labs, Medical and Life Sciences Faculty, Institute of Precision Medicine, Furtwangen University, Jakob-Kienzle-Str. 17, 78054 Villingen-Schwenningen, Germany.
[2]Institute of Agricultural Technology, University of Hohenheim, Schloß Hohenheim 1, 70599 Stuttgart, Germany.
[3]EXIM Department, Fraunhofer Institute IZI (Leipzig), Schillingallee 68, 18057 Rostock, Germany.
[4]Faculty of Science, Eberhard Karls University Tuebingen, Auf der Morgenstelle 8, 72076 Tübingen, Germany.

Abstract:
In this research peptide arrays, synthesized with combinatorial solid-phase peptide synthesis (SPPS), have been used to detect CO_2 binding in an artificial CO_2 atmosphere by the technique of thermographic measurements using a high-resolution infrared thermographic camera. Thereby, endo- or exothermic reaction heat release can be detected in mk range indicating successful CO_2 binding to possible active peptides.

1 Introduction / Objectives

- Biocatalysts such as RubisCO play an important role in the conversion of CO_2 into organic molecules. Certain amino acids are crucial for CO_2 fixation in the binding site of carboxylases/oxygenases [1].
- To investigate this process, we performed a combinatorial peptide array synthesis of peptides on functionalized glass slides, followed by screening for CO_2-binding-affinity of the peptide library with an infrared camera in a CO_2 containing environment (see Figure 1).

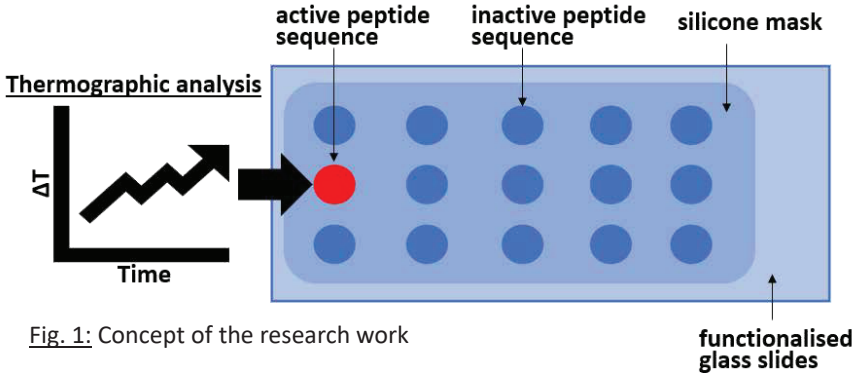

Fig. 1: Concept of the research work

2 Methods

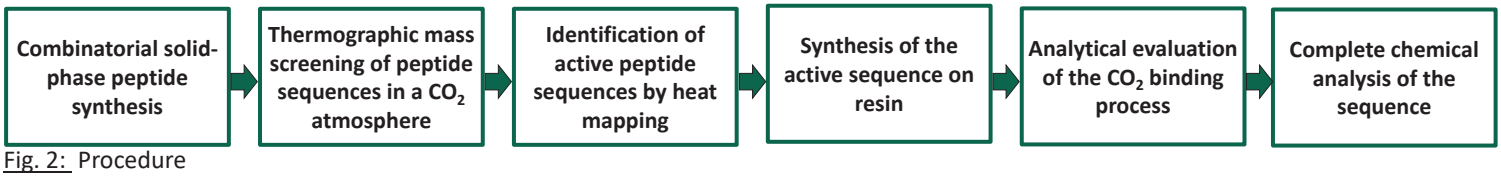

Fig. 2: Procedure

3 Results

- The temperature abnormality in the His-Phe-Asn sequence was reproducible.
- The temperature abnormality in the Phe-His-His sequence was not reproducible.

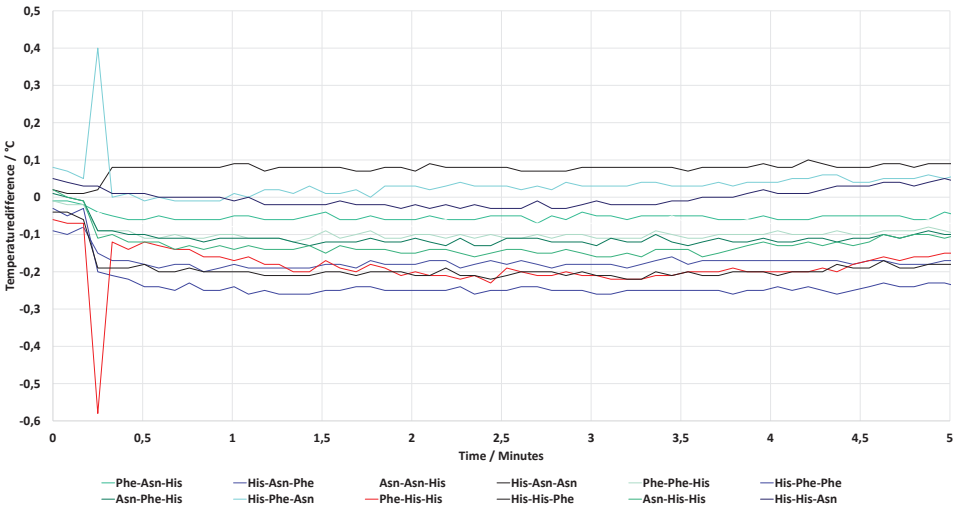

Fig. 3: Example of a thermographic examination of a slide with tripeptides

4 Outlook

- We are currently in the process of transferring the synthesis of the potential HIT sequence to resin beads.
- Gaining higher amounts of peptides for the evaluation of the CO_2 binding process.
- Technical applications of the sequence are to be tested.

5 Literature

[1] Stoffel, G. M. M., Saez, D. A., DeMirci, H., Vögeli, B., Rao, Y., Zarzycki, J., Yoshikuni, Y., Wakatsuki, S., Vöhringer-Martinez, E., & Erb, T. J. (2019). Four amino acids define the CO2 binding pocket of enoyl-CoA carboxylases/reductases. Proceedings of the National Academy of Sciences of the United States of America, 116(28), 13964–13969. https://doi.org/10.1073/pnas.1901471116

Stabilization of a miniprotein fold by an unpuckered proline surrogate

Madison M. Wright[a], Benjamin H. Rajewski[a], Taylor A. Gerrein[a], Lorna J. Smith[b], W. Seth Horne[c], Juan R. Del Valle[a]*
[a]Department of Chemistry & Biochemistry, University of Notre Dame ◆ [b]Department of Chemistry, University of Oxford
[c]Department of Chemistry, University of Pittsburgh

https://doi.org/10.17952/37EPS.2024.P1257

BACKGROUND and OBJECTIVES

The installation of unnatural monomers into proteins can augment their thermal stability, resistance to proteolysis, and biological activity.[1,2] Proline (Pro) is a unique proteinogenic residue due to isoenergetic *cis/trans* amide rotamers and constrained backbone torsions. Given its ability to modulate protein folding and dynamics, there is considerable interest in the development of unnatural and tunable Pro surrogates.[3,4] We recently described an unpuckered Pro surrogate, γ,δ-dehydro-δ-azaproline (ΔaPro), with unusually high *trans* amide rotamer bias, low amide isomerization barrier, and backbone torsions typical of a polyproline II (PPII) fold.[5] We hypothesized that ΔaPro could enhance miniprotein stability upon incorporation into PPII and loop domains.

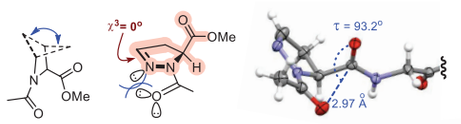

Ac-**Pro**-OMe (γ-endo/exo pucker, ~ 5:1 *trans:cis*) | Ac-Δ**aPro**-OMe (no pucker, ~ 44:1 *trans:cis*) | Ac-Δ**aPro**-Gly-OBn (X-ray): ΔaPro ϕ,ψ = -60°, +151°; PPII ϕ,ψ = -75°, +150°

Study Objectives: [1] Develop an efficient synthetic protocol to incorporate ΔaPro into peptides and proteins; **[2]** Evaluate the effect of ΔaPro substitution on the folding and stability of the avian pancreatic polypeptide (aPP).

RESULTS

1) Synthesis of ΔaPro precursor dipeptides and incorporation of ΔaPro into host structures by SPPS

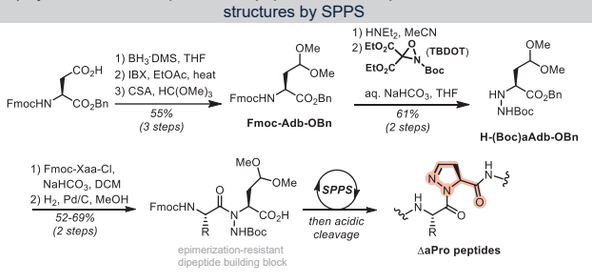

2) A single-strand PPII model peptide featuring an ΔaPro guest residue gives an anomalous CD signature but undergoes two-state thermal transition

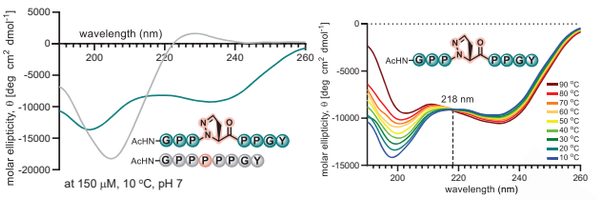

3) aPP miniproteins featuring ΔaPro substitution in the PPII helix adopt wild-type tertiary structure by CD

sequence (X = ΔaPro)	yield %
GPSQPTYPGDDAPVEDLIRFYDNLQQYLNVVTRHRY	8
GXSQPTYPGDDAPVEDLIRFYDNLQQYLNVVTRHRY	6
GPXQPTYPGDDAPVEDLIRFYDNLQQYLNVVTRHRY	6
GPSXPTYPGDDAPVEDLIRFYDNLQQYLNVVTRHRY	7
GPSQXTYPGDDAPVEDLIRFYDNLQQYLNVVTRHRY	8
GPSQPXYPGDDAPVEDLIRFYDNLQQYLNVVTRHRY	6
GPSQPTXPGDDAPVEDLIRFYDNLQQYLNVVTRHRY	14
GPSQPTYXGDDAPVEDLIRFYDNLQQYLNVVTRHRY	3
GPSXPXYPGDDAPVEDLIRFYDNLQQYLNVVTRHRY	13
GPSPPTYPGDDAPVEDLIRFYDNLQQYLNVVTRHRY	10
GPSQPPYPGDDAPVEDLIRFYDNLQQYLNVVTRHRY	7
GPSGPTYPGDDAPVEDLIRFYDNLQQYLNVVTRHRY	10

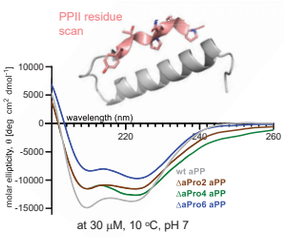

4) ΔaPro4 and ΔaPro6 substitutions in the aPP PPII helix maintain or enhance thermal stability

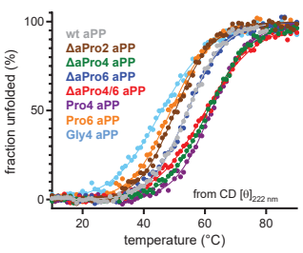

peptide	T_m (°C)
wt aPP	54.2 ± 0.8
ΔaPro2 aPP	49.7 ± 0.9
ΔaPro4 aPP	61.9 ± 1.2
ΔaPro6 aPP	53.6 ± 1.1
ΔaPro4/6 aPP	60.9 ± 0.9
Pro4 aPP	62.7 ± 0.6
Pro6 aPP	47.7 ± 1.6
Gly4 aPP	47.6 ± 2.4

5) NMR-derived ensembles reveal wild-type tertiary and quaternary structure but greater conformational disorder in the case of a di-substituted ΔaPro4/6 aPP analogue

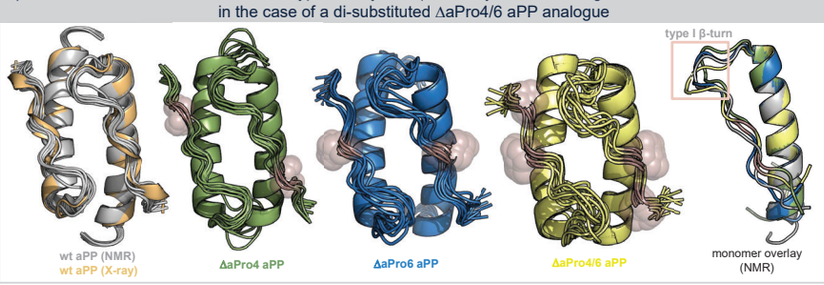

6) ΔaPro4/6 aPP exhibits loss of a dimer-stabilizing π-π interaction but gains intramonomer π-π interactions

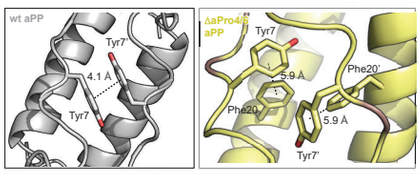

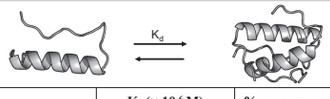

peptide	K_d (× 10^{-6} M) from AUC	% monomer at 30 μM
wt aPP	1.31	19%
ΔaPro4/6 aPP	4.71	33%

7) Loss of a wild-type intramonomer H-bond in ΔaPro4 aPP allows for Pro2-Tyr27 CH-π interaction and a more ordered PPII strand

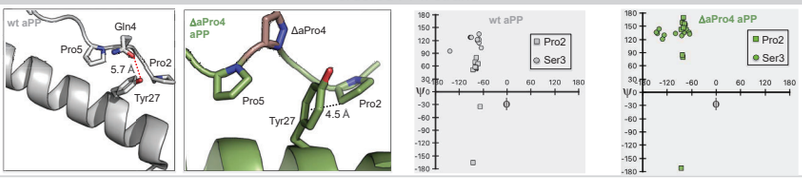

8) Substitution of the loop Pro13 residue for ΔaPro significantly enhances thermal stability

sequence	yield %
GPSQPTYGGDDAXVEDLIRFYDNLQQYLNVVTRHRY	6
GPSQPTYGGDDAAVEDLIRFYDNLQQYLNVVTRHRY	6
GPSXPXYGDDAXVEDLIRFYDNLQQYLNVVTRHRY	5

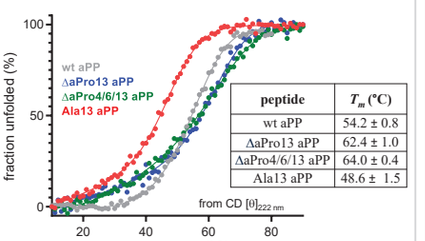

peptide	T_m (°C)
wt aPP	54.2 ± 0.8
ΔaPro13 aPP	62.4 ± 1.0
ΔaPro4/6/13 aPP	64.0 ± 0.4
Ala13 aPP	48.6 ± 1.5

9) ΔaPro13 substitution stabilizes the aPP tertiary fold despite reduced dimer population

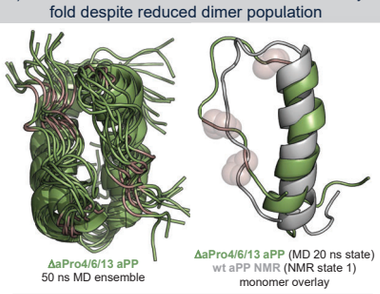

peptide	K_d (× 10^{-6} M) from AUC	% monomer at 30 μM
wt aPP	1.31	19%
ΔaPro13 aPP	24.4	58%
ΔaPro4/6/13 aPP	58.2	73%

CONCLUSIONS

We developed a convenient method for the incorporation of a novel, unpuckered proline surrogate into peptides and proteins. ΔaPro substitution of solvent-exposed PPII residues, and the key "Pro switch" residue in the loop of aPP, can stabilize the miniprotein while substitutions in the hydrophobic core destabilize the fold. NMR-derived structures reveal that ΔaPro readily adopts canonical PPII backbone torsions in all cases. Our most stable analogue, whose melting temperature is 10°C higher than wild-type aPP, features incorporation of three ΔaPro residues (positions 4, 6, and 13). Notably, this stabilization of tertiary structure is attended by a significant increase in monomer population. Our results suggest that ΔaPro is an effective conformational surrogate of Pro for use in the design of thermostable proteomimetics.

ACKNOWLEDGEMENTS

We thank Prof. Yichun Wang for access to CD instrumentation; Dr. Giselle Jacobson and the ND Biophysical Instrumentation Core Facility for assistance with AUC; and Dr. Evgenii Kovriguine and the ND NMR Facility for assistance with NMR acquisitions. This work was supported by a grant from the National Science Foundation (NSF 2109008).

REFERENCES

[1] Gellman et al., *Acc. Chem. Res.* **1998**, *31*, 173; [2] Baker et al., *Acc. Chem. Res.* **2017**, *50*, 2085; [3] Yaron et al., *Crit. Rev. Biochem. Mol Biol.* **1993**, *28*, 31; [4] Kubyshkin and Rubini, *Chem. Rev.* **2024**, *124*, 8130; [5] Elbatrawi et al., *J. Org. Chem.* **2020**, *85*, 4207.

Exploring the potential of CXCR4 mimetic peptides to target cancer cells

Showmika Srirangan[1], Chafia Chiheb[2], Sebastian Stäbler[2], Anja Bosserhoff[2] and Jutta Eichler[1]

[1]Department of Chemistry and Pharmacy, Friedrich-Alexander-Universität Erlangen-Nürnberg, 91058 Erlangen, Germany
[2]Institute of Biochemistry, Friedrich-Alexander-Universität Erlangen-Nürnberg, 91054 Erlangen, Germany

https://doi.org/10.17952/37EPS.2024.P1259

showmika.srirangan@fau.de

The chemokine receptor CXCR4 plays crucial roles in various physiological processes and is implicated in diseases such as HIV-1 infection and cancer[1]. In cancer, the interaction between CXCR4 and the chemokine CXCL12 has been shown to stimulate multiple oncogenic processes[2]. In HIV-1 infection, CXCR4 serves as a coreceptor for viral entry into the host cell[3]. Previously, we designed a peptide that presents the three extracellular loops (ECLs) of CXCR4, which was shown to inhibit both HIV-1 infection[4] and CXCR4 signaling[5]. We have now optimized the sequence of this peptide, CX4M1, to enhance its affinity for CXCL12 by truncation, among other modifications. The optimized CX4M1 variants bind to CXCL12 with higher affinity while being considerably shorter than the original peptide.

These peptides have been shown to interfere with the migration of CXCR4-dependent cancer cells and inhibit the binding of CXCL12 to CXCR4-expressing cancer cells.

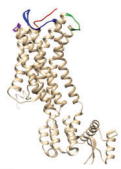

CXCR4
PDB ID: 3ODU

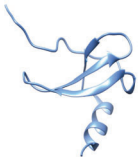

CXCL12
PDB ID: H3P3

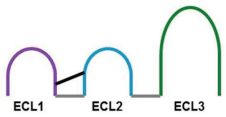

CX4M1

Results & Discussion

Design & Optimization

Created with BioRender.com

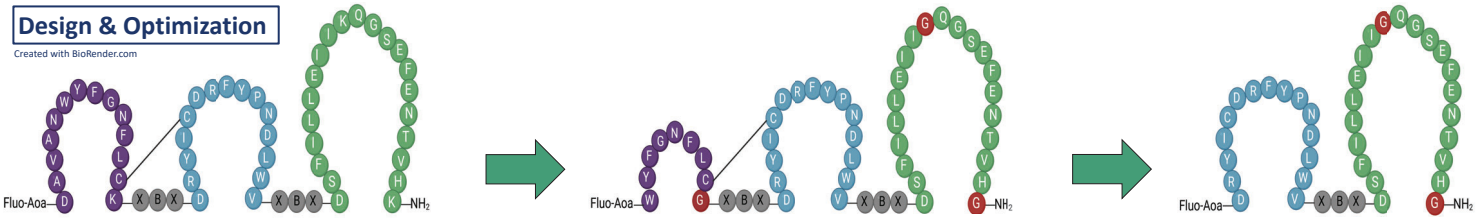

CX4M1 | KMF18-7 (-5N) | SRI_14.2 (-ECL1)

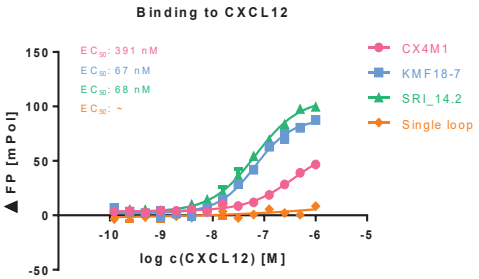

- Replacement of basic amino acids by glycine & N-terminal truncation up to 5 amino acids (**KMF18-7**)
- Truncation of ECL1 (**SRI_14.2**) binding affinity towards CXCL12 is preserved

Proteolytic stability of KMF18-7

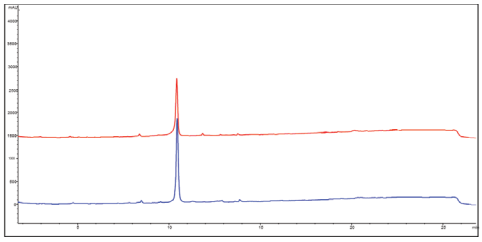

KMF18-7 after 0 h (blue) and 24 h(red) incubation with human serum

- KMF18-7 exhibited significant resistance to enzymatic degradation in human serum → can be tested in cell-based Assays

Investigation of Cancer Cell processes

Disruption of CXCL12-Binding to CXCR4

Via FACS

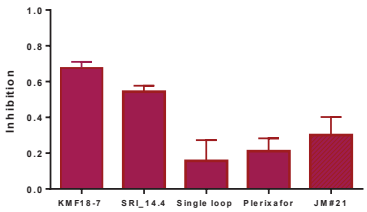

- CXCR4-expressing cells were incubated with CXCL12-Fc, CXCR4 mimetic peptides, Plerixafor[6]and JM#21[7] (each at 1 µM) and analyzed via FACS
- KMF18-7 and SRI_14.2 strongly disrupted binding of CXCL12 to CXCR4

Inhibition of Migration

Via Boyden chambers

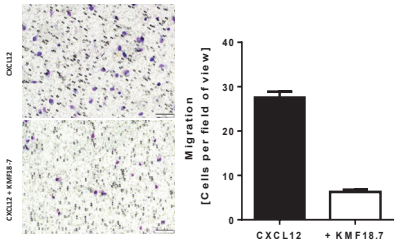

- Cancer cell migration was analyzed using Boyden chambers
- CXCR4-expressing cells were seeded in the upper chamber
- CXCL12 and a CXCR4 mimetic peptide were added to the lower chamber
- The migration duration was 4 hours

Via Real-Time Cell Analysis (RTCA)

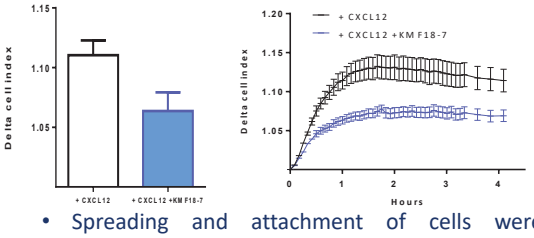

- Spreading and attachment of cells were detected using RTCA and expressed as the cell index (CI) value
- CXCR4-expressing cells were stimulated with CXCL12, leading to increased cell spreading and attachment
- This response was reduced by the CXCR4 mimetic peptide

Outlook

- Further truncation to find minimal active peptide length
- Investigating the CXCR4 mimetic peptides in an *in vivo* model
- Introducing the N-terminal tail as a CXCR4 mimetic peptide → testing in cancer cell based assays

References

[1]M. Z. Ratajczak et al., Leukemia. **2006**, 20, 1915-1924.
[2] A. Zlotnik et al., Int. J. Cancer 119. **2006**, 2026–2029.
[3] Brelot, A. et al., Journal of Biological Chemistry. **2000**, 23736-23744.
[4] K. Möbius et al., Chem. Eur. J. **2012**, 18, 8292-8295.
[5] A. Groß et al., Bioorg. Med. Chem. **2015**, 23, 4050–4055.
[6]De Clercq, Erik et al., Pharmacology & therapeutics 128.3. **2010**, 509-518.
[7] Harms, Mirja, et al. Acta Pharmaceutica Sinica B 11.9. **2021**, 2694-2708.

The ornithine-based siderophore as a potential carrier of peptide nucleic acid into *Escherichia coli* cells

U. Tsylents, M. Burmistrz, P. Maj, M. Wojciechowska, J. Trylska

Centre of New Technologies, University of Warsaw, Warsaw, Poland

https://doi.org/10.17952/37EPS.2024.P1260

Research goal

The rapid spread of antimicrobial resistance, especially in the case of gram-negative bacteria, encourages searching for new alternative delivery ways through the restrictive outer membrane, which is an outer layer of the bacterial envelope [1].

Iron chelators, known as **siderophores**, are secreted, recognized and later transported through the outer membrane by the TonB-dependent transport system (**TBDT**) [2].

Peptide nucleic acid (PNA) is a nucleic acid mimic with high affinity towards natural nucleic acids. PNA can be used as an antisense oligonucleotide, which binds to the target mRNA in a complementary manner regulating its expression. Gene-targeting is a promising approach against various diseases, including bacterial infections. However, due to poor cellular permeability, PNA cannot act as a gene silencing agent on its own [3].

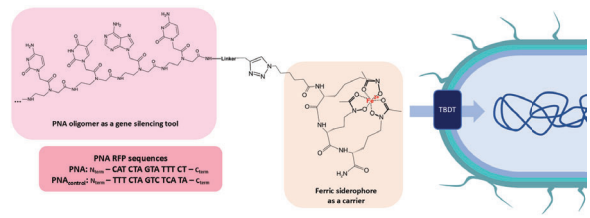

Figure 1: The Trojan horse strategy which uses the bifunctional conjugate of the synthetic siderophore and a PNA oligomer enables the passage through the *E. coli* membrane.

Our goal is to synthesize an ornithine-based siderophore, which upon conjugation with a PNA oligonucleotide will ensure non-invasive transport of PNA into *E. coli* cells. To confirm that, PNA anti-rfp sequence was used to target the reporter gene *mrfp1* expressing red fluorescent protein (RFP) inside *E. coli* cells (Figure 1).

Synthesis

Modified ornithine derivative (N^{δ}-hydroxy-N^{δ}-acetyl-ornithine) was used as a building block, because it provides hydroxamate groups capable of binding ferric iron.
S_L siderophore was synthesized using the solid-phase peptide synthesis (SPPS) technique with appropriate Fmoc strategy (Figure 2).

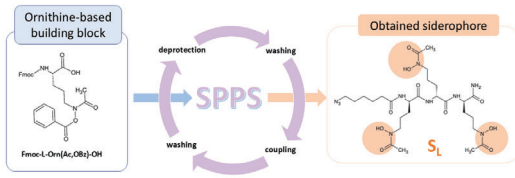

Figure 2: Chemical structures of the Fmoc-protected modified ornithine derivative used for the S_L siderophore synthesis. Hydroxamate groups are highlighted.

In order to verify its carrier potential S_L was later used for conjugation with PNA oligomers via copper-catalyzed azide-alkyne cycloaddition (also known as "click reaction"), which resulted in S_L–PNA conjugates connected via uncleavable triazole ring (Figure 1).

PNA oligomers (Figure 1) used for conjugation were synthesized manually using appropriate SPPS protocol.

Circular Dichroism (CD) Spectroscopy

CD spectra of the synthesized siderophore mimic - S_L were recorded to verify iron(III)-coordination properties and later were compared to CD spectra of two natural siderophores - coprogen and ferrichrome (Figure 3). Upon binding iron(III) siderophores obtain structure, which can be assigned to Δ or Λ optical isomer structure using CD analysis. Ferrichrome complex represents Λ configuration and coprogen obtains structure for Δ isomer. [4]

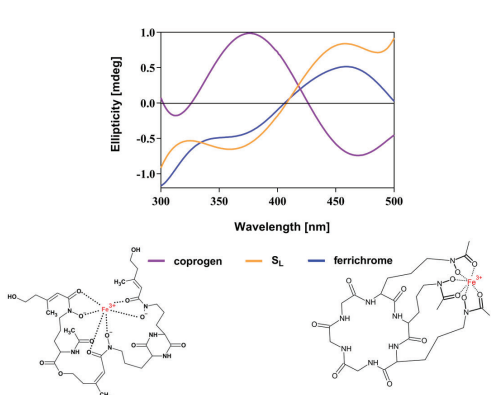

Figure 3: CD spectra of the natural and S_L siderophores in the presence of Fe^{3+} salt. Ferric complex structure of coprogen (left) and ferrichrome (right) are included. CD spectra of a natural cyclic siderophore – ferrichrome (and its ferric complex structure included on the right) is detected as Λ optical isomer (blue line).

Based on the CD spectra obtained for S_L, this siderophore chelates ferric iron adopting the structure of the isomer (Figure 3). Similar positions of the minima and maxima in the Fe(III)-S_L complex and ferrichrome spectra suggest that, while capturing iron, S_L adopts a structure comparable to the cyclic ferrichrome.

Microbial assays

After confirming the iron coordination properties of the S_L siderophore, uptake of PNA conjugates with S_L was tested on *E. coli* Δ*fur* mutant with continuous iron uptake (Figure 4, left). Bacteria were cultured in iron limiting conditions. RFP fluorescence was measured using the flow cytometry with two control cultures: bacteria carrying plasmids expressing RFP (with RFP) and bacteria lacking the RFP gene (without RFP).

Additionally, unconjugated S_L was used for the growth recovery assays. Several *E. coli* mutants lacking various TBDT receptors, proteins or reductases were used in order to investigate the S_L pathway through outer membrane receptors.

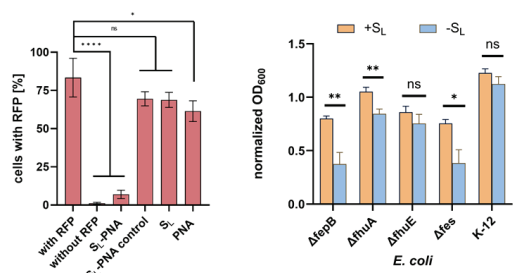

Figure 4: RFP fluorescence silencing in the *E. coli* Δ*fur* mutant cultured in iron limiting conditions (left). Growth recovery assay with various *E. coli* mutants with or without 16 μM S_L in iron limiting conditions (right). Statistical significance was determined by the two-way ANOVA test (****: $p<0.0001$, *: $p<0.05$, ns: non-significant)

Conclusions

- As shown by CD analysis, S_L efficiently binds ferric iron achieving the structure (Λ configuration) similar to natural cyclic siderophore - ferrichrome (Figure 3, orange and purple lines).
- The growth recovery assays on various *E. coli* mutants confirms the uptake of the linear siderophore mimic via the *E. coli* receptors recognizing the hydroxamate-type siderophores.
- Conjugates with S_L siderophore are recognized by *E. coli* iron uptake system and allow to transport PNA inside the bacterial cell.

Acknowledgements

We acknowledge support from National Science Centre Poland (OPUS UMO-2020/37/B/NZ1/02904).

References

[1] Z. Breijyeh, B. Jubeh, and R. Karaman. Resistance of gram-negative bacteria to current antibacterial agents and approaches to resolve it. *Molecules*, 25(6), 2020.

[2] P. Delepelaire. Bacterial abc transporters of iron containing compounds. *Research in Microbiology*, 170(8):345–357, 2019.

[3] U. Tsylents, I. Siekierska, and J. Trylska. Peptide nucleic acid conjugates and their antimicrobial applications—a mini-review. *European Biophysics Journal*, 52:533–544, 2023.

[4] G. Winkelmann. *CRC handbook of microbial iron chelates*. CRC Press Boca Raton, 1991.

Full study here:

Iron uptake pathway of *Escherichia coli* as an entry route for peptide nucleic acids conjugated with a siderophore mimic, U. Tsylents, M. Burmistrz, M. Wojciechowska, J. Stepień, P.Maj, J. Trylska, DOI: `https://doi.org/10.3389/fmicb.2024.1331021`

https://doi.org/10.17952/37EPS.2024.P1261

STEPWISE CHEMICAL CONTROL IN THE FORMATION OF BETA-PEPTIDE ASSEMBLIES

Imola Cs. Szigyártó[1], Kristóf Ferentzi[2], Kamal el Battioui[1], Olivér Pavela[1], András Wacha[1], Viktor Farkas[2] and Tamás Beke-Somfai[1]

[1]HUN-REN Research Centre for Natural Sciences, Institute of Materials and Environmental Chemistry, Budapest, Hungary
[2]HUN-REN - ELTE Protein Modeling Research Group, Institute of Chemistry, Eötvös Loránd University, Budapest, Hungary

szigyarto.imola.csilla@ttk.hu

ABSTRACT

Peptidic foldamers are an important class of synthetic macromolecules and have gained high attention in different areas of nanotechnology, drug delivery and molecular biology. Small **manipulations in peptide sequences**: length, charge or amino acid chirality can lead to the formation of different morphological assemblies. We have recently demonstrated[1,2] that acyclic, lysine-rich, short beta-peptides can achieve nanostructures that closely mimic both the oligomerization and the filament formation of natural peptides. **Here, we show** how systematic small variations could affect assemblies formation. **Molecular dynamics simulations** combined with **electron microscopy** confirmed distinct levels of macromolecular structures: from oligomers to fibrillar bundles, by applying **single point mutations** or **N-terminal chemical modifications** in the sequences. These results suggest that the self-assembly process could be fine-tuned by sequence modification, allowing widespread applications where specific levels of assembly stages need to be maintained.

EXPERIMENTAL DESIGN

- lysine-rich, acyclic, **beta-hexapeptide** sequences, with alternating side chain chirality

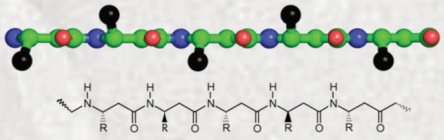

β³-heterochiral

- synthesized **β³-sequences**

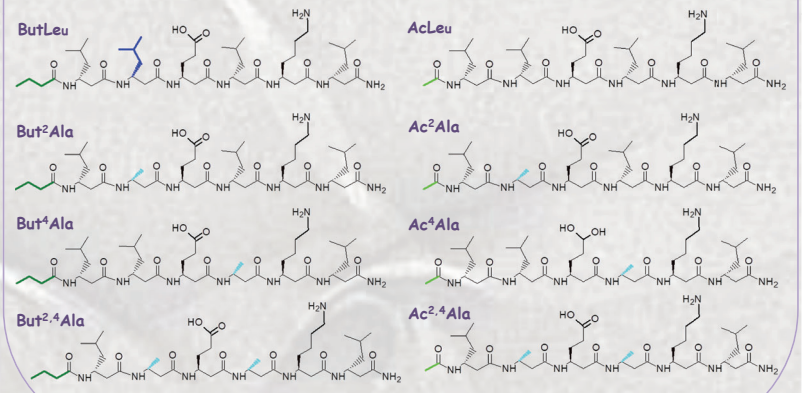

RESULTS – STRUCTURE & MORPHOLOGY

* MD simulations

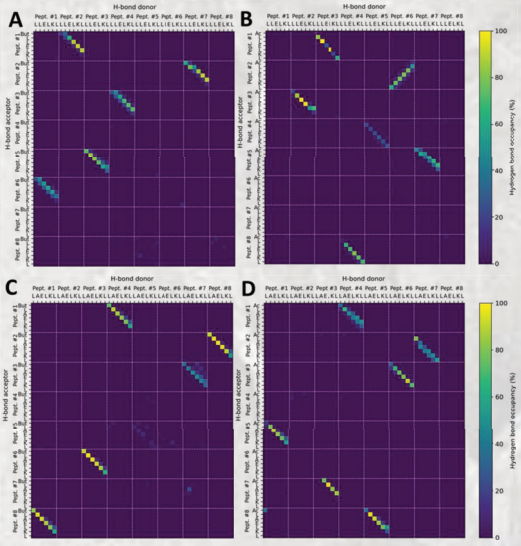

Interchain hydrogen bonds occupancy in octameric oligomers: ButLeu (A), AcLeu (B), ButAla (C) and AcAla (D).

* Molecular Spectroscopy secondary structure

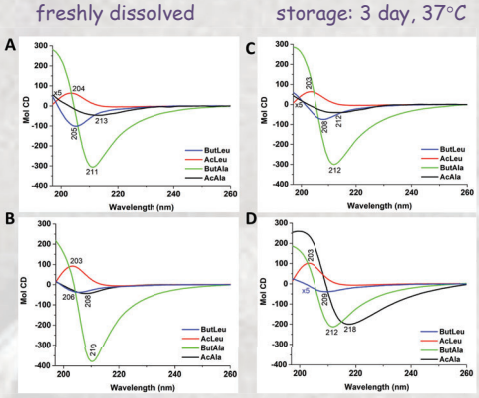

CD spectra at a nominal peptide concentration of 100 μM (A and C) and 500 μM (B and D), respectively.

* Electron microscopy

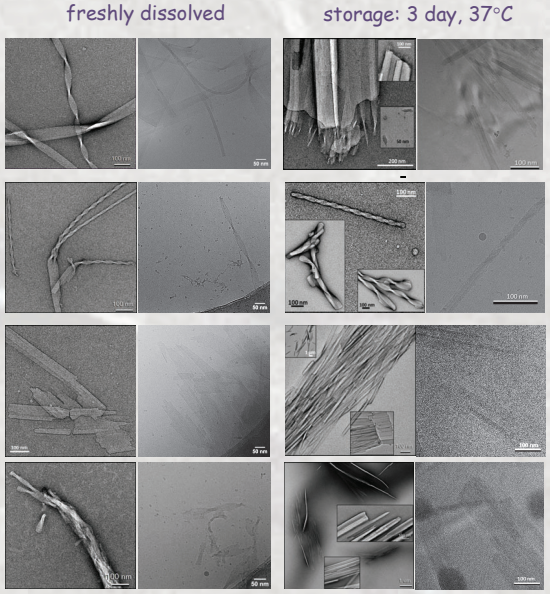

TEM & cryo-EM images of ButLeu (A), AcLeu (B), ButAla (C) and AcAla (D).

ACKNOWLEDGEMENTS

- ✓ Momentum Programme (LP2016-2) of the Hungarian Academy of Sciences
- ✓ TKP2021-EGA-31 and 2020-1-1-2-PIACI-KFI_2020-00021 from Ministry of Innovation and Technology (Hungary), NRDIF
- ✓ SA-87/2021 from Eötvös Loránd Research Network

REFERENCES

1. Szigyártó, I.Cs. *et al.*: Membrane active Janus-oligomers of β³ -peptides. **Chem. Sci.** 11, 6868-6881, **2020**
2. el Battioui, K. *et al.*: In situ captured antibacterial action of membrane-incising peptide lamellae. **Nat. Comm.** 15, Paper: 3424, **2024**

https://doi.org/10.17952/37EPS.2024.P1262

Low-Molecular α-Amino Acid-Based Derivatives as Nanocarriers of Plant Growth Regulators

Vasilena Kondova[1], Borislav Anchev[1], Konstantin Dochev[1], Daniela S. Tsekova[1], Mariana Sichanova[2], Maria Geneva[2]

[1]University of Chemical Technology and Metallurgy, Sofia, Bulgaria, [2] Institute of Plant Physiology and Genetics, Bulgarian Academy of Sciences, Sofia, Bulgaria

Purpose:

The development of nanocarriers, suitable to deliver biologically active compounds, is a modern interdisciplinary field. These substances can be designed as carriers of active compounds for delivery in plants, for example plant growth regulators. Our research is related to design and synthesis of α-amino acid-based amphiphiles and study of their ability to form supramolecular complexes in aqueous solution under specific conditions. Here, we present newly synthesized derivatives of L-Asp and the decanoic acid, which have the structure of either a monomeric or a gemini surfactant [1, 2]. The supramolecular complexes of the sodium salt of the gemini derivative were loaded with thidiazuron (TDZ) and tested *in vitro* on *Stevia rebaudiana* Bertoni to evaluate the effectiveness of the release of the regulator and to monitor the result growth changes. The same surfactants have been used as carriers of silver cations and have shown beneficial effect on the plant development [3].

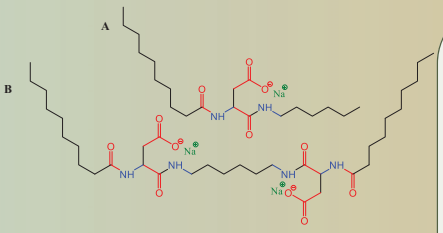

Fig. 1. Structure of the sodium salt of the monomeric l-Asp surfactant MA6N1CNa (A) and the double sodium salt of the gemini L-Asp surfactant A6N10CNa (B).

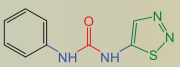

Fig. 2. Structure of thidiazuron (TDZ).

Materials and methods:

The compounds used for this study have been synthesized applying TBTU condensing approach in solution [1, 2]. As sodium salts, the L-Asp derivatives (Fig. 1) behave as anionic surfactants in aqueous media. The gemini surfactant representative was loaded with the plant growth regulator thidiazuron (TDZ, Fig. 2) through a dispersion technique. Supramolecular complexes formed by surfactant solely and the surfactant with TDZ were investigated and confirmed by DLS analysis (Fig. 3). Our experiments showed that the best results for nanoaggregates are obtained at concentrations of the surfactant three times higher than its critical aggregation concentration [1] and for complexes with TDZ in molar ratio: 3:1. The work solutions were analyzed with UV-Vis spectroscopy (Fig. 4). The solid obtained from the solution with the supramolecular complexes of TDZ after solvent removal was applied as an additive to the culture medium Murashige and Skoog for *in vitro* experiments on plant species in several concentrations.

Tab. 1. The average size and z-potential values of the complexes, according the data obtained from the DLS analysis.

Compound	Average size [nm]		Average z-potential [mV]	
	3xCAC	6xCAC	3xCAC	6xCAC
MA6N10CNa	361.3	128.5	-67.47	-59.23
A6N10CNa	134.5	2.6	-52.55	-61.26

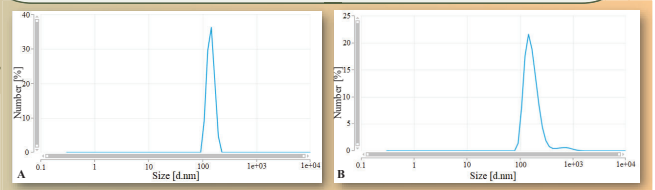

Fig. 3. Size distribution by number of A6N10CNa with three times its CAC (A) and the same compound loaded with TDZ with concentration of the regulator 0.333 mg/mL (B).

Results and discussion:

Low-molecular weight organic compounds derived from L-Asp that belong to the anionic monomeric (Fig. 1A) and gemini surfactants (Fig. 1B) were synthesized. The study of the supramolecular structures by DLS is summarized in Tab. 1, which presents the average size of the complexes distributed by number along with their average z-potential values. It can be well noticed that for both of the compounds, the higher the concentration, the lower the sizes of the aggregates, which may be due to the number of sodium cations in the solution and the concentration of the compound. More experiments should be carried out to clarify the reason for these results.

The gemini surfactant A6N10CNa was chosen for further experiments. The size distribution by number of the aggregates of either A6N10CNa alone and the complex A6N10CNa-TDZ, are shown on the graphics in Fig. 3 A and B. In both cases the majority of the aggregates are of around 130 nm in diameter.

The UV-Vis spectra of the compounds TDZ and A6N10CNa, as well as of the complex A6N10CNa-TDZ are presented in Fig. 4. The UV-Vis analysis of the loaded molecules showed that there is a significant change in the absorption signals of TDZ after the addition of the nanocarriers, such as a bathochromic effect along with a hyperchromic effect of the TDZ peak in 290 nm. This confirms the effectiveness of the loading technique.

The results of the *in vitro* testing of the loaded nanocarriers show insignificant change in the growth of *Stevia rebaudiana* Bertoni at the lowest concentration (1 mg/L), while at higher concentrations there is a negative effect on the plants growth compared to the control plant (Fig. 5). Also, some non-typical morphological changes appear as a result of the treatment, such as thick and curved leaves.

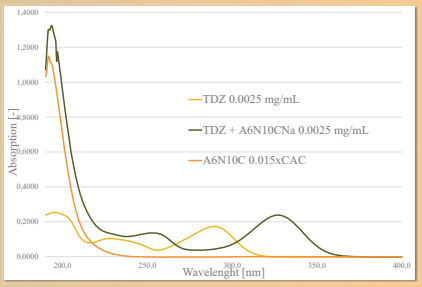

Fig. 4. UV-Vis spectra of TDZ (0.0025 mg/mL) A6N10CNa (0.015xCAC) and A6N10CNa loaded with TDZ (0.0025 mg/mL).

Conclusions:

The sodium salt of the newly synthesized A6N10C self-aggregates into supramolecular complexes in the nanoscale. The changes of the spectra of the probes loaded with TDZ suggest that the molecules of the compound act as potential nanocarriers of TDZ, although the *in vitro* analysis shows that the complex A6N10C-TDZ has a negative effect on the plants growth. Our previous studies with the same organic compound used as a carrier of Ag+ show that the effect of the carrier is not limited only to transferring an active compound, but the process is more complicated and depends also on the complexes formed. More experiments are planned to be carried out in order to explain these results.



Fig. 5. Photographs of in vitro plants of Stevia rebaudiana Bertoni after three weeks treatment with TDZ (A) and A6N10CNa loaded with TDZ – 1 mg/L (B), 10 mg/L (C), 50 mg/L (D).

References:

[1] Anchev, Borislav A., et al. "Monolayer formed by L-Asp-based gemini surfactants self-assembled in 1D nanostructures." *RSC advances* 9.57 (2019): 33071-33079.

[2] Anchev, Borislav, et al. "On the synthesis, surface activity and supramolecular structures of pseudo double-chained L-Asp based amphiphiles." *J. Chem. Technol.* 55.1 (2020).

[3] Sichanova, Mariana, et al. "Influence of the Abiotic Elicitors Ag Salts of Aspartic Acid Derivatives, Self-Organized in Nanofibers with Monomeric and Dimeric Molecular Structures, on the Antioxidant Activity and Stevioside Content in Micropropagated Stevia rebaudiana Bert." *Plants* 12.20 (2023): 3574.

Acknowledgments:

This research was funded by the National Science Fund at the Bulgarian Ministry of Education and Science, Project КП-06-Н56/8 12.11.21. The authors also acknowledge prof. G. Staneva's group at the IBPhBME-BAS for the opportunity to study solution nanoformations by applying DLS analysis.

https://doi.org/10.17952/37EPS.2024.P1264

From Peptides to Bioactive Lactam-constrained Foldamers

Maxime Fillaudeau[1], Alexandre Messerschmitt[1], Arie Van der Lee[2], Lubomir Vezenkov[1], Luc Brunel[1], Young Kee Kang[3], Jean Martinez[1], Baptiste Legrand[1], Muriel Amblard[1]

[1]Institute of Biomolecules Max Mousseron, Montpellier, France
[2]European Institute for Membranes, Montpellier, France
[3]Chungbuk National University, Cheongju Chungbuk, Republic of Korea

Introduction

α-amino-γ-lactam-amino acids (Agl-AA), so-called Freidinger's lactams, are bridged dipeptides that stabilize type II' β-turn conformation.[1] Widely used in modified peptides, they successfully lead to bioactive molecules.[2] Our group developed a straightforward synthesis to generate Agl-AA oligomers from peptide sequences and investigated their structural and physicochemical properties. We demonstrated that Agl-αAA oligomers adopt stable ribbon-like structures[3] and exhibit higher cellular uptake and proteolytic resistance than the well-known cell-penetrating peptides (CPPs), making them suitable for drug delivery.[4]

Further investigating the α-amino-γ-lactam motif in peptide sequences, we focused on Agl oligomers with alternating β-aminoacids (Agl-βAA). Structural studies using nuclear magnetic resonance (NMR), X-ray diffraction (XRD) and circular dichroism (CD) revealed that this new family of oligomers adopts an original 12-Helix with an elliptical cross-section, stabilized by a zigzag hydrogen bond network. Surprisingly, these oligomers display high water solubility despite exclusively containing hydrophobic side-chains such as Trp, Phe and Ile.

Synthesis of Agl oligomers

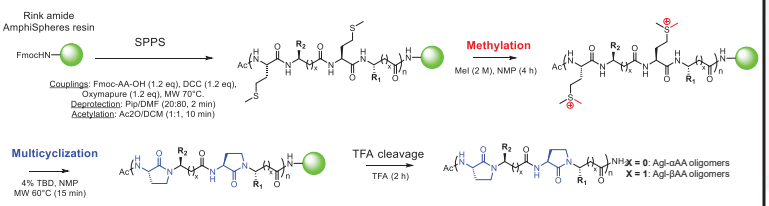

Figure 1: Agl oligomers synthesis pathway. Oligomers are generated on solid support directly from peptide sequences allowing a wide range of side chain diversity.[3]

Agl-αAA oligomers

Physicochemical properties of Agl-AA oligomers can be easily modulated by the peptide sequence and the location of side chains on each face of the ribbon. We identified cell-penetrating Agl-AA oligomers, by alternating Trp and Arg residues along the sequence that displays higher cellular uptake and proteolytic resistance than the well-known R6W3 (RRWWRRWRR) cell-penetrating peptide (Figure 3 and 4). [4]

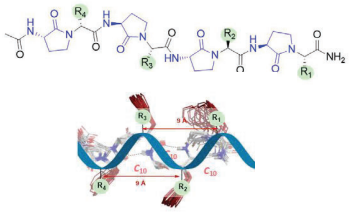

Figure 2: Schematic representations and NMR structure of Agl-αAA oligomers.

Agl-αAA oligomers adopt ribbon-like structures orchestrated by a repetition of β-II' turns which are stabilized by hydrogen bonds, forming 10-membered pseudocycles (C_{10}). The ribbon displays two faces, with side chains aligned and separated by a distance of 9 Å.

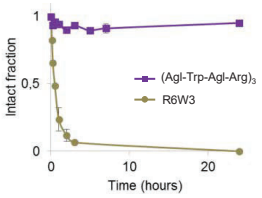

Figure 3: Stability in human blood serum.
37°C, 250 µM of compound

Figure 4: Cellular uptake of Agl-αAA-based foldamers.

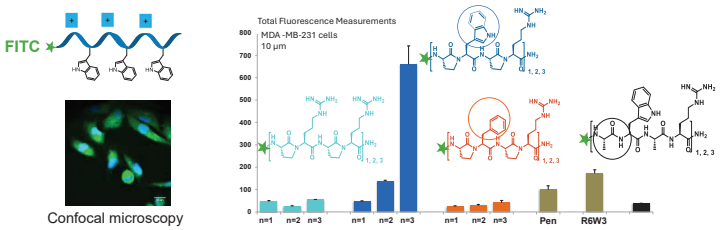

Figure 5: Vectorization potency of (Agl-Trp-Agl-Arg)$_3$ oligomer. Vectorization of the KLA proapoptotic peptide. Conjugate displayed cytotoxicity against MDA-MB-231 cancer cell line compared to KLA and vector alone.

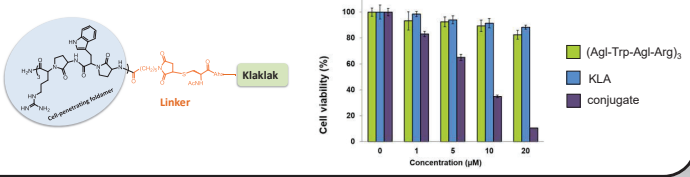

Agl-βAA oligomers

To investigate the impact of Agl motif in different peptide sequences, a new series of oligomers was designed by alternating Agl with β-amino acids and synthesized in the same way as the Agl-αAA oligomers by substituting α-amino acids with β-amino acids. This design strategy was implemented to explore how the additional methylene group in β-amino acids would locally disrupt the Agl-AA β-turn conformation and potentially lead to novel structures. The oligomers' structures were investigated by NMR in various solvents. The solid-state structure of compound **2a** was obtained through slow evaporation in MeOH. These two studies allowed for a comparison between the solution and solid-state structures. The CD signatures of this family of molecules were also reported.

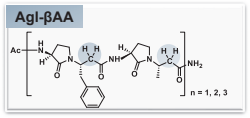

Model Agl-βAA oligomers of different sizes

1a: Ac-**Agl**-β^{3}F-**Agl**-β^{3}A-NH$_2$
2a: Ac-**Agl**-β^{3}F-**Agl**-β^{3}A-**Agl**-β^{3}F-**Agl**-β^{3}A-NH$_2$
3a: Ac-**Agl**-β^{3}F-**Agl**-β^{3}A-**Agl**-β^{3}F-**Agl**-β^{3}A-**Agl**-β^{3}F-**Agl**-β^{3}A-NH$_2$
4a: Ac-**Agl**-β^{3}F-**Agl**-β^{3}A-**Agl**-β^{3}F-**Agl**-β^{3}A-**Agl**-β^{3}F-**Agl**-β^{3}A-**Agl**-β^{3}F-**Agl**-β^{3}A-NH$_2$

➢ DRX

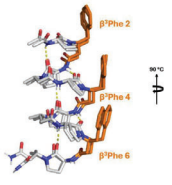

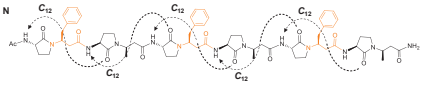

Figure 7: X-ray crystal structure of 3a. Hydrogen bonds are shown in yellow dashed lines. β^3-Phe residues are colored in orange.

The 12-Helix has an elliptical cross-section and is stabilized by zigzag hydrogen bonds network with a macrodipole directed from C-ter to N-ter (Figure 7).

➢ NMR & CD

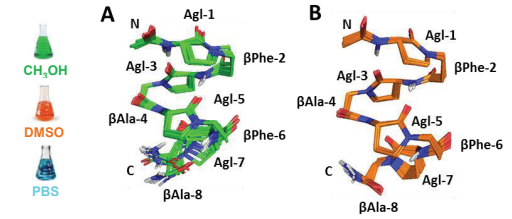

Figure 8: NMR solution structures of 2a in MeOH-d_3, DMSO-d_6 and PBS (10% D_2O, pH 6.5). Agl-βAA oligomers are highly stable and adopt a 12-Helix in chaotropic and aqueous media (Figure 8).

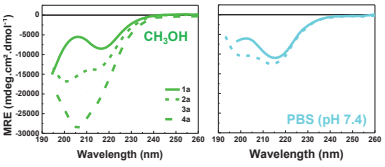

Figure 9: CD spectra at 20 °C of 4-mer 1a, 8-mer 2a and 12-mer 3a in methanol and PBS (pH 7.4).

The 12-Helix CD signature is characterized by negative maxima near 204 and 215 nm. Signal intensities show that longer oligomers further stabilized the 12-Helix and the latter is more stable in methanol than in PBS (Figure 9).

➢ Solubility

Oligomers with exclusive hydrophobic side chains such as Ile and Trp were synthetized to evaluate the solubility of Agl-βAA oligomers (Figure 10).

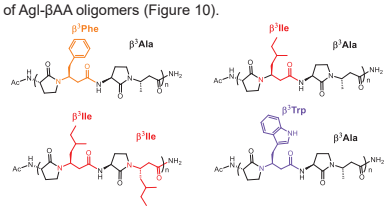

Sequence	n	s (µM)	LogP
Ac-Agl-βPhe-Agl-βAla-NH$_2$	1	>200	-0.94
Ac-(Agl-βPhe-Agl-βAla)$_2$-NH$_2$	2	>200	-0.60
Ac-(Agl-βPhe-Agl-βAla)$_3$-NH$_2$	3	>200	-0.42
Ac-Agl-βIle-Agl-βAla-NH$_2$	1	>200	-1.01
Ac-(Agl-βIle-Agl-βAla)$_2$-NH$_2$	2	>200	-0.82
Ac-(Agl-βIle-Agl-βAla)$_3$-NH$_2$	3	>200	-0.45
Ac-Agl-βIle-Agl-βIle-NH$_2$	1	>200	0.15
Ac-(Agl-βIle-Agl-βIle)$_2$-NH$_2$	2	173±5	1.00
Ac-(Agl-βIle-Agl-βIle)$_3$-NH$_2$	3	172±2	2.13
Ac-Agl-βTrp-Agl-βAla-NH$_2$	1	>200	-0.72
Ac-(Agl-βTrp-Agl-βAla)$_2$-NH$_2$	2	>200	-0.15
Ac-(Agl-βTrp-Agl-βAla)$_3$-NH$_2$	3	167±5	0.43

Sequence	s (µM)	LogP
Ac-(Agl-αPhe-Agl-αAla)$_4$-NH$_2$	117 ± 5	0.30
Ac-(Agl-βPhe-Agl-βAla)$_4$-NH$_2$	860 ± 5	0.42

x 8

Figure 10 : Series of hydrophobic sides chains Agl-βAA oligomers (left) and solubility and LogP values (right).

Most of the oligomers exhibit excellent water solubility and possess LogP values ≤ 0. Only the full Ile series possesses LogP > 0. Oligomers containing β-Ala and β-Phe are 8 times more soluble in phosphate buffer compared to Agl-αAA oligomers.

Conclusion and Perspectives

A new family of foldamers based on the Agl motif has been developed. When the oligomers contain α-amino acids, a ribbon-like structure is formed. The presence of Trp and Arg side chains on each face of the ribbon grants the oligomers the ability to penetrate cells. This property has been utilized to successfully vectorize the KLA proapoptotic peptide in MDA-MB-231 cells. Replacing α-amino acids with β-amino acids results in a novel structure, a 12-Helix that is stable in water. Surprisingly, this family of oligomers exhibits high solubility in water despite the exclusive presence of hydrophobic side chains. We further investigate these unique physicochemical properties to attempt to link specific structures to their solubility.

References

[1] Roger M. Freidinger, Debra Schwenk Perlow, Daniel F. Veber (**1982**), *J. Org. Chem.*, 47, 104-10
[2] a) Andrej Perdih; Danijel Kikelj (**2006**), *Current Medicinal Chemistry*, *1525-1556*. b) Rob M J Liskamp, Dirk T S Rijkers, John A W Kruijtzer, Johan Kemmink (**2011**), *Chembiochem.*, 12, 1626-1653.
[3] Vincent Martin, Baptiste Legrand, Lubomir Vezenkov, Mathéo Berthet, Gilles Subra, Monique Calmès, Jean-Louis Bantignies, Jean Martinez, Muriel Amblard (**2015**), *Angew. Chem. Int. Ed.*, 54, 13966-13970.
[4] Lubomir Vezenkov, Vincent Martin, Nadir Bettache, Matthieu Simon, Alexandre Messerschmitt, Baptiste Legrand, Jean-Louis Bantignies, Gilles Subra, Marie Maynadier, Virginie Bellet, Marcel Garcia, Jean Martinez, Muriel Amblard (**2017**), *ChemBioChem*, 18, 2110-2114.

https://doi.org/10.17952/37EPS.2024.P1265



Development of Neurotensin(8-13) Analogs as Potent NTS1/NTS2 Receptor Ligands with Enhanced Effects on a Mouse Model of Parkinson's Disease

Nikolay T. Tzvetkov[1,*], Toni Kühl[2], Maya G. Georgieva[1], Harald Hübner[3], Maria Lazarova[4], Polina Petkova-Kirova[4], Tamara I. Pajpanova[1], Reni Kalfin[4], Lyubka Tancheva[4], Aneliya A. Balacheva[2], Peter Gmeiner[3], Diana Imhof[2]

1) Department of Biochemical Pharmacology and Drug Design, Institute of Molecular Biology, Bulgarian Academy of Sciences, Acad. G. Bonchev Str., Bl. 21, 1113 Sofia, Bulgaria
2) Pharmaceutical Biochemistry and Bioanalytics, Pharmaceutical Institute, University of Bonn, An der Immenburg 4, 53121 Bonn, Germany
3) Department of Chemistry and Pharmacy, Medicinal Chemistry, Friedrich-Alexander-Universität Erlangen-Nürnberg, Nikolaus-Fiebiger-Straße 10, 91058 Erlangen, Germany
4) Institute of Neurobiology, Bulgarian Academy of Sciences, Acad. G. Bonchev Str., Bl. 23, 1113 Sofia, Bulgaria

Corresponding author:** ntzvetkov@bio21.bas.bg **(NTT)

Introduction

The tridecapeptide Neurotensin (NT, **1**) is widely expressed throughout the central nervous system (CNS) and periphery [1,2]. NT exerts its neurophysiological effects mainly by interactions with the human NT receptors type 1 (hNTS1) and 2 (hNTS2) [1]. In the brain, NT modulates directly or indirectly dopamine (DA) neurotransmission through different neuronal mechanisms, including antagonistic NT/D_2 receptor interaction and second messenger-dependent receptor alteration [3,4]. Moreover, both NTS1 and NTS2 receptors are also found in high concentrations on dopaminergic neurons in substantia nigra (SN), suggesting that the activation of both NTS1 and NTS2 receptors in this brain region by NT may stimulate the DA release [3,4]. Accordingly, the main effect of NT binding in SN is a D_2 autoreceptor inhibition with a subsequent increase of DA signaling [5,6]. Therefore, both receptor subtypes are promising targets for the development of novel NT-based analogs for the treatment of Parkinson's disease (PD).

In the current study we aim at:

- Developing NT(8-13) peptidomimetics by using virtually guided two-step protein structure homology/molecular modelling approach (Fig. 1 and 2, Scheme 1, and Table 1) [2].
- Identifying of NTS1/NTS2 dual-specific NT(8-13) analogues with *in vitro* (by radioligand binding studies) and *in vivo* (in a MPTP-induced mouse model of PD) confirmed efficacy against PD (Fig. 3).

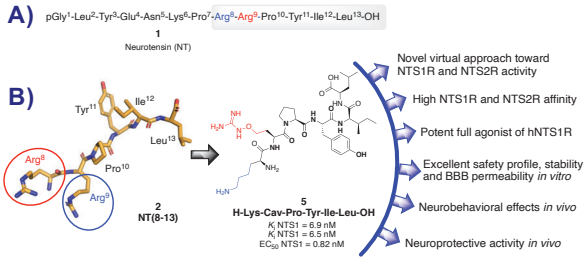

Figure 1: A) Amino acid sequences of neurotensin (NT); B) NT(8-13) (**2**, left), the biologically active fragment of neurotensin (NT, **1**), and the most potent C-terminal hexapeptide H-Arg^8-Arg^9-Pro^{10}-Tyr^{11}-Ile^{12}-Leu^{13}-OH as dual NTS1R/NTS2R ligand (middle) as well as the investigated herein in vitro and in vivo properties (right).

Homology modeling of hNTRs and synthesis

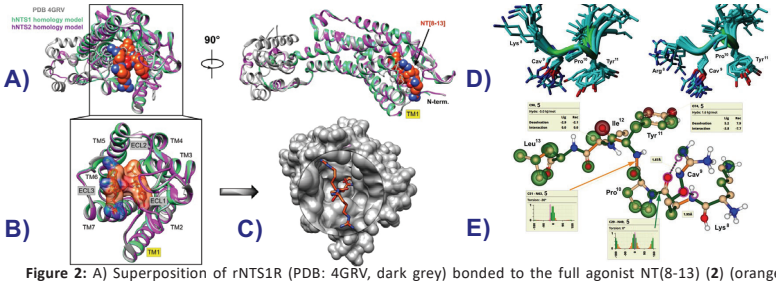

Figure 2: A) Superposition of rNTS1R (PDB: 4GRV, dark grey) bonded to the full agonist NT(8-13) (**2**) (orange spheres) with the homology models of hNTS1R (green) and hNTS2R (magenta). B) Extracellular receptor side of rNTS1R and hhNTRs with the binding side of **2**. C) Space filling model of the superimposed receptors (dark grey) with **2** (orange sticks) [5]. D) NMR structures of **5** (left) and **8** (right). E) HYdrogen DEsolvation (HYDE) visual assessment of **5** into the hhNTS1R. HYDE coloring and torsion analysis: **green** = good, **red** = bad for affinity [6].

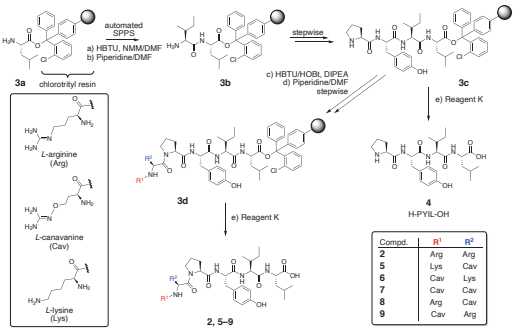

Scheme 1: Synthesis of H-PYIL-OH (**4**), NT(8-13) (**2**) and its analogs **5–9**.

Prediction *vs.* Experiment

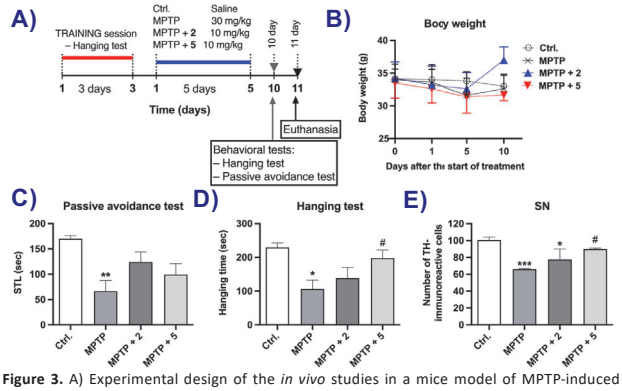

Figure 3. A) Experimental design of the *in vivo* studies in a mice model of MPTP-induced PD. B) Body weight change in mice. C) Effects of **2** and **5** on the memory and motor (D) disturbances. E) Attenuation of the MPTP-induced nigrostriatal neuronal damage in SN [2].

Peptide	K_i binding (nM ± SEM) [1] (experiment)		$K_{i\,HYDE}$ ranges (nM) (SeeSAR/HYDE prediction)			G-protein activation [5]
	*h*NTS1	*h*NTS2	*hh*NTS1	*hh*NTS2	SI [4]	EC_{50} (nM ± SEM
NT(8-13) (2)	0.68 ± 0.04 [2] 1.07 ± 0.05 [3]	1.8 ± 0.17 [2] 6.6 ± 2.18 [3]	0.13–12.6	4.28–425	0.38 0.16 [3]	0.88 ± 0.10
4	>50,000	>50,000	n.a.	n.a.	n.a.	3,200 ± 320
5	**6.9 ± 0.59**	**6.5 ±0.63**	**0.10–10.3**	**3.23–321**	**1.06**	**0.82 ± 0.16**
6	15 ± 4.5	14 ± 4.4	0.15–15.0	0.31–30.5	1.07	0.85 ± 0.06
7	60 ± 5.4	54 ± 11	0.35–34.7	3.47–344	1.11	1.30 ± 0.26
8	5.5 ± 1.7	5.6 ± 1.0	2.35–233	2.94–292	0.98	0.74 + 0.19
9	4.2 ± 0.62	5.8 ± 0.65	1.19–118	1.56–154	0.72	0.89 ± 0.15

Table 1. Receptor binding data for human (h) and HYDE estimated *binding affinity* for human homolog (hh) NTS1 and NTS2 receptor of NT(8-13) (**2**) and ligands **4–9** [2].
[1] Determined by radioligand competition binding with [^{3}H]**2** at HEK293T cells (N = 3). [2] K_D value in nM ± SEM.[3] Data are from Ref. [6]. [4] Selectivity index: SI = K_i (hNTS1R)/K_i (hNTS2R). [5] IP-One® assay (Ciscbio) with HEK293T cells transiently transfected with hNTS1R [2]. n.a. = not applicable.

Conclusions

SeeSAR/HYDE concept: An innovative drug design concept combining a homology modeling of hNTS1/2 receptors with the molecular modelling platform SeeSAR/HYDE was used to predict the binding affinities ($K_{i\,HYDE}$ ranges) towards both hNTRs of a small set of NT(8-13) (**2**) analogs (peptides **5–9**).

Proof-of-concept: Consequently, we synthesized such series of NT(8-13) analogs **5–9** with modifications at positions 8 and/or 9 in NT(8-13) and determined the 3D-structures of **5** and **8** using 2D-NMR. The experimental binding affinities (K_i values) for peptides **5–9** reproduced their predicted $K_{i\,HYDE}$ ranges. I*n vivo* evaluation of **5** suggested that dual NTS1/NTS2-acting NT(8-13) peptidomimetics represent an attractive strategy for the treatment of PD and possibly other CNS disorders.

Acknowledgments: This work is supported by the Bulgarian National Science Fund (BNSF) under Grant No. **KP-06-N59/2 (КП-06-Н59/2)**.

Literature

[1] A. W. K. Yeung et al. *Future Med. Chem.* **2020**.
[2] T. Kühl et al. *Eur. J. Med. Chem.* **2023**.
[3] M. Boules et al. *Front. Endocrinol.* **2013**.
[4] S. Tanganelli et al. *Curr. Med. Chem.* **2012**.
[5] www.cgl.ucsf.edu/chimera (UCSF Chimera v.15.1, **2020**)
[6] www.biosolveit.de/SeeSAR (SeeSAR v.12.1, **2022**).

https://doi.org/10.17952/37EPS.2024.P1266

SYNTHESIS AND BIOLOGICAL APPLICATION OF A SHORT PEPTIDOMIMETICS BASED ON BACTERIAL CELL WALL PEPTIDOGLYCAN MONOMER

Marcela Šišić[1], Leo Frkanec,[2] Ruža Frkanec [1]

[1]University of Zagreb, Zagreb, Croatia;
[4]Ruđer Bošković Institut, 10 000 Zagreb, Croatia
E-mail: *msisic@unizg.hr*

INTRODUCTION

Bacterial peptidoglycan (PG) (Figure 1.) plays a vital role in both bacterial viability and in the response of human physiology to bacterial infection. A large number of novel synthetic compounds representing smaller parts of original peptidoglycan molecules have been synthesized and found to possess versatile biological activity [1]. Peptidoglycan monomer (PGM) was isolated from the cell wall of the non-pathogenic bacterium *B. divaricatum* by a procedure described in the literature, and its significant immunomodulating activity was confirmed [2]. It was previously reported that bacterial cell wall fragments play important roles in the immune response of higher organisms against bacterial infections, and mediate the innate immune response. Furthermore, it is known that bacterial cell wall biosynthesis is a major target of antibiotics, including beta-lactam and glycopeptide antibiotics, such as vancomycin, which represent the last line of defense against antimicrobial resistance (AMR). Hence, based on the facts that peptides are increasingly becoming key therapeutic agents for a wide range of applications and that the introduction of triazolyl or lipidic moieties into the peptides as well as cyclization could stabilize the molecule to hydrolysis, oxidation, or reduction [3], the new PGM peptidomimetics are designed. The structure and conformation of the PGM molecule in solution, in DMSO, and in an aqueous medium, were studied in detail through molecular modeling and chemical calculations and were confirmed by ^{1}H NMR spectroscopy [4] (Figure 2.). Numerous PGM derivatives with an adamantane moiety, the amino acid tyrosine [5], and adamantyltripeptides have been synthesized. All the derivatizations were performed on the amino group present in the side chain of diaminopimelic acid. Still, no cyclic derivative has been synthesized, nor has a new functional group been introduced to the C-terminal end of the peptide.

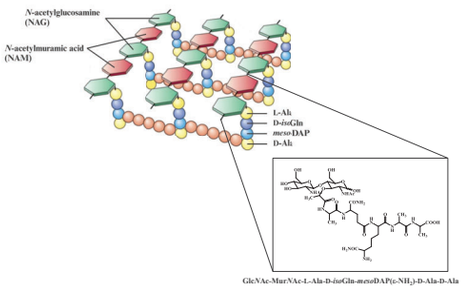

Figure 1. Schematic representation of bacterial peptidoglycan.

AIM

The aim of the present study is the synthesis of new peptidomimetics of the peptidoglycan monomer (PGM), Glc*N*Ac-Mur*N*Ac-L-Ala-D-*iso*Gln-*meso*DAP(ε-NH_2)-D-Ala-D-Ala, cyclic derivative (tail-to-side chain cyclization of Tyr-PGM), cyTyr-PGM (Figure 3.), and lipophilic derivative, PGM-DOPE (Figure 4.).

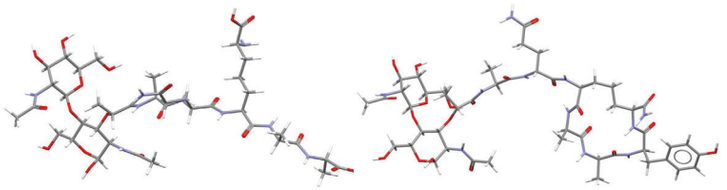

Figure 2. Minimized chemical structure of PGM [4] and designed cyTyr-PGM derivative.

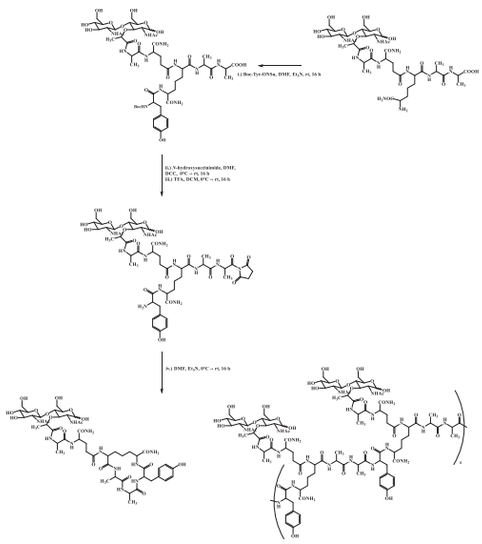

Figure 3. Synthesis route for the cyclic derivative of peptidoglycan monomer, cyTyr-PGM.

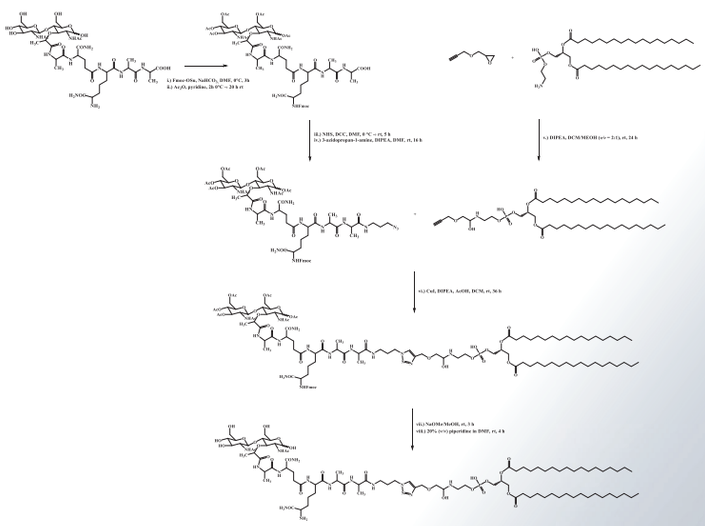

Figure 4. Synthesis route for the lipophilic derivative of peptidoglycan monomer, PGM-DOPE.

METHODS

The design of new peptidomimetics is carried out using molecular modeling and chemical calculations using a numerical/graphical workstation HP-620 (Linux) equipped with a software package for molecular modeling (MM) and molecular dynamics (MD) *Sybyl*-X (Tripos Inc. Certara). The peptidomimetics were synthesized in solution. PGM-DOPE synthesis is carried out by cycloaddition catalyzed by copper(I) ions, which leads to the formation of 1,4-disubstituted 1,2,3-triazoles under very mild reaction conditions. For the design of cyclic peptidomimetics, obtained clusters of conformations with minimum energy were analyzed, and tyrosine-PGM was selected as the starting molecule for cyclization. DCC and NHS crosslinking agents were used for introducing "zero-length" amide cross-links between a carboxylic group of terminal D-Ala and the amino group of tyrosine which is attached to *meso*DAP in the molecule Tyr-PGM. In the cyclization reaction, along with the cyclization of the tetrapeptide, polymerization was observed. The described synthetic protocols should be optimized and the antibacterial and immunostimulating effects of the synthesized peptidomimetics should be tested.

CONCLUSION

- ❑ Design of peptidomimetics by molecular modeling and structure optimization with particular emphasis on the possibility of cyclization of the peptide part of the PGM molecule is performed
- ❑ The protocol for the introduction of new substituents by the click-chemistry method at the carboxyl end of the peptide part of the PGM is established and PGM-DOPE is synthesized
- ❑ The synthetic route using copper(I)-catalyzed azide-alkyne cycloaddition for the synthesis of triazolyl-containing PGM-DOPE peptidomimetic was developed
- ❑ The preliminary protocol for tail-to-side chain cyclization of the Tyr-PGM molecule is established

REFERENCES

[1] C. M. Vacariu, M. E. Tanner, *Eur. J.* 2022, 28, e202200788.
[2] J. Tomašić, I. Hršak, *Peptidoglycan monomer originating from B. divaricatum: its metabolism and biological activities in the host*, in: E. Schrinner, M.H. Richmond, G. Seibert, U. Schwartz, Surface structures of microorganisms and their interaction with mammalian host, Wiley-VCH, 1987 Weinheim; pp.: 113–121.
[3] A. Staśkiewicz, P. Ledwoń, P. Rovero, A. M. Papini, R. Latajka, *Front. Chem.* 2021, 9, 674705.
[4] H. Matter, L. Szilagyi, P. Forgo, Ž. Marinić, B. Klaić, *J. Am. Chem. Soc.* 1997, 119, 2212-2223.
[5] Đ. Ljevaković, J. Tomašić, V. Šporec, B.Halassy Špoljar, I. Hanzl-Dujmović, *Bioorg. Med. Chem.* 2000, 8, 2441-2447.

ACKNOWLEDGEMENTS: *We acknowledge the financial support of the Croatian Science Foundation (HrZZ, Project No: IP-2018-01-6910*

https://doi.org/10.17952/37EPS.2024.P1267

University of Gdańsk

Antimicrobial peptidomimetics against methycillin-resistant *Staphylococcus aureus* (MRSA)

Katarzyna Łada[1], Maria Dzierżyńska[1], Agnieszka Gajewicz-Skrętna[2], Łukasz Grabowski[3], Alicja Węgrzyn[4], Franciszek Kasprzykowski[1], Sylwia Rodziewicz-Motowidło[1]

[1] Department of Biomedical Chemistry, Faculty of Chemistry, University of Gdansk, Gdansk, Poland
[2] Department of Enviromental Chemistry and Radiochemistry, University of Gdansk, Gdansk, Poland
[3] Department of Molecular Microbiology, Faculty of Biology, University of Gdansk, Gdansk, Poland
[4] Phage Therapy Center, University Center for Applied and Interdiscyplinary Science, University of Gdansk, Gdansk, Poland

E-mail: katarzyna.lojewska@phdstud.ug.edu.pl

INTRODUCTION

Staphylococcus aureus is considered the leading cause of human diseases not only in hospitalized individuals, but also in individuals living in the community. *Staphylococcus aureus* mainly causes skin infections, such as purulent wounds, soft tissue inflammation, impetigo, and may also cause inflammation of the endocardium, lungs, and bone marrow. The number of infections caused by MRSA strains is increasing around the world. WHO predicts that by 2050, mortality caused by AMR (antimicrobial resistance) will be one of the main causes of death. [1]
In this work, we report the development of novel peptidyl derivatives based upon the structure of the *N*-terminal fragment ($R^8L^9V^{10}G^{11}$) of the human cystatin C protein. A derivative called Cystapep 1 (A-20) has a strong activity against Gram-positive bacteria, including MRSA strains. [2] We synthesized analogues of Cystapep 1 with modifications at the highlighted site on Scheme 1.

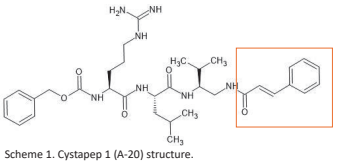

Scheme 1. Cystapep 1 (A-20) structure.

QSAR STUDIES

The QSAR analysis of Cystapep 1 and its derivatives was essential to establish which elements of the molecule are crucial for its antibacterial activity. Analysis was carried out based on 80 Cystapep 1 derivatives with established antibacterial activity for *Staphylococcus aureus* and computed descriptors. The calculated descriptors represented different levels of chemical structures/properties and therefore different theoretical dimensions (0-3D).
The simplest, constitutional and topological descriptors (ON1V, GNar, ZM1V), which encode information about molecular weight, size and shape, were obtained using the Dragon-7 software. More complex electronic descriptors related to the 3D conformation of the molecule, were calculated using the MOPAC2016 package. These descriptors were used for principal component analysis (PCA) (Figure 2). This graph shows that ON1V, volume, ZM1V, LogS and Molecular weight are the most influential variables in PC1, while MLOGP, TPSA, LogP, and LogKp form PC2. The classification tree shown in Figure 1 reveals four descriptors as being the most effective in determining the high activity against *Staphylococcus aureus*. These descriptors are lipophilicity, TPSA (topological polar surface area), Hy (hydrophilic factor) and ZM1V (topological/structure descriptor). On this basis, we designed new derivatives with potentially high antibacterial activity. By using a classification tree, we were able to predict, which peptidomimetic has high (Klasa-3) or low (Klasa 1) activity against *Staphylococcus aureus.*

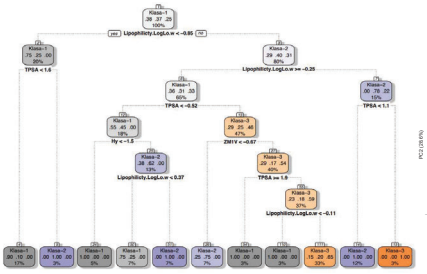

Figure 1. Classification tree.

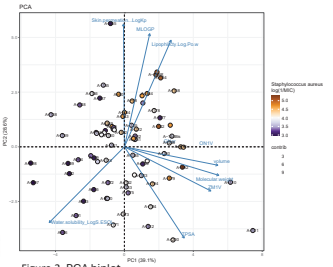

Figure 2. PCA biplot.

ANIMICROBIAL ACITIVITY

The most promising molecules A-75, A-76, A-238, A-241, A-243, and the leading structure A-20 were examined on MRSA isolates: RA636, O2449, 342, 124, 115, 44, 343, O2229, RA532, RA604, 352 (clinical and laboratory strains) by measuring the growth of bacterial cells for 20h (Figure 3). The peptidomimetics have strong inhibitory effect on MRSA growth. No differences were observed between concentrations inhibiting bacterial cells growth, only one strain MRSA 342 was more resistant, and inhibition concentration was one fold higher.

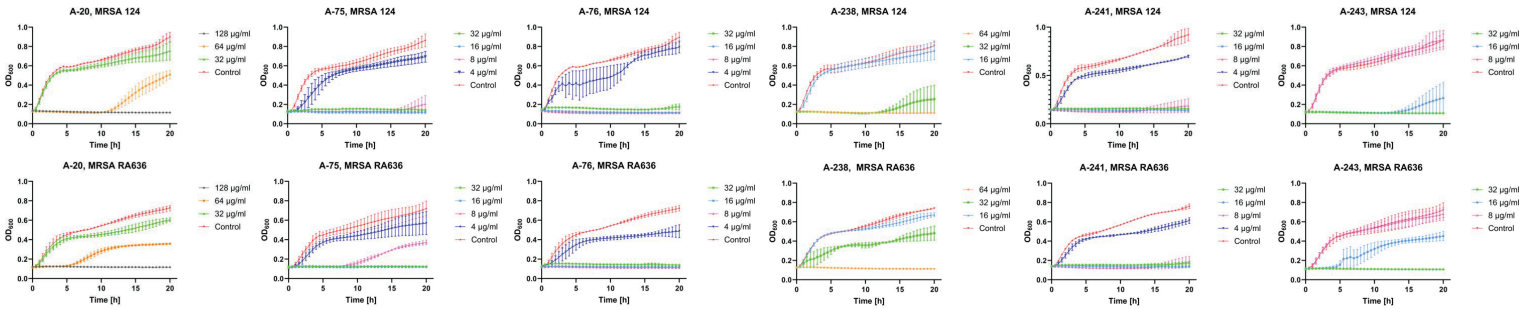

Figure 3. A-20, A-75, A-76, A-238, A-241, A-243 effect on MRSA 124 (clinical strain) and MRSA RA636 (laboratory strain) growth in different concentrations.

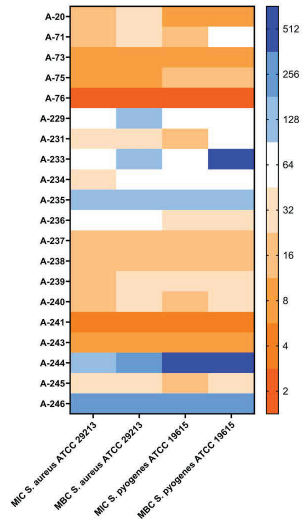

Figure 4. A-20 and its analogues antimicrobial activity against *Staphylococcus aureus* and *Streptococcus pyogenes.*

The susceptibility of bacterial strains of *S. aureus* and *S. pyogenes* has been examined by broth microdilution tests. The most active peptidomimetics are A-73, A-75, A-76, A-241, A-243 (Figure 4). Most of these compounds have similar activity on both tested bacterial strains. There was no difference between MIC (minimal inhibitory concentration) and MBC (minimal bactericidal concentration) value is two fold higher than MIC value.

CYTOTOXICITY

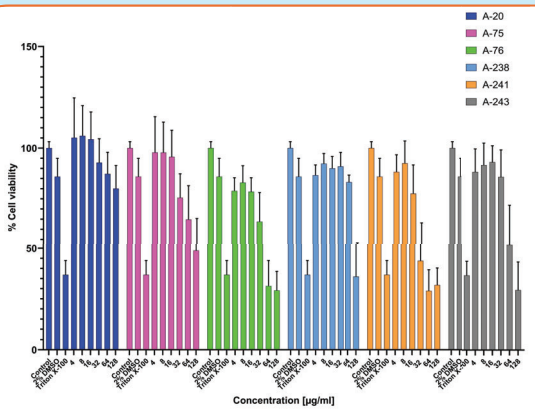

Figure 5. A-20, A-75, A-76, A-238, A-241, A-243 cytotoxicity effect on HaCaT cells.

To investigate the cytotoxicity of the peptidomimetics (Figure 5), a Neutral Red assay was performed on human keratinocytes (HaCaT cells). Cells were cultured with compounds at different concentrations for 24h. Maximum cytotoxicity was determined as 0.1% Triton X-100 solution, and a control for the 2% DMSO solution was performed, in which the compounds were dissolved. A-20 show no negative effect on HaCaT cells. The analogues A-75, A-238, A-243 do not show cytotoxicity at concentrations below 32 µg/ml, A-76, A-241 at concentrations below 16 µg/ml.

CONCLUSIONS

- Principal component analysis (PCA) showed that the more lipophilic molecule is, the more antimicrobial activity it has. Water-soluble molecules are characterized by low activity.
- A-20 and its analogues have a strong inhibitory effect on the growth of MRSA (both clinical and laboratory strains). There is no difference in MRSA growth inhibition between laboratory and clinical strains.
- The tested peptidomimetics do not show cytotoxicity concentrations at which they inhibit the growth of MRSA.

[1] J. O'Neill, Tackling drug-resistant infections globally : final report and recommendations, The Review on Antimicrobial Resistance, 2016
[2] [2] Dzierżyńska M., Sikorska E., Pogorzelska A., Mulkiewicz E., Sawicka J., Wyrzykowski D., Małuch I., Grubb A., Kasprzykowski F., Rodziewicz-Motowidło S., *Prot Pep Letters*, 2019, *26*, 1-12.

This work was supported by the grant PRELUDIUM BIS „*New class of antimicrobial compounds. Design, synthesis and biological studies.*" no. UMO-2020/39/O/NZ7/00430

National Science Centre Poland

https://doi.org/10.17952/37EPS.2024.P1268

Synthesis of 5-member heteroaromatics containing peptide backbones: *pro* and *cons* of structural constraints induced by amide bond surrogates

Francesco Brenzini Biagioni[1, 2], Corentin Layec[1], Karine Porte[1], Pierre-Yves Renard[1], Anna Maria Papini[2,3]

[1]*Normandie Univ, UNIROUEN, INSA Rouen, CNRS, COBRA (UMR 6014) IRCOF, Mont-Saint-Aignan Cedex, France.*
[2]*Interdepartmental Research Unit of Peptide and Protein Chemistry and Biology, University of Florence, Sesto Fiorentino (FI), Italy.*
[3]*Department of Chemistry "Ugo Schiff", University of Florence, Sesto Fiorentino (FI), Italy.*

XL-Chem thesis in cotutelle between University of Rouen Normandie and University of Florence

Background

Increasing the stability and bioavailability of short peptides *in vivo* is crucial for the development of peptide-based drugs. The main challenges to address are the low metabolic stability and the high conformational flexibility of peptides, which can lead to inactivation and a decrease in their activity. To avoid these issues, one strategy is the use of peptidomimetics, where the peptide bond is replaced by surrogate bonds with similar structural features (bioisostere).[1] One of the most common bioisostere of the amide bond is the [1,2,3] triazole moiety, which presents structural features similar to the peptide bond, resulting in an improvement in metabolic stability and an increase in structural constraints. Moreover, this moiety is easily obtained by 1,3-dipolar cycloaddition reaction, and proved particularly resistant to several types of cleavage. Finally, an additional benefit of peptidotriazoles is their low toxicity.

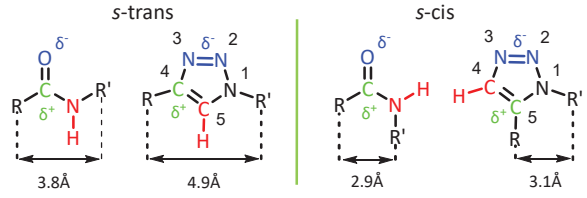

Objectives

The main objective is to develop mimetics of the *s*-cis peptide bond using 1,5-disubstituted [1,2,3] triazole in order to stabilize β-turns where a **glycine** is present in the i+1 or i+2 position. This aims to improve the low rigidity of glycine, thereby increasing the activity and selectivity against specific targets.

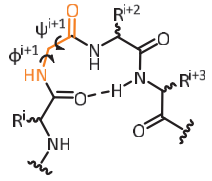

➢ Orientation of heterocycle ←→conformational behavior

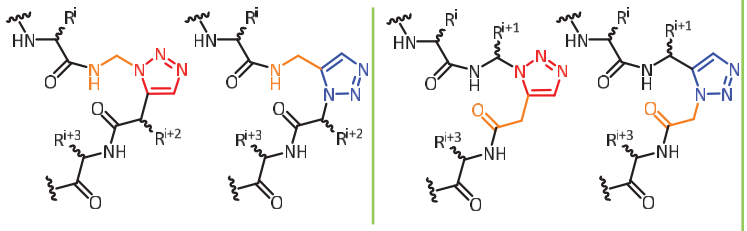

1,5 disubstituted [1,2,3] triazole peptidomimetic

5,1 disubstituted [1,2,3] triazole peptidomimetic

Research and development[2]

Mimetic containing 1,5 disubstituted [1,2,3] triazole

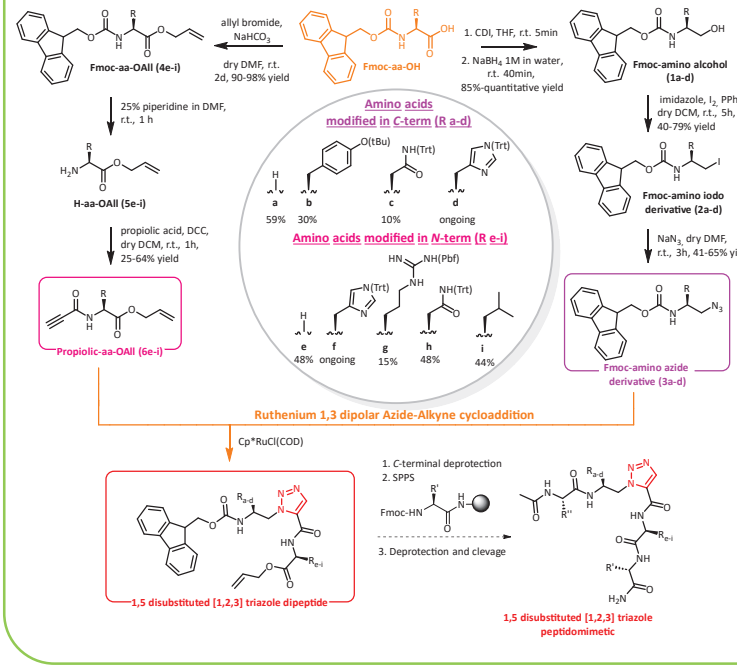

Mimetic containing 5,1 disubstituted [1,2,3] triazole

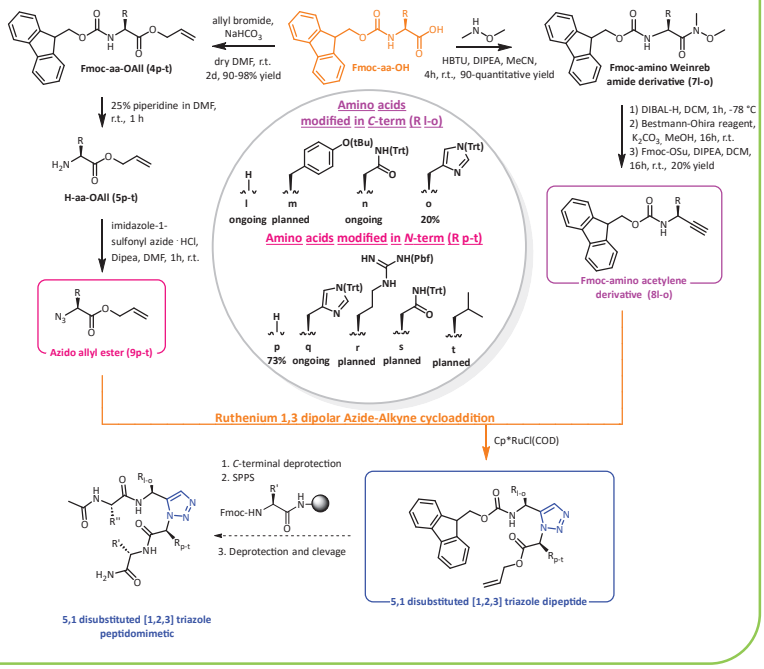

Results and Future perspectives

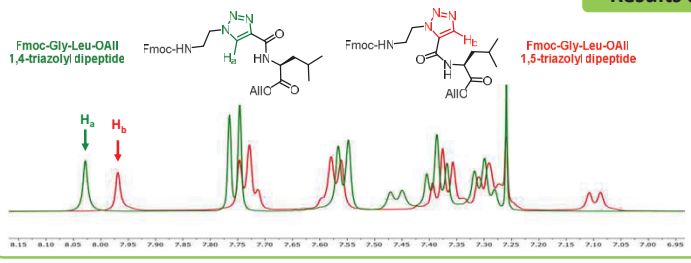

- Study of the conformational behavior
- Biological properties
- Comparison with side chain-to-side chain triazolyl bridged peptides[3]

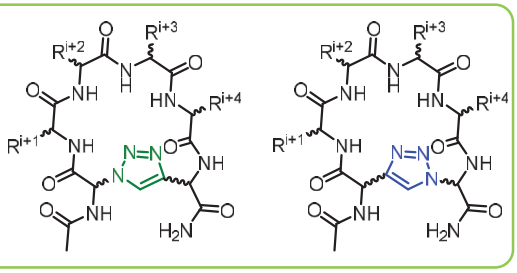

[1]Li, H.; Aneja, R.; Chaiken ,I. *Molecules* **2013**, *18* (8), 9797–9817.
[2]Bruyat, P.; Gautier, A.; Jean, L.; Renard, P. *J. Org. Chem.* **2018**, 83, 13515−13522
[3]Testa, C.; Scrima, M.; Grimaldi, M.; D'Ursi, A. M.; Dirain, M. L.; Lubin-Germain, N.; Singh, A.; Haskell-Luevano, C.; Chorev, M.; Rovero, P.; Papini, A. M. *J. Med. Chem.* **2014**, *57* (22), 9424–9434.

Looking for EPS-IPS 2024
www.eps2024.com
37th EPS European Peptide Symposium
14th IPS International Peptide Symposium
25 - 30 August 2024 Florence, Italy

PepFuNN: Novo Nordisk open-source toolkit to enable peptide *in silico* analysis

Rodrigo Ochoa[1], Kristine Deibler[2]

[1]Novo Nordisk A/S, Novo Nordisk Park, Måløv, DK-2760, Denmark

[2]Novo Nordisk Research Center Seattle, Novo Nordisk A/S, 818 Stewart St. Suite #910, Seattle, WA, 98101, USA

Source code

https://doi.org/10.17952/37EPS.2024.P1270

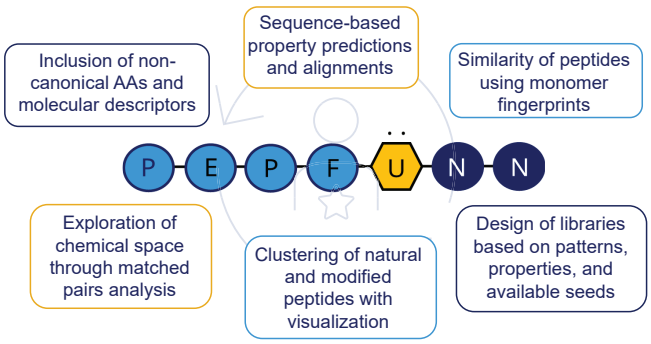

Open computational protocols for peptide analysis

- We present PepFuNN, a new open-source version of the PepFun package with functions to study the chemical space of peptide libraries and perform structure-activity relationship (SAR) analysis.
- PepFuNN modules allow calculating physicochemical properties, performing similarity analysis using different peptide representations, running SAR exploration studies adapted for peptides, and functions to support the design of peptide libraries based on specific requirements.

What input do you need?

Simple linear peptides can be represented using FASTA format. For non canonical elements, line notations to allow the representation of complex peptides are suggested (i.e., BILN format*).

*Fox, Bieler, Haebel, Ochoa, Peters, Weber. *J. Chem. Inf. Model.* 2022

Description	FASTA	BILN
Simple linear peptide	PEPTIDE	P-E-P-T-I-D-E
Peptide with internal C-C disulfide bridge and amidation at the C-terminus	ACGAGCD	A-C(1,3)-G-A-G-C(1,3)-D-NH2
C-term to N-term cyclic peptide	CYCLIC	C(1,1)-Y-C-L-I-C(1,2)

What new methodologies are included in PepFuNN?

For complex peptides, it is possible to generate monomer-based fingerprints to run similarity analysis.

- A line notation sensible to complex chemical structures is used to represent the peptides.
- The complex peptide is represented as a graph, which is decomposed into fragments up to a defined radius.
- Per each combination, a numerical token is generated based on a combination of physicochemical properties per monomer.
- Each token is converted into a bit that will be part of a fixed-size fingerprint used to run similarity searches.

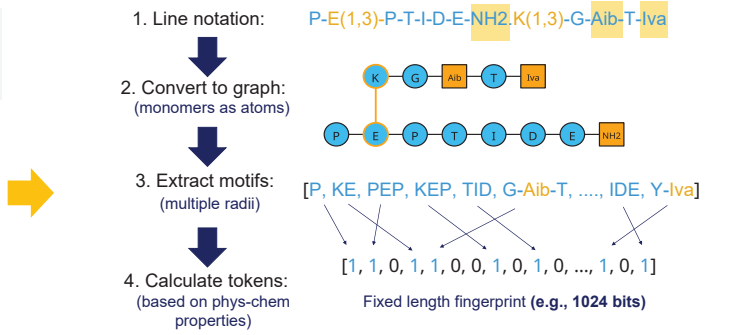

How to run SAR analysis?

For peptides, we allow the option to calculate molecular matched pairs to identify single modifications that can have a positive or negative impact in an experimental assay.

- The matched pairs methodology compares the properties of two molecules that differ by a single chemical transformation.
- The method is relevant to deeply exploring SAR data and collecting ideas for designing optimized molecules.

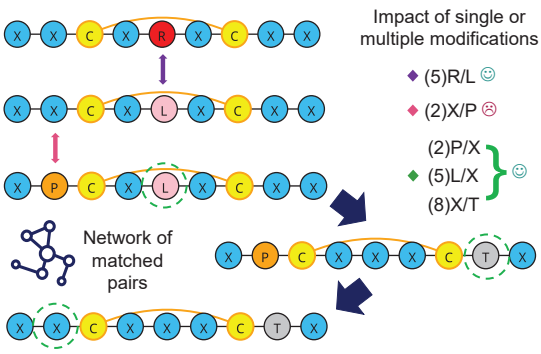

Matched pairs analysis of a library built with PepFuNN, using a peptide scaffold as a reference

Library design using a scaffold

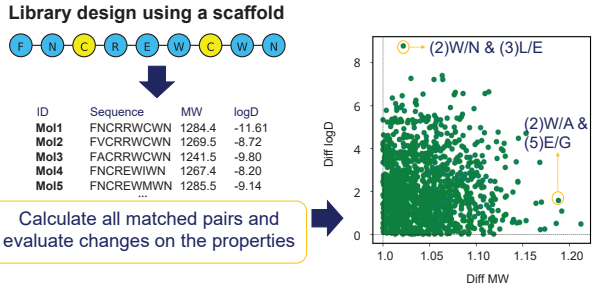

How to check the similarity between simple and/or complex peptides?

We can use different notations and representations to compare the peptides. In this case, the chemical similarity strategy can rely on the use of Morgan fingerprints (used also for small molecules) or monomer-based fingerprints. The latest are obtained from the BILN representations of the sequences.

- Strategy to cluster and compare cyclic head-to-tail peptides from the ChEMBL database.
- We can generate a Principal Component Analysis (PCA) plot of the descriptors, with arrows showing the properties with higher importance in the dataset.

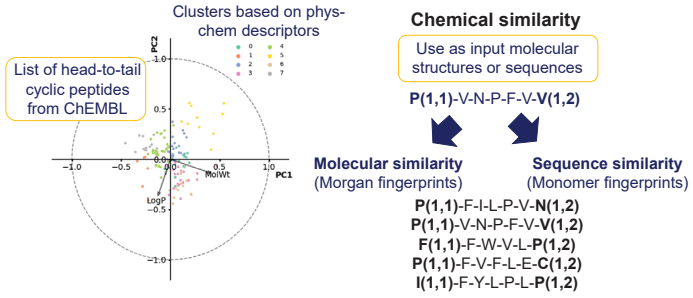

Availability

- Project name: PepFuNN (version 1.0)
- Project home page: https://github.com/novonordisk-research/pepfunn
- Operating system(s) tested: Linux
- Programming language: Python 3.9 or higher
- Other requirements: RDKit 2020 or later; Biopython 1.7.9 recommended
- License: MIT

Computational Drug Design • Molecular AI
raoc@novonordisk.com

Digital Science & Innovation DSI.

A peptide database from human feces to foster the discovery of novel bioactive peptides

Armando A. Rodriguez[1,2], Nico Preising[1], Merve Karacan[1], Thomas Seufferlein[3], Martin Wagner[3], Frank Kirchhoff[4], Jan Münch[4], Ludger Ständker[1], Sebastian Wiese[2]

armando.rodriguez-alfonso@uni-ulm.de

https://doi.org/10.17952/37EPS.2024.P1271

[1] Core Facility Functional Peptidomics, Ulm University Medical Center, Ulm, Germany. [2] Core Unit Mass Spectrometry and Proteomics, Ulm University Medical Center, Ulm, Germany. [3] Institute of Molecular Virology, Ulm University Medical Center, Ulm, Germany. [4] Section of Nephrology, Ulm University Medical Center, Ulm, Germany. [5] Anesthesiology and Intensive Medicine Clinic, Ulm University Medical Center, Ulm

Abstract

Fecal microbiota transplantation (FMT) is known for its high efficacy in addressing gastrointestinal, metabolic, and neurological disorders, as well as various types of cancer. However, sterile stool filtrates (SSF) have also been proven effective in the treatment of a variety of diseases[1,2], posing a lower risk for bacterial infection than FMT treatment, particularly in immunocompromised patients[1]. SSF consists mainly of microbiota-derived polypeptides and gut metabolites, but the nature and identity of antimicrobial or immunomodulatory factors are largely unknown. We have previously shown that body fluid filtrates are a rich source of novel anticancer and antimicrobial peptides with diagnostic and therapeutic potential[4]. Therefore, in the present work, we focused on the generation and analysis of a peptide bank from human feces for the identification of novel antimicrobial, immunomodulatory, and anticancer peptides, either using *in silico* approaches or bioassay-guided isolation and characterization of specific peptide components. A liquid sample (2L) of human feces from healthy donors was filtered through a membrane with a cut-off of 30 kDa. The filtered sample was subjected to reversed-phase HPLC; 36 fractions were collected and stored at -80ºC until further use. A 0.1 mL aliquot of each fraction was used to form six small pools of adjacent fractions for sample preparation and mass spectrometry. All pools of fractions were processed for heme group removal by either cold acetone extraction or C18-SPE and then subjected to sequencing analysis by LC-MSMS and bioinformatics. Several hundred peptides were identified as bacterial or human protein fragments, as well as many *de novo*-sequenced peptides. An *in silico* approach was also used to predict antimicrobial peptides among them. We expect that our methodology, which includes the generation of the human feces peptide bank, sample processing, and bioinformatics analyses, will facilitate the discovery of novel human peptides of therapeutic interest.

[1]Ott SJ *et al.* Gastroenterology. 2017 Mar;152(4):799-811.
[2]Gedgaudas R *et al.* J Gastrointestin Liver Dis. 2023 Sep 28;32(3):332-338.
[3]Bosso M *et al.* Bioorg Med Chem. 2018 Jun 1;26(10):2719-2726.

General strategy

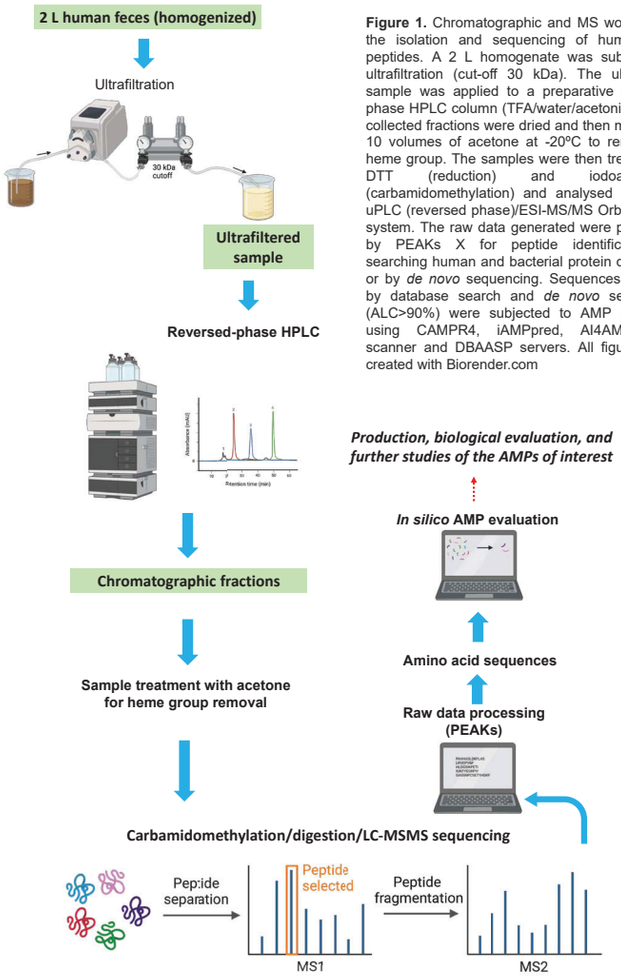

Figure 1. Chromatographic and MS workflow for the isolation and sequencing of human fecal peptides. A 2 L homogenate was subjected to ultrafiltration (cut-off 30 kDa). The ultrafiltered sample was applied to a preparative reversed-phase HPLC column (TFA/water/acetonitrile). The collected fractions were dried and then mixed with 10 volumes of acetone at -20ºC to remove the heme group. The samples were then treated with DTT (reduction) and iodoacetamide (carbamidomethylation) and analysed by nano-uPLC (reversed phase)/ESI-MS/MS Orbitrap Elite system. The raw data generated were processed by PEAKs X for peptide identification by searching human and bacterial protein databases or by *de novo* sequencing. Sequences obtained by database search and *de novo* sequencing (ALC>90%) were subjected to AMP prediction using CAMPR4, iAMPpred, AI4AMP, AMP scanner and DBAASP servers. All figures were created with Biorender.com

Conclusions

- Combining ultrafiltration, liquid chromatography, mass spectrometry and bioinformatics, we discovered a total of 578 peptides in human faeces (from database searches and de novo sequencing), most of which are fragments of gut bacterial proteins.
- These peptides are predominantly small, with molecular masses between 1-2 kDa and a wide range of isoelectric points and retention times in RPC (hydrophobicity).
- Approximately 20% of these peptides were predicted to be antimicrobial by the AMP servers.

What's next?

- Further *in silico* analysis of antimicrobial-predicted peptides and biological evaluation of the most interesting candidates on a variety of pathogens.

Results

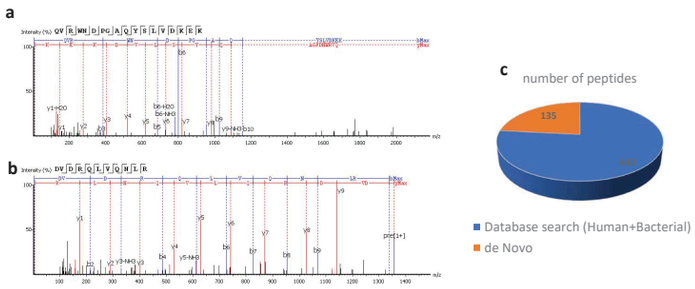

Figure 2. Mass spectrometry sequencing of fecal peptides. a) Fragmentation spectrum (MS2) of a peptide identified by database search as a fragment of cadherin-17 (Q12864|CAD17_HUMAN). b) Fragmentation spectrum (MS2) of a *de novo* peptide. Raw data were processed by PEAKs X, considering FDR=1%, Cys carbamidomethylation as fixed modification and Met oxidation as variable modification. The database search was performed against human proteins and gut (134) bacterial proteins from the UniProt database. c) Distribution of the number of peptides found in the present study: 23% *de novo* peptides vs. 77% database search peptides.

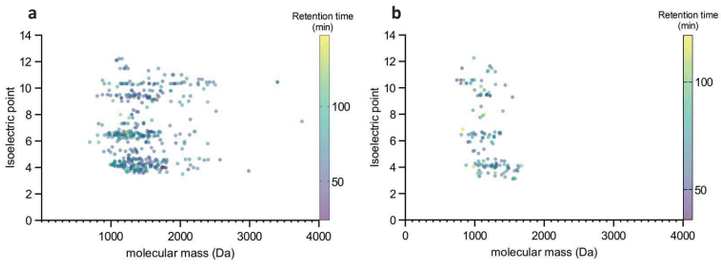

Figure 3. Isoelectric point/molecular mass/retention time (nanoLC-RP) distribution of human fecal peptides found in this study. a) Peptides found by database search. b) Peptides found by *de novo* sequencing. Graphs were generated using GraphPad Prism v10.2.3.

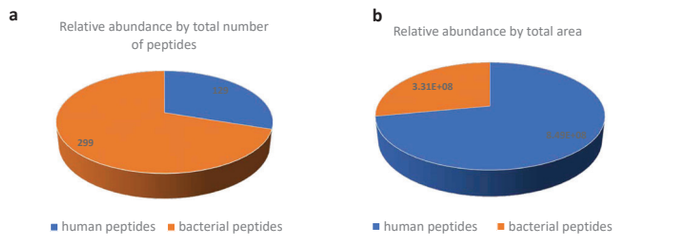

Figure 4. Distribution of total number of peptides and total area between peptides of human and bacterial origin. a) Relative abundance by total number: 70% bacterial peptides vs. 30% human peptides. b) Relative abundance by total area: 28% bacterial peptides vs. 72% human peptides.

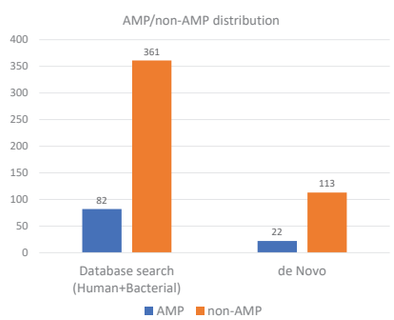

Figure 5. AMP prediction of fecal peptides using the AMP servers CAMPR4, iAMPpred, AI4AMP, AMP scanner, and DBAASP. A fasta file was created with all non-redundant sequences and subjected to *in-silico* evaluation. The results were similar for both groups of peptides, with AMP/non-AMP 18.5%/81.5% for database-found peptides and 19.4%/80.6% for *de Novo* peptides.

Acknowledgements

The authors gratefully acknowledge the German Research Foundation (DFG) for funding the present study within the CRC1279 framework.

https://doi.org/10.17952/37EPS.2024.P1272

Application of the MALDI-MS and MALDI-IMS in the identification of the GPR146 receptor in tissue preparations

Joanna Waśko[1], Aleksandra Ryk[2], Wojciech Fendler[2], Beata Kolesińska[1]

[1]Institute of Organic Chemistry, Lodz University of Technology, Zeromskiego 116, 90-543 Lodz, Poland,

[2]Department of Biostatistics and Translational Medicine, Medical University of Lodz, Mazowiecka 15, 92-215 Lodz, Poland

Introduction

G protein-coupled receptor 146 (GPR146, PGR8) belongs to membrane protein with molecular mass around 36.6 kDa. Its activity is regulated by seven typical transmembrane domains (Fig. 1). GPR146 is highly expressed in the livers (especially in hepatocytes) and adipose tissues of humans and mice. The activation of a G-protein coupled receptor can trigger a number of intracellular signalling cascades and responses. Which pathway is activated varies depending on the class of the coupled protein. Regardless of class, the G proteins initiate interactions and relocation of cellular components.

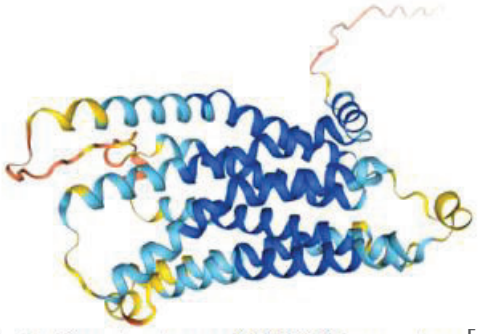

Fig.1. The structure of GPR146 receptor. [5]

Despite the fact that signalling mechanisms have been well studied and established, it has been increasingly clear that GPR146 signalling biology is remarkably more complex than originally thought. Moreover, the number of potential ligands, compatible to GPR146 receptor could be also more, which makes it possible to expand the use of this protein in the diagnosis and treatment of many diseases. Based on human genetic findings and on mouse studies, the G protein-coupled receptor emerges as a promising target against hypercholesterolemia and atherosclerosis [1,2]. It is also known their potential in diabetes treatment – current GPR-targeting therapies include glucagon-like peptide 1 (GLP-1) based agonists, the related DPP4 antagonists, bromocriptine, and serotonin agonists [3]. In turn, proinsulin C-peptide has gained recognition as a potential therapeutic target for the treatment of metabolic disorders and there are some reports indicate on their correlation with GPR146 receptor activity [1,2,4]. Therefore, in order to develop more effective methods of treating type I and II diabetes, it is important to know the correlation between receptor expression and the stage of disease advancement.

Results and Discussion

The attempts were made to detect the transmembrane receptor GPR146 in biological material (fresh tissue and tissue homogenates) collected from various organs of patients with known insulin resistance using matrix-assisted laser desorption/ionization spectrometry (MALDI-MS) and imaging mass spectrometry (MALDI-IMS) equipped in time of flight analyzer (TOF). Sinapic acid (SA) was used as a matrix in both techniques, and a mixture of water and acetonitrile with addition of 1% trifluoroacetic acid as the solvent (in a volume ratio of 1:1).

In the first stage, MALDI-MS measurements were performed for tissue homogenates, collected from patients with known insulin resistance, from: the saphenous vein (Z), right atrium of the heart (U), para-aortic fat tissue (TKO), epicardial fat tissue (TKN) and postthymic fat tissue

(TKP). Furthermore, MS spectra for the standard sample of GPR146 were also recorded and compared with homogenates results (Fig.2).

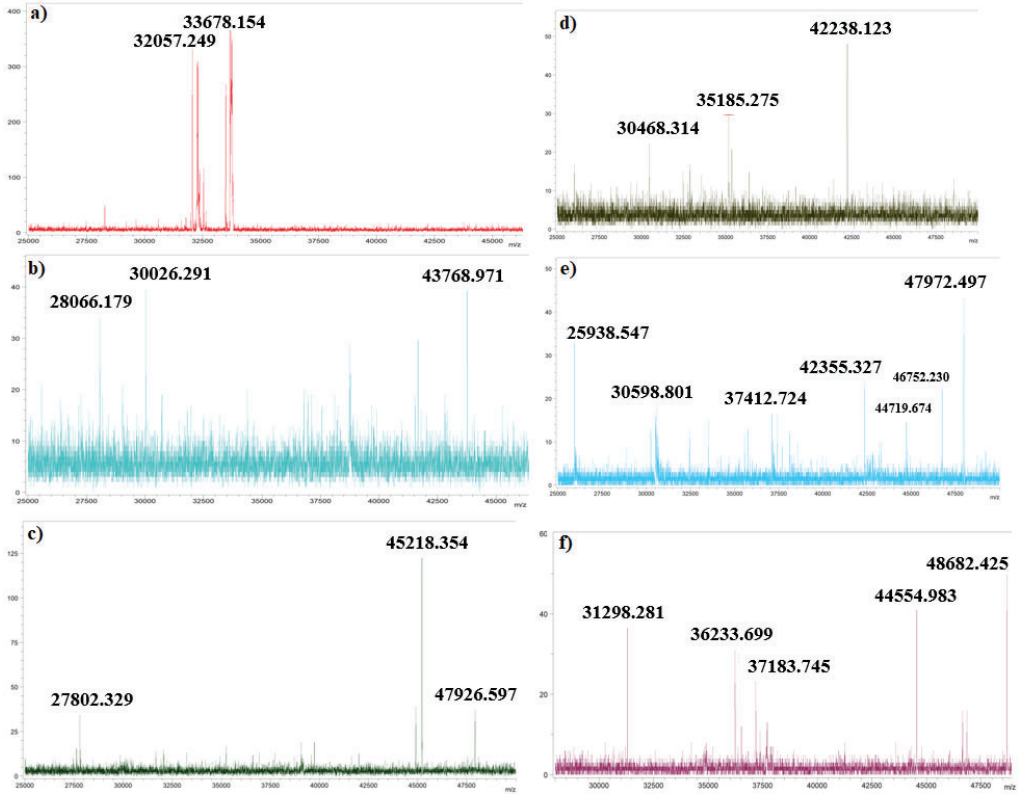

Fig.2. The MALDI-MS spectra registered for the following homogenates: a) TKN, b) TKO, c) Z; d) TKP; e) U and for f) GPR146 standard sample. SA concentration 20 mg/ml.

The presence of GPR146 depends on the type of homogenate – for that receptor the most characteristic and repetitive peaks in MALDI-MS analyses were detected in postthymic fat tissue (TKP) and right atrium of the heart (U). On the other hand the results registered for the saphenous vein (Z) didn't confirm expression of the receptor within tissue homogenate. Nextly, MALDI-IMS imaging was performed for tissue specimens taken from a healthy patient (reference sample) and from a patient with diagnosed metabolic disorders (Fig.3). It was compared occurrence and intensity of peaks characteristic for GPR146 within both of them. Firstly, the ionization efficiency was higher in the case of healthy tissue – probably, changes occurring in the diabetic's body definitely

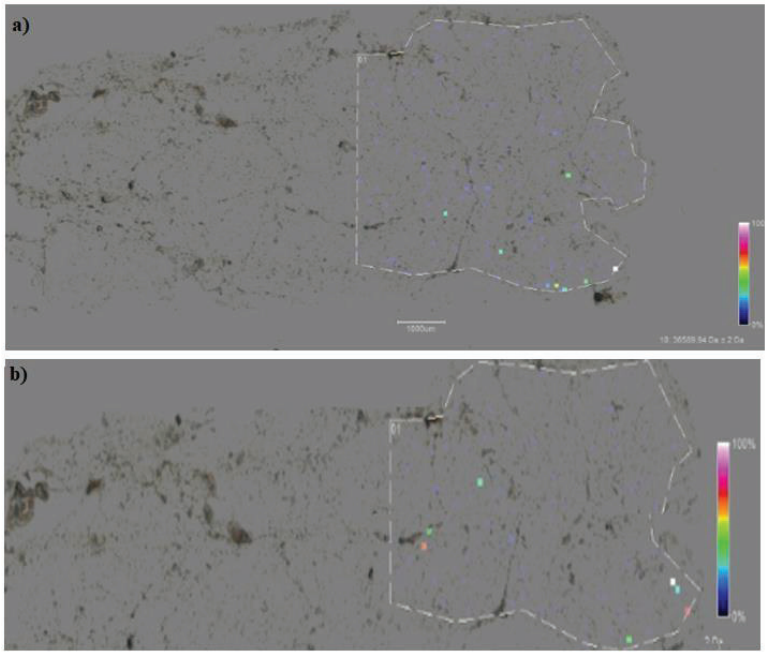

Fig.3. GPR146 distribution within: a) diabetic tissue, b) healthy tissue.

modify its structure. In addition, the occurrence of GPR146 was more intensive and visible in the pancreas section taken from a patient with diagnosed insulin resistance.

Conclusions

Based on the presented results we concluded that GPR146 expression within human tissues may be higher during metabolic disorders. Moreover the same tendency we observed for peptide C in previous studies, thus both of them should be take into account during designing innovative and more effective methods for treatment of diabetes mellitus. In samples collected from circulatory system the largest number of peaks corresponding to transmembrane protein were identified, which confirms the relationship between diabetes and heart diseases. Moreover, increased expression of the receptor in tissue taken from a patient with known insulin resistance may also indicate possible correlations between the amount of C-peptide and the GPR146 receptor.

Literature

[1] Lindfors, L., Sundström, L., Fröderberg Roth, L., Meuller, J., Andersson, S., Kihlberg, J. (2020). Is GPR146 really the receptor for proinsulin C-peptide? Bioorganic and Medicinal Chemistry Letters, 30, 127208. doi: 10.1016/j.bmcl.2020.127208

[2] Kolar, G.R., Grote, S.M., Yosten, G.L.C. (2017). Targeting orphan G protein coupled receptors for the treatment of diabetes and its complications: C-peptide and GPR146. J Intern Med. 281(1), 25–40. doi:10.1111/joim.12528.

[3] Ahren, B. (2009). Islet G protein-coupled receptors as potential targets for treatment of type 2 diabetes. Nat Rev Drug Discov. 8(5), 369–385.

[4] Yosten, G.L.C., Kolar, G.R. (2015). The Physiology of Proinsulin C-Peptide: Unanswered Questions and a Proposed Model. PHYSIOLOGY, 30, 327–332. doi:10.1152/physiol.00008.2015

[5] https://www.proteinatlas.org/ENSG00000164849-GPR146/structure (accsess date: 02.07.2024)

Proceedings of the 37th European Peptide Symposium
Michal Lebl, Editor
European Peptide Society, 2024 *http://doi.org/10.17952/37EPS.2024.P1273*

Searching for biomarkers characteristic for severe stage of COVID-19 disease

Aleksandra Czerchawy[1], Joanna Waśko[1], Beata Kolesińska[1]

[1] *Institute of Organic Chemistry, Faculty of Chemistry, Lodz University of Technology, Zeromskiego 116, Lodz, 90-543, Poland*

Introduction

Biomarkers, also known as biological markers, are defined as objectively measured and evaluated molecules (e.g. amino acids, peptides, proteins, enzymes, lipids, sugars, antibodies, hormones etc.) that act as indicators of typical biological processes, pathogenic processes or pharmacological responses. Their estimation can provide a valuable source of information about a patient's health condition, thus allowing for better diagnosis, prognosis and treatment options. Biomarkers analysis in physiological fluids (e.g. blood, urine, saliva, sweat, tears, faeces or exhaled air) can also offer a quick, painless, non-invasive and cost-effective method for disease detection and monitoring. However, this approach so far has many limitations due to the complexity and wide dynamic range of compounds present in bodily fluids. A promising alternative could be the direct identification of characteristic compounds from tissue sections, which would provide a comprehensive molecular view in a histology-related context [1].

Proteomics as a large-scale study of interactions, function, composition and structures of proteins could offer extensive insights into the molecular and cellular mechanisms of diseases. Nevertheless, the diversity of protein sequences and post-translational modifications makes it a challenging discipline. Fortunately, impressive technological advancements combined with bioinformatics have significantly progressed proteomics, aiding in compound characterization. The most commonly applied methods contain electrophoresis and high-throughput technologies such as liquid chromatography with mass spectrometry (tandem MS, MALDI-TOF) [2].

Under these circumstances, MALDI-MSI has gained particular attention due to its many advantages. This label-free technique generates two-dimensional ion density maps, enabling a spatial distribution of various biomolecules, including pharmaceuticals, lipids, peptides and proteins, through a tissue section in a single run. It allows for the simultaneous screening of hundreds of biological compounds, even low molecular weight compounds fig(e.g. drugs, metabolites) with a high sensitivity for multiple samples placed in a single target plate What's more, an easy sample preparation and a soft-ionization process simplifies data collection and interpretation [3].

The COVID-19 pandemic highlighted the need for accurate diagnostic tools. Utilizing modern techniques in biomarker search and recognition would help indicate the disease, assess the infection severity, and identify at-risk patients. The collected information could help in making treatment decisions and determining admission or intensive care criteria [4].

Results and Discussion

The aim of the studies conducted in the Institute of Organic Chemistry was the search and identification of potential protein and peptide biomarkers indicating the SARS-CoV-2 virus infection. The research focused on analysing the lung tissues that could indicate characteristic compounds for the COVID-19 disease, the advancement stage or other complications related to the disease course (e.g. lung fibrosis) and involved preparing lung tissue samples taken from a person who died of severe SARS-CoV-2 virus infection for MALDI-MSI imaging studies. Firstly, the samples were covered with two matrices, α-cyano-4-hydroxycinnamic acid (CHCA) and 2,5-dihydroxybenzoic acid (DHB) to detect compounds with low and high molecular masses, respectively. Matrix-coated samples were next subjected to MALDI-MSI analysis [5]. For some values revealed in a range of molecular ions, MALDI-MSI imaging was performed to show compound distribution within the tissue sample (Figure 1). Results combined with bioinformatic methods allowed for the identification of protein fragments involved in the process of replication and degradation of the SARS-CoV-2 genome, as well as other peptides associated with inflammatory processes, or even the fragment of hACE2 enzyme, which serves as a receptor for coronavirus particles (Table 1).

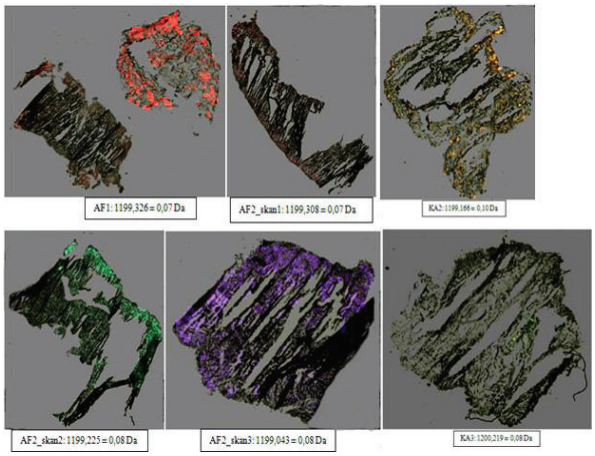

Fig. 1. *Picture showing the distribution of a ~1199 Da peptide identified in lung tissue using MALDI-MSI*

Table 1. *Representation of peptides identified during MALDI-MSI analysis as potential biomarkers for COVID-19 disease.*

	Protein	Fragment	m/z	Commentary
Inflammation	Vitamin K-dependent protein C (PROC)	HSSLER	729,29	May be involved in the pathogenesis of COVID-19 (lung damage and thrombogenicity). Involved in the coagulation process and the metabolism of elastic fibres
	Pulmonary surfactant-associated protein A1 (SFTPA1)	NCLYSR	755,37	Binding surfactant phospholipids lowering the surface tension in alveoli. Associated with lung fibrosis, a side effect of SARS-CoV-2 infection
	Fibrinogen alpha chain (FGA)	DSGEGDFL AEGGGVR	~1464	Increased levels observed for COVID-19 cases correlating with excessive inflammation and disease severity [6]
	Serum amyloid A-1/ A-2 protein (SAA1/ SAA2)	FFSFLGEAF DGAR	~1464	Increased levels of amyloid A observed in human serum of patients with severe SARS-CoV-2 virus infection [7]
	Complement component 6 (C6)	ALNHLPLEY NSALYSR		Constituent of the membrane attack complex playing a role in the innate and adaptive immune response
	Apolipoprotein A-II (APOA2)	VKSPELQAE AK	~1199	Decreased level of APOA1, APOA2 and APOC2 in COVID-19 plasma patients [8]
	Apolipoprotein A-I (APOA1)	DSGRDYVS QFEGSALG K	~1816	
	Apolipoprotein C-II (APOC2)	ESLSSYWES AK	~1286	
hACE2	Angiotensin-converting enzyme type 2 (ACE2)	LFNMLR; HEGPLHK	793,44 817,50	Receptor interacting with RBD of the S1 protein subunit of SARS-CoV-2
Replication and Replication and degradation of the viral genome	Replicase polyprotein 1ab (fragment)	NLYDK	651,64	Involved in the transcription and replication of viral RNAs
	Cystic fibrosis transmembrane conductance regulator (CFTR)	WFQMR	769,35	CFTR expression/function is involved in the regulation of SARS-CoV-2 replication
	E3 ubiquitin-protein ligase HUWE1 (HUWE1)	SMLNFLK; HLGYTLCK	853,78 935,74	Protein inducing ubiquitination and degradation of the MERS-CoV protein ORF3 (important for SARS-CoV-2 infection)

Conclusions

Progress in biomarker recognition and proteomic technologies shows great promise for a better understanding of disease pathologies and improving diagnostic procedures, particularly in the context of COVID-19. Nonetheless, it is still a developing field of study and involves significant costs and long-term examination. The analysis of samples is highly dependent on the sample collection and preparation, and the longevity of probes is also a consideration. Result interpretation is not an easy task and requires in-depth knowledge of multiple inflammatory processes. Currently, analyses are so far compared with standard approaches, but ongoing advancements may simplify the process.

Acknowledgements

The research was founded by “Young Scientist Fund” no. W-3D/FMN/16G/2023.
Samples of lung tissues and respiratory filters were taken from the Military Institute of Medicine in Warsaw and the Infectious Diseases Hospital in Lodz.

References

[1] Minerva, L., Ceulemans, A., Baggerman, G., Arckens, L. *Proteomics Clin. Appl*. **6**, 581-595 (2012), https://doi.org/10.1002/prca.201200033
[2] Al-Amrani S., Al-Jabri, Z., Al-Zaabi, A., Alshekaili, J., Al-Khabori, M. *World J Biol Chem.* **12(5)**, 57-69 (2021), https://doi.org/10.4331/wjbc.v12.i5.57
[3] Zhu, X., Xu, T., Peng, C. *Front. Chem.* **9**, 782432 (2022), https://doi.org/10.3389/fchem.2021.782432
[4] Samprathi, M., Jayashree, M. *Front. Pediatr.* **8**, 7607647 (2021), https://doi.org/10.3389/fped.2020.607647

[5] Aichler, M., Walch, A. *Lab. Invest.* **95**, 422-431 (2015), https://doi.org/10.1038/labinvest.2014.156
[6] Sui, J., Noubouossie, D.F., Gandotra, S., Cao, L. *Front. Cell. Infect. Microbiol*. **11**, 734005 (2021), https://doi.org/10.3389/fcimb.2021.734005
[7] Jana, A.K., Greenwood, A.B., Hansmann, U.H.E. *J. Phys. Chem. B.* **125 (32)**, 9155–9167 (2021), https://doi.org/10.1021/acs.jpcb.1c04871
[8] Faguer, S., Del Bello, A., Danet C., Renaudineau Y., Izotep J., Kamar, N. *Front. Pharmacol.* **13,** 936659 (2022), https://doi.org/10.3389/fphar.2022.936659

Identification of *Delftia lacustris* Proteins in Response to Cadmium Stress.

[1]Ximena Carolina Pulido Villamil, [1,2]Jefferson Beltrán, [2]Maryeimy Varón-López, [1]Cesar Augusto Jaramillo.

[1]Grupo de Química Aplicada a Procesos Ecológicos (QUAPE), Universidad del Tolima, Ibagué, Colombia. [2]Grupo de Genética y Biotecnología Vegetal y Microbiana (GEBIUT), Universidad del Tolima, Ibagué, Colombia.

xpulido@ut.edu.co

37th EPS European Peptide Symposium · 14th IPS International Peptide Symposium
25 - 29 August 2024 Satellite Workshop 30 - 31 August 2024 Florence, Italy- 2024

https://doi.org/10.17952/37EPS.2024.P1274

1. INTRODUCTION

Heavy metal contamination such as cadmium, has a negative impact on ecosystems; in the soil it reduces the fertility and the agricultural productivity, additionally it presents serious effects on human health, as the increase of the carcinogenic activity, can also affect kidney function, the immune response promotes and the development of cardiovascular and skeletal diseases. Bacteria have different stress tolerance mechanisms due to the presence of heavy metals, including the production of siderophores, proteins and exopolysaccharides. The aim of this work was to identify *Delftia lacustris* B11CM strain [1] proteins in response to cadmium using nano LC/MSMS proteomic analysis of the bacterial extract without and with cadmium at a concentration of 150 ppm. This research contributes to the fulfillment of sustainable development objectives 3 and 6.





2. MATERIALS AND METHODS

1. Cells growth of *Delftia lacustris* without and with Cd(II) to 150 ppm
2.Protein extraction
3. Electrophoresis (Tricine-SDS-PAGE)-based protein separation
4. In-Gel Protein digestion with trypsin

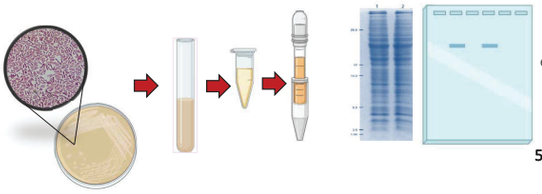

5. nano LC-MS/MS Analysis:

6. Protein ID

Mascot (Matrix Science, London, UK; version 2.8.0). Database *Delftia lacustris* Uniprot (11103 entries).

Scaffold (version Scaffold_5.1.2) was used to validate MS/MS based peptide and protein identifications. criteria: At least 2 unique peptides identified sum score greater than 2X p<0,01 (0.0001% error rate).

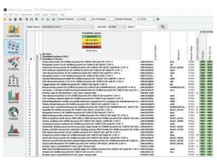

7. Functional Bioinformatic Analysis

The analysis by gene ontology (Gene Ontology) was derived from the UniProt-GO database, the proteins were classified into the categories: Biological Process, Molecular Function and Cellular Component.

3. RESULTS AND DISCUSSION

Protein Identification

The results obtained allowed us to identify 81 differentially present proteins of *Delftia lacustris* extract with Cd(II) to 150 ppm as shown in figure 1A.

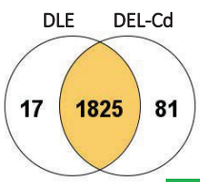

Figure 1. A. Venn diagram provides an overview of key proteins of *Delftia lacustris* extract without (DLE) and with Cd(II) to 150 ppm (DEL-Cd). **B.** Gene Ontology (GO) classification of *Delftia lacustris* proteins in response to Cd(II) stress in the categories: Biological Process, Molecular Function and Cellular Component.

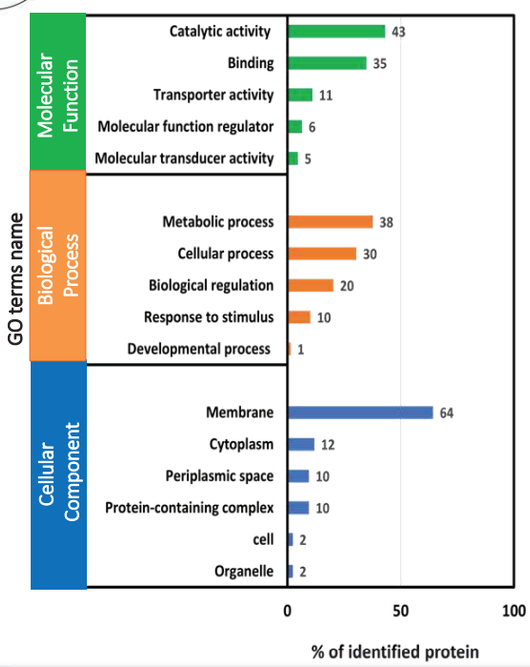

Functional Bioinformatic Analysis

In the functional analysis, regarding the *Molecular Function*, these proteins are involved in catalytic activity (43%), metalloproteins or proteins that bind to different molecules (35%), protein that participate in the transport system of ions or molecules (11%); in *Biological Processes* involved in metabolic processes (38%), cellular processes (30%), biological regulation (20%) and proteins that respond to stimuli (10%). Regarding the *Cellular Component*, the majority of the proteins identified in this category are found in the plasma membrane (64%) (Figure 1B), among others. It is evident that these proteins possibly allow this bacterium to survive in environments contaminated with cadmium, and they are directly related to the tolerance effect, conditions that make them potential to be used as a bioinoculant with agronomic interest or in bioremediation processes.

Proposed Molecular Mechanisms in the response of *Delftia lacustris* to Cd(II) at proteomic level

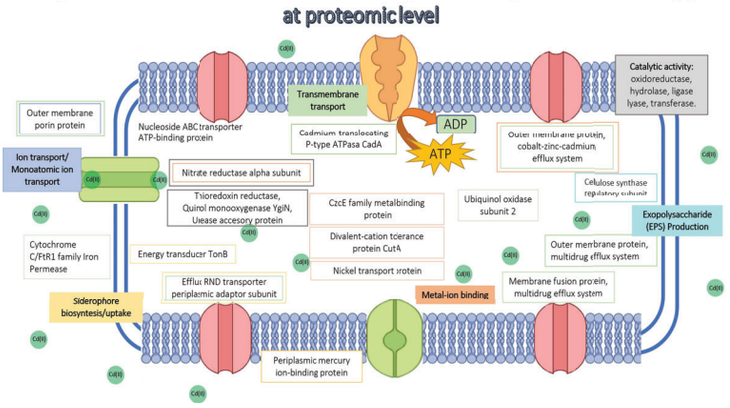

The molecular mechanisms proposed in response of *Delftia lacustris* to cadmium at the proteomic level, it was done only proteins in the extract with cadmium at a concentration of 150 ppm

CONCLUSION

The identification of proteins in *Delftia lacustris* extracts and proposed molecular mechanisms possibly allow this bacterium to survive in environments contaminated with cadmium, and they are directly related to the tolerance effect, conditions that make them potential to be used as a bioinoculant with agronomic interest or in bioremediation processes.

Universidad del Tolima

QUAPE

ACKNOWLEDGMENTS

We thank to the University of Tolima for its financial support under the research project "Proteomic analysis of protein extracts obtained from a cadmium-tolerant bacterial strain and its removal capacity using a bioadsorbent" code: 470121.

REFERENCE

1. Ortiz Ortiz, J. C. ; Ramirez, R. A. ; Pulido, X. ; Varon López, M. 2021. Evaluación de la tolerancia a cadmio y plomo y su capacidad promotora de crecimiento vegetal de microorganismos aislados de relaves mineros . Memorias XXX Reunión Latinoamericana de Rizobiología V Conferencia Latinoamericana de Microorganismos Promotores del Crecimiento Vegetal.

Proteins Involved in the Plant Growth Promotion of *Pseudomonas orientalis* in the Presence of Cadmium.

https://doi.org/10.17952/37EPS.2024.P1275

[1]Ximena Carolina Pulido Villamil, [1,2]Jefferson Beltrán, [2]Maryeimy Varón-López, [1]Cesar Augusto Jaramillo.

[1]Grupo de Química Aplicada a Procesos Ecológicos (QUAPE), Universidad del Tolima, Ibagué, Colombia.
[2]Grupo de Genética y Biotecnología Vegetal y Microbiana (GEBIUT), Universidad del Tolima, Ibagué, Colombia.

xpulido@ut.edu.co



1. INTRODUCTION

Cadmium is considered a heavy metal that has effects on human health and also on ecosystems. In the soil, it reduces fertility and agricultural productivity. Bacteria have different stress tolerance mechanisms due to the presence of this metal, including the production of siderophores, proteins and exopolysaccharides. The objective of this study was to identify *Pseudomonas orientalis* B06CM strain [1] proteins in response to cadmium using nano LC/MSMS proteomic analysis of the bacterial extract with and without cadmium at a concentration of 150 ppm. The bioinformatic analysis of the proteins was carried out with the Gene Ontology (GO) annotation from the UniProt database, which allowed the protein to be classified into three categories such as *Molecular Function*, *Biological Process* and *Cellular Component*. These findings contribute to the fulfillment of sustainable development objectives 3 and 15.





2. MATERIALS AND METHODS

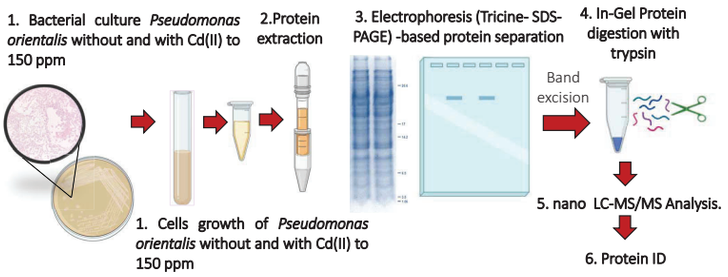

Mascot (Matrix Science, London, UK; version 2.8.0). Database *Pseudomonas orientalis* Uniprot (19009 entries).
Scaffold (version Scaffold_5.1.2) was used to validate MS/MS based peptide and protein identifications. criteria: At least 2 unique peptides identified sum score greater than 2X p<0,01 (0.0001% error rate).

7. Functional Bioinformatic Analysis

The analysis by gene ontology (Gene Ontology) was derived from the UniProt-GO database, the proteins were classified into the categories: Biological Process, Molecular Function and Cellular Component.



3. RESULTS AND DISCUSSION

Protein Identification

The results obtained allowed us to identify 5 differentially present proteins, which may be related to the effect of tolerance on the growth of bacteria in the presence of cadmium as shown in figure 1.

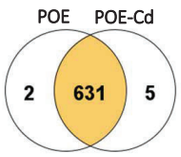

Figure 1. Venn diagram provides an overview of key proteins of *Pseudomonas orientalis* extract without (POE) and with Cd(II) to 150 ppm (POE-Cd).

Table 1. Identified proteins of *Pseudomonas orientalis* extract with Cd possibly associated with the response to this metal (green) and both extract involved in the Plant Growth Promotion of by LC-MS/MS

Activity	Identified protein	Entry name UniProt	Molecular mass (kDa)
Tolerance in presence of cadmium	4-hydroxytetrahydrobiopterin dehydratase	A0A2L0S3R6	46
	4-hydroxythreonine-4-phosphate dehydrogenase	A0A1H2G0Q6	35
	50S ribosomal protein	A0A4Q7D568	5
	Formyltetrahydrofolate deformylase	A0A0R2ZXH8	32
	Ferredoxin	A0A0R3A2T1	12
Phosphate solubilization	dITP/XTP pyrophosphatase	A0A3G7X6U5	21
	Exopolyphosphatase	A0A0R3A3Q0	56
	Inorganic pyrophosphatase	A0A0R2ZTP5	19
Nitrogen fixation/Nitrogen ciclation	Cysteine desulfurase	A0A1H2FJN3	45
	Nitrogen regulatory protein P-II family	A0A0R2ZXC0	12
Sulfur metabolism	Sulfate ABC transporter ATP-binding protein	A0A0R2ZPQ3	37
	Sulfite reductase	A0A2L0RY68	62
	Sulfate transport system substrate-binding protein	A0A1H2I5V4,	37
GSH biosyntesis/ Metabolisms	Glutathione S-transferase	A0A1H2EYI0	23
	S-(Hydroxymethyl)glutathione dehydrogenase / alcohol dehydrogenase	A0A1H2HTS8	39
	Glutathione synthetase	A0A2L0S3Q2	35
Siderophore Biosynthesis	Bacterioferritin	A0A3G7WTM2	20
	Ferric uptake regulation protein	A0A0R2ZTQ2	15
	Chorismate synthase	A0A0R3A5P1	39
	Bifunctional chorismate mutase/prephenate dehydratase	A0A4Q7D396	40
Synthesis of the phytohormone indole acetic acid	Anthranilate synthase component I	A0A3G7X759	54
	Anthranilate synthase, component II	A0A3G7XNG7	22
	Tryptophan synthase beta chain	A0A3G7WSN2	45
	Anthranilate phosphoribosyltransferase	A0A0R2ZYL9	37
	Indole-3-glycerol phosphate synthase	A0A1H2G078	30
Oxidative stress response	Superoxide dismutase	A0A0R2ZYT5	22
	Catalase	A0A1H2FY57	54
	Thiol peroxidase	A0A0R3A1L2	18
	Alkyl hydroperoxide reductase C	A0A0R2ZU27	22
	Alkylhydroperoxidase AhpD domain protein	A0A3G7X046	20
	Alkyl hydroperoxide reductase C	A0A0R3A3V0	20
	Thioredoxin peroxidase	A0A1H2HY76	17
	Alkyl hydroperoxide reductase	A0A3G7X6Y1	24

Functional Bioinformatic Analysis

Furthermore, approximately 30 common proteins were identified in the two bacterial extracts involved in the activities of nitrogen fixation, phosphate solubilization, sulfur metabolism, siderophore production, synthesis of the phytohormone indole acetic acid, metal resistance, exopolysaccharide biosynthesis and oxidative stress response (Table 1).

Figure 2. Gene Ontology (GO) classification of *Pseudomonas orientalis* proteins in presence to Cd(II) stress in the categories: Biological Process, Molecular Function and Cellular Component.

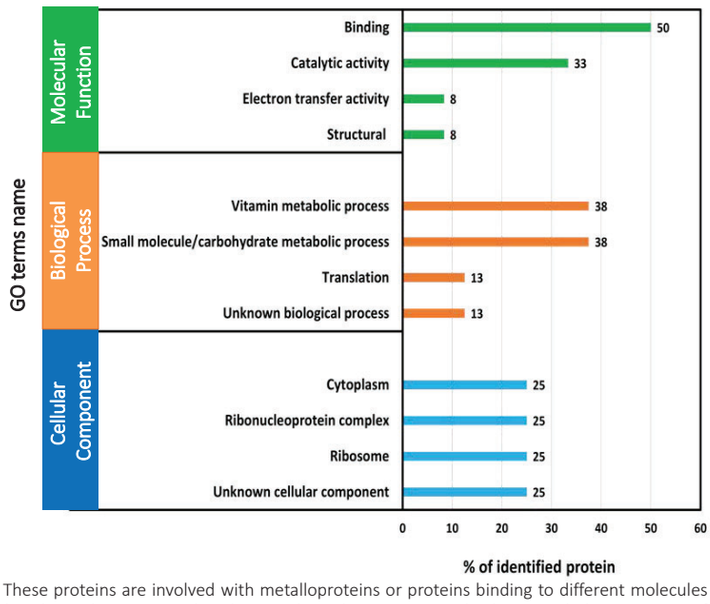

These proteins are involved with metalloproteins or proteins binding to different molecules (50%), catalytic activity (33%). In *Biological Processes* involved in metabolic processes of vitamins (38%) and small molecules or carbohydrates (38%). Regarding the Cellular Component, most proteins are part of the cytoplasm, ribosome and ribonucleoprotein complex (Figure 2).

CONCLUSION

The identification and functional classification of proteins in extracts of *Pseudomonas orientalis* with and without cadmium associated with plant growth promoting traits, make it a future candidate to potentially be used as a bioinoculant in contaminated soils.

ACKNOWLEDGMENTS

We thank to the University of Tolima for its financial support under the research project “Proteomic analysis of protein extracts obtained from a cadmium-tolerant bacterial strain and its removal capacity using a bioadsorbent” code: 470121.

Universidad del Tolima

QUAPE

REFERENCE

1. Ortiz Ortiz, J. C. ; Ramirez, R. A. ; Pulido, X. ; Varon López, M. 2021. Evaluación de la tolerancia a cadmio y plomo y su capacidad promotora de crecimiento vegetal de microorganismos aislados de relaves mineros . Memorias XXX Reunión Latinoamericana de Rizobiología V Conferencia Latinoamericana de Microorganismos Promotores del Crecimiento Vegetal.

Identification of protease inhibitors from the human peptidome to develop novel antivirals

https://doi.org/10.17952/37EPS.2024.P1276

Armando A. Rodríguez[1,2], Jan Lawrenz[3], Nico Preising[2], Merve Karacan[2], Bernd Schröppel[4], Rene van Erp[4], Eberhard Barth[5], Marion Schneider[5], Ludger Ständker[2], Frank Kirchhoff[3], Jan Münch[3], Sebastian Wiese[1]

armando.rodriguez-alfonso@uni-ulm.de

[1] Core Facility Functional Peptidomics, Ulm University Medical Center, Ulm, Germany. [2] Core Unit Mass Spectrometry and Proteomics, Ulm University Medical Center, Ulm, Germany. [3] Institute of Molecular Virology, Ulm University Medical Center, Ulm, Germany. [4] Section of Nephrology, Ulm University Medical Center, Ulm, Germany. [5] Anesthesiology and Intensive Medicine Clinic, Ulm University Medical Center, Ulm

Abstract

Protease inhibitors are potent modulators of the viral replication cycle by selectively interfering with host cell and viral protease functions, thus effectively preventing the propagation of infectious progeny virions. The human body produces a myriad of peptides and proteins of physiological relevance1; some play critical roles in controlling viral pathogens. Exploration of the human peptidome by body fluid analyses has revealed new therapeutic candidates against bacteria and viruses[1]. Protease inhibitors have also been found in the search for antiviral agents by bioassay-guided purification from body fluids[2,3]. However, the isolation and further analysis of low-abundance protease inhibitors can be challenging, and a different approach may often be needed to remove the impurities and concentrate the active molecules. In the present work, we used affinity chromatography and mass spectrometry to discover the main serine-protease inhibitors from a human hemofiltrate pool. Chromatographic fractionation of 1000L HF using pH-gradient cation-exchange chromatography yielded four pools by stepwise elution in increasing order of pH. A sample of each pool and the non-retained fraction were subjected to affinity chromatography on an immobilized-Trypsin gel based on a cheap and available protease used as a prototype to capture serine-protease inhibitors. Subsequently, the eluates were analyzed using a bottom-up mass spectrometry approach to sequence the peptides/proteins. Several serine-protease inhibitors were identified, with Kazal-type 1 showing the highest abundance in HF. Although much less abundant, serine-protease inhibitor Kazal-type 5 and the cysteine-protease Cystatin C3 were also found among the major inhibitors. Further analyses will reveal their antiviral activity and whether these molecules are composed of full-length proteins or fragments that can display antiviral activity. We expect this approach to be applied not only to serine-protease inhibitors but also extended to other relevant proteases for discovering novel protease inhibitors with antiviral activity.

[1]Bosso M *et al.* Exploiting the human peptidome for novel antimicrobial and anticancer agents. Bioorg Med Chem. 2018 Jun 1;26(10):2719-2726.

[2]Wettstein L *et al.* Alpha-1 antitrypsin inhibits TMPRSS2 protease activity and SARS-CoV-2 infection. Nat Commun. 2021 Mar 19;12(1):1726.

[3]Hayn M *et al.* Natural cystatin C fragments inhibit GPR15-mediated HIV and SIV infection without interfering with GPR15L signaling. Proc Natl Acad Sci USA. 2021 Jan 19;118(3).

General strategy

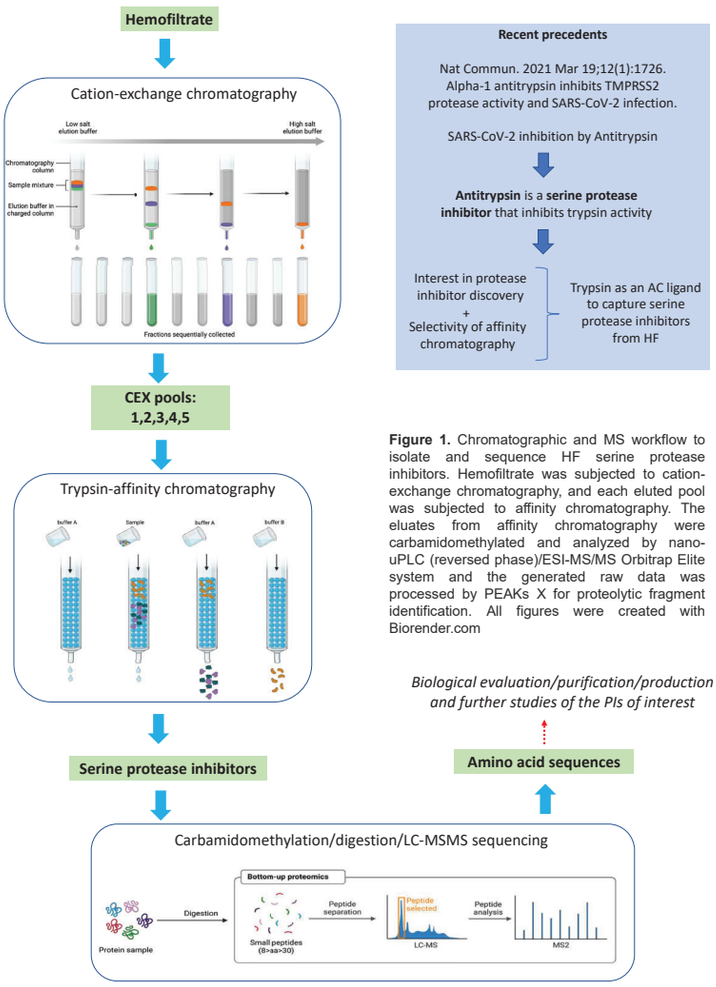

Recent precedents

Nat Commun. 2021 Mar 19;12(1):1726. Alpha-1 antitrypsin inhibits TMPRSS2 protease activity and SARS-CoV-2 infection.

SARS-CoV-2 inhibition by Antitrypsin

Antitrypsin is a **serine protease inhibitor** that inhibits trypsin activity

Interest in protease inhibitor discovery + Selectivity of affinity chromatography

Trypsin as an AC ligand to capture serine protease inhibitors from HF

Figure 1. Chromatographic and MS workflow to isolate and sequence HF serine protease inhibitors. Hemofiltrate was subjected to cation-exchange chromatography, and each eluted pool was subjected to affinity chromatography. The eluates from affinity chromatography were carbamidomethylated and analyzed by nano-uPLC (reversed phase)/ESI-MS/MS Orbitrap Elite system and the generated raw data was processed by PEAKs X for proteolytic fragment identification. All figures were created with Biorender.com

Biological evaluation/purification/production and further studies of the PIs of interest

Conclusions

- Our approach, based on trypsin affinity chromatography and mass spectrometry, allowed us to specifically capture and identify the serine protease inhibitors from the hemofiltrate, mainly represented by the serine protease inhibitor Kazal-type 1, in contrast to blood/plasma studies where alpha-1-antitrypsin is highly dominant.

What's next?

- Combination of Trypsin affinity chromatography with other purification techniques and biological activity screening.
- Additional LC-MSMS analyses to define whether these are full-length peptides or fragments.
- Screening of synthetic/recombinant protease inhibitors or their fragments for antiviral activity.

Results

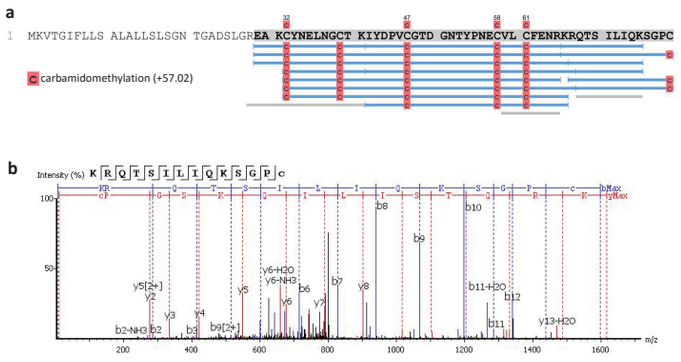

Figure 2. Mass spectrometric identification of protease inhibitors. a) Sequence coverage of the serine protease inhibitor Kazal-type 1. The blue lines represent the fragments identified by database search, while the gray lines are *de novo* peptides that were fully matched. b) MS/MS spectra of one of its peptide fragments. Both figures were generated by the proteomics software PEAKs X.

Table 1. List of protease inhibitors found in hemofiltrate by Trypsin-affinity chromatography and mass spectrometry identification

Protease inhibitor	Accession (Uniprot)	Classification
Serine protease inhibitor Kazal-type 1	P00995|ISK1_HUMAN	Serine protease inhibitor
Serine protease inhibitor Kazal-type 5	Q9NQ38|ISK5_HUMAN	Serine protease inhibitor
Cystatin-C	P01034|CYTC_HUMAN	Cysteine protease inhibitor
Kunitz-type protease inhibitor 1	O43278|SPIT1_HUMAN	Serine protease inhibitor
Antileukoproteinase	P03973|SLPI_HUMAN	Serine protease inhibitor
Tissue factor pathway inhibitor	P10646|TFPI1_HUMAN	Serine protease inhibitor
Serine protease inhibitor Kazal-type 6	Q6UWN8|ISK6_HUMAN	Serine protease inhibitor
Cystatin-M	Q15828|CYTM_HUMAN	Cysteine protease inhibitor
Alpha-1-antitrypsin	P01009|A1AT_HUMAN	Serine protease inhibitor
Cystatin-B	P04080|CYTB_HUMAN	Cysteine protease inhibitor
Kunitz-type protease inhibitor 2	O43291|SPIT2_HUMAN	Serine protease inhibitor
Elafin	P19957|ELAF_HUMAN	Serine protease inhibitor
Cystatin-SN	P01037|CYTN_HUMAN	Cysteine protease inhibitor

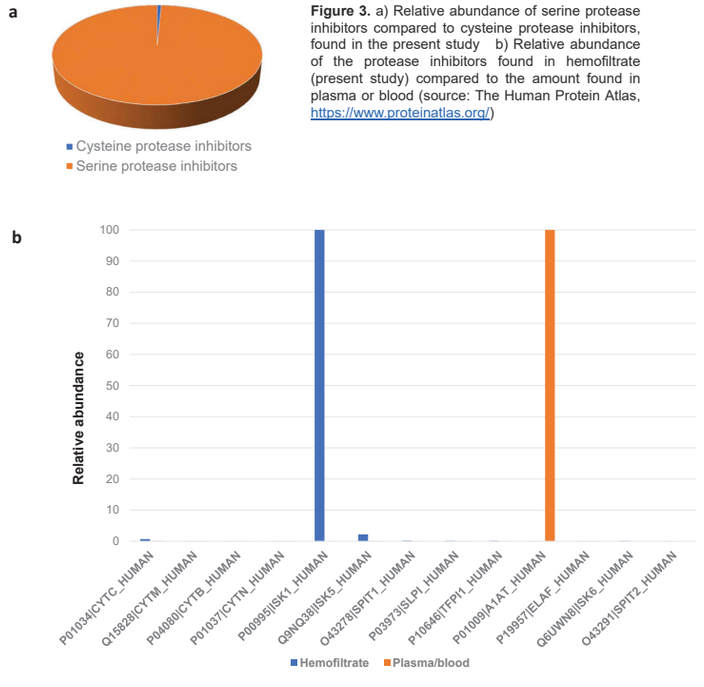

Figure 3. a) Relative abundance of serine protease inhibitors compared to cysteine protease inhibitors, found in the present study b) Relative abundance of the protease inhibitors found in hemofiltrate (present study) compared to the amount found in plasma or blood (source: The Human Protein Atlas, https://www.proteinatlas.org/)

Acknowledgements

The authors gratefully acknowledge the German Research Foundation (DFG) for funding the present study within the CRC1279 framework.

https://doi.org/10.17952/37EPS.2024.P1277

An Advanced Database for GlycoPeptide Structure Exploration to build GlycoPeptideStructure Hub: GPS Hub

Michele Casoria[1,2,3], Marina Macchiagodena[1,3], Carla Bazzicalupi[1,3], Claudia Andreini[1,3,4], Gianni Cardini[1,3], Anna Maria Papini[2,3], Marco Pagliai[1,3]

1 Research Unit of Computational Chemistry, University of Florence, 50019 Sesto Fiorentino, Italy

2 Interdepartmental Research Unit of Peptide and Protein Chemistry and Biology, University of Florence, 50019 Sesto Fiorentino, Italy

3 Department of Chemistry "Ugo Schiff", University of Florence, 50019 Sesto Fiorentino, Italy

4 Magnetic Resonance Center - University of Florence, 50019 Sesto Fiorentino, Italy

e-mail: michele.casoria@unifi.it

Using PDB experimental structures, a new database named GPS Hub is proposed. We define a sequon as an 11-mer peptide that spans from positions -5 to +5 relative to the central glycosylation site. We identified 87050 sequons and using machine learning techniques, in particular UMAP and DBSCAN algorithms, we clustered them into 2625 distinct groups. Below, we present the key findings for three of these clusters.

GPS Hub Overview

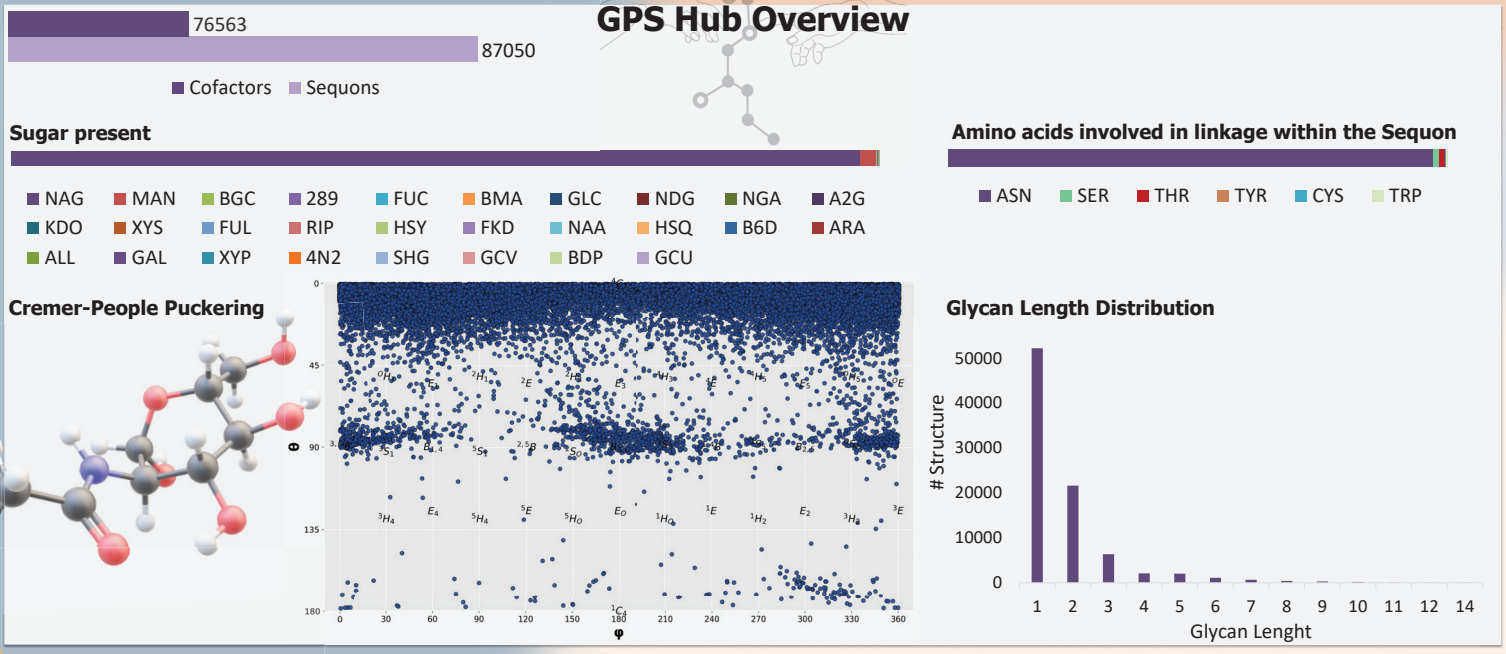

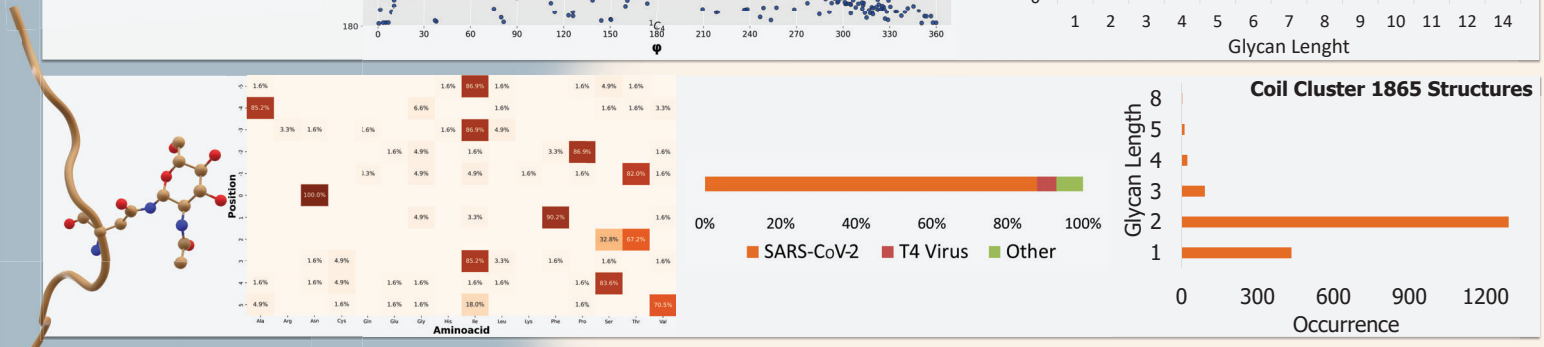

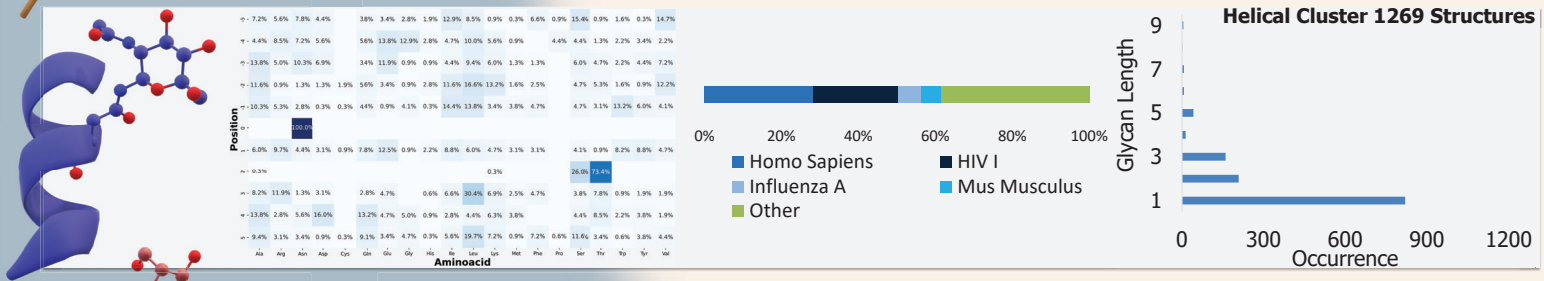

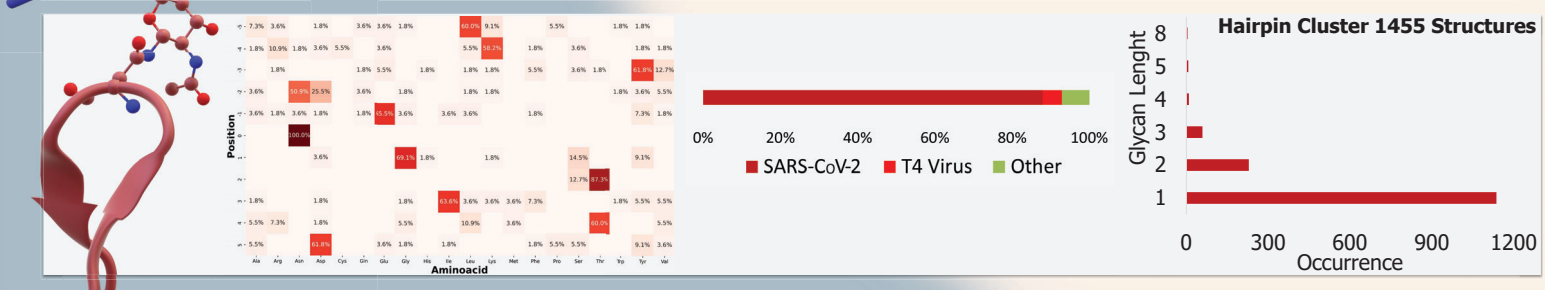

Conclusions

We have developed a database that consolidates comprehensive information on sequon and Glycan structures, starting from experimental data. We employed a machine learning approach to categorize these structures into clusters, uncovering common patterns hidden within glycan sequences.

Acknowledgments

European Peptide Society is kindly acknowledged for the awarded registration grant to Mr. Michele Casoria

MUR is kindly acknowledged for Michele Casoria's PhD scholarship

https://doi.org/10.17952/37EPS.2024.P1278

Machine Learning Reveals Structural Properties of Monosaccharides and their Peptide Conjugates

Michele Casoria[1,2,3], Marina Macchiagodena[1,3], Carla Bazzicalupi[1,3], Claudia Andreini[1,3,4], Gianni Cardini[1,3], Anna Maria Papini[2,3], Marco Pagliai[1,3]

1 Research Unit of Computational Chemistry, University of Florence, 50019 Sesto Fiorentino, Italy
2 Interdepartmental Research Unit of Peptide and Protein Chemistry and Biology, University of Florence, 50019 Sesto Fiorentino, Italy
3 Department of Chemistry "Ugo Schiff", University of Florence, 50019 Sesto Fiorentino, Italy
4 Magnetic Resonance Center - University of Florence, 50019 Sesto Fiorentino, Italy
e-mail: michele.casoria@unifi.it

Introduction

The Protein Data Bank (PDB) is a valuable resource for investigating the three-dimensional conformations of glycoproteins, facilitating our understanding of the impact of glycosylation on proteins. It is important to note that the glycan components in these structures frequently contain inaccuracies, which can range from subtle irregularities to major errors. Projects such as PDB-REDO [1] aim to enhance precision through experimental validation. Previous studies [2] on carbohydrates report that PDB database lack precise categorization and only a limited set of structural parameters are present. For these reasons we conducted a systematic analysis of the complete PDB proteins set, aiming to categorize sugars with precision based on their glycosidic linkages

Methods

On April 2024 213239 pdb files are available on Protein Data Bank.

We developed a python script, which allows us to parse all files and collect the data in Json format files.
From each file resolution, taxonomy and owab are stored.
All residues within each protein chain have been analyzed, collecting relative atom coordinates and filtering the residues based on their 'resname' values.
To identify carbohydrate structures, we employed the 'HETNAME' value, specifically selecting 1724 three-letter code entries from the PDB HET Group Dictionary.
To ensure a standard procedure to determine the local structure of glycopeptides, particularly within the glycosylated regions, we deliberately selected 11-mer peptides spanning from the -5 to +5 positions with respect to the glycosylation site strategically positioned at the centre.
We computed the relative Solvent Accessible Surface Area (SASA) and secondary structures using the Shrake-Rupley and Define Secondary Structure Proteins (DSSP) algorithms respectively.

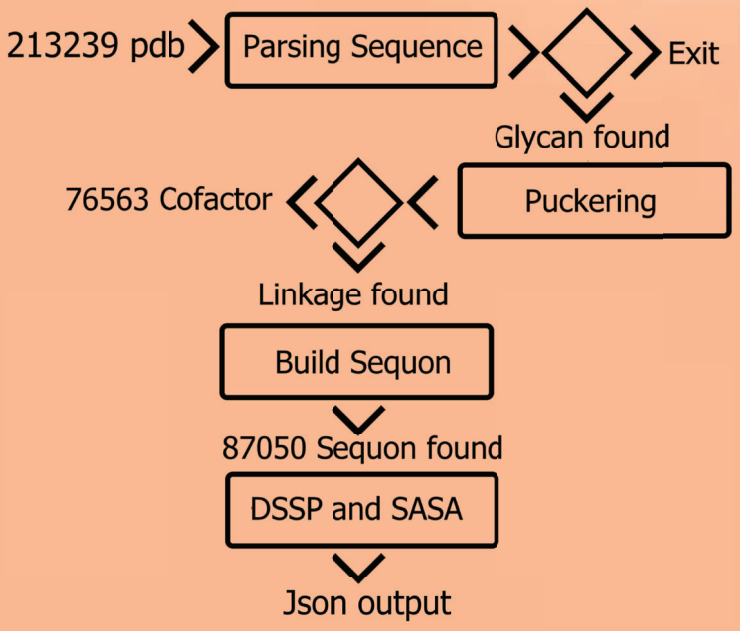

Clustering

We characterized the structures as a sequence of local conformations, which are delineated by forming eight tetrahedrons over four consecutive Cα atoms (Gap 0), five tetrahedra using alternate C_α atoms (Gap 1) and two tetrahedra with two alternate C_α atoms (Gap 2). Each tetrahedron is subsequently employed to calculate 12 geometric indices (GI parameters) as features. In total, we have 15 tetrahedra, each contributing 12 features, resulting in a collective description of 180 features for a given structure.

Tetrahedra Gap 0	Tetrahedra Gap 1	Tetrahedra Gap 2
1 2 3 4	1 3 5 7	1 4 7 10
2 3 4 5	2 4 6 8	2 5 8 11
3 4 5 6	3 5 7 9	
4 5 6 7	4 6 8 10	
5 6 7 8	5 7 9 11	
6 7 8 9		
7 8 9 10		
8 9 10 11		

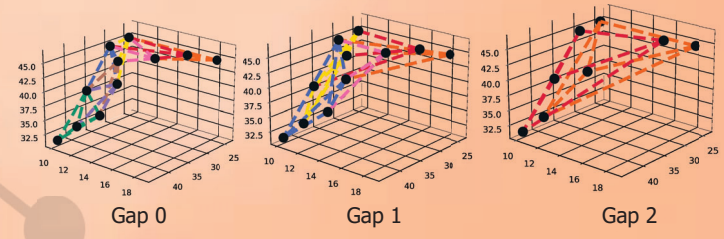

GI Parameters

Feature	Description
1	$dist(i, i+2)$
2	$dist(i, i+3)$
3	$dist(i+1, i+3)$
4	$\sqrt[3]{volume(i, i+1, i+2, i+3)}$
5	$\text{perimeter}(i, i+1, i+2, i+3)$
6	$\sum_{i=0, i\neq j}^{3} variance(i)\ x\ variance(j)$
7	$area(i, i+1, i+2)$
8	$area(i+1, i+2, i+3)$
9	$area(i, i+2, i+3)$
10	$\text{perimeter}(i, i+1, i+2)$
11	$\text{perimeter}(i+1, i+2, i+3)$
12	$\text{perimeter}(i, i+2, i+3)$

These 180 features were collected into a matrix describing all the sequons, UMAP reduction to three dimensions was applied, followed by clustering of the structure using the DBSCAN algorithm, with an epsilon value of 0.4 and a minimum sample size of 4.
The resulting evaluation metrics are as follows: Silhouette Score: 0.69, Cluster Compactness: 0.04, and Cluster Separation: 12.35. Additionally, we identified 2625 clusters and 21 structures in cluster -1 as noise.

Future Developments

We are developing a database named GPS-Hub (GlycoPeptideStructure Hub), created by M. Casoria et al., which will compile comprehensive information about sequons. This database will include the biological significance of the organisms in which these peptides are found. Additionally, it will contribute to enhancing classical force fields used in molecular modeling and simulations.

Reference and Acknowledgments

1. V. Beusekom, Acta Cryst. F **2018**, 74, 463–472.
2. J. L. de Meirelles, J. Chem.Inf. Model. **2020**, 60, 684−699

European Peptide Society is kindly acknowledged for the awarded registration grant to Mr. Michele Casoria
MUR is kindly acknowledged for Michele Casoria's PhD scholarship

Mechanistic basis for the role of acidic tail of Rad6 (ubiquitin-conjugating enzyme) in Bre1 (E3 ligase) mediated recognition of histones in Saccharomyces cerevisiae

Pawan Yadav[1], Manish Gupta[2], Mohan Kamthan[1], Pankaj Kumar[1,#]

[1]Department of Biochemistry, School of Chemical and Life Sciences, Jamia Hamdard University, New Delhi 110062, India
[2]Department of Medicine, Johns Hopkins University, Baltimore, MD 21231, USA

[#]Pankaj Kumar, pankajimtech@gmail.com

https://doi.org/10.17952/37EPS.2024.P1279

Abstract

Mono-ubiquitation at histone $H2B_{K123}$ in yeast ($H2B_{K120}$ in humans) plays an important role in gene activation and regulation. It is a highly conserved process which involves E2 conjugating enzyme (Rad6) and E3 Ligase (Bre1). Previous studies have highlighted the role of Rad6 and Bre1 in mono-ubiquitination at histone $H2B_{K123}$ site in yeast, however the mechanistic basis of Rad6/Bre1 dependent histone H2B mono-ubiquitination was unknown. In our present study, we aim to characterize the role of a C-terminal acidic tail of Rad6 and its interaction with Bre1 for site-specific H2B mono-ubiquitination. Through solution-based structural biology, *in-vitro* assays and binding studies we have shown that Rad6 acidic tail binds to positively charged surface on H2B restricting the access of Rad6 to 15 A˚ radii on NCP surface. This allows only promiscuous ubiquitination of various lysine residues present in the vicinity in absence of Bre1.Using different structural and biophysical approaches, this study for the first time uncovers the direct role of Rad6-acidic tail in interaction with the Bre1 Rad6-Binding Domain (RBD) and recognition of histones surface to facilitate histone H2B mono-ubiquitination. On the other hand, RBD (Rad6 Binding Domain) along with RING domain in Bre1 inhibits non-specific transfer of ubiquitin by Rad6 on histones by modulating the dynamics of acidic tail and restricting only H2BK123 mono-ubiquitination. Taken together, we aim to reveal the mechanistic basis of constrains in E2:E3 and E2:NCP recognition that ensure the fidelity of histone H2B monoubiquitination reaction.

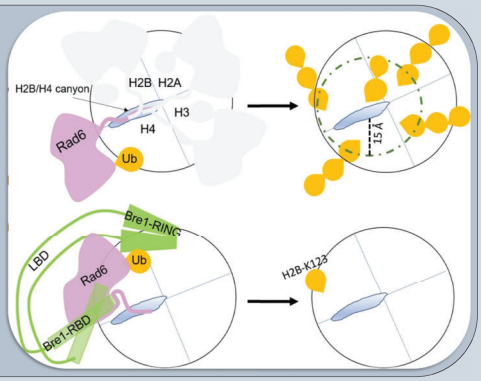

Results

Acidic tail in Rad6 is critical in mediating ubiquitin transfer to histone lysine

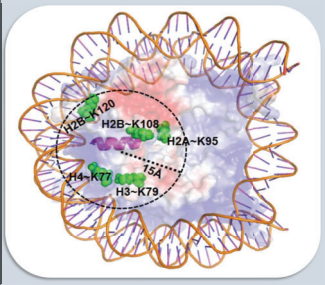

Figure 1-Model of recombinant *Xenopus laevis* nucleosome with positively charged region of H2B

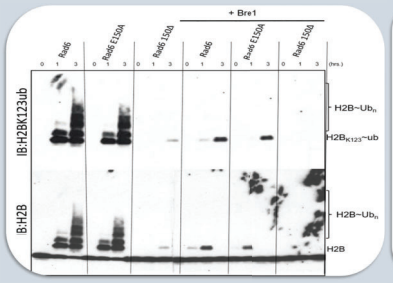

Figure 2-Ubiquitination of natural nucleosome by Rad6 and mutants with and without Bre1 enzyme

Rad6 acidic tail and a positively charged histone H2B region are involved in E2:NCP recognition

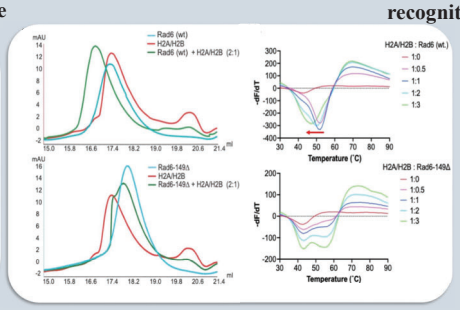

Figure 3-Size-Exclusion chromatography and DSF of Rad6 and Rad6-149Δ with H2A/H2B heterodimer

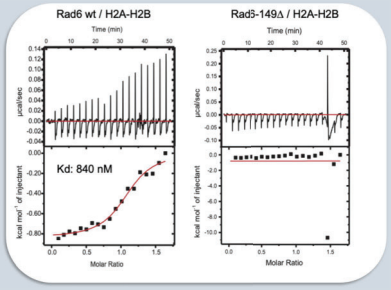

Figure 4- Interaction study of H2A/H2B heterodimer with full-length Rad6 and Rad6-149Δ using ITC

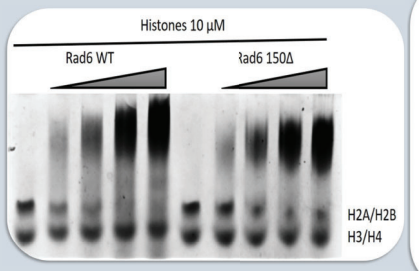

Figure 9- Rad6(wt) or Rad6-149Δ with histones complex (H2A/H2B + H3/H4)

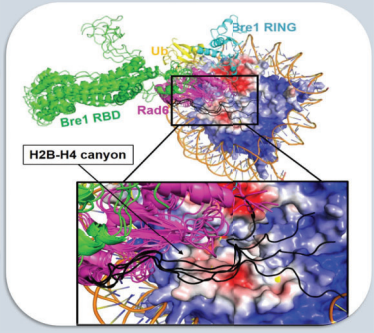

Figure 12- Docking of Rad6 acidic tail over the yeast nucleosome

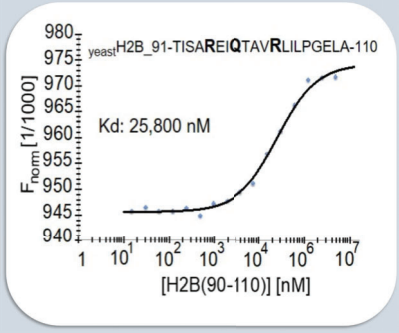

Figure 5- Interaction study between Rad6 and peptide from yeast H2B using Microscale Thermophoresis

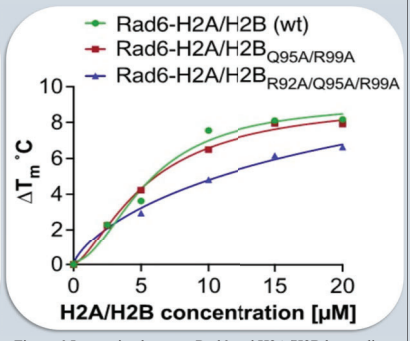

Figure 6-Interaction between Rad6 and H2A/H2B heterodimers using ThermoFluor assay

Bre1 RBD domain prevents non-specific ubiquitin transfer to histone lysine residues

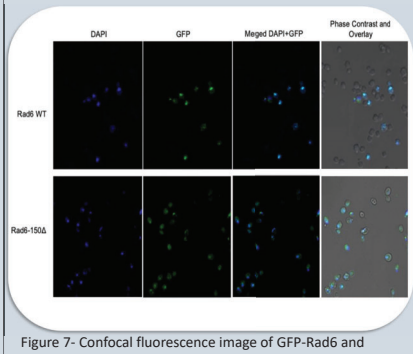

Figure 7- Confocal fluorescence image of GFP-Rad6 and GFP-Rad6-150Δ expressed in *Saccharomyces cerevisiae*

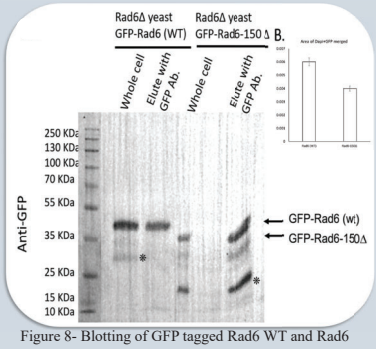

Figure 8- Blotting of GFP tagged Rad6 WT and Rad6 150Δ and intensity graph of confocal images

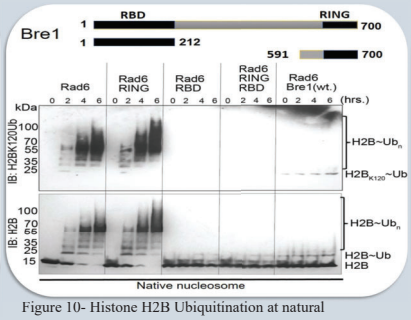

Figure 10- Histone H2B Ubiquitination at natural nucleosome by Rad6 alone and in the presence of Bre1 full-length and its domains RBD and RING

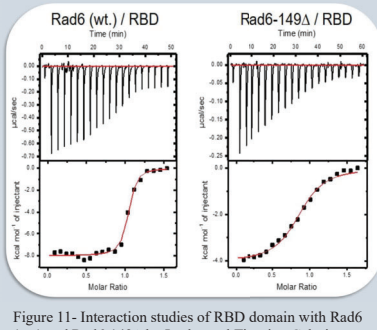

Figure 11- Interaction studies of RBD domain with Rad6 (wt.) and Rad6-149Δ by Isothermal Titration Calorimetry

Conclusion

E2 Rad6 and E3 Bre1 are indispensable for $H2B_{K123}$ monoubiquitination in budding yeast however, the mechanistic basis for the fidelity of the ubiquitination reaction was not clear. The present study reveals two important findings: (i)) the involvement of Rad6 acidic tail and a positive charged surface of histone H2B in E2-NCP recognition prior to ubiquitin transfer, and (ii) direct interaction of Bre1 RBD with Rad6 prevents promiscuous ubiquitin transfer to histone lysine residues, allowing site-specific monoubiquitination in conjunction with the RING domain

Acknowledgment

We thank Department of Biotechnology, Government of India (BT-RLF/Re-entry/68/2017 to P.K.) for funding this project and Department of Biochemistry, School of Chemical and Life Sciences, Jamia Hamdard University, New Delhi for providing the infrastructure and ICMR for the travel grant [3/2/TG-1 31 /HRD-2024(70)]

Refferences

- P. Yadav, M. Gupta, R. Wazahat, Z. Islam, S.E. Tsutakawa, M. Kamthan, P. Kumar, Structural basis for the role of C-terminus acidic tail of Saccharomyces cerevisiae ubiquitin-conjugating enzyme (Rad6) in E3 ligase (Bre1) mediated recognition of histones, Int. J. Biol. Macromol. 254 (2024). https://doi.org/10.1016/j.ijbiomac.2023.127717
- Kumar P, Magala P, Geiger-Schuller KR, Majumdar A, Tolman JR, Wolberger C. Role of a non-canonical surface of Rad6 in ubiquitin conjugating activity. Nucleic Acids Res. 2015 Oct 15;43(18):9039-50. doi: 10.1093/nar/gkv845. Epub 2015 Aug 18. PMID: 26286193; PMCID: PMC4605308.

Publication

Contact Details

https://doi.org/10.17952/37EPS.2024.P1280

Arginine-rich peptides vs. lysine-rich peptides: interaction with differently charged lipid bilayers

Andreja Jakas[1]*, Lea Pašalić[1], Danijela Bakarić[1]
[1]Divison of Organic Chemistry and Biochemistry, Ruđer Bošković Institute, Zagreb, Croatia
*andreja.jakas@irb.hr

BACKGROUND

Cell penetrating peptides

- short peptides built up from dominatly cationic and hydrophobic amino acid residues
- distinguished ability to pass through the cell membrane with molecular cargo
- uptake mechanism of CPPs still remain unclear
- **arginine** and **lysine** contained CPPs can be used to cross cell membranes

Liposomes

- spherical vesicles made by self-assembly of phospholipids
- simplified models of cell membrane
- important for understanding of fundamental biological processes such as **peptide-lipid interactions**

THE AIM OF THE STUDY

- investigate interaction of short cationic-hydrophobic peptides with lipid membranes and adsorption of petpides on lipid membranes as first step in cell penetration

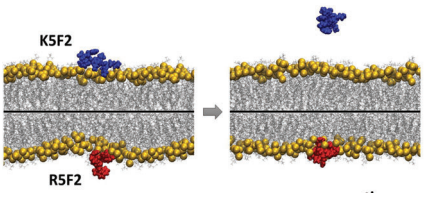

RESULTS

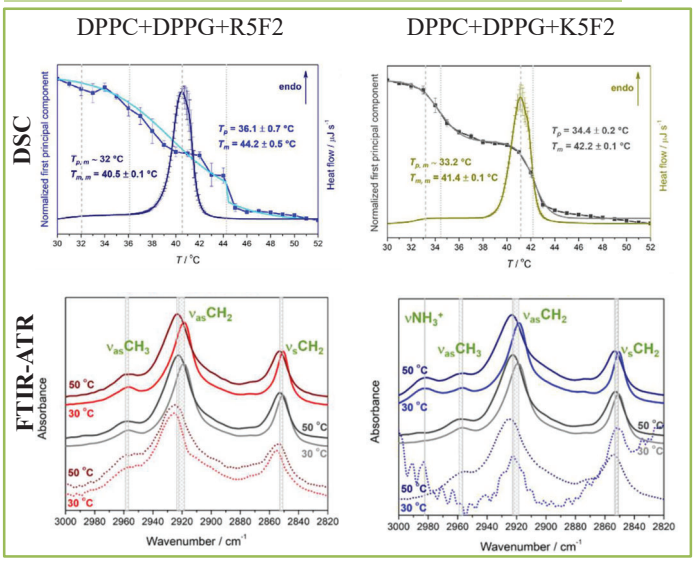

This work was suported by Croatian Science Fundation (HrZZ UIP- 2020-02-7669) and The Scientific Centre of Excellence for Marine Bioprospecting-BioProCro project K.K.01.1.1.0002

solid-phase synthesis

- synthesis of R5F2 and K5F2 heptapeptides
- perforemed automatically using Fmoc-protected amino acids
- structure of peptides confirmed by:

i) high-resolution mass spectrometry (HR-MS)
ii) nuclear magnet resonance spectroscopy (NMR spectroscopy)

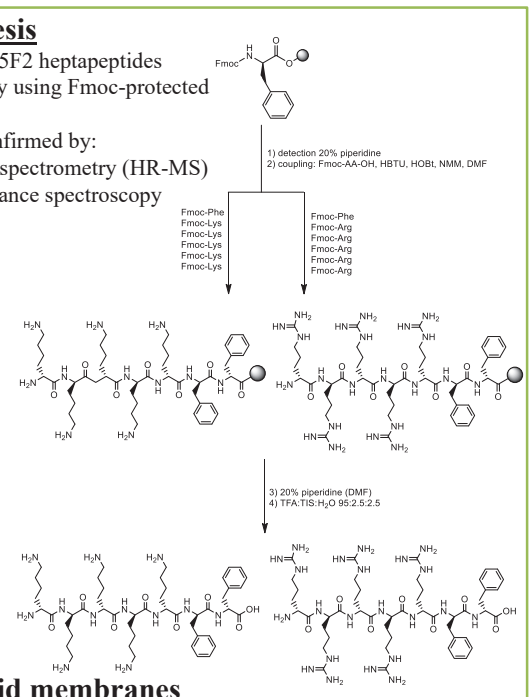

preparation of lipid membranes

- large unilamellar vesicles (LUVs) composed of phosphatidylcholine (DPPC) and phosphatidylglycerol (DPPG) lipids
- addition of peptides to liposome suspensions
- investigation:

i) impact of peptides on thermotropic behaviour of lipids with **differential scanning calorimetry** (DSC) and **UV-Vis spectroscopy**
ii) molecular-level details of interaction with **infrared spectroscopy** (FTIR-ATR)

CONCLUSION

- adsorption of R5F2 and K5F2 peptides on DPPC+DPPG lipid bilayer was examined
- alternation of DPPC+DPPG thermotropic properties caused because of different mechanism of peptides
- R5F2 is adsorbed on DPPC+DPPG lipid bilayer (proton transfer-carboxylic moiety)

FOLLOW-UP

- examination of interaction of differently charged lipid bilayers with other heptapeptides (R5W2, K5W2, R5I2, K5I2)
- investigate which peptide is best potential cell penetrating peptide

REFERENCES

1. Vivès, E., Schmidt, J. & Pèlegrin, A. Cell-penetrating and cell-targeting peptides in drug delivery. Biochimica et Biophysica Acta-Reviews on Cancer vol. 1786 126-138 (2008).
2. 2. Böhmová, E. et al. Cell-penetrating peptides: A useful tool for the delivery of various cargoes into cells. Physiological Research vol. 67 267–279 (2018)
3. Pašalić, L., Jakas, A., Pem, B. & Bakarić, D. Adsorption/Desorption of Cationic-Hydrophobic Peptides on Zwitterionic Lipid Bilayer Is Associated with the Possibility of Proton Transfer.Antibiotics vol.12 1216 (2023)

Scan me!

TOWARDS PEPTIDE-BASED THERAPEUTICS AGAINST CARDIAC DISEASE

Prediction and simulation of the S100A1ct peptide with a membrane environment

Tommaso Bartoloni[1,2,6], Manuel Glaser[1,2], Julia Ritterhof[2,3,4] Patrick Most[2,3,4] , Rebecca C. Wade[1,2,5]

[1] Molecular and Cellular Modeling (MCM) Group, Heidelberg Institute for Theoretical Studies (HITS), 69118 Heidelberg, Germany ; [2] Informatics for Life (I4L) consortium, Klaus Tschira Foundation ; [3] Division of Molecular and Translational Cardiology, Department of Medicine III, Heidelberg University Hospital, 69120 Heidelberg, Germany ; [4] German Center for Cardiovascular Research (DZHK), Partner site Heidelberg, 69120 Heidelberg, Germany ; [5] Center for Molecular Biology of Heidelberg University (ZMBH), DKFZ-ZMBH Alliance and Interdisciplinary Center for Scientific Computing (IWR), 69120 Heidelberg, Germany ; [6] Faculty of Biosciences and Heidelberg Biosciences International Graduate School (HBIGS), Heidelberg University, Heidelberg, Germany

https://doi.org/10.17952/37EPS.2024.P1283

Introduction

Cardiovascular diseases are the leading cause of death worldwide according to WHO estimates[1]. Heart failure accounted for over 60 million deaths in 2017[2] and can be classified into Heart Failure with reduced (HFrEF), preserved (HFpEF) and mid-range (HFmrEF) Ejection Fraction, with HFrEF accounting for many of these hospitalizations [3]. S100A1ct is a peptide derived from S100A1, a member of the Ca^{2+} binding EF-hand protein family, that has been observed to exert an inotropic effect on cardiomyocytes, both *in vivo and in vitro*, influencing with RyR2 and SERCA2a similarly to the parent protein[4,5].

DKDDPP-YVVLVAALTVACNNFFWENS



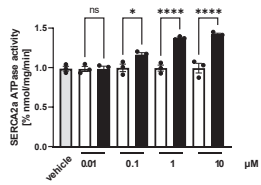

On the left: S100A1ct sequence. In bold the S100A1-derived sequence, with red and yellow colours representing the polar and apolar portions. Below, the peptide is highlighted with the same colour scheme on the parent protein[5]. On the right: dose-dependent augmentation of SERCA2a activity by different concentrations of S100A1ct in cardiac SR vesicles, compared to control[5].

Peptide drugs can achieve a high degree of selectivity and specificity, however they come with drawbacks such as difficulties in oral and nasal administration in the absence of modifications or carriers [6]. S100A1ct is not immune to such weaknesses, therefore further modifications are needed to improve its potency and pharmacokinetics. In order to do so, a deeper characterization of S100A1ct interactions is needed.

S100A1ct conformations in a membrane bilayer model

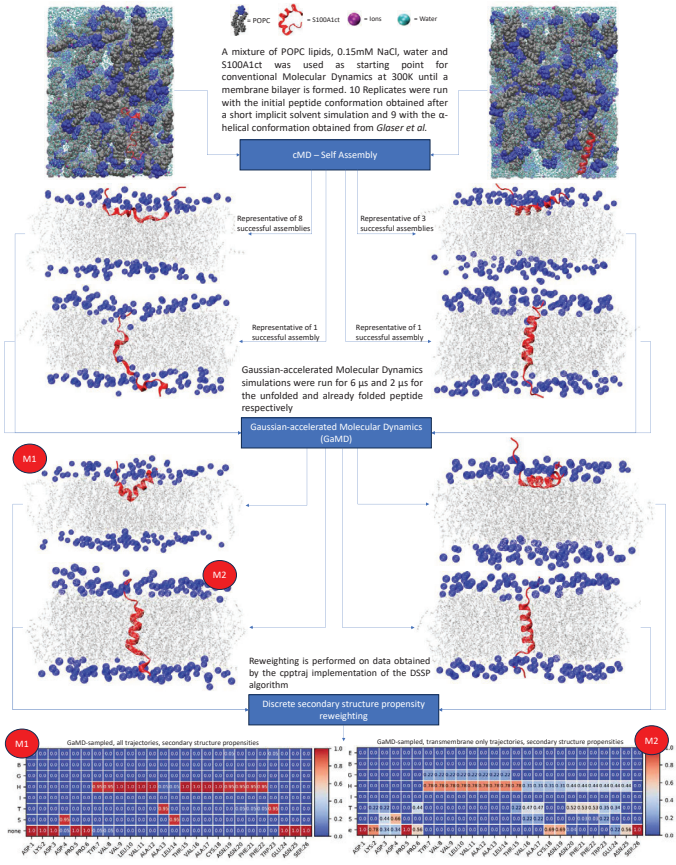

Confirmation of helical propensity in different force fields

In each force field, conventional Molecular Dynamics simulations were run for 600 ns from 8 starting points, each with two replicates. Four starting points with "M1"-like and "M2"-like conformations inserted in the membrane leaflet and transmembrane and other four with an helical conformation inserted in the same positions.

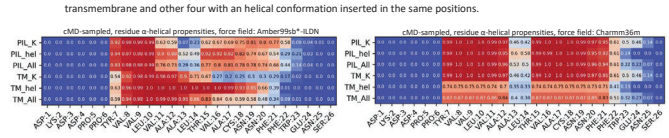

Outlook/Ongoing

- Evaluation of the impact of amino acid mutations on the peptide's preferred conformations in membrane with Monte Carlo simulations
- Simulation of both insertion and passage through the phospholipid bilayer in a more realistic cardiomyocyte model
- Clarify the role of the different kinked states in the peptide pharmacological properties
- Design and evaluation of peptidomimetics derived from such peptide.
- Investigating the possible role of cooperative effects in the switch between stable conformations

Acknowledgement

This study was supported by the Klaus Tschira Foundation Informatics for Life consortium (subproject 2 to RCW and PM)

Monte Carlo simulations in implicit membrane

80 different runs were obtained from Monte Carlo (MC) simulations, 20 for each starting point (S100A1ct in the leaflet, transmembrane, in water and in the middle of the implicit membrane). The simulations were run at 310K using SLIM implicit membrane model[6] and Amber99sb*-ILDN force field using SIMONA software[8]. The obtained conformations were clustered by energy after high energy outliers (over 3 times the standard deviation) were removed.

Conformation Ensemble	Mean energy Kcal/mol *	Standard Deviation Kcal/mol*
TOP_100_PIL	679.21	1.55
TOP_100_TM	645.26	1.18
TOP_20_WATER	602.00	9.0

PIL = Peptide in the leaflet
TM = Transmembrane

* The energy here reported comes from the force field and can be used to compare different mutants, it does not represent the real one

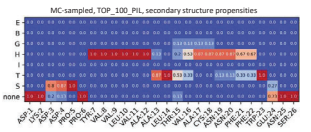

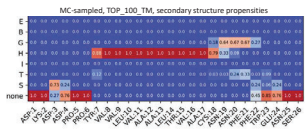

S100A1ct insertion in a membrane bilayer model

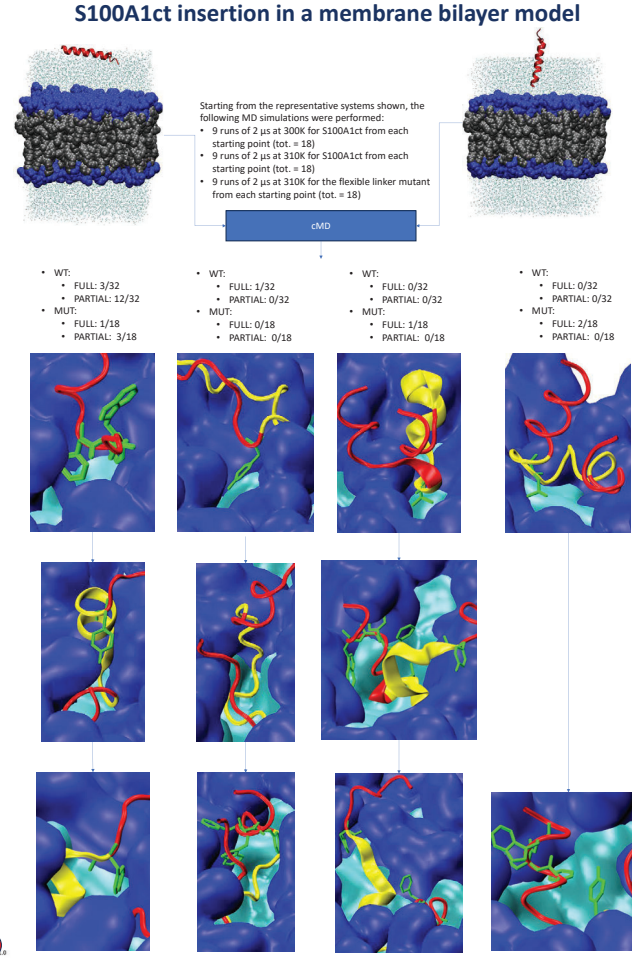

Conclusions

S100A1ct peptide has been observed to interact with SERCA2a and predicted to do so with a transmembrane (TM) helical conformation. Here we show that:

- A TM peptide arrangement can be found using an unbiased "assembly" approach and it is stable across the GaMD trajectories
- S100A1ct appears, however, to be found more frequently at the interface between a single membrane leaflet and the aqueous environment
- These findings were confirmed with short MD simulations in two different force fields
- Monte Carlo simulations employing an implicit membrane model also show agreement with these results, providing an efficient means to quickly explore how mutations and different chemical modifications can impact the identified states

The process of insertion in the membrane follows a pathway that relies on the appearance of gaps between the polar heads, as recently observed for another peptide[9]. Importantly:

- Aromatic residues play a major role in the process, especially when a rigid linker is present at the N-terminus
- When such linker is more flexible, pathways relying on hydrophobic stretches appear, highlighting the importance of carefully designing the 'non-active' parts of the peptide

References

1. The top 10 causes of death [Internet]. World Health Organization; [cited 2023 Sept 8]. Available from: https://www.who.int/news-room/fact-sheets/detail/the-top-10-causes-of-death
2. Savarese G, Becher PM, Lund LH, Seferovic P, Rosano GM, Coats AJ. Global burden of heart failure: A comprehensive and updated review of Epidemiology. Cardiovascular Research. 2022;118(17):3272–87. doi:10.1093/cvr/cvac013
3. Murphy SP, Ibrahim NE, Januzzi JL. Heart failure with reduced ejection fraction. JAMA. 2020;324(5):488. doi:10.1001/jama.2020.10262
4. Rohde D, Ritterhoff J, Voelkers M, Katus HA, Parker TG, Most P. S100A1: A multifaceted therapeutic target in cardiovascular disease. Journal of Cardiovascular Translational Research. 2010;3(5):525–37. doi:10.1007/s12265-010-9211-9
5. Kehr D, Ritterhoff J, Glaser M, Jarosch L, Salazar RE, Spaich K, et al. S100A1CT: A synthetic peptide derived from human S100A1 protein improves cardiac contractile performance and survival in pre-clinical heart failure models. 2023; doi:10.1101/2023.03.04.531024
6. Setzler J, Seith C, Brieg M, Wenzel W. Slim: An improved generalized born implicit membrane model. Journal of Computational Chemistry. 2014 Sept 22;35(28):2027–39. doi:10.1002/jcc.23717
7. Glaser M, Bruce NJ, Han SB, Wade RC. Simulation of the positive inotropic peptide S100A1ct in aqueous environment by gaussian accelerated molecular dynamics. The Journal of Physical Chemistry B. 2021 May 4;125(18):4654-66.doi:10.1021/acs.jpcb.1c00902
8. Strunk T, Wolf M, Brieg M, Klenin K, Biewer A, Tristram F, et al. Simona 1.0: An efficient and versatile framework for stochastic simulations of Molecular and Nanoscale Systems. Journal of Computational Chemistry. 2012 Aug 10;33(32):2602–13. doi:10.1002/jcc.23089
9. Linker SM, Schellhaas C, Kamenik AS, Veldhuizen MM, Waibl F, Roth H-J, et al. Lessons for oral bioavailability: How conformationally flexible cyclic peptides enter and cross lipid membranes. Journal of Medicinal Chemistry. 2023;66(4):2773–88. doi:10.1021/acs.jmedchem.2c01837

Engineering Stable Miniproteins: The Journey from Computational Design to Tertiary Structure Stability

Natalia Miodowska[1], Ewa Rudzińska-Szostak[1], Vitaly Kovalenko[1], Łukasz Berlicki[1]

[1]Department of Bioorganic Chemistry, Faculty of Chemistry, Wrocław University of Science and Technology, Wybrzeże Wyspiańskiego 27, 50-370 Wrocław, Poland

https://doi.org/10.17952/37EPS.2024.P1285

BACKROUND

Recent advances in miniproteins containing β-amino acid residues have changed the understanding and manipulation of helical structures, facilitated by the use of cycloalkane-based β-building blocks. These α/β-peptides exhibit unique structural features and have demonstrated promising biological activities, such as antimicrobial properties and protein interaction inhibition[1]. Additionally, miniproteins containing β-residues, have been studied extensively for their well-defined three-dimensional structures, making them attractive candidates for various applications due to their precise conformation control and resistance to enzymatic proteolysis[2].

While secondary structure studies have been successful, research on more extended systems is limited, especially of peptide foldamers composed of *cis*-aminocyclopentanecarboxylic acid. Initially, miniproteins were designed by naturally excreting proteins. Since then, however, the field has evolved into a rational design approach that respects not only biochemical and physicochemical principles but also empirical data. Nowadays, the use of computational methods that rely on fragment-based design is crucial in *de novo* design of most miniproteins[3].

OBJECTIVES

De novo design of conformationally stable miniproteins that fold cooperatively in an absence of cross-links and binding metal using computational methods and the rational approach.

Synthesis of the series of miniproteins composed of three helices, that have well-defined tertiary structure and high thermal stability.

Inclusion of unnatural *cis*-(1R,2S)-ACPC and *cis*-(1S,2R)-ACPC residues as building blocks to induce the folding due to their torsion angles and rigidity.

HHH MINIPROTEINS

The structural design of the miniproteins, composed of three helices (HHH), ensures their stability solely due to the precise arrangement of the hydrophobic core.

Helical fragments based on the 9/12/9/10-helix structure[4] were designed maintaining the αααββ motif. This was achieved by alternating L- and D-α-amino acid residues with cyclic β-amino acid building blocks of different stereochemistry (*cis-(1R,2S)*-ACPC *and cis-(1S,2R)*-ACPC) following the stereochemical patterning approach[5]. The α-residues were selected using the Rosetta FastDesign protocol[6] to optimise the packing of the hydrophobic core.

c3H1 miniprotein: s D s W l N GGGn Kq Wy VEGT Ha Fs

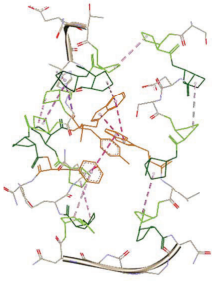

Model of **c3H1**

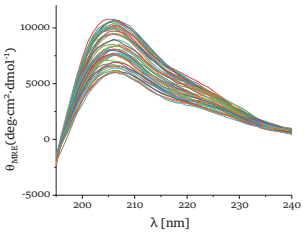

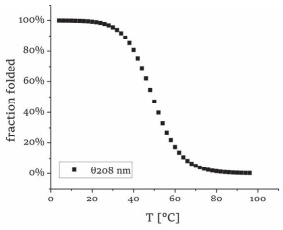

Thermal denaturation plot of **c3H1**, water pH 10.5

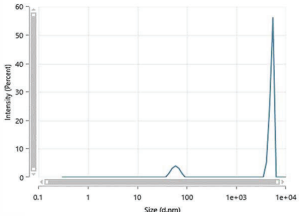

DLS analysis of **c3H1,** water pH 10.5

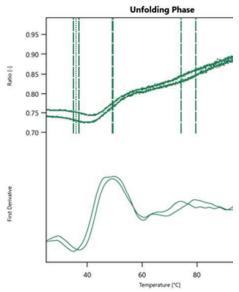

nanoDSF analysis of **c3H1,** water pH 10.5

The CD and nanoDSF measurements confirmed that the designed miniprotein folds cooperatively and indicates high thermal stability – the estimated melting temperature is close to 50°C.

Since the presence of hydrophobic building blocks inducing peptide folding significantly reduces its solubility, initially designed peptides tend to aggregate and precipitate in the pH value lower than 10.5. Thus, the designed miniproteins were subsequently modified to improve the physicochemical properties.

STRUCTURE OPTIMISATION

c3H3 miniprotein: k N L W k N GKGD KF Wk VK GS Ha Fe

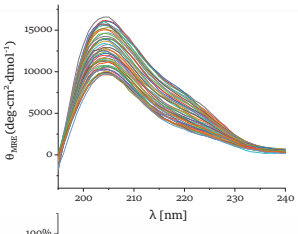

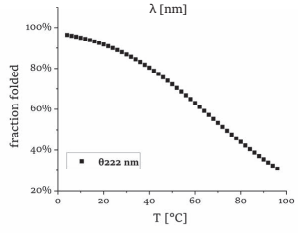

Thermal denaturation plot of **c3H3**, potassium phosphate buffer 25 mM pH 7.5

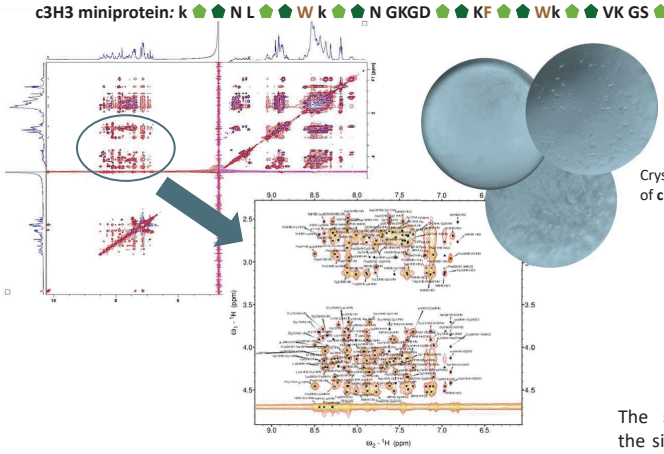

NMR spectrum of **c3H3**, potassium phosphate buffer 25 mM pH 7.5

Crystalline products of **c3H3** miniprotein

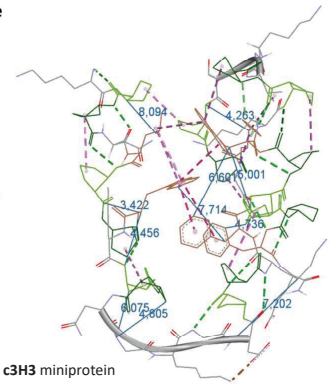

Model of **c3H3** miniprotein

The sequence of **c3H3** miniprotein was resolved and all the signals have been assigned. Thirty four long-range contacts were found, selected few are marked on the model above.

SUMMARY

The use of fragment assembling has proven to be an excellent tool for the design of miniproteins. The series of stable oligomers that fold cooperatively was successfully designed and synthesised. Obtained peptides are accessible through the solid phase synthesis, facilitating reachable analysis.

The possibility of controlling the folding process of the synthesised miniproteins, as well as their rigidity and specific physicochemical, and pharmacokinetic properties, such as high proteolytic stability and biocompatibility, make the obtained oligomers attractive scaffolds for drug design and other biomedical applications.

1. Haase H.S., Peterson-Kaufman K.J.,. Lan Levengood S.K, Checco J.W., Murphy W.L., Gellman S.H.: *J. Am. Chem. Soc.* (2012) 134, 7652-7655
2. Fortuna P., Twarda-Clapa A., Skalniak Ł., Ożga K., Holak T.A., Berlicki Ł.: *Eur. J. Med. Chem.* (2020) 208, 112814
3. Woolfson D.N.: *Journal of Molecular Biology* (2021) 433, 20, 167160
4. Zasloff M.: *Proc. Natl. Acad. Sci. USA* (1987) 15, 5449-5453
5. Mandity I.M., Weber E., Martinek T.A., Olajos G., Toth G.K., Vass E., Fulop F.: *Angew. Chem. Int. Ed.* (2009) 48, 2171-2175
6. Chevalier A. et al.,:*Nature* (2017) 550, 74-79

natalia.miodowska@pwr.edu.pl

Research was financed by the National Science Centre GRANT ID.: 2021/43/B/ST4/01837

(1R,2S)-aminocyclopentanecarboxylic acid [*cis-(1R,2S)*-ACPC]

(1S,2R)-aminocyclopentanecarboxylic acid [*cis-(1S,2R)*-ACPC]

Enhancing computational peptide therapeutic design with quantum chemistry and quantum computing

Vikram K. Mulligan[1], Tristan Zaborniak[2], P. Douglas Renfrew[1], and Benjamin Brown[3].

1. Biomolecular Design Group, Center for Computational Biology, Flatiron Institute, New York, NY 10010, United States of America.
2. Department of Computer Science, University of Victoria, Victoria, BC V8W 2Y2, Canada.
3. Department of Chemistry, Vanderbilt University, Nashville, TN 37240, United States of America.

https://doi.org/10.17952/37EPS.2024.P1286

Introduction

Advances in synthetic chemistry have greatly increased the number of amino acid and amino acid-like monomers that can be incorporated into a synthetic heteropolymer, creating exciting opportunities for the rational design of peptide and peptide-like drugs, nanomaterials, and catalysts. In recent years, we have worked to generalize the Rosetta software suite to permit its application to the design of synthetic peptides and heteropolymers built from non-canonical amino acids and other artificial building-blocks, and to allow validation of designs by simulation of molecules' folding properties and propensities [1–7]. Examples of synthetic peptides designed with our pipeline and validated by X-ray crystallography or NMR spectroscopy are shown in **Fig. 1**.

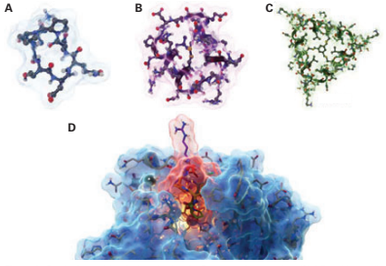

Figure 1: Synthetic peptides designed using the Rosetta software suite. (**A**) A 7-residue cyclic peptide, made from a mixture of D- and L-amino acids, that folds into a rigid, designed fold [2,4,7]. (**B**) A 26-residue cyclic peptide made from D- and L-amino acids that folds into a tertiary fold with helices of opposite handedness packing against each other, a fold impossible for any natural protein made from canonical amino acids alone [1]. (**C**) A 60-residue cyclic polypeptide with a fold stabilized by 1,3,5-tris(bromomethyl) benzene that serves both as a covalent three-way crosslink and as a component of a small hydrophobic core [3]. (**D**) An 8-residue cyclic peptide inhibitor (pink) of the New Delhi metallo-β-lactamase 1 (blue), an enzyme involved in antibiotic resistance. This peptide, also built from a mixture of D- and L-amino acids, folds rigidly into its binding-competent conformation, largely eliminating the entropic cost associated with ordering a disordered peptide on binding to a target [5].

However, this chemical diversity creates two challenges for rational design. First, force field-based design methods generalize poorly, and must be reparameterized as new chemical building blocks are added. More exotic building-blocks often have few experimental data available for empirically calibrating force fields. Second, the expansion in the number of possible building blocks vastly increases the number of combinatorial possibilities, creating an intractably large search space for computational optimization-based design approaches. Here, we describe recent work to address both of these challenges. To achieve greater accuracy and generality, we have developed *RosettaQM*, a set of software tools allowing quantum chemistry calculations to be incorporated into any existing Rosetta protocol. To tackle the combinatorial problem, we have developed a new open-source software library that extends Rosetta or other peptide modelling packages, which we call *Masala*. Masala provides diverse high-efficiency solvers for combinatorial optimization problems like the sequence design problem. Beyond traditional Monte Carlo based solvers for classical computing hardware, we have mapped these problems to current-generation quantum annealers and gate-based quantum computers, which may offer scaling advantages as the combinatorial space continues to balloon. We believe that these computational tools will be an important complement to experimental screening and other approaches.

Introducing Quantum Chemistry in Peptide Design and Validation Pipelines

Historically, the Rosetta software (used for macromolecular design and structure prediction) has been limited by its reliance on classical force fields, which are of limited accuracy and which are difficult to extend to support synthetic chemical building-blocks. Quantum mechanics-based (QM) calculations permit far greater accuracy and generality, albeit at greater computational cost depending on the level of approximation used to solve the multi-body Schrödinger equation. Historically, these have been laborious to set up, however. We have developed the RosettaQM communications bridge to allow Rosetta to communicate with GAMESS, Orca, or other quantum chemistry software, permitting QM energy calculations in the context of any Rosetta protocol. **Fig. 2A** illustrates how a user may use low-cost, low-accuracy force fields, medium-cost, medium accuracy semi-empirical methods, and high-cost, high-accuracy DFT calculations in the context of a single protocol, reserving the more expensive calculations for samples that pass intermediate filters. **Fig. 2B** shows RosettaQM features that facilitate its application to large peptides and proteins, including fragment molecular orbital (FMO) calculations that use a "divide and conquer" approach to get around the scaling of full DFT calculations, as well as the RosettaQM MultiScoreFunction, which allows different levels of QM theory to be applied to different regions of a structure.

We demonstrate some of RosettaQM's many applications by showing the computation of main-chain potentials (Ramachandran maps) for different canonical and non-canonical amino acids (**Fig. 2C**). Precomputed lookup tables for the mainchain potential are essential for the force fields used in peptide design and validation, so this provides facile means of generating these for new non-canonical amino acids [8]. In addition, RosettaQM permits QM-based energy calculations in the context of existing protocols, including peptide conformational sampling and structure prediction protocols. **Fig. 2D** shows how even approximate semi-empirical methods, such as DFTB, offer accuracy and generality well beyond those of force fields, permitting the accurate prediction of the folded structure of cyclosporine A in organic solvent for the first time. RosettaQM also generalizes well to more exotic chemical building blocks. We are currently applying it to the design and validation of peptoid polymers (N-functionalized poly-glycine) with secondary and tertiary folds (**Fig. 2E**).

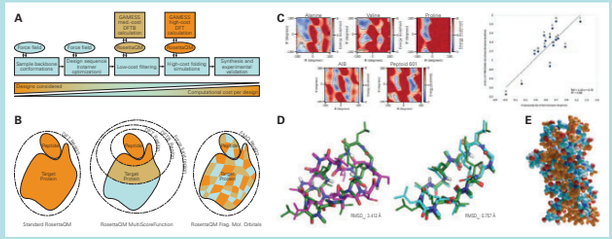

Figure 2: Quantum mechanics-based (QM) energy calculations in peptide design and validation pipelines using RosettaQM. (**A**) Existing design and validation pipelines enhanced with RosettaQM. While force fields can continue to be used for steps that must be fast, where accuracy is of finite importance, semi-empirical calculations or full DFT calculations can be performed at later stages. RosettaQM permits a QM calculation to be configured from within Rosetta, sent to GAMESS or Orca, executed, and the result imported into Rosetta, all without user intervention. (**B**) Modes of operation of RosettaQM. Left: a basic RosettaQM calculation treats a molecular structure as a quantum-mechanical system. Middle: the RosettaQM "MultiScoreFunction" permits regions of a structure to be scored with force fields or with different levels of QM theory, using mechanical or electrostatic embedding schemes. Right: RosettaQM supports fragment molecular orbital (FMO) calculations in GAMESS [12], in which separate QM calculations performed on individual amino acids or on pairs of interacting amino acids are combined to produce an estimate of the overall energy of the system. (**C**) Computation of Ramachandran potentials with RosettaQM (using the 6-311++G** level of theory and MP2). Left: Ramachandran potentials for alanine, proline, and valine, plus non-canonical amino acid 2-aminoisobutyric acid and peptoid monomer (S)-N-(1-phenylethyl)-glycine. Right: Correlation between computed and experimentally-determined helical propensity of amino acids [11]. (**D**) Prediction of the folded state of cyclosporine A in organic solvent. Left: overlay of prediction using Rosetta ref2015 energy function (magenta) on the X-ray crystal structure (green). The predicted structure has no resemblance to the reality. Right: overlay of prediction using RosettaQM DFTB semi-empirical method (cyan) on the X-ray crystal structure (green), showing excellent agreement. (**E**) Designed peptoid helical bundle fold using RosettaQM for validation. Polar groups are shown in cyan, and apolar groups in orange. Work to make peptoids that fold into intricate tertiary folds as proteins do is ongoing.

Mapping the Sequence Design Problem to Quantum Computers

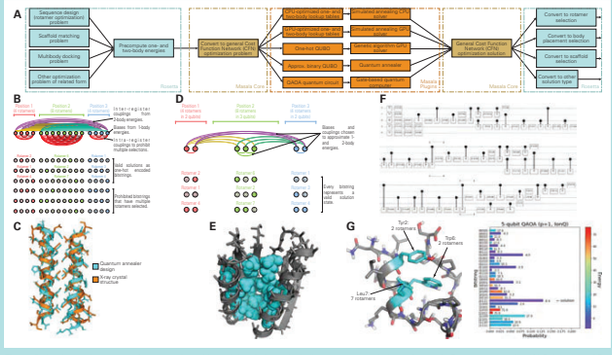

Figure 3: Implementing support for external combinatorial optimizers, including quantum optimizers, for use in Rosetta protocols. (**A**) Schematic of Rosetta's communication with the Masala libraries. Rosetta precomputes one- and two-body energies for rotamer optimization or related problems, then sends the problem description to Masala expressed as a generic cost function network optimization (CFN) problem. Masala's core detects available plug-in optimizer (CPU, GPU, or QPU-based) at runtime, sends the CFN problem to a user-selected optimizer. The CFN solution is transmitted back to Rosetta and converted to a rotamer optimization solution. (**B**) Mapping of the rotamer optimization problem to the quantum annealer, using *ND* qubits to represent *D* candidate rotamers at each of *N* possible positions. Final solutions are expressed as a bitstring with one-hot encoding of selected rotamers [9,10]. (**C**) A self-assembling heterochiral helical bundle peptide designed on the quantum annealer using the hybrid classical-quantum QBSolv algorithm. The design (cyan) is shown superimposed on the X-ray crystal structure (orange). (**D**) An approximate binary encoding of the rotamer optimization problem for the quantum annealer, using $N \log_2(D)$ qubits. This encoding uses far fewer qubits, but introduces some error in states' scores. (**E**) A well-packed protein core (cyan) designed entirely on the quantum annealer with the approximate binary encoding. (**F**) Mapping of the rotamer optimization problem to a gate-based quantum computer, using the quantum approximate optimization algorithm (QAOA). (**G**) A small rotamer optimization problem solved on the IonQ quantum computer. Left: three side-chains in the core of the Top7 protein were optimized with 7, 2, and 2 rotamers (28 total combinations). Right: with repeated sampling, the lowest-energy solution was found most frequently and showed considerable enrichment.

Given *D* possible synthetic building blocks in an N-residue peptide, how is one to choose which of the D^N possible sequences to synthesize? Even supercomputers cannot exhaustively enumerate possible sequences as *D* or *N* grow large. Historically, Rosetta has used simulated annealing as a heuristic for finding good sequences likely to produce a desired fold and function, at the expense of any guarantees of finding the best. However, Rosetta's simulated annealer lacks support for modern hardware (multi-core CPUs, GPUs), extensibility (support for alternative search algorithms), or versatility (support for optimization problems other than sequence design). We have built the Masala software library as an extension library against which software like Rosetta can be linked. Masala has versatile plug-in architecture, allowing easy development of plug-in Masala optimizers that can be detected at runtime and used by Rosetta without recompilation. **Fig. 3A** shows Rosetta's interaction with Masala's solvers. The sequence design problem is separable into a energy calculation step, in which the energies of candidate rotamers (amino acid identities with fixed side-chain conformations) and pairs of rotamers are pre-computed and stored, and a combinatorial optimization step, in which the precomputed one- and two-body energies are used to try to find a selection of one rotamer per position that minimizes energy. The first step can be performed by Rosetta, and the second by a general-purpose solver provided by Masala.

Quantum computers offer a possible means of surmounting the scaling obstacles of difficult combinatorial optimization problems. We have implemented solvers in Masala that allow Rosetta design using quantum computers. Our initial implementation (described in [9]) used an exact one-hot encoding of rotamer selections, requiring ***ND*** qubits to represent *D* rotamers at *N* positions (**Fig. 3B**). As a proof of principle, we used this to design a self-assembling mixed-chirality peptide helical bundle on the D-Wave quantum annealer, which we synthesized by solid-phase methods and validated by x-ray crystallography (**Fig. 3C**). However, this required more qubits than were available on the then-current D-Wave 2000Q quantum annealer, so that it was necessary to use a hybrid classical-quantum algorithm called QBSolv to divide the problem into pieces that could be solved on the annealer. We subsequently developed an approximate binary encoding (**Fig. 3D**) that compresses the problem to use $N \log_2(D)$ qubits at the expense of some accuracy in energy values. This has permitted the direct design of much larger polypeptides (*e.g.* **Fig. 3E**) entirely on the QPU. We have also explored a mapping to gate-based quantum computers using the QAOA algorithm for optimization (**Fig. 3F**). On current devices, such as systems built by IBM or IonQ, this allows only very small rotamer optimization problems to be solved; nevertheless, it is able to rapidly find lowest-energy solutions (**Fig. 3G**). Since we have previously shown that the multibody docking problem, another NP-hard problem, maps to the same functional form [10], we anticipate that these solvers will be broadly useful.

Conclusions

Robust computational peptide design faces challenges of accuracy, generality, and tractability. By introducing quantum mechanical energy calculations into design and validation pipelines through the RosettaQM bridge, we have addressed the major sources of inaccuracy in energy calculations, and have greatly improved our ability to generalize the methods to new chemical building-blocks. By mapping design problems to quantum annealers and gate-based quantum computers, we have met tractability challenges head-on, and opened the door to tackling design problems involving far more candidate building-blocks as quantum computers improve.

References

[1] G. Bhardwaj*, V.K. Mulligan*, C.D. Bahl*, J.M. Gilmore, P.J. Harvey, O. Cheneval, G.W. Buchko, S.V.S.R.K. Pulavarti, Q. Kaas, A. Eletsky, P.-S. Huang, W.A. Johnsen, P.J. Greisen, G.J. Rocklin, Y. Song, T.W. Linsky, A. Watkins, S.A. Rettie, X. Xu, L.P. Carter, R. Bonneau, J.M. Olson, E. Coutsias, C.E. Correnti, T. Szyperski, D.J. Craik, D. Baker, Accurate de novo design of hyperstable constrained peptides, *Nature* 538 (2016) 329–335. (*Co-primary authors.)
[2] P. Hosseinzadeh*, G. Bhardwaj*, V.K. Mulligan*, M.D. Shortridge, T.W. Craven, F. Pardo-Avila, S.A. Rettie, D.E. Kim, D.-A. Silva, Y.M. Ibrahim, I.K. Webb, J.R. Cort, J.N. Adkins, G. Varani, D. Baker, Comprehensive computational design of ordered peptide macrocycles, *Science* 358 (2017) 1461–1466. https://doi.org/10.1126/science.aap7577. (Co-primary authors.)
[3] B. Dang*, H. Wu*, V.K. Mulligan*, M. Mravic, Y. Wu, T. Lemmin, A. Ford, D.-A. Silva, D. Baker, W.F. DeGrado, De novo design of covalently constrained mesosize protein scaffolds with unique tertiary structures, *Proc. Natl. Acad. Sci. U.S.A.* 114 (2017) 10852–10857. https://doi.org/10.1073/pnas.1710695114. (Co-primary authors.)
[4] V.K. Mulligan, C.S. Kang, M.R. Sawaya, S. Rettie, X. Li, I. Antselovich, T.W. Craven, A.M. Watkins, J.W. Labonte, F. DiMaio, T.O. Yeates, D. Baker, Computational design of mixed chirality peptide macrocycles with internal symmetry, *Protein Sci.* 29 (2020) 2433–2445. https://doi.org/10.1002/pro.3974.
[5] V.K. Mulligan, S. Workman, T. Sun, S. Rettie, X. Li, L.J. Worrall, T.W. Craven, D.T. King, P. Hosseinzadeh, A.M. Watkins, P.D. Renfrew, S. Guffy, J.W. Labonte, R. Moretti, R. Bonneau, N.C.J. Strynadka, D. Baker, Computationally designed peptide macrocycle inhibitors of New Delhi metallo-β-lactamase 1, *Proc. Natl. Acad. Sci. U.S.A.* 118 (2021) e2012800118. https://doi.org/10.1073/pnas.2012800118.
[6] P. Hosseinzadeh, P.R. Watson, T.W. Craven, X. Li, S. Rettie, F. Pardo-Avila, A.K. Bera, V.K. Mulligan, P. Lu, A.S. Ford, B.D. Weitzner, L.J. Stewart, A.P. Moyer, M. Di Piazza, J.G. Whalen, P.J. Greisen, D.W. Christianson, D. Baker, Anchor extension: a structure-guided approach to design cyclic peptides targeting enzyme active sites, *Nat. Commun.* 12 (2021) 3384. https://doi.org/10.1038/s41467-021-23609-6.
[7] G. Bhardwaj, J. O'Connor, S. Rettie, Y.-H. Huang, T.A. Ramelot, V.K. Mulligan, G.G. Alpkilic, J. Palmer, A.K. Bera, M.J. Bick, M. Di Piazza, X. Li, P. Hosseinzadeh, T.W. Craven, R. Tejero, A. Lauko, R. Choi, C. Glynn, L. Dong, R. Griffin, W.C. van Voorhis, J. Rodriguez, L. Stewart, G.T. Montelione, D. Craik, D. Baker, Accurate de novo design of membrane-traversing macrocycles, *Cell* 185 (2022) 3520–3532.e26. https://doi.org/10.1016/j.cell.2022.07.019.
[8] V. Mironov, Y. Alexeev, V.K. Mulligan, D.G. Fedorov, A systematic study of minima in alanine dipeptide, *J. Comput. Chem.* 40 (2019) 297–309. https://doi.org/10.1002/jcc.25589.
[9] V.K. Mulligan, H. Melo, H.I. Merritt, S. Slocum, B.D. Weitzner, A.M. Watkins, P.D. Renfrew, C. Pelissier, P.S. Arora, R. Bonneau, Designing Peptides on a Quantum Computer, *bioRxiv* (2019) 752485. https://doi.org/10.1101/752485.
[10] M. Pandey, T. Zaborniak, H. Melo, A. Galda, V.K. Mulligan, Multibody molecular docking on a quantum annealer, *arXiv* (2022). https://doi.org/10.48550/arXiv.2210.11401.
[11] A. Chakrabartty, T. Kortemme, R.L. Baldwin, Helix propensities of the amino acids measured in alanine-based peptides without helix-stabilizing side-chain interactions, *Protein Sci. Publ. Protein Soc.* 3 (1994) 843–852. https://doi.org/10.1002/pro.5560030514.
[12] D.G. Fedorov, The fragment molecular orbital method: theoretical development, implementation in GAMESS, and applications, *WIREs Comput. Mol. Sci.* 7 (2017) e1322. https://doi.org/10.1002/wcms.1322.

Collaboration Opportunity

The Biomolecular Design Group seeks collaborators interested in working together to develop macromolecules for binding to targets of therapeutic interest, for functional nanomaterial applications, or for catalysis of reactions of interest. In particular, we seek experimental collaborators interested in recombinant expression of proteins, chemical synthesis of peptides, peptoids, or other heteropolymers, or experimental screening of designed macromolecules in in vitro or in vivo assays. Please contact vmulligan@flatironinstitute.org if you are interested.

Biomolecular Design Group
Center for Computational Biology,
Flatiron Institute,
162 5th Ave, New York, NY 10010

simonsfoundation.org/flatiron/

Formation of native disulfide bond patterns in small antifungal proteins and their γ-core optimized analogs

https://doi.org/10.17952/37EPS.2024.P1287

György Váradi[1], László Galgóczy[2,3], András Czajlik[4,5], Attila Borics[6], Gábor Bende[2], Csaba Papp[7], Zoltán Kele[1], Gyula Batta[4], Gábor K. Tóth[1,8]

[1]Department of Medical Chemistry, University of Szeged, Hungary, [2]Department of Biotechnology, University of Szeged, Hungary, [3]Fungal Genomics and Evolution Lab, Institute of Biochemistry, HUN-REN Biological Research Centre, Szeged, Hungary, [4]Department of Organic Chemistry, University of Debrecen, Hungary, [5]Department of Biochemistry, Institute of Biochemistry and Molecular Biology, Semmelweis University, Budapest, Hungary, [6]Laboratory of Chemical Biology, Institute of Biochemistry, HUN-REN Biological Research Centre, Szeged, Hungary, [7]Department of Microbiology, University of Szeged, Hungary, [8]MTA-SZTE Biomimetic Systems Research Group, University of Szeged, Hungary

Introduction

The increasing number of fungal infections makes the development of new antifungal agents essential. Small proteins from filamentous fungi can be promising lead compounds. The *Penicillium chrysogenum* antifungal protein (PAF) and the *Neosartorya fischeri* antifungal protein 2 (NFAP2) are representatives of this family. These proteins have different locations for the evolutionary-conserved γ-core motif.

PAF AKYTGKCTKSKNECKYKNDAGKDTFIKCPKFDNKKCTKDNNKCTVDTYNNAVDCD

NFAP2 IATSPYYACNCPNNCKHKKGSGCKYHSGPSDKSKVISGKCEWQGGQLNCIAT

Our previous studies showed that substitutions in small peptides representing the γ-cores of PAF [1] and NFAP2 [2] led to more effective antifungal agents. Therefore, the γ-cores of the proteins were replaced by an optimized peptide sequence, and the modified protein analogs were attempted to be prepared by chemical methods. In the case of NFAP2, knowledge of the native disulfide bond pattern was the prerequisite for the synthesis. The sequences of the modified proteins are the following:

PAF^{impγ} AKYTGKCKTKKNKCKYKNDAGKDTFIKCPKFDNKKCTKDNNKCTVDTYNNAVDCD

NFAP2^{impγ} IATSPYYACNCPNNCKHKKGSGCKYHSGPSDKSKVISGKCKTKKNKCIAT

Aims

- Development of synthetic strategies for the preparation of PAF and NFAP2 analogs containing optimized γ-cores and having native disulfide bridge patterns.
- Determination of native disulfide connectivity of NFAP2.
- Investigation of the antifungal effects of modified PAF and NFAP2.

NFAP2 - determination of the disulfide pattern

Since there are no tryptic or chymotryptic cleavage sites between Cys[9] and Cys[15], common mass spectrometry-based methods cannot be used to determine the disulfide bridge pattern of NFAP2. *In silico* predictions based on NMR results suggested two possible disulfide connectivities: *abbcac* and *abbacc* [4]. Both proteins were synthesized by chemical methods applying orthogonal protection to the cysteine thiols. Cleavage from the resins resulted in the following proteins:

NFAP2^{abbcac} IATSPYYACNCPNNCKHKKGSGCKYHSGPSDKSKVISGKCEWQGGQLNCIAT (SH, Mob, Mob, Acm, SH, Acm)

NFAP2^{abbacc} IATSPYYACNCPNNCKHKKGSGCKYHSGPSDKSKVISGKCEWQGGQLNCIAT (SH, Mob, Mob, SH, Acm, Acm)

The pair of free sulfhydryl groups were oxidized by air oxygen in a pH 7.5 NH_4OAc buffer. Acetamidomethyl (Acm) groups were removed, and the formed thiol functions were oxidized by iodine in an acidic solution. Cleavage of 4-methoxybenzyl (Mob) groups with trifluoromethanesulfonic acid (TFMSA) in the presence of trifluoroacetic acid (TFA) and anisole was followed by air oxidation in a pH 7.5 NH_4OAc buffer.

RP-HPLC analysis, ECD measurements, NMR investigations, and antifungal susceptibility tests against *Candida albicans* proved the identity of NFAP2^{abbcac} with recombinant NFAP2. Consequently, the disulfide bridge pattern of NFAP2 is ***abbcac***.

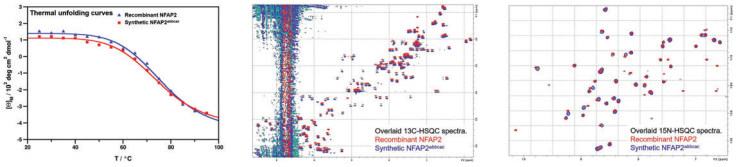

PAF^{impγ}

Synthesis and folding

Since stepwise solid-phase synthesis of PAF^{impγ} failed, native chemical ligation (NCL) was used. The thioester of the N-terminal part was prepared on a preloaded Cys-SH resin using Boc chemistry [3], while the C-terminal part of the protein was synthesized on a preloaded Wang resin using Fmoc chemistry. NCL was carried out in a pH 7.5 ammonium acetate (NH_4OAc) buffer containing 3% thiophenol.

After purification, oxidation was performed in a 1 mM reduced glutathione (GSH)-oxidized glutathione (GSSG) (1:1) buffer at pH 7.5, which resulted in the formation of a native disulfide bridge pattern.

AKYTGKCKTKKNKC + KYKNDAGKDTFIK—S—CH_2—CH(NHAc)(CONH$_2$) + CPKFDNKKCTKDNNKCTVDTYNNAVDCD

↓ 3% thiophenol; 0.1 M NH_4OAc buffer, pH=7.5; 3 h

AKYTGKCKTKKNKCKYKNDAGKDTFIKCPKFDNKKCTKDNNKCTVDTYNNAVDCD

↓ 1 mM GSH-GSSG (1:1); 0.2 mg/ml peptide concentration; 0.1 M NH_4OAc buffer, pH=7.5; 24 h

AKYTGKCTKSKNECKYKNDAGKDTFIKCPKFDNKKCTKDNNKCTVDTYNNAVDCD

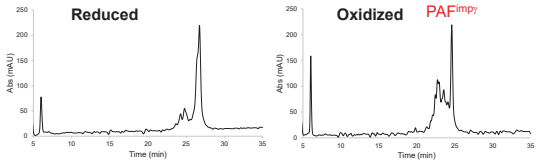

Antifungal activity

The minimum inhibitory concentration (MIC) determined on *Candida albicans* with a broth microdilution assay was found to be 5.0 μM for PAF and 1.3 μM for PAF^{impγ}. That is, in the case of PAF, appropriate modification of the γ-core increased the antifungal effect.

NFAP2^{impγ} - uniform protection of cysteines

Synthesis and folding

NFAP2^{impγ} was prepared by microwave-assisted solid-phase peptide synthesis and Fmoc chemistry.

The following methods were tested for the oxidation of cysteine thiols:

- Air oxygen in a 0.1 M NH_4OAc buffer at pH 7.5.
- 1 mM GSH-GSSG (1:1) in 0.1 M NH_4OAc buffer at pH 7.5.

None of these methods resulted in the formation of a native disulfide bond pattern.

NFAP2^{impγ} - selective protection of cysteines

With the disulfide bridge pattern of NFAP2 in hand, the γ-core modified analog of the protein was synthesized. The same procedure was followed as for NFAP2^{abbcac}.

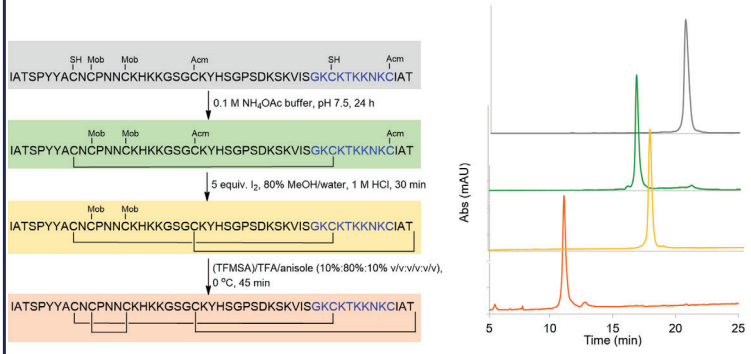

ECD analysis of NFAP2^{impγ} showed an unordered structure. Although, the applied modification improved the antifungal activity of the 14-mer peptide representing the γ-core against *Candida albicans*, the MIC of the modified protein was found to be two-fold higher (12.5 μg/mL) than NFAP2 (6.25 μg/mL). This proves that in the case of NFAP2, the γ-core does not affect the antifungal effect, but rather the formation of the structure.

Discussion

The γ-cores of the PAF and NFAP2 antifungal proteins were replaced by an optimized peptide sequence, and the modified analogs were synthesized by chemical methods.

PAF^{impγ} could only be prepared by NCL from two fragments, and oxidation in a GSH-GSSG buffer led to native disulfide connectivity. The PAF^{impγ} protein showed stronger inhibitory activity against *Candida albicans* compared to PAF, proving the role of γ-core in the antifungal effect.

NFAP2^{impγ} was prepared by stepwise solid-phase synthesis, applying orthogonal thiol protection. For this, the native disulfide bond pattern of NFAP2 was determined first, and it was found to be *abbcac*. The disulfide bridges were formed regioselectively. The produced NFAP2^{impγ} was less effective against *Candida albicans* than NFAP2, pointing to the importance of the γ-core in stabilizing the structure and not in the antifungal activity.

References

[1] Sonderegger C, Váradi G, Galgóczy L, Kocsubé S, Posch W, Borics A, Dubrac S, Tóth GK, Wilflingseder D, and Marx F, *Front. Microbiol.*, 2018, **9**, Article 1655.
[2] Tóth L, Poór P, Ördög A, Váradi G, Farkas A, Papp C, Bende G, Tóth GK, Rákhely G, Marx F, and Galgóczy L, *BioControl*, 2022, **67** (2), 249-262.
[3] Váradi G, Tóth GK, Kele Z, Galgóczy L, Fizil Á, Batta G, *Chem. Eur. J.*, 2013, **19**, 12684-12692.
[4] Váradi G, Kele Z, Czajlik A, Borics A, Bende G, Papp C, Rákhely G, Tóth GK, Batta G, Galgóczy L, *Protein Sci.*, 2023, **32**, e4692

Acknowledgements

The present work of L.G. was financed by the Hungarian National Research, Development and Innovation Office - NKFIH, FK 134343 project. G.V. and G.K.T. were supported by the TKP2021-EGA-32 fund of the Hungarian National Research, Development, and Innovation Office – NKFIH.

https://doi.org/10.17952/37EPS.2024.P1290

Alanine scanning analysis of the antimicrobial peptide lyp1987 using a template-based approach

Jomari C. Fernando[a], Jeremiah D. Batucan[b], Jacquelyn E. Peran[b], Lilibeth A. Salvador-Reyes[b], Aaron Joseph L. Villaraza*[a]

[a]Institute of Chemistry, College of Science, University of the Philippines – Diliman, Quezon City, Metro Manila 1101, Philippines
[b]Marine Science Institute, University of the Philippines – Diliman, Quezon City, Metro Manila 1101, Philippines
*corresponding author: alvillaraza@up.edu.ph

ABSTRACT

A preference for several amino acids is observed to occur at particular positions of cationic α-helical antimicrobial peptides (AMPs), which ensures the formation of amphipathic regions once they assume their correct secondary structure in membranes or membrane-mimicking environments and makes them active against pathogens. This study determined the effect of alanine mutations on the secondary structure and bioactivity of lyp1987 (GRLQAFLAKMKEIAAQTL-NH_2), a cationic α-helical AMP obtained from the venom of Lycosa poonaensis which exhibits broad range activity against Gram-positive and Gram-negative bacteria with micromolar minimum inhibitory concentrations (MIC). CD spectroscopy revealed no significant difference in the secondary structure, with all alanine-substituted analogs exhibiting predominantly α-helical structure in buffered 2,2,2-trifluoroethanol solution. Alanine substitution at Glu12 and Thr17 increased the activity of lyp1987 against Gram-positive and -negative bacteria, while alanine substitution at Lys9 increased its selectivity against Gram-positive bacteria. Further investigation can be done to determine positions and substitutions that will give less cytotoxic analogs.

Background

Most antimicrobial peptides (AMPs) are composed of up to 50 amino acids and have a net positive charge due to the presence of lysine and arginine and around 50% hydrophobic residues, which form separate domains in the secondary structure.(1) Studies have actually shown a preference for several amino acids to occur at certain positions in the primary sequence of naturally-occurring α-helical AMPs which form their amphipathic regions that are implied in their antimicrobial activity once they assume their correct secondary structure.(2-3)

The AMP lyp1987 (GRLQAFLAKMKEIAAQTL-NH_2), isolated from the venom of Lycosa poonaensis, is an 18-mer α-helical cationic AMP with an amidated C-terminus that exhibits broad range activity against bacteria, with MIC values of 15-20 μM against E. coli NBRC 3972, 75-100 μM against S. aureus NBRC 13276, and 2.5-5 μM against B. subtilis NBRC 3009.(4) It has a secondary structure containing three positively-charged residues (Arg2 and Lys9, and Lys11) effectively flanking a predominantly hydrophobic face which is observed and hypothesized to be involved in improved cell-penetrating ability of model AMPs, but might be implied in other undiscovered bioactivities of lyp1987.(5)

Methodology

Automated microwave-assisted solid-phase peptide synthesis of lyp1987 and alanine-monosubstituted analogs
Fmoc chemistry, DIC/Oxyma coupling agents, Rink amide MBHA resin

↓

HPLC purification
Gradient elution using 0.1% TFA in diH_2O and 0.1% TFA in acetonitrile
Up to ≥95% purity

↙ ↓ ↘

MALDI-TOF-MS
α-cyano-4-hydroxycinnamic acid as matrix

Antimicrobial assay
Resazurin-based broth microdilution assay using P. aeruginosa ATCC 27853 and S. aureus ATCC 6538

CD spectroscopy
In 0.2 M phosphate buffer (pH 7.0) and in 50% 2,2,2-trifluoroethanol

↓

Cytotoxicity assay
MTT-based colorimetric assay using HK2 (ATCC® CRL 2190) normal human kidney cell line
For lyp1987 and active analogs

Analog Design

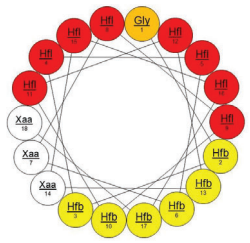

Predominant nature of amino acids of each position of an 18-mer α-helical AMP. Hfl = hydrophilic, Hfb = hydrophobic, Xaa = no specific amino acid

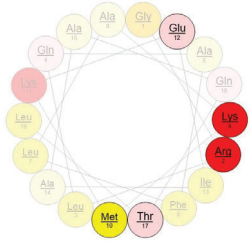

α-helical conformation of lyp1987, with positions of alanine monosubstitution highlighted.

lyp1987	GRLQAFLAKMKEIAAQTL#
R2A	G**A**LQAFLAKMKEIAAQTL#
K9A	GRLQAFLA**A**MKEIAAQTL#
M10A	GRLQAFLAK**A**KEIAAQTL#
E12A	GRLQAFLAKMK**A**IAAQTL#
T17A	GRLQAFLAKMKEIAAQ**A**L#

Primary sequences of lyp1987 and synthesized analogs. Positions of alanine substitution for each peptide written in red, boldface and underlined. # indicates C-terminal amidation for all peptides.

Results

Peptide	MIC[a] (μM)		IC_{50}[b] (μM)
	P. aeruginosa ATCC 27853	S. aureus ATCC 6538	HK2 kidney cells
lyp1987	25	>200	41.14
R2A	>50	>200	n.d.
K9A	25	50	8.8
M10A	>50	>200	n.d.
E12A	6.25	50	31.6
T17A	12.5	100	30.6

Abbreviation: n.d.: not determined. [a]MIC refers to the lowest concentration causing ≥99% inhibition of microbial pathogens. Data presented as average MIC (n=3). [b]IC_{50} refers to the concentration causing 50% inhibition of cell viability. Data presented as average IC_{50} (n=3).

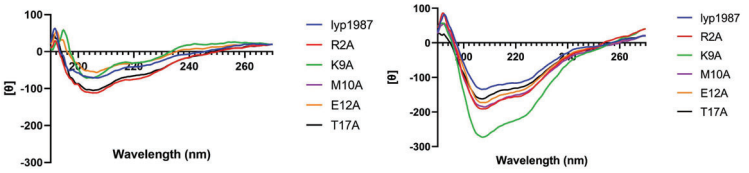

CD spectra of lyp1987 and selected analogs in 0.2 M phosphate buffer (pH 7.0) (left) and in 50% 2,2,2-trifluoroethanol in 0.2 M phosphate buffer (pH 7.0) (right).

Conclusions

- Arg2 and Met10 are essential to the antimicrobial activity of lyp1987.
- Alanine mutation at Lys9 increases its activity against Gram-positive bacteria.
- Alanine mutation at Glu12 and Thr17 increases its activity for both Gram-negative and -positive bacteria.
- lyp1987 can be further engineered to increase its antimicrobial activity and reduce its cytotoxicity.

References

(1) Microbial Biotechnology, **2023**, 16, 757–777.
(2) Trends in Food Science & Technology, **2021**, 109, 103–115.
(3) Biochimica et Biophysica Acta (BBA) - Biomembranes, **2006**, 1758, 1436–1449.
(4) Bioscience, Biotechnology, and Biochemistry, **2021**, 85, 1348–1356.
(5) Quart. Rev. Biophys., **2022**, 55, e10.

Acknowledgments

ROYAL SOCIETY OF CHEMISTRY

Royal Society of Chemistry
Research Fund
R22-0607145454

Access the full paper:

ChemMedChem, **2024**, article accepted
doi: 10.1002/cmdc.202400488

https://doi.org/10.17952/37EPS.2024.P1292

Synthesis and assessment of amyloidogenic activity of the C-peptide fragments

Joanna Waśko[1], Beata Kolesińska[1]

[1]Institute of Organic Chemistry, Faculty of Chemistry, Lodz University of Technology, Zeromskiego 116, 90-543 Lodz, Poland

Introduction

In the recent years, the research on amyloidogenic peptides have become a key area of scientific research in the field of biotechnology and medicine. The amyloidogenic peptides have significantly contribution in understanding the pathological mechanisms associated with neurodegenerative disorders such as Alzheimer's and Parkinson's disease. Moreover, it has been found that undesirable aggregation of metabolic hormones (insulin and amylin) could be also a source of the progress of type I and II diabetes. It is known that the diabetes mellitus is a group of physiological dysfunctions characterized by hyperglycaemia resulting directly from insulin resistance (in the case of type 2 diabetes mellitus-T2DM), inadequate insulin secretion/production, or excessive glucagon secretion (in type 1 diabetes mellitus-T1DM) [1,2]. Although the aetiology of diabetes may differ from T1DM to T2DM, common features, namely formation of insoluble amyloid deposits within different tissue, may occur during the progression of the both diseases. It has been proven that amyloid deposits consist largely of aggregated insulin molecules (especially during long-term subcutaneous application of the hormone during T1DM) and both insulin and amylin chains in the case of T2DM. Amylin is co-secreted with insulin from pancreatic β cells, and due to its tendency to aggregate within pancreatic islet cells in type 2 diabetes mellitus (T2DM) is so-called as human amyloid polypeptide (hIAPP) [3,4]. The amyloidogenic properties of peptides could be also favoured by factors like acidic pH, drastic changes in temperature, contact with hydrophobic surfaces or variations in ionic strength of solution. Although there are reports which put hypothesis that amyloid deposits may also include other structures. Currently, researchers are increasingly focusing on the tendency to aggregate C-peptide and its input on another metabolic disorders [5,6].

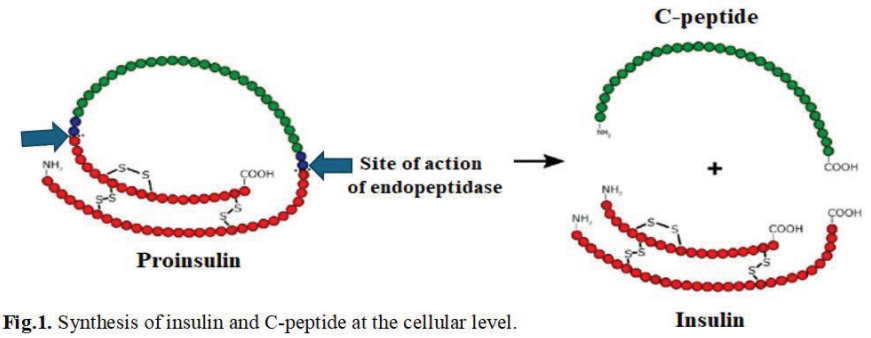

Fig.1. Synthesis of insulin and C-peptide at the cellular level.

Initially, peptide C, produced in the cell during the proteolytic transformation of proinsulin into insulin and co-secreted in equimolar amounts into the circulatory system together with insulin, was considered as a by-product whose action did not significantly affect the functioning of the body. However, its activity has now been confirmed at the stage: a) promoting proper folding of proinsulin; b) initiating the process of creating disulphide bridges within the hormone; c) supporting interactions enabling controlled secretion of insulin from the pancreas. On the other hand, there is some controversy regarding reported effects of the C-peptide. Its beneficial effects have been demonstrated in long-term treatment in type 1 diabetes. In contrast to this, C-peptide in type 2 diabetes could induce proinflammatory and proatherogenic effects.

Results and Discussion

Based on these inconsistencies, one of the directions of our research includes studies on the tendency to aggregation of C-peptide fragments under *in vitro* conditions.

To verify this hypothesis, C-peptide was divided into five shorter fragments (Table 1). As it was identified for insulin [7], we also would like to detect the shortest potential sequences within C-peptide responsible for the growth of amyloid fibril (so-called hot-spot fragments).

Table 1. The synthesized C-peptide fragments.

(1)	H_2N-^{57}EAEDLQV^{63}-OH
(2)	H_2N-^{64}GQVELG^{69}-OH
(3)	H_2N-^{70}GGPGAG^{75}-OH
(4)	H_2N-^{76}SLQPLA^{81}-OH
(5)	H_2N-^{82}LEGSLQ^{87}-OH

The proposed peptide chains were synthesized according to the Fmoc/tBu methodology on a 2-chlorotrityl chloride resin using a triazine coupling reagent [8]. In the second stage of the research, a spectrophotometric and microscopic tests were carried out to assess their tendency to aggregation.

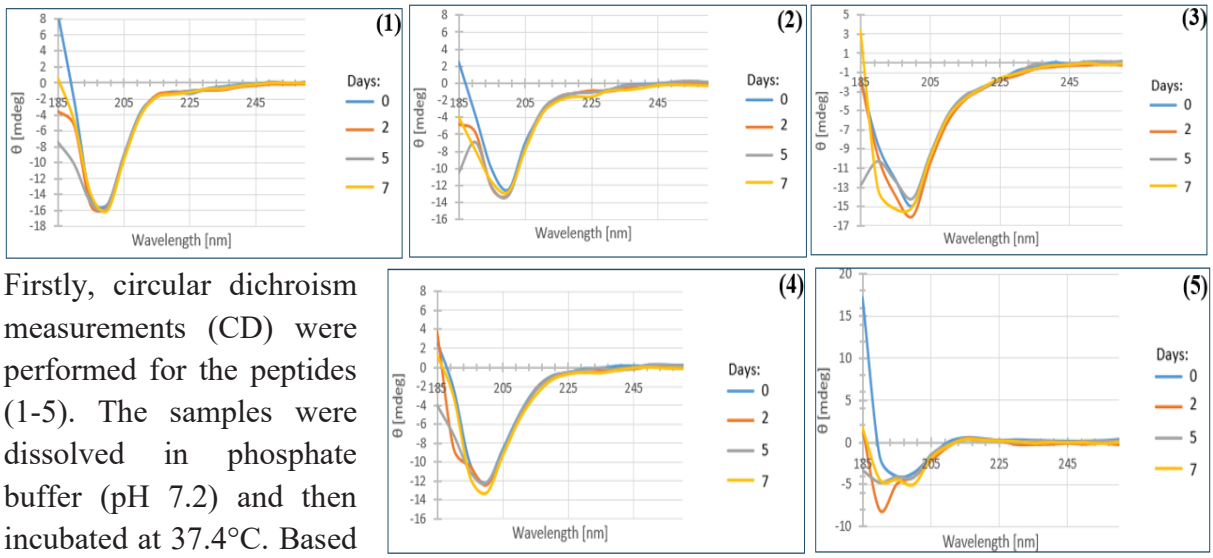

Figure 1. CD measurements registered for the analyzed C-peptide frgaments.

Firstly, circular dichroism measurements (CD) were performed for the peptides (1-5). The samples were dissolved in phosphate buffer (pH 7.2) and then incubated at 37.4°C. Based on the registered CD spectra we conclude that first four peptides (1-4) showed stable secondary structure during 7 days. In turn, the fragment (5) was the most susceptible to conformational changes. For the

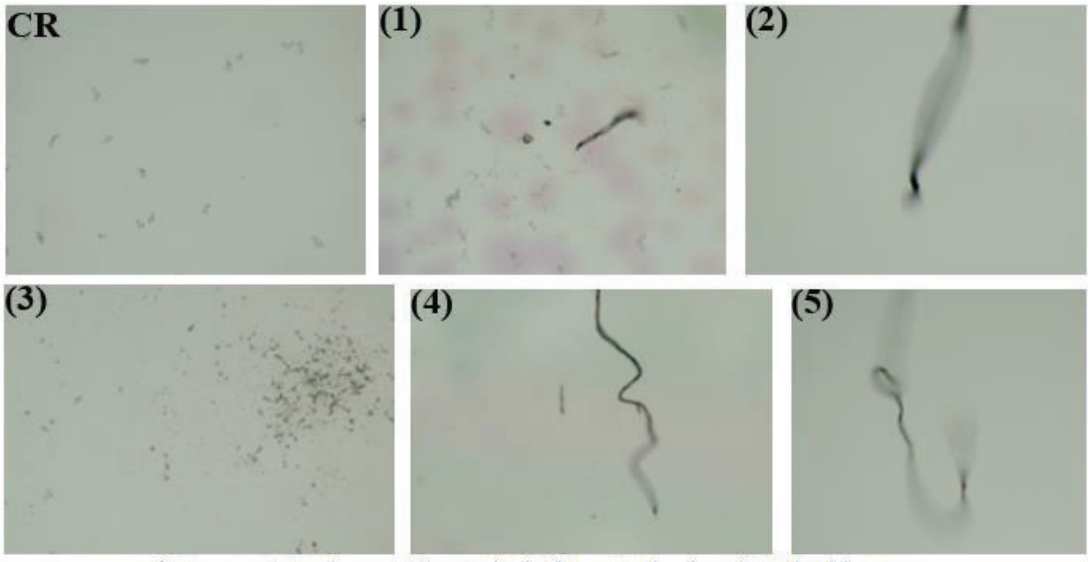

Figure 2. The microscopic analysis for samples incubated with CR.

microscopic studies carried out for the incubated samples, additionally stained with a dye that selectively interacts with amyloid fibers (namely Congo red, CR), the highest density of fibrillar structures was also identified in the fifth, C-terminal sequence, marked in locants 82-87. This is most likely related to the presence of the active site in this area, information about which can be found in the literature [9].

Moreover, the unmature amyloid fibers were observed for the samples (1), (2) and (4) but there were unstable. On the other hand, in the case of the third peptide (70-75), the predisposition to form aggregates was the weakest compared to the rest of the synthesized amino acid chains.

Conclusions

The research carried out so far point out the tendency to aggregate some of the analyzed sequences, while opening a new research approach to searching for new functions of C-peptide as a biomarker in the diagnosis of diseases related to metabolic disorders. As part of further experiments, it is planned to repeat the aggregation tests for structures composed of at least seven amino acids and at a reduced pH.

Literature

[1] Wahren, J., Ekberg, K., & Jörnvall, H. (2007). C-peptide is a bioactive peptide. Diabetologia, 50, 503-509. https://doi.org/10.1007/s00125-006-0559-y

[2] Krause, M., De Vito, G. (2023). Type 1 and type 2 diabetes mellitus: commonalities, differences and the importance of exercise and nutrition. Nutrients, 15, 4279. https://doi.org/10.3390/nu15194279

[3] Alrouji, M., Al-Kuraishy H.M., Al-Gareeb, A.I., Alexiou, A., Papadakis, M., Saad, H.M., El-Saber Batiha, G. (2023). The potential role of human islet amyloid polypeptide in type 2 diabetes mellitus and Alzheimer's diseases. Diabetology & Metabolic Syndrome, 15 (101), 1-16. https://doi.org/10.1186/s13098-023-01082-1

[4] Das, A., Shah, M., Saraogi, I. (2022). Molecular aspects of insulin aggregation and various therapeutic interventions. ACS Bio Med Chem Au, 2, 205−221. https://doi.org/10.1021/acsbiomedchemau.1c00054

[5] Vasic, D., Walcher, D. (2012). C-Peptide: A new mediator of atherosclerosis in diabetes. Mediators of Inflammation, 2012, 1-8. https://doi:10.1155/2012/858692

[6] Tsiolaki, P.L., Louros, N.N., Zompra, A.A., Hamodrakas, S.J., Iconomidou, V.A. (2016). Unraveling the aggregation propensity of human insulin C-Peptide. PeptideScience, 108 (2), 1-8. https://doi.org/10.1002/bip.22882

[7] Swiontek, M., Fraczyk, J., Wasko, J., Chaberska, A., Pietrzak, L., Kaminski Z.J., Szymanski, L., Wiak, S., Kolesinska, B. (2019). Search for new aggregable fragments of human insulin. Molecules, 24, 1600, 1-20. https://doi.org/10.3390/molecules24081600

[8] Kolesińska B., Rożniakowski K.K., Frączyk J., Relich I., Papini A.M., Kamiński Z.J. (2015). The Effect of Counterion and Tertiary Amine on the Efficiency of N-Triazinylammonium Sulfonates in Solution and Solid-Phase Peptide Synthesis. Eur. J. Org. Chem., 401-408. doi.org/10.1002/ejoc.201402862

[9] Munte, C. E., Vilela, L., Kalbitzer, H. R., & Garratt, R. C. (2005). Solution structure of human proinsulin C-peptide. The FEBS Journal, 272 (16), 4284-4293. https://doi.org/10.1111/j.1742-4658.2005.04843

High-Throughput Synchrotron Radiation Circular Dichroism (HT-SRCD) for the screening of G-quadruplex ligands

Martina Rotondo[1], Claudia Honisch[2], Barbara Biondi[2], Pietro Spanu[3], Fausta Ulgheri[3], Giovanni Loriga[3], Andrea Beccu[3], Rohanah Hussain[4], Giuliano Siligardi[4], Paolo Ruzza[2]

[1]*Università Degli Studi di Napoli Federico II, Napoli, Italy,*
[2]*Institute of Biomolecular Chemistry of CNR, Padova Unit, Padova, Italy,*
[3]*Institute of Biomolecular Chemistry of CNR, Sassari Unit, Sassari, Italy,*
[4]*Diamond Light Source, Harwell Science and Innovation Campus, Didcot, United Kingdom*

https://doi.org/10.17952/37EPS.2024.P1293

G-quadruplexes (G4) are stable DNA/RNA structures formed by stacking guanine tetrads, supported by Hoogsteen hydrogen bonds and metal cations like K^+ and Na^+. Found in proto-oncogenes, telomeres, and various organisms, G4s are crucial in gene expression. Research aims at finding specific ligands, including peptides, for therapeutic use.

CD spectroscopy and HT-SRCD at Diamond Light Source was used to study G4 topologies and ligand binding. The stability and binding of three G4-forming strands were examined in **10 mM TRIS HCl buffer, pH 7.4, in the presence of either sodium or potassium ions**.

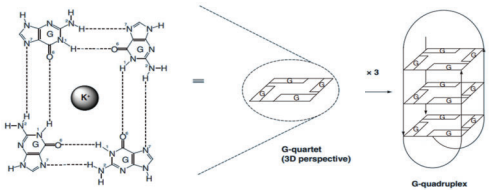

SYNCHROTRON RADIATION

The use of **synchrotron radiation** (SR) of third-generation synchrotrons as a light source has overcome the limitation of the lower photon flux of benchtop CD instruments extending the range of analysis in the vacuum-UV region. The highly collimated SR micro-beam allows measurement of small volume cells of appropriate pathlength whereas the high photon flux improves signal-to-noise ratio, allowing to record just one or few repeated scan per sample with optimal signal quality.

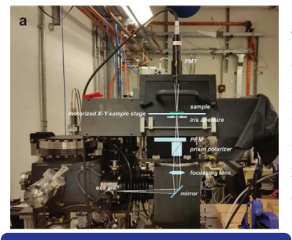

The flexible sample compartment enables various experimental setups, such as a vertical sample compartment designed for multi-well plates used in **high-throughput analysis**. These plates are placed on a motorized X-Y stage for precise and automated movement. Monochromatic light is directed upwards by a plane mirror inside the chamber, which then reflects the light to a photo elastic modulator that creates circularly polarized light before it passes through the sample. **Using multi-well plates allows simultaneous analysis of many samples, significantly accelerating data collection**.

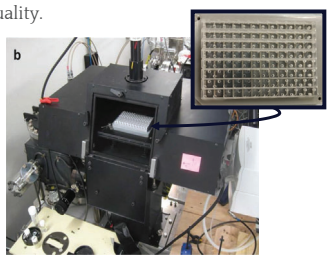

HT-SRCD ANALYSIS

Htelo1
5'-TAGGGTTAGGGTTAGGGTTAGGG-3'
T95-2T
5'-TTGGGTGGGTGGGTGGGT-3'
G3T3
5'-GGGTTTGGGTTTGGGTTTGGG-3'

The binding properties **of seven peptides** and **eleven peptidomimetics** to three selected G4 strands were screened in **two different buffers**, testing 18 different ligands for each G4 strand. **This approach allowed the collection of 360 spectra in just two days.**

EXAMPLE 60-WELL PLATES

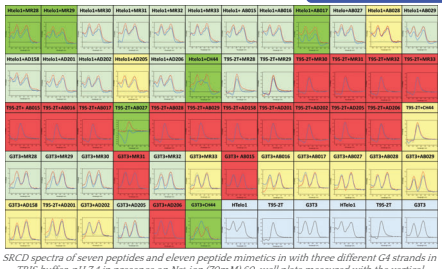

SRCD spectra of seven peptides and eleven peptide mimetics in with three different G4 strands in TRIS buffer, pH 7.4 in presence on Na^+ ion (70mM) 60-well plate measured with the vertical chamber for HT-SRCD. The green boxes highlights the spectra in which there is a greater signal variation, the yellow boxes highlights the spectra in which there is a smaller conformational variation, the red boxes highlights the spectra in which there isn't any modification, and the blue boxes highlights the spectra of the G4 alone.

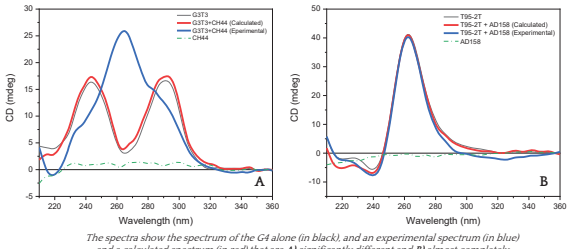

*The spectra show the spectrum of the G4 alone (in black), and an experimental spectrum (in blue) and a calculated spectrum (in red) that are **A)** significantly different and **B)** almost completely overlapping. The dashed line represents the spectrum of the ligand alone*

FURTHMORE ANALYSIS WITH CH44 LIGAND

CIRCULAR DICHROISM

The ligand CH44 is the peptide RAU25, a fragment of the N-terminal domain of the RHAU protein, a RNA helicase.

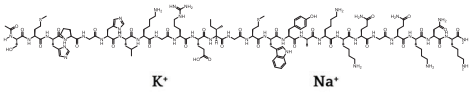

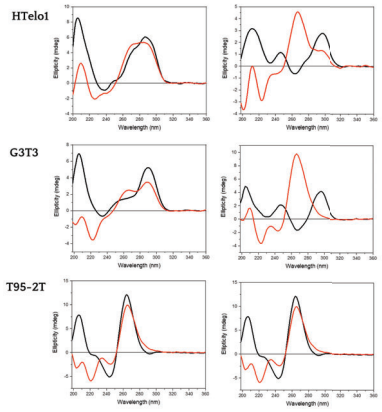

CD spectra of the three different G4 strands (13,5μM) alone (black lines) and in the presence of the RAU-25 peptide (2eq) (red lines) in TRIS buffer, pH 7.4 in presence of K^+ ion (left) or Na^+ ion (right) (70mM)

MELTING ANALYSIS

Sample	Melting Temperature T_m (°C) KCl	NaCl
G3T3 alone	69 ± 0.3	51 ± 0.4
G3T3 + peptide	n.d. *	69 ± 0.3
Htelo1 alone	66 ± 0.3	53 ± 0.3
Htelo1 + peptide	n.d. *	59 ± 0.4 *,#
T95-2T alone	>90	61 ± 0.2
T95-2T + peptide	>90	>90

n.d. not determinable because of high stability of the structure. * observed conformational conversion. # determined after 5 h equilibration time.

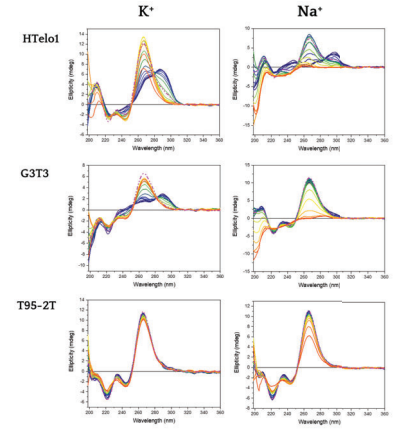

CD Spectra of G4 forming sequences (13.5 μM) in 10 mM Tris-HCl buffer, pH 7.4, containing 70 mM potassium ions (left) or sodium ions (right) during the annealing process 10°C to 90°C every 5°C. The dashed line represents the oligonucleotide cooled to 20 C after heating at 90°C.

CALORIMETRY

The binding constant and thermodynamic values for the T95-2T-RAU25 complex were calculated. Other ligand-G4 couples with significant changes in CD spectra produce ITC data under the same conditions with large errors, making the measurements unreliable.

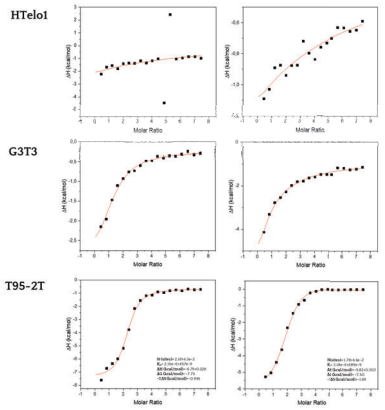

ITC curves of G4 forming sequences (25 μM) in 10 mM Tris-HCl buffer, pH 7.4, containing 70 mM potassium ions (left) or sodium ions (right) in presence of increasing amount of RAU-25 peptide (25mM).

CONCLUSION

In this study, we used HTCD by means of synchrotron light as a rapid system for investigating the binding ability of a wide panel of ligands with three different G4s in two different environments (presence of Na+ or K+), allowing us to quickly assess the potential presence of interactions. Subsequent studies with the chosen ligand allowed us to confirm the interactions identified by HTCD. Obviously, these interaction studies will be continued for the other promising ligands found during the screening analyses.

REFERENCES

[1] Del Villar-Guerra R, Trent JO, Chaires JB. *Angew Chem Int Edit.* **2018**;57(24):7171-5.
[2] Ji D, Juhas M, Tsang CM, Kwok CK, Li Y, Zhang Y. *Brief Bioinform.* **2021**;22(2):1150-60.
[3] Honisch C, Ragazzi E, Hussain R, Brazier J, Siligardi G, Ruzza P. *Pharmaceutics.* **2021**; 13(8):1104.

AKNOLEDGEMENT

This work was carried out with the support of Diamond Light Source, Beamline B23 (proposal SM34241-1), EU funding within the MUR PNRR "National Center for Gene Therapy and Drugs based on RNA Technology" (Project no. CN00000041 CN3 RNA) and MUR PRIN 2020 progetto AEX4TA Natural Products-Assisted Organic Synthesis.

Design and Synthesis of a Diamino Diacid-based Short Cyclic Peptide with Tunable Self-Assembly

Devki Nandan and Dr. Ramesh Ramapanicker

Department of Chemistry, Indian Institute of Technology Kanpur, Uttar Pradesh, India.

https://doi.org/10.17952/37EPS.2024.P1295

Introduction

- Cyclic peptide nanostructures are thought to be potential candidates for biomedical applications because of their biocompatibility. The diamino diacid residues are formed from two α-amino acid units, which are coupled with a linker. They have been used as external templates for synthesizing short cyclic peptides (CP).
- We have used a diamino diacid for the preparation of a cyclic heptapetide with an aliphatic chain connecting the two terminal α-amino acid units.
- The properties of this cyclic peptide were compared with that of the corresponding linear peptide (LP). It was found that the CP showed concentration dependent self-assembly resulting in the formation of different nanostructures at different concentrations.
- These self-assembled nanostructures were characterized using FESEM, AFM, DLS, and FTIR. The study showed that the self-assembling behaviors of the cyclic and linear peptides are significantly different. Both the CP and the LP have very low critical aggregation concentrations (CAC), which were measured using fluorescence and DLS. The conformations of the CP and LP were analyzed at different concentrations using CD spectroscopy and marked differences were observed in their native conformations at different concentrations and solvents.

Literature reports

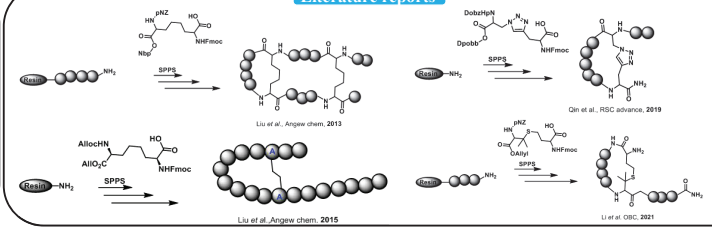

Results and discussion

Design and synthesis of diamino diacid (DADA) and cyclic peptide (CP)

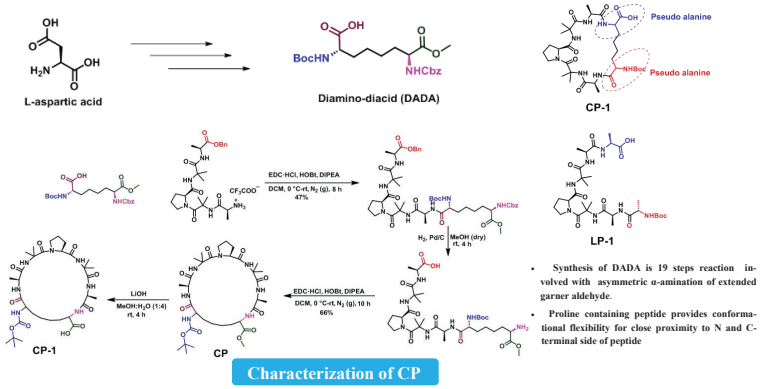

- Synthesis of DADA is 19 steps reaction involved with asymmetric α-amination of extended garner aldehyde.
- Proline containing peptide provides conformational flexibility for close proximity to N and C-terminal side of peptide

Characterization of CP

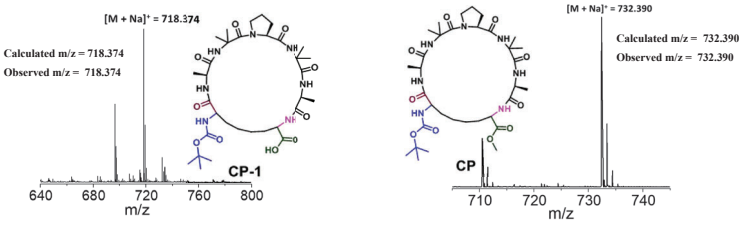

CD analysis of CP and LP

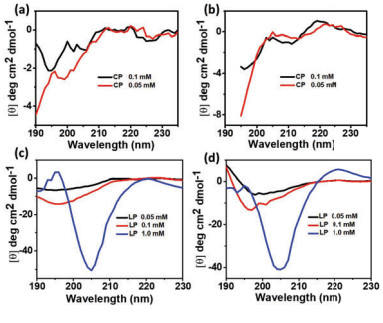

CD spectra of (a) CP in trifluoroethanol with two different concentrations and (b) CP in methanol at two different concentrations. (c) LP in trifluoroethanol and (d) in methanol at three different concentrations

Determination of CAC for CP-1 and LP-1

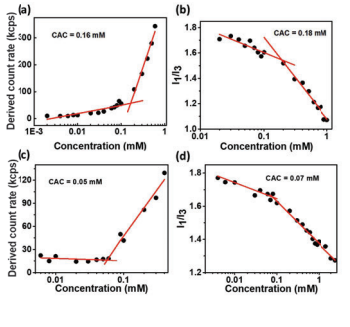

Aggregation behavior of CP and LP (a) determination of critical aggregation concentration of CP-1 using fluorescence intensity measurement of pyrene and (b) by dynamic light scattering (DLS). (c) determination of critical aggregation concentration of LP-1using fluorescence intensity measurement of pyrene and (d) by dynamic light scattering

Morphology study

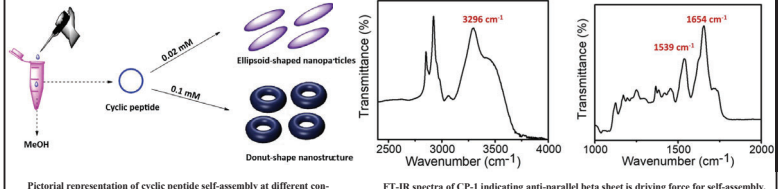

Pictorial representation of cyclic peptide self-assembly at different concentrations.

FT-IR spectra of CP-1 indicating anti-parallel beta sheet is driving force for self-assembly.

Self-assembly behaviors of CP-1 and LP-1

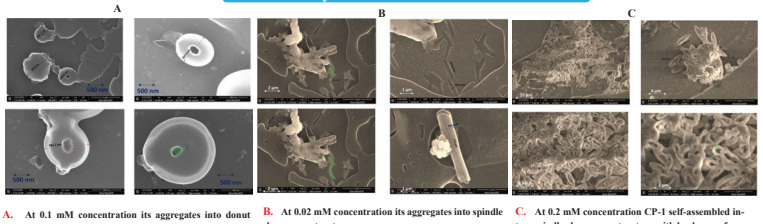

A. At 0.1 mM concentration its aggregates into donut shape nanostructure.

B. At 0.02 mM concentration its aggregates into spindle shape nanostructure.

C. At 0.2 mM concentration CP-1 self-assembled into spindle shape nanostructure with broken surface.

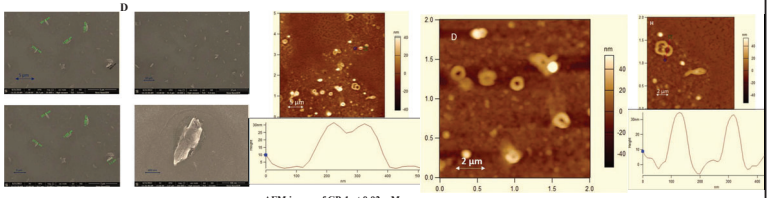

D. Irregular morphology with undefined structures of Linear peptide (LP-1).

AFM image of CP-1 at 0.02 mM

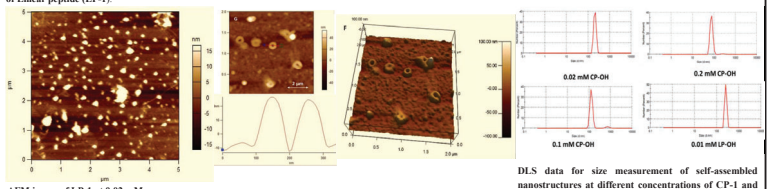

AFM image of LP-1 at 0.02 mM

DLS data for size measurement of self-assembled nanostructures at different concentrations of CP-1 and

References

Ramapanicker, *et al.*, *Tetrahedron*, **2014**, **70**, 9554–9563

Advanced imaging center and MSE (IITK) for the AFM and FESEM facility, Dr. A. Thakur for the DLS facility.

Conclusions

- A short cyclic peptide was synthesized using diamino diacid (DADA) as a external templet.
- The CAC value was found to be quite low for both linear and cyclic peptides.
- CD analysis confirmed that CP in methanol exist in β-sheet conformation which is likely a driving force for self-assembly whereas linear peptide was found in α and β-turn conformations.
- In comparison of self-assembly behavior of CP-1 and LP-1. The well ordered self-assembled nanostructures were observed for Cyclic peptide but in linear peptide there is no

Effect of lipid peroxidation on protein conformational stability

Honisch C.[1], Rotondo M.[2], Tartaggia S.[1],Hussain R.[3], Siligardi G.[3], Ruzza P.[1]

[1]Institute of Biomolecular Chemistry of CNR, Padua Unit, Padova, Italy,
[2]University of Napoli Federico II, Dept. of Biology, Napoli, Italy
[3]Diamond Light Source Ltd., Harwell Science and Innovation Campus, Didcot, UK

https://doi.org/10.17952/37EPS.2024.P1296

Introduction

Lipid oxidation can occur in vivo during oxidative stress and redox imbalance conditions, such as inflammation or environmental toxicity. This process generates reactive oxygen species (ROS), including the superoxide anion and hydroxyl radical within cells. Unsaturated fatty acids in tissues are particularly prone to oxidation by these ROS through non-enzymatic mechanisms. Lipid peroxidation, operating via a chain mechanism, produce a wide range of oxygenated small molecules, which significantly affects membrane organization and can modify proteins and DNA, leading to functional changes [1]. To study the effects of lipid peroxidation on the conformational stability of model proteins, BSA, HEWL, Ubiquitin, and rabbit IgG were solubilized in phosphate buffer and examined alone or in the presence of DMPG-DOPC (at a 1:1 molar ratio) small unilamellar vesicles (SUVs) at either 20°C or 40°C.

Synchrotron Radiation Circular Dichroism (SRCD) and the SRCD UV-denaturation assay



Oxidative conditions were created by collecting 30 consecutive repeated synchrotron radiation circular dichroism (SRCD) spectra at beamline B23 of the Diamond Light Source synchrotron (Didcot, UK).
The synchrotron radiation, besides increasing the S/N ratio and expanding the available spectral window, due to its high photon flux and brilliance is able to induce water photolysis and production of ROS, which can denature protein/peptide folding [2].
This method is used to quantify the UV photostability of proteins/peptides with and without ligands as a function of the environment [3].

Effect of lipids and temperature

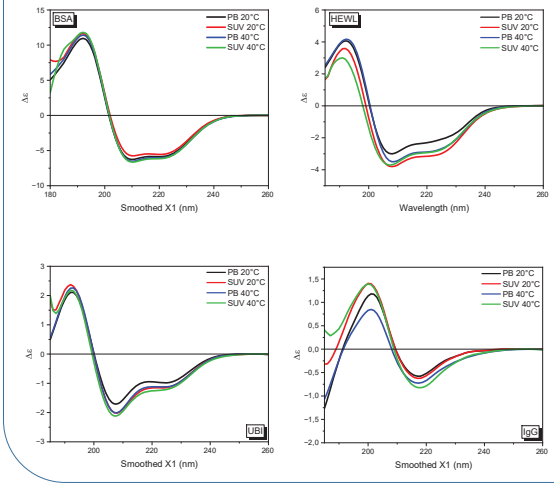

Three mainly helical proteins were analysed in different environments, and taking the spectrum of proteins in phosphate buffer at 20°C as reference,

- BSA is the least influenced by the change of solvent polarity and temperature, as all spectra are almost superimposable
- UBI shows a slight increase in the intensity of both negative bands, comparable in all other environments
- HEWL shows increased intensity of the negative bands with temperature, and a similar effect with lipid presence, while the intensity of the positive band is decreased both with lipids and with temperature

IgG is characterized by a predominant β-sheet folding, with a positive band at ~205 nm and a negative one at ~220 nm.
The intensity of these bands is affected differently by heating or the presence of phospholipids.
In PB at 40°C the intensity of the positive band decreases, and the negative one increases. The latter is not affected by lipids at 20°C, while it is slightly increased in lipids at 40°C. On the contrary, the positive band increased in intensity at both temperatures studied when in presence of lipids.

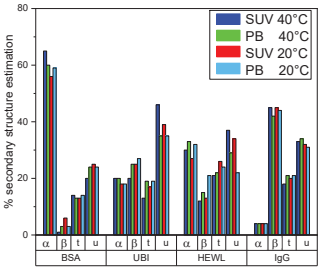

The secondary structure content estimation performed using both CONTILL and CDSSTR algorithms implemented in the CDApps software [5] shows no significant variation in protein conformation related to heating and/or addition of phospholipids.

SRCD UV-denaturation

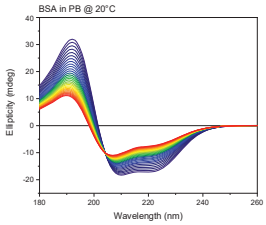

Protein UV-denaturation assays were performed in the presence or not of DMPG:DOPC SUVs.
30 consecutive SRCD scans were recorded at 20° or 40°C. The progressive decrease in the intensity and/or change in shape of the CD bands indicates a progressive loss of the native structure of proteins due to the action of reactive oxygen species generated by the photolysis of water molecules as previously demonstrated [3].

The change in the CD spectra is more evident in the buffer solution than in the presence of DMPG:DOPC SUVs. The increment of temperature (40°C) has a positive effect on the rate of denaturation in the presence of only the buffer. In the presence of SUVs a decrease in the rate of change of the SRCD was detected at the increasing of temperature.

Plotting the ellipticity values at λ_{max} vs the scan number:

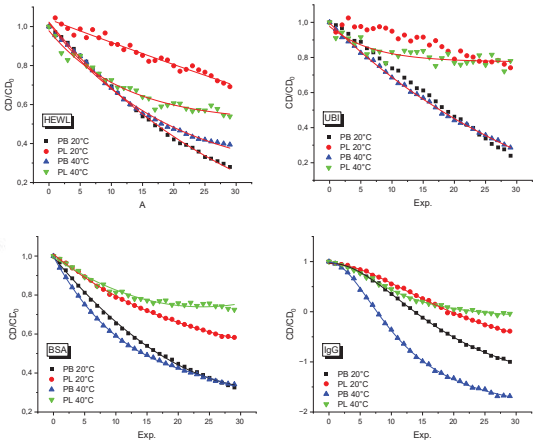

Fitting the ellipticity values at λ_{max} vs the scan number with an exponential decay function (Origin ExpDec1: $y = y_0 + Ae^{-x/t}$), allows to determine both the decay rate ($k = 1/t$) and the half-life ($t½ = t * \ln 2$) from the time constant parameter (t). Linear (UBI in PB and PL 20°C) or sigmoidal (IgG) fitting do not allow to estimate k or t½.
Higher decay rate and lower half-life reveal a rapid process.

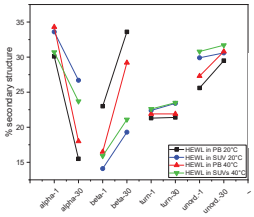

The estimation of secondary structure before and at the end of the UV-denaturation experiment shows that the loss of native conformation is mitigated in the presence of SUVs.

	k = 1/t				t½ = t * ln2			
	HEWL	UBI	BSA	IgG	HEWL	UBI	BSA	IgG
PB 20°C	3,08	n.d.	5,06	Sigmoidal fit	22,52	n.d.	13,70	Sigmoidal fit
PB 40°C	5,368	2,66	8,27		12,89	26,08	8,38	
SUVs 20°C	0,38	n.d.	4,53		n.d.	n.d.	15,31	
SUVs 40°C	8,33	14,60	11,30		8,32	4,74	6,16	

Conclusions

For the investigated proteins, CD spectra revealed that their conformation is not affected by temperature change or lipid presence.
The SRCD UV-denaturation assay showed that the presence of lipids seems to prevent the denaturation of proteins, which opens new questions on the effects of the synchrotron light on the lipids structure, stability and reactivity, which will be addressed by future studies.

References

1. Viedma-Poyatos Á, González-Jiménez P, Langlois O, Company-Marín I, Spickett CM, Pérez-Sala D. Protein Lipoxidation: Basic Concepts and Emerging Roles. Antioxidants (Basel). **2021** Feb 16;10(2):295.
2. Ruzza P, Honisch C, Hussain R, Siligardi G. Free Radicals and ROS Induce Protein Denaturation by UV Photostability Assay. Int J Mol Sci. **2021** Jun 17;22(12):6512.
3. Hussain R, Longo E, Siligardi G. UV-Denaturation Assay to Assess Protein Photostability and Ligand-Binding Interactions Using the High Photon Flux of Diamond B23 Beamline for SRCD. Molecules. **2018** Jul 31;23(8):1906.

https://doi.org/10.17952/37EPS.2024.P1297

Three-dimensional structure and membrane permeability relationship of cyclopropane-restricted cyclic peptides

Yuki Yamazaki[1], Hiroyuki Kumeta[2], Satoshi Shuto[1] and Mizuki Watanabe[1]

[1]Faculty of Pharmaceutical Sciences and [2]Faculty of Advanced Life Science, Hokkaido University, Sapporo, Hokkaido 060-0812, Japan

Background

Cyclic peptides improve

✓ the stability against proteolytic degradation.

✓ bioactivity and selectivity for the target protein.

Cyclic peptides are expected to be effective for regulating "undruggable" targets.

But

The control of cell membrane permeability is a major issue.

Membrane permeability of cyclic peptides is strongly related to the 3D structure.

cyclo[D-Leu-D-Leu-Leu-D-Leu-Pro-Tyr] cyclo[Leu-D-Leu-Leu-Leu-D-Pro-Tyr]

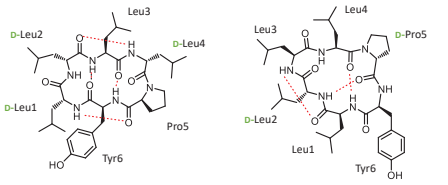

High permeability
Pe : 0.63 × 10⁻⁶ cm/s
(PAMPA)

Low permeability
Pe : <0.01 × 10⁻⁶ cm/s
(PAMPA)

Lokey, R. S. *et al. J. Am. Chem. Soc.* **2006**, *128*, 2510.

Previous work

α,δ-Disubstituted cyclopropane δ-amino acid (CPA)

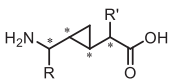

The conformation of CPA is strongly restricted by the properties of cyclopropane.

***cis/trans* restriction**



Cyclopropylic strain

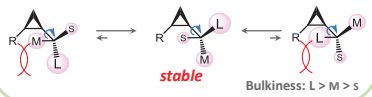

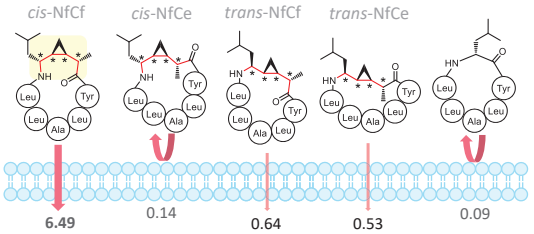

Chem. Eur. J. **2017**, *23*, 3034.

✓ CPAs can regulate the conformation of the peptide backbone.

✓ The cyclic peptide that contains a particular stereoisomer of CPAs showed remarkably high membrane permeability.

This work

Design and synthesis of cyclic hexapeptides introducing a ***cis*-NfCf**, the specific stereoisomer of CPA.

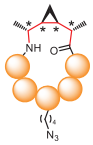

✓ The number of polar amino acids is 0 to 2.
→ Ser, Tyr, Thr, Gln, Asn and Arg

✓ The clogP range is 4.4 to 7.4.

✓ Evaluation of membrane permeability



✓ Analysis of 3D structure using NMR and the computational calculation



Synthesis of the cyclopropane δ-amino acid

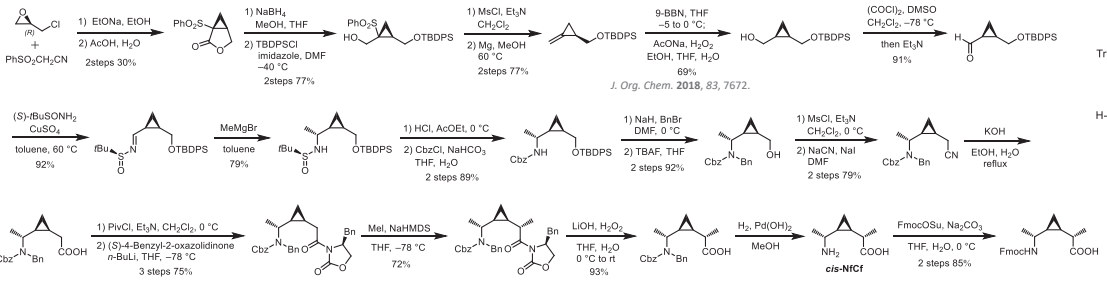

Synthesis of cyclic peptides

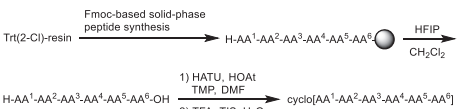

Thirty cyclic peptides with different amino acid sequences and azido group positions were synthesized.

Evaluation of membrane permeability using PAMPA

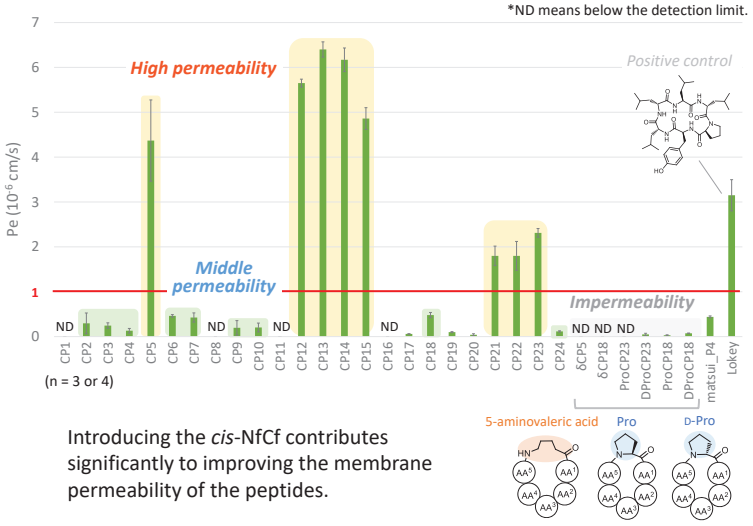

Introducing the *cis*-NfCf contributes significantly to improving the membrane permeability of the peptides.

NMR Analysis of 3D structure (DMSO-d_6 or $CDCl_3$, 600 MHz)

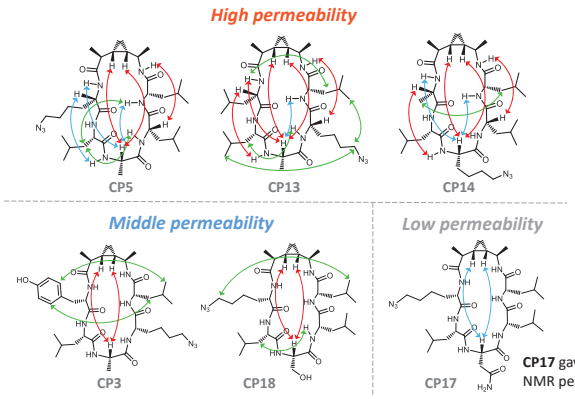

CP17 gave no assignable NMR peaks in $CDCl_3$.

The backbone conformation of cyclic peptides would be similar in DMSO-d_6 and $CDCl_3$ despite passive permeability.

3D structural calculations based on NMR

CP5 in DMSO-d_6 vs $CDCl_3$

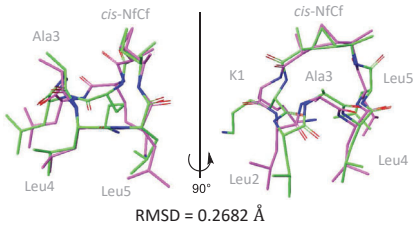

RMSD = 0.2682 Å

CP5 vs CP18 in DMSO-d_6

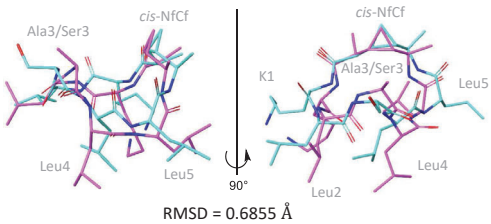

RMSD = 0.6855 Å

(Calculation: CYANA ver 2.1, Conditions: distance constraints of ROE signals; < 5Å, View: MacroModel 13.2)

3D structures of the cyclic peptide's main chains had a **similar "closed" conformation** regardless of the amino acid sequences and environments.

✓ We succeeded in controlling the 3D structure in a sequence-independent manner by introducing the *cis*-NfCf into cyclic peptides.

✓ These results indicate that cyclic peptides don't have sufficient passive permeability even when controlled to a "closed" conformation.

Vienna-DNP:

Methyl-based NMR methods for characterization of large peptide self-assemblies

https://doi.org/10.17952/37EPS.2024.P1298

Dörte Brandis[1,2], Fanny Kozak[1,2], Christian W. F. Becker[1], Dennis Kurzbach[1]

1. Institute of Biological Chemistry, Faculty of Chemistry, University of Vienna, Währingerstraße 38, 1090 Vienna, Austria.

2. Vienna Doctoral School in Chemistry (DoSChem), University of Vienna, Währinger Str. 42, 1090 Vienna, Austria

Email: doerte.brandis@univie.ac.at

Find us at: www.Kurzbach-group.univie.ac.at

Nuclear Magnetic Resonance (NMR) spectroscopy is a key method for studying the structural dynamics of peptides and proteins in their native aqueous environment. However, due to weak signal intensities, in particular for high molecular weights, its application to peptide self-assemblies still needs to be improved. Our group previously described an NMR-based approach for real-time monitoring of assembly of the biomimetic R5 peptide,[1,] which forms supramolecular structures upon exposure to phosphate and co-precipitates upon silicate exposure.[2] Herein, we present a new approach utilizing methyl groups as intrinsic spin labels, with favorable relaxation properties resulting in improved sensitivity and a smaller sampling rate of 1 min^{-1}. This enables us to extend our approach to even bigger supramolecular assemblies of Elastin-like Polypeptide (ELP) – R5 fusion constructs, also providing a silica precipitation mechanism.[3]

$[PGXGV]_{90}$ – ENLYFQ – GSSKKSGSYSGSKGSKRRIL

X = 27 × G, 18 × A, 44 × V

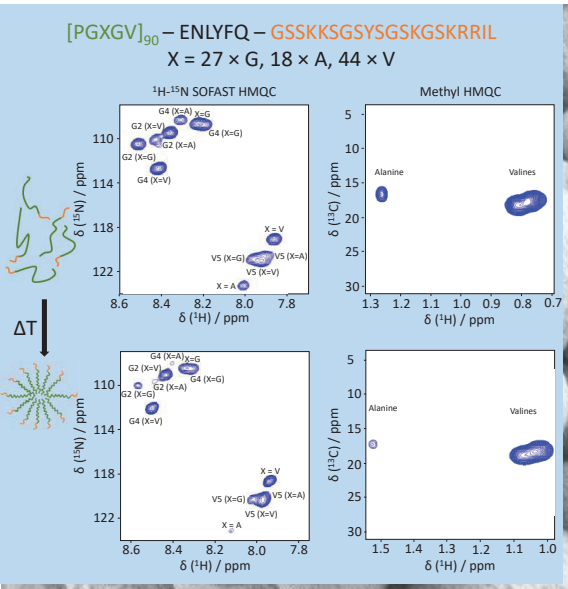

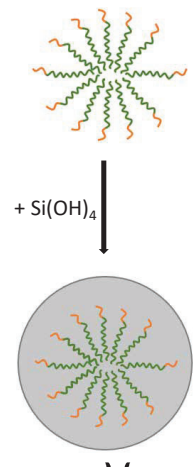

Real-time monitoring of silica precipitation process with methyl NMR.

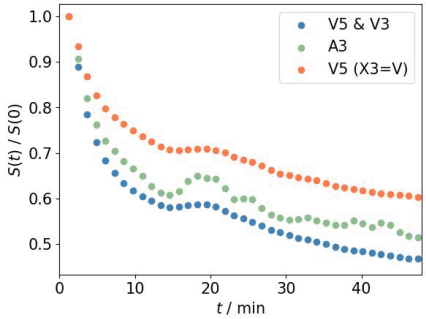

Real-time monitoring of silica precipitation process with conventional backbone NMR.

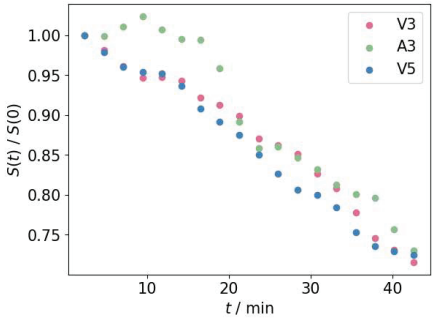

Bimodal size distribution of Particles formed by ELP-R5.

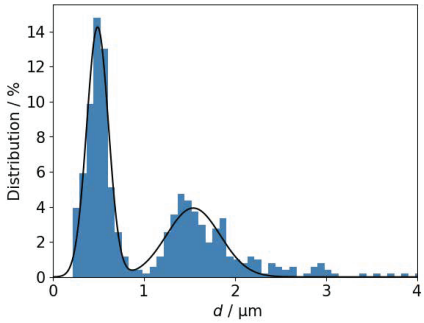

References:

[1] Strobl, J., Kozak, F., Kamalov, M., Reichinger, D., Kurzbach, D., Becker, CFW., Advanced Materials 2207586 (2023).
[2] Kozak, F., Brandis, D., Pötzl, C., Epasto, L. M., Reichinger, D., Obrist, D., Peterlik, H., Polyansky, A., Zagrovic, B., Daus, F., Geyer, A., Becker, C. F., Kurzbach, D., Adv. Sci. 2401239 (2024).
[3] Han, W., MacEwan, S. R., Chilkoti, A. & López, G. P. Nanoscale 7, 12038–12044 (2015).

INSTITUT FÜR BIOLOGISCHE CHEMIE

FWF Der Wissenschaftsfonds.

erc European Research Council Established by the European Commission

Silaffin 1A$_1$: Insights to the Processes of Tailored Silica Precipitation

Fanny Kozak[1,2], Fabian Daus[3], Dörte Brandis[1,2], Armin Geyer[3], Christian W. F. Becker[1], Dennis Kurzbach[1]

[1]Institute of Biological Chemistry, Faculty of Chemistry, University of Vienna, Währingerstraße 38, 1090 Vienna, Austria.
[2]University of Vienna, Doctoral School of Chemistry (DoSChem), Währingerstraße 42, 1090 Vienna, Austria
[3]Faculty of Chemistry, Philipps-Universität Marburg 35032, Marburg, Germany

E-Mail: fanny.kozak@univie.ac.at,
Find us at: www.Kurzbach-group.univie.ac.at

https://doi.org/10.17952/37EPS.2024.P1299

1) Introduction

The variety and intricate beauty of diatom algaes' typical silica shells inherently demands to pose the question of how these organisms are capable of shaping silica from the intrinsically low silicic acid concentration in seawater. Further than the urge to understand **biomineralization** on a deeper level, the ability to develop **tailored silica particles** allows for new approaches to drug delivery and provides a further step in rational materials design. Peptide Silaffin 1A$_1$, isolated from marine diatom species ***Cylindrotheca fusiformis***, is one of the molecules enabling controlled silica precipitation in the presence of positively charged ions.[1] Still, the mechanism leading to controlled silica precipitation under mild conditions is scarcely understood.

2) Diatoms

Their intricate silica shells served as inspiration for designing mimetic peptides and sparked further interest in unraveling biomineralisation processes. Shown: *Mastogloia binotata* (Grun.) [4,]

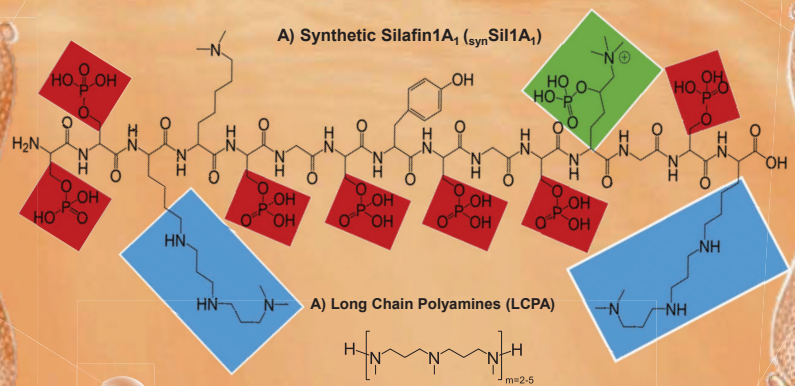

3) Synthetic Silafin1A$_1$

Synthetic Silafin1A$_1$ (synSil1A$_1$) differs from its natural scaffold by the homogeneous length of the polyamine **post-translational modifications**. Still, to yield homogeneously sized particles, adding **long-chain polyamides** LCPA) is necessary. Structures are shown in Figure A). This facilitates **supramolecular assembly** necessary for the precipitation event. Depending on the conditions chosen, influence is taken on the morphology of the precipitate [2]. This process is closely related to similar biomineralization processes, which are debated to not follow the classical scheme of nucleation. But rather to form **prenucleation species**, which are subject to growth until sizes susceptible for solid formation are formed [3] (Fig.B)

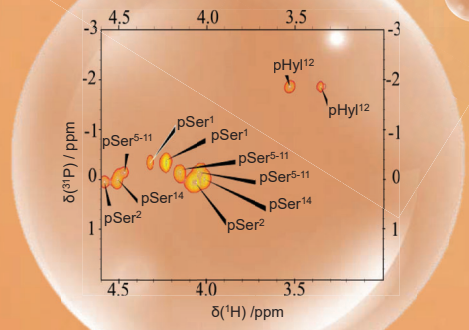

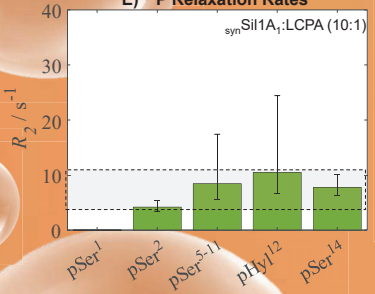

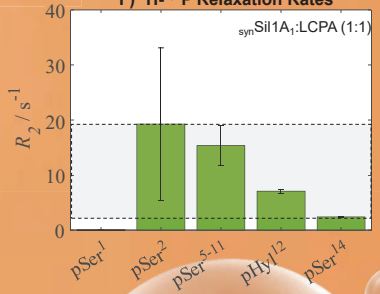

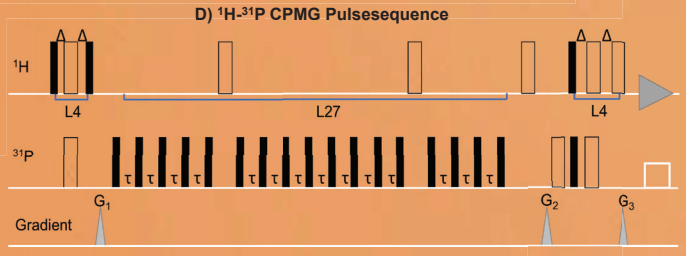

4) ^{1}H-^{31}P CPMG Pulsesequence

To allow for residue resolution, we detected the **post-translational phosphorylations** by a specifically designed pulse sequence. Therefore, we traced ^{1}H-^{31}P T_2 relaxation rates in different conditions. Pulse sequence, as well as extracted relaxation rates (E& F) and ^{1}H ^{31}P correlation spectrum, can be seen in Figure C+D. The sequence contains an additional CPMG train during the magnetization transfer as devised by Luy and Marino [5] for **enhanced sensitivity** (L4) combined with a traditional Carr-Purcell-Meiboom-Gill sequence for T_2 determination.

5) ^{1}H-^{31}P CPMG

Figure E and F show the changes depending on LCPA additive concentration. Upon adding different concentrations of LCPA, we observe an increase in R2 rates with increasing LCPA availability. This points towards decreasing mobility and indicates, combined with DOSY-data (not shown) **supramolecular assemblies** varying in structure, depending on additive presence.

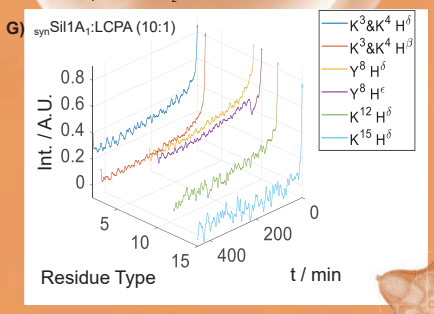

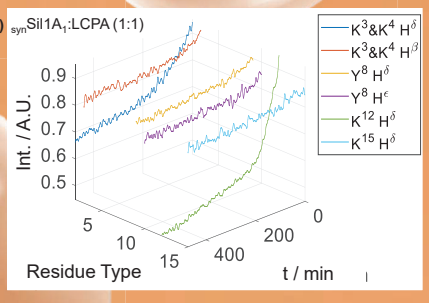

6) Real-time Precipitation Assay

The precipitation is triggered by the addition of silicic acid to the formed assemblies. To observe the influence of different LCPA concentration in the precipitation event, we traced the change in intensity by real-time 1D proton spectroscopy (Figure G and H). **Kinetic constants** were extracted by **exponential fitting** and can be seen in figure G) for synSil1A$_1$:LCPA (10:1) and in figure H) for synSil1A$_1$:LCPA (1:1).

The extracted kinetic constants are shown in the respective panels below, showing different involvement of different residues, depending on the concentration of LCPA. These differences in kinetic involvement and in the dynamic behavior of the R_2 rates, are conserved in the morphology of the precipitate. By **Scanning Electron Microscopy** (SEM), we observed smaller particle sizes for synSil1A$_1$:LCPA (10:1) (Figure I) than for synSil1A$_1$:LCPA (1:1) (shown in Figure K). Concluding, bridging further the gap between **liquid precursors** and precipitate, insights contribute to a deeper understanding of the events leading to bio(mimetic) mineralization. [6,7]

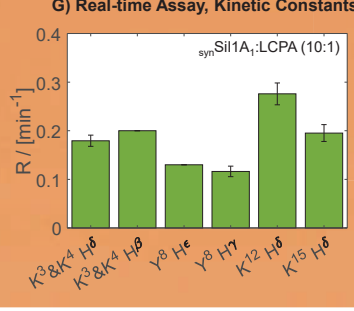

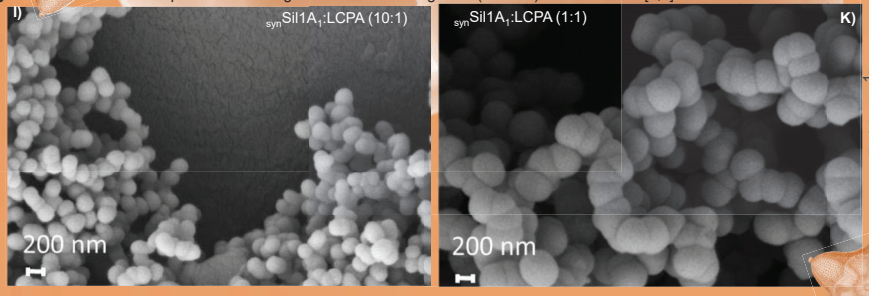

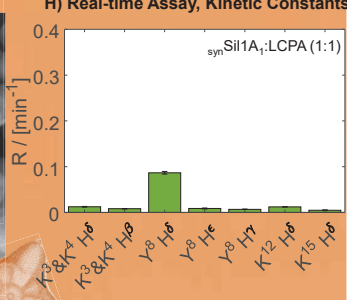

[1] Lechner CC, Becker CFW. *J Pept Sci* **2014**;20:152–8.
[2] Daus F, Xie X, Geyer A. *Org Biomol Chem* **2022**;3:3387–96.
[3] Gebauer D, Völkel A, Cölfen H. *Science* (80-) **2008**;322:1819–22.
[4] A. Falciatore, C. Bowler, *Annu. Rev. Plant Biol.* **2002**, *53*, 109–130.
[5] B. Luy, J. P. Marino, *J. Am. Chem. Soc.* **2001**, *123*, 11306–11307.
[6] F. Kozak, D. Brandis, C. Pötzl, L. M. Epasto, D. Reichinger, D. Obrist, H. Peterlik, A. Polyansky, B. Zagrovic, F. Daus, A. Geyer, C. F. Becker, D. Kurzbach, *Adv. Sci.* **2024**, 2401239.
[7] J. Strobl, F. Kozak, M. Kamalov, D. Reichinger, D. Kurzbach, C. F. Becker, *Adv. Mater.* **2023**, 35, 2207586.

INSTITUT FÜR BIOLOGISCHECHEMIE
erc European Research Council
FWF Der Wissenschaftsfonds.
universität wien

Fluorine-Specific Interactions

FREIE UNIVERSITÄT BERLIN

Rational design of polyfluorinated peptide-based materials: Self-assembly of an amphiphilic motif

Maurizio Iannuzzi[1], Suvrat Chowdhary[1], Holly Fiedler[1], Kilian Haoues[1], Dr. Boris Schade[2], Dr. Andreas F. Thünemann[3], Elisa Quaas[1] and Prof. Dr. Beate Koksch[1]

[1]Institute of Chemistry and Biochemistry, Freie Universität Berlin, Arnimallee 20, 14195, Berlin, Germany
[2]Institute of Chemistry and Biochemistry and Core Facility BioSupraMol, Freie Universität Berlin, Fabeckstraße 36a, 14195 Berlin, Germany
[3]Federal Institute for Materials Research and Testing (BAM), Unter der Eichen 87, 12205 Berlin, Germany

https://doi.org/10.17952/37EPS.2024.P1302

AIM

- Characterization of polyfluorinated **pH sensitive amphiphilic peptides for prospective receptor-specific drug delivery applications**
- Evaluation of self-assembly properties through **fluorine-specific interactions**

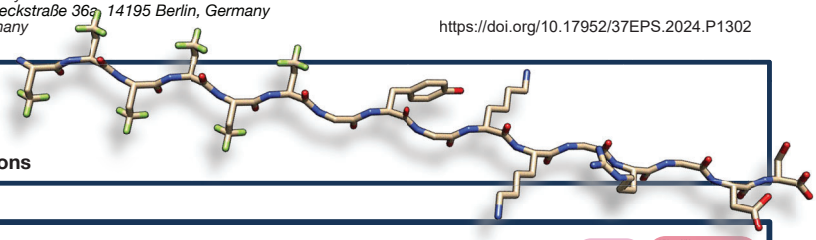

INTRODUCTION

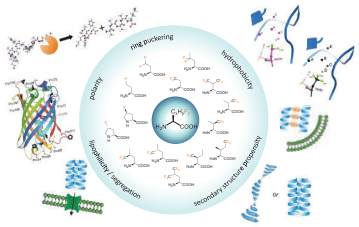

Generation of a pH sensitive amphiphilic block oligopeptide containing the bioactive function RGD and a library of derivatives varying the length of the hydrophobic core and the degree of side chain fluorination. [4] Peptide rational design enables us to obtain desired features (pH sensitivity etc.). [1] The introduction of fluorine alters a wide range of peptide properties such as secondary structure propensity, folding, thermal and metabolic stability and proteolytic resistance. [2] The **RGD function** is highly effective at promoting the attachment of numerous cell types to a plethora of materials. This small sequence is the principal integrin-binding domain present within ECM proteins such as fiobronectin, vibronectin and fibrinogen. For this reason, RGD containing peptides offer several advantages for biomaterials applications. The use of RGD compared with native ECM proteins, minimized the risk of immune reactivity or pathogen transfer[3].

Herein in this work, we present the peptide motif X6RGD and its fluoro-derivates for prospective receptor-specific drug delivery in cancer theraphy. Overall, our results demonstrate that high degree of fluorination achieved triggers a selective modification of peptide self-assembly dramatically improving the structural properties, the carrier suitability,enzimatic degradation profiles and cytotoxic features of the fluoropeptide conjugate(s).

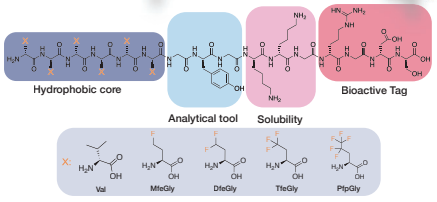

Sructure of the amphiphilic block co-polypeptide X6RGD (X6GYGKKGRGDS) and chemical structures of the (fluorinated) amino acids incorporated in the hydrophobic core.

RESULTS AND DISCUSSION

Hydrophobicity and secondary structure determination

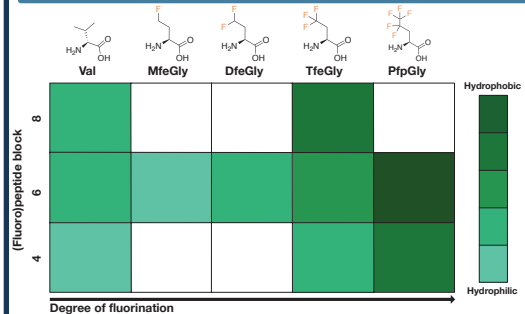

Heatmap giving an idea of the hydrophobicity of the peptides in the library. For (fluoro)peptide blocks: shorter than 6 residues no self-assembly was detected; longer than six residues the intrinsic aggregation propensity of the amphiphile made the process of sythesis and purification too complex.

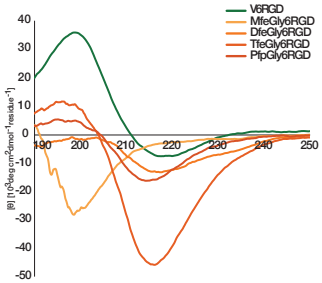

CD spectras of amphiphilic (fluoro)peptides in phosphate buffer 10 mM pH 7.4 . Enhancing the content of fluorine in the hexapeptide hydrophobic core the secondary structure transitions from a canonical β-sheet conformation to a non-canonical one where the intensity of the bands is inverted in favor of the n -> π* UV transition

Carrier suitability

In oder to determine which peptide in the library was able to self-assemble incorporating a small molecule in the hydrophobic inner core, a fluorescence-based investigation through addition of water-insoluble probe pyrene was conducted. An enhancement in fluorescence intensity indicates the encapsulation and solubilization of pyrene in the core of the molecule.

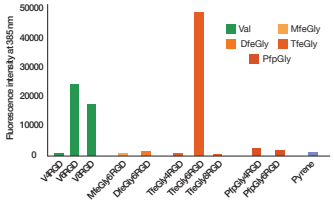

Among the whole library, V6RGD and TfeGly6RGD were the most suitable for carrier applications and therefore were subsequently tested for their drug release abilities. It's important to notice that PfpGly6RGD was also able to self-assemble but not to incorporate pyrene. A possible explanation is that due to the very strong fluorine-specific interaction that drives the assembly of this specific sequence it cannot accomodate molecules.

Morphology and self-assembly properties

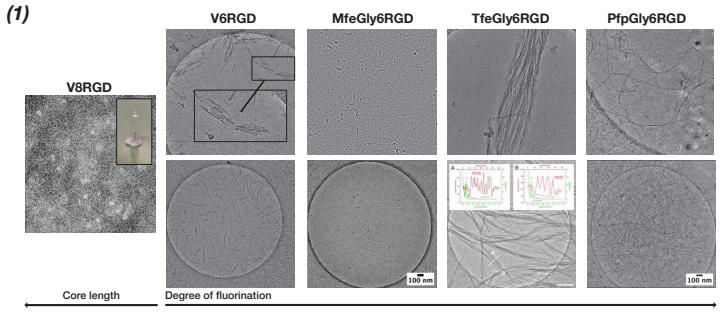

Cryo-EM micrographs (1) of amphiphilic (fluoro)peptides 1 wt% (diluted to 0.33 wt%) dissolved in phosphate buffer 10mM pH 7.4. V6RGD show platelet architectures compared to amyloid-like fibrils. Enhancing the fluorine content MfeGly6RGD forms a hint of fibrils probably at the air/water interface making difficult the capture of the image. TfeGly6RGD forms an homogeneous and highly organized elongated morphology, with a medium diameter centered around 6-7nm (zoom A,B). The single fibers tend to aggregate in bundles and twist. PfpGly6RGD forms instead a "snowflake"-like architecture consisting of shorter and more flexible fibers. On the other hand, elongating the chain of the hydrophobic core V8RGD forms a stiff hydrogel of bundled short and flexible fibrils. The rod-like architectures have been confirmed via SAXS measures revealing cilindrical structures with compact internal diameters according to the degree of fluorination. ThT fluorescence spectroscopy assay to confirm the amyloid nature of V6RGD (2). This dye display a strong fluorescence upon binding amyloid cross-β-sheet structures due to rotational immobilization. SAXS results confirmed the absence of assembled species of at least 1nm diameter at pH 5 (3) and CD spectra show a clear transition from β-sheet conformation in neutral medium (pH 7.4) to random coil in acidic (pH 5) conditions confirming the pH sensitivity of the motif.

Ezyme degradability

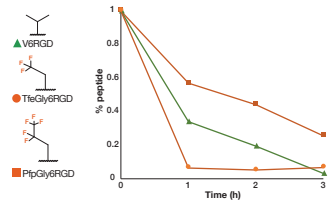

Digestion profiles of V6RGD, TfeGly6RGD, PfpGly6RGD 100uM in phosphate buffer 10 mM upon digestion with serine protease elastase 0.1 mg/mL during 3 hours of incubation time. Valine and TfeGly amino acids share similar hydrophobicity and van der vaals radius values. For this reason the substrate can accomodate the enzyme pocket resulting in an even faster digestion times in favor of the fluorinated peptide. Extending the sidechain length and fluorination content the enzyme is less selective towards the active site resulting in a much slower degradation kinetic.

Cytotoxicity

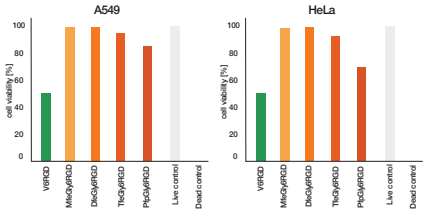

Cell viability (%) A549 and HeLa cell cultures treated with different amphiphilic oligopeptides V6RGD, MfeGly6RGD, DfeGly6RGD, TfeGly6RGD and PfpGly6RGD 1 mg/mL (circa 0.5mM) after 24h incubation. Values of viability are obtained via software automated quantification of fluorescence-imaged live/dead assays. The results are the media of two independent experiments. Countrary to any expectations, the non fluorinated V6RGD is the solely peptide to show a marked toxicity against both cell lines. The integration of even one fluorine atom is enough to bring the cell viability to safe values. For a very high fluorination degree (PfpGly6RGD - 26.6% in fluorine content of the total mw) a slighlty toxic effect is shown in the case of HeLa cells due to the intrinsic sensitivity ot the cell line.

Drug release: mechanism and in vitro experiment

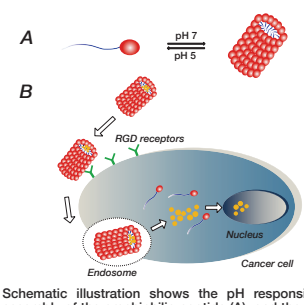

Schematic illustration shows the pH responsive self-assembly of the amphiphilic peptide (A) and the targeted release of anti-tumor drug from the self-assembled architectures of the amphiphilic peptide (B).

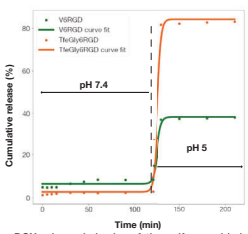

DOX release behavior of the self-assembled amphiphilic peptides V6RGD and TfeGly6RGD in neutral (pH 7.4) or acidic medium (pH 5.0) at physiological temperature (37°C)

Outlook

MD simulations to determine the impact of fluorine-specific interactions on the self-assembly properties of the peptide motif.

References

[1] J. Liang, W.L. Wu, X.D. Xu, R.X. Zhuo, X.Z. Zhang Colloids and Surfaces B: Biointerfaces, 2014. 114: p. 398-403
[2] A. A. Berger, J.S. Völler, N. Budisa, B. Koksch, Acc. Chem. Res. 2017, 50, 2093–2103.
[3] S.L. Bellis, Biomaterials, 2011. 32(18): p. 4205-4210.
[4] U. I. M. Gerling, M. Salwiczek, C. D. Cadicamo, H. Erdbrink, C. Czekelius, S. L. Grage, P. Wadhwani, A. S. Ulrich, M. Behrends G. Haufe, B. Koksch, Chem. Sci. 2014, 5, 819–830.
[5] Y. Chen, Y. Hua, W. Zhang, C. Tang, Y. Wang, Y. Zhang and F. Qiu, Int. J. Nanomed,. 2018, 13, 2477–2489.
[6] A. Bertolani, L. Pirrie, L. Stefan, N. Houbenov, J. S. Haataja, L. Catalano, G. Terraneo, G. Giancane, L. Valli, R. Milani, O. Ikkala, G. Resnati and P. Metrangolo, Nat. Commun,.2015, 6, 7574.

Let's do the Twist - Chiral Information Transfer in Supramolecular Peptide Complexes

Danielle Aria Liebnitz, P.Vosbein-Christensen and A. R. Thomson

University of Glasgow, School of Chemistry, Joseph Black Building, University Avenue, Glasgow, G12 8QQ, United Kingdom
Email: 2261781L@student.ac.uk

https://doi.org/10.17952/37EPS.2024.P1303

INTRODUCTION

Chirality is inherent in nature from molecular to macroscales.[1,2]
How this information is transferred is still poorly understood.[3] A model system using the well documented inbuilt chirality of peptides is being used to investigate this phenomena.



AMINO ACIDS
L-Configuration in nature, ***left-handed***.
Point Chiral.



PRIMARY STRUCTURE
Easily synthesised by SPPS. Chirality retained from the amino acids.



SECONDARY STRUCTURE
Helices comprised of L-AA's are ***right-handed***.[4,5]
Axially Chiral



SUPRA-SECONDARY STRUCTURE
Coiled-Coils display supercoiling with a ***left-handed*** helical sense.[6]

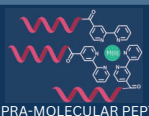

SUPRA-MOLECULAR PEPTIDE ASSEMBLY
Will there be supramolecular chirality?

PEPTIDE SEQUENCES

All peptides are designed **3-heptad homotrimeric coiled-coils** and have been synthesised by microwave assisted **SPPS** and further functionalised on resin with a bipyridine (bpy, **X**) group at the N-terminus. All sequences have been tabulated below, except **1b** all other **b** control sequences have been omitted.

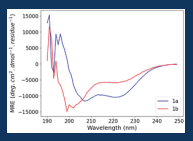

bpy at the N-term stabilises the secondary structure

1a	X-GQ**EIAAIKK**EIAAIKKEIAAIKYG-NH2 *d-efgabcdef*	**5a**	X-αQ**EIAAIKK**EIAAIKKEIAAIKYG-NH2 *d-efgabcdef*	**9a**	X-**IAAIKKE**IAAIKKEIAAIKKEYG-NH2 *g-abcdefg*
1b	Ac-GQ**EIAAIKK**EIAAIKKEIAAIKYG-NH2 *d-efgabcdef*	**6a**	X-PQ**EIAAIKK**EIAAIKKEIAAIKYG-NH2 *d-efgabcdef*	**10a**	X-**AAIKKEI**AAIKKEIAAIKKEIYG-NH2 *a-bcdefga*
2a	X-AQ**EIAAIKK**EIAAIKKEIAAIKYG-NH2 *d-efgabcdef*	**7a**	X-Q**EIAAIKK**EIAAIKKEIAAIKYG-NH2 *e-fgabcdef*	**11a**	X-**AIKKEIA**AIKKEIAAIKKEIAYG-NH2 *b-cdefgab*
3a	X-GG**EIAAIKK**EIAAIKKEIAAIKYG-NH2 *d-efgabcdef*	**8a**	X-**EIAAIKK**EIAAIKKEIAAIKKYG-NH2 *f-gabcdef*	**12a**	X-**IKKEIAA**IKKEIAAIKKEIAAYG-NH2 *c-defgabc*
4a	X-PEG-**EIAAIKK**EIAAIKKEIAAIKYG-NH2 *gabcdef*			**13a**	X-**QKEIAAI**KKEIAAIKKEIAAIYG-NH2 *d-efgabcd*

EFFECT OF METAL AND COUNTERION ON THE FORMATION OF CHIRAL PEPTIDE-BPY COMPLEXES

To investigate the relationship between the chirality of the secondary structure and the supramolecular bpy-peptide complex, peptide **1a** was titrated against a series of 1st row TMs.

EFFECT OF ACHIRAL LINKER ON THE FORMATION OF CHIRAL PEPTIDE-BPY COMPLEXES

To investigate the limits of the chiral effect of the peptide on the bpy-peptide complex peptides **1a-6a** with differing lengths of achiral spacer were titrated against **Zn(II)**.

EFFECT OF N-TERMINAL REGISTER POSITION ON THE FORMATION OF CHIRAL PEPTIDE-BPY COMPLEXES

To investigate the spacial requirements for the formation of the chiral bpy-peptide complex peptides **7a-13a** with systematically varied N-terminal register position were titrated against **Zn(II)**.

1a CD Titration with Co(II)

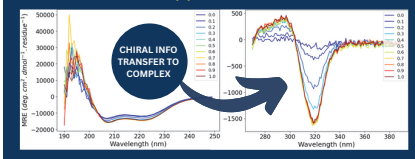

4a CD Titration with Zn(II)

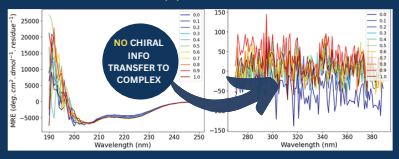

7a and 13a CD Titrations with Zn(II)

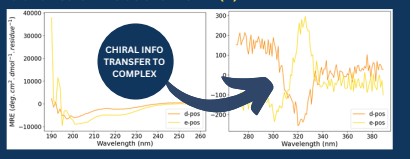

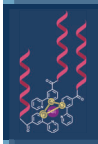

For helix to form the complex must be ***fac***

Signal at 222 nm intact except Co(II) and Cu(II) Co(II) **stabilised** Cu(II) **destabilised**

Cu(II) octahedral complexes are distorted so break down **after 0.3 eq**

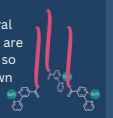

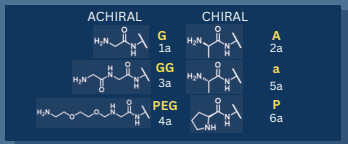



Helical wheel representation of a homotrimer

a, d, e **bpy pointed inward**
b, c, f, g **bpy pointed outward**



Superimposed vectors indicating bpy directionality

Octahedral - 320 nm signal increases rapidly until 0.3 eq (Zn(II), Co(II) Cu(II) and Ni(II))

Favours Right-handed[7,8] - Signal has a negative Cotton-Effect

Signal at 320 nm - G > **A** > GG > a > P > PEG

Signal at 222 nm - **A** > G > GG > a > P > PEG

Only d and e positions formed bpy-peptide complex with chiral preference.

d position - ***right-handed*** *e* position - ***left-handed***

Plots of the CD signals at 222 nm and 320 nm for all peptides allows the relationship between the bpy-complex and the helicity of the peptide to be observed.

DIFFERENT TMs

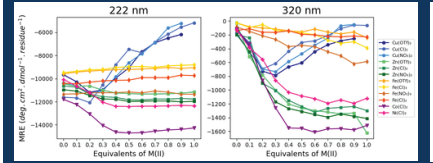

DIFFERENT LINKERS

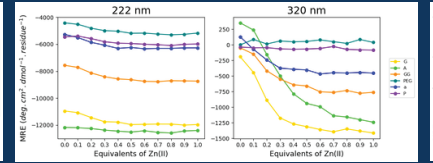

DIFFERENT REGISTER POSITION

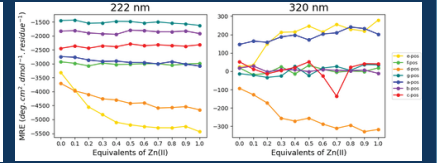

CONCLUSION
Zn(II), Ni(II) or Co(II) appear to have the strongest preferences for forming octahedral complexes.

CONCLUSION
Distance from chiral centre should be no more than 7 atoms.

CONCLUSION
d or *e* position preferred for attachment BUT will give preference for opposite handedness.

CHIRAL PREFERENCE CAN BE INDUCED

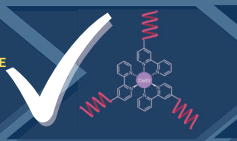

FUTURE WORK

NMR studies to determine ratios of isomers
Titration with a 2nd row TM

REFERENCES

1. A. H. G. David and J.F. Stoddart, *Is. J. Chem.*, 2021, **61**, 608-621
2. J. Dong, Y.Liu and Y.Cui, *Accounts of Chem. Res.*, 2021, **54**, 194-206
3. S. M. Morrow, A. J. Bissette and S. P. Fletcher, *Nat. Nanotechnol.* 2017, **12**, 410-419
4. M. Liu, L. Zhang and T. Wang, *Chem. Rev.*, 2015, **115**, 7304-7397
5. N. E. Shepherd, H. N. Hoang, G. Abbenante and D. P. Fairlie, *J. Am. Chem. Soc.*, 2009, **131**, 15877-15886.
6. A. N. Lupas, J. Bassler and S. Dunin-Horkawicz, *Subcell. Biochem.*, 2017, **82**, 96-129
7. Y. Kobayashi *et al*, *Inorg. Chem.* , 2018, **5**, 5475-5485
8. N. Ousaka, Y. Takeyama, H. Iida, E. Yashima, *Nat. Chem.* 2011, **3**, 856-861

ACKNOWLEDGEMENTS

I would like to thank the Thomson Group, our collaborators in the Forgan Group, the Chemical Biology Laboratory, Captain, Skipper and Matthew.

LEVERHULME TRUST

https://doi.org/10.17952/37EPS.2024.P1306

Tailoring the self-assembly of cyclic peptide scaffolds for prostate cancer imaging

Fátima Santillán,[1] Carlie Charron,[2] Betty C. Galarreta,[3] Leonard G. Luyt[4]

[1] Department of Chemistry, University of Western Ontario, 1151 Richmond St, London, Ontario N6A 5B7, Canada
[2] Department of Chemistry, Dalhousie University, 6274 Coburg Road, Halifax, Nova Scotia B3H 4R2, Canada
[3] Departamento Académico de Ciencias - Sección Química, Pontificia Universidad Católica del Perú, Av. Universitaria 1801, San Miguel, Lima 15088, Perú
[4] Departments of Chemistry and Departments of Medical Imaging and Oncology, University of Western Ontario, University of Western Ontario, Centre; 1151 Richmond St, London, ON, N6A 3K7, Canada. Verspeeten Family Cancer Centre, London Health Sciences, 800 Commissioners Rd. E., London, ON, N6A 5W9, Canada.

Introduction

Advancements in the design of peptide self-assemblies have opened the potential for nanostructuresto be used in cancer diagnosis and imaging. The use of peptide nanomaterials as imaging probes represents a promising alternative owing to its tailorable design that provides specificity towards molecular targets.[1-4] In the context of cancer diagnostics, optical imaging holds immense potential, where precise targeting of biomarkers, like the prostate-specific membrane antigen (PSMA), is crucial for cancer detection.

In our exploration of optical imaging agents for cancer, we focused on the design and co-assembly of cyclic peptide templates that generate nanotubes. These nanotubes were fabricated through the pH-triggered self-assembly of D/L-alternating cyclic octapeptides.[1] The main sequence is derived from cyclo-(L-Leu-Lys-D-Leu-Tyr)$_2$. The surface of the peptide was modified to enhance its functionality, leading to three additional peptides that were critical for building the nanoprobe. The first modification involves the attachment of polymeric chains (m-PEG) to reduce nanotube aggregation. The second peptide featured the conjugation of a fluorescent dye as a signaling component. Lastly, our targeting peptide incorporated a modified PSMA-targeting ligand for cancer imaging. All the peptides were purified by reverse-phase high-performance liquid chromatography (LC-MS) and analyzed using high-resolution mass spectrometry.

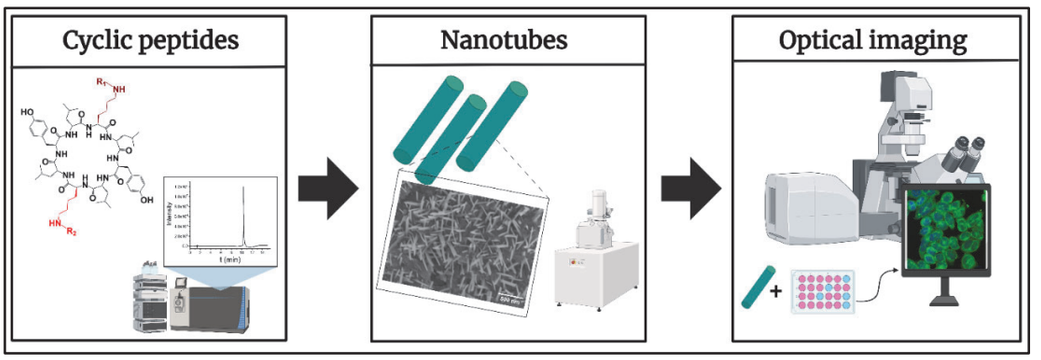

Fig. 1 General schematic representation of the research conducted

Editar con WPS Office

Results and Discussion

The self-assembly behavior of all the cyclic peptides and the co-assembled systems was assessed using field emission scanning electron microscopy (FESEM). FESEM imaging revealed diameters ranging from 13 to 30 nm and lengths of 100-300 nm for most peptide systems. Notably, our targeting nanotubes, formed through the co-assembly of all four peptides, exhibited an average diameter of 28 nm and length values of 100-400 nm (Figure 2b). Circular dichroism spectroscopy revealed the presence of β-sheet-like assemblies, which were stable under room and physiological temperature conditions (Figure 2c).

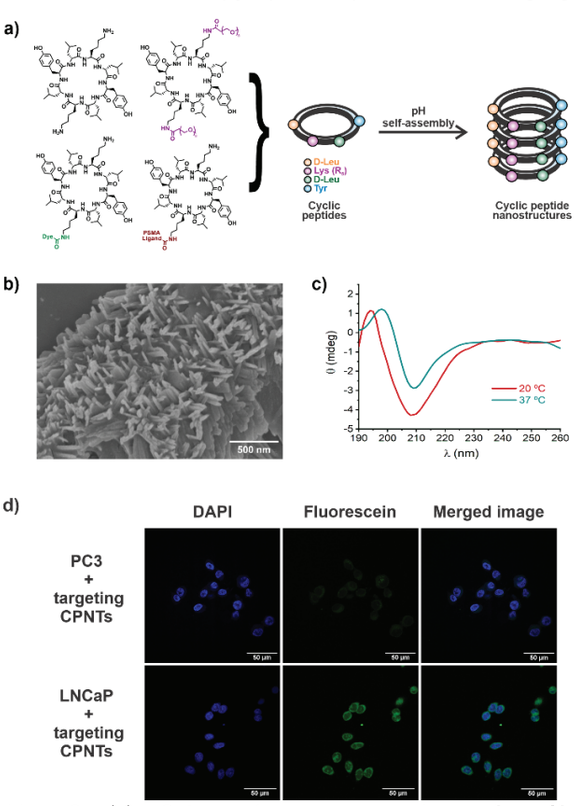

Fig. 2 (a) Schematic representation of self-assembly. (b) FESEM images of targeting nanotubes. (c) CD spectra at room and physiological temperatures. (d) Confocal fluorescence microscopy images of PC3 and LNCaP cells with targeting nanotubes after incubation for 2 h at 37 °C.

Confocal fluorescence microscopy evaluated the targeting capabilities of the co-assembled cyclic peptides nanotubes (Figure 2d). To this end, two cancer cell lines, PC3 (PSMA-low) and LNCaP (PSMA-high) were selected. Confocal fluorescence images of LNCaP cells, treated with our targeting nanotubes, exhibited a significantly heightened fluorescence signal on cell membranes compared to non-targeting nanotubes. This confirms the interaction of our developed nanoprobes with PSMA overexpressed in LNCaP cells. Further analysis via Z-stacking indicated partial internalization of the targeting nanotubes, suggesting a potential endocytic mechanism. Confocal fluorescence images of PC3 cells, treated with our targeting nanotubes, exhibited low fluorescence signal as was expected due to the reduced presence of PSMA in this cell line.

In conclusion, our findings underscore the enhanced target specificity that can be achieved by engineering peptide nanotubes with tailorable functionalities, expanding the use of co-assembled peptide nanoprobes to the realm of molecular imaging and offering possible pathways towards clinical translation.

Editar con WPS Office

Acknowledgments

This research was supported by the Natural Sciences and Engineering Research Council of Canada (NSERC) and the Collaborative Program in Molecular Imaging (Western University). The authors would like to thanks Surface Science Western for the training and access to field emission scanning electron microscopy.

References

1. Insua, I., Montenegro, J. *J. Am. Chem. Soc.* **142**, 300-307 (2020). https://doi.org/10.1021/jacs.9b10582
2. A. Méndez-Ardoy, A. Bayón-Fernández, Z. Yu, C. Abell, J. R. Granja, J. Montenegro, *Angewandte Chemie* **132,** 6969 (2020). https://doi.org/10.1002/anie202000103
3. S. Díaz, I. Insua, G. Bhak, J. Montenegro, *Chem. Eur. J.* **26,** 14765 (2020). https://doi.org/10.1002/chem.202003265
4. Panigrahi, B., Singh, R.K., Suryakant, U., Mishra, S., Potnis, A.A., Jena, A.B., Kerry, R.G., Rajaram, H., Ghosh, S.K., Mandal, D. *Eur. J. Pharm. Sci.* **171**, 106125 (2022). https://doi.org/10.1016/j.ejps.2022.106125

Editar con WPS Office

Computational/Experimental Symbiosis in the Design of Supramolecular Peptide Architectures

Ivan R. Sasselli,[1,2] Laura Perez-Chirinos,[2] Aitziber L. Cortajarena,[2,3] & Zaida Alvarez.[4]

i.sasselli@csic.es

[1]**Materials Physics Center (MPC-CFM)**, CSIC-UPV/EHU, San Sebastian, Spain. [2]**CIC biomaGUNE**, Basque Research and Technology Alliance (BRTA), San Sebastian, Spain. [3]**Ikerbasque**, Basque Foundation for Science, Bilbao, Spain. [4]**Institute for Bioengineering of Catalonia (IBEC)**, Barcelona, Spain.

https://doi.org/10.17952/37EPS.2024.P1307

Supramolecular Peptide Assemblers (SPAs)

- Short peptides able to self-assemble into fibres[1]
- Form networks with excellent performance as artificial extracellular matrices (ECMs)[2]

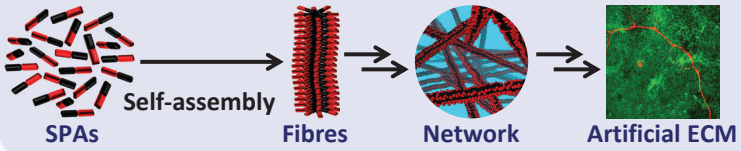

Design & Understanding Challenges

- Experimental characterization from proteins
  → challenging interpretation

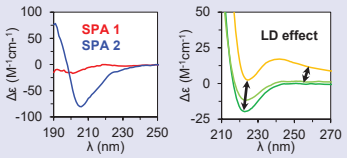

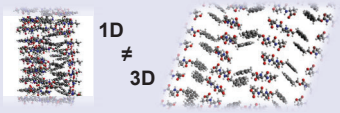

- Lack of representative crystal structures to benchmark experimental and computational methods

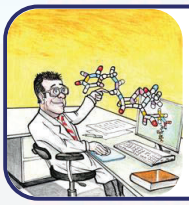

We propose: Computational/Experimental Symbiosis

- Computational work:
  - Improves experimental data interpretation
  - Gives intermolecular detail

Side-by-side implementation
Continuous feedback
Iterative process

- Experimental work:
  - Starting and final point
  - Determines model set-up
  - Validates computational data



Amyloid Like Peptides (ALPs)

- $(FE)_n$ repeats:
  - Hydrophilic surface
  - Hydrophobic core

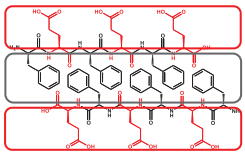

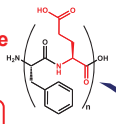

- Crystallinity prediction (effect of *n*)
- Converges → *n* = 6

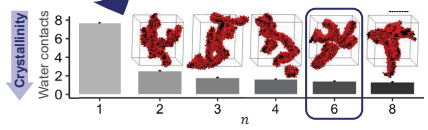

Short Branched Peptides (SBPs) ► nPods

- Branching in peptides → hydrogen bonding patterns
- Number (*n*) of *Pods* determines order/cohesion

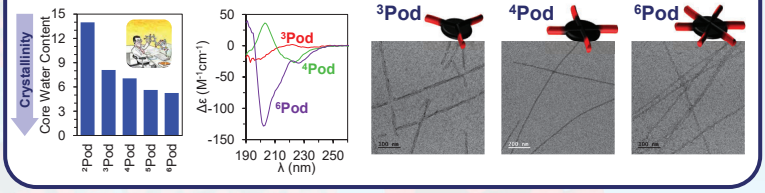

Charge Density Effect in Bioactivity

- Assess the effect of charge density on bioactivity
- ALP Library of Charges -3 to -9/peptide

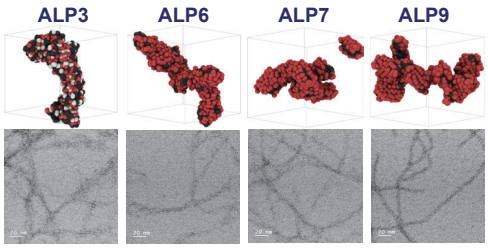

Fibres with strong intermolecular order

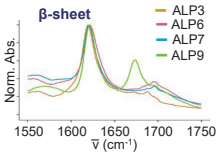

- Neuronal differentiation from Neuronal Progenitor Cells (NPCs)

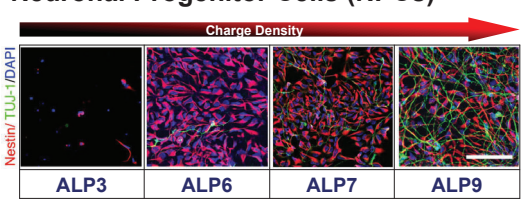

TUJ1= Neurons

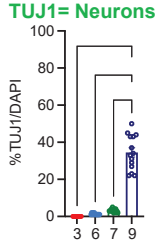

Protein-ALP Hybrid Assemblies

- Tetratricopeptide Repeat (TPR) protein[3] + ALPs
- 1 *vs* 2 ALPs → Controls material dimensionality

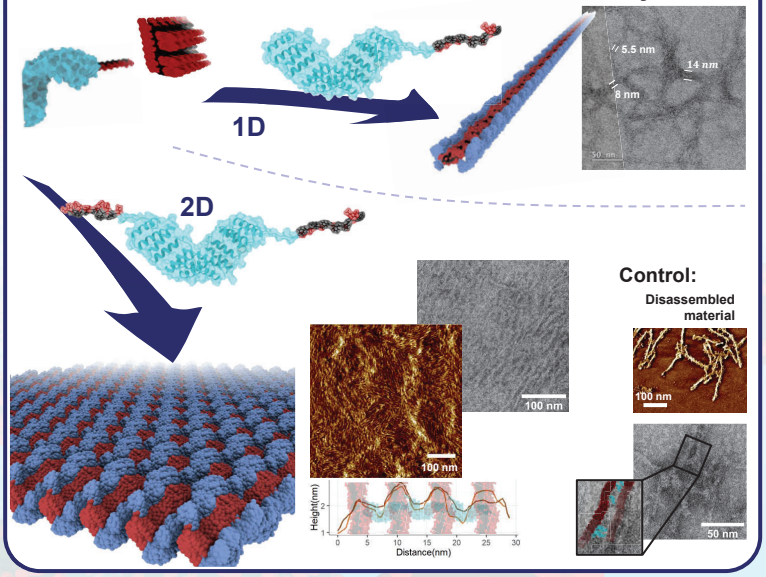

Conclusions

- nPod: new parameter to control intermolecular cohesion.
- ALP libraries: key role of charge density in the bioactivity of SPAs.
- Hybrid assemblies: control dimensionality and nanoscale morphology.
- ***The Computational/Experimental Symbiosis is a powerful approach to design materials with novel features and understand their function.***

References

1. Sasselli, Syrgiannis. *Eur. J. Org. Chem.* **2020**, *2020, 5305.*
2. Alvarez, Kolberg-Edelbrock, Sasselli, Stupp *et al. Science*, **2021**, *374*, 848.
3. Cortajarena, Sasselli, *et al. Acc. Chem. Res.* **2021**, *54*, 3836.

Acknowledgements

- Ramon y Cajal (RYC2021-033294-I)
- Gipuzkoa Fellow (2019-FELL-000017-01)
- Maria de Maeztu Units of Excellence (MDM-2017-0720)

https://doi.org/10.17952/37EPS.2024.P1310

Ultrasound-assisted formation of therapeutic peptide microcapsules

G. Rossi,[1] E. Belforte,[1] F, Cavalieri,[1] H. G. Peres,[2] A. Aguilera,[2] and M. Venanzi[1]

[1]Tor Vergata University of Rome, Rome, Italy; [2]Center for Genetic Engineering and Biotechnology, Havana, Cuba

CIGB-500: A therapeutic formulation

Researchers at the Centre of Genetic Engineering and Biotechnology (CIGB) of Havana (Cuba) have developed an original approach for the treatment of cardiovascular diseases based on the use of the growth hormone releasing hexapeptide (GHRP-6), a peptide targeting specifically GHSR-1a and CD36, two receptors involved in cardiovascular diseases.

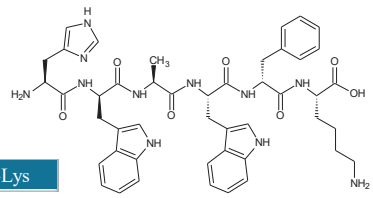

His-(**D-Trp**)-Ala-**Trp**-(D-Phe)-Lys

CIGB treatment of Acute Myocardial Infarction

- reduce necrosis
- reduce heart failure
- reduce systemic toxic complications

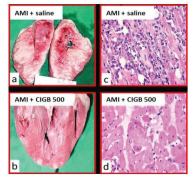

CIGB-500 aggregation in water

Pyrene assay

The CAC is the critical concentration at which peptide supramolecular structures, capable to embed the pyrene fluorophores in a hydrophobic environment, form.

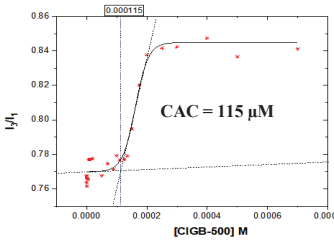

Oil/water CIGB-500 microcapsules

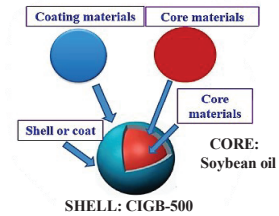

Using ultrasound-induced oil-in-water emulsification, CIGB-500 formed stable microcapsules characterized by a peptide shell embedding an oily inner phase.



Sonication

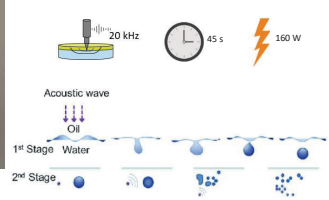



Spectroscopic and morphological characterization of CIGB-500 microcapsules

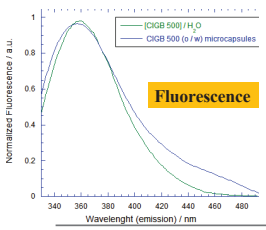

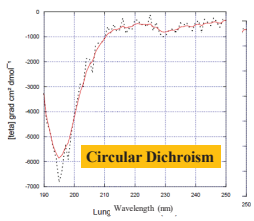

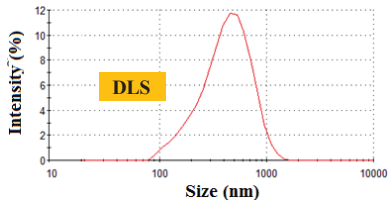

Optical Microscopy

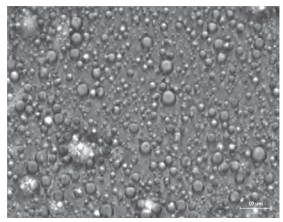

Fluorescence Anisotropy

CIGB-500 (µM)	r	V_H (nm³)
40	0.028 ± 0.007	1.4±0.08
1000	0.096 ± 0.001	6.3 ± 0.2
microcapsules	0.127± 0.002	

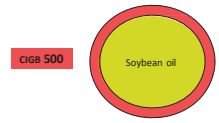

CIGB-500 (Rhodamine B)

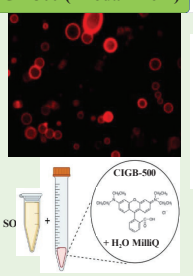

SO-Nile Red

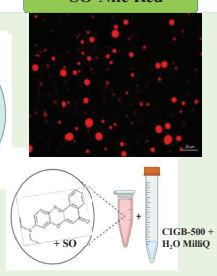

CIGB-500 (Rhodamine B)

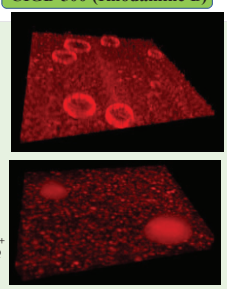

Confocal Microscopy

CIGB-500 (Rhodamine B)

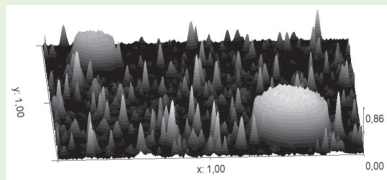

CIGB-500(FITC)

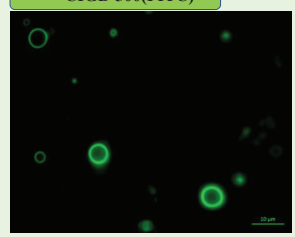

Temperature stability of CIGB-500 microcapsules

Rayleigh Light Scattering

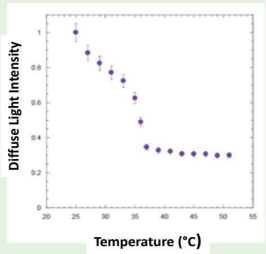

Optical microscopy

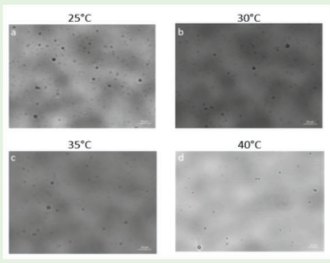

DLS

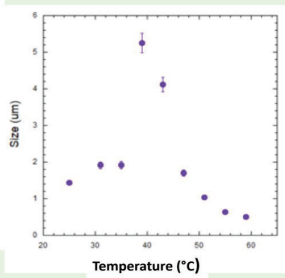

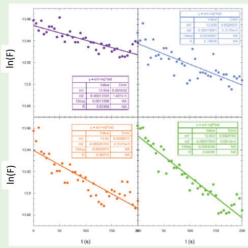

Temperature/K	$k_d(s^{-1})$ [x10⁻⁴]
303	1.3
307	1.9
311	2.6
315	3.7

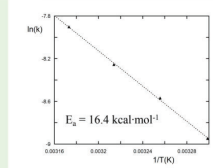

The temperature stability of CIGB-500 microcapsules was investigated by Rayleigh and Differential Light Scattering techniques, measuring a critical dissolution temperature at around 40°C.

Encapsulation of "1 primary wound dressing" (OPWD)

OPWD inclusion

"100% natural" spray used to treat diverse types of wounds.



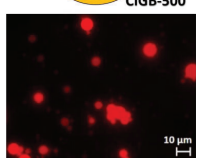

OPWD release by Temperature

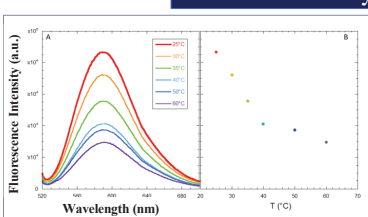

OPWD was released with the temperature, as measured by the NLR fluorescence intensity decrease.

Temperature/K	$k_d(s^{-1})$ [x10⁻³]
303	1.3
307	1.7
311	1.9
315	2.4

E_a = 9.3 kcal·mol⁻¹

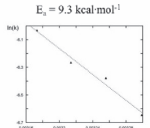

OPWD release by pH

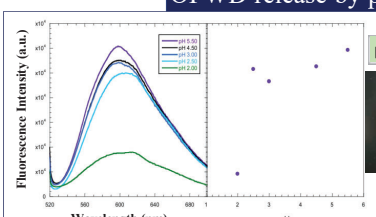

pH=5.5 pH=2.0

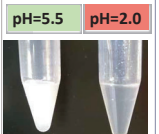

OPWD was released at pH=2, as measured by the NLR fluorescence intensity decrease and the decrease of scattered light.

Tailoring Peptide Self-Assembly with Electron Donor Functionalization Towards Formation of Vesicles, Helical Ribbons, and Fibers

Laura Brüchle, Thomas Heim, Milan Kivala,* Franziska Thomas*

Institute of Organic Chemistry, Heidelberg University, Im Neuenheimer Feld 270, 69120 Heidelberg

* *E-Mail: franziska.thomas@oci.uni-heidelberg.de; milan.kivala@oci.uni-heidelberg.de*

UNIVERSITÄT HEIDELBERG ZUKUNFT SEIT 1386

https://doi.org/10.17952/37EPS.2024.P1311

Studying the self-assembly of peptides is of high interest for research and medical applications. Different short peptides have already shown self-assembly into distinct morphologies ranging from ribbons to vesicles. Here, we present a set of tripeptides, functionalized with nitrogen-containing electron donors, introducing tunable (opto-)electronic properties. Our tripeptides show self-assembly in aqueous solution and were characterized by fluorescence spectroscopy, cyclic voltammetry, dynamic light scattering, fluorescence and electron microscopy. Additionally, one of the presented tripeptides shows promise for cargo transportation in aqueous media as irradiation with UV-light led to decomposition of the formed vesicles.

Synthesis

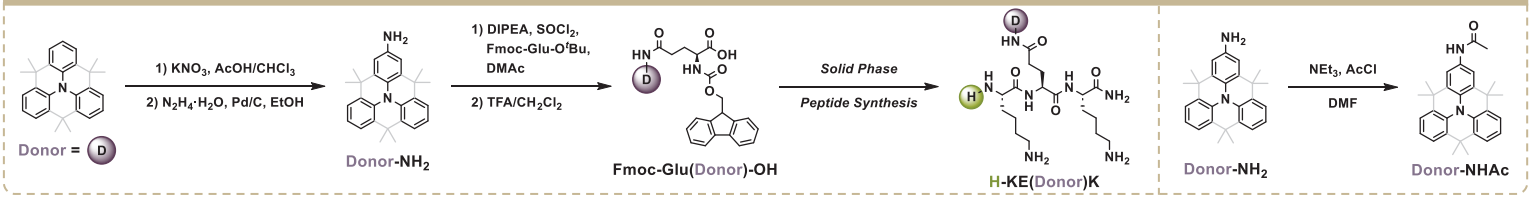

Self-Assembly

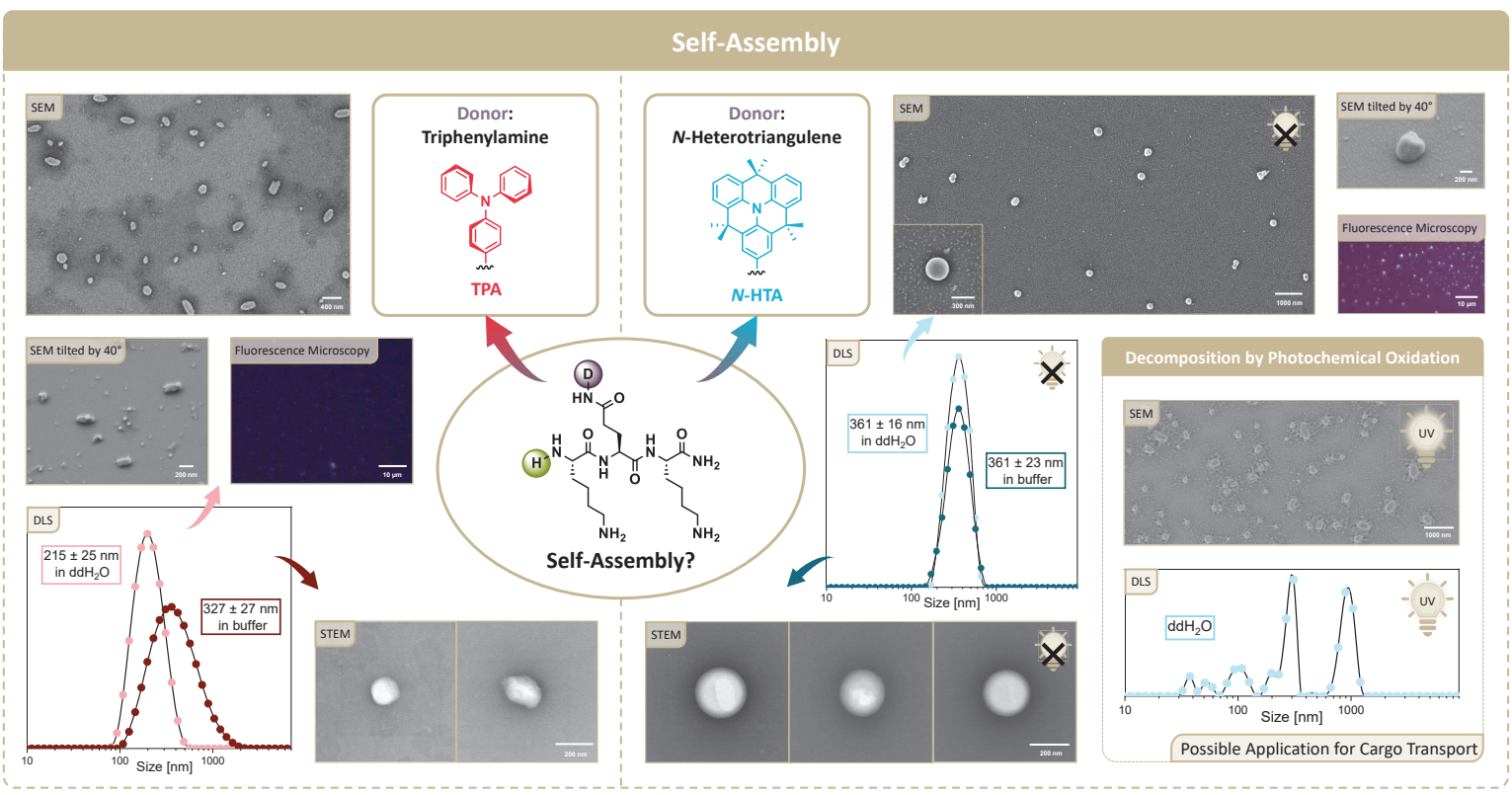

Cyclic Voltammetry

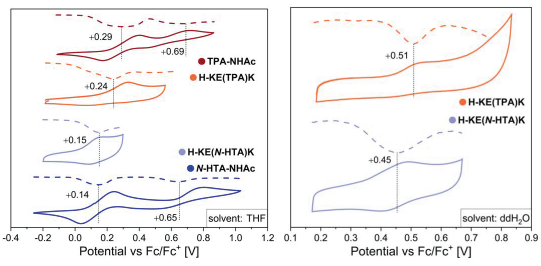

X-Ray Analysis

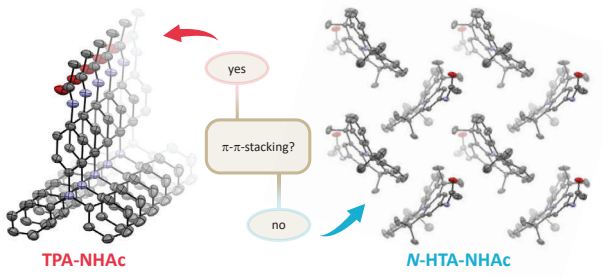

Sneak Peak

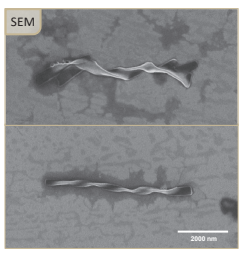

References

[1] *Bioactive Materials* **2022**, *11*, 268.
[2] *Chem. Commun.* **2012**, *48*, 8481.
[3] *Langmuir* **2019**, *35*, 12460.
[4] *Chem. Rec.* **2015**, *15*, 1119.

Acknowledgements

We want to thank Prof. Rasmus Schröder, Dr. Irene Wacker and Ronald Curticean for the support with SEM imaging.

Contact

laura.bruechle@oci.uni-heidelberg.de
+49 6221 54 4379
Laura Brüchle

ORGANISCH-CHEMISCHES INSTITUT OCI

Federal Ministry of Education and Research

Baden-Württemberg MINISTRY OF SCIENCE, RESEARCH AND ARTS

FLAGSHIP INITIATIVE ENGINEERING MOLECULAR SYSTEMS

UNIVERSITÄT HEIDELBERG ZUKUNFT SEIT 1386

Crosslink reaction of α-/ω-substituted diacrylate polyethylene-glycol in Fmoc-FF hydrogel matrices

Carlo Diaferia[1], Paolo Pellegrino[2], Giancarlo Morelli[1], Rosaria Rinaldi[2], Antonella Accardo[1]

[1]University of Naples «Federico II», Department of Pharmacy, Via de Amicis 95, Naples. [2] Institute for Microelectronics and Microsystems (IMM), CNR, 73100 Lecce, Italy.

email: carlo.diaferia@unina.it

TOPIC: **Peptide materials**

https://doi.org/10.17952/37EPS.2024.P1312

Abstract: Peptides can form **supramolecular gels,** as N$^{\alpha}$-9-fluorenylmethoxycarbonyl protected diphenylalanine (**Fmoc-FF).** [1] The Fmoc-FF hydrogel functional properties are modified incorporating additional entity. Multicomponent matrices of Fmoc-FF and diacrylate **α-/ω-substituted polyethylene glycol derivatives (PEGDAs)** were formulated, by using **two different PEGDA** molecular weight (575 and 250 Da for **PEGDA1** and **PEGDA2**, respectively) at **different molar peptide/polymer ratio (1/1, 1/2, 1/5 ,1/10).**[2] The acrylate moieties were **cross-linked by UV irradiation at 365 nm**, thus production no-covalent/covalent interpenetrated networks (IPNs). The properties of final materials (in terms of permeability, rheological response, and topography) were modulated by tuning the polymerization time. [3]

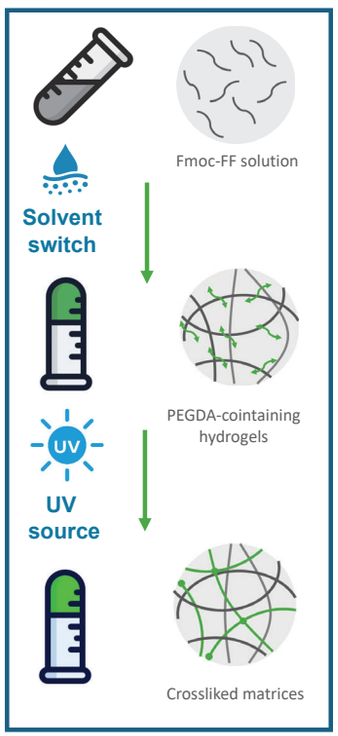

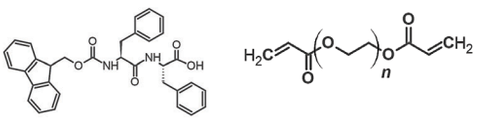

Chemical structures of hydrogel components

Hydrogel components: Fmoc-FF and α-/ω-substituted polyethylene glycol derivatives (PEGDAs, Mw 575 and 250 Da for PEGDA1 and PEGDA2, respectively). Different molar peptide/polymer ratio (1/1, 1/2, 1/5 ,1/10) were tested Fmoc-FF was dissolved in DMSO at 100 mg/mL. PEGDA solution were obtained in water.

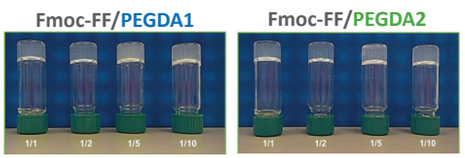

Inverted test tube for mixed matrices

Multicomponent hydrogel formulation: For all the tested experimental conditions, self-supporting hydrogels are formed, using a **solvent switch** approach (dilution of Fmoc-FF stock with PEGDA solutions in water at 0.5 wt%). Both PEGDAs are quantitatively included (no syneresis effects). Gelation kinetics are not affected

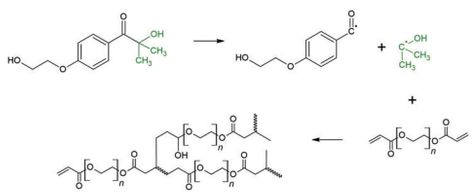

α-HP supported PEGDA crosslink reaction

Crosslinking PEGDAs: acrylic groups can cross-link under **UV–vis irradiation (365 nm)** *via* a radical mechanism favored by a photoinducer (α-HP, Irgacure 2959). Two **irradiation times (5 and 15 min)** were tested. The cross-linked matrices have been characterized from different points of view to emphasize the emergent properties of the proposed materials, expanding their possible applicative scenario.

Fmoc-FF/PEGDA1

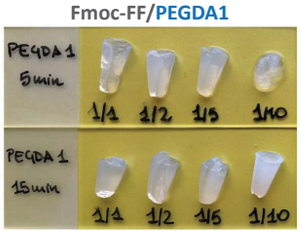

Fmoc-FF/PEGDA2

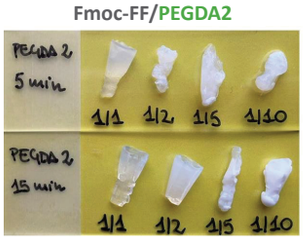

Macroscopical PEGDAs gels. A progressive transparency decreases with the increase in time exposure is detected (UV–vis). This evidence was correlated with the formation of light scattering supramolecular elements mainly resulting from the density of acrylic mesh.

FT-IR analysis

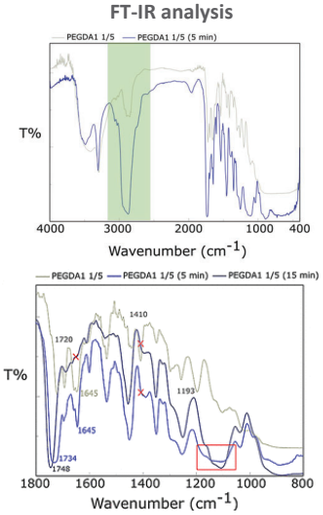

FT-IR analysis. Increase band at 2920–2880 cm^{-1} (green region C–H stretching); modification of 1410 cm^{-1} band (deformation C=CH$_2$) and the decrease in the intensity of acylic C=O signal (1193 cm^{-1}). Broad band (1190–1050 cm^{-1}) of primary alcohols post-reaction.

Rheological characterization: Extrapolated storage modulus (G') and loss modulus (G'') from oscillation strain sweeps, tan δ (G''/G'), breakage point of strain (ωc), and frequency (νc).

		5min					15 min				
	Ratio	G'(Pa)	G''(Pa)	tanδ	ωc (%)	νc (Hz)	G'(Pa)	G''(Pa)	tanδ	ωc (%)	νc (Hz)
PEGDA1	1/1	3224	560	0.173	16	32	3600	620	0.172	20	35
	1/2	2172	334	0.154	17	35	2460	380	0.154	28	35
	1/5	1660	225	0.135	9	39	1760	236	0.134	11	43
	1/10	960	114	0.118	26	49	1476	179	0.121	30	60
PEGDA2	1/1	5380	782	0.145	16	-	5941	855	0.144	27	-
	1/2	4590	605	0.132	18	-	8321	812	0.117	31	-
	1/5	2160	263	0.122	14	-	5590	1255	0.224	43	-
	1/10	4060	45	0.100	38	-	9390	1428	0.152	54	-

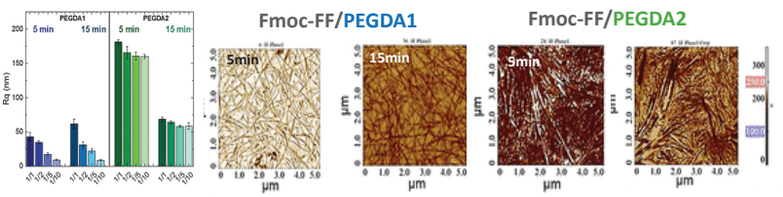

AFM analysis. Rq roughness histograms (left). AFM semicontact phase-contrast mode images. The number of fibers decreases with the increase of PEGDA1 ratio, independently from the UV exposure time. A similar trend was found in the PEGDA2 samples. However, in all the PEGDA2 samples, an increase in the fiber number, as well as in the fiber dimension, was detected. OrientationJ tool analysis showed also a preferential orientation for all the PEGDA2-cointaining gels (θ~0 deg). **Topography is influenced by PEGDA molecular weight and UV-exposure.**

References: [1] Diaferia C. *et al.* J. Mater. Chem. B, 2019,7, 5142-5155. [2] Rosa E. *et al* Gels, 2022, 8(12), 831. [3] Rosa E. *et al* ACS Appl. Polym. Mater. 2024, 6, 12, 7197–7208

Innovative Strategies for Sustainable Materials: Developing Protein-Based Bioplastics from Rapeseed By-Products for a Circular Economy

Sara Aquilia,[1,2,3] Michele Pinna,[3] Anna Maria Papini,[1,2] Francesco Ciardelli,[3] Luca Rosi,[2] Claudia Bello.[1,2]

[1] *Interdepartmental Research Unit of Peptide and Protein Chemistry and Biology, University of Florence, Italy*

[2] *Department of Chemistry "Ugo Schiff", University of Florence, Italy*

[3] *Spin-PET s.r.l., Pontedera, Italy*

Sara Aquilia email: *sara.aquilia@unifi.it*

https://doi.org/10.17952/37EPS.2024.P1313

Bioplastics derived from coproducts or waste materials offer the advantage of exploiting pre-existing, underutilized resources.[1] Among these, natural biopolymers, specifically proteins, emerge as an attractive alternative to petroleum-based materials both in terms of potential applications and environmental impact.[2] The presented study is a proof-of-concept of the development of a protein-based cross-linked material with plastic response for multiple applications. Whole rapeseed protein-rich meal has been chosen as main ingredient and pression-moulding process was evaluated as an efficient method to produce a protein-based material.

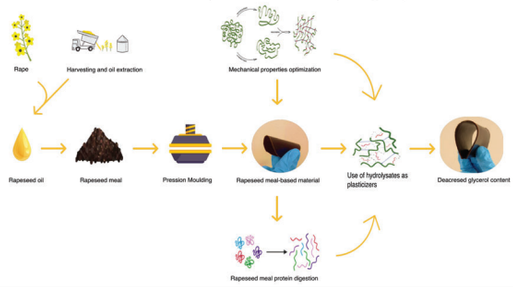

Samples were collected from a by-product of the crude oil production after oil pressing and hexane extraction process.[3] Meal/glycerol/cross-linker/protein-based compatibilizer blends (RM) were mixed with sodium sulfite (Na_2SO_3) and different denaturants (SDS, urea, guanidine) to obtain protein denaturation during thermal processing, thereby enhancing the strength and toughness of the final materials. Furthermore, this research extends its focus to the proteolysis of rapeseed proteins using specific proteases directly on rapeseed meal, generating peptide mixtures. These hydrolysates have been used as components of the protein-rich materials, with the aim of achieving a full eco-sustainability.

USE OF HYDROLYSATES AS PLASTICIZERS

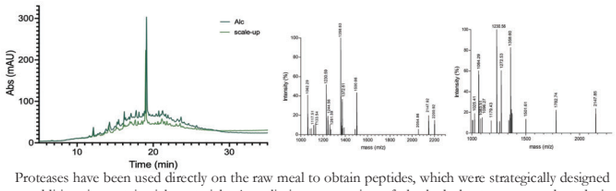

Proteases have been used directly on the raw meal to obtain peptides, which were strategically designed as additives in protein-rich materials. A preliminary screening of the hydrolysates was conducted via RP-HPLC and MALDI-TOF-MS, revealing the formation of hydrophilic peptides with masses ranging between 1000 and 1500 Da. Scale-up of the process was set-up in semi-industrial scale.

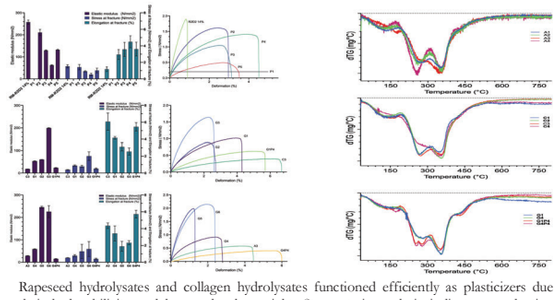

Rapeseed hydrolysates and collagen hydrolysates functioned efficiently as plasticizers due to their hydrophilicity and low molecular weight. Stress-strain analysis indicates a reduction in Young's modulus and a significant increase in elongation at break. Thermogravimetric analysis (TGA) revealed enhanced thermal stability, particularly in materials with a reduced glycerol content in the mixtures.

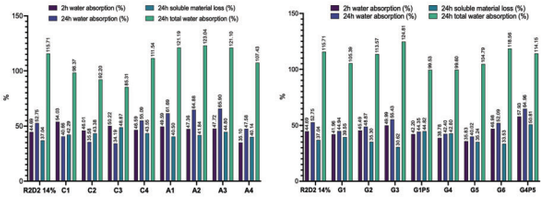

All the specimens exhibited improved water absorption, attributed to the increased formation of entanglements due to hydrogen bonding between the protein matrix and the hydrolysates.

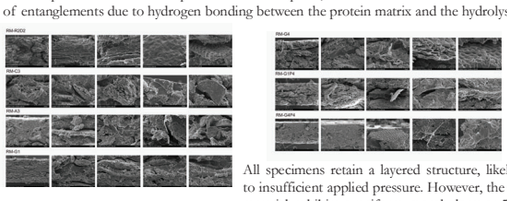

All specimens retain a layered structure, likely due to insufficient applied pressure. However, the G4P4 material exhibits a uniform morphology at 50 and 100 µm. Particles of the raw material are still visible to varying degrees.

USE OF PROTEIN DENATURING AND S-S REDUCING AGENTS

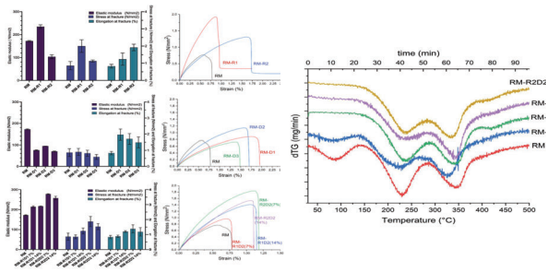

Different S-S reducing and denaturing agents were tested at various concentrations to induce protein denaturation and to understand the role of the molecular feature on the material ultimate properties. The polypeptide chain became so more flexible and, at the same time, made functional groups more accessible for crosslinking reactions. Moreover, Thermogravimetric analysis (TGA) revealed improved thermal stability of the material containing both the reducing and the denaturing agent (RM-R2D2 14%).

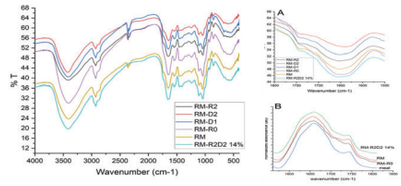

A change in protein structure was evidenced by the FT-IR analysis when comparing the amide I bands of the specimens with different composition to each other and to the one of rapeseed meal, indicating effective protein denaturation. The presence of the reduced disulfide bond and of the denaturing agents causes partial unfolding of the proteins and led to a major exposure of the amino acid side chains in the protein.

In all specimens, there was an approximate 40% loss of soluble material, with glycerol being the likely primary contributor to this material loss due to migration issues. Additionally, the water absorption remained above 100%

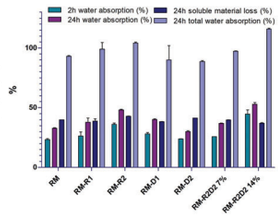

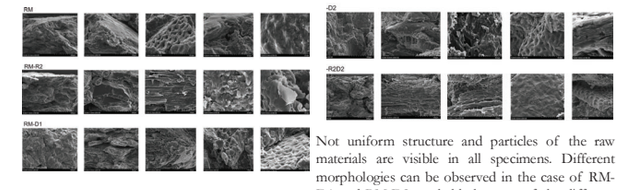

Not uniform structure and particles of the raw materials are visible in all specimens. Different morphologies can be observed in the case of RM-D1 and RM-D2, probably because of the different effect of the denaturing agent used. Among all the specimens analyzed RM-R2D2 is the one that looks as the most compact and uniform material.

CONCUSIONS

Rapeseed meal has a high potential for the use in the production of sustainable materials for multiple applications. Different reducing and denaturing agents were tested to induce protein denaturation. The polypeptide chain became so more flexible and, at the same time, led functional groups more accessible for crosslinking reactions. Enzymatic digestion process on the raw meal has been scaled-up and plasticizers effect of hydrolysates mixtures has been also studied. The study is certainly innovative and informative but the mechanical properties are not yet industrially competitive. However, our study suggests a promising pathway to develop a protein-rich material for industrial applications.[4]

1.Hatti-Kaul, R. et al. Trends Biotechnol 2020, 38 (1), 50–67. 2.DeFrates, K. G. et al. Nanomaterials 2018, 8 (7), 457.
3.Newson, W. R. Industrial Oil Crops 2012, 59-65. 4. Aquilia, S. et al. Biomolecules 2024, 14, 982 (accepted on August 9, 2024).

PON Research and Innovation 2014–2020 (D.M 1061/2021) XXXVII Cycle in Chemical Sciences funded by MUR/EU-FSE.

https://doi.org/10.17952/37EPS.2024.P1314

清華大學
Key Laboratory of Bioorganic Phosphorus Chemistry
& Chemical Biology (Tsinghua University), Ministry of Education

Self-assembled Peptides for Biomimetic Mineralization and Enamel Repair

Yue Li, Rong Chang, Yang-Jia Liu, Feng Chen* and Yong-Xiang Chen*

Yue Li, Rong Chang and Yong-Xiang Chen: Department of Chemistry, Key Lab of Bioorganic Phosphorus Chemistry & Chemical Biology (Ministry of Education), Tsinghua University, Beijing, 100084, P.R. China.
Yang-Jia Liu and Feng Chen: Central Laboratory, Peking University Hospital of Stomatology, Beijing, 100081 China.

Biomimetic mineralization strategy based on self-assembling scaffolds plays a vital role in the formation of highly mineralized organic–inorganic hybrid complexes, which possesses great potential for elucidating the mechanism of biomineralization. Herein, we have developed three self-assembled peptides including a phosphorylated protein segment (LCPS-OP), a phosphonated protein segment (LCPS-CP) and a branched amphipathic polypeptide ($CAMP_{15}$), which are utilized as biocompatible scaffolds to template epitaxial growth of HAP in situ on demineralized enamel surfaces, forming new remineralized enamel layers while reducing the adhesion of *Streptococcus mutans*. These results demonstrate the promising performance of these novel polypeptides in the regulation of biomimetic mineralization interfaces and hold great biomedical potential in the effective repair of defected enamel, as well as in the prevention of dental caries regeneration.

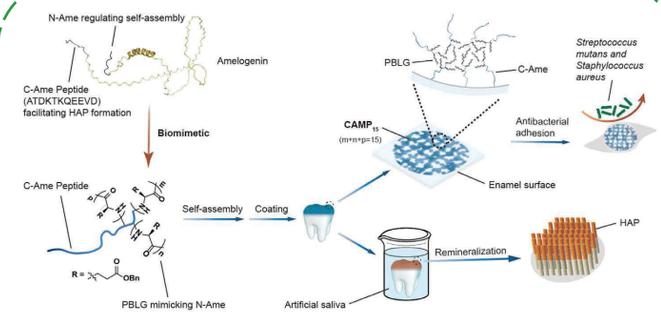

Figure 1. Schematic illustration of a novel self-assembled branched polypeptide ($CAMP_{15}$) as an Ame mimic for enamel repair and antibacterial adhesion.

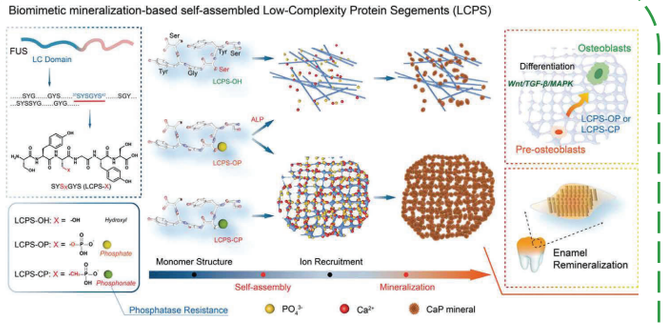

Figure 2. Schematic illustration of phosphorylated and phosphonated LCPSs for biomimetic mineralization and repair of tooth enamel.

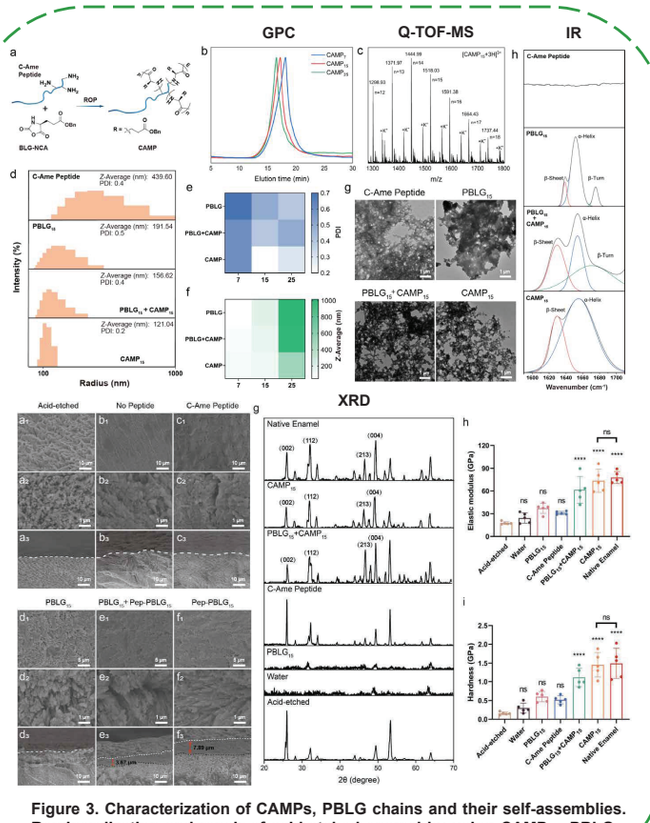

Figure 3. Characterization of CAMPs, PBLG chains and their self-assemblies. Remineralization and repair of acid-etched enamel by using $CAMP_{15}$, $PBLG_{15}$ and C-Ame Peptide assemblies in artificial saliva.

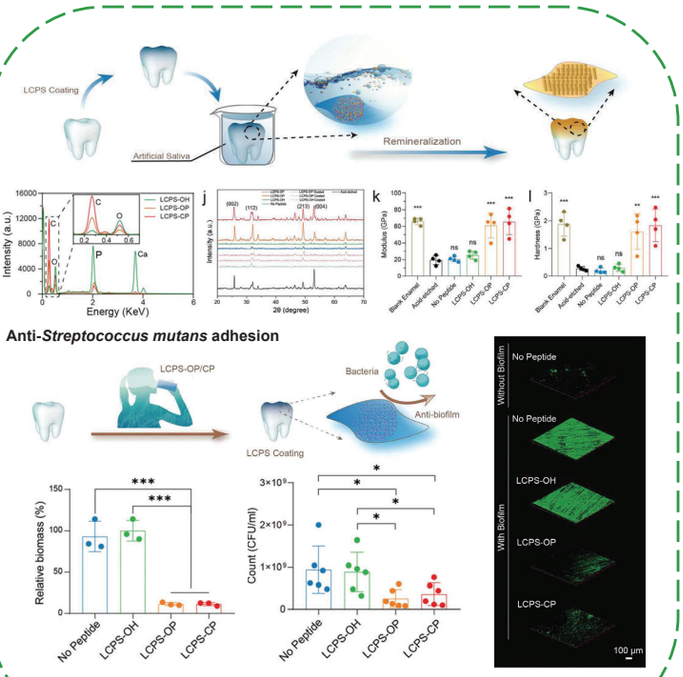

Figure 4. Remineralization and repair of demineralized enamel by LCPS coating. Antibacterial adhesion of enamel coated with LCPS in vitro.

References:

[1] Y. Li, R. Chang, Y.-J. Liu, F. Chen, Y.-X. Chen, *J. Mater. Chem. B* **2024,** *12* (26), 6452.
[2] R. Chang, Y.-J. Liu, Y.-L. Zhang, S.-Y. Zhang, B.-B. Han, F. Chen, Y.-X. Chen, *Adv. Sci.* **2022,** *9* (6), 2103829.

Acknowledgements: This work was supported by grants from the National Key R&D Program of China (2021YFC2103900) and National Natural Science Foundation of China (22177059 and 92353302), and the Tsinghua University Initiative Scientific Research Program to Y.X.C.

Finanziato dall'Unione europea NextGenerationEU
Ministero dell'Università e della Ricerca
Italiadomani PIANO NAZIONALE DI RIPRESA E RESILIENZA
Dipartimento di Farmacia
Università degli Studi di Napoli Federico II
https://doi.org/10.17952/37EPS.2024.P1315

RNA &GENETHERAPY

National Center for Gene Therapy and Drugs based on RNA Technology

Cationic amphiphilic peptide-based delivery platforms for negatively charged active pharmaceutical ingredients including short interfering RNA

M. Rosa,[a] C. Diaferia,[a] A. Accardo[a], G. Morelli[a]
[a] *Department of Farmacy, University of Naples "Federico II", Naples, Italy.*
E-mail: mariangela.rosa@unina.it

TOPIC: peptide materials

ABSTRACT

Peptide sequences have been recently proposed as suitable building blocks for the formulation of supramolecular aggregates that can be used to deliver diagnostic or therapeutic agents. The encapsulation of these active molecules into nanoparticles allows them to overcome some *in vivo* drawbacks (e.g. degradation, inability to cross barriers).[1] Positively charged nanoparticles, such as micelles or polymeric nanoparticles, have been proposed as suitable delivery carriers for RNA-based therapeutics.[2] Here we report the preparation of novel peptide based nanovectors as promising delivery systems for short interfering RNA (siRNA). We synthesized a **library of eighteen cationic lipopeptides** that were explored as charge modifier of peptide **gels** and **nanogels**.[3] In any case, the presence of a variable number of positive charges were exploited to favor **non-covalent electrostatic interactions** of model siRNA.

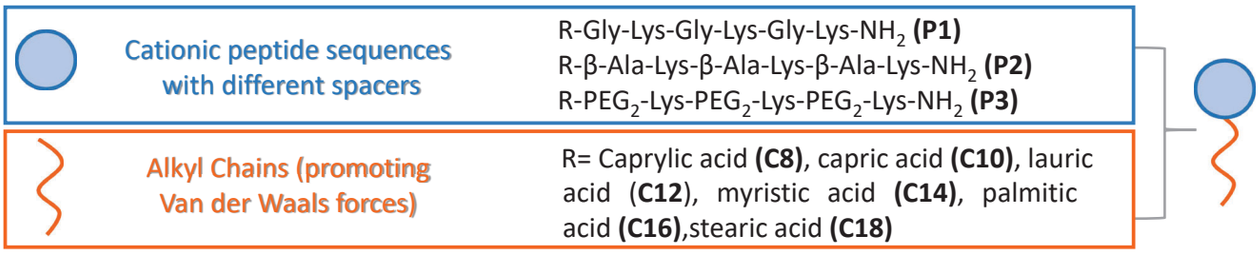

HYDROGELS

Mixed hydrogels were prepared using **DMSO/H_2O solvent-switch method**: a Fmoc-FF stock DMSO (100 mg mL^{-1}) solution was used to dissolve the cationic peptides. The mixed stock was then rehydrated with water and vortexed to ensure homogeneity of the sample. Secondary structural and topography characterization were performed via CD, FTIR and AFM. Gels were tested as reservoirs for 5-carboxyfluorescein (5-FAM).

Inverted test tube for Fmoc-FF/Cn-P1

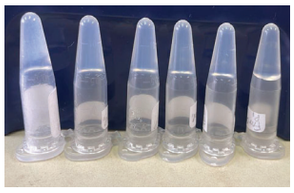

AFM characterization

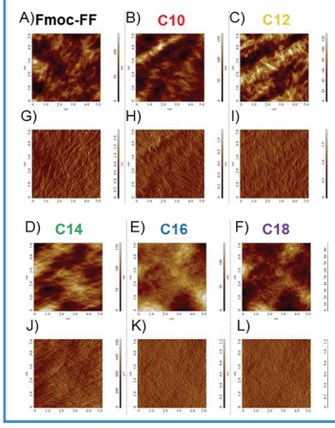

CD and FTIR of mixed HGs

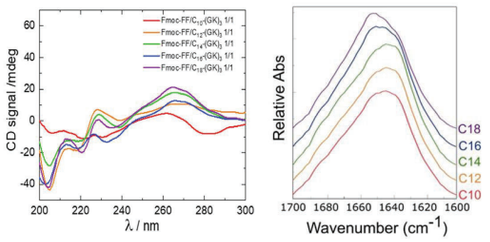

Encapsulation and release of 5-FAM overtime

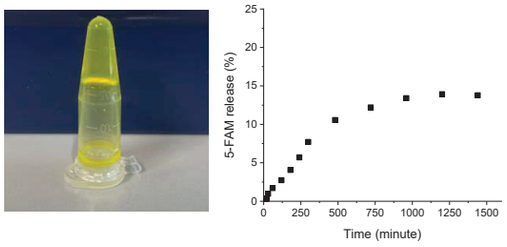

NANOGELS

Nanogels were prepared using the **top-down** method: an aqueous filtered solution of TWEEN® 80/SPAN® 80 at a w/w ratio of 53/47 was added to the preformed hydrogels. The resulting suspensions were homogenized and tip sonicated.

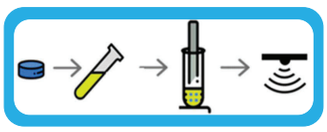

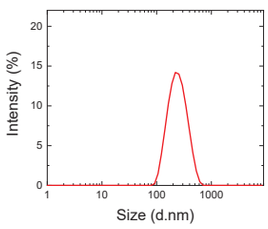

Main diameter: 190 nm
ζ potential: +33 mV

Next step was the **encapsulation** of **siRNA** into NGs

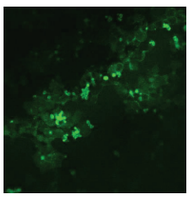

The internalization of the obtained formulations into cells was estimated through **confocal microscopy**.

(1) R. Zhong et al, Nature Materials, 2023, 811-831. **(2)** J.A. Kulkarni et al, ACS Nano, 2018, 12, 4787-4795. **(3)** E.Rosa et al, Soft Matter, 2023, 19, 4686-4696.

https://doi.org/10.17952/37EPS.2024.P1316

Synthesis of peptidomimetics using Diaryl-β^{2,3} amino acids for the preparation of smart materials

Dulce A. Quintana-Romero[1], Raffaella Bucci[1], Merve Gul[2], Maria M. Pérez-Madrigal[2], Carlos Alemán[2], M. Luisa Gelmi[1]

[1] Università degli Studi di Milano, Department of Pharmaceutical Science, Sez A. Marchesini, via Venezian 21, 20133, Milano; [2]Universitat Politècnica de Catalunya, Department of Chemical Engineering, Campus Diagonal Besòs, Building A (EEBE). Av. Eduard Maristany, 16 08019, Barcelona

Introduction

α-Amino acids are at the basis of the living world, being the building blocks of peptides and proteins. The advantages of α-peptides, *i.e.* versatility, biocompatibility and ease of preparation, make them the perfect candidates in different applications, for example biology and pharmaceutical science. However, they show some drawbacks mainly due to their protease sensitivity. To overcome this limitation, non-standard amino acids such as β-amino acids are inserted in peptide sequences to produce peptidomimetics, molecules with the same biological activity of the natural peptides but with enhanced proteolytic and conformational stability.[1] In addition, the ability of peptides or amino acids alone to self-assemble and self-organize, allows their use in wide and variable applications, from nanomedicine to electrochemistry and catalysis, as well as bioelectronic materials.[2]

Synthesis of unnatural fluorine-substituted β^{2,3}-diarylamino acid

Stereoselective Mannich-like reaction[3]

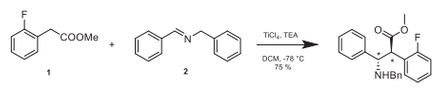

L-Ala used to resolve the racemic mixture

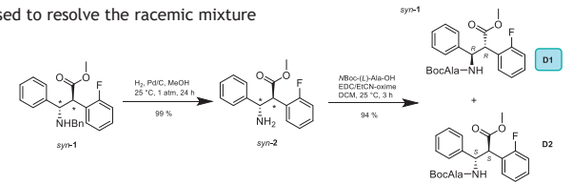

Peptide synthesis

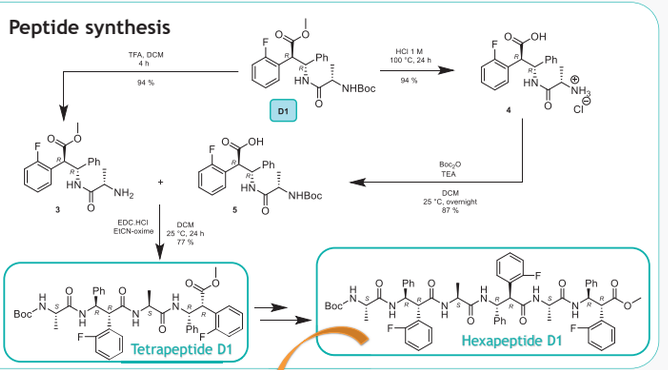

β^{2,3}-Syn Diaryl AA

This β-amino acid triggers the formation of different bioinspired architectures, depending on the peptide sequence in which it is inserted. So far, different nanomaterials such as nanotubes,[4] supramolecular conductive ropes,[5] and cationic nanospheres,[6] were obtained and characterized.

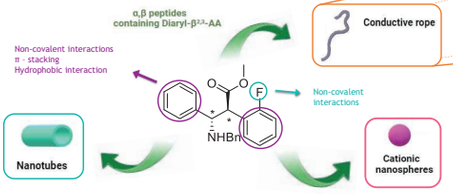

Extended conformation → self-assembles to form an antiparallel β-sheet structure

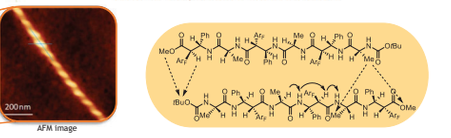

Conductive Nanorope

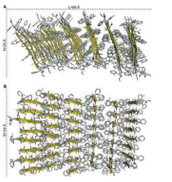

D1

ROESY zoom of Boc and Me region spectrum

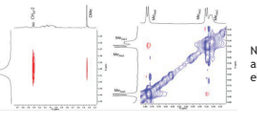

Nanorope structure where the aromatic groups are close to each other allowing to have electron conduction properties.[5]

In collaboration with Prof. Gatto University of Tor Vergata

Electrochemical characterization

In collaboration with D.C. 13, Merve Gul NanoReMedi programme Polytechnic University of Catalonia

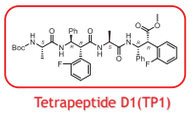

Tetrapeptide D1(TP1)

Cyclic Voltammetry (CV)

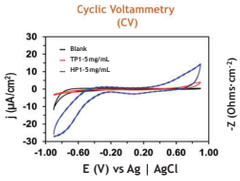

Electrochemical Impedance Spectroscopy (EIS)

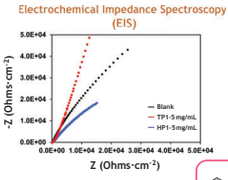

Working Electrode: Stainless Steel

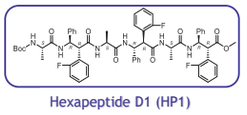

Hexapeptide D1 (HP1)

- Hexapeptide showed a good electroactivity → Biosensor for biomolecule detection
- Tetrapeptide showed good capacitive behavior → Bio-supercapacitor

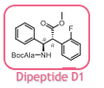

Dipeptide D1

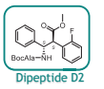

Dipeptide D2

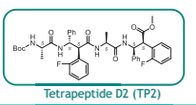

Tetrapeptide D2 (TP2)

Modification of Working Electrode:

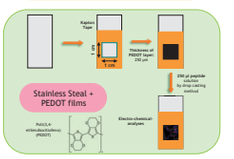

Factors influencing the electrochemical behavior:

- Spatial disposition of the amino and carboxyl groups.
- Spatial disposition of the phenyl and flourobenzene.
- Length and surface area according to dipeptides, tetrapeptides and hexapeptide.

CV

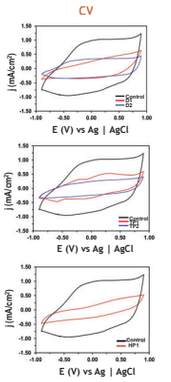

EIS - Nyquist Plot

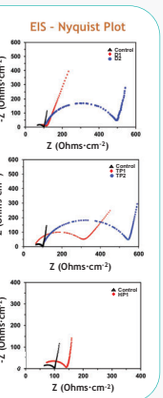

Applications and future work

- Self-assembly studies.
- Study of the relationship between self-assembly and electrochemical activity.
- Development of electrically responsive peptides able to prevent bacterial contamination on implants.
- Controlled release of drugs and antimicrobials by electrostimulation.

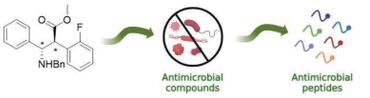

*This project has received funding from the European Union's research and innovation programme under the Marie Skłodowska-Curie grant agreement No 101072645

References:

1. R. Bucci, F. Foschi, C. Loro, E. Erba, M.L. Gelmi, S. Pellegrino, Eur. J.O.C. (2021), 20, 2887-2900.
2. F. Clerici, E. Erba, M.L. Gelmi, S. Pellegrino,Tetrahedron Lett. (2016), 57, 5540-5550.
3. A. Bonetti, F. Foschi, D. Nava, S. Pellegrino, M. Penso, R. Soave, M.L. Gelmi, Eur. J.O.C. (2014), 15, 3203-3209.
4. A. Bonetti, S. Pellegrino, P. Das, S. Yuran, R. Bucci, N. Ferri, F. Meneghetti, C. Castellano, M. Reches, M. L. Gelmi, Org. Lett. (2015), 17, 4468-4471.
5. N. Forlano, R. Bucci, A. Contini, M. Venanzi, E. Placidi, M.L. Gelmi, R. Lettieri, E. Gatto, Nanomaterials. (2023), 13, a.n. 333.
6. R. Bucci, P. Das, F. Iannuzzi, M. Feligioni, R. Gandolfi, Gelmi M. L., Reches M., Pellegrino S. Org. Biomol. Chem. (2017), 15, 6773-6779.

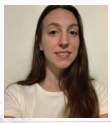

Conformational and self-assembly studies of a protein-mimetic peptide from *Pseudomonas aeruginosa*'s YeaZ protein

Elettra Fasola[1], Giulia Alboreggia [1], Stefano Pieraccini[2], Francesco Oliva [2], Fatima Ezzahra Agharbaoui[2], Michela Bollati[3], Giovanni Bertoni[4], Sandro Recchia[1], Marcello Marelli[5], Umberto Piarulli[1], Sara Pellegrino[6] and Silvia Gazzola[1]

1 Science and High Technology Department, University of Insubria, Como, Italy; 2 Chemistry Department, University of Milan, Milan, Italy; 3 CNR and Department of Biosciences, Institute of Biophysics, University of Milan, Milan, Italy; 4 Department of Bioscience, University of Milan, Milan, Italy; 5 CNR-SCITEC—Istituto di Scienze e Tecnologie Chimiche "Giulio Natta", Milan, Italy; 6 Pharmaceutical Science Department, University of Milan, Milan, Italy. email: efasola@uninsubria.it

https://doi.org/10.17952/37EPS.2024.P1317

BACKGROUND

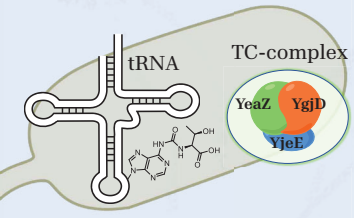

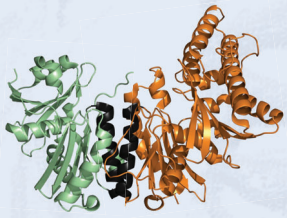

YeaZ-YgjD complex (6z81)

Protein-mimetic peptides (PMPs):
shorter sequences of proteins and biocompatible building blocks with multiple applications.

Self-assembly:
association process of individual building block units into highly ordered structures.

PaYeaZ:
self-assembling protein from *P. aeruginosa*, involved in the formation of an essential protein complex.

PaYeaZ shows protein-protein interactions thanks to an α-helical surface domain → **Study of aggregation properties of the PMP for material science applications**

STUDY

Peptides' design

- Identification of the shortest sequence mainly responsible of **protein-protein interactions** in YeaZ homodimer
- Determination of the essential residues for **interactions and helicity**

METHODS

Computational studies

- Identification of the **surface accessible residues** in the homodimer of YeaZ (4y0w)

Vecchietti, Davide, *et al. BBRC* 470.2 (**2016**): 460-465

- **Hot spots** identification by Computational Alanine Scanning (CAS)
- Introduction of a **polar group** at the C-terminal to enhance hydrophilicity and aggregation properties

Peptides' synthesis and characterization

- **PMP2** and shorter derivatives **PMP3-5**
- Secondary structure by Circular Dichroism

Solid Phase Peptide Synthesis

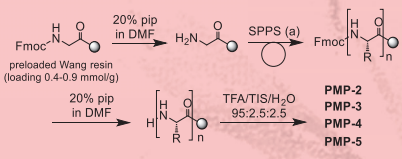

[a] Coupling conditions – 1: Fmoc-aa-OH 3-5 eq, DIPEA 9-15 eq, COMU 3-5 eq. Coupling conditions – 2 : Fmoc-aa-OH 3-5 eq, DIC 3-5 eq, Oxyma 3-5 eq.

Supramolecular aggregates morphology studies

- Comparison between hydrophilic and hydrophobic environment
- Dependance on concentration
- Aggregates stability in DMSO

- **Scanning and Transmission Electron Microscopy (solvent displacement DMSO to water)**
- **Thioflavin T assay**
- **Dynamic Light Scattering**
- **Attenuated Total Reflectance**

RESULTS

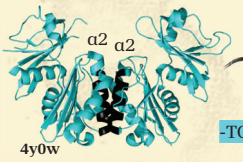

Arg73 – Leu86 in the YeaZ protein is the main responsible domain for protein-protein interactions

First Subhunit	
Mutation	ΔΔG (kcal/mol)
THR70ALA	-0.5497
VAL72ALA	0.0956
ARG73ALA	-13.0972
ILE74ALA	3.5133
ILE76ALA	0.2629
VAL78ALA	2.1032
GLN80ALA	-0.1673
LEU82ALA	3.2982
PHE84ALA	7.5524
LEU86ALA	1.6491

Second Subhunit	
Mutation	ΔΔG (kcal/mol)
THR70ALA	0.3585
VAL72ALA	0.0717
ARG73ALA	-8.6279
ILE74ALA	0.6214
ILE76ALA	0.8843
VAL78ALA	1.5774
GLN80ALA	-1.434
LEU82ALA	2.2705
PHE84ALA	10.6594
LEU86ALA	1.3862

ΔΔG < 0 : more stable with Ala
ΔΔG > 0 : less stable with Ala

- **Ile74, Val78, Leu82, Phe84:** hot spots
- **Arg73:** substituted with Ala

AIAIGVVQGLAFAL **PMP1**

↓

AIAIGVVQGLAFALGGKKKG **PMP2**

Name	Sequence	Yield	Purity	Helix%
PMP-2	AIAIGVVQGLAFALGGKKKG	60%	96%	35%
PMP-3	VVQGLAFALGGKKKG	42%	97%	7%
PMP-4	LAFALGGKKKG	25%	95%	8%
PMP-5	AIAIGVVQGGKKKG	36%	98%	12%

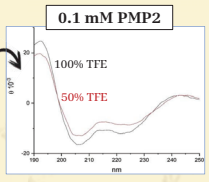

Only **PMP2** is α-helical and able to form supramolecular aggregates.

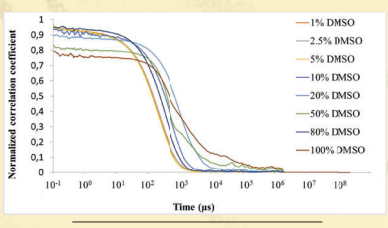

- **PMP2** is stable to all DMSO conditions

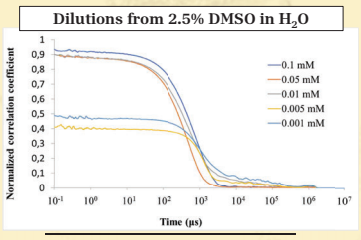

- Stable aggregates are formed above 0.01 mM

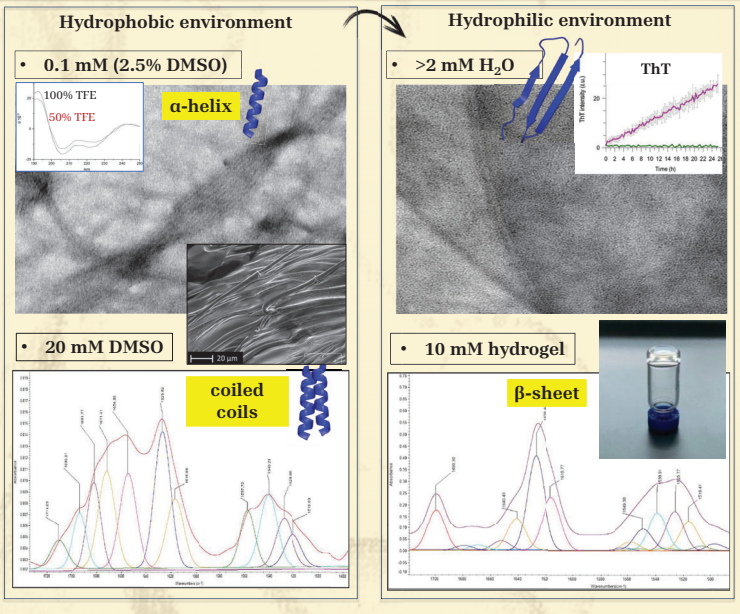

Fasola, Elettra, *et al.*, *Front. Chem.* (**2022**) 10:1038796

OUTLOOK AND CONCLUSION

- **PMP1** is the main sequence responsible for YeaZ-YeaZ and YeaZ/YgjD interactions
- **PMP2** is an amphiphilic, more soluble derivative of **PMP1**, and the shortest sequence able to maintain helicity outside the protein environment
- The secondary structure is related to aggregation abilities: only the helical **PMP2** forms aggregates
- The secondary structure and type of aggregates depends on the environment (hydrophobic vs hydrophilic)
- **PMP2** aggregates are stable to DMSO, and in water a stable hydrogel is formed

Overall, we were able to obtain a biocompatible protein-mimetic building block, able to maintain α-helix and to form aggregates. A conformational switch to β-sheet occurs in hydrophilic conditions.

A comparative study between phenylglycine- and phenylalanine-derived peptide hydrogels

https://doi.org/10.17952/37EPS.2024.P1318

Jolien Bertouille[1], Ulrich Hennecke[1], Charlotte Martin[1], Ana V. Cunha[2], Steven Ballet[1]

[1]Research Group of Organic Chemistry, Department of Chemistry, Vrije Universiteit Brussel, Pleinlaan 2, 1050 Brussels, Belgium
[4]Laboratory of Molecular Spectroscopy, Department of Chemistry, University of Antwerp, Groenenborgerlaan 171, B-2020 Antwerp, Belgium
email: Jolien.Bertouille@vub.be

INTRODUCTION

Peptide hydrogels are soft materials which, due to their biocompatibility, are excellent candidates for the development of **controlled drug delivery** matrices and wound healing applications. The properties of the gel materials are directly linked to the peptide sequence. However, minor alterations in the sequence can entail major differences in the **assembly mode** and hence material characteristics. Many of the well-known hydrogelators self-assemble solely by non-covalent interactions; it is known that hydrophobic effects, π-π stacking, ionic interactions and hydrogen bonding play major roles. Nevertheless, the extent and tunability of each of these interactions in the self-assembly process is not fully understood. To further elucidate the role of **aromatic interactions** in this process, the amino acids **phenylalanine (Phe)** and **phenylglycine (Phg)** were interchanged in a short amphipathic peptide hydrogelator with sequence H-FQFQFK-NH_2 [1-2]. This substitution resulted in four new hydrogelators in which the aryl rings are oriented differently [3]. The novel soft materials were **characterized at different levels** and additionally, **atomic models** were obtained of the stacking modes by molecular dynamics (MD) simulations.

SCOPE

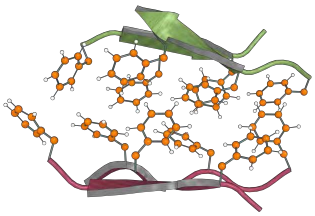

SBL-HG-063

Principally T-shaped π-π stacking

MD

Code	Sequence
SBL-HG-063	H-Phe-Gln-Phe-Gln-Phe-Lys-NH_2
SBL-HG-085	H-**Phg**-Gln-**Phg**-Gln-**Phg**-Lys-NH_2
SBL-HG-086	H-**Phg**-Gln-Phe-Gln-Phe-Lys-NH_2
SBL-HG-087	H-Phe-Gln-**Phg**-Gln-Phe-Lys-NH_2
SBL-HG-084	H-Phe-Gln-Phe-Gln-**Phg**-Lys-NH_2

MD

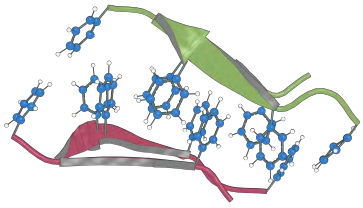

SBL-HG-085

Principally parallel-slipped π-π stacking

SPPS conditions: Rink amide AM resin – Coupling with Fmoc-AA/COMU/DMP in DMF, 45 min – Fmoc-deprotection with 20% 4-Me-piperidine in DMF, 20 min – Cleavage with TFA/TIS/H_2O (95:2.5:2.5 v/v/v), 3 h.

DYNAMIC RHEOLOGY

- 2% w/v gels in physiological saline

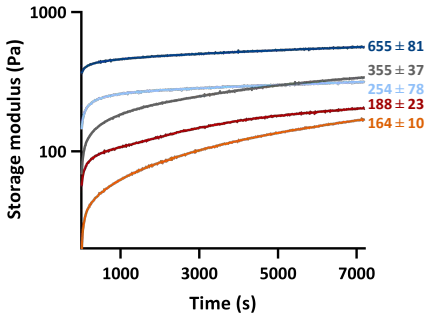

- 3-fold increase in gel strength for **SBL-HG-085**
- Thixotropic materials
- **SBL-HG-085** more stable upon injection

ATOMIC FORCE MICROSCOPY

- 0.5% w/v solutions in physiological saline, adsorbed on mica surface [4]

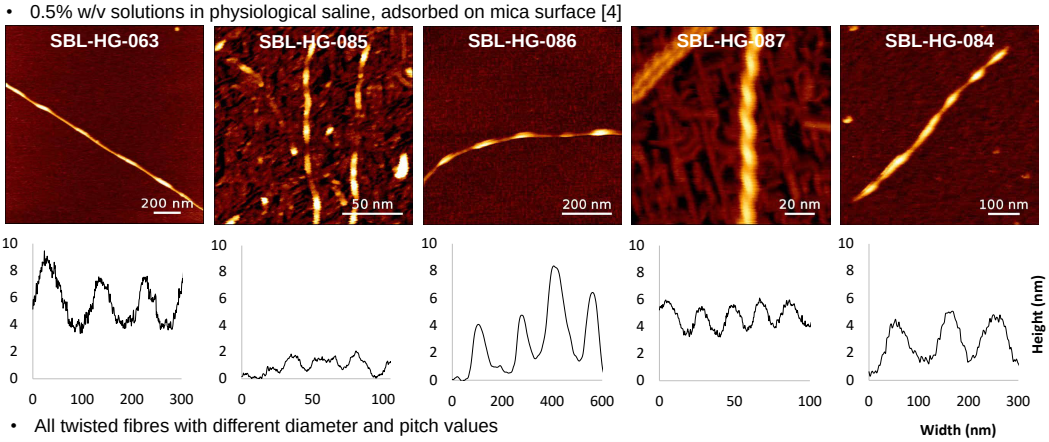

- All twisted fibres with different diameter and pitch values

CIRCULAR DICHROISM

- 2% w/v gels in physiological saline

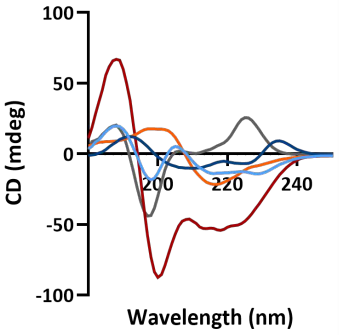

- Red-shifted β-sheet profile
- Indication of aromatic clustering
- Clear nanoribbons for **SBL-HG-087**

MOLECULAR DYNAMICS SIMULATIONS

A. V. Cunha

- Antiparallel β-sheet double layer of 36 peptide strands
- 100 ns all-atom MD simulation (GROMACS)

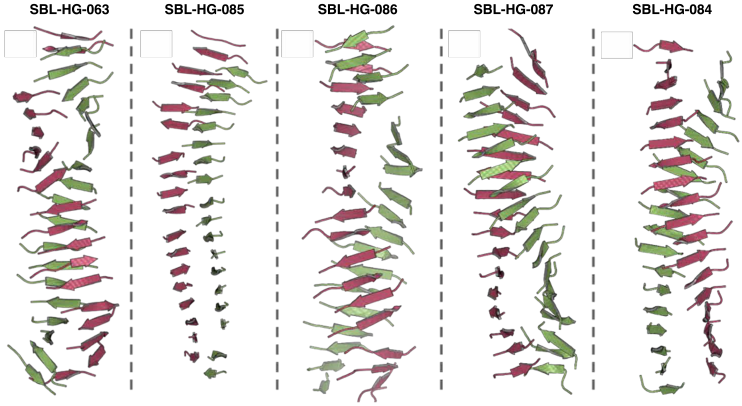

- **SBL-HG-085**: lowest RMSD variation → most conserved structure
- High correlation between computed and experimental infrared spectra

HYDROGEL STABILITY

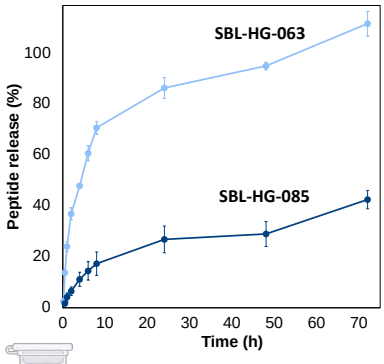

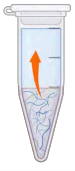

- *In vitro* release experiment
- 37°C, saline supernatants

- Phg-rich hydrogel remains more intact than Phe-rich hydrogel

CONCLUSION

The substitution of Phe with Phg in a previously described peptide hydrogelator led to the formation of four **new soft biomaterials**. The aromatic side chain of Phg reduced the side chain flexibility of the peptide sequence, leading to a different π-π stacking orientation during self-assembly. One of the studied hydrogels (**SBL-HG-085**) showed a three-fold increase in gel strength and more rapid recovery after disruption. Based on atomic force microscopy experiments, this system contained the smallest, yet most interacting fibres. Additionally, the Phg-rich hydrogel remained more intact during *in vitro* release studies. The antiparallel β-sheet double layer assembly was subjected to MD simulations and the assembled model was validated by means of calculated and experimental IR spectroscopy. Overall, **reducing the aromatic flexibility stabilized the assemblies** by modified **π-π stacking** interactions.

[1] C. Martin, E. Oyen, J. Mangelschots, M. Bibian, T. B. Haddou, J. Andrade, J. Gardiner, B. Van Mele, A. Madder, R. Hoogenboom and S. Ballet. *MedChemComm,* **2016**, 7, 542.
[2] C. Martin, E. Oyen, Y. Van Wanseele, T. B. Haddou, H. Schmidhammer, J. Andrade, L. Waddington, A. Van Eeckhaut, B. Van Mele, J. Gardiner and S. Ballet. *Mater. Today Chem.,* **2017**, 3, 49.
[3] J. Bertouille, R. Van Lommel, R. Aerts, L. Dockx, N. Van Den Brande, R. G. Willaert, U. Hennecke, C. Martin, F. De Proft, W. Herrebout, T. L.C. Jansen, S. Ballet, A. V. Cunha. *Manuscript in preparation.*
[4] J. Bertouille, S. Kasas, C. Martin, U. Hennecke, S. Ballet, R. G. Willaert. *Small* **2023**, 19, 2206795.

We thank the Research Foundation Flanders (FWO, 1SD7321N and OZR3939) and the Strategic Research Programme (SRP50 and SRP95) of the VUB for the financial support.

https://doi.org/10.17952/37EPS.2024.P1319

Peptides stapling as a tool for improving molecular recognition of C-reactive protein

Katarzyna Szot-Karpińska[1*], Marta Lubos[2], Natalia Cwalina[1], Jan Pícha[2], Jakub Kaminský[2], Jiří Jiráček[2], Magdalena Majewska[3], Magdalena Narajczyk[4], Joanna Niedziółka-Jönsson[1]

1 Institute of Physical Chemistry, Polish Academy of Sciences, 01-224 Warsaw, Poland
2 Institute of Organic Chemistry and Biochemistry of the CAS, 166 10 Prague, Czech Republic
3 Faculty of Chemistry, University of Warsaw, 02-093 Warsaw, Poland
4 Bioimaging Laboratory, University of Gdansk, 80-308 Gdansk, Poland

kszot@ichf.edu.pl

In our previous study, we identified several new CRP binding peptides (P2, P3, P9) using experimental (biological and physicochemical) methods supported by theoretical simulations (computational modelling analysis) [1]. The linear P3 peptide was successfully applied as a sensing element in a microfluidic sensing device for CRP recognition [2]. However, we are aware that linear peptides have some limitations, e.g. conformational instability. Thus, we have applied the stapling approach to solve that problem. We started with an in silico analysis to evaluate which of the studied peptides retain their recognition activity towards CRP. The calculations performed showed that the P9 peptide with a staple has a significantly higher affinity for CRP than linear peptides without a staple. The calculated binding energy for this stapled P9 peptide, which was lower than the values obtained for the linear form of the peptides (P2, P3, P9) or the stapled P2 and P3. The ring-closing olefin metathesis reaction was used to obtain the stapled P9 peptide. The new stapled peptide differs structurally from the linear form what was demonstrated using transmission electron microscopy and circular dichroism. The stapled P9 peptide was used for CRP recognition on silicate-modified indium tin oxide-coated glass electrodes. The obtained electrodes exhibit a better affinity towards CRP than electrodes modified with the linear form of this peptide. Moreover, the conformational stability of the P9 stapled peptide was also evaluated in the presence of proteases using CD and electrochemical studies.

GOAL

To identify new receptors (peptides) for various disease markers and characterize their interactions



CRP - marker of inflammatory processes in human body
>10 mg/L inflammation
10-30 mg/L viral infection
>30 mg/L bacterial infection
Higher in cardiovascular, chronic and autoimmune diseases, tumors and COVID19

Phage dispaly - CRP clones selection

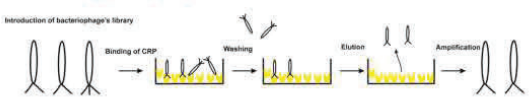

Stapling reaction

Ring-closing olefin metathesis [3]

SWFSDWDLELHA
P9 peptide

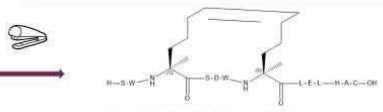

Stapled (St.) P9 peptide

Amino acids sequence analysis, synthesis of selected peptides

CRP peptides	Amino acids sequence												
P2	G	G	S	D	P	E	G	M	Q	G	N	Y
P3	V	H	W	D	F	R	Q	W	W	Q	P	S
P9	S	W	F	S	D	W	D	L	E	L	H	A

Molecular docking analysis

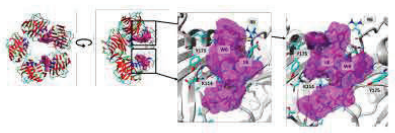

The binding energy of selected peptides in complex with CRP.

CRP- P9 peptide -51.7 kcal/mol
CRP- St. P9 peptide -79.1 kcal/mol

Transmisson electron microscopy analysis

P9 peptide



Stapled P9 peptide

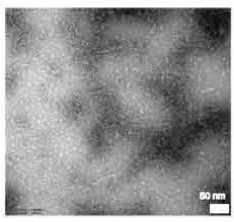

After treatment with proteases

P9 peptide



Stapled P9 peptide

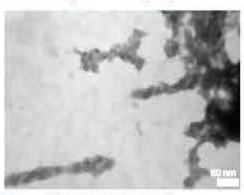

Circular dichroism analysis

P9 peptide

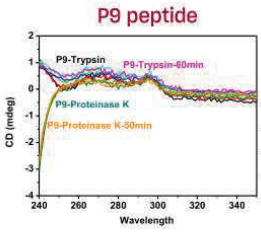

Stapled P9 peptide

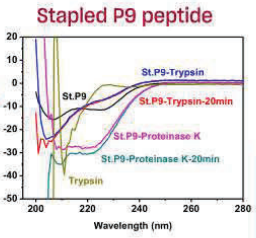

Circular dichroism analysis

Temperature stability

P9 peptide

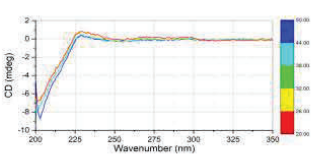

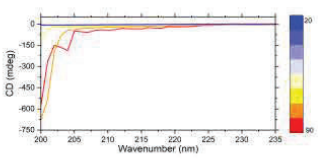

Stapled P9 peptide

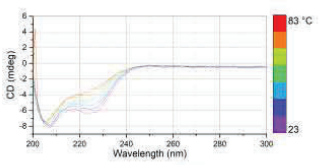

Electrochemical studies of CRP recognition by P9 peptide and St. P9 peptide

Schematic illustration of ITO electrode modification

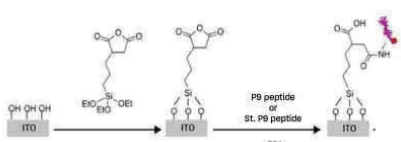

1mM 1,1'-ferrocenodimethanol/PBS

ITO/TESPSA/P9

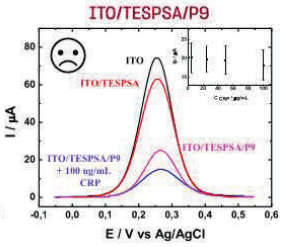

ITO/TESPSA/St. P9

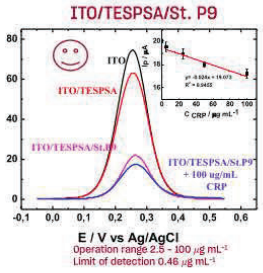

10-30 mg/L - VIRUS



> 30 mg/L - BACTERIA



Effect of trypsin on electrochemical activity towards CRP

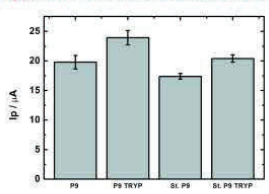

CRP (2.5 µg mL-1)
Trypsin - TRYP (200 ng mL-1)

Conclusions

Three CRP binding peptides were found based on the phages display technique.

The result shows that the stapled P9 peptide exhibits higher affinity toward CRP than linear P9.

The conformational structure of the stapled P9 peptide is more resistant to external factors (temperature, protease activity) than linear P9 peptide.

The stapled P9-based electrode exhibits response towards the CRP in a wide range of concentration and in the presance of proteases.

It is possible to use P3 peptide to distinguish between virial and bacterial infection.

References:

[1] K. Szot-Karpińska, P. Kudła, U. Orzel, M. Narajczyk, M. Jönsson-Niedziółka, B. Palys, S. Filipek, A. Ebner, J. Niedziółka-Jönsson. Analytical Chemistry, 95 (2023) 14475. [2] S. Boonkaew, K. Szot-Karpińska, J. Niedziółka-Jönsson, B. Palys, M. Jönsson-Niedziółka, Sensors and Actuators B: Chemical 387 (2023) 134659. [3] Lubos, M.; Mrázková, L.; Gwozdiaková, P.; Pícha, J.; Budéšínský, M.; Jiráček, J.; Kaminský, J.; Žáková, L. Org. Biomol. Chem. 2022, 20, 2446-2454.

Acknowledgments

This work was funded by the Polish National Science Centre under the SONATA 13 grant UMO 2017/26/D/ST5/00980 to Dr Katarzyna Szot-Karpińska.

A structural sight on peptides forming stable LLPS: a combined experimental and computational investigation

Gianfranco Bocchinfuso[1], Francesca Cavalieri[1] , Daniel O. Cicero[1], Annachiara Ferrara[1], Hilda Garay-Perez[2], Greta Petrella[1], Marco Savioli[1], Mariano Venanzi[1]

[1]Department of Chemical Sciences and Technology, University of Rome Tor Vergata, 00133, Rome, Italy;
[2]Centre for Genetic Engineering and Biotechnology, PO Box 6162, 10600, Havana, Cuba;
https://doi.org/10.17952/37EPS.2024.P1320

PAS peptides

- PAS-based polypeptides are recombinant or synthetic peptides
- Typically, PASs lack any secondary structure
- Recently proposed as an alternative to polyethylene glycol (PEG)
- Used as components of nanoparticles for different applications

Breibeck J. and Skerra A. Biopolymers. 2018, 109:e23069

Liquid Liquid Phase Separation (LLPS)

- Important in the organization and function of cellular components
- Considered for designing new biomolecular dynamic condensates
- Described also for peptides
- Little studied in peptides lacking charges or aromatic residues

Brangwynne, C. P. et al. Science 2009, 324:1729 Leshem, B. et al. Nature Communications 2023; 14:421

Investigated systems

PAS sequences containing short repeating sequences.

PAS20 : (PASPAAPAPSAPAASPAAPA)–COOH
PAS40: $(PASPAAPAPSAPAASPAAPA)_2$–COOH
PAS80: $(PASPAAPAPSAPAASPAAPA)_4$–COOH

Possibility to investigate the effect of chain length.

Monomers populate two conformations

Molecular Dynamics Simulations at different temperatures

Gyration Radius (Rg)

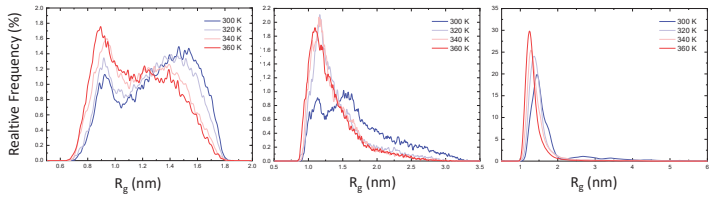

Secondary Structure (Coil B-sheet B-Bridge Bend Turn 3-Helix)

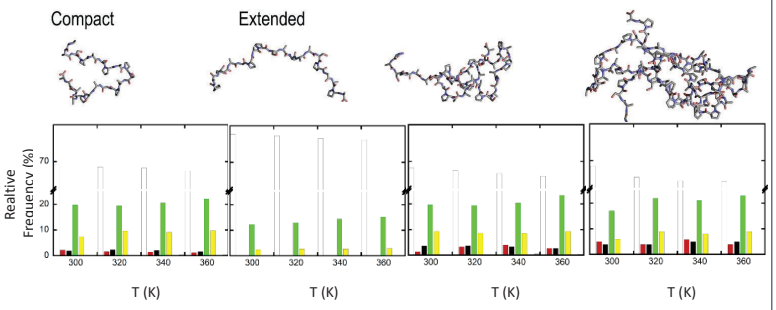

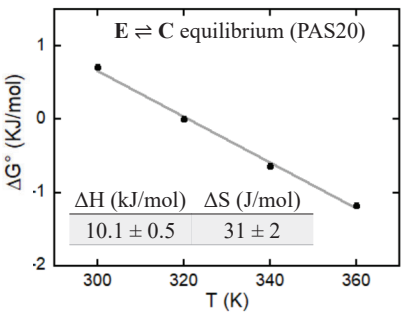

- An equilibrium between extended (**E**) and compact (**C**) conformations exists
- **C** are favored at higher T and high MW
- **C** are characterized by the presence of β motifs
- The equilibrium toward **C** is entropically driven
- CD spectra (not shown) at low concentrations confirm MD results

PASs exhibit high mobility in the aggregates (LLPS)

Changing in the **CD spectra** with concentration is due to PAS aggregation.

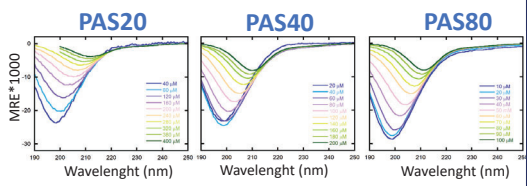

Aggregation depends on the concentration of amino acid units in the solution.

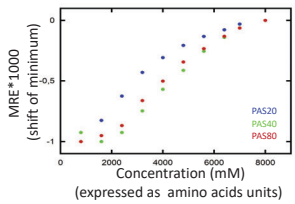

MD simulations of systems containing 8 replicas of PAS20 and PAS40 show **high flexibility** of the peptides in the aggregates. Peptides in the aggregates populate preferentially compact conformations.

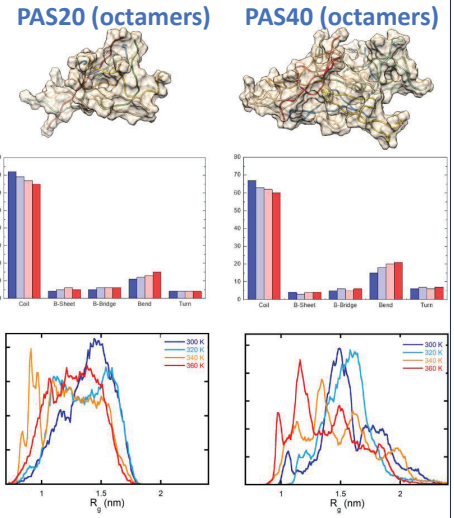

NMR data of PAS80 at high concentrations confirm the **extreme mobility** of peptides in the aggregates

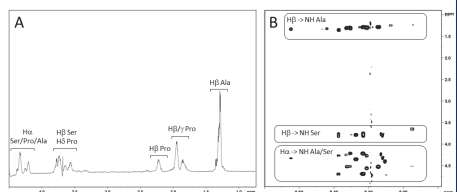

Confocal microscopy images with 3D reconstruction of FITC labeled PAS show the formation of condensates 3-5 microns in size

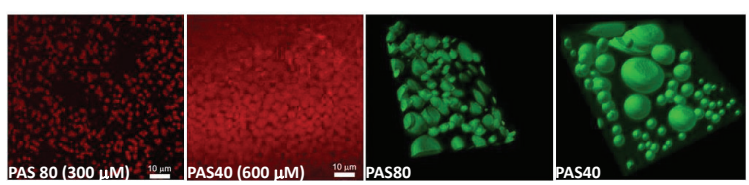

Conclusions

- Under the C.A.C., an equilibrium between extended and compact conformations exists
- PAS peptides aggregate at critical concentrations of amino acid units in the solution, almost independently by the chain length
- PAS sequences remain extremely flexible in the aggregate and the aggregates form condensates 3-5 microns in size.

Despite the absence of charges and aromatic rings, the investigated PAS sequences show LLPS

PEPSA-MATE
Nanopeptides and Nanosaccharides for Advanced and Sustainable Materials

FROM SYNTHESIS TO APPLICATION: PEPTIDE-FUNCTIONALIZED NANOFORMULATIONS FOR BIOMEDICAL APPLICATIONS

S. Joshi[1,2], G. Verma[2,3], A. Saini[1*]
[1]Department of Biophysics, Panjab University, Sector 25, Chandigarh, India
[2]Energy Research Centre, Panjab University, Chandigarh, India
[3]Dr. S. S. Bhatnagar University Institute of Chemical Engineering & Technology, Chandigarh, India
Email correspondence at avneet@pu.ac.in

https://doi.org/10.17952/37EPS.2024.P1321

37th EPS European Peptide Symposium | 14th IPS International Peptide Symposium
Florence, Italy-2024

Background

- **Healthcare-Associated Infections** (HAI) are nosocomially acquired infections that are not present or incubating at the time of admission to a hospital.
- One out of every 100 patients in acute-care hospitals, seven patients in high-income countries and 15 patients in low- and middle-income countries acquire at least one HAI during their hospital stay (WHO).
- **Need of the hour:** Development of antibacterial nanocoating's to prevent the spread of infections.
- **Antimicrobial peptides** have the potential of exhibiting broad-spectrum antibacterial and immunomodulatory activity with a low propensity of bacteria to develop resistance towards them.
- **In this study, a novel cationic peptide DP1 (RFGRFLRKILRFLKK) was covalently conjugated with nano sized graphene oxide (GO) and reduced graphene oxide (rGO) to synthesize a biotic-abiotic platforms (GO-DP1 and rGO-DP1) that are biocompatible and at the same time demonstrates significant antibacterial and antibiofilm activity**[1-3].
- These peptide based nanoformulations were explored for their ability to function as an antibacterial additive for commercial paint production (Indian Patent Office, Application No. 202211011934 A), anti-pseudomonal bandage and as an antibiofilm coating on indwelling catheters[4,5].

Objectives

- Synthesis and biophysical characterization of a stable peptide-functionalized GO/rGO nanoformulations.
- *In-vitro* biological evaluation of peptide-functionalized nanoformulations.
- Evaluation of anti-bacterial and anti-biofilm efficacy of the nanoformulations.
- Biomedical application of the nanoformulation in *P. aeruginosa* contaminated hypodermic needle model.

Methodology

Synthesis of peptide-functionalized GO nanoformulation

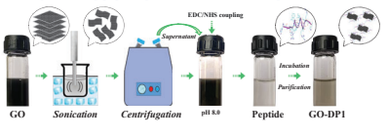

Evaluation of physico–chemical properties



Evaluation of bio nano conjugates as an effective antimicrobial and antibiofilm platform

Evaluation of hemolytic toxicity against red blood cells

Evaluation of cytotoxicity by 3-(4,5-dimethyl-thiazol-2-yl)-2,5-diphenyl-tetrazolium bromide (MTT) assay

Peptide-functionalized nanoformulations based biomedical applications to control the spread of healthcare-associated infections

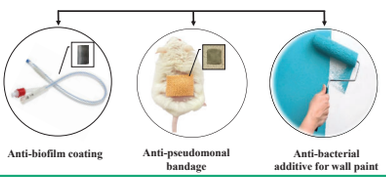

Results and Discussion

Characterization of GO-DP1 nanoformulation

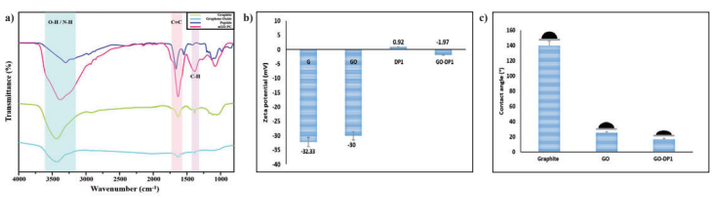

Fig. 1: Characterization of GO-DP1 nanoformulation by fourier-transform infrared spectroscopy (a), zeta potential (b) and water contact angle (c)[1].

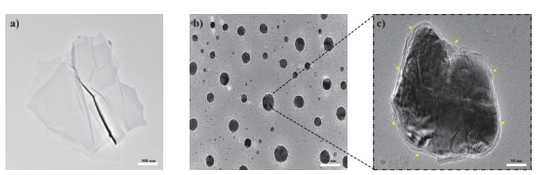

Fig. 2: High-resolution transmission electron micrographs of graphene oxide (d) and GO-DP1 nanoformulation (b,c)[1].

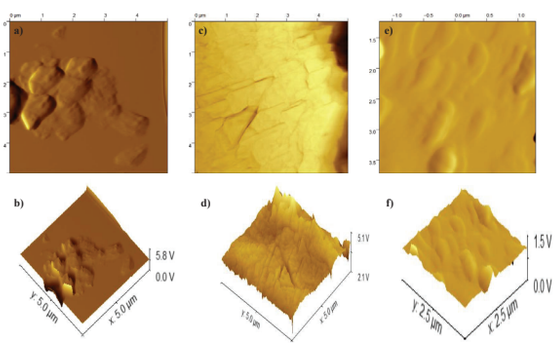

Fig. 3: AFM micrographs and 3D topology of graphite (a-b), GO (c-d) and GO-DP1 (e-f)[1].

Biomedical applicability of GO-DP1 nanoformulation as an antibiofilm coating

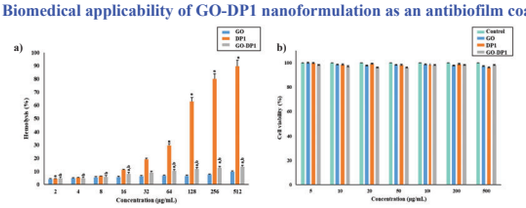

Fig. 4: *In-vitro* biocompatibility assessment via determination of hemolytic activity (a) and cell viability towards 3T3-L1(b) at different concentrations. Values represent mean ± SD (n = 6)[1].

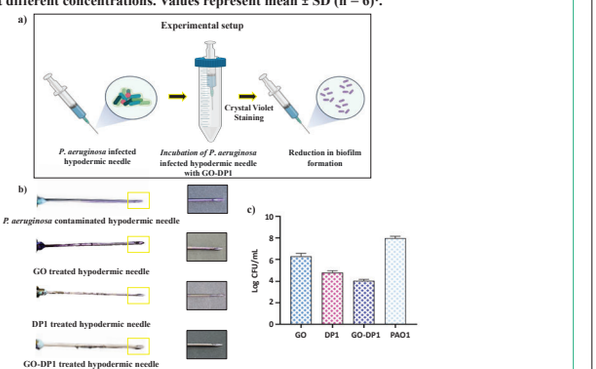

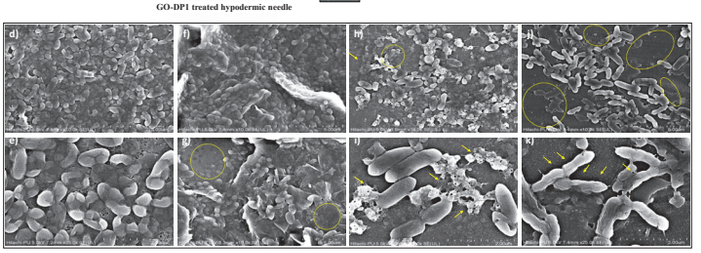

Fig. 5: Experimental setup for evaluation of antibiofilm activity in *P. aeruginosa* infected hypodermic needle model (a). Crystal violet-stained hypodermic needles incubated with GO, DP1 and GO-DP1, respectively (b). Antibacterial (c) and antibiofilm (d-k) effect of GO, DP1 and GO-DP1 incubated *P. aeruginosa* infected hypodermic needles[1].

Conclusion

- Biocompatible nanoformulations of GO-DP1 and rGO-DP1 with superior antibacterial properties against Gram-positive, Gram-negative and multidrug-resistant bacterial strains has been developed.
- Peptide DP1 and graphitic materials (GO and rGO) complimented each other in terms of antibacterial activity and hemolytic toxicity. The peptide imparts its antibacterial property to the conjugate while GO/rGO contributes by lowering the hemolytic toxicity.
- The synergy between the two materials led to the development of a one-of-a-kind non-hemolytic, antibacterial nanoformulations that displays broad-spectrum antibacterial as well as antibiofilm property. The study reports biomedical applicability of GO-DP1 as an antibiofilm nanocoating in *P. aeruginosa* infected hypodermic needles.
- Overall, the nanoformulations constitute highly promising system to combat bacterial infections that are difficult to treat by conventional methods.

References

1. Joshi, S., Chadha, J., Harjai, K., Verma, G., & Saini, A. (2024). Synthetic peptide (DP1) functionalized graphene oxide: A biocompatible nanoformulation with broad-spectrum antibacterial and antibiofilm activity. FlatChem, 44, 100626.
2. Sharma, P., Sharma, S., Joshi, S., Barman, P., Bhatt, A., Maan, M., Singla, N., Rishi, P., Ali, M.E., Preet, S., & Saini, A. (2022). Design, characterization and structure-function analysis of novel antimicrobial peptides based on the N-terminal CATH-2 fragment. Scientific Reports, 12(1), 12058.
3. Joshi, S., Siddiqui, R., Sharma, P., Kumar, R., Verma, G., & Saini, A. (2020). Green synthesis of peptide functionalized reduced graphene oxide (rGO) nano bioconjugate with enhanced antibacterial activity. Scientific Reports, 10(1), 9441.
4. Joshi, S., Sharma, D., Saini, A., & Verma, G. (2024). Peptide-reduced graphene oxide based functional paint: A sustainable alternative to toxic biocides. Progress in Organic Coatings, 195, 108636.
5. Verma, G., Saini, A., Joshi, S., & Sharma, D. (2022) Process and development of nano-bio composite anti-bacterial additive for commercial paint production. Indian Patent Office, Application No. 202211011934 A.

Acknowledgement

S. Joshi and A. Saini acknowledge Department of Science and Technology (DST), India for granting Women Scientist Scheme-B fellowship. G. Verma acknowledges the financial support given by Technical Education Quality Improvement Programme (TEQIP)-III funding conferred to Dr. SSBUICET, Panjab University, India. Authors would also like to like to express gratitude to the Sophisticated Analytical Instrumentation Facility (SAIF) and Central Instrumentation Lab (CIL), Panjab University, Chandigarh, India for providing instrumentation facilities.

https://doi.org/10.17952/37EPS.2024.P1322

Sustainable Development of Cross-Linked Films from Rapeseed Meal

Sara Aquilia,[1,2,3] Michele Pinna,[3] Anna Maria Papini,[1,2] Francesco Ciardelli,[3] Luca Rosi,[2] Claudia Bello.[1,2]

[1] *Interdepartmental Research Unit of Peptide and Protein Chemistry and Biology, University of Florence, Italy*

[2] *Department of Chemistry "Ugo Schiff", University of Florence, Italy*

[3] *Spin-PET s.r.l., Pontedera, Italy*

Sara Aquilia email: *sara.aquilia@unifi.it*

The availability of proteins from agricultural by-products and their favourable properties fostered a renewed interest in protein-based materials, fuelling research on innovative technologies for the preparation of bioplastics.[1] Proteins from rapeseed meal have been chosen as first candidates for our bio-plastics main ingredient due their low cost and biodegradability.[2] Herein, we present our preliminary results toward the development of biocompatible and renewable protein-based film.

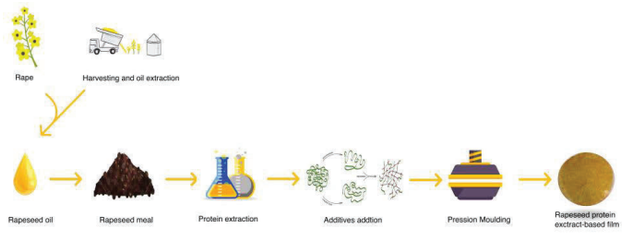

A novel protein extraction method was set up, yielding a protein-enriched extract with high efficiency, showing its potential for industrial application. Utilizing this protein extract, films were fabricated through pression moulding. Blends incorporating the protein extract, glycerol, cross-linker, and protein-based compatibilizer (RM) were formulated. The addition of sodium sulfite (Na_2SO_3) and different denaturants (SDS, urea, guanidine) aimed to induce protein denaturation during thermal processing. Enzymatic proteolysis of the protein-enriched extract with selected proteases lead to hydrolysates that will be employed as additives in the rapeseed protein-based film.

RAPESEED PROTEIN EXTRACTION AND CHARACTERIZATION

The main rapeseed protein component is cruciferin, representing about 60% of the total protein content. Cruciferin is a globular protein with a molecular mass of 300-360 kDa.[3]

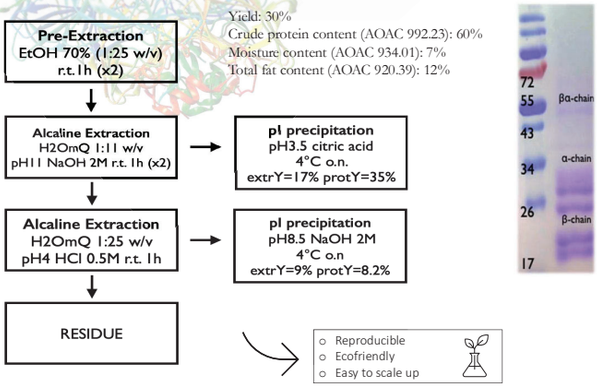

Yield: 30%
Crude protein content (AOAC 992.23): 60%
Moisture content (AOAC 934.01): 7%
Total fat content (AOAC 920.39): 12%

A protein-rich extract was obtained as shown by the IR spectra and RP-HPLC chromatogram. The process is reproducible, scalable, and eco-friendly, demonstrating its potential for industrial applications.

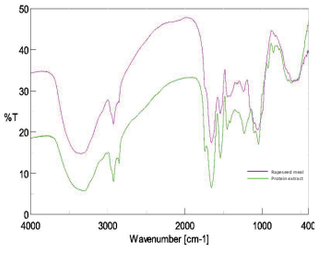

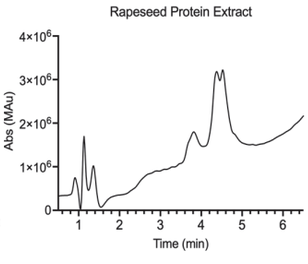

PRELIMINARY STUDIES

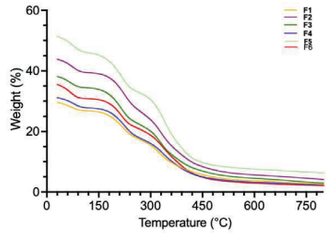

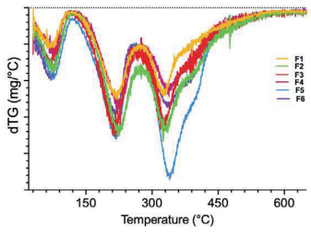

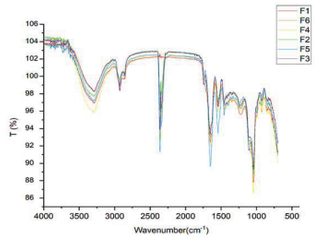

Change in shape in the range of 1600-1625 cm^{-1} were observed in the IR spectrum due to changes in the secondary structure of the protein. TGA indicates an enhanced thermal stability for the material containing both the reducing and the denaturing agent (*F6*).

ENZYMATIC PROTEOLYSIS

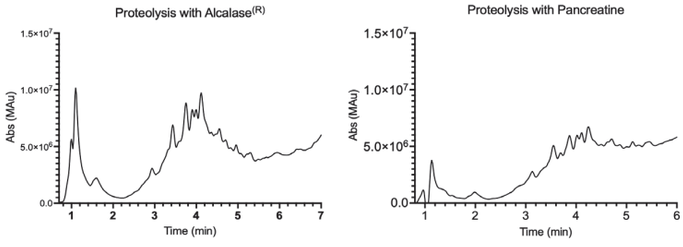

Formation of hydrophilic peptides has been showed by RP-HPLC.

CONCLUSIONS AND FUTURE PROSPECTIVES

Rapeseed protein extract has a high potential for its use in the production of sustainable films. First studies on the thermal stability and on the protein structural changes have been done, showing an enhanced thermal stability when both reducing and the denaturing agents (*F6*) are used. The study is certainly innovative and informative but the mechanical properties not industrially competitive. However, our study suggests a promising pathway to develop a protein-rich material for industrial application.

The conditions for proteolysis have been optimized, and ongoing tests are being conducted to assess their impact on the rapeseed protein-based film properties. Purification and characterization of the most promising peptides will be performed in order to understand the relationship between the peptide structures and their influence on the features of the film.

1. Hatti-Kaul, R. et al. Trends Biotechnol 2020, 38 (1), 50–67.
2. DeFrates, K. G. et al. Nanomaterials 2018, 8 (7), 457.
3. Newson, W. R. Industrial Oil Crops 2012, 59.

PON Research and Innovation 2014–2020 (D.M 1061/2021) XXXVII Cycle in Chemical Sciences funded by MUR/EU-FSE.

https://doi.org/10.17952/37EPS.2024.P2002

Suspension Bead Loading (SBL): An Economical Protein Delivery Platform to Study URM1's Behavior in Live Cells

Reem Mousa‡ , Abhishek Saha‡ , Yam Alalouf, Pradeep Sadhu, Mahdi Hasan, Shaswati Mandal, Guy Mann, and Ashraf Brik*

Schulich Faculty of Chemistry, Technion-Israel Institute of Technology, Haifa, 3200008, Israel.
Reem.mousa@campus.Technion.ac.il

Abstract

Uniquely modified synthetic proteins are difficult to produce in large quantities, which could limit their use in various *in vitro* settings and in cellular studies. In this study, we developed a method named "suspension bead loading" (SBL), to deliver protein molecules into suspended living cells using glass beads, which significantly reduces the amount of protein required for effective delivery. We investigated the delivery efficiency of functionally different proteins and evaluated the cytotoxic effect of our method and the chemical and functional integrity of the delivered protein. We utilized SBL to address questions related to ubiquitin-related modifier 1 (URM1). Employing minimal protein quantities, SBL has enabled us to study its behavior within live cells under different redox conditions, including subcellular localization and conjugation patterns. We demonstrate that oxidative stress alters both the localization and conjugation pattern of URM1 in cells, highlighting its possible role in cellular response to such extreme conditions.

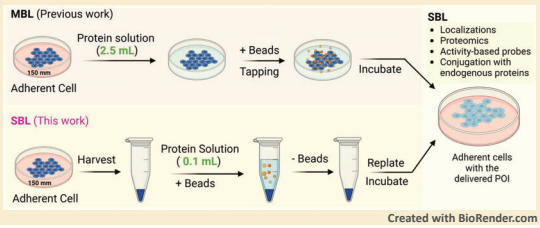

Results

The synthetic proteins employoed in SBL development

All protein were prepared chemically by Fmoc-SPPS

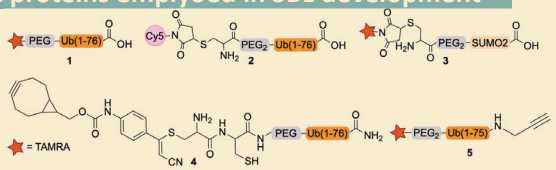

Cellular uptake of TAMRA-Ub (1)

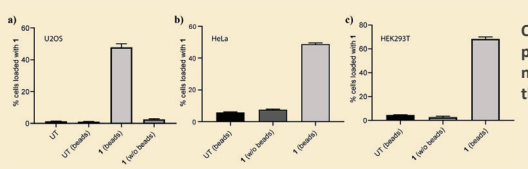

Our developed SBL method produces a considerable number of cells containing the protein cargo

Cytotoxcicity studies of SBL

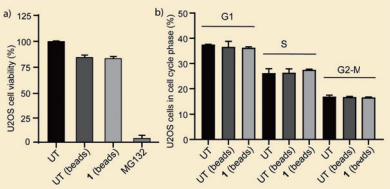

a) MTT cell proliferation assay on U2OS cells showed more than 85% of the cells remained viable after SBL
b) Propidium iodide (PI) based cell cycle assay shows no impact on the cell cycle phases

Live cells LCSM images of U2OS cells loaded with SUMO2 and EGFP

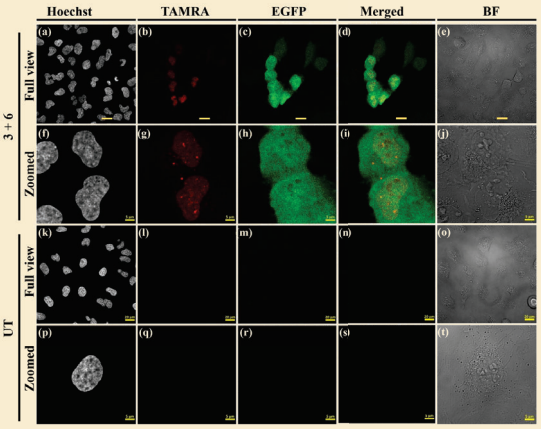

- SUMO2 (3) localized in both the cytosol nucleus, and EGFP (6) is distributed all over the cell.
- Multiplexed bead loading in suspention showed also reproducible results.

Chemical and functional charctrization of Ub cargos

Fluorecent intensity analysis of cargo (4) using SPAAc reaction confirms the intigerity of our synthetic Ub in live cells

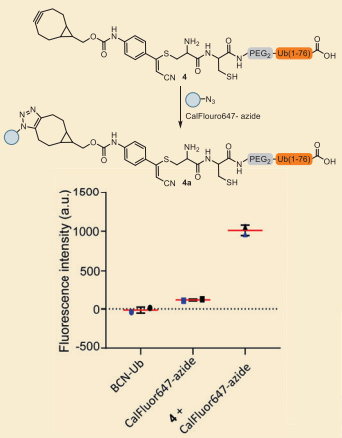

Florecent gel analysis of the conjugation pattern of synthetic Ub (1), and for Ub-PA (5) caputring DUBs in live cells

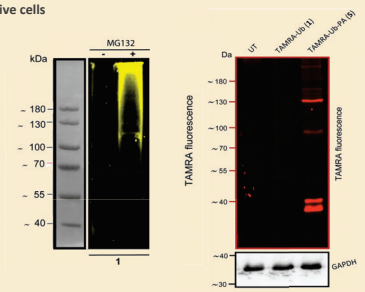

All functional analyses confirm that SBL didn't affect the integrity and functioanlity of our delivered proteins

Volcano plot of enriched DUBs captured by Biotin-Ub-PA

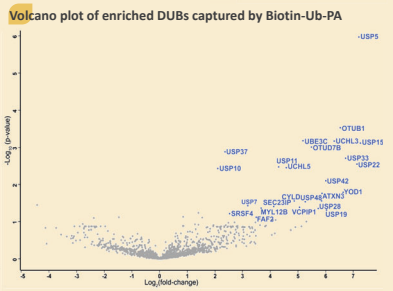

Applying SBL to study ubiquitin like modifier-1 (URM1)

Chemical protein synthesis of URM1

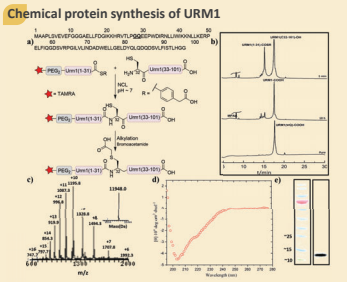

Live cell LSCM images of U2OS cells loaded with URM1-COOH using the SBL

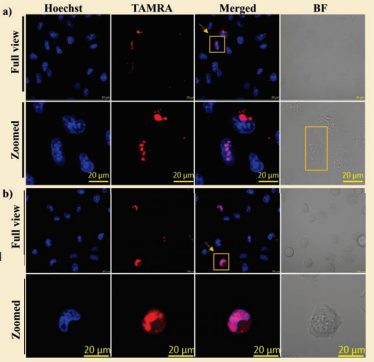

Live cell LSCM images of U2OS cells loaded with URM1-COOH using bead loading

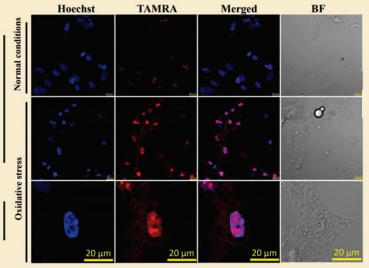

All URM1 analogs localize in the nucleoles under normal condition and diffuse out under oxidative stress.

Fluorecent gel analysis of U2OS cells loaded with URM1 analogs under normal and oxidative stress conditions

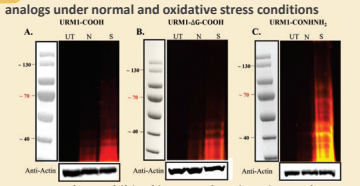

URM1 analogs exhibited increased conjugation under oxidative stress

Conclusions

- We developed a new general approach for delivering different functional proteins, in suspension phase, applying small amounts of protein(s).
- SBL is also suitable for multiplexed loading of proteins without requiring any special machinery or equipment.
- SBL allowed accessing for the first time URM1, and study some of its cellular properties. Despite challenges in URM1 synthesis, SBL enabled applying minimal quantities (0.1 ml vs. 1ml of protein solution).
- URM1 localizes in the nucleoli under normal conditions and diffuses out under oxidative stress, emphasizing its role and involvement in stress damage response.
- Regardless of its C-terminal functionality, URM1 forms fewer conjugates under normal conditions compared to oxidative stress.

1. Abhishek Saha‡ , Reem Mousa ‡, *et.al.* Suspension Bead Loading (SBL): An Economical Protein Delivery Platform to Study URM1's Behavior in Live Cells, *Angew. Chem. Int. Ed. Under revision* .
2. Mann, G.; Sadhu, P.; Brik, A. Multiplexed Delivery of Synthetic (Un) Conjugatable Ubiquitin and SUMO2 Enables Simultaneous Monitoring of Their Localization and Function in Live Cells. *ChemBioChem* 2022, *23*, e202200122.
3. Mann, G.; Sadhu, P.; Brik, A. Synthetic Proteins behind the Plasma Barrier: Molecular Spies. *Acc. Chem. Res.* 2022, *55*, 2055−2067.

https://doi.org/10.17952/37EPS.2024.P2003

Synthesis and Conformational Analysis of β,β-Diaryl-α-Amino Acids: on the Way to Molecular Gearing

Timo Zimmer and Armin Geyer
Department of Chemistry, Philipps-University Marburg, Germany

Introduction

Unnatural amino acids are useful building blocks for the synthesis of custom-made peptides and other complex molecules in drug discovery, medicinal, or material chemistry among other fields. β-branched-α-amino acids allow the conformational control of side chain orientation and thus can shape a peptide in a predictable way. We previously synthesized unsymmetric β,β-diaryl-α-amino acids, combining phenylalanine and tryptophan in one amino acid.[1] Depending on the side chain orientation the biologic function of short ghrelin peptides could be switched between agonism and antagonism towards its receptor.[2] We present the synthesis of even larger β,β-dinaphthyl-α-amino acids, their conformational analysis, and incorporation into peptides.

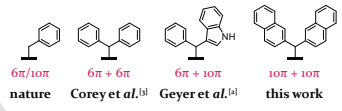

Design

Combining different aromatic groups leads to a squared number of possible substitution patterns. Shown is the combination of 3 different naphthyl moieties, resulting in 9 different amino acids, that have been synthesized.

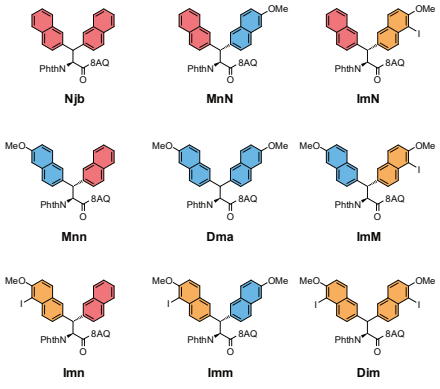

Synthesis

The amino acids are synthesized *via* palladium catalyzed, directed C-H activation. Therefore alanine is decorated with a phtalimide (Phth) protecting group on the nitrogen and the amide of 8-aminoquinoline (8AQ) at the *C*-terminus. Depending on the reaction conditions only one or two aryl groups are installed in β-position. In the former case a second aryl group can be incorporated stereoselectively, thus giving access to different diasteromers of the same amino acid. The amino acid can consecutively be transformed into a building block for solid phase peptide synthesis (SPPS), as previously reported by our group.[2]

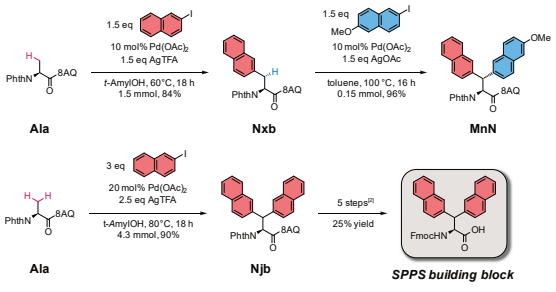

Applications in SPPS

The dinaphthyl amino acids are incorporated into peptides via SPPS. Due to their high hydrophobicity and their distinct sidechain orientation they can shape a peptide in a specific way, while the mobility of each napthyl group allows for adaptation to the environment. Furthermore, a possibly cooperative conformational exchange between the naphthyl groups would allow the design of allosteric interactions in a complex environment.

In the examples shown below the Njb amino acid (red) replaces phenylalanine in a short ghrelin receptor binding peptide. Structure determinaton based on NMR derived restraints reveal the helical structure of the peptide. Another example shows the incorporation of Njb into the foldon miniprotein, a well known trimeric structure. This way the interaction between three Njb residues can be studied, as they are brought into spatial proximity.

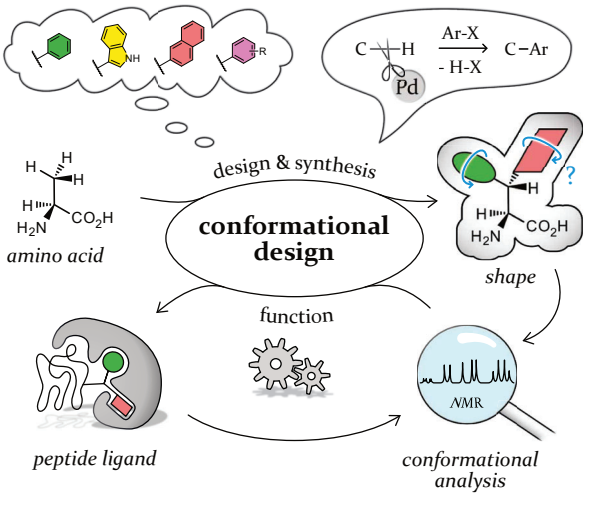

Analysis of Side Chain Conformation

The conformation of β,β-diaryl amino acids is usually restricted along the Cα-Cβ (χ1) axis due to steric reasons, with Hα and Hβ oriented anti-periplanar. The aromatic side chains may rotate along the χ2 and χ2' axis (indicated with blue arrows), although due to steric reasons the two conformations in which the aromatic ring is in the same plane as the Cβ-Hβ bond should be preferred (a). For each of those conformations a specific NOE pattern is expected (b). An analysis of the averaged pattern (c) indicates to what extent the conformations are populated and, more interestingly, if a correlation between the conformations exists. Such a gearing type interaction between the aromatic rotors, as observed for Phth-Njb-8AQ (d) can potentially be used for the design of allosteric interactions.

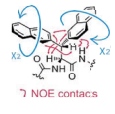

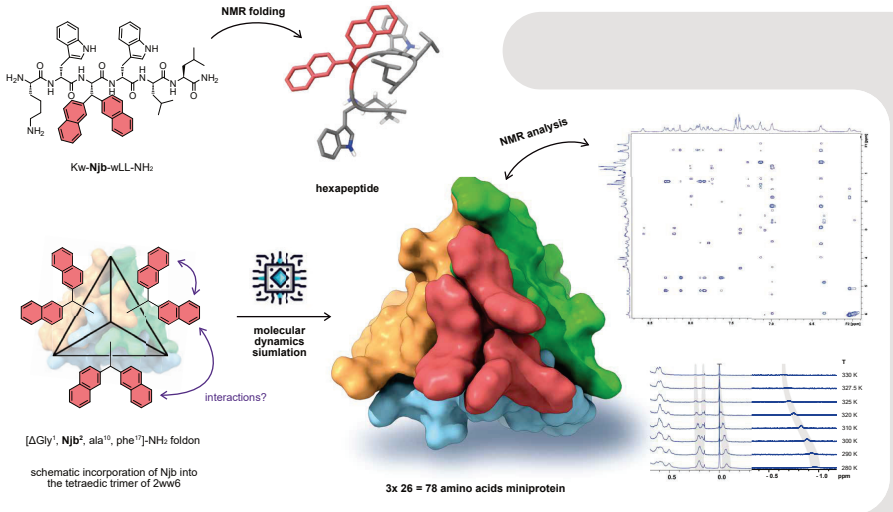

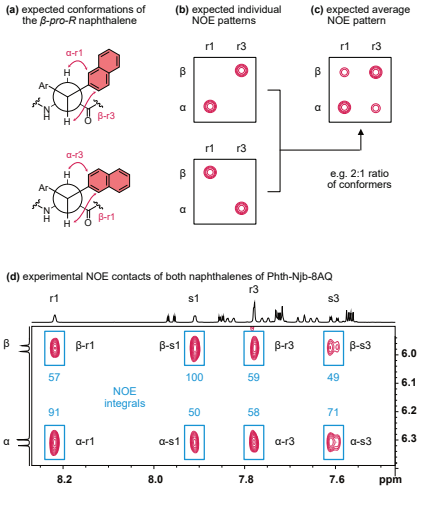

References

[1] L. Nicke, P. Horx, R. Müller, S. Els-Heindl, A. Geyer, *ChemBioChem* **2021**, *22*, 330-335.
[2] L. Nicke, P. Horx, K. Harms, A. Geyer, *Chem. Sci.* **2019**, *10*, 8634.
[3] B. V. S. Reddy, L. R. Reddy, E. J. Corey, *Org. Lett.* **2006**, *8*, 3391.

Conclusion and Outlook

The synthesis of a novel β,β-diaryl-α-amino acids featuring two naphthyl moieties was achieved by a palladium catalyzed C-H activation strategy with consecutive transformation into a SPPS building block[2]. The conformation of the Njb amino acid was studied in peptidic environment, showing promising first results on the way to molecular gearing.



A green peptide synthesis protocol for improving peptide production: a new approach

L. Lastella[1], B. Biondi[2] , I. Guryanov[3] , F. Formaggio[1,2] , M. Macis[3] and A. Ricci[3]

[1]Department of Chemistry, University of Padova, 35131 Padova, Italy [2]Institute of Biomolecular Chemistry, Padova Unit, CNR, 35131 Padova, Italy
[3]Fresenius Kabi iPSUM Srl, 45010 Villadose, Italy

https://doi.org/10.17952/37EPS.2024.P2004

Co-funded by the European Union

Introduction

Peptides play important roles in many fields, but especially in the pharmaceutical one, as they have numerous advantages. On both a laboratory and industrial scale, peptides are synthesised according to the Solid Phase Peptide Synthesis (SPPS) protocol, which involves the use of an insoluble solid support on which the peptide chain is grown. Despite the numerous advantages that make this protocol the most widely used methodology for peptide production, SPPS has some disadvantages: it is necessary both to use a large excess of reagents to obtain excellent yields and good purity of the final product, and to use a large quantity of organic solvent, especially in the washing steps.

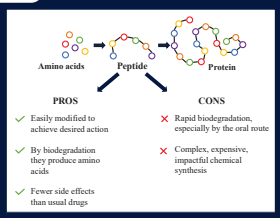

New Scaffolds

The main objective is to develop an alternative route for peptide synthesis.
The idea is to replace the common insoluble polystyrene substrates (resins) used for SPPS with soluble and biodegradable ones that allow the homogeneous phase to be used for peptide synthesis.

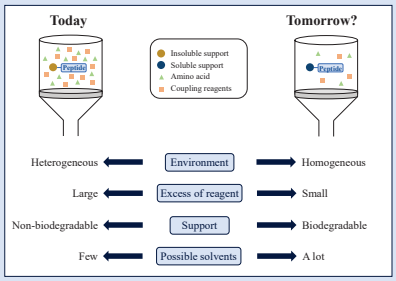

Heterogeneous phase synthesis has numerous advantages (such as the easiness with which excess reagents and by-products are removed by filtration) but also numerous disadvantages as mentioned above.

By exploiting synthesis protocols in a homogeneous environment, where reactivity is higher, it would be possible to reduce reagent excess and solvent volume. Furthermore, by using homogeneous phase synthesis, different types of organic solvents will be exploited.

The designed and synthesised scaffold (**S**) was then functionalised to allow subsequent synthesis of the peptide sequence.
Fmoc Rink Amide Linker was chosen to obtain the peptide with an amide at the C-terminal (**S***) but several other linkers can be used to achieve different functionalities on the C-terminal.

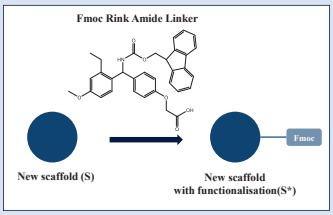

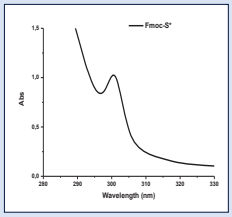

The UV absorption of the Fmoc group was used to confirm the presence of the linker on the scaffold.

The graph on the left shows the UV absorption spectrum of the soluble scaffold synthesised and functionalised with the linker (**S***).

Organic Nanofiltration

Crucial is the development of an organic nanofiltration (**ONF**) procedure that separates (i) the by-products and excess reagents present after the coupling reactions and (ii) the dibenzofulvene, generated during the Fmoc removal from the growth chain.

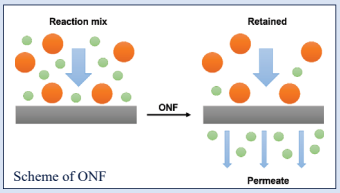

Scheme of ONF

MetCell System



The nanofiltration system used is the MetCell System (Evonik Industries), a system that uses membranes with a cutoff of 600Da.



The membranes identified are stable to various organic solvents of low polarity (alcohols, ethyl acetate, hexane, toluene).

	EtOH		ACN		DCM		DMF				
	Compatibility	Optimal flow rate	Compatibility	Optimal flow rate	Compatibility	Optimal flow rate	Compatibility	5% in DCM Optimal flow rate	10% in DCM Optimal flow rate	15% in DCM Optimal flow rate	20% in DCM Optimal flow rate	100% Optimal flow rate
Type of membranes												
Performance	✓	✓	✓	✓	✓	✓	✗	✓	✓	✓	✓	✗

The best solvents are ACN and DCM, which allow rapid filtration with a flow rate of about 3mL/min. DMF (excluded anyway due to its high environmental impact) has been tested for comparison but is not compatible with the membranes used unless it is mixed with one of the other solvents (20% DMF in DCM). Alcohols, on the other hand, were excluded because they generate high back pressure during filtration and, being good nucleophiles, are avoided in peptide synthesis processes because they are competitive in peptide bond formation.

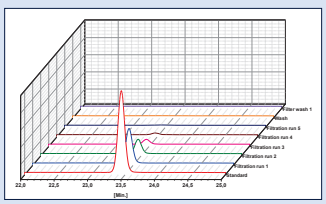

To use ONF, filtration conditions were first developed on a model system consisting of **S*** and Fmoc-Ala-OH 2mM. Numerous filtration cycles were performed and for each of them, an HPLC-MS analysis was conducted to detect the presence or absence of alanine in the filtrate and retained solution. From the results shown in the graph on the left, it can be concluded that four filtration cycles are sufficient to completely remove the low molecular weight components.

Synthesis of a model peptide

Fmoc-LLVF-NH$_2$

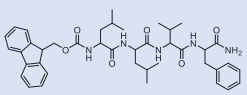

The model peptide **Fmoc-Leu-Leu-Val-Phe-NH$_2$** was synthesised according to the scheme on the left. The couplings were conducted with an excess of 3eq of amino acid, OxymaPure and DIC as coupling reagents. At the end of the reaction, excess reagents and by-products were removed by ONF. Fmoc removal was performed with 20% piperidine in the solvent used and also in this case an ONF step is necessary to remove the dibenzofulvene from the scaffold with the growing peptide.
The scaffold-peptide conjugate was then isolated in each step.

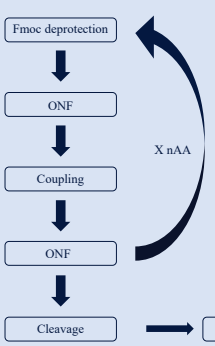

After each coupling, UV-Vis experiments were conducted on the isolated scaffold-peptide conjugate to verify the actual formation of the peptide bond between the chain present on the support and the amino acid. This was possible by detecting the presence of the Fmoc absorption band at λ=298nm. For comparison, the absorption spectrum of the scaffold-peptide conjugate isolated after ONF , after removal of the protective Fmoc group from the growing chain, was also recorded, which shows no UV absorption due to the presence of the free amine.

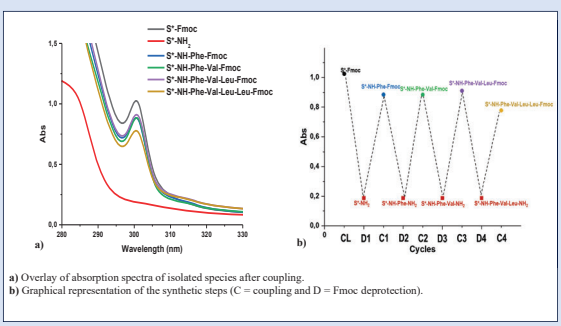

a) Overlay of absorption spectra of isolated species after coupling.
b) Graphical representation of the synthetic steps (C = coupling and D = Fmoc deprotection).

When the peptide has been completely synthesised, the chain was detached from the support. This product comprises the model peptide chain and the scaffold from which the chain was detached.

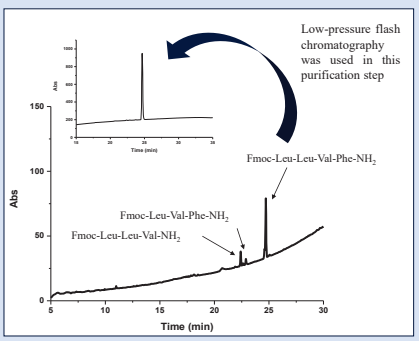

HPLC chromatogram shows the target model peptide and two by-products that confirm the results of the UV-Vis analysis.

Conclusions

- Soluble, biodegradable and non-toxic supports have been synthesised that can be used instead of common polystyrene resins.
- On these scaffolds, it was possible to synthesise a model peptide chain.
- The ONF procedure developed made it possible to separate the scaffold with the growing peptide from the mixture of by-products and excess reagents.
- Throughout the new process, we moved away from the use of DMF as a solvent.

However, due to solubility issues and some limitations of ONF, the developed scaffolds are still being studied.

References

Chemical Communications, **2010**, *46*, 2808-2810

Fmoc solid phase peptide synthesis: a practical approach, Oxford University Press, **1999**

Green Chemistry, **2016**, *18*, 3879-3890

Nature, **1972**, *237*, (5357), 512-513

Chemical reviews, **2014**, *114*, 10735-10806

Please do not hesitate to contact me for questions and curiosities!!!

luana.lastella@phd.unipd.it

https://doi.org/10.17952/37EPS.2024.P2005

A Rapid and Efficient Photochemical Modification Strategy for Late-Stage Peptide and Protein Functionalization

Meng-Qian Zhang, Yan-Mei Li*

Department of Chemistry, Key Lab of Bioorganic Phosphorus Chemistry & Chemical Biology(Ministry of Education), Tsinghua University, Beijing, 100084, P.R. China.

Corresponding author Email: liym@mail.tsinghua.edu.cn

Abstract

As an easily introduced noncoded amino acid with unique electrophilicity distinct from 20 natural amino acids, dehydroalanine (Dha) is a promising multifunctional labeling site for peptides and proteins. However, achieving a balance between reaction rate and mild reaction conditions has been a major challenge in developing novel Dha-modification strategies. Rapid, efficient, and mild Dha modification strategies are highly desired. Here, we present a photoinitiated 1,3-dipolar cycloaddition reaction between Dha and 2,5-diaryl tetrazoles. Under low-power UV irradiation, this reaction completes rapidly without catalysis, yielding a fluorescent pyrazoline-modified peptide or protein with exceptional Dha residue chemoselectivity. This reaction demonstrates complete site-specificity in thiostrepton modification within 20 minutes, making it the fastest Dha16-specific reaction in thiostrepton. Furthermore, this photoinitiated reaction provides a chemoselective strategy for the precise functionalization of proteins. Additionally, when combined with the fluorogenic property of the pyrazoline-modified product, this photo-controllable methodology can be applied to live cell imaging, further expanding the application scope of Dha modification techniques.

Photoinitiated 1,3-dipolar cycloaddition between dehydroalanines and tetrazoles

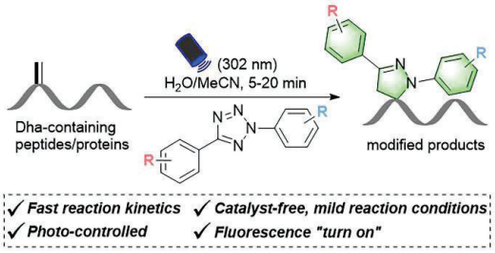

An efficient strategy for dehydroalanine cycloaddition modification was presented, which enables rapid generation of fluorescent pyrazoline-modified peptides and proteins under mild, non-catalytic reaction conditions.

Chemoselective labelling of *α*-synS129Dha

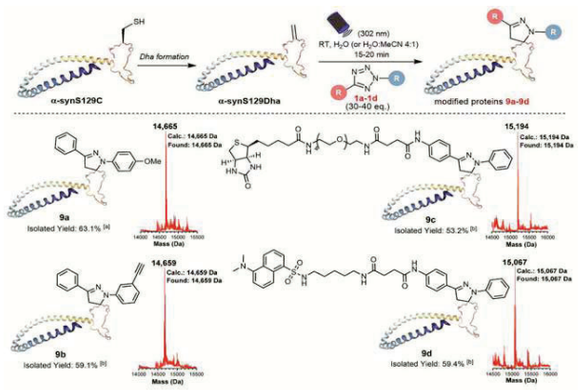

[a] The reaction was performed in H_2O. [b] The reactions were conducted in the H_2O-MeCN mixed solvent (4:1, v/v).

Site-selective labelling of thiostrepton

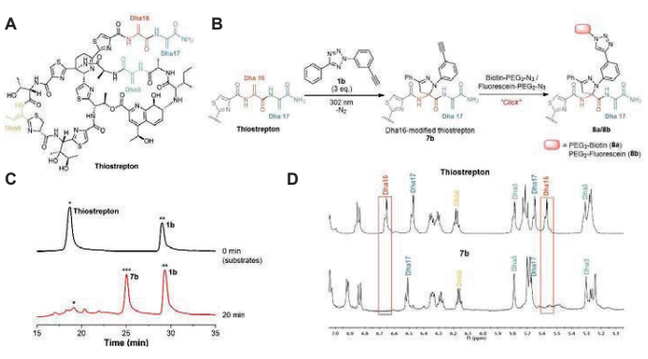

A) Chemical structure of thiostrepton. B) Two-step reaction for site-specific labelling of Dha16 on thiostrepton. C) HPLC analysis of the reaction mixture of thiostrepton and tetrazole **1b** at 0 min (top) and 20 min (bottom). D) ^{1}H NMR spectra of thiostrepton and Dha16-labelling product **7b**. Chemical shifts of signals from the C(sp^2)-H of Dha3, Dha16, Dha17, and Dhb8 are assigned.

In-situ imaging of tumour cells

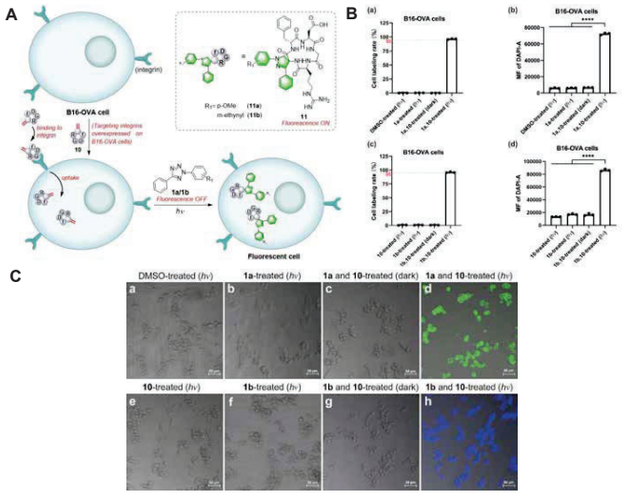

A) Schematic illustration. B) Flow cytometry analysis of B16-OVA cells. C) Merged images of DAPI and T-PMT channels of B16-OVA cells captured by confocal laser scanning microscope.

References

1. Zhang, M.-Q.; He, P.-Y.; Li, Y.-M., Light-initiated 1,3-dipolar cycloaddition between dehydroalanines and tetrazoles: application to late-stage peptide and protein modifications, *Chem. Sci.,* **2023**, *14*, 9418-9426.

Novel Selectively Cleavable Dmb-Based Protecting Groups for Side Chain Amino Groups of Amino Acids

Raimund Maier[1], Karin Rustler[1], Thomas Bruckdorfer[1], Udo Kalejs[2], Vilnis Liepins[2], Kai Holland-Nell[3], Jacqueline Dalski[3], Stephan Pritz[3]

[1] Iris Biotech GmbH, Adalbert-Zoellner-Str. 1, 95615 Marktredwitz, Germany ; Bapeks Ltd., Rupnicu 4, Nordic Industrial Park, Olaine, LV-2114, Latvia ; Biosyntan Gesellschaft für bioorganische Synthese mbH, Robert-Roessle-Straße 10, 13125 Berlin, Germany

https://doi.org/10.17952/37EPS.2024.P2008

Abstract

We are presenting a **novel selectively cleavable protecting group** for the side-chain amino groups of lysine or other diamino acids, which play an important role during peptide synthesis, e.g., for modification of a particular side chain on the synthesis resin.

Trityl-based, mildly acidic cleavable protecting groups such as Mtt or Mmt are incompatible with strongly acid-labile resin linkers like trityl. Therefore, amino acid derivatives carrying the **hydrazinolysis-susceptible protecting group Dde or ivDde**[A] are frequently used for the synthesis of branched, cyclic, or side chain-modified peptides. However, **Dde might migrate to free lysine epsilon-amino groups ("scramble")**[B] and for the more robust **ivDde, total removal is hardly possible**.

A newer group for the orthogonal protection of amino groups is **MeDmb (methyl dimethylbarbituric acid)**.[C]

In our study we present the possibilities and limitations of the novel lysine Dmb derivatives **(MeDmb, EtDmb, ivDmb)** and compare their properties with the existing protecting groups Dde and ivDde.

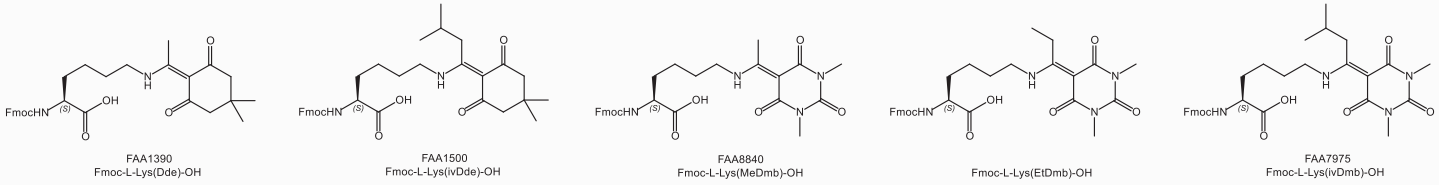

FAA1390 Fmoc-L-Lys(Dde)-OH | FAA1500 Fmoc-L-Lys(ivDde)-OH | FAA8840 Fmoc-L-Lys(MeDmb)-OH | Fmoc-L-Lys(EtDmb)-OH | FAA7975 Fmoc-L-Lys(ivDmb)-OH

Results & Discussion

- **Stability**

  → Fmoc-Lys(MeDmb/EtDmb/ivDmb)-OH are clearly soluble in DMF (0.5 M), stable for > 3d in closed vials at RT in DMF, and stable in TFA/H_2O for at least 4.5h

- **Scrambling on side chains**

  → Synthesis of Boc-Lys(Fmoc)-Ala-Lys(**X**)-Pro-Lys(**X**)-Ala-(2CT-resin); 50% Pip/DMF, 30 min; cleavage 20% HFIP/DCM; LCMS: Boc-Lys-Ala-Lys(**X**)-Pro-Lys(**X**)-Ala-OH

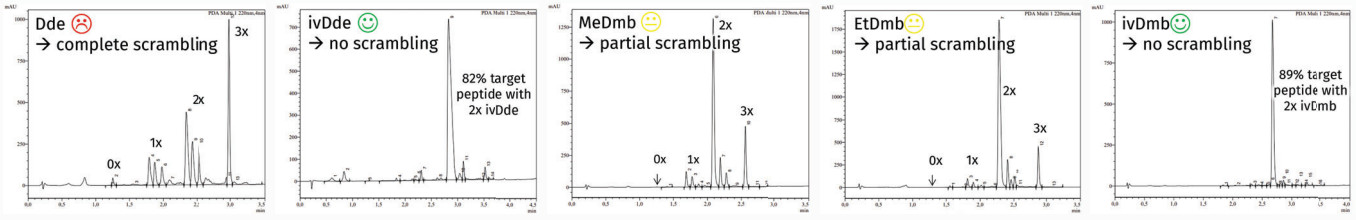

- **Stability during synthesis/cleavage**

  → Synthesis of Boc-Gly-Ser(tBu)-Ala-Leu-Gly-Lys(**ivDmb**)-Ala-Phe-Gly-Phe-Ser(tBu)-Glu(OtBu)-TG S Trt resin; treatment with various solvents; TFA cleavage

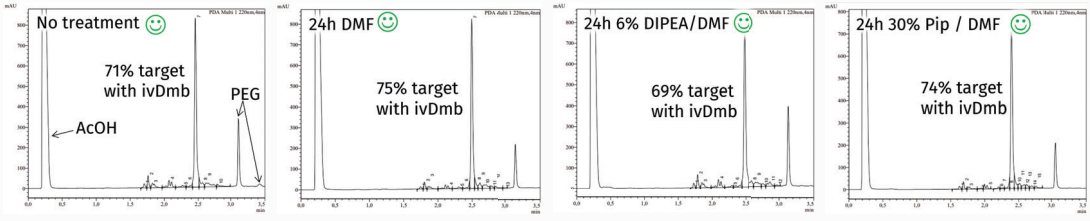

- **Cleavage of the side chain protecting group**

  → „Standard" protocol 2% hydrazine monohydrate 3x3 min (left); „stronger" protocol 4% hydrazine monohydrate 5x5 min (right)

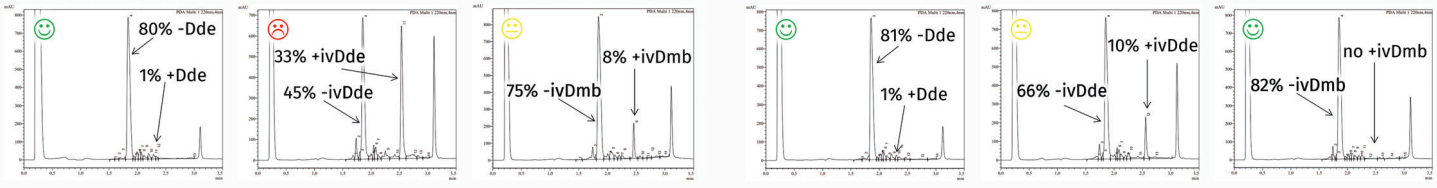

- **„Real" example**

  → Synthesis of Boc-Gly-Ser(tBu)-Ala-Leu-Gly-Lys(**X**)-Ala-Phe-Gly-Phe-Ser(tBu)-Glu(OtBu)-TG S Trt resin (HATU/NMM; 30% piperidine/DMF; 200 mg Glu-TG; 0.19 mmol/g); cleavage of ivDmb/ivDde („stronger" protocol); coupling of 5-carboxyfluorescein; TFA cleavage; HPLC purification (RP18, ACN/H_2O/0.05% TFA)

	ivDde 😐	ivDmb ☺
Crude yield	31 mg	37 mg
Crude purity	82% 5-Fluo + 4% ivDde	86% 5-Fluo + no ivDmb detectable
Isolated yield	10.9 mg (>95%) + 7.8 mg (82%) (repurification)	23.6 mg (>95%)

Summary

- Fmoc-Lys(ivDmb)-OH performs better than previously known orthogonally protected Lysines with regards to scrambling avoidance, deprotection completion, and peptide yield.

References:

[A] S.R. Chhabra, B. Hothi, D.J. Evans, P.D. White, B.W. Bycroft, W.C. Chan; *Tetrahedron Lett.* 1998, **39:** 1603-1606.

[B] R.R. Wilhelm, A. Srinivasan, M.A. Schmidt; in *„Peptides for the New Millennium, Proc. 16th American Peptide Symposium"*, G.B. Fields, J.P. Tam, G. Barany (Eds.), Kluwer Academic Publishers, Dordrecht, p. 58f.

[C] S. Ramkisson, H. H. Al-Rasheed, K. A. Dahlous, B. G. de La Torre, A. El-Faham, F. Albericio; *ChemistrySelect* 2021, **6:** 6626-6630.

https://doi.org/10.17952/37EPS.2024.P2009

Conformational editing and intracellular delivery of intrinsically disordered protein domain

Alexis Jouin,[1] Alastair McEwen,[2] Pierre Poussin-Courmontagne[2], Bruno Kieffer[2], Vladimir Torbeev[1]

[1]UMR7242 : Biotechnologie et signalisation cellulaire (BSC) , Laboratoire chimie des biosystèmes, École Supérieure de Biotechnologie de Strasbourg (ESBS), Illkirch, France

[2] Department of Integrated Structural Biology, Institut de Génétique et de Biologie Moléculaire et Cellulaire (IGBMC), CNRS, INSERM, University of Strasbourg, Illkirch France

Introduction: In this study, we proposed an approach to target complex formation that involves IDPs that is based on conformational editing of the IDP domain by utilizing backbone conformational constraints (α-methylation) to facilitate binding and stabilize or destabilize helical structures. (1) Non-canonical modifications can also stabilize against proteolytic degradation—an advantage for intracellular activity of peptides.

Biological context

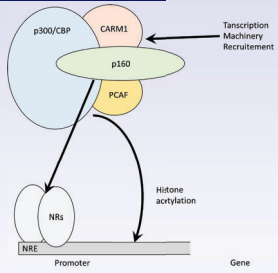

Our system of study:

NCBD of CBP/p300 (2066-2112)

H_2N-SALQDLLRTLKSPSSPQQQQQVLNILKSNPQL-Nle-AAFIKQRTAKYVAN-$CONH_2$

AD1-ACTR/p160 (1040-1086)

H_2N-EGQSDERALLDQLHTLLSNTDATGLEEIDRALGIPELVNQGQALEPK-$CONH_2$

Mutation site : X→α-methylation ; G→d-Ala

CBP/p300 interact with the promoter of **≈25%** of the human genome and more than **400** transcription factors.

Implication in numerous diseases such as estrogen-dependent (ER+) breast cancer, neurodegenerative diseases.(2)

ACTR/p160 is implicated in the **estrogen production and response** and known to be overexpressed in **breast cancer ER+** and be involved in the **tamoxifen resistance.**(3)

Cell culture

All experiments have been done on U2OS cells.

Variants used : Pen-cys(IAF)-peg5-aMex3

Confocal microscopy

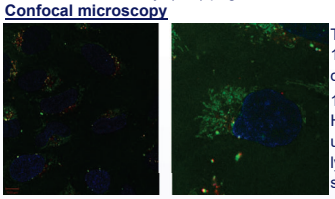

Three concentration tried : 10µM, 5µM, 2,5µM in media

1h incubation (Blue: Hoechst 33342 for nucleus, red: LysoTracker for lysosome and late endosome)

Endoplasmic reticulum? Golgi apparatus? Mitochondria ? Bind to CBP ? Aggregation ?

Flow cytometry

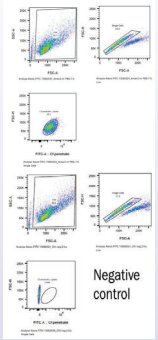

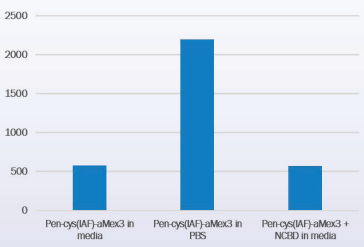

The use of PBS instead of media to make the incubation seems to increase the uptake of the peptide (interaction with media component ?).

Circular dichroism characterization

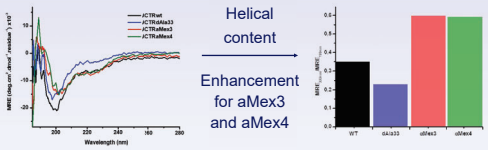

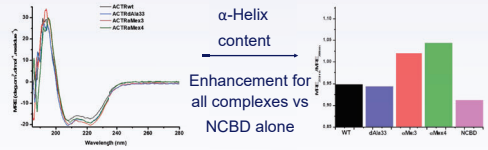

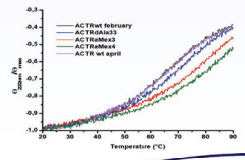

The thermal denaturation of complex NCBD/ACTR$_{Variants}$ shows that all the variants induce more stable complex with NCBD than WT.

Reproducibility of the data.

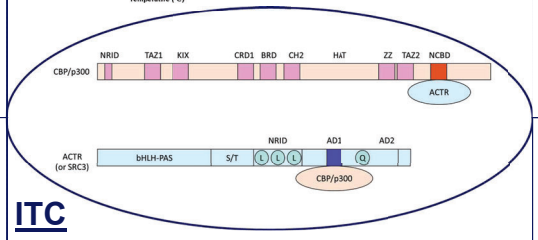

ITC

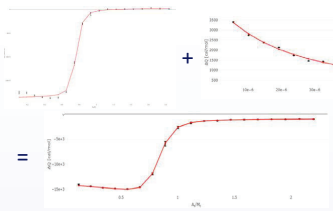

New model :

A+B ↔ AB + A+A ↔A2

Variant	Kd (nM)	ΔH (kcal/mol)	ΔG (kcal/mol)	-TΔS (kcal/mol)	ΔS (kcal/mol/deg)	ΔCp (kcal/deg,mol)
wt	260	-13,6	-9,16	4,48	-0,0147	
aMex4	119	-16,1	-9,63	6,44	-0,0212	
aMex3	97,7	-20,6	-9,75	10,9	-0,0358	-0,975
dAla33	188	-16,0	-9,36	6,64	-0,0218	-0,748

ΔG is nearly constant whereas ΔH and ΔS change a lot => **enthalpy-entropy compensation** (EEC).

ΔH = more contact or more tighter ones between both peptide.

New questions :

⇒ Does the EEC can be explain only by conformational entropy ?

⇒ Role of solvation ?

⇒ Role of hydrogen bonding ?

⇒ Role of ionic interactions ?

} New experiments needed. D_2O in place of water, different pH, different buffers...

Crystallography

Quasi-racemic crystallography

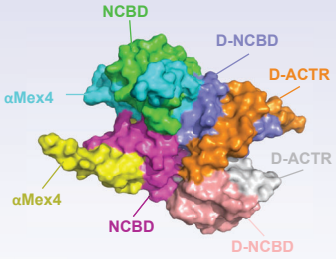



In each data set (n=8) we can see the two types of ACTR/NCBD complexes

ACTRαMex4 adopts **two different conformations** in each crystal and it is very stable in a large pH range (4.5 to 9.0).

The backbone angle variability between two conformations.

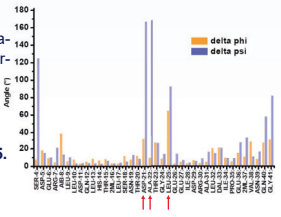

Higher flexibility area between **Asp21** and **Leu25.**

NMR

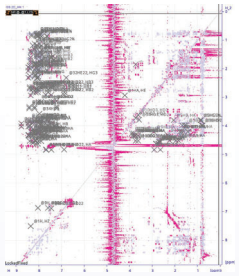

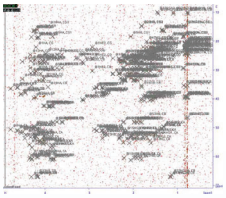

Amino-acid assignment, and sequential attribution of aMex3 done.

We recognized the signature of α-Helix in NOESY experiment.

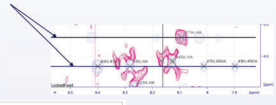

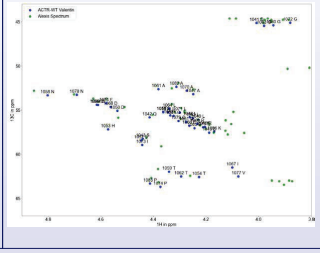

Comparison of Cα/Hα correlation between ACTR WT and aMex3 in ^{13}C-HSQC spectra.

Conclusion: In this study, we enhanced helical content in free ACTR or in the complex with NCBD. We observed the presence of two distinct structures by X-ray crystallography. Their presence in the same crystal can indicate a dynamic interconversion between them. Furthermore, NMR on the three-methylated variant displayed a pattern of α-Helix which is coherent with the increase of the helical content observed in CD. In ongoing experiments, notably in NMR, the complex of NCBD with the three-methylated variant will be studied to characterize its solution dynamics. Another point that needs to be explored further is the energetic implication of solvation, hydrogen bonds and ionization during the complexation. We also started to explore the intracellular delivery of a construct to determine pathways it uses to go inside cells and if it can have an effect on breast cancer ER+ cell line.

References :

(1)Bauer, V.; Schmidtgall, B.; Gógl, G.; Dolenc, J.; Osz, J.; Nominé, Y.; Kostmann, C.; Cousido-Siah, A.; Mitschler, A.; Rochel, N.; Travé, G.; Kieffer, B.; Torbeev, V. Conformational Editing of Intrinsically Disordered Protein by α-Methylation. Chem. Sci. 2021, 12 (3), 1080–1089. https://doi.org/10.1039/D0SC04482B.

(2)Dyson, H. J.; Wright, P. E. Role of Intrinsic Protein Disorder in the Function and Interactions of the Transcriptional Coactivators CREB-Binding Protein (CBP) and P300 *. *Journal of Biological Chemistry* **2016**, *291* (13), 6714–6722. https://doi.org/10.1074/jbc.R115.692020 .

(3)Karmakar, S.; Foster, E. A.; Blackmore, J. K.; Smith, C. L. Distinctive Functions of P160 Steroid Receptor Coactivators in Proliferation of an Estrogen-Independent, Tamoxifen-Resistant Breast Cancer Cell Line. *Endocrine-Related Cancer* **2011**, *18* (1), 113–127. https://doi.org/10.1677/ERC-09-0285.

Palladium-mediated *S*-arylation and *S*-allylation for late-stage peptide functionalization and protein conjugation

https://doi.org/10.17952/37EPS.2024.P2010

Ross D. Ballantine[a], Mingxiang Zhu[b], Ameni Hadj Mohamed[b], Aromal Asokan[a], Linhuan Shen[b], Mélanie Chenon[a], Ana Novak[a], Vincent Robert[c], Séverine Morisset-Lopez[a], Massimiliano Beltramo[c], Carlo Pifferi[a], Vincent Aucagne[a] & Samir Messaoudi[b].

[a] CBM, CNRS UPR4301, Rue Charles Sadron – 45071 Orléans, France, [b] BioCIS, CNRS UMR8076, 19 Avenue des Sciences – 91400 Orsay, France, [c] PRC, INRA UMR85 – 37380 Nouzilly, France

Chemoselective Functionalization *via* Buchwald-Hartwig-Migita

The chemoselective functionalization of peptides and proteins through manipulation and modification of the integral within a complex polyfunctional system, represents a key area of research for the elucidation of biological mechanisms and generation of potential pharmaceuticals. Messaoudi *et al*. recently reported the palladium catalysed Buchwald-Hartwig-Migita (BHM) coupling of thiosugars as well as aryl- and alkyl-thiols with various iodoarenes at room temperature under remarkably mild conditions. The coupling involves the use of the XantPhos Pd G3 as a precatalyst and exhibits a high functional group tolerance.[1] The synthetic utility of this method was subsequently expanded by using semi-aqueous conditions to perform various conjugation reactions on unprotected para-iodophenylalanine (pIPhe) containing peptides, with various glycosyl thiols.[2] The reactions were fast and highly chemoselective, allowing the use of unprotected thiosugars and unprotected polypeptides.

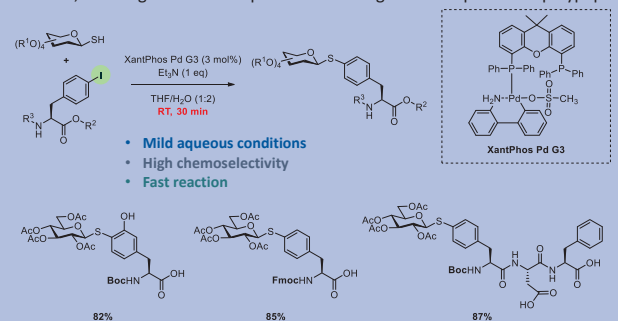

Scheme 1 – General conditions for synthesis of thioglyco-amino acids by Messaoudi *et al.*[1]

S-Arylation of pIPhe containing unprotected peptides

While *S*-arylation *via* BHM had previously been demonstrated for the synthesis of thioglycopeptides,[2] herein we extend the scope of this method to include the thiomethylation of a biologically relevant model peptide. The methodology is unprecedented in terms of mild reaction conditions which allow controlled late-stage peptide diversification. Importantly, an unreactive tag (iodo-aryl moiety) can be incorporated into peptide synthesis or protein expression[3] until the addition of palladium catalyst, conferring excellent bioconjugative control. Kisspeptin-10 (KP-10) (**1**) is a potent neural decapeptide that binds to G-protein-coupled receptor 54 (GPR54) in order to stimulate the release of gonadotropin-releasing hormone (GnRH). KP-10 (**1**) contains two aromatic residues which are crucial for target binding, therefore we sought to synthesise analogues whereby these residues were substituted for thiomethylated phenylalanine to potentially modulate activity for improved binding, higher selectivity towards related receptors or antagonistic activity.

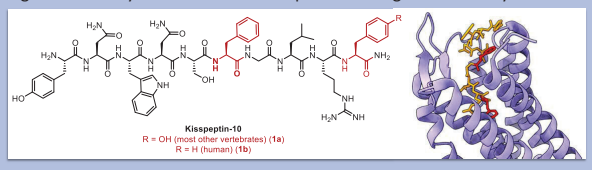

Figure 1 – Left: Structure of kisspeptin-10 (1) with residues important for binding in red, Right: Cryo-EM structure of kisspeptin receptor (purple) bound to KP-10 (1) PDB: 8ZJD[4]

Three analogues (**2** – **4**) were synthesized via automated Fmoc solid-phase peptide synthesis (SPPS) on Rink amide (RA) ChemMatrix resin (0.36 mmol/g), incorporating pIPhe alternately at position 6 (**2**) and 10 (**3**) and a double substituted analogue (**4**). The crude mono-iodopeptides were then reacted with Xantphos Pd G3 (3 eq) and trimethylamine (3 eq) for 30 minutes before addition of sodium thiomethoxide (10 eq). The reagents were doubled for crude di-iodopeptide (**4**). After 15 minutes, the reactions had proceeded to near quantitative yields as observed by RP-HPLC (Figure 2).

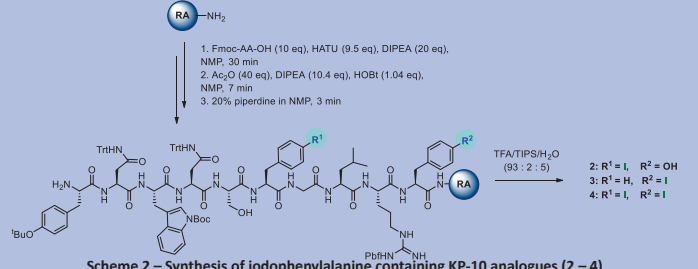

Scheme 2 – Synthesis of iodophenylalanine containing KP-10 analogues (2 – 4)

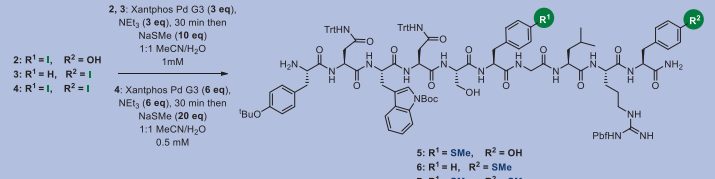

Scheme 3 – S-Arylation of iodopeptides (2 – 4) with Pd G3 Xantphos as precatalyst and sodium thiomethoxide as thiolate source

Peptides (**5** – **7**) were purified by semi-preparative RP-HPLC and obtained with an overall yield of 9 – 12%. Since KP10 has significant hydrophobic character and the reaction profiles are clean (> 99% conversion), it is likely that the loss of yield is due to aggregation of the peptides prior to purification. The yield was improved three-fold for KP10 6,10-SMe (**7**) by using 20% DMSO in the work-up, in order to disrupt any hydrophobic aggregation.

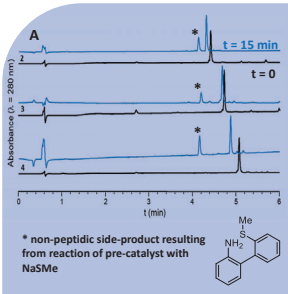

B

Analogue	Conversion %	Isolated Yield %	Isolated Yield % (20% DMSO workup)
KP10 6-SMePhe (5)	> 99	12	N/A
KP10 10-SMePhe (6)	> 99	9	N/A
KP10 6,10-SMePhe (7)	> 99	12	36

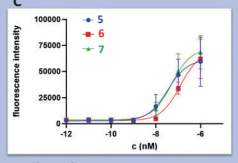

D

Analogue	EC50 / nM
KP10 (1)	2.5[5]
KP10 6-SMePhe (5)	50
KP10 10-SMePhe (6)	122
KP10 6,10-SMePhe (7)	33

Figure 2 – A: RP-HPLC traces of iodopeptides (2 – 4) in black, reaction profile after 15 minutes in blue (5-50% MeCN in H_2O with 0.1% TFA over 5 min) B: Percentage yields of thioaryl peptides (5 - 7) after purification, C: Fluorescence-based Ca^{2+} mobilization assay of compounds 5 – 7 against cells expressing the GPCR and D: Determined EC50 of analogues 5 – 7 compared with native KP10 (1)

The activity of compounds **5** – **7** was assessed *via* a fluorescence-based Ca^{2+} assay, whereby activation of the GPCR increases intracellular levels of calcium which are then detected by a calcium sensitive fluorophore resulting in fluorescence. Preliminary results show the analogues maintain nanomolar binding to GPR54, albeit slightly reduced compared to natural KP10 (**1**).

S-Arylation vs *S*-allylation

In addition to the BHM coupling, herein we demonstrate a Tsuji-Trost reaction mediated by tris(dibenzylideneacetone) dipalladium (0) ($Pd_2[dba]_3$) in the presence of a thiol source and an allyl carbamate. The two reactions are orthogonal to each other with chemoselectivity being controlled by the palladium catalyst, presenting a potential novel method for late stage peptide functionalization and protein conjugation. Preliminary results using bifunctional linker **8** under Tsuji-Trost conditions followed by BHM coupling afforded the desired product (**10**) in 75% yield over 2 steps. Inversely, initial BHM coupling followed by Tsuji-Trost resulted in **10** with a 55% yield.

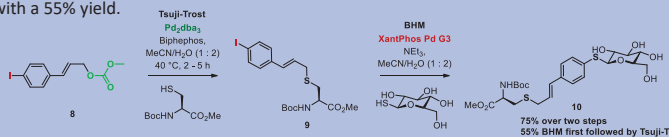

Scheme 3 – Sequential Tsuji-Trost and BHM coupling on bifunctional linker 8

The methodology has since been applied to labelling an optimized anti-HER2 affibody (**11**) which was synthesized via automated Fmoc SPPS, installing a cysteine at the *C*-terminus.[6] A catalyst system was prepared by mixing Biphephos with $Pd_2(dba)_3$ in deoxygenated acetonitrile and heated to 60 °C for 1 hour. The catalyst solution was added to a solution containing affibody **11** and 7-nitrobenz-2-oxa-1,3-diazole (NBD) functionalized with an allyl carbamate (**12**) (prepared *via* BHM of **8**), then the reaction was deoxygenated and stirred at 40 °C.

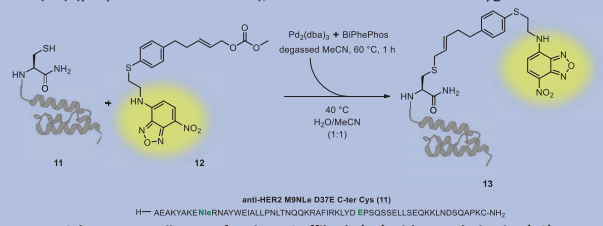

Scheme 4 – Tsuji-Trost of anti-HER2 affibody (11) with NBD derivative (12)

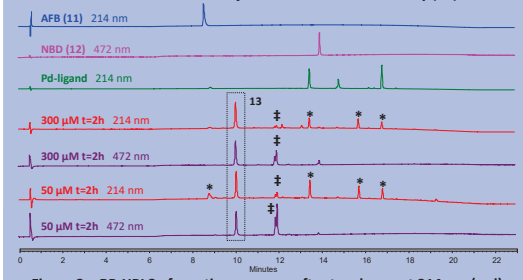

* Catalyst

‡ NBD hydrolysis side-product

Figure 3 – RP-HPLC of reaction progress after two hours at 214 nm (red) and 472 nm (purple) compared to affibody 11 (blue), NBD derivative 12 (pink) and Pd-ligand solution (green) (15% MeCN in H_2O w/ 0.1% TFA over 5 min then 15 – 95% MeCN in H_2O with 0.1% TFA over 15 min)

At an affibody concentration of 300 µM, total conversion was achieved at 2 hours with **13** being obtained in a 71% yield following purification by semi-preparative RP-HPLC. As low as 50 µM, **13** was obtained in a good yield of 50% after 2 hours with almost complete conversion observed by RP-HPLC. Conversion was incomplete at 10 µM after 18 hours.

Future work and perspectives

- Full biological evaluation of KP-10 analogues (**5** – **7**) against G-protein coupled receptor 54, compared to native KP-10.
- Expansion of late stage diversification to include other thiol sources (ethyl-, isopropyl-) and oxidation to sulfones allowing facile access to a large library of compounds
- Demonstrate the ability to utilise the methodology for isotopic labelling (^{14}C) to access radiolabelled analogues for pharmacokinetic and pharmacodynamics studies
- Exploiting NBD fluorescence for cellular internalization assays of compound **13**
- Dual labelling of peptide/protein using sequential BHM/Tsuji Trost system

References

1. A. Bruneau, M. Roche, A. Hamze, J.-D. Brion, M. Alami, S. Messaoudi, *Chem. Eur. J.*, 2015, **21**, 8375 – 8379.
2. D. Montoir, M. Amoura, Z. El Abidine Ababsa, T. M. Vishwanatha, E. Yen-Pon, V. Robert, M. Beltramo, V. Piller, M. Alami, V. Aucagne, S. Messaoudi, *Chem. Sci.*, 2018, **9**, 8753 – 8759.
3. K. Kirshenbaum, I. S. Carrico and D. A. Tirrell, *ChemBioChem.*, 2002, **3**, 235 – 237.
4. S. Shen, D. Wang, H. Liu, X. He, Y. Cao, J. Chen, S. Li, X. Cheng, H. E. Xu and J. Duan, *Cell Rep.*, 2024, **43** (7), 114389.
5. M. Beltramo, V. Robert, M. Galibert, J-B. Maunier, P. Marceau, H. Dardente, C. Decourt, N. De Roux, D. Lornet, A. F. Delmas, A. Caraty and V. Aucagne, *J. Med. Chem.* 2015, **58** (8), 3459 – 3470.
6. A. Novak, F. Kersaudy, S. Berger, S. Morisset-Lopez, F. Lefoulon, C. Pifferi and V. Aucagne, *Eur. J. Med. Chem.*, 2023, **260**, 115747.

TOTAL CHEMICAL SYNTHESIS OF NANOBODIES FOR TARGETED CANCER THERAPY

Keziah Poggenpoel[a], Kevin Beijerling[b], William Kelton[b], Jiwon Hong [c], Margaret A. Brimble,[a] Iman Kavianinia[c]

[a] School of Chemical Sciences and Maurice Wilkins Centre for Molecular Biodiscovery, The University of Auckland, 3A Symonds Street, Auckland 1010, New Zealand
[b] School of Health, The University of Waikato, Hamilton, Hillcrest Road, Hillcrest, Hamilton 3216, New Zealand.
[c] School of Biological Sciences and Maurice Wilkins Centre for Molecular Biodiscovery, The University of Auckland, 3A Symonds Street, Auckland 1010, New Zealand

https://doi.org/10.17952/37EPS.2024.P2011

Introduction:

Nanobodies (Nbs) are fragments isolated from heavy-chain-only antibodies (HcAbs) in the sera of the Camelidae family.

Nbs encompass superior characteristics when compared to full-size antibodies including, **low immunogenicity**, **exquisite antigen-binding affinity** (0.1 – 10 nM), and **small size** (MW 15 kDa; dimensions: 4 nm × 2.5 nm × 3 nm)

Their implementation has been hindered by the limited flexibility of existing production methods (e.g., challenges in incorporating non-natural amino acids) and manufacturing/purification challenges (e.g., removing bacterial endotoxins).

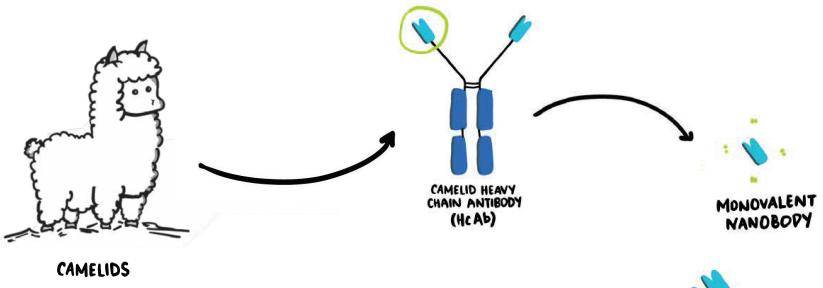

Total chemical synthesis of Nbs poses significant challenges due to the propensity of proteins to **self associate into oligomeric aggregates**, especially those rich in β-sheet structures like Nbs.

However, overcoming these challenges could **unlock new avenues for synthetic production of Nbs** and advance cancer therapy through **enhanced tumor penetration** and **targeted drug delivery.**

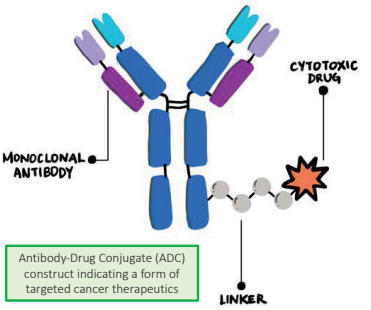

Antibody-Drug Conjugate (ADC) construct indicating a form of targeted cancer therapeutics

Results:

Two-fragment Native Chemical Ligation

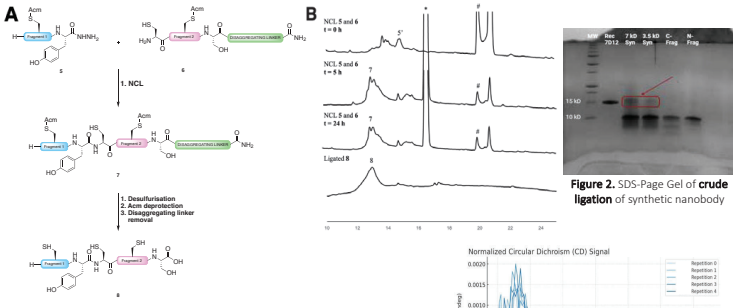

Figure 1. A. Synthetic strategy for obtaining the synthetic Nb. **B.** HPLC analysis of the NCL of **5** and **6**. **5'** peptide azide, • indicates MPAA, **#** indicated MPAA disulfide adduct.

- Challenging synthesis and purification
- Low yield and recovery
- Inability to track via analytical HPLC and ESI-MS

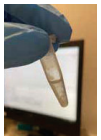

1-24 amino acid residues of highly β-sheet containing Nb fragment without disaggregating linker

Biological Results

Figure 2. SDS-Page Gel of **crude ligation** of synthetic nanobody

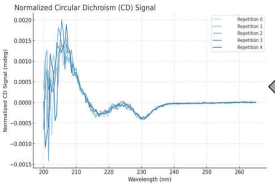

Figure 3. Normalized Circular Dichroism (CD) signal of recombinant Nb.

CD Data to confirm the β-sheet nature of the recombinant Nb for comparison with the synthetically produced Nb

Four-fragment Native Chemical Ligation

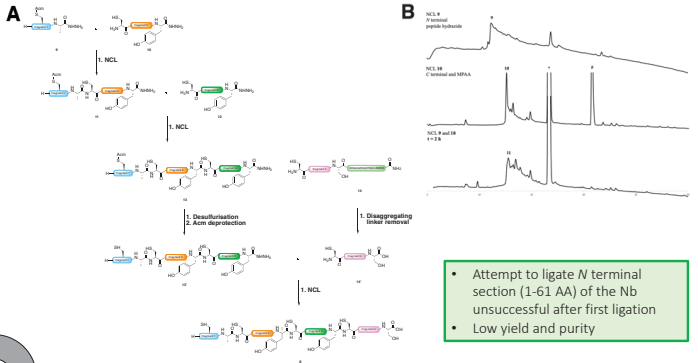

Figure 4. A. A multi-fragment synthetic strategy for obtaining the synthetic Nb. **B.** HPLC analysis of the NCL of **9** and **10**. • indicates MPAA, **#** indicated MPAA disulfide adduct.

- Attempt to ligate *N* terminal section (1-61 AA) of the Nb unsuccessful after first ligation
- Low yield and purity

Future:

Standard SPPS

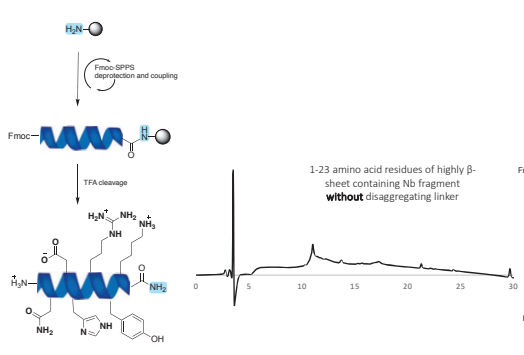

1-23 amino acid residues of highly β-sheet containing Nb fragment **without** disaggregating linker

Our methodology

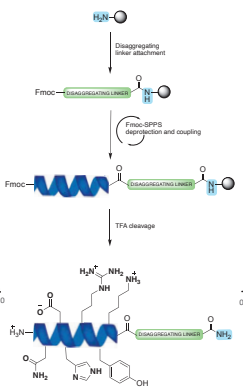

- Improved synthesis and purification
- High yield and recovery

1-23 amino acid residues of highly β-sheet containing Nb fragment **with** disaggregating linker

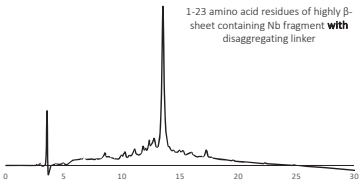

Conclusion:

In summary, synthetic access to Nbs holds major significance in the field of cancer therapeutics and diagnostics.

Our work shows contribution to the field thus towards the total chemical synthesis of Nbs.

In future, we hope to develop a novel and robust synthetic route to produce nanobodies.

References:

(1) Dawson, P. E.; Muir, T. W.; Clark-Lewis, I.; H Kent, S. B. Synthesis of Proteins by Native Chemical Ligation; **1994**; Vol. 266
(2) Kasim, J. K.; Kavianinia, I.; Ng, J.; Harris, P. W. R.; Birch, N. P.; Brimble, M. A. Efficient Synthesis and Characterisation of the Amyloid Beta Peptide, Aβ 1-42 , Using a Double LinkerSystem. *Org Biomol Chem* **2019**, 17 (1), 30–34. https://doi.org/10.1039/c8ob02929f
(3) Fang, G. M.; Li, Y. M.; Shen, F.; Huang, Y. C.; Li, J. Bin; Lin, Y.; Cui, H. K.; Liu, L. Protein Chemical Synthesis by Ligation of Peptide Hydrazides. *Angew. Chem. – International Edition* **2011**, 50 (33), 7645–7649. https://doi.org/10.1002/anie.201100996
(4) Huppelschoten, Y.; Elhebieshy, A. F.; Hameed, D. S.; Sapmaz, A.; Buchardt, J.; Nielsen, T. E.; Ovaa, H.; van der Heden van Noort, G. J. Total Chemical Synthesis of a Functionalized GFP Nanobody. *ChemBioChem* **2022**, 23 (19). https://doi.org/10.1002/cbic.202200304
(5) Tong, J. T. W.; Harris, P. W. R.; Brimble, M. A.; Kavianinia, I. An Insight into FDA Approved Antibody-Drug Conjugates for Cancer Therapy. *Molecules*. MDPI October 1, **2021**. https://doi.org/10.3390/molecules26195847.
(6) Pentelute, B. L.; Kent, S. B. H. Selective Desulfurization of Cysteine in the Presence of Cys(Acm) in Polypeptides Obtained by Native Chemical Ligation. *Org Lett* **2007**, 9 (4), 687–690. https://doi.org/10.1021/ol0630144
(7) Kang, W.; Ding, C.; Zheng, D.; Ma, X.; Yi, L.; Tong, X.; Wu, C.; Xue, C.; Yu, Y.;Zhou, Q. Nanobody Conjugates for Targeted Cancer Therapy and Imaging. *Technology in cancer research & Treatment*. **2021**.
(8) Mong, S. K.; Vinogradov, A. A.; Simon, M. D.; Pentelute, B. L. Rapid Total Synthesis of DARPin PE59 and Barnase. *ChemBioChem* 2014, 15 (5), 721–733. https://doi.org/10.1002/cbic.201300797

Green Synthesis of a Novel Primary Amine Protecting Group for Solid-phase Peptide Synthesis

Clouie Justin Aguilar,[a] Makhdoom Sarwar[b], Margaret A. Brimble,[a] Iman Kavianinia*[a]
[a] Iman Kavianinia – School of Biological Sciences, School of Chemical Sciences and Maurice Wilkins Centre for Molecular Biodiscovery, The University of Auckland, 3A Symonds Street, Auckland 1010, New Zealand;https://orcid.org/0000-0002-2446-1376; Email: i.kavianinia@auckland.ac.nz
[b] Department of Obstetrics and Gynaecology, University of Otago, Christchurch, 2 Riccarton Avenue, Christchurch 8011, New Zealand.

https://doi.org/10.17952/37EPS.2024.P2012

INTRODUCTION

Orthogonal protecting groups are vital in the chemo-selective modification of biologically active peptides and proteins, especially in solid-phase peptide synthesis (SPPS). Existing protecting groups for the temporary protection of the reactive ε-amino group of lysine sidechain, such as Alloc, mtt, iNoc, Dde, and ivDde, often require harsh conditions for their removal and involve complex synthesis with suboptimal yields.

Our new protecting group (**Dty**) offers a more efficient and environmentally friendly alternative for the temporary masking of reactive side-chain functionalities in amino acids, particularly lysine's ε-amino group (sidechain). We present a novel primary amine protecting group, developed via a one-pot, two-step reaction in water using a known cross-linking agent. This method offers high yields, good atom economy, and minimal waste, addressing the need for greener synthetic pathways.

Dty protecting group

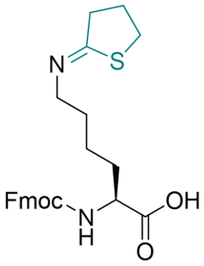

- Water-based synthesis
- Small and polar group
- No amino scrambling
- Gram-scale synthesis
- Orthogonal to Fmoc

SYNTHESIS

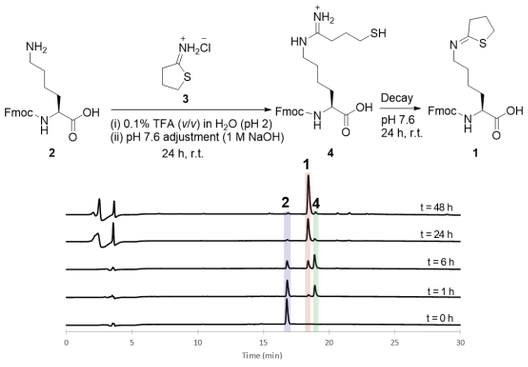

Figure 1. Synthesis of Fmoc-Lys(Dty)-OH in water at pH 7.6 via a one pot two-step reaction.

REMOVAL

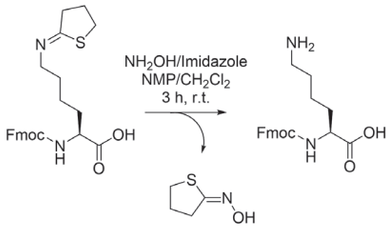

Figure 2. Removal of the Dty protecting group using a mixture of NH_2OH and imidazole.

APPLICATIONS IN SPPS

Scenario 1: Compared to Dde, the Dty group does not exhibit intramolecular migration between ε-amino groups of lysine side-chains.

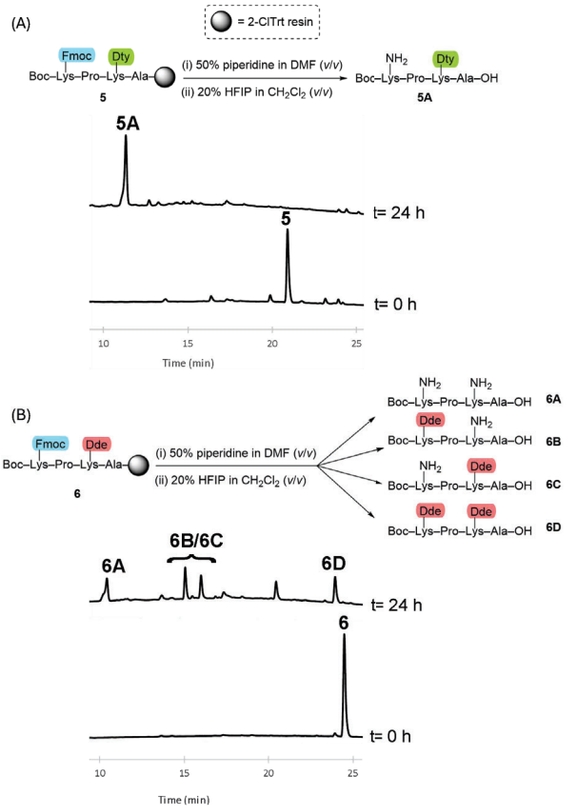

Figure 3. **(A)** Testing Dty migration after removal of Fmoc from a neighbouring lysine sidechain using 50% piperidine in DMF (*v*/*v*) for 24 h. **(B)**Testing the migration of Dde after removal of Fmoc from a neighbouring lysine sidechain using 50% piperidine in DMF (*v*/*v*) for 24 h

Scenario 2: Selective removal of the Dty protecting group through the use of NH_2OH, allows for the site-selective modification of biologically relevant peptides.

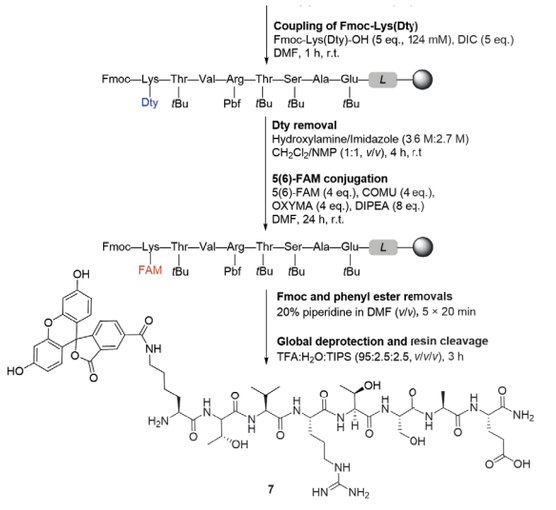

Figure 4. Synthesis and site-selective modification of folate binding peptide TVRTSAE. Dty protected lysine is coupled at the *N*-terminus and the Dty protecting group is selectively removed and was subsequently conjugated with a fluorophore, 5(6)-FAM.

BIOLOGICAL RESULTS

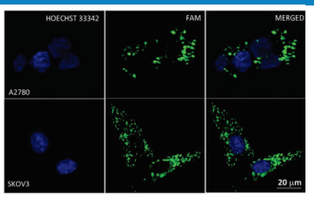

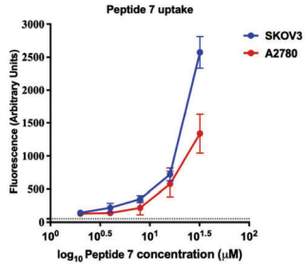

CONCLUSION

In summary, we herein introduce the Dty amino protecting group and demonstrate its suitability for conducting Fmoc SPPS. Our findings indicate that Dty meets the criteria as an ideal lysine ε-amino protecting group, displaying excellent compatibility with standard peptide synthesis procedures and efficient removal under mild nucleophilic conditions.

ACKNOWLEDGEMENTS

The authors wish to acknowledge the Leather and Shoe Research Association (LASRA), the Strategic Science Investment Fund (SSIF) [LSRX-1801] from the Ministry of Business, Innovation and Employment (MBIE), The University of Auckland doctoral scholarship, the Maurice Wilkins Centre for Molecular Biodiscovery, the Health Research Council of New Zealand (Sir Charles Hercus Health Research Fellowship; ref: 24/195), and Dr. Sujay Prabakar from LASRA for their support.

REFERENCES

[1] I. Vecchio, C. Tornali, N. L. Bragazzi, M. Martini, *Front. Endocrinol* **2018**, *9*, 613.
[2] L. Wang, N. Wang, W. Zhang, X. Cheng, Z. Yan, G. Shao, X. Wang, R. Wang, C. Fu, *Signal Transduct. Target. Ther.* **2022**, *7*, 1–27.
[3] L. A. Carpino, G. Y. Han, *J. Am. Chem. Soc.* **1970**, *92*, 5748–5749.
[4] R. Behrendt, P. White, J. Offer, *J. Pept. Sci.* **2016**, *22*, 4–27.
[5] A. Isidro-Llobet, M. Álvarez, F. Albericio, *Chem. Rev.* **2009**, *109*, 2455–2504.
[6] J. Almaliti, M. Alhindy, M. C. Yoon, V. Hook, T. F. Molinski, A. J. O'Donoghue, W. H. Gerwick, *ACS Omega* **2024**, *9*, 3997–4003.
[7] a) C. Azevedo, A. Saiardi, *Adv. Biol. Regul.* **2016**, *60*, 144–150; b) J. N. deGruyter, L. R. Malins, P. S. Baran, *Biochemistry* **2017**, *56*, 3863–3873; c) M. Haque, N. Forte, J. R. Baker, *Chem. Commun.* **2021**, *57*, 10689–10702; d) A. Tantipanjaporn, M.-K. Wong, *Molecules* **2023**, *28*, 1083; e) J. A. Shadish, C. A. DeForest, *Matter* **2020**, *2*, 50–77; f) J. Rizo, F. Albericio, E. Giralt, E. Pedroso, *Tetrahedron Lett.* **1992**, *33*, 397–400.
[8] N. Thieriet, J. Alsina, E. Giralt, F. Guibé, F. Albericio, *Tetrahedron Lett.* **1997**, *38*, 7275–7278.
[9] B. W. Bycroft, W. C. Chan, S. R. Chhabra, N. D. Hone, *J. Chem. Soc. Chem.Commun.* **1993**, 778–779.
[10] S. R. Chhabra, B. Hothi, D. J. Evans, P. D. White, B. W. Bycroft, W. C. Chan, *Tetrahedron Lett.* **1998**, *39*, 1603–1606.
[11] a) S. Chithanna, S. Vyasamudri, D.-Y. Yang, *Org. Lett.* **2020**, *22*, 2391–2395; b) R. R. Wilhelm, A. Srinivasan, M. A. Schmidt, in *Pept. New Millenn. Proc. 16th Am. Pept. Symp. June 26–July 1 1999 Minneap. Minn. USA* (Eds.: G.B. Fields, J.P. Tam, G. Barany), Springer Netherlands, Dordrecht, **2002**, pp. 58–59.
[12] a) Y.-K. Qi, Q. Qu, D. Bierer, L. Liu, *Chem. – Asian J.* **2020**, *15*, 2793–2802; b) M. Staderini, A. Gambardella, A. Lilienkampf, M. Bradley, *Org. Lett.* **2018**, *20*, 3170–3173.
[13] a) K. Augustyns, W. Kraas, G. Jung, *J. Pept. Res.* **1998**, *51*, 127–133; b) O. A. Shepperson, P. W. R. Harris, M. A. Brimble, A. J. Cameron, *Antibiotics* **2024**, *13*, 615.
[14] R.R. Traut, A. Bollen, T.-T. Sun, J. W. B. Hershey, J. Sundberg, L. R. Pierce, *Biochemistry* **1973**, *12*, 3266–3273.
[15] R. Singh, L. Kats, W. A. Blättler, J. M. Lambert, *Anal. Biochem.* **1996**, *236*, 114–125.
[16] a) M. Mokotoff, Y. m. Mocarski, B. I. Gentsch, M. Miller, J.-H. Zhou, J. Chen, E. d. Ball, *J. Pept. Res.* **2001**, *57*, 383–389; b) C. J. Aguilar, M. Sarwar, S. Prabakar, W. Zhang, P. W. R. Harris, M. A. Brimble, I. Kavianinia, *Org. Biomol. Chem.* **2023**, *21*, 9150–9158; c) M. G. Bartlett, K. L. Busch, *Biol. Mass Spectrom.* **1994**, *23*, 353–356.
[17] a) L. Bialy, J. J. Díaz-Mochón, E. Specker, L. Kenicke, M. Bradley, *Tetrahedron* **2005**, *61*, 8295–8305; b) J. J. Díaz-Mochón, L. Bialy, M. Bradley, *Org. Lett.* **2004**, *6*, 1127–1129.
[18] S. L. Hulin-Curtis, J. A. Davies, D. Nestić, E. A. Bates, A. T. Baker, T. G. Cunliffe, D. Majhen, J. D. Chester, A. L. Parker, *Cancer Gene Ther.* **2020**, *27*, 785–798.
[19] a) K. Siwowska, R. M. Schmid, S. Cohrs, R. Schibli, C. Müller, *Pharmaceuticals* **2017**, *10*, 72; b) Y. Wen, W. S. Graybill, R. A. Previs, W. Hu, C. Ivan, L. S. Mangala, B. Zand, A. M. Nick, N. B. Jennings, H. . J. Dalton, V. Sehgal, P. Ram, J.-S. Lee, P. E. Vivas-Mejia, R. L. Coleman, A. K. Sood, *Clin. Cancer Res. Off. J. Am. Assoc. Cancer Res.* **2015**, *21*, 448–459; c) N. R. Patel, A. Pilvoyan, S. Ganta, A. B. Morse, K. M. Candiloro, A. L. Solon, A. H. Nack, C. A. Galati, C. Bora, M. A. Magtaty, S. W. O'Brien, S. Litwin, B. Davis, D. C. Connolly, T. P. Coleman, *Cancer Biol. Ther.* **2018**, *19*, 554–564; d) M. K. Y. Siu, D. S. H. Kong, H. Y. Chan, E. S. Y. Wong, P. P. C. Ip, L. Jiang, H. Y. S. Ngan, X.-F. Le, A. N. Y. Cheung, *PloS One* **2012**, *7*, e47201.
[20] a) S. K. Vashist, *Diagnostics* **2012**, *2*, 23–33; b) C. R. Cammarata, M. E. Hughes, C. M. Ofner, *Mol. Pharm.* **2015**, *12*, 783–793; c) S. A. Madison, J. O. Carnali, *Ind. Eng. Chem. Res.* **2013**, *52*, 13547–13555.

Created with BioRender Poster Builder

https://doi.org/10.17952/37EPS.2024.P2013

Faculty of Chemistry - Organic and Bioorganic Chemistry - OCIII

UNIVERSITÄT BIELEFELD

New Opportunities for Side-Chain Functionalization of Halogenated Amino Acids

***Laura Cerveson* and Norbert Sewald**

Organic and Bioorganic Chemistry, Faculty of Chemistry, Bielefeld University, Germany.

laura.cerveson@uni-bielefeld.de

- Chemical modifications of amino acids and peptides embody a vast and significant field of biochemical research because they permit to obtain arrays of functionalised derivatives with modified properties or biological effects.
- One particularly attractive method for diversification is provided by **transition-metal catalysed cross-coupling** reactions. However, the functionalisation of amino acids and peptides is considered **challenging** and not all cross-couplings are suitable.[1]

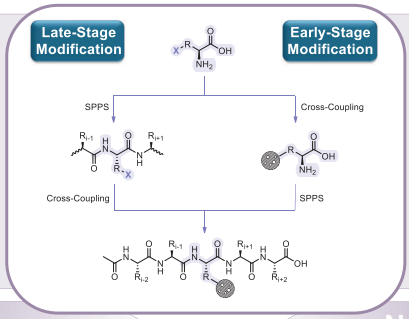

- **Phenylalanine** and **tryptophan** are considered interesting substrates to be used for chemical modification. They show, indeed, noteworthy fluorescence properties and take part in important biological processes. In particular, tryptophan participates in the determination of protein folding and protein-protein interactions.[2]
- Here in we present cross-coupling reactions that can be used for both **early-** and **late-stage modification** of peptides containing **halogenated amino acids** such as 6-bromo-tryptphane and 4-iodo-phenylalanine.

Vinylation of Halogenated Trp and Phe

- Halogenated amino acids can be cross-coupled with triethoxyvinylsilane in water to give the corresponding **vinylated** product.[3]
- One advantage of this kind of reaction is that **no protecting groups** are needed since it proved to be compatible with functional groups such as amines and carboxylic acids.
- Even if strong basic conditions are required for the course of the reaction, no perceptible racemization occurred. However, this represents a problem when moving to peptides as it leads to epimerization.

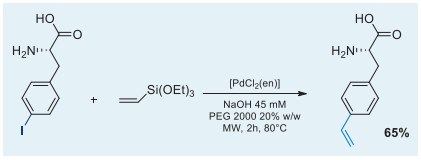

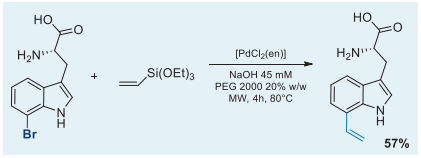

Late-Stage Modification of Peptides

- Late-stage vinylation of iodophenylalanine containing peptides is possible at certain conditions: the reaction must be conducted in diluted conditions but keeping the same equivalents of NaOH and the halogenated amino acid must occupy the **last position** in the peptide sequence.

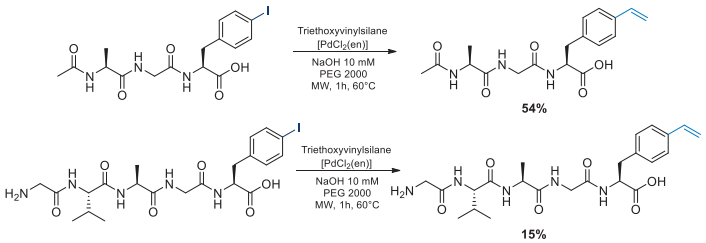

Early-Stage Modification of Peptides

- 4-vinyl-phenylalanine can be directly Fmoc-protected, **without purification** from prior reaction, and used for solid phase peptide synthesis.

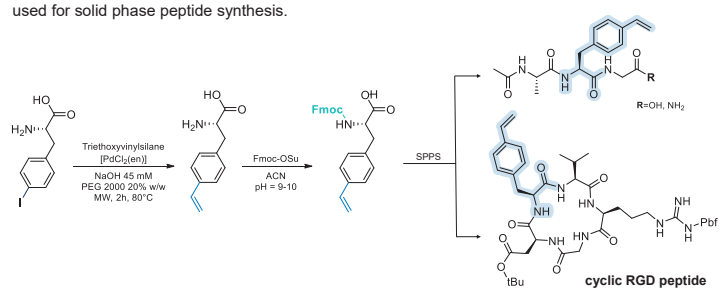

Further Modifications

- Vinylated amino acids or peptides can undergo further reactions, such as **Heck cross-coupling**.[4]

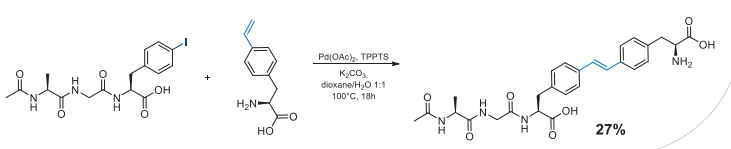

Negishi Cross-Coupling: Alkylation of Trp

- In a previous work, Negishi cross-coupling was used for diversification of protected 7-bromo-tryptophan enabling its **selective alkylation**.[5]
- The reaction is carried out using mild conditions without preformation of the metal organyls.

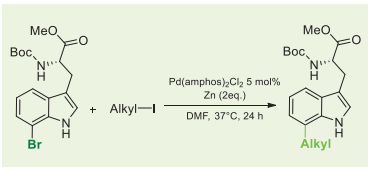

- Different types of alkyl iodides were employed for a **substrate screening**.

Entry	Alkyl iodide	T [°C]	Yield [%]	Entry	Alkyl iodide	T [°C]	Yield [%]
1		20	26	4	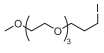	20	0
		37	83			37	0
2	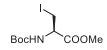	20	21	5		20	n.d.[a]
		37	52			37	73
3		20	37	6		20	0
		37	81			37	0

Table 1 – Substrate screening at 20°C and 37°C. [a] not detected due to low conversion

Late-Stage Modification of Tripeptides

- For the late-stage functionalization of 6-bromo-tryptophan containing peptides some **modifications** from the previous procedure were necessary to obtain acceptable yields.

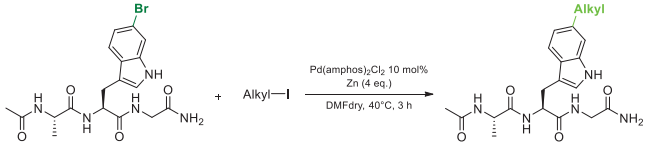

- Different alkyl iodides and pentapeptides are currently being tested in order to prove the validity of this reaction for late-stage alkylation of bromotryptophan containing peptides.

Entry	Alkyl iodide	Yield [%]
1		44
2		45

Conclusion

- We reported here **two strategies** for the early- and late-stage functionalization of halogenated amino acids containing peptides.
- The first one permits to selectively vinylate 6-bromotryptophan and 4-iodophenylalanine and works for both early- and late-stage.
- Vinylated compounds can be used for further modifications, such as Heck cross-coupling. A development of the latter would be its application for the synthesis of **cyclic peptides**.
- Negishi cross-coupling between bromotryptophan and different alkyl iodides provides alkylated derivatives and it's being tested for late-stage modification.

References

1. Gruß, H.; Sewald, *N. Chem. Eur. J.* **2020**, 26, 5328-5340.
2. Rose, G.,D.; Geselowitz, A., R.; Lesser, G., J.; Lee, R., H.; Zehfus, M., H. *Science* **1985**, 229, 834-838.
3. Gordillo, A.; Ortuno, M., A.; Lòpez-Mardomingo, C.; Lledòs, A.; Ujaque, G.; de Jesùs, E. *J. Am. Chem. Soc.* **2013**.
4. Gruß, H.; Belu, C.; Bernhard, L., M.; Merschel, A.; Sewald, *N. Chem. Eur. J.* **2019**, 25, 5880-5883.
5. Dachwitz, S.; Scharkowski, B.; Sewald, N. *Chem. Eur. J.* **2021**, 27, 18043.

https://doi.org/10.17952/37EPS.2024.P2014

Sculpting cavities in alpha-helical bundles to accommodate ligands of different size and shapes

Katarzyna Ozga[a], Rokas Petrenas[a], Joel J. Chubb[a], and Derek N. Woolfson[a,b,c,d]

[a] School of Chemistry, University of Bristol, Cantock's Close, Bristol BS8 1TS, UK ,
[b] Max Planck-Bristol Centre for Minimal Biology, University of Bristol, Cantock's Close, Bristol BS8 1TS, UK ,
[c] School of Biochemistry, Biomedical Sciences Building, University of Bristol, University Walk, Bristol BS8 1TD, UK,
[d] BrisEngBio, School of Chemistry, University of Bristol, Cantock's Close, Bristol BS8 1TS, UK

Abstract

The advancement of AI methods, including RoseTTAFold and AlphaFold (structure prediction from sequence), RFdiffusion (backbone design), ProteinMPNN (sequence design), and more comprehensive tools like Chroma (backbone and sequence design), has made protein structure and function design highly accessible (e.g. through platforms like Colab notebooks) and remarkably successful. However, **rational design** still offers two significant advantages: it minimizes the need for extensive sequence sampling and enhances understanding. In the **Woolfson lab**, we employ a hybrid approach that combines rational and computational methods to design functional and complex coiled-coil proteins, beginning with a deep understanding of the **sequence design rules** for coiled-coil peptide assemblies.

Coiled-coil protein design

The relationship between sequence and structure for coiled-coil peptides was uncovered through bioinformatic analysis of natural coiled coils, complemented by extensive biochemical studies (1). This understanding paved the way for the ***de novo*** design of larger, more complex assemblies (**barrels**), which are rare in nature. In recent work, these coiled-coil peptide assemblies have been further utilized as seeds for template-based loop design using MASTER and ProteinMPNN (2). This approach enables the creation of robust, highly thermostable proteins with varying pore sizes and chemistries, which can be easily functionalized (desymmetrized).

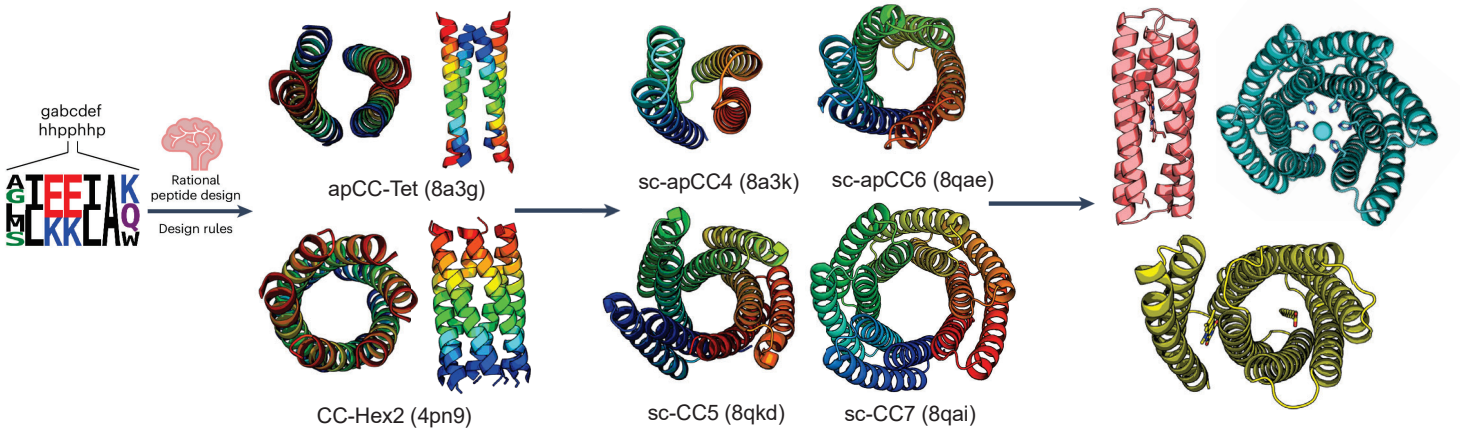

RASSCoL: introducing binding sites within coiled coils

In this work, we introduce the **R**apid **A**ssessment of **S**ize, **S**hape, and **C**omplementarity of **L**igand (**RASSCoL**) as an **ultra-fast protocol** for designing binding sites for various small molecules, including metals, cofactors, and transition states, within coiled-coil proteins. The process begins with a significant reduction of the sequence space by applying **design specifications** that can be quickly assessed at the **sequence level**, e.g. rough estimation of whether the introduced side chains volumes will cumulatively sum up to the target volume of ligand. Next, the filtered sequences are packed onto a scaffold using FASPR and pre-scored with AutoDock Vina, achieving a computing time of just **0.3 seconds per sequence** on a single CPU. The top 100 sequences are then selected for a series of short molecular dynamics (MD) simulations with the ligand to more accurately calculate binding affinity and predict the stability of the mutants. The two best designs for each ligand were subsequently tested experimentally, demonstrating specificity and binding affinities in the low to sub-micromolar range.

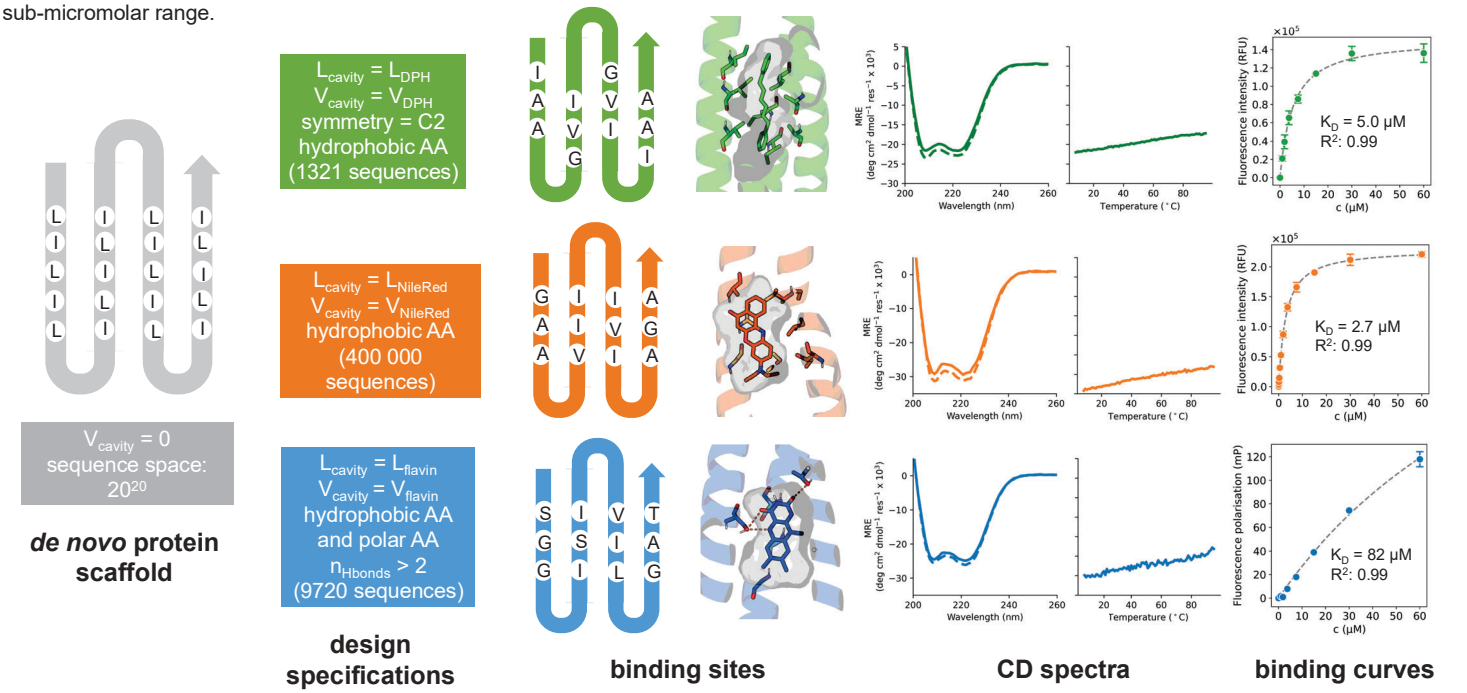

References

1. D.N. Woolfson, 2023, *JBC Reviews*, 299(4):104579; 2. K.I. Albanese, R. Petrenas, F. Pirro, E.A. Naudin, U. Borucu, W.M. Dawson, D.A. Scott, G.J. Legget, O.D. Weiner, T.A.A. Oliver, D.N. Woolfson, 2024, *Nat. Chem. Bio*, 20:991-999; 3. E.A. Naudin, K.I. Alanese, A.J. Smith, B. Mylemans, E.G. Baker, O.D. Weiner, D.M. Andrews, N. Tigue, N.J. Savery, D.N. Woolfson, 2022, Chem. Sci., 13:11330-11340.

Efficient and glycoeconomic synthesis of densely clustered mucin glycopeptides

Arseniy Galashov, Ekaterina Kazakova, Oliver Seitz*

Humboldt-Universität zu Berlin, Germany

oliver.seitz@chemie.hu-berlin.de

https://doi.org/10.17952/37EPS.2024.P2015

Introduction

Mucins are known for fully O-glycosylated multiple tandem repeats (TRs), like the PTTSTTS motif found in MUC5AC, which has ~240 copies and 6 glycosylation sites per TR. The lack of methods to access long, glyco-defined multi-TRs limits our understanding of how mucin glycosylation impacts its functional properties. While solid-phase synthesis (SPS) is a viable approach, its disadvantage is the requirement of excess amounts of costly and potentially delicate glycoamino acids. We strive to improve access to glycoamino acid building blocks and develop methods allowing glycoeconomic synthesis of densely clustered mucin glycopeptides.

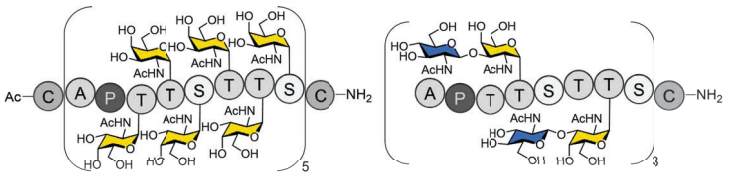

Chemical structures of exemplar synthesized glycopeptides.

Multigram synthesis of mono[1]- and di-glycosylated building blocks

✓ **Azidophenylselenylation** of galactal instead of azidonitration.

✓ **Acid-base extraction** as the purification method of choice at the final step.

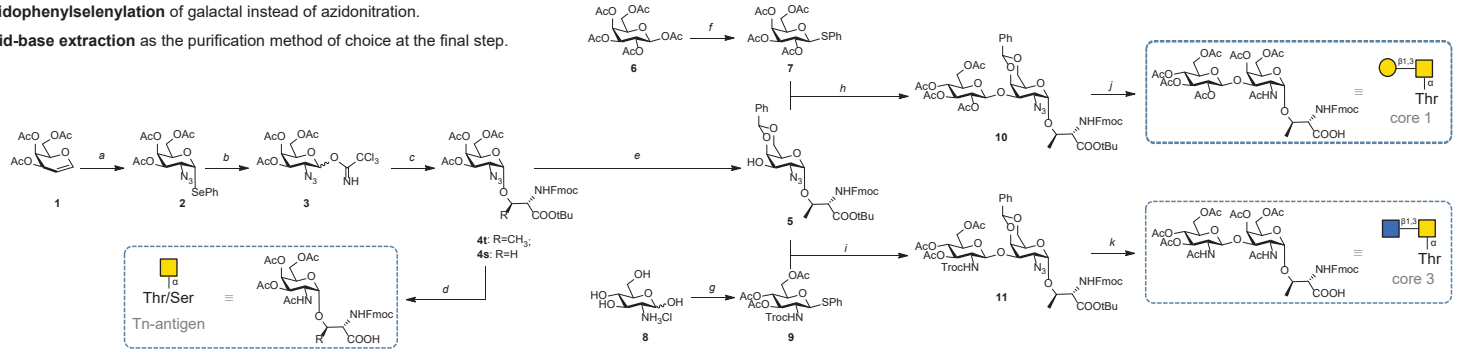

Conditions. (a) Se_2Ph_2, $TMSN_3$, (diacetoxyiodo)benzene, CH_2Cl_2, -30°C (55%); (b) i. NIS, acetone, H_2O, RT (quant.); ii. CCl_3CN, Cs_2CO_3, CH_2Cl_2, RT (84%); (c) Fmoc-Thr/Ser(OH)-tBu, TMSOTf, CH_2Cl_2, Et_2O, 0°C; (d) i. Zn, THF, AcOH, Ac_2O, RT (47-51% for 2 steps); ii. TFA, CH_2Cl_2, RT (95-97%); (e) i. 1M NaOMe, MeOH; ii. $PhCH(OMe)_2$, CSA, CH_3CN (82% for 2 steps); (f) $BF_3{\cdot}Et_2O$, PhSH, CH_2Cl_2 (83%); (g) i. TrocCl, $NaHCO_3$, H_2O; ii. Ac_2O, Py (50% for 2 steps); iii. $BF_3{\cdot}Et_2O$, PhSH, CH_2Cl_2 (84%); (h) NIS, TMSOTf, CH_2Cl_2 (55%); (i) NIS, TMSOTf, CH_2Cl_2 (76%); (j) i. CSA, DTT, CH_2Cl_2; ii. Zn, AcOH, THF; iii. Ac_2O, Py (70% for 3 steps); iv. anisole, TFA (97%); (k) i. 80% AcOH, 80°C; ii. Zn, AcOH, THF; iii. Ac_2O, Py (64% for 3 steps); iv. anisole, TFA (91%).

Solid-Phase Synthesis of mucin glycopeptides

Semi-automated synthesis of partially monoglycosylated MUC5AC peptides[1]

✓ Development of fast and clean coupling of Fmoc-Thr/Ser(αAc_3GalNAc) with only **1.5 eq**.
→ DIC/Oxyma in **2-MeTHF** instead of DMF, **10 min** coupling time, **no microwave**.

x Due to low viscosity of 2-MeTHF, coupling of glycoamino acid must be performed manually.

Peptide	Fmoc deprotection	Coupling	Capping	Sugar deprotection	Yield[a]
Ac-C-(APTTSTTS)$_5$-N_2H_4	20% Piperidine in DMF	AA: 5 eq. AA/HATU/Oxyma, 15 eq. DiPEA in DMF; **GlycoAA**: 1.5 eq. AA/DIC/Oxyma in 2-MeTHF	Ac_2O/ DiPEA in DMF	$N_2H_4{\cdot}H_2O$ in DMF (50:50)	17%
Ac-C-(APTTSTTS)$_5$-N_2H_4					9%
CPTTSTTS-(APTTSTTS)$_4$					9%

[a]Yields calculated after HPLC purification

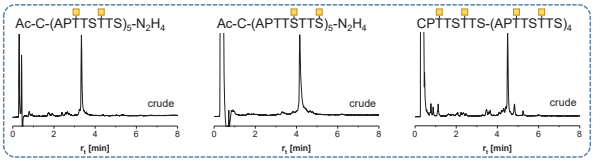

Automated synthesis of partially and fully monoglycosylated MUC5AC peptides

✓ Automated DMF-free synthesis with green solvent **1,3-dioxolane (DOL)/Tween-20** furnishes high yields of isolated material.

✓ **Tween-20** is added with the intention to prevent on-resin aggregation, allowing the synthesis of difficult MUC5AC peptide.

X However, synthesis of highly glycosylated peptides remains challenging.

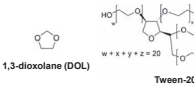

1,3-dioxolane (DOL) Tween-20

Peptide	Fmoc deprotection[a]	Coupling[a]	Capping	Sugar deprotection	Yield[b]
Ac-C-(APTTSTTS)$_5$-C	20% Pyrrolidine in DOL	1.5 eq. AA/DIC/Oxyma in DOL	Ac_2O/ DiPEA in DOL	$N_2H_4{\cdot}H_2O$ in DMF (50:50)	18%
Ac-C-(APTTSTTS)$_5$-C					16%
Ac-C-(APTTSTTS)$_5$-C					2%
UPTTSTTS-(APTTSTTS)$_2$-C					5%
Ac-C-(APTTSTTS)$_2$-N_2H_4					27%

[a]1% Tween-20 (v/v) was added to all synthetic mixtures; [b]Isolated yields calculated after HPLC purification

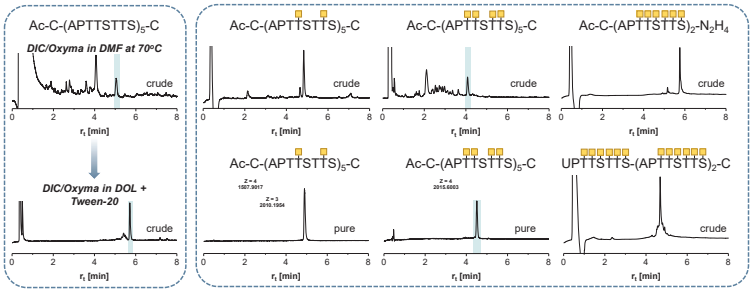

Manual synthesis of partially diglycosylated MUC5AC peptides

X Core-3 diglycosylated peptides with only two glycoamino acids per TR **behave similarly** to fully monoglycosylated peptides during SPS.

✓ Changing GlcNAc to Gal in the disaccharide (core-3 → core-1) **enables the elongation** of peptides up from 2 TRs to 3 TRs.

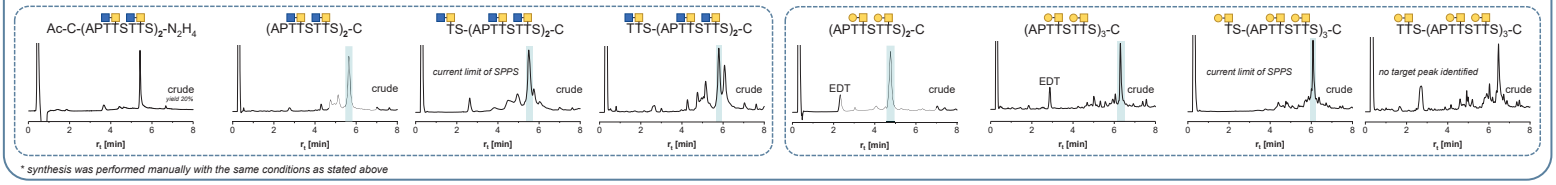

* synthesis was performed manually with the same conditions as stated above

Ligation techniques to obtain long mucin glycopeptides

✓ C-terminal glyco-serine **does not interfere** with either ligation or dechalcogenation methods

Native Chemical Ligation with C-terminal glycoamino acid[1]

Ac-(APTTSTTS)$_5$-NH-NH_2 → (1. MPAA, acac, Gd-HCl buffer; 2. MPAA extraction with EtOAc, then $NaBEt_4$/TCEP) → CPTTSTTS-(APTTSTTS)$_4$

Ac-(APTTSTTS)$_5$-(APTTSTTS)$_5$ with 80 aa, 20 GalNAc, yield 17%

Diselenide-Selenoester Ligation with C-terminal glycoamino acid

Ac-C-(APTTSTTS)$_2$-NH-NH_2 → (1. Ph_2Se_2, TCEP, acac, buffer A, pH 3, 37°C; 2. Gd-HCl buffer, pH 7, RT; 3. Ph_2Se_2 extraction with hexane, then TCEP/DTT) → (UPTTSTTS-(APTTSTTS)$_2$-C)$_2$

Ac-C-(APTTSTTS)$_5$-C with 42 aa, 30 GalNAc, yield 22%

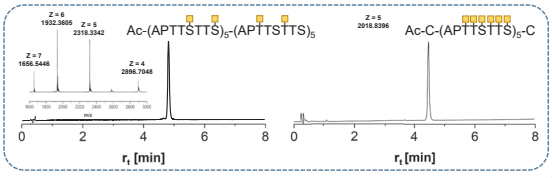

Conclusions

✓ Replacing azidonitration of galactal with azidophenylselenylation facilitated multi-gram scale (16 g) access to glycoamino acids.

✓ Employment of DOL/Tween-20 mixture allows DMF-free synthesis of fully glycosylated mucin-like peptides with high purity.

✓ Highly monoglycosylated peptides are difficult to access by SPS. Diglycosylated peptides are especially hard to extend.

✓ Core-3 (GlcNAcβ(1→3)GalNAc) glycopeptides are more challenging to extend than core-1 (Galβ(1→3)GalNAc) glycopeptides.

✓ High glycosylation degree and glycosylation at the ligation junction do not interfere with ligation and dechalcogenation.

References

[1] Galashov, A., Kazakova, E., Stieger, C. E., Hackenberger, C. P. R., Seitz, O. (2024). *Chemical Science, 15*(4), 1297-1305.

Acknowledgements

Funded by the Deutsche Forschungsgemeinschaft (DFG, German Research Foundation) – Project ID 431232613 – SFB 1449.

CRC 1449

HUMBOLDT-UNIVERSITÄT ZU BERLIN

P2.017

Targeting LAT1 with technetium(I)-99m-labeled tryptophan derivatives for SPECT imaging

https://doi.org/10.17952/37EPS.2024.P2017

Rúben D.M. Silva[1*], Cristina P. Matos[1], Catarina I.G. Pinto[1], Joana F. Guerreiro[1], Lurdes Gano[1,2], Filipa Mendes[1,2], João D.G. Correia[1,2]

[1] C²TN – Centro de Ciências e Tecnologias Nucleares, Instituto Superior Técnico, Universidade de Lisboa, Portugal

[2] DECN – Departamento de Engenharia e Ciências Nucleares, Instituto Superior Técnico, Universidade de Lisboa, Portugal

*ruben.silva@ctn.ist.ulisboa.pt

Cancer

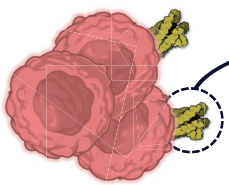

- **UNCONTROLLED** and **UNLIMITED** proliferation and growth are benchmark characteristics of cancer[1]
- Metabolic reprogramming leads to an increase in nutritional needs of the cell[2]

Large Amino acid Transporter 1 (LAT 1)

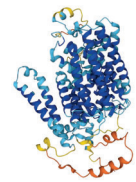

- LAT1 belongs to the solute carrier 7 family and is overexpressed in many types of cancers, including some of the most common, such as prostate, breast and lung cancer[3]
- LAT1 has been increasingly explored as a drug target for imaging and therapy of cancers

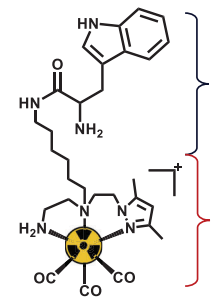

Tryptophan (Trp) derivative

Radiometal Core[4]

= [^{99m}Tc]Tc

Tryptophan-based radiocomplexes

Trp-based radiocomplexes of the type *fac*-[^{99m}Tc(CO)$_3$(k^3-Pz-Trp)]$^+$ for targeting LAT1: Design and biological evaluation of potential tools for non-invasive cancer imaging

Cellular uptake of [^{99m}Tc]Tc-complexes based on the *L*/*D*-enantiomers of Trp

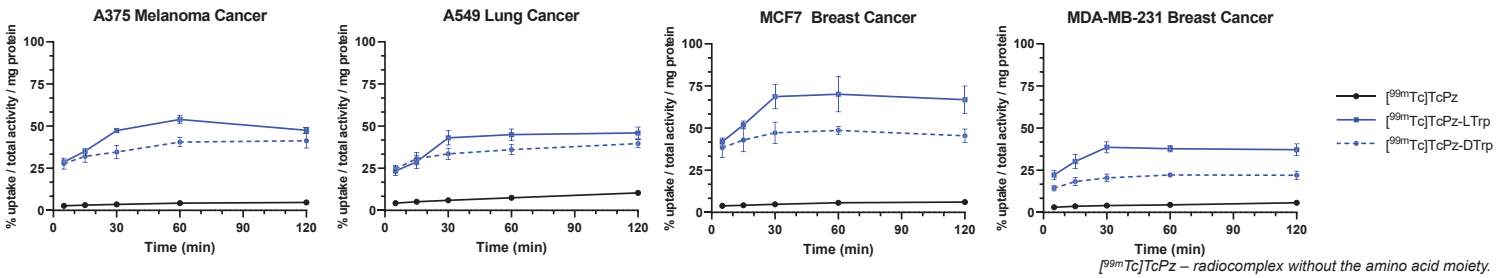

[^{99m}Tc]TcPz – radiocomplex without the amino acid moiety.

Results (N = 4) were normalized by protein content

Cellular internalization

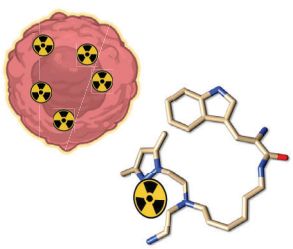

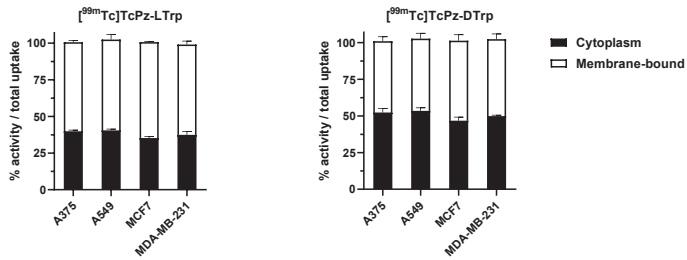

40 to 50% of the total cell-related activity is found intracellularly

Activity measured after 2h incubation. Results normalized to the total cell-related activity (N = 4).

Biodistribution studies of [^{99m}Tc]TcPz-LTrp in mice bearing A549 lung cancer xenografts

[^{99m}Tc]TcPz-LTrp presents tumor accumulation but poor contrast



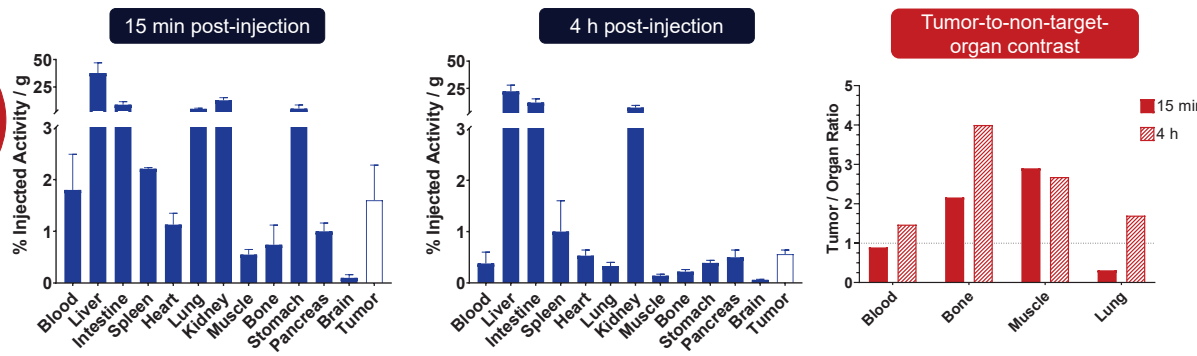

Biodistribution studies were performed on female Balb/c-Nude mice bearing A549 Lung Cancer xenografts (N = 3).

Conclusions

- **The cellular uptake depends on the enantiomeric form of Trp, with the L-Trp-bearing radiocomplex presenting the highest values.**
- **MCF7 breast cancer cell line shows the highest overall uptake.**
- **40 to 50% of the total cell-related activity is found intracellularly.**
- **[^{99m}Tc]TcPz-LTrp shows fast tumor uptake in tumor-bearing mice but poor tumor-to-non-target organs contrast.**

References:

[1] Vaupel et al., *J. Physiol.* **2021** *599*(6),1745

[2] Yasuhiro et al. *Cancer Sci.* **2021** *112*(8), 2958

[3] Wei et al. *Front. Cell Dev. Biol.* **2021**, *8*, 603837

[4] Morais et al., *Dalton Trans.* **2017**, *46*, 14537

The authors would like to thank the Fundação para a Ciência e Tecnologia (FCT), Portugal, for financial support through projects PTDC/QUI-NUC/30147/2017, PTDC/BTM-TEC/29256/2017 and UIDP/04349/2020. FCT is also acknowledged for PhD fellowships to RDMS (DFA/BD/4978/2020) and CIGP (DFA/BD/07119/2020).

https://doi.org/10.17952/37EPS.2024.P2018

Applications of Thiol-ene and Thiol-yne Chemistry for Peptide Stapling and Bioconjugation

Inés Rabadán González,[a] Joshua Mclean,[a] Nikitas Ostrovitsa,[a] Sheila Fitzgerald,[b] Andrea Mezzeta,[c] Lorenzo Guazzelli,[c] Donal O'shea,[b] Eoin M. Scanlan[a]*

[a]School of Chemistry, Trinity College Dublin, Ireland, [b]Department of Chemistry, Royal College of Surgeons in Ireland, Dublin, Ireland, [c]University of Pisa, 56126 Pisa, Italy

rabadngi@tcd.ie,

Introduction

- **Peptide modification** is gaining significance across a range of biomedical applications.
- Modified peptides have been used as **drug candidates** in the treatment of cancer, enzyme deficiency or metabolic disorders and infectious diseases.[1]
- The radical mediated **thiol-ene click (TEC) reaction** exhibits high atom economy, excellent yields and good regiocontrol.[2]
- Therefore, the **thiol-yne click (TYC) reaction** expands the chemistry of thiol-ene, providing access to a broad range of new properties.[3]

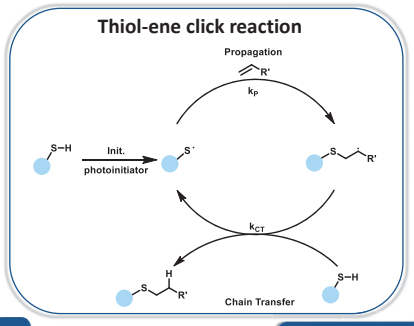

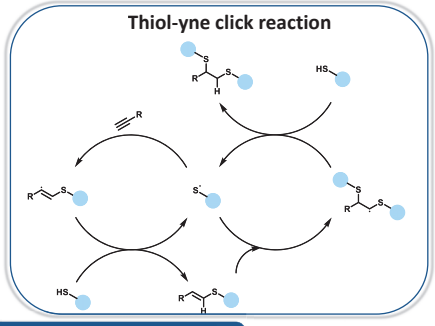

Green Continuous-Flow Bioconjugation

- **Flow chemistry** possesses a multitude of advantages, such as greater control over selectivity and reproducibility, less hazardous reaction setups and easier scale-up, and is therefore ideal for pharmaceutical and industrial applications.[4]
- **Deep Eutectic Solvents (DESs) and bio-based solvents** are promising candidates to provide significantly greener solvent options.
- The goals of flow chemistry and green chemistry are **ideally aligned** in prioritising the development of highly efficient synthetic approaches.

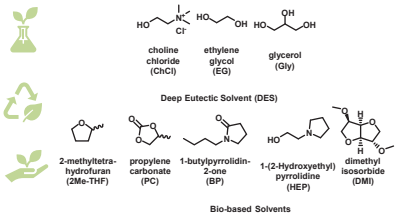

Green Optimisation

TEC was optimised with 2 different alkenes in batch and under continuous flow, utilising DES and Bio-based solvents. Glutathione (GSH) was selected as a model thiolated peptide substrate due to its therapeutic potential.

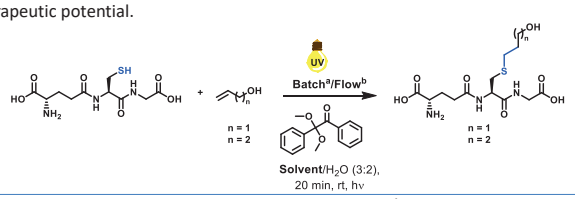

Entry	DES	n = 1 Conv.[a]	n = 1 Conv.[b]	n = 2 Conv.[a]	n = 2 Conv.[b]
I	ChCl: EG (2:1)	>99%	83%	98%	91%
II	ChCl: Gly (2:1)	Quant.	84%	>99%	Quant.
III	2Me-THF + BHT	>99%	95%	>99%	86%
IV	PC	Quant.	96%	>99%	>99%
V	BP	Quant.	93%	>99%	>99%
VI	HEP	98%	96%	Quant.	Quant.
VII	DMI	>99%	96%	Quant.	Quant.

Scale-up examples

One of the peptide glycosylation reactions reported in this study was this RGD peptide with DES and water under continuous flow along with a tumour homing peptide and an AFP peptide.

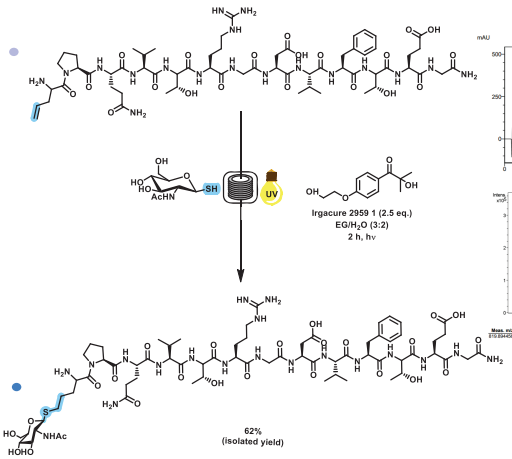

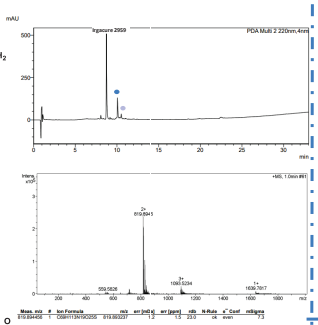

Disulfide rebridging

- **Essential disulfides** present a target that is known to be susceptible to topological changes upon reduction, and thus deactivation.
- Surface exposed disulfide bonds allow for the in-situ generation of unique functionalization sites through mild reduction, followed by selective chemical rebridging with unnatural linkers.[5]

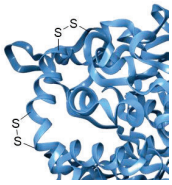

Project aim

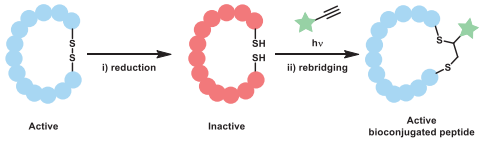

i) >99% reduction of the disulfide by $NaBH_4$ (2.0 eq.) was observed in 30 min.

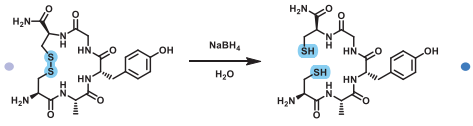

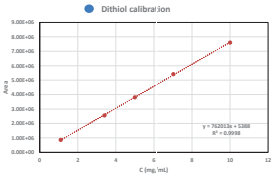

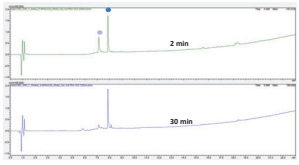

ii) TYC stapling

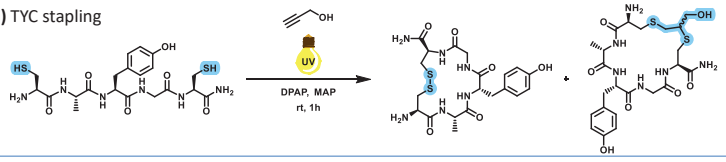

Entry	SH : alkyne (eq.)	Dithiol Concentration (mM)	Solvent	Additive	Disulfide conversion	Product conversion	Starting Dithiol
1	1 : 1	4.86	H_2O:ACN (9:1)	FA	45%	52%	>3%
2	1 : 2	4.86	H_2O:ACN (9:1)	FA	34%	58%	8%
3	1 : 4	4.86	H_2O:ACN (9:1)	FA	34%	50%	16%
4	**1 : 1**	**9.72**	**H_2O:ACN (9:1)**	**FA**	**29%**	**71%**	**0%**
5	1 : 1	19.4	H_2O:ACN (8:2)	FA	50%	25%	25%
6	1 : 1	4.86	PBS:ACN (9:1)	pH 7.4	73%	27%	0%
7	1 : 1	4.86	DMF	FA	95%	>3%	>2%
8	1 : 1	9.72	H_2O:ACN (9:1)	No additives	60%	40%	0%

*FA = Formic acid

Ongoing work

Disulfide rebridging in **one-pot reaction** will be performed to synthesise a bioconjugated active peptide for further therapeutic aims.

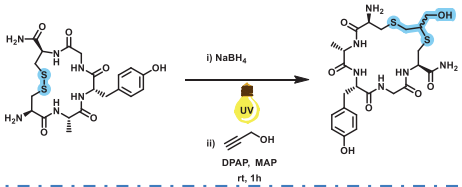

Conclusion

In this work, we report TEC mediated reactions under continuous-flow in both aqueous conditions, using 'green' solvents and furnishing biologically active glycopeptides in high yield. We also report a highly efficient TYC-mediated approach for peptide rebridging that can be applied to disulfide containing peptides. Following disulfide reduction, the radical-mediated crosslinking of the free thiol moieties via sequential thiol-yne ligation furnishes the covalently bound peptide macrocycle. TEC and TYC proved to be a promising and novel green strategy in the functionalisation of active peptide derivatives.

[1] I. Rabadán González, E. M. Scanlan et al., *Org. Biomol. Chem.*, 2024, **22**, 2203-2210. [2] M.D. Nolan, R. Petrarca *et al.*, *Org. Biomol. Chem.*, 2022, **20**, 8192-8196. [3] C. N. Bowman *et al.*, J. *Mater. Chem.*, 2010, **20**, 4745–4750. [4] F. Chen, *et al.*, *Green Synth. Catal.*, 2022, **3**, 243-258. [5] D. A. Richards, J. R. Baker *et al.*, *Org. Biomol. Chem.*, 2016, **14**, 455–459.

Greening Peptide Purification Through Use of Elevated Temperatures

European Peptide Symposium
August 25-29, 2024

Colin Simpson, Drew Cesta, Sandeep Singh, Jon Collins
CEM Corporation, Matthews, NC, USA, support@cem.com

https://doi.org/10.17952/37EPS.2024.P2019

Abstract

With increasing global demand for peptide therapeutics, there have been significant efforts towards improving the sustainability of peptide production, to include both synthesis and purification. Even as much of the recent efforts towards greener and more efficient peptide purification workflows have focused on the development of continuous chromatography approaches (e.g. MCSGP), there remains a need to further improve batch chromatography approaches, particularly for lab scale purification. In this work, we explore the use of elevated temperatures (using a novel integrated heating system) to enable both improved purity and/or recovery as well as improved access to greener, though more viscous solvents, such as ethanol. A set of 11 crude synthetic peptides ranging from 9-42 amino acids in length (and a range of hydrophobicities and isoelectric points) were purified at elevated temperatures (60 °C) using either acetonitrile or ethanol as the organic modifier. Despite a minor loss of chromatographic efficiency using ethanol, the final purity and recovery were nearly identical when using either mobile phase (Acetonitrile: 95% purity, 55% recovery; Ethanol: 95% purity, 53% recovery), and significantly improved as compared to ambient conditions using acetonitrile (90% purity, 37% recovery). This finding in addition to similar eluotropic strength (average target elution of 26.1% acetonitrile, and 27.5% ethanol) and selectivity suggests wider applicability of the use of ethanol as a green solvent alternative, particularly in the context of elevated temperature conditions.

Integrated Heating System

Despite the established performance benefits of HPLC purification at elevated temperatures, including improved peak shape and solubility and lower overall system pressures, lab scale purification continues to be performed nearly exclusively at ambient temperatures. Traditional heating approaches (e.g. water baths and heating jackets) at the preparative scale are cumbersome and generally don't provide an effective means for eluent preheating, which is critical for maximizing peak shape and chromatographic efficiency (**Figure 1**) [1].

We present here a novel heating system (**Figure 2**; used in this work as a component of the Prodigy (CEM) preparative HPLC system) for semi-preparative and preparative applications, which is comprised of a forced air column oven with an integrated mobile phase heater. Rapid temperature equilibration along with easily accessible bulkhead fluid connections provide a facile means for accessing elevated temperatures, reminiscent of approaches commonly employed at the analytical scale.

Figure 1. Effect of Column Heating, With or Without Mobile Phase Heating, on Chromatographic Efficiency. A: Illustration Depicting the Influence of Temperature Mismatch (between mobile phase and column) on Band Broadening. B: Effect of Integrated Heating System on Resolution for 18-mer Crude Peptide

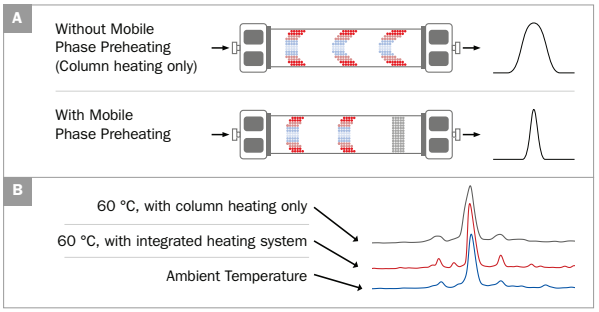

Figure 2. Renderings and Image of Novel Integrated Heating System

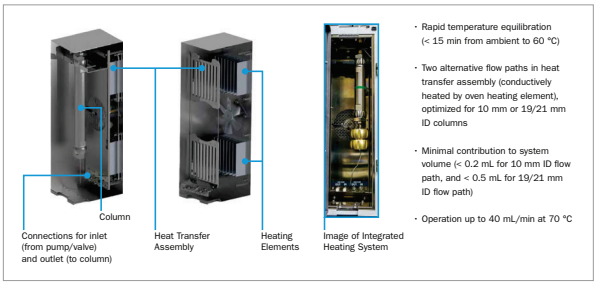

Use of Ethanol for Purification at Elevated Temperatures

Ethanol has been identified as a greener alternative to acetonitrile for reversed-phase HPLC of peptides [2], due both to a similar eluotropic strength as well as a low UV cutoff (205 nm), but its significantly higher viscosity (1.1 cP, as compared to 0.38 cP for acetonitrile) has generally precluded application for routine lab scale purification. Particularly when using columns packed with 5 µm media (often used to achieve the required resolution, as compared to larger 10 µm media), the backpressure generated using ethanol in ambient conditions can exceed typical column pressure limits as well as place significant demands on HPLC hardware. System backpressure is directly related to solvent viscosity (**Eq. 1**), so the backpressure using ethanol can be nearly 3-fold higher than that using acetonitrile (**Figure 3**). Additionally, the increased viscosity results in slower diffusion ("*D*") in the mobile phase (**Eq. 2**), which can result in an increased resistance to mass transfer ("*C*") between the mobile phase and stationary phase. This can result in broader peaks and reduced resolution according to the Van Deemter equation (**Eq. 3**), whereby chromatographic plate height is directly related to the resistance to mass transfer. However, since viscosity is indirectly related to temperature, increases in temperature can reduce viscosity such that system backpressure can become more manageable (**Figure 3**) and the impact of broadening due to reduced mass transfer kinetics can be minimized.

In this work, a set of 11 peptides (9 – 42 amino acids in length) with a range of hydrophobicities and isoelectric points were screened on an analytical HPLC system using mobile phases with either acetonitrile or ethanol (denatured), both at 60 °C. The average elution % was nearly identical for both mobile phases (**Table 1**), enabling the use of the same (or similar) focused gradient methods for purification. Additionally, while the selectivity was similar for both mobile phases, there was a slight loss of efficiency (broader peaks) using ethanol due to the increased viscosity. However, after purifying each sequence on the Prodigy HPLC system (CEM) using 15 minute focused gradient methods (0.4%B/CV slope; custom gradients calculated according to analytical HPLC retention times), the final purities and recoveries using elevated temperatures were significantly improved over 25 °C conditions (90% purity, and 37% recovery), and the results were nearly identical when using acetonitrile (95% purity, 55% recovery) or ethanol (95% purity, 53% recovery) (**Figure 4**).

$$\Delta P = \frac{\eta F L}{K^0 \pi r^2 d_p^2} \quad \textbf{Eq. 1}$$

$$D = \frac{k_B T}{\eta} \quad \textbf{Eq. 2}$$

$$h = A + \frac{B}{v} + Cv \quad \textbf{Eq. 3}$$

Figure 3. Relative System Pressure Using Either Acetonitrile or Ethanol at Both 25 and 60 °C

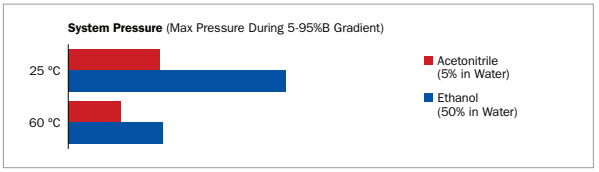

Table 1. Test Sequences and Analytical Elution %

#	Sequence	pI	Hydrophobicity	60 °C	
				Acetonitrile Elution %	Ethanol Elution %
1	GWVKPIIIGHHAYGDQYRAT	9.6	35.4	25.2	27
2	HGSRKNITDMVEGAKKANG	10.3	15.5	17.8	17.8
3	SLLNQPKAV	10.1	21.6	20.4	20.4
4	ALAVLSNYDA	3.1	25.2	24.7	25.8
5	TMEDKIYDQQVTKQCLCF	4.3	32.1	27.3	29.1
6	YSYPETPLYMQTASTSYYE	3.1	36.3	26.4	25.4
7	KVGYTERQRWDFLSEASIM	7.1	42.2	30.8	32.9
8	IVQENNTPGTYLLSVSARD	4.1	31.8	26.5	27.5
9	RFHMKVSVYLLAPLREALS	10.4	45.3	36.7	41.2
10	ENLKQNDISAEFTYQTKDA	4.1	29	21.1	21.9
11	DAEFRHDSGYEVHHQKLVFFAEDVGSNKGAIIGLMVGGVVIA ($^{1-42}$β-amyloid)	5.2	54.8	30.2 (70 °C)	34.0 (70 °C)
			Average Elution %	**26.1**	**27.5**

*#s 1-10 are neoantigen peptides described in a recent clinical trial for glioblastoma [3]

Figure 4. Screening and Purification at Elevated Temperatures Either Acetonitrile or Ethanol-Based Mobile Phases

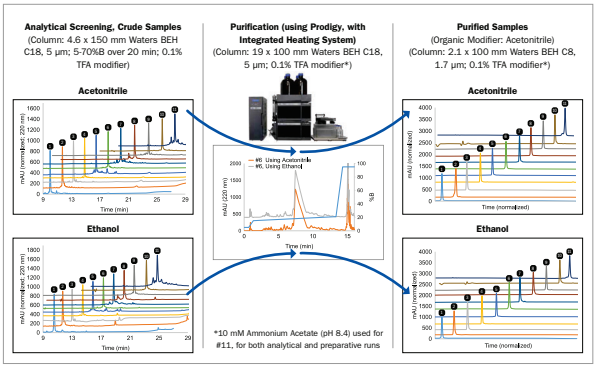

Table 2. Final Purity and Recovery

#*	Sequence	Crude Purity %	25 °C (150 mm column length; 1%B/CV gradient; 0.3% column loading)		60 °C (100 mm column length; 0.4%B/CV gradient; 0.5% column loading)*			
			Water / Acetonitrile Gradient		Water / Acetonitrile Gradient		Water / Ethanol Gradient	
			Purity %	Recovery %	Purity %	Recovery %	Purity %	Recovery %
1	GWVKPIIIGHHAYGDQYRAT	74	93	34	97	48	97	48
2	HGSRKNITDMVEGAKKANG	68	94	44	91	41	96	36
3	SLLNQPKAV	75	97	64	98	57	99	62
4	ALAVLSNYDA	79	95	66	97	63	95	72
5	TMEDKIYDQQVTKQCLCF	55	89	22	92	42	96	44
6	YSYPETPLYMQTASTSYYE	56	94	23	97	78	95	77
7	KVGYTERQRWDFLSEASIM	56	91	22	95	52	93	45
8	IVQENNTPGTYLLSVSARD	66	93	34	96	44	96	52
9	RFHMKVSVYLLAPLREALS	59	96	57	97	66	98	47
10	ENLKQNDISAEFTYQTKDA	71	87	30	93	52	91	46
11	DAEFRHDSGYEVHHQKLVFFAEDVGSNKGAIIGLMVGGVVIA	31	62	7	88	60	89	56
	Average	**63**	**90**	**37**	**95**	**55**	**95**	**53**

*Conditions for #11: 70 °C, 150 mm length column, 1%B/CV gradient

Conclusions

The application of elevated temperature conditions (using a novel integrated heating system) to enable the routine use of ethanol as an organic modifier for peptide purification was investigated. A set of 11 crude peptides (with varying lengths, hydrophobicities, and isoelectric points) were purified using either acetonitrile or ethanol-based mobile phases at 60 °C, and compared to purification using acetonitrile-based mobile phases at 25 °C. We found that purity and recovery were significantly improved using elevated temperatures and that the use of ethanol provided nearly identical results to that of acetonitrile, suggesting that any apparent loss of chromatographic efficiency using ethanol can be considered negligible in the context of purification using focused gradients and relatively high column loadings. Additionally, the eluotropic strength and chromatographic selectivity are nearly identical for ethanol and acetonitrile, suggesting wider applicability for the use of ethanol as an alternative green solvent.

References

[1] Brandt, A., Mann, G., and Arlt, W. Temperature gradients in preparative high-performance liquid chromatography columns. *J. Chrom A.* 769 (1997), 109-117.
[2] Brettschneider, F. et al. Replacement of acetonitrile by ethanol as solvent in reversed phase chromatography of biomolecules. *J. Chrom B.* 878 (2010), 763-768.
[3] Hilf, N. et al. Actively personalized vaccination trial for newly diagnosed glioblastoma. *Nature* 565 (2019), 240–245.

Faculty of Chemistry - Organic and Bioorganic Chemistry - OCIII

UNIVERSITÄT BIELEFELD

Enzymatic Peptide and Protein Bromination: The BromoTrp Tag

Nicolai Montua and Norbert Sewald

Organic and Bioorganic Chemistry, Faculty of Chemistry, Bielefeld University, Germany

Email: nicolai.montua@uni-bielefeld.de

https://doi.org/10.17952/37EPS.2024.P2020

Introduction: Flavin-Dependent Halogenases

- Flavin-dependent tryptophan halogenases (FDHs) catalyze the chlorination, bromination or iodination of the Trp-sidechain indole at C5, C6 or C7.[1,2]
  - Environmentally-friendly conditions: aqueous buffer, neutral pH, halide-salt, ambient temp.
  - Remarkable regioselectivity, no oversubstitution
- Poor catalytic parameters, narrow substrate scope, stability and process scalability[3-5]
- FDHs require $FADH_2$ in stochiometric amounts
  - Cofactor regeneration strategy required!
- Halotryptophan is part of many bioactive natural products & peptides.[4,5]
- Br-Trp: useful chemical handle for transition metal catalyzed cross-coupling reactions

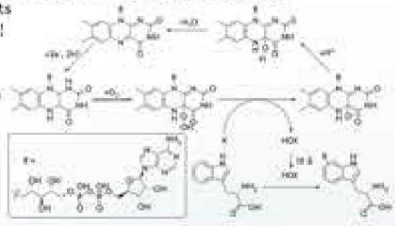

Fig. 1: Mechanism of FDH-catalyzed halogenation. $FADH_2$ reacts with molecular oxygen, forming a C4a-hydroperoxyflavin intermediate. This is attacked by a halide ion ($X^- = Cl^-$, Br^-). It's generate hypohalous acid as an activated halogen transfer reagent. After diffusion through an approx. 10 Å long tunnel, catalytically essential Lys and Glu residues further activate HOX to generate the active halogenation species. Aryl halogenation proceeds via electrophilic aromatic substitution.

Summary & Outlook

- Enzyme engineering campaign over three rounds of mutagenesis improved conversion of peptides with C-terminal Trp by up to 25-fold.
  - Regioselectivity for indole-C6 fully retained
  - conversion of N-protected Trp-derivatives also greatly improved
  - triple mutant Thal-AAC → strong bromide preference vs. chloride
  - YNIW as a viable protein tag → "BromoTrp Tag"
- Post-translational protein bromination
  - Successful for three model proteins (66-93% conversion)
- Suzuki coupling of brominated DARPin-E01 with phenyl boronic acid
- Potential applications:
  - Novel bioconjugation technique (e.g. for ADCs) → SMC yields stable C-C-Bond
  - Fluorogenic protein labelling[10]
  - Protein macrocyclization,[12] Palladium-catalyzed protein-protein cross-coupling[13]
  - Radiobromine labelling[14] → positron emitters (^{75}Br, ^{76}Br), Auger emitters (^{77}Br, ^{80m}Br)

Late-Stage Enzymatic Halogenation

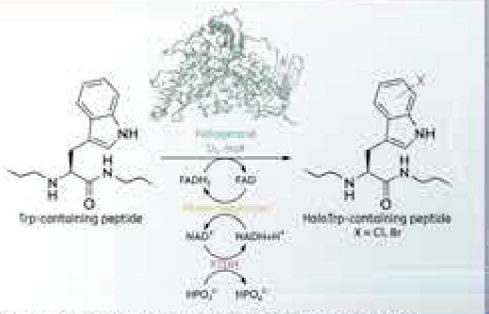

- We previously described effective peptide halogenation of N-terminal Trp-residues.[6]
- Halogenation of internal or C-terminal Trp → poor conversion

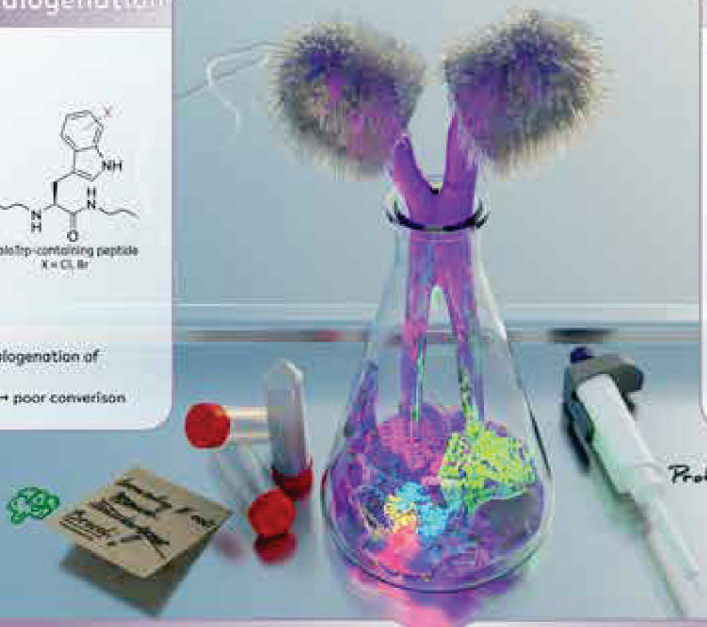

Bioconjugation by Suzuki-coupling

- Pd-catalyzed Suzuki-Miyaura coupling of brominated DARPin-E01 → successful with both Pd-ADHP and Pd-nanoparticles.[8,9]

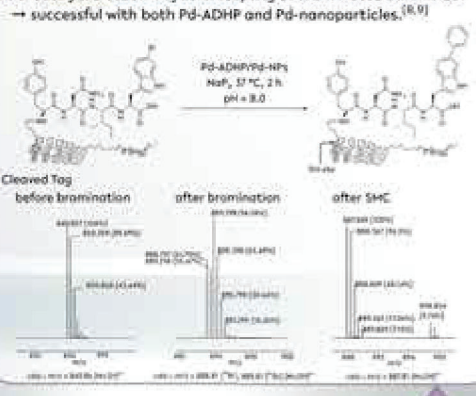

Protein Engineering of Thal:
Peptide Bromination? ☑
Extended Trp? ☑
tagged Proteins? ☑

Enzyme Engineering Campaign

- Enzyme engineering extended the substrate scope of Thal to peptides with Trp at the C-terminus and N^{in}-protected Trp derivatives; Conversions improved up to 25× using a triple mutant variant of Thal.
- Thal-AAC exhibits a pronounced halide preference for bromide over chloride.

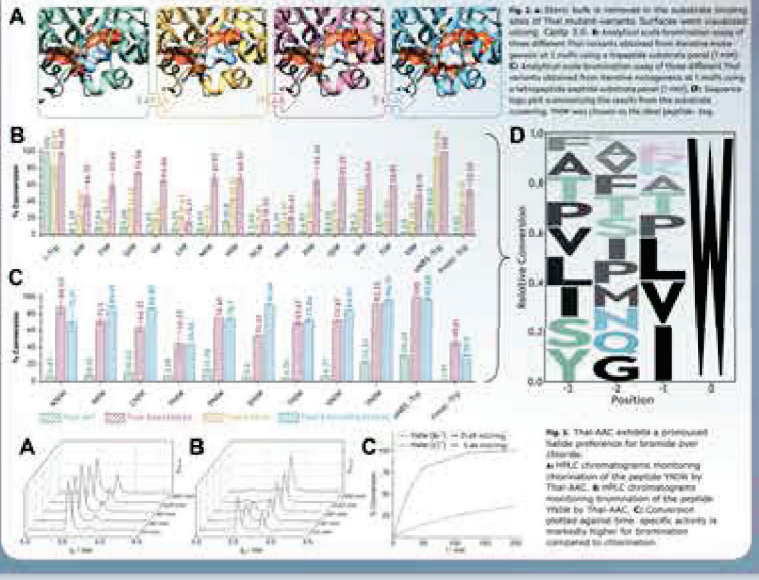

Fig. 3: A: Steric bulk is removed in the substrate binding sites of Thal mutant variants. Surfaces were visualized using Cavity 3.0. B: Analytical scale bromination assay of three different Thal variants obtained from iterative mutagenesis on 5 motifs using a tetrapeptide acetride substrate panel (1 mM). C: Analytical scale bromination assay of three different Thal variants obtained from iterative mutagenesis at 5 motifs using a tetrapeptide acetride substrate panel (1 mM). D: Sequence logo plot summarizing the results from the substrate screening. YNIW was chosen as the ideal peptide tag.

Fig. 5: Thal-AAC exhibits a pronounced halide preference for bromide over chloride. a: HPLC chromatograms monitoring chlorination of the peptide YNIW by Thal-AAC. b: HPLC chromatograms monitoring bromination of the peptide YNIW by Thal-AAC. c: Conversion plotted against time: specific activity is markedly higher for bromination compared to chlorination.

The BromoTrp Tag: Selective Protein Bromination

- The BromoTrp tag YNIW was appended to model proteins via a flexible linker peptide → Coexpression with halogenase cascade in one *E. coli* cell → selective monobromination

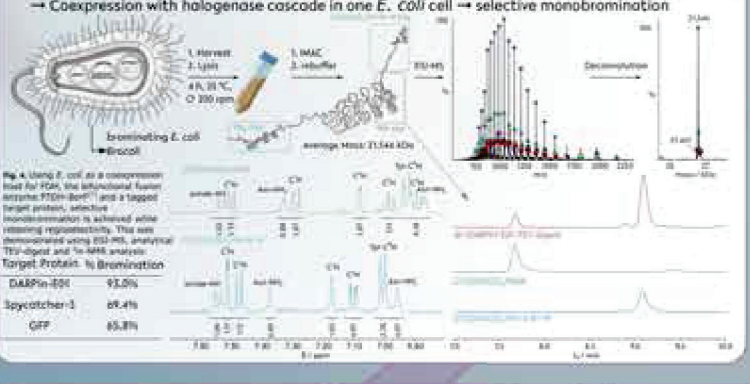

Fig. 4: Using *E. coli* as a coexpression host for FDH, the bifunctional fusion enzymes FDH-BorF[11] and a tagged target protein, selective monobromination is achieved while retaining regioselectivity. This was demonstrated using ESI-MS, analytical TEV-digest and ^{1}H-NMR analysis.

Target Protein	% Bromination
DARPin-E01	93.0%
Spycatcher-3	69.4%
GFP	65.8%

References & Acknowledgements

[1] v. Hooijdonk, M. Sewald, ChemCatChem 2020, 12, 4478–4479.
[2] C. Schnepel, J. Sewald, Chem. Eur. J. 2017, 23, 12689–12707.
[3] A. Pimviriyakul, A. Thobhirak, M. Jaruwat, M. Lapsen, S. Thongkongkaew, P. Wongnate, Angew. Chem. Int. Ed. 2020, 59, 16207–16211.
[4] C. M. Dobbs, Synthesis 2021, 53, 1941–1952.
[5] C. Schnepel, J. Sewald, ChemBioChem 2017, 18, 486–501.
[6] N. Montua, M. Sewald, ChemBioChem 2021, e202100408.
[7] N. Montua, M. Sewald, Org. Biomol. Chem. 2022, 20, 4478–4479.
[8] J. Sewald, N. Montua, M. Sewald, ChemBioChem 2023, e202300439.
[9] N. Montua, M. Sewald, ChemBioChem 2023, e202300439.
[10] M. Sewald, Chem. – Eur. J. 2024, 30, e202314364.
[11] J. Sewald, M. Sewald, Angew. Chem. Int. Ed. 2024, 63, e202317455.
[12] J. Sewald, M. Sewald, Chem. Sci. 2024, 15, 1–10.
[13] J. Sewald, M. Sewald, Nat. Commun. 2024, 15, 1–12.
[14] J. Sewald, M. Sewald, Nat. Chem. 2024, 16, 1–10.

This work was supported by the DFG (SE 1808/9-1) and the Fonds der Chemischen Industrie. The work was also supported by the BMBF (Unterstützer-Netzwerk Bioinformatics-Infrastructure, DA 1380 TP3+TP4B, 031L0102C, 031L0102A). We thank Prof. Dr. Norbert Sewald for his support and helpful discussions.

Scan to read more!

https://sewaldlab.de

Combining Quaternary Ammonium Compounds and Peptides- Its Application to Antimicrobials and Beyond

Rolland Lin[1,2,3], Margaret A. Brimble[1,2,3], Brian H. Northrop[4], Alan J. Cameron[1,2,3]

[1]School of Chemical Sciences, University of Auckland, [2]School of Biological Sciences, University of Auckland, [3]Maurice Wilkins Centre for Molecular Biodiscovery, University of Auckland, [4]Chemistry, Wesleyan University

https://doi.org/10.17952/37EPS.2024.P2021

UNIVERSITY OF AUCKLAND
Waipapa Taumata Rau
NEW ZEALAND

What are Quaternary Ammonium Compounds?

Also known as **quats**- a tetravalent nitrogen bonded to four alkyl/aryl substituents

- **Permanent positive charge**

Broad spectrum antimicrobial activity

- In disinfectants, antiseptics, preservatives



Quats' Mode of Action involve...

Initial **electrostatic interaction** between quats and negatively charged bacterial membranes

- Penetration of quat hydrophobic tails into the hydrophobic membrane core leads to:
  - Loss of membrane integrity
  - Leakage of cellular contents
  - Cell death

Similar MOA to cationic antimicrobial peptides

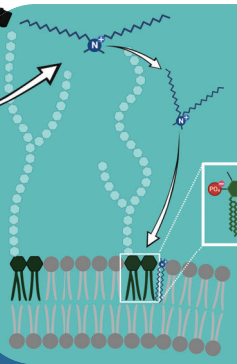

Serendipitous Finding...

While developing allenamide handles for peptides,[1] we observed quat by-products resulting from the **aza–Michael addition of tertiary amines** to allenamides.

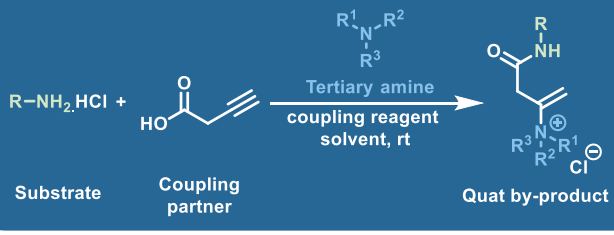

Why are We Interested?

1. **Interesting chemistry**- a new way to prepare quats
2. Aza-Michael reaction is a **"click" reaction**
   - No alkylating agents!
3. Could be adapted for **solid-phase peptide synthesis** (SPPS)
   - Given our established method to introduce allenamides during SPPS[1]

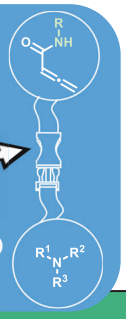

The Research

1 Reaction Optimization And Scope

Solvent was critical

- **Green solvents** were best performing
  - Propylene carbonate
  - Water

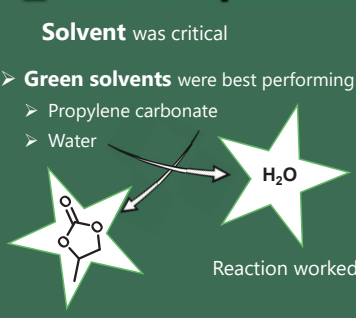

Reaction worked for 12 different tertiary amines

2 Preparation of Quat Mimics

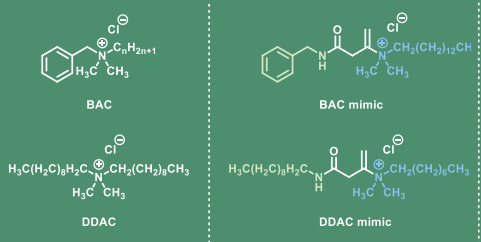

Bacteria	Minimum inhibitory concentrations (μM)			
	BAC	BAC mimic	DDAC	DDAC mimic
E. coli	32	(32)	16	(32)
S. aureus	8	(4)	4	(8)
C. albicans	16	(8)	8	(8)

BAC and DDAC- two of the most common quat disinfectants

3 Application to Antimicrobial Peptides

Previous literature showed **incorporation of quats to polymyxin B (PMB) broadens activity towards Gram-positive bacteria**[2]
-may infer activity against resistant strains

∴ **Quaternization was adapted for Fmoc-SPPS**

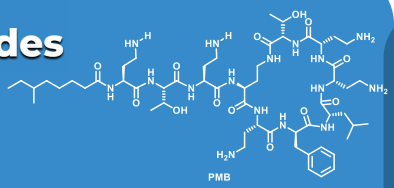

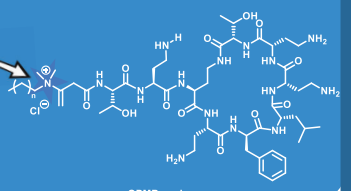

Bacteria	Minimum inhibitory concentrations (μM)			
	PMB	QPMB1 (n=4)	QPMB2 (n=8)	QPMB3 (n=12)
E. coli	0.125	2	(0.25)	1
S. aureus	>64	>64	32	(2)

4 Computational Chemistry Corroborates...

Aza-Michael addition of 3° amines to allenamide **uniquely favours product formation**, due to RDS

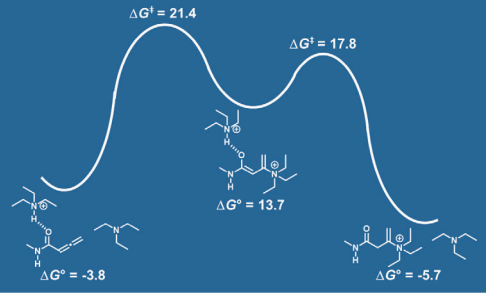

5 Reaction is selective in the presence of peptide-related functional groups

Side chains of Asn, Met, Ser, Trp, Tyr and **Lys**

Experimental selectivity of 3° amines over 1° amines supported by DFT

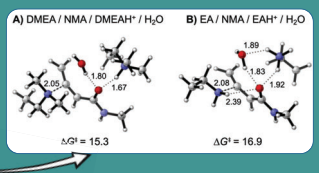

6 Future Work

- Application as **prodrug**- in progress
- More PMB analogues
- More QAC disinfectant analogues
- Test against resistance strains

References:

1. Cameron, A. J.; Harris, P. W. R.; Brimble, M. A. On-Resin Preparation of Allenamidyl Peptides: A Versatile Chemoselective Conjugation and Intramolecular Cyclisation Tool. *Angewandte Chemie International Edition* **2020**, *59* (41), 18054–18061. https://doi.org/10.1002/anie.202004656.
2. Ongwae, G. M.; Morrison, K. R.; Allen, R. A.; Kim, S.; Im, W.; Wuest, W. M.; Pires, M. M. Broadening Activity of Polymyxin by Quaternary Ammonium Grafting. *ACS Infect. Dis.* **2020**. https://doi.org/10.1021/acsinfecdis.0c00037

Also check out:

Na, T. U.; Sander, V.; Davidson, A. J.; Lin, R.; Hermant, Y. O.; Hardie Boys, M. T.; Pletzer, D.; Campbell, G.; Ferguson, S. A.; Cook, G. M.; Allison, J. R.; Brimble, M. A.; Northrop, B. H.; Cameron, A. Allenamides as a Powerful Tool to Incorporate Diversity: Thia-Michael Lipidation of Semisynthetic Peptides and Access to β-Ketoamides. *Angewandte Chemie International Edition*, **2024** e202407764. https://doi.org/10.1002/anie.202407764.

Emails:
rlin655@aucklanduni.ac.nz
alan.cameron@auckland.ac.nz

MAURICE WILKINS CENTRE FOR MOLECULAR BIODISCOVERY

SCAN ME

*Graphic Created with Biorender.com

https://doi.org/10.17952/37EPS.2024.P2022

Department of Chemistry - Organic and Bioorganic Chemistry - OCIII

UNIVERSITÄT BIELEFELD

Fluorescent Amino Acids with large STOKES Shift

Nicolas Schnatmann and Norbert Sewald

Organic and Bioorganic Chemistry, Department of Chemistry, Bielefeld University, Germany.

Contact: nicolas.schnatmann@uni-bielefeld.de

Introduction

- Classic method for fluorescent peptide modification uses active esters or isothiocyanates
- Recently fluorescent modification of bromotryptophan containing peptides by cross-couplings has been demonstrated[1]
- Biaryl coupling leads to an extension of π-system
- Excitation wavelength does not shift as expected for π-system extension
- This hints to biaryl rotation around formed σ-bond
- For 7-bromotryptophan this can be suppressed by cyclisation with the indole-nitrogen

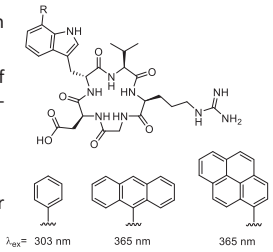

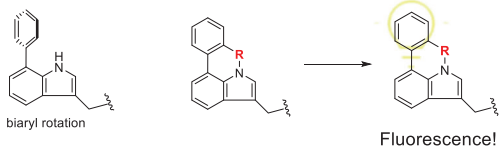

Dye Synthesis

Bor Coordination

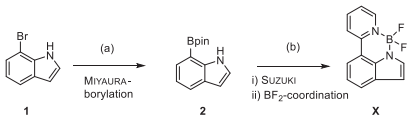

λ_{ex}: max 360 nm (DCM)
till 420 nm excitation possible
λ_{em}: max 490/520 nm
Φ < 0.27 (DCM)

Scheme 1: (a) B_2pin_2, KOAc, $PdCl_2(dppf)$, dioxane, 92 °C (b) i) 2-Bromopyridine, $PdCl_2(dppf)$, K_2CO_3, dioxane/H_2O, 90 °C ii) DIPEA, BF_3·OEt_2, DCM, rt.

Lactam Cyclisation

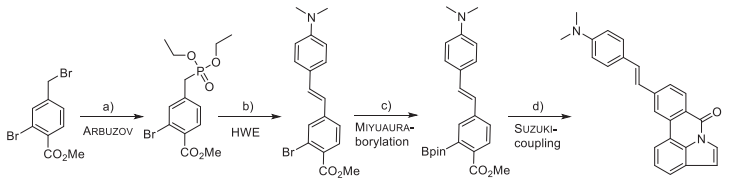

λ_{ex}: max 415 nm (MeOH)
till 450 nm excitation possible
λ_{em}: max 650 nm
Φ =0.28 (MeOH)

Scheme 2: (a) $P(OEt)_3$, dioxane, 100 °C. (b) *p*-dimethylaminobenzaldehyde, NaH, THF, 0 °C -> rt. (c) $PdCl_2(dppf)$, B_2pin_2, KOAc, dioxane, 90 °C. (d) 7-Br-indole, $PdCl_2(dppf)$, K_2CO_3, DME/MeOH, 90 °C.

Fluorescence Spectra

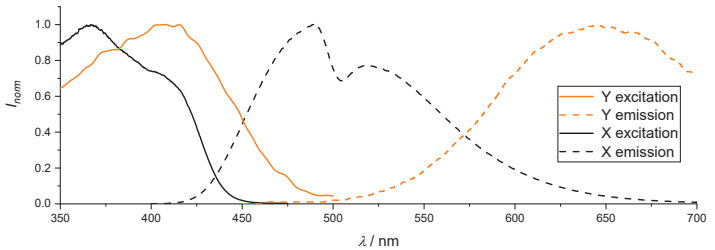

Figure 1: Fluorescence spectra of diazaborinin-structure **X** in DCM and lactam-structure **Y** in MeOH. Both dyes have bright fluorescence mit quantum yields of ~28 % with STOKES-shifts of 130 and 220 nm.

Amino Acid Modification

- 7-borylated Trp is accessable via Ir-catalysed C-H borylation[2]
- Since other diazaborinin-structures (BODPIY) are known to be unstable during peptide synthesis, bor coordination is the last step



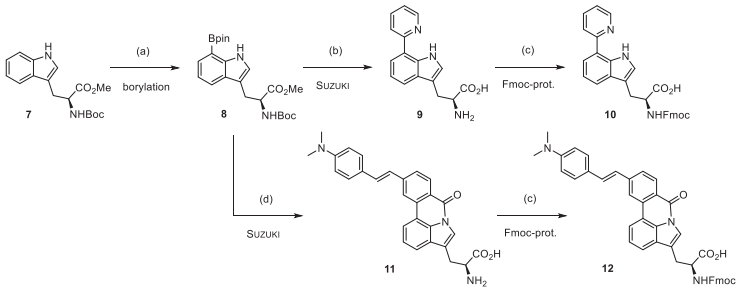

Scheme 3: (a) i) $[Ir(cod)OMe]_2$, dtbpy, HBpin, THF, 60 °C ii) $Pd(OAc)_2$, AcOH, 70 °C. (b) i) 2-Bromopyridine, $PdCl_2(dppf)$, K_2CO_3, dioxane/H_2O, 90 °C. ii) TFA/TIS/H_2O. (c) Fmoc-OSu, Na_2CO_3, ACN/H_2O. (d) **5**, $PdCl_2(dppf)$, K_2CO_3, DME/MeOH, 90 °C.

Amyloid-affine Peptide Modified with new Dye

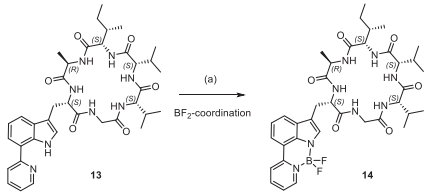

Scheme 4: (a) BF_3·OEt_2, DIPEA, 1,4-dioxane, rt.

Late Stage Peptide Modification: Lactam

- Late stage SUZUKI-couplings with peptides are well known in the literature[1,3]
- To prevent saponification of ester **6** water-free conditions are necessary
- Lactam cyclisation reaction needs temperature of min. 90°C
- Due to peptide solubility, solvent was changed to DMF/MeOH
- Based on DACHWITZ *et al.*, pentapeptides for test reactions have been synthesized[3]

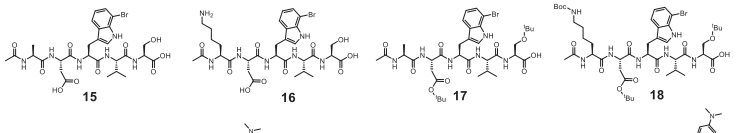

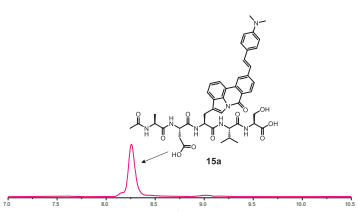

Figure 2: HPLC-chromatogramm of coupling with **15** after 30 min: SUZUKI-coupling with free aspartic acid leads to desired product

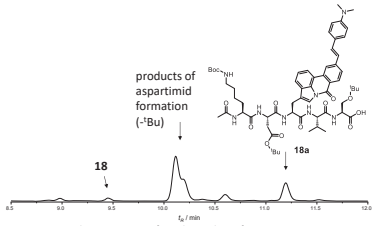

Figure 3: HPLC-chromatogramm of coupling with **18** after 30 min: SUZUKI-coupling protected aspartic acid leads to aspartimid formation, proven by a shouldered peak with am mass [M-tBu+H]+

- Coupling with free amine (peptide **16**) showed bad conversion

Conclusion:

- Coupling of amines needs Boc-protection
- Deprotection of Asp prevents aspartimid formation

Mechanism Aspartimid Formation

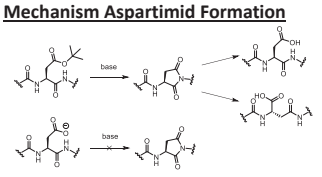

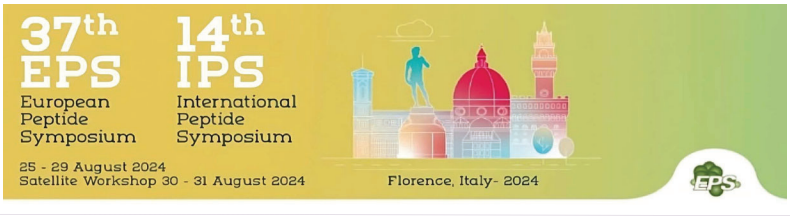

References

[1] I. Kemker, D. C. Schröder, R. C. Feiner, K. M. Müller, A. Marion, N. Sewald, *J. Med. Chem.* **2021**, *64*, 586.
[2] R. P. Loach, O. S. Fenton, K. Amaike, D. S. Siegel, E. Ozkal, M. Movassaghi, *J. Org. Chem.* **2014**, *79*, 11254.
[3] S. Dachwitz, D. H. Duwe, Y. H. Wang, H. Gruß, Y. Hannappel, T. Hellweg, N. Sewald, *Chem. Eur. J.* **2020**, *26*, 16357.

https://doi.org/10.17952/37EPS.2024.P2023

Propargylamine Amino Acids as Constrained N^{ε}-Substituted Lysine Mimetics

Kevin Van holsbeeck, Mathias Elsocht, Steven Ballet

Research Group of Organic Chemistry, Vrije Universiteit Brussel, Brussels, Belgium

Email: kevin.van.holsbeeck@vub.be

INTRODUCTION

Lysine (Lys) is an essential amino acid playing a **crucial role in a plethora of biologically active proteins and peptides**, due to its primary amine moiety connected to a hydrophobic alkyl side chain. Naturally, Lys undergoes **various reversible post-translational modifications** (e.g. methylations), which affect the functioning of proteins such as histones.[1]

Therefore, N^{ε}-alkylated and constrained Lys derivatives (e.g. **1-8a-e**, **Figure 1**) have been developed for application in peptides targeting these proteins, such as peptide inhibitors of methylated lysine reader proteins.[2] In this context, we developed an efficient synthetic pathway towards **lysine analogues rigidified in their side chain** by an internal alkyne functionality and decorated with various **substituents at the ε-amine** (**9**).[3] Solution syntheses of this type of lysine mimetics were only reported for aza-Lys-D-Phe dipeptides (Lubell Group) and racemic α-CF3 substituted propargylglycine (Osipov Group), both protected at their *N*- and *C*-termini.[4,5]

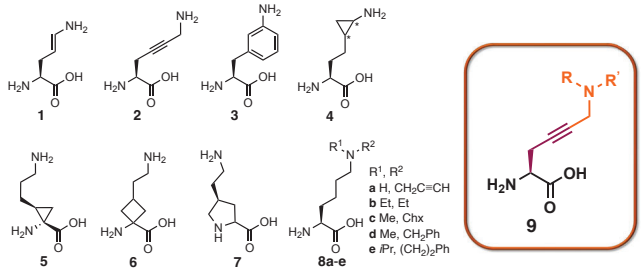

Figure 1. Examples of reported constrained and alkylated lysine derivatives.

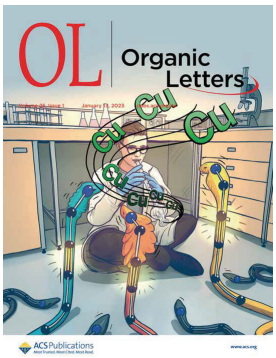

Copper(I)-catalyzed A³-reaction on Fmoc-Pra-OH

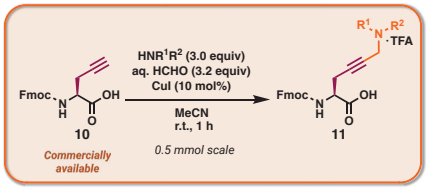

- **Fast conversions**
- Longer reaction times with sterically demanding amines
- Aqueous formaldehyde: limits allene formation
- Preformation of iminium: limits *N*-Fmoc removal
- **75-90% isolated yields** (RP chromatography)

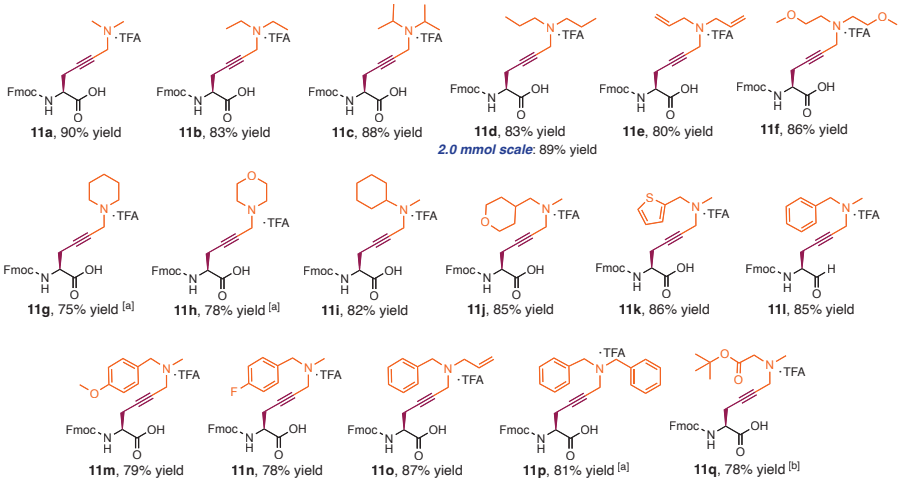

[a] 2 h reaction time. [b] Additional DIPEA (3.0 equiv) and CuI (1.5 equiv).

Diversification of the internal alkyne towards 1,2,3-triazoles

- Internal alkyne moiety: further functionalization via **ruthenium-catalyzed azide-alkyne cycloadditions** (RuAAC)
- Ester protection needed

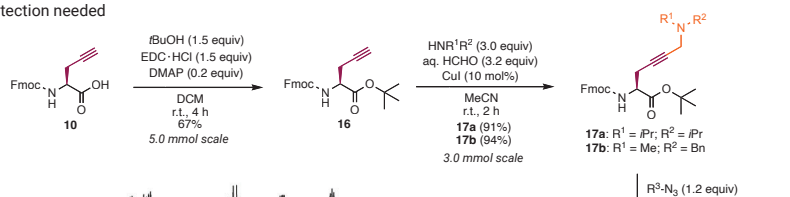

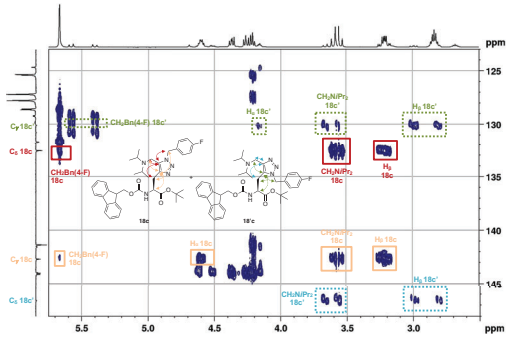

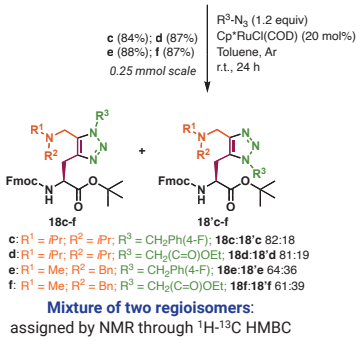

c: R^1 = *i*Pr; R^2 = *i*Pr; R^3 = $CH_2Ph(4\text{-}F)$; **18c**:**18'c** 82:18
d: R^1 = *i*Pr; R^2 = *i*Pr; R^3 = $CH_2(C{=}O)OEt$; **18d**:**18'd** 81:19
e: R^1 = Me; R^2 = Bn; R^3 = $CH_2Ph(4\text{-}F)$; **18e**:**18'e** 64:36
f: R^1 = Me; R^2 = Bn; R^3 = $CH_2(C{=}O)OEt$; **18f**:**18'f** 61:39

Mixture of two regioisomers: assigned by NMR through ^{1}H-^{13}C HMBC

Application of the A³-reaction during SPPS

- **Direct incorporation** in peptides of **11a-q** by Fmoc-based SPPS
- Diversification **during SPPS assembly**: pre-assembled **12**
  - Purification not jeopardized by less efficient conversions
  - Higher conversions: DMSO, 50 mol% CuI and extended reaction times

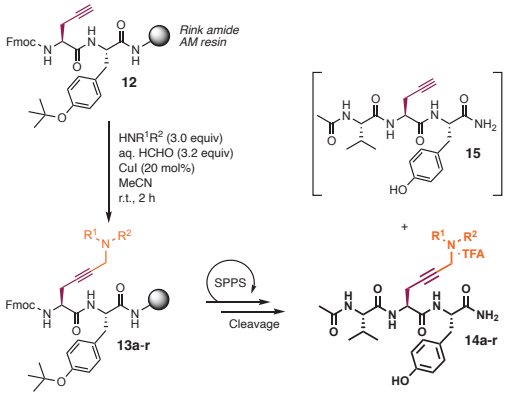

Code	HNR^1R^2 used for A³-coupling	Amount of **14a-r** (%) [c]	Amount of **15** (%) [c]
14a	Dimethylamine	71	23
14b	Diethylamine	n.d.[d]	n.d.[d]
14c	Di*iso*propylamine	91	1
14d	Dipropylamine	89	4
14e	Diallylamine	70	25
14f	Bis(2-methoxyethyl)amine	57	25
14g [a]	Piperidine	84	10
14h [a]	Morpholine	52	43
14i	*N*-Methylcyclohexylamine	90	4
14j	*N*-Methyl(tetrahydro-2*H*-pyran-4-yl)methanamine	89	5
14k	*N*-Methyl-*N*-(thien-2-yl-methyl)amine	66	26
14l	*N*-Methylbenzylamine	78	13
14m	4-Methoxy-*N*-methyl-benzylamine	83	10
14n	4-Fluoro-*N*-methyl-benzylamine	82	12
14o	*N*-Allylbenzylamine	62	34
14p [a]	Dibenzylamine	65	30
14q [b]	*Tert*-butyl sarcosinate hydrochloride	56	24

[a] Performed for 4h. [b] Additional DIPEA (3.0 equiv) and CuI (1.5 equiv). [c] Determined by analytical HPLC of the crude peptides. [d] Not determined due to overlap.

CONCLUSION & PERSPECTIVES

- **Efficient pathway toward N^{ε}-alkylated propargylamine amino acids as lysine mimetics**
- **Synthetic accesibility by A³-reaction on Fmoc-protected building blocks and during solid phase assembly**
- **Additional functionalization of internal alkyne by the RuAAC towards 1,2,3-triazoles**
- **Diversification of azide substitutent: additional linkage point for peptide cyclizations or late-stage functionalization**

REFERENCES

[1] Wang, Z.; Cole, P. *Cell Chem. Biol.* **2020**, *27*, 953-969. [2] Lamb, K.; Bsteh, D. *et al. Cell Chem. Biol.* **2019**, *26*, 1365-1379. [3] Van holsbeeck, K.; Elsocht, M.; Ballet, S. *Org. Lett.* **2023**, *25*, 130-133. [4] Zhang, J.; Proulx, C. *et al. Org. Lett.* **2013**, *16* (1), 298-301. [5] Philippova, A. N.; Vorobyeva, D. *et al. Mendeleev Commun.* **2022**, *32* (2), 260-261.

ACKNOWLEDGEMENTS

K.V.h. and S.B thank the Research Foundation Flanders (FWO Vlaanderen) for providing a PhD fellowship to K.V.h. S.B. thanks the Research Council of the Vrije Universiteit Brussel for financial support through the Strategic Research Programme (SRP50). Giulia Atza is acknowledged for performing preliminary work.

Synthesis and structural characterization of trifluoromethylated tetrahydroisoquinolines as new constrained aromatic amino acid surrogates

Lilian Loisons,[1] Steven Ballet,[2] Thierry Brigaud,[1] Simon Gonzalez.[1]

[1] CNRS, BioCIS, CY Cergy-Paris Université, 95000 Neuville sur Oise, France;
[2] Research Group of Organic Chemistry, Vrije Universiteit Brussel, Brussels, Belgium.

simon.gonzalez1@cyu.fr

https://doi.org/10.17952/37EPS.2024.P2024

Introduction

It is often necessary to apply **conformational restrictions** to peptides in order to fine tune their activity in vivo.
Local constrains, such as **cyclization**, applied to (aromatic) amino acids can restrain **dihedral angles** and the so-called **χ-space**, and improve peptides' **activity, selectivity, or stability**.[1]

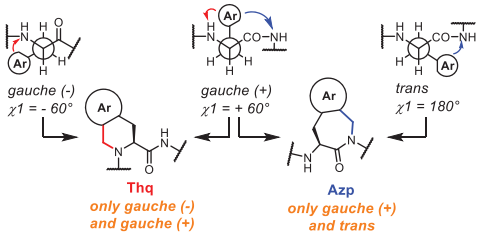

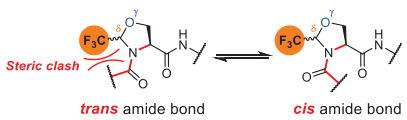

In addition to enhancement of peptide's **stability**,[2] and membrane permeation due to **increased hydrophobicity**,[3] introduction of **fluorine** in peptides and amino acids can have remarkable effects on their **structure**. Notably, we demonstrated that a **trifluoromethyl** (**Tfm**) group, introduced in δ position of proline derivatives, exerts a stereoelectronic effect lowering the *cis*/*trans* isomerization barrier and **favors the *cis* amide bond** conformer.[4]

We herein invistigate the combination of **cyclic constrains** and the **stereoelectronic effect of Tfm** on aromatic amino acids. Cyclization on the *N*$^{\alpha}$ *via* **Pictet-Spengler type reactions** should provide the desired trifluoromethylated **tetrahydro-β-carboline** or **tetrahydroisoquinolines** (**Thq**).

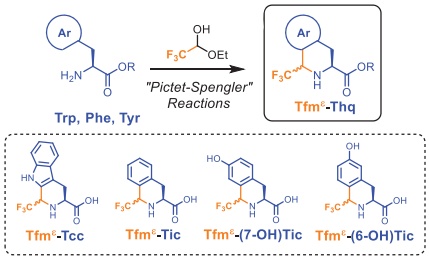

Synthesis

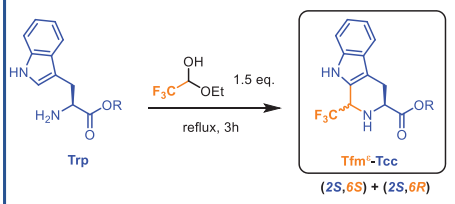

R	Yield	dr
Me	62%	52/48
Et	75%	54/46
Bn	62%	71/29
*t*Bu	81%	51/49

- First on Trp **without solvent** as published by Nishida.[5]
- Different protecting groups are **well tolerated**.
- **No significant diastereoselectivity**, except for the (**2*S*,6*S***) isomer with Bn as protecting group.
- Two diastereomers **separable on silica gel**.

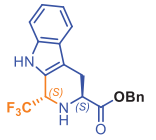

H-(**2*S*,6*S***)-Tfm$^{\varepsilon}$-Tcc-OBn

Acidic hydrolysis of esters failed while saponification **led to fast epimerization** (with NaOH or LiOH) or no conversion (NaOH + $CaCl_2$).

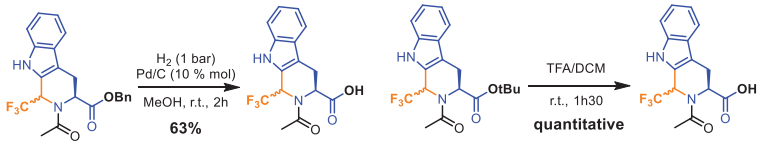

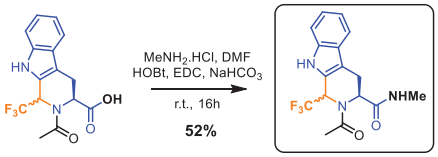

- Bn or *t*Bu ester deprotection **proceeded smoothly**.
- Coupling with methyl amine afforded the expected models for both diastereomers.

Derivatization and acetylated models synthesis

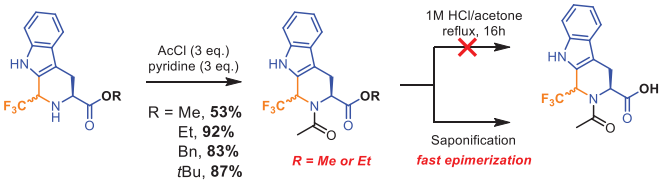

Other amino acids

- Only **traces obtained with Phe or Tyr**. Complex mixture of side products.
- **Decent result with *m*Tyr** but also side reactions.

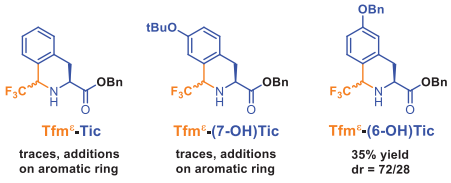

Require milder conditions

Structural characterization

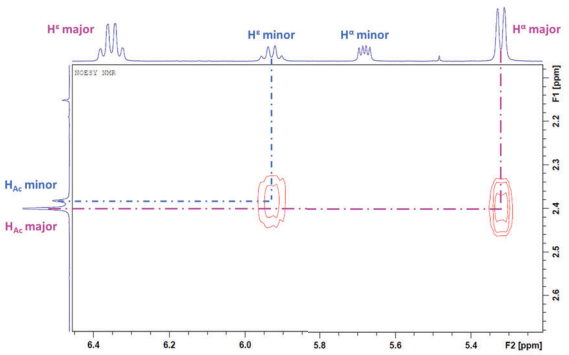

NOESY NMR in CD_3OD

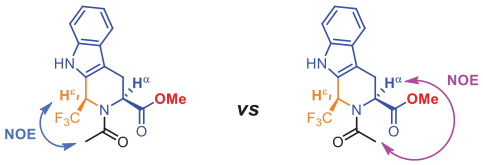

Ac-(**2*S*,6*R***)-Tfm$^{\varepsilon}$-Tcc-OMe with *trans* amide bond conformation

Ac-(**2*S*,6*R***)-Tfm$^{\varepsilon}$-Tcc-OMe with *cis* amide bond conformation

Amino acid	Cis/trans ratio
Ac-(**2*S*,6*R***)-Tfm$^{\varepsilon}$-Tcc-OMe	58/42
Ac-(**2*S*,6*S***)-Tfm$^{\varepsilon}$-Tcc-OMe	70/30
Ac-Tcc-OMe	45/55
Ac-(**2*S*,6*R***)-Tfm$^{\varepsilon}$-Tcc-NHMe	61/39
Ac-(**2*S*,6*S***)-Tfm$^{\varepsilon}$-Tcc-NHMe	69/31

- Both diastereomers show a **preference for the *cis* conformation**, especially the (**2*S*,6*S***) analog.
- **Remarkable effect of the CF_3** compared to the non fluorinated Tcc (*trans* as major conformer).
- No clear influence of the *C*-terminus.

Conclusion

- Cyclization was **performed efficiently on Trp** with various tolerated protecting groups, but **no clear diastereoselectivity** except with Bn esters.
- Derivatization more difficult than expected since the product quickly **undergo complete epimerization in basic conditions**.
- Cyclization worked with the **activated *m*Tyr** but not with Tyr or Phe, probably due to side reactions on the aromatic ring. **Milder conditions** should be attempted.
- Effect of Tfm on the *cis*/*trans* ratio with an **increased *cis* population** compared to the non fluorinated analog.

Incorporation into peptides and structural implications

References

[1] ***(a)*** De Neve, J. *et al. J. Med. Chem.* **2024**, *67* (9), 7603-7619, ***(b)*** Lozada, C. *et al. Bioorg. Chem.* **2023**, *139*, 106731, ***(c)*** Gonzalez, S. *et al., J. Med. Chem.* **2020**, *63* (21), 12929-12941. [2] Huhmann, S. *et al. Eur. J. Org. Chem.* **2018**, *2018* (27-28), 3667-3679. [3] Oliver, M. *et al. RSC Adv.* **2018**, *8*, 14597-14602. [4] Chaume, G. *et al. J. Org. Chem.* **2017,** *82* (24), 13602-13608. [5] Maki, Y. *et al. J. Fluor. Chem.* **1989,** *43* (2), 189-205.

Aknowledgements

The CY Initiative of Excellence (grant « Investissement d'Avenir » INEX 2022 CArACT-R) is thanked for the financial support.

Cysteine Thioaldehydes : Photolytic Generation and Reactivity

Ardra Karthika,*[1] Matthew Murray,[1] Guillermo Palop,[1] Lee-Ann Keane,[1] Patrick McArdle,[1] Luke Crehan,[1] Nicholas Yates,[2] Alison Parkin,[2] Martin Fascione,[2] Eddie L. Myers[1]

[1]School of Biological and Chemical Sciences, University of Galway, Ireland, [2]Department of Chemistry, University of York, York, UK.

A.Karthika1@universityofgalway.ie, Eddie.Myers@universityofgalway.ie

https://doi.org/10.17952/37EPS.2024.P2025

Formylglycine Generating Enzyme[1]

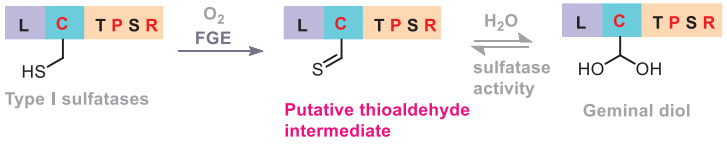

Lowe's Chemical Mutation of Papain[2]

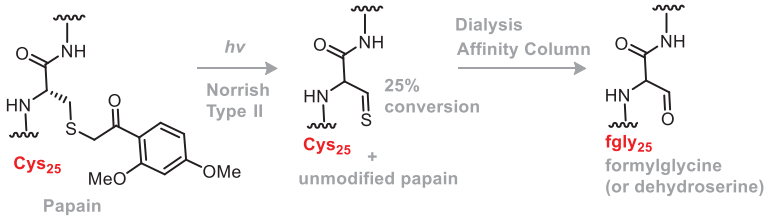

Coenzyme A Biosynthesis[3]

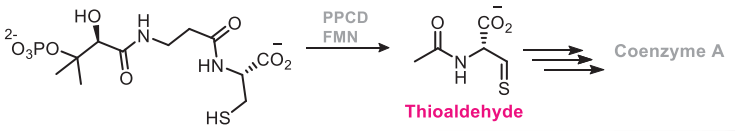

- Products characterised through enzyme turnover assay
- Multiple rounds needed for complete alkylation and photolysis

Photolytic generation of thioaldehyde[4]

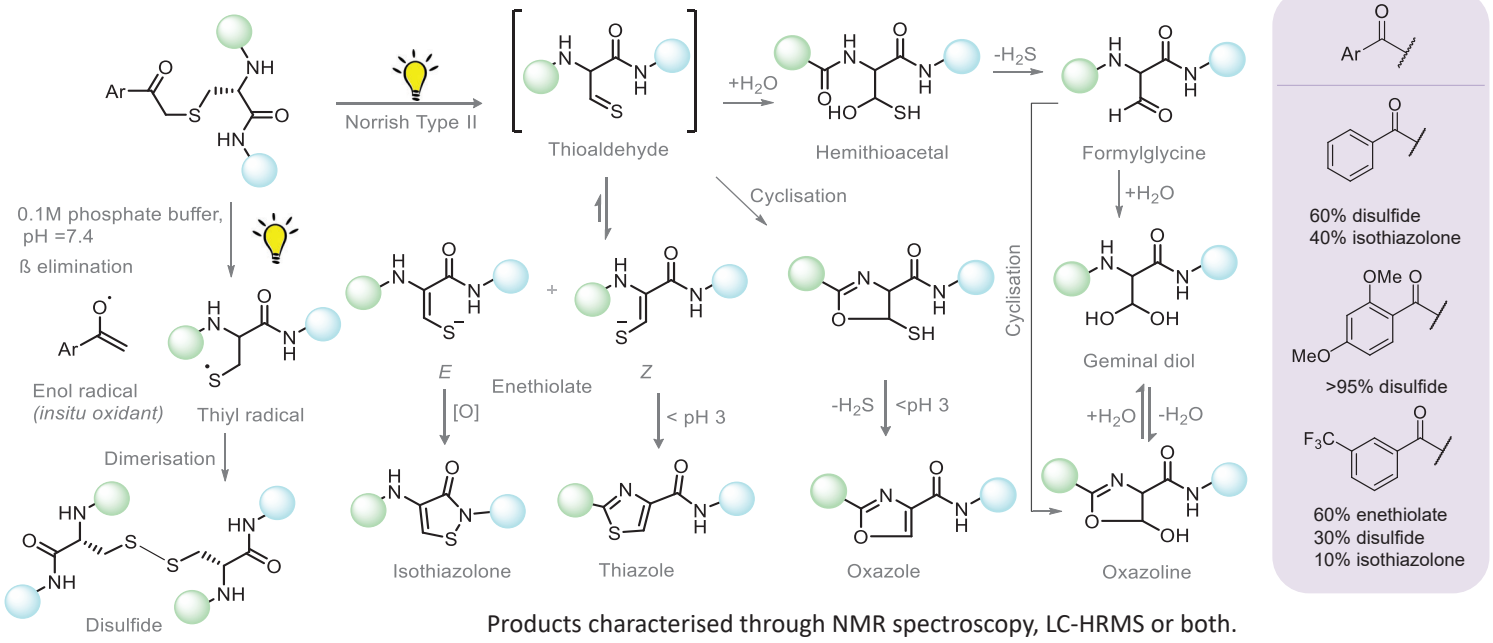

Products characterised through NMR spectroscopy, LC-HRMS or both.

Photolysis of alkylated peptide – AACTPSRGSLFTGRG

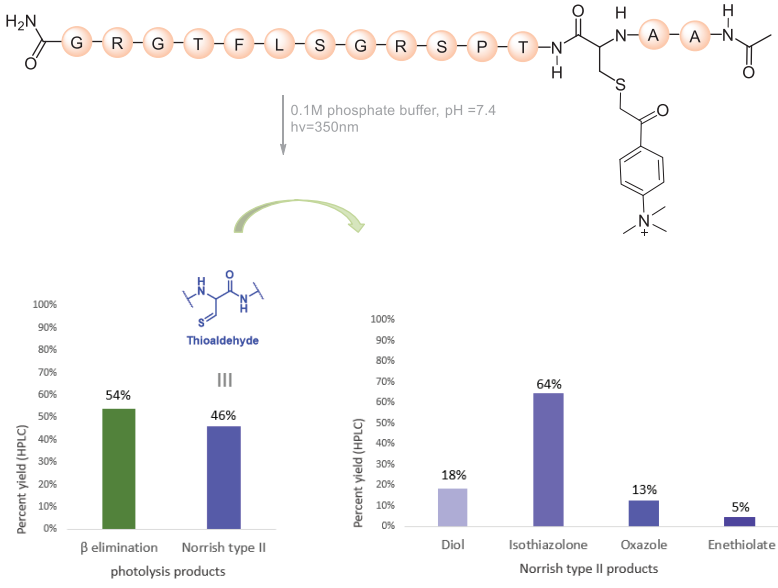

Figure 1: (Left) Partitioning of photolysis pathways, (Right) Distribution of products arising from further reaction of thioaldehyde.

Efficiency of thioaldehyde hydrolysis depends on sequence of peptide.

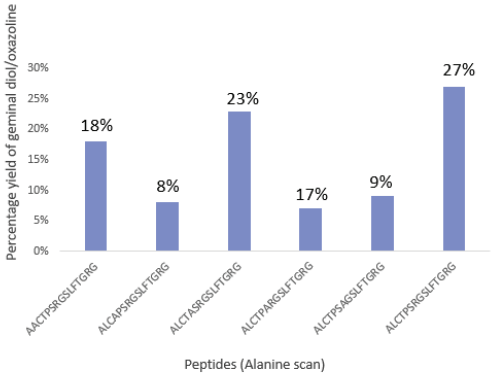

Figure 2: Percentage yield of geminal diol/oxazoline for peptides having the consensus sequence of FGE substrate, where each amino acid in the consensus sequence is replaced by alanine.

Conclusion

1. Cysteine thioaldehydes are highly reactive, undergoes rapid hydrolysis to thiohemiacetals and then to formylglycine. They also undergo tautomerisation to the enethiolate E, which is susceptible to oxidation to form isothiazolone and enethiolate Z, which undergoes cyclisation under acidic conditions to form thiazole.
2. Structure of the peptides have a profound effect on the yield of geminal diol/oxazoline formed from thioaldehyde, where each amino acid contributes to the formation and stability of geminal diol/oxazoline.
3. Hydrolysis of thioaldehyde to formylglycine by FGE is not trivial but carefully designed by enzyme in such a way that the thioaldehyde formed is completely hydrolysed to formylglycine/geminal diol in the active site in the presence of a water molecule thereby preventing all other possible reaction pathways.

References

1. B. Schmidt, T. Selmer, A. Ingendoh, K. von Figura, *Cell*. *82*, 271–278 (1995)
2. P. I. Clark and G. Lowe, *J. Chem. Soc. Chem. Commun*. 923–924 (1977)
3. E. Strauss, T. Begley, *J. Am. Chem. Soc.123*, 6449–6450 (2001)
4. P. J. Wagner and E.J. Siebert, *J. Am. Chem. Soc.* 103, 7329–7335 (1981)

https://doi.org/10.17952/37EPS.2024.P2026

Application of a new green protocol in Solid-Phase Peptide Synthesis: identification of a new green solvent mixture compatible with ETT/TBEC

Vivenzio, G.; Scala, M. C.; Campiglia, P. and Sala, M.

Department of Pharmacy, University of Salerno, Fisciano, SA, Italy

Introduction

Solid Phase Peptide Synthesis (SPPS) is the preferred technique for synthesizing bioactive peptides. However, traditional SPPS generates significant waste and employs hazardous solvents like DMF and DCM. The aim of this research is to investigate solvents that align with the green chemistry and are suitable for all stages of SPPS.
Some solvents, such as p-cymene and anisole, taken into consideration in this work, can be derived from renewable sources like plants and biomass, rendering them environmentally sustainable choices. However, many of these alternative solvents possess different physicochemical properties compared to DMF. To overcome this challenge, solvent mixtures are employed. In this study, we identified a novel green solvent mixture by combining anisole with NOP; its ability to swell different resins and its capability to solubilize all Fmoc protected amino acids was investigated. The same mixture was also assessed in combination with a pair of coupling reagents, TBEC and ETT and model peptides Aib-enkephalin and Aib-ACP were synthesized resulting in favorable outcomes in terms of peptide synthesis efficiency.

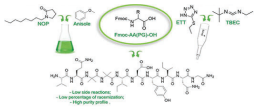

Methods

The solubility test was performed by adding 1 mL of either mixture into 10 mL test tubes containing 0.2 mmol of Fmoc-AA(PG)-OH or coupling agents. The tubes were then placed on a shaker at room temperature until complete dissolution.
For swelling test, 0.1 g of several resins were weighed and placed in a 5 mL reactor equipped with a polypropylene filter, which occupied a volume of 0.4 mL. The desired solvents, was added to the resin, and the mixture was stirred at room temperature for 45 minutes.
Deprotection kinetics test
Fmoc-Val-OH (0.2 mmol) was dissolved in a solution consisting of 20% piperidine and anisole/NOP (75:25). The reaction mixture was stirred at room temperature, and 2 µL were extracted at t=0 (before adding the base), and after 2, 4, 6, 8 minutes. These samples were analyzed using HPLC system.
Racemization study
The synthesis of Z-Phg-Pro-NH2 was performed by dissolving Z-Phg-OH (0.05 mmol) in a glass vial with 0.625 mL of DMF or anisole/NOP (75:25). The desired reagents were then added to the following order: H-Pro-NH2 (0.05 mmol), and ETT/TBEC (0.05 mmol, 1:2). The solution was stirred at room temperature for 3 h.
SPPS of Aib-enkephalin and Aib-ACP
Peptides synthesis was performed according to the solid phase approach using standard Fmoc methodology by Biotage Initiator + Alstra automated microwave synthesizer.

Results

The main goal is to replace the most common solvent used, DMF, with solvents or solvent mixtures that have a high score in the GSK Green Solvents Guide and, at the same time, are effective in all the steps of SPPS. Among these, the green solvents such as p-cymene and anisole[1] have been selected. As shown in Table 1, both anisole and p-cymene exhibit a low dielectric constant and dipole moment value, making them poor candidates for dissolving all amino acids and coupling agents. To address this issue, it was necessary to use mixtures with other green solvents to enhance these properties. Indeed, ethanol, butanol, ethyl acetate, and NOP[2], besides being classified as green solvents, exhibit better hydrophilic characteristics.

Table 1. Physical-chemical properties and cost of p-cymene, anisole, and co-solvents.

Physical-chemical properties	Solvent			Co-solvent			
	DMF	p-Cymene	Anisole	Ethyl acetate	Butanol	Ethanol	NOP
Boiling point	153°C	178°C	154°C	77°C	83°C	78°C	172°C
Density	0.95 g/cm³	0.86 g/cm³	0.99 g/cm³	0.90 g/cm³	0.77 g/cm³	0.78 g/cm³	0.92 g/cm³
Viscosity	0.85 mm²/s	0.81 mm²/s	0.78 mm²/s	0.44 mm²/s	2.95 mm²/s	1.1 mm²/s	6.6 mm²/s
Dielectric constant	36.7	2.24	4.33	6.02	10.90	24.5	32.0
Dipole moment	3.86	0.18	1.38	1.88	1.7	1.69	-
Melting point	-31°C	-68°C	-37°C	-84°C	25°C	-114°C	-25°C
Flash point	58°C	47°C	51°C	-4°C	35°C	12°C	142°C
Cost	72.50 €/L	49.00 €/L	97.10 €/L	55.60 €/L	109.00 €/L	169.00 €/L	195.00 €/L

Solubility test



To evaluate the effectiveness of the chosen solvents in solid-phase peptide synthesis (SPPS), we first examined their ability to dissolve amino acids and coupling agents. Some amino acids were not completely soluble in mixtures tested, only mixture anisole/NOP (75:25) was able to solubilize all Fmoc protected amino acids and coupling agents, such as, TBEC[3] and ETT.[4]

Swelling test

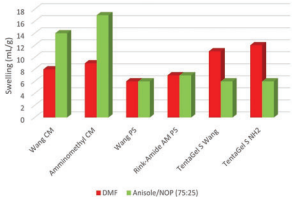

Figure 1. Swelling results of several resins in DMF and anisole/NOP (75:25).

A suitable solvent should have the ability to effectively swell the most used resins. In this study, we selected different types of resins and linkers. Subsequently, after removing the solvent and drying the resin, we evaluated the degree of swelling using the following formula: (ml/g) = (measured – volume 0.4)/0.1 g. As illustrated in Figure 1, TG resins showed a less degree of swelling than DMF, while PS resins behaved similarly in both solvents. On the other hand, CM resins showed better swelling in the green mixture than DMF.

Therefore, PS based resin and ChemMatrix resin showed a good degree of swelling in anisole/NOP (75:25) so the morphology of polystyrene and ChemMatrix resin beads was analyzed through scanning electron microscopy (SEM) using a Carl Zeiss EVOMA10 microscope (Figure 2). In particular, our SEM images at higher magnification show that the ChemMatrix® resin swells significantly in the green selected mixture.

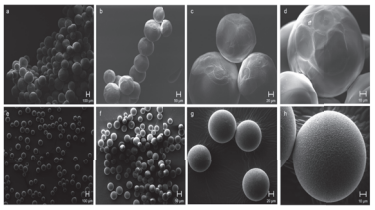

Figure 2. SEM pictures of PS and CM resin: (**a**) CM resin beads before swelling, (**b-d**) CM resin beads after swelling, and (**e**) polystyrene resin beads before swelling (**f-h**) polystyrene resin beads after swelling.

Deprotection kinetics test

In SPPS, it is common to use a solution of piperidine in DMF to remove the Fmoc group from the α-amino function. The experiment involved a 20% piperidine solution in anisole/NOP (75:25) and the formation of dibenzofulvene (DBF) was monitored using HPLC at time points of 0, 2, 4, 6 min. The peak corresponding to Fmoc-Val-OH disappeared after 4 minutes, so the Fmoc cleavage reaction is complete in few minutes, and this is very similar to when performed in DMF.

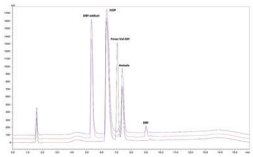

Figure 3. Chromatogram of Fmoc-Val-OH deprotection Kinetics test. t_0=0 min (black), t_1=2 min (purple), t_2=4 min (blue).

Racemization study

Racemization represents a fundamental side reaction in peptide synthesis. The couplings were performed using (L)-amino acids and the crude was analyzed by HPLC-MS injection after 3 h, in order to determine the formation of the dipeptide and the degree of racemization. Table 2 illustrates the degree of racemization. The green solvent mixture, Anisole/ NOP (75:25), provided only about 0.16% of racemization (entry **1**), which is lower than that observed in DMF (entry **2**).

Table 2. Racemization ratio (%) in the synthesis of Z-Phg-Pro-NH_2.[a]

Entry	Solvent	Agents of coupling	Dipeptide (%)	DL[b] (%)
1	Anisole/ NOP (75:25)	TBEC/ETT (2:1)	99.84	0.16
2	DMF	TBEC/ETT (2:1)	99.6	0.40

[a] Racemization was calculated by HPLC.
[b] Defined as (Z-D-Phg-Pro-NH_2/ Z-L-Phg-Pro-NH_2) x 100.

SPPS of Aib-enkephalin and Aib-ACP

As mentioned before, to apply the selected mixture to SPPS, it is important to test it throughout the synthetic process. In this case, a reference pentapeptide, Aib-enkephalin (H-Tyr-Aib-Aib-Phe-Leu-OH/NH2) (16), was chosen. The effectiveness of the new method is evaluated by measuring the amount of des-Aib. The synthesis was carried out on Wang PS and Rink-Amide AM PS, using microwave-assisted synthesis and mixture anisole/ NOP (75:25) and DMF in all steps..

Table 3. HPLC purities of Aib-enkephalin pentapeptide assembled on different resins with Anisole/ NOP (75:25) as solvent for all steps.

Entry	Solvent	Agents of coupling	Resin	Pentapeptide (%)	Des-Aib (%)	Other (%)
1	DMF	TBEC/ETT (2:1)	Wang PS	91.56	-	29.69
2	Anisole/ NOP (75:25)	DIC/ETT (2:1)	Wang PS	99.63	-	0.37
3	Anisole/ NOP (75:25)	TBEC/ETT (2:1)	Wang PS	97.81	-	2.19
4	DMF	TBEC/ETT (2:1)	Rink-Amide PS	85.35	-	14.65
5	Anisole/ NOP (75:25)	DIC/ETT (2:1)	Rink- Amide PS	66.20	-	33.8
6	Anisole/ NOP (75:25)	TBEC/ETT (2:1)	Rink-Amide PS	89.64	-	10.36

Purity values of Aib-enkephalin were calculated by HPLC. As shown in Table 3, the highest values of purity were obtained for pentapeptide synthesized on Wang PS resin with new selected green mixture (entries **2** and **3**) compared to that obtained with the synthesis performed in standard solvent, DMF (entry **1**). Another interesting result was obtained using TBEC/ETT, as coupling agents, and Rink-Amide PS, as resin (entry **6**), in fact, the percentage of side reactions was lower than that obtained during the synthesis performed in DMF (entry **4**). Considering these results, entry **3** and **6** can be considered the best method for further investigations.

The same protocol was applied for the synthesis of a longer and difficult sequence, Aib-ACP decapeptide (H-Val-Gln-Aib-Aib-Ile-Asp-Tyr-Ile-Asn-Gly-OH/NH_2). HPLC purities of Aib-ACP are shown in Table 4. The highest values of purity were obtained for decapeptide synthesized on Rink-Amide PS resin with new selected green mixture (entry **4**). Its value is approximately double that of the decapeptide synthesized with standard solvent (entry **3**).

Table 4. HPLC purities of Aib-ACP decapeptide assembled on Rink-Amide CM.

Entry	Agents of coupling	Solvent	Resin	Decapeptide (%)	Des-Aib (%)	Other (%)
1	TBEC/ETT (2:1)	DMF	Wang PS	96.64	3.36	-
2	TBEC/ETT (2:1)	Anisole/ NOP (75:25)	Wang PS	77.21	22.79	-
3	TBEC/ETT (2:1)	DMF	Rink-Amide PS	48.40	50.01	1.59
4	TBEC/ETT (2:1)	Anisole/ NOP (75:25)	Rink-Amide PS	98.86	1.14	-

Conclusion

In this work, we identified a new green solvent mixture for solid-phase peptide synthesis as a valid alternative to standard solvents, DMF. In particular, mixture of Anisole/NOP (75:25) was able to solubilize all Fmoc amino acids and showed a good property of swelling for Rink amide PS and Wang PS resins. Furthermore, we used a pairs of coupling agents, TBEC and ETT, able to reduce side reaction and improve the percentage of purity of synthetized peptides. We obtained satisfactory results synthesizing the pentapeptide, Aib-enkephalin and a longer peptide, Aib-ACP. Thus demonstrating that the new green protocol may replace the traditional DMF-based one for industrial peptide synthesis.

References

1. Delolo, F. G.; dos Santos, E. N.; Gusevskaya, E. V. Anisole: a further step to sustainable hydroformylation. *Green Chem.* **2019**, 21, 109.
2. Martelli, G.; Cantelmi, P.; Tolomelli, A.; Corbisiero, D.; Mattellone, A.; Ricci, A.; Fantoni, T.; Cabri, W.; Vacondio, F.; Ferlenghi, F.; Mor, M.; Ferrazzano, L. Steps towards sustainable Solid Phase Peptide Synthesis: use and recovery of N-octyl pyrrolidone. *Green Chemistry*. **2021**, 23, 4095.
3. Manne, S. R.; Luna, O.; Acosta, G. A.; Royo, M.; El-Faham, A.; Orosz, G.; De la Torre, B.; Albericio, F. Amide Formation: Choosing the Safer Carbodiimide in Combination with OxymaPure to Avoid HCN Release. *Org. Lett.* **2021**, 23, 6900–6904.
4. Nzama, H.; Manne, S. R.; Akintayo, D. C.; de la Torre, B. G.; Albericio, F. Ethylthio-1H-tetrazole (ETT) as coupling additive for the solid-phase synthesis (SPS) of hindered amino acid-containing peptides. Tetrahedron Letters **2024**, 142, 155108.

gvivenzio@unisa.it

Modular Access to Structurally Defined Ubiquitin Chains

Moritz Urschbach[1], Susanne Huhmann[1], Luca Ferrari[2], Dominik Vogl[1], Dominik Appel[1], Sascha Martens[2] & Christian F. W. Becker[1]

[1]University of Vienna, Faculty of Chemistry, Institute of Biological Chemistry, Währinger Straße 38, 1090 Vienna, Austria

[2]University of Vienna, Center for Molecular Biology, Department of Biochemistry and Cell Biology, Dr.-Bohr-Gasse 9, 1030, Vienna, Austria

Contact: moritz.urschbach@univie.ac.at // christian.becker@univie.ac.at

https://doi.org/10.17952/37EPS.2024.P2029

universität wien

TARGETED PROTEIN DEGRADATION

Introduction

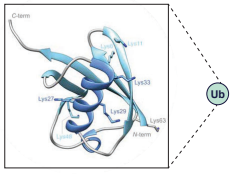

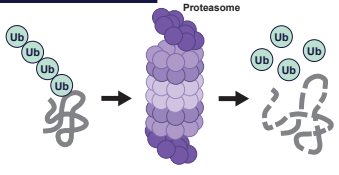

Exact molecular composition of Ubiquitin (Ub) tags is critical for executed function like degradation signalling for the ubiquitin-proteasome system (UPS) or autophagy-lysosomal pathway.
High complexity by 8 different linkage types within Ub, chain length variability, PTM of Ub means challenging assembly of defined Ub chains and ubiquitylated proteins.
Methods and strategies to generate ubiquitin chains: enzymatic approaches,[2] genetic code expansion, (semi)-synthesis.[3, 4]
Fully defined Ub chains are unique tools in deciphering complex degradation signals at a high molecular resolution.

Building Blocks

- Monomeric Ub building blocks for high flexibility in modular chain assembly
- Efficient generation of Ub-Intein fusions by recombinant expression up to 60 mg/L
- Activated Ubiquitin for universal C-terminal modification[5]/elongation

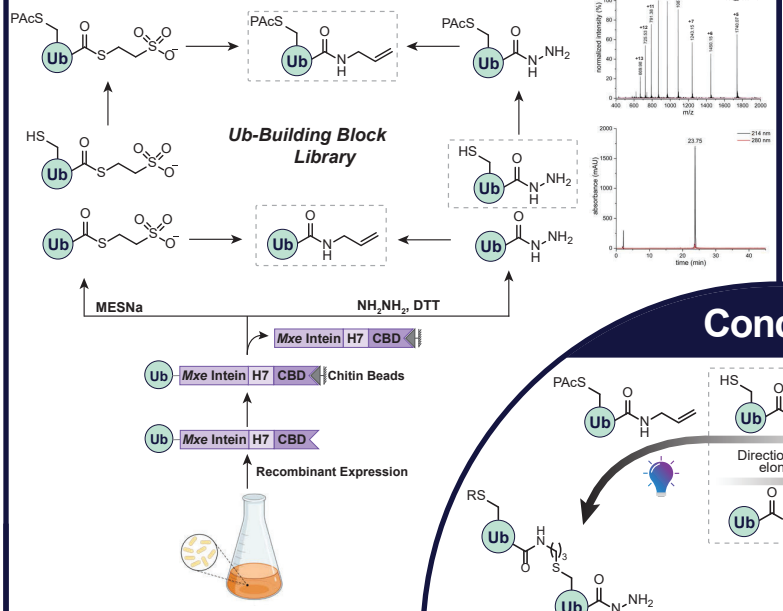

Analysis of Ub[K48C(PAc)]-AA. HPLC chromatogram and ESI+ mass spectrum.

3. Artificial linkage is recognized by ubiquitin processing machinery

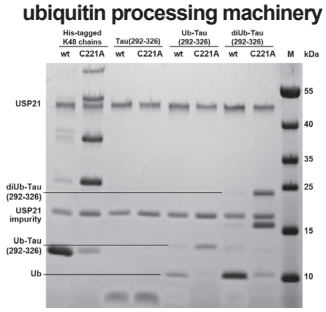

DUB-assay. SDS-PAGE after incubation of Ub-Tau(292-326) and diUb-Tau(292-326) with USP21 @37°C for 60 min. Substrate-DUB ratio 3:2. C221A mutant as inactive control. Coomassie stain.

Concept

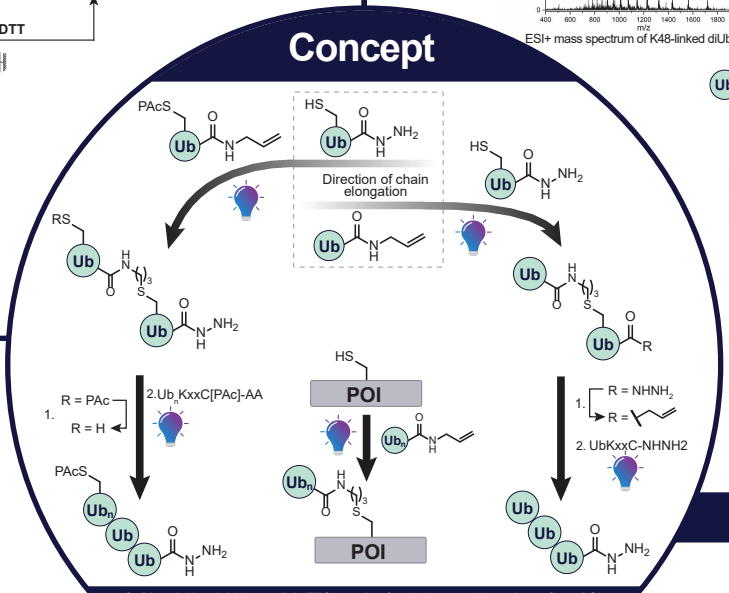

- Photoinitiated thiol-ene click (TEC) reaction for chain assembly and transfer to POI.
- Rapid, mild, chemoselective connection chemistry.
- Modular approach gives access to homotypic and heterotypic structures.
- Protection group and masking strategy for flexible bidirectional elongation.

2. Construction of protein with site-selective ubiquitylation

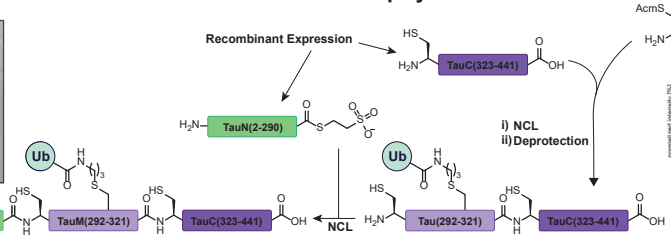

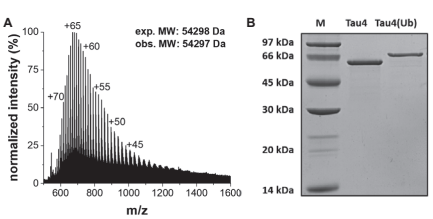

Analysis of site-selectively ubiquitylated Tau4. (A) ESI+ mass spectrum; (B) SDS-PAGE of native Tau4 and Tau4(Ub), coomassie stain.

Chain Assembly

- Iterative TEC + activation or deprotection towards Ub oligomers
- 6 mM Ub-AA + 7.5 mM UbKxxC-NHNH2 + 4 mM LAP + 1.5 mM TCEP < 1 min irradiation, up to 40% isolated diubiquitin
- Probed for UbK63C, UbK29C, UbK48C, UbK27C, UbK11C

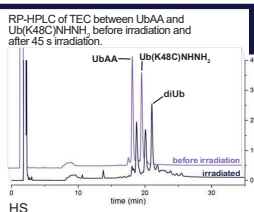

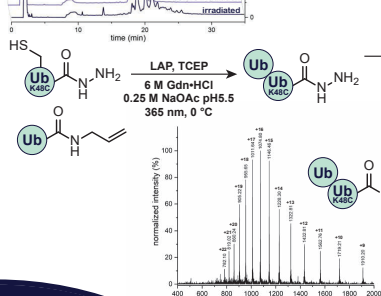

ESI+ mass spectrum of K48-linked diUb-AA.

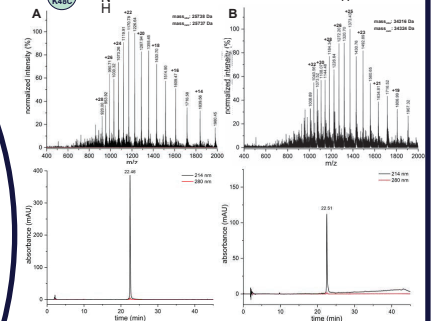

a) HPLC chromatogram and ESI+ mass spectrum of K48-linked triUb.
b) HPLC chromatogram and ESI+ mass spectrum of K48-linked tetraUb.

Protein Modification

1. Ubiquitylation of peptides via TEC

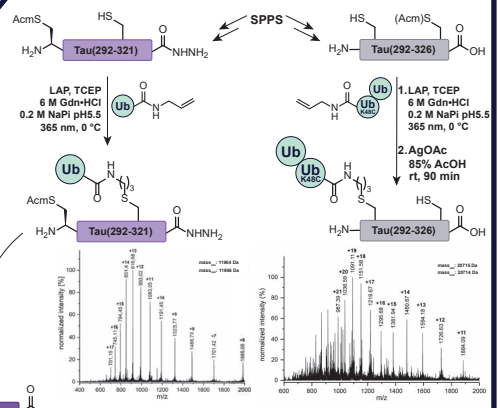

Analysis of site-selectively ubiquitinated peptides.
(A) ESI+ mass spectrum of monoubiquitinated TauM(292-321);
(B) ESI+ mass spectrum of diUb(K48)-Tau(292-326).

References

[1] D. Komander, M. Rape, Annu Rev Biochem **2012**, 81, 203-229.
[2] K. Martinez-Fonts, A. Matouschek, Biochemistry **2016**, 55, 1898-1908.
[3] Y. Huppelschoten, G. J. Van der Heden van Noort, Semin. Cell Dev. Biol. **2022**, 132, 74-85.
[4] E. M. Valkevich, R. G. Guenette, N. A. Sanchez, Y. Chen, Y. Ge, E. Strieter, J. Am. Chem. Soc. **2012**, 134, 6916-6919.
[5] K. R. Love, R. K. Pandya, E. Spooner, H. L. Ploegh, ACS Chem. Biol. **2009**, 4, 275-287.

Funded by

FWF Österreichischer Wissenschaftsfonds

Acknowledgements

We gratefully acknowledge support from Gerhard Niederacher with initial expression experiments and from Manuel Felkl with peptide synthesis. We thank the mass spectrometry center of the university of Vienna for analytical support.

Tetrahydropyranyl and Tetrahydrofuranyl as New Backbone Protecting Groups For Enhanced Fmoc SPPS

Samuel J. Paravizzini, Craig A. Hutton*, John A. Karas*

THE UNIVERSITY OF MELBOURNE

Introduction

9-Fluorenylmethyloxycarbonyl (Fmoc) solid-phase peptide synthesis (SPPS) is the most reliable method for preparing a wide range of peptide targets. However, synthetic efficiency often declines as chain elongation proceeds, making it difficult to routinely obtain pure peptides with >40 residues. This loss of efficiency is caused by poor chain solubility and aggregation via β-sheet formation (Figure 1a).[1]

Acid-labile amide backbone protecting groups (PGs), such as the 2,4-dimethoxybenzyl (Dmb)[2] group, improve peptide chain solubility and disrupt hydrogen bonding networks (Figure 1b), which can significantly improve crude purity. However, benzyl-based protecting groups are often difficult to remove and the benzyl cations that form during trifluoroacetic acid (TFA) cleavages can alkylate sensitive side chains; this limits their use because multiple protecting groups are needed for the synthesis of longer sequences. Pseudoproline[3] and *N,O*-benzylidene[4] dipeptides avoid this deprotection issue, although they are largely limited to serine and threonine containing peptides.

Ideally, backbone protecting groups should be highly acid-labile and easily incorporated into a broad range of amino acid residues. Therefore, we have evaluated the use of tetrahydropyranyl (THP)[5] and tetrahydrofuranyl (THF) groups as backbone protection for Fmoc SPPS, introduced via prepared dipeptide building blocks.

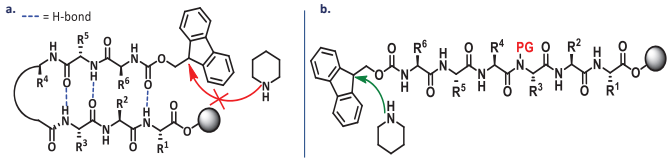

Figure 1. (a.) Backbone hydrogen bonding can cause steric crowding of the N-terminus during Fmoc SPPS. **(b.)** Backbone protection improves solubility and blocks hydrogen bonding, improving synthetic yields.

Objectives

To address these limitations, we are developing new highly acid-labile backbone protecting groups that can be introduced via dipeptide precursors. Our objectives are:

- To explore the synthesis of THP and THF protected dipeptides.
- To investigate the kinetics of these protecting groups in TFA mediated cleavages.
- To evaluate their effectiveness in improving crude peptide purity during SPPS.

Synthesis of Backbone Protected Dipeptides

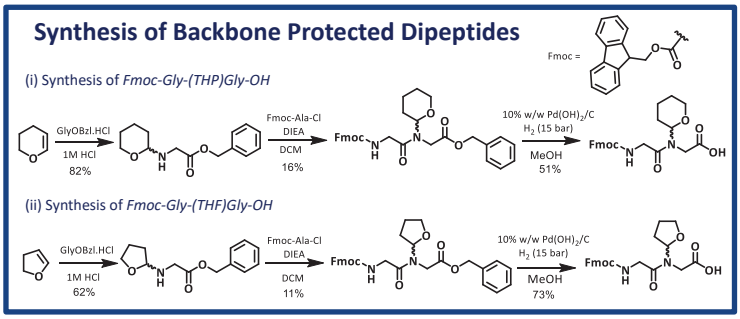

Acidic Cleavage Deprotection Kinetics

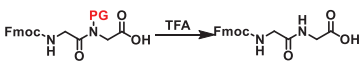

THP and THF protected dipeptides with general structure Fmoc-Gly-(PG)Gly-OH, were reacted in cleavage solutions containing various amounts of TFA, monitored over a 3-hour period. They were compared to the Dmb group and a pseudoproline (Ser($\psi^{Me,Me}$Pro))* motif.

Results:

- Tetrahydrofuran (THF) is hyper acid-labile
- Tetrahydropyran (THP) can be removed in mild cleavage cocktails
- Order of reactivity; THF > $\psi^{Me,Me}$Pro > THP > Dmb

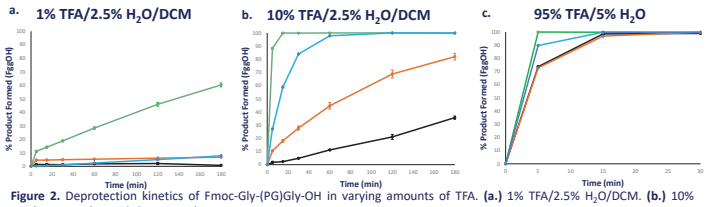

Figure 2. Deprotection kinetics of Fmoc-Gly-(PG)Gly-OH in varying amounts of TFA. **(a.)** 1% TFA/2.5% H_2O/DCM. **(b.)** 10% TFA/2.5% H_2O/DCM. **(c.)** 95% TFA/ 5% H_2O. All experiments were conducted in triplicate; error bars are calculated as standard error. * The pseudoproline was tested in the sequence Fmoc-Gly-(Ser($\psi^{Me,Me}$Pro)-OH.

SPPS of Amyloid Aβ(32-43): Fmoc-IGLMVG(PG)GVVIAT-OH

The dipeptide building blocks (Fmoc-Gly-(PG)Gly-OH) were incorporated in the SPPS of a fragment of amyloid Aβ protein (Figure 3.) and their improvement on the crude product purity was compared to an unprotected dipeptide control (Fmoc-Gly-Gly-OH).

Results:

- THP and Dmb provide equal improvement to crude product purity.
- THF was worse, presenting more deletion sequences closer to the site of protection.
- All the protected dipeptides provided improvement over the unprotected control.

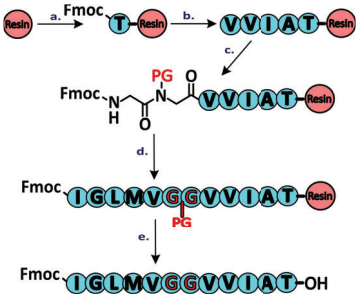

Figure 3. SPPS of amyloid Aβ (32-43). **(a.)** Loading Wang resin; 4 eq. Fmoc-Thr(OtBu)-OH, 6 eq. DIC, 0.1 eq. DMAP, DCM, 4hrs. **(b.)** Standard SPPS conditions; Fmoc deprotection (20% piperidine/DMF, 15 mins), then coupling (4 eq. Fmoc-Xxx-OH, 4eq. HATU, 8eq. DIEA.) **(c.)** Protected dipeptide coupling. (2 eq. Fmoc-Gly-(PG)Gly-OH, 2eq. HATU, 4eq. DIEA.) **(d.)** Standard SPPS conditions. **(e.)** Resin cleabage; 95% TFA / 2.5% H_2O / 2.5% TIPS

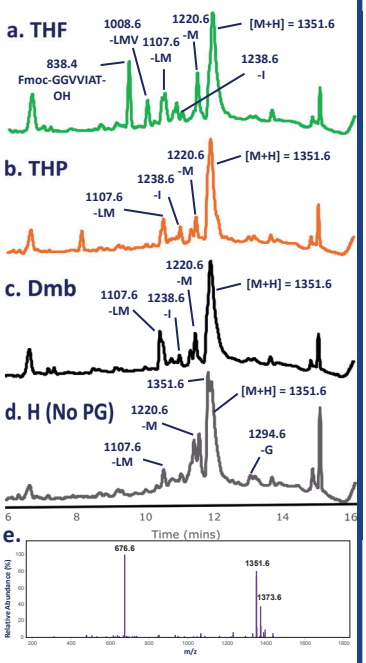

Figure 4. LCMS trace of Fmoc-IGLMVGGVVIAT-OH after SPPS. Dipeptides used are; **(a.)** Fmoc-Gly-(THF)Gly-OH. **(b.)** Fmoc-Gly-(THP)Gly-OH, **(c.)** Fmoc-Gly-(Dmb)Gly-OH, **(d.)** Fmoc-Gly-Gly-OH. **(e.)** Mass spectrum of target peak, [M+H] = 1351.6.

Conclusion

Backbone protected dipeptide building blocks are an effective way to introduce tertiary amide bonds during the SPPS of aggregation-prone sequences and provide an extended solubilising effect that greatly improves crude peptide purity. For the protecting groups investigated it was found that:

- both the THP and THF groups are exceptionally acid-labile.
- they both provide an improvement to the crude product purity during SPPS.
- the THP group can provide the same improvement to crude product purity as Dmb during SPPS.
- the THF performed worse than THP during the SPPS of Aβ(32-43).

Future Work

- Exploring higher yielding synthetic routes of the THP and THF protected dipeptides.
- Incorporating protecting groups into different dipeptide structures.
  (i.e. Fmoc-Xxx-(PG)Gly-OH or Fmoc-Xxx-(PG)Ala-OH)
- Further evaluation of side reactions occurring during SPPS.
  (epimerisation or diketopiperazine formation)

References

(1) Behrendt, R.; White, P.; Offer, J. Advances in Fmoc solid-phase peptide synthesis. *J. Pept. Sci.* 2016, *22* (1), 4-27.

(2) Cardona, V.; Eberle, I.; Barthélémy, S.; Beythien, J.; Doerner, B.; Schneeberger, P.; Keyte, J.; White, P. D. Application of Dmb-Dipeptides in the Fmoc SPPS of Difficult and Aspartimide-Prone Sequences. *Int. J. Pept. Res. Ther.* 2008, *14* (4), 285-292.

(3) Wöhr, T.; Wahl, F.; Nefzi, A.; Rohwedder, B.; Sato, T.; Sun, X.; Mutter, M. Pseudo-Prolines as a Solubilizing, Structure-Disrupting Protection Technique in Peptide Synthesis. *J. Am. Chem. Soc.* 1996, *118* (39), 9218-9227.

(4) Wu, H.; Sun, Z.; Li, X. N,O-Benzylidene Acetal Dipeptides (NBDs) Enable the Synthesis of Difficult Peptides via a Kinked Backbone Strategy. *Angew. Chem.* 2023, *62* (44).

(5) Sharma, A.; Ramos-Tomillero, I.; El-Faham, A.; Nicolas, E.; Rodriguez, H.; de la Torre, B. G.; Albericio, F. Understanding Tetrahydropyranyl as a Protecting Group in Peptide Chemistry. *ChemistryOpen.* 2017, 6 (2), 168-177.

Acknowledgements

University of Melbourne: Masson Travel Award (2023), GI Feutrill Award (2023 + 2024)

Australian Research Council

Australian Government
Australian Research Council

https://doi.org/10.17952/37EPS.2024.P2034

Sam Paravizzini:
paravizzinis@unimelb.edu.au

THE UNIVERSITY OF MELBOURNE

Exploring Innovative Liquid-Phase Peptide Synthesis Strategies with Silane-Containing Molecules

[1]Nissan Chemical Corporation, Chiba, Japan, [2]PeptiDream, Inc., Kanagawa, Japan

https://doi.org/10.17952/37EPS.2024.P2035

Naoki Nishizawa[1], Akihiro Nagaya[1], Shota Murase[1], Yuji Mimori[1], Michiharu Handa[1], Ayumu Matsuda[2], Yutaka Kobayashi[2], Haruaki Kurasaki[2], Douglas R. Cary[2], Keiichi Masuya[2]

Introduction

Convergent liquid-phase peptide synthesis (LPPS) is a powerful method for producing short and medium-sized peptides. However, traditional LPPS is limited by side reactions, necessitating an extended period for process development. To address this challenge, we have developed a novel coupling method, new protecting groups, and novel solubilizing tags for LPPS, utilizing silane-containing molecules.

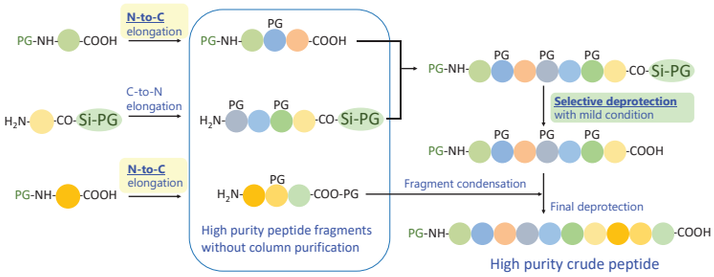

N-to-C coupling (R-Coupling)[1]

Our newly developed coupling method 'R-Coupling' employs isostearyl halide (ISTA-X) and a silylation reagent to facilitate peptide elongation in a non-conventional N-to-C direction.

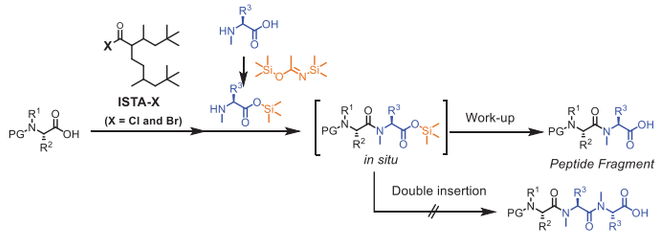

This inverse approach significantly reduces production time by eliminating deprotection steps, thereby minimizing overall synthesis steps. R-Coupling enables the rapid synthesis of high-quality peptide fragments, including those containing *N*-methyl amino acids.

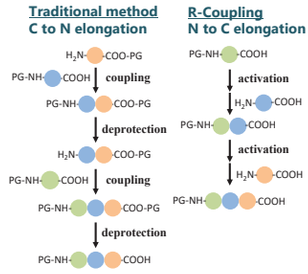

Silyl ester protecting group (SIPS)[2]

Traditional LPPS process development is time-consuming and labor-intensive, primarily due to the limitations of C-terminal carboxylic acid-protecting groups. Commonly used methyl and ethyl esters are prone to epimerization during basic deprotection, while diketopiperazine (DKP) formation is a significant challenge when proline or *N*-methyl amino acids are at the C-terminus. Our novel silyl-based protecting groups offer several advantages for peptide fragment synthesis:

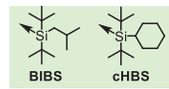

- Compatibility with Fmoc, Boc, and Cbz chemistries
- Prevention of DKP formation
- Selective removal without affecting other protecting groups
- Enhanced solubility of protected peptides

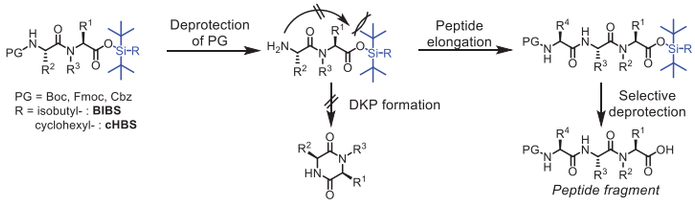

Example of cyclic peptide synthesis using R-Coupling and SIPS[2]

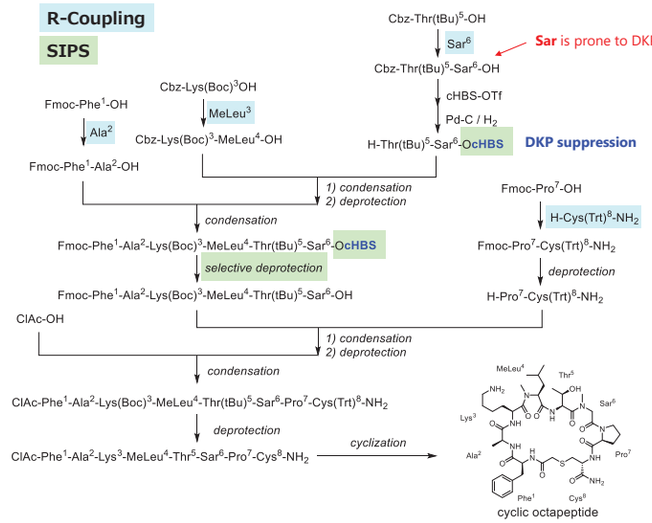

Intermediate peptide fragments bypassed column chromatography purification. The synthetic process was refined to minimize impurity generation near the main peak, enabling highly efficient purification through impurity management.

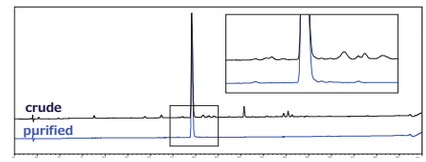

Alkyl silane solubilizing tag

Tag-assisted LPPS efficiently extends peptide chains sequentially. We developed a novel, alkyl-silane-based solubilizing tag (FMSE) for this process.

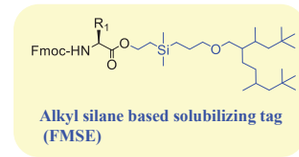

FMSE imparts exceptional solubility to peptides during synthesis. Uniquely, FMSE is selectively removable without affecting other protecting groups, generating peptide fragments.

This property enables diverse C-terminal modifications, including amidation, esterification, thioesterification, and conjugation with biotin, fluorophores, or chelators. Additionally, the C-terminal free peptide fragment serves as a versatile building block for fragment condensation, producing larger peptides.

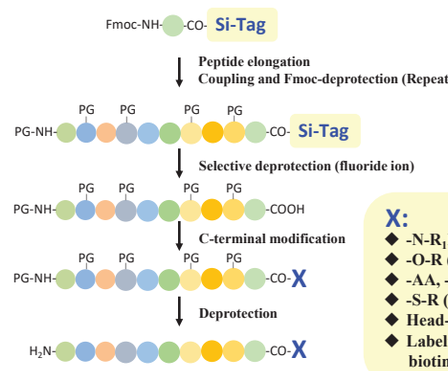

X:

- -N-R_1R_2 (amide)
- -O-R (ester)
- -AA, -peptide (fragment condensation)
- -S-R (thioester)
- Head-to-tail cyclization
- Labeling with; biotin, fluorophore, and chelator

Summary

We developed a novel convergent LPPS platform, SYNCSOL, employing silane-containing molecules. SYNCSOL incorporates N-to-C coupling, a new protecting group, and a detachable solubilizing tag. This platform efficiently produces high-quality peptide fragments, enabling fragment condensation and C-terminal modifications. SYNCSOL enhances LPPS flexibility and promises to improve peptide manufacturing productivity.

Reference: 1. Kurasaki, H. *et al*., (2020), *Org. Lett*. **20**, 8039–8043. 2. Nagaya, A. *et al.*, (2021) *Org. Process Res. Dev.* **25**, 2029–2038.

Influence of tryptophan insertion on the fibrillation capacity and antimicrobial efficacy of β-Hairpin Antimicrobial Peptides

Dhanya Mahalakshmi Murali, Jian Xu, Dai Thien Nhan Tram and Pui Lai Rachel Ee

Department of Pharmacy and Pharmaceutical Science, National University of Singapore, Singapore

https://doi.org/10.17952/37EPS.2024.P2037

Introduction

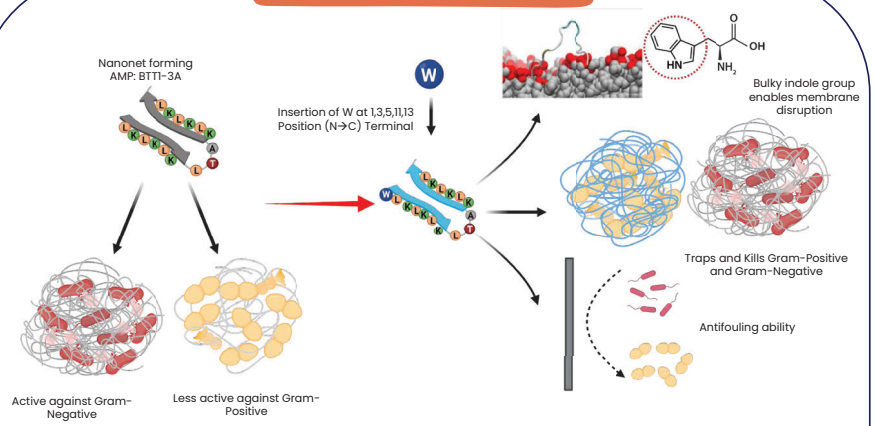

- Antimicrobial Peptides (AMPs) have gained attention for combating bacterial infections due to their unique mechanisms of action and low tendency to induce resistance.
- However, a major challenge in utilizing AMPs is their inherent selectivity, against either Gram-negative or Gram-positive bacteria.
- To address this limitation, we modified our existing bacteria-responsive nanonet forming AMP: BTT1-3A by incorporating hydrophobic-aromatic tryptophan (W) at specific positions (1,3,5,11 and 13), named as 1W, 3W, 5W, 11W and 13W respectively.
- Since, tryptophan's bulky aromatic indole ring can enhance interactions with the thick peptidoglycan layer in the gram-positive bacterial membrane.

Fibrillation of W-Peptides

1)

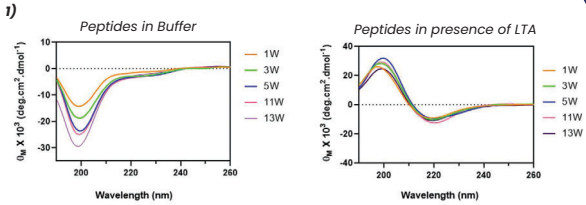

- CD spectroscopy was used to evaluate the secondary structures of w-inserted peptides.
- In buffer: Random coiled structures (minima 196nm) but in the presence of LTA, **anti-parallel β-sheet** and **β-turn secondary structures** present → folding of the peptides when in contact with LTA, forms the preface for their mechanism of action.

2)

- K114 amyloidophillic assay evaluates the nanonet-forming ability of the modified peptides as it undergoes a red shift when it binds to amyloid-like fibrils.
- Both **1W and 3W show the highest fluorescence intensity with LTA**, similar to that of the parent peptide

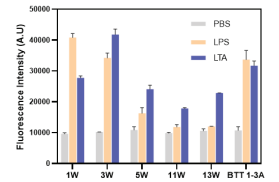

Expansion of Bacteria Spectrum

1)

- The antibacterial efficacy of W-inserted peptides was assessed via the Minimum Inhibitory Concentration (MIC) assay, targeting model gram-positive strains; ***S. aureus*** and ***E. faecalis***.
- The findings demonstrate that peptides **1W** and **13W** exhibit enhanced antibacterial activity, surpassing the parent peptide and other W-inserted peptides by at least 2-fold.

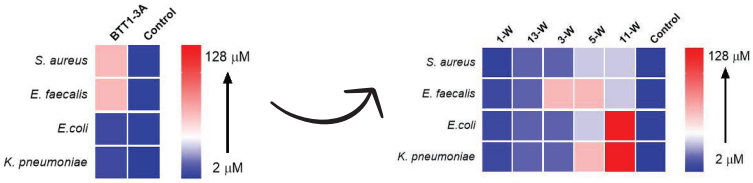

2)

- Agglutination assay performed to evaluate the fibrillation capacity in the presence of bacteria→ bacteria form clusters in the presence of peptide, reducing the absorbance of the suspension.
- **1W and 13W show the highest clustering for *E. faecalis*.**

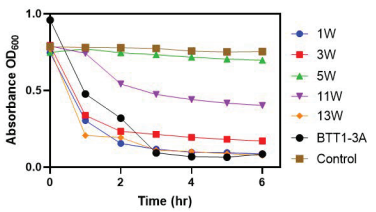

3)

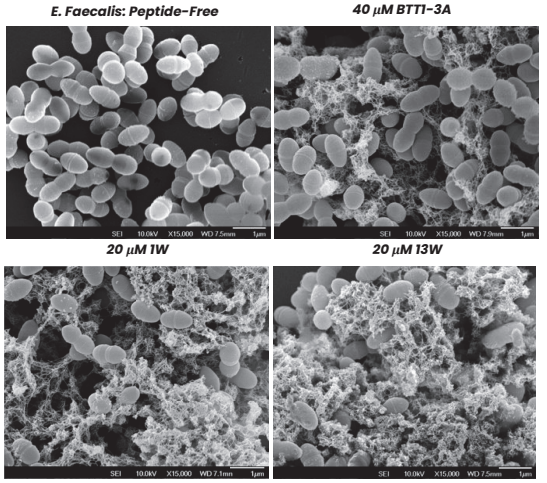

Scanning Electron Microscope (SEM) showed **an increase in the fibrillation tendency of both 1W and 13W peptides** compared to the parent peptide at their MICs.

Antifouling Ability

1)

- In clinical settings, the antifouling ability of peptides is crucial in preventing biofilms and improving the longevity and functionality of medical devices.
- The antifouling ability of W-peptides was studied using confocal microscopy. *E. faecalis* biofilms were initiated in the presence of W-peptide and stained to perform a live/dead assay
- Volume of bacterial cells in the presence of **W-peptide decreased by approximately 90%.**

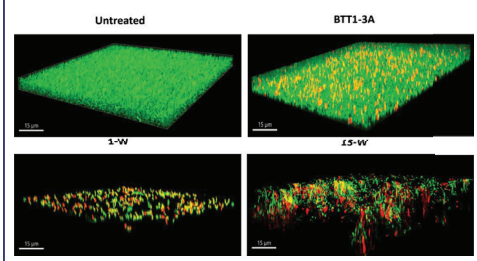

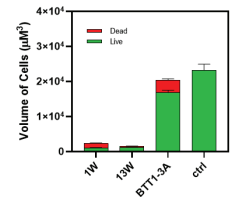

2)

- The antifouling ability of W-peptides was evaluated on polymer substrates and 0.1% crystal violet staining (2) and SEM (3) were used to visualize the bacterial adhesion of *E. faecalis* after biofilms were initiated.
- Overall, it indicates a **decrease in bacterial adhesion and trapped bacteria were observed on these solid surfaces**.

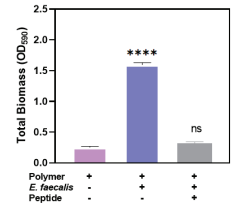

3)

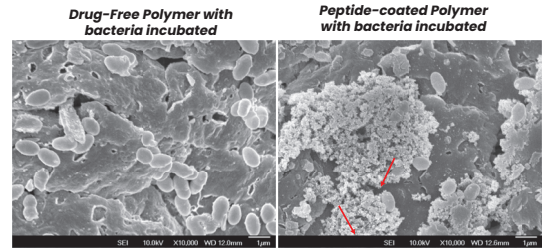

Key Insights

- Incorporating tryptophan into BTT1-3A significantly enhances its antimicrobial activity against Gram-positive bacteria while maintaining efficacy against Gram-negative bacteria.
- The strategic incorporation of tryptophan enhances fibrillation capacity against gram-positive compared to the parent peptide.
- Additionally, the modified W-peptides show potential antifouling ability and may act as an effective solution for preventing biofilm-related complications in medical settings.

Reference

1. Tram, N. D. T., et. al., Bacteria-Responsive Self-Assembly of Antimicrobial Peptide Nanonets for Trap-and-Kill of Antibiotic-Resistant Strains. *Adv. Funct. Mater.* 2023, 33, 2210858.
2. Nhan D.T. Tram, et. Al., Manipulating turn residues on de novo designed β-hairpin peptides for selectivity against drug-resistant bacteria, Acta Biomaterialia, Volume 135, 2021
3. *Drug repurposing for next-generation combination therapies against multidrug-resistant bacteria. Theranostics*, 2021; 11(10):4910-4928

Contact Information

National University of Singapore
Department of Pharmacy
18 Science Drive 4,
Singapore 117543

Email: phaeplr@nus.edu.sg (A/Prof Rachel Ee)
e0606578@u.nus.edu (Dhanya Murali))

https://doi.org/10.17952/37EPS.2024.P2040

Cyclic Antimicrobial Peptides Guanidino-based Analogues of Temporin L

Boccino I.[1], **Bellavita R.**[1], **Loffredo M.R.**[2], **Cappiello F.**[2], **Casciaro B.**[2], **Mangoni M.L.**[2], **Grieco P.**[1], **Merlino F.**[1]

[1]*Department of Pharmacy, University of Naples Federico II, Naples, Italy.*

[2]*Department of Biochemical Sciences, Laboratory affiliated to Istituto Pasteur Italia-Fondazione Cenci Bolognetti, Sapienza University of Rome, Rome, Italy.*

Introduction

Antimicrobial Resistance (**AMR**) occurs when microorganisms such as bacteria, viruses, fungi and parasites change in ways that render ineffective the medications used to cure the infections they cause.

Antimicrobial peptides (**AMPs**) have recently been identified as promising targets for novel drug development, due to their properties: *i)* short sequence length, *ii)* activity against a wide range of pathogens, *iii)* additional chemotactic activity and immunomodulatory effects.[1].

Among these, Temporin L (TL) peptide is a 13-mer cationic peptide derived from skin of Rana Temporaria.[2] TL has high antimicrobial potency against Gram negative and Gram positive bacteria strains, but it also has hematotoxic effect.

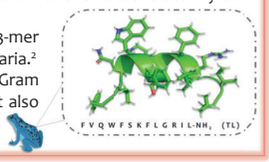

Aim

Local modifications, *stereoinversion* have been made on **TL**, subsequently, different cyclization were made to optimize antimicrobial activity but especially to reduce toxicity. [2,3]



Based on previous results, a new library of ***cyclic derivatives*** was designed and synthesized, which bear a **guanidino group** in key positions of the TL peptide sequence.

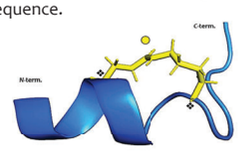

F V P W F c[K K F / E]R I L (1)

- Lactam bridge or guanidino bridge
- ❖ D-amino acids
- ▪ Guanidino group in lateral chain

FVPWF[KKF/*e*]RIL	(2)
$(H_2N)_2C$=N-FVPWF[KKF/*e*]RIL	(3)
$(H_2N)_2C$=N-βAla-FVPWF[KKF/*e*]RIL	(4)
$(H_2N)_2C$=N-GABA-FVPWF[KKF/*e*]RIL	(5)
F[*p*-NHC(=NH)NE_2]VPWF[KKF/*e*]RIL	(6)
FVP[*p*-NHC(=NH)NH_2]WF[KKF/*e*]RIL	(7)
FVPWF[*p*-NHC(=NH)NH_2][KKF/*e*]RIL	(8)
FVPWF[KRF/*e*]RIL	(9)
FVPWF[KKF[*p*-NHC(=NH)NH_2]/*e*]RIL	(10)
FVPWF[KKF/K]RIL	(11)
FVPWF[KKF/*k*]RIL	(12)
FVPWF[OrnKF/Orn]RIL	(13)

Methods

Peptides were assembled by an ultrasonic-assisted solid phase peptide synthesis (US-SPPS) approach.[4] The cyclization of peptides **1-10** occurs via the formation of the lactam bridge (Scheme **1**), due to orthogonal protection of the residues involved. For peptides **11-13**, the synthesis of the side chain-to-side chain guanidino bridge proceeded according to Scheme **2.**

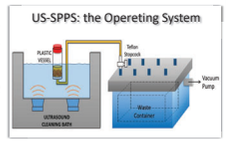

Scheme 1 synthesis of **lactam bridged**

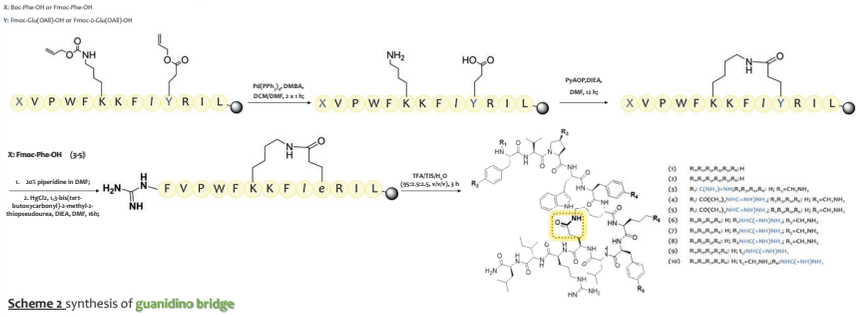

Scheme 2 synthesis of **guanidino bridge**

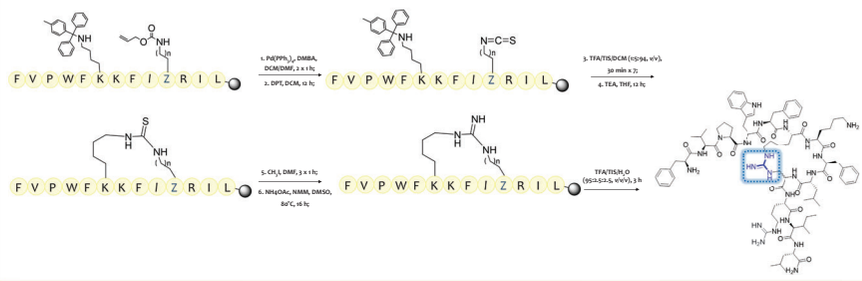

Results

☑ Minimum Inhibitory Concentration

Biological assays on selected bacterial strains suggest the major activity, especially, against **Gram negative** bacteria when the **guanidino group** is located in the *N*-term region or when it is involved in the cyclization bridge.

MIC (μM)

ID	Gram positive			Gram negative		
	S. aureus ATCC 25923	*S. epidermidis* ATCC 12228	*Bac.megaterium* Bm11	*E. coli* ATCC 25922	*P. aeruginosa* ATCC 27853	*Ac. baumannii* ATCC 19606
(1)	3.12	3.12	1.56	25	100	3.12
(2)	*n.a*	3.12	*n.a.*	6.25	50	6.25
(3)	6.25	3.12	0.78	6.25	100	3.12
(4)	3.12	1.56	0.78	3.12	25	3.12
(5)	3.12	3.12	0.78	6.25	50	3.12
(6)	25	3.12	0.78	6.25	25	3.12
(7)	6.25	3.12	0.78	3.12	12.5	3.12
(8)	25	6.25	0.78	12.5	50	6.25
(9)	6.25	3.12	1.56	6.25	100	3.12
(10)	100	12.5	0.78	6.25	50	6.25
(11)	3.12	1.56	1.56	6.25	50	1.56
(12)	6.25	1.56	0.39	6.25	12.5	1.56
(13)	6.25	1.56	0.39	6.25	50	1.56

☑ Membrane Interaction

- Thioflavin T assay studied the **peptide aggregation** on LUVs (large unilamellar vesicles) composed by DOPE/DOPG/CL, mimicking Gram negative membrane, is significant for peptide **12**, also at low concentration.
- Laurdan assay studied the membrane fluidity by calculating the GP value in the presence of LUVS mimicking Gram negative bacteria. The value increased for all tested peptides at at 50 μM, indicating a shift towards more ordered membranes.

Thioflavin T assay

F_0= fluorescence before peptide addition
F= fluorescence after peptide addition

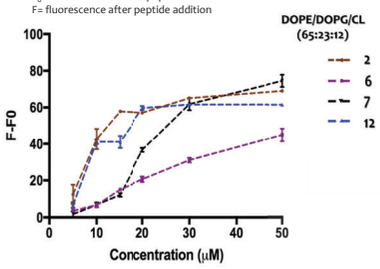

Laurdan assay

Membrane fluidity evaluation using the generalized polarization value (GP)

$$GP = \frac{I_{440} - I_{490}}{I_{440} + I_{490}}$$

I_{440} and I_{490} are the emission intensities of Laurdan

GP value

ID	Unloaded LUVs	LUVs + 20μM Compound	LUVs + 50μM Compound	LUVs + 100μM Compound
Gram negative mimicking membranes				
(2)	-0.21	-0.18	0.07	0.02
(6)	-0.22	-0.05	0.05	0.06
(7)	-0.20	-0.02	0.08	0.07
(12)	-0.18	-0.04	0.06	0.06

☑ Serum Stability

The **guanidino group**, like as pendant or bridge, confer greater stability to proteases, also after 4h or 8h (see analogues **6**, **11** and **12**).

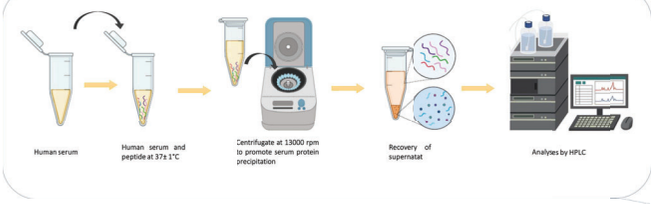

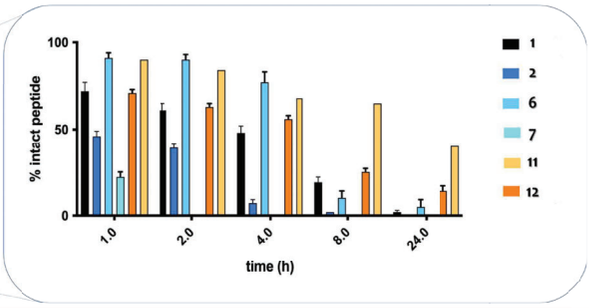

Conclusions and Future Directions

The results suggest that the increase in antimicrobial activity is potentially related to the introduction of a further **positive charge**. The preliminary results of the **antimicrobial activity** and on **modes of interaction with membrans** obtained for these derivatives will guide the development of further cyclic analogues.

References

1. L.D. D'Andrea et al. *Int. J. Mol.* **2023**, 24, 5426.
2. F. Merlino et al., *Eur. J. Med. Chem.* **2017**, 139, 750–761.
3. R. Bellavita, et al. *J. Med.Chem.* **2021**, 64, 11675–11694.
4. F. Merlino et al., *Org. Lett.* **2019**, 21,6378–6382.

ida.boccino@unina.it

Department of Pharmacy — Università degli Studi di Napoli Federico II

Sapienza Università di Roma

From clotting to calcification: Gla-domains as guardians of vascular remodeling

S.M. Agten, A. Gentier, D.P.L. Suylen, S. Peijenborgh, M. Hochstenbach, L.J. Schurgers, T.M. Hackeng

Department of Biochemistry, Cardiovascular Research Institute Maastricht, University of Maastricht, the Netherlands

https://doi.org/10.17952/37EPS.2024.P2041

Funded by Hartstichting

Vitamin-K dependent proteins and calcification

Coagulation and mineralization have little in common, proteins from both subfamilies can affect the critical pathological process of **vascular calcification**. Mechanisms by which they modulate calcification, however, are largely unknown. Therapeutic interventions are unavailable, and diagnosis can only be performed at a late stage of disease, hampering possible intervention.

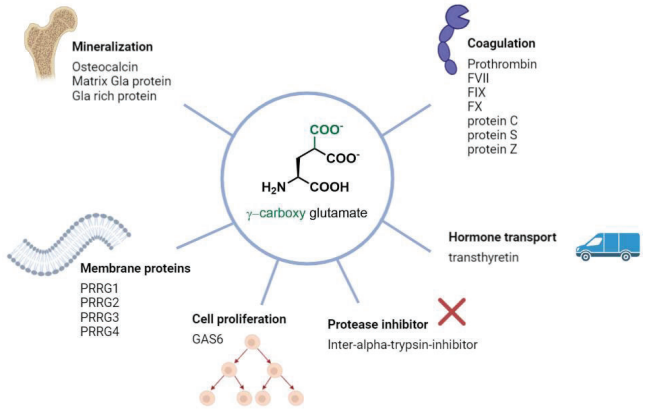

Aims

- Provide access to post-translationally modified variants of VKD proteins
- Elucidate modulatory mechanism of action of VKD proteins in vascular calcification
- Enable early detection and repair of vascular calcification

Calcium phosphate precipitation inhibition

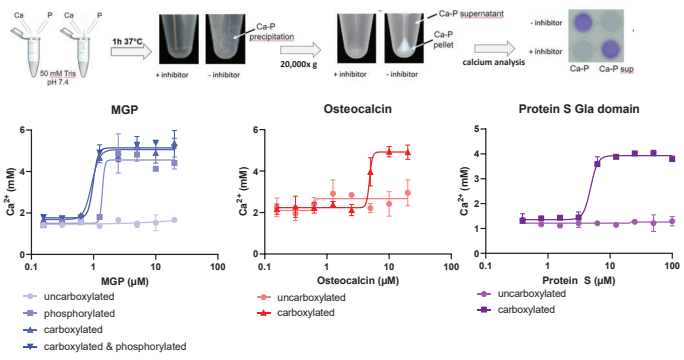

Protein structure determination using CD

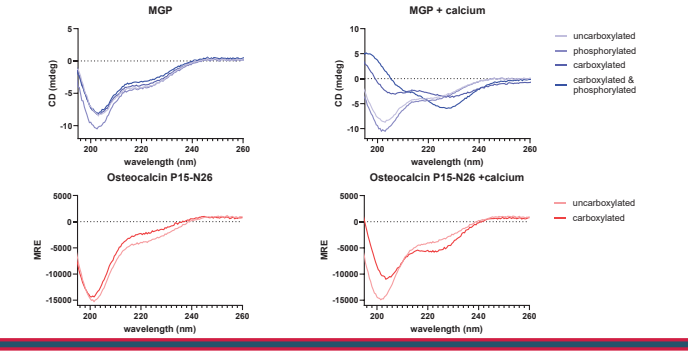

Bulk RNA sequencing

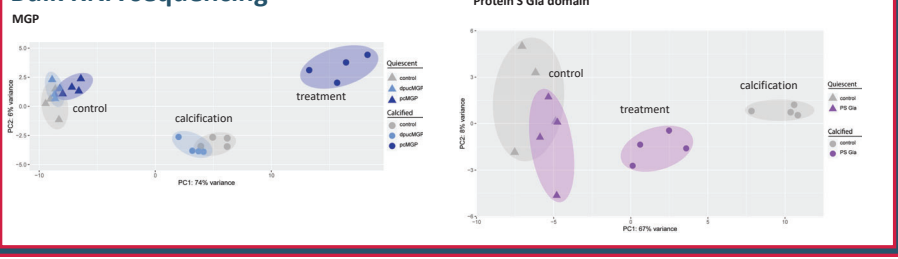

Chemical protein synthesis

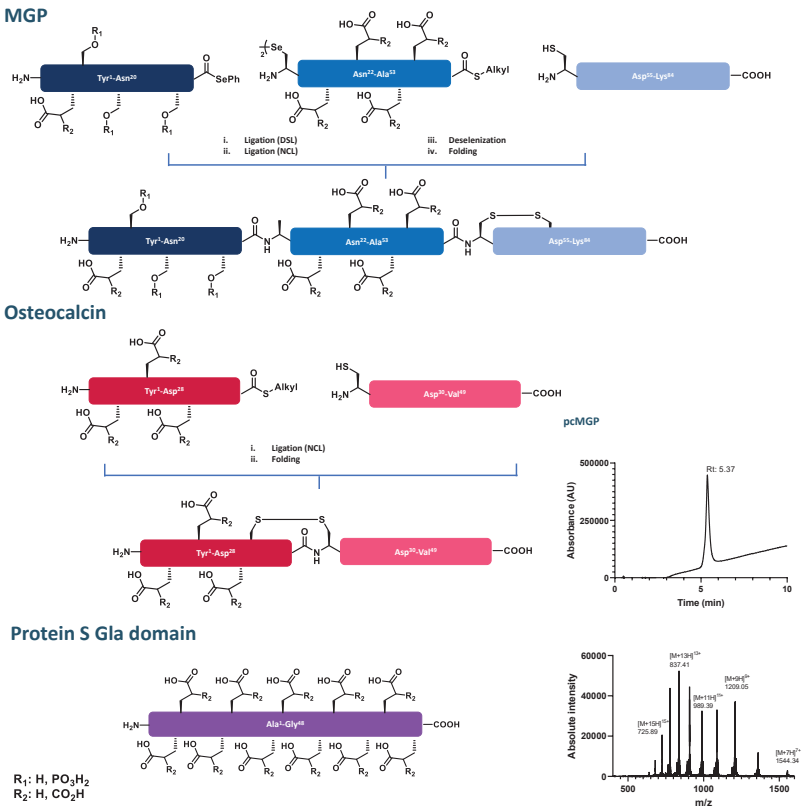

Calcification modulation of hVSMCs

Cellular model of vascular calcification using primary human vascular smooth muscle cells (hVSMC) cultured under calcifying conditions of increased calcium and phosphate.

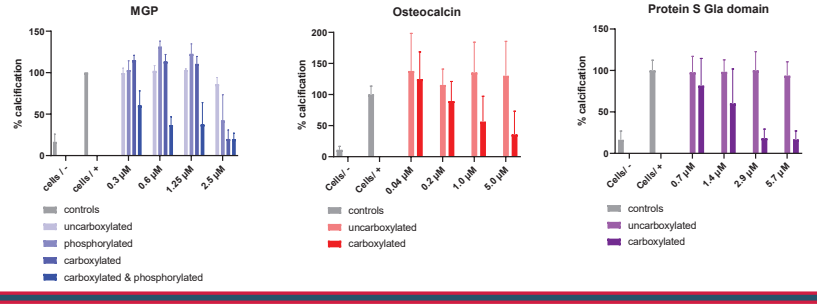

Detection of calcifying cells using protein S Gla domain

Protein S Gla was used to identify calcifying cells; hVSMC were exposed to either stringent calcification conditions or control conditions for 24 hours in the presence of 1.5 μM protein S in uncarboxylated (Glu) or carboxylated (Gla) form.

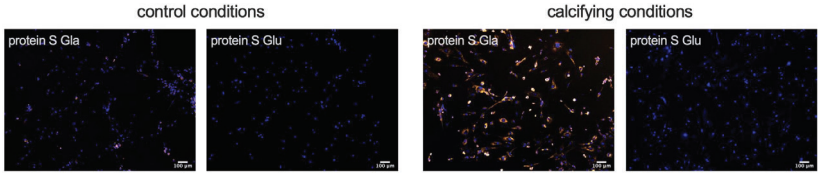

Conclusions

- Three different VKD proteins in multiple variants were synthesized
- In vitro calcium phosphate precipitation can be inhibited by all post-translationally modified VKD proteins
- Calcification of human vascular smooth muscle cells was inhibited by phosphorylated and carboxylated variants of VKD proteins
- Structure of carboxylated proteins is influenced by addition of calcium
- RNA sequencing may point to two distinct mechanisms of action of VKD proteins from the mineralization and coagulation group

https://doi.org/10.17952/37EPS.2024.P2042

Design and Synthesis of Peptide Modulators of Gαi/s Proteins

Anna Pepanian[1], Sabriye Aydoğdu[1], F. Ayberk Binbay[1], Pradipta Ghosh[2], Dehua Pei[3], and Diana Imhof[1]

[1]Pharmaceutical Biochemistry and Bioanalytics, Pharmaceutical Institute, University of Bonn, Bonn, Germany, [2]Department of Cellular and Molecular Medicine, University of California San Diego, La Jolla, USA, [3]Department of Chemistry and Biochemistry, The Ohio State University, Columbus, USA.

Introduction

The stimulation of G protein-coupled receptors (GPCRs) by ligand binding initiates the shuttle of heterotrimeric G proteins (Gαβγ) between the active (Gα-GTP) and inactive (Gα-GDP) state[1]. Subsequently, the active Gα-GTP subunit and the Gβγ dimer interact with downstream effectors that trigger several intracellular pathways. These can provoke cellular alterations that account for severe diseases. Such cellular changes can be investigated through peptides targeting specifically the Gα subunits[2-3]. For instance, the discovery of the macrocyclic depsipeptides YM-254890 and FR900359, inhibitors of the Gαq subfamily, evoked curiosity in developing linear and cyclic peptides against other Gα subunits. Interestingly, procedures such as the screening of **combinatorial peptide libraries** revealed the KB-752, GIV-Girdin, and GPM-1c/d (G protein modulator) peptides, which exhibit novel GEM (guanine nucleotide exchange modulator)-like activities by inhibiting Gαi and activating the Gαs signaling cascades[3-9].

Workflow

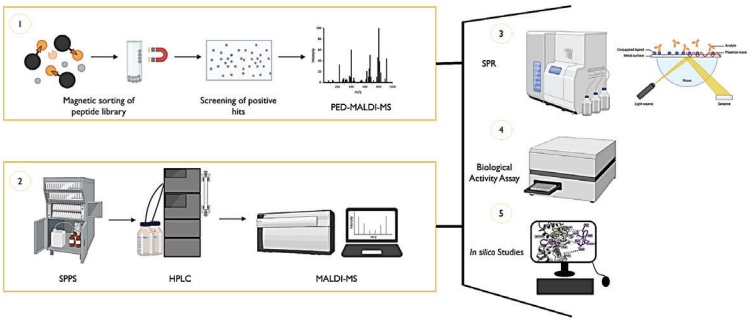

Figure 1. The methodology includes (1) peptide library screening, (2) synthesis, (3) binding analysis, (4) cellular activity assays, and (5) computational modeling and docking studies. Created with BioRender.com.

Results

- We previously identified a linear nonapeptide, GPM-1, from the screening of a one-bead-one-compound (OBOC) library against Gαi-GDP[3-5], which revealed high binding affinities to Gαi and Gαs, resulting in a bifunctional GEM-like activity. Chemical modifications of the GPM-1 lead compound, such as cyclization and conjugation with a cell-penetrating peptide (series GPM-1b/c/d), resulted in modulators with enhanced proteolytic stability and cell permeability.
- Second, an advanced **one-bead-two-compound (OBTC)** library was screened towards both activity states of the Gαi protein and revealed bicyclic peptides containing non-proteinogenic and D-amino acids (GPM-2, GPM-3, peptide 10, (*Fig. 2a-c*)). Cellular studies showed that the GPM-2/3 compounds bind to novel sites on the protein surface influencing thereby their biological properties (GPM-2 as GEF-like and GPM-3 as a GAP-like modulator of the Gαi signaling (*Fig. 2d*)).

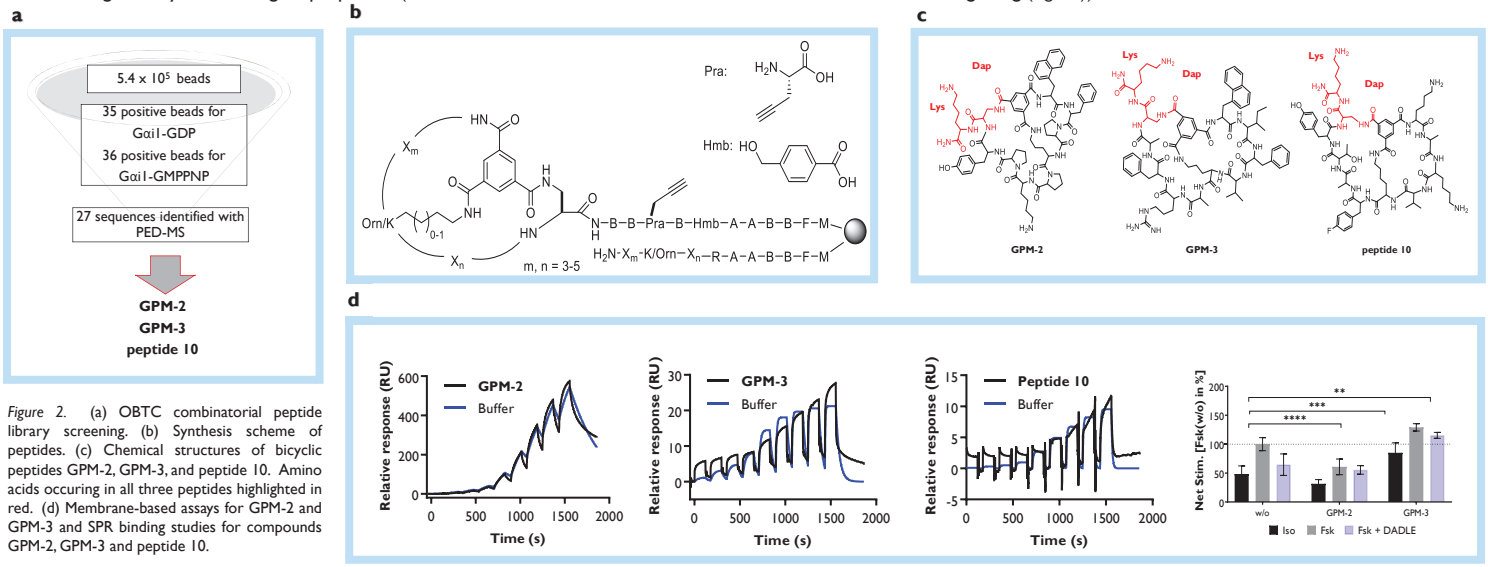

Figure 2. (a) OBTC combinatorial peptide library screening. (b) Synthesis scheme of peptides. (c) Chemical structures of bicyclic peptides GPM-2, GPM-3, and peptide 10. Amino acids occuring in all three peptides highlighted in red. (d) Membrane-based assays for GPM-2 and GPM-3 and SPR binding studies for compounds GPM-2, GPM-3 and peptide 10.

- *In silico* studies of the peptides GPM-2, GPM-3, and peptide 10 defined the structural similarities and differences between them (*Fig. 3a, b*). Protein-ligand docking studies also revealed similarities in the binding site between peptide 10 and GPM-3, which were found to interact between the α-helical and switch III region (SWIII) (*Fig. 3a*).

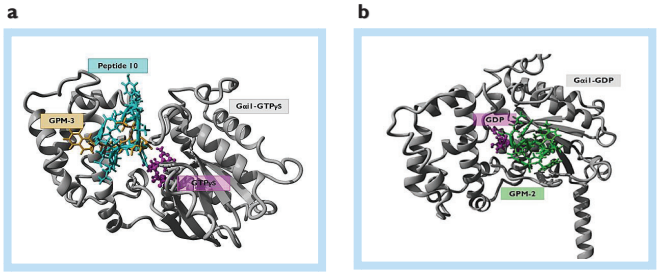

- Despite the binding site similarity, the K_D value (9.077 µM) was higher for peptide 10 compared to GPM-2 (5.0 µM) and GPM-3 (0.7 µM) (*Fig. 2d*). The reduced binding affinity may be a result of the positioning of the high numbers of hydrogen bond donor and acceptor residues (Lys, Thr, Tyr, Dap).
- Additionally, the interaction of both rings of peptide 10 with the protein might introduce unfavorable interactions, contributing to the overall weaker binding affinity.

Figure 3. Computational superimposition of peptides on the Gαi1 protein (a) Comparison of interaction sites of the peptides GPM-3 (yellow) and peptide 10 (cyan) on Gαi1-GTPγS (PDB: 1GIA[9]) (gray). (b) The superimposed position of GPM-2 on Gαi1-GDP[3] (gray). Nucleotides are shown in magenta.

Summary & Outlook

Our studies with different combinatorial peptide libraries revealed novel Gαi/s modulators with distinct guanine nucleotide exchange activities. Compounds GPM-2, GPM-3, and peptide 10 were identified from an OBTC peptide library with promising selectivity for Gαi. *In silico* studies unveiled new important structural features for Gαi binding, which were confirmed by comparison of peptide 10 to the Gαi modulators GPM-2 and GPM-3. These findings provide fundamental knowledge for deeper investigations of peptide 10, and optimization of the biological properties of the obtained compounds to achieve higher pharmacological potencies.

References

1. Campbell et al. Nat. Rev. Drug Discov., (2018), 17(11), 789-803
2. Johnston et al. FEBS Letters, (2005), 579(25) , 5756-5750
3. Nubbemeyer et al. ACS Chem. Biol., (2022), 17(2) , 463–473
4. Pepanian et al. J. Med. Chem., (2023), 66(17) , 12396-12406
5. Pepanian et al. J. Pept. Sci., (2024), 30(6), e3565
6. Upadhyaya et al. Tetrahedron, (2014), 70(42), 7714-7720
7. Kalogriopoulos et al. PNAS, (2019), 116(33), 16394-16403
8. Lian et al. JACS, (2014), 136(28), 9830-9833
9. Coleman et al. Science (1994), 265, 1405-1412

Acknowledgment

DFG Deutsche Forschungsgemeinschaft
heinrichhertzstiftung
DAAD Deutscher Akademischer Austauschdienst German Academic Exchange Service
GDCh

Check Imhof Lab Publications

Synthesis of Macrocyclic Thiolactone Peptides via Radical Acyl Thiol-Ene

Alby Benny, Eoin M. Scanlan

Trinity Biomedical Sciences Institute (TBSI), Trinity College Dublin, The University of Dublin, 152-160 Pearse St., Dublin, Ireland

Contact: bennya@tcd.ie, scanlae@tcd.ie

https://doi.org/10.17952/37EPS.2024.P2045

1. Peptide Thiolactones - AIPs

Thiolactones are found in several bioactive natural peptides, including the **autoinducing peptides (AIPs)** found in Gram-positive bacteria such as *Staphylococcus aureus*. AIPs play a key role in the regulation of the quorum sensing system.[1-2] Thus, analogues of AIPs have been investigated as modulators of the quorum sensing system to attenuate and treat *S. aureus* infections.[3-4]

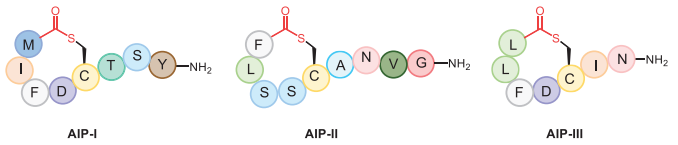

2. Peptide Thiolactone Synthesis

The traditional synthesis of peptide thiolactones has relied on the thiolactonisation of fully protected peptides using coupling reagents, or the displacement of activated groups (thioesters, Dbz, MeDbz) by Cys. Both require elevated temperature (50 °C) and extended reaction times (2–12 h).[5] The aim of this project is to **develop a photochemical acyl thiol-ene method to rapidly synthesise peptide thiolactones**.

This work

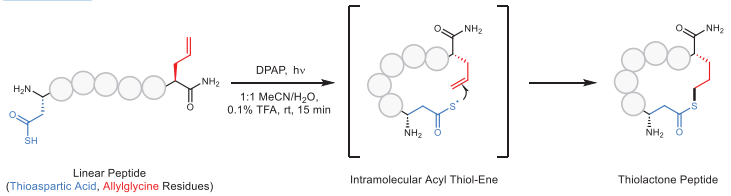

- Standard Fmoc SPPS synthesis of linear peptide.
- Compatible with aqueous conditions.
- Compatible with fully unprotected peptides.
- Rapid reaction time (15 min)

3. Thioaspartic Acid SPPS Monomer Synthesis

Thioacid was introduced during standard Fmoc SPPS as the **acid-labile *S*-trityl group**, which can be deprotected during global deprotection/resin cleavage. **Overall, 51% yield over 6 steps**, with two chromatographic purifications.

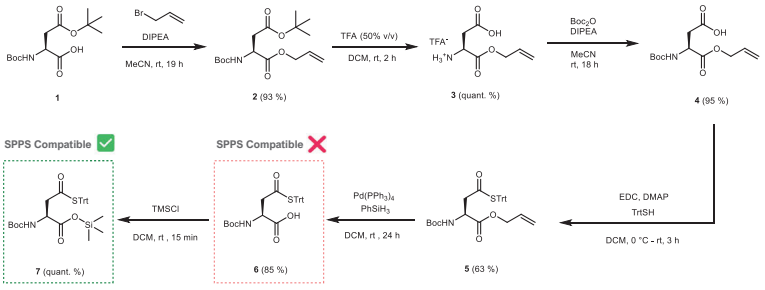

Carboxylic acid (**6**) prone to base catalysed lactonisation during amino acid activation. Silyl ester (**7**) masks carboxylic acid.[6]

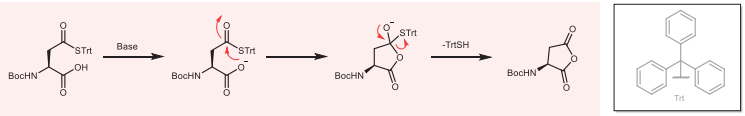

4. SPPS of Linear Thioacid/Alkene Peptide

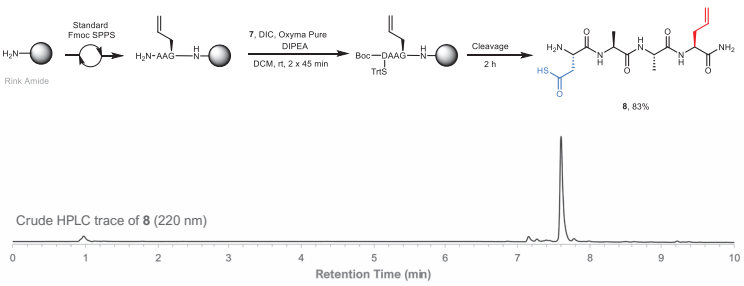

5. Model Acyl Thiol-Ene Thiolactonisation Reaction

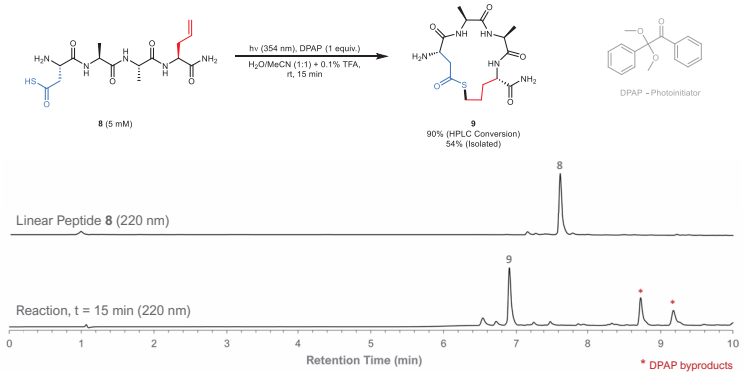

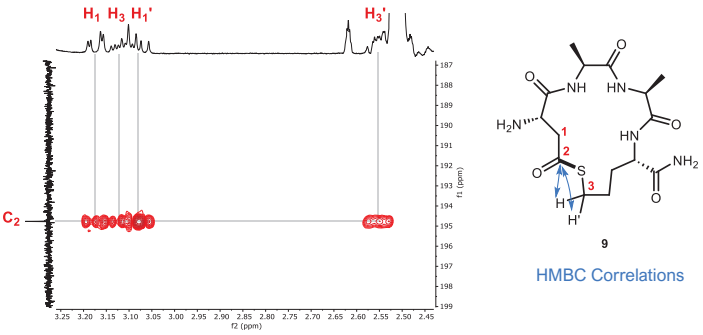

Cyclisation confirmed by Heteronuclear Multiple Bond Correlation (HMBC) NMR spectroscopy.

6. Acyl Thiol-Ene Macrothiolactonisation Scope

Series of linear peptides were synthesised by SPPS and cyclised using the conditions above. Compatibility with various ring sizes and functional groups was demonstrated. All reported yields are isolated yields after semi-preparative HPLC purification.[7]

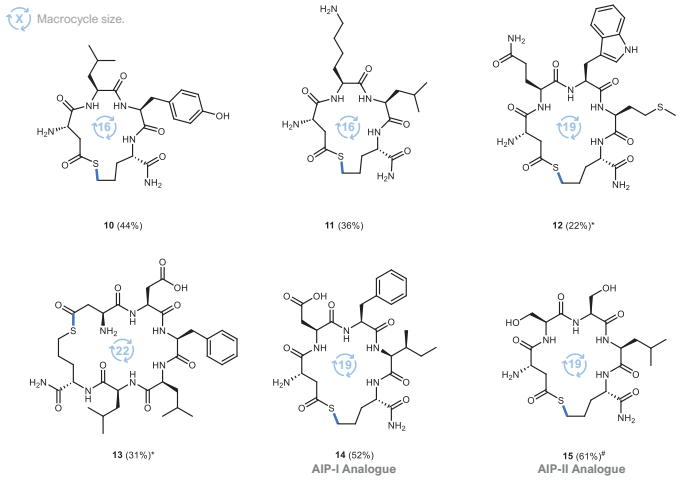

* 80% pure by ^{1}H NMR due to inseparable impurity. #6 M guanidinium hydrochloride added to reaction mixture.

References and Acknowledgements

1. B. Wang and Tom W. Muir, *Cell Chem. Biol.*, **2016**, 23, 214-224.
2. B. H. Gless, M. S. Bojer, P. Peng, M. Baldry, H. Ingmer and C. A. Olsen, *Nat. Chem.*, **2019**, 11, 463-469.
3. J. K. Vasquez and H. E. Blackwell, *ACS Infect. Dis.*, **2019**, 5, 484-492.
4. K. H. J. West, C. G. Gahan, P. R. Kierski, D. F. Calderon, K. Zhao, C. J. Czuprynski, J. F. McAnulty, D. M. Lynn and H. E. Blackwell, *Angew. Chem. Int. Ed.*, **2022**, 61, e202201798
5. C. P. Gordon, *Org. Biomol. Chem.*, **2020**, 18, 379-390.
6. R. Joseph, M. Morales Padilla and P. Garner, *Tetrahedron Lett.*, **2015**, 56, 4302-4304.
7. A. Benny, E. M. Scanlan, *Chem. Commun.*, **2024**, 60, 7950-7953.

SCAN ME

Trinity College Dublin
Coláiste na Tríonóide, Baile Átha Cliath
The University of Dublin

IRISH RESEARCH COUNCIL
An Chomhairle um Thaighde in Éirinn

Fondúireacht Eolaíochta Éireann
Dá bhfuil romhainn
Science Foundation Ireland
For what's next

https://doi.org/10.17952/37EPS.2024.P2046

Divalent metal ions-directed release of *C*-terminally modified peptides at 60 °C under mild conditions

Rebeca G. Moura, Thiago de Souza Freire, M. Terêsa Machini

Department of Biochemistry, Institute of Chemistry, University of São Paulo, Av. Prof. Lineu Prestes, 748, 05508-900, São Paulo, Brazil
rebeca.garcia.moura@usp.br; mtmachini@iq.usp.br

Introduction

C-terminally modified peptides (*C*-TMPs) are of great interest in the field of therapeutic peptides as modification of such macromolecules can favorably impact its potency, chemical stability, hydrophobicity and biological barriers permeability.[1] The synthesis of *C*-TPMs can be complex and time-consuming. In fact, some steps of the synthetic routes employ acidic or basic conditions, leading to *C*-terminal amino acid enantiomerization[2a,b] and other side-reactions.

In the 1990s, Machini-Miranda et al. first observed transesterification of the *N*-acylated *C*-esterified tripeptide Moz-Asn-Leu-Gly-OEt in MeOH/H_2O containing calcium salts. These authors also proved the applicability such Ca^{2+}-promoted transesterification by using this new procedure to produce various di- and tripeptide esters.[3a] Soon after, they first demonstrated that the peptide-resin (PR) ester bond present in growing PRs made by Boc chemistry was susceptible to Ca^{2+}-promoted methanolysis, releasing the corresponding the *N*- and side-chain protected peptide methyl ester.[3b] In the following years, the group investigated Ca^{2+}- or Zn^{2+}-promoted peptide detachment from the Kaiser oxime resin (KOR) to give the corresponding *C*-TMPs. Examples included: i) transesterification of X-KOR bond from Ac-Ala-Gly-X-KOR (X: Gly, Ala, Phe or Lys (2-Cl-Z)) and from Ac-Ile-Ser(Bzl)-Asp(OZ)-KOR (Z: Bzl or cHex) to yield 85-96 % of the corresponding Ac-peptide-OMe;[4] ii) aminolysis of the Asp(X)-KOR bond from Ac-Ile-Ser(Bzl)-Asp(X)-KOR (X: OBzl or OcHex) to yield > 50 % of the corresponding Ac-peptide-amide;[4] iii) hydrolysis of X-KOR bond from Ac-Ile-Ser(Bzl)-X-KOR (X: Gly, Asp, Phe, Lys or Leu (2-Cl-Z)) to yield 19–90 % of the corresponding Ac-peptides-OH;[5] iv) thiolysis of the Asp(OcHx)-KOR bond from Ac-Ile-Ser(Bzl)-Asp(OcHx)-KOR to yield > 90 % of the corresponding Ac-peptide-SR.[6]

Objectives

With the intention of expanding this alternative single-step synthetic approach to SPPS-Fmoc chemistry, we have been studying peptide detachment from HMBA resins because the ester bond P-HMBA from these PRs is also susceptible to nucleophilic attack[7] and could be promoted by Ca^{2+}, Zn^{2+} or Cu^{2+} ions.

Experimental

The synthesis of aminoacyl (Fmoc-Asp(O^{t}Bu)-HMBA; Fmoc-Phe-HMBA, and Fmoc-Gly-HMBA) and PRs (Fmoc-Ile-Ser(But)-Asp(O^{t}Bu)-HMBA, Ac-Met-Ser-Leu-Phe-HMBA, and Fmoc-Gly-Gly-His(Trt)-Gly-HMBA) were performed using traditional or microwave-assisted synthesis at 60 °C and our customized protocols for Fmoc chemistry.[8] Their substitution levels (SL) were determined by total acidic hydrolysis of PRs at 130 °C for 24 h followed by amino acid analysis of the hydrolysates. The alcoholysis reactions were performed using Ca^{2+}, Zn^{2+} or Cu^{2+} ions as additive and RP-HPLC/LC-MS for monitoring. Identities of the *C*-esterified side-chain protected peptides formed were confirmed by electrospray ionization mass spectrometry (ESI-MS). Reaction yields were calculated from the difference between initial and final SLs.

Results and Discussion

Initially, we investigated alcoholysis of the ester bond of Fmoc-aminoacyl or Fmoc-peptidyl-resin varying the HMBA resins, the divalent metal ion (Ca^{2+} and Zn^{2+}), and the solvent system (20–50 % ROH/DMF; R: Et, ^{i}Pr and $(CH_2)_2CH_3$). The results showed that HMBA-AM and HMBA-PEGA resins were appropriate, $ZnCl_2$ was better metal salt than

$Ca(OAc)_2$ in 50% ROH/DMF at 60 °C for 48 h at molar ratio of 1:2 (peptide: metal ion). The Zn^{2+}-promoted alchoholyis of amino acid-resin ester bond from Fmoc-Gly-HMBA-AM produced the desired Fmoc-Gly-OR with yields > 97 % and methanolysis of the PR ester bond from Fmoc-Ile-Ser(^{t}Bu)-Asp(O^{t}Bu)-HMBA-AM furnished the desired product Fmoc-Ile-Ser(^{t}Bu)-Asp(O^{t}Bu)-OMe with yield of 87 %. All reactions were monitored by RP-HPLC; it was observed slow formation of the DBF (dibenzofulvene) resulting from removal of Fmoc group that led to little amounts of contamination. Aiming to overcome this undesirable side-reaction, the Fmoc group was replaced by acetyl group, so Zn^{2+}-promoted alcoholyses of the PR ester bond from Ac-Ile-Ser(^{t}Bu)-Asp(O^{t}Bu)-HMBA-AM using 50 % MeOH, EtOH, ^{i}PrOH, butan-1-ol or benzyl alcohol/DMF at 60 °C for 48 h formed the corresponding Ac-peptides-OR with yields of 73–95%, except for ^{i}PrOH that yielded only 20 % of the product due to sterical hindrance.

Afterwards, we studied the Zn^{2+}-promoted transesterification of Ac-Ile-Ser-Asp-OMe in Ac-Ile-Ser-Asp-OR (R:Et, But, Benzyl and ^{i}Pr)] under the same conditions. Such reactions produced the desired *C*-esterified peptides with yields of 73 – 92 %, except for that using ^{i}PrOH that formed the product with yield of 30 %. At last, to verify the tolerance of other functional groups, such as sulfur, in peptide sequences by our alternative method, we synthesized Ac-Met-Ser-Leu-Phe-HMBA, sequence analogous to that of the anti-inflammatory tripeptide For-Met-Ser-Leu-Phe.[9] Zn^{2+}-promoted methanolysis in 50 % MeOH/DMF, at 60 °C for 48 hfurnished the Ac-Met-Ser-Leu-Phe-OMe with yield of 93.5 % and high purity (83 %).

Currently, we are studying Shepherin I (Shep I)-derived PRs because this unique Gly- and His–rich peptide has 7 repetitions of the ATCUN motif GGH in its structure. which chelates Cu^{+2} and Ni^{2+} ions.[10] Once again, Cu^{2+}, Ca^{2+} and Zn^{2+}-promoted methanolyses of the PR ester bond from Fmoc-Gly-Gly-His(Trt)-Gly-HMBA-PEGA were effectively carried-out in 20% MeOH/DMF at 60 °C for 24 h to give the desired products with reaction yields >50 %.

In short, our alternative single-step method to produce *C*-TMPs based on divalent metal ion-promoted detachment of the peptide from resins showed to be compatible to Fmoc chemistry and HMBA resins, is efficient, quite selective, employs very mild conditions and neutral pH, being greener than the traditional.

Acknowledgments

The authors thank FAPESP (2022/01825-2) and CNPq (314470/2023-9) for the research grant and scholarship to MTM and TSF, Dr. Cleber W. Liria for the mass spectrometry and amino acid analyses and Matheus M. P. Landim for total acidic hydrolysis of PRs (undergraduate student).

References

1. Tanaka, S.; Kanno, M; Tashiro, Y. *Explor Drug Sci.* **2023**, *1*, 322.

2. a) Halpern, B.; Chew, L.; Close, V. et al. *Tetrahedron Lett.* **1968**, 5163. b) Weber, J. R.; Lokey, R. S. *Org. Letters.* **2010**, *12*, 1852.

3. a) Miranda, M. T. M.; Morita, H.; Tominaga, M. *Int. J. Peptide Prot. Res.* **1991**, *37*, 299. b) Miranda, M. T. M.; Theobaldo, F.C.; Tominaga, M. *Int. J. Peptide Prot. Res.* **1991**, *37*, 451.

4. Moraes, C.M., Bemquerer, M.P. & Miranda, M.T.M. *J. Peptide Res.* **2000**, *55*, 279.

5. Proti, P. B.; Remuzgo, C. Miranda, M. T. M. *J. Pept. Sci*. **2007**, *13*, 386.

6. Proti, P. B. & Miranda, M. T. M. *Tetrahedron Lett.* **2008**, *49*, 3853.

7. Alsina, J. & Albericio, F. *Biopolymers (Peptide Science)*, **2003**, *71*, 454-477.

8. Loffredo, C. et al. *J. Pept. Sci.* **2009**, *15*, 808.

9. Freire, T. S., Master Dissertation, Institute of Chemistry, University of São Paulo, **2013**.

10. a) Park. C. J. et al. *Plant Mol. Biol*. **2000**, *44*, 187. b) Remuzgo. C. et al. *Amino Acids*. **2014**, *46*, 2573. c) Nunes, L.G.P. et al., *Int. J. Pept. Res. Ther.* **2021**, *27*, 2945.

https://doi.org/10.17952/37EPS.2024.P2047

P2047

Exploring the Three-Dimensional Structures and Activity Relationships of *N*-Methyl and *N*-Desmethyl Analogues of Cyclodepsipeptide Destruxin E

Takayuki Doi,[1] Hiroshi Sato,[1,2] Hiroshi Nakagawa,[3] and Masahito Yoshida[4]
(1 Pharm Sci, Tohoku Univ., 2 Mitsubishi Tanabe Pharma Co.
3 Dept Appl Biol Chem, Chubu Univ, 4 Dept Chem, Univ. Tsukuba, Japan)

I. Introduction

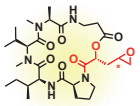



Destruxin E Inhibits bone resorption by inducing morphological changes without affecting the viability of osteoclasts, indicating destruxin E would be a novel anti-resorptive agent for osteoporosis therapy.

Destruxin E was isolated from *Metarhidium anisopliae* in 1989 based on insecticidal activity along with other derivatives [Phytochemistry, **1981**, *20*, 715–723.]. It inhibits V-ATPase at the IC_{50} value of 0.40 μM, which is the most potent among destruxin derivatives [*Chem. Biodivers.* **2005**, *2*, 123–130]. According to the Nakagawa group, destruxins have shown to inhibit osteoclast bone resorption activity. Destruxin E reversibly induce morphological changes in osteoclast-like multinucleated cells (OCLs) at concentrations lower than those exhibiting the V-ATPase inhibitory activity [*Bone*, **2003**, 33, 443]. We investigated the total synthesis of destruxin E and its analogs, as well as their biological activity, to elucidate structure-activity relationships (SAR) for morphological changes in OCLs.

II. Results and Discussion

Combinatorial Synthesis of Side Chain-Modified Destruxin E Analogues

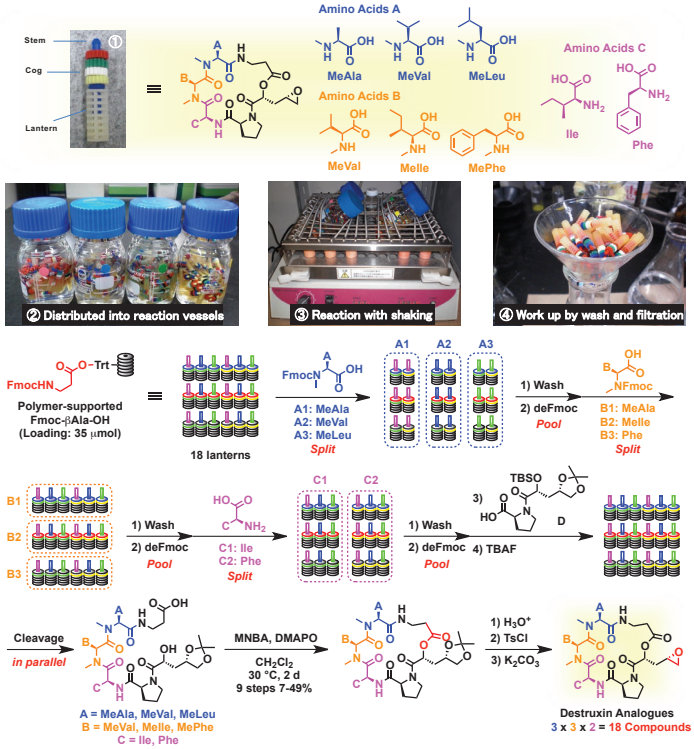

Biological Evaluation of Side Chain-Modified Destruxin E Analogues

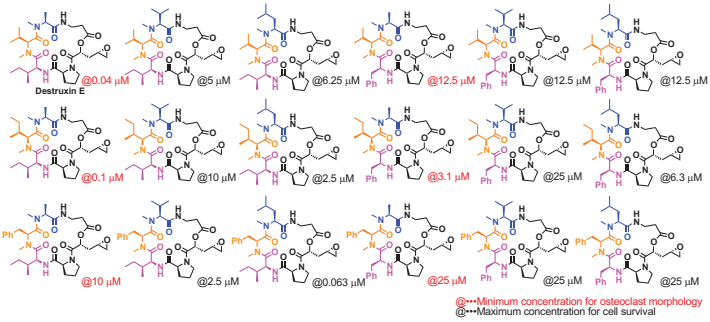

Yoshida, M.; Ishida, Y.; Adachi, K.; Murase, H.; Nakagawa,H.; Doi, T. *Chem. Eur. J.* **2015**, *21*, 18417–18430.

Solid-Phase Total Synthesis of Destruxin E

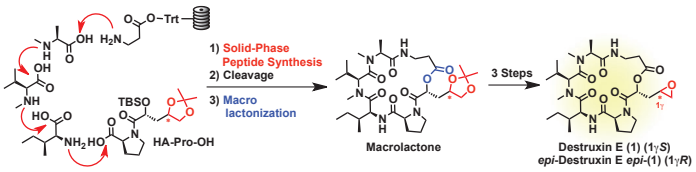

Our laboratory has achieved the first total synthesis of destruxin E and determined the absolute stereochemistry. They have also shown that the stereochemistry of the side chain epoxide is important for V-ATPase inhibitory activity [*Org. Lett.* **2010**, 12, 3792].

Conformational Analysis of Destruxin E

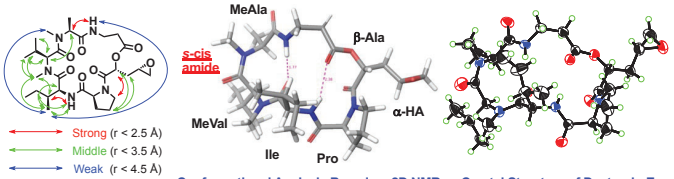

- Calculating program : Macromodel 9.9
- Conformational search method : Monte Carlo based-torsional sampling
- Constraints : 21 distances based on NOESY analysis in $CDCl_3$
- Force field (OPLS2005), Solvent for calculation ($CHCl_3$), Iteration : 50000

- Conditions: from hexane-benzene

The conformational analysis by using the NMR experiments can be utilized to expect the tertiary structure of destruxin analogues.

Design and Synthesis of *N*-Methylated or Desmethylated Destruxin E Analogues

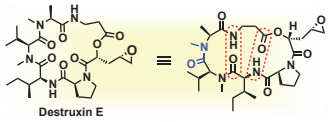

The *cis*-amide between *N*-Me-Ala and *N*-Me-Val and two intramolecular hydrogen bonds could play crucial roles for maintaining the conformation to induce osteoclast morphology.

Synthesis and biological evaluation of the following analogues would lead us to understand the role of *cis*-amide and intramolecular hydrogen bond in the osteoclast morphology.

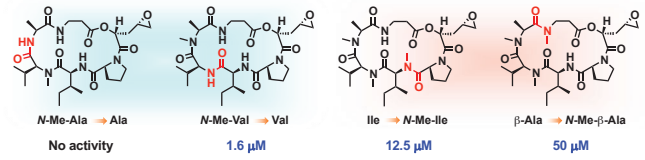

The *cis*-amide between *N*-Me-Ala and *N*-Me-Val is required to induce osteoclast morphology.

Intramolecular hydrogen bonds are important for potent biological activity.

Sato, H.; Murase, H.; Ishida, Y.; Sugiyama, H.; Uekusa, H.; Nakagawa, H.; Yoshida, M.; Doi, T. *Bioorg. Med. Chem.* **2024**, *108*, 117777.

III. Summary

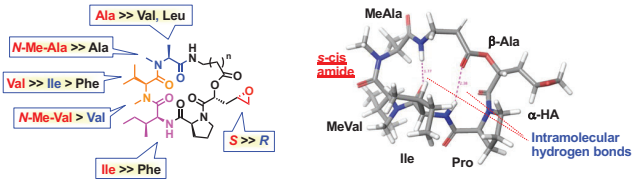

★ (*S*)-Epoxide, 19-membered ring, and N-MeAla are important.
★ *S-cis* amide bond and two intramolecular hydrogen bonds are important.

Yoshida, M.; Nakagawa, H.; Doi, T. *J. Antibiot.* **2022**, *75*, 420–431.

IV. Acknowledgement

This work was supported by JSPS KAKENHI, Uehara Memorial Foundation, and Protein Research Foundation.

Green solvents and Safe Reagents in SPPS taking advantage of induction heating and automation:

Synthesis and HPLC-free Purification of Difficult Sequences

https://doi.org/10.17952/37EPS.2024.P2048

Lorenzo Pacini[1,2], Manoj Kumar Muthyala[3], Oleg Marder[4], Luísa Aguiar[3], Robert Zitterbart[3], Paolo Rovero[1,5], Anna Maria Papini[1,2]

[1] Interdepartmental Research Unit of Peptide and Protein Chemistry and Biology, University of Florence, Sesto Fiorentino (FI), Italy;
[2] Department of Chemistry "Ugo Schiff", University of Florence, Sesto Fiorentino (FI), Italy;
[3] Gyros Protein Technologies Inc., Tucson, AZ, United States;
[4] Luxembourg Bio Technologies, Ness Ziona, Israel;
[5] Department of Neurosciences, Psychology, Drug Research and Child Health, University of Florence, Sesto Fiorentino (FI), Italy.
Presenting author e-mail: L.Pacini@unifi.it

DMF Issue: a high toxic gold standard solvent for SPPS

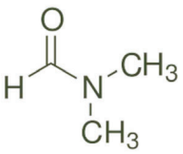

Flammable liquid and vapor

May damage the unborn child

Harmful in contact with skin or if inhaled.
Causes serious eye irritation

Thus, on December 12th, 2023, the European Commission has taken regulatory action to amend Annex XVII of REACH (Registration, Evaluation, Authorization and Restriction of Chemicals), imposing restrictions on the utilization of the solvent *N,N*-dimethylformamide (DMF) within the EU market, owing to its well-established high toxicity.

DMF replacement: Search of Neat or Binary Solvents

Selection Criteria

Non-toxic
Polarity
Reagent Solubility
Boiling point
Viscosity
Polar & Aprotic

Sustainable efficient Green SPPS

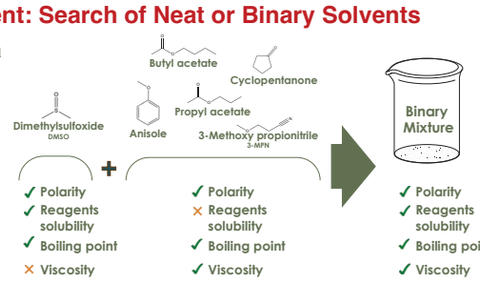

Binary Mixtures - Solubility and Swelling test

Neat Solvents – Fmoc Amino Acids solubility

	Fmoc-His(Trt)-OH (M)	Fmoc-Gln(Trt)-OH (M)	Fmoc-Gly-OH (M)	Fmoc-Phe-OH (M)	Fmoc-Arg(Pbf)-OH (M)
cyclopentanone	< 0.1	≥ 0.4	> 0.4	0.3	< 0.1
3-methoxypropionitrile	< 0.1	≥ 0.4	< 0.1	< 0.1	< 0.1
anisole	< 0.1	< 0.1	< 0.1	< 0.1	< 0.1
propyl acetate	< 0.1	0.2	< 0.1	< 0.1	< 0.1
butyl acetate	< 0.1	< 0.1	< 0.1	< 0.1	< 0.1
DMSO	≥ 0.4	≥ 0.4	≥ 0.4	≥ 0.4	≥ 0.4

Binary SolventMixtures – Fmoc Amino Acids solubility

	Fmoc-His(Trt)-OH (M)	Fmoc-Arg(Pbf)-OH (M)	Fmoc-Gln(Trt)-OH (M)	Fmoc-Gly-OH (M)	Fmoc-Phe-OH (M)
cyclopentanone/DMSO 7:3	≥ 0.4	≥ 0.4	≥ 0.4	≥ 0.4	≥ 0.4
butyl acetate/DMSO 7:3	≥ 0.4	≥ 0.4	≥ 0.4	≥ 0.4	≥ 0.4
propyl acetate/DMSO 7:3	≥ 0.4	≥ 0.4	≥ 0.4	≥ 0.4	≥ 0.4
3-MPN/DMSO 7:3	0.2	≥ 0.4	≥ 0.4	0.2	< 0.1
anisole/DMSO 8:2	≥ 0.4	≥ 0.4	≥ 0.4	≥ 0.4	≥ 0.4

Binary Solvent Mixtures – Coupling Reagents solubility

		HATU (M)	Oxyma Pure (M)	DIC (M)
Neat Solvents	anisole	< 0.1	≥ 1	≥ 1
	butyl acetate	< 0.1	≥ 1	≥ 1
	propyl acetate	< 0.1	≥ 1	≥ 1
Binary Mixtures	anisole/DMSO 8:2	0.2	≥ 1	≥ 1
	butyl acetate/DMSO 7:3	< 0.1	≥ 1	≥ 1
	propyl acetate/DMSO 7:3	< 0.1	≥ 1	≥ 1

Binary Solvent Mixtures – Resin Swelling test

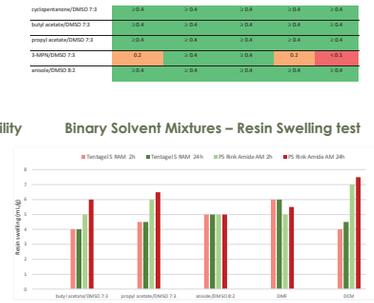

SPPS Experiment Design

Reagent System

Coupling: Fmoc-AA/DIC/Oxyma Pure 5/5/5 equivalents
Fmoc- deprotection: 20% (v/v) Piperidine in Binary Mixture(1:1)
Coupling: r.t., 45' *vs* 90°C, 2'
Fmoc- deprotection: r.t., 5'+5' *vs* 90°C, 1'

Model Peptides

ACP(Acyl Carrier Protein) (65-74): H-VQAAIDYING-NH_2
$A_{10}K$: H-AAAAAAAAAAK-NH_2
GPTStd: H-AKADEVSLHKWYG-NH_2

Resin

PS Rink Amide Am resin 0.64mmol/g

Instrument



PurePep® Chorus
GYROS PROTEIN Technologies

1 run = 6 syntheses
3 vessels: r.t. syntheses
3 vessels: 90°C induction
Assisted solid phase syntheses

Solvents

Operation	Solvent mixture	ratio	Solvent mixture	ratio	Solvent mixture	ratio
Fmoc-deprotection	PrOAc/DMSO/Piperidine	2:2:1	BuOAc/DMSO/piperidine	2:2:1	anisole/DMSO/piperidine	2:2:1
Coupling*	PrOAc/DMSO	7:3	BuOAc/DMSO	7:3	anisole/DMSO	8:2
Capping	PrOAc/pyridine/ acetic anhydride	15:16:19	BuOAc/pyridine/ acetic anhydride	15:16:19	anisole/pyridine/ acetic anhydride	15:16:19
Washing	EtOAc/DMSO	8:2	EtOAc/DMSO	8:2	EtOAc/DMSO	8:2

* Fmoc-amino acid 0.4M, DIC 1M, Oxyma pure 1M. Fmoc-His(Trt)-OH and Fmoc-Asn(Trt)-OH were solubilized in 6:4 acetate/DMSO and 7:3 anisole/DMSO mixtures because we observed precipitation after few hours from complete solubilization.

Model Peptides: Results at r.t.

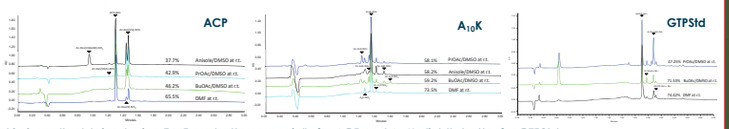

At r.t. results obtained using DMF are better, especially for ACP and $A_{10}K$, slightly better for GTPStd.

Model Peptides: Results at 90C°

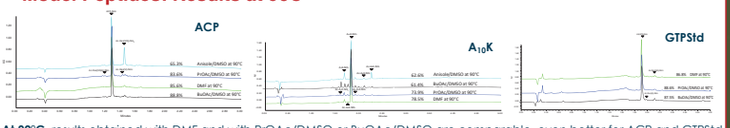

At 90°C, results obtained with DMF and with PrOAc/DMSO or BuOAc/DMSO are comparable, even better for ACP and GTPStd.

Testing T-Bec, A safe and green SPPS reagent

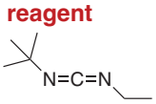

Peptide		DMF 90°C, 2'	BuOAc DMSO 90°C, 2'	Anisole DMSO 90°C, 2'	PrOAc DMSO 90°C, 2'
		HPLC Purity (% A/A)			
ACP	VQAAIDYING-NH_2	89.1	77.0	78.6	78.4
A10K	AAAAAAAK-NH_2	77.4	72.4	79.9	62.1
GTPstd	AKADEVSLHKWYG-NH_2	89.6	93.3	83.9	74.1

Let's stress the system with difficult sequences!

β-Amyloid(1-42)

DAEFRHDSGYEVHHQKLVFFAEDVGSNKGAIIGLMVGGVVIA-NH_2

Length: 42 amino acids

Resin: Tentagel S RAM 0.20mmol/g

Synthesis at 90°C using BuOAc/DMSO or DMF

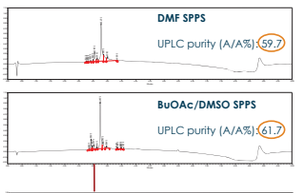

Sars CoV 2 Spike $RBM_{436-507}$

WNSNNLDSKVGGNYNYLYRLFRKSNLKPFERDISTEIYQAGSTPCNGVEGFNCYFPLQSYGFQPTNGVGYQP-NH_2

Length: 72 amino acids

Resin: Tentagel R RAM 0.19mmol/g

Synthesis at 90°C using BuOAc/DMSO or DMF

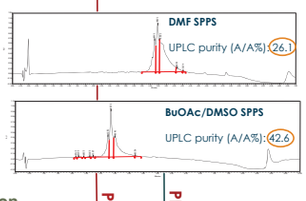

PEC - a catch and release HPLC-free purification

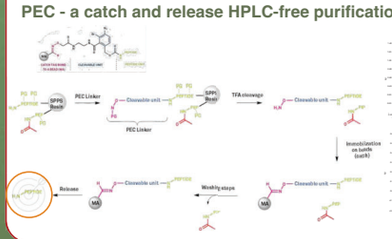

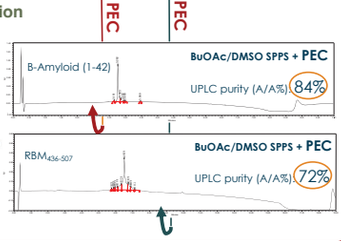

References & Acknowledgments

- https://echa.europa.eu/it/substance-information/-/substanceinfo/100.000.617
- Pawlas J, Rasmussen JH. ReGreen SPPS: Enabling Circular Chemistry in Environmentally Sensible Solid-Phase Peptide Synthesis. Green Chemistry, **2019**; *21*. 5990–5998. DOI: 10.1039/c9gc02775k.
- Pratesi F, Errante F, Pacini L, et al. A SARS–CoV-2 Spike Receptor Binding Motif Peptide Induces Anti-Spike Antibodies in Mice and Is Recognized by COVID-19 Patients. Frontiers in Immunology, **2022**, *13*, DOI: 10.3389/fimmu.2022.879946.
- Zitterbart R, Berger N, Reimann O, et al. Traceless Parallel Peptide Purification by a First-in-Class Reductively Cleavable Linker System Featuring a Safety-Release. Chemical Science, **2021**; *12*. 2389–2396. DOI: 10.1039/d0sc06285e.
- Pawlas, Jan, et al. "Elevating 1-tert-butyl-3-ethylcarbodiimide (TBEC) as a reagent for sustainable peptide synthesis: quality assessment and minimizing racemization, precipitation, and radical-induced side reactions by TBEC/Oxyma couplings in an environmentally sensible solvent." Organic Process Research & Development, **2023**, 27.7. 1348-1364. DOI: 10.1021/acs.oprd.3c00120
- Pacini, Lorenzo, et al. Optimization of peptide synthesis time and sustainability using novel eco-friendly binary solvent systems with induction heating on an automated peptide synthesizer. Journal of Peptide Science, **2024**, e3605. DOI: 10.1002/psc.3605

L.P. gratefully acknowledges: **MUR and EU-FSE** for financial support of the PhD fellowship PON Research and Innovation 2014-2020 (D.M 1061/2021) XXXVII Cycle in Chemical Sciences regarding the Development of green technologies for the automated synthesis of peptide active ingredients, **Gyros Protein Technologies** for cotutoring the PhD fellowship.

SIMPLE ONE-POT PEPTIDE CLEAVAGE AND SPONTANEOUS MACROCYCLIZATION THROUGH PAAL-KNORR-LIKE REACTIONS USING 2,5-DIALKYLFURAN DERIVATIVES

Alex Manicardi,[a,b*] Atiruj Theppawong,[b] Marleen Van Troys,[c] Annemieke Madder[b]

[a] Department of Chemistry, Life Sciences and Environmental Sustainability, University of Parma, Parco Area delle Scienze, 17/A, Parma, I-43124, Italy
[b] Department of Organic and Macromolecular Chemistry, Organic and Biomimetic Chemistry Research Group, Ghent University, Krijgslaan 281 S4, Ghent, B-9000, Belgium
[b] Department of Biomedical Molecular Biology, Ghent University, Technologiepark-Zwijnaarde 71, B-9052 Ghent, Belgium

alex.manicardi@unipr.it

https://doi.org/10.17952/37EPS.2024.P2049

1 INTRODUCTION
WHAT'S THE PROBLEM?

Macrocyclic peptides show enhanced properties as compared to linear peptides (e.g., enhanced target affinity, resistance toward degradation), making them attractive candidates for therapeutic applications and for interfering with protein-protein interactions (PPIs). Synthetic techniques have revolutionized peptide macrocyclizations, relying on the use of both natural and unnatural amino acids to achieve chemoselective ligations on protected or unprotected peptides. Recently, research has been oriented toward one-pot chemistries that rely on simple reaction conditions or reagent-less approaches. Despite the notable progress in peptide stapling techniques, challenges persist in existing methodologies, particularly in controlling the reaction order at multiple sites and achieving precise positional selectivity.

Our idea: use **2,5-disubstituted furans** as **stable** handles to generate **γ-diketones** that can be exploited for the one-pot peptide macrocyclization in the presence of **α-effect nucleophilic** moieties.

2 THE STRATEGY
A RESUSPEND-AND-WAIT PROTOCOL FOR PEPTIDE CYCLIZATION

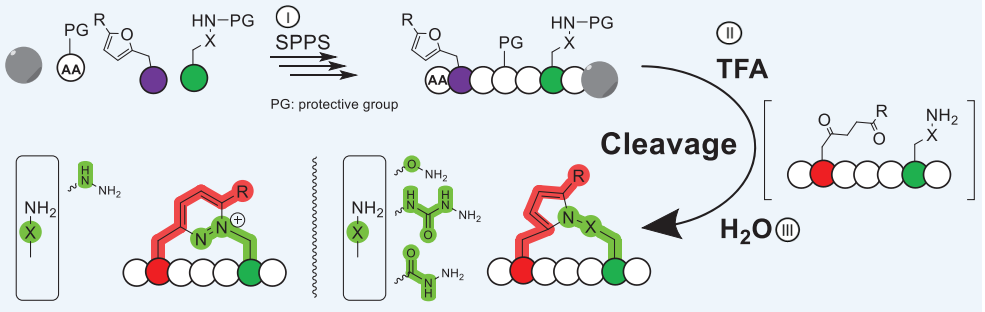

① Standard SPPS using Fmoc-protected monomers
② Standard peptide cleavage
③ Crude resuspension, waiting for reaction, HPLC purification

3 FURAN OPENING
PRO-ELECTROPHILE ACTIVATION

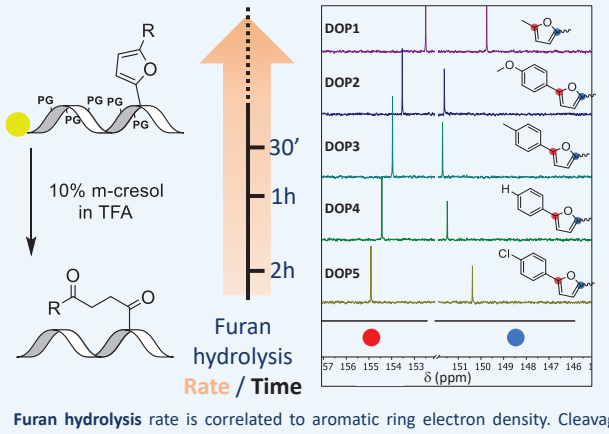

Furan hydrolysis rate is correlated to aromatic ring electron density. Cleavage duration can be predicted by simple ^{13}C-NMR (●).

4 REACTION KINETICS
PROXIMITY-INDUCED BIORTHOGONAL REACTION

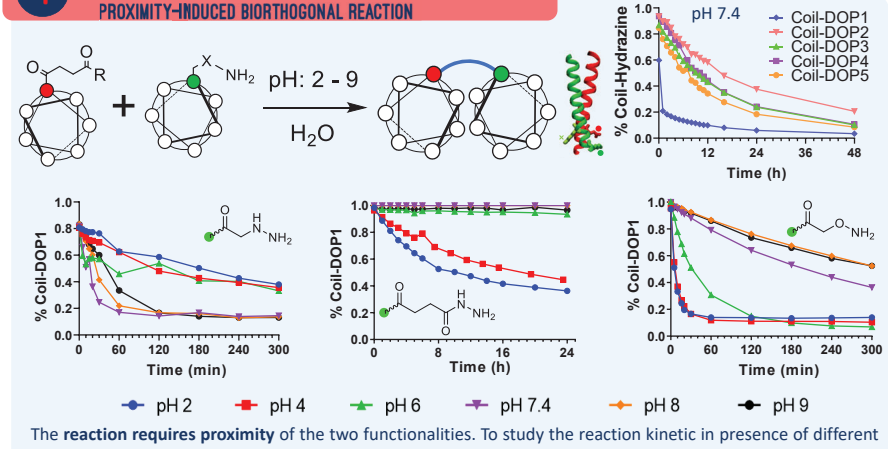

The **reaction requires proximity** of the two functionalities. To study the reaction kinetic in presence of different nucleophiles and under different experimental conditions, a supramolecular coiled-coil architecture was exploited. Reaction conditions: 5 μM coils in buffered solution, T= 25°C.

5 SCOPE
2 COILED SYSTEMS, 8 G4-BINDERS, 8 CYCLIC RGD MODELS

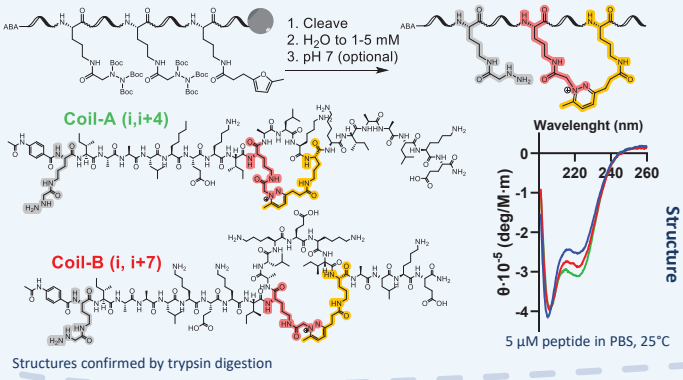

Structures confirmed by trypsin digestion

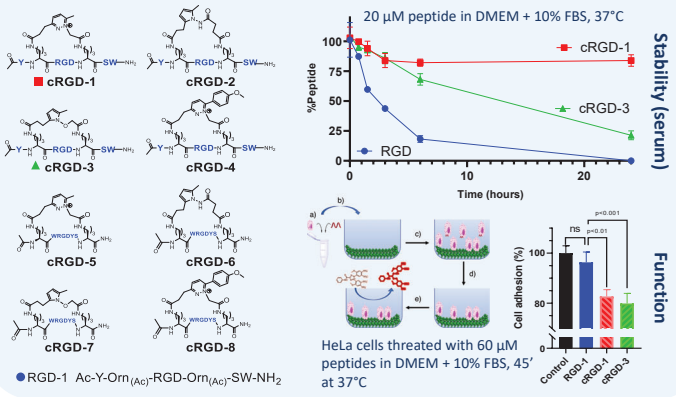

●RGD-1 Ac-Y-Orn$_{(Ac)}$-RGD-Orn$_{(Ac)}$-SW-NH$_2$

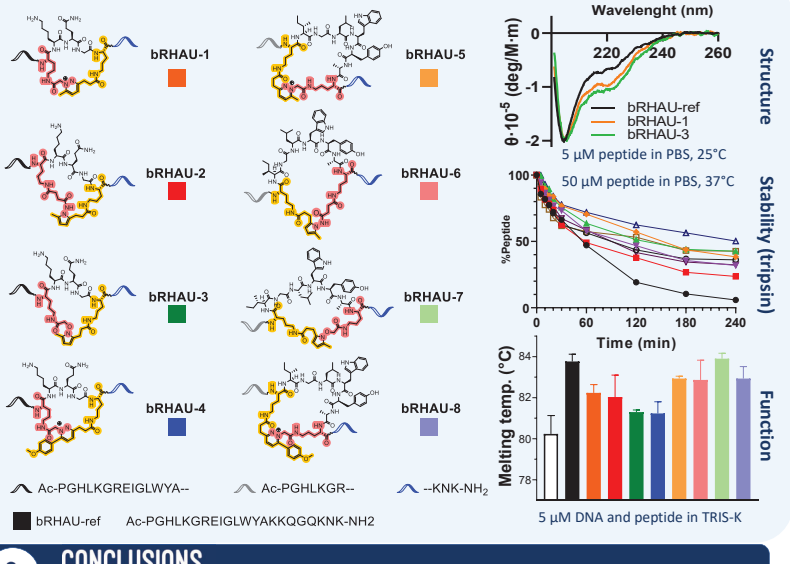

6 CONCLUSIONS
AND ACKNOWLEDGEMENTS

- Pro-electrophile and nucleophile can be included using standard SPPS protocols
- Pro-electrophile is activated during peptide cleavage
- Reaction after simple peptide resuspension in water/buffer
- Stable bond formation, orthogonal to other available chemistries

This work was supported by UGent Industrieel Onderzoeksfonds projects F2019/IOF-ConceptT/188, F2020/IOF-ConceptT/111, and by the University of Parma through the action 'Bando di Ateneo 2021 per la ricerca' co-funded by MUR-Italian Ministry of Universities and Research - D.M. 737/2021 - PNR - PNRR - NextGenerationEU (Al.M). A.T. is indebted to Research Foundation Flanders (FWO) for support of his postdoctoral fellowship (1273521N). MVT is supported by a concerted research action grant from Ghent University (GOA-028-19).

This work was partially supported by a cascade call issued within the framework of the "National Center for Gene Therapy and Drugs based on RNA Technology (CN RNA & Gene Therapy)" program, using the resources of the National Recovery and Resilience Plan (PNRR), Mission 4 "Education and Research", Component 2 "From research to business", Investment Line 1.4 "Strengthening research structures and creation of national R&D champions on some Key Enabling Technologies", Call Code 00000041_1, CUP [C93C22002780006]; funded by the European Union – NextGenerationEU.Project CASN_A_24_PNRR_BAC-HERMES_01 PNRR–M4C2–BAC–Notice, Title "Highly Efficient and selective RNA delivery systems for the treatment of MEtabolic and cardiovascular diseaseS – HERMES" codeCN00000041 – CUP CUPC93C22002780006.

Sustainable Scale-Up of GLP-1 Agonist Peptides through Green Solid Phase Peptide Synthesis

https://doi.org/10.17952/37EPS.2024.P2050

Lorenzo Pacini[1,2], Manoj Kumar Muthyala[3], Robert Zitterbart[3], Paolo Rovero[1,4], Anna Maria Papini[1,2]

[1] Interdepartmental Research Unit of Peptide and Protein Chemistry and Biology, University of Florence, Sesto Fiorentino (FI), Italy;
[2] Department of Chemistry "Ugo Schiff", University of Florence, Sesto Fiorentino (FI), Italy;
[3] Gyros Protein Technologies Inc., Tucson, AZ, United States;
[4] Department of Neurosciences, Psychology, Drug Research and Child Health, University of Florence, Sesto Fiorentino (FI), Italy.
Presenting author e-mail: L.Pacini@unifi.it

An insatiable Appetite

GLP-1 agonists are a transformative class of drugs used in managing **type 2 diabetes and obesity**, mimicking the GLP-1 hormone to enhance insulin secretion, reducing glucagon release, slowing gastric empty, and promoting satiety. Their dual efficacy in glycemic control and weight loss has positioned them as crucial in treating these conditions. Over the next decade, the GLP-1 agonist market is expected to grow significantly due to expanding indications, novel formulations, combination of therapies, and increasing recognition of their cardiovascular benefits. As pharmaceutical companies invest in research and development, these drugs are likely to become more accessible, revolutionizing chronic disease management and **positioning GLP-1 agonists as central to future metabolic and cardiovascular disorder treatments.**

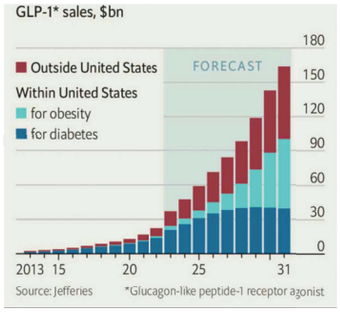

Liraglutide: a case study for green SPPS

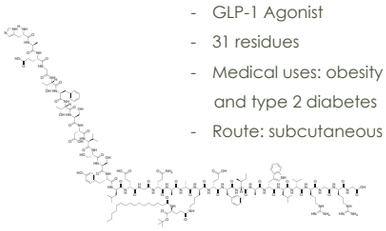

- GLP-1 Agonist
- 31 residues
- Medical uses: obesity and type 2 diabetes
- Route: subcutaneous
- Dosage: 0.6-3 mg daily
- Produced via traditional SPPS, using DMF and DCM and introducing a further orthogonality degree (Dde group) for a selective acylation on lysine

Experimental Set Up

Resin
Fmoc-Gly 2-CTC resin 0.33 mmol/g
Fmoc-Gly Wang TG resin 0.19mmol/g

Instrument
PurePep® Chorus
GYROS PROTEIN Technologies

Reagent System
Coupling: Fmoc-AA/DIC/Oxyma Pure 5/5/5 equivalents
Fmoc-Lys(Palm-Glu-OtBu)-OH/DIC/Oxyma Pure 2/2/2
in **BuOAc/DMSO** 7:3 (v/v)
Fmoc deprotection: 20% (v/v) Piperidine in **BuOAc/DMSO** (1:1)
Capping: 4M Pyridine + 4M Ac_2O in **BuOAc/DMSO** 7:3 (v/v)
Main washing solvent: **EtOAc/DMSO** 8:2 (v/v)
Coupling: r.t., 60' till 8th residue then 60'+60'
Fmoc deprotection: r.t., 5'+5'

Liraglutide green synthesis: strategy A

PEC® technology for purification

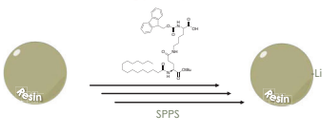

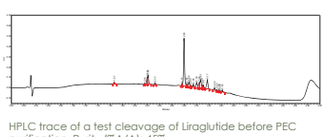

HPLC trace of a test cleavage of Liraglutide before PEC purification. Purity (%A/A): 45%

PEC-Linker coupling
4 eq. Linker
6 eq. Oxyma Pure
6 eq. DiPEA
16h, r.t. in BuOAc/DMSO 7:3
→ Liraglutide-PEC-Linker

Cleavage
83% TFA
5% H_2O 5% EDT
5% Thioanisole 2% TIS
2h, r.t.
Et_2O, 10', -20°C.
→ Liraglutide-PEC-Linker

Immobilization
On functionalized Agarose beads
16h, r.t.
→ Liraglutide-PEC-Linker (Agarose bead)

Release → **Liraglutide**

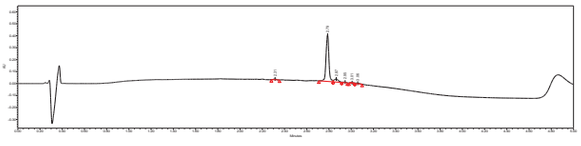

HPLC trace of Liraglutide after PEC purification, strategy A. Purity (%A/A): 83%, Overall Yield: 25%

Liraglutide green synthesis: strategy B scaled from 10µmol to 100µmol

PEC® technology for acylation and purification

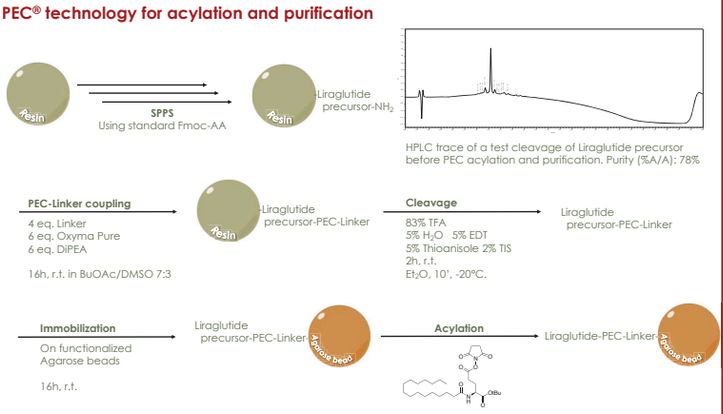

Acylation optimization

Building Block	Additive	Base	Time	Conv. (%A/A)	Purity after release (%A/A)
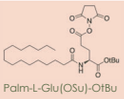 Palm-L-Glu(OSu)-OtBu (4 eq.)	Oxyma Pure (4 eq.)	DiPEA (6 eq.)	5'	97	73
	HOAt (4 eq.)	DiPEA (6 eq.)	PreActivation	99	78
	Oxyma Pure (4 eq.)	Pyridine (6 eq.)	5 hours, r.t.	86	61

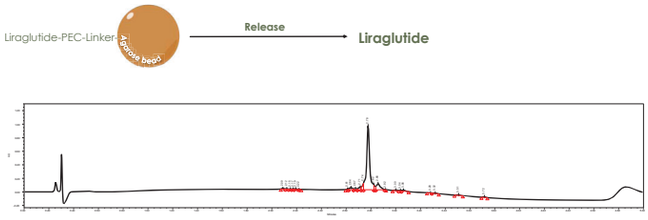

HPLC trace of Liraglutide after PEC acylation and purification. Purity (%A/A): 78%, Overall Yield: 27%



Totally **scalable** on Gyros Protein Technologies SONATA + (work in progress)

No need of a further **orthogonality degree**

Green solvent mixtures

PEC® used for acylation and purification can be automated

Decreasing efforts for **final purification**

Suitable also for many **other GLP-1 agonist** (Semaglutide, Tirzepatide)

It can be futher improved by the use of **pseudoprolines**

The **excess** of expensive **building blocks** can be recovered and restored

References & Acknowledgments

- Pawlas J, Rasmussen JH. ReGreen SPPS: Enabling Circular Chemistry in Environmentally Sensible Solid-Phase Peptide Synthesis. Green Chemistry, **2019**; *21*. 5990–5998. DOI: 10.1039/c9gc02775k.
- Martin V, Jadhav S, Egelund PHG, et al. Harnessing Polarity and Viscosity to Identify Green Binary Solvent Mixtures as Viable Alternatives to DMF in Solid-Phase Peptide Synthesis. Green Chemistry, **2021**; *23*. 3295–3311. DOI: 10.1039/d1gc00603g.
- Carbajo, Daniel, et al. Optimized stepwise synthesis of the API Liraglutide using BAL resin and pseudoprolines. ACS omega4.5, **2019**, 8674-8680. DOI: 10.1021/acsomega.9b00974
- Zitterbart R, Berger N, Reimann O, et al. Traceless Parallel Peptide Purification by a First-in-Class Reductively Cleavable Linker System Featuring a Safety-Release. Chemical Science, **2021**; *12*. 2389–2396. DOI: 10.1039/d0sc06285e.
- Pacini, Lorenzo, et al. Optimization of peptide synthesis time and sustainability using novel eco-friendly binary solvent systems with induction heating on an automated peptide synthesizer. Journal of Peptide Science, **2024**, e3605. DOI: 10.1002/psc.3605
- Barredo-Vacchelli, Gabriela R., et al. A Novel Method for Liraglutide Synthesis and Purification. Peptide Science, **2024**, e24351. DOI: 10.1002/pep2.24351

L.P. gratefully acknowledges: **MUR and EU-FSE** for financial support of the PhD fellowship PON Research and Innovation 2014-2020 (D.M 1061/2021) XXXVII Cycle in Chemical Sciences regarding the DEVELOPMENT OF GREEN TECHNOLOGIES FOR THE AUTOMATED SYNTHESIS OF PEPTIDE ACTIVE INGREDIENTS, **Gyros Protein Technologies** for cotutoring the PhD project.

Searching for peptide inhibitors of TNFR2/TNFα complex formation using a virtual "phage display"

Paulina Stencel[1] *, Artur Giełdoń[2,4], Beata Gromadzka[3], Sylwia Rodziewicz-Motowidło[1], Marta Spodzieja[1]

*email: paulina.stencel@phdstud.ug.edu.pl

https://doi.org/10.17952/37EPS.2024.P2051

[1] *Department of Biomedical Chemistry, University of Gdańsk, Wita Stwosza 63, 80-308 Gdańsk, Poland,* [2] *Department of Theoretical Chemistry, University of Gdansk, Wita Stwosza 63 Street, 80-308 Gdansk, Poland,* [3] *Next Generation Therapeutics, Kładki 24/25 Street, 80-819 Gdansk, Poland,* [4] *QSAR Lab Ltd., Trzy Lipy 3 Street, Building B, 80-172 Gdansk, Poland*

INTRODUCTION

- New hope for cancer treatment comes from immunotherapy, which is based on blocking immune checkpoints (ICPs). ICPs are proteins (receptors and their ligands) found on the surface of immune cells. To maintain homeostasis, the body forms receptor-ligand interactions that can both stimulate and inhibit the immune response.

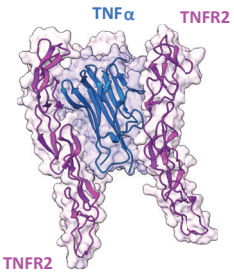

Fig. 1. Crystal structure of TNFR2/TNFα complex [PDB: 3alq]

- The receptor for tumor necrosis factor 2 (TNFR2) and its ligand, tumor necrosis factor (TNFα), constitute a stimulatory immune checkpoint.
- TNFR2 is mainly expressed on malignant cells and T-regulatory cells (Tregs). Its interaction with TNFα leads to the activation and proliferative expansion of Tregs, which subsequently suppress the immune response. This suppression interferes with the activation of cytotoxic T lymphocytes (Tc), whose function is the elimination of malignant cells.
- Moreover, ligation of TNFα on TNFR2 expressed on tumor cells initiates signaling pathways that promote tumor cell survival, proliferation, and metastasis. Consequently, the TNFR2/TNFα interaction contributes to tumor immuneevasion and development (Fig. 2A).

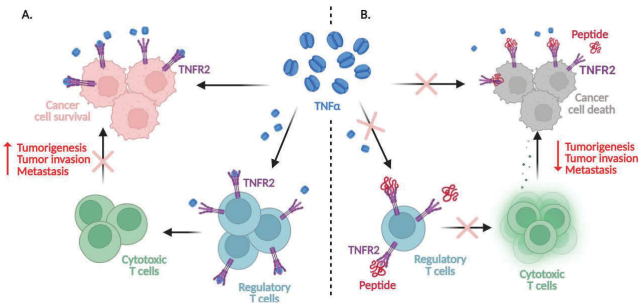

***Fig. 2. A)** Tumorigenesis from TNFR2/TNFα complex formation; **B)** Inhibitor application obstructs TNFR2/TNFα complex formation and promotes tumor regression*

- Blockade of the TNFR2/TNFα interaction with peptide inhibitors can inhibit the activation of Tregs. Furthermore, the expression level of TNFR2 on the cell surface is reduced by the TNFR2 antagonist. As a result, the quantity and functionality of Tc are enhanced, leading to a more robust antitumor immune response (Fig. 2B).

RESULTS AND DISCUSSION

- The main objective of this research is to identify peptide inhibitors of TNFR2/TNFα complex formation. To achieve this, we utilized QSAR - PeptAIm software, which employs machine learning (ML) and artificial intelligence (AI) methods. The software conducted a virtual 'phage display' experiment, generating a peptide-ligands candidate referred to as Pep(1) (Fig. 3).

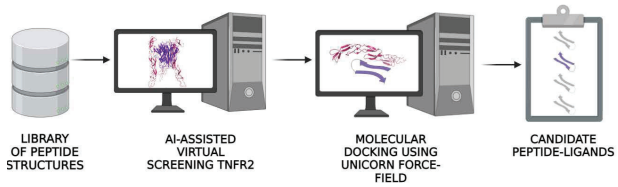

Fig. 3. Scheme of virtual screening PeptAIm

- Peptide Pep(1) was synthesized using solid-phase peptide synthesis (SPPS) with Fmoc/tBu chemistry and subsequently subjected to a biotinylation reaction. However, Pep(1) has not been obtained in pure form. Consequently, Pep(1) was modified to yield the Pep(2) - Pep(6) peptides.

***Tab. 1.** Amino acid sequences of peptides selected for further research*

Peptide name	Amino acid sequence
Pep(1)	Biotin-^{1}SWNYNLDMGTWERS^{14}-NH_2
Pep(2)	Biotin -^{1}SWNYNLDSGTWERS^{14}-NH_2
Pep(3)	Biotin -^{1}SYNYNLDSGTYERS^{14}-NH_2
Pep(4)	Biotin -^{1}SYNYNLDSGTYRRS^{14}-NH_2
Pep(5)	Biotin -^{1}SYNYNLDSGTYRES^{14}-NH_2
Pep(6)	Biotin -^{1}SYNYNLDSGTYEES^{14}-NH_2

- Pep(2) - Pep(6) peptides were modified at positions 2, 8, and 11 due to the high propensity of Met and Trp for oxidation.

  In the Pep(4) - Pep(6) compounds, the peptide charge was also altered at positions 12 and 13. These changes occurred due to the substitution of acidic residues with basic ones in Pep(3) and Pep(4), and basic residues with acidic ones in Pep(5) and Pep(6).
- Peptides were synthesized using SPPS, subjected to a biotinylation reaction, and then purified and analyzed using RP-HPLC and MS techniques.
- The ability of Pep(2) - Pep(6) peptides to interact with the TNFR2 protein was assessed using an indirect enzyme-linked immunosorbent assay (Fig. 4).
- The biotinylated peptides (40µg/ml) were pre-coated on a streptavidin plate. In the next step, TNFR2-Fc was added at various concentrations. The addition of a secondary anti-human IgG antibody conjugated with HRP (horseradish peroxidase) enabled the detection of the Fc region in TNFR2. In the final step, TMB (3,3′,5,5′-tetramethylbenzidine) substrate was added to catalyze the enzymatic color reaction.

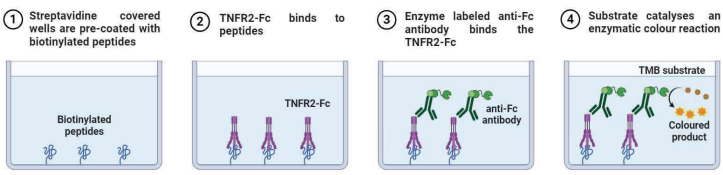

Fig. 4. Scheme of indirect ELISA

- The titration assay demonstrated that TNFR2 binds to all tested peptides in a concentration-dependent manner (Fig. 5). The strongest binding was observed with Pep(4), while a slightly weaker interaction was noted for Pep(5).

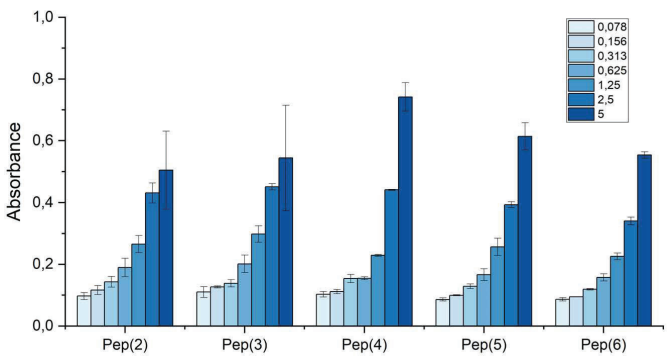

Fig. 5. Binding of Pep(2) - Pep(6) peptides analysed using indirect ELISA. Data are depicted as mean with SD (Mean +/- SD).

CONCLUSION

- The ELISA assay demonstrated that Pep(4) exhibited the strongest binding affinity for the TNFR2 receptor. These findings suggest that basic amino acid residues may enhance the interaction with TNFR2.
- The next step is to assess the ability of these peptides to inhibit the formation of the TNFR2/TNFα complex.
- The innovation of this research lies in the use of a specialized algorithm based on ML and AI, which reduces the costs and computational power required to develop receptor-binding sequences.

NATIONAL SCIENCE CENTRE POLAND

Acknowledgements

Research reported in this poster was financed by NCN (UMO2021/41/B/NZ7/03312) "Blocking TNF-TNFR2 interactions as a new treatment for ovarian cancer"

[1] Gołąb J, Jakóbisiak M, Lasek W, Stokłosa T. Immunologia. wyd. 7. Wydawnictwo Naukowe PWN; 2017

[2] Siminiak N, Czepczyński R, Zaborowski MP, Iżycki D. Immunotherapy in Ovarian Cancer. Arch Immunol Ther Exp (Warsz). 70(1):19 (2022)

[3] Mukai Y, Nakamura T, Yoshikawa M, i in. Solution of the structure of the TNF-TNFR2 complex. 2010;3(148). doi:10.1126/scisignal.2000954

[4] Torrey H, Kühtreiber WM, Okubo Y, i in. A novel TNFR2 agonist antibody expands highly potent regulatory T cells. 2020;13(661). doi:10.1126/scisignal.aba9600

[5] Nie Y, He J, Shirota H, et al. Blockade of TNFR2 signaling enhances the immunotherapeutic effect of CpG ODN in a mouse model of colon cancer. 2018;11(511):1-10. doi:10.1126/scisignal.aan0790

[6] Chen X, Subleski JJ, Kopf H, Howard OMZ, Männel DN, Oppenheim JJ. Cutting Edge: Expression of TNFR2 Defines a Maximally Suppressive Subset of Mouse CD4+CD25+FoxP3+ T Regulatory Cells: Applicability to Tumor-Infiltrating T Regulatory Cells. J Immunol. 2008;180(10):6467-6471. doi:10.4049/jimmunol.180.10.6467

Core-shell Type Resins for SPPS

Kwanwoo Kim[1], Seok-In Kim[1], Yoon-Sik Lee[1,*]
[1] BeadTech Inc. 49 Wonsi-ro, Danwon-gu, Ansan-si, Gyeonggi-do, 15610 Korea ;
*School of Chemical and Biological Engineering, Seoul National University, Seoul, 08826 Korea
E-mail : yslee@snu.ac.kr, yslee@beadtech.co.kr

https://doi.org/10.17952/37EPS.2024.P2054

Abstract

Since Merrifield developed the solid-phase peptide synthesis (SPPS) method, gel type PS based resins, which still possess various short comings, have been used for peptide synthesis. For efficient peptide synthesis, various core-shell (CS) type resins [2-CTC resin, AM SURE resin, HiCore resin, etc] have been developed so that the reactive functional groups are mainly located on the shell layer of the resin for easy accessibility of reagents as well as efficient washing during SPPS. Due to this special structural feature, the CS type resins have shown high efficiency in various type of peptide synthesis, especially the difficult sequences, and photolytic cleavage reactions. When water compatible polymers such as polyethylene glycol (PEG) is grafted on PS resins they can be also used for on-bead screening of peptide ligand libraries. Recently, we have developed commercial scale production (~Kg scale) of CS PEG-g-PS resin (HiCore resin). Also, when properly designed, the HiCore resin could also be used for the purification of biomolecules.

Core-Shell Type Resins for Solid-phase Peptide Synthesis

Introduction: Ideal Resins for Peptide Synthesis

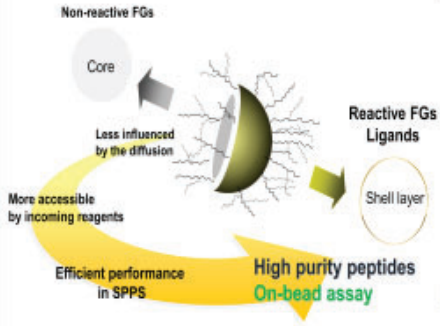

Various Types of Core-Shell Type Resins

▷ Core-Shell Type BTCORE™ CTC

- Structure

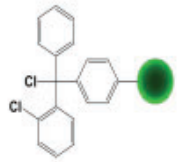

- Production Scale : Multi-ton/ year
- Loading level : 0.8 ~1.0, 1.2~1.4 mmol/g resin

Cross-sectioned images of FITC-Trp-(Boc)-CTC resin

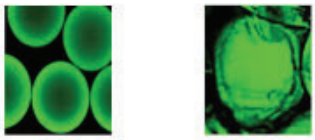

• 2-CTC (BTCORE™ CTC) • 2-CTC (A Company)

- Performance

1. Synthesis of fully protected 3 fragments of T20 on BTCORE™ CTC

Sequence	Starting resin	Loading level (mmol/g)	Crude Yield	HPLC Purity
1-16	Fmoc-Gln-O-2-CTC-L	0.54	76%	84%
17-26	Fmoc-Leu-O-2-CTC-L	0.74	96%	95%
27-35	Fmoc-Trp(Boc)-O-2-CTC-L	0.69	92%	91%

• Fmoc-AA-OH (2eq.), HBTU/HOBt (2eq.), 30°C, 1h, without double coupling
• Cleavage : 1%TFA/DCM

▷ Core-Shell Type BTCORE™ CTC(continued)

2. Comparison of Peptide Fragment Synthesis (27-35mer of T20)

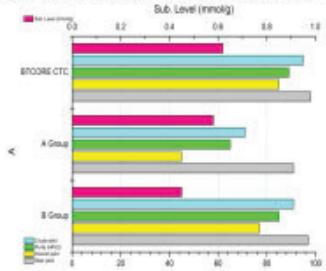

▷ AM SURE™ resin

- Structure

Thickness can be controllable in AM SURE™ resin

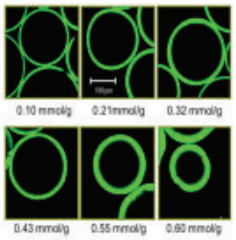

Cross-sectioned images of FITC-Trp(Boc)-CTC-AM Resins



Preparation of the Fmoc-Trp(Boc)-OH loaded CTC AM resins



- Performance

1. Synthesis of ACP (65-74) on Fmoc-Gly-CTC-AM resins

• Sequence : Val-Gln-Ala-Ala-Ile-Asp-Tyr-Ile-Asn-Gly
• Condition : purity after cleavage: 99% (CS) vs 79% (non CS)

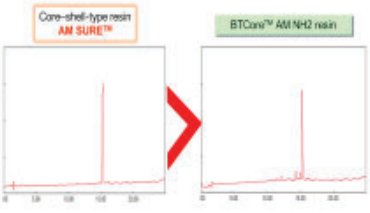

▷ HiCore™ resin

- Structure & Property

J. Comb. Chem. 8, 280 (2006)

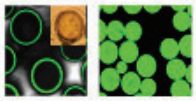

Confocal & cross-sectioned (inlet) images of FITC-HiCore & TentaGel.

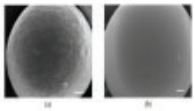

Scanning electron microscopy images of the resins
(a) TentaGel resin and (b) HiCore resin. Each scale bar represents 10 μm.

Nonspecific Protein Bindings on HiCore™ Resin

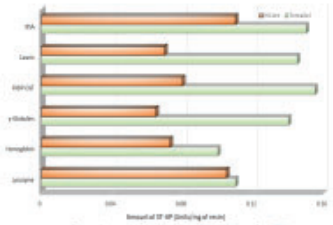

Bound proteins on HiCore (■) & TentaGel (■)

- Performance

Photocleavage Reactions on HiCore™ Resin

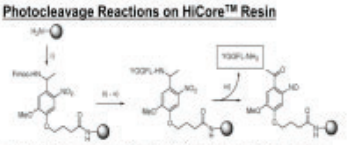

i) Fmoc-photolabile linker (PLL), BOP, DIPEA, NMP; ii) 20% Pip/NMP; iii) Fmoc-AA, BOP, HOBt, DIPEA, NMP; repeat (ii) and (iii); iv) 25% Pip/NMP; (v) 95% TFA, 2.5% TES, 2.5% H2O; (vi) hv, 360 nm, MeOH.

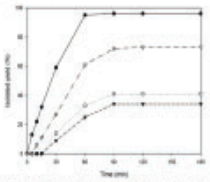

Kinetic profiles of photolytic cleavage on each resin: from the top, (●) HiCore resin, (▷) TG resin, (○) LL PS resin, (▶) HL PS resin

➢ **Core-shell structure : high efficiency in photo-cleavage reaction.**

Fishing proteins with peptide ligand on HiCore™ Resin

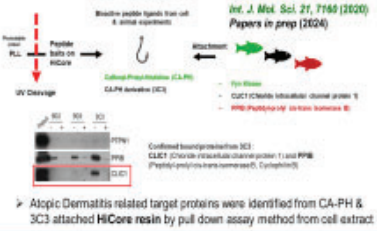

➢ Atopic Dermatitis related target proteins were identified from CA-PH & 3C3 attached **HiCore resin** by pull down assay method from cell extract

Summary

- Core-shell type resins are ideal solid supports for the peptide synthesis.
- Various kinds of core-shell type resins were developed for solid-phase peptide synthesis and bio-assay.
- Reaction kinetics of AA loading, couplings, and photolysis are superior compared to gel type resin because FGs are mostly located on the surface layer.
- Peptides with difficult amino acid sequences can be synthesized well on core-shell type resins with high purity.
- Peptide libraries can be assembled and screened successfully on HiCore resin.
- BeadTech Inc. is currently producing multi-ton scale BTCORE™ CTC and multi-kg scale HiCore™ Resin.

* **Acknowledgement: part of this work is supported by Ministry of Industry, Trade and Energy: No 20018608**

We are your solid partner on TIDES **Oligonucleotide and Peptide Therapeutics** **BeadTech Inc.**



WALLENBERG CENTRE FOR MOLECULAR AND TRANSLATIONAL MEDICINE

UNIVERSITY OF GOTHENBURG

https://doi.org/10.17952/37EPS.2024.P2055

Nature-inspired unique antimicrobial peptides from Chilean marine sediments

L. I. Beyer, A.-B. Schäfer[1], A. Undabarrena[2], I. Mattsby-Baltzer[3], D. Tietze, E. Svensson[1], A.Stubelius[1], M. Wenzel[1] , B. Camara[2], and A. A. Tietze*

University of Gothenburg, Department of Chemistry and Molecular Biology, Wallenberg Centre for Molecular and Translational Medicine, Göteborg, Sweden

[1]Chalmers University of Technology, Department of Biology and Biological Engineering, Göteborg, Sweden

[2]Universidad Técnica Federico Santa María, Laboratorio de Microbiología Molecular y Biotecnología Ambiental, Valparaíso, Chile

[3]University of Gothenburg, Department of Infectious Diseases, Institute of Biomedicine, Sahlgrenska Academy at University of Gothenburg, Göteborg, Sweden

Secondary Metabolite Prediction

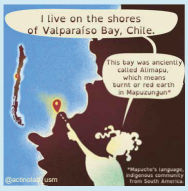

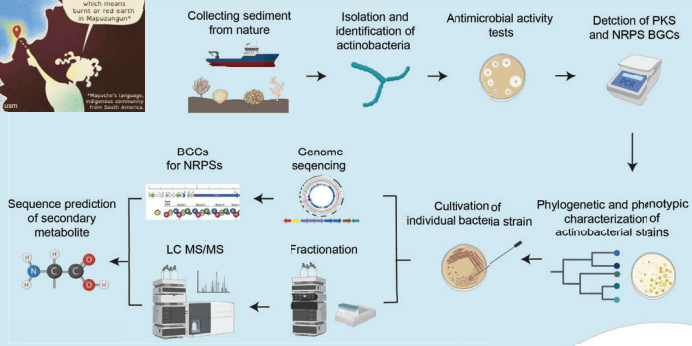

This project focuses on the discovery of AMPs from natural sources. An ambiguous cyclic **non-ribosomal peptide sequence** was predicted from ***actino*bacteria** isolated from **marine sediments in Chilean *Comau fjord***.

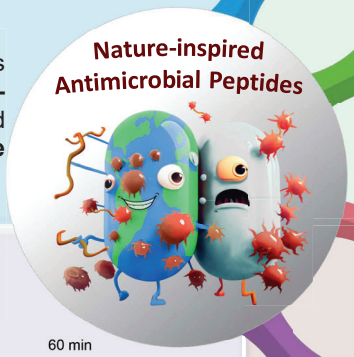

Peptide Design

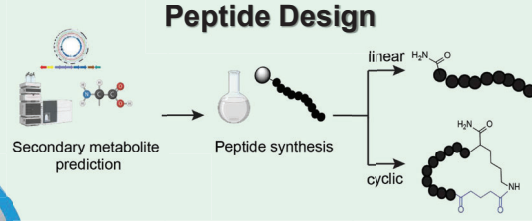

Based on ambiguous sequence three different **peptides** in their **linear and cyclic** form were **designed** and **synthesized** by automated Fmoc-based solid-phase peptide synthesis (SPPS) and manual on-resin head-to-tail cyclization.

Name	N-terminus	1	2	3	4	5	6	7	8	9	10	11
L1	free	-	dA	yV	pA	W	pD	T	pD	dV	-	K
C1	cyclic	-	dA	yV	pA	W	pD	T	pD	dV	-	K
L2	free	-	dA	yV	pA	W	Orn	T	Om	dV	-	K
L2-K	free	-	dA	yV	pA	W	Orn	T	Om	dV	-	-
C2	cyclic	-	dA	yV	pA	W	Orn	T	Orn	dV	-	K
L3	free	W	dA	yV	pA	W	Orn	T	Orn	dV	Y(-NO2)[1]	K
L3-K	free	W	dA	yV	pA	W	Orn	T	Om	dV	Y(-NO2)[1]	-
C3	cyclic	W	nA	yV	nA	W	Orn	T	Orn	nV	Y(-NO2)[1]	K

[1] 3-Nitrotyrosine

Bioactivity Evaluation

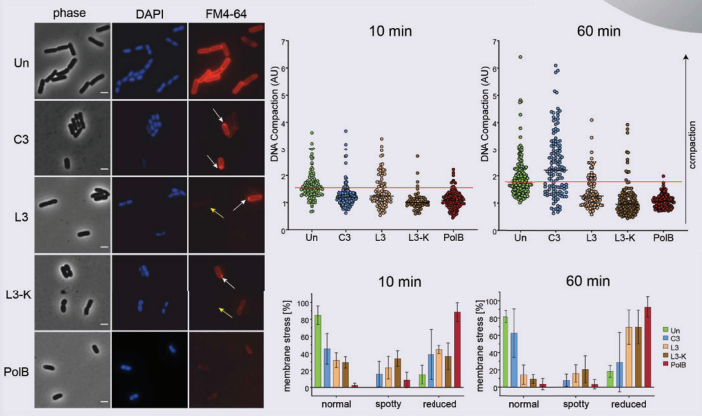

Mode of action studies performed by **live cell imaging** suggests that these peptides potentially act on the **cell membrane** *via* a **novel mechanism** allowing the passage of **small ions** resulting in the dissipation of the membrane potential.

Peptide	MMC$_{99}$ [µg/mL]								
	S. aureus			*E. coli*			*C. albicans*		
	2h	6h	24h	2h	6h	24h	2h	6h	24h
L1	>	>	>	>	>	>	>	>	>
C1	>	>	>	>	>	>	>	>	>
L2	(100)[2]	(100)[2]	>	>	>	>	50	25	25
L2-K	>	>	>	>	>	>	>	>	>
C2	>	>	>	>	>	>	>	>	>
L3	12.5	12.5	25	12.5	6.3	6.3	12.5	6.3	12.5
L3-K	25	25	25	50	25	25	25	25	12.5
C3	>	>	>	>[3]	>[3]	100	>	>	>

[1] Minimum microbicidal concentration killing ≥99% of the inoculum (MMC$_{99}$) at 2, 6, and 24 h of incubation in 100-fold diluted brain-heart infusion medium (BHI$_{100}$). Two-fold dilutions series were performed on all peptides, starting at 100 ug/mL. Peptides with a MMC$_{99}$ of ≤100 µg/ml were repeated on two or four additional occasions (median values are reported).
[2] Just below 99% killing (98.5%) at 100 µg/mL.
[3] MMC$_{99}$ achieved at 200 µg/mL.

Secondary Structure Analysis

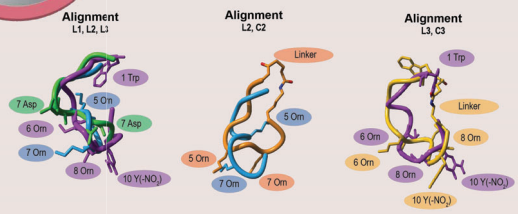

Secondary structure analysis was performed by solution NMR spectroscopy using CCPN for **NMR assignment** and YASARA for **structural calculations**. The rigidity of the structures are calculated by **RMSD** values.

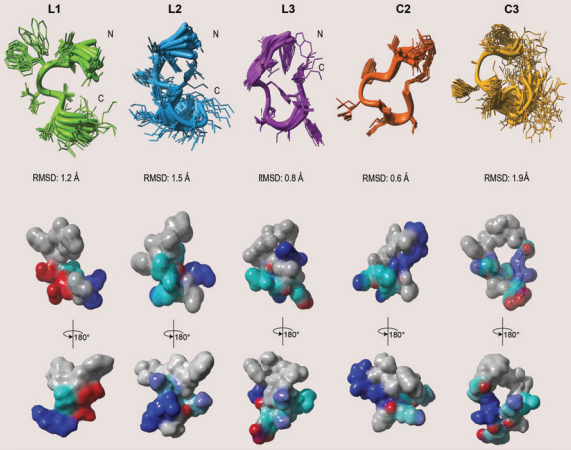

Beyer, L., *et al., ACS Infect Dis* **2024**, *10*, 79-92.

For additional information, please contact:
Luisa Beyer
E-mail: **luisa.beyer@gu.se**
alesia.a.tietze@gu.se

The role of quorum sensing peptide PlnA in the gut microbiome-sarcopenia axis

Amélie Descamps[1,2], Anton De Spiegeleer[1,2,3,4], Liesbeth Crombez[1,3,4], Morten Kjos[5] and Evelien Wynendaele[1,2]

[1] Translational Research in Immunosenescence, Gerontology and Geriatrics (TRIGG) group, Ghent University Hospital, Ghent, Belgium.
[2] Drug Quality and Registration (DruQuaR) group, Faculty of Pharmaceutical Sciences, Ghent University, Ghent, Belgium.
[3] VIB Inflammation Research Center, Unit for Molecular Immunology and Inflammation, Ghent University, Ghent, Belgium.
[4] Department of Geriatrics, Faculty of Medicine and Health Sciences, Ghent University Hospital, Ghent, Belgium.
[5] Faculty of Chemistry, Biotechnology and Food Science, Norwegian University of Life Sciences, Ås, Norway.

https://doi.org/10.17952/37EPS.2024.P2056

SARCOPENIA

- Accelerated loss of **muscle mass, muscle strength and physical function** associated with ageing
- Increased **mortality** and **decreased quality of life**
- Underlying pathophysiological mechanisms unclear
- No targeted therapies

More than 10% of the people aged >65y suffer from sarcopenia

QUORUM SENSING PEPTIDES

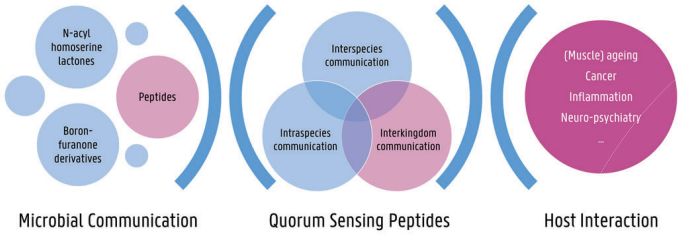

QUORUM SENSING PEPTIDES

GUT MICROBIOTA SARCOPENIA AXIS

The bacterial quorum sensing peptide PlnA plays a pivotal role in sarcopenia.

In vitro screening

Cell specificity

Mice grip strength

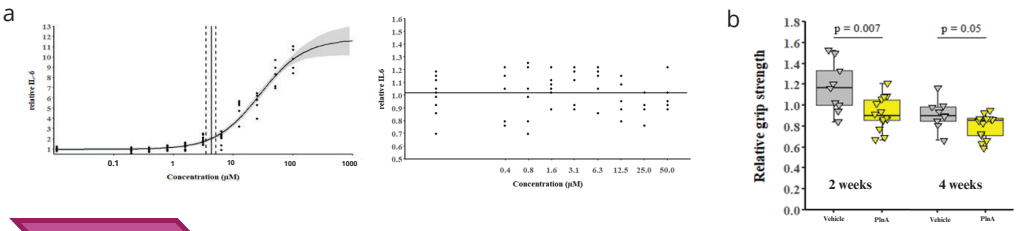

Peptide detection

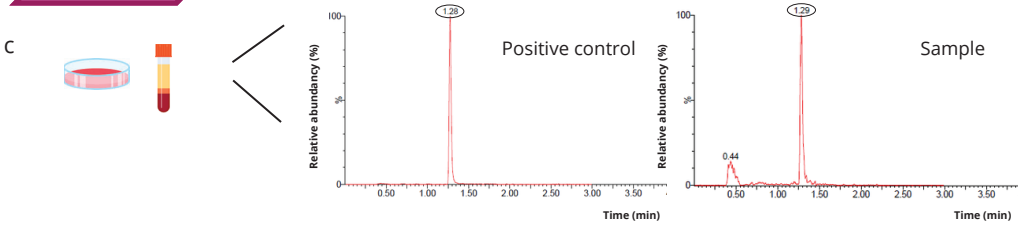

a. IL-6 dose response curves of PlnA in C2C12 (left) and splenocytes (right). b. *In vivo* mice experiments demonstrating a decrease in grip strength after daily injection of PlnA. c. PlnA detection, using UPLC-MS/MS, in human plasma and *L. plantarum* supernatant.

FUTURE PERSPECTIVES

Our study will provide new insights into a **causal association between gut microbiota, i.e. the quorum sensing peptides, and sarcopenia** leading to:

- New **diagnostic** possibilities
- New **therapeutic** dimensions

Unlocking Mango's Peptide Potential: Exploring Bioactive Peptides in Pulp, Peel and Seed

Mahya Bahmani [1,2], Michelle L. Colgrave [2,3], Cassandra L. Pegg [3], Angéla Juhász [2]

1 Commonwealth Scientific and Industrial Research Organisation (CSIRO), Western Australia, Floreat, Australia
2 Australian Research Council Centre of Excellence for Innovations in Peptide and Protein Science (CIPPS), Edith Cowan University, Australia
3 Commonwealth Scientific and Industrial Research Organisation (CSIRO), Queensland, St. Lucia, Australia

https://doi.org/10.17952/37EPS.2024.P2058

Introduction

Mango (*Mangifera indica* L.), known as "the king of fruits" for its delectable taste and nutritional richness, belongs to the *Anacardiaceae* family and is a widely cherished tropical fruit. Throughout the process of mango processing, a significant portion of the fruit, ranging from 35-60%, is disposed of, often without any treatment, resulting in environmental challenges and financial setbacks. Peels and seeds, accounting for 40-50% of the fruit's weight, are typically discarded as by-products[1]. This waste holds potential for conversion into valuable resources. Although mango is known to have various bioactive compounds, the understanding of bioactive peptides within different mango tissues remains limited. This research aims to explore mango tissues to uncover potential bioactive peptide-encoding genes present in the pulp, peel, and seed using publicly available genomic data resources in combination with discovery proteomic.



Figure 1: Mango fruit is a potential candidate for food waste valorisation.

Materials and Methods

Employing bioinformatics tools, we conducted an *in-silico* analysis of published mango genomic data[2]. We evaluated gene expression patterns and mapped an in-house bioactive database to translated gene models, identifying bioactive peptides and their corresponding coding genes. Then, we conducted proteomics and peptidomics experiments on two mango varieties, Kensington Pride (KP) and R2E2. Mango flesh, peel, and seed tissues from these varieties were prepared and proteins were extracted using different extraction protocols. In Protocol 1 we used a solvent mixture of acetonitrile, water, and formic acid (25:24:1) to extract native proteins and peptides. Protocol 2 involved the use of urea (8M) in Tris-HCl, followed by the application of trypsin enzyme for digestion. The samples were then subjected to discovery proteomics and bioactive peptide screening as shown in Figure 2.

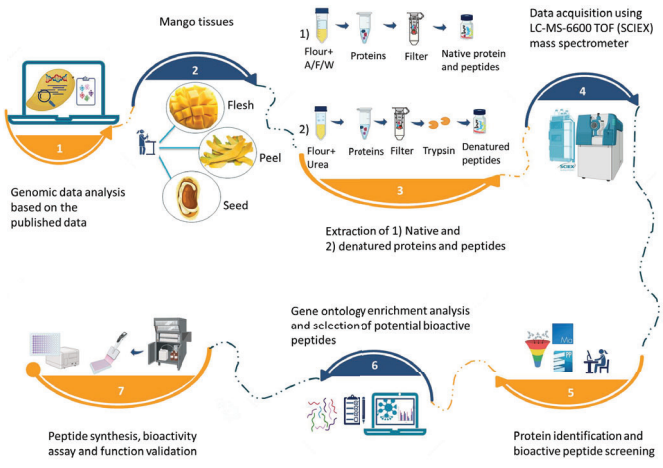

Figure 2: Workflow of protein and peptide extraction and identification of bioactive proteins and peptides in three different mango tissues using mass spectrometry-based techniques.

Results

As a result of the *in-silico* analysis, from the mango reference proteome (52,078 proteins), we identified 1,586 proteins with a 100% match mapped to regions of our in-house database of known bioactive peptides. Proteomic experiments were then conducted using two protocols (native and denaturing) to extract bioactive proteins and peptides from three different tissues (flesh, peel and seed). Across all tissues and varieties, 1,195 proteins were identified that produce bioactive peptides with >80% sequence similarity match to reported bioactive peptides (Table 1).

Table 1: Proteomic and peptidomic results using two protocols and two mango varieties and three different tissues.

Protocol	Variety	Tissue	# of identified proteins	# of Peptide >95% conf	# Bioactive peptide (>80%)	# of Bioactive peptides (Normalised)
P1	KP	F	226	598	277	0.46
P1	KP	P	142	329	163	0.49
P1	KP	S	57	289	105	0.36
P1	R2E2	F	226	599	105	0.17
P1	R2E2	P	174	294	210	0.71
P1	R2E2	S	50	383	73	0.19
P2	KP	F	1455	6074	1617	0.26
P2	KP	P	911	2822	997	0.35
P2	KP	S	178	506	218	0.43
P2	R2E2	F	1506	6386	1634	0.25
P2	R2E2	P	887	2756	917	0.25
P2	R2E2	S	204	777	234	0.30

We performed gene ontology enrichment analysis on the identified proteins with bioactive peptides common to both varieties in each tissue (flesh, peel and seed) (Figure 3).

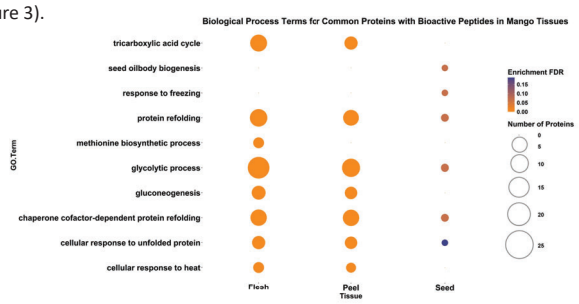

Figure 3: Gene ontology enrichment analysis of common proteins with bioactive peptides in flesh, peel, and seed of two mango varieties (KP and R2E2) based on the results of protocol 2.

Distribution of bioactive peptides across both varieties and three different tissues showed that in R2E2 variety, protocol 1 extracted more bioactive peptides from peel (compared to the flesh) in all six bioactive functions (Figure 4). In protocol 2, the highest number of bioactive peptides was found in flesh, followed by peel, and seed, with antimicrobial, antibacterial functions being most represented.

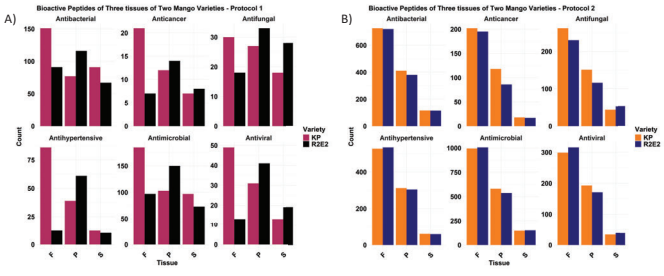

Figure 4: Distribution of bioactive peptides in two varieties and three different tissues based on their functions in protocol 1 (A) and 2 (B).

Next step

In the subsequent phase of this analysis, bioactive peptides will be quantified using targeted proteomics. Selected peptides will be synthesized and then tested in bioactivity assays to evaluate their functions and effects.

FOR FURTHER INFORMATION
Mahya Bahmani
Postdoctoral Fellow | CSIRO Agriculture & Food | Applied Proteomics
Mahya.bahmani@csiro.au



REFERENCES
[1] Owino, W. O., & Ambuko, J. L. (2021). Mango fruit processing: Options for small-scale processors in developing countries. Agriculture, 11(11), 1105.
[2] NCBI BioProject: PRJNA983966

ACKNOWLEDGEMENTS
Special thanks to the European Peptide Symposium (EPS) organizing committee for the opportunity to present and share our work at this exceptional event.

COLLABORATORS

Alca1, a cyclotide extracted and isolated from *Allexis cauliflora* (Violaceae): Synthesis and biological activities

Olivier Ndogo Eteme[1], Letícia Oliveira Catarin Nunes[2], Marcela Nunes Argentin[3], Norival Alves Santos-Filho[2], Ilana Lopes Baratella da Cunha Camargo[3], Eduardo Festozo Vicente[1]

[1]School of Science and Engineering, Sao Paulo State University (Unesp), Tupã 17602-496, São Paulo, Brazil.
[2]São Paulo State University (Unesp), Institute of Chemistry, Araraquara, 14800-900, São Paulo, Brazil.
[3]University of São Paulo, São Carlos Institute of Physics, São Carlos, 13566-590, São Paulo, Brazil.
eduardo.vicente@unesp.br

https://doi.org/10.17952/37EPS.2024.P2059

INTRODUCTION

Bacterial resistance to conventional antibiotics is a serious public health problem. The research of molecules with bactericidal activity is always current event with increase of multi-resistance. Over the past decade, small proteins known as antimicrobial peptides (AMPs), natural compounds produced by all prokaryotic and eukaryotic cells have shown promising results in overcoming the growing problems of antibiotic resistance. In parallel, there are the so-called cyclotides, which are cyclic peptides, rich in cysteines and originated from plants, showing potent antimicrobial activities with a very reduced toxicity. They are considered promising molecules for peptide drug design, due to their stable circular structure.

OBJECTIVES

In this work, the Alca1, cyclotide from the plant *Allexis cauliflora* (Fig. 1), were fully synthesized, purified, characterized, and the antibacterial activities were evaluated against multi-resistant bacteria and biofilm growth.

Figure 1. *Alexis cauliflora* (left). On the right, primary structure of cyclotide Alca1, showing the three disulfide brigdes between the cysteine residues. Also, the scheme provides the loops' location in the cyclotide.



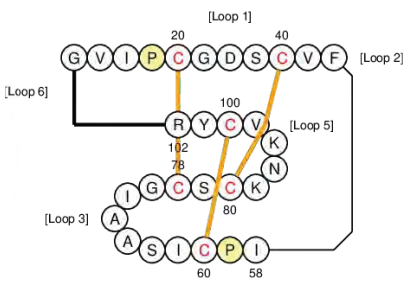

METHODOLOGY

The methodology are fully described in Akcan and Craik (2013) [1]. Synthesis of cyclotide Alca1 were evaluated for the first time in our lab and was achieved employing the solid phase peptide synthesis (SPPS) method using Fmoc chemistry, with a final yield of 40%. The synthesis reaction was monitored by combined HPLC and LC-MS methods, with the evaluation of the antibacterial property of cyclotide Alca1 from *Allexis cauliflora*. The antibacterial test was perform using microdilution method on many species of bacteria, such as *Staphylococcus epidermidis* (ATCC 35984), *S. aureus* (ATCC 25923), *S. aureus* (ATCC 8095), *Enterococcus faecalis* (ATCC 29212), *E. faecium* (ATCC 700221), *Klebsiella pneumoniae* (ATCC 700603), *Escherichia coli* (ATCC 25922), *Acinetobacter baumannii* (ATCC 19606) and *Pseudomonas aeruginosa* (ATCC 27853). Also, for hemolytic essays, a volume of 100 µL of the erythrocyte solution were added to the tubes containing the peptide dilutions and incubated at 37ºC for 1 hour. The tubes were then centrifuged at 500 g for 5 minutes. The supernatants were pipetted into microplates for later reading at 540 nm in a microplate reader.

RESULTS

Table 1. MIC and MBC results for Alca1.

Bacterial strains	MIC (mg/L)	MBC (mg/L)	MBC/ MIC	Activity*
S. epidermidis ATCC 35984	128	256	2	Bactericide
S. aureus ATCC 25923	256	512	2	Bactericide
S. aureus ATCC 8095	256	256	1	Bactericide
E. faecalis ATCC 29212	256	256	1	Bactericide
E. faecium ATCC 700221	64	128	2	Bactericide
K. pneumoniae ATCC 700603	256	256	1	Bactericide
E. coli ATCC 25922	64	512	8	Bactericide
A. baumannii ATCC 19606	64	128	2	Bactericide
P. aeruginosa ATCC 27853	>512	*N. R.*	*N. R.*	*N. R.*

**Activity defined by the CBM/CIM ratio. For results = 4 or < 4, the activity is considered bactericidal, above this value, the activity is considered bacteriostatic, according to Pankey and Sabath (2004). Activity not determined (N.D.) and N. R.: Test not carried out as the compound did not show activity against the strain.*

Figure 3: Alca1 hemolytic activity curve.

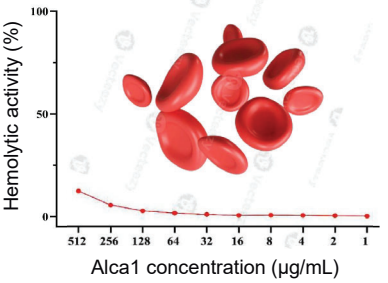

Table 2. Reduction of *S. epidermidis* ATCC 35984 biofilm by using the compound at a concentration of 512 mg/L.

Compound (512 mg/L)	Biofilm eradication ability (%)
Alca1	-26,2 ± 9,4

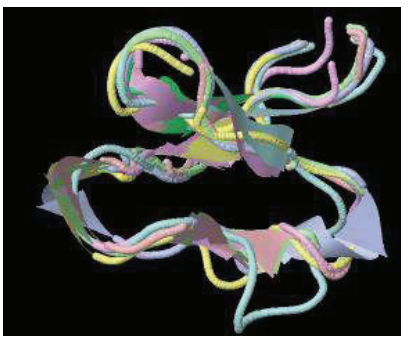

Figure 4. Overlay model. The superposition is carried out using the MaxSub algorithm. This algorithm attempts to find the maximum subset of atoms between two structures that can be superposed within a radius of 4.5 Å. Typically, one would choose as master either the top-ranked model or a model judged to be the most interesting based on some prior basic biological knowledge.

RESULTS

Figure 2. Chromatogram profile (left) and Alca1 peptide mass spectrometry spectra of the synthesized cyclotide. Retention time at 18,2 min and purity greater than 95%. The monoisotopic lion peak of Alca1 is 3,210.43 Da. From the analysis of the LC-MS spectrum, it was able to detect the peaks of the [M+2H] and [M+3H] ions, respectively: 1,606.73 and 1,071.49, which confirms the material obtaining.

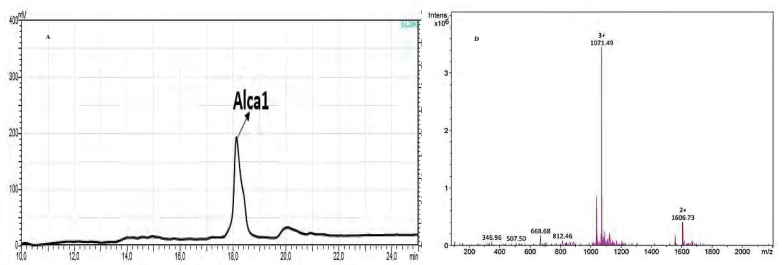

CONCLUSIONS

Therefore, the biological activities combined with its already reported high stability, the Alca1 antimicrobial cyclotide has demonstrated to be an excellent molecule for combating multi-resistant bacteria with low toxicity to erythrocytes.

REFERENCES

Akcan, M., & Craik, D. J. (2013). Synthesis of cyclic disulfide-rich peptides. *Peptide Synthesis and Applications*, 89-101.

ACKNOWLEDGEMENTS

FAPESP Grant process number 2021/06706-9 and 2022/02808-4

37th European Peptide Symposium and 14th International Peptide Symposium

Florence, Italy
25-31 august 2024

Microporous Scaffold-Mediated Myeloid Cell Activation in Situ for Robust Peptide-Based Cancer Vaccine

https://doi.org/10.17952/37EPS.2024.P2060

Shao-Hua Zhuo[1] , Wen-Hao Li[1] , Jing-Yun Su[1] , Yan-Mei Li [1]*
Key Laboratory of Bioorganic Phosphorus Chemistry & Chemical Biology (Ministry of Education),
Department of Chemistry, Tsinghua University, Beijing, 100084, China.
*Email: liym@mail.tsinghua.edu.cn

Abstract

Neoantigen research is crucial for advancing custom cancer vaccines and immunotherapies, offering tumor-specific immune responses. Despite their potential, these therapies have had limited success due to challenges in neoantigen prediction and cancer's immune evasion. Neoantigen vaccines, like peptide and dendritic cell vaccines, effectively boost anti-tumor immunity but face manufacturing complexities. In vivo cell engineering simplifies this process, with myeloid cells showing promise for enhancing immune responses. We developed an injectable microporous scaffold for in vivo monocyte and DC vaccine generation, promoting antigen presentation and T-cell activation. Furthermore, the production of intracellular neoantigens in DCs can be achieved generally via mRNA transfection or mRNA electroporation, which are not suitable for in vivo cell engineering. Subsequently, surface-modified but not encapsulated peptide antigen or neoantigen are released and ingested by extensive antigen presenting cells, regardless of their phagocytic abilities, via cell membrane sulfhydryl group-promoted disulfide bond exchange. Consequently, this promotes cell differentiation, activation, and migration from the produced monocyte and DC vaccines (MASVax) to stimulate antitumor T-cell immunity. Neoantigen-based MASVax combined with immune checkpoint blockade induces rejection of established tumors and long-term immune protection.

Design of MAS and its function

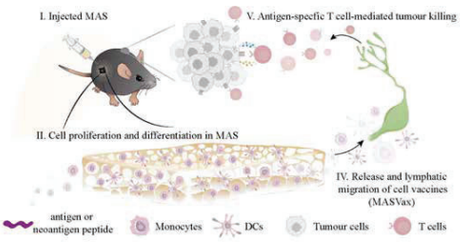

We designed an injectable macroporous myeloid cell adoptive scaffold (MAS) that acts as *in vivo* monocyte and DC vaccine.

Poly(disulfide) (PDS) modification on MAS

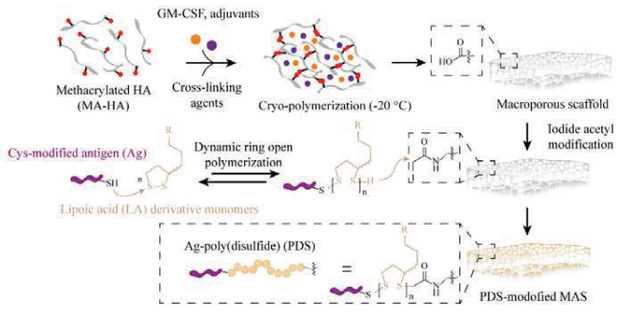

Antigen loading and release through dynamic disulfide exchange

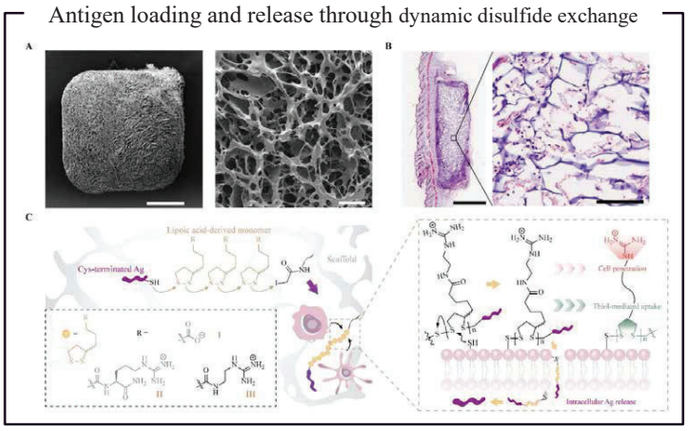

Optimized MAS components activate monocytes and DCs and enhance their dLN accumulation

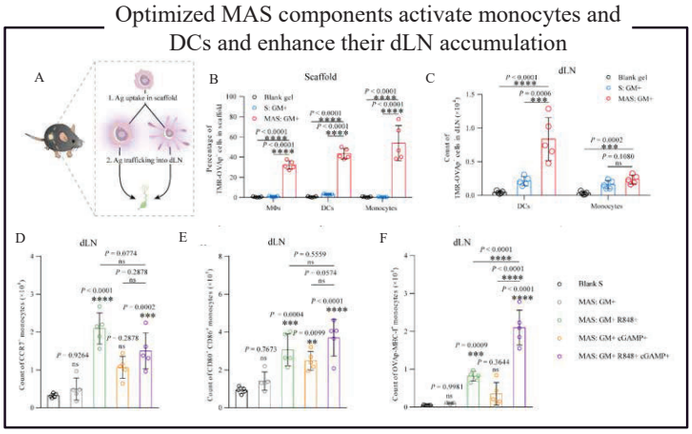

MASVax-based neoantigen therapies eradiate tumors in an MC38 tumor mouse model

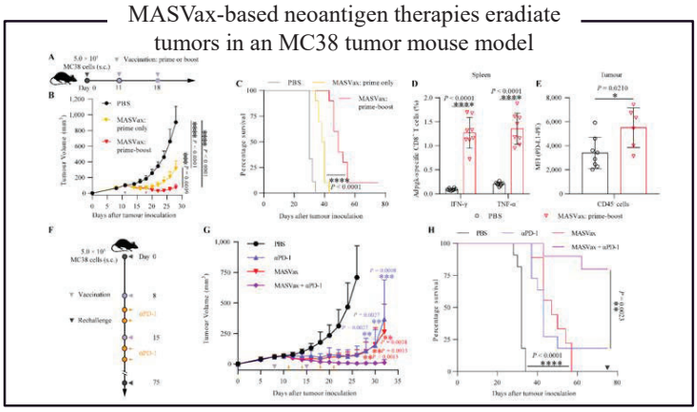

Depletion of PMN-MDSC by αLy-6G augments MASVax-based neoantigen therapies

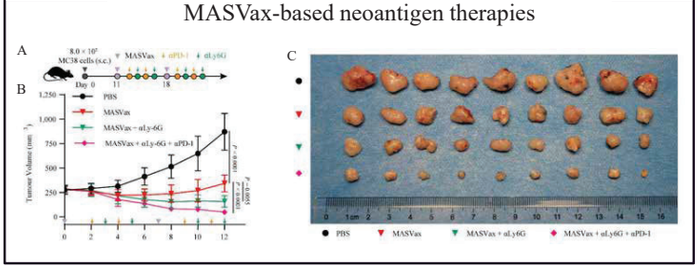

Acknowledgement

This work was supported by the National Key R&D Program of China (2019YFA0904200, 2018YFA0507600), Tsinghua University Spring Breeze Fund (2020Z99CFY042) and the National Natural Science Foundation of China (92053108).

[1] W.-H. Li, J.-Y. Su, B.-D. Zhang, L. Zhao, S.-H. Zhuo, T.-Y. Wang, H.-G. Hu, Y.-M. Li, Adv. Mater. 2024, 36, 2308155.

https://doi.org/10.17952/37EPS.2024.P2062

The "Sand in a gearbox" effect of antimicrobial peptides: beyond pore formation on model membranes and real bacteria cells

D. Roversi,[1] Z. Vaezi,[1,2] A. Bortolotti,[1] C. Di Stefano,[1] S. Bonacorsi,[1] V. Santucci,[1] C. Aisenbrey,[3] M. M. Konai,[4] Y. Acharya,[4] R. Khosravi-Far,[5] B. Bechinger,[3] J. Haldar,[4] and L. Stella,[1]

[1]Tor Vergata University of Rome, Rome, Italy; [2]Tarbiat Modares University, Tehran, Iran; [3]Institut de Chimie de Strasbourg, Strasbourg, France; [4]Jawaharlal Nehru Centre for Advanced Scientific Research, Bengaluru, India; [5]Harvard Medical School and Beth Israel Deaconess Medical Center, Boston, MA, United States

Antimicrobial peptides: the « Sand in a gearbox» hypothesis

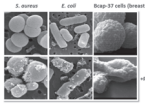

- Rapid and broad spectrum activity
- Selective toward bacterial membranes
- Kill pathogens by making their membrane permeable

~10 million bound peptides/cell

«Sand in a gerabox»

AMPs might perturb bilayer dynamics and interfere with cellular functions involving membrane proteins



Systems investigated

Antimicrobial peptides

PMAP-23	RIIDLLWRVRRPQKPKFVTVWVR
Alamethicin	AcUPUAUAQUVUGLUPVUUQQFol
Magainin 2	GIGKFLHSAKKFGKAFVGEIMNS
LAH4	KKALLALALHHLAHLALHLALALKKA-NH_2
Melittin	GIGAVLKVLTTGLPALISWIKRKRQQ-NH_2

Membrane-active compounds

Killer-FLIP GRKKRRQRRRFFWSLCTA

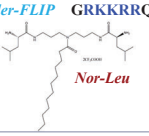

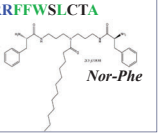

Membrane viscosity: fluorescence anisotropy

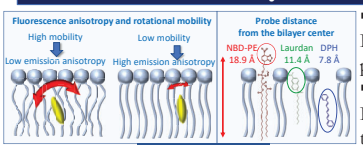

- **Steady state**

Increase in anisotropy: decreased mobility of the probes

- **Time-resolved**

Increase in both the average rotational correlation time and in the fraction of residual anisotropy.

Steady state

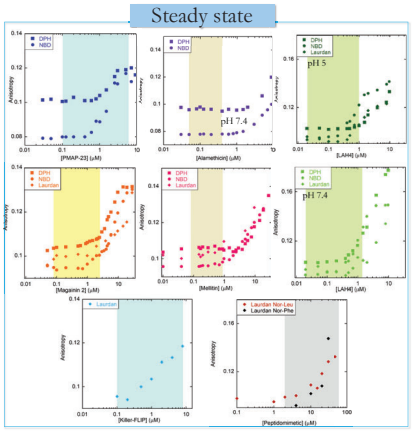

Time-resolved

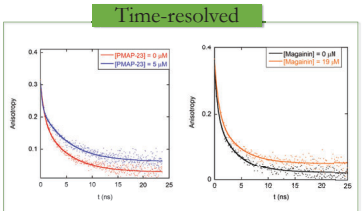

$$r(t) = r_0\left[f_1 e^{-t/\phi_1} + f_2 e^{-t/\phi_2} + f_\infty\right]$$

Probe: **NBD-PE**

	<ϕ> (ns)	f_∞
[PMAP-23]=0 μM	3.2±0.2	0.10±0.02
[PMAP-23]=5 μM	3.8±0.1	0.20±0.04
[Magainin]=0 μM	2.2±0.1	0.06±0.03
[Magainin]=19 μM	2.5±0.1	0.13±0.04

Probes motions are slower and more hindered: increase of membrane viscosity

Membrane hydration: generalized polarization

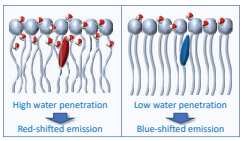

Red shift of Laurdan emission spectrum of 50 nm when water molecules surround the naphthalene moiety.

$$GP = \frac{I_{435\text{nm}} - I_{500\text{nm}}}{I_{435\text{nm}} + I_{500\text{nm}}}$$

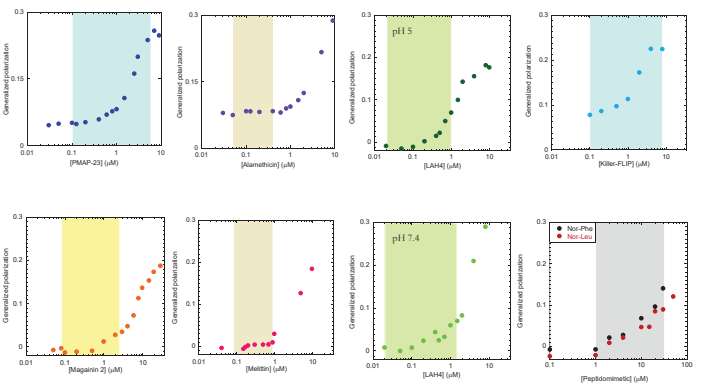

Reduction of the degree of water penetration inside the bilayer for all the compounds

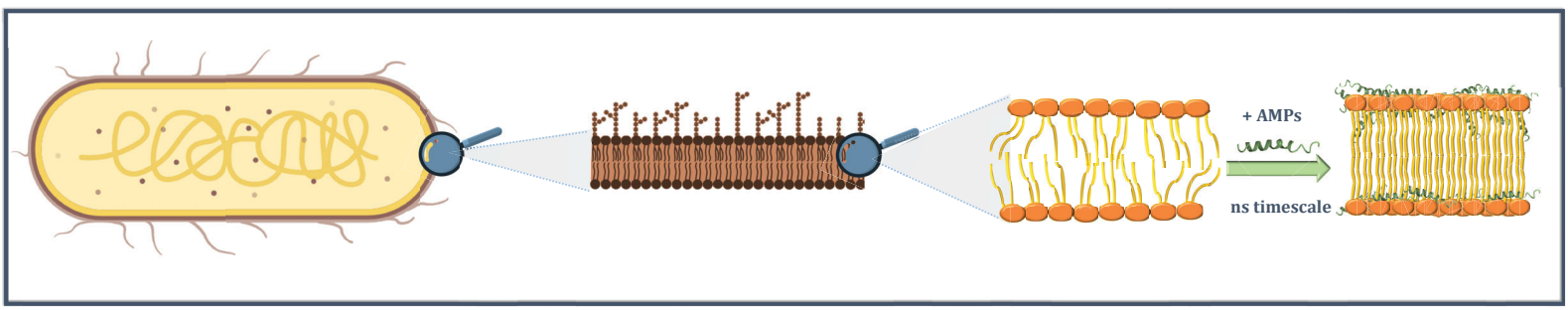

Lipid lateral mobility: excimer formation

- Excited-state dimer formation is diffusion-limited: Information on the lateral diffusion of pyrene-labelled lipids

$$\frac{Excimer\ (\lambda_{em} = 475nm)}{Monomer(\lambda_{em} = 397nm)}$$

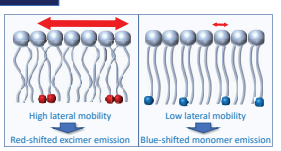

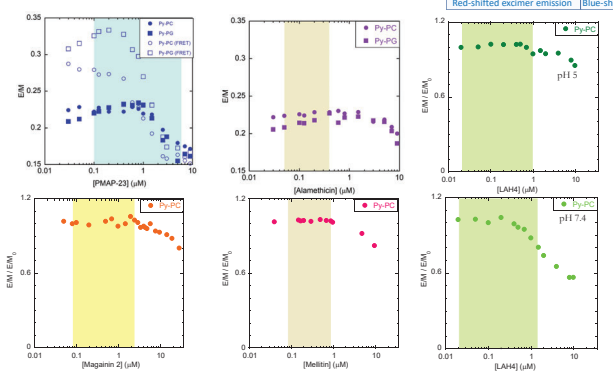

Reduction of the lipid lateral diffusion observed with all the compounds analyzed

Membrane dynamics in live bacterial cells

- PMAP effects were measured on the dynamics of membranes of live *E. coli* cells

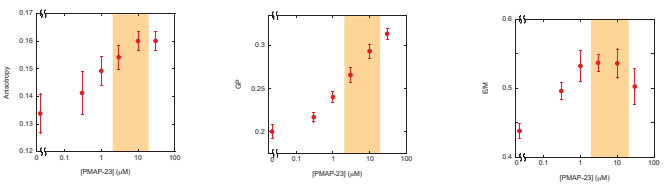

Increase in DPH anisotropy and laurdan GP, and an initial rise, followed by a decrease in pyrene excimer to monomer intensity ratio.

Lipid order parameters: ^{2}H ssNMR spectroscopy

- ^{2}H ssNMR spectroscopy studies to measure peptide effects on lipid order parameter of POPC/POPG 2/1 liposomes.

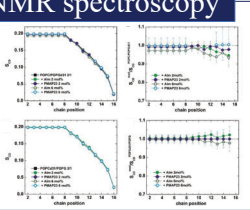

No significant peptide effects were observed on the order parameter of the zwitterionic or anionic lipids.

All the compounds induce an increase of membrane viscosity, a reduction of water penetration and of lipid lateral mobility. The overall effect is a membrane stiffening of the vesicle.

PMAP-23 affects membrane dynamics also in real, live cells

Roversi *et al*, Biophys. Chem. **300**, 107060 (2023)

https://doi.org/10.17952/37EPS.2024.P2064

Design and Structural Analysis of Fluorinated Polyproline-Type Foldamers and their Ability to Interact with Membrane Models

Chloé Cayrou,[1,2] Simon Gonzalez,[1,2] Astrid Walrant,[3] Delphine Ravault,[3] Karine Guitot,[1,2] Sylvie Noinville,[3] Françoise Illien,[3] Sandrine Sagan,[3] Thierry Brigaud,[1,2] Olivier Lequin,[3] Sandrine Ongeri,[2] Grégory Chaume[1,2]

[1] BioCIS, CNRS, CY Cergy-Paris Université, 5 mail Gay-Lussac, 95000 Cergy-Pontoise, France; [2] BioCIS, CNRS, Paris Saclay Université, Bat. Henri Moissan, 17 av. des Sciences, 91400 Orsay, France; [3] Laboratoire des Biomolécules, Sorbonne Université, École normale supérieure, PSL University, CNRS, 4 place Jussieu, 75005 Paris, France

chloe.cayrou@cyu.fr

INTRODUCTION

Foldamers are oligomers with a strong tendency to fold into a well-defined secondary structure.[1] Among peptidic foldamers, oligomers of prolines are known to adopt a **polyproline type II helix (PPII)** in water where amide bonds are **all-*trans*** and a more compact helix (PPI) in organic solvent with all-*cis* amide bonds (fig. 1).

In this work, we report the incorporation of the trifluoromethyl pseudoproline (CF_3ΨPro) into a polyproline backbone and the **structural analysis** of the resulting oligomers. Then, in order to increase the interaction with membranes, **amphipathic oligomers** are synthesized with the addition of a guanidyl group on prolines.

all-*trans* PolyProline II helix
Extended left-handed helix
(φ = -75°, ψ = 146°, ω = 180°)
Favored in water

High energy of interconversion ⇌

all-*cis* PolyProline I helix
Compact right-handed helix
(φ = -75°, ψ = 160°, ω = 0°)
Favored in organic solvent (*n*-propanol)

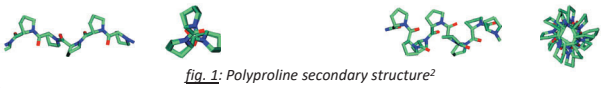

fig. 1: Polyproline secondary structure[2]

SYNTHESIS

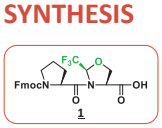

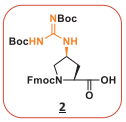

As the CF_3 group decreases the nucleophilicity of the amine, the coupling of the **CF_3ΨPro** is performed in solution to access the ready-to-use **building block 1** for SPPS.[3]

The **guanidylated proline 2** is synthesized as reported.[4]

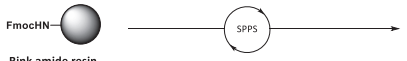

i. *Fmoc cleavage*: pip. (20% in DMF, v/v)
ii. *Coupling*: DIC (2 or 5 eq), Oxyma (2 or 5 eq), Pro (5 eq), **1** (2.5 eq), **2** (3 eq)
Optional *iii.* *Acetylation*: Ac_2O (10 eq), DIPEA (10 eq)
iv. *Cleavage*: TFA/TIS/H_2O (95:2.5:2.5)

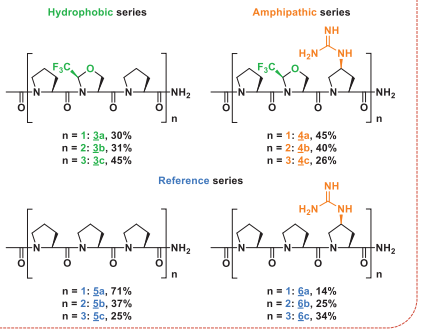

Polyproline oligomers are obtained in good yield
(MW activation is used for oligomers 3 and 5)
(Oligomers 4 and 6 are TFA salt)

NMR ANALYSIS

- Determination of the rotamer populations (**^{19}F NMR**).
- Full characterization of fluorinated oligomers (**^{1}H, ^{13}C and 2D NMR**).
- Assignment of amide bond conformation (**NOESY and ROESY NMR**, fig. 2 and 3).

	n = 1	n = 2	n = 3
3	All-*trans* (>95%)	All-*trans* (>95%)	All-*trans* (>95%)
4	All-*trans* (>95%)	All-*trans* (>95%)	All-*trans* (>95%)

fig. 2: Amide bond ratio of synthetized fluorinated oligomers determined in D_2O at 20°C

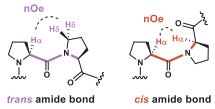

trans amide bond *cis* amide bond

fig. 3: Assignment of amide bonds with nOe effect

all-*trans* amide bond conformation is strongly favored as expected for PPII helix

CIRCULAR DICHROISM (CD) ANALYSIS

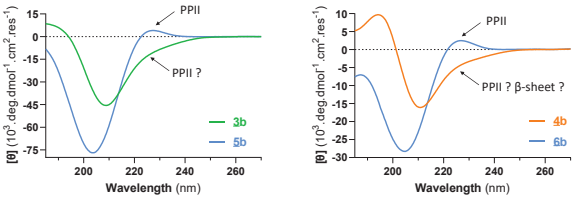

fig. 4: CD spectra of hydrophobic (left) and amphipathic (right) hexamers with their respective non fluorinated reference (100 µM in PBS 20 mM (pH = 7.0) at 4°C)

CD spectra of fluorinated oligomers do not reveal typical PPII signature (absence of positive band at 226 nm)

PPII CD SIGNATURE CONCEPT QUESTIONED FOR OLIGOMERS 3

Impact of the solvant on the CD signature

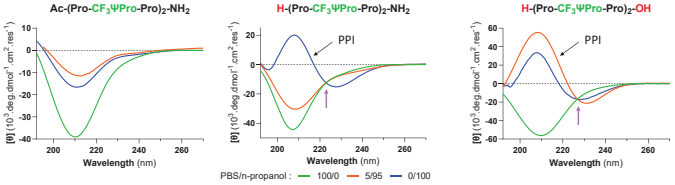

fig. 5: Impact of the n-propanol depending on the termini (100 µM at 4°C); ⟶ : isobestic point

By increasing *n*-propanol content, **PPI signature is observed** with charged termini (*N*-term: H, *C*-term: OH). Neutral termini (*N*-term: Ac, *C*-term: NH_2) are known to stabilize PPII helix.[5] Moreover, the presence of **isobestic points** reveal that **only two conformations** are involved in this equilibrium: **PPI ⇌ PPII**.[6]

X-ray structure of 3c

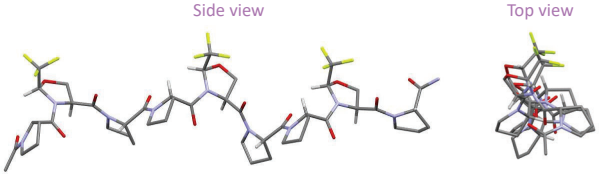

fig. 6: X-ray structure of 3c (obtained in MeOH with an accuracy of 0.04 Å for bond C-C, against the 0.01 Å expected)

X-ray structure of 3c reveals a **left handed helix** with **slightly distorted C_3 symmetry**.

Conclusion

We have assembled a set of CD and X-ray diffraction data consistent with hydrophobic fluorinated oligomers 3 adopting a helical structure close to a PPII helix

INTERACTION WITH MEMBRANE MODELS MONITORED BY ^{19}F NMR (LEFT) AND DSC (RIGHT)

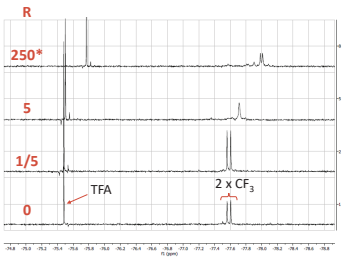

*fig. 7: Interaction with SDS micelles monitored by ^{19}F NMR of 4b with different concentration of SDS (foldamer as TFA salt at 200 µM in H_2O/D_2O (90/10), *: above CMC, R = [SDS]/[foldamer])*

As **^{19}F is very sensitive** to its environment, we assume that the chemical shift displacement is due to **interaction with micelles**. This is confirmed by DOSY ^{1}H-^{19}F assay.

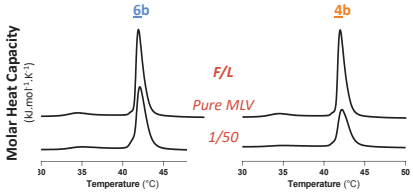

fig. 8: Interaction of hexamers 4b and 6b with Multi-Lamellar Vesicles, MLV, of DPPG (anionic lipid) monitored by DSC (1 mg/mL MLV, F/L: molar ratio of foldamers on lipids)

DSC experiments reveal that **foldamers 6b and 4b disrupt MLV thermal transitions**, with the decrease of the area under the curve, providing evidence of an **interaction**. A **more significant effect of the fluorinated foldamer** can be highlighted.

Foldamer 4b interacts with membrane models, SDS micelles and DPPG MLV

CONCLUSION

- X-ray crystallography, CD and NMR spectroscopies are consistent with **3 adopting a helical secondary structure close to PPII**. The presence of the **CF_3 group** in δ position of the oxazolidine ring **may cause steric clashes** that can partially (or locally) disrupt PPII helix structure.
- Concerning the amphipathic series **4**, more **experiments** have to be done **to decipher the secondary structure**, between **PPII helix** or **β-sheet**.
- The introduction of cationic groups on our fluorinated oligomers leads to **foldamers able to interact with membrane models**. Moreover, **^{19}F NMR** revealed to be a **useful tool** to investigate these **interactions**.

REFERENCES

1: Gellman, S. H. *Acc. Chem. Res.* **1998**, *31*, 173.
2: Moradi, M. *et al. J. Chem. Phys.* **2010**, *133*, 125104.
3: Chaume, G. *et al. J. Org. Chem.* **2013**, *78*, 10144.
4: Hruby, V. J., *et al. J. Org. Chem.* **2001**, *66*, 1038.
5: Wennemers, H., *et al. J. Am. Soc.* **2009**, *131*, 15471.
6: Horng, J.-C., *et al. Protein Science*. **2009**, *18*, 1967.

Acknowledgements

The CY Initiative of Excellence (grant « Investissement d'Avenir » INEX 2021 Biomol) is thanked for the financial support of Chloé Cayrou. Part of this work is also supported by the ANR FluFOLD N°ANR-22-CE44-0020-01.

Cyclic peptides as Connexin43 and Pannexin1 inhibitors for the treatment of inflammatory disorders

https://doi.org/10.17952/37EPS.2024.P2065

Debora Iaculli,[1] Arthur Lamouroux,[1] Malaury Tournier,[2] Jade Montgomery,[2] Anne Caufriez,[1,3] Mathieu Vinken,[3] Filippo Molica,[2] Brenda R. Kwak,[2] Steven Ballet[1]

[1] Research Group of Organic Chemistry, Vrije Universiteit Brussel, Brussels, Belgium; [2] Department of Pathology and Immunology, University of Geneva, Geneva, Switzerland; [3] Department of in Vitro Toxicology and Dermato-Cosmetology, Vrije Universiteit Brussel, Brussels, Belgium.

Debora.iaculli@vub.be

CONNEXIN43 AND PANNEXIN1

Connexins (Cxs) and Pannexins (Panxs) are ubiquitous channel-forming membrane proteins which play an important role in a variety of both physiological and pathological processes. In the cardiac system, Connexin43 (**Cx43**) hemichannels (HCs) and Pannexin1 (**Panx1**) channels have shown to be critical mediators of inflammation in the context of **cardiovascular diseases**, including **ischemia-reperfusion (I/R) injury** and **atherosclerosis**. Selective modulation of Cx43 HCs and Panx1 channels represents then a potential therapeutic approach.[1]

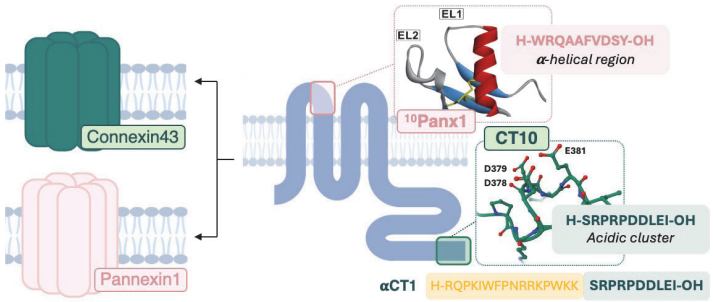

CT10 AND ^{10}Panx1

Peptide inhibitors mimicking a segment of the sequences of the proteins, in particular **CT10** and **αCT1** (including a cell-penetrating peptide (CPP)) for Cx43 and ^{10}Panx1 for Panx1, have shown to be promising **therapeutic agents** both by *in vitro* and *in vivo* experiments.[2] However, their rapid proteolytic cleavage and low bioavailability make them poor systemically-applied drug candidates.[3] To overcome these limitations and fine-tune the properties of the ^{10}Panx1 and **CT10** peptides, a series of chemical strategies, including **cyclization** and the introduction of **lipidic motifs**, were investigated.[4,5]

DESIGN AND SYNTHESIS

CT10 H-SRPRPDDLEI-OH

- **Alanine scan** did not pinpoint any residues as essential for biological activity
- Cyclic peptide **SBL-Cx43-125** designed based on the NMR solution structure of the *C*-terminal domain[6]

Variation of linker position and flexibility allowed for generation of a set of cyclic peptide inhibitors

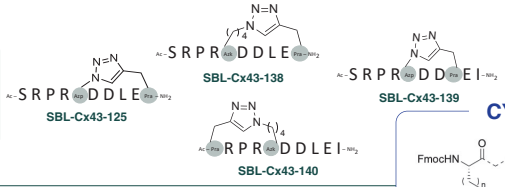

- The use of **lipidic motifs** to improve cell permeability was investigated
- **SBL-Cx43-135** shows reduced water solubility

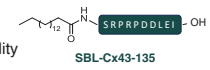

- Different polar linkers were introduced to **improve solubility**
- The best linker was used to design **SBL-Cx43-157**, a **water-soluble**, lipidated cyclic peptide based on **SBL-Cx43-125**

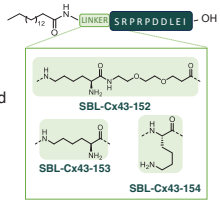

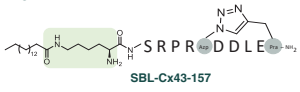

CYCLIZATION STRATEGY

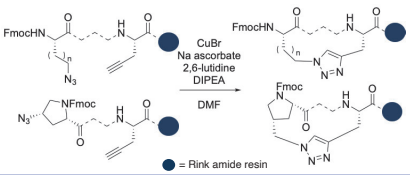

^{10}Panx1 H-WRQAAFVDSY-OH

- **Cyclization scan** at (*i*,*i*+4) distance to stabilize helical conformation

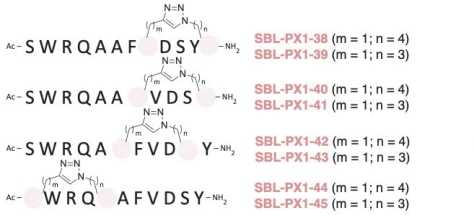

- Lead peptides **SBL-PX1-42** and **SBL-PX1-44**
- Variation of linker orientation, stereochemistry and length

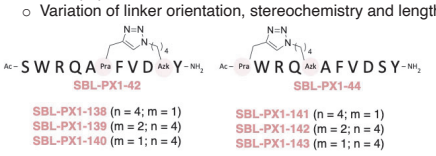

SBL-PX1-138 (n = 4; m = 1)
SBL-PX1-139 (m = 2; n = 4)
SBL-PX1-140 (m = 1; n = 4)

SBL-PX1-141 (n = 4; m = 1)
SBL-PX1-142 (m = 2; n = 4)
SBL-PX1-143 (m = 1; n = 4)

- The structures of lead peptides **SBL-PX1-42** and **SBL-PX1-44** were combined into a "**double stapled**" structure

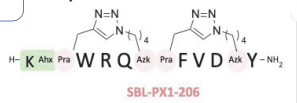

The addition of a **solubilizing tail** (H-K-Ahx) led to the generation of a proteolytically stable, water-soluble bicyclic peptide

The α-helical secondary structure is stabilized

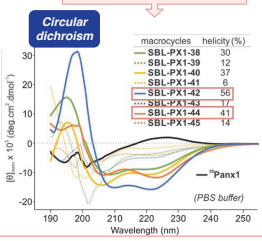

BIOLOGICAL ACTIVITY

Cx43

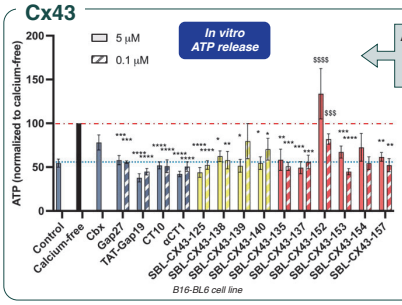

At **5 μM**, all the cyclic peptides have an inhibitory activiity comparable to that of **αCT1** without a CPP.
SBL-Cx43-125 retains its activity at a concentration as low as **100 nM.**

The **length** of the linker affects activity of the lipidated peptides **SBL-Cx43-157** shows a higher inhibitory capacity compared to the peptide based on **CT10 (SBL-Cx43-135).**

The cyclic, lipidated peptide was linked to a **cardiac endothelium-targeting peptide**[7] and binding was tested by flow cytometry together with two control peptides in different cardiac cell lines. **SBL-Cx43-158** binds preferentially to a mouse cardiac endothelial cell line (MCEC).

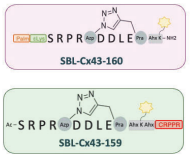

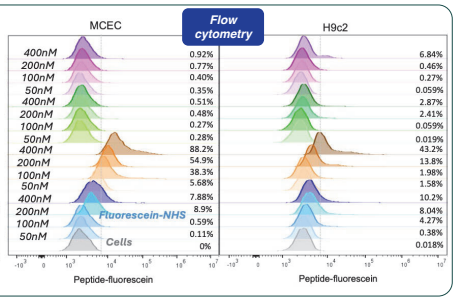

Panx1

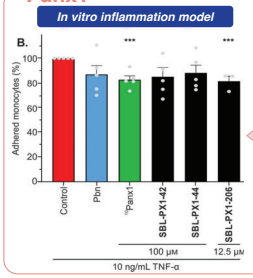

SBL-PX1-42 and **SBL-PX1-44** reduce the adhesion of THP-1 monocytes to a TNF-α-activated endothelial monolayer by about 20% at 100 μM, similarly to **^{10}Panx1**. The same effect was reached by the water-soluble "double stapled" **SBL-PX1-206** at **12.5 μM**.

SBL-PX1-42 was tested in an *in vivo* mouse model of I/R injury. 30 min ischemia followed by 24h reperfusion was induced in WT and Panx1-/- mice by ligation of the left anterior descending coronary artery. 90μM **SBL-PX1-42** was injected intravenously at 5 min before reperfusion.

SBL-PX1-42 decreased the infarct size by 40% in 7 out of 10 WT mice. No reduction in infarct size was observed in Panx1-/- mice.

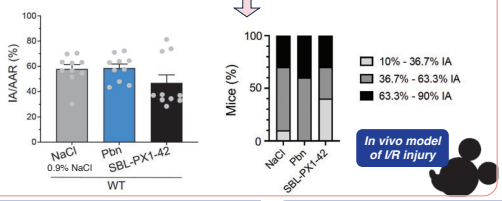

PLASMA STABILITY

CT10 t½ = 75.86 ± 4.01 min

The half-life of **SBL-Cx43-125** largely **exceeds 24h**

^{10}Panx1	t½ = 2.27 ± 0.11 min
SBL-PX1-42	t½ = 66.13 ± 0.52 min
SBL-PX1-44	t½ = 62.42 ± 2.51 min

For **SBL-PX1-206**, after **24h**, **20%** of the intact peptide is still intact in the blood plasma. The only metabolite is the peptide without the solubilizing tail. The stability of the bicyclic structure **exceeds 24h**.

CONCLUSIONS

- **SBL-Cx43-125** is a potent and proteolytically stable inhibitor of Cx43 HC activity *in vitro*, showing an activity comparable to that of **αCT1** at submicromolar concentrations **without requiring a CPP.**
- The designed **solubilizing linkers** allowed to obtain **water-soluble lipidated peptides** of increased lipophilicity, which might be favourable for *in vivo* bioavailability.
- The presence of an endothelial cell-targeting motif in **SBL-Cx43-158** increased the binding of this peptide to MCECs compared to the cardiomyocyte-like cell line H9c2.
- Cyclic peptides **SBL-PX1-42** and **SBL-PX1-44** **reduce monocyte adhesion to the endothelium** (the first step in the inflammatory cascade) by 20%, similarly as ^{10}Panx1, with a 30-fold **longer half-life**.
- The combination of the staples in the peptides led to **SBL-PX1-206**. This bicyclic peptide reaches a similar anti-inflammatory activity *in vitro* at **low concentration (12.5 μM).**
- Preliminary *in vivo* results on **SBL-PX1-42** show its ability to **decrease infarct size by 40%** in 7 out of 10 WT mice in an acute model of **myocardial I/R injury.**

REFERENCES

[1] Meens, M. J., Kwak, B. R., Duffy, H. S. *Cell. and mol. life sci.* **2015**, *72*, 2779
[2] Caufriez, A., Böck, D., Martin, C., Vinken, M., Ballet, S. *Exp. Opin. Drug Disc.* **2020**, *15*, 1213
[3] Caufriez, A., Lamouroux, A., Martin, C., Iaculli, D., Ergüç, E. I., Gozalbes, R., ... & Ballet, S. *Bioorg. Chem.* **2023**, *138*, 106612
[4] Lamouroux, A.,° Tournier, M., ° Iaculli, D., Caufriez, A., Rusiecka, O. M., Martin, C., ... & Ballet, S. *J. Med. Chem.* **2023**, *66*, 13086
[4] Iaculli, D., Montgomery, J., Lamouroux, A., Caufriez, A. ... & Ballet, S. *Manuscript under review*
[6] Sorgen, P. L., Duffy, H. S., Sahoo, P., Coombs, W., Delmar, M., & Spray, D. C. *J. Biol. Chem.* **2004**, *279*, 54695
[7] Zhang, L., Hoffman, J. A., & Ruoslahti, E. *Circulation* **2005**, *112*, 1601

ACKNOWLEDGEMENTS

PANACHE
Funded by the Horizon 2020 Framework Programme of the European Union

This project has received funding from the European Union's Horizon 2020 Future and Emerging Technologies programme under grant agreement number 858014

We thank Horizon2020 and the Research Council of the VUB for financial support through the Strategic Research Programme (SRP50 and SRP95). We also thank the Rode Kruis Vlaanderen for supplying human plasma. We thank the EPS organization for the reception of a registration waiver.

Antimicrobial Peptidomimetics: Design, Synthesis, and Surface Binding

Virginie Briguet and Marc Mathieu

HES-SO//Valais, Institute of Life Technologies, CH-1950 Sion, Switzerland

https://doi.org/10.17952/37EPS.2024.P2066

Issue

- Antibiotic resistance[1] -> Thread to global health
- Effectiveness of antibiotics -> Need of innovation
- Repeated use -> Promotion of resistant strains

Objectives

- Synthesis of antimicrobial peptides (NON DISCLOSED) with -SH functionality (N-term & C-term)
- Covalent Immobilisationon titanium plates (> 99.6% purity, *Grade II*).
- Characterize through different techniques: FTIR, SEM & XPS

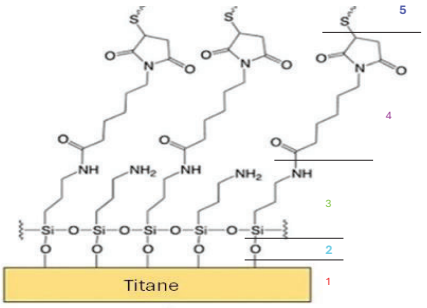

Figure 1: Assembly process on Titanium Surfaces [2]

Data & Discussion

- Solid phase peptide synthesis on **PurePep Chorus**, Gyros Protein Technologies.
- Peptide purification on **Agilent 1260 Infinity II** HPLC-preparative.
- Characterization of the peptide on UPLC-MS **Agilent 1290 Infinity II** UPLC-MS.
- Covalent immobilisation of the peptide on a Titanium plate according to strategy **Figure 1** [2].
- Characterization of the peptide by FTIR-ATR, XPS and FEG-SEM.

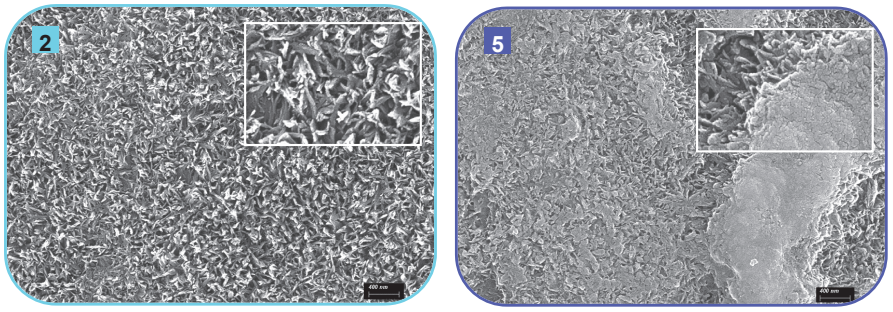

FEG-SEM : Ti-OH (2) and crosslinked with Peptide (5) @20'000x and 100'000x (inserts) ; by Hervé Girard, internal service platform HES-SO//Valais

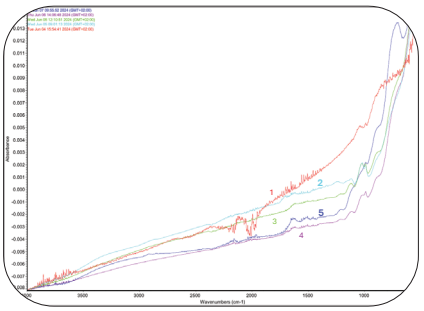

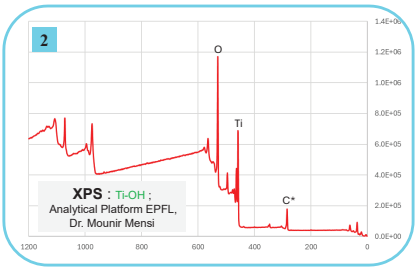

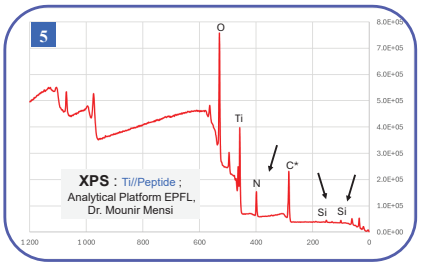

The surface binding strategy went smoothly, confirming the binding of the peptides to the titanium surface. Following immobilisation, the sequences with C-Term Cys gave better binding to the titanium surface, while our sequences with N-Term Cys had tendency to form mainly dimers, which limited its binding efficiency to the plate. Of the three characterization methods used, XPS proved to be the most effective. Thanks to its high resolution and accuracy, XPS enabled in particular precise identification of the elements present on the surfaces, although initial carbon (C*) traces remained visible throughout the different analyses, likely an original contamination.

Litterature

1. www.who.int/news-room/fact-sheets/detail/antibiotic-resistance
2. B. Mishra et G. Wang, vol. 33, no 7, p. 544-555 (2017), doi: 10.1080/08927014.2017.1332186.
3. **Bachelor Thesis HES-SO//Valais** by Virginie Briguet, August 2024 , « *Peptides antimicrobiens adhésifs : synthèse et caractérisation* »

https://doi.org/10.17952/37EPS.2024.P2067



NEW INSIGHTS INTO ANTIBACTERIAL AND ANTITUMOR EFFECTS OF STRUCTURALLY VERSATILE AMINO ACID-BASED AND NON-PROTEINOGENIC COMPOUNDS

Martina I. Peeva[1], Maya G. Georgieva[1], Aneliya A. Balacheva[1], Svetoslav Dimov[2] , Nikolay T. Tzvetkov[1,*]

1) Department of Biochemical Pharmacology and Drug Design, Institute of Molecular Biology, Bulgarian Academy of Sciences, Acad. G. Bonchev str. Bl. 21, Sofia 1113, Bulgaria
2) Faculty of Biology, Sofia University "St. Kliment Ohridski", Sofia, Bulgaria

Corresponding author:** ntzvetkov@bio21.bas.bg **(NTT)

Introduction

The honey bee (*Apis mellifera*) has been known to mankind since ancient times. The last few decades, honey bee populations have been declining dramatically worldwide due to various causes including pesticides, bacterial diseases and parasites [1]. That leads to a pressing problem with a huge global economic, environmental, social, and public health impact.

The American Foulbrood disease (AFB) is an infection that still belong to the most deleterious honey bee diseases (Fig. 1) [1,2]. Herein we investigate the cytotoxic potential of new small molecules against the Gram-positive bacterium *Paenibacillus larvae*, the causative agent of the American Foulbrood disease (AFB). Furthermore, we were interested to study the activity of these compounds against different cancer cell lines.

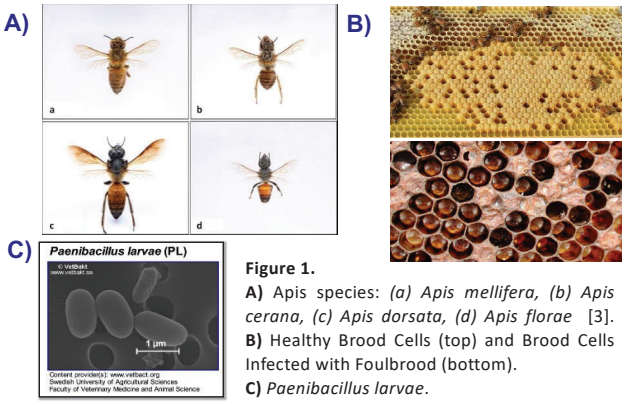

Figure 1.
A) Apis species: *(a) Apis mellifera, (b) Apis cerana, (c) Apis dorsata, (d) Apis florae* [3].
B) Healthy Brood Cells (top) and Brood Cells Infected with Foulbrood (bottom).
C) *Paenibacillus larvae*.

Anti-bacterial and antitumor efficacy

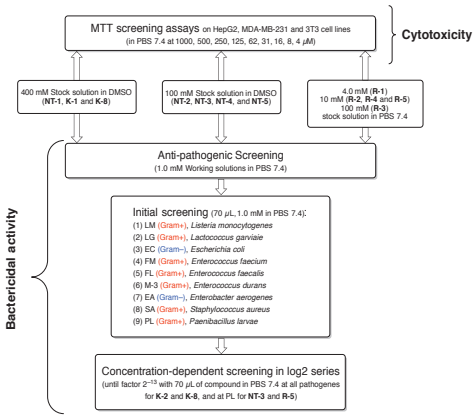

Figure 2: Work-flow of the screening procedure.

Until now, we have investigated the anti-bacterial and antitumor efficacy of a series of novel, small molecule-based compounds and compared their biological effects with those of well-known reference drugs, including cis-Pt, carbo-Pt, etoposide, and doxorubicin (Fig. 2). All compounds were further tested for their cytotoxicity on various tumor cell lines, including HepG2, MDA-MB-231, HT-29, and the non-tumor 3T3. A two-step screening procedure was applied in order to identify highly selective compounds against the target pathogen *Paenibacillus larvae* in comparison with the standard antibiotic lincomycin (Fig. 2 and 3).

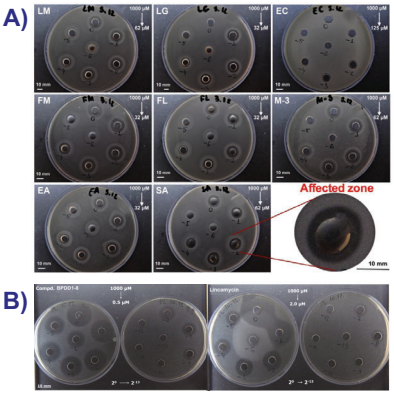

Figure 3. Anti-bacterial effects of Cmpd. **PBDD1-8** (**K-8**) on eight bacterial types (A) and against *Paenibacillus larvae* (PL) in comparison with **lincomycin** (B).

New insights into cytotoxicity

To further investigate the possible mechanism of action (MoA) of compound **BPDD1-8** (**K-8**), for example apoptotic effects, we performed initial time- and concentration-dependent fluorescence spectroscopy (Axio fluorescent microscope) using HepG2 cancer cells (Fig. 4).

After 4 h incubation time, the cells were stained with the respective fluorescence dye (DAPI, 4',6-diamidino-2-phenylindole) which showed appearance of a cytotoxic effect compared with non-treated cells. This method allowed us to obtain the appropriate effective concentrations of **BPDD1-8** in the subsequent apoptosis and cell cycle studies.

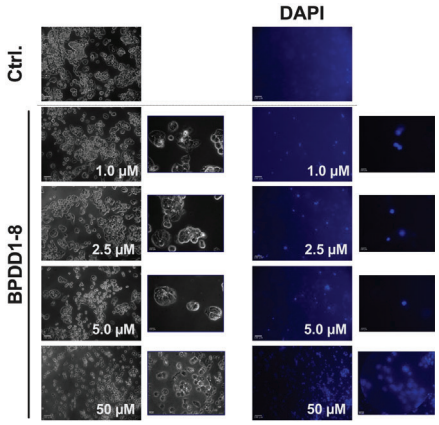

Figure 5. Representative photos of the fluorescent microscopy experiments with **BPDD1-8** on HepG2 cell line. The cells were treated for 4h at 37°C at different compound's concentrations (1.0, 2.5, 5.0, and 50 µM).

Conclusions

The biological effects of these new compounds are comparable to those of the approved antibiotic **lincomycin** and the anti-cancer drug **doxorubicin**. Based on their cytotoxic and antiproliferative activity two of the new drug candidates (designated as **BPDD1-3** / **NT-3** and **BPDD1-8** / **K-8**) were chosen for further studies identifying their mechanisms of action, e.g., apoptosis and cell cycle on cancer cells.

Acknowledgments: The authors acknowledge the financial support by the Bulgarian National Science Found (BNSF) under Grant No. KP-06-N59/2.

Literature

[1] Ebeling, J. et al. *Appl. Microbiol. Biotechnol.* **2016**, 100(17), 7387–95.
[2] Matović, K. et al. *Vet. Sci.* **2023**, 10(3), 180.
[3] Makkar, G.S. et al. Vegetos **2020**, 33, 538–544.

https://doi.org/10.17952/37EPS.2024.P2068

Chemical Synthesis and Intracellular Delivery of P53 Transactivation Domain (TAD) Constructs

Mo'ath Yousef and Vladimir Torbeev

Laboratory of Biosystems Chemistry, École supérieure de biotechnologie de Strasbourg, UMR7242, CNRS and Université de Strasbourg

The tumor suppressor (P53) is a well-known oncoprotein, known for its involvement in majority of cancers. This protein consists of several domains, one of which is the Transactivation domain (TAD-P53). TAD-P53 is an intrinsically disordered region, that is responsible for the binding of P53 with numerous targets. Upon cellular stress, phosphorylation leads to the release of P53 from its negative regulators, HDM2 and CBP[1,2]. To understand the various interactions of TAD-P53, modifications can be effected such as α-methylation[3], or phosphorylation[4]. We have already demonstrated the chemical synthesis of TAD-P53 via three segments using various approaches[4,5]. To enable in vitro studies of TAD-P53, the intercellular delivery of chemically synthesized variants of TAD-53 is considered. Herein, we demonstrate the chemical synthesis of TAD-P53 analogues, conjugated to a cell penetrating peptide (CPP) and Nuclear localization signals (NLS) to aid the intracellular to delivery of TAD-P53 constructs. The inclusion of a CPP already proved to be an effective method, to enhance the delivery of various cargo, and in this project, Penetratin sequence was introduced at N-terminus. Even though TAD maybe delivered, it may not reach the nucleus. Therefore, to overcome this obstacle, the NLS of TAD-P53 (305-322) was attached at C-terminus. The chemical synthesis of the constructs was accessed via native chemical ligation, joining 4 segments to yield a 106 amino acids-long protein.

Strategy

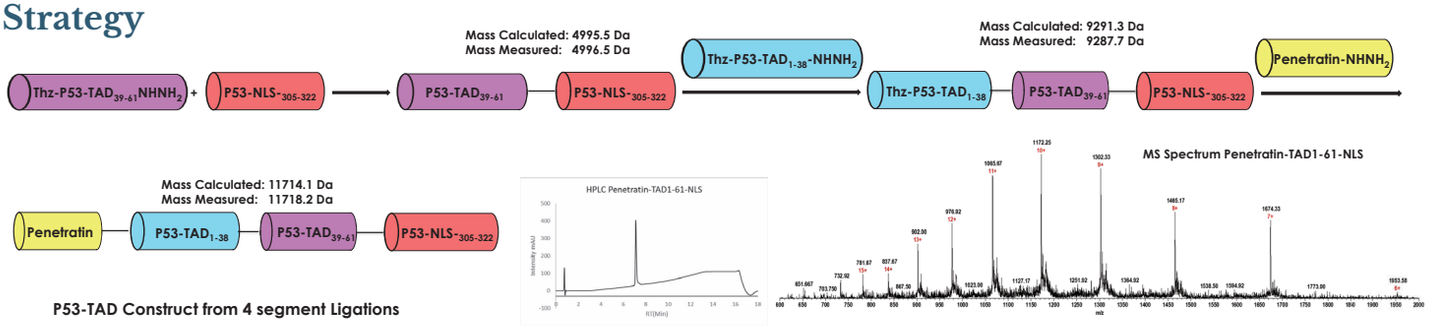

Methods

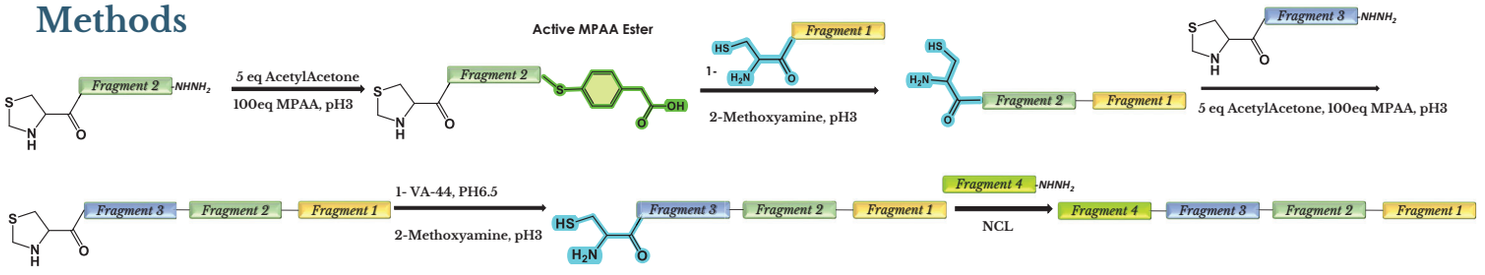

The use of NCL is the backbone of this work, allowing the chemical synthesis of the target product, from several peptide segments. Newer and more sophisticated methods, such as Knorr pyrazole[6] synthesis were adopted. The use of this method preserves the thiazolidine moiety (Thz) from any side reaction, as would take place in a classical thioester formation method with $NaNO_2$.

The resulting thioester from the Knorr Pyrazole method undergoes a ligation reaction, joining two segments (1+2). Thz can be subsequently deprotected to cysteine via methoxyamine treatment, and reacted with the next segment (1-2 +3). A subsequent desulfurization reaction, using VA-044 converts the Cys residue to an Ala residue. The final step involves a classical NCL reaction to yield the desired product.

Results

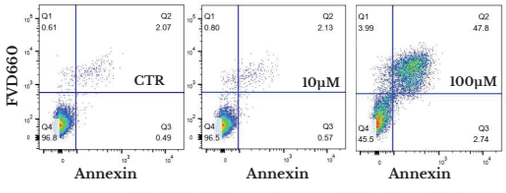

Apoptosis assay of CPP-TAD-NLS with Annexin PCP-eFluor 710. Late apoptosis is evident at 100µM

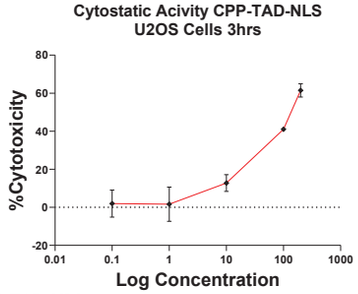

Effect of CPP-TAD-NLS on cell proliferation, cells were treated for 3Hrs and incubated for 3 days, preceding the MTT assay.

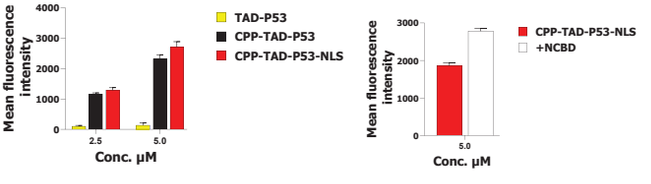

Flow Cytometry experiment showing the relative uptake of the constructs, second graph shows the increased uptake upon the introduction of NCBD protein in the cell media.

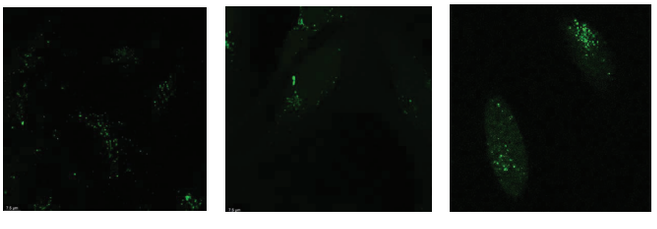

$TAD_{1\text{-}61}$ $CPP\text{-}TAD_{1\text{-}61}$ $CPP\text{-}TAD_{1\text{-}61}\text{-}NLS_{305\text{-}322}$

Live Confocal Microscopy showing the increased uptake of fluorescent TAD-P53 $_{1\text{-}61}$ constructs when CPP is introduced. U2OS Cells are treated for 3Hrs at 37°C.

References

[1] C. W. Lee, M. Arai, M. A. Martinez-Yamout, H. J. Dyson, and P. E. Wright. *Biochemistry*, **2009**, *48*, 2115–2124,

[2] J. C. Ferreon, C. W. Lee, M. Arai, M. A. Martinez-Yamout, H. J. Dyson, and P. E. Wright. *Proc Natl Acad Sci USA*,**2009**, *106*, 6591–6596.

[3] V. Bauer *et al.*, *Chem Sci*, **2021**,12, 1080–1089.

[4] Margiola, S., Gerecht, K., & Müller, M. M. *Chem. Sci.* **2021**, 12(24), 8563-8570.

[5] A. Baral, A. Asokan, V. Bauer, B. Kieffer, and V. Torbeev. *Tetrahedron*, **2019**,*75*, 703–708.

[6]D. T. Flood, J. C. J. Hintzen, M. J. Bird, P. A. Cistrone, J. S. Chen, and P. E. Dawson, *Angewandte Chemie International Edition*, **2018**,57, 11634–11639.

CONCLUSIONS

TAD of P53 was chemically synthesized using modern methods. This allows further modifications in the structure of TAD-P53 permitting the investigation of its interactions. The prepared constructs were successfully delivered, and their biological studies prove that our design permitted increased permeability. The biological activity of CPP-TAD-P53-NLS instigates that TAD can solely affect the cell survival.

37th EPS European Peptide Symposium
14th IPS International Peptide Symposium
25 - 29 August 2024
Satellite Workshop 30 - 31 August 2024
Florence, Italy- 2024

Development of a retro-inverso tetrapeptide collagen modulator as anti-aging active principle

Fosca Errante [a,b,c], Marco Pallecchi [b], Gianluca Bartolucci [b], Elena Frediani [d], Francesca Margheri [d], Lisa Giovannelli [e], Anna M. Papini [a,f], Paolo Rovero [a,b*]

a) Interdepartmental Research Unit of Peptide and Protein Chemistry and Biology, University of Florence, Sesto Fiorentino (FI), 50019, Italy
b) Department of Neurosciences, Psychology, Drug Research and Child Health, University of Florence, Sesto Fiorentino (FI), 50019, Italy
c) Espikem s.r.l., Prato (PO), 59100, Italy
d) Department of Experimental and Clinical Biomedical Sciences "Mario Serio", University of Florence, Firenze (FI), 50139, Italy
e) Department of Neurosciences, Psychology, Drug Research and Child Health, University of Florence, Firenze (FI), 50139, Italy
f) Department of Chemistry "Ugo Schiff", University of Florence, Sesto Fiorentino (FI), 50019, Italy

https://doi.org/10.17952/37EPS.2024.P2071

UNIVERSITÀ DEGLI STUDI FIRENZE
PeptLab
INTERDEPARTMENTAL RESEARCH UNIT OF PEPTIDE AND PROTEIN CHEMISTRY AND BIOLOGY

fosca.errante@unifi.it

BACKGROUND

Serpin A1 or Alpha1-antitrypsin is the physiological inhibitor of elastase, one of the main enzymes involved in collagen degradation.
Congote et al.[1] have shown that the C-terminal portion of Serpin A1 is able to stimulate type I collagen production.
We previously showed that a shorter portion of Serpin A1, termed SA1-III[2], is a collagen turnover modulator and the activity of SA1-III is based on inhibition of collagen degradation, as described by Cipriani et al.[3].

RESULTS

We developed new peptide analogues, acting on the following parameters:
- Size of the molecule (n° of amino acids);
- Chemical stability (presence of Met);
- Enzymatic stability (retro-inversion).

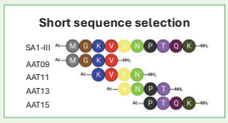

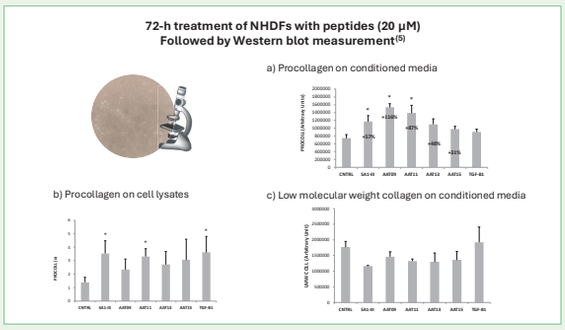

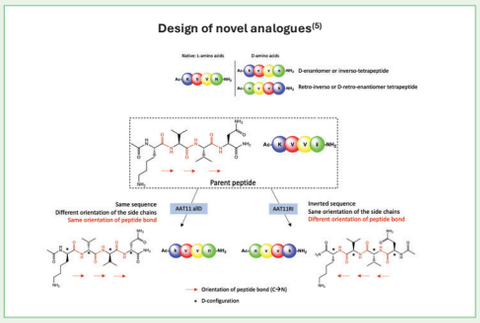

Among all the tested sequences, peptide **AAT11RI** was found to be the most active and a family of peptides was patented[4].

The activity of peptide AAT11RI in **decreasing collagen degradation** was evaluated trough Western Blot experiments (procollagen measurement) and Invasion experiments (migration of fibroblasts in Boyden chambers)[5].

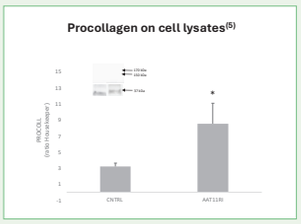

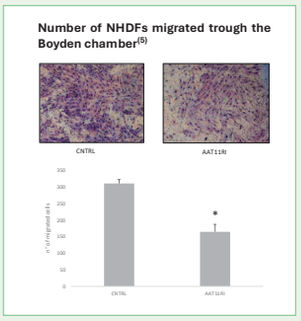

Peptide **enzymatic stability** towards skin proteases was evaluated in ex-vivo experiments on human skin homogenates in comparison with a well-known cosmeceutical peptide[5].

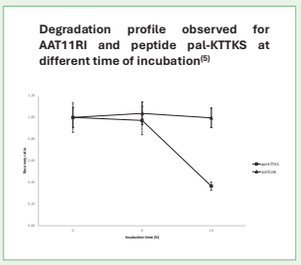

METHODS

Peptide synthesis:
Solid Phase Peptide Synthesis (SPPS)
Flash chromatography and semi-preparative HPLC
UHPLC-MS characterization
Cell treatments:
In Neonatal Normal Human Dermal Fibroblasts (Neo-NHDFs)
Collagen quantification:
Western Blot
Stability evaluation:
LC-MS/MS using human skin homogenates (HSH)
Invasion assay:
Boyden chambers

CONCLUSIONS

Second-generation peptides were designed, starting from SA1-III, as novel cosmeceutical ingredients. A *retro-inverso* peptide, named AAT11RI was synthetized, tested and patented. Further studies described AAT11RI mechanism of action as a collagen degradation protector[5]. Moreover, the use of D-amino acids induced in peptide AAT11RI high stability to dermal proteases. Besides the use in cosmeceuticals, there is evidence indicating that serine proteases play a pathogenic role in some diseases (e.g. chronic inflammatory lung disorders) characterized by elevated protease activity. This suggests a potential interest in further investigating the pharmaceutical applications of short sequences derived from serpin A1 such as AAT11RI.

(1) Congote, L. F.; Temmel, N.; Sadvakassova, G.; Dobocan, M. C. Comparison of the Effects of Serpin A1, a Recombinant Serpin A1-IGF Chimera and Serpin A1 C-Terminal Peptide on Wound Healing. *Peptides* 2008, *29* (1), 39–46. https://doi.org/10.1016/j.peptides.2007.10.011.
(2) Pascarella, S.; Tiberi, C.; Sabatino, G.; Nuti, F.; Papini, A. M.; Giovannelli, L.; Rovero, P. Serpin A1 C-Terminal Peptides as Collagen Turnover Modulators. *ChemMedChem* 2016, *11* (16), 1850–1855. https://doi.org/10.1002/cmdc.201500472.
(3) Cipriani, C.; Pascarella, S.; **Errante, F.**; Menicacci, B.; Magnelli, L.; Mocali, A.; Rovero, P.; Giovannelli, L. Serpin A1 and the Modulation of Type I Collagen Turnover: Effect of the C-Terminal Peptide 409-418 (SA1-III) in Human Dermal Fibroblasts: Serpin-A1 C-Terminal Modulates Collagen Levels. *Cell Biol. Int.* 2018, *42* (10), 1340–1348. https://doi.org/10.1002/cbin.11018.
(4) **Errante, F.**; Giovannelli, L.; Papini, A. M.; Rovero, P. Bioactive Peptides and Compositions Comprising Them. WO/2020/245772, December 10, 2020.
(5) **Errante F.**, Pallecchi M., Bartolucci G., Frediani E., Margheri F., Giovannelli L., Papini A.M., Rovero P., Retro-Inverso Collagen Modulator Peptide Derived from Serpin A1 with Enhanced Stability and Activity In Vitro. *J. Med. Chem.* 2024 67 (6), 5053-5063. https://doi.org/10.1021/acs.jmedchem.4c00137

Regione Toscana
This work was supported by Tuscany Region [PORCREOFESR 2007-2013]

European Peptide Society is kindly acknoledged for the awarded registration grant to Dr. Fosca Errante

https://doi.org/10.17952/37EPS.2024.P2076

37th EPS European Peptide Symposium
14th IPS International Peptide Symposium
25 - 29 August 2024
Florence, Italy

A BMP-2-derived bioactive peptide conjugated to chitosan improves osteoblast proliferation and antibacterial properties of membranes for oral surgery

Cristian Balducci[1], Annj Zamuner[1,2], Martina Todesco[2], Andrea Bagno[2], Antonella Pasquato[1], Giovanna Iucci[3], Federica Bertelà[3], Chiara Battocchio[3], Luca Tortora[3,4], Luca Sacchetto[5], Paola Brun[6], Eriberto Bressan[5], Monica Dettin[1]

[1] Department of Industrial Engineering, University of Padova, [2] Department of Civil, Architectural and Environmental Engineering, University of Padova, [3] Department of Science, Roma Tre University, [4] National Institute for Nuclear Physics, INFN Roma Tre, [5] Department of Neurosciences, Section of Dentistry, University of Padova, [6] Department of Molecular Medicine, University of Padova

INTRODUCTION

About 3 billion people suffer from partial or total edentulism and alveolar bone resorption. To achieve a favourable prognosis in implant-supported rehabilitations, it is crucial to have adequate peri-implant bone volume [1].
Guided Bone Regeneration (GBR) uses **barrier membranes** in combination with bone substitutes to block out non-osteogenic cells, thereby improving bone recovery and growth at defect sites [2]. Commercial **OsseoGuard® membranes**, made of formaldehyde-cross-linked bovine type I collagen, are resorbable in 6-9 months and can be moulded and applied dry or wet. Despite their benefits, these membranes sometimes fail to adequately promote vertical alveolar bone growth, leading to suboptimal bone quality and density.

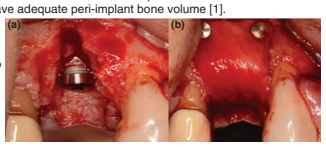

(a) implant insertion with persistence of bone defect and exposure of implant coils (b) defect correction with GBR technique: compensation of the defect with particulate heterologous bone and covering with collagen membrane fixed with 2 titanium pins.

BACKGROUND

Chitosan (CS) is known for its biocompatibility and antibacterial features; it supports coagulation, hemostasis, and osteoblast proliferation and differentiation. In previous studies, we demonstrated that **the fragment (48-69) of BMP-2 (GBMP1α)** enhances human osteoblast calcium deposition, adhesion, proliferation, and the expression of important osteoblast genes, and guides mesenchymal stem cells differentiation towards an osteoblastic phenotype [3].

AIM

This study aimed to engineer and evaluate the efficacy of modified barrier membranes by enhancing their bioactivity for alveolar bone tissue regeneration and their antibacterial properties. Specifically, membranes covalently functionalised with **chitosan (CS)** and **chitosan functionalized with the peptide GBMP1α (CS + GBMP1α)** were investigated to promote bone growth.

METHODS

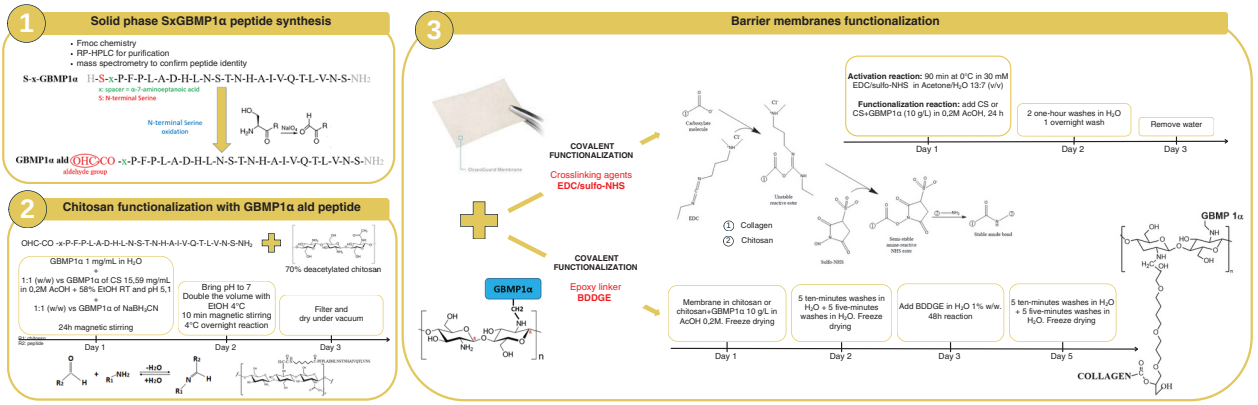

RESULTS

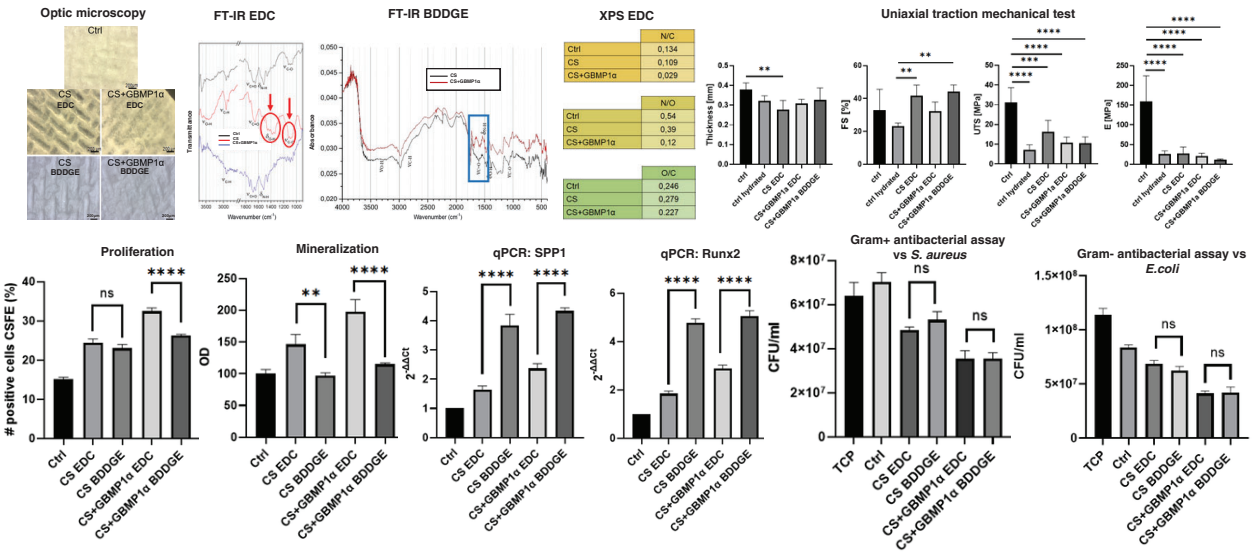

CONCLUSIONS

the modification of membrane surfaces was confirmed through optical microscopy, FT-IR, and XPS analyses. Biological *in vitro* tests (proliferation, mineralization, gene expression assays) with human osteoblasts showed notable enhancements in functionalized membranes, especially those with GBMP1α that in addition showed antibacterial activity against S. aureus and *E. coli.* EDC/sulfo-NHS method gave better results in proliferation and mineralization, while BDDGE method outperformed in SPP1 and Runx2 genes expression. Mechanical tests indicated functionalizations did not vary the mechanical properties of the membranes.

REFERENCES

[1] R. Gupta, et al, *Dental Implants*, StatPearls Publishing, Aug 2023
[2] I. A. Urban, et al, *Guided Bone Regeneration in Alveolar Bone Reconstruction*, Oral and Maxillofacial Surgery Clinics of North America, May 2019, pp. 331-338
[3] P. Brun, et al, *Chitosan Covalently Functionalized with Peptides Mapped on Vitronectin and BMP-2 for Bone Tissue Engineering*, Nanomaterials (Basel), Nov 2021; pp.2784.

CONTACTS

Cristian Balducci, PhD student - cristian.balducci@phd.unipd.it
Prof. Monica Dettin - monica.dettin@unipd.it



https://doi.org/10.17952/37EPS.2024.P2077

UNIVERSITY OF GOTHENBURG

Transmembrane peptide-loaded ionic liquid nanocarriers targeting ErbB2-positive cancer

Helal Abujubara[1], **Pankaj Bharmoria**[2], **Samantha W. Alvarez**[3], **Enoch Appiah**[1], **Kasper Moth-Poulsen**[2], **Volkan I. Sayin**[3], **and Alesia A. Tietze**[1]*

[1]University of Gothenburg, Department of Chemistry and Molecular Biology, Wallenberg Centre for Molecular and Translational Medicine, Gothenburg (Sweden)
[2]The Autonomous University of Barcelona, Institute of Materials Science of Barcelona, ICMAB-CSIC, Barcelona (Spain)
[3]University of Gothenburg, Department of Surgery, Wallenberg Centre for Molecular and Translational Medicine, Sahlgrenska Center for Cancer Research, Gothenburg (Sweden)

Peptide and Nanocarrier formulation

Project concept

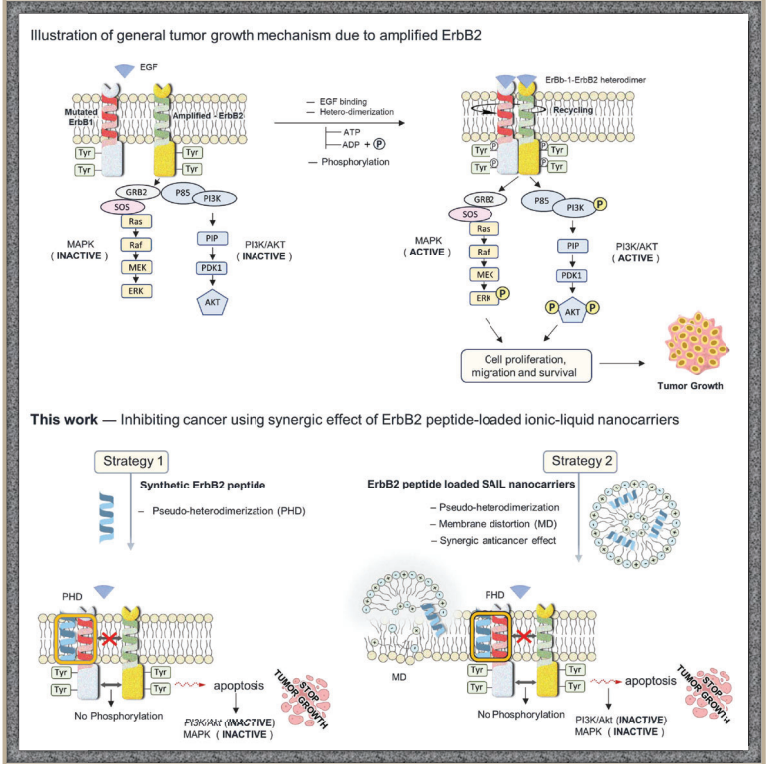

Peptides for the study

Peptide variant	Representation of amino acids sequence	Experimental Mw[a] [g/mole]	ppm	tR[b] [min]
ErbB2_TM		-	-	-
V1	Solubilizing tag	984.3067	12.6	4.7
V2	Dye, Solubilizing tag	1103.6897	19.4	4.6
V3	Dye, Spacer, Solubilizing tag	1186.6244	485	4.8

(a) Mass peaks detected as [M+3H]$^{3+}$. (b) Retention time (tR) based on LC-UV 214 nm detection.

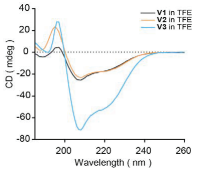

TM peptides synthesized via SPPS and characterized using LC-MS displayed α-helical structures

Ionic Liquid-based Nanocarriers

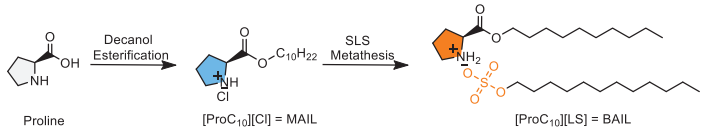

Self-assembly of MAIL and BAIL in aqueous buffer solution

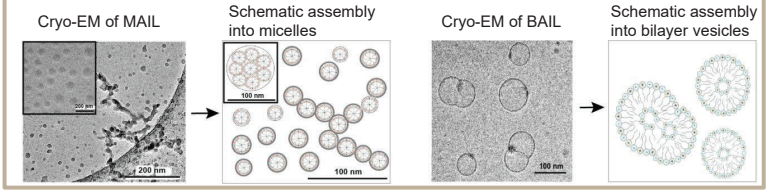

Anti-cancer activity

Effect on cancer cells viability

Cell line	Cancer type	Molecular Subtype	ERBB2 expression (RNA)	ERBB2 CRISPER Effect
BT-474	Breast	HER2 overexpressed	10.5	N/A
AU565	Breast	HER2 overexpressed	11.6	-1.09
A549	Lung	-	4.2	-0.78
CFPAC-1	Pancreatic	-	5.7	-0.87

- Cancer cells with varying ErbB2 protein expression levels
- CellTiter-Glo assay
- TM peptides were cytotoxic at low micromolar concentrations (1.25 μM)
- Cytotoxic nanocarriers at CMC

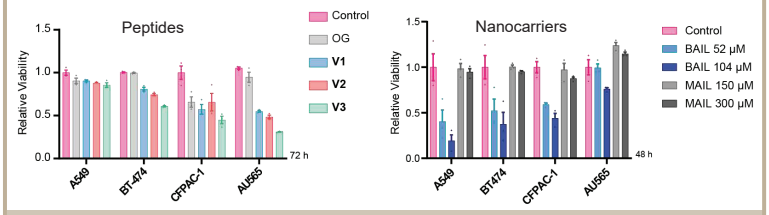

Synergetic effect of nanocarriers on ErbB2 positive cancer cells

- TM peptides were incorporated into nanocarriers via reverse phase evaporation technique
- Substantial reduction in viabilities in all cell lines with a dose-dependent effect
- TM peptide-nanocarrier suppressed both the ErbB2 MAPK and PI3K/Akt intracellular pathways (Western blot)
- Synergistic anticancer activity of TM peptides in combination with MAIL or BAIL nanocarrier

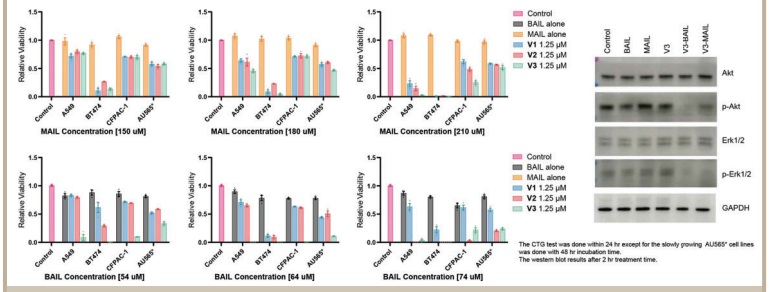

Localization of nanocarriers in cancer cell lines

TM peptide **V3** showed membrane localization following 24 h incubation with stained BT474 cells

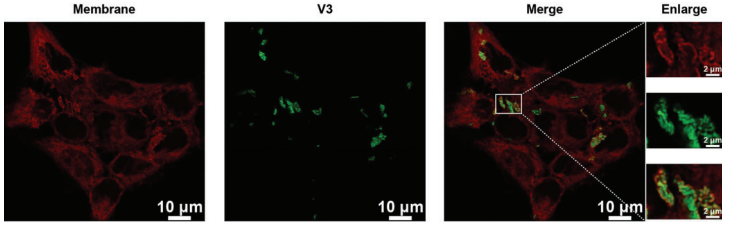

Conclusion

- New approach for synthesis and characterization of a series of transmembrane domain-derived hydrophobic peptides
- Design of novel surface-active ionic liquids nanocarriers
- Novel strategy for targeting ErbB2 receptors in cancer by combining transmembrane peptide and nanocarriers

Acknowledgment

The Knut and Alice Wallenberg Foundation via the Wallenberg Centre for Molecular and Translational Medicine (AT), Swedish Research Council (2020-04299) (AT) and Cancerfonden (AT) are gratefully acknowledged.

For additional information, please contact:
Alesia Tietze
alesia.a.tietze@gu.se
Helal Abujubara
Helal.abu93@gmail.com

Interested in more from the Tietze Lab research? Follow this QR code

https://doi.org/10.17952/37EPS.2024.P2078

Characterization of Aurora-A Activation and Allosteric Regulation by TACC-3 Peptidomimetics

Diana Gimenez,[a,b] Martin Walko,[b,d] Jennifer A. Miles,[c,d] Richard Bayliss,[c,d] Megan H. Wright[b,d] and Andrew J. Wilson[a,b,d,*]

[a] School of Chemistry. University of Birmingham, Birmingham B15 2TT, UK.
[b] School of Chemistry and [c] Faculty of Biological Sciences, University of Leeds, Leeds, LS2 9JT, UK.
[d] Astbury Centre for Structural Molecular Biology, University of Leeds, Leeds LS2 9JT, UK.

E-mail: d.gimenez-ibanez@bham.ac.uk

TACC3 / Aur A Protein-Protein Interaction

Aurora-A is a Ser/Thr protein kinase that regulates key mitotic events by recruiting and phosphorylating a range of different intrinsically disordered proteins. Among them, the Aurora-A interaction with TACC-3 (Transforming Acidic Coiled-Coil Containing Protein 3) is instrumental for spindle assembly and chromosome segregation,[2,3] and is frequently up-regulated in many different types of cancer.[4]

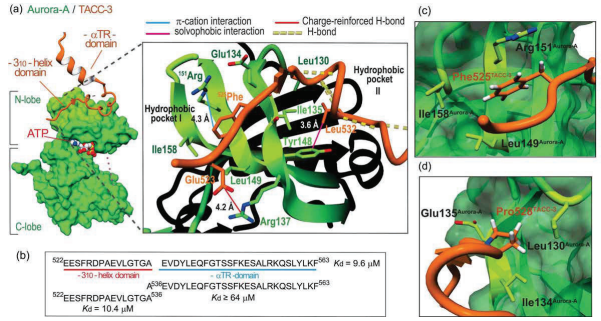

Figure 1. Key features of the Aurora-A/TACC-3 complex. (a) Crystal structure of the Aurora-A catalytic domain (green) in complex with TACC-$3_{522-563}$ (orange; PDB: 5ODT). **(b)** Sequence of TACC-3 docking region to Aurora-A, TACC-3 $_{522-563}$, and individual FA dissociation constants (K_d) for each domain. **(c-d)** MD calculated energy minimum structure of WT TACC-$3_{522-536}$ in the presence of Aurora-A, showing the key $Phe525^{TACC-3}$ and $Pro528^{TACC-3}$ *exo*-pucker conformation.

TACC3 / Aur A Protein-Protein Interaction

We used sequence truncation and fluorescence anisotropy (FA) to optimize the TACC3 docking segment.

TACC3 522-536 **EESFRDPAEVL**GTGA IC_{50}= 163 ± 37 μM

TACC3 518-532 LELK **EESFRDPAEVL** **IC_{50}= 124 ± 33 μM**

Stapled TACC3 518-532 L/R

LECKEESFCDPAEVL

X= IC_{50} (Bph)= 36 ± 5 μM

IC_{50} (PEG)= 380 ± 13 μM

IC_{50} (Oct)= 65 ± 6 μM

Stapled TACC3 518-532 S/E

LELKEECFRDPACVL

X= IC_{50} (Bph)= 31 ± 5 μM

IC_{50} (PEG)= 320 ± 52 μM

IC_{50} (Oct)= N/D

NMR structure analysis

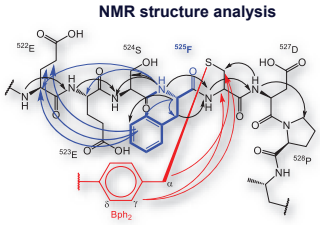

Schematic showing the observed NMR nOE contacts in stapled TACC3 518-532 L/R at the ^{525}F region.

Bph constraints restrict the conformational landscape and orientates the key ^{525}Phe predisposing the peptide towards Aur A binding

Optimization of Phe525 and Pro528 interaction with Aur-A

By using unnatural phenylalanine analogs and exploiting stereo-electronic effects (i.e. gauche effect) twelve-fold improved Kd values were measured for new constrained peptides when compared to the linear sequences, with all variants showing low micromolar/high nanomolar affinities.

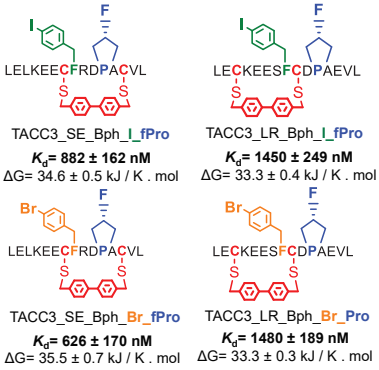

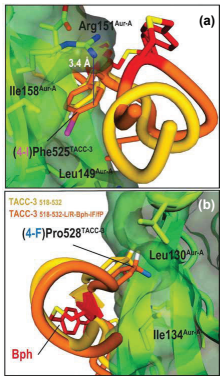

Figure 2. Key features of TACC-3 constrained peptidomimetics. (a) Iodinated (4-I)-$Phe525^{TACC-3}$ in its binding pocket. **(b)** Exo-pucker conformation of fluorinated *trans*-(4-F)$Pro528^{TACC-3}$ in its binding pocket.

TACC-$3_{518-532}$ peptidomimetics stimulate Aur-A

Linear WT variants are relatively poor activators of the kinase, whereas the constrained peptidomimetics stimulate Aurora-A and promote substrate phosphorylation in a dose-dependent manner by up to 160-190%.

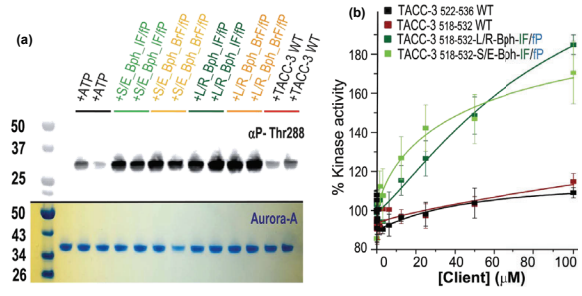

Figure 3. Kinase activation by peptidomimetics. (a) Qualitative kinase assay monitoring the autophosphorylation of unphosphorylated Aurora-A in the presence of TACC-$3_{522-536}$ and constrained peptides (all peptides 10 μM). (b) % Kinase activation of Aurora-A (10 nM) in the presence of linear and constrained TACC-3 peptides as measured in ADP-Glo assays.

Enhanced binding of peptidomimetics to Aur-A is entropically driven

To explore how restricting the accessible conformations influences the thermodynamics of binding, we carried out isothermal titration calorimetry (ITC) and variable-temperature FA experiments. Constrained variants exhibited a more favorable entropy of binding in comparison to the linear variants.

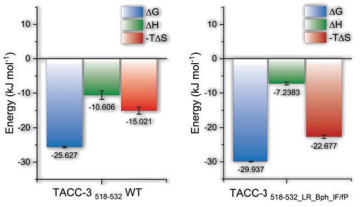

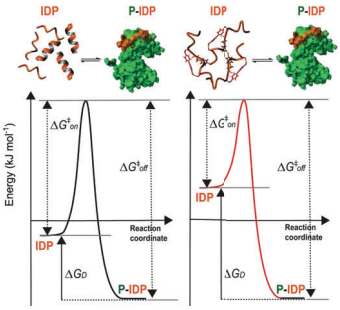

Figure 3. Thermodynamics of binding in the presence of Aurora-A. (a) ITC thermodynamic signatures of linear TACC-$3_{518-532}$ and **(b)** constrained TACC-$3_{518-532-S/E-Bph-I/fP}$ binding to Aurora-$A_{122-403-C290A/C393A}$; **(c)** Diagram schematically illustrating the hypothetical free energy profile of a one-step/one-barrier peptide-protein binding event for a linear and a constrained peptide.

TACC-$3_{518-532-L/R-Bph-I/fP}$ as an allosteric inhibitor of the N-MYC/Aur-A interaction

Constrained peptidomimetics exhibited limited evidence of TPX2 displacement, indicating promising specificity for the TACC-3 binding site (IC50 >> 200 μM). Surprisingly, the constrained variants were observed to out-compete N-MYC.

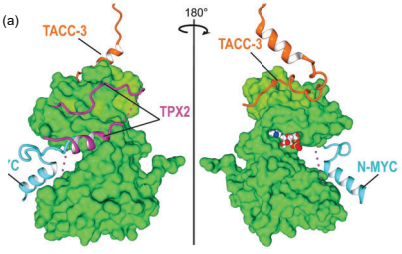

ALLOSTERIC MECHANISM

$$IC_{50} = K_B\left[\frac{[A] + K_A}{\alpha[A] + K_A}\right]$$

$$\alpha = 1$$

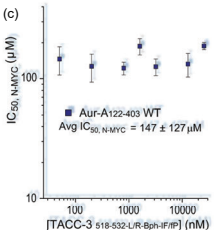

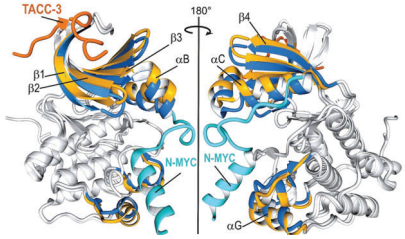

Figure 7. Constrained TACC-$3_{518-532_Bph_LR_IF/fP}$ as an allosteric inhibitor of N-MYC/Aurora-A PPI: (a) Aligned x-ray crystal structures of TACC-3/Aurora-A complex (PDB: 5ODT), TPX2 (PDB: 1OL5), and N-MYC (PDB: 5G1X); **(b)** FA competition assay of control N-MYC_{61-89} (black line) and constrained TACC-3 $_{518-532_Bph_LR_IF/fP}$ (forest green) against FAM-Ahx-N-MYC_{61-89} (200 nM), and reverse assay in the presence of Aurora-A; **(c)** Competition FA N-MYC IC50's values for N-MYC_{61-89} at increased TACC-$3_{518-532_Bph_LR_IF/fP}$ concentrations; **(d)** X-ray crystal structures of TACC-3/Aurora-A and N-MYC/Aurora-A complexes..

Conclusions

We have developed a series of **constrained peptides that inhibit TACC3/Aurora A PPI with up to 12-fold enhanced IC_{50}/K_d values**. NMR and MD analysis of the peptides show that improved affinities are achieved due to the combined effect of **restricting the conformational landscape of the peptide** (Bph constraints), **fine-tunning the orientational preference of the key Phe525** (4I and 4Br-Phe substitutions) and **conformational pucker-ring selection at the Pro528 level** (4F-Pro). Our minimal peptidomimetics are sufficient to induce the conformational changes needed to **activate the kinase by binding only the "F" pocket on the N-lobe, and to allosterically displace N-MYC from its binding site**. Knocking-out the TACC-3/Aurora-A interaction without affecting kinase activity represents a promising alternative to active-site kinase inhibition. Similarly, inhibition of the Aurora-A/N-MYC interaction without downregulating other Aurora-A essential functions also represents a major target for anticancer drug-development.

References

1. Barr, A. R.; Gergely, F. *J Cell Sci.* **2007**, 120 (Pt 17), 2987–2996.
2. Burgess, S. G.; Peset, I.; Joseph, N.; Cavazza, T.; Vernos, I.; Pfuhl, M.; Gergely, F.; Bayliss, R. *PLOS Genetics.* **2015**, 36.
3. Burgess, S. G.; Mukherjee, M.; Sabir, S.; Joseph, N.; Gutiérrez-Caballero, C.; Richards, M. W.; Huguenin-Dezot, N.; Chin, J. W.; Kennedy, E. J.; Pfuhl, M.; Royle, S. J.; Gergely, F.; Bayliss, R. *The EMBO Journal*. **2018**, 37 (8).
4. Ha, G.-H.; Kim, J.-L.; Breuer, E.-K. Y. *Cancer Letters*. **2013**, 336 (1), 24–335.

Acknowledgements
This work is financed by the Biotechnology and Biological Sciences Research Council (BBSRC) BB/V003577/1

Biotechnology and Biological Sciences Research Council

Synthesis, conformational analysis and biological activity evaluation of novel antiviral peptides blocking the SARS-CoV-2 cell-entry

M. Quagliata[1,2], M.A. Stincarelli[3], A. Di Santo[1,4], L. Pacini[1,2], F. Real-Fernandez[1,5], R. Arvia[3], S. Rinaldi[5], S. Giannecchini[3], A.M Papini[1,2], P. Rovero[1,4]

[1]Interdepartmental Research Unit of Peptide and Protein Chemistry and Biology, University of Florence, Sesto Fiorentino (FI), Italy
[2]Department of Chemistry "Ugo Schiff", University of Florence, Sesto Fiorentino (FI), Italy
[3]Department of Experimental and Clinical Medicine, University of Florence, Florence, Italy
[4]Department of Neurosciences, Psychology, Drug Research and Child Health, University of Florence, Sesto Fiorentino (FI), Italy
[5]CNR – Istituto di Chimica dei Composti Organometallici (CNR-ICCOM), Sesto Fiorentino (FI), Italy
E-mail: michael.quagliata@unifi.it

Introduction

ACE2-RBD interaction

The infection pathway starts when the RBD of the viral spike protein interacts with the ACE2, which acts as a host receptor for the RBD expressed on the host cell surface.

Most of ACE2 residues involved in the interaction with RBD are located in the α-helix α1, namely the portion ACE2(24-42).
In particular, the key residues are: Q24, T27, D30, K31, H34, E35, E37, D38, Y41 e Q42

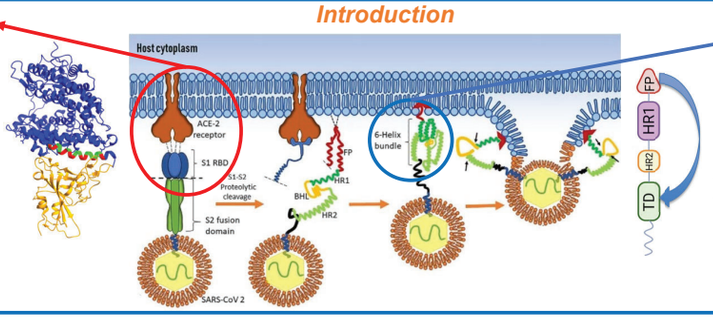

IFP-MPER interaction

Once the subunit S1 is primed by the proteases, the Fusion Peptide (FP) is free to insert into the host membrane, then the HR1 and HR2 start to interact each other forming the so-called 6-Helix Bundle (6-HB), pulling the viral and the host membrane closer. [1]

The Internal Fusion Peptide (IFP) plays a key role in the bundle formation because it interacts with the Membrane Proximity External Region (MPER) contained in the Transmembrane Domain (TD). [2]

Design and antiviral activity of the novel peptides

Possible antiviral peptide ?

ACE2(24-42): capable of interacting with RBD...

...but

Computational studies have shown that α1 unfolds rapidly and therefore the binding with RBD is weak.[3]

Cu(I) catalyzed Azide-Alkyne Cycloaddition (CuAAC) was exploited to obtain conformational stable analogs [4,5]

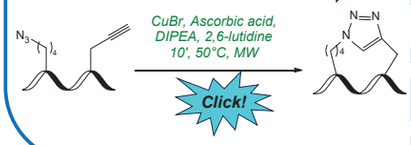

Peptide	Sequence	IC_{50} (mean ± SD) μM[a]	Sequence	Peptide
		2.80±2.68	Ac-SGWTFGAGAALQIPFAMQMAYRF-NH_2	**IFP**
		0.71±2.11	Ac-WTFGAGAALQIPFAMQMAYRF-NH_2	**PN21**
ACE2(24-42)	Ac-QAKTFLDKFNHEAEDLFYQ-NH_2	>100		
		0.20±1.11	Ac-FGAGAALQIPFAMQMAYRF-NH_2	**PN19**
		2.79±1.96	Ac-AGAALQIPFAMQMAYRF-NH_2	**PN17**
P1	 Ac-QAKT-NHCHCO-LDK-NHCHCO-NHEAEDLFYQ-NH_2	>100		
		8.33±3.60	Ac-SGWTFGAGAALQIPFAMQMAY-NH_2	**PC21**
		9.43±2.44	Ac-SGWTFGAGAALQIPFAMQM-NH_2	**PC19**
P2	 Ac-QAKTFLDK-NHCHCO-NHE-NHCHCO-EDLFYQ-NH_2	>100		
		97.94±21.84	Ac-SGWTFGAGAALQIPFAM-NH_2	**PC17**
		46.83±9.97	Ac-WTFGAGAALQIPFAMQMAY-NH_2	**PNC19**
P3	Ac-QAKTFLDKFNHE-NHCHCO-EDL-NHCHCO-YQ-NH_2	8.89±6.03		
		>100	Ac-FGAGAALQIPFAMQM-NH_2	**PNC15**
		1.70±0.52	Ac-LQIPFAMQMAYRF-NH_2	**PN13**
P4	Ac-QAKT-NHCHCO-LDK-NHCHCO-NHE-NHCHCO-EDL-NHCHCO-YQ-NH_2	>100		
		5.93±9.74	Ac-FAMQMAYRF-NH_2	**PN9**

[a]IC_{50} values are measured by inhibitory viral plaque reduction assay (PRA) on Vero E6 cells.

Conformational analysis

IFP peptide: capable of interacting with MPER...

...but

IFP has a promising antiviral activity against SARS-CoV-2 (IC_{50} = 2,80 ± 2,68 μM) but it is a 23mer peptide.

Shortening the IFP to find the minimal active sequence

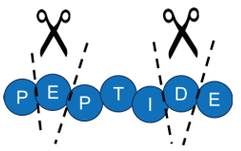

Ala-scan and conformational analysis

Results

CD spectra of the peptides to evaluate their secondary structure. The experiment were performed both in neat H_2O and in H_2O:TFE 1:1 mixture. Simulation of percentage of secondary structure in H_2O:TFE (1:1) and in H_2O (in bracket) evaluated using online tool BestSel.

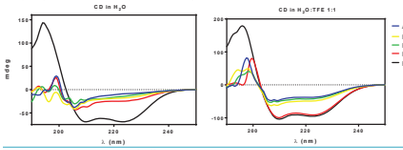

Peptide	α-helix	β-strand	β-turn	Random coil
ACE2(24-42)	63.3 (8.8)	23.6 (15.1)	13.1 (14.7)	0.0 (61.3)
P1	40.1 (5.4)	13.5 (22.9)	8.5 (16.9)	37.9 (54.7)
P2	37.3 (7.7)	15.7 (25.8)	10.2 (14.6)	36.8 (51.9)
P3	57.0 (34.6)	32.8 (31.7)	5.2 (25.1)	5.0 (8.6)
P4	96.2 (49.5)	0.0 (1.5)	3.8 (7.0)	0.0 (42.0)

Peptides affinity constant with the sequence MPER by SPR

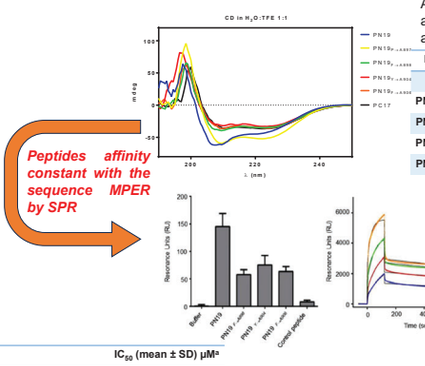

Ala-scan of the peptide PN19 to evaluate the importance of each residue for the antiviral activity and CD spectra to find a correlation between secondary structure and biological activity.

Peptide	Sequence	IC_{50} (mean ± SD) μM	α-helix	β-strand	β-turn	random
PN19	Ac-FGAGAALQIPFAMQMAYRF-NH_2	0.20±1.11	56,3	19,2	13,1	11,5
$PN19_{F\rightarrow A897}$	Ac-FGAGAALQI*A*FAMQMAYRF-NH_2	0.24 ± 0.10	61,3	28,5	10,2	0
$PN19_{F\rightarrow A898}$	Ac-FGAGAALQIP*A*AMQMAYRF-NH_2	57.64 ± 66.15	26,2	22,1	13,8	37,9
$PN19_{Y\rightarrow A904}$	Ac-FGAGAALQIPFAMQMA*A*RF-NH_2	28.32 ± 47.96	50,7	5,4	12,3	31,6
$PN19_{F\rightarrow A906}$	Ac-FGAGAALQIPFAMQMAYR*A*-NH_2	2,65 ± 4.45	47,4	26,0	26,6	0
PC17	Ac-SGWTFGAGAALQIPFAM-NH_2	97.94 ± 21.84	23,5	21,7	38,9	15,9

Surface Plasmon Resonance (SPR) experiments to measure the affinity constant of the peptides with the sequence MPER25c (CLIDLQELGKYEQYIKWPWYIWLGF). Only the peptide PN19 has a well establish interaction with MPER peptide, with a K_D= 9,44 nM

Derivatization with Cholesterol

Synthesis of cholesteryl analogs of peptide PN19, to exploit the lipidic rafts present in the viral membrane.[6] Moreover, different types of spacers were introduced, i.e. PEG_5 and/or GSGSG pentamer, to evaluate the importance of the distance between the active peptide and the cholesterol moiety for the antiviral activity.

Peptide	Sequence	IC_{50} (mean ± SD) μM[a]
[C^1(chol)]PN19	Ac-C(chol)FGAGAALQIPFAMQMAYRF-NH_2	0.38 ± 0.11
[C^{20}(chol)]PN19	Ac-FGAGAALQIPFAMQMAYRFC(chol)-NH_2	0.08 ± 0.04
[C^1(chol)]PN19-spacer	Ac-C(chol)-GSGSG-FGAGAALQIPFAMQMAYRF-NH_2	0.98 ± 0.12
[C^{25}(chol)]PN19-spacer	Ac-FGAGAALQIPFAMQMAYRF-GSGSG-C(chol)-NH_2	0.74 ± 0.34
[C^1(chol)]PN19-PEG_5	Ac-C(chol)-*PEG_5*-FGAGAALQIPFAMQMAYRF-NH_2	3.70 ± 1.01
[C^{20}(chol)]PN19-PEG_5	Ac-FGAGAALQIPFAMQMAYRF-*PEG_5*-C(chol)-NH_2	0.14 ± 0.12
[C^1(chol)]PN19-spacer-PEG_5	Ac-C(chol)-*PEG_5*-GSGSG-FGAGAALQIPFAMQMAYRF-NH_2	1.75 ± 0.71
[C^{25}(chol)]PN19-spacer-PEG_5	Ac-FGAGAALQIPFAMQMAYRF-GSGSG-*PEG_5*-C(chol)-NH_2	0.04 ± 0.02

[a]IC_{50} values are measured by inhibitory viral plaque reduction assay (PRA) on Vero E6 cells.

Antiviral activity evaluation

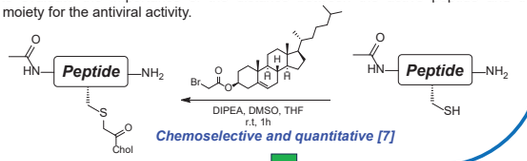

Chemoselective and quantitative [7]

Conclusions

The stabilizing effect increased by shifting the bridge position towards the C-terminal part or by increasing the number of stapled, but the too high rigid structure appears to hamper the antiviral activity.
In this scenario, the peptide **P3** represents a model peptide, with a flexible N-terminal and rigid C-terminal part. [8]

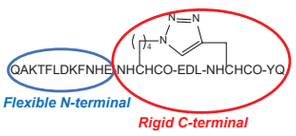

The studies on shortened sequences of the IFP peptide allows to find a shorter and more active peptide termed **PN19** with a nanomolar IC_{50}. Moreover, this screening point out the key role played by the aromatic residues in the sequence, as confirmed also by the Ala-scan.[9]

The addition of a cholesterol moiety in the N-terminal part of the peptide PN19 increases dramatically the antiviral activity, reaching nanomolar range of IC_{50}. On the other hand, the cholesterol moiety in the C-terminal is detrimental. Regarding the distance between cholesterol and the active peptide sequence, only the addition of the pentamer GSGSG alone seems to decrease the activity.

References

[1] Shekhar, N. et al. *mSystems*, **2020**,5, 5, e00382-e00320. DOI: 10.1128/mSystems.00382-20
[2] Liao, Y. et al. *Biochemistry*, **2015**, 54, 1819–1830. DOI: 10.1021/bi501352u
[3] Han, Y. et al. *ACS Nano*, **2020**, 14, 5143–5147. DOI:10.1021/acsnano.0c02857
[4] Tornøe, C.W. et al. *J. Org. Chem*. **2002**, 67, 9, 3057–3064. DOI: 10.1021/jo011148j
[5] D'Ercole, A. et al. *Pept Sci*, **2020**,112, 4. DOI: 10.1002/pep2.24159
[6] Quagliata, M. et al. *J. Pept. Sci*., **2024**, 30, 2, e3541. DOI: 10.1002/psc.3541
[7] Ingallinella, P. et al. *Proc. Natl. Acad. Sci*., **2009**, 106, 14, 5801-5806. DOI: 10.1073/pnas.0901007106
[8] Quagliata, M. et al. *ACS Omega*, **2023**, 8, 25, 22665-22672. DOI: 10.1021/acsomega.3c01436
[9] Stincarelli, M.A. et al. *Virus Research*, **2023**, 334, 199170. DOI: 10.1016/j.virusres.2023.199170

https://doi.org/10.17952/37EPS.2024.P2080

Acknowledgment

For travel grant to Michael Quagliata

For Michael Quagliata's PhD scholarship

https://doi.org/10.17952/37EPS.2024.P2083

SYNTHESIS, CHARACTERIZATION AND BIOLOGICAL ACTIVITY EVALUATION OF A DUAL-DRUG BASED ON THE ANTIBACTERIAL PEPTIDE LUGDUNIN FUNCTIONALIZED WITH THE CARBONIC ANHYDRASE SULFONAMIDE INHIBITOR ACETAZOLAMIDE.

M. Quagliata[1, 2], F. Brenzini Biagioni[1, 2, 3], S. Giovannuzzi[4], V. De Luca[5], C. Capasso[5], A. Nocentini[4], C. T. Supuran[4], P. Rovero[1, 4], A.M Papini[1, 2]

[1]*Interdepartmental Research Unit of Peptide and Protein Chemistry and Biology, University of Florence, Sesto Fiorentino (FI), Italy*

[2]*Department of Chemistry "Ugo Schiff", University of Florence, Sesto Fiorentino (FI), Italy*

[3]*Normandie Université, UNIROUEN, INSA Rouen, CNRS, COBRA (UMR 6014) IRCOF, Mont-Saint-Aignan Cedex, France*

[4]*Department of Neurosciences, Psychology, Drug Research and Child Health, University of Florence, Sesto Fiorentino (FI), Italy*

[5]*Department of Biology, Agriculture and Food Sciences, Institute of Biosciences and Bioresources, CNR, Naples, Italy*

E-mail: michael.quagliata@unifi.it

Acetazolamide (AAZ)



AAZ is a therapeutic used to treat glaucoma, epilepsy, acute mountain sickness, periodic paralysis, idiopathic intracranial hypertension, heart failure and to alkalinize urine. Moreover, acetazolamide is a first-generation carbonic anhydrase inhibitor

Potent inhibitor

Carbonic anhydrase (CA)



CA is a zinc-containing enzyme that plays a crucial role in various physiological processes by catalyzing the reversible hydration of carbon dioxide (CO_2) into carbonic acid (H_2CO_3). This family of metal enzymes is a promising target for the development of antibacterial compounds because it plays a key role for the survival of the microorganism.

Three major classes

α → Primarily found in animals but also present in some bacteria (Gram negative) and green algae. These are carbonic anhydrases present in humans and sulfonamides are powerful inhibitors.

β → Widely found in microorganisms, algae, plants, and invertebrates.

γ → Primarily found in bacteria [1]

β and γ are more difficult to inhibit with sulfonamides [2]

Dual drug Lugdunin-Acetazolamide

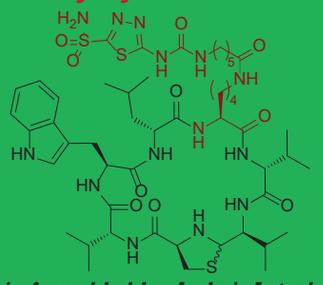

Synthesis of a novel dual drug Lugdunin-Acetazolamide, by replacing L-Val[1] with L-Lys[4] and exploiting the amino function for subsequent coupling.

Lugdunin

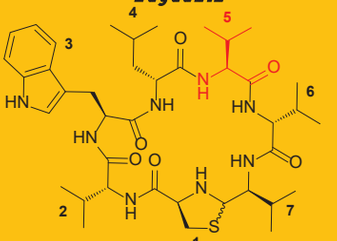

Lugdunin is an antibiotic thiazolidine-containing cyclopeptide. It was isolated in 2016 from *Staphylococcus lugdunensis*. This cyclopeptide displays potent antimicrobial activity against a broad spectrum of Gram-positive bacteria, including challenging-to-treat methicillin-resistant Staphylococcus aureus (MRSA) (MIC = 3.9 μM). In particular, it inhibits target bacteria by dissipating their membrane potential, forming supramolecular peptide channels [3,4].

An Ala-scan performed by Schilling et al. showed that changing **L-Val[5]** with an **L-Ala[5]** residue does not influence the antimicrobial activity [5].

Building blocks synthesis

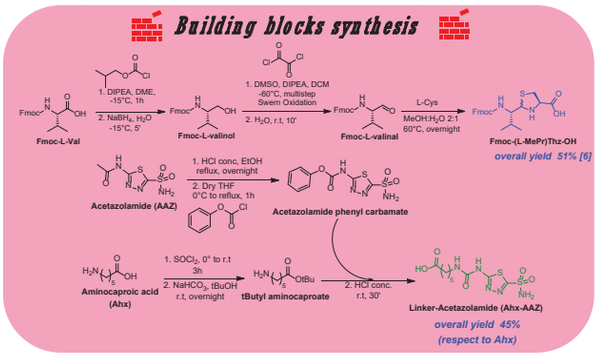

Cyclopeptide synthesis

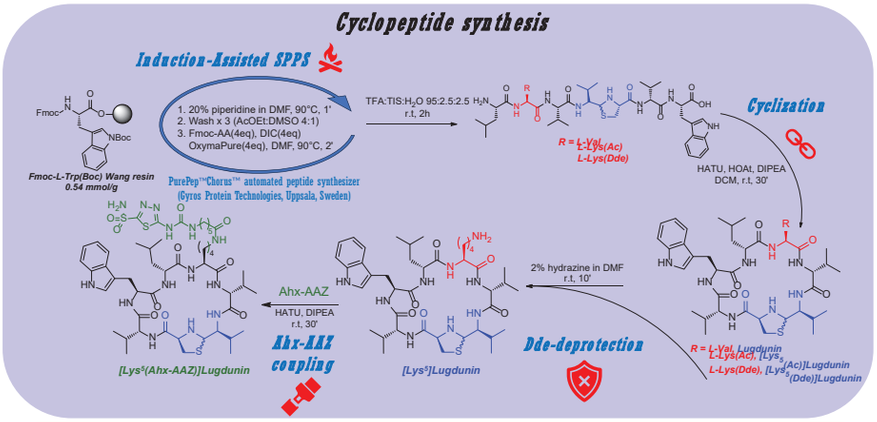

Pathogenic carbonic anhydrases tested

Carbonic anhydrase	Pathogen	Gram
MtbCA1, CA2, CA3	*Mycobacterium tuberculosis*	+
MscCA	*Mammaliicoccus sciuri*	+
PgiCA	*Porphyromonas gingivalis*	-
EcoCA	*Escherichia coli*	-
HpCA	*Helicobacter pylori*	-
VchCA	*Vibrio cholerae*	-
BpsCA	*Burkholderia pseudomallei*	-
SmuCA	*Streptococcus mutans*	+
NgCA	*Neisseria gonorrhoea*	-
EfCA	*Enterococcus faecalis*	+

Analytical characterization of Lugdunin analogs

Cyclopeptide	HPLC gradient (% B)ª, Rf (min)	HPLC purity (%)	Yield[b] (%)	ESI-MS (m/z) found[c] (calcd)
Lugdunin	30-90, 4.60-4.82	91	60	783.80 (783.45)
[Lys5(Ac)]Lugdunin	30-90, 3.72-3.87	95	45	854.85 (854.49)
[Lys5(Ahx-AAZ)]Lugdunin	30-90, 3.52-3.62	90	20	1132.10 (1132.52)

The cyclopeptides were characterized by RP-HPLC Alliance Chromatography system (Waters, Milford Massachusetts, USA) with a BEH C18 (1.7 μm, 2.1× 50 mm) column at 35°C, 0.6 mL/min, coupled to a single quadrupole ESI-MS Micromass ZQ (Waters, Milford Massachusetts, USA). Eluents: 0.1% (v/v) TFA in H_2O (A) and 0.1% (v/v) TFA in ACN (B), λ 215 nm. Gradient times: [a]5min. [b]Calculated as the ratio of obtained mass to theoretical mass. ESI-MS: detected as [c][M+H]⁺.

Inhibition by Stopped-Flow technique

Inhibition of different carbonic anhydrases

Inhibitory constant (K_I) expressed in nM concentration, using Acetazolamide (AAZ) as standard drugs. Mean from 3 different assays, by a stopped Flow-Technique (errors were in the range of ± 5-10 % of the reported values).

	α Carbonic anhydrase						β Carbonic anhydrase									γ Carbonic anhydrase				
Inhibitor	**hCA I**	**hCA II**	**HpCAα**	**VchCAα**	**NgCAα**	**EfCAα**	**MtbCA1β**	**MtbCA2β**	**MtbCA3β**	**MscCAβ**	**PgiCAβ**	**EcoCAβ**	**HpCAβ**	**VchCAβ**	**BpsCAβ**	**SmuCAβ**	**PgiCAγ**	**EcoCAγ**	**VchCAγ**	**BpsCAγ**	**EfCAγ**
[Lys5(Ac)]Lugdunin	>100000	>100000	>100000	>100000	>100000	>100000	>100000	>100000	>100000	>100000	>100000	>100000	>100000	>100000	>100000	>100000	>100000	>100000	>100000	>100000	>100000
[Lys5(Ahx-AAZ)]Lugdunin	332.9	88.9	23.4	19.3	34.9	70.2	373.4	33.6	59.0	184.9	81.4	343.6	70.6	1125	612.4	170.3	478.5	432.5	445.2	288.2	427.1
AAZ	250.0	12.0	21.0	6.8	74.1	56.7	480.0	9.1	104.0	628.0	214.0	227.0	40.0	4512	745.0	344.0	324.0	248.0	473.0	149.0	322.8

In-vitro assays against E.coli

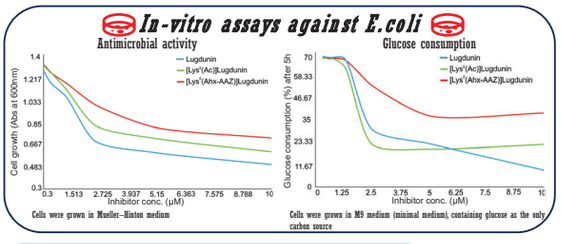

Conclusions

The Lugdunin-acetazolamide conjugate showed promising inhibitory activity in several pathogenic carbonic anhydrases. In particular, compared to acetazolamide, the conjugate shows greater activity in β carbonic anhydrases and comparable activity in α and γ ones.

Regarding the assays against *E.coli*, all three Lugdunin analogs interfered with both bacterial growth and glucose consumption at different concentrations. This demonstrates that Lugdunin-based derivatives are also active against Gram-negative bacteria.

Perspectives

The synthetic Lugdunin analogs will be tested against various pathogenic Gram-positive and Gram-negative bacteria. In addition, the synthesis of Lugdunin analogs with benzensulfonamide replacing sulfonamide will be performed.

In addition, we will explore a triazolyl-based linker between Lugdunin and the inhibitor, formed via Cu(I)-catalyzed azide–alkyne cycloaddition (CuAAC).

References

[1] Supuran, C.T. *Nat. Rev. Drug. Discov.* **2008**, 7, 168-181. DOI: 10.1038/nrd2467

[2] Zimmermann, S.A. et al. Curr. Pharm. Des. 2008, 14, 716-721. DOI: 10.2174/138161208783877929

[3] Zipperer, A. et al. *Nature* **2016**, 535, 511-516. DOI: 10.1038/nature18634

[4] Ruppelt, D. et al. *Nat. Commun.* **2024**, 15, 3521. DOI: 10.1038/s41467-024-47803-6

[5] Schilling, N.A. et al. *Angew. Chem. Int. Ed* **2019**, 58, 9234-9238. DOI: 10.1002/anie.201901589

[6] Saur, J.S. et al. *J. Med. Chem.* **2021**, 64, 4034−4058. DOI: 10.1021/acs.jmedchem.0c02170

Acknowledgments

For travel grant to Michael Quagliata

For Michael Quagliata's PhD scholarship

Phosphorylation and GlcNAcylation of the RNA polymerase II C-Terminal domain and their effect on recognition by Pin1 and Protein Phosphatase 1

Alina Herfort[1], **Emanuele Piemontese**[1], **Corina Maller**[2], **Maja Köhn**[2], **Oliver Seitz**[1]*

[1] Institut für Chemie, Humboldt-Universität zu Berlin, Brook-Taylor-Str. 2, 12489 Berlin (Germany)

[2] BIOSS Centre for Biological Signaling, Schänzlestr. 18, 79104 Freiburg (Germany)

https://doi.org/10.17952/37EPS.2024.P2085

INTRODUCTION

C-terminal domain (CTD) of the RNA polymerase II subunit RBP1 consists of 52 multiple repeats of the consensus ($Y_1S_2P_3T_4S_5P_6S_7$)-unit.[1]

CTD landing hub for proteins to regulate[2]

- Transcription
- Splicing
- Chromatin remodeling

CTD (consensus) undergoes posttranslational modifications (PTMs)

- **Phosphorylation** (Y_1, $S_{2/5/7}$, T_4)
- Glycosylation (GlcNAc) ($S_{5/7}$)
- *Cis/trans*-Isomerization ($P_{3/6}$)

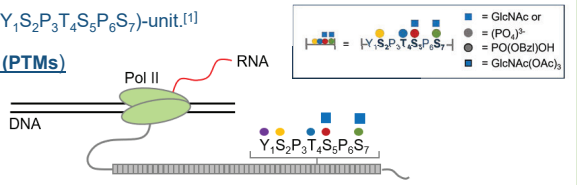

CONCEPT

Unknown if CTD readers and CTD modifiers:

- engage in **multivalent interactions**
- recognize specific **multiphosphorylation** patterns
- are affected by **glycosylation (GlcNAC)**

Idea:

But: No indication how many and which of the 52 repeats carry PTMs

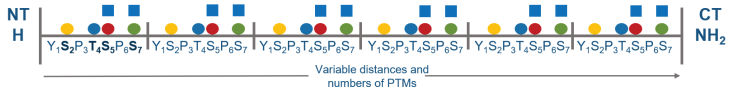

- **Chemical synthesis (SPPS)** of CTD-like peptides with **defined** multiple variations of **phospho-(glyco) sites**
- **Screening** to decipher the multiphoshorylation(-glycosylation)-specific recognition patterns (**FP – Assay**)

RESULTS

1. Positional scan of monophoshorylated CTD-peptides (FP-Assay)

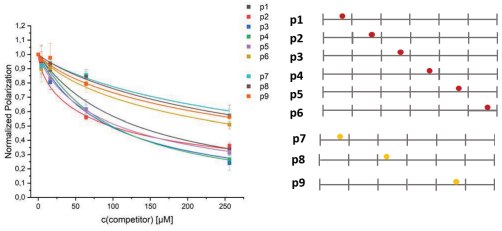

	IC_{50} [µM]
p1	**131 ± 22**
p2	97 ± 9
p3	**96 ± 9**
p4	99 ±3
p5	107 ± 2
p6	**273 ± 25**
p7	416 ± 186
p8	**360 ± 44**
p9	342 ± 38

→ **Pin1 prefers pS_5** over pS_2

→ Pin1 has **lower affinity** for pS_5 near **C-terminus**

3. Optimization of Synthesis of phospho-glyco peptides



S P

	Method I	Method II	Method III	Method IV	Method V
Fmoc-Ser(β-Ac_3GlcNAc)-OH	2,5 eq.	2,5 eq.	10 eq.	10 eq.	10 eq.
Activator System	HCTU/HOBt (2,5/2,5 eq.)	HATU/HOAt (2,5/2,5 eq.)	HATU/HOAt (10/10 eq.)	HATU/HOAt (10/10 eq.)	HATU/HOAt (10/10 eq.)
Base	DIEA (5 eq.)	DIEA (5 eq.)	NMM (10 eq.)	TMP (10 eq.)	TMP (10 eq.)
Time/Temp.	12 h/rt	12 h/rt	12 h/rt	12 h/rt	**1 h**/40 °C
Isomerization	18:82	10:90	7:93	7:93	7:93
Yield* [%]	63	55	85	95	**100**

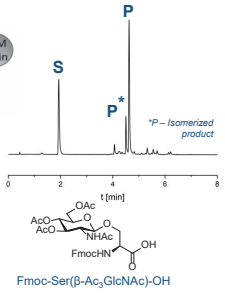

*Based on UPLC data

2a. Spatial screening for homobivalency-enhanced binding (FP-Assay)

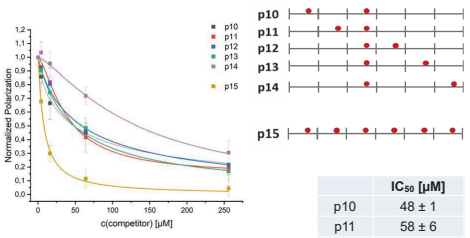

	IC_{50} [µM]
p10	48 ± 1
p11	58 ± 6
p12	59 ± 3
p13	49 ± 3
p14	137 ± 11
p15	8 ± 0,3

→ No bivalency-enhanced binding

→ No multivalency-enhanced binding of Pin1

4a. GlcNAcylated (S_7) phospho-peptides (FP-Assay)

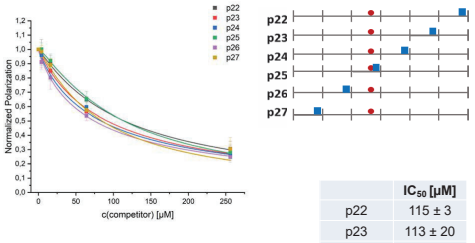

	IC_{50} [µM]
p22	115 ± 3
p23	113 ± 20
p24	**91 ± 8**
p25	**83 ± 5**
p26	**114 ± 5**
p27	74 ± 2

→ GlcNAcylation at S_7 does not influence recognition of pS_5 by Pin1

4b. GlcNAcylated (S_5) phospho-peptides (FP-Assay)

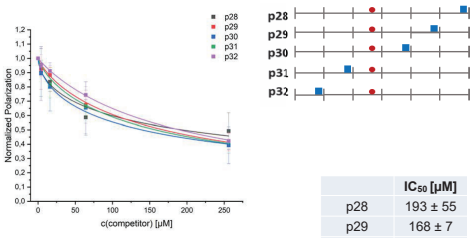

	IC_{50} [µM]
p28	193 ± 55
p29	168 ± 7
p30	**139 ± 10**
p31	**158 ± 16**
p32	190 ± 9

→ Minor but significant weakening of Pin1 binding due to GlcNAcylation at S_5

2b. Spatial screening for heterobivalency-enhanced binding (FP-Assay)

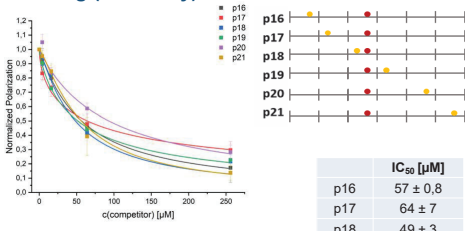

	IC_{50} [µM]
p16	57 ± 0,8
p17	64 ± 7
p18	49 ± 3
p19	52 ± 2
p20	93 ± 12
p21	57 ± 4

→ Negligible influence of second phosphorylations ($pS_{2/5}$) on binding of Pin1

5a. Phosphatase (PP1) activity:

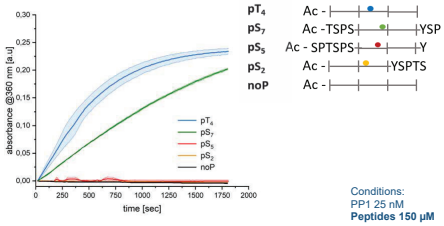

Conditions:
PP1 25 nM
Peptides 150 µM

→ PP1 acts on **pT_4** and **pS_7**

5b. Phosphatase (PP1) activity: positional scan

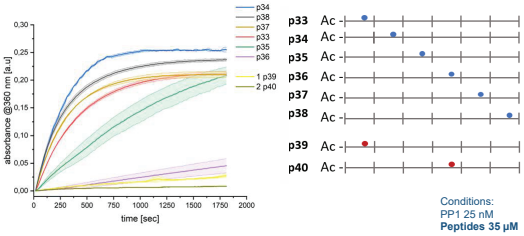

Conditions:
PP1 25 nM
Peptides 35 µM

→ High activity on **longer** (42 AA) peptides

CONCLUSION & OUTLOOK

The CTD modifier Pin1 prefers pS_5 over pS_2. Contrary to previous report[3], bivalency-enhanced binding was not observed. Current data suggests remarkable tolerance of Pin1 for *O*-GlcNAcylation at gS_7, though binding to gS_5 is slightly reduced. This modification may hinder future phosphorylation at this site. Future work will examine the effect of *O*-GlcNAcylation at T_4 (reported to induce turn-like structures[4]), at gS_7 in biphosphorylated (pS_5) peptides and the influence of multi-*O*-GlcNAcylation. Furthermore, the influence of a third phospho site (pS_2) on the recognition of Pin1 will be explored.

The phosphatase PP1 has a preference for removing phosphorylation at pT_4 and pS_7 residues and showed higher activity on longer peptides. For the phosphatase PP1 the effect of *O*-GlcNAcylation on the activity of CTD-like peptides with pT_4 residues is not known and needs also to be tested. Other phosphatases like Ssu7 that dephosphorylates pS_5 residues and interact together with Pin1 will be used to decipher which phosphorylation patterns are important for the recognition of Pin1.

[1] D. Eick, *et al.*, *Chem. Rev.* **2013**, 113, 8456–8490.
[2]. D. E. Lyons, *et al.*, *Transcription* **2020**, *11*, 66–82.
[3] M. A. Verdecia, *et al.*, *Nat Strut Biol.* **2000**, 7, 639–643.
[4] E. Simanek, *et al.*, *J. Am. Chem. Soc* **1998**, *120*, 11567–11575.

alina.herfort.1@hu-berlin.de
oliver.seitz@hu-berlin.de
Alina Herfort

SYN BIO RESEARCH TRAINING GROUP OF BIOACTIVE PEPTIDES
Gefördert durch DFG Deutsche Forschungsgemeinschaft
HUMBOLDT-UNIVERSITÄT ZU BERLIN

How a single non-conventional amino acid can modify the effectiveness of amphibian antimicrobial peptides

Maria Rosa Loffredo[1], Bruno Casciaro[1], Giacomo Cappella[1], Rosa Bellavita[2], Diego Brancaccio[2], Floriana Cappiello[1], Francesco Merlino[2], Paolo Grieco[2], Lorenzo Stella[3], Alfonso Carotenuto[2], Maria Luisa Mangoni[1]

[1]Department of Biochemical Sciences, Laboratory Affiliated to Istituto Pasteur Italia-Fondazione Cenci Bolognetti, Sapienza University of Rome, 00185 Rome, Italy;
[2]Department of Pharmacy, University of Naples "Federico II", Via D. Montesano 49, 80131 Naples, Italy.
[3] Department of Chemical Science and Technologies, University of Rome Tor Vergata, 00133 Rome, Italy.

https://doi.org/10.17952/37EPS.2024.P2086

Background

Esculentin(1-21) [Esc(1-21)] is a short-sized cationic antimicrobial peptide (AMP) corresponding to the N-terminal region of the frog-skin AMP esculentin-1a. It is endowed with a fast rate of killing activity, especially against Gram-negative bacteria, by a membrane perturbing mechanism of action.

Esculentin-1a

GIFSKLAGKKIKNLLISGLKNVGKEVGMDVVRTGIDIAGCKIKGEC

Esc(1-21) GIFSKLAGKKIKNLLISGLKG-NH_2 +6 Basic residues

- **Short size**
- **A large spectrum of activity (Gram$^-$, Gram$^+$, fungi)**
- **A potent activity against planktonic and biofilm forms of *Pseudomonas aeruginosa* (Gram$^-$).**



Rana esculenta

Antimicrobial activity of Esc(1-21) against reference strains and clinical isolates of *P. aeruginosa*

[PEPTIDE] CAUSING 99,9% KILLING OF PLAKTONIC CELLS	[PEPTIDE] CAUSING 95% KILLING OF BIOFILM CELLS
1 μM	12.5-25 μM

RESULTS

Design and Synthesis of Glycine-Replaced Derivative of Esc(1-21)

Fig. 1 Primary structure of Esc(1-21) and its derivative

GIFSKLAGKKIKNLLISGLKG-NH_2 Esc(1-21)

GIFSKLAAibKKIKNLLISGLKG-NH_2 [Aib[8]]

Residue variation is highlighted in red.
The last glycine is amidated on the C-terminus.

With the aim to increase the biological activity of Esc(1-21) against Gram-positive bacteria we explored the effect of the **replacement** of Glycine amino acid residue in **position 8** with a non-coded amino acid, (**Fig. 1**) **α-aminoisobutyric acid, [Aib[8]].**

Antimicrobial activity of [Aib[8]]

Strain	MIC (μM) Esc (1-21)	MIC (μM) [Aib[8]]
Gram-Negative		
E. coli ATCC 25922	1.56	0.78
A. baumannii ATCC 19606	1.56	0.78
P. aeruginosa ATCC 25853	3.12	3.12
Gram-Positive		
S. epidermidis ATCC 12228	3.12	0.78
S. aureus ATCC 25923	>100	12.5
S. aureus MDR #1	>100	12.5
S. aureus MDR #2	100	12.5
S. aureus MDR #3	100	12.5
S. aureus MDR #4	>100	6.25

Tab. 1 Antimicrobial activity of Esc-peptides

The parent peptide Esc (1-21) did not show any antibacterial effect against *S. aureus*. On the contrary, **[Aib[8]]** showed strong activity against the Gram-positive *S. epidermidis* strain, and it was also effective against the Gram-positive *S. aureus* ATCC 25923 and multi-drug resistant strains **(Tab. 1)**.

Effect of [Aib[8]] on Cell Viability

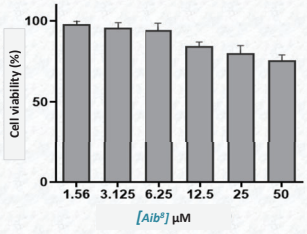

[Aib[8]] did not induce any significant cytotoxic effect on HaCaT cells up to a concentration of 25 μM after 24h of treatment on metabolically active cells **(Fig. 2)**.

Fig. 2 Effect of [Aib[8]] on the viability of HaCaT cells was evaluated using the MTT assay after 24 h treatment. All data are expressed as percentage with respect to the untreated control cells.

Antibiofilm activity of [Aib[8]]

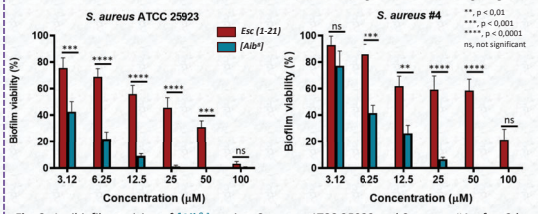

Fig. 3. Antibiofilm activity of [Aib[8]] against S. aureus ATCC 25923 and S. aureus #4, after 2 h of treatment. Biofilm viability was evaluated by MTT assay and expressed as percentage compared to that of untreated samples (bacterial biofilm not treated with the peptide, 100% viability).

Esc (1-21) was able to reduce ~90% of biofilm viability at 100 μM against the reference strain of *S. aureus* ATCC 25923. On the contrary, **[Aib[8]]** was able to reduce more than 90% biofilm viability of both reference and clinical isolates at concentrations of 25 μM, which are only 2- or 4-fold higher than the corresponding MIC against the two strains **(Fig. 3)**.

Stability of [Aib[8]] in Serum

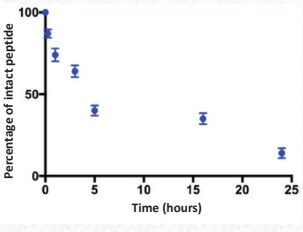

Fig. 4 Stability of [Aib[8]] in 50% bovine at different incubation times at 37°C. The percentage of non degraded peptide (%) after 1, 3, 4, 5, 16, and 24h incubation.

To investigate the stability of the promising **[Aib[8]]** derivate in biological fluids, the amount of intact peptide was monitored within 24h of incubation at 37°C in the presence of 50% fresh bovine serum **(Fig 4)**.

The percentage of intact peptide was ~90%, ~75%, and ~65% after 1, 3, and 4h of incubation, respectively. Interestingly, after 5h treatment the nondegraded amount of peptide was ~40% and the same percentage of intact peptide was detected even after 16h.

Structural Characterization of [Aib[8]]

Circular Dichroism Analysis in POPG/POCL LUVs

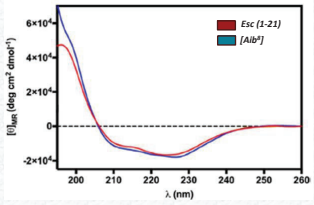

Fig 5. *Circular dichroism spectra of Esc-(1-21) and [Aib[8]] at 20 μM measured in the presence of POPG/POCL (6:4 mol/mol) LUVs (500 μM).* **POPG**: 1-palmitoyl-2-oleoyl-sn-glycero-3-phosphoglycerol **POCL**: 1',3'-bis[1-palmitoyl-2-oleoyl-sn-glycero-3-phospho]-glycerol

In the presence of liposomes mimicking the Gram-positive bacterial membrane, both CD spectra were characteristic of a helical structure. The intensity ratio between the two minima was greater than 1.0, indicating a helical conformation in its oligomeric state **(Fig. 5)**.

NMR analysis in the presence of POPG/POCL bicelles

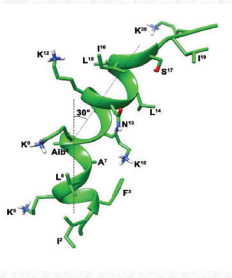

Fig.6. Representative structure of [Aib[8]] peptide. Backbone is shown as ribbon and helical axes are shown as dotted lines.

An α-helix from Phe^3 to Leu^6 can be observed followed by a 3_{10} helix from Ala^7 to Lys^9 and again by an α-helix from Lys^{10} to Ile^{16};
C-terminal tail has also tendency to the helix but turns out to be more flexible.
The structure can be described as a distorted helix, bent on the Aib^8 residue **(Fig. 6)**.

Characterization of Mechanism of Action of [Aib[8]]

Cytoplasmic Membrane Perturbation

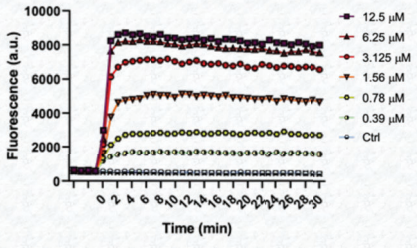

Fig 7. Kinetics of cytoplasmic membrane permeabilization of S. aureus ATCC 25923. Sytox Green probe (1 μM) was able to bind nucleic acids upon the impairment of the cytoplasmic membrane, resulting in an increase of fluorescence intensity. Control is given by microbial cells without peptide.

To verify the membrane perturbation mechanism of action of **[Aib[8]]** against Gram-positive bacteria, the fluorescent probe Sytox Green was employed to carry out fluorescence studies on *S. aureus* ATCC 25923 during the first 30 minutes (**Fig.7**).
[Aib[8]] induced a fast, and dose-dependent membrane perturbation process. Already within the first minutes from its addition, the highest values of fluorescence intensity were recorded at the concentration range of 6.25-12.5 μM.

Membranolytic Mechanism by CF Leakage from POPG/POCL LUVs

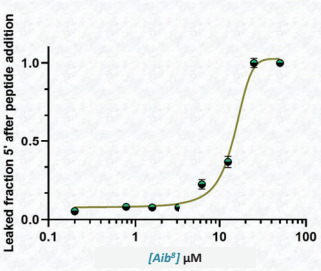

Fig 8. Effect of different concentrations of [Aib[8]] on the leakage of CF encapsulated into POPG/POCL (6:4, mol:mol) LUVs. LUVs were used at a final lipid concentration of 100 μM.

The membranolytic mechanism of **[Aib[8]]** and the extent of peptide-induced membrane injury were also explored by using artificial large unilamellar vesicles (LUVs), mimicking the composition of the membrane of Gram-positive bacteria and loaded with fluorescent probe carboxyfluorescein (CF).
[Aib[8]] displayed a fast membrane-perturbing activity with a total CF leakage within 5 min from its addition to the LUVs at 25 μM **(Fig. 8)**.

References

Luca, V. et al. Esculentin(1−21), an amphibian skin membrane-active peptide with potent activity on both planktonic and biofilm cells of the bacterial pathogen Pseudomonas aeruginosa. *Cell. Mol. Life Sci.* 2013, *70*, 2773−2786.
Loffredo, MR. Et al. Strategic Single-Residue Substitution in the Antimicrobial Peptide Esc(1-21) Confers Activity against Staphylococcus aureus, Including Drug-Resistant and Biofilm Phenotype. ACS Infect Dis. 2024 Jun 7. doi: 10.1021/acsinfecdis.4c00130.
Di Grazia, A. et al. D-Amino acids incorporation in the frog skin-derived peptide esculentin-1a(1−21)NH2 is beneficial for its multiple functions. Amino Acids 2015, 47, 2505−2519.

Conclusion

Our findings have contributed to explain how the incorporation of unconventional amino acids is a valid strategy to obtain promising candidates for the development of new anti-infective therapies.

Acknowledgements

This research was partially supported by EU funding within the NextGeneration EU-MUR PNRR Extended Partnership initiative on Emerging Infectious Diseases (Project no. PE00000007, INF-ACT) to M.L.M and Fondazione Italiana per la Ricerca Cistica (Project FFC#4/2022) Delegazione FFC Ricerca di Roma e della Franciacorta e Val Camonica

DEVELOPMENT OF BIOACTIVE PEPTIDES OF COSMETIC INTEREST THROUGH ENVIRONMENTALLY SUSTAINABLE PROCESSES

LUCREZIA SFORZI [a,b] ; FOSCA ERRANTE [a,b] ; JOANNA MAKOWSKA [d] ; PAOLO ROVERO [a,b] ; ANNA MARIA PAPINI [a,c] .

a) Interdepartmental Research Unit of Peptide and Protein Chemistry and Biology, University of Florence, Sesto Fiorentino (FI), 50019, Italy;
b) Department of Neurosciences, Psychology, Drug Research and Child Health, University of Florence, Sesto Fiorentino (FI), 50019, Italy;
c) Department of Chemistry "Ugo Schiff", University of Florence, Sesto Fiorentino (FI), 50019, Italy;
d) Faculty of Chemistry, University of Gdańsk, Gdańsk, Poland.

https://doi.org/10.17952/37EPS.2024.P2087

lucrezia.sforzi@unifi.it

INTRODUCTION:

Peptides are more and more used in the cosmeceutical field to enhance skin beauty, health and appearance. Their synthesis is mainly performed by Solid Phase Peptide Synthesis (SPPS) that usually involves large quantities of harmful reagents and solvents like DMF, which has been recently banned by EU. This project aims to design, synthesize, and characterize metabolically stable peptides for cosmeceutical use, employing greener solvents and reagents to minimize environmental impact.

We focused our attention on **Waglerin-1**, a 22-mer peptide derived from tropical snake *Tropidolaemus wagleri*, characterized by an intramolecular disulfide bond that forms a rigid cysteine loop. The flexible N- and C- terminal parts as well as the disulphide bond contribute to the interaction of the toxin with the muscle nicotinic acetylcholine receptors (nAChR), classifying this toxin as cosmeceutical neurotransmitter-inhibiting peptide, endowed with botox-like activity.

WTX-1	GGKPDLRPc[CHPPC]HYIPRPKPR *Native peptide*
WTX-L	GGKPDLRPCHPPCHYIPRPKPR *Reduced peptide*
WTX-S	GGKPDLRPSHPPSHYIPRPKPR *Serine-containing peptide*

Stabilizing the structure of Waglerin-1 via CuAAC:

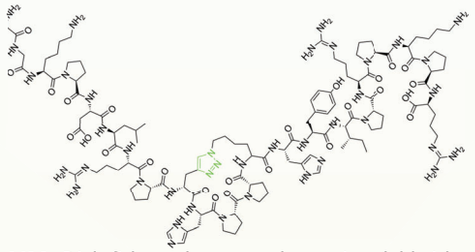

AIM: *Dislufide replacement by a triazolyl bridge*

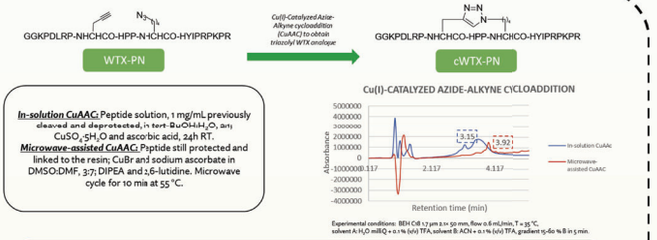

Greening N-terminal Fmoc removal:

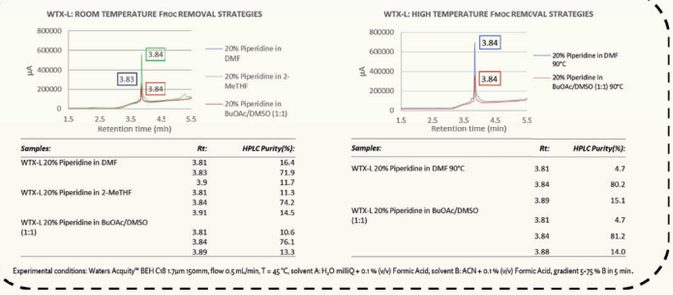

Samples:	Rt:	HPLC Purity(%):
WTX-L 20% Piperidine in DMF	3.81	16.4
	3.83	71.9
	3.9	11.7
WTX-L 20% Piperidine in 2-MeTHF	3.81	11.3
	3.84	74.2
	3.91	14.5
WTX-L 20% Piperidine in BuOAc/DMSO (1:1)	3.81	10.6
	3.84	76.1
	3.89	13.3

Samples:	Rt:	HPLC Purity(%):
WTX-L 20% Piperidine in DMF 90°C	3.81	4.7
	3.84	80.2
	3.89	15.1
WTX-L 20% Piperidine in BuOAc/DMSO (1:1)	3.81	4.7
	3.84	81.2
	3.88	14.0

Experimental conditions: Waters Acquity™ BEH C18 1.7µm 150mm, flow 0.5 mL/min, T = 45 °C, solvent A: H_2O milliQ + 0.1 % (v/v) Formic Acid, solvent B: ACN + 0.1 % (v/v) Formic Acid, gradient 5-75 % B in 5 min.

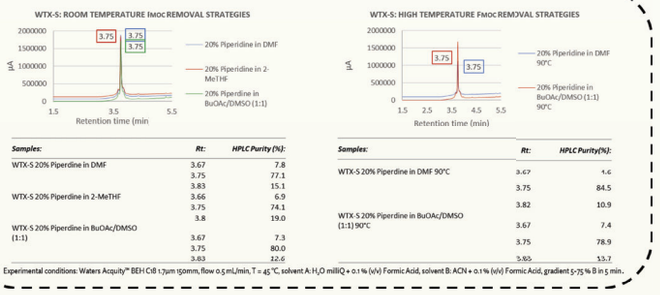

Samples:	Rt:	HPLC Purity (%):
WTX-S 20% Piperdine in DMF	3.67	7.8
	3.75	77.1
	3.83	15.1
WTX-S 20% Piperdine in 2-MeTHF	3.66	6.9
	3.75	74.1
	3.8	19.0
WTX-S 20% Piperdine in BuOAc/DMSO (1:1)	3.67	7.3
	3.75	80.0
	3.83	12.6

Samples:	Rt:	HPLC Purity(%):
WTX-S 20% Piperdine in DMF 90°C	3.67	4.6
	3.75	84.5
	3.82	10.9
WTX-S 20% Piperdine in BuOAc/DMSO (1:1) 90°C	3.67	7.4
	3.75	78.9
	3.85	13.7

Experimental conditions: Waters Acquity™ BEH C18 1.7µm 150mm, flow 0.5 mL/min, T = 45 °C, solvent A: H_2O milliQ + 0.1 % (v/v) Formic Acid, solvent B: ACN + 0.1 % (v/v) Formic Acid, gradient 5-75 % B in 5 min.

Greening the precipitation step:

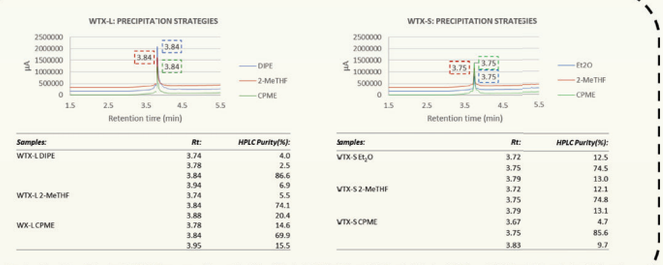

Samples:	Rt:	HPLC Purity(%):
WTX-L DIPE	3.74	4.0
	3.78	2.5
	3.84	86.6
	3.94	6.9
WTX-L 2-MeTHF	3.74	5.5
	3.84	74.1
	3.88	20.4
WX-L CPME	3.78	14.6
	3.84	69.9
	3.95	15.5

Samples:	Rt:	HPLC Purity(%):
WTX-S Et_2O	3.72	12.5
	3.75	74.5
	3.79	13.0
WTX-S 2-MeTHF	3.72	12.1
	3.75	74.8
	3.79	13.1
WTX-S CPME	3.67	4.7
	3.75	85.6
	3.83	9.7

Experimental conditions: Waters Acquity™ BEH C18 1.7µm 150mm, flow 0.5 mL/min, T = 45 °C, solvent A: H_2O milliQ + 0.1 % (v/v) Formic Acid, solvent B: ACN + 0.1 % (v/v) Formic Acid, gradient 5-75 % B in 5 min.

RESULTS:

Greening the N-terminal Fmoc removal; for both WTX-L and WTX-S, deprotection at RT and HT using 20% Piperidine in BuOAc/DMSO (1:1) gave better results, the only exception being the deprotection of WTX-S at high temperature.

Greening the precipitation step; WTX-L and WTX-S displayed opposite behavior. In both cases 2-MeTHF could be a good compromise between efficiency and yield.

FUTURE PERSPECTIVES:

- Application of the greener Fmoc removal strategy during the full synthesis and final comparison of the results with the one obtained by classic SPPS, combined with a further investigation on greener precipitation solvents.
- Optimization of the bioactive sequence by conformational analysis and structure-activity relationship studies.
- Development of an efficient method to prepare constrained triazolyl bridged analogues.

REFERENCES:

1. Errante, F., Ledwoń, P., Latajka, R., Rovero, P. & Papini, A. M. Cosmeceutical Peptides in the Framework of Sustainable Wellness Economy. Front. Chem. 8, 572923 (2020).
2. Schmidt, J. J., Weinstein, S. A. & Smith, L. A. Molecular properties and structure-function relationships of lethal peptides from venom of Wagler's pit viper, Trimeresurus wagleri. Toxicon 30, 1027–1036 (1992).
3. Al Musaimi, O., de la Torre, B. G. & Albericio, F. Greening Fmoc/ t Bu solid-phase peptide synthesis. Green Chem. 22, 996–1018 (2020).
4. Pacini, L. et al. Optimization of peptide synthesis time and sustainability using novel eco-friendly binary solvent systems with induction heating on an automated peptide synthesizer. J. Pept. Sci. 30, e3605 (2024).
5. Roice, M., Johannsen, I. & Meldal, M. High Capacity Poly(ethylene glycol) Based Amino Polymers for Peptide and Organic Synthesis. QSAR Comb. Sci. 23, 662–673 (2004).
6. Tornøe, C. W., Christensen, C. & Meldal, M. Peptidotriazoles on Solid Phase: [1,2,3]-Triazoles by Regiospecific Copper(i)-Catalyzed 1,3-Dipolar Cycloadditions of Terminal Alkynes to Azides. J. Org. Chem. 67, 3057–3064 (2002).
7. D'Ercole, A. et al. On-resin microwave-assisted copper-catalyzed azide-alkyne cycloaddition of H1-relaxin B single chain 'stapled' analogues. 10.
8. Le Chevalier Isaad, A., Papini, A. M., Chorev, M. & Rovero, P. Side chain-to-side chain cyclization by click reaction: CLICKED CYCLOPEPTIDES. J. Pept. Sci. 15, 451–454 (2009).
9. Testa, C. et al. Design, synthesis, and conformational studies of [DOTA]-Octreotide analogs containing [1,2,3]triazolyl as a disulfide mimetic. Pept. Sci. 110, e24071 (2018).

Thermodynamic and kinetic effects on the activity and selectivity of antimicrobial peptides

F. Carneri[1], E. Franci[1], C. Troiano[1], G. Giaquinto[1], A. Leoci[1], D. Roversi[1], M. R. Loffredo[2], Y. Park[3], A. Toto[2], S. Gianni[2], M. L. Mangoni[2], H. Franzyk[4], L. Stella[1,]*

[1] Deparment of Chemical Science and Technologies, University of Rome Tor Vergata, 00133 Rome, Italy

[2]Deparment of Biochemical Sciences, Sapienza University of Rome, Istituto Pasteur Italia-Fondazione Cenci Bolognetti, 00185 Rome, Italy

[3]Department of Biotechnology, Chosun University, 501-759 Gwangju, Korea

[4]Department of Drug Design and Pharmacology, University of Copenhagen, DK-2100 Copenhagen, Denmark

Email: stella@stc.uniroma2.it

https://doi.org/10.17952/37EPS.2024.P2088

What have we learned about antimicrobial peptides (AMPs)?

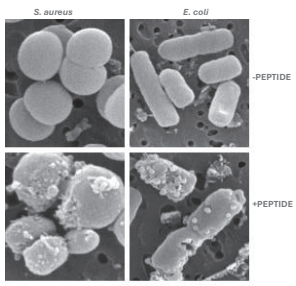

FEBS Lett. 1999, 463: 58

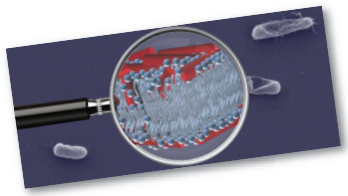

- Liposomes are a good model to study AMPs
- Spectroscopic methods can be applied to live bacterial cells
- The active concentration depends on cell density (both for bacteria and host cells)
- Microbiological assays should be modified to better represent realistic conditions

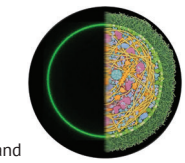

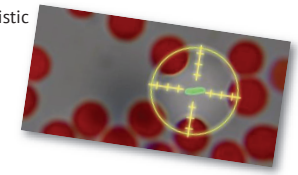

- Produced by all organism
- Short sequences (10-50 a.a.)
- Cationic and amphipatic
- Kill pathogens rapidly by making their membrane permeable
- Selective (due to the different composition of bacterial and host membranes)

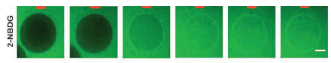

Biophysical journal, 110(1), 176-187

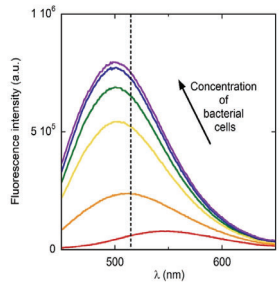

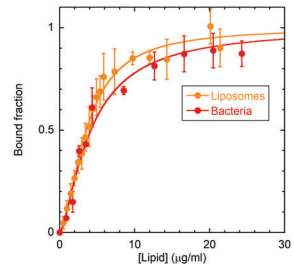

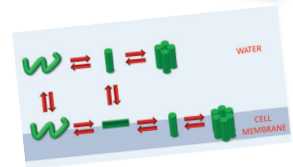

Roversi ACS Chem Biol 2014 9: 2003; Savini BBA 2020 1862: 183291; Loffredo PNAS 2021 118: e2014363118

Open questions

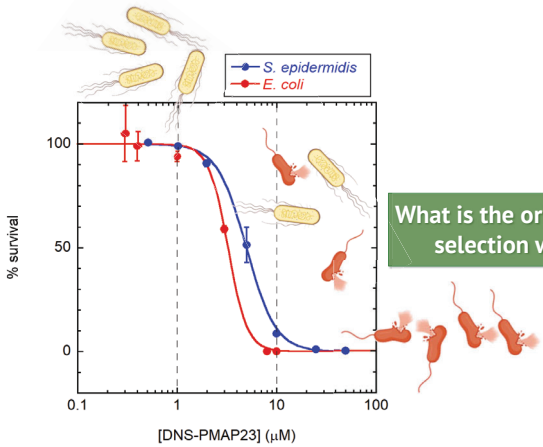

What is the origin of the mutant selection window (MSW)

What is the sequence of events involved in bacterial killing

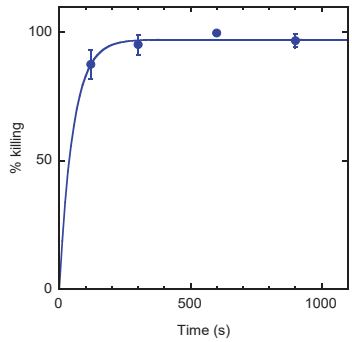

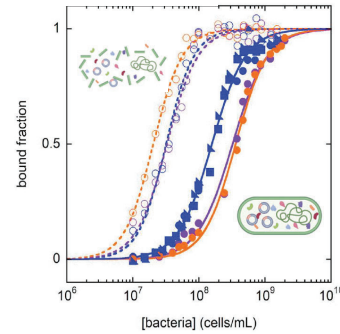

Mutant selection window: the role of water-membrane partition

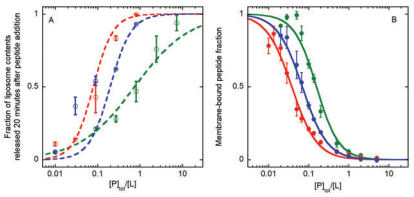

	Sequence	AA[a]	Q[b]
Novicidin	KNLRRIIRKGIHIIKKYF-NH_2	18	+8
P9-4	KWRRWIRWL-NH_2	9	+5
Sub3	RRWRIVVIRVRR-NH_2	12	+7

- We followed spectroscopically the membrane-perturbing activity of different antimicrobial peptides in model membranes and we found the same heterogeneous response observed in bacteria (**A**)
- In an extremely wide range of $[P]_{tot}/[L]$ values (10^{-2} to 10) only a fraction of the liposomes released their contents: these peptides have an "all or none" mechanism of action (**C**)

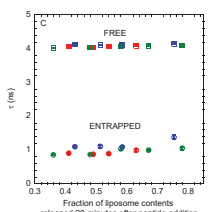

- By measuring the membrane-bound peptide fraction at different lipid concentrations (**B**), we reported the curves (**A**) as a function of the peptide actually bound to the membranes (**D**,**E**)

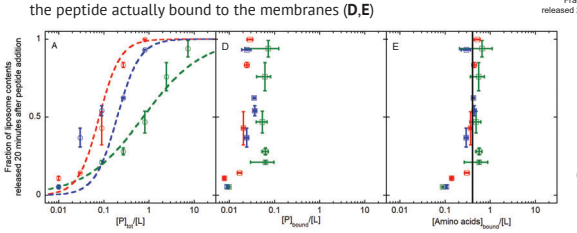

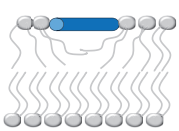

- **Different peptides show the same threshold necessary to form pores: steric mechanism of action**
- **Heterogeneous response determined only by the variation of the fraction of membrane-bound peptides**

Sequence of events in bacterial killing: kinetics of peptide/cell interaction

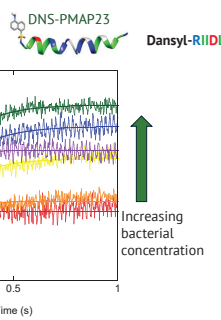

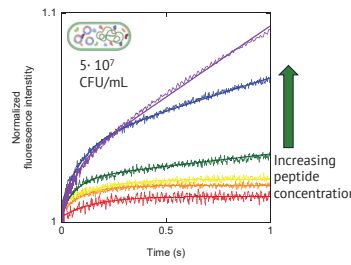

- **Cell-binding is complete in less than 1 s**
- **Additional slower process only at peptide concentration causing killing**

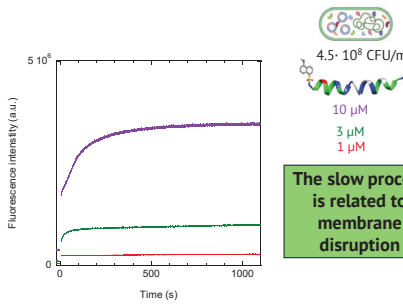

The slow process is related to membrane disruption

DIFFERENT APPROACHES IN OPTIMISATION OF MINIPROTEIN STRUCTURE FOR IMPROVEMENT OF AFFINITY TOWARDS TARGET AND INHIBITORY ACTIVITY

Paweł Noceń[1], Łukasz Berlicki[1]

[1]Department of Bioorganic Chemistry, Wrocław University of Science and Technology, Wybrzeże Wyspiańskiego 27, 50-370 Wrocław

e-mail: pawel.nocen@pwr.edu.pl

https://doi.org/10.17952/37EPS.2024.P2091

Abstract

The interaction between PD-1 protein (programmed death receptor 1), present on the surface of the immune response system cells, especially T lymphocytes, and PD-L1 (programmed death ligand 1), exposed on the surface of various cancer cells, is thoroughly described in the literature[1,2].

The interplay between these two proteins mediates the modulation of the tumour microenvironment and, as a consequence, leads to the inhibition of the apoptotic process.
PD-L1 binds to PD-1 and displays high affinity, described by a dissociation constant equal to 8 μM[3].

In the pursuit of inhibitors targeting the PD-1/PD-L1 interaction, Rosetta Protein Design software[4] and rational drug design[5] methodologies were employed to generate novel miniproteins. Designed sequences underwent synthesis and evaluation to assess their efficacy in disrupting the aforementioned interaction. The optimisation process focused on leveraging the physicochemical properties of the exposed amino acid residues towards the target protein surface and the mutual position of those residues in spatial arrangement.

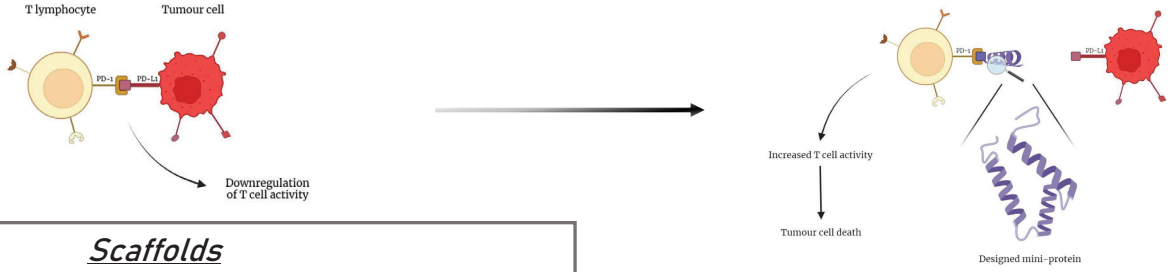

Scaffolds

In the beginning, two different scaffolds of well described topologies, ENH and MvaT, were applied to the Rosetta Protein Design software[4] to better fit to the PD-1 protein cavity which is known to bind PD-L1. Rational drug design was in use to suggest further modifications. More than 86 miniproteins were obtained and investigated in terms of affinity towards the target molecule, folding pattern and thermal stability.

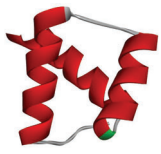

Figure 1 - Structure of the *Drosophila melanogaster* engrailed homeodomain [4] (pdb: 1enh)

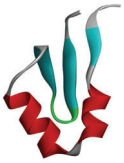

Figure 2 - C-terminal domain of MvaT protein [3] (pdb: 2mxe)

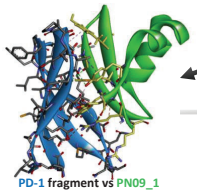

Figure 3 - Result of the Rosetta Protein Design Software optimization [Discovery Studio Visualizer]. Green ribbon represents PN09_1 miniprotein derived from MvaT scaffold. It is shown in complex with PD-1 (light blue ribbon). Yellow sticks represent residues which are introduced in PN09_1 instead of those which are originally placedin the MvaT sequence.

Rational drug design strategies were then applied to propose further structural modifications. The changes in sequences included single and multiple substitutions of residues at certain positions and the alteration of the total resultant charge of the miniprotein being designed.
Considering the observation that positively charged miniproteins were shown to have a greater attraction to the PD-L1 surface, a hypothesis regarding altering the resultant charge to negative was tested, in terms of potentially obtaining a highly effective PD-1 protein inhibitor.
Over 80 miniproteins were synthesized and subjected to comprehensive analysis to determine their affinity towards the PD-1 receptor, folding characteristics, and thermal stability.

Sequences

Table 1 - List of selected MvaT-derived sequences and their physico-chemical properties. Residues of MvaT highlighted in bold blue indicate the substituted spots. Residues in bold red did not improve the measured parameters, whereas those in bold black are proven to have positive influence - either giving lower dissociant contant value (K_d) or higher thermal stability point of the product.

name	sequence	CD		BLI
		proper folding pattern	thermal stability point [°C]	K_d [μM]
mvaT	KVKQYKNPHT GEVIETKGGN HKTLKEWKAK WGPEAVESWA TLL			
PN01	KRKMYSNPHT GAAIYTRGGN HKTLKEWKAK WGPEAVESWA YLE	Y	36	231
PN06	KRKMYYNPHT GAAIYTRGGN HKTLKEWKAK WGPEAVESWA YLE	Y	49	6.61
PN09	KRKMYSNPHT GAAIYTRGGN HKLLKEWKAK WGPEAVESWA YLE	Y	36	2.63
PN09_1	KRKMYYNPHT GAAIYTRGGN HKLLKEWKAK WGPEAVESWA YLE	Y	50.6	11.22
PN09_2	KRKMYYNPHH GAAIYTRGGN HKLLKEWKAK WGPEAVESWA YLE	N	<30	n/a
PN09_4	KRKMYYNPHT GAAIYTQGGN HKLLKEWKAK WGPEAVESWA YLE	Y	46.4	12
PN91_H17	KRKMYYNPHT GAAIYTHGGN HKLLKEWKAK WGPEAVESWA YLE	Y	55	250
PN91_N21	KRKMYYNPHT GAAIYTRGGN NKLLKEWKAK WGPEAVESWA YLE	Y	51.5	26.5
PN91_S21	KRKMYYNPHT GAAIYTRGGN SKLLKEWKAK WGPEAVESWA YLE	Y	49.5	24.6
PN91_F13	KRKMYYNPHT GAFIYTRGGN HKLLKEWKAK WGPEAVESWA YLE	Y	55.5	404.7

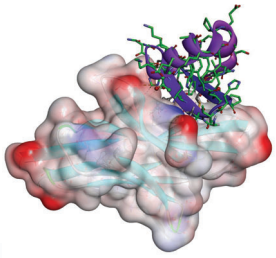

Figure 4 - Docking of MvaT mini-protein structure (violet ribbon) to PD-1 protein molecule.

Results

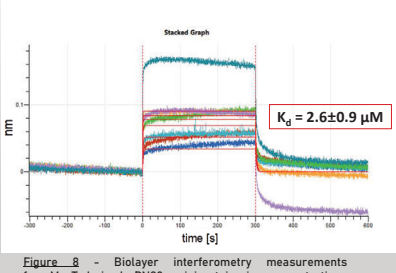

Figure 8 - Biolayer interferometry measurements for MvaT-derived PN09 miniprotein in concentrations from 1.25to 30 μM [Octet K2, Sartorius]. The calculated K_d value is close to 2.6 μM.

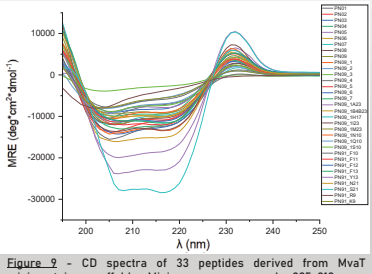

Figure 9 - CD spectra of 33 peptides derived from MvaT mini-protein scaffold. Minima seen around 205-210 nm and 215-220 nm indicate on the proper folding pattern due to presence of α-helices and β-sheet in the structures.

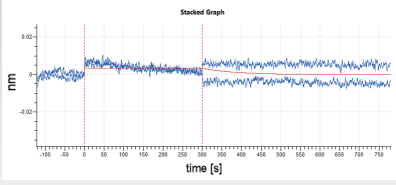

Figure 10 - Example of biolayer interferometry measurement: PN91_QEE shows no specificity towards the PD-1 protein. Unfortunately, all the other peptides with lower resultant charge showed the tendency to lose the specificity even though the changes in the sequence were not made in the binding fragment of mini-protein and the CD spectra have proven that the folding pattern is preserved.

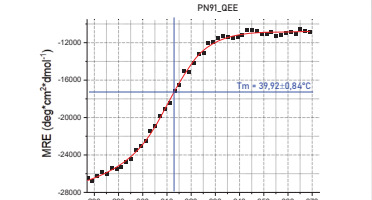

Figure 12 - Thermal stability point is calculated basing on the CD spectra measured in various temperatures - interval measurements from 4°C to 96°C. Here the value for PN91_QEE, of lower resultant charge than PN09_1, is presented.
For the calculation of the parameter a normalised fitting method is applied [OriginLab software], but the the highest temperature in which the mini-protein preserves the folding pattern might be also estimated from the curve: in the half of the slope in between two plateaux.
In general, as seen in the Table 2, the changes in non-binding region applied for lowering the resultant charge, seemed to decrease the thermal stability of designed mini-proteins.

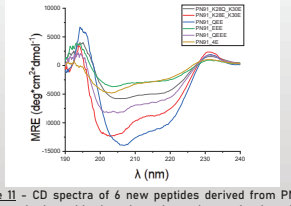

Figure 11 - CD spectra of 6 new peptides derived from PN09_1 mini-protein, but with altered resultant charge. As the minima are present, it is stated that the folding pattern is preserved.

Table 2 - List of PN09_1-derived mini-proteins with lowered resultant charge. The substitutions in sequences were made stepwise by altering the amino acid residue with positively charged side chain to amino acid residue with negatively charged side-chain.

name	sequence	CD		BLI	resultant charge
		proper folding pattern	thermal stability point [°C]	K_d [μM]	z
PN09_1	KRKMYYNPHT GAAIYTRGGN HKLLKEWKAK WGPEAVESWA YLE	Y	50.6±1.3	11.2±5.1	+3.217
PN91_K28Q_K30E	KRKMYYNPHT GAAIYTRGGN HKLLKEWQAE WGPEAVESWA YLE	Y	39.0±1.2	n/a	+0.226
PN91_K28E_K30E	KRKMYYNPHT GAAIYTRGGN HKLLKEWEAE WGPEAVESWA YLE	Y	41.7±1.2	n/a	-0.773
PN91_QEE	KRKMYYNPHT GAAIYTRGGN HKLLQEWEAE WGPEAVESWA YLE	Y	39.9±0.8	n/a	-1.769
PN91_EEE	KRKMYYNPHT GAAIYTRGGN HKLLEEWEAE WGPEAVESWA YLE	Y	38.0±2.5	n/a	-2.768
PN91_QEEE	KRKMYYNPHT GAAIYTRGGN HQLLEEWEAE WGPEAVESWA YLE	Y	35.6±1.9	n/a	-3.764
PN91_4E	KRKMYYNPHT GAAIYTRGGN HELLEEWEAE WGPEAVESWA YLE	Y	34.0±4.5	n/a	-4.762

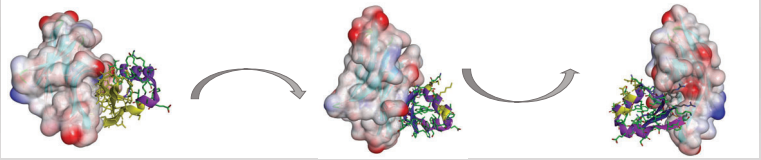

Figure 5 - PN09_1 docked to PD-1 protein, displayed from the perspective showing the region that had to remain unchanged (yellow colour)

Figure 6 - Another visual representation of PD-1 vs PN09_1 after rotation and with highlighting of four residues submitted to substitution with negatively charged side chain.

Figure 7 - Visualization displaying PN91_4E docked to the PD-1 protein, with four Glu residues instead of positively charged amino acid side chains.

Conclusions

To make the picture complete, it must be underlined that the data presented above constitute a fragment of the whole idea, initially thought to be presented. This work is mainly focused on the issue of the resultant charge modulation and its influence on the physicochemical properties of the products. On the way to these parameters and results, two different scaffolds, ENH and MvaT, were tested. Besides these two statregies, also peptides based on short helices similar to 7ARR (pdb: 7arr) were synthesised and investigated. In eight sets of mini-proteins and peptides, a total number of products will soon reach circa one hundred different sequences.

Based on the data presented here, it can be concluded that the modulations made in order to make the resultant charge lower - knowing that resultant charge of the PD-1 protein is positive - did not serve to obtain an inhibitor of PD-1/PD-L1 interaction. Probably the main problem is the fact that the substituted residues, even though they were not playing crucial role in the mode of binding, had too significant impact on the thermal stability of the next products and that, in turn, made the new mini-proteins unable to display any inhibitory activity. The research will be continued in order to possibly find a solution to this problem.

Acknowledgement

The presented work was supported by the project entitled "Minigrants for doctoral students of the Wroclaw University of Science and Technology".

References

[1] Okazaki T., Honjo T., Int Immunol., 2007, 19(7):813-24.
[2] Magnez R, et al. Sci Rep., 2017, 7(1):17623.
[3] Chamoto K. et al., Curr Top Microbiol Immunol., 2017, 410:75-97.
[4] Kuhlman B., J Biol Chem., 2019, 294(50):19436-19443.
[5] Helmer D, Schmitz K., Adv Exp Med Biol. 2016;917:147-183.

CENTER FOR BIOPHARMACEUTICALS
DEPARTMENT OF DRUG DESIGN AND PHARMACOLOGY
FACULTY OF HEALTH AND MEDICAL SCIENCES
UNIVERSITY OF COPENHAGEN

https://doi.org/10.17952/37EPS.2024.P2092

Developing autoinducing peptides for regulating the quorum sensing system in *S. lugdunensis*

Iben Jensen, Benjamin S. Bejder, Martin S. Bojer, Hanne Ingmer, Christian A. Olsen

1 Background

Bacteria are highly adaptable microorganisms able to change their gene expression based on environmental changes such as pH or nutrient availability. Quorum sensing (QS) is a system used by many bacteria to sense the population density, and make corresponding changes in the gene expression pattern. This is done through a signaling molecule known as an autoinducing peptide (AIP). In *Staphylococcus aureus* the system causes an up-regulation in virulence related genes and a down-regulation of genes relevant for biofilm formation.[1]

In most staphylococcal bacteria, the QS system functions similarly to what is seen in *S. aureus*, however, cellular processes regulated by the quorum sensing system is different in different species. Substantial efforts have already been focused on developing inhibitors of the QS system in *S. aureus*, however, other species are under-represented in this regard. Our aim is therefore to synthesize an inhibitor of QS in *S. lugdunensis* to investigate the system further in this organism.

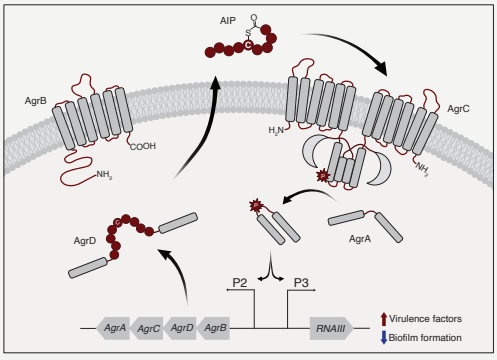

Figure 1: Schematic overview of the quorum sensing system in *S. aureus*. After translation of the accesory gene regulator (*agr*) locus, the precursor AgrD peptide is posttranslationally cleaved and cyclized into the final AIP. The AIP is then transported into the extracellular environment where it interacts with the receptor kinase AgrC. Activation of AgrC leads to phosphorylation of AgrA which can then bind to the P2 and P3 promoters, causing changes in gene expression.

2 QS cross-talk

Gless et al[2] have carried out extensive studies regarding the cross-inhibitory profile of a number of native AIPs from different species of *Staphylococcus*. The purpose of the study is to investigate how different species interfere with QS in case of co-habitation.

Testing the AIPs under the same conditions, makes it possible to directly compare the potency of different AIPs on the same reporter strain.

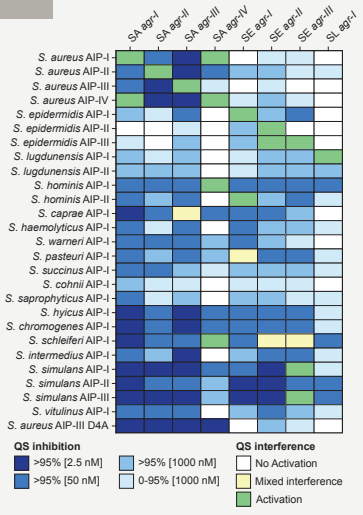

Figure 2: Synthetic AIPs were tested at multiple concentrations (1 µM, 50 nM, 2.5 nM) against eight fluorescent reporter strains of *S. aureus* (SA), *S. epidermidis* (SE), and *S. lugdunensis* (SL).[2]

3 Sequence alignment

In the heatmap from Gless et al, we found that only a small number of native AIPs inhibit *S. lugdunensis* to a significant extent. These sequences were aligned to identify any common motif. The alignment showed high sequence similarity in the ring with a more variable tail region.



Figure 3: Alignment of peptide sequences from *S. lugdunensis* AIP-I, *S. hominis* AIP-II, *S. schleiferi* AIP-I, *S. simulans* AIP-II, and *S. simulans* AIP-III.

4 AIP synthesis

The characteristic thioester motif, found in most of the natural AIPs, can be installed by employing the chemistry introduced by Dawson and coworkers.[3] This chemistry was further optimized in our group by Gless et al[4] for simplified synthesis of AIPs.

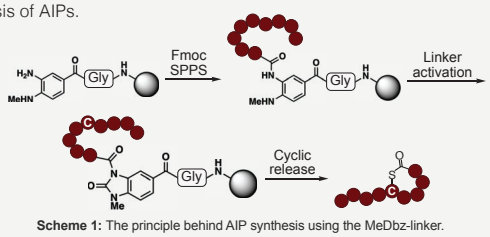

Scheme 1: The principle behind AIP synthesis using the MeDbz-linker.

5 Results

From the alignment of *S. lugdunensis* inhibiting AIPs, we decided to base our inhibitor series on the sequence KYNPC-**X**-GYF, where **X** represents a variable amino acid residue. Using this sequence, we investigated what functionalities were tolerated at position **X**. A representative selection of compounds, including the most potent, were then tested in a dose-response assay. As a control, we also tested an *S. lugdunensis* QS inhibitor reported previously.[5]

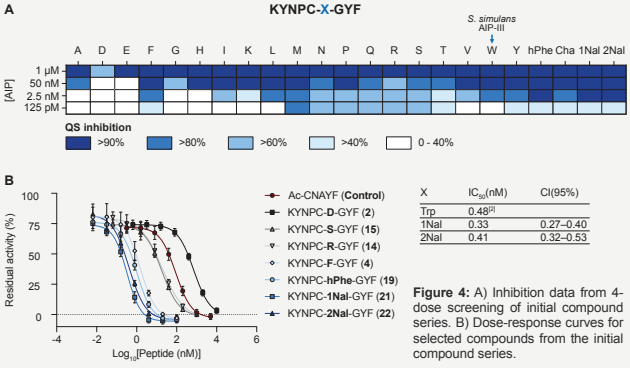

X	IC_{50}(nM)	CI(95%)
Trp	0.48[2]	
1Nal	0.33	0.27–0.40
2Nal	0.41	0.32–0.53

Figure 4: A) Inhibition data from 4-dose screening of initial compound series. B) Dose-response curves for selected compounds from the initial compound series.

6 Summary & outlook

- We designed a compound series to test against our *S. lugdunensis* fluorescent reporter strain.
- We found two lead candidates which showed potent inhibition.
- The next step is to test compounds **21** & **22** against our other reporter strains, and compare cross-interference with what is observed for *S. simulans* AIP-III.
- It would be interesting to then investigate what phenotype would result from *S. lugdunensis* QS inhibition, and if possible also activation.

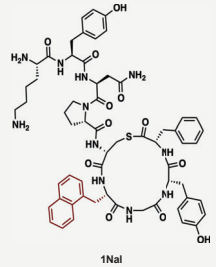

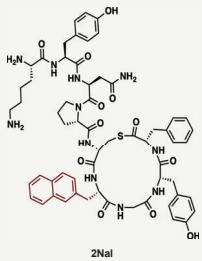

References
[1] Wang et al, *Cell Chem. Bio.* 2016, 23(2), 214–224
[2] Gless et al, *bioRxiv.* **2021** (preprint)
[3] Blanco-Canosa et al, J. Am. Chem. Soc. **2015**, 137(22), 7197–7209
[4] Gless et al, *Nat. Chem.* **2019**, 11(5), 463–469
[5] Gordon et al, *J. Med. Chem.*, **2016**, 59(19), 8879–8888

LEO FOUNDATION

Design of fluorinated Aib foldamers: synthesis, structural study and capacity to interact with amyloid proteins

Marine Pietri[1,2], Olivier Monasson[1,2], Julia Kaffy[2], Sandrine Ongeri[2], Elisa Peroni[1,2], Nathalie Lensen[1,2], Grégory Chaume[1,2]

[1]CY Cergy Paris Université, CNRS, BioCIS (UMR 8076), Cergy Pontoise, France
[2]Université Paris-Saclay, CNRS, BioCIS (UMR 8076), Orsay, France
marine.pietri@cyu.fr

https://doi.org/10.17952/37EPS.2024.P2093

Protein misfolding and **aggregation** and their subsequent dysfunction are associated with more than 30 serious **and incurable human diseases**.[1] **Amyloid protein** aggregation occurs through misfolding and a cascade of protein-protein interactions, leading to oligomeric precursors and **fibrillar species**, both responsible for **cellular dysfunction**.
α-Helical and 3_{10} helical structures have been described for Tau, α-synuclein (α-Syn), amyloid β (Aβ) and human Islet Amyloid PolyPeptide (hIAPP) amyloid proteins and $\mathbf{3_{10}}$ **helices** have been proposed as probable **intermediates** in the conversion of **α-helix to β-sheet** during the $\mathbf{A\beta_{1\text{-}40}}$ **and hIAPP amyloidogenesis**. [2]

Therefore, the rational design of **peptidomimetic scaffolds** able to promote a **well-defined helical structure** and interact with monomeric or small amyloid protein oligomers to **inhibit** their aggregation constitutes a promising approach.

Oligopeptides containing α-aminoisobutyric acid residue (Aib) have been reported as mimics of 3_{10}, mixed $3_{10}/\alpha$, or α-helical structure.[3] Our group has recently reported the synthesis of fluorinated Aib foldamers incorporating (*R*)- and (*S*)-α-trifluoromethylalanine (α-TfmAla) and demonstrated their ability to stabilize the 3_{10} helical conformation.[4;5] The 3_{10} helix is characterized by the a 3-fold rotational symmetry with three residues per turn and therefore 3 faces.
In this work, we engineered a promising α-TfmAla-containing peptidomimetic template to interact with amyloid proteins in their helical conformation and inhibit their aggregation. Here, we will present the synthesis of a first generation of fluorinated peptides through adapted SPPS methodology, their conformational studies using NMR and CD spectroscopy as well as our preliminary results on ThT assay of amyloid protein aggregation inhibition.

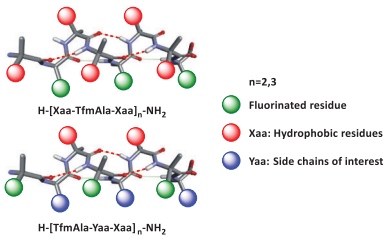

Assessing the impact of the position of TfmAla in hydrophobic hexamers

Synthesis of Leu-oligomers

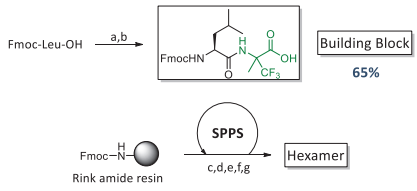

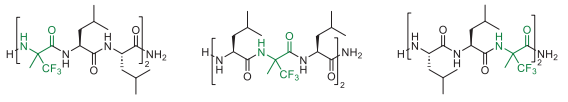

H-[TfmAla-Leu-Leu]$_2$-NH$_2$
1R 18%
1S 22%
***N*-terminal**

H-[Leu-TfmAla-Leu]$_2$-NH$_2$
2R 24%
2S 37%
Middle

H-[Leu-Leu-TfmAla]$_2$-NH$_2$
3R 15%
3S 9%
***C*-terminal**

(a) $SOCl_2$, dry DCM,))), r.t., 1 h 30; (b) H-TfmAla-OH, dry THF, 100 W, 100 °C, 20 min; (c) Fmoc-Leu-OH, HATU, DIPEA, DMF, r.t., 40 min; (d) Piperidine/DMF 20 % r.t., 5 min, 15 min; (e) Building block, PyAOP, NMM, DMF, 50 W, 75 °C, 1 h; (f) Fmoc-TfmAla-OH, PyAOP, NMM, DMF, 50 W, 75 °C, 1 h; (g) TFA:H_2O:TIS 95:2.5:2.5 1h30

Conformational studies

Intramolecular (i ← i+3) **H-bonding pattern** of 3_{10} helix structure has been confirmed by temperature coefficients (Δδ/ΔT) of -NH protons for compounds **1-3**. Sequential NH_i-NH_{i+1} and $H\alpha_i$-NH_{i+2} **ROE** correlations are also in support of the $\mathbf{3_{10}}$ **helix conformation**.

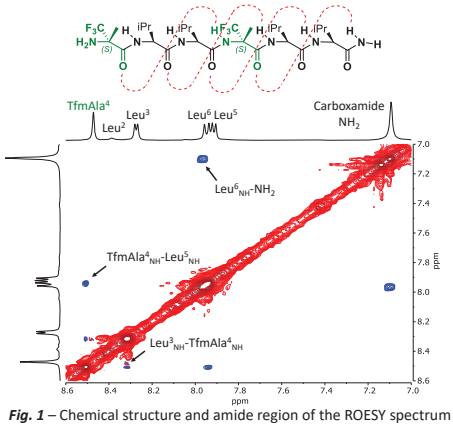

Fig. 1 – Chemical structure and amide region of the ROESY spectrum of peptide **1*S*** (5 mM CD_3OH, 20 °C).

Circular dichroism has been performed on peptides **1-3** and all spectra show the typical $\mathbf{3_{10}}$ **helix signature**.[6] A **negative band** around **205 nm** is characteristic of a **right-handed** helicity (*P*) while a positive band refers to a left-handed helicity (*M*).

Perturbations in the CD profile are observed as the TfmAla is moved within the repetition unit. At ***N*-terminal** position, (*S*)- and (*R*)-TfmAla configurations lead to a **difference in curve amplitude**. When placed in the **middle**, the configuration of the TfmAla has **no significant impact** on the CD signature. However, when incorporated in ***C*-terminal** position, (*S*)-TfmAla induces a **inversion of the helicity** of the peptide from a *P* to a *M* helix. Peptide **1*S***, containing the (*S*)-TfmAla in *N*-terminal position seems to have **the greatest helical content**.

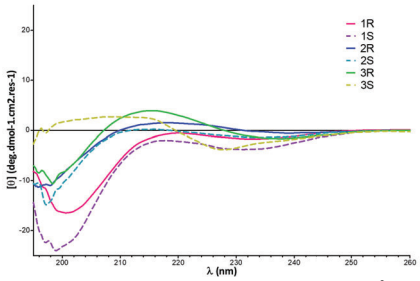

Fig. 2 – CD spectra of peptide **1-3** (300 µM, MeOH, 20°C).

Amphipathic nonamers

Design's rational

The 3_{10} helix is characterized by the a 3-fold rotational symmetry with three residues per turn and therefore 3 faces.

A rational repetition of a **triplet TfmAla-Yaa-Aib** has been designed to lead to original **nonameric foldamers** presenting a highly hydrophobic fluorinated face on the helix. The second face, carrying the Aib residues, is expected to strengthen the helicity of the foldamer. Finally, the third face exposing **selected side chain** of amino acids (Yaa) will be responsible for the **specific** and potent **interactions** (hydrophobic, aromatic or electrostatic) with an amyloid protein.

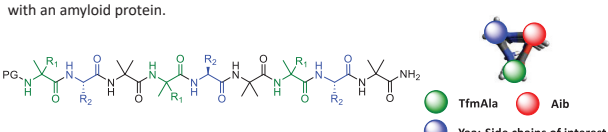

Fig. 3 – General design of inhibitors.

Series	PG	Xaa	Peptide name	Yield
Anionic	H-	(*R*)TfmAla	**4*R***	7 %
		(*S*)TfmAla	**4*S***	6 %
		Aib	**4-Aib**	32 %
	Ac-	(*R*)TfmAla	**5*R***	9 %
		(*S*)TfmAla	**5*S***	7 %
Cationic	H-	(*R*)TfmAla	**6*R***	13 %
		(*S*)TfmAla	**6*S***	12 %
		Aib	**6-Aib**	30 %
		(*R*)TfmAla	**7*R***	17 %
		(*S*)TfmAla	**7*S***	13 %
		Aib	**7-Aib**	23 %

All peptides were synthetized using previously reported SPPS method to obtain generic sequence
PG-[Xaa-Yaa-Aib]$_3$-NH$_2$
(PG = H- or Ac-; R_1 = CF_3, Xaa = TfmAla; R_1= CH_3, Xaa = Aib).

Conformational studies were carried out using both NMR and CD spectroscopy and revealed a $\mathbf{3_{10}}$ **helix** or a **mixed** $\mathbf{\alpha/3_{10}}$ helix structure for all nonamers.

Interaction with amyloid protein

Thioflavin T (ThT) dye fluorescence is commonly used to quantify the formation and inhibition of amyloid fibrils in the presence of anti-amyloidogenic compounds. When bounded to b-sheet-rich structures, such as those in amyloid aggregates, the dye displays enhanced fluorescence and a characteristic red shift of its emission spectrum.[7]

We first investigated the activity of our inhibitors towards **hIAPP** amyloid protein involved in type II diabetes.

As preliminary results, 10 nonamers were tested via ThT assays at a peptide/hIAPP ratio of 10 : 1. None of the inhibitors tested showed any fluorescence that would indicate the presence of β-sheet-like aggregates.

For both series, fluorinated peptides show slightly better activity compared to their non fluorinated analogs. In the case of anionic series, the configuration of TfmAla does not appear to have a direct influence on the inhibition while it does for the cationic series.

Our **preliminary results** show a **reduction** of hIAPP **fibrils** by our inhibitors **between 40 % and 80 %**.

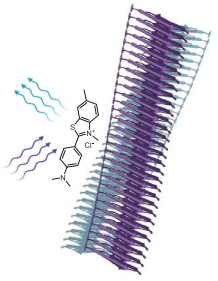

Fig. 4 – ThT binding on amyloid fibrils.

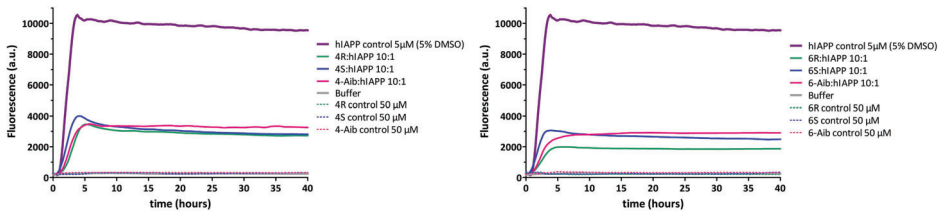

Fig. 5 – Preliminary results of ThT assays on hIAPP fibrillation (Buffer 10 mM Tris/HCl, 100 mM NaCl, pH 7.4). Triplicate average.

Conclusion

- ❑ The introduction of (*R*)- and (*S*)-TfmAla into hydrophobic hexamer using SPPS and microwave activation is a success.
- ❑ Both NMR and CD results tend to a 3_{10} helix. The peptide's conformation is impacted by both the configuration and the position of the fluorinated amino acid.
- ❑ A first generation of nonameric amphipathic inhibitors has been synthetised using the previously optimised SPPS method.
- ❑ The ThT assays evaluating their activity towards hIAPP are promising and other tests will be carried out at different ratios. Inhibition of other amyloid targets will also be tested through these assays.
- ❑ Investigation needs to be done towards the different side chains of Yaa to evaluate the impact regarding the interaction with different amyloid protein.

References

[1] Ke, P. C. et al. *Chem. Soc. Rev.* **2017**, *46* (21), 6492–6531.
[2] Bram, Y. et al. Sci. Rep. 2017, 7, 14031
[3] Jones, J. E. et al *J. Am. Chem. Soc.* **2016**, *138* (2), 688–695.
[4] Bodero, L. et al. *Chem. Eur. J.* **2022**, e202103887.
[5] Picois, N. et al. *Chem. Eur. J.* **2024**, e202400540.
[6] Toniolo, C. et al. *J. Am. Chem. Soc.* **1996**, *118*, 2744–2745.
[7] Khurana, R. et al. *J. Struct. Biol.* **2005**, *151*, 229–238.

Acknowledgements

The authors are grateful to Agence Nationale de la Recherche for financial support (ANR-22-CE44-0020). Marine Pietri is grateful to the European Peptide Society for the waived registration.

Antimicrobial peptides with varied chemical compositions trigger hyperpolarization of the bacterial membrane

Anasztázia Hetényi,[a] Kaushik Nath Bhaumik,[a] Réka Spohn,[b] Anett Dunai,[b] Lejla Daruka,[b] Csaba Pál,[b] Tamás A. Martinek[a,c]

[a]Department of Medical Chemistry, University of Szeged, Dóm tér 8, Szeged HU-6720, Hungary

[b]Synthetic and Systems Biology Unit, Institute of Biochemistry, Biological Research Centre, National Laboratory of Biotechnology, Hungarian Research Network; Szeged, HU-6726, Hungary [c]HUN-REN–SZTE Biomimetic Systems Research Group, Dóm tér 8, Szeged HU-6720, Hungary

https://doi.org/10.17952/37EPS.2024.P2094

Introduction

Alleviating the impact of antimicrobial resistance is an ongoing medical necessity and one of the biggest hurdles. Striking is directed towards the introduction of expedited methodologies for antibiotic development, but new compounds rarely manifest a diminished predisposition to resistance. Consequently, adjuvant strategies to maintain or improve the efficacy of current antibiotic treatments are attractive approaches, and new complementary mechanisms are in demand. Several previous observations point to hyperpolarization as a potentially useful adjuvant approach.

Results

In search of the bacterial hyperpolarization effects, we chose 17 AMP sequences (Table 1). The selection was based on the secondary structure, including α-helix, polyproline helix, disulfide-stabilized β-sheet, and disordered sequences.

Table 1

Peptides	Abbreviation	Sequence
Apidaecin 1B	AP	GNNRPVYIPQPRPPHPRL-OH
Protegrin-1	PROT1	RGGRLCYCRRRFCVCVGR-NH_2
Tachyplesin II – Lys	TP2K	KWCFKVCYKGICYKKCK-NH_2
Tachyplesin II	TP2	RWCFRVCYRGICYRKCR-NH_2
Indolicidin-OH	IND	ILPWKWPWWPWRR-OH
LL37	LL37	LLGDFFRKSKEKIGKEFKRIVQRIKDFLRNLVPRTES-OH
Indolicidin	INDa	ILPWKWPWWPWRR-NH_2
R8	R8	FLGKVFKLASKVFKAVFGKV-OH
PGLa – Arg	PGRLa	GMASRAGAIAGRIARVALRAL-NH_2
PGLa	PGLa	GMASKAGAIAGKIAKVALKAL-NH_2
PGLa-OH	PGL	GMASKAGAIAGKIAKVALKAL-OH
Guavanin 2	GUA2	RQYMRQIEQALRYGYRISRR-NH_2
Cecropin P1	CP1	SWLSKTAKKLENSAKKRISEGIAIAIQGGPR-OH
Buforin II	BUF2	TRSSRAGLQFPVGRVHRLLRK-OH
Bactenecin 5	BAC5	RFRPPIRRPPIRPPFYPPFRPPIRPPIFPPIRPPFRPPLGPFP-OH
Magainin II-OH	MAG2	GIGKFLHSAKKFGKAFVGEIMNS-OH
Magainin II	MAG2a	GIGKFLHSAKKFGKAFVGEIMNS-NH_2

We assessed alterations in the polarization of the cytosolic membrane potential of E. coli cells in reaction to antimicrobial peptides (AMPs) in Table 1. To prevent complete membrane disruption, we administered subinhibitory concentrations, consistently at 0.5 MIC. Polarization was tracked through flow cytometric analysis utilizing the membrane potential-sensitive dye $DiOC_2(3)$ (Figure 1a-c). All measurements was performed after 15 minutes of incubation.

Figure 1

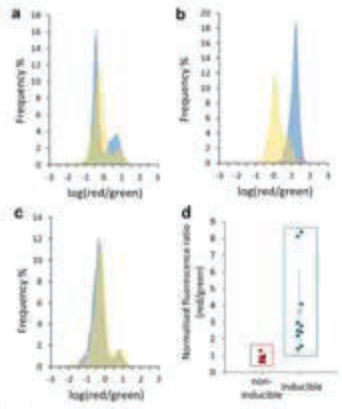

Our results demonstrated that several AMPs could induce hyperpolarization in a sequence-dependent manner. We calculated the average hyperpolarization effect across biological replicates and compared the results with the structural characteristics of the sequences (Figure 1d). AMPs with membrane-induced helical structures typically generate hyperpolarization at subinhibitory concentrations without causing bacterial depolarization. Conversely, sequences with membrane-insensitive conformations fail to shift the bacterial population to a predominantly hyperpolarized state. A specific side chain pattern is required, which creates distinct hydrophobic and ionic faces on the helices, allowing for sufficient residual flexibility without self-aggregation. We found no correlation with known non-membrane lytic targets.

Figure 1. Bacterial hyperpolarization effects of AMPs at subinhibitory concentrations. Representative histograms of the log ratio calculated from the red and green channels for LL37 (**a**) MAG2 (**b**) and AP (**c**) (yellow untreated, blue AMP treated). (**d**) Population means of the red/green fluorescence ratios normalised to the values obtained for the untreated cells. Ratios below one correspond to depolarisation, and values above one indicate hyperpolarization. Values are displayed against the inducibility of the secondary structure.

We hypothesized that the disruption of polarization in bacteria is also driven by direct interactions between the membrane and AMPs. To investigate this, we developed a cytosolic bacterial membrane mimetic system using DOPG:DOPC large unilamellar vesicles (LUVs), where AMP-induced changes in membrane potential could be monitored with the voltage-sensitive fluorescent dye oxonol VI. LUV samples were prepared with varying ion gradients at a constant pH of 7.2 to enhance the detection of any dynamic polarization effects. Specifically, we used 100 mM NaCl inside and 100 mM KCl outside for the cation gradient, and 100 mM NaCl inside with either 100 mM NaH_2PO_4 or $NaNO_3$ outside for the anion gradient. We recorded the membrane potential changes induced by AMPs at 0.5 MIC in the presence of the cation gradient.

The ion gradient-dependent fluorescence intensity curves showed that most AMPs generated an inside-positive diffusion potential. This indicates that AMPs enhance cross-membrane permeability for K^+ more than Na^+, suggesting that AMPs act as K^+-selective ionophores at sublethal concentrations. However, AP and CP1 did not induce diffusion potential in the cation gradient LUV model. Measurements using an inside Cl^- gradient against $H_2PO_4^-$ also generally produced an inside-positive diffusion potential, pointing to a higher cross-membrane permeability for Cl^- over $H_2PO_4^-$, indicating Cl^- selective anion transport, with the exception of AP.

Figure 2

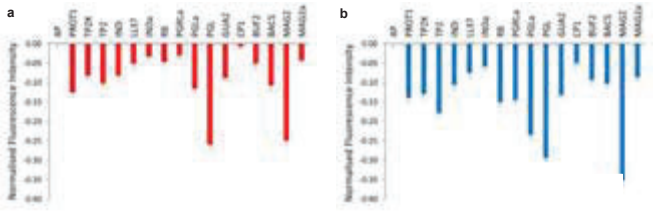

Figure 2. Membrane polarisation measurements in large unilamellar vesicles. AMP-induced fluorescence intensity decreases, implying the diffusion potential for the K^+/Na^+ gradient model (red) (**a**). AMP-induced fluorescence intensity decreases, indicating the diffusion potential for the $Cl^-/H_2PO_4^-$ gradient model (blue) (**b**).

We concluded that the AMPs induced diffusion potential in the LUV model in a sequence-dependent manner (Figure 2). The observed changes in fluorescence intensity demonstrated that AMPs create diffusion potential through selective cross-membrane ion transport for K^+ or Cl^- (over Na^+ and $H_2PO_4^-$, respectively), or both. These findings suggest that direct membrane–AMP interactions at subinhibitory concentrations can influence diffusion potential across a lipid bilayer.

We hypothesized that AMPs enable voltage generation through subtle electrogenic transport without fully disrupting the ion concentration gradients across the membrane. To examine the extent of macroscopic ion exchange across the bilayer, we directly measured time-dependent ion concentration levels in LUVs using NMR spectroscopy. We monitored Na^+ and $H_2PO_4^-$ by detecting ^{23}Na and ^{31}P NMR signals in LUVs, $Dy(PPP)_2^{7-}$ was employed as an NMR shift reagent to distinguish between internal and external Na^+, while external and internal phosphate signals were discernible without a shift reagent. After 20 minutes, ion exchange either halted or slowed significantly, resulting in a stable, steady-state ion gradient or a slow drift. This finding confirms that AMPs do not rapidly dissipate the ion gradient, thereby sustaining a quasi-steady-state membrane potential. The rate-limiting step in this exchange is the slow transport of the less preferred ion.

Figure 3

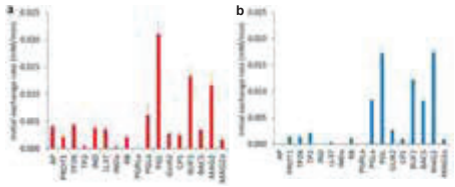

Figure 3. Ion transport measurements in large unilamellar vesicles. Initial exchange rates observed for AMPs in the Na^+/K^+ gradient model (**a**). Initial exchange rates observed for AMPs in the $Cl^-/H_2PO_4^-$ gradient model (**b**).

Conclusion

Our findings underscore the potential of AMPs as a valuable tool for chemically hyperpolarising bacteria, with significant implications for antimicrobial research and bacterial electrophysiology.

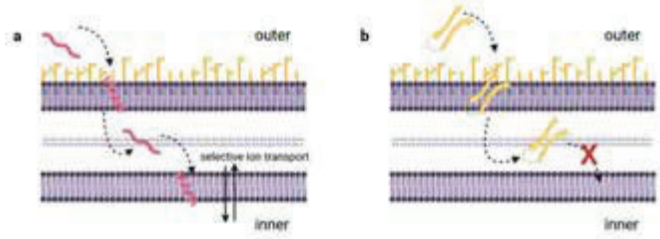

Acknowledgement

Supported by the Ministry of Innovation and Technology of Hungary from the National Research, Development and Innovation Fund (NKFIH K134754). Project no. TKP2021-EGA-32 has been implemented with the support provided by the Ministry of Culture and Innovation of Hungary from the National Research, Development and Innovation Fund, financed under the TKP2021-EGA funding scheme.

Synthetic glucosylated peptide antigens of the bacterial protein adhesin of nontypeable Haemophilus influenzae to detect antibodies in Multiple Sclerosis

F. Nuti[1,2*], F. Real-Fernandez[1,3], H. Berhane Tesfaya[2], P. Strauss[4], R. Aharoni[5], M. Hurevich[4], P. Rovero[1,6], and A.M. Papini[1,2]

***e-mail: francesca.nuti@unifi.it**

https://doi.org/10.17952/37EPS.2024.P2095

[1]Interdepartmental Research Unit of Peptide and Protein Chemistry and Biology, University of Florence, Sesto Fiorentino, Italy
[2]Department of Chemistry "Ugo Schiff", University of Florence, Sesto Fiorentino, Italy
[3] CNR - Istituto di Chimica dei Composti Organometallici (CNR-ICCOM), Sesto Fiorentino, Italy
[4]The Institute of Chemistry, The Hebrew University of Jerusalem, Edmond J. Safra Campus, Givat Ram, Jerusalem, Israel
[5] Department of Immunology, The Weizmann Institute of Science, Rehovot, Israel
[6] Department of Neurosciences, Psychology, Drug Research and Child Health, University of Florence, Sesto Fiorentino, Italy

Introduction

In previous studies, we demonstrated that antibodies in Multiple Sclerosis (MS), initially identified by a type I' β-turn glucopeptide, cross-reacted with the hyperglucosylated adhesin C-terminal fragment HMW1ct(1205-1536) of non-typeable Haemophilus influenzae [1]. The aberrant glucosylated moiety Asn(Glc), that is the common element between the glucopeptide and the bacterial adhesin protein, turned out to be the fundamental epitope to discriminate between sera of a subtype of MS patients and healthy individuals [2]. Since *N*-glucosylation is not present in eukaryotes as a post-translational modification, the hypothesis is that such a bacterial infection, can have an impact in triggering the autoimmune response in an MS patient subpopulation. The non-typeable Haemophilus influenzae (NTHi) bacterium was reported to express an glucosylated protein, the adhesin high molecular weight protein 1 (HMW1), which contains *N*-glucosyl moieties on asparagine residues in consensus *N*-glycosylation sites N-X-(S/T) (where X≠Pro) on β-turns. The HMW1ct(1205-1536), (Figure 1), was isolated and expressed as a 1:1:1 ratio of three *N*-glucosylated versions having 7, 8, and 9 glucose moieties on asparagines in N-X-(S/T) sequons. In HMW1ct(1205-1536) 12 glycosylation sequon sites are present, but only some of them appear to be located on the exposed loops of β-turns (sites 1, 2, 3, 5, 6, 7, 8 and 9). This is also in accordance with the computational model of the protein. (Figure 1).

Selected HMW1ct glucopeptides sequences

With the idea in mind to investigate the role of shorter peptides of hyperglucosylated HMW1ct adhesin protein in antibody recognition in MS, *N*-glucopeptides of adhesin bearing multiple *N*-Glc moieties were designed. In virtue of their spatial proximity and their optimal exposition on the same side of the protein, glucosylated asparagines could be preferentially targeted by anti-HMW1(Glc) antibodies. The selected fragments correspond to the peptide HMW1ct(1390-1403) including the glucosylation sites N^{1348}(Glc) and N^{1352}(Glc), and to the peptide HMW1ct(1345-1357) including the glucosylation sites N^{1393}(Glc) and N^{1398}(Glc). In particular the following adhesin peptide fragments specifically *N*-glucosylated were also synthesized by High-Temperature Fast-Stirring Solid-Phase Synthesis (HTFS-PS) (Table 1).

AHHHHHHVWTANSGALTTLAGSTIKGTESVTTSSQSGDIGGTISGGT
VEVKATESLTTQSNSKIKATTGEAN(1)VTSATGTIGGTISGNTVN(2)VT
ANAGDLTVGNGAEIN(3)ATEGAATLTTSSGKLTTEASSHITSAKGQVN
(4)LSAQDGSVAGSI**NAAN(5)VTLN(6)TTGTL**TTVKGSNIN(7)ATSGTL
VINAKDAELNGAALGN(8)H**TVVN(9)ATNAN(10)GSGSV**IATTSSRV
N(11)ITGDLITINGLNIISKNGINTVLLKGVKIDVKYIQPGIASVDEVIEA
KRILEKVKDLSDEREALAKLGVSAVRFIEPN(12)NTITVDTQNEFATR
PLSRIVISEGRACFSNSDGATVCVNIADNGR

Table 1. NTHi adhesin peptide analogs synthesized

Peptide	*N*-Glc moieties	Sequence
GP1 -[Asn^{1352}(Glc)]HMW1ct(1349-1357)	1 N-Glc	Ac-VTL**N(Glc)**TTGTL-NH_2
GP2- [Asn^{1348}(Glc), Asn^{1352}(Glc)]HMW1ct(1348-1357)	2 N-Glc	Ac-**N(Glc)**VTL**N(Glc)**TTGTL-NH_2
GP3-[Asn^{1348}(Glc), Asn^{1352}(Glc)]HMW1ct(1347-1357)	2 N-Glc	Ac-A**N(Glc)**VTL**N(Glc)**TTGTL-NH_2
GP4-[Asn^{1348}(Glc),Asn^{1352}(Glc)]HMW1ct(1345-1357)	2 N-Glc	Ac-NAA**N(Glc)**VTL**N(Glc)**TTGTL-NH_2
GP5-[Asn^{1398}(Glc)]HMW1ct(1390-1403)	1 N-Glc	Ac-TVVNATNA**N(Glc)**GSGSV-NH_2
GP6-[Asn^{1393}(Glc),Asn^{1398}(Glc)]HMW1ct(1390-1403)	2 N-Glc	Ac-TVV**N(Glc)**ATNA**N(Glc)**GSGSV- NH_2

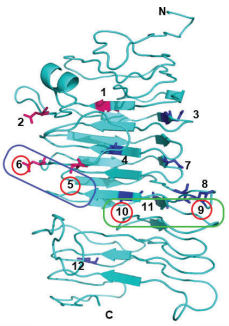

Figure 1. Structural model of the HMW1ct fragment calculated by ITASSER server [1] (right) and the corresponding amino acid sequence (left), with the 12 putative N-glucosylation sites.
The sequence HMW1ct(1345-1357) including the glucosylation sites N^{1393}(Glc) and N^{1398}(Glc) is highlighted in blue; HMW1ct(1390-1403) including the glucosylation sites N^{1348}(Glc) and N^{1352}(Glc), is highlighted in green.

Synthesis of a model glycopeptide bearing multiple copies of *N*-Glc moieties

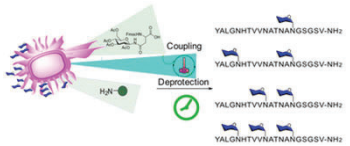

Synthetic protocols for the synthesis of glycosylated peptides by high-temperature fast stirring-solid phase synthesis (HTFS-PS) [3]
All syntheses were carried out in the same reactor, using of TentaGel R RAM resin (100 mg, loading 0.18 mmol/g). All the steps in the process were performed at 90 °C with a stirring of 1200 rounds per minute (rpm).
Resin swelling. swelling in DMF for 30 min.
Fmoc-deprotection procedure. Washing with DMF (1 × 3 mL) for 30 sec. Fmoc-deprotection by 20% (v/v) piperidine/DMF in 30 sec Washing with DMF (1 × 3 mL) for 30 sec.
Coupling procedure. Coupling volume (3mL):1 ml of 7.2mM Fmoc-AA-OH in DMF was added to 1 mL, 6.6mM HATU in DMF and 1 mL of 14.4mM DIPEA in DMF. The reaction was stirred for 60 sec.
Fmoc-L-Asn[β-D-Glc(OAc)4]-OH were synthesized as previously described [4]
Final washing procedure. At the end of synthesis, the reactor was cooled to RT. Washings with DMF (1 × 3 mL), DCM (3 × 3 mL), MeOH (3 × 3 mL), and Et_2O (2 × 3 mL). The resin was dried under a vacuum.
Cleavage. Peptide cleavage was performed with a solution of TFA (5.5 mL), H_2O (0.3 mL), and TIPS (0.2 mL). The glycopeptides were precipitated in cold diethyl ether and lyophilized. After deacetylation of hydroxyl groups on glucose moieties, **GP1-6** peptides were purified by semi-preparative RP-HPLC and the glycopeptides purity was determined by HPLC and characterized by ESI-MS analysis. The analytical data are reported in details in Table 2.

Table 2. Analytical characterization of peptides

No	HPLC (Rt, min)[a]	ESI-MS (m/z) Found/calcd	HPLC Purity (%)	Yield (%)	Quantity (mg)
GP1	3.73	1123.00/1123.25[b]	95	1.5	2
GP2	3.40	1399.26/1399.50[b]	96	8.36	12
GP3	3.42	1470.38/1470.56[b]	96	6.0	8.8
GP4	3.35	1655.40/1655.76[b]	95	2	2
GP5	2.27	1494.29/1494.56[b]	95	1.54	2.5
GP6	1.43	1656.38/1656.71[b]	95	4.1	7

Peptides **GP 1-6** were purified by Reversed-Phase Flash Liquid Chromatography on a Biotage® Isolera™ (Biotage, Uppsala, Sweden) and Semi-preparative RP-HPLC on a Waters 600 chromatograph with solvent system A (0.1% TFA in H_2O) and B (0.1% TFA in CH_3CN). Analytical characterization of peptides **GP 1-6** was performed by analytical HPLC using a Waters Alliance instrument (model 2695, Milford, Massachusetts) coupled to a single quadrupole ESI-MS (Waters® ZQ Detector, Waters Milford, MA, USA) supplied with a BEH C18 (1.7 µm, 2.1× 50 mm) column at 35 °C, at 0.6 mL/min using solvent systems A (0.1% TFA in H_2O) and B (0.1% TFA in ACN). [a]Gradient elution was performed with a flow of 0.6 mL/min and started at 10% B, with a linear increase to 90% B in 5 min. [b]ESI-MS detected as $[M+H]^+$, $[M+2H]^{2+}$

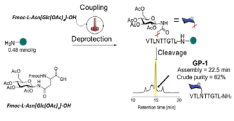

Figure. 2 HTFS-PS of **GP-1** on Rink Amide MBHA resin (0.48 mmol g^{-1} loading) solid support. Couplings were performed using 1.2 equiv. of all Fmoc-AAs, including Fmoc-L-Asn[Glc(OAc)4]-OH for 1 min at 90 °C using HATU/DIPEA as coupling system.

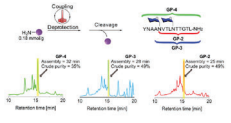

Figure 3. HTFS-PS of **GP-2**, **GP-3**, and **GP-4** on TentaGel R RAM resin (0.18 mmol g^{-1} loading). Coupling was performed using 1.2 equiv. of all Fmoc-AAs, including Fmoc-L-Asn[Glc(OAc)4]-OH and HATU/DIPEA coupling system for 1 min at 90 °C. HPLC analysis of the crude peptides were recorded at 220 nm.

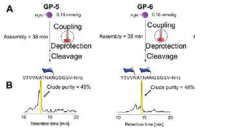

Figure 4. HTFS-PS of **GP-5** and **GP-6** on TentaGel R RAM resin (0.18 mmol g^{-1} loading) solid support (**A**). Couplings were performed using 1.2 equiv. of all Fmoc-AAs, including Fmoc-L-Asn[Glc(OAc)4]-OH and HATU/DIPEA as coupling system for 1 min at 90 °C. HPLC of crude (**B**) were recorded at 220 nm.

Results of the screening of Antibodies to the bacterial HMW1ct(Glc) peptides in Multiple Sclerosis patient sera

SP-ELISA:

- Peptides derived from NTHi adhesin bacterial protein HMW1ct(Glc) exhibited **no significant responses**, neither IgGs nor IgMs, in MS patient sera. We hypothesized that the sequences are **not long enough to coat** and recognize antibodies in the ELISA plate. In accordance with previous results, the antibody titre decreases in parallel with the length of the peptide immobilized [5].

COMING SOON **Inhibition Experiments in representative MS patient sera**

Conclusions

•HTFS-PS can become a prominent strategy to accelerate the synthesis of post-translationally modified peptides
•Antibody response is strictly influenced by the length of the immobilized peptide.

Acknowledgments:

The study is part of the Rita Levi Montalcini Award 2018-2019 for the binational Italian-Israel Scientific Research Collaboration with the Hebrew University of Jerusalem, the Azrieli Faculty of Medicine and the Weizmann Institute of Science (Israel).

REFERENCES: [1] Walvoort MT, Testa C, Eilam R, Aharoni R, Nuti F, Rossi G, Real-Fernandez F, Lanzillo R, Brescia Morra V, Lolli F, Rovero P, Imperiali B, Papini AM. Sci Rep. 2016, 6:39430. doi: 10.1038/srep39430; **[2]** Mazzoleni A, Real-Fernandez F, Nuti F, Lanzillo R, Brescia Morra V, Dambruoso P, Bertoldo M, Rovero P, Mallet JM, Papini AM. Chembiochem. 2022, 23(3):e202100515. doi: 10.1002/psc.3281; **[3]** Strauss P, Nuti F, Quagliata M, Papini AM, Hurevich M. Org Biomol Chem. 2023, 21(8):1674-1679. doi:10.1039/d2ob01886a; **[4]** Paolini I, Nuti F, Pozo-Carrero MC, Barbetti F, Kolesinska B, Kaminski ZJ, Chelli M, Papini AM. Tetrahedron Letters 2007, 48(16), 2901-2904. doi.org/10.1016/j.tetlet.2007.02.087; **[5]** Nuti, F.; Fernandez, F.R.; Sabatino, G.; Peroni, E.; Mulinacci, B.; Paolini, I.; Pisa, M.D.; Tiberi, C.; Lolli, F.; Petruzzo, M.; et al. Brain Sci. 2020, *10*, 453. doi.org/10.3390/brainsci10070453.

UNIVERSITÀ DEGLI STUDI FIRENZE

PeptLab
INTERDEPARTMENTAL RESEARCH UNIT OF PEPTIDE AND PROTEIN CHEMISTRY AND BIOLOGY

iCCOM Istituto di Chimica dei Composti Organometallici
Consiglio Nazionale delle Ricerche

Design, synthesis, and biological activity of tumor necrosis factor-alpha peptides for adalimumab recognition

Feliciana Real-Fernandez[1], Andrea Di Santo[2,3], Kalina Kirilova Kirilova[2], Silvia Rinaldi[1], Gabriele Simonini[3,4], Paolo Rovero[2,3]

[1]Institute of Chemistry of Organometallic Compounds – National Research Council of Italy (ICCOM-CNR), Sesto Fiorentino (Florence), Italy; [2]Interdepartmental Research Unit of Peptide and Protein Chemistry and Biology, University of Florence, Sesto Fiorentino, Italy; [3]Department of NeuroFarBa, University of Florence, Sesto Fiorentino, Italy; [4]Pediatric Rheumatology Unit, AOU Meyer, Florence, Italy;

https://doi.org/10.17952/37EPS.2024.P2098

Biologics targeting the **tumor necrosis factor alpha (TNF-α)** have revolutionized treatments in a wide variety of diseases, including juvenile idiopathic arthritis (JIA). Unfortunately, a significant proportion of patients fail to reach any therapeutic response owing to drug ineffectiveness (primary failure) and/or acquired therapeutic resistance eliciting anti-drug antibodies (ADAbs) as immunoresponse (secondary failure) [1]. Despite immunogenicity drawbacks have been addressed by using fully human antibodies as **adalimumab (ADL)**, this is still an open issue. Monitoring both ADL and anti-drug antibodies is fundamental in the follow-up of patients.

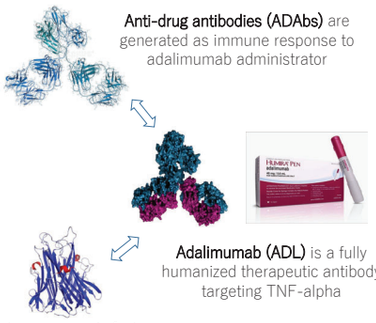

Anti-drug antibodies (ADAbs) are generated as immune response to adalimumab administrator

Adalimumab (ADL) is a fully humanized therapeutic antibody targeting TNF-alpha

tumor necrosis factor alpha (TNF-α)

TNF-α sequence uniprot code P01375 (TNFA_HUMAN)

MSTESMIRDVELAEEALPKKTGGPQGSRRCLFLSLFSFL
IVAGATTLFCLLHFGVIGPQREFPRDLSLISPLAQAVRSSS
RTPSDKPVAHVVANPQAEGQLQWLNRRANALLANGVEL
RDNQLVVPSEGLYLIYSQVLFKGQGCPSTHVLLTHTISRI
AVSYQTKVNLLSAIKSPCQRETPEGAEAKPWYEPIYLGG
VFQLEKGDRLSAEINRPDYLDFAESGQVYFGIIAL

Aim of the project:
Set up a new method to monitor ADL using TNF-α peptides

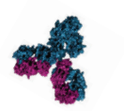

During ADL treatment, the symptoms of the autoimmune disease can re-emerge in a percentage of patients due to two possible reasons: anti-drug antibodies formation and decreasing drug concentration in the blood. In this context, adalimumab concentration quantification becomes necessary during treatment monitored together with ADAbs presence. Up to now ADL quantification is performed using TNF-α or monoclonal antibodies against ADL as antigens. The use of peptides mimicking the appropriate epitopes of the TNF-α could display enhanced ADL recognition specificity eliminating or minimizing potential cross-reactivity between structurally homologous or non relevant protein epitopes improving detection. With all these considerations in mind, the aim of the project is the design and synthesis of TNF-α peptides to be used as antigens in solid-phase ELISA and surface plasmon resonance for ADL quantification.

TNF-α and adalimumab interaction

The interaction between TNF-α and the light and heavy chains of the Adalimumab is stable and strong because of the hidrogen bonds. Hu et al. previously described the interaction identificating Adalimumab conformational epitope on TNF-α, the binding sites are composed of four discontinuous segments [2].

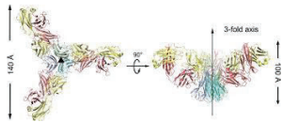

Crystal structure of TNF-α(77-233) binding adalimumab protein data bank 3WD5 [2]

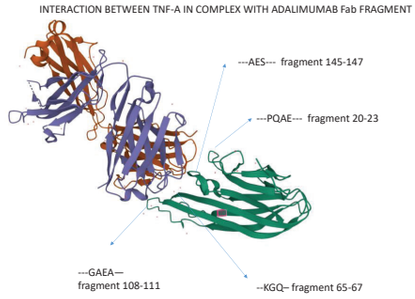

Peptides design and synthesis

1.- Chimeric strategy

A chimera with the fragments 20-23 and 145-147 maintaining the distances between the two residues of the TNF-α has been designed. Both peptides were selected using Chembio3D Ultra by calculating the number of amino acids between the proline (P,20) of the fragment 20-23 and the serine (S, 23) of the fragment 145-147 to maintain the real distance in the adalimumab-TNF-α complex of 9,1 Å. Finally, it was decided to lengthen the sequence of the fragments as necessary, resulting two different peptides:

TNF-α-(17-26)-(142-150) → VANPQAEGQLLDFAESGQV
TNF-α-(15-28)-(140-150) → HVVANPQAEGQLQDYLDFAESGQV

2.- Molecular modelling strategy

A linear peptide on TNF-α C-terminal targeting the H chain of adalimumab has been designed (PeptC).

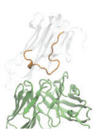

PeptC → INRPDYLDFAESGQVYFGIIAL

A new peptide trying to maximize the binding interation site has been designed, targeting both the L and H chains of ADL (FUSpept)

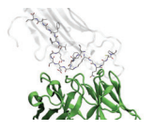

FUSpept → KGQGCPLNFAESGQVYFGIIAL

Synthesis of peptides were performed by using solid phase peptide synthesis in manual combined with microwave assisted synthesis following the Fmoc/tBu strategy, starting from 200 mg of Wang resin.

Analytical characterization of peptides

Peptide	Retention time (min)	HPLC gradient B (%)	ESI-MS (m/z) $[M+2H]^{2+}$ found (calc.)	Molecular weight (g/mol)
TNF-α-(17-26)-(142-150)	1,48	30-90	987,57 (987,54)	1791.96
TNF-α-(15-28)-(140-150)	3,43	20-80	1308,91 (1309,27)	2615.20
PeptC	2.92	35-55	1252 (1251.13)	2501.78
FUSpept	3.05	35-60	1157 (1156.59)	2312.64

Peptides were purified by Reversed-Phase Flash Liquid Chromatography on a Biotage® IsoleraTM (Biotage, Uppsala, Sweden) and Semi-preparative RP-HPLC on a Waters 600 chromatograph with solvent system A (0.1% TFA in H_2O) and B (0.1% TFA in CH_3CN). The purity of the peptides was analyzed by analytical HPLC using a Waters HPLC coupled to a single quadrupole ESI-MS (Waters ZQ Mass Detector)

Biological experiments



All peptides were tested in solid phase ELISA as antigens for adalimumab identification. Unfortunately, no significance signals were observed. We strongly hypothesized that binding sites of peptides were also involved in the coating to the ELISA plate. For this reason, inhibition ELISA experiments and surface plasmon resonance binding experiments will be proposed.

First inhibition experiments with peptides TNF-α-(17-26)-(142-150) and TNF-α-(15-28)-(140-150) showed no inhibitory activity for both peptides, whereas TNF-α was able to inhibit adalimumab interaction in solution.

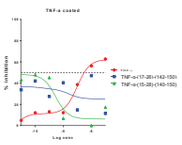

Conclusions

- A series of peptides reproducing binding sites of TNF-α have been design and proposed for adalimumab identification.
- Peptides have been successfully synthesized and purified by solid phase peptide synthesis following the Fmoc/tBu strategy.
- Peptides were not able to identify adalimumab in solid phase ELISA used as antigens. A second round of molecular modelling calculations will be performed.
- You can find more details of adalimumab quantification using surface plasmon resonance visiting the poster number P2.134.

References

[1] Real-Fernández, F. et al. *Analytical and bioanalytical chemistry* (2015):407.24, 7477-7485 [2] *Hu, S., Liang, S.Y., Guo, Y.J., Lou, Z.Y. (2013) J Biol Chem 288: 27059–27067*

Laboratory details: https://www.peptlab.unifi.it/

Corresponding author contact details: feliciana.realfernandez@iccom.cnr.it
http://www.iccom.cnr.it/

https://doi.org/10.17952/37EPS.2024.P2099

Computational design of ultrashort peptide inhibitors for the RBD of the SARS-CoV-2 S-protein

Pengfei Pei, Shi-Zhong Luo*

State key Laboratory of Chemical Resource Engineering, College of Life Science and Technology,

Beijing University of Chemical Technology, Beijing, 100029, China

***Corresponding author Email: luosz@mail.buct.edu.cn**

Abstract

Targeting the interaction between severe acute respiratory syndrome-coronavirus 2 (SARS-CoV-2) receptor-binding domain (RBD) and angiotensin-converting enzyme 2 (ACE2) is believed to be an effective strategy for drug design to inhibit the infection of SARS-CoV-2. Herein, several ultrashort peptidase inhibitors against the RBD-ACE2 interaction were obtained by a computer-aided approach based on the RBD-binding residues on the protease domain (PD) of ACE2. The designed peptides were tested on a model coronavirus GX_P2V, which has 92.2 and 86% amino acid identity to the SARS-CoV-2 spike protein and RBD, respectively. Molecular dynamics simulations and binding free energy analysis predicted a potential binding pocket on the RBD of the spike protein, and this was confirmed by the specifically designed peptides SI5alpha and SI5alpha-b. They have only seven residues, showing potent antiviral activity and low cytotoxicity. Enzyme-linked immunosorbent assay result also confirmed their inhibitory ability against the RBD-ACE2 interaction. The ultrashort peptides are promising precursor molecules for the drug development of SARS-CoV-2, and the novel binding pocket on the RBD may be helpful for the design of RBD inhibitors or antibodies against SARS-CoV-2.

Results and Discussion

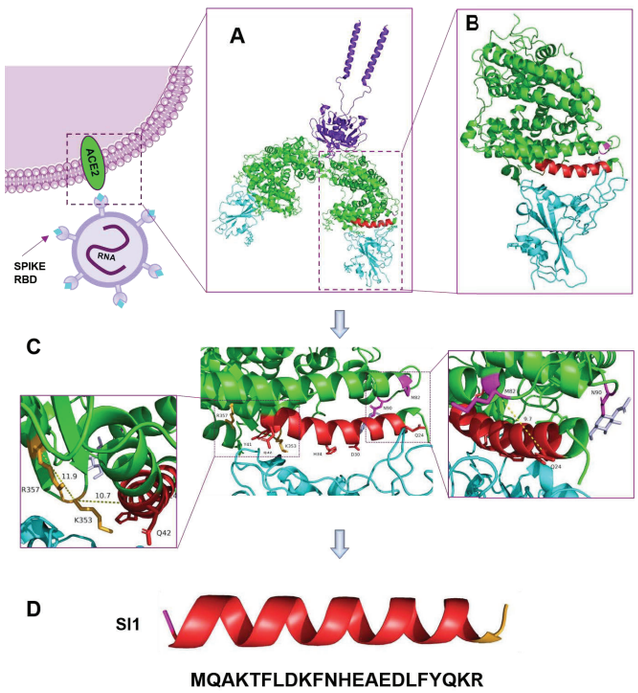

Figure 1. Design of RBD inhibitor SI1. (A) The structure of ACE2–RBD complex (split from RBD–ACE2–B0AT1 complex, PDB ID: 6M17). The PD is colored in green, the C-terminal collectrin-like domain (CLD) is colored in purple and the RBD of SARS-CoV-2 is colored in cyan. (B) The structure of the PD–RBD complex that separated from the ACE2–RBD complex. (C) The key residues on ACE2 that bound by the RBD, which were derived from the crystal structure analysis7. The distance between residues was measured by PyMol. (D) Designed sequence of the starter peptide inhibitor SI1. Single-letter abbreviations for the amino acid residues are as follows: A, Ala; D, Asp;E, Glu; F, Phe; H, His; I, Ile; K, Lys; L, Leu; M, Met; N, Asn; P, Pro; S, Ser; T, Thr; V, Val; W, Trp and Y, Tyr.

The first peptide inhibitor was designed in a structure-based manner, by analyzing the RBD-ACE2 complex (PDB ID: 6M17), and extract the critical residues in ACE2. Then the molecular docking and simulation technologies were applied for the sequence evolution, and several ultrashort peptides were obtained, namely SI4, SI4-b, SI5α and SI5α-b.

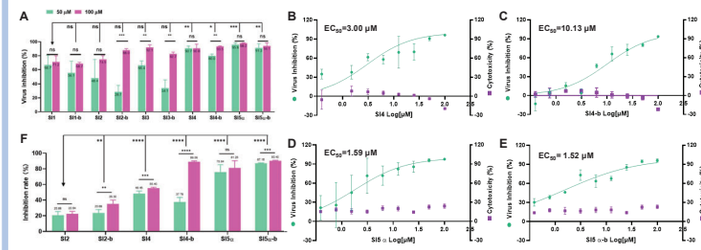

Figure 2. Antiviral activity and cytotoxicity of the peptide inhibitors. (A) Antiviral tests of the peptide inhibitors at concentrations of 100 and 50 μM using the model coronavirus GX_P2V. (B–E) EC50 and cytotoxicity of the high potency peptide inhibitors on GX_P2V virus and Vero E6 cells were determined. (B) SI4; (C) SI4-b; (D) SI5α and (E) SI5α-b. (F) ELISA for the determination on the ability of the peptides to inhibit the binding between RBD and ACE2. The data are shown as mean ± SD. Two-way ANOVA was used for the comparisons between the shorter peptides with SI1. Student's t-test was used to compare between two concentrations of a peptide (∗P < 0.05, ∗∗P < 0.01, ∗∗∗P < 0.001, ∗∗∗∗P < 0.0001).

The antiviral activity of the designed peptides was firstly tested on GX_P2V, a model coronavirus of SARS-CoV-2. The ultrashort peptides showed high antiviral activity, with the EC50 = 3.00, 1.59, and 1.52 μM for SI4, SI5α and SI5α-b (Figure 2 A-E). The ability of the peptides to inhibit the RBD-ACE2 binding was confirmed by a competitive ELISA kit (Figure 2 F). Moreover, MD simulation and binding energy calculation indicated an important binding pocket that located between E484 and Y505 on the RBD, which is critical for the activity of RBD inhibitors.

Conclusion

In conclusion, several ultra-short peptide inhibitors against the interaction between the RBD and ACE2 were designed by a computer-aided method, and confirmed to be potent in antiviral test using a model coronavirus of SARS-CoV-2 and an ELISA kit. MD simulation and binding energy calculation on the interaction between the peptides and the RBD indicated an important binding pocket on the RBD, which may be helpful for the design of RBD inhibitors or antibodies in future.

Acknowledgements

This work was supported by the National Natural Science Foundation of China (grant numbers 91853116, 21672019); Joint Project of BRC-BC (Biomedical Translational Engineering Research Center of BUCT-CJFH) (grant number XK2020-09); National Key Research and Development Program of China (grant numbers 2020YFA0712100, 2020YFC0840805).

Reference

Pei P, Qin H, Chen J, Wang F, He C, He S, Hong B, Liu K, Qiao R, Fan H, Tong Y, Chen L, Luo SZ. Brief Bioinform 2021, 22 (6), bbab243.

In vitro effect of the acidic pH on the susceptibility of the antimicrobial peptide Esc(1-21) against respiratory pathogens in cystic fibrosis lung environment

Giacomo Cappella[1], Maria Rosa Loffredo[1], Bruno Casciaro[1], Floriana Cappiello[1], Arianna Turchini[1], Maria Luisa Mangoni[1]

[1]Department of Biochemical Sciences, Laboratory Affiliated to Istituto Pasteur Italia - Fondazione Cenci Bolognetti, Sapienza University of Rome, Rome, Italy

https://doi.org/10.17952/37EPS.2024.P2100

Background

Esculentin(1-21) [Esc(1-21)] is a short-sized cationic antimicrobial peptide (AMP) corresponding to the N-terminal region of the frog-skin AMP esculentin-1a. It is endowed with a fast rate of killing activity, especially against Gram-negative bacteria, with a membrane perturbing mechanism of action.

Esculentin-1a

GIFSKLAGKKIKNLLISGLKNVGKEVGMDVVRTGIDIAGCKIKGEC

Esc(1-21) GIFSKLAGKKIKNLLISGLKG-NH_2 +6 Basic residues

- Short size
- A large spectrum of activity (Gram$^-$, Gram$^+$, fungi)
- A potent activity against planktonic and biofilm forms of *Pseudomonas aeruginosa* (Gram$^-$).



Rana esculenta

Antimicrobial activity of Esc(1-21) against reference strains and clinical isolates of *P. aeruginosa*

[PEPTIDE] CAUSING 99,9% KILLING OF PLAKTONIC CELLS	[PEPTIDE] CAUSING 95% KILLING OF BIOFILM CELLS
1 μM	12.5-25 μM

Premise and aim of the work

The number of antibiotic-resistant microbial infections is dramatically increasing, while the discovery of new antibiotics is significantly declining. Furthermore, the activity of antibiotics is negatively influenced by the ability of bacteria to form sessile communities, called biofilms, and by the microenvironment of the infection, characterized by an acidic pH, especially in the lungs of patients suffering from cystic fibrosis (CF). AMPs represent interesting alternatives to conventional antibiotics, and with expanding properties. Here, we explored the effects of an acidic pH on the antimicrobial and antibiofilm activities of the AMP Esc(1-21).

1. Antimicrobial Activity of AMPs and Antibiotics at Different pH Values, against Reference Gram-Negative Bacterial Strains

The capability of Esc(1-21) and various AMPs in inhibiting microbial growth of three reference Gram-negative bacterial strains was studied compared to conventional antibiotics, in 10% TSB (Tryptic soy Broth) pH 7.5.

	MICs (μg/mL)		
Compound	*A. baumannii* ATCC 19606	*E. coli* ATCC 25922	*P. aeruginosa* ATCC 27853
Esc(1-21)	4.3	4.3	8.7
Bombinin H2	15.3	61.3	245
Temporin L	3.25	6.5	6.5
LL-37	9.0	9.0	4.5
Colistin	0.5	0.5	0.25
Tobramycin	2.0	1.0	0.125
Ciprofloxacin	0.25	0.25	0.125

Table 1. The data are the modal values from three independent experiments. Table taken from ref. **[1]**

The MIC values were then determined in media with increasing acidity.

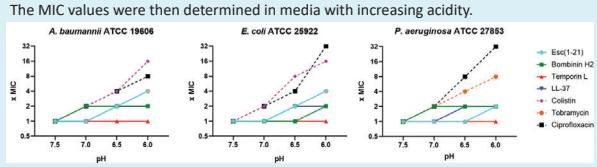

Figure 1. Variation in the MIC (**expressed as fold-change in MIC value**) of AMPs and antibiotics against the same strains as above, in 10% TSB at different pH values. The plotted data represent the modal values of three independent experiments. Graph taken from ref **[1]**

Subsequently, the activity of Esc(1-21) was evaluated against a panel of different Gram-negative strains, including reference and multidrug-resistant clinical isolates. Tobramycin was also included for comparison.

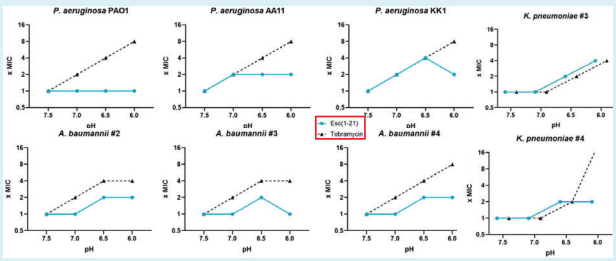

Figure 2. Variation in the MIC values (**expressed as fold-change in MIC value**) of Esc(1-21) and tobramycin at different pH values against several Gram-negative strains, in 10% TSB at different pH values. The data are the modal values from three independent experiments. Graph taken from ref **[1]**

Overall, these experiments underline the capability of Esc(1-21) to better withstand acidic conditions, retaining its antimicrobial activity more effectively than conventional antibiotics.

2. Antibiofilm Activity of Esc(1-21) Compared to Tobramycin against Preformed Biofilm in Luria–Bertani Broth (LB)

Gram-negative bacteria easily colonize biological surfaces by creating matrix-enclosed aggregates, called biofilms, in which the pH can vary within the biofilm microenvironment. Therefore, it is crucial to investigate the activity of antibiotic compounds against the sessile form of bacteria at different pH levels.

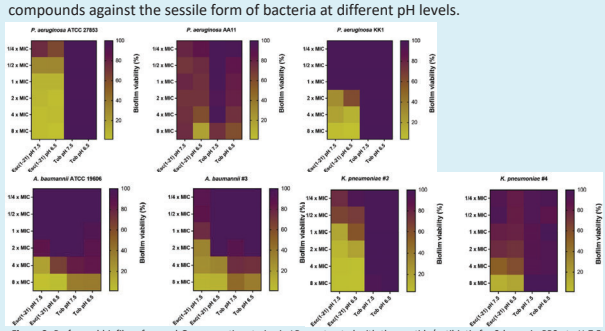

Figure 3. Preformed biofilm of several Gram-negative strains in LB was treated with the peptide/antibiotic for 2 hours in PBS at pH 7.5 and 6.5. The colors represent the percentage of biofilm viability from 0% (yellow) to 100% (purple). Graph taken from ref **[1]**

Notably, the activity of the peptide remained almost unchanged in the trend. These results highlight the potential of AMPs as novel antimicrobial agents, considering the enhanced resistance to antibiotics of the bacteria embedded in biofilms.

References

[1] Loffredo, M.R.; Cappiello, F.; Cappella, G.; Capuozzo, E.; Torrini, L.; Diaco, F.; Di, Y.P.; Mangoni, M.L.; Casciaro, B. The pH-Insensitive Antimicrobial and Antibiofilm Activities of the Frog Skin Derived Peptide Esc(1-21): Promising Features for Novel Anti-Infective Drugs. *Antibiotics* **2024**, *13*, 701.
[2] Luca, V.; Stringaro, A.; Colone, M.; Pini, A.; Mangoni, M.L. Esculentin(1-21), an amphibian skin membrane-active peptide with potent activity on both planktonic and biofilm cells of the bacterial pathogen Pseudomonas aeruginosa. Cell. Mol. Life Sci. **2013**,70, 2773–2786.
[3] Batoni, G.; Maisetta, G.; Esin, S. Antimicrobial peptides and their interaction with biofilms of medically relevant bacteria. Biochim.Biophys. Acta **2016**, 1858, 1044–1060.

Acknowledgements

The authors thank Alessandra Bragonzi (San Raffaele Institute, Milan, Italy) and Burkhard Tummler (Klinische Forschergruppe, OE 6710, Medizinische Hochschule Hannover, Germany) for the *P. aeruginosa* clinical isolates.

3. Antibiofilm Activity of Esc(1-21) Compared to Tobramycin against Preformed Biofilm Grown in m63 Medium

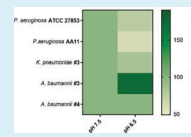

The acidic pH is also known to influence biofilm formation. For this reason, we also investigated the capability of different strains to form biofilm at two different pH conditions, pH 7.5 and 6.5. To ensure a constant pH during biofilm formation, m63 medium was used.

Figure 4. Percentage of biofilm viability of different Gram-negative strains in m63 at pH 6.5 with respect to pH 7.5 (set as 100%). The colors represent the percentage of biofilm viability from 0% (light green) to 100% (dark green). The statistical analysis was conducted with the *t* test for all strains between the two different pH values: all differences were found to be significant ($p < 0.05$), with the sole exception of *A. baumannii* #4 ($p = 0.765$). Graph taken from ref **[1]**

Then, Esc(1-21) was tested against these preformed biofilms for two hours in PBS at the corresponding pH, while tobramycin was used as the antibiotic control.

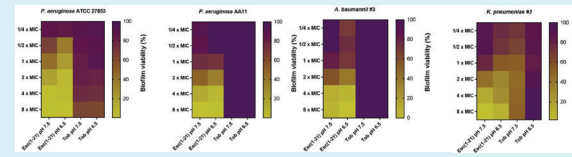

Figure 5. The effect of Esc(1-21) and tobramycin (Tob), against preformed biofilms of several Gram-negative bacterial strains in m63 medium at two different pHs, i.e., 7.5 and 6.5. Data were collected from three independent experiments. Graph taken from ref **[1]**

The activity of Esc(1-21) was enhanced against the biofilms of all the tested strains at pH 6.5. On the contrary, tobramycin had a significantly weaker activity at the two different pHs.

4. Activity of Esc(1-21) at pH 7.5 and 6.5 against Model Membranes of Gram-Negative Bacteria

Esc(1-21)'s primary mechanism of action is membrane disruption, leading to cell death. To assess the impact of pH variations, Esc(1-21) was tested at pH 7.5 and 6.5 on large unilamellar vesicles (LUVs), mimicking Gram-negative bacterial membranes and loaded with the fluorescent probe carboxyfluorescein (Cyf).

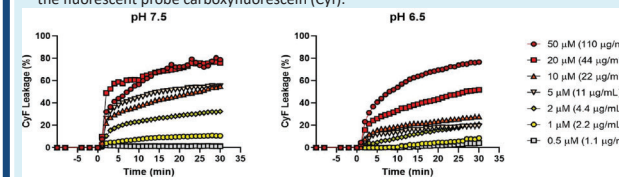

Figure 6. Kinetics of the effect of different concentrations of Esc(1-21) at pH 7.5 and 6.5, on the leakage of CyF encapsulated into POPE/POPG (ratio 7:3 mol-mol) LUVs. LUVs were used at a final lipid concentration of 100 μM. Data points are the mean of three different experiments. Graph taken from ref **[1]**

After peptide addition (time 0), a fast and dose-dependent increase in the fluorescence signal was recorded, according to the membrane-perturbing mechanism of action of Esc(1-21).
At pH 7.5, the percentage of CyF leakage was >60% at 50 and 25 μM, while 20–50% leakage was recorded for the lowest concentrations. At pH 6.5, the peptide retained its membrane-perturbing activity, albeit to a lower intensity, with a CyF leakage of about 60% at 25 μM.

5. Cytotoxic Activity of Esc(1-21) at Different pH against Mammalian Cell Lines

We previously reported the safety profile of Esc(1-21) against several mammalian cell lines through the tetrazolium bromide reduction assay (MTT).
Here, the effect of Esc(1-21) on the viability of different mammalian cell lines, i.e., HaCaT and A549 cells, was studied in acidic conditions by the CCK-8 assay.

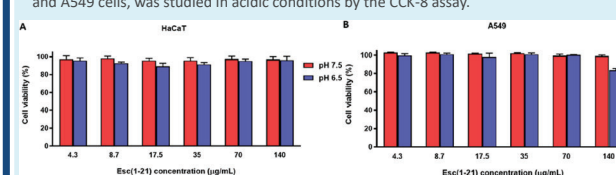

Figure 7. Viability of HaCaT (**A**) and A549 (**B**) cells after 24 h treatment with different concentrations of Esc(1-21) in DMEMg at pH 7.5 and 6.5. Cells not treated with peptides were used as controls. All data are the means of three replicates. Graph taken from ref **[1]**

Esc(1-21) did not markedly reduce the percentage of viable cells at concentrations up to 140 μg/mL; only a slight reduction in cell viability (~20%) was recorded at the highest concentration tested, at pH 6.5 against A549 cells.

Conclusion

The antimicrobial/antibiofilm activity of the AMP Esc(1-21) was explored when used at a pH lower than 7.5. It was found that when tested at pH 6.5, the peptide is practically insensitive to pH changes, highlighting the great potential of Esc(1-21) in the designing and developing of new antimicrobials to fight Gram-negative biofilm bacterial infections.

Funding

This research was supported by EU funding within the NextGeneration EU-MUR PNRR. Extended Partnership initiative on Emerging Infectious Diseases (Project no. PE00000007, INF-ACT), and also partially supported by Sapienza University (RP1221816191F624E), by Fondazione Italiana per la Ricerca sulla Fibrosi Cistica (Project FFC#4/2022) Delegazione FFC Ricerca di Roma e della Franciacorta e Val Camonica, and National Institutes of Health Grant No. R01 AI176537. M.R.L. is grateful to Pasteur Italia-Fondazione Cenci Bolognetti, as a postdoctoral fellow holder of this Institute.

Bismaleimidohexane-Stapled Anoplin Analogs

Magdalena N. Bobier [1,2], Aaron Joseph L. Villaraza [1], and Portia Mahal G. Sabido [1]

[1] Institute of Chemistry, University of the Philippines, Diliman
[2] Bicol University, Legazpi City

https://doi.org/10.17952/37EPS.2024.P2103

Abstract

The indiscriminate use of antimicrobials has led to the emergence of pathogenic organisms that have developed resistance strategies to these drugs. This necessitates the development of novel antimicrobial agents to add to our current therapeutic arsenal. **Anoplin (GLLKRIKTLL-NH2)** is a cationic, **α-helical antimicrobial peptide (AMP)** that was first isolated from the solitary spider wasp, *Anoplius samariensis*, by Konno and colleagues (2001). It **exhibits broad-spectrum antibacterial activity and low hemolytic activity**. The ease and economy in the synthesis of the short peptide chain, and the manipulability of the peptide structure for chemical modification make anoplin a practicable candidate for developing antibacterial agents. In this study, cysteine-substituted anoplin analogs were synthesized by solid-phase peptide synthesis (SPPS), and stapled with bismaleimidohexane (BMH) via the formation of thioether linkage between the sulfhydryl groups of substituted cysteine residues with the terminal maleimides of BMH. The secondary structure of the peptides and the effect of the BMH-stapling on the antibacterial activity were investigated. The circular dichroism (CD) spectra indicated the helical characteristics of the peptides. The peptides showed variable activities against Staphylococcus aureus and Escherichia coli. The BMH-stapled anoplin analog, Ano-4C8C(BMH), exhibited a more potent activity against S. aureus than anoplin. To the best of our knowledge, this study is the first report on the use of BMH for stapling cysteine-substituted anoplin analogs, and the potential of the novel BMH-stapled peptides as antibacterial agents.

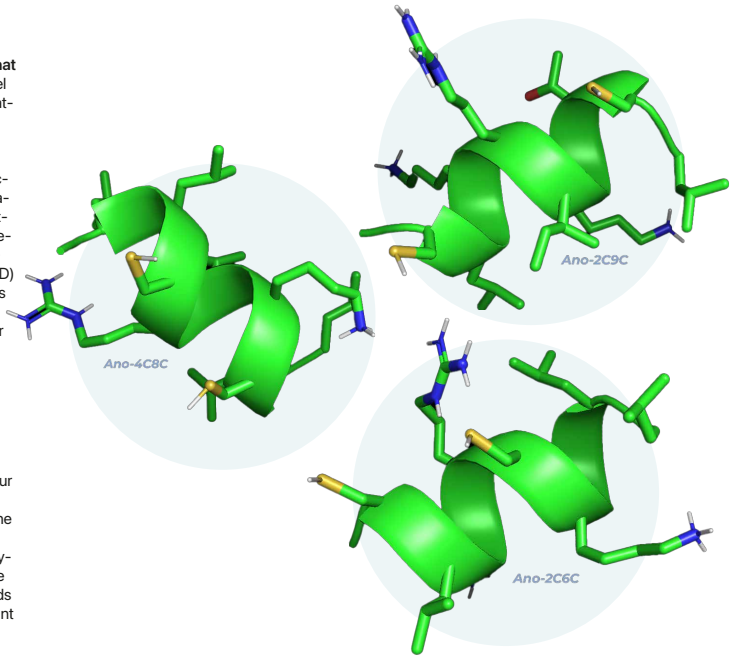

Introduction

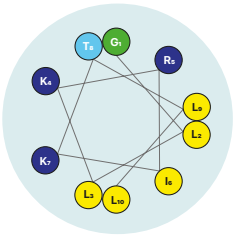

- **Anoplin** is **an amidated decapeptide** with a positive four **(+4) charge**. It is randomly coiled in water and in buffer solutions but folds into an α-helical structure in membrane mimicking solvents, TFE and SDS. The amphipathicity of anoplin is apparent from its helical wheel diagram. The hydrophobic amino acids, leucine and isoleucine are on one side of the α-helical axis while the hydrophilic amino acids are on the other side (Konno, et al., 2001). This is important in the mechanism of action of anoplin.

- **Bis(maleimido)hexane** (BMH) is a homobifunctional crosslinker with a non-cleavable, six-atom spacer arm between terminal maleimides. It finds application in protein labelling and bioconjugation.

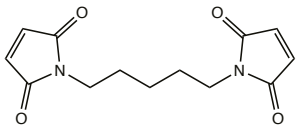

Objectives

1. Synthesize anoplin and the cysteine-substituted anoplin analogs by SPPS; and staple the cysteine-substituted analogs with BMH.
2. Characterize the secondary structure of the anoplin and the BMH-stapled analogs.
3. Evaluate the antibacterial activity of anoplin and the BMH-stapled analogs.

Methodology

Synthesis
- Solid Phase Peptide Synthesis (SPPS)
- BMH Stapling

Purification
- High-Performance Liquid Chromatography (HPLC)

Characterization
- Mass Determination: MALDI TOF
- Secondary Structure Determination: Spectroscopy
- MIC Determination: Broth Microdilution Assay

Results and Discussion

A. Mass Spectrometry Data and Percentage Yields of the Stapled Peptides

Peptides	Monoisotopic Mass (Da)	Observed Mass[a] (Da)	% Yield	Net Charge	Retention Time[b] (min)
Anoplin	1152.8	1153.4	24.58	+4	19.9
Ano-2C6C(BMH)	1408.8	1409.9	9.29	+4	18.7
Ano-2C9C(BMH)	1408.8	1409.6	11.03	+4	19.3
ANO-4C8C(BMH)	1405.8	1406.8	11.32	+3	24.8

[a] Based on the [M+H]+ m/z
[b] from RP-HPLC in a Phenomenex Luna C18 analytical column with a linear gradient of 5-95% CH3CN/H2O/0.1% TFA

- The mass data from the MALDI analyses of the cysteine-substituted peptides indicate that they have been stapled by BMH. It is apparent from the retention time of the stapled peptides in RP-HPLC that the most hydrophobic among the peptides is Ano-4C8C(BMH), followed by anoplin and then Ano-2C9C(BMH) which has comparable hydrophobicity to that of anoplin. The increase in hydrophobicity of Ano-4C8C(BMH) is expected considering the decrease in the hydrophilicity of the peptide backbone coming from the mutation of lysine and threonine to cysteine, and the additional hydrophobicity conferred by the BMH staple.

B. CD Spectra

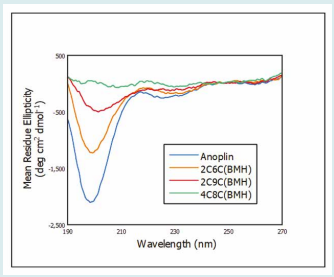

Phosphate Buffer

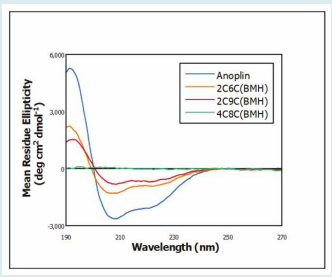

50% TFE

- The CD spectra of anoplin and the stapled peptides in buffer indicate that they are in a random coil conformation, exhibiting a negative band between 190 and 210 nm. In 50% TFE, anoplin folded into an α-helical structure, exhibiting the characteristic absorption at around 190 nm for the intense π-π* transition of the amide bonds, and the weak but broad absorbance at around 210 nm for the n-π* transition. Ano-2C6C (BMH) and Ano-2C9C(BMH) also adopted the helical structure exhibiting the same maxima at 190 nm and minima at around 210 and 220 nm. The CD spectra of Ano-4C8C(BMH) indicate that it did not form helical structure.

C. Minimum Inhibitory Concentrations (MIC) of BMH-stapled anoplin analogs against E. coli and S. Aureus

- Anoplin, with its broad spectrum antimicrobial activity, inhibited both the Gram–positive and Gram-negative bacteria. Ano-4C8C(BMH) inhibited S. aureus better than anoplin at a range of 5.5-11 μM. Ano-2C9C(BMH) selectively inhibited E. coli at a concentration of 22.7 μM.

Peptides	MIC (μM)	
	E. Coli ATCC 25922	*S. Aureus* ATCC 25923
Anoplin	13.9	28
Ano-2C6C(BMH)	>90.8	>90.8
Ano-2C9C(BMH)	22.7	>90.8
Ano-4C8C(BMH)	>22	5.5 - 11

Conclusions

- Anoplin and the cysteine-substituted analogs were synthesized by SPPS using an orthogonal group protecting strategy on a Rink amide resin.
- The BMH-stapled anoplin analogs were synthesized by stapling the cysteine-substituted peptides with BMH under ambient conditions.
- All peptides had a random coil conformation in phosphate buffer but took on the helical conformation in TFE solution, except Ano-4C8C(BMH) which did not exhibit the helical structure even in TFE.
- Ano-4C8C(BMH) exhibited better activity against S. aureus compared to anoplin.
- Ano-2C9C(BMH) was also found to be active against E. coli.

References

Konno, K. et.al. (2001). Anoplin, a novel antimicrobial peptide from the venom of the solitary wasp *Anoplius samariensis*. *Biochimica et Biophysica Acta*, 1550, 70-80.

Wojciechowska, M., Miszkiewicz, J. and Trylska, J. (2020). Conformational Changes in Anoplin, W-MreB1-9, and (KFF)3K Peptides near the Membranes. *International Journal of Molecular Sciences*, 21, 9672. https://doi.org/10.3390/ijms21249672

Proceedings of the 37th European Peptide Symposium
Michal Lebl, Editor
European Peptide Society, 2024 *http://doi.org/10.17952/37EPS.2024.P2104*

Glycine- and histidine-rich peptides derived from Shepherin I: study of candidacidal activity, metal-chelation properties and mode of action

Gustavo Nunes[1], Lohanna Lopes[1], Ernani Lacerda[2], Ana M. C. Ferreira[2], Carlos Marques[3], Breno P. Esposito[2] and M. Terêsa Machini[1]

Departments of Biochemistry[1] and Fundamental Chemistry[2], Institute of Chemistry, University of São Paulo, São Paulo, Brazil; [3]CNRS, Ecole Normale Supérieurie (ENS)[3], Lyon, France
gnunes@usp.br; mtmachini@iq.usp.br

Introduction

Antimicrobial Peptides (AMPs) have been considered very promising candidates for the development of new drugs capable of killing antibiotic-resistant pathogens, a global public health problem. Thus, it is important to explore the structure, properties and mode of actions of this class of bioactive peptides [1]. Glycine- and Histidine-Rich AMPs (GRH-AMPs) are rare in nature and very little studied. This small group includes Shepherin I (Shep I) [1,2], which is found in the roots of the Korean plant *Capsella bursa-pastoris* (*Brassicaceae* family) as a cationic product of *shep*-GRP polypeptide proteolysis [3] and contains 28 amino acid residues (67.9% glycine and 28.6 histidine) with 7 repetitions of the ATCUN motif GGH. In 2014, we reported that Shep I and fragments are more efficient in inhibiting the growth of *Candida* cells in the presence of $ZnCl_2$ [4].

Objectives

The present study is part of our ongoing research focused on Shep I. We developed and studied amidated Shep I and new short truncated analogues aiming to better understand Shep I´s structure-antifungal activity relationship, mode of action, and ability to chelate Zn^{2+} and Cu^{2+} ions [1,4]. The results could also inform on potential applications of these peptides in the fight against two major global public health problems: candidiasis and neurodegenerative diseases related to Cu^{2+}-promoted amyloid plaque formation [5].

Experimental and Results

Peptide synthesis employed microwave-assisted solid phase at 60 ºC and customized protocols. The purified peptides presented high purity degrees and the predicted amino acid contents. As expected, Shep Ia, truncated analogues, and their corresponding N-carboxyfluorescein (FAM)-forms inhibited the growth of *C. parapsilosis* ATCC 22019 (MICs of 25-100μM), *C. krusei* ATCC 6258 (MICs of 6.25-100 μM) and *C. albicans* ATCC 90028 (MICs ≥ 6.25 μM). Some of them also killed the fungal cells (MFCs of 6.25-100 μM) and became more potent in the presence of Zn^{2+} ions, confirming our previous observations [4]. Experiments using fluorescence spectroscopy, special metal-chelators and ESI-MS showed that the active FAM-peptides bind Cu^{+2} and Zn^{+2} ions with molar ratios of 1 Peptide:2 Cu^{2+} ions and 1 Peptide:10 Zn^{2+} ions. To speculate possible mode of actions for such efficient candidacidals, phase contrast and epifluorescence images were obtained using them and very simplified models of *Candida* plasma membrane (Giant Unilamellar Vesicles produced by *natural swelling* [6]); the results showed that the active fluorescent peptides strongly interact with the vesicles and penetrate and/or disrupt them after exposure of 20 min. *In vitro*, Shep I and new truncated analogues also competed with synthetic β-amyloid peptides for Cu^{+2} ions and prevented the formation of reactive oxygen species [7], findings highly suggestive of potential ability to interfere in Cu^{+2}-assisted amyloid plaques formation typical of neurodegenerative diseases. Preliminary *in vivo* experiments using FAM-octapeptide

 http://doi.org/10.17952/37EPS.2024.P2104

showed penetration not only into *Candida* cells into *Caenohabditis elegans*, used as used as model organism for Blood Brain Barrier penetration [8].

Conclusions

C-amidated Shep I, some of the new short analogues and their corresponding FAM-forms are efficient candidacidals, potent chelators of divalent metal ions, and/or cell-penetrating peptides. Such functional versatility suggests that these Shep I-derived peptides find applications in science, human health and nutrition, agriculture, chemical and environmental activities.

Acknowledgments

The authors thank FAPESP (2022/01825-2) for the research grant to MTM, CNPq for research and doctoral scholarships to MTM (314470/2023-9) and LGPN (141836/2018-0), and to Dr. Cleber W. Liria for all mass spectrometry and amino acid analyses.

References

1. Nunes, L.G.P. et al. *Int J Pept Res Ther*. 2021, *27*, 2945.
2. Wang. G. et al. *Nucleic Acid Res*., 2016, *44*, 1087.
3. Park. C. J. et al. *Plant Mol. Biol*., 2000, *44*, 187.
4. Remuzgo, C. et al. *Amino Acids*., 2014, *46*, 2573; Reichert, T. Masters Dissertation, IQ-USP, 2018.
5. Oikonomou, G. & Shaham, S. *GLIA*, 2011, *59*, 9, 1253.
6. Conte-Daban et al. *Chemistry – A European Journal*, 2018, *24*, 33, 8447.
7. Dimova, R. & Marques, C. The Giant Vesicle Book (1st Ed.), CRC Press, p.676, 2019.
8. Kim, Y. et al. Physiol. Genomics, 2018, 50, 1002.

ReCHEMbinant Protein Engineering – Synthetically Enhanced Protein Therapeutics for Myc Targeting

Jan Pascal Kahler, Brecht D. Ellenbroek and Sebastian Pomplun
Division of Medicinal Chemistry, LACDR, Leiden University, The Netherlands

https://doi.org/10.17952/37EPS.2024.P2107

Myc dimerizes with MAX to bind E-Box DNA and initiate gene transcription

Myc modulates 15% of the genome and **is involved in >50% of all cancers**

Under abnormal Myc levels, otherwise silent genes become activated. This eventually leads to Myc's implication in cancer

Max can homodimerize and acts as endogenous Myc inhibitor

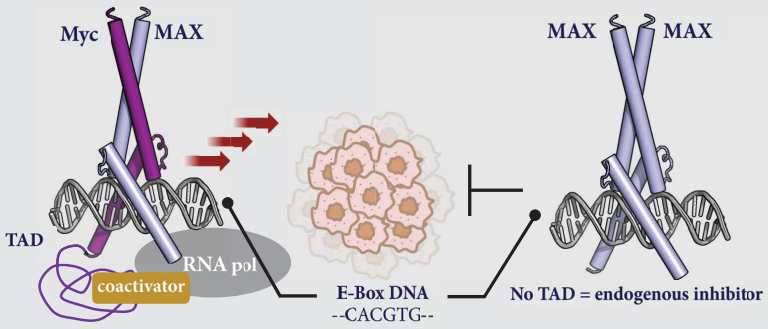



SCAN ME

Concept and Design

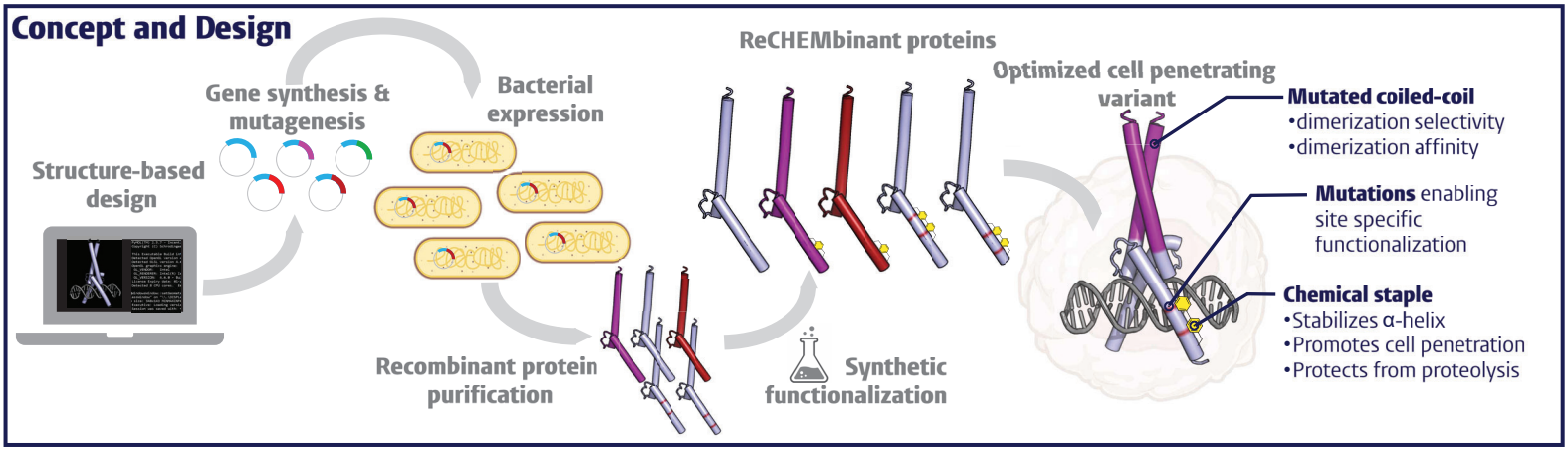

Protein Modification and DNA Binding

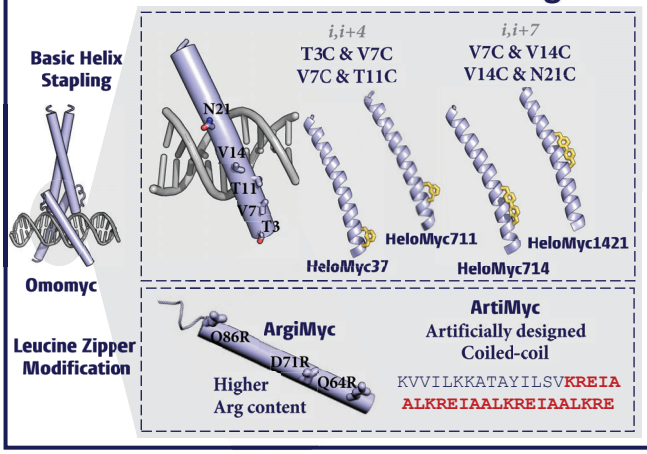

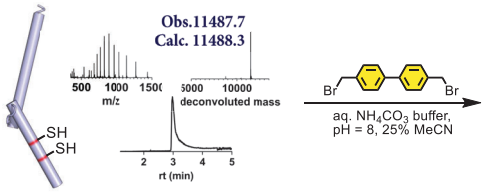

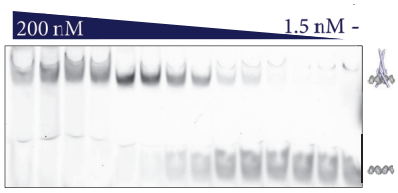

EMSA of HeloMyc1421

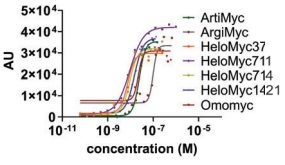

Protein	K_D (nM)
HeloMyc1421	15
HeloMyc714	9
HeloMyc37	8
HeloMyc711	9
ArgiMyc	99
ArtiMyc	24
Omomyc	22

Physical Properties

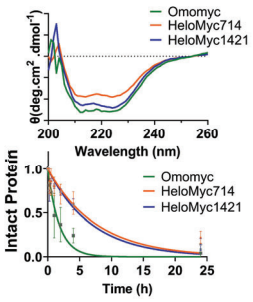

Protein	Tm (°C)	$t_{0.5}$ (h)
HeloMyc714	71.9	5.3
HeloMyc1421	74.3	4.8
Omomyc	76.0	1.2

HeloMyc714 and 1421 display good stability

Myc Reporter Gene Assay

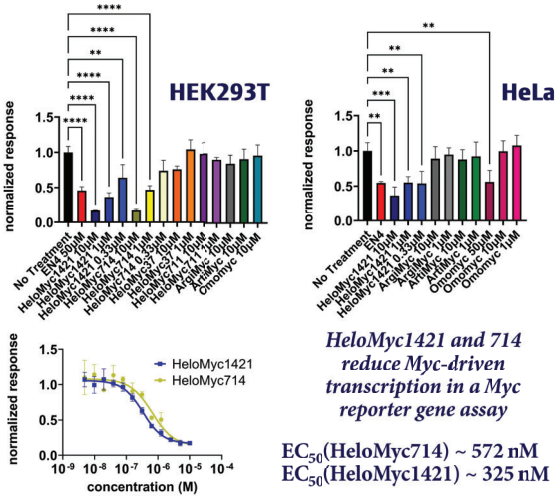

HeloMyc1421 and 714 reduce Myc-driven transcription in a Myc reporter gene assay

EC_{50}(HeloMyc714) ~ 572 nM
EC_{50}(HeloMyc1421) ~ 325 nM

Cell Penetration of HeloMyc1421

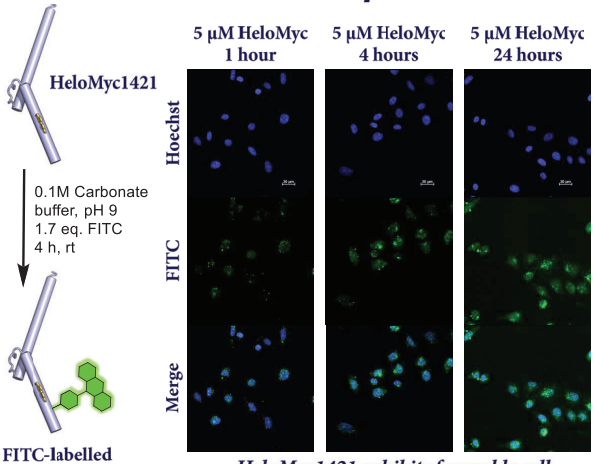

HeloMyc1421 exhibits favorable cell penetrating properties

PDB 5I50 used for all structures

Cecropin A-Melittin B Hybrid CA(1-7)M(2-9) Analogs with Improved Antibacterial Activity, Low Toxicity, and Good Protease Stability

Talia Chetty,[1] Jessica T. Mhlongo,[1,2] Ayman Y. Waddad,[1] Fernando Albericio,[1,3,4] Beatriz G. de la Torre[2]

[1] Peptide Science Laboratory, School of Chemistry and Physics, University of KwaZulu-Natal, Westville, Durban 4000, South Africa.
[2] KwaZulu-Natal Research Innovation and Sequencing Platform (KRISP), School of Laboratory Medicine and Medical Sciences, College of Health Sciences, University of KwaZulu-Natal, Durban 4041, South Africa.
[3] Institute for Advanced Chemistry of Catalonia (IQAC-CSIC), 08034 Barcelona, Spain.
[4] CIBER-BBN, Networking Centre on Bioengineering, Biomaterials and Nanomedicine, and Department of Organic Chemistry, University of Barcelona, 08028 Barcelona, Spain.

https://doi.org/10.17952/37EPS.2024.P2108

Introduction:

Cetropin A and Mellitin peptide hybrids have been a distinguished study for many decades. Cecropin A (1) compromises 37 amino acid and shows good antibacterial activity and is not toxic, however, it is too large to produce at a reasonable cost. Melittin is a 26-residue peptide that shows antibacterial activity, among others, but it is highly toxic to eukaryotic cells (2,3). Previously, it has been established that the hybridization of cecropin A and melittin has the optimal strategy with the combination of residues 1–13 of cecropin A (CA) followed by residues 1–13 of melittin (M), (4) which leads to an antibacterial peptide [CA (1–13)M(1–13)] of broad spectrum with a low hemolytic effect. However, this peptide sequence was still long (26 amino acid residues). Our group has managed to shortened the hybrid sequence even further to 15 amino acid residues, CA(1–7)M(2–9). Managed to synthesize this peptide with its analogs using solid phase peptide synthesis, characterized these peptides using reverse phase High Performance Liquid Chromatograpy (HPLC) and Liqiud Chromatography Mass Spectrometry (LC-MS). According to our findings CA(1–7)M(2–9) and its analogs have good antimicrobial activity, low hemolysis, and have good stability in tryptic digestion. These peptide properties solely depend on the construction of the hybrids, keeping in mind the fragment order, its amino acid composition, length, replacing of certain amino acids and the structure (linear/cyclic).

CA(1-7)M(2-9): H-KWKLFKKIGAVLKVL-NH_2

NaCme	Short name	Sequence	MW
CA(1-7)M(2-9)	CAM	H-KWKLFKKIGAVLKVL-NH_2	1770.3
CA(1-7)	CA	H-KWKLFKK-NH_2	976.3
M(2-9)	M	H-IGAVLKVL-NH_2	811.1
M(2-9)CA(1-7)	MCA	H- IGAVLKVL KWKLFKK-NH_2	1770.3
R_1-CA(1-7)M(2-9)	R_1-CAM	H-RWKLFKKIGAVLKVL-NH_2	1798.4
R_3-CA(1-7)M(2-9)	R_3-CAM	H-KWRLFKKIGAVLKVL-NH_2	1798.4
R_6-CA(1-7)M(2-9)	R_6-CAM	H-KWKLFRKIGAVLKVL-NH_2	1798.4
R_7-CA(1-7)M(2-9)	R_7-CAM	H-KWKLFKRIGAVLKVL-NH_2	1798.4
R_{13}-CA(1-7)M(2-9)	R_{13}-CAM	H-KWKLFKKIGAVLRVL-NH_2	1798.4
R-CA(1-7)M(2-9)*	R-CAM	H-RWRLFRRIGAVLRVL-NH_2	1910.4
O-CA(1-7)M(2-9)*	O-CAM	H-OWOLFOOIGAVLOVL-NH_2	1700.3
Cyclic C-CA(1-7)M(2-9)-C	Cyc-CAM		1974.6

Figure 1: The table above shows the amino acid sequence of CA(1–7)M(2–9) peptide hybrid and its analogs that were synthesized by our group. All peptides were synthesized using Rink-amide resin following Fmoc/tBu strategy in SPPS both in both automated and manual modes. After their cleavage all of them were purified by semi-preparative HPLC. The purities of the tested compounds ranged from 90–99% characterized by HPLC and LCMS.

Cyclization:H-CKWKLFKKIGAVLKVLC-NH_2

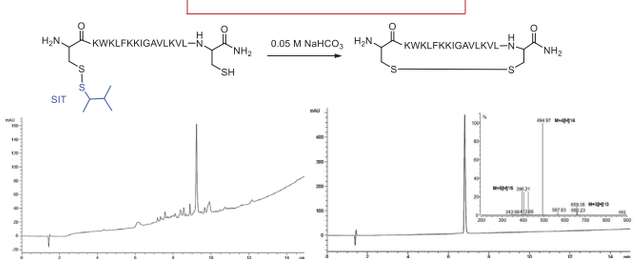

Figure 2: The disulfide cyclic version of CA(1–7)M(2–9) was obtained by adding a Cys residue to each end of the peptide and carrying out a chemoselective thiol–disulfide interchange using sec-isoamylmecaptan as protecting group of one of these residues. After peptide cleavage and precipitation, the crude peptide, was dissolved in a 0.05 M NaHCO3 solution to a dilution of 0.1 mM at a pH of approximately 8. The reaction was quenched by acidification to pH 2–3 using TFA and then required only a straightforward purification step in which a >99% purity was achieved.

MIC

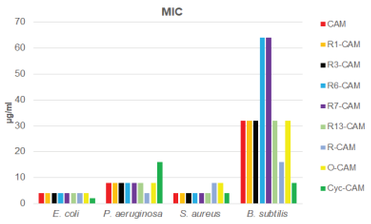

Figure 3: MIC (minimal inhibitory concentration) of peptides tested against gram negative (E. coli and P. aeruginosa) and Gram-positive S. aureus and B. subtilis) reference bacterial strains (ATCC strains). All nine peptides showed low MIC values against the four bacterial strains in a range from 2 to 64 μg/mL, the highest MICs being against B. subtilis.

% Hemolysis

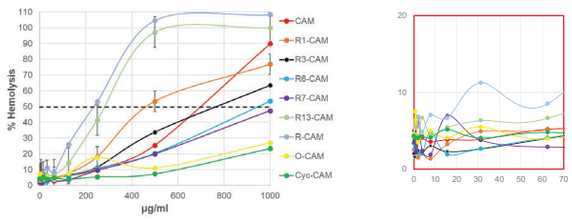

Figure 4: The graph is showing hemolytic activity of the peptides tested in Sheep Red Blood Cells. The R-CAM (high Arg content) showed the highest percentage of hemolysis as expected. The least hemolytic peptide was the disulfide-cycled version of CAM and O-CAM. However, of note, in the range of concentrations where the peptides showed antibacterial activity, the hemolysis value was below 10% for all of them, see the magnified part.

HC_{50} and Selectivity Index

	CAM	R_1-CAM	R_3-CAM	R_6-CAM	R_7-CAM	R_{13}-CAM	R-CAM	O-CAM	Cyc-CAM
SRBC (HC_{50} μg/ml)	690	450	750	935	>1000	280	230	>1000	>1000
SI *E. coli*	173	113	188	234	>250	70	58	>250	>500
SI *P. aeruginosa*	86	56	94	117	>125	35	58	>125	>63
SI *S. aureus*	173	113	188	234	>250	70	29	>125	>250
SI *B. subtilis*	22	14	23	15	>16	9	14	>31	>125

Figure 5: The table above is showing the R6-CAM, R7-CAM, O-CAM, and cyclic-CAM, had SI values that were significantly higher than that of the parent compound CAM. In contrast, as expected, the most hemolytic peptides, namely R13-CAM and R-CAM, presented the lowest SI values in comparison to CAM.

Trypsin Enzymatic Stability

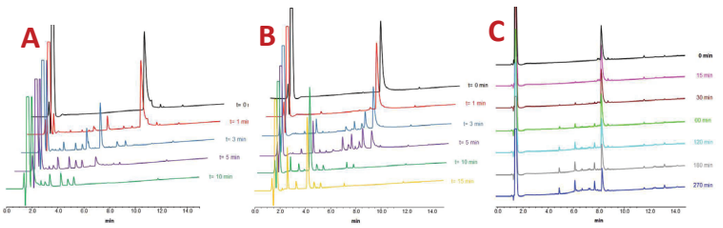

Figure 6: Time course of trypsin digestion of (A) CAM, (B) Cyc-CAM, and (C) O-CAM. In the case of linear CAM, there were no traces of the full-length peptide after 3 min. In contrast, for Cyc-CAM, the full-length peptide was still present at 5 min. The O-CAM showed the presence of 58% of the initial O-CAM in the medium after 4.5 h of tryptic digestion.

CONCLUSION:

- ✓ **CA(1-7)M(2-9):KWKLFKKIGAVLKVL** has good antibacterial activity and hemolysis, however they are easily digested by enzymes.
- ✓ **Cyclic C-CA(1-7)M(2-9)-C: CKWKLFKKIGAVLKVLC** has good antibacterial activity and hemolysis, has improved resistance to enzyme digestion
- ✓ **O-CA(1-7)M(2-9): OWOLFOOIGAVLOVL** has good antibacterial activity and hemolysis, has good resistance to enzyme digestion

References:

1. Steiner H.; Hultmark D.; Engström Å.; Bennich H.; Boman H. G. *Nature*. 1981, 292, 246–248.
2. Fennell J. F.; Shipman W. H.; Cole L. J. *Proc. Soc. Exp. Biol. Med*. 1968, 127, 707–710.
3. Habermann E. *Science*. 1972, 177, 314–322.
4. Boman H. G.; Wade D.; Boman I. A.; Wåhlin B.; Merrifield R. B. *FEBS Lett*. 1989, 259, 103–106.
5. T. Chetty T.; Mhlongo J. T.; Waddad A. Y.; Albericio F.; de la Torre B. G. *ACS Med. Chem. Lett*. 2022, 13, 1370

ACKNOWLEDEGMENT

Luxembourg Bio Technologies

MARIE CURIE ACTIONS

SUPRO-GEN

UKZN INSPIRING GREATNESS

Optimizing Ham Curing Process: Impact of overripening and the use of nitrifying salts on Peptide Bioactivity.

Noelia Hernández Correas*, Cindy Bande-De León*, Adela Abellán Guillén*, Teresa Muela Clemente*, Eva Salazar Serna*, Jose María Cayuela García*, Luis Tejada Portero*
*Universidad Católica de San Antonio de Murcia - UCAM, Guadalupe de Maciascoque

https://doi.org/10.17952/37EPS.2024.P2109

1 INTRODUCTION

Bioactive peptides are short chains of amino acids that can trigger specific effects in the human body, making them of great interest in the development of functional foods. For ham, which is often limited in consumption due to its high salt content, this study aims to improve its quality and health benefits by using alternative curing processes and salts to increase the concentration of bioactive peptides. The number and evolution of these peptides during ham maturation depend on a balance between proteolytic processes and factors such as temperature and maturation time. The study investigates how over-ripening and the use of different nitrifying salts during the salting process affect the final quality of the ham in relation to the biological activity of peptides.

2 METHODOLOGY

The study analyzed 9 treatments of nitrifiers and salt types in deboned cured ham, focusing on how these changes affect bioactivity. Treatments included NO3 nitrifiers with reduced salt (T1, T3), NO3 with normal salt (T4), NO2 with reduced salt (T6), and NO4 with either reduced (T7) or normal salt (T9). The goal was to identify which treatment provides the highest bioactivity in the final product.

Six batches of cured ham, each treated with a different nitrifying salt and over-ripened to a 42% weight loss, were evaluated. Bioactive peptides were identified using mass spectrometry, and their quantification was normalized using peptide spectral matches (PSM). The identified peptides were compared with the BIOPEP-UWM database to confirm their bioactive potential.

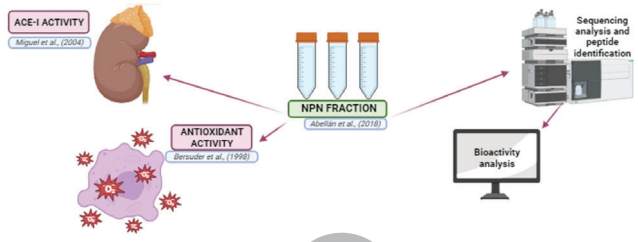

3 RESULTS

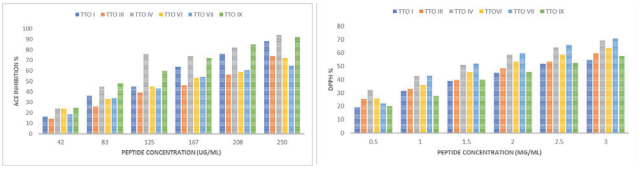

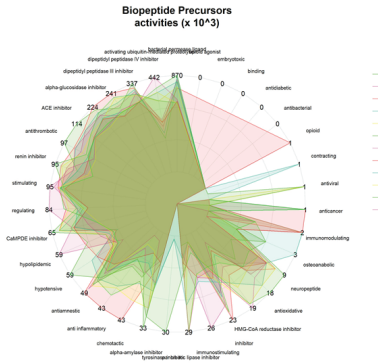

The analysis of hams matured to a 38% weight loss (SIV) versus those over-ripened to 42% (SV) reveals distinct bioactive properties. SIV hams exhibit stronger inhibition of DPP IV and ACE, indicating greater antidiabetic and antihypertensive potential, along with moderate antithrombotic effects. In contrast, SV hams show improved antibacterial and consistent antioxidant activities, despite a slight decrease in enzyme inhibition. Overall, SIV hams are more effective in enzyme inhibition, while SV hams emphasize antibacterial properties.

4 CONCLUSIONS

Some samples (such as SIV4 and SV4) exhibit high activity in inhibiting DPP IV (dipeptidyl peptidase IV), which is associated with antidiabetic effects. Inhibition of ACE enzyme, which affects blood pressure, is notable in several samples. Antiviral, antioxidant, and anti-inflammatory activities are present to a lesser extent in most samples. There is variation in activity between SIV and SV samples, suggesting differences in biopetide precursors depending on the maturation or curing conditions of the ham.

BIBLIOGRAPHY

Sentandreu, M. A., & Toldrá, F. (2006). A fluorescence-based protocol for quantifying angiotensin-converting enzyme activity. Nature Protocols, 1, 2423-2427.
Bersuder, P., Hole, M., & Smith, G. (1998). Antioxidants from a heated histidine- glucose model system. I: Investigation the antioxidant role histidine and isolation of antioxidants by high-performance liquid chromatography. Journal of the American Oil Chemists' Society, 75(2), 181-187.
Escudero, E., Aristoy, M. C., Nishimura, H., Arihara, K., & Toldrá, F. (2012). Antihypertensive effect and antioxidant activity of peptide fractions extracted from Spanish dry-cured ham. Meat Science, 91(3),

Financiado por la Unión Europea NextGenerationEU
GOBIERNO DE ESPAÑA MINISTERIO DE CIENCIA, INNOVACIÓN Y UNIVERSIDADES
Plan de Recuperación, Transformación y Resiliencia
UCAM UNIVERSIDAD CATÓLICA DE MURCIA

FUNCTIONAL AND STRUCTURAL UNDERSTANDING OF THE ANGIOTENSIN II RECEPTOR TYPE 1 (AT1R) BIASED SIGNALING

Margot Hadjadj[a], Alexandre Murza[a], Brian Holleran[a], Yoon Namkung[b], Stéphane Laporte[b], Richard Leduc[a], Mannix Auger-Messier[c] and Pierre-Luc Boudreault[a]

[a] *Department of Pharmacology-Physiology, Faculty of Medicine and Health Sciences, Université de Sherbrooke, Sherbrooke, Québec, J1H 5N4, Canada*
[b] *Department of Medicine, Research Institute of the McGill University Health Center(RI-MUHC), McGill University, Montréal, QC H4A 3J1, Canada*
[c] *Department of Medicine,Division of Cardiology, Faculty of Medicine and Health Sciences, Université de Sherbrooke, Sherbrooke, Québec, J1H 5N4, Canada*

https://doi.org/10.17952/37EPS.2024.P2110

INTRODUCTION

AT1R belongs to the large family of G protein-coupled receptors (GPCRs) and is a central component of the renin-angiotensin system (RAS) with a major influence on **blood pressure regulation**. Its endogenous ligand angiotensin II (AngII), an octapeptide **Asp-Arg-Val-Tyr-Ile-His-Pro-Phe**, triggers both G protein-dependent and independent signaling pathways such as, **Gαq, Gαi, Gα12/13 and β-arrestins.**[1-2]

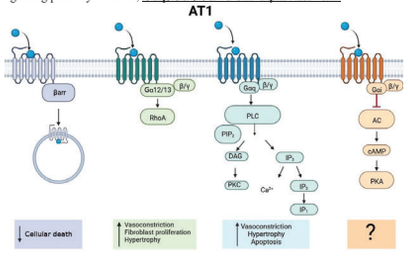

HYPOTHESIS

Selectively activating specific pathways would permit having positive effects (βarr) without the undesirable effects (Gαq). These types of ligands are called biased ligands. [3]

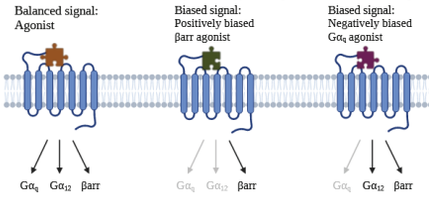

Objective: **Understand the structure-signaling relationship of the Gq pathway.**

METHODOLOGY

The peptide analogs' synthesis is carried out on solid phase (SPPS) following the Fmoc strategy.

Peptides are purified on PREP-HPLC.

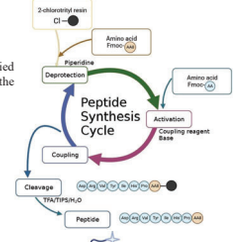

The activation of the different pathways is studied using biosensors based on Bioluminescence Resonance Energy Transfer (BRET) technology in HEK cells.[4]

BRET is a method based on the proximity of a luminescent donor and a fluorescent acceptor; the transfer only occurs when the distance between the two is between 10-100 Å.

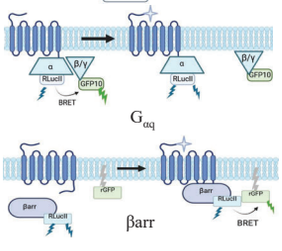

Using a calculation relating the potency and efficacy of the compound for each pathway, taking AngII as the reference point, we obtain a **quantification of the bias**.

Quantification of bias:

$$\Delta\Delta log R = \Delta log\left(\frac{\tau}{\alpha_2}\right) = log\left(\frac{\tau}{\alpha_2}\right)_{ligand} - log\left(\frac{\tau}{\alpha_2}\right)_{AngII} \quad or\ simplified\ as\ \Delta log\left(\frac{Emax}{EC50}\right) = log\left(\frac{Emax}{EC50}\right)_{ligand} - log\left(\frac{Emax}{EC50}\right)_{AngII}$$

RESULTS

We replaced the Phe8 with a structural diversity of natural and unnatural amino acids. The Phe8 is known to play a crucial role in activating the Gq pathway without affecting βarr2 recruitment.[5]

We aim to understand which ligand-receptor interactions are involved in the activation of the Gq pathway.

The replacement of Phe8 with lipophilic amino acids led to negatively Gαq-biased ligands able to recruit βarr to similar extent as AngII.

Polar or charged amino acids induce weak recruitment of βarr, owing to a potential lack of binding.

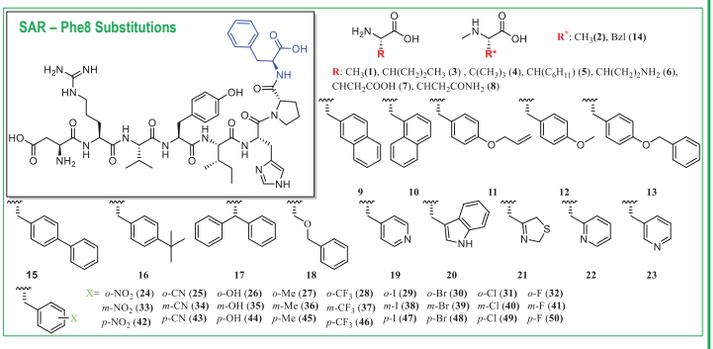

Spider plot Gq and βarr

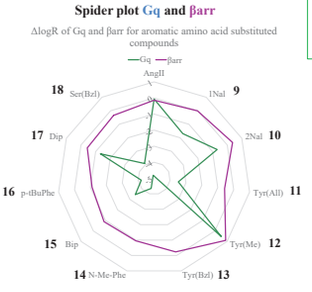

The size seems important, indeed amino acids with longer side chains lower proportionally the activation of Gaq. Moreover, expanding the width appears to result in a less pronounced impact on the activation of Gq ➔ Space in the interactions pocket

Spider plot Gq and βarr

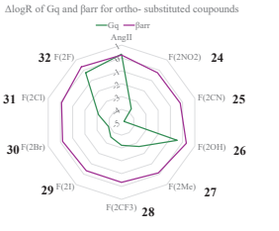

Gq activation is maintained only **F(2F)** and **F(2OH).** ***Ortho is highly sensitive.***

Spider plot Gq and βarr

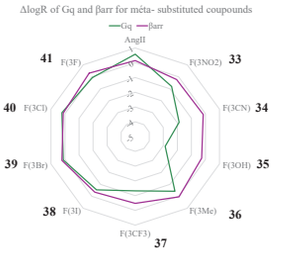

Molecular Modeling

3D representation of 500 ns molecular dynamic simulations of AT1R (PDB 7F6G) with F(3CN) and F(3OH) Angiotensin II analogs

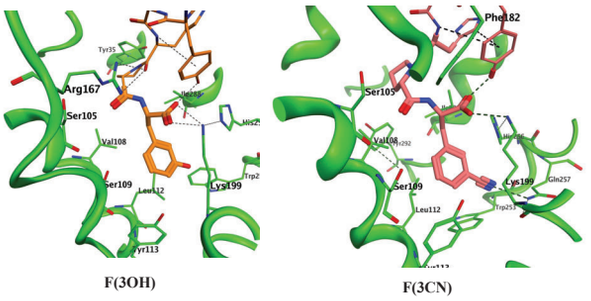

F(3OH) F(3CN)

Meta: ***H-bond donor group is detrimental***
Interaction with Gln257 could be implicated in Gq signaling

Protein Kinase C (PKC) downstream signaling

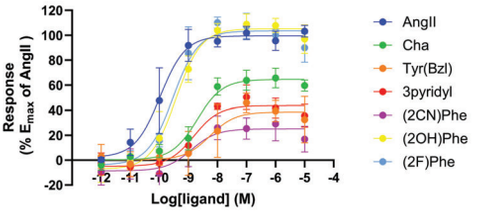

F(2CN), Tyr(Bzl), and 3pyridyl analogs of AngII exhibiting the lower activation of Gq protein also weakly trigger PKC signaling (Emax 20-40%).

CONCLUSION

We synthesized novel AngII analogs exhibiting various degrees of Gq protein and PKC activation, unraveling a chemical switch related to Gq signaling. Molecular modeling also provided new hypotheses about the interactions between ligand-AT1R restraining Gq activation.

PERSPECTIVES

- Biological tests: BRET in VSMCs, Blood Pressure Analysis in rats
- Crystallography: To understand which receptor conformation leads to the activation of Gq pathway

Acknowledgments

BOUDREAULT MEDICINAL CHEMISTRY LAB
M4M's LAB
INSTITUT DE PHARMACOLOGIE DE SHERBROOKE UdS
IRSC CIHR Instituts de recherche en santé du Canada Canadian Institutes of Health Research
NSERC CRSNG

References

1. Forrester et al. Physiol Rev 2018
2. Guo et al., 2022
3. Rominger et al., 2014
4. Hiroyuki Kobayashi *et. al* Biophysical Journal 2659-Pos B675 2018
5. Namkung et al, Sci. Sign. 2018

Proceedings of the 37th European Peptide Symposium
Michal Lebl, Editor
European Peptide Society, 2024 *http://doi.org/10.17952/37EPS.2024.P2111*

Molecular determinants of the anti-amyloid function of the cross-interaction of the human cathelicidin LL-37 with islet amyloid polypeptide

Valentina Armiento, Hendrik Wunderlich, and Aphrodite Kapurniotu
Division of Peptide Biochemistry, TUM School of Life Sciences, Technical University of Munich (TUM), Freising, D-85354, Germany

Introduction

Islet amyloid polypeptide (IAPP) is a 37-amino acid long neuroendocrine hormone which is secreted from the pancreatic β-cells [1]. IAPP is a highly amyloidogenic polypeptide. Its self-assembly into cytotoxic oligomers and amyloid fibrils is linked to inflammation, β-cell degeneration, and the pathogenesis of type 2 diabetes (T2D). Cathelicidins are a large group of multifunctional host-defense peptides (HDP) which are expressed by various cells including pancreatic β-cells and play important roles in inflammatory processes. The only known human cathelicidin is the 37-residue polypeptide LL-37. LL-37 has been long known for its broad-spectrum antimicrobial activity and its potent immunomodulatory effects [2]. Intriguingly, recent studies of our group showed that LL-37 is able to interact with IAPP with nanomolar affinity and to effectively suppress its amyloid self-assembly and related pancreatic β-cell-damaging effects *in vitro*. Our results suggested that the LL-37/IAPP interaction may play a protective role in T2D [3].

We asked which are the molecular and structural requirements of the anti-amyloid function of the LL-37/IAPP interaction. To address this, we first studied the effects of systematic N-terminal shortening of LL-37 on its structure, interactions with IAPP, and related anti-amyloid function.

Results and Discussion

Various different N-terminal truncated LL-37 analogues were synthesized by Fmoc-based solid phase peptide synthesis (SPPS) methodology. Their effects on fibril formation of IAPP were studied by using the amyloid specific thioflavin T (ThT) binding assay in combination with transmission electron microscopy (TEM). Their effects on formation of cytotoxic IAPP assemblies were determined using the MTT reduction assay in cultured rat insulinoma cells (RIN5fm). Of note, full length LL-37 was included in the studies for comparison.

We found that the deletion of the N-terminal dipeptide segment from LL-37 does not affect its ability to inhibit IAPP amyloid self-assembly and cytotoxicity. This suggests that residues Leu1 and Leu2 are not necessary for its anti-amyloid function. However, further N-terminal truncation up to LL-37(7-37) resulted in a loss of anti-amyloid activity. Thus, residues within LL-37(3-6) seem to play an important role in the anti-amyloid activity of LL-37. Interestingly, fluorescence spectroscopic titrations of fluorescently labeled IAPP with the truncated LL-37 analogues revealed that N-terminal truncation of LL-37 up to residue 14 does not impair binding affinity to IAPP.

Thus, the binding affinities of the LL-37 variants to IAPP did not correlate with their effects on IAPP amyloid formation suggesting that additional factors might be involved. Finally, far-UV CD spectroscopic studies were consistent with nearly identical secondary structure contents for LL-37 and LL-37(3-37) while further N-terminal truncation affected the secondary structure. The results of our studies should assist in deciphering the molecular basis of the anti-amyloid function of the LL-37/IAPP interaction and the design of novel molecules targeting pathogenic IAPP amyloid self-assembly in T2D.

Acknowledgments

This work was supported by Deutsche Forschungsgemeinschaft (DFG) grant SFB1035 B06 (part of SFB1035, project number 201302640).

References

1. Westermark, P., et al. *Physiol Rev* **91**, 795-826 (2011), https://doi.org/10.1152/physrev.00042.2009
2. Durr, U. H., et al. *Biochim Biophys Acta* **1758**, 1408-1425 (2006), https://doi.org/10.1016/j.bbamem.2006.03.030
3. Armiento, V., et al. *Angew Chem Int Ed Engl* **59**, 12837-12841 (2020), https://doi.org/10.1002/anie.202000148

https://doi.org/10.17952/37EPS.2024.P2114

USE OF ALTERNATIVE CURING SALTS IN THE CURED HAM PRODUCTION PROCESS. EFFECT ON THE GENERATION OF BIOACTIVE PEPTIDES.

Cindy Bande-De León*, Noelia Hernández Correas*, Manuel Hernández Lorca*, Pablo Gómez San Miguel*, Gregorio Molina Valero*, Estefanía Bueno Gavilá*, María Dolores Gil Martínez*, Adela Abellán Guillén*
*Universidad Católica de San Antonio de Murcia - UCAM, Guadalupe de Maciascoque

1 INTRODUCTION

The curing process of ham not only affects its sensory characteristics but also influences the bioactive peptide profile of the final product. Bioactive peptides generated during curing have shown potential health benefits. This study explores how different types of curing salts affect the concentration and bioactivity of peptides produced in boneless dry-cured white ham, using six different salt formulations.

2 METHODOLOGY

Six batches of boneless dry-cured white ham were cured with a different type of salt and nitrifying agent (NA):

-SIV1: NA n°3 (+60%) with reduced salt (RS) (Salt n°5).
-SIV2: NA n°3 (x2 dose) with RS (Salt n°5).
-SIV3: NA n°3 (x2 dose) with regular salt (Salt n°1).
-SIV4: NA n°2 (reduced nitrates) with RS (Salt n°5).
-SIV5: NA n°4 (traditional nitrification but reduced in salt) with RS of special granulometry (Salt n°4).
-SIV6: NA N°4 (traditional nitrification but reduced in salt) with regular salt (Salt n°1).

Peptide identification was carried out by tandem mass spectrometry (MS) from the non-protein nitrogen fraction. Quantification values were normalized, focusing on the total peptide spectral matches (PSM) for all peptides in the sample.

3 RESULTS

*1: PEPTIDE INTERSECTIONS BY FREQUENCY AND DEGREE.
*2: ACTIVITY HEATMAP.
*3: QUANTIFICATION OF BIOPEPTIDE PRECURSORS.

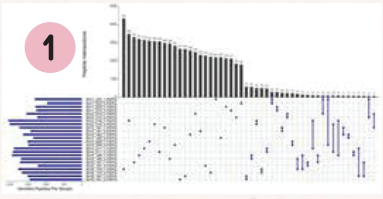

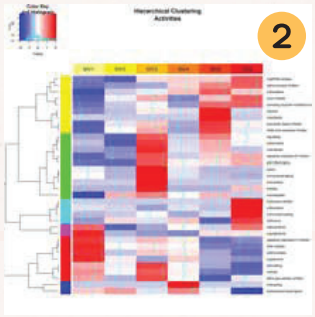

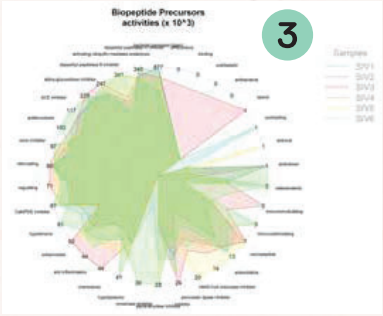

The analysis revealed significant differences in bioactive peptide concentration and types among the hams. Hams cured with SIV3 (Nitrifying agent N03 with regular salt) and SIV6 (Nitrifying agent N04 with regular salt) exhibited higher bioactive activity, suggesting that regular salt with higher nitrifying agents enhances peptide bioactivity. SIV3 and SIV6 also showed the highest concentrations of bioactive precursors, with SIV6 particularly noted for antioxidant and antihypertensive peptides. Additionally, SIV6 displayed a unique diversity of bioactive peptides, indicating its superior bioactive profile.

4 CONCLUSION

The type of curing salt significantly influences the bioactivity of dry-cured hams. SIV6 (Nitrifying agent N04 with regular salt) optimizes bioactive peptide production, making it the most effective choice for enhancing the functional properties of cured meats. Reduced salt formulations, like SIV1 and SIV4, produce lower bioactivity levels, suggesting some trade-offs with salt reduction.

5 BIBLIOGRAPHY

Aliño, M., Grau, R., Fuentes, A., & Barat, J. M. Influence of low-sodium mixtures of salts on the post-salting stage of dry-cured ham process. 2010. Journal of Food Engineering, 99, 198–205.
Arihara, K. (2006). Strategies for designing novel functional meat products. Meat Science, 74 (1), 219–229.

Financiado por la Unión Europea NextGenerationEU
GOBIERNO DE ESPAÑA MINISTERIO DE CIENCIA, INNOVACIÓN Y UNIVERSIDADES
Plan de Recuperación, Transformación y Resiliencia
UCAM UNIVERSIDAD CATÓLICA DE MURCIA

https://doi.org/10.17952/37EPS.2024.P2116

Development of a potent and specific peptide inhibitor for the *E. coli* MazF toxin

Luiz R. Pizzolato-Cezar, Phelipe Vitale, Carolina D. Lacerda, Mario A. R. Pineda, Roberto K. Salinas, M. Terêsa Machini*

Department of Biochemistry, Institute of Chemistry, University of São Paulo, Av. Prof. Lineu Prestes, 748, 05508-900, São Paulo, Brazil

Corresponding author: mtmachini@iq.usp.br

Introduction

Antibiotics are compounds capable of interfering in active metabolic processes, such as transcription, translation, and cell wall synthesis. Therefore, in a population of pathogenic microorganisms, the cells that temporarily assume a dormant state are less susceptible to antibiotics. Cells displaying this phenotype are called persistent [1]. Although different pathways lead to this state, toxin-antitoxin systems (TAs) are assumed to play an important role in persistence [2].

TAs are abundant in the chromosome of prokaryotes, being composed of two types of protein: a toxin with cell growth inhibitory activity and a cognate antitoxin that keeps the toxin inactive under basal conditions. Through toxins, microorganisms enter a state of low metabolic activity and great resilience to different types of stress. Among the well-known TAs, a few have more prominent effects on bacterial physiology, such as the mazEF module. MazF is a 12 KDa-toxin with endoribonucleolytic action that inhibits cell growth through mRNA cleavage, while MazE is the cognate 9 KDa-antitoxin that keeps MazF inactive by blocking its catalytic site. MazEF complex, a heterohexamer, has a central role in several bacteria since it is involved in the formation of biofilm and increase of fitness in face of stress situations, such as phage infection, antibiotics, extreme temperatures and oxidative stress [3,4].

Inspired on such information, we designed this study aiming to discover a potent and specific peptide inhibitor for the toxin MazF [5].

Experimental

Briefly, peptide sequences of 12 amino acid residues interacting with *E. coli* His-MazF immobilised in a 96-well plate were selected with the Ph.D.TM-12 Phage Display Peptide Library kit (NEB, MA/USA). The best candidates were synthesized by microwave-assisted solid-phase synthesis at 60 °C using customized protocols [6], purified by RP-HPLC and characterized by ESI-MS and amino acid content. Cloning, expression, purification, and protein refolding technologies provided the recombinant *E. coli* MazE, His-MazF, and its mutant MazF(E24A). The synthetic peptides and MazE were compared in the capacity of inhibiting the endoribonuclease activity of His-MazF. Mapping of the interaction between the peptide inhibitor and the recombinant toxin or its mutant was performed by ITC, peptide analogues and NMR spectroscopy. 3D-structure analyses and calculations of toxin-P1 and toxin-antitoxin complexes by 800 MHz-NMR are in progress. Recently, effects of MazF inhibition on *E. coli* cells were also examined by bacterial growth, antibiotic surviving, oxygen consumption and resazurin assays [5,7].

Results and Discussion

The results obtained so far demonstrate that a potent and specific peptide inhibitor for *E. coli* MazF toxin (Fig. 1A) was discovered and studied. P1 contains 12-amino acid residues and acts as a reversible competitive inhibitor (Fig. 1B). Extensive scanning of P1 amino acid sequence using different techniques and a few synthetic analogues allowed mapping the interactions of the synthetic P1 with the recombinant His-MazF and comparing the points of contact with those already described for the MazEF complex. P1 proved to be also functional *in vivo* as it prevented the deterministic activation of the toxin that causes a strong metabolic inhibition with consequent acquisition of bacterial tolerance to antibiotics. Overall, these results indicated that MazF is a possible regulator of bacterial persistence.

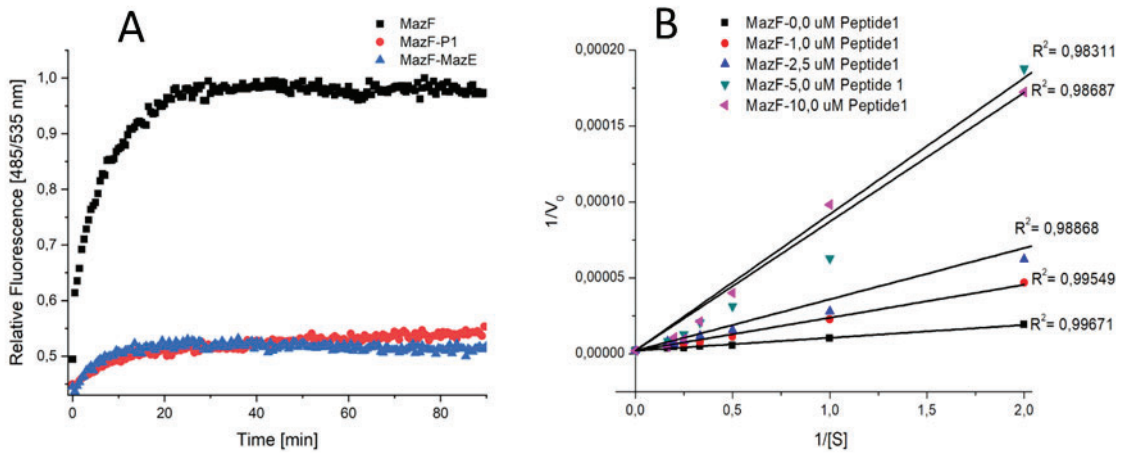

Fig. 1. I*n vitro* catalytic profiles of *E. coli* His-MazF using a specific fluorescent substrate in the absence and presence of MazE or the synthetic peptide (**A**). Plot of Lineweaver-Burk in the presence of P1(**B**).

Acknowledgments

The authors thank FAPESP (2022/01825-2) for the research grant to MTM, CNPq for research and doctoral scholarships to MTM (314470/2023-9) and LRPC (141141/2016-6), respectively, Dr. Cleber W. Liria for all mass spectrometry and amino acid analyses, Prof. German Sgro (FCFRP-USP) for discussion and help with protein cloning, expression and purification, Jose D. Rivera and A. Davalos for help with 800-MHz NMR analyses, Profs. S.R. Marana, I.M. Cuccovia, S.C. Farah, C.O. Columbano, and A. Kowaltosvski (IQ-USP) for advices and/or sporadic use of their equipments.

References

1. Kumar, A. Rahal, J. S. Sohal, V. K. Gupta, *Expert Rev. Anti. Infect. Ther.*, 19, 2, 121–127, 2021.
2.Singh, G.; Yadav, M.; Ghosh C.; Rathore, J. S. *Curr. Res. Microb. Sci.*,2, 1000472, 2021
3. Pizzolato-Cezar, LR; Spira, B.; Machini, M.T. *Curr. Res. Microb. Sci.,* 5 100204, 2023
4. Al-Hinai et al. Appl. Environ. Microbiol. 78(22), 8112-8121, 2012
5. Loffredo, C.; Assunção, N.A.; Miranda, M.T.M. *J. Pept. Sci.*, *15*, 808-817, 2009.
6. Pizzolato-Cezar, L.R. Ph.D. Thesis, Institute of Chemistry, University of São Paulo, 2023
7. Pizzolato-Cezar, L.R. *et al.* Development of a potent and functional *in vivo* inhibitor peptide for the toxin MazF (*in preparation*)

https://doi.org/10.17952/37EPS.2024.P2120

AUREL VLAICU UNIVERSITY of ARAD

37th EPS European Peptide Symposium
14th IPS International Peptide Symposium
25 - 29 August 2024
Florence, Italy

BUFORIN-DERIVED SYNTHETIC PEPTIDES WITH POTENTIAL APPLICATIONS IN MEDICINE

Dana Maria Copolovici[1*], Cristian Moisa[1], Andreea Ioana Lupitu[1], Oana Gavriliuc[1,2,3], Florina Bojin[1,2,3], Mihaela Dochia[1], Dorina Chambre[1], Lucian Copolovici[1]

[1] *Aurel Vlaicu University of Arad, Faculty of Food Engineering, Tourism and Environmental Protection; and Institute for Interdisciplinary Research, 310330, Arad, Romania*

[2] *"Victor Babes" University of Medicine and Pharmacy, Department of Functional Sciences, Immuno-Physiology and Biotechnologies Center, 300041 Timisoara, Romania*

[3] *Timis County Emergency Clinical Hospital "Pius Brînzeu" Timisoara, Center for Gene and Cellular Therapies in the Treatment of Cancer—OncoGen, No. 156 Liviu Rebreanu, 300723 Timisoara, Romania*

[*] *dana.copolovici@uav.ro*

Introduction

Efforts to find efficient and specific treatments for cancer have prompted the investigation of novel approaches that utilize the distinctive characteristics of antimicrobial peptides. Bioconjugates containing peptides, including antimicrobial peptides and cell-penetrating peptides, have emerged as an intriguing and effective therapy for cancer [1,2,3]. They can be used to treat cancer, genetic disorders, cardiovascular diseases, infectious diseases, and inflammatory diseases.

Materials and Methods

Ten newly designed buforin derivatives were synthesized using solid-phase peptide synthesis (including microwave-assisted SPPS) by Fmoc chemistry strategy. The purified peptides were analyzed using MALDI-TOF-MS (Table 1 and Fig. 1). The antimicrobial activity of the new peptides was determined by broth microdilution method in several Gram-negative bacteria (*Escherichia coli, Pseudomonas aeruginosa, Salmonella typhimurium*) and Gram-positive bacteria (*Staphylococcus aureus, Bacillus subtilis subsp. spizizenii*). Microscopy and Alamar Blue assays were used to measure cytotoxicity, cell proliferation, and cellular metabolic activity of the peptides in tumor cells: U266B1, Jurkat, MDA-MB-231, MCF-7 breast cancer cells, and in normal PBMC and mesenchymal stem cells (Fig. 2).

Results and discussions

Table 1. Peptides obtained and analyzed.

Name	Composition	M_w calc (Da)	M_w det (Da)
CPP-1	(C18-13 aa)	1752.36	878.81*
CPP-2	(13 aa)	1480.89	1482.94
CPP-3	(C18-17 aa)	2285.73	2289.11
CPP-4	(17 aa)	2019.27	2022.21
CPP-5	(C18-21 aa)	2700.33	2701.88
CPP-6	(21 aa)	2432.43	2435.25
CPP-8	(21 aa)	2559.20	2559.28
CPP-10	(21 aa)	2499.95	2500.31
CPP-14	(13 aa)	1547.85	1548.99
CPP-18	(17 aa)	2086.55	2086.97

*double deprotonated ion observed in TOF-MSMS

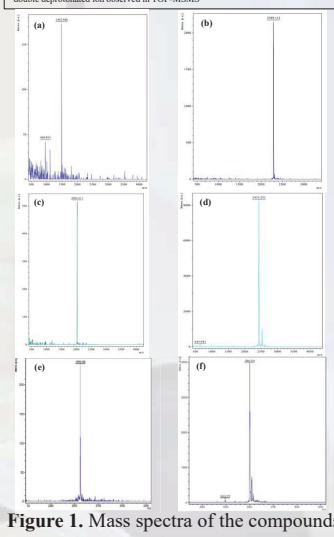

Figure 1. Mass spectra of the compounds: CPP-2 (a), CPP-3 (b), CPP-4 (c), CPP-6 (d), CPP-8 (e), CPP-10 (f).

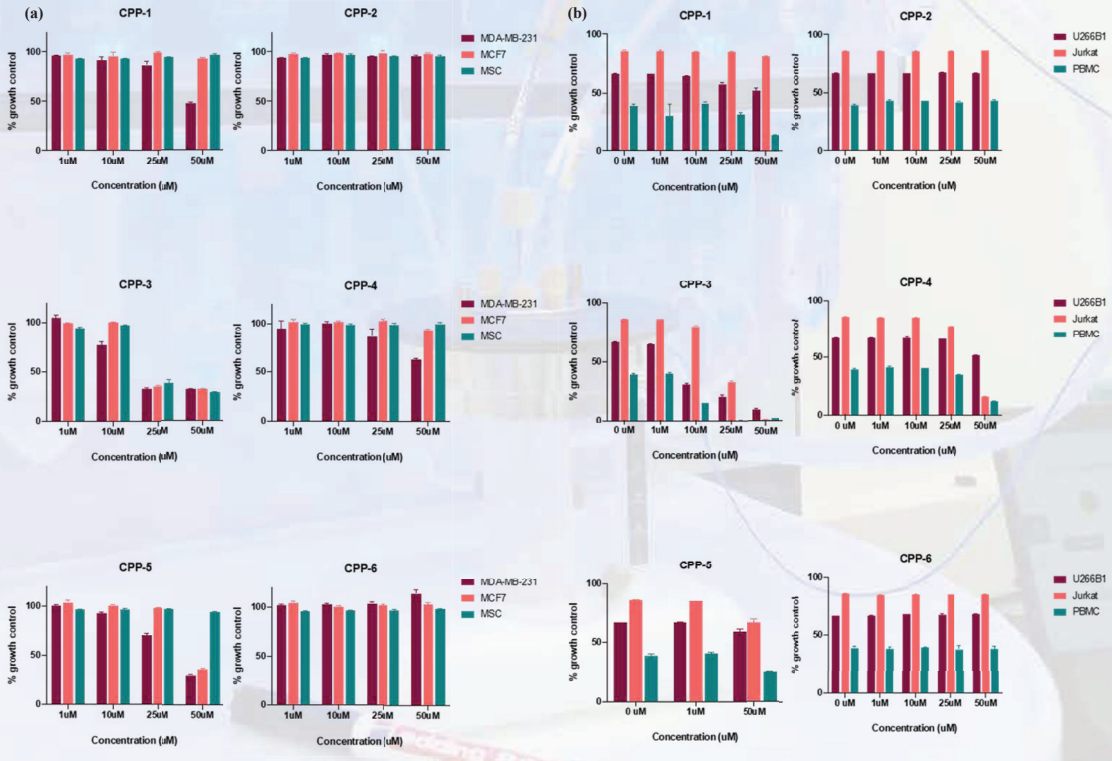

Figure 2. *In vitro* toxicity: cell proliferation assays in (a) breast cancer cells (MDA-MB-231, MCF-7), mesenchymal stem cells, and (b) multiple myeloma cells (U266B1 cells), Jurkat, and human peripheral blood mononuclear cells (PBMC) for CPP-1 – CPP-6.

Conclusions

To accelerate the progress of peptide-based medication systems, it is crucial to create peptides that can cross cell membranes or biological barriers, have an extended duration in the bloodstream, and are non-toxic and non-immunogenic to humans. The peptides presented selective toxicity in the tested cell lines in a dose-dependent manner. CPP-1, 2, 4, 6 are not toxic to breast cancer and normal cells (MSC) and could be further investigated as delivery vectors of biomolecules. CPP-3 and CPP-5 are toxic in tested breast cancer cells at min. 25 µM.

References

1. A. Gostaviceanu, S. Gavrilas, L. Copolovici, D. M. Copolovici, *Pharmaceutics*, 2023, 15(8), 2091.
2. D. M.Copolovici, K. Langel, E. Eriste, Ü. Langel. 2014, *ACS Nano*, 8(3): 1972.
3. A. M.Tolos (Vasii), C. Moisa, M. Dochia, C. Popa, L. Copolovici, D.M. Copolovici, *Polymers*, 2024, 16, 728.

Acknowledgment

This work was supported by a grant of the Ministry of Research, Innovation and Digitization, CNCS - UEFISCDI, project number PN-III-P4-PCE-2021-0639, within PNCDI III.

https://cpps-cancer.uav.ro/

https://doi.org/10.17952/37EPS.2024.P2121

AUREL VLAICU UNIVERSITY of ARAD

37th EPS European Peptide Symposium
14th IPS International Peptide Symposium
25 - 29 August 2024
Florence, Italy

EXPLORING ANTIMICROBIAL PEPTIDES: A NEW FRONTIER IN CANCER TREATMENT INNOVATION

Lucian Copolovici, Cristian Moisa, Andreea Ioana Lupitu, Dorina Chambre, Dana Maria Copolovici

Faculty of Food Engineering, Tourism and Environmental Protection and Institute for Interdisciplinary Research, "Aurel Vlaicu" University of Arad, 310330, Arad, Romania; e-mail: lucian.copolovici@uav.ro

Introduction

Antimicrobial peptides (AMPs) have emerged as promising candidates for the development of alternative cancer therapies. These naturally occurring peptides are produced by a wide array of living organisms, including plants, vertebrates, invertebrates, bacteria, and fungi[1,2,3]. Most AMPs possess amphiphilic structures and positive charges. Cationic AMPs are capable of killing bacteria by specifically disrupting their membranes. However, cationic cell-penetrating peptides (CPPs) can enter bacterial cells without damaging the membrane and target intracellular components, demonstrating their antimicrobial capabilities.

Materials and Methods

For the bibliometric study, we searched articles published in PubMed, ScienceDirect, and Web of Science, Clarivate, in the last two decades [1,2,3,4,5,6,7,8].

Results and discussions

The mechanisms of cell-penetrating of AMPs with dual effects may be used either on their own or as part of combination therapy (for example, with antibiotics). These AMPs represent an alternative platform of therapeutic agents that can be used to treat intracellular infections (Figure 1)[1,2,3,4,5,6,7,8,9].

Data was collected about the use of peptides as antibacterial agents, antitumoural substances, and vaccines (Table 1). The bibliometric study illustrates the increasing significance of anticancer peptides in the treatment of cancer during the past two decades. Membrane-active peptides encompass categories of antimicrobial peptides and cell-penetrating peptides (CPPs). One significant obstacle in cancer treatment is the unfavorable outlook, particularly for pancreatic cancer, glioma, and lymph metastases.

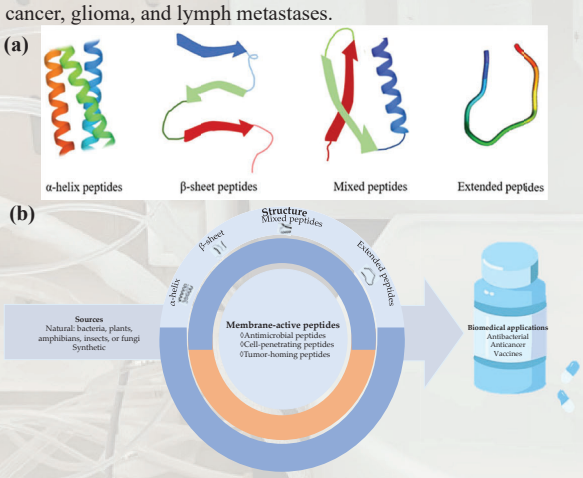

Figure 1. (a) 3D structures of different classes of AMPs. (b) Schematic information on peptides' origin and potential biomedical applications.

Table 1. Peptides with applications in medicine [8].

Peptide	Commercial Drug Name	Applications	Trial Phase
		Antibacterial	
Gramicidin	Neosporin®	Treating bacterial conjunctivitis	Admitted to the market
Vancomycin	Vancocin®HCl	Treatment of Gram-positive bacterial infections	Admitted to the market
Daptomycin	Cubicin®	Treatment for skin infections and *Staphylococcus aureus* infections	Admitted to the market
Telavancin	Orbactiv®	Treatment of Gram-positive bacterial infections	Admitted to the market
Nisin	Nisaplin®, Chrisin® and Delvo®Nis	Biopreservative	Admitted to the market
Streptococcus salivarius K12	BLIS K12	Protection against oral pathogenic bacteria in humans	Admitted to the market
		Antitumoral	
Microcin E492	-	Cervical adenocarcinoma, acute T-cell leukemia, Burkitt's lymphoma, B-lymphoblastoid cells	Preclinical
Colicin A and E1	-	Breast carcinoma, osteosarcoma, leiomyosarcoma, fibrosarcoma	Preclinical
Azurin-Derived Peptide p28	-	Breast cancer	Phase I of clinical trials
Nisin A	-	Head and neck squamous cell carcinoma, breast adenocarcinoma, liver hepatocellular carcinoma, acute T-cell leukemia	Preclinical
Pediocin CP2	-	Mammary gland adenocarcinoma, hepatocarcinoma, cervical adenocarcinoma	Preclinical
Peptide	Commercial Drug Name	Used for	Trial Phase
		Vaccines	
Combination of 25 amino acids from several immune mutations of the repetitive region of MUC1 combined with immunoadjuvant monophosphoryl lipid A	Liposomal BLP-25	Anticancer	Phase III of clinical trials
Combination of 16 peptides	ISA101	HPV immunization	Phase II of clinical trials
Combination of nucleoprotein, matrix 1, and both B- and T-cell linear epitopes from HA into a single recombinantly synthesized polypeptide	Multimeric-001	Influenza and HIV-1 immunization	Phase I of clinical trials
Synthesized peptide immunogens of the SARS-CoV-2 S protein conjugated to a carrier protein and absorbed on aluminum hydroxide	EpiVacCorona	Coronavirus disease 19 (COVID-19) immunization	Phase II of clinical trials
Short C-terminal fragments of Aβ40 and an aluminum hydroxide adjuvant	ABvac40	Treatment for Alzheimer's disease	Phase II of clinical trials

Conclusions

Peptide-based treatments have revolutionized drug delivery and enhanced clinical outcomes in cancer treatment through the utilization of cutting-edge peptide-based assembly techniques. They exhibit anti-cancer effects via disrupting cell membranes and by processes that do not disturb cell membranes. These mechanisms include inducing necrosis or apoptosis in cancer cells, inhibiting the growth of new blood vessels (angiogenesis), attracting immune cells, and activating specific regulatory proteins. Similar to many typical polymeric compositions, these macromolecules have the potential to significantly reduce the rate of drug release. Peptides, unlike other polymeric formulations, can be precisely tailored to a specific sequence through the use of genetic engineering. This renders them a compelling alternative to conventional formulations. Combinations of peptide-based strategies and conventional therapies are being investigated for their potential synergistic effects in developing anticancer drugs.

References

1. I.P. Encalada, L.M.C. Cocom, N.D.Q. Bojórquez, M.R.S. Campos, *Int. J. Pept. Res. Therapeut.*, 2023, 29:62.
2. D.M. Copolovici, K. Langel, E. Eriste, Ü. Langel. *ACS Nano*, 2014, 8, 1972.
3. L. Diao, M. Liu, *Adv. Sci*. 2023, 2300121.
4. M. Mahlapuu, M., J. Hakansson, L. Ringstad, C. Bjorn, *Front. Cell Infect. Microbiol*., 2016, 6,194.
5. J. Xie, Y. Bi , H. Zhang, S. Dong, L. Teng, R.J. Lee, Z. Yang. Front. *Pharmacol*. 2020, 11, 697.
6. D.F. Buccini, M.H. Cardoso, O.L. Franco, *Front. Cell. Infect. Microbiol*. 2021, 10, 612931.
7. H.K. Kang, J. Park, Chan, C.H. Seo, Y. Park, *ACS Infectious Diseases*, 2021, 7, 2620.
8. A. Gostaviceanu, S. Gavrilas, L. Copolovici, D.M. Copolovici, *Pharmaceutics,* 2023, 15(8), 2091.
9. M. Tolos (Vasii), C. Moisa, M. Dochia, C. Popa, L. Copolovici, D. M. Copolovici, *Polymers*, 2024, 16, 728.

Acknowledgment

This work was supported by a grant of the Ministry of Research, Innovation and Digitization, CNCS - UEFISCDI, project number PN-III-P4-PCE-2021-0639, within PNCDI III.

https://cpps-cancer.uav.ro/

uefiscdi

P2.122 – High level soluble expression of human Glucagon-Like Peptide-1 (GLP-1) analogue as a recombinant peptide in *E. coli*

Sushmita, Esha Shukla, and Gaurav Pandey*
Bioprocess and Bioproduct Development Lab
Guru Gobind Singh Indraprastha University, New Delhi, India
gpandey@ipu.ac.in

https://doi.org/10.17952/37EPS.2024.P2122

Abstract

Human GLP-1 is an incretin gut peptide hormone produced by proteolytic cleavage of proglucagon. The 31 amino acid peptide GLP-1 stimulates postprandial insulin secretion and treats Type II diabetes mellitus. This drug is currently marketed as Liraglutide, an acetylated GLP-1 analogue produced in *S. cerevisiae*. The goal of this study is to develop a bioprocess for producing GLP-1 analogues for Type II diabetics that are affordable. It has been attempted to express GLP-1 analogues on an *E. coli* host platform due to its advantages in yield and productivity. An expression construct has been designed in which an analogue of GLP-1 is fused with GST and an enterokinase (EK) site is sandwiched between them. Using a medium, inducer concentration, temperature, pH, and strains, we optimized expression in shake flask experiments to improve fusion protein expression in soluble form. In a series of batch fermenters, the kinetics of GLP-1 analogue production have been studied. We investigated how the growth stage before induction affects GLP-1 expression. We induced cultures during early, mid, and late log phases of growth, which were measured at optical densities (at 600nm) of 1, 10, and 20 respectively. We then monitored the expression for 12 hours after induction. Using information from previous batches, the fed-batch was designed to maintain a pre-induction specific growth rate (μ) of 0.35 h^{-1} and a post-induction specific growth rate (μ) of 0.15 h^{-1}. Fed-batch fermentation resulted in approximately 88.9 g/L dry cell weight at 8 hours post induction with GST-GLP-1 analogue. A volumetric yield of 10.3 g/L was obtained at an OD600 of 180. Purification of the GLP-1 analogue from the fusion tag was achieved by affinity chromatography followed by enzymatic cleavage with enterokinase. Affinity chromatography was used to purify the cleaved GLP 1 analogue, which was then identified by western blotting and mass spectrometry.

Introduction

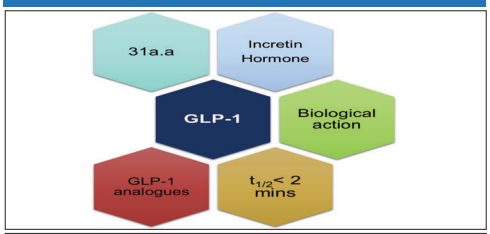

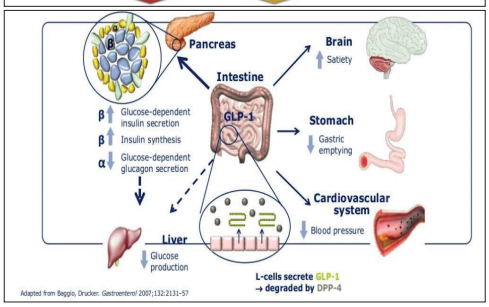

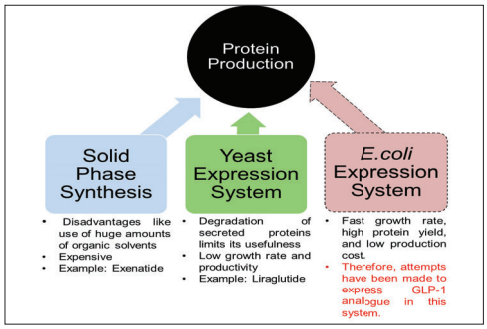

Methodology

Workflow

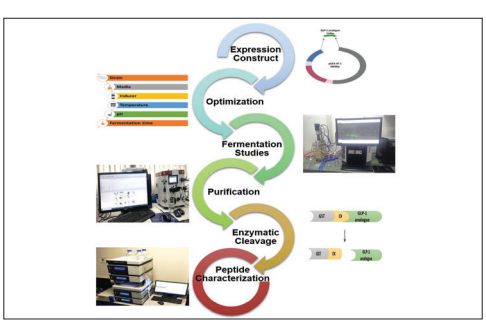

Results

(A) Growth kinetics and expression of GST-GLP-1 analogue in Batch fermentation

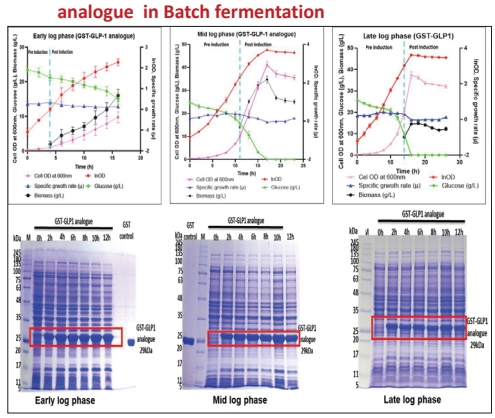

Table showing the specific product yield and volumetric yield of GST-GLP-1 analogue in Batch mode fermentation

S.No	Log phase	Induction at OD_{600} nm	Final Biomass (OD at 600nm)	Total GST-GLP1 analogue yield (mg/L)	Specific GST-GLP1 analogue yield (mg/g)
1	Early log phase	1	~10	~1800	~110
2	Mid log phase	10	~35	~2100	~90
3	Late log phase	20	~32	~650	~52
4	Uninduced culture	-	~35	-	-

(B) Growth kinetics and expression of GST-GLP-1 analogue in Batch fermentation

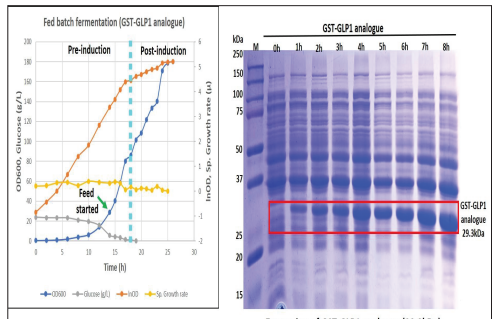

Batch	Time (h)	Induction point	Final OD	Biomass (g/L)	Volumetric yield (g/L)	Specific yield (g/g)
Fed Batch	8	86	180.3	88.9	10.37641	0.11672

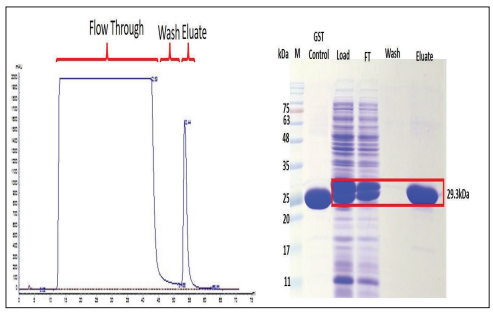

(D) Enzymatic cleavage of GST-GLP1 analogue and its identity confirmation wtih western blot

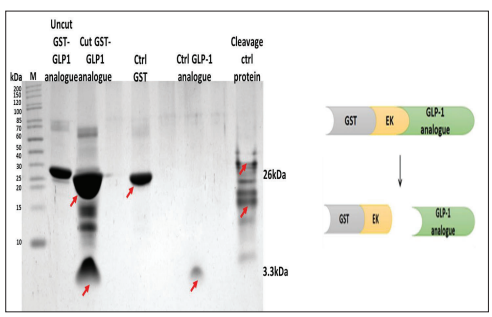

(E) Purification of cleaved GLP-1 analogue

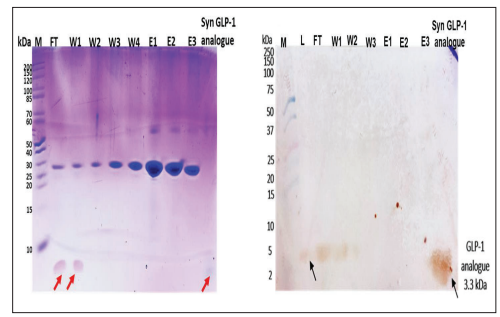

(F) Confirmation of Molecular weight of cleaved GLP-1 analogue by mass spectrometry

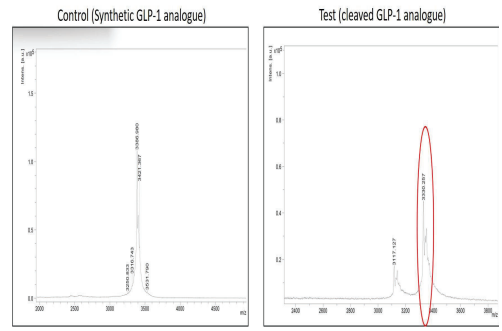

(G) Confirmation of cleaved GLP-1 analogue by RP-HPLC

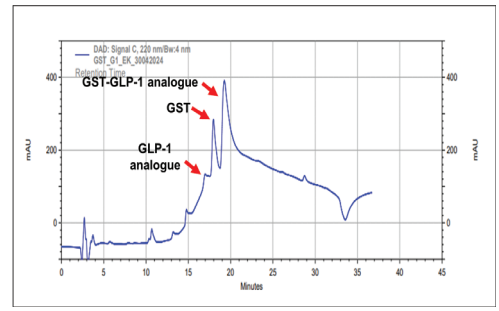

Conclusion

- GLP-1 analogue was successfully cloned in pGEX4T1 vector with N-terminal GST tag for expression. High expression of GST-GLP1 was achieved in BL21(DE3) strain in the synthetic medium at temperature of 22°C and after induction with 0.5mM IPTG.
- In Batch fermentations, high specific activity and volumetric yield are observed when the culture was induced at mid-log phase that is OD_{600} of 10.
- In fed-batch fermentation, the volumetric yield of GST-GLP1 analogue was 6270 mg/L and specific GST-GLP-1 analogue yield was 116 mg/g.
- Fusion protein GST-GLP-1 was purified by affinity chromatography and cleaved with r-Enterokinase enzyme to confirm the peptide identity with western blot.
- Intact mass of the cleaved GLP-1 analogue was confirmed.
- Confirmation of cleaved GLP-1 was confirmed by RP-HPLC.

References

- Liu, Y., Ren, L., Ge, L., Cui, Q., Cao, X., Hou, Y., ... & Bai, G. (2014). A strategy for fusion expression and preparation of functional glucagon-like peptide-1 (GLP-1) analogue by introducing an enterokinase cleavage site. *Biotechnology letters*, *36*(8), 1675-1680.
- Zhang, Z. Z., Yang, S. S., Dou, H., Mao, J. F., & Li, K. S. (2004). Expression, purification, and C-terminal amidation of recombinant human glucagon-like peptide-1. *Protein expression and purification*, *36*(2), 292-299

Acknowledgments

We would like to acknowledge GGS Indraprastha University (for FRGS grant) for funding the research work and University Grants Commission (UGC) for fellowship.

Combining peptide fragments for the high-throughput generation and screening of large libraries

Contact information
linktr.ee/annezarda

Anne Zarda, Xingwang Deng, Edward Will, Maylin Romero, Christian Heinis*

Laboratory of Therapeutic Proteins and Peptides, EPFL, SB ISIC LPPT, CH-1015 Lausanne, Switzerland.
Presenting author: anne.zarda@epfl.ch; *Corresponding author: christian.heinis@epfl.ch

https://doi.org/10.17952/37EPS.2024.P2124

Established method to synthesize thiol peptides

Special resin for solid phase peptide synthesis that yields C-terminal thiol [1]

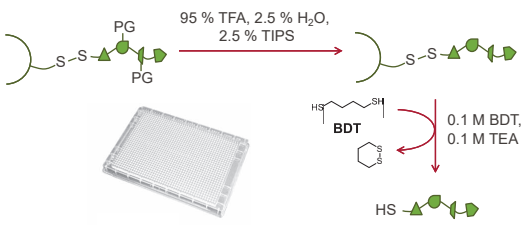

Reduced thiol peptides are stored in 1536 microwell plate



Peptide synthesizer with upgrade for parallel synthesis of 1536 peptides[2]

1536 highly diverse thiol peptides
Ready to screen, no purification needed!

Testing dimerization reaction

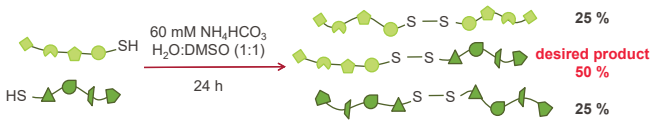

LCMS chromatograms of test dimerizations and analysis of results

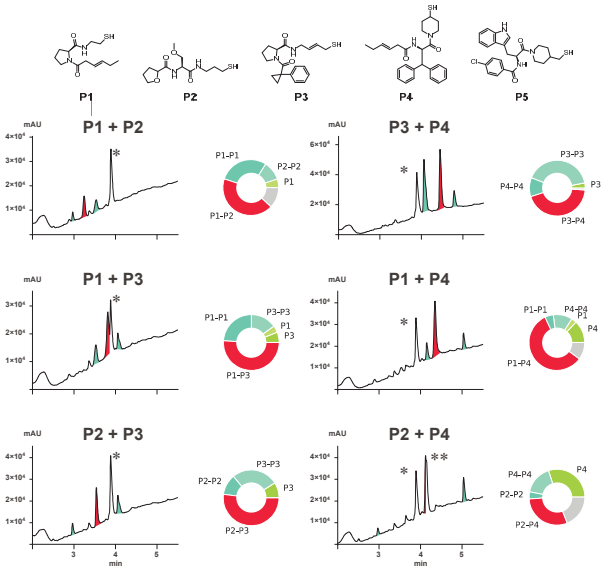

Transfer of 2 nmol per peptide, final concentration of peptides 100 µM
* Impurity on the column, ** overlapping product peak

Workflow for synthesizing dimer libraries

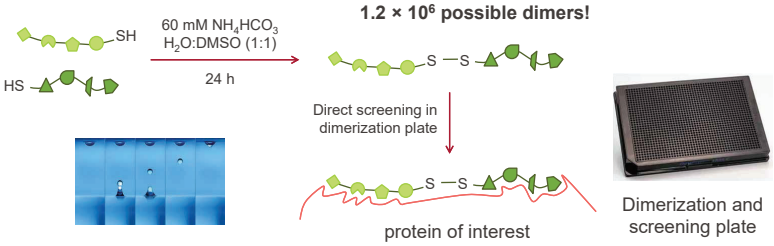

Acoustic droplet ejection to transfer nanoliter volumes of peptides to dimerization plate

Dimerization and screening plate

Synthesis of dimer library and screening against thrombin

1 To facilitate screening of a large library, dimers are screened in mixtures. Peptides are organized in groups of 6. In each screening well, two groups are pooled resulting in a mixture of 12 peptides forming 72 dimers. In total a library of **853 471 dimers** was screened.

2 Mixtures that decreased the proteolytic activity of thrombin in the first step are deconvoluted by resynthesizing and screening all 72 dimers of the mixture in parallel.

3 After identification of the active dimer in the mixture, the compound is resynthesized and purified for characterization and IC_{50} determination.

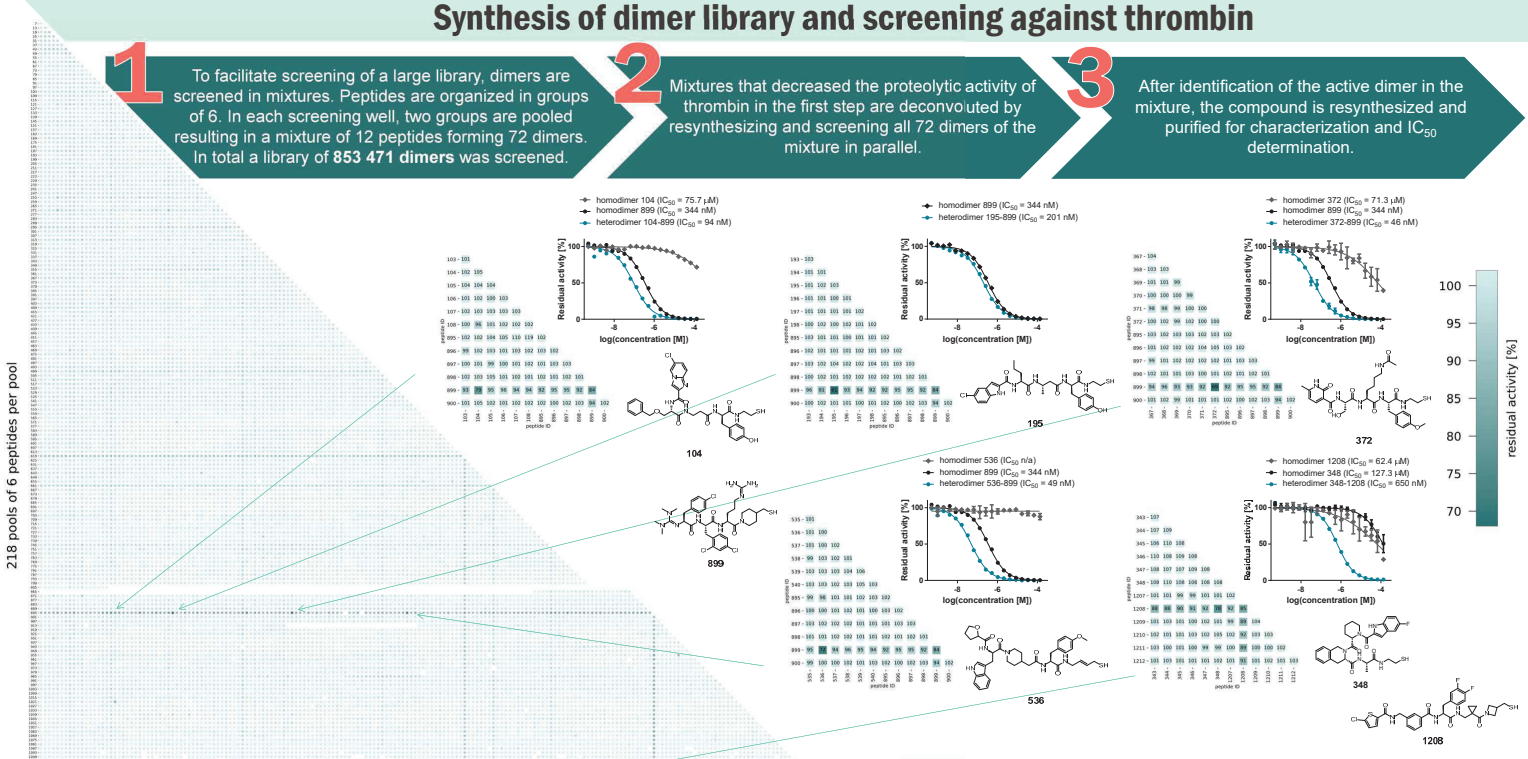

218 pools of 6 peptides per pool

Large screen: Transfer of 10 pmol per peptide → screening concentration for each individual dimer ~ 100 nM
Deconvolution: Transfer of 2.5 pmol per peptide → screening concentration for each individual dimer ~ 170 nM

Conclusion

- New method to easily and purification-free synthesize peptide libraries.
- A library of 853 471 peptides was screened against the model target thrombin.
- Nanomolar thrombin inhibitors were identified.

References

[1] Schüttel, M., et al. "Solid-phase peptide synthesis in 384-well plates." Journal of Peptide Science 30.4 (2024): e3555.
[2] Bognar, Z., et al. "Solid-phase peptide synthesis on disulfide-linker resin followed by reductive release affords pure thiol-functionalized peptides." Organic & Biomolecular Chemistry 20.29 (2022): 5699-5703.

https://doi.org/10.17952/37EPS.2024.P2126

Designed Peptide based on Plant Original Cyclic Scaffold facilitate Rheumatoid Arthritis Diagnosis

Mingshu Zhang,[1] Sunithi Gunasekera,[1] Liyan Mei,[2,3] Erik Jakobsson,[1] Camilla Eriksson,[1] Helena Idborg,[2] Per-JohanJakobsson,[2] Ulf Göransson[1]
[1]Department of Pharmaceutical Biosciences, Uppsala University, Uppsala, Sweden.
[2]Division of Rheumatology, Department of Medicine Solna & Karolinska University Hospital, Karolinska Institutet, Stockholm, Sweden.
[3]The Second Affiliated Hospital, Guangzhou University of Chinese Medicine (Guangdong Provincial Hospital of Chinese Medicine),Guangzhou, China.

- Plant based peptide scaffold SFTI-1 can sufficiently display various anti-citrullinated peptide autoantibody (ACPA) antigen epitopes, and present higher binding efficiency towards ACPAs.
- Grafted peptides (GP) are optimized as detection tool of ACPA for affinity purification and ELISA.
- ACPA fine-specificity profile differs between RA patients.
- Grafted peptides described can be used to screen large RA cohort.
- Physical and Functional characterization *in vivo* will help to understand correlation between fin-specificity and pathogenesis.

Study Design

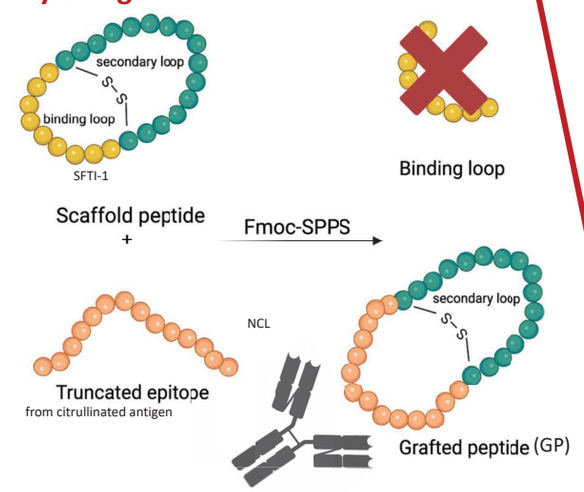

Application 1

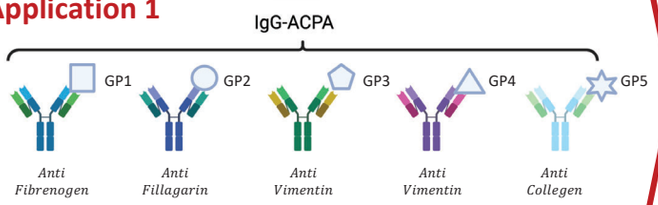

Application 2

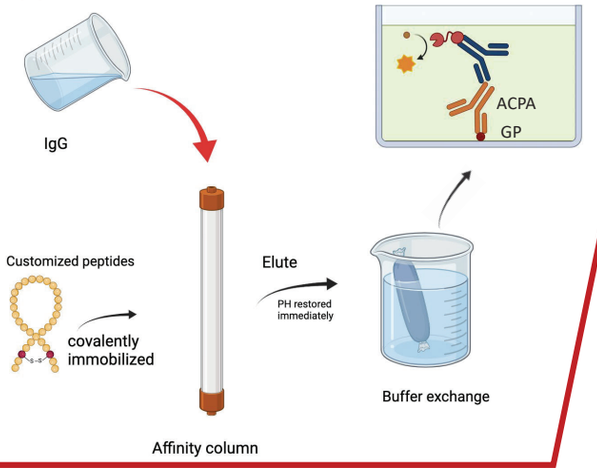

Fine-specific ACPA purification Chromatogram of ACPA purification and SDS-PAGE for IgG and Fib-ACPA

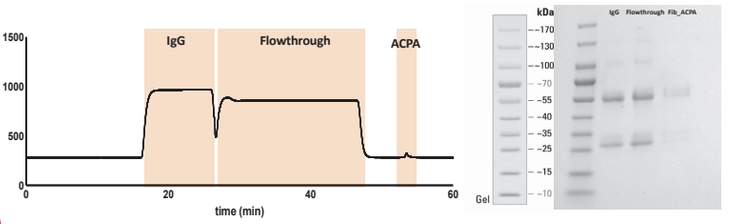



Individual ACPAs Fine-specificity Mapping indicates reactivity of individual IgG against designed antigen peptides.

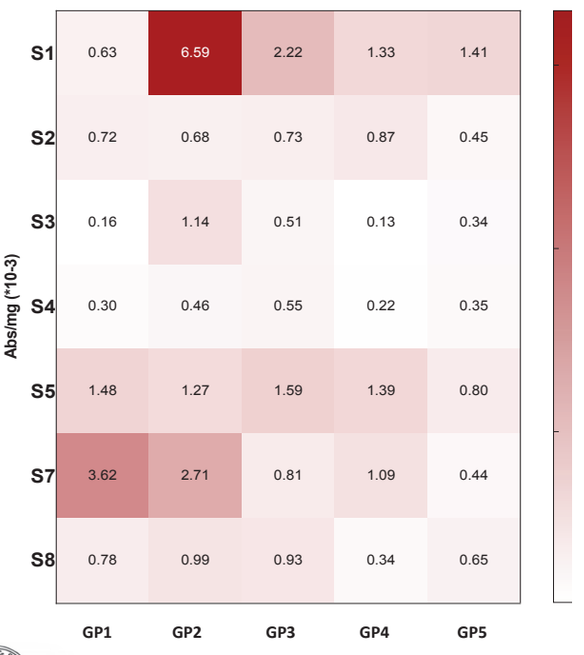

Acknowledgement

✓ Supports from prof. Göransson, prof. Jakobsson and all the collegues working together with me.
✓ Sample collection from Rheumatology, Karolinska Institutet.

UPPSALA UNIVERSITET
Karolinska Institutet

Highway to Cell: Internalization of CFTR–Stabilizing Peptides as Potent Cystic Fibrosis Treatment

https://doi.org/10.17952/37EPS.2024.P2127

prisca.boisguerin@inserm.fr

Clémentine Teko-Agbo[1], Emilie Josse[1], Quentin Seisel[2], Dean R. Madden[3], Magali Taulan Cadars[1], Prisca Boisguérin[1]

(1) PhyMedExp, University of Montpellier, INSERM U1046, CNRS UMR 9214, 34295 Montpellier, France (2) University of Montpellier, 34090 Montpellier, France
(3) Geisel School of Medicine at Dartmouth, 7200 Vail Building, Hanover, NH 03755-3844, USA

Abstract

Cystic fibrosis (CF) is due to loss-of-function mutations in the CFTR chloride channel. The consequences on the airways are:
- impairment of mucociliary clearance
- higher prevalence of chronic bacterial infections [1]

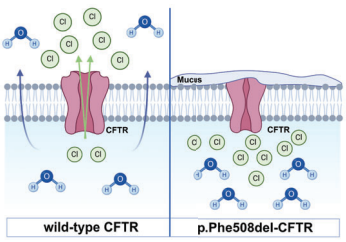

One of the three known functional defects associated with the most prevalent mutation, p.Phe508del-CFTR, concerns the stability of this chloride channel at the apical membrane of endothelial cells. Previously, our group has reported the development of CAL inhibiting peptides (iCAL36) which rescue CFTR activity (11% increase in chloride efflux) [4, 5].

Indeed, both wt- and p.Phe508del-CFTR can be degraded through a lysosomal pathway involving the CFTR:CAL protein-protein interaction [2], hence reducing its lifetime. In contrast, NHERF1/2 proteins anchor the CFTR channel at the apical membrane of epithelial cells.
Thus, our strategy thus consists of the development of an interfering iCAL peptide targeting specifically the CAL protein. As a consequence of the CFTR:CAL inhibition, CFTR rescuing at the apical cell membrane should be observed resulting in increased physiological functionality.
To improve iCAL activity, the presented work concerns the optimization of the iCAL36 interfering peptide via different cell-penetrating peptides (CPP) [6] as a delivery system.

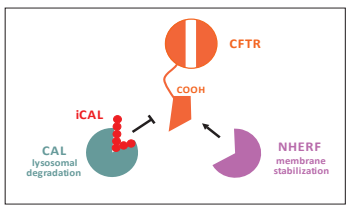

CONCLUSION

Interfering iCAL peptide as CFTR stabilizer

- Cell-penetrating peptides for iCAL36 internalization
- Penetratin showing optimal internalization
- Internalization involve endocytosis-dependent pathways
- TRI-iCAL36 as optimal peptide for cell internalization
- TRI-iCAL36 increase CFTR amount (accumulation)
- But needs a VX pre-incubation

I – Improvement of iCAL36 cellular delivery

Cell-penetrating peptides (CPP) can cross biological membranes, alone or while being associated to another molecule called cargo. We selected seven CPP (MPG & Penetratin [9],Tat [10], its D- and retro-inverso isoform [11], C6M1 [12] and WRAP5 [13] to improve cellular internalization and thus biological activity of the iCAL36 peptide. Resulting CPP-iCAL36 conjugates were evaluated in terms of their cellular internalization on epithelial cells (Caco-2) expressing wt-CFTR as a model [14].

FIGURE 1

A

Name	Structure	Residues
iCAL36	ANSRWPTSII	10
MPG-iCAL36	GALFLGWLGAAGSTMGAWSQPKKKRKV-ANSRWPTSII	37
Pen-iCAL36	RQILIWFQNRRMKWKK-ANSRWPTSII	26
Tat-iCAL36	GRKKRRQRRRPPQ-ANSRWPTSII	23
dTat-iCAL36	grkkrrqrrrppq-ANSRWPTSII	23
TRI-iCAL36	qpprrrqrrkkrg-ANSRWPTSII	23
C6M1-iCAL36	RLWRLWRLWRRLWRLL-ANSRWPTSII	28
WRAP5-iCAL36	LLRLLRWWWRLLRLL-ANSRWPTSII	25

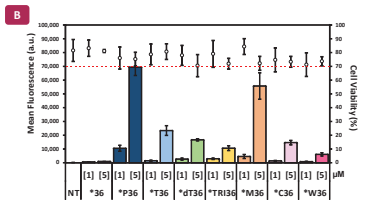

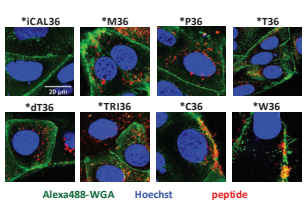

Internalization properties are assayed by flow cytometry and by confocal microscopy using TAMRA-labelled peptides (denoted by *) on Caco-2 cells. **Left panel:** Cells were incubated with TAMRA-CPP-iCAL36 and mean fluorescence values corresponding to the internalized peptides were quantified by flow cytometry. DAPI staining allow the acquisition of the cell viability. **Right panel:** Representative images of TAMRA-CPP-iCAL36 cellular distribution in living Caco-2 cells. Co-staining with Hoechst (blue, nucleus) and Alexa488-WGA (green, cell membrane) were performed for better visualization. Both secondary amphipathic peptides (C36 and W36) are mainly sticking at the cell membrane. All other CPP-iCAL conjugates are visible as punctuated patterns in the cytosol which could be an indication for an endocytosis-dependent internalization.

FIGURE 2

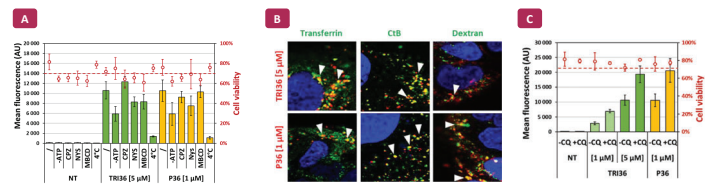

Left panel: Cells were incubated with the peptide at 4°C or co-incubated with endocytosis inhibitors (-ATP = NaN3/DG, CPZ = Chlorpromazine, NYS = Nystatin, MbCD = methyl-beta-cyclodextrin) and compared to the standard condition (37°C). Two conditions induced an internalization reduction (~85% for 4°C and ~45% for ATP depletion) suggesting an energy-dependent internalization. **Middle panel:** Representative images of TAMRA-labelled peptides co-transfected with endocytosis markers (Transferrin, Cholera toxin, and Dextran - in green) in living Caco-2 cells. Yellow staining revealed a colocalization of the peptide with the markers. Cholera toxin colocalization seems to be unspecific. White bar = 20 µm. **Right panel:** Cells were incubated with the peptide alone or in the presence of chloroquine (CQ) an endosomolytic reagent. Increased fluorescence level after CQ treatment suggests an endosomal encapsulation of the peptide.

II — TRI–iCAL36 increase CFTR amount

The stabilizing property of TatRI-iCAL36 was evaluated indirectly. Because the peptide might inhibit the interaction of the CAL protein with the C-terminus of the mutated p.Phe508del-CFTR, CFTR degradation via the endosomal–lysosomal pathway should be reduced or abolished. As a consequence, an increase in the total CFTR amount should be detected in the 16HBEge cells.
Indeed, for the first time, we were able to reveal in p.Phe508del-CFTR 16HBE epithelial cells an additive increase in the CFTR amount in the presence of VX-445/VX-809 compared to VX-445/VX-809 treatment alone.

FIGURE 3

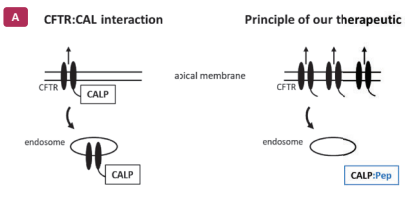

Left panel: Scheme highlighting the activity of the interfering iCAL peptide. **Right panel:** Representative images of living 16HBEge cells imaged by CLSM after 3 h incubation with Tamra-iCAL36 (10 µM) or Tamra-TRI-iCAL36 (10 µM)) in OptiMEM. Nuclei are labeled with Hoechst dye. Bars represent 10 µm.

FIGURE 4

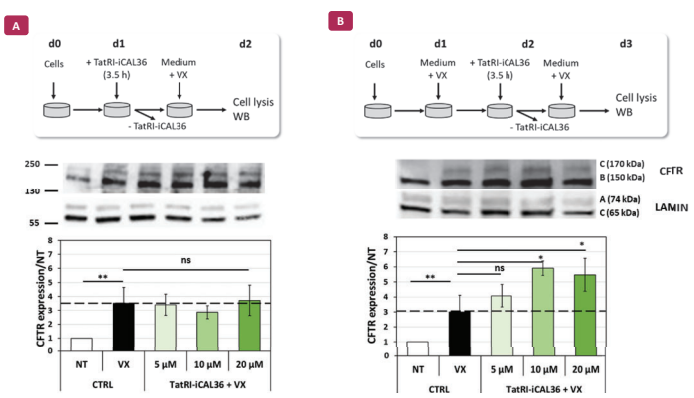

Activity of TatRI-iCAL36 in 16HBEge cells. Left panel: 16HBEge cells were incubated with TatRI-iCAL36 (5 µM, 10 µM, or 20 µM) in the presence of the corrector VX-445/VX-809 cocktail as indicated in the scheme. On day 2 (d2), the cells were lysed and p.Phe508del-CFTR was quantified by Western blot. **Right panel:** 16HBEge cells were pre-incubated with the correction VX-445/VX-809 for 24 h. Afterward, the cells were incubated with TatRI-iCAL36 (5 µM, 10 µM, or 20 µM) in the presence of the VX-445/VX-809 corrector cocktail as indicated in the scheme. On day 3 (d3), cells were lysed and p.Phe508del-CFTR was quantified by Western blot.

References

[1] Kerem et al., Science, 245, 1073 (1989). - [2] Wolde et al., J Biol Chem, 282, 8099 (2007). - [3] Vouilleme et al., Angew Chem Int Ed Engl, 49, 9912 (2010). - [4] Cushing et al., Angew Chem Int Ed Engl, 49, 9907 (2010). - [5] Frank, J Immunol Methods, 267, 13 (2002). - [6] Heitz et al., Br J Pharmacol, 157, 195 (2009). - [7] Boisguerin et al., Chem Bio Chem, 8, 2302 (2007). - [8] Seisel et al., Bioorg Med Chem Lett, 27, 3111 (2017). - [9] Müller et al., J Pep Sci, 18, 293 (2012). - [10] Vivès et al., J Biol Chem, 272, 16010 (1997). - [11] Meloni et al., Cell Mol Neurobiol, 34, 173 (2014). - [12] Jafari et al., PLoS ONE, 9, e97797 (2014). - [13] Konate et al., Bioconjug Chem, 30(3), 592 (2019). - [14] Seisel et al., Pharmaceitics, 14(4), 808 (2022).

Financial support

anr agence nationale de la recherche
RECHERCHE EN SANTÉ RESPIRATOIRE
VAINCRE LA MUCOVISCIDOSE

This work is currently in press for J. Phys. Chem. Letters https://doi.org/10.1021/acs.jpclett.4c01767

Effects of peptide labeling on fluorescence binding assays to Src homology 2 domains: the case of protein-protein interactions inhibitors of the oncogenic phosphatase SHP2

Sara Bobone[1], Chiara Fulci[1], Chiara Innamorati[1], Alessia Damiani[1], Claudia Storti[1,5], Paolo Calligari[1], Daniela Roversi[1], Luca Pannone[3], Simone Martinelli[3], Gianfranco Bocchinfuso[1], Fernando Formaggio[2], Cristina Peggion[2,4], Barbara Biondi[4], Lorenzo Stella[1,]*

[1]*Department of Chemical Science and Technologies, Tor Vergata University of Rome, 00133 Rome, Italy*
[2]*Department of Chemical Sciences, University of Padova, 35131 Padova, Italy;*
[3]*Dipartimento di Oncologia e Medicina Molecolare, Istituto Superiore di Sanità, 00161 Rome, Italy;*
[4]*Institute of Biomolecular Chemistry (Padova Unit), CNR, 35131 Padova, Italy;*
[5]*Department of Public Health, Experimental and Forensic Medicine, University of Pavia, Pavia, 27100, Italy*

chiara.innamorati@uniroma2.it

https://doi.org/10.17952/37EPS.2024.P2128

Introduction

Due to their role in numerous signaling pathways, Src homology 2 (SH2) domains have garnered significant attention as potential targets for pharmaceutical intervention. Their primary biochemical function is to recognize polypeptide sequences containing phosphotyrosine (pTyr). Tyrosine phosphorylation plays a critical role in eukaryotic cell regulation; hence, mutations in the genes for at least 23 distinct SH2 domain proteins contribute to various human disorders, including cancers, leukemias, developmental disorders, diabetes, and immunodeficiencies. Peptide-based drugs targeted to SH2 domains are a powerful tool to inhibit therapeutically relevant protein-protein interactions [1]. Fluorescence-based assays, such as anisotropy/polarization measurements [2], or quantitative microarrays [3] are commonly used to determine the affinity and selectivity of these molecules for their target domain. We recently developed protein-protein interaction (PPI) inhibitors targeted at the N-terminal Src homology 2 (SH2) domain of the oncogenic phosphatase SHP2 [1].

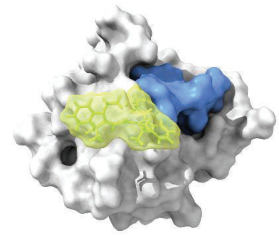

Our PPI inhibitors

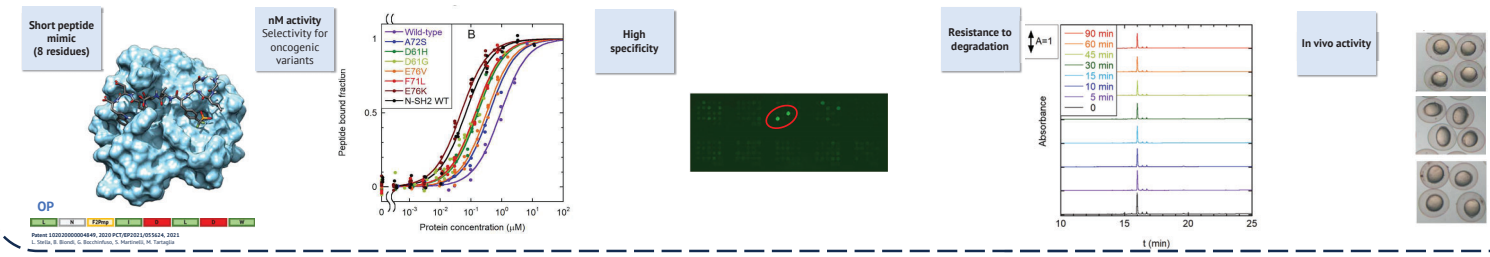

1. Quantitative analysis of the microarray data

While highly active and selective, these molecules showed a weaker unwanted interaction with the SH2 domain of another protein, called APS, in a fluorescence microarray assay [1].

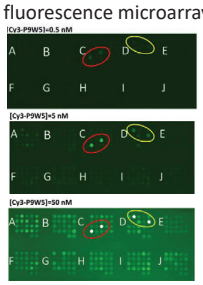

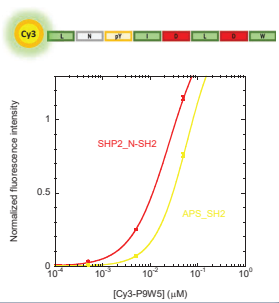

2. Fluorescence anisotropy binding assays

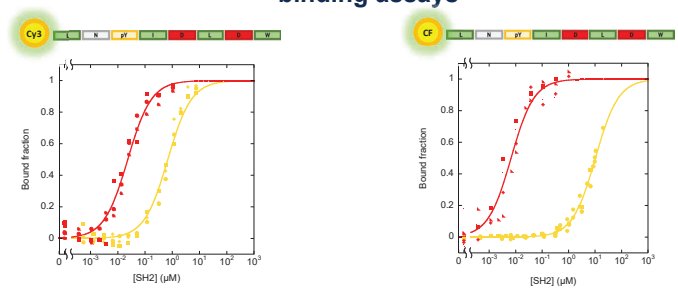

Labeling can enhance or inhibit binding by more than one order of magnitude.

3. Displacement binding assays

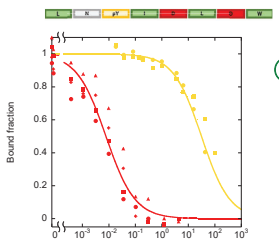

Competition displacement assays can be used to determine the dissociation constants of unlabeled peptides

$$\frac{K_d\ APS}{K_d\ NSH2} = 10000 \pm 2000$$

Molecular modeling

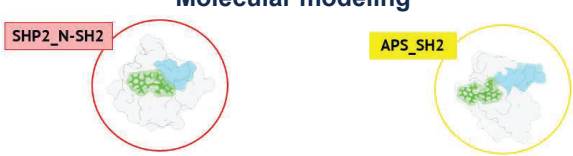

The fluorophore interacts significantly with the protein surface of both domains, thus providing a structural rationale for the observed effects of labeling on the binding affinity.

Conclusions

Protein-protein association can be perturbed by any chemical modification (ex. the insertion of a **fluorescent probe**), to one of the binding partner. This is particularly true when one of the two molecules is relatively small, as in the case of peptides.

Peptide	K_d (APS_SH2) (μM)	K_d (SHP2_N-SH2) (μM)	Selectivity (K_d APS/K_d SHP2)
Cy3-P9W5	$(6.9 \pm 0.3)\ 10^{-1}$	$(2.3 \pm 0.2)\ 10^{-2}$	30 ± 3
CF-P9W5	5.8 ± 0.2	$(3.3 \pm 0.2)\ 10^{-3}$	1700 ± 100
P8W5	$(1.6 \pm 0.2)\ 10^{1}$	$(1.6 \pm 0.2)\ 10^{-3}$	10000 ± 2000
OP	$(7.0 \pm 1.0)\ 10^{1}$	$(1.5 \pm 0.3)\ 10^{-2}$	5000 ± 1000

- ✓ The perturbation of the dissociation constant caused by labeling can be significant (more than an order of magnitude).
- ✓ The effect can depend strongly on the specific fluorophore used, and even on the protein domain.
- ✓ Our findings suggest that displacement binding assays should always be employed to obtain binding data free from labeling artifacts.

References

1. S. Bobone et al., *Journal of Medicinal Chemistry*, **2021**, 64, 15973-15990.
2. S. Bobone, P. Calligari and L. Stella, *Methods in Molecular Biology*, **2023**, 2705, 93-112.
3. J. Chen, C. Sagum and M.T. Bedford, *Methods*, **2020**, 184, 4-12.

Acknowledgements

The authors gratefully acknowledge the Protein Array and Analysis Core at The University of Texas M. D. Anderson Cancer Center for performing the SH2 array experiments, and Prof. Shwan Li (Schulich School of Medicine and Dentistry, Western University, London, Ontario) for providing the APS SH2 plasmid. This work was supported by the AIRC Foundation for Cancer Research in Italy (Grant IG24940 to L.S.), the Italian Ministry of Education, University and Research (MIUR, Grant PRIN 2020833Y75_005 to L.S., Dipartimento di Eccellenza 2023-27 X-CHEM project, to the Department of Chemical Science and Technologies, Tor Vergata University of Rome), Regione Lazio (Grant A0375-2020-36719 to L.S.), CINECA (Grant ISCRA-B HP10B3TIMH, to G.B.), the European Union (PNRR, Project CN_00000013 "National Center for HPC, Big Data and Quantum Computing", to GB and LS, and PNRR – M4C2-I1.3 Project PE_00000019 "HEAL ITALIA", to LS)

https://doi.org/10.17952/37EPS.2024.P2129

Bicyclic peptidomimetics enable efficient transport of proteins across brain endothelium

Maria C. Lucana, Roberta Lucchi, Fabien Gosselet, Cristina Díaz-Perlas, Benjamí Oller-Salvia

Institut Químic de Sarrià - Universitat Ramon Llull (IQS-URL)

benjami.oller@iqs.url.edu, www.chemsynbio@iqs.edu

Brain shuttle peptides

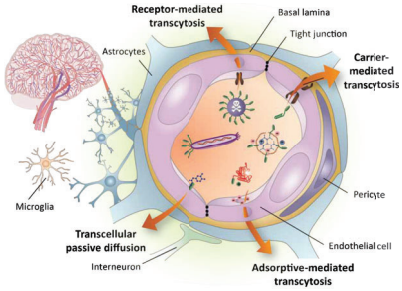

Transport across the **blood-brain barrier** (BBB) is one of the most challenging obstacles in the development of biotherapeutics for brain diseases. **Brain shuttles** are molecules capable of transporting cargoes across the BBB by hijacking endogenous transport mechanisms, including receptor-mediated transcytosis.[1] Most protease-resistant peptide brain shuttles available have low affinity for target receptors & limited protein transport capacity.[2-4]

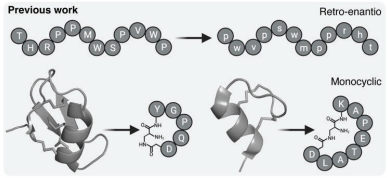

Objectives

The main goal of this study was to obtain a novel family of bicyclic protease-resistant peptide shuttles, **BrainBikes**, targeting the **transferrin receptor 1 (TfR1)**. We aimed to develop shuttles with high resistance to proteases and suitable affinity for the **transport of therapeutic proteins**.

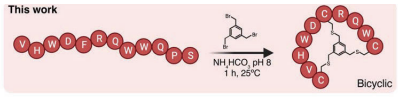

BrainBikes: a new family of brain shuttles

Design of bicyclic peptidomimetics

Starting from a sequence identified via phage display against TfR1, Y1, bicyclic variants were obtained by reacting three cysteines with a trifunctional linker. Several analogs were designed enhancing or disrupting the alpha helical conformation of Y1.

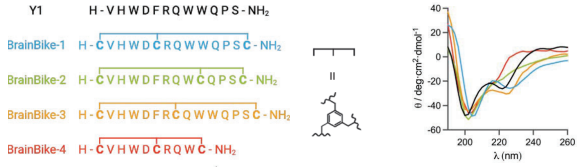

Affinity for cells with high levels of TfR1

All bicyclic peptidomimetics display affinity for cells with high levels of TfR1, especially those with the least alpha helical character. BrainBike-4 (BB4) shows a **7-fold increased cell association** with respect to the parent peptide. Even higher binding was confirmed by further overexpressing TfR1.

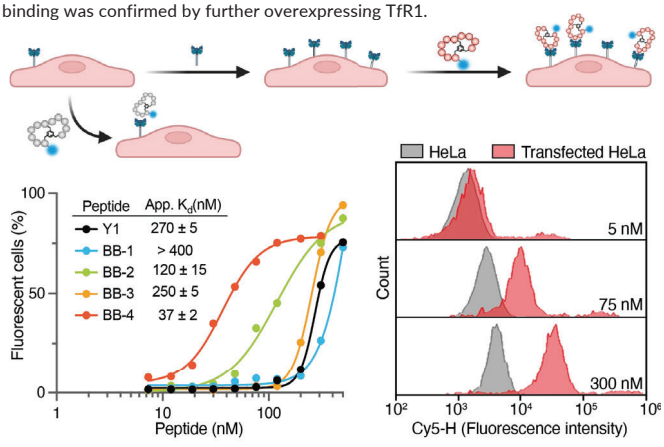

Stability to serum proteases

BrainBikes present **high metabolic resistance**, with half-lives ranging from 3.5 to 7.7 h in human serum. Bicyclization leads to 2- to 4-fold increase in half-life with respect to the parent peptide.

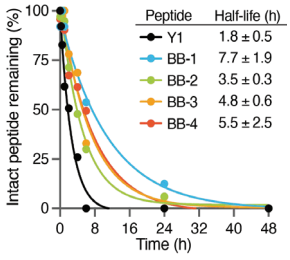

BrainBike-4 increases the transport of proteins

Site-specific conjugation of BrainBike-4 to a single chain antibody

BBB-shuttle peptides were conjugated to a single chain variable fragment (scFv) against a brain tumour target via chemoenzymatic ligation. Peptides were derivatized with an *N*-terminal azide and conjugated to the scFv bearing a complementary reactive handle via an inverse electron-demand Diels-Alder cycloaddition.

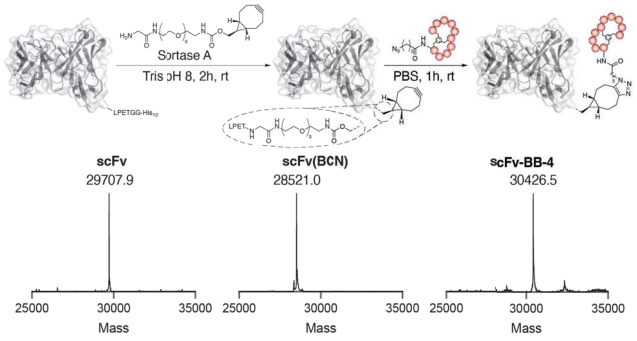

Transport of an scFv-BB4 conjugate across brain endothelium

The transport of the conjugate was assessed on a tight monolayer of human brain endothelial cells seeded on Transwell® membranes. **BrainBike-4 enables a 5-fold increase** in the transport of the scFv. This is significantly higher than the transport enhancement provided by Angiopep-2, the current gold-standard peptide brain shuttle. A similar enhancement was observed for other proteins such as GFP.

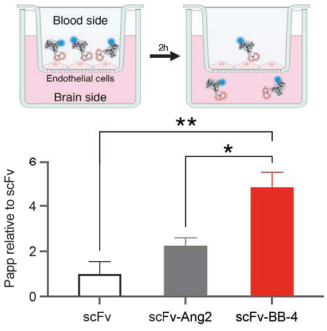

Conclusions and perspective

Here we report a new class of bicyclic brain shuttle peptidomimetics, BrainBikes. We have shown that linear peptide shuttles binding TfR1 can be turned into BrainBikes utilizing a trifunctional linker. These peptides have enhanced half-lives and BrainBike-4 presents 7-fold higher affinity for cells expressing high levels of TfR1. BrainBike-4 site-specifically conjugated to an scFv enables a 5-fold increase in the transport capacity in a cell-based model of the BBB.[5] We are now assessing the transport of therapeutic protein conjugates *in vivo* and developing new brain shuttles.

What next?

Brain shuttle development is limited by little knowledge on receptor-mediated transcytosis. We are currently developing orthogonal transport systems to shed light on this transport mechanism.

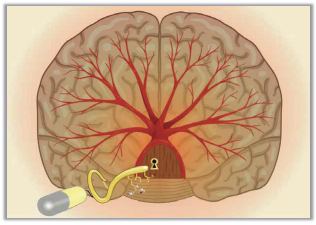

References

1. B Oller-Salvia, M Sánchez-Navarro, M Teixidó, E Giralt. BBB-shuttle peptides: an emerging paradigm for brain delivery. *Chem Soc Rev.* **2016**, 45, 4631.
2. R Prades, B Oller-Salvia, ..., M Teixidó, E Giralt. Applying the retro-enantio approach to obtain a peptide capable of overcoming the BBB. *Angew Chem Int Ed.* **2015**, *54*, 3967.
3. Oller-Salvia, M Sánchez-Navarro, ..., E Giralt, M Teixidó. MiniAp-4: a venom-inspired peptidomimetic for brain delivery. *Angew Chem Int Ed.* **2016**, *55*, 572.
4. MC Lucana, Y Arruga, E Petracchi, A Roig, C Díaz-Perlas, Oller-Salvia. Protease-resistant peptides for targeting and intracellular delivery of therapeutics. *Pharmaceutics.* **2021**, 13, 2065.
5. **MC Lucana, R Lucchi, F Gosselet, C Díaz-Perlas, B Oller-Salvia. BrainBike peptidomimetic enables efficient transport of proteins across the brain endothelium. *RSC Chem Biol.* 2024, *5*, 7.**

Acknowledgements

B.O.-S., C.D.-P., and R. L. hold "la Caixa" Junior Leader (ID 100010434), MSCA-PF, and FPU (FPU19/03216) fellowships, resp. We acknowledge support from the MCIN/AEI/10.13039/501100011033 (No PID2020-117486RA-I00), from Universitat Ramon Llull (No 2021-URL-Proj-028), and from AGAUR (SGR2017 1559).

https://doi.org/10.17952/37EPS.2024.P2132

Faculty of Chemistry - Organic and Bioorganic Chemistry - OCIII

UNIVERSITÄT BIELEFELD

Synthesis of Halogenated Cyclic RGD-Peptides as Potent SMDC-ligands

Beate Nachtigall* and *Norbert Sewald

Organic and Bioorganic Chemistry, Faculty of Chemistry, Bielefeld University, Germany. E-Mail: b.nachtigall@uni-bielefeld.de

Selective Halogenation of Tryptophane

- FAD-dependent halogenases PyrH, Thal or RebH enable regioselective bromination or chlorination in C5, C6 or C7 position under mild reaction conditions
- Co-immobilization of the halogenase with cofactor regenerating enzymes enable production of halotryptophane on gram-scale.[1]
- Tryptophan synthase (TrpS) was used for the synthesis of 5-halotryptophan as the PyrH *combi*CLEAs (cross-linked enzyme aggregates) are less efficient.

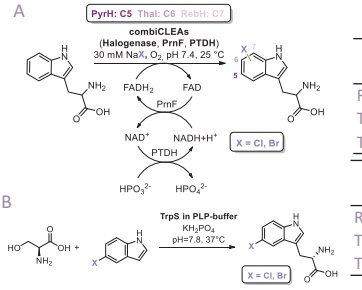

Fig. 1: *Biocatalytic synthesis of halogenated tryptophan by means of selective halogenation in the combiCLEAs process* ***(A)*** *or starting from halogenated indole and serine* ***(B)****.*

Tab. 1: *Determined conversion to halogenated tryptophan with halogenases RebH, Thal or TrpS.*

	L-Trp [mM]	Br-Indol [mM]	Conv. RP-HPLC Br-Trp[%]
RebH	1	-	100
Thal	1	-	100
TrpS	-	1	100

	L-Trp [mM]	Cl-Indol [mM]	Conv. RP-HPLC Cl-Trp[%]
RebH	1	-	100
Thal	1	-	100
TrpS (TmAzul)	-	1	100

Late-Stage Modification

- Attachment of fluorescent residues to brominated indole function by selective C-C linkage such as by palladium-catalyzed HECK- or SUZUKI-MIYAURA cross-coupling[2,3]
- Investigation of the conversion via LC-ESI-MS
- Measurement of absorption spectra to prevent cell damage from overly energetic radiation in subsequent biological tests

➔ Identify fluorescent coupling reagents - extension of the π-system often leads to a desired redshift

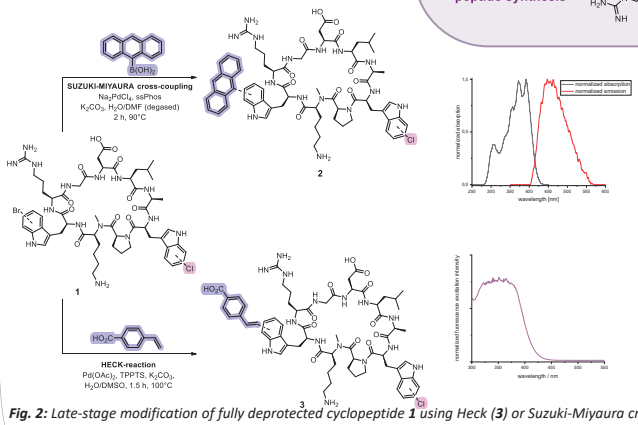

Fig. 2: *Late-stage modification of fully deprotected cyclopeptide* ***1*** *using Heck* ***(3)*** *or Suzuki-Miyaura cross-coupling* ***(2)*** *and measured absorption spectra after derivatization of one halogenated indole ring.*

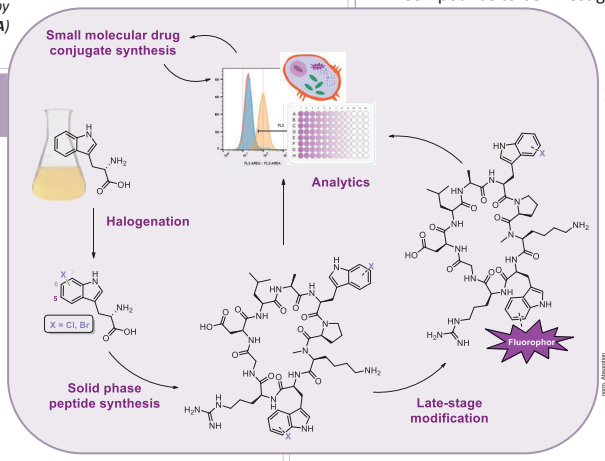

Biological Evaluation of RGD-Peptides

- $\alpha_v\beta_6$ and $\alpha_v\beta_8$ integrin as proteins of interest, due to frequent expression in cells of viral and cancerogenic diseases
- Replacement of hydrophobic phenylalanine of the published nonapeptide c(DLAFp(NMe)KFRG) with halogenated tryptophan allows investigations due to its influence on bioactivity and increases affinity for $\alpha_v\beta_6$ and may improve selectivity toward $\alpha_v\beta_8$.[4,5]
- Halogenated compounds are often essential for biological activity and, on the other hand, have a positive effect on metabolic stability, modulation of lipophilicity, hydrophobic interactions and pharmacological features
- N-Methylation on lysine increases affinity[4]
- **ELISA** (enzyme-linked immunosorbent assay) with isolated integrins to determine selective affinity towards individual integrins.

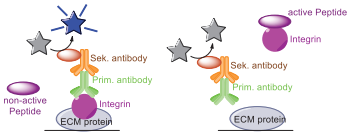

Fig.3: *Schematic representation of the ELISA assay for determination of IC_{50} values of peptides, left: EMC protein binds to the integrin.*

- Internalization investigation via **flow cytometry measurement** to ensure receptor-mediated cell uptake
- Compounds to be investigated must be fluorescently labeled in this respect

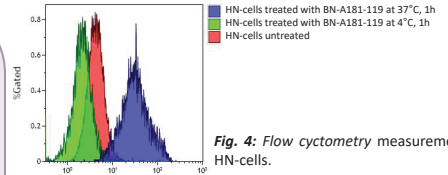

Fig. 4: *Flow cytometry* measurement of treated HN-cells.

- Determination of IC_{50} values in **competitive adhesion assay**
- 96-well plate previously coated with the natural ligand TGF-ß1
- HN cells were seeded, which were cultivated on fibronectin
- Using Mn^{2+} (2mM) in buffer for integrin activation
- Cell lysis in DMSO, absorbance measurements at 570 nm

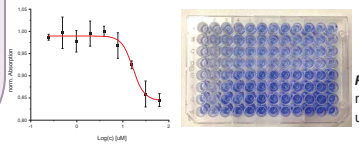

Fig. 5: *Flow cytometry* measurement and evaluation using sigmoidal fit.

Peptide	IC_{50} $\alpha_v\beta_6$ [nM]	IC_{50} $\alpha_v\beta_8$ [nM]	IC_{50} $\alpha_v\beta_3$ [nM]	$\alpha_v\beta_8/\alpha_v\beta_6$ ratio	$\alpha_5\beta_1$ [nM]	$\alpha_{IIb}\beta_1$ [nM]	IC_{50} [nM] cell adhesion HN-cells
c(DLAFp(NMe)KFRG)	0.26[8]	23.6[8]	632[8]	91:1	72.9	>10^4	22.34±4.30
c(DLA(5-Br)Wp(NMe)KFRG)	0.083±0.03	14.0±0.8	242±67	169:1	0.82±0.85	>10^4	6.80±2.69
c(DLA(6-Br)Wp(NMe)KFRG)	0.036±0.01	39.7±3.4	247±132	1102:1	4.57±0.03	>10^4	4.24±1.24
c(DLA(7-Br)Wp(NMe)KFRG)	0.24±0.06	26.2±9.3	38±17	109:1	0.036±0.001	>10^4	3.75±0.77
c(DLA(6-(4-Vinyl-benzoic acid)Wp(NMe)KFRG	4.75±0.95	191.6±69.5		40:1			
c(DLA(5-(anthr-9-yl)Wp(NMe)KFRG)	18.11±0.38						
c(DLA(5-Cl)Wp(NMe)K(6-(anthr-9-yl)WRG	0.289± 0.02						
c(DLA(6-Cl)Wp(NMe)K(6-(anthr-9-yl)WRG	0.279± 0.05						

Analysis of integrin-expression

- Screening of different cancer cell lines and culture conditions to increase and analyze the expression of individual integrins.
- Immunofluorescence imaging different $\alpha_v\beta_6$–integrins such α_v, $\alpha_v\beta_3$, $\alpha_v\beta_6$ or $\alpha_v\beta_8$ and investigation via flow cytometry or widefield deconvolution microscopy after fixation of the cells and labeling of the cell nucleus with DAPI

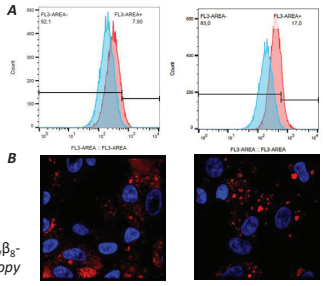

Fig. 3: A) *Flow cytometric measurement of* $\alpha_v\beta_6$- and $\alpha_v\beta_8$-expression in HN-cells. ***B)*** *Fluorescence spectroscopy*

Conclusion

- Synthesis of high-affinity halogenated peptide ligands for selective targeting of $\alpha_v\beta_6$ integrin
- Halotryptophane-containing peptides exhibit higher affinity and selectivity than the known lead structure
- Late-stage modification by cross-coupling reactions like HECK- or SUZUKI-MIYAURA at the tryptophane of fully deprotected cyclopeptides containing different halogens
- Fluorogenic peptides allow Exzitation in the wavelength range above 350 nm and exhibit only a moderate reduction in IC_{50}value

References

[1] M. Frese, P. H. Guzowska, H. Voß, N. Sewald, *ChemCatChem* **2014**, *6*, 1270-1276.
[2] H. Gruß, C. Belu, L. M. Bernhard, A. Merschel, N. Sewald, *Chemistry* **2019**, *25*, 5880.
[3] Q.-L. Luo, J.-P. Tan, Z.-F. Li, W.-H. Nan, D.-R. Xiao, *J. Org. Chem.* **2012**, *77*, 8332.
[4] O. V. Maltsev, U. K. Marelli, T. G. Kapp, F. S. Di Leva, S. Di Maro, M. Nieberler, U. Reuning, M. Schwaiger, E. Novellino, L. Marinelli et al., *Chem. Int. Ed.* **2016**, *55*, 1535
[5] I. Kemker, D. C. Schröder, R. C. Feiner, K. M. Müller, N. Sewald, *J. Med. Chem.* **2021**, *64*, 1, 586–601.

37th EPS European Peptide Symposium
14th IPS International Peptide Symposium
25 - 29 August 2024
Satellite Workshop 30 - 31 August 2024
Florence, Italy- 2024

https://doi.org/10.17952/37EPS.2024.P2301

Theoretical and biological studies of oxytocin containing conformationally fixed analogue of Tyrosine Tic(OH) (1,2,3,4-Tetrahydro-7-hydroxyisoquinoline-3-carboxylic acid)

Michal Lebl, Jiří Jiráček, Marta Lubos and Jakub Kaminský
Institute of Organic Chemistry and Biochemistry, Flemingovo náměstí 542/2, Prague, Czech Republic
Markus Muttenthaler and Monika Perisic
Institute of Biological Chemistry, Faculty of Chemistry, Währingerstr. 38, University of Vienna, 1090 Vienna, Austria

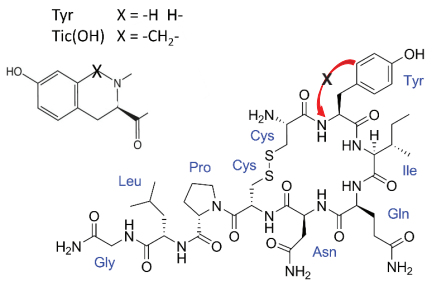

Introduction:

The most efficient tool for studying the effect of conformational stabilization of peptides is the cyclization of the peptide chain or replacement of the natural amino acid with an analog which has limited flexibility. While the cyclization inevitably modifies the functionality of the side chains and results in drastic conformational changes, introduction of modified amino acids brings less disturbance of the peptide chain. One of the example of conformationally stabilized amino acids is Tic (tetrahydroisoquinoline carboxylic acid) as a replacement of Phe. We studied earlier the effect of replacement of Phe by Tic on the biological activity of analogs of oxytocin (OXT)[1]. However, just the replacement of the native Tyr in position 2 of OXT by Phe has very pronounced effect on the biological activity of this hormone and therefore the effect of the stabilization of the conformation of this analog does not necessarily predict the effect of the same type of stabilization in the native molecule of OXT. We have developed the strategy to prepare the stabilized Tyr – 7-hydroxy-tetrahydroisoquinoline carboxylic acid (Tic(OH))[2] and made this amino acid commercially available (https://www.5z.com/spyderinstitute/unnaturals.html).

Earlier we speculated[3] about the interaction of the aromatic side chain of Tyr in OXT with the sulfur atoms in the cysteine in the disulfide bridge of this cyclic peptide based on the NMR studies of OXT carba analogs and about steric hindrance of the analogs with methyl groups attached to the cysteine methylene side chain in penicillamine containing analogs of OXT. In this study we wanted to answer the fundamental question whether the addition of one CH_2 group into the molecule of OXT will turn this hormone onto its antagonist.

1. Lebl, M.; Hill, P.; Kazmierski, W.; Karaszova, L.; Slaninova, J.; Fric, I.; Hruby, V. J. Conformationally restricted analogs of oxytocin; stabilization of inhibitory conformation. Int. J. Peptide Prot. Res. 1990, 36 (4), 321-330.
2. Verschueren, K.; Toth, G.; Tourwe, D.; Lebl, M.; Van Binst, G.; Hruby, V. J. Facile synthesis of 1,2,3,4-tetrahydro-7-hydroxyisoquinoline-3-carboxylic acid, a conformationally constrained tyrosine analogue. Synthesis-Stuttgart 1992, 458-460.
3. Lebl, M.; Sugg, E. E.; Hruby, V. J. Proton NMR spectroscopic evidence for sulfur-aromatic interactions in peptides. Int. J. Peptide Prot. Res. 1987, 29 (1), 40-45.

Strategy:

Here we present the alternative approach to our earlier structure activity studies of the neurohypophysial hormones:

- Computational modelling of solution structure of two proposed analogs of oxytocin - [L-Tic(OH)^2]OXT and [D-Tic(OH)^2]OXT
- Docking of the selected conformations into oxytocin receptor
- Synthesis of an analog with higher probability of interaction with the receptor
- Biological evaluation of oxytocin receptor response.

Computational approach:

The approach for in silico screening of the structure and binding activity of oxytocin ligands involves molecular dynamic simulations of free ligands (oxytocin and its variants) and subsequent docking of the ligands to the oxytocin receptor. Finally, the estimated free binding energies for each ligand to the receptor were used to compare the binding activity of oxytocin with its analogues. The NMR solution structure of oxytocin (pdb code 2MGO) was used as a template for the ligand structures. The first five structures stored in the pdb file were used.

The prepared ligands were surrounded by explicit waters (TIP3P) in an orthorhombic periodic box and subjected to 100 ns MD simulations in Desmond. The OPLS4 force field was used to define the ligand atoms. Ten thousand ligand geometries were regularly sampled during the simulation. The obtained MD trajectories (5) were analyzed using the Desmond Trajectory Clustering tool and the sampled ligand geometries were clustered according to their backbone conformation. Furthermore, only the twenty most abundant clusters were considered. For each cluster, a representative structure (5 trajectories x 20 clusters = 100 total / ligand) was stored and further used in docking.

The 100 stored geometries for each ligand were then docked into the oxytocin receptor using Glide. The binding site in the oxytocin receptor was defined according to the 7RYC pdb structure as a centroid within 10 Å of oxytocin. More than 1000 ligand-receptor poses (ligand conformations/orientations within the binding site) were docked and ranked according to their Glide SP score for oxytocin ligand. All poses were then rescored by estimating their binding energies (DG_{bind}) according to the MM-GBSA approach in Prime at the OPLS4/VSGB level.

Figure below displays [L-Tic(OH)^2]OXT and [D-Tic(OH)^2]OXT docked into the oxytocin receptor. As for oxytocin, two different poses (selection based on the Glide score or DG_{bind}) are shown for each ligand. The best oxytocin pose according to DG_{bind} is shown for comparison. We can see from Figure 4 that both considered poses of [L-Tic(OH)^2]OXT in the receptor differ from the best pose of oxytocin, while the best pose of [D-Tic(OH)^2]OXT selected according to DG_{bind} is relatively similar. Note that the orientation of [D-Tic(OH)^2]OXT in the best pose according to the Glide score is basically opposite.

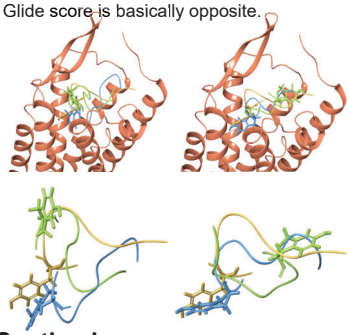

Zoom in on the two best poses (according to the Glide score in green, according to the MM-GBSA DG_{bind} in blue) of [L-Tic(OH)^2]OXT (A) and [D-Tic(OH)^2]OXT (B) in the oxytocin receptor (A). The best predicted structure of oxytocin in the receptor (according to the MM-GBSA DG_{bind}), shown for comparison, is in yellow.

Synthesis:

Since [D-Tic(OH)^2]OXT showed higher probability of interaction with the oxytocin receptor, it was synthesized using classical solid phase strategy on an automatic centrifugal solid phase synthesizer Spyder Mark IV (https://www.5z.com/spyderinstitute/synthesizer.html).

Finally, we can compare the predicted structures of all studied ligands in the oxytocin receptor in terms of energy and ligand-receptor interactions. Figure below compares interactions between amino acids of the receptor and the ligand for the best ligand-receptor poses selected according to DG_{bind}. We can see four H-bonding and one p-p interaction between oxytocin and the receptor. In the case of the modified oxytocins, we see five H-bonds for [L-(Tic(OH)2]OXT and even seven H-bonds for [D-Tic(OH)^2]OXT. No p-p stacking was observed for the modified analogues. Most of the interactions involve different amino acids of the receptor. The binding energies DG_{bind} of individual oxytocin ligands in the oxytocin receptor are -63.4 kcal/mol for oxytocin, -41.2 kcal/mol for [L-Tic(OH)^2]OXT and -53.9 kcal/mol for [D-Tic(OH)^2]OXT. By definition, the more negative the binding energy, the stronger the affinity of the ligand for the receptor. Although MM-GBSA DG_{bind} energies are often overestimated in absolute values, they can usually be used for qualitative comparison of individual ligands. Thus, oxytocin seems to have the highest affinity towards the oxytocin receptor, followed by [D-Tic(OH)^2]OXT and the weakest [L-Tic(OH)^2]OXT.

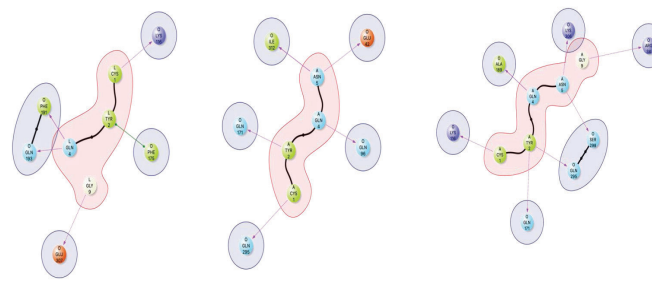

Hydrogen bonding (magenta) and p-p (green) interactions of oxytocin (left), [L-Tic(OH)^2]OXT (middle) and [D-Tic(OH)^2]OXT (right) with the oxytocin receptor. The best predicted poses according to their MM-GBSA DG_{bind} energies were used.

Biological activity:

[D-Tic(OH)^2]OXT was tested at 10 μM concentration as agonist (no activation) and as antagonist (the whole dose-response, no right-shift of the curve hence no displacement of oxytocin), both n=2.

Since the compound doesn't displace OXT in the antagonist assay it seems that the compound doesn't interact with the orthosteric binding pocket of the receptor. Based on the antagonist curve it doesn't seem to be an allosteric modulator either.

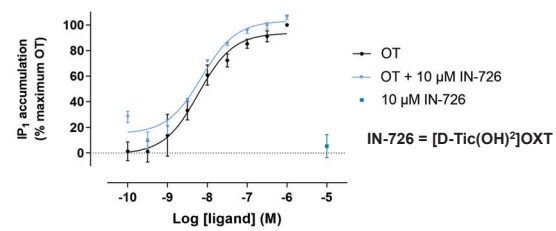

Conclusion:

Even though the theoretical studies predicted possible interaction of an analog of oxytocin containing only one additional carbon atom to interact with the oxytocin receptor, the prepared analog did not show any interaction with the oxytocin receptor.

37th EPS European Peptide Symposium
14th IPS International Peptide Symposium
25 - 29 August 2024 Satellite Workshop 30 - 31 August 2024
Florence, Italy- 2024

UNIVERSITÀ DEGLI STUDI FIRENZE
NEUROFARBA
DIPARTIMENTO DI NEUROSCIENZE, PSICOLOGIA, AREA DEL FARMACO E SALUTE DEL BAMBINO

https://doi.org/10.17952/37EPS.2024.P2134

UNIVERSITÀ DEGLI STUDI FIRENZE
PeptLab
INTERDEPARTMENTAL RESEARCH UNIT OF PEPTIDE AND PROTEIN CHEMISTRY AND BIOLOGY

ADALIMUMAB AND ANTI-ADALIMUMAB ANTIBODIES: A NOVEL METHOD OF DETECTION AND QUANTIFICATION IN HUMAN SERA BASED ON SURFACE PLASMON RESONANCE TECHNIQUE

Andrea Di Santo[1, 2], Fosca Errante[1, 2], Manuela Capone[3], Alessandra Vultaggio[3, 4], Matteo Accinno[3], Lorenzo Cosmi[3, 4], Francesco Annunziato[3, 5], Anna Maria Papini[1, 6], Paolo Rovero[1, 2], Feliciana Real-Fernandez[1, 7]

1 Interdepartmental Research Unit of Peptide and Protein Chemistry and Biology, University of Florence, Sesto Fiorentino (FI), Italy, 2 Department of Neurosciences, Psychology, Drug Research and Child Health, University of Florence, Sesto Fiorentino (FI), Italy, 3 Department of Experimental and Clinical Medicine, University of Florence, Florence, Italy, 4 Immunoallergology Unit, Careggi University Hospital, Florence, Italy, 5 Immunology and Cell Therapy Unit, Careggi University Hospital, Florence, Italy, 6 Department of Chemistry "Ugo Schiff", University of Florence, Sesto Fiorentino (FI), Italy, 7 Institute of Chemistry of Organometallic Compounds (ICCOM), National Research Council of Italy (CNR), Sesto Fiorentino (FI), Italy

email: andrea.disanto@unifi.it

Adalimumab

Biologics targeting the tumor necrosis factor alpha (TNF-a) have revolutionized treatments in a wide variety of autoimmune diseases, such as rheumatoid arthritis and juvenile idiopathic arthritis. **Adalimumab (ADL)** is the most widely used drug in this field, but, despite being a fully human antibody, **anti-adalimumab antibodies (AAA)** are reported at a rate up of 8% after 8 weeks and 24% after 60 weeks of treatment.[1] Their presence is correlated to an inadequate response to initial treatment (primary failure), the loss of response over time (secondary failure), and the development of potentially therapy-limiting adverse events.[2]

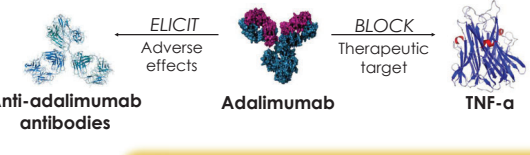

Anti-adalimumab antibodies (AAA) monitoring

Problems caused by:[3,4]
- Proper secondary reagent to discriminate AAA and ADL
- Drug-antibody complexes and complexity of the matrix (serum)
- Heterogenicity of the assays and lack of a gold standard

Aim of the study

The purpose of this work is to overcome the problems of AAA monitoring, proposing a novel method able to **detect and quantify** AAA as well as the free drug ADL

SPR-based biosensor

Surface plasmon resonance (SPR) allows the detection of mass changes on the chip surface in real-time, registering the binding between the immobilized ligand and the analyte in solution.
- ✓ No sample pre-treatment
- ✓ No need for secondary reagent
- ✓ Parallel measurement exploiting different channels
- ✓ Fully automatized
- ✓ Able to detect low-affinity antibodies



SPR for detection of both ADA and ADAbs
Biacore™ X100 from Cytiva (Uppsala, Sweden)

- ❖ Immobilization of an anti-ADL mAb to detect ADL
- ❖ Immobilization of ADL o detect AAA
- ❖ Reference subtraction using an immobilized human pAb

Materials and methods

Patients and samples, materials and reagents, immobilization and analysis conditions, statistics

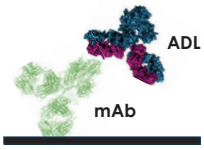

Adalimumab quantification

SPR signal correlated with increased concentration of ADL with a 4-parameters polynomial correlation

	C ADL (ng/mL)	n	Mean (ng/mL)	CV (%)	SD (ng/mL)	Accuracy (%)	Precision (%)
Intraday	100	3	103.5	3.2	3.3	103.5	96.8
	800	3	832.1	3.8	32.0	104.0	96.2
Interday	100	7	99.0	1.6	1.6	99.0	98.4
	800	7	800.3	0.1	0.8	100.0	99.9

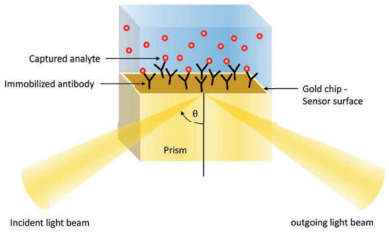

Anti-adalimumab antibodies quantification

SPR signal linearly correlated with increased concentration of mAb ($r^2 > 0.998$)



	C AAA (ng/mL)	n	Mean (ng/mL)	CV (%)	SD (ng/mL)	Accuracy (%)	Precision (%)
Intraday	100	3	102.0	7.8	8.0	102.0	92.2
	800	3	805.0	1.0	8.2	100.6	99.0
Interday	100	11	99.2	4.7	4.7	99.2	95.3
	800	11	791.2	0.8	6.3	98.9	99.2

Analysis of human sera samples

ADL-treated patients (n = 47) and controls (n = 13)

Data distribution of ADL serum titers measured. Cut-off was set at 5 µg/mL.

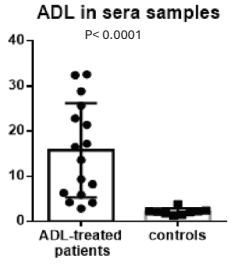

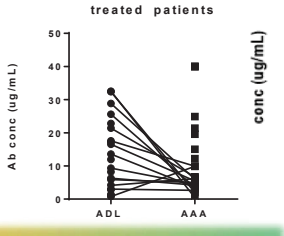

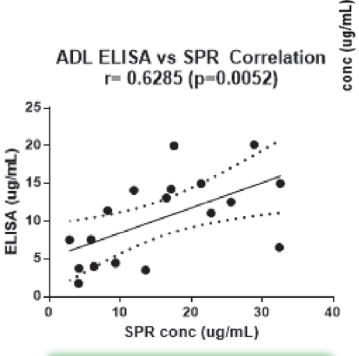

Comparison with commercially available ELISA kit

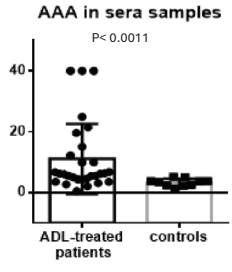

Data distribution of AAA serum titers measured. Cut-off was set at 7.5 µg/mL.

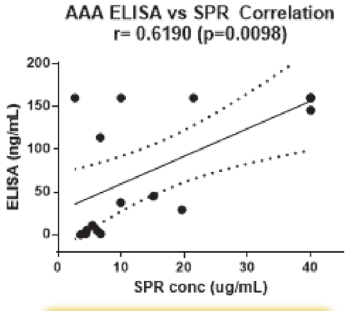

Comparison with commercially available ELISA kit

ADL and AAA coupled titres

Conclusions

- Methods developed
- Samples presenting AAA titres revealed lower traces of ADL
- ADL overall agreement with ELISA: 77%
- AAA overall agreement with ELISA: 79%

Acknowledgments

Thanks to MiUR for Andrea Di Santo PhD scholarship

Thanks to European Peptide Society for Andrea Di Santo awarded registration

Thanks to THE Tuscany Health Ecosystem for the grant ECS_00000017 and the Azienda USL Toscana Centro for the financial support to the project "Progetto ADA" (No. 1043/16-09-2022)

References

1. Imagawa, T.; *et al.* Clin Rheumatol 2012, 31 (12), 1713–1721.
2. van Schouwenburg, P. A.; *et al.* Ann Rheum Dis 2013, 72 (1), 104–109.
3. Real-Fernández, F; *et al.* Anal Bioanal Chem 2015, 407 (24), 7477–7485
4. Rusche, H.; et al. Sci Rep 2021, 11 (1), 16393.

Innovative liquid chromatographic-mass spectometric technologies to purify and identify biologically active antibody-drug conjugates.

Margherita Marino,[a] Paolo Rovero,[a] Walter Mier[b], Hendrik Rusche,[c] Anna Maria Papini.[a]

[a]*Interdepartmental Research Unit of Peptide & Protein Chemistry & Biology, Departments of Chemistry "Ugo Schiff" and NeuroFarba, University of Florence, 50019-Sesto F.no, Italy*
[b] Radiopharmaceutical Chemistry, University Clinic of Heidelberg, Neuenheimer Feld 400 69120 Heidelberg Gebaude 6400, Germany
[c]*Fischer Analytics GmbH, Saarlandstrasse 377, 55411-Bingen, Germany*

E-mail: margherita.marino@unifi.it

https://doi.org/10.17952/37EPS.2024.P2136

Background

Antibody-Drug Conjugates (ADCs) [Fig.1] are the most powerful tools in cancer treatment [1,2] [Fig. 2] combining targeted therapy and chemotherapy exploiting two fundamental aspects: **SELECTIVITY** and **CYTOTOXICITY.**[3]

ADCs are extremely complex proteins since their *heterogeneity depends* of the monoclonal antibody (mAb) and of the *physico-chemical properties* of the conjugation site, linker chosen and ultimately of the payload.
It is imperative, then, develop an easy, fast and efficient methodology to characterize and purify these molecules.
For this reason, in the past few years the pharmaceutical industry has more and more been interested in exploring the variety of liquid chromatography (LC) techniques by putting more effort and attention in exploring the possibility of combing different LC together a multi dimension liquid chromatography (**mD-LC**). [5]
There are great advantages in performing an mD-LC:

- it is possible to combine different and even complementary separation systems,
- it is possible to achieve a higher resolution,
- it has been proven to be a faster and more convenient system,
- it allows also coupling mass spectrometry (MS) with some chromatography techniques that are not MS-compatible enabling to combine information otherwise not possible.

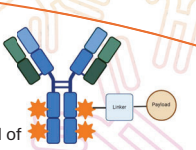

Fig.1: General structure of ADC

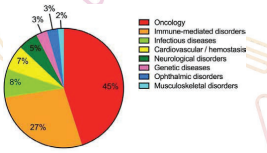

Fig. 2: Therapeutic antibodies approved or in regulatory review in USA and EU. Based on data publicly available on November 15, 2021 [4]

Aim of the work & results

The goal of this work is to develop an innovative 3D LC technology coupled to a high-performance MS system to purify and characterize ADCs.

To achieve this goal a model ADC has been produced. We divided the work in four main parts (as shown in the scheme on the right).

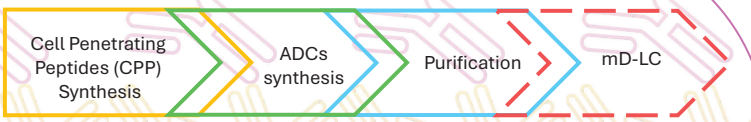

Synthesis and purification of Cell Penetrating Peptides, such as short polyarginines sequences composed of three and six units of arginine and bearing a cysteine in C-terminal, necessary for the cross linking, H-R_6C-NH_2 and H-R_3C-NH_2.

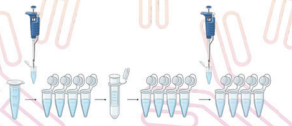

Synthesis of the model ADC: by linking through a **non-specific lysine conjugation** a mAb (Rituximab, Matuzumab and Trastuzumab) with units of sSMCC (Sulfosuccinimidyl-4-(N-maleimidomethyl)cyclohexan-1-carboxylate), a cross-linker commonly used in ADC production and the CPP previously prepared. The conjugation procedure has been optimized to use the less amount of linker (2eq) and payload (1,2, 5, 7 eq) necessary to observe a change in the chromatographic profile.
The success of the the conjugation has been checked by electrophoretic gel by a 12% SDS-PAGE Gel.
(Fig. 3 SDS-Page gel of Rituximab conjugation with 2eq sSMCC and 1, 2, 5, 7 eq of R3C and R6C)

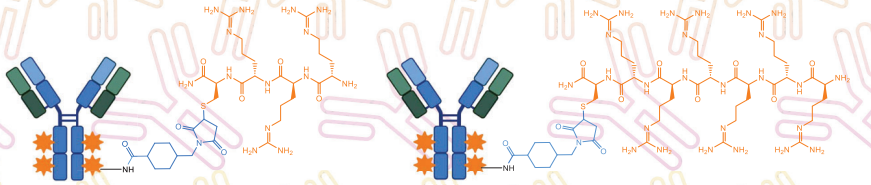

Model ADC bearing R3C as CPP

Model ADC bearing R6C as CPP

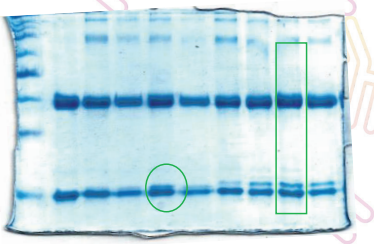

Fig. 3: From left to right: marker, RM, ADC(2eq sSMCC+1eqR3C), ADC(2eq sSMCC+2eqR3C), ADC(2eq sSMCC+5eqR3C), ADC(2eq sSMCC+7eq R3C), ADC(2eq sSMCC+1eqR6C), ADC(2eq sSMCC+2eqR6C), ADC(2eq sSMCC+5eqR6C), ADC(2eq sSMCC+7eqR6C),

Purification, NON DENATURATING CHROMATOGRAPHY TECHNIQUES such as Size Exclusion Chromatography (SEC), Weak Cation Exchange (WCX) and Hydrophobic Interaction Chromatography (HIC) and DENATURATING CHROMATOGRAPHY as Reverse Phase Liquid Chromatography (RP-LC) have been tested by using different columns and changing the chromatographic parametrers.
The best separation has been observed by using WCX
The chromatograms showed the presence of new peaks with higher retention time («ADCs' peaks») but since the couplings happen on random mAb's lysine residues the new peaks could not be sharper and separated.

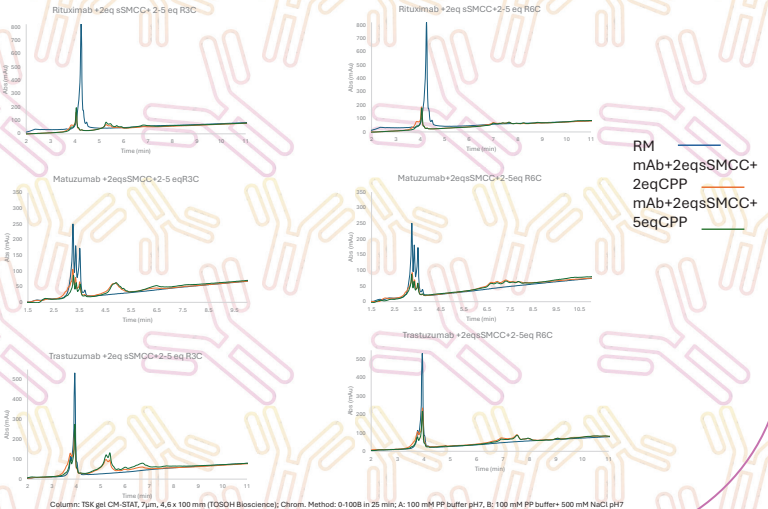

Column: TSK gel CM-STAT, 7µm, 4,6 x 100 mm (TOSOH Bioscience); Chrom. Method: 0-100B in 25 min; A: 100 mM PP buffer pH7, B: 100 mM PP buffer+ 500 mM NaCl pH7

Conclusions

Model ADCs have been designed and synthesized by using sSMCC as cross-linker and two different length polyarginines as CPPs with a new optimised method and monitored by SDS-PAGE gels.
Both non-denaturating and denaturing chromatography have been used to analyse the complex matrix obtained by the coupling steps and among them WCX showed the best separation and resolution.

Future studies will be aimed to improve the chromatographic separation and coupling LC techniques to build a 3D LC-MS purification system.

References

[1] Birrer MJ, Moore KN, Betella I, Bates RC. Antibody-Drug Conjugate-Based Therapeutics: State of the Science. J Natl Cancer Inst. 2019 Jun 1;111(6):538-549. doi: 10.1093/jnci/djz035. PMID: 30859213.

[2] Matsuda Y. Current approaches for the purification of antibody-drug conjugates. J Sep Sci. 2022 Jan;45(1):27-37. doi: 10.1002/jssc.202100575. Epub 2021 Sep 16. PMID: 34473399.

[3] D'Atri V, Imiołek M, Quinn C, Finny A, Lauber M, Fekete S, Guillarme D. Size exclusion chromatography of biopharmaceutical products: From current practices for proteins to emerging trends for viral vectors, nucleic acids and lipid nanoparticles. J Chromatogr A. 2024 May 10;1722:464862. doi: 10.1016/j.chroma.2024.464862. Epub 2024 Apr 1. PMID: 38581978.

[4]Kaplon H, Chenoweth A, Crescioli S, Reichert JM. Antibodies to watch in 2022. MAbs. 2022 Jan-Dec;14(1):2014296. doi: 10.1080/19420862.2021.2014296. PMID: 35030985; PMCID: PMC8765076.

[5] L.N. Tumey, Antibodies-Drug Conjugates, Human Press, Methods in Molecular Biology 2078, 2020

Acknowledgments

Thanks to the European Peptide Society for the Registration fee to attend 37th European and 14th International Peptide Symposium (August 25-31, 2024).

Thanks to National Recovery and Resilience Plan (NRRP), D.M.352/2022, for the PhD fellowship XXXVIII Cycle in Chemical Sciences funded by MUR/NextGenerationEU



High-Throughput Permeability Assay for the Discovery of Cell Penetrating Cyclic Peptides

Hanna Stokes[1], Noora Azadvari[1,2], Parisa Hosseinzadeh[1,2]

[1]University of Oregon, [2]Knight Campus Department of Bioengineering

https://doi.org/10.17952/37EPS.2024.P2140

Abstract

★ We aim to unravel the underlying rules of cell permeation of cyclic peptides and develop novel high-throughput methods for screening their cell penetration

★ We aim to develop computational methods to predict the permeability of cyclic peptides based on their sequence

Research Question

★ How can we use mRNA display technology to develop a high-throughput permeability assay for the discovery of cell-penetrating cyclic peptides?

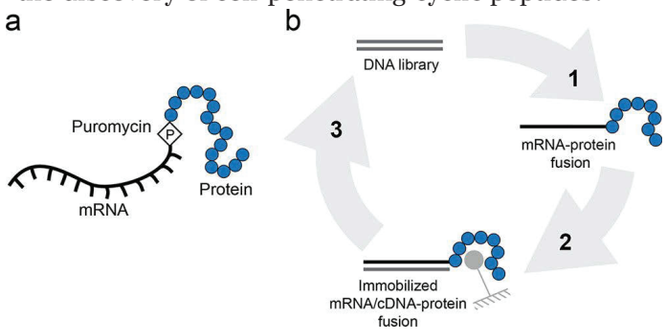

(1) mRNA Display

Introduction

★ Cell Penetrating Peptides (CPPs) are a promising tool in the delivery of therapeutic drugs to cells

★ Cyclic peptides have a large surface area and higher conformational rigidity and stability relative to their linear counterparts that potentiate them to have a higher affinity and specificity for any target of interest

★ Cyclic CPPs have higher resistance to degradation, unlike their linear counterparts

★ A high-throughput assay of cyclic CPPs could increase the efficiency of the discovery of the features of CPPs and screen their permeation

★ Understanding the core features of cell-penetrating peptides will allow for great advancements in therapeutics and the development of less invasive oral bioavailable treatments

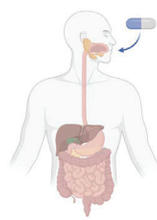

(2) Diagram of Oral Bioavailability

Methodology and Roadmap

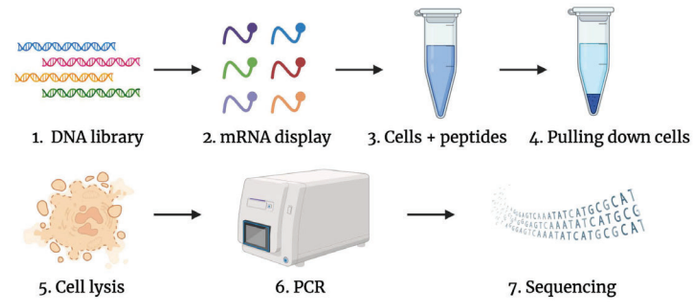

(3) Roadmap

★ By amplifying the DNA from within the cell and within the buffer we can determine which peptides stayed in the buffer and which penetrated through to the cell. Preferentially, the peptides are selectively permeable and prefer to permeate diseased cells. Then the peptides can be used as vehicles for the drug to deliver the therapeutic to its target within the cell.

Results

Fluorescence Reading Across Cell Types

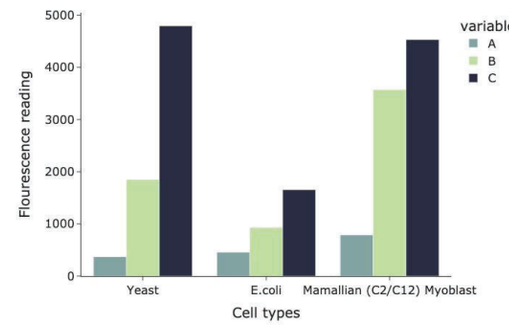

Future Directions

★ TAT was the first cyclized CPP. High-throughput assay would increase the ability to discover and create more CPPs such as this one

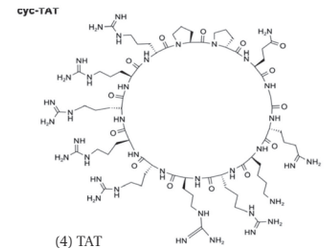

(4) TAT

References

(1) *ACS Synth. Biol.* 2020, 9, 2, 181-190
(2) Created with biorender.com
(3) Created with biorender.com
(4) Zhang, H.; Zhang, Y.; Zhang, C.; Yu, H.; Ma, Y.; Li, Z.; Shi, N. Recent Advances of Cell-Penetrating Peptides and Their Application as Vectors for Delivery of Peptide and Protein-Based Cargo Molecules. *Pharmaceutics* **2023**, *15*, 2093. https://doi.org/10.3390/pharmaceutics15082093

UL144-derived peptides as modulators of the BTLA/HVEM signaling pathway

Magdalena Lipińska[1], Piotr Ciura[2], Sylwia Rodziewicz-Motowidło[1], Anna Wardowska[3], Marta Spodzieja[1]

[1]Department of Biomedical Chemistry, Faculty of Chemistry, University of Gdańsk, Wita Stwosza 63, 80-308 Gdańsk, Poland
[2]Department of Theoretical Chemistry, Faculty of Chemistry, University of Gdańsk, Wita Stwosza 63, 80-308 Gdańsk, Poland
[3]Department of Physiopathology, Faculty of Medicine, Medical University of Gdańsk, Dębinki 7, 80-211 Gdańsk, Poland
email: magdalena.lipinska@phdstud.ug.edu.pl
https://doi.org/10.17952/37EPS.2024.2143
https://doi.org/10.17952/37EPS.2024.P2143

INTRODUCTION

Immune checkpoint blockade is one of the strategies used to treat cancer and autoimmune diseases. One of the immune checkpoint receptors is B and T lymphocyte attenuator (BTLA), which forms a complex with herpes virus entry mediator (HVEM) (Fig. 1A). It is confirmed that the BTLA/HVEM complex plays a negative role in the tumor microenvironment and some autoimmune diseases [1,2].

BTLA also interacts with the human cytomegalovirus glycoprotein UL144 (Fig. 1C), which exhibits noticeable homology to the HVEM protein (Fig. 1B). UL144 binds to a site on BTLA that overlaps with HVEM's binding site, and in consequence is capable of disrupting the interaction of BTLA/HVEM [3].

This study aimed to design and synthesize peptide analogues of the UL144 protein based on the crystal structure of the BTLA/UL144 complex and molecular mechanics/generalized Born surface area (MM/GBSA) analysis conducted for this complex. To determine the inhibitory properties of the peptides, we performed enzyme-linked immunosorbent assays (ELISAs). Besides, we evaluated binding properties of the peptides to BTLA protein with microscale thermophoresis (MST). These results can help determine the therapeutic potential of the examined compounds.

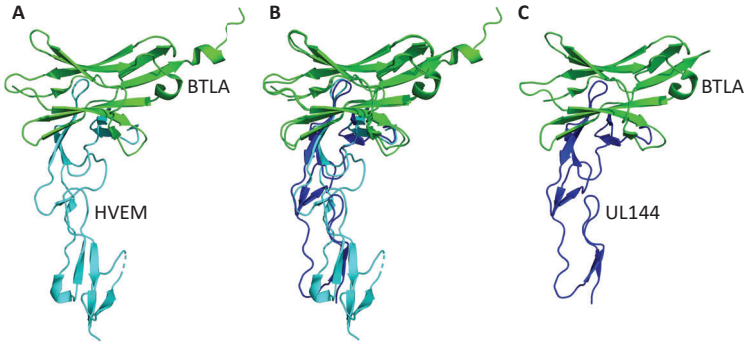

Fig. 1. The crystal structure of (A) BTLA/HVEM complex (PDB code: 2AW2), (B) alignment of both complexes and (C) BTLA/UL144 complex (PDB code: 6NYP).

METHODS AND RESULTS

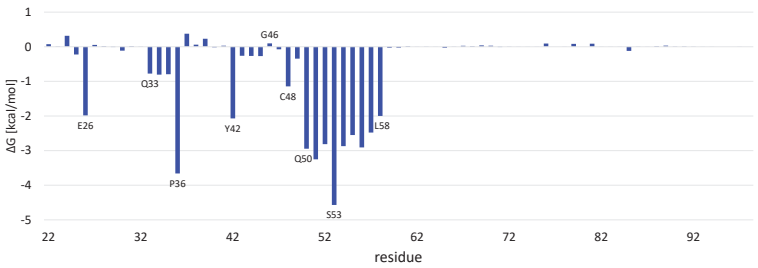

Fig. 2. Representation of the key UL144 amino acid residues involved in the BTLA/UL144 complex formation, determined by per-residue energy decomposition.

1. Design and synthesis of the peptides

To define which amino acid residues of the UL144 protein are crucial for binding to BTLA, we performed the MM/GBSA analysis. The results showed that residues E26, Q33-P36, Y42, C48, and Q50-L58 in UL144 are significant for the interaction with BTLA (Fig. 2). According to Šedý et al., mutation of residue G46 to lysine (G46K) in the UL144 protein significantly increases binding affinity to BTLA, due to a new salt bridge formation [4].

Considering the crystal structure of the BTLA/UL144 complex, MM/GBSA results and reference data, we designed eight peptides containing 0, 1, or 2 disulfide bonds – potential inhibitors of the BTLA/HVEM complex formation (Tab. 1).

The designed peptides were synthesized using solid-phase peptide synthesis (SPPS) and Fmoc/tBu strategy. The synthesis was conducted with an automated microwave peptide synthesizer (Liberty Blue, CEM Corporation). Peptides were then purified with RP-HPLC, oxidized to obtain disulfide bonds (except linear peptides), and purified again.

Tab. 1. Comparison of the designed UL144-derived peptides and their dissociation constants (K_d) obtained with microscale thermophoresis (MST).

Abbreviation	UL144(1)	UL144(2)	UL144(3)	UL144(4)
Disulfide bonds	0	1	1	2
K_d obtained with MST	46,9 µM	500 µM	119 µM	201 µM
Abbreviation	**UL144(K1)**	**UL144(K2)**	**UL144(K3)**	**UL144(K4)**
Disulfide bonds	0	1	1	2
K_d obtained with MST	1,23 mM	15,9 µM	182 µM	236 µM

2. Inhibitory properties of the peptides

To investigate whether the peptides are able to inhibit BTLA/HVEM complex formation, we performed enzyme-linked immunosorbent assays. We used Thermo Scientific™ 96-well NUNC™ Maxisorp™ Immuno Plates for that purpose. First, the BTLA-His protein was immobilized in microplates. After adding the blocking agent (5% BSA), the peptides were added at four different concentrations (300 µM, 150 µM, 75 µM and 37,5 µM) and incubated with BTLA. Unbound peptides were then removed, and HVEM-Fc protein was added. To detect HVEM-Fc, a goat anti-human IgG (H+L)-HRP conjugate and TMB ULTRA substrate (3,3',5,5'-tetramethylbenzidine) were applied.

The results show that all peptides except UL144(K1) have concentration-dependent inhibitory properties towards the BTLA/HVEM complex formation (Fig. 3). The most efficient inhibition display UL144(K2) and UL144(1).

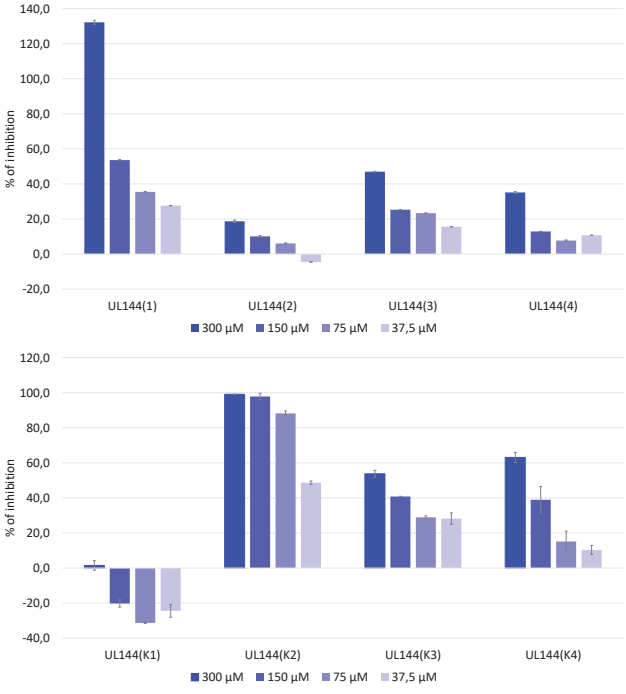

Fig. 3. The inhibitory properties of UL144-derived peptides, obtained from ELISAs.

3. Binding affinity assays

To check the binding affinity of evaluated peptides to BTLA protein, we performed microscale thermophoresis (MST) with Monolith X (Nanotemper). The findings of the assays correspond to ELISAs. Peptides UL144(K2) and UL144(1) have the highest binding affinity to BTLA. Table 1 sums up all the obtained dissociation constants (K_d).

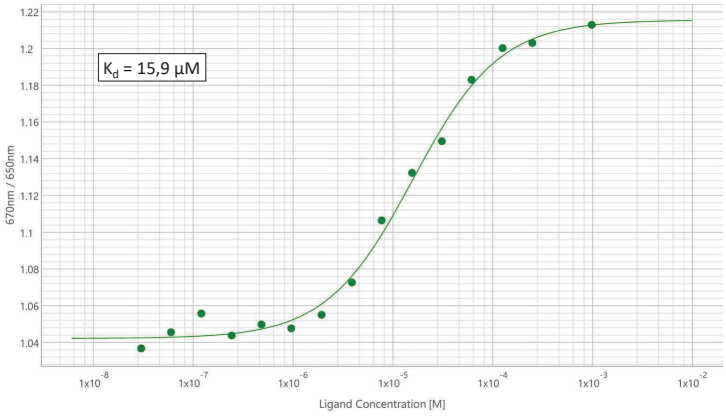

Fig. 4. Dissociation constant (K_d) obtained for UL144(K2) with MST.

CONCLUSIONS

- ✓ BTLA/HVEM protein complex is an interesting molecular target in the field of immune checkpoint blockade.
- ✓ MM-GBSA analysis showed that amino acid residues of the UL144 protein E26, Q33-P36, Y42, C48, and Q50-L58 are crucial for the interaction with BTLA.
- ✓ ELISAs and MST assays showed that UL144(K2) and UL144(1) bind most strongly to the BTLA protein and have the best inhibitory properties.
- ✓ UL144-derived peptides have the potential to become inhibitors of the BTLA/HVEM complex formation, and further investigation, including cellular assays, will determine its therapeutic properties.

Acknowledgments: Research reported in this poster was financed by the National Science Center (Poland), OPUS 22 grant (No. UMO-2021/43/ B/NZ7/01022) and Young Scientists' Research financed by the University of Gdańsk (No. 539-T070-B135-24).

References: [1] C. Demerlé et al. (2021), *Frontiers in oncology*, 11, 682007, [2] K. Wojciechowicz et al. (2022), *Cellular Immunology*, 376, 104532, [3] A. Bitra et al. (2019), *Journal of Biological Chemistry*, 294(27), 10519–10529, [4] J. R. Šedý et al. (2013), *The Journal of Immunology*, 191(2), 828–836

β-HAIRPIN PEPTIDE FIBRILLATION AND BACTERIA TRAPPING IN HYDROGEL

Peiyan YU[1], Mrunmayee DESHPANDE[1], Nhan Dai Thien TRAM[1] and Pui Lai Rachel EE[1]*

[1]Department of Pharmacy and Pharmaceutical Sciences, National University of Singapore, Singapore
*Corresponding author

https://doi.org/10.17952/37EPS.2024.P2144

Peptide fibrillation protects organisms against bacterial infections

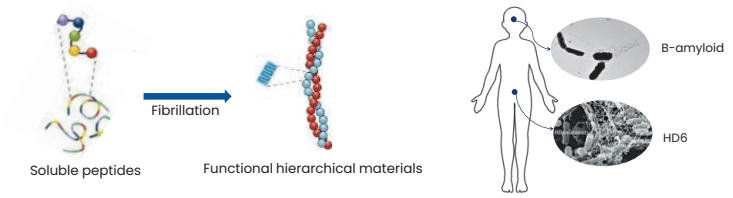

Peptide fibrillation is a process in which short chains of peptides self-assemble into organized structures. Originally studied in the context of misfolding that can lead to human disorders, increasing evidence now suggests that controlled fibrillation is involved in normal physiological processes. For example, the secretion of fibrillating human α-defensin 6 (HD6) by intestinal Paneth cells which fights infection by forming nanonets that entrap the microbial cells; and amyloid-β peptide whose expression protects against fungal and bacterial infections in animal models of Alzheimer's disease.

Bacteria-responsive nanonet forming peptides (BTT peptide)

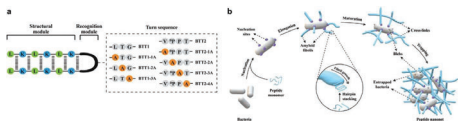

Inspired by nature, we have designed a library of β-hairpin peptides (BTT). The sequences of BTT peptides are rationally designed with two functional modules: (i)a hairpin turn as the "recognition module"; and (ii) side stands as the "structure module".

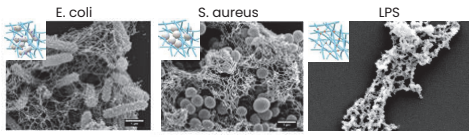

BTT peptides are capable of self-assembling into nanonets in response to bacteria, and form nanonets that trap and kill bacteria.

How does BTT peptide interact, fibrillate and trap bacteria in hydrogels?

Materials



Techniques & Methods



1 Bacteria motility is negatively affected by hydrogel stiffness

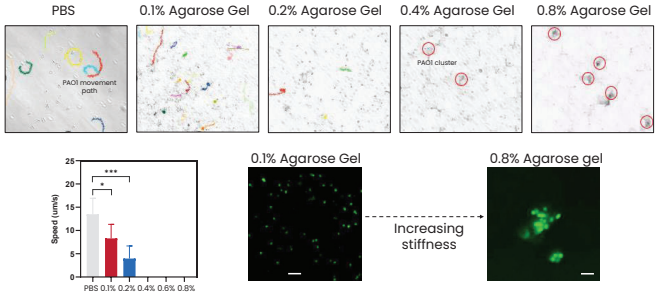

PAO1 cells swim freely in PBS solution but adopt curved paths and become transiently trapped when they are in a gel matrix. Moreover, as gel stiffness increases, the swimming path lengths decrease to the point where cells are locally confined and restricted to rotational movements.

2 Matrix porosity affects the extensiveness and distribution of BTT-bacteria clusters

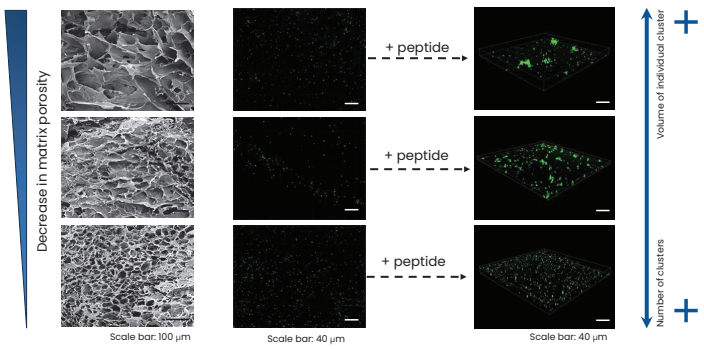

Without BTT peptide, PAO1 cells are uniformly distributed in agarose. Under the action of BTT peptide, PAO1 cells form clusters within the agarose matrix. The size of bacteria cluster is positively correlated with the pore size, while the number of observable clusters increases as pore size decreases.

3 BTT peptide-laden hydrogel attracts and entraps bacteria

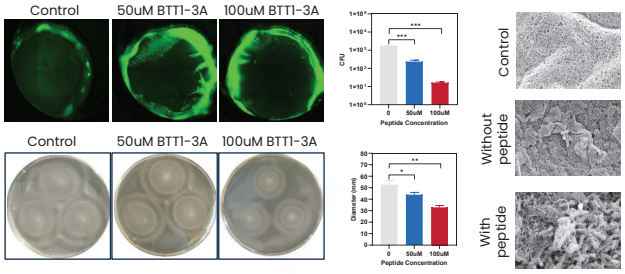

When BTT peptide is loaded in agarose gel, more PAO1 cells are attracted to and entrapped within the gel matrix. Moreover, BTT peptide forms fibrils around PAO1 cells inside the gel, restricting their motility.

4 Conclusion and Perspectives

By using agarose as a model material, we have demonstrated that BTT peptide can attract and entrap bacteria by forming nanonets within hydrogel. The stiffness and pore size of the matrix affect the motility of bacterial cells and the morphology of BTT-bacteria clusters. Our ongoing work has two focus:

- To investigate the effect of matrix charges on BTT fibrillation.
- To evaluate the *in vivo* anti-microbial efficacy of in-gel nanonets in animal model.

References:
1. Tram, N. D. T., et. al., Bacteria-Responsive Self-Assembly of Antimicrobial Peptide Nanonets for Trap-and-Kill of Antibiotic-Resistant Strains. *Adv. Funct. Mater.* 2023, 33, 2210858.
2. Nhan D.T. Tram, et. Al., Manipulating turn residues on de novo designed β-hairpin peptides for selectivity against drug-resistant bacteria, Acta Biomaterialia, Volume 135, 2021
3. Yuk, H., Zhang, T., Lin, S. *et al.* Tough bonding of hydrogels to diverse non-porous surfaces. *Nature Mater* 15, 190–196 (2016).
4. Song, F and Ren, D, Stiffness of Cross-Linked Poly(Dimethyl siloxane) Affects Bacterial Adhesion and Antibiotic Susceptibility of Attached Cells, Langmuir 30 (34), 10354-10362 (2014)

Contact Information
Associate Professor: Pui Lai Rachel EE
Email: phaeplr@nus.edu.sg

Peptide Nanonets as Antimicrobial and Anti-inflammatory Agents

Pui Lai Rachel Ee[a], Nhan Dai Thien Tram[a], Jian Xu[a], Dhanya Mahalakshmi Murali[a], Peiyan Yu[a], Wai Shiu Fred Wong[b], Lakshminarayanan Rajamani[a,c]

[a] *Department of Pharmacy and Pharmaceutical Sciences, National University of Singapore,*
[b] *Department of Pharmacology, National University Health System*
[c] *Ocular Infections and Anti-Microbials Research Group, Singapore Eye Research Institute*

https://doi.org/10.17952/37EPS.2024.P2145

De novo design of beta-hairpin peptides

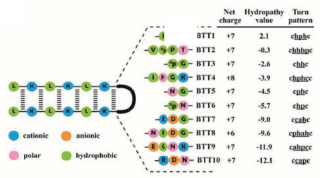

We have designed a series of de novo β-hairpin peptides with identical side strands but varied turns. We demonstrated that mutations of only 2 to 4 amino acids at the turn region could impart a wide range of antimicrobial profiles among synthetic β-hairpin AMPs.

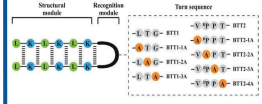

Through turn sequence modification by Ala scanning, we identified specific analogues capable of forming bacteria-responsive nanonets.

Nanonet forming analogues have anti-microbial activity

Peptide	MIC [μM]	
	E. coli	*S. aureus*
BTT1	4	8
BTT1-3A	8	16

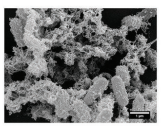

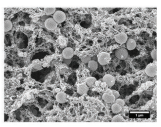

BTT1-3A was found to be the only analogue capable of forming bacteria-responsive nanonets. We successfully converted the kill-only BTT1 to the trap-and-kill BTT1-3A.

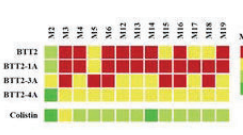

By replacing single amino acid at the run segment of BTT2, we obtained BTT2-4A with improved antimicrobial potency against clinically relevant antibiotic-resistant strains, while preserving the ability to form bacteria-trapping nonets.

Nanonet forming analogues are anti-inflammatory

BTT2-4A and BTT1-3A nanonets also displayed selective trapping activity toward pro-inflammatory cytokines while not affecting anti-inflammatory cytokines

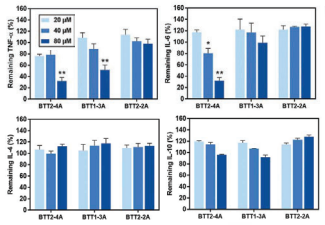

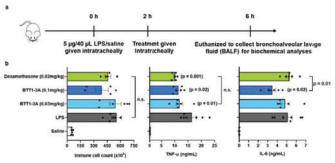

In endotoxin-induced acute lung injury mice model, BTT1-3A via intratracheal administration, significantly lowered the level of pro-inflammatory cytokines.

Nanonet-forming peptides inhibit TLR4 and TLR9 activations in cells by inflammatory mediators

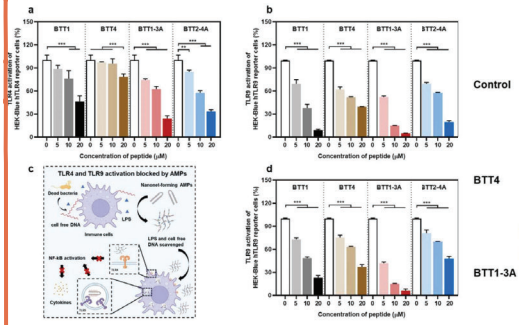

(a) BTT peptides inhibited TLR4 activation in HEK-Blue™ hTLR4 cells by entrapping extracellular LPS. (b, d) BTT peptides inhibited TLR9 activation in HEK-Blue™ hTLR9 cells by scavenging extracellular (b) and intracellular (d) CpG DNA. (c) Scheme of nanonet-forming AMPs blocking TLR4 and TLR9 activations and the downstream NF-κB pathway.

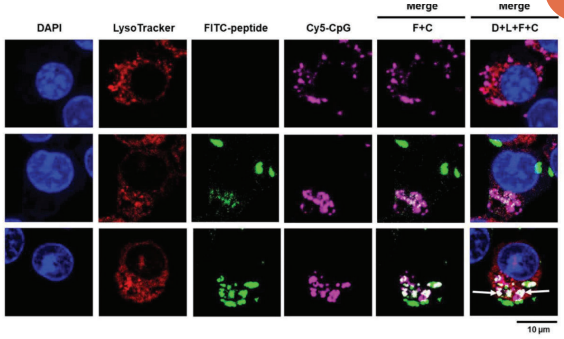

Co-localization of BTT peptides with intracellular CpG DNA in RAW264.7 cells. Most of FITC-BTT1-3A but less of FITC-BTT4 intracellularly co-localized with CpG DNA and endo-lysosomes, demonstrating that BTT1-3A had stronger capacity of entering cells and competitively binding with intracellular CpG DNA than BTT4.

1 Objective: To explore anti-inflammatory activity via inhibition of TLR4 and TLR9 pathways

Methodology:

- CpG DNA binding assay

CpG DNA was incubated with PicoGreen and peptide solutions. Fluorescence intensity was measured.

- Cellular co-localization of peptides with CpG DNA

Overnight culture of RAW 264.7 cells were incubated with 1 μg/mL of Cy5-CpG DNA for 1 hour. FITC-peptides were then added in the medium and incubated for 4 hours. The cells were stained by LysoTracker Red DND-99, followed by fixation with 4% formaldehyde in PBS and staining with DAPI.

2 Objective: To improve the proteolytic stability of β-hairpin antimicrobial peptide

Methodology:

- Minimum inhibitory concentration (MIC) determination

MIC of peptides was determined by broth microdilution method. The MIC presented the lowest peptide concentration at which at least 90% of OD600 was reduced compared to control without peptide treatment.

- Field-emission scanning electron microscope (SEM) was employed for the observation of bacteria-trapping nanostructures.

- NPN (N-phenylnaphthalen-1-amine) uptake assay for outer membrane permeability; SYTOX green uptake assay for indication of inner membrane permeability.

Pan-substitution with Ornithine confer robust enzymatic stability to BTT1-3A while retaining activity

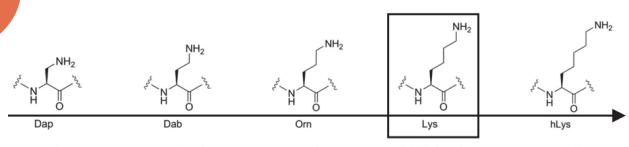

Design scheme for pan-substitution of Lysine residue in BTT1-3A using unnatural amino acids with unaltered stereochemistry but different side chain chemistry.

Peptide	MIC against *E. coli* (μM)	
	Pre-trypsin	Post-trypsin
pan-hLys	128	> 128
BTT1-3A	16	> 128
pan-Orn	8	8
pan-Dab	64	> 128
pan-Dap	>128	> 128

Without trypsin treatment, only pan-Orn displayed better antimicrobial potency relative to BTT1-3A; following trypsin treatment, pan-Orn retains antimicrobial activity with unchanged MIC, suggesting excellent trypsin stability.

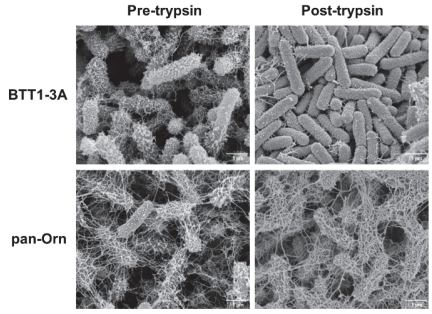

In contrast to BTT1-3A whose nanonet-forming capacity drastically degraded post-trypsin, pan-Orn formed expansive bacteria-trapping nanonets both pre- and post-trypsin, further strengthening the claim on superior proteolytic stability of pan-Orn.

References:
1. Tram, N. D. T., et. al., Bacteria-Responsive Self-Assembly of Antimicrobial Peptide Nanonets for Trap-and-Kill of Antibiotic-Resistant Strains. *Adv. Funct. Mater.* 2023, 33, 2210858.
2. Nhan D.T. Tram, et. Al., Manipulating turn residues on de novo designed β-hairpin peptides for selectivity against drug-resistant bacteria, Acta Biomaterialia, Volume 135, 2021
3. N. D. T. Tram, Q. T. N. Tran, J. Xu, J. C. T. Su, W. Liao, W. S. F. Wong, P. L. R. Ee, Multifunctional Antibacterial Nanonets Attenuate Inflammatory Responses through Selective Trapping of Endotoxins and Pro-Inflammatory Cytokines. Adv. Healthcare Mater. 2023, 12, 2203232.

Contact Information
Associate Professor: Pui Lai Rachel EE
Email: phaeplr@nus.edu.sg

https://doi.org/10.17952/37EPS.2024.P2146

Protein-Protein Interactions: Unraveling the link between HTLV-1 Tax-1 oncoprotein and human *Drosophila discs* large tumor suppressor

Wael El Yazidi Mouloud[1], Sibusiso B. Maseko [2], Yasmine Brammerloo [2], Inge Van Molle [3], Adria Sogues Castrejon [3], Charlotte Martin[1], Han Remaut[3], Steven Ballet[1], Oleksandr Volkov [3,4], Jean-Claude Twizere [2, 5, 6]

[1] Research Group of Organic Chemistry – Vrije Universiteit Brussel (VUB) – Brussels (BE)
[2] Laboratory of Viral Interactomes, Unit of Molecular Biology of Diseases, GIGA Institute – University of Liege – Liège (BE)
[3] VIB-VUB Center for Structural Biology, Flemish Institute of Biotechnology (VIB) – Brussels (BE)
[4] Jean Jeener NMR Centre – Brussels (BE)
[5] TERRA research and teaching centre, Microbial Processes and Interactions (MiPI), Gembloux Agro Bio-tech – University of Liege – Liège (BE)
[6] Laboratory of Algal Synthetic and Systems Biology, Division of Science and Math – New York University of Abu Dhabi – Abu Dhabi (UAE)

e-mail: wael.el.yazidi.mouloud@vub.be

INTRODUCTION [I]

Tax-1 is the most pathogenic protein of the **human T-cell leukemia virus type 1 (HTLV-1)**, an oncogenic virus responsible for the onset of an aggressive form of cancer, **adult T-cell leukemia (ATL)**. The oncoprotein undergoes **protein-protein interactions (PPI)** with a plethora of host proteins, such as the human homologue of the ***Drosophila discs large* (hDlg1) tumor suppressor** which is implicated in HTLV-1's oncogenic abilities.[1]This study aimed at the characterization of the interaction between **HTLV-1 Tax-1** and **hDlg1 PDZ domains**.[2]

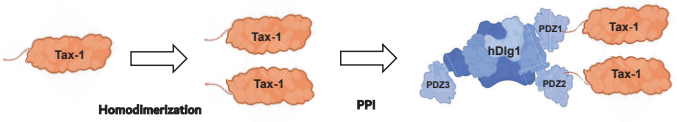

The interaction was characterized through **nuclear magnetic resonance** (NMR) and **X-ray crystallography**, additionally **isothermal titration calorimetry** (ITC) was utilized to quantify the strength of the respective interactions. Our work provides structural insights essential in the pursuit of **PPI inhibitors**.

X-RAY CRYSTALLOGRAPHY [III]

PDZ1 co-crystallization

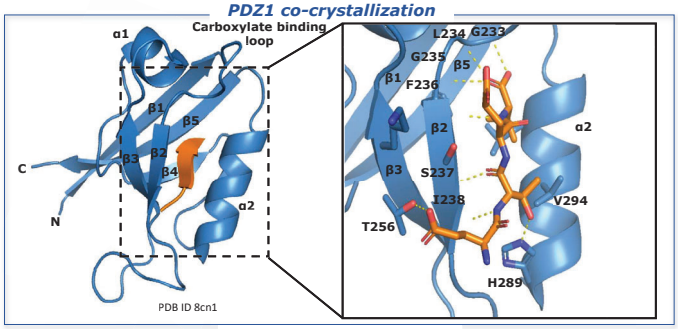

PDZ2 co-crystallization

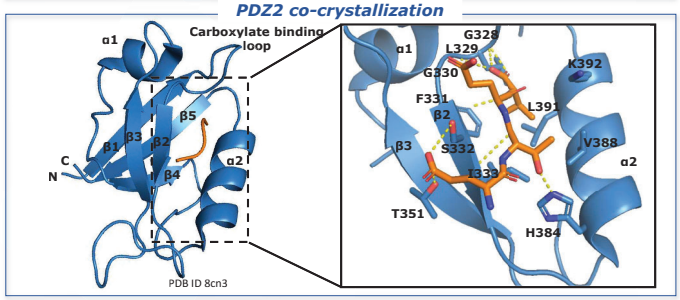

➢ Residues experiencing the largest spectral changes in NMR (**G235**, **F236** and **S237** for PDZ1 & **G330**, **F331** and **S332** for PDZ2) are accounted for in the crystal structure.

➢ Binding observed in the crystal structure is **compatible** with the measured spectral changes by solution NMR.

ISOTHERMAL TITRATION CALORIMETRY [IV]

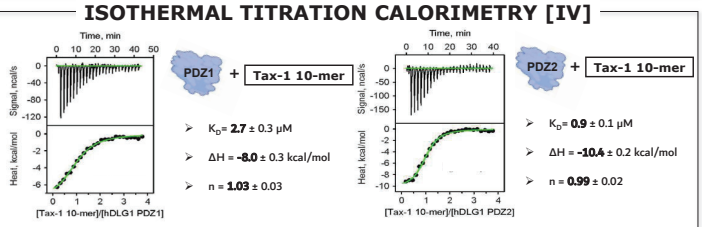

➢ Both interactions are **enthalpically** driven, with the decamer binding stronger to **PDZ2**.

CONCLUSIONS [V]

➢ Solution NMR revealed the binding hotspots to be located in the **β1/β2 loop**, **β2 strand** and **α2 helix.**

➢ Only the last four amino acids (**H-Glu-Thr-Glu-Val-OH**) of the Tax-1 10-mer seem to be essential for the binding.

➢ Tetramer bound PDZ domains crystals revealed a binding modality congruent with the hotspots observed by NMR.

PERSPECTIVES [VI]

➢ Structural insights gained by X-ray crystallography and NMR could be utilized to find potential PPI inhibitors (**small molecules and peptides**).

NUCLEAR MAGNETIC RESONANCE [II]

PDZ domains predominantly interact with the *C*-terminal tail of their binding partners, appropriately called **PDZ-binding motif (PBM)**,[3] thus a similar interaction was expected with Tax-1. Peptides mimicking the *C*-terminal tail of the Tax-1 protein were synthetized and their respective interactions with the PDZ domains was evaluated through **[^{1}H,^{15}N] heteronuclear single-quantum correlation (HSQC)**.

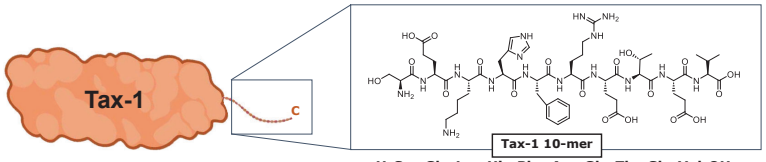

H-Ser-Glu-Lys-His-Phe-Arg-Glu-Thr-Glu-Val-OH

Tandem PDZ1+2

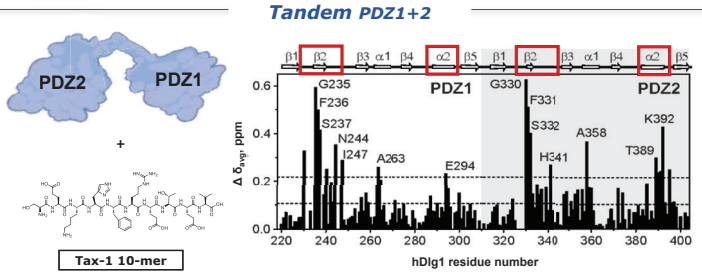

➢ Significant spectral changes for residues located in **β1/β2 loop**, **β2 strand** and **α2 helix**

Individual domains

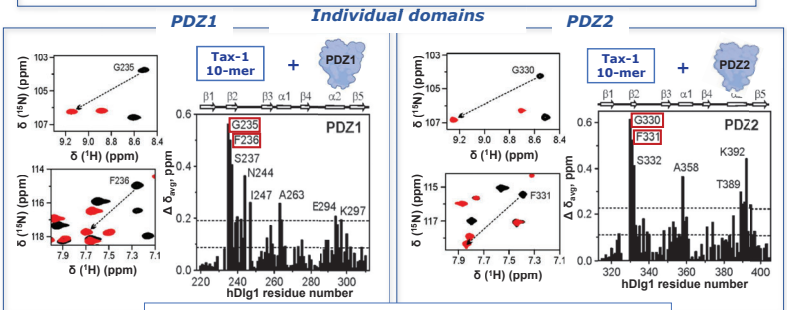

➢ Highly similar binding modalities between the tandem and the individual domains.

➢ Residues G235, F236, G330 and F331 experience the largest **spectral changes**.

Essential amino acids

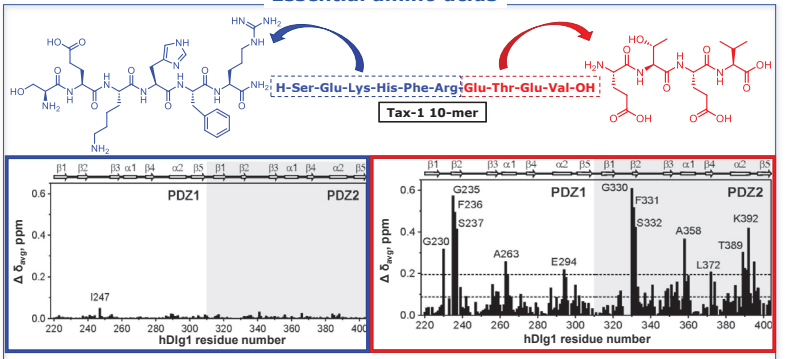

➢ When split in two parts, only the last four amino acids cause spectral changes

H-Glu-Thr-Glu-Val-OH is the essential part for the interaction.

ACKNOWLEDGEMENTS

We thank the Research Council of the VUB for financial support through the Strategic Research Programmes (SRP50 & SRP95), the Research Foundation Flanders (FWO) through FWO Hercules (OZR3939) and the Fund for Scientific Research (FNRS) for the financial support.

REFERENCES

(1) Suzuki, T.; Ohsugi, Y.; Uchida-Toita, M.; Akiyama, T.; Yoshida, M. *Oncogene*. **1999**, *18* (44), 5967-5972
(2) Maseko, S. B.; Brammerloo, Y.; Van Molle, I.; Sogues, A.; Martin, C.; Gorgulla, C.; Olivet, J.; Blavier, J.; Ntombela, T.; Delvigne, F.; Arthanari, H.; Salehi-Ashtiani, K.; Remaut, H.; Ballet, S.; Volkov, A., N.; Twizere, J. *Antiviral Research*. **2023**, *217*, 105675
(3) Songyang, Z.; Fanning, A., S.; Fu, C.; Xu, J.; Marfatia, S., M.; Chishti, A., H.; Crompton, A.; Chan, A., C.; Anderson, J., M.; Cantley, L., C. *Science*. **1997**, *275* (5296), 73-77

Esc peptides for novel therapeutics against *Pseudomonas aeruginosa* pulmonary infections: beyond antimicrobial activity

Maria Rosa Loffredo[1], Loretta Ferrera[2], Floriana Cappiello[1], Bruno Casciaro[1], Giacomo Cappella[1], Ivana D'Angelo[3], Y. Peter Di[4] , Maria Luisa Mangoni[1]

[1]Department of Biochemical Sciences, Sapienza University of Rome; [2]U.O.C. Genetica Medica, Istituto Di Ricovero e Cura a Carattere Scientifico, Istituto Giannina Gaslini, Genova; [3]Department of Biotechnology, DiSTABiF, University of Campania Luigi Vanvitelli, Caserta, Italy; [4]Department of Environmental and Occupational Health, University of Pittsburgh, USA

Email: marialuisa.mangoni@uniroma1.it

https://doi.org/10.17952/37EPS.2024.P2148

BACKGROUND & RESULTS

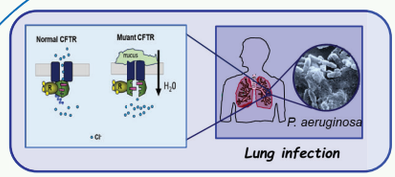

- Cystic fibrosis (CF) is a genetic disorder due to mutations in the gene encoding the CFTR channel at the apical membrane of epithelia, including those at the airways [1,2].
- The most prevalent mutation is the loss of phenylalanine 508 (F508del CFTR) which severely impairs CFTR trafficking to the cell surface and alters the mechanisms of channel opening. Despite the clinical efficacy of present CFTR modulators in restoring the activity of defective CFTR, some patients remain untreatable or continue to experience chronic pulmonary infections, presenting considerable challenges.
- In the last years, we identified two antimicrobial peptides (AMPs), Esc peptides [3-5] (scheme 1), that (i) rapidly kill *P. aeruginosa* and eradicate its biofilm with a membrane-perturbing activity that prevents bacteria from developing resistance; (ii) accelerate recovery of damaged bronchial epithelium; (iii) reduce lung bacterial burden in C57BL/6 mice upon intra-tracheal instillation at a very low dosage (0.1 mg/kg) (Figure 1).

Note that complete activation of CFTR with gating mutations can be achieved upon addition of forskolin (FSK), which promotes the phosphorylation of the channel, and genistein (GEN) to prolong the open channel probability [6,7].

Esculentin-1a: GIFSKLAGKKIKNLLISGLKNVGKEVGMDVVRTGIDIAGCKIKGEC (Basic residues, Acid residues)

Esc(1-21): GIFSKLAGKKIKNLLISGLKG-NH_2 +6 (L-Leu, L-Ser)

Esc-1c: GIFSKLAGKKIKNLLISGLKG-NH_2 +6 (D-amino acids)

Esc peptides

Scheme 1.

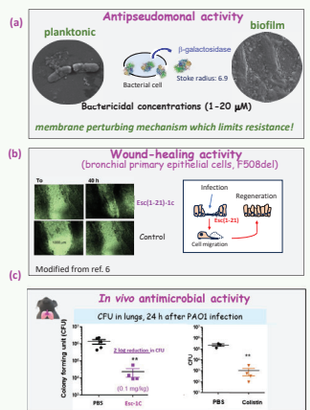

Figure 1. (a) Scanning electron microscopy images showing the effect of Esc(1-21) on *P. aeruginosa*; (b) Effect of Esc-1c on the wound healing activity in primary bronchial epithelial cells homozygous for F508del-CFTR; (c) *In vivo* antimicrobial efficacy of Esc-1c in a mouse model of acute *P. aeruginosa* induced lung infection. The peptide was intratracheally instilled at 0.1 mg/kg, 2 h after infection and the number of colony forming units in the lungs was evaluated after 24 h and compared to that of colistin, under the same conditions.

Recently, the ability of Esc peptides to increase the F508del CFTR-mediated transepithelial conductance (TEEC) was studied in combination with FSK. This effect was higher for Esc-1C at 10 μM and comparable to that of GEN when used at the same concentration (Figure 2). We also found that this effect is highly dependent on the primary structure of Esc peptides and the presence of Ser-17 (Figure 3).
The CFTR potentiating activity of Esc peptides was well preserved in primary airway epithelial cells from homozygous F508del patients (Figure 4).

To verify whether the effect of Esc peptides on the ion currents was controlled by CFTR, patch clamp experiments (*inside-out configuration*) were carried out on Fisher Rat Thyroid cells (FRT) expressing F508del CFTR. The increased peptide-induced ion current is due to activation of CFTR and likely mediated by direct interaction of the peptides with CFTR (Figure 5).

To achieve the lungs, it is fundamental the development of pharmaceutical formulations able to assist the peptide diffusion through extracellular barriers and to provide a gradual peptide release at the infectious site.
Peptide-loaded PLGA-PVA nanoparticles (NPs) were able to improve the diffusion of the encaspulated peptide through the bronchial mucus and simulated biofilm (Figure 6).

Note also that peptide-loaded NPs were found to be more efficient in reducing the number of *P. aeruginosa* in a mouse model of acute lung infection compared to the results found when the peptides were i.t. instilled in their soluble free form (Figure 7).

CFTR-DEPENDENT TRANSEPITHELIAL CONDUCTANCE (ΔG) BY ESC PEPTIDES

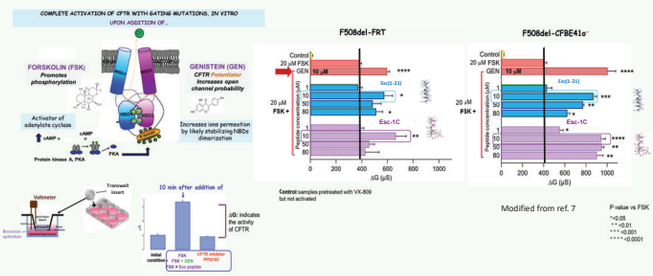

Figure 2. Fisher Rat Thyroid (FRT) cells or bronchial epithelial cells (CFBE41o-) expressing F508del-CFTR were pre-incubated with the corrector VX-809 (to deliver the mutated protein to the membrane) for 24h and then with Esc peptides for 10 min at different concentrations, in the presence of FSK. Then, CFTR channel activity was fully inhibited by the CFTR specific inhibitor PPQ-102 (30 μM) and CFTR-mediated transepithelial electrical conductance was calculated.

CFTR-DEPENDENT TRANSEPITHELIAL CONDUCTANCE (ΔG) BY ANALOGS OF ESC PEPTIDES

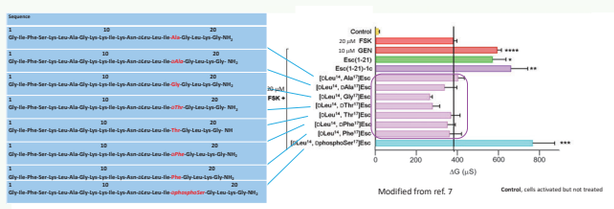

Figure 3. CFTR-mediated transepithelial conductance upon treatment of F508del-CFTR FRT cells with Esc analogues (10 μM) for 10 min in the presence of 20 μM FSK. Data are expressed as mean ± SEM from 3 independent experiments.
*, $p < 0.01$; ** $p < 0.001$; ** p<0.0001, vs FSK.

CFTR-DEPENDENT TRANSEPITHELIAL CONDUCTANCE (ΔG) IN PRIMARY BRONCHIAL EPITHELIA

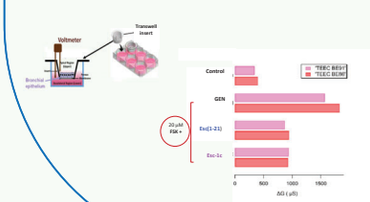

Figure 4. Effect of peptides on CFTR-mediated TEEC in primary airway epithelial cells obtained from a CF patient homozygous for the mutation F508del. TEEC was evaluated as the difference between the conductance measured after 10 min addition of 20 μM FSK alone or after addition of the combination FSK + GEN or peptides to Vx-809 pre-incubated epithelia, and the conductance measured after CFTR inhibition (delta conductance, ΔG) upon addition of PPQ102, as reported in Fig. 2. Epithelia pre-incubated with VX-809 but not activated (control) were included for comparison.

EFFECT OF PEPTIDES ON IONS CURRENT BY PATCH CLAMP EXPERIMENTS (inside-out configuration)

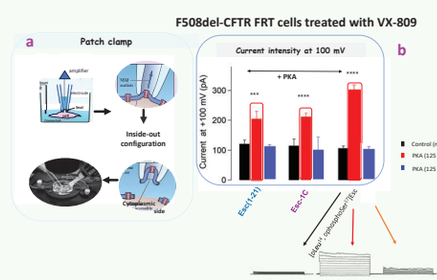

Figure 5.
a. Current intensity at +100 mV for indicated treatment. ****, $p < 0.0001$ vs control. Superimposed currents elicited at different membrane potential are also indicated for the phosphorylated peptide. b. Current ratio at +100 mV upon addition of protein kinase A (pKA) and ATP.

NPs DIFFUSION THROUGH ARTIFICIAL BIOLOGICAL BARRIERS & KINETICS OF PEPTIDE RELEASE

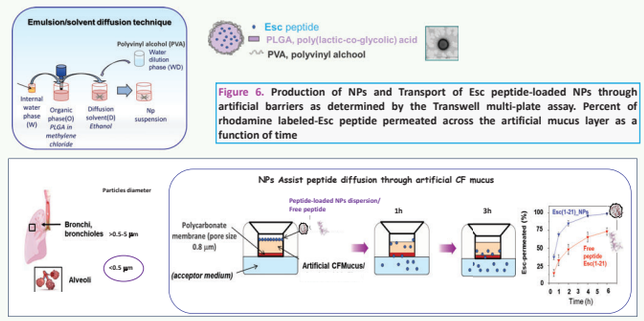

Figure 6. Production of NPs and Transport of Esc peptide-loaded NPs through artificial barriers as determined by the Transwell multi-plate assay. Percent of rhodamine labeled-Esc peptide permeated across the artificial mucus layer as a function of time

EFFICACY IN MURINE MODELS OF ACUTE LUNG INFECTION AT 24h AFTER BACTERIAL CHALLENGE

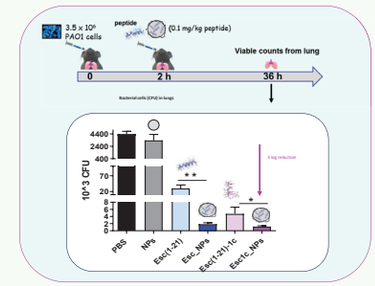

Figure 7. Comparison among bare NPs, Esc peptides and peptides-loaded NPs on the number of viable *P. aeruginosa* cells (CFU) in mouse lungs at 36 h after their administration. Results are the mean ± SEM from three independent experiments. The t-test was used to compare the means of peptide-treated infected mice versus animals treated with the corresponding peptide-loaded NPs. The levels of statistical significance are *p* values of< 0.05 (*) and < 0.01 (**).

CONCLUSIONS & PERSPECTIVES

These studies should allow the development of new peptide-based therapeutic agents able to:

- Defeat *P. aeruginosa* lung infection
- Heal damaged bronchial epithelium
- Restor the function of mutated CFTR

Advantageous properties for treatment of Lung pathology in CF !

References

1. Cuthbert AW (2011). *Br J Pharmacol* 163(1):173–183.
2. Liu F, et al. (2017) Cell 169(1):85-95
3. Luca V et al. (2013) *Cell Mol Life Sci* 70, 2773-2786
4. Cappiello F. et al. (2021) *Int J Mol Sci.* 2021, 22, 557
5. Chen C et al. (2017) *Sci Rep*, Sci Rep 7(1):8548
6. Mangoni ML et al. (2024) *Int. J. Mol Life Sci,* 25, 4400
7. Ferrera L et al. (2022) *Cell Mol Life Sci*, 79:67

Acknowledgments:

Fondazione per la Ricerca sulla Fibrosi Cistica - Onlus
italian cystic fibrosis research foundation

Finanziato dall'Unione europea NextGenerationEU

Ministero dell'Università e della Ricerca

Italiadomani

FFC Project 4/2022 adopted by Delegazione FFC Ricerca di Roma; Delegazione FFC Ricerca della Franciacorta e Val Camonica.
EU funding within the NextGeneration EU-MUR
PNRR Extended Partnership initiative on Emerging Infectious Diseases (Project no.PE00000007, INF-ACT) .

Synthesis and antimicrobial activity of hybrid peptides as dual inhibitor of intracellular targets in ESKAPE pathogens

Aman Kumar Mahto, Rikeshwer Prasad Dewangan*

Affiliation: Department of Pharmaceutical Chemistry, School of Pharmaceutical Education and Research (SPER), Jamia Hamdard (Deemed to be University), New Delhi- 110062, India

https://doi.org/10.17952/37EPS.2024.P2150

Background

❑ The infections caused by ESKAPE pathogens are a global challenge in clinical settings due to their multidrug resistance and even last-resort antibiotics ineffective for treatment.

❑Advances in science have shown that bacteria adapt and mutate to resist antibiotics. To combat this, new antibiotics with novel targets and mechanisms are needed.

❑Antimicrobial peptides (AMPs), which have evolved over millennia as natural antimicrobial agents and immune response mediators, are one of the promising candidates in this fight.

Rationale &Objectives

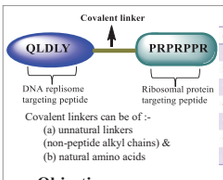

Proline &Arginine rich antimicrobial peptides (PrAMPs)

S.no	PrAMPs	Peptide Sequence
1.	Onc72	VDKPPYL**PRPRPPR**OIVNO
2.	Api88	Gu-ONNRPVYI**PRPRPP**HPRL
5.	Api134	Gu-ONNRPVYI**PRPRPP**HPOL
4.	A3-APO	(zRPDKPRPYL**PRPRPPR**PVR)2
5.	CheX1-R20	ZRPDKPRPYL**PRPRPPR**PVR
6.	Pyrrhocoricin	VDKGSYL**PRPTPPR**IYNRN
7.	PR-39 (1-18)	RRRPRPPYL**PRPRPPP**FF

Objectives:

- Synthesis of the designed hybrid analogues of proline rich antimicrobial peptides.
- Purification & Characterization of the peptide through HPLC and LC-MS
- Determination of anti-bacterial potency of the peptides against ESKAPE pathogens.
- Evaluation of *in vitro* cell cytotoxicity and hemolytic activity of the peptides.

Methodology

❑ Design and synthesis of peptides

- Natural host defense cationic antimicrobial peptides (AMPs) are effective against multidrug-resistant (MDR) pathogens, but their membrane-disruptive action can be toxic to mammalian cells, limiting systemic use.
- However, intracellular-targeting AMPs, which can inhibit DNA or protein synthesis, bypass these restrictions. This study proposes the design of such AMPs to target enzymes involved in DNA replication and protein synthesis.
- The peptides were synthesized using standard solid-phase Fmoc chemistry and characterized by HPLC and ESI-MS.

❑ Antimicrobial potency

- Modified serial broth dilution method was used.
- The peptides were tested against a range of gram-negative and gram-positive pathogens, revealing lead sequences with potential against drug-resistant bacteria.

❑ Cell cytotoxicity assay

- Hemolytic activity of the designed peptides were determined on fresh human red blood cells (hRBC) and were found non-hemolytic even at the concentration of 0.5 mg/mL.
- We conducted cytotoxicity study of the lead peptides by MTT assay method against HEK-293T cell lines at higher concentrations of the calculated MIC value obtained from antibacterial assay (as depicted as in Figure 3.2).

❑ Drug resistance studies

- Resistance development studies of the peptides till 17 passages of bacteria. a) for *E. coli* ATCC 11775 and b) for *S. aureus* ATCC 33591.

❑ Mode of action studies

- Peptide internalization studies (using confocal microscopy).
- Bacterial membrane depolarization assay.

Results

1. Characterisation: HPLC, UPLC & ESI-MS

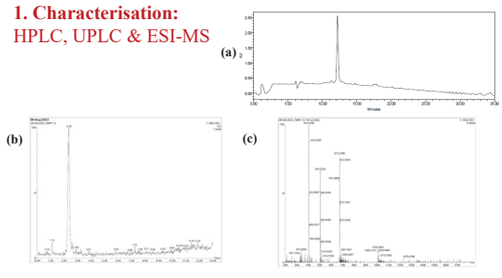

Fig 1: (a) HPLC, (b) UP-LC chromatogram, and (c) ESI-Mass spectra of peptides.

2. Antibacterial Assay

Table 1: Peptide name, sequence, and MIC of the synthesized peptides.

Sr. No	Sequence of peptides	Sample Code	S. aureus ATCC 33591	S. aureus ATCC BAA-44	S. aureus ATCC 43300	MRSE ATCC 6093	B. subtilis ATCC 6633	S. epidermidis ATCC 51625	E. coli ATCC 11775	E. coli ATCC BAA-427	P. aeruginosa ATCC 35667	E. faecium ATCC 19606	A. baumannii ATCC 19606	K. pneumoniae ATCC BAA-1705	E. faecalis ATCC 7080
1	Ac-PRPRPPR- $CONH_2$	Prn	>500	>500	>500	>500	>500	>500	>500	>500	>500	>500	>500	>500	>500
2	Ac-QLDLY-R-PRPRPPR- $CONH_2$	NHP-11	500	500	500	500	500	500	>500	500	500	500	500	500	500
3	Ac-QLDLY-RR-PRPRPPR- $CONH_2$	NHP-12	250	500	500	>500	500	250	500	250	250	500	250	250	500
4	**Ac-QLDLY-RRR-PRPRPPR- $CONH_2$**	**NHP-13**	**31.2**	**31.2**	**62.5**	**62.5**	**31.2**	**15.1**	**62.5**	**31.2**	**31.2**	**125**	**125**	**125**	**125**
5	Ac-QLDLY-Spermine	Spn-1	62.5	31.2	62.5	62.5	31.2	250	250	250	250	250	250	250	250
6	**Lauric acid-QLDLY-Spermine**	**Spn-4**	**7.8**	**7.8**	**15.1**	**7.8**	**7.8**	**31.2**	**62.5**	**31.2**	**31.2**	**125**	**62.5**
7	Vancomycin	Van	0.4	1.9	1	ND	1	**62.5**	**125**	**62.5**	**125**	**ND**	**125**
8	Ciprofloxacin	Cipro	0.2	62.5	0.03	ND	0.03	**0.02**	**0.8**	**0.5**	**0.8**	**ND**	**0.8**

3. Cell cytotoxicity and Hemolytic assay

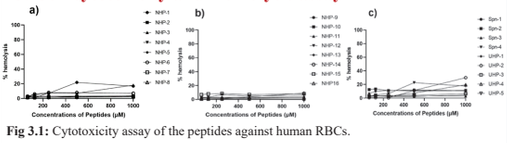

Fig 3.1: Cytotoxicity assay of the peptides against human RBCs.

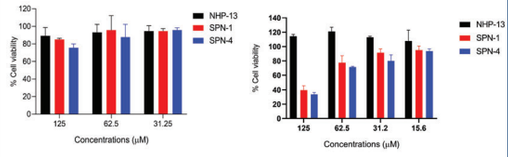

Fig 3.2: (a)Cytotoxicity assay of the peptides against HEK-293T cell lines.
(b) Cytotoxicity assay of the peptides against peripheral blood mononuclear cells (Primary cells). The assay was performed based on reduction of alamar blue dye.

4. In-vitro antiendotoxin neutralization assay

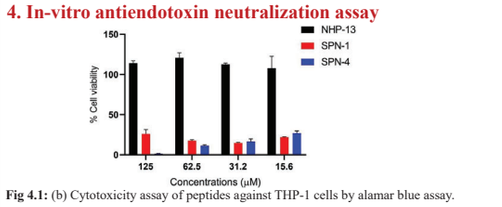

Fig 4.1: (b) Cytotoxicity assay of peptides against THP-1 cells by alamar blue assay.

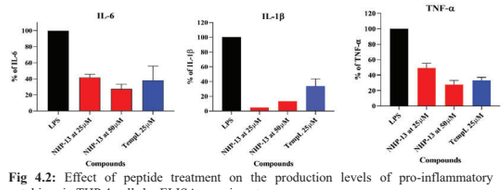

Fig 4.2: Effect of peptide treatment on the production levels of pro-inflammatory cytokines in THP-1 cells by ELISA experiments.

Results

5. Drug resistance studies

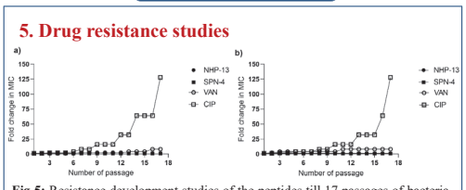

Fig 5: Resistance development studies of the peptides till 17 passages of bacteria. a) for E. coli ATCC 11775 and b) for S. aureus ATCC 33591.

6. Mode of action studies

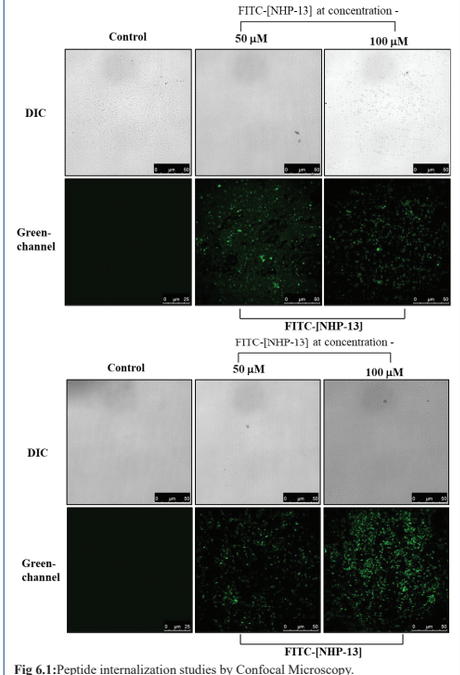

Fig 6.1: Peptide internalization studies by Confocal Microscopy.

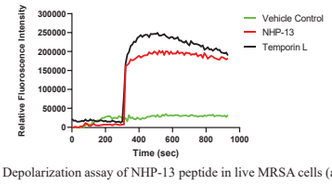

Fig 6.2: Depolarization assay of NHP-13 peptide in live MRSA cells (at 2 × MIC).

Key findings

❑The peptide templates, PRPRPPR and QLDLY were employed to design for dual inhibition of protein and DNA synthesis, respectively.

❑Peptide NHP-13 and SPN-4 was found to be active in the MIC range of 7.8-125 µM concentrations against tested strains with no hemolytic activity observed up to 500 µM concentrations.

❑Further studies was performed to evaluate peptide internalization in bacteria by labelling with FITC.

❑The most active peptide (NHP-13) was hybrid of above two templates with linker of triple arginine, highlighting arginine's role in cell penetration and enhancing antibacterial activity.

❑In vitro LPS neutralization activity of NHP-13 shown potential effects on reduction in inflammatory cytokines in human monocytes.

❑Further studies are going on for evaluation of protein synthesis by interaction with 70s ribosomes and DNA replisomes.

AKNOWLEDGEMENT:

- Dr. Shalini Kumari (CSIR-IGIB, Mathura Road, New Delhi),
- Dr. Pradeep Kumar (CSIR-IGIB, Mall road, New Delhi),
- Central Instrumentation Facility, SPER, Jamia Hamdard (Hamdard Nagar, New Delhi.
- ICMR-EMR adhoc project (OMI/ECD-001/2021)
- Science Engineering Research Board (SERB) travel grant to attend EPS-2024

Disrupting the RANK-TRAF6 Interface: A Novel Approach for Bone Metastases Treatment

https://doi.org/10.17952/37EPS.2024.P2152

Sofia A. Martins[1], Cátia Rosa[1], Marco Cavaco[2], Rita Melo[1], David Andreu[3], Javier Valle[3], Vera Neves[2], Miguel A. R. B. Castanho[2], João D.G. Correia[1,4]

[1] Centro de Ciências e Tecnologias Nucleares, Instituto Superior Técnico, Universidade de Lisboa, Estrada Nacional 10, ao km 139,7; 2695-066 Bobadela LRS, Portugal;

[2] Instituto de Medicina Molecular João Lobo Antunes, Faculdade de Medicina, Universidade de Lisboa, Avenida Professor Egas Moniz 1649-028 Lisboa, Portugal;

[3] Department of Medicine and Life Sciences, Pompeu Fabra University, Dr. Aiguader 88, Barcelona Biomedical Research Park, 08003 Barcelona, Spain;

[4] Departamento de Engenharia e Ciências Nucleares, Instituto Superior Técnico, Universidade de Lisboa, Estrada Nacional 10, ao km 139,7; 2695-066 Bobadela LRS, Portugal

A. Background

Most **cancer deaths** are prompted by **incurable metastases**[1]

Bone is one of the most frequent **metastasis** sites[1]

Bone metastasis entails **unbalanced bone remodelling**[1]

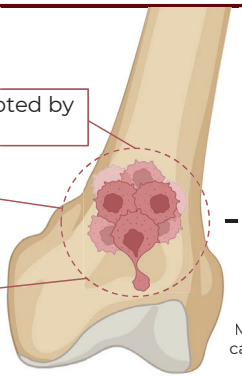

Vicious cycle of bone metastasis

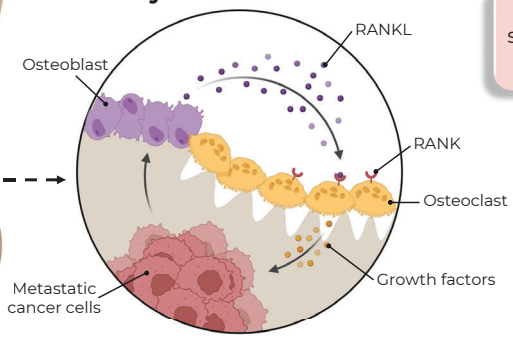

Cancer cells induce **osteoblasts** to secrete receptor activator of nuclear factor kappa B ligand (**RANKL**)[1]

RANKL binds to **RANK** in **osteoclasts** and increases **proliferation**[1]

Osteoclasts promote **resorption** and secrete **growth factors**[1]

B. Proposal

Develop **bone-seeking peptides** that **disrupt** the **RANK/TRAF6** axis and thus **hinder osteoclastogenesis** and **metastatic potential**

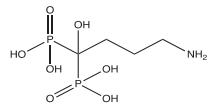

Bone-targeting unit → A bisphosphonate (**alendronate**) with high affinity for **bone mineral**[2]

\+ **Fragment A** — Cathepsin K-sensitive linkers → **Cathepsin K** is an abundant **protease** in the **bone microenvironment**[3]

\+ **Fragment B** — Cell-penetrating peptides (CPPs) → **Peptide sequences** able to promote **cell entry** of different cargos[4]

\+ **Fragment C** — RANK-derived sequences → **Bind** to tumor necrosis factor receptor associated factor 6 (**TRAF6**)[5]

C. Approach and Results

Selected sequences

Linker1	GGPNle	CPP1	AAVALLPAVLLALLAP	RANK-derived sequences: RQMPTEDEY, RQMATADEA, RKIPTEDEY, RKIATADEA
Linker2	PR	CPP2	KLFMALVAFLRFLT	
Linker3	GPR			

PEG – Polyethylene glycol **Ahx** – 6-aminohexanoic acid

Constructed peptides

PepA	PEG2-Linker1-Ahx-CPP1-NH2	PepF	PEG2-Linker3-Ahx-CPP2-NH2
PepB	PEG2-Linker2-Ahx-CPP1-NH2	3A	CPP2-RQMPTEDEY
PepC	PEG2-Linker3-Ahx-CPP1-NH2	3B	CPP2-RQMATADEA
PepD	PEG2-Linker1-Ahx-CPP2-NH2	5A	CPP1-RKIPTEDEY
PepE	PEG2-Linker2-Ahx-CPP2-NH2	5B	CPP1-RKIATADEA

Circular Dichroism

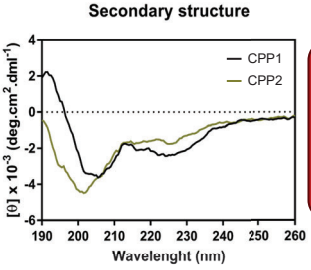

The **secondary structure** of these peptides is mainly **α-helix**

Cell Internalization

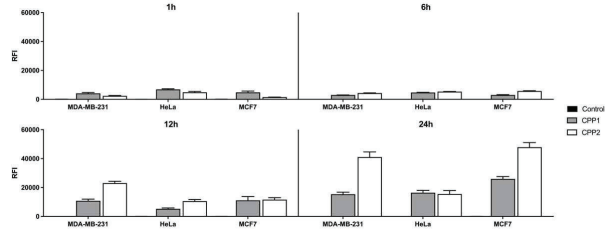

Flow cytometry

Higher internalization was observed for **CPP2** over 24 hours in **MDA-MB-231** and **MCF7** cells

Confocal microscopy

Higher internalization was observed for **CPP1**, when in comparison with **CPP2** in **MDA-MB-231** cells

CPP1 – MDA-MB-231 cells | CPP2 – MDA-MB-231 cells

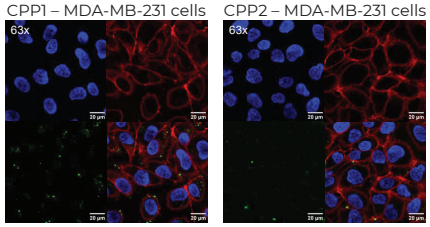

Cathepsin K Assay

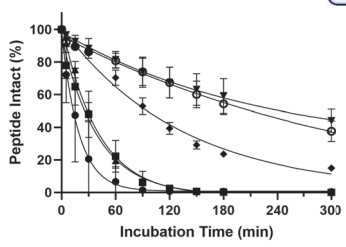

Enzymatic cleavage

Cleavage was confirmed by electrospray ionization mass spectrometry

Cleavage kinetics strongly depends on the CPP sequence and less on the linker type

Peptides **A, B and C** exhibit a **more favorable kinetic** when compared with peptides **D, E and F**

Cell Viability

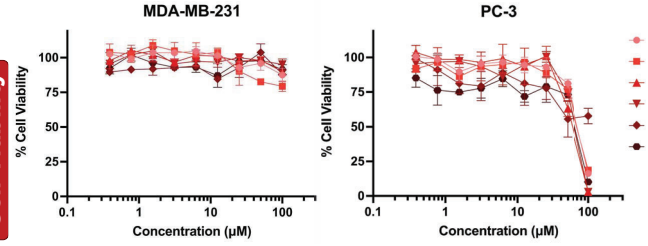

Peptide	IC50 (μM) 24 h MDA-MB-231	PC-3
3A	>100	69.08±2.82
3B	>100	67.67±3.37
5A	>100	54.64±2.30
5B	>100	58.52±3.56
CPP1	>100	>100
CPP2	>100	61.64±30.73

Peptides **5A** and **5B** exhibit the **highest cytotoxicity** towards **PC-3** cells

D. Conclusions

- **PepA**, which combines **CPP1** and **Linker1**, exhibits the most favorable kinetic profile in terms of enzymatic cleavage, and will be used for assembling novel bone-seeking peptides that interfere with the RANK/TRAF6 interface.
- Peptides that combine **CPPs** with **TRAF6-binding sequences** are cytotoxic towards TRAF6-expressing prostate cancer cells.

REFERENCES

1. Zhang, Y. *et al.* Front. Endocrinol. 13: 1063815 (2022).
2. Dionísio, M. R. *et al.* Brit J Clin Pharm. 85.6: 1114-1124 (2019).
3. Qian, D. *et al.* Curr. Oncol. 29.8: 5963-5987 (2022).
4. Zorko, M. *et al.* Adv. Drug Deliv. Rev. 180: 114044 (2022).
5. Park, J. H. *et al.* Mol. Cells. 40.10: 706-713 (2017).

ACKNOWLEDGEMENTS

This work was supported by FCT through PTDC/QUI-OUT/3854/2021, UI/BD/154474/2022 and UID/Multi/04349/2020.

Targeting MRGPRX2 with venom peptide P17: A therapeutic avenue for DSS-Induced colitis

Karthi Duraisamy,[1,2] Mukesh Kumar,[1] Abdullah Nawabjan,[1] Emily Kwun Kwan Lo,[1] Benjamin Lefranc,[2] Elsa Bonnafé,[3] Michel Treilhou,[3] Hani El-Nezami,[1,4] Billy K.C. Chow, *[1] Jérôme Leprince.*[2]

[1]*School of Biological Sciences, The University of Hong Kong, Hong Kong, China;* [2]*INSERM U1239 NorDiC, PRIMACEN, Université Rouen Normandie, Rouen, France;* [3]*EA7417 BTSB, Université Fédérale Toulouse Midi-Pyrénées, INU Champollion, Albi, France;* [4]*Institute of Public Health and Clinical Nutrition, University of Eastern Finland, Kuopio, Finland.*

Karthi.duraisamy@univ-Rouen.fr

https://doi.org/10.17952/37EPS.2024.P2154

Introduction

Inflammatory Bowel Disease

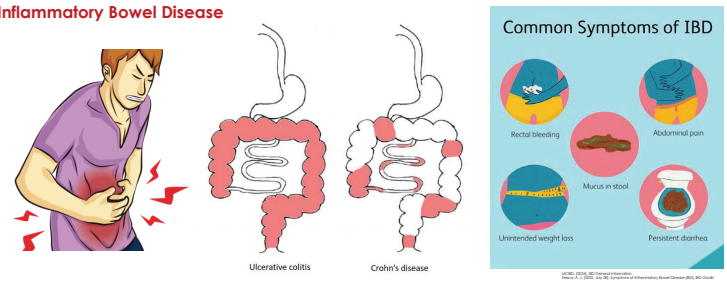

Peptide P17

Novel Anti Microbial Peptide (AMP) from the venom of *Tetramorium bicarinatum*

LFKEILEKIKAKL-NH2

Known to activate an unknown GPCR



Results & discussion

Identification of P17 receptor

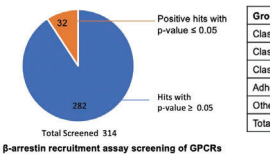

β-arrestin recruitment assay screening of GPCRs

Group	GPCRs
Class A	262
Class B	16
Class C	17
Adhesion	17
Other	2
Total	314

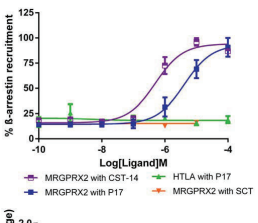

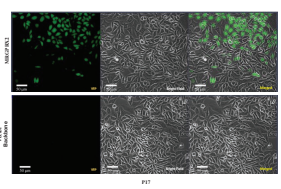



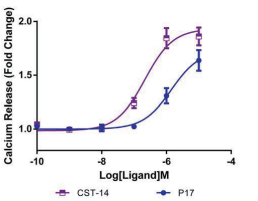

Structure-Activity Relationship of P17 and MRGPRX2 Activation

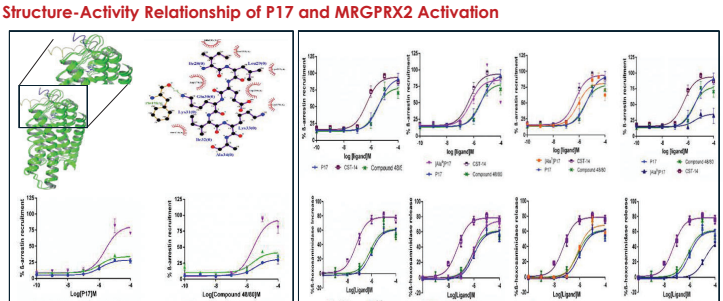

MRGPRX2 Activation in Mast Cells Promotes Monocyte Recruitment and Differentiation

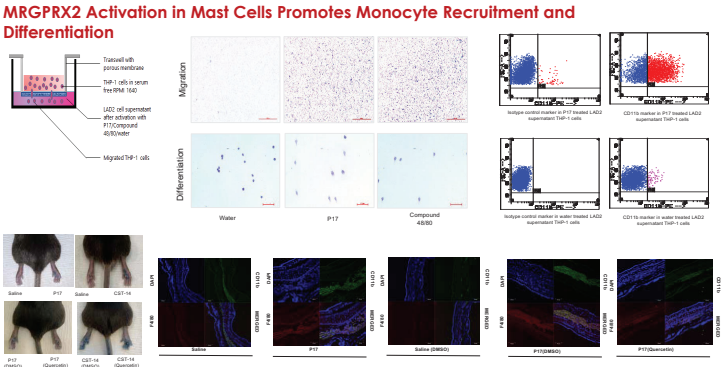

Acknowledgements & affiliations

The WINNINGNormandy Marie Skłodowska-Curie Fellowship Programme

Recipient of the WINNINGNormandy Program supported by the Normandy Region

MRGPRX2/B2 deficiency exacerbates colitis in DSS mouse model

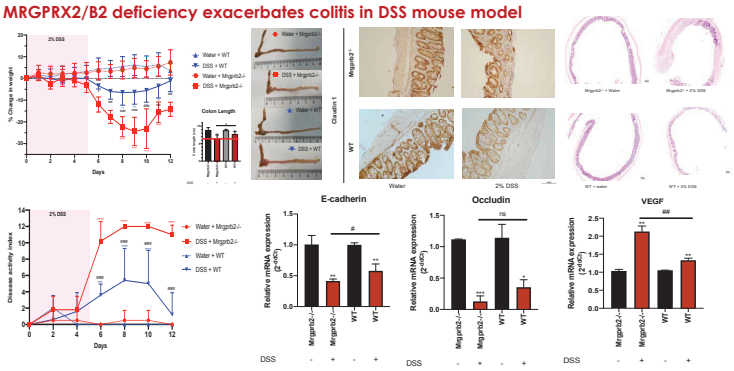

MRGPRB2 ameliorates severity of colitis in DSS mouse model

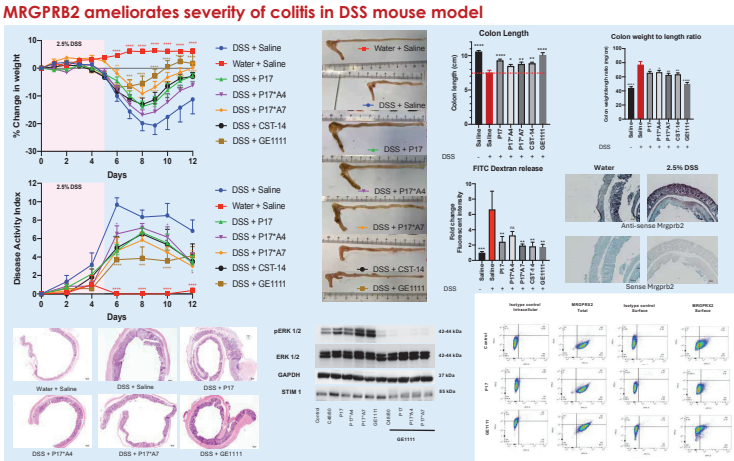

MRGPRB2 ligands reduce inflammatory cytokines and immune cell infiltration in DSS-Induced Colitis mice model

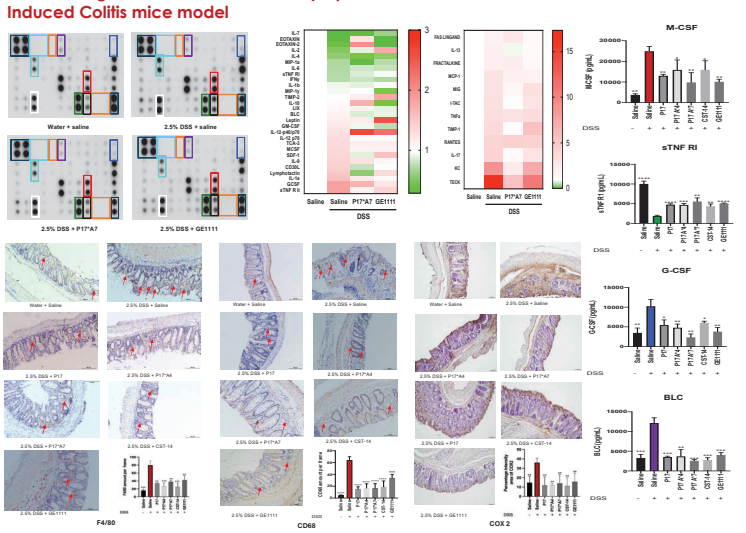

Conclusion & future prospective

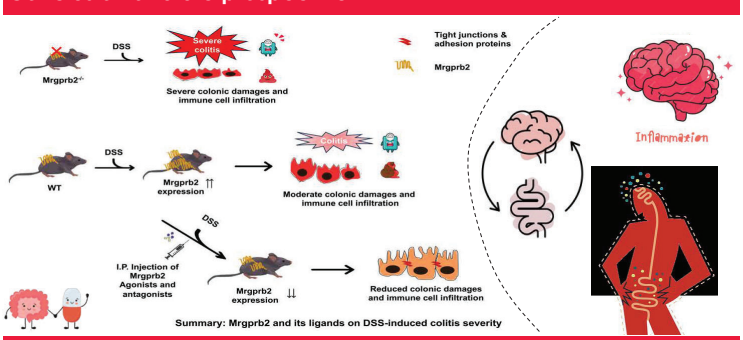

References

1. Duraisamy, K., Singh, K., Kumar, M., Lefranc, B., Bonnafé, E., Treilhou, M., ... & Chow, B. K. (2022). P17 induces chemotaxis and differentiation of monocytes via MRGPRX2-mediated mast cell–line activation. *Journal of Allergy and Clinical Immunology*, *149*(1), 275-291.
2. Duraisamy, K., Kumar, M., Nawabjan, A., Lo, E. K. K., Hui Un, M., Lefranc, B., ... & Chow, B. K. (2024). MRGPRB2/X2 and the analogous effects of its agonist and antagonist in DSS-induced colitis in mice. *Biomedicine & Pharmacotherapy*, *174*, 116471.
3. Kumar, M., Duraisamy, K., Annapureddy, R. R., Chan, C. B., & Chow, B. K. (2023). Novel small molecule MRGPRX2 antagonists inhibit a murine model of allergic reaction. *Journal of Allergy and Clinical Immunology*, *151*(4), 1110-1122.
4. do Nascimento, R. D. P., da Fonseca Machado, A. P., Gálvez, J., Cazarin, C. B. B., & Júnior, M. R. M. (2020). Ulcerative colitis: Gut microbiota, immunopathogenesis and application of natural products in animal models. *Life sciences*, *258*, 118129.
5. Lakhan, S. E., & Kirchgessner, A. (2010). Neuroinflammation in inflammatory bowel disease. *Journal of neuroinflammation*, *7*, 1-12.
6. Talley, S., Vallaguga, R., Anderson, L., Cannon, A. R., Choudhry, M. A., & Campbell, E. M. (2021). DSS-induced inflammation in the colon drives a proinflammatory signature in the brain that is ameliorated by prophylactic treatment with the S100A9 inhibitor paquinimod. *Journal of Neuroinflammation*, *18*, 1-14.
7. Bernuzzo, K., Authier, H., Prat, M., Alsdadine, M., Lefèvre, L., Rizhabi, M. C., ... & Coste, A. (2017). P17, an original host defense peptide from ant venom, promotes antifungal activities of macrophages through the induction of C-type lectin receptors dependent on LTB4-mediated PPARγ activation. *Frontiers in immunology*, *8*, 1650.

https://doi.org/10.17952/37EPS.2024.P2158

FIGHT-TB: DESIGN OF NOVEL VACCINE ANTIGENS TO FIGHT TUBERCULOSIS

Marina Sala[1], Giovanni Barra[2], Maria Carmina Scala[1], Pietro Campiglia[1], Rita Berisio[2] and Alessia Ruggiero[2]

[1]Department of Pharmacy, University of Salerno, Fisciano (SA), Italy

[2]Institute of Biostructures and Bioimaging, IBB, CNR, Napoli, Italyl

INTRODUCTION

Tuberculosis (TB) is the leading cause of death worldwide due to an infectious disease, causing around 1.6 million deaths each year (Fihure 1). This situation has become more complicated by the emergence of drug-resistant M. tuberculosis (Mtb) and HIV-TB co-infection, which has significantly worsened TB prognosis and treatment. Vaccination has been considered the best approach to reduce the TB burden. Since 1923, the Bacillus Calmette–Guérin (BCG) vaccine, an attenuated form of Mycobacterium bovis, remains the only licensed vaccine; Its efficacy against severe and extrapulmonary forms of paediatric TB is well recognized, but highly variable and poor protection at all ages against pulmonary TB remains a major concern [1]. Therefore, a safer and more effective vaccine to replace BCG or BCG-prime boosting is urgently required.

Following the establishment of primary infection, infected dendritic cells (DCs) and recruited monocytes transport Mtb to draining lymph nodes, which initiate T-cell priming and acquired immunity. T lymphocytes, in particular CD4+ T helper 1 (TH1) lymphocytes, and IFN-γ produced by these cells are necessary to control Mtb. Mtb infection elicits both effector and memory T cells. TB vaccine research has focused largely on identifying strong IFN-γ/TH1-inducing vaccine candidates for several years. Likewise, polyfunctional T cells that co-express multiple TH1 cytokines (TNF-α, IL-6, and IL-12) have been considered qualitatively superior to T cells expressing a single cytokine and are being investigated with much interest in ongoing vaccine trials. Although strong T-cell-stimulating antigens induce robust protective immunity in mice, these antigens cannot induce complete sterilizing immunity . It has been suggested that Mtb subverts CD4 T-cell dependent immunity by delaying initiation of T-cell responses via modulation of DC functions and survives in a dormant form [2,3].

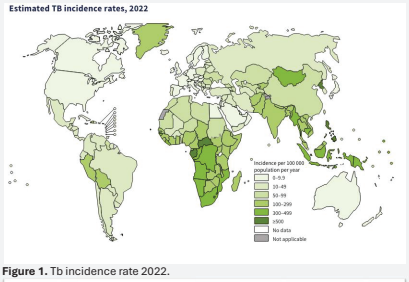

Figure 1. Tb incidence rate 2022.

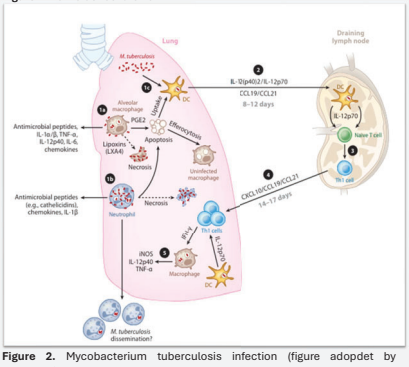

Figure 2. Mycobacterium tuberculosis infection (figure adopdet by https://doi.org/10.1038/nrdp.2016.76)

Therefore, early activation and migration of DCs to draining lymph nodes together with stimulation of T cells are key factors for inducing effective and durable protection against Mtb infection. These observations suggest that a mycobacterial antigen that elicits effective host protective immunity via DC activation is a promising target for development of a TB vaccine [3].

METHODS

The main purpose of FIGHT_TB project is to use structural vaccinology (SV) as a rational tool to improve immunogenic properties of some Mtb antigenic proteins (table 1) either to replace or boost BCG vaccine.
Structural vaccinology or structure-based antigen design is a rational approach that uses three-dimensional structural information to design novel and enhanced vaccine antigens.

The typical SV approach (Figure 3), involves the determination of the three-dimensional structure of the antigen or antigen–antibody complex using structural biology tools. This is achieved by combining the benefits of RV, with advancements in X-ray crystallography, NMR spectroscopy and single particle Cryo-Electron Microscopy, and novel computational approaches [4, 5].

Structural vaccinology offers a tangible tool to antigen improvement and the development of multi epitope vaccines. So FIGHT_TB combines different methodologies, like molecular and structural biology and chemical synthesis, with computational and experimental tools aimed at epitope identification.

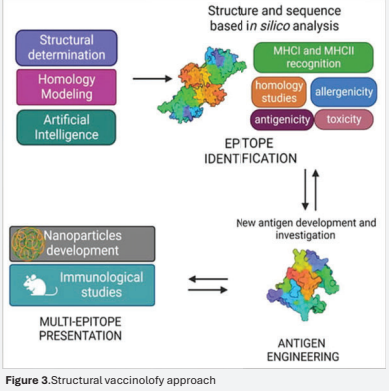

Figure 3.Structural vaccinolofy approach

OBJECTS of the research

We will focus on four proteins [6,7] that shown a promising vaccine potential and constitute valid starting points for antigen improvement (Table 1) .

Mtb protein	Putative function/annotation	Immunogenic function	Structural information
Rv2299c	Mycobacterial Chaperone **HtpG**	DC maturation Boosting BCG when fused with ESAT6	No structure available
Rv2450c	Cell Wall hydrolase/Virulence Factor **RpfE**	DC maturation	4CGE The recombinant Rv3463 is folded and Stable.
Rv1009	Cell Wall hydrolase/Virulence Factor **RpfB**	DC maturation	4KL7, 4KPM, 4EMN, 3EO5, 5E27
Rv3463	Putative oxidoreductase	Macrophage-activator Bactericidal activity	No structure available

Table 1. Protein antigens involved in this project

Production of the rationally designed antigen: Peptide synthesis

We used computational approaches to identify the most immunogenic region of Rv3463, we identified the fragment **Rv3463 68-96** able to intercat with HLA.
Mimicking natural antigens through peptides which mimic their epitope region is a promising strategy, named as (mimotope)-based, for vaccine development. In order to identify the epitope of the fragment , we synthesized a library of overlapping peptides (figure 5), with specific length and specific offset covering the entire fragment.



Figure 5 . Overlapping peptide library

Peptides synthesis was performed according to the solid phase approach using standard Fmoc methodology by CEM liberty blue 2.0 automated microwave synthesizer. The peptides purification was achieved using a preparative RP-HPLC C-18 bonded silica column. The purified peptides were 98% pure as determined by analytical RP-HPLC and molecular weights were confirmed by ESI-MS.

RESULTS

To date we focused our attention on **Rv2299c**, a mycobacterial chaperone named also HtpG. its activity depends on its nucleotide-binding state, we planned to solve the structure of HtpG, still unavailable, in its different nucleotide-binding states. To reach this goal, we performed a biophysical characterization and crystallisation trials by using a high-throughput crystallisation facility available at CNR [6]. Structural characterisation is still in progress (Scheme 1).

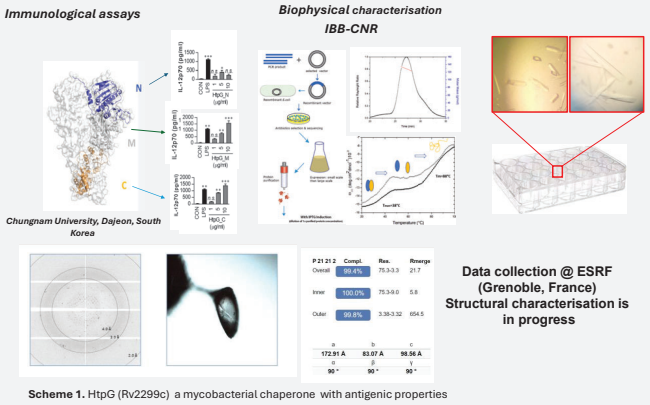

Scheme 1. HtpG (Rv2299c) a mycobacterial chaperone with antigenic properties

Then we studied **Rv3463** , a novel macrophage-activating protein recently identified from a multidimensional fraction of Mtb culture filtrate. It is a TB conserved protein (a putative flavin dependent oxidoreductase) with macrophage activating properties and bactericidal activity. Rv3463 mainly interact with TLR4 while only slightly interacting with TLR2 [7]. These results suggest that Rv3463 induces macrophage activation through the TLR2 and TLR4 pathways.

In this framework, an ongoing study is aimed at the functional and structural characterization of Rv3463 (Figure 4).

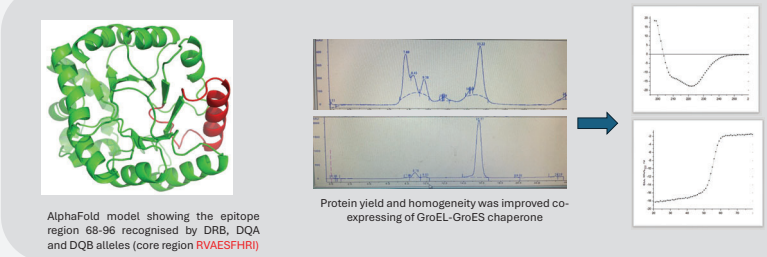

AlphaFold model showing the epitope region 68-96 recognised by DRB, DQA and DQB alleles (core region RVAESFHRI)

Protein yield and homogeneity was improved co-expressing of GroEL-GroES chaperone

Figure 4 . IBB-CNR/UNISA → Recombinant protein expression and its biophysical characterisation

CONCLUSION

Aims to improve the immunogenic properties of the investigated proteins using a structuralvaccinology approach. Structural vaccinology combines information from immunology with the benefits of the structural biology.
Indeed, structural data are used to determine the epitope region of each antigenic protein, either through structure-based prediction or through experimental epitope identification. This information is key to the re-design of vaccine antigens for a selectively enhancement of antigenic properties, using several strategies like (i) conjugation of antigens stimulating different immunomodulatory roots and (ii) multi-epitope presentation, a strategy that typically enhances the immune response, (iii) design of cross-reactive antigens, able to act on more bacterial species.

REFERENCES
[1] Mangtani, P. et al, Clin. Infect. Dis. Off. Publ. Infect. Dis. Soc. Am, 2014.
[2]O'Garra, A et al, Annu. Rev. Immunol., 2013
[3]Griffiths, K. L. et al, Nat. Commun. 2016
[4]Ruggiero A et al, Front. Mol. Biosci. 2022
[5]Berisio R et ak, Biomolecules 2024
[6]Choi HG et al, Oncotarget 2017
[7]Park FS et al, SciREP 2019
[8]Sala, M. et al. Front. Microbiol, 2016

msala@unisa.it

https://doi.org/10.17952/37EPS.2024.P2161

Advances on the green synthesis of Etelcalcetide

[1]Koula Achilleos, [2]Andreas Sergides, [1]Styliana Mirallai, [2]Charalambos Ioannou, [3]Vicky Nicolaidou, [1]Christos Petrou, [2]Christakis Sergides, [1]Yiannis Sarigiannis

[1] Department of Health Sciences, School of Life & Health Sciences, University of Nicosia, Nicosia, Cyprus
[2] Biogena API LTD, Limassol, Cyprus
[3] Department of Life Sciences, School of Life & Health Sciences, University of Nicosia, Nicosia, Cyprus

Introduction

Background

Treatment of Secondary Hyperparathyroidism (SHPT) includes Etelcalcetide (ETC), a calcium-sensing receptor (CaSR) agonist, which reduces the levels of Parathyroid Hormone (PTH) levels in serum leading to increased bone mass. However, the effects of combined treatment with osteoporosis drugs such as teriparatide (TPTD) remain unclear. Meanwhile ETC is under investigation for the treatment of other rare diseases caused from abnormal calcium sensing and signaling like autosomal dominant hypocalcemia (ADH) or Bartter-syndrome type V.

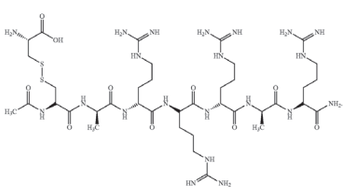

Objective

Etelcalcetide is a linear octapeptide with a disulfide bridge consisting of seven D-amino acids, four of them are D-Arginine, while at the N terminal site there is a D-Cysteine which forms a disulfide bridge with an L-Cysteine. It is really a synthetic challenge because of the three arginine in a row. Arginine is a sensitive amino acid which produces epimerization or other side reactions. This demands special treatment during synthesis and particular purifications steps as reported in most of the patents. The new EU regulations restrict the use of DMF (Dec 2023), a commonly used solvent in SPPS for manufacturing of peptides. This green wind of change presents challenges and opportunities for peptide manufactures. Solvents which is among the crucial parameters are especially considered as they may affect the total process. Here, we present some of our efforts for the synthesis of etelcalcetide in a greener way.

Materials - Methods

Our plan was to use ChemMatrix ® resin which is an established PEG type resin and exhibits great performance especially in high temperatures and stability under Microwave irradiation. However, this resin became recently unavailable for industrial scale. So, it was decided to work with other resins currently available in the market in bulk quantities making the future transfer from lab to industrial scale easier. In short and ultra short peptides like Etelcalcetide in industrial scale resins should have high loading capacity or else the peptide should be synthesized in liquid phase. We tried several combinations of resins (Polystyrene or PEG type or Hybrids) and green solvents and Fmoc-deprotection solutions. For the protection of Cysteine side group Trt or Mmt protecting group was selected. Depending on the side group selection of Cysteine, different way of disulfide bridge formation was selected. Here we present some of our findings elaborating with the following solid supports: Rink Amide Protide ®, PL-Rink Amide (Fmoc-Rink Amide AMS), Rink Amide MBHA, and PL Rink Amide. All couplings for Arg and Cys had been performed at temp 40-45 min while Fmoc deprotections occurred in similar conditions. The peptides were cleaved from the resin with TFA:TIS:H_2O (92:4:4, v/v).

Results

Swelling test

Swelling of the resin is crucial for the success of a synthesis in Solid Phase Peptide Synthesis as it permits the molecules to come closer and easily react. In the following figures we present an example of the swelling tests. **A remarkable notice is that the green solvents swell better PEG Type resins than PS type resins like the Amphispheres 20 RAM (PS PEG600 Fmoc-Rink Amide).**

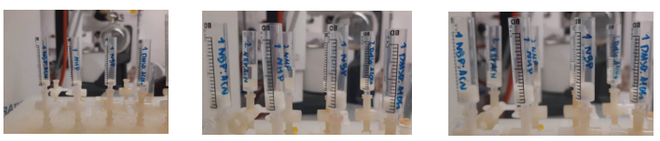

Fig 1. Swelling test for 50mg resin Amphispheres 20 RAM (loading 0.6mmoL/g) and 1 mL of solvent for 15min and 30min

Table 1 (left) presents the combinations of Rink Amide MBHA resin and solvents systems for the synthesis of Etelcalcetide as well as occurred problems during synthesis while **Table 2** (right) presents combinations of PEG Type resins as well as problems occurred during synthesis.

Resins	Coupling conditions	Solvent Systems	Deprotection Conditions	Results
Rink Amide MBHA resin (200-400 mesh)	Fmoc-D-Arg (Pbf)-OH: Coupling: 1 min 40°C, 4 min 45°C	DMSO: EtOAc (1:9)	5% piperazine + 2% DBU in NMP	Arg and Cys needed recouplings
Rink Amide MBHA resin (200-400 mesh)	Fmoc-D-Arg (Pbf)-OH: Coupling: 1 min 40°C, 4 min 45°C	DMSO: EtOAc (1:9)	5% piperazine + 2% DBU in NMP	*Increase of coupling time resolve the previous problem*
Rink Amide MBHA resin (200-400 mesh)	Fmoc-D-Arg (Pbf)-OH: Coupling: 1 min 40°C, 4 min 45°C	NBP	5% piperazine + 2% DBU in NMP	The 3rd Arg need recoupling. *Elongation of the coupling time resolve the problem*
Rink Amide MBHA resin (200-400 mesh)	Fmoc-D-Arg (Pbf)-OH Coupling: 3 min 40°C, 7 min 45 °C	NBP: ACN (5:5)	5% piperazine + 2% DBU in NMP	After 3rd arginine each AA needed recoupling
Rink Amide MBHA resin (200-400 mesh)	Fmoc-D-Arg (Pbf)-OH Coupling: 3 min 40°C, 7 min 45 °C	NMP	5% piperazine + 2% DBU in NMP	Each Arginine demands recoupling

Resins	Coupling conditions	Solvent Systems	Deprotection Conditions	Results
PL-Rink: Fmoc Rink amide AMS resin	Fmoc-D-Arg (Pbf)-OH: Coupling: 3 min 40°C, 7 min 45°C	NBP: ACN (5:5)	5% piperazine + 2% DBU in NMP	**No need for any recoupling**
PL-Rink: Fmoc Rink amide AMS resin	Fmoc-D-Arg (Pbf)-OH: Coupling: 3 min 40°C, 7 min 45°C	NMP	5% piperazine + 2% DBU in NMP	*Repeat couplings*
Rink Amide Protide Resin	Fmoc-D-Arg (Pbf)-OH: Coupling: 3 min 40°C, 7 min 45°C	NBP: ACN (5:5)	5% piperazine + 2% DBU in NMP	**No need for any recoupling**
PS PEG600 Fmoc Rink amide	Fmoc-D-Arg (Pbf)-OH Coupling: 3 min 40°C, 7 min 45 °C	NBP: ACN (5:5)	5% piperazine + 2% DBU in NMP	**No need for recoupling**
Rink Amide Protide Resin	Fmoc-D-Arg (Pbf)-OH Coupling: 1 min 40°C, 5 min 45 °C	NBP: ACN (5:5)	5% piperazine + 2% DBU in NMP	**No need for recoupling**

Under these conditions we didn't manage to obtain products of the heptapeptide without epimerization. Another issue is the high polarity of the acetyl heptapeptide which is responsible for the early elution of the peptide (~ 2 min). This demands other analytical approach which is under investigation.

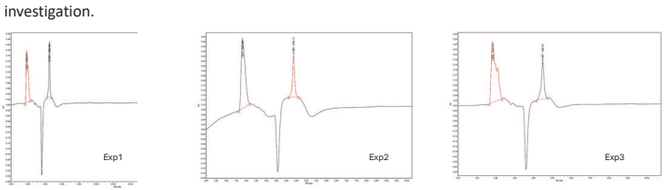

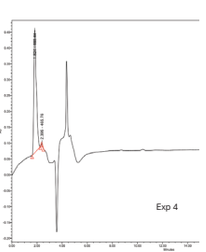

It is obvious how the resin selection and the rest conditions affect the synthesis of the linear heptapeptide. **Figure 3** presents the synthesis of heptapeptide with Rink Amide MBHA (200-400 mesh) and using NMP as solvent. **On the opposite PL Rink Amide resin either with NMP or NBP-ACN reduces the epimerization of the heptapeptide. Moreover, Rink Amide Protide also displays high epimerization level under these conditions. We have some preliminary results of other conditions at higher temperatures limiting the epimerization. Soon we are going to present them.**

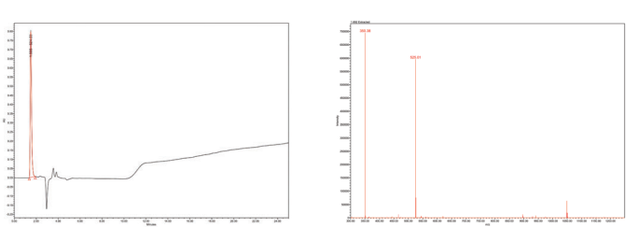

LC-MS of isolated Etelcalcetide

LC-PDA-MS analysis was performed using a Luna 5um C18 100 A (150 x 3 mm, 5um) column and eluents A: H_2O 0.1FA% v/v, B: MeCN 0.1FA % v/v (5% B to 65% B in 25min);
Detection at 220 nm. $[M+H]^{+}$: 1047.53, $[M+2H]^{2+}$: 525.01, $[M+3H]^{3+}$: 350.38

Acknowledgements
The Project "Development and Scale-Up Manufacturing of Therapeutic Peptides (CYTIDES) is funded by the European Union – Next GenerationEU, through the call of Research and Innovation Foundation CODEVELOP-ICT-HEALTH/0322/0038
Also we thank Agilent and especially Janice Qian Li, Products and Applications Manager for providing some of the used solid supports.

Determination of the Oligomerization States of the Transmembrane Domains from SARS-CoV-2 Membrane Proteins

Tyler G. Hobart, Andrew M. Rehak, and Timothy M. Reichart

Department of Chemistry, Hampden-Sydney College, Hampden-Sydney, VA

https://doi.org/10.17952/37EPS.2024.P2163

Abstract

SARS-CoV-2 is the third highly infectious, highly deadly coronavirus to make the jump to humans in the last two decades. SARS-CoV-2, like other coronaviruses, is an enveloped virus with a small number of integral membrane proteins embedded in a lipid membrane. Each of these proteins has a transmembrane (TM) domain, a portion of the protein approximately 20 amino acids in length. Several proteins, including the Spike protein, are functional proteins only when trimeric–that is, three copies of the protein must self-assemble in order to carry out their function. Six proteins present in SARS-CoV-2 are known or hypothesized to have TM domains. These TM domains are highly conserved, and they are an underexplored region for potential drug discovery.

To examine the oligomerization state, three versions of each peptide of several of the TM proteins have been synthesized. One has a nitrobenzodiazole (NBD) fluorophore active in membranes, one has tetramethylrhodamine (TAMRA), a quencher of NBD, and one is unlabeled. These peptides are dissolved in a detergent above its CMC, which presents the peptides in micelles previously shown to be accurate mimics of membranes for the analysis of oligomerization states of TM domains. The three variants are used in a fluorescence-based assay which monitors the change in fluorescence as a function of added quencher peptide. The shape of the resulting fluorescence curve describes the oligomerization state. We describe the results of this experiment for two TM proteins, ORF 7a and ORF 3a.

Membrane Proteins in SARS-CoV-2

Protein	Function(s)	TM Domain Sequences	Literature Oligomerization State of Full Protein
Spike	Cell entry	1	Trimer
Envelope	Viral assembly, budding	1	Pentamer
Membrane	Viral assembly	3	Dimer
ORF 3a	Ion channel	3	Dimer or tetramer
ORF 7a	Immunomodulation, possibly structural	1	Monomer
ORF 7b	Structural	1	Dimer or tetramer

TM Domains Are Highly Conserved



A LogoPlot of the TM domain of the Spike protein of all β-coronaviruses ever sequenced from human hosts.

Peptides Synthesized

ORF 3a helix 1	IPIQASLPFGWLIVGVALLAV-KKKK
ORF 7a	LYSPIFLIVAAIVFITLCFTL-KKKK

- C-terminal lysines added for solubility and handling
- Synthesized by undergraduates using manual Fmoc SPPS
- Synthesized 3 variants of each: NBD-labeled, TAMRA labeled, and unlabeled
- Purified by HPLC and analyzed by LCMS

Determining the Peptide Oligomerization State

- Peptide dissolved in C14 betaine previously showed to be a good mimic for membrane bilayers in analyzing TM peptide biophysics
- Constant concentration of peptide and of NBD
- Titrate in solution of NBD/TAMRA labeled
- Shape of curves yields oligomerization state

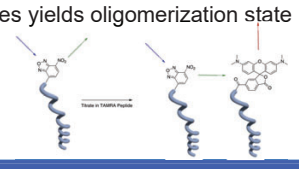

ORF3a Data Fits Trimer

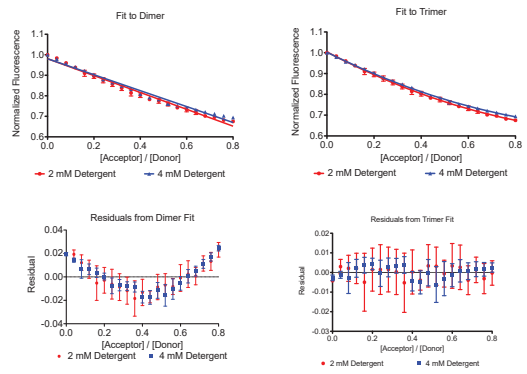

ORF7a Data Fits Dimer

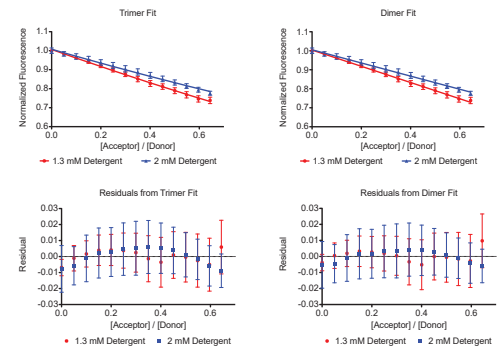

Conclusions

- Undergraduates successfully synthesized and purified 25 amino-acid peptides
- Used fluorescence-based assay to determine peptide oligomerization state in a model membrane
- ORF3a TM domain a trimer
- ORF7a TM domain a dimer

Future Directions

- Synthesize other TM domains and determine their oligomerization states
- Analyze intermolecular determinants of oligomerization
- Use variant of fluorescence assay to determine intermolecular TM domain interactions

Acknowledgments

This research was supported by the VFIC Mednick Fellowship and the Hampden-Sydney Summer Research Program.

References

DeGrado, W. F.; Nanda, V.; Lear, J. D.; and Tatko, C. D. Polar Networks Control Oligomeric Assembly in Membranes. *Journal of the American Chemical Society* **2006**, *128* (13), 4170–4171.

Narayanan, K.; Huang, C.; and Makino, S. SARS Coronavirus Accessory Proteins. *Virus Research* **2007**, *133* (1), 113–121.

Redondo, N.; Zaldívar-López, S.; Garrido, J. J.; and Montoya, M. SARS-COV-2 Accessory Proteins in Viral Pathogenesis: Knowns and Unknowns. *Frontiers in Immunology* **2021**, *12*.

Reichart, T.; Leaman, D.; Sands, D.; Zwick, M.; Dawson, P. The Conserved Positive Charge in the Transmembrane Domain of HIV GP41 Contributes to Its Intrinsic Preference for Trimerization. **2020**.

Yan, W.; Zheng, Y.; Zeng, X.; He, B.; and Cheng, W. Structural Biology of SARS-CoV-2: open the door for novel therapies. *Signal Transduction and Targeted Therapy* **2022**, 26.

37th European Peptide Symposium, 14th International Peptide Symposium, 25th-29th August 2024, Florence, Italy
https://doi.org/10.17952/37EPS.2024.P2164

Exploiting the features of short peptides to recognize specific cell surface markers

Michela Buonocore[1,2], Angelo Santoro[3], Enza Napolitano[3], Elena Ciaglia[4], Francesco Montella[4], Francesca Boccafoschi[5], Valeria Perugini[6], Matteo Santin[6], Anna Maria D'Ursi[3]

[1]Department of Chemical Sciences, University of Naples Federico II, Naples, Italy, [2]Research Centre on Bioactive Peptides (CIRPeB), University of Naples Federico II, Naples, Italy, [3]Department of Pharmacy, University of Salerno, Fisciano, Italy, [4]Department of Medicine, Surgery and Dentistry "Scuola Medica Salernitana", University of Salerno, Baronissi, Italy, [5]Department of Health Sciences, University of Piemonte Orientale, 28100, Novara, Italy, [6]Centre for Regenerative Medicine and Devices, School of Applied Sciences, University of Brighton, Brighton, UK

Introduction

Stem cells have an unlimited potential for cell division and the ability to transdifferentiate into other cell types. In recent years they grew to be a first-line weapon of regenerative medicine for repairing tissue and organic abnormalities caused by diseases, congenital deficiencies, and age-related effects[1]. Bone marrow-derived mesenchymal stem cells (MSCs) mainly develop in adipocytes, chondroblasts, and osteoblasts but also show the property to successfully transdifferentiate in neural, myocyte, and epidermal cells when engrafted in endogenous tissues under specific conditions[2]. Efficient isolation of MSCs from other cell components in the bone marrow is fundamental to obtaining valuable MSC clinical applications. Currently, the most widespread purification methods include the isolation of MSCs based on the expression of precise surface markers, thus involving specific antibodies[3]. In this work, we aimed to develop a fast and affordable method for the phenotypic characterization and isolation of MSCs from bone marrow without using immunoglobulins. To this purpose, we designed short peptides based on the deposited 3D structures of two specific MSCs surface markers, CD44 and CD271, in complex with their natural ligands. The peptides were selected by computational modeling, synthesized by solid-phase peptide synthesis, and tested in cell assays. Interestingly the data show that starting from a small set of peptides, using a protocol based on molecular simulations, it is possible to obtain small ligands endowed with a significant specificity in targeting CD44 and CD271 in place of their antibody, bypassing the common challenges and issues due to the use of immunoglobulins.

Results

Computational modelling

CD44

PDB ID: 4MRD
Residues: 23-173
Organism: Mus musculus
Ligand: Hyaluronic acid (HA) (in blue)

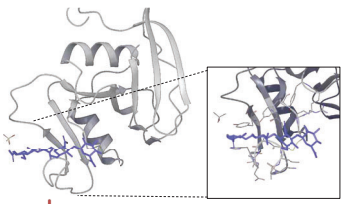

Residues involved in binding with HA:
R45 Y46 C81 R82 Y83 I92 N98 A99 I100 C101 A102 A103 N104 H105 Y109

Grid box built on these residues

Screening of 250 random peptide sequences

CFNAS
QDWTQ
DTYCF
AGVF
SHYPH
PNHSE
QSFST

Polar uncharged amino acids
Hydrophobic amino acids
Positively charged amino acids
Negatively charged amino acids
Special amino acids

Redocking

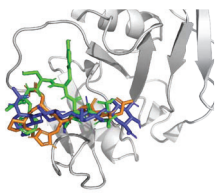

HA
DTYCF
PNHSE

Ligand	HA	DTYCF	PNHSE
Docking score (kJ/mol)	-10.3	-9.6	-8.6

CD271

PDB ID: 3IJ2
Residues: 30-190
Organism: Rattus norvegicus
Ligand: Neurotrophin 3 (Neu3) (in blue)

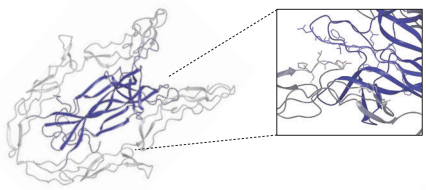

Residues involved in binding with Neu3:
P67 C68 L69 D70 N71 M96 P99

Grid box built on these residues

Peptide sequences selected from Neu3 residues interacting with CD271.

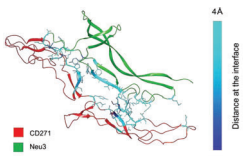

VFQYFF
RGEFSVCD
DGKQAAWRF
NSPVKQYF
KSHRGEY
KEARPVK
HMGEF
DSVSVW
SVFRQYFF
RGIDSKHW
QAAWRF

NSPVKQYF
VFQYFF

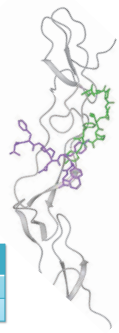

Ligand	Score (kJ/mol)	Poses with RMSD < 6 (out of 100)
VFQYFF	-7.3	18
NSPVKQYF	-8.1	6

Solid Phase Peptide Synthesis

DTYCF, PNHSE, NSPVKQYF and VFQYFF were synthesized by classical Merrifield SPPS[4] using the N-α-fluorenylmethoxycarbonyl-protected amino acids and a Rink-amide resin as a solid support.
In order to detect these peptides for FACS assays, the same sequences were synthesized, attaching as the last residue in the C->N peptide synthesis a fluorophore tag; we used the 7-nitrobenz-2-oxa-1,3-diazol-4-yl (NBD) conjugated to the 2,3-Diaminopropionic acid (Dap). NBD excitation is at 480 nm and the emission is at 540 nm.

Cell assays

CD44

FACS

hBM-MSC CD44^{bright} (> 96%)

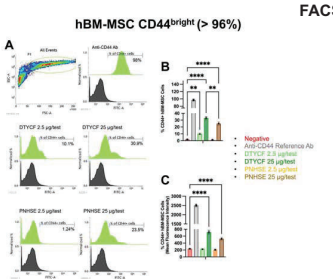

MEG-01 CD44^{dim} (< 57%)

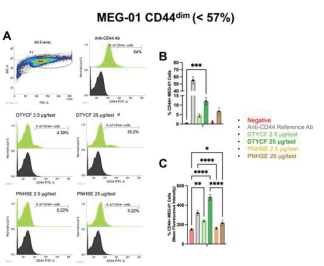

Cytofluorometric analysis of h-BM-MSC CD44^{bright} and MEG-01 CD44^{dim} cells stained with NBD-DTYCF, NBD-PNHSE or FITC-Anti-CD44 Ab as control. Panel (**A**) reports a representative FACS histogram profile of surface staining with reference Ab (upper right) and the two peptides (middle and bottom) at different concentrations. Black-filled curves referred to the negative control cells. Bars graph in panels (**B**,**C**) report, respectively, the % ± SD of fluorescent positive cells and mean fluorescence intensity (MFI) values ± SD on viable gated cells. Pairwise comparisons statistically significant are indicated (ANOVA; * $p < 0.05$; ** $p < 0.01$; *** $p < 0.001$, **** $p < 0.0001$).

The dose-response increase in fluorescence proportional to the expression of the CD44 marker might suggest that both DTYCF and PNHSE peptides can bind the surface receptor CD44.

Immunostaining

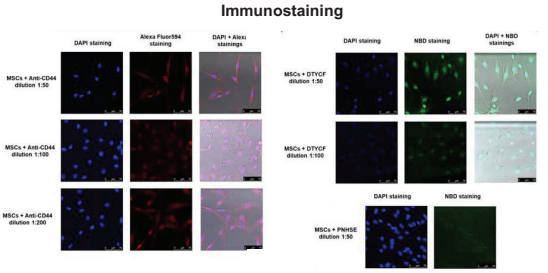

Immunostaining results: On the left, DAPI-stained human bone marrow mesenchymal stem cells (MSCs) with Alexa Fluor594 stained anti-CD44 in three different dilution ratios (1:50, 1:100, 1:200); on the top right, MSCs with NBD conjugated DTYCF in two different dilution ratios (1:50, 1:100); on the bottom right, MSCs with NBD conjugated PNHSE in 1:50 dilution ratio.

These data support a more significant interaction of DTYCF with MSCs compared to PNHSE, confirming the results we previously collected in the FACS experiments.

CD271

FACS – preliminary results

NSPVKQYF

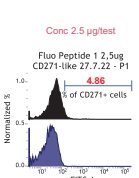

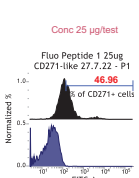

VFQYFF

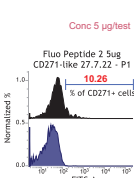

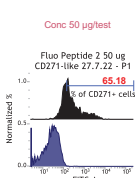

→ ***Work in progress***

Conclusions. In this poster, we report a methodology for the use of short peptide sequences as a tool for phenotypic characterization and the isolation of cell bodies, exploiting their binding of surface cell markers. Taken together, the data show that using an ad hoc designed computational protocol, it is possible to obtain short peptide sequences with adequate specificity to study the expression of the CD44 and CD271 receptors by an antibody-free assay. Replacing antibodies with short peptides can be a viable strategy in all procedures that require the use of antibodies to preserve sensitivity and specificity while avoiding high costs and complex laboratory protocols. This work paves the way towards the identification of a range of peptide aptamers targeting biomarkers relevant to existing or emerging biomedical applications such as regenerative medicine. In the latter case, the availability of these aptamers will enable the selection of specific cell populations suitable for tissue regeneration as such or in combination with nanoparticles.

References: [1]Mason, C.; Dunnill, P. A brief definition of regenerative medicine. Future Medicine 2008, 3; [2]Samsonraj, R.M.; Raghunath, M.; Nurcombe, V.; Hui, J.H.; van Wijnen, A.J.; Cool, S.M. Concise review: multifaceted characterization of human mesenchymal stem cells for use in regenerative medicine. Stem cells translational medicine 2017, 6, 2173-2185; [3]Pittenger, M.F. Multilineage Potential of Adult Human Mesenchymal Stem Cells. Science 1999, 284, 143-147.[4]Merrifield, Robert B. "Solid phase peptide synthesis. I. The synthesis of a tetrapeptide." Journal of the American Chemical Society 85.14 (1963): 2149-2154.

https://doi.org/10.17952/37EPS.2024.P2167

Obtaining, Optimizing, and Evaluating the Activity of Anticancer LfcinB-Derived Peptides on in vitro Models against Melanoma

Karla Rodriguez[1] , Jose Mendoza[1], Javier García[1], Zuly Rivera[1], Joel Lopez[2], Ricardo Fierro[1]

[1]*Universidad Nacional de Colombia, Bogotá D.C, Colombia,* [2]*Universidad Michoacana de San Nicolás de Hidalgo, Michoacan, Mexico*

Abstract: Melanoma, a leading cause of cancer-related deaths, is expected to see a 50% increase in diagnoses and a 68% rise in mortality by 2040. This study focuses on evaluating and optimizing anticancer peptides derived from Bovine Lactoferricin and Buforin II in human (A-375) and murine (B16-F10) melanoma models. Peptide bioactivity was assessed using MTT assays and microscopy, followed by optimization through sequence modifications. Characterization was performed using RP-HPLC and LC-QTOF MS. The results of this study showed that the strategy of enhancement activity contributes to the development of new therapeutic agents for Melanoma treatment.

INTRODUCTION

Cancer incidence in 2022

- 01 Lung cancer — 2 480 675 (12.4%)
- 02 Breast cancer — 2 296 840 (11.5%)
- 05 Skin cancer — 1 234 533 (6.2%)
- Melanoma — 331 722 (1.6%)

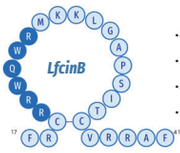

- **Animal Origin:** Bovine
- **Source:** Gastric pepsin hydrolysis of LFB
- **Activity:** Equal to or higher than LFB
- **Spectrum:** Broad-spectrum homologues

BFII



- **Animal Origin:** Asian Toad *Bufo gargarizans*
- **Source:** Proteolysis of histone H2A
- **CPPs** (Cell-Penetrating Peptides)
- **Spectrum:** Broad-spectrum PAM (Antimicrobial peptide)

METHODS

1. Solid-Phase Peptide Synthesis (SPPS)

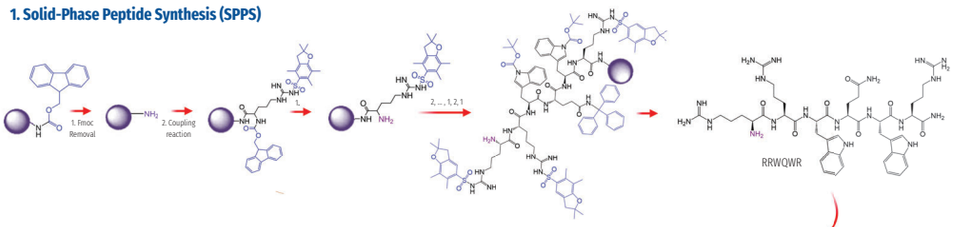

2. Solid-phase extraction (SPE)

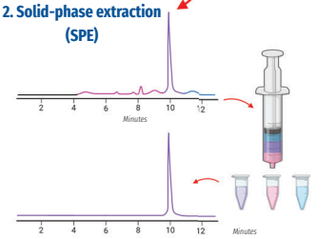

3. Peptide Characterization

RP-HPLC
LC-QTOF MS

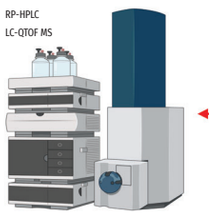

4. MTT Viability Assay

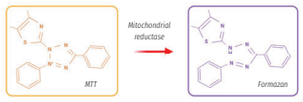

5. Hemolytic Activity Assay



RESULTS AND DISCUSSION

Code	Sequence	IC_{50} (μM)	
		A-375	B16-F10
LfcinB-1	**RRWQWR**	>203	>203
LfcinB-2	Ahx-**RRWQWR**	>182	>182
LfcinB-3	**RWQWRWQWR**	35	43
LfcinB-4	Ahx-**RWQWRWQWR**	>125	>125
LfcinB-5	(**RWQWRWQWR**)$_2$K-Ahx	>63	>63
LfcinB-6	**RWQWRWQW**O	>139	>139
LfcinB-7	R**RWQWRWQWR**	>111	>111
LfcinB-8	RGD-Ahx-**RRWQWRWQWR**	>96	>96
LfcinB-9	OOO**RWQWRWQWR**	97	>109
LfcinB-10	**RRWQWRMKKLG**	>130	>130
LfcinB-11	(**RRWQWRFKKLG**)$_2$K-Ahx	41	46
LfcinB-12	(**RRWQWR**-1-Nal-**KKLG**)$_2$K-Ahx	>58	>58
LfcinB-13	(**RRWQWR**-Hphe-**KKLG**)$_2$K-Ahx	8	41
LfcinB-14	(**ROWQWRFKKLG**)$_2$K-Ahx	>61	>61
LfcinB-15	KK**WQW**K-Ahx-**RLLRRLLR**	22	166
LfcinB-16	KK**WQW**K-Ahx-KL**L**KKL**L**K	>96	>96
LTX-315	KKWWKKW-Dip-K	9.7	53
LfcinBOp-1	(**RRWQWRRLLR**)$_2$-K-Ahx	15	18
LfcinBOp-2	**WW**KK**WQW**K-Ahx-**RLLRRLLR**	ND	88
LfcinBOp-3	**WW**KK**WQW**K-Ahx-**RLLRRLLR**	ND	70
LfcinBOp-4	**WWW**KK**WQW**K-Ahx-**RLLRRLLR**	ND	41
LfcinBOp-5	**RTS**KK**WQW**K-Ahx-**RLLRRLLR**	ND	52
LfcinBOp-6	**KTS**KK**WQW**K-Ahx-**RLLRRLLR**	ND	52

Table 1. Cytotoxic activity of peptides derived from Bovine Lactoferricin and Buforin II against Melanoma cell lines A-375 and B16-F10. Data are presented as mean ± SE. (n=3)

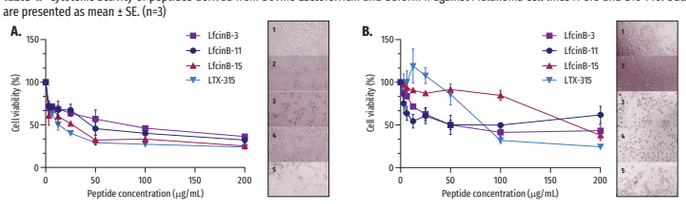

Figure 1. Cytotoxic Effect of Peptides with Enhanced Activity Against Melanoma Cell Lines: (A) A-375 and (B) B16-F10. Data are presented as mean ± SE. (n=3) . Microscopic images (100x) show: (1) negative control (no treatment), (2) LfcinB-3, (3) LfcinB-11, (4) LfcinB-15, and (5) LTX-315.

Peptide Chimera Dimer Containing Minimal Motifs from LfcinB and BFII (LfcinBOp-1)

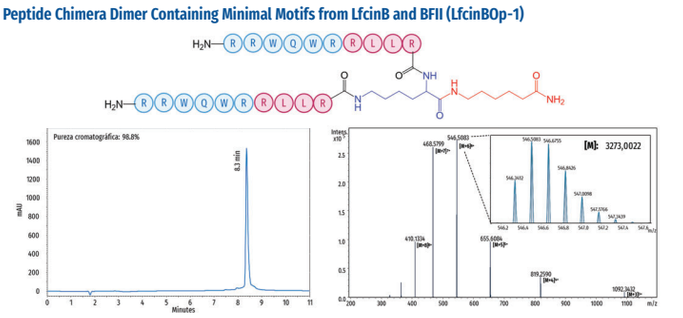

Figure 2. Characterization of the peptidic chimera dimer containing minimal motifs from LfcinB and BFII by RP-HPLC (left) and LC-ESI-QTOF Mass Spectrometry (right).

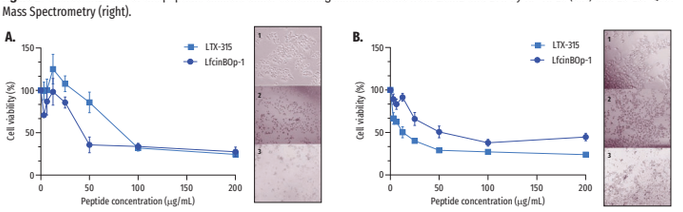

Figure 3. Cytotoxic Effect of the LfcinBOp-1 Peptide Against Melanoma Cell Lines: (A) A-375 and (B) B16-F10. Data are presented as mean ± SE. (n=3). Microscopic images (100x) show: (1) negative control (no treatment), (2) LfcinBOp-1, and (3) LTX-315.

Code	Sequence	%Hemolisis
LfcinBOp-1	(**RRWQWRRLLR**)$_2$-K-Ahx	18.9*

Table 2. Hemolytic Activity of the LfcinBOp-1 Peptide. *Percentage of Hemolysis at IC_{50} Concentration in A-375 Cells (15 μM)

CONCLUSION

Bioactivity screening showed that the peptides derivated of LfcinB and Buforin II have cytotoxic activity against melanoma cell lines derivated from human and murine sources (A-375 and B16-F10 respectively). Consequently, a variety of optimization strategies, such as sequence conjugation and W-tagging, were explored. Peptide design focused on identifying suitable locations for modifications that would maintain or enhance cytotoxic activity. Peptides analogous to RRWQWR and RLLR, exhibited equal or improved cytotoxic activity in melanoma cell lines, generated through modifications involving functionalization with these sequences, the KTS/RTS tripeptide or W-tagging at the N-terminus. The peptide LfcinBOp-1: (RRWQWRRLLR)$_2$-K-Ahx exhibit a potent cytotoxic activity at 2 hours of treatment in both cell lines, with no significant differences in IC_{50} values. Furthermore, it was shown that the inclusion of the W_8 or the KTS/RTS motif generated sequences with increased anticancer effect against the more resistant cell line, murine melanoma cell line. These results suggest that these strategies could be considered in development of peptide sequences with cytotoxic activity against melanoma.

REFERENCES

- Arnold, M., Singh, D., Laversanne, M., Vignat, J., Vaccarella, S., Meheus, F., Cust, A. E., de Vries, E., Whiteman, D. C., & Bray, F. (2022). Global Burden of Cutaneous Melanoma in 2020 and Projections to 2040. JAMA Dermatology, 158(5), 495–503. https://doi.org/10.1001/jamadermatol.2022.0160
- Arias, M., Hilchie, A. L., Haney, E. F., Bolscher, J. G. M., Hyndman, M. E., Hancock, R. E. W., & Vogel, H. J. (2017). Anticancer activities of bovine and human lactoferricin- derived peptides. Biochemistry and Cell Biology = Biochimie et Biologie Cellulaire, 95(1), 91–98. https://doi.org/10.1139/bcb-2016-0175
- Lee, H. S., Park, C. B., Kim, J. M., Jang, S. A., Park, I. Y., Kim, M. S., Cho, J. H., & Kim, S. C. (2008). Mechanism of anticancer activity of buforin IIb, a histone H2A-derived peptide. Cancer Letters, 271(1), 47–55. https://doi.org/10.1016/j.canlet.2008.05.041
- Solarte, V. A., Conget, P., Vernot, J.-P., Rosas, J. E., Rivera, Z. J., García, J. E., & Arango-Rodriguez, M. L. (2017). A tetrameric peptide derived from bovine lactoferricin as a potential therapeutic tool for oral squamous cell carcinoma: A preclinical model. PloS One, 12(3), e0174707. https://doi.org/10.1371/journal.pone.0174707
- Kozar, I., Margue, C., Rothengatter, S., Haan, C., & Kreis, S. (2019). Many ways to resistance: How melanoma cells evade targeted therapies. Biochimica et Biophysica Acta. Reviews on Cancer, 1871(2), 313–322. https://doi.org/10.1016/j.bbcan.2019.02.002
- Duong, D. T., Singh, S., Bagheri, M., Verma, N. K., Schmidtchen, A., & Malmsten, M.(2016). Pronounced peptide selectivity for melanoma through tryptophan end-tagging. Scientific Reports, 6, 24952. https://doi.org/10.1038/srep24952


PhD. Zuly Rivera


PhD. Javier García

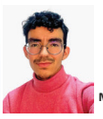
Jose David Mendoza


PhD. Ricardo Fierro


PhD. Joel López

37th EPS European Peptide Symposium
14th IPS International Peptide Symposium
UNIVERSIDAD NACIONAL DE COLOMBIA
SAMP

Proceedings of the 37th European Peptide Symposium
Michal Lebl, Editor
European Peptide Society, 2024
https://doi.org/10.17952/37EPS.2024.P2169

Design and characterization of a multistage peptide-based vaccine platform to target *Mycobacterium tuberculosis* infection

C. Bellini[1,2,‡], E. Vergara3, F. Bencs[4], Sz. Bősze[5], D. Krivić[6], B. Bacsa[6], S.E. Surguta[7], J. Tóvári[7], R. Reljic[3], and K. Horváti[1*]

*[1]MTA-HUN-REN TTK Lendület Peptide-Based Vaccines Research Group, Institute of Materials and Environmental Chemistry, HUN-REN Research Centre for Natural Sciences, Budapest, Hungary, *email address: horvati.kata@ttk.hu*
[2]Hevesy György PhD School of Chemistry, Eötvös Loránd University, Budapest, Hungary;
[3]Institute for Infection and Immunity, St. George's, University of London, London, UK;
[4]Laboratory of Structural Chemistry and Biology, Institute of Chemistry, Eötvös Loránd University, Budapest 1117, Hungary
[5]HUN-REN-ELTE Research Group of Peptide Chemistry, Budapest, Hungary;
[6]Division of Medical Physics and Biophysics, Gottfried Schatz Research Center, Medical University of Graz, Graz, Austria;
[7]Department of Experimental Pharmacology and National Tumor Biology Lab., National Institute of Oncology, Budapest, Hungary.
[‡]Present address: Interdepartmental Laboratory of Peptide and Protein Chemistry and Biology, Department of NeuroFarBa, University of Florence, Sesto Fiorentino (FI), 50019, Italy.

Tuberculosis (TB) is the second leading cause of death by a single infectious agent worldwide. The Bacille Calmette-Guérin (BCG), the only available vaccine against TB, provides inconsistent protection against pulmonary TB in adults, the primary source of disease transmission. Thus, a more effective vaccine is urgently needed to stop the TB epidemic. The development of a new vaccine is hindered by the complex immunopathology of *Mycobacterium tuberculosis* (*Mtb*), especially in eliciting protection against both active and latent stages of infection.

Multistage subunit vaccines, which incorporate antigens expressed in both phases, are designed to address different stages of a pathogen's life cycle or diverse aspects of the immune response in one construct. This strategy may be particularly advantageous when dealing with complex pathogens characterized by high antigen variability or propensity for mutagenesis, such as *Mtb*. However, their main limitation is that they often elicit a less robust immune response compared to traditional vaccines. In addition, they may face challenges related to bioavailability, including rapid clearance or undesired post-injection degradation. Consequently, developing subunit vaccines requires a well-designed formulation, incorporating immunostimulatory adjuvants and a delivery system to address these limitations [**1**].

Epitope selection:
A set of validated T cell epitopes was chosen from the available literature and synthesized using solid-phase peptide synthesis. After the screening, the 4 epitopes contained in the peptide mixture PM1 were selected for the inclusion in the vaccine platform.

Sequence selection workflow for multi-epitope vaccine antigens

1 Database Research
Selection of MHC I and MHC II-restricted validated epitope peptides expressed in the active or latent TB stages.

2 Epitope Peptides Synthesis
Solid Phase Peptide Synthesis (SPPS) - Fmoc/^{t}Bu strategy

3 Cellular Uptake in Antigen-Presenting Cells (APCs) Model
Internalization efficiency

4 Epitope Peptides Pools
The epitope peptides selected from the preliminary screening were pooled in two peptide mixtures (**PM1** and **PM2**)

PM1			
Gene name	**Epitope name**	**Stage**	**MHC**
Rv3874	$CFP10_{32-39}$	Active	MHC I
Rv3908c	$GlfT2_{4-12}$	Active	MHC I
Rv0475	$HBHA_{185-194}$	Latent	MHC I and MHC II
Rv1039c	$PPE15_{1-15}$	Latent	MHC II

PM2			
Gene name	**Epitope name**	**Stage**	**MHC**
Rv3874	$CFP10_{32-39}$	Active	MHC I
Rv1886c	$Ag85B_{41-48}$	Active	MHC I
Rv0125	$Mtb32a_{309-318}$	Latent	MHC I
Rv0341	$IniB_{33-45}$	Latent	MHC I and MHC II

5 Antigenicity
Antigen-recall assay on human PBMCs from *Mtb*-sensitized donors

Lipopeptide-based vaccine platform:
The peptides included in PM1 were used to synthesize the peptide-based vaccine platforms. $CFP10_{32-39}$, $GlfT2_{4-12}$, and $HBHA_{185-194}$ were combined in one linear peptide chimera, which was derivatized with a maleimide moiety by orthogonal reaction. The $PPE15_{1-15}$ was elongated with a cysteine residue at the *C*-terminal and then conjugated to the linear peptide through the thiol-maleimide reaction. The *N*-term of the peptide chimera was either acetylated or palmitoylated to obtain the final branched conjugates (Ac-CGHP and Pal-CGHP). Palmitoylation previously demonstrated to improve the cellular uptake and the immunogenicity of peptide-based vaccines [**2**].

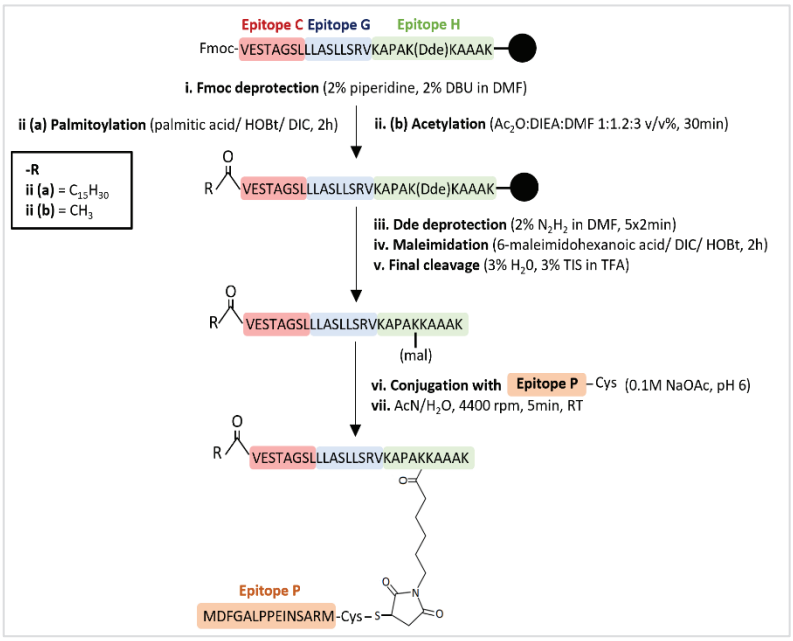

Immunological evaluation.
The Pal-CGHP conjugate, the peptide mixture PM1 in PBS, and PM1 formulated with the Sigma Adjuvant System (SAS) were administered subcutaneously to BALB/c mice three times, two weeks apart. We then measured antigen-specific splenic T cell proliferation and cytokine secretion among immunised and unimmunised animals. As expected, PM1 did not produce a noticeable immune response, likely due to intrinsic poor immunogenicity and *in vivo* stability of short synthetic peptides. Pal-CGHP immunization produced significant T cell proliferation, which slightly increased over time, with the highest levels observed four weeks post-immunization. Similarly, IFNγ and TNFα concentrations followed a time-dependent increase. In contrast to the SAS-formulated candidate, Pal-CGHP induced significant IL-22 and IL-10 production but no IL-17 response. When splenocytes from Pal-CGHP immunized mice were restimulated with the individual C/G/H/P peptides, bearing the original sequences, epitope-specific antigenicity was observed, suggesting that their chemical modification occurred in the conjugation did not compromise the epitope recognition. Thus, the results suggest that Pal-CGHP is more promising than the two tested candidates and it merits further investigation as a multi-epitope self-adjuvating vaccine platform [**3**].

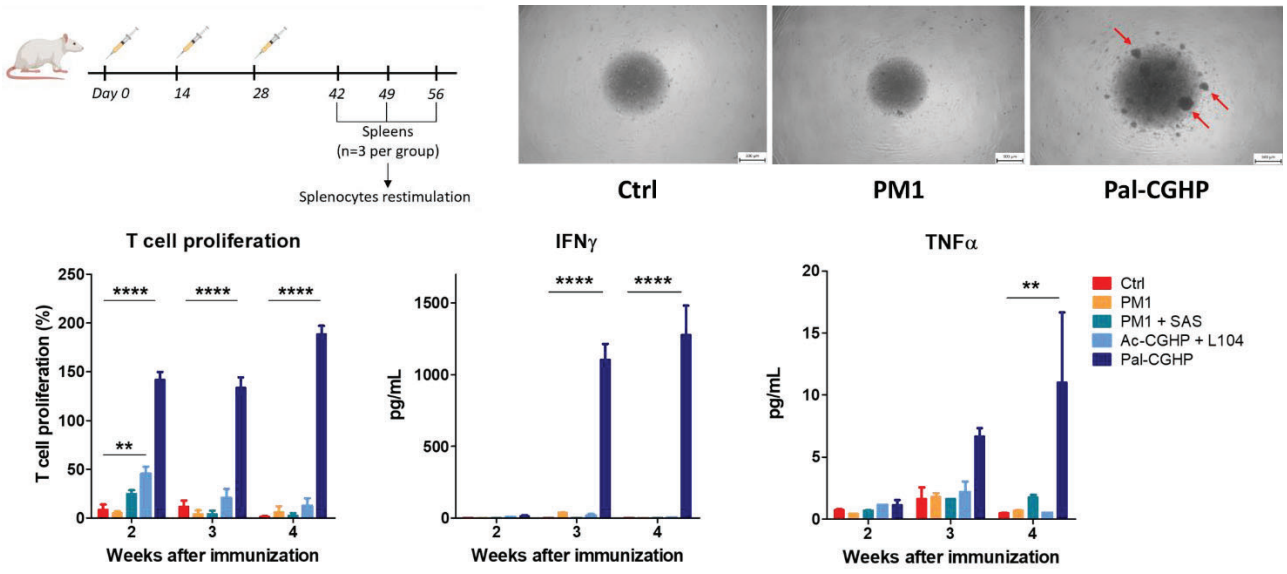

Acknowledgements
Authors thank the European Union's H2020-MSCA-ITN programme BactiVax (No. 860325) and the Momentum Program (LP2021-28) of the Hungarian Academy of Sciences.

References
[**1**] *Bellini C, Horváti K. Cells. 2020, 2673;* [**2**] *Horváti, K. et al. Vaccines. 2019, 7, 101;* [**3**] *Bellini C. et al. Bioconjugate Chem. 2023, 34, 10, 1738–1753*

Engineering mRNA display for GPCR drug discovery – de novo discovery of cyclic peptide GLP1R binders.

https://doi.org/10.17952/37EPS.2024.P2171

Authors

Esther Meron[1,2], Jens C. Nielsen[1], Mads M. Nygaard[1], Dennis Worm[1], Ulrike Leurs[1], Morten Lundh[1], Joseph M. Rogers[2]

[1]Gubra, Hørsholm, Denmark

[2]University of Copenhagen, Copenhagen, Denmark

Corresponding author
Esther Meron - eme@gubra.dk

Background & Aim

mRNA display enables screening of large (>10^{13}) randomized *in vitro* translated peptide libraries against a target of interest. Through several rounds of screening there will be an enrichment of sequences of highly potent and selective peptide binders of the target. These peptides can further be cyclised by disulphide bond formation during the translation step, which is advantageous for the potential for higher binding affinity.

The aim of this study was to explore the use of mRNA display for discovering disulphide-cyclised peptides that act against a family B GPCR, which naturally binds a linear helical peptide. We show how mRNA display can be used for screening against the GLP1R extracellular domain (ECD). By using clustering analyses, we aim to select sequences from distinct sequence families to better cover the scope of sequences for further functional screenings.

Methods

The mRNA library was transcribed from a DNA library encoding 4-15 randomised amino acids flanked by cysteines. Peptides were transcribed using the PURE system (Protein synthesis Using Recombinant Elements) and cyclised through disulphide bonds. Cyclisation was confirmed by UPLC-HR-MS. Five selection rounds of mRNA display were performed against the GLP1R ECD; positive and negative binders were sequenced using NGS.

Sequences of binders from round 5 were clustered based on their Levenshtein distances. Top peptides from each cluster were selected for preliminary affinity screenings, and selected peptides were tested in functional assays for inhibition of cAMP accumulation.

Conclusion

- mRNA display allows for screening of large libraries of randomised disulphide-bonded cyclic peptides.
- Sequences selected based on clustering criteria provided basis for further functional testing.
- Unexpectedly, linear isoforms showed increased function with µM potencies in cAMP inhibition assays.

www.gubra.dk

1 mRNA display protocol outline

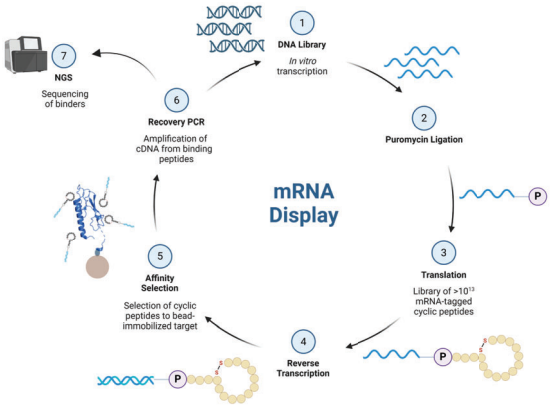

Figure 1. Protocol outline for mRNA display.

2 In vitro translation of disulphide-bonded peptides

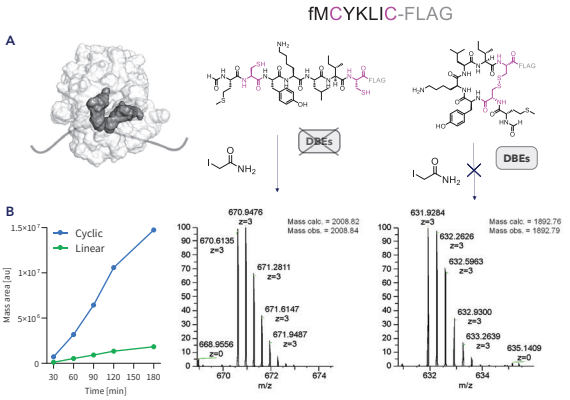

Figure 2. *In vitro* translation and cyclisation. (A) Translation of test-peptide fMCYKLIC using the PURE cell free translation system with and without disulphide-bond enhancers (DBEs). Free cysteines could react with iodoacetamide, and mass difference was measured using UPLC-HR-MS. Cyclised peptide was observed with addition of DBEs. **(B)** Amount of cyclic and linear peptide detected over time of fMCYKLIC translated in the presence of DBEs.

3 mRNA display selections were performed against hGLP1R ECD

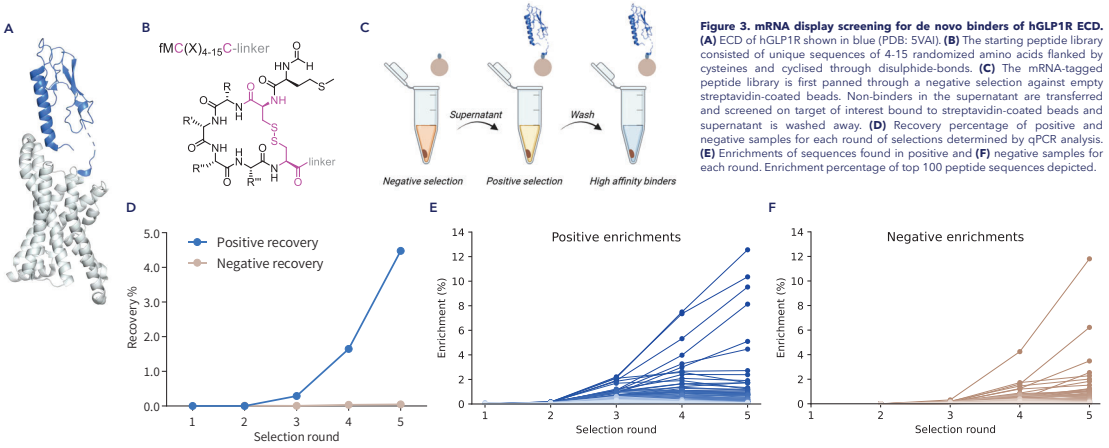

Figure 3. mRNA display screening for de novo binders of hGLP1R ECD. (A) ECD of hGLP1R shown in blue (PDB: 5VAI). **(B)** The starting peptide library consisted of unique sequences of 4-15 randomized amino acids flanked by cysteines and cyclised through disulphide-bonds. **(C)** The mRNA-tagged peptide library is first panned through a negative selection against empty streptavidin-coated beads. Non-binders in the supernatant are transferred and screened on target of interest bound to streptavidin-coated beads and supernatant is washed away. **(D)** Recovery percentage of positive and negative samples for each round of selections determined by qPCR analysis. **(E)** Enrichments of sequences found in positive and **(F)** negative samples for each round. Enrichment percentage of top 100 peptide sequences depicted.

4 Clustering analysis of binding sequences

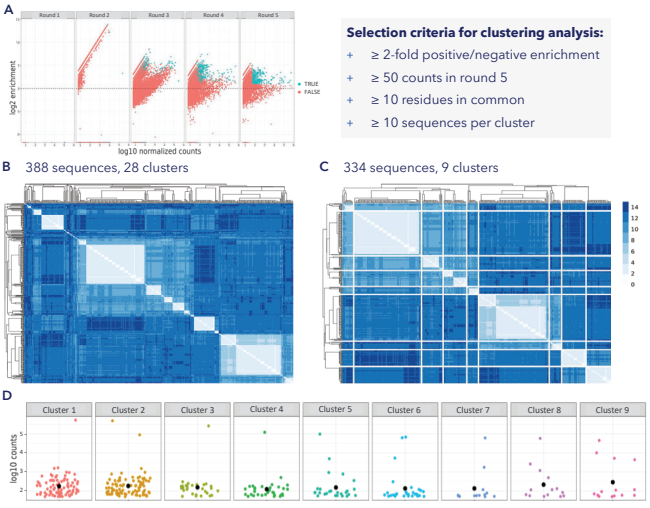

Selection criteria for clustering analysis:

- ≥ 2-fold positive/negative enrichment
- ≥ 50 counts in round 5
- ≥ 10 residues in common
- ≥ 10 sequences per cluster

Figure 4. Clustering analysis of binding peptides. (A) Sequences with ≥ 50 counts found in positive selection round 5, and ≥ 2-fold positive/negative enrichment in round 5 were included for clustering analysis. **(B)** Heatmap of clustering based on Levenshtein distanced with ≥ 10 residues in common resulted in 388 sequences in 28 clusters. **(C)** Excluding clusters with < 10 sequences resulted in 334 sequences in 9 clusters. **(D)** Count in positive selection round 5 for each sequence per cluster. Black dot denotes average count per cluster. Top 5 ranking sequences from each cluster selected for preliminary crude screenings and from these, selected peptide sequences were chosen for further evaluations.

5 Functional inhibition of hGLP1R

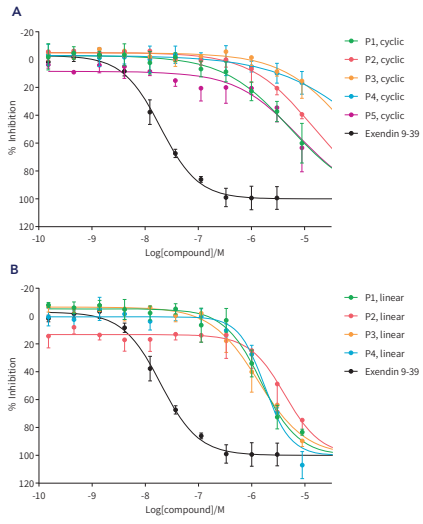

Figure 5. Functional inhibition of hGLP1R cAMP accumulation in cells. cAMP measurements in CHO-K1 cells transfected with hGLP1R and incubated for 30 minutes at room temperature with a concentration gradient of peptides 1-5 in purified cyclic **(A)** or linear **(B)** form along with a fixed concentration of 0.3 µM GLP1. Exendin 9-39 is a known hGLP1R antagonist. n=4.

DEPARTMENT OF CHEMISTRY
UNIVERSITY OF COPENHAGEN

https://doi.org/10.17952/37EPS.2024.P2172

Novel functionalized acylation reagents for Gly- and Lys-His tag acylation on proteins

Delphine N. Møller, Christian Kofoed, Mikkel B. Thygesen, Kasper K. Sørensen, Tuule Treiberg, Knud J. Jensen

Department of Chemistry, Faculty of Science, University of Copenhagen, Denmark

ABSTRACT

Chemical modification of protein amines is often performed by acylation of amines using NHS-esters. Due to the high reactivity of NHS-esters, mixtures of products are formed. Highly selective chemical modification of a protein was performed using an N-terminal histidine based peptide tag, the Gly-His tag (GHHHHHH–), which has been developed in our lab. New acylating reagents which facilitate the introduction of functionalities such as biotin, fluorophores, or half-life extending moieties were designed and synthesized using well-known organic chemistry. This was demonstrated by the synthesis of an array of activated biotin esters. We compared them to our previous biotinylation reagent, and a biotin ester with X = H. The reactivity and solubility of the esters were tuned by varying the substituents on the α-carbon, X and Y, and including a carboxylate on the phenolic side. Our optimized esters reacted with very high selectivity towards GH_6-Protein X.

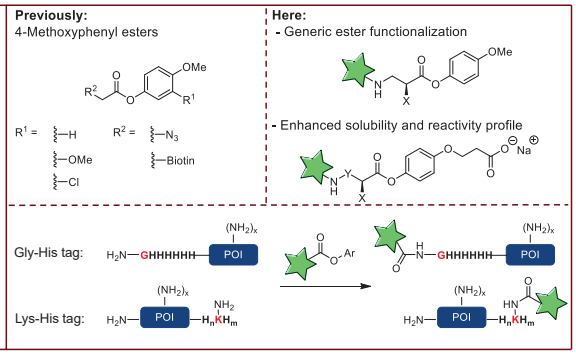

EXPERIMENTAL

Step 1: Organic synthesis

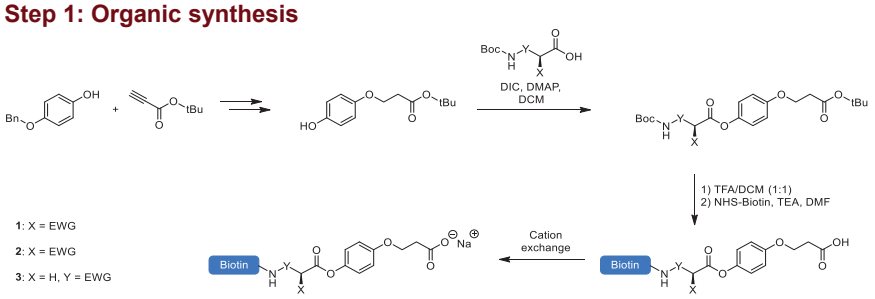

Step 2: Protein modification

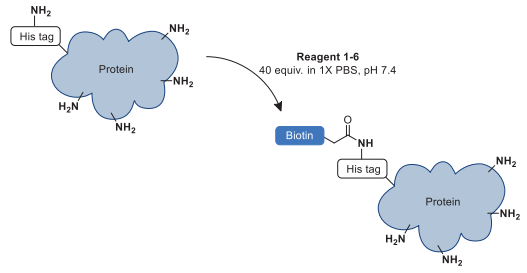

RESULTS AND DISCUSSION

- Increasing the sum of Hammett parameters of the phenol substituents in the esters give a linear decrease in hydrolysis half-life of esters
- This also gave more non-specific acylation of model peptides

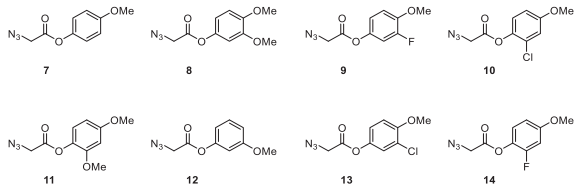

Improved biotin esters

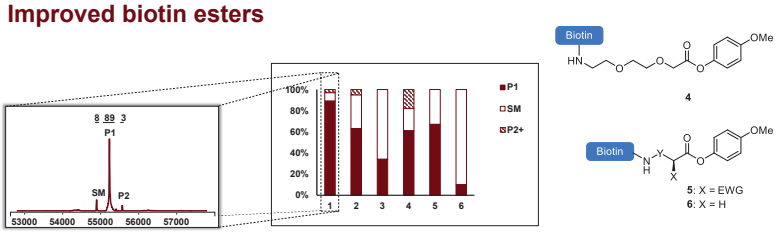

Conditions: 30 μM GH_6-Protein X in PBS, pH 7.4 at 4°C was reacted with the ester for 48 h (5% DMSO was used to dissolve **4-6**). The relative abundances of products were derived from deconvoluted mass spectra (ESI-TOF).

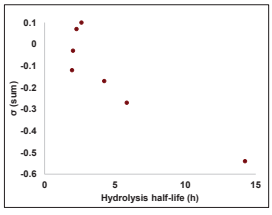

Conditions: 2.5 mM ester **7-14** in 200 mM HEPES (10% acetonitrile), pH 7.5 at 4°C was monitored on UPLC for 24 h. The areas under the curve for the ester signals were used to estimate the hydrolysis.

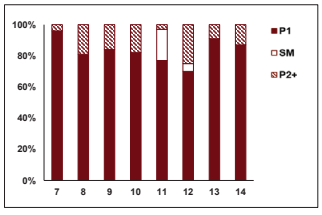

Conditions: 2.5 equiv. ester **7-14** in acetonitrile was reacted with 1 mM GHHHHHHG-DWLKAFYDKVAEKLKEAF in 200 mM HEPES, pH 7.5 at 4°C for 24 h. The relative abundances of monofunctionalized (P1) and multi-functionalized (P2+) products were derived from UPLC traces (215 nm).

CONCLUSIONS

Esters with a higher sum of Hammett parameters of the phenol substituents hydrolyzed more rapidly and gave more formation of P2+. The increased electronegativity at the α-carbon in **5** relative to **4** and **6** resulted in enhanced formation of P1 and improved the selectivity of the protein acylation reaction. Incorporation of a carboxylate on the phenolic side of the ester increased the solubility and selectivtiy of the protein functionalization. Further, it did not affect the pH of the reaction mixture (data not shown). Esters with an EWG at the α-carbon showed the highest selectivity in Gly-His tag acylation of GH_6-Protein X. We expect an increase in the applications of our Gly- and Lys-His tag acylations following this development of a highly selective reagent for protein functionalization.

CONTACT

Delphine Nørgaard Møller
dnm@chem.ku.dk

UCPH Nanobioorganic Chemistry – KJJ lab

ACKNOWLEDGEMENTS

We gratefully acknowledge our collaborator Dr. Sanne Schoffelen for her contribution to the design of these experiments and protocols for the expression of N-terminally Gly-His tagged proteins. We thank Independent Research Fund Denmark for a grant (2035-00277B) to KJJ.

References

1) M. C. Martos-Maldonado, C. T. Hjuler, K. K. Sørensen, M. B. Thygesen, J. E. Rasmussen, K. Villadsen, S. R. Midtgaard, S. Kol, S. Schoffelen, K. J. Jensen, *Nat. Commun.* **2018**, 9, 3307.
2) C. Kofoed, S. Wu, K. K. Sørensen, T. Treiberg, J. Arnsdorf, S. P. Bjorn, T. L. Jensen, B. G. Voldborg, M. B. Thygesen, K. J. Jensen, S. Schoffelen, *Chem. Eur. J.* **2022**, 28, e202200147.
3) K. J. Jensen, M. B. Thygesen, K. K. Sørensen, S. Wu, T. Treiberg, S. Schoffelen, *ChemBioChem* **2022**, 23, e202200359.
4) C. Hansch, A. Leo, R. W. Taft, *Chem. Rev.*, **1991**, 91, 165-195.

KLVFF peptide functionalization of graphene oxide as suitable Aβ biomarker detection platform

Rita Turnaturi[a], Giuseppina Sabatino[a], Giuseppe Di Natale[a], Giuseppe Nocito[b], Angela Scala[c], Viviana Scuderi[d], Simona Filice[d], Antonino Mazzaglia[b], Silvia Scalese[d], Giuseppe Pappalardo[a].

[a]CNR-IC Catania, Italy [b]CNR-ISMN URT Messina, Italy
[c]Dip ChiBioFarAm, Università di Messina, Messina, Italy [d]CNR-IMM Catania, Italy

https://doi.org/10.17952/37EPS.2024.P2173

Background

Accurate diagnosis of the preclinical stages of Alzheimer's disease (AD), by means of biomarker early detection, is considered crucial for therapeutic advancements.
Current AD diagnosis relies on the combinatorial use of biomarkers detection, derived from cerebrospinal fluid (CSF), with advanced molecular imaging and cognitive assessment tools [1].
However, the invasiveness and the difficult access to routine diagnosis, due to high costs of these tools, represent some challenges that need to be overcome.
Low-cost and non-invasive alternatives, such as plasma, saliva, or urine biomarkers, could be a valid substitute in AD screening and diagnosis.

Aim

Nanomaterial-based biosensors development for recognition of AD biomarkers, such as amyloid beta Aβ(1–40) and the more toxic form Aβ (1–42), could pave the way for early diagnosis of AD [2].

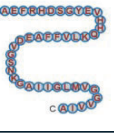

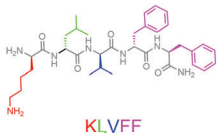

KLVFF

In this scenario, KLVFF (H_2N-Lys-Leu-Val-Phe-Phe-COOH, Aβ (16–20)), a peptide fragment deputed to interact with the homologous region of full-length Aβ(1–40) or Aβ (1–42), was selected as molecular recognition element of the selected Aβ biomarkers [3].

Graphene oxide (GO) was chosen as nanomaterials-based sensing layer

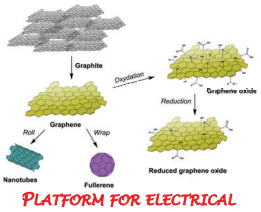

PLATFORM FOR ELECTRICAL BIO-SENSORS

GO surface decorated with amphiphilic cyclodextrin SC16OH nanovesicles entangling KLVFF conjugates

MW-SPPS and characterization of Ada-PEG_4-KLVFF (Ada-Pep) and Fc-PEG_4-KLVFF (Fc-Pep)

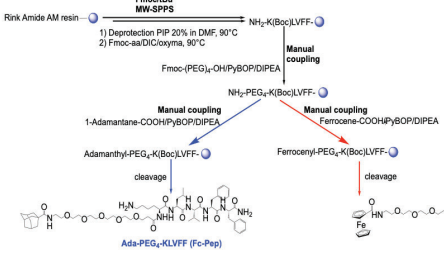

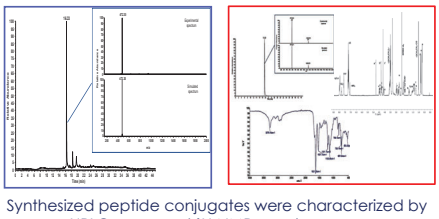

Synthesized peptide conjugates were characterized by HPLC, mass and ^{1}H-NMR spectroscopy.

The amphiphilic cyclodextrin/graphene oxide/KLVFF nanohybrids (Ada-Pep and the Fc-Pep) were prepared following the thin film hydration method [4] and characterized from Scanning Electron Microscopy and Dynamic Light Scattering analyses

Nanohybrid preparation

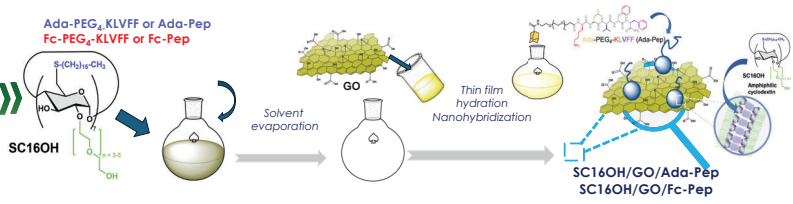

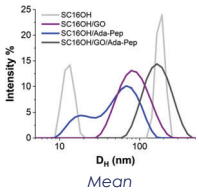

Mean hydrodynamic diameter (D_H) from DLS analysis

SC16OH/GO/Ada-PEG_4-KLVFF and SC16OH/GO/Fc-PEG_4-KLVFF analisys

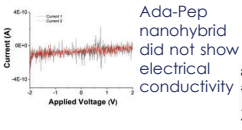

Ada-Pep nanohybrid did not show electrical conductivity

SEM imaging

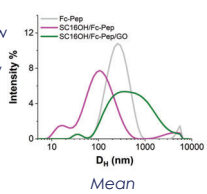

Mean hydrodynamic diameter (D_H) from DLS analysis

Cyclic voltammetry (CV) from SPGE (10 mV/s)

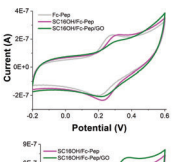

CV from modified SPGE (10 mV/s)

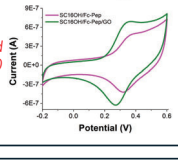

The Fc-Pep inclusion onto SC16OH was confirmed from CV.

The SC16OH/GO/Fc-Pep modified screen printed gold electrode showed 30 % current increase.

GO surface covalently functionalized with NH_2-PEG_4-KLVFF

MW-SPPS of NH_2-PEG_4-KLVFF

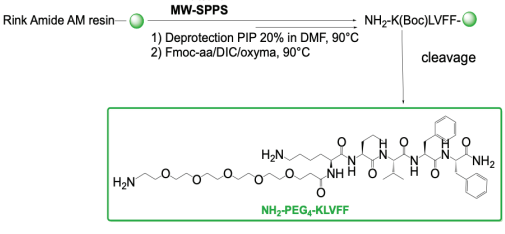

Peptide NH_2-PEG_4-KLVFF was covalently conjugated with GO by EDC/NHS coupling protocol.

GO functionalization with NH_2-PEG_4-KLVFF by means EDC/NHS protocol

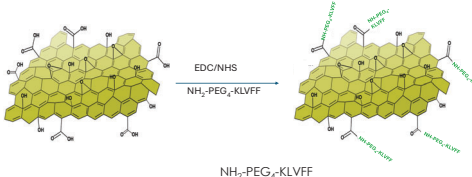

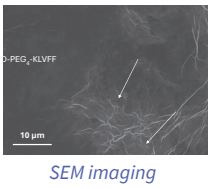

SEM imaging

In the GO ATR-FTIR spectrum (black) are clearly distinguishable the bands at 1) 1710 cm^{-1} (C=O vibration of the –COOH), 2) 1626 cm^{-1} (aromatic C=C stretching). 3) 1069 cm^{-1} (epoxy vibrations). The spectrum of peptide conjugate NH_2-PEG_4-KLVFF (red) shows a strong Amide I band (at 1632.23 cm^{-1}) and the Amide II band (at 1537.47 cm^{-1}). PEG characteristic bands found in the spectra NH_2-PEG_4-KLVFF are that due to CH_2 twisting and CH_2 wagging (1276.07 and 1399.49 cm^{-1}, respectively) and C-C and C-O stretching at 835.68 cm^{-1}.

In the ATR-FTIR spectrum of GO-PEG_4-KLVFF (blue) the band at 1710 cm^{-1} disappears whereas it tuns appreciable the band at 1648-1560 cm^{-1} (amide group).

ATR-FTIR

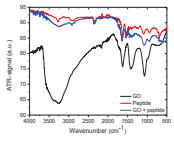

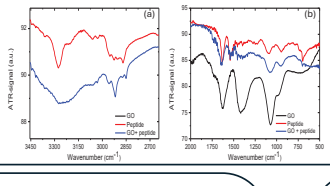

XPS analysis

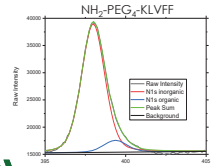

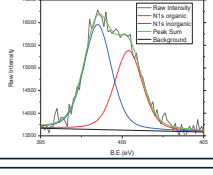

	GO		NH_2-PEG_4-KLVFF		GO-PEG_4-KLVFF	
Bond type	BE (eV)	%	BE (eV)	%	BE (eV)	%
–NC(=O)–	400,380	*	399,359	8,5	400,390	43,1
–C–NR_2	398,298	*	397,984	91,5	398,491	56,9

N1s XPS spectra of NH_2-PEG_4-KLVFF reports two main peaks related to -N-(C=O)- and -C-NR_2. The former contribute is at higher binding energy with respect to the latter.
When the peptide is grafted to GO layers, the -N-(C=O)- contribution increases because of the formation of amide bonding between carboxyl groups of GO and amine groups of NH_2-PEG_4-KLVFF.

Conclusions

- Ada-Pep nanohybrid did not show electrical conductivity, probably for an extensive shielding operated by cyclodextrins.
- The inclusion of Fc-Pep onto SC16OH amphiphilic cyclodextrin was confirmed from cyclic voltammetry and the modified screen printed gold electrode showed 30 % current increase.
- β-amyloid detection with SC16OH/GO/Fc-Pep modified SPGE is in validation.
- Preliminary results with Fc-Pep (control without cyclodextrin) indicated the electrochemical sensing of β-amyloid.
- Preliminary investigations show the nanoconjugate GO-$(PEG)_4$-KLVFF potential as a multifunctional platform for biomedical applications as biosensing layers for Alzheimer's biomarker detection.

References

[1] Zhou, Y., Liu, L., Hao, Y., & Xu, M. Detection of Aβ Monomers and Oligomers: Early Diagnosis of Alzheimer's Disease. *Chemistry, an Asian journal* **2016**, *11*, 805–817.
[2] Chen, G. F., Xu, T. H., Yan, Y., Zhou, Y. R., Jiang, Y., Melcher, K., & Xu, H. E. Amyloid beta: structure, biology and structure-based therapeutic development. *Acta pharmacologica Sinica* **2017**, *38*, 1205–1235.
[3] Tjernberg, L. O., Näslund, J., Lindqvist, F., Johansson, J., Karlström, A. R., Thyberg, J., Terenius, L., & Nordstedt, C. Arrest of beta-amyloid fibril formation by a pentapeptide ligand. *The Journal of biological chemistry* **1996**, *271*, 8545–8548.
[4] Mazzaglia, A., Di Natale, G., Tosto. R., Scala, A., Sortino, G., Piperno, A., Casaletto, M. P., Riminucci, A., Giuffrida, M.L., Mineo, P.G., Villari, V., Micali, N., Pappalardo, G. KLVFF oligopeptide-decorated amphiphilic cyclodextrin nanomagnets for selective amyloid beta recognition and fishing *Journal of Colloid and Interface Science* **2022**, *613*, 814–826.

samothrace
Finanziato dall'Unione europea NextGenerationEU
ICCI CNR Istituto di Cristallografia
IMM Istituto per la Microelettronica e Microsistemi
Consiglio Nazionale delle Ricerche
CNR ISMN ISTITUTO PER LO STUDIO DEI MATERIALI NANOSTRUTTURATI
37th EPS European Peptide Symposium 14th IPS International Peptide Symposium

On-Resin Synthesis and Modification of Novel Peptide Heterocycles

Ciaran McGrory, Eddie Myers

University of Galway, Ireland

https://doi.org/10.17952/37EPS.2024.P2174

Previous Work On Cysteine Thioaldehydes in the Myers Group[1, 2]

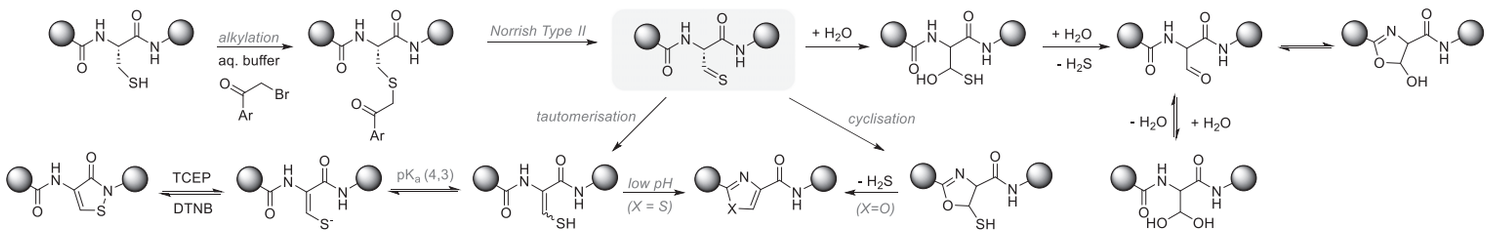

On-Resin Synthetic Investigations of Heterocycles

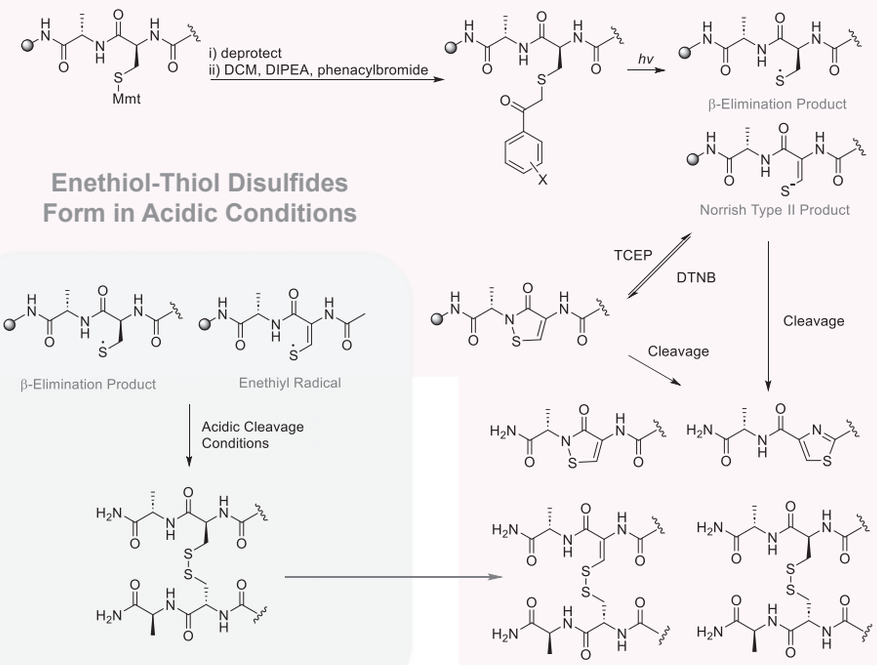

Medical Applications of Isothiazolones[3, 4]

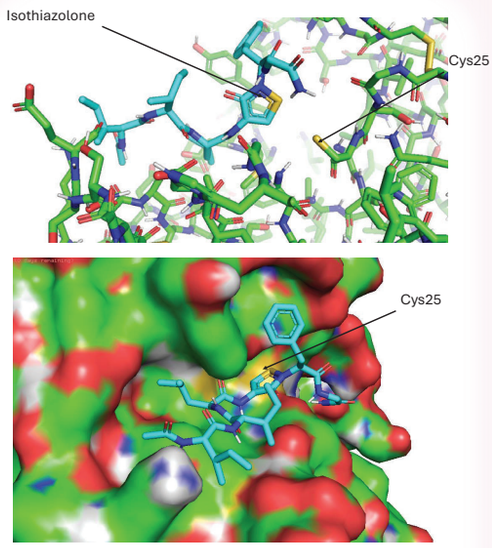

- Isothiazolones could be potential inhibitors of cysteine proteases
- The S–N bond is weak and the sulfur forms disulfides easily

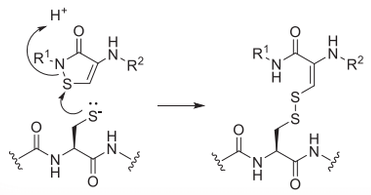

DTT Treatment Before Cleavage Stops Disulfide Formation

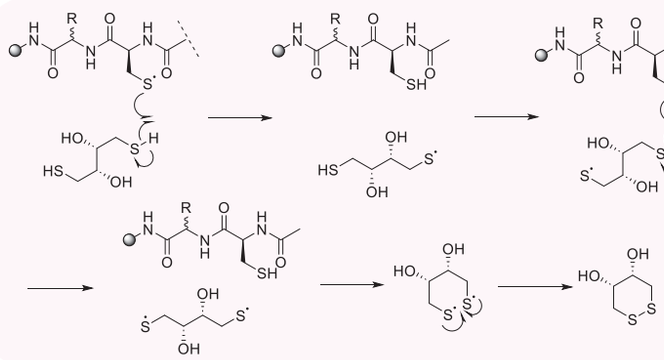

Enethiolate oxidation by phenacylbromides

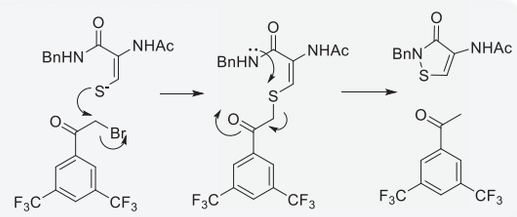

- Enethiolate can be oxidized by DTNB or phenacylbromides

Results and Future Work

- Isothiazolone has been made on-resin but in low yield after cleavage
- Disulfides can form between enethiyl and thiyl radicals during cleavage
- DTT treatment prior to cleavage reduces disulfide formation and increases the amount of thiol that can react with isothiazolone
- Thiazole peptides are known bioactive molecules, and the conditions tested thus far are more suitable for their synthesis than isothiazolone containing peptides
- Thiazole has been formed in cleavage with up to 30% conversion and is less reactive to other species in solution than isothiazolone

1. P. I. Clark and G. Lowe, *Journal of the Chemical Society, Chemical Communications*, 1977, 923-924
2. P. J. Wagner, *Accounts of Chemical Research*, 1971, **4**, 168-177.
3. N. Hayakawa, K. Nozawa, A. Ogawa, N. Kato, K. Yoshida, K.-i. Akamatsu, M. Tsuchiya, A. Nagasaka and S. Yoshida, *Biochemistry*, 1999, **38**, 11501-11507
4. Y.-H. Chen, H.-Y. Hsu, M.-T. Yeh, C.-C. Chen, C.-Y. Huang, Y.-H. Chung, Z.-F. Chang, W.-C. Kuo, N.-L. Chan and J.-H. Weng, *Journal of Medicinal Chemistry*, 2016, **59**, 9906-9918.

Ollscoil na Gaillimhe University of Galway

Science Foundation Ireland sfi For what's next

https://doi.org/10.17952/37EPS.2024.P2175

Use of Green Solid Phase Peptide Synthesis to Obtain Tripeptide-85

Brasil, M. C. O. A.[1]; Princival, C. R.[2]; Kuchenbecker, V.[2]; Katekawa, E.[2]; Magalhães, W. V.[2]; Cilli, E. M.[1]

mcoa.brasil@unesp.br; eduardo.cilli@unesp.br

[1]São Paulo State University (UNESP), Institute of Chemistry, Araraquara; [2]R&D, Chemyunion (Brasil)

ABSTRACT

Peptides have increasingly attracted the attention of the industry due to their applicability, safety profile, and possibility of conjugation with other molecules. Most peptides currently produced are obtained through solid phase peptide solid phase peptide synthesis (SPPS), but this methodology still uses solvents that are considered problematic from an ecological point of view, such as dimethylformamide (DMF)[1-3]. The objective of this study was to test green solvents in the SPPS protocol.

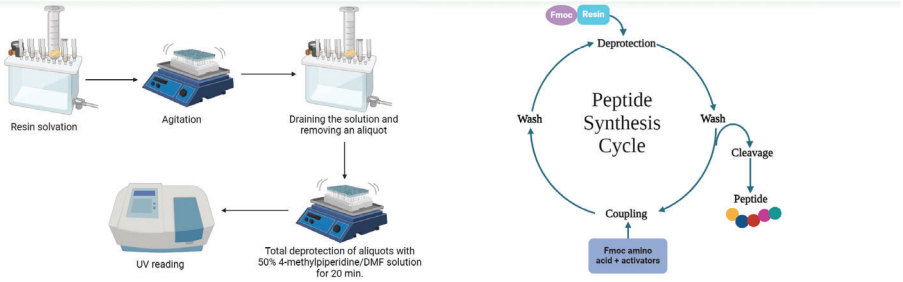

RESULTS

Deprotection analysis

Table 1: First amino acid deprotection analysis

Solvent	Temperature	% Deprotection Time						
		5	25	45	65	85	105	125
20% 4-methylpiperidine/DMF	Room temperature	100	-	-	-	-	-	-
50% Morpholine/ 2-MeTHF	Room temperature	63	83	96	100	-	-	-
	50°C	89	100	-	-	-	-	-
30% Imidazole/ DMF	Room temperature	18	36	52	66	78	90	100
	50°C	21	40	57	72	82	92	100
30% imidazole/ DMF	Room temperature	18	36	52	66	78	90	100
	50°C	21	40	57	72	82	92	100
25% Aminoethanol/ DMF	Room temperature	79	100	-	-	-	-	-
	50°C	100	-	-	-	-	-	-
25% 2-amino-2-methyl-1-propanol/ DMF	Room temperature	88	100	-	-	-	-	-
	50°C	79	91	100	-	-	-	-
25% 2-amino-2-methyl-1-propanol/ 2-MeTHF	Room temperature	26	46	62	75	85	93	100
	50°C	73	90	97	99	100	-	-

Peptide synthesis

Figure 1: Synthesis of the EVF peptide using the standard SPPS protocol.

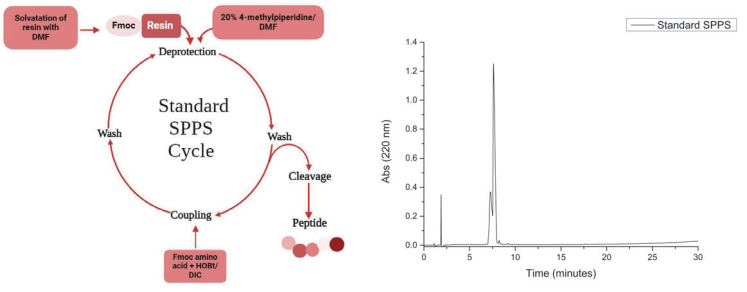

Figure 2: Synthesis of the EVF peptide using the partial GSPPS protocol with aminoethanol.

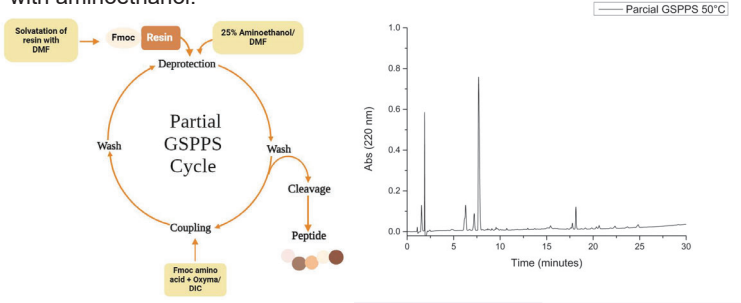

Figure 3: Synthesis of the EVF peptide using the partial GSPPS protocol with 2-amino-2-methyl-1-propanol.

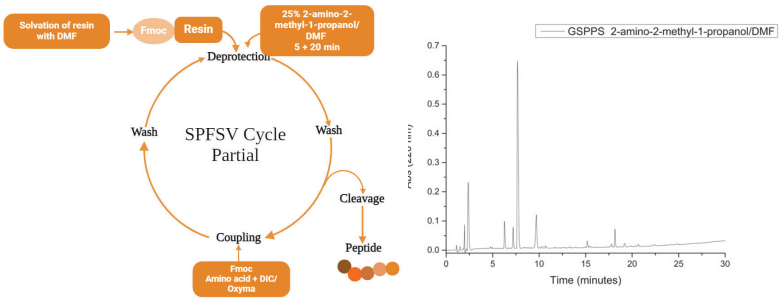

Figure 4: Synthesis of the EVF peptide using the GSPPS protocol with 2-amino-2-methyl-1-propanol in 2-MeTHF.

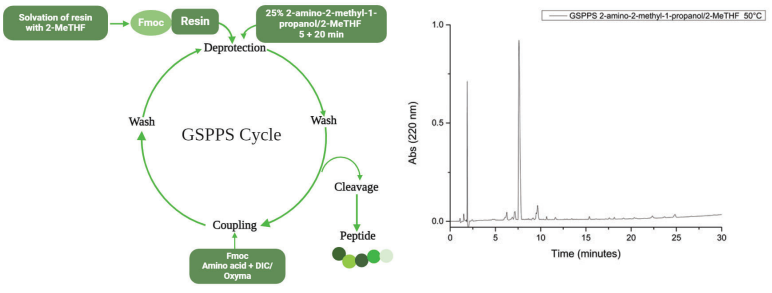

Figure 5: Synthesis of the EVF peptide using the GSPPS protocol with morpholine in 2-MeTHF.

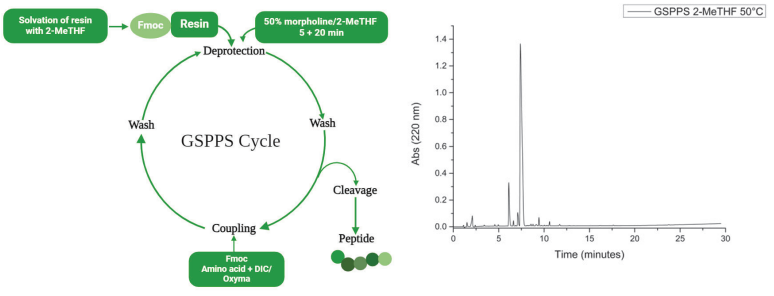

CONCLUSION

The deprotection methods evaluated were efficient in deprotecting the Fmoc group, and the peptides obtained from the new protocols applied for synthesis presented a higher degree of purity than the peptide synthesized by the standard SPPS protocol.

REFERENCE

(1) AL MUSAIMI, O.; JAD, Y. E.; KUMAR, A.; EL-FAHAM, A.; COLLINS, J. M.; BASSO, A.; LA TORRE, B. G.; ALBERICIO, F. Greening the solid-phase peptide synthesis process. 2-methf for the incorporation of the first amino acid and precipitation of peptides after global deprotection. **Organic Process Research & Development**, v. 22, n. 12, p. 1809-1816, 2018.

(2) AL MUSAIMI, O.; TORRE, B. G.; ALBERICIO, F. Greening Fmoc/t Bu solid-phase peptide synthesis. **Green Chemistry**, v. 22, n. 4, p. 996-1018, 2020.

(3) FERRAZZANO, L.; CATANI, M.; CAVAZZINI, A.; MAETELLI, G.; CORBISIERO, D.; CANTELMI, P.; FANTONI, T.; MATTELLONE, A.; DE LUCA, C.; FELLETI, S.; CABRI, W. TOLOMELLI, A. Sustainability in peptide chemistry: current synthesis and purification technologies and future challenges. **Green Chemistry**, v. 24, n. 3, p. 975-1020, 2022.

ACKNOWLEDGMENTS

FAPESP · CNPq Conselho Nacional de Desenvolvimento Científico e Tecnológico · LASEBio · CHEMYUNION Inspiring Innovation

https://doi.org/10.17952/37EPS.2024.P2176

Affinity Peptide Extraction Using Small-Molecule, Thermoresponsive Zwitterionic Liquid Materials

Yu-Hsin Chung and Yen-Ho Chu*

Department of Chemistry, National Chung Cheng University, 168 University Road, Chiayi 62102, Taiwan, Republic of China. E-mail: cheyhc@ccu.edu.tw; Tel: +886 5 2729139

The zwitterionic liquid materials are small-molecule newfangled organic salts and can be used as biocompatible solvents for biomolecule extraction. This poster presents the use of thermoresponsive ionic materials with LCST (lower critical solution temperature) properties for water-ionic liquid extraction aiming at both biomolecule enrichment and affinity extraction. Additionally, in affinity extraction, a small amount of **CIL1** (crowned ionic liquid) is added to utilize its crown ether cavity and cation-chelating ability for extracting biomolecules from aqueous solutions.

Synthesis of Zwitterionic Liquid Materials (ZMs)

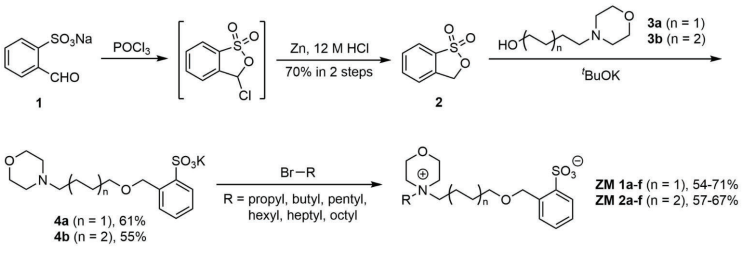

Scheme 1. Synthesis of **ZM 1a-f** and **ZM 2a-f**.

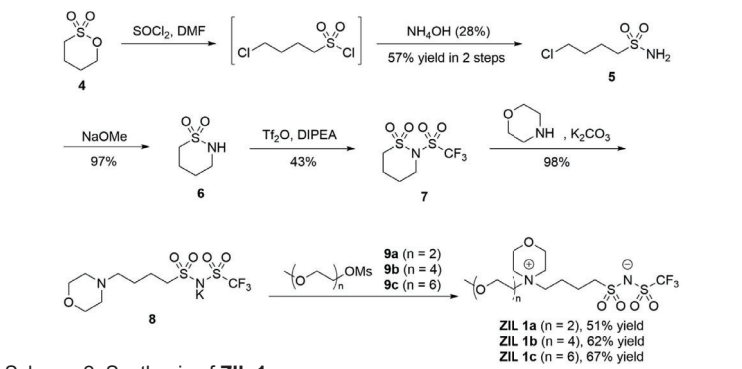

Scheme 2. Synthesis of **ZIL 1a-c**.

Results and Discussion

We successfully synthesized a small library of 12 ZMs, and discovered 3 ZMs (**ZM 1e**, **ZM 1f**, and **ZM 2d**) carrying LCST phase separation in water. A QR code allows to readily view the video actions of LCST phase transition with heating and cooling of **ZM 1f** in water.

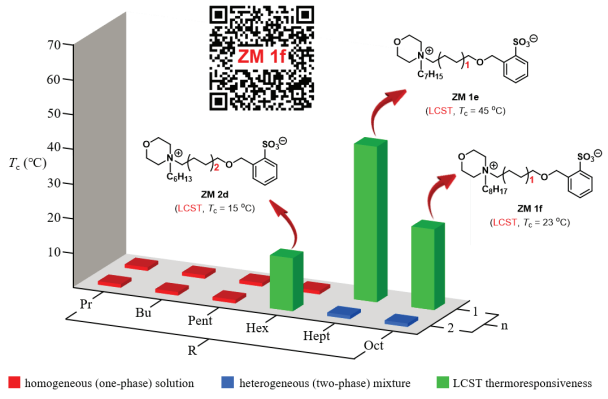

Figure 1. Thermoresponsive materials screening of a small library of 12 zwitterionic morpholinium sulfonates (**ZM 1a-f** and **ZM 2a-f**) upon mixing with water at temperatures between 4 ℃ and 90 ℃. With this library, three ZMs (labeled in green) show LCST phase transitions: **ZM 1e** (T_c = 45 ℃), **ZM 1f** (T_c = 23 ℃) and **ZM 2d** (T_c = 15 ℃).

Concentration enrichment of cytochrome c by ZM 2d

Figure 2 shows that **ZM 2d** is miscible with an aqueous cytochrome c solution (1:10, w/w) at low temperature (4 ℃) but undergoes LCST phase separation upon heating to 37 ℃. The result suggested that a highly diluted protein solution was readily enriched 16-fold. Furthermore, after the enrichment, cytochrome c maintains its original structure (no change of the Soret absorption) and is not destroyed.

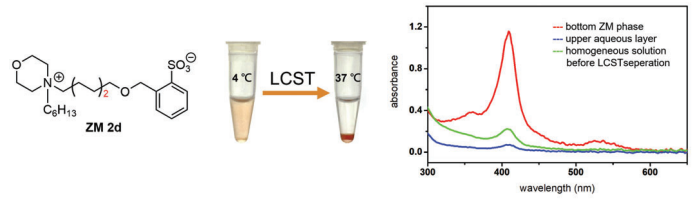

Figure 2. Photos and UV-vis spectra of **ZM 2d** enriched cytochrome c during its transition from the aqueous phase to ionic liquid phase via LCST mixing and separation.

Affinity extraction of peptides and protein by CIL 1

Figure 4 shows the extraction of peptides (Dab-$(R)_6$) and proteins (cytochrome c) using **ZIL 1b** (immiscible with water) and **ZIL 1c** (with LCST properties, T_c = 26 ℃). First, the ZILs are mixed with the aqueous solution containing biomolecules for extraction, where the biomolecules remain in the aqueous phase. Next, the affinity ionic liquid **CIL 1** is added for a chemoselective extraction based on biomolecular recognition, eventually resulting in the transfer of the biomolecules into the ionic liquid layer. Finally, by adding KCl (for peptides) or NH_4CO_2 (for cytochrome c), the biomolecules can be back-extracted into the aqueous phase while retaining their original structures.

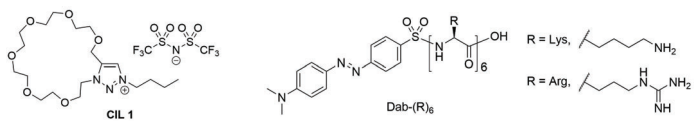

Figure 3. The structure of **CIL 1** and Dab-$(R)_6$

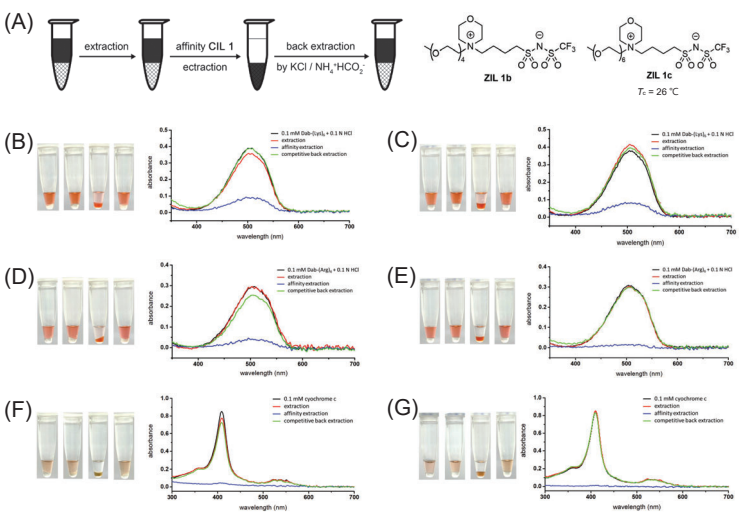

Figure 4. (A) presents the process of affinity extraction. (B) and (C) are the results of Dab-$(Lys)_6$ extraction using **ZIL1b** and **ZIL1c**, respectively. (D) and (E) are the results of Dab-$(Lys)_6$ extraction using **ZIL1b** and **ZIL1c**, respectively. (F) and (G) are the results of cytochrome c extraction using **ZIL1b** and **ZIL1c**, respectively.

Summary

We successfully developed zwitterionic thermoresponsive ionic liquid materials (LCST). We utilized their water-ionic liquid extraction system for the enrichment and affinity extraction of biomolecules containing Lys- and Arg-rich residues. Throughout the extraction process, the protein structure was preserved, demonstrating the potential of this biocompatible system for biomolecule separation and purification.

Acknowledgments

This research was supported by the Ministry of Science and Technology Council (NSTC 111-2113-M-194-010-MY2) and National Chung Cheng University in Taiwan, Republic of China.

Development of visceral smooth muscle

Optimization of pDNA delivery by WRAP cell–penetrating–peptide

Karidia Konate[1], **Sébastien Deshayes**[1], **Prisca Boisguérin**[1], **Eric Vivès**[1], **Sandrine Faure**[1], **Pascal De Santa Barbara**[1].

1 - *PhyMedExp - Université de Montpellier, INSERM U1046, CNRS UMR 9214, CHU Arnaud de Villeneuve, 371 av. doyen Giraud, 34295 Montpellier Cedex 5, France*

karidia.konate@inserm.fr

https://doi.org/10.17952/37EPS.2024.P2178

CCP	Sequence	Length	Charge	Nb W	Nb R	Nb L
WRAP1 (W1)	LLWRLWRLLWRLWRLL	16	5	4	4	8
WRAP5 (W5)	LLRLLRWWWRLLRLL	15	5	3	4	8
NLS-WRAP1 (WIN)	KKKRKV-LLWRLLWRLLWRLWRLL	22	10	3	5	8

Introduction

WRAP peptides are short tryptophan and arginine-rich amphipathic cell-penetrating peptides (CPPs) first dedicated to the delivery of short interfering RNA (siRNA) [1]. By a non-covalent strategy, the peptide and the siRNA form spontaneously peptide-based nanoparticles (PBNs) with a size of around 100 nm and able to silence efficiently the targeted protein in numerous cell lines but also *in vivo* [1,2]. Transfection that introduces DNA plasmid (pDNA) in cells represents a promising tool for fundamental, translational and therapeutic fields. The difference in size and flexibility between small, rigid siRNA and larger, more flexible pDNA poses a challenge for WRAP-based PBNs in improving cellular transfection and protein expression.

In the present study, we optimize formulation and internalization conditions for pDNA to obtain effective transfection with WRAP peptides. This fine-tuning between PBN formation and delivery implies the definition of an optimal charge of ratio and the final quantity applied on cells to avoid cytotoxicity. By employing a model plasmid that expresses and addresses fluorophores exclusively in the nuclei trough a Nuclear Localization Sequence (NLS), we successfully demonstrated significant GFP and mCHERRY expression levels in HEK293 and HELA cell lines through flow cytometry experiments and confocal microscopy. In order to obtain protein expression even in non-dividing cells, WRAP peptides were functionalized with a NLS sequence to obtain PBNs able to cross the nuclear envelope. This conducts to the efficient delivery and expression of GFP into non-dividing cells [3].

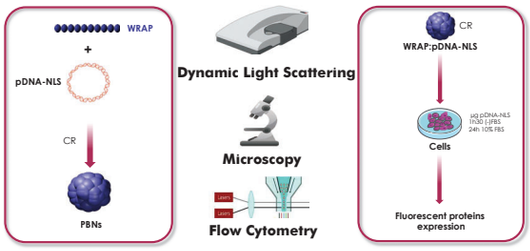

1. WRAP5 for Plasmid Delivery

FIGURE 1

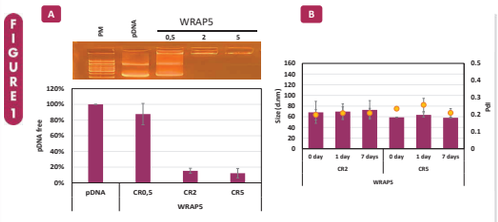

PBNs Formation

A/ By gel shift assay we determined a fully complexation of the plasmids from CR2 with WRAP5. B/ W5-PBNs are characterized as homogeneous nanoparticles around 60 nm and stable until 7 days by DLS.

FIGURE 2

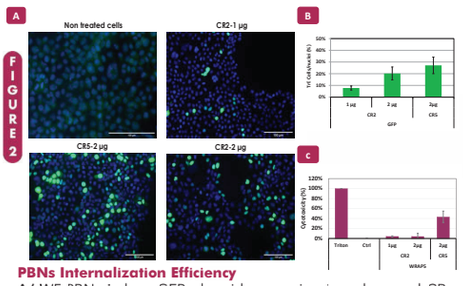

PBNs Internalization Efficiency

A/ W5-PBNs induce GFP plasmid expression in a dose and CR-dependent manner in HEK293 cells. B/ Quantification of GFP-expressing cells (ratio between GFP-expressing cells and total number of nuclei stained by DAPI - approximately 30% of the cells expressed GFP. C/ LDH cytotoxicity test (W5-PBNs toxicity reached 40% for the highest CR and dose applied).

FIGURE 3

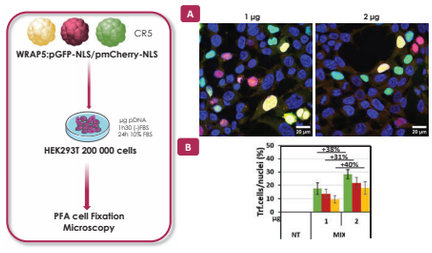

PBNs Encapsulating pDNA–NLS for Multi–Protein Expression

A/ W5 can internalize both plasmids in one PBN that conducts the co-expression of GFP and mCherry in the same nuclei in HEK293 cells.

B/ Quantification reveals a dose-dependent expression of GFP, mCherry, or both proteins (approximately 30% of the cells expressed the GFP).

2. Ajusting of parameters to optimize efficiency and to reduce cytotoxicity

FIGURE 4

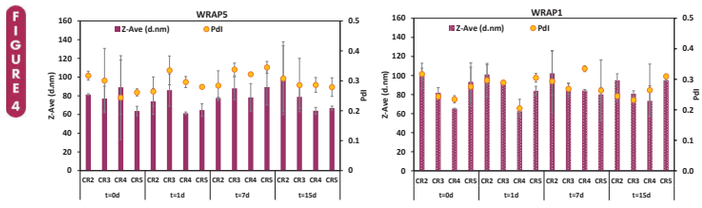

Comparison of WRAP5 and WRAP1 PBN Formation at different charge ratios (CR)

PBNs formation was compared at CR of 2, 3, 4 and 5 for W5 and W1. Both harbor constant size, homogeneous, and stable over time nanoparticles whatever CR of formulation. Globally sizes are under 100 nm.

FIGURE 5

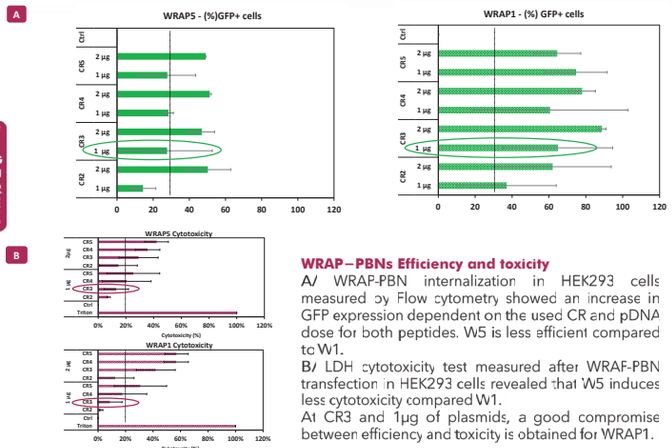

WRAP–PBNs Efficiency and toxicity

A/ WRAP-PBN internalization in HEK293 cells measured by Flow cytometry showed an increase in GFP expression dependent on the used CR and pDNA dose for both peptides. W5 is less efficient compared to W1.

B/ LDH cytotoxicity test measured after WRAP-PBN transfection in HEK293 cells revealed that W5 induces less cytotoxicity compared W1.

At CR3 and 1µg of plasmids, a good compromise between efficiency and toxicity is obtained for WRAP1.

3. Internalization in confluent cell condition

FIGURE 6

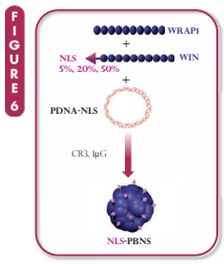

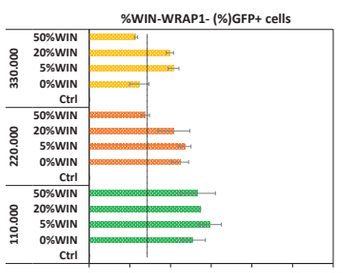

WRAP1 functionalized PBNs on HELA cells

W1- PBNs functionalized with 0%, 5%, 20%, or 50% of WIN-peptide were applied on HeLa cells at different cell confluence (110 000 cells = ~70% confluence compared to 220 000 cells = ~85% confluence, and 330 000 cells = full confluence / non-divinding cells).

CONCLUSION

- WRAP peptides can fully complexed plasmids at CR ≥2
- WRAP1 and WRAP5 form homogeneous and stable nanoparticles (<100 nm)
- WRAP-PBNs are able to internalize two plasmids for multi protein expression
- WRAP-PBNs internalize plasmid for gene expression in a CR and dose-dependent manner
- Efficient delivery with lowest toxiciy are obtained for PBNs at CR3 using 1 µg of plasmid
- Functionalization of WRAP1 with NLS allows efficient delivery in non-dividing cells

References

[1] Konate K. *et al.* Peptide-Based Nanoparticles to Rapidly and Efficiently "Wrap 'n Roll" siRNA into Cells. *Bioconjug Chem*. **2019** Mar 20;30(3):592-603.

[2] Ferreiro I. *et al.* In Vivo Follow-Up of Gene Inhibition in Solid Tumors Using Peptide-Based Nanoparticles for siRNA Delivery. *Pharmaceutics*. **2021** May 19;13(5):749.

[3] Guerin A. *et al.* LIX1-mediated changes in mitochondrial metabolism control the fate of digestive mesenchyme-derived cells. *Redox Biol*. **2022** Oct,56:102431

https://doi.org/10.17952/37EPS.2024.P2180

mascot "pep"

Application of coumarin-type chemiluminophore toward *in vivo* detection

Yukie Nohara[1], Keiko Taniguchi[2], Hiromi Ii[3], Shun Masuda[1], Hiroko Kawakami[1], Masakatsu Matsumoto[4], Susumu Nakata[3], and Toshiyuki Sakai[2], Taku Yoshiya[1, 5]

[1]Peptide Institute, Inc., [2]Department of Drug Discovery Medicine, Kyoto Prefectural University of Medicine, Kyoto Pharmaceutical University, [3]Department of Clinical Oncology, [4]Department of Chemistry, Kanagawa University, [5]Institute for Protein Research, Osaka University.

Chemiluminogenic compound "BDU"

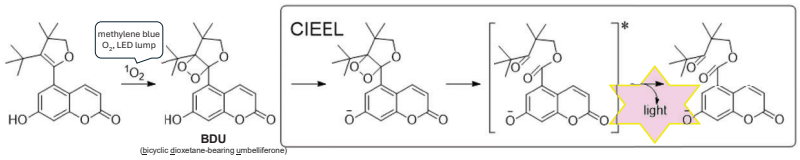

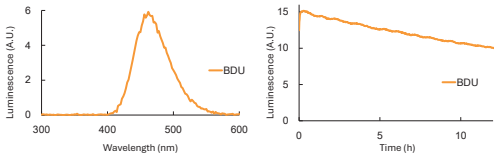

Luminescence spectrum and time course (Em:476 nm, 10 μM in PBS/DMSO(9/1)).

✓ Dioxetane-containing compounds flash without the assistance of any enzymes, such as luciferases.
✓ Long-lasting chemiluminescence ($T_{1/2}$=20 h, in PBS, 40℃)

Dioxetanes (-C-C-O-O- 4-membered ring) are known to 'accessible high-energy chemiluminogenic intermediates'. In chemiluminogenic probes, dioxetane moiety is positioned at the meta-position of the phenolic hydroxy group, and upon dissociation of the proton of the hydroxy group, chemically initiated electron exchange luminescence (CIEEL) occurs immediately to cast light.

OFF-ON probe

: Hydroxy groups are masked by O-acylation and de-masked enzymatically or chemically.

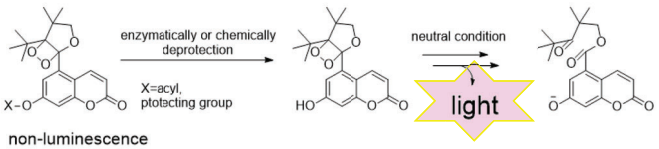

Always ON probe

: As a tracer molecule, like a radioisotope or fluorophore.

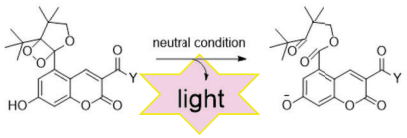

We synthesized the chemiluminogenic probes containing BDU (bicyclic dioxetane-bearing umbelliferone) moiety. BDU moiety is a long-lasting chemiluminophore, where our group discovered that the bicyclic structure is crucial for protecting sensitive dioxetane moiety. Using this characteristic, here we desined two types of probes: i) OFF-ON type, and ii) always ON type.

OFF-ON type: *GGCT* probe "LISA-103"

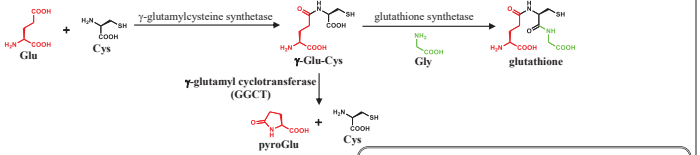

GGCT recognizes **γ-Glu-Xaa** as a substrate but **not γ-Glu-peptide**.

The tumor-related protein "C7orf24" is a γ-glutamylcyclotransferase (GGCT). And GGCT involved in regulation of the glutathione homeostasis.

・ Characteristics of GGCT:
(I) a diagnostic marker of bladder urothelial carcinoma
(II) silencing of the gene by siRNA showed an antiproliferative effect on cancer cell
(III) over-expressed in a range of cancers

A novel tumor-related protein, C7orf24, identified by proteome differential display of bladder urothelial carcinoma.

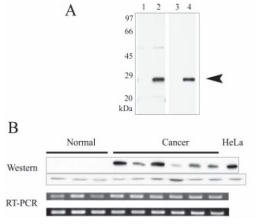

S. Kageyama *et al.*, *Proteomics Clin. Appl.* **2007**, *1*, 192; 特許 第4712692号.

Prevention of tumor growth by needle-free jet injection of anti-C7orf24 siRNA

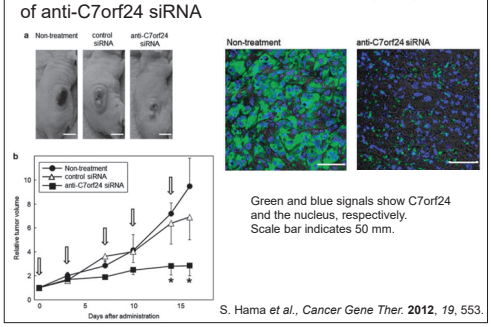

Green and blue signals show C7orf24 and the nucleus, respectively. Scale bar indicates 50 mm.

S. Hama *et al.*, *Cancer Gene Ther.* **2012**, *19*, 553.

Chemiluminogenic GGCT probe "LISA-103"

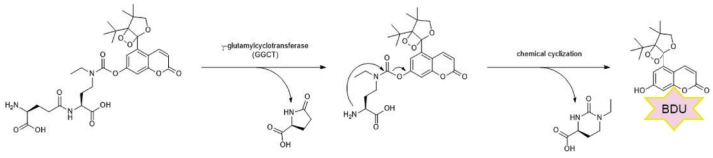

・ Quantification of GGCT activity using recombinant protein

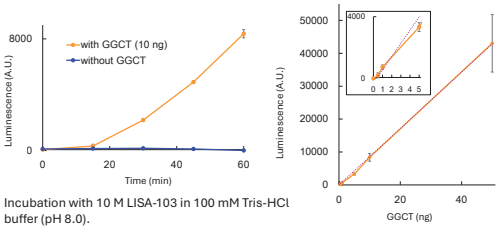

Incubation with 10 M LISA-103 in 100 mM Tris-HCl buffer (pH 8.0).

LISA-103 contains a masked *O*-acylated BDU. The luminescence from BDU was efficiently suppressed (less than 1%) by its *O*-acylation, and increased by time in the presence of GGCT.

Cell-permeable GGCT probe "MAM-LISA-103"

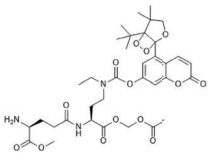

LISA-103 couldn't penetrate cell membrane, so we developed a new probe, methyl and acetoxy methyl esters (MAM)-LISA103. As expected, MAM-LISA-103 successfully enabled monitor of intracellular GGCT activity, and also, in vivo GGCT imaging was achieved.

・ GGCT activity in living cell

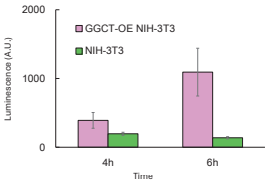

Cells were treated with 25 μM of LISA-103. The luminescence was measured without cell-wash.

・ Imaging of tumor-bearing mouse

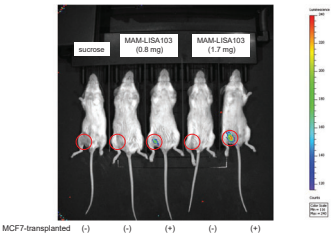

MAM-LISA-103 was injected in tumor and imaging was performed after 10 min.

Y. Nohara *et al. Org. Biomol. Chem.* **2023**, *21*, 5977.

Always ON type: Glucose tracer "2-DGU"

*Collaboration with Dr. K. Kaneda-Nakashima and Dr. Y.Shirakami at Osaka University.

・ Synthesis of 2-DGU

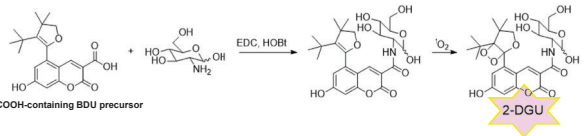

To achieve the synthesis of "always ON type" probe, we designed and synthesized **COOH-containing BDU precursor**, the novel chemiluminophore-introducing reagent, which enables simple chemiluminogenic decoration of an amine-containing compound.
2-DGU casted light with the half-life of 26 h at 40℃. In bioimaging study, 2-DGU was visible after intratumor injection. We are now applying it to *i.v.* injections.

・ Luminescence of 2-DGU

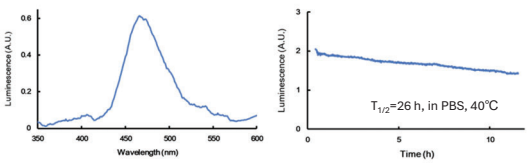

Luminescence spectrum and time course (Em:476 nm, 10 μM in PBS/DMSO(9/1)).

Imaging by IVIS.

・ Imaging of tumor-bearing mouse

Intratumor injection

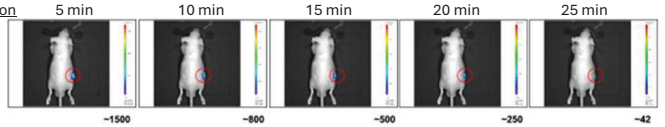

2-DGU was injected in 0.5 mg /*i.t.* Mouse images were taken at the times indicated in each figure after injection.

Y. Nohara *et al. ChemBioChem* **2022**, *23*, e202200556.

Take-home message: BDU-probes would accelerate biological/disease research.

DEVELOPMENT OF NOVEL AUTOMATED SOLID PHASE PEPTIDE SYNTHESIZERS ENSURING ECONOMIC, EFFECTIVE, SCALABLE AND GREEN SYNTHESIS

https://doi.org/10.17952/37EPS.2024.P2181

Krisztina Kiss[1,2], Soma Ránky[2], László Molnár[2]

[1] HUN-REN-ELTE Research Group of Peptide Chemistry, Budapest, Hungary,
[2] SolidScience Plc, Budapest, Hungary / www.solidscience.eu

Introduction

Peptide-based pharmaceutics are at the forefront of pharmaceutical innovation and academic research. However, the high costs associated with solid phase peptide synthesis pose a significant financial challenge to this research domain, due to the costly instruments involved and the extensive use of expensive raw materials. To tackle these challenges, further optimization of synthesizers is crucial to reduce the costs, time, and manual labor of peptide synthesis. These ideal instruments should be efficient, flexible, economical, scalable, robust, and aligned with green chemistry principles. Such advancements could accelerate peptide-based pharmaceutical research in academic and in industrial R&D settings.

Custom doser

- ▶ Fast and efficient dosing
- ▶ Reagent handling with disposable syringes:
  - Cleaning free
  - Minimal waste of raw materials
- ▶ 36 places for reagents
- ▶ 3 special places for large quantity and even heated liquid dosing from external reservoirs
- ▶ User friendly
- ▶ EXTREMELY REDUCED FOOTPRINT
- ▶ We developed a new synthesizer adapted to the new doser:
  - 1 to 6 synthesis vials
  - Optional heating/cooling
  - Optional UV readout
  - Synthesis monitoring



Flow based synthesizer

- ▶ Though our batch technology based syntesizers fulfiled our requirements, we thought that FLOW techology could offer new opportunities:
  - Better heat transfer and very effective mixing
  - Radically decreased synthesis time
  - Straightforward scale-up possibility
  - Continuous flow-through UV readout for reaction monitoring
- ▶ We implemented a recirculation based flow system, with high (>500mL/min) flow-rates
- ▶ Reagent dosing with our doser or even with Tecan liquid handler or manually

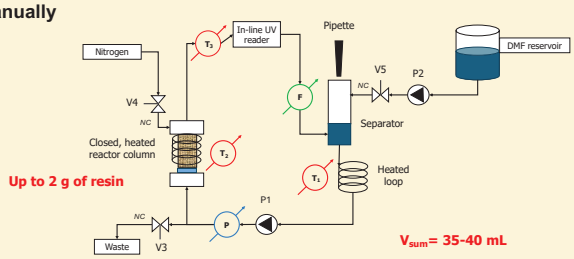

Table 3: Reproducing the results of a marketed synthesizer with our system

Sequence	Our custom FLOW synthesizer	CEM Liberty 2.0
	Yield (%)	
YSYPETPLYMQTASTSYYE	37	47
ALAVLSNYDA	84	84

- ▶ Recirculation offers longer cycle times (if needed), without the extensive use of raw materials
- ▶ Despite the high flow-rates, the pressure in the system is still low (<3bar), resulting that all types of resin is applicable in the system
- ▶ All synthesis parameters are monitored and stored in database





Classical batch technology

- ▶ Classical SPPS methodology – no pressure or heat
- ▶ Fully automated
- ▶ 1 to 12 reactor – 1 to 12 parallel synthesis
- ▶ Scale: 0.1-1.0 g resin with capacity of 0.2-0.9 mmol/g
- ▶ Inert atmosphere
- ▶ Constant good mixing
- ▶ Minimal solvent usage – Total solvent usage per steps 3.5-4.0 mL
- ▶ Relatively fast synthesis (compared to manual synthesis): 30-60 min cycle time

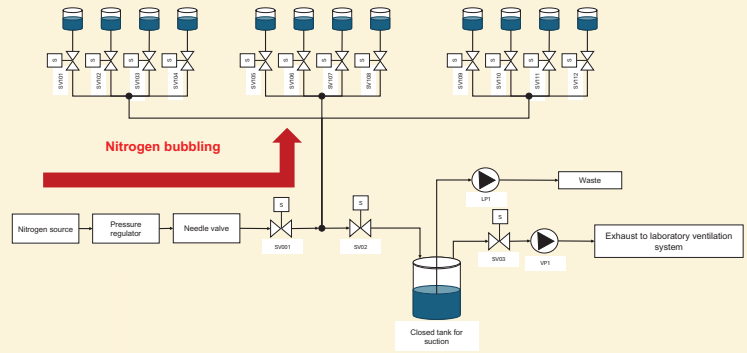

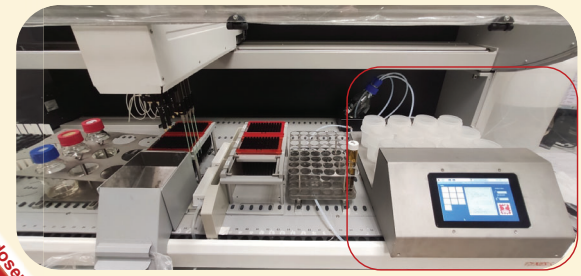

*First iteration as a **Tecan add-on** **Tecan Worktable** was mandatory which slowed down and limited some functions*

	Procedure	Solvent usage (mL)	Time (min)
0. Initialization step	Resin swelling	8	30-60
	4 x Fmoc-removal (deprotection)	4 x 3.5	4 x 1 (4 x 2 if 20% pip. was used)
	6 x Wash after deprotection	6 x 4	6 x 1
1. step	AA Coupling	3.5	15-30
2. step	3 x Wash after coupling	3 x 4	3 x 1
3. step	2 x Fmoc-removal (deprotection)	2 x 3.5	2 x 1 (2 x 2 if 20% pip. was used)
4. step	6 x Wash after deprotection	6 x 4	6 x 1

Table 1: Typical synthesis parameters

Coupling reagent		AA	t	Solvent	Crude Yield (%)	Purity (%)	Yield (%)	Cost (EUR/mg)
PyAOP/DIPEA	2/4 eq	2 eq	30 min	DMF	96.59	80.71	77.96	0.18
PyAOP/DIPEA	3/6 eq	3 eq	30 min	DMF	91.21	81.01	73.90	0.25
PyAOP/DIPEA	3/6 eq	3 eq	15 min	DMF	89.98	81.25	73.11	0.25
PyAOP/DIPEA	3/6 eq	1.2 eq	30 min	DMF	88.95	72.90	64.85	0.19
Oxyma/DIC	3/6 eq	3 eq	30 min	DMF	82.35	84.83	69.86	0.13
PyAOP/DIPEA	2/4 eq	2 eq	15 min	DMF	86.53	62.72	54.27	0.27
Oxyma/DIC	3/6 eq	3 eq	30 min	GVL	61.48	72.00	44.27	0.47
PyAOP/DIPEA	1.2/2.4 eq	1.2 eq	30 min	DMF	80.28	55.03	44.18	0.18

Table 2: Synthesis of ipAoa-LRRY-VHLFYLT-NH2 on RinkAmide MBHA (0,65 mmol/g) resin

Color coding: Hybrid ratio in coupling step, Synthesis with green solvent (GVL)

Summary

With our recent developments, we aimed to address the challenges highlighted in the introduction: reducing costs, time, and manual labor associated with peptide synthesis. By eliminating expensive components such as microwave heating from our synthesizers, the total cost of ownership for these products becomes manageable even for peptide research labs with limited budgets.

https://doi.org/10.17952/37EPS.2024.P2183

Discovery and Characterization of a Short Peptide Possessing a Latent Warhead Undergoing Intramolecular Cyclization in the Aqueous Environment

○Riku Katsuki and Masumi Taki
The University of Electro-Communications (UEC), Tokyo, Japan
E-mail: k2343004@edu.cc.uec.ac.jp, taki@pc.uec.ac.jp

Abstract

Peptidic targeted covalent inhibitor (TCI) can form a specific covalent bond to a target protein and show semi-permanent drug effects. Such a TCI should possess a latent reactive group (i.e., warhead), which can react only in a bioactive site of the target protein(i.e., matchmaking microenvironment). We hypothesize that even a simple peptide without needing a complex protein would create the matchmaking microenvironment. This peptide had a geometry in which a nucleophilic tyrosine and the electrophilic AFS are supposed to be stacked each other by π-π interaction. In addition, the reactivity of an AFS was increased in a hydrophilic environment, rather than a hydrophobic environment.

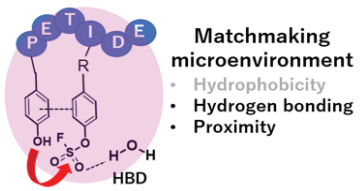

Background

Targeted Covalent Inhibitor (TCI)[1]

TCIs form a specific covalent bond to a target protein and show semi-permanent drug effects.

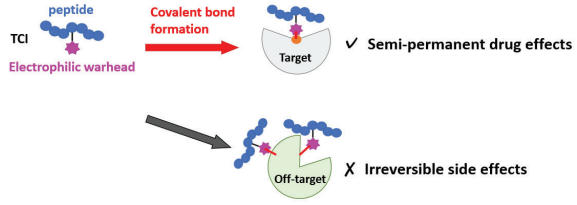

[1] Tabuchi Y., Yang J. and Taki M., *Int. J. Mol. Sci.*, **23**, 7778 (2022).

Latent warhead[2]

Aryl-fluorosulfate has a latent reactivity; it is activated only in a matchmaking microenvironment.

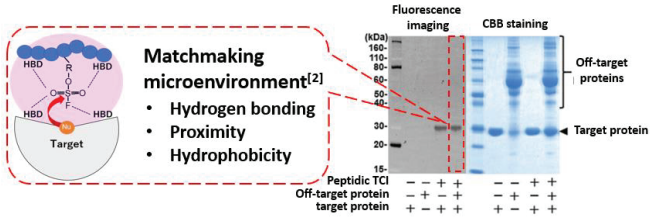

[2] Yang J., Tabuchi Y., ○Katsuki R. and Taki M., *Int. J. Mol. Sci.*, **24**, 3525 (2023).

Result and discussion

Characterization of the intramolecular cyclization

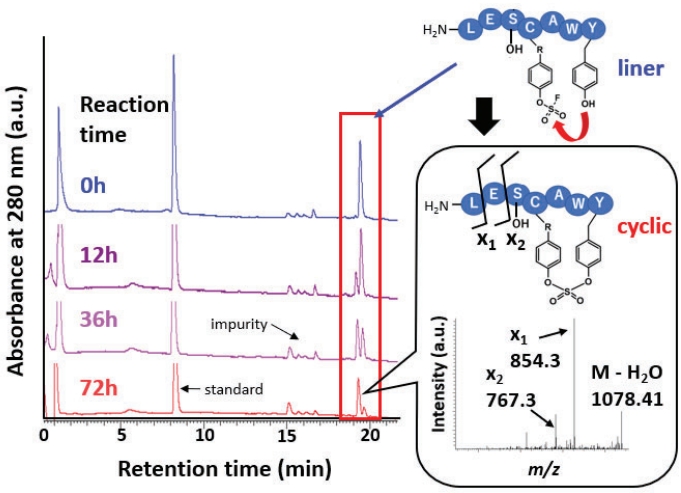

Solvent effects

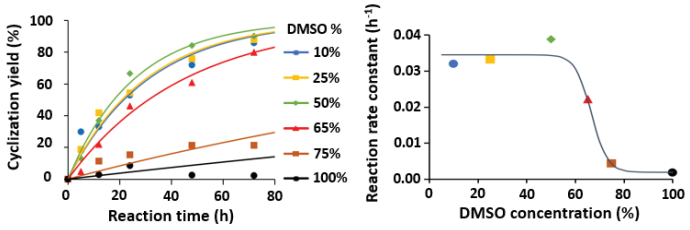

MD simulation in the aqueous environment

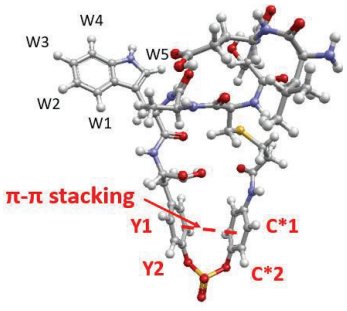

Position selectivity of cyclization

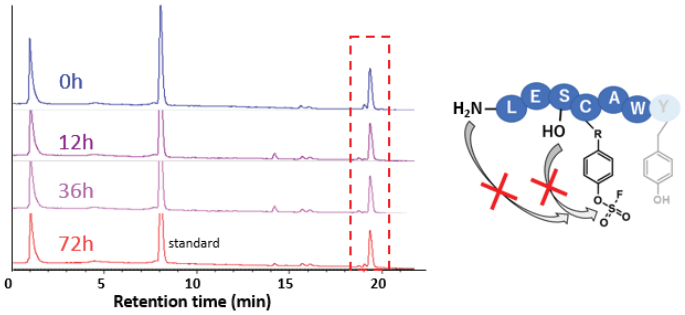

^{1}H-NMR spectra of the cyclic peptide

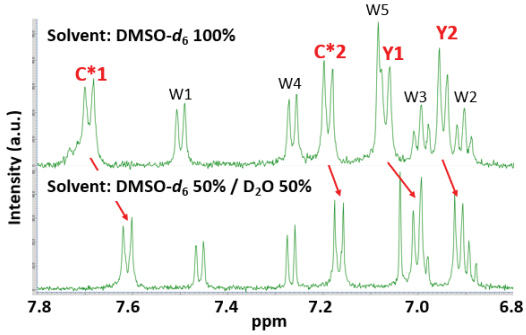

Future perspective

We will investigate the sequence dependency of this activation. Also, we wonder that we would construct a staple peptide library by the demonstrated tyrosine-selective cyclization.

A fishing technology of glycated peptides

F. Nuti[1,2*], M. Marino[1,2], P. Ledwon,[1,3,4] R. Latajka[4], A. Lapolla[5], M. Chorev[6], P. Rovero[1,3], A.M. Papini[1,2]

*e-mail: francesca.nuti@unifi.it

https://doi.org/10.17952/37EPS.2024.P2186

[1]Interdepartmental Research Unit of Peptide and Protein Chemistry and Biology, University of Florence, Sesto Fiorentino, Italy
[2]Department of Chemistry "Ugo Schiff", University of Florence, Sesto Fiorentino, Italy
[3]Department of Neurosciences, Psychology, Drug Research and Child Health, University of Florence, Sesto Fiorentino, Italy
[4]Department of Bioorganic Chemistry, Faculty of Chemistry, Wrocław University of Science and Technology, Wrocław, Poland
[5]Diabetology and Dietetics, Department of Medicine (DIMED), University of Padova, Padova, Italy
[6]Laboratory for Translational Research, Department of Medicine, Brigham & Women's Hospital, Harvard Medical School, Boston, MA, U.S.A.

Introduction

Glycation is a non enzymatic post-translational reaction between glucose and amino functions in proteins at *N*-terminus and/or on Lys or Arg side-chains. Amadori products are well known in food chemistry, but also as intermediates of Advanced Glycation End Products (AGEs) involved in complications of Diabetes and other neurodegenerative diseases [1]. The non enzymatic glycation of peptides and proteins in human beings occurs spontaneously in vivo but is highly pronounced when persistent and excessive levels of glucose are present in blood as in the case of diabetes: the sugar-modified peptides may modify their functional conformation and lead to lose of their normal activity. Thus, detection, isolation and sequencing of glycated peptides is crucial. Solid supports modified with a phenyl boronate (PhB) moiety can be useful tools to fish out peptide-sugar conjugates in biological fluids.

In our previous work ChemMatrix® Rink (CMRR) resin modified with a lysine substituted two PhB units, PhB-Lys(PhB)-CMRR was found to be able to capture selectively peptides containing deoxyfructosyl-lysine moieties, which then can be efficiently and specifically detected by MS experiments [2]. In order to optimize this "fishing" methodology, in terms of efficiency and selectivity, we studied the capturing of deoxyfructosylated peptides (**1-8**) by (i) comparing the above mentioned the ChemMatrix® Rink resin (CMRR) with ω-Aminohexyl–Agarose resin (ω-AHA) and by (ii) comparing the same two resins, CMRR and ω-AHA, modified with mono- or di-PhB substituted Lys moieties.

Resin Synthesis

To compare the different capture properties of both resins, the ω-AHA was functionalized on the amino function with the Rink Linker present in the commercially available ChemMatrix® Rink resin and called this new solid support Agarose Rink Resin (AGRR).

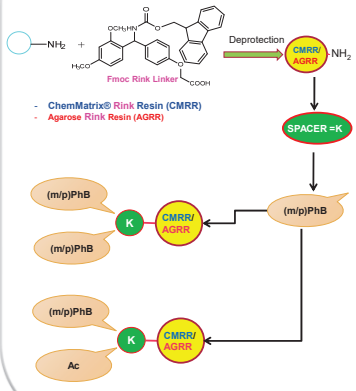

Table 1 Functionalized resins to capture glycated peptides.

CMRR - ChemMatrix® Rink resin; AGRR - Agarose Rink resin

No.	Resin			Loading (mmol/g)	Quantity (g)
1	CMRR	di-modified	*p*-PhB-Lys(*p*-PhB)-CMRR	0.462	0.961
2			*m*-PhB-Lys(*m*-PhB)-CMRR	0.354	0.533
3		mono-modified	Ac-Lys(*p*-PhB)-CMRR	0.298	0.549
4			Ac-Lys(*m*-PhB)-CMRR	0.151	0.487
5			*p*-PhB-Lys(Ac)-CMRR	0.274	0.478
6	AGRR	di-modified	*p*-PhB-Lys(*p*-PhB)-AGRR	0.524	0.0284
7			*m*-PhB-Lys(*m*-PhB)-AGRR	0.406	0.0698
8		mono-modified	Ac-Lys(*p*-PhB)-AGRR	0.317	0.0252
9			Ac-Lys(*m*-PhB)-AGRR	0.203	0.0702

Table 2 List of the Amadori CD59 peptides and the glycosylated peptides to test.

No.	Name	Sequence	MW [g/mol]	Quantity available (mg)
1	***"Amadori" Peptide 1***	Ac-YNKSWK(ε(Nε-1-deoxyFru)FEHSNFNDVC-OH	2236	5
2	***Non-modified Peptide 1***	Ac-YNKSWKFEHSNFNDVC-OH	1930	5
3	***Scrambled Peptide 1***	Ac-**VSEND**K(Nε-1-deoxyFru)YNFHKSWNFC-OH	2236	5
4	***Amadori GCD-59 Surrogate Calibrator***	Ac-NKAWK(Nε-1-deoxyFru)FEHANFNDC(OH)-***PEG LINKER***-Ac-ACFNDVTTRLRENELTYYCAAK	5940	5
5	***Glucitol GCD-59 Surrogate Calibrator***	**Ac-A[CNFNDVTTRLRENELTYYC]AAK-NH$_2$** (dPEG$_{24}$-Succ) **Ac-NKAWK (Glucitol) FEHANFNDC-OH**	5944	PCS-32532-PI:5 x 1mg, PCS-30321-PI1 x 5mg
6	**[Ser^7(Glc)]CSF114**	H-TPRVERS^7(β-D-Glc)GHSVFLAPYGWMVK-OH	2579	-
7	**[Asn^7(Gal)]CSF114**	H-TPRVERN^7(β-D-Gal)GHSVFLAPYGWMVK-OH	2606	-
8	**[(Nε-1-deoxyFru)]CSF114**	H-TPRVERK^7(Nε-1-deoxyFru)GHSVFLAPYGWMVK-OH	2621	10
	Glycated CD59 peptides(**1-5**) were provided by Prof. Michael Chorev (Mellitus, LLC)			

Procedure description:

- Resin swelling in 1 mL of ammonium bicarbonate buffer (**B**) for 1 h, filtration.
- Dissolving a peptide in **B**. Solutions for the capturing will be in saturating concentrations, relatively equal to the amount of dry resin used and calculated taking into account the resin loading value.
- Capturing reaction, shaking continuously (1-1.5 h).
- Filtration.
- Washing the resin with **B** – filtrates should contain the uncoupled peptide.
- Cleavage reaction in 1 mL of acidic buffer **A** (1 h).
- Filtration.
- Washing the resin with buffer **A** – filtrates should contain the captured peptide.
- Lyophilizing both solutions.
- Dissolving the peptide residues in each tube in precise volume of H_2O.
- UV-Vis analysis of both samples – measurement of Abs values, summing them up and calculation of capture percentage. Use of LC-MS analysis in case of peptide mixtures (>1 peptide).

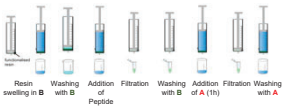

B (basic): 30 min in ammonium bicarbonate buffer (50 mM) at pH 8 in H_2O/MeCN 1:1 (*v/v*)

A (acidic): 0.1% HCOOH in H_2O/MeCN 1:1 (v/v) for 1h

Capturing of naturally occuring sequences of glycated and glycosylated peptides by the new functionalized resin

With the aim to select and optimize a resin to fish out deoxyfructosylated peptides, as early glycation biomarkers of diabetes, in terms of efficiency and selectivity, we selected 8 peptides (**Table 2**): 4 Amadori peptides (**1-4,** and **8**), 1 negative control (**5**) and 2 glycosylated peptides (**6-7**). Herein, we report, the capturing results of glycated peptides by (i) two different resins: the ChemMatrix® Rink resin (CMRR) and the ω-Aminohexyl–Agarose (ω-AHA), and by (ii) the same resins, CMRR and ω-AHA, modified by either mono- or di-PhB substituted Lys moieties (**Table 1**).

mono- or bifunctionality on the capturing ?

Schematic Capturing experiment

Experiment 1. In our previous investigations we tested the *para*-analogues of the CMRR resin (data not shown). Now, a set of 8 peptides (**1-8**) was tested with each *meta*-resin (**Table 1:** Resins **2, 4, 7, 9**) :



Meta or para PhB orientation on the capturing ?

Experiment 2. After completing the **Experiment 1**, a set of 8 peptides (**1-8**), each one separately, was tested with *para*-analogue resin (**Table 1:** Resins **1, 3, 6, 8**) and the most efficient *meta*-analogue resin selected previously.



para analogue of the most efficiently capturing CMRR (**3**) resin
para analogue of the most efficiently capturing AGRR (**8**) resin

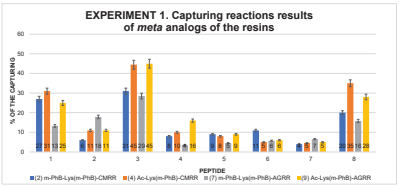

("the percentage of capturing was calculated using the sum of peak areas in „captured" and „uncaptured" samples as 100%)

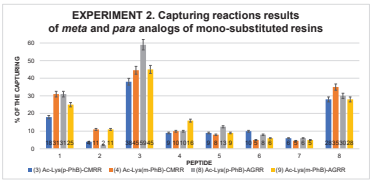

("the percentage of capturing was calculated using the sum of peak areas in „captured" and „uncaptured" samples as 100%)

Conclusions from Experiments 1 and 2.

1. The results suggest **better binding of the Amadori-containing peptides to the mono-substituted CMRR and AGRR resins**
2. Mono-*m*-PhB substituted resins **4-CMRR** and **9-AGRR** demonstrated to be better in terms of efficiency

Comparison of CMRR Resin and AGRR Resin capturing ability once containing only one PhB moiety

Experiments 3 (A-C) were designed in order to determine the **selectivity of AGRR and CMRR** resins toward the Amadori product when presented in a peptide mixture. Three solid supports were examined: Ac-Lys(*m*-PhB)-CMRR (**4**), Ac-Lys(*m*-PhB)-AGRR (**9**) and the commercially available AGRR (A8530-Sigma Aldrich). Ad hoc aqueous solutions containing the synthetic peptides were prepared as follows: solution of [(Nε-1-deoxyFru)]CSF114 and [(N(Glc)]CSF114 at the same concentration (mg/ml) in the **exp 3A**; the same solution but at 5% of [(Nε-1-deoxyFru)]CSF114 in the **exp 3B**; equimolar solution (mM) of eight synthetic peptides with two Amadori peptides in the **exp 3C**. These peptides were selected for the following characteristics: amino acid sequence, hydrophobicity, different length and bearing post-translational modification (DeoxyFru, Ac, PO_3H_2, and Pam). The mixtures were dissolved in an ammonium bicarbonate buffer solution at pH 8 and then subjected to the capturing reaction conditions described above

Experiments 3A and 3B (n=2)		
	RESINS	**PEPTIDES**
A	(**4**) Ac-Lys(*m*-PhB)-CMRR (**9**) Ac-Lys(*m*-PhB)-AGRR *m*-Aminophenylboronic acid–Agarose (A8530)	**Nε-1-deoxyFru *vs* Glc (1:1)** [Lys^7(Nε-1-deoxyFru)]CSF114 *vs* Asn^7(Glc)CSF114
B	(**4**) Ac-Lys(*m*-PhB)-CMRR (**9**) Ac-Lys(*m*-PhB)-AGRR *m*-Aminophenylboronic acid–Agarose (A8530)	**Nε-1-deoxyFru *vs* Glc (0.1 :1)** [Lys^7(Nε-1-deoxyFru)]CSF114 *vs* Asn^7(Glc)CSF114

RESIN	Amount	Captured peptide	CONCLUSION
(**4**) Ac-Lys(*m*-PhB)-CMRR **Captured**	1:1	**Nε-1-deoxyFru**	**Resin (4) is able to capture selectively the glycated peptide, even at low concentrations**
	1:0.1	**Nε-1-deoxyFru**	
(**9**) Ac-Lys(*m*-PhB)-AGRR **Captured**	1:1	**Nε-1-deoxyFru**	Resin (**9**) is able to capture selectively the glycated peptide only when the peptide is present in high excess
	1:0.1	**Nε-1-deoxyFru** & Glc	
m-Aminophenylboronic acid–Agarose (A8530) **Captured**	1:1	**Nε-1-deoxyFru**	Commercial agarose resin (A8530) is able to capture selectively the glycated peptide only when the peptide is present in high excess
	1:0.1	**Nε-1-deoxyFru** & Glc	

Experiment 3C (n=2)	
RESINS	**PEPTIDES**
(**4**) Ac-Lys(*m*-PhB)-CMRR (**9**) Ac-Lys(*m*-PhB)-AGRR *m*-Aminophenylboronic acid–Agarose (A8530)	equimolar amounts (1:1) **in a peptide mixture**

RESIN	CONCLUSION
(**4**) Ac-Lys(*m*-PhB)-CMRR	Only these three peptides are captured by Resin (4): hydrofobic peptide, Amadori peptide 1, and amadori peptide 2
(**9**) Ac-Lys(*m*-PhB)-AGRR	Resin (**9**) captures hydrophobic peptide, Amadori peptide 1, and Amadori peptide 2, but also other non-Amadori peptides Resin (**9**) is not selective when other, unmodified sugars are present in the MIX
m-Aminophenylboronic acid–Agarose (A8530)	Agarose resin (A8530) resin captures hydrophobic peptide, Amadori peptide 1, and Amadori peptide 2, but also other, non-Amadori peptides. Commercial AGRR resin is not selective when other, glycosylated peptides are present in the MIXTURE.

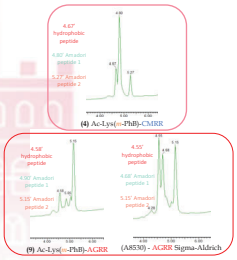

Conclusions

•Monofunctionalized (mono-PhB) resins more than bifunctionalized (di-PhB) resins are capable to capture the tested peptides;
•Among CMRR resins, *meta* analogue (*m*-PhB) is more efficient and more selective than *para* (*p*-PhB) analogue;
•Among all the monosubstituted resins, **(4)** Ac-Lys(*m*-PhB)-CMRR seems to present the consensus between the efficacy AND the selectivity.
•AGRR – solid support containing –OH groups. CMRR– a polymer non containing –OH groups. In case of CMRR, the presence of the –OHs may affect specificity of capturing that depends only on the interaction with the PhB groups. AGRR beads may interact non-specifically → lower specificity.

Perspectives

•Optimization work will look at the further modifications probing the spatial relationship between the two *m*-PhB substituting the Lys.
•Ac-Lys(*m*-PhB)-CMRR resin **(4)** will be tested in fishing the Amadori-modified peptide fragments from an enzymatic digest of a glycated protein

REFERENCES: **[1]** D'Aronco S, Crotti S, Agostini M, Traldi P, Chilelli NC, Lapolla A. Mass Spectrom Rev. 2019 Jan;38(1):112-146. doi: 10.1002/mas.21576; **[2]** Kijewska M, Nuti F, Wierzbicka M, Waliczek M, Ledwoń P, Stańkiewicz A, Real-Fernandez F, Sabatino G, Rovero P, Stefanowicz P, Szewczuk Z, Papini AM. Molecules. 2020 Feb 10;25(3):755. doi: 10.3390/molecules25030755.

https://doi.org/10.17952/37EPS.2024.P2188

Programmable Chemical Synthesis & in-situ Modifications of Peptides

University of Glasgow

Jacopo Zero, Tristan Tyler, Leroy Cronin*

Advanced Research Centre, The University of Glasgow, Glasgow, G12 8QQ, UK - Email:lee.cronin@glasgow.ac.uk

digital chemistry programming matter

Introduction

In this work, we **fully automated** all stages of solid-phase peptide synthesis (SPPS) including peptide assembly, cleavage, precipitation, and further **chemical modifictions**. Syntheses were carried out on the **Chemputer** platform, a modular batch synthesiser, operated via the standardised chemical programming language **χDL**.

Workflow

Chemical

Reagents

Fmoc-AA$_n$-OH | HATU | DIPEA | Piperidine | Ac_2O | TIPS | TFA | ... | H_2O | DMF | DCM | Et_2O | MeCN

SPPS

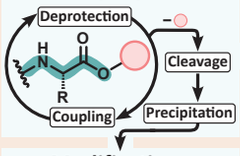

Modifications

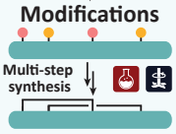

Physical

Procedure

- Deprotection and coupling
- Cleavage and precipitation
- Chemical modifications

Chemputer hardware



Digital

χDL

```
<Add
  vessel="spps_reactor"
  reagent="amino_acid"
  amount="2 mL"/>
...
```

Graph

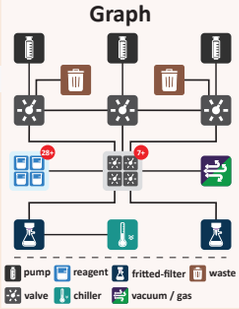

Benchmark results

ACP(65-74)
H-VQAAIDYING-OH

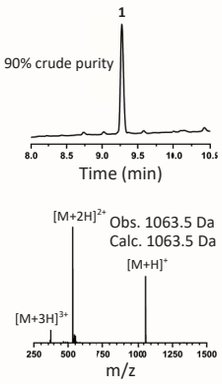

18A
Ac-DWLKAFYDKVAEKLKEA-NH$_2$

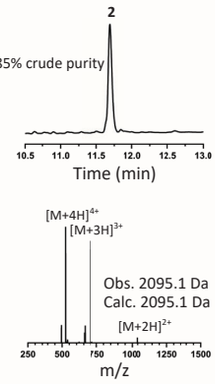

GHRH(1-29)
H-YADAIFTNSYRKVLGQLSAR KLLQDILSA-NH$_2$

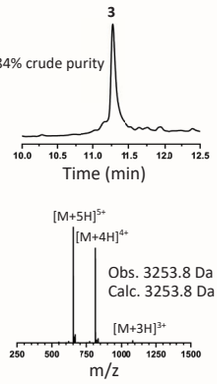

Fully automated peptide assembly, cleavage, precipitation, and chemical modifications

Bismuth mediated bicycle formation

= CHGFKCDGFKCS

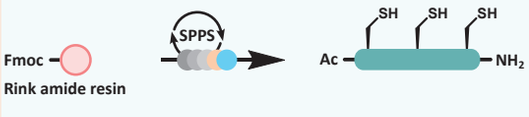

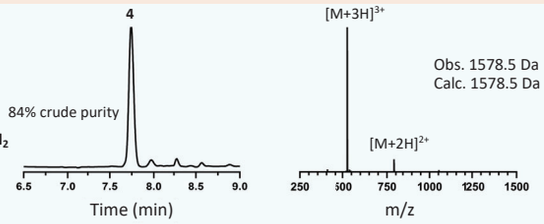

1,3-Dipolar cycloaddition "click" reaction

= RQIKIWFQNRRMKWKK

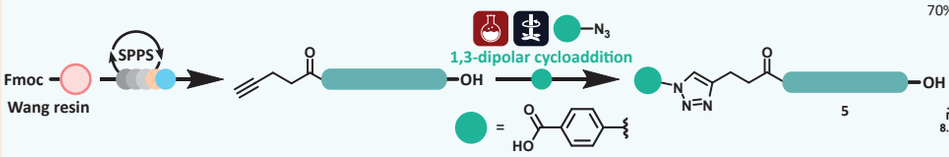

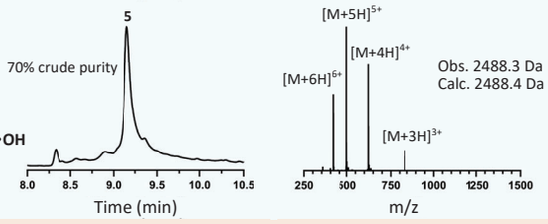

Chemoselective cyclisation and one-pot functionalisation

= CPIEDRPMK



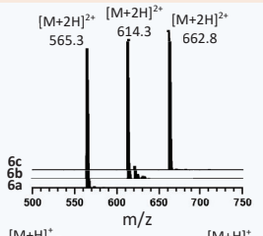

Intramolecular native chemical ligation

= CNPIWIGF



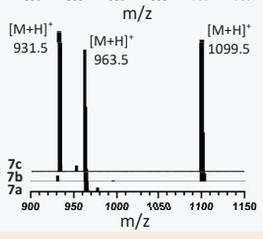

Peptide stapling diversification

= YCGGGCAL

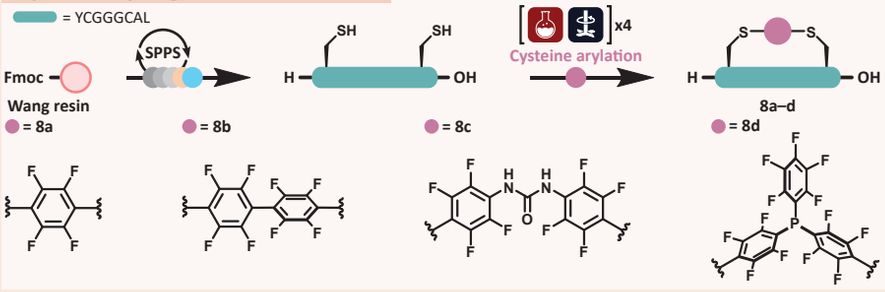

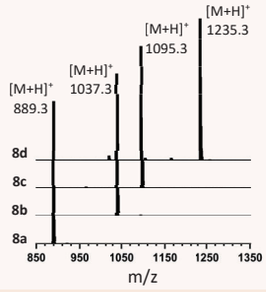

Conclusion

A universal workflow using **χDL** on the **Chemputer** platform was established to synthesise increasingly complex peptides from commercially available building blocks.

EPSRC Pioneering research and skills
erc

Peptide-based Coacervates as Evolutionary Roads of Catalytic Function

David Reis[1], Sara Pereira[1], Ana P. Ramos[1], Pedro M. Pereira[1], Leonor Morgado[2] and Ana S. Pina[1]

Drq.reis@itqb.unl.pt

[1] Instituto de Tecnologia Química e Biológica António Xavier, Universidade Nova de Lisboa, Av. da República,, 2780-157 Oeiras, Portugal
[2] Associate Laboratory i4HB – Institute for Health and Bioeconomy and UCIBIO – Applied Molecular Biosciences Unit, NOVA School of Science and Technology, Universidade NOVA de Lisboa, 2829-516 Caparica, Portugal

INSTITUTO DE TECNOLOGIA QUÍMICA E BIOLÓGICA ANTÓNIO XAVIER | ITQB.UNL.PT

Bioinspired Peptide Systems Laboratory

https://doi.org/10.17952/37EPS.2024.P2191

Introduction

Scientists suggest that cooperative interactions among peptides facilitated the formation of enzymes, introducing functionality through sequence diversification[1]. While peptides serve as effective chiral catalysts in organic reactions, their utilization in aqueous reactions is still limited and remains a challenge in molecular engineering, arising from their conformational heterogeneity[2,3]. Coacervates, formed through liquid-liquid phase separation (LLPS), are considered primitive models of protocells, linked to the origin of life, shielding and concentrating oligomers[3]. Therefore, the compartmentalization of catalytic peptides appears to have great potential as a route to evolve catalytic function in small catalytically modest peptides, by constraining their conformational flexibility observed in aqueous solutions.

Methodology

- Coacervation was achieved by mixing 5 mg/mL of P7 peptide[4] in 100mM of sodium phosphate buffer, containing 1M NaCl, at pH 8.0, to final peptide concentration of 1mg/mL
- This is followed by 1h of incubation at 27°C, leading to the formation of a milky-like state
- Lastly microscopy imaging is proceeded

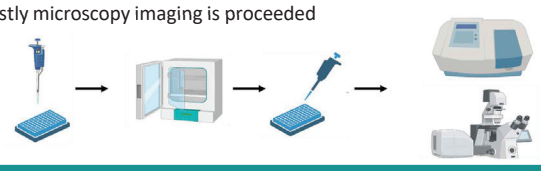

Results and Discussion

LLPS Propensity

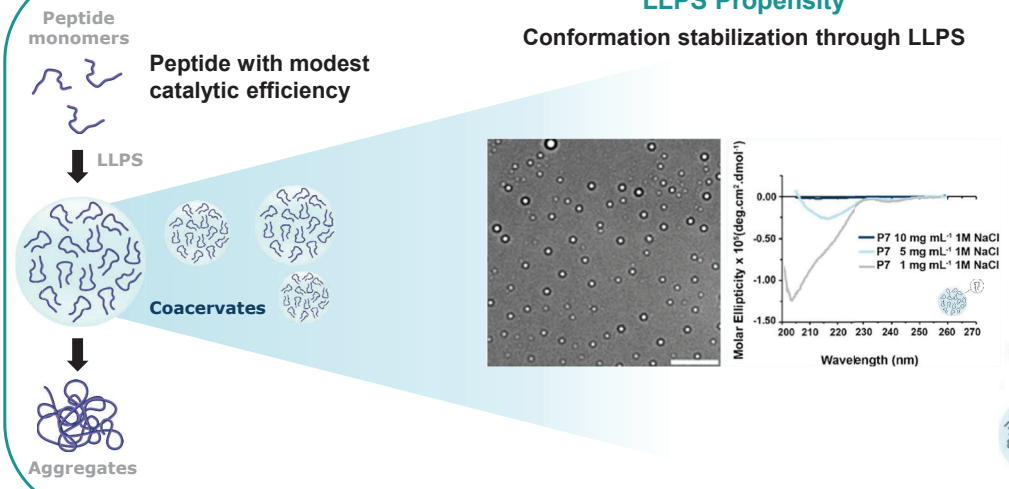

Enhancement of the catalytic efficiency

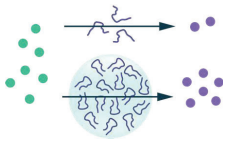

15.000-fold improvement!

Affinity-mediated molecular uptake

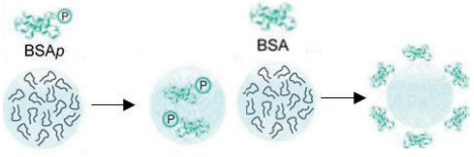

Affinity-mediated Sequestration

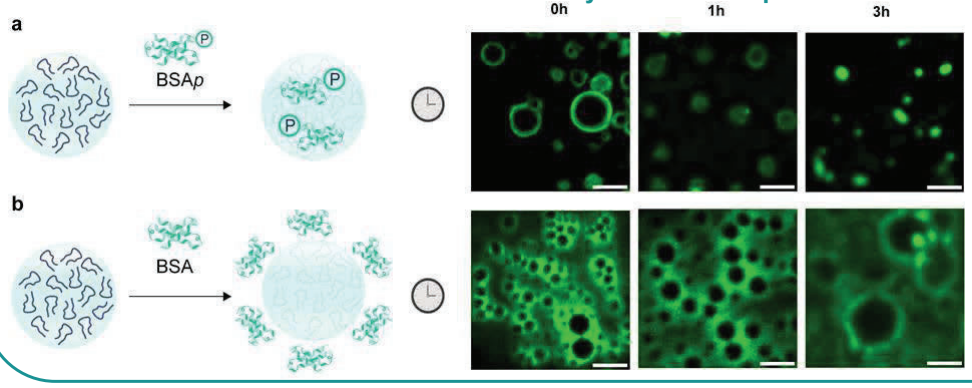

- Upon coacervate formation, P7's affinity for phosphorylated assemblies facilitates the sequestration of phosphorylated supramolecules (BSA*p*).
- P7 coacervates demonstrate a faster sequestration of phosphorylated BSA*p* compared to non-phosphorylated BSA.

Catalytic Microreactors

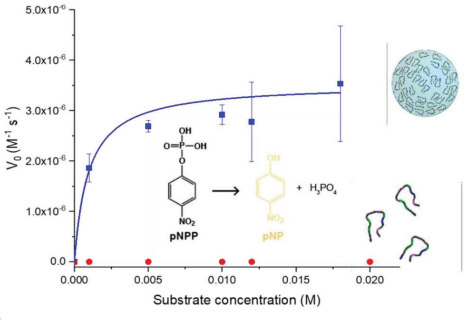

Catalyst	k_{cat} (s^{-1})	K_M (M)	k_{cat}/K_M (M^{-1} s^{-1})
P7-based Peptide Coacervates	(4.9 ± 0.6) x10^{-3}	(8.2 ± 3.2) x 10^{-4}	5.9 ± 0.2
P7 Peptide in solution	(1.0 ± 0.0) x10^{-5}	(1.4 ± 3.2) x 10^{-2}	(4.0 ± 0.3) x 10^{-4}

- 15,000-fold increase when P7 peptide coacervates are formed
- The catalytic reaction takes place within P7 coacervates

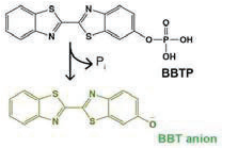

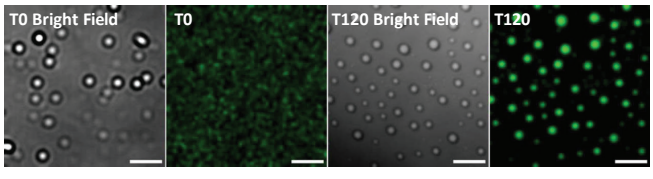

Acknowledgements

References

1. Frenkel-Pinter M, Samanta M, Ashkenasy G, Leman LJ. Prebiotic Peptides: Molecular Hubs in the Origin of Life. Chemical Reviews 2020, 120(11): 4707-4765.
2. Carvalho S, Peralta Reis DQ, Pereira S V., Kalafatovic D, Pina AS. Catalytic Peptides: the Challenge between Simplicity and Functionality. Isr J Chem. Published online 2022. doi:10.1002/ijch.202200029
3. Mann S. Life as a Nanoscale Phenomenon. Angewandte Chemie International Edition 2008, 47(29): 5306-5320.
4. Pina AS, Morgado L, Duncan KL, et al. Discovery of phosphotyrosine-binding oligopeptides with supramolecular target selectivity. Chem Sci. 2022;13(1):210-217. doi:10.1039/D1SC04420F

An all-in-one automated peptide purification and synthesis solution

PurePep®

Luísa Aguiar, M. Muthyala, S. Lüdtke, Dominik Sarma, Robert Zitterbart

Gyros Protein Technologies, 4675 South Coach Drive, Tucson, Arizona, 85714, U.S.A.

https://doi.org/10.17952/37EPS.2024.P2194

Introduction

Rapid parallel production of high-quality synthetic peptide sequences by solid-phase peptide synthesis (SPPS) and subsequent purification is a challenging yet essential pursuit. Neoantigen peptides, in particular, with medium to long lengths used in cancer immunotherapies need to be manufactured rapidly and with high purity. However, conventional batch-synthesis is slow and purification with sequential high-pressure liquid chromatography (HPLC) offers low throughput, leading to extended production times and potential product loss requiring repeated synthesis. Shorter and more reliable production timelines are essential to ensure the rapid delivery of life saving personalized medicine to patients. This study presents a PurePep® solution to improve neoantigen production for cancer therapy. The integrated approach includes induction heating (IH) for rapid automated peptide synthesis followed by automated orthogonal PurePep EasyClean (PEC™) purification on the PurePep Chorus synthesizer.[1]

Methods

We chose a set of six neoantigen sequences (#1-#6) from the literature that are severely challenging to synthesize and purify (Table 1).[2] Induction-heated solid-phase peptide synthesis (IH-SPPS) at 0.1 mmol scale was performed with 17 min synthesis cycle time (incl. capping):

- Coupling: DIC/Oxyma 3 min at 90°C
- Capping: Ac_2O/Pyr. 2 min at 50°C
- Fmoc-deprotection: DMF/Pip. 1 min at 90°C
- PEC-Linker coupling on the synthesizer with Oxyma/DMF for 15 min at 60°C.
- On-board TFA cleavage at RT for 2 h (83:5:5:5:2 TFA/H_2O/PhSH/EDT/TIS)

Purification was performed using the PEC Auto Kit with the pre-configured protocol for automated peptide purification on the PurePep Chorus synthesizer.

A final HPLC polish with Knauer Semi-prep. HPLC, C18 column 15 x 2 cm was applied to obtain clinical grade peptides

Table 1. Sequences of neoantigen peptides used in this study.

ID	Sequence
#1	SNLDITPDDPRWIRAWWGGFLLCGA
#2	DWGGQHHGLREVLAAALFASCLWGA
#3	YSLDSSGNQNLYAMYQLSHFQSISVL
#4	FTLQIRGRERFEMYRELNEALELKD
#5	TLQIRGRERFEMYRELNEALELK
#6	TMLVSSLRDHFPDLPLHIHTHDTS

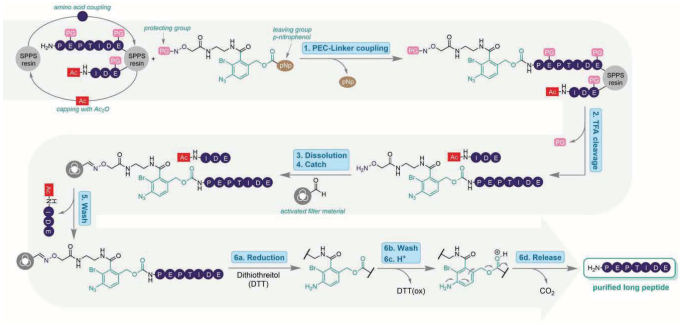

Figure 1. Chemical steps of the PEC technology used in the PEC Auto Kit, utilizing the universal linker system and its reduction-triggered safety release.

Results & Discussion

Table 2 displays the results after IH-SPPS as well as PEC purification in comparison to reported purities by Truex et al. who synthesized these peptides with the help of flow-chemistry. According to the literature, five of six peptides couldn't be delivered from an external vendor, proving their challenging profile.[2]

Table 2. Reported and gained UV-purities at 210 nm.

ID	Crude IH-SPPS	Flow-SPPS + HPLC	IH-SPPS + PEC	IH-SPPS + PEC + HPLC
#1	46%	45%	78%	94%
#2	59%	69%	80%	95%
#3	16%	53%	72%	96%
#4	60%	56%	78%	94%
#5	65%	92%	89%	94%
#6	16%	99%	74%	93%
Mean	**44%**	**69%**	**79%**	**94%**

- IH-SPPS enabled sequences that failed using batch synthesis thus providing a means to highly reliable synthesis of most difficult peptides
- Orthogonal purification with the PEC Auto Kit yielded superior PEC-grade mean purity versus flow-SPPS with subsequent HPLC using the routine protocol
- HPLC polish after PEC yielded >90% final purity for all reported difficult sequences.

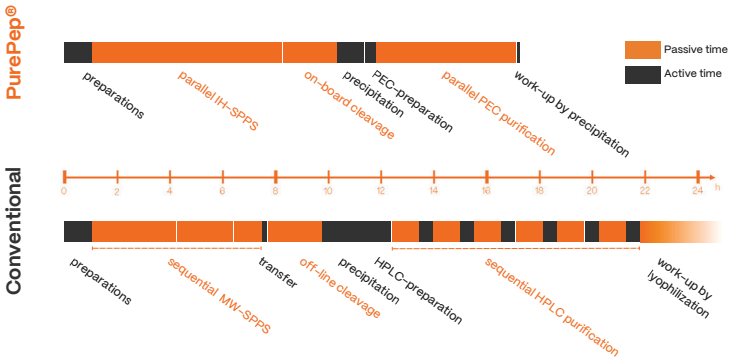

Figure 2. Time needed for parallel IH-SPPS, automated on-board cleavage and subsequent automated purification with the PEC Auto Kit for 6 peptides at 0.1 mmol scale.

- 17 min synthesis cycle time with induction heating resulted in ~7 h total time per set of 6 25-mer peptides (incl. capping)
- On-board cleavage enables hands-off workflows to obtain final product over night
- Automated purification of 6 peptides "ready to collect" in 5.2 h with only 26 minutes total hands-on time for preparation of the PEC run
- 20% faster with only one manual intervention compared to a sequential microwave synthesis and HPLC purification workflow with 7 manual interventions

PurePep Solution



- PurePep Chorus combines IH-SPPS, automated cleavage and purification in one instrument
- The PurePep Pathway features zero cross-contamination for maximum purity
- Upgradable design for 2, 4 or 6 reaction vessels and independent induction heating and UV-monitoring
- Save reagent cost with Single-Shot™ delivery with no dead volume and zero priming

Download the poster

References

[1] R. Zitterbart et al. Chem Sci 2021, 12, 2389
[2] N. L. Truex, B. Pentelute et al. Sci Rep 2020, 10, 723

D0049568

GYROS PROTEIN Technologies

www.gyrosproteintechnologies.com/peptides peptides@gyrosproteintech.com

Gyros Protein Technologies logo, Intellisynth, Prelude, PS3, PurePep, Single-Shot, Sonata, Symphony, PEC, and Tribute are trademarks of Gyros Protein Technologies Group. COMU, OxymaPure, PyClock, K-Oxyma and Py-Oxim are trademarks owned by Luxembourg Bio Technologies Ltd. All other trademarks are the property of their respective owners. © Gyros Protein Technologies 2024

Riding new Tides: Synthesis of oligonucleotides on PurePep® Chorus

PurePep®

Luísa Aguiar, Dominik Sarma, Robert Zitterbart

Gyros Protein Technologies, 4675 South Coach Drive, Tucson, Arizona, 85714, U.S.A.

https://doi.org/10.17952/37EPS.2024.P2195

Introduction

Modern drug discovery incorporates novel modalities such as oligonucleotides, RNA, protein degraders, as well as next-generation peptides. Therefore, quick access to these molecules through flexible synthesis platforms is crucial for competitive drug development. This application note highlights the successful synthesis of short oligonucleotides (18–24 bases) on the PurePep® Chorus, showcasing its versatility beyond peptide synthesis.

Methods

We adopted all steps of the phosphoramidite approach on the PurePep Chorus peptide synthesizer at a 5 µmol scale to synthesize different oligonucleotides shown in Table 1.

- Coupling was performed using 0.5 mL of 0.1M nucleotide phosphoramidite in ACN and 0.5 mL of 0.5M 5-ethylthio-H-tetrazole in ACN for 2 x 2 min.
- Capping was performed with a mixture of 0.5 mL of Ac2O/Lutidine/THF 1:1:8 v/v and 0.5 mL of 20% v/v N-Me-imidazole in THF for 2 minutes after coupling and 1 min 10 s after the oxidation step.
- Oxidation was achieved with 0.1 M iodine in THF/pyridine/water 88:10:2 v/v for 2 min.
- Detritylation was performed with 3% trichloroacetic acid (TCA) in dichloromethane (DCM) for 2 x 2 min.

Cleavage was performed using a 1:1 v/v mixture of 30% aqueous NH4OH and 40% aqueous methylamine for 1 hour at RT.

Purification was performed with the DMT-on method with reversed-phase solid phase extraction using Glen-Pak DNA Purification cartridges (PN 60-5200-10) at a scale of 1 µmol.

Table 1. Oligonucleotides synthesized during this study.

ID	Name	Sequence	DMT-on (crude)	DMT-off (purified)
#1	pBluescript SK primer	5′-CGC TCT AGA ACT AGT GGA TC-3′	68.9%	86.4%
#2	Genasense G3139	5′-TCT CCC AGC GTG CGC CAT-3′	64.0%	77.7%
#3	GAL1 Forward primer	5′-AAT ATA CCT CTA TAC TTT AAC GTC-3′	66.2%	90.3%
#4	3′-pBabe-Seq Primer	5′-ACC CTA ACT GAC ACA CAT TCC-3′	68.3%	93.9%
#5	Fomivirsen	5′-GCG TTT GCT CTT CTT CTT GCG-3′	87.9%	97.3%
#6	U6 Primerc	5′-GGG CAG GAA GAG GGC CTA C-3′	65.3%	83.2%
#7	M13 Reverse* (-48)	5′-A*G*C* G*GA TAA CAA TTT CA*C* A*C-3′	13.0%	98.7%
#8	Intein Forward*	5′-CCC GC*C* G*C*T GCT TTT GCA CGT* G*A*G-3′	25.3%	98.9%
#9	pBAD Reverse* (F)	5′-G*A*T TTA ATC TGT AFC* A*G*G-3′	29.3%	92.6%

a – DMT protected oligo nucleotide; b – fully deprotected oligo nucleotide; c – mutated: first T changed to C; '*' indicates multiple phosphorothioate linkages; F – 2′-Fluoro-dU

Results & Discussion

- During the synthesis of #1, the growing oligonucleotide chain has been monitored by LC/MS after each extension up to the length of 8–10 nucleotides (Figure 1).
- The chromatograms demonstrate an efficient elongation of the target sequence through automated oligo synthesis on the PurePep Chorus synthesizer.

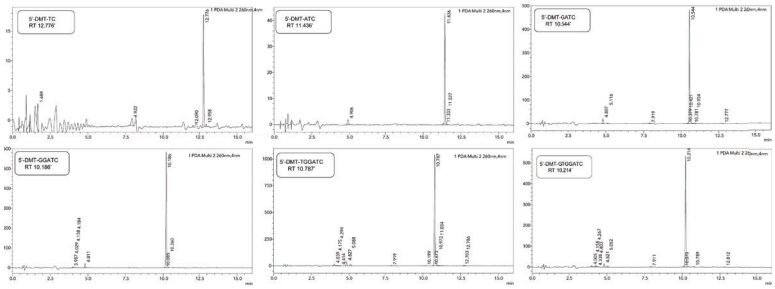

Figure 1. UV260 nm chromatogram of the universal pBluescript SK primer synthesis progress, steps 1 through 6 (crude, microcleavage).

- Encouraged by the initial results from our coupling studies, we continued the synthesis of oligos #2. In this example we highlight how impurities can easily be removed with the DMT-on method.
- Figure 2 shows the crude DMT-on oligo before the purification (A and C) and DMT-off after purification (B and D).
- While the improvement becomes apparent from the UV chromatogram, remaining truncation sequences are observed with MS analysis (D).

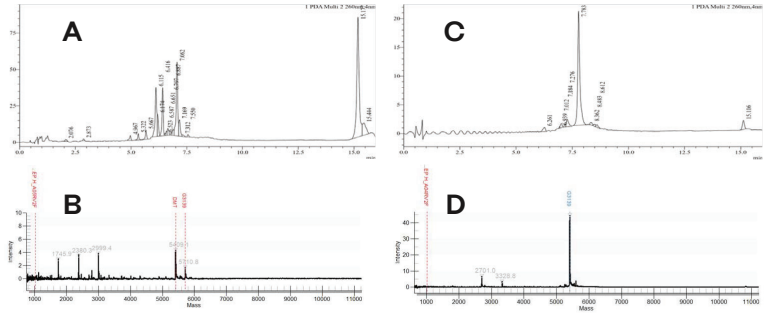

Figure 1. UV260 nm chromatogram of crude Genasense G3139 (DMT on) [A] and desalted Genasense G3139 (DMT off) [B] and their respective MALDI-TOF mass-spectra [C] and [D].

- Oligonucleotides #3 to #7 were synthesized automatically on the PurePep Chorus and purified with the DMT-on method in very good purity as depicted in Table 1.
- The PurePep® Chorus peptide synthesizer allows the successful synthesis of several short (18–24 bases) oligonucleotides due to the operation under inert conditions.
- We have also demonstrated the synthesis of phosphorothioates and other labeled and specially substituted nucleotide-containing oligonucleotides with the same platform.

Conclusions

- Expand the synthesis capabilities from peptides to oligonucletides on the PurePep Chorus
- Efficiently optain high-quality short oligonucleotide sequences with DMT-on purification
- Apply sulfurization in the automated synthesis process to expand the chemical flexibility

PurePep Chorus



- PurePep Chorus is a versatile instrument for the synthesis of peptides, peptide-nucleic acids, peptoids, oligonucleotides, and other polymers assembled on the solid phase
- The PurePep Pathway features zero cross-contamination for maximum purity
- Upgradable design for 2, 4 or 6 reaction vessels and independent induction heating and UV-monitoring
- Save reagent cost with Single-Shot™ delivery with no dead volume and zero priming

Download the poster

References

[1] M.-J. Blanco et al., ACS Med. Chem. Lett. 2022, 13, 1691 - 1698
[2] https://www.lslabs.com/resources/universal-primer-list

D0049566

GYROS PROTEIN Technologies

www.gyrosproteintechnologies.com/peptides peptides@gyrosproteintech.com

Gyros Protein Technologies logo, Intellisynth, Prelude, PS3, PurePep, Single-Shot, Sonata, Symphony, PEC, and Tribute are trademarks of Gyros Protein Technologies Group. COMU, OxymaPure, PyClock, K-Oxyma and Py-Oxim are trademarks owned by Luxembourg Bio Technologies Ltd. All other trademarks are the property of their respective owners. © Gyros Protein Technologies 2024

The first endocrine-disrupting chemical inhibiting a coactivator peptide's binding



Masaki Iwamoto, Takahiro Masuya, Mari Hosose, Tomaka Ishibashi, and Ayami Matsushima

Laboratory of Structure-Function Biochemistry, Department of Chemistry, Faculty of Science, Kyushu University, Fukuoka 819-0395, Japan

https://doi.org/10.17952/37EPS.2024.P2196

Bisphenol A (BPA) is a chemical that has gained significant attention due to its well-known endocrine-disrupting properties. As a result, BPA has been replaced with its derivatives, next-generation BPAs, which prioritize environmental and human safety. However, the safety of these next-generation BPAs is not fully evaluated. We have assumed that bisphenol's chemical structure is a privileged structure for nuclear receptors; therefore, we have screened a library of ca. 200 bisphenol derivatives for ERα and ERβ. We found that many next-generation BPAs, including BPAF and BPC, acted as antagonists for ERβ, despite being agonists for ERα. We confirmed that these chemicals act as coactivator-binding inhibitors for ERβ by surface plasmon resonance analysis using a coactivator peptide.

Background

BPA has garnered widespread attention as one of the most well-known EDCs. BPA induces adverse effects on experimental animals, even at low doses, especially on their reproductive organs and nervous systems. However, the molecular mechanisms of these BPA's low-dose effects are still yet clarified. These circumstances have facilitated replacing BPA with its derivatives, next-generation BPAs aiming at environmental and human safety.

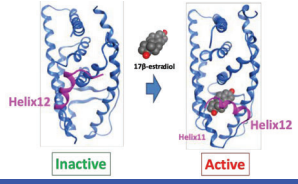

BPA binds to both estrogen receptor α (ERα) and ERβ, although its binding ability is much weaker than that of natural female hormone, 17β-estradiol.

We have assumed that bisphenol's chemical structure is a privileged structure for nuclear receptors; therefore, we have screened a library of ca. 200 bisphenol derivatives for ERs.

Experimental & Results

① Competitive radio-ligand binding assay

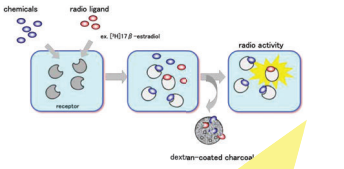

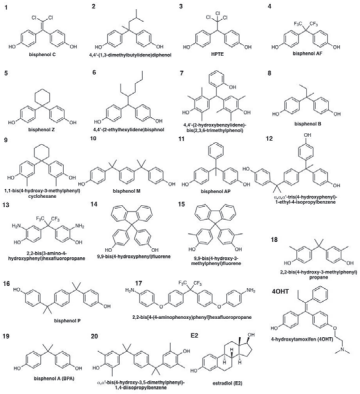

ca. 20 next-generation BPAs bind to ERα and ERβ stronger than BPA.

② Reporter gene assay

Agonist activity evaluated by reporter gene assay

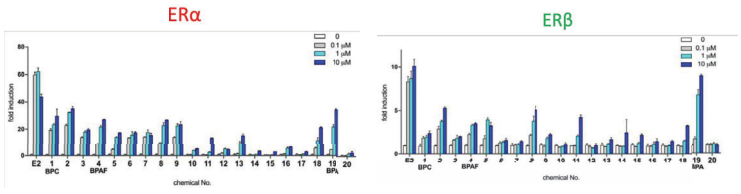

Antagonist activity evaluated by reporter gene assay

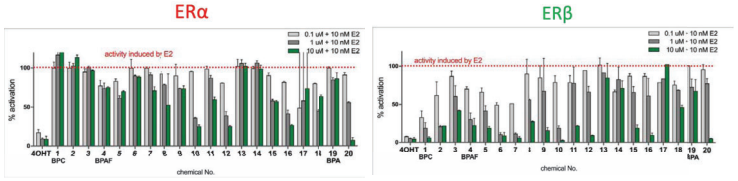

- Tri-cyclic bisphenols (ex. BPM) act as antagonists both for ERα and ERβ .
- Next-generation BPAs that strongly bind both to ERα and ERβ are ERα-agonists and ERβ-antagonists.

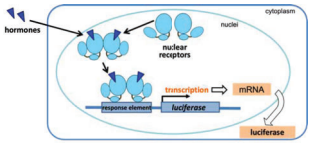

③ Docking simulation & binding ability of ERβ(W335A)

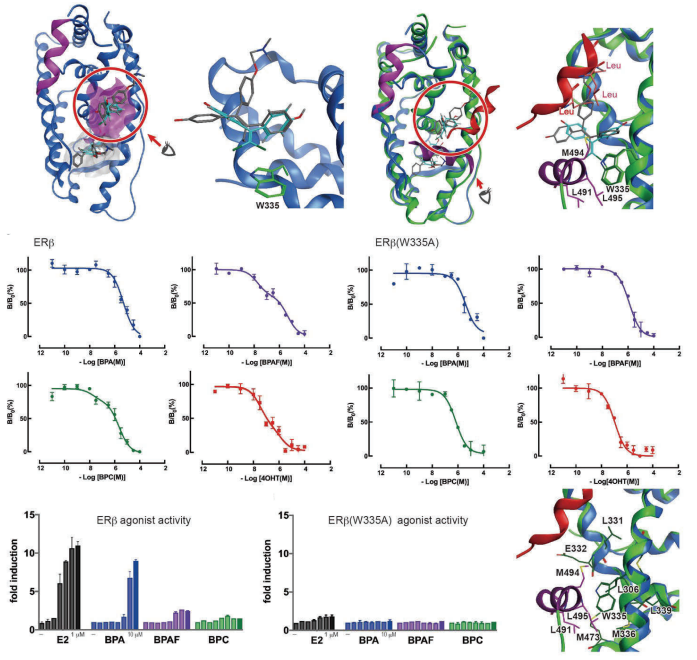

④ Surface plasmon resonance analysis using a coactivator peptide fragment (ERHKILHRLLQEG)

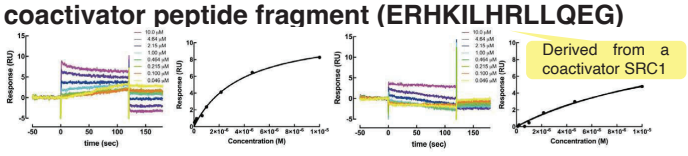

Conclusion

- ✓ Bisphenol AF (BPAF) and bisphenol C (BPC) bind to ERα much more strongly than does BPA itself.
- ✓ Tricyclic bisphenols, which have three benzene rings, are antagonists for ERβ, as they are as well for ERα.
- ✓ Many next-generation BPAs, including BPAF and BPC, acted as antagonists for ERβ despite being agonists for ERα.
- ✓ Next-generation BPAs act as coactivator-binding inhibitors for ERβ by surface plasmon resonance analysis using a coactivator peptide.

Iwamoto, M. et al. Bisphenol a derivatives act as novel coactivator-binding inhibitors for estrogen receptor β. *Journal of Biological Chemistry* **297**, 101173 (2021).

PYY peptides and Fc-PYY conjugates selectively agonise Y2R

https://doi.org/10.17952/37EPS.2024.P2197



Elise Bernard[1], Siobhan O'Brien[2], Nicole Burmeister[1], Jacqueline Naylor[3], Stephanie Oldham[4], Arthur Suckow[4], Hamid Salari[4] and Maria A. Bednarek[1]

[1] Hit Discovery, Discovery Sciences, BioPharmaceuticals R&D, AstraZeneca, Cambridge, UK ; [2] Biologics Engineering, Oncology R&D, AstraZeneca, Cambridge, UK ; [3] Cardiovascular Renal and Metabolism, BioPharmaceuticals, R&D, AstraZeneca, Gothenburg, Sweden ; [4] Cardiovascular Renal and Metabolism, BioPharmaceuticals, R&D, AstraZeneca, Gaithersburg, USA

Introduction

- Type 2 Diabetes (T2D) is a disease characterized by hyperglycemia and increased cardiovascular (CV) risk.
- Over 540 million people are afflicted with diabetes worldwide and the International Diabetes Federation projects that this number will increase to 783 million in 2045 [1].
- Bariatric surgery like Roux-en-Y gastric bypass (RYGB) surgery produces long term remission of T2D and reduces CV risk factors [2].
- After diabetic patients undergo RYGB surgery, rapid improvement in blood glucose and insulin levels occur before any significant weight loss is observed. PYY3-36 secretion is also acutely increased after surgery and may act as an effector for reversal of T2D [3].
- PYY peptides and PYY conjugated peptides with improved stability have the potential to serve as beneficial therapeutics.

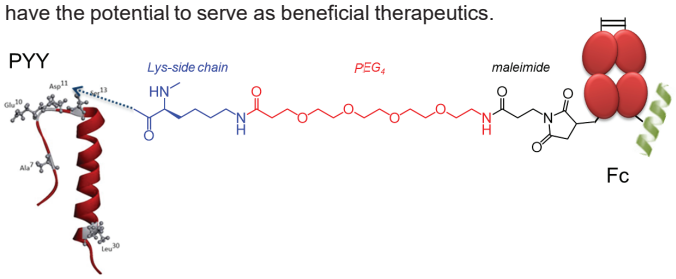

Methods

- PYY peptides with a PEG_4 linker on the side chain of a Lys in position 11 are **conjugated to the Fc domain** at amino acid position 442 via maleimide-thiol conjugation.
- For **cAMP activity assays**, forskolin was used to stimulate cAMP production in cells expressing recombinant human neuropeptide Y1, Y2, Y4 or Y5 receptors. Receptor stimulation by agonist ligands results in the inhibition of FSK stimulated cAMP production, which provides a measure of biological activity of the PYY ligands.
- **Pharmacokinetic studies** were conducted with 8-10 weeks old C57BL/6 lean, male mice fed a standard chow diet. They were given a subcutaneous injection of PY095 or PY132 peptide (Figure 1A, dosed at 100nmol/kg) or Fc-PY095 or Fc-PY132 (Figure 1B, dosed at 1 mg/kg) and blood was collected at various time points depending on the expected half-life of the drugs investigated.
- For **BioDaq food intake (FI) study,** on the day of the study mice were fasted for the 6-8 hours preceding lights out. Compounds were dosed approximately 1 hour prior to lights out at the indicated doses at a dose volume of 5-10 mL/kg. Food was given back 30 min prior to lights out and food intake was monitored in real-time in the BioDaq system for at least 48 hours.

Results

Table 1: Potency and selectivity of PYY peptides and Fc-PYY conjugates in the cAMP assay, where unAA is an unnatural amino acid.

Alias	Sequence	cAMP EC_{50} nM			
		Y2R	Y1R	Y4R	Y5R
PYY 3-36	IKPEAPGEDASPEELNRYYASLRHYLNLVTRQRY-amide	**0.15**	83	98	25
Fc-PYY3-36	IKPEAPGEK[PEG_4-MAL-442C]ASPEELN RYYASLRHYLNLVTRQRY-amide	**0.143**	>1000	>1000	183
PY095	PKPEAPGEDASPEELARYYASLRAYINLITRQRY-amide	**0.029**	490	198	37
Fc-PY095	PKPEHPGE K[PEG_4-MAL-442C] ASPEELARYYASLRAYINLITRQRY- amide	**0.039**	>1000	>1000	113
PY132	PKPEAPGEDASPEELARYYASLRAYINLITRQ(unAA)Y-amide	**0.022**	>1000	>2000	19.9
Fc-PY132	PKPEHPGE K[PEG_4-MAL-442C] ASPEELARYYASLRAYINLITRQ(unAA)Y- amide	**0.005**	>1000	>1000	161

- Selectivity of the PYY peptides and Fc-PYY conjugates: PYY3-36, PY095 and PY132 were conjugated to the Fc domain at position 442C and all constructs were tested for potency in the cAMP Y2R assay and for selectivity in the cAMP Y1R, Y4R and Y5R assays (Table 1).
- All PYY peptides conjugated to Fc gained Y2R selectivity over Y1R, Y4R and Y5R versus the unconjugated PYY peptide.
- Unconjugated peptides PY095 and PY132 were more selective than PYY3-36 across all the receptors.
- The unconjugated PY132 showed similar selectivity for Y2R over Y1R and Y4R as observed for conjugated molecules. However, the peptide lost selectivity over Y5R compared to PY095: this loss in selectivity over Y5R was gained on conjugation and the unnatural amino acid containing conjugate Fc-PY132 shows the best Y2R selectivity profile.

Figure 1: plasma concentrations of (A) unconjugated PYY peptides PY095 and PY132, and (B) Fc-PYY molecules Fc-PY095 and Fc-PY132 from PK studies in lean mouse

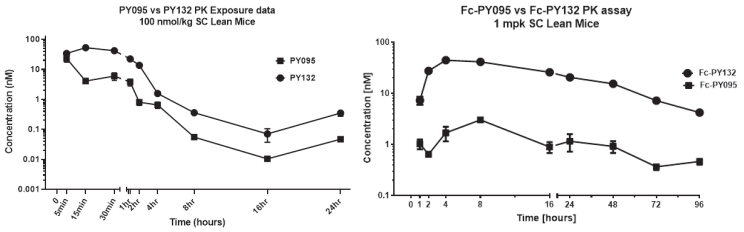

Figure 2: *in vivo* data from a single dose food intake study in mouse comparing unconjugated PYY peptides PYY3-36, PY095 and PY132 (fig. 2A) and Fc-PYY molecules Fc-PY095 and Fc-PY132 (fig. 2B). Data for Fc-GLP-1 is also provided.

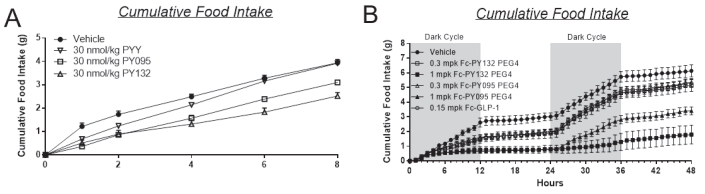

- Biological stability of PYY analogue molecules: mouse PK and FI studies were carried out using both conjugated and unconjugated PYY peptides.
- PK studies showed that when dosed at 100 nmol/kg PY132 was more stable than PY095 which has previously been shown to be more stable than PYY3-36 (Fig. 1A). PYY3-36 efficacy was lost after 4 hrs, while PY095 and PY132 showed efficacy for up to 8 hrs (Fig. 2A).
- When conjugated to Fc, the PK data clearly indicate that Fc-PY132 is more stable than Fc-PY095 (Fig. 1B). The food intake studies in lean mice showed efficacy up to 48 hrs for Fc- PY132 and Fc-PY095. Fc-PY132 showed more durable effects than Fc-PY095 (Fig. 2B).
- Conjugation to Fc domain provides 20 times more plasma stability than keeping the naked PYY sequence.

Conclusions

- PYY peptides and Fc-PYY conjugates activate Y2R receptor and reduce food intake.
- All Fc-PYY conjugates retained potency and gained Y2R selectivity upon conjugation to Fc.
- Peptide-conjugates proved to be better than peptides alone on stability and half-life but modifying Arg35 gave an unconjugated peptide with an equivalent if not better selectivity on Y2R receptor.
- Substitution of Arg 35 with the unnatural amino acid clearly resulted in more stable molecules.
- For these peptides, conjugation improves selectivity toward Y5R.

References

1. https://idf.org/about-diabetes/diabetes-facts-figures/
2. Brethauer et al., *Ann. Surg.*, **2013**, 258(4), 628-636.
3. Ramracheya et al. *Cell Reports*, **2016**, 15, 944-950.

Supported by AstraZeneca

Presented at the 37th European Peptide Symposium, Florence, Italy, 25-29 August 2024

https://doi.org/10.17952/37EPS.2024.P2200

Pipeline for development of acylated peptide-based CGRP receptor antagonist with extended half-life for migraine treatment

Authors
Jens Bjelke Kristensen [1,2], Lisbeth Elster[1], Morten Lundh[1], Borja Ballarín-González[3], Flora Alexopoulou[3], Martin Kræmer[1], Ditte Marie Jensen[1], Ulrike Leurs[1], Jens Christian Nielsen[1], Henrik H. Hansen[1], Matilda Degn[1] and Kristian A. Haanes[2]

Gubra, [1]Gubra, Hørsholm, Denmark
[2]Sensory Biology Unit, Translational Research Centre, Copenhagen University Hospital - Rigshospitalet, Glostrup, Denmark.
[3]Novo Nordisk, Måløv, Denmark

Corresponding author
Jens Bjelke Kristensen (jbj@gubra.dk)

Background & Aim

Migraine is a debilitating headache disorder. The disease has neurovascular origin and migraine attacks can be elicited by vasodilative neuropeptides such as alpha calcitonin gene-related peptide (αCGRP). Antagonizing αCGRP actions in migraine patients has proven clinically efficient. Here, we present a pipeline for development of a peptide-based αCGRP receptor antagonist with increased half-life capable of antagonising the vasodilatory effect of αCGRP.

Methods

A series of αCGRP8-37 analogues carrying a C18-or C20-diacid lipidation were screened in vitro for CGRP receptor antagonism. An αCGRP8-37 analogue protracted with a C20 diacid at position 25 was subjected to an amino acid substitution screen to identify mutations that could further enhance antagonism. Average purity of peptides included in the lipidation scan, and the mutation scan ranged between 30-50%. Findings from lipidation scan and mutation scans were subsequently confirmed by characterising potency of selected antagonists with a purity of >95 %.

Conclusion

- Antagonism of αCGRP8-37 is maintained with C20DA-γGlu protraction at N25K.
- A ~4-fold gain of potency is observed by substituting alanine with serine at position 36 increase.
- αCGRP8-37 analogues carrying a C20 diacid lipidation antagonized vasodilative actions of αCGRP

www.gubra.dk

1 Lipidation scan

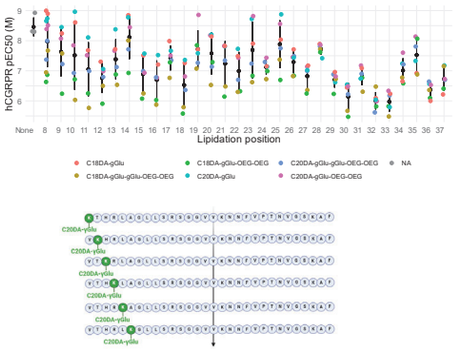

Figure 1. Greatest losses of potency were observed in the C-terminal region of αCGRP8-37. Potency might be maintained with N25K-C20DA-γGlu protraction.
Six lipidation moieties were applied to a lysine substitution at every amino acid residue of αCGRP8-37. A γGlu linker connects the peptide to C18DA or C20DA. The peptides were incubated with a fixed concentration of αCGRP corresponding to EC90 of αCGRP. Five-point concentration response curves were generated with antagonist concentrations of 30 nM, 100 nM, 300 nM, 1 µM and 3 µM. Antagonist potency was determined measuring cAMP applying HTRF Technology, CisBio. Black dots represent means. Error bars denote standard deviations.

2 Validation of lipidation

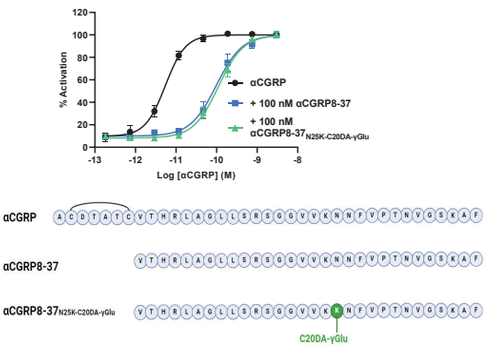

Figure 2. Antagonism of αCGRP8-37 is maintained with N25K-C20DA-γGlu protraction.
Inhibition of αCGRP-stimulated cAMP generation using a hCGRP-R CHO-K1 stable cell system. Concentration-response curves of αCGRP were generated in the absence or presence of 100 nM αCGRP8-37 or αCGRP8-37$_{N25K\text{-}C20DA\text{-}\gamma Glu}$.

3 Mutation scan

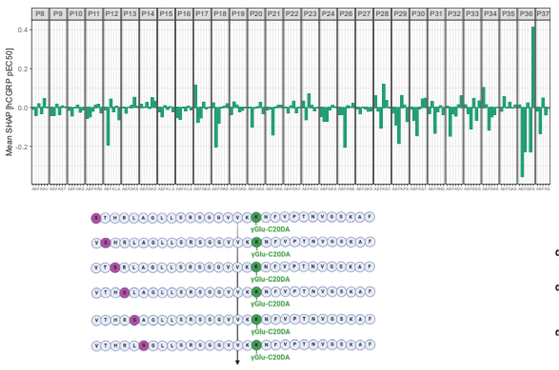

Figure 3. Mutations in the C-terminal region is generally associated with losses of potency. Serine at position 36 might induce a gain of potency.
Antagonist potency was evaluated with the cAMP HTRF technology (CisBio) applying five-point concentration response curves (30 nM to 3 µM). Each position was mutated to five different amino acids, either alone or in combination, resulting in a total data set consisting of 950 peptides. Lysine (K), glutamic acid (E), phenylalanine (F), serine (S), and alanine (A) were applied as substitutions. A random forest model was computed based on the relationship between the pEC50 values and the amino acid sequences. SHAP values were computed to determine the potency contribution of each mutation, where a positive SHAP value correspond to a positive contribution and a negative SHAP value corresponds to a negative contribution.

4 Validation of amino acid mutation

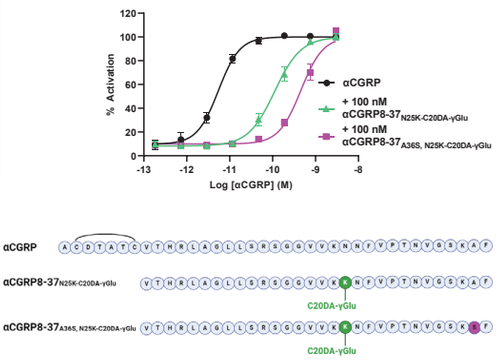

Figure 4. Serine at position 36 results in a 4-fold gain of potency to αCGRP8-37$_{N25K\text{-}C20DA\text{-}\gamma Glu}$.
Inhibition of αCGRP-stimulated cAMP generation using a hCGRP-R CHO-K1 stable cell system. Concentration-response curves of αCGRP were generated in the absence or presence of 100 nM αCGRP8-37$_{N25K\text{-}C20DA\text{-}\gamma Glu}$ or αCGRP8-37$_{A36S,\ N25K\text{-}C20DA\text{-}\gamma Glu}$.

5 Demonstration of ex vivo efficacy

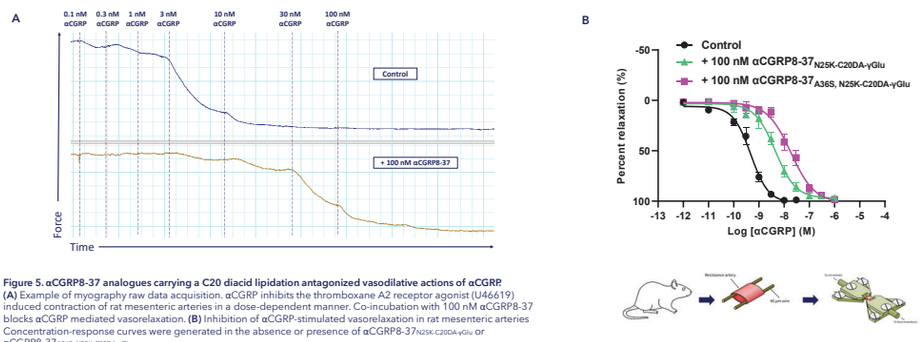

Figure 5. αCGRP8-37 analogues carrying a C20 diacid lipidation antagonized vasodilative actions of αCGRP
(A) Example of myography raw data acquisition. αCGRP inhibits the thromboxane A2 receptor agonist (U46619) induced contraction of rat mesenteric arteries in a dose-dependent manner. Co-incubation with 100 nM αCGRP8-37 blocks αCGRP mediated vasorelaxation. **(B)** Inhibition of αCGRP-stimulated vasorelaxation in rat mesenteric arteries Concentration-response curves were generated in the absence or presence of αCGRP8-37$_{N25K\text{-}C20DA\text{-}\gamma Glu}$ or αCGRP8-37$_{A36S,\ N25K\text{-}C20DA\text{-}\gamma Glu}$.

https://doi.org/10.17952/37EPS.2024.P2201

PEPTIDE-CONJUGATES DERIVED FROM BACTERIAL ParE TOXIN: SYNTHESIS AND BIOLOGICAL STUDIES

J. G. M. Bedoya; N. M. Pereira and R. Marchetto*

UNESP – Institute of Chemistry – Department of Biochemistry and Organic Chemistry, Araraquara, São Paulo, Brazil

* reinaldo.marchetto@unesp.br

INTRODUCTION

Antimicrobial resistance represents the major public health problem of the 21st century. New therapeutic agents, with innovative modes of action, are urgently needed given the seriousness of the problem. Peptides derived from bacterial toxins could be considered as a way to avoid this global health threat. ParELC3, a peptide derived from bacterial toxin ParE was reported to be a good inhibitor of bacterial topoisomerases *in vitro* and therefore a potential antibacterial agent [1]. However, a permeability limitation prevents its use as a new therapeutic agent. For circumvent this permeability limitation and promote a dual inhibitory targeting, we decided to design and synthesize molecular structures resulting from the conjugation of a ParELC3 analog with quinolone and coumarin groups to permeate the bacterial membrane and act synergistically in the inhibition of different topoisomerases. The peptide ParELC3M and respective conjugates CJHOAc, CJCOQ, CJCFX and CJNCFX (Figure 1b) were chemically synthesized by Solid Phase methodology, purified by RP-HPLC and characterized by mass spectrometry. (ESI-MS). The obtained peptide-conjugates were evaluated for their ability to inhibit topoisomerases activity and prevent the bacterial growth. In standard supercoiling and relaxation assays, the peptide ParELC3M and its conjugates did not inhibit the *E. coli* and *S. pneumoniae* DNA gyrase activity. On the other hand, all conjugates were able to inhibit completely the *M. tuberculosis* DNA gyrase activity and relaxation reaction of *E. coli* and *S. pneumoniae* topo IV with expressive IC_{100} values. In addition, CJCFX and CJNCFX conjugates inhibited *E. coli* topo IA with IC_{100} smaller than 6.25 μmol.L^{-1}. For yeast topoisomerase II, the inhibition was even more effective. The conjugates were effective against *E. coli* and *S. aureus* with MIC values of 25 μmol.L^{-1}. The results also showed low cytotoxicity for both peptide and peptide-conjugates with a cell viability greater than 75% even under the highest tested concentration. The results showed that the insertion of coumarin and fluoroquinolones groups to a peptide chain increase its capacity to permeate the bacterial plasma membrane and reach the cytoplasm, where can exert its activity.

METHODOLOGY

Synthesis, purification and characterization

The peptide ParELC3M and its conjugates (Figure 1) were synthesized by solid-phase methodology, using Fmoc/tBu chemistry with a RinK amide MBHA resin (0.55 mmol.g^{-1}) and DIC/HOBt activation. After deprotection and cleavage with TFA/water/EDT/TIS (94.5:2.5:2.5:0.5) for 2h at RT, the peptides were precipitated, solubilized and dried under vacuum. Analysis and purification was performed by RP-HPLC and the identity of the peptide and peptide-conjugates was confirmed by ESI-MS.

Antimicrobial activity assays

The antimicrobial activity on standard strains of *Staphylococcus aureus* (ATCC 14458) and *Escherichia coli* (ATCC 43895) and *Candida albicans* (ATCC 90028) was evaluated by broth microdilution assay performed in 96-well microplates, as described in the Clinical and Laboratory Standards Institute, reference guide M7-A10 and M27-A3 [2,3] with modifications as previously described [4]. The plates were submitted to spectrophotometric analysis, using a Biotek Instruments EPOCH microplate reader, at a wavelength of 595 nm. This assay was performed in triplicate.

Cytotoxicity assays

The cytotoxicity was investigated by MTT assay in MRC-5 cells (ATCC CCL-171). Briefly, 100 μL of a cell suspension in DMEM-C (DMEM medium supplemented with 10% (v/v) FBS, 40 μg.mL^{-1} gentamicin and 1 μL.mL^{-1} streptomycin) at 5 x 10^4 cells/mL density were added to each well of a sterile 96-wells plate and incubated for 24 h at 37°C in 5% CO_2 for cell adhesion. The cells were washed with PBS buffer, pH 7.4. Aliquots of 100 μL of peptide and conjugates solutions serially diluted in DMEM-C (200 to 25 μmol.L^{-1}) were added to each well, followed by incubation for 72 h at 37°C. The solution was removed and the cells were washed with PBS buffer. Subsequently, 180 μL of DMEM:PBS (1:4) and 20 μL of MTT (1.0 mg.mL^{-1}) solutions were added, followed by incubation for 4 h at 37°C in 5% CO_2. The supernatant was discarded and 100 μL of isopropyl alcohol:DMSO (1:1) was added and the absorbance read at 540 nm. DMEM-C and cells in DMEM-C were the negative and positive controls, respectively. Cell viability was obtained by the ratio between the optical density (OD) of the treated cells and that of the negative control. This assay was performed in triplicate (Figure 2).

Topoisomerase inhibition assays

The ability of peptides inhibits the topoisomerase supercoiling and relaxation reactions were investigated by gel electrophoresis assays [1].

The standard supercoiling reaction (30 μL) contained relaxed pBR322 DNA (500 ng), *E. coli, S. pneumoniae or M. tuberculosis* DNA gyrase (3.4 nmol L^{-1}) and indicated amounts of samples were carried out in the assay buffer and incubated at 37°C for 1 hour. The reaction was stopped by adding 15 μL of STEB and 60 μL of chloroform: isoamyl alcohol (24:1 v/v). The mixture was centrifuged and the supernatant was analyzed on a 1% agarose gel in TBE buffer. The samples were electrophoresed at 50V for 2 h. The gel was stained with ethidium bromide solution (1 mg mL^{-1}) and analyzed by an Alpha Imager EP System of Alpha Innotech. The ImageJ software was used to process the gel images and quantify the bands (Figure 3).

The *E. coli* or *S. pneumoniae* topoisomerase IV (topo IV) relaxation reactions were carried out in the assay containing supercoiled pBR322 DNA (400 ng), topo IV (5.0 nmol L^{-1}) and indicated amounts of samples, at 37°C for 1 hour. The mixture treatment and the gel analysis were made as described for the gyrase inhibition assay (Figure 4).

The reaction catalyzed by *E.coli* topoisomerase IA (topo IA) was carried out in 30 μL of assay containing supercoiled pBR322 DNA (0.5 μg), topo IA (1U) and indicated amounts of samples, at 37°C for 20 min The gel was analyzed as described for the gyrase and Topo IV inhibition assay (Figure 5A).

For yeast topo II inhibition assay, 30 μL of a standard reaction contained supercoiled pBR322 DNA (0.5 μg), topo II (1U), ATP solution (1 μL) and indicated amounts of each sample, in the assay buffer, was prepared. The mixture was incubated at 37°C for 30 min. The mixture treatment and the gel analysis were made as above (Figure 5B).

RESULTS

Synthesis and Structures

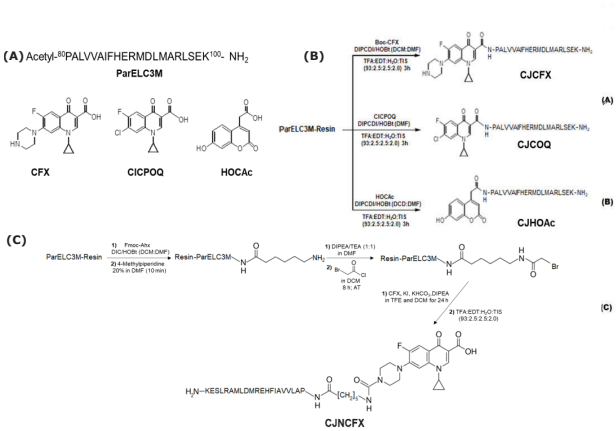

Figure 1. ParELC3M, CFX, ClCPOQ and HOCAc structures (A); Synthesis scheme of peptide-conjugates CJCFX, CJCOQ, CJHOAc (B) and CJNCFX (C)

Characterization

Sample	Calculated MW (g.mol^{-1})	ES+	ES m/z (g.mol^{-1})	Obtained MW (g.mol^{-1})
ParELC3M	2,467.99	+3 +4	824.00 618.49	2,469.18
CJCCFX	2,739.30	+3 +4	914.71 686.09	2,740.74
CJCOQ	2,689.61	+3 +4	898.35 674.02	2,692.05
CJHOAc	2,628.13	+3 +4	877.67 658.27	2,629,54
CJNCFX	2,910.77	+3 +4	971.46 728.86	2,911.41

Antimicrobial Assays

Sample	Minimal inhibitory concentration (MIC)					
	E. coli		*S. aureus*		*C. albicans*	
	μmol.L^{-1}	%	μmol.L^{-1}	%	μmol.L^{-1}	%
ParELC3M	100	ND	100	ND	100	ND
CJHOAc	100	ND	100	ND	100	ND
CJCOQ	100	ND	100	ND	100	ND
CJCFX	100	96	50	96	100	ND
CJNCFX	100	95	25	98	100	ND

Cytotoxicity Assays

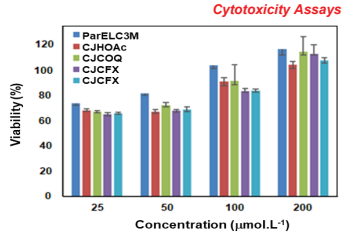

Figure 2. Cell viability assay for MRC-5 cells for ParELC3M peptide and its conjugates. Incubation time =72 h. Standard deviation are indicates by vertical bars.

Gel electrophoresis assays

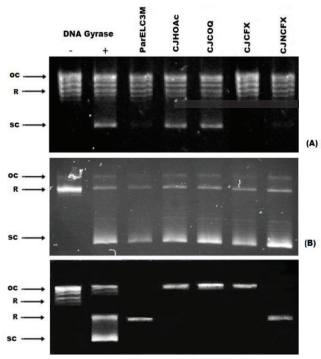

Figure 3. Initial screening at 100 μmol.L^{-1} of ParELC3M, CJHOAc, CJCOQ, CJCFX and CJNCFX for the DNA supercoiling reaction catalyzed by **DNA Gyrase** from (A) *E. coli*, (B) *S. pneumoniae* and (C) *M. tuberculosis.* (OC=nicked open circular; R=relaxed topoisomers; SC= supercoiled topoisomers

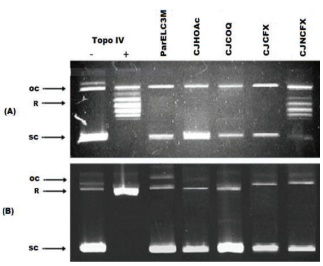

Figure 4. Initial screening at 100 μmol.L^{-1} of ParELC3M, CJHOAc, CJCOQ, CJCFX and CJNCFX for the DNA supercoiling reaction catalyzed by **Topo IV** from (A) *E. coli* and (B) *S. pneumoniae.* OC= nicked, open circular; R=relaxed topoisomers; SC= supercoiled topoisomers

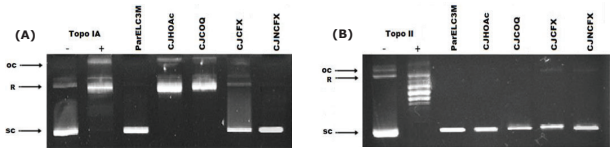

Figure 5. Initial screening at 100 μmol.L^{-1} of ParELC3M, CJHOAc, CJCOQ, CJCFX and CJNCFX for the DNA relaxation reaction catalyzed by **Topo IA** from *E. coli* **(A)** and DNA supercoiling reaction catalyzed by Topo II from Yeast **(B)**. OC= nicked, open circular; R=relaxed topoisomers; SC= supercoiled topoisomers

Sample	IC_{100} (μmol.L^{-1})						
	DNA Gyrase			Topo IV		Topo IA	Topo II
	E. coli	*S. pneumoniae*	*M. tuberculosis*	*E. coli*	*S. pneumoniae*	*E. coli*	*yeast*
ParELC3M	75	ND	50	25	50	100	12.5
CJHOAc	ND	ND	50	50	50	ND	3.125
CJCOQ	ND	ND	50	50	50	ND	6.25
CJCFX	75	ND	12.5	25	50	6.25	3.125
CJNCFX	75	ND	25	25	50	6.25	3.125

IC_{100} = Concentration of the peptide required for complete inhibition of topoisomerase activity;
ND = No detectable inhibitory activity.

CONCLUSIONS

- The primary target of the ParELC3M conjugate with CFX is Topo IV enzyme unlike free CFX that is DNA gyrase.
- In Gram-negative bacteria, the main targets of peptide conjugates are Topo IV and Topo IA enzymes while for Gram-positives the target is DNA gyrase.
- Peptide-CFX conjugates showed bactericidal activity, with CJNCFX as the most active. This fact may be related to the C3/C4 ketoacid region of the quinolone, which is free in this conjugate.
- Peptide-CFX conjugates inhibited the yeast Topo II activity with very expressive IC_{100} values, but were unable to inhibit the growth of *C. albicans*, basically due the inability to permeate the fungal cell membrane.
- The results showed that the insertion of coumarin and fluoroquinolones groups to ParELC3M increase its capacity to permeate the bacterial (but not the fungal) plasma membrane and reach the cytoplasm, where exert its activity.

REFERENCES

[1] Barbosa, L.C.B., Garrido, S.S., Garcia, A. Delfino, D.B., Santos, L.N., Marchetto, R. *Eur. J. Med. Chem.* 2012, 54, 591–596.

[2] CLSI. Methods for Dilution Antimicrobial Susceptibility Tests for Bacteria That Grow Aerobically; Approved Standard - Tenth Edition. CLSI document M07-A10. Wayne, PA: 2015.

[3] CLSI. Reference methods for broth dilution antifungal susceptibility tests for yeasts; Approved standards - 4ª ed. CLSI document M27-A3. Wayne, PA: 2017

[4] Almeida, C.V., Oliveira, C.R.F., Santos, E.L. et al. *BBA General Subjects.* 2021, 1865, 129937.

Support

CAPES

CNPq grant 310774/2021-7

FAPESP grant 2018/19468-6

Identification and Characterization of Small Molecule Nucleotide Binding and Oligomerization Domain 2 (NOD2) Receptor Agonists

Liora E. Wittle[1], Karl L. Ocius[1], and Marcos M. Pires[1]

[1]Department of Chemistry, University of Virginia, Charlottesville, VA

https://doi.org/10.17952/37EPS.2024.P2202

Background

The nucleotide binding and oligomerization domain protein 2 (NOD2) is an innate immune receptor that detects fragments a portion of the bacterial cell wall, known as peptidoglycan (PG).[1] PG is a polymer of crosslinked units of N-acetyl glucosamine (GlcNac) and N-acetyl muramic acid (MurNac), with a short peptide chain attached to MurNac. The peptide chain typically has the sequence L-Ala-D-isoGlu-L-Lys-D-Ala-D-Ala, with some organisms having a mesodiaminopimelic acid instead.[1]

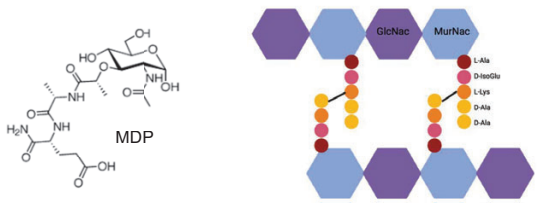

NOD2 activation has been shown to have many beneficial effects, such as protecting against bacterial infections,[2] aiding in recovery from malnutrition,[3] reducing symptoms of irritable bowel diseases,[4] and increasing the efficacy of cancer immunotherapy.[5] The minimal active fragment of peptidoglycan, muramyl dipeptide (MDP), composed of MurNac and the first two amino acids in the stem peptide, has been shown to cause these beneficial effects.

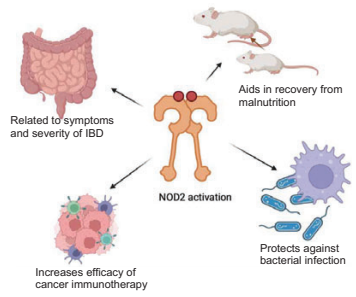

However, MDP is pyrogenic and difficult to use as a treatment in clinical settings. Other avenues to increase NOD2 activation, such as probiotic bacteria, are difficult to control in the body and hard to elucidate the exact effects from treatment. Many synthetic variations on MDP are currently available and used, but no unrelated small molecule activators are options for widespread use.

Project Aims

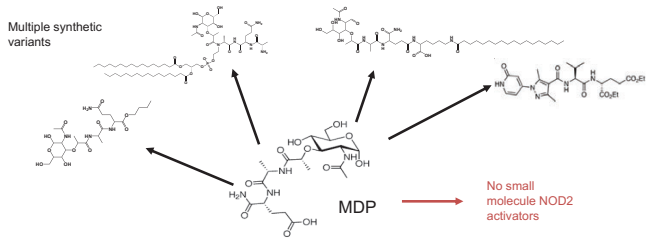

DISCOVER SMALL MOLECULE ACTIVATORS OF NOD2 THAT POTENTIATE THE SAME EFFECTS AS MDP

Methods and Results

Method Overview: HEK-Blue™ NOD2 cells

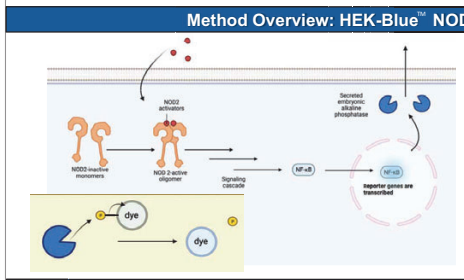

- HEK cells that express a reported gene downstream of NF-kB
- NOD2 activation causes expression of reporter genes
- Dye compound in media is dephosphorylated, causing color change
- Read results at 655 nm on UV-vis spectrophotometer

Discovery and Characterization of a Small Molecule NOD2 Activator

Screen of FDA Approved Compound Library

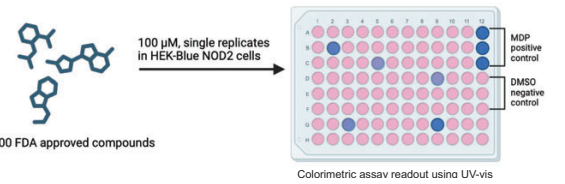

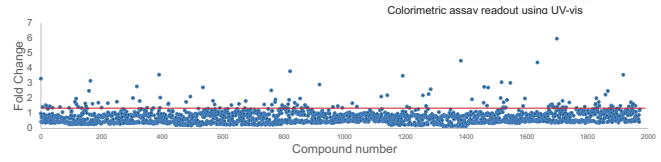

At a cutoff of fold change 1.5, several NOD2 agonists were identified

Further Analysis of Screen Hits

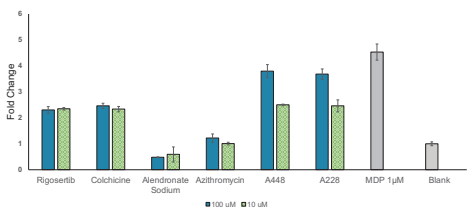

Strongest hits 14-48 and 20-28 share major structural similarities.

Expansion of Structurally Similar Screening Hits

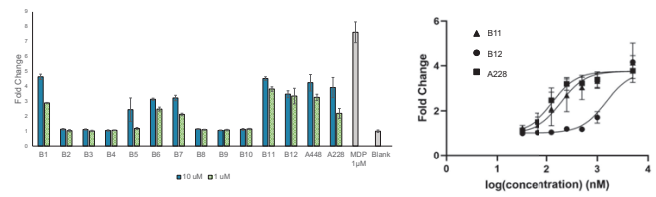

Several compounds with a similar core chemical structure activate NOD2. Two especially potent agonists (B11, B12) were identified

Methods and Results

Inhibition and Cytokine Release Small Molecule NOD2 Activator

Cytokine Release by Screen Hits in THP-1 cells

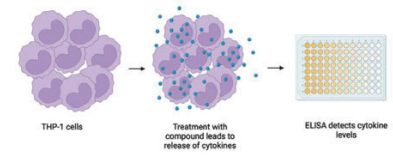

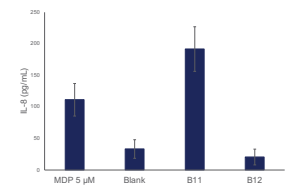

B11 induces cytokine release more strongly than B12

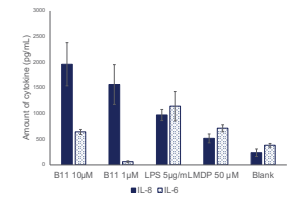

B11 induces IL-8 and IL-6 production

Inhibition by Specific NOD2 Inhibitor GSK717

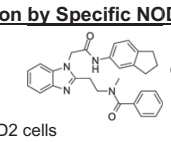

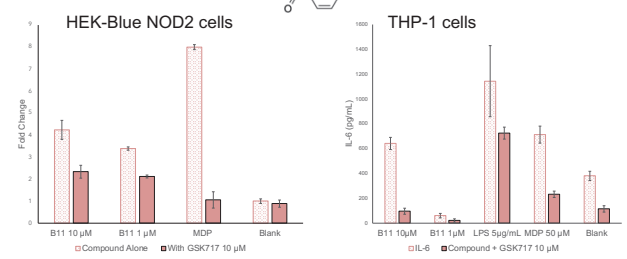

GSK717 inhibits activation of NOD2 by B11 in HEK-Blue NOD2 cells, and blocks cytokine release in THP-1 cells, indicating that B11 works through NOD2

Ongoing Work

- ❑ **Structural activity relationship studies with hit compounds to improve activation**
- ❑ **Cytokine panel using bone marrow derived macrophages**
- ❑ **Photocrosslinking assays to better demonstrate specific interaction with NOD2**

References

1. Crump, G. M.; Mashayekh, S.; Zhou, J.; Grimes, C. L. Revisiting Peptidoglycan Sensing: Interactions with Host Immunity and Beyond. *Chem Commun (Camb)* **2020**, *56* (67), 13313–13322. https://doi.org/10.1039/d0cc02605k.
2. Rangan, K. J.; Pedicord, V. A.; Wang, Y.-C.; Kim, B.; Lu, Y.; Shaham, S.; Mucida, D.; Hang, H. C. A Secreted Bacterial Peptidoglycan Hydrolase Enhances Tolerance to Enteric Pathogens.
3. Schwarzer, M.; Gautam, U. K.; Makki, K.; Lambert, A.; Brabec, T.; Joly, A.; Šrůtková, D.; Poinsot, P.; Novotná, T.; Geoffroy, S.; Courtin, P.; Hermanová, P. P.; Matos, R. C.; Landry, J. J. M.; Gérard, C.; Bulteau, A.-L.; Hudcovic, T.; Kozáková, H.; Filipp, D.; Chapot-Chartier, M.-P.; Šinkora, M.; Peretti, N.; Boneca, I. G.; Chamaillard, M.; Vidal, H.; De Vadder, F.; Leulier, F. Microbe-Mediated Intestinal NOD2 Stimulation Improves Linear Growth of Undernourished Infant Mice. *Science* **2023**, *379* (6634), 826–833. https://doi.org/10.1126/science.ade3767.
4. Gao, J.; Zhao, X.; Hu, S.; Huang, Z.; Hu, M.; Jin, S.; Lu, B.; Sun, K.; Wang, Z.; Fu, J.; Weersma, R. K.; He, X.; Zhou, H. Gut Microbial DL-Endopeptidase Alleviates Crohn's Disease via the NOD2 Pathway. *Cell Host & Microbe* **2022**, *30* (10), 1435-1449.e9. https://doi.org/10.1016/j.chom.2022.08.002.
5. Griffin, M. E.; Espinosa, J.; Becker, J. L.; Luo, J.-D.; Carroll, T. S.; Jha, J. K.; Fanger, G. R.; Hang, H. C. Enterococcus Peptidoglycan Remodeling Promotes Checkpoint Inhibitor Cancer Immunotherapy. *Science* **2021**, *373* (6558), 1040–1046. https://doi.org/10.1126/science.abc9113.

PIRES lab

https://doi.org/10.17952/37EPS.2024.P2203

Influence of Hydrophobic Moieties on the Formation and Stability of Collagen Heterotrimers

Maša Stopinšek, Valdrin Islami, Giuseppe Antoniazzi, Philipp Bittner, Renato Zenobi, Helma Wennemers*
Laboratory of Organic Chemistry, ETH Zürich, Switzerland

1 Introduction

- Collagen, the main component of the extracellular matrix, and its triple helical structure provide strength and stability to connective tissues.[1] Synthetic collagen model peptides (CMPs) are useful for studying the structure and stability of natural collagen and exploring the effect of functional groups on the properties and function of collagen. Our group has shown that CMPs bearing hydrophobic moieties form fast-folding and hyperstable homotrimeric triple helices in water.[2,3]
- In nature, most collagens consist of two or three different strands. Our lab showed that the controlled assembly of synthetic heterotrimers can be achieved through an interstrand salt bridge between (4*S*)aminoproline and aspartic acid.[4,5] The folding rate is however slower compared to that of homotrimers.
- Here, we investigate whether lipidation can accelerate the folding of heterotrimeric collagen and assess how the number of lipids and their position within the CMPs affect the thermal stability and formation specificity of collagen heterotrimers.

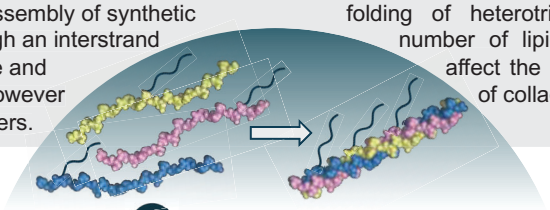

2 Design of ABC-type Heterotrimers

Unfunctionalized

1	POGP**D**GPOGPOG**X**PGPOGPOGPOG
2	POG**X**PGPOGPOGPOGPOGP**D**GPOG
3	POGPOGPOGP**D**GPOGPOG**X**PGPOG

D aspartic acid, **X** (4*S*)aminoproline

Functionalized with palmitic acid

At the same position

4P	POGP**D**G**Z**OGPOG**X**PGPOGPOGPOG
5P	POG**X**PG**Z**OGPOGPOGPOGP**D**GPOG
6P	POGPOG**Z**OGP**D**GPOGPOG**X**PGPOG

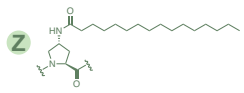

Distributed along the triple helix

7P	POGP**D**GPOGPOG**X**PGPOG**Z**OGPOG
8P	POG**X**PGPOG**Z**OGPOGPOGP**D**GPOG
9P	POG**Z**OGPOGP**D**GPOGPOG**X**PGPOG

3 Thermal Stability Studies with CD Spectroscopy

		T_m [°C]
unfunctionalized	**1·2·3**	42
one functional moiety	**4P·2·3**	45
	1·5P·3	43
	1·2·6P	44
two functional moieties	**1·5P·6P**	40
	4P·2·6P	36
	4P·5P·3	39
three functional moieties	**4P·5P·6P**	34
one functional moiety	**7P·2·3**	43
	1·8P·3	43
	1·2·9P	44
two functional moieties	**1·8P·9P**	37
	7P·2·9P	38
	7P·8P·3	41
three functional moieties	**7P·8P·9P**	40

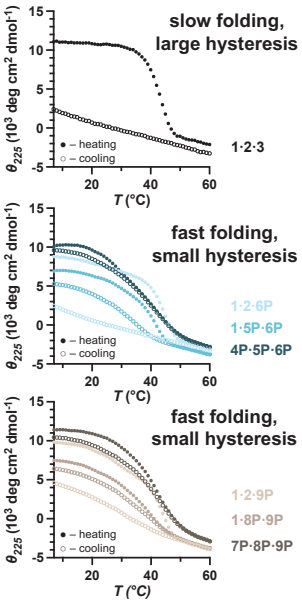

- Slight decrease of thermal stability and **reduction of the hysteresis** by increasing the number of fatty acid appendages
- The position and the relative distance between lipidated residues does not affect thermal stability and folding rate of triple helices significantly

4 Temperature Jump Experiments

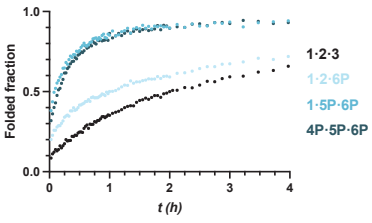

monitored by CD spectroscopy

		$t_{1/2}$ [h]
unfunctionalized	**1·2·3**	16
one functional moiety	**1·2·6P**	1.8
two functional moieties	**1·5P·6P**	0.4
three functional moieties	**4P·5P·6P**	0.7

40-fold decrease

- Shortest $t_{1/2}$ and fastest folding for the **difunctionalized** triple helix

5 Native ESI-MS Measurements

Example of analysis of two different samples

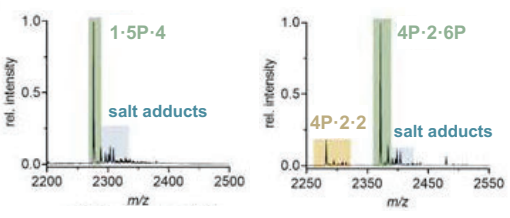

- Confirmed formation of all desired heterotrimers
- All mixtures except **4P·2·6P** and **7P·8P·3** assembled with high selectivity

6 Conclusion

- Functionalization of CMPs with palmitic acid does not increase the thermal stability of collagen heterotrimers.
- Addition of more than one palmitic acid appendage allows for a faster assembly of individual strands into a triple helix.
- Thermal stability and folding rate of triple helices are independent of the position of the lipidated residue within the triple helix.

References

1. M. D. Shoulders, R. T. Raines, *Annu. Rev. Biochem.* **2009**, *78*, 929.
2. J. Egli, C. Siebler, M. Köhler, R. Zenobi, H. Wennemers, *J. Am. Chem. Soc.* **2019**, *141*, 5607.
3. J. Egli, C. Esposito, M. Muri, S. Riniker, H. Wennemers, *J. Am. Chem. Soc.* **2021**, *143*, 5937.
4. N. B. Hentzen, V. Islami, M. Köhler, R. Zenobi, H. Wennemers, *J. Am. Chem. Soc.* **2020**, *142*, 2208.
5. V. Islami, P. Bittner, T. Fiala, N. B. Hentzen, R. Zenobi, H. Wennemers, *J. Am. Chem. Soc.* **2024**, *146*, 1789.

Swiss National Science Foundation

Let's connect!

Exploring Novel Peptide-Based Natural Products as a Payload for the Generation of Antibody and Peptide-Assisted Targeted Cancer Therapy

Suzie M. Chan[ab], Makhdoom Sarwar[cd], João Vitor Silva[e], Jeanine Giarolla Vargas[e], Margaret A. Brimble[abc], Iman Kavianinia[abc]

[a]School of Biological Sciences, The University of Auckland, Waipapa Taumata Rau, Auckland, New Zealand,
[b]School of Chemical Sciences, The University of Auckland, Waipapa Taumata Rau, Auckland, New Zealand,
[c]Maurice Wilkins Centre for Molecular Biodiscovery, The University of Auckland, Waipapa Taumata Rau, Auckland, New Zealand,
[d]Department of Obstetrics and Gynaecology, University of Otago, Christchurch, New Zealand,
[e]Department of Pharmacy, Faculty of Pharmaceutical Sciences, University of São Paulo, São Paulo, Brazil

https://doi.org/10.17952/37EPS.2024.P2207

Background

- Targeted cancer therapy is a growing field in research due to its improvements to reducing adverse effects by widening the therapeutic index of cytotoxic payloads
- Antibody-drug conjugates (ADCs) are a leading field in targeted cancer therapy with 12 FDA-approved ADCs
- However, among these 12, there are 7 different types of payloads used representing 3 unique mechanisms of action (microtubule inhibitors, topoisomerase I inhibitors, or DNA-damage)
- This ultimately leads to an issue of **drug resistance**

MoA: Inhibition of oxidative phosphorylation

Aminolipopeptides: An Attractive Anticancer Drug



Folate Receptor-α (FRα): The Ideal Target

- Glycosyl-phosphatidylinositol (GPI) anchored cell-surface protein
- Normal tissues:
  - Minimal role post-embryogenesis
  - Low expression
  - Restricted to apical surface
- Cancer cells:
  - Exposed to blood circulation
  - Overexpressed in many cancer types including endometrial carcinoma, **ovarian**, and lung cancer

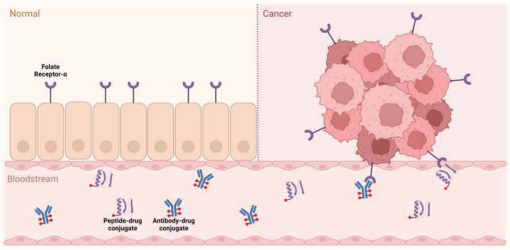

Solid Phase Peptide Synthesis of Aminolipopeptides

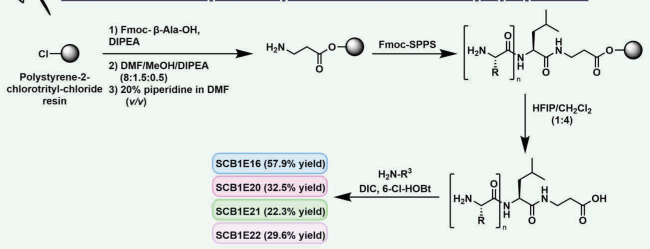

Biological Evaluation of Aminolipopeptide Analogues in Ovarian Cancer Cell Lines

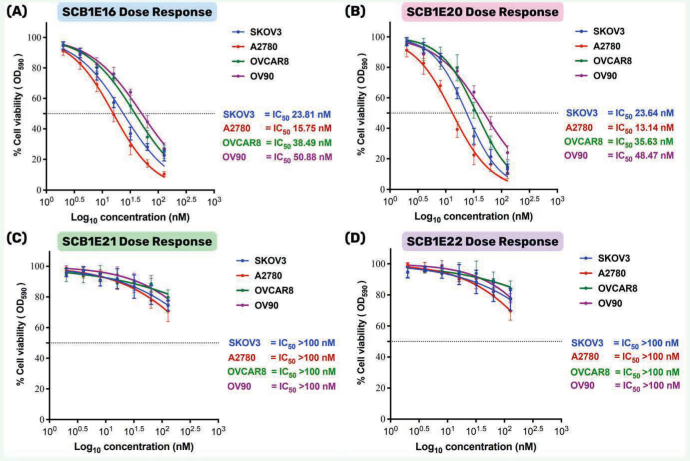

Figure 1. Cell viability (%) as evaluated by Crystal Violet assay after 48 h incubation of SKOV3 (FRα +ve, EGFR -ve), A2780 (FRα -ve), OVCAR8 (FRα +ve, EGFR -ve), and OV90 (EGFR -ve) cells with Compounds (A) SCB1E16, (B) SCB1E20, (C) SCB1E21, and (D) SCB1E22

FRα-Binding Peptides

Molecular Modelling

- Molecular models and predicted free binding energy of analogues of the C7 peptide and the binding site of FRα gave insight as to which peptides would have the best selectivity for FRα

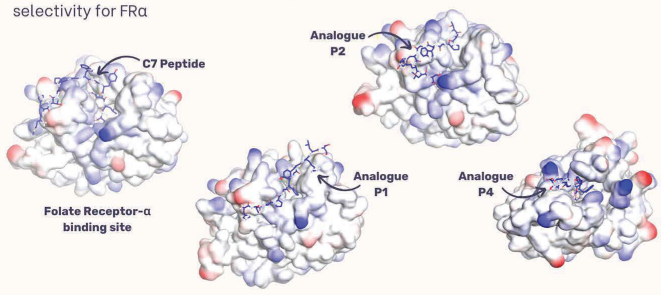

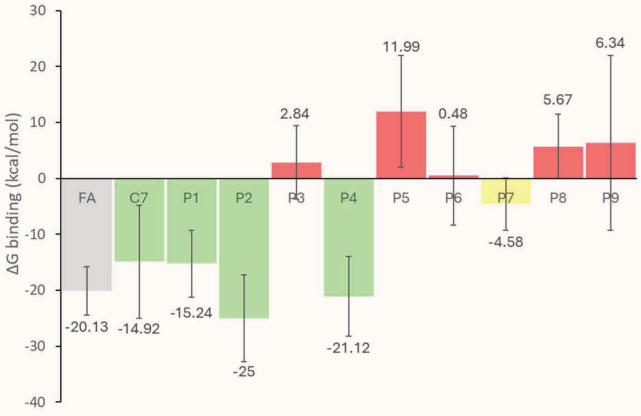

Figure 2. Predicted free binding energy of the modelled FRα-binding peptide C7, its analogues P1-9, and the native ligand folic acid (FA)

Synthesis of FRα-binding Peptides for Internalisation Studies

- 5(6)-carboxyfluorescein (5(6)-FAM) for visualisation inside cells
- PEG_8 spacer to prevent interference of 5(6)-FAM with peptide binding

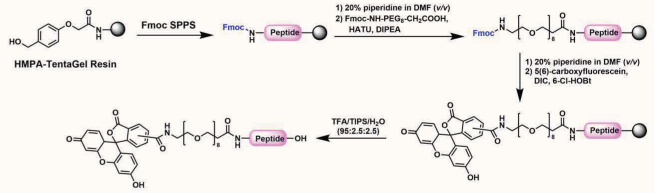

Future Work

- Conjugate SCB1E20 to the most selective FRα binding peptide to form a peptide-drug conjugate (PDC)
- Conjugate SCB1E20 to an anti-FRα antibody to give an antibody-drug conjugate (ADC)
- Biologically evaluate the PDC and ADC for selective toxicity of ovarian cancer cells expressing FRα

SCAN ME

Key References:

1. Stubbing, L. A.; Kavianinia, I.; Brimble, M. A. Synthesis of AHMOD-containing aminolipopeptides, unique bioactive peptaibiotics. *Org. Biomol. Chem.* **2017**, 15, 3542–3549 DOI:10.1039/C7OB00541E.
2. Scaranti, M.; Cojocaru, E.; Banerjee, S.; Banerji, U. Exploiting the folate receptor α in oncology. *Nature Reviews Clinical Oncology* **2020**, *17* (6), 349–359. DOI: 10.1038/s41571-020-0339-5.
3. Xing, L.; Xu, Y.; Sun, K.; Wang, H.; Zhang, F.; Zhou, Z.; Zhang, J.; Zhang, F.; Caliskan, B.; Qiu, Z.; et al. Identification of a peptide for folate receptor alpha by phage display and its tumor targeting activity in ovary cancer xenograft. *Scientific Reports* **2018**, *8* (1), 8426. DOI: 10.1038/s41598-018-26683-z.

Bispecific DNA-Peptide Conjugates for Targeting Cancer Cells

Pritam Ghosh‡, Huyen Dinh‡, Oliver Seitz*

Department of Chemistry, Humboldt-Universität zu Berlin, Brook-Taylor-Str. 2, 12489 Berlin

‡: Equal contribution, E-Mail: oliver.seitz@chemie.hu-berlin.de

https://doi.org/10.17952/37EPS.2024.P2208

Introduction

Cells of a given tissue express a unique "fingerprint" of surface receptors. By targeting two oncogenic receptors that are uniquely overexpressed in a cancer cell of interest and displaying their peptide ligands in the proper arrangement, it is possible to achieve high-avidity, highly selective binding to cancerous cells over surrounding healthy cells. Herein, we demonstrate that the programmable base-pairing interactions make DNA an ideal scaffold[1-3] to direct the presentation of peptide ligands binding pairs of receptors, such as the VEGFR/$\alpha_v\beta_3$ integrin and the EGFR/MET pairs.

Aim

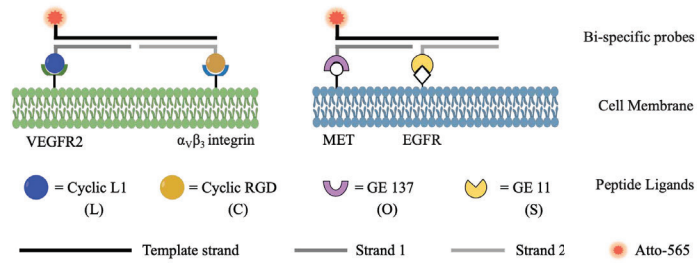

Designing the probes

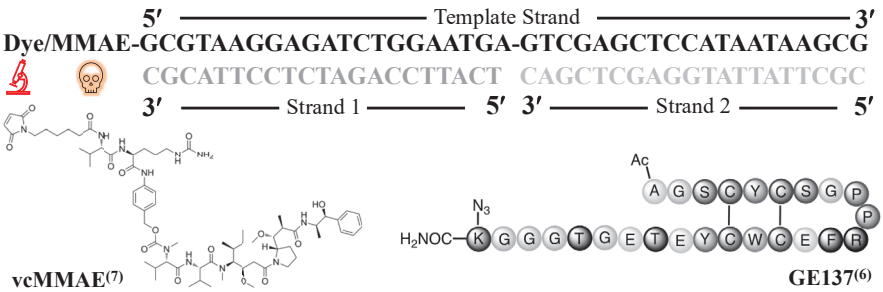

vcMMAE[7]

GE137[6]



GE11[6]

Peptide Ligands

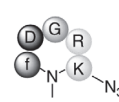

Cyclic RGD[4]

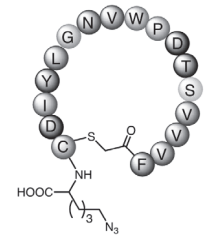

Cyclic L1[5]

Targeting VEGFR2-$\alpha_v\beta_3$

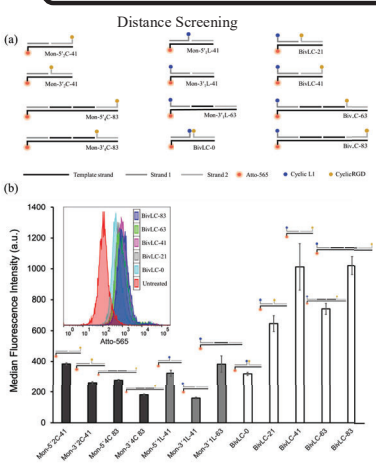

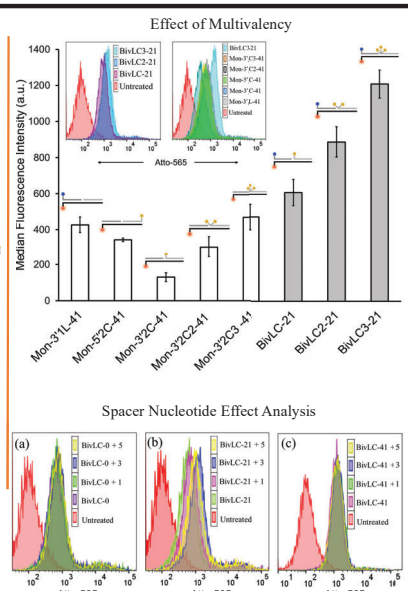

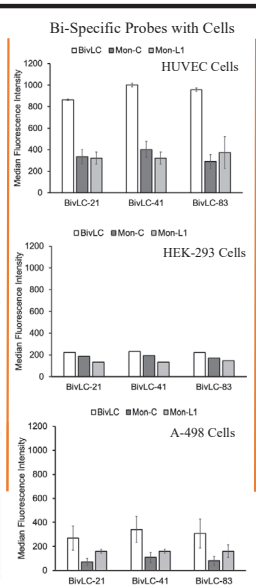

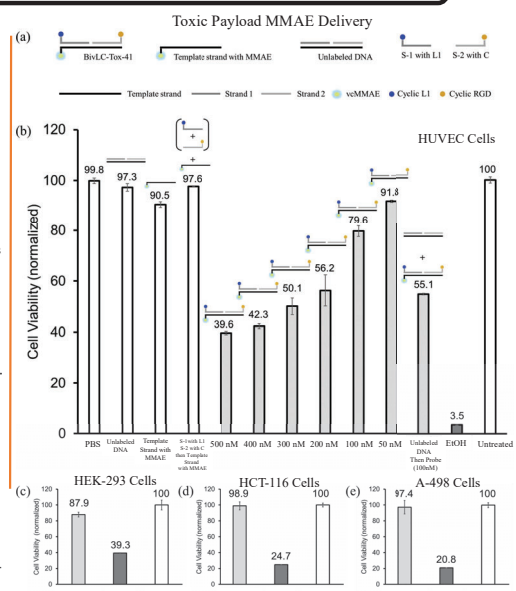

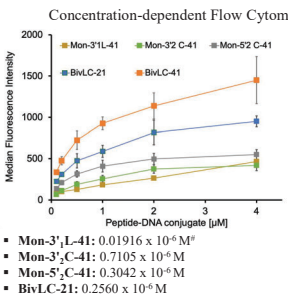

- **Mon-3'$_1$L-41:** 0.01916 x 10^{-6} M#
- **Mon-3'$_2$C-41:** 0.7105 x 10^{-6} M
- **Mon-5'$_2$C-41:** 0.3042 x 10^{-6} M
- **BivLC-21:** 0.2560 x 10^{-6} M
- **BivLC-41:** 0.2098 x 10^{-6} M

The plateau was not reached within the concentration range

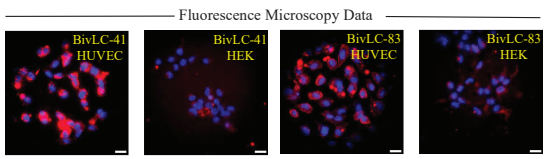

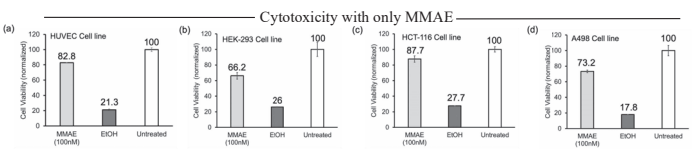

Targeting EGFR-MET

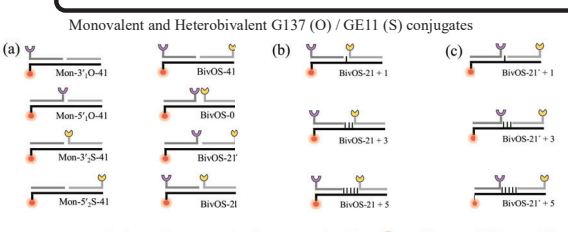

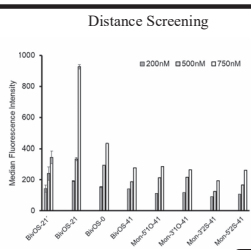

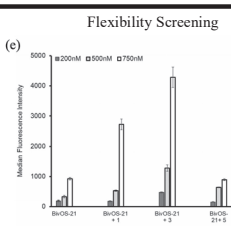

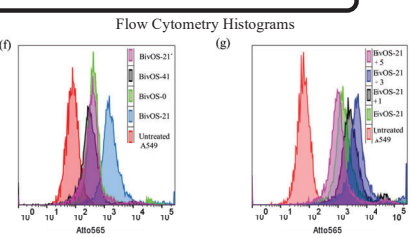

Conclusions

- Distance-controlled arrangement of peptide-DNA conjugates enhances the specificity of cancer cell recognition.
  - VEGFR2-$\alpha_v\beta_3$ (HUVEC): high affinity for distances > 135 Å
  - EGFR-MET (A549): high affinity for distance ≈ 70 Å
- Bispecific DNA-peptide probes can deliver cytotoxic agent (MMAE) selectively to cells expressing oncogenic receptor pairs

References and Acknowledgement

(1) Seitz et al. Angew. Chem. Int. Ed. 2011, 50, 4146 –4150; **(2)** Seitz et al. Angew. Chem. Int.Ed. 2019, 58,907 –911; **(3)** Seitz et al. Angew. Chem. 2020, 132,21202 –21208; **(4)** Appella et al, Nat Commun. 2012, 3, 614; **(5)** Murakami et al, ACS Chem. Biol. 2013, 8, 1205-1214; **(6)** Hardwick et al, Nat. Med. 2015, 21, 955-961; **(7)** Parren et al, Nat. Med. 2018, 24, 203-212.

We acknowledge support from **Deutsche Forschungsgemeinschaft** (Se819/24-1)

Memantine and Adamantine KLVFF Conjugates: Synthesis, Aβ interaction and Effects on Recognition Memory in Mice.

Giuseppe Pappalardo,[a] Eleonora Bocchieri,[a,b] Stefania Zimbone,[a] Maria Laura Giuffrida,[a] Giuseppe Di Natale,[b] Giuseppina Sabatino,[b] Graziella Vecchio,[c] Santina Chiechio.[b,d]

[a] *Institute of Crystallography, National Research Council (CNR-IC), 95126 Catania, Italy;* [b] *Department of Drug and Health Sciences, Pharmacology and Toxicology Section, University of Catania, Italy;* [c] *Department of Chemical Sciences, University of Catania, Catania, Italy;* [d] *Oasis Research Institute – IRCCS, Troina (EN), Italy.*

https://doi.org/10.17952/37EPS.2024.P2209

INTRODUCTION

Adamantane derivatives, such as memantine (Mem) and amantadine (Ada), are clinically active drugs with distinct mechanisms of action and therapeutic applications. While Ada is primarily used as an antiviral and anti-Parkinson drug and is not reported to have significant pro-cognitive effects, Mem has been demonstrated to be effective in various clinical conditions characterized by cognitive deficits, including Alzheimer's disease (AD). In our mind, preserving Aβ monomers from being recruited into oligomers may represent a viable therapeutic approach in AD. We designed and characterized two peptide conjugates of the KLVFF fragment bearing a memantinyl (Mem-Succ-KLVFF; Mem=3,5-dimethyladamantan-1-amine,) or an amantadinyl (Ada-Succ-KLVFF; Ada=Adamantan-1-amine) moiety, linked to the KLVFF sequence through a succinyl spacer. Their ability to counteract in vitro Aβ fibrillogensis and in vivo enhancement of memory performance was investigated

METHODS

Here we report the synthesis and structural characterization of two KLVFF peptide conjugates with the adamantane derivative drugs memantine or adamantine. Time course Circular Dichroism (CD) were carried out to investigated on the ability of the conjugated peptides to interfere with the $A\beta_{42}$ fibril formation. Complementary Th-T fluorescence and western blot experiments provided further information about the capacity of the conjugated peptides to impact the Aβ's fibrillogenic process. analyses. The interaction of these conjugates with β-CyD was also considered in view of their administration to CD1 mice as inclusion complexes to carry out Novel Object Recognition (NOR) tests. The whole of the results are discussed in terms of Structure Activity Relationships (SAR) based on the in vivo observation in comparison with the evoked cellular pathways connected with memory as well as HR-ESI-MS analyses carried out on the brain homogenates of the treated mice.

SYNTHESIS AND MOLECULAR CHARACTERIZATION OF THE CONJUGATES

MW-Assisted SPPS

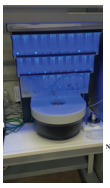

Novabiochem TGR resin

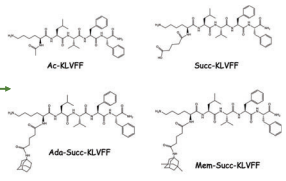

Coupling: TBTU / HOBT / DIEA activation method. MW power 25W, coupling reaction temperature 75 °C, coupling reaction time 300 sec

Deprotection: 20% piperidine in DMF. MW power 25Watt, temperature 75 °C, reaction time 180 sec.

Mem/Ada Conjugation: manually on peptidyl-resin using DIC/Oxima and free-base Mem (1:4) or HATU, DIEA and Ada•HCl (1:5)

Cleavage: TFA/TIS/H_2O (95/2.5/2.5; v/v/v), 1h RT

Inclusion complexes with β-cyclodextrins

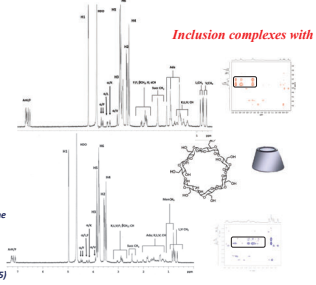

^1H NMR spectrum of Ada-Succ-KLVFF (A) and Mem-Succ-KLVFF (B) peptides in the presence of β-CyD.

Interaction with Amyloid -β

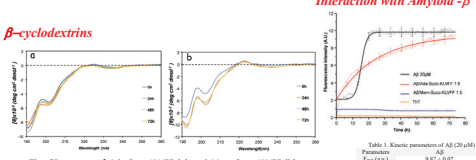

The CD spectra of Ada-Succ-KLVFF (a) and Mem-Succ-KLVFF (b) at different intervals of time as reported in the graphics. Spectra were recorded at 25 °C, in 10 mM phosphate buffer pH 7.4 and at 25 mM sample concentration

Time course of Th-T fluorescence assay of the $A\beta_{42}$/Ada-Succ-KLVFF and $A\beta_{42}$/Mem-Succ-KLVFF mixtures in a 1/5 ratio. $A\beta_{42}$ aggregation curve is reported for comparison

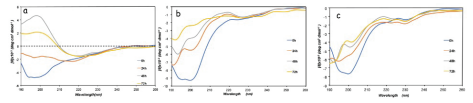

Table 1. Kinetic parameters of Aβ (20 μM) and conjugates at 1:5 molar ratio (100 μM)

Parameters	Aβ	Aβ/Ada-Succ-KLVFF	Aβ/Mem-Succ-KLVFF
T_{lag} (min)	9.82 ± 0.02	9.49 ± 0.1	6.79 ± 0.01
$k_1(h^{-1})$	1.76 ± 0.05	24.86 ± 3.2	2.28 ± 1.2
$k_2(h^{-1})$	15.49 ± 0.02	N.A.	29.35 ± 1.4
t_{50} (h^{-1})	11.97 ± 0.04	N.A.	24.79 ± 1.0

The CD spectra of $A\beta_{42}$ (a); $A\beta_{42}$/Ada-Succ-KLVFF 1:5 molar ratio(b); $A\beta_{42}$/Mem-Succ-KLVFF 1:5 molar ratio (c). Spectra were acquired at different intervals of time, at 25 °C, in 10 mM phosphate buffer pH 7.4.

IN VIVO STUDIES: NOVEL OBJECT RECOGNITION TASK

Novel Object Recognition Task

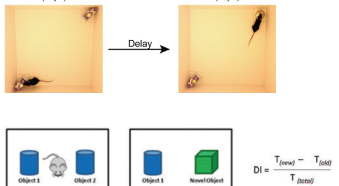

$$DI = \frac{T_{(new)} - T_{(old)}}{T_{(total)}}$$

The test was performed according to Ennaceur and Delacour (1988) with slight modifications. To reduce the stress associated with the novel environment, mice received one habituation session 24 hours before testing. During this session, each mouse was placed in a behavioral box for 10 minutes without objects (habituation). Twenty-four hours later each mouse received the treatment and was placed in the housing cage. After 15 minutes the mouse was returned to the behavioral box. In this first trial, each mouse was exposed to two identical objects (familiarization) and allowed to explore the identical objects for 10 minutes before being returned to the housing cage. Three hours later, in the testing trial, one of the two objects was replaced by a new one and the mouse was allowed to explore the novel and the familiar object for 10 minutes. Each trial was analyzed by a researcher blind to the treatment. Exploration of the object was characterized by sniffing and touching the object. The time spent exploring the familiar and novel object was measured and expressed in seconds for each mouse. The results are expressed as discrimination index (DI) calculated as follows: DI = [(time spent exploring the novel object) – (time spent exploring the familiar object)]/[(time spent exploring the novel object) + (time spent exploring the familiar object)]. The DI represents the ability to discriminate the novel object from the familiar one.

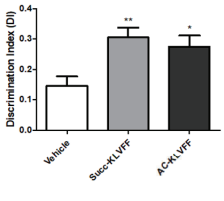

Effects of Succ-KLVFF and Ac-KLVFF in the NOR task. Succ-KLVFF and Ac-KLVFF (27.9 mM, 1ml/kg, ip), injected 15 minutes before the training session significantly increased the exploration of the novel object compared to the vehicle group. Results are expressed as discrimination index (DI) calculated as follows: DI = [(time spent exploring the novel object) – (time spent exploring the familiar object)]/[(time spent exploring the novel object) + (time spent exploring the familiar object)]. DI represents the ability to discriminate a novel object from the familiar one. Results are the MEAN ± SEM of 12-15 mice per group.
One-way ANOVA, followed by Tukey's test. *p<0.05 ; **p<0.01; vs vehicle group.

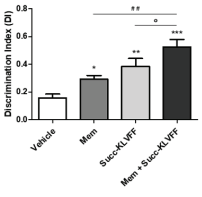

Effects of the combination treatment with Mem and Succ-KLVFF in the NOR task. The combined treatment with Mem (27.9 mM, 1 ml/kg, ip) and Succ-KLVFF (27.9 mM, 1ml/kg, ip) injected 15 minutes before the training session significantly increased the exploration of the novel object compared to the vehicle group and showed a synergic effect when compared to MEM or Succ-KLVFF alone. Results are expressed as discrimination index (DI) calculated as follows: DI = [(time spent exploring the novel object) – (time spent exploring the familiar object)]/[(time spent exploring the novel object) + (time spent exploring the familiar object)]. DI represents the ability to discriminate a novel object from the familiar one. Results are the MEAN ± SEM of 12-15 mice per group. One-way ANOVA, followed by Tukey's test. *p<0.05; **p<0.01; vs vehicle group.

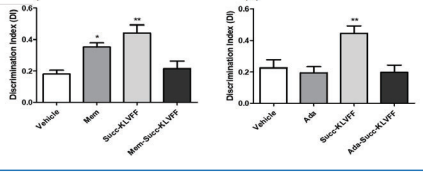

Effects of Mem (A) or Ada (B) alone or conjugated with Succ-KLVFF in the NOR task. Mem (27.9 mM, 1ml/kg, ip) and Succ-KLVFF (A: 27.9 mM, 1ml/kg, ip; B: 330 mM, 1 ml/kg, ip) alone 15 minutes before the training session significantly increased the exploration of the novel object compared to the vehicle group. Neither Mem-Succ-KLVFF (27.9 mM, 1ml/kg, ip) nor Ada-Succ-KLVFF (330 mM, 1 ml/kg, ip) or Ada (330 mM, 1 ml/kg, ip) affected the DI compared to the vehicle group. Results are expressed as discrimination index (DI) calculated as follows: DI = [(time spent exploring the novel object) – (time spent exploring the familiar object)]/[(time spent exploring the novel object) + (time spent exploring the familiar object)]. DI represents the ability to discriminate a novel object from the familiar one. Results are the MEAN ± SEM of 12-15 mice per group. One-way ANOVA, followed by Tukey's test. *p<0.05; **p<0.01; vs vehicle group.

IN VITRO STUDIES: MTT AND WESTERN BLOT

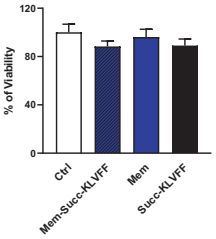

MTT Assay of fully differentiated SH-SY5Y treated for 48 hours with Mem-Succ-KLVFF, Mem, and Succ-KLVFF at the concentration of 5 μM. Bars represent means ±SEM of three independent experiments with n=3 each

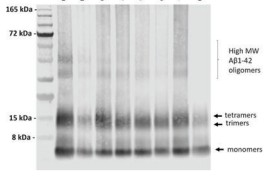

1. oAβ1-42/Mem-Succ-KLVFF (l:1)
2. oAβ1-42/Mem-Succ-KLVFF (l:5)
3. oAβ1-42/Mem (1:1)
4. oAβ1-42/Mem (1:5)
5. oAβ1-42/Succ-KLVFF (1:1)
6. oAβ1-42/Succ-KLVFF (1:5)
7. oAβ1-42
8. mAβ1-42

Representative western blot of Aβ oligomers (oAβ) prepared in the presence or absence of different molar ratios (1:1, 1:5) of Mem-Succ-KLVFF, Memantine (Mem) and Succ-KLVFF. Samples were separated into a 4-12% Bis-Tris SDS-PAGE gel and blotted with anti-Aβ N-terminal1-16 mouse monoclonal antibody 6E10 (1:800).

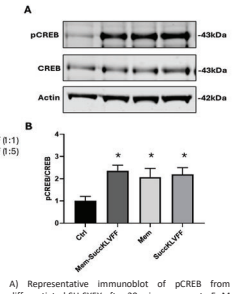

A) Representative immunoblot of pCREB from differentiated SH-SY5Y after 30 min exposure to 5μM Memantine (Mem), Memantine-Succ-KLVFF (Mem-Succ-KLVFF) and Succ-KLVFF. B) Densitometric values of pCREB, normalized on CREB signals, are represented in the respective graph bars. Bars represent means ±SEM of 4 independent experiments with n=3 each.

IN VITRO STUDIES: HR-ESI-MS

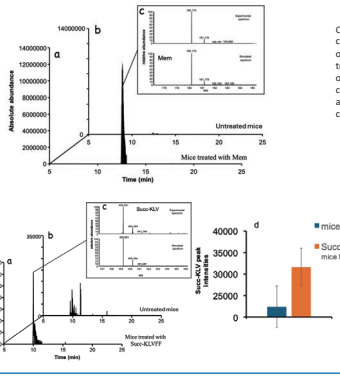

Chromatographic profiles reported as extracted-ion chromatograms (XIC) of Mem (m/z=180.17-180.18) of a) homogenate brain tissue obtained from mice treated with Mem and b) homogenate brain tissue obtained from mice not treated with Mem. The inset c) shows the comparison between the experimental and theoretical isotopic distribution of the m/z peak corresponding to the Mem.

Chromatographic profiles reported as extracted-ion chromatograms (XIC) (m/z=459.27–459.29) of a) homogenate brain tissue obtained from mice treated with Mem + Succ-KLVFF and b) homogenate brain tissue obtained from mice not treated with Mem + Succ-KLVFF. The inset c) shows the comparison between the experimental and theoretical isotopic distribution of the m/z peak corresponding to the Succ-KLV. d) comparative analysis of the chromatographic peak intensities averaged over 3-6 replicate measurements.

CONCLUSIONS

The results suggest that co-administration of Mem and KLVFF-based peptides behave as cognitive enhancers in normal cognition and therefore might have great potential to treat cognitive impairment resulting from neurodevelopmental and neurodegenerative disorders.

REFERENCES

Hardy J., Selkoe D.J., The amyloid Hypothesis of Alzheimer's disease: progress and problems on the road to therapeutics. Science, 2002, 297, 353-356

Giuffrida M.L., Caraci F., Pignataro B., Cataldo S., De Bona P., Bruno V., Molinaro G., Pappalardo G., Messina A., Palmigiano A., Garozzo D., Nicoletti F., Rizzarelli E., Copani A. β-amyloid monomers are neuroprotective. J Neurosci. 2009, 29 (34), 10582-10587

CONTACTS

Dr. Giuseppe Pappalardo : Giuseppe.pappalardo@cnr.it
Prof. Santina Chiechio: Chiechio@unict.it

www.PosterPresentations.com

UNIVERSITY OF COPENHAGEN

https://doi.org/10.17952/37EPS.2024.P2210

Chemoselective arylation of amino acids, peptides and proteins

Ahmed M. Embaby, Sanne Schoffelen, Christian Kofoed, Morten Meldal and Frederik Diness*

Center for Evolutionary Chemical Biology, Department of Chemistry, University of Copenhagen, Copenhagen, Denmark. *fdi@chem.ku.dk

1. Introduction

Methods for identification and regulation of cysteine containing proteins are essential as these proteins have key roles in diseases, including parasite infections, osteoporosis and cancer. Within this area many chemical tools for covalent protein modification have been developed. However, the traditional applied electrophiles (e.g. iodoacetamide), have in general little room for tuning of the reactive carbon. Benzene, on the other hand, is interesting as a core for developing selective reactive probes, as it provides five positions for tuning of reactivity, and attachment of other functionalities of interests, in addition to the electrophilic carbon. Based on our experience with nucleophilic aromatic substitution (S_NAr) reactions, we hypothesized that molecular tools for selective cysteine labeling in water could be developed through fine tuning the reactivity of fluorobenzenes by variation of number of fluorine atoms in combination with other substituents.[1,2,3]

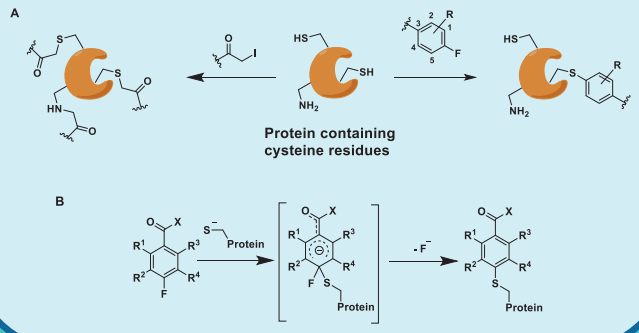

2. Reactivity screening of fluorobenzenes

As a model system, the reactivity of fluorobenzene derivatives towards *tert*-butyloxycarbonyl protected cysteine was tested. Under promoting reaction conditions using DMF and DIPEA the compounds presented in red and blue reacted. The remaining derivatives (in black) did not react. Under less promoting reaction condition, in aqueous buffer only the examples presented in red reacted. The reactivity of the fluorobenzene derivatives could be linked to the electron withdrawing capacity (Hammett σ_p-constant) of the substituents as well as the number of fluoro substituents. To test for selectivity towards cysteine over other amino acids, peptide **4** was reacted with an excess (3 eq.) of **2a** under aqueous condition (see Scheme 3). Only a the monosubstituted adduct **5** was observed and identified by LC-MS and MSMS.

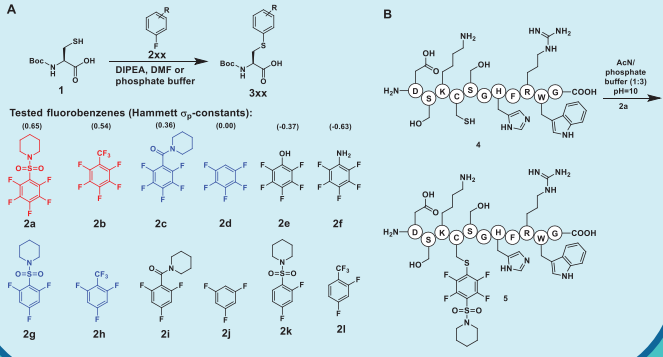

3. Selective cysteine protease inhibition

Selective inhibition of papain (cysteine protease) over subtilisin (serine protease) was explored using an on-bead inhibition assay. The enzymes were pre-incubated with the fluorobenzenes and then added to polymer bound FRET substrates. Compound **2a** and pentafluoronitrobenzene (**2aa**) completely inhibited papain, whereas subtilisin was still fully active under identical conditions.

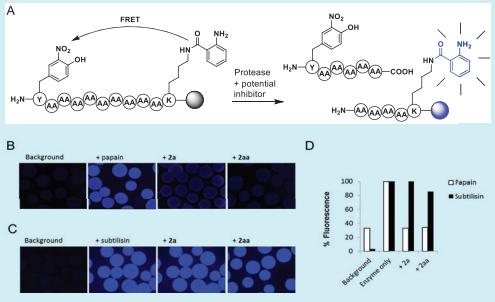

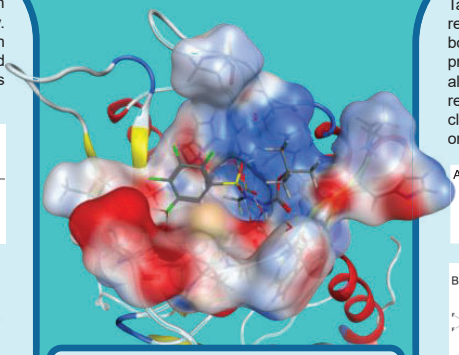

Model of cysteine protease with covalent bound inhibition

4. Protein labelling

Tag-containing probes based on **2a** were synthesized and then reacted with enhanced green fluorescent protein (eGFP) or with bovine serum albumin (BSA). All three types of reporter-linked probes were capable of labeling the free thiols of eGFP and albumin in a concentration-dependent manner. Gratifyingly, the reactive fluorobenzene probes did not interfere with the functional click, the fluorescence or the affinity tag under the protein labeling or the detection conditions.

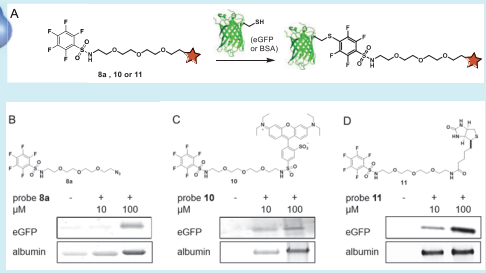

5. Selective reaction among cysteine residues

Three fluorobenzene derivatives with different reactivities (**2a**, **2g** and **2i**) were investigated for their ability to react selectively with only one of the unpaired cysteine residues in Tobacco Etch Virus (TEV) protease. After tryptic digest of the native TEV protease (negative control), the peptide fragment with cysteine in the active site (Cys170) was found at 1219.59 and that of the fragment with a surface exposed cysteine (Cys129) at 1267.68 Da. The signal at 1219.59 Da disappeared upon pre-treatment with **2g**, and a new mass peak at 1478.65 corresponding to the modified fragment appeared. The fragment with Cys129 remained unchanged. In contrast, both of the native signals completely disappeared upon reaction with compound **2a** and the mass peaks corresponding to modified peptide fragments appeared. On the other hand **2i** (not shown) did not react all.

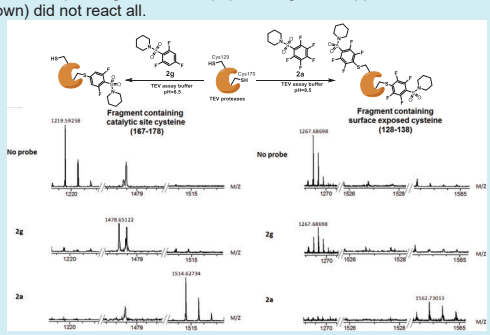

6. Activity Based Protein Profiling

To investigate the applicability of fluorobenzenes for activity-based protein profiling (ABPP), native or heat-denatured TEV protease was treated with compound **8a**, **8b**, **8c** or **8d**. Probe **8b** and **8c** proved able to label TEV protease in an activity-dependent manner. In contrast, probe **8a** was able to label both active and denatured TEV protease, while probe **8d** did not label any of the samples.

The probes were also tested towards bacterial cell lysates, with or without pretreatment with iodoacetamide. The most reactive probe (**8a**), labeled many bands with great intensity, whereas probe **8b** appeared much more selective and probe **8d** did not label any protein in the cell lysate. The pre-treatment with iodoacetamide inhibited the labeling with the active probes completely, supporting that these probes selectively target cysteine residues. A major labeled protein band around 25 kDa was analyzed by mass spectrometry after tryptic digestion. Gratifyingly, the protein proved to be chloramphenicol acetyltransferase (CAT), an enzyme containing a cysteine in the catalytic site.

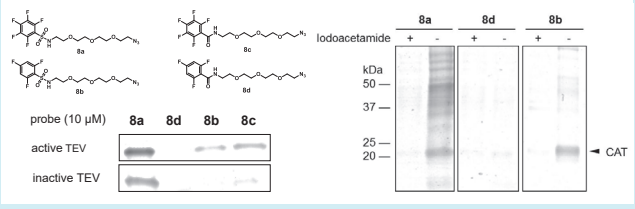

1) Embaby, A. M.; Schoffelen, S.; Kofoed, C.; Meldal, M.; Diness, F. *Angewandte Chemie International Edition*, **2018**, *57*, 8022-8026
2) Diness, F.; Fairlie, D. P. *Angewandte Chemie International Edition*, **2012**, *51*, 8012-8016
3) de Araujo, A. D.; Hoang, H. N.; Kok, W. M.; Diness, F.; Gupta, P.; Hill, T. A.; Driver, R. W.; Price, D. A.; Liras, S.; Fairlie, D. P. *Angewandte Chemie International Edition*, **2014**, *53*, 6965-6969

https://doi.org/10.17952/37EPS.2024.P2211

Glycopeptides as synthetic antigenic probes for MOG Antibody-Associated Disease

Silvia Bracci[a,b], Feliciana Real-Fernandez,[c] Christine Patte-Mensah[d], Christian Klein[d], Nicolas Collongues[d,e,f,g], Jérôme de Sèze[d,e,f], Paolo Rovero[a,h], and Anna Maria Papini[a,b]

[a] Interdepartmental Research Unit of Peptide and Protein Chemistry and Biology - PeptLab, University of Florence, 50019 Sesto Fiorentino, Italy
[b] Department of Chemistry "Ugo Schiff", University of Florence, Via della Lastruccia 3-13, 50019 Sesto Fiorentino, Italy
[c] Institute of Chemistry of Organometallic Compounds (ICCOM), National Research Council of Italy (CNR), 50019 Sesto Fiorentino, Italy
[d] Biopathology of Myelin, Neuroprotection and Therapeutic Strategies, INSERM U1119, Federation of Translational Medicine of Strasbourg, Université of Strasbourg, 1, Rue Eugène Boeckel, 67000 Strasbourg, France
[e] Department of Neurology, University Hospital of Strasbourg, 1 Avenue Molière, 67200 Strasbourg, France
[f] Center for Clinical Investigation, INSERM U1434, Strasbourg, France
[g] Department of Pharmacology, Addictology, Toxicology, and Therapeutics, Strasbourg University, Strasbourg, France
[h] Department of NeuroFarBa, University of Florence, Via Ugo Schiff 6, 50019 Sesto Fiorentino, Italy
E-mail: silvia.bracci@unifi.it

Ministero dell'Università e della Ricerca
Italiadomani PIANO NAZIONALE DI RIPRESA E RESILIENZA
Funded by the European Union NextGenerationEU
THE Tuscany Health Ecosystem
UNIVERSITÀ DEGLI STUDI FIRENZE
PeptLab INTERDEPARTMENTAL RESEARCH UNIT OF PEPTIDE AND PROTEIN CHEMISTRY AND BIOLOGY
DICUS DIPARTIMENTO DI CHIMICA "UGO SCHIFF"
37th EPS 14th IPS

Introduction

Myelin-oligodendrocyte glycoprotein antibody-associated disease (MOG-AD) has been recently identified as an antibody-mediated demyelinating autoimmune disorder of the CNS, distinct from multiple sclerosis (MS) of which it was long considered a subtype, due to some clinical and radiological overlaps. However, a specific diagnosis is essential due to the different clinical features, treatment considerations, and prognoses compared to MS[1].

Autoantibodies targeting myelin-oligodendrocyte glycoprotein (MOG), in particular anti-MOG IgGs, are considered biomarkers of the disease. Cell-based assays are (CBAs) the recommended method for testing anti-MOG antibodies, according to international consensus[2]. Despite being considered the gold standard, CBAs have not yet been standardized, and low positive results show poor agreement. Moreover, CBAs are time-consuming and require expertise both in the interpretation of results and in working with cells[3].

Conversely, **ELISAs** are user-friendly, cost-effective, and, with the potential to be automated, are ideal for simultaneous screening of larger numbers of patients[3]. However, ELISAs using linear or refolded recombinant full-length MOG have thus far given inconsistent results.

Myelin-oligodendrocyte glycoprotein (MOG) is a 218 amino acid glycoprotein (molecular mass 26–28 kDa). MOG is uniquely expressed on the surface of the myelin sheath, specifically on oligodendrocytes membrane, in the central nervous system (CNS), but it is a quantitatively minor component of myelin (0.05%).
The biological role of MOG is still unknown. The N-terminal region of MOG forms an Ig-V fold consisting of two antiparallel β-sheets. It also presents one N-linked glycosylation site on asparagine 31[4].
MOG is known to be an encephalitogenic protein that can elicit a demyelinating immune response in numerous experimental models of inflammatory demyelinating diseases.
Conflicting results have been obtained when using full-length MOG in ELISAs to test MS patient sera.

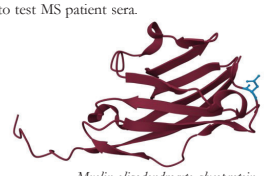

Myelin-oligodendrocyte glycoprotein
PDB: 1PKO

Protein **post-translational modifications** (PTMs), such as phosphorylation, glycosylation, citrullination, and ubiquitination, are essential for increasing proteome diversity and regulating protein activity, structure, localization, and interactions, thus influencing numerous vital biological processes. However, dysregulation of the spontaneous or enzymatic reactions that generate PTMs, triggered by processes such as inflammation, can cause a lack or abundance of modifications that lead to the generation of neoantigens, that can be targeted by antibodies, generating an autoimmune response[5,6].

In this context, recombinant or extracted protein antigens often used in immunoassays may not reproduce the correct modifications, as well as the correct folded conformation, essential for antibody recognition.

On the other hand, synthetic **peptides** can be produced as specific chemical entities in high quality and quantity through standard and reproducible solid-phase synthesis protocols. SPPS also enables the straightforward introduction of modifications in the sequence to mimic the native epitope, using non-standard, modified amino acids corresponding to the target PTM.

Non-typeable *Haemophilus influenzae* adhesin

The Asn(Glc) modification is virtually absent in humans but is found in prokaryotes in surface proteins such as adhesins. It was found that a hyperglucosylated protein domain from adhesin protein of nontypeable *Haemophilus influenzae* (NTHi) termed HMW1, is preferentially recognized by antibodies from sera of an MS patient subpopulation, supporting the hypothesis of the involvement of an infection by an exogenous pathogen in MS pathophysiology[7].

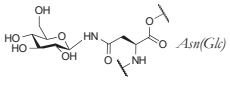

Asn(Glc)

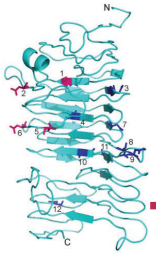

I-TASSER model of HMW1ct

Aim of the work

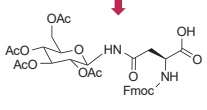

Fmoc-Asn[Glc(OAc)$_4$]-OH

SPPS

	Peptides	Sequence
1	hMOG(25-55)	RISPGKNATGMEVGWYRPPFSRVVHLYRNGK
2	[N^{31}]hMOG(25-55)	RISPGKN^{31}(Glc)ATGMEVGWYRPPFSRVVHLYRNGK
3	[N^{53}]hMOG(25-55)	RISPGKNATGMEVGWYRPPFSRVVHLYRN^{53}(Glc)GK
4	[N^{31},N^{53}]hMOG(25-55)	RISPGKN^{31}(Glc)ATGMEVGWYRPPFSRVVHLYRN^{53}(Glc)GK

Cleavage, purification and characterization of peptides

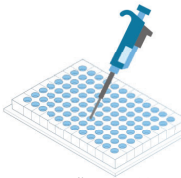

Indirect ELISA



MS vs. MOGAD

Peptides	HPLC R$_t$ (min)	HPLC purity (%)	ESI-MS (m/z) found (calcd)
1	4.28	>95	1192.89 (1192.63)
2	3.88	>95	1245.69 (1245.98)
3	3.62	>95	1245.56 (1245.98)
4	3.75	>95	1300.90 (1300.99)

Peptide characterization by RP-HPLC-MS on Waters Alliance™ Chromatography system (Separation Module 2695, Detector Diode Array 2996) equipped with an online single quadrupole ESI-MS Waters Micromass ZQ using a Supelco BIOshell A160 Peptide C18 (10 cm x 3.0 mm, 2.7 µm) column. Analytical HPLC flow at 0.6 mLmin^{-1}; temperature 35 °C. Eluents: 0.1% (v/v) TFA in H_2O (A) and 0.1% (v/v) TFA in ACN (B), λ 215 nm. 10-90% gradients of B solvent were performed in 5min. ESI-MS: detected as $[M+3H]^{3+}$.

Anti-Hyperglucosylated Adhesin Ab recognition

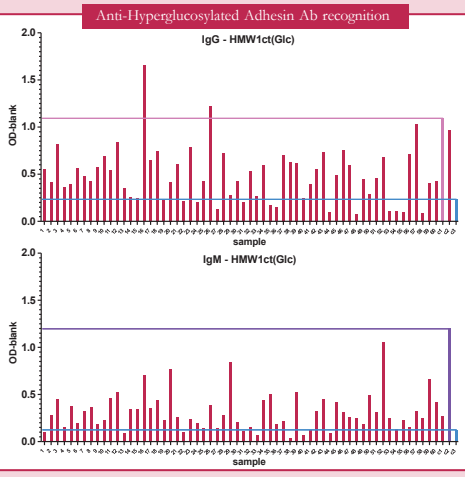

Preliminary results on MS patient sera

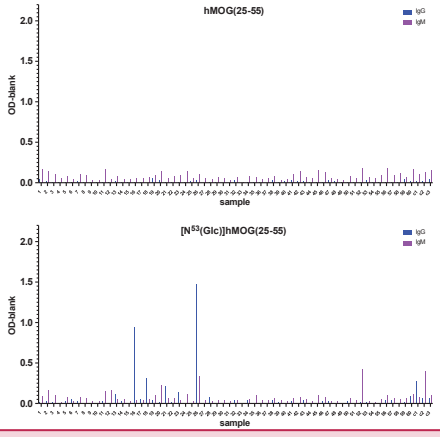

Role of N-glucosylation in Ab recognition

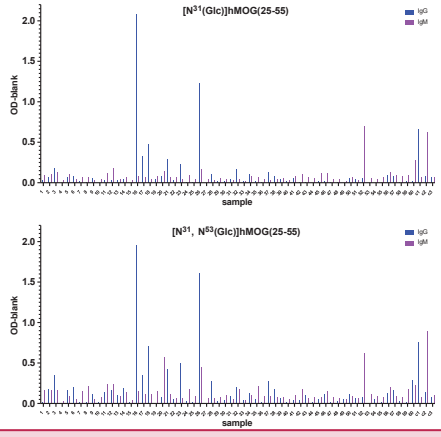

Conclusions and future perspectives

- ✓ Confirmed preferential recognition of N-glucosylated human MOG peptides over the non-glucosylated ones in a subpopulation of a new cohort of MS patients, from which MOG-AD patients are excluded according to recent classification criteria.
- ✓ Confirmed recognition of hyperglucosylated adhesin of non-typeable *Haemophilus influenzae* in a new cohort of MS patients, from which MOG-AD patients are excluded according to recent classification criteria.

- ► Comparative evaluation of the results obtained with MOG-AD patient serum following equal protocols to study the role of N-glucosylation in antigen-antibody recognition and optimize the synthetic peptide antigenic probes for specific recognition of MOG-AD patients.
- ► Comparative evaluation of the results obtained with MOG-AD patient serum following equal protocols to determine whether non-typeable *Haemophilus influenzae* could be involved in MOG-AD pathogenesis.

References

1. L. Cacciaguerra, E. P. Flanagan, *Neurologic Clinics*. **42**, 77–114 (2024).
2. B. Banwell *et al.*, *The Lancet Neurology*. **22**, 268–282 (2023).
3. M. Tampoia *et al.*, *Autoimmun Highlights*. **10**, 5 (2019).
4. C. Breithaupt *et al.*, *Proceedings of the National Academy of Sciences*. **100**, 9446–9451 (2003).
5. A. C. Conibear, *Nat Rev Chem*. **4**, 674–695 (2020).
6. M. G. Zavala-Cerna *et al.*, *Clinic Rev Allerg Immunol*. **47**, 73–90 (2014).
7. M. T. C. Walvoort *et al.*, *Sci Rep*. **6**, 39430 (2016).

Acknowledgments

This research was supported by the European Union by the Next Generation EU Project ECS00000017 "Ecosistema dell'Innovazione" THE - Tuscany Health Ecosystem (Spoke 6: Precision medicine & personalized healthcare) for Silvia Bracci's PhD fellowship.

Funded by the European Union NextGenerationEU
THE Tuscany Health Ecosystem

We thank the Euroepan Peptide Society for Silvia Bracci's awarded registration at 37th EPS/14th IPS.

P2.212 - Designing self-assembling lipopeptide for tissue regeneration

Dhriti Shenoy[1,2], Lauren Roberts[1,2], Michela Pesenti[1], Kaliroi Peqini[1], Stefania Crespi[3], Cécile Echalier[2], Gilles Subra[2], and Sara Pellegrino[1]

[1]Dipartimento di Scienze Farmaceutiche, Università degli Studi di Milano, Italy
[2]IBMM, University of Montpellier, CNRS, ENSCM, France
[3]Dipartimento di Scienze della Terra Ardito Desio,Università degli Studi di Milano, Italy

dhriti.shenoy@unimi.it

https://doi.org/10.17952/37EPS.2024.P2212

1. INTRODUCTION

Lipopeptides are one class of biosurfactant materials, which have been widely studied in the past decade for tissue engineering applications. Their biocompatibility and flexibility make them ideal scaffold materials for tissue regeneration[1]. The hydrophobic lipid tail propels the self assembly and exposes the functional peptide sequences on the surface of the supramolecular structure. In our work, we've combined stearic acid with bioactive peptides which can imitate the structure and function of native ECM[2]. Here, the self-assembly propensity of these compounds are reported.

Bioactive peptides	Biological activity
IKVAV	Encourages vascularization and differentiation factors
REDV	Promoted endothelial cell adhesion and proliferation
GFOGER	Promotes cell adhesion, proliferation and differentiation of stem cells (hMSCs) (present in collagen type 1)

2. Methodology

The peptide sequences were *synthesized* using microwave assisted solid phase peptide synthesis technique on CEM liberty blue instrument.

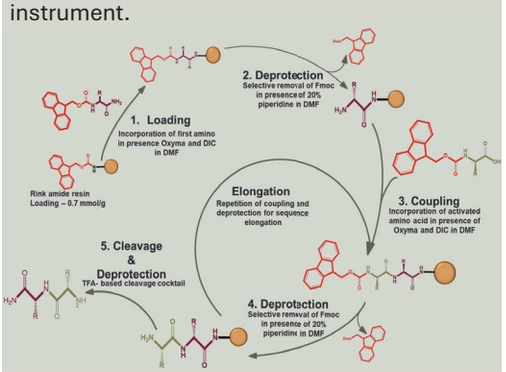

The peptides were then purified by RP-HPLC and freeze dried.

The *self-assembly studies* were done using solvent displacement technique in pure water and phosphate buffer saline solution (PBS).

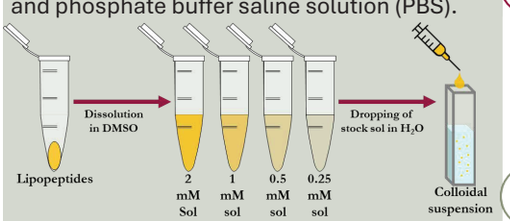

3. Results

DLS results of colloidal suspensions of the lipopeptides in pure water at different peptide concentrations and solvent ratios are reported below

Peptide sequence	pH		9:1 (50 µM)	9.5:0.5 (50 µM)	9:1 (25 µM)	9.5:0.5 (25 µM)
Stearic acid-IKVAV-NH_2	6.93	PDI	0.4443±0.04	0.6717±0.21	0.7981±0.17	0.6277±0.62
		Size (nm)	191±18.9	870.1±147	782.3±500	383.2±382
Stearic acid-REDV-NH_2	7.29	PDI	0.2698±0.02	0.319±0.048	0.4018±0.03	0.3431±0.021
		Size (nm)	291±10.02	450.4±8.4	497.1±12.4	659.3±18
Stearic acid-GFOGER-NH_2	7.19	PDI	0.2625±0.02	0.3017±0.06	0.2661±0.008	0.1692±0.015
		Size (nm)	1116±35.4	1418±62.9	414.2±12.4	250±0.88

PDI- Polydispersity index

Below the DLS graphs and SEM images of the lipopeptides in H_2O/DMSO (9.5:0.5) are reported (for 25 µM concentration)

Stearic acid-IKVAV-NH_2

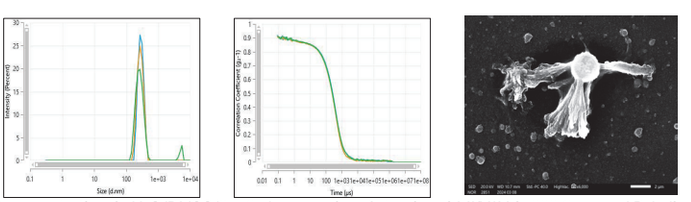

For 25 µM concentration, in H_2O/DMSO(9.5:0.5), mean size of stearic acid-IKVAV is 383.2 nm and Polydispersity Index is 0.6277

Stearic acid-REDV-NH_2

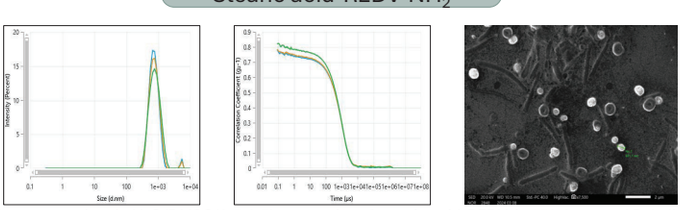

For 25 µM concentration, in H_2O/DMSO(9.5:0.5), mean size of stearic acid-REDV is 659.3 nm and Polydispersity Index is 0.3431

Stearic acid-GFOGER-NH_2

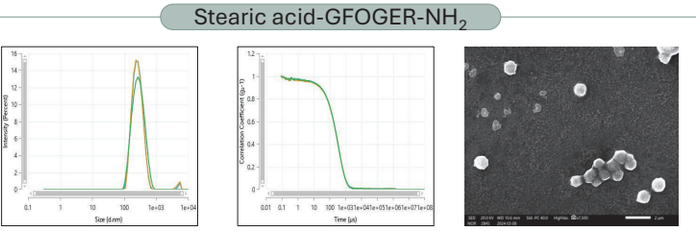

For 25 µM concentration, in H_2O/DMSO(9.5:0.5), mean size of stearic acid-GFOGER is 250 nm and Polydispersity Index is 0.1692

4. Conclusion

Our results showed that all lipopeptides self-assemble in aqueous environment. The best results were obtained with the higher percentage of water (95%) at the lowest concentration (25 µM). In PBS, an increase in the dimension was observed, probably due to the higher pH and salt concentration.

5. Future perspectives

The lipopeptides will be combined with low temperature gelling biopolymers like agarose to develop composite hydrogels which will then be used for 3D printing. The obtained scaffolds will be tested for their rheological properties and then seeded with L929 cells to evaluate their cytotoxicity and cell viability.

References

(1) Hutchinson, J. A.; Burholt, S.; Hamley, I. W. Peptide Hormones and Lipopeptides: From Self-Assembly to Therapeutic Applications. Journal of Peptide Science 2017, 23 (2), 82–94. https://doi.org/10.1002/psc.2954.
(2) Sun, W.; Gregory, D. A.; Zhao, X. Designed Peptide Amphiphiles as Scaffolds for Tissue Engineering. Advances in Colloid and Interface Science 2023, 314, 102866. https://doi.org/10.1016/j.cis.2023.102866.

"This project has received funding from the European Union's research and innovation programme under the Marie Skłodowska-Curie grant agreement No 101072645".

Optimizing biological activity of Lactoferricin derived peptides: Conjugation with non peptidic motifs as a strategy

Daniel Castellar [1] , Javier García [1] , Zuly Rivera [2] , Ricardo Fierro [2]

[1] Pharmacy Department, Universidad Nacional de Colombia– Bogotá D.C, Colombia
[2] Chemistry Department, Universidad Nacional de Colombia– Bogotá D.C, Colombia

https://doi.org/10.17952/37EPS.2024.P2213

37th EPS European Peptide Symposium
14th IPS International Peptide Symposium
Florence, Italy 25 - 29 August 2024

INTRODUCTION

Synthetic peptides derived from Bovine Lactoferricin have been established as promising molecules against multiple cancers. The palindromic sequence RWQWRWQWR has demonstrated selective cytotoxic activity against breast and cervical cancers, establishing this peptide as a potential anticancer agent. To broaden the biological applications of this sequence, we utilized three different functional moieties to enhance the peptide's biological activities: i) non-steroidal anti-inflammatory Drugs (NSAID) , which could optimize the anticancer activity of the sequence by modulating anti-inflammatory signals; ii) fluorescent probes, enabling the peptide to be used as a bioanalytical tool in cancer cell imaging; and iii) ferrocene, which could enhance redox reactions within cancer cells. Some of these motifs proved useful for optimizing the cytotoxic activity of the core sequence and for enabling the peptide to be used in other applications such as cancer cell imaging.

METHODS

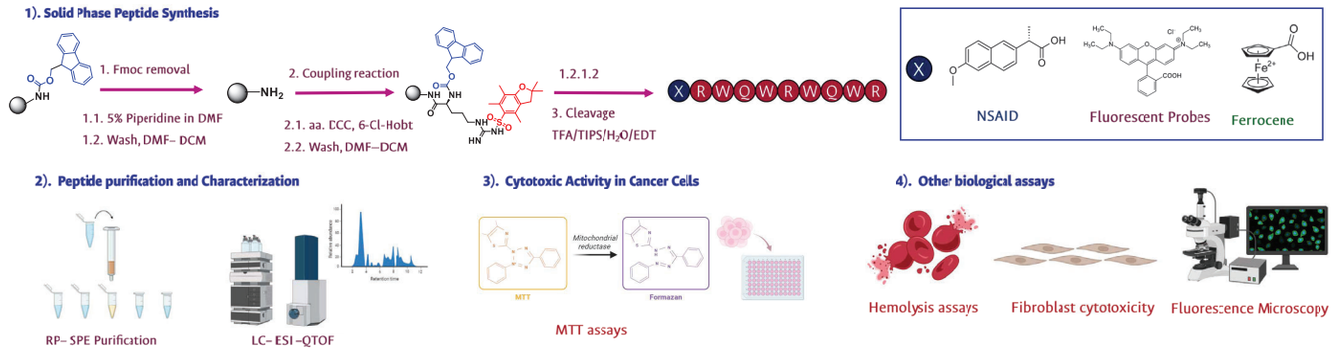

RESULTS AND DISCUSSION

NSAID– LfcinB conjugates

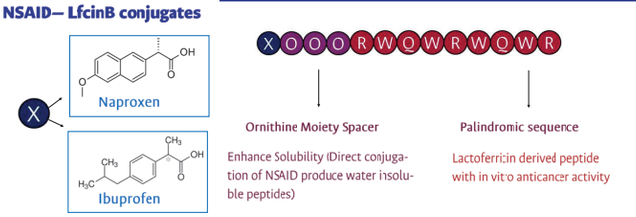

Code	Sequence	t_R (min)	Purity (%)	Expected mass (amu)	Experimental mass (amu)
$(Orn)_3$-$(LfcinB)_{Pal}$	OOORWQWRWQWR	5,7	99,9	1828,0000	1828,0125
NAP $(Orn)_3$-$(LfcinB)_{Pal}$	NAP-OOORWQWRWQWR	7,0	94,3	2040,0900	2040,1200
IBU $(Orn)_3$-$(LfcinB)_{Pal}$	IBU-OOORWQWRWQWR	7,5	97,7	2016,1200	2016,1340

Table 1. Characterization of NSAID conjugated peptides optimized with a polar Ornithine moiety spacer

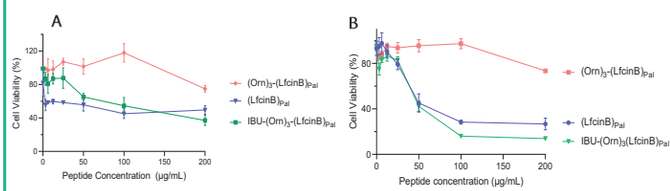

Figure 1. Cytotoxic activity of the Ibuprofen conjugated peptide IBU $(Orn)_3$-$(LfcinB)_{Pal}$ compared to the activity of the palindromic sequence and its non conjugated ornithine deivate against A) MCF-7 (breast cancer) and B) HeLa (cervical cancer) cells. Experiments were conducted in triplicates (n=3)

Code	Sequence	IC 50 µM (HeLa)	IC50 µM (MFC-7)	IC50 µM Fibroblast (L929)	Hemolysis (%) *	Selectivity Index
$(Orn)_3$-$(LfcinB)_{Pal}$	OOORWQWRWQWR	>109	> 109	>109	< 10 %	N.A
NAP $(Orn)_3$-$(LfcinB)_{Pal}$	NAP-OOORWQWRWQWR	85	> 98	> 98	<10 %	>1
IBU $(Orn)_3$-$(LfcinB)_{Pal}$	IBU-OOORWQWRWQWR	29	55	> 81	<10 %	>2

Table 2. Summary of the cytotoxic activity of the NSAID conjugated peptides against cancer cells, fibroblast and erythrocytes. *Percentage of hemolysis is reported at a maximum concentration of 200 µg/mL

Ferrocene– Lfcin B conjugates

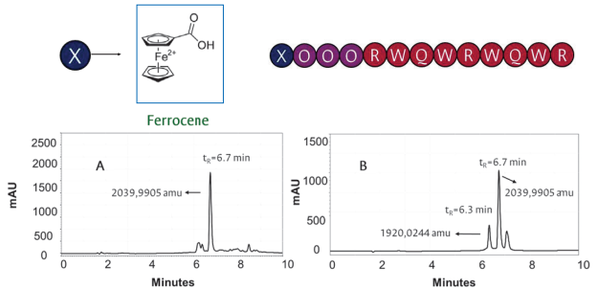

Figure 4. Representative RP-HPLC-chromatogram depicting the degradation process of the Ferrocene conjugated peptide optimized with an Ornithine moiety. A) Crude peptide B) Peptide after RP-SPE purification process

Fluorescent probes– Lfcin B conjugates

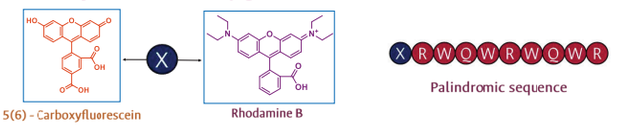

Code	Sequence	t_R (min)	Purity (%)	Expected mass (amu)	Experimental mass (amu)
(5(6) FAM)-$(LfcinB)_{Pal}$	(5(6) FAM)-RWQWRWQWR	8,2	96,9	1843,8100	1843,8088
(RhodB)-$(LfcinB)_{Pal}$	(RhodB)-RWQWRWQWR	*9,8 and 10,1	30,2 and 65,0	1910,9900	1910,9800

Table 3. Characterization of the fluorescent peptides obtained.* Rhodamine B peptide is a mixture of two isomers

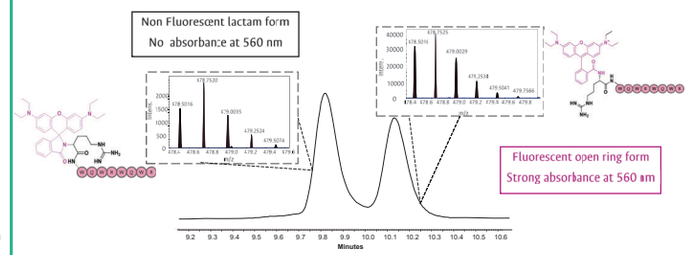

Figure 2. Representative RP-HPLC-chromatogram of the Rhodamine B conjugated peptide presenting the pair of isomers detected by LC-ESI-QTOF (isotopic distribution showed) which correspond to an open ring–lactam equilibrium

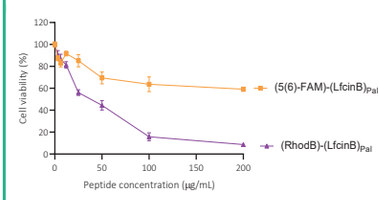

Figure 3. Cytotoxic activity of the fluorescein and Rhodamine B conjugated peptides against MCF-7. Experiments were conducted in triplicates (n=3)

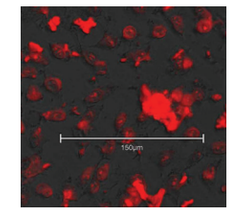

Figure 4. Fluorescence Microscopy images of MCF-7 cells incubated with 200 µg/mL of the RhodB conjugated peptide

CONCLUSION

The fluorescent probe Rhodamine B was successfully conjugated to the amino terminal region of the palindromic peptide, and the resulting fluorescent product retained the cytotoxic activity of the core sequence. Fluorescence microscopy revealed colocalization of the fluorescent peptide with MCF-7 cells, demonstrating its potential for cancer cell imaging.

Moreover, the conjugation of NSAID to the palindromic sequence was effectively achieved using an ornithine moiety, which enhanced the solubility profile. The ibuprofen-conjugated peptide exhibited enhanced selective cytotoxic activity against MCF-7 and HeLa cells, in contrast to the non-conjugated ornithine counterpart, which lost its cytotoxic activity.

For the case of the organometallic–LfcinB conjugates, a degradation process was observed in solution for the ferrocene-conjugated peptide with the same ornithine spacer, preventing this molecule from being evaluated in biological assays. Further experiments are required to study the stability of this organometallic conjugate.

Overall we succesfully obtained novel Ibuprofen-LfincB conjugates with enhanced selective cytotoxic activity against cervical and breast cancer cells. Additionally, we demonstrated the effect of conjugating the fluorescent probe Rhodamine B on the cytotoxic activity of the palindromic peptide and its utility for future experiments involving cell distribution and imaging.

ACKNOWLEDGEMENTS

We thank PhD students Karla Rodriguez , Natalia Ardila and PhD Andrea Barragan for their support with cytotoxic activity assays. We also thank Fernando Chavez and Dennis Salazar for their support with peptide synthesis and the research group leaders for their assessment

REFERENCES

Ardila-Chantré, N., Hernández-Cardona, A. K., Pineda-Castañeda, H. M., Estupiñan-Torres, S. M., Leal-Castro, A. L., Fierro-Medina, R., ... & García-Castañeda, J. E. (2020). RSC advances, 10(49), 29580-29586.

Barragán Cárdenas, A., Insuasty Cepeda, D. S., Niño Ramírez, V. A., Umaña Pérez, A., Ochoa Zarzosa, A., López Meza, J. E., ... & García Castañeda, J. E (2020). ChemistrySelect, 5(31), 9691-9700.

https://doi.org/10.17952/37EPS.2024.P2215

Introducing Novel Titanium Binding Peptides; Effect of the Sequence of Amino Acids on Their Adsorption Energy to TiO_2

Roja Rahmani[1*], Alexander P. Lyubartsev[1]

[1]*Dept. of Materials and Environmental Chemistry, Stockholm University, Sweden*

Abstract

Standard inert materials used in the production of orthopedic and dental implants include titanium (Ti) and titanium alloys due to their mechanical qualities, biocompatibility and corrosion resistance. A layer of titanium dioxide (TiO_2) forms when the Ti is in contact with oxygen or water, which is intact and stable at physiological pH and improves the biocompatibility of titanium used as implants. However, the absence of recognizable moieties on the implant prevents cell activities from being regulated and may induce a foreign body reaction to the implant causing infections due to biofilm formation and bacterial adhesion. Solid-binding peptides are short amino acid sequences that can specifically recognize and bind by one end to solid surfaces like titanium while the other end can be used to link with various bioactive molecules. No specific binders have evolved in nature for TiO_2. Therefore, it is important to design novel peptides that specifically bind to TiO_2. An established titanium-binding peptide (TBP), RKLPDA (min TBP-1), introduced by Sano and Shiba using the phage display method, has shown significant antimicrobial effect and enhanced bone formation activities in osteoblasts-like (bone synthesizing) cells [1].

Achieving binding and selectivity at the interface of peptide-TiO_2 is vital for constructing well-organized hybrid materials. One of the important determinants in the binding process is the composition of peptides, encompassing the sequence of amino acids, structural conformation, and charge. The aim of this work is to find new TBPs which bind to TiO_2 stronger than the min TBP-1 using computational methods. We mainly focused on two aspects: one is the selection of potential titanium binding peptides by reordering the amino acid sequences in min TBP-1 using atomistic molecular dynamics (MD) simulations, and the other is to quantify the functionality of these potential peptides by calculating their adsorption free energy to TiO_2 using enhanced sampling MD simulations. We discovered several peptides which show much stronger affinity to titanium than the established min TBP-1. We also investigated the conformation of these peptides on the surface of TiO_2 which is crucial for their functionality in the vicinity of bioactive molecules on cells.

Results

- 20 peptides showed potential adsorption affinity to TiO_2 in unbiased atomistic MD simulations.
- By employing the enhanced sampling multiple-walker metadynamics method, we calculated the adsorption free energy of these 20 potential peptides to TiO_2. After 10-16 microseconds of simulations, 13 peptides showed adsorption energies higher than min TBP-1 (see table on the right) implying better affinities toward TiO_2 than the min TBP-1.
- **K2R**, **R1D**, **A1D**, **L1D**, **K1L** peptides adsorb 2-6 times stronger than min TBP-1.

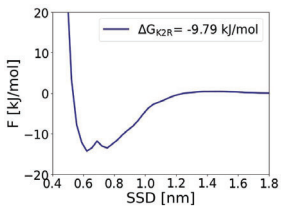

Peptides	ΔG (kJ/mol)
K1L	-29.31
L1D	-18.84
A1D	-14.32
R1D	-12.81
K2R	-9.79
K3D	-8.92
R2D	-8.91
L2P	-8.77
P1D	-8.31
L3D	-7.87
K4P	-7.74
A2R	-6.50
L4R	-5.47
min TBP-1	-5.08

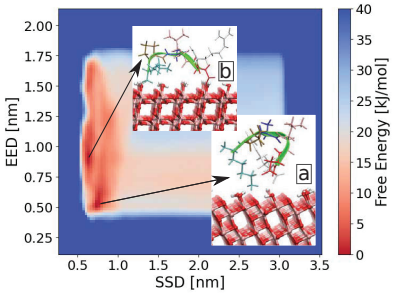

- We have done cluster analysis to extract the bound state conformations of these 13 peptides. Some peptides have several favorable conformations when they are adsorbed on the surface.
- We show a 1D free energy profile of K2R peptide along SSD (see plot above) and its 2D free energy surface along the SSD and EED (to the left), together with the compact (a) and stretched (b) bound states of K2R on TiO_2 (inner pictures).

Can we introduce new peptides having higher affinity to titanium by reordering the sequence of amino acids in min TBP-1?

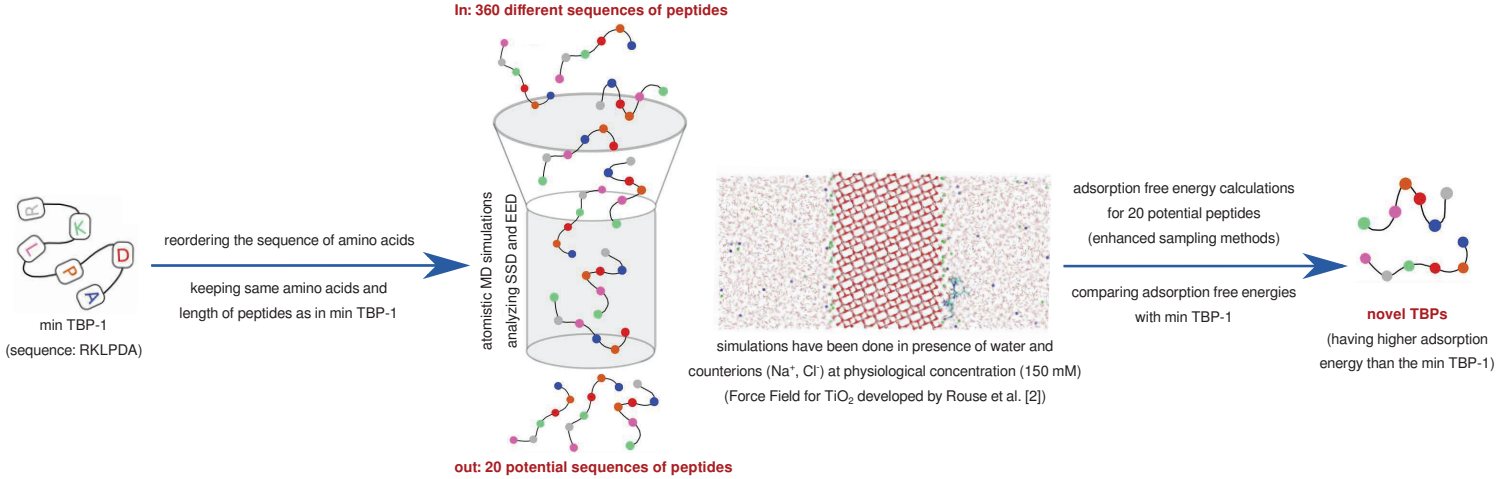

Methods

We started from 360 peptides each possesses six amino acids (Arg, Lys, Leu, Pro, Asp, Ala) in its structure and is distinctive in its sequence. Given the computational cost associated with calculating the free energy of adsorption directly, we implemented a two-step approach to narrow down our choices of potential TBPs efficiently. First, we used unbiased atomistic MD simulations to select peptides that might potentially have affinities to TiO_2 by analyzing the separation distance of each peptide from the surface of TiO_2 (SSD) and end-to-end distance of the peptides (EED). In the second step, to quantify their adsorption strength, we employed the multiple-walker well-tempered metadynamics (MW WT-MetaD) method to calculate the adsorption free energies of these potential peptides [3]. We used the GROMACS and PLUMED softwares for the simulations [4, 5].

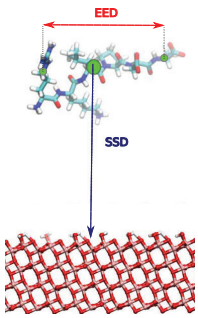

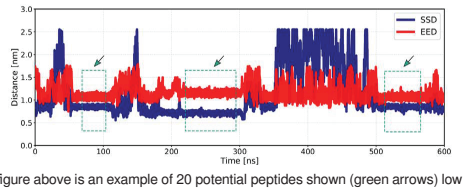

figure above is an example of 20 potential peptides shown (green arrows) low separation distance from surface (SSD) and stable end-to-end distance (EED)

$$C_{ads} = \frac{1}{z_0 - z_{min}} \int_{z_{min}}^{z_0} \exp(-\beta G(z))\, dz$$

$$C_{bulk} = \frac{1}{z_{max} - z_0} \int_{z_0}^{z_{max}} \exp(-\beta G(z))\, dz$$

$$\Delta G = -k_B T \ln \frac{C_{ads}}{C_{bulk}}$$

$$\mathrm{SSD} = |\mathbf{x}_{\mathrm{COM}} - \mathbf{x}_i|$$

$$\mathrm{EED} = |\mathbf{x}_N - \mathbf{x}_C|$$

Summary

- This work aimed to introduce novel titanium-binding peptide (TBP)s which have higher affinity to titanium dioxide (TiO_2) than the already reported TBP called min TBP-1 by reordering the sequences of the min TBP-1 and calculating the adsorption free energy of new sequences to TiO_2 using computational methods.

- We found 13 novel sequences having higher affinities to TiO_2 than the intial sequences in min TBP-1. Some of these novel sequences adsorb to 2-6 times stronger than min TBP-1. Further investigations showed several bound state conformations for peptides when they are adsorbed on the TiO_2.

- These novel sequences promise much better specificity toward TiO_2 than min TBP-1 and their performance and selectivity could be explored experimentally.

References

[1]. Sano KI, Shiba K. A hexapeptide motif that electrostatically binds to the surface of titanium. Journal of the American Chemical Society. 2003 Nov 26;125(47): 14234-5.

[2]. Rouse I, Power D, Brandt EG, Schneemilch M, Kotsis K, Quirke N, Lyubartsev AP, Lobaskin V. First principles characterisation of bio–nano interface. Physical Chemistry Chemical Physics. 2021;23(24):13473-82.

[3]. Raiteri P, Laio A, Gervasio FL, Micheletti C, Parrinello M. Efficient reconstruction of complex free energy landscapes by multiple walkers metadynamics. The journal of physical chemistry B. 2006 Mar 2;110(8):3533-9.

[4]. Páll S, Abraham MJ, Kutzner C, Hess B, Lindahl E. Tackling exascale software challenges in molecular dynamics simulations with GROMACS. InSolving Software Challenges for Exascale: International Conference on Exascale Applications and Software, EASC 2014, Stockholm, Sweden, April 2-3, 2014, Revised Selected Papers 2 2015 (pp. 3-27). Springer International Publishing.

[5]. Tribello GA, Bonomi M, Branduardi D, Camilloni C, Bussi G. PLUMED 2: New feathers for an old bird. Computer physics communications. 2014 Feb 1;185(2):604-13.

Contact me:

Peptides Conjugated to Sugars as Therapeutics for Ebola & Cancer disease

Fayna García-Martín,[1] Óscar Suárez,[1] Gonzalo Millán,[1] Filipa Marcelo,[2] Ana Gimeno,[3] Elena Lalinde,[1] Jesús R. Berenguer,[1] Juan Anguita,[3] Héctor Busto,[1] Jesús Manuel Peregrina,[1] Asuka Nanbo,[4] Jesús Jiménez-Barbero,[3] and Francisco Corzana[1]

(1) Department of Chemistry, Research Center in Chemical Synthesis (CISQ), University of La Rioja, 26006 Logroño, Spain.
(2) Universidade Nova de Lisboa (Portugal), (3) CIC Biogune (Bilbao, Spain), (4) University of Nagasaki (Japan)

E-mail: fayna.garcia@unirioja.es

https://doi.org/10.17952/37EPS.2024.P2216

The use of synthetic biomolecules emulating biological systems has emerged as a promising frontier in therapy and medicine. Research presented here explores diverse strategies to target both Cancer and Ebola disease.

MUC1 Glycopeptide as Cancer Vaccine

Mucin 1 or (MUC1) is a membrane-associated protein highly *O*-glycosylated through Ser/Thr residues. This protein is highly glycosylated in healthy cells, whereas in tumour cells it carries simple and truncated carbohydrates and exposes fragments, such as APDTRP or Tn antigen [Thr/Ser(α-GalNAc)], which can trigger the production of anti-MUC1 antibodies. Vaccines incorporating these structures are a promising field of research (Asín *et al. Curr Med Chem*, **2022**).

MUC1



Synthesis and Conjugation

Using SPPS with microwave energy, we synthesized a multi-epitope with MUC1 epitope (PDT(GalNAc)RP) without and with a Thelper attached, and then conjugated to mesoporous silica nanoparticles (siNPs) by copper-free click chemistry.
The compounds were evaluated *in vivo* through biological assays, both alone and in combination with an aluminum adjuvant.

Glycopeptides Conjugation via Click reaction

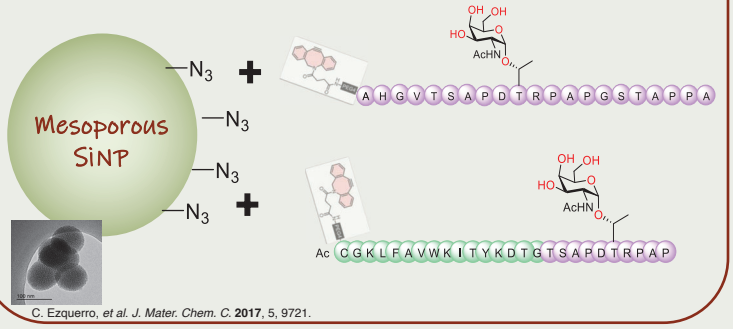

C. Ezquerro, *et al. J. Mater. Chem. C.* **2017**, 5, 9721.

Glycopeptides-SiNP compounds

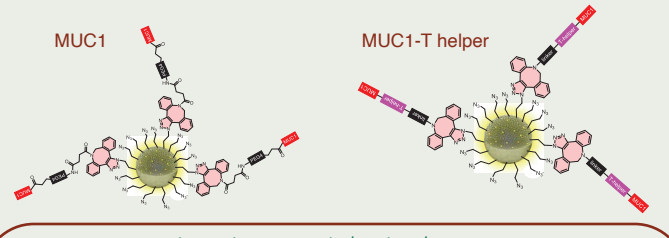

Vaccination & Biological Assays

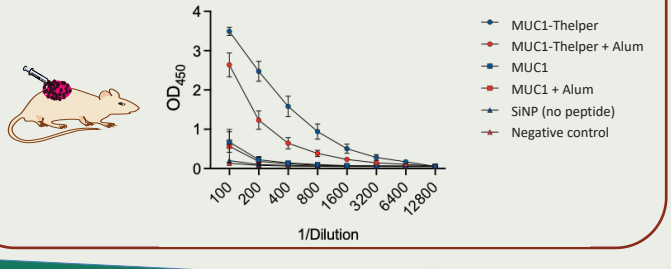

Peptides conjugated to sugars as Inhibitors of Ebola virus

Ebola virus utilizes glycoproteins of the extracellular capsid for host cellular entry, to attach to several receptors such as Macrophage Galactose Lectin (MGL).

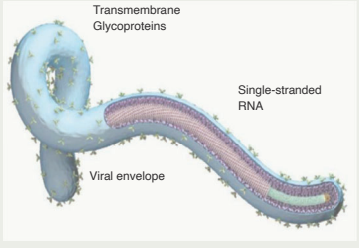

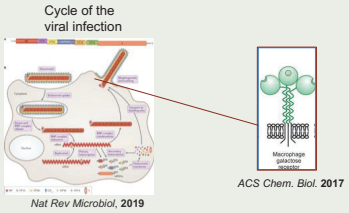

Nat Rev Microbiol, **2019**

ACS Chem. Biol. **2017**

Multiantenna Ligands Design & Synthesis

To create entry inhibitors, we aim to mimic the virus using the Lys multiantigenic peptide system (MAP) (Tam *et al. J Immunol Meth*, **1989**).

Our compound of interest is the sugar *N*-acetylgalactosamine (GalNAc) linked to Ser, a ligand for one of the main viral entry receptors.

We synthesized a small library with varying Ser(GalNAc) repetitions to assess ligand density influence.

In characterization, NMR structure analyses revealed a symmetric dendritic shape for the multi-antenna platforms with the ligand.

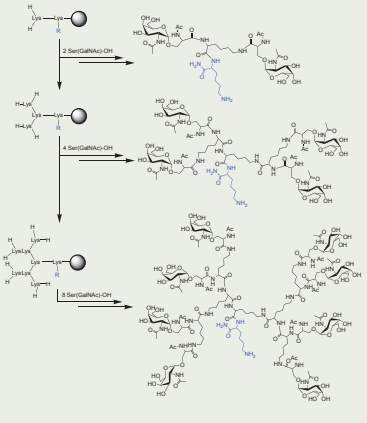

Affinity Assays

Affinity assays by calorimetry and NMR competition assays with the Ebola virus receptor, demonstrated higher ligand display correlating with increased affinity.

NMR Competition Assays

HSQC NMR using 15N-labeled MGL can be a powerful technique to study ligand binding and interactions in competition assays.

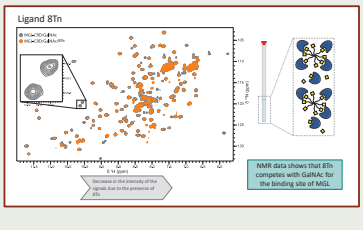

Calorimetry ITC assays

	GalNAc*	2Tn	4Tn	8Tn
N		0.4±0.01	0.2±0.02	0.1±0.01
ΔG (kcal/mol)		-8.2±0.1	-8.5±0.08	-9.0±0.1
ΔH (kcal/mol)	-14.7	-23±2	-40.1±0.4	-121±11
-TΔS (kcal/mol)		15±2	32.0±0.5	112±12
K_D (μM)	1400	1.1±0.2	0.6±0.1	0.3±0.04

* A Gabba *et al. J Am Chem Soc* , **2023**

CONCLUSIONS & FUTURE PROSPECTS

- We could obtain MUC1 derivatives and Ebola virus inhibitors in high purity.
- Biological assays of SiNP-MUC1 demonstrated a significant enhancement of the immune response following vaccination.
- Studies include binding affinity with MGL lectin by HSQC NMR & calorimetry assays.
- Best candidates will be proven as pathogen entry inhibitors.
- Peptides conjugated to sugars serve as highly effective probes for therapeutic applications.

ACKNOWLEDGEMENT

- This work is supported by Spanish National plan PID2020-120099RA-I00.
- FGM acknowledges to Beatriz Galindo senior program at University of La Rioja.

https://doi.org/10.17952/37EPS.2024.P2217

Synthetic strategies to prepare novel bioactive lysine and peptide conjugates with triazolium derivatives

Claudia Bello,[a,c] Michał Jewginski,[d] Patrycja Ledwon,[a,b,d] Francesca Nuti ,[a,c] Paolo Rovero,[a,b] Rafal Latajka,[d] and Anna Maria Papini[a,c]

a) Interdepartmental Research Unit of Peptide and Protein Chemistry and Biology, University of Florence, Sesto Fiorentino (FI), 50019, Italy
b) Department of Neurosciences, Psychology, Drug Research and Child Health, University of Florence, Sesto Fiorentino (FI), 50019, Italy
c) Department of Chemistry "Ugo Schiff", University of Florence, Sesto Fiorentino (FI), 50019, Italy
d) Department of Bioorganic Chemistry, Faculty of Chemistry, Wrocław University of Science and Technology, Wybrzeze Wyspianskiego 27, 50370 Wrocław, Poland

Introduction

Peptide conjugates with small molecules are increasingly used, particularly in pharmaceutical applications, and can be designed as carriers, stabilizing agents, or active ingredients per se. In many conjugates a drug-like molecule is responsible for the activity, but the efficacy can be enhanced by the peptide sequence, e.g. by providing an additional binding specificity. Research for new peptide- and peptidomimetic drug conjugates is leading to the development of novel compounds with anticancer and antimicrobial activity and for diagnostic applications. Dihydro-[1,2,4]triazolo [4,3-a]pyridine-2-ium carboxylates known as *Safirinium* dyes, have been previously investigated as antibacterial and imaging agents.[1] Heterocyclic compounds, such as N-benzoylpyrazoles and N-benzoylindazoles were found to be good inhibitors of human neutrophil elastase (HNE). To the best of our knowledge, *Safirinium* derivatives and conjugates were not tested as enzyme inhibitors. Making available a straightforward synthesis strategy to prepare lysine and peptide conjugates with *Safirinium* dyes is key to enable their exploitation for pharmaceutical and cosmeceutical applications, and as building blocks for the synthesis of novel bioactive peptides.

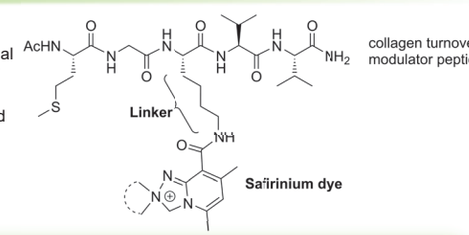

Synthesis of *Safirinium* derivatives



Safirinium derivatives 8'-carboxy-4,5',7'-trimethyl-3'H-spiro[piperidine-1,2'-[1,2,4] triazolo[4,3-a]pyridin]-1-ium inner salt (**1**), 8'-carboxy-5',7'-dimethyl- 3'H-spiro [pyrrolidine-1,2'-[1,2,4]triazolo[4,3-a]pyridin]-1-ium inner salt (**2**), 8'-carboxy-5',7'-dimethyl- 3'H-spiro[morpholine-4,2'-[1,2,4]triazolo[4,3-a] pyridin]-4-ium inner salt (**3**), and 8-carboxy-2-ethyl-2-(1-methylethyl)-5,7-dimethyl-2,3-dihydro-1,2,4] triazolo[4,3-a] pyridin-2-ium inner salt (**4**) were synthesised by reacting 4,6-dimethylisoxazolo [3,4-] pyridin-3(1H)-one with amine **A**-**D** respectively

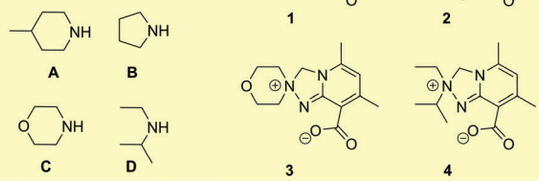

Solid phase synthesis of *Safirinium*-lysine building blocks and conjugates

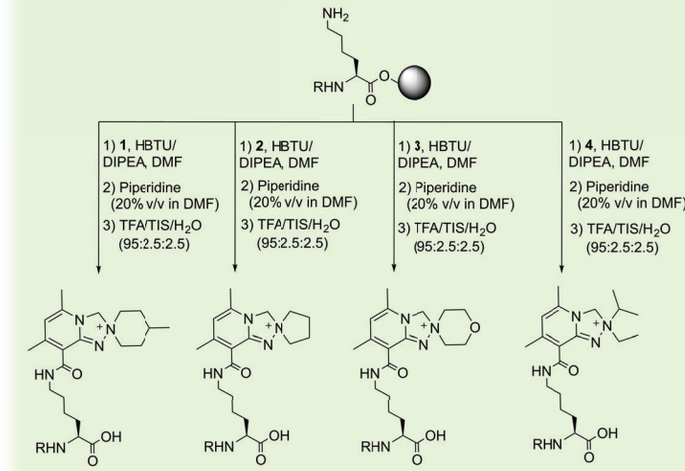

1a R = H (steps 1, 2, 3) **2a** R = H (steps 1, 2, 3) **3a** R = H (steps 1, 2, 3) **4a** R = H (steps 1, 2, 3)
1a' R = Fmoc (steps 1,3) **2a'** R = Fmoc (steps 1, 3) **3a'** R = Fmoc (steps 1, 3) **4a'** R = Fmoc (steps 1, 3)

Use of building blocks 1a'-4a' for the SPPS of *Safirinium*-peptide conjugates and evaluation of elastase inhibitory activity of *Safirinium*-lysine and peptide conjugates

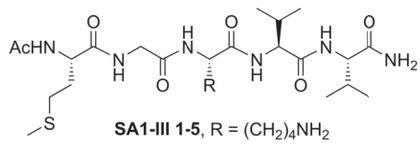

SA1-III 1-5, R = $(CH_2)_4NH_2$

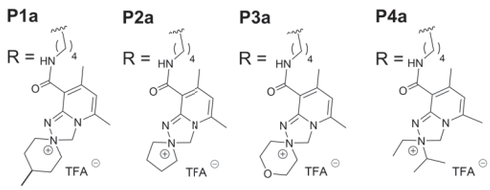

The building blocks were used in the synthesis of peptide conjugates (**P1a**-**P4a**) as Human Neutrophil Elastase (HNE) inhibitors for potential cosmeceutical applications, using the collagen turnover modulator **SA1-III 1-5**[2] as model peptide. All the new lysine and peptide conjugates were tested on Porcine Pancrease Elastase (PPE), commonly used as model of HNE. Lysine conjugates **1a**-**4a** showed moderate inhibitory activity on PPE, with **2a** being the most potent among the tested compounds. Peptide conjugates **P1a**-**P4a** are, instead, only weak inhibitors of PPE, probably because their affinity for the active site of the enzyme is reduced by steric hindrance.

C_M	1a	2a	3a	4a
10 μM	2%	8%	3%	0%
20 μM	5%	11%	10%	2%
30 μM	11%	18%	9%	10%
40 μM	12%	15%	20%	9%
50 μM	9%	25%	19%	12%

Conclusions and outlook

- *Safirinium* derivatives **1**-**4** as payloads for amino acid/peptide-drug conjugates acting as potential elastase inhibitors have been designed and efficiently synthesized.
- Their facile conjugation to amino acids was demonstrated by developing a straightforward solid phase synthesis of new lysine conjugates (**1a-4a**) and building blocks (**1a'-4a'**).
- Versatile conjugation to peptides has been proved by using building blocks **1a'-4a'** in the solid phase synthesis of the model peptide Ac-MGKVV-NH2 via Fmoc/tBu orthogonal strategy.
- All the *Safirinium* conjugates have been tested for their inhibitory activity toward porcine pancreas elastase. **2a** gave the best results, being a moderate elastase inhibitor.
- The described Lys-based *Safirinium* conjugates are good starting point for the development of novel elastase inhibitors which can be further used as new seedbed for the design of bioactive conjugates for pharmaceutical and cosmeceutical applications, and as building blocks for the synthesis of bioactive peptides.

Acknowledgements

The authors declare the support from the Polish Ministry of Science and Higher Education for the Faculty of Chemistry of Wroclaw University of Science and Technology, and from the University of Florence. PL is the participant of "BioTechNan" project–Interdisciplinary Environmental Doctoral Studies KNOW in the field of Biotechnology and Nanotechnology, co-financed by the European Union.

References

[1] J. Sączewski, K. Hinc, M. Obuchowski, M. Gdaniec, Chem. Eur. J. 2013, 19, 11531–11535
[2] F. Errante, L. Giovannelli, A. M. Papini, P. Rovero, Bioactive Peptides and Compositions Comprising Them / Peptidi Bioattivi e Composizioni Che Li Contengono, 2020, WO 2020/245772 A1
[3] P. D. Ledwoń, M. Jewginski, C. Bello, F. Nuti, P. Rovero, R. Latajka, and A. M. Papini Eur JOC 2024, e20240039

Contact information

Claudia Bello, PhD
email: claudia.bello@unifi.it
University of Florence, Department of Chemistry "Ugo Schiff", via della Lastruccia 13 50019 Sesto Fiorentino

https://doi.org/10.17952/37EPS.2024.P2222

EFFECT OF AZAGLYCINE ON THE INTERNALIZATION OF PENETRATIN DERIVATIVES



Karima Tarchoun[1,2], Dóra Soltész[1,2], Ildikó Szabó[3], Zoltán Bánóczi[1,*]

KARIMA TARCHOUN
Email: tarchoun.karima14@gmail.com

[1]Institute of Chemistry, Faculty of Science, ELTE Eötvös Loránd University, Budapest, Hungary,
[2]Hevesy György PhD School of Chemistry, Institute of Chemistry, ELTE Eötvös Loránd University, Budapest, Hungary
[3]HUN-REN-ELTE Research Group of Peptide Chemistry, 1117 Budapest, Hungary
* Correspondence: zoltan.banoczi@ttk.elte.hu

INTRODUCTION

Delivering therapeutic and imaging agents into cells is still challenging. Cell-penetrating peptides (CPPs); short, mainly positively charged peptides, are promising tools to transport biologically active compounds into cells. The firstly discovered and well-known member of CPP family is the Penetratin (R^{43}QIKIWFQNRRMKWKK^{58}) [1–3]. The structure-activity results showed that replacement of Trp at position 48 with Phe revealed lower cellular uptake [4]. Although it is very efficient CPP, many efforts were made to improve its properties [5-8]. Penetratin and its derivatives are potentially useful as an uptake enhancer for intracellular drug delivery [9]. Among the possible structural modifications one is the substitution of one or more amino acids by an aza-amino acid in which C^{α} is replaced by nitrogen results in an aza-peptide **(Figure 1).** This modification may change the structure of the original peptide and thus can increase its biological activity [10].

AIMS

Our aim was to investigate the effect of aza-glycine substitution of tryptophan residues (Trp48, Trp56, or both) on the internalization of Penetratin, and to assess how these modifications influence the cellular uptake and the internalization mechanism, utilizing 5(6)-carboxyfluorescein labeling of the peptide N-terminus for flow cytometry analysis.

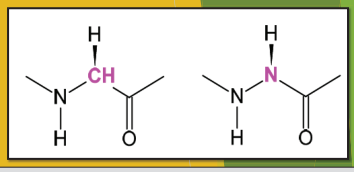

Figure 1. The structure of glycine and aza-glycine moiety

RESULTS

1) Synthesis of Peptides

Peptides were synthesized by SPPS on Rink-Amide MBHA resin using standard Fmoc/^{t}Bu protocol. The azaglycine was introduced using CDI and Fmoc-hydrazide dissolved in DMF and in the presence of 2 eq. of DIEA **(Figure 2).**

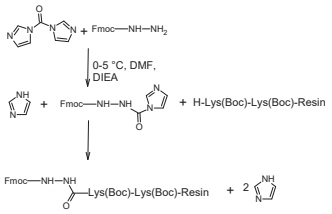

Figure2. The introduction of azaGlycine into the peptide sequences

The crude peptides were purified by RP-HPLC and the peptides were characterized by analytical RP-HPLC and ESI-MS **(Table 1).**

Table 1. Chemical Characterization of Peptides

Sequence	Code	Rt [a]	M_{Calc}	M_{meas} [b]
Cf-RQIKIWFQNRRKWKK	Pen(desMet) [c]	15.1	2472.9	2472.2
Cf-RQIKIWFQNRRK-**azaGly**-KK	Trp56aGlyPen(desMet)	14.8	2344.7	2344.2
Cf-RQIKI-**azaGly**-FQNRRKWKK	Trp48aGlyPen(desMet)	13.4	2344.7	2344.1
Cf-RQIKI-**azaGly**-FQNRRK-**azaGly**-KK	Trp48,56aGlyPen(desMet)	12	2216.5	2216.2
Cf-RQIKIWFQNRRK**G**KK	Trp56GlyPen(desMet)	15	2343.7	2343.2
Cf-RQIKI**G**FQNRRKWKK	Trp48GlyPen(desMet)	13.6	2343.7	2343.2
Cf-RQIKI**G**FQNRRK**G**KK	Trp48,56GlyPen(desMet)	13.2	2214.5	2214.1

[a] The analytical chromatogram was obtained using Hypersil Hypurity C18 column (4.6 mm × 150 mm, 5 µm, 190 Å). Linear gradient elution (0 min 0% B, 2 min 0% B, 22 min 90% B) was used at 1 mL/min flow rate. [b] ESI-MS on a Bruker Amazon SL (Bremen, Germany). [c] Pen(desMet) refers to a penetratin derivative which does not have Met in its sequence.

2) Cellular Uptake of Peptides

A-431 human skin squamous cancer cells were treated with a solution of peptides at 5 µM concentration at 37 °C for 90 min. The cellular uptake was measured by flow cytometry **(Figure 3).**

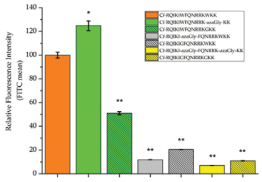

Figure 3. Cellular uptake of the labelled penetratin derivatives into A-431 cells.

- Trp56aGlyPen(desMet) peptide had higher internalization (124.8%) than Pen(desMet) (100%).
- The internalization of Trp56aGlyPen(desMet) peptide was 2.4-fold higher than that of Trp56GlyPen(desMet) peptide (50.0%).
- Substitution of the Trp residue near the N-terminus (Trp48aGlyPen(desMet) and Trp48GlyPen(desMet)) or in both positions (Trp48,56aGlyPen(desMet) and Trp48,56GlyPen(desMet)) resulted in markedly decreased internalization (it was between 6% and 20.5%).

3) Mechanism of the Internalisation

To study the mechanism of internalisation, cells were pretreated with the solution of inhibitors (EIPA (500 µM) as macropinocytosis, CPZ (300 µM) as clathrin-mediated endocytosis; mBCD (36 mM) as caveolae/lipid raft-mediated endocytosis and COL (200 mM) as microtubular inhibitor) for 30 min, followed by the treatment of the most promising peptides solution at 5 µM for 90 min. To inhibit all endocytosis routes, NaN_3 (500 µM) and DOG (250mM) was used. **(Figure 4)**.

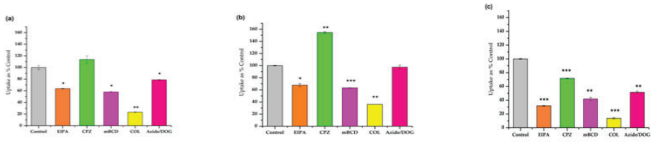

Figure 4. Effect of endocytosis inhibitors on the internalization of peptides (a) Pen(desMet), (b) Trp56aGlyPen(des), and (c) Trp56GlyPen(des).

- The EIPA, mβCD, and COL had the same effect on the cellular uptake in case of all peptides.They significantly inhibited their uptake by 14% - 68%.
- The Gly substituted derivative was more sensitive to these inhibitors, showing reductions of 32%, 42%, and 14% respectively.
- CPZ had varied effects: no influence on internalization of Pen(-Met), decreased cellular uptake of Trp56GlyPen and increased internalization of Trp56aGlyPen derivative.
- Pretreatment with NaN_3 and DOG resulted in significant decrease in uptake of Trp56GlyPen(50%), moderate decrease in uptake of Pen(-Met) (79%) and no effect on the uptake of Trp56aGlyPen (97%).

CONCLUSIONS

- The substitution of Trp48 dramatically reduced the internalization, showing the importance of Trp48 in cellular uptake.
- Trp56 (Trp56aGlyPen(desMet)) is the most active CPPs.
- The Trp56GlyPen(desMet) and Trp56aGlyPen(desMet) peptides demonstrated altered internalization pathways, suggesting that the difference in their backbone - natural or aza-amino acid - significantly influence their cellular uptake mechanisms.
- Our results suggest that aza-amino acid insertion may be a useful modification to alter the internalization of a CPP.

ACKNOWLEDGEMENT

We are grateful and kindly acknowledge the support from the Hevesy György Ph.D. School of Chemistry, Eötvös Loránd University, and the support from the ELTE Thematic Excellence Program supported by the Hungarian Ministry for Innovation and Technology.

ABBREVIATIONS

CDI: 1,1′-carbonyldiimidazole; DIEA: N,N-diisopropylethylamine; EIPA: 5-(N-Ethyl- N-isopropyl)amiloride; CPZ: chlorpromazine; mBCD: methyl-β-cyclodextrin; Col: colchicine; DOG: 2-Deoxyglucose.

REFERENCES

[1] Derossi, D. et al. Trends Cell Biol. **1998**, 8, 84–87.
[2] Bánoczi, Z. et al. Bioconjug. Chem. **2007**, 18, 130–137.
[3] Watson, G.M. et al. ACS Omega **2017**, 2, 670–677.
[4] Dom, G. et al. Nucleic Acids Res. **2003**, 31, 556–561.
[5] Khafagy, E. et al. *Int. J. Pharm.* **2009**, *381* (1), 49–55.
[6] Keum, T. et al *Int. J. Nanomedicine*. **2022**, *17*, 697–710.
[7] Garibotto, F. et al. *J. Med. Chem.* **2011**, *46* (1), 370–377.
[8] Thorén, P. E. G. et al. *Biochem. Biophys. Res. Commun.* **2003**, *307* (1), 100–107.
[9] Liu, C. et al. Mol. Pharm. **2014**, *11*, 1218–1227.
[10] Tarchoun, K. et al. Futur. Pharmacol. **2022**, *2*, 293–305.

https://doi.org/10.17952/37EPS.2024.P2223



Molecular Design for Cytosolic Delivery of Antibodies Using an Intracellular Delivery Peptide

○Yoshimasa Kawaguchi[1], Shiroh Futaki[1] [1]Institute for Chemical Research, Kyoto University

Introduction

Cytosolic Antibody Delivery

☺ High antigen recognition ability
☹ Lack of membrane permeability



Cytosolic antibody delivery methods are required to expand the target of antibodies in the cells

L17E : Attenuated Cationic Amphiphilic Lytic Peptide

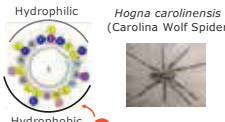

Hogna carolinensis (Carolina Wolf Spider)

Peptide	Sequence	CC50 (μM)
M-Lycotoxin	IWLTALKFLGKHAAKHLAKQQLSKL-amide	1.36
L17E	IWLTALKFLGKHAAKHEAKQQLSKL-amide	> 40

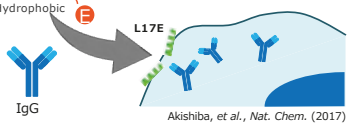

Akishiba, *et al.*, *Nat. Chem.* (2017)

☺ Cytosolic antibody delivery was achieved by mixing L17E and antibodies
☹ Both L17E and antibodies require high concentrations

Created L17E trimer to improve the cytosolic delivery ability

Cytosolic Antibody Delivery by Coacervate

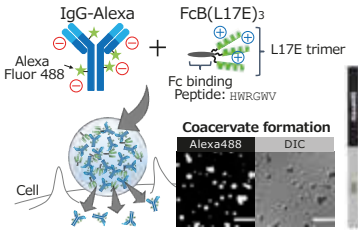

Influx occurs approximately 1 min after attach with the cell.

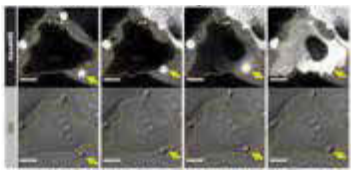

Iwata, *et al.*, *Angew. Chem. Int. Ed.* (2021)

☹ Requires random fluorescent labeling
- Affects antigen recognition and reproducibility
- Difficult to analyze interaction patterns

Research aim

Development of antibody molecules that form coacervates and achieve cytosolic delivery without fluorescent labeling.

Strategy

Design of Anion Antibody Scaffold

✻ Attaching a Negatively Charged Tag to the C-termini of IgG

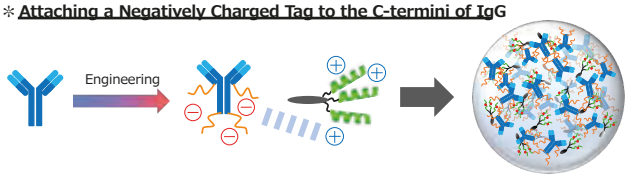

✻ Design of the Negatively Charged Tag Sequence

Interaction mode for LLPS*

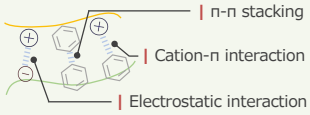

Anionic tag	Sequence
E10	EEEEEEEEEE
E20	EEEEEEEEEEEEEEEEEEEE
$(EY)_{10}$	EYEYEYEYEY
$(E_4Y)_2$	EEEEYEEEEY
$(E_4Y)_4$	EEEEYEEEEYEEEEYEEEEY

*LLPS: liquid-liquid phase separation

Results & Discussion

Coacervate Formation

✻ Anion-tagged antibody scaffold

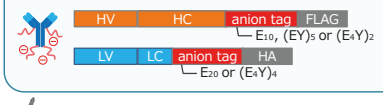

Light chain	Heavy chain	Light chain	Heavy chain
E20	E10	(E4Y)4	E10
	(EY)5		(EY)5
	(E4Y)2		(E4Y)2

Observation of Coacervate

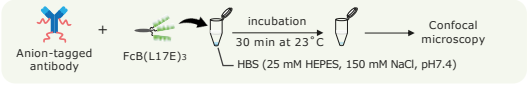

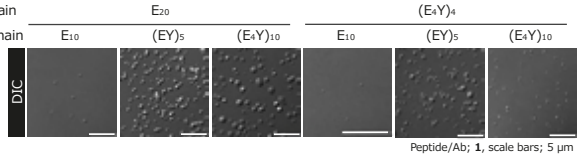

Peptide/Ab; **1**, scale bars; 5 μm

Formation of stable coacervates in HBS by introducing negatively charged tags into the heavy and light chains.

Results & Discussion

Intracellular Delivery of Antibodies by Coacervate

Cytosolic Antibody Delivery

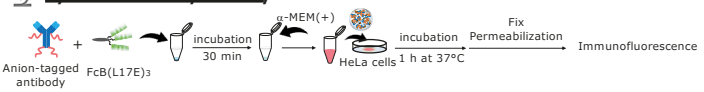

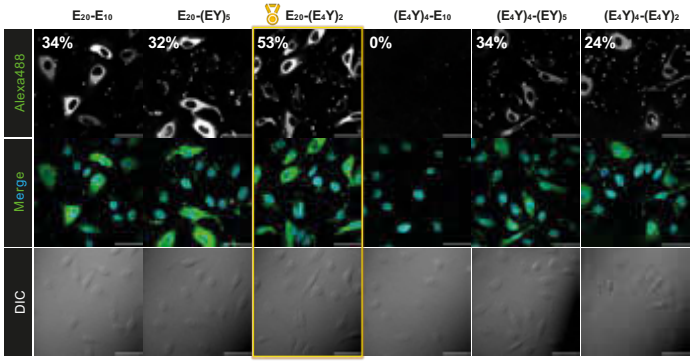

FcB(L17E)3 final conc. 1 μM, IgG final conc. 1 μM, (Peptide/Ab; **1**), scale bars; 50 μm

✻ The delivery efficiency differed depending on the tag sequence
✻ Coacervate composed of E20-$(E_4Y)_2$ demonstrated the highest delivery efficiency

Physical Properties of Coacervates

Turbidity: Stability

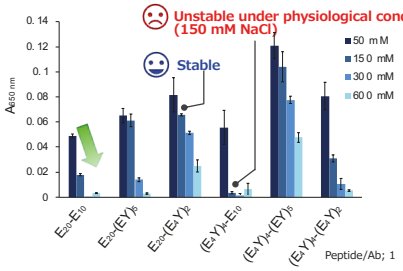

✻ Electrostatic interactions are important for coacervate formation
✻ Coacervate formation under physiological condition is crucial for cytosolic delivery of Antibodies.

Fluorescence Recovery After Photobleaching: Fluidity

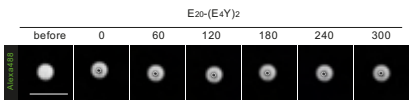

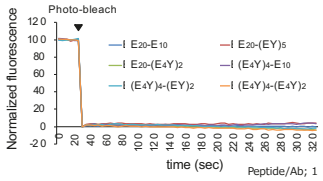

✻ Fluorescence recovery was not observed.
✻ Coacervates may be gel-like particles with low fluidity

Unique Intracellular Uptake of Coacervate

Timelapse imaging: lifeact-mCherry-expressing cells (Actin stain)

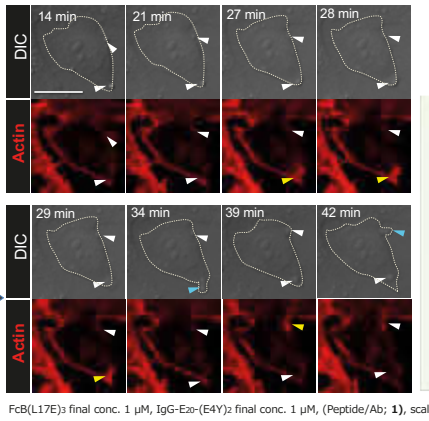

✻ Observation of accumulation of actin around particles after being taken up by cells (Yellow arrowheads)
✻ Following the actin acculation, an arm-like structure emerged. (blue arrowheads)

New mechanism of cellular uptake ?

FcB(L17E)3 final conc. 1 μM, IgG-E20-(E4Y)2 final conc. 1 μM, (Peptide/Ab; **1**), scale bars; 50 μm

Summary

✻ A negatively charged antibody scaffold was created to form a coacervate with FcB(L17E)3 and achieve intracellular delivery of antibodies.
✻ The stability of coacervate at physiological salt concentrations was important for intracellular delivery by the coacervates.
✻ Intracellular uptake of the coacervate may be a novel uptake mechanism.

Proceedings of the 37th European Peptide Symposium
Michal Lebl, Editor
European Peptide Society, 2024
http://doi.org/10.17952/37EPS.2024.P2224

Synthesis and characterization of nucleolin receptor recognizing F3 peptide fragment-drug conjugates

Bettina Basa[1, 2, 3], Diána Vári-Mező[3, 4, 5], Kata Nóra Enyedi[1, 3], József Tóvári [5], Szilvia Bősze[3, 6], Krisztina Kiss[3], Gábor Mező[1, 3]

[1]ELTE Eötvös Loránd University, Faculty of Science, Institute of Chemistry, Department of Organic Chemistry, Budapest, 1117 Hungary, [2]ELTE Hevesy György PhD School of Chemistry, Budapest, 1117 Hungary, [3]HUN-REN-ELTE Research Group of Peptide Chemistry, Budapest, 1117 Hungary, [4]School of Ph.D. Studies, Doctoral School of Pathological Sciences, Semmelweis University, Budapest, 1085 Hungary; [5]Department of Experimental Pharmacology and the National Tumor Biology Laboratory, National Institute of Oncology, Budapest, 1122 Hungary; [6]Department of Genetics, Cell- and Immunobiology, Faculty of Medicine, Semmelweis University, Budapest, 1089 Hungary

Introduction

Chemotherapy remains the most widely used approach in cancer treatment. Despite its widespread use, the frequency of tumor relapse, and the associated severe toxic side effects, require continuous methodological development. Targeted tumor therapy has emerged as a promising route for this development. This strategy involves conjugating drugs with targeting molecules that exhibit high specificity and selectivity towards tumor-selective proteins or receptors. By doing so, the drug delivery becomes tailored to tumor cells, minimizing the impact on healthy cells [1]. Nevertheless, a pervasive challenge in targeted therapeutic methods is the limited number and types of tumor-specific markers. This is particularly true for tumor subtypes, called tumor stem-like cells (CSCs) [2], where the lack of overexpression of common tumor markers impedes methodological progress. In addition, because of their high self-renewal properties, CSCs are also implicated in cancer relapse. Thus, the development of effective compounds for targeted tumor therapy is necessary that can recognize not only the conventional tumor cells but the resistant CSCs, too. Nucleolin is a protein that is expressed both on sensitive cells and resistant CSCs, which makes it a suitable target in tumor therapy. The 31-mer peptide (F3), selectively binds to the nucleolin receptor, offering a novel approach for targeted tumor therapy [3]. This research endeavors to optimize the F3 peptide structure for the development of a more cost-effective drug candidate.

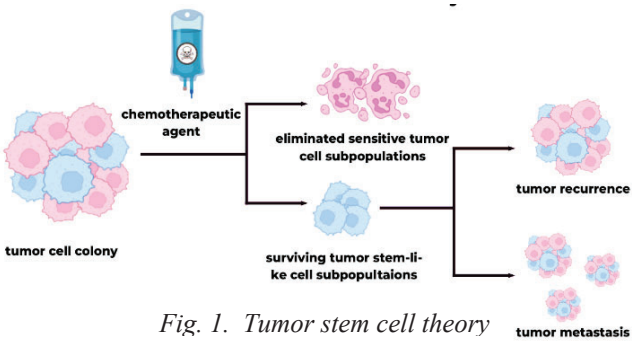

Fig. 1. Tumor stem cell theory

Results and Discussion

In this study, we aimed to develop peptide-daunomycin conjugates with enhanced targeting activity. To ensure uniform drug release we inserted the cathepsin-B enzyme labile GFLG spacer between the peptide and daunomycin. Daunomycin was selected as the chemotherapeutic agent due to its intrinsic autofluorescence, which allowed for simultaneous evaluation of cellular uptake and cytostatic effect. The efficacy of the conjugates was measured using MTT assays on human melanoma (A2058) and human colorectal adenocarcinoma (HT-29) cell lines. To optimize the peptide sequence for nucleolin receptor binding, we synthesized eight overlapping decapeptides that cover the entire F3 peptide. The *in vitro* cytostatic activity studies demonstrated that the peptide-daunomycin conjugate, that contains the first 10 amino acids of the N-terminal of the F3 peptide, exhibited higher antitumor activity compared to the full-length conjugate. To identify the shortest, most effective targeting sequence we synthesized peptides containing the first 7,13, and 20 amino acids of the N-terminal. The cytotoxicity results indicated, that shortening the sequence reduced the efficacy of the conjugate, while elongating the sequence did not improve the effectiveness.

Table 1. – Length optimization of the targeting sequence

Sequence	*Cytostatic effect* IC_{50} *(μM)*	
	A2058	*HT-29*
Dau-Aoa-GFLG-^{1}KDEPQRRSARLSAKPAPPKPEPKPKKAPAKK^{31}-NH_2	2,99 ± 0,37	11,78 ± 0,12
Dau-Aoa-GFLG-^{1}KDEPQRRSARLSAKPAPPKP^{20}-NH_2	3,35 ± 0,12	87,85 ± 0,13
Dau-Aoa-GFLG-^{1}KDEPQRRSARLSA^{13}-NH_2	3,60 ± 0,09	90,91 ± 0,15
Dau-Aoa-GFLG-^{1}KDEPQRRSAR^{10}-NH_2	**3,78 ± 0,12**	**28,32 ± 0,09**
Dau-Aoa-GFLG-^{1}KDEPQRR^{7}-NH_2	17,15 ± 0,10	> 100

Further optimization was carried out using alanine scanning, in which each amino acid was systematically substituted with apolar alanine, to evaluate its role in the conjugate's activity. This approach identified critical residues, like the DEPQ sequence and the C-terminal arginine, whose modification significantly diminished the conjugate's efficacy, which means these amino acids could be important in the attachment to the nucleoline receptor. Conversely, substitutions at the N-terminal lysine, and the 8th position serine improved the conjugate effectiveness, suggesting that these positions tolerate modifications.



Fig. 2. Results of the alanine scan

Table 2. – Alanine scan

Sequence	*Cytostatic effect* IC_{50} *(μM)*	
	A2058	*HT-29*
Dau-Aoa-GFLG-^{1}KDEPQRRSAA^{10}-NH_2	32,0 ± 3,4	> 50
Dau-Aoa-GFLG-^{1}KDEPQRRAAR^{10}-NH_2	**11,0 ± 1,2**	**17,2 ± 9,1**
Dau-Aoa-GFLG-^{1}KDEPQRASAR^{10}-NH_2	22,8 ± 2,8	26,7 ± 3,6
Dau-Aoa-GFLG-^{1}KDEPQARSAR^{10}-NH_2	15,1 ± 1,0	33,0 ± 16,9
Dau-Aoa-GFLG-^{1}KDEPARRSAR^{10}-NH_2	> 50	> 50
Dau-Aoa-GFLG-^{1}KDEAQRRSAR^{10}-NH_2	> 50	> 50
Dau-Aoa-GFLG-^{1}KDAPQRRSAR^{10}-NH_2	39,1 ± 8,4	> 50
Dau-Aoa-GFLG-^{1}KAEPQRRSAR^{10}-NH_2	> 50	> 50
Dau-Aoa-GFLG-^{1}ADEPQRRSAR^{10}-NH_2	**3,3 ± 0,3**	**9,7 ± 3,4**

Additionally, to improve both the efficacy and serum stability of the conjugates, non-natural amino acids and intramolecular cyclization were introduced. Although the incorporation of a disulfide bridge slightly reduced the cytotoxicity of the peptide-drug conjugate, it could increase the serum stability, ultimately enhancing the overall therapeutic potential of the conjugate. The preliminary in vivo experiments confirmed that the shorter peptides with optimized sequences might be better drug conjugates than the F3-drug conjugate.

Table 3. – Incorporation of non-natural amino acids and intracellular rings

Sequence	*Cytostatic effect* IC_{50} *(μM)*	
	A2058	*HT-29*
Dau-Aoa-GFLG-^{1}KDEPQRCitSAR^{10}-NH_2	19,70 ± 0,10	> 50
Dau-Aoa-GFLG-^{1}KDEPQCitRSAR^{10}-NH_2	18,20 ± 0,14	> 50
Dau-Aoa-GFLG-^{1}NleDEPQRRSAR^{10}-NH_2	20,30 ± 0,07	> 50
Dau-Aoa-GFLG-^{1}KDEPQF$_{(pCl)}$RSAR^{10}-NH_2	**10,13 ± 0,15**	**> 50**
Dau-Aoa-GFLG-^{1}CDEPARRCAR^{10}-NH_2 **-S---------S-**	**8,17 ± 0,11**	**30,23 ± 0,07**
Dau-Aoa-GFLG-^{1}KDEAQRRCAR^{10}-NH_2 HN-CO-CH_2-S	12,94 ± 0,12	> 50

Acknowledgments

The research was supported by the National Research, Development and Innovation Office under grants NKFIH K146039.

References

1. G. Mező, M. Manea - Receptor-mediated tumor targeting based on peptide hormones - Expert Opinion in Drug Delivery, 2010; 7; 79-96; https://doi.org/10.1517/17425240903418410
2. L. S. Carvalho, N. Grançalves, N. A. Fonseca, J. N. Moreira: Cancer Stem Cells and Nucleolin as Drivers of Carcinogenesis - Pharmaceuticals - 2021; 14(1); 60; 1-21; https://doi.org/10.3390/ph14010060
3. K. Prokka, P. Laakkonen, J. A. Hoffman, M. Bernsconi, E.Ruoslathi. - A fragment of the HMGN2 protein homes to the nuclei of tumor cells and tumor endothelial cells in vivo - Proceedings of the National Academy of Sciences of the United States of America, Biochemistry, 2002, 99, 7444-7449 https://doi.org/10.1073/pnas.062189599

https://doi.org/10.17952/37EPS.2024.P2225

Leuprorelin Peptide Drug Complexes with Permeability Enhancers to Increase Bioavailability

Adel Penhasi[✉,1,2], Zeina Zaatari[1], Moustafa Ghanyem[1], Deborah E. Shalev[✉,1,3]

[1]Department of Pharmaceutical Engineering, Azrieli College of Engineering Jerusalem, Israel, [2]Department of Research and Development, Polycaps Holdings Ltd, Atidim Technology Park, Tel Aviv, Israel and [3]Wolfson Centre for Applied Structural Biology, The Hebrew University of Jerusalem, Israel

One in eight men will develop prostate cancer during their lifetime and it is the second-leading cause of cancer death in men in the world.

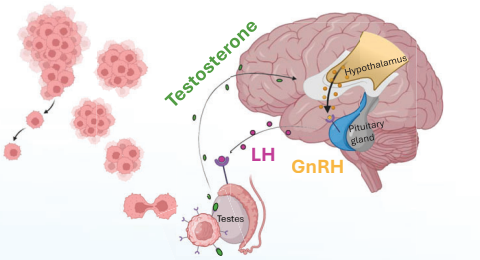

Testosterone-dependent prostate cancer is currently treated by desensitizing the gonadotropin hormone-releasing hormone (GnRH) receptor which stops testosterone production. This is done with the GnRH agonist, leuprorelin. The drug is also used to treat breast cancer, endometriosis, uterine fibroids, and premature puberty.

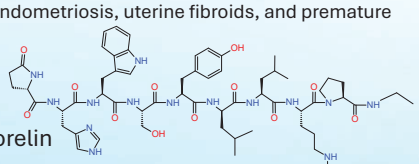

Leuprorelin

Leuprorelin, and all peptide drugs, suffer from extreme metabolic and chemical instability, since the body identifies them as food. Therefore, the drug is administered by injection, which reduces compliance.



An oral formulation of leuprorelin is being prepared using alginate with calcium crosslinking to protect it until it reaches the colon.

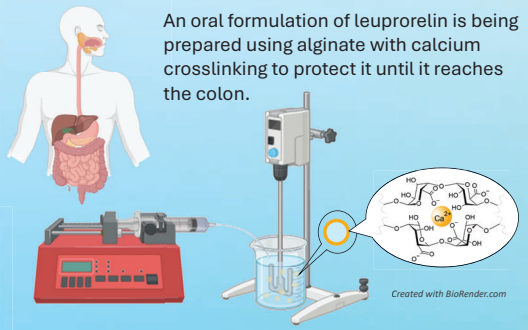

Permeability enhancers are necessary for leuprorelin to traverse the membrane of the gastrointestinal tract since it is too large to do so by itself.

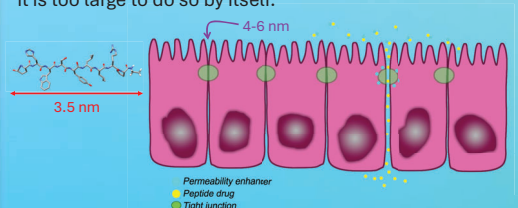

NMR was used to measure interactions between leuprorelin and permeability enhancers: Six known permeability enhancers showed significant interactions, and five showed no significant interactions.

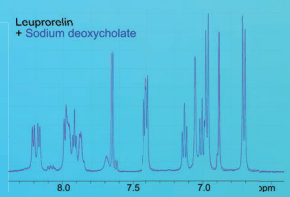

Leuprorelin titration with sodium deoxycholate, showing no interaction.

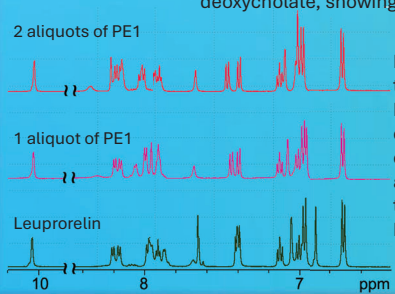

Leuprorelin titration with PE1 showing changes in chemical shift as a function of titration in ^{1}H-NMR spectra.

Leuprorelin titration with all permeability enhancers (PE): 2D NMR ^{1}H COSY spectra (right). As seen below, the changes in chemical shift for the various permeability enhancers were significant both for HN and Hα resonances, indicating a significant degree of complexation of leuprorelin with the permeability enhancer.

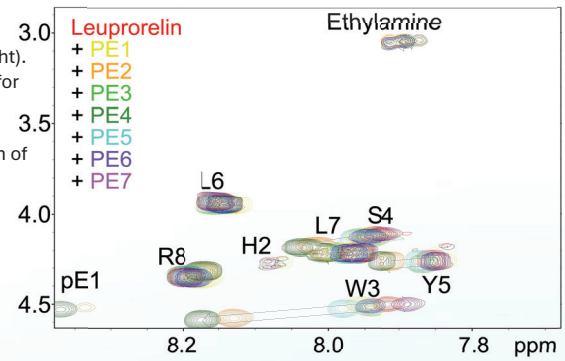

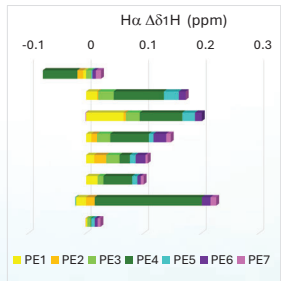

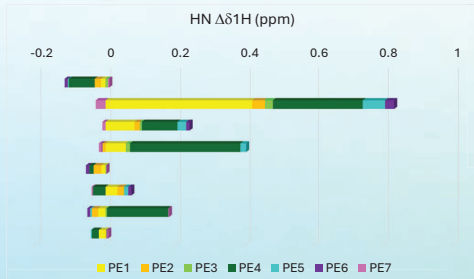

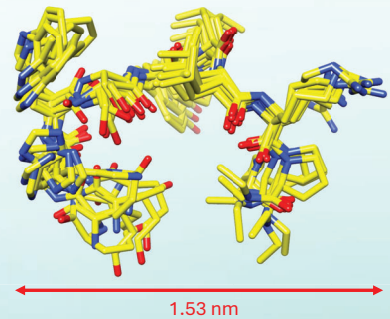

The low energy ensemble of leuprorelin (yellow) bound to PE1 (not shown) showing a structure that has a radius of 1.53 nm, which is significantly smaller than the 3.5 nm measured for the extended peptide and also smaller than the 4-6 nm passage through the tight junctions, even without the aid of the permeability enhancer itself.

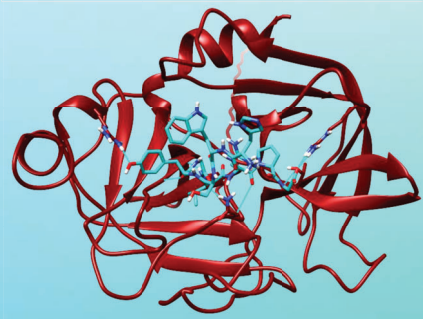

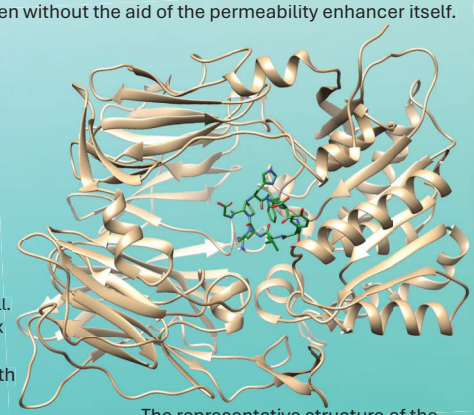

AlphaFold2-multimer on ColabFold (Mirdita, M., Schütze, K., Moriwaki, Y. et al. ColabFold: making protein folding accessible to all. *Nat Methods* **2022**) was used to calculate (above) the complex of GnRH hormone peptide (cyan) and Chymotrypsin C (red), and (right) the GnRH hormone peptide (green) in complex with dipeptidyl peptidase (tan).

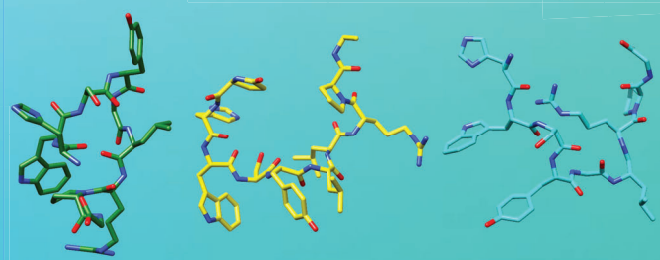

The representative structure of the low energy ensemble of leuprorelin bound to PE1 (yellow) compared to the structure of GnRH hormone from the complex with chymotrypsin C (cyan), and GnRH from the complex with dipeptidyl peptidase (green), showed significant differences in structure that should prevent the PE-bound peptide from entering the enzyme binding sites.

Release profiles (below) from calcium-crosslinked alginate microsphere formulations of leuprorelin bound to permeability enhancers PE2, PE5 and PE6 showed significant extended release relative to leuprorelin itself.

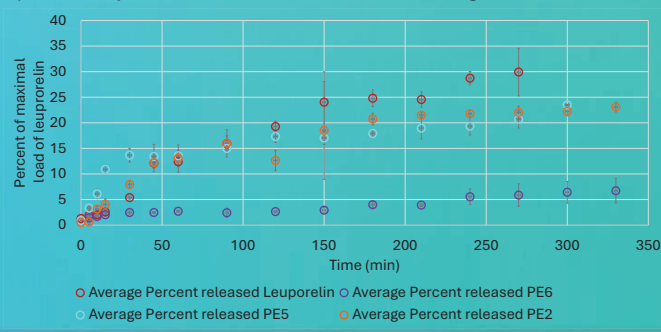

Conclusion: NMR can be used to identify and qualify the interaction between leuprorelin and the various permeability enhancers. The upfield shift seen for the interaction with PE6 may suggest enhanced shielding that correlates the degree of binding and subsequent extended release profile.

Designing selective peptide binders for Methicillin resistance *Staphylococcus aureus*

Yaara Zandany, Ph.D. student (yaara.zandany@mail.huji.ac.il)
Prof. Zvi Hayouka

Institute of Biochemistry, Food Science and Nutrition, The Robert H. Smith Faculty of Agricultural, Food & Environment, The Hebrew University of Jerusalem, Rehovot, 76100, Israel.

THE HEBREW UNIVERSITY OF JERUSALEM

The Robert H Smith Faculty of Agriculture, Food and Environment

https://doi.org/10.17952/37EPS.2024.P2226

Abstract

The growing global crisis of antibiotic resistance highlights the need for novel approaches in diagnosing and treating bacterial infections. Methicillin-resistant *Staphylococcus aureus* (MRSA) presents a particularly severe threat, especially in healthcare environments. This study aims to advance the development of rapid and selective peptide binders for MRSA as a model bacterium. Peptides, with their potential for modification and cost-effectiveness, offer significant promise for creating effective bacterial binders. We employed phage display technology to identify unique peptide binders with high affinity for MRSA cells. This method involved using whole bacterial cells in suspension during the assay, which increased the diversity of the selection process. During the phage display screening, the peptide library was exposed to various types of bacteria (negative selection) to enhance selectivity towards MRSA (the target bacteria). Subsequent Next Generation Sequencing and bioinformatics analysis allowed us to select sequences that were present in high abundance in the MRSA treatment compared to the negative selection bacterial cells.

The identified lead peptides were synthesized, purified, and characterized using two methods: Flow Cytometry for suspension-based interactions and gold surface immobilization for interactions on surfaces. The lead peptides demonstrated strong binding affinities for MRSA in both immobilized and suspension conditions, with promising specificity. Chemical modifications further enhanced the binding affinities, resulting in peptides that showed even greater affinity for MRSA than the original sequences. Notably, the two leading peptide binders, WPG and TST, along with the modified peptide WPG11A, exhibited high selectivity for MRSA, even in mixed bacterial populations. Importantly, these peptides showed no toxicity towards either bacterial or mammalian cells, highlighting their potential for safe application in diagnostic and therapeutic settings.

Our study successfully identifies selective peptide binders for MRSA using innovative phage display technology. The characterized peptides demonstrate promising selectivity and high binding affinity for MRSA, laying the basis for the development of rapid and specific bacteria detection technologies.

1. Peptide screening and isolation

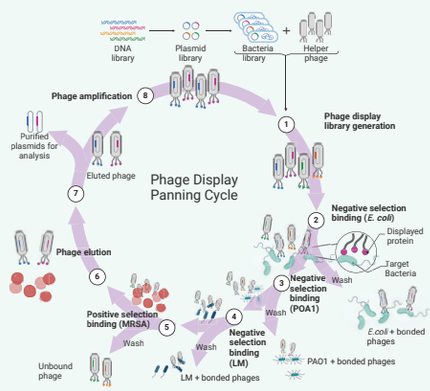

Phage display methodology that was Used at the current study:

1. **Initial Phage Library Preparation:** A diverse library of phage-displayed peptides was created, featuring a broad spectrum of peptide sequences.
2. **First Negative Selection:** The phage library was incubated with *Escherichia coli* (*E. coli*) cells. Phages that bind to *E. coli* are removed, leaving only those that did not interact with *E. coli*.
3. **Second Negative Selection:** The remaining phages were then incubated with *Pseudomonas aeruginosa* (PAO1) bacterial cells. Phages that bind to PAO1 were removed, isolating those that did not interact with PAO1.
4. **Third Negative Selection:** The process was repeated with *Listeria monocytogenes* (LM) bacterial cells. Phages that bind to LM were discarded, retaining only those that did not bind to LM.
5. **Positive Selection:** The remaining phages were incubated with Methicillin-resistant *Staphylococcus aureus* (MRSA) cells. Phages that specifically bind to MRSA were kept, while unbound phages were removed.
6. **Elution:** Bound phages were eluted from MRSA cells to isolate those as a candidate as the peptide binders.
7. **Phage Amplification:** The eluted phages were amplified in *E. coli* DH5α bacteria to increase the quantity of the selected phages.
8. **Iteration:** Steps 2 through 7 were repeated three times independently to enrich for phages with the highest specificity and affinity for MRSA.

This refined process enhanced the selection and enrichment of peptide binders that specifically target MRSA, while minimizing non-specific interactions with other bacterial species.

2. Characterizing the binding affinity of the lead peptides

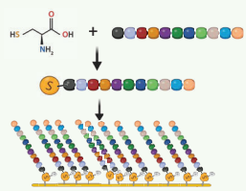

Schematic Illustration for the Immobilization of Peptides on a Gold Surface:

All peptides were synthesized with a linker at the N-terminus, consisting of three glycine residues followed by a cysteine residue (Gly-Gly-Gly-Cys) to covalently immobilize the peptides on the gold surfaces through the thiol group (-SH) in the cysteine side chain. This thiol-gold interaction covalently attaches the peptide to the gold surface, resulting in a peptide-coated gold surface.

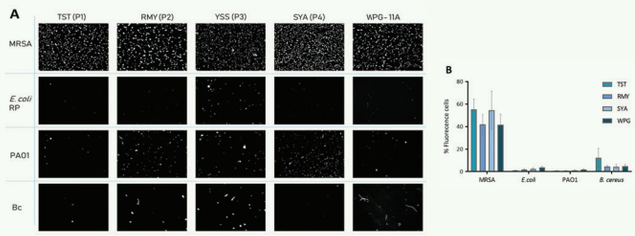

Peptide-Bacteria Binding Affinity Detection:

Peptide sequences identified from phage display as having high copy numbers for Methicillin-resistant *Staphylococcus aureus* (MRSA) and low copy numbers in negative control bacteria were assessed for bacterial affinity against MRSA, *Pseudomonas aeruginosa* (PAO1), *Escherichia coli* (E. coli RP), and *Bacillus cereus* (Bc). **(A). Immobilized peptide binding analysis:** peptides were covalently attached to a gold surface at a concentration of 10 μM using a thiol-gold interaction. Bacterial cells were then stained with 4′,6-diamidino-2-phenylindole (DAPI) and observed using Evos fluorescence microscopy to visualize binding. **(B). flow cytometry analysis:** bacterial cells at a density of approximately 10^8 CFU/mL were incubated with 10 μM fluorescein-tagged peptide. After removing unbound peptides, flow cytometry was used to measure the proportion of fluorescein-labeled bacteria relative to the total bacterial population, providing quantitative data on peptide binding (mean of three replicates ± standard error).

3. Chemical modification of the lead peptide

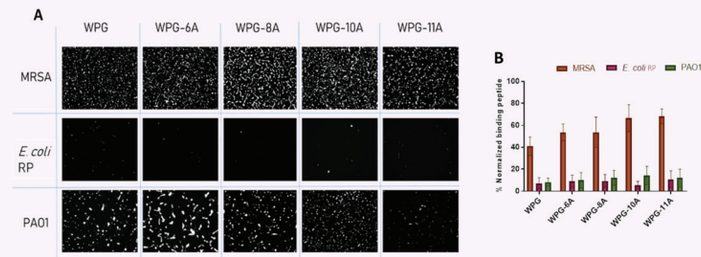

WPG lead peptide chemical modifications:

The WPG peptide and four derivatives were evaluated for bacterial affinity against Methicillin-resistant *Staphylococcus aureus* (MRSA), *Pseudomonas aeruginosa* (PAO1), and *Escherichia coli* (E. coli RP). **(A). Immobilized peptide binding analysis:** peptides were covalently attached to a gold surface at a concentration of 10μM via a thiol-gold interaction. Bacterial cells were stained with 4′,6-diamidino-2-phenylindole (DAPI) and visualized using Evos fluorescence microscopy to assess bacterial cells binding. **(B). Flow cytometry analysis:** bacterial cells at an approximate density of 10^8 CFU/mL were incubated with 10μM fluorescein-tagged peptide. Following the removal of unbound peptides, flow cytometry measured the proportion of fluorescein-labeled bacteria relative to the total bacterial population, providing quantitative analysis on peptide binding, expressed as the mean of three replicates ± standard error.

4. Quantifying the binding affinities of the lead peptides

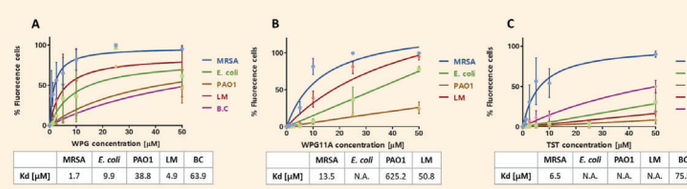

	MRSA	*E. coli*	PAO1	LM	BC
Kd [μM]	1.7	9.9	38.8	4.9	63.9

	MRSA	*E. coli*	PAO1	LM
Kd [μM]	13.5	N.A.	625.2	50.8

	MRSA	*E. coli*	PAO1	LM	BC
Kd [μM]	6.5	N.A.	N.A.	N.A.	75.5

Binding curves for lead peptide bacterial binders:

The binding curves for peptides WPG (A), WPG11A (B), and TST (C) are shown. Fluorescently labeled peptides were used at varying concentrations: 0.65, 1.25, 2.5, 5, 10, 25, and 50 μM. Each peptide concentration was incubated with bacteria at a density of 10^8 CFU/ml in PBS for 30 minutes. After incubation, the bacteria were washed twice with PBS and fixed with 4% glutaraldehyde. Flow cytometry was then employed to measure the proportion of FITC-labeled bacteria at each peptide concentration. The dissociation constant (K*d*) for each peptide-bacteria interaction was calculated using PRISM software. Data are presented as the mean of three replicates ± standard error (S.E.).

5. Competition binding assay

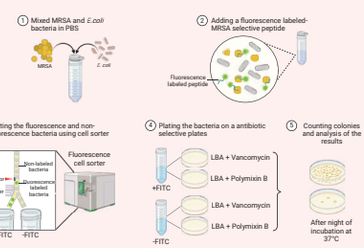

Competition assay of the lead peptide bacterial binders:

1. **Bacterial Preparation:** Methicillin-resistant *Staphylococcus aureus* (MRSA) and *Escherichia coli* (*E. coli*) were cultured separately in LB medium to a density of 10^8 CFU/ml, then washed three times with PBS. The bacteria were mixed in equal ratios.
2. **Peptide Incubation:** Fluorescence-labeled peptides were added to the bacterial mixture at concentrations of 10 and 50 μM and incubated for 30 minutes. After incubation, the bacteria were washed with PBS.
3. **Separation by FACS:** Fluorescence-activated cell sorting (FACS) was used to distinguish between FITC-labeled bacteria and non-labeled bacteria.
4. **Plating and Incubation:** Both labeled and non-labeled bacteria were plated on LB agar plates separately containing selective antibiotics and incubated overnight at 37°C.
5. **Colony Counting:** Colonies were counted the following day to determine the proportion of each bacterial type.

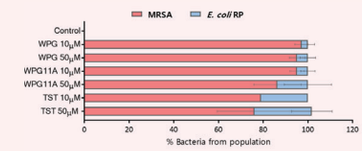

Quantification of MRSA and *E. coli* cells that the lead peptides bind:

The distribution of bacteria within the FITC-positive population was assessed as follows. MRSA and *E. coli* were cultured and processed as described. After separation by fluorescence-activated cell sorting (FACS) and plating on LB agar plates with selective antibiotics, colonies were counted the following day. The bacterial load for each type was normalized to the total number of FITC-positive cells. Data are presented as the mean of three replicates ± standard error (S.E.).

Conclusions

Our study successfully identified selective peptide binders for Methicillin-resistant *Staphylococcus aureus* (MRSA) using a phage display technique that utilized whole bacterial cells in suspension to enhance peptide diversity. This method led to the discovery of peptides with good specificity and high binding affinity for MRSA cells. The chemically modified peptides, including WPG and its derivatives, demonstrated enhanced binding affinities compared to the original sequence. Importantly, these peptides exhibited no toxicity towards either bacterial or mammalian cells, highlighting their safety for potential diagnostic and therapeutic applications.

In conclusion, our findings highlight the potential of our approach as a basis for developing rapid and specific any pathogenic bacterial detection abilities for various applications.

Created with BioRender Poster Builder

https://doi.org/10.17952/37EPS.2024.P2228

Phosphopeptides as a replacement of bisphosphonates for bone targeting

HEIDELBERG FACULTY OF MEDICINE

Mazen Jamous, Barbara Roether, Uwe Haberkorn and Walter Mier

Heidelberg University Hospital, Department of Nuclear Medicine, Germany

INTRODUCTION

The advancements in tumor biology have led to the development of highly specific therapies, notably in nuclear medicine, precisely targeting tumor-specific epitopes [1]. Bone-targeting agents utilize bisphosphonates, which bind farnesyl pyrophosphate synthase. Due to the enzyme's heightened activity this allows an effective targeting of metastatic bone disease [2,3]. Bisphosphonates are highly resistant to degradation. This results in long *in vivo* half-lives. While this is beneficial for inhibiting bone resorption, it is problematic for use in drug conjugates [4]. This study aimed to design novel bone-targeting peptides to increase their bone targeting affinity. NCPs (non-collagenous proteins) of the SIBLING (small integrin-binding ligand, N-linked glycoprotein) family are known for their high affinity to hydroxyapatite and their role in bone mineralization. Peptides derived from osteopontin (OPN) and matrix extracellular phosphoglycoprotein (MEPE, also known as OF45) with phosphorylated serine residues show inhibitory effects on mineralization and increased affinity for hydroxyapatite [5].

METHODS

Solid-Phase Peptide Synthesis

The peptides with unmodified serine or tyrosine residues were synthesized through solid-phase peptide synthesis (SPPS) employing the Fmoc strategy on a TentaGel resin. The protected chelator was coupled to the N-terminus using HATU as the activating agent.

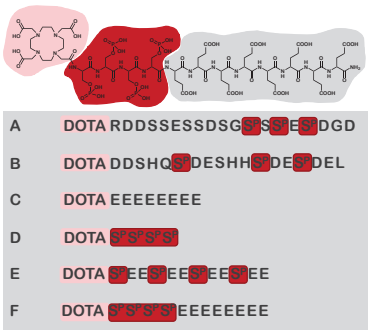

The subsequent post-synthetic phosphorylation step was carried out using dibenzyl-N,N-diisopropylphosphoramidite. The deprotection, along with the cleavage of the peptide, was achieved under standard conditions. The phosphopeptides were purified by preparative HPLC utilizing a Gilson 321 pump HPLC system and lyophilized, resulting in white solids. The yields ranged from 20% to 25%.

In vivo Small Animal PET Imaging

Positron emission tomography (PET) measurements were performed with female Wistar rats aged 8-10 weeks, weighing approximately 250 g. The rats were anesthetized with 2% sevoflurane (Abbott, Wiesbaden, Germany) and oxygen at a flow rate of 0.5 L/min. They were scanned in a prone position using a Siemens Inveon micro-PET scanner (Siemens, Knoxville, TN, USA) at 1 hour and 2 hours after the injection of the respective ^{68}Ga-radiolabeled conjugate (100 to 150 MBq). Each scanning session included a 15-minute transmission scan followed by a 20-minute emission scan. PET images were reconstructed using the Ordered Subset Expectation Maximization (OSSEM) 3D Maximum A Posteriori (MAP) algorithm with the Inveon Research Workplace system software (Siemens, Knoxville, TN, USA).

SUMMARY

The newly developed phosphopeptides demonstrate pharmacokinetic characteristics comparable to those of bisphosphonates. Given their promising safety profile and low toxicity, these peptide compounds merit additional research as potential agents for targeting bone metastases in cancer therapy.

REFERENCES

[1] Banerjee SR, Pullambhatla M, Byun Y, et al. 68Ga-Labeled Inhibitors of Prostate-Specific Membrane Antigen (PSMA) for Imaging Prostate Cancer. *Journal of Medicinal Chemistry.* 2010;53(14):5333-5341.

[2] Sartor O, Hoskin P, Bruland ØS. Targeted radio-nuclide therapy of skeletal metastases. *Cancer Treatment Reviews.* 2013;39(1):18-26.

[3] Love C, Din AS, Tomas MB, Kalapparambath TP, Palestro CJ. Radionuclide Bone Imaging: An Illustrative Review. *RadioGraphics.* 2003;23(2):341-358.

[4] Lin JH. Bisphosphonates: A review of their pharmacokinetic properties. *Bone.* 1996;18(2):75-85.

[5] Rowe PS, Kumagai Y, Gutierrez G, et al. MEPE has the properties of an osteoblastic phosphatonin and minhibin. *Bone.* 2004;34(2):303-319.

RESULTS

Effect of the Absence of Phosphorylation of MEPE-ASARM on Bone Hydroxyapatite-Binding *in vivo*

In Wistar rats, biodistribution studies were conducted using non-phosphorylated MEPE-ASARM peptide (^{177}Lu-DOTA-ASARM). The results showed that the radioactivity was primarily eliminated through the kidneys and bladder, with no significant bone accumulation observed one hour post-injection..

Bone Hydroxyapatite-Binding of Phosphorylated OPN-ASARM Peptide *in vivo*

Phosphorylated OPN-ASARM peptides inhibit crystal growth and matrix mineralization in osteoblast cultures. The phosphorylated OPN-ASARM peptide shares 60% homology with MEPE-ASARM and both contain three phosphoserine residues. While both peptides showed maximal inhibition at 20 µM, their pharmacokinetics differed, with fast blood clearance for both conjugates. Phosphorylation increased bone accumulation of ^{68}Ga-DOTA-OPN-ASARM compared to the non-phosphorylated version.

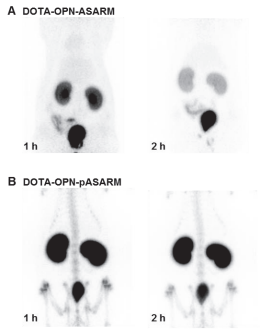

FIGURE 2.

PET-images of the ^{68}Ga-labeled non-phosphorylated (A) and phosphorylated (B) OPN-derived-DOTA-ASARM conjugate at 1h and 2 h post injection into female Wistar rats.

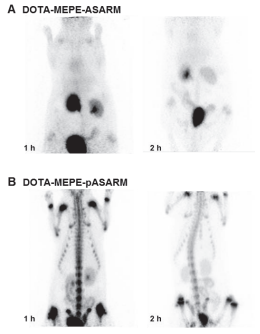

FIGURE 1.

PET-images of the ^{68}Ga-labeled non-phosphorylated MEPE-derived DOTA-ASARM conjugate (A) and its phosphorylated derivative (B) at 1h and 2 h post injection into female Wistar rats.

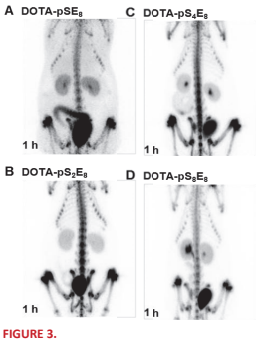

FIGURE 3.

PET-images of the ^{68}Ga-labeled phosphorylated conjugates with different sequence length DOTA-pS_nE_8 n=1 (A), 2 (B), 4 (C), 8 (D) at 1 h post injection into female Wistar rats.

Phosphopeptides of Aspartic Acid, Glutamic Acid, or DSS Repeats

Synthesized phosphorylated model peptides (DOTA-pS_4D_8, DOTA-pS_2E_8, DOTA-pS_4E_8, and DOTA-$pS_2(DSS)_4$) were tested in Wistar rats. Results indicated that phosphate groups enhance hydroxyapatite affinity, with ^{177}Lu-DOTA-pS_4D_8 and ^{177}Lu-DOTA-$pS_2(DSS)_4$ showing similar bone-binding potency to ^{177}Lu-DOTA-MEPE-pASARM. Replacing DSS repeats with glutamic acid significantly increased binding affinity, while aspartic acid did not alter it, confirming the specific binding of glutamic acid repeats to hydroxyapatite.

The Effect of Sulfation on Binding to Hydroxyapatite

The phosphorylated model peptides (DOTA-pS_4D_8, DOTA-pS_2E_8, DOTA-pS_4E_8, and DOTA-$pS_2(DSS)_4$) were studied in Wistar rats. Results indicated that phosphate groups strongly enhance bone affinity, with ^{177}Lu-DOTA-pS_4D_8 and ^{177}Lu-DOTA-$pS_2(DSS)_4$ showing similar bone-binding potency to ^{177}Lu-DOTA-MEPE-pASARM. Replacement of the DSS repeats with glutamic acid significantly increased binding affinity, while aspartic acid did not alter it, confirming the specific binding of glutamic acid repeats to hydroxyapatite.

The Effect of Phosphopeptide Length on its Pharmacokinetic Profile

We studied phosphorylated glutamic acid repeat peptides and found varying bone uptake levels, ranging from 0.85 ± 0.10 %ID/g for ^{177}Lu-DOTA-D_8 to 1.94 ± 0.17 %ID/g for ^{177}Lu-DOTA-pS_2D_8. Notably, kidney uptake increased proportionally with phosphopeptide length. Unexpectedly, ^{177}Lu-DOTA-pS_8D_8, despite having more phosphorylated serine residues, showed lower bone accumulation, potentially due to enhanced renal excretion. PET imaging of ^{68}Ga-labeled phosphorylated conjugates with varying sequence lengths (DOTA-$pSnE_8$) corroborated these findings.

Phosphoserine Position within the Peptide Sequence of Glutamic Acid Repeats

We compared two phosphorylated peptides: DOTA-$(pSE_2)_4$, with alternating phosphoserine and glutamic acid residues, and DOTA-pS_4D_8, differing only in phosphoserine positions. In vivo PET imaging in Wistar rats showed that DOTA-$(pSE_2)_4$ had higher kidney and bladder signals but lower bone uptake (SUVmax 10.1) compared to DOTA-pS_4D_8 (SUVmax 13.7).

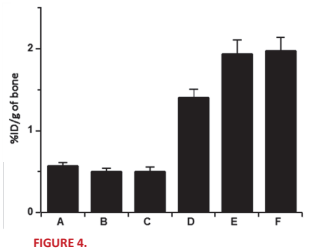

FIGURE 4.

The percentage of accumulation (%ID/g) of different ^{177}Lu-labeled phosphorylated peptides of DOTA-MEPE-pASARM (A), DOTA-$pS_2(DSS)_4$ (B), DOTA-pS_4D_8 (C), DOTA-pS_2E_8 (D), DOTA-pS_4E_8 (E) and ^{99m}Tc-MBP as reference (F) in the bone at 1 h post injection into female Wistar rats.

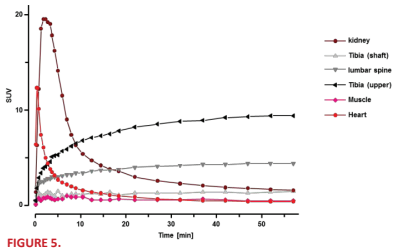

FIGURE 5.

Dynamic PET study of the ^{68}Ga-labeled phosphorylated conjugate DOTA-pS_4E_8.

Our Findings suggest:

- phosphorylated serine residues in the MEPE-ASARM peptide sequence are essential for bone accumulation
- serine phosphorylation is more effective for bone-binding than tyrosine phosphorylation
- binding potency depends on more than just net negative charge
- sulfation does not substantially improve peptide affinity to hydroxyapatite
- the bone targeting is dependent on both peptide sequence and net charge

Site-specific Conjugation of Cell-penetrating Peptides: A Strategy to Ameliorate Antibody Therapy

https://doi.org/10.17952/37EPS.2024.P2231

HEIDELBERG FACULTY OF MEDICINE

Niklas van den Bergh[a], Verena Merke[a], Sabrina Wohlfart[a], Philipp Uhl[b] and Walter Mier[a]

[a] Department of Nuclear Medicine, Heidelberg University Hospital, Germany
[b] Institute of Pharmacy and Molecular Biotechnology, Heidelberg University, Germany

niklas.vandenbergh@med.uni-heidelberg.de

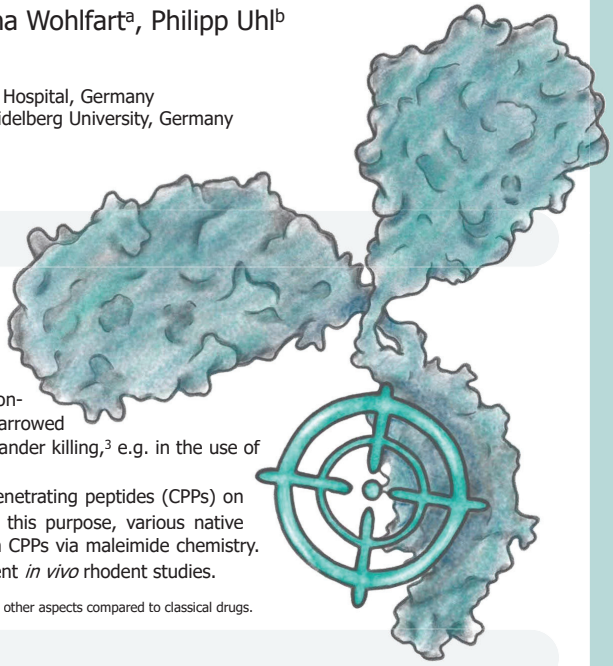

Motivation and Objective

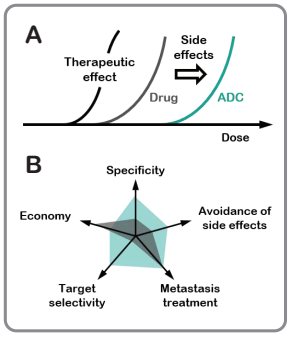

Antibody drug conjugates (ADCs) have emerged as innovative therapeutics for the targeted therapy of cancer,[1] inflammation and infection.[2] To date, their synthesis mostly relies on random and heterogenous conjugation of the payload since site-specific labeling of monoclonal antibodies (mAbs) remains challenging and tedious.[3] As a consequence, broad drug-antibody ratio (DAR) distributions can lead to a narrowed therapeutic index[4,5] and cause undesired side-effects as a result of bystander killing,[3] e.g. in the use of cytostatic ADCs.

In this work, we aim to exploit the reported benefitial effects of cell-penetrating peptides (CPPs) on mAb internalization and biodistribution[6] under strict DAR control. For this purpose, various native off-the-shelf mAbs are conjugated site-specifically to a library of known CPPs via maleimide chemistry. The conjugates are characterized and labeled radioactively for subsequent *in vivo* rhodent studies.

Figure 1. ADCs are able to (A) broaden the therapeutic window and (B) enhance treatment in many other aspects compared to classical drugs.

Methods and Concept

To be able to obtain high yields of conjugates with defined DARs, the recently established AJICAP™ approach[7] was chosen. It relies on proximity-induced site-specific labeling of distinct lysine residues using affinity peptides equipped with a reactive organic moiety. For the analysis of the conjugates, Hydrophobic Interaction Chromatography (HIC) and Ellman's Assay are used.

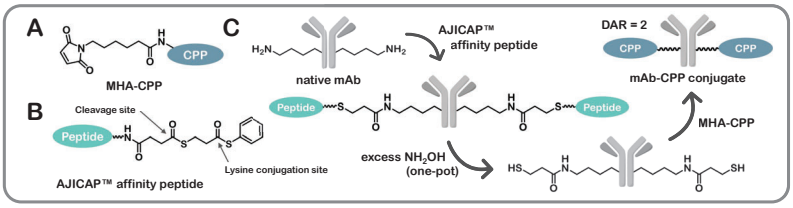

Figure 2. (A) Schematic general structure of CPPs coupled to maleimidohexanoic acid (MHA) for thiol conjugation. (B) Schematic structure of the AJICAP™ affinity peptide used in this work. (C) Modification of native mAbs is carried out in a three-step protocol.

Results

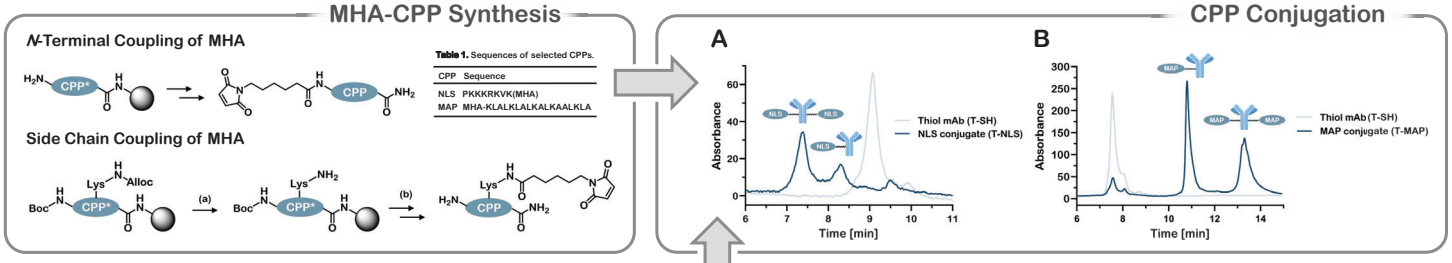

Figure 3. Alternative approaches for the solid phase synthesis of MHA-labeled CPPs. *N*-Terminal labeling of resin-bound peptide is achieved in two steps: HBTU-mediated coupling of MHA followed by simultaneous deprotection and resin cleavage using TFA and scavengers. Side chain coupling via lysine residues is carried out using orthogonal protection: (a) The *N*-allyloxycarbonyl (Alloc) protecting group is reductively cleaved from the Boc-protected resin-bound peptide using Pd(0) and BH_3NHMe_2; (b) MHA coupling is then performed prior to deprotection and resin cleavage using TFA and scavengers. *Indicates that the CPP side chains are protected with Fmoc/*t*Bu-compatible protecting groups.

Figure 5. HIC chromatograms (TSKgel HIC-ADC column, 5 µm, 4.6 x 100 mm from Tosoh Bioscience) of Trastuzumab CPP conjugates (crude mixtures) show a decrease in retention times for (A) hydrophilic NLS and an increase for (B) hydrophobic MAP. Gradient: A: 1.1 M $(NH_4)_2SO_4$ in 100 mM phosphate buffer (pH 7.0) to B: 25% iPrOH in 100 mM phosphate buffer (pH 7.0); (A) 0% B for 2 min, then 0 to 30% B in 11 min; 1 mL/min; 5 µg sample. (B) 0% B for 2 min, then 0 to 50% B in 11 min and 50% B for 2 min; 1 mL/min; T-SH: 5 µg sample, T-MAP: 17.5 µg sample.

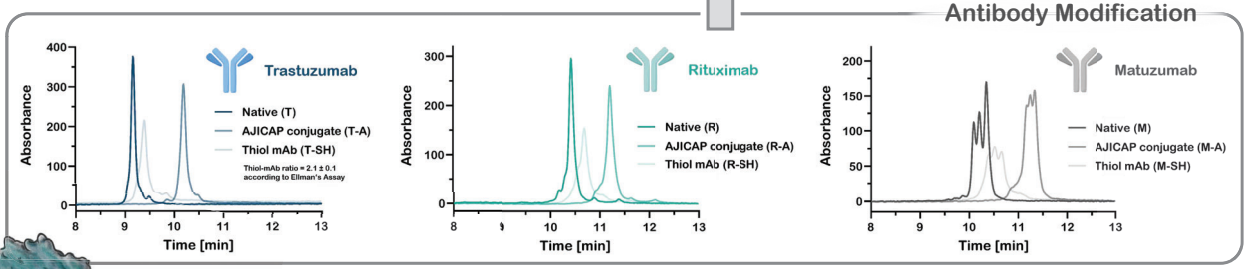

Figure 4. HIC chromatograms (TSKgel HIC-ADC column, 5 µm, 4.6 x 100 mm from Tosoh Bioscience) of different native off-the-shelf mAbs as well as their AJICAP™ derivatves. Gradient: A: 1.5 M $(NH_4)_2SO_4$ in 25 mM phosphate buffer (pH 6.0) to B: 25% iPrOH in 25 mM phosphate buffer (pH 6.0); 0% B for 2 min, then 0 to 50% B in 11 min; 1 mL/min; 5 µg sample.

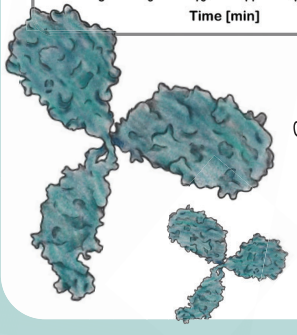

Contact me

Summary and Outlook

Site-specific modification of different CPPs using the AJICAP™ approach was accomplished for Trastuzumab, Rituximab and Matuzumab. Next, purification and *in vivo* testing of the CPP conjugates will be performed. We anticipate to obtain valuable data for the amelioration of ADC-based therapies.

References

1. S. Jin *et al.*, *Sig. Transduct. Target Ther.* **2022**, *7*, 39.
2. A. Casadevall *et al.*, *mBio* **2021**, *12* (2), e03372-20.
3. P. Gogia *et al.*, *Cancers* **2023**, *15* (15), 3886.
4. Y. Matsuda *et al.*, *Mol. Pharm.* **2021**, *18* (11), 4058-4066.
5. J. Junutula *et al.*, *Nat. Biotechnol.* **2008**, *26*, 925-932.
6. M. Sauter *et al.*, *J. Control. Release* **2020**, *322*, 200-208.
7. T. Fujii *et al.*, *Bioconjug. Chem.* **2023**, *34* (4), 728-738.

https://doi.org/10.17952/37EPS.2024.P2234

Faculty of Chemistry - Organic and Bioorganic Chemistry - OCIII

UNIVERSITÄT BIELEFELD

Synthesis of cell-penetrating peptides with peroxisomal targeting signal 1

Christine Krofta[1], Anne Sophie Hammann[2], Sven Thoms[2] and Norbert Sewald[1]

[1] Organic and Bioorganic Chemistry, Faculty of Chemistry, Bielefeld University, Germany.
[2] Biochemistry and Molecular Medicine, Medical School EWL, Bielefeld University, Germany.

Christine.krofta@uni-bielefeld.de

Peroxisomes

- Peroxisomes play a unique role in metabolism and signalling pathways in all tissues.[1]
- Peroxisomes are involved in many metabolic pathways and thus influence numerous bodily functions.[2]
- Serious diseases such as Zellweger spectrum disorders examplify the importance of peroxisomes and thus the urgency of research in this area.[2]
- The delivery of various non-cellular molecules into the peroxisome is an important tool in peroxisome research.[2]



*adapted from R.J.A. Wanders et al.[2]

CPPs

- Cell penetrating peptides (CPPs) can effectively cross the cell membrane and act as a transporter for cargo molecules up to 200 nm in size.[3]
- CPPs are often positively charged peptides consisting of 2-40 amino acids.[4]
- The different transport mechanisms of CPPs into the cell are divided into two categories: the passive/ direct pathway and the energy-dependent/ endocytotic pathway.[4]

PTS1

- Peroxisomal targeting signal 1 (PTS1) is a C-terminal targeting sequence of peroxisomal matrix proteins.[5]
- PTS1 is recognized in the cytosol by the peroxisomal transport machinery and inserted posttranslationally into the peroxisome.[6]
- Earlier research suggested that PTS1 is a simple tripeptide, with -SKL-OH being a common Sequence. Recent research has shown the influence of the following amino acids and it is now assumed that the effective PTS1 sequence consists of 10-12 amino acids.[7]

Design of a potential transporter

- A CPP and PTS1 were combined to develop a potential in vitro carrier with the goal of being able to penetrate the cell membrane and enter the peroxisomes.

Fluorophore-(G)G-CPP-GG-PTS1-OH

cTAT	Fluorophore-G-G-K-r-R-R-G-r-K-k-R-r-E-G-G-P-V-I-G-S-L-K-S-K-L-OH	1
cR8	Fluorophore-G-G-K-r-R-r-R-r-R-r-R-E-G-G-P-V-I-G-S-L-K-S-K-L-OH	2
KW	Fluorophore-G-K-R-K-R-W-H-W-G-G-P-V-I-G-S-L-K-S-K-L-OH	3
Asparagutin	Fluorophore-G-R-R-W-F-R-R-R-R-R-R-G-G-P-V-I-G-S-L-K-S-K-L-OH	4

Synthesis

- Through manual SPPS difficulties in the synthesis were optimized
- The final oligopeptides were synthesized via SPPS on a synthesizer
- Cyclisation of the CPP sequence is assumed to enhance the cell penetrating properties and the stability in the cell.[3] A side chain to side chain cyclisation between lysine and glutamic acid was performed for 2 peptides.
- All peptides were labelled with 5(6)-FAM and peptide 3 was also labelled with Sulfo-Cy3 to visualise the subcellular localization of test molecules in human cells.

5(6)-FAM

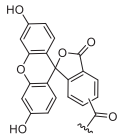

λ_{ex} = 498 nm
λ_{ex} = 517 nm

Sulfo-Cy3

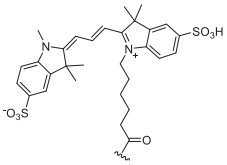

λ_{ex} = 548 nm
λ_{ex} = 563 nm

Cell tests

1 h Incubation, 5 µM CPP concentration

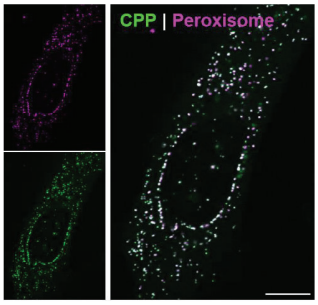

U-2 OS, scale bar 10 µm

- Cell tests were performed and analysed with fluorescence microscopy
- All peptides showed low efficiency of peroxisomal localization < 1% (5 µM)
- The peptides entered the cells, but were probably transported endosomally and could not escape from the endosomes
- CPP concentrations of 10 µM showed to be cytotoxic
- CPP conentrations of 0.1 µM showed low signals in the cells

Conclusion and outlook

- The goal was the development of peroxisomal transporters which can penetrate the plasma membrane and are recognized inside the cell to initiate import into the peroxisome. A peptide library of 4 peptides was created with a PTS1 and a CPP part.
- The synthesized transporter 1-4 were tested with cells and analysed with fluorescence microscopy. The analysis indicated a problem with endosomal entrapment of all peptides
- The cell penetrating properties need enhancement to optimize the transporter:
  - The cell penetrating properties of a CPP are influenced by the cargo, the sequence and the concentration of the CPP.[3]
  - Determination of the influence of the PTS1 on the cell penetrating properties on the peptide.
  - Analysis of the structure of the transporters could show if the CPP part is blocked
  - Optimization tests in regards of transporter concentration could be performed.
  - Optimization of the CPP sequence.

Reference

[1] K. Soliman, F. Göttfert, H. Rosewich et al., *Sci Rep* **2018**, 8, 7809.
[2] R. J. A. Wanders et al., *Physiol. Rev.* **2023**, 103, 957-1024.
[3] H. Derakhshankhah, S. Jafari, *Biomed Pharmacother.* **2018**, 108, 1090-1096.
[4] M. Zorko, Ü. Langel, *Methods Mol. Biol.* **2022**, 2383,3-32.
[5] T. Francisco et al., *Bioessays* **2017**, 39.
[6] C. Nötzel et al., *Traffic* **2016**, 17, 1110-1124.
[7] C. Brocard, A. Hartig, *Biochim Biophys Acta.* **2006**, *1763*, 1565-1573.



清華大學
Key Laboratory of Bioorganic Phosphorus Chemistry
& Chemical Biology (Tsinghua University), Ministry of Education
https://doi.org/10.17952/37EPS.2024.P2235

Surface peptide-modified black phosphorus nanosheets: a novel multifunctional nanoadjuvant

Tian-Yang Wang,[a] Wen-Hao Li,[a] Xue-Feng Yu,[b]* Yan-Mei Li[a]*

a Department of Chemistry, Key Lab of Bioorganic Phosphorus Chemistry & Chemical Biology (Ministry of Education), Tsinghua University, Beijing, 100084, P.R. China.
b Materials and Interfaces Center, Shenzhen Institute of Advanced Technology, Chinese Academy of Sciences, Shenzhen, 518055, P.R. China.
E-mail addresses: xf.yu@siat.ac.cn (Xue-Feng Yu), liym@mail.tsinghua.edu.cn (Yan-Mei Li).

The basic components of cancer vaccines include antigens and adjuvants. Antigens determine the specificity of cancer vaccines, while adjuvants can enhance the immunogenicity of antigens and activate immune responses. Nanoplatforms can effectively enhance the lymph node targeting, antigen presentation and immune activation of vaccines. Black phosphorus nanosheets (BPs) are novel two-dimensional nanomaterials with good biodegradability and biosafety. However, the immunogenicity and application of BPs themselves remain to be further studied. Here, we developed a method for peptide modification on the surface of BPs. FKF tripeptide modification increases the loading capacity of BPs for antigens peptide, forming a simplified component nanovaccine (FKF-OVAp@BP). Surface peptide modification improved the lymph node enrichment and T cell activation of BPs. The photothermal effects of BPs also effectively enhanced their ability to activate immune responses. In addition, FKF-OVAp@BP had a good synergistic effect with immune checkpoint therapy.

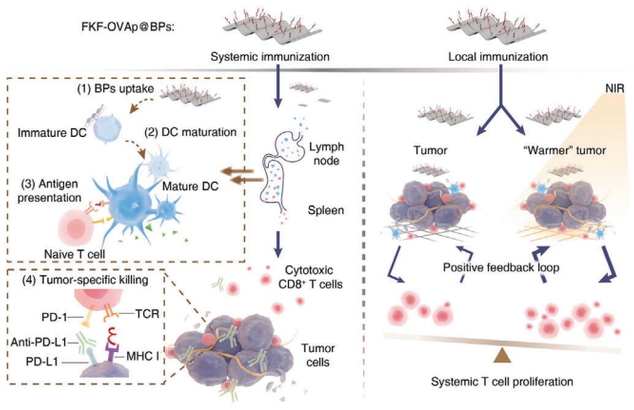

Scheme 1. Black phosphorus nanosheets (BPs) as novel adjuvant nanomaterials for cancer vaccines.

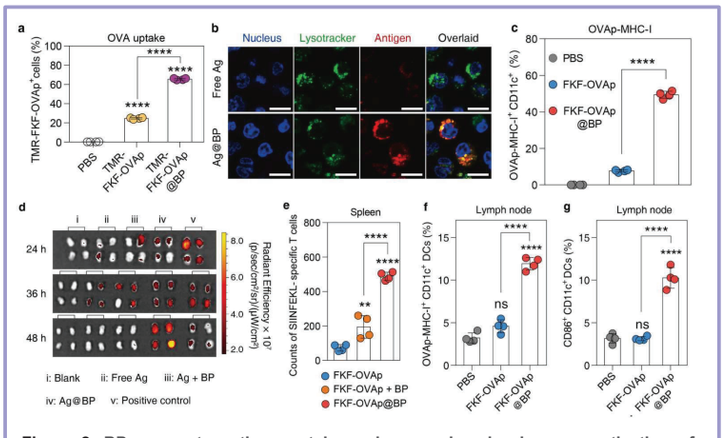

Figure 2. BPs promote antigen uptake and comprehensive immune activation of cytotoxic T lymphocyte (CTL) responses *in vivo*.

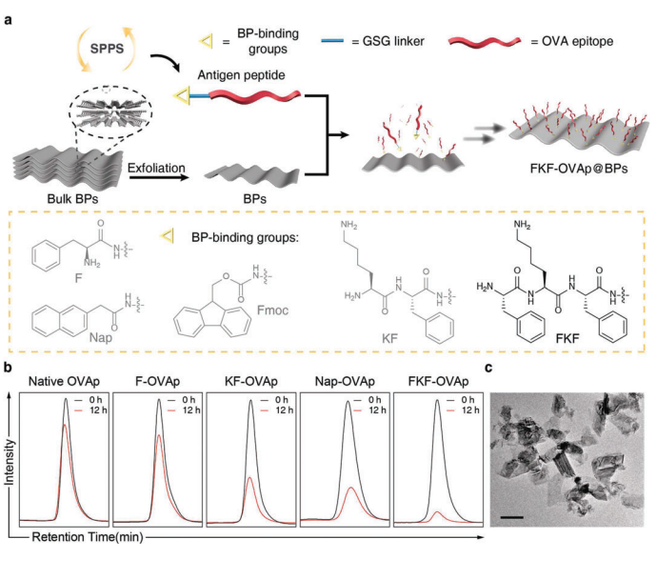

Figure 1. BPs serve as a high loading platform for peptide antigen.

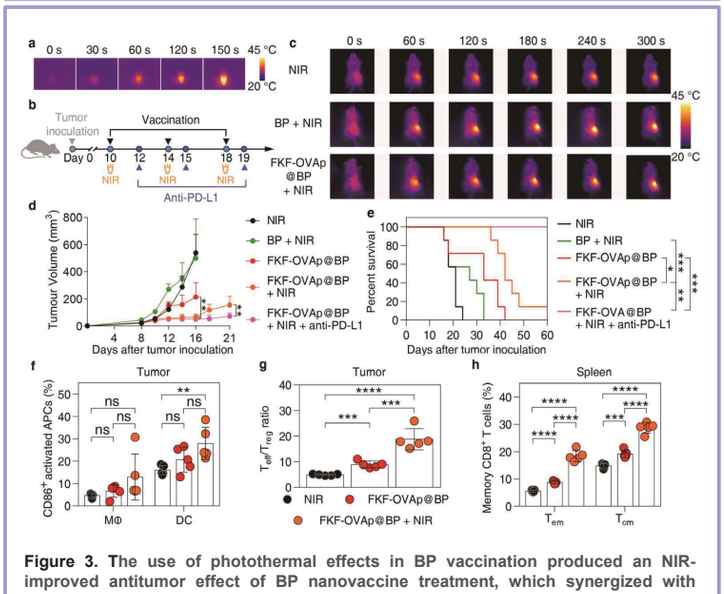

Figure 3. The use of photothermal effects in BP vaccination produced an NIR-improved antitumor effect of BP nanovaccine treatment, which synergized with checkpoint blockade therapy.

Acknowledge: This work was supported by the National Key R&D Program of China (2019YFA0904200, 2018YFA0507600), and the National Natural Science Foundation of China (21672126, 21975280), and Guangdong Special Support Program (2017TX04C096).

Reference: ［1］Li, W. H.; Yu, X. F.; Li, Y. M., et al., *Biomaterials* **2021,** *273*, 120788.

Proceedings of the 37th European Peptide Symposium
Michal Lebl, Editor
European Peptide Society, 2024 *10.17952/37EPS.2024.P2236*

Non-ionic surfactants for the solubilisation of lipopeptides and enhancement of their biological activity

Ágnes Ábrahám [a,b], Gergő Gyulai [a,b], Judith Mihály [c], Andrea Horváth [d], Orsolya Dobay [d], Éva Kiss [b] and Kata Horváti [a]*

[a] *MTA–HUN-REN TTK Lendület "Momentum" Peptide-Based Vaccines Research Group, Institute of Materials and Environmental Chemistry, Research Centre for Natural Sciences, Budapest, Hungary,* *email address: horvati.kata@ttk.hu
[b] *Laboratory of Interfaces and Nanostructures, Eötvös Loránd University, Budapest, Hungary*
[c] *HUN-REN TTK Biological Nanochemistry Research Group, Institute of Materials and Environmental Chemistry, Research Centre for Natural Sciences, Budapest, Hungary*
[d] *Institute of Medical Microbiology, Semmelweis University, Budapest, Hungary*

Lipopeptides have been extensively explored for their antimicrobial, anticancer and hormone activity, as well as promising fully synthetic self-adjuvanted vaccine candidates. However, lipopeptides tend to violate classical medicinal chemistry filters, mainly due to their high molecular weight and LogP characteristics. Lipopeptides usually form heterogenic aggregates in the micrometre range, therefore filtration is not an appropriate method to ensure sterility of the suspension. In addition, low aqueous solubility is a challenge when performing cell-based assays and often leads to failure in drug development. Besides, the often occurring haemolytic and cytotoxic side effects of lipopeptides may also be a serious limitation for their *in vitro* and *in vivo* use.

Table 1. *Modell lipopeptides selected for this study*

Name	Composition	Molecular weight	Net charge	Biological activity
pL1	palmitoyl-LLRK	766.1	2	Short antibacterial lipopeptide
pCM15	palmitoyl-KWKLFKKIGAVLKVL	2008.6	5	Hybrid peptide with anticancer activity
pATIPC	palmitoyl-KLVANNTRLTKPK-(FFGINTIPIAC)-GGLIDIAPHQISSV	4496.8	4	Branched-chained vaccine antigen

Non-ionic surfactants: poloxamers

In this study, self-assembling triblock copolymers, namely poloxamers were investigated to control the size of aggregates and i*n vitro* properties of biologically active lipopeptides (***Table 2***). Poloxamers are non-ionic amphiphilic copolymers consisting of poly(ethylene-oxide)—poly(propylene-oxide)—poly(ethylene-oxide) blocks. Their versatility arises from their tunable properties, which are linked to the length of their hydrophilic and hydrophobic chains. They are applied in various fields, serving as drug matrices and carriers, surfactants, solubilizers, wetting agents, emulsifiers, and adsorption enhancers. Due to their biocompatibility the U.S. Food and Drug Administration (US FDA) and European Medicines Agency (EMA) have approved numerous poloxamers for human use. Moreover, polymer micelles, which are more resistant to dilution than conventional surfactants, can be produced on a large scale. Poloxamers can encapsulate molecules within the core, constructed by the hydrophobic PPO segment, while the hydrophilic PEO region acts as a protective shield. The formed micelles have small size (10-100 nm), and exhibit spherical or rod-like shapes. In this study, the below listed poloxamers were investigated and the Critical Micelle Concentration (CMC) together with the cytotoxicity effect was determined. Based on our results, three poloxamers were selected (P-104, P-123, F-127) that have relatively low CMC values and can be used in high concentrations without toxicity.

Table 2. *Characteristics of the used poloxamers*

Poloxamer name	Pluronic name	Molecular weight	EO units	PO units	HLB values	CMC literature (g/L)	CMC experimental (g/L) [1]	Cytotoxicity IC50 (g/L) [2]
334	P-104	5900	27	56	13	0.02-0.08	0.02	2.731
403	P-123	5800	20	70	8	0.01-0.02	0.02	>2.9
407	F-127	12600	97	63	22	0.03-0.2	0.08	>6.3

The state of the poloxamer is marked with liquid (L), flakes (F), and paste (P). EO: ethylene oxide; PO: propylene oxide.HLB: hydrophilic-lipophilic balance.
[1] Critical micelle concentration (CMC) values of the poloxamers at 37°C in PBS, determined by pyrene fluorescence probe method
[2] Half-maximal inhibitory concentration (IC_{50}) values of the poloxamers, measured on HepG2 human cell-line, using AlamarBlue viability assay.

Characteristics of the poloxamer – lipopeptide mixed micelles

Mixed micelles of poloxamers with model lipopeptides were prepared by a simple solvation method and through dynamic light scattering (DLS) measurements, the production of small particles (diameter of around 20 nm) and reproducible, storable systems were demonstrated. Besides, these micelles can also tolerate freeze-thaw and lyophilisation-resolution cycles.

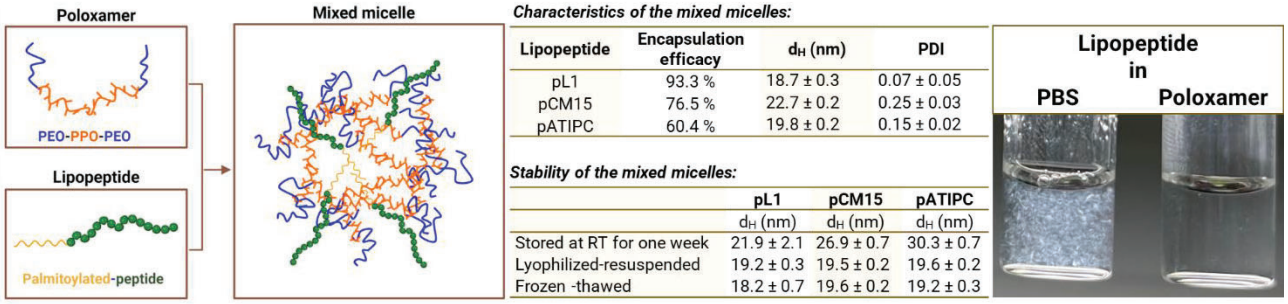

Characteristics of the mixed micelles:

Lipopeptide	Encapsulation efficacy	d_H (nm)	PDI
pL1	93.3 %	18.7 ± 0.3	0.07 ± 0.05
pCM15	76.5 %	22.7 ± 0.2	0.25 ± 0.03
pATIPC	60.4 %	19.8 ± 0.2	0.15 ± 0.02

Stability of the mixed micelles:

	pL1	pCM15	pATIPC
	d_H (nm)	d_H (nm)	d_H (nm)
Stored at RT for one week	21.9 ± 2.1	26.9 ± 0.7	30.3 ± 0.7
Lyophilized-resuspended	19.2 ± 0.3	19.5 ± 0.2	19.6 ± 0.2
Frozen -thawed	18.2 ± 0.7	19.6 ± 0.2	19.2 ± 0.3

Improved effectivity and selectivity

During the biological assessments, the properties of lipopeptide and lipopeptide–poloxamer systems were compared. The results showed that selectivity of pL1 lipopeptide was significantly improved by the poloxamers, increasing its antibacterial activity while reducing its haemolytic activity. The cytostatic effect of pCM15 colorectal tumor cells in the presence of poloxamers was approximately twice as high as that of the unformulated lipopeptide. For the self-adjuvanted vaccine antigen pATIPC, the rate of cellular uptake by antigen presenting model cells increased several-fold in the presence of poloxamers. Among the poloxamers, the highest biological activity was observed when Plur123 was used.

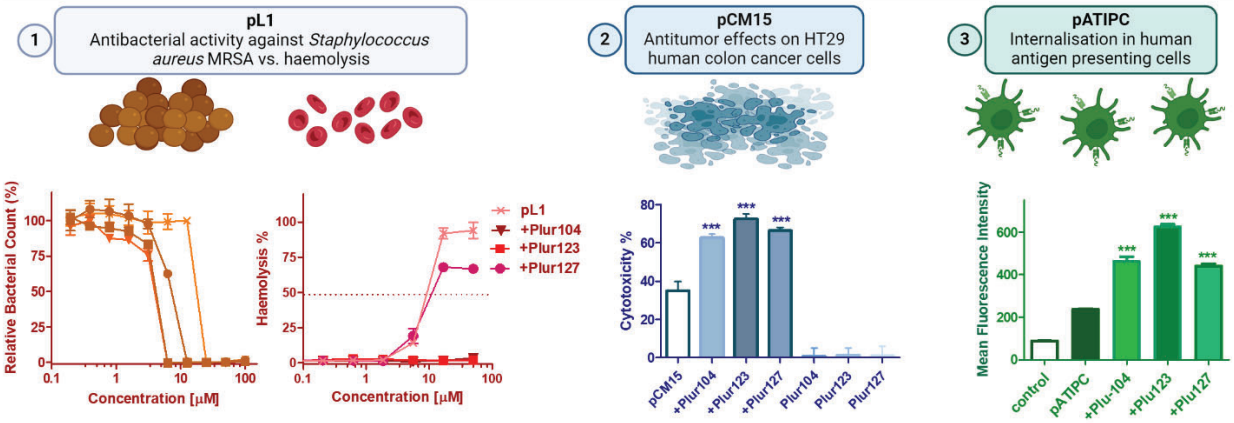

Figure 1. *Biological effect of the unformulated lipopeptides ans their mixed micelles with poloxamers*

Overall, it is concluded that poloxamer formulation is effective in optimizing the effect of lipopeptides, but the final properties of the mixed micelles are highly dependent on the length and structure of the peptide chain. It is believed that the optimal peptide chain length that can still be hidden in the PEO chains of Plur123 is around 10–12 amino acids.

Acknowledgements
This work was supported by the Lendület (Momentum) Programme of the Hungarian Academy of Sciences (LP2021-28).

Reference
Ábrahám, Á. et al. Optimizing lipopeptide bioactivity: The impact of non-ionic surfactant dressing. *J Pharm Analysis*, 2024, 101020.

https://doi.org/10.17952/37EPS.2024.P2238

Nanobody CDR3 loop peptidomimetic improves binding on living *Acinetobacter baumannii*

Kevin Van holsbeeck,[1] Anke Breine,[2,3] Charlotte Martin,[1] Morganne Mannes,[1]
Els Pardon,[3] Jan Steyaert,[3] Han Remaut,[3] Charles Van der Henst,[2,3] Steven Ballet[1]

[1] Research Group of Organic Chemistry, Vrije Universiteit Brussel, Brussels, Belgium
[2] Microbial Resistance and Drug Discovery, Vrije Universiteit Brussel, Brussels, Belgium
[3] Structural Biology Brussels, VIB-VUB Center for Structural Biology, Brussels, Belgium

Email: kevin.van.holsbeeck@vub.be

INTRODUCTION

Acinetobacter baumannii represent one of the **most persistent, highly virulent and multidrug-resistant bacterial species** that threaten human life. These are Gram-negative capsulated and nonflagellated bacteria producing multiple types of lipooligosaccharides which **widely vary between clinical isolates** due to its highly dynamic genome.

Nanobodies (ca. 15 kDa) are interesting, downsized variants of monoclonal antibodies (ca. 150 kDa) displaying remarkable specificity and high affinity binding capabilities. Nevertheless, only a ***limited number* of nanobodies able to bind or neutralize bacteria have been reported to date. Recently, we discovered a nanobody able to bind *Acetinobacter baumannii* bacterial cells**, but only upon formaldehyde fixation. To overcome this fixation step, peptides (ca. 1-2 kDa) representing the nanobody complementarity-determining regions (CDR) were considered as downsized alternatives enabling increased membrane access.[1,2]

NbD4 binding properties

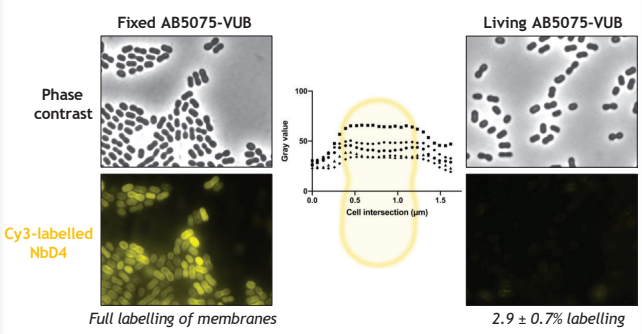

- Paraformaldehyde alters bacterial surface facilitating access of NbD4 to target
- Target unknown: inconclusive pull-down and MS experiments

Nanobody miniaturization through its CDR loops

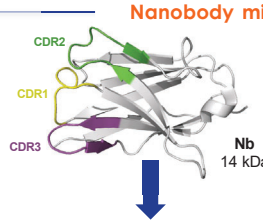

- Target not identified: no structural data available
- **Nb CDR definitions: classical Ab numbering schemes insufficient**
- Structural comparison to overlapping experimental structures (extended IMGT CDR definitions)

Code	Nb CDR	Sequence
1	CDR1	SulfoCy3-β-Ala-Gly-Ile-Ser-Lys-Ser-Ile-Thr-Ile-NH_2
2	CDR2	SulfoCy3-β-Ala-Thr-Ile-Thr-Ser-Gly-Gly-Thr-Thr-Asn-NH_2
3	CDR3	SulfoCy3-β-Ala-Asn-Ala-Arg-Arg-Leu-Arg-Glu-Tyr-Trp-NH_2

- SPPS of linear peptides
- In solution labelling using NHS ester of SulfoCy3

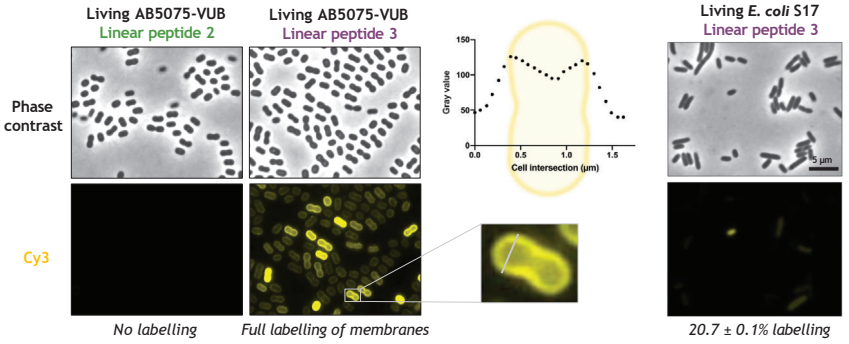

- **CDR3 as minimal required element** for membrane binding
- Peptide size allows **enhanced accessibility** on living capsulated *A. baumannii* bacteria

Linear CDR3 peptide binds a variety of A. baumannii isolates

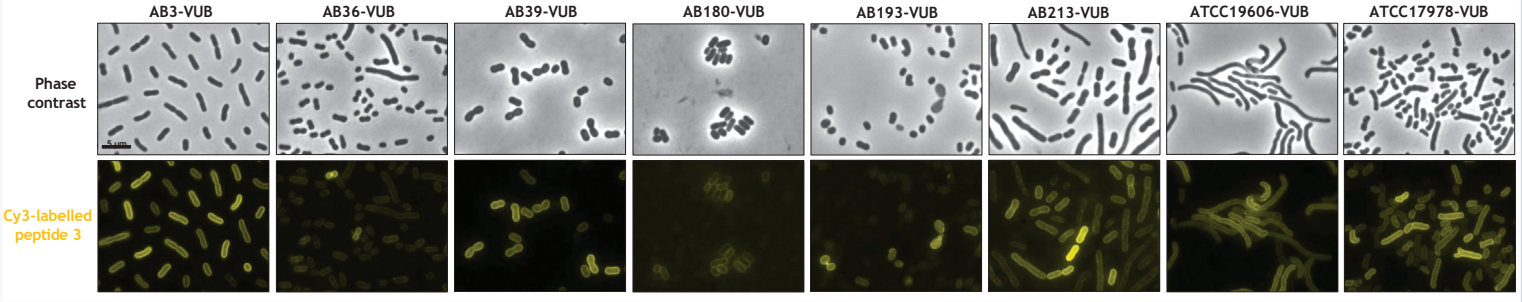

Going cyclic: preserved binding

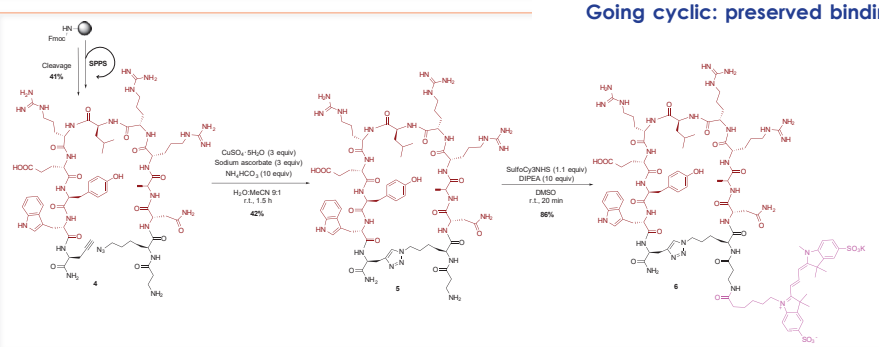

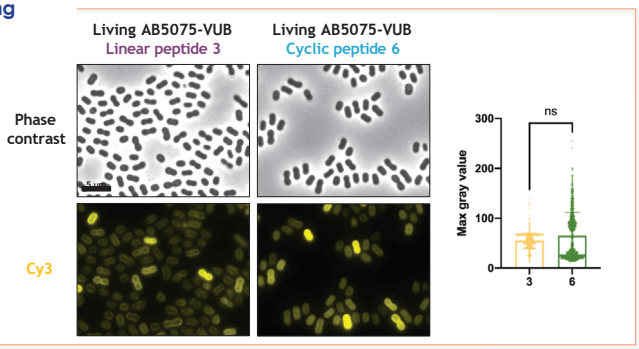

Proteolytic stability

- *In vitro* human plasma assay by HPLC analysis
- Acetylated variants of:
  - Linear peptide 3: $t_{1/2}$ 36.3 ± 0.5 min
  - Cyclic peptide 6: $t_{1/2}$ 55.7 ± 0.3 min

No bacterial cytotoxicity

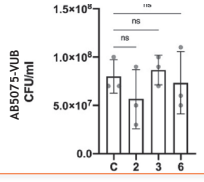

CONCLUSION & PERSPECTIVES

- Necessity of cell fixation for Nb membrane labelling
- Downsized CDR3 peptide enables full membrane labelling of unaltered living capsulated *A. baumannii*
- CDR3 peptide binds variety of living MDR *A. baumannii* isolates, despite high genetic diversity
- Peptide cyclization increases proteolytic stability, while preserving labelling potential
- Benefit of smaller peptide (1-2 kDa) size vs Nb (14 kDa)
- Peptides as targeting tags (visualization, peptide-drug conjugates)

ACKNOWLEDGEMENTS

K.V.h. and S.B. thank the Research Foundation–Flanders (FWO Vlaanderen) for providing a PhD fellowship to K.V.h. K.V.h., M.M., and S.B. thank the Research Council of the Vrije Universiteit Brussel for financial support through the spearhead (SRP50) program. A.B., C.V.d.H., and H.R. thank the FWO for providing a PhD SB fellowship to A.B. C.V.d.H. acknowledges the Flemish Institute of Biotechnology (VIB) for their support. E.P. and J.S. acknowledge the support and the use of resources of Instruct-ERIC, part of the European Strategy Forum on Research Infrastructures (ESFRI), and the FWO for their support to the nanobody discovery.

REFERENCES

1 Van holsbeeck, K.; Martins, J.C.; Ballet, S. *Bioorg. Chem.* **2022**, *119* (105563), 1-14.

2 Breine, A.; Van holsbeeck, K. *et al. Bioconjug. Chem.* **2023**, *34*, 1234-1243.

P2. 239 High-Throughput Analysis of Peptide Accumulation in Mammalian Cells

Sobika Bhandari, George Ongwae, Marcos M. Pires*
Department of Chemistry, University of Virginia, Charlottesville, Virginia, United States
https://doi.org/10.17952/37EPS.2024.P2239

Background

Peptides as Potential Drugs

- Since the first commercial use of insulin in 1923, proteins and peptides have been emerged as potentially effective therapeutic scaffolds[1]
- However, a molecule's effectiveness as a therapeutic target is largely determined by its ability to reach its intended target

Peptide drug approvals[2]

Major Challenges

- Cell membrane acts as a **major barrier** for intracellular transport of biologically active molecules
- Given the **larger size**, peptides face difficulty entering the cytosol successfully instead, their delivery relies on endocytic pathway

How is Permeability Being Measured?

Tag-free assay

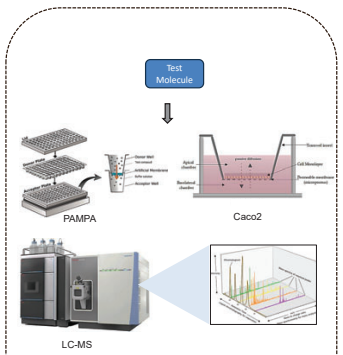

Limitation

Unable to distinguish sub-cellular localization[3]

Tag-based assay

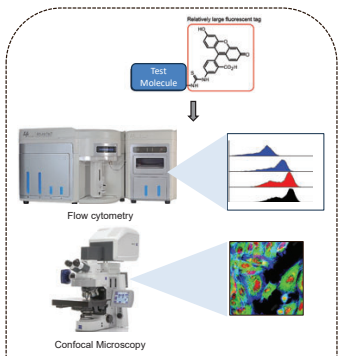

Limitation

Structural modification of molecule due to large fluorescent tag

Chloroalkane Penetration Assay (CAPA)[4]

- Relies on genetically encoded stably expressed "**HaloTag**" GFP-fusion protein

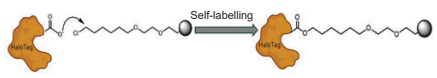

Self-labelling of HaloTag protein to HaloTag ligands

- Pulse-chase assay

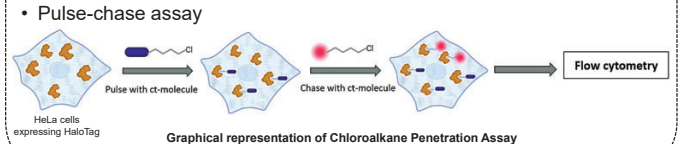

Graphical representation of Chloroalkane Penetration Assay

Limitation : Presence of long chloroalkane tag

Approach and Design

- Use a small azide tag,[5] comparatively less disruptive to molecules; named **CHAMP** (**Ch**loroalkane **A**zide-tagged **M**embrane **P**ermeability) Assay
- **DBCOcl** first binds irreversibly with HaloTag protein followed by SPAAC
- HaloTag-bound DBCO helps measure access of azide-bearing test molecules into the cytosol

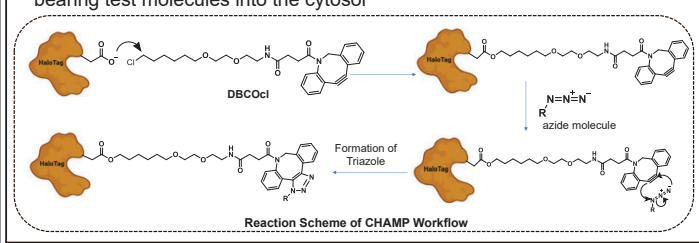

Reaction Scheme of CHAMP Workflow

CHAMP Assay Workflow

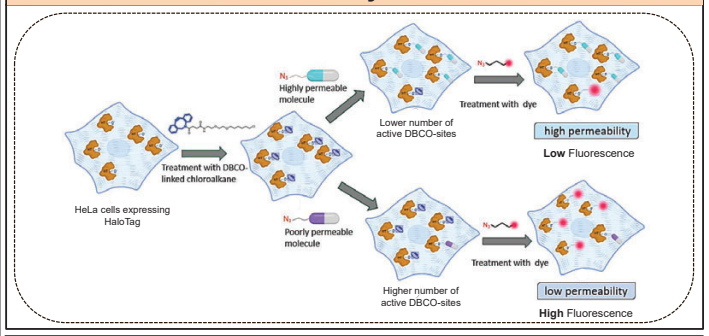

Results

Expression of HaloTag in HeLa cells

- Unmodified HeLa cells not expressing HaloTag were used as a negative control
- Significant differences in signal confirmed chloroalkane-tagged fluorophore in the cytoplasm of mammalian cells is captured by the cells that express HaloTag protein

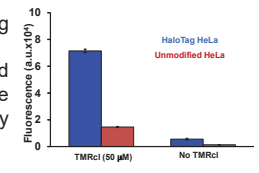

Parameter Optimization

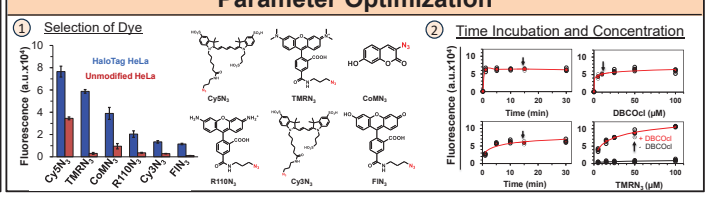

Results

Assay Development with Peptides

- Peptides were synthesized using solid phase peptide synthesis (SPPS)
- Permeability of polyarginine peptides were analyzed to probe optimal assay conditions

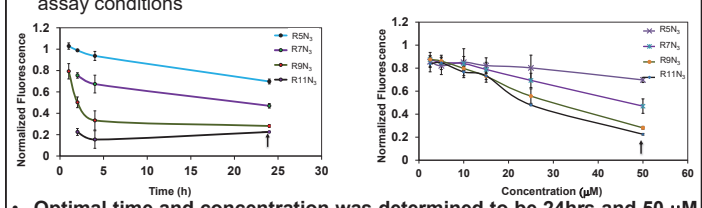

- **Optimal time and concentration was determined to be 24hrs and 50 μM respectively**.

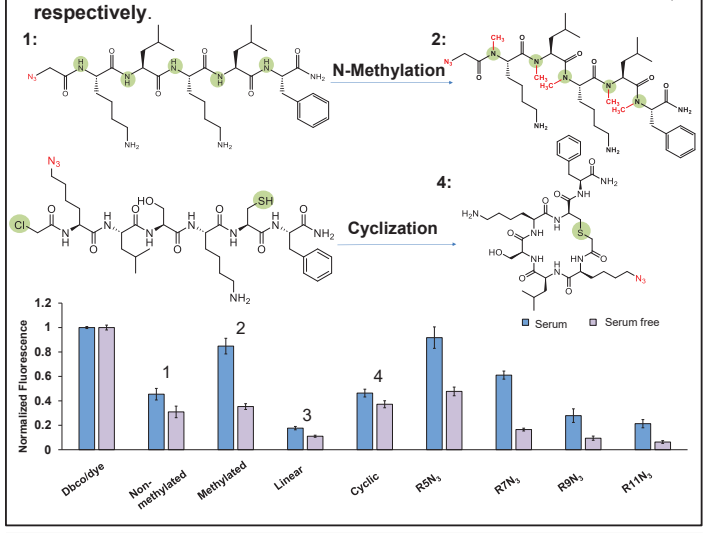

Conclusions

- Allows for comparative accumulation of azide-tagged peptides inside the cytosol of mammalian cells
- Significant decrease in signal corresponds to increase in accumulation of peptides in serum free media.
- Effective and high-throughput method to determine the cytosolic accumulation of peptides in mammalian cells.

References and Acknowledgements

1. Chandni, C et al *Current Drug Research Reviews*, **2024,** 16 (3), 381-394.
2. Muttenthaler, M et al, *Nature Reviews Drug Discovery*, **2021**, 20 (4), 309-325
3. Kritzer, J. A. et al *Methods in Enzymology; Elsevier*, **2020**, 641, 277-309.
4. Kritzer J. A. et al *Science Direct; Elsevier*, **2024**, 81
5. Ongwae, G. M et al *ACS Infect. Dis*, **2023,** 9 (1), 97-110.

Pires research lab
NIH National Institutes of Health

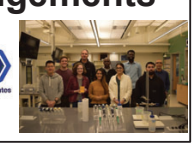

37th EPS European Peptide Symposium
14th IPS International Peptide Symposium

Electrostatically modulated peptide-based drug delivery against resistant cancer

Yvonne Christian[1], Amay Sanjay Redkar[1], Naveen Kumar[1], Shine Varghese Jancy[3], Aneesh Chandrasekharan[3], T.R. Santhoshkumar[3*] and Vibin Ramakrishnan[1,2,*]

[1]*Department of Biosciences and Bioengineering, Indian Institute of Technology Guwahati, India*
[2]*Mehta Family School of Data Science & Artificial Intelligence, Indian Institute of Technology Guwahati, India*
[3]*Cancer Research Program, Rajiv Gandhi Centre for Biotechnology, Thiruvananthapuram, India*

Email: christia@iitg.ac.in

https://doi.org/10.17952/37EPS.2024.P2240

BACKGROUND AND MOTIVATION

Problems of cancer drug resistance and side-effects of conventional therapies

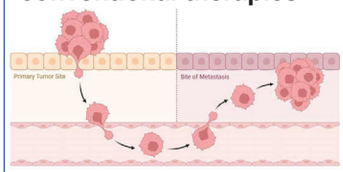

Cancer drug resistance

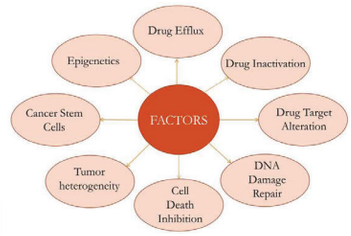

Why the need for drug delivery vehicles ??

Specificity → Dosage reduction

Cell-penetrating peptides (CPPs)

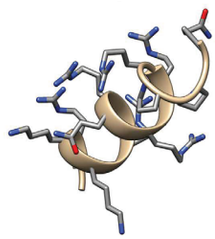

Pros
- ✓Internalize efficiently
- ✓Biocompatible
- ✓Easy to synthesize
- ✓Wide variety cargo
- ✓Non-toxic

Objectives:
- Designing novel and stable CPPs for drug delivery
- Tuning the electrostatics and structure of the peptides for specificity to cancerous cells
- Developing peptide-based drug delivery targeting cancer drug resistance

METHODOLOGY

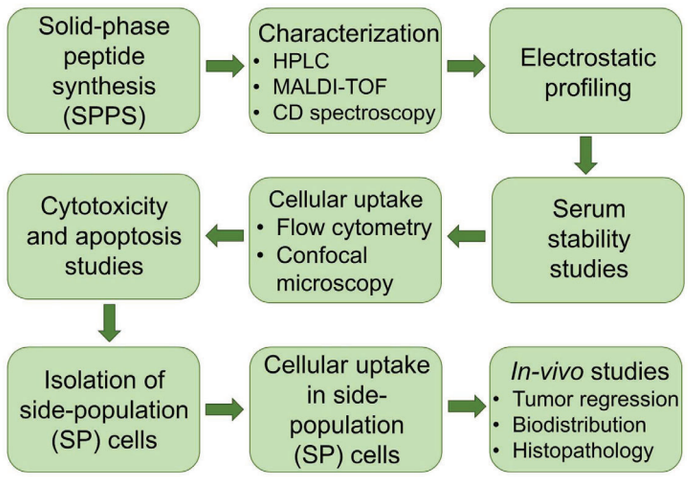

RESULTS

(a) Peptide design and electrostatic potential mapping

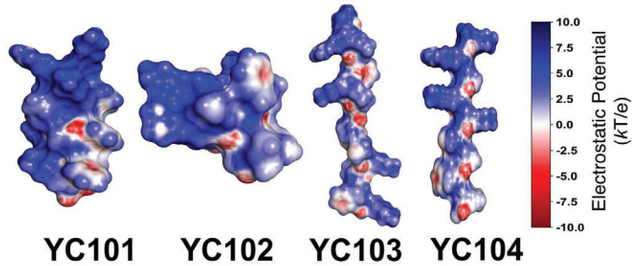

(b) Cellular uptake of peptides

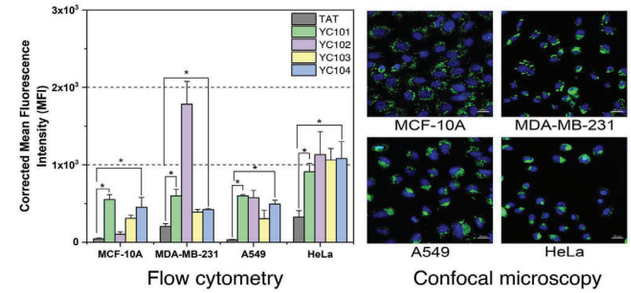

Flow cytometry | Confocal microscopy

(c) Cytotoxicity of peptide-drug conjugates

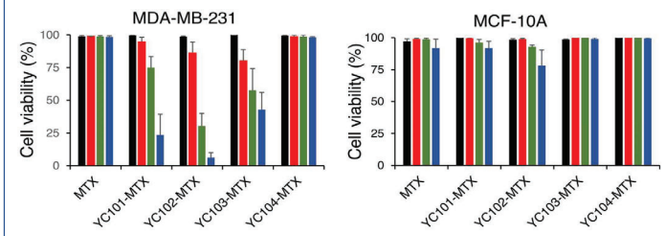

(d) Isolation and cellular uptake in SP cells

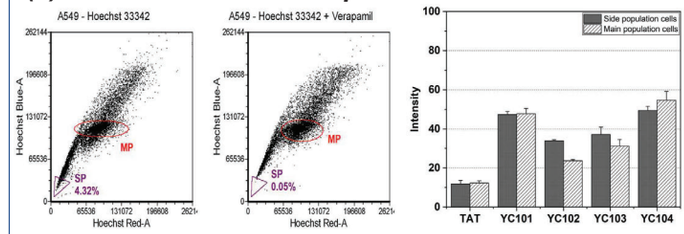

(e) In-vivo mice model studies

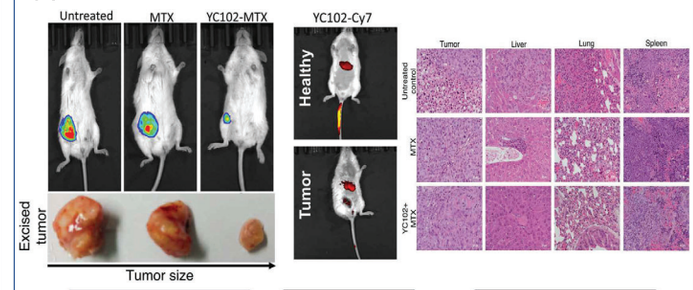

Tumor regression | Biodistribution | Histopathology

SUMMARY

- Peptides are stable and covalently conjugated to methotrexate (MTX) drug
- Varying electrostatic signatures of the peptides causes differential cellular uptake
- Enhanced cytotoxicity to cancer cells
- Comparable cellular uptake in side-population (SP) and main-population (MP) of tumor cells
- Significant tumor reduction in mice models

ACKNOWLEDGEMENTS

Department of BioTechnology, Government of India
MHRD
BSBE IITG
RGCB

REFERENCES

1. Christian Y, Redkar AS, Kumar N, Jancy SV, Chandrasekharan A, Retnabai Santhoshkumar T, Ramakrishnan V. Structural regression modelling of peptide based drug delivery vectors for targeted anti-cancer therapy. *Drug Deliv Transl Res.* **2024** Aug 8.
2. Jerath G, Darvin P, Christian Y, Trivedi V, Kumar TRS, Ramakrishnan V. Delivery of Small Molecules by Syndiotactic Peptides for Breast Cancer Therapy. *Mol Pharm.* **2022** Aug 1; 19(8):2877-2887.
3. Goyal R, Jerath G, Chandrasekharan A, Christian Y, Kumar TRS, Ramakrishnan V. Molecular hybridization combining tumor homing and penetrating peptide domains for cellular targeting. *Drug Deliv Transl Res.* **2022** May; 12(5):1285-1292.

Proceedings of the 37th European Peptide Symposium
Michal Lebl, Editor
European Peptide Society, 2024
http://doi.org/10.17952/37EPS.2024.P2241

Novel viral peptide-based tandemized carriers: Structure prediction and *in vitro* evaluation

Katalin Uray[1], Martin Krátký[2], Jiří Horčic[2], Levente Lakatos[1,3], Előd Méhes[4], Bálint Jezsó[5,6], Jarmila Vinšová[2], Szilvia Bősze[1,7]

1 HUN-REN–ELTE Research Group of Peptide Chemistry, Hungarian Research Network, Eötvös Loránd University, H-1117 Budapest, Hungary, 2 Department of Organic and Bioorganic Chemistry, Faculty of Pharmacy, Charles University, CZ-50005 Hradec Králové, Czech Republic, 3 Doctoral School of Biology, Institute of Biology, Eötvös Loránd University, H-1117 Budapest, Hungary,4 Institute of Physics, Department of Biological Physics, Eötvös Loránd University, H-1117 Budapest, Hungary, 5 "Momentum" Motor Enzymology Research Group, Department of Biochemistry, Eötvös Loránd University, H-1117 Budapest, Hungary, 6 HUN-REN Research Centre for Natural Sciences, H-1117 Budapest, Hungary, 7 Department of Genetics, Cell- and Immunobiology, Semmelweis University, Faculty of Medicine, H-1089 Budapest, Hungary

Introduction

Previously we have shown the efficacy of a modified synthetic peptide (RF) derived from the Herpes simplex virus-1 gD glycoprotein (^{228}QRTVAVYSLRIAGFHG^{243}) (Fig. 1) ([1] in internalization into epithelial or neural cells. Tuftsin derivatives (OT5(P), OT5) can deliver cargo into different cells via neuropilin receptors [2-4]. Positively charged penetratin, the most studied cell-penetrating peptide (Pen), can rapidly enter cells.
We aimed to modify the RF peptide's cellular uptake rate and intracellular localization by tandemizing it with tuftsin or penetratin derivatives (Table 1, Fig. 2).
Internalization was evaluated on VERO E6 non-human primate kidney epithelial and A431 human skin squamous carcinoma cells.

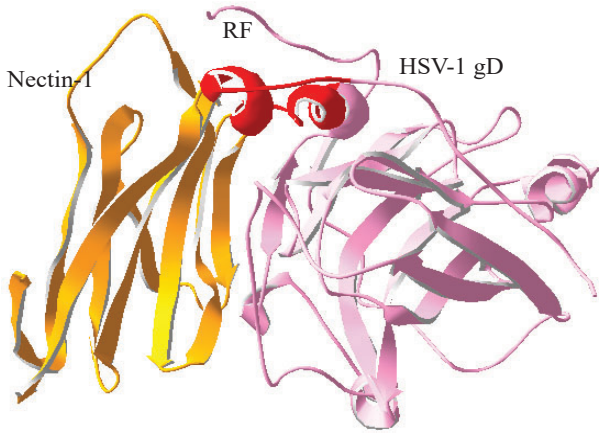

Figure 1. Secondary structure of HSV-1 gD–nectin-1 cell adhesion complex (PDB: 3U82) for virus entry. HSV gD 228-243 region show cellular entry ability as a synthetic peptide (Cf-RF).

Results and Discussions

Internalization of synthetic Cf-labeled peptides and tandems was measured by BD LSR II flow cytometer. All Cf-peptides containing the RF sequence internalize in a concentration-dependent manner (UC_{50} concentration value for Cf-positivity in 50% of the live cells: 0.1 – 5 µM) (Figure 2, Table 1). No cytotoxicity was detected (Figure 2, inserts). According to confocal laser scanning microscopy Cf-RF showed cytoplasmic localization; its tandemization with the tuftsin derivative resulted in compartmentalized localization to different degrees (data not shown).

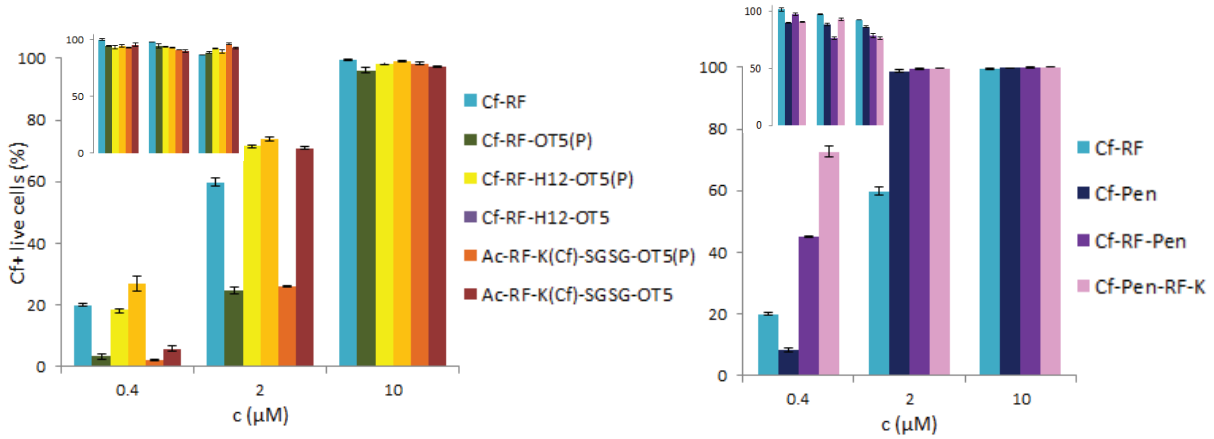

Figure 2. Internalization of Cf-peptides into A431 epithelial cells (B), represented by Cf+ live cell percentage. Inserts: relative viability (%).

Table 1. Analytical data, and internalization of Cf-labeled peptides characterized by UC_{50} (concentration value for Cf-positivity in 50% of the live cells)

Peptide code	*Mw, average*[a]		*UC_{50} (μM)*[b]	
	calc.	*meas.*	*A431*	*VERO E6*
Cf-RF	2132.36	2132.17	1.34	4.72
Cf-RF-OT5(P)	2712.10	2710.81	3.54	1.36
Cf-RF-H12-OT5(P)	3859.31	3857.33	1.04	1.08
Cf-RF-H12-OT5	3791.23	3790.98	0.88	2.37
Ac-RF-K(Cf)-SGSG-OT5(P)	3170.49	3169.44	3.41	0.51
Ac-RF-K(Cf)-SGSG-OT5	3102.41	3101.13	1.19	1.23
Cf-Pen	2605.06	2603.08	0.84	0.10
Cf-RF-Pen	4361.11	4361.42	0.46	0.60
Cf-Pen-RF-K	4489.28	4489.82	0.24	0.54

[a] *ESI-MS (Bruker Amazon SL ESI Mass Spectrometer, Bremen, Germany)*
[b] *Concentration value for Cf-positivity in 50% of the live cells (BD LSR II flow cytometer, data evaluation: FACSDiva 5.0 software.*

The secondary structure of tandem peptides (Pep-Fold 3) [5] depends on the linker moiety. The H12 rigid spacer may help the RF region to adopt its native helical structure, thus helping internalization in VERO E6 cells.
Penetratin derivatives and tandems internalize the most effectively; in A431 cells, nectin-binding HSV gD RF peptide enhances the internalization. Different spacers and tuftsin vs. tuftsin agonists in the tandemized peptides showed opposite orders of internalization in A431 and VERO E6 cells. Internalization into VERO E6 cells is favored by the presence of linker, preferably a shorter, more flexible one. On the other hand, in A431 cells the rigid linker proved more effective.

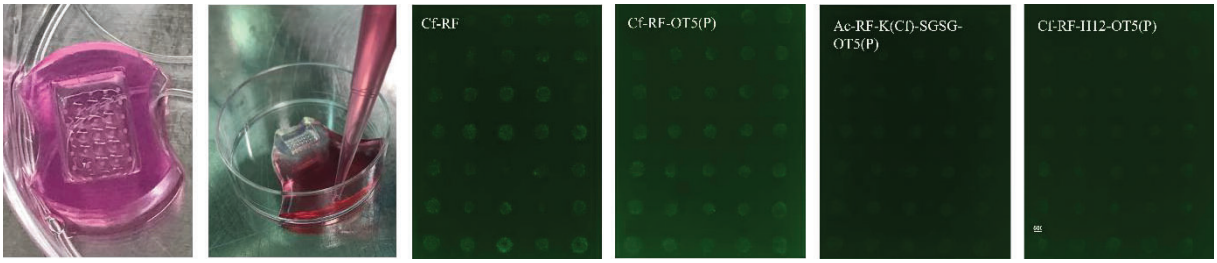

Figure 3. Penetration studies on agarose dish-based A431 spheroids, treatment applying 12.5 μM Cf-peptides, 3h.

The tandem peptides' penetration (with low UC_{50} values) was evaluated on spheroids as simple *in vitro* tissue-mimicking milieu, and all tandems demonstrated fair penetration ability (Figure 3).
These peptides are promising carrier candidates with variable intracellular trafficking depending on their sequence.

Acknowledgements

Grants OTKA 142904; VEKOP-2.3.3-15-2017-00020; EFOP-1.8.0-VEKOP-17-2017-00001; 2018-1.2.1-NKP-2018-00005; TKP2020-IKA-05; Gedeon Richter Talentum Foundation (LL).

References

1. Bősze. S., et al. *Biomolecules*, **10(5),** 721. (2020), https://doi.org/10.3390/biom10050721
2. Horváth, L.B., et al. *Eur J Pharm Biopharm.,* **174**, 111-130. (2022), https://doi.org/10.1016/j.ejpb.2022.03.009
3. Baranyai, Z., et al. *J Med Chem.,* **64(6),** 2982-3005. (2021), https://doi.org/10.1021/acs.jmedchem.0c01399
4. Horváth, L.B., et al. *ACS Omega.,* **9(15),** 16927-16948 (2024), https://doi.org/10.1021/acsomega.3c05727
5. Lamiable, A., et al. *Nucleic Acids Research*, **44,** W449-454 (2016), https://doi.org/10.1093/nar/gkw329

Small Additive Molecules to Enhance the Effective Accessibility of Delivered Nucleic Acid by Cell-Penetrating Peptide

https://doi.org/10.17952/37EPS.2024.P2242

Geeta Arya, Ly Porosk, Chigozie Nkwocha, Margus Pooga
Institute of Technology, University of Tartu, Tartu, Estonia
e-mail: geeta.arya@ut.ee

Introduction and Objective

- **Cell-penetrating peptides (CPPs)** are short peptides (up to 30 aa) with cell membrane permeability.
- With **nucleic acids**, CPPs form electrostatic complexes in the nanometer range: nanoparticles (NPs).
- Still, the efficiency of transfection with CPP NPs is usually lower than of lipid-based particles.
- The reason for the inefficient transfection of NAs is predominantly due to the **endosomal entrapment** of the particles.
- In this work, we have introduced several additive molecules in complexes to improve the accessibility of the NAs.
- We screened several FDA-approved compounds, categorized into groups: fusogenic lipids, endosomotropic agents, inhibitors of exocytosis, and autophagy.
- PF14 with sequence stearyl-AGYLLGKLLOOLAAAALOOLL-NH_2 was used as model CPP for our work.

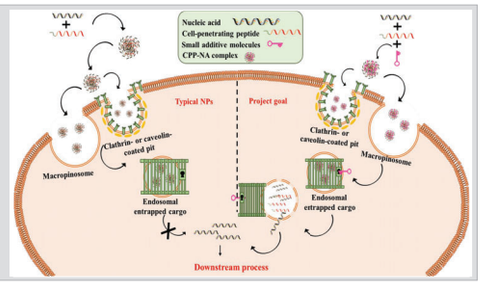

Methodology and Transfection Efficiency Evaluation Assays

Methodology:

1. Mixed CPP with nucleic acid: splice-correcting oligonucleotide (**SCO**) or **siRNA to form NPs**.
2. After 15 min of incubation, **additive**s were added in different concentrations.
3. After 15 min, the complexes were added to the cells for treatment.
4. After 24 hr, **measured** the luminescence or fluorescence.

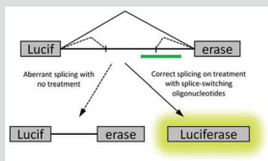

Restoration of luminescence of luciferase gene with **SCO-705** in HeLa pLuc-705

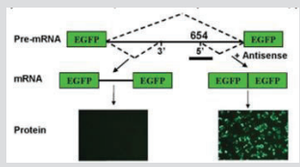

Restoration of fluorescence of EGFP gene with **SCO-654** in HeLa EGFP-654

Reporter cell lines

- **HeLa pLuc-705 (**having mutated luciferase gene**)**
- **HeLa EGFP-654 (**having mutated EGFP gene**)**
- **U87 MG-Luc2 (**having luciferase encoding gene**)**

Characteristics of Nanoparticles

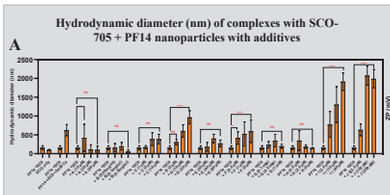

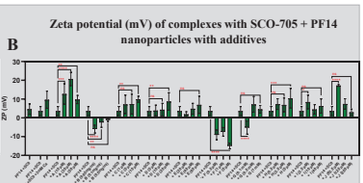

- The inclusion of additives into NPs changed the hydrodynamic diameter of the complexes.
- Compounds I and J significantly increased the size up to 2000 nm at higher concentrations.

- The addition of additives also affects the zeta potential of the complexes towards a more positive charge.
- Compounds B and F addition resulted in negative zeta potential.

Effect of Additives on Reporter Gene Expression

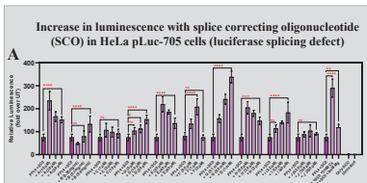

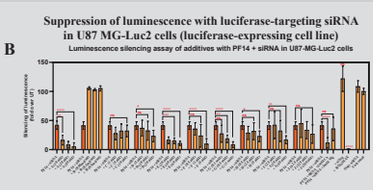

- Expression of **luciferase** was enhanced by supplementing additives along with PF14 + SCO nanoparticles.
- Concentration-dependent effect with high significance can be seen here.

- Silencing of **luciferase** expression was observed by supplementing additives along with PF14 + SCO nanoparticles.
- Concentration-dependent effect with high significance can be seen here.

Cell Viability Profiles of Additives

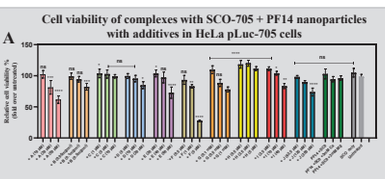

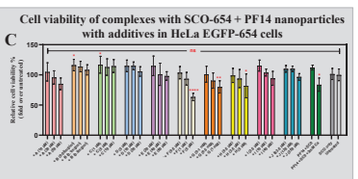

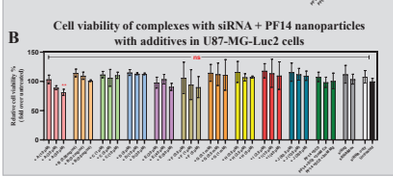

- Additives have different effects depending on the cell line.
- Compounds A and F showed reduced cell viability at higher concentrations in HeLa pLuc-705 cells.
- In the case of U87 MG-Luc2, none of the additives showed reduced viability except compound A at the highest tested concentration.
- Similarly, HeLa EGFP-654 showed reduced viability with some compounds at the highest tested concentration.

Cellular Association and Internalization

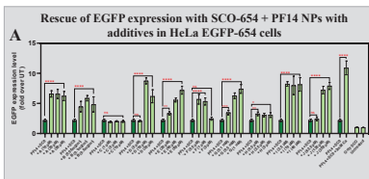

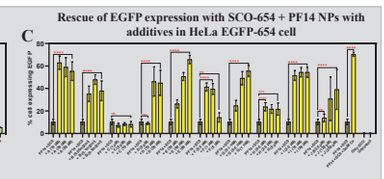

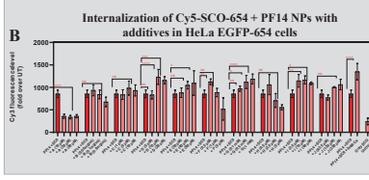

- Higher levels of cellular association were observed with the addition of additives as shown in figure A.
- With HeLa EGFP, almost all the additives are showing a significant increase in the expression level of EGFP except compound C.
- Figure B shows the association of Cy5 labeled SCO, which is also enhanced by introducing additives.
- Figure C shows the % of cells expressing eGFP protein, which is significantly correlating with Figure A.

Conclusion

- Additives enhance the PF14-mediated transfection of SCO and siRNA into all the used cell lines.
- All the studied additives positively contributed to the accessibility of NAs in cells in a concentration-dependent manner.
- Most of the PF14-NA + additives NPs did not significantly affect the cell viability.

Future Plan

- These additives will be screened with other types of Nas and onther CPPs too.
- Study of mechanism of action of additives-NAs-PF14 will be performed.
- Confocal microscopy imaging will be performed.

Funding

Eesti Teadusagentuur
Estonian Research Council
European Union
European Regional Development Fund
Investing in your future
M-ERA.NET

Fluorogenic cell surface labelling using fluorescent molecular rotor-labelled peptide boronic acid conjugates

Alen Koçak[ϕ], Pritam Ghosh[ϕ], Oliver Seitz*

Department of Chemistry, Humboldt-Universität zu Berlin, Brook-Taylor-Straße 2, 12489 Berlin, Germany, E-mail: oliver.seitz@chemie.hu-berlin.de

ϕ: equal contribution, *Corresponding author

https://doi.org/10.17952/37EPS.2024.P2244

CRC 1449

Abstract

Abnormally viscous mucus hydrogel layers represent the key pathological characteristic of chronic, muco-obstructive respiratory and gastrointestinal disorders such as Cystic Fibrosis (CF), Chronic Obstructive Pulmonary Disease (COPD) and Inflammatory Bowel Disease (IBD). To date, quantifying and mapping spatial nanoviscosity on living cells/tissues poses a major challenge. Our aim is to probe viscosity by anchoring fluorescent molecular rotor (FMR) dyes to cell surface glycans. For this purpose, the FMRs are attached to peptide-multiboronic acid conjugates. We show the development of fluorogenic probes that have high affinity for cell surfaces and demonstrate ratiometric imaging with an FMR and a non-FMR probe to characterize cell surface nanoviscosities.

Background

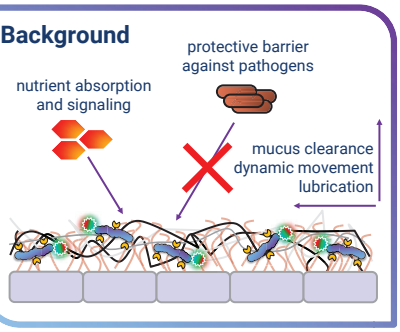

Concept

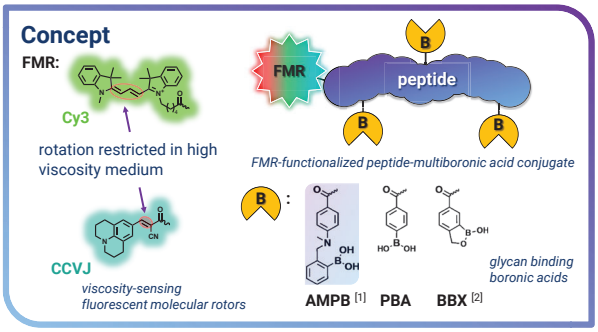

Developing FMR-functionalized peptide-multiboronic acid conjugates for cell surface labeling

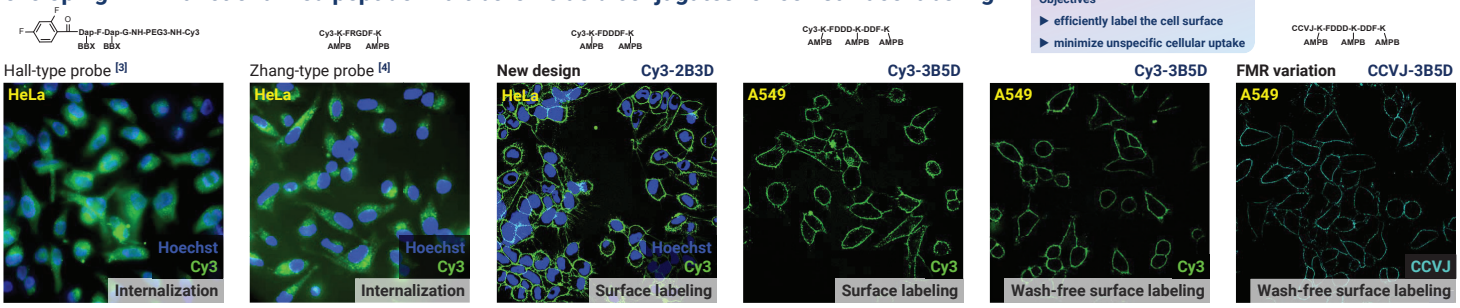

Objectives
- efficiently label the cell surface
- minimize unspecific cellular uptake

- boronates can facilitate cellular uptake [5]
- starting point of screening campaign of approx. 50 different probes with three different boronate receptors
- 2 boronates (B) with 3 aspartates (D) sufficient for staining of HeLa surface, but not A549 (data not shown)
- increase number to 3 boronate receptors and 5 aspartates for successful staining of A549 cell surface
- Cy3 and CCVJ are fluorogenic
- probes light up under high viscosity [6] - [8]

Influence of boronic acid receptor on cell surface affinity

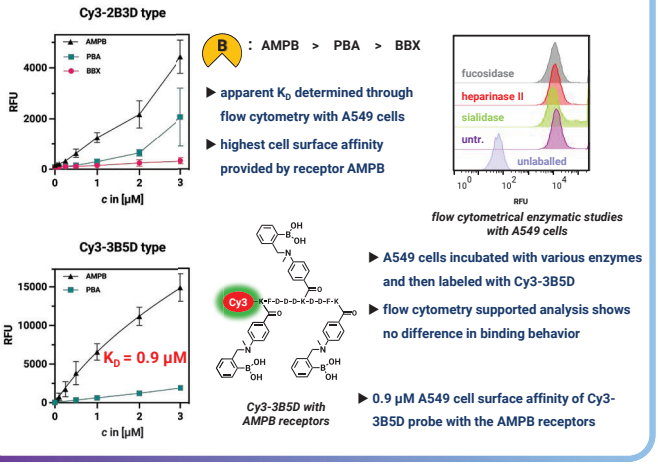

- apparent K_D determined through flow cytometry with A549 cells
- highest cell surface affinity provided by receptor AMPB

flow cytometrical enzymatic studies with A549 cells

- A549 cells incubated with various enzymes and then labeled with Cy3-3B5D
- flow cytometry supported analysis shows no difference in binding behavior
- 0.9 µM A549 cell surface affinity of Cy3-3B5D probe with the AMPB receptors

Ratiometric imaging of A549 cell surfaces

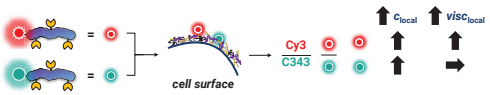

dual labeling of the A549 cell surface yields fluorescence ratios of Cy3/C343

Objectives
- nanoviscosity on A549 cell surface/glycocalyx
- regular fluorescence microscope without relying on specialized FLIM setup

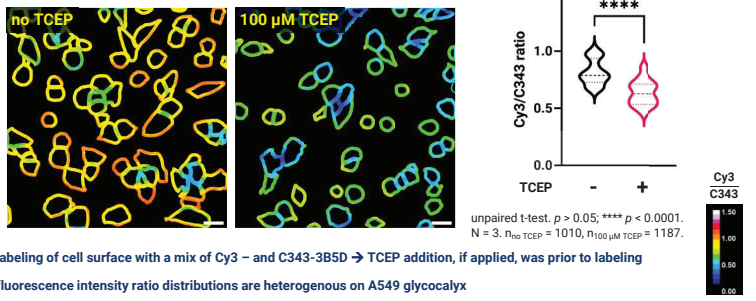

- labeling of cell surface with a mix of Cy3 – and C343-3B5D → TCEP addition, if applied, was prior to labeling
- fluorescence intensity ratio distributions are heterogenous on A549 glycocalyx
- upon treatment with 100 µM TCEP for 1h at 37°C ratios were reduced significantly

Fluorogenic cell surface glycan labelling with fluorescence molecular rotor dyes and nucleic acid stains [8]

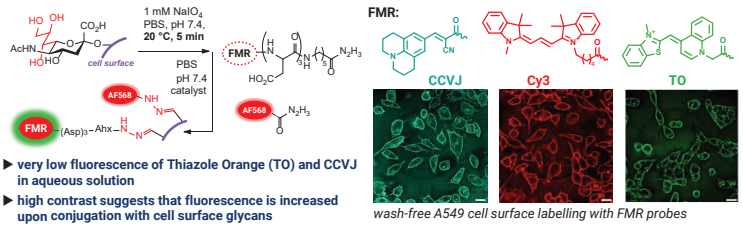

- very low fluorescence of Thiazole Orange (TO) and CCVJ in aqueous solution
- high contrast suggests that fluorescence is increased upon conjugation with cell surface glycans

wash-free A549 cell surface labelling with FMR probes

Mucin bound FMR-3D-Ahx-N_2H_3 sensitive to changes of viscosity/crowding

- successfully labeled porcine mucin in PBS with CCVJ – or TO-3D-Ahx-N_2H_3
- probes are sensitive to TCEP induced cross-linking changes and changes in viscosity

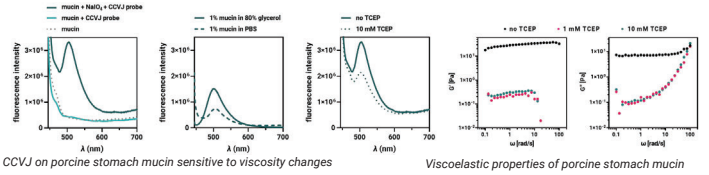

CCVJ on porcine stomach mucin sensitive to viscosity changes

Viscoelastic properties of porcine stomach mucin

Ratiometric imaging of A549 cells upon dual covalent labeling with FMR-probe and non-FMR

- heterogenous fluorescence intensity ratio distributions on A549 cell surface (also with HeLa and CEM cell surface, data not shown)
- CCVJ/AF568 fluorescence intensity ratio respond to TCEP treatment, and the same effect was observed with TO/AF568 fluorescence intensity ratio

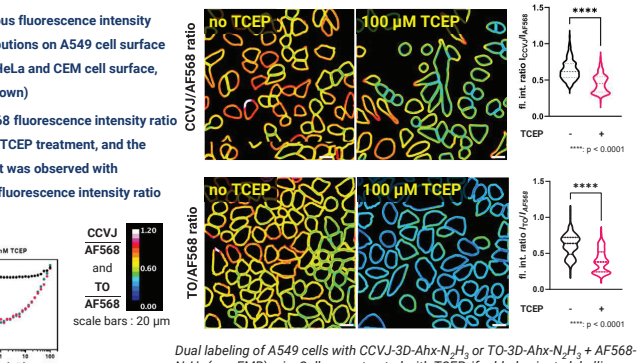

Dual labeling of A549 cells with CCVJ-3D-Ahx-N_2H_3 or TO-3D-Ahx-N_2H_3 + AF568-N_2H_3 (non-FMR) mix. Cells were treated with TCEP, if added, prior to labelling.

References

[1] G. Wulff, *Pure Appl. Chem.* **1982**, *54*, 2093-2102.
[2] M. Dowlut, D. G. Hall, *J. Am. Chem. Soc.* **2006**, *128*, 4226-4227.
[3] A. Pal, M. Bérubé, D. G. Hall, *Angew. Chem. Int. Ed. 2010*, 49, 1492-1495.
[4] X.-D. Xu, H. Cheng, W.-H. Chen, S.-X. Cheng, R.-X. Zhuo, X.-Z. Zhang, *Sci. Rep., 2013*, 3, 2679.
[5] K. A. Andersen, T. P. Smith, J. E. Lomax, R. T. Raines, *ACS Chem. Biol.* **2016**, 11, 319-323.
[6] S. C. Lee, J. Heo, H. C. Woo, J. A. Lee, Y. H. Seo, C. L. Lee, S. Kim, O. P. Kwon, *Chemistry* **2018**, 24, 13706-13718.
[7] M. A. Haidekker, E. A. Theodorakis, *Org. Biomol. Chem.* **2007**, 5, 1669-1678.
[8] A. Koçak, A. K. Homer, A. Feida, F. Telschow, J. L. Gorenflos López, C. Baydaroğlu, M. Gradzielski, C.P. R. Hackenberger, U. Alexiev, O. Seitz, *Chem. Commun.* **2024**, 60, 4785-4788.

Funded by the Deutsche Forschungsgemeinschaft (DFG, German Research Foundation) – Project ID 431232613 – SFB 1449.

Proceedings of the 37th European Peptide Symposium
Michal Lebl, Editor
European Peptide Society, 2024
http://doi.org/10.17952/37EPS.2024.P2247

Synthesis and application of β-amino γ-lactam (Bgl) residues

Charity D. Yongo-Luwawa[1] and William D. Lubell.[1]
[1]*Department of Chemistry, Université de Montréal. Montréal, H2V 0B3, Canada*

Introduction

α-Amino γ-lactam (Agl), so-called Freidinger-Veber lactam residues have garnered significant interest in the realm of peptide mimicry due to ability to introduce backbone constraint (Figure 1)[1,2]. In peptides, the Agl residue prefers the *i*+1 position of β-turn conformers and can thereby stabilize a bioactive conformation that is commonly found in natural peptides[1,2]. Compared to Agl residues, β-amino γ-lactam (Bgl) analogs have been less frequently explored in spite potential to favor turn geometry. For example, Bgl residues have been utilized in the study of growth hormone-releasing peptide-6 (GHRP-6, H-His-D-Trp-Ala-Trp-D-Phe-Lys-NH_2) to gain insight into a turn conformer about the Ala[3] residue[3]. Moreover, a Bgl scan of 101.10 (H-D-Arg-D-Tyr-D-Thr-D-Val-D-Glu-D-Leu-D-Ala-NH_2) illustrated the relevance of turn conformers for interleukin-1 receptor modulation[4]. Highlighting utility for stabilizing biologically active peptide conformers, such studies spur interest in synthetic methods for making Bgl residues. Previously, Bgl peptides have been synthesized using aspartate-derived cyclic sulfamidates as bis-electrophiles[4]. Towards an alternative method for Bgl peptide synthesis, commercially available (*S*)-(–)-β-hydroxy-γ-butyrolactone has now been employed as precursor.

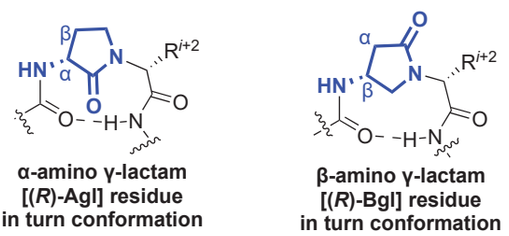

Figure 1. Agl and Bgl residues at i+1 position of β-turn conformations

Results and Discussion

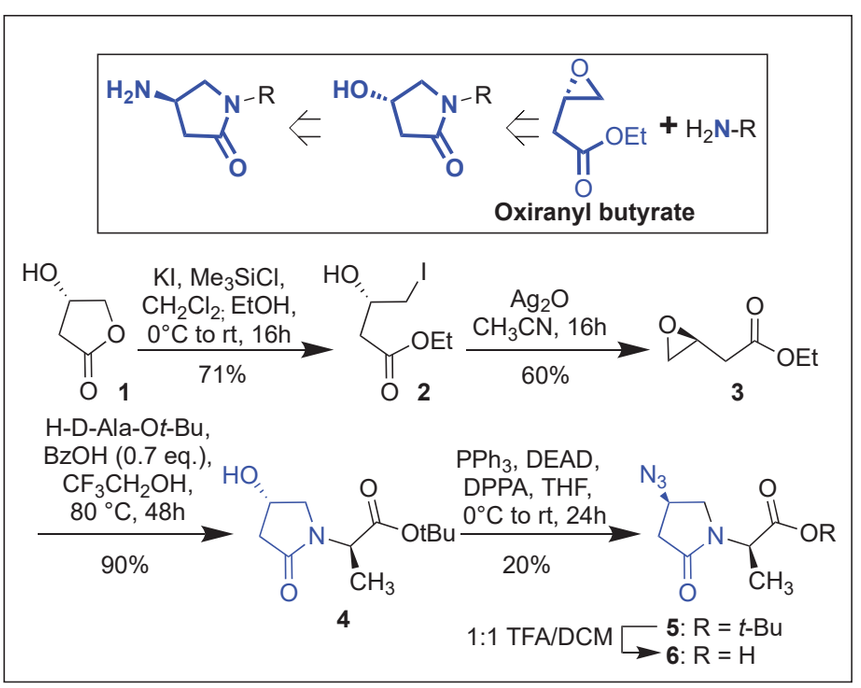

Figure 2. Conceptual and actual applications of oxiranyl butyrate in Bgl residue synthesis.

Proceedings of the 37th European Peptide Symposium
Michal Lebl, Editor
European Peptide Society, 2024 *http://doi.org/10.17952/37EPS.2024.P2247*

(*S*)-(–)-β-Hydroxy-γ-butyrolactone undergoes a ring-opening reaction in the presence of potassium iodide, trimethylsilyl chloride and ethanol to provide iodo ester **2** in 71% yield[5] (Figure 2). Oxiranyl butyrate **3** is prepared from iodo alcohol **2** on treatment with silver oxide in acetonitrile in 60% yield[5]. In proof-of-concept studies, oxiranyl butyrate **3** was employed as a bis-electrophile in the alkylation and acylation of D-alanine *tert*-butyl ester. Employing benzoic acid as catalyst in trifluoroethanol at 80°C for 48 h gave β-hydroxy lactam **4** in 90% yield[6]. An initial attempt to displace the alcohol by azide using diethyl azo dicarboxylate (DEAD), diphenyl phosphoryl azide (DPPA) and triphenyl phosphine in THF provided Bgl analog **5** (20% unoptimized), which after removal of the *tert*-butyl ester with trifluoroacetic acid in dichloromethane is suitable for incorporation into peptides. The scope of this approach is currently being developed with interest in expanding the synthesis of Bgl analogs in peptides including GHRP-6 and 101.10 to study further biological activities.

Acknowledgments

We thank the Canadian Institutes of Health Research (CIHR) for project PJT-190158, the Natural Sciences and Engineering Research Council of Canada (NSERC) for funding Discovery Research Project RGPIN-2019-04079, and the Fonds de Recherche du Québec - Nature et Technologie (FRQNT) for support of the Centre in Green Chemistry and Catalysis (CGCC, FRQNT-2020-RS4-265155-CCVC). The authors acknowledge the assistance of members of the Université de Montréal facilities: Dr. P. Aguiar (NMR spectroscopy) and Dr. A. Fürtös (mass spectrometry). CYL is grateful for a doctoral fellowship from the FRQNT.

References

1. Freidinger, R. M.; Veber, D. F.; Perlow, D. S.; Brooks, J. R.; Saperstein, R., Bioactive conformation of luteinizing hormone-releasing hormone: evidence from a conformationally constrained analog. *Science* **1980,** *210* (4470), 656-665.
2. St-Cyr, D. J.; García-Ramos, Y.; Doan, N. D.; Lubell, W. D., Aminolactam, N-Aminoimidazolone, and N-Aminoimdazolidinone Peptide Mimics. In Peptidomimetics I; Springer, 2017; pp 125−175.
3. Boutard, N.; Jamieson, A. G.; Ong, H.; Lubell, W. D., Structure–Activity Analysis of the Growth Hormone Secretagogue GHRP-6 by α- and β-Amino γ-Lactam Positional Scanning. *Chem. Biol. Drug Des.* **2010,** *75* (1), 40-50.
4. Jamieson, A. G.; Boutard, N.; Beauregard, K.; Bodas, M. S.; Ong, H.; Quiniou, C.; Chemtob, S.; Lubell, W. D., Positional Scanning for Peptide Secondary Structure by Systematic Solid-Phase Synthesis of Amino Lactam Peptides. *J. Am. Chem. Soc.* **2009,** *131* (22*),* 7917-7927.
5. Sunnapu, R.; Rajendar, G., A Concise Stereoselective Total Synthesis of Methoxyl Citreochlorols and Their Structural Revisions. *Eur. J. Org. Chem.* **2021,** *2021* (11), 1637-1642.
6. St-Cyr, D. J., Jamieson, A. G.; Lubell, W. D., α-Amino-β-hydroxy-γ-lactam for constraining peptide Ser and Thr residue conformation. *Org. Lett.* **2010**, *12* (8), 1652–1655.

Development of Cyclopropane-Based Foldamers Mimicking Protein Secondary Structures

https://doi.org/10.17952/37EPS.2024.P2250

Makoto Nagata, Nanase Ochiai, Akiko Yoshida, Satoshi Shuto, Mizuki Watanabe

Faculty of Pharmaceutical Sciences, Hokkaido University, Sapporo, Hokkaido 060–0812, Japan

E-mail (M.W.) mwatanab@pharm.hokudai.ac.jp

α-Helix & β-Strand : protein secondary structures

✓ forming hot spots of protein–protein interactions (PPI).

MDM2/p53 interaction

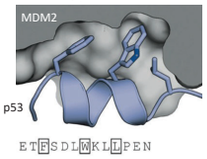

Grossmann, T. N. *et al. ACIE* **2015**, *54*, 8896.

Raf1/Rap1 interaction

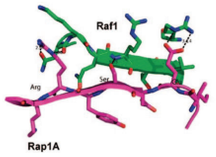

Hamilton, D. *et al. JACS* **2009**, *131*, 4566.

Foldamers : synthetic oligomers forming a specific secondary structure

✓ It can mimic the 3D structures and functions of natural α-peptides in proteins.
✓ It can be one of the candidates for PPI inhibitors.
✓ A great many helical peptide-based foldamers have been reported.

β-peptides

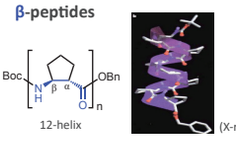

Gellman, S. H. *et al. Nature* **1997**, *387*, 381.

γ-peptides

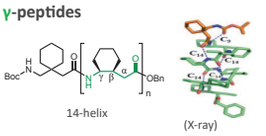

Gellman, S. H. *et al. ACIE* **2016**, *55*, 11096.

aromatic δ-peptides

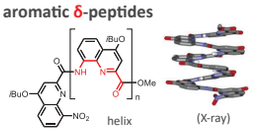

Huc, I. *et al. JACS* **2003**, *125*, 3448.

On the other hand, there are **few reports on aliphatic δ-peptide & β-strand-like foldamers.**

Structural properties of cyclopropane

Cyclopropane can control the molecular conformation.

✓ *Trans/cis* restriction



✓ Cyclopropylic strain



✓ Bisected conformation preference

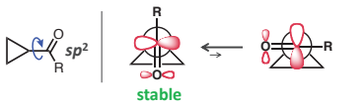

Shuto, S. *et al. Chem. Eur. J.* **2017**, *23*, 14394.

Design of helical δ-peptide foldamer

When adapting a 14-helix...

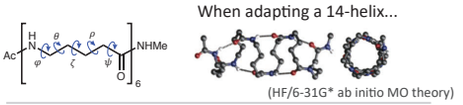

compounds	Torsion angles (°) φ	θ	ζ	ρ	ψ
14-helical unsubstituted linear δ-hexapeptide	106.5	–72.8	171.6	–76.9	113.7

Hofmann, H.-J. *et al. J. Org. Chem.* **2004**, *69*, 6214.

δ-Disubstituted cyclopropane δ-amino acid (Cp-δ-aa)

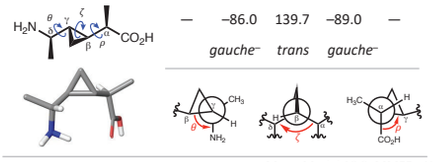

MacroModel 10.9, MMFFs; H_2O

Oligomer of Cp-δ-aa

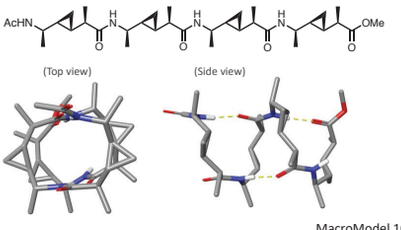

Predicted 3D structure

MacroModel 10.9 MMFF94s; H_2O

right-handed 14-helical structure

Structural analysis of Cp-δ-peptides

by X-ray diffraction of crystal

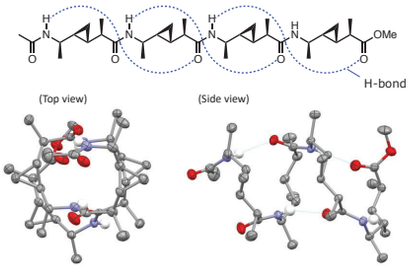

by 2D NMR spectra (CD_3OH, 600 MHz)

: Observed NOE correlations

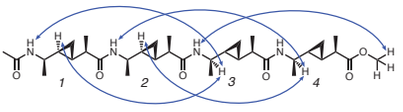

The lowest-energy 3D structure from the NMR-based calculations

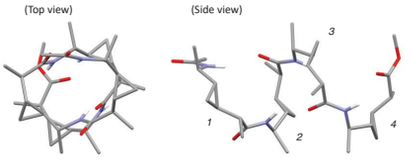

The Cp-δ-peptides were the 14-helices, as expected by the molecular design, in solution and crystal.

Watanabe, M.; Shuto, S. *et al. Org. Biomol. Chem.* **2023**, *21*, 970.

Design of β-strand-like foldamer

γ-Substituted cyclopropane γ-amino acid (Cp-γ-aa)

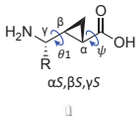

Predicted stable conformation

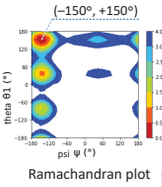

Ramachandran plot

DFT : B3LYP/6-31+G*

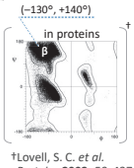

†Lovell, S. C. *et al. Proteins* **2003**, *50*, 437.

Oligomer : Alternate coupling of a pair of enantiomers of Cp-γ-aa

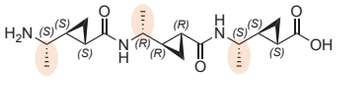



Predicted 3D structure

MacroModel 10.9 MMFF94s; H_2O

β-strand-like structure

with the oriented side chain to the same face, corresponding to the *i*, *i*+2, *i*+4 residues of β-strand

Structural analysis of Cp-γ-peptides

by Micro ED method

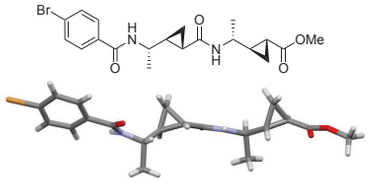

by 2D NMR spectra (DMSO-d_6, 800 MHz)

: Observed ROE or NOE correlations

2-mer : (TFA salt)

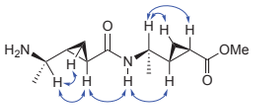

3-mer : (HCl salt)

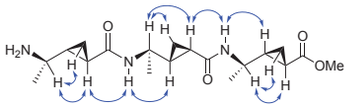

α/Cp-δ-mixed peptides as PPI inhibitors

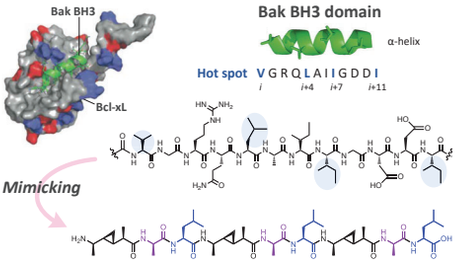

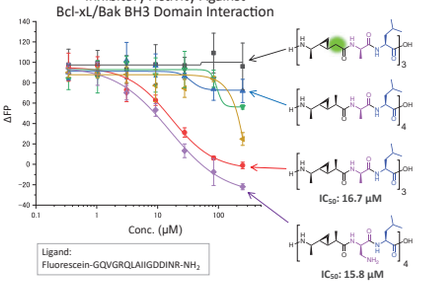

Acknowledgements

Special thanks to Prof. Koh Takeuchi (The Univ. of Tokyo) & Dr. Hiroyuki Kumeta (Hokkaido Univ.) for their help in conducting the NMR measurements

Special thanks to Ms. Marin Yokomine & Assoc. Prof. Jumpei Morimoto (The Univ. of Tokyo) for their help in conducting the inhibitory activity assay

Gq protein peptidomimetics as allosteric modulators of the ghrelin receptor

Morgane Mannes[1], Esaü Vangeloven[1], Charlotte Martin[1], Marjorie Damian[2], Sonia Cantel[2], Jean-Alain Fehrentz[2], Julie Kniazeff[2], Jean-Louis Banères[2*], Steven Ballet[1*]

[1]Research Group of Organic Chemistry, Vrije Universiteit Brussel, Pleinlaan 2, 1050 Brussels, Belgium.

[2]Institut des Biomolécules Max Mousseron IBMM, UMR-5247, Université de Montpellier, CNRS, ENSCM, Montpellier, France.

morgane.mannes@vub.be

https://doi.org/10.17952/37EPS.2024.P2253

INTRODUCTION

G protein-coupled receptors (GPCRs) represent an important family of membrane receptors that play a central role in modern medicine. Unfortunately, it is quite challenging to gain insights into the structure and functioning of GPCRs due to their **intrinsic dynamics** and **high instability** when extracted from the cell membrane.

In past years, **Nanobodies** (Nbs) were discovered to lock GPCRs in active signaling states and these have been recognized to be of extreme value in the search of specific orthosteric GPCR agonist ligands.[1] However, to overcome the limitations associated to Nbs, in terms of development costs for the discovery and purification, a set of **peptidomimetics** stabilizing the active state conformation of G protein-coupled receptors, was developed.[2,3] Herein, a peptide mimicry approach was used to **mimic the G protein**, an endogenous allosteric modulator of GPCRs, by synthesizing rigidified variants of the helical *C*-terminal Gα protein epitope (α_5 helix), which interacts with the GPCR.[4]

DESIGN OF G_s PROTEIN PEPTIDOMIMETICS

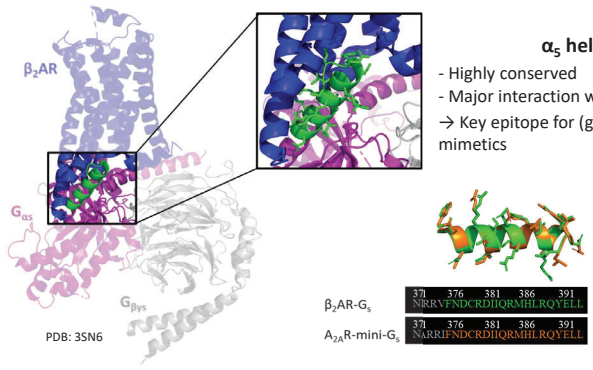

SYNTHESIS AND PHARMACOLOGICAL EVALUATION OF G_s PROTEIN PEPTIDOMIMETICS

***N*-terminus modification**
-> To improve solubility

***C*-terminus modification**
-> To improve affinity for receptor

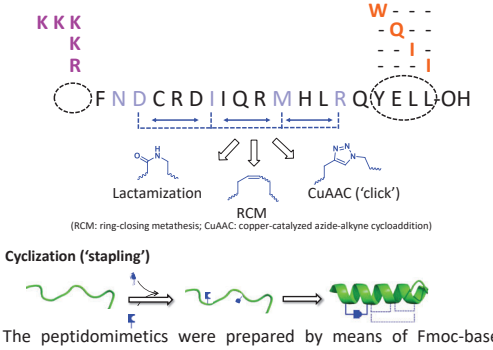

(RCM: ring-closing metathesis; CuAAC: copper-catalyzed azide-alkyne cycloaddition)

Cyclization ('stapling')

The peptidomimetics were prepared by means of Fmoc-based solid phase peptide synthesis (**SPPS**) and the α-helical conformation was stabilized using '**stapling**' strategies. Based on the X-ray crystal structure of the β_2AR in complex with the G_s protein, **point mutations** were introduced at the *C*-terminus.[5]

Radioligand displacement assay (RLA) on β_2AR

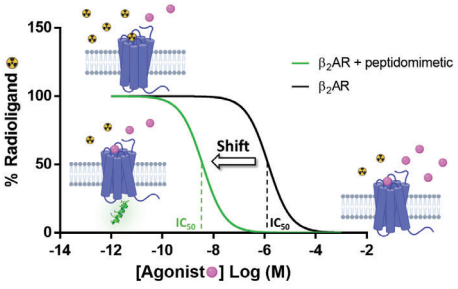

Optimization cycles of peptidomimetics were guided by radioligand binding assays, that quantify the stabilization of the receptor in active conformation.

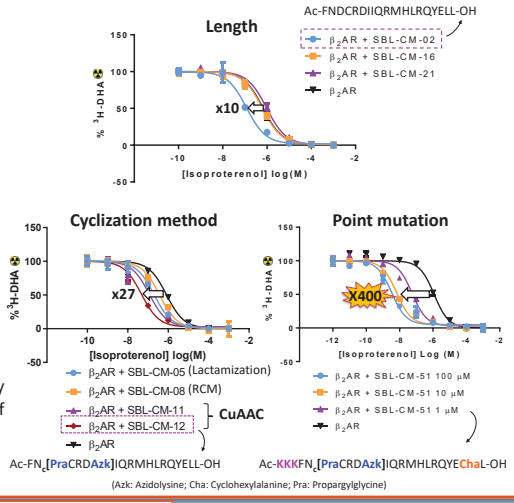

(Azk: Azidolysine; Cha: Cyclohexylalanine; Pra: Propargylglycine)

EXPLORE OTHER G PROTEIN FAMILIES

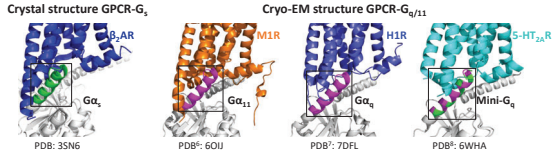

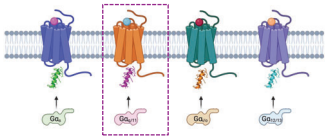

⇨ **Insert best modifications of G_s peptide into (mini-)$G_{q/11}$ peptides**[9,10]

SBL-CM-51 (G_s peptide)
Ac-KKKFNε[PraCRDAzk]IQRMHLRQYEChaL-OH

$G_{q/11}$	Mini-G_q
SBL-GQ-05 Ac-KKKFAε[PraVKDAzk]ILQLNLKEYNLV-OH	**SBL-GQ-11** Ac-KKKFNε[PraCKDAzk]ILQMNLREYNLV-OH
SBL-GQ-06 Ac-KKKFAε[PraVKDAzk]ILQNLKEYNChaV-OH	**SBL-GQ-12** Ac-KKKFNε[PraCKDAzk]ILQMNLREYNChaV-OH

CONCLUSIONS

Proof-of-concept: G_s peptidomimetics

- Stabilize active state of GPCR
- Generic toolset for G_s-coupled receptors
- ✓ Validation on Dopamine 1 receptor (D1R)
- Identification of agonist-like fragments by fragment-based screening

⇨ **Same methodology used to develop G_q peptidomimetics**

PERSPECTIVES

- Explore other G protein epitopes ($G_{i/o}$, $G_{12/13}$)
  -> Drug discovery
  -> Further unveil GPCR:G protein coupling
- Investigate cell permeability of the G protein peptidomimetics

PHARMACOLOGICAL EVALUATION OF G_q PEPTIDOMIMETICS

Bimane fluorescence assay

⇨ Detect conformational changes associated with receptor activation

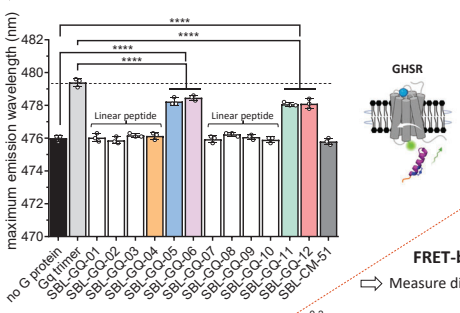

- Increase in maximum emission wavelength with stapled G_q peptides
- No change with linear G_q peptides

-> Staple required to affect receptor conformation

BODIPY-GTPγS assay

⇨ Investigate competition with G_q protein (measure GTP uptake)

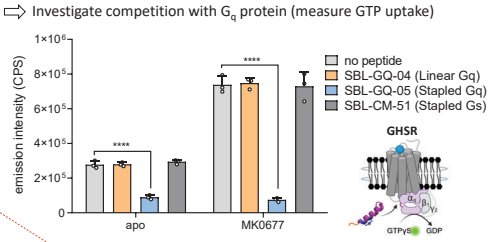

Receptor activation: GDP-to-GTP exchange

- SBL-GQ-05 compete with receptor-catalyzed G protein activation
  - Linear G_q peptide and stapled G_s peptide do not affect GTPγS binding

-> Specificity of the constrained *C*-terminal helix of Gα$_q$

FRET-based assay

⇨ Measure direct binding to receptor

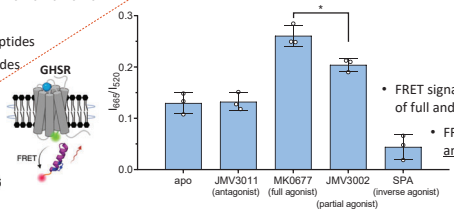

- FRET signal increased in presence of full and partial agonist
  - FRET signal not affected by neutral antagonist
  - FRET signal completely abolished in presence of inverse agonist

REFERENCES

1. Rasmussen, S. G. *et al. Nature* **2011**, *469*, 175.
2. Mannes, M. *et al. Angew. Chem. Int. Ed.* **2021**, *60*, 10247.
3. Mannes, M. *et al.* International Patent Application No. PCT/EP2021/086733.
4. Mannes, M. *et al. Trends Pharmacol. Sci.* **2022**, *43*, 406.
5. Rasmussen, S. G. *et al. Nature* **2011**, *477*, 549.
6. Maeda, S. *et al. Science* **2019**, *364*, 552.
7. Xia, R. *et al. Nat. Commun.* **2021**, *12*, 1.
8. Kim, K. *et al. Cell* **2020**, *182*, 1574.
9. Mannes, M. *et al.* European Patent Application No. 22180492, **2022**
10. Mannes, M. *et al. Science Signaling* (Under revision)

ACKNOWLEDGEMENT

innoviris.brussels empowering research · cnrs · Fondation Recherche Médicale · fwo · anr · VUB · confo

https://doi.org/10.17952/37EPS.2024.P2255

A reductive amination approach for the synthesis of catalytic peptide foldamers

M. Pollastrini[1,2] and A. Moretto[1]

1. University of Padova, Department of Chemical Sciences, 35131 – Padova
2. CNR, Institute of Biomolecular Chemistry, 35131 – Padova

I look a lot like...

Intro

Enzymatic catalysis often depends on the proper spatial organization of two or more reactive groups within an active site.

Foldamers are synthetic, conformationally defined mimics of proteins and other biopolymers. The exploration of new moieties and new geometries for sets of reactive side chains is enabled by the modular nature of foldamers at the covalent level.

We report a reductive amination approach as a general synthetic strategy for the assembly of helical catalytic peptide foldamers.

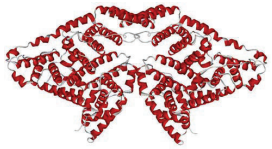

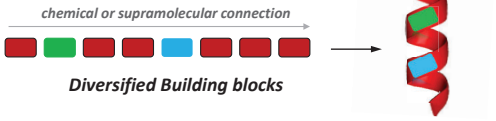

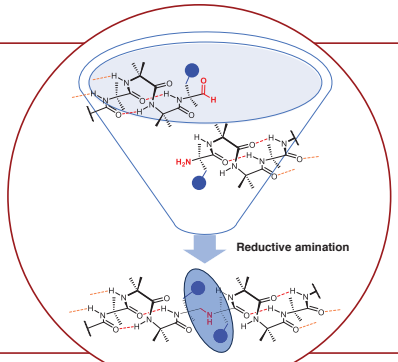

Secondary amine backbone modification

As a preliminary step, we explored the reductive amination reaction and conformational effects of the Ψ[CH_2NH] backbone modification in a model compound.

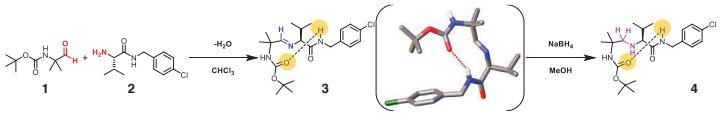

- first crystallographic characterization of an imino surrogate for a peptide bond between two amino acids;
- β-turn conformation stabilized by an intramolecular N-H···O=C hydrogen bond;
- reduction of the imino group allows the formation of the Ψ[CH_2NH] moiety.

To explore the effect of the introduction of the secondary amine backbone modification in structured peptides, surrogate foldamers Boc-(L-Ala-Aib)$_n$Ψ[CH_2NH]-(L-Ala-Aib)$_n$-OMe were synthesized.

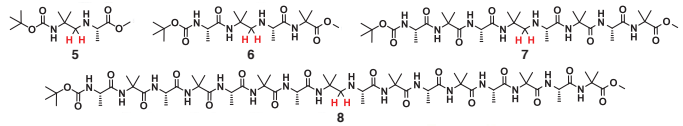

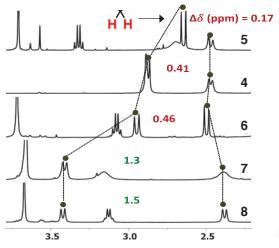

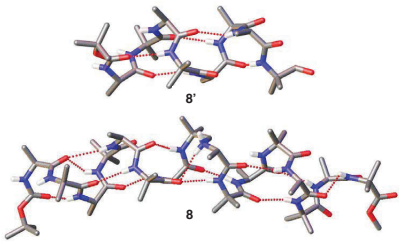

Helical foldamers with tri-dimensional catalytic centres

A set of helical peptide foldamers was synthesized with different reactive side chains in proximity of the newly-formed secondary amine for the creation of catalytic diads and triads.

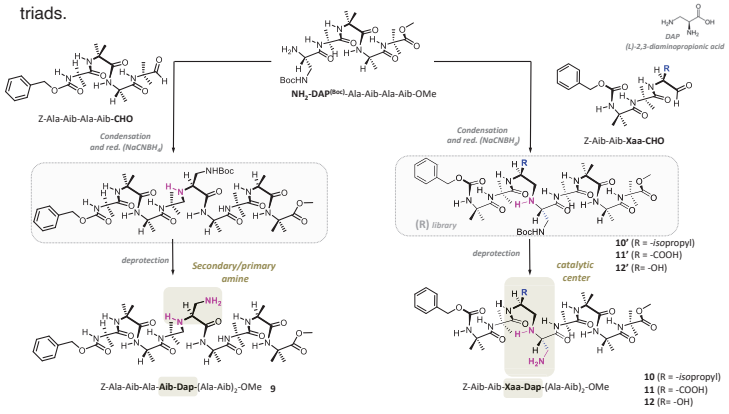

We tested the catalytic performance of these foldamers to efficiently template C-C bond formation through imine/enamine type catalysis

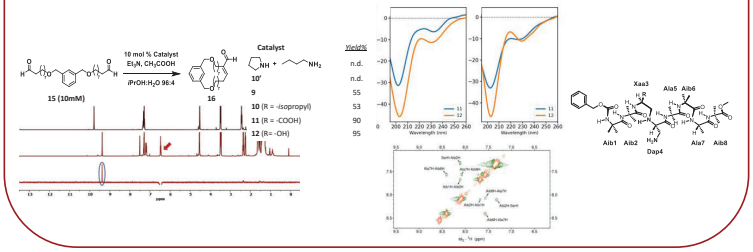

Synthesis and screening of screw-sense preferences of helical foldamers

We applied the reductive amination approach for the functionalization of the N-termini of Aib oligomers synthesized by ROP of his NCA.

Firstly, we studied polymerization conditions and chromatographic methods.

Now, we are trying to develop catalysts for stereoselective enamine catalysis, where the N-terminal reactive site could be influenced by chiral residues located at the C terminus.

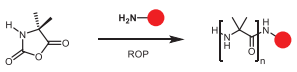

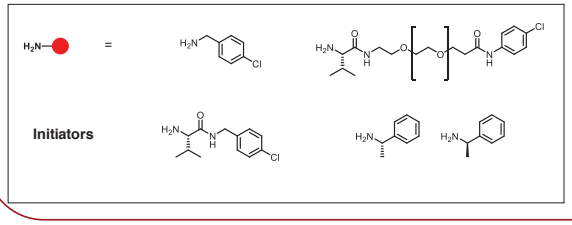

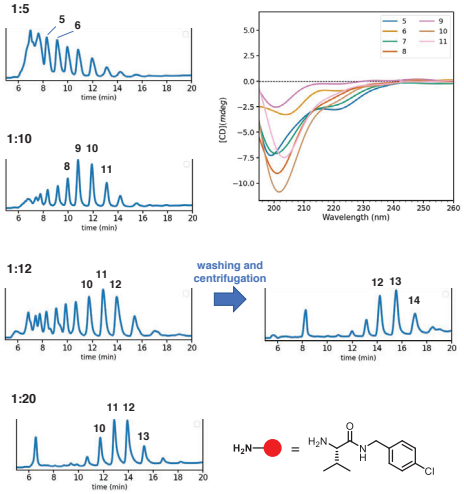

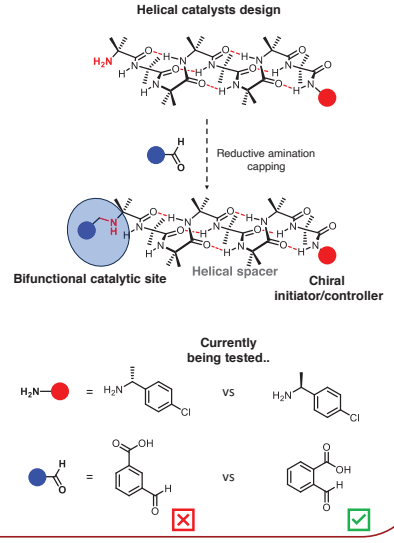

1) Z. C. Girvin and S. H. Gellman, J. Am. Chem. Soc. **2020**, 142, 17211

2) Z. C. Girvin and S. H. Gellman *J. Am. Chem. Soc.* **2018** *140*, 12476

3) M. Pollastrini, G. Marafon, J. Clayden, A. Moretto Chem. Commun. **2021**, 57, 2269

https://doi.org/10.17952/37EPS.2024.P2257

DARPin-based Pretargeting: Zeroing in on Cancer

PNA-guided delivery of ^{177}Lu enhances tumor uptake and spares vital organs in HER2+ xenograft mice

Westerlund K[1]., Oroujeni M[2]., Van Deventer A[1]., Wang Z[2]., Clinton J[1]., Zelepukin I[2]., Papalanis E[2]., Liu Y[2]., Orlova A[2]., Tolmachev V[2]. and Eriksson Karlström A[1].

1. Department of Protein Science, KTH Royal Institute of Technology, Stockholm, Sweden
2. Department of Immunology, Uppsala University, Uppsala, Sweden

Presenting author: Kristina Westerlund, PhD
krw@kth.se

Pretargeting: A Two-Step Approach to Radiotherapy

Challenge:
Conventional targeted radiotherapy often results in unwanted radiation exposure to healthy tissues.

Our solution:
Two-Step DARPin-Based Pretargeting

Aim:
Improve tumor-targeting while mimizing off-target effects in mice with HER2-expressing xenografts

Key Benefits:
- Enhanced tumor specificity
- Reduced radiation to healthy tissues
- Potential for improved therapeutic window

Step1: Primary agent G3-HP1
- Non-radioactive DARPin-PNA conjugate
- Binds specifically to HER2-expressing tumors
- Carries HP1: a 15-mer PNA-based recognition sequence
- Is allowed to clear from bloodstream

Step 2: Secondary probe ^{177}Lu-HP2
- Radiolabeled with Lutetium-177 for therapy and imaging
- Administred after optimized interval
- Either:
  - Binds specifically to primary agent at tumor site via complementary PNA-sequence, or
  - Rapidly clears through the kidneys

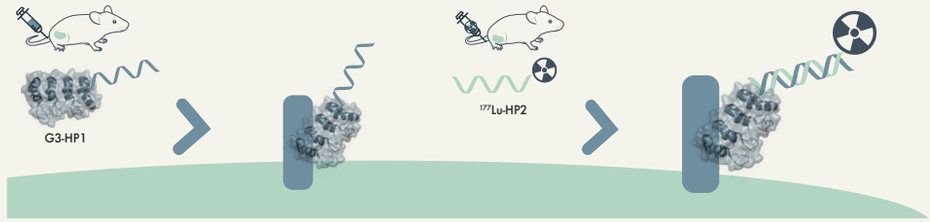

Two-Step DARPin-based PNA-guided Pretargeting

Results and Discussion

1. PRODUCTION OF PRETARGETING PROBES

Primary agent:

I a) Expression in *E. coli*. b) IMAC purification
II Automated solid-phase synthesis (SPS)
III a) Sortase A mediated ligation b) IMAC and RP-HPLC purification

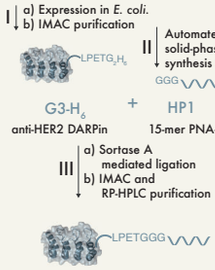

G3-H$_6$ anti-HER2 DARPin + HP1 15-mer PNA-probe

G3-HP1 (22 kDa)
DARPin-PNA conjugate

Secondary probe:

a) Automated SPS b)RP-HPLC purification

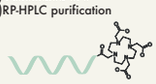

HP2 (5.2 kDa)
Complementary 15-mer PNA-probe, carrying a DOTA-chelator for radiometal-labeling

G3-HP1 and HP2 are both:
>95% pure
after final purification

2. AFFINITY DETERMINATION USING SURFACE PLASMON RESONANCE (SPR)

A

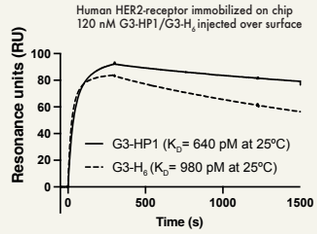

B

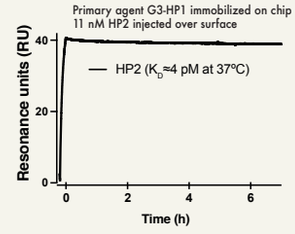

The DARPin-PNA primary agent, G3-HP1, is capable of high affinity binding in vitro to both:
- human HER2 receptor (K_D=640 pM), and
- secondary probe HP2 (K_D≈4 pM at 37°C)

3. BIODISTRIBUTION STUDIES IN BALB/c-nu IMMUNODEFICIENT MICE

Pretargeting specificity:
4h p.i.

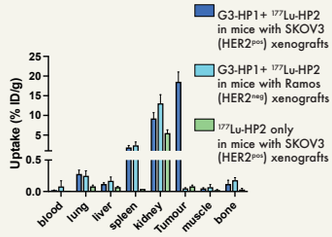

Factors Influencing ^{177}Lu-HP2 Tumor Uptake:
- preinjection of G3-HP1 (PNA-mediated)
- HER2 expression level (HER2-specific)

Influence of pretargeting:
Pretargeting vs. direct DARPin-based tumor-targeting, 4h p.i.

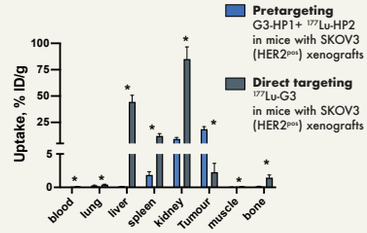

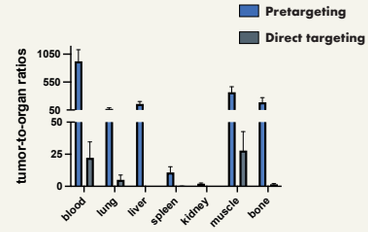

Impact of DARPin-Based and PNA-Guided Delivery of ^{177}Lu-HP2:
- ▲ Tumor: 8-fold higher uptake
- ▼ Kidney: 9-fold lower uptake
- ▼ Liver: 370-fold lower uptake
- ▼ Spleen: 7-fold lower uptake

Key Conclusions:
- Our two-step approch achieves an 8-fold increase in tumor uptake of ^{177}Lu
- Off-target accumulation is markedly reduced, with up to 370-fold decrease in liver uptake
- Results suggest potential for improved efficacy and reduced toxicity in treatment of HER2-positive cancers

Future Implications:
This pretargeting method may pave the way for more effective and safer targeted radionuclide therapies, improving treatment options for HER2-positive cancers.

Rational design of novel peptidomimetics against influenza a virus: biological and computational studies

Scala, M. C.;[a] Agamennone, M.;[b] Marchetti, M;[c] Superti, F.;[c] Campiglia, P.[a] and Sala, M.[a]

[a] Department of Pharmacy, University of Salerno, Fisciano, SA, Italy;
[b] Department of Pharmacy, University of Chieti "G. d'Annunzio", Via dei Vestini 31, Chieti, Italy;
[c]Department of Technology and Health, National Institute of Health, Viale Regina Elena 299, Rome, Italy.

https://doi.org/10.17952/37EPS.2024.P2258

INTRODUCTION

Influenza is a highly contagious, acute respiratory illness, which represents one of the main plagues worldwide. Even though some antiviral drugs are available, the alarming increase of virus strains resistant to them, highlights the need to find new antiviral compounds.[1]

Pep.	Sequence	IC_{50} (nM) A/Parma/24/09 H1N1
1	SLDC	6 ± 1.23
2	SKHS	1.5 ± 0.71

Table 1. HI activity of peptides **1**-**2**.

Previously, Superti et al. have deeper investigated the mechanism of the anti-influenza virus effect of bovine Lactoferrin (bLf) and the role of its tryptic fragments (the N and C-lobes) in the antiviral activity.[2] In particular, they evaluated the influence of bLf on hemagglutinin-mediated functions. Recently, through a truncation library, we identified the tetrapeptides, SKHS (**1**) and SLDC (**2**), derived from Blf C-lobe fragment 418-429, which were able to bind hemagglutinin (HA) and inhibit cell infection in a concentration range of femto- to picomolar (*table 1, 2*).[3]

Pep.	A/Parma/24/09 H1N1 EC_{50} (pM)	SI
1	4.6±0.05	>5.4.10^6
2	0.048±0.0012	>5.2.10^8

Table 2. I*n vitro* antiviral activity against influenza virus infection of peptides **1**-**2**.

DESIGN

It is well known that the direct application of peptides as medicinal entities has some severe limitations, including high degradation by proteolytic enzymes and poor cell mem-brane permeability. We designed new peptidomimetics starting from tetrapeptide sequences SLDC (**1**) and SKHS (**2**). To increase metabolic stability and improve bioavailability, receptor affinity, and selectivity to overcome these drawbacks. Two different strategies were used to reduce the conformational freedom of the peptide backbone and increase the affinity towards the target: N-methylation and synthesis of peptoids.[4,5] Then, we carried out binding affinity measurements by microscale thermophoresis (MST) and hemagglutination inhibition assay on peptide synthesized.

CHEMISTRY

Peptides synthesis was performed according to the solid phase approach. The crude peptides were purified by preparative RP-HPLC and purity monitored by analytical HPLC. Molecular weights were confirmed by ESI-MS.

Synthesis of N-Methyl peptides

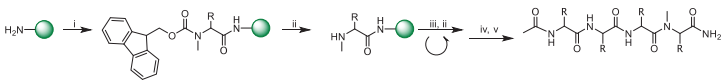

Scheme 1. General synthesis of N-methylated peptide. Reagent and conditions: (i) Fmoc-N-Me-aa(PG)-OH (3 eq.), OxymaPure (3 eq.), DIC (6 eq.), 5 min, MW 75 °C; (ii) piperidine/DMF (2:8, v/v), 1 min, MW 90 °C; (iii) Fmoc-L-aa(PG)-OH (3 eq.), OxymaPure (3 eq.), DIC (6 eq.), 2 min, MW 90 °C; (iv) Ac_2O/DCM (1:3, v/v) 2 min, MW 65 °C; (v) TFA/TIS/H_2O (95:2.5:2.5 v/v).

Synthesis of peptoids

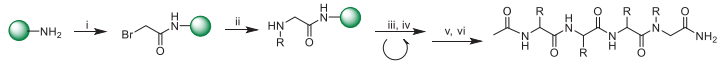

Scheme 2. General synthesis of peptoids. Reagent and conditions: (i) bromoacetic acid/DMF (2M) and DIC (2.4 M), 5 min, MW 75 °C; (ii) R-NH_2/DMF (1M), 5 min, MW 75 °C; (iii) Fmoc-L-aa(PG)-OH (3 eq.), OxymaPure (3 eq.), DIC (6 eq.), 2 min, MW 90 °C; (iv) piperidine/DMF (2:8, v/v) 1 min, MW 90 °C; (v) Ac_2O/DCM (1:3, v/v) 2 min, MW 65 °C; (vi) TFA/TIS/H_2O (95:2.5:2.5 v/v).

RESULTS and DISCUSSION

We decided to investigate the direct binding of peptides **1**, **2**, and the peptidomimetics library to HA protein by two complementary techniques: microscale thermophoresis and surface plasmon resonance.

MicroScale Thermophoresis analysis

The 16 compounds were subjected to MST screening and the results are shown in Table 3. According to analysis, every peptide interacts with HA with different dissociation constants. Compounds **4**, **9**, **16**, and **18** bind HA more effectively than compounds **1** and **2**, showing an equilibrium dissociation constant (K_D) value in a two-digits nanomolar concentration range (figure 1).

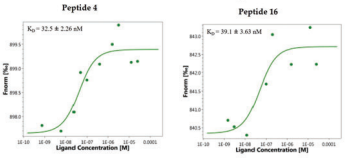

Figure 1. MST binding curve of peptides **4** and **16** to HA.

Pep.	Sequence	MST K_D (μM)	SPR K_D (μM)
1	SLDC	10.4 ± 0.23	7.12 ± 0.26
2	SKHS	7.26 ± 0.06	4.53±0.08
3	(N-Me)SLDC	24.8±0.71	7.60±2.69
4	S(N-Me)LDC	0.0325±0.002	0.58±0.34
5	SL(N-Me)DC	8.8±0.23	NPD
6	SLD(N-Me)C	0.142±0.03	3.80±1.06
7	(N-Me)SKHS	0.336±0.02	4.19±0.86
8	S(N-Me)KHS	7.93±0.73	8.33± 1.73
9	SK(N-Me)HS	0.0528±0.005	1.26±0.36
10	SKH(N-Me)S	3.04±0.85	NPD
11	ΛhSLDC	0.0672±0.002	6.55±1.52
12	SΛLDC	0.701±0.03	3.81±2.13
13	SLΛDC	1.34±0.02	NPD
14	SLDΛhC	0.0459±0.01	NPD
15	ΛhSKHS	7.4±0.35	2.09±2.41
16	SΛKHS	0.0391±0.003	1.70±0.13
17	SKΛHS	3.07±0.79	NPD
18	SKHΛhS	0.0491±0.001	0.43±0.21

Table 3. Sequence and binding affinities between HA and peptides **1**-**18** determined using MST and SPR.

SPR-based binding assays

The affinity of peptidomimetics for HA was determined by SPR. SPR study revealed that synthesized peptides effectively interact with the immobilized protein. The sensorgrams of the compounds **4** and **18** bound to HA in HBS-P buffer are shown in Figure 2. Interestingly, these peptidomimetics bind HA with higher efficiency with respect to **1** and **2**, showing a K_D value in a three-digits nanomolar concentration range.

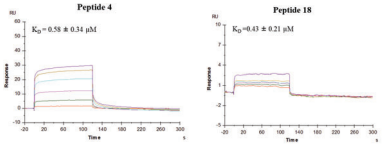

Figure 2. Sensorgram of compound **4** and **18**. Each compound was injected at four different concentrations (from 1 μM to 20 μM).

Hemagglutination assay

The capability of compounds **4**, **9**, **16**, and **18** to inhibit the hemagglutinating activity was evaluated by HI. The inhibitory activity of peptides **1** and **2** is shown as a reference. The oseltamivir-resistant A/Parma/24/09 H1N1 virus strain was used. As shown in Table 4, compounds **4** and **16** prevented the hemagglutination of the oseltamivir-resistant strain A/Parma/24/09 H1N1 at quite similar concentrations than the reference peptides.

Pep.	Sequence	IC_{50} (nM) A/Parma/24/09 H1N1
1	SLDC	6 ± 3
2	SKHS	1.5 ± 0.7
4	S(N-Me)LDC	4.6 ± 2.3
9	SK(N-Me)HS	3.2 ± 1.6
16	SΛKHS	1.2 ± 0.6
18	SKHΛhS	3.3 ±1.7

Table 4. Sequence and HI activity of peptides **1**. **2**. **4**. **9**. **16**. **18**.

Neutralization assay

Next, we evaluated the ability of the four compounds to inhibit viral infection by neu-tralization assay. All compounds were able to prevent viral infection in a dose range of roughly 50 to 140 pM, corresponding to selectivity indices ≈ 10^3/10^5. In particular, com-pound 4 inhibited the virus replication at a concentration similar to that of the reference peptide (Table 5).

Pep.	Sequence	EC_{50} (μM)	SI
1	SLDC	4.6 ± 0.05 × 10^{-6}	>5.4 × 10^6
2	SKHS	4.8 ± 0.12 × 10^{-8}	>5.2 × 10^8
4	S(N-Me)LDC	8.5 ± 0.04 × 10^{-5}	>2.9 × 10^5
9	SK(N-Me)HS	1.425 ± 0.02 × 10^{-4}	>1.78 × 10^3
16	SΛKHS	4.7 ± 0.02 × 10^{-4}	>5.3 × 10^4
18	SKHΛhS	5 ± 0.04 × 10^{-5}	>5 × 10^5

Table 5. Sequence and Nt activity of peptides and peptoids.

Computational study

To get more clues on the tetrapeptide interaction with studied HAs, a structure-based computational analysis was carried out. Compound **4** is the derivative of SLDC where the Leu2 NH is methylated. Its docked interactions are driven by the hydrophobic contact of the Leu2 side chain in the most lipophilic region of the RBS. To satisfy this contact, the ligand inverts its binding mode with respect to the hit SLDC.

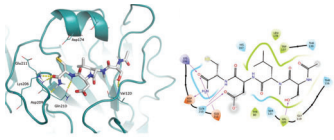

Figure 3. Docked poses of N-methyl peptide **4** represented as sticks (light orange and white C atoms, respectively) in the RBS of A/Parma/24/09 H1N1 (deep-cyan cartoon).

CONCLUSION

In this paper, we synthesized a library of peptidomimetics, N-methyl peptides and peptoids, starting from the most promising tetrapeptides previously identified.[3] Direct binding assays were carried out by two biophysical techniques (MST and SPR). Both demonstrated specific binding between compounds **4**, **9**, **16**, and **18** and HA. Therefore, the antiviral activity of these compounds was assessed through biological assays, such as HI and NT. Results from hemagglutination inhibition assay confirmed the specific interaction with HA. The neutralization test showed that S(N-Me)LDC (**4**) and SKHΛhS (**18**) are the most active derivatives. Computational analysis allowed us to envision the putative interactions of these ligands with HA, where they establish conserved interactions with residues of the RBS as already observed for peptides **1** and **2**.[3]
All applied methods agreed upon the identification of N-methyl peptide, S(N-Me)LDC, able to bind hemaggluˈtinin with high affinity and inhibit Influenza virus hemagglutination and cell infection at nano- and picomolar concentration, respectively. This small sequence can represent a valuable starting point for the design of small molecules.[6]

References

1. Hale, B. G. et al. (2010) *Future Microbiol.*, **5**, 23-41.
2. Ammendolia, M. G. et al. (2012) *Pathog. Glob. Health.*, **106**, 12-19.
3. Scala, M.C. et al. (2017) *Sci Rep.*, **7**, 10593.
4. Zuckermann, R.N. et al. (1992) *J. Am. Chem. Soc.*, **114**, 10646-10647.
5. Rajeswaran, W.G., et al. (2001) *J. Med. Chem.*, **44**, 1305–1311.
6. Scala, M. C., et al. (2023) *Int J Mol Sci.*, **24**(18), 14268.

mscala@unisa.it

Development of peptide nucleic acids-based molecules targeting non-canonical nucleic acids structures

Matilde Rossi[a,b,c], Paola Gratteri[c], Anna Maria Papini[a,b] and Carla Bazzicalupi[a]

[a] *Department of Chemistry "Ugo Schiff", University of Florence, Via della Lastruccia 3, 50019 Sesto F.no (IT)*
[b] *Interdepartmental Research Unit of Peptide and Protein Chemistry and Biology, University of Florence, 50019 Sesto Fiorentino (IT)*
[c] *Department of NeuroFarBa, Via Ugo Schiff 6, 50019 Sesto Fiorentino (IT)*
matilde.rossi@unifi.it

37th EPS European Peptide Symposium — 14th IPS International Peptide Symposium — Florence, Italy — 25 - 29 August 2024

https://doi.org/10.17952/37EPS.2024.P2259

Introduction

Peptide nucleic acids

- Nucleobases linked to an **achiral**, **uncharged**, **flexible** polyamide backbone (generally N-2-aminoethylglycine units) through methylene carboxylic linkers.
- High **affinity** towards nucleic acids sequences.
- High PNA-nucleic acids **complex stability**.
- **Watson-Crick** and **Hoogsteen** base pairing.
- **Stability** towards nucleases and proteases.[1]

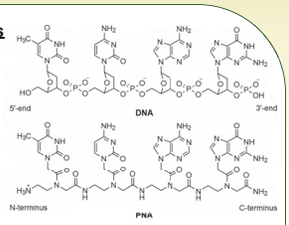

G-quadruplex (G4)

- Non-canonical nucleic acids structures abundant in guanine-rich sequences.
- Stacked guanine-based tetrads stabilized by Hoogsteen-hydrogen bonds.
- G-tracts arranged in different topologies: parallel, anti-parallel, hybrid.
- Abundant in proto-oncogenic promoters and in telomeric sequences, being deeply correlated with crucial cellular processes.
- Telomeric G4-stabilizing ligands are candidates for cancer therapy, despite challenges in **selectivity** and **specificity**.[2,3]

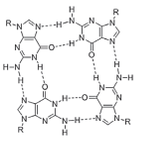

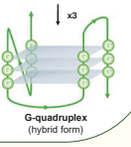

Synergize the base-pairing selectivity of PNA molecules with the capability of G4-ligands to stabilize G4 structures

Need for structural information about G4 PNA-DNA adducts

Design and synthesis

Design:

DNA Tel23 sequence:	5'- **TAGGGTTAGGGTTAGGGTTAGGG** -3'	**Homologous PNAs** able to form stable PNA-DNA G4 adducts.[4]
PNA1 sequence:	H- **TTAGGGTTAGGG** -NH_2	
PNA2 sequence:	H- **TAGGGTTAGGGT** -NH_2	
PNA3 sequence:	H- **GGGTTAGGGT** -Lys-Lys-NH_2	

DNA Tel23 sequence:	5'- **TAGGGTTAGGGTTAGGGTTAGGG** -3'	**Hybrid PNA** hybrid complex by forming both a double helix and a G-quadruplex
PNA4 sequence:	H_2N-Lys-**ATCCCAATGGG** –H	

Solid Phase Synthesis

Fmoc/t-Bu orthogonal protection strategy

PNA1, PNA2

- Resin: TentaGel® S RAM (0.23 mmol/g)
- Deprotection: 20% piperidine in DMF 5'+10'
- PNA monomers coupling: PNA monomer (4 eq), PyOxim (4 eq), DIPEA (8 eq) for 30' at room temperature. Double coupling for 1st, 10th, 11th, 12th residues.
- Capping: after each coupling step, 10% Ac_2O in DMF

PNA3, PNA4

- Resin: TentaGel® R RAM (0.20 mmol/g)
- Deprotection: 20% piperidine in DMF 5'+10'
- Lys-coupling: Lys (5 eq), HBTU (5 eq), DIPEA (10 eq) for 30' at room temperature.
- PNA monomers coupling: PNA monomer (6 eq), PyOxim (6 eq), DIPEA (12 eq) for 40 min at room temperature.

Conformational and stability studies

Circular dichroism analysis

Samples with 4.7 μM DNA in the absence and presence of PNA were prepared to per form CD analyses at 20°C. Spectra were recorded in 80 mM KH_2PO_4 (pH 7.0). PNA1 and PNA2 were solubilized in DMSO (20 mM PNA).

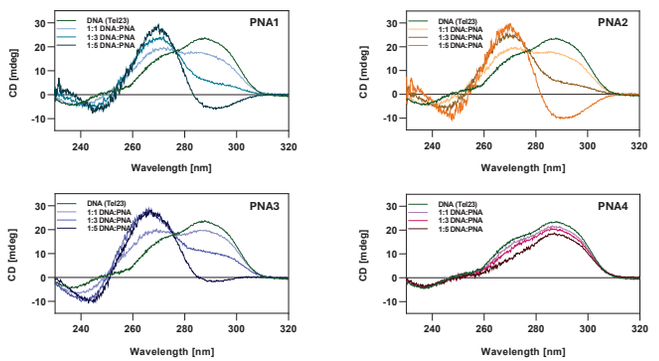

DNA Tel23 → Hybrid G-quadruplex shape

PNA1, PNA2, PNA3 → 1:5 DNA:PNA parallel G-quadruplex shape

PNA4 → The decrease in signal around 270 nm, coupled with the absence of a minimum at 260 nm, might suggest the presence of an antiparallel G-quadruplex whose signal is overlapping with a duplex structure signal.

Melting temperatures

were determined using circular dichroism spectroscopy. Temperature gradient of 1°C from 20°C to 90°C. Heating rate of 0.2 °C/min, data pitch of 0.1 nm. For PNA1, PNA2, and PNA3, CD spectra were recorded from 266 nm to 266.5 nm, for DNA and PNA4 measurements were taken between 290 nm and 289.5 nm. DNA:PNA 1:5.

	T_m (°C)	ΔT_m (°C)
DNA	63.9 ± 0.1	-
PNA1	71.7 ± 0.2	+7,8
PNA2	70.7 ± 0.3	+6.8
PNA3	68.8 ± 0.2	+4,9
PNA4	65.5 ± 0.1	+1,6

CD analysis and melting temperatures suggest an interaction between DNA and PNAs that determines in all cases a conformational change of the Tel23 G-quadruplex and an increase in stability.

In silico studies

In silico studies (Maestro - Schroedinger suite) for the DNA-PNA complexes

Construction

- Templates used for the homologous complexes:
  - Bimolecular parallel-stranded human telomeric quadruplex in complex (PDB: 3CE5)
  - PNA template: gamma-methylated PNA duplex (PDB: 2KVJ)
- Complex Features:
  Two bimolecular parallel-stranded DNA-PNA antiparallel G-quadruplexes (assuming the same topology that characterized the 3CE5 complex for all the G4s and the PNA N-terminus, aligns with DNA 5' -terminus)

- Templates used for the Hybrid complex:
  - Biomolecular telomeric G4 structure: (3+1) assembly of three human telomeric DNA repeats into an asymmetrical dimeric G-quadruplex (PDB: 2AQY)
  - PNA template: gamma-methylated PNA duplex (PDB: 2KVJ)
  - DNA duplex template: CK14 DNA duplex (PDB: 1K8J)
- Complex Features:
  DNA-PNA double helix + (3+1) DNA-PNA antiparallel G-quadruplex (assuming the same topology that characterized the 2AQY complex and the PNA N-terminus, aligns with DNA 3' -terminus)

Molecular dynamics (MD) study:

Force Field: OPLS4
Time 100ns
Essemble class: NPT
Temperature: 300K
Pressure : 1.01325 bar

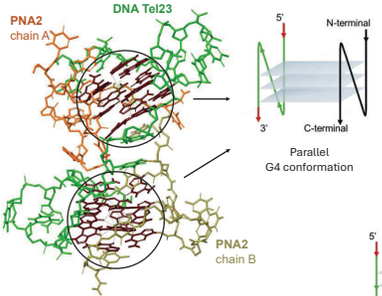

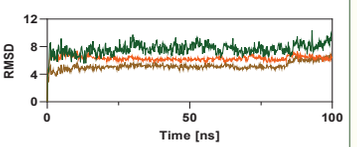

RMSD analysis of **PNA2** (orange, chain A, and ochre, chain B) and DNA (green) relative to the initial frame of the MD simulation. PNA RMSD fluctuates around 6.31 Å (chain A) and 5.20 Å (chain B), DNA RMSD fluctuates around 7.66 Å

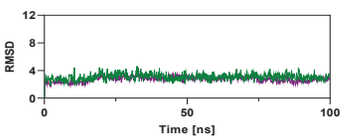

RMSD analysis of **PNA4** (magenta) and DNA (green) relative to the initial frame of the MD simulation. PNA RMSD fluctuates around 2.76 Å, DNA RMSD fluctuates around 3.06 Å.

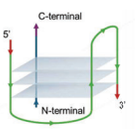

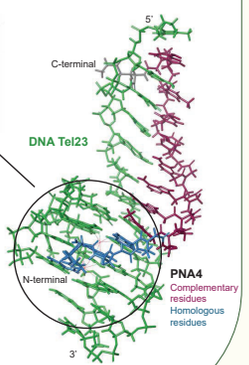

Final conformation of the PNA and DNA complexes obtained from the last frame of the 100 ns MD simulation

Conclusions and perspectives

- PNA1, PNA2, PNA3 determine a conformational change of Tel23 DNA from hybrid G4 to parallel G4. MD studies performed on PNA1 and PNA2 with Tel23 DNA with a 1:2 DNA:PNA ratio and with parallel G4 conformation returned RMSD values that appear to converge, suggesting that the system has reached a stable structural equilibrium during the simulation.
- Molecular dynamics studies performed on PNA4 and Tel23 returned convergent RMSD values suggesting that the system has reached a stable structural equilibrium during the simulation. CD studies on PNA4 and Tel23 DNA showed a conformational change of Tel23 DNA from hybrid G4 to possibly antiparallel G4 with additional formation of a double helix as observed in MD studies.
- All DNA-PNA complexes in 1:5 ratio showed higher melting temperatures than the DNA-DNA adduct suggesting a greater stability of the complexes.
- **Mass Spectrometry Analysis**: Perform precise mass spectrometry studies to determine the molecularity of the PNA-DNA complexes.
- **NMR and X-ray Crystallography**: Utilize nuclear magnetic resonance spectroscopy and X-ray crystallography to elucidate the conformations of the complexes and characterize the interactions crucial for complex formation.
- **Molecular Dynamics Simulations**: Conduct MD simulations to guide the structural modifications of hybrid and homologous PNAs, including amino acid conjugation, aimed at identifying molecules with enhanced interaction properties.
- **Ligand-PNA Conjugation**: Explore the design of ligand-PNA conjugated molecules to achieve selective and stable interactions with quadruplex DNA.

References

1. Brodyagin, Nikita et al. "Chemical approaches to discover the full potential of peptide nucleic acids in biomedical applications." *Beilstein journal of organic chemistry* vol. 17 (2021) 1641-1688.
2. Cadoni, Enrico et al. "Beyond small molecules: targeting G-quadruplex structures with oligonucleotides and their analogues." *Nucleic acids research* vol. 49 (2021): 6638-6659.
3. Pirota, Valentina et al. "Chapter Six - An overview of quadruplex ligands: Their common features and chemotype diversity." *Annual Reports in Medicinal Chemistry* vol. 54 (2020).
4. Panyutin, Igor et al. "Targeting DNA G-quadruplex structures with peptide nucleic acids." *Current Pharmaceutical Design* vol. 18 (2012) 1984-91.

Florence, 25 – 29 August 2024

Macrocyclic mimetics of the Suppressor of Cytokine Signaling 1 and 3 proteins (SOCS1-SOCS3)

A. Cugudda[1], S. La Manna[1], D. Florio[1], D. Marasco[1]

[1]University of Naples "Federico II", Department of Pharmacy, 80131, Naples, Italy.
alessia.cugudda@unina.it

https://doi.org/10.17952/37EPS.2024.P2260

BACKGROUND and AIM

In numerous inflammatory, immune, and oncogenic processes, the Janus kinase (JAK)/signal transducer and activator of transcription (STAT) pathway is selectively upregulated in response to cytokine stimulation. Of particular interest are the endogenous proteins that modulate this pathway: the suppressors of cytokine signaling (SOCS) proteins, which operate via a negative feedback mechanism [1] . Notably, SOCS1 and SOCS3 are downregulated in chronic inflammatory diseases and cancer [2] . In this study, aiming to develop SOCS1 and SOCS3 mimetics, we designed and synthesized cyclic analogues using the CLIPS strategy. This method involves the formation of non-native bonds between the thiol side chains of cysteines and xylene-based scaffolds [3].

METHODS

Peptides were prepared by the Solid Phase Peptide Synthesis (SPPS) on a 25μmol scale following the fluorenylmethoxycarbonyl (Fmoc) strategy. Cyclization was performed by mixing crude linear peptidomimetics (1mM) with 1.1 equivalents of xylene scaffolds in 50% CH_3CN and 50% K_2HPO_4 buffer 0.1M pH 7.6, under stirring overnight at room temperature (RT). The purity and identity of the peptides were confirmed by LC-MS. The cyclic peptides were then characterized by Circular Dichroism (CD) and Nuclear Magnetic Resonance (NMR) spectroscopies. In addition, Micro Scale Thermophoresis (MST) experiments, serum stability studies and phosphorylation inhibition assays were performed.

DESING OF CYCLIC ANALOGUES OF SOCS1 AND SOCS3 PROTEINS

For the design of these new xylene-based cyclic analogues of SOCS1, two different scaffolds were used: α,α'-dibromo-m-xylene and 1,3,5-tribromomethylbenzene to provide a monocyclic and a bicyclic version of previously identified lead compounds, in this case icPS5(Nal1) (**Figure 1A**). In the case of SOCS3, KIRCONG chim was used as a template and reacted with α,α'-dibromo-m-xylene to form partially flexible cycles by cyclizing only the N-terminal (KIR region) or C-terminal (CONG region), allowing the development of monoright and monoleft cycles, respectively. As these new cycles are highly insoluble, one or two PEG were inserted sequentially to give monoright PEG_1 and PEG_2 and monoleft PEG_1 and PEG_2 (**Figure 1B**).

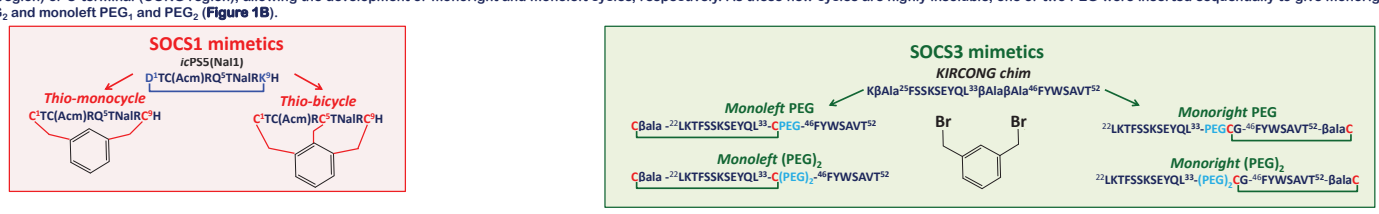

Figure 1. Template sequence (**A**) (*ic*PS5(Nal1)) for the design of thio-analogues of SOCS1 protein (**B**) (KIRCONG chim) for the design of monocyclic mimetics of SOCS3 protein.

RESULTS OF THIO-ANALOGUES OF SOCS1 PROTEIN

Binding Assay-MicroScale Thermophoresis (MST)

Fitting the experimental data for the thio-monocycle PS5(Nal1) (**Figure 2A**) resulted in a very good K_D in the low Micromolar range (~7μM), even 5-fold lower than the *ic*PS5(Nal1) template (K_D ~ 36μM), whereas the thio bicycle PS5(Nal1) has a high K_D value of 130 μM and does not reach full saturation (**Figure 2B**). It is hypothesized that the introduction of a bicyclic scaffold reduces the ability to recognize JAK2 due to partial masking of the interaction hotspots [4] .

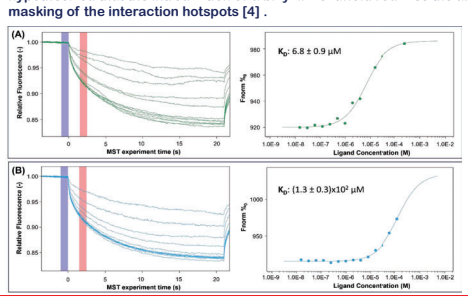

Figure 2. In vitro binding assays. Binding isotherms for MST signals versus peptides concentrations (left) and thermophoretic traces of MST assays for the binding to JAK2 (right) of peptide (**A**) thio-monocycle PS5(Nal1) and (**B**) thio-bicycle PS5(Nal1).

Inhibition of Phosphorylation Assay

The SOCS1 mimetic activity of two thio-analogues was studied using phosphorylation inhibition assays on a substrate called Srctide. LC-MS experiments measured the decrease in p-Srctide peak area with increasing amounts of thio-analogues. The IC_{50} for the thio-monocycle was found to be 2.2 ± 0.3 μM, and for the thio-bicycle, it was 1.0 ± 0.5 x 102 μM (**Figure 3**) [4] .

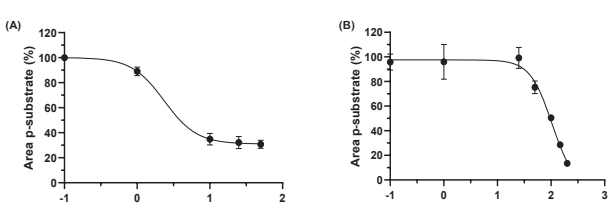

Figure 3. The SOCS1 mimetic activity of thio-analogues PS5(Nal1) was measured by analyzing the percentage area of phosphorylated Srctide (p-Srctide) at different concentrations for both (**A**)thio-monocycle and (**B**)thio-bicycle forms. The data, averaged from two experiments and expressed in logarithmic form, use 100% as the p-Srctide area without the inhibitor.

Circular Dichroism

The thio-monocycle PS5(Nal1) lacks an aromatic band and shows two minima at 224 nm and 203 nm, which shift to 218 nm and 197 nm with 50% TFE, indicating no helical structure (**Figure 4 A**). The thio-bicycle has a minimum below 200 nm and a band at 230 nm, indicating an aromatic contribution enhanced by the naphthyl group of Nal1 (**Figure 4 B**). The addition of 50% TFE does not significantly alter the CD profiles or increase the secondary structure content [4] .

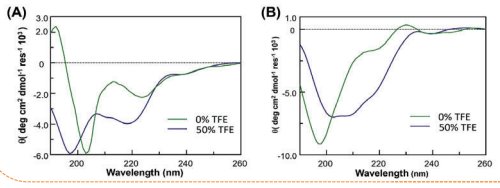

Figure 4. Overlay of CD spectra of (**A**) thio-monocycle PS5(Nal1); (**B**) thio-bicycle PS5(Nal1) compounds.

Serum stability

Serum stability assays showed that the new thio-cyclic analogues of icPS5(Nal1) degraded faster over time compared to icPS5(Nal1) (**Figure 5**). Nevertheless, both analogues retained 25% of their presence after 30 Hours [4] .

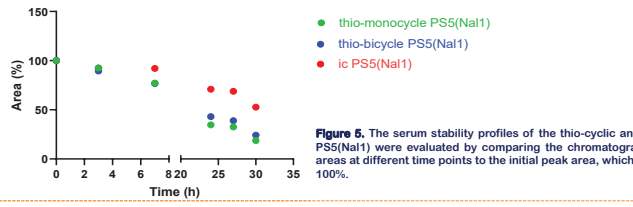

Figure 5. The serum stability profiles of the thio-cyclic analogues of PS5(Nal1) were evaluated by comparing the chromatographic peak areas at different time points to the initial peak area, which was set at 100%.

RESULTS OF MACROCYCLIC MIMETICS OF SOCS3 PROTEIN

ONGOING studies

The main problem with these mimetics is their poor solubility, which has made purification difficult and led to low synthetic yields. Of the MST assays (**Table 1**), only *Monoright* PEG_1 gave a good K_D (**Figure 6**), while the other compounds showed no binding, and even *Monoright* PEG_2 showed aggregation (**Figure 7**) . In view of the above issues, macro-cycle characterization studies are still ongoing.

Table 1. Results of MST binding assays of macrocyclic mimetics of SOCS3 protein

PEPTIDE	BINDING
Monoleft PEG	No binding
Monoleft $(PEG)_2$	No saturation
Monoright PEG	K_D= (5±2)*10 μM
Monoright $(PEG)_2$	Insoluble

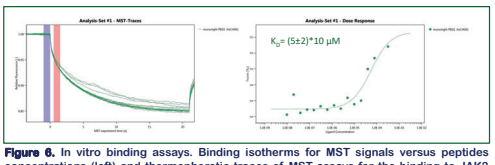

Figure 6. In vitro binding assays. Binding isotherms for MST signals versus peptides concentrations (left) and thermophoretic traces of MST assays for the binding to JAK2 (right) of peptide *Monoright* PEG_1 .

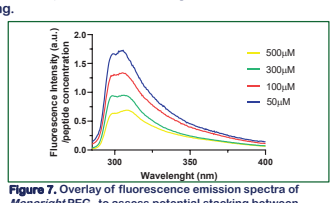

Figure 7. Overlay of fluorescence emission spectra of *Monoright* PEG_2 to assess potential stacking between monomers.

CONCLUSION

In summary, with respect to SOCS1 protein mimetics, the results demonstrated that the *ic*PS5 peptide is a bioactive sequence, making it highly adaptable and ideal for the chemical modifications necessary to convert KIR-SOCS1 peptidomimetics into specific JAK2 inhibitors. For SOCS3 mimetics, synthetic difficulties and poor solubility have slowed down studies, but MST suggest that cyclization at the CONG end is more favorable for interaction with JAK2.

REFERENCES

[1] S. La Manna, L. Lopez-Sanz, S. Bernal, S. Fortuna, F.A. Mercurio, M. Leone, C. Gomez-Guerrero, and D. Marasco, Cyclic mimetics of kinase-inhibitory region of Suppressors of Cytokine Signaling 1: Progress toward novel anti-inflammatory therapeutics. Eur J Med Chem 221 (2021) 113547.
[2] T. Wang, S. Kaneko, E. Kriukov, D. Alvarez, E. Lam, Y. Wang, S. La Manna, D. Marasco, A. Fernandez-Gonzalez, S.A. Mitsialis, S. Kourembanas, A. Stahl, M. Chen, H. Xu, P. Baranov, G. Cai, U.H. von Andrian, and Y. Sun, SOCS3 regulates pathological retinal angiogenesis through modulating SPP1 expression in microglia and macrophages. Mol Ther (2024).
[3] D.E. Hacker, M. Almohaini, A. Anbazhagan, Z. Ma, and M.C. Hartman, Peptide and peptide library cyclization via bromomethylbenzene derivatives. Methods Mol Biol 1248 (2015) 105-17.
[4] A. Cugudda, S. La Manna, M. Leone, M. Vincenzi and D.Marasco, Design of macrocyclic proteomimetics of SOCS1 protein. The European Journal of Medicinal Chemistry (2024) (Submitted).

https://doi.org/10.17952/37EPS.2024.P2262

Modulation of the antagonistic properties of an insulin mimetic peptide by disulfide bridge modifications

Marta Lubos, Jan Pícha, Irena Selicharová, Jiří Žák, Miloš Buděšínský, Katarína Mitrová, Lenka Žáková and Jiří Jiráček

Institute of Organic Chemistry and Biochemistry, Czech Academy of Sciences, Prague, Czech Republic

INTRODUCTION

Insulin is a peptide crucial for maintaining metabolic balance within the organism, it elicits its effects through binding to the transmembrane insulin receptor (IR). Investigating insulin mimetics, which can either stimulate or inhibit the receptor, presents a promising field of research for diabetes and cancer treatments. We synthesized five variants of a previously reported 20-amino acid insulin-mimicking peptide S592 (Table 1) [1]. These new peptides **1**-**5** (Table 2) differ from each other by the structure of the covalent bridge connecting positions 11 and 18. In addition to the peptide with a disulfide bridge, we prepared a derivative with a dicarba bridge and three derivatives with a 1,2,3-triazole, differing from each other by the presence of sulfur or oxygen in their staples.

Table 1. Sequences of referred peptides.

Code	Sequence
S592	SLEEEWAQIECEVWGRGCPSY
S371	GSLDESFYDWFERQLGKK
S661	GSLDESFYDWFERQLGGGSGGSSLEEEWAQIQCEVWRGCPSY-amide
S961	GSLDESFYDWFERQLGGGSGGSSLEEEWAQIQCEVWGRGCPSY
S519	SLEEEWAQVECEVYGRGCPSGSLDESFYDWFERQLG
Cys→Ser in S661	GSLDESFYDWFERQLGGGSGGSSLEEEWAQIQSEVWGRGSPSY-amide
Cys→Ser in S592	SLEEEWAQIQSEVWGRGSPSYC
peptide 1	SLEEEWAQIECEVWGRGCPS-amide
IM459	#SLEQEWaKIECEVYGKCPPKKAyKWFERQLK-amide
IM172N22	#SLEEEWAQIECEVYGRCPPSES-amide
S597-N20	SLEEEWAQIECEVYGRGCPS-amide

The Cys residues forming the disulfide bridge are highlighted in red. # denotes *N*-terminal phenylacetylation, a means 2-aminoisobutyric acid, y is *O*-methyltyrosine

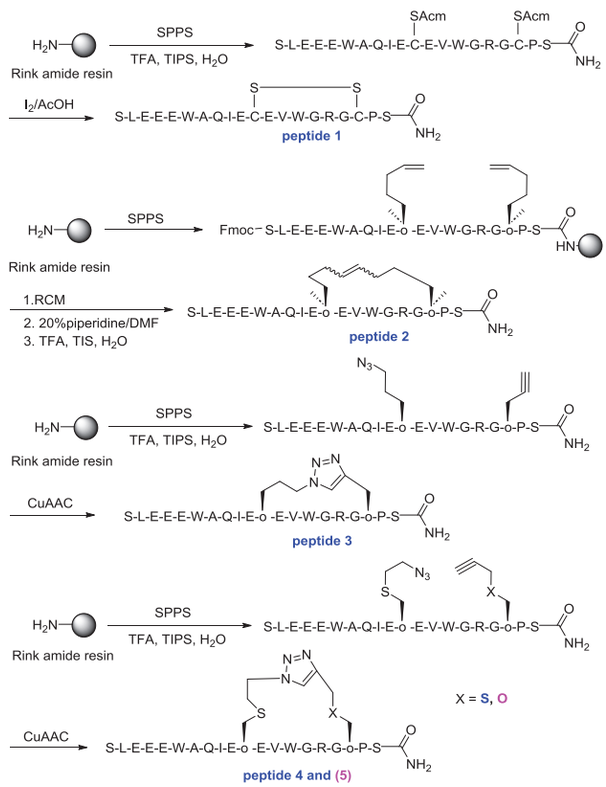

Figure 1. Synthetic route for cyclic peptides preparation. o denotes C^{α} atom of non-standard amino acids.

SYNTHESIS

Peptides were synthesized by the solid-phase peptide synthesis (SPPS) on Rink Amide AM resin using standard Fmoc protocol on the multiple Peptide Synthesizer Spyder Mark IV (EP 17206537.7) developed in the Development Center of the IOCB (Figure 1). Cleavage of peptides was achieved by treatment with TFA:TIS:H_2O. Peptide with Acm-protected cysteines was dissolved in 40% AcOH at 10^{-3} M. Iodine (25 eq.) in AcOH was added, and the solution was stirred at RT. Then, 1 M ascorbic acid was added until the iodine colour disappeared. Ring-closing olefin metathesis (RCM) was performed on resin-bound peptide with the N-terminal amino acid protected with Fmoc. RCM was carried out using 6 mM Grubbs catalyst 1st generation (20 mol% regarding the resin substitution) in DCE. The resin was agitated under nitrogen at rt for 2 h, protected from light. A Cu(I)-catalyzed azide-alkyne cycloaddition (click reaction) was conducted on the linear peptide, which was dissolved in H_2O/tBuOH (2 : 1, v/v), and then $CuSO_4 \cdot 5H_2O$ (14 eq.) and ascorbic acid (13 eq.) were added. The reaction was stirred overnight, without light at RT.

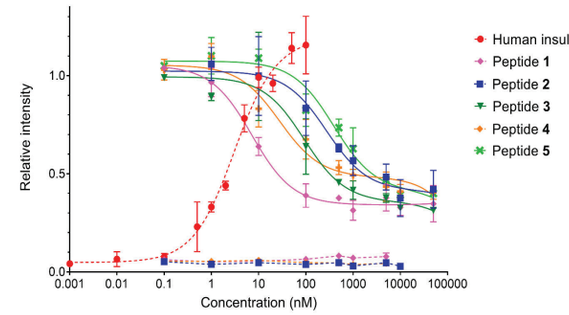

Figure 2. Relative abilities of peptides **1**–**5** to antagonize insulin-stimulated receptor phosphorylation (full lines). Dashed lines show stimulation of IR-A with insulin and selected peptides **1**, **2** and **4** alone.

Table 2. Binding affinity for IR-A and ability to stimulate IR-A autophosphorylation by human insulin and peptides **1**-**5**.

Peptide	Type of the intramolecular staple (number of atoms in the staple)	K_d ± S.D. [nM] for binding to IR-A (n≥3)	EC_{50} [nM] (best fit values) for stimulation (S) or antagonism (A)	EC_{50}/K_d
Insulin		0.31 ± 0.02	3.0 (S)	10
1	disulfide (4)	3.9 ± 1.0	7.2 (A)	1.8
2	dicarba (8)	49 ± 6	274 (A)	5.6
3	triazole (7)	15 ± 3	92 (A)	6.1
4	triazole-sulfur-sulfur (10)	25 ± 7	28 (A)	1.1
5	triazole-sulfur-oxygen (10)	75 ± 29	389 (A)	5.5

CONCLUSIONS

We prepared five variants of a 20-amino acid insulin-mimicking peptide targeting Site 2 of the insulin receptor (IR). Peptide **1**, with a natural disulfide bridge, exhibited the strongest binding, with affinity only 13 times lower than human insulin (Table 2). Other derivatives had 4–19 times weaker binding than peptide **1**, indicating a correlation between increased bridge length and reduced affinity. Although none of the peptides activated IR, all inhibited insulin-induced activation, behaving as partial antagonists with about 30% residual receptor activity at high concentrations (Figure 2). Peptides with sulfur in their bridges showed better binding and antagonistic effects, while those without sulfur had lower affinity and reduced antagonism. This study demonstrates that functional properties of IR peptide ligands can be modulated using unnatural disulfide bridge mimetics, potentially leading to effective nonpeptide insulin mimetics in the future.

REFERENCES

1. M. Lubos, J. Pícha, I. Selicharová, J. Žák, M. Buděšínský, K. Mitrová, L. Žáková, J. Jiráček, *J. Pept. Sci.*, 2023, 29:e3478.

ACKNOWLEDGEMENTS

This work was supported by the National Institute for Research of Metabolic and Cardiovascular Diseases (Program EXCELES, ID Project No. LX22NPO5104, Funded by the European Union-Next Generation EU), by the Czech Science Foundation (project No. 22-17978S) and by the Academy of Sciences of the Czech Republic (Research Project RVO:6138963).

MINISTERSTVO ŠKOLSTVÍ, MLÁDEŽE A TĚLOVÝCHOVY
CarDia
Funded by the European Union
NextGenerationEU
CZECH RECOVERY PLAN

ÚOCHB AV ČR
IOCB PRAGUE

Combinatorial Libraries of Bipodal Binders of the Insulin Receptor

https://doi.org/10.17952/37EPS.2024.P2263

Irena Selicharová, Benjamin Fabre, María Soledad Garre Hernández, Marta Lubos, Jan Pícha, Zdeněk Voburka, Katarína Mitrová and Jiří Jiráček
Institute of Organic Chemistry and Biochemistry, AS CR, Prague, Czech Republic

Background

Treatment of diabetes with insulin is complicated by its narrow therapeutic index. Efforts are devoted to develop insulin analogs/mimetics with altered properties that would bring better comfort to patients.

We designed and prepared combinatorial libraries of bipodal compounds consisting of two distinct peptides linked to a molecular scaffold. The libraries were searched for specific insulin receptor (IR) binders.

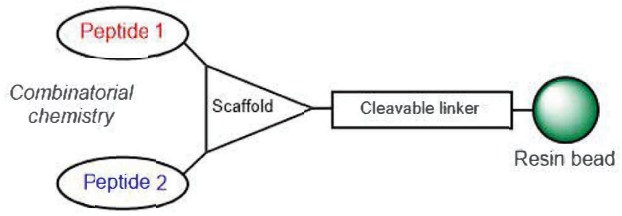

Figure 1. General structure of resin-bound construct.

Synthesis of Library

Trimesic-acid scaffold was attached to bi-layered TentaGel beads and modified with equimolar mixture of D-amino acids (x1-x6). Azido groups of the scaffold and reporter linker (inner sphere) were reduced to amines and modified by a split-combine technique to yield unique peptide sequence on each bead (a1-a6).

Scheme 1:

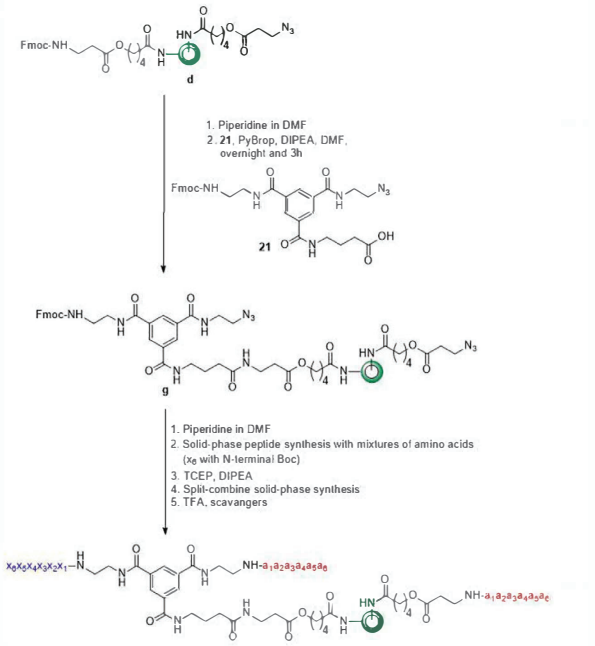

Active beads selection workflow

Beads modified with compound libraries were incubated with IR and fluorescent antibody sandwich and sorted on large-particle BioSorter. Fluorescent beads were manually re-sorted for specific IR binders.

Figure 2:

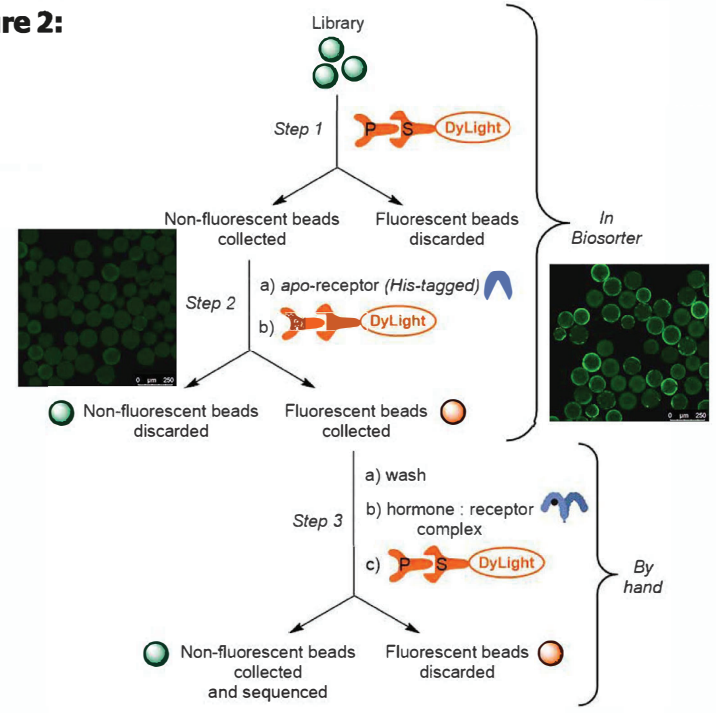

New IR binding compounds

- Peptides „slyfys" (IR Site-1) **Figure 3**, „GeeepaGG" (IR Site-2) and „yyaypGG" (IR Site-2) were discovered within libraries of nearly 3 x 10_6 peptides.
- Similarity with peptides discovered through phage display Ac-FYDFWERQ (IR Site-1) and SLEEEWAQ (IR Site-2)

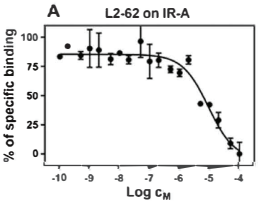

Figure 3: IR-A binding of L2-62 having a slyfys sequence of one arm of the trimesic acid scaffold and all possible hexapeptide sequences (selection of 12 D-amino acids).

Challenges encountered

- Robust non-specific interactions with basic and hydrophobic peptides.
- Inevitable looses of beads throught the selection proces.
- No highly potent compounds were found.

Reference: Selicharova et al., ChemMedChem 2024, 19, e202400145

Supported by: Nat.Inst.Res. of Metabolic and Cardiovascular Diseases (Program EXCELES, No. LX22NPO5104, Funded by the European Union-Next Generation EU), OP RDE, Project: "ChemBioDrug" (No. CZ.02.1.01/0.0/0.0/16_019/0000729), Czech Sci.Fund (No.22-17978S) and RVO:6138963 from AS CR

EUROPEAN UNION
European Structural and Investment Funds
Operational Programme Research, Development and Education
CarDia
MINISTERSTVO ŠKOLSTVÍ, MLÁDEŽE A TĚLOVÝCHOVY
CZECH RECOVERY PLAN

AI-DRIVEN DESIGN OF β-SECRETASE 1 INHIBITORS

MARKO NJIRJAK[1,2], DANIELA KALAFATOVIC[2,3], GORAN MAUŠA[1,2]

[1]Faculty of Engineering, University of Rijeka, Rijeka, Croatia
[2]Center for Artificial Intelligence and Cybersecurity, University of Rijeka, Rijeka, Croatia
[3]Faculty of Biotechnology and Drug Development, University of Rijeka, Rijeka, Croatia

https://doi.org/10.17952/37EPS.2024.P2266

INTRODUCTION

12

EVERY 12 SECONDS, SOMEONE IN THE WORLD IS DIAGNOSED WITH DEMENTIA

Alzheimer's disease and other dementias have become the **7th leading cause of death worldwide**. With a 181% rise in the global mortality rate between 2000 and 2019, and with population aging occurring at an unprecedentedly fast pace, **dementia is expected to become the predominant factor of disability and dependency** [1].

ESTIMATED NUMBER OF PEOPLE WITH DEMENTIA

55 M (2019) | **139 M** (2050)

Disrupting the Amyloid-beta precursor protein (APP) processing pathway has been proven to be a viable way of tackling Alzheimer's [2]. However, **designing drugs** that can cross the blood-brain barrier (BBB) and act upon a specific mechanism in the brain **is a challenging endeavor**, encompassing lead identification, optimization, and experimental validation, **requiring a substantial amount of effort with success rates as low as 1%** [3].

METHODOLOGY

Due to the established capability of **artificial intelligence** (AI) to efficiently search through extensive chemical spaces [4], we used it in this study **to rapidly identify lead compounds with a high probability of inhibiting β-secretase 1 enzyme**.

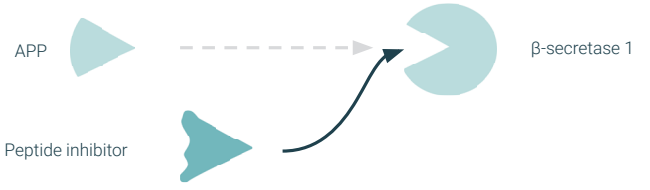

We utilized **NSGA-II genetic algorithm** as a backbone of our AI system [5], **guided by the following criteria**:

1. **Binding affinity of a peptide towards β-secretase 1**
2. **ML-estimated probability of a peptide crossing the BBB** [6]
3. **Wildman-Crippen logP value indicating peptide's lipophilicity**

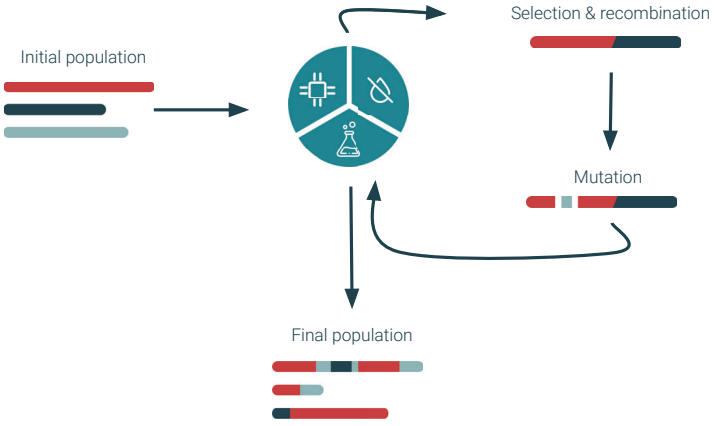

RESULTS

AI-DESIGNED INHIBITORS

Peptide	Binding affinity towards β-secretase 1 [kcal/mol]	Probability of BBB penetration	LogP
WLWWWPF	-9.4	75.4%	6.00
WWWPF	-10.2	72.9%	4.26
GIHAYWT	-7.8	91.7%	-0.98
MHLAFKW	-7.9	89.7%	1.19

PATENTED INHIBITORS FROM THE LITERATURE

Peptide (source: [7])	Binding affinity towards β-secretase 1 [kcal/mol]	Probability of BBB penetration	LogP
NEESMYCRLLGIGCG	-6.1	14.8%	-7.36
PEESLYCRLLALGCG	-6.3	10.6%	-5.13

COMPARISON OF DESIGNED AND PATENTED INHIBITORS

67% INCREASE IN BINDING AFFINITY TOWARDS β-SECRETASE 1

5X INCREASE IN BBB PENETRATION PROBABILITY

11.62 HIGHER LOGP VALUE

DISTRIBUTION OF AMINO ACIDS IN THE POPULATION



REFERENCES

[1] World Health Organization. "Global status report on the public health response to dementia." (2021).

[2] Hampel, H., Hardy, J., Blennow, K. et al. "The Amyloid-β Pathway in Alzheimer's Disease." Molecular Psychiatry 26, 5481–5503 (2021).

[3] Das, P., Sercu, T., Wadhawan, K. et al. "Accelerated antimicrobial discovery via deep generative models and molecular dynamics simulations." Nature Biomedical Engineering 5, 613–623 (2021).

[4] Sadybekov, A.V., Katritch, V. "Computational approaches streamlining drug discovery." Nature 616, 673–685 (2023).

[5] Mauša, G., Njirjak, M., Otović, E. et al. "Configurable soft computing-based generative model: The search for catalytic peptides." MRS Advances 8(19), 1068-1074 (2023).

[6] Dai, R., Zhang, W., Tang, W. et al. "BBPpred: sequence-based prediction of blood-brain barrier peptides with feature representation learning and logistic regression." Journal of Chemical Information and Modeling 61(1), 525-534 (2021).

[7] Lazarus, R. A., Zhang, Y., Wang, W. (Genentech Inc.) "Peptide inhibitors of BACE1", US patent US9624269B2 (2017).

ACKNOWLEDGEMENTS

- Design of short catalytic peptides and peptide assemblies (grant no. UIP-2019-04-7999)
- Deep Learning - based Prediction of Therapeutic Peptides (grant no. uniri-23-78)
- Funded by:

HRZZ Croatian Science Foundation

uniri

Proprietary

Application of Deep Learning Imputation to Peptide Bioactivity and Property Prediction

Samar Mahmoud[1], Himani Tandon[1], Matthew Segall[1], Ruibo Zhang[2], Robert Thompson[3], Jeffrey Schubert[4], Dipannita Kalyani[5], Dan Sindhikara[2]

[1]R&D, Optibrium Ltd, Cambridge, United Kingdom, [2]Department of Modeling and Informatics, Merck & Co., Inc., Rahway, NJ, USA, [3]Department of Discovery Chemistry, Merck & Co., Inc., South San Francisco, CA, USA, [4]Department of Discovery Chemistry, Merck & Co., Inc., West Point, PA, USA, [5]Department of Discovery Chemistry, Merck & Co., Inc., Rahway, NJ, USA

https://doi.org/10.17952/37EPS.2024.P2267

Introduction

Predicting bioactivities and properties is pivotal for advancing peptide-based therapeutics. It facilitates the rapid virtual screening of large peptide libraries and prioritisation of candidates with high target activity, stability, and permeability. However, accurate prediction is challenging due to the complex structure-activity relationships between peptide sequence, conformation and diverse biological activities, which current models often struggle to fully capture. Also, limited resources and diverse peptide libraries complicate testing, leading to sparse and noisy datasets.

In this context, we introduce the application of a deep learning platform, which employs an imputation approach to derive valuable insights from such noisy experimental data. This platform generates reliable predictions of peptide properties and provides valuable insights that can be used for peptide optimisation.

Deep Learning Imputation

Cerella™ [1,2] is a deep learning platform which accepts both molecular descriptors and sparse experimental data as inputs to impute (fill-in) the missing values, exploiting the **assay-assay correlations**, as well as structure-activity relationships (SAR).

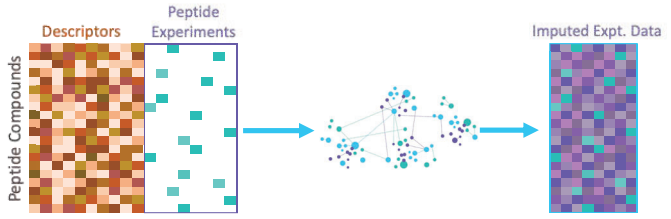

Cerella further provides a robust estimate of the **uncertainty** in each prediction, enabling the most accurate results to be identified.

In combination, these provide **more accurate predictions** of activity and property values, enabling additional insights, such as identifying experimental outliers and the most valuable experimental data measure with which to improve a model's predictions.

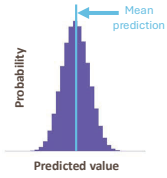

Dataset and Methods

Cerella platform was applied to model two proprietary datasets of peptidic compounds, provided by Merck & Co., Inc., Rahway, NJ, USA. The peptides were mostly **macrocycles,** and **6-15 'mers** in length.

Project 1: 33 experimental endpoints and 5168 peptides

Project 2: 39 experimental endpoints and 1125 peptides

Model performances were compared with other methods including Random Forests, ChemProp, and KNN imputation.

Results

Model performance

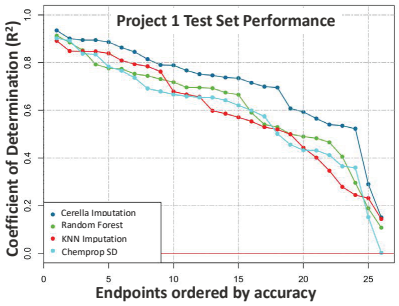

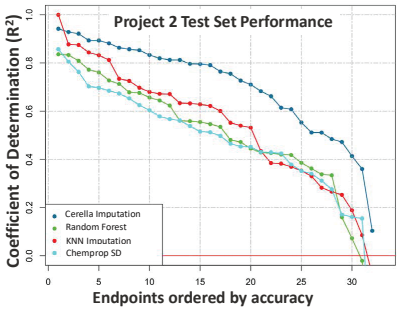

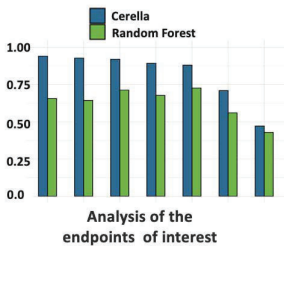

Figure 1: Imputation models outperform QSAR models for both the Projects (paired t-test p-values < 0.05), with a **substantial** improvement in **Project 2**. The bar chart illustrates the **significant** performance differences between the Imputation model and the Random Forest models for the endpoints of interest in **Project 2**. The models were built using 2D StarDrop™ descriptors. Insignificant performance differences are observed between different QSAR models (paired t-test p-values >0.05) for both Project 1 and 2

Uncertainty correlates well with accuracy

Cerella's uncertainty estimates correlate well with accuracy, highlighting the model's ability to identify accurate predictions, as shown for a peptide activity endpoints in **Project 2**. This provides **greater confidence** in decisions based on model predictions.

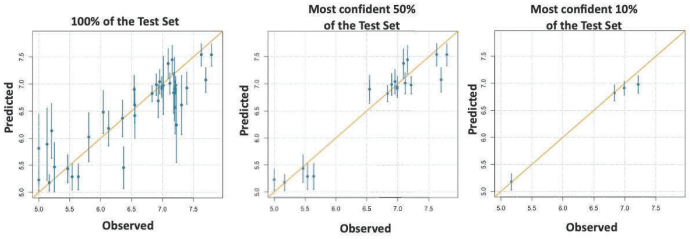

Figure 2: Correlation between uncertainty (error bars) and model accuracy: Model accuracy increases when focusing on the most confident predictions

Importance analysis guides design and optimisation

Importance analysis shows which experiments and/or descriptors contribute most to the accurate predictions of others. The heatmaps show the most informative inputs for prediction of Project 1 and 2 endpoints.

Figure 3: Sequence-based descriptors, derived from PepSeA [3] alignments using interpretable monomer descriptors, were used to enhance the imputation model.

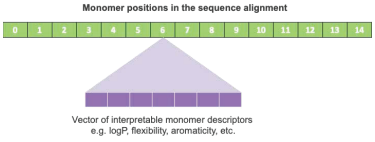

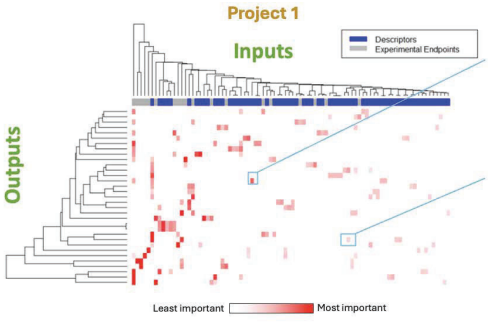

Figure 4: Experimental **Endpoint X** is influenced by the **number of aromatic atoms** at **position 4** in the peptide sequence alignment

Experimental **Endpoint Y** is informed by the monomer **logP** at **position 12** in the peptide sequence alignment

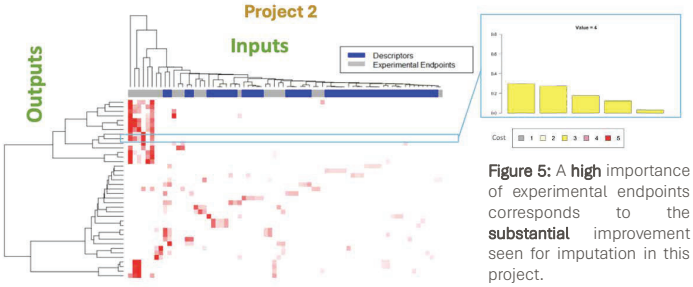

Figure 5: A **high** importance of experimental endpoints corresponds to the **substantial** improvement seen for imputation in this project.

Moderate cost experiments inform high-value outcomes, guiding the prioritisation of running the lower-cost yet informative experimental measurements to accurately impute expensive, late-stage endpoints

Conclusion

1. Cerella Imputation generates reliable predictions of peptide properties and activities by leveraging assay-assay relationships.
2. Strong correlation are confirmed between estimated uncertainties and observed accuracy of predictions.
3. Cerella guides the design of peptides and the prioritisation of experimental resources.

References

[1] B. Irwin et al. J. Chem. Inf Model. (2020) 60(6), pp. 2848–2857

[2] B. Irwin et al. Appl. AI Lett. (2021) 2(3) pp. e31-2689

[3] J. Baylon et al. J. Chem. Inf Model. (2022) 62(5) pp. 1259-1267

Learn more on our webpage

© 2024 Optibrium Ltd. Optibrium™, StarDrop™, Inspyra™, Augmented Chemistry®, Cerella™, Glowing Molecule™, WhichP450™, WhichEnzyme™, Auto-Modeller™, Nova™, MPO Explorer™ and Card View® are trademarks of Optibrium Ltd.

https://doi.org/10.17952/37EPS.2024.P2268

PICKAPEP

Visualization and Calculation of Cyclized and Modified Peptidomimetics Made Easy

Erckes, V.[1]; Hilleke, M.[2]; Isert, C.[2]; Steuer, C.[1]

1 Laboratory of Pharmaceutical Analytics, Department of Chemistry and Applied Biosciences, ETH Zurich, Switzerland

2 Laboratory of Computer-Assisted Drug Design, Department of Chemistry and Applied Biosciences, ETH Zurich, Switzerland

INTRODUCTION

Recently, the interest in peptides and peptidomimetic structures has risen enormously.[1] Novel modification strategies including nonnatural amino acids, sophisticated cyclization strategies, and side chain modifications to improve the pharmacokinetic properties of peptides are continuously arising. However, a calculator tool accompanying the current development in peptide sciences towards modified peptides is missing. Herein, we present the application **PICKAPEP**, enabling the virtual **construction** and **visualization** of peptidomimetics with regular and self-designed amino acids.[2] **Calculated** parameters include the molecular weight, the **LogP**, the **TPSA**, and the peptide **SMILES code**.[3] To our knowledge, **PICKAPEP** is the first tool allowing users to add custom amino acids (**AA**) as building blocks and also the only tool giving the possibility to process **large peptide libraries** and calculate parameters for multiple peptides at once.

USER FRIENDLY GRAPHICAL INTERFACE

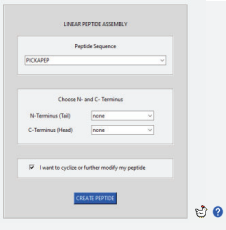

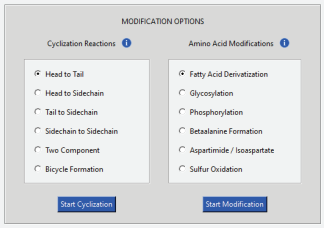

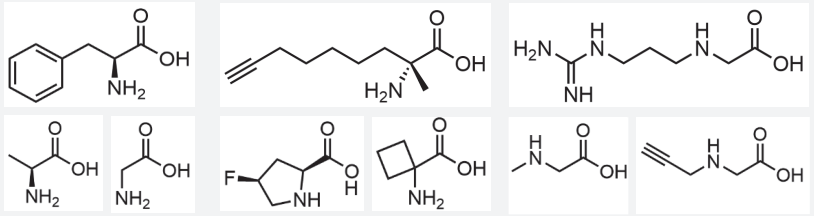

- Enter sequence
- Modify N- & C-terminus
- Cyclize your peptide

AMINO ACID BUILDING BLOCKS

Non-Natural Amino Acids
- D- or N-methylated
- Peptoid building blocks
- Various

Own Amino Acids
Backbone template

Natural Amino Acids
One or three letter code

Beta alanine

Post-Translational Modifications
- Glycosylation
- Phosphorylation

Fatty Acid Derivatization
Spacer + Linker + Fatty (di)acid

AMINO ACID MODIFICATIONS

Common Side Products from Synthesis
- Sulfur oxidation
- Formation of aspartimide and isoaspartate

CYCLIZATIONS

Backbone Involved
- Head to tail
- Head to sidechain
- Tail to sidechain

Multiple Cyclizations
- Bicycle formation
- Stitched peptides

Sidechain to Sidechain
- Natural and nonnatural
- Two component

C-/N-TERMINUS MODIFICATIONS

- > 100 predefined AAs
- Create your own AAs
- Modify side chains

- Efficiently calculate multiple peptides at once

- Visualize your peptides in 2D and 3D
- Get all important parameters

MULTIPLE PEPTIDE PROCESSING

	A	B	C	D	E	F	G	H	I
1	Name	Input Linear Sequence	Nterm	Cterm	Cyclizations	Modifications	Status	Sequence	Linea
2	Angiotensin I	D-R-V-Y-I-H-P-F-H-L					Done	N-Term ,	D-R-\
3	Angiotensin II	Asp-Arg-Val-Tyr-Ile-His-Pro-I					Done	N-Term ,	D-R-\
4	Ciclosporin A	V-Lnme-A-Ad-Lnme-Lnme-V			Head, Tail		Done	N-Term ,	*V-Lnı
5	Linaclotide	CCEYCCNPACTGCY			1, 6, disulfide; 2 , 10, c		Done	N-Term ,	C-C-E
6	Liraglutide	HAEGTFTSDVSSYLEGQAAKEFI				20, fa, 1, y-glu, c16ac	Done	N-Term ,	H-A-I
7	Semaglutide	HAibEGTFTSDVSSYLEGQAAKE				20, fa, 2, ado, 1, y-glu, c1	Done	N-Term ,	H-Aib
8	Motixafortide	Motix1-R-Motix3-C-Y-Cit-K-K		Am	4, 13, disulfide		Done	N-Term ,	Moti
9	Zilucoplan	K-V-E-R-F-D-Dnme-Ziluc8-Y-;	Ac		1, 6, amide	15, fa, 1, y-glu, c16 ac	Done	N-Term ,	Ac-K-
10									
11	Peptide 1	P-J-C-K-A-P-E-P					Unknown aminoacid: J		
12	Peptide 2	P-I-C-K-A-P-E-P			2, 8 , disulfide		Reaction 1 not possible		
13	Peptide 3	P-I-C-K-A-P-E-P				3, sulfiac; 7, a-D-GalNac	Glycosylation not possible		
14	Peptide 4	P-I-C-K-A-P-E-P	Am				N-Terminus not available		
15									

OUTPUT AND VISUALIZATION

Chemical Formula: $C_{38}H_{63}N_9O_{11}S$	Number of Amino Acids: 8
Molecular Weight: 854.04	LogP: -1.78
Exact Weight: 853.4368	TPSA: 298.77
$[M+H]^{+}$: 854.4446	Rotatable Bonds: 23
$[M+2H]^{2+}$: 427.7262	Number of HBA: 12
$[M+3H]^{3+}$: 285.4867	Number of HBD: 10
$[M+4H]^{4+}$: 214.367	Aromatic Rings: 0

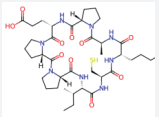

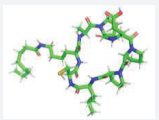

CONCLUSION

With **PICKAPEP**, we provide an open-source tool which can be used to generate numerous types of cyclized and modified peptidomimetics. Combined with its user-friendly comprehensive GUI and various options, **PICKAPEP** can be used **without** substantial **computational expertise** or **knowledge in peptide chemistry**.

Resources and contact information

Resources

Open source software: ETH research collection

Source code: Github

Contact:

Vanessa Erckes: ETH Zurich, Institute of Pharm. Sciences, Pharm. Analytics; Email: vannessa.erckes@pharma.ethz.ch

Christian Steuer: ETH Zurich, Institute of Pharm. Sciences, Pharm. Analytics; Email: christian.steuer@pharma.ethz.ch

References

[1] PepTherDia: database and structural composition analysis of approved peptide therapeutics and diagnostics, V. D'Aloisio, P. Dognini 1 , G. A. Hutcheon 1 , C. R. Coxon, Drug Disc. Today, 2021, **6**, 1409

[2] PICKAPEP: An Application for Parameter Calculation and Visualization of Cyclized and Modified Peptidomimetics, V. Erckes, M. Hilleke, C. Isert, C. SteuerJ. of Pept.Science,2024, epub ahead of print

[3] A story of peptides, lipophilicity and chromatography – back and forth in time, V. Erckes, C. Steuer, RSC Med Chem., 2022, **13**, 676

ACKNOWLEDGEMENT

The authors thanks the organizing committee for giving a waiver for registration fee to V. Erckes.

Metalloproteins Investigation for the Development of new Inhibitors

Matteo Orlandi [a, b], Piero Procacci [a], Marina Macchiagodena [a], Fabrizio Carta [b], Claudiu T. Supuran [b] and Marco Pagliai [a].

[a] Department of Chemistry "Ugo Schiff", University of Florence, via della Lastruccia 13, 50119- Sesto F.no (FI), Italy
[b] Department of NeuroFarBa, University of Florence, Via Ugo Schiff 6, 50019- Sesto Fiorentino, Italy
E-mail: matteo.orlandi1@unifi.it
https://doi.org/10.17952/37EPS.2024.P2274

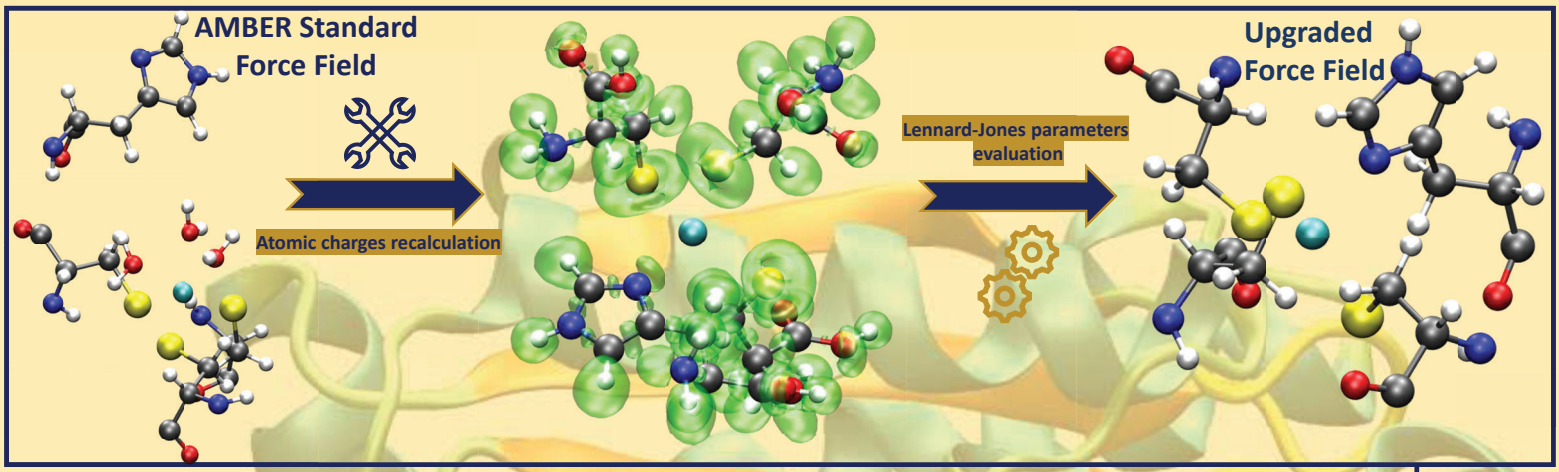

Metalloproteins Modelling

Molecular Dynamics (MD) simulations are a pivotal tool in computational chemistry and biophysics that allow to study the behavior of molecules at the atomic level. The accuracy of these simulations heavily relies on the force fields used to model the interactions between particles. We focused on the development of tailored Force Fields (**Fig. 1**)[1] for the metal-ligand interactions to simulate more accurately the behavior of metalloproteins as potential drug targets and to computationally design innovative and effective inhibitors for these targets. Simulating metal-containing systems with MD is inherently challenging due to the complex electronic and bonding properties of metals. For example, we focused on capturing the polarization effect induced by the cations on the ligands surrounding through accurate QM/MM MD (**Fig. 2**) simulations (CP2K/GROMACS interface) to reparameterize their atomic charges and Lennard-Jones parameters.



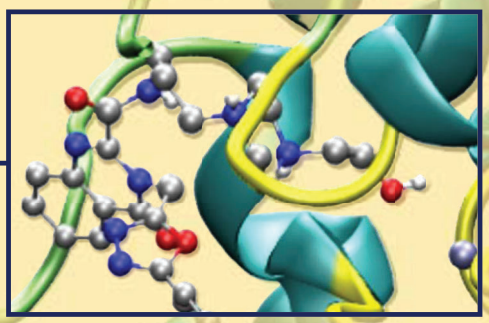

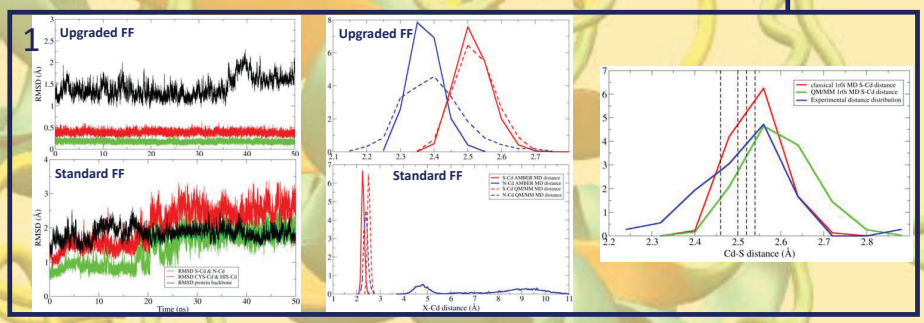

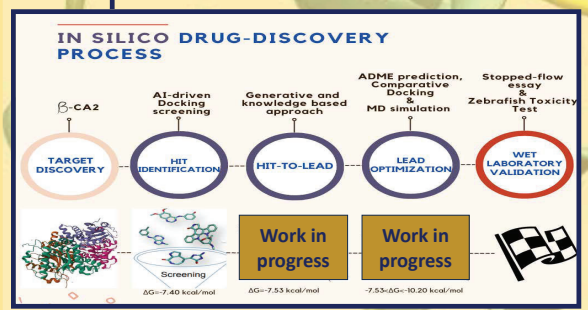

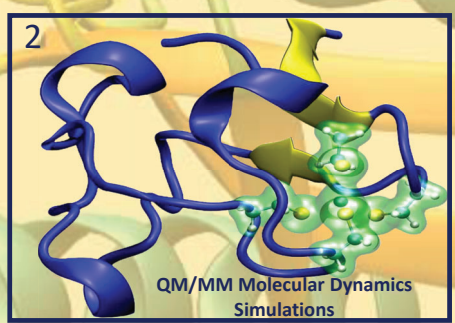

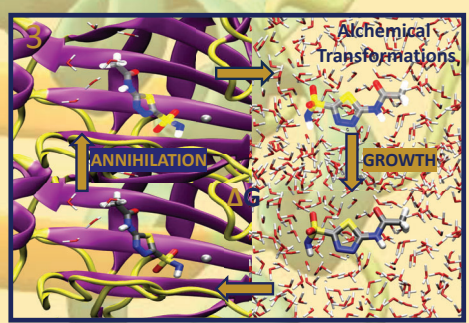

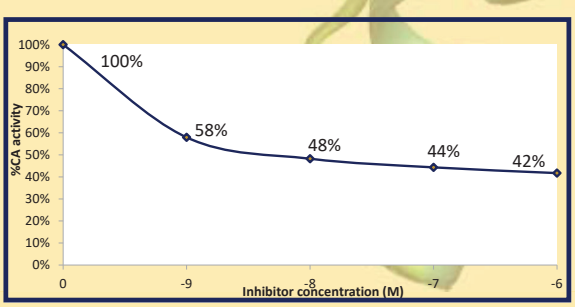

Drug Design

The drug discovery pipeline involves a multifaceted process, spanning from the validation of biological targets to in vivo testing. Computational chemistry tools play a crucial role in accelerating drug development. Their focus lies in minimizing false positive hits and lead compounds that may progress to in vivo experimentation, ultimately mitigating economic losses for the pharmaceutical industry. We focused on the design of a new class of antitubercular drugs effective against the **β Carbonic Anhydrases** of drug-resistant *Mycobacterium tuberculosis*[2]. To develop the new chemical entities both *deep learning generative models*[3] and chemical intuition were exploited. Binding affinities calculation schemes (**Fig. 3**) were also tuned on metalloproteins complex, since the modeling complexity of these systems poses arduous challenges in the feasibility of accurate predictions.

Acknowledgments

We acknowledge the **CINECA** under the ISCRA initiative(project **ISCRA-C MiP**), for the availability of high-performance computing resources and support.

European Peptide Society is kindly acknowledged for the awarded registration grant to Mr. Matteo Orlandi.

[1] Macchiagodena,.. **Upgrading and Validation of the AMBER Force Field for Histidine and Cysteine Zinc(II)-Binding Residues in Sites with Four Protein Ligands** JCIF, 2021.
[2]Fabrizio Carta, ...Claudiu T. Supuran **Carbonic anhydrase inhibitors. Characterization and inhibition studies of the most active β-carbonic anhydrase from Mycobacterium tuberculosis, Rv3588c**, Bioorganic & Medicinal Chemistry Letters, 2009.
[3] Miha Skalic,...Gianni De Fabritiis **LigVoxel: inpainting binding pockets using 3D-convolutional neural networks**, Bioinformatics, 2019

https://doi.org/10.17952/37EPS.2024.P2275

Deep learning for Peptide Classification: From Data to Effective Models

Marko Njirjak[1], Marko Babić[2], Patrizia Jankovic[2], Erik Otović[1], Daniela Kalafatovic[2,3], Goran Mauša*[1,3]

[1] University of Rijeka, Faculty of Engineering, Rijeka, Croatia
[2] University of Rijeka, Faculty of Biotechnology and Drug Development, Rijeka, Croatia
[3] University of Rijeka, Center for Artificial Intelligence and Cybersecurity, Rijeka, Croatia

1. Overview of the proposed research pipeline

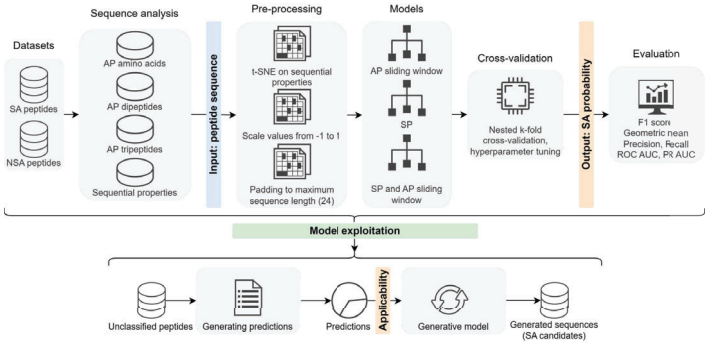

Fig. 1. The models are based on heterogeneous data obtained by applying sliding windows of varying lengths: from single amino acids to di- and tripeptides. Three models were trained on peptides with experimentally validated SA status. Data pre-processing based on t-SNE was performed for dimensionality reduction while padding shorter sequences to a maximum length of 24 residues was used to expedite training. The models were optimized and evaluated using the nested 5-fold cross-validation sampling technique before yielding the final model ready for exploitation. With the aim of discovering sequences with high self-assembly propensity, the hybrid AP-SP model was used as a guideline in a genetic algorithm-based generative approach.

2. Neural network data pre-processing and hyperparameter optimisation

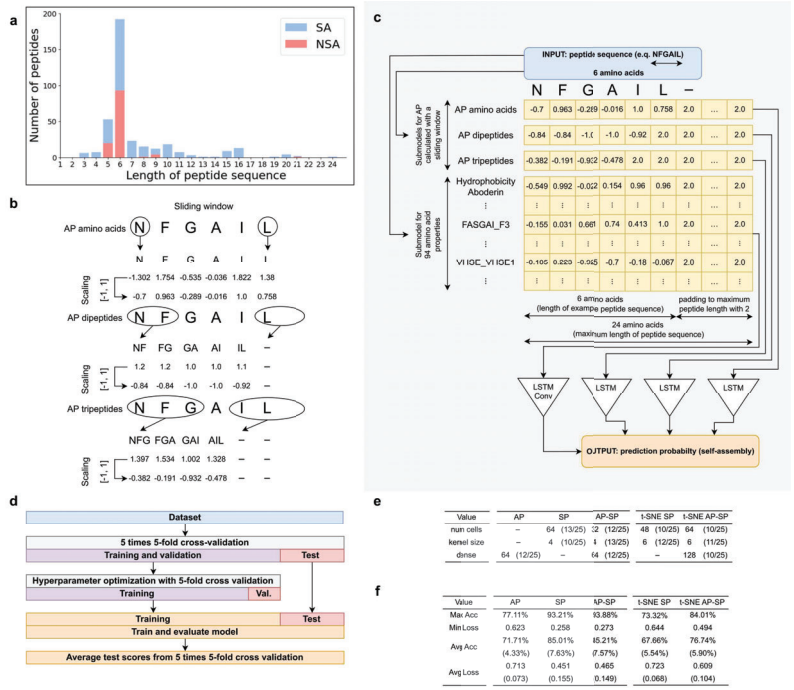

Fig. 2. **a** The distribution of peptides lengths within the dataset. The sequences were labelled by their experimentally confirmed self-assembly status. **b** Schematic representation of the sliding window pre-processing procedure identifying individual amino acids, di- and tri- peptides within the sequence. **c** Structure of the input data for an example sequence NFGAIL and a hybrid AP-SP RNN model. **d** Model construction workflow diagram. **e** Hyperparameter values selected by grid-search optimisation, along with the number of occurrences. 'Num cells' represents the number of cells in a bidirectional LSTM layer, 'kernel size' is the kernel size used in the convolutional layer, while 'dense' presents the number of units in the final densely connected layer of the model. **f** Maximum accuracy, minimal loss, and average accuracy and loss during training, along with standard deviations.

3. Architectures and respective performance assessments

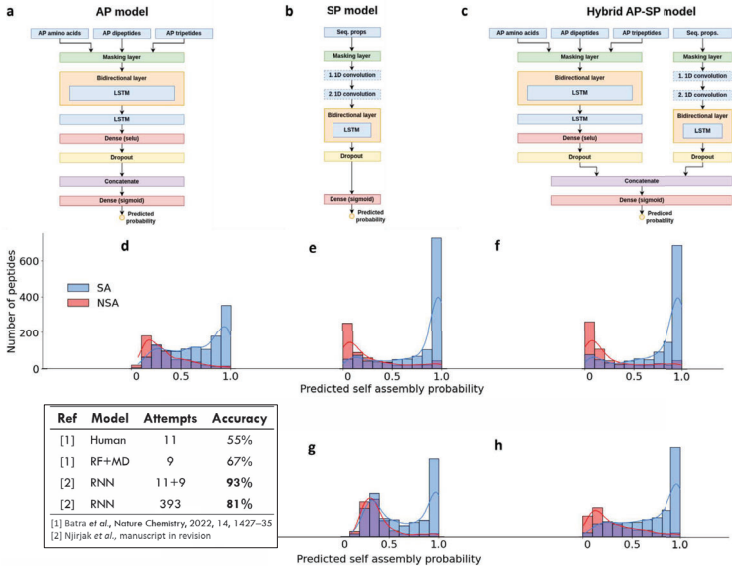

Ref	Model	Attempts	Accuracy
[1]	Human	11	55%
[1]	RF+MD	9	67%
[2]	RNN	11+9	**93%**
[2]	RNN	393	81%

[1] Batra *et al.*, Nature Chemistry, 2022, 14, 1427–35
[2] Njirjak *et al.*, manuscript in revision

Fig. 3. Schematic representations of the architectures of the RNN models for **a** the AP model, **b** the SP model, and **c** the hybrid AP-SP model. Histograms of the self-assembly prediction probability distribution on the aggregated test folds for **d** the AP model, **e** the SP model, **f** the hybrid AP-SP model, **g** the SP model with t-SNE, and **h** the hybrid AP-SP model with t-SNE, for the experimentally confirmed SA peptides (blue) and NSA peptides (red).

4. Applicability of the proposed model: Self-assembly potential in unexplored sequence space

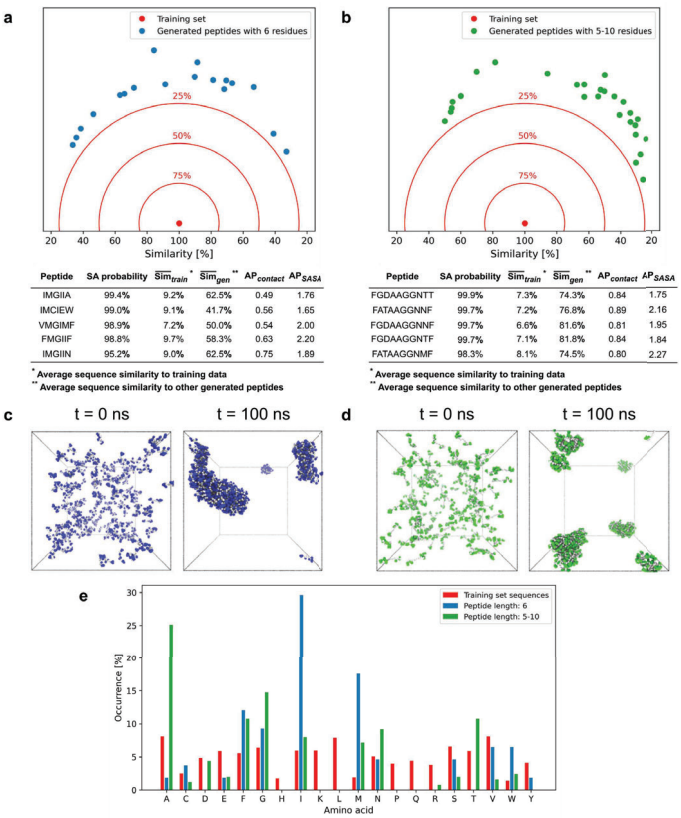

Peptide	SA probability	$\overline{Sim}_{train}$ *	$\overline{Sim}_{gen}$ **	$AP_{contact}$	AP_{SASA}
IMGIIA	99.4%	9.2%	62.5%	0.49	1.76
IMCIEW	99.0%	9.1%	41.7%	0.56	1.65
VMGIMF	98.9%	7.2%	50.0%	0.54	2.00
FMGIIF	98.8%	9.7%	58.3%	0.63	2.20
IMGIIN	95.2%	9.0%	62.5%	0.75	1.89

* Average sequence similarity to training data
** Average sequence similarity to other generated peptides

Peptide	SA probability	$\overline{Sim}_{train}$ *	$\overline{Sim}_{gen}$ **	$AP_{contact}$	AP_{SASA}
FGDAAGGNTT	99.9%	7.3%	74.3%	0.84	1.75
FATAAGGNNF	99.7%	7.2%	76.8%	0.89	2.16
FGDAAGGNNF	99.7%	6.6%	81.6%	0.81	1.95
FGDAAGGNTF	99.7%	7.1%	81.8%	0.84	1.84
FATAAGGNMF	98.3%	8.1%	74.5%	0.80	2.27

* Average sequence similarity to training data
** Average sequence similarity to other generated peptides

Fig. 4. **The peptides were generated using a genetic algorithm guided by the hybrid AP-SP model and validated using MD simulations.** A plot depicting the similarities between the generated peptides and the sequences used for model training, along with the accompanying table containing five generated sequences with the highest probability of self-assembly for **a** hexapeptides and **b** peptides with lengths between five and ten residues. The ability of the generated peptides to aggregate was validated using MD simulations where the initial (0 ns) and final (200 ns) frames of the simulation are shown for an example **c** hexapeptide (FMGIIF) and **d** decapeptide (FATAAGGNNF). **e** Comparison of amino acid distributions within the training dataset, generated sequences with six residues, and generated sequences with five to ten residues.

5. Consensus motifs

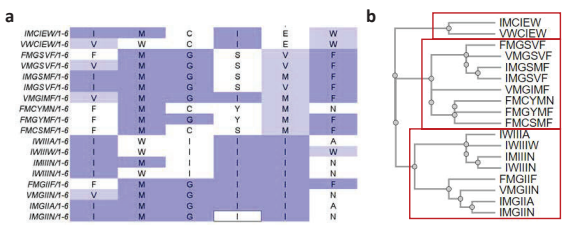

Fig. 5. **Sequences from the final population of an example generative run**, aimed at investigating the convergence of the generative approach. Only a single occurrence of each peptide in the final population was retained to prevent redundancy. Distinct motifs can be observed: **a** BLOSUM62 coloring, ClustalW multiple sequence alignment; **b** main motif groups and **c** sequence logo showing the main consensus motif obtained by an example generative run for hexapeptides.

References:

1. P. Janković, I. Šantek, A.S. Pina, D. Kalafatovic. Exploiting Peptide Self-Assembly for the Development of Minimalistic Viral Mimetics. ***Front. Chem., 2021; 9:723473***
2. G. Mauša, M. Njirjak, E. Otović, D. Kalafatovic. Configurable soft computing-based generative model: The search for catalytic peptides. ***MRS Adv., 2023;8: 1068–74.***
3. E. Otović, M. Njirjak, D. Kalafatovic, G. Mauša. Sequential Properties Representation Scheme for Recurrent Neural Network-Based Prediction of Therapeutic Peptides. ***J. Chem. Inf. Model. 2022;62(12): 2961-72.***
4. M. Negovetić, E. Otović, D. Kalafatovic, G. Mauša. Efficiently solving the curse of feature-space dimensionality for improved peptide classification. ***Digit. Discov., 2024,3, 1182-93***
5. M. Njirjak, L. Žužić, M. Babić, P. Janković, E. Otović, D. Kalafatovic, G. Mauša. AI-driven generative approach guided by hybrid deep learning. 2024; *in revision in* ***Nat. Mach. Intell.***

Acknowledgements:

1. *Croatian Science Foundation (UIP-2019-04-7999, DOK-2021-02-3496, DOK-2020-01-4659)*
2. *University of Rijeka (uniri-23-78, uniri-23-16, UNIRI-INOVA-3-23-2)*

Scoring the Synthesizability of Any Novel Non-natural Amino Acid

Gökçe Geylan[ab*], Mikhail Kabeshov[a], Samuel Genheden[a], Christos Kannas[a], Thierry Kogej[a], Ola Engkvist[ac], Leonardo De Maria[d]

a. Molecular AI, Discovery Sciences, BioPharmaceuticals R&D, AstraZeneca, Gothenburg, Sweden.
b. Division of Systems and Synthetic Biology, Department of Life Sciences, Chalmers University of Technology, Gothenburg, Sweden.
c. Department of Computer Science and Engineering, Chalmers University of Technology and University of Gothenburg, Gothenburg, Sweden
d. Medicinal Chemistry, Research and Early Development, Respiratory & Immunology, BioPharmaceuticals R&D, AstraZeneca, Gothenburg, Sweden

* Email: gokce.geylan@astrazeneca.com



https://doi.org/10.17952/37EPS.2024.P2276

Abstract

The introduction of solid-phase peptide synthesis (SPPS) has transformed peptide design and synthesis. While nowadays dozens of non-natural amino acids (NNAAs) are available from vendors to be used in peptide synthesizers, the NNAA chemical space is vast and still unexplored. Enabling any in-silico screened NNAAs for solid-phase synthesis requires to: i) introduce the right protecting groups and ii) synthesize them in adequate amounts. In this work, we introduce tools for cheminformatically protect any novel amino acid to be used in solid-phase synthesis and to score the synthesizability of the so obtained molecule. Our tool not only offers a synthesizability retrosynthesis score of the NNAAs but also can be used for ranking of the potential protection strategies, thus increasing the synthetic feasibility.

1. Introduction

While dozens of NNAAs are currently available for peptide synthesizers, there is still a vast unexplored chemical space awaiting discovery. We have recently shown how this space can be significantly expanded, enumerating ~400000 novel alpha NNAAs and using 10,000 representatives to predict improved peptide binding affinities and solubility (Fig 1).[1,2] In this work we show how to add synthesizability considerations in our computational workflow.

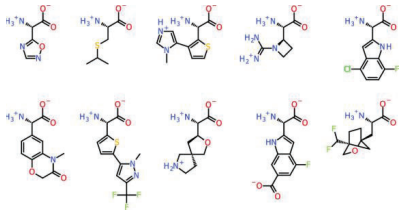

Figure 1. Examples of novel non-natural amino acids from our virtual library[2]

Computational protocols work on un-protected amino-acids and incorporating a novel NNAA on a peptide requires the synthesis of the SPPS specifically protected compound. The protection strategy requires careful consideration of the protecting groups for sidechains and backbones. Here, we introduce a tool for evaluating the synthetic feasibility of any protected non-natural amino acid, after finding the optimal protection strategy. The proposed synthesizability score can be used as additional in-silico parameter for compound selection.

2. Methods

I. Generate Protected Compounds. A cheminformatics tool was built to obtain multiple protected versions of each NNAA, suitable for SPPS.[3]

II. Retrosynthesis scoring. We used our single-step retrosynthesis model (AiZynthFinder[4]) trained on USPTO data and the stocks for eMolecules[5]. The generated routes were scored by accumulating scores for the reactions in the route and were filtered with the feasibility predicted by a forward Chemformer model[6]. Finally, the routes were scored with a rank score for reaction class based on historical data, referred as the Synthetic Feasibility (SF) score.

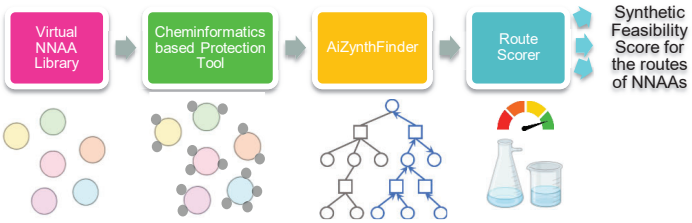

Figure 2. Schematic representation of the scoring workflow

3. Results

A. Retrosynthesis Planning for a novel NNAA

Problem: A peptide designed *in-silico* included a novel NNAA. Next, the NNAA must be synthesized and protected to be used in SPPS for experimental testing the predicted improved peptide.

Solution: Our tool enables ranking and choosing the most feasible protection strategy for a novel NNAA upon retrosynthesis planning.

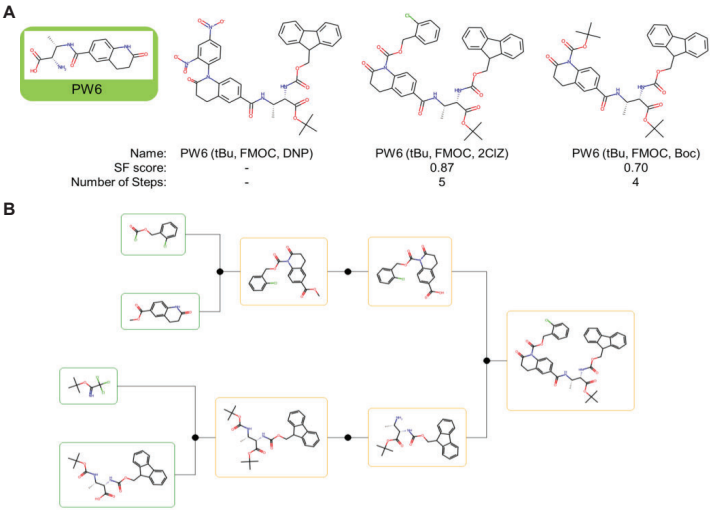

Figure 4. Route Enumeration & Scoring
A) The protected series for amino acid "PW6" and B) the most synthesizable route of the protected PW6

B. Application to Virtual Screening

Problem: Adding a synthesizability score to binding-affinity predictions for compound selection. We used as model system the N-acetylated 9-mer peptide, $^{(76)}$LDEETGEFL$^{(84)}$ and targeted the Glu78 position to find novel NNAAs leading to improve its binding affinity to KEAP1. A site-specific mutation docking protocol was used for the 10,000 representative novel a-NNAAs[2].

Outcome: Our tool facilitates synthesizability-aware compound selection.

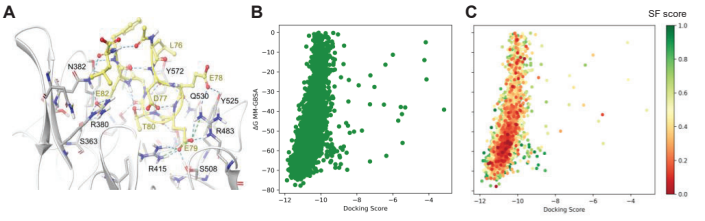

Figure 3. Virtual Screening plus Synthetic Feasibility (SF) Score
The docking of the NNAA library to position Glu78 in A) Keap1 in Keap1−Neh2 binding site structure, adapted from Amarasinghe et al[2]. The plots showing B) the docking scores for NNAAs, C) the docking scores colored by the SF score.

Conclusions & Future Directions

- Our synthesizability tool:
  - Creates multiple protected versions of a given non-natural amino acid
  - Considers SPPS specifical protection groups
  - Scores the synthesizability of each route
  - Facilitates the evaluation of retrosynthesis planning
- Our tool can be used to:
  - Rank the synthetic feasibility of all the protection strategies for a given novel NNAA
  - In addition to other peptide optimization scoring functions

We are conducting validation studies on the synthesis and characterization of some of the non-natural amino acids for the KEAP1-NEH2 model system.

References

1. Oeller et al (2023) *Sequence-based prediction of the intrinsic solubility of peptides containing non-natural amino acids* Nat. Comm. **14**, 1. DOI: 10.1038/s41467-023-42940-w
2. Amarasinghe et al (2022) *Virtual Screening Expands the Non-Natural Amino Acid Palette for Peptide Optimization* J. Chem. Inf. Mod. **62**, 2999. DOI: 10.1021/acs.jcim.2c00193
3. Wuts & Greene (2006) *Greene's Protective Groups in Organic Synthesis* DOI: 10.1002/0470053488
4. Saigiridharan et al (2024) AiZynthFinder 4.0: developments based on learnings from 3 years of industrial application. J. Cheminf. **16**, 1. DOI: 10.1186/s13321-024-00860-x
5. eMolecules (https://www.emolecules.com)
6. Westerlund et al (2024) Do Chemformers Dream of Organic Matter? Evaluating a Transformer Model for Multistep Retrosynthesis. J Chem. Inf. Model. **64**, 3021. DOI: 10.1021/acs.jcim.3c01685

Supported by AstraZeneca

Presented at the 37th European Peptide Symposium and 14th International Peptide Symposium, Florence, Italy 25-29 August 2024

https://doi.org/10.17952/37EPS.2024.P2277

Chemoenzymatic synthesis of protein pseudo-[2]rotaxane

Elodie Soehnlen,[1] Shalene Ofner,[1] Judit Osz,[2] Natacha Rochel, [2] Vladimir Torbeev, [1]

[1]*Équipe de Chimie des Biosystèmes, ESBS, UMR 7242 Biotechnologie et Signalisation Cellulaire, Illkirch, France*

[2]*Équipe de Chimie biophysique de la signalisation transcriptionnelle, Institut de Genetique et de Biologie, Moleculaire et Cellulaire (IGBMC), INSERM (U1258), University of Strasbourg, CNRS, UMR 7104, Illkirch, France*

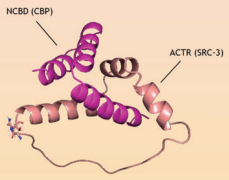

Introduction :

Intrinsically disordered proteins (IDPs) display enhanced conformational flexibility and structural heterogeneity. They are able to recognize diverse molecular targets and engage in multivalent interactions[1]. For instance, transcriptional co-activators ACTR (p160) and p300/CBP contain IDP regions which are involved in the formation of multiprotein complexes with nuclear receptors regulating the transcription of many genes. These proteins are overexpressed in breast and ovarian cancers[2,3].

Goal of the project :

Target and disrupt protein-protein interactions between ACTR and NCBD. To do this, we want to increase the stability of the ACTR/NCBD complex by linking the two domains through non-covalent interactions enhanced by non-classical topology (pseudo-[2]rotaxane protein complex) .

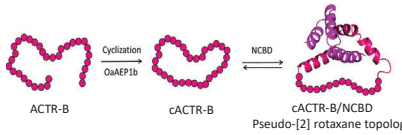

Complex :

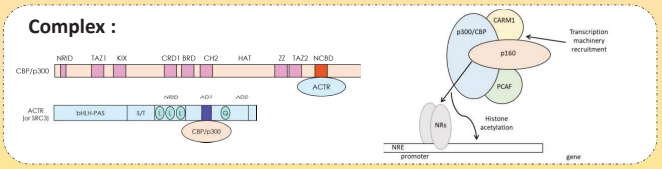

Chemoenzymatic synthesis

Native Chemical Ligation (NCL)

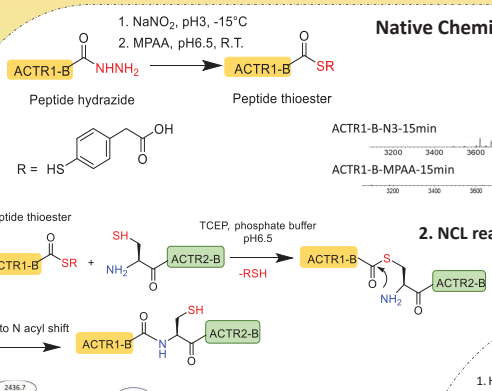

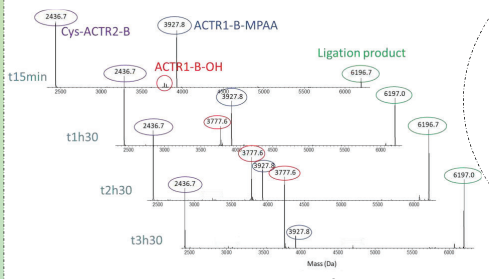

Enzyme asparaginyl endopeptidase



Motif of recognition for cyclization by OaAEP1b

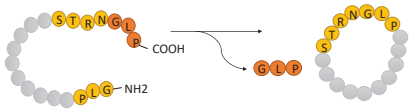

Proposed mechanism of AEPs catalysis

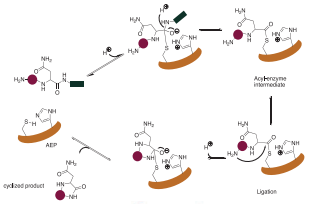

AEP activation and improvement of the catalytic efficiency with AEP C247A mutant

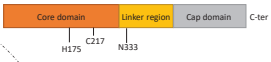

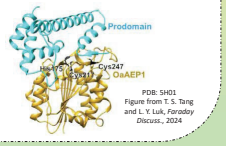

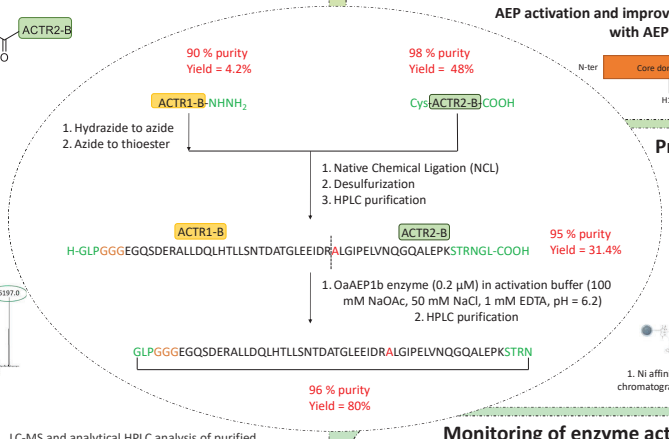

Production and purification of AEP C247A mutant

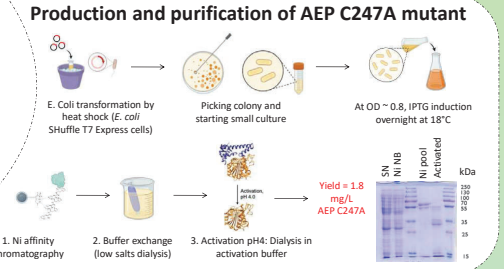

Cyclization

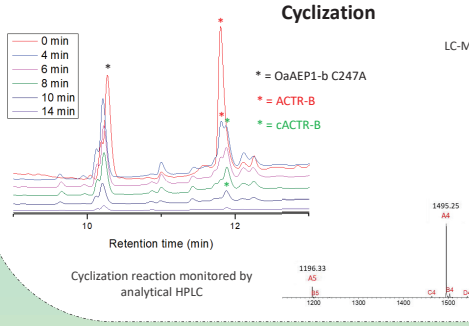

Cyclization reaction monitored by analytical HPLC

LC-MS and analytical HPLC analysis of purified cACTR-B (MW = 5978.55 g/mol)

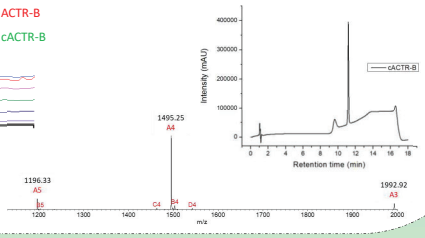

Monitoring of enzyme activation by FRET

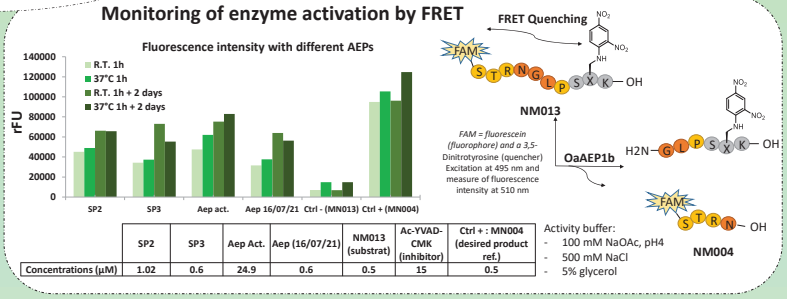

	SP2	SP3	Aep Act.	Aep (16/07/21)	NM013 (substrat)	Ac-YVAD-CMK (inhibitor)	Ctrl + : MN004 (desired product ref.)
Concentrations (µM)	1.02	0.6	24.9	0.6	0.5	15	0.5

Activity buffer:
- 100 mM NaOAc, pH4
- 500 mM NaCl
- 5% glycerol

Biophysical characterization and cell penetration studies

Circular Dichroism (CD)

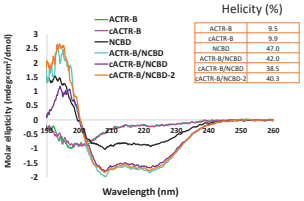

Helicity (%)

ACTR-B	9.5
cACTR-B	9.9
NCBD	47.0
ACTR-B/NCBD	42.0
cACTR-B/NCBD	38.5
cACTR-B/NCBD-2	40.3

Thermal Denaturation (TD)

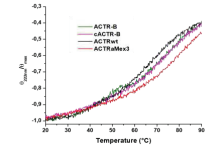

Variant	Thermal denaturation
ACTR-B/NCBD	86°C
cACTR-B/NCBD	79°C
ACTR/NCBD W.T.*	67°C
ACTRαMex3*	110°C

* Data from Alexis Jouin, PhD student in the team of Biosystem chemistry

Isothermal Titration Calorimetry (ITC) of cACTR-B

Series of 23 injections of cACTR-B solution into NCBD solution

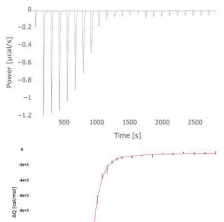

Variant	K_d (nM)	ΔH (cal.mol^{-1})	ΔG (kcal.mol^{-1})	-TΔS (kcal.mol^{-1})
cACTR-B	170.0	-16344	-9.4	6.9
ACTRwt	206.0	-12700	-9.3	3.4

→ Better binding for cACTR-B than W.T.
→ Decreasing of enthalpy and increasing of entropy → More interaction that stabilize the complex and destabilization because less freedom of conformation degree (enthalpy-entropy compensation)

Fluorescence polarization measurement (FP measurement)

Direct FP measurement: Binding study of cACTR-B/NCBD complex (N=3)

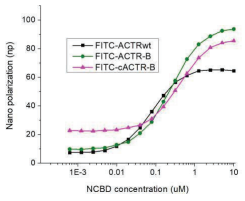

Variant	K_d (nM)
ACTR-B	167.7
cACTR-B	102.1
ACTRwt	57.7

FITC is not in the same place for ACTRwt than ACTR-B and cACTR-B

Competition binding experiment: Targeting NCBD domain in full length 265 kDa CBP (N=3)

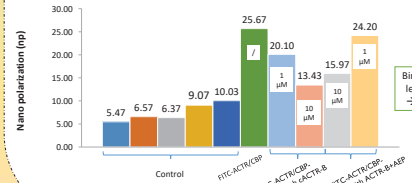

Binding of cACTR-B to full lenght CBP is confirmed → Binding mechanism ?

Cell penetration studied by confocal microscopy

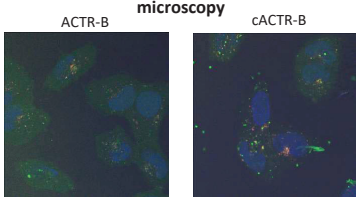

Cell uptake of ACTR-B and cACTR-B (10 µM peptide, 1h treatment in PBS, U2OS cell line)

Quantitative determination of cell uptake by flow cytometry

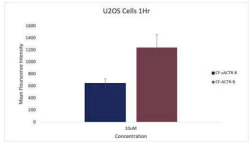

Mean fluorescence intensity of CF-cACTR-B (10 µM) and CF-ACTR-B (10 µM) (p-value = 0.014) (1 h treatment at 37°C in PBS)

Conclusion and perspectives

ACTR-B could be chemically synthesized and cyclized enzymatically via the ligase asparaginyl endopeptidase. cACTR-B/NCBD pseudo-[2]rotaxane complex was formed. CD analysis shown an helical structure similar for ACTR-B/NCBD and cACTR-B/NCBD complex. We proved that complex cACTR-B/NCBD and ACTR-B/NCBD have an higher thermal denaturation than ACTRwt/NCBD. It was found that cACTR-B is a better binding with NCBD compare to ACTRwt. Fluorescence polarization measurement allowed us to see a binding between cACTR-B and NCBD, but also full length CBP. For the future it would be interesting to determine the binding mechanism between this cyclic cACTR-B and NCBD (and CBP) and get a cristal structure of the complex. The next step will be to study the biological impact of cACTR-B into cells.

References

1. *Oldfield C. J. and Dunker A. K. , Annu. Rev. Biochem., 2014, 83, 553–584*
2. Demarest S.J., Martinez-Yamout M., Chung J., Chen H., Xu W., Dyson H. J., Evans R. M., and Wright P. E., *Nature*, 415, 549–553, 2002
3. *Shammas S. L. , Curr. Opin. Struct. Biol., 2017, 42, 155–161*
4. *Harris K. S., Durek T., Kaas Q., Poth A. G., Gilding E. K., Conlan B. F., Saska I., Daly N. L., van der Weerden N. L., Craik D. J., Anderson M. A., Nat. Commun., 2015*

https://doi.org/10.17952/37EPS.2024.P2279



Structural and Mechanistic Insights Into the Advances of FXIIIa Inhibitors

Ivan P. Bogdanov[1], Arijit Biswas[2], Diana Imhof[3], Nikolay T. Tzvetkov[1,*]

1) Institute of Molecular Biology, Bulgarian Academy of Sciences, Acad. G. Bonchev str. Bl. 21, Sofia 1113, Bulgaria
2) Institute of Experimental Hematology and Transfusion Medicine, University Hospital Bonn, Venusberg Campus-1, D-53127 Bonn, Germany
3) Pharmaceutical Biochemistry and Bioanalytics, Pharmaceutical Institute, University of Bonn, An der Immenburg 4, D-53121 Bonn, Germany

***Corresponding author:** ntzvetkov@bio21.bas.bg*

Introduction

Cardiovascular diseases (CVDs) represent a major problem to humanity, having the highest mortality rates (above 85% of the deaths caused are due to heart attacks and strokes) in the category of natural causes [1]. The fast treatment with anticoagulants inhibiting the activity of blood clotting factors represents a promising approach to stop the clot formation (thrombosis), and therefore, to protect the patients from fatal consequences. Inhibitors targeting blood clotting factor XIIIa (FXIIIa), that is involved in the last step of coagulation process, have been considered as a new generation of anticoagulants [2]. Plasma FXIIIa is an enzyme, belonging to the family of transglutaminases (TGase), which is primary responsible for stabilization of the fibrin network by stabilizing the preformed clot.

In the current study we aim at:

- Performing a three-step virtual screening (VS) approach in order to estimate binding affinities (steps 1–3, Fig. 1) of a rationally selected set of small drug-like compounds using Single Crystal X-Ray Diffraction (SCXRD) technique in combination with the molecular modelling platform SeeSAR [3].
- Identifying of a set of FXIIIa inhibitors based on their predicted affinity ranges ($K_{i\ HYDE}$ scores), physicochemical and drug-like properties (see Table 1 and 2, Fig. 2 and 3).

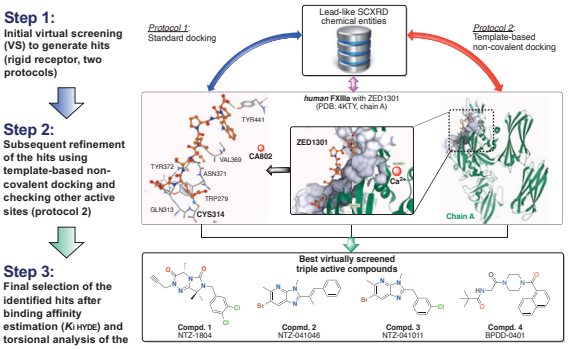

Figure 1. Three-step VS approach of SCXRD chemical entities on human FXIIIa leading to the best scored compounds **1–4**.

SeeSAR visualization and HYDE analysis

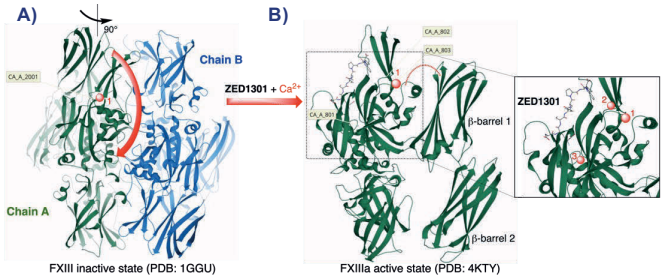

Figure 2: A) SeeSAR visualization of the inactive state of FXIII (PDB: 1GGU) [4], in which FXIII exists as a dimer (Chain A in green and Chain B in blue). B) After binding of the substrate **ZED1301** (off-white, *cf.* Fig. 1) the β-barrel 1 and 2 moved (red arrow) and together with Ca^{2+}-binding (three Ca^{2+} instead one in FXIII) is activated to its active form FXIIIa (PDB: 4KTY) [5].

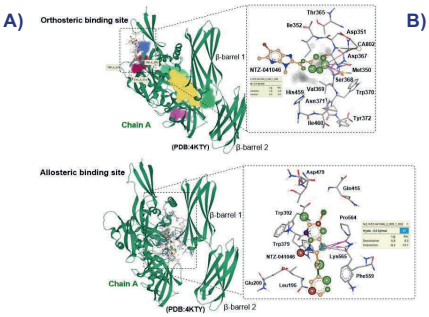

Figure 3: A) SeeSAR visualization of orthosteric and allosteric binding of **NTZ-041046** to *h*FXIIIa. B) HYDE analysis of desolvation effects (lipophilic interactions) and torsions for **NTZ-041046** within the catalytic domain of the activated form of FXIIIa. HYDE coloring and torsion analysis: **green** = good, **red** = bad for affinity.

Modeling of transitional states and predicted energies of FXIII

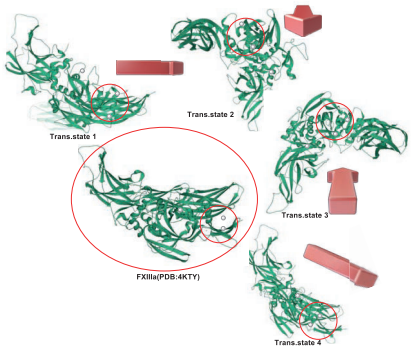

Figure 4. Transitional state models of FXIII generated with HADDOCK 2.4 web server.

Cluster№	Van Der Waals energy [kcal/mol]	Desolvation energy [kcal/mol]	Electrostatic energy [kcal/mol]	RMSD [Å]	Restraints violation energy [kcal/mol]	HADDOCK score [a.u.]
12.1-12.4	-33.8 ± 11.5	12.1 ± 3.8	-275.0 ± 66.6	32.5 ± 0.1	9.9 ± 9.3	-75.7 ± 17.7

PDB Energy and Energy minimization (kJ/mol)							
Cluster 12.1		Cluster 12.2		Cluster 12.3		Cluster 12.4	
Energy[1]	Minimized[2] Energy	Energy[1]	Minimized[2] Energy	Energy[1]	Minimized[2] Energy	Energy[1]	Minimized[2] Energy
-76.681	-80.806	-65.661	-82.090	-66.514	-81.585	-66.677	-81.897

Transition state models



Table 1. Top scored cluster according to HADDOCK combining the different energies (the more negative the better). Energy optimization was performed to determine the lowest energies of the structures. [1] initial and [2] minimized energy.

Ligands	$K_{i\ HYDE}$ lower boundaries (μM) (SeeSAR/HYDE prediction)		
	*h*FXIIIa	*Trans.state* *h*FXIIIa (Cl. 12.2)	*TG2* (2Q3Z)
ZED1301	0.07 **100 [6]**	0.09	2000 **3000 [6]**
Compd. 1	0.75	340	2315
Compd. 2	1.22	31.3	5.56
Compd. 3	1.53	0.03	188
Compd. 4	0.55	336	16.7

Table 2. Receptor binding data and HYDE estimated binding affinity for the human FXIIIa and FXIII generated models as well as the transglutaminase 2 (TG2) enzymes of **ZED1301** inhibitor and ligands **1–4**.

Conclusions

SCXRD/SeeSAR/HYDE concept: An innovative drug design concept combining a X-ray (SCXRD) technique and a protein target (human FXIIIa enzyme) that is related to CVDs pathophysiology with a molecular modeling platform SeeSAR/HYDE was used to identify a small set of promising ligands (compounds **1–4**).

Proof-of-concept: The estimated binding affinities ($K_{i\ HYDE}$ ranges) combining both physicochemical and drug-like properties, as well as torsional and thermodynamic analysis, suggested that these four compounds may be used for further development of new FXIIIa inhibitors as anticoagulants against thrombosis. However, the subsequent experiments partly confirmed their estimated (predicted) inhibitory potencies against FXIIIa.

Acknowledgments: This work is supported by the Bulgarian National Science Fund (BNSF) under Grant No. **KP-06-N59/2 (КП-06-Н59/2)**.

Literature

[1] World Health Organization. *WHO* 2021-22.
[2] R. A. Al-Horani & S. Kar *Eur. J. Med. Chem.* **2020**.
[3] www.biosolveit.de/SeeSAR (SeeSAR v.13.0, **2024**).
[4] B. A. Fox et al. *J. Biol. Chem.* **1999**.
[5] M. Stieler et al. *Angew. Chem. Int. Ed. Engl.* **2013**.
[6] Oertel et al. *Anal. Biochem.* **2007**.

Can large scale structural modeling be applied to peptide screening and deorphanization?

Shaima Hashem[a], Jérôme Leprince[b], Pierre Tuffery[a]

[a]BFA, Université Paris Cite, CNRS UMR 8251, Inserm U1133, Paris, France
[b]University Rouen Normandie, Inserm, NorDiC UMR 1239, F-76000 Rouen, France

Contact: pierre.tuffery@u-paris.fr

https://doi.org/10.17952/37EPS.2024.P2280

Background and objectives

– Peptides are ubiquitous in all living organisms and associated with varied fundamental physiological and biochemical processes. They are also becoming valuable therapeutic candidates, especially to modulate targeted protein-protein interactions.
– Thanks to the progress of techniques such as mass spectrometry, or large-scale genome analysis, more and more endogenous peptides are identified but frequently, their targets remain unknown. Their identification is referred to as the ***peptide deorphanization problem (1 peptide, n targets)***. It has motivated efforts in the past years, either from the experimental [1] or theoretical side [2].
– Conversely, for peptide therapeutic development, the target is usually known and one wishes to identify the best peptide targeting it among a collection of candidates. This is referred to as the ***peptide screening problem (1 target, n peptides)***.
– Recent advances in deep learning-based protein structure prediction [3,4] suggest it is possible to predict the effective interaction of protein (and peptides ?) thanks to their associated confidence scores, which motivates the development for in silico protocols to address peptide screening and deorphanization (e.g. [2]).

Here, our objectives are:
1: assess Alphafold2 performance for peptide deorphanization and screening for known binders of G Protein Coupled Receptors (GPCRs).
2: assess Alphafold2 performance for the ranking of peptides identified *in vitro* using PEPscan.

Materials

– **GPCR test set (GPCRts)**: It consists of 366 GPCR sequences corresponding to sequences extracted from the IUPHAR resource [5] on date of September 22nd, 2022.
– **GPCR peptide binders (GPCRpb)**: a set of 14 peptides known as GPCR binders, where the GPCR belongs to the GPCR test set (see Table 1)
– **PEPscan dataset**: a collection of peptides identified in vitro using PEPscan, scanning 7 protein complexes of known structures, as in [6].

Name	Sequence	Target
alphaMSH	SYSMEHFRWGKPV	Q01727
angiotensin II	FDPRHVIY* / DRVYIHPF (*: scramble)	P35351
apelin	KFRRQRPRLSHKGPMPF	Q9JHG3
bradykinin	RPPGFSPFR	P25023/ P97583
Cholecystokinin	DYMGWMDF	P30551
CRH	SEEPPISLDLTFHLLREVLEMARA EQLAQQAHSNRKLMEII	P47866
Galanin	GWTLNSAGYLLGPHAIDNHRSFS DKHGLT	O08726
Ghrelin	GSSFLSPEHQKAQQRKESKKPP AKLQPR	O08725
glucagon	HSQGTFTSDYSKYLDSRRAQDF VQWLMNT	P30082
NeuromedinB	GNLWATGHFM	P24053
NeuromedinU	FFLFRPRN	Q9JJI5
NeuropeptideS	SFRNGVGSGV / SFRNGVGSGVKKTSFRRAKQ	P0C0L6
NeuropeptideW	WYKHVASPRYHTVGRASGLLMG LRRSPYLW	P48146
Oxytocin	CYIQNCPLG	P70536

Table 1: *GPCR binders (GPCRpb), with their sequences and the Uniprot Id of their true receptor*

Methods

To evaluate if a peptide interacts with a protein, we generate 3D models using the Alphafold2 framework [3], and analyze the scores associated with the complexes. We assume that the best scores will make it possible to identify the best pairs of partners.

– **Peptide-protein complex generation**: We have used Colabfold [7] version 1.5, using *multimer_v3* weights, enabling dropout, using 5 recycles and 5 seeds (resulting in 25 models). For the PEPScan analyses, the number of seed was increased to 20 (100 models). Given the size of some sequences, calculation have been performed using A100 GPUs thanks to the RPBS platform [8].

– **Peptide-protein complex scoring:** For each model we have then extracted the alphafold's **ipTM** (observed best score in [2]), the **pDockQ** and **pDockQ2** scores.

– **Deorphaning**: For each peptide of the **GPCRpb** set, we have considered the models generated with each member of the GPCRts collection (25 x 366 = 9150 models), and ranked them according to several confidence indexes (Alphafold2' ipTM, pDockQ and pDockQ2 [9]). The **Comb** score corresponds to a combination of the rankings obtained using ipTM and pDockQ2, with the assumption that if both scores rank a GPCR well, then it is more likely to truly interact with a peptide. In practice, we average the ranks (between 1 and 366) obtained using the ipTM and pDockQ2, but cases for which at least one score ranks the GPCR at a position greater than a value (200 here) are considered as too unlikely to be a binder, and the GPCR is removed from the list.

– **Screening**: For each peptide of the **GPCRpb** set, we have considered the models generated with each of their true binders in the GPCRts collection (25 x 14 = 350 models), and ranked them as for the deorphaning experiment.

– **PEPscan candidate validation**: Assess the ranking of the candidate peptide at protein-protein interface among all candidates identified using PEPscan for the target protein.

Results (1)
Peptide deorphanization

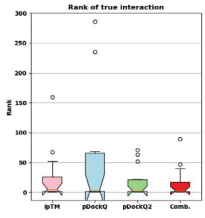

Figure 1: *Distribution of ranks for different scores.*

	ipTM	pDockQ	pDockQ2	Comb
mean	24.8	55.2	17.6	16.0
median	5	3.5	2.0	2.5
top10	9	9	9	9

Table 2: *Mean, median ranks of the true binders. Top10: number of targets for which the true binder is ranked 10 or less (over 366).*

Main observations:
- The true binders are in the best 10% for all cases but 2 (86%)
- The protocol ranks in the top10 the true receptor for 9 out of 14 cases (64%), independently of the score.
- The pDockQ2 improves largely over the pDockQ

- The different scores rank poorly the same targets. For alphaMSH and NeuropeptideS, the rank of the true receptor is of more than 40. For Ghrelin and NeuromedinU, the scores vary the most, one of the score only ranking the true target in the best 10%.
- Consequently, combining the rankings obtained using the ipTM and the pDockQ2 (Comb) improves only marginally the performance.

Results (2)
Peptide screening

Name	Rank			Target
	ipTM	pDockQ2	Comb	
alphaMSH	3	3	2	Q01727
angiotensin II	2	2	2	P35351
apelin	2	1	1	Q9JHG3
bradykinin	1	1	1	P25023
Cholecystokinin	1	1	1	P30551
CRH	1	1	1	P47866
Galanin	1	1	1	O08726
Ghrelin	**12**	**4**	**9**	O08725
glucagon	1	1	1	P30082
NeuromedinB	1	1	1	P24053
NeuromedinU	2	4	2	Q9JJI5
NeuropeptideS	**4**	**8**	**5**	P0C0L6
NeuropeptideW	2	1	1	P48146
Oxytocin	1	2	1	P70536

Table 3: *Rank of the true binder according to different scores (see methods)*

Main observations:
- The natural binders are ranked in the top 3 for all cases but 2.
- Ranking heterogeneity depending on the scores is observed for the 2 poorly predicted targets.
- The pDockQ2 values are usually very low, suggesting pDockQ2 is irrelevant for peptides/protein interactions.
- The number of cases is however too limited to draw general conclusions.

Results (3)
In-Silico PEPscan validation

Motivation: PEPscan is an *in vitro* approach to identify candidate interfering peptides to modulate protein-protein interactions. In previous studies, we have shown that it returns a limited number of candidates among which some are located in the vicinity of protein-protein interface. Here, we assess if Alphafold2 is able to discriminate the best interfering candidate among all the candidates.

PDB	Name	#ip	Rank		#if	Name	#ip	Rank		#if
			ipTM	pDQ2				ipTM	pDQ2	
1e96	NCF2	7	N/A	N/A	N/A	Rac1	4	**1**	**1**	4
1ktz	TGFβ3	12	12	12	9	TGFR2	8	**1**	**1**	0
1m27	SAP	4	3	3	0	FynSH3	4	2	**1**	0
1lfd	RalGDS	2	2	**1**	2	Ras	8	3	3	2
2j0t	MMP-1	5	3	4	3	TIMP1	2	**1**	**1**	2
3bx7	NGAL	8	2	2	6	CTLA-4	2	**1**	**1**	2
1eer	EPO	1	N/A	N/A	N/A	EPOR	8	4	3	8

Table 4: *Rank of the peptide at interface according to different scores among candidate peptides identified using PEPscan. Lines present the results for the each partner of the 3D complex of the PDB entry. N/A: no peptide identified at the interface. #ip: number of peptides identified using PEPscan #if: number of peptides contacting the experimental interface over #ip*

Main observations:
- Scores best rank peptides at complex interface in only 6 cases over 12 (50%)
- For 9 cases out of 12, the poses overlap the experimental binding site.
- All peptides tend to bind to the same position on protein, suggesting a very poor specificity to identify the binding interface.

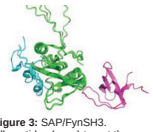

Figure 3: SAP/FynSH3. All peptides (cyan) target the same spot, not at the experimental interface

Discussion/Conclusions

Present analyses rely on the assumption that the scoring of models generated using Alphafold2 is able to discriminate models containing different entities. Note that peptides are free to bind to any place on the protein surface.
- For the GPCR deorphanization, varied receptors are confronted with a given peptide, and the results are rather satisfactory, consistently with the results in [2].
- For the GPCR peptide screening, different peptides are confronted with a given receptor. Here again, the results are encouraging.
- For the PEPscan candidate validation, the results are more ambiguous. In some cases, no pose of the peptide targets the protein-protein interface. Furthermore, all peptides tend to bind the same location on protein surface (see Figure 3), which is possibly not the desired one.

Overall, the specificity of the protein-peptide modeling is at stake, and our results suggest that it is really poor.
- When peptides are confronted with the same protein, it is possible the scores lose effectiveness due to the smaller size of the peptides compared to their target protein.
- Ranking heterogeneity is possibly an indicator of the poor performance of the scoring.

Why such a difference between PEPscan candidate validation and GPCR peptide screening ? Different hypotheses under investigation are:
- All peptides confronted with GPCRs are naturally occurring peptides whereas PEPscan candidates might exhibit different properties and correspond to a class of peptides not learnt by AlphaFold2.
- PEPscan peptides that correspond to protein fragments could be more hydrophobic than natural peptides selected during evolution, and thus be more sticky. It is however surprizing that in some cases such peptides do not target the protein-protein interface which should be more hydrophobic.

Overall our results suggest the need to develop peptide-protein specific scores to discriminate the true binders from the incorrect ones. Another challenge is that of protein-peptide binding specificity, but this supposes to go back to AlphaFold2 internal prediction scheme, especially to increase the diversity of the poses.

Acknowledgements/Funding

The authors thank R. Guerois and J. Andreani for useful discussions.

This project is supported by the MSD Avenir foundation, MSD being a trade name of Merck & Co.

References

[1] Foster, S. R., Hauser, A. S., Vedel, L., Strachan, R. T., Huang, X. P., Gavin, A. C., ... & Gloriam, D. E. (2019). Discovery of human signaling systems: pairing peptides to G protein-coupled receptors. Cell, 179(4), 895-908.
[2] Teufel, F., Refsgaard, J. C., Kasimova, M. A., Deibler, K., Madsen, C. T., Stahlhut, C., ... & Madsen, D. (2023). Deorphanizing peptides using structure prediction. Journal of chemical information and modeling, 63(9), 2651-2655.
[3] Jumper J, Evans R, Pritzel A. et al. (2021) Highly accurate protein structure prediction with AlphaFold. *Nature* 596, 583–589
[4] Bryant, P., Pozzati, G., & Elofsson, A. (2022). Improved prediction of protein-protein interactions using AlphaFold2. Nature communications, 13(1), 1265.
[5] Harding SD, Armstrong JF, Faccenda E, Southan C, Alexander SPH, Davenport AP, Spedding M, Davies JA. (2023) The IUPHAR/BPS Guide to PHARMACOLOGY in 2024. Nucl. Acids Res. 2024; 52(D1):D1438-D1449.
[6] Rebollo, A., Fliedel, L., & Tuffery, P. (2022). PEPscan: A Broad Spectrum Approach for the Characterization of Protein-Binder Interactions?. Biomolecules, 12(2), 178.
[7] Mirdita M, Schütze K, Moriwaki Y, Heo L, Ovchinnikov S and Steinegger M. (2022) ColabFold: Making protein folding accessible to all. *Nature Methods*. doi: 10.1038/s41592-022-01488-1.
[8] Alland, C., Moreews, F., Boens, D., Carpentier, M., Chiusa, S., Lonquety, M., ... & Tuffery, P. (2005). RPBS: a web resource for structural bioinformatics. Nucleic acids research, 33(suppl_2), W44-W49.
[9] Zhu, W., Shenoy, A., Kundrotas, P., & Elofsson, A. (2023). Evaluation of AlphaFold-Multimer prediction on multi-chain protein complexes. Bioinformatics, 39(7), btad424.

https://doi.org/10.17952/37EPS.2024.P2281

Impact of backbone N-amination on the stability of parallel β-sheets

Syrah K. Starnes[a], W. Seth Horne[b], Juan R. Del Valle[a]*

[a]Department of Chemistry & Biochemistry, University of Notre Dame ◆ [b]Department of Chemistry, University of Pittsburgh

BACKGROUND and OBJECTIVES

Homotypic interactions between parallel β-strands are characteristic of amyloids that underlie several neurodegenerative diseases.[1] Minimalist approaches to stabilize parallel sheet conformation can inform the design of β-strand mimics and selective ligands of pathological amyloids. Backbone amide substitution can be used to enforce specific peptide conformations without sacrificing side chain content. We previously demonstrated that backbone N-amination of linear peptides stabilizes antiparallel β-sheet folds through increased torsional strain, *cis* amide lone pair repulsion, and intraresidue hydrogen bonding.[2] Here, we investigate the impact of backbone amide N-amination on parallel β-sheet stability in a peptide parallel hairpin model, as well as in a miniprotein that exhibits a βαβ tertiary fold.

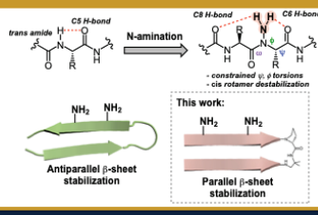

Study Objectives: (1) Determine the effect of α-hydrazino acid substitution on the folded population of a parallel β-hairpin model peptide[3]; **(2)** Incorporate α-hydrazino acids into the β-strand region of DS119 analogues and assess their impact on thermal stability[4]

RESULTS

1) A parallel β-hairpin (Pbh) model for investigating the impact of backbone amide substitution

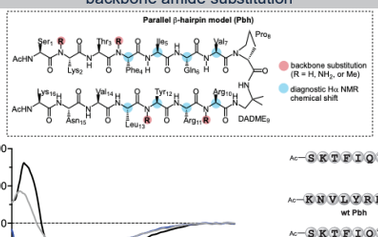

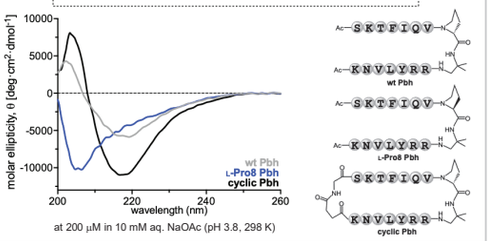

at 200 μM in 10 mM aq. NaOAc (pH 3.8, 298 K)

2) Synthesis of N-amino dipeptide building blocks suitable for SPPS

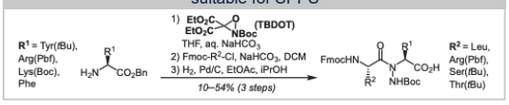

3) Synthesis of the resin-bound turn D-Pro-DADME motif

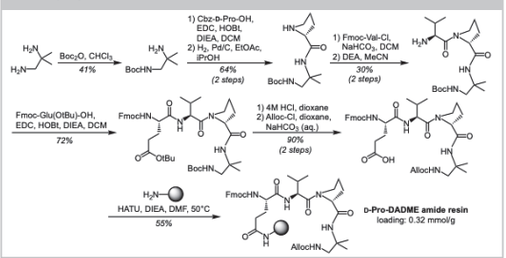

4) SPPS of parallel β-hairpin peptides featuring backbone amide substitutions

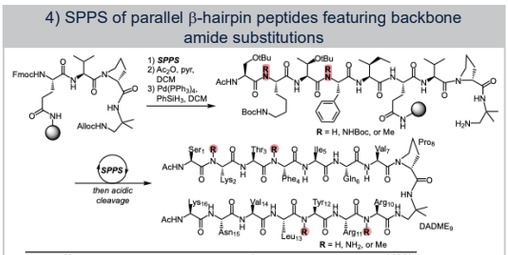

peptide	sequence*	yield %
wt Pbh	Ac–S K T F I Q V–^{D}P–dadme–R R Y L V N K–Ac	30
L-Pro8 Pbh	Ac–S K T F I Q V–**^{L}P**–dadme–R R Y L V N K–Ac	32
cyclic Pbh	**c[**G–S K T F I Q V–^{D}P–dadme–R R Y L V N K–**suc]**	10
aLys2 Pbh	Ac–**SaK** T F I Q V–^{D}P–dadme–R R Y L V N K–Ac	23
MeLys2 Pbh	Ac–**SMeK**T F I Q V–^{D}P–dadme–R R Y L V N K–Ac	31
aPhe4 Pbh	Ac–S K **TaF** I Q V–^{D}P–dadme–R R Y L V N K–Ac	15
MePhe4 Pbh	Ac–S K **TMeF**I Q V–^{D}P–dadme–R R Y L V N K–Ac	19
aTyr12 Pbh	Ac–S K T F I Q V–^{D}P–dadme–R **aY L** V N K–Ac	12
MeTyr12 Pbh	Ac–S K T F I Q V–^{D}P–dadme–R **MeYL** V N K–Ac	8
aArg10 Pbh	Ac–S K T F I Q V–^{D}P–dadme–**aRR** Y L V N K–Ac	11
MeArg10 Pbh	Ac–S K T F I Q V–^{D}P–dadme–**MeRR**Y L V N K–Ac	19

* aX = Nα-amino Xaa, MeX = Nα-methyl Xaa

5) Backbone N-amino and N-methyl peptides retain a parallel β-sheet CD signature

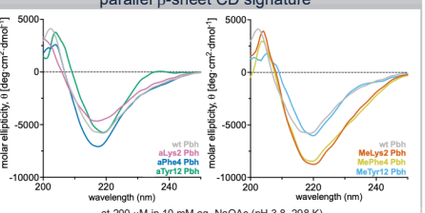

at 200 μM in 10 mM aq. NaOAc (pH 3.8, 298 K)

6) Hα NMR chemical shift deviations define the folded core of amide-substituted β-hairpin peptides

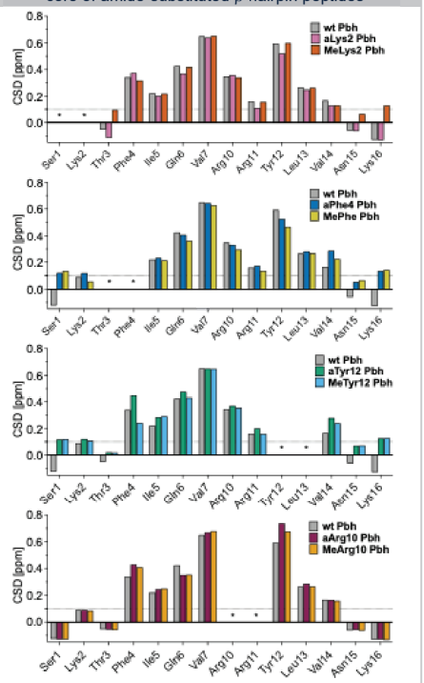

7) N-amination of core residues enhances folded population relative to parent and N-methyl peptides

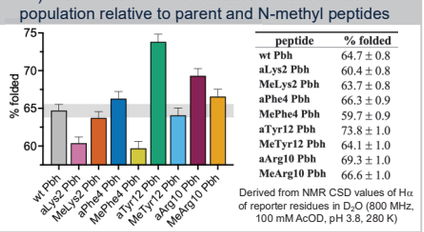

peptide	% folded
wt Pbh	64.7 ± 0.8
aLys2 Pbh	60.4 ± 0.8
MeLys2 Pbh	63.7 ± 0.8
aPhe4 Pbh	66.3 ± 0.9
MePhe4 Pbh	59.7 ± 0.9
aTyr12 Pbh	73.8 ± 1.0
MeTyr12 Pbh	64.1 ± 1.0
aArg10 Pbh	69.3 ± 1.0
MeArg10 Pbh	66.6 ± 1.0

Derived from NMR CSD values of Hα of reporter residues in D_2O (800 MHz, 100 mM AcOD, pH 3.8, 280 K)

8) NMR-derived structures of wt Pbh reveal significant fraying at the termini and the Lys2 substitution site

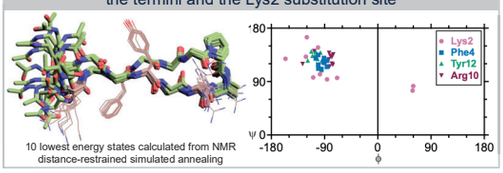

10 lowest energy states calculated from NMR distance-restrained simulated annealing

9) Backbone substituted analogues of DS119: a miniprotein featuring a βαβ parallel sheet fold

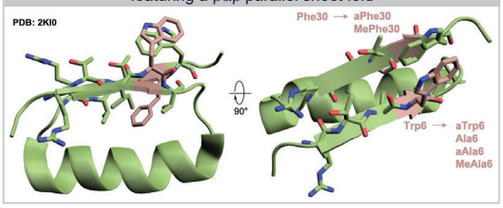

10) N-Aminated DS119 analogues retain wild-type fold and thermal stability in 1M Gdn·HCl

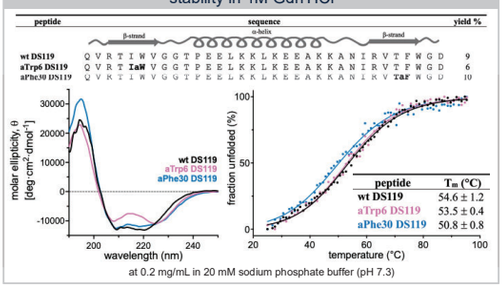

at 0.2 mg/mL in 20 mM sodium phosphate buffer (pH 7.3)

11) Backbone N-amination restores thermal stability in DS120

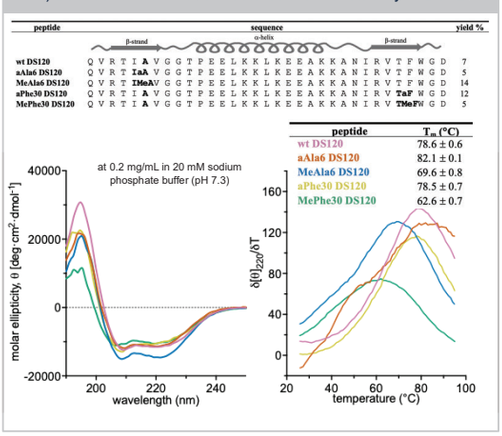

CONCLUSIONS

We incorporated α-hydrazino acids into models of folded secondary and tertiary structure. In the parallel β-sheet hairpin model, N-amination was well tolerated at residues in the structured core, but not at the frayed N-terminus. N-Amination of Arg10 and Tyr12 resulted in a significant increases in folded population relative to unsubstituted and N-methylated analogues. In the DS119 miniprotein, N-amination at Trp6 and Phe30 preserved the βαβ fold and had minimal effect on miniprotein stability. DS120, a DS119 analogue with a lower melting temperature, was stabilized upon N-amination of the Trp6 residue. As in the parallel β-hairpin model, α-hydrazino acids were better tolerated in the strand regions relative to N-methyl amino acids.

ACKNOWLEDGEMENTS

This work was supported by the National Science Foundation (CHE2109008) and the National Institute on Aging (NIH R01AG074570). SKS was supported by a Notre Dame CBBI fellowship through the NIH (T32GM145773). We thank the ND Nuclear Magnetic Resonance and Mass Spectrometry Core Facilities for access to instrumentation.

REFERENCES

[1] Taylor and Staniforth, *Front. Neurosci.* **2022**, *16*, e878869; [2] Angera et al., *Acc. Chem. Res.* **2024**, *57*, 1287; [3] Fisk et al., *J. Am. Chem. Soc.* **2006**, *128*, 7148; [4] Liang et al., *Angew. Chem.* **2009**, *48*, 3301.

https://doi.org/10.17952/37EPS.2024.P2283

How do Disulfide, Thioacetal and Lanthionine Bridges Influence the Conformations of Macrocyclic Peptides?

William T. P. Darling,[a] Lianne H. E. Wieske,[b] Declan T. Cook,[a] Abil E. Aliev,[a] Laurent Caron,[c] Emily J. Humphrys,[c] Angelo Miguel Figueiredo,[d] D. Flemming Hansen,[d] Máté Erdélyi[b] and Alethea B. Tabor[a]

[a]Department of Chemistry, UCL; [b]Department of Chemistry – BMC, Uppsala University; [c]Biosynth Laboratories (formerly Cambridge Research Biochemicals Ltd); [d]Department of Structural and Molecular Biology, UCL

Understanding the effects of different side-chain bridges on the conformations of cyclic peptides

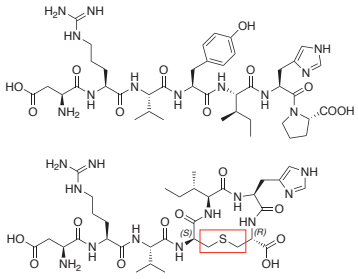

nAng(1-7):
potent GPCR agonist
rapidly inactivated *in vivo*

cAng(1-7) **1**
potent GPCR agonist
protease resistant
active via oral and pulmonary delivery[1]

Thioether (lanthionine) bridge
13 membered ring

What are the structural effects of the lanthionine bridge? How do these compare with disulfide and methylene thioacetal bridges?

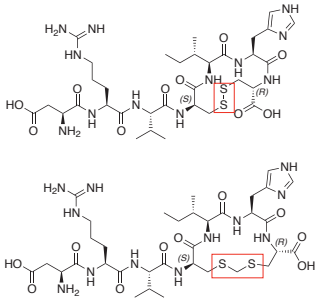

peptide **2**
disulfide bridge
14 membered ring

peptide **3**
methylene thioacetal bridge
15 membered ring

Peptide Synthesis

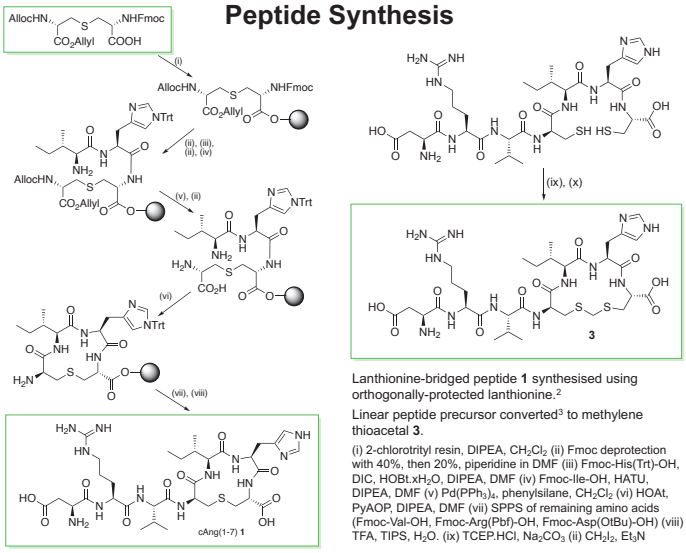

Lanthionine-bridged peptide **1** synthesised using orthogonally-protected lanthionine.[2]

Linear peptide precursor converted[3] to methylene thioacetal **3**.

(i) 2-chlorotrityl resin, DIPEA, CH_2Cl_2 (ii) Fmoc deprotection with 40%, then 20%, piperidine in DMF (iii) Fmoc-His(Trt)-OH, DIC, HOBt.xH_2O, DIPEA, DMF (iv) Fmoc-Ile-OH, HATU, DIPEA, DMF (v) $Pd(PPh_3)_4$, phenylsilane, CH_2Cl_2 (vi) HOAt, PyAOP, DIPEA, DMF (vii) SPPS of remaining amino acids (Fmoc-Val-OH, Fmoc-Arg(Pbf)-OH, Fmoc-Asp(OtBu)-OH) (viii) TFA, TIPS, H_2O. (ix) TCEP.HCl, Na_2CO_3 (ii) CH_2I_2, Et_3N

NAMFIS

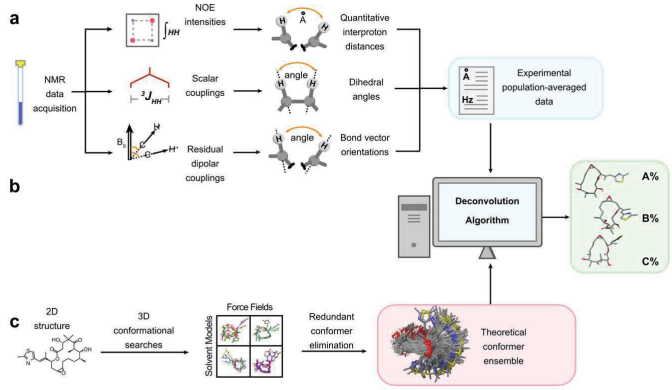

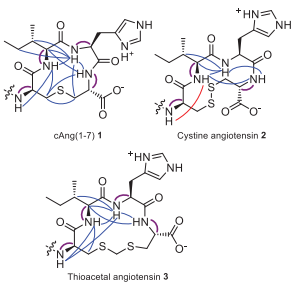

cAng(1-7) **1** Cystine angiotensin **2**

Thioacetal angiotensin **3**

NAMFIS uses NOE-derived interproton distances and $^3J_{HH}$ scalar coupling constants to find the best fit solution between a population weighted combination of theoretical conformations and experimentally determined distances and coupling constants.[4]

NMR experiments carried out in 9:1 H_2O:D_2O mixtures.

Solvent suppression obscured and altered the integrals of some α protons: for these, interproton distances were instead determined in D_2O with EASY ROESY without solvent suppression.

MCMM conformational searches were performed using MacroModel as implemented within the Schrödinger suite[5] to create the theoretical input ensembles.

Inter-residue interproton distances (blue lines) and scalar couplings (purple lines) used in the NAMFIS analyses are shown.

The red line indicates an interproton distance that when removed during validation causes an 18% change in the solution ensemble of peptide **2**.

Results

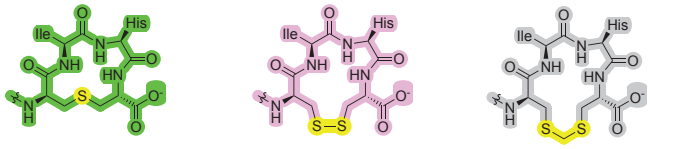

Peptide **1** Peptide **2** Peptide **3**

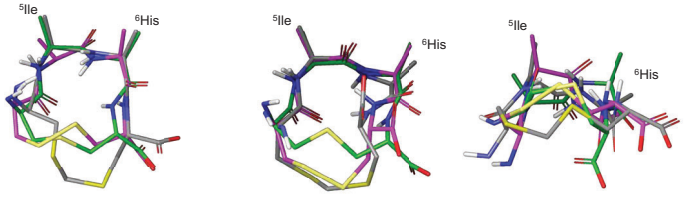

Conformer A1	**Conformer A2**	**Conformers B1-3**
Peptide **1** : 51%	Peptide **1** : 35%	Peptide **1** : 8%
Peptide **2** : 19%	Peptide **2** : 61%	Peptide **2** : 7%
Peptide **3** : 26%	Peptide **3** : 31%	Peptide **3** : 8%
RMSD 0.57 – 0.58 Å	RMSD 0.57 – 0.77 Å	RMSD 1.12 – 1.73 Å

For each of the peptides, two conformational families, **A** and **B**, are observed.

In **A** the [4]Xaa NH is oriented towards the macrocyclic R groups.

Larger rings have more sub-conformers.

The flexible side-chains of [5]Ile and [6]His, and the methylene thioacetal, cannot be accurately determined.

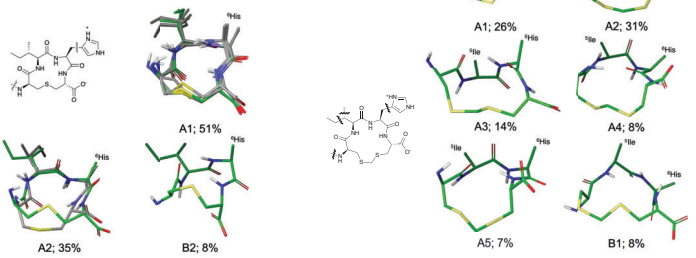

Conclusions

- Changing the length of the bridge appears to have almost no effect on the conformational families seen[6]
- The molar fraction of each conformation changes between analogues (by up to 35%)
- The three conformations are more equally distributed in the thioacetal, likely due to increased flexibility
- Receptor binding conformation is unknown at present
- Will this apply to other cyclic peptides?

(1) L. D. Kluskens *et al., J. Pharmacol. Exp. Ther.* **2009**, *328*, 849
(2) R. Dickman *et al., J. Org. Chem.* **2019**, *84*, 11493
(3) C. M. B. K. Kourra, N. Cramer, *Chem. Sci.* **2016**, *7*, 7007
(4) L. H. E. Wieske, S. Peintner, M. Erdélyi, *Nature Rev. Chem.* **2023**, *7*, 511
(5) F. Mohamadi *et al., J. Comput. Chem.* **1990**, *11*, 440
(6) W. T. P. Darling *et al., Chem. – Eur. J.* **2024**, *30*, e202401654

Biotechnology and Biological Sciences Research Council
Wenner-Gren Stiftelserna
Vetenskapsrådet
UPPSALA UNIVERSITET

Characterizing bradykinin-derived membrane-sensing peptides through Molecular Dynamics

C. Guardiani[1], A. Giacomello[1]

[1] Dipartimento di Ingegneria Meccanica e Aerospaziale, Sapienza Università di Roma, Rome, Italy;
carlo.guardiani@uniroma1.it

https://doi.org/10.17952/37EPS.2024.P2284

Finanziato dall'Unione europea
NextGenerationEU

1. Abstract

Curvature-sensing peptides are peptides capable of recognizing high-curvature membranes like those of the Exosomes. Exosomes are extracellular vesicles that have raised a huge interest for their biomedical applications. The main challenge in the use of exosomes is the difficulty of purification by means of standard monoclonal antibodies. Alternative approaches, like those exploiting their membrane curvature are thus actively explored. In a recent work Cretich and coworkers tested three bradykinin-derived (BK) peptides (single, tandem and branched) showing that they recognize exosomes from the blood serum. NMR optimization simulations were first run on the BK-single peptide, using NMD-derived distance and torsion restraints. The parameters of a H-REMD simulation were tuned so as to reproduce the results of the NMR optimization, and the protocol was then used to study the conformations of the BK-tandem and BK-branched peptides. H-REMD simulations showed that the BK-single peptide adopts a W-shaped conformation that segregates hydrophobic and charged residues. While hydrophobic residues are mostly exposed on the convex side of the W-motif and might fit into the crevices of the membrane, charged residues are on the opposite side of the molecule. This arrangement is reminiscent to that of alpha-synuclein but BK-peptides realize residue segregation employing a structural motif alternative to the amphypathic helix of alpha-synuclein and ALPS motifs.

2. The Exosomes

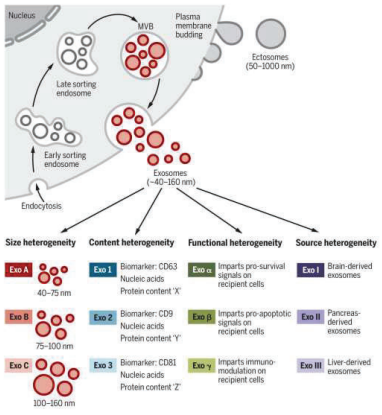

3. Curvature sensing

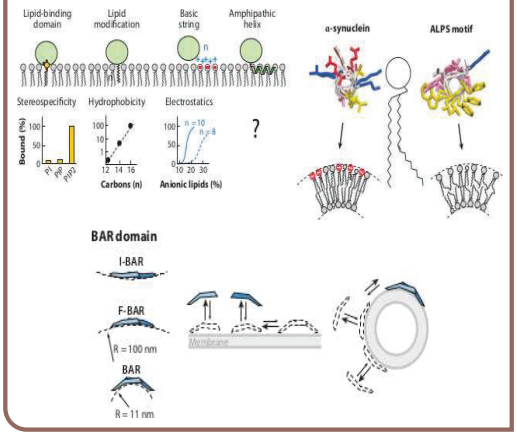

4. BK peptides: structure

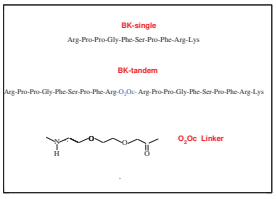

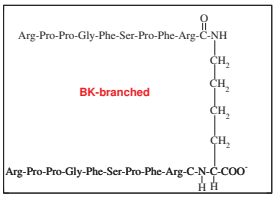

5. BK peptides: properties

- Three variants of BK peptides:
  - BK-single decapeptide
  - BK-tandem peptide: two BK-decapeptides connected by a PEG linker O_2Occ
  - BK-branched peptide: Lys10, uses both the α and ϵ amine groups to bind two peptide chains
- BK-peptides interact with small (150 nm) but not large ($\lesssim$450 nm) liposomes
- BK-peptides successfull in purification of exosomes from blood serum.
- Exosome purification successfull even after protein digestion with trypsin.
- Multivalent peptides more effective than monovalent one in exosome but not in liposome recognition.

6. NMR optimization

Intensity of cross-peaks from NOESY spectrum

Res1	Atom1	Res2	Atom2	Intensity	Dist (Å)
Pro3	Hγ 2	Pro2	Hα	Strong	2.4
Phe5	Hβ	Phe5	H(2,6)	Strong	2.5
Phe8	Hα	Phe8	H(3,5)	Medium	3.0
Phe8	H(2,6)	Pro7	Hβ1	Weak	4.0
Phe8	H(3,5)	Pro7	Hβ1	Weak	4.1
Phe5	Hβ	Phe5	H(3,5)	Weak	4.3
Phe8	Hβ1	Phe8	H(3,5)	Weak	4.6
Phe8	Hβ2	Phe8	H(3,5)	Weak	4.6

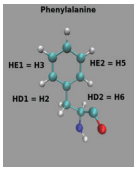

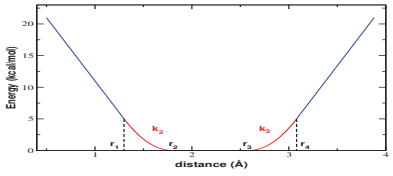

7. Annealing structures

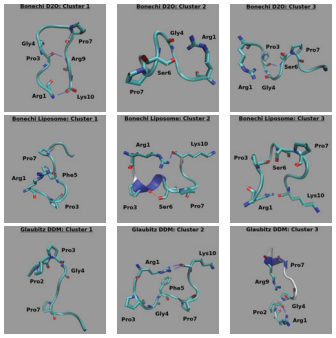

8. The REMD method

- Replicas are simulated in parallel at different temperatures with exchanges accepted based on Metropolis criterium.

$$\begin{matrix}(T_1,\dots,T_i,T_j,\dots,T_N)\\(q_1,\dots,q_m,q_n,\dots,q_N)\\\Downarrow\\(T_1,\dots,T_j,T_i,\dots,T_N)\\(q_1,\dots,q_m,q_n,\dots,q_N)\end{matrix} \qquad P=\min[1,e^{-(\beta_i-\beta_j)(E(q_n)-E(q_m))}]$$

- Poor scaling with system size: $p_{acc}\propto\exp(\Delta\beta\Delta E)$
- Large systems $\Longrightarrow$ Large $\Delta E\Longrightarrow$ Small $\Delta\beta$
- Hamiltonian REMD:replicas simulated at the same temperature but with different potential energy functions
- p_{acc} becomes function of a small subset of variables

9. H-REMD structures: 1

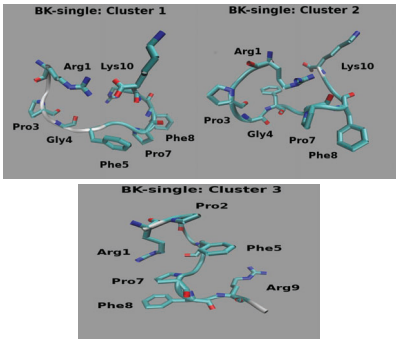

10. H-REMD structures: 2

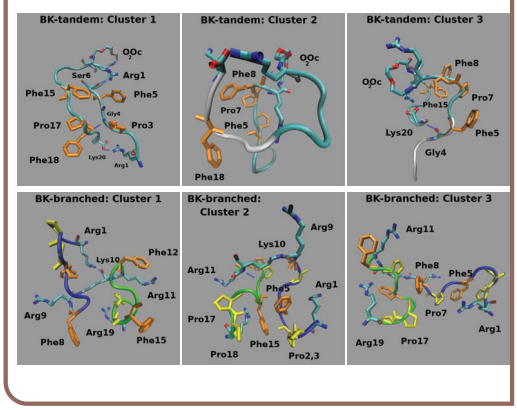

11. Acknowledgements

Financially supported by the European Union - Next Generation EU

Title:

The virtual EV (v-EV): A digital twin of extracellular vesicles for health and food

(P2022EKHKL)

12. Conclusions

- Exosomes are promising tools both in diagnostics and therapeutics.
- Curvature-sensing peptides can be used to purify exosomes.
- Bradykinin proved successfull in the recognition of exosomes and its efficacy is enhanced by multivalency.
- In pure water the prevalent NMR structure of BK-single is a hairpin. The structure shifts to S- and W-shaped motifs in the neighborhood of a lipid micelle.
- H-REMD simulations show that both BK-single and the tandem and branched constructs adopt a conformation with segregation of a hydrophobic and a basic face similarly to α-synuclein and ALPS motifs.

Effect of antifreeze activity and lipid interaction of tryptophan scanning of 11-residue lysine homopeptide

Rojas R. 12, Aróstica M. 23, Cardenas.C. 2, Aguilar L 4 , Albericio F. 5 , Guzmán F. 2.

1 Universidad de las Américas (UDLA), Viña del Mar, Chile. 2 Núcleo de Biotecnología Curauma, PUCV, Valparaíso, Chile. 3Doctorate Program in Biotechnology. Universidad Técnica Federico Santa María and PUCV , Valparaíso, Chile. 4 Institute of Chemistry, PUCV.

5 Department of Organic Chemistry, University of Barcelona, Martí i Franqués 1-11, Barcelona 08028, Spain

rrojasg@udla.cl

https://doi.org/10.17952/37EPS.2024.P2285

ABSTRACT

Antifreeze peptides and proteins play crucial roles in the survival of organisms that thrive in cold environments, such as polar fish [1]. These compounds serve diverse functions, including cryopreservation, which is essential for organisms facing freezing conditions. Peptides exhibit varied primary and secondary structures, offering a range of functionalities in cold adaptation.

In our study, we focused on an 11-residue lysine homopeptide, K11, where each position was substituted with Trp using a scanning technique. Peptides were synthesized using the Fmoc/tBu strategy [2], followed by purification and characterization via RP-HPLC and mass spectrometry.

Antifreeze activity of peptide was evaluated using differential scanning calorimetry (DSC) and quantifying ice recrystallization inhibition, known as thermal hysteresis (THA). Results showed a slightly increased antifreeze activity with fewer remaining nucleation points across all peptides in the scanning sequence. Substituting internal residues whit Trp, enhanced ice recrystallization inhibition, highlighting the significance of peptide structure.

However, Trp substitution disrupted the secondary structure of K11, as obtained by circular dichroism, notably affecting the type II polyproline helix of K11 and resulting in decreased antifreeze activity compared to the K11 homopeptide. This highlights the intricate relationship between peptide structure and functionality in antifreeze mechanisms.

INTRODUCTION

Antifreeze proteins (AFPs) are expressed in fish that inhabit the polar zones, allowing them to survive in environments at temperatures below zero. This physical property is considered of enormous importance in the cryopreservation of cells, tissues and organisms. There are different types of secondary structure for AFPs. The exact mechanism by which these molecules exert the antifreeze effect has not been fully clarified at present. In order to appreciate changes in the structure of proteins, a study of lysine peptide (K11) is carried out as well a series in which each position of the peptide K11 chain was replaced by tryptophane (Scan-W) (Fig. 1). They present secondary polyproline II structure (PPII) that has diehedral angles ϕ = -75 and ψ = +145 and ϕ = -75 and ψ +160 for PPI (Fig. 2A).

METHODOLOGY

- All lysine peptides were synthesized by Fmoc solid phase synthesis (Fig. 1) [3].
- The peptides were purified at 95% purity and analyzed by high performance liquid chromatography (HPLC).
- The molecular mass of the peptides was confirmed by mass spectroscopy MALDI-TOF and HPLC-MS [4].
- The secondary structure of the peptides was determined by circular dichroism spectroscopy (CD), Jasco J-815 equipment.
- The effects of thermal hysteresis of all the peptides synthesized was evaluated in a DSC1 METTLER-TOLEDO calorimeter, the antifreeze activity was quantified with reference to a water control with the STARe 10.0 program (Fig. 2B).

0	KKKKKKKKKKK	K11
1	WKKKKKKKKKK	W1
2	KWKKKKKKKKK	W2
3	KKWKKKKKKKK	W3
4	KKKWKKKKKKK	W4
5	KKKKWKKKKKK	W5
6	KKKKKWKKKKK	W6
7	KKKKKKWKKKK	W7
8	KKKKKKKWKKK	W8
9	KKKKKKKKWKK	W9
10	KKKKKKKKKWK	W10
11	KKKKKKKKKKW	W11

Figure 1: Synthesized peptides of Scan-W of K11 homopeptide.

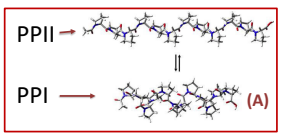

Temperature program for measurements of DSC. (B)

- ✓ Preliminary method (below).
- ✓ Inhibition of recrystallization (on the right).

Step	T° Start (°C)	T° End (°C)	Rate (°C/min)	Time (min)
1	10	-25	2	17,5
2	-25	10	1	35,0

Step	T° Start (°C)	T° End (°C)	Rate (°C/min)	Time (min)
1	10	-25	3	11,7
2	-25	-10	3	35,0
3	-10	THo	1	
4	THo	THo	0	10,0
5	THo	-10	1	
6	-10	-25	3	5,0
7	-25	10	3	11,7

Figure 2: (A) Poliproline structures type I and II. (B) Temperature program for DSC measurements.

REFERENCES

[1] Bang J.,Lee J.,Murugan R.,Lee S.,Do H.,Koh H.,Shim H.,Kim H.y Kim H. 2013.Antifreeze peptides and glycopeptides, and their derivatives: potential uses in biotechnology. Drugs 11(6): 2013-2041.

[2] Houghten RA. 1985. General method for the rapid solid-phase synthesis of large numbers of peptides: specificity of antigen-antibody interaction at the level of individual amino acids. Proceedings of the National Academy of Sciences of the United States of America, 82: 5131-5135.

[3] Guzmán F., Barberis S., Illanes A. 2007 Peptide Synthesis: Chemical or Enzymatic. Electronic Journal of Biotechnology, 10(2).

[4] Jofré C., Guzmán F., Cárdenas C., Albericio F. y Marshall S.H.2011. A natural peptide and its variants derived from the processing of infectious pancreatic necrosis virus (IPNV) displaying enhanced antimicrobial activity: A novel alternative for the control of bacterial diseases. Peptides, 328:852-858.

RESULTS

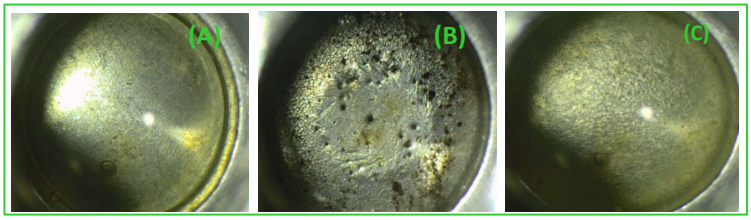

Figure 3: (A) Liquid phase sample, (B) Spike crystallization, (C) Recrystallization of partially fused sample on DSC

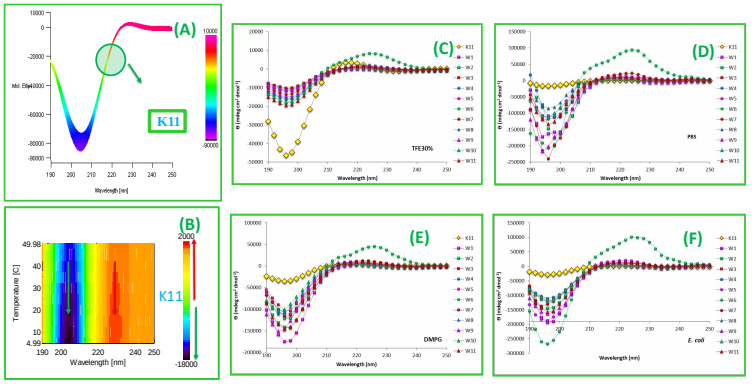

Figure 4 : (A, B) Peptide K11 CD spectrum between 5 ° C and 50 ° C, (C) Scan-W series CD results in 30% Trifluoroethanol, (D) Scan-W series CD results in PBS, (E) results Scan-W series in DMPG and (F) results Scan-W series in lipidic extract from *E.Coli*

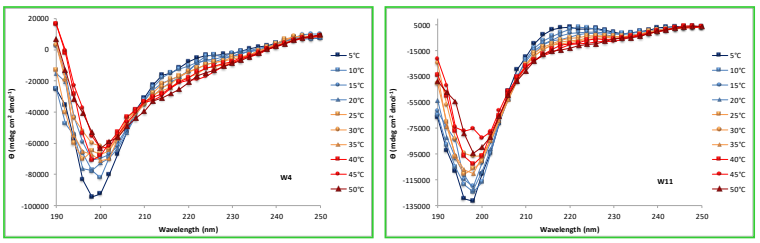

Figure 5 : (A) Peptide K11W4 CD spectrum between 5 ° C and 50 ° C, (B) Peptide K11W11 CD spectrum between 5 ° C and 50 ° C.

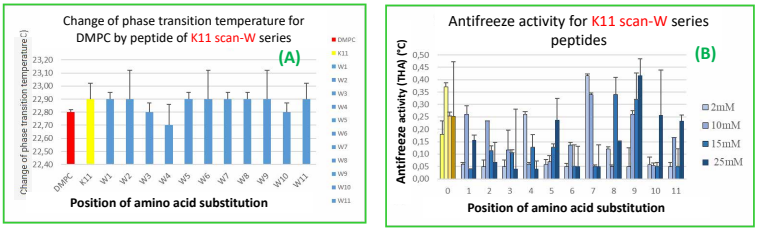

Figure 6 : (A) Change of the transition temperature of DMPC due to the peptide, (B) inhibition of recrystallization of ice for peptides at 2,10,15 & 25 mM of 11 residues measured by differential scanning calorimetry

CONCLUSIONS

✓**The presence of peptides in the solution produces a morphological change of the ice crystals. (Fig. 3A-C)**

✓**The results obtained by circular dichroism show that the series of peptides have a more defined structure when the substitution by tryptophane (Scan-W) than homopeptide K11 (Fig. 4 A-B), in different medium (Fig. 4 C-F).**

✓ **When comparing the effect of temperature on the definition of the secondary structure type Polyproline II, a common isodichroic point is observed between all temperatures. (Fig. 4A-B) for K11, but not in Scan-W.**

✓**In the peptides studied, the antifreeze activity is increased by substituting lysine for tryptophane at positions other than the amino and carboxyl ends of the peptide (Fig. 6B).**

✓**The interaction with ice is not directly related to the interaction with lipid model of 1,2-dimyristoyl-sn-glycero-3-phosphocholine (DMPC) that slightly increased the phase transition because of peptide (Fig. 5A).**

Acknowledgments

Fondecyt Grant Nr 1140926; Internal project UDLA DI- 11/21 of Dr. R. Rojas;

Structural Ensemble of Peptide-induced Membrane Poration by Heterogeneous Magainin Peptides

Author: *Bing Zan, Charles Chen*, Martin Ulmschneider*, Jakob Ulmschneider-Mayer**
Department of Chemistry, King's College London, UK
School of Physics and Astronomy, Shanghai Jiao Tong University, China
https://doi.org/10.17952/37EPS.2024.P2286

Introduction

Antimicrobial resistance has emerged as a significant global public health concern. Antimicrobial peptides (AMPs) hold potential as alternative therapeutic agents. However, a primary obstacle resides in the absence of effective experimental methodologies capable of investigating transient behaviors at the atomic scale.

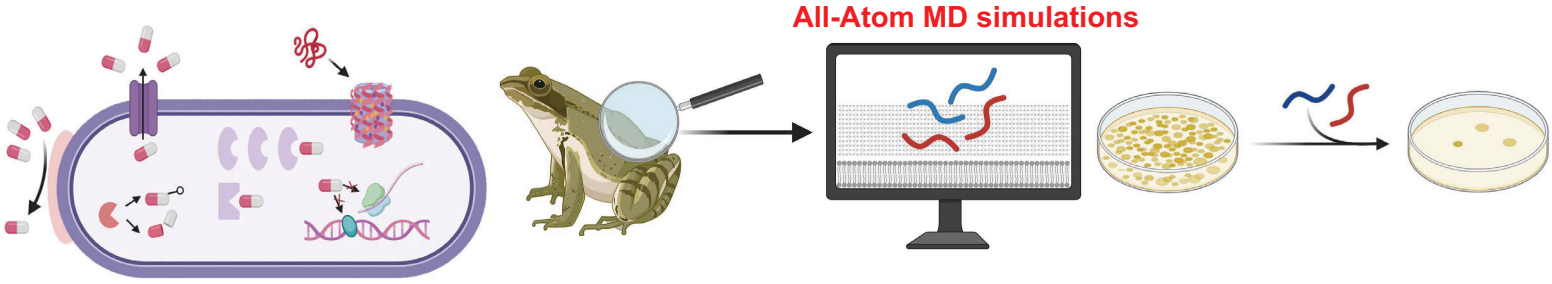

Result1: Ab-initial microsecond-scale all-atom folding-assembly simulations can capture the spontaneous behavior of AMPs exhibiting membrane-disrupting activity.

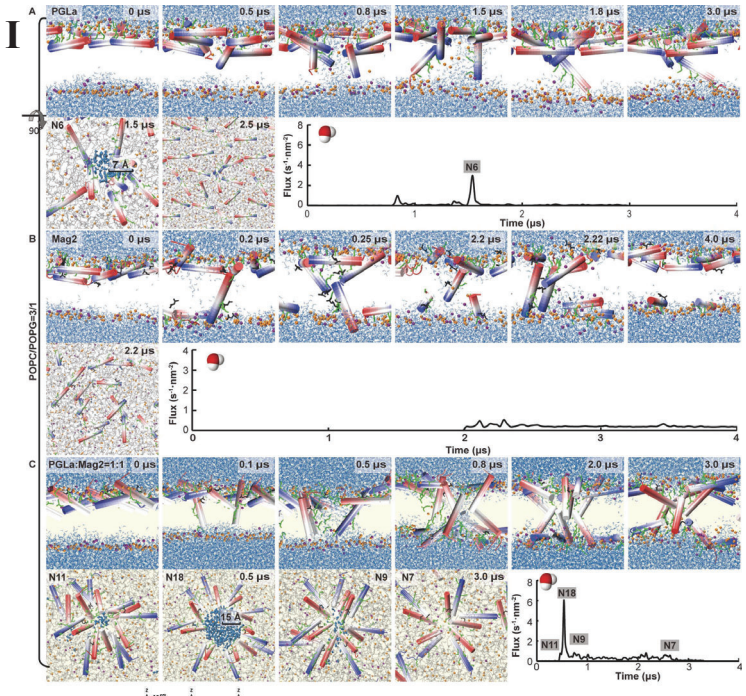

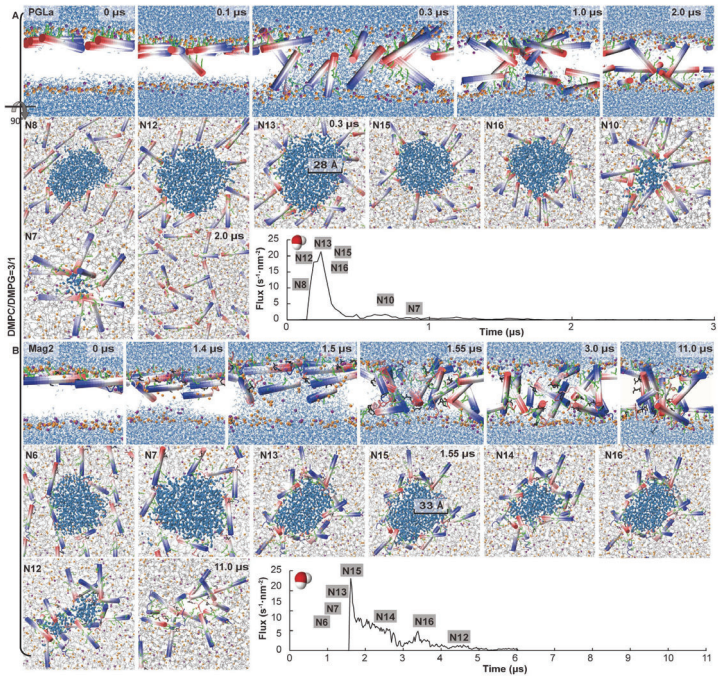

Result2: Dynamic ensemble of pore architectures may explain the low potential of resistance development of AMPs.

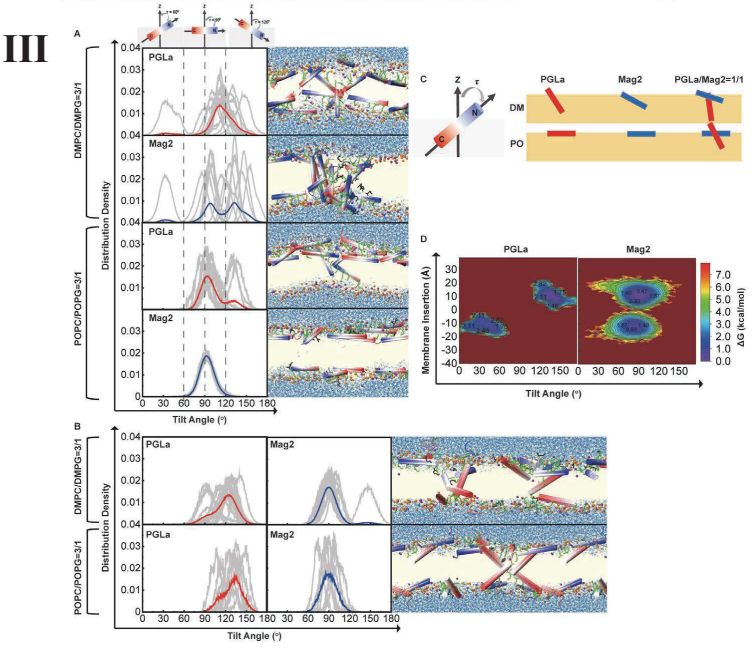

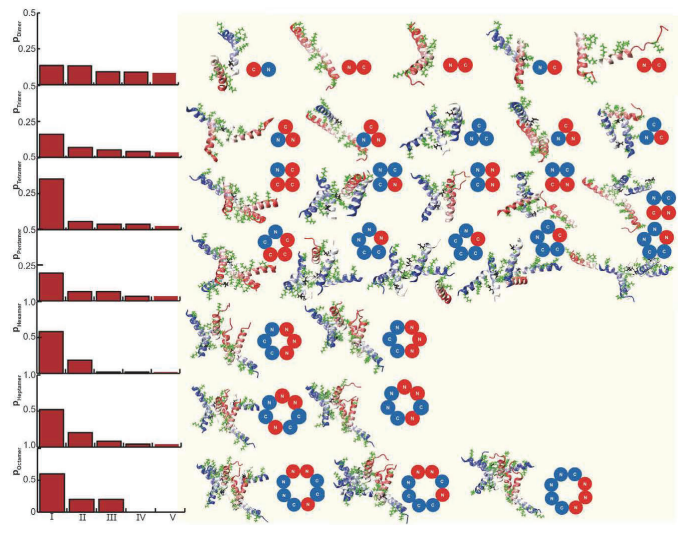

Helical Peptides Bearing Dual Triplet-spin/Fluorescent Labels Enable the First Parallel Distance Measurements by Electron Spin Resonance and Förster Resonance Energy Transfer

Arnau Bertran,[a] Laura Morbiato,[b] Jack Sawyer,[a] Chiara Dalla Torre,[b] Derren J. Heyes,[a] Sam Hay,[a] Christiane R. Timmel,[a] Marilena Di Valentin,[b] Alice M. Bowen,[a] Marta De Zotti[b]

[a] The National Research Facility for Electron Paramagnetic Resonance, Department of Chemistry, The University of Manchester, Oxford Road, Manchester M13 9PL, United Kingdom.
[b] Department of Chemistry, University of Padova, 35131 Padova, Italy
marta.dezotti@unipd.it

https://doi.org/10.17952/37EPS.2024.P2288

INTRODUCTION

Comparison between different methods in structural biology can be important to identify structural changes or prevent interpretation of structural artifacts related to sample conditions or preparation. Electron spin resonance (ESR) pulsed dipolar spectroscopy (PDS) is a set of techniques for the study of conformational flexibility and disorder in complex biological macromolecular systems.

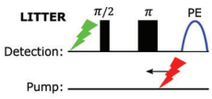

The light-induced triplet–triplet electron resonance (**LITTER**) technique, enables the measurement of the dipolar interaction between two photogenerated triplets, in chromophore-containing molecules, which are ESR silent in their ground state, eliminating the need for permanent spin centers [1]. LITTER pulse sequence: π/2 and π MW detection pulses (**black**) preceded by laser 1 (green) form a primary spin-echo (PE). The intensity is modulated by the formation of the second triplet by time-variant laser 2 (pump, red).

RESULTS & DISCUSSION

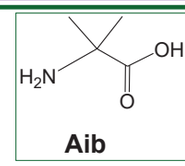

Peptide Synthesis.

1. **Bis-labeled model peptides [1] and [2] containing orthogonal chromophore pairs**, TPP with Zn(II)TPP (ZnTPP) and TPP with erythrosine B (EB), respectively, were synthesized by SPPS to have a rigid α-helical structure resulting from alternating L-leucine-α-aminoisobutyric acid (Leu-**Aib**) residues.
2. **A sarcosine (Sar) linker** was used to attach the labels to the N-terminus, **avoiding the formation of colorless EB spiro-lactam**. This is advantageous over previous strategies as it uses the more affordable non-derivatized chromophore and introduces a shorter linker.
3. **Zn(II) complexation was achieved directly with resin-bound TPP peptide**, by several treatments with a saturated solution of $Zn(Ac)_2$ in a DMF/Ethanol mixture 1:1, thus reducing the number of purification steps. Quantitative complexation on resin required two overnight treatments with fresh solutions of $Zn(Ac)_2$ (Zinc Acetate, 50 equiv.).

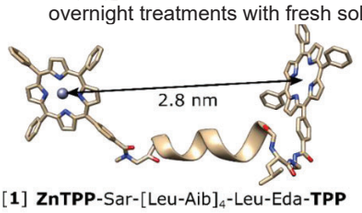

[**1**] **ZnTPP**-Sar-[Leu-Aib]$_4$-Leu-Eda-**TPP**

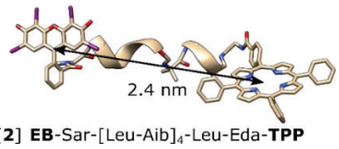

[**2**] **EB**-Sar-[Leu-Aib]$_4$-Leu-Eda-**TPP**

Either 5-(4-Carboxyphenyl)-10,15,20-(triphenyl)porphyrin (**TPP**-COOH) or Erythrosin B (**EB**) was successfully inserted at the N-terminus by coupling reactions repeated three times (1h, 1h, and overnight, respectively) with three equivalents of the chosen chromophore.

1,2-Diaminoethane-trityl resin [thus preloaded with the C-terminal linker ethylenediamine (Eda)] was used, and the C-terminal **TPP** group was added in solution.

Light-induced pulsed dipolar spectroscopy methods have been developed based on the photogenerated triplet state of a **TPP** moiety as photoswitchable spin-label.

Chromophore center-to-center distances determined by in vacuo DFT optimization.

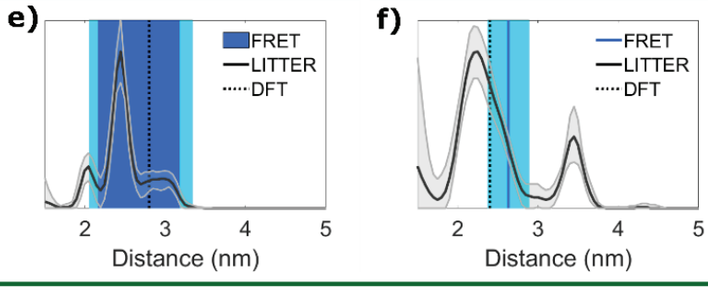

The first LITTER experiments with optically orthogonal chromophores and 2-color photoexcitation resulted in larger modulation depths corresponding to a **4-fold shortening of the acquisition time** with respect to previous 1-color measurements are reported.

Comparison of the distances determined for [**1**] (**e**) and [**2**] (**f**) by FRET (blue) with error bounds (cyan), LITTER (solid black line) with 95% confidence intervals (gray), which include analysis of the uncertainty in the background correction, and DFT (dotted black line).

CONCLUSIONS

The 2-color LITTER represents a dramatic step forward in biological structural determination in systems where FRET labels can be added or innate chromophores used. The choice of orthogonal chromophores provides a significant improvement in data quality compared to the initial homo-LITTER experiments. Furthermore, the selective optical addressability of each chromophore has the potential to enable **unambiguous determination of the PDS distance in systems with more than two labels**, without the interference of multi-spin effects. Optical orthogonality is easier to achieve and allows a wider choice of labels than spin-label orthogonality. There is also potential for increasing the modulation depth by further reducing the spectral overlap and unwanted excitations by choosing different chromophore pairs and excitation wavelengths. LITTER requires low concentrations and is likely suitable for in-cell ESR studies, where conventional nitroxide labels degrade rapidly. When combined with fluorescence microscopy, LITTER could provide location-specific structural infor-mation for labelled biomolecules inside cells.

REFERENCES

[1] Bertran A., Henbest K.B., De Zotti M., Gobbo M., Timmel C. R., Di Valentin M., Bowen A. M. J. Phys. Chem. Lett. **2021**, 12, 80-85.
[2] Bertran A., Morbiato L., Sawyer J., Dalla Torre C., Heyes D.J., Hay S., Timmel C.R., Di Valentin M., De Zotti M., Bowen A.M. J. Am. Chem. Soc. **2023**, 145, 22859−22865.

ACKNOWLEDGMENTS

MINISTERO DELL'ISTRUZIONE, DELL'UNIVERSITÀ E DELLA RICERCA

PRIN 2022LBZM2
P-DiSC#04BIRD2021-UNIPD
PoC@UNIPD

https://doi.org/10.17952/37EPS.2024.P2289

Department of Chemistry - Organic Chemistry – C317

Indian Institute of Science Education and Research-Pune
IISER PUNE

Antiparallel β-Double Helices from α,γ-Hybrid Peptides

DRGKoppalu R. Puneeth Kumar, Gijo George, Uddipan Bhattacharya, Arnab Mukherjee and Hosahudya N. Gopi*

[1] Department of Chemistry, Indian Institute of Science Education and Research, Dr. Homi Bhabha Road, Pashan, Pune-411008, India. E-mail: puneeth.dr@uni-Bielefeld.de

Introduction

- Heterooligomers of $(\alpha\beta)_n$-sequences have demonstrated the adoption of 11-, 14/15- and 11/9 helices.
- $(\alpha\gamma)_n$-sequences have exhibited the ability to form 12- and 12/10- helical structures.
- In contrast to the prevalent protein secondary structures such as α-helix and β-sheets, β-double helices are rare in proteins.

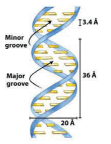

DNA duplex

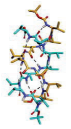

Benedetti *et al.*
Nature **1979**, *282*, 630

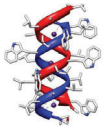

Gramicidin A

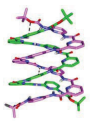

Lehn *et al.*
Nature **2000**, *407*, 720

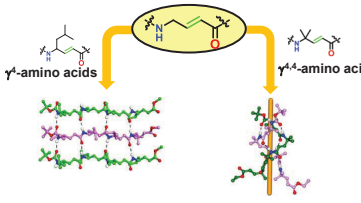

Org. Biomol. Chem., **2019**,17, 9226 *Angew. Chem. Int. Ed.* **2018**, *57*, 1057

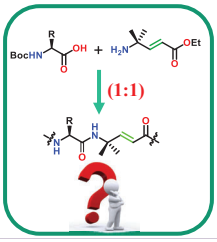

Synthesis Scheme

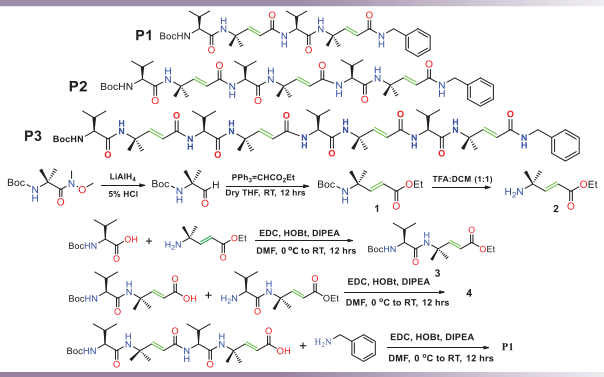

CD Study of the Peptides P1-P3

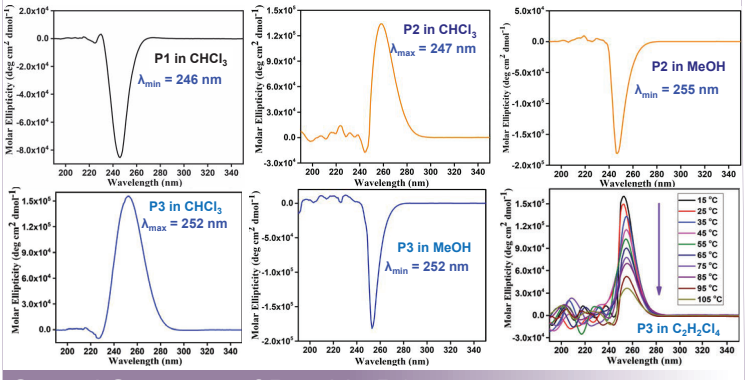

Crystal Structure of Peptide P1

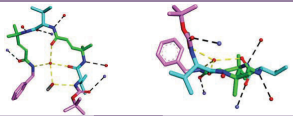

Torsion Angles of P1

Peptide Unit	ϕ	θ1	θ2	Ψ
Val (1)	-88.60	-	-	-127.54
dyAic (2)	45.68	-155.21	-178.24	171.65
Val (3)	-71.92	-	-	143.78
dyAic (4)	81.56	-0.04	177.46	-179.95

Structural Analysis of Peptide P3

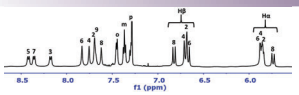

Partial ROESY spectrum of Peptide P3

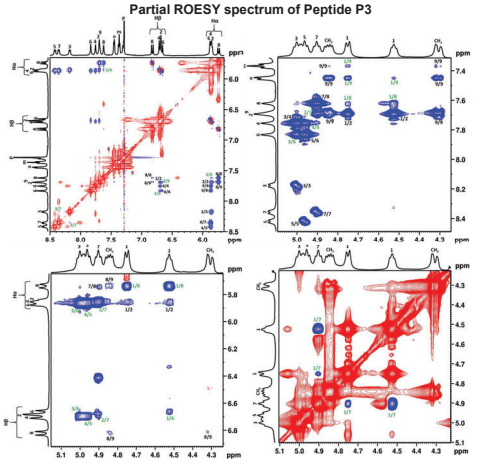

Inter-molecular NOEs – Green
Intra-molecular NOEs – Black

Inter-NOEs	Type
Boc/Pro-S CH_3 (0/7)	Strong
Boc/Pro-R CH_3 (0/7)	Medium
Pro-R CH_3/Pro-S CH_3 (3/8)	Medium
Pro-S CH_3/Pro-R CH_3 (4/7)	Medium
Pro-R CH_3/Pro-S CH_3 (5/6)	Medium
Hβ/NH (2/6)	Weak
Hα/NH (2/8)	Weak
NH/NH (3/7)	Weak
Hβ/NH (6/2)	Weak
NH/Hα (1/7)	Weak
Hα/Hα (1/7)	Very Strong

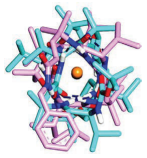

Top View

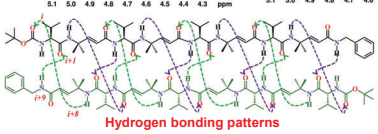

Hydrogen bonding patterns

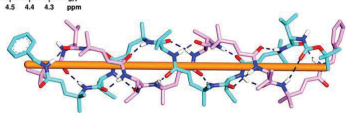

Anti-Parallel β-Double Helix

Computational Studies of Peptide P3 in $CHCl_3$

Simulations of Peptide P3 in $CHCl_3$

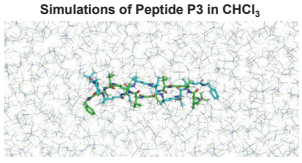

P3 solvated with 9019 molecules of $CHCl_3$ & their stability upto 300 ns

Density Fluctuation of P3

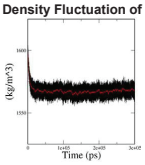

RMS Deviation of P3

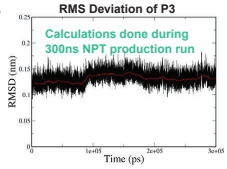

Red line shows the running average of the density & RMS deviation for 1 ns.

Number of inter strand H-bonds

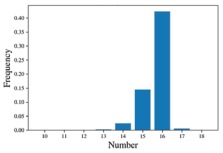

MM-GBSA free energy (101.87 kJ/mol)

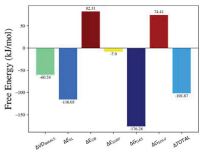

Unbinding Mechanism

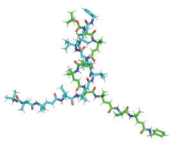

Conclusion

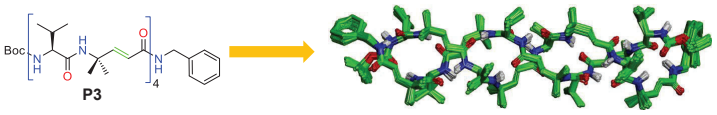

- This is the first example demonstrating that α,γ-hybrid peptides can adopt into anti-parallel β-double helical structures.
- Both NMR structural analysis and computational studies revealed the anti-parallel orientation of α,γ-hybrid peptides strand of β-double helix.
- The anti-parallel β-double helical structure is stabilized through 16-inter strand H-bonds and its total free energy is around -101.87 kJ/mol.

Reference

1) Misra, R.; Dey, S.; Reja, R. M.; Gopi, H. N. Artificial β-Double Helices from Achiral γ-Peptides. *Angew. Chemie - Int. Ed.* **2018**, *57*, 1057–1061.
2) Pahan, S.; Dey, S.; George, G.; Panda Mahapatra, S.; **Puneeth Kumar, D. R.**; Gopi, H. N. Design of Chiral β-Double Helices from γ-Peptide Foldamers. *Angew. Chemie - Int. Ed.* **2024**, *63*, e202316309.
3) Benedetti, E.; Di Blasio, B.; Pedone, C.; Lorenzi, G. P.; Tomasic, L.; Gramlich, V. A Double-Stranded β-Helix with Antiparallel Chains in a Crystalline Oligo-L-D-Peptide. *Nature* **1979**, *282*, 630.
4) Berl, V.; Huc, I.; Khoury, R. G.; Krische, M. J.; Lehn, J. M. Interconversion of Single and Double Helices Formed from Synthetic Molecular Strands. *Nature* **2000**, *407*, 720–723.

Alexander von HUMBOLDT STIFTUNG

IISER PUNE

37th EPS European Peptide Symposium
14th IPS International Peptide Symposium
25 - 29 August 2024
Satellite Workshop 30 - 31 August 2024
Florence, Italy- 2024

http://sites.iiserpune.ac.in/%7Ehn.gopi/gopi.html

Aromatic-aromatic interactions as an intrinsic modulator of amyloid formation

https://doi.org/10.17952/37EPS.2024.P2290

Artem Pavlov, Beate Koksch

Freie Universität Berlin, Arnimallee 20, 14195 Berlin

artem.pavlov@fu-berlin.de

Introduction

Amylin (hIAPP) sequence: H_2N–KCNTATCATQ RLANFLVHSS NNFGAILSST NVGSNTY–C(=O)–NH_2

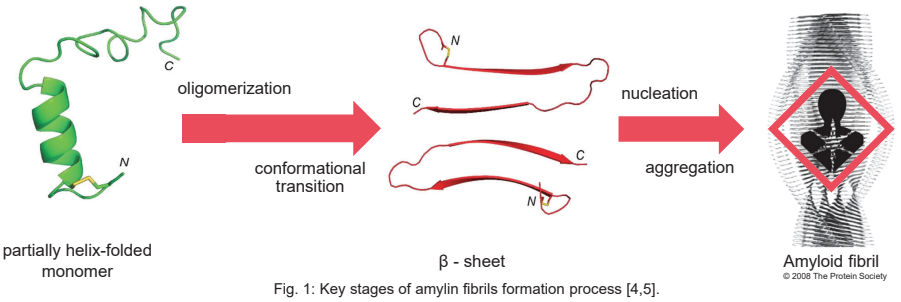

Fig. 1: Key stages of amylin fibrils formation process [4,5].

- Amyloid fibrils formed by amylin play a crucial role in the development of type 2 diabetes [1].
- The formation of these structures depends on the peptide's amino acid sequence with its internal propensities to the particular secondary structures and specific interactions involved in the process [2].
- Aromatic-aromatic interactions contribution remains debated [3].

Aim and Methods

This study examines how substituting aromatic residues in the amylin peptide influences amyloid fibril formation kinetics. Prior studies involving fluorinated Phe and Leu highlighted the importance of hydrophobics and secondary structure propensity. By selectively altering these contributions, the research aims to isolate and analyze the role of aromatic-aromatic interactions in amyloidogenesis, while maintaining other structural aspects of the peptide.

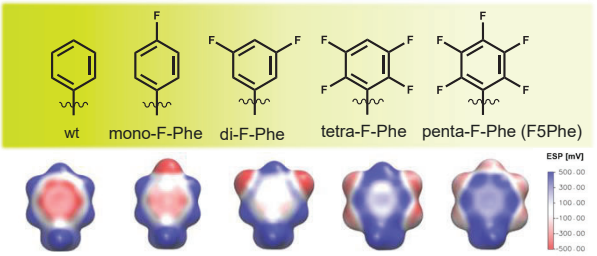

Fig. 2: Aromatic ring fragment of Phe variants of our **first set** amylin analogues and its electrostatic potential maps [6].

Position with penta-F-Phe	15	23	37
peptide 15F	✓		
peptide 23F		✓	
peptide 37F			✓
peptide 15/23F	✓	✓	
peptide 23/37F		✓	✓
peptide 15/37F	✓		✓

Tables of the peptide **second set** with individual and pair substitution of Phe/Tyr with pentafluoro-Phe.

Two sets of full-length amylin variants were obtained: first one – with different fluoro-Phe analogues inside the hydrophobic core of the sequence (NFGAIL); second one – contains individual and pair substitution of Phe/Tyr with pentafluoro-Phe.

State of the art

Short-fragment model studies stated:

- ↑Hydrophobicity of Phe analogues → ↑rate of fibril formation.
- Amyloidogenesis independence of specific π-stacking geometries, and by extension, aromaticity.[6]

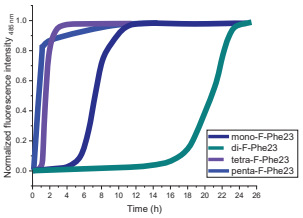

Fig. 3: Thioflavin T assay of fibrils formation kinetics of NFGAIL and its Phe_{23} variants [6]. (peptide conc. 3/4 mmol, pH 7.4)

Phe/Tyr → Leu amylin mutants model studies:

- Shift from discussing aromatic-aromatic interactions
- Highlight the importance of α-helix and β-sheet propensities of amino acids, which influence oligomerization and β-sheet formation as key steps in the fibril formation process [3].

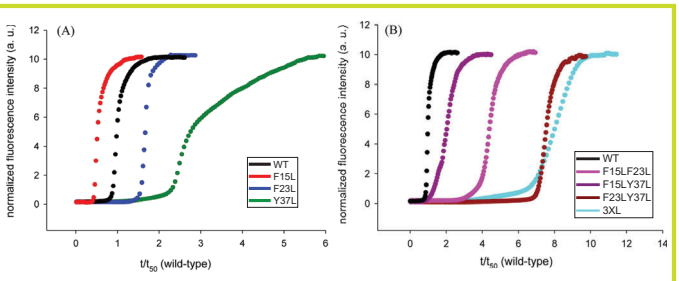

Fig. 4: Thioflavin T assay of fibril formation kinetics of amylin Phe/Tyr → Leu mutants [3]. (peptide conc. 16 μmol, pH 7.4)

Results

Full-length model probing the hydrophobic core:

- ↑ Aromatic-aromatic interactions → ↓rate of fibril formation.
- Amyloidogenesis independence of hydrophobicity changes at the Phe_{23}.

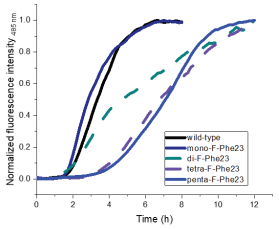

Fig. 5: Thioflavin T assay of fibrils formation kinetics of hIAPP and its Phe_{23} variants. (peptide conc. 15 μmol, pH 7.4)

Phe/Tyr → F5Phe amylin mutants model studies:

- Challenge the α-helix propensity of AA_{15} as a key factor in amyloidogenesis enhancement.
- Reveal complex interplay where certain aromatic interactions enhance, disrupt, or compensate for each other to amyloidogenesis.

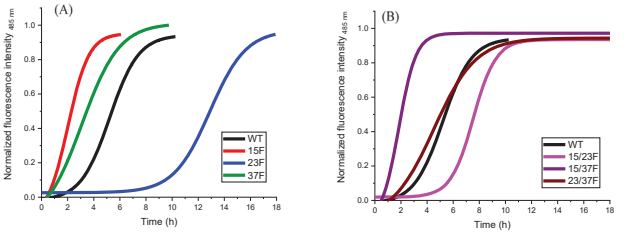

Fig.6 : Thioflavin T assay of fibril formation kinetics of amylin Phe/Tyr → F5Phe analogues (peptide conc. 15 μmol, pH 7.4)

Conclusions and Outlook

- Our study demonstrated distinct effects of aromatic-aromatic interactions on amyloidogenesis, highlighting its critical role.
- Substitution of Phe/Tyr with pentafluoro-Phe, which has reversed electrostatic potential of the ring, favors π-stacking with natural aromatic rings. In case of double substitution experiments, it emphasizes the divergent contribution of aromatic-aromatic interactions to amyloidogenesis Fig.6 (B).
- Based on the obtained data and the comparative analysis of previous studies we hypothesize new features of **molecular mechanism** specifically: Phe_{23} with Tyr_{37} may engage in specific π-stacking interactions leading to amyloid formation, meanwhile, Phe_{15} acts as a stabilizer, potentially preventing this process. This hypothesis opens up new avenues for further investigation in future studies.

References

[1] Clark, A. et al., The Lancet, **1987**, 330, 231-234
[2] Gai Liu, et al., J. Am. Chem. Soc., **2010** 132 (51), 18223-18232
[3] Ling-Hsien Tu, D.P. Raleigh, Biochemistry, **2013**, 52, 2, 333–342
[4] D. C Rodriguez. et al., eLife, **2017**, 6:e31226
[5] J.J. Wiltzius, et al. Protein Sci, **2008**, 17 (9), 1467-1474
[6] S. Chowdhary, et al., ChemBioChem, **2020**, 21, 3544-3554

Acknowledgments: We gratefully acknowledge financial support by the DFG 1114 and assistance of DFG CoreFacility BioSupraMol, especially the director of the NMR department Dr. Mario Schubert.

AG Koksch

Freie Universität Berlin

SYN PeP BIO
RESEARCH TRAINING GROUP OF BIOACTIVE PEPTIDES

@KokschGroup

Structure-Activity Relationship Study of β-Hairpin Peptides with Antibiotic Activity

Aparna Palakkurussi Rathessan[1], Suvrat Chowdhary[1], Johannes Kupke[2], Marcus Fulde[2,3], Beate Koksch[1]

[1]Institute of Chemistry and Biochemistry, Freie Universität Berlin, Berlin, Germany
[2]Institute of Microbiology and Epizootics, Center of Infection Medicine, Freie Universität Berlin, Berlin, Germany
[3]Veterinary Center for Resistance Research (TZR), Freie Universität Berlin, Berlin, Germany

https://doi.org/10.17952/37EPS.2024.P2291

Introduction

- The increasing resistance of pathogenic microbes to antibiotics poses a major threat and calls for methods to improve the pace of antibiotic discovery.[1] Antimicrobial peptides (AMPs) are effective against antibiotic-resistant bacteria in many cases.
- The peptide SAJO-2 developed by Sarojini and coworkers represents a tryptophan zipper-like motif involving a central D-Phe-Abz unit which is a peptidomimetic beta turn including the conformationally inflexible ortho-aminobenzoic acid. [2]
- By fine-tuning the intrinsic hydrophobicity of SAJO-2 by distinctive degrees of fluorination, Chowdhary and coworkers enhanced antimicrobial activity; however, undesired proteolytic degradation by β-trypsin was also enhanced. [3]

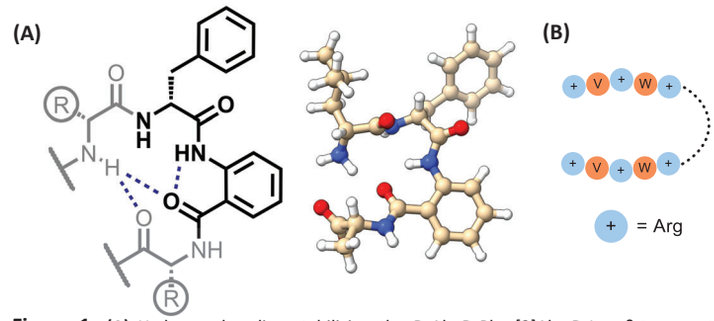

Figure 1. **(A)** Hydrogen bonding stabilizing the D-Ala-D-Phe-[2]Abz-D-Leu β-turn motif **(PDB Code: 6ANM), (B)** Cartoon of SAJO-2 peptide with positive charge denoting arginine residue and V and W denoting valine and tryptophan, respectively.

Results – Proteolytic Studies and Antimicrobial Susceptibility Testing

Amino acids employed

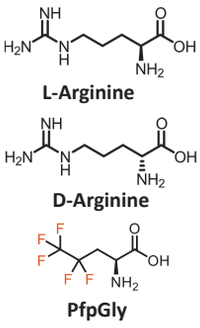

Scientific Aim

- Improve SAJO-2 stability against proteolytic degradation by the introduction of D-arginine or PfpGly amino acids
- Study the relationship between structural conformation and biological activity

ANTIMICROBIAL PEPTIDE	APPLIED ENZYMES
SAJO-2	**α- chymotrypsin:** Preferentially cleaves at aromatic residues at position P1 (Phenylalanine, Tryptophan, and Tyrosine)
SAJO-D	
SAJO-1D	**β- trypsin:** Specifically cleaves the C-terminal side of lysine and arginine residues
SAJO-2D	
SAJO-PfpGly-DArg	**Carboxypeptidase B:** Perform diverse physiological functions by removing C-terminal amino acids (preferably arginine) **Proteinase K:** Broad specificity and cleaves peptide bonds adjacent to the carboxylic group of aliphatic and aromatic amino acids

(A) Minimum Inhibitory Concentration (MIC) Assay

Antimicrobial Peptide	S. Typhimurium ATCC 14028	E. Coli ATCC 25922	S. Aureus ATCC 29213	P. Aeruginosa ATCC 27853	K. pneumoniae ATCC 700603	C. Albicans IMT 9655
SAJO - 2	32	16	64	64	64	32
SAJO - D	32	16	256	512	64	32
SAJO - 1D	32	32	128	1024	64	32
SAJO - 2D	16	32	256	1024	128	32
SAJO - PfpGly-DArg	32	32	64	512	64	32

(B) Proteolytic Digestion

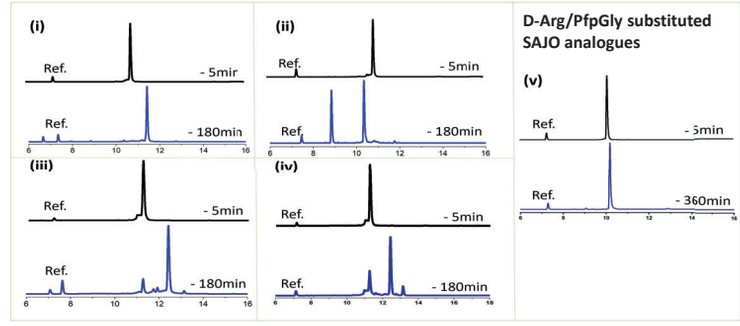

Figure 2. **(A)** MIC analysis of different library members, all experiments carried out in triplicate with three internal measurements **(B)** Proteolytic degradation profile of native peptide SAJO-2 (1mM stock concentration) observed by HPLC when incubated against **(i)** β-trypsin, **(ii)** α-chymotrypsin, **(iii)** Carboxypeptidase B and **(iv)** Proteinase K (All 20μM stock concentration) at 30°C for 3hours and **(v)** after introducing D-arginine and PfpGly amino acids (1mM stock concentration).

Conclusion

- A library of the turn motif SAJO-2 was synthesized with varying non-canonical amino acid substitutions
- All peptides were found to be stable against enzymatic degradation against β-trypsin and α-chymotrypsin due to altered stereochemistry that prohibits sufficient enzyme-substrate binding
- MIC values of D- analogues were comparable with their L counterparts against *E. coli*, *S. typhimurium,* and fungal pathogen *C. albicans*

Outlook

- Cytotoxicity and hemolysis studies
- Mode of action studies
- MIC assays with resistant strains of *S. typhimurium*
- Structural conformation studies with circular dichroism (CD) experiments

References
[1] K. Lewis, *Nature Reviews Drug Discovery*, 2013, 12, 371-387
[2] A.J Cameron, K.G Varnava, P.J.B Edwards, R. Harjes and V. Sarojini, *Journal of Peptide Science*, 2018, 24, e3094
[3] S. Chowdhary, T. Pelzer, M. Saathoff, E. Quaas, J. Pendl, M. Fulde, B. Koksch, *Peptide Science*, e24306, 2023
[4] S. Chowdhary, T. Pelzer, M. Fulde, B. Koksch, "Peptide With Antimicrobial Activity", int. patent, EP4375289A1

Acknowledgments
This work has been generously supported by the Research Training Group (RTG) on Bioactive Peptides – Innovative Aspects of Synthesis and Biosynthesis. My deepest gratitude goes out to Dr. Suvrat Chowdhary and Prof. Dr. Beate Koksch for their valuable support throughout the research, Johannes Kupke and Prof. Dr. Marcus Fulde for their assistance and knowledge in performing the MIC tests at the Institute of Microbiology and Epizootics, Freie Universität Berlin.

https://doi.org/10.17952/37EPS.2024.P2293

MOLECULAR INSIGHTS INTO THE LIPID BILAYER INTERACTIONS OF THE CYCLIC LIPODEPSIPEPTIDE TOLAASIN

B. Kovács[1], T. Juhász[1], N. Geudens[2], José C. Martins[2] and T. Beke-Somfai[1]

[1]*BIOMOLECULAR SELF-ASSEMBLY GROUP, HUN-REN RESEARCH CENTRE FOR NATURAL SCIENCES, BUDAPEST, HUNGARY*

[2]*NMR AND STRUCTURE ANALYSIS RESEARCH UNIT, DEPARTMENT OF ORGANIC AND MACROMOLECULAR CHEMISTRY, GHENT UNIVERSITY*

Tolaasin – not your average AMP

- Bacterial secondary metabolite of rhizosphere-dwelling *Pseudomonas tolaasii*
- Cyclic lipodepsipeptide with *non-proteinogenic* amino acids[1]

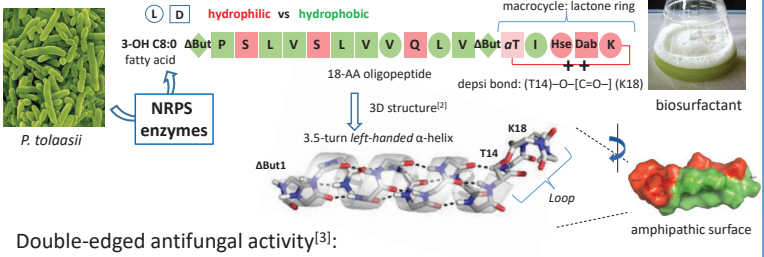

- Double-edged antifungal activity[3]:

Crop Protecting Agent[4] ✓ *vs* Toxin of Brown Blotch Disease[5] ✗



Few (left) vs many (right) tolaasin producers in soil of cocoyam crop fields in Cameroon



Decreases production in edible mushroom farms of *Agaricus bisporus* by 8–15% in Europe

Figure adapted from [5]

- Antifungal activity via *cell membrane* interactions. Main mode of action?

→ Mixed reports i.e. barrel-staved pore formation[2,6] *vs* asymmetry stress[7]

Adapted from [6d]

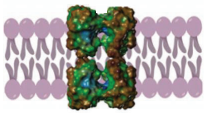

Oligomer vs Monomer (high *P/L*) (low *P/L*)

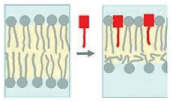

Adapted from [7b]

Via Ion Channel Measurements + ATR-IR — *Via Fluorescence Leakage*

→ Objective: molecular insights into the interaction of tolaasin and the lipid bilayer using novel biophysical and computational approaches.

I) Revisiting the tolaasin conformation using *J*-coupling based NMR spectroscopy with membrane mimic detergent micelles

1) $^3J[\phi]$-couplings

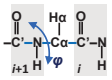

E.COSY, QJ spectroscopy
e.g. HNHA[8]→ $^3J_{H-H\alpha}$
$^3J_{H-H\alpha}$ → φ angle (Karplus)

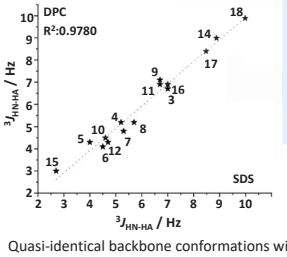

Quasi-identical backbone conformations with SDS(–) vs DPC (+/–) micelles

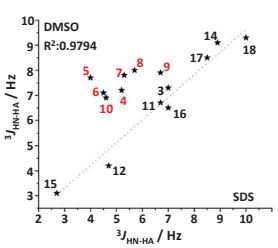

Last helical turn (11-14) + loop (14-18) preserved but α-helix disrupted in DMSO

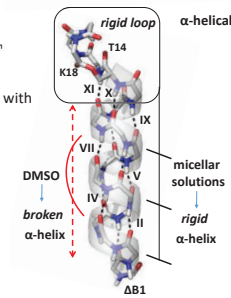

2) H-bond coupling

donor ^{15}N–H ↔ acceptor ^{13}C'=O
[^{15}N–H]-^{13}C' frequencies correlated

→ LR-HNCO[9] experiment

$^{3h}J_{N-C'}$ (< 1Hz)

if detected: $\tau \geq \frac{1}{|^{3h}J_{NC'}|}$

τ ~ ms–s

α-helical (*i*+4;*i*) hydrogen bonds detected:

Bond	SDS	DPC	DMSO
I	✓	✓	✗
II	✗	✗	✗
III	✓	✓	✗
IV	✓	*overlap*	✗
V	*overlap*	✓	✗
VI	✓	✓	✗
VII	✓	✓	✗
VIII	✓	✓	✗
IX	✗	✗	✗
X	✗	✗	✗
XI	✓	✓	✓

Results I

- The backbone conformation of tolaasin as determined with SDS micelles is fully maintained with DPC despite the charge difference.
- Long-lived hydrogen bond network detected @water:lipid interface.
- Loop + last helix turn most rigid, maintained in organic solvents too.

tolaasin ^{13}C,^{15}N isotope labeling : $^{12}C_{94}H_{163}O_{25}{}^{14}N_{21}$ → ~100% $^{13}C_{94}H_{163}O_{25}{}^{15}N_{21}$ → **C and N spins for NMR!**

Nucleus	%	NMR
^{1}H	99.97	✓
^{12}C	98.90	✗
^{14}N	99.60	✗
^{13}C	1.10	✓
^{15}N	0.40	✓

Recipe:

bacterial growth in M9 salt medium[10]

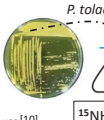

$^{15}NH_4Cl$
U-^{13}C-glucose

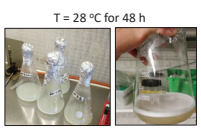

II) Tolaasin membrane interaction characterized by polarized light spectroscopy with membrane mimic liposome SUVs

1) Circular Dichroism (CD)

for chiral elements

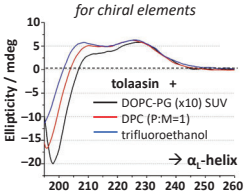



~100 nm

DOPC (+/–) or DOPC-DOPG (–)

↓ effect of charge

2) Linear Dichroism (LD)

for orientation[11]

LD: $A_{\parallel(z)} - A_{\perp(z)}$ → orientation of μ_e → orientation of molecule

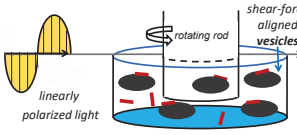

2) LD (a.u.)

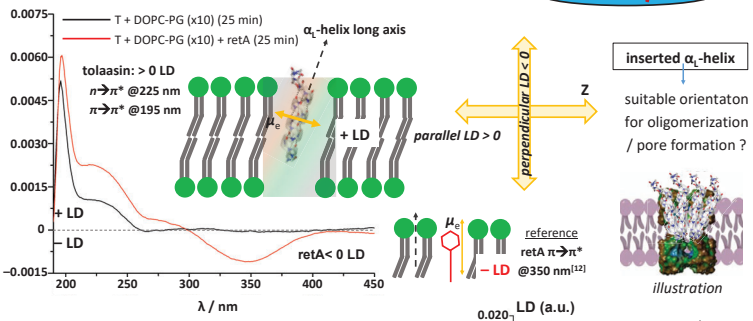

The system and time dependence of the tolaasin LD signal

- liposomes: pure DOPC (+/–)or mixed (4:1) DOPC-DOPG (–) SUVs
- peptide:lipid ratios (*P/L*): 1:10–50 (with [Tol]= 75 μM in PBS)

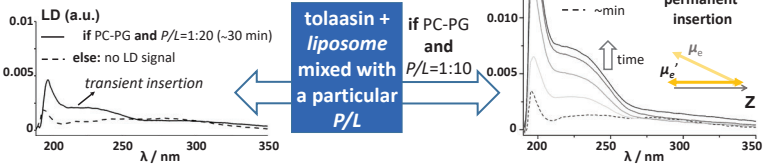

Results II

- Tolaasin maintains its α_L-helical conformation upon interaction with lipid bilayers regardless of their charge.
- With negatively charged, (4:1) mixed DOPC-DOPG vesicles the α-helix of tolaasin is inserted into the lipid bilayer more parallel with its surface norm. Using *P/L*=1:10 LD signal of tolaasin shows gradual increase that plateaus on the timescale of hours and remains constant.
- Conditions are crucial! Using zwitterionic liposomes or lower *P/L* ratio tolaasin remains weakly aligned suggesting more random orientation within the lipid bilayer or transient alignment.

Discussion and Outlook

- Isotopically labeled NMR methods allowed to quantify backbone torsion angles and directly detect long-lived backbone hydrogen bonds for the cyclic lipodepsipeptide tolaasin. These data can now be implemented as novel restraints to improve the current model of tolaasin oligomerization and pore formation processes.
- Polarized light spectroscopy confirmed that the tolaasin helix is able to insert itself into the lipid bilayer parallel with the surface norm which agrees with ATR-IR results[6c]. The full insertion process takes place gradually on the timescale of *hours* and shows irreversible provided that, in our setup, 20% negatively charged SUVs and high peptide-to-lipid ratio (1:10) are used. To demonstrate potential oligomerization and pore formation processes under these conditions imaging techniques are planned to be involved. However, in general, at low *P/L* values or min timescale insertion of the tolaasin helix into the lipid bilayer is yet inefficient and no pore formation is expected.[7b]

III) Initial molecular dynamics simulations of the lipid bilayer interactions of tolaasin

- AMBER ff14SB force field[13], TIP3P water solvent, lipid bilayer builder: CHARMM-GUI Membrane Builder[14]

→ setup: 2 tolaasin +128 POPC molecules (*P/L*=64), 100 ns

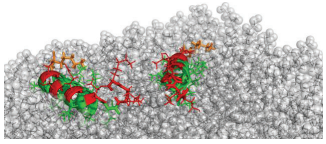

Observations

- The tolaasin molecules remain parallel with the surface.
- They interact with the lipid headgroup region mostly.
- No dimerization takes place in the applied setup.

Abbreviations

ΔBut – dehydroaminobutyril, AMP – antimicrobial peptide, ATR-IR – attenuation total reflection infrared spectroscopy DAB – 2,4 diaminobutyril, DMSO – dimethyl sulfoxide, DOPC – 1,2-dioleoyl-sn-glycero-3-phosphocholine or (18:1) PC, DOPG – 1,2-dioleoyl-sn-glycero-3-phosphoglycerol or (18:1) PG, DPC – dodecyl phosphocholine, HNHA – experiment [8], Hse – homoseryl, LD – linear dichroism, LR-HNCO – long-range HNCO experiment [9], MOA – mode of action, NRPS – non-ribosomal peptide synthetase, NMR – nuclear magnetic resonance, PBS – phosphate buffer saline solution, *P/L* – molar peptide to lipid ratio, retA – retinoic acid, SDS – sodium dodecyl sulfate, SUV – small unilamellar vesicle

References

[1] Nutkins, J.C. *et al., JACS*, 1991, **113**, 2621–2627. [2] Jourdan, F. *et al., Proteins: Struct., Funct., Genet.*, 2003, **52**, 534–543 [3] Geudens, N., Martins., J.C. *Front. Miroblol.* 2018, **9**, 1–18 C. [4] Olorunleke, F.E. *et al.* unpublished data [5] Soler-Rivas, S. *et al., FEMS Microbiol. Rev.*, 1999, **23**, 591–614. [6] a) Cho, K.H. and Kim, Y. K., *FEMS Microbiol. Lett.*, 2003, **221**, 221–226. b) Brody, C.L. *et al., Mol. Plant Microb. Interact.* 1991, **4**, 407–411. c) Coraiola, M. *et al., BBA*, 2006, **1758**, 1713–1722. d) Jo, G. *et al., J. Microbiol. Biotechnol.*, 2011, **21**, 1097–1100. [7] a) Andolfi, A. *et al., Perspect. Med. Chem.*, 2008, **2**, 1177391X0800200–112. b) Steigenberger, J. *et al., Front., Mol., Biosci.*, 2022, **9**, 2296-889X. [8] Vuister, G.W. and Bax, A., *JACS*, 1993, **115**, 7772–7777. [9] Cordier, F. *et al., Nat. Protoc.*, 2008, **3**, 235–241. [10] Geudens, N. *et al. Molecules*, 2019, **24**, 2257. [11] Nordén, B. *et al.*, Linear Dichroism and Circular Dichroism: A Textbook on polarized-light spectroscopy, *RSC Books*, Cambridge, UK, 2010. [12] Svensson, F.R. *et al., J. Phys. Chem. B, 2007*, **111**, 10839–48. [13] Maier, J.A. *et al., J. Chem. Theory Comput.*, 2015, **11**, 3696–3713. [14] a) Jo, S. *et al., PLoS ONE*, 2007, **2**, e880. b) Jo, S. *et al., Biophys J.*, 2009, **97**, 50–58.

Group platform: http://bionano.ttk.mta.hu/ **e-mail: kovacs.benjamin@ttk.hu**

Proceedings of the 37th European Peptide Symposium
Michal Lebl, Editor
European Peptide Society, 2024 *http://doi.org/10.17952/37EPS.2024.P2294*

A comprehensive structural study on AT1 Receptor Variants: Towards the Design of Potent Biased Agonists

Malihe Hassanzadeh(1), Audrey Collette(1), Brian Holleran(1), Stéphane Laporte(2), Richard Leduc(1) and Pierre-Luc Boudreault(1)*

(1) Department of Pharmacology-Physiology, Faculty of Medicine and Health Sciences, Institute de Pharmacologie de Sherbrooke, Université de Sherbrooke, 3001 12th Ave North, Sherbrooke, Qc, J1H 5N4, Canada
(2) Department of Pharmacology and Therapeutics, McGill University, Montréal, Québec, H3G 1Y6, Canada

The angiotensin II type 1 receptor (AT_1R) is a crucial component of the renin-angiotensin system (RAS), which plays a significant role in regulating blood pressure, and cardiovascular health [1]. Biased agonism is an emerging concept that activates specific signaling pathways of G protein-coupled receptors (GPCRs). It involves selectively targeting the receptor with a ligand that stimulates one pathway while inhibiting others, leading to more precise treatments with fewer side effects. To gain a deeper understanding of GPCR functional selectivity at a molecular level, this study focuses on the use of AT_1R mutants and biased agonists. The activation of the AT_1R by different agonists leads to different signaling pathways which is known as functional selectivity [2]. Understanding this mechanism can help to develop more effective and targeted treatments for hypertension and other cardiovascular diseases. To assess the activation of Gq and the recruitment of β-arrestin in response to the stimulation of AT_1R with angiotensin II (AngII), [Sar^1Ile8], AngII [Sar^1LBpa^8]AngII, and [Sar^1DBpa^8]AngII ligands, we opted to substitute position $W253^{6.48}$, also referred to as the rotamer toggle switch, with alanine (W253A-AT_1R). The activation of G_q and recruitment of β-arrestin were quantified using BRET-based biosensors. Our results indicate that the mutant W253A-AT_1R was able to activate Gq and recruit β-arrestin when stimulated with AngII. However, upon stimulation with [Sar^1Ile^8]AngII or [Sar^1DBpa^8]AngII, which are β-arrestin-biased ligands on AT_1R, W253A-AT_1R mutant failed to recruit β-arrestin. Interestingly, [Sar^1LBpa^8]AngII could activate β-arrestin in the W253A-AT_1R mutant background.

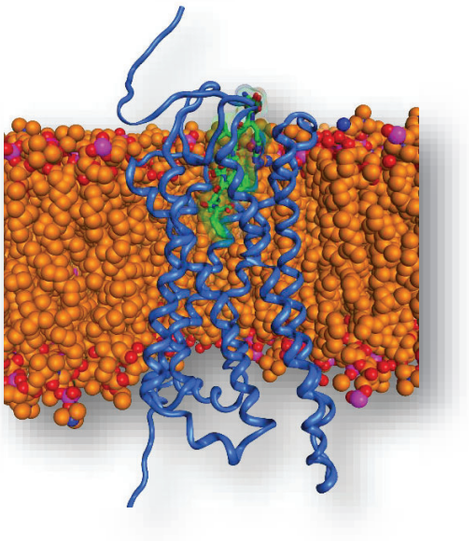

This study proposes significant interactions exist between the mutant W253A-AT_1R and specific determinants of the different peptide ligands, which are involved in stabilizing the receptor in a conformation capable of recognizing β-arrestin. To investigate the structural dynamics of the native AT_1R and W253A-AT_1R mutant receptor, we utilized molecular dynamics (MD) simulations. Our study incorporated interactions with the native endogenous ligand and the three modified peptides. Our simulations revealed distinct conformational landscapes for each receptor-ligand pairing, with particular emphasis on regions of flexibility and interaction. Significantly, these unique conformational tendencies, lead to a better understanding of the molecular determinants responsible for selecting a given biased pathway. This information provides opportunities to design biased agonists with great therapeutic promise, as they may offer the potential for enhanced efficacy and reduced side effects.

References:

1. Van Haaster, McDonough, Gurley, Curr Opin Nephrol Hypertens, 2018, 27, 1-7.
2. Wingler, Skiba, McMahon, Staus, Kleinhenz, Suomivuori, Latorraca, Dror, Lefkowitz, Kruse, 2020,367, 888-892.

37th European Peptide Symposium, 14th International Peptide Symposium, 25th-29th August 2024, Florence, Italy https://doi.org/10.17952/37EPS.2024.P2295

Structural analysis of a peptide-based simplified model reproducing SARS-CoV-2 S RBD/ACE2 binding site

Michela Buonocore[1,2], Rosanna Lucignano[1], Angelo Santoro[3], Anna Maria D'Ursi[3], & Delia Picone[1,2]

[1]Department of Chemical Sciences, University of Naples Federico II, Naples, Italy, [2]Research Centre on Bioactive Peptides (CIRPeB), University of Naples Federico II, Naples, Italy, [3]Department of Pharmacy, University of Salerno, Fisciano, Italy

Introduction

SARS-CoV-2, the pathogen causing the COVID-19 outbreak, is an RNA virus which infects lung cells through the binding of its surface glycoprotein spike (S) with the angiotensin-converting enzyme 2 (ACE2). The moiety of S involved in the interaction – namely receptor binding motif (RBM) – has been subjected to a remarkable number of point mutations throughout the rapid evolution of the virus. Therefore, the description of a model that individuates the interacting residues between S and ACE2 needs to be updated as soon as new variants of interest emerge. To this aim, the synthesis of peptide molecules reproducing short moieties involved in the interaction, rather than the production of the full protein construct, allowed the development of a simplified system that would afford to study the change in the SARS-CoV-2 S RBD/ACE2 binding related to the frequent mutations.[1-3]

In this work, we synthesized and studied the structure of short amino acid sequences, mimicking the two proteins' critical portions. Variations in the residues were easily managed through the one-point alteration of the sequences. Nuclear magnetic resonance (NMR) spectroscopy provides insights into ACE2 and SARS-CoV-2 S RBD deriving peptides' structures with their related variants (Alpha, Beta, and Gamma). Moreover, these sequences proved to be highly immunogenic, as many monoclonal antibodies target this moiety and give an individual susceptibility to the different variants. To study this effect, we used these peptides to functionalize the monomers of H-chain of human ferritin (hHFt), a protein able to assemble in an ordered 24-mer nanocage with high thermal and chemical stability in physiological conditions. The decoration of the outer surface of the nanocage with the S-derived epitopes can provide a tool able to elicit an immune answer in view of the development of novel vaccine strategies that can also be applied to other critical pathologies, for which there is no therapeutical strategy.

Results

Peptides

Analysis of the SARS-CoV-2 S/ACE2 complex

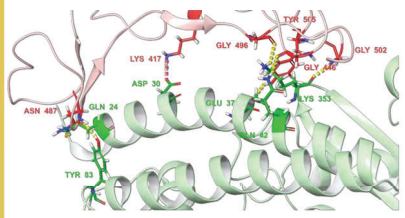

ACE2 $_{21}$I-Q$_{42}$ sequence

$_{21}$IEEQAKTFLDKFNHEAEDLFYQ$_{42}$

S RBD $_{482}$G-Q$_{506}$ sequences

Original (SMIMIC$_{OR}$)	$_{482}$GVEGFNCYFPLQSYGFQPTNGVGYQ$_{506}$
B.1.1.7 (SMIMIC$_{\alpha}$)	$_{482}$GVEGFNCYFPLQSYGFQPT**Y**GVGYQ$_{506}$
P.1/B.1.351 (SMIMIC$_{\beta\gamma}$)	$_{482}$GV**K**GFNCYFPLQSYGFQPT**Y**GVGYQ$_{506}$

Synthesis of the peptides and characterization by solution NMR

Solvent mixture: HFIP/water 50/50 v/v

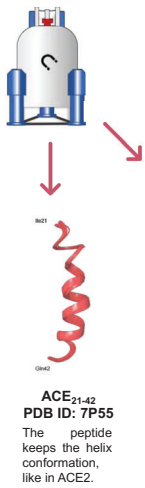

ACE$_{21-42}$ PDB ID: 7P55

The peptide keeps the helix conformation, like in ACE2.



SMIMIC$_{OR}$ PDB ID: 7P5G



SMIMIC$_{\alpha}$ PDB ID: 7P5Q



SMIMIC$_{\beta\gamma}$ PDB ID: 7P5S

Effect of the mutations on the secondary structures

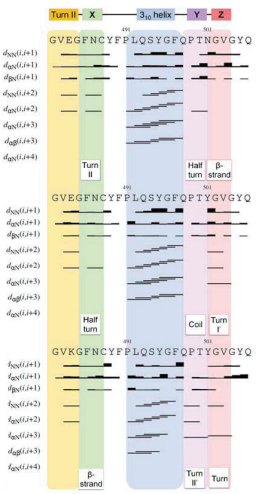

NOE connectivities bar plot shows a common pattern Turn II–X–3$_{10}$ helix–Y–Z for the three peptides, where the X, Y and Z conformations are affected by the mutated residues: in particular the mutation N501Y has a strong effect both on N and C terminus.

Analysis of the binding ACE$_{21-42}$/SMIMIC$_{OR}$

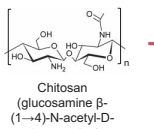

Chitosan (glucosamine β-(1→4)-N-acetyl-D-glucosamine)



Chitosan beads



Functionalization of chitosan beads with SMIMIC$_{OR}$ (EDC/NHS strategy) and analysis of the binding with ACE$_{21-42}$

STD-NMR

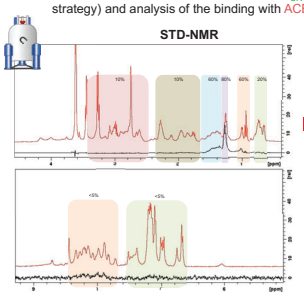

STD-NMR experiments on SMIMIC$_{OR}$ functionalized chitosan beads with ACE$_{21-42}$ (1:50 molar ratio) show a clear effect on the aliphatic protons of ACE$_{21-42}$, confirming the presence of binding driven by the peptide's side chains.

Fuctionalization of ferritin

Selection of the peptide sequences



Name	Sequence	Note
S3	$_{327}$VRFPNITNL$_{335}$	Highly immunogenic and conserved epitope[4]
S6	$_{482}$GVEGFNSYF PLQ**S**YGFQPTN GVGYQ$_{506}$	SMIMIC$_{OR}$ with the mutation C494S to provide more stability
S7	$_{482}$GVEGFYSYFP LQ**S**YGFQPTYG VGYQ$_{506}$	SMIMIC$_{\alpha}$ with the mutation C494S to provide more stability
S8	$_{482}$GVKGFYSYFP LQ**S**YGFQPTYG VGYQ$_{506}$	SMIMIC$_{\beta\gamma}$ with the mutation C494S to provide more stability
S9	$_{482}$GVAGFNSYF PLR**S**YSFRPTY GVGHQ$_{506}$	482-506 residues from the Delta variant with the C494S mutation
S10	$_{896}$IPFAMQMAYR FNGIG$_{910}$	Highly immunogenic and conserved epitope[5]

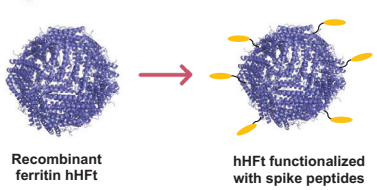

Recombinant ferritin hHFt → **hHFt functionalized with spike peptides**

We engineered 10 plasmids of hHFt sequence including the S-deriving peptides (in the table above we reported only the most promising). The spike peptides were added at the **C-terminus** of hHFt and separated using a (GGGGS)$_3$ linker.[6-7]

Protein expression in E.coli and purification

The recombinant proteins were expressed following the previously described protocols[7], but the temperature of the thermal treatment was lowered from 75°C to 65°C due to their lower stability compared to the native hHFt.

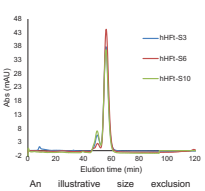

An illustrative size exclusion chromatography (SEC) run of hHFt-S3, S6 and S10 using a Superdex™ S200 column, which manages to separate proteins from 10 to 600 kDa.

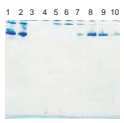

Native gel electrophoresis of hHFt-S10 after the SEC run: we loaded a native hHFt as standard (lane 1), the mixture loaded in the column (lane 2), and the product eluted from the column after 40 (lane 3), 48 (lane 4) 50 (5), 52 (6), 54 (7), 58 (8), 60 (9) and 62 (10) minutes.

CD

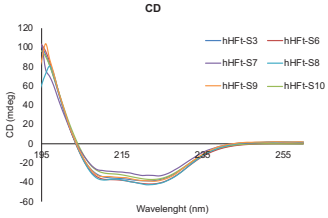

CD spectra of the modified ferritins in phosphate buffer at pH 7.4 suggest that the proteins tend to assume a helix structure, as also reported in a previous work of characterization of hHFt in native conditions[8].

Characterization of the products of gene expression by SEC, native PAGE, and CD spectroscopy reported that the hHFt proteins modified with the spike sequences behave similarly to the parent hHFt in native conditions, with the successful formation of the super-assembled nanocage.

Binding analysis of hHFt-spike proteins with ACE$_{21-42}$

1D ^{1}H CMPG

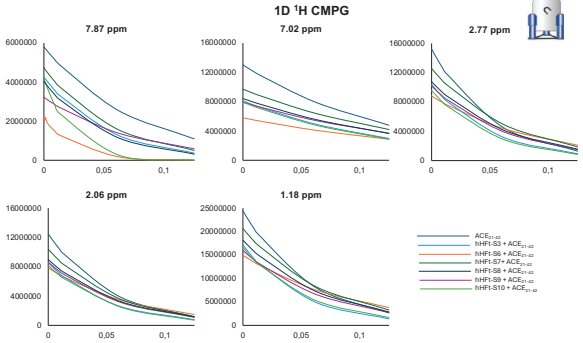

	T2 (s)						
ppm	ACE$_{21-42}$	hHFt-S3 + ACE$_{21-42}$	hHFt-S6 + ACE$_{21-42}$	hHFt-S7 + ACE$_{21-42}$	hHFt-S8 + ACE$_{21-42}$	hHFt-S9 + ACE$_{21-42}$	hHFt-S10+ ACE$_{21-42}$
7.87	0.075±1.2e^{-3}	0.051±1.3e^{-3}	0.025±1.3e^{-3}	0.056±1.2e^{-3}	0.049±1.4e^{-3}	0.074±2.2e^{-3}	0.023±6.0e^{-4}
7.02	0.12±7.9e^{-4}	0.13±1.3e^{-4}	0.18±3.3e^{-4}	0.150±1.4e^{-3}	0.151±1.6e^{-3}	0.164±1.9e^{-3}	0.124±1.3e^{-3}
2.80	0.050±3.0e^{-4}	0.0517±4.8e^{-4}	0.088±8.5e^{-4}	0.066±4.6e^{-4}	0.065±5.4e^{-4}	0.065±5.5e^{-4}	0.051±4.8e^{-4}
2.06	0.053±3.4e^{-4}	0.0504±49e^{-4}	0.076±7.4e^{-4}	0.058±4.3e^{-4}	0.061±5.5e^{-4}	0.061±5.8e^{-4}	0.053±5.4e^{-4}
1.18	0.056±2.3e^{-4}	0.0502±3.2e^{-4}	0.61±6.1e^{-4}	0.068±3.5e^{-4}	0.068±4.3e^{-4}	0.071±4.6e^{-4}	0.055±3.5e^{-4}
Prot.	-	6.8e^{-3}±1.9e^{-4}	0.026±7.7e^{-4}	0.015±4.8e^{-4}	0.053±2.0e^{-3}	0.132±5.0e^{-3}	0.014±8.8e^{-4}

1D ^{1}H CPMG acquired with different delays from 0 to 0.125 ms of hHFt-spike proteins in the presence of ACE$_{21-42}$ peptide showed that respect to the reference value of T_2 measured on the free peptide (dark blue line in the plots, first column in the table), the T_2 of ACE$_{21-42}$ decreases in the presence of the proteins, resulting in a faster relaxation that indicates an interaction of the peptide with the protein.

Conclusions. In this poster, we report a methodology for studying large binding complexes using short peptide sequences. The starting model was the SARS-CoV-2 S RBD/ACE2 complex. We extracted two sets of peptide sequences mimicking the binding domains of the two proteins (including the mutations of the variants of concern in SARS-CoV-2 S) and studied the peptides' conformation in solutions. Moreover, we functionalized chitosan beads with SMIMICS$_{OR}$ and tested their binding potential with ACE$_{21-42}$ using STD-NMR, reporting a sizeable binding. With the aim of using these S-deriving sequences in a pharmacological active tool, we functionalized the human H chain of the ferritin (hHFt) with the spike peptides, which is a very interesting molecule for the drug delivery and for the development of immunoreactive devices. We successfully produced six modified hHFt sequences and tested their binding with ACE$_{21-42}$ using 1D CPMG. These preliminary results will be used as the basis for a thorough study of the potential of these macromolecules in novel vaccine development strategies.

References: [1]Grubaugh, et al. Cell 184 (2021) 1127–1132.; [2]Sanyaolu, et al. Therapeut. Adv. Infect. Dis. 8 (2021), 20499361211024372; [3]Buonocore, et al., Heliyon 8.11 (2022); [4]Bagherzadeh, et al. Scientific reports 12.1 (2022): 14017; [5]Tarke, et al. Cell 185.5 (2022): 847-859; [6]Ma, et al. " ACS Applied Bio Materials 4.3 (2021): 2654-2663; [7]Rodrigues, et al. " Pharmaceutics 13.10 (2021): 1621. [7]Lucignano, et al. International Journal of Biological Macromolecules (2024): 134373. [8]Lucignano, et al. Frontiers in Molecular Biosciences 10 (2023): 1008985.

Funding: M.B. was recipient of a fellowship FRA2022 financed by the Italian Ministry of University and Research (MUR).

Planar aggregation of the influenza viral fusion peptide alters membrane structure and promotes poration

NIH National Heart, Lung, and Blood Institute

Richard W. Pastor, Amy Rice, Paul S. Blank, Joshua Zimmerberg

https://doi.org/10.17952/37EPS.2024.P2296

Background

The **fusion peptide** (FP) domain of influenza A hemagglutinin is the only portion of the virus that interacts directly with the target membrane of the host organism; its primary function is to facilitate fusion between the viral membrane and the host.

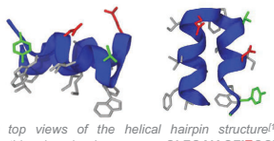

Side and top views of the helical hairpin structure[1] of Influenza A fusion peptide domain (sequence: GLFGAIAGFIEGGWTGMIDGWYG). Side chain coloring: red – anionic; green – polar; grey – nonpolar.

Previous experiments and simulations have shown the ability of the isolated FP domain to aggregate when membrane-bound, and form pores in model membrane systems[2,3]; poration was demonstrated to be inhibited by cholesterol. It was hypothesized that FP clustering promotes poration by decreasing the hydrophobic thickness a pore must span in order to form.

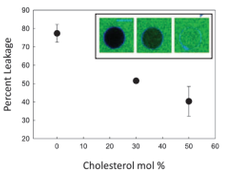

FP-induced dye leakage in GUVs as a function of cholesterol content. The inset depicts a typical dye leakage experiment, where fluorescent dye leaks into the GUV after FP is added. Adapted from ref. [2].

However, in subsequent simulations cholesterol appeared to enhance FP clustering, seemingly in conflict with the original hypothesis. Here, we aim to resolve this apparent discrepancy by characterizing the energetic landscape of FP–FP interactions and elucidating the role that membrane-specific properties play in FP clustering and poration.

Simulation Details

- CHARMM 36 force field
- Unbiased long timescale MD simulations
  - 10 FP in POPC, 1:1 chol:POPC, 7:3 OPC:POPC
    - 21 μs each
  - 21 FP in POPC and 1:1 chol:POPC
    - 3x10 μs each
  - 10 FP dimers in POPC and 1:1 chol:POPC
    - 3x10 μs each
- Free energy calculations – Umbrella Sampling
  - POPC, 1:1 chol:POPC, 7:3 OPC:POPC, & 24:76 DOG:POPC
  - Dimerization PMFs
    - 35 windows, 1 μs per window
  - Tetramerization PMFs
    - 26 windows, 1 μs per window
- Simulation packages
  - OpenMM [4] and Anton 2 [5]
- Analysis
  - PMFs – WHAM [6]1
  - RDFs – LOOS [7]

Results

1 Dimers are favored regardless of bilayer constituents

***Potentials of mean force (PMF)**, for antiparallel dimer formation in four membrane compositions. The minima at a peptide COM distance of 12.2 Å corresponds to the antiparallel dimer structure.*

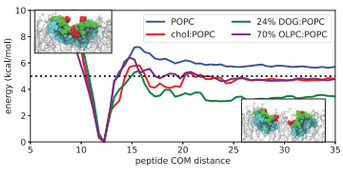



Antiparallel dimer stabilized, with ΔG ≈ −5 kcal/mol in the four membranes simulated, indicating population at equilibrium should primarily be antiparallel dimers

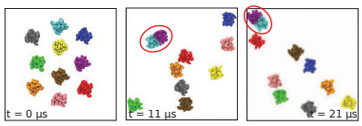

***Simulation snapshots**, depicting an antiparallel dimer (circled) that forms at t = 4 μs and remains stable through the remainder of the 21 μs simulation. Top down view of bilayer; lipids and water omitted. Taken from Ref [2]*

2 Tetramer formation is largely membrane-dependent

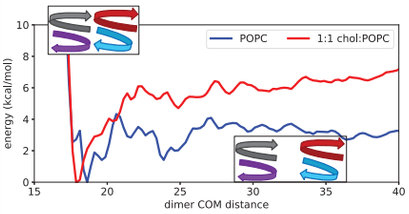

***Potentials of mean force (PMF)**, for tetramer formation from two antiparallel dimers. Both have a minima at a dimer COM distance ~17.7 Å, which corresponds to dimers with no lipid separating them. The PMF in **POPC has a second minimum at ~24 Å**, corresponding to separation by a single layer of lipids, a feature which is absent from the chol:POPC PMF.*

Dimer-dimer interfaces in POPC often include lipids, whereas in chol:POPC direct contact between dimers is more likely

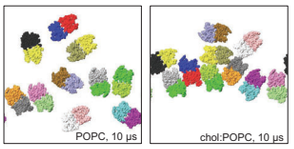

***Simulation snapshots**, depicting arrangement of ten antiparallel FP dimers in POPC (left) and chol:POPC (right) after 10 μs of equilibration. Top down view of bilayer, lipids and water omitted.*

3 Spontaneous curvature drives lipid enrichment in the bottom leaflet

***Lipid radial distribution functions**, demonstrating lipid-dependent enrichment underneath an FP dimer. Lipids that generate negative spontaneous curvature (DOG and cholesterol) are enriched while lysolipid which generates positive spontaneous curvature is depleted. The gray shaded regions represent the approximate extent of one FP, along its shorter and longer axes.*

DOG – enriched
chol – enriched
OPC – depleted
POPC – enriched
POPC – depleted
POPC – depleted

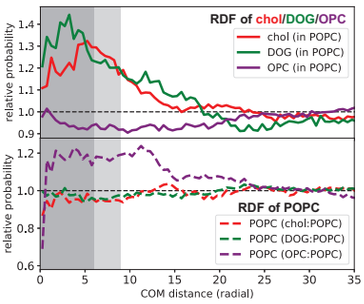

Lipids that generate negative spontaneous curvature are enriched under FP aggregates, while lipids that generate positive spontaneous curvature are depleted, consistent with predictions from theory [8]

Hypothesis

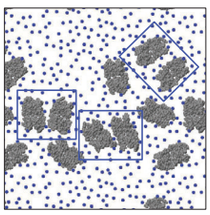

In pure **POPC** membranes, dimer-dimer interfaces typically include several lipids. These lipids are highly perturbed by the neighboring FP, destabilize the bilayer, and represent a weak point in the bilayer, thus acting as sites of pore nucleation.

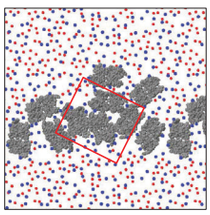

In **chol:POPC** membranes, cholesterol is excluded from dimer-dimer interfaces and many interfaces contain no lipids. These direct peptide-peptide contacts prevent water from penetrating into the bilayer, potentially stabilizing the bilayer and inhibiting pore formation.

References

[1] Lorieau, Louis, Bax, *PNAS* **2010**, *107*, 11341–11346
[2] Rice et al. *Nat. Comm.* **2022**, *13*(1), 7336
[3] Rice, Zimmerberg, Pastor, *Biophys. J.* **2023**, *122*(6), 1018–1032
[4] Eastman et al. *PLOS Comp. Biol.* **2017**, *13*, e1005659
[5] Shaw et al. *IEEE* **2014**, 41–53
[6] Grossfield, "WHAM : the weighted histogram analysis method" v. 2.0.9
[7] Romo, Grossfield, *Conf. Proc. IEEE Eng. Med. Biol. Soc.* **2009**
[8] Barnoy, Parton, Kozlov, *bioRxiv*, doi: 10.1101/2024.07.09.602763
[9] Humphrey, Dalke, Schulten, *J. Molec. Graphics* **1996**, *14*, 33–38

Acknowledgements

This work was supported by the Intramural Program of the National Heart Lung and Blood Institute of the National Institutes of Health, Bethesda MD, USA, and utilized high performance computational resources at the National Institutes of Health (NHLBI LoBoS and HPC Biowulf clusters) and Anton 2 (PSC). Simulation snapshots rendered using VMD [9].

Conclusions

- Formation of antiparallel FP dimers is highly favorable, driven primarily by peptide-peptide contacts, and not strongly influenced by membrane composition
- Higher order clustering of FP is membrane dependent:
  - Cholesterol presence favors large aggregates with little lipid separating dimers
  - In POPC, interfaces separated by a single lipid layer are also favorable
- In all systems, POPC is enriched around FP
- Lipid composition under peptide aggregates is influenced by spontaneous curvature generation of lipids:
  - Lipids that generate negative spontaneous curvature are enriched
  - OPC (generates positive spontaneous curvature) is depleted
  - Enrichment of chol or DOG under FP may generate negative curvature, stabilizing tetramer formation
- Hypothesize that a single layer of lipids between adjacent peptides destabilizes the bilayer, facilitating poration – potentially explaining why cholesterol inhibits poration

Unlocking HIV's Secrets: Synthesis of Histone H3K36Me3 to Investigate LEDGF Protein Binding to Modified Nucleosomes using Cryo-Electron Microscopy

Ramesh M. Chingle[1], Samanthreddy Kedika[1], Tao Jing[2], Dmitry Lyumkis[2,*] and Terrence R. Burke, Jr. [1,*]

[1]*Chemical Biology Laboratory, National Cancer Institute, Frederick, Maryland, 21702, United States*

[2]*The Salk Institute for Biological Studies, Laboratory of Genetics, La Jolla, California 92037, United States*

https://doi.org/10.17952/37EPS.2024.P2298

Background: Nucleosome structure and histone

Histone post-translational modifications (PTMs) intricately orchestrate the epigenetic landscape, profoundly influencing chromatin dynamics and functional gene expression. Among PTMs, methylation of histone lysine residues emerges as a pivotal regulator in diverse biological processes, notably gene transcription. Our research endeavors to engineer modified histones with augmented affinity for the methyl-lysine binding site within the PWWP domain of LEDGF/p75, a pivotal cellular cofactor of HIV-1 integrase (IN). Leveraging native chemical ligation (NCL), we introduce non-standard amino acid residues into histone 3.3, facilitating subsequent structural and functional investigations. This study unveils optimized protocols merging solid-phase peptide synthesis with sequential NCL, enabling the synthesis of fully synthetic variants of the methylated 135-residue protein, H3.3K36(Me)3, featuring trimethylated and dimethylated lysine at residue 36. These tailored histones are envisioned to form nucleosomes with heightened LEDGF affinity, poised for cryo-electron microscopy (cryo-EM) elucidation. Our work not only advances the synthetic accessibility of modified histones but also paves the way for unraveling intricate chromatin-LEDGF interactions, holding promise for understanding HIV-1 integration mechanisms at a molecular level.

Role of LEDGF protein in HIV integration

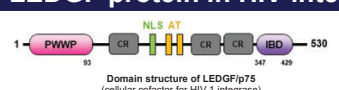

Domain structure of LEDGF/p75
(cellular cofactor for HIV-1 integrase)

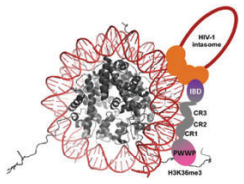

Fig 1. Representation of H3K36(Me)3-modified nucleosome bound to the PWWP domain of LEDGF.

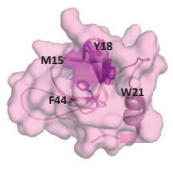

Fig 2. PWWP aromatic cage to recognize H3K36(Me)3 (cation-π interaction).

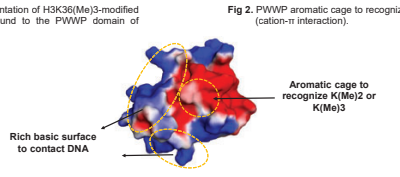

Fig 3. Rich basic surface to contact DNA (H3K36Me3 binding pocket).

cryo-EM structure of the PWWP domain with H3Kc36(Me3) modified nucleosome

Fig 4. A) cryo-EM structure of the H3K36(Me)3-modified nucleosome bound to the PWWP domain of LEDGF. **B)** Pull-down of LEDGF from crude nuclear extract by using nucleosomes bearing wild-type (WT) H3, MLA (H3Kc36Me3), or H3K36(Me)3, H3K36(Me)3 peptide (panel b Figure adopted from Ruthenburg, et. al., *Chem. Bio. Chem.* **2014**, *15*, 2071-2075).

Goal : Integrated approach to generate H3K36(Me)3 for incorporation into nucleosomes

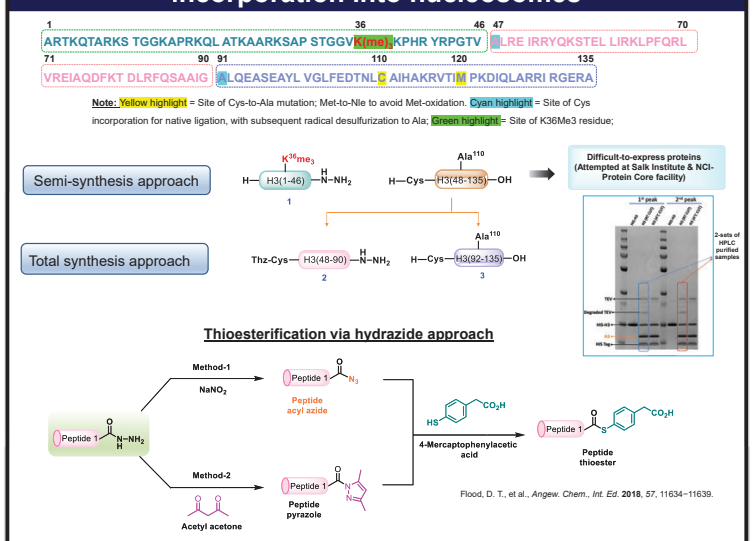

Results: Three segment C-to-N synthesis strategy for H3K36(Me3)

Sequential native chemical ligation

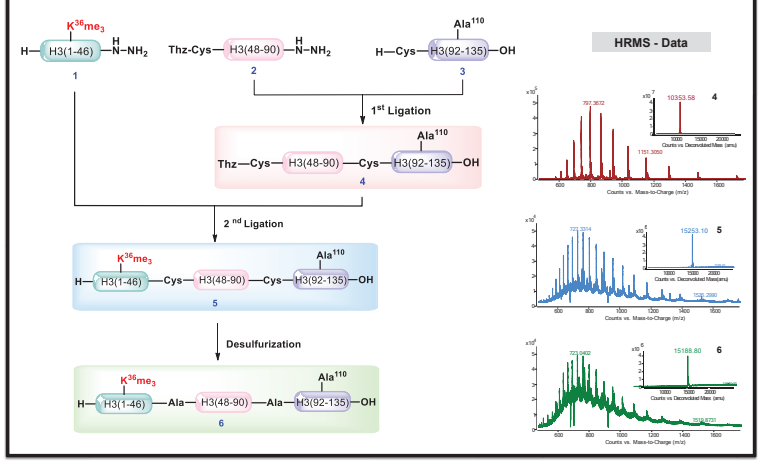

Conclusion and Future Perspective

- Optimized robust methodology for total synthesis of H3K36(Me)3 with an excellent overall yield.
- Native chemical ligation (NCL) technique used for stitching together peptide fragments.
- The final 135-mer constructs will be used to prepare nucleosomes for cryo-EM studies.

Acknowledgements

CBL (Chemical Biology Laboratory)
- Terrence R. Burke Jr.*
- Xue Zhi Zhao
- Steve Smith
- Pankaj Mahajan
- Samanthreddy Kedika
- Anand Kulkarni

NCI Biophysics Resource
- Sergey G. Tarasov
- Marzena Dyba

NCI Administration
- Patricia Beard
- Debbie Perone

Salk Institute
- Dmitry Lyumkis*
- Tao Jing

Elucidating the role of phosphoserines in Tau protein by combined computational and synthetic methods

Martina Tuberti[1,2], Fintan Kelleher[1] and Gemma K. Kinsella[2]

[1]Molecular Design & Synthesis Group, TU Dublin, Tallaght, Ireland

[2] School of Food Science and Environmental Health, TU Dublin, Grangegorman, Ireland

D21128574@mytudublin.ie

https://doi.org/10.17952/37EPS.2024.P2300

Introduction

- The cause of Alzheimer's disease (AD) is still unknown but is correlated with alteration of neuron proteins like Tau, which functions by the assembly and stabilization of microtubules, which helps normal neuronal functions. In AD, Tau loses that capacity and does not bind microtubules, due to posttranslational modifications such as hyper-phosphorylation at serine residues, resulting in misfolding.[1]

- In some bacteria, enzymatic β-elimination of phosphoserines by the amine of a nearby Lys sidechain is reported (**Figure 1**).[2] This leads to a Dha intermediate which is then capable of undergoing crosslinking reactions with Lys, His and Cys residues, as well as glutathione.

- Is it possible: ➢ to apply this type of mechanism to Tau protein in human brain?
  ➢ that a proximal Lys amine sidechain could lead to Dha formation, cross-linking, and subsequent misfolding of Tau protein?

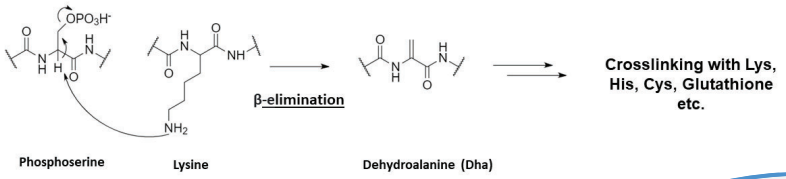

Figure 1. Mechanism of β-elimination of phosphoserine by Lys, with Dha formation

Solid–Phase Peptide Synthesis (SPPS)

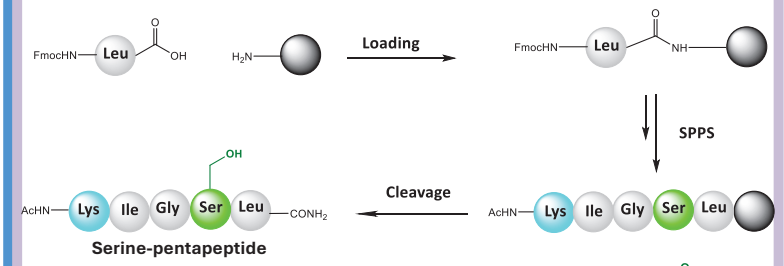

Similar method used to synthesise phosphoserine and Ala-containing pentapeptide. This one is used to check if β-elimination occurred without Lys side chain.

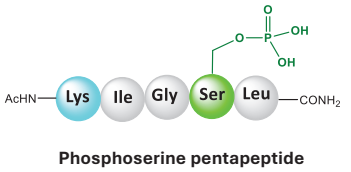

Scheme 1. SPPS of Serine, Phosphoserine and Ala - pentapeptides.

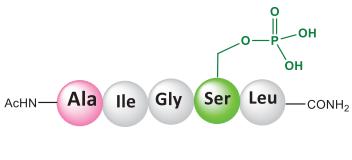

Molecular Dynamics (MD) Simulations

A library of Tau (PDB entries) was prepared and the distance between Ser and Lys was measured with a Python script **(Fig. 2)**.

All-atom MD simulations were performed using *NAMD 2.14* on (i) pentapeptide (Lys^{353}-Leu^{357}) of Tau and on (ii) the same fragment with $pSer^{356}$ **(Figure 3)**

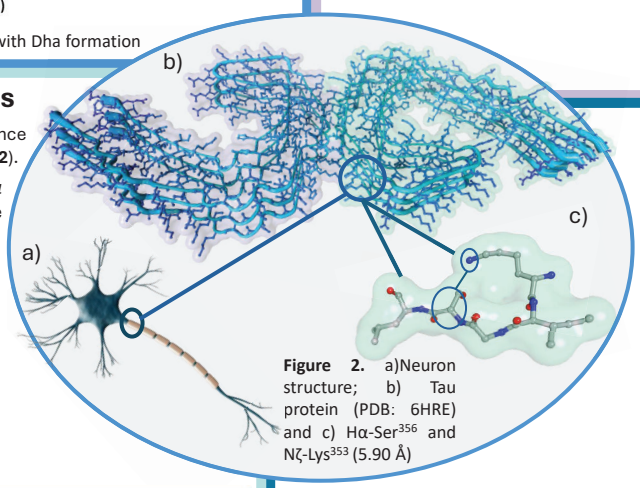

Figure 2. a)Neuron structure; b) Tau protein (PDB: 6HRE) and c) Hα-Ser^{356} and Nζ-Lys^{353} (5.90 Å)

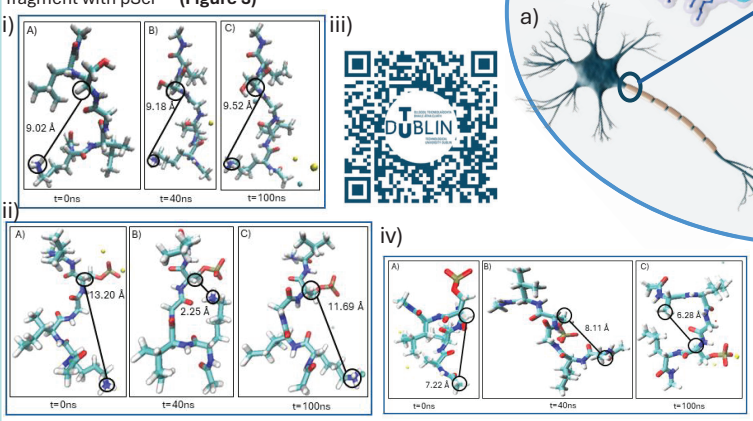

Figure 3. Snapshots of **i)** non-phosphorylated chain versus;**ii)** phosphorylated chain $pSer^{356}$ and $Lys^{353}$and; **iii)** phosphorylated chain $pSer^{356}$ and Ala^{357} are highlighted; **iv)** QR code of phophopentapeptide simulation movie

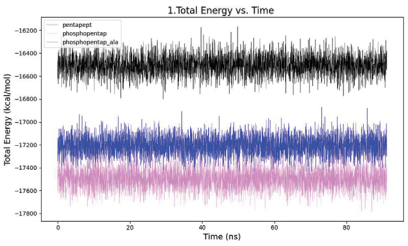

MD simulation	% of Occupancy
Pentapeptide	0.11
Phosphopentaptide	35.92

Table 1. % of Occupancy of interaction with a cut off < 4 Å between Nζ-Lys^{353} of and Hα-Ser^{356} of the first MD simulation and Hα-$pSer^{356}$ for the second.

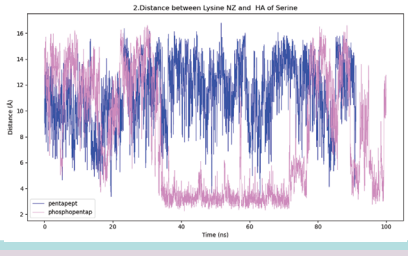

1. Total Energy is a measure of how the system is stable after heating at 310K and equilibrating after 5ns

2. Average distance between Hα-Ser^{356} and Nζ-Lys^{353} and Hα-$pSer^{356}$ and Nζ-Lys^{353}

(blue) Pentapeptide
(pink) Phosphopentapeptide
(black) Phosphopentapeptide with K353A

LC-MS Analysis of synthesised fragments

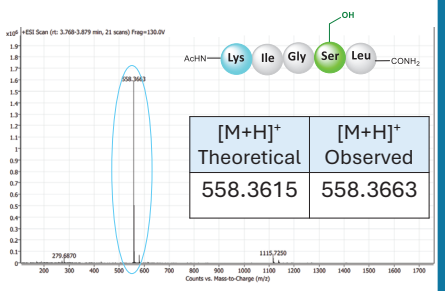

[M+H]+ Theoretical	[M+H]+ Observed
558.3615	558.3663

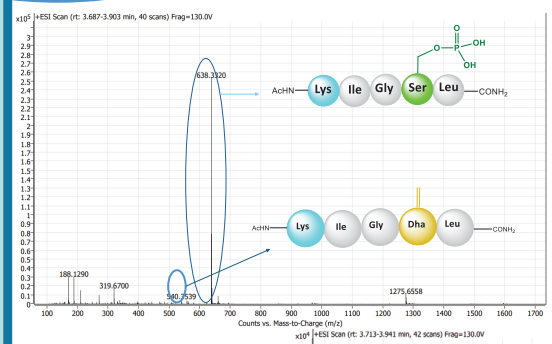

[M+H]+ Theoretical	[M+H]+ Observed
638.3278	638.3320

[M+H]+ Theoretical	[M+H]+ Observed
540.3509	540.3539

[M+H]+ Theoretical	[M+H]+ Observed
581.2700	581.2756

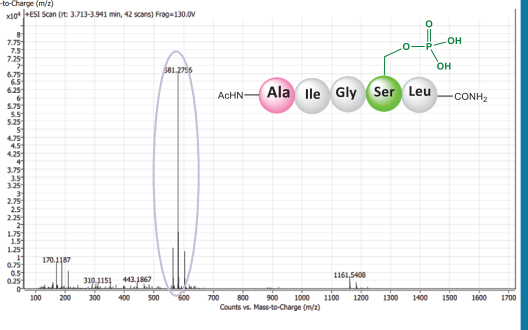

- *Column Poroshell 120 RP18, 3.0x 50mm, 2,7; eluent H_2O/ACN (90% : 10%-100%) +Formic acid, flow rate 0.400 ml/min, UV-VIS detection 208nm.*

Figure 4: Serine pentapeptide fragment (top); Phosphoserine and Dha-containing peptide fragment (middle); Phosphoserine with alanine instead of lysine (end).

Conclusions Structural analysis, and computational studies identified a phosphoserine-containing Tau protein pentapeptide fragment, that was synthesised by SPPS. LC-MS analysis shows the desired phosphopeptide fragment, along with a minor amount of the Dha-containing peptide being detected. Future work will study the aqueous stability of the phosphopeptide fragments at varied pH values and computational studies will focus on the Dha peptide, and pH.

1. Sirai, G. et al., Tau Protein Hyperphosphorylation and Aggregation in Alzheimer's Disease and Other Tauopathies, and Possible Neuroprotective Strategies. *Biomolecules*.**2016**, 6,6(1):6
2. Goto, Y. et al., Mechanistic Studies of Ser/Thr Dehydration Catalyzed by a Member of the Lanl, Lanthionine Synthetase Family, *Biochemistry*, **2011**, 50, 891-898

Acknowledgement :
Irish Centre for High –End Computing (ICHEC) and TU Dublin

https://doi.org/10.17952/37EPS.2024.P2301

Theoretical and biological studies of oxytocin containing conformationally fixed analogue of Tyrosine Tic(OH) (1,2,3,4-Tetrahydro-7-hydroxyisoquinoline-3-carboxylic acid)

Michal Lebl, Jiří Jiráček, Marta Lubos and Jakub Kaminský
Institute of Organic Chemistry and Biochemistry, Flemingovo náměstí 542/2, Prague, Czech Republic
Markus Muttenthaler and Monika Perisic
Institute of Biological Chemistry, Faculty of Chemistry, Währingerstr. 38, University of Vienna, 1090 Vienna, Austria

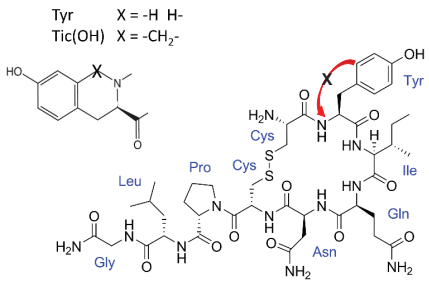

Introduction:

The most efficient tool for studying the effect of conformational stabilization of peptides is the cyclization of the peptide chain or replacement of the natural amino acid with an analog which has limited flexibility. While the cyclization inevitably modifies the functionality of the side chains and results in drastic conformational changes, introduction of modified amino acids brings less disturbance of the peptide chain. One of the example of conformationally stabilized amino acids is Tic (tetrahydroisoquinoline carboxylic acid) as a replacement of Phe. We studied earlier the effect of replacement of Phe by Tic on the biological activity of analogs of oxytocin (OXT)[1]. However, just the replacement of the native Tyr in position 2 of OXT by Phe has very pronounced effect on the biological activity of this hormone and therefore the effect of the stabilization of the conformation of this analog does not necessarily predict the effect of the same type of stabilization in the native molecule of OXT. We have developed the strategy to prepare the stabilized Tyr – 7-hydroxy-tetrahydroisoquinoline carboxylic acid (Tic(OH))[2] and made this amino acid commercially available (https://www.5z.com/spyderinstitute/unnaturals.html).

Earlier we speculated[3] about the interaction of the aromatic side chain of Tyr in OXT with the sulfur atoms in the cysteine in the disulfide bridge of this cyclic peptide based on the NMR studies of OXT carba analogs and about steric hindrance of the analogs with methyl groups attached to the cysteine methylene side chain in penicillamine containing analogs of OXT. In this study we wanted to answer the fundamental question whether the addition of one CH_2 group into the molecule of OXT will turn this hormone onto its antagonist.

1. Lebl, M.; Hill, P.; Kazmierski, W.; Karaszova, L.; Slaninova, J.; Fric, I.; Hruby, V. J. Conformationally restricted analogs of oxytocin; stabilization of inhibitory conformation. Int. J. Peptide Prot. Res. 1990, 36 (4), 321-330.
2. Verschueren, K.; Toth, G.; Tourwe, D.; Lebl, M.; Van Binst, G.; Hruby, V. J. Facile synthesis of 1,2,3,4-tetrahydro-7-hydroxyisoquinoline-3-carboxylic acid, a conformationally constrained tyrosine analogue. Synthesis-Stuttgart 1992, 458-460.
3. Lebl, M.; Sugg, E. E.; Hruby, V. J. Proton NMR spectroscopic evidence for sulfur-aromatic interactions in peptides. Int. J. Peptide Prot. Res. 1987, 29 (1), 40-45.

Strategy:

Here we present the alternative approach to our earlier structure activity studies of the neurohypophysial hormones:

- Computational modelling of solution structure of two proposed analogs of oxytocin - [L-Tic(OH)^2]OXT and [D-Tic(OH)^2]OXT
- Docking of the selected conformations into oxytocin receptor
- Synthesis of an analog with higher probability of interaction with the receptor
- Biological evaluation of oxytocin receptor response.

Computational approach:

The approach for in silico screening of the structure and binding activity of oxytocin ligands involves molecular dynamic simulations of free ligands (oxytocin and its variants) and subsequent docking of the ligands to the oxytocin receptor. Finally, the estimated free binding energies for each ligand to the receptor were used to compare the binding activity of oxytocin with its analogues. The NMR solution structure of oxytocin (pdb code 2MGO) was used as a template for the ligand structures. The first five structures stored in the pdb file were used.

The prepared ligands were surrounded by explicit waters (TIP3P) in an orthorhombic periodic box and subjected to 100 ns MD simulations in Desmond. The OPLS4 force field was used to define the ligand atoms. Ten thousand ligand geometries were regularly sampled during the simulation. The obtained MD trajectories (5) were analyzed using the Desmond Trajectory Clustering tool and the sampled ligand geometries were clustered according to their backbone conformation. Furthermore, only the twenty most abundant clusters were considered. For each cluster, a representative structure (5 trajectories x 20 clusters = 100 total / ligand) was stored and further used in docking.

The 100 stored geometries for each ligand were then docked into the oxytocin receptor using Glide. The binding site in the oxytocin receptor was defined according to the 7RYC pdb structure as a centroid within 10 Å of oxytocin. More than 1000 ligand-receptor poses (ligand conformations/orientations within the binding site) were docked and ranked according to their Glide SP score for oxytocin ligand. All poses were then rescored by estimating their binding energies (DG_{bind}) according to the MM-GBSA approach in Prime at the OPLS4/VSGB level.

Figure below displays [L-Tic(OH)^2]OXT and [D-Tic(OH)^2]OXT docked into the oxytocin receptor. As for oxytocin, two different poses (selection based on the Glide score or DG_{bind}) are shown for each ligand. The best oxytocin pose according to DG_{bind} is shown for comparison. We can see from Figure 4 that both considered poses of [L-Tic(OH)^2]OXT in the receptor differ from the best pose of oxytocin, while the best pose of [D-Tic(OH)^2]OXT selected according to DG_{bind} is relatively similar. Note that the orientation of [D-Tic(OH)^2]OXT in the best pose according to the Glide score is basically opposite.

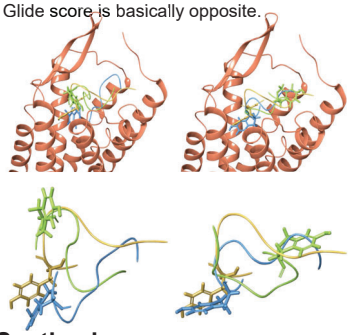

Zoom in on the two best poses (according to the Glide score in green, according to the MM-GBSA DG_{bind} in blue) of [L-Tic(OH)^2]OXT (A) and [D-Tic(OH)^2]OXT (B) in the oxytocin receptor (A). The best predicted structure of oxytocin in the receptor (according to the MM-GBSA DG_{bind}), shown for comparison, is in yellow.

Synthesis:

Since [D-Tic(OH)^2]OXT showed higher probability of interaction with the oxytocin receptor, it was synthesized using classical solid phase strategy on an automatic centrifugal solid phase synthesizer Spyder Mark IV (https://www.5z.com/spyderinstitute/synthesizer.html).

Finally, we can compare the predicted structures of all studied ligands in the oxytocin receptor in terms of energy and ligand-receptor interactions. Figure below compares interactions between amino acids of the receptor and the ligand for the best ligand-receptor poses selected according to DG_{bind}. We can see four H-bonding and one p-p interaction between oxytocin and the receptor. In the case of the modified oxytocins, we see five H-bonds for [L-(Tic(OH)2]OXT and even seven H-bonds for [D-Tic(OH)^2]OXT. No p-p stacking was observed for the modified analogues. Most of the interactions involve different amino acids of the receptor. The binding energies DG_{bind} of individual oxytocin ligands in the oxytocin receptor are -63.4 kcal/mol for oxytocin, -41.2 kcal/mol for [L-Tic(OH)^2]OXT and -53.9 kcal/mol for [D-Tic(OH)^2]OXT. By definition, the more negative the binding energy, the stronger the affinity of the ligand for the receptor. Although MM-GBSA DG_{bind} energies are often overestimated in absolute values, they can usually be used for qualitative comparison of individual ligands. Thus, oxytocin seems to have the highest affinity towards the oxytocin receptor, followed by [D-Tic(OH)^2]OXT and the weakest [L-Tic(OH)^2]OXT.

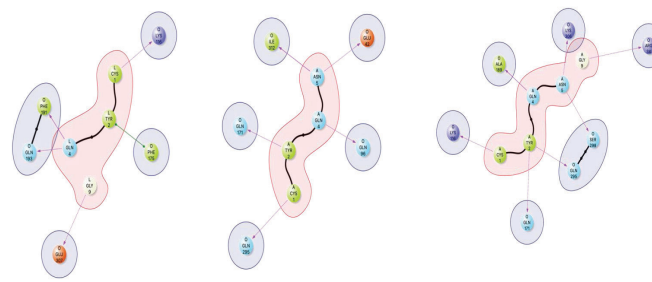

Hydrogen bonding (magenta) and p-p (green) interactions of oxytocin (left), [L-Tic(OH)^2]OXT (middle) and [D-Tic(OH)^2]OXT (right) with the oxytocin receptor. The best predicted poses according to their MM-GBSA DG_{bind} energies were used.

Biological activity:

[D-Tic(OH)^2]OXT was tested at 10 μM concentration as agonist (no activation) and as antagonist (the whole dose-response, no right-shift of the curve hence no displacement of oxytocin), both n=2.

Since the compound doesn't displace OXT in the antagonist assay it seems that the compound doesn't interact with the orthosteric binding pocket of the receptor. Based on the antagonist curve it doesn't seem to be an allosteric modulator either.

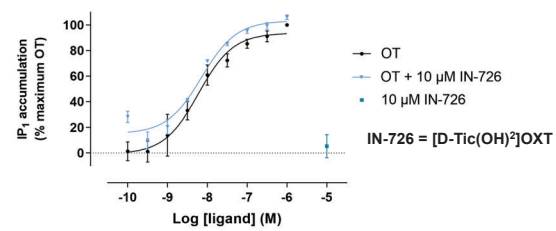

Conclusion:

Even though the theoretical studies predicted possible interaction of an analog of oxytocin containing only one additional carbon atom to interact with the oxytocin receptor, the prepared analog did not show any interaction with the oxytocin receptor.

Can we improve Coarse-Grained simulations of peptide self-assembly and aggregation by cluster analysis inputs?

Marko Babić[1], Daniela Kalafatović[1]

[1]Faculty of Biotechnology and Drug Development, University of Rijeka

https://doi.org/10.17952/37EPS.2024.P2305

Motivation

Peptide-based nanomaterials have applications in both medicine and industry. Designing accurate molecular dynamics (MD) systems to test supramolecular behavior of peptide assemblies will help develop these materials by providing fast and low-cost screening for new design ideas.

Methods

Three types of atomistic PDB files were generated:
1) **Linear** peptide (standard PyMol output)
2) Conformations from a **cluster** analysis of 10 ns atomistic simulations
3) Top model of a **PEPFOLD3** structure prediction

The structures were converted to Coarse-grained (CG) representatons using the secondary structure flag "E" for the **linear** input, representing an extended beta-sheet conformation. The **cluster** and **PEPFOLD3** generated structures had no secondary structure flags added.
The system was then populated by either 120 or 200 instances of the same deca- or hexapeptide, resprctively. This system was then minimized, equilibrated and run as shown in Figure 1.

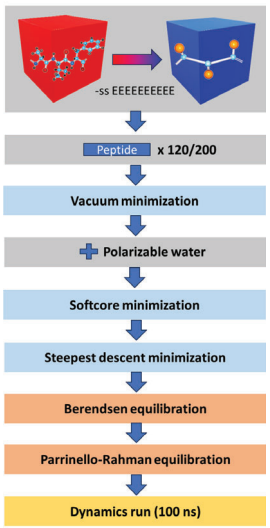

Figure 1 – Showing the method of testing aggregation in molecular dynamics simulattions used in this work.

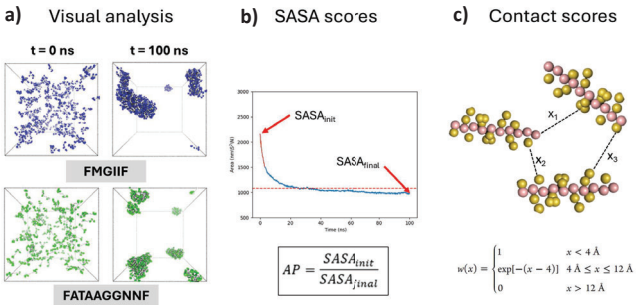

Figure 2 – To prove peptides aggregated 3 tests were done; **a)** a visual analysis of the frames in the simulation. **b)** The AP_{SASA} score is based on solvent accessible surface area (SASA) and its ratio between the first and last frame. **c)** The $AP_{contact}$ score calculates the shortest distances between the peptides, scores them based on the provided formula between 0 an 1, and takes the average score of the last 10 ns of the simulation.

Ramachandran plots were used to obsereve the retention of distinct structural features of the input PDBs. They were made by converting CG files back into all atom systems using the cg2all algorithm and GROMACS for creating the dihedral data that was plotted. The AP_{SASA} and $AP_{contact}$ scores (Figure 2) were compared between peptides to detect the impact of input PDBs, secondary structure flags or both.

Results

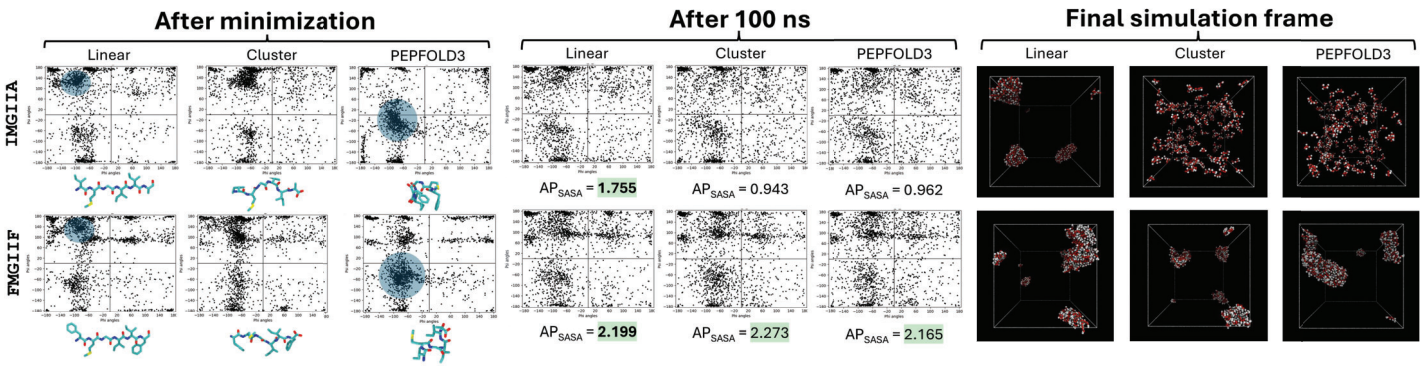

Figure 3 – After minimizing the systems peptides retain their distinct structures. After running the simulations most dihedrals across all systems are similar, regardless of aggregation. The input structures are shown under the Ramachandran plots on the left. On the right, green are marked AP_{SASA} scores indicating aggregation. The final simulation frame provides visual confirmation of aggregation behavior. The two peptides were chosen because of having the smallest (FMGIIF) and largest (IMGIIA) AP score variaton.

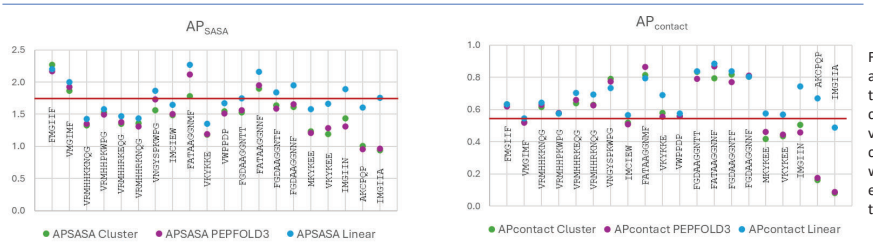

Figure 4 – The comparison of AP scores across 20 peptides. The red line represents the threshold above which peptides are considered as prone to aggregation. Its visible that cluster and PEPFOLD3 inputs are closely grouped while the linear molecule with the set secondary structure flag as an extended beta sheet shows deviation from the results.

Conclusions:

Secondary structure flags defined in the all-atom to CG conversion change the behavior of peptides in molecular dynamics simulations while structural factors and dihedral angles have minimal impact on the overall aggregation in large peptide systems.

HRZZ Croatian Science Foundation
DOK-2021-02-3496
UIP-2019-04-7999
Sveučilište u Rijeci
Zaklada Sveučilišta u Rijeci
RSC INTEREST GROUP CHEMICAL BIOLOGY AND BIOORGANIC

Download the poster using the QR code:

Design and Exploration of Tubular Assemblies of Hybrid Cyclic Peptides

Souvik Panda Mahapatra* and Hosahudya N. Gopi

Department of Chemistry, Indian Institute of Science Education and Research, Pune, 411008, India

panda.mahapatrasouvik@students.iiserpune.ac.in and hn.gopi@iiserpune.ac.in

https://doi.org/10.17952/37EPS.2024.P2306

Abstract

Self-assembling cyclic peptides are important building blocks to construct synthetic nanotubes. They can be primarily classified into cyclic α-alt(D,L)-peptides, cyclic β-peptides, cyclic α,γ-peptides, and cyclic peptides incorporating δ- or ε-amino acids based on their composition.[1] Our research focuses on design of novel cyclic peptides derived from β(O)-δ^5 -amino acid residues, consisting of a hybrid structure of crown ether and peptide macrocycles. These peptides exhibit unique self-assembly, forming hollow sub-nanotubular structures with unidirectional hydrogen bonds. These cyclic dipeptides, adopting non-centrosymmetric space groups, display significant anisotropy, suggesting potential macroscopic dipole extensions.[2] Furthermore, their inherent macrodipole orientation inspires investigation into their piezoelectric properties, opening new avenues for diverse applications. Additionally, we have synthesized size-variant macrocycles featuring β(O)-δ^5 amino acid residues which also fold into self-assembled nanotubes in solution and gas phase. This apparent supramolecular size-variant nanotube acts as an anion-selective transporter. The ion channel activity and selective transport of these structures are examples of the great potential that cyclic peptide nanotubes show for the construction of functional artificial transmembrane transporters.[3]

Background

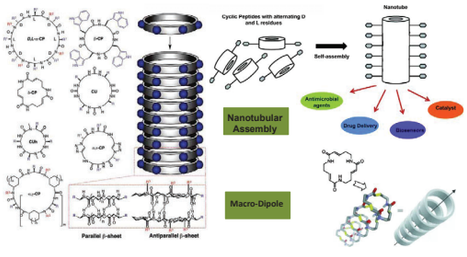

Chemical Reviews **2021**, *121*, 13936–13995. *Angew. Chem. Int. Ed.* **2001**, *113*, 24.

δ-amino Acid Foldamers

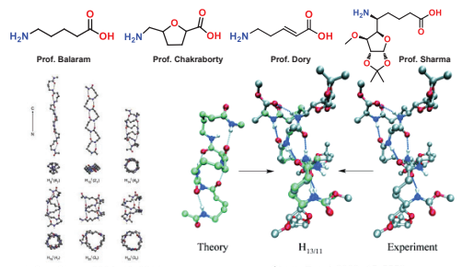

J. Org. Chem. **2004**, *19*, 6214. *Chem. Eur. J.* **2009**, *15*, 5552.

Our Design

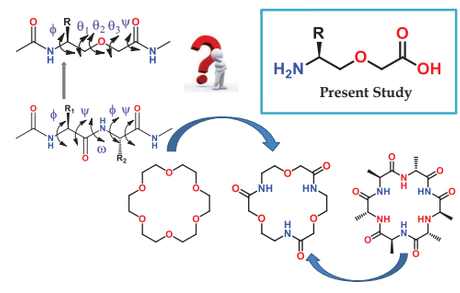

Synthesis of the Monomer

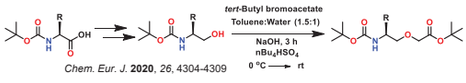

Chem. Eur. J. **2020**, *26*, 4304-4309

Crystal Analysis of Cyclic Dipeptides

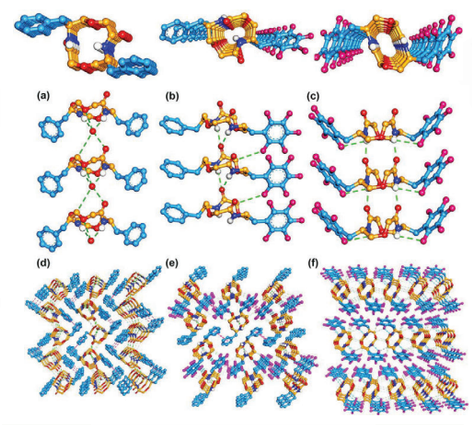

Crystal Analysis of Cyclic Tripeptide

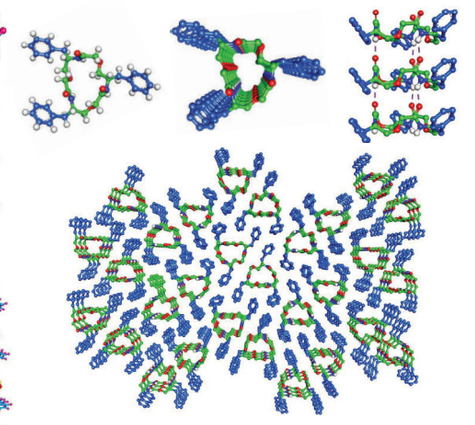

CPs Library Synthesis

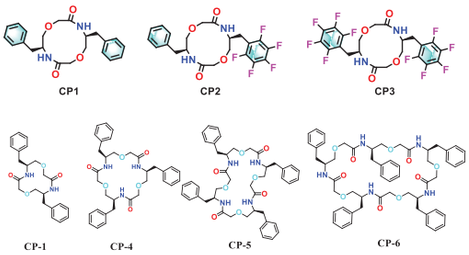

Solution Structure Analysis

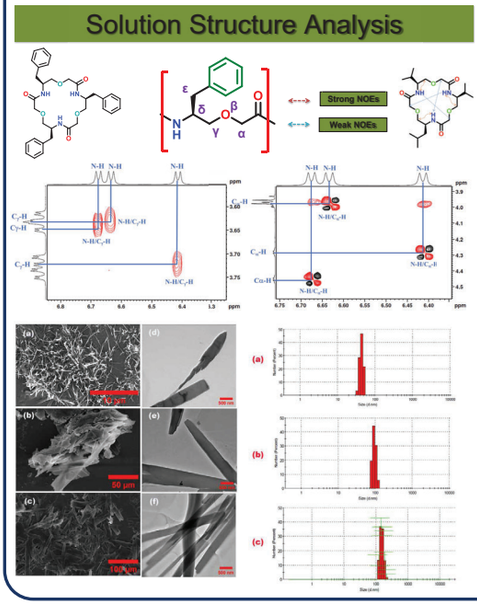

PFM Analysis of CPs

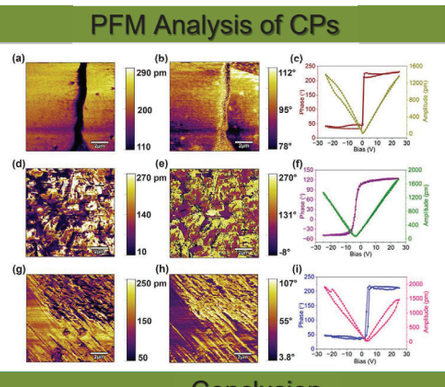

Vesicle Leakage Assay

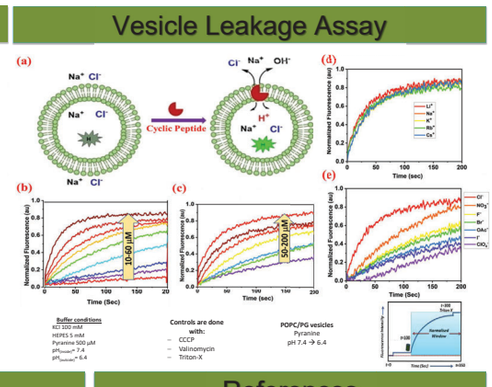

Conclusion

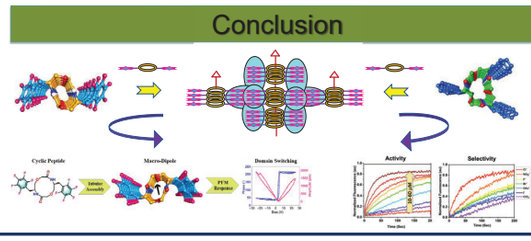

References

[1] D. Gauthier, Y. L. Dory, *Angew. Chem. Int. Ed.* **2001**, *113*, 24.

[2] S. Panda Mahapatra, S.Pahan. A.Chatterjee, S.Roy, D. R. Puneeth Kumar, H. N. Gopi, *Angew. Chem. Int. Ed.* **2024,** e202409969.

[3] T. D. Clark, L. K. Buehler, M. R. Ghadiri, *J. Am. Chem. Soc.* **1998**, *120*, 651-656.

Acknowledgements

SERB INDIA

DST

IISER PUNE

https://doi.org/10.17952/37EPS.2024.P2307

Antimicrobial and cell-adhesive peptide-based hydrogels for biomedical applications

N. Mehwish[1,2], P. López-Gómez[1,2], M.P. Ginebra[1-4], C. Mas-Moruno[1-3]

[1] Department of Materials Science and Engineering, Biomaterials, Biomechanics and Tissue Engineering Group (BBT), Universitat Politècnica de Catalunya, Spain, [2] Barcelona Research Center in Multiscale Science and Engineering, Universitat Politècnica de Catalunya, Spain, [3] Biomedical Engineering Research Center (CREB), Barcelona 08028, Spain, [4] Centro de Investigación Biomédica en Red, Bioingeniería, Biomateriales y Nanomedicina (CIBER-BBN), Madrid, Spain.

Email: nabila.mehwish@upc.edu

Background

In the ever-evolving landscape of biomaterials, the demand for multifunctional hydrogels has intensified due to their pivotal role in addressing simultaneous challenges associated with bacterial infections and inadequate cell adhesion in various biomedical applications [1-3].

Amphiphilic peptide sequence design

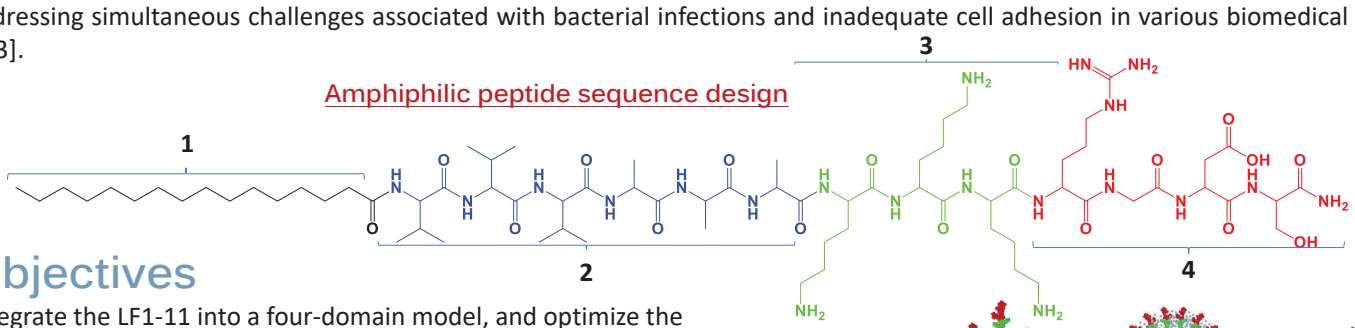

Objectives

- Integrate the LF1-11 into a four-domain model, and optimize the gelation of as prepared peptides.
- Design peptide-based hydrogels with cell-instructive properties.
- Incorporate antibacterial peptides to reduce bacterial viability.

Results and discussion

1. Generation of the hydrogels

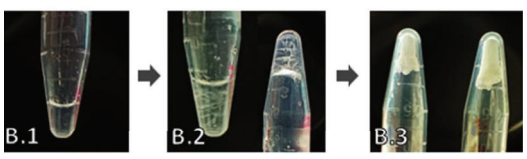

2. CD

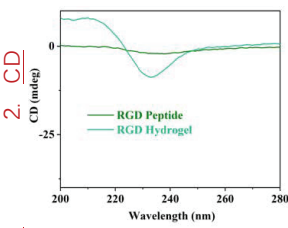

3. FTIR

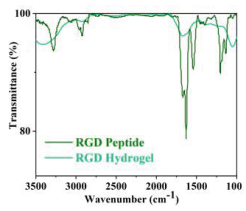

4. Swelling

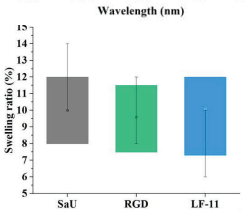

5. Fiber length

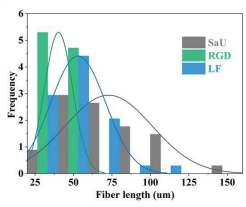

6. Morphology of the hydrogels

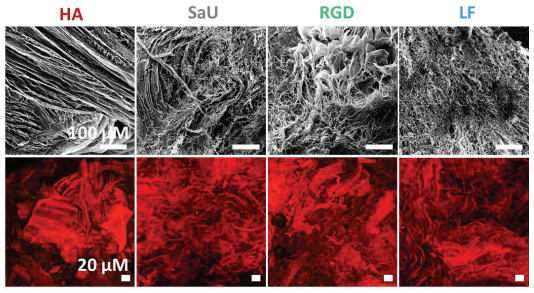

7. Human osteosarcoma cell line (Saos-2)

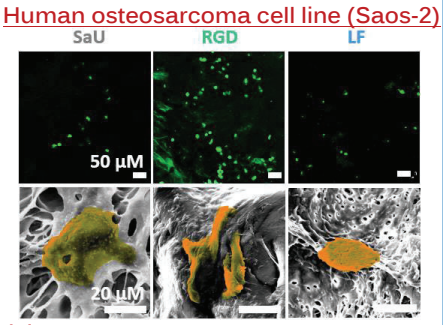

8. Antibacterial activity

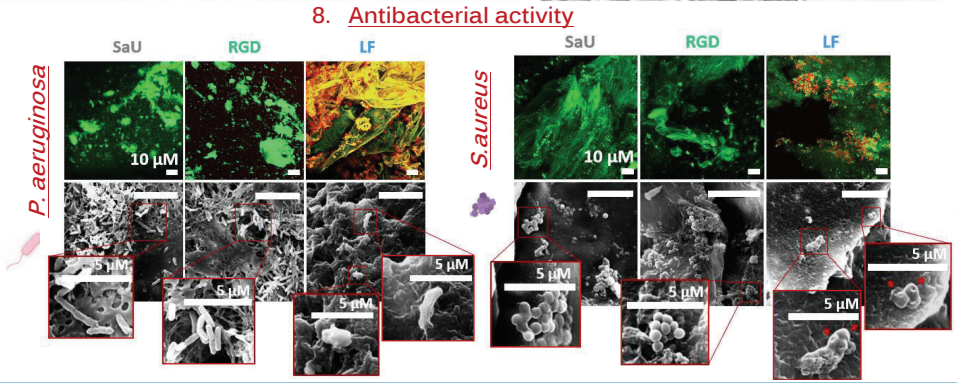

Conclusions

Developed peptide-derived hydrogels support excellent Saos-2 viability and reduce the risk of bacterial infection for both Gram-positive and Gram-negative models. The study successfully integrated LF1-11 into a four-domain peptide model for the first time, highlighting the potential for tailored hydrogels with diverse bioactivities.

References

1. Sun et al, Journal of materials chemistry. 2024, B, 12(9), 2253–2273.
2. Hoyos et al, ACS applied materials & interfaces, 2017, 9(26), 21618–21630.
3. Godoy et al, Biomacromolecules. 2015;16(2):483-496.

Acknowledgements

- Agencia Estatal de Investigación through grant PID2020-114019RB-I00 (Smart-Gel)
- Marie Skłodowska-Curie grant Agreement No. 872869 (RISE Project Bio-TUNE)
- Generalitat de Catalunya (AGAUR 2021 FI_B 00889 predoctoral fellowship of P.L.-G.)

https://doi.org/10.17952/37EPS.2024.P2309

De novo design of collagen-like peptides for cell-based technologies

Maryana Baran[1, 2], Eileen Gentleman[1, 3], Maxim Ryadnov[2]

[1] Centre for Craniofacial and Regenerative Biology, King's College London, London, United Kingdom
[2] National Physical Laboratory, Teddington, United Kingdom
[3] Department of Biomedical Sciences, University of Lausanne, Lausanne, Switzerland

maryana.baran@npl.co.uk

Background

Native collagen, a structural protein of 300 kDa, folds into triple helix self-assembling into microns long fibres forming extracellular matrices (ECMs) (Figure 1). This ability to form hierarchical structures from the molecule up has inspired the development of collagen-like peptides (CLPs), typically of 3 kDa, to mimic the native collagen and ECMs. CLPs form collagen like fibres, but also nanoscale spheres, which is particularly the case for sequences with aromatic amino acids at their termini, and ring-like particles. All these assemblies are underpinned by the triple helix formation, which emphasises the potential of CLPs to broaden a range of collagen-like materials and their applications.

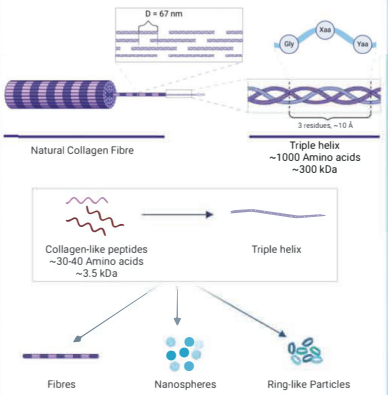

Figure 1: *Representation of collagen's hierarchical architecture and of CLPs' higher order structures. The artwork has been created with www.biorender.com.*

Challenges

Collagen-like peptides tend to assemble into both fibres and particles. Here we show that shorter sequences can form both structures simultaneously. However:

- Can shorter CLPs maintain polyproline II helical structure and fibre formation?
- What is the shortest peptide sequence required to form a triple helix and assemble into higher-order structures?
- Does the density and abundance of fibre formation depend on the sequence length of CLPs?
- Is the fibre formation necessary for gelation?
- What is the length cut-off of CLPs required to form fibres and particles or particles only?

CLPs fold as a collagen triple helix

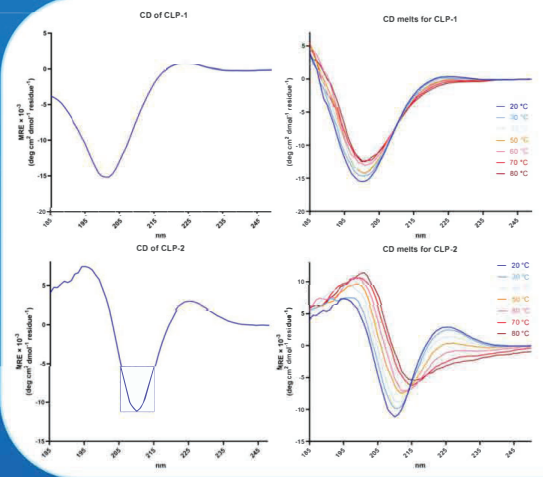

Circular Dichroism spectra show **polyproline II** conformations, characteristic of the triple helix, for **CLP-1** and CLP-2, with expected **maximum at 225 nm** and a strong **minimum at 200 nm**.

Upon thermal denaturation the CLPs undergo a fully reversable conformational transition with a single **iso-dichroic point** around 215 nm.

CLPs assemble into fibre and spherical structures

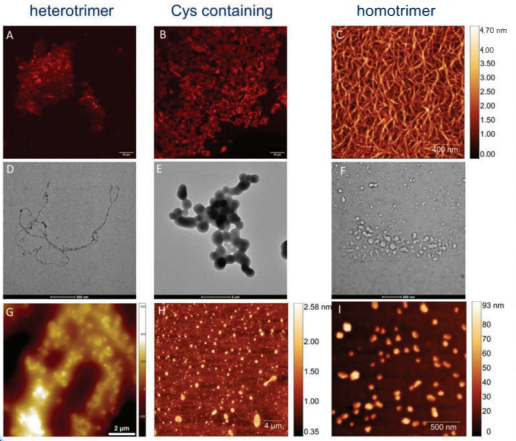

Confocal, electron and atomic-force micrographs revealed that **CLP-2**, a peptide with N-terminus cysteine, self-assembles into **nanospheres** approximately 1 µm in size whereas **CLP-1** and **CLP-3**, formed both **spherical** and **fibrous structures**.

Figure 2: *The observed higher ordered CLP structures. A) CLP-1 and B) CLP-2 confocal images, CLPs stained with Congo Red; D) CLP-1, E) CLP-2 and F) CLP-3 electron micrographs, with samples stained with uranyl acetate (2% w/v); G) CLP-1, H) CLP-2, C) and F) CLP-3 atomic force micrographs.*

Conclusion

- Fibre formation is not dominant in collagen-like peptides that are 15 amino acids long.
- Cysteine promotes the assembly into spherical particles via disulfide bridges.
- Both particle and fibre formation are present in short and medium-length CLPs.
- The longer the collagen sequence, the more predominant fibre formation is over particle formation.

Future Work

- Investigate the use of CLP particles for cell transfection applications.
- Determine the conditions under which both fibres and particles co-form.
- Develop CLP-based hydrogels or integrate CLPs into existing hydrogels to study their cell-ECM cues.

References

1. Yu, L. T. et al. Hollow Octadecameric Self-Assembly of Collagen-like Peptides. J. Am. Chem. Soc. 145, 5285–5296 (2023).
2. Sun, X. et al. Peptide-triggered self-assembly of collagen mimetic peptides into nanospheres by Cejas, M. A. et al. Thrombogenic collagen-mimetic peptides. Self-assembly of triple helix-based fibrils driven by hydrophobic interactions. Proc. Natl. Acad. Sci. U. S. A. 105, 8513–8518 (2008).
3. O'Leary, L. E. R., Fallas, J. A., Bakota, E. L., Kang, M. K. & Hartgerink, J. D. Multi-hierarchical self-assembly of a collagen mimetic peptide from triple helix to nanofibre and hydrogel. Nat. Chem. 3, 821–828 (2011).
4. Noble, J. E. et al. Folding-Mediated DNA Delivery by α-Helical Amphipathic Peptides. ACS Biomater. Sci. Eng. 9, 2584–2595 (2023).

Funded by
Department for Science, Innovation & Technology

Centre for Craniofacial and Regenerative Biology

www.npl.co.uk

©NPL Management Limited 2023

Self-assembling dipeptides as vehicles for the delivery of peptide therapeutics

Peter Divanach[1,2], Eirini Fanouraki[1,2], Vagelis Harmandaris[3,4,5], Anastassia N. Rissanou[3,5,6], and Anna Mitraki[1,2]

https://doi.org/10.17952/37EPS.2024.P2310

1. Department of Materials Science and Technology, University of Crete, Voutes Campus, Greece.
2. Institute of Electronic Structure and Laser / Foundation for Research and Technology-Hellas, (FORTH), Nikolaou Plastira 100, Vassilika Vouton, Heraklion, Crete, Greece.
3. Institute of Applied and Computational Mathematics (IACM), Foundation for Research and Technology Hellas, (FORTH), IACM/FORTH, GR-71110 Heraklion, Crete, Greece.
4. Department of Mathematics and Applied Mathematics, University of Crete, GR-71409, Heraklion, Crete, Greece.
5. Computation-based Science and Technology Research Center; The Cyprus Institute, Nicosia 2121, Cyprus.
6. Theoretical & Physical Chemistry Institute, National Hellenic Research Foundation, 48 Vassileos Constantinou Avenue, 11635 Athens, Greece.

ABSTRACT

Self-assembling peptides consist of short chains of amino acids capable of spontaneously forming higher-order structures such as fibers, tubes, and hydrogels. Combination of computational and experimental approaches allow rational design of peptide materials with increasing complexity. While peptides ranging from 6-12 amino acids allow the insertion of targeting functionalities, their length results in increased cost and limits wider applicability. On the other hand, ultrashort peptides ranging from 2-6 amino acids, are more tractable and still amenable to interesting applications. One such application is the controlled delivery of peptide therapeutics from structurally similar hydrogelating peptides. **In recent studies we combined both theoretical and experimental approaches for the thorough investigation of the structural and conformational properties of biocompatible aliphatic-aromatic and aromatic dipeptide hydrogels for the controlled release of the peptide drug Bortezomib**. Bortezomib is a modified, Phenylalanine-BoroLeucine dipeptide (N-pyrazino-Phe-BoroLeu) that acts as proteasome inhibitor for the treatment of multiple myeloma, approved by the U.S. Food and Drug Administration (FDA) in 2003. It has also shown potential in the treatment of other malignancies. The self-assembly of Bortezomib in water was examined computationally for the first time, as well as its tendency to bind to similar dipeptides with hydro-gelating capacities, using a series of all-atom molecular dynamics simulations [1]. Our aim was to obtain a quantitative prediction of the Bortezomib-Peptides conformational, dynamical and structural properties at the molecular level, while also performing a comparison between dipeptides in order to find the most suitable candidates for Bortezomib controlled release. **Our results suggested that the protected Phe-Phe category is qualified and between its two members, Fmoc-Phe-Phe looks more promising. This study paves the way towards optimal peptide carrier selection for the encapsulation and controlled delivery of Bortezomib in future experimental studies.**

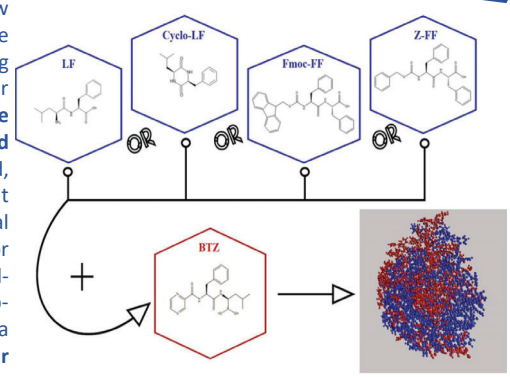

SIMULATION DETAILS

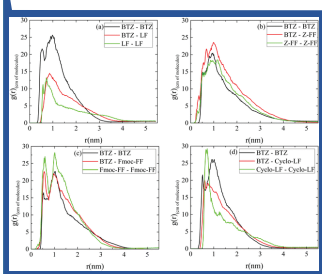

Pair radial distribution functions between the centers of mass of molecules for the pairs: Bortezomib–Bortezomib; dipeptide–dipeptide and Bortezomib–dipeptide in the aqueous solutions at T = 300 K in all systems: (a) LF system; (b) Z-FF system; (c) Fmoc-FF system; and (d) Cyclo-LF system.→ No big differences observed amongst the 3 curves for the systems except LF.

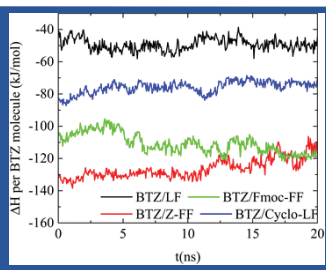

Binding enthalpy per BTZ molecule as a function of time between the dipeptides and BTZ.→ lowest energy indicates the energetically most stable association to BTZ which is Z-FF, followed closely by Fmoc-FF.

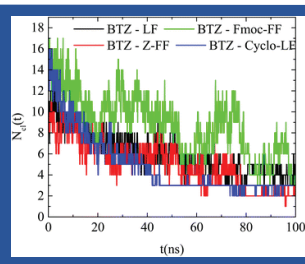

Number of clusters formed by BTZ and dipeptides as a function of time in the examined systems.→ Large fluctuations imply a dynamic equilibrium between the association & dissociation of molecules in the formed clusters. Fluctuations are most pronounced for the Fmoc-FF/BTZ system, indicating a continuous restructuring of the clusters.

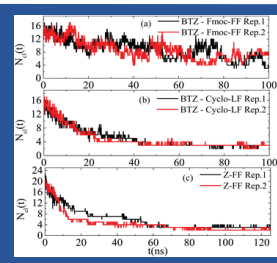

Number of clusters formed by molecules as a function of time in the (a) Fmoc-FF with BTZ; (b) Cyclo-LF with BTZ; and (c) Z-FF bulk systems.→ Accounting for the trapping in metastable states, the number of clusters formed by BTZ / dipeptides as a function of time has been recalculated with new replicas, showing similar pathway towards the "equilibrated state". Hence physicochemical association characteristics are captured whether or not the system reaches a local (metastable state) or the global (final state) energetic minimum.

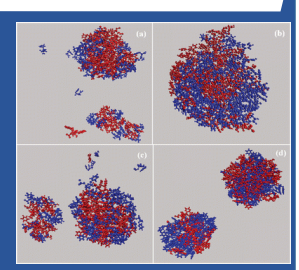

Characteristic snapshots of dipeptide–BTZ complexes (a) LF; (b) Z-FF; (c) Cyclo-LF; and (d) Fmoc-FF. Bortezomib molecules are presented in red and dipeptides in blue color. Water molecules are omitted for clarity.→ Clusters of various sizes are observed, which are classified in one or two clusters case with few individual molecules dispersed in the solution.

EXPERIMENTAL STUDIES



FESEM pictures of bortezomib spheres, following H2O evaporation after 24h incubation at room temperature, at a concentration of c=4 mg/ml, along with an inverted vial showing that the solution flows to the bottom and does not form a self-supporting gel.

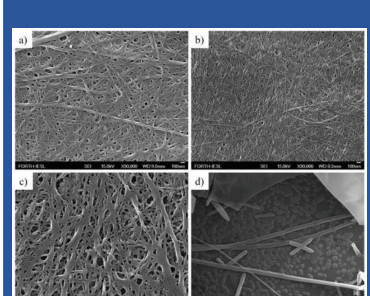

FESEM images peptides in (EtOH/H2O 3:7) with BTZ at a 1:1 ratio at a concentration of c= 4 mg/ml after 24h at room temperature. Scale bars are 1 μm. a) Z-FF with BTZ b) Fmoc-FF with BTZ c) Cyclo-LF with BTZ and d) LF with BTZ.

CONCLUSIONS

Evaluating all the measures, we can claim that the protected FF category is qualified and between its two members, Fmoc-FF looks more promising. However, Z-FF also has various features that could make it a potential candidate carrier for Bortezomib and a promising candidate for future studies.

REFERENCES

[1] P. Divanach, E. Fanouraki, A. Mitraki, V. Harmandaris, and A. N. Rissanou, Soft Matter, 2023, 19, 8684-8697

ISSN 1744-6848 CODEN SMOABF 19(45) 8671-8920 (2023)



Cover
See Anna Mitraki, Anastassia N. Rissanou *et al.*, pp. 8684–8697. Image reproduced by permission of Peter Divanach, Eirini Fanouraki, Anna Mitraki, Vagelis Harmandaris, Anastassia N. Rissanou from *Soft Matter*, 2023, **19**, 8684. Artwork by first author, Peter Divanach.

https://doi.org/10.17952/37EPS.2024.P2314

Self-assembly of histidine-containing peptides and applications

C.P Apostolidou[1,2], Chrysoula Kokotidou[1,2], Varvara Platania[1,2], Vasilis Nikolaou[1,3], Georgios Landrou[1,3], Emmanouil Nikoloudakis[1,3], Georgios Charalambidis[1,3], Maria Chatzinikolaidou[1,2], Athanassios G. Coutsolelos[1,3], A. Mitraki[1,2].

[1] Department of Materials Science and Technology, University of Crete,
[2] Institute for Electronic Structure and Laser, IESL-FORTH, Vassilika Vouton, 71003 Heraklion, Crete, Greece
[3] Department of Chemistry, University of Crete, Laboratory of Bioinorganic Chemistry
*chrysana@materials.uoc.gr

Abstract

Self-assembling peptides consist of short chains of amino acids capable of spontaneously forming higher-order structures such as fibers, tubes, and hydrogels [1]. Among these, histidine peptides are widely studied since histidine is an essential amino acid with a unique property. Its imidazole side chain exhibits pH sensitivity, allowing histidine peptides to undergo conformational changes and self-assemble into supramolecular structures in response to environmental factors like pH or salinity. Such versatility holds promise for pharmaceutical applications. Expanding on prior research [2,3], recent studies have focused on evaluating the effectiveness of coordinating histidine-containing peptides with copper and zinc to produce Zn and Cu nanoparticles. Through studying the morphology of these His-peptide NPs (**Cyclo-(His-Phe)**, cHF NPs) using techniques such as FESEM, TEM, and FTIR, our ultimate goal is to evaluate the **antimicrobial properties** of the synthesized materials against selected Gram-positive and Gram-negative bacterial strains, as well as their potential as **anticancer metal-based drugs and antibiotics**. Preliminary experiments have shown promising results in both directions, underscoring the versatility of these nanostructures in biomedical applications.

Structural Characterization of the peptide

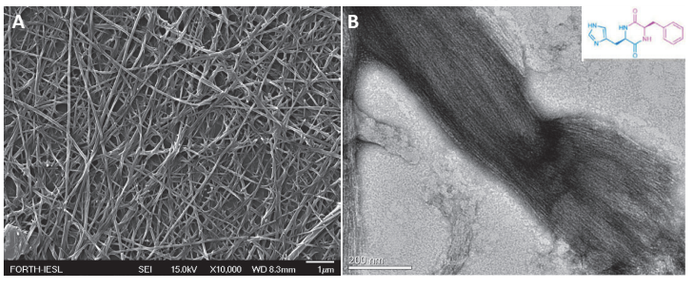

Figure 1: Cyclo-(His-Phe) (cHF) at the concentration of 1 mg/mL in PBS 1X under **A)** Field-emission SEM **B)** TEM microscope.

Preparation of cHF-CuNPs and cHF- ZnNPs

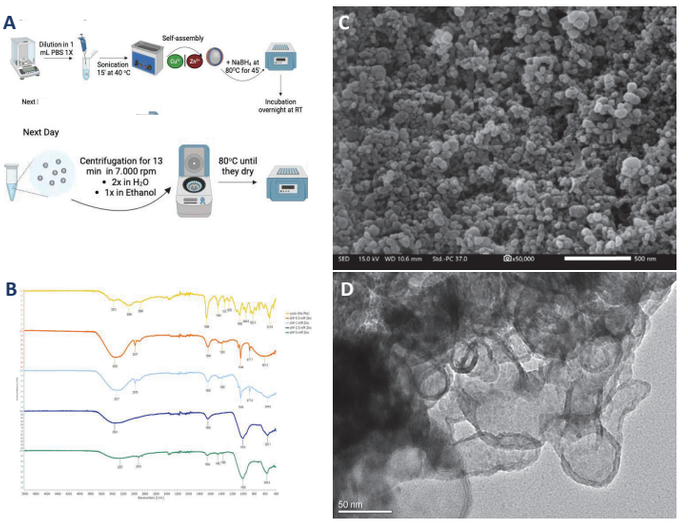

Figure 2: **A)** Schematic representation of the preparation of cHF-NPs **B)** FTIR analysis of cHF-ZnNPs at different metal concentrations **C, D)** Field-emission SEM images of cHF-ZnNPs (initial metal concentration was 1mM).

Evaluation of the antimicrobial potency of cHF-CuNPs and cHF-ZnNPs

The cHF-CuNPs and cHF-ZnNPs were prepared with different metal concentrations. Then, all the prepared samples were tested for their antimicrobial efficiency against *E. coli* and *S. aureus.*

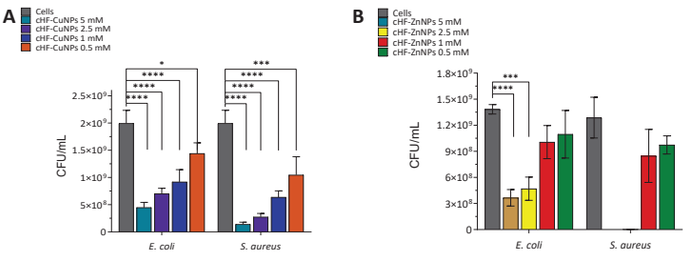

Figure 3: The graph depicts bacterial growth expressed as colony forming unit per mL (CFU/mL) of *E. coli* and *S. aureus* after 24 hours **A)** cHF-CuNPs and **B)** cHF-ZnNPs.

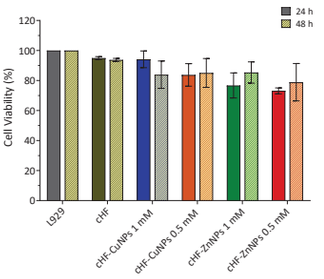

Figure 4: Cytotoxicity assessment at 24 and 48 hours on L929 fibroblast cell line. cHF NPs exhibit high cytocompatibility at lower metal concentrations.

Evaluation of the cytotoxicity of cHF-CuNPs and cHF-ZnNPs under different pH on MG-63 osteosarcoma cell line

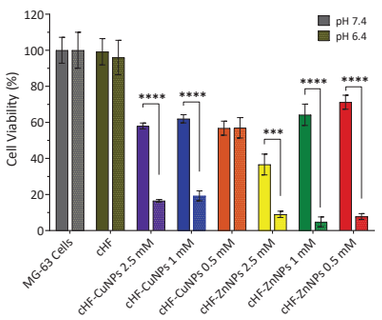

Figure 5: Cell viability in the presence of cHF-NPs after 24 h at **pH 6.4** and **pH 7.4** was studied by MTT test**.**

Conclusions

•Cyclic-(His-Phe) can spontaneously self-assemble into **amyloid fibrils**
•Cyclic-(His-Phe) can coordinate successfully with metal ions**, zinc**, and **copper**, due to the presence of **histidine** residue (FESEM and FTIR), and form peptide-metal NPs.
•Antimicrobial potency: The cHF–CuNPs (1 mM) showed limited cytotoxicity on L929 cells and strong antimicrobial effects against *E.coli* and *St. aureus.*
•Anticancer potency: The cHF-ZnNPs showed strong cytotoxicity against the MG-63 osteosarcoma cell line.

References

[1] G. Fichman, E. Gazit, Acta Biomater, 2014, 10, (4), 1671–1682.
[2] E. Glymenaki, et. al., ACS Omega, 2022, 7, (2), 1803–1818.
[3] C.P. Apostolidou, et. al., Biomolecules, 2024, 14, (2), 226.

Ευρωπαϊκή Ένωση European Social Fund
Operational Programme Human Resources Development, Education and Lifelong Learning
Co-financed by Greece and the European Union
ΕΣΠΑ 2014-2020
H.F.R.I. Hellenic Foundation for Research & Innovation

https://doi.org/10.17952/37EPS.2024.P2315

TUNING THE ASSEMBLY OF PROTEINS AND PEPTIDES IN LIPID BILAYERS

S. Jiménez Millán[1], I. R. Sasselli[1], A. Maestro[1,2]

[1] Centro de Física de Materiales (CSIC, UPV/EHU) - Materials Physics Center MPC, Paseo Manuel de Lardizabal 5, E-20018 San Sebastián, Spain
[2] IKERBASQUE—Basque Foundation for Science, Plaza Euskadi 5, Bilbao, 48009 Spain

Viral fusion proteins facilitate membrane binding of the viral envelope to the host cell, enabling the release of the viral genetic material into the cell. Within the fusion domain of the SARS-CoV-2 Spike protein, several peptides have been identified to interact with the cell membrane. We aim to understand the viral infection role of these fusion peptides by studying their interaction with biomimetic model membranes.

SARS-CoV-2 Spike protein

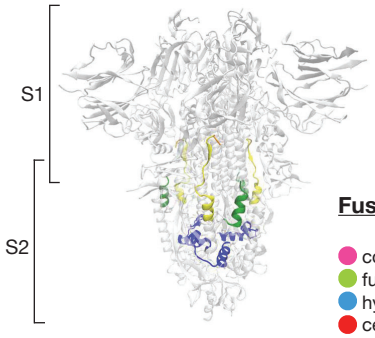

PDB: 6VXX[1]

Sequence



Fusion Peptides

- conserved motifs
- fusion tripeptide
- hydrophobic
- central proline

FP1 816 - SFIEDLLFNKVTLADAGFIKQY - 837
FP2 835 - KQYGDCLGDIAARDLICAQKFN - 856
FP3 854 - KFNGLTVLPPLLTDEMIAQYT - 874
FP4 885 - GWTFGAGAALQIPFAMQMAYRFNGI - 909

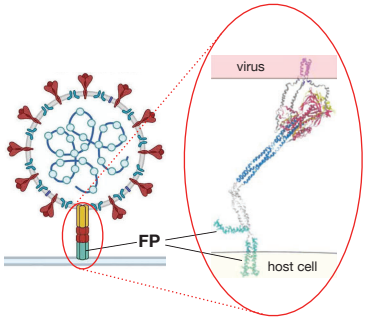

The fusion peptides bind to the host cell membrane driving the cell and virus together to initiate membrane fusion[2,3]

COARSE-GRAINED (CG) MOLECULAR DYNAMICS (MD)

Fusion peptides in bulk

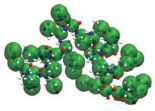

- Martini 2 force field[4,5]
- 4-1 mapping

$$AP = \frac{SASA_0}{SASA_f}$$

$SASA$ = solvent accessible surface area

Aggregation Propensity

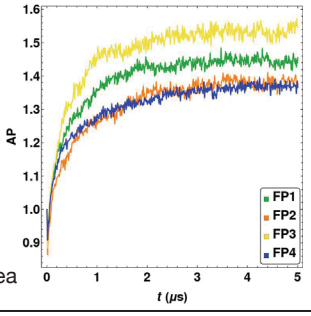

Interaction of fusion peptides with lipid bilayers

Density profile along z axis FP1

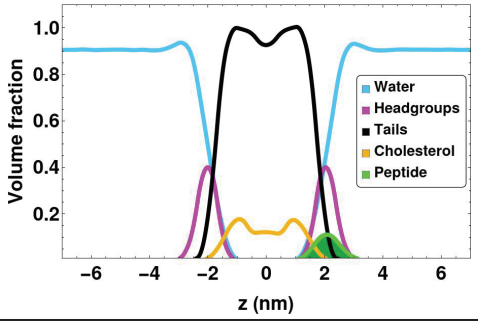

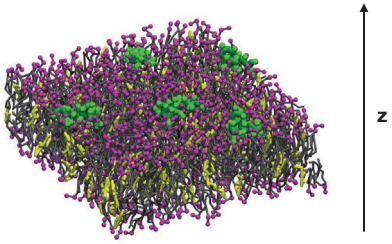

Representation of the peptides and lipid bilayer system after 5μs of simulation. Solvent omitted for clarity.

Interaction of fusion peptides with lipid monolayers

Surface tension - area isotherms at 300K

lipid monolayer surface tension

$$\gamma = L_z \frac{P_N - P_L}{2}$$

Lz = box normal size
$P_L = (P_{xx}+P_{yy})/2$
A_L = average area per lipid

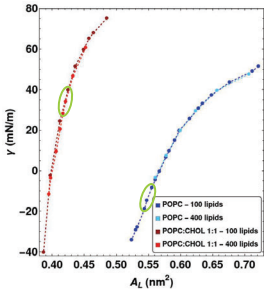

Density profiles along z axis FP2

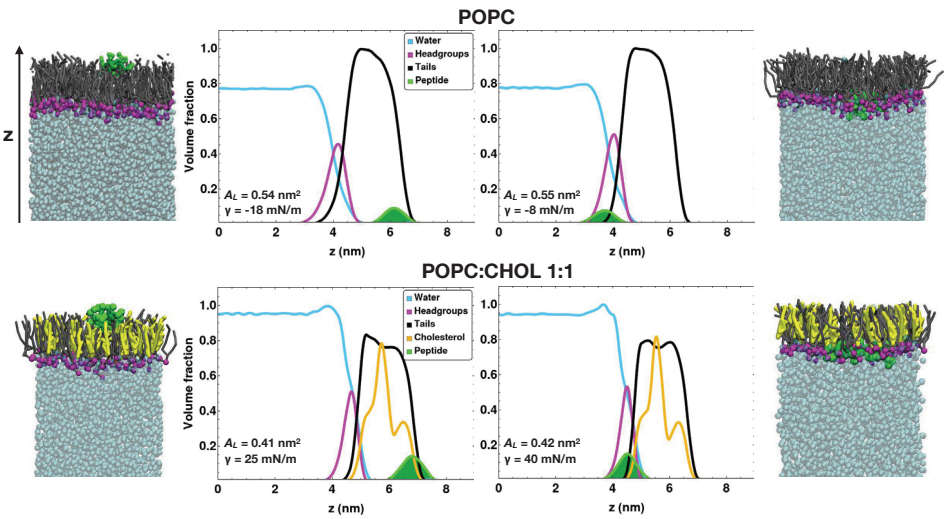

RDF POPC

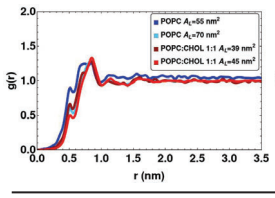

RDF cholesterol

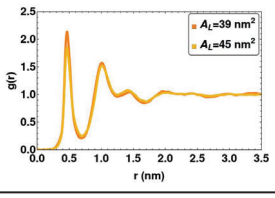

References

1. A.C. Walls *et al.*, Seattle Structural Genomics Center for Infectious Disease (SSGCID), Structure of the SARS-CoV-2 spike glycoprotein (closed state) (2020) https://doi.org/10.2210/pdb6vxx/pdb
2. D.A. Jamison *et al.*, *Eur J Hum Genet* **8**, 889-898 (2022)
3. E. Dodero-Rojas *et al.*, *eLife* **10**:e70362 (2021)
4. S. J. Marrink *et al.*, *The Journal of Physical Chemistry B* **111**, 7812-7824 (2007)
5. L. Monticelli, *et al.*, *Journal of Chemical Theory and Computation* **4**, 819-834 (2008)

Acknowledgements

- Ramon y Cajal (RYC2021-033294-I)
- Spanish State Research Agency (PID2022-136392NA-I00)

Conclusions

- The fusion peptides tend to aggregate in solution
- They interact with lipid bilayers at the head group level
- In monolayers they are able to insert and bind to the lipid headgroups at a certain surface tension and average area per lipid
- Cholesterol reduces the amount of area per lipid and thus a higher surface tension is needed for the peptides to be able to cross the monolayer

Centro de Física de Materiales | sjimenez037@ikasle.ehu.eus | Polymers and Soft Matter Group

Design of fluorinated peptide-based hydrogels for sustained drug release application

Aurélie Honfroy[1,2,3,4], Jolien Bertouille[1], Ana-Maria Turea[1], Thibault Cauwenbergh[1], Jessica Bridoux[2], Nathalie Lensen[3,4], Jessica Mangialetto[5], Niko Van den Brande[5], Jacinta F. White[6], James Gardiner[6], Thierry Brigaud[3,4], Steven Ballet[1], Sophie Hernot[2], Grégory Chaume[3,4], Charlotte Martin[1]

[1]VUB, Research Group of Organic Chemistry (ORGC), 1050 Brussels, Belgium; [2]VUB, In Vivo Cellular and Molecular Imaging (ICMI), 1090 Jette, Belgium; [3]CY Cergy Paris Université, CNRS, BioCIS, 95000 Cergy-Pontoise, France; [4]Université Paris-Saclay, CNRS, BioCIS, 91400 Orsay, France; VUB, Research group Sustainable Materials Engineering (SUME), Physical Chemistry and Polymer Science (FYSC), 1050 Brussels, Belgium; [6]CSIRO Manufacturing, Bayview Avenue, Clayton, VIC 3169, Australia.

aurelie.jeanne.vivane.honfroy@vub.be

https://doi.org/10.17952/37EPS.2024.P2318

Introduction

- **Amphipathic peptides** alternating hydrophobic and hydrophilic amino acids have shown to form **self-assembled hydrogels.**[1]
- Alternative system for **chronic pain treatment** as **extended-release drug delivery platforms** of pharmaceutical cargoes when injected subcutaneously.
- Subcutaneous injections can **increase patient compliance** by limiting the number of injections required for therapeutic efficiency. The drug release window is **limited to 3 to 4 days** and has to be extended for optimal use in clinical setting.[2,3]

Thus, two strategies are considered to incorporate fluorinated amino acids into the consensus sequence and provide access to a new class of injectable controlled-delivery systems that incorporates favorable properties of fluorine.

Peptide-based Hydrogelator Design[2,3]



Gelation: 2%w/v in PBS

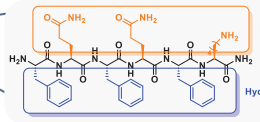

H-FQFQFK-NH_2

→ How to increase drug release properties of the system?

FLUORINE INTRODUCTION[4,5]

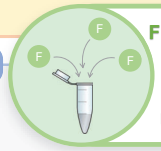

Increases the local hydrophobicity

Stabilizes and promotes secondary structures

Improves pharmacological properties

Strategy 1: Fluorinated hexapeptide Hydrogelators

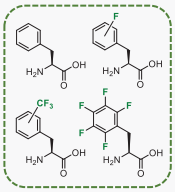

(Fluorinated) amino acids

To investigate the impact of different fluorinated groups



To investigate the importance of aromatics vs. hydrophobicity[7]

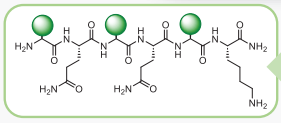

Reference H-FQFQFK-NH_2

Strands and turn modulations

Strategy 2: β-hairpin Peptide Hydrogelators

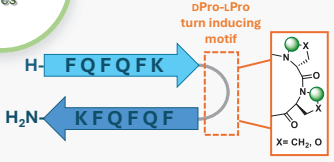

To help the alignment between strands

To investigate conformational restriction with fluorinated amino acid

HYDROGEL MECHANICAL PROPERTIES (DYNAMIC RHEOMETRY)

Among **13 fluorinated hexamer** analogues synthesized, three formed the strongest hydrogels:

Hydrogel	*G'* (Pa)	*G'* (Pa)
H-FQFQFK-NH_2	1792 ± 236	162 ± 31
H-FQFQ(**oCF$_3$**)FK-NH_2	**13039** ± 8206	**921** ± 319
H-FQFQ(**F$_5$**)FK-NH_2	**16649** ± 1644	**1546** ± 205
H-FQFQ(**CF$_3$**)MK-NH_2	**33875** ± 4949	**1354** ± 403

HAIRPIN DESIGN
Higher gel rigidity (G')

Among **14 analogues synthesized**, H-FQFQFK-pP-FQFQFK-NH_2 formed the strongest hydrogel:

Hydrogel	*G'* (Pa)	*G'* (Pa)
H-FQFQFK-pP-FQFQFK-NH_2	2557 ± 546	178 ± 82
H-FQFQFK-p(**CF$_3$ΨPro**)-FQFQFK-NH_2	**1094** ± 92	**107** ± 3
H-FQFQFK-(**pCF$_3$ΨPro**)P-FQFQFK-NH_2	**225** ± 117	**15** ± 8

HAIRPIN DESIGN
Higher gel rigidity (G')

FLUORINATED TURN
CF_3ΨPro ↓ gel rigidity (G')

SECONDARY STRUCTURE (CIRCULAR DICHROISM) & FIBER NETWORK (AFM, TEM)

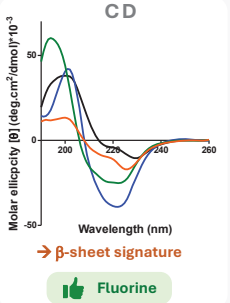

→ β-sheet signature

Fluorine

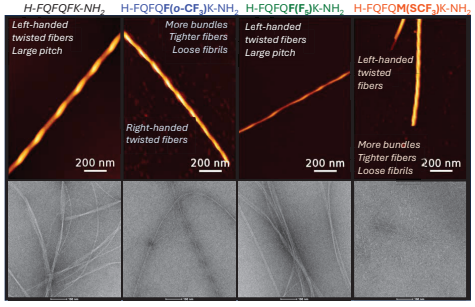

Fluorine incorporation: more bundled fibrils, tighter twisted fibers

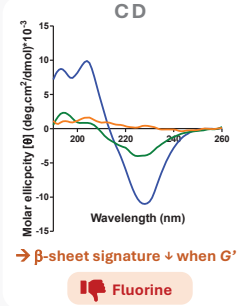

→ β-sheet signature ↓ when *G'* ↓

Fluorine

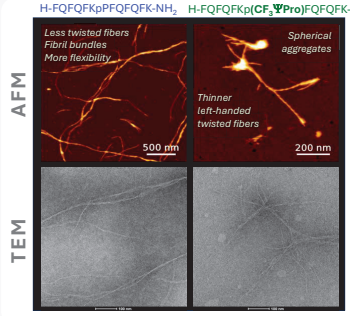

Hairpin hydrogels: More flexible fiber network and thicker fibrils than the linear hexamer

RELEASE KINETIC: *IN VITRO* DRUG RELEASE STUDY (ANALYTICAL RP-HPLC)

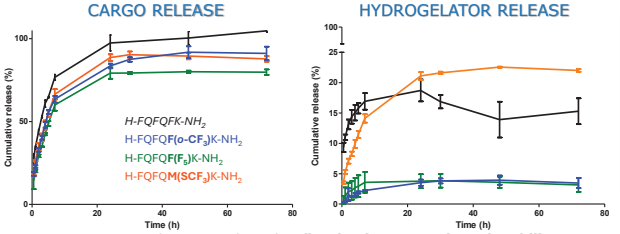

Similar cargo release but **fluorine increases the gel stability**

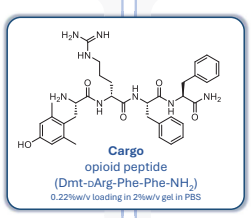

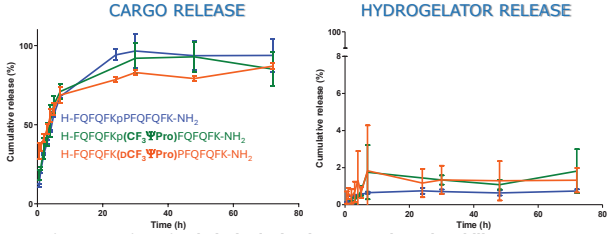

Similar cargo release but **hairpin design increases the gel stability**

IN VIVO HYDROGEL STABILITY (SPECT/CT IMAGING)

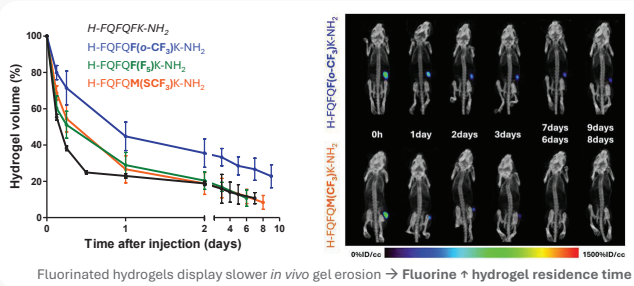

Fluorinated hydrogels display slower *in vivo* gel erosion → **Fluorine** ↑ **hydrogel residence time**

***In vivo* formulation:**
^{111}In-labelled-hydrogelator :
Unlabelled hydrogelator (1:20)

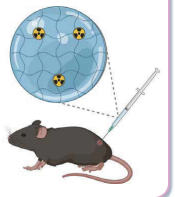

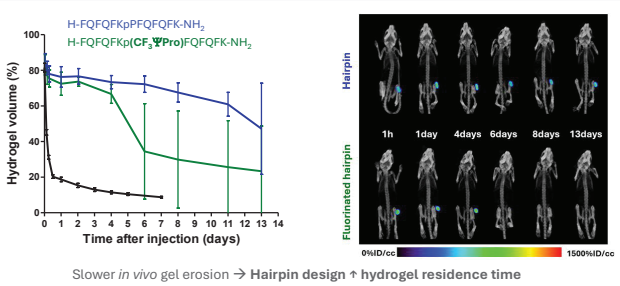

Slower *in vivo* gel erosion → **Hairpin design** ↑ **hydrogel residence time**

Conclusion & Perspectives

- **Fluorine incorporation in hexapeptide hydrogel** increases gels mechanical properties, impact the fibrils alignment and twist characteristics in the gel network.
- **Hairpin designed peptide hydrogel** show improved mechanical properties with more flexible fiber network **BUT** fluorine introduction in the turn is detrimental on physico-chemical properties of the gel.
- **Design of fluorinated hexamer hydrogels and β-hairpin hydrogels** allow to increase the hydrogel residence time *in vivo* after subcutaneous injection.
- Next: ***In vivo* drug release** properties of the different hydrogels.

ACKNOWLEDGEMENTS

We thank the CY Initiative of Excellence for their financial support through the EUTOPIA - PhD co-tutelle program 2020 (EXPLORE, 2020-166) and through the grant « Investissements d'Avenir » ANR-16-IDEX-0008). We thank the Research Council of VUB for the financial support through the Strategic Research Programme (SRP50 and SRP95). We thank the Research Foundation Flanders through FWO Hercules (OZR3939)

REFERENCES

[1] Chang, H. *et al, J. Mater. Chem. B*, **2019**, *7*, 2899
[2] Martin, C. *et al, J. Med. Chem.*, **2018**, *61*, 9784-9789.
[3] Heremans, J. *et al, J. Control. Release.*, **2022**, *350*, 514-524.
[4] Meanwell *et al, J. Med. Chem.*, **2018**, *61*, 5822
[5] Sloand, J. N. *et al, Pept. Sci.*, **2020**, *113*, e24184.
[6] Bettens, T. *et al, Mater. Adv*, **2021**, *2*, 4792
[7] Gadais, C. *et al, ChemBioChem*, **2018**, *19*, 1026
[8] Terrien, A. *et al, Biomacromolecules* **2023**, *24*, 4, 1555–1562

CRC 1449
Dynamic Hydrogels at Biointerfaces

FREIE UNIVERSITÄT BERLIN

Single glycans shape viscoelastic properties of a mucin-inspired peptide hydrogel

Jonas Proksch[1], Marlene Dal Colle[1,2], Frederick Heinz[2], Jacqueline Gottwald[3], Robert Schmidt[4], Dr. Martina Delbianco[2], Prof. Dr. Bettina Keller[1], Prof. Dr. Ulrike Alexiev[3], Prof. Dr. Michael Gradzielski[4], Prof. Dr. Beate Koksch[1]*

[1] Freie Universität Berlin, Institute of Chemistry and Biochemistry – Organic Chemistry, Berlin, Germany
[2] Max Planck Institute of Colloids and Interfaces, Department of Biomolecular Systems, Potsdam, Germany
[3] Freie Universität Berlin, Institute of Experimental Physics, Berlin, Germany
[4] Technische Universität Berlin, Stranski-Laboratory of Physical and Theoretical Chemistry, Berlin, Germany

https://doi.org/10.17952/37EPS.2024.P2319

Introduction

The main component of mucus are mucins, highly glycosylated proteins.[1] Building relevant experimental models for mucins is hindered by their vast size, glycan content and structural complexity.[2] Biologic mucus samples differ strongly depending on the donor.[3]

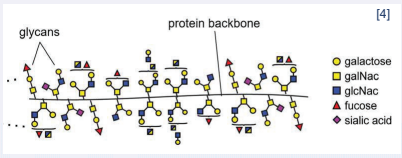

Aim

- Establish a simple and straightforward model for some key properties of mucus
- Systematically study the effect of glycan decoration on structure and viscoelastic properties
- Establish structure-property relations
- Identify key features for interactions with pathogens

Tool: A self-assembling peptide hydrogel scaffold for glycan-presentation

The peptide scaffold

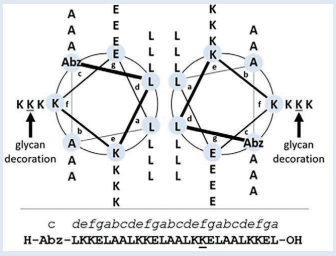

Glycan library

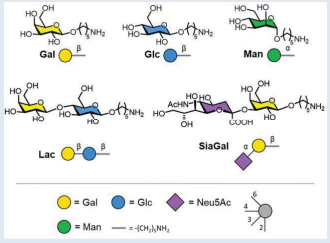

Glycopeptide library

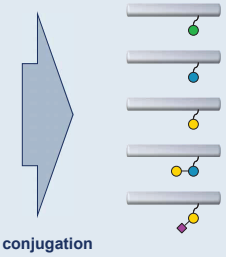

conjugation

self-assembly

Mucin-like hydrogel

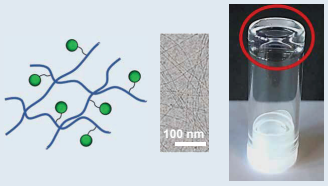

Results

Synthesis

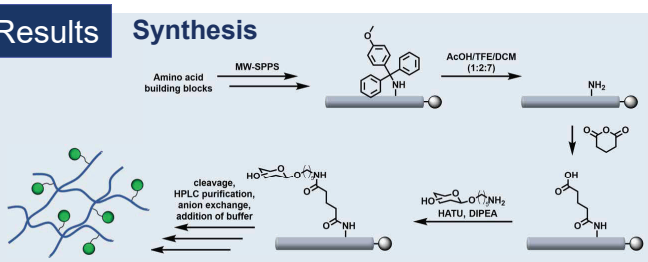

Structural properties

Circular dichroism

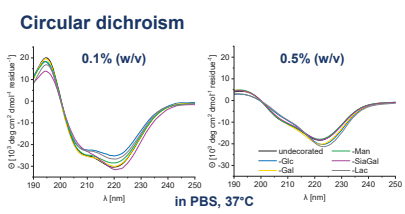

in PBS, 37°C

✓ Fibre formation with increasing concentration

Cryo-TEM

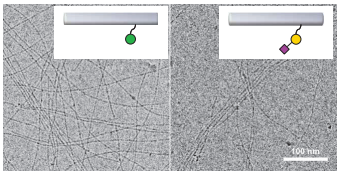

✓ Fibre formation unhindered by glycans

Mechanical properties

Macrorheology

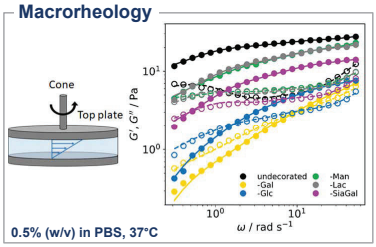

0.5% (w/v) in PBS, 37°C

Microrheology

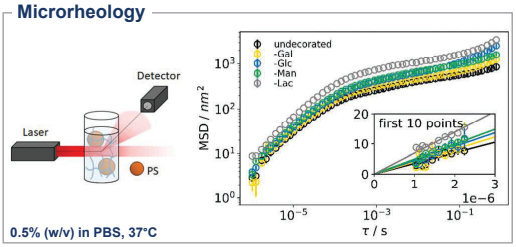

0.5% (w/v) in PBS, 37°C

Nanorheology

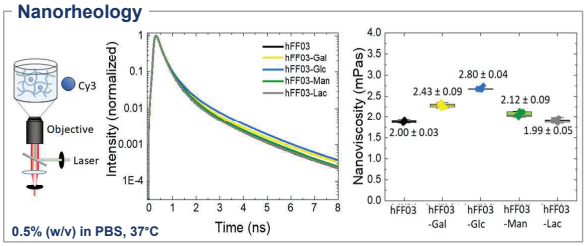

0.5% (w/v) in PBS, 37°C

✓ Rheology characterised over three techniques and length scales

✓ Rheology tuneable via glycan modification and pH

✓ Key properties (e.g. mesh size, G') comparable to native mucus[9]

Understanding the differences

✓ Hydrogel structure formation robust regardless of glycan

✓ Differences in viscoelastic behaviour depending on the glycan

✓ MD suggests importance of dynamic processes and the linker

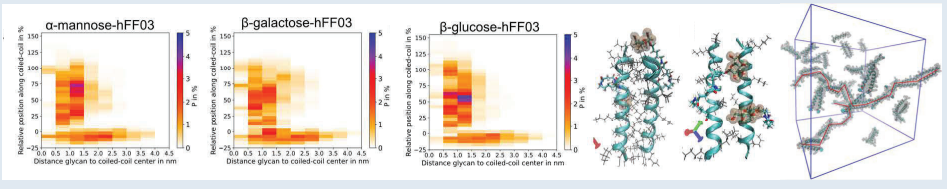

Outlook

Library expansion

Complex glycans

Multiple decoration

Mixed decoration

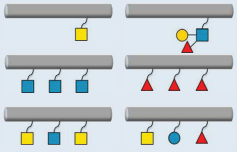

➢ Move closer to native mucus

Determine the influence of the linker

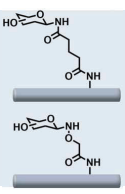

➢ "Long" vs "short"

Interactions with surroundings

Particle permeation



Pathogen interaction



➢ Identify key features for interactions with pathogens

References:
[1] R. Bansil, B. S. Turner, *Advanced Drug Delivery Reviews*, **2018**.
[2] C. E. Wagner, M. Krupkin, K. B. Smith-Dupont, C. M. Wu, N. A. Bustos, J. Witten, K. Ribbeck, *Biomacromolecules*, **2023**.
[3] S. K. Lai, Y.-Y. Wang, D. Wirtz, J. Hanes, *Advanced Drug Delivery Reviews*, **2009**.
[4] B.X. Wang, C.M. Wu, K. Ribbeck, *The FEBS Journal*, **2021**.
[5] K. S. Hellmund, B. von Lospichl, C. Böttcher, K. Ludwig, U. Keiderling, L. Noirez, A. Weiß, D. J. Mikolajczak, M. Gradzielski, B. Koksch, *Peptide Science*, **2021**.
[6] E. Zacco, J. Hütter, J. L. Heier, J. Mortier, P. H. Seeberger, B. Lepenies, B. Koksch, *ACS Chemical Biology*, **2015**.
[7] J. Proksch, M. C. S. Dal Colle, F. Heinz, R. F. Schmidt, J. Gottwald, M. Delbianco, B. G. Keller, M. Gradzielski, U. Alexiev, B. Koksch, *Journal of Peptide Science*, **2024**.
[8] F. Heinz, J. Proksch, R.F. Schmidt, M. Gradzielski, B. Koksch & B. G. Keller, *Biomacromolecules*, **2024**.
[9] R. Bej & R. Haag, *Journal of the American Chemical Society*, **2022**.

Acknowledgements: Funded by the Deutsche Forschungsgemeinschaft (DFG, German Research Foundation) through the CRC 1449 *Dynamic Hydrogels at Biointerfaces* (ID 431232613). The authors acknowledge the assistance of the core facility BioSupraMol supported by the DFG.

Contact: jonas.proksch@fu-berlin.de

@KokschGroup

Cardiolipin-specific peptides, designed to possess cell penetrating ability, rescue mitochondrial dysfunction[1]

Gwangsu Shin,[#] Dongwoo Kim, Yoonhwa Choi, Hyeong woon Choe, and Seung Hee Yang,[¶] Jaehoon Yu[#,*]

[#]Department of Chemistry & Education, Seoul National University, Seoul, Korea; [*]CAMP Therapeutics, Seoul, Korea;

[¶]Kidney Research Institute, Seoul National University Hospital, Seoul, Korea

https://doi.org/10.17952/37EPS.2024.P2330

Pathogenic CL-remodeling makes leaky IMM, resulting in mitochondrial dysfunction[2]

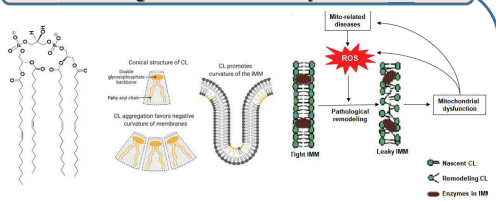

- Nascent CL (20% of total IMM) makes negative curvature, increasing surface area & fluidity of IMM, helps for proteins carrying out most chemical reactions in mitochondria
- CL is oxidized to be pathogenic remodeling, affording leaky IMM, where proteins begins to lose their functions
- Owing to the leaky IMM, dysfunctional mitochondria triggers a variety of degenerative diseases

Mitochondrial dysfunction can be restored by peptides, binding strongly to CLs, keeping tight IMM

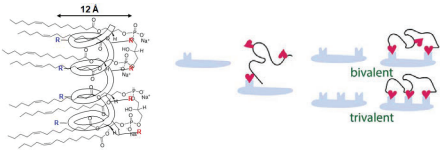

- More than 4 positive charges in amphipathic α-helix interacts with 4 negative charged phosphates in bivalent or trivalent CLs, increasing avidity
- α-Helical peptide has wider diameter to afford strong hydrophobic interactions with those parts in CLs
- Repairing all defective IMM is not necessary; A portion of active IMM is enough to restore normal tissue function; a small amount of CL-specific peptide may give enough efficacy

We have cell penetrable bundled α-helical peptides,[3] but lack of specificity to mitochondria

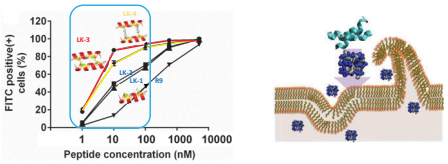

- α-Helical monomers are oxidized to form "dimer bundle" via 2 disulfide bonds[3]
- The "dimer bundle" has nano-molar cell penetrating ability, forming oligomers to facilitate endocytosis[4]
- It has >100-fold ability than the corresponding monomer peptides, which is penetrable only at micro-molar concentrations
- Introduction of mitochondria-specific residues in "dimeric bundle" would not ruin the cell penetrating ability

Synthesis of the deconvolution peptide library & selection for inhibition of ROS production

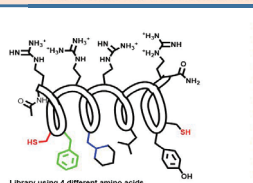

	hdf1	hdf2	hdf3	hdf4	
Ac-	Phe	Hdf	Hdf	Hdf	-amide
Ac-	Leu	Hdf	Hdf	Hdf	-amide
Ac-	Tyr	Hdf	Hdf	Hdf	-amide
Ac-	Cha	Hdf	Hdf	Hdf	-amide
Ac-	Hdf	Phe	Hdf	Hdf	-amide
Ac-	Hdf	Leu	Hdf	Hdf	-amide
Ac-	Hdf	Tyr	Hdf	Hdf	-amide
Ac-	Hdf	Cha	Hdf	Hdf	-amide
Ac-	Hdf	Hdf	Phe	Hdf	-amide
Ac-	Hdf	Hdf	Leu	Hdf	-amide
Ac-	Hdf	Hdf	Tyr	Hdf	-amide
Ac-	Hdf	Hdf	Cha	Hdf	-amide
Ac-	Hdf	Hdf	Hdf	Phe	-amide
Ac-	Hdf	Hdf	Hdf	Leu	-amide
Ac-	Hdf	Hdf	Hdf	Tyr	-amide
Ac-	Hdf	Hdf	Hdf	Cha	-amide

- Hdf; a mixture of known mitochondrial specific AA (Phe, Leu, Tyr & Cha) to increase diversity
- Each hydrophobic AA was position-scanned to make 16 sub-libraries (each sub-library contains 64 kinds, total 1,024 kinds of peptides)
- CMP001 was selected for the best inhibitor of ROS production

Maintaining mitochondrial function & protecting by CMP001 in oxidative damaged cells

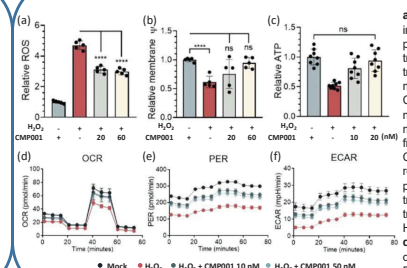

a and b, CMP001 inhibits ROS (a) production. Peptide pre-treated (3 h) cells were treated with H_2O_2 (0.5 mM) for 30 min. **b,** CMP001 preserves mitochondria membrane potential (ψ) from H_2O_2 stimulus. **c,** CMP001 causes resumption of ATP production. Peptide pre-treated (3 h) cells were treated with 1 mM of H_2O_2 for 1 h. **d-f,** CMP001 protects cellular respiration from ROS stimulus

CMP001 goes to the damaged (donut-shape) mitochondria

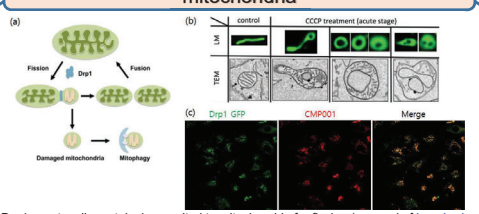

- Drp1, a cytosolic protein, is recruited to mitochondria for fission (removal of impaired mitochondria, (a)
- If CCCP is treated, mitochondria goes to donut- or blub-shape, less & shorter cristae (b)
- Drp1-GFP was transfected to cells; it went to the damaged mitochondria (c)
- CMP001 is colocalized with Drp1, suggesting that CMP001 goes to the damaged or dysfunctional mitochondria (c)

Mitochondrial fractionation of CMP001 & other peptides

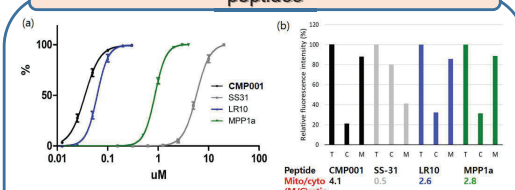

Peptide	CMP001	SS-31	LR10	MPP1a
Mito/cyto (M/C)ratio	4.1	0.5	2.6	2.8

- For the fair comparison, cell penetrating ability (EC_{50}, concentration of a peptide, at which it is inserted to 50% of the cells) of peptides (SS-31[5]; a typical CPP, LR10[6]; Kelley's MPP[7]; CMP001) were determined
- CMP001 shows the lowest EC_{50} value; It has the best cell penetrating ability
- After peptides were inserted into cells, mitochondria were fractionated
- CMP001 shows the highest mito/cyto ratio (4.1) to compare with other peptides

CMP001 protects and rejuvenates cristae depleted by H_2O_2

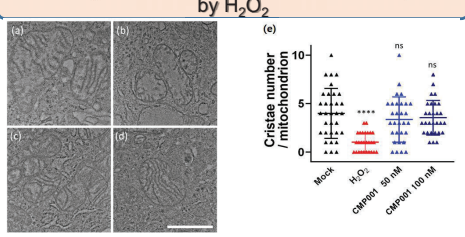

TEM images were observed after the following treatment conditions; (a) mock, (b) HeLa cells were treated with 0.5 mM of H_2O_2 for 2 h, (c-d) cells were pretreated with CMP001 (50 nM for c and 100 nM for d, respectively) for 2 h, followed by H_2O_2 for another 2 h, (e) more than 0.5 μm-long cristae was counted from at least 50 independent mitochondrial images. Scale bar = 1 μm.

CMP001m binds to the remodeled DLCL, possibly promoting dysfunctional mitochondria

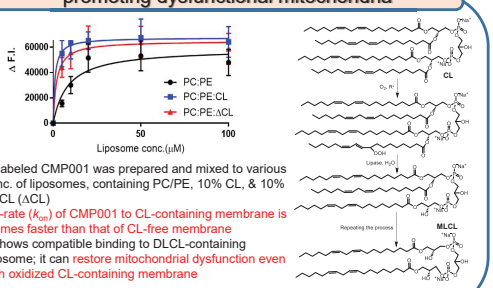

- FI-labeled CMP001 was prepared and mixed to various conc. of liposomes, containing PC/PE, 10% CL, & 10% DLCL (ΔCL)
- On-rate (k_{on}) of CMP001 to CL-containing membrane is 8-times faster than that of CL-free membrane
- It shows compatible binding to DLCL-containing liposome; it can restore mitochondrial dysfunction even with oxidized CL-containing membrane

CMP001m strongly binds to membrane w/ > 5% CL & dissociates slowly from CL-containing membrane

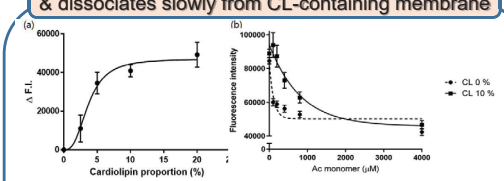

(a) To a solution of NBD-labelled CMP001m (1 μM in PBS) in black 96-well plate, CL-containing liposomes (POPC:POPE = 2:1, 0 to 20 % various contents of CL) were added; After mixing for 10 min, fluorescent NBD was measured (Final liposome concentration = 5 μM); λ_{ex} = 467 nm, λ_{em} = 536 nm; n = 3; strong affinity between CMP001m & membrane is maintained if the membrane contains 5-20% CL

(b) A competition assay using non-labeled CMP001m was carried out for dissociation of the peptide from CL-containing or CL-free membrane; same as above conditions; Off-rate (k_{off}) of CMP001 monomer from CL-containing membrane is 8-times slower than that of CL-free membrane

CMP001 attenuates nephrotoxicity induced by colistin in mouse model

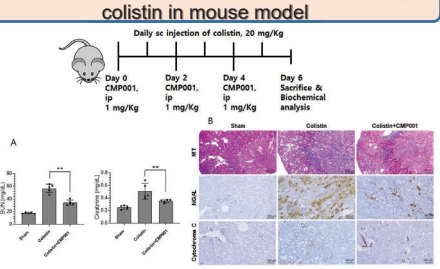

- AKI induced by colistin was rescued by small amount of CMP001 (1mg/Kg)
- BUN & creatinine levels are significantly reduced
- Biomarkers, such as NGAL & cytochrome C are greatly reduced

CMP001 protects mitochondria in the kidney section of colisitin induced kidney injury mice

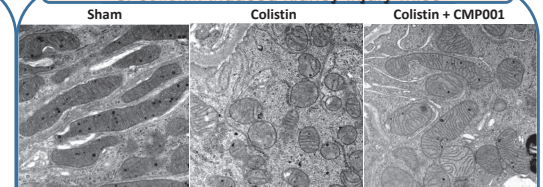

- TEM images were observed after sacrificing colistin-induced nephrotoxicity (CIN) mice. Scale bar = 1 mm. TEM images were observed after sacrificing colistin-induced nephrotoxicity (CIN) mice. Scale bar = 1 μm.
- In the CIN mouse model, CMP001 rejuvenates the kidney's morphology and cristae of mitochondria.

The survival curves of CMP001 treated on the colistin-induced nephrotoxicity (CIN) mouse model

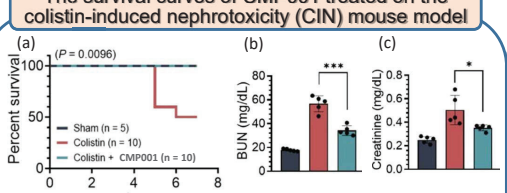

- Five mice (5 days = 4 and 6 days =1) without CMP001 treatment died of nephrotoxicity-associated renal failure, with a percentage of survival of 50% (Long-rank, p-value = 0.0096), respectively
- CMP001-treated mice live beyond CIN mice, **showing a rate the same as the control**
- A dose of CMP001 promotes colistin-induced acute kidney injury reductions and is beneficial in mortality
- CMP001 protects the kidney function (BUN, Cr levels) on the CIN mouse model.

CMP001 increases anti-inflammatory effects on the Ischemia-reperfusion injury (IRI) mouse model

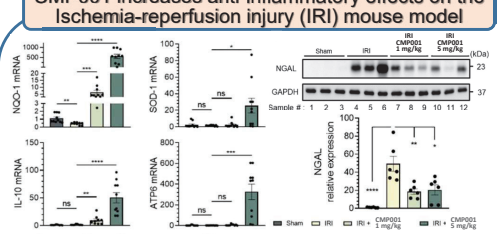

- In IRI mouse model, CMP001 increases mRNA of anti-inflammatory enzymes such as NAD(P)H dehydrogenase 1 (NQO-1), superoxide dismutase-1 (SOD-1).
- CMP001 decreases Neutrophil Gelatinase-Associated Lipocalin (NGAL), which is a early marker of kidney injury and inflammation.

Summary; CL-specific peptide holds IMM structure

- Chemically important events in mitochondria occur in the inner membrane, where cardiolipin (CL), a specific phospholipid, causes curvature needed for functional proteins to function properly
- Pathological CL remodeling, however, destroys the curvature, resulting in mitochondrial dysfunction
- The amphipathic dimeric α-helical peptide, CMP001, penetrates into cells, binds to multiple CLs, and regenerates mitochondrial curvature
- This results in gathering of mitochondrial proteins and correction of mitochondria dysfunction in many human diseases

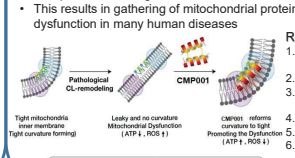

References

1. Shin G et al., *Journal of Medicinal Chemistry* **2024**, 67, 3385.
2. Zhang J, Shi Y. *Cells* **2022**, *11*, 1906.
3. Jang SM et al., *Angew. Chem.* **2014**, *53*, 10086.
4. Hyun S et al., *ACS Cent. Sci.* **2018**, *4*, 885.
5. Szeto HH. *Protein Pept. Lett.* **2018**, *25*, 1108.
6. Hyun S et al., *Bioconjug. Chem.* **2022**, *33*, 2420.
7. Jean SR et al., *Acc. Chem. Res.* **2016**, *49*, 1893.

https://doi.org/10.17952/37EPS.2024.P2331

Efficient synthesis of three-helix bundle proteins using ligase-mediated trimerization of HIV-1 fusion inhibitor T20 on a dendrimer scaffold

Xiaohong Zhang, Yiyin Xia, Chuan-Fa Liu and James P. Tam

School of Biological Sciences, Synzymes and Natural Products Center, Nanyang Technological University, Singapore 637551

INTRODUCTION

Helix bundles are stable quaternary proteins and hold promise for developing therapeutics and synthetic vaccines. However, their synthesis, particularly by enzymatic methods, continues to be challenging. Peptide asparaginyl ligases (PAL) have been shown to be useful for precision protein conjugations, modifications and semi-synthesis. Butelase-1, which is the prototype PAL discovered in 2014 [1], is a transpeptidase because the reverse reaction could decrease the ligation yield in certain applications. To overcome this drawback, we have recently developed PAL-QC enzymatic cascade method in which a second enzyme, glutaminyl cyclase (QC) is added in the reaction mixture to prevent the reverse reaction by a glutaminyl dipeptide liberated from the PAL-mediated reactions as an inactive pyroglutamyl dipeptide [2]. Here, we report a successful synthesis of a highly stable three-helix bundle (3HB) of an HIV-1 fusion inhibitor using a PAL-QC cascade ligation approach. We used a modified 41-residue T20 (enfuvirtide) on a dendrimeric lysine-based scaffold to form a 3HB-T20 quaternary mimics by the PAL-QC ligation. Addition of QC resulted in a 78% ligation yield in 3 h, and which is much higher than a reaction without QC. A combination of CD analysis and proteolytic stability showed that the T20-trimer exhibits a 3HB structure that is highly stable to proteolytic degradation, and which was not observed in the monomer.

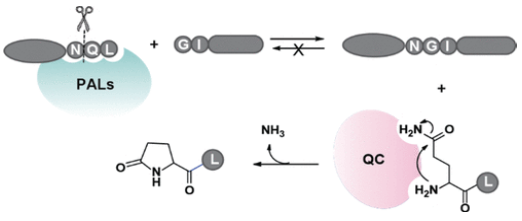

General scheme of PAL-QC enzymatic cascade method

SCHEMES

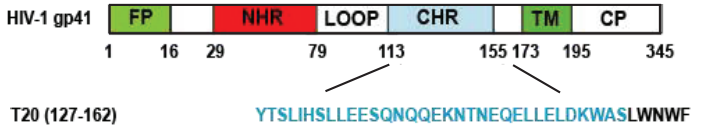

Scheme 1. Schematic illustration of HIV-1 gp41 and amino acid sequence of T20

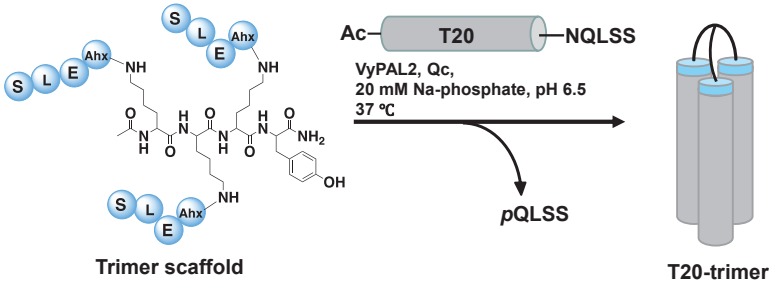

Scheme 2. The synthesis of T20-trimer using the PAL-QC cascade ligation method

RESULTS

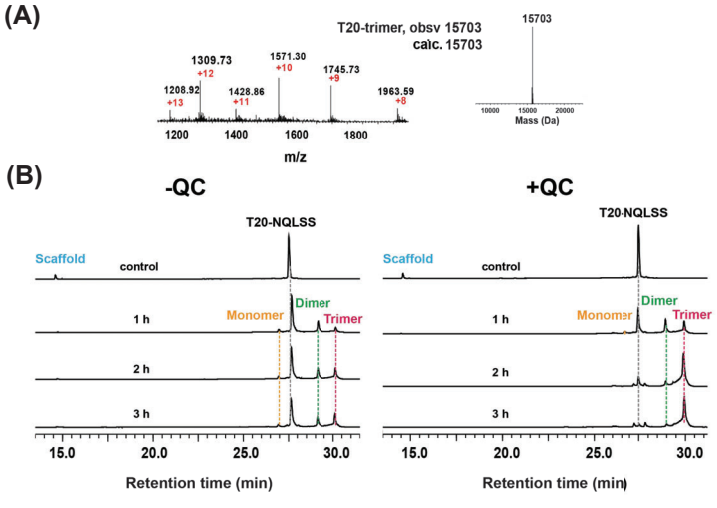

Figure 1. VyPAL2-mediated T20 trimerization with and without QC. Reaction conditions: T20-NQLSS 0.7 mM, scaffold 0.15 mM, 1.4 uM VyPAL, 0.7 uM QC in 20 mM Na-phosphate buffer, pH 6.5, 37 °C. (A). Mass of T20-trimer. (B). HPLC profile of conjugation reaction.

RESULTS

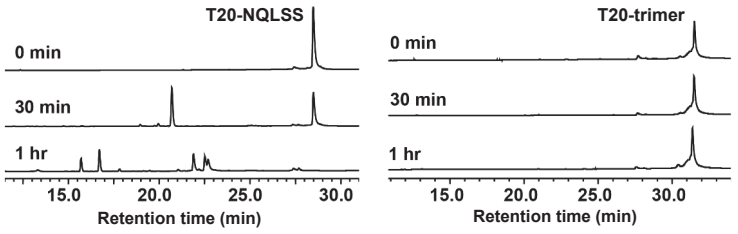

(A) Monomer T20-NQLSS digestion (B) T20-trimer digestion

Figure 2. Stability test of T20-NQLSS and T20-trimer against proteinase K digestion. 0.1 eq. of Proteinase K was added to the testing solution for 0, 30 and 60 min digestion.

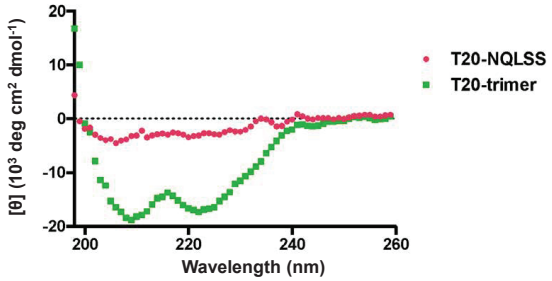

Figure 3. CD spectra of monomer- and trimer-T20 indicate that the trimer adopts an α-helix structure while the monomer does not. Solutions of 10 μM of peptides were prepared in phosphate buffer pH 7.4.

SUMMARY

In sum, our results demonstrated that PAL-QC cascade enzymatic ligation is an effective method to prepare protein multimers for therapeutic, diagnostic and biotechnological applications.

REFERENCES

1. G. K. T. Nguyen, S. Wang, Y. Qiu, X. Hemu, Y. Lian, and J. P. Tam (2014). Butelase 1 is an Asx-specific ligase enabling peptide macrocyclization and synthesis. *Nat. Chem. Biol.*, **10** (9), 732-738.
2. Y. Xia, F. Li, X. Zhang, S. Balamkundu, F. Tang, S. Hu, J. Lescar, J. P. Tam, C.-F. Liu (2023). A Cascade Enzymatic Reaction Scheme for Irreversible Transpeptidative Protein Ligation. *J. Am. Chem. Soc.*, **145** (12), 6838–6844.

ACKNOWLEDGEMENT

This research was supported in part by the Nanyang Technological University Internal Funding Synzymes and Natural Products (SYNC) and Ministry of Education Singapore (MOE-T2EP30222-0004).

https://doi.org/10.17952/37EPS.2024.P2332

Broaden the Applications of Peptidyl Asparaginyl Ligases

Yiyin XIA, Hongxia LI, Jiayong LIU, James P.TAM, Chuan Fa LIU
School of Biological Sciences, Nanyang Technological University, Singapore

INTRODUCTION

Peptidyl asparaginyl ligases (PALs) are transpeptidases that recognize substrates with an Asx-Xaa-Yaa (P1-P1'-P2') tripeptide motif, where P1-Asx is Asn or Asp. PALs cleave the peptide bond after the Asx residue to form an acyl-enzyme thioester intermediate which is subsequently resolved by the N$^{\alpha}$-amine of an incoming nucleophile peptide, forming a new Asx-peptide bond. Owning to their short recognition motifs and high catalytic efficiency, PALs have been used in many applications, such as peptide/protein macrocyclization, protein C- or N-terminal conjugation and cell-surface labelling. In our previous work, we have discovered that PALs can accept an unnatural amino acid as the P1 residue [1] or a non-aminoacid nucleophile substrate [2]. We have also established a method that overcomes the reversibility of PAL-mediated ligation – a major shortcoming of the transpeptidation reaction – by coupling it to glutaminyl cyclase (QC)-catalysed pyroglutamyl formation (Scheme 1) [3]. By quenching the nucleophilic α-amine of a P1'-Gln in a lactam, PAL-mediated ligation becomes irreversible and can achieve near-quantitative yields. Thus, this cascade reaction scheme greatly improves the efficiency of PAL-mediated ligation. Recently, we show that the ligation yields of non-aminoacid nucleophiles with antibody can also be improved using QC-PAL cascade reaction scheme. In this poster, we will present various examples of bioconjugates, including antibody-drug conjugates, that are prepared by PAL-mediated ligation. These examples further establish PALs as precision biomanufacturing tools for protein-based biologics.

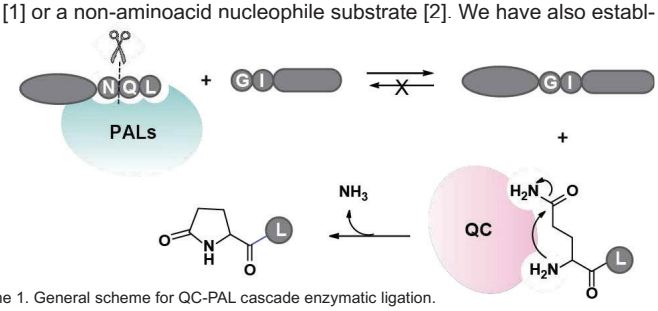

Scheme 1. General scheme for QC-PAL cascade enzymatic ligation.

RESULTS

1. Protein-peptide ligation

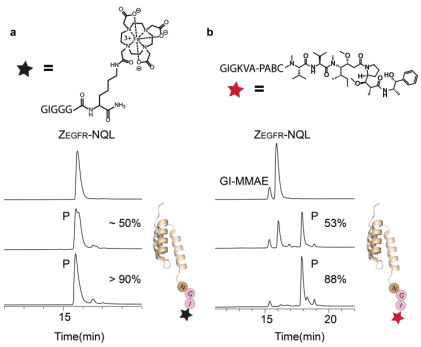

Figure 1. PAL-QC coupled cascade ligation of affibody Z_{EGFR} with DOTA and MMAE peptides. Yields are estimated by HPLC analysis, in the presence or absence of QC. Black and red stars refer to DOTA and MMAE peptides, respectively.

2. Protein-protein ligation

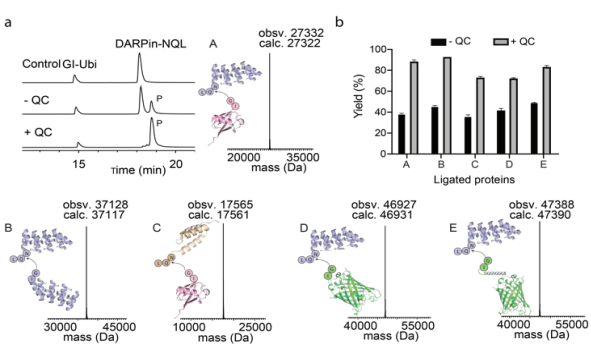

Figure 2. PAL-QC coupled cascade protein-protein ligation. (a) HPLC monitoring of VyPAL2-mediated ligation between DARPin and ubiquitin. (b) Yields of various protein−protein ligations in the presence or absence of QC [DARPin (purple), ubiquitin (pink), Z_{EGFR} (yellow), GFP (green)].

3. Large protein ligation

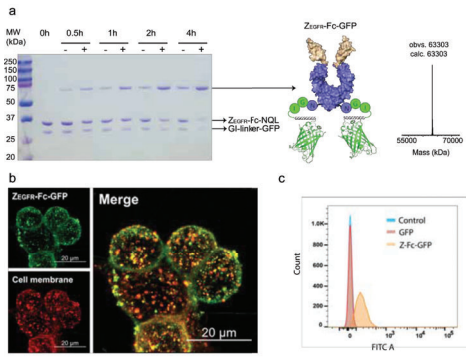

Figure 3. PAL-QC coupled cascade ligation of large proteins. a) SDS-PAGE of the ligation reaction. b). Confocal microscopy image of ZEGFR-Fc-GFP binding to A431 cells c). Flow cytometry analysis of ZEGFR-Fc-GFP targeting A431.

4. Antibody-drug conjugation

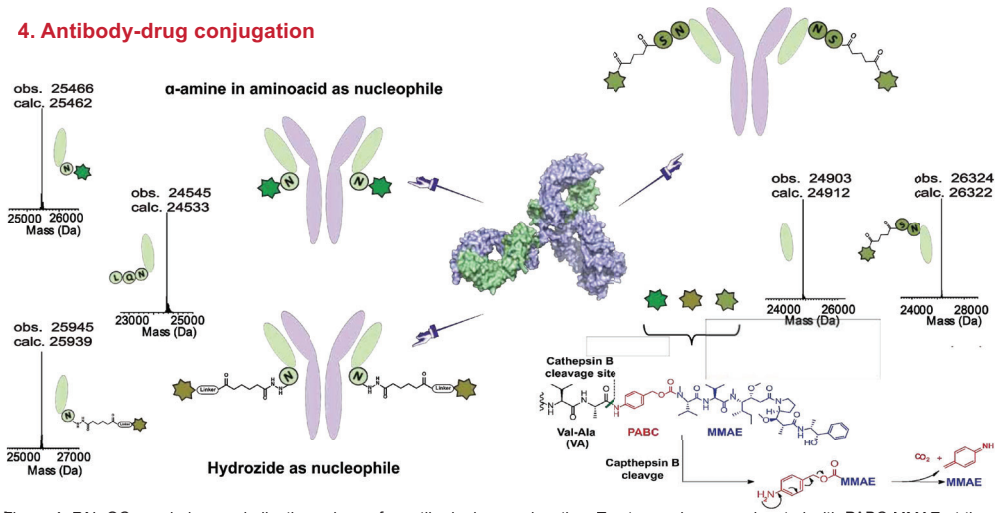

Figure 4. PAL-QC coupled cascade ligation scheme for antibody-drug conjugation. Trastuzumab was conjugated with PABC-MMAE at the N or C terminal of the light chains of Trastuzumab.

5. Cytotoxicity of protein-drug conjugates

Compound	IC_{50} (nM) BT-474	MCF7
MMAE	0.05 ± 0.01	0.08 ± 0.02
Trastuzumab	> 100	> 100
MMAE-PABC-Trastuzumab (DAR2)	2.49 ± 0.05	> 100
Trastuzumab-PABC-MMAE (DAR2)	0.16 ± 0.01	> 100
Compound	**A431**	**MCF7**
Z_{EGFR}-Fc-PABC-MMAE	69.53 ± 28.9	> 100
Z_{EGFR}-PABC-MMAE	12.89 ± 3.02	> 100

Table 1. IC_{50} of MMAE-labelled proteins on A431 (EGFR+), BT-474 (HER2+) and MCF7 (EGFR-/HER2-) cells. IC_{50} values were presented as mean ± SEM.

CONCLUSION

To sum up, we successfully used the PAL and QC enzymes for ADC preparation. The synthetic ADCs showed high selectivity towards HER2+ cell lines (BT-474). These results show that the PAL-QC cascade ligation scheme is a powerful tool for ADC generation.

ACKNOWLEDGEMENTS

This research was supported by Ministry of Education Singapore (MOE-T2EP30222-0004 and AcRF Tier 1 RG9/23)

REFERENCES

1. Y. Xia, *et al.* (2021). Nγ-Hydroxy-asparagine: A Multifunctional Unnatural Amino Acid That is a Good P1 Substrate of Asparaginyl Peptide Ligases. *Angew. Chem. Intl. Ed.*, **60** (41), 22207–22211.
2. D. Zhang. *et al.* (2022). Asparaginyl Endopeptidase-Mediated Protein C-Terminal Hydrazinolysis for the Synthesis of Bioconjugates. *Bioconj. Chem.*, **33** (1), 238–247.
3. Y. Xia, *et al.* (2023). A Cascade Enzymatic Reaction Scheme for Irreversible Transpeptidative Protein Ligation. *J. Am. Chem. Soc.*, **145** (12), 6838–6844.